University of Agronomic Sciences
and Veterinary Medicine of Bucharest
Faculty of Land Reclamation
and Environmental Engineering

# SCIENTIFIC PAPERS

## Series E

## LAND RECLAMATION, EARTH OBSERVATION & SURVEYING, ENVIRONMENTAL ENGINEERING

## Volume XV




2026
BUCHAREST

# SCIENTIFIC PAPERS

Series E

LAND RECLAMATION, EARTH OBSERVATION &
SURVEYING, ENVIRONMENTAL ENGINEERING

Volume XV



University of Agronomic Sciences
and Veterinary Medicine of Bucharest
Faculty of Land Reclamation
and Environmental Engineering

# SCIENTIFIC PAPERS

## Series E

## LAND RECLAMATION, EARTH OBSERVATION & SURVEYING, ENVIRONMENTAL ENGINEERING

## Volume XV

2026
BucharesT

**EDITORIAL BOARD**

**General Editor:** Razvan Ionut TEODORESCU

**Executive Editor:** Ana VIRSTA

**Managing Editor:** Augustina Sandina TRONAC

**Members:** Maria Jose ORUNA CONCHA, Radu Claudiu FIERASCU, Jana ŠIC ŽLABUR, Maria POPA, Fulvio CELICO, Catalina ITICESCU, Rupesh Kumar SINGH, Jelena LUBURA STOŠIĆ, Petrica VIZUREANU, Orhan ERCAN, Denis MIHAILESCU, Deodato TAPETE, Lucian COPOLOVICI, Jesus SIMAL-GANDARA, Alina ORTAN

**PUBLISHERS:**
**University of Agronomic Sciences and Veterinary Medicine of Bucharest, Romania - Faculty of Land Reclamation and Environmetal Engineering**
Address: 59 Marasti Blvd, District l, Zip code 011464, Bucharest, Romania
Phone: + 40 213 1830 75, E-mail: conference@fifim.ro, Webpage: www.fifim.ro

**CERES Publishing House**
Address: 106 Izbiceni Street, District 1, Bucharest, Romania
E-mail: edituraceres@yahoo.com, Webpage: www.editura-ceres.ro

**Copyright 2026**
*To be cited: Scientific Papers. Series E. LAND RECLAMATION, EARTH OBSERVATION & SURVEYING, ENVIRONMENTAL ENGINEERING, Vol. XV, 2026*

*The publishers are not responsible for the content of the scientific papers and opinions published in the Volume. They represent the authors' point of view.*

**Print ISSN 2285-6064, CD-ROM ISSN 2285-6072, Online ISSN 2393-5138, ISSN-L 2285-6064**

**International Database Indexing:**
Web of Science Core Collection (Emerging Sources Citation Index)
Index Copernicus; Ulrich's Periodical Directory (ProQuest); PNB (Polish Scholarly Bibliography); Scientific Indexing Service; Cite Factor (Academic Scientific Journals) Scipio; OCLC; Research Bible

**SCIENTIFIC & REVIEW COMMITTEE**

**SCIENTIFIC CHAIRMAN**
Prof. univ. dr. Sorin Mihai CIMPEANU

**MEMBERS***

- Stefano CASADEI – University of Perugia, Italy
- Carmen CIMPEANU – University of Agronomic Sciences and Veterinary Medicine of Bucharest, Romania
- Sorin Mihai CIMPEANU – University of Agronomic Sciences and Veterinary Medicine of Bucharest, Romania
- Andrea DOMINIJANNI – Politecnico di Torino, Italy
- Claudiu DRAGOMIR - University of Agronomic Sciences and Veterinary Medicine of Bucharest/ National Institute for Research and Development - URBAN-INCERC, Bucharest, Romania
- Eric DUCLOS-GENDREU – Spot Image GEO-Information Services, France
- Jean-Luc HORNICK – Université de Liège, Belgium
- Hossein KAZEMI – GUASNR, Gorgan, Iran
- Bela KOVACS – University of Debrecen, Hungary
- Raluca MANEA – University of Agronomic Sciences and Veterinary Medicine of Bucharest, Romania
- Tamara van OMMEREN-MYSLYVA – Ministry of Spatial Planning and Environment of Suriname
- Jovan Br. PAPIC – Ss. Cyril and Methodius University, Skopje, R. N. Macedonia
- Nelson PÉREZ-GUERRA – University of Vigo, Spain
- Nicolae PETRESCU – Valahia University Targoviste, Romania
- Dorin Dumitru PRUNARIU – Romanian Space Agency, Romania
- Andrei Victor SANDU – "Gheorghe Asachi" Technical University of Iași, Romania
- Simona MARCU-SPÎNU – University of Agronomic Sciences and Veterinary Medicine of Bucharest, Romania
- Umut Gunes SEFERCIK – Gebze Technical University, Turkey
- Ando SHIN – Tokyo University of Science, Japan
- Marisanna SPERONI – Centro di Ricerca Zootecnia e Acquacoltura, Consiglio per la Ricerca in Agricoltura e L'analisi Dell'economia Agraria (CREA), Italy
- Razvan Ionut TEODORESCU – University of Agronomic Sciences and Veterinary Medicine of Bucharest, Romania
- Péter UDVARDY – Óbuda University, Hungary
- Neven VOĆA – University of Zagreb, Croatia

**alphabetically ordered by family name*

# CONTENTS

## ENVIRONMENTAL SCIENCE AND ENGINEERING


1 NICKEL SPECIATION AND BIOAVAILABILITY IN SERPENTINE SOILS OF THE EASTERN AND SOUTHERN RHODOPES, BULGARIA - **Violina ANGELOVA** ..... 15

2 POTENTIAL OF SELECTED AROMATIC ASTERACEAE SPECIES FOR THE PHYTOREMEDIATION OF HEAVY METAL - CONTAMINATED SOILS - **Violina ANGELOVA, Maria IHTYAROVA**..... 23

3 INVESTIGATION OF HYDROCARBON POLLUTION IN THE OIL TERMINAL CONSTANȚA AREA USING ELECTRICAL RESISTIVITY METHODS AND HYDROSTATIC REGIME ANALYSIS - **Sorin ANGHEL, Andrei Gabriel DRAGOS, Gabriel IORDACHE, Bogdan Marius BARAITAREANU, Constanta Alexandra DUDU**..... 30

4 MINERAL COMPOSITION OF *VACCINIUM VITIS-IDAEA* FRUITS ACROSS DIFFERENT MOUNTAIN HABITATS - **Carla-Maria APARASCHIVE, Alina TRUTA, Irina MORAR, Tania MIHAIESCU, Claudia BALINT, Alexandra MURESAN, Catalina DAN, Adriana SESTRAS**..... 36

5 FROM WASTE TO RESOURCE: IMPLEMENTING SPENT GARNET (SG) AS A PARTIAL FINE AGGREGATE IN CEMENT-BASED MATERIALS — TECHNICAL, LEGAL AND COMMERCIAL PERSPECTIVES - **Cornelia BAERA, Aurelian GRUIN, Ana Cristina VASILE, Caius LUMINOSU, Ana-Andreea MIHARTESCU, Alexandra Marina BARBU** ..... 45

6 TECHNICAL FRAMEWORK FOR SUSTAINABLE VALORIZATION OF VINEYARD BY-PRODUCTS THROUGH SMALL-SCALE PROCESSING TECHNOLOGIES - **Carmen BALTATU, Gabriel Valentin GHEORGHE, Dragos MANEA, Larisa-Bianca IONICA**..... 59

7 SUSTAINABLE UNFIRED CLAY MASONRY INCORPORATING AGRICULTURAL WASTE: PHYSICAL AND MECHANICAL PROPERTIES - **Alexandra-Marina BARBU, Aurelia BRADU, Claudiu-Sorin DRAGOMIR, Augustina-Sandina TRONAC**..... 69

8 EFFECT OF SOIL TYPE AND MANAGEMENT ON POTENTIALLY TOXIC ELEMENTS (As, Cu, Zn) IN SOILS OF OLIVE GROVES IN DALMATIA, CROATIA - **Aleksandra BENSA, Nikolina JURKOVIĆ BALOG, Aleksandra PERČIN**..... 79

9 THE DUAL CHALLENGE OF CO2 AND OZONE: INSIGHTS INTO PHOTOSYNTHESIS, VOC EMISSION AND BIOCHEMICAL RESPONSES - **Flavia BORTES, Lucian COPOLOVICI, Cristian MOISA, Andreea LUPITU, Dana Maria COPOLOVICI** ..... 89

10 MOISTURE, LIPID CONTENT, AND MERCURY IN FRESHWATER FISH MUSCLE: INDICATORS OF ECOLOGICAL CONDITION IN THE LOWER DANUBE RIVER - **Andreea-Miruna CODREANU, Ștefania-Adelina MILEA, Cristina Mihaela LUNTRARU, Alin Constantin DÎRȚU, Cătălina ITICESCU** ..... 97

11 *DAPHNIA MAGNA* INDICATOR OF WATER POLLUTION WITH ZINC – **Paula COJOCARU, Alexandra-Andreea STRUNGARU, Gabriela BIALI, Maria Cătălina PASTIA** ..... 105

12 CARBON STORAGE IN FOREST STANDS ON DEGRADED LANDS - **Cristinel CONSTANDACHE, Ciprian TUDOR, Laurențiu POPOVICI, Raul RADU**..... 113

13 SEASONAL AND DIURNAL DYNAMICS OF SIZE-RESOLVED PARTICULATE MATTER IN AN URBAN AREA OF GALAȚI, ROMANIA, BASED ON CONTINUOUS RAPID-E MONITORING - **Mădălin CRISTEA, Adrian ROȘU, Sorin FRĂSÎNĂ, Bogdan ROȘU, Daniel-Eduard CONSTANTIN, Mirela VOICULESCU, Silvia DRĂGAN**..... 121

14 BACTERIAL MICROBIOTA IN AQUATIC ENVIRONMENTS AND THE BIODEGRADATION POTENTIAL OF SUSTAINABLE MATERIALS: INSIGHTS INTO ENVIRONMENTAL FATE - A REVIEW - **Andreea DOROFTE, Ira-Adeline SIMIONOV, Ștefan-Mihai PETREA, Cătălin PLATON, Cătălina ITICESCU** ..... 131
15 FOREWARNING ON SOME POLLUTANTS AND THEIR EFFECTS ON WATERFOWL - **Cristina Alina DUMITRACHE** ..... 144
16 MOBILITY AND TOXICOLOGICAL RELEVANCE IN THE EVALUATION OF HEAVY METAL TRANSFER FROM SOIL TO PLANTS - **Claudiu-Denis FILIP, Mirela Ana COMAN** ..... 151
17 ENVIRONMENTAL AND SOIL IMPACTS OF END-OF-LIFE LITHIUM-ION BATTERIES: QUANTITATIVE POLLUTION SCENARIOS, EMERGING CONTAMINANTS AND RECYCLING-ROUTE ASSESSMENT - **Roxana-Elena FRÎNCU, Carmen Otilia RUSĂNESCU, Ana VÎRSTA, Elena-Denisa PREDESCU, Daniela MIHAI, Sabrina Maria BĂLĂNESCU, Ionela Alexandra ION** 163
18 ELECTROCHEMICAL SENSORS FOR DETECTING ENVIRONMENTAL POLLUTANTS - A REVIEW - **Andrei-Daniel GEMAN, Andreea-Loredana COMĂNESCU, Constantin APETREI, Cătălina ITICESCU, Puiu-Lucian GEORGESCU** ..... 172
19 TREE COMMUNITY PATTERNS IN RELATION TO EDGE INFLUENCE IN A PERI-URBAN FOREST NEAR CLUJ-NAPOCA, ROMANIA - **Ioana-Loredana GHIURCO, Carla-Maria APARASCHIVE, Adela-Maria NEAG, Iulia-Ecaterina MORA, Păunița BOANCĂ, Sonia BODEA, Denisa JUCAN, Catalina DAN, Adriana ESTRAS** ..... 184
20 STUDY OF THE DYNAMICS OF SOME WATER QUALITY PARAMETERS IN THE PRUT RIVER AREA DURING 2014-2023 - **Dinu GÎRNEȚ, Lorena DELEANU, Gabriel MURARIU, Laura DANILESCU, Romana DRASOVEAN** ..... 193
21 DYNAMICS OF AIRBORNE MICROORGANISMS ACCORDING TO ENVIRONMENTAL CONDITIONS - **Bilyana GRIGOROVA-PESHEVA, Asen PESHEV, Georgi KADINOV, Ekaterina TODOROVA, Boyka MALCHEVA** ..... 202
22 *IN VITRO* PROPAGATION OF *EUONYMUS FORTUNEI* CULTIVARS FOR SUSTAINABLE URBAN GREENING AND DEGRADED LAND REHABILITATION - **Tatiana GROPA, Ion ROȘCA, Ioana-Cătălina NICOLAE** ..... 211
23 HYBRID RENEWABLE ENERGY SUPPLY SYSTEM - STORAGE REQUIREMENTS CONSIDERING SEASONAL VARIATION OF PV OUTPUT - **Mirela Laura IEREMCIUC, Ioan DAVID, Camelia ȘTEFĂNESCU, Mihai NEGURA, Dorina-Gabriela IONESCU, Mircea VIȘESCU** ..... 222
24 A LOW-COST, OPEN-SOURCE APPROACH FOR SENSOR-BASED LIGHT MANAGEMENT IN PROTECTED CULTIVATION SYSTEMS - **Bogdan ILIE, Yuxin TONG, Ana BUTCARU, Tiberiu ION, Ionuț Ovidiu JERCA** ..... 231
25 THE INFLUENCE OF INOCULATION WITH SYNTHETIC MICROBIOMES ON THE EVOLUTION OF SOIL CARBON SEQUESTRATION UNDER THERMAL STRESS - **Sorin MATEI, Gabi Mirela MATEI, Sorina DUMITRU, Victoria MOCANU, Monica DUMITRAȘCU** ..... 246
26 TRACING PESTICIDES AND PHARMACEUTICALS IN WATER AND SEDIMENTS OF THE DANUBE DELTA - **Stefania-Adelina MILEA, Valentina-Andreea CALMUC, Andreea-Miruna CODREANU, Catalina ITICESCU, Silvia DRAGAN** ..... 258
27 INACTIVATION OF GRAM-POSITIVE AND GRAM-NEGATIVE BACTERIA BY USING ARGON COLD ATMOSPHERIC PRESSURE PLASMA - **Cristina MOISESCU, Ovidiu STOICAN, Ana Valentina ZAMFIRESCU, Mihaela Marilena STANCU** ..... 266
28 OZONE STRESS IN PLANTS: SIGNALLING AND RESPONSE - **Senad MURTIĆ** ..... 274
29 PHYSICOCHEMICAL STABILITY AND EMULSIFYING ACTIVITY OF A BIOSURFACTANT OF SALINE ORIGIN - **Simona NEAGU, Mihaela Marilena STANCU** ..... 287
30 PLANT TISSUE CULTURE STRATEGIES FOR SUSTAINABLE MULTIPLICATION OF BLACK CHOKEBERRY (*ARONIA MELANOCARPA*) GERMPLASM - **Ioana - Cătălina NICOLAE, Maria TABĂRA, Nina CIORCHINĂ, Natalia ONICA, Melania GHEREG, Liliana BĂDULESCU** ..... 296

31 NATURA 2000 SITE DEALURILE STREHAIA–BÂTLANELE - UPDATED INFORMATION ON SPECIES AND HABITATS OF COMMUNITY INTEREST - **Marilena ONETE, Florian Paul BODESCU, Roxana-Georgiana NICOARĂ, Minodora MANU, Monica Angela NEBLEA** ..... 309
32 ASSESSMENT OF THE STATE OF ATMOSPHERIC AIR IN AN URBAN ENVIRONMENT DURING A FIRE AT A SOLID WASTE LANDFILL AND COMPARISON WITH AIR QUALITY INDICES - **Georgi PATRONOV, Diana KIRIN, Kenan SEZER, Petya ZAHARIEVA, Radoslava ZAHARIEVA**..... 319
33 INTERRELATIONSHIP BETWEEN SOIL MICROORGANISMS AND AIRBORNE MICROFLORA IN URBAN ENVIRONMENT - **Asen PESHEV** ..... 327
34 BIOMATERIALS – BASED COATINGS WITH INDOOR EMISSION CONTROL PROPERTIES - **Irina POPA, Vasilica VASILE, Claudiu-Sorin DRAGOMIR, Alexandra-Marina BARBU** ..... 335
35 PHYSICAL AND MECHANICAL CHARACTERISTIC ASPECTS FOR CLADDING PRODUCTS BASED ON RICE HUSKS AND HEMP STALKS - **Irina POPA, Vasilica VASILE, Claudiu-Sorin DRAGOMIR, Cristian GRIGORAȘENCO**..... 342
36 CORRELATION BETWEEN THE PHYSICAL PROPERTIES AND NPK NUTRIENT CONTENT OF ORCHARD SOILS FOR THE SELECTION OF APPROPRIATE SOIL DECONTAMINATION TECHNOLOGIES - **Maria POPA**..... 349
37 OCCURRENCE AND LEVELS OF HAZARDOUS ORGANIC COMPOUNDS IN SOILS FROM INDUSTRIAL AREAS - **Mihaela PREDA, Veronica TĂNASE, Nicoleta Olimpia VRÎNCEANU, Florența JAFRI**..... 357
38 IDENTIFYING THE NATURAL AND ANTHROPOGENIC SOURCES OF PARTICULATE MATTER: AN ANALYSIS OF POLLUTION ORIGINS AND ENVIRONMENTAL IMPACT - **Elena-Denisa PREDESCU, Carmen Otilia RUSĂNESCU, Roxana-Elena FRÎNCU, Sabrina Maria BĂLĂNESCU, Daniela MIHAI, Ionela Alexandra ION**..... 365
39 DETERMINATION OF CONCRETE PERMEABILITY WITH CERAMIC WASTE CONTENT - **Mircea SĂLCUDEAN, Maria POPA, Mirel GLEVITZKY, Daniela ONITA, Mihai Teopent CORCHEȘ** ..... 371
40 EXPERIMENTAL STUDY ON BRICKS MADE WITH BRICK WASTE AND SAWDUST - **Mircea SĂLCUDEAN, Maria POPA, Mirel GLEVITZKY, Mihai Teopent CORCHEȘ** ..... 378
41 DETERMINATION OF SPLITTING TENSILE STRENGTH OF PAVING BLOCKS CONTAINING CERAMIC WASTE - **Mircea SĂLCUDEAN, Mihai Teopent CORCHEȘ, Maria POPA, Mirel GLEVITZKY**..... 386
42 HYDROCARBON TOLERANCE AND BIODEGRADATION IN ENVIRONMENTAL *PSEUDOMONAS* STRAINS - **Mihaela Marilena STANCU, Simona NEAGU** ..... 393
43 SEASONAL VARIATION OF $CO_2$ SOIL FLUX AND VEGETATION RESPONSE AT BODOC AND BĂILE LĂZĂREȘTI - **Lia STELEA, Alexandra-Constanța DUDU, Corina AVRAM, Marius-Bogdan BĂRĂITĂREANU, Andrei-Gabriel DRAGOȘ, Gabriel IORDACHE** 403
44 EVALUATION OF THE PERFORMANCE OF WHEAT VARIETIES UNDER MINIMUM TILLAGE SYSTEM IN THE PEDOCLIMATIC CONDITIONS OF SĂCELE AREA, CONSTANȚA COUNTY (2021-2024) - **Traian Ciprian STROE, Oana MIHAI FLOREA, Liliana PANAITESCU**..... 416
45 ON THE IMPORTANCE OF ENVIRONMENTAL FACTOR PROTECTION IN KEY AREAS OF THE BORDER ZONE. CASE STUDY ROMANIA-UCRAINA, MARAMUREȘ MOUNTAINS - **Maria ȘEVERA, Mirela COMAN**..... 429
46 GEOTECHNICAL ENGINEERING AND SOIL MANAGEMENT: LEGAL GAPS AND ENVIRONMENTAL CONSIDERATIONS – **Daniel-Dumitru TOADERE, Nicoleta-Maria ILIEȘ, Ioan PETRAN**..... 436
47 MONITORING ENVIRONMENTAL QUALITY VIA NITRATE ACCUMULATION IN GREENHOUSE LETTUCE (*LACTUCA SATIVA* L.) - **Irina TOMASU, Mihaela DRAGOI CUDALBEANU, Simona MARCU SPINU, Zina PARASCHIV, Augustina Sandina TRONAC, Alina ORTAN** ..... 446

48 VALORIZATION OF STEEL FURNACE SLAG FOR CONSTRUCTION APPLICATIONS: TECHNICAL CHALLENGES AND OPPORTUNITIES - **Ana-Cristina VASILE, Raul ZAHARIA, Cornelia BAERA, Aurelian GRUIN, Paula SFIRLOAGA, Adelin STIRB, Alexandru ION** ..... 458
49 CULTIVABLE MICROALGAE FROM PEATLAND WATERS: MORPHOLOGICAL FEATURES AND PIGMENT PROFILES - **Ana Valentina ZAMFIRESCU, Cristina MOISESCU, Sorin ȘTEFĂNUȚ, Miruna-Maria ȘTEFĂNUȚ, Ana-Maria MOROȘANU** ..... 470

## DISASTER RESILIENCE AND SUSTAINABLE DEVELOPMENT

1 INTEGRATED GEOTECHNICAL AND STRUCTURAL APPROACHES FOR REDUCING SEISMIC VULNERABILITY OF HERITAGE BUILDINGS - **Stefan Florin BALAN, Bogdan Felix APOSTOL** 482
2 ASPECTS RELATED TO VEGETATION SUCCESSION, ON AGRICULTURAL LANDS, IMPROPERLY EXPLOITED AND ABANDONED, AFFECTED BY DROUGHT, IN NON-COLLECTIVIZED AREAS - **Flavia-Mălina CIOFLAN, Călin Ioan IOVAN, Sorin Lucian DOROG, Călin Gheorghe PĂȘCUȚ, Eugenia ȘERBAN** ..... 492
3 THE CHALLENGES OF CLIMATE CHANGE ADAPTATION IN ROMANIA'S LAND RECLAMATION SYSTEMS: BETWEEN GREY INFRASTRUCTURE AND NATURE-BASED SOLUTIONS - **Mihai Teopent CORCHES, Mirel GLEVITZKY, Mircea SĂLCUDEAN** ..... 506
4 SEISMIC RESPONSE ANALYSIS OF A LONG-TERM MONITORED BUILDING USING CO-LOCATED STRUCTURAL AND FREE-FIELD RECORDS - **Iolanda-Gabriela CRAIFALEANU, Claudiu-Sorin DRAGOMIR, Daniela DOBRE, Emil Sever GEORGESCU, Alexandra-Marina BARBU** ..... 518
5 A NOVEL CONCEPT FOR A SUBMERGED WAVE ENERGY CONVERTER - **Alexandru DIMACHE, Iulian IANCU** ..... 530
6 A DATA-DRIVEN ANALYSIS OF SEISMIC RESPONSE AND STRUCTURAL PERFORMANCE - **Daniela DOBRE, Iolanda-Gabriela CRAIFALEANU, Claudiu-Sorin DRAGOMIR, Emil-Sever GEORGESCU, Cornelia-Florentina DOBRESCU** ..... 537
7 STRUCTURAL PERFORMANCE ASSESSMENT OF ECOLOGICALLY STABILIZED ROAD LAYERS - **Daniela DOBRE, Lidia-Rodica RADU, Nicoleta-Adaciza IONESCU, Cornelia-Florentina DOBRESCU** ..... 545
8 CORRELATION BETWEEN DENSITY, ULTRASONIC PULSE VELOCITY, AND DRYING SHRINKAGE IN ECO-CLAY POURED-EARTH - **Aurelian GRUIN, Sorin DAN, Cornelia BAERĂ, Bogdan BOLBOREA, Ana-Cristina VASILE, Claudiu-Sorin DRAGOMIR, Evelin Anda LAZA** ... 551
9 INTERNAL AIR RECIRCULATION FOR CONDENSATION RISK CONTROL IN PASSIVE SOLAR GREENHOUSES: A DEW MARGIN-BASED ZONAL APPROACH - **Bogdan ILIE, Yuxin TONG, Ana BUTCARU, Tiberiu ION, Ionuț Ovidiu JERCA** ..... 560
10 INFLUENCE OF CONSTITUTIVE MODELS ON DEEP EXCAVATIONS: A COMPARATIVE STUDY - **Daniel-Marcel MANOLI, Nicolae RĂDULESCU-SINGURAN, Adrian Alexandru SAVU, Elena-Mihaela STAN, Cristian-Ștefan BARBU** ..... 574
11 THERMAL AND MECHANICAL PERFORMANCE OF GROUTING MATERIALS IN GEOTHERMAL BOREHOLES: IMPLICATIONS FOR HEAT TRANSFER EFFICIENCY AND ENVIRONMENTAL PERSPECTIVE - **Daniel-Marcel MANOLI, Alina TATOMIR, Elena-Mihaela STAN, Cristian-Stefan BARBU, Andrei-Dan SABAU** ..... 580
12 ASPECTS REGARDING CLIMATE RESILIENCE AND URBAN HEAT ISLAND EFFECT MITIGATION IN URBAN AREAS RENOVATION PROJECTS - **Izabella MARIN LAZĂR** ..... 586
13 INFLUENCE OF TESTING METHODS ON THERMAL PERFORMANCE CHARACTERIZATION OF SHEEP WOOL-BASED INSULATION - **Cristian PETCU, Andreea HEGYI, Horia PETRAN, Florin BĂLTĂREȚU** ..... 598
14 AQUIFER THERMAL ENERGY STORAGE SYSTEMS FOR NEARLY ZERO ENERGY BUILDINGS: A CASE STUDY ASSESSMENT FOR ROMANIAN CLIMATE CONDITIONS - **Cristian PETCU, Horia PETRAN, Andreea HEGYI, Florin BĂLTĂREȚU, Ciprian ENE** ..... 610

15 CASE STUDY ON THE ASSESSMENT OF THE EFFECTS OF CONTROLLED BLASTING DEMOLITION ON NEARBY BUILDINGS - **Adrian SIMION** ..... 624
16 COMPARATIVE STUDY ON DETERMINING THE FIRE RESISTANCE OF MASONRY WALLS - **Adrian SIMION, Augustina-Sandina TRONAC, Claudiu-Sorin DRAGOMIR, Laurențiu Denis CHERPEC** ..... 632

## WATER RESOURCES MANAGEMENT

1 LONG-TERM CHANGES IN AREAS EQUIPPED WITH DRAINAGE AND DEWATERING SYSTEMS UNDER DIFFERENT LAND USES - **Mihaela BALAN, Oana Alina NIȚU, Cristian POPESCU** ..... 637
2 MOBILE WASTEWATER TREATMENT SYSTEMS FOR CIRCULAR WATER REUSE: TECHNOLOGIES, APPLICATIONS AND THE ROMANIAN GAP IN THE EUROPEAN CONTEXT - **Sabrina-Maria BĂLĂNESCU, Carmen Otilia RUSĂNESCU, Ana VÎRSTA, Daniela MIHAI, Ionela Alexandra ION, Elena Denisa PREDESCU, Elena Roxana FRÎNCU** ..... 645
3 PROCESS STABILITY IN LIVESTOCK WASTEWATER TREATMENT: A COMPARATIVE REVIEW OF CONVENTIONAL SYSTEMS AND MEMBRANE BIOREACTORS FOR DECENTRALIZED APPLICATIONS - **Sabrina-Maria BĂLĂNESCU, Carmen Otilia RUSĂNESCU, Ana VÎRSTA, Nicoleta-Alina UDROIU, Bogdan-Dumitru ȚIGĂNOAIA, Nicolae FARCAȘ** ..... 657
4 SALT LAKE MICROBIAL ECOSYSTEMS: IMPORTANCE AND CONSERVATION CHALLENGES - **Lucia-Roxana COJOC, Mirela-Mădălina MOLDOVEANU, Larisa-Isabela FLORESCU, Mădălin-Iancu ENACHE, Anca-Ioana LUCACI** ..... 667
5 INCREASING THE EFFICIENCY OF BIOLOGICAL SLUDGE STABILIZATION PROCESSES WITHIN WASTEWATER TREATMENT PLANTS - **Dragos DRACEA, Alin HAPCA, Sebastian MUSTATA, Augustina Sandina TRONAC** ..... 675
6 *CYANOBACTERIA* AS KEY FACTORS IN STRUCTURING PLANKTONIC COMMUNITIES IN THE DANUBE DELTA - **Larisa Isabela FLORESCU, Maria Iasmina MOZA, Mirela Mădălina MOLDOVEANU** ..... 685
7 SPATIAL VARIATION OF MICROBIAL COMMUNITIES IN THE BAHLUI RIVER ACROSS THE URBAN AREA OF IASI - **Andrei-Mihai GAFENCU, Andreea-Mihaela FLOREA, Florin-Daniel LIPȘA, Eugen ULEA** ..... 697
8 HYDRO-MECHANICAL ANALYSIS AND NUMERICAL SIMULATION OF WATER INFILTRATION PROCESSES IN RAILWAY EMBANKMENTS - **Dorian HAUSLER COZMA, Eugen Teodor MAN, Robert Florin BEILICCI, Erika Beata Maria BEILICCI** ..... 704
9 HYDRAULIC MODELING APPLIED TO THE DETERMINATION OF SANITARY PROTECTION ZONES FOR LAKE BUHUI - **Mirela Laura IEREMCIUC, Ioan DAVID, Robert Florin BEILICCI, Erika Beata Maria BEILICCI** ..... 710
10 RISK ASSESSMENT OF THE USE OF *RUTILUS RUTILUS* FOR FOOD FROM TWO ANTHROPOGENICALLY INFLUENCED DAMS - **Nikolina ILIEVA, Viliana PASKALEVA, Diana KIRIN, Radoslava ZAHARIEVA, Petya ZAHARIEVA, Georgi PATRONOV, Doychin TERZIYSKI** ..... 717
11 MONITORING THE ECOLOGICAL STATE AND ANTHROPOGENIC LOADING OF THE LUDA YANA RIVER THROUGH THE USE OF INDICATOR MACROZOOBENTHOS - **Diana KIRIN, Radoslava ZAHARIEVA, Petya ZAHARIEVA** ..... 725
12 MICROBIAL PATTERNS IN URBAN AND PERI-URBAN LAKES FROM SOUTHERN ROMANIA: IMPLICATIONS FOR WATER QUALITY AND ECOSYSTEM HEALTH - **Anca-Ioana LUCACI, Larisa Isabela FLORESCU, Mirela Mădălina MOLDOVEANU, Roxana-Lucia COJOC** ..... 736

13 XRF-BASED ASSESSMENT OF ELEMENT ACCUMULATION IN *PHRAGMITES AUSTRALIS* ACROSS FRESHWATER, URBAN, AND SALINE AQUATIC ECOSYSTEMS: IMPLICATIONS FOR NATURAL FILTRATION AND ENVIRONMENTAL RISK – **Mirela Mădălina MOLDOVEANU, Larisa Isabela FLORESCU, Raluca Alexandra MIHAI, Cristian BANCIU, Maria Iasmina MOZA, Doru Simon DOBRE, Cristina Alina DUMITRACHE, Rodica Daniela CATANĂ** ..... 749

14 GLOBAL CHALLENGES CONCERNING WATER RESOURCES AND THEIR MANAGEMENT: CASE STUDY – THE DANUBE - **Aurelia NICA, Isabelle METAXA, Alina ANTACHE, Adeline-Ira SIMIONOV, Cătălina ITICESCU, Ștefan-Mihai PETREA** ..... 761

15 METALS CONTENT IN THE SYSTEM WATER - SEDIMENTS - CHIRONOMIDAE - *PERCA FLUVIATILIS* - *PROTEOCEPHALUS PERCAE* FROM TOPOLNITSA DAM, BULGARIA - **Viliana PASKALEVA, Diana KIRIN, Petya ZAHARIEVA, Radoslava ZAHARIEVA, Marian VARBANOV** ..... 767

16 PHYSICOCHEMICAL DYNAMICS OF WATER QUALITY IN SAND AND GRAVEL POST-EXPLOITATION LAKES - **Karoly Alexandru RACZ, Emilia Valentina PANTEA, Nicu Cornel SABĂU** ..... 775

17 PHOTOCHEMICAL DEGRADATION OF IMIDACLOPRID IN WATER UNDER UV RADIATION THROUGH CFD MODELING **- Alexandru Florin SIMION, Angelica Nicoleta GĂMAN, Sorin SIMION, Marius KOVACS** ..... 788

18 COMPARATIVE ASSESSMENT OF ANNUAL DYNAMICS IN WATER QUALITY OF HERASTRAU LAKE, ROMANIA - **Iuliana VOICU, Mihaela DRAGOI CUDALBEANU, Andreea Adriana MAN, Nicoleta Daniela SARBU, Teodor COSTACHIOIU, Daniela FAUR, Carmen Laura CIMPEANU** ..... 803

19 STATE-OF-THE-ART APPLICATIONS FOR THE REHABILITATION OF IRRIGATION MAIN-CANAL CROSSINGS - **Elena-Maria VORNICESCU, Sorin Mihai CIMPEANU, Nicolae MARACINE, Marco MORARU** ..... 815

## REMOTE SENSING AND GEOINFORMATICS

1 COMPARATIVE ANALYSIS OF ALTIMETRIC VARIATIONS IN THE SLĂNIC PRAHOVA AREA BASED ON LEVELING MEASUREMENTS **- Mihai AVADANEI, Tiberiu POPESCU, Florina ȚERLE BURESCU, Florin SALA, Mihai Valentin HERBEI** ..... 821

2 INTEGRATED COMPENSATION OF TERRESTRIAL GEODETIC AND GNSS NETWORKS USING A MODULAR 3D SOFTWARE PLATFORM. CASE STUDY: UCC MĂNECIU NETWORK - **Gabriel BĂDESCU, Mihail SUSINSKI, Cristian VASILE, Emilia CONSTANTINESCU, Petre SĂVESCU, Gabriel TĂNASIE** ..... 832

SEISMIC SURVEY FOR SHALLOW INVESTIGATION OF $CO_2$ MIGRATION PATHWAYS IN BĂILE LĂZĂREȘTI, ROMANIA - **Marius-Bogdan BĂRĂITĂREANU, Ionelia PANEA, Alexandra Constanța DUDU, Andrei Gabriel DRAGOȘ, Gabriel IORDACHE, Lia STELEA, Sorin ANGHEL** 846

4 SMART INTEGRATED E-PERMITTING PLATFORM FOR URBAN PLANNING AND CONSTRUCTION MANAGEMENT - **Andreea BEGOV-UNGUR, Liana Luminita BOCA** ..... 853

5 A METHODOLOGICAL FRAMEWORK FOR TERRAIN MORPHOLOGICAL ANALYSIS IN RISK MAPPING BASED ON DEM-DERIVED GEOMORPHOMETRIC PARAMETERS - **Liviu BUZILA, Silvia Alexandra DREGHICI, Ciprian CORPADE, Levente DIMEN, Zoltan NYIKES** ..... 862

6 GIS-BASED NOISE MAPPING OF NATURA 2000 SITES EXPOSED TO A1 MOTORWAY TRAFFIC IN ROMANIA - **Cristina CĂLIN, Răzvan Lucian VOICU, Sorin Mihai CÎMPEANU** ..... 870

7 DIGITAL TRANSFORMATION OF TREE INVENTORY THROUGH GIS: OPTIMIZING FORESTRY PROCESSES VIA SPATIAL DATA COLLECTION, INTEGRATION AND ANALYSIS **- Silvia CHIOREAN, Tudor SĂLĂGEAN, Mircea-Emil NAP, Ioana POP, Florica MATEI, Răzvan PLOSCAR, Steluța-Maria SÎNGEORZAN, Vasile ȘIMONCA** ..... 877

8 REAL-TIME PATHOGEN RISK MAPPING IN CEREAL FIELDS THROUGH INTEGRATED UAV, GIS AND SMART FORECASTING TOOLS - **Dragoș Andrei CÎRCIUMARIU, Mirela PARASCHIVU, Constantin ȘULEA-IORGULESCU, Dorin SENDRESCU** ..... 885
9 APPLICATION OF PHOTOGRAMMETRIC TECHNOLOGIES FOR CROP MONITORING IN PRECISION AGRICULTURE - **Silvia Alexandra DREGHICI, Levente DIMEN, Liviu BUZILA, Tudor BORȘAN, Gianmarco PITTON** ..... 903
10 ASSESSING WINTER MICROCLIMATES AND URBAN-RURAL THERMAL DIFFERENCES: A MOBILE MONITORING PILOT STUDY IN SOUTH-EASTERN ROMANIA - **Sorin FRĂSINA, Adrian ROȘU, Bogdan ROȘU, Maxim ARSENI, Daniel-Eduard CONSTANTIN, Mădălin CRISTEA, Lucian SFÎCĂ, Cătălina ITICESCU, Silvia DRAGAN** ..... 912
11 SATELLITE-DERIVED TURBIDITY AS AN INDICATOR OF SMALL-SCALE GOLD MINING ACTIVITY AROUND THE BROKOPONDO RESERVOIR, SURINAME - **Tamara MYSLYVA, Christiaan Max HUISDEN, Marek MROZ, Gerald TJON A SAN, Fauzia Gatoen ABDOELRAHMAN** ..... 925
12 HIGH-RESOLUTION MAPPING OF VEGETATION TYPES, STRUCTURE, HEIGHT, AND DENSITY IN THE UASVM CLUJ-NAPOCA CAMPUS USING LiDAR, PHOTOGRAMMETRY AND MULTISPECTRAL SENSING - **Mircea Emil NAP, Tudor SĂLĂGEAN, Silvia CHIOREAN, Ioana POP, Florica MATEI, Cătălin VÂRBAN, Simion BRUMĂ, Elemer Emanuel ȘUBA** ..... 937
13 DEFORESTATION PREDICTIONS IN NORTHERN ROMANIA USING LONG SHORT-TERM MEMORY NEURAL NETWORKS - **Adina NITULESCU** ..... 946
14 THE ALTGORITHMIC LANDSCAPE OF A.I BASED LAND USE INTERPRETATION - **Ioana Delia POP, Tudor SĂLĂGEAN, Mircea-Emil NAP, Elemer-Emanuel ȘUBA, Cristian MALINAS, Lucia-Adina TRUTA, Silvia CHIOREAN, Ferenc KAITAR, Adela-Maria NEAG, Florica MATEI** 952
15 LAND USE CHANGES INDUCED BY CONSTRUCTION MATERIAL EXTRACTION IN SURFACE QUARRIES WITHIN THE INEU ADMINISTRATIVE TERRITORY (BIHOR COUNTY, ROMANIA) - **Karoly Alexandru RACZ, Claudia Simona TIMOFTE, Nicu Cornel SABĂU** ..... 967
16 HIGH-DENSITY AIRBORNE LiDAR POINT CLOUD FOR DIGITAL TERRAIN MODELS IN SMALL STREAM ASSESSMENT AND REHABILITATION - **Tudor SĂLĂGEAN, Ioana POP, Florica MATEI, Silvia CHIOREAN, Mircea-Emil NAP, Catalin-Stefanel SABOU, Andreea-Catalina MOSNEAG** ..... 976
17 UAV-DERIVED VEGETATION INDICES FOR SPATIAL ASSESSMENT OF WEED INFESTATION IN ARABLE CROPS - **Claudiu-Daniel UTOIU, Bogdan DRAGANCEA, Elena UTOIU, Catalin LAZAR, Mihai GIDEA** ..... 988
18 GIS-BASED SCREENING OF ROAD-INDUCED SPATIAL FRAGMENTATION IN NATURA 2000 SITES IN ROMANIA - **Răzvan Lucian VOICU, Cristina CĂLIN, Sorin Mihai CÎMPEANU** ..... 997

## MISCELLANEOUS

1 RESEARCH ON FREE SURFACE ENERGY DISSIPATION - **Nicolae ALBOIU, Daniel CORNEA, Georgiana Daniela VULPE** ..... 1003
2 EFFICIENT USE OF AGRICULTURAL LAND BY ORGANIZING AND DIMENSIONING CROP ROTATION - **Marius Nicolae CIOBOATĂ, Dragomir BRUMAR, Marilena Alina PRIOTEASA** 1011
3 THREE-DIMENSIONAL BUILDING MODELING AS A DIGITAL STRATEGY FOR ENHANCING RURAL TOURISM PROMOTION - **Levente DIMEN, Silvia Alexandra DREGHICI, Tudor BORȘAN, George COZA** ..... 1021
4 A DECISION-SUPPORT FRAMEWORK FOR SUSTAINABLE MANAGEMENT OF NATURAL SPORTS TURF UNDER TEMPERATE-CONTINENTAL CONDITIONS - A REVIEW AND CASE STUDY - **Alexandru DUMITRU, Mihai Sorin CÎMPEANU** ..... 1030
5 SPECIFIC REHABILITATION WORKS OF DEGRADED AGROSILVOPASTORAL SYSTEMS, IN NONCOLLECTIVIZED AREAS - **Călin Ioan IOVAN, Sorin Lucian DOROG, Călin Gheorghe PĂȘCUȚ, Flavia-Mălina CIOFLAN, Eugenia ȘERBAN** ..... 1039

6 THE *SPHAGNUM* PEATBOGS OF MOLHAȘUL DE LA RÂȘCA - DEALUL NEGRU, CLUJ COUNTY - **Ana-Maria MOROȘANU, Miruna-Maria ȘTEFĂNUȚ, Sorin ȘTEFĂNUȚ** ..... 1053
7 GEOMETRY AND PHYSICS **- Cosmin-Constantin NIȚU**..... 1060
8 THE USE OF FUNCTIONAL APPROACHES TO ANALYZE THE DIFFERENCES IN LAKE WATER MICROBIOME ASSEMBLAGES - **Paula POP, Vlad STOIAN, Bianca POP, Alexandra GHEORGHIȚĂ, Roxana VIDICAN** ..... 1065
9 ASSESSING STUDENTS' COMPETENCIES IN ADVANCED TECHNOLOGIES FOR A SUSTAINABLE GREEN FUTURE IN ENERGY, AGRICULTURE, AND INDUSTRY **- Nicoleta RADU, Mihai Dan CARAMIHAI, Francisca BLANQUEZ CANO, Adrian SILVA, Narcisa BABEANU, Laura IOSUB, Razvan Ionut TEODORESCU**..... 1073
10 GAMIFICATION AS A TOOL FOR ENHANCING PARTICIPATION AND LEARNING IN GREEN DIGITISATION EDUCATION **- Nicoleta RADU, Mihai Dan CARAMIHAI, Francisca BLANQUEZ CANO, Adrian SILVA, Narcisa BABEANU, Laura IOSUB, Razvan Ionut TEODORESCU**..... 1081
11 NUTRITIONALLY RELEVANT MINERALS IN PARSLEY ROOT: AN X-RAY FLUORESCENCE STUDY **- Laura RADULESCU, Calin JIANU, Ersilia ALEXA, Ariana-Bianca VELCIOV, Virgil-Dacian LALESCU, Antoanela COZMA, Corina Iuliana MEGYESI, Daniela STOIN, Diana MOIGRADEAN, Simion ALDA, Mariana-Atena POIANA, Carmen-Daniela PETCU, Viorica BOACA, Despina-Maria BORDEAN** ..... 1087
12 ANALYSIS OF SPATIAL GEODETIC METHODS FOR MONITORING MINING GEOSYSTEMS - **Gabriel TĂNASIE, Nicolae DIMA, Larisa-Ofelia FILIP, Gabriel BĂDESCU** ..... 1093
13 COST EFFECTIVE SYSTEM FOR HUMAN PRESENCE DETECTION IN RURAL ENVIRONMENT **- Peter UDVARDY, Levente DIMEN, Gergely VAKULYA**..... 1101

Scientific Papers. Series E. Land Reclamation, Earth Observation & Surveying, Environmental Engineering. Vol. XV, 2026
Print ISSN 2285-6064, CD-ROM ISSN 2285-6072, Online ISSN 2393-5138, ISSN-L 2285-6064

# NICKEL SPECIATION AND BIOAVAILABILITY IN SERPENTINE SOILS OF THE EASTERN AND SOUTHERN RHODOPES, BULGARIA

**Violina ANGELOVA**

Agricultural University Plovdiv, 12 Mendeleev Blvd, Plovdiv, Bulgaria

Corresponding author email: vileriz@yahoo.com

***Abstract***

*Serpentine soils in the Eastern and Southern Rhodopes, Bulgaria, exhibit elevated nickel (Ni) concentrations and distinct mineralogical characteristics, dominated by serpentine minerals (antigorite, lizardite) and the Ni-rich willemseite. This study assesses Ni speciation, mobility, and potential bioavailability by analysing soil physicochemical properties, iron oxide mineralogy, and selective chemical extractions targeting exchangeable, DTPA-extractable, and iron oxide-associated Ni fractions. Results indicate that Ni distribution depends on pedogenetic development: in moderately developed soils, Ni preferentially associates with amorphous and poorly crystalline iron oxides, while in more advanced soils, well-crystallised oxides stabilise Ni and limit its mobility. The Feo/Fed ratio reflects oxide crystallinity and pedogenic stage, serving as a key control on Ni behaviour. Multivariate analyses, including PCA and cluster analysis, reveal a pedogenetic continuum linking mineralogical inheritance, iron oxide transformation, and Ni fractionation. This framework enables the prediction of potential Ni bioavailability and highlights the importance of pedogenesis and secondary mineral phases in regulating Ni dynamics. The findings improve understanding of Ni behaviour in temperate ultramafic soils and provide a basis for ecological risk assessment and sustainable management of serpentine ecosystems.*

***Key words****: bioavailability, nickel (Ni), Rhodopes Mountains, serpentine soils, soil geochemistry.*

## INTRODUCTION

Nickel (Ni) is widely distributed in the Earth's crust and plays an important role in biogeochemical processes in the soil environment. It is essential for plants and microorganisms, as it participates in the structure and activity of the enzyme urease and other key metabolic processes (Kabata-Pendias, 2011). At the same time, elevated nickel concentrations can be toxic, disrupting plant physiological functions, inhibiting nutrient uptake, and reducing soil microbial activity (Alloway, 2013). Therefore, understanding the factors controlling nickel distribution, mobility, and potential bioavailability in soils is crucial.

Nickel content strongly depends on the geological substrate. The highest concentrations are observed in soils formed on ultramafic and ultrabasic rocks such as peridotites, dunites, and serpentinites (Brooks, 1987). These rocks contain high levels of magnesium and heavy metals, including nickel, chromium, and cobalt. Weathering of these rocks leads to the formation of serpentine soils, characterised by high concentrations of potentially toxic elements, low Ca/Mg ratios, and limited content of essential nutrients (Alexander et al., 2007). The specific geochemical conditions of these soils strongly influence the plant and microbial communities typical of serpentine ecosystems.

The geochemical behaviour of nickel depends not only on its total content but also on its chemical forms. It can be adsorbed on clay minerals, associated with iron and manganese oxides, complexed with organic matter, or structurally incorporated into mineral lattices (Kabata-Pendias, 2011; Alloway, 2013). These forms differ in stability and mobility, determining their potential bioavailability to plants and their role in soil geochemical processes.

Quantitative assessment of metal mobility and bioavailability is commonly achieved using selective chemical extractions. Different extractants allow operational definition of metal fractions associated with specific soil components or characterised by varying mobility (McLean & Bledsoe, 1992). For example, the chelating agent diethylenetriaminepentaacetic acid (DTPA) extracts potentially bioavailable trace metal forms (Lindsay & Norvell, 1978), whereas neutral salts such as $Sr(NO_3)_2$ extract

exchangeable and weakly adsorbed forms. These approaches provide a more realistic assessment of the ecological significance of nickel compared to total concentrations.

Iron oxides also play a key role in nickel retention and distribution. They act as effective sorbents, limiting metal mobility and strongly influencing their stability (Alloway, 2013). Amorphous and poorly crystalline iron oxides can retain more labile nickel forms, while well-crystallised oxides stabilise the metal pool. Oxalate extraction targets nickel associated with amorphous and poorly crystalline Fe and Al oxides, while the sodium dithionite-citrate-bicarbonate (DCB) method dissolves free crystalline iron oxides (Mehra & Jackson, 1960; Schwertmann, 1964). Comparison of these fractions and the $Fe_o/Fe_d$ ratio provide valuable information on soil development and nickel stability.

Serpentinites and ultramafic rocks are widespread across the Balkans, including Bulgaria. The Rhodope Massif is a key area with localised bodies of serpentinites and ultrabasic rocks. In the Eastern and Southern Rhodopes, these lithological features form soils with elevated nickel and other trace elements (Angelova & Kovacheva, 2023). However, information on nickel distribution among soil fractions and the influence of iron oxides on its potential bioavailability remains limited.

Investigating nickel speciation and potential bioavailability in the serpentine soils of the Rhodopes is crucial for understanding the processes controlling its behaviour. A combined approach integrating selective chemical extractions, soil physicochemical properties, and mineralogical composition provides a comprehensive, process-oriented interpretation of nickel dynamics.

This study aims to analyse nickel speciation, mobility, and potential bioavailability in serpentine soils of the Eastern and Southern Rhodopes, with a focus on the role of iron oxides, pedogenesis, and mineralogical composition. To achieve this, the study evaluates total nickel content, its spatial variability, distribution among different chemical fractions via selective extractions, the influence of iron oxides and their crystallinity, and the relationship between soil physicochemical and mineralogical properties and nickel's potential bioavailability. Multivariate statistical analyses are applied to identify pedogenetic and functional soil groups that reflect gradients in soil development and nickel bioavailability.

## MATERIALS AND METHODS

### *Study area and sampling*

The study was conducted in ultramafic regions of the Central and Eastern Rhodope Mountains, southern Bulgaria. The investigated sites included Kazak, Goljamo Kamenyane, Avren, Chernichevo, Kardzhali, Fotinovo, Dyulitsa, Dobromirtsi, Asenovgrad, Cherven, Parvenets, and Gornoslav. The region is characterized by a transitional Mediterranean-continental climate, contributing to considerable spatial variability in environmental conditions.

Surface soil samples (0-20 cm) were collected from each site. Prior to analysis, the samples were air-dried, homogenized, and sieved to <2 mm.

### *Physicochemical soil analysis*

Soil physicochemical properties were determined using standardized analytical procedures. Soil pH was measured potentiometrically in water according to ISO 10390 (2021). Organic matter content was determined following BS EN 13039 (2011). Cation exchange capacity and exchangeable cations were determined using $BaCl_2$ extraction in accordance with ISO 11260 (1994).

Pseudo-total metal concentrations were determined after acid digestion following ISO 11466 (1995). Potentially available nickel was extracted using diethylenetriaminepentaacetic acid (DTPA) according to ISO 14870 (2001), while exchangeable nickel was obtained using 0.1 M $Sr(NO_3)_2$ extraction (van der Ent et al., 2019).

Iron oxide fractions were differentiated by selective chemical extraction. Amorphous iron oxides ($Fe_o$) were extracted using ammonium oxalate, whereas free iron oxides ($Fe_d$) were determined using the citrate-bicarbonate-dithionite method (Sparks, 1996). The crystalline iron oxide fraction ($Fe_{cr}$) was calculated as the difference between Fed and Feo. The Feo/Fed ratio was used as an indicator of pedogenic development and weathering

intensity. Elemental concentrations were measured using ICP-OES.

***Mineralogical characterization***

Mineralogical composition was analyzed by X-ray diffraction (XRD). Powder diffraction patterns were recorded over an angular range of 5-80° 2θ using Cu Kα radiation. Phase identification was performed using standard reference databases, and quantitative phase analysis was carried out by Rietveld refinement.

***Statistical analysis***

Differences among sampling sites were evaluated using one-way analysis of variance (ANOVA). Correlation analysis was applied to assess relationships between soil properties and the distribution of nickel fractions. Statistical significance was considered at $p < 0.05$.

## RESULTS AND DISCUSSIONS

***Soil physicochemical properties and total nickel content***

The main physicochemical characteristics of the serpentine soils from the Eastern and Southern Rhodopes are summarised in Table 1. Soil reaction varies within a relatively narrow range, from slightly acidic to slightly alkaline (pH 6.05-7.62), with a mean value of 6.84. Such pH conditions are typical for serpentine-derived soils and reflect the buffering effect of the Mg-rich ultramafic parent material (Brooks, 1987; Kabata-Pendias, 2011).

Organic matter content (LOI) is generally low to moderate (2.27-8.30%), characteristic of ultramafic soils with limited biological productivity and reduced potential for humus accumulation (Alexander et al., 2007). The cation exchange capacity (CEC) shows substantial variability (83.1-434.5 mmolc/kg), indicating differences in soil texture, mineralogical composition and degree of pedogenic development across the studied sites. Total Ni concentrations are high across all samples, ranging from 919.9 to 2397.2 mg/kg, with a mean of 1667.9 mg/kg. These values greatly exceed background concentrations typical for non-serpentine soils and clearly indicate a dominant geogenic control on Ni accumulation derived from the ultramafic parent material (Brooks, 1987; Alloway, 2013). Similar concentrations have been reported for serpentine soils into other ultramafic regions worldwide reflecting the structural incorporation of Ni in primary silicate minerals of the parent rock (Alexander et al., 2007; Bani et al., 2009).

Table 1. Descriptive statistics of physicochemical properties, iron oxides and nickel fractions in serpentine soils of the Eastern and Southern Rhodopes

| Variable | Mean±SD | Min. | Median | Max. |
|---|---|---|---|---|
| pH | 6.84±0.50 | 6.05 | 6.8 | 7.62 |
| LOI, % | 5.27±1.87 | 2.27 | 5.23 | 8.30 |
| CEC, mmolc/kg | 220.61±87.94 | 83.1 | 201.6 | 434.5 |
| Exch. Ca, mmolc/kg | 100.60±75.33 | 26.57 | 96.60 | 379.64 |
| Exch. Mg, mmolc/kg | 117.25±67.09 | 25.96 | 119.14 | 328.22 |
| Exch. K, mmolc/kg | 2.75±1.77 | 0.47 | 2.09 | 6.16 |
| Mg/Ca | 1.62±1.14 | 0.1 | 1.3 | 4.7 |
| Fine sand (0.2–0.02 mm), % | 30.50±14.43 | 7.01 | 29.63 | 62.65 |
| Silt (0.02–0.002 mm), % | 15.52±8.64 | 5.27 | 13.06 | 35.14 |
| Clay (<0.002 mm), % | 17.53±5.53 | 7.70 | 17.16 | 28.00 |
| Physical clay (<0.02 mm), % | 33.05±12.61 | 12.97 | 31.43 | 54.97 |
| $Fe_o$ (oxalate), mg/kg | 4153.9±1543.4 | 1512.0 | 4166.3 | 6552.0 |
| $Fe_d$ (DCB), mg/kg | 19392.2±10779.7 | 3318.8 | 16453.8 | 41096.3 |
| $Fe_o/Fe_d$ | 0.30±0.27 | 0.09 | 0.23 | 1.27 |
| $Ni_o$ (oxalate), mg/kg | 398.3±170.1 | 103.5 | 427.5 | 667.5 |
| $Ni_d$ (DCB), mg/kg | 335.84±155.68 | 61.3 | 346.9 | 583.8 |
| $Ni_o/Ni_d$ | 1.352±0.569 | 0.407 | 1.219 | 3.135 |
| Ni ($Sr(NO_3)_2$), mg/kg | 1.212±1.37 | 0.012 | 0.601 | 4.32 |
| Ni (DTPA), mg/kg | 46.96±33.11 | 6.08 | 40.16 | 125.28 |
| Ni (total), mg/kg | 1667.9±390.8 | 919.9 | 1603.9 | 2397.2 |
| Fe (total), mg/kg | 63298.1±13794.6 | 36302.4 | 64110.4 | 93194.5 |
| Antigorite, % | 60.55±20.27 | 19.0 | 66.0 | 86.0 |
| Lizardite, % | 1.55±4.99 | 0.0 | 0.0 | 20.0 |
| Clinochlore, % | 12.7±11.63 | 0.0 | 11.0 | 48.0 |
| Willemseite, % | 7.0±6.82 | 0.0 | 6.5 | 24.0 |
| Quartz, % | 9.45±11.77 | 1.0 | 8.0 | 55.0 |

***Distribution of nickel among chemical fractions and indicators of mobility***

Selective extraction results reveal a pronounced fractionation of nickel among the investigated soil phases (Figure 1). Boxplots show minimum, first quartile (Q1), median, third quartile (Q3), and maximum values for total Ni, oxalate extractable Ni (Ni–Ox; associated with amorphous Fe oxides). The potentially bioavailable fraction, determined by DTPA extraction, represents only a small proportion of the total Ni pool. Ni-DTPA concentrations vary widely (6.08-125.28 mg/kg), with an average of

46.96 mg/kg, indicating that despite the very high total Ni concentrations, its mobility and immediate bioavailability remain limited.

Nickel associated with amorphous and poorly crystalline iron oxides (Ni-oxalate) ranges from 103.5 to 667.5 mg/kg (mean 398.3 mg/kg). In contrast, nickel bound to free crystalline iron oxides (Ni-DCB) varies between 61.3 and 583.8 mg/kg (mean 335.8 mg/kg). This distribution indicates that a significant portion of Ni has been secondarily incorporated into Fe-oxide phases during pedogenesis.

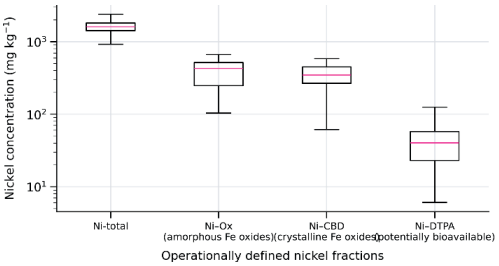



Figure 1. Nickel speciation in serpentine soils from the Eastern and Southern Rhodopes, Bulgaria

The exchangeable fraction extracted with $Sr(NO_3)_2$ is extremely low (0.01-4.32 mg/kg), confirming that easily mobile Ni forms represent only a negligible component of the overall Ni pool in these soils. These results highlight that total Ni content alone is not a reliable indicator of ecological risk or plant availability, as nickel speciation exerts a fundamental control on its environmental behaviour (Kabata-Pendias, 2011; Alloway, 2013).

### *Iron oxides and the $Fe_o/Fe_d$ pedogenic indicator*

Amorphous ($Fe_o$) and free crystalline ($Fe_d$) iron oxide contents show substantial variability among the studied serpentine soils. $Fe_o$ concentrations range from 1,512 to 6,552 mg/kg, while $Fe_d$ reaches values up to 41,096 mg/kg. Consequently, the $Fe_o/Fe_d$ ratio - commonly used as an indicator of iron oxide crystallinity and pedogenic development - varies widely between 0.09 and 1.27.

This variability indicates that the investigated soils represent a broad pedogenic spectrum, ranging from weakly developed serpentine regoliths dominated by crystalline Fe oxides to more evolved soils characterised by a greater contribution of amorphous and poorly crystalline Fe phases. Such variability reflects progressive transformations of Fe oxides during pedogenesis and highlights the dynamic role of these phases in regulating Ni stabilisation.

The relationship between $Fe_o/Fe_d$ and potentially bioavailable nickel (Ni-DTPA), illustrated in Figure 2, suggests that higher Ni-DTPA values occur mainly in soils exhibiting intermediate $Fe_o/Fe_d$ ratios. In this figure, boxplots show the minimum, first quartile (Q1), median, third quartile (Q3), and maximum values for oxalate-extractable iron ($Fe_o$), dithionite-citrate-bicarbonate-extractable iron ($Fe_d$), and their ratio ($Fe_o/Fe_d$), used as an indicator of iron oxide crystallinity and degree of pedogenetic development, with the y-axis presented on a logarithmic scale.

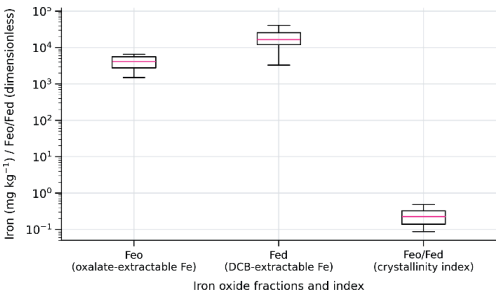



Figure 2. Distribution of iron oxide fractions and $Fe_o/Fe_d$ ratio in the investigated serpentine soils

These systems are characterised by a substantial presence of amorphous and poorly crystalline iron oxides, which act as highly reactive sorbents that temporarily retain nickel in relatively labile forms. This observation is consistent with mechanisms described in the literature, in which amorphous Fe oxides function as transitional reservoirs that control Ni mobility before its stabilisation in more crystalline phases (Chardot et al., 2007; Echevarria, 2018). Overall, iron oxides play a central role in regulating nickel mobility in serpentine soils. The wide variability of the Feo/Fed ratio reflects different stages of oxide transformation and soil ageing (Blume & Schwertmann, 1969; Schwertmann & Taylor, 1989). Amorphous and poorly crystalline Fe oxides provide large reactive surfaces and bind nickel less strongly than well-crystallised oxides, potentially enhancing its availability

(Chardot et al., 2007; Echevarria, 2018). With progressive pedogenic development and increasing crystallinity of Fe oxides, nickel becomes more efficiently stabilised, and its mobility decreases, in agreement with the conceptual model proposed by Echevarria (2018), which emphasises the role of amorphous Fe phases as key Ni buffers in moderately developed ultramafic soils.

***Multivariate analysis (PCA and cluster analysis)***

Principal component analysis (PCA; Figure 3), presented as a biplot with PC1 and PC2 axes showing both variable loadings and sample scores, integrates soil physicochemical parameters, Ni fractions, iron oxide characteristics, and mineralogical composition, revealing a clear pedogenic gradient that controls Ni speciation and potential bioavailability. The first principal component (PC1) is dominated by variables related to Fe oxides ($Fe_o$, $Fe_d$, $Fe_o/Fe_d$) and associated Ni fractions, highlighting the central role of iron oxide dynamics in Ni retention and redistribution. The second principal component (PC2) primarily reflects variations in pH, texture, and mineralogical composition, indicating the influence of lithogenic control and soil physicochemical conditions.

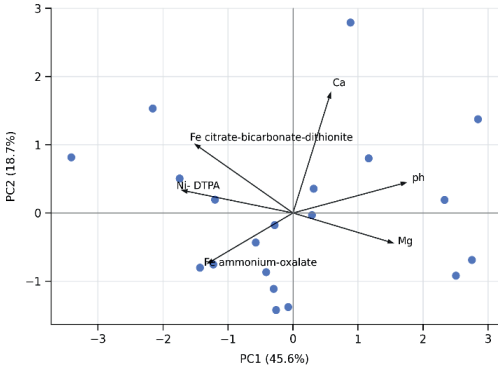



Figure 3. Principal component analysis (PCA) of serpentine soils from the Eastern and Southern Rhodope Mountains.

Cluster analysis (Figure 4), displayed as a hierarchical dendrogram based on standardized physicochemical parameters, Ni fractions, and iron oxide indicators, further supports the PCA results by grouping soils into several functional clusters that reflect differences in pedogenic development, mineralogical inheritance, and Ni mobility. These clusters form a pedogenic sequence ranging from weakly developed soils with relatively higher proportions of labile Ni to more stabilised systems where Ni is increasingly fixed in crystalline Fe oxides and secondary mineral phases. Soils at intermediate developmental stages form distinct clusters characterised by higher Ni-DTPA and Ni-oxalate values. In contrast, both less developed and more stabilised systems show a dominance of structurally and oxide-bound Ni. The consistency between PCA and cluster analysis confirms the existence of a pedogenic continuum controlling Ni stabilisation mechanisms in serpentine soils.

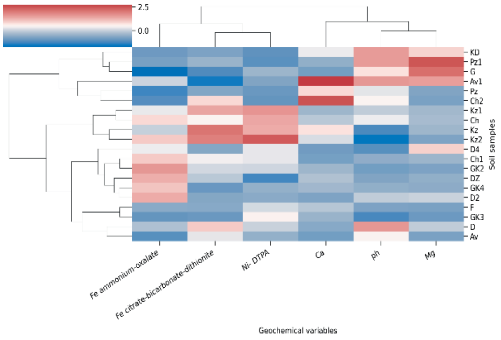



Figure 4. Hierarchical cluster analysis (HCA) of serpentine soils from the Eastern and Southern Rhodope Mountains

***Mineralogical composition and its influence on nickel mobility and bioavailability***

X-ray diffraction (XRD) analysis indicates that the mineralogical composition of the studied soils is dominated by primary ultramafic minerals typical of serpentinised parent materials. The dominant mineral phase in all soils is antigorite, with contents ranging from 19 to 86% and an average of approximately 60.6%. In several sites (Gornoslav, Dyulitsa, Parvenets) antigorite reaches particularly high proportions, indicating strong lithogenic control and relatively limited chemical weathering.

Lizardite occurs in fewer samples, with contents reaching up to 20%. Its presence, together with antigorite, indicates different serpentinisation pathways and variable stability of serpentine phases during pedogenesis. Both minerals belong to the serpentine group and represent

major structural hosts of Ni through isomorphic substitution of $Mg^{2+}$ by $Ni^{2+}$ within octahedral positions of the crystal lattice (Brooks, 1987; Kabata-Pendias, 2011).

A particularly important mineralogical observation is the identification of willemseite (Ni-rich serpentine) in several soils, with contents reaching up to 24%. Willemseite provides direct evidence for structurally bound nickel incorporated within the primary mineral lattice during rock formation. This mineralogical control explains the combination of high total Ni concentrations and very low exchangeable and DTPA-extractable fractions observed in the studied soils. Similar mineralogical controls on Ni behaviour have been reported in other ultramafic regions (Alexander et al., 2007; Bani et al., 2009).

Among the secondary phases, clinochlore plays an important role, reaching up to 48% in some samples (e.g., Golyamo Kamenyane). Clinochlore forms during secondary transformation of serpentine minerals and may retain Ni through surface sorption and partial structural incorporation. Quartz occurs as a secondary component (up to 55%), reflecting silica enrichment during weathering but contributing little to Ni retention. Montmorillonite is present only in minor amounts (< 9%), indicating limited development of advanced clay mineral phases and a relatively moderate pedogenic intensity.

Mineralogical composition, therefore, exerts a fundamental control on Ni behaviour by determining both the initial geochemical reservoir and its subsequent transformation during pedogenesis. The dominance of serpentine minerals indicates that a large proportion of Ni remains structurally bound within primary ultramafic silicate phases, exhibiting extremely low mobility and minimal bioavailability (Brooks, 1987; Kabata-Pendias, 2011).

With progressive weathering, part of the Ni released from primary minerals becomes incorporated into secondary phases. Clinochlore and Fe oxides act as intermediate geochemical reservoirs, temporarily retaining Ni. Amorphous and poorly crystalline Fe oxides function as reactive sorbents, whereas well-crystallised oxides provide more stable long-term fixation (Schwertmann & Taylor, 1989; Chardot et al., 2007).

This mineralogical-geochemical evolution forms a pedogenic continuum in which structurally bound Ni dominates in early stages of serpentine minerals, intermediate stages involve redistribution toward amorphous Fe oxides and clinochlore, and more advanced stages lead to the stabilisation of Ni in crystalline oxides and secondary mineral phases. Similar pedogenic sequences have been documented in temperate and Mediterranean ultramafic systems and provide a key framework for explaining the observed spatial variability in Ni mobility and plant accumulation (Chardot et al., 2007; Bani et al., 2013; Echevarria, 2018).

***Conceptual model of Ni stabilisation in serpentine soils***

The results obtained in this study allow the development of a conceptual model describing the mechanisms controlling nickel stabilisation in serpentine soils of the Eastern and Southern Rhodopes (Figure 5). The conceptual diagram illustrates the role of serpentine minerals (antigorite, lizardite, willemseite) as primary Ni reservoirs through structural incorporation, and highlights the contribution of secondary minerals and iron oxides in regulating Ni mobility. The model integrates mineralogical inheritance from ultramafic parent material with pedogenic transformations affecting Ni speciation and mobility.

In the initial stage, nickel is predominantly structurally incorporated into primary serpentine minerals such as antigorite, lizardite, and willemseite, where it substitutes for $Mg^{2+}$ in the octahedral positions of the crystal lattice. Under these conditions, Ni is largely immobile and poorly available for biological uptake.

During progressive weathering and pedogenesis, partial dissolution of serpentine minerals releases Ni into the soil system. A significant portion of this Ni is subsequently associated with amorphous and poorly crystalline Fe oxides, which act as highly reactive sorbents and temporary geochemical reservoirs. This stage is characterised by relatively higher proportions of labile Ni fractions, reflected in increased Ni-DTPA and Ni-oxalate concentrations.

With further pedogenic development, iron oxides progressively transform into more crystalline phases, enhancing the long-term stabilisation of nickel through stronger sorption and co-precipitation mechanisms. Consequently, Ni becomes increasingly immobilised in crystalline Fe oxides and secondary mineral phases, leading to reduced mobility and lower potential bioavailability.

Overall, this conceptual framework highlights the combined influence of lithogenic inheritance and pedogenic transformation processes on the distribution, mobility, and environmental behaviour of nickel in serpentine soils.

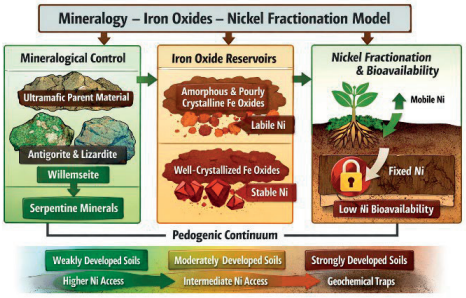



Figure 5. Conceptual model of nickel (Ni) behaviour in serpentine soils of the Eastern and Southern Rhodopes (Generated using Microsoft Copilot)

## CONCLUSIONS

This study provides a comprehensive assessment of nickel (Ni) speciation, mobility, and potential bioavailability in serpentine soils of the Eastern and Southern Rhodopes, highlighting the key role of mineralogical inheritance and pedogenetic processes.

The soils are characterised by high total nickel concentrations, confirming the dominant geogenic control exerted by the ultramafic parent material. However, the potentially bioavailable fraction of Ni is limited, indicating that total element content alone does not reflect ecological risk.

Mineralogical analysis shows that serpentine minerals - antigorite and lizardite - serve as the primary reservoirs of nickel through structural incorporation. The detection of willemseite provides direct evidence for stably fixed nickel and explains its low mobility. Secondary mineral phases, primarily clinochlore and iron oxides, act as intermediate geochemical sinks, modifying nickel distribution and regulating its mobility. Amorphous and poorly crystalline Fe oxides retain Ni in more labile pools, while well-crystallised oxides provide long-term stabilisation.

Multivariate analysis identifies a pedogenetic continuum, where intermediately developed soils exhibit higher potential Ni bioavailability, whereas poorly or highly developed soils function as stable geochemical “traps”. This continuum indicates that plant-accessible nickel is spatially heterogeneous and strongly controlled by mineralogy and iron oxide dynamics rather than total Ni content.

The proposed conceptual model, "mineralogy – iron oxides – nickel fractionation", provides a process-oriented framework for predicting Ni behaviour in temperate ultramafic ecosystems. The results are of both fundamental significance for understanding Ni biogeochemistry and practical value for ecological risk assessment and management of serpentine soils.

## ACKNOWLEDGEMENTS

This work has been carried out in the framework of the National Science Program "Critical and strategic raw materials for a green transition and sustainable development", approved by the Resolution of the Council of Ministers no. № 508/18.07.2024 and funded by the Ministry of Education and Science (MES) of Bulgaria.

## REFERENCES

Alexander, E. B., Coleman, R. G., Keeler Wolf, T., & Harrison, S. P. (2007). *Serpentine geoecology of western North America: Geology, soils, and vegetation*. Oxford University Press, Oxford, UK.

Alloway, B. J. (2013). *Heavy metals in soils: Trace metals and metalloids in soils and their bioavailability* (3rd ed.). Springer, Dordrecht.

Angelova, V., & Kovacheva, D. (2023). Characterisation of serpentine soils from Eastern and Southern Rhodope Mountains (Bulgaria). *Comptes rendus de l’Académie bulgare des Sciences*, 76(1), 141–152.

Bani, A., Echevarria, G., Mullaj, A., Reeves, R. D., & Morel, J. L. (2009). Nickel hyperaccumulation by Brassicaceae in serpentine soils of Albania and Northwestern Greece. *Northeastern Naturalist*, 16(Special Issue 5), 385–404.

Bani, A., Imeri, A., Echevarria, G., Pavlova, D., Reeves, R.D., Morel, J.L., & Sulçe, S. (2013). Nickel hyperaccumulation in the serpentine flora of Albania. *Fresenius Environmental Bulletin*, 22(6), 1792–1801.

Blume, H. P., & Schwertmann, U. (1969). Genetische Evaluierung der Eisenoxide in Profilen überwiegend aus Sedimenten. *Journal of Soil Science*, 20, 164–174.

Brooks, R. R. (1987). Serpentine and its vegetation: A multidisciplinary approach. Dioscorides Press, Portland, OR.

BS EN 13039 (2011) Soil improvers and growing media-determination of organic matter content and ash. BSI, London.

Chardot, V., Echevarria, G., Gury, M., Massoura, S., & Morel, J. L. (2007). Nickel bioavailability in an ultramafic toposequence in the Vosges Mountains (France). *Plant and Soil*, 293(1–2), 7–21.

Echevarria, G. (2018). Genesis and behaviour of ultramafic soils and consequences for nickel biogeochemistry. *Environments*, 5(6), 1–27.

ISO 10390 (2021) Soil, treated biowaste and sludge-determination of pH. International Organization for Standardization, Geneva.

ISO 11260 (1994) Soil quality-determination of effective cation exchange capacity and base saturation level using barium chloride solution. ISO, Geneva.

ISO 11466 (1995) Soil quality - extraction of trace elements soluble in aqua regia. ISO, Geneva.

ISO 14870 (2001) Soil quality - extraction of trace elements by buffered DTPA solution. ISO, Geneva.

Kabata-Pendias, A. (2011). Trace elements in soils and plants (4th ed.). CRC Press, Boca Raton, FL.

Lindsay, W. L., & Norvell, W. A. (1978). Development of a DTPA soil test for zinc, iron, manganese, and copper. *Soil Science Society of America Journal*, 42(3), 421–428.

McLean, J. E., & Bledsoe, B. E. (1992). Behavior of metals in soils. EPA Ground Water Issue, U.S. Environmental Protection Agency.

Mehra, O. P., & Jackson, M. L. (1960). Iron oxide removal from soils and clays by a dithionite citrate system buffered with sodium bicarbonate. *Clays and Clay Minerals*, 7, 317–327.

Schwertmann, U. (1964). Differenzierung der Eisenoxide des Bodens durch photochemische Extraktion mit saurer Ammoniumoxalat Lösung. Zeitschrift für Pflanzenernährung, *Düngung und Bodenkunde*, 105, 194–202.

Schwertmann, U., & Taylor, R. M. (1989). Iron oxides. In J. B. Dixon & S. B. Weed (Eds.), Minerals in soil environments (2nd ed., pp. 379–438). Soil Science Society of America, Madison, WI.

Sparks, D. L. (1996) Methods of Soil Analysis. Part 3: Chemical Methods. Soil Science Society of America, Madison, WI.

van der Ent, A., Nkrumah, P.N., Tibbett, M., & Echevarria, G. (2019). Evaluating soil extraction methods for chemical characterization of ultramafic soils in Kinabalu Park (Malaysia). *Journal of Geochemical Exploration*, 196, 235–246.

Scientific Papers. Series E. Land Reclamation, Earth Observation & Surveying, Environmental Engineering. Vol. XV, 2026
Print ISSN 2285-6064, CD-ROM ISSN 2285-6072, Online ISSN 2393-5138, ISSN-L 2285-6064

# POTENTIAL OF SELECTED AROMATIC ASTERACEAE SPECIES FOR THE PHYTOREMEDIATION OF HEAVY METAL - CONTAMINATED SOILS

**Violina ANGELOVA, Maria IHTYAROVA**

Agricultural University Plovdiv, 12 Mendeleev Blvd, Plovdiv, Bulgaria

Corresponding author email: vileriz@yahoo.com

***Abstract***

*Aromatic plants of the Asteraceae family have significant potential for phytoremediation due to their rapid growth, high biomass production, and resilience in contaminated soils. This study evaluated the capacity of Artemisia absinthium, Achillea millefolium, Tanacetum balsamita, Tanacetum vulgare, and Artemisia dracunculus to accumulate heavy metals in soils contaminated by industrial activities in Bulgaria. Field experiments were conducted at contaminated sites, where soil and plant tissues (roots, stems, leaves, and flowers) were analysed for Pb, Cd, and Zn using ICP-OES. Bioconcentration (BCF) and translocation (TF) factors were calculated to assess metal uptake and distribution from roots to aboveground biomass. The results demonstrate considerable accumulation of Pb and Zn, with A. absinthium and A. millefolium exhibiting the highest BCF and TF values, indicating their suitability as the most effective species for phytoextraction. T. balsamita and T. vulgare displayed moderate accumulation with limited translocation, suggesting their potential for phytostabilisation, whereas A. dracunculus showed minimal uptake. These findings provide important insights into metal accumulation and translocation in Asteraceae species and identify the most promising species for the sustainable management of industrially contaminated soils.*

***Key words****: Asteraceae, aromatic plants, heavy metals, phytoremediation, bioaccumulation, soil contamination.*

## INTRODUCTION

Soil contamination with heavy metals represents one of the most pressing environmental challenges resulting from industrialisation, mining, metallurgical activities, and intensive agriculture. Among the most prevalent soil pollutants are lead (Pb), cadmium (Cd), and zinc (Zn), which are highly persistent in the environment because they are not subject to biological degradation and can remain in soils for extended periods. Accumulation of these elements in soil ecosystems can reduce soil fertility, disrupt plant growth and development, and exert toxic effects on soil microorganisms. Furthermore, heavy metals can enter the food chain, posing a serious risk to human health (Raskin & Ensley, 2000; Terry & Banuelos, 2000; Ali et al., 2013; Yan et al., 2020).

Conventional remediation methods, such as excavation, soil washing, and chemical stabilisation, are often associated with high costs, substantial technical resources, and significant disruption of soil structure and ecosystem functions. Consequently, in recent decades, there has been growing interest in phytoremediation as an environmentally friendly and cost-effective technology for restoring contaminated sites. Phytoremediation employs plants to extract, stabilise, or transform contaminants in soil and water and is considered a sustainable alternative to conventional cleanup methods (Terry & Banuelos, 2000; Angelova, 2023; Angelova & Ihtyarova, 2023; Angelova, 2025; Bhat et al., 2025). Depending on the mechanism, phytoremediation may involve phytoextraction, phytostabilisation, rhizofiltration, or phytovolatilisation, each of which differs in how plants interact with contaminants (Bhat et al., 2025).

The effectiveness of phytoremediation largely depends on selecting suitable plant species. Ideal plants should exhibit rapid growth, high biomass production, well-developed root systems, and tolerance to elevated contaminant concentrations. Recently, there has been increasing scientific interest in using medicinal and aromatic plants for phytoremediation. These plants typically show high resilience to abiotic stress and can thrive on margminal or degraded soils. Moreover, their economic value associated with bioactive compounds, enables

the integration of environmental and economic benefits (Deng et al., 2024; Yadav et al., 2025). Particular attention has been given to species from the Asteraceae family, which are widely distributed and well-adapted to diverse environmental conditions. Many members exhibit high ecological plasticity, rapid growth, and substantial biomass production - key traits for successful phytoremediation. Genera such as Achillea, Artemisia, and Tanacetum include species used in traditional medicine and the production of pharmaceutical products. Studies indicate that these plants can accumulate significant amounts of heavy metals in various organs while maintaining resilience in contaminated environments (Salt et al., 1998; Sharma et al., 2023; Zhang et al., 2024; Bhat et al., 2025).

Despite growing interest in using aromatic plants for phytoremediation, several aspects remain underexplored. Most research has focused on classical hyperaccumulator or energy crop species, while the potential of aromatic plants, particularly Asteraceae, remains relatively poorly investigated. Information on the distribution of heavy metals among different plant organs and the efficiency of translocation from roots to shoots under naturally contaminated conditions is limited.

This knowledge gap is especially relevant for regions with long-term industrial and mining activities, where soils are often heavily contaminated with Pb, Cd, and Zn. In Bulgaria, numerous industrial and mining areas face significant environmental challenges from heavy metal accumulation, underscoring the need for sustainable, effective remediation strategies.

The present study addresses this gap by systematically evaluating the phytoremediation potential of selected aromatic Asteraceae species grown on industrially contaminated soils in Bulgaria. By analysing Pb, Cd, and Zn concentrations in roots, stems, and leaves and calculating bioconcentration (BCF) and translocation (TF) factors, the study provides a comprehensive assessment of these species' capacity to accumulate and translocate heavy metals.

The objectives of this study are: (i) to determine Pb, Cd, and Zn concentrations in different plant organs (roots, stems, leaves, flowers); (ii) to evaluate the species' ability to accumulate and translocate metals through BCF and TF calculations; and (iii) to identify species with the highest potential for application in the phytoremediation of heavy metal-contaminated soils.

The results will contribute to a better understanding of the mechanisms of metal accumulation and translocation and support the development of sustainable strategies for the management and restoration of industrially contaminated soils.

## MATERIALS AND METHODS

The study was conducted on soils located in the vicinity of a major industrial pollution source - the Non-Ferrous Metal Works near Plovdiv, Bulgaria. The sampling sites are situated at approximately 0.5 km from the emission source, where long-term industrial activity has resulted in significant accumulation of trace metals in the surface soil layer.

This site has been extensively investigated in previous studies focused on plant-based phytoremediation (Angelova, 2020; Angelova & Ihtyarova, 2023; Angelova & Ihtyarova, 2025), and is therefore considered a well-characterised system for assessing heavy metal behaviour under field conditions.

Seedlings of selected medicinal plants - costmary (*Tanacetum balsamita* L.), tansy (*Tanacetum vulgare* L.), yarrow (*Achillea millefolium* L.), wormwood (*Artemisia absinthium* L.), and tarragon (*Artemisia dracunculus* L.) - were obtained from a commercial nursery and planted in spring. Plant samples were collected during the flowering stage in the second and third years after planting and dried at room temperature to a constant air-dry mass.

Pseudo-total metal content in the soil was determined following ISO 11466. At the same time, concentrations of Pb, Zn, and Cd in plant organs (roots, stems, leaves, and flowers) were analysed after microwave-assisted acid digestion. Quantitative measurements were performed using inductively coupled plasma optical emission spectrometry (ICP-OES; Jobin Yvon Emission JY 38 S, France), with analytical accuracy validated using apple leaves as a certified reference material (SRM 1515, NIST).

Phytoremediation potential was evaluated using quantitative indices describing metal uptake, translocation, and accumulation in plant tissues (Raskin & Ensley, 2000; Terry & Banuelos, 2000). The phytoremediation assessment focused on three key indicators: the bioconcentration factor (BCF), the translocation factor (TF), and the aboveground accumulation factor (BAF). These parameters are widely applied in studies of heavy metal uptake and phytoextraction efficiency (Yoon et al., 2006; Kabata-Pendias, 2011; Ali et al., 2013). BCF quantifies root uptake relative to soil concentrations (BCF = Croot/Csoil). TF evaluates internal metal mobility and is calculated for individual organs (TF_stem = Cstem/Croot; TF_leaf = Cleaf/Croot; TF_flower = Cflower/Croot) as well as a total value (TF_total = Caboveground/Croot). BAF represents the accumulation of metals in the aboveground biomass relative to soil concentration (BAF = Caboveground/Csoil).

Together, these metrics provide a concise evaluation of metal uptake, translocation, and accumulation efficiency. BCF reflects the efficiency of metal uptake by roots relative to soil concentrations; values >1 indicate effective extractors, whereas values <0.1 denote stabilisers or metal excluders. TF characterises internal metal translocation, with TF_total summarising transport from roots to all aboveground tissues; TF_total >1 indicates efficient translocation, while TF_total <1 suggests predominant root retention and potential for phytostabilisation. BAF integrates uptake and translocation into a direct indicator of phytoextraction potential. Together, these metrics enable robust classification of species as accumulators, intermediates, stabilisers, or excluders, supporting their targeted application in sustainable soil remediation strategies.

## RESULTS AND DISCUSSIONS

### *Soil Contamination Characteristics*

Soils at the investigated site show markedly elevated concentrations of heavy metals as a result of long-term industrial activity in the region. The measured concentrations of Zn, Pb and Cd considerably exceed commonly accepted guideline values for agricultural soils reported in the literature, indicating severe contamination (Kabata-Pendias, 2011).

Zinc concentrations generally fall within the range typical for metal-impacted soils in proximity to metallurgical facilities, while lead and cadmium levels also indicate strong anthropogenic influence. Such elevated concentrations reflect the long-term accumulation of trace elements derived from emissions of the nearby Non-Ferrous Metal Works and associated industrial activities.

Similar contamination patterns for this site have been previously reported (Angelova et al., 2025), confirming that the studied soils represent a characteristic example of chronically polluted industrial areas. Under such conditions, only plant species with high tolerance to metal stress are able to persist, often developing adaptive physiological and biochemical mechanisms that enable survival in highly contaminated environments.

Measured concentrations (Table 1) further confirm that Zn, Pb and Cd levels exceed regulatory limits by several-fold. Such contamination levels are characteristic of soils affected by mining and metallurgical activities, where prolonged anthropogenic inputs lead to the accumulation of trace metals (Alloway, 2013). Elevated concentrations of Pb, Cd and Zn impose strong selective pressure on vegetation, favoring species capable of tolerating metal stress and regulating metal uptake. Plants growing under such conditions typically activate complex physiological and biochemical defense mechanisms, including metal binding, antioxidant responses and intracellular compartmentalization, which allow them to maintain metabolic function despite high soil contamination (Al-Khayri et al., 2023).

### *Heavy Metal Accumulation in Plant Organs*

Analysis of metal concentrations in different plant organs revealed substantial interspecific and metal-specific differences. The highest concentrations of Pb, Cd, and Zn were generally observed in leaves and roots, while stems contained considerably lower amounts (Table 1). This pattern is characteristic of plants actively translocating metals to aerial tissues (Angelova, 2020; Angelova & Ihtyarova, 2023; Ihtyarova & Angelova, 2023; Angelova, 2023; Angelova, 2025). Roots serve as the primary site of metal uptake from the soil solution, after which ions are transported to aboveground tissues via the xylem, where they accumulate in

leaves and other photosynthetically active organs. In some cases, leaf metal accumulation may also result from atmospheric deposition of metal particles, especially in industrially contaminated areas (Rahman et al., 2024). Similar accumulation patterns have been documented in aromatic Asteraceae, which demonstrate enhanced metal tolerance and the ability to regulate intracellular concentrations through detoxification and compartmentalisation mechanisms (Ali et al., 2013; Kumar et al., 2016).

Table 1. Concentrations of Pb, Cd, and Zn (mg/kg) in soils and different plant organs (roots, stems, leaves, flowers) of selected Asteraceae species grown on industrially contaminated sites

| Species/Element | | Soils | Roots | Stems | Leaves | Flowers |
|---|---|---|---|---|---|---|
| *Artemisia absinthium* | Pb | 2509.1 | 1913.0 | 123.5 | 4414.9 | 1223.3 |
| | Cd | 64.3 | 102.7 | 19.9 | 225.1 | 163.9 |
| | Zn | 2423.9 | 1495.2 | 76.1 | 2026.6 | 911.5 |
| *Achillea millefolium* | Pb | 2509 | 1000.3 | 230.8 | 405.6 | 1170.9 |
| | Cd | 64.3 | 102.6 | 82.7 | 133.0 | 89.8 |
| | Zn | 2423.9 | 506.4 | 196.1 | 737.6 | 1035.3 |
| *Tanacetum balsamita* | Pb | 2966.9 | 676.3 | 495.1 | 566.0 | 244.1 |
| | Cd | 92.0 | 58.4 | 77.1 | 59.7 | 18.4 |
| | Zn | 3196.1 | 500.7 | 395.1 | 664.6 | 159.7 |
| *Tanacetum vulgare* | Pb | 2966.9 | 237.1 | 71.8 | 425.0 | 310.6 |
| | Cd | 92.0 | 56.3 | 75.4 | 99.4 | 56.5 |
| | Zn | 3196.1 | 112.8 | 73.9 | 508.0 | 312.4 |
| *Artemisia dracunculus* | Pb | 2509.1 | 91.1 | 56.5 | 742.8 | 294.3 |
| | Cd | 64.3 | 3.9 | 15.5 | 39.0 | 35.1 |
| | Zn | 2423.9 | 50.9 | 68.5 | 556.1 | 304.6 |

### *Metal-Specific Uptake and Translocation Patterns*

*Artemisia absinthium* exhibited the highest Pb accumulation among the studied species, with leaf concentrations exceeding 4415 mg/kg and root concentrations of around 1913 mg/kg. The high translocation factor (TF_leaf > 2) indicates effective transport to aerial parts. This is unusual, as Pb generally has low mobility and is largely retained in roots due to strong binding to cell walls and limited xylem transport (Rahman et al., 2024). Enhanced mobility may involve organic ligands, such as phenolics and terpenoids, which facilitate Pb translocation. *Achillea millefolium* also accumulated considerable Pb, particularly in flowers, suggesting active translocation to reproductive organs (Salt et al., 1998; Angelova & Ihtyarova, 2023; Yadav et al., 2025). *T. balsamita* and *T. vulgare* retained Pb mainly in roots, characteristic of phytostabilisation strategies (Ali et al., 2013; Nikolić & Stević, 2015; Angelova & Ihtyarova, 2023; Angelova, 2025). *Artemisia dracunculus* showed minimal Pb uptake (BCF = 0.04) (Table 2), indicating limited Pb accumulation under the studied conditions.

Cd exhibited higher mobility than Pb. The highest concentrations were observed in leaves of *A. absinthium* (225.1 mg/kg) and *A. millefolium* (133.0 mg/kg), indicating efficient translocation to aboveground tissues. High Cd accumulation reflects effective detoxification mechanisms, including complexation with organic acids, amino acids, and phytochelatins (Clemens et al., 2013). Cd is relatively easily transported via the xylem to photosynthetic tissues (Tao & Lu, 2022). In *A. dracunculus*, Cd accumulated primarily in leaves and flowers despite low root concentrations, demonstrating efficient internal metal transport (Nagajyoti et al., 2010).

Table 2. Bioconcentration (BCF), translocation (TF), and aboveground accumulation (BAF) factors for Pb, Cd, and Zn in selected Asteraceae species cultivated on industrially contaminated soils

| Element | BCF | TF stem | TF leaf | TF flower | TF total | BAF |
|---|---|---|---|---|---|---|
| *T. balsamita* | | | | | | |
| Pb | 0.23 | 0.73 | 0.84 | 0.36 | 1.93 | 0.44 |
| Cd | 0.64 | 1.32 | 1.02 | 0.32 | 2.66 | 1.69 |
| Zn | 0.16 | 0.79 | 1.33 | 0.32 | 2.43 | 0.38 |
| *T. vulgare* | | | | | | |
| Pb | 0.08 | 0.30 | 1.79 | 1.31 | 3.41 | 0.27 |
| Cd | 0.61 | 1.34 | 1.77 | 1.00 | 4.11 | 2.51 |
| Zn | 0.04 | 0.66 | 4.51 | 2.77 | 7.93 | 0.28 |
| *A. millefolium* | | | | | | |
| Pb | 0.40 | 0.23 | 0.41 | 1.17 | 1.81 | 0.72 |
| Cd | 1.60 | 0.81 | 1.30 | 0.88 | 2.98 | 4.75 |
| Zn | 0.21 | 0.38 | 1.46 | 2.04 | 3.89 | 0.81 |
| *A. absinthium* | | | | | | |
| Pb | 0.76 | 0.06 | 2.30 | 0.64 | 3.01 | 2.30 |
| Cd | 1.60 | 0.19 | 2.19 | 1.60 | 3.98 | 6.36 |
| Zn | 0.62 | 0.05 | 1.36 | 0.61 | 2.02 | 1.24 |
| *A. dracunculus* | | | | | | |
| Pb | 0.04 | 0.62 | 8.15 | 3.23 | 12.01 | 0.44 |
| Cd | 0.06 | 3.97 | 9.96 | 8.95 | 22.87 | 1.39 |
| Zn | 0.02 | 1.34 | 10.93 | 5.99 | 18.26 | 0.38 |

Zn is an essential micronutrient with tightly regulated uptake. The highest concentrations were observed in *A. absinthium* leaves (>2000 mg/kg). Relatively high concentrations were also detected in *A. millefolium*, especially in leaves and flowers, indicating that Asteraceae species can accumulate Zn without visible toxicity symptoms, likely through intracellular compartmentalisation (Broadley et al., 2007; Balafrej et al., 2020).

### *Species-Specific Phytoremediation Strategies*

*Artemisia absinthium* demonstrated the highest capacity for heavy metal accumulation. The genus Artemisia is known for resilience to

abiotic stress, including metal contamination, activating protective mechanisms through enhanced synthesis of secondary metabolites such as terpenes and phenolics (Balafrej et al., 2020). *Achillea millefolium* also showed considerable potential for Pb, Cd, and Zn accumulation, making it promising for phytoextraction (Angelova & Ihtyarova, 2023). *T. balsamita* and *T. vulgare* exhibited moderate BCF and limited translocation, suitable for phytostabilisation (Nikolić & Stevović, 2015). *Artemisia dracunculus* showed low accumulation potential and is suitable for cultivation on moderately contaminated soils.

***Morphological Determinants of Metal Uptake***

Morphological traits significantly influence metal accumulation. Species with deep, branched roots, such as *A. absinthium* and *A. millefolium*, showed higher efficiency in metal ion uptake. Dense leaf trichomes enhance deposition of atmospheric metal particles, leading to higher Pb concentrations in leaves, particularly in industrial areas (Rahman et al., 2024). High transpiration rates facilitate transport of mobile metals such as Cd and Zn to aerial organs (Tao & Lu, 2022).

***Bioconcentration and Translocation Factors***

Bioconcentration and Translocation Factors BCF indicates a plant's ability to extract metals from soil, while TF reflects the efficiency of transport to aboveground tissues (Yoon et al., 2006). *A. absinthium* and *A. millefolium* exhibited BCF > 1 for Cd and Zn, along with high TF values (Table 2), confirming their phytoextraction potential (Angelova & Ihtyarova, 2023). In the case of Pb, although BCF values in *A. absinthium* were moderate, the high TF_leaf and TF_total values indicate efficient translocation from roots to aboveground tissues. This results in enhanced accumulation in leaves, which may exceed soil concentrations and reflects the strong accumulator behaviour of the species. As shown in Table 2, although the BCF value (0.76) indicates moderate uptake from soil, the translocation factors, particularly TF_leaf (2.30) and TF_total (3.01), demonstrate highly efficient transport of Pb from roots to aboveground tissues. In addition, the BAF value (2.30) indicates significant accumulation in the aerial biomass. This combination of moderate uptake and strong translocation results in the enrichment of Pb in leaves, leading to concentrations exceeding those in soil. Therefore, this behavior confirms the classification of *Artemisia absinthium* as an accumulator species rather than indicating an inconsistency. Furthermore, the contribution of atmospheric deposition in industrially affected areas may also enhance Pb levels in leaves. *T. balsamita* and *T. vulgare* had lower BCF and TF, typical of stabilisers (Nikolić & Stevović, 2015). A. dracunculus showed low BCF and TF, confirming limited metal uptake.

***Implications for Phytoremediation***

The results indicate that aromatic Asteraceae species can be integrated into sustainable strategies for managing metal-contaminated soils. High-accumulating species, such as *A. absinthium* and *A. millefolium*, are suitable for phytoextraction, whereas moderately accumulating species may serve in phytostabilisation (Ali et al., 2013; Nikolić & Stevović, 2015; Angelova, 2020; Angelova & Ihtyarova, 2023). An integrated analysis of BCF, TF_total, and BAF revealed clear differences among species. *A. absinthium* and *A. millefolium* showed the highest potential for Cd and Zn extraction, with elevated BCF, TF_total > 1, and BAF > 1 (Table 3). *T. balsamita* and *T. vulgare* exhibited moderate or partial extraction, while *A. dracunculus* displayed typical excluder behavior with low uptake but maintained internal translocation, suitable for stabilisation. These findings demonstrate the differentiated phytoremediation potential of *Asteraceae* species, indicating their promise as sustainable, multifunctional crops that combine metal tolerance with high aboveground biomass production.

From a practical perspective, the utilization of the resulting biomass depends on the level of metal accumulation and the target element. For species with high accumulation in aboveground tissues, such as *A. absinthium* and *A. millefolium*, direct use for food, feed or medicinal purposes is not recommended due to the risk of metal transfer. However, the biomass can be directed toward non-food applications, such as bioenergy production or essential oil extraction, where metals are not transferred into

the distilled product. In contrast, low-accumulating species such as *A. dracunculus* may be suitable for controlled use in moderately contaminated soils.

Table 3. Phytoremediation classification of selected Asteraceae species for Pb, Cd, and Zn, based on metal accumulation and translocation patterns.

| Species | Pb | Cd | Zn |
|---|---|---|---|
| *Artemisia absinthium* | Accumulator | Strong accumulator / Hyperaccumulator | Accumulator |
| *Achillea millefolium* | Intermediate accumulator | Strong accumulator | Accumulator |
| *Tanacetum balsamita* | Intermediate accumulator | Accumulator | Intermediate accumulator |
| *Tanacetum vulgare* | Mixed behavior | Accumulator | Mixed |
| *Artemisia dracunculus* | Metal excluder | Mixed behavior | Metal excluder |

Note: Classification is based on BCF, TF_total, and BAF values. Species with BCF > 1 and TF_total > 1 are considered potential phytoextractors, whereas species with BCF > 1 but TF_total < 1 are classified as phytostabilisers. Species with BCF < 1 are considered metal excluders. "Mixed" indicates species exhibiting contrasting behaviour depending on the metal or showing inconsistent BCF and TF patterns.

## CONCLUSIONS

The present study demonstrates clear interspecific differences among Asteraceae species in their capacity for heavy metal uptake, accumulation, and translocation under conditions of severe industrial soil contamination. *Artemisia absinthium* and *Achillea millefolium* exhibited the highest phytoextraction potential, characterised by efficient accumulation of Pb, Cd, and Zn and effective translocation to the aboveground biomass. In contrast, *T. balsamita* and *T. vulgare* showed moderate metal accumulation and limited translocation, indicating a phytostabilisation-oriented strategy. *Artemisia dracunculus* displayed minimal metal uptake and typical excluder behaviour, suggesting its suitability for cultivation on moderately contaminated soils rather than for active phytoextraction.

Morphological traits, particularly a well-developed root system, leaf surface characteristics, and high transpiration capacity, appear to play a critical role in regulating metal uptake and internal transport within plant tissues. Overall, the findings highlight the significant potential of aromatic Asteraceae species as multifunctional crops for the sustainable management of metal-contaminated soils. Their capacity to combine metal tolerance with productive aboveground biomass supports their inclusion in future phytoremediation strategies aimed at the ecological restoration of industrially impacted landscapes.

## ACKNOWLEDGEMENTS

This research was supported by the Bulgarian National Science Fund [grant number KP-06-H54/7].

## REFERENCES

Ali, H., Khan, E., & Sajad, M.A. (2013). Phytoremediation of heavy metals - Concepts and applications. *Chemosphere*, 91(7), 869-881.

Alloway, B.J. (2013). *Heavy metals in soils: trace metals and metalloids in soils and their bioavailability*. Dordrecht: Springer.

Al-Khayri, J. M., Banadka, A. B. A., Rashmi, R. R., Nagella, P., Alessa, F. M., & Almaghasla, M. I. (2023). Cadmium toxicity in medicinal plants: An overview of the tolerance strategies, biotechnological and omics approaches to alleviate metal stress. *Frontiers in Plant Science*, 13, 1047410. https://doi.org/10.3389/fpls.2022.1047410

Angelova, V. (2020). Heavy metal accumulation and chemical composition of essential oils of wormwood (*Artemisia absinthium* L.) cultivated on heavy metal contaminated soils. *Scientific Papers. Series E. Land Reclamation, Earth Observation & Surveying, Environmental Engineering*, IX, 44-52

Angelova, V. (2023). Heavy metal accumulation and chemical composition of essential oils of tansy (*Tanacetum vulgare* L.) cultivated on heavy metal-contaminated soils. *Medicinal Plants - International Journal of Phytomedicines and Related Industries*, 15(4), 754-762.

Angelova, V., & Ihtyarova, M. (2023). Heavy metal accumulation a nd chemical composition of the essential oils of yarrow (*Achillea millefolium* L.) cultivated on heavy metal-contaminated soils. *Agricultural sciences*, 15(36), 67-76.

Angelova, V. (2025). Evaluation of chemical composition of essential oil and toxic metal accumulation of tarragon (*Artemisia dracunculus* L.) cultivated on metal-contaminated soils. *Scientific Papers. Series E. Land Reclamation, Earth Observation & Surveying, Environmental Engineering*. XIV, 17-23.

Angelova, V., & Ihtyarova, M. (2025). Evaluation of phytoremediation potential of Asteraceae species grown on heavy metal-contaminated soils. *Proceedings of the 60th Croatian and 20th International Symposium on Agriculture. Faculty of Agrobiotechnical Sciences Osijek*, 247-251, ISSN 2459-5543.

Balafrej, H., Bogusz, D., Triqui, Z.-E. A., Guedira, A., Bendaou, N., Smouni, A., & Fahr, M. (2020). Zinc

Hyperaccumulation in Plants: A Review. Plants, 9(5), 562. https://doi.org/10.3390/plants9050562

Bhat, B. A., Rather, M. A. M. A., Bilal, T., Nazir, R., Qadir, R. U., & Mir, R. R. (2025). Plant hyperaccumulators: A state-of-the-art review on mechanisms of heavy metal transport and sequestration. *Frontiers in Plant Science*, 16 https://doi.org/10.3389/fpls.2025.1631378

Broadley, M.R., White, P.J., Hammond, J.P., Zelko, I., Lux, A. (2007). Zinc in plants. *New Phytol*., 173. 677-702.

Clemens, S., Aarts, M.G.M., Thomine, S., & Verbruggen, N. (2013). Plant science: the key to preventing slow cadmium poisoning. *Trends Plant Sci*, 18(2), 92-99.

Deng, S., Zhang, X., Zhu, Y., & Zhuo, R. (2024). Recent advances in phyto-combined remediation of heavy metal pollution in soil. *Biotechnology Advances*, 72, 10837

Ihtyarova, M., & Angelova, V. (2023). Heavy metal accumulation and chemical composition of essential oils of costmary (*Tanacetum Balsamita L*.) cultivated on heavy metal contaminated soils. *Scientific Papers. Series E. Land Reclamation, Earth Observation & Surveying, Environmental Engineering*, XII, 320-329

ISO 11466 (1995). Soil Quality-Extraction of Trace Elements Soluble in Aqua Regia.

Kabata-Pendias A. (2011). *Trace Elements in Soils and Plants*. 4th ed. CRC Press.

Kumar, R., Mishra, R.K., Mishra, V., Qidwai, A., Pandey, A., Shukla, S.K., Pandey, M., Ashutosh Pathak, A. & Dikshit, A. (2016). *Detoxification and tolerance of heavy metals in plants*. In P. Ahmad (Ed.), Plant metal interaction (pp. 335-359). Elsevier.

Nagajyoti, P.C., K.D. Lee, K.D., T.V.M., & Sreekanth, T.V.M. (2010). Heavy metals, occurrence and toxicity for plants: a review. *Environ. Chem. Lett*., 8, 199-216.

Nikolić, M., & Stevović, S. (2015). Family Asteraceae as a sustainable planning tool in phytoremediation and its relevance in urban areas. *Urban Forestry & Urban Greening,* 14(4), 782-789. https://doi.org/10.1016/j.ufug.2015.08.002

Rahman, S., Qin, A., Zain, M., Mushtaq, Z., Mehmood, F., Riaz, L., Naveed, S., Ansari, M.J., Saeed, M., Ahmad, I., & Shehzad, M. (2024). Pb uptake, accumulation, and translocation in plants: Plant physiological, biochemical, and molecular response: A review. *Heliyon*, 10(6), e27724.

Raskin, I., & Ensley, B. D. (2000). *Phytoremediation of Toxic Metals: Using Plants to Clean Up the Environment*. Wiley-Interscience. ISBN 978 0471192541.

Salt, D. E., Smith, R. D., & Raskin, I. (1998). Phytoremediation. *Annual Review of Plant Physiology and Plant Molecular Biology*, 49, 643-668. https://doi.org/10.1146/annurev.arplant.49.1.643.

Sharma, J. K., Kumar, N., Singh, N. P., & Santal, A. R. (2023). Phytoremediation technologies and their mechanism for removal of heavy metals from contaminated soil. *Frontiers in Plant Science*, 14, 1076876.

Terry, N., & Bañuelos, G. S. (2000). *Phytoremediation of Contaminated Soil and Water*. CRC Press: Lewis Publishers.

Tao, J., & Lu, L. (2022). Advances in Genes-Encoding Transporters for Cadmium Uptake, Translocation, and Accumulation in Plants. *Toxics*, 10(8), 411. https://doi.org/10.3390/toxics10080411

Yadav, K., Kumar, D., Gupta, A.K., Gupta, B., Tyagi, P., Sharma, A., Patra, P.K., Patra. P.K., & Chaitanya, A.K. (2025). Heavy metals contamination and their phytoremediation in soil and water for sustainable environmental restoration. *Discover Environment,* 3, 201. https://doi.org/10.1007/s44274-025-00390-9

Yan, A., Wang, Y., Tan, S. N., Mohd Yusof, M. L., Ghosh, S., & Chen, Z. (2020). Phytoremediation: A promising approach for revegetation of heavy metal polluted land. *Frontiers in Plant Science*, 11, 359.

Yoon, J., Cao, X., Zhou, Q., & Ma, L.Q. (2006). Accumulation of Pb, Cu, and Zn in native plants growing on a contaminated Florida site. *Sci Total Environ*., 368, 456-464.

Zhang, L., Zhu, Y., Gu, H., Lam, S.S., Chen, X., Sonne, C., & Peng, W. (2024). A review of phytoremediation of environmental lead (Pb) contamination, *Chemosphere*, 362, 142691.

Scientific Papers. Series E. Land Reclamation, Earth Observation & Surveying, Environmental Engineering. Vol. XV, 2026
Print ISSN 2285-6064, CD-ROM ISSN 2285-6072, Online ISSN 2393-5138, ISSN-L 2285-6064

# INVESTIGATION OF HYDROCARBON POLLUTION IN THE OIL TERMINAL CONSTANȚA AREA USING ELECTRICAL RESISTIVITY METHODS AND HYDROSTATIC REGIME ANALYSIS

**Sorin ANGHEL, Andrei Gabriel DRAGOS, Gabriel IORDACHE, Bogdan Marius BARAITAREANU, Constanta Alexandra DUDU**

National Institute for Research and Development on Marine Geology and Geo-ecology – GeoEcoMar, 23-25 Dimitrie Onciu Str, District 2, Bucharest, Romania

Corresponding author email: soanghel@geoecomar.ro

***Abstract***

*Soil and groundwater contamination with hydrocarbons represents a major environmental issue in port–industrial areas, with direct impacts on agricultural ecosystems and the quality of life of local populations. This study investigates the degree of pollution in the Oil Terminal Constanța North area, located outside the industrial enclosure, within a residential zone where the persistent smell of hydrocarbons indicates active contamination. Geophysical investigations were carried out using the Vertical Electrical Sounding (VES) method along four electrical profiles (P1, P2, P3, and P4), with a spacing of 10 m between measurement points. The main objective was to determine the geological structure, identify the groundwater table, and highlight its relationship with the hydrocarbon pollution plume. The inverted geoelectrical sections, characterized by low RMS values, reveal low-resistivity anomalies associated with hydrocarbon-saturated materials, predominantly located at the groundwater level. Correlation of the geoelectrical results with the hydrostatic level map indicates a groundwater flow direction oriented toward the Black Sea, facilitating pollutant migration. The results confirm the presence of active hydrocarbon pollution, with potential impacts on agricultural soils and the coastal environment.*

***Key words****: coastal environment, electrical resistivity sounding, groundwater migration, hydrocarbon contamination, pollution plume.*

## INTRODUCTION

One of the most persistent and difficult-to-control forms of environmental contamination is soil and groundwater pollution with hydrocarbons, particularly in port-industrial areas and in the vicinity of petroleum storage and transfer facilities. Hydrocarbons can persist in the environment for long periods, affecting groundwater quality, the physicochemical properties of soils, and consequently agricultural land use, food safety, and ecosystem health.

Hydrocarbon pollution presents an additional risk in coastal areas due to the direct interaction between continental hydrogeological systems and the marine environment. The groundwater table plays a key role in contaminant transport, as hydrocarbons preferentially migrate at this level in the direction of groundwater flow, forming a pollution plume (Ali et al., 2025). Under such conditions, contamination does not remain localized but can spread over large areas, affecting both agricultural soils and the receiving marine environment.

One of the most important industrial hubs for handling and storing petroleum products in Romania is the Oil Terminal Constanța area. Over time, long-term industrial activities have generated significant environmental contamination risks, particularly in areas adjacent to the industrial enclosure. Outside the site boundary, in the northern part of the Oil Terminal, a residential area characterized by apartment buildings and green spaces has developed, where the persistent smell of hydrocarbons indicates the presence of major subsurface pollution sources.

In this context, assessing the degree of contamination and the mechanisms of hydrocarbon migration becomes essential for the sustainable management of land with agricultural potential, as well as for environmental protection in the vicinity of industrial areas. Electrometric methods represent efficient, non-destructive tools for investigating subsurface structure, identifying the groundwater table, and delineating contaminated zones through electrical resistivity

contrasts (Alao et al., 2025). Vertical Electrical Sounding (VES) is frequently used in environmental studies aimed at characterizing hydrocarbon-saturated environments, which are typically associated with lower electrical resistivity values compared to unaffected materials. The correlation of geoelectrical results with hydrogeological data allows for the delineation of the pollution plume and the determination of contaminant migration direction.

The present study aims to investigate the degree of hydrocarbon pollution in the Oil Terminal Constanța North area by applying the Vertical Electrical Sounding method along multiple electrometric profiles (Figure 1), correlated with hydrostatic regime analysis.



Figure 1. Acquisition of electrometric data using an AGI MiniSting system

The objective is to determine the geological structure of the area, highlight its relationship with the movement of the pollution plume, and identify the groundwater level, with particular emphasis on migration toward the Black Sea and its implications for the environment and soils.

## MATERIALS AND METHODS

In the northern area of the Oil Terminal Constanța, geophysical investigations were carried out outside the industrial enclosure, within a residential area characterized by apartment buildings and green spaces, where persistent hydrocarbon odors were identified. The area is located in close proximity to the port zone and is influenced by the historical activities of storage and transfer of petroleum products.

The Vertical Electrical Sounding (VES) method was used to assess the subsurface structure and the degree of pollution, this electrometric method being well established in environmental and hydrogeological studies (Goldman & Neubauer, 1994). Measurements were performed along four electrical profiles, labelled P1, P2, P3, and P4 (Figure 2), arranged in the northern extremity of the Oil Terminal, both parallel and perpendicular to the main structural directions and to the estimated groundwater flow direction. To validate the geoelectrical interpretation, two control boreholes (F1 and F2), each reaching a depth of 4 m, were drilled at representative locations within the study area (Figure 2). The borehole information was used to correlate the interpreted electrical resistivity anomalies with the local lithology and groundwater table depth, thereby increasing the reliability of the geophysical interpretation.




Figure 2. Profile layout map

A spacing of 10 m between VES points was applied in order to achieve adequate spatial resolution for identifying lateral variations in electrical resistivity (Eze & Chinemelu, 2025). The electrode configuration was designed to allow investigation of the upper meters of the subsurface, where the groundwater table develops and where the presence of a hydrocarbon pollution plume is assumed. To characterize the saturated zone, the investigation depth reached approximately 4-5 m.

Two-dimensional electrical resistivity inversion was applied to process the field data, resulting in inverted geoelectrical sections for each measured profile (Figures 3-6). The quality of the inversion was assessed using the root mean square (RMS) error, which showed low values of 3.1% for Profile 1, 4.53% for Profile 2, 5.9%

for Profile 3, and 7.07% for Profile 4. These values indicate a good agreement between the measured and calculated apparent resistivity data. Overall, the obtained RMS errors confirm the stability of the inversion solutions and the reliability of the geoelectrical interpretation. For all four profiles, the obtained RMS values confirm the stability of the inversion solutions and the reliability of the geoelectrical interpretation (Loke, 2010).

The interpretation of the geoelectrical sections involved correlating local lithology with electrical resistivity values, borehole information, and hydrogeological conditions. Zones characterized by low resistivity values were interpreted as electrically conductive materials, which may represent water-saturated fine-grained sediments, saline groundwater, wastewater infiltration, and/or hydrocarbon-contaminated horizons. The anomalies detected in this study were interpreted as hydrocarbon-affected zones only where they spatially coincide with the groundwater table, the groundwater flow direction, and the known history of petroleum-related activities in the Oil Terminal Constanța area. Higher resistivity values generally correspond to drier, coarser-grained, or more compact deposits. Particular attention was given to identifying the groundwater table and its lateral variations. Particular attention was given to identifying the groundwater table and its lateral variations.

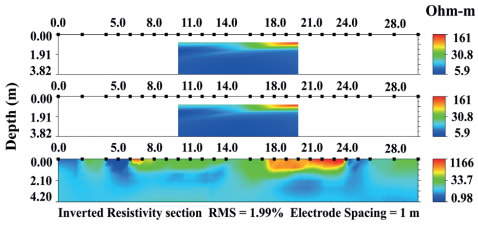



Figure 3. Inverted resistivity section - Profile 1

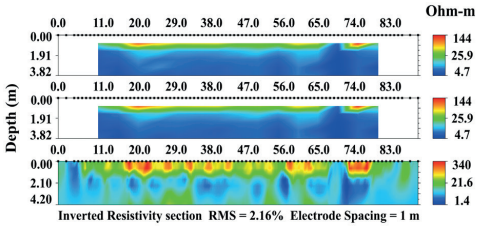



Figure 4. Inverted resistivity section - Profile 2

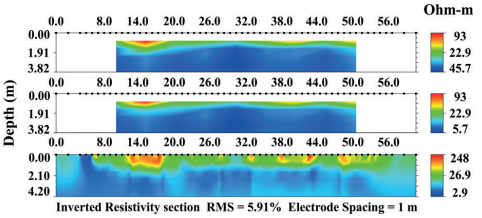



Figure 5. Inverted resistivity section - Profile 3

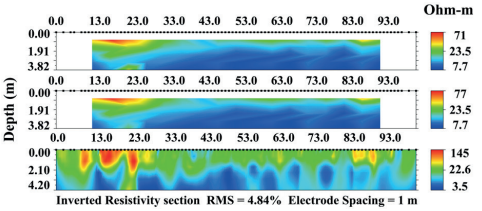



Figure 6. Inverted resistivity section - Profile 4

The analysis of pollutant migration direction was based on correlating the electrometric results with the hydrostatic level map, developed using available piezometric measurements. This correlation allowed the relationship between groundwater table position and resistivity anomaly distribution to be defined, as well as the identification of the dominant groundwater flow direction, oriented toward the coastal area of the Black Sea.

The study, based on electrometric methods and hydrostatic analysis, enabled a detailed assessment of subsurface structure and hydrocarbon transport pathways, providing a solid basis for interpreting the degree of pollution and its potential impact on the environment and on residential land use in the investigated area.

## RESULTS AND DISCUSSIONS

During the interpretation stage of the inverted geoelectrical sections obtained for the four Vertical Electrical Sounding (VES) profiles (P1, P2, P3, and P4), detailed information was obtained regarding the subsurface geology and the surface distribution of electrical resistivity anomalies within the investigated area. The results reveal significant lateral and vertical variations in resistivity values, which are related to lithological changes, hydrocarbon contamination, and groundwater distribution (Ali et al., 2025).

Zones represented by red shades, corresponding to high electrical resistivity values, are observed on all profiles and are predominantly located in the upper parts of the sections (Atekwana et al., 2000). These zones are associated with unsaturated soils, more compact deposits, and anthropogenic fill materials characteristic of residential environments. Such units are characterized by low moisture conditions and a low degree of contamination. Beneath these layers, zones represented by blue shades, corresponding to low electrical resistivity values, are systematically identified at depths ranging from approximately 1.5 to 4-5 m. These low-resistivity anomalies coincide with the groundwater table and are interpreted as water-saturated horizons contaminated with hydrocarbons. Similar geoelectrical responses have been reported in hydrocarbon-contaminated environments, where contamination may modify the electrical properties of saturated sediments through physicochemical and biogeochemical processes (Abdel Aal et al., 2004). The interpretation obtained in the present study is also consistent with the findings of Eze and Chinemelu (2025), who demonstrated that electrical resistivity techniques provide reliable information for identifying groundwater contamination and delineating the spatial extent of hydrocarbon-affected zones. Similar to their observations, the low-resistivity anomalies detected in the investigated area coincide with the saturated zone and reflect the influence of contaminant migration on the electrical properties of the subsurface. This agreement further confirms the applicability of the Vertical Electrical Sounding (VES) method as an effective tool for preliminary environmental investigations and hydrocarbon contamination assessment in petroleum-impacted areas. The inverted apparent resistivity sections corresponding to profiles P1, P2, and P3 display laterally continuous low-resistivity anomalies (blue shades), indicating the presence of a pollution plume developed over a large area along the groundwater table. The spatial extent of these anomalies suggests that contamination is not localized but distributed throughout the investigated area, following natural groundwater flow pathways. The low RMS values obtained for these profiles confirm the reliability of the inversion models and the accuracy of the geoelectrical interpretation. In the case of profile P4, a similar resistivity structure is observed, but with variations in the thickness and intensity of the low-resistivity zones (blue shades). These variations may reflect differences in permeability, local lithological heterogeneities, or hydrocarbon concentration. Extremely low resistivity values are interpreted as sectors where hydrocarbons are mixed with fine-grained sediments and groundwater, resulting in a marked increase in electrical conductivity. The geoelectrical results correlate well with the hydrostatic level map, revealing a clear relationship between the position of the groundwater table and the distribution of low-resistivity anomalies. The hydrostatic gradient indicates (Fetter, 2001) a dominant groundwater flow direction oriented toward the Black Sea (Figure 7).

According to the hydrogeological principles described by Fetter (2001), groundwater flow is primarily controlled by hydraulic gradients, which govern the transport of dissolved and free-phase contaminants within saturated porous media. The groundwater flow direction identified in the present study therefore provides a logical explanation for the observed distribution of low-resistivity anomalies and supports the interpretation that the hydrocarbon plume is migrating from the industrial area toward the coastal environment.

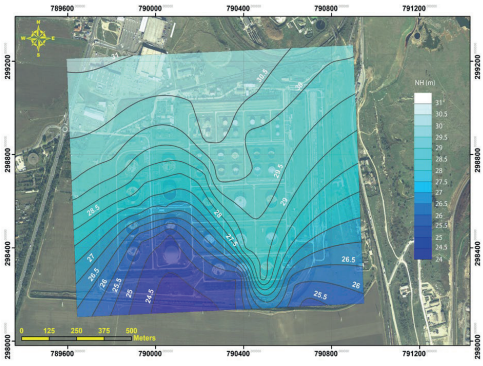



Figure 7. Hydrostatic water level map based on borehole data and piezometric studies

Consequently, the hydrocarbon pollution plume, highlighted by the low-resistivity zones (blue shades), is interpreted as migrating along the

groundwater flow direction from the industrial source area toward the coastal zone.

The migration of the pollution plume represents a significant environmental risk, as it facilitates the transport of hydrocarbons into residential areas, potentially affecting soils used for agricultural purposes as well as the coastal marine environment.

The integrated interpretation of the geoelectrical sections and the hydrostatic level map provides a consistent conceptual model of hydrocarbon migration in the investigated area. The spatial coincidence between the low-resistivity anomalies and the groundwater table indicates that contaminant transport is primarily controlled by the local hydrogeological regime rather than by isolated leakage points. The lateral continuity of the anomalies observed along profiles P1, P2, and P3 suggests the development of an extensive pollution plume migrating in the direction of groundwater flow toward the Black Sea. These findings confirm that the integration of electrical resistivity investigations with hydrogeological information represents a reliable approach for identifying hydrocarbon contamination pathways and provides valuable support for environmental monitoring and remediation planning in coastal industrial areas. These findings are consistent with previously reported geoelectrical models of hydrocarbon plumes in saturated sediments (Sauck, 2000). Furthermore, the migration pattern identified in the present study agrees with observations reported for other hydrocarbon-contaminated coastal and industrial sites, where groundwater acts as the dominant transport pathway and geoelectrical methods effectively delineate contamination plumes (Alao et al., 2025; Ali et al., 2025). The integration of VES data with hydrogeological information also reduces the ambiguity of geophysical interpretation by distinguishing lithological variations from contamination-related anomalies, thereby improving the reliability of environmental assessments and supporting remediation prioritization in complex industrial environments. The geoelectrical response observed in the investigated area is also consistent with previous studies reporting that hydrocarbon contamination modifies the electrical properties of subsurface materials, particularly within the saturated zone where contaminant migration is closely controlled by groundwater dynamics (Atekwana et al., 2000; Abdel Aal et al., 2004). In addition, the relatively low RMS errors obtained for all investigated profiles increase confidence in the inversion models and support the interpretation of the detected anomalies as environmentally significant features rather than inversion artefacts. Similar approaches have been successfully applied in contaminated industrial sites, demonstrating that electrical resistivity techniques provide reliable information on the geometry and lateral continuity of pollution plumes while minimizing environmental disturbance compared with intrusive investigation methods (Goldman & Neubauer, 1994; Loke, 2010). Consequently, the integrated application of geoelectrical investigations and hydrogeological analysis represents a robust methodology not only for contamination assessment but also for planning future monitoring campaigns and evaluating the effectiveness of remediation measures in areas affected by long-term petroleum-related activities.

## CONCLUSIONS

The Vertical Electrical Sounding (VES) investigations successfully characterized the shallow geological structure and identified the groundwater table within the investigated area.

Low electrical resistivity anomalies indicate the presence of hydrocarbon-contaminated saturated horizons, confirming active contamination in the northern part of the Oil Terminal Constanța area.

Correlation between the geoelectrical results and the hydrostatic level map demonstrates that contaminant migration is controlled by groundwater flow toward the Black Sea.

The integration of electrical resistivity investigations with hydrogeological analysis provides an effective approach for identifying hydrocarbon migration pathways and supporting environmental monitoring and remediation activities.

## ACKNOWLEDGEMENTS

This work was funded under the CORE Program, projects no. 23300403, 23300404.

## REFERENCES

Abdel Aal, G. Z., Atekwana, E. A., Slater, L. D., & Atekwana, E. A. (2004). Effects of microbial processes on electrolytic and interfacial electrical properties of unconsolidated sediments. *Geophysics, 69*(4), 1073–1084, https://doi.org/10.1029/2004GL020030.

Alao, J. O., Balarabe, B., Ayejoto, D. A., Abubakar, F., Otorkpa, O. J., & Eze, S. U. (2025). Evaluation of hydrocarbon and co-contaminants in groundwater and associated public health risks using electrical resistivity and hydrochemical data. *Water Research & Industry, 15*, 100319. https://doi.org/10.1016/j.wri.2025.100319.

Ali, N., Chappuies, J. C. J., Sloan, G., Rouland, G., Rai, A. R., & Dong, Y. (2025). A global perspective on electrical resistivity tomography, electromagnetic and ground penetration radar methods for estimating groundwater recharge zones. *Frontiers in Water*, 7, 1636613, https://doi.org/10.3389/frwa.2025.1636613.

Atekwana, E. A., Sauck, W. A., & Werkema, D. D. (2000). Investigations of geoelectrical signatures at a hydrocarbon contaminated site. *Journal of Applied Geophysics, 44*(2–3), 167–180. https://doi.org/10.1016/S0926-9851(98)00033-0.

Eze, S. U., & Chinemelu, E. S. (2025). Evaluation of hydrocarbon contamination in groundwater through electrical resistivity imaging and geochemical techniques. *Earth Sciences Malaysia*, 9(1), 23–29, https://doi.org/10.26480/esmy.01.2025.23.29.

Fetter, C. W. (2001). *Applied hydrogeology* (4th ed.). Upper Saddle River, NJ: Prentice Hall.

Goldman, M., & Neubauer, F. M. (1994). Groundwater exploration using integrated geophysical techniques. *Surveys in Geophysics*, 15(3), 331–361. https://doi.org/10.1007/BF00690176

Loke, M. H. (2010). *Electrical imaging surveys for environmental and engineering studies: A practical guide.* Penang, Malaysia: Geotomo Software.

Sauck, W. A. (2000). A model for the resistivity structure of LNAPL plumes and their environs in sandy sediments. *Journal of Applied Geophysics*, 44(2-3), 151–165. https://doi.org/10.1016/S0926-9851(00)00005-9.

Scientific Papers. Series E. Land Reclamation, Earth Observation & Surveying, Environmental Engineering. Vol. XV, 2026
Print ISSN 2285-6064, CD-ROM ISSN 2285-6072, Online ISSN 2393-5138, ISSN-L 2285-6064

# MINERAL COMPOSITION OF *VACCINIUM VITIS-IDAEA* FRUITS ACROSS DIFFERENT MOUNTAIN HABITATS

**Carla-Maria APARASCHIVE, Alina TRUTA, Irina MORAR, Tania MIHAIESCU, Claudia BALINT, Alexandra MURESAN, Catalina DAN, Adriana SESTRAS**

University of Agricultural Sciences and Veterinary Medicine of Cluj-Napoca,
3-5 Calea Manastur, Cluj-Napoca, Romania

Corresponding author email: adriana.sestras@usamvcluj.ro

***Abstract***

*The present study investigated the mineral composition of Vaccinium vitis-idaea fruits collected from five mountain regions of the Romanian Carpathians, characterized by distinct environmental and geological conditions. Fruit samples were analyzed using portable X-ray fluorescence spectrometry (pXRF) to determine the concentrations of macro-, micro- and trace elements, including K, Ca, Fe, Mn, Zn, Cu, Ni, Sr and Rb. Climatic parameters describing the environmental context of the sampling sites were also considered. The results revealed clear differences in elemental profiles among the studied provenances. Potassium was the dominant macronutrient in all samples, whereas Ca, Mn and Rb exhibited noticeable spatial variability. Multivariate analyses (HCA and PCA) indicated that the elemental profile of lingonberry fruits reflects both environmental gradients and site-specific geochemical characteristics. In particular, rubidium showed the strongest differentiation among sites, suggesting a possible relationship between berry elemental composition and the geological characteristics of the habitats. The results highlight spatial variability in the mineral profile of wild V. vitis-idaea fruits across mountain environments and provide baseline information on their elemental composition in the Romanian Carpathians.*

***Key words****: Carpathians, environment, mineral composition, Vaccinium vitis-idaea, variability.*

## INTRODUCTION

*Vaccinium vitis-idaea* L. (lingonberry) is a perennial evergreen shrub of the *Ericaceae* family that is widely distributed throughout boreal forests and alpine regions of the Northern Hemisphere. The species typically grows in nutrient-poor, acidic soils and the berries are traditionally harvested from wild populations and are widely consumed in Northern and Central Europe due to their nutritional value and characteristic sour taste (Hjalmarsson & Ortiz, 2001; Nestby et al., 2019). Lingonberry fruits have received considerable scientific attention due to their high content of bioactive constituents, including phenolic acids, flavonoids and anthocyanins, which contribute to their high antioxidant capacity and potential health-promoting properties (Bujor et al., 2018; Kowalska, 2021). In addition to these compounds, lingonberry fruits also contain several mineral elements that contribute to their nutritional value and play important roles in plant physiological processes (Toncheva et al., 2016).

The concentration of mineral elements in wild berries can vary significantly depending on environmental conditions (Ekholm et al., 2007). Soil properties, nutrient availability and geographical location may influence the uptake and accumulation of macro- and micronutrients in plant tissues. Studies on lingonberries have shown that the concentration of elements such as K, Mn, Fe, Zn and Cu can vary between plant organs and sampling sites, reflecting differences in soil chemistry and environmental conditions (Lazarenko et al., 2021).

Environmental factors such as temperature, precipitation and altitude can influence plant physiological processes involved in nutrient uptake, transport and allocation within plant tissues. In mountainous ecosystems, these factors interact with soil characteristics and geological substrate to determine nutrient availability in the rhizosphere. As a result, plants growing under different habitat conditions may exhibit distinct patterns of mineral allocation between vegetative organs and fruits, reflecting both environmental constraints and species-

specific physiological regulation (Broadley et al., 2007; Luginina & Egoshina, 2013).

Despite the increasing interest in the nutritional and biochemical properties of lingonberries, information regarding the variability of mineral elements in fruits collected from different natural populations remains relatively limited. Investigating the mineral composition of lingonberries from different provenances can improve our understanding of spatial variation in element accumulation in wild populations and may also provide useful information on the nutritional value of these fruits. Therefore, the aim of this study was to characterize the mineral composition of *V. vitis-idaea* fruits collected from five mountain habitats in Romania and to examine whether differences in elemental profiles are associated with local environmental and lithological conditions. In this context, the study provides baseline data on the mineral profile of wild lingonberry fruits from the Romanian Carpathians.

## MATERIALS AND METHODS

### Study area and fruit sampling

Lingonberry (*Vaccinium vitis-idaea* L.) fruits were collected from five natural populations located in mountainous regions of Romania, each representing a distinct geographical area. The sampling sites were Groșii Țibleșului (GT; 47.551° N, 24.136° E), Valea Vinului (VV; 47.513° N, 24.851° E), Bilbor (BI; 47.115° N, 25.496° E), Cheia (CH; 45.427° N, 25.846° E) and Doda Pilii (DP; 46.662° N, 22.861° E). The coordinates represent the central point of the sampled area, while the abbreviations are used throughout the text to indicate the sampling site. Altitude was expressed as the midpoint of the reported elevation range for each sampling site (m a.s.l.).

Lithological information for each location was determined using geological maps and literature describing the geological structure of the Romanian Carpathians (Peters et al., 2018). These locations differ in terms of altitude, lithology and local environmental conditions, as presented in Table 1. Fruit sampling was conducted in August 2023, when berries had reached full ripeness (Figure 1).

The fruits were cleaned to remove visible impurities and dried in a ventilated oven at 60°C until constant weight was reached. The dried material was subsequently ground into a fine homogeneous powder using a laboratory grinder.

Table 1. Geographic and environmental characteristics of the sampling sites

| Site | County | Altitude | Lithology |
|---|---|---|---|
| Groșii Țibleșului | Maramureș | 1250 | Sedimentary |
| Valea Vinului | Bistrița-Năsăud | 1550 | Metamorphic |
| Bilbor | Harghita | 1150 | Metamorphic |
| Cheia | Prahova | 1450 | Sedimentary |
| Doda Pilii | Cluj | 1150 | Metamorphic |

At each location, three independent composite samples were collected to account for within-site variability. Each sample consisted of berries harvested from several individual plants distributed within an area of approximately 100 m² in order to obtain representative material for the local population. The fruits from each sampling point were pooled to form a composite sample representing that site replicate. After collection, the samples were transported to the laboratory for further processing.



Figure 1. Fully ripe *V. vitis-idaea* berries at the time of sampling

The powdered samples were stored in airtight containers at room temperature until analysis. Elemental analysis was performed using an ElvaX Mobile Portable XRF Spectrometer (Elvatech Ltd., Kyiv, Ukraine). Prior to analysis, the powdered material was loaded into sample cups and analyzed directly using X-ray fluorescence spectroscopy (Sapkota et al., 2019; Zhou et al., 2023). To ensure analytical reliability, all measurements were performed under identical instrumental conditions and each sample was analyzed in replicate scans. The instrument calibration and element quantification were carried out using the

manufacturer's software and factory calibration settings. Detection limits were estimated based on the lowest detectable concentrations recorded during the measurements. Quality control was evaluated through repeated measurements of selected samples, which showed consistent elemental readings within the expected analytical variability of portable XRF measurements.

**Climatic variables**

Environmental data for each location were obtained from the ERA5-Land reanalysis dataset provided by the Copernicus Climate Data Store (Muñoz-Sabater et al., 2021).

Climatic variables included mean daily air temperature (°C), representing the near-surface air temperature measured at approximately 2 m above ground level; cumulative precipitation (mm), corresponding to the total precipitation reaching the land surface during the analyzed period; mean daily surface solar radiation (MJ $m^{-2}$ $day^{-1}$), describing the incoming solar energy received at the land surface; and mean volumetric soil water content ($m^3$ $m^{-3}$), representing the proportion of water in the upper soil layer (0-7 cm).

These parameters were calculated for the period May-July by averaging daily values (temperature, solar radiation and soil moisture) and summing precipitation totals. This period corresponds to the main fruit development stage of *V. vitis-idaea*, when active nutrient transport and accumulation occur in developing berries, making it particularly relevant for assessing the mineral elements analyzed in this study.

The values were extracted based on the geographic coordinates of each sampling site, and the resulting parameters are presented in Table 2.

Table 2. Climatic variables of the sampling sites

| Site | Temperature (°C) | Precipitation (mm) | Solar radiation (MJ $m^{-2}$) | Soil moisture ($m^3$ $m^{-3}$) |
|---|---|---|---|---|
| GT | 15.6 | 379.09 | 20.07 | 0.35 |
| VV | 13.9 | 291.82 | 19.73 | 0.23 |
| BI | 14 | 359.35 | 19.62 | 0.29 |
| CH | 14.4 | 482.76 | 20.1 | 0.38 |
| DP | 15.1 | 497.83 | 19.57 | 0.38 |

The analyzed elements were grouped into three categories: macronutrients, micronutrients, and trace elements. Elemental concentrations were expressed on a dry weight basis (mg $kg^{-1}$ DW). Values below the detection limit were replaced by half of the detection limit (LOD/2) prior to statistical analysis in order to avoid bias caused by non-detectable values. Detection limits were estimated based on the lowest detectable concentrations obtained during the analytical measurements.

**Statistical analysis**

Differences in elemental concentrations among sites were evaluated using analysis of variance (ANOVA), followed by a post hoc multiple comparison test to identify statistically significant differences between means ($p < 0.05$).

To explore relationships between mineral composition and environmental variables, multivariate statistical analyses were performed. Principal component analysis (PCA) was used to identify patterns in the distribution of mineral elements and to assess the influence of climatic parameters on elemental variability. In addition, hierarchical cluster analysis (HCA) was applied to evaluate similarities among provenances and to visualize relationships between elements.

All statistical analyses and graphical representations were performed using PAST software - Paleontological Statistics, version 4.17 (Hammer et al., 2001).

## RESULTS AND DISCUSSION

**Macronutrient concentrations**

Potassium (K) was the predominant macronutrient in *V. vitis-idaea* fruits across all sampling sites (Figure 2a). The highest concentrations were recorded at Bilbor and Doda Pilii, exceeding 12,000 mg $kg^{-1}$ DW, while lower values were observed at the other three provenances. Comparable K levels have been reported for lingonberry fruits (approximately 6,400-6,700 mg $kg^{-1}$ FW) (Lazarenko et al., 2021), indicating that potassium represents the dominant mineral component in these berries. This high K content reflects its key physiological role in osmotic regulation and carbohydrate transport during fruit development.

Calcium (Ca) concentrations showed a different pattern among the sampling sites (Figure 2b), with the highest values recorded at Valea Vinului and Cheia (approximately 1,200-1,300 mg $kg^{-1}$ DW), while lower levels were observed

at Groșii Țibleșului, Doda Pilii and Bilbor. Similar Ca levels have been reported in fruits of other *Vaccinium* species, such as *V. oxycoccos* and *V. macrocarpon*, where concentrations range from approximately 480-1,160 mg kg$^{-1}$ DW (Karlsons et al., 2018). Calcium is primarily associated with structural functions in plant tissues, and its relatively moderate concentration in fruits reflects its limited mobility within the plant.

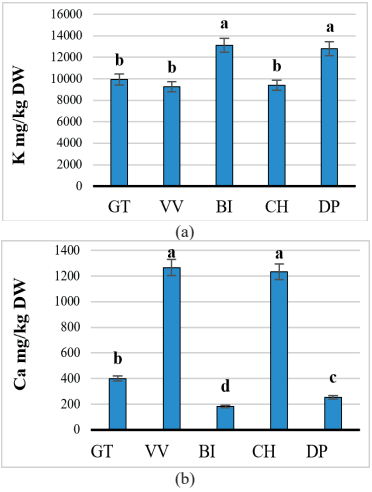



Figure 2. Macronutrient concentrations in *V. vitis-idaea* fruits: (a) potassium (K); (b) calcium (Ca). Mean ± SD (n = 3). Different letters indicate significant differences ($p < 0.05$)

**Micronutrient concentrations**

Iron (Fe) concentrations in lingonberry fruits were highest at Cheia and Bilbor, reaching approximately 150 mg kg$^{-1}$ DW (Figure 3a), whereas slightly lower values were observed at Doda Pilii and intermediate concentrations at Valea Vinului. The lowest Fe levels were recorded at Groșii Țibleșului, remaining below 100 mg kg$^{-1}$ DW. Although Fe is an essential element involved in electron transport processes and chlorophyll synthesis, its accumulation in fruits is generally limited because iron is preferentially retained in vegetative tissues such as leaves and roots. This pattern is consistent with previous studies on *V. vitis-idaea*, where Fe concentrations were substantially higher in leaves, stems and roots than in reproductive organs, indicating restricted translocation of Fe toward fruits (Kobayashi & Nishizawa, 2012; Kandziora-Ciupa et al., 2017).

Manganese (Mn) concentrations were highest at Valea Vinului and Bilbor, approaching 90-100 mg kg$^{-1}$ DW (Figure 3b), while the lowest values were observed at Groșii Țibleșului (40-50 mg kg$^{-1}$ DW). These concentrations are in line with previously reported Mn levels in lingonberries (Rodushkin et al., 1999) (approximately 87-160 mg kg$^{-1}$ DW). Manganese plays an essential role in photosynthetic processes and is often more strongly accumulated in vegetative organs than in fruits in *V. vitis-idaea*.

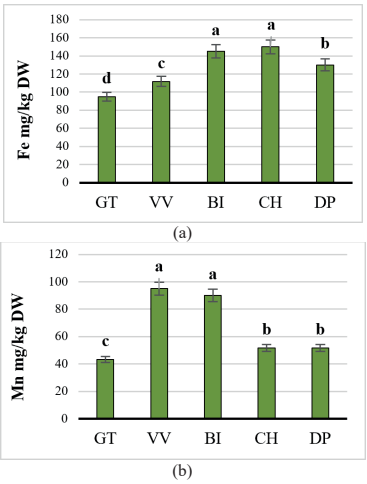



Figure 3. Micronutrient concentrations in *V. vitis-idaea* fruits: (a) iron (Fe); (b) manganese (Mn). Mean ± SD (n = 3). Different letters indicate significant differences ($p < 0.05$)

Zinc (Zn) concentrations ranged between approximately 10 and 18 mg kg$^{-1}$ DW (Figure 4a). The highest levels were recorded at Bilbor and Doda Pilii, while intermediate concentrations were observed at Valea Vinului and Groșii Țibleșului. The lowest Zn content was found at Cheia, with values close to 10 mg kg$^{-1}$ DW. These values fall within the range commonly reported for plant tissues, where adequate Zn concentrations are typically around 15-20 mg kg$^{-1}$ DW (Broadley et al., 2007). Zinc is an essential micronutrient involved in numerous enzymatic and metabolic processes in plants, and differences in its concentration may reflect variations in soil availability and environmental conditions among the sampling sites (Jungová et al., 2021).

Copper (Cu) concentrations ranged from less than 1 to about 6.5 mg kg$^{-1}$ DW (Figure 4b). The

highest value was measured at Bilbor, followed by slightly lower concentrations at Valea Vinului and Cheia, while the lowest Cu content was recorded at Doda Pilii. The generally low concentrations observed are consistent with the limited mobility of Cu in plants and its tendency to accumulate mainly in vegetative tissues rather than fruits. Copper plays an important role in plant metabolism as a cofactor of several redox enzymes involved in photosynthesis and oxidative stress regulation. Comparable Cu levels have been reported for *V. vitis-idaea* fruits, ranging from approximately 0.29 to 1.14 mg kg$^{-1}$ fresh weight (Drózdz et al., 2018).

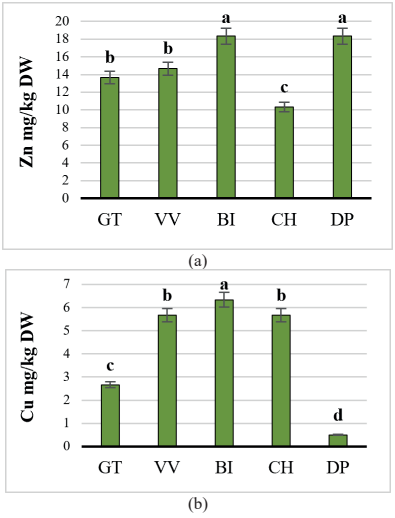



Figure 4. Micronutrient concentrations: (a) zinc (Zn); (b) copper (Cu). Mean ± SD (n = 3). Different letters indicate significant differences ($p < 0.05$)

## Trace element content

Nickel (Ni) concentrations were highest at Grosii Țibleșului, reaching approximately 1.1 mg kg$^{-1}$ DW, while lower values were observed at Cheia (Figure 5a). In the other sampling sites, Ni concentrations were below the limit of detection (LOD) of the analytical method. These concentrations are lower than those previously reported for lingonberries, where Ni levels ranged from 1.81 to 12.9 mg kg$^{-1}$ DW (Zeiner & Juranović Cindrić, 2018). Nickel occurs in plants at trace levels and functions as a cofactor of urease involved in nitrogen metabolism, while its accumulation in fruits is generally limited.

Strontium (Sr) concentrations were highest at Valea Vinului, and lower levels were observed at Bilbor while the other locations were below the limit of detection (Figure 5b). Strontium behaves chemically similar to calcium and can enter plant tissues through the same uptake pathways. Consequently, differences in Sr concentrations among sites may reflect variations in the geochemical composition of the underlying substrates and soil mineralogy (Capo et al., 1998; Burger & Lichtscheidl, 2019).

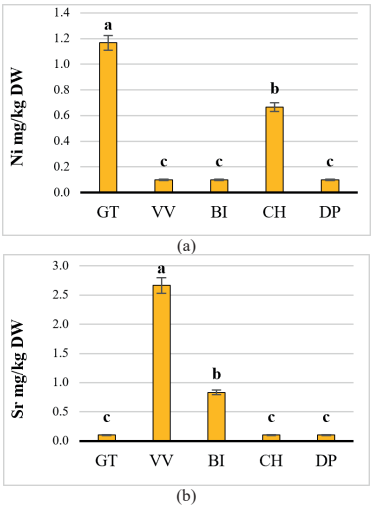



Figure 5. Trace element content in lingonberry fruits: (a) nickel (Ni); (b) strontium (Sr). Mean ± SD (n = 3). Different letters indicate significant differences ($p < 0.05$)

Rubidium (Rb) content was highest at Doda Pilii, reaching approximately 24-25 mg kg$^{-1}$ DW (Figure 6). Lower values were recorded at Grosii Țibleșului, Valea Vinului, and Bilbor, whereas Rb concentrations at Cheia were below the limit of detection (LOD) of the method. Rubidium behaves chemically similar to potassium and can be absorbed by plants through the same transport pathways. Consequently, variations in Rb concentrations among sampling sites are likely influenced primarily by differences in soil geochemistry rather than plant metabolic requirements. Elevated Rb levels, such as those observed at Doda Pilii, may therefore reflect differences in the mineral composition of the underlying substrate, particularly the presence of Rb-bearing silicate minerals in the soil (Kabata-Pendias & Pendias, 1992).

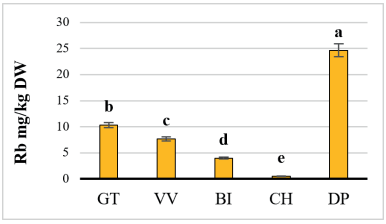



Figure 6. Rubidium (Rb) content in lingonberry fruits. Mean ± SD (n = 3). Different letters indicate significant differences ($p < 0.05$)

Several additional elements were detected sporadically and at very low concentrations. Arsenic and bromine were identified only in samples from Groșii Țibleșului, while molybdenum was detected only in Cheia. Given their rare occurrence and low concentrations, these elements were not included in further analyses.

**Multivariate analysis of mineral composition**

The hierarchical clustering analysis highlighted clear differences in the mineral profiles of *V. vitis-idaea* fruits among the sampling sites (Figure 7). Bilbor and Doda Pilii formed a closely related cluster characterized by relatively higher levels of K, Zn and Rb, indicating similar elemental signatures in the fruits collected from these locations. In contrast, Valea Vinului was clearly separated from the other sites due to elevated Sr concentrations, suggesting a distinct geochemical influence on the mineral composition of the berries.

A different elemental pattern was observed at Groșii Țibleșului, where comparatively higher Ni levels contributed to its separation from the other sampling sites. These clustering patterns indicate that the mineral composition of lingonberry fruits varies substantially among locations and likely reflects differences in local soil geochemistry and environmental conditions. Similar site-dependent variability in elemental composition of lingonberries has been reported in previous studies (Kabata-Pendias & Pendias, 1992; Rodushkin et al., 1999).

Principal component analysis (PCA) provided further insight into the relationships between mineral elements and environmental variables influencing the composition of *V. vitis-idaea* fruits (Figure 8). The first principal component (PC1), explaining 42.24% of the total variance, was associated with soil moisture, temperature and precipitation, together with higher contributions from K, Zn and Rb, suggesting a potential relationship between environmental conditions and the observed elemental variability. The alignment of these variables may indicate that soil water availability could influence the mobility and transport of these elements in the soil, potentially facilitating their uptake by plants. This relationship is particularly plausible for potassium and rubidium, which are known to be highly mobile in the soil solution and are commonly transported to plant roots through water-driven mass flow processes (Kabata-Pendias & Pendias, 1992). The position of Doda Pilii along this axis reflects higher contributions of these elements, suggesting that both climatic conditions and local substrate characteristics may influence nutrient accumulation in the berries. Differences in altitude among the sampling sites may also contribute indirectly to this pattern by influencing local climatic conditions such as temperature, precipitation and soil moisture.

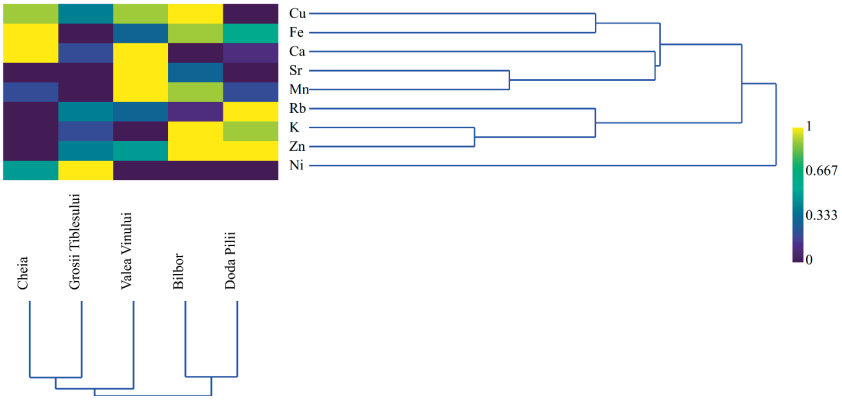



Figure 7. Heatmap and hierarchical clustering of mineral elements in *V. vitis-idaea* fruits from five sampling sites

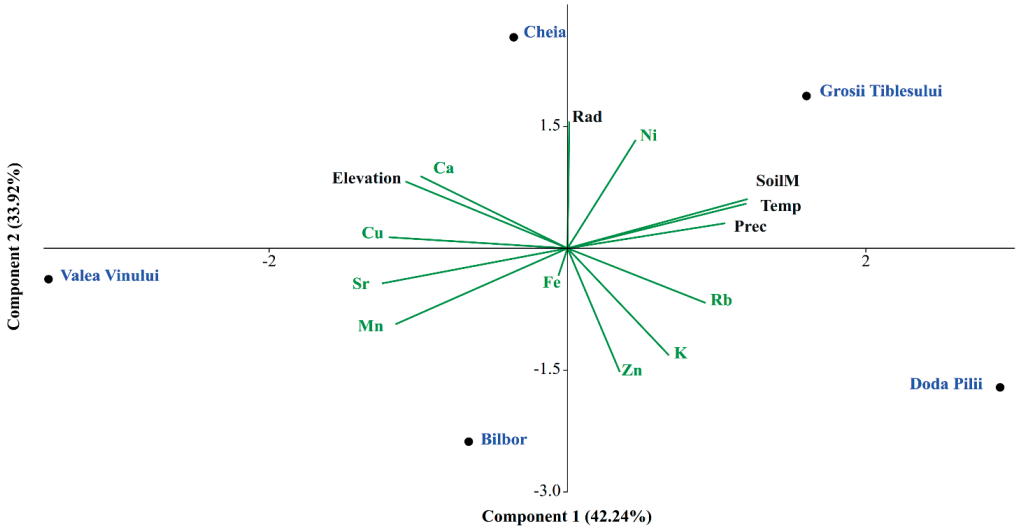



Figure 8. PCA biplot of mineral elements, environmental variables, and sampling sites in lingonberry fruits

The second principal component (PC2), accounting for 28.32% of the variance, was mainly associated with Ni, Ca and solar radiation, while Sr, Mn and Cu were oriented in the opposite direction. The separation of Sr from Ca, despite their chemical similarity, suggests that strontium accumulation in lingonberry fruits may be influenced more strongly by geochemical characteristics of the substrate than by plant physiological regulation. Considering the lithological differences among the studied sites, including sedimentary substrates at Grosii Țibleșului and Cheia and metamorphic substrates at Valea Vinului, Bilbor and Doda Pilii, the observed elemental patterns may partly reflect differences in the mineral composition of soils derived from these parent materials. Sites developed on similar lithological backgrounds may therefore exhibit comparable geochemical influences on element availability, while differences between sedimentary and metamorphic substrates may contribute to the variability observed in the mineral composition of the berries. The PCA indicates that the elemental profile of *V. vitis-idaea* fruits reflects the combined influence of climatic gradients, altitude-related environmental variation and lithological characteristics of the habitats, a pattern also observed in studies investigating mineral composition of wild berries using multivariate approaches (Vilkickyte & Raudone, 2021; Amundsen et al., 2023)

## CONCLUSIONS

This study provides new insights into the mineral composition of *V. vitis-idaea* fruits collected from different mountainous regions of Romania and highlights the influence of local environmental conditions on elemental accumulation in berries. The results confirm that potassium is the dominant macronutrient in lingonberry fruits, while other macro- and micronutrients occur in moderate concentrations consistent with previously reported ranges for the genus *Vaccinium*. The observed differences in elemental composition among sites indicate that the mineral profile of lingonberry fruits reflects site-specific environmental and geochemical conditions. In particular, the multivariate analyses revealed distinct elemental signatures associated with certain locations, suggesting that both climatic conditions and local substrate characteristics may influence nutrient accumulation in berries. The study also highlights the relevance of trace elements such as rubidium, strontium and nickel as potential indicators of geochemical variability in lingonberry habitats. Among these, rubidium showed the most pronounced spatial variation, which may be related to differences in soil mineral composition and the chemical similarity between rubidium and potassium during plant uptake. These findings indicate that the mineral composition of *V. vitis-idaea* fruits

reflects the combined influence of climatic gradients and lithological background across mountain habitats. The integration of elemental profiles with environmental variables highlights the potential of wild lingonberries as indicators of local geochemical conditions in natural ecosystems.

Although the present study provides useful baseline information on the mineral composition of wild lingonberry fruits from different mountain habitats, further studies including a larger number of sampling sites and complementary analyses of soil properties would help to better clarify the environmental and geochemical factors influencing elemental accumulation in the berries. Such approaches could contribute to a more comprehensive understanding of the relationships between habitat characteristics and mineral profiles in wild *Vaccinium* populations.

## ACKNOWLEDGEMENTS

The research was carried out with the partial support of the Doctoral School of the University of Agricultural Sciences and Veterinary Medicine of Cluj-Napoca (USAMVCN) for C.M.A.

## REFERENCES

Amundsen, M., Jaakola, L., Aaby, K., Martinussen, I., Kelanne, N., Tuominen, S., Laaksonen, O., Yang, B., & Hykkerud, A. L. (2023). Effect of ripening temperature on the chemical composition of lingonberries (*Vaccinium vitis-idaea* L.) of northern and southern origin. *Food Research International*, 167, 112738. https://doi.org/10.1016/j.foodres.2023.112738

Broadley, M. R., White, P. J., Hammond, J. P., Zelko, I., & Lux, A. (2007). Zinc in plants: Tansley review. *New Phytologist*, 173(4), 677–702. https://doi.org/10.1111/j.1469-8137.2007.01996.x

Bujor, O. C., Ginies, C., Popa, V. I., & Dufour, C. (2018). Phenolic compounds and antioxidant activity of lingonberry (*Vaccinium vitis-idaea* L.) leaf, stem and fruit at different harvest periods. *Food Chemistry*, 252, 356–365. https://doi.org/10.1016/j.foodchem.2018.01.052

Burger, A., & Lichtscheidl, I. (2019). Strontium in the environment: Review about reactions of plants towards stable and radioactive strontium isotopes. *Science of the Total Environment*, 653, 1458–1512. https://doi.org/10.1016/j.scitotenv.2018.10.312

Capo, R. C., Stewart, B. W., & Chadwick, O. A. (1998). Strontium isotopes as tracers of ecosystem processes: Theory and methods. *Geoderma*, 82(1-3), 197-225.

Drózdz, P., Sežiene, V., Wójcik, J., & Pyrzyńska, K. (2018). Evaluation of bioactive compounds, minerals and antioxidant activity of lingonberry (*Vaccinium vitis-idaea* L.) fruits. *Molecules*, 23(1). https://doi.org/10.3390/molecules23010053

Ekholm, P., Reinivuo, H., Mattila, P., Pakkala, H., Koponen, J., Happonen, A., Hellström, J., & Ovaskainen, M. L. (2007). Changes in the mineral and trace element contents of cereals, fruits and vegetables in Finland. *Journal of Food Composition and Analysis*, 20(6), 487–495. https://doi.org/10.1016/j.jfca.2007.02.007

Hammer, Ø., Harper, D. A. T., & Ryan, P. D. (2001). PAST: Paleontological statistics software package for education and data analysis. *Palaeontologia Electronica*, 4(1), 9.

Hjalmarsson, I., & Ortiz, R. (2001). Lingonberry: Botany and horticulture. *Horticultural Reviews*, 27, 79–123.

Jungová, M., Asare, M. O., Jurasová, V., & Hejcman, M. (2021). Distribution of micro (Fe, Zn, Cu, and Mn) and risk (Al, As, Cr, Ni, Pb, and Cd) elements in the organs of *R. alpinus* L. https://doi.org/10.21203/rs.3.rs-570070/v1

Kabata-Pendias, A., & Pendias, H. (1992). *Trace elements in soils and plants.* CRC Press.

Kandziora-Ciupa, M., Nadgórska-Socha, A., Barczyk, G., & Ciepał, R. (2017). Bioaccumulation of heavy metals and ecophysiological responses to heavy metal stress in selected populations of *Vaccinium myrtillus* L. and *Vaccinium vitis-idaea* L. *Ecotoxicology*, 26(7), 966–980. https://doi.org/10.1007/s10646-017-1825-0

Karlsons, A., Osvalde, A., Čekstere, G., & Pormale, J. (2018). Research on the mineral composition of cultivated and wild blueberries and cranberries. *Agronomy Research*, 16(2), 454–463. https://doi.org/10.15159/AR.18.039

Kobayashi, T., & Nishizawa, N. K. (2012). Iron uptake, translocation, and regulation in higher plants. *Annual Review of Plant Biology*, 63, 131–152. https://doi.org/10.1146/annurev-arplant-042811-105522

Kowalska, K. (2021). Lingonberry (*Vaccinium vitis-idaea* L.) fruit as a source of bioactive compounds with health-promoting effects - a review. *International Journal of Molecular Sciences*, 22(10). https://doi.org/10.3390/ijms22105126

Lazarenko, V., Babiča, K., Balcerbule, Z., Bērtiņš, M., & Vīksna, A. (2021). Variations of some metallic elements in different parts of lingonberries (*Vaccinium vitis-idaea* L.). *Key Engineering Materials*, *903*, 9–14.

Luginina, E. A., & Egoshina, T. L. (2013). The peculiarities of heavy metals accumulation by wild medicinal and fruit plants. *Annals of Warsaw, University of Life Sciences*, Agriculture and Forest Engineering, 61, 97–103.

Muñoz-Sabater, J., Dutra, E., Agustí-Panareda, A., Albergel, C., Arduini, G., Balsamo, G., Boussetta, S., Choulga, M., Harrigan, S., Hersbach, H., Martens, B., Miralles, D. G., Piles, M., Rodríguez-Fernández, N. J., Zsoter, E., Buontempo, C., & Thépaut, J. N. (2021). ERA5-Land: A state-of-the-art global reanalysis dataset for land applications. *Earth System Science*

*Data*, 13(9), 4349–4383. https://doi.org/10.5194/essd-13-4349-2021

Nestby, R., Hykkerud, A. L., & Martinussen, I. (2019). Review of botanical characterization, growth preferences, climatic adaptation and human health effects of *Ericaceae* and *Empetraceae* wild dwarf shrub berries in boreal, alpine and arctic areas. *Journal of Berry Research*, 9(3), 515–547. https://doi.org/10.3233/JBR-190390

Peters, S. E., Husson, J. M., & Czaplewski, J. (2018). Macrostrat: A platform for geological data integration and deep-time earth crust research. *Geochemistry, Geophysics, Geosystems*, 19(4), 1393–1409. https://doi.org/10.1029/2018GC007467

Rodushkin, I., Ödman, F., & Holmström, H. (1999). Multi-element analysis of wild berries from northern Sweden by ICP techniques. *Science of The Total Environment*, 231(1), 53-65.

Sapkota, Y., McDonald, L. M., Griggs, T. C., Basden, T. J., & Drake, B. L. (2019). Portable X-ray fluorescence spectroscopy for rapid and cost-effective determination of elemental composition of ground forage. *Frontiers in Plant Science*, 10, 317. https://doi.org/10.3389/fpls.2019.00317

Toncheva, G., Nikolova, K., Boyadzhiev, D., Alexieva, I., Georgieva, D., Antova, G., Aladjadjiyan, A., & Buhalova, D. (2016). Differentiation of Bulgarian wild fruits according to their mineral content. *Bulgarian Journal of Agricultural Science*, *22*(5), 857–861.

Vilkickyte, G., & Raudone, L. (2021). *Vaccinium vitis-idaea* L. fruits: Chromatographic analysis of seasonal and geographical variation in bioactive compounds. *Foods*, 10(10), 2243. https://doi.org/10.3390/foods10102243

Zeiner, M., & Juranović Cindrić, I. (2018). Harmful elements (Al, Cd, Cr, Ni, and Pb) in wild berries and fruits collected in Croatia. *Toxics*, 6(2). https://doi.org/10.3390/toxics6020031

Zhou, S., Wang, J., Wang, W., & Liao, S. (2023). Evaluation of portable X-ray fluorescence analysis and its applicability as a tool in geochemical exploration. *Minerals*, 13(2). https://doi.org/10.3390/min13020166

Scientific Papers. Series E. Land Reclamation, Earth Observation & Surveying, Environmental Engineering. Vol. XV, 2026
Print ISSN 2285-6064, CD-ROM ISSN 2285-6072, Online ISSN 2393-5138, ISSN-L 2285-6064

# FROM WASTE TO RESOURCE: IMPLEMENTING SPENT GARNET (SG) AS A PARTIAL FINE AGGREGATE IN CEMENT-BASED MATERIALS - TECHNICAL, LEGAL AND COMMERCIAL PERSPECTIVES

**Cornelia BAERA[1, 2], Aurelian GRUIN[1, 3], Ana Cristina VASILE[1, 3], Caius LUMINOSU[2], Ana-Andreea MIHARTESCU[2], Alexandra Marina BARBU[4]**

[1]NIRD URBAN-INCERC Timisoara Branch, 2 Traian Lalescu, Timisoara, Romania
[2]Faculty of Management in Production and Transportation, Politehnica University of Timisoara, 14 Remus Street, Timisoara, Romania
[3]Faculty of Civil Engineering, Politehnica University of Timisoara, 2 Traian Lalescu Street, Timisoara, Romania
[4]NIRD URBAN-INCERC Bucharest Branch, 266 Pantelimon Road, District 2, Bucharest, Romania

Corresponding author email: cornelia.baera@upt.ro

***Abstract***

*The growing demand for natural aggregates and stricter environmental regulations are driving the construction sector toward the valorisation of industrial by-products. This study investigates the technological transfer potential of Garnet sand waste (SG) as a partial substitute for natural fine aggregates in cement-based building materials, including mortars and concrete. Experimental results at laboratory and preliminary pilot scale demonstrate that controlled replacement levels of SG can achieve comparable or improved fresh and hardened properties relative to reference mixes, while meeting durability and performance requirements. Beyond technical validation, the paper examines the legislative framework governing waste reuse in construction, with particular attention to aggregate standards, waste-to-product transition, and conformity assessment procedures. Finally, commercial and market aspects are addressed, identifying barriers and drivers for industrial uptake, stakeholder acceptance, and potential business models within a circular economy context. The results provide an integrated pathway proposal for transforming Spent Garnet (SG) sand waste from an industrial residue into a viable construction resource, supporting sustainable material innovation and market implementation.*

***Key words****: cement-based materials, circular economy, fine aggregate substitution, market adoption, spent garnet (SG), sustainable construction, technology transfer, waste regulation.*

## INTRODUCTION

The construction industry remains one of the largest consumers of natural resources worldwide, particularly mineral aggregates used in concrete and mortar production. The growing demand for infrastructure and urban development has significantly increased the extraction of natural aggregates, generating environmental concerns related to landscape degradation, energy consumption, and greenhouse gas emissions (Corbu et al., 2014; Mattra et al., 2025). At the same time, industrial activities produce substantial quantities of mineral waste streams that are often disposed of in landfills, despite their potential reuse as secondary raw materials.

Within this context, the circular economy paradigm promotes the transformation of industrial by-products and waste into valuable resources (Potting et al., 2017; Morseletto, 2020). By closing material loops and reducing dependency on virgin raw materials, circular economy strategies can contribute to both environmental protection and resource efficiency in the construction sector. The reuse of mineral residues in cement-based materials has therefore gained increasing attention in recent years.

One such industrial residue is spent garnet sand generated from abrasive waterjet (AWJ) cutting operations. Garnets are widely used as abrasives medium due to their high hardness, chemical stability, and cutting efficiency (Perianu et al., 2014; 2017). However, after repeated use in AWJ processes, the material becomes contaminated with fine particles and loses its suitability for further abrasive applications. As a result, large quantities of spent garnet (SG) are

generated globally and are commonly classified as industrial waste, leading to disposal costs and environmental impacts (Baera et al., 2026a).

Previous studies have demonstrated that garnet residues generated by AWJ processes (AWJ-SG), with suitable granulometry and mineralogical composition, can partially replace natural aggregates in cement-based materials without compromising mechanical performance. AWJ spent garnets (AWJ-SGs) show considerable potential for application in cement-based materials (Ab Kadir et al., 2019; Lim et al., 2020; Budiea et al., 2021; Jamaludin et al., 2021; Kanta et al., 2022) as well as in alkali-activated concrete (Muttashar et al., 2017; 2018a, 2018b; Huseien et al., 2019), mortars (Kunchariyakun et al., 2020; Baera et al., 2025; 2026a), plasters, fibre-reinforced composites, and other construction materials.

Nevertheless, the transition from laboratory - scale investigations to practical implementation remains limited. In many cases, technological feasibility is demonstrated but the broader aspects required for industrial adoption - such as regulatory compliance, certification procedures, and market acceptance are insufficiently addressed (Baera et al., 2026a). In this context, the present study investigates the potential valorisation of single cycle AWJ spent garnets as partial substitute for natural fine aggregates in cement-based materials, including mortars and concrete. Beyond the technical evaluation of substitution viability, the study also addresses complementary dimensions, including technological transfer challenges, the legislative framework governing waste reuse in construction and product certification, and broader commercial and market-related considerations, all of which influence the practical implementation of circular economy principles. By combining these dimensions, the paper proposes an integrated pathway for transforming spent garnet from an industrial residue into a viable construction resource, supporting sustainable material innovation within a circular economy framework.

## CIRCULAR ECONOMY (CE) CONTEXT FOR AWJ SPENT GARNET (AWJ-SG)

The transition toward a circular economy requires the development of strategies that reduce waste generation and promote the efficient use of resources across industrial sectors. The integration of sustainable materials and innovative techniques in civil engineering contributes to environmental protection while enhancing resource efficiency and structural reliability, thereby supporting the transition toward more sustainable construction practices (Olinic et al., 2024). In the construction industry, one of the most promising approaches involves the integration of secondary materials derived from industrial processes into building materials. Such practices can simultaneously reduce waste disposal and decrease the consumption of natural aggregates.

Abrasive waterjet (AWJ) cutting is widely applied in manufacturing industries for the precise cutting of metals, ceramics, composites, and stone materials (Perianu et al., 2023). Garnet is commonly used as the abrasive medium due to its favourable mechanical and chemical properties (Chassé et al., 2018). During the AWJ process, garnet particles progressively fracture and become mixed with removed material and fine debris. In some cases, SG waste can be recycled and reused for its original application as AWJ abrasive, although few initiatives have focused on this type of material recovery. In most cases, after one AWJ use the resulting SG material is discharged as spent garnet waste.

From a material flow perspective, the lifecycle of garnet in AWJ operations typically includes four stages: extraction of natural garnet, use as an abrasive medium, generation of spent garnet waste, and final disposal. In many industrial facilities, the spent material is collected as sludge or dried sand and transported to landfill sites. This linear disposal pathway results in both environmental impacts and additional operational costs. Within a circular economy framework, spent garnet can be considered a secondary mineral resource. Several potential valorisation routes have been explored, including reuse as abrasive media after processing, use in sandblasting operations, and incorporation into construction materials. Among these options, the use of AWJ-SG as a fine aggregate substitute in cement-based materials presents significant potential, considering its proven suitability for integration and the large volumes of aggregates required in the construction sector. The integration of spent

garnets into mortar and concrete production can therefore represent a form of industrial symbiosis, offering a dual advantage, as illustrated in Figure 1: first, it diverts waste from disposal pathways, generating positive environmental and economic impacts from a waste management perspective. Second, it partially replaces natural aggregates, thereby reducing the pressure on natural resource extraction.

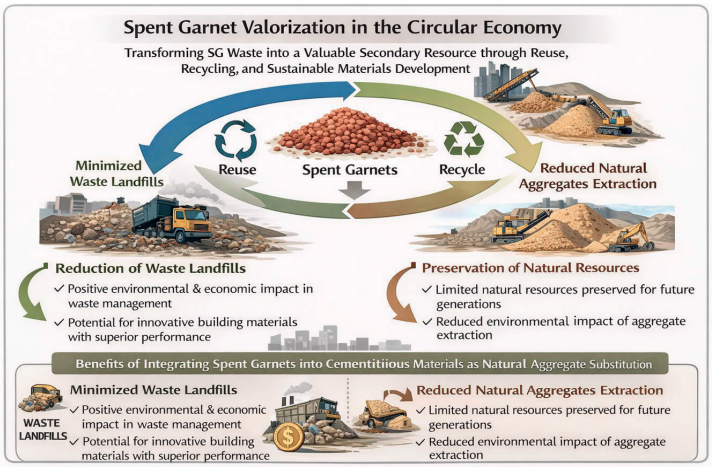



Figure 1. Circular Economy Framework for Spent Garnet Waste Valorization in Cementitious Materials (AI-generated image)

In Romania, the valorization of AWJ-SG waste in construction materials and products through the innovative substitution of fine aggregates was investigated within one of the research axes of project PN 23 35 04 01 (Figure 2), entitled "Development of innovative engineering solutions for eco-intelligent construction products through the efficient valorization of additions generated by local industries".

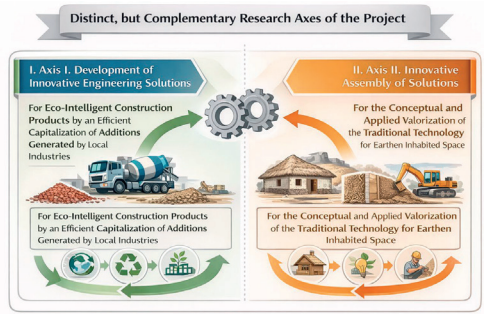



Figure 2. Schematic representation of the research axes of project PN 23 35 04 01 (AI-generated image)

The project is part of the Nucleu Programme under the National Research, Development and Innovation Plan 2022-2027 (ECODIGICONS), funded by the Romanian Ministry of Research, Innovation and Digitalization, and is aligned with European Union objectives and national strategic frameworks such as Romanian National Strategy on the Circular Economy (SNEC, 2022) and the National Strategy for Research, Innovation and Smart Specialization (SNCISI 2022-2027, 2022).

The project's main goal is to facilitate technological transfer and enable the practical implementation of the developed materials, products, and technologies through sustained collaboration among key stakeholders, including academia and research institutions, entrepreneurs, industrial users and end-consumers, suppliers, and social, economic, and political actors, as well as local and central authorities.

## MATERIALS AND METHODS

The procedure-based transition of abrasive waterjet spent garnet (AWJ-SG) from industrial waste to a construction resource is conceptualized through *a three-layer circular economy framework*, represented by a *technology-transfer diagram structured around three complementary layers* (Figure 3):

(i) *Technical layer*, addressing material characterisation, mix design optimisation, prototype validation, pilot-scale trials, and the transition from laboratory research to field implementation;
(ii) *Regulatory layer*, covering compliance with relevant standards, waste legislation, and the procedures required for product certification and conformity assessment; and
(iii) *Commercial layer*, focusing on supply-chain integration, stakeholder engagement, and the market adoption of AWJ-SG-based construction materials.

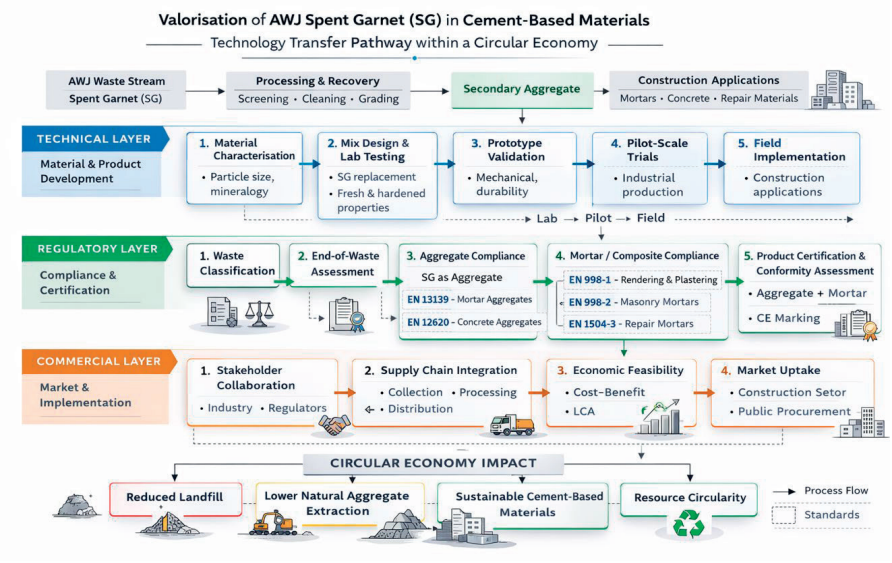



Figure 3. Spent Garnet Waste Valorization in Cementitious Materials:
Three-Layer Circular Economy Structure (AI-generated image)

The figure illustrates the transition of AWJ SG material from industrial residue to construction resource through three complementary implementation layers. The technical layer describes the progression from material characterization to field application. The regulatory layer distinguishes between compliance of SG as aggregate and compliance of the final mortar-based product, including relevant European standards for aggregates, rendering/plastering mortars, masonry mortars and repair mortars. The commercial layer captures the supply-chain and market conditions needed for industrial uptake. Together, these layers define the practical pathway for circular economy implementation of AWJ-SG in cement-based materials.

**I. Technical Layer: SG as Fine Aggregate Substitute in Cement-Based Mortars**

The technical implementation of abrasive waterjet spent garnet (AWJ-SG) as a secondary aggregate in cement-based mortars follows a progressive validation pathway that includes specific technical stages like *material characterization, mix design optimization, prototype validation and pilot-scale assessment* (Figure 4). The proposed methodological framework aims to verify the feasibility of transforming AWJ-SG from an industrial waste stream into a functional construction material within a CE context, while ensuring consistent performance and reproducibility of results.

***Material Characterisation***

The initial stage focuses on the *physical, chemical and mineralogical characterisation of AWJ-SG* in order to evaluate its suitability as a fine aggregate substitute in cement-based composites. Key parameters include particle size distribution (PSD), particle morphology, density and potential impurities resulting from the abrasive cutting process.

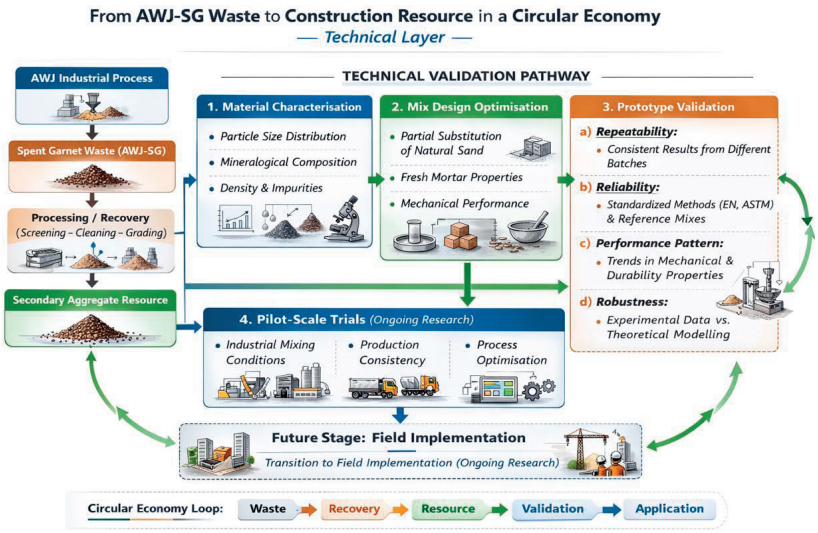



Figure 4. Circular economy pathway for valorisation of AWJ spent garnet (AWJ-SG) as a secondary aggregate: from waste generation to technical validation and pilot-scale implementation (AI-generated image)

These characteristics were analysed (Baera et al., 2026a) and identified the expected compatibility with the grading requirements of conventional mortar aggregates; also, the potential effects on fresh and hardened properties were also identified and discussed. Proper processing steps, such as screening and cleaning, were also considered to ensure consistent material quality before incorporation into mortar mixtures. market adoption of SG-based construction materials.

***Mix Design Optimisation***

To assess the feasibility of using spent garnets (SG) as a fine aggregate substitute, mortar mixtures were prepared with varying partial replacement levels (30% and 50%) of natural sand while maintaining acceptable aggregate grading. Conventional cement binders and typical water-to-binder ratios were used. Reference mixtures containing only natural aggregates were produced for comparison. SG was introduced by replacing a portion of the natural sand while keeping the binder content and overall mix proportions constant. This approach enabled evaluation of the influence of SG on fresh and hardened properties while minimizing the impact of other variables; the expected SG to cementitious matrix compatibility was identified (Baera et al., 2025; 2026a).

***Prototype Validation***

Prototype validation was conducted to confirm the feasibility and consistency of incorporating spent garnet (SG) as a partial fine aggregate substitute in cement-based mortars. The validation procedure was initiated and further developed (Baera et al., 2025; 2026a) to follow a structured methodology based on four general criteria. *Repeatability* was assessed by verifying that comparable performance results were obtained for successive SG batches collected at different times, both from the same and from different sources. *Reliability* was ensured through testing performed according to standardized procedures (e.g., EN and ASTM methods) and by comparing the results with those obtained from reference cement–sand control mixtures. *Performance pattern* was evaluated by analysing systematic trends in mechanical and durability properties as a function of SG substitution levels and the characteristics of the waste material. Finally, *robustness* was examined by correlating experimental observations with theoretical modelling in order to minimise the influence of uncontrolled experimental variability and confirm the consistency of the proposed material system.

The results (Baera et al., 2026a) are validating the SG mortar prototypes and the viability of the proposed integrating concept, at laboratory scale

and also are founding the technological transfer to the industry, ensuring the transitioning to pilot scale assessments.

***Pilot-scale assessment***

Pilot-scale assessment represents the next stage in the implementation pathway for the valorisation of AWJ spent garnet (AWJ-SG) as a secondary aggregate in cement-based mortars. This stage aims to verify the reproducibility of laboratory results under industrial mixing conditions, including *batching procedures, mixing energy, and material handling practices* typically encountered in mortar production facilities. Particular attention is given to *production consistency*, ensuring that the incorporation of AWJ-SG does not introduce variability in fresh or hardened properties across successive batches. Monitoring of parameters such as aggregate dosing, moisture control, and mixing duration is therefore required to maintain stable production quality. In parallel, process *optimisation measures* are being investigated, including adjustments to mixing sequences, particle grading control, and potential pre-treatment steps (e.g., screening or drying) to ensure uniform material behaviour at scale. These ongoing investigations aim to confirm that the performance trends observed in laboratory conditions can be reliably reproduced in industrial environments, thereby supporting the transition of AWJ-SG from experimental validation toward industrial implementation.

**II. Regulatory and Legal Layer for AWJ-SG Waste-to-Product Transition**

The regulatory layer establishes the legal and conformity framework required for the transition of AWJ spent garnet (AWJ-SG) from waste status to a construction resource. The corresponding regulatory validation pathway, illustrated in Figure 5, includes waste classification, evaluation of end-of-waste/by-product conditions, compliance with aggregate and mortar standards, and product certification in accordance with Regulation (EU) No. 305/2011.

***Waste Classification***

The first regulatory step involves the classification of abrasive waterjet spent garnet (AWJ-SG) within the waste management framework. In Romania, this process follows HG nr. 856/2002 regarding waste management records and the approval of the waste list, which is aligned with European waste legislation, particularly Commission Decision 2000/532/EC establishing the European List of Waste (LoW). Within this framework, AWJ spent garnet can be classified under code 12 01 17 - "waste blasting materials other than those mentioned in 12 01 16". *This classification establishes the regulatory basis for waste handling, traceability, and further evaluation of potential recovery or valorisation pathways*.

***End-of-Waste/By-Product Assessment***

Following waste identification, an end-of-waste or by-product assessment is required to determine whether AWJ-SG can transition from a waste material to a secondary resource suitable for construction applications. This evaluation considers criteria such as the intended use of the material, *compliance with technical specifications, absence of environmental or health risks, and the existence of a stable market demand*. Demonstrating that the processed material can be safely and consistently used as an aggregate substitute is essential for enabling its transition from waste status to a recoverable construction resource.

***AWJ-SG Aggregate Compliance***

Once the material is considered suitable for recovery, AWJ-SG must demonstrate technical compliance with relevant aggregate standards. For applications in cement-based mortars, the material must meet the requirements specified in EN 13139 - Aggregates for mortars, including particle size distribution, density, and cleanliness parameters. For potential applications in concrete, compliance with EN 12620 - Aggregates for concrete must also be assessed. These standards ensure that the recovered material meets the necessary physical and mechanical properties required for use as a construction aggregate.

***Mortar/Composite Compliance***

In addition to aggregate-level compliance, the performance of the final cement-based composite containing AWJ-SG must satisfy the relevant mortar standards, depending on the intended application.

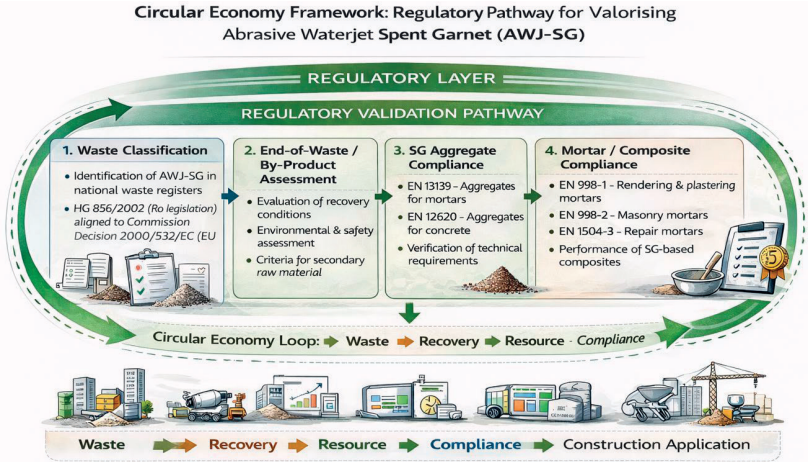



Figure 5. Circular economy pathway of AWJ-SG Waste-to-Product transition (as a secondary aggregate): Regulatory and Legal layer (AI-generated image)

Rendering and plastering mortars must comply with EN 998-1, masonry mortars with EN 998-2, and repair mortars used for concrete structures with EN 1504-3. Compliance with these standards requires the evaluation of mechanical strength, durability, and other performance characteristics to ensure that the incorporation of SG does not negatively affect the functional behaviour of the mortar.

***Product Certification & Conformity Assessment***

The final regulatory step involves product certification and conformity assessment, ensuring that both the aggregate component and the final mortar-based product meet the requirements for placing construction products on the market. This process is carried out in accordance with Regulation (EU) No. 305/2011 (Construction Products Regulation – CPR) and may involve testing, factory production control, and conformity verification procedures. Certification therefore addresses both aggregate compliance and mortar/composite performance, enabling the resulting product to be marketed as a compliant construction material within the European regulatory framework.

## III. Commercial Layer for AWJ-SG Waste-to-Product Transition

After establishing the regulatory framework for the valorization of AWJ-SG, the focus moves to the commercial layer, which examines supply-chain organization, stakeholder engagement, business model development, and the conditions necessary for market adoption of SG-based construction materials (Figure 6).

***Supply-Chain Integration***

The commercial implementation of AWJ spent garnet (AWJ-SG) valorisation requires the integration of the material into existing construction material supply chains. This involves *establishing logistical connections between abrasive waterjet processing facilities, waste recovery operators, and construction material producers*. Efficient supply-chain integration ensures that SG can be collected, processed, and delivered in a consistent form suitable for use as a secondary aggregate in cement-based materials.

***Stakeholder Engagement***

Successful market implementation depends on the active involvement of key stakeholders, including AWJ operators, waste management companies, construction material manufacturers, regulatory authorities, and end users. Stakeholder engagement is essential for building trust in the technical performance and environmental safety of SG-based materials, as well as for facilitating knowledge exchange and promoting acceptance within the construction sector.

***Supply-Chain Organisation***

The development of a reliable supply chain structure *is necessary to ensure the consistent availability and quality of AWJ-SG*.

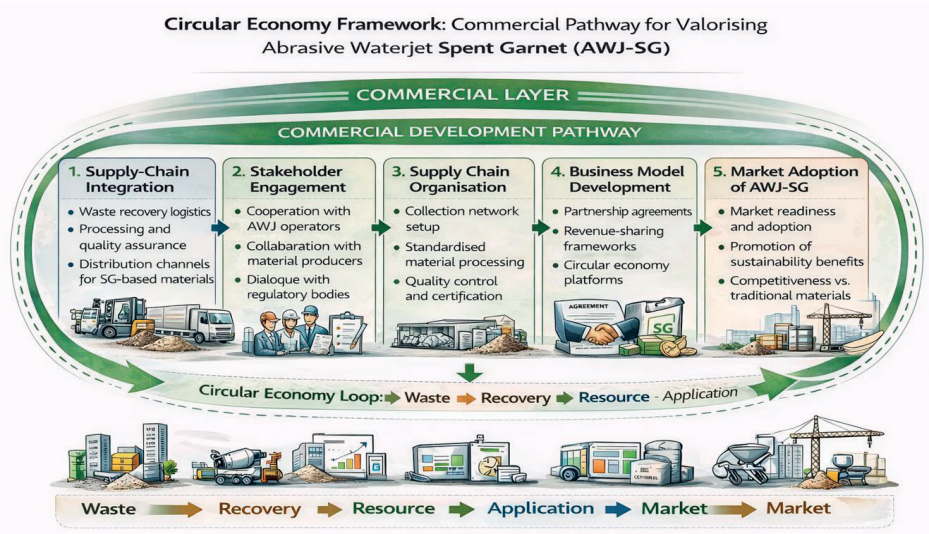



Figure 6. Circular economy pathway of AWJ-SG Waste-to-Product transition: Commercial layer (AI-generated image)

This includes the establishment of *standardized collection procedures, material processing operations, and quality control mechanisms* to guarantee that the recovered aggregate meets technical and regulatory requirements before entering the construction materials market.

***Business Model Development***

The valorisation of AWJ-SG also requires the identification of *sustainable business models* that balance economic feasibility with environmental benefits. Potential models may include partnerships between AWJ service providers and construction material producers, waste recovery agreements, or circular economy platforms that promote the reuse of industrial by-products. In addition, *social entrepreneurship initiatives* may represent a viable approach, particularly where waste recovery and material processing activities can generate local employment and support community-based circular economy practices. Such models combine environmental value creation with social impact, contributing to both resource efficiency and regional socio-economic development (Baera et al., 2026b) Overall, these approaches aim to reduce disposal costs while creating additional value from recovered materials.

***Market Adoption of AWJ-SG-Based Construction Materials***

The final stage involves the market uptake of construction materials incorporating AWJ-SG. This process depends on demonstrating *technical reliability, regulatory compliance, and economic competitiveness* compared to conventional materials. As confidence in the performance and sustainability benefits of SG-based mortars increases, their adoption may contribute to reducing the consumption of natural aggregates and supporting CE practices within the construction sector.

Together, the technical validation, regulatory compliance, and commercial integration layers form a coherent circular economy framework that enables the sustainable transition of AWJ spent garnet from an industrial waste stream to a viable construction resource.

## RESULTS AND DISCUSSIONS

### I. Technical Layer: SG as Fine Aggregate Substitute in Cement-Based Mortars

The results obtained from the experimental investigations confirm the technical feasibility of incorporating abrasive waterjet spent garnet (AWJ-SG) as a partial fine aggregate substitute in cement-based mortars. The evaluation followed the staged validation pathway described in the methodology section, including material characterisation, mix design optimisation, prototype validation, and preparation for pilot-scale assessment.

The *physical, chemical and mineralogical characterisation of AWJ-SG* performed in previous studies (Baera et al., 2026a) confirmed

via PSD determination, Scanning Electron Microscopy (SEM) analysis, X-Ray Diffraction (XRD) analysis and Fourier Transform Infrared Spectroscopy FTIR technique that the material exhibits properties compatible with the requirements of conventional mortar aggregates, that they are inert and safe for use in regular mixtures. The particle size distribution (PSD) of the processed SG fractions was found to fall within the grading range suitable for fine aggregates used in cement-based mortars. In addition, the angular particle morphology, typical of abrasive materials, may contribute to enhanced mechanical interlocking within the cementitious matrix. The density and mineralogical composition of the material were also consistent with the characteristics expected for silicate-based abrasive sands. Potential impurities associated with the cutting process are removed using the proposed specific procedure, which includes collection, screening and sorting, cleaning and verification, and storage operations, ensuring a stable and reproducible material suitable for mortar formulations.

Based on the material characterisation results, *the Mix Design Optimisation* stages led to mortar mixtures prepared using partial replacement levels of natural sand with AWJ-SG at 30% and 50%, while maintaining consistent binder content and water-to-binder ratios. The experimental results (Baera et al., 2026a) indicated that the incorporation of SG within these substitution ranges did not adversely affect the fresh properties of the mortars (visual aspect, consistency and fresh state density), while mechanical performance (compressive and flexural strength at early, regular and late ages) offered superior performance when compared to reference mixtures containing only natural aggregates. These observations confirm the compatibility between SG particles and the cementitious matrix, supporting findings reported in previous studies (Baera et al., 2025). The optimisation of the mix design therefore demonstrated that SG can be effectively integrated into mortar formulations without significant modifications to conventional mixture proportions.

The *prototype validation stage* aimed to verify the reproducibility and reliability of SG-based mortar formulations. Experimental testing carried out according to standardized methods (EN and ASTM procedures) confirmed that the incorporation of SG produces consistent performance trends across different batches of material. The validation procedure followed a structured framework based on four criteria: repeatability, reliability, performance pattern and robustness. Comparable results were obtained for SG batches collected from different sources and time periods, confirming the repeatability of the material behaviour. Reliability was ensured through the comparison of SG-based mixtures with conventional cement–sand reference mortars. Furthermore, systematic performance trends were observed with respect to SG substitution levels, while correlations between experimental results and theoretical expectations confirmed the robustness of the proposed material system. Overall, the results reported by Baera et al., (2026) validate the SG mortar prototypes at laboratory scale and demonstrate the technical viability of the proposed valorisation concept.

Following laboratory validation, the next stage *involves pilot-scale assessment*, aimed at verifying the reproducibility of the experimental results under industrial production conditions. This stage focuses on evaluating industrial mixing procedures, batching practices and material handling conditions typically encountered in mortar production facilities.

The current research phase developed a mixing procedure different from the standardized method (paddle mixer, rotational speed 140/280 rpm; revolutionary motion 61.5/123 rpm, according to EN 196-1). The objective was to create a simpler and more accessible manufacturing approach, better suited for technology transfer to industrial operators. The proposed technology involves mixing with a mortar mixer in a standard container (bucket/mixing vat) and includes the following steps: Step 1 - Dry mixing (natural sand + SG-AWJ addition); Step 2 - Dry mixing (aggregate + cement); Step 3 - Addition of water (and additive, if applicable); Step 4 - Visual inspection for proper consistency and absence of lumps.

The *critical characteristics* of standard AWJ-SG mortars required for calibrating the proposed technological transfer, as well as *the validation criteria*, are defined in the proposed ***Primary Validation Procedure***:

1 Properties in the fresh state: Visual appearance; Consistency; Bulk density (fresh state);
2. Properties in the hardened state: Bulk density (hardened state) and water absorption; Compressive strength (at 7 and 28 days); Flexural strength (at 7 and 28 days).

**Validation criterion:** Similar performance trends (a stable pattern) must be obtained, even if absolute values vary slightly between batches, within an acceptable margin of ±15%.

Ongoing study considers particular attention for ensuring production consistency, for preventing variability in fresh and hardened properties when AWJ-SG is incorporated into mortar formulations at larger scales. In parallel, process optimisation measures are being investigated, including adjustments to mixing sequences, aggregate grading control and potential pre-treatment operations such as additional screening or drying of the SG material. The successful scaling of these processes would support the *transition from experimental validation to industrial implementation*, enabling AWJ-SG to be integrated into cement-based materials as a secondary aggregate. From a circular economy perspective, this transition contributes to reducing landfill disposal of industrial abrasive waste while simultaneously lowering the demand for natural aggregate resources in the construction sector.

## II. Regulatory and Legal Layer for AWJ-SG Waste-to-Product Transition

The regulatory assessment indicates that the valorisation of abrasive waterjet spent garnet (AWJ-SG) as a secondary aggregate in cement-based mortars can be supported by the existing European and national regulatory framework. This stage of the research focuses on identifying the legal conditions under which AWJ-SG can transition from an industrial waste stream to a construction resource, while ensuring compliance with applicable waste management legislation and construction product standards. The results presented here outline the proposed regulatory pathway, which will be further investigated and validated in subsequent stages of the research.

### *Waste Classification*

The regulatory pathway begins with the identification of AWJ-SG within the waste management framework. In Romania, this process is governed by HG nr. 856/2002, which regulates waste management records and establishes the national waste list, aligned with the European List of Waste defined by Commission Decision 2000/532/EC. Under this classification system, AWJ spent garnet can be assigned to code 12 01 17 – waste blasting materials other than those specified in 12 01 16, providing the legal basis for its traceability and further evaluation for recovery.

### *End-of-Waste/By-Product Assessment*

A key step in the regulatory transition involves assessing whether AWJ-SG can satisfy the conditions required for end-of-waste or by-product status. This evaluation considers the intended application of the material, compliance with technical standards, and the absence of environmental or health risks. Preliminary technical results (Baera et al., 2026a) indicate that, following appropriate processing and grading, AWJ-SG may meet these conditions, supporting its potential recognition as a secondary resource within circular construction practices.

### *AWJ-SG Aggregate Compliance*

For construction applications, the processed material must demonstrate compliance with the relevant European aggregate standards. In the case of cement-based mortars, this includes EN 13139 - Aggregates for mortars, while potential applications in concrete require evaluation according to EN 12620 - Aggregates for concrete.

The application of these standards, in conjunction with Regulation (EU) No. 305/2011 (CPR) and relevant national legislation, entails:

- initial type testing (ITT) for essential characteristics (grain size, fines content, sand equivalent, absorption, chloride content, sulfate content, total sulfur, hazardous substances, etc.);
- implementation of a Factory Production Control (FPC) system;
- obtaining FPC certification through the AVCP 2+ system;
- issuing the Declaration of Performance (DoP) and affixing the CE marking.

Therefore, artificial/recycled aggregate cannot be lawfully used in construction mixtures without demonstrating, through documented evidence, compliance with the requirements of

the applicable harmonized standards and the consistency of its performance. Ongoing research aims to further assess the conformity of AWJ-SG with these standards and to define the quality control measures required for its use as a secondary aggregate.

***Mortar/Composite Compliance***

Beyond aggregate-level requirements, the performance of mortars incorporating AWJ-SG must comply with the relevant product standards, depending on the intended application. The incorporation of 30-50% of recycled garnet aggregate AWJ-SG into hydraulic-binder-based mortars results in a new product that is distinct from a regulatory standpoint and must be evaluated and certified separately from the raw material used. Depending on the mortar's intended use, the following harmonized standards apply: EN 998-1 for rendering and plastering mortars, EN 998-2 for masonry mortars, and EN 1504-3 for repair mortars used in concrete structures.

In this context, certification of the final product involves:

- determination of mechanical performance (compressive strength, adhesion, modulus of elasticity, etc.);
- evaluation of physical properties (density, capillary absorption, vapor permeability, shrinkage);
- verification of durability (freeze-thaw cycles, compatibility with the substrate);
- determination of the performance class (e.g., M5, M10, CS II, R3, R4, etc., as applicable);
- implementation of the system for assessing and verifying the constancy of performance appropriate to the product;
- issuing a separate Declaration of Performance for the resulting mortar.

It is essential to emphasize that the aggregate's compliance with EN 12620 or EN 13139 does not automatically imply the resulting mortar's compliance with EN 998 or EN 1504. The performance of the final product must be demonstrated experimentally and certified independently.

Preliminary laboratory results suggest that SG-based mixtures can achieve the required performance levels, although further testing is necessary to confirm compliance under broader application scenarios.

***Product Certification and Conformity Assessment***

The final stage of the regulatory pathway concerns product certification and conformity assessment in accordance with Regulation (EU) No. 305/2011 (Construction Products Regulation – CPR). This process addresses both the certification of the aggregate component and the verification of the performance of the final mortar-based product. Future research will therefore focus on identifying the appropriate certification procedures and factory production control requirements necessary for the market placement of AWJ-SG-based construction materials.

Overall, the regulatory layer highlights the legal and conformity conditions required to enable the circular valorisation of AWJ-SG, while also defining the main directions for further investigation needed to support its transition from waste management practices toward certified construction products.

**III. Commercial Layer: AWJ-SG Waste-to-Product Transition**

The commercial dimension of AWJ-SG valorisation addresses the practical conditions required to move from laboratory validation and regulatory compliance toward market implementation. At the current stage of the research project, the commercial layer remains *exploratory*, identifying potential pathways for integrating AWJ-SG into construction material value chains. The results presented here therefore outline preliminary directions for further investigation, reflecting the multidisciplinary approach adopted within the project.

The cost-benefit analysis of AWJ-SG Valorisation in construction materials and products is currently ongoing, based on comparative assessments against conventional aggregates. No definitive conclusions are available at this stage.

***Supply-Chain Integration***

Initial assessments indicate that the effective valorisation of AWJ-SG requires the integration of abrasive waterjet processing facilities with waste recovery operators and construction material producers. Establishing these logistical links is essential to ensure that the recovered material can be collected, processed, and

supplied in a consistent form suitable for use as a secondary aggregate. Further investigations will focus on identifying the most efficient configurations for such supply-chain integration at regional or industrial scales.

***Stakeholder Engagement***

Preliminary consultations highlight the importance of involving key stakeholders, including AWJ operators, waste management companies, construction material manufacturers, and regulatory bodies. Stakeholder engagement is particularly relevant for building confidence in the technical performance and environmental safety of SG-based materials. Continued dialogue with these actors will be necessary to support knowledge exchange and to facilitate acceptance of secondary aggregates within the construction sector.

***Supply Chain Organisation***

The analysis also suggests that the establishment of a structured supply chain is required to ensure the consistent availability and quality of AWJ-SG. This includes defining standardized collection, processing, and quality control procedures for the recovered material. Future work will therefore examine potential operational models capable of maintaining stable supply while meeting the technical and regulatory requirements identified in the previous layers.

***Business Model Development***

Several potential business models have been identified as promising directions for the valorisation of AWJ-SG. These include collaborative arrangements between AWJ service providers and mortar producers, waste recovery partnerships, or circular economy platforms promoting the reuse of industrial by-products. In addition, social entrepreneurship initiatives may represent a viable pathway, particularly where waste recovery and processing activities can generate local employment and support community-based circular economy practices. Further research will evaluate the economic feasibility and scalability of these models.

***Market Adoption of AWJ-SG-Based Construction Materials***

The market uptake of SG-based construction materials will ultimately depend on demonstrating technical reliability, regulatory compliance, and economic competitiveness compared with conventional materials. Although preliminary results indicate that SG-based mortars meet the required performance levels, broader market acceptance will require additional validation, pilot-scale production, and stakeholder engagement. Consequently, the commercial layer remains an ongoing research direction, aimed at identifying the conditions under which AWJ-SG can be successfully integrated into construction markets and contribute to circular economy practices in the sector.

## CONCLUSIONS

This study investigated the potential valorisation of abrasive waterjet spent garnet (AWJ-SG) as a secondary fine aggregate in cement-based mortars, adopting a multidisciplinary approach that integrates technical validation, regulatory assessment, and commercial considerations. The results confirm that the transition of AWJ-SG from an industrial waste stream to a construction resource is technically feasible and conceptually supported by the existing legal and market frameworks, although further investigations are required to advance toward full industrial implementation.

From a technical perspective, the laboratory investigations demonstrate that processed AWJ-SG exhibits physical and mineralogical characteristics compatible with conventional fine aggregates used in cement-based mortars. Mortar mixtures incorporating SG at partial replacement levels showed acceptable fresh and hardened performance, confirming the compatibility between SG particles and the cementitious matrix. The validation framework based on repeatability, reliability, performance pattern, and robustness further confirmed the consistency of SG-based mortar prototypes at laboratory scale, providing a solid basis for subsequent pilot-scale investigations.

Beyond the material performance assessment, this study contributes to the integration of circular economy principles into construction material design. By proposing the reuse of AWJ abrasive residues as secondary aggregates, the research demonstrates the potential for industrial symbiosis between manufacturing processes and construction material production, contributing to reduced landfill disposal and decreased consumption of natural aggregate resources.

A key contribution of the work lies in the analysis of the regulatory pathway for waste-to-product transition. The study identifies the legal framework governing the classification, recovery, and certification of AWJ-SG-based materials within the European construction sector, highlighting the relevance of waste classification procedures, end-of-waste or by-product assessments, compliance with aggregate and mortar standards, and product certification in accordance with Regulation (EU) No. 305/2011. This regulatory mapping clarifies the conditions under which SG-based materials could be placed on the market as compliant construction products.

In addition, the research explores the commercial dimension of SG valorisation, identifying key elements required for practical market integration. These include supply-chain organisation, stakeholder engagement, the development of viable business models-including potential social entrepreneurship initiatives-and the gradual market adoption of SG-based construction materials. Although this component of the study remains at an exploratory stage, it provides an initial framework for understanding the economic and organisational conditions necessary for successful implementation. One limitation of this study is that the economic assessment of AWJ-SG valorisation has not yet been completed. Comparative analyses with conventional aggregates are currently underway, and definitive conclusions regarding the cost–benefit performance are therefore beyond the scope of the present work.

Overall, the research proposes a three-layer technology-transfer framework-technical, regulatory, and commercial-designed to support the practical implementation of AWJ-SG valorisation within a circular economy context. By combining laboratory validation with regulatory analysis and preliminary commercial considerations, the study contributes to bridging the gap between experimental material research and real-world industrial application.

Future work will focus on pilot-scale assessments and industrial implementation, further evaluation of regulatory compliance pathways, and the development of operational supply chains capable of supporting the market introduction of SG-based construction materials. Through these continued investigations, AWJ spent garnet may evolve from an industrial waste stream into a valuable resource for sustainable construction practices.

## ACKNOWLEDGEMENTS

This work was carried out within the Nucleu Programme of the National Research Development and Innovation Plan 2022-2027, supported by MCID, "ECODIGICONS" project no. PN 23 35 04 01, financed by the Romanian Government.

The authors acknowledge the use of AI-based tools, including ChatGPT, for the generation of figures, language editing, and structural refinement of the manuscript. All scientific content, interpretations, and conclusions remain the sole responsibility of the authors.

## REFERENCES

Ab Kadir, M. A., Khiyon, M. I., Sam, A. R. M., Kueh, A. B. H., Lim, N. H. A. S., Mastor, M. N. M. A., Zuhan, N., & Mohamed, R. N. (2019). Performance of spent garnet as a sand replacement in high-strength concrete exposed to high temperature, *Journal of Structural Fire Engineering,* 10(4), 468-481.

Baera, C., Gruin, A., Vasile, A.C., Bolborea, B., Ion, A., Varga, L., & Barbu, A.M. (2025). Preliminary results validation on the theoretical and experimental approach for using spent garnet residues of Romanian local industries in construction materials. *Scientific papers. Series e. Land Reclamation, Earth Observation & Surveying, Environmental Engineering*, vol. XIV, print ISSN 2285-6064, 59-72.

Baera, C., Vasile, A. C., Gruin, A., Sfirloaga, P., Dragomir, C. S., Zaharia, R., Balcu, I., Macarie, C., & Buzatu, D. (2026a). Sustainable valorization of spent garnet wastes in construction eco-materials: Validation stage of performance assessment. *Sustainability*, 18(2), 1000.

Baera, C., Draghici, A., Gruin, A., Sandu, I., Zaharia, R., Dragomir, C. D., Vasile, A. C., Luminosu, C., Negru, A. C., Stanciu, V., & Varga, L. (2026b). The

preservation of Romanian vernacular urban heritage through social entrepreneurship. A debate based on university–research center-community collaboration. *International Journal of Conservation Science*, 17(1), 155-180.

Budiea, A. M. A., Sek, W. Z., Mokhatar, S. N., Muthusamy, K., & Yusoff, A. R. M. (2021). Structural performance assessment of high strength concrete containing spent garnet under three point bending test, In *IOP Conference Series: Materials Science and Engineering,* 1144(1), 012018.

Chassé, M., Griffin, W. L., Alard, O., O'Reilly, S. Y., & Calas, G. (2018). Insights into the mantle geochemistry of scandium from a meta-analysis of garnet data. *Lithos,* 310, 409-421.

Corbu, O., Szilagyi, H., Puskas, A., Popovici, A., Baera, C., & Moga, L. (2014). Recycling and waste recovery in the construction field. *Proceedings of the 14th International Multidisciplinary Scientific GeoConference & EXPO-SGEM, Albena, Bulgaria*, 259-265.

European Committee for Standardization. (2002). EN 12620: Aggregates for concrete. *CEN*.

European Committee for Standardization. (2013). EN 13139: Aggregates for mortar. *CEN*.

European Committee for Standardization. (2005). EN 1504-3: Products and systems for the protection and repair of concrete structures - Definitions, requirements, quality control and evaluation of conformity - Part 3: Structural and non-structural repair. *CEN*.

European Committee for Standardization. (2016). EN 196-1: Methods of testing cement - Part 1: Determination of strength. *CEN*.

European Committee for Standardization. (2016). EN 998-1: Specification for mortar for masonry - Part 1: Rendering and plastering mortar. *CEN.*

European Committee for Standardization. (2016). EN 998-2: Specification for mortar for masonry - Part 2: Masonry mortar. *CEN.*

Huseien, G. F., Sam, A. R. M., Shah, K. W., Budiea, A. M. A., & Mirza, J. (2019). Utilizing spent garnets as sand replacement in alkali-activated mortars containing fly ash and GBFS, *Construction and Building Materials,* 225, 132-145.

Jamaludin, N. F. A., Muthusamy, K., Isa, N. N., Jaafar, M. F. M, & Ghazali, N. (2021). Use of spent garnet in industry: A review. *Materials Today: Proceedings,* 48(4), 728-733.

Kanta, N. R., & Ponnada, M. R. (2022). Performance of spent garnet sand and used foundry sand as fine aggregate in concrete. *World Journal of Engineering,* 19(5), 632-638.

Kunchariyakun, K., & Sukmak, P. (2020). Utilization of garnet residue in radiation shielding cement mortar. *Construction and Building Materials,* 262*,* 120122.

Lim, N. H. A. S., Alladin, N. F. N, Mohammadhosseini, H., Ariffin, N.F., & Mazlan, A. N. (2020). Properties of Mortar Incorporating Spent Garnet as Fine Aggregates Replacement, International *Journal of Integrated Engineering 12(9),* 96-102.

Mattra, M. M., Sujauddin, M., Hossain, M. M., Yu, J., Liu, X., & Manago, G. (2025). Navigating the Sustainability Conundrum of Construction Sand. *Sustainability*, 17(18), 8255.

Morseletto, P. (2020). Targets for a circular economy. *Resources, conservation and recycling*, 153, 104553.

Muttashar, H. L., Ali, N. B., Ariffin, M. A. M., & Hussin, M. W. (2018a). Microstructures and physical properties of waste garnets as a promising construction material. *Case studies in construction materials,* 8, 87-96.

Muttashar, H. L., Ariffin, M. A. M., Hussein, M. N., Hussin M. W., & Ishaq, S. B. (2018b). Self-compacting geopolymer concrete with spent garnet as sand replacement. *Journal of Building Engineering,* 15, 85-94.

Muttashar, H. L., Hussin, M. W., Ariffin, M. A. M., Mirza, J., Hasanah, N., & Shettima, A. U. (2017). Mechanical properties of self-compacting geopolymer concrete containing spent garnet as a replacement for fine aggregate. *Jurnal Teknologi (Sciences & Engineering)*, 79(3).

Olinic, T., Olinic, E. D., & Butcaru, A. C. (2024). Integrating Geosynthetics and Vegetation for Sustainable Erosion Control Applications. *Sustainability, 16(23),* 10621.

Perianu, I. A., Ionescu, D., & Verbitchi, V. (2017). Method of measuring the abrasive-water jet diameter, for the cutting process control. *Welding and Material Testing,* 1.

Perianu, I. A., Marin-Corciu, M., Geana, A. A., Duma, I., & Baeră, C. (2023). CFD simulation study for abrasive waste management using water eductors for abrasive waterjet cutting collector tanks. *Key Engineering Materials,* 952, 43-49.

Perianu, I. A., Mitelea, I., & Şerban, V. A. (2014). The effect of water pressure variation on cut surfaces quality during abrasive waterjet cutting of austenitic steels. *Advanced Materials Research,* 1029, 176-181.

Potting, J., Hekkert, M. P., Worrell, E., & Hanemaaijer, A. (2017). Circular economy: measuring innovation in the product chain.

Romanian Government (September 27, 2022). National Strategy on the circular economy (SNEC 2022), Government Decision No. 1172/2022 *The official monitor of Romania*, Part I, No. 943. https://sgg.gov.ro/1/wp-content/uploads/2022/08/Strategia-economie-circulara_18.08.2022.pdf.

Romanian Ministry of Research, Innovation and Digitalization (July 25, 2022). National Strategy for Research, Innovation and Smart Specialization 2022-2027 (SNCISI 2022-2027), Government Decision No. 933/2022, *The Official Monitor of Romania*, Part I, 744. https://www.mcid.gov.ro/wp-content/uploads/2022/12/strategia-na-ional-de-cercetare-inovare-i-specializare-inteligent-2022-2027.pdf.

Scientific Papers. Series E. Land Reclamation, Earth Observation & Surveying, Environmental Engineering. Vol. XV, 2026
Print ISSN 2285-6064, CD-ROM ISSN 2285-6072, Online ISSN 2393-5138, ISSN-L 2285-6064

# TECHNICAL FRAMEWORK FOR SUSTAINABLE VALORIZATION OF VINEYARD BY-PRODUCTS THROUGH SMALL-SCALE PROCESSING TECHNOLOGIES

**Carmen BALTATU, Gabriel Valentin GHEORGHE, Dragos MANEA, Larisa-Bianca IONICA**

INMA-Bucharest, 6 Ion Ionescu de la Brad Blvd, District 1, Bucharest, Romania

Corresponding author email: carmen.vasilachi@gmail.com

***Abstract***

*The management of vineyard by-products represents an important environmental challenge in viticultural regions, where large quantities of organic residues are generated annually. From an environmental engineering perspective, the sustainable valorization of these by-products offers significant opportunities for reducing waste streams while improving resource efficiency. This paper proposes a technical framework for the sustainable valorization of vineyard by-products through the implementation of small-scale processing technologies. The framework integrates engineering criteria such as processing efficiency, energy demand, and technological adaptability with environmental considerations including waste reduction, resource recovery, and alignment with circular economy principles. The proposed approach is illustrated through a representative application scenario focusing on grape seed processing for oil production, highlighting the potential of small-scale technologies to convert viticultural residues into value-added products. The results emphasize the role of appropriately selected processing technologies in minimizing environmental pressure associated with vineyard waste and supporting sustainable agricultural systems. The framework provides a structured basis for further applied research and technology development in viticulture-related waste management.*

***Key words****: environmental engineering, grape seed valorization, sustainable processing, vineyard by-products, waste reduction.*

## INTRODUCTION

The expansion of the global wine industry has led to a substantial increase in the generation of organic residues, particularly vineyard by-products such as grape pomace, stalks, and lees. These materials, which may account for up to 30% of the initial processed grape mass, represent a significant environmental challenge due to their high organic content and rapid biodegradability (Bustamante et al., 2008; Nirmal et al., 2025).

The accumulation of such residues, especially during harvest seasons, creates pressure on local waste management systems and raises concerns related to greenhouse gas emissions, soil contamination, and inefficient resource utilization (Moletta, 2005; Beres et al., 2017). Romania ranks among the top ten wine-producing countries in the European Union, with approximately 180,000 hectares of vineyard area and an annual wine production exceeding 4 million hectolitres (OIV, 2023). This production volume generates substantial quantities of grape pomace estimated at over 150,000 tons per year, the management of which represents a persistent challenge for small and medium-sized wine producers, particularly in viticultural regions such as Muntenia, Moldova, and Oltenia where processing infrastructure remains limited.

From an environmental engineering perspective, the management of vineyard by-products requires a transition from conventional disposal practices to integrated valorization strategies. Traditional approaches, including composting, distillation, or uncontrolled land spreading, often fail to fully exploit the resource potential of these materials and may generate secondary environmental impacts if not properly controlled (Negro et al., 2003; Provenzano et al., 2024). In addition, the high moisture content and biochemical activity of grape pomace can accelerate fermentation processes, leading to greenhouse gas emissions and the formation of leachates containing organic acids and phenolic compounds (Dwyer et al., 2014; Teixeira et al., 2014).

Recent advances in circular economy research emphasize the importance of transforming agri-food residues into value-added products, thereby reducing waste streams and improving overall system efficiency (Galanakis, 2012; Mirabella et al., 2014). In the context of viticulture, vineyard by-products are increasingly recognized as a source of valuable compounds, including lipids, polyphenols, dietary fibers, and antioxidants, which can be recovered through appropriate processing technologies (Rockenbach et al., 2011; Fontana et al., 2013). Such approaches contribute not only to waste reduction but also to the development of sustainable bio-based value chains aligned with European circular economy policy objectives (Puglia et al., 2021; Abbate et al., 2025).

Grape pomace, the main residue of the winemaking process, consists of seeds, skins, and stems that retain a significant fraction of the original grape constituents after juice extraction. Its composition varies depending on grape variety, climatic conditions, and processing techniques, but consistently includes compounds with high industrial and nutritional value (Pardo et al., 2009; Martin et al., 2020). Among these fractions, grape seeds are of particular interest due to their oil content, typically ranging from 8% to 15% on a dry matter basis, and the presence of bioactive molecules with antioxidant properties (Malićanin et al., 2014; Kapcsándi et al., 2021). These characteristics make grape seeds suitable for valorization through mechanical or physico-chemical extraction processes, with cold-pressed grape seed oil increasingly recognized as a high-value functional food ingredient.

Various technological pathways have been explored for the recovery of valuable compounds from vineyard residues, including solvent extraction, supercritical fluid extraction, enzymatic treatment, and mechanical pressing (Passos et al., 2010; Mushtaq et al., 2020). While these methods demonstrate high recovery efficiencies under controlled conditions, their implementation is often limited to industrial-scale operations requiring significant capital investment, energy input, and specialized infrastructure (Cerutti et al., 2013; Spigno et al., 2017). Consequently, their applicability in small and medium-sized vineyards remains restricted, and access to valorization technologies for farm-level operators continues to be a barrier to sustainable by-product management.

In contrast, small-scale processing technologies offer a promising alternative by enabling decentralized valorization directly at the source of biomass generation. Such systems can reduce transportation requirements, lower associated emissions, and facilitate the integration of valorization processes into local agricultural practices (Laufenberg et al., 2003; Ahmad et al., 2020). Mechanical screw pressing, for example, represents a relatively simple and energy-efficient method for oil extraction that can be adapted to farm-level applications without the use of chemical solvents, with specific energy consumption values reported below 0.15 kWh per kilogram of processed seeds under optimized conditions (Kamal-Eldin, 2006; Bjelica et al., 2019).

Despite the increasing interest in vineyard by-product valorization, existing studies tend to address either the physicochemical characterization of grape pomace fractions (Rockenbach et al., 2011; Martin et al., 2020) or the optimization of individual extraction technologies under laboratory conditions (Passos et al., 2010; Mushtaq et al., 2020), without integrating engineering performance with environmental assessment at the process level. Kokkinomagoulos and Kandylis (2023) provide a comprehensive review of winery waste valorization pathways, yet no unified framework combining processing efficiency, energy demand, technological adaptability, and environmental indicators has been proposed specifically for small-scale. In particular, the interaction between processing efficiency, energy demand, technological adaptability, and environmental impact is not sufficiently explored within a unified analytical framework applicable to farm-level or regional valorization scenarios (Dimić et al., 2020).

Addressing this gap requires the development of structured methodologies capable of supporting decision-making in the selection and implementation of appropriate technologies. The integration of engineering indicators, such as processing efficiency and specific energy consumption, with environmental metrics including waste reduction and resource recovery, is essential for evaluating the

sustainability of valorization pathways (Mironeasa et al., 2010; Orsavova et al., 2015). Such an approach enables a more comprehensive understanding of the trade-offs involved in biomass processing systems and provides a quantitative basis for comparing alternative technological configurations at the same scale of operation.

The aim of this study is to develop and validate a technical framework for the sustainable valorization of vineyard by-products through the application of small-scale processing technologies, integrating engineering indicators: processing efficiency, specific energy consumption, and technological adaptability, with environmental metrics including waste reduction rate, resource recovery index, and circularity coefficient. The applicability of the framework is demonstrated through a representative scenario involving mechanical grape seed oil extraction using the NF80 screw press, applied to Riesling 1 and Fetească Regală 1 grape varieties sourced from the Research and Development Station for Viticulture and Oenology (ICDVV) Valea Călugărească, Romania.

## MATERIALS AND METHODS

### Vineyard by-products considered in the study

The present study focuses on vineyard by-products generated during the winemaking process, particularly grape pomace, which consists of seeds, skins, and stems remaining after the pressing stage. These residues may represent approximately 20-30% of the initial grape mass processed in wineries and contain valuable biochemical components such as oils, phenolic compounds, fibers, and proteins (Laufenberg et al., 2003; Martin et al., 2020).

Among the different fractions of grape pomace, grape seeds were considered the most relevant component for the representative application scenario analyzed in this study. Grape seeds are characterized by a significant content of lipids and bioactive compounds, which makes them suitable for valorization through mechanical oil extraction technologies (Pardo et al., 2009; Kapcsándi et al., 2021). In addition to oils, grape seeds contain antioxidants, polyphenols, and essential fatty acids, contributing to their potential use in food, cosmetic, and pharmaceutical applications (Malićanin et al., 2014; Bjelica et al., 2019).

Prior to processing, grape seeds are typically separated from grape pomace using mechanical separation equipment and may undergo conditioning stages such as drying and cleaning in order to reduce moisture content and remove impurities. Literature data indicate that the optimal moisture content for mechanical oil extraction generally ranges between 6% and 10%, depending on the grape variety and the extraction technology used (Mushtaq et al., 2020).

In addition to grape seeds, the framework also considers the potential utilization of secondary residues generated during processing, such as press cake. This by-product may be further used as organic fertilizer, soil amendment, or raw material for bioenergy production, contributing to improved resource recovery within vineyard systems (Puglia et al., 2021) content. It only contains example text and proper formatting.

### Representative processing technology

To illustrate the proposed framework, a representative small-scale processing technology was considered, namely a mechanical screw press used for oil extraction from grape seeds. Mechanical pressing technologies are widely applied for processing oil-bearing materials due to their relatively simple construction, moderate energy consumption, and the absence of chemical solvents (Passos et al., 2010). The main processing stages considered in the framework, together with the associated input and output streams, are summarized in Figure 1.

Small-scale screw presses are particularly suitable for decentralized agricultural systems because they allow on-site processing of biomass with relatively low investment costs and minimal infrastructure requirements. Such systems are typically composed of several main components: a feeding hopper, a screw conveyor placed inside a cylindrical pressing chamber, an outlet nozzle for solid residues, an oil collection system, and an electric motor that provides the mechanical energy required for operation.

For this study, experimental data obtained at INMA Bucharest were used, involving the NF80 mechanical screw press (0.37 kW, 220V)

equipped with interchangeable screw configurations (pitch 16 mm and 22 mm) and outlet nozzles with diameters of 10, 12, and 15 mm.

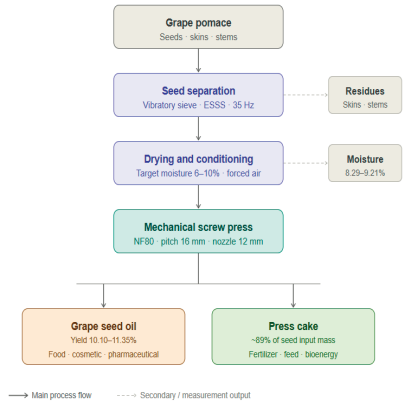



Figure 1. Conceptual process flow for grape seed valorization using the NF80 small-scale screw press, from pomace conditioning to the recovery of oil and press cake.

The separation of seeds from conditioned pomace was performed using the ESSS vibrating screen separator operated at frequencies between 25 and 45 Hz. The grape pomace was obtained from two Romanian research institutes: ICDVV Valea Călugărească (Prahova County) and INCDBH Ștefănești (Argeș County). Two white grape varieties were selected for the representative application scenario: Riesling and Fetească Regală. The conceptual process flow for grape seed valorization using the NF80 small-scale screw press, from pomace conditioning to the recovery of oil and press cake, is presented in Figure 2.

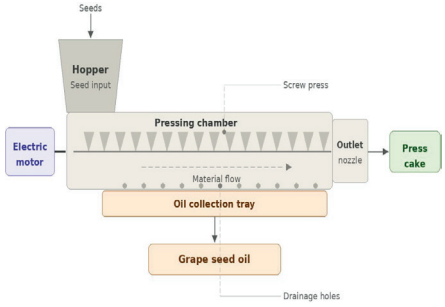



Figure 2. Schematic representation of the main components of the NF80 small-scale screw press: hopper (seed input), pressing chamber with screw press, drainage holes for oil extraction, oil collection tray, outlet nozzle, and press cake discharge.

During the pressing process, the biomass is transported along the screw channel while being progressively compressed. As pressure increases, the oil contained in the seeds is released and collected through small openings in the pressing chamber. The remaining solid fraction, commonly referred to as press cake, is discharged through the outlet of the press. Mechanical extraction methods are often preferred for small-scale operations because they ensure a relatively high oil quality and do not involve chemical solvents that may generate environmental concerns (Kamal-Eldin, 2006).

**Engineering performance indicators**

In order to evaluate the performance of small-scale processing technologies used for the valorization of vineyard by-products, several engineering indicators were considered.

*Processing efficiency* ($\eta_p$) represents the ratio between the mass of valuable product obtained during processing and the mass of biomass introduced into the system.

$$\eta_p = \frac{M_{valuable\ product}}{M_{input\ bionass}} \times 100$$

where: $M_{valuable\ product}$ - mass of recovered product (e.g., grape seed oil), $M_{input\ bionass}$ - mass of processed biomass.

This indicator is commonly used in biomass processing systems to evaluate the efficiency of conversion processes (Laufenberg et al., 2003).

*Specific energy* ($E_s$) consumption represents the amount of energy required to process a unit mass of biomass.

$$E_s = \frac{E_{total}}{M_{processed}}$$

where: $E_{total}$ - total electrical energy consumed during processing, $M_{processed}$- mass of biomass processed.

Energy demand is considered an important engineering parameter for evaluating the sustainability of biomass processing technologies.

*The technological adaptability index* (TAI) evaluates the suitability of the processing technology for decentralized agricultural applications.

$$TAI = \frac{S_c + S_o + S_m}{3}$$

where: $S_c$- equipment complexity score, $S_o$- operational simplicity score, $S_m$- maintenance

requirements score. Each parameter is evaluated on a qualitative scale from 1 to 5.

**Environmental performance indicators**

In addition to engineering parameters, environmental indicators were used to assess the sustainability of vineyard by-product valorization.

The *waste reduction* (WR) rate indicates the proportion of initial biomass converted into valuable products.

$$WR = \frac{M_{initial\,waste} - M_{residual\,waste}}{M_{initial\,waste}} \times 100$$

Waste reduction indicators are frequently used in environmental engineering studies evaluating resource recovery systems (Puglia et al., 2021).

The *resource recovery index* (RRI) reflects the proportion of by-products that can be converted into useful resources.

$$RRI = \frac{M_{recovered\,resources}}{M_{total\,byproducts}}$$

The *circularity coefficient* (CC) expresses the degree to which biomass-derived products are reintegrated into the economic cycle.

$$CC = \frac{M_{reintroduced\,resources}}{M_{total\,biomass}}$$

Such indicators are commonly applied in circular economy assessments related to agricultural residue valorization (Abbate et al., 2025).

The framework indicators defined above were applied to experimental data obtained from the NF80 screw press trials and are discussed in the following section.

## RESULTS AND DISCUSSIONS

**Development of the technical framework**

Based on the engineering and environmental indicators defined in the materials and methods section, a technical framework for the sustainable valorization of vineyard by-products was developed. The framework integrates process-level performance criteria with environmental assessment metrics in order to support decision-making in the selection and implementation of small-scale processing technologies. The overall structure of the proposed framework is presented in Figure 3.

The framework is organized around four interconnected stages. The first stage, *biomass assessment*, involves the identification and characterization of vineyard residues, including quantity estimation, moisture content determination, and compositional analysis. For the representative scenario analyzed in this study, the initial moisture content of Riesling (R) pomace was 56.98% and that of Feteasc Regală (FR) was 62.61%, reduced to 24.12% and 27.35% respectively following a two-stage drying protocol combining natural air-drying and forced convection at 30-40°C (Mushtaq et al., 2020). Physical characterization of the separated seeds revealed mean diameters of 3.65 mm for Riesling (sphericity 0.643) and 3.75 mm for Feteasc Regală (sphericity 0.696), with oil contents of 9.52% and 9.72% respectively - both within the 6-10% optimal moisture range for mechanical pressing (Mushtaq et al., 2020).

The second stage focuses on the *selection of appropriate processing technologies* based on engineering criteria. In this context, small-scale screw pressing was identified as a suitable solution for decentralized applications due to its relatively low energy requirements, absence of chemical solvents, and operational simplicity (Kamal-Eldin, 2006; Passos et al., 2010). The NF80 screw press, evaluated across six configurations, achieved a technological adaptability index (TAI) of 4.0 out of 5, reflecting its simple construction and ease of deployment at farm level.

**Application of the framework to grape seed oil extraction**

The third stage of the framework, *process implementation*, was applied to the grape seed oil extraction scenario using the NF80 screw press. Seed separation from conditioned pomace was performed at 35 Hz using the ESSS vibratory screen separator, recovering 6.52 kg of seeds from 20 kg of Riesling pomace (32.6%) and 6.34 kg from Feteasc Regală pomace (31.7%), exceeding the 18-25% range commonly cited in the literature (Laufenberg et al., 2003). The crude oil yield and extraction efficiency across all six press configurations are presented in Figure 4.

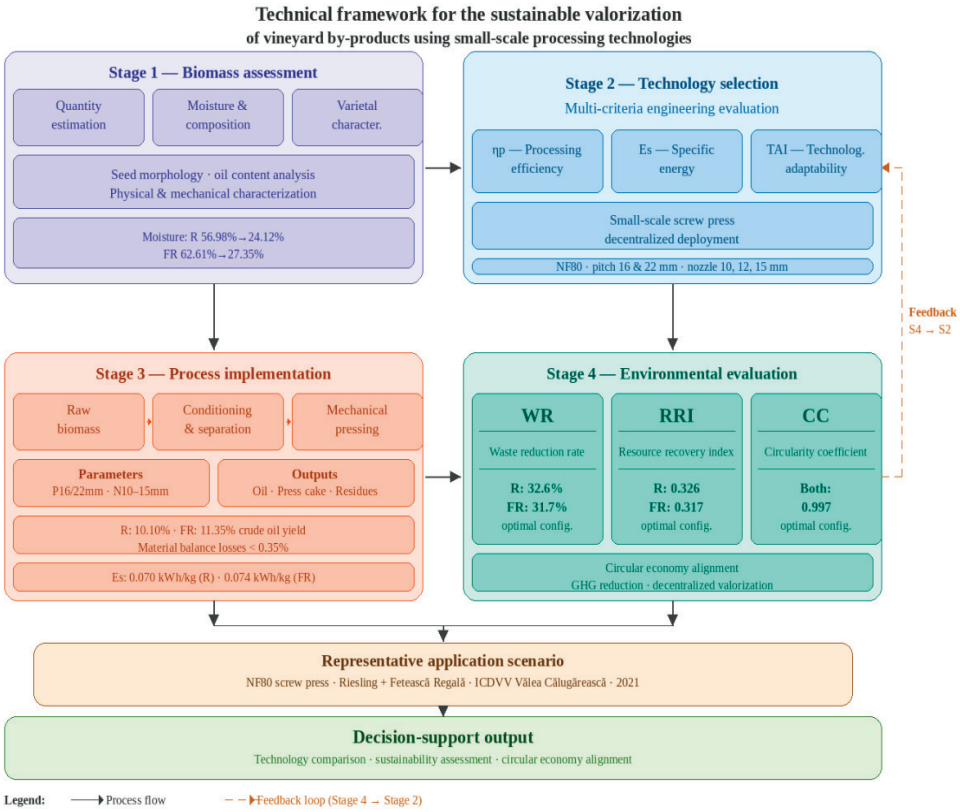



Figure 3. Technical framework for the sustainable valorization of vineyard by-products using small-scale processing technologies, structured around four interconnected stages and integrating engineering and environmental performance indicators

The highest performance was obtained with the pitch (P) 16 mm, nozzle (N) 12 mm, and speed 10 rpm configuration for both varieties, yielding 10.10% crude oil and 83.81% extraction efficiency for Riesling, and 11.35% crude oil with 92.23% extraction efficiency for Fetească Regală. Specific energy consumption was 0.070 kWh/kg and 0.074 kWh/kg respectively - values significantly lower than solvent-based extraction systems and competitive with cold-pressing technologies at comparable scales (Kamal-Eldin, 2006). The pitch 22 mm configurations showed a marked performance decrease, with yields falling to 7.43-8.65%, attributable to the reduced compression ratio and incomplete cell wall rupture (Passos et al., 2010). These results confirm trends reported for cold-pressed grape seed oil, where mechanical pressing yields of 8-12% are typical (Kapcsándi et al., 2021).

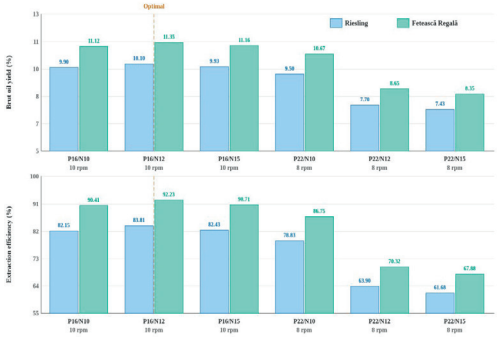



Figure 4. Brut oil yield (top) and extraction efficiency (bottom) across six NF80 press configurations for Riesling and Feteasca Regala (3 kg seed input). P = screw pitch (mm), N = nozzle diameter (mm)

From an energy perspective, the low specific energy consumption confirms the suitability of the NF80 system for decentralized applications

where energy efficiency is a critical operational constraint. The material balance for the complete valorization chain is presented in Figure 5. From a 3 kg seed input, 303 g of crude oil and 2,687 g of press cake were recovered for Riesling (losses 0.33%), and 340 g of crude oil with 2,650 g of press cake for Feteasc Regală (losses 0.32%). The press cake fraction, representing 89.6% and 88.3% of seed input respectively, constitutes a valorizable secondary stream for fertilizer, animal feed, or bioenergy applications (Puglia et al., 2021).

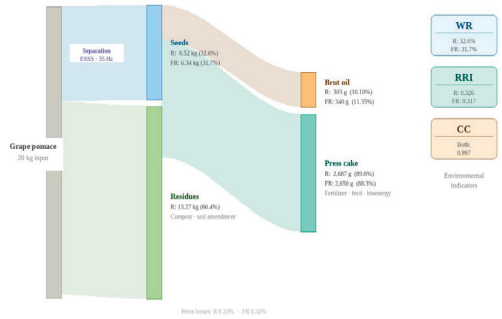



Figure 5. Sankey diagram of the material balance for the grape seed valorization chain: from 20 kg pomace input through seed separation to mechanical pressing. Band width is proportional to mass flow. Environmental indicators (WR, RRI, CC) are presented for Riesling (R) and Feteasc Regală (FR) under the optimal processing configuration

## Environmental performance assessment

The fourth stage of the framework was applied through the calculation of the three *environmental indicators*. The complete set of engineering and environmental performance indicators under the optimal configuration is presented in Table 1, and the comparative performance profiles for both varieties are illustrated in Figure 6.

The waste reduction rate (WR) reached 32.6% for Riesling and 31.7% for Feteasc Regală, reflecting the proportion of pomace input converted into the recoverable seed fraction. These values confirm that approximately one third of the pomace mass can be systematically redirected from the waste stream into a productive valorization chain (Kokkinomagoulos & Kandylis, 2023). The resource recovery index (RRI) was 0.326 and 0.317 respectively.

Table 1. Environmental performance indicators for grape seed valorization under optimal processing configuration

| Indicator | Symbol | Riesling | Feteasc regală | Unit |
|---|---|---|---|---|
| Waste reduction rate | wr | 32.6 | 31.7 | % |
| Resource recovery index | rri | 0.326 | 0.317 | – |
| Circularity coefficient | cc | 0.997 | 0.997 | – |
| Overall circular performance | – | high | high | quali-tative |

The residual pomace fraction retains further valorization potential through composting or anaerobic digestion pathways, contributing to overall system circularity. The circularity coefficient (CC) was 0.997 for both varieties, indicating near-complete reintegration of all biomass-derived fractions, oil and press cake, into productive use pathways, consistent with circular economy objectives for agri-food by-product valorization (Abbate et al., 2025).

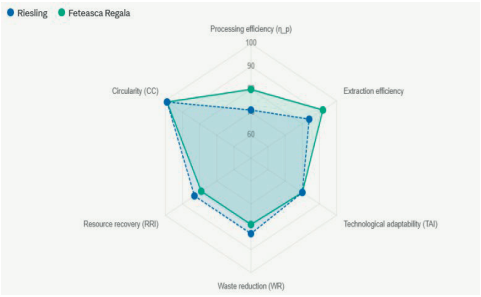



Figure 6. Normalized performance profile (0–100 scale) of all framework indicators for Riesling and Feteasca Regala under optimal configuration (pitch 16 mm, nozzle 12 mm, 10 rpm)

Furthermore, the implementation of small-scale pressing directly at source eliminates the need for transportation of raw pomace to centralized processing facilities, reducing associated greenhouse gas emissions - an aspect particularly relevant in viticultural regions with dispersed farm structures such as Muntenia and Oltenia in Romania.

## Correlation analysis and framework applicability

The relationships between engineering and environmental performance indicators across all

six configurations and both varieties are presented in Figure 7. Processing efficiency ($\eta_p$) shows a strong positive correlation with the circularity coefficient (CC, r = +0.96) and moderate correlations with WR (r = +0.72) and RRI (r = +0.58), confirming that configurations maximizing oil yield simultaneously maximize environmental performance. Conversely, specific energy consumption (E s) shows strong negative correlation with CC (r = −0.89), WR (r = −0.61), and RRI (r = −0.48). The TAI showed no correlation with environmental indicators (r = 0.00), confirming its role as an independent equipment-level criterion in the framework.

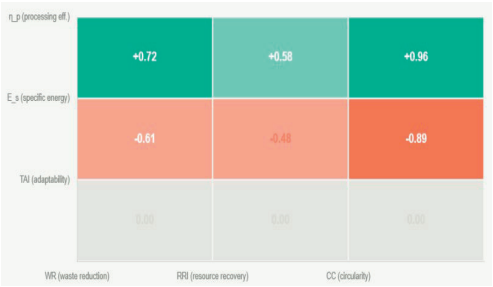



Figure 7. Pearson correlation matrix between engineering and environmental framework indicators across all processing configurations (n = 12). Values range from −1 (strong negative) to +1 (strong positive)

These findings demonstrate a convergence of engineering and environmental optima under the pitch 16 mm configurations, making them simultaneously optimal from both technical and sustainability perspectives. Compared to centralized industrial solutions, the proposed framework applied to small-scale systems offers advantages in flexibility, reduced transport requirements, and improved local resource utilization. Limitations include variability in raw material characteristics across harvest years and the need for future validation through life cycle assessment (LCA) and techno-economic analysis to quantify environmental benefits more precisely across diverse viticultural contexts.

## CONCLUSIONS

The present study proposed and applied a technical framework for the sustainable valorization of vineyard by-products through the integration of engineering and environmental performance indicators. The framework proved to be a structured and effective approach for supporting decision-making in small-scale processing applications, particularly in decentralized viticultural systems.

The results obtained from the representative application scenario demonstrated that grape pomace can be efficiently valorized through mechanical processing, with grape seeds representing a key resource for oil extraction. The application of the NF80 screw press confirmed the technical feasibility of small-scale processing, achieving satisfactory processing efficiency and low specific energy consumption under optimized operating conditions.

From an environmental perspective, the implementation of the proposed framework enabled a significant reduction in waste streams and an efficient recovery of valuable resources. The calculated values of waste reduction rate and resource recovery index indicate that a substantial fraction of vineyard residues can be redirected into productive use, while the high circularity coefficient highlights the potential for reintegrating both oil and press cake into the economic cycle.

The integration of engineering indicators (processing efficiency, specific energy consumption, and technological adaptability) with environmental metrics (waste reduction, resource recovery, and circularity) provides a comprehensive tool for evaluating valorization pathways. This approach allows the identification of optimal processing configurations that simultaneously meet technical and sustainability criteria.

Furthermore, the results emphasize the advantages of small-scale processing technologies in reducing transportation needs, lowering associated emissions, and improving local resource utilization. These aspects are particularly relevant for small and medium-sized vineyards, where access to centralized processing infrastructure is limited.

Although the framework was validated using a representative case study, further research is required to extend its applicability through larger datasets, multi-seasonal analysis, and integration with life cycle assessment and techno-economic evaluation methods. Such

developments would enhance the robustness of the framework and support its implementation across different viticultural regions.

Overall, the proposed technical framework contributes to the advancement of sustainable vineyard by-product management by providing a practical and adaptable model aligned with circular economy principles and environmental engineering objectives.

## ACKNOWLEDGEMENTS

This research was supported by the National Institute of Research-Development for Machines and Installations Designed for Agriculture and Food Industry – INMA Bucharest and funded by the Romanian Ministry of Agriculture and Rural Development through the Nucleus Programme, Contract no. 4N/2023, Project PN 23 04 02 03, entitled *"Innovative technology for grassing the inter-row space in vineyards and fruit orchards to prevent soil structure degradation"*.

## REFERENCES

Abbate, S., Centobelli, P., & Di Gregorio, M. (2025). Wine waste valorisation: Crushing the research domain. *Review of Managerial Science*, 19(3), 963-998, doi:10.1007/s11846-024-00779-5

Ahmad, B., Yadav, V., Yadav, A., Rahman, M. U., Yuan, W. Z., Li, Z., & Wang, X. (2020). Integrated biorefinery approach to valorize winery waste: A review from waste to energy perspectives. *Science of The Total Environment*, 719, 137315. https://doi.org/10.1016/j.scitotenv.2020.137315

Beres, C., Costa, G. N., Cabezudo, I., da Silva-James, N.K., Teles, A.S.C., Cruz, A.P.G., Mellinger-Silva, C., Tonon, R.V., Cabral, L.M.C, & Freitas, S.P. (2017). Towards integral utilization of grape pomace from winemaking process: A review; *Waste Management*, 68, 581–594. https://doi.org/10.1016/j.wasman.2017.07.017

Bjelica, M., Vujasinović, V., Rabrenović, B., & Dimić, S. (2019). Some Chemical Characteristics and Oxidative Stability of Cold Pressed Grape Seed Oils Obtained from Different Winery Waste. *European Journal of Lipid Science and Technology*, 121(8), 1800416. https://doi.org/10.1002/ejlt.201800416

Bustamante, M. A., Moral, R., Paredes, C., Pérez Espinosa, A., Moreno-Caselles, J., & Perez-Murcia, M.D. (2008). Agrochemical characterisation of the solid by-products and residues from the winery and distillery industry. *Waste Management*, 28(2), 372–380. https://doi.org/10.1016/j.wasman.2007.01.013

Cerutti, A. K., Bruun, S., Donno, D., Beccaro, G. L., & Bounous, G. (2013). Environmental sustainability of traditional foods: The case of ancient apple cultivars in Northern Italy assessed by multifunctional LCA. *Journal of Cleaner Production*, *52*, 245–252. https://doi.org/10.1016/j.jclepro.2013.03.029

Dimić, I., Teslić, N., Putnik, P., Bursać Kovačević, D., Zeković, Z., Šojić, B., Mrkonjić, Ž., Čolović, D., Montesano, D., & Pavlić, B. (2020). Innovative and Conventional Valorizations of Grape Seeds from Winery By-Products as Sustainable Source of Lipophilic Antioxidants. *Antioxidants*, 9(7), 568. https://doi.org/10.3390/antiox9070568

Dwyer, K., Hosseinian, F., & Rod, M. (2014). The market potential of grape waste alternatives. *Journal of Food Research,* 3(2), 91–106. doi: 10.5539/jfr.v3n2p91

Fontana, A. R., Antoniolli, A., & Bottini, R. (2013). Grape pomace as a sustainable source of bioactive compounds. Journal of Agricultural and Food Chemistry: Extraction, Characterization, and Biotechnological Applications of Phenolics. *Journal of Agricultural and Food Chemistry*, 61(38), 8987–9003. https://doi.org/10.1021/jf402586f

Galanakis, C. M. (2012). Recovery of high added-value components from food wastes: Conventional, emerging technologies and commercialized applications. *Trends in Food Science & Technology*, 26(2), 68–87. https://doi.org/10.1016/j.tifs.2012.03.003

Kamal-Eldin, A. (2006). Effect of fatty acids and tocopherols on the oxidative stability of vegetable oils. *European Journal of Lipid Science and Technology*, 108(12), 1051–1061. https://doi.org/10.1002/ejlt.200600090

Kapcsándi, V., Lakatos, E. H., & Sik, B. (2021). Characterization of fatty acid, antioxidant, and polyphenol content of grape seed oil from different *Vitis vinifera* L. varieties. *OCL*, 28. https://doi.org/10.1051/ocl/2021017.

Kokkinomagoulos, E., & Kandylis, P. (2023). Grape pomace, an undervalued by-product: Industrial reutilization within a circular economy vision. *Reviews in Environmental Science and Bio/Technology*, *22*(3), 739–773. https://doi.org/10.1007/s11157-023-09665-0

Laufenberg, G., Kunz, B., & Nystroem, M. (2003). Transformation of vegetable waste into value-added products. *Bioresource Technology*, 87(2), 167–198. https://doi.org/10.1016/S0960-8524(02)00167-0

Malićanin, M., Rac, V., Antić, V., Antić, M., Palade, L. M., Kefalas, P., & Rakić, V. (2014). Content of Antioxidants, Antioxidant Capacity and Oxidative Stability of Grape Seed Oil Obtained by Ultra Sound Assisted Extraction. *Journal of the American Oil Chemists' Society*, 91(6), 989–999. https://doi.org/10.1007/s11746-014-2441-2

Martin, M. E., Grao-Cruces, E., Millan-Linares, M. C. & Montserrat-de La Paz, S. (2020). Grape (*Vitis vinifera* L.) Seed Oil: A Functional Food from the Winemaking Industry. *Foods*, 9(10), 1360. https://doi.org/10.3390/foods9101360

Mirabella, N., Castellani, V., & Sala, S. (2014). Current options for the valorization of food manufacturing waste: A review. *Journal of Cleaner Production*, 65, 28–41. https://doi.org/10.1016/j.jclepro.2013.10.051

Mironeasa, S., Leahu, A., Codina, G., Stroe, S.G., & Mironeasa, C. (2010). Grape Seed: Physico-chemical, structural characteristics and oil content. *Journal of Agroalimentary Processes and Technologies*, 16(1), 1-6. http://journal-of-agroalimentary.ro

Moletta, R. (2005). Winery and distillery wastewater treatment by anaerobic digestion. *Water Science and Technology,* 51(1), 137–144. https://doi.org/10.2166/wst.2005.0022

Mushtaq, A., Roobab, U., Denoya, G. I., Inam-Ur-Raheemet, M., Gullón, B., Lorenzo, J.M., Barba, F. J., Zeng, X.A., Wali, A., & Aadil, R.M. (2020). Advances in green processing of seed oils using ultrasound-assisted extraction: A review. *Journal of Food Processing and Preservation,* 44(10), e14740. https://doi.org/10.1111/jfpp.14740

Negro, M. J., Manzanares, P., Oliva, J. M., Ballesteros, I., & Ballesteros, M. (2003). Changes in various physical/chemical parameters of *Pinus pinaster* wood after steam explosion pretreatment. *Biomass and Bioenergy,* 25(3), 301–308. https://doi.org/10.1016/j.psep.2024.11.106

Nirmal, N., Mahale, K. R., Rathod, N. B., Siddiqui, S. A., & Dhar, B.K. (2025). Winery waste: A sustainable approach for bioactive compound extraction and various industrial applications. *Process Safety and Environmental Protection*, 193, 760-771 https://doi.org/10.1016/j.psep.2024.11.10

Orsavova, J., Misurcova, L., Ambrozova, J.V., Vicha, R., & Mlcek, J. (2015). Fatty Acids Composition of Vegetable Oils and Its Contribution to Dietary Energy Intake and Dependence of Cardiovascular Mortality on Dietary Intake of Fatty Acids. *International Journal of Molecular Sciences,* 16(6), 12871–12890. https://doi.org/10.3390/ijms160612871

Passos, C. P., Silva, R. M., Da Silva, F., Coimbra, M. A., & Silva, C. M. (2010). Supercritical fluid extraction of grape seed (*Vitis vinifera* L.) oil. Effect of the operating conditions upon oil composition and antioxidant capacity. *Chemical Engineering Journal,* 160(2), 634–640. https://doi.org/10.1016/j.cej.2010.03.087

Pardo, J. E., Fernández, E., Rubio, M., Alvarruiz, A., & Alonso, G. L. (2009). Characterization of grape seed oil from different grape varieties (*Vitis vinifera*). *European Journal of Lipid Science and Technology*, 111(2), 188–193. https://doi.org/10.1002/ejlt.200800052

Provenzano, M., Pacchera, F., Silvestri, C., & Ruggieri, A. (2024). From vineyard to value: A circular economy approach to viticulture waste. *Resources* 2024, 13(12), 172; https://doi.org/10.3390/resources13120172

Puglia, D., Pezzolla, D., Gigliotti, G., Torre, L., Bartucca, M.L., & Del Buono, D. (2021). The Opportunity of Valorizing Agricultural Waste, Through Its Conversion into Biostimulants, Biofertilizers, and Biopolymers. *Sustainability*, 13(5), 2710, https://doi.org/10.3390/su13052710

Rockenbach, I. I., Rodrigues, E., Gonzaga, L. V., Caliari, V., Genovese, M. I., Gonçalves, A. E. D. S. S., & Fett, R. (2011). Phenolic compounds content and antioxidant activity in pomace from selected red grapes (*Vitis vinifera* L. and *Vitis labrusca* L.) widely produced in Brazil. *Food Chemistry*, 127(1), 174–179. https://doi.org/10.1016/j.foodchem.2010.12.137

Spigno, G., Marinoni, L., & Garrido, G. D. (2017). State of the Art in Grape Processing By-Products. In Handbook of Grape Processing By-Products (pp. 1–27). Elsevier. https://doi.org/10.1016/B978-0-12-809870-7.00001-6

Teixeira, A., Baenas, N., Dominguez-Perles, R., Barros, A., Rosa, E., Moreno, D., & Garcia-Viguera, C. (2014). Natural Bioactive Compounds from Winery By-Products as Health Promoters: A Review. *International Journal of Molecular Sciences*, 15(9), 15638–15678. https://doi.org/10.3390/ijms150915638

International Organisation of Vine and Wine (OIV). (2023). State of the World Vine and Wine Sector in 2022. https://www.oiv.int

Scientific Papers. Series E. Land Reclamation, Earth Observation & Surveying, Environmental Engineering. Vol. XV, 2026
Print ISSN 2285-6064, CD-ROM ISSN 2285-6072, Online ISSN 2393-5138, ISSN-L 2285-6064

# SUSTAINABLE UNFIRED CLAY MASONRY INCORPORATING AGRICULTURAL WASTE: PHYSICAL AND MECHANICAL PROPERTIES

**Alexandra-Marina BARBU[1], Aurelia BRADU[1], Claudiu-Sorin DRAGOMIR[1, 2], Augustina-Sandina TRONAC[2]**

[1]National Institute for Research and Development in Construction, Urban Planning and Sustainable Spatial Development - URBAN-INCERC,
266 Pantelimon Road, 021652, District 2, Bucharest, Romania
[2]University of Agronomic Sciences and Veterinary Medicine of Bucharest,
59 Mărăști Blvd, District 1, 011464, Bucharest, Romania

Corresponding author email: alexandra.barbu@incd.ro

***Abstract***

*Sustainable societal development requires practical solutions that promote the use of traditional and locally available materials, particularly for vulnerable rural communities. In this context, unfired clay represents an environmentally friendly construction material due to its low embodied energy, recyclability, and local availability. Compared to conventional fired materials, it reduces energy consumption and environmental impact, supporting sustainable construction practices. At the same time, the valorization of plant-based waste generated by agricultural and wood-processing activities represents an effective strategy for improving resource efficiency and reducing environmental pollution. According to the National Institute of Statistics, agriculture accounted for approximately 2.5% of Romania's GDP in 2025 and generated over 50% of total municipal waste as vegetal residues. As consumption increases, the management of such waste becomes increasingly challenging, while its decomposition releases greenhouse gases such as methane, contributing to climate change. The incorporation of plant-based waste into clay-based construction materials represents a promising approach for waste valorization and the development of sustainable building materials. This study investigates the effect of hemp fibers and sawdust on the physical and mechanical properties of unfired clay mixtures.*

***Key words****: hemp fibers, plant-based waste, sawdust, sustainable construction, unfired clay.*

## INTRODUCTION

The development of sustainable construction materials has become a strategic research direction in civil engineering, driven by the urgent need to reduce the environmental impact of the construction sector and to address the growing challenges associated with global climate change (Hegyi et al., 2016). Over the past decades, the construction industry has been identified as a major contributor to global greenhouse gas emissions, both through the industrial processes involved in material production and through the extensive consumption of natural resources required for construction activities.

In particular, the production of conventional construction materials such as cement and fired bricks involves energy-intensive technological processes that generate significant amounts of carbon dioxide emissions. These environmental concerns have stimulated increasing research efforts aimed at identifying alternative construction materials and technologies capable of reducing environmental impact while maintaining adequate structural performance and energy efficiency (Bradu et al., 2025).

Within this context, the use of locally available natural materials has gained considerable attention as part of sustainable construction strategies. Materials such as unfired earth, wood, and other natural resources offer significant advantages in terms of reduced embodied energy and lower carbon footprint during production. Moreover, the use of local materials reduces transportation-related environmental impacts and facilitates the adaptation of buildings to specific climatic and geographical conditions (Walker et al., 2005; Minke, 2012).

Masonry elements produced from natural materials such as clay soil, sand, local aggregates, and plant-based waste represent one of the oldest construction technologies used

worldwide (Hegyi et al., 2023). These materials provide several sustainability-related advantages, including local availability, low energy consumption during processing, recyclability, and environmental compatibility. In addition, unfired clay masonry elements contribute to improved hygrothermal comfort in buildings due to their ability to regulate indoor humidity and their high thermal inertia, which helps stabilize indoor environmental conditions (Houben & Guillaud, 1994; Tomaževič, 1999).

The use of clay soil for masonry construction has a long tradition in Romania, particularly in rural areas where traditional building techniques have been developed according to local climatic conditions and available resources (Petcu et al., 2023). The geological diversity of Romania provides significant reserves of clay soils, sands, and natural aggregates that can be utilized for producing environmentally friendly masonry materials (Calatan et al., 2020).

At the same time, the agricultural sector and the wood-processing industry generate considerable amounts of plant-based waste, including sawdust resulting from timber processing and hemp fibers obtained from the cultivation of this traditional crop (Mircea et al., 2021). The incorporation of these materials into masonry compositions can lead to the development of natural composite materials with improved thermal insulation performance and enhanced mechanical behavior. Furthermore, this approach supports the valorization of renewable resources while reducing the amount of biodegradable waste that could otherwise contribute to greenhouse gas emissions during decomposition (Walker et al., 2005; Ashour et al., 2010).

Hemp is characterized by high ecological adaptability, being able to grow under a wide range of climatic and soil conditions without requiring intensive use of fertilizers or pesticides. Due to its ability to absorb and neutralize certain soil contaminants, hemp cultivation can contribute to reducing soil pollution and improving soil quality. In addition, the deep root system of this plant improves soil structure and promotes aeration, facilitating the development of subsequent agricultural crops (Binici et al., 2007).

Moreover, hemp plays an important role in carbon sequestration, capturing atmospheric carbon dioxide from the early stages of plant growth. Hemp-based products are non-toxic, biodegradable, and renewable, making them particularly attractive for the development of sustainable construction materials (Lachheb et al., 2023).

Historically, Romania was one of the major global producers of industrial hemp. In the 1990s, with a production exceeding 72,000 tons, Romania ranked third worldwide in hemp production. However, increasingly restrictive regulations significantly reduced interest in this crop. In recent years, a gradual revival of hemp cultivation has been observed in Romania, supported by investments in processing facilities, access to European Union funding, and its higher economic potential compared to traditional crops such as cereals and oilseeds (Neacșu, 2022).

In parallel, Romania has a well-developed forestry and wood-processing sector, generating significant quantities of wood residues, particularly sawdust. This type of waste represents an important resource within the framework of the circular economy and is increasingly used in various applications, including energy production, wood-based panel manufacturing, and sustainable construction materials (Bailly et al., 2024). The incorporation of sawdust into construction materials contributes both to the efficient reuse of industrial by-products and to the improvement of certain physical properties such as density reduction and enhanced thermal insulation.

In recent years, increasing research interest has been directed toward the use of sawdust in ecological construction materials. The integration of this by-product into building materials not only facilitates the valorization of wood waste but also improves certain physical and mechanical properties of composite materials. Furthermore, this approach supports the development of locally sourced, low-cost construction materials while promoting environmentally sustainable building solutions, particularly in rural areas (Toader et al., 2025).

Despite the growing interest in plant-based additives for earthen construction materials, limited research has been conducted on the combined use of locally available clay soils with vegetal residues such as sawdust and hemp fibers in masonry elements. In particular, there

is still insufficient experimental data regarding the influence of these additives on the physical and mechanical properties of clay-based composites produced from locally available materials.

Therefore, the present study aims to investigate the influence of plant-based waste additives on the performance of clay masonry materials. A comparative experimental study was conducted on clay-based compositions intended for masonry elements, produced from locally available sustainable materials and modified by the addition of plant-based waste in the form of sawdust and hemp fibers. The main objective of this research is to evaluate the influence of these vegetal additives on the physical and mechanical properties of the resulting composites and to identify sustainable construction solutions based on locally available natural resources.

## MATERIALS AND METHODS

The mixtures used for the production of masonry elements were composed of locally available materials, including clay soil, sand, aggregates, and agricultural waste in the form of sawdust and hemp fibers, together with a natural additive (Figure 1). The formulations of the mixtures are presented in Table 1.

Table 1. Composition of the evaluated clay-based mixtures

| Constituents | Unit | S1 | S2 | H1 | H2 |
|---|---|---|---|---|---|
| Clay soil | g | 10,758 | 10,758 | 10,758 | 10,758 |
| Sand 0-1 mm | g | 220 | 220 | 220 | 220 |
| Sand 0-4 mm | g | 2,289 | 2,289 | 2,289 | 2,289 |
| Aggregate 4-8 mm | g | 2,102 | 2,102 | 2,102 | 2,102 |
| Hemp | g | - | - | 1,537 | 3,074 |
| Sawdust | g | 1,537 | 3,074 | - | - |
| Additive | g | 107.6 | 107.6 | 107.6 | 107.6 |
| Clay/water ratio | - | 0.28 | 0.29 | 0.28 | 0.22 |
| Spread | mm | 108.9 | 106.9 | 110.6 | 105.1 |

The clay soil used as a binder consisted of 52% clay fraction, 44% silt, and 4% sand.

The sand incorporated into the clay mixture was coarse construction sand with particle size distributions of 0-1 mm and 0-4 mm. In addition, natural alluvial aggregates with particle sizes ranging from 4 to 8 mm were used.

The amount of water was determined experimentally for each mixture in order to ensure optimal workability of the fresh material. To obtain smoother and more uniform surfaces of the self-supporting elements and to improve the workability of the mixtures, rabbit glue was used as a natural additive. This additive enhances the elasticity and cohesion of the clay matrix.

Plant-based waste in the form of hemp fibers and sawdust was incorporated into the material composition as additives in order to valorize renewable resources.



a) Hemp fibers



b) Sawdust



c) Rabbit glue

Figure 1. Constituent materials

The incorporation of fibers in a saturated state improves the adhesion between the fibers and the clay matrix. Moistening the fibers helps eliminate entrapped air, reducing the risk of void formation and ensuring a stronger bond between the constituent materials.

The preparation of the clay mixture followed several stages. First, the clay soil and the vegetal waste were mixed in a large container until a homogeneous mixture was obtained. The rehydrated rabbit skin glue was dissolved in the required amount of water and added to the composition, while mixing continued until a uniform consistency was achieved. Finally, sand with particle sizes of 0-1 mm and 0-4 mm, together with aggregates (4-8 mm), were added to the mixture, and mixing was continued until a homogeneous texture was obtained.
The consistency of the fresh clay mixture was determined according to SR EN 1015-3:2001/A2:2007 (Figures 2 and 3).



a) 10% sawdust content



b) 20% sawdust content

Figure 2. Spread of the clay mixture with sawdust addition

The principle of this method is as follows: the conical mold is placed on the circular flow table, using a manual flow table manufactured by MATEST (Italy), and filled with the fresh mixture in two layers. Each layer is compacted using a metal tamper. After removing the mold, 15 drops are applied to the flow table within 15 seconds, after which the average diameter of the spread specimen is measured.



a) 10% hemp fiber content



b) 20% hemp fiber content

Figure 3. Spread of the clay mixture with hemp fiber addition

The mixture was cast into standardized molds, using cubic molds for concrete sample preparation manufactured by UTEST (Turkey), with dimensions of 150 × 150 × 150 mm, intended for compressive strength testing after 28 days. In addition, part of the mixture was cast into molds measuring 300 × 300 × 50 mm for thermal conductivity testing.
The specimens were demolded after 5 days and conditioned at a temperature of 23 ± 5°C. The stages of specimen preparation are illustrated in Figure 4.
The drying time of the specimens varies depending on the mixture composition and environmental conditions. Mixtures containing sawdust or hemp tend to require a longer drying period due to their higher moisture retention capacity.
This time can be reduced by exposing the mixtures to air circulation or controlled temperatures; however, excessive acceleration of the drying process should be avoided in order to prevent cracking.



a) Mixing of the materials



b) Casting of the specimens



c) Conditioning of the specimens

Figure 4. Stages of specimen preparation

The density of the elements was determined in accordance with SR EN 1015-10:2002/A1:2007 - Methods of test for mortar for masonry. Part 10: Determination of the apparent density of hardened mortar.
The density of the hardened material was calculated using Eq. (1):

$$\boldsymbol{D = \frac{m}{V}} \quad (1)$$

where:
$D$ - density of the hardened material, kg/m³;
$m$ - mass of the specimen in saturated state, kg;
$V$ - volume determined by measurement, m³.
The compressive strength was calculated using Eq. (2):

$$\boldsymbol{f_c = \frac{F_c}{A}} \quad (2)$$

where:
$f_c$ - compressive strength, MPa;
$F$ - maximum load at the moment of rupture, N;
$A$ - area of speciment, mm².

The thermal conductivity was determined in accordance with SR EN 12667:2002 - Thermal performance of building materials and products. Determination of thermal resistance by means of guarded hot plate and heat flow meter methods, using a thermal conductivity measuring device (HESTO Lambda Control A 90) manufactured by HESTO Elektronik GmbH (Germany). Products of high and medium thermal resistance. The thermal resistance was calculated using Eq. (3):

$$\boldsymbol{R = \frac{d}{\lambda}} \quad (3)$$

where:
$R$ - thermal resistance, m²K/W;
$d$ - thickness of the layer, mm;
$\lambda$ - thermal conductivity of the material, W/mK.

## RESULTS AND DISCUSSIONS

The determination of the geometric characteristics of unfired clay specimens after the drying process is essential for evaluating the shrinkage behavior of the material and its ability to maintain the initial mold geometry. The dimensional stability of masonry elements plays an important role in ensuring proper placement within masonry structures, contributing to the uniform distribution of vertical loads and adequate contact with the bonding mortar. Significant dimensional deviations may lead to local stress concentrations, crack initiation, and a reduction in the overall structural stability.
The experimental measurements indicated relatively small dimensional deviations compared to the initial nominal dimensions of the specimens, suggesting a good dimensional stability of the studied mixtures. For specimens containing 10% vegetal waste addition, both sawdust and hemp fibers exhibited a maximum shrinkage of 3.5 mm, corresponding to 2.33% of the initial dimension.
For mixtures incorporating 20% sawdust, the measured shrinkage was 3.2 mm, while specimens containing 20% hemp fibers showed

a slightly higher shrinkage value of 4.1 mm. This behavior may be associated with the higher water absorption capacity and greater volumetric variability of hemp fibers compared to sawdust, which can influence the drying process and dimensional stability of the clay matrix (where H represents the specimen height, l the specimen width, L the specimen length, and Δ the longitudinal/transversal shrinkage of the specimen).

The corresponding experimental results are presented in Tables 2 and 3, where samples 1, 2, and 3 represent the three tested specimens for each composition (10% and 20% addition of sawdust or hemp fibers).

Table 2. Geometrical characteristics of the specimens with sawdust addition after 28 days

| Sample no. | Dimensions, mm | | | | |
|---|---|---|---|---|---|
| | 10% sawdust | | | | |
| | H mm | l mm | L mm | % $\Delta_l$ | % $\Delta_L$ |
| 1 | 142.2 | 147.5 | 146.9 | 2.5 | 3.1 |
| 2 | 143.4 | 146.9 | 146.5 | 3.1 | 3.5 |
| 3 | 143.1 | 146.7 | 146.9 | 3.3 | 3.1 |
| Sample no. | Dimensions, mm | | | | |
| | 20% sawdust | | | | |
| | H mm | l mm | L mm | % $\Delta_l$ | % $\Delta_L$ |
| 1 | 143.8 | 146.9 | 147.1 | 3.1 | 2.9 |
| 2 | 143.1 | 146.8 | 146.8 | 3.2 | 3.2 |
| 3 | 142.9 | 147.0 | 147.2 | 3.0 | 2.8 |

Table 3. Geometric characteristics of the specimens with hemp fiber addition after 28 days

| Sample no. | Dimensions, mm | | | | |
|---|---|---|---|---|---|
| | 10% hemp | | | | |
| | H mm | l mm | L mm | % $\Delta_l$ | % $\Delta_L$ |
| 1 | 145.6 | 147.3 | 147.2 | 2.7 | 2.8 |
| 2 | 145.9 | 147.1 | 146.5 | 2.9 | 3.5 |
| 3 | 145.7 | 147.1 | 147.1 | 2.9 | 2.9 |
| Sample no. | Dimensions, mm | | | | |
| | 20% hemp | | | | |
| | H mm | l mm | L mm | % $\Delta_l$ | % $\Delta_L$ |
| 1 | 142.0 | 146.2 | 146.1 | 3.8 | 3.9 |
| 2 | 141.8 | 145.9 | 145.9 | 4.1 | 4.1 |
| 3 | 142.6 | 146.3 | 146.0 | 3.7 | 4.0 |

The determination of the density of clay-based mixtures represents an important indicator in the evaluation of the physical and mechanical performance of construction materials, as it directly influences both the structural behavior and the thermal insulation properties of the material. The analysis of density allows the assessment of the degree of compaction and homogeneity of the mixture, as well as the identification of an optimal balance between mechanical strength and thermal insulation capacity.

An increase in material density is generally associated with a higher degree of compaction of the clay matrix and improved mechanical strength. However, it simultaneously leads to an increase in thermal conductivity, which reduces the material's insulating capacity. From a practical perspective, construction elements with densities exceedingly approximately 1200 kg/m³ become more massive and more difficult to handle and install, potentially requiring additional construction measures to prevent settlement or deformation during construction.

Therefore, optimizing the density of the material represents an important aspect in the design of clay-based mixtures intended for construction applications.

The experimental density results obtained for the four analyzed mixtures indicate a coefficient of variation below 5%, highlighting a relatively high degree of homogeneity of the materials produced under laboratory conditions.

The highest density value was recorded for the sample containing 10% sawdust addition, reaching 1643 kg/m³, with a coefficient of variation of 2.92%. Increasing the amount of sawdust to 20% of the total aggregate mass led to a density reduction of approximately 8%, resulting in a value of 1509 kg/m³.

The specimens produced with 20% hemp fiber addition exhibited the lowest density among all analyzed samples, namely 1383 kg/m³, with a coefficient of variation of 3.43%, representing a 14.3% decrease compared to the values recorded for the specimens containing 10% hemp fibers.

The overall range of experimentally determined densities, illustrated in Figure 5, varies between approximately 1362 and 1642 kg/m³. These values fall within the range characteristic of conventional construction materials, being comparable to the density of solid bricks (approximately 1600-1900 kg/m³) and close to the density range of hollow ceramic blocks (700-1400 kg/m³).

This comparison suggests that the analyzed clay-based materials may present significant

potential for use in construction applications, offering a favorable balance between mechanical performance and thermal insulation properties.

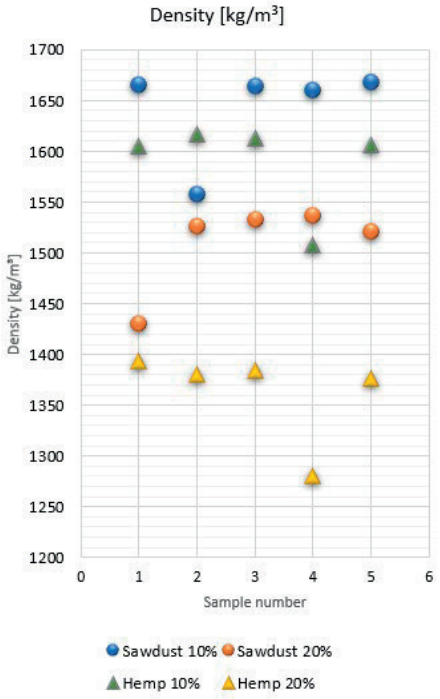



Figure 5. Density of clay-based mixtures

The compressive strength of clay-based elements is influenced by several factors, including the type and quantity of clay, the particle size distribution of the mixture, the preparation technology of the mixture, and the casting process of the specimens. These parameters determine the degree of cohesion of the matrix and the way stresses are transmitted within the material. According to data reported in the literature, the compressive strength of unfired clay materials generally ranges between 0.2 and 5 N/mm², depending on the composition and production conditions of the mixture (Ashour et al., 2011).

The compressive strength values obtained experimentally are presented in Figure 6. The compositions containing sawdust recorded the lowest compressive strength values, particularly in the case of the 20% addition, for which the experimentally determined average value was 1.46 MPa, with a coefficient of variation of 4.02%. The specimens containing 10% sawdust showed an average compressive strength of 1.602 MPa and a coefficient of variation of 8.95%.

Mixtures incorporating hemp fibers exhibited better mechanical behavior, with compressive strength values slightly varying depending on the proportion of fibers added. The compressive strength reached 2.03 N/mm² for the composition containing 10% hemp fibers and 1.912 MPa for the mixture with 20% hemp fiber addition.

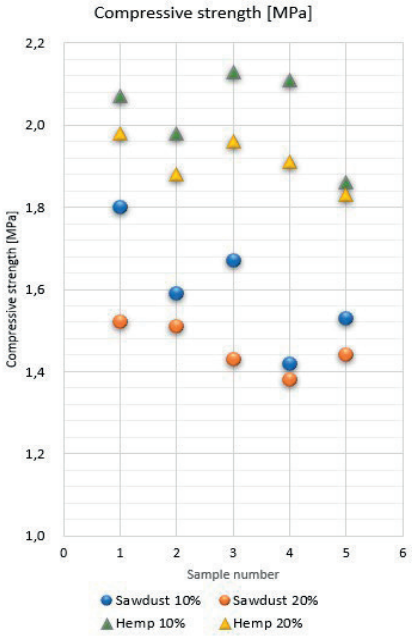



Figure 6. Compressive strength of clay-based mixtures

The comparative analysis of the results reveals a general trend of decreasing compressive strength with the increase in the percentage of vegetal material incorporated into the clay matrix. This behavior can be explained by the reduction in the structural continuity of the clay phase and by the occurrence of discontinuities or additional porosity within the material, which lead to a reduced capacity of the material to uniformly absorb and transmit mechanical stresses.

Following the compressive strength tests, all clay specimens containing vegetal additives exhibited a failure mode characterized by the appearance of vertical cracks distributed over the entire surface of the tested elements, a phenomenon typical for brittle materials subjected to axial compressive loading. This type of cracking indicates the progressive

development of internal stresses and the propagation of cracks in the direction of the applied load until the structural integrity of the specimens is lost.

The failure mode of the specimens subjected to axial compression is illustrated in Figures 7 and 8.




Figure 7. Failure mode of the specimens containing hemp fibers under axial compression




Figure 8. Failure mode of the specimens containing sawdust under axial compression

The determination of the thermal conductivity of materials is essential for the design and efficient use of building products and structures involving heat transfer, ensuring optimal thermal performance, safety, and energy efficiency.

In the construction sector, the evaluation of the thermal conductivity of unfired clay-based materials with fiber additives is particularly important for assessing their thermal insulation performance.

Such materials can contribute to improving the energy efficiency of buildings by reducing heat losses during winter and limiting heat gains during summer.

Consequently, thermal conductivity represents a key parameter in determining indoor thermal comfort and reducing energy consumption associated with heating and cooling.

The experimentally determined values of thermal conductivity and thermal resistance for the analyzed clay-based specimens are presented in Table 4.

Table 4. Experimental values of thermal conductivity and thermal resistance

| Specimen type | Dimensions | Thickness | Thermal conductivity λ | Thermal resistance |
|---|---|---|---|---|
| | [mm] | [mm] | λ[W/mK] | [$m^2$K/W] |
| R1 (10% sawdust) | 280x295 | 26.67 | 0.19099 | 0.140 |
| R2 (20% sawdust) | 290x295 | 31.16 | 0.18369 | 0.169 |
| R3 (10% hemp) | 294x292 | 26.12 | 0.17503 | 0.149 |
| R4 (20% hemp) | 295x260 | 26.39 | 0.17258 | 0.152 |

The data presented in Table 4 indicate that the specimens containing sawdust exhibited higher thermal conductivity values (λ). At the same time, increasing the content of vegetal additives contributed to improved thermal insulation performance of the clay-based composite.

## CONCLUSIONS

The incorporation of vegetal waste into the composition of construction materials influences both the physical behavior and the mechanical and thermal insulation properties of the material. Based on the comparative study of the clay-based mixtures, the following conclusions can be drawn:

- From the perspective of the dimensional stability of the specimens, the relatively small deviations of the geometric characteristics, ranging between 1.98% and 2.6%, indicate a relatively uniform shrinkage during the drying process, suggesting good dimensional stability of the analyzed mixtures.
- The density coefficient of variation below 5% confirms the production of relatively homogeneous materials. The determined density values, ranging between 1362 and 1642 kg/m³, demonstrate that the studied materials fall within the density range characteristic of commonly used construction materials. The results indicate that vegetal additives contribute to reducing the density of the clay matrix, an effect more pronounced in the case of hemp fiber compositions, while the addition of sawdust leads to comparatively higher density values.
- From the perspective of mechanical behavior, a general tendency of decreasing compressive strength was observed with increasing vegetal additive content. This phenomenon can be associated with increased porosity and the presence of discontinuities within the clay matrix structure. Nevertheless, the mixtures containing hemp fibers exhibited slightly higher compressive strength values compared to the specimens containing sawdust. The observed failure mode, characterized by vertical cracks distributed across the surface of the specimens, confirms the typical behavior of brittle materials subjected to axial compressive loading.
- Regarding thermal insulation performance, the experimental results indicate that increasing the vegetal additive content contributes to the reduction of thermal conductivity for both types of vegetal additives, although this improvement is accompanied by a reduction in mechanical performance.

Overall, the experimental data suggest the existence of a trade-off between density, mechanical strength, and thermal conductivity, highlighting the need to optimize the proportion of vegetal additives in order to obtain a clay-based material with balanced properties suitable for construction applications.

## ACKNOWLEDGEMENTS

This paper was supported by the Program Advanced research on the development of eco-innovative solutions, composite materials, technologies and services, in the concept of a circular economy and increased quality of life, for a sustainable digitized infrastructure in a built and urban environment resilient to climate change and disasters, "ECODIGICONS", Program code: PN 23 35 03 01: "Integrated system of development and scientific research of constructions and vital infrastructures exposed to extreme seismic and climatic environmental actions and the exploitation of sustainable resources of materials and energy", financed by the Romanian Government.

## REFERENCES

Ashour, T., Wieland, H., Georg, H., Bockisch, F., & Wu, W. (2010). The influence of natural reinforcement fibres on insulation values of earth plaster for straw bale buildings. *Materials & Design*, *31*(10), 4676–4685.

Ashour, T., Georg, H., & Wu, W. (2011). Performance of straw bale wall: A case of study. *Energy and Buildings*, *43*(8), 1960–1967.

Bailly, G. C., El Mendili, Y., Konin, A., & Khoury, E. (2024). Advancing Earth-Based Construction: A Comprehensive Review of Stabilization and Reinforcement Techniques for Adobe and Compressed Earth Blocks. *Eng*, *5*(2), 750-783.

Binici, H., Aksogan, O., & Shah, T. (2007). Investigation of fibre reinforced mud brick as a building material. *Construction and Building Materials*, *21(4)*, 901–906.

Bradu, A., Andon, A. E., Barbu, A. M., & Dragomir, C. S. (2025). Evaluating aggregate content and its effect on clay mortar performance. *Scientific Papers. Series E: Land Reclamation, Earth Observation & Surveying, Environmental Engineering*, XIV.

Calatan, G., Hegyi, A., Dico, C., & Szilagyi, H. (2020). Opportunities regarding the use of adobe bricks within contemporary architecture. *Procedia Manufacturing*, 46, 150–157.

Hegyi, A., Dico, C., & Calatan, G. (2016). Construction sustainability with adobe bricks type elements. *Urbanism. Architecture. Constructions*, 7(2), 147–156.

Hegyi, A., Petcu, C., Ciobanu, A. A., Calatan, G., & Bradu, A. (2023). Development of clay-composite plasters integrating industrial waste. *Materials*, 16(14), 4903.

Houben, H., & Guillaud, H. (1994). *Earth construction: A comprehensive guide*. London, UK: Intermediate Technology Publications.

Lachheb, M., Youssef, N., & Younsi, Z. (2023). A comprehensive review of the improvement of the thermal and mechanical properties of unfired clay bricks by incorporating waste materials. *Buildings*, 13(9), 2314.

Minke, G. (2012). *Building with earth: Design and technology of a sustainable architecture* (3rd ed.). Basel, CH: Birkhäuser.

Mircea, C., Toader, T. P., Hegyi, A., Ionescu, B. A., & Mircea, A. (2021). Early age sealing capacity of structural mortar with integral crystalline waterproofing admixture. *Materials*, 14(17), 4951.

Neacșu, M. (2022). Cânepa – o soluție reală pentru un viitor sustenabil. Retrieved from https://www.infoclima.ro/articole/cnepa-o-soluie-real-pentru-un-viitor-sustenabil

Petcu, C., Dobrescu, C. F., Dragomir, C. S., Ciobanu, A. A., Lăzărescu, A. V., & Hegyi, A. (2023). Thermophysical characteristics of clay for efficient rammed earth wall construction. *Materials*, 16(17), 6015.

SR EN 1015-3:2001/A2:2007 (2007). *Methods of test for mortar for masonry – Part 3: Determination of consistence of fresh mortar (by flow table)*.

SR EN 1015-10:2002/A1:2007 (2007). *Methods of test for mortar for masonry. Part 10: Determination of the apparent density of hardened mortar*.

SR EN 12667:2002. (2002) *Thermal performance of building materials and products – Determination of thermal resistance by means of guarded hot plate and heat flow meter methods – Products of high and medium thermal resistance*.

Tomaževič, M. (1999). *Earthquake-resistant design of masonry buildings*. London, UK: Imperial College Press.

Toader, T. P., Moldoveanu, M. I., Boca, D. M., Iștoan, R., Lupan, L. M., Bradu, A., Hegyi, A., & Boga, A. (2025). Sustainable investments in construction: Cost–benefit analysis between rehabilitation and new building in Romania. *Buildings*, *15*(15), 2770.

Walker, P., Keable, R., Martin, J., & Maniatidis, V. (2005). *Rammed earth: Design and construction guidelines*. Watford, UK: BRE Press.

Scientific Papers. Series E. Land Reclamation, Earth Observation & Surveying, Environmental Engineering. Vol. XV, 2026
Print ISSN 2285-6064, CD-ROM ISSN 2285-6072, Online ISSN 2393-5138, ISSN-L 2285-6064

# EFFECT OF SOIL TYPE AND MANAGEMENT ON POTENTIALLY TOXIC ELEMENTS (As, Cu, Zn) IN SOILS OF OLIVE GROVES IN DALMATIA, CROATIA

**Aleksandra BENSA, Nikolina JURKOVIĆ BALOG, Aleksandra PERČIN**

University of Zagreb Faculty of Agriculture, Svetošimunska cesta 25 10000, Zagreb, Croatia

Corresponding author email: abensa@agr.hr

***Abstract***

*The objectives of the study were to (i) establish and compare As, Cu, and Zn concentrations in two contrasting soil types under different management and (ii) assess soil pollution of the study area by the mentioned potentially toxic elements. A 40 composite topsoil samples were collected in Middle Dalmatia, Croatia, out of which 20 were from Terra rossa and 20 from Regosols. On each soil type, 10 samples were taken from intensive olive groves (IOG) and 10 from traditional low-input olive groves (TOG). The total concentrations of As, Cu, and Zn were obtained using the pXRF method. The mean As, Cu, and Zn concentrations in Terra rossa were 21.9, 112.7, and 124.5 mg/kg, respectively. In Regosols, mean As, Cu, and Zn concentrations were 6.3, 55.0, and 63.6 mg/kg, respectively. Significantly higher ($p<0.05$) As, Cu, and Zn concentrations were determined in Terra rossa compared to Regosols. Significantly higher ($p<0.05$) Cu concentrations were found in IOG compared to TOG (124.5 and 43.2 mg/kg, respectively). Terra rossa under IOG was polluted with Cu, while the other soils were not. The studied soils were not polluted with As and Zn.*

***Key words****: olive groves, potentially toxic elements, Regosol, soil pollution, Terra rossa.*

## INTRODUCTION

Potentially toxic elements (PTE) represent a threat to soil fertility, quality, health, and security, as recognized in various studies e.g. Kibblewhite et al. (2007), Hou et al. (2020). The PTE distribution in soils is governed by natural conditions and anthropogenic inputs. Among the natural reasons for PTE variability, soil properties, parent material, climate, and geomorphology stand out (Mottese et al., 2020). The most important areas of olive production in Dalmatia, Croatia, are widespread on soils derived from limestones (Terra rossa and Calcocambisols) and flysch deposits (Regosols). These are two contrasting parent materials on which soils with different properties develop. Soils developed over limestones contain elevated levels of PTE (Kabata-Pendias & Pendias, 2001; Halamić & Miko, 2009). Furthermore, high clay content and abundance of Fe and Al oxides contribute to strong adsorption and retention of PTE in the top-soil horizon of Terra rossa (Miloš & Bensa, 2021). PTE concentrations are typically lower in soils formed on flysch sediments, though this varies depending on the nature and sedimentation processes of the rock-derived material (Lovrenčić Mikelić et al., 2013). Also, since these soils contain lower clay and humus content, they retain less PTE. Anthropogenic inputs of PTE in soils involve different types of emissions from the industrial areas, as well as from agricultural activities (Zhang et al., 2019). Fertilizers and plant production products are the primary agricultural sources of PTE in agricultural soils (Pathak et al., 2002; Wyszkowski & Brodowska, 2020). Since the late 19$^{th}$ century, viticulture in Europe extensively used Cu-based fungicides (Komarek et al., 2010). Furthermore, nitrogen and phosphate fertilizers can be significant sources of As and Zn in cultivated soils (Kabata Pendias & Mukherjee, 2007; Sachdeva et al., 2025). Given its impact on food safety, PTE pollution in agricultural soils is especially concerning (Antoniadis et al., 2017; Edelstein & Ben-Hur, 2018) considering negative consequences for all agroecosystems (Kibblewhite et al., 2007). Elevated Cu concentrations in soil diminish microbial growth and biomass (Díaz Raviña et al., 2007) as well as development of plant roots (Ambrosini et al., 2015).

Increased concentrations of Cu are predominantly reported for soils of permanent crops, particularly vineyards (Komarek et al., 2010) and olive groves (Avramidis et al., 2019). Pollution of agricultural soils by As (Jimenez Balesta et al., 2023) and Zn (Fernández-Calviño et al., 2012) was also stated in earlier literature findings. Excessive concentrations of arsenic can induce aberrant plant growth and disturb ecological equilibrium (Kabata-Pendias & Pendias, 2001). Soil organisms such as earthworms (Lev et al., 2010) and bacterial communities (Pan et al., 2020) are negatively affected by high Zn concentrations. We hypothesized that Terra rossa and Regosols differ in PTE concentrations, and that soil management in olive groves affects PTE concentrations in soil. The objectives of this study were (i) to establish and compare As, Cu, and Zn concentrations in two contrasting soil types under different management and (ii) to assess soil pollution of the study area by the mentioned PTE.

## MATERIALS AND METHODS

The study was conducted in Middle Dalmatia, Croatia (Figure 1A), distinguished by a Mediterranean type of climate (Csa), commonly referred to as an "olive climate" (Filipčić, 1998). The western part of the study area is built up of Cretaceous platy and massive limestones with pronounced stratification, while the eastern part consists of Eocene flysch deposits (Figure 1B). The limestones are of Senonian and Turonian age and are characterized by dominant biocalcarenites. Flysch deposits are predominantly classified as calcarenites, breccia-conglomerates, calcirudites, and marls (Marinčić et al., 1967).

This area is characterized by typical karst geomorphology, with the steeper slopes in the northern part and the gentler ones in the southern part. Therefore, the northern part of the area is subject to erosion processes and characterized by shallow soils, while in the southern parts, colluvial processes are present and deeper soils dominate. The dominant soil types on limestones are Terra rossa, while Regosols are developed on Flysch deposits (Figure 1C; Čolak & Martinović, 1974). Terra rossa is a Mediterranean soil distinguished by its red colour, heavy texture and inconstant depth. Regosols on flysch deposits are calcareous silty soils highly susceptible to erosion and characterized by alkaline reaction and low humus content. The correlation analogs of Terra rossa and Regosol are Leptic Chromic Cambisols (Clayic) and Regosols (Calcaric, Siltic/Loamic), respectively (IUSS Working Group of WRB, 2015). This area is under long-term anthropogenic influence, which is evident in the numerous terraces and dry-wall enclosures (Miloš & Bensa, 2021). Olive growing in the study area is characterized by dry farming, encompassing traditional low-input (TOG) and intensified olive growing systems (IOG). The traditional low-input growing system is characterized by periodic soil cultivation, fertilization with low doses of fertilizers, and rare application of pesticides. In a more intensive olive growing system, fertilization and plant protection are more often applied, including larger quantities of fertilizers and pesticides.

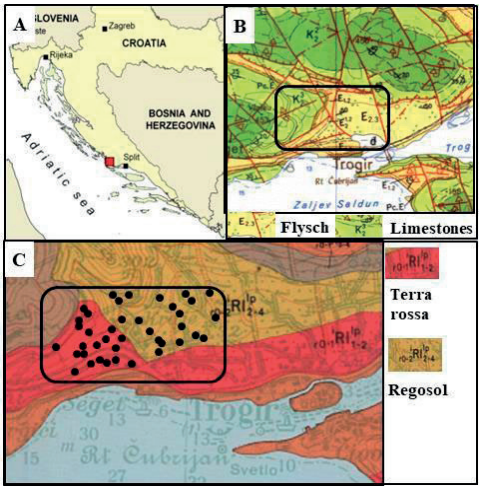



Figure 1. Location of the study area (A), Basic geological map of Croatia at scale 1:100 000 section Split (Marinčić et al., 1967) with indicated study area (B) and Basic soil map of Croatia at scale 1:50 000 section Šibenik 4 (Čolak & Martinović, 1974) with indicated study area and sampling locations (C)

A 40 composite topsoil samples (0-20 cm) were taken in currently productive private olive groves in the study area (Figure 1C). The composite soil samples consisted of 3 sub-samples taken at a distance of 1 m in a cross

arrangement. The 20 samples were taken from Terra rossa and 20 samples from Regosols. On each soil type, 10 samples were taken from traditional low-input olive groves (TOG) and 10 from intensive ones (IOG).

The disturbed soil samples were prepared according to ISO 11464:2006. Soil particle size distribution was analyzed by the pipette method using wet sieving and sedimentation. Soil pH in $H_2O$ and KCl (c=1M) was measured after ISO 10390:2005. A modified volumetric method (ISO 10693:1995) was used for determination of $CaCO_3$ content. Humus content was dteremined using the Tjurin method (JDPZ, 1966) and subsequently converted to soil organic carbon (SOC) by dividing by the Van Bemmelen factor (1.724). The $P_2O_5$ and $K_2O$ concentrations were determined using lactate-acetate as the extraction solution (Egner et al., 1960).

The total concentrations of As, Cu, and Zn were determined using the Vanta handheld XRF analyser C Series (Olympus, Waltham, MA, USA, 2019) according to the loose powder method (Takahashi, 2015). The certified (SRM 2711) and reference soil samples (ISE 989) were used to control accuracy and precision of the analyses. The results of the analyses were acceptable (accuracy: RPD < 5% and recovery 95%-105%; precision: RSD < 5%).

The Ordinance on the protection of agricultural land from pollution (Official Gazette 71/19) was used to evaluate the pollution of the studied soils. When agricultural land contained more PTE than the maximum permissible concentrations (MPC) (mg/kg), it was considered polluted. The MPC of PTE in agricultural soils is prescribed considering $pH_{KCl}$ values (Table 1).

Table 1. Maximum permissible concentrations (MPC) (mg/kg) of selected PTE in agricultural soils in Croatia (Official Gazette 71/19)

| | $pH_{KCl}$ | | |
|---|---|---|---|
| Element | < 5 | 5-6 | >6 |
| As | 15 | 25 | 30 |
| Cu | 60 | 90 | 120 |
| Zn | 60 | 150 | 200 |

Descriptive statistics (minimum, maximum, mean, coefficient of variation, and skewness) were used to process obtained data of basic chemical soil properties and PTE concentrations. A two-way analysis of variance (ANOVA) was carried out for statistical comparison of analysed PTE concentrations. All statistical analysis was performed using MS Excel.

## RESULTS AND DISCUSSIONS

Basic soil properties govern adsorption processes in soils. Adsorption and retention of PTE in soils dominantly depend on soil texture, especially clay minerals (Bradl, 2004; Uddin, 2017; Huang et al., 2020), organic matter content (Kabata-Pendias & Pendias, 2001; Wan et al., 2024), and pH values (Elzahabi & Yong, 2001; Romić et al., 2014).

Particle size analysis has shown differences between the studied soil types (Table 2).

Table 2. Descriptive statistic for particle size distribution of Terra rossa and Regosols

| Soil type | Min. | Max. | Mean | CV | Skew |
|---|---|---|---|---|---|
| | Coarse sand (2.0-0.2 mm) | | | | |
| Terra rossa | 0.1 | 0.7 | 0.3 | 80.7 | 1.08 |
| Regosol | 1.9 | 12.3 | 5.7 | 55.7 | 1.14 |
| | Fine sand (0.2-0.063 mm) | | | | |
| Terra rossa | 1.9 | 3.1 | 2.6 | 14.3 | 0.09 |
| Regosol | 4.8 | 15.7 | 9.2 | 33.4 | 0.66 |
| | Coarse silt (0.063-0.02 mm) | | | | |
| Terra rossa | 15.9 | 22.3 | 19.6 | 9.5 | -0.43 |
| Regosol | 14.3 | 23.8 | 19.2 | 13.89 | -0.18 |
| | Fine silt (0.02-0.002 mm) | | | | |
| Terra rossa | 35.6 | 50.2 | 43.4 | 8.1 | -0.38 |
| Regosol | 31.1 | 51.1 | 42.4 | 13.8 | -0.42 |
| | Clay (< 0.002 mm) | | | | |
| Terra rossa | 27.6 | 46.0 | 34.2 | 14.0 | 1.47 |
| Regosol | 18.2 | 29.1 | 23.5 | 14.6 | 0.04 |

Min. - minimum; Max. - maximum; CV - coefficient of variation; Skew - skewness

Terra rossa soils are composed predominantly of fine silt (mean value 43.4%), followed by clay particles (mean value 34.2%). Sand particles (coarse and fine) form less than 3% on average. In Regosols, fine silt particles also dominate (mean value 42.4%). However, a lower content of clay particles (mean value 23.5%) was observed in comparison to Terra rossa soils. Furthermore, a higher content of sand was recorded in Regosols in comparison to Terra rossa soils (Table 2).

Terra rossa has mainly a silty clayey loamy texture, while Regosols are mainly silty loams, but silty clayey loams also occur (Figure 2). The

determined texture of the studied soils is consistent with literature findings for Terra rossa (Bellanca et al., 1996; Vingiani et al., 2018; Miloš & Bensa, 2021) and soils on flysch deposits (Bogunović et al., 2009; Miloš & Bensa, 2019; Bensa & Jurković Balog, 2023).

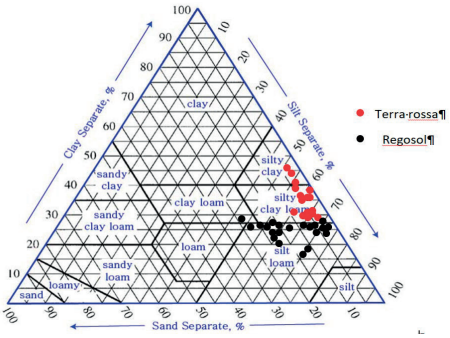



Figure 2. Display of soil samples on texture triangle (FAO/UNESCO, 1990)

Terra rossa soils under both management types have a slightly acidic to neutral reaction and low $CaCO_3$ content (Table 3).

Table 3. Descriptive statistic for basic chemical properties of Terra rossa soils under traditional (TOG) and intensive olive groves (IOG)

| Management type | Soil property | Min. | Max. | Mean | CV | Skew |
|---|---|---|---|---|---|---|
| TOG | pH (KCl) | 6.07 | 6.90 | 6.61 | 4.33 | -1.10 |
| | pH (H2O) | 7.11 | 7.78 | 7.43 | 3.22 | 0.02 |
| | $CaCO_3$ | 1.50 | 3.00 | 1.94 | 23.1 | 1.31 |
| | SOC | 2.52 | 4.45 | 3.44 | 17.4 | 0.08 |
| | $P_2O_5$ | 0.59 | 5.85 | 1.98 | 78.3 | 1.73 |
| | $K_2O$ | 25.5 | 57.3 | 36.4 | 30.2 | 0.72 |
| IOG | pH (KCl) | 5.62 | 7.01 | 6.53 | 6.46 | -1.07 |
| | pH (H2O) | 6.51 | 7.77 | 7.25 | 5.18 | -0.47 |
| | $CaCO_3$ | 1.90 | 4.34 | 2.88 | 24.5 | 0.75 |
| | SOC | 3.31 | 7.20 | 4.59 | 23.5 | 1.38 |
| | $P_2O_5$ | 21.8 | 49.4 | 34.4 | 26.1 | 0.09 |
| | $K_2O$ | 71.3 | 252 | 111.6 | 43.0 | 2.86 |

Min. - minimum; Max. - maximum; CV - coefficient of variation; Skew - skewness

The SOC content in Terra rossa under TOG was in the range of 2.52-4.45% with symmetric data distribution (skew 0.08), while Terra rossa under IOG had higher SOC content (3.31-7.20%), with asymmetric data distribution (skew 1.38). This suggests various organic fertilizations in Terra rossa soils under IOG, as well as different soil tillage systems. Several authors have noted an increase in SOC content after the application of organic amendments (Perez Lomas et al., 2010; Aranda et al., 2015; Mekki et al., 2017; Mbarek et al., 2020). Conversely, soil tillage promotes mineralization and lowers SOC content (Haddaway et al., 2017; Hashimi et al., 2022). In Terra rossa soils under TOG a lower $P_2O_5$ concentrations (0.59-5.85 mg/100 g of soil) were established, compared to soils under IOG (21.8-49.4 mg/100 g of soil). The supply of $K_2O$ was rich and very rich in soils under both management types, although Terra rossa soils under IOG contained much higher $K_2O$ concentrations compared to TOG (mean values 111.6 and 36.4 mg/100 g of soil, respectively) (Table 3).

The Regosols under both management types were highly calcareous and had an alkaline soil reaction with minor differences (mean $pH_{(KCl)}$ values of 7.28 and 7.41, respectively) (Table 4).

Table 4. Descriptive statistic for basic chemical properties of Regosol under traditional (TOG) and intensive olive groves (IOG)

| Management type | Soil property | Min. | Max. | Mean | CV | Skew |
|---|---|---|---|---|---|---|
| TOG | pH (KCl) | 7.19 | 7.40 | 7.28 | 0.90 | 0.62 |
| | pH (H2O) | 7.63 | 7.98 | 7.88 | 1.29 | -1.60 |
| | $CaCO_3$ | 15.0 | 23.0 | 18.3 | 13.9 | 0.14 |
| | SOC | 1.13 | 1.97 | 1.46 | 17.0 | 0.73 |
| | $P_2O_5$ | 0.29 | 1.96 | 1.09 | 47.7 | 0.30 |
| | $K_2O$ | 9.80 | 23.0 | 18.3 | 21.3 | -0.87 |
| IOG | pH (KCl) | 7.23 | 7.58 | 7.41 | 1.77 | -0.07 |
| | pH (H2O) | 7.73 | 8.47 | 8.26 | 2.68 | -1.71 |
| | $CaCO_3$ | 14.3 | 25.0 | 19.0 | 16.7 | 0.19 |
| | SOC | 1.39 | 2.12 | 1.79 | 12.8 | -0.07 |
| | $P_2O_5$ | 4.42 | 13.0 | 7.57 | 38.6 | 0.57 |
| | $K_2O$ | 27.5 | 66.0 | 40.4 | 25.7 | 1.54 |

Min. - minimum; Max. - maximum; CV - coefficient of variation; Skew - skewness

The SOC content was lower in Regosols under TOG compared to IOG (mean values 1.46% and 1.79%, respectively). The Regosols under TOG were poorly supplied with $P_2O_5$, while soils under IOG were moderately supplied (mean values 1.09 and 7.57 mg/100 g of soil, respectively). The $K_2O$ concentrations were also lower in Regosols under TOG than in IOG (mean values 18.3 and 40.4 mg/100 g of soil, respectively) (Table 4).

The obtained results correspond to earlier studies of Terra rossa (Durn, 1999; Vingiani et al., 2018; Miloš & Bensa, 2021) and Regosols on flysch deposits (Bogunović et al., 1999; Miloš & Bensa, 2019). Higher concentrations of $P_2O_5$, $K_2O$ and SOC in soils under IOG, in both soil types, confirmed application of mineral and

organic fertilizers in much higher doses compared to TOG.

Descriptive statistics for PTE (As, Cu, and Zn) in the studied soils are presented in Table 5. A two-way ANOVA has shown the effect of soil type, soil management, and their interaction on PTE concentrations in the studied soils (Table 6).

Table 5. Descriptive statistic for As, Cu and Zn concentrations in Terra rossa and Regosol under traditional (TOG) and intensive olive groves (IOG)

| ST | MT | Element | Min. | Max. | Mean | CV | Skew |
|---|---|---|---|---|---|---|---|
| Terra rossa | TOG | As | 21.7 | 26.6 | 23.4 | 6.6 | 0.73 |
| | | Cu | 33.9 | 85.7 | 48.9 | 30.9 | 1.74 |
| | | Zn | 114.0 | 135.5 | 124.6 | 5.7 | -0.02 |
| | IOG | As | 16.1 | 24.1 | 20.3 | 14.0 | -0.17 |
| | | Cu | 68.7 | 290.8 | 176.4 | 45.2 | 0.11 |
| | | Zn | 42.5 | 165.0 | 124.5 | 33.6 | -1.56 |
| Regosols | TOG | As | 4.50 | 6.52 | 5.58 | 10.8 | -0.18 |
| | | Cu | 19.8 | 63.5 | 37.4 | 40.5 | 0.48 |
| | | Zn | 32.3 | 66.7 | 52.7 | 24.5 | -0.67 |
| | IOG | As | 5.38 | 8.50 | 7.03 | 15.3 | -0.21 |
| | | Cu | 43.4 | 107.1 | 72.6 | 31.4 | 0.15 |
| | | Zn | 55.7 | 95.7 | 74.5 | 16.5 | 0.19 |

ST - soil type; MT - management type; Min. - minimum; Max. - maximum; CV - coefficient of variation; Skew - skewness

Soil type and the interaction effect of soil type and management significantly influenced As concentrations in the studied soils, while soil management had no significant impact (Table 6). Significantly higher As concentrations ($p$<0.05) were detected in Terra rossa soils in comparison to Regosols (16.1-26.6 and 4.50-8.50 mg/kg, respectively) (Table 5).

The As concentrations in Terra rossa soils and Regosols (16.1-26.6 mg/kg and 4.50-8.50 mg/kg, respectively) are analogous to findings from the Geochemical Atlas of Croatia (Halamić & Miko, 2009) which indicated As level over 25 mg/kg in soils derived from limestones and below 12 mg/kg in soils on flysch deposits. Peh et al. (2003) also reported higher As concentrations in Terra rossa soils than in flysch-derived soils in Istria (mean values 20.31 and 7.83 mg/kg, respectively).

The As concentrations in Terra rossa soils in current study are also in accordance with previous findings for a broader study area in Dalmatia (Miko et al., 2001; Bensa et al., 2025). Although As concentrations in soils under different land management types did not differ significantly (Table 6), Regosols under IOG contained higher As concentrations than Regosols under TOG (mean values 7.03 and 5.58 mg/kg, respectively) (Table 5). The increased level of As in agricultural soils may be attributed to the application of mineral fertilizers as emphasized by Kabata Pendias & Mukherjee (2007).

Table 6. Summary statistics of the two-way ANOVA for PTE concentrations in the studied soils

| Source of variation | SS | df | MS | $F_{exp}$ | p value | $F_{crit}$ |
|---|---|---|---|---|---|---|
| As | | | | | | |
| **Soil type** | **2417** | **1** | **2417** | **723.6** | **1.97E-25** | **4.11** |
| Soil management | 6.66 | 1 | 6.66 | 1.99 | 0.16666 | 4.11 |
| **Interaction** | **51.26** | **1** | **51.26** | **15.35** | **0.000383** | **4.11** |
| Within | 120.26 | 36 | 3.34 | | | |
| Total | 2595.4 | 39 | | | | |
| Cu | | | | | | |
| **Soil type** | **33287** | **1** | **33287** | **16.33** | **0.000267** | **4.11** |
| **Soil management** | **66183.7** | **1** | **66183.7** | **32.47** | **1.76E-06** | **4.11** |
| **Interaction** | **21258.3** | **1** | **21258** | **40.43** | **0.002648** | **4.11** |
| Within | 73376.8 | 36 | 2038.2 | | | |
| Total | 194105.9 | 39 | | | | |
| Zn | | | | | | |
| **Soil type** | **37161** | **1** | **37161** | **63.36** | **1.89E-09** | **4.11** |
| Soil management | 1171.5 | 1 | 1171.5 | 1.997 | 0.166176 | 4.11 |
| Interaction | 1204.1 | 1 | 1204.1 | 2.053 | 0.160537 | 4.11 |
| Within | 21115.3 | 36 | 586.5 | | | |
| Total | 60652.1 | 39 | | | | |

SS - the sum of squares, df - degrees of freedom, MS - mean square

The Cu concentrations in Terra rossa soils and Regosol displayed wide ranges (33.9-290.8 and 19.8-107.1 mg/kg, respectively), (Table 5). Data distributions for Cu concentrations in Regosols under both management types, as well as in Terra rossa soils under IOG were approximately symmetric (skew<0.5). However, Terra rossa soils under TOG revealed positively skewed data distribution (skew 1.74), (Table 5). This can be attributed to the fact that some low-input olive groves were planted on former vineyard soils with accumulated Cu (Miloš & Bensa, 2021), although recent use of Cu-based fungicides is rare or completely absent on these soils. Significantly higher Cu concentrations ($p$<0.05) were established in Terra rossa soils compared to Regosols, as well as in soils under IOG in comparison to TOG (Tables 5 and 6). Significantly higher Cu concentrations in Terra rossa soils than in Regosol can be linked to higher SOC and clay content (Tables 2 and 3). Soil colloids (organic matter and clay minerals) adsorb copper strongly (Parat et al., 2002). Organically complex Cu is particularly firmly bound, inhibiting its mobilization and leading to

Cu accumulation in topsoil (Cerqueira et al., 2011). Additionally, amorphous and crystalline Fe and Al oxides readily adsorb Cu (Romić et al., 2014), leading to increased Cu concentrations in Terra rossa soils. Significantly higher Cu concentrations in soils under IOG compared to TOG can be ascribed to the increased application of Cu-based fungicides. Nevertheless, the Cu concentrations in the current study are lower compared to those reported by Avramidis et al. (2019) for intensive olive groves in Greece (mean value 286.2 mg/kg).

Soil type significantly influenced Zn concentrations in the studied soils, while soil management and the interaction effect of soil type and management did not have a statistically significant impact (Table 6). Significantly higher Zn concentrations ($p$<0.05) were determined in Terra rossa soil than in Regosol (42.5-165.0 and 32.3-95.7 mg/kg, respectively), (Table 5). The obtained results are in line with previous findings for the studied soil types. Peh et al. (2003) also stated lower Zn concentrations in flysch derived soils in comparison to soils on limestones (45-130 and 59-186 mg/kg, respectively).

A similar range of Zn concentrations in a broader study area in Dalmatia was reported for the studied soil types. Miloš & Bensa (2019) established a range of 24.1-105.9 mg/kg in anthropogenic terraced soils on flysch deposits in the Kaštela bay coastal area. A study of former vineyard soils on Terra rossa in Middle Dalmatia under natural vegetation and olive groves revealed Zn mean values similar to the current study (118.1 and 138.0 mg/kg, respectively) (Bensa et al., 2025).

**Soil pollution by PTE**

All studied soils exhibited As concentrations below the maximum permissible concentrations (MPC) of 30 mg/kg (Official Gazette 71/19 (Figure 3). Obtained results are comparable to previous studies of As concentrations in a broader study area in Croatia (Lovrenčić Mikelić et al., 2013; Bensa et al., 2025) which similarly found no evidence of arsenic pollution of agricultural soils. Grattacaso et al. (2025) documented an As concentration range of 5.55-14.6 mg/kg in olive grove soils derived from various parent materials in Italy, which were not contaminated with arsenic.

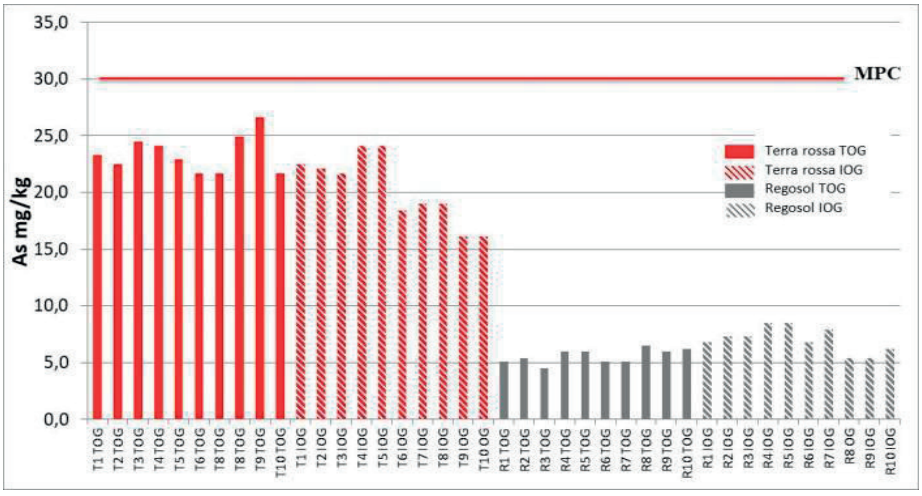



Figure 3. As concentrations in studied soils and MPC (Official Gazette 71/19)

The majority of the studied Terra rossa soils under IOG (70%) exhibited pollution by Cu, but the remaining portion (30%), along with Terra rossa soils under TOG, showed no pollution (Figure 4). The Cu concentrations in Regosols under both management types were below the MPC of 120 mg/kg (Official Gazette 71/19) (Figure 4).

Pollution of olive grove soils by Cu was reported in many studies. Avramidis et al. (2019) reported a range of 58.4 -671.6 mg/kg in various soils of Aetoliko lagoon in Greece developed

over limestones and clastic sediments, out of which 88% of samples were polluted by Cu. Similarly, Bensa et al. (2025) established pollution by Cu in 90% of the samples from Terra rossa soils under olive groves planted on former vineyard soils. However, Miloš & Bensa (2021) reported only 10% of Cu-polluted Terra rossa soils under olive groves in Middle Dalmatia. In olive groves on terraced soils on flysch deposits, Miloš & Bensa (2019) established much lower Cu concentrations (mean value 38.1 mg/kg) far below MPC, that are comparable to the current study.

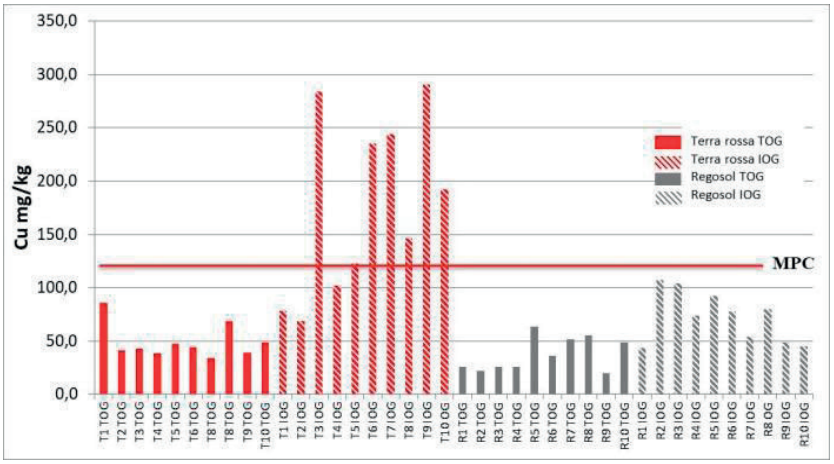



Figure 4. Cu concentrations in studied soils and MPC (Official Gazette 71/19)

The Zn concentrations in Terra rossa soils and Regosol under both management types were below the MPC of 200 mg/kg (Official Gazette 71/19) (Figure 5). Obtained results are in line with previous studies on broader study areas for Terra rosa soils (Miko et al., 2001, Bensa et al., 2025) and Regosols (Miloš & Bensa, 2019). However, previous study of olive grove soils (Doğan & Gülserr, 2020) pointed out higher Zn concentrations, and the authors stated that studied soils can be considered polluted. Additionally, Lovrenčić Mikelić et al. (2013) found elevated Zn concentrations in agricultural soils of the Kaštela Bay coastal area in Dalmatia that may be considered polluted.

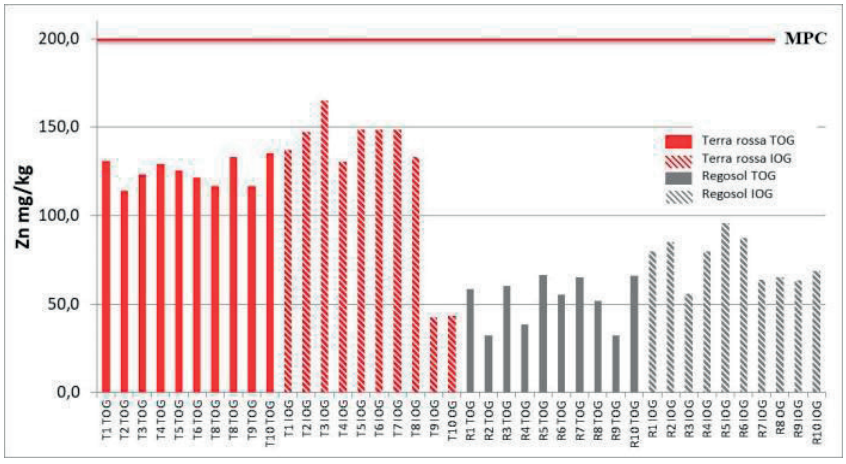



Figure 5. Zn concentrations in studied soils and MPC (Official Gazette 71/19)

## CONCLUSIONS

A study of PTE concentrations in Terra rossa soils and Regosols under traditional low-input and intensive olive groves showed significantly higher As, Cu, and Zn concentrations in Terra rossa soils compared to the Regosols. Furthermore, significantly higher Cu concentrations were found in soils under intensive olive groves than in soils under traditional low-input management. The soil management type did not significantly influence As and Zn concentrations. According to Croatian legislation (Official Gazette 71/19), only Terra rossa soils under intensive olive groves were polluted with Cu, while other studied soils were not polluted with Cu. Likewise, the studied soils were not polluted by As and Zn. The obtained results indicate the need for further, more detailed study on copper in olive grove soils in Dalmatia, especially on Terra rossa soils.

## REFERENCES

Ambrosini, V.G., Rosa, D.J. Prado, J.P.C., Borghezan, M., Melo, G.W.B., Fonsêca de Sousa Soares, C.R., Comin, J.J., Simao, D.G., & Brunetto, G. (2015). Reduction of copper phytotoxicity by liming: A study of the root anatomy of young vines (*Vitis labrusca* L.). *Plant physiology and biochemistry,* 96. 270-280.

Antoniadis, V., Shaheen, S.M., Boersch, J., Frohne, T., Du Laing, G., & Rinklebe, J. (2017). Bioavailability and risk assessment of potentially toxic elements in garden edible vegetables and soils around a highly contaminated former mining area in Germany. *Journal of Environmental Management*, 186(2). 192-200.

Aranda, V., Macci, C., Peruzzi, E., & Masciandaro, G. (2015). Biochemical activity and chemical-structural properties of soil organic matter after 17 years of amendments with olive-mill pomace co-compost. *Journal of Environmental Management*, 147. 278-285.

Avramidis, P., Barouchas, P., Dünwald, T., Unkel, I., & Panagiotaras, D. (2019). The Influence of Olive Orchards Copper-Based Fungicide Use, in Soils and Sediments - The Case of Aetoliko (Etoliko) Lagoon Western Greece. *Geosciences,* 9(6). e267.

Bellanca, A., Hauser, S., Neri, R., & Palumbo, B. (1996). Mineralogy and geochemistry of Terra Rossa soils, western Sicily: insights into heavy metal fractionation and mobility. *Science of The Total Environment*, 193(1). 57–67.

Bensa, A., & Jurković Balog, N. (2023). Humus quality of anthropogenic soils from flysch deposits. Case study: Kaštela bay, Croatia. In D. Kovačević (Ed.), *Book of proceedings XIV International Scientific Agriculture Symposium "Agrosym 2023"* (pp. 877-883). Jahorina, Bosnia and Herzegovina: Faculty of Agriculture University of East Sarajevo

Bensa, A., Jurković Balog, N., Matan, K., & Perčin, A. (2025). Potentially toxic elements (As, Cu, Pb and Zn) in former vineyard soils under olive groves and natural vegetation. *Journal of Central European Agriculture,* 26(3). 772-784.

Bogunović, M., Bensa, A., Husnjak, S., & Miloš, B. (2009). Suitability of Dalmatian soils for olive tree cultivation. *Agronomski glasnik*, 5-6. 367-404.

Bradl, H.B. (2004) Adsorption of heavy metal ions on soils and soil constituents. *Journal of Colloid and Interface Science*, 277(1). 1-18.

Cerqueira, B., Covelo, E.F., Andrade, L., & Vega F.A. (2011). The influence of soil properties on the individual and competitive sorption and desorption of Cu and Cd. *Geoderma*, 162(1-2). 20-26.

Čolak, A., & Martinović, J. (1974). *Basic soil map of Croatia 1: 50 000 section Šibenik 4*. Croatia, Split: Institute for Adriatic Crops and Karst Reclamation

Díaz-Raviña, M., Calvo de Anta, R., & Bååth, E. (2007). Tolerance (PICT) of the bacterial communities to copper in vineyard soils from Spain. *Journal of Environmental Quality,* 36(6). 1760-1764.

Doğan, B., & Gülser, C. (2020). Soil quality assessment for olive groves areas of Menderes district, Izmir-Turkey. *Eurasian Journal of Soil Science,* 9(4). 298-305.

Durn, G., Ottner, F., & Slovenec, D. (1999). Mineralogical and geochemical indicators of the polygenetic nature of terra rossa in Istria, Croatia. *Geoderma,* 91(1-2). 125-150.

Edelstein, M., & Ben-Hur, M. (2018). Heavy metals and metalloids: Sources, risks and strategies to reduce their accumulation in horticultural crops. *Scientia Horticulturae*, 234. 431-444.

Egner, H., Riehm, H., & Domingo, W.R. (1960). Untersuchungen uber die chemische Bodenanalyse als Grundlage fur die Beurteilung des Nahrstoffzustandes der Boden, II: Chemische Extractionsmetoden zu Phosphorund Kaliumbestimmung. *Kungliga Lantbrukshugskolans Annaler,* 26. 199-215.

FAO/UNESCO (1990). *Guidelines for soil description*. Rome, Italy: FAO/UNESCO

Elzahabi, M., & Yong, R.N. (2001). pH influence on sorption characteristics of heavy metal in the vadose zone. *Engineering Geology,* 60(1-4). 61-68.

Fernández-Calviño, D., Pateiro-Moure, M., Nóvoa-Muñoz, J.C., Garrido-Rodríguez, B., & Arias – Estévez, M. (2012). Zinc distribution and acid-base mobilisation in vineyard soils and sediments. *Science of the Total Environment*, 414. 470-479.

Filipčić, A. (1998). Climatic regionalization of Croatia according to W. Köppen for the standard period 1961–1990 in relation to the period 1931–1960. *Acta Geographica Croatica*, 34. 1–15.

Grattacaso, M., Canali, G., Vannini, A., Protano,G., Nannoni, F., De Lucia, V., Di Lella, L.A., Biagiotti, S., & Loppi, S. (2025). Health and ecological risk from potentially toxic elements in soils and extra virgin oils from Valdichiana Senese, Tuscany (Italy). *Journal of Plant Nutrition and Soil Science*, 188(2). 241-250.

Haddaway, N.R., Hedlund, K., & Jackson, L.E. (2017). How does tillage intensity affect soil organic carbon? A systematic review. *Environmental evidence*, 6. 30.

Halamić, J., & Miko, S. (2009). *Geochemical Atlas of the Republic of Croatia.* Zagreb, Croatia: Croatian Geological Survey

Hashimi, R., Kaneko, N., & Komatsuzaki, M. (2022). Impact of no-tillage on soil quality and crop yield in Asia: a meta-analysis. *Land, Degradation & Development*, 34(4). 1004-1018.

Hou, D., O'Connor, D., Igalavithana, A.D. *et al.* (2020). Metal contamination and bioremediation of agricultural soils for food safety and sustainability. *Nature Reviews Earth & Environment,* 1. 366–381.

Huang, B., Yuan, Z., Li, D., Zheng, M., Nie, X., & Liao, Y., (2020). Effects of soil particle size on the adsorption, distribution, and migration behaviours of heavy metal(loid)s in soil: a review. *Environmental science*: *Processes & Impacts,* 22(8). 1596-1615.

ISO (1995). *Soil quality. Determination of carbonate content. Volumetric method (ISO 10693:1995).* Geneva, Switzerland: International organization for standardization

ISO (2005). *Soil quality. Determination of pH (ISO 10390:2005)*. Geneva Switzerland: International organization for standardization

ISO (2006). *Soil quality, "Pretreatment of samples for Physico-chemical analysis" (ISO 11464:2006)* Geneva Switzerland: International organization for standardization

IUSS Working Group WRB (2015). World Reference Base for Soil Resources 2014, Update 2015. International Soil Classification System for Naming Soils and Creating Legends for Soil Maps. World Soil Resources Reports No. 106, Rome: FAO.

JDPZ (1966). *Handbook for soil analysis. Book I. Chemical methods for soil analysis*. Beograd, Yugoslavia. Yugoslav Soil Science Society

Jimenez-Ballesta, R., Bravo, S., Perez-de-los-Reyes, C., Amoros, J.A., & Garcia-Navarro, F.J. (2023). Contents and spatial distribution of arsenic in vineyard soils in Mediterranean environment. *Water, Air, Soil Pollution*, 234. e83.

Kabata Pendias, A., & Mukherjee, A.B. (2007). *Trace elements from soil to human.* Berlin, Germany: Springer Verlag

Kabata-Pendias, A., & Pendias, H. (2001) *Trace Elements in Soils and Plants. 3rd edition*. London, United Kingdom: CRC Press.

Kibblewhite, M.G., Ritz, K., & Swift M.J. (2007). Soil health in agricultural systems. *Philosophical Transactions of the Royal Society B*, 363. 685-701.

Komarek, M., Čadkova, E., Chrastny, V., Bordas, F., & Bollinger, J.C. (2010). Contamination of vineyard soils with fungicides: A review of environmental and toxicological aspects. *Environment International*, 36(1). 138-151.

Lev, S.M., Matthies, N., Snodgrass, J.W., Casey, R.E., & Ownby, D.R. (2010). Effects of zinc exposure on earthworms, *Lumbricus terrestris* in an artificial soil. *Bulletin of Environmental Contamination and Toxicology*, 84. 687-691.

Lovrenčić Mikelić, I., Oreščanin, V., & Barišić, D. (2013). Distribution and origin of major, minor, and trace elements in sediments and sedimentary rocks of the Kaštela Bay (Croatia) coastal area. *Journal of Geochemical Exploration,* 128. 1–13.

Marinčić, S., Magaš, N., & Borović, I. (1967). *Basic geological map SFRJ 1:100000, List Split i Primošten K 33-20 i K 33-21*. Zagreb, Croatia: Geological Survey Zagreb

Mbarek, H.B., Gargouri, K., Mbadra, C., Chaker, R., Souidi, Y., Abbas, O., Baeten, V., & Rigane, H. (2020). Change and spatial variability of soil organic matter humification after long-term tillage and olive mill wastewater application in arid regions. *Soil research*, 58(4). 388-399.

Mekki, A., Aloui, F., & Sayadi, S. (2017). Influence of biowaste compost amendment on soil organic carbon storage under arid climate. *Journal of the Air & Waste Management Association*, 69(7). 867-877.

Miko, S., Halamić, J., Peh, Z., & Galović, L. (2001). Geochemical baseline mapping of soils developed on diverse bedrock from two regions in Croatia. *Geologia Croatica,* 54(1). 53-118.

Miloš, B., & Bensa, A. (2019). Cd, Cu, Pb and Zn on terraced soil on flysch deposits of Kaštela bay coastal area Croatia. *Journal of Central European Agriculture*, 20(3). 974-985.

Miloš, B, & Bensa, A. (2021). The copper content in soil of olive orchards from Dalmatia, Croatia. *Eurasian Soil Science*, 54. 865-874.

Mottese, A.F., Sabatino, G., Di Bella, M. *et al.* (2020). Environmental screening for the assessment of potentially toxic elements content in PGI soils from the Mediterranean region (Italy and Turkey). *Environment Earth Science,* 79. 499.

Official Gazette (2019). *Ordinance on the protection of agricultural land from pollution* (in Croatian). Zagreb, Croatia: Government of Republic of Croatia, Ministry of Agriculture and Forestry

Pan, X., Zhang, S., Zhong, Q., Gong, G., Wang, G., Guo, X., & Xu, X. (2020). Effect of soils chemical properties and fractions of Pb, Cd and Zn on bacterial and fungal communities. *Science of The Total Environment*, 715. e 136904

Parat, C., Chaussod, R., Leveque, J., Dousset, S., & Andreux, F. (2002). The relationship between copper accumulated in vineyard calcareous and soil organic matter and iron. *European Journal of Soil Science*, 53(4). 663-670.

Pathak, V.M., Verma, V.K., Rawat, B.S., Kaur, B., Babu, N., Sharma, A., Dewali, S., Yadav, M., Kumari, R., Singh, S., Mohapatra, A., Pandey, V., Rana, N., & Cunill, J.M. (2022). Current status of pesticide effects on environment, human health and its eco-friendly management as bioremediation: A comprehensive review. *Frontiers in Microbiology*, 13. e 962619

Peh, Z., Miko, S., & Bukovec D. (2003). The geochemical background in Istrian soils. *Natura Croatica*, 12(4). 195-232.

Perez Lomas, A.L., Delgado, D., Parraga, J., Delgado, R., Almendros, G., & Aranda, V. (2010). Evolution of organic matter fractions after application of co-compost of sewage sludge with pruning waste to four

Mediterranean agricultural soils. A soil microcosm experiment. *Waste Management*, 30(10). 1957-1965.

Romić, M., Matijević L., Bakić, H., & Romić, D. (2014). Copper accumulation in vineyard soils: distribution, fractionation, and bioavailability assessment. In: M.C. Hernandez-Soriano (Ed.), *Environmental risk assessment of soil contamination* (pp 845-859). InTech

Sachdeva, S., Varshney, A., Barman, H.C., Powell, M. A., & Sahoo, P.K. (2025). Potentially toxic elements in different inorganic and organic fertilizers: A comprehensive review on global perspective and fertilizer-wise differences. *Applied Soil Ecology,* 209. e 105996.

Takahashi, G. (2015). Sample preparation for X- ray fluorescence analysis. *Rigaku Journal*, 31(1). 26-30.

Uddin, M.K. (2017). A review on the adsorption of heavy metals by clay minerals, with special focus on the past decade. *Chemical Engineering Journal,* 308. 438-462.

Vingiani, S., Di Iorio, E., Colombo C., & Terribile F. (2018). Integrated study of Red Mediterranean soils from Southern Italy. *Catena*, 168. 129-140.

Zhang, Z., Zheng, D., Xue, Z., Wu, H., & Jiang, M., (2019). Identification of anthropogenic contributions to heavy metals in wetland soils of the Karuola Glacier in the Qinghai – Tibetan plateau. *Ecological Indicators,* 98. 678-685.

Wan, Y., Liu, J., Zhuang, Z., Wang, Q., & Li, H. (2024). Heavy metals in agricultural soils: sources, influencing factors, and remediation strategies. *Toxics*, 12(1). 63.

Wyszkowski, M., & Brodowska, M.S. (2020). Content of trace elements in soil fertilized with potassium and nitrogen, *Agriculture,* 10(9). e 398.

Scientific Papers. Series E. Land Reclamation, Earth Observation & Surveying, Environmental Engineering. Vol. XV, 2026
Print ISSN 2285-6064, CD-ROM ISSN 2285-6072, Online ISSN 2393-5138, ISSN-L 2285-6064

# THE DUAL CHALLENGE OF $CO_2$ AND OZONE: INSIGHTS INTO PHOTOSYNTHESIS, VOC EMISSION AND BIOCHEMICAL RESPONSES

**Flavia BORTES[1, 2], Lucian COPOLOVICI[1, 3], Cristian MOISA[2], Andreea LUPITU[2], Dana Maria COPOLOVICI[3]**

[1]Interdisciplinary Doctoral School of "Aurel Vlaicu" University of Arad, 2 Elena Dragoi Street, Arad, Romania
[2]Institute for Interdisciplinary Research, "Aurel Vlaicu" University of Arad, 2 Elena Dragoi Street, Arad, Romania
[3]Faculty of Food Engineering, Tourism and Environmental Protection, "Aurel Vlaicu" University of Arad, 2 Elena Dragoi Street, Arad, Romania

Corresponding author email: lucian.copolovici@uav.ro

***Abstract***

*Human activities release various pollutants into the atmosphere, many of which directly affect plants. Among these pollutants are carbon dioxide ($CO_2$), which serves as the essential substrate for photosynthesis, and ozone ($O_3$), which acts as a harmful oxidant. With a particular emphasis on photosynthetic parameters, pigment content, volatile organic compound emissions, and biochemical features, this research investigates the responses of Raphanus sativus plants to increased exposure to $CO_2$ and $O_3$, focusing on three different varieties: Johanna, Helga, and Rozaria. To create conditions similar to those in the real world, the plants were grown under varying $CO_2$ concentrations (400, 800, and 1200 ppmv) and subjected to high ozone levels (100 ppb). Photosynthetic parameters were assessed through a gas exchange system, while volatile organic compound (VOC) emissions were analyzed using gas chromatography-mass spectrometry (GC-MS). Additionally, photosynthetic pigments were identified and quantified using the UHPLC-DAD system. Higher $CO_2$ levels initially enhanced net photosynthesis, but ozone severely reduced photosynthesis, leading to partial recovery after 24 hours. Ozone degraded chlorophyll a and b at all $CO_2$ concentrations, whereas zeaxanthin protected the photosynthetic system.*

***Key words****: abiotic stress, climate changes, ozone fumigation, secondary metabolites.*

## INTRODUCTION

Atmospheric carbon dioxide ($CO_2$) levels continue to rise steadily, altering photosynthetic processes, carbon allocation, and physiological responses in terrestrial ecosystems. At the Mauna Loa Observatory, the annual mean $CO_2$ concentration is projected to increase by 2.37 ± 0.55 ppm in 2026 relative to 2025, reaching a record level of 429.4 ± 0.6 ppm.

Numerous studies show that higher $CO_2$ levels stimulate photosynthetic carbon assimilation and can also modify respiration, with robust responses reported in $C_3$ species (Leakey et al., 2006; Zheng et al., 2010; 2019; Ainsworth & Long, 2021; Li et al., 2023). However, the magnitude and persistence of this growth stimulation are highly context-dependent. In particular, plant responses to elevated $CO_2$ vary with nutrient supply, and the fertilization effect often weakens as nutrient availability declines (Menge & Field, 2007; Lenka & Lal, 2012; Pandey et al., 2015). As rising $CO_2$ can increase plant nutrient demand, nutrient limitation may therefore attenuate or even offset $CO_2$-driven gains in growth, especially under low-fertility conditions (Lenka & Lal, 2012; Pandey et al., 2015; Jin et al., 2025).

Tropospheric ozone ($O_3$) is a secondary pollutant formed through sunlight-driven photochemical reactions involving volatile organic compounds (VOCs) and nitrogen oxides ($NO_x$). It has been observed that free-tropospheric ozone levels have risen since the mid-1990s, with reported rates ranging from approximately 2% to 12% per decade, depending on the region. The biggest increases are usually seen in developing and quickly industrialising areas, such as East Asia, the Persian Gulf, India, northern South America, the Gulf of Guinea, and Malaysia/Indonesia. In Europe and North America, on the other hand, trends are usually

weaker and more mixed. The health effects of ozone exposure are most reliably recorded for the respiratory and cardiovascular systems (Kim et al., 2020). However, studies indicate potential links to respiratory mortality, the onset of asthma in children, and heightened respiratory symptoms in individuals with asthma (Kim et al., 2020; Hua et al., 2025).

Ozone primarily impacts above-ground plant tissues through direct leaf uptake, yet some of the earliest detectable responses can occur below ground (Nakadera et al., 2024). Root growth may be suppressed, respiratory costs can increase, and symbiotic interactions (e.g., with mycorrhizae) may be disturbed (Agathokleous et al., 2020; Zhang et al., 2024). With sufficiently high or prolonged exposure, ozone can reduce overall plant growth and alter typical plant-parasite relationships (Duque et al., 2019). Recent open-field enrichment experiments simulating future atmospheric conditions have emphasized the complex interplay between elevated carbon dioxide and tropospheric ozone in determining crop performance. In mustard (*Brassica juncea* L.), a major oilseed crop of economic and nutritional importance, elevated $CO_2$ (550 ppm) has been reported to enhance yield by stimulating photosynthesis and increasing photosynthate accumulation. In contrast, elevated ozone (65 ppb) significantly reduces yield by impairing branching patterns, biomass production, and seed formation. Importantly, when both factors co-occur, $eCO_2$ may partially mitigate ozone-induced yield losses, suggesting a buffering interaction under future climate scenarios characterized by rising atmospheric $CO_2$ and persistent ozone pollution. Moreover, varietal differences in responsiveness indicate that selecting ozone-tolerant and $CO_2$-responsive genotypes could be critical for sustaining mustard productivity under projected climate change conditions (JawaharJothi et al., 2025). Recent studies in wheat (*Triticum aestivum* L.) indicate that stomatal $O_3$ flux - a key determinant of ozone injury - varies substantially across different $O_3$ and $CO_2$ regimes and plays a central role in shaping physiological performance and yield. In two Indian wheat cultivars differing in $O_3$ sensitivity, elevated $CO_2$ reduced stomatal $O_3$ flux and partially mitigated $O_3$-induced yield losses. Notably, the $O_3$-sensitive cultivar exhibited greater yield protection under the combined $eCO_2$ + $eO_3$ treatment, likely due to enhanced allocation of photosynthates to reproductive structures, as reflected in a higher harvest index. Moreover, yield responses were more strongly correlated with stomatal $O_3$ flux in the sensitive cultivar than in the tolerant one, underscoring the importance of flux-based approaches for predicting crop performance under future atmospheric conditions (Mishra et al., 2024).

Given the concurrent rise in atmospheric $CO_2$ and tropospheric ozone under ongoing climate change, understanding their interactive effects on crop physiology is essential. Therefore, the present study aimed to evaluate how elevated $CO_2$ (800 and 1200 ppm) modulates ozone-induced stress (100 ppb) in three radish (*Raphanus sativus* L.) cultivars (Johanna, Helga, and Rozaria). We specifically assessed photosynthetic performance, chlorophyll content, and the accumulation of antioxidant-related secondary metabolites (total phenolics and flavonoids) to determine (i) whether elevated $CO_2$ mitigates ozone-induced physiological impairment and oxidative stress, and (ii) whether genotypic variability influences stress resilience under combined atmospheric conditions.

## MATERIALS AND METHODS

The impact of increased $CO_2$ concentrations and ozone exposure on plant growth was studied by selecting and cultivating seeds from three *Raphanus sativus* (Brassicaceae) varieties. Those varieties included *Raphanus sativus* var. Johanna (Agrosel, Romania), *Raphanus sativus* var. Helga (Agrosel, Câmpia-Turzii, Romania) and *Raphanus sativus* var. Rozaria (Agrosel, Campia-Turzii, Romania).

A combination of commercial garden soil and sand was used to plant the seeds in 0.8-liter plastic containers. The plants were cultivated under artificial light from LED lamps at 800 $\mu mol\ m^{-2}s^{-1}$. We kept the daytime and nighttime temperatures at 25°C and 22°C, respectively, and the relative humidity at 65%. The light and dark cycles were set at 12 hours each. Every two days, the plants were watered until the soil was saturated. An ambient level of 400 ± 20 ppm $CO_2$ was used for plant cultivation, along with two higher levels of 800 and 1200 ppm $CO_2$,

respectively. Ozone gas at 100 ppb was used to fumigate the plants for 5 minutes.
The experiments were conducted on plants at least 4 weeks old, with at least 3 fully formed leaves throughout their growth cycle. The plants were fertilized with foliar fertilizers (Bionat Plus, Panetone SRL, Timisoara, Romania) and root fertilizers (Cropcare 11-11-21, YaraMila, Oslo, Norway).

***Determination of photosynthetic parameters***
A portable gas-exchange system (GFS-3000, Heinz Walz GmbH, Effeltrich, Germany) was employed to assess photosynthetic parameters, including $CO_2$ assimilation rate and stomatal conductance to water vapor. The device features an environment-controlled cuvette with an 8 $cm^2$ aperture and a complete-window leaf-chamber fluorimeter for sample illumination. A 4 $cm^2$ segment of radish leaf was positioned in the chamber for each measurement. All conditions remained constant except for $CO_2$, which was varied at 400, 800, and 1200 ppm during the experiment. The constant parameters were: air flow at 750 µmol $s^{-1}$, incident light at 1000 µmol $m^{-2}$ $s^{-1}$, relative humidity at 65%, and cuvette temperature at 25 °C (Niinemets et al., 2010).

***Chromatographic analysis of photosynthetic pigments***
To identify and quantify photosynthetic pigments, a high-performance liquid chromatography (HPLC) system (NEXERA 8030, Shimadzu, Japan) in conjunction with a diode-array detector (DAD) was utilized following the procedures described in (Opriş et al., 2013).

***Total Phenolic Content Determination***
The extracts were obtained from fresh leaves using static maceration in a methanol-water mixture (60-40%) for 7 days at +4°C. All extracts were filtered using a 0.45 µm PTFE membrane. The total phenolic content of radish leaves, quantified as gallic acid equivalents (GAE), was assessed utilizing the Folin-Ciocalteu method as described (Lupitu et al., 2022).

***Flavonoid Content Analysis***
Total flavonoids were quantified by the $AlCl_3$ colorimetric method as described in our previous work (Copolovici et al., 2021), measuring absorbance at 434 nm and expressing results as rutin equivalents (calibration curve: 0.02-0.4 mg $mL^{-1}$).

***Total Volatile Organic Compounds Determination***
Total VOCs were collected and analyzed by GC–MS according to the protocol described in our previous study (Lupitu et al., 2025). Briefly, VOC emissions were sampled under the experimental treatments and quantified as the sum of identified compounds.

***Statistical Analysis and Data Handling***
All analyses were performed in triplicate, and results are presented as mean ± SD. Statistical significance was assessed by two-way ANOVA followed by Tukey's post hoc test using GraphPad Prism (v. 11.0.1), with $p < 0.05$ considered significant.

## RESULTS AND DISCUSSIONS

***Photosynthetic Parameters under Elevated $CO_2$ and Ozone Exposure***
Figure 1a illustrates the effects of elevated carbon dioxide (800 and 1200 µmol $mol^{-1}$) and ozone exposure on the photosynthetic assimilation rate of the three radish cultivars (Johanna, Helga, and Rozaria). Under control conditions, assimilation rate increased progressively with rising $CO_2$ concentration in all cultivars, with the highest values recorded at 1200 µmol $mol^{-1}$, indicating strong $CO_2$ fertilization (Chen et al., 2022). Ozone exposure significantly reduced assimilation at all $CO_2$ levels, with the strongest inhibition observed at ambient $CO_2$.
However, increasing $CO_2$ partially alleviated ozone-induced suppression, particularly at 800 and 1200 µmol $mol^{-1}$, suggesting a protective interaction between elevated $CO_2$ and ozone stress. The same behaviour has been observed across different Indian mustard cultivars under strong $CO_2$ fertilization (Mishra et al., 2024). Across the three radish cultivars, both $CO_2$ concentration and ozone exposure had a significant effect on stomatal conductance ($g_s$) (Figure 1b).

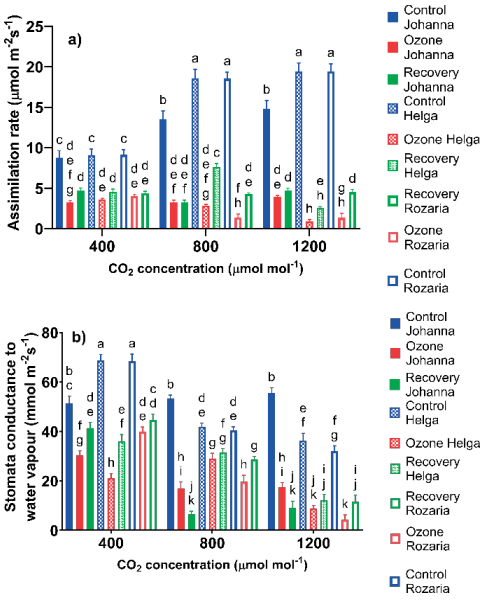



Figure 1. Effects of carbon dioxide (400, 800 and 1200 μmol mol$^{-1}$) and ozone exposure (100 ppb) on the net photosynthetic assimilation rate (μmol m$^{-2}$ s$^{-1}$) (a) and stomatal conductance to water vapour (b) in three radish (*Raphanus sativus* L.) cultivars: Johanna, Helga, and Rozaria. Plants were subjected to control, ozone stress, and recovery treatments under each $CO_2$ concentration. Bars represent mean values ± SD. Different letters indicate statistically significant differences among treatments within each $CO_2$ level ($p < 0.05$)

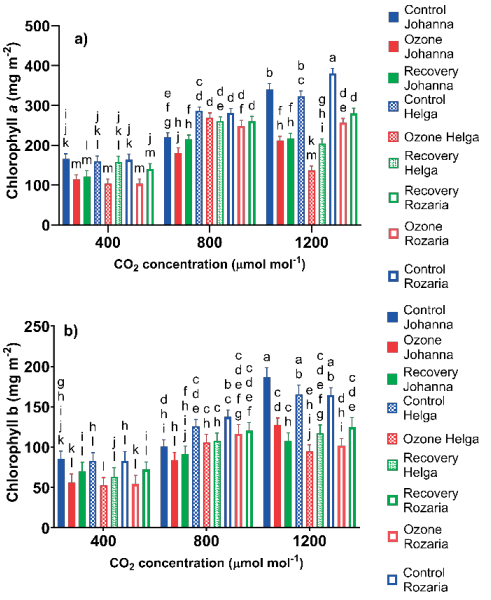



Figure 2. Effects of elevated $CO_2$ (400, 800 and 1200 μmol mol$^{-1}$) and ozone (100 ppb) on chlorophyll *a* (a) and chlorophyll *b* (b) content in three radish (*Raphanus sativus* L.) cultivars (Johanna, Helga, Rozaria). Plants were subjected to control, ozone stress, and recovery treatments under each $CO_2$ level. Bars represent mean ± SD. Different letters indicate significant differences among treatments within each $CO_2$ concentration ($p < 0.05$)

In controlled conditions, $g_s$ decreased progressively with increasing $CO_2$ concentration, indicating partial stomatal closure in response to elevated $CO_2$ levels. A lot of research has shown that similar reactions occur when $CO_2$ levels rise (Ainsworth & Rogers, 2007; Franks et al., 2013; Ainsworth & Long, 2021), as elevated $CO_2$ typically triggers a reduction in stomatal aperture and conductance through both hydraulic and ABA-related signaling, resulting in lower $g_s$ and reduced stomatal diffusion of gases (Xu et al., 2016). At higher $CO_2$ levels, the ozone-induced drops in $g_s$ were less noticeable. It indicates that $CO_2$ enrichment altered stomatal responses and may have limited the amount of ozone they could take in (Bhatia et al., 2021).

***Photosynthetic Pigment Responses***

Chlorophyll content was significantly affected by both $CO_2$ concentration and ozone exposure in all three radish cultivars (Figure 2).

Under control conditions, chlorophyll *a* and chlorophyll *b* increased progressively with rising $CO_2$ levels, indicating enhanced photosynthetic capacity under $CO_2$ enrichment. The increase in chlorophyll content under elevated $CO_2$ may be linked to increased Rubisco carboxylation capacity, suggesting coordinated upregulation of the photosynthetic machinery under $CO_2$ enrichment (Wang et al., 2025).

Both chlorophyll fractions decreased significantly upon ozone exposure, especially at ambient $CO_2$ levels, indicating oxidative damage to the photosynthetic apparatus. However, the ozone-induced decrease in chlorophyll content was lessened under high $CO_2$, suggesting a buffering or protective effect of $CO_2$ enrichment (Férriz et al., 2025).

Among cultivars, Johanna and Helga generally maintained higher chlorophyll levels under combined treatments than Rozaria, which showed a more pronounced decline under ozone stress, especially at lower $CO_2$ concentrations.

Recovery treatments partially restored chlorophyll content, although values did not always reach control levels. It is still not clear whether the higher chlorophyll content is due to structural changes in the photosynthetic apparatus or to slower pigment breakdown. The interaction between increased carbon assimilation and modulation of oxidative stress is likely to affect the stability of photosynthetic pigments under multiple atmospheric stressors (Ainsworth & Rogers, 2007; Ainsworth & Long, 2021).

### *Antioxidant Compounds: Total Phenolics and Flavonoids*

The total phenolic content was significantly influenced by both $CO_2$ concentration and ozone exposure among the three radish cultivars (Figure 3a).

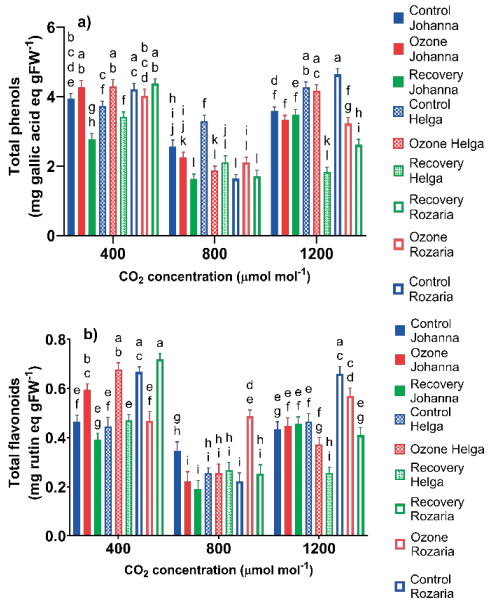



Figure 3. Effects of $CO_2$ concentration (400, 800 and 1200 µmol $mol^{-1}$) and ozone exposure (100 ppb) on (a) total phenolic content and (b) total flavonoid content in three radish (*Raphanus sativus* L.) cultivars (Johanna, Helga and Rozaria) under control, ozone and recovery treatments. Values are means ± SD (n = 3). Different letters indicate significant differences among treatments within each $CO_2$ level (two-way ANOVA followed by Tukey's test, $p < 0.05$)

Ozone treatment typically increased phenolic accumulation relative to control plants, especially under ambient carbon dioxide, suggesting the activation of antioxidant defense mechanisms in response to oxidative stress (Winyard et al., 2005).

Phenolic levels exhibited greater variability among cultivars under elevated $CO_2$ conditions. In some cases, $CO_2$ enrichment alone led to a marginal decrease in phenolic concentration compared to ambient conditions. Conversely, under the combined $eCO_2$ and $eO_3$ treatment, phenolic accumulation was consistently higher than in control plants, yet frequently lower than in conditions with ozone alone. This implies that increased $CO_2$ may partially influence ozone-induced oxidative stress responses (Bhatia et al., 2021). There were clear differences between cultivars. For example, Johanna showed the strongest increase in phenolics under ozone stress, while Rozaria showed a more moderate response.

The increase in total phenolics during ozone exposure indicates the activation of secondary metabolic pathways that are responsible for scavenging reactive oxygen species (ROS) (Jin et al., 2025). Phenolic compounds are important non-enzymatic antioxidants that help protect membranes and maintain the stability of the photosynthetic apparatus under high oxidative stress (Tamaoki, 2008; Piechowiak et al., 2026). The diminished phenolic response in elevated $CO_2$ conditions may indicate reduced oxidative stress, potentially resulting from decreased stomatal ozone absorption and enhanced carbon availability, which facilitate metabolic equilibrium. The interplay between carbon enrichment and ozone stress seems to govern the equilibrium between growth and defense allocation in radish cultivars.

For all three radish cultivars, $CO_2$ concentration and ozone exposure significantly affected total flavonoid content (Figure 3b). Compared with control plants, ozone treatment generally increased flavonoid accumulation, especially under ambient $CO_2$, suggesting that antioxidant defense mechanisms were activated in response to oxidative stress. At elevated $CO_2$ levels, flavonoid levels varied across cultivars. In some instances, $CO_2$ enrichment alone did not significantly enhance flavonoid content relative to ambient conditions; however, under the combined $eCO_2$ + $eO_3$ treatment, flavonoid accumulation persisted at elevated levels,

indicating that secondary metabolism remained active under stress.

Helga had the highest flavonoid levels when exposed to ozone, especially at 400 and 800 µmol mol$^{-1}$ $CO_2$. Rozaria, on the other hand, had lower values when exposed to both stress treatments. Johanna's responses were in the middle. These results indicate that flavonoid biosynthesis represents an important component of the oxidative stress response in radish, and its modulation under elevated $CO_2$ suggests a complex balance between carbon availability and defense allocation. These findings demonstrate that flavonoid biosynthesis is a significant aspect of the oxidative stress response in plants, and its alteration in response to increased $CO_2$ indicates a complex equilibrium between carbon availability and defense distribution (Falcone Ferreyra et al., 2012; Ibrahim & Jaafar, 2012).

### *Volatile organic compound emissions*

Ozone exposure significantly affected total VOC emissions, with clear patterns that depended on cultivar and $CO_2$ levels. Under controlled conditions, VOC emissions remained relatively low across all $CO_2$ levels (Figure 4). Conversely, ozone treatment resulted in a significant increase in total VOCs across all cultivars, consistent with the activation of stress-related volatile emission pathways under oxidative stress.

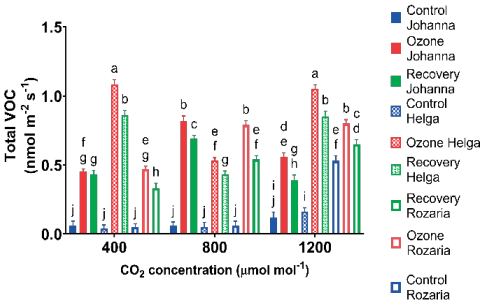



Figure 4. Effects of $CO_2$ concentration (400, 800 and 1200 µmol mol$^{-1}$) and ozone exposure (100 ppb) on total VOC emissions in three radish (*Raphanus sativus* L.) cultivars (Johanna, Helga and Rozaria) under control, ozone and recovery treatments. Values are means ± SD (n = 3). Different letters indicate significant differences among treatments within each $CO_2$ level (two-way ANOVA followed by Tukey's test, $p < 0.05$)

Higher levels of $CO_2$ altered VOC responses to ozone. At 800 and 1200 µmol mol$^{-1}$ $CO_2$, VOC emissions under ozone differed from those under ambient $CO_2$. This suggests that the amount of carbon available and the way stomata function when $CO_2$ levels are high affect volatile release. Recovery treatments showed VOC levels midway between those of plants stressed by ozone, indicating that the plants partially recovered physiological status after the stress was removed, but differences between cultivars persisted. In general, the data show that total VOC emissions are a good indicator of ozone stress and that higher $CO_2$ levels can alter this response, with differences among Johanna, Helga, and Rozaria.

Total VOC emissions increased significantly in the presence of ozone, supporting the idea that $O_3$ is a strong oxidative stressor that triggers the release of stress-related volatiles used for defense and signaling (Li et al., 2017). The modulation of this response under elevated $CO_2$ suggests that the two atmospheric drivers do not exert simply additive effects, but rather interact in a more complex manner. This is in line with evidence that multiple concurrent stresses can significantly alter the size and composition of plant VOC emissions (Holopainen & Gershenzon, 2010). One possible explanation is that $CO_2$-Induced stomatal regulation reduces the amount of $O_3$ that stomata take in, thereby lowering oxidative pressure within the plant and partially blocking ozone-driven volatile signaling. However, changes in carbon availability under elevated $CO_2$ may still allow the formation of *de novo* VOCs (Himanen et al., 2009; Holopainen & Gershenzon, 2010).

## CONCLUSIONS

Higher levels of $CO_2$ improved the physiological performance of radishes by increasing net $CO_2$ assimilation and raising the levels of chlorophyll a and b in all cultivars. This is consistent with a $CO_2$ fertilization response. On the other hand, exposure to 100 ppb of ozone clearly induced oxidative stress, lowering chlorophyll content and assimilation, and altering stomatal conductance. This showed that the photosynthetic machinery was not working properly.

Significantly, increased $CO_2$ levels (800-1200 ppm) partially alleviated ozone damage, as evidenced by a diminished ozone-induced reduction in assimilation, stomatal conductance, and pigment pools relative to ambient $CO_2$, indicating a buffering interaction among concurrent atmospheric change factors. Ozone also triggered secondary metabolism associated with antioxidants, as evidenced by higher levels of total phenolics and flavonoids. The fact that these levels changed when $CO_2$ levels rose suggests that the balance between growth and defence allocation is changing. Total VOC emissions rose sharply when ozone was present, and $CO_2$ levels also affected them. This shows that volatile release is a sensitive indicator of ozone stress, and its strength depends on how $CO_2$ affects stomatal regulation and carbon availability. Lastly, cultivar-specific response patterns (for example, Johanna had a stronger phenolic induction, Helga had a higher flavonoid accumulation, and Rozaria was generally more sensitive under combined stress) show that there is a lot of genotypic variability and support the idea that cultivar selection could help crops do well in the future when $CO_2$ levels are rising.

## ACKNOWLEDGEMENTS

This work was supported by a grant from the Ministry of Research, Innovation, and Digitization, CNCS -UEFISCDI, project number PN-IV-P8-8.3-ROMD-2023-0022, within PNCDI IV.

## REFERENCES

Agathokleous, E., Feng, Z., Oksanen, E., Sicard, P., Wang, Q., Saitanis, C.J., Araminiene, V., Blande, J.D., Hayes, F., Calatayud, V., Domingos, M., Veresoglou, S.D., Peñuelas, J., Wardle, D.A., De Marco, A., Li, Z., Harmens, H., Yuan, X., Vitale, M., & Paoletti, E. (2020). Ozone affects plant, insect, and soil microbial communities: A threat to terrestrial ecosystems and biodiversity. *Science Advances 6*, eabc1176.

Ainsworth, E.A., & Long, S.P. (2021). 30 years of free-air carbon dioxide enrichment (FACE): What have we learned about future crop productivity and its potential for adaptation? *Global Change Biology, 27*, 27-49.

Ainsworth, E.A., & Rogers, A. (2007). The response of photosynthesis and stomatal conductance to rising $CO_2$: mechanisms and environmental interactions. *Plant, Cell & Environment, 30*, 258-270.

Bhatia, A., Mina, U., Kumar, V., Tomer, R., Kumar, A., Chakrabarti, B., Singh, R.N., & Singh, B. (2021). Effect of elevated ozone and carbon dioxide interaction on growth, yield, nutrient content and wilt disease severity in chickpea grown in Northern India. *Heliyon, 7*(1). e06049.

Chen, C., Riley, W.J., Prentice, I.C., & Keenan, T.F. (2022). $CO_2$ fertilization of terrestrial photosynthesis inferred from site to global scales. *Proceedings of the National Academy of Sciences, 119*, e2115627119.

Copolovici, L., Lupitu, A., Moisa, C., Taschina, M., & Copolovici, D.M. (2021). The effect of antagonist abiotic stress on bioactive compounds from basil (*Ocimum basilicum*). *Applied Sciences, 11*, 9282.

Duque, L., Poelman, E.H., & Steffan-Dewenter, I. (2019). Plant-mediated effects of ozone on herbivores depend on exposure duration and temperature. *Scientific Reports, 9*, 19891.

Falcone Ferreyra, M.L., Rius, S., & Casati, P. (2012). Flavonoids: biosynthesis, biological functions, and biotechnological applications. *Frontiers in Plant Science, 3,* 222.

Férriz, M., Aranda, I., Gea-Izquierdo, G., & Martin-Benito, D. (2025). $CO_2$ enrichment does not alter the relative physiological performance of seedlings of two close pine species under water stress. *European Journal of Forest Research, 144*, 591-606.

Franks, P.J., Adams, M.A., Amthor, J.S., Barbour, M.M., Berry, J.A., Ellsworth, D.S., Farquhar, G.D., Ghannoum, O., Lloyd, J., McDowell, N., Norby, R.J., Tissue, D.T., & von Caemmerer, S. (2013). Sensitivity of plants to changing atmospheric $CO_2$ concentration: from the geological past to the next century. *New Phytologist*, *197*, 1077-1094.

Himanen, S.J., Nerg, A.-M., Nissinen, A., Pinto, D.M., Stewart Jr, C.N., Poppy, G.M., & Holopainen, J.K. (2009). Effects of elevated carbon dioxide and ozone on volatile terpenoid emissions and multitrophic communication of transgenic insecticidal oilseed rape (*Brassica napus*). *New Phytologist*, *181*, 174-186.

Holopainen, J.K., & Gershenzon, J. (2010). Multiple stress factors and the emission of plant VOCs. *Trends in Plant Science 15*, 176-184.

Hua, Q., Meng, X., Gong, J., Qiu, X., Shang, J., Xue, T., & Zhu, T. (2025). Ozone exposure and cardiovascular disease: A narrative review of epidemiology evidence and underlying mechanisms. *Fundamental Research 5*, 249-263.

Ibrahim, M.H., & Jaafar, H.Z.E. (2012). Impact of elevated carbon dioxide on primary, secondary metabolites and antioxidant responses of *Eleais guineensis* Jacq. (oil palm) seedlings. *Molecules 17*, 5195-5211.

JawaharJothi, G., Sharma, D.K., Kovilpillai, B., Bhatia, A., L. Antille, D., Padnilay Chidambaram, P., Vasudev, S., Taak, Y., Pradipsingh Pardeshi, P., & Kumar, S. (2025). Could elevated $CO_2$ ameliorate the negative effects of elevated $O_3$ on yield and quality of mustard (*Brassica juncea* (L.))? *Ozone: Science & Engineering 47*, 393-410.

Jin, Z., Tan, J., Zhang, X., Li, X., Guan, W., Liu, P., & Chen, A. (2025). Ozone Treatment Modulates Reactive Oxygen Species Metabolism Regulation and Enhances Storage Quality of Kiwifruit During Cold Storage. *Horticulturae 11*, 911.

Kim, S.-Y., Kim, E., & Kim, W.J. (2020). Health effects of ozone on respiratory diseases. *Tuberculosis and Respiratory Diseases 83*, S6-S11.

Leakey, A.D.B., Uribelarrea, M., Ainsworth, E.A., Naidu, S.L., Rogers, A., Ort, D.R., & Long, S.P. (2006). Photosynthesis, productivity, and yield of maize are not affected by open-air elevation of $CO_2$ concentration in the absence of drought. *Plant Physiology 140*, 779-790.

Lenka, N.K., & Lal, R. (2012). Soil-related constraints to the carbon dioxide fertilization effect. *Critical Reviews in Plant Sciences 31*, 342-357.

Li, F., He, C., Chang, Z., Ma, C., Yu, J., Liu, L., Zhang, Y., & Hao, L. (2023). Effects of elevated carbon dioxide on plant growth and leaf photosynthesis of annual ryegrass along a phosphorus deficiency gradient. *Frontiers in Plant Science 14,* 1271262.

Li, S., Harley, P.C., & Niinemets, Ü. (2017). Ozone-induced foliar damage and release of stress volatiles is highly dependent on stomatal openness and priming by low-level ozone exposure in Phaseolus vulgaris. *Plant, Cell & Environment 40*, 1984-2003.

Lupitu, A., Bortes, F., Moisa, C., Copolovici, D.M., & Copolovici, L. (2025). The impact of *Eurydema Ventralis* infestation on *Brassica oleracea* var. *Botrytis* grown at Different $CO_2$ concentrations in Romania. *Journal of Soil Science and Plant Nutrition 25*, 9863-9877.

Lupitu, A., Moisa, C., Gavrilaş, S., Dochia, M., Chambre, D., Ciutină, V., Copolovici, D.M., & Copolovici, L. (2022). The influence of elevated $CO_2$ on volatile emissions, photosynthetic characteristics, and pigment content in *Brassicaceae* plants species and varieties. *Plants 11*.

Menge, D.N.L., & Field, C.B. (2007). Simulated global changes alter phosphorus demand in annual grassland. *Global Change Biology 13*, 2582-2591.

Mishra, A.K., Gupta, G.S., Agrawal, S.B., & Tiwari, S., (2024). Understanding the impact of elevated $CO_2$ and $O_3$ on growth and yield in Indian wheat cultivars: Implications for food security in a changing climate. *Environmental Pollution 362*, 124990.

Nakadera, M., Endo, W., Oi, N., Yagita, A., Tanaka, R., Izuta, T., & Watanabe, M. (2024). Differences of stomatal ozone uptake in leaves of mature trees and seedlings of *Zelkova serrata*. *Environmental Research 261*, 119673.

Niinemets, Ü., Copolovici, L., & Hüve, K. (2010). High within-canopy variation in isoprene emission potentials in temperate trees: implications for predicting canopy-scale isoprene fluxes. *Journal of Geophysical Research - Biogeosciences 115*, G04029.

Opriş, O., Copaciu, F., Soran, M.L., Ristoiu, D., Niinemets, Ü., & Copolovici, L. (2013). Influence of nine antibiotics on key secondary metabolites and physiological characteristics in *Triticum aestivum*: leaf volatiles as a promising new tool to assess toxicity. *Ecotoxicology and Environmental Safety 87*, 70-79.

Pandey, R., Zinta, G., AbdElgawad, H., Ahmad, A., Jain, V., & Janssens, I.A. (2015). Physiological and molecular alterations in plants exposed to high $CO_2$ under phosphorus stress. *Biotechnology Advances 33*, 303-316.

Piechowiak, T., Kapusta, I., Rak, M., & Balawejder, M. (2026). Ozone treatment enhances antioxidant status and energy metabolism in radish (*Raphanus sativus*) aprouts. *Food and Bioprocess Technology 19*, 52.

Tamaoki, M., (2008). The role of phytohormone signaling in ozone-induced cell death in plants. *Plant Signaling & Behavior 3*, 166-174.

Wang, L., Chen, Y., Jin, H., Huang, S., Wu, H., Cheng, J., Rong, J., Zhang, Y., Chen, Y., Wang, J., Jin, S., & Li, X. (2025). Enhancing photosynthesis and starch accumulation enable *Torreya grandis* seedlings to benefit from $CO_2$ enrichment and warming. *Industrial Crops and Products 237*, 122178.

Winyard, P.G., Moody, C.J., & Jacob, C. (2005). Oxidative activation of antioxidant defence. *Trends in Biochemical Sciences 30*, 453-461.

Xu, Z., Jiang, Y., Jia, B., & Zhou, G. (2016). Elevated-$CO_2$ response of stomata and its dependence on environmental factors. *Frontiers in Plant Science 7,* 657.

Zhang, K., Zentella, R., Burkey, K.O., Liao, H.-L., & Tisdale, R.H. (2024). Long-term tropospheric ozone pollution disrupts plant-microbe-soil interactions in the agroecosystem. *Global Change Biology 30*, e17215.

Zheng, Y., Li, F., Hao, L., Yu, J., Guo, L., Zhou, H., Ma, C., Zhang, X., & Xu, M. (2019). Elevated $CO_2$ concentration induces photosynthetic down-regulation with changes in leaf structure, non-structural carbohydrates and nitrogen content of soybean. *BMC Plant Biology 19*, 255.

Zheng, Y., Xie, Z., Rimmington, G.M., Yu, Y., Gao, Y., Zhou, G., An, P., Li, X., Tsuji, W., & Shimizu, H. (2010). Elevated $CO_2$ accelerates net assimilation rate and enhance growth of dominant shrub species in a sand dune in central Inner Mongolia. *Environmental and Experimental Botany 68*, 31-36.

Scientific Papers. Series E. Land Reclamation, Earth Observation & Surveying, Environmental Engineering. Vol. XV, 2026
Print ISSN 2285-6064, CD-ROM ISSN 2285-6072, Online ISSN 2393-5138, ISSN-L 2285-6064

# MOISTURE, LIPID CONTENT, AND MERCURY IN FRESHWATER FISH MUSCLE: INDICATORS OF ECOLOGICAL CONDITION IN THE LOWER DANUBE RIVER

**Andreea-Miruna CODREANU[1], Ștefania-Adelina MILEA[1], Cristina Mihaela LUNTRARU[2], Alin Constantin DÎRȚU[3], Cătălina ITICESCU[1, 4]**

[1]"Dunărea de Jos" University of Galați, REXDAN Research Infrastructure,
98 George Coșbuc Street, Galați, Romania
[2]SC Hofigal Export Import SA, 2 Intrarea Serelor Street, District 4, Bucharest, Romania
[3]"Alexandru Ioan Cuza" University of Iași, Faculty of Chemistry, 11 Carol I Blvd, Iași, Romania
[4]"Dunărea de Jos" University of Galați, Faculty of Sciences and Environment,
111 Domnească Street, Galați, Romania

Corresponding author email: miruna.codreanu@ugal.ro

***Abstract***

*The composition of fish muscle is influenced by environmental factors and can be used to assess the status of the aquatic ecosystems. This study explores the relationship between moisture and lipid content in the muscle tissue of selected freshwater fish species from the Lower Danube River, aiming to evaluate their potential as ecological indicators. Eight edible fish species, asp, vimba bream, perch, wels catfish, zander, pontic shad, common roach, and common carp, were included in the analysis. Moisture content was determined by freeze-drying and total lipid content was assessed on the dry fish using the Soxhlet extraction method. Lipid content was expressed both as dry and wet weight to allow an extensive interpretation in a biological and environmental context. Total mercury concentrations were also determined in fish samples, ranging from 0.15 ± 0.02 mg/kg in pontic shad to 1.04 ± 0.62 mg/kg in wels catfish. The results for moisture content ranged from 73.67 ± 2.52 % to 81.25 ± 1.06%, while lipid content (expressed as wet weight) showed high variability among species (0.4 ± 0.00% to 17.67 ± 5.42%). A strong inverse correlation was observed between moisture and lipid content (r ≈ -0.929), which suggests that fish muscle composition reflects differences in energy storage and environmental conditions. The findings of this study support the use of biochemical parameters as complementary indicators in aquatic environmental assessment, particularly in freshwater systems subject to environmental variability.*

***Key words:*** *Danube River, freshwater fish, freeze-drying, lipids, mercury.*

## INTRODUCTION

Aquatic ecosystems evaluation is based on the integration of physicochemical and biological indicators that show both natural diversity and environmental stresses. This evaluation is closely linked to water quality monitoring, which provides essential information regarding the environmental status and the anthropic pressures, especially for the large rivers like Danube (Iticescu et al., 2014). In addition, environmental monitoring is strongly connected to broader sustainability goals and policy frameworks (Georgescu et al., 2025). Moreover, recent studies emphasize the importance of conventional and emerging pressures on water ecosystems, highlighting their role in supporting water security and the socio-economic development (Goswami & Bisht, 2017; Wang et al., 2024; Zlati et al., 2024; Cadieux, 2026; Moon et al., 2026).

Within this perspective, identifying complementary indicators capable of evaluating the ecosystem regarding the environment quality and trophic dynamics remains a key objective in environmental research and monitoring.

Even though physicochemical characteristics provide an overview of water quality and biological communities are an indicator of long-term responses to ecological changes, biochemical parameters of fish tissues can reflect environmental changes over time and contribute to the assessment of the physiological state of the aquatic organisms. Therefore, fish are considered relevant bioindicators of

ecological condition in water environments due to their sensitivity to environmental pressures and can be complementary to physicochemical and biological monitoring by integrating trophic interactions and environmental quality (Maceda-Veiga & De Sostoa, 2011; Wannas & Mohammed, 2025). The principal constituents of fish muscle are generally water, lipids and proteins, while carbohydrates and ash are present in low levels. Since the protein concentrations tend to vary less than the lipid content, fluctuations in fat content are linked to interchanges between water and lipid fractions. As a consequence, an inverse relationship between moisture and lipid content in fish species was reported, with greater lipid depositions corresponding to lower water content (Naeem & Salam, 2010; Ahmed et al., 2022; Warret Rodrigues et al., 2023). Lipid and moisture content can offer valuable insight about energy storage and other physiological characteristics and may reflect the adaptive response to environmental conditions in freshwater ecosystems like the Lower Danube River (Petricorena, 2014; Martin et al., 2017; Ahmed et al., 2022).

Furthermore, the assessment of total mercury can be included alongside fish muscle composition, as mercury is known for its persistence in the aquatic ecosystems, and for its bio-accumulative and bio-magnification character across the trophic chain (Tolkou et al., 2023; Rock et al., 2025). Therefore, monitoring total mercury in fish from different trophic levels can give additional data on the ecosystem quality (Zillioux, 2015; Bernal-Alviz et al., 2025).

The selected fish species are representative for different trophic positions and feeding habits within the lower Danube River, and permit a more extensive evaluation of the biochemical interspecific variation in fish muscle. The study includes omnivorous species such as common carp (*Cyprinus carpio carpio*) and common roach (*Rutilus rutilus*); benthic-omnivorous vimba bream (*Vimba vimba*); predatory species including perch (*Perca fluviatilis*), pontic shad (*Alosa immaculata*), asp (*Leuciscus aspius*), zander (*Sander lucioperca*), and wels catfish (*Silurus glanis*) (Okgerman et al., 2013; Gerasimov & Strel'nikova, 2016; Mazlum & Akgumus, 2019; Olsson, 2019; Pfauserová et al., 2019; Nahon et al., 2020; Santos et al., 2025).

The aim of the present study was to evaluate the relationship between moisture and lipid content in muscular tissue of selected freshwater fish species from the Lower Danube River and to investigate their potential as indicators of ecological status. Furthermore, mercury concentrations were assessed to provide supplementary information on the extent of metal contamination in the aquatic environment. This work highlights the importance of fish muscle composition in ecological evaluation. It also provides preliminary data for the Lower Danube River, contributing to the relatively limited research regarding the use of simple compositional analysis in freshwater monitoring.

## MATERIALS AND METHODS

Fish samples were collected in spring 2023 from local fishermen in the Lower Danube and Danube Delta regions. The biometric characteristics of the analysed fish were as follows: asp, total length 37.00 cm and body weight 386.00 g (n=1); vimba bream, 44.40 ± 31.89 cm and 265.70 ± 34.02 g (n=3); perch, 22.33 ± 1.51 cm and 169.33 ± 22.05 g (n=3); wels catfish, 74.83 ± 3.67 cm and 2916.67 ± 633.11 g (n=2); zander, 23.35 cm and 151.50 g (n=1); pontic shad, 25.93 ± 1.40 cm and 167.67 ± 21.94 g (n=3); common roach, 30.00 cm and 290.00 g (n=1); common carp, 59.10 ± 4.45 cm and 2800 ± 1255.99 g (n=3). Two of the eight analysed species are represented in Figure 1. All specimens were eviscerated immediately after collection. Muscle samples were collected from the dorsal white muscle. The fish muscles were frozen, and stored at –20°C until analysis.

Ten grams of each muscle sample were first pre-frozen at −80°C for 24 hours, then freeze-dried for 24 hours at a condenser temperature of −80°C and a vacuum pressure of 200 Pa to remove all water content, allowing accurate determination of the moisture level in the fish tissues (Figure 2); the lyophilization was performed on a Table Top Freeze Dryer BK-FD10PT (BioBase, Shandong, China).



Figure 1. Examples of analysed species: perch and Pontic shad

Moisture was calculated by the gravimetric method using the formula:

$$\text{Moisture (\%)} = \frac{wet\ weight - dry\ weight}{wet\ weight} \times 100$$

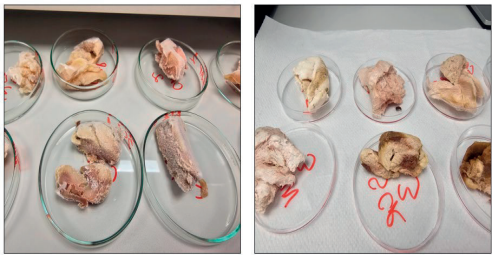


Figure 2. Fish muscle before and after freeze-drying

Subsequently, lipid determination was carried out on the dried samples. The total lipids were analysed by the modified Soxhlet method, with 30 minutes of hot extraction, 60 minutes of rinsing time and 30 minutes of solvent recovery. The samples were extracted with 150 mL n-hexane, with the heating block set to 180°C. The samples were weighed in the cellulose thimble. Each extraction beaker contained 2 boiling stones to ensure constant boiling. The extract was evaporated to dryness, permitting the gravimetric determination of fat content. The total lipid content was determined using a Soxtherm SOX414 (C. Gerhardt Analytical Systems, Königswinter, Germany) fully automated extraction unit. Lipids were expressed on dry weight, using the gravimetric method:

$$\text{Lipids (dry weight, \%)} = \frac{final\ mass - initial\ mass}{sample\ mass} \times 100$$

The results were further used for conversion to wet weight:

$$\text{Lipids (wet weight, \%)} = \text{Lipids (dry weight, \%)} * (1 - \text{Moisture}/100)$$

The data have been statistically processed and interpreted in Python (version 3.12) using the pandas, matplotlib, and SciPy libraries within the Spyder IDE.

Pearson's Correlation analysis was used to evaluate the relationship between lipids content and moisture.

Approximately 50 milligrams of fresh, non-lyophilized muscle was weighed in nickel sample boat and submitted to the analysis using DMA-80 evo Direct Mercury Analyzer (Milestone, Sorisole, Italy). Samples were analysed directly without previous digestion. Total mercury (THg) was assessed by thermal decomposition of the sample, followed by catalytic removal of by-products, gold amalgamation and quantification by atomic absorption spectroscopy (AAS).

One-way statistical analysis (ANOVA) was performed using Data Analysis ToolPak in Microsoft Excel (Microsoft Corporation, WA, USA) to evaluate differences among species regarding total mercury concentrations, lipids content and moisture. Only fish with duplicate or triplicate measurements were included in the analysis. Statistical significance was accepted at $p<0.05$.

## RESULTS AND DISCUSSIONS

Results for moisture and lipid content in freshwater fish from the Danube River are presented in Table 1.

Moisture content was fairly constant among the species, ranging from 73.67 ± 2.52 % to 81.25 ± 1.06 %; these results are in accordance with a study conducted by Xia (2025) on freshwater fish. However, Pontic shad showed lower levels of 65.70 ± 8.00%, consistent with its high lipid content.

One-way ANOVA indicated significant differences in moisture content among fish species ($F = 5.09$; $p = 0.024$).

The differences in total lipid content observed between the analysed fish species can indicate different feeding behaviour, distinct habitats and environmental characteristics in the Lower Danube River ecosystem. Lipids can be used as an indicator of energy storage and fish physiological characteristics and can be

influenced by food resource availability and trophic interactions. Fish species that have increased lipid concentrations have access to more energy-rich food resources, whereas decreased lipid levels can indicate accelerated metabolism or environmental pressures.

Pontic shad showed the highest lipid levels, 17.67 ± 5.42% wet weight (ww), which can reflect energy reserves for migration (Misir et al., 2016). Common carp also showed relatively high lipid concentrations of 7.57 ± 2.34% ww, due to their omnivorous feeding behaviour and efficient accumulation of energy reserves (Ayalew et al., 2025). Lower lipid levels were exhibited by perch (0.4 ± 0.00% ww), zander (0.6% ww) and asp (0.7% ww), which can be explained by their predatory feeding character, intense swimming activity or habitat conditions. These species use most of their energy for locomotion, resulting in lower lipid deposition in their fish muscle tissue. Intermediate lipid values were obtained for common roach, wels catfish and vimba bream (2.1% ww, 2.35 ± 0.35% ww, 3.13 ± 0.91% ww, respectively). These results indicate species-specific feeding behaviour and resource management (Łuczyńska et al., 2020; Simeanu et al., 2022). Lipid levels remained highest in Pontic shad when expressed on a dry weight basis, suggesting that inter-species differences were present even after normalising for moisture content.

These findings suggest that fish muscle composition, especially lipid and moisture content, indicate species-specific adaptive response and can represent useful information on energy usage, availability of food resources, and ecological stress, supporting its use as a bioindicator within the Lower Danube River ecosystem.

One-way ANOVA revealed significant differences in lipid content between fish species ($F = 14.33$; $p = 0.001$).

Table 1. Moisture and lipid content in freshwater fish from the Danube River

| Fish species | Abbreviation | Number of specimens | Moisture (%) | Total lipids (% dry weight) | Total lipids (% wet weight) |
|---|---|---|---|---|---|
| common carp (*Cyprinus carpio carpio*) | CRP | 3 | 73.67 ± 2.52 | 28.77 ± 8.93 | 7.57 ± 2.34 |
| perch (*Perca fluviatilis*) | BIB | 3 | 78.90 ± 1.04 | 1.87 ± 0.15 | 0.4 ± 0.00 |
| vimba bream (*Vimba vimba*) | MOR | 3 | 76.77 ± 2.05 | 13.33 ± 2.95 | 3.13 ± 0.91 |
| pontic shad (*Alosa immaculata*) | SCR | 3 | 65.70 ± 8.00 | 51.03 ± 5.67 | 17.67 ± 5.42 |
| wels catfish (*Silurus glanis*) | SMN | 2 | 81.25 ± 1.06 | 12.65 ± 1.06 | 2.35 ± 0.35 |
| zander (*Sander lucioperca*) | SL | 1 | 79.9 | 3.0 | 0.6 |
| common roach (*Rutilus rutilus*) | BAB | 1 | 77.7 | 9.6 | 2.1 |
| asp (*Leuciscus aspius*) | AVAT | 1 | 78.0 | 3.0 | 0.7 |

The negative correlations between moisture and lipid content across the analysed muscles (wet weight basis; r=-0.929, n=17, $p<0.001$) are represented in Figure 3. The linear regression equation was y=-1.020x+82.550, $R^2$=0.864, indicating a statistically significant inverse relationship. As lipid levels increase, moisture content decreases as a result of intracellular water being replaced by high-energy lipidic deposits (Huss, 1995). The obtained results align with the well-documented moisture-lipid relationship described for muscle (Zhang et al., 2014; Matos et al., 2019; Ahmed et al., 2022).

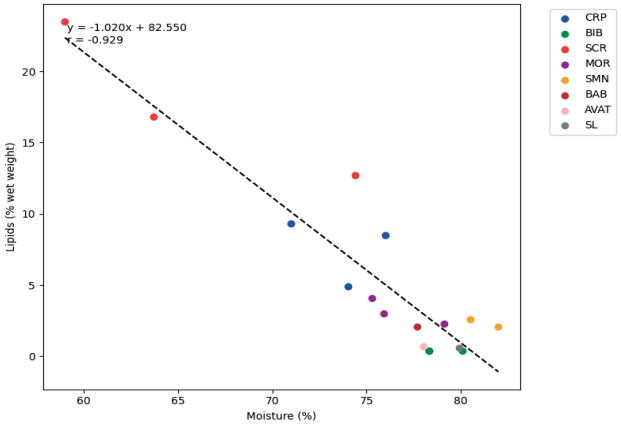



Figure 3. Correlations between lipids content and moisture

Mercury (Hg) is a widespread environmental pollutant that is extremely toxic and bioavailable. It accumulates in aquatic food chains and poses serious health concerns to consumers who eat seafood (Fioravanti et al., 2025). In all fish samples (Figure 4), the total mercury concentration varied between 0.15 ± 0.02 to 1.04 ± 0.62 mg/kg. Catfish recorded the highest concentration of 1.044 ± 0.62 mg/kg and at the opposite pole, the pontic shad determination recorded values of 0.15 ± 0.02 mg/kg.

Catfish from Danube are predator species which can accumulate high mercury levels by consuming other fish species. They are freshwater omnivores and consume substrate that is found at the bottom of water bodies (Cadieux, 2026).

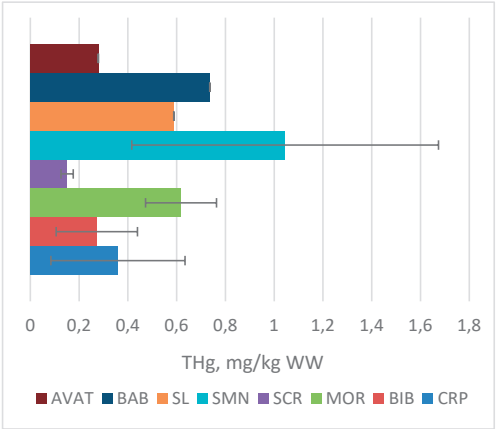



Figure 4. Total mercury (THg) concentrations (mg/kg) in fish muscle

Moreover, they have a potential to bioaccumulate this toxic element in time. Usually, the mercury level within the catfish reflects very well the degree of pollution from that environment. Pontic shad usually feed with smaller plankton, so their position into the food chain is lower and has a much shorter average lifespan compared to catfish. According to Brodziak-Dopierała & Fischer (2023), mercury levels in catfish from river Po ranged from 0.51 to 1.43 mg/kg. The observed levels are similar, which means that support the comparability between studies. Milea (2023) measured the mercury in pontic shad and obtained 0.21 mg/kg DW and Brodziak-Dopierała & Fischer (2023) stated that fish from the Danube, which passes through Croatia, have approximately 0.191 mg/kg (omnivorous species) and 0.441 mgHg/kg (plankton eaters). Regarding the other analysed samples, common roach, vimba bream, and zander exhibited high concentrations of mercury, followed by smaller concentrations in common carp, asp, and perch. Excepting pontic shad, all fish samples presented an increased intra-species variability in terms of mercury concentration. All these differences could be due to specific environmental factors, diet, age, size of each individual fish (Rock et al., 2025). Mercury levels in fish are important because for humans, eating fish is typically the main source of mercury (Dang & Wang, 2012). Additionally, they are indicators for the environmental pollution status (Tolkou et al., 2023).

One-way ANOVA showed a statistically significant difference in total mercury

concentration among fish species at the 0.05 significance threshold ($F = 3.70$; $p = 0.050$).

## CONCLUSIONS

The present study showed interspecific variability for moisture and lipid content in muscle tissue of freshwater fish species from the Lower Danube River. The highest lipid accumulation was observed in Pontic shad and common carp, while perch, zander, and asp exhibited lower lipid reserves, highlighting differences in feeding strategies, metabolic activity, and habitat adaptations.

A strong inverse relationship between moisture and lipid content was identified ($r=-0.929$), confirming that lipid deposition is associated with lower tissue moisture across the investigated samples.

After determining the concentration of mercury in all fish species, it can be concluded that the highest levels were observed in the predatory species, in catfish. The presence of mercury in fish from the Danube highlights the need for continuous monitoring in order to preserve the quality of the aquatic ecosystem, but also to control the possibility of human exposure to contaminated food.

The findings of this study represent baseline data for the Lower Danube River area and reinforce the use of biochemical parameters as ecological indicators in aquatic environmental assessment in freshwater ecosystems. However, sampling was limited to a single season, and annual variations could not be accounted for. Seasonal changes in the lipid reserves and tissue moisture content can influence the mercury bioaccumulation. Future research should include seasonal sampling and the assessment of other pollutants and stressors to better understand the determinants of biochemical variations. These investigations would consolidate the use of these biomarkers in ecological monitoring programs and would contribute to the Water Framework Directive implementation, while contributing to broader freshwater management and sustainability strategies.

## ACKNOWLEDGEMENTS

This work was supported by the Fondo Proserpina S.R.L., grant number 2506/2022, "The impact of heavy metals and microplastics from aquatic organisms on human health", and by the project "HORIZON-MISS-2021-OCEAN-02, DANUBE REGION WATER LIGHTHOUSE ACTION," Project No. 101094070 - DALIA, funded by the European Union's Horizon Europe programme.

## REFERENCES

Ahmed, I., Jan, K., Fatma, S., & Dawood, M. A. O. (2022). Muscle proximate composition of various food fish species and their nutritional significance: A review. *Journal of Animal Physiology and Animal Nutrition*, *106*(3), 690–719. https://doi.org/10.1111/jpn.13711

Ayalew, T., Teshome, M., & Aemro, D. (2025). Food and feeding habits of the introduced common carp (*Cyprinus carpio* L. 1758) in Lake Ardibo, Ethiopia. *Heliyon*, *11*(4), e42596. https://doi.org/10.1016/j.heliyon.2025.e42596

Bernal-Alviz, J., Córdoba-Tovar, L., Pastrana-Durango, D., Molina-Polo, C., Buelvas-Soto, J., Cruz-Esquivel, Á., Marrugo-Negrete, J., & Díez, S. (2025). Influence of environmental and biological factors on mercury accumulation in fish from the Atrato River Basin, Colombia. *Environmental Pollution*, *366*, 125345. https://doi.org/10.1016/j.envpol.2024.125345

Brodziak-Dopierała, B., & Fischer, A. (2023). Analysis of the Mercury Content in Fish for Human Consumption in Poland. *Toxics*, *11*(8), 717. https://doi.org/10.3390/toxics11080717

Cadieux, J. (2026). *What Do Catfish Eat? A Pond Owner's Guide to Feeding & Management*. Midwest Ponds. https://midwestponds.com/blogs/midwestponds-blog/what-do-catfish-eat-a-pond-owner-s-guide-to-feeding-management

Dang, F., & Wang, W.-X. (2012). Why mercury concentration increases with fish size? Biokinetic explanation. *Environmental Pollution*, *163*, 192–198. https://doi.org/10.1016/j.envpol.2011.12.026

Fioravanti, R., Muzzioli, L., Maurel, E., Palma, G., Calabrese, G., Angioni, A., La Rocca, C., Mantovani, A., Pezzana, A., & Donini, L. M. (2025). Bioaccumulation and Biomagnification of Mercury Along the Seafood Chain in Europe: A Systematic Review. *Foods*, *14*(21), 3752. https://doi.org/10.3390/foods14213752

Georgescu, P.-L., Barbuta-Misu, N., Zlati, M. L., Fortea, C., & Antohi, V. M. (2025). Quantifying the Performance of European Agriculture Through the New European Sustainability Model. *Agriculture*, *15*(2), 210. https://doi.org/10.3390/agriculture15020210

Gerasimov, Yu. V., & Strel'nikova, A. P. (2016). Specific features of feeding in underyearlings of zander (Sander lucioperca) (Percidae) of the Rybinsk reservoir in various years. *Journal of Ichthyology*, *56*(3), 390–396. https://doi.org/10.1134/S0032945216030036

Goswami, K. B., & Bisht, P. (2017). The Role of Water Resources in Socio-Economic Development. *International Journal for Research in Applied Science & Engineering Technology (IJRASET)*, *5*(12), 1669–1674.

Huss, H. H. (1995). *Quality and quality changes in fresh fish—4. Chemical Composition*. Food and Agriculture Organization of the United Nations. https://www.fao.org/4/v7180e/v7180e05.htm

Iticescu, C., Georgescu, L., Topa, M.C. & Murariu, G. (2014). Monitoring the Danube water quality near the Galati city. *Journal of Environmental Protection and Ecology*, *15*, 30–38.

Łuczyńska, J., Paszczyk, B., Łuczyński, M. J., Kowalska-Góralska, M., Nowosad, J., & Kucharczyk, D. (2020). Using *Rutilus rutilus* (L.) and *Perca fluviatilis* (L.) as Bioindicators of the Environmental Condition and Human Health: Lake Łańskie, Poland. *International Journal of Environmental Research and Public Health*, *17*(20), 7595. https://doi.org/10.3390/ijerph17207595

Maceda-Veiga, A., & De Sostoa, A. (2011). Observational evidence of the sensitivity of some fish species to environmental stressors in Mediterranean rivers. *Ecological Indicators*, *11*(2), 311–317. https://doi.org/10.1016/j.ecolind.2010.05.009

Martin, B. T., Heintz, R., Danner, E. M., & Nisbet, R. M. (2017). Integrating lipid storage into general representations of fish energetics. *Journal of Animal Ecology*, *86*(4), 812–825. https://doi.org/10.1111/1365-2656.12667

Matos, Â., Matos, A., & Moecke, E. (2019). Polyunsaturated fatty acids and nutritional quality of five freshwater fish species cultivated in the western region of Santa Catarina, Brazil. *Brazilian Journal of Food Technology*, *22*. https://doi.org/10.1590/1981-6723.19318

Mazlum, R., & Akgumus, S. (2019). Stomach content analysis and length-weight relationship of the Pontic shad *Alosa immaculata* Bennett, 1835 (Pisces: Clupeidae), from the eastern Black Seacoast of Turkey. *Indian Journal of Fisheries*, *66*, 39–45. https://doi.org/10.21077/ijf.2019.66.4.79747-05

Milea, Ș.-A., Lazăr, N.-N., Simionov, I.-A., Petrea, Ș.-M., Călmuc, M., Călmuc, V., Georgescu, P.-L., & Iticescu, C. (2023). Effects of cooking methods and co-ingested foods on mercury bioaccessibility in pontic shad (*Alosa immaculata*). *Current Research in Food Science*, *7*, 100599. https://doi.org/10.1016/j.crfs.2023.100599

Misir, G., Tufan, B., & Köse, S. (2016). Variations in Total Lipid and Fatty Acid Contents of Edible Muscle, Liver, and Roes of Spotless Shad, Alosa Immaculata, During Catching Season in Black Sea. *Journal of Aquatic Food Product Technology*, *25*(1), 2–14. https://doi.org/10.1080/10498850.2013.816402

Moon, S. R., Rahman, M. M., Rahman, A., Khan, A. A., Nazir, M. A., Islam, M. A., & Abdulla-Al-Mamun, M. (2026). Water Resources and Environmental Sustainability: Current Challenges and Future Perspectives. *Resources*, *15*(2), 31. https://doi.org/10.3390/resources15020031

Naeem, M., & Salam, A. (2010). Proximate composition of fresh water bighead carp, *Aristichthys nobilis*, in relation to body size and condition factor from Islamabad, Pakistan. *Afr. J. Biotechnol.*, *9*, 8687–8692.

Nahon, S., Roussel, J.-M., Jaeger, C., Menniti, C., Kerhervé, P., Mortillaro, J.-M., & Aubin, J. (2020). Characterization of trophic niche partitioning between carp (*Cyprinus carpio*) and roach (*Rutilus rutilus*) in experimental polyculture ponds using carbon (δ13C) and nitrogen (δ15N) stable isotopes. *Aquaculture*, *522*, 735162. https://doi.org/10.1016/j.aquaculture.2020.735162

Okgerman, H., Yardimci, C., Dorak, Z., & Yilmaz, N. (2013). Feeding ecology of vimba (*Vimba vimba* L., 1758) in terms of size groups and seasons in Lake Sapanca, Northwestern Anatolia. *Turkish Journal of Zoology*, *37*, 288–297. https://doi.org/10.3906/zoo-1107-1

Olsson, J. (2019). Past and Current Trends of Coastal Predatory Fish in the Baltic Sea with a Focus on Perch, Pike, and Pikeperch. *Fishes*, *4*(1), 7. https://doi.org/10.3390/fishes4010007

Petricorena, Z. C. (2014). *Chemical Composition of Fish and Fishery Products*. In Handbook of Food Chemistry (pp. 1–28). Springer, Berlin, Heidelberg. https://doi.org/10.1007/978-3-642-41609-5_12-1

Pfauserová, N., Slavík, O., Horký, P., Kolářová, J., & Randák, T. (2019). Migration of Non-Native Predator Asp (*Leuciscus aspius*) from a Reservoir Poses a Potential Threat to Native Species in Tributaries. *Water*, *11*(6), 1306. https://doi.org/10.3390/w11061306

Rock, K. D., Bhoothapuri, S., Lassiter, E., Segedie, L., & Belcher, S. M. (2025). Variability of Mercury Concentrations Across Species, Brand, and Tissue Type in Processed Commercial Seafood Products. *Toxics*, *13*(6), 426. https://doi.org/10.3390/toxics13060426

Santos, G. S., Ribeiro, F., Pereira, E., Silva, A. F., Almeida, P. R., Ribeiro, D., & Quintella, B. R. (2025). Behaviour of the Apex Predator European Catfish (Silurus glanis) on a Recently Invaded Reservoir. *Ecology of Freshwater Fish*, *34*(1), e12817. https://doi.org/10.1111/eff.12817

Simeanu, C., Măgdici, E., Păsărin, B., Avarvarei, B.-V., & Simeanu, D. (2022). Quantitative and Qualitative Assessment of European Catfish (*Silurus glanis*) Flesh. *Agriculture*, *12*(12), 2144. https://doi.org/10.3390/agriculture12122144

Tolkou, A. K., Toubanaki, D. K., & Kyzas, G. Z. (2023). Detection of Arsenic, Chromium, Cadmium, Lead, and Mercury in Fish: Effects on the Sustainable and Healthy Development of Aquatic Life and Human Consumers. *Sustainability*, *15*(23), 16242. https://doi.org/10.3390/su152316242

Wang, Z., Liu, X., Liu, T., Wang, W., & Liu, J. (2024). Towards the sustainable development of water security: A new copula-based risk assessment system. *Ecological Indicators*, *166*, 112489. https://doi.org/10.1016/j.ecolind.2024.112489

Wannas, A., & Mohammed, S. (2025). The role of environmental stress in fish health: A review. *GSC Biological and Pharmaceutical Sciences*, *32*, 017–027. https://doi.org/10.30574/gscbps.2025.32.2.0304

Warret Rodrigues, C., Armstrong, D., Wang, F., & Roth, J. D. (2023). Tissue composition and storage duration affect the usefulness of generic wet-to-dry mass conversion factors in toxicology studies. *Environmental Research*, *236*, 116727. https://doi.org/10.1016/j.envres.2023.116727

Xia, B., Zhang, J., Li, C., Wu, S., Huang, L., Qin, D., Hao, Q., & Gao, L. (2025). Texture, Nutrition, and Flavor of Different Freshwater Fish Muscles: Comparative Study and Molecular Docking. *Foods*, *14*(13), 2258. https://doi.org/10.3390/foods14132258

Zhang, Z., Liu, L., Xie, C., Li, D., Xu, J., Zhang, M., & Zhang, M. (2014). Lipid Contents, Fatty Acid Profiles and Nutritional Quality of Nine Wild Caught Freshwater Fish Species of the Yangtze Basin, China. *Journal of Food and Nutrition Research*, *2*, 388–394. https://doi.org/10.12691/jfnr-2-7-10

Zillioux, E. (2015). Mercury in Fish: History, Sources, Pathways, Effects, and Indicator Usage. *Environmental Indicators*, *Environmental Indicators, RH Armon&O Hänninen, eds.DOI 10.1007/978-94-017-9499-2_42, Springer, New York.* https://doi.org/10.1007/978-94-017-9499-2_42

Zlati, M. L., Antohi, V.-M., Ionescu, R.-V., Iticescu, C., & Georgescu, L. P. (2024). Quantyfing the impact of the water security index on socio-economic development in EU27. *Socio-Economic Planning Sciences*, *93*, 101912. https://doi.org/10.1016/j.seps.2024.101912

Scientific Papers. Series E. Land Reclamation, Earth Observation & Surveying, Environmental Engineering. Vol. XV, 2026
Print ISSN 2285-6064, CD-ROM ISSN 2285-6072, Online ISSN 2393-5138, ISSN-L 2285-6064

# *DAPHNIA MAGNA* INDICATOR OF WATER POLLUTION WITH ZINC

**Paula COJOCARU, Alexandra-Andreea STRUNGARU, Gabriela BIALI, Maria Cătălina PASTIA**

"Gheorghe Asachi" Technical University of Iasi, Faculty of Hydrotechnics, Geodesy and Environmental Engineering, 63-65 Prof. dr. docent Dimitrie Mangeron Blvd, Iasi, Romania

Corresponding author email: paula.cojocaru@academic.tuiasi.ro

***Abstract***

*Heavy metal contamination represents a persistent threat to aquatic ecosystems due to its toxicity and long-term environmental persistence. Among these metals, zinc plays a dual role as an essential micronutrient at low concentrations but becomes toxic when present in excess. The present study evaluates the acute toxicity of zinc on the freshwater crustacean Daphnia magna, a widely used bioindicator species in ecotoxicological assessments. Toxicity experiments were conducted using standardized Daphtoxkit bioassays in which neonates of D. magna were exposed to zinc concentrations ranging from 1.0 to 6.0 mg/L under controlled laboratory conditions. Mortality rates were recorded at four-hour intervals over an exposure period of 36 hours. The results revealed a strong concentration- and time-dependent increase in mortality. At the lowest concentration tested (1.0 mg/L), mortality reached 20% after 16 hours and increased to 60% after 36 hours. In contrast, the highest concentration (6.0 mg/L) induced rapid toxicity, producing 80% mortality within four hours and complete mortality after twelve hours of exposure. These findings highlight the high sensitivity of D. magna to elevated zinc concentrations and confirm its suitability as an effective biological indicator for monitoring heavy metal contamination in freshwater ecosystems. The results contribute to a better understanding of zinc-induced toxicity mechanisms in aquatic invertebrates and provide valuable information for environmental monitoring and risk assessment of metal pollution.*

***Key words****: Daphnia magna, mortality rate, toxicity, zinc.*

## INTRODUCTION

The contamination of aquatic environments with heavy metals represents one of the most persistent environmental challenges associated with industrialization and modern agricultural activities. Due to their chemical stability and limited biodegradability, heavy metals tend to accumulate in aquatic ecosystems and can exert long-term toxic effects on living organisms (Ali et al., 2019; Pandey & Keshavkant, 2021). Their presence in water bodies may disrupt ecological balance and pose risks to aquatic biodiversity as well as to human health through the contamination of water resources.

Among heavy metals, zinc occupies a particular position because it plays a dual role in biological systems. At low concentrations, zinc is considered an essential micronutrient involved in numerous physiological processes, including enzyme activation, gene expression, and protein synthesis (King, 2011). Several studies have highlighted the importance of zinc in maintaining cellular metabolism and proper organismal functioning (Bellido et al., 2022; Paylar et al., 2022; Oprea et al., 2024). However, when present in elevated concentrations, zinc may become toxic and cause adverse effects on aquatic organisms (DeForest & van Genderen, 2012; Clearwater et al., 2002).

The detection and monitoring of aquatic pollution can be effectively achieved using biological indicators, also known as bioindicators. These are living organisms that respond to environmental changes and can provide valuable information about ecosystem health. Bioindicators may include microorganisms, plants, and animals whose physiological responses can signal the presence of pollutants even at low concentrations (Zaghloul et al., 2020; Simionov et al., 2022). Their use is particularly valuable because they can detect the early stages of environmental contamination and provide insights into the biological effects of pollutants (Wang & Guan, 2010; Parmar et al., 2016; Kadim & Risjani, 2022).

Several aquatic organisms have been widely employed in ecotoxicological testing to assess water pollution. Among these are the freshwater crustacean *Thamnocephalus platyurus*, the

rotifer *Brachionus calyciflorus*, the protozoan *Tetrahymena thermophila*, the cladoceran *Ceriodaphnia dubia*, the aquatic plant *Spirodela polyrhiza*, and the microalga *Pseudokirchneriella subcapitata*. While a variety of aquatic organisms are used as bioindicators, they are mentioned here to provide context, with the present study specifically focusing on *Daphnia magna* due to its high sensitivity and established role in standardized ecotoxicological testing.

One of the most widely used organisms in freshwater ecotoxicology is the cladoceran *Daphnia magna*, commonly known as the water flea. This species plays a crucial ecological role in freshwater ecosystems such as ponds and lakes, where it acts as a primary consumer by filtering suspended particles and microorganisms from the water column. Through this filtering activity, *Daphnia magna* contributes significantly to water clarity and nutrient cycling within aquatic ecosystems

Acute toxicity tests involving freshwater daphnids have become internationally recognized tools for evaluating the toxic effects of chemical substances and for monitoring contaminated water and industrial effluents (Persoone et al., 2009; Fekete-Kertész et al., 2016; Sönmez et al., 2022). The extensive use of *Daphnia magna* in ecotoxicological studies is mainly due to its high sensitivity to pollutants, rapid reproduction, short life cycle, and parthenogenetic reproduction (Koivisto, 1995). In addition, it offers practical advantages such as low experimental costs, standardized protocols, and reproducible results within short testing periods (Kim et al., 2003).

Considering the increasing presence of heavy metals in aquatic ecosystems and the potential ecological consequences of their accumulation, it is essential to evaluate their effects on sensitive aquatic organisms. Therefore, the main objective of the present study was to investigate the toxic effects of zinc at different concentrations on *Daphnia magna* and to assess the relationship between pollutant concentration, exposure time, and mortality rate in this bioindicator species.

## MATERIALS AND METHODS

The experimental study was carried out using the *Daphtoxkit F magna toxicity test system,* produced by MicroBioTests Inc. (Belgium, Figure 1). This standardized bioassay kit contains the necessary materials for performing acute toxicity tests on *Daphnia magna*, including concentrated salt solutions used for preparing the test medium, micropipettes, a microsieve, Petri dishes, spirulina owder for feeding the organisms, and dormant ephippial eggs of *Daphnia magna*.

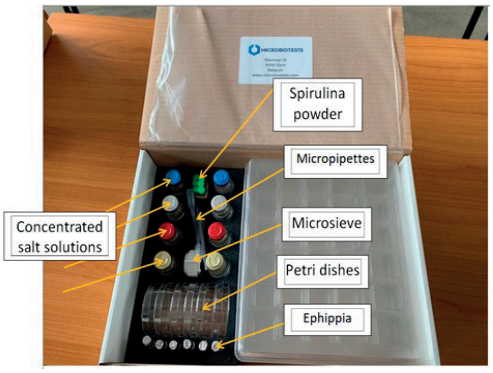



Figure 1. Daphtoxkit *F magna*

### *Preparation of standard freshwater*

A Standard Freshwater solution was prepared according to the protocol described in ISO 6341:2012, which is commonly used in acute toxicity tests involving freshwater crustaceans.

The solution was obtained by adding the following concentrated salt solutions to one liter of distilled water: $NaHCO_3$ with a concentration of 64.75 mg/L (12 mL), $CaCl_2 \cdot 2H_2O$ with a concentration of 294 mg/L, $MgSO_4 \cdot 7H_2O$ with a concentration of 123.25 mg/L, KCl with a concentration of 5.75 mg/L.

After the addition of these components, the solution was diluted with distilled water to obtain a final volume of 2000 mL, and the mixture was thoroughly homogenized to ensure uniform distribution of the salts.

This prepared solution served both as the hatching medium for ephippia and as the dilution medium for preparing pollutant concentrations.

### *Preparation of zinc pollutant solution*

The pollutant solution used in the experiments consisted of zinc sulfate ($ZnSO_4$) dissolved in distilled water. The physicochemical parameters of the test solutions (pH, dissolved oxygen, and conductivity) were maintained within the recommended ranges specified by ISO

6341:2012. A stock solution with a concentration of 104.5184 mg/L $ZnSO_4$ was prepared and subsequently used to obtain the experimental concentrations through serial dilution with Standard Freshwater.

From the stock solution, six working concentrations of zinc sulfate ($ZnSO_4$) were prepared: 1.0 mg/L, 2.0 mg/L, 3.0 mg/L, 4.0 mg/L, 5.0 mg/L, 6.0 mg/L.

Each concentration represented a separate experimental treatment. All experimental variants were performed in four independent replicates in order to ensure reliability and reproducibility of the results.

The prepared solution served both as the hatching medium for ephippia and as the dilution medium for preparing pollutant concentrations.

***Hatching of Daphnia magna ephippia***

Dormant eggs (*ephippia*) of *Daphnia magna* were first rinsed using tap water in order to remove any residues of the storage medium. The ephippia were then placed in a microsieve and transferred into Petri dishes containing 10 mL of pre-aerated Standard Freshwater.

The Petri dishes were covered with lids and incubated for approximately 80 hours at a controlled temperature of 20–22°C under continuous illumination. These conditions allowed the hatching of the ephippial eggs and the emergence of neonate individuals.

***Feeding of Neonates***

After the hatching process was completed, the newly emerged *Daphnia magna* neonates were provided with spirulina powder as a food source. Feeding was performed shortly after hatching in order to ensure the physiological stability of the organisms before the toxicity testing began. Two hours after feeding, the neonates were selected for use in the toxicity experiments (Figure 2).

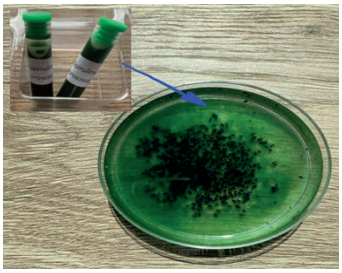


Figure 2. Spirulina feeding

***Toxicity testing procedure***

For each experimental condition, five neonates of *Daphnia magna* were introduced into test plates containing 10 mL of zinc-contaminated Standard Freshwater at the predetermined concentrations. The experimental procedure followed the standardized protocol described in ISO 6341:2012. The use of five neonates per test plate is consistent with Daphtoxkit guidelines and contributes to the reproducibility and reliability of the results. To prevent evaporation of the test solution during the incubation period, the plates were sealed with parafilm strips and covered with a transparent lid.

The experimental plates were then incubated under controlled conditions in darkness at a constant temperature of approximately 22°C (Figure 3).

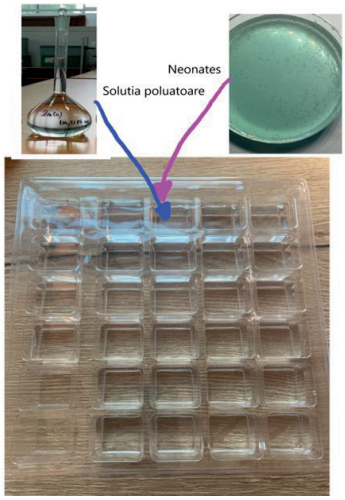



Figure 3. Testing plates

***Monitoring of organism response***

The response of *Daphnia magna* to zinc exposure was monitored throughout the experimental period. Observations were conducted every four hours, during which the number of surviving and dead organisms was recorded.

Mortality was determined based on the absence of movement of the organisms when observed under standard laboratory conditions.

***Calculation of mortality rate***

The mortality rate of the organisms was calculated using the following equation:

$$R_m = \frac{N_i - N_f}{N_i} \cdot 100\ (\%) \quad (1)$$

where:
Rm represents the mortality rate expressed as a percentage (%);
Ni represents the initial number of *Daphnia magna* individuals introduced into the test plate;
Nf represents the number of surviving individuals recorded during observation.
In addition to mortality rate, the inhibitory effect of the pollutant was evaluated by comparing the results obtained in the contaminated samples with those observed in the control group, where the organisms were maintained in uncontaminated Standard Freshwater.

## RESULTS AND DISCUSSIONS

### *Effects of zinc exposure on the survival of Daphnia magna*

After the hatching period and the initial feeding stage, the newly emerged *Daphnia magna* neonates were transferred to freshwater containing different concentrations of zinc (Figure 4).



Figure 4. *Daphnia magna* (water fleas)

During the experimental exposure period, the organisms were not provided with additional food. The survival of the water fleas was monitored throughout the experiment in order to evaluate the influence of zinc concentration and exposure time on organism mortality.
The observations revealed that *Daphnia magna* individuals were able to survive in zinc-contaminated freshwater for a maximum exposure period of approximately 36 hours. However, their number progressively decreased as both the zinc concentration and exposure duration increased.
The experimental results, summarized in Table 1, indicate a clear concentration-dependent reduction in the number of surviving organisms. The values presented represent mean results obtained from four independent replicates for each concentration and exposure time.

Table 1. Zinc toxicity on *Daphnia magna*

| Concentration (mg/L) | Number of *Daphnia magna* in test plates | | | | | | | | |
|---|---|---|---|---|---|---|---|---|---|
| | Day 1 | | | | | Day 2 | | | |
| | Hour | | | | | Hour | | | |
| | 8 h | 12 h | 16 h | 20 h | 24 h | 4 h | 8 h | 12 h | 16 h |
| 1.0 | 5 | 5 | 5 | 4 | 4 | 4 | 4 | 3 | 2 |
| 2.0 | 5 | 5 | 4 | 4 | 3 | 2 | 2 | 1 | 0 |
| 3.0 | 3 | 3 | 2 | 2 | 2 | 1 | 1 | 1 | 0 |
| 4.0 | 2 | 2 | 2 | 1 | 1 | 1 | 0 | 0 | 0 |
| 5.0 | 2 | 1 | 1 | 0 | 0 | 0 | 0 | 0 | 0 |
| 6.0 | 1 | 1 | 0 | 0 | 0 | 0 | 0 | 0 | 0 |

For example, at the lowest tested concentration (1.0 mg/L Zn), all five individuals survived during the first 12 hours of exposure. After 16 hours, the number of surviving organisms decreased to four individuals, and after 36 hours, only two organisms remained alive.
At a zinc concentration of 2.0 mg/L, the number of surviving individuals began to decrease earlier. While five organisms were initially present, survival declined progressively to zero by the end of the exposure period.
At 3.0 mg/L, the toxic effects became more pronounced. Only three individuals remained alive after the initial exposure period, and the population gradually declined until complete mortality occurred by the end of the experiment.
Higher zinc concentrations caused even faster reductions in survival. At 4.0 mg/L, only two organisms remained alive after the first observation interval, and the entire population was eliminated within the experimental timeframe.
Similarly, at 5.0 mg/L, mortality increased rapidly, with only one organism surviving after the early observation intervals and complete mortality occurring shortly afterward.
The most severe toxic effects were observed at the highest concentration tested (6.0 mg/L). In this case, only one individual survived during the initial observation period, and all organisms died within a few hours of exposure.

These results clearly demonstrate that zinc toxicity in *Daphnia magna* increases significantly with increasing pollutant concentration.

***Mortality rate of water fleas***

The mortality rate of the water fleas was calculated based on the recorded number of surviving individuals at each observation interval. The results are illustrated in Figures 5 and 6, which show the mortality rates recorded after the first and second days of exposure.

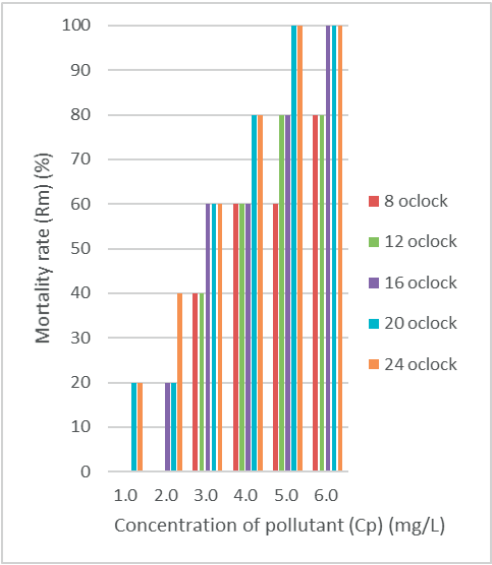



Figure 5. Mortality rate of water fleas after Day 1 of exposure to the pollutant

During the first day of exposure, the mortality rate remained relatively low at the lower zinc concentrations. At concentrations of 1.0 mg/L and 2.0 mg/L, mortality reached approximately 20% only after 16 hours and 12 hours of exposure, respectively.

In contrast, the mortality rate increased substantially at higher zinc concentrations. At the maximum concentration tested (6.0 mg/L), mortality reached approximately 80% after only four hours of exposure and increased to 100% after twelve hours.

The results also indicate that mortality increased significantly during the second day of exposure (Figure 6). After 36 hours, the mortality rate reached 60% at the lowest tested concentration (1.0 mg/L), while at all higher concentrations complete mortality (100%) was observed.

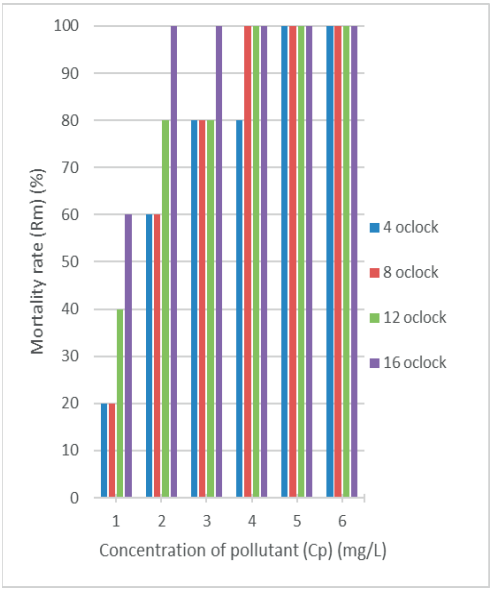



Figure 6. Mortality rate of water fleas after Day 2 of exposure to the pollutant

These findings demonstrate that both exposure time and zinc concentration strongly influence the survival of *Daphnia magna*.

After calculating the mortality rate of water fleas, the $LC_{50}$ (lethal concentration for 50% of organisms) was determined, a standard toxicology indicator used to measure the acute toxicity of a substance. $LC_{50}$ is calculated using statistical methods and is used to compare toxicity and assess ecological and human risks. A lower $LC_{50}$ value indicates higher toxicity.

To calculate the $LC_{50}$ value, the logarithmic method was applied. Using the AAT Bioquest $LC_{50}$ calculator, the concentrations (X values) and the corresponding responses expressed as percentage mortality (Y values) were entered to obtain the equations required for determining the $LC_{50}$ for Zn exposure on Day 1 and Day 2. The resulting equations and $LC_{50}$ values are presented in Table 2.

Table 2. The $LC_{50}$ values for Zn pollution used in the experiment

| Type of Pollutant | Equation | | $LC_{50}$ | |
|---|---|---|---|---|
| $Zn^{2+}$ | *Day 1* | *Day 2* | *Day 1* | *Day 2* |
| | $Y = 0.034 + \frac{1.019 - 0.034}{1 + \left(\frac{X}{2.96}\right)^{4.623}}$ | $Y = -0.053 + \frac{4.969 + 0.053}{1 + \left(\frac{X}{0.434}\right)^{1.596}}$ | 2.969±0.032 | 0.434±0.063 |

All values are mean values of repetitions ± S.D.

***Relationship between zinc concentration and population inhibition***

In addition to mortality rate, the inhibitory effect of zinc exposure on *Daphnia magna* populations was also evaluated by comparing the survival of organisms in contaminated water with that observed in the control sample maintained in uncontaminated freshwater.

Graphical analysis of the relationship between pollutant concentration and inhibition of the organisms revealed a clear correlation between increasing zinc concentration and increasing levels of inhibition. This relationship is illustrated in Figures 7, 8, and 9, which show the correlation between pollutant concentration (Cp) and the inhibition of *Daphnia magna* (I) after 12 hours, 24 hours, and 36 hours of exposure, respectively.

The results indicate that inhibition increased with both zinc concentration and exposure time.

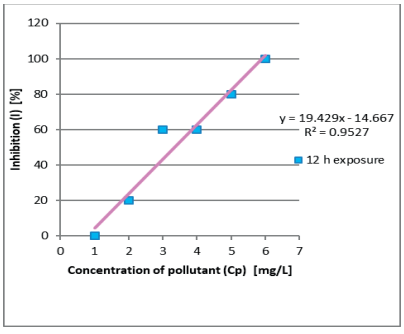



Figure 7. Correlation between the concentration of pollutant (Cp) and inhibition (I) of *Daphnia magna* under the influence of water pollution with Zn after 12 hours of exposure

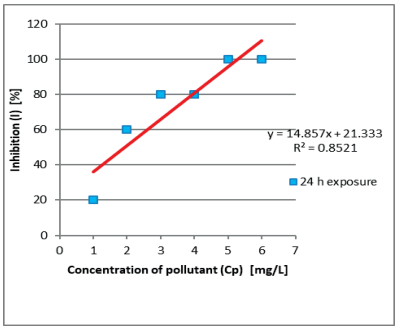



Figure 8. Correlation between the concentration of pollutant (Cp) and inhibition (I) of *Daphnia magna* under the influence of water pollution with Zn after 24 hours of exposure

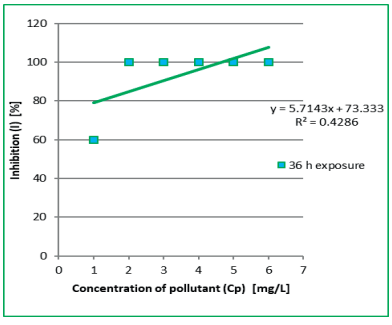



Figure 9. Correlation between the concentration of pollutant (Cp) and inhibition (I) of *Daphnia magna* under the influence of water pollution with Zn after 36 hours of exposure

The relationship between pollutant concentration and inhibition was quantified using the correlation coefficient ($R^2$), which showed a decreasing trend over time, with values of 0.9527 after 12 hours, 0.8521 after 24 hours, and 0.4286 after 36 hours. This decline suggests that, at longer exposure times, the strength of the correlation weakened due to the high mortality observed, with surviving organisms recorded only at the lowest zinc concentration tested (1.0 mg/L).

***Toxicological interpretation***

Zinc is widely recognized as a metal that can exert both beneficial and harmful effects on aquatic organisms depending on its concentration in the environment. At low concentrations, zinc functions as an essential

trace element and plays an important role in enzymatic activity and metabolic regulation.
However, when present in elevated concentrations, zinc may become toxic and disrupt important biological processes in aquatic organisms.
From an ecological perspective, increased mortality of *Daphnia magna* may disrupt trophic interactions, as this species represents a key link between primary producers and higher trophic levels. A decline in its population could lead to algal overgrowth and reduced water quality. Prolonged exposure to high zinc concentrations can affect growth, reproduction, and overall physiological functioning. Toxic accumulation of the metal may interfere with essential biological processes such as cellular respiration, ionic balance, and metabolic regulation, ultimately leading to organism mortality.
The results obtained in the present study are consistent with those reported by De Schamphelaere et al. (2004), who demonstrated that excessive zinc exposure can negatively affect the development and reproduction of *Daphnia magna* due to metal accumulation within the organism.
Furthermore, previous research conducted by Simionov et al. (2022) suggests that the toxicity of zinc in aquatic environments can be influenced by environmental parameters such as water alkalinity and salinity, which affect the bioavailability and uptake of metals by aquatic organisms.
The findings of the present study confirm that *Daphnia magna* populations are highly sensitive to zinc exposure. A significant reduction in organism survival was observed as zinc concentrations increased. After 32 hours of exposure, the population decreased by approximately 40% at the lowest concentration (1.0 mg/L), while reductions of approximately 80% were observed at concentrations of 2.0 mg/L and 3.0 mg/L.
At 4.0 mg/L, the population was completely eliminated, resulting in 100% mortality. At the highest concentration tested (6.0 mg/L), toxicity reached its maximum level within only 12 hours of exposure, indicating a rapid and severe toxic effect on the organisms.

## CONCLUSIONS

The present study demonstrates that *Daphnia magna* exhibits a pronounced sensitivity to zinc contamination, reinforcing its relevance as a reliable bioindicator for evaluating heavy metal pollution in freshwater environments. Experimental results clearly show that both exposure duration and zinc concentration significantly influence mortality rates in *D. magna*. Even relatively low concentrations of zinc (1.0 mg/L) produced measurable toxic effects within a short exposure period, while higher concentrations caused rapid and complete mortality.
The observed concentration-dependent toxicity confirms that zinc, although biologically essential in trace amounts, can severely disrupt physiological processes when present in elevated concentrations. The observed toxicity could be related to potential disruptions in physiological processes such as ion regulation and metabolic activity; however, these mechanisms were not directly measured and therefore remain speculative. These findings are consistent with previous ecotoxicological studies demonstrating that metal bioavailability and exposure time are critical determinants of toxic responses in aquatic invertebrates.
From an environmental perspective, the results underline the importance of monitoring zinc levels in freshwater systems, particularly in areas influenced by industrial activities, mining operations, or urban wastewater discharges. The rapid toxic response observed in *D. magna* suggests that this organism can serve as an early warning indicator of metal contamination in aquatic ecosystems.
Future research should focus on evaluating the influence of environmental parameters such as water hardness, pH, temperature, and dissolved organic matter on zinc toxicity. These factors may significantly affect metal bioavailability and consequently modify toxic responses in aquatic organisms. Additionally, further studies involving sublethal endpoints such as reproduction, growth, and behavioral changes could provide a more comprehensive understanding of long-term ecological impacts.

Overall, the findings contribute to the growing body of knowledge on metal toxicity in freshwater organisms and support the use of *Daphnia magna* in ecotoxicological monitoring and environmental risk assessment programs.

## REFERENCES

Ali, H., Khan, E., & Ilahi, I. (2019). Environmental chemistry and ecotoxicology of hazardous heavy metals: Environmental persistence, toxicity, and bioaccumulation. *Journal of Chemistry*, 2019, 6730305.

Bellido Valencia, O., Alca, J.J., & Núñez Alberca, M. (2022). Incidence of heavy metals in water, soil, alfalfa (*Medicago sativa* L.) and sheep (*Ovis aries* L.) along the Quilca - Vitor - Chili Basin in Arequipa, Peru. *Carpathian Journal of Earth and Environmental Sciences*, 17(1), 21–34.

Clearwater, S.J., Farag, A.M., & Meyer, J.S. (2002). Bioavailability and toxicity of dietborne copper and zinc to fish. *Comparative Biochemistry and Physiology Part C: Toxicology & Pharmacology*, 132(3), 269–313.

DeForest, D.K., & van Genderen, E.J. (2012). Application of U.S. EPA guidelines in a bioavailability-based assessment of ambient water quality criteria for zinc in freshwater. *Environmental Toxicology and Chemistry*, 31, 1264–1272

De Schamphelaere, K.A.C, Canli, M., Van Lierde, V., Forrez I., Vanhaecke F., & Janssen C.R. (2004). Reproductive toxicity of dietary zinc to *Daphnia magna. Aquatic Toxicology*, 70(3), 233-244.

Fekete-kertész, I., Kunglné-Nagy, Z., & Molnár, M. (2016). Ecological impact of micropollutants on aquatic life determined by an innovative sublethal endpoint *daphnia magna* heartbeat rate. *Carpathian Journal of Earth and Environmental Sciences*, 11(2), 345-354.

Kadim, M.K., & Risjani, Y. (2022). Biomarker for monitoring heavy metal pollution in aquatic environment: An overview toward molecular perspectives. *Emerging Contaminants*, 8, 195–205.

King, J.C. (2011). Zinc: An essential but elusive nutrient. *The American Journal of Clinical Nutrition,* 94, 679S–684S.

Kim, B.C., Park, K.S., Kim, S.D., & Gu, M.B. (2003). Evaluation of a high throughput toxicity biosensor and comparison with a *Daphnia magna* bioassay. *Biosensors and Bioelectronics*, 18(5-6), 821-826.

Koivisto, S. (1995). Is *Daphnia magna* an ecologically representative zooplankton species in toxicity tests? *Environmental Pollution*, 90(2), 263-267.

Oprea, B.Ș., Vrînceanu, N.O., Carabulea, V., Motelică, D.M., Costea, M., & Plopeanu, G.I. (2024). Soil heavy metals content variation depending on the distance from pollution source and uptake by the *Trifolium pratense* L. species harvested from Copșa Mică area, Central Romania. *Scientific Papers. Series E. Land Reclamation, Earth Observation & Surveying, Environmental Engineering*, XIII, 719-726.

Pandey, N., & Keshavkant, S. (2021). Chapter 1 - Mechanisms of heavy metal removal using microorganisms as biosorbents. *New Trends in Removal of Heavy Metals from Industrial Wastewater*, 1–21.

Parmar, T.K., Rawtani, D., & Agrawal, Y.K. (2016). Bioindicators: The natural indicator of environmental pollution. *Frontiers in Life Science*, 9(2), 110–118.

Paylar, B., Asnake, S., Sjöberg, V., Ragnvaldsson, D., Jass, J., & Olsson, P.E. (2022). Influence of water hardness on zinc toxicity in *Daphnia magna*. *Journal of Applied Toxicology*, 42(9), 1510–1523.

Persoone, G., Baudo, R., Cotman, M., Blaise, C., Thompson, K.Cl., Moreira-Santos, M., Vollat, B., Törökne, A., & Han, T. (2009). Review on the acute *Daphnia magna* toxicity test – Evaluation of the sensitivity and the precision of assays performed with organisms from laboratory cultures or hatched from dormant eggs. *Knowledge and Management of Aquatic Ecosystems*, 393.

Simionov, I.A., Călmuc, M., Antache, A., Călmuc, V., Petrea, Ș.M., Nica, A., Cristea, V., & Neculiță, M. (2022). The use of *Pectinatella magnifica* as bioindicator for heavy metals pollution in Danube Delta. *Scientific Papers. Series E. Land Reclamation, Earth Observation & Surveying, Environmental Engineering*, XI, 181-186.

Sönmez, V.Z., Ercan, N., & Sivri, N. (2022). Toxic effects of ester based polymers on *Daphnia magna*: a laboratory microcosm study. *Carpathian Journal of Earth and Environmental Sciences*, 17(1), 35–47.

Zaghloul, A., Saber, M., Gadow, S., & Awad, F. (2020). Biological indicators for pollution detection in terrestrial and aquatic ecosystems. *Bulletin of the National Research Centre*, 44(1), 127.

Wang, W.X., & Guan, R. (2010). Subcellular distribution of zinc in *Daphnia magna* and implication for toxicity. *Environmental Toxicology and Chemistry*, 29(8), 1841–1848.

ISO 6341 (2012). *Water quality. Determination of the inhibition of the mobility of Daphnia magna Straus (Cladocera, Crustacea). Acute toxicity test.*

Scientific Papers. Series E. Land Reclamation, Earth Observation & Surveying, Environmental Engineering. Vol. XV, 2026
Print ISSN 2285-6064, CD-ROM ISSN 2285-6072, Online ISSN 2393-5138, ISSN-L 2285-6064

# CARBON STORAGE IN FOREST STANDS ON DEGRADED LANDS

**Cristinel CONSTANDACHE, Ciprian TUDOR, Laurențiu POPOVICI, Raul RADU**

"Marin Drăcea" National Institute for Research and Development in Forestry,
128 Eroilor Blvd, Voluntari, Ilfov County, Romania

Corresponding author email: ciprian.tudor@icas.ro

***Abstract***

*In the context of expanding environmental degradation processes, degraded lands represent potential areas for forest plantations that help reduce soil erosion, increase carbon storage and biodiversity. Research conducted in 2025 aimed to determine the carbon stock (in soil, litter, forest biomass and deadwood) and the annual carbon sequestration capacity in forest stands established on degraded lands in the Curvature Subcarpathians region. The results indicate that soil and living biomass are essential components for storing organic carbon. Soil carbon stock is relatively stable (between 70 and 120 t/ha), while carbon in living biomass shows greater variation (between 45.78 and 258.24 t/ha). The distribution of carbon in soil, litter, forest biomass and deadwood reflects the influence of environmental conditions and stand structure on carbon storage dynamics. The results demonstrate that forest plantations on degraded lands represent an effective tool for carbon storage and for mitigating the effects of climate change, capable of providing significant ecosystem and socio-economic services.*

***Key words****: carbon storage, degraded lands, forest biomass, stands.*

## INTRODUCTION

Beyond their traditional production and protective roles, forests play an important part in carbon storage and mitigation of greenhouse gas (GHG) concentrations, functions that have gained particular importance in Romania following its accession to the Kyoto Protocol (1997). In recent years, the role of forests in carbon storage and the mitigation of greenhouse gas emissions (GHG) has emerged as a global priority, as emphasized in the EU Green Book on forest protection and information (European Commission, 2010). The report highlights that European forests have the capacity to act as efficient absorbers for gases such as $CO_2$, $NH_3$ and $NO_x$ but this is not yet fully understood.. Given that substantial reductions in GHG emissions are difficult to achieve in the short term, carbon sequestration is increasingly considered as a viable long-term solution.

Forests represent the most important terrestrial ecosystem in the carbon (C) cycle and also play a key role in carbon storage (Schulze et al., 2010; Konôpka et al., 2025). Phytomass, or tree biomass, by definition, refers to the organic mass of trees (Koch, 2010), and carbon storage in tree biomass has become an effective measure for mitigating climate change (Somogyi et al., 2007). More than 80% of aboveground biomass is stored in forest ecosystems and also accounts for over 70% of the carbon present in soils (Jandl et al., 2007).

Therefore, in addition to their traditional production and protection roles, forest ecosystems contribute significantly to carbon sequestration by functioning as important carbon pools.

In the context of ongoing climate change conditions and increasing environmental degradation processes, degraded lands represent potential sites for establishing tree plantations (Constandache et al., 2023). Afforesting degraded lands can provide multiple benefits, such as biodiversity, strengthening ecosystem stability, preventing soil erosion, offering recreational opportunities, and enhancing carbon storage (Maestre & Cortina, 2004; Semwal et al., 2013; Moscatelli et al., 2017; Oprică et al., 2022). Soil organic carbon dynamics have been widely investigated across different forest ecosystems, with particular attention given to pines species (*Pinus* spp.) due to their significant ecological and economic importance (Dincă et al., 2015; Torres et al., 2021).

Pine species have often been studied both in monocultures and in mixture with other forest

species, offering valuable information on their carbon sequestration potential (Tudor et al., 2025). Studies comparing pure pine stands with mixed-species forests suggest that, while pine stands accumulate substantial amounts of carbon in their aboveground biomass, mixed forests may provide a more even distribution of carbon between belowground and aboveground components (Rodríguez de Prado et al., 2023).

Soil organic carbon is a fundamental component of forest ecosystems (Nadelhoffer, 2004; Batjes, 2014). On a global scale, soils store almost three times more carbon than the atmosphere and about 4.5 times more than the total terrestrial carbon pool in the biosphere (Lajtha et al., 2014), surpassing the combined carbon found in both the atmosphere and vegetation (Jobbágy et al., 2000). Forest soils have significant role in the global carbon cycle, containing roughly 1.5 times more carbon than the biomass of isolated standing trees (Baritz et al., 2010).

Soil carbon also representing a critical factor in the balance of greenhouse gases (GHGs), contributing to the mitigation of rising GHG emissions (Janssens et al., 2003; Jandl et al., 2007; Baritz et al., 2010). However, measuring soil organic carbon stocks over time and space is challenging due to specific local conditions and the differing results obtained in various studies, which makes harmonization of data being difficult for the development of predictive models (Grüneberg et al., 2014; Dincă et al., 2015).

Data from the National Greenhouse Gas Inventory, compiled under the United Nations Framework Convention on Climate Change (UNFCCC), indicate that Romanian forest lands absorbed an average of around 25 million tons of $CO_2$ equivalent over the last 10 years (2011-2020), accounting about 25% of the total national greenhouse gas emissions (Dragostin et al., 2022).

Given the importance of quantifying carbon dioxide fluxes from forests for greenhouse gas (GHG) inventory reporting (Braga, 2018), and considering that this represents a novel research direction in Romania, it was deemed appropriate to carry out a study focusing on degraded lands as well. The results obtained can provide an initial basis for evaluating the annual carbon dioxide pools from plantations established on degraded lands within the country.

The aim of the research was to quantify the total carbon stored in the soil, litter, aboveground biomass, and deadwood of forest plantations established on degraded lands in the Curvature Subcarpathians region.

## MATERIALS AND METHODS

The research was carried out in permanent experimental plots (PEP), located in representative situations of stands on degraded lands in three experimental perimeters (EP) in the Subcarpathian Curvature area (Figure 1): Caciu-Bârseşti (CB), Pârâul Sărat-Valea Sării (PS) located from a phytoclimatic point of view in the hilly storey of sessile oak, beech and sessile oak-beech codified as $FD_3$ and Livada-Râmnicu Sărat (LV), located in internal forest-steppe site codified as Ssd (Table 1).

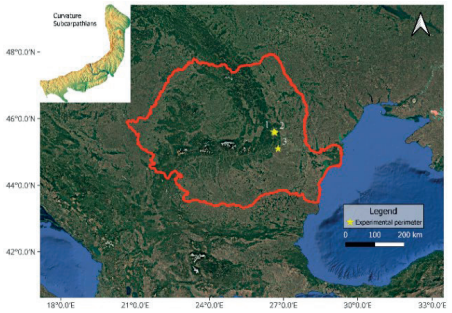



Figure 1. Location of the study (marked on the map with yellow stars: 1 - EP Caciu-Bârseşti; 2 - EP Pârâul Sărat-Valea Sării; 3 - EP Livada-Râmnicu Sărat)

The researches consisted in observations, measurements, field data collection, processing and interpretation regarding the determination of carbon stored in the soil, litter, living biomass and deadwood.

In the laboratory, soil samples were collected from soil profiles at depths of 0-10 cm, 11-20 cm, and 21-40 cm to determine organic carbon (%) and bulk density (BD, g/cm³). Litter samples consisting of dried leaves, fruits, plant residues, and twigs, were collected from each research plot over an area of 1 m² to determine organic carbon content (C%) and mass (g/m²).

To determine the amount of carbon (C) accumulated at different soil depths, the following formula was used:

$$C = SOC\ \% * BD * d * CFst$$

where: C - soil carbon stock (kg/m² × 10 = t/ha); SOC % - soil organic carbon concentration determined in the laboratory (%); BD - bulk density of the soil (kg/dm³);
d - depth or thickness of the analyzed horizon (cm); CFst - correction factor for skeletal fraction (= 1).

Table 1. General information on the studied permanent experimental plots (PEP)

| Name/Location | | Phyto-climatic zone | Stand composition | Age (years) | Degradation form |
|---|---|---|---|---|---|
| EP | PEP | | | | |
| Caciu-Bârsești (CB) | PEP8 | $FD_3$ | 93Pi 7Pi.n | 50 | E3 |
| | PEP11 | $FD_3$ | 33Pi 67Pi.n | 51 | E3 |
| Pârâul Sărat-Valea Sării (PS) | PEP1 | $FD_3$ | 44Pi 48Pi.n 8 Dt | 68 | E3 |
| | PEP9 | $FD_3$ | 8Pi 92 Pi.n | 70 | E1 |
| Livada-Râmnicu Sărat (LV) | PEP10 | Ssd | 52 Pi 48 Dt | 71 | E1 |
| | PEP12 | Ssd | 95 Pi.n 5 Dt | 73 | E1 |
| | PEP13 | Ssd | 100 St.r | 73 | E1 |
| | PEP14 | Ssd | 81 St.b 19 Dt | 73 | E1 |

**Legend:** PEP - Permanent Experimental Plot; EP - Experimental Perimeter; $FD_3$ - the hilly storey of sessile oak, beech and sessile oak-beech; Ssd - internal forest-steppe site; Pi - Scots Pine; Pi.n - Black pine; Dt - diverse hardwood species; St.r - red oak; St.b - greyish oak; E3 - very strong erosion; E1 - moderate erosion.

The organic carbon in litter (OC_L) stock was calculated as the product of litter mass and the carbon percentage (C %) determined in the laboratory.
Data collection for trees and deadwood to determine the organic carbon stored in wood, involved inventories of tree numbers by species, dendrometric characteristics of trees (DBH-diameter at the breast height, H- height) or deadwood (DBH, length and so on) and sampling of wood samples using a "Pressler" increment borer to determine wood density.
The organic carbon stored in wood (CW) was calculated by first estimating tree volume (m³) using allometric equations. To convert tree volume (m³) into biomass (t), species-specific wood density (WD) values were used, determined gravimetrically (Chave et al., 2006) based on analyses of wood samples extracted from trees of each species. The carbon stock (C, t/ha) corresponding to aboveground biomass (AGB) and deadwood biomass (DWB) was calculated according to standard recommendations (IPCC, 2003; Penman et al., 2003; Eggleston, 2006; IPCC, 2006). Depending on the species, the carbon content in wood ranges between 46% and 59% of the tree biomass (Thomas & Malczewski, 2007). The carbon content in wood (CW), whether living or dead (C_DW), was assumed to be 50% of the biomass (Innes, 2004) and was obtained by multiplying the total biomass by 0.5.

## RESULTS AND DISCUSSIONS

### Soil carbon stock

Based on the research data obtained (Table 2), it was found that the highest soil organic carbon stocks at a depth of 0-40 (20) cm ranged between 99.57-120 t/ha. In some cases, particularly on degraded lands, the total soil depth was only 20 cm. These values were recorded in Scots pine plantations mixed with black pine, aged 50-51 years, on very strongly eroded lands. The lowest values (70.96-71.76 t/ha) were recorded in deciduous plantations or in mixed pine (Scots and black pine) and deciduous stands, aged 71-73 years, on moderately to strongly eroded lands.

Table 2. Soil organic carbon stock, by depth intervals and total values

| PEP-EP | Soil depth | Bulk density | Soil organic carbon | |
|---|---|---|---|---|
| | Cm | g/cm³ | % | (t/ha) |
| PEP8-CB | 0-10 cm | 1.058 | 3.74 | 39.54 |
| | 10-20 cm | 1.406 | 2.31 | 32.48 |
| | 20-40 cm | 1.627 | 1.48 | 47.98 |
| | **Total** | | **7.52** | **120.00** |
| PEP11-CB | 0-10 cm | 1.121 | 4.41 | 49.39 |
| | 10-20 cm | 1.483 | 1.25 | 18.47 |
| | 20-40 cm | 1.613 | 0.98 | 31.72 |
| | **Total** | | **6.64** | **99.57** |
| PEP1-PS | 0-10 cm | 1.224 | 2.39 | 29.27 |
| | 10-20 cm | 1.308 | 1.26 | 16.50 |
| | 20-40 cm | 1.520 | 0.89 | 26.89 |
| | **Total** | | **4.54** | **72.67** |
| PEP9-PS | 0-10 cm | 1.251 | 3.13 | 39.15 |
| | 10-20 cm | 1.501 | 1.43 | 21.39 |
| | 20-40 cm | 1.485 | 0.93 | 27.73 |
| | **Total** | | **5.49** | **88.27** |
| PEP10-LV | 0-10 cm | 1.029 | 4.01 | 41.30 |
| | 10-20 cm | 1.266 | 2.39 | 30.28 |
| | **Total** | | **6.41** | **71.58** |
| PEP12-LV | 0-10 cm | 1.224 | 3.33 | 40.71 |
| | 10-20 cm | 1.185 | 2.62 | 31.05 |
| | **Total** | | **5.95** | **71.76** |
| PEP13-LV | 0-10 cm | 1.324 | 1.98 | 26.26 |
| | 10-20 cm | 1.511 | 1.13 | 17.08 |
| | 20-40 cm | 1.469 | 1.10 | 32.26 |
| | **Total** | | **4.21** | **75.60** |
| PEP14-LV | 0-10 cm | 1.065 | 2.16 | 23.04 |
| | 10-20 cm | 1.109 | 1.36 | 15.09 |
| | 20-40 cm | 1.237 | 1.33 | 32.84 |
| | **Total** | | **4.85** | **70.96** |

In the soil profile, the highest carbon content values were generally recorded in the upper 10 cm (Figure 2).

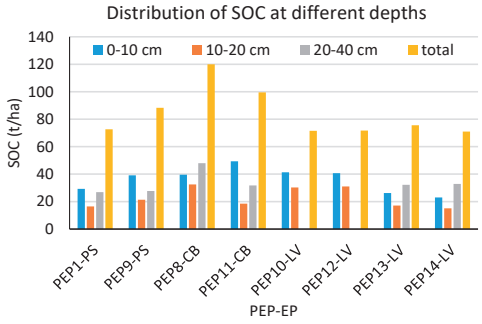



Figure 2. Distribution of soil organic carbon (SOC) stock

In the first 10 cm of the soil profile, carbon stock values ranged between 23.04 t/ha and 49.39 t/ha, whereas in the 10-20 cm layer they ranged from 15.09 t/ha to 32.48 t/ha. The minimum and maximum values by soil horizon were recorded in the same plots/stands as for total carbon stock. In a previous study conducted on eutricambosol soils (Dincă et al., 2012), the following organic carbon stocks were determined by geometric horizons: 42 t/ha (0-10 cm), 26 t/ha (10-20 cm), 33 t/ha (20-40 cm), and 40 t/ha (>40 cm), giving a total of 140 t/ha. For soils in Germany of the cambisol class, Grüneberg et al. (2014) compared periodic values of carbon stock in the mineral layer at a depth of 30 cm, finding 68.3 ± 2.2 t/ha, which is lower than the average value determined in Romania. Batjes (2002) reported that cambisol soils in central and southern Europe have a carbon stock of 69 t/ha for the first 30 cm and 118 t/ha at 100 cm depth. The same author (Batjes, 2014) determined a global carbon stock of 88 t/ha in eutricambosol soils for the first 100 cm.

Compared with values reported by the aforementioned authors, the average carbon stock in soils on degraded lands in the studied plots was 36 t/ha (0-10 cm), 23 t/ha (10-20 cm), and 33 t/ha (20-40 cm), which is lower (in the first 20 cm) or similar (20-40 cm) to those determined for eutricambosols.

According to the guidelines elaborated by ICPA (Dumitru et al., 2011), in the soils analyzed on degraded lands, carbon content in the upper 20 cm is considered good to very good (3.65-6.41%) in all pine-containing stands, and medium (3.11-3.52%) in deciduous stands (oaks). The total carbon stock (throughout the entire soil depth) is generally classified as medium in most of the analyzed cases.

## Litter carbon stock

Litter represents the organic matter on the soil surface, which, due to its characteristics, is an ecologically important component.

The determination of the total litter quantity, such as the organic carbon stock in litter for the analyzed research plots, revealed differences between plots depending on stand composition, age, and the degree of land degradation. According to the summary data (Table 3), the highest litter carbon stock (OC_L) values (12.24-13.04 t/ha) were recorded in pine stands (Scots pine or black pine) mixed with deciduous species, aged 71-73 years, on moderately to strongly eroded lands. Lower values were found in deciduous stands (4.99-7.9 t/ha) and in pine stands on very strongly to excessively eroded lands (4.72-8.60 t/ha), (Table 3).

Table 3. Organic carbon stock in litter (OC_L)

| PEP - EP | Litter horizon | C % | Mass t/ha | OC_L t/ha |
|---|---|---|---|---|
| PEP8 - CB | OL | 42.54 | 5.17 | 2.20 |
| | OF+OH | 24.99 | 10.07 | 2.52 |
| | **Total** | | 15.24 | 4.72 |
| PEP11 - CB | OL | 51.06 | 10.08 | 5.15 |
| | OF+OH | 32.97 | 10.48 | 3.46 |
| | **Total** | | 20.56 | 8.60 |
| PEP1 - PS | OL | 47.76 | 4.41 | 2.10 |
| | OF+OH | 31.99 | 14.26 | 4.56 |
| | **Total** | | 18.67 | 6.67 |
| PEP9 - PS | OL | 56.16 | 6.82 | 3.83 |
| | OF+OH | 25.02 | 6.26 | 1.57 |
| | **Total** | | 13.08 | 5.40 |
| PEP10 - LV | OL | 36.24 | 7.40 | 2.68 |
| | OF+OH | 29.63 | 34.97 | 10.36 |
| | **Total** | | 42.36 | 13.04 |
| PEP12 - LV | OL | 47.70 | 8.41 | 4.01 |
| | OF+OH | 29.90 | 27.53 | 8.23 |
| | **Total** | | 35.94 | 12.24 |
| PEP13 - LV | OL | 38.88 | 6.83 | 2.66 |
| | OF+OH | 23.94 | 9.74 | 2.33 |
| | **Total** | | 16.57 | 4.99 |
| PEP14 - LV | OL | 42.60 | 11.56 | 4.93 |
| | OF+OH | 25.12 | 11.82 | 2.97 |
| | **Total** | | 23.38 | 7.90 |

**Legend:** PEP - Permanent Experimental Plot; EP - Experimental Perimeter; C - organic carbon stock (%); OL - organic horizon of litter; OF - fermentation horizon; OH - Humification Horizon; OC_L - organic carbon in litter.

## Carbon Stock in Tree Biomass

Research indicates that carbon stock in biomass on degraded lands varies depending on stand age, species composition, stand structure, and the type of degradation. It is determined by the accumulated wood volume of the different

species, as well as by the wood density or specific gravity. For the studied plots (Table 4), in pine-containing stands, carbon stock in biomass ranged from 45.78 t/ha in a Scots pine plantation mixed with black pine, aged 50 years, on very strongly to excessively eroded land, up to 213.45 t/ha in a predominantly black pine plantation mixed with Scots pine, aged 70 years, on moderately eroded land.

In deciduous stands, biomass carbon stock was 135.44 t/ha in a late pedunculate oak (*Quercus pedunculiflora*) stand and 258.24 t/ha in a red oak (*Quercus rubra*) stand, both aged 73 years and located on moderately eroded land.

Table 4. Carbon stock in tree biomass (CW)

| PEP-EP | SP | WD, kg/mc | WD, t/mc | V, mc/ha | AGB, t/ha | CW, t/ha |
|---|---|---|---|---|---|---|
| PEP8 - CB | Pi | 45.84 | 0.45 | 190.00 | 86.23 | 43.11 |
| | Pi.n | 471.71 | 0.47 | 11.28 | 5.32 | 2.66 |
| | **total** | | | **201.28** | **91.55** | **45.78** |
| PEP11 - CB | Pi | 413.87 | 0.41 | 118.60 | 49.08 | 24.54 |
| | Pi.n | 471.41 | 0.47 | 237.85 | 112.12 | 56.06 |
| | **total** | | | **356.45** | **161.21** | **80.60** |
| PEP1 - PS | Pi | 522.97 | 0.52 | 137.84 | 72.09 | 36.04 |
| | Pi.n | 687.90 | 0.69 | 159.98 | 110.05 | 55.03 |
| | **total** | | | **297.82** | **182.14** | **91.07** |
| PEP9 - PS | Pi | 522.97 | 0.52 | 64.70 | 33.84 | 16.92 |
| | Pi.n | 531.04 | 0.53 | 740.17 | 393.06 | 196.53 |
| | **total** | | | **804.87** | **426.90** | **213.45** |
| PEP10 - LV | Pi | 404.71 | 0.40 | 418.04 | 169.18 | 84.59 |
| | Dt | 669.12 | 0.67 | 45.79 | 30.64 | 15.32 |
| | **total** | | | **463.83** | **199.82** | **99.91** |
| PEP12 -LV | Pi.n | 452.47 | 0.45 | 494.46 | 223.73 | 111.86 |
| | St | 669.12 | 0.67 | 4.84 | 3.24 | 1.62 |
| | **total** | | | **499.30** | **226.97** | **113.48** |
| PEP13 - LV | St.r | 600.52 | 0.60 | **860.06** | **516.48** | **258.24** |
| PEP14 - LV | St.b +Dt | 669.12 | 0.67 | **404.83** | **270.88** | **135.44** |

**Legend:** PEP - Permanent Experimental Plot; EP - Experimental Perimeter; SP - species; WD - wood density; V - volume per hectare; AGB- aboveground biomass; CW - carbon stock for living biomass of the tree; Pi - Scots pine; Pi.n - black pine; Dt - diverse hardwood species; St - common oak; St.r- red oak; St.b - greyish oak.

The results indicate that the rate of carbon accumulation in living biomass of the tree increases proportionally with wood density (WD) and unit volume (V). The exponential model used captures the nonlinear nature of carbon stock growth (Figure 3), suggesting that substantial amounts of carbon can be accumulated as tree diameter increases. Moreover, the model parameters allow efficient estimation of the carbon accumulation rate in relation to both tree diameter and species.

In comparison, in the internal forest-steppe site (EP Livada - Râmnicu Sărat), deciduous species (greyish oak - St.b; red oak - St.r) exhibit higher carbon accumulation than conifers (Scots pine - Pi; black pine - Pi.n), due to higher wood density (WD) and favorable dimensional characteristics (DBH, H), which promote greater biomass growth (Figure 3).

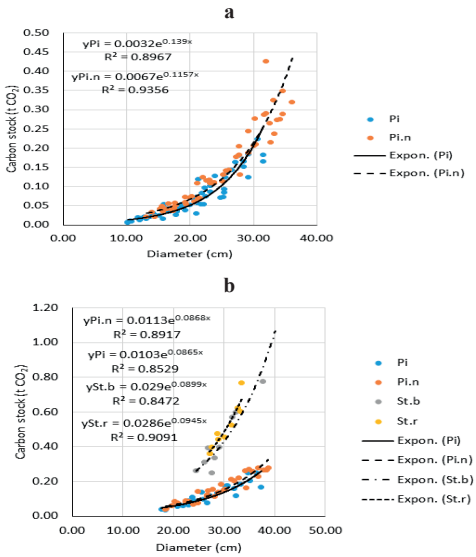



Figure 3. Distribution of soil organic carbon stock in relation to diameter at breast height (DBH) for the main species within the experimental perimeter: **a** - EP Caciu Bârseşti and EP Pârâul Sărat-Valea Sării; **b** - EP Livada-Râmnicu Sărat (**Legend**: Pi - Scots pine; Pi.n - Black pine; St.b - greyish oak; St.r - red oak)

## Carbon Stock in Deadwood

To evaluate the biomass derived from deadwood (DWB), the volume of deadwood in the analyzed plots was considered, determined according to the dimensions of the identified pieces by species, along with the average values of deadwood density ($WD_m$) determined for different decay classes (Weggler et al., 2012). These values range from 315.42 to 481.04 kg/m³ for pine species and 534.24-558.55 kg/m³ for manna ash (*Fraxinus ornus*). Scots pine (*Pinus sylvestris*) shows higher wood density and slower decay compared to black pine (*Pinus nigra*), which has lower wood densities and faster decay across the classes.

The carbon stock in deadwood (C_DW) ranges from 17-18 t/ha (Table 5), representing 16-17% of the carbon stock in living tree biomass in the analyzed plots. This is explained by the high proportion of damage (such as drying and

breakage) in pines caused by abiotic stress factors, including drought and wind.

In the analyzed experimental plots where deadwood was identified (Table 5), coniferous species (Scots pine and black pine) represent the main source of deadwood biomass, while the contribution of deciduous species (manna ash) is low, representing less than 5% of the total. This distribution reflects a forest structure dominated by pines, with deadwood accumulation primarily from these species.

The differences observed between the two analyzed plots are associated with stand composition, stand density, the history of ecosystem disturbances and the decay stage of the wood, with slightly higher carbon storage in deadwood from stands dominated by black pine.

Table 5. Carbon stock per hectare in deadwood

| PEP - EP | SP | DWB (t/ha) | C_DW (t/ha) |
|---|---|---|---|
| PEP10 - LV | Pi | 32.38 | 16.19 |
| | Mj | 1.68 | 0.84 |
| | **Total** | **34.06** | **17.03** |
| PEP12 - LV | Pi.n | 35.47 | 17.74 |
| | Mj | 0.17 | 0.09 |
| | **Total** | **35.64** | **17.83** |

**Legend**: PEP- Permanent Experimental Plot; EP -Experimental Perimeter; DWB - deadwood biomass; C_DW - Carbon stock in deadwood; Pi - Scots pine; Pi.n - black pine; Mj - manna ash.

**Total Organic Carbon Stock (Soil, Litter, Living and Dead Biomass)**

The data summarized in Figure 4 reveal considerable variations in carbon stocks across the permanent experimental plots (PEPs).

Higher total carbon values were recorded in PEPs dominated by species with high productive potential relative to environmental conditions (land degradation), such as black pine and xerophytic oaks. These results are consistent with accumulated living biomass, stand age, forest structure and vegetation conditions.

The contribution of soil carbon remains relatively stable, ranging between 70 and 120 t/ha, whereas litter carbon exhibits greater variability. The highest litter carbon stock (13.04 t/ha) was observed in well-balanced pine with deciduous mixtures of older age (PEP10-LV), likely due to more substantial accumulation of organic matter.

Experimental plots with pine stands (PEP10 and PEP12-LV) in the internal forest-steppe site (Ssd) are notable for the presence of a significant deadwood component (~17.00 t/ha), which further contributes to total carbon stock. In contrast, in other plots, deadwood is absent or insignificant, indicating either low tree mortality dynamics or rapid decomposition of deadwood.

Overall, total carbon stock is primarily determined by living biomass and soil carbon, highlighting the influence of stand composition and structure (depending on pedological conditions) on carbon storage capacity.

From the graphical analysis (Figure 4), the following characteristics emerge:

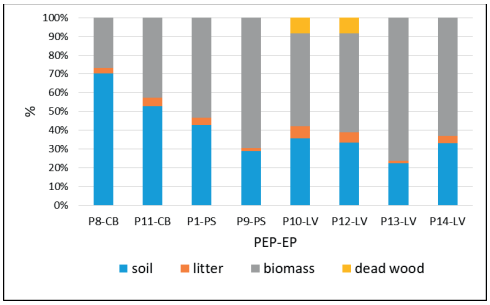



Figure 4. Carbon Stock Structure (%) by component (soil, litter, biomass, deadwood) for different experimental plots

- Pine stands store more carbon in the soil than deciduous (quercine) stands. Conversely, deciduous stands accumulate more carbon in the aboveground living biomass;
- Stands from internal forest-steppe site (Ssd), particularly pine stands, accumulate more carbon in litter and deadwood compared to stands from the hilly storey of sessile oak, beech and sessile oak-beech ($FD_3$) phytoclimatic level;
- Pines on very strongly eroded lands in the $FD_3$ level accumulate less carbon in the aboveground living biomass, with a greater proportion stored in the soil. In contrast, pine stands in internal forest-steppe site (Ssd) on moderately eroded lands accumulate more carbon in the aboveground living biomass.

## CONCLUSIONS

The determination of organic carbon stock in forest plantations on degraded lands involved quantifying carbon accumulated in the main storage compartments of forest ecosystems: soil, litter, living tree biomass and deadwood.

Higher values of soil carbon stock were determined in younger pine stands on very heavily

eroded lands, compared to older deciduous stands on moderately eroded lands. In the litter, the largest amount of carbon was accumulated by mixed pine and deciduous trees of older ages, on moderately-severely eroded lands.

The carbon stock in tree biomass varies depending on the age, composition, structure of the stands and the degree of soil degradation, being almost 5 times lower in younger stands on heavily eroded lands (45.78 t/ha) compared to those of older age and on moderately eroded lands (>200 t/ha).

The carbon stock in dead wood differs according to species and phytoclimatic zone, with higher values being recorded in pine stands in the forest-steppe zone, as a result of damage caused by abiotic factors.

Total carbon stock is generally given by living biomass and soil carbon. The proportion of carbon stored in dead wood and litter becomes significant only in certain ecological contexts, such as the case of stands in the hilly forest-steppe area.

The complexity represented by environmental conditions revealed differences between the analyzed areas, highlighting the role of stand structure and composition in carbon storage. These results highlight the importance of species diversity and forest structure for the carbon sequestration capacity of forest ecosystems.

The aim of the study to know the total carbon stock in stands on degraded lands was achieved, this being limited to stands in the Curvature Subcarpathian area with the possibility of being used in similar situations. The results obtained make an important contribution to the assessment of the carbon stock in forests and the monetization of their ecosystem services, reflecting the importance of forest ecosystems in carbon sequestration and climate change mitigation.

In the next stage, new research is needed to determine the annual carbon flux, which is a dynamic, variable and complex process in relation to the characteristics of the stands, the silvicultural works applied, the impact of damaging abiotic factors, etc.

## ACKNOWLEDGEMENTS

This research was conducted as part of the NUCLEU Research Program, Project PN 23090203, funded by the Ministry of Education and Research and implemented by the ”Marin Drăcea” National Institute for Research and Development in Forestry (INCDS).

## REFERENCES

Baritz, R., Seufert, G., Montanarella, L., & Van Ranst, E. (2010). Carbon concentrations and stocks in forest soils of Europe. *Forest Ecology and Management*, *260*(3), 262-277.

Batjes, N. H. (2002). Carbon and nitrogen stocks in the soils of Central and Eastern Europe. *Soil Use and Management*, *18*(4), 324-329.

Batjes, N. H. (2014). Total carbon and nitrogen in the soils of the world. *European journal of soil science*, *65*(1), 10-21.

Braga, C. I. (2018). *The analysis of the main factors that influence the soil carbon dioxide efflux in beech forests on hills from the South of Muscelele Argeşului Region*. Doctoral dissertation, Universitatea Transilvania din Brasov, Facultatea de Silvicultura si Exploatari Forestiere.

Chave, J., Muller-Landau, H. C., Baker, T. R., Easdale, T. A., Steege, H. T., & Webb, C. O. (2006). Regional and phylogenetic variation of wood density across 2456 neotropical tree species. *Ecological applications*, *16*(6), 2356-2367.

Constandache, C., Tudor, C., Popovici, L., & Vlad, R. (2023). The state and behavior of some forestry cultures installed on degraded lands in the forest-steppe site. *Scientific Papers, Series E. Land Reclamation, Earth Observation & Surveying, Environmental Engineering, 12*, 215-223.

Dincă, L. C., Spârchez, G., Dincă, M., & Blujdea, V. N. (2012). Organic carbon concentrations and stocks in Romanian mineral forest soils. *Annals of Forest Research*, *55*(2), 229-241.

Dincă, L. C., Dincă, M., Vasile, D., Sparchez, G., & Holonec, L. (2015). Calculating organic carbon stock from forest soils. *Notulae Botanicae Horti Agrobotanici Cluj-Napoca*, *43*(2), 568-575.

Dragostin, C., Tobescu, C., Hapa, M., Badea, O., Radu, R., Chivulescu, S., (2022), *The forest-wood sector in the context of climate change and its contribution to the development of the socio-economic system* (Sectorul pădure-lemn în contextul schimbărilor climatice și contribuția acestuia la dezvoltarea sistemului socio-economic), Silvica Publishig House.

Dumitru, M., Manea, A., Ciobanu, C., Dumitru, S., Vrînceanu, N., Calciu, I., ... & Eftene, M. (2011). Soil quality monitoring in Romania. *Institutul Național de Cercetare-Dezvoltare pentru Pedologie, Agrochimie și Protecția Mediului-ICPA*, SITECH Publishing House, Craiova.

Eggleston, S. (2006). Estimation of emissions from CO2 capture and storage: the 2006 IPCC guidelines for national greenhouse gas inventories. In *Presentation at the UNFCCC workshop on carbon dioxide capture and storage,* (20).

European Commission (2010). *Green Papaer on Forest Protection and Information in the EU: Preparing forests for climate change*, Brussels, 1.3.2010 66 final.

Grüneberg, E., Ziche, D., & Wellbrock, N. (2014). Organic carbon stocks and sequestration rates of forest soils in Germany. *Global change biology*, *20*(8), 2644-2662.

Innes, J. L. (2004). Forests And Forest Plants – Vol. I - *Forests in Environmental Protection*, University of British Columbia, Canada.

IPCC (2003). *Good Practice Guidance for Land Use, Land-Use Change and Forestry*. Intergovernmental Panel on Climate Change (IPCC), IPCC/IGES, Hayama, Japan.

IPCC (2006). 2006 IPCC guidelines for national greenhouse gas inventories. *Institute for global environmental strategies, Hayama, Kanagawa, Japan*.

Jandl, R., Lindner, M., Vesterdal, L., Bauwens, B., Baritz, R., Hagedorn, F., Johnson, D. W., Minkkinen, K., & Byrne, K. A. (2007). How strongly can forest management influence soil carbon sequestration? *Geoderma*, *137*(3-4), 253-268.

Janssens, I. A., Freibauer, A., Ciais, P., Smith, P., Nabuurs, G. J., Folberth, G., Schlamadinger, B., Hutjes, R.W.A., Ceulemans, R., Schulze, E.D., Valentini, R., & Dolman, A. J. (2003). Europe's terrestrial biosphere absorbs 7 to 12% of European anthropogenic CO2 emissions. *Science*, *300*(5625), 1538-1542.

Jobbágy, E. G., & Jackson, R. B. (2000). The vertical distribution of soil organic carbon and its relation to climate and vegetation. *Ecological applications*, *10*(2), 423-436.

Koch, B. (2010). Status and future of laser scanning, synthetic aperture radar and hyperspectral remote sensing data for forest biomass assessment. *ISPRS Journal of Photogrammetry and Remote sensing*, *65*(6), 581-590.

Konôpka, B., Pajtík, J., & Šebeň, V. (2025). Biomass Modeling in European Beech and Norway Spruce Plantations: An Opportunity to Enhance the Carbon Market and Climate Sustainability. *Sustainability*, *17*(9), 4198.

Lajtha, K., Townsend, K. L., Kramer, M. G., Swanston, C., Bowden, R. D., & Nadelhoffer, K. (2014). Changes to particulate versus mineral-associated soil carbon after 50 years of litter manipulation in forest and prairie experimental ecosystems. *Biogeochemistry, 119*(1), 341-360.

Maestre, F. T., & Cortina, J. (2004). Insights into ecosystem composition and function in a sequence of degraded semiarid steppes. *Restoration Ecology, 12,* 494-502.

Moscatelli, M. C., Bonifacio, E., Chiti, T., Cudlín, P., Dinca, L., Gömöryova, E., Grego, S., Porta, N. L., Karliński, L., Pellis, G., Rudawska, M., Squartini, A., Zhiyanski, M., & Broll, G. (2017). Soil properties as indicators of treeline dynamics in relation to anthropogenic pressure and climate change. *Climate Research*, *73*(1-2), 73-84.

Nadelhoffer, K. J., Colman, B. P., Currie, W. S., Magill, A., & Aber, J. D. (2004). Decadal-scale fates of 15N tracers added to oak and pine stands under ambient and elevated N inputs at the Harvard Forest (USA). *Forest Ecology and Management*, *196*(1), 89-107.

Oprică, R. F., Tudose, N. C., Davidescu, Ş. O., Zup, M., Marin, M., Comănici, A. N., Criț, M. N., & Pitar, D. (2022). Gender inequalities in Transylvania's largest peri-urban forest usage. *Annals of Forest Research*, *65*(2), 57-69.

Penman, J., Gytarsky, M., Hiraishi, T., Krug, T., Kruger, D., Pipatti, R., Buendia, L., Miwa, K., Ngara, T., Tanabe, K., & Wagner, F. (2003). Definitions and methodological options to inventory emissions from direct human-induced degradation of forests and devegetation of other vegetation types. *Hayama Kanagawa: IPCC National Greenhouse Gas Inventories Programme-Technical Support Unit,* 32.

Rodríguez de Prado, D., Vázquez Veloso, A., Quian, Y. F., Ruano, I., Bravo, F., & Herrero de Aza, C. (2023). Can mixed forests sequester more $CO_2$ than pure forests in future climate scenarios? A case study of Pinus sylvestris combinations in Spain. *European Journal of Forest Research, 142*(1), 91–105.

Schulze, E. D., Ciais, P., Luyssaert, S., Schrumpf, M., Janssens, I. A., Thiruchittampalam, B., Theloke, J., Saurat, M., Bringezu, S., Lelieveld, J., Lohila, A., Rebmann, C., Jung, M., Bastviken, D., Abril, G., Grassi, G., Leip, A., Freibauer, A., Kutsch, W., Don, A., Nieschulze, J., Borner, A., Gash, J. H., & Dolman, A. J. (2010). The European carbon balance. Part 4: Integration of carbon and other trace-gas fluxes. *Global Change Biology*, *16*(5), 1451-1469.

Semwal, R. L., Nautiyal, S., Maikhuri, R. K., Rao, K. S., & Saxena, K. G. (2013). Growth and carbon stocks of multipurpose tree species plantations in degraded lands in Central Himalaya, India. *Forest Ecology and Management*, *310*, 450-459.

Somogyi, Z., Cienciala, E., Mäkipää, R., Muukkonen, P., Lehtonen, A., & Weiss, P. (2007). Indirect methods of large-scale forest biomass estimation. *European Journal of Forest Research*, *126*(2), 197-207.

Thomas, S. C., & Malczewski, G. (2007). Wood carbon content of tree species in Eastern China: Interspecific variability and the importance of the volatile fraction. *Journal of Environmental Management*, *85*(3), 659-662.

Torres, I., Moreno, J. M., Morales-Molino, C., and Arianoutsou, M. (2021). *Ecosystem services provided by pine forests. Pines and their mixed forest ecosystems in the Mediterranean Basin*. Springer International Publishing, 617–629.

Tudor, C., Constandache, C., Dinca, L., Murariu, G., Badea, N. O., Tudose, N. C., & Marin, M. (2025). Pine afforestation on degraded lands: a global review of carbon sequestration potential. *Frontiers in Forests and Global Change*, *8*, 1648094.

Weggler, K., Dobbertin, M., Jüngling, E., Kaufmann, E., & Thürig, E. (2012). Dead wood volume to dead wood carbon: the issue of conversion factors. *European Journal of Forest Research*, *131*(5), 1423-1438.

Scientific Papers. Series E. Land Reclamation, Earth Observation & Surveying, Environmental Engineering. Vol. XV, 2026
Print ISSN 2285-6064, CD-ROM ISSN 2285-6072, Online ISSN 2393-5138, ISSN-L 2285-6064

# SEASONAL AND DIURNAL DYNAMICS OF SIZE-RESOLVED PARTICULATE MATTER IN AN URBAN AREA OF GALAȚI, ROMANIA, BASED ON CONTINUOUS RAPID-E MONITORING

**Mădălin CRISTEA[1], Adrian ROȘU[1, 2], Sorin FRĂSÎNĂ[1], Bogdan ROȘU[2], Daniel-Eduard CONSTANTIN[1, 2], Mirela VOICULESCU[1, 2], Silvia DRĂGAN[3]**

[1]"Dunărea de Jos" University of Galaţi, Faculty of Sciences and Environment, Department of Chemistry, Physics and Environment, 111 Domnească Street, Galaţi, Romania
[2]"Dunărea de Jos" University of Galaţi, REXDAN Research Infrastructure, 98 George Coşbuc Street, Galaţi, Romania
[3]EnviroEcoSmart S.R.L., 189 Tecuci Street, Galaţi, Romania

Corresponding author email: adrian.rosu@ugal.ro

***Abstract***

*Fine and ultrafine particulate matter (PM) is a major environmental and public health issue, particularly in densely populated urban areas exposed to significant anthropogenic emissions. This study presents an analysis of PM concentrations based on size in a high-traffic area of Galați, Romania, using the REXDAN Research Center monitoring system and the RAPID-E real-time analyzer. The continuous measurements were carried out between December 31, 2023 (10:00 p.m.) and December 31, 2025 (10:00 p.m.), covering the particle size fractions of 0.3, 0.5, 1 and 5 µm. In addition to an earlier study of daily and weekly variations, this work examines seasonal variability as well as diurnal (day/night) contrasts. Statistical and temporal analyses were used to characterize fluctuations in PM concentrations and to identify trends related to weather conditions and anthropogenic activities. The results improve the understanding of particulate dynamics in urban settings and support the development of effective air quality management strategies.*

***Key words:*** *diurnal variation, particulate matter (PM), RAPID-E monitoring system, seasonal variability, urban air quality.*

## INTRODUCTION

Atmospheric pollutants, such as particulate matter (PM), $NO_2$, $SO_2$, $CO_2$, CO and $O_3$, have a significant influence on air quality and originate from a wide range of sources and processes, including atmospheric and chemical reactions, mechanical resuspension, biological activity, industrial emissions, agricultural activities and other pollution-generating processes (Manisalidis et al., 2020; World Health Organization, 2021; European Environment Agency, 2024).

These pollutants require continuous monitoring and control due to their effects on the environment, ecosystems and, most importantly, public health. Among them, particulate matter is considered one of the most harmful air pollutants, as it can directly or indirectly affect multiple internal organs. Fine and ultrafine particles, particularly those with diameters below 1 µm, may penetrate deep into the respiratory system, enter the bloodstream and reach sensitive organs such as the heart and brain, potentially causing severe and long-term health effects (Ngoc et al., 2017; Yang et al., 2021; Garcia et al., 2023). The most vulnerable population groups include elderly people, children and individuals with pre-existing health conditions, for whom exposure to particulate matter may act as an aggravating factor (Kirešová et al., 2023; Hamanaka & Mutlu, 2025).

In urban areas, the main sources of pollutants such as $NO_2$, $SO_2$ and particulate matter are fossil fuel combustion, road traffic and industrial activities (Karagulian et al., 2015; Roșu et al., 2020; World Health Organization, 2021). However, atmospheric particles may also originate from natural sources, including desert dust, volcanic eruptions and sea salt aerosols, which are difficult or impossible to control directly (Lonati & Giugliano, 2006; Ramgolam et al., 2008; Baldacchini et al., 2019). Atmospheric particles can occur in different physical states: some are entirely liquid, others are solid, while certain particles consist of a solid core surrounded by a liquid layer. Their

chemical composition is complex and may include inorganic ions, metallic compounds, elemental carbon, organic substances and crustal materials (Wilson et al., 2002; Mugica et al., 2009; Tao et al., 2017). In addition, many atmospheric particles are hygroscopic, meaning that they can absorb atmospheric moisture and retain water within their structure.

At the European level, air quality limit values are already established for $PM_{10}$ and $PM_{2.5}$, requiring continuous monitoring and data collection. However, as previously mentioned, particles with diameters below 1 μm may have particularly important health implications. To address the need for high-resolution monitoring of fine and ultrafine airborne particles, the Rapid-E+ device, developed as an advanced version of the Rapid-E system, has become a valuable tool for monitoring airborne particles such as pollen, fungal spores and bacteria (Sikoparija et al., 2024; Bruffaerts et al., 2025). This device employs optical detection technology combined with laser illumination to measure particles within the 0.3-100 μm size range with high accuracy. Therefore, Rapid-E+ provides a rapid and reliable method for the continuous monitoring of airborne particles (Šauliene et al., 2019).

The present article represents a continuation of a previous study that investigated the variation of particulate matter during weekdays and weekends (Cristea et al., 2025). In addition to the earlier analysis of daily and weekly variability, the present work investigates seasonal variability and differences between diurnal and nocturnal intervals. Statistical and temporal analyses were applied to characterize fluctuations in suspended particle concentrations and to identify trends associated with meteorological conditions and anthropogenic activities. The results contribute to a better understanding of atmospheric particle dynamics in urban environments and provide support for the development of effective air quality monitoring and management strategies.

## MATERIALS AND METHODS

### Study area and localization

For this study, continuous measurements of suspended particle concentrations were carried out in the municipality of Galați, one of the most important urban centers in north-eastern Romania. The monitoring campaign was conducted over a two-year period, from December 31, 2023, to December 31, 2025. The measurements were performed at the REXDAN Research Infrastructure (REXDAN RI), located on George Coșbuc Boulevard no. 98, Galați, Romania (45°26'6.66"N, 28°2'14.02"E).

The monitoring site was selected because it is in an urban area characterized by intense road traffic and active urban dynamics, both of which may influence local particulate matter concentrations. In addition, the location provided suitable conditions for the simultaneous operation of the aerosol monitoring system and the meteorological station within the same research infrastructure.

To obtain relevant data on atmospheric particle concentrations and local meteorological conditions, two complementary monitoring systems were used: the Rapid-E+ aerosol monitoring device and the ACTRIS RADO Galați meteorological station. The Rapid-E+ device was installed in the courtyard of the REXDAN RI, while the meteorological station was located on the rooftop of the same facility. This configuration allowed the continuous acquisition of particle concentration data together with meteorological parameters representative of the local urban environment from Galati city. The location of the Rapid-E+ device was previously presented in Cristea et al. (2025).

The main objective of this study was to assess the temporal variability of suspended particles in an urban environment and to investigate their relationship with local atmospheric parameters.

### Equipment and data used

The particulate matter measurements were performed using the Rapid-E+ system, an advanced real-time bioaerosol sensor developed for the detection, characterization and classification of individual airborne particles. During the two-year monitoring period, the Rapid-E+ system and the ACTRIS RADO Galați meteorological station operated simultaneously, enabling the direct comparison and correlation of particle concentration data with local meteorological parameters.

The instrument uses proprietary laser-based optical technology, combining scattered light pattern analysis with fluorescence spectroscopy,

which allows the characterization of aerosols in complex atmospheric environments (Plair SA, 2025a; 2025b). The integration of GPU-based processing improves the speed of data acquisition and processing, enabling efficient real-time monitoring of ambient air (Plair SA, 2025b).

The Rapid-E+ sensor continuously detects and characterizes airborne particles with diameters ranging from 0.3 to 100 µm (Plair SA, 2025a). The raw particle counts provided by the instrument are cumulative and correspond to particles above specific size thresholds. Thus, the 0.3 µm channel represents particles between 0.3 and 100 µm, the 0.5 µm channel corresponds to particles between 0.5 and 100 µm, the 1 µm channel includes particles between 1 and 100 µm, and the 5 µm channel represents particles between 5 and 100 µm (Plair SA, 2025b). These cumulative data were subsequently used to derive size-resolved particle fractions for further analysis.

The device can operate autonomously and remotely, allowing continuous data acquisition and access to measurements from any location. Rapid-E+ is designed for the real-time monitoring of airborne biological and non-biological particles, including pollen, fungal spores and bacteria, and is therefore suitable for applications in air quality assessment, biological risk monitoring, public health studies and environmental research (Plair SA, 2025b). The main technical specifications and operational features of the instrument are described in the previous study by Cristea et al. (2025) and on the official Rapid-E+ webpage (Plair SA, 2025a).

Figure 1 shows the Rapid-E+ system installed at the REXDAN RI. The instrument is placed inside a climate-controlled protective enclosure, which reduces direct exposure to external environmental factors, while the air intake tube is positioned externally to ensure continuous sampling of ambient air.

The ACTRIS RADO Galati meteorological station was used to continuously monitor local atmospheric conditions during the study period. The station recorded meteorological data at a temporal resolution of 5 minutes, providing detailed information on short-term atmospheric variability. The monitored parameters included air temperature, relative humidity, atmospheric pressure, visibility, wind speed and wind direction.

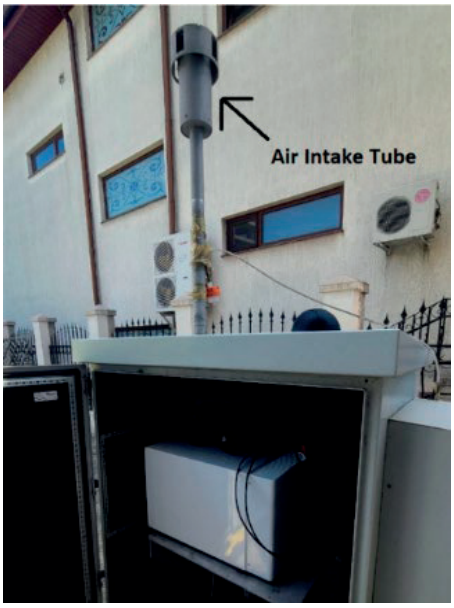



Figure 1. Rapid-E+ equipment installed at the REXDAN RI, showing the protective enclosure and the external air intake tube used for ambient air sampling of PM during 2024-2025 measurements

The meteorological data were used to evaluate the influence of local atmospheric conditions on airborne particle concentrations and size distribution. Continuous monitoring allowed the identification of temporal variations and supported the analysis of possible relationships between meteorological parameters and aerosol concentrations. The collected meteorological datasets were further used for comparison and correlation analyses with the Rapid-E+ measurements in order to assess the influence of atmospheric conditions on urban particle dynamics.

Figure 2 presents the ACTRIS RADO Galați meteorological station installed on the rooftop of the REXDAN RI. More technical specifications of the meteorological sensors can be found in the corresponding ACTRIS and Cloudnet instrument database entries (DJUG CS106, 2026; DJUG Ultrasonic Anemometer 2D, 2026; DJUG Weather Station, 2026).



Figure 2. ACTRIS RADO Galați meteorological station installed on the rooftop of the REXDAN RI used for continuous records of local atmospheric parameters for the 2024-2025 measurements

The Rapid-E+ system and the ACTRIS RADO Galați meteorological station operated simultaneously, enabling the direct comparison and correlation of particle concentration data with local meteorological parameters.

**Data processing and statistical analysis**

The analysis was based on particle number concentrations measured by the Rapid-E+ system within the 0.3-100 µm size range and on meteorological data recorded by the ACTRIS RADO Galați meteorological station. Since the Rapid-E+ instrument provides cumulative particle counts above specific diameter thresholds, a subtraction method was applied between consecutive cumulative channels to obtain size-resolved particle fractions.

Therefore, the broad measurement range was divided into four distinct size intervals: 0.3-0.5 µm, 0.5-1 µm, 1-5 µm and 5-100 µm. Each interval represents the isolated contribution of particles within the corresponding diameter range. If the instrument provides cumulative counts above each size threshold, namely $N_{\geq 0.3}$, $N_{\geq 0.5}$, $N_{\geq 1}$and $N_{\geq 5}$, the size-resolved fractions were calculated as follows:

$$N_{0.3-0.5} = N_{\geq 0.3} - N_{\geq 0.5} \quad (1)$$

$$N_{0.5-1} = N_{\geq 0.5} - N_{\geq 1} \quad (2)$$

$$N_{1-5} = N_{\geq 1} - N_{\geq 5} \quad (3)$$

$$N_{5-100} = N_{\geq 5} \quad (4)$$

where $N_{(\geq x)}$ represents the cumulative particle number concentration measured for particles with diameters greater than or equal to $x$ µm, while $N_{a-b}$ represents the particle number concentration calculated for the size interval between $a$ and $b$ µm.

All meteorological datasets were filtered and averaged to hourly values to ensure temporal compatibility with the particulate matter dataset. Pearson correlation analysis was then applied to evaluate the relationships between meteorological parameters and particle concentrations for each size fraction. The resulting correlation coefficients were represented as heatmaps to visualize the strength and direction of the relationships. The strength of the Pearson correlations was interpreted based on the absolute value of the correlation coefficient: weak correlations were considered for $|r| < 0.30$, moderate correlations for $0.30 \leq |r| < 0.50$, and strong correlations for $|r| \geq 0.50$. Positive values indicate that particle concentrations increase with the corresponding meteorological parameter, whereas negative values indicate an inverse relationship. Although statistical significance was assessed using $p$-values, only moderate and strong correlations were considered relevant for physical interpretation. Very weak correlations, even when statistically significant, were not interpreted as physically meaningful.

To assess the statistical significance of the observed correlations, a $p$-value analysis was performed for the Pearson correlation coefficients. This allowed the identification of statistically significant relationships and helped determine whether the observed correlations were unlikely to have occurred due to random variation in the dataset. Statistical significance was indicated directly on the Pearson correlation heatmaps using asterisks: $p < 0.05$, $p < 0.01$, and $p < 0.005$. Only moderate and strong correlations were considered relevant for physical interpretation.

## RESULTS AND DISCUSSIONS

The results are presented in three complementary stages to evaluate the relationships between meteorological parameters and size-resolved particulate matter fractions. First, the overall Pearson correlation

patterns were analyzed for the entire 2024-2025 monitoring period, as shown in Figure 3. Second, the dataset was divided by season to identify seasonal differences in the strength and direction of the correlations. Finally, daytime and nighttime conditions were analyzed separately to assess whether diurnal atmospheric variability influenced the relationships between meteorological parameters and particle concentrations. For each condition an explanation attempt is done based on the recorded data for weather (meteorological parameters) corellated with the PM classes. Figure 3 summarizes the overall correlations between local meteorological parameters and the size-resolved particulate matter fractions derived from the Rapid-E+ measurements. Positive correlation coefficients indicate that particle concentrations tend to increase with increasing values of the corresponding meteorological parameter, whereas negative coefficients indicate an inverse relationship.

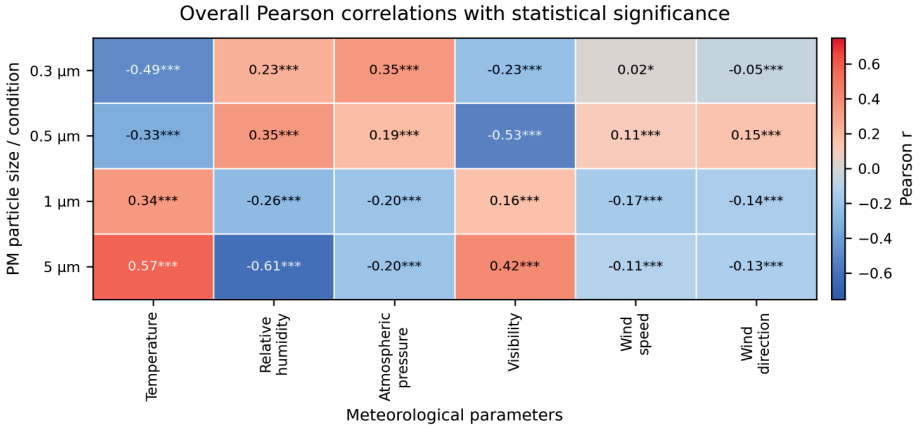



Figure 3. Overall Pearson correlation heatmap between meteorological parameters and size-resolved particulate matter fractions during the 2024-2025 monitoring period in Galați, Romania. Asterisks indicate statistical significance: ***$p < 0.005$, *$p < 0.01$, $p < 0.05$

Figure 3 shows the overall Pearson correlations between meteorological parameters and particle size fractions for the entire 2024-2025 monitoring period. The strongest negative correlation was observed between relative humidity and the 5 µm fraction (r = −0.61), suggesting that higher humidity was generally associated with lower concentrations of coarse particles, possibly due to particle removal, deposition or hygroscopic growth effects. A strong positive correlation was observed between temperature and the 5 µm fraction (r = 0.57), while visibility was negatively correlated with the 0.5 µm fraction (r = −0.53), indicating that fine particles may contribute to reduced atmospheric visibility. The 0.3 µm and 0.5 µm fractions generally showed correlation patterns opposite to those of the 1 µm and 5 µm fractions, especially for temperature, relative humidity, pressure and visibility. In contrast, wind speed and wind direction showed weak correlations with all particle fractions, suggesting a limited influence on the overall dataset. Most correlations were statistically significant, with *p*-values generally below 0.005 as presented in Figure 3 with asterisks that indicate the statistical significance: ***$p < 0.005$, *$p < 0.01$, $p < 0.05$. Similar approach was conducted for the other correlation heat maps presented in below figures.

Figure 4 highlights the seasonal variability of the relationships between meteorological parameters and particle size fractions. Stronger correlations were generally observed during winter, spring and autumn, while summer showed weaker and more variable associations, indicating that the influence of meteorological conditions on particulate matter is season dependent.

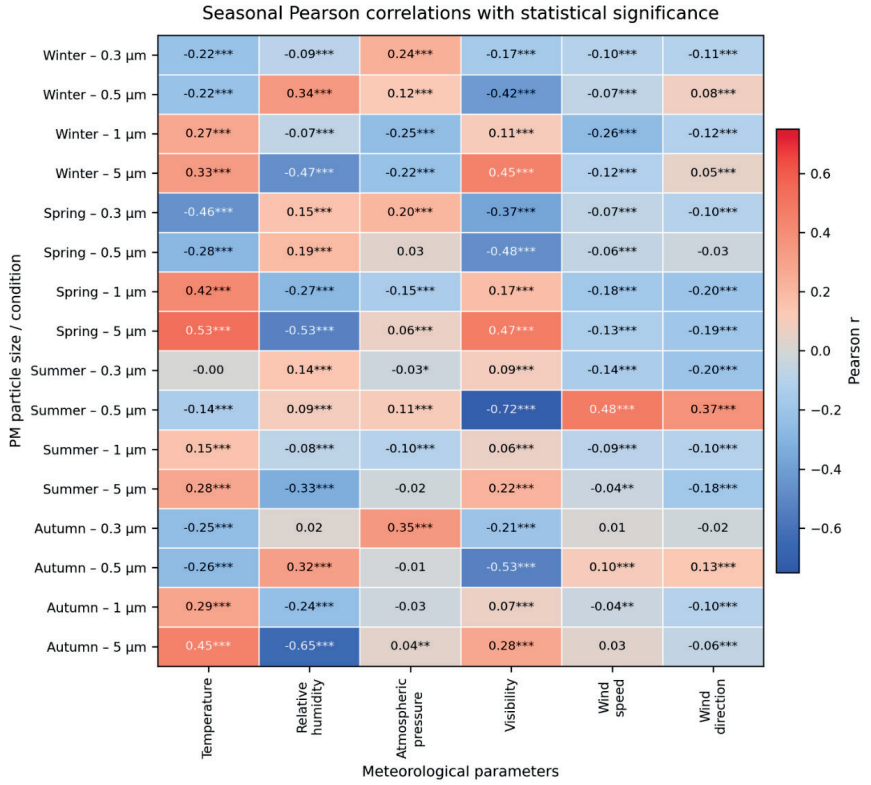



Figure 4. Seasonal variability of Pearson correlations between meteorological parameters and size-resolved particulate matter fractions during the 2024-2025 monitoring period in Galați, Romania. Asterisks indicate statistical significance: ***$p < 0.005$, *$p < 0.01$, $p < 0.05$

In winter, the 5 µm fraction showed a moderate positive correlation with visibility (r = 0.45) and a moderate negative correlation with relative humidity (r = −0.47). In spring, the strongest positive correlation was observed between temperature and the 5 µm fraction (r = 0.53), suggesting that warmer and drier conditions may favor coarse particle resuspension. During summer, most correlations were weak, except for the strong negative relationship between visibility and the 0.5 µm fraction (r = −0.72), indicating a strong optical effect of fine particles. In autumn, the 5 µm fraction was positively correlated with temperature (r = 0.45) and strongly negatively correlated with relative humidity (r = −0.65), again suggesting the sensitivity of coarse particles to humidity-related processes. The *p*-value analysis presented in Figure 4 (asterisks) indicated that most seasonal correlations were statistically significant, although weaker relationships involving pressure, wind speed and wind direction should be interpreted with caution.

Figure 5 presents the seasonal Pearson correlations calculated for daytime conditions. In winter, the 5 µm fraction showed a strong positive relationship with visibility (r = 0.52) and a moderate negative relationship with relative humidity (r = −0.43). This pattern suggests that coarse particles were less abundant under more humid daytime conditions, possibly due to humidity-related removal processes, while clearer atmospheric conditions were associated with higher coarse particle concentrations. In spring, the 5 µm fraction was moderately correlated with temperature (r = 0.48) and visibility (r = 0.45), indicating that warmer and clearer conditions may favor the presence or resuspension of coarse particles.

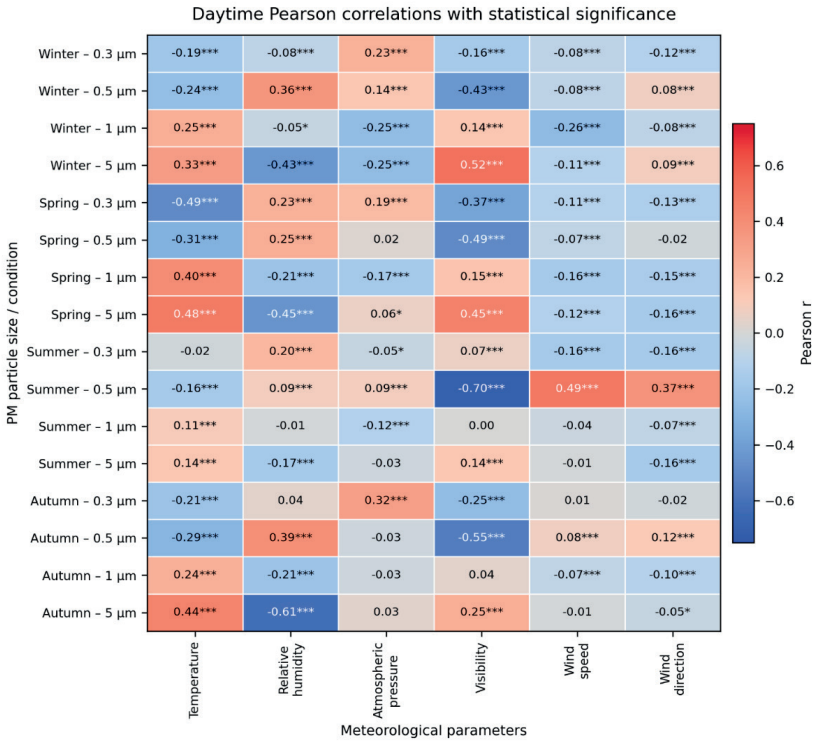



Figure 5. Daytime seasonal variability of Pearson correlations between meteorological parameters and size-resolved particulate matter fractions during the 2024–2025 monitoring period in Galați, Romania. Asterisks indicate statistical significance: ***$p < 0.005$, *$p < 0.01$, $p < 0.05$

During summer, most correlations were weak, except for the strong negative relationship between visibility and the 0.5 µm fraction (r = −0.70), suggesting that fine particles had an important role in reducing atmospheric visibility through light scattering. Moderate positive correlations were also observed between the 0.5 µm fraction and wind speed (r = 0.49), as well as wind direction (r = 0.37), which may indicate the influence of local transport processes. In autumn, the 5 µm fractions showed a moderate positive correlation with temperature (r = 0.44) and a strong negative correlation with relative humidity (r = −0.61), again indicating the sensitivity of coarse particles to humidity-related atmospheric processes.

Figure 6 shows the seasonal Pearson correlations calculated for nighttime conditions. In winter, the 5 µm fraction was moderately positively correlated with visibility (r = 0.41) and moderately negatively correlated with relative humidity (r = −0.48), showing a pattern like that observed during daytime. In spring, the 5 µm fractions showed a strong positive correlation with temperature (r = 0.53) and a strong negative correlation with relative humidity (r = −0.56), suggesting that warmer and drier nighttime conditions may favor the persistence of coarse particles.

During summer, the strongest nighttime relationship was observed between visibility and the 0.5 µm fraction (r = −0.74), indicating a strong influence of fine particles on visibility reduction. In autumn, the 5 µm fraction was strongly negatively correlated with relative humidity (r = −0.65), while temperature remained moderately positively correlated with the same fraction (r = 0.36). These results suggest that nighttime particle dynamics are strongly influenced by humidity and atmospheric stability, which may reduce vertical mixing and favor particle accumulation near the surface.

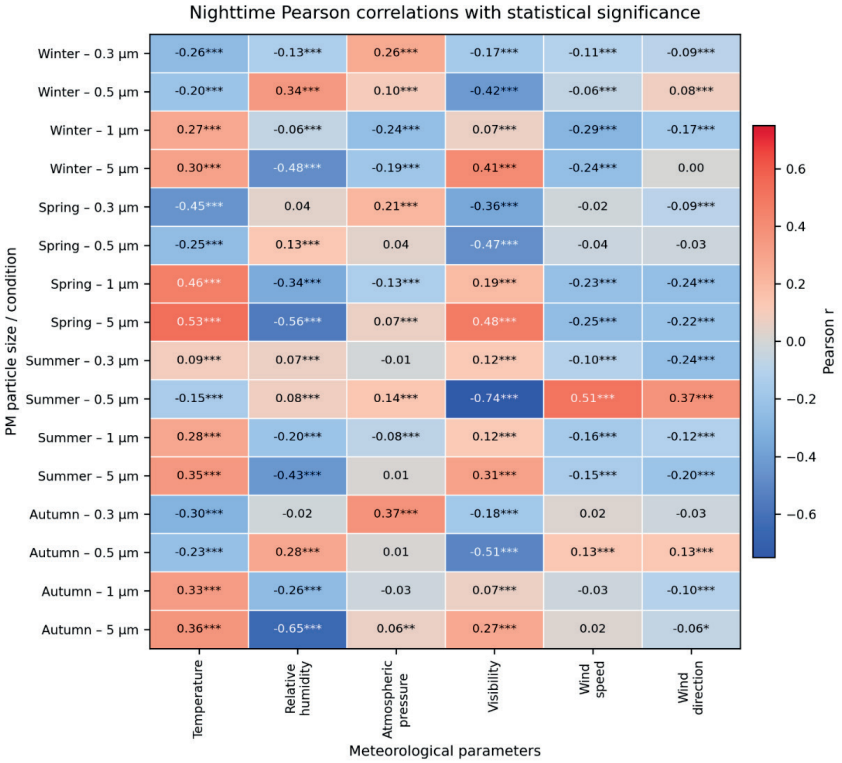



Figure 6. Nighttime seasonal variability of Pearson correlations between meteorological parameters and size-resolved particulate matter fractions during the 2024-2025 monitoring period in Galați, Romania. Asterisks indicate statistical significance: ***$p < 0.005$, *$p < 0.01$, $p < 0.05$

Overall, the daytime and nighttime patterns were broadly similar, but several correlations were slightly stronger during nighttime, particularly those involving relative humidity, visibility and the 5 µm fractions.

This may reflect more stable nocturnal atmospheric conditions, reduced dispersion and enhanced particle accumulation.

The *p*-value analysis presented in Figure 6 (asterisks) indicated that several correlations were statistically significant, especially those involving temperature, relative humidity and visibility, whereas weaker correlations involving atmospheric pressure, wind speed and wind direction should be interpreted with caution.

As shown in Table 1, most moderate and strong correlations were statistically significant, with *p*-values below 0.005.

Table 1. Main statistically significant moderate and strong correlations identified during the 2024-2025 monitoring period

| An. | Cond. | PM | Par. | r | *p*-value |
|---|---|---|---|---|---|
| Ov. | Full | 5 µm | RH | −0.61 | <0.005 |
| Ov. | Full | 5 µm | T | 0.57 | <0.005 |
| Ov. | Full | 0.5 µm | Vis. | −0.53 | <0.005 |
| Seas. | Sum. | 0.5 µm | Vis. | −0.72 | <0.005 |
| Seas. | Aut. | 5 µm | RH | −0.65 | <0.005 |
| Day | Sum. | 0.5 µm | Vis. | −0.70 | <0.005 |
| Night | Sum. | 0.5 µm | Vis. | −0.74 | <0.005 |
| Night | Spr. | 5 µm | T | 0.53 | <0.005 |
| Night | Spr. | 5 µm | RH | −0.56 | <0.005 |
| Night | Aut. | 5 µm | RH | −0.65 | <0.005 |

**Note.** An. = analysis; Cond. = condition; Ov. = overall analysis; Seas. = seasonal analysis; Day = daytime; Night = nighttime; Full = full monitoring period; Spr. = spring; Sum. = summer; Aut. = autumn; PM = particulate matter fraction; Par. = meteorological parameter; T = temperature; RH = relative humidity; Vis. = visibility. The table includes only strong correlations, defined as $|r| \geq 0.50$. The sign of r indicates the direction of the relationship.

The strongest and most consistent relationships were observed for relative humidity, temperature and visibility, especially in relation to the 0.5 µm and 5 µm particle fractions.

## CONCLUSIONS

The results of this study highlight the influence of local meteorological conditions on size-resolved particulate matter dynamics in the urban area of Galați during the 2024-2025 monitoring period. The strongest relationships were observed for temperature, relative humidity and visibility, particularly in relation to the 0.5 µm and 5 µm particle fractions. The 5 µm fraction showed strong sensitivity to humidity-related processes, with negative correlations with relative humidity, while its positive correlations with temperature suggest that warmer and drier conditions may favor the persistence or resuspension of coarse particles.

The negative correlations between visibility and the 0.5 µm fraction, especially during summer and nighttime conditions, indicate that fine particles may play an important role in reducing atmospheric visibility through light scattering. Seasonal analysis showed that the relationships between meteorological parameters and particulate matter were not constant throughout the year, with stronger correlations generally observed during winter, spring and autumn, and weaker or more variable associations during summer.

The comparison between daytime and nighttime conditions indicated broadly similar patterns, but several correlations were slightly stronger during nighttime. This suggests that more stable nocturnal atmospheric conditions, reduced vertical mixing and lower dispersion may contribute to particle accumulation near the surface. In contrast, atmospheric pressure, wind speed and wind direction showed weaker and less consistent relationships with particle concentrations and should therefore be interpreted with caution.

Overall, the combined use of the Rapid-E+ monitoring system and the ACTRIS RADO Galați meteorological station proved suitable for continuous, high-resolution investigation of urban aerosol dynamics. The results provide useful insight into the interaction between meteorological variability and particle size distribution and support the use of integrated monitoring systems for urban air quality assessment.

## ACKNOWLEDGEMENTS

This work was financed by Smart Growth, Digitization and Financial Instruments Program (PoCIDIF) 2021-2027, Action 1.3 Integration of the national RDI ecosystem in the European and international Research Space, project "Supporting the operation of facilities in Romania within the ACTRIS ERIC research infrastructure", SMIS code 309113. We acknowledge that the equipment used in this study is part of the REXDAN Research Infrastructure (REXDAN RI).

## REFERENCES

Baldacchini, C., Sgrigna, G., Clarke, W., Tallis, M., & Calfapietra, C. (2019). An ultra-spatially resolved method to quali-quantitative monitor particulate matter in urban environment. *Environmental Science and Pollution Research*, 26, 18719–18729. https://doi.org/10.1007/s11356-019-05160-8

Bruffaerts, N., Graf, E., Matavulj, P., Tiwari, A., Pyrri, I., Zeder, Y., Erb, S., Plaza, M., Dietler, S., Bendinelli, T., D'hooge, E., & Sikoparija, B. (2025). Advancing automated identification of airborne fungal spores: Guidelines for cultivation and reference dataset creation. *Aerobiologia*, 41(2), 505–525. https://doi.org/10.1007/s10453-025-09864-y

Cristea, M., Roșu, A., Roșu, B., Constantin, D.-E., Condurache-Bota, S., Voiculescu, M., Iticescu, C., Georgescu, P.-L., & Drăgan, S. (2025). Comprehensive analysis of particulate matter variability in an urban environment using Rapid-E monitoring. *Land Reclamation, Earth Observation & Surveying, Environmental Engineering.* https://landreclamationjournal.usamv.ro/pdf/2025/Art17.pdf

DJUG CS106. (2026). Retrieved February 5, 2026, from https://instrumentdb.out.ocp.fmi.fi/instrument/3dd19a6e-e22e-4720-a458-0c765dc74d36

DJUG Ultrasonic Anemometer 2D. (2026). Retrieved February 5, 2026, from https://instrumentdb.out.ocp.fmi.fi/instrument/07441608-a3af-42ad-938f-f7d80a859463

DJUG weather station. (2026). Retrieved February 5, 2026, from https://instrumentdb.out.ocp.fmi.fi/instrument/8ca6674e-ad02-4d5f-bf8c-feccf2d11c3b

European Environment Agency. (2024). Europe's air quality status 2024. EEA Briefing No. 06/2024. Publications Office of the European Union. doi:10.2800/5970

Garcia, A., Santa-Helena, E., De Falco, A., de Paula Ribeiro, J., Gioda, A., & Gioda, C. R. (2023).

Toxicological effects of fine particulate matter (PM2.5): Health risks and associated systemic injuries—Systematic review. *Water, Air, and Soil Pollution,* 234(6), 346. https://doi.org/10.1007/s11270-023-06278-9

Hamanaka, R. B., & Mutlu, G. M. (2025). Particulate matter air pollution: Effects on the respiratory system. *The Journal of Clinical Investigation*, 135(17). https://doi.org/10.1172/JCI194312

Karagulian, F., Belis, C. A., Dora, C. F. C., Prüss-Ustün, A. M., Bonjour, S., Adair-Rohani, H., & Amann, M. (2015). Contributions to cities' ambient particulate matter (PM): A systematic review of local source contributions at global level. *Atmospheric Environment*, 120, 475–483. https://doi.org/10.1016/j.atmosenv.2015.08.087

Kirešová, S., Guzan, M., & Sobota, B. (2023). Using low-cost sensors for measuring and monitoring particulate matter with a focus on fine and ultrafine particles. *Atmosphere*, 14(2), 324. https://doi.org/10.3390/atmos14020324

Lonati, G., & Giugliano, M. (2006). Size distribution of atmospheric particulate matter at traffic exposed sites in the urban area of Milan (Italy). *Atmospheric Environment,* 40, 264–274. https://doi.org/10.1016/j.atmosenv.2005.11.077

Manisalidis, I., Stavropoulou, E., Stavropoulos, A., & Bezirtzoglou, E. (2020). Environmental and health impacts of air pollution: A review. *Frontiers in Public Health*, 8, 14. https://doi.org/10.3389/fpubh.2020.00014

Mugica, V., Ortiz, E., Molina, L., De Vizcaya-Ruiz, A., Nebot, A., Quintana, R., Aguilar, J., & Alcántara, E. (2009). PM composition and source reconciliation in Mexico City. *Atmospheric Environment*, 43(32), 5068–5074. https://doi.org/10.1016/j.atmosenv.2009.06.051

Ngoc, L. T. N., Park, D., Lee, Y., & Lee, Y. C. (2017). Systematic review and meta-analysis of human skin diseases due to particulate matter. *International Journal of Environmental Research and Public Health*, 14(12), 1458. https://doi.org/10.3390/ijerph14121458

Plair SA. (2025a). Rapid-E+ and accessories brochure [Brochure]. Retrieved February 5, 2026, from https://www.plair.ch/assets/pdf/Brochure/Rapid-E+%20and%20its%20accessories.pdf

Plair SA. (2025b). Rapid-E+: Intelligent real-time bioaerosol sensing. Retrieved February 5, 2026, from https://www.plair.ch/Rapid-E+.html

Ramgolam, K., Chevaillier, S., Marano, F., Baeza-Squiban, A., & Martinon, L. (2008). Proinflammatory effect of fine and ultrafine particulate matter using size-resolved urban aerosols from Paris. *Chemosphere*, 72, 1340–1346. https://doi.org/10.1016/j.chemosphere.2008.04.025

Roșu, A., Constantin, D. E., Voiculescu, M., Arseni, M., Merlaud, A., Van Roozendael, M., & Georgescu, P. L. (2020). Observations of atmospheric NO2 using a new low-cost MAX-DOAS system. *Atmosphere*, 11(2), 129. https://doi.org/10.3390/atmos11020129

Šauliene, I., Šukiene, L., Daunys, G., Valiulis, G., Vaitkevičius, L., Matavulj, P., Brdar, S., Panic, M., Sikoparija, B., Clot, B., Crouzy, B., & Sofiev, M. (2019). Automatic pollen recognition with the Rapid-E particle counter: The first-level procedure, experience and next steps. *Atmospheric Measurement Techniques*, 12(6), 3435–3452. https://doi.org/10.5194/amt-12-3435-2019

Sikoparija, B., Matavulj, P., Simovic, I., Radisic, P., Brdar, S., Minic, V., Tesendic, D., Kadantsev, E., Palamarchuk, J., & Sofiev, M. (2024). Classification accuracy and compatibility across devices of a new Rapid-E+ flow cytometer. *Atmospheric Measurement Techniques,* 17(17), 5051–5070. https://doi.org/10.5194/amt-17-5051-2024

Tao, J., Zhang, L., Cao, J., & Zhang, R. (2017). A review of current knowledge concerning PM2.5 chemical composition, aerosol optical properties and their relationships across China. *Atmospheric Chemistry and Physics,* 17(15), 9485–9518. https://doi.org/10.5194/acp-17-9485-2017

Wilson, W., Chow, J., Claiborn, C., Fusheng, W., Engelbrecht, J., & Watson, J. (2002). Monitoring of particulate matter outdoors. *Chemosphere*, 49(9), 1009–1043. https://www.sciencedirect.com/science/article/pii/S0045653502002709

World Health Organization. (2021). WHO global air quality guidelines: Particulate matter ($PM_{2.5}$ and $PM_{10}$), ozone, nitrogen dioxide, sulfur dioxide and carbon monoxide. World Health Organization. ISBN 978-92-4-003422-8

Yang, L., Zhang, Y., Qi, W., Zhao, T., Zhang,L., Zhou, L., & Ye, L. (2021). Adverse effects of PM2.5 on cardiovascular diseases. *Reviews on Environmental Health*, 37(1), 71–80. https://doi.org/10.1515/reveh-2020-0155

Scientific Papers. Series E. Land Reclamation, Earth Observation & Surveying, Environmental Engineering. Vol. XV, 2026
Print ISSN 2285-6064, CD-ROM ISSN 2285-6072, Online ISSN 2393-5138, ISSN-L 2285-6064

# BACTERIAL MICROBIOTA IN AQUATIC ENVIRONMENTS AND THE BIODEGRADATION POTENTIAL OF SUSTAINABLE MATERIALS: INSIGHTS INTO ENVIRONMENTAL FATE - A REVIEW

**Andreea DOROFTE[1], Ira-Adeline SIMIONOV[1, 2], Ștefan-Mihai PETREA[1, 2], Cătălin PLATON[3], Cătălina ITICESCU[1, 4]**

[1]"Dunărea de Jos" University of Galaţi, REXDAN Research Infrastructure, 98 George Coşbuc Street, Galaţi, Romania
[2]"Dunărea de Jos" University of Galaţi, Faculty of Food Science and Engineering, 111 Domnească Street, Galaţi, Romania
[3]"ROMFISH" National Association of Fish Producers, 12A Nicolae Iorga Blvd, Iaşi, Romania
[4]"Dunărea de Jos" University of Galaţi, Faculty of Sciences and Environment, 111 Domnească Street, Galaţi, Romania

Corresponding author email: andreea.dorofte@ugal.ro

***Abstract***

*In recent years, a global strategy to replace petroleum-based polymers has been the development of durable, innovative and sustainable alternatives, namely biodegradable materials. This review provides a narrative synthesis of studies published between 2009 and 2026 investigating the interactions between biodegradable polymers and bacterial microbiota from aquatic environments. It focuses on major classes of biodegradable materials, including PLA, PHA, starch-based polymers and commercial blends and examines their behaviour in freshwater and marine environments. Current literature highlights that environmental conditions strongly influence biodegradation rates and microbial colonization patterns, yet the relationships between biodegradable materials and aquatic microbiomes remain insufficiently characterized. According to published studies, biodegradable polymers generally support more extensive bacterial colonization than conventional plastics, promoting higher microbial diversity and facilitating polymer breakdown into final metabolic products. This review identifies key knowledge gaps regarding the long-term environmental fate of biodegradable materials, synthesizes evidence on microbial drivers of biodegradation, and outlines implications for future research priorities, environmental monitoring strategies and the design of next-generation biomaterials.*

***Key words****: aquatic ecosystem, bacterial microbiota, biodegradable materials, biodegradation, environmental risk.*

## INTRODUCTION

Nowadays, one of the biggest global challenges is represented by plastic pollution with a negative impact on the aquatic environment and on the development of natural biological processes. Waste that reaches the environment interacts with it, leading to the release of harmful substances or altering the composition and structure of existing microbial communities, which can contribute to the reduction of water quality and increase the risk of toxicity for humans and the environment (Zlati et al., 2023). The advantages of petroleum-based plastics are represented by lower costs and better mechanical properties, but the disadvantage is their slow degradation capacity and persistence in the environment, which leads to the accumulation of pollutants (Wang et al., 2026). Specialists' forecasts estimate that by 2050, approximately 12 billion tons of plastic waste will be released into natural environments, having a negative effect on the balance of aquatic ecosystems (Amelia et al., 2025).

The solution that arouses interest and comes to meet this problem of excessive plastic use is represented by its replacement with new biodegradable materials. Materials that can be bio-based, biodegradable or can meet both characteristics at the same time are called bioplastics and are considered to be durable and sustainable substitutes that can replace conventional polymers (Lavagnolo et al., 2024). It is worth noting that the biodegradability of a material is not a universally valid characteristic for all polymers obtained from biological

sources, and not all plastic materials derived from fossil sources are non-biodegradable (Ahsan et al., 2023). For example, recent analyses confirm that bio-based polyethylene (bio-PE) remains chemically identical to conventional polyethylene and therefore non-biodegradable (Burelo et al., 2023), whereas fossil-derived polycaprolactone (PCL) continues to be recognized as a clearly biodegradable polyester in natural environments (Ntrivala et al., 2025).

Biodegradable materials are numerous and among the most commonly used are polylactic acid (PLA), polyhydroxy-alkanoates (PHA/PHB), polybutylene adipate terephthalate (PBAT) and polybutylene succinate (PBS), which are most widely used in the packaging industry due to their remarkable properties (Meyer-Cifuentes et al., 2020; Chen, 2022; Ahsan et al., 2023; Amelia et al., 2025).

However, despite their promise as sustainable alternatives, recent evidence indicates that biodegradable materials may also exhibit incomplete degradation, environmental persistence and ecological risks under natural aquatic conditions.

The biodegradation process of materials that reach the aquatic environment is usually not complete, being influenced by the bacterial communities present and their degradation capacity. An important role is also played by environmental, biological, physical and chemical factors such as water temperature, salinity, pH, dissolved oxygen concentration, ultraviolet radiation and the presence of nutrients, on which the dynamics of material degradation in the aquatic environment depend (Eronen-Rasimus et al., 2022; Jiao et al., 2026; Velayudhan et al., 2026). These environmental parameters not only influence polymer degradation rates but also shape the composition and activity of microbial taxa colonizing biodegradable materials, with certain genera becoming dominant under specific physicochemical conditions.

The microbial community of the aquatic environment has the property of colonizing biodegradable materials from the moment they are released into the aquatic environment (Amaral-Zettler et al., 2020). Microorganisms such as species belonging to the genera *Pseudomonas*, *Bacillus*, *Rhodococcus*, *Variovorax* or the families *Comamonadaceae* and *Xanthobacteraceae* have a remarkable role in the biodegradation process of biodegradable materials through the secretion of extracellular enzymes capable of cleaving polymer chains into low molecular weight compounds (Peng et al., 2022; Ahsan et al., 2023). Recent findings show that the incomplete degradation of biodegradable materials under natural conditions of aquatic ecosystems leads to their prolonged persistence and the potential emergence of unwanted ecological impacts (Zhang et al., 2025).

In this context, understanding the interactions between bacterial microbiota and biodegradable materials becomes essential for assessing the ecological impact and behaviour of these materials in the natural environment. This review synthesizes current information on the impact of aquatic bacterial communities on the degradation of biodegradable materials in both freshwater and marine environments, the dynamics of the plastisphere, a distinct microhabitat, in where bacteria, fungi and other microorganisms adhere to the surface of polymers and actively participate in biodegradation processes. This biofilm provides protection primarily for the microorganisms themselves, offering a stable micro-environment that shields them from environmental stressors while enabling enzymatic activity on the polymer surface (Amaral-Zettler et al., 2020).

The successional colonization pattern of the plastisphere - comprising early, intermediate and advanced stages - has been described in detail by Šerá et al. (2026), and is broadly consistent with observations from other studies reporting shifts from early colonizers consisting of fast-growing, surface-attaching microorganisms, including species of *Pseudomonas*, *Vibrio* and *Alteromonas* to mature biofilms enriched in taxa like *Burkholderiaceae*, *Comamonadaceae* and *Rhodococcus* (Zettler et al., 2013; Danso et al., 2019; Amaral-Zettler et al., 2020).

Although microbial colonization follows a predictable successional trajectory, the extent of biofilm development and the composition of the resulting microbial community depend strongly on the type of polymer. Compared to conventional plastics, biodegradable materials favor higher microbial diversity and biomass and more intense enzymatic activity than that formed on conventional materials such as polyethylene, polypropylene and polystyrene

(PE, PP and PS) due to their hydrophilic properties and the release of low molecular weight organic compounds (Zheng et al., 2025). Studies have shown that the average microbial biofilm biomass on biodegradable materials such as PHA and PLA was consistently, although modestly, higher (1.08-1.26 fold) than that on non-biodegradable plastics (PE, PP and PS), indicating an enhanced potential for microbial colonization and biodegradation (Peng et al., 2022; Zhang et al., 2025).

## BIODEGRADABLE MATERIALS IN AQUATIC ENVIRONMENTS

Biodegradability is defined as the ability of a material to be decomposed by microorganisms into $CO_2$, water and biomass under aerobic conditions, or into $CO_2$, $CH_4$ and biomass under anaerobic conditions. The biodegradation process generally involves three sequential stages: biodeterioration, biofragmentation and microbial assimilation, culminating in the mineralization of polymer-derived compounds (Ahsan et al., 2023; Cerbule et al., 2023).

Figure 1 shows the disintegration process of biodegradable materials, under the action of external environmental factors of degradation but also through internal mechanisms such as enzymatic cleavage.

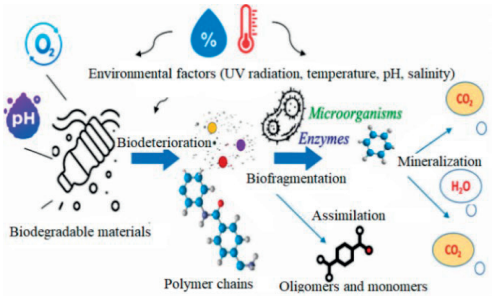



Figure 1. Schematic representation of the biodegradation process of biodegradable polymers, illustrating the sequential stages of biodeterioration, biofragmentation, microbial assimilation and final mineralization (adapted from Amelia et al., 2025)

During the biodeterioration stage, abiotic factors, including UV radiation, oxidation and temperature fluctuations, together with microbial colonization, alter the surface properties of the polymer, facilitating subsequent degradation. In the biofragmentation stage, extracellular enzymes degrade polymer chains into oligomers and monomers that can subsequently be assimilated by microorganisms. Polyesters such as PLA, PBAT and PHA are mainly hydrolysed by esterases, lipases and cutinases, whereas starch-based materials are primarily degraded by amylases. During the assimilation stage, these degradation products are utilized as carbon and energy sources and are ultimately converted into biomass and inorganic products through mineralization (Amelia et al., 2025).

Although the fundamental mechanisms of biodegradation are similar across environments, degradation generally proceeds more slowly in aquatic ecosystems than in terrestrial or industrial composting environments because of lower temperatures, reduced nutrient availability, lower microbial abundance and other environmental constraints that limit microbial activity and enzymatic degradation (Ahsan et al., 2023; Tantawi et al., 2025).

The biodegradability of different polymers therefore depends not only on environmental conditions but also on their chemical composition and physicochemical properties.

Due to their chemical composition, biodegradable materials are more hydrophilic and more susceptible to hydrolysis, which generates oligomers and monomers that can be utilized as carbon and energy sources by microorganisms (Zhang et al., 2025).

Compared with conventional polyolefins such as polyethylene (PE) and polypropylene (PP), biodegradable polyesters including PLA and PBAT exhibit greater biodegradation potential. However, their degradation rates differ substantially depending on environmental conditions, with PLA generally degrading efficiently under industrial composting conditions but much more slowly in natural freshwater and marine environments (Chen, 2022; Ahsan et al., 2023). PHB and PHA are considered among the most biodegradable materials in aquatic environments, both in freshwater and marine systems (Chen, 2022).

Starch-based materials also exhibit high biodegradation potential; however, their degradation rates vary considerably depending on starch content, polymer blending ratio, plasticizer composition, crystallinity and environmental moisture, all of which influence

microbial accessibility and enzymatic hydrolysis (Ahsan et al., 2023).

## ENVIRONMENTAL FACTORS INFLUENCING BIODEGRADATION

Biodegradation of materials in aquatic ecosystems is influenced by the complex interaction of physical, chemical and biological factors, which control both the activity of microorganisms and the properties of polymers. Indicators of biodegradation include mass loss, surface erosion, changes in molecular weight and chemical modifications of the polymer. In particular, oxidative processes generate carbonyl-containing functional groups, which increase surface polarity and consequently reduce hydrophobicity, thereby promoting microbial colonization and further biodegradation (Amelia et al., 2025).
Temperature is one of the most important factors, as low temperatures slow down microbial metabolic activity. For this reason, materials such as PLA exhibit efficient degradation under industrial composting conditions, but much slower degradation under natural conditions of aquatic ecosystems (Ahsan et al., 2023).
Oxygen levels also influence aerobic and anaerobic biodegradation processes. Under aerobic conditions, degradation mainly leads to the formation of $CO_2$, water and biomass, while anaerobic conditions favour fermentative processes and methane production. Aquatic sediments and the water-sediment interface represent areas of intense microbial activity, which favour depolymerization and mineralization processes (Amelia et al., 2025). Ultraviolet radiation promotes surface modification of polymers and increases their susceptibility to microbial colonization. Salinity, pH, and nutrient availability shape the composition of bacterial communities and the microbial succession within the plastisphere, indirectly influencing the efficiency of biodegradation (Eronen-Rasimus et al., 2022). Physico-chemical and biological parameters determine the integrity of the aquatic ecosystem, and an integrated approach to these parameters is essential for managing surface and groundwater used in agriculture, industry, and daily life (Iticescu et al., 2014).
Recent studies suggest that the variability of environmental conditions represents one of the main reasons why the biodegradation of materials labelled as “biodegradable” often remains incomplete in natural ecosystems.

## BACTERIAL COMMUNITIES IN BIODEGRADATION PROCESSES

Among the most frequently reported bacterial genera involved in the degradation of biodegradable materials in aquatic environments are *Pseudomonas*, *Bacillus*, *Rhodococcus*, *Variovorax*, *Alcaligenes*, *Comamonas*, *Shewanella*, and *Vibrio*. These microorganisms adhere to polymer surfaces and secrete extracellular enzymes capable of hydrolyzing polymer chains into oligomers and monomers that are subsequently assimilated and mineralized by the microbial community (Danso et al., 2019; Ru et al., 2020; Amelia et al., 2025).
The biodegradability of biodegradable polymers differs considerably according to polymer chemistry and environmental conditions. Polyhydroxyalkanoates (PHA), including polyhydroxybutyrate (PHB), are consistently reported among the most readily biodegradable biopolymers in aquatic environments, whereas materials such as poly(butylene succinate) (PBS) may exhibit very high degradation rates under specific sediment conditions. For example, Amelia et al. (2025) reported degradation rates approaching 100% for PBS and approximately 70% for PHB in aquatic sediments; however, these values should be interpreted as study-specific rather than universal rankings, as biodegradation strongly depends on environmental conditions, exposure time and experimental design.
The degradation of PLA has been associated with shifts in microbial community composition, including the enrichment of denitrifying bacteria that utilize lactic acid released during polymer hydrolysis as a carbon source and electron donor. Changes in the abundance of anammox bacteria have also been reported during PLA degradation, although their role appears to be linked to nitrogen cycling rather than the direct metabolism of lactic acid (Chen, 2022; Nie et al., 2022). According to studies, among bio-based materials, PHB was the most readily biodegradable, both in freshwater and in seawater (Chen, 2022). Biodegradable starch-based materials also

exhibit a significant degree of biodegradation in seawater; however, the process shows high variability, being influenced by factors such as material properties and environmental conditions (Chen, 2022; Ahsan et al., 2023).
Table 1 summarizes the principal biodegradable polymers investigated in aquatic environments, the dominant bacterial taxa associated with their degradation, the enzymes involved and the reported biodegradation outcomes, based on data compiled from the scientific literature.

Table 1. Biodegradable Materials (BM) in Aquatic Systems - Processes and Mechanisms of Their Degradation Under the Influence of the Plastisphere

| BM | Plastisphere | Effects | Reference |
|---|---|---|---|
| PLA | *Vibrionaceae*<br>*Actinomycetaceae*<br>*Flavobacteriaceae*<br>*Flavobacteriales*<br>*Planctomycetaceae* | Slow biodegradation; mass loss detected; no consistent % reported. | (Peng et al., 2022; Amelia et al., 2025) |
| PHA | *Actinomyces*<br>*Acinetobacter*<br>*Arthrobacter*<br>*Aspergillus*<br>*Bacillus*<br>*Clostridium*<br>*Comamonas*<br>*Enterobacter*<br>*Klebsiella*<br>*Variovorax*<br>*Mycobacterium*<br>*Streptomyces*<br>*Pseudomonas,*<br>*Rhodococcus* | Degradation in multiple aquatic conditions, including extreme habitats. | (Du et al., 2022; Amelia et al., 2025) |
| PHB | *Pseudomonas*<br>*Bacillus*<br>*Rhodococcus*<br>*Variovorax*<br>*Comamonas*<br>*Alcaligenes*<br>*Xanthomonas*<br>*Klebsiella*<br>*Streptomyces* | Very high; up to ~100% in sediments ~8.5% mass loss in 365 days at 25ºC. | (Du et al., 2022; Ahsan et al., 2023; Šerá et al., 2026) |
| PBS | *Actinomicete*<br>*Proteobacteria*<br>*Maribus*<br>*Neptunibacter*<br>*Bacillus* | Microbial degradation in the aquatic environment. | (Brakstad et al., 2022; Peng et al., 2022) |
| PHBH | *Acidovorax,*<br>*Undibacterium*<br>*Chitinimonas* | Signs of deterioration are visible after two weeks. | (Peng et al., 2022; Šerá et al., 2026) |
| Corn starch | *Capitella capitata* | 1.5% mass loss in 90 days at 25°C; up to 69% mass loss in 236 days. | (Ahsan et al., 2023) |

PLA - polylactic acid, PHA - polyhydroxyalkanoate, PHB - poli-3-hidroxibutirat, PHBV - poly(3-hydroxybutyrate-co-3-hydroxyvalerate), PHBH - poly(3-hydroxybutyrate-co-3-hydroxyhexanoate), PBS - poly (butylene Succinate).

Although numerous bacterial and fungal taxa have been identified on the surface of biodegradable materials, their actual contribution to polymer degradation in natural aquatic environments remains poorly understood. The presence of a microorganism in the plastisphere does not necessarily demonstrate that it actively participates in polymer depolymerization, as many taxa may simply exploit degradation products released by other microorganisms or colonize the biofilm without directly degrading the polymer. Consequently, most studies describe the composition of the microbial community rather than experimentally confirming the biodegradation potential of individual taxa under environmentally relevant conditions. This lack of functional validation represents one of the main knowledge gaps in understanding the fate of biodegradable plastics in aquatic ecosystems and highlights the need for field studies that combine microbial community analyses with measurements of enzymatic activity and polymer degradation (Peng et al., 2022).

## ECOLOGICAL LIMITATIONS AND RISKS IN NATURAL BIODEGRADATION

Although biodegradable materials represent promising alternatives to conventional polymers, they may also generate undesirable ecological effects.
Incomplete biodegradation can lead to the formation of biodegradable fragments that persist in aquatic ecosystems and interact with pollutants and living organisms (Amelia et al., 2025). These fragments can adsorb organic pollutants and trace metals from surrounding waters and subsequently release them after ingestion by aquatic organisms, thereby acting as vectors that increase contaminant transport and bioavailability within aquatic food webs (Catarci Carteny et al., 2023; Lu et al., 2024).
The plastisphere developing on biodegradable materials may also provide a favourable habitat for opportunistic and potentially pathogenic microorganisms. The close spatial organization of microbial cells within biofilms facilitates cell-to-cell interactions and horizontal gene transfer, thereby promoting the dissemination of antibiotic resistance genes (ARGs) and other mobile genetic elements.

Several opportunistic and potentially pathogenic bacteria have been reported in plastisphere biofilms associated with biodegradable materials (Amaral-Zettler et al., 2020; Zhang et al., 2023). Their occurrence and ecological significance are discussed in the following section.

These issues demonstrate that the environmental benefits of biodegradable materials cannot be assessed solely based on their biodegradation potential. A comprehensive assessment should also consider the persistence of degradation products, their interactions with contaminants and microorganisms, and their long-term ecological effects under natural environmental conditions. Addressing these knowledge gaps through long-term field studies will be essential for accurately assessing the environmental sustainability of biodegradable polymers in aquatic ecosystems.

## SUSTAINABLE WATER PURIFICATION IN AQUACULTURE

Aquaculture systems represent an increasingly important source of plastic and biodegradable polymer inputs into aquatic environments. Operational materials such as nets, ropes, feed bags, and filtration components introduce both conventional plastics and emerging biopolymers into surrounding waters, where they rapidly become colonized by microbial communities. These biofilm-covered surfaces form localized plastisphere niches, influencing nutrient cycling, pathogen proliferation, and antibiotic-resistance dynamics- all central themes of this review.

At the same time, aquaculture wastewater itself contains high nitrogen and phosphorus loads, suspended organic matter, pathogenic bacteria, antibiotic-resistant strains, and mobile resistance genes (Sun et al., 2025). These pollutants interact with plastic debris present in the system, creating complex microbial consortia that affect both water quality and the degradation pathways of plastic and biodegradable materials. For this reason, sustainable purification strategies are increasingly exploring biodegradable materials as filtration media, microbial carriers, or components of circular-economy remediation technologies.

The link between pollutant accumulation and insufficient recycling or reuse practices is well documented, particularly in systems where circular-economy principles are not implemented (Georgescu et al., 2025). As aquaculture expands, untreated wastewater discharge intensifies environmental pressures (Raza et al., 2025), reinforcing the need for purification methods that align with biodegradation processes and reduce plastisphere-associated risks.

To illustrate current directions in sustainable aquaculture remediation - including microbial consortia, advanced material-based treatments, and energy-efficient systems - Table 2 summarizes several high-efficiency purification methods and highlights their relevance for biodegradable-material applications, plastisphere management, and circular-economy integration.

Table 2. Sustainable aquaculture purification solutions with relevance to biodegradable materials and plastisphere dynamics

| Solution | Description | Effect | Relevance to biodegradable materials & plastisphere | Reference |
|---|---|---|---|---|
| Symbiotic bacteria-algae system | Nitrogen-fixing bacteria isolated from *Penaeus albus* used synergistically with *Tetraselmis suecica* microalgae to remove nutrients and suppress pathogens. | Removes >93% ammonia; reduces total N and P by 67-95% in 4 days; suppresses *Vibrio* and *Aeromonas* by 97-99%; reduces ARGs by 57.9%. | Supports microbial consortia similar to plastisphere communities, offering a model for biofilm-mediated degradation on biodegradable polymer surfaces; algae-bacteria systems can be immobilized on biopolymer carriers for circular-economy wastewater treatment. | (Sun et al., 2025) |
| Ag-ZnO/graphene composite | Photocatalytic and antimicrobial composite designed for antibiotic removal and inactivation of resistant bacteria. | Inactivates 99% *A. baumannii* and 97% *S. aureus* within 24 h; rapid antibiotic degradation and ARG reduction in both ultrapure and real wastewater. | Demonstrates how advanced materials can be integrated with biodegradable polymer matrices to create hybrid purification media; reduces microbial pressures that shape plastisphere biofilms and influence biodegradation kinetics. | (Li et al., 2025) |

| Solution | Description | Effect | Relevance to biodegradable materials & plastisphere | Reference |
|---|---|---|---|---|
| Energy-efficient electrochemical system | Floating ecological bed combined with a closed-loop microbial electrochemical system. | Enriches functional taxa (*Aeromonas*, *Stenotrophomonas*, *Dechloromonas*, *Thioalkalivibrio*, *Clostridium*, *Thermodesulfovibrio*, *Desulfobulbus*) supporting carbon and nitrogen removal and electron transfer. | Electroactive microbial communities resemble those colonizing biodegradable plastics, offering insights into electron-transfer-driven polymer degradation; floating beds can incorporate biopolymer substrates to reduce plastic pollution in aquaculture. | (Liao et al., 2025) |
| Microalgae-based purification | Microalgae added to aquaculture systems for nutrient assimilation and biomass production. | Efficient assimilation of dissolved inorganic carbon, nitrogen, and phosphorus; reduces eutrophication potential. | Microalgal biomass can be used to produce biodegradable bioplastics, linking aquaculture purification to circular-economy material loops; microalgae also colonize plastic surfaces, influencing plastisphere succession. | (Raza et al., 2025) |

## ANTIBIOTIC EFFECTS ON AQUATIC BACTERIAL COMMUNITIES AND THEIR ROLE IN PLASTISPHERE DYNAMICS

Antibiotics are widely used in aquaculture to manage bacterial infections in fish and shellfish. While they provide short-term health benefits, their excessive or prophylactic use has accelerated the emergence of antibiotic-resistant bacteria, disrupting the ecological balance of aquatic systems (Haque et al., 2024). Multiple antibiotic classes, including sulphonamides, fluoroquinolones, and macrolides, are routinely detected in effluents from livestock farms, medical facilities, and wastewater treatment plants. Their presence in aquatic environments alters the structure of bacterial communities, often promoting shifts toward resistant taxa (Zhang et al., 2023).

Freshwater case studies illustrate the scale of this issue: in the upper Danube River, approximately one-third of microorganisms sampled were resistant to one or two antibiotic classes, and over 10% exhibited multi-resistance. Similarly, Swedish data show that *E. coli* populations in rivers and clinical settings share comparable resistance profiles (Leopold et al., 2024). Although these examples come from European freshwater systems, they reflect broader global patterns observed across marine, estuarine, and freshwater environments, where antibiotic contamination shapes microbial community composition and resistance dynamics.

A critical connection to the present review is the role of antibiotics in plastisphere formation. Both conventional plastics and biodegradable materials rapidly develop biofilms when submerged in aquatic environments. Antibiotic exposure influences these biofilms by selecting for resistant strains, modifying microbial succession, and enhancing horizontal gene transfer. As a result, plastisphere biofilms can act as reservoirs and vectors for ARGs, facilitating their spread across ecosystems. This has direct implications for the environmental safety of biodegradable materials, whose degradation depends on microbial activity that may be altered by antibiotic pressure.

In modern aquaculture, intensive antibiotic use also promotes the formation of persistent biofilms. These three-dimensional microbial structures, embedded in an extracellular matrix, exhibit elevated tolerance to antibiotics, disinfectants, and environmental stressors (Haque et al., 2024).

Because plastics and bioplastics serve as ideal substrates for biofilm attachment, antibiotic-selected communities can colonize polymer surfaces, influencing biodegradation rates, polymer fragmentation, and the ecological behaviour of biodegradable materials.

Certain taxa, such as ε-proteobacteria, are frequently associated with environments experiencing high contaminant pressure. Their correlation with antibiotic resistance arises from metabolic versatility, stress-response pathways, and efficient horizontal gene transfer mechanisms (Barra Caracciolo et al., 2019). These traits also make ε-proteobacteria relevant to plastisphere studies, where biofilm-associated microbes encounter complex mixtures of

pollutants, including antibiotics, microplastics, and biodegradable polymer fragments.

The spread of antibiotic resistance in water bodies is largely driven by anthropogenic pollution-wastewater discharges, agricultural runoff, manure applications, and hospital effluents (Callejas et al., 2024). These same pressures influence plastisphere formation and microbial colonization on biodegradable materials.

Understanding antibiotic impacts is therefore essential for evaluating how biodegradable polymers interact with microbial communities, how ARGs propagate within plastisphere biofilms, and how environmental contamination affects biodegradation efficiency and ecological risk.

## PATHOGENIC BACTERIA AND AQUATIC BACTERIAL COMMUNITIES

While previous sections discussed the role of bacterial communities in biodegradation and the ecological risks associated with plastisphere formation, it is equally important to consider the occurrence of pathogenic bacteria within these microbial assemblages. Beyond their contribution to polymer degradation, plastisphere-associated biofilms may provide suitable habitats for opportunistic pathogens, with potential consequences for aquatic ecosystem functioning, aquaculture and public health.

Therefore, this section focuses on representative pathogenic bacteria found in aquatic environments and discusses how their interactions with native bacterial communities and biodegradable-material associated biofilms may influence their persistence and dissemination.

Although bacteria play a major role in maintaining the stability of aquatic environments, the evolution of pathogens has become a threat to the aquatic environment, causing infections if they reach the human body. In aquatic environments, fecal indicator bacteria, particularly *Escherichia coli* and intestinal enterococci, are widely used to assess fecal contamination and associated public health risks. These microorganisms are routinely monitored because their presence reflects recent fecal pollution and the potential occurrence of enteric pathogens. In the context of biodegradable materials, monitoring these indicator bacteria is also relevant for evaluating whether plastisphere biofilms associated with biodegradable polymers provide suitable habitats for fecal-associated microorganisms and other opportunistic pathogens (Li et al., 2021; Schneier et al., 2024).

Besides serving as indicators of fecal contamination, the presence of fecal indicator bacteria on the surfaces of biodegradable materials can give valuable information about the potential of these materials to act as carriers for fecal-associated microorganisms.

Another relevant pathogen is *Salmonella enterica* which can enter aquatic environment through sewage discharges, urban and agricultural runoff and animal waste. Once introduced, it can persist for extended periods in soil and surface water contributing to diseases such as typhoid fever and gastroenteritis. At the same time, these pathogens also interact with the bacterial community, often competing for resources. High bacterial diversity generally inhibits pathogenic species through competitive exclusion, whereas depleted bacterial communities weaken this antagonistic effect, facilitating pathogen spread (Díaz et al., 2024).

Studies have identified various potential pathogens, including *Vibrio*, *Acinetobacter*, *Aeromonas*, *Klebsiella*, *Legionella*, *Arcobacter*, and members of the Campylobacteraceae, colonizing plastisphere biofilms on plastic materials, including biodegradable polymers, in marine and freshwater ecosystems worldwide.

Among these, *Vibrio* species are of particular concern because they can cause diseases in aquatic organisms and humans (Amaral-Zettler et al., 2020; Zhang et al., 2023).

Lactococcosis is caused by *Lactococcus garvieae*, an emerging disease that affects many fish species and causes large economic losses in both marine and freshwater aquaculture particularly in summer, when temperatures above approximately 15-18°C favor bacterial proliferation and disease transmission (Callejas et al., 2024; Khalil et al., 2024; Vendrell et al., 2006). Higher temperatures boost microbial growth and biofilm formation on submerged polymers surfaces showing why it's important to study plastisphere-related microbial communities in conditions that match the

environment. *Bacillus cereus* has a wide spectrum of phenotypic traits, can be a source of contamination in food processing chains, representing a severe risk to human health (Callejas et al., 2024).

As discussed in earlier sections on antibiotic effects and aquaculture wastewater, antibiotic contamination, nutrient loads, and pollutant stressors further shape plastisphere communities, often selecting resistant or opportunistic pathogens. Biodegradable materials, while designed to reduce long-term pollution, also undergo biofilm-mediated degradation, meaning their ecological behavior is tightly coupled to the composition and stability of surrounding microbial communities. Therefore, interactions between pathogens and aquatic bacterial communities highlight the need for approaches that minimize the risks of contaminants in water while preserving the native microbial diversity that supports stability of aquatic ecosystems.

Understanding these relationships is imperative because diverse and functionally balanced microbial communities provide an important ecological barrier against pathogen establishment, whereas disturbances in community structure may facilitate pathogen persistence and the dissemination of antibiotic resistance genes.

In this context, biodegradable materials should not be evaluated solely according to their degradation rates, but also according to their influence on plastisphere development and microbial community assembly. Determining whether plastisphere formation supports native microbial functions or promotes the enrichment of opportunistic and pathogenic microorganisms remains a major research challenge that requires long-term investigations under environmentally relevant conditions.

## KNOWLEDGE GAPS AND FUTURE DIRECTIONS

The dynamics of the plastisphere and the succession of microbial communities associated with biodegradable materials remain insufficiently investigated, even though numerous studies have identified dominant bacterial taxa involved in polymer colonization and degradation (Peng et al., 2022). As discussed throughout this review, particularly in the sections addressing microbial colonization, bacterial biodegradation processes and ecological risks, understanding the functional role of these microbial communities under natural environmental conditions remains one of the major challenges for predicting the environmental fate of biodegradable materials.

### Methodological gaps

Research efforts are directed toward improving the end-of-life biodegradation capacity of commercially available biomass-derived materials such as polylactic acid, polybutylene succinate, and polyhydroxyalkanoates. Although interest in biodegradable materials is steadily increasing, many aspects of their long-term behaviour remain poorly understood, as most studies are conducted under controlled laboratory conditions, using constant temperatures, simplified microbial communities, and relatively short experimental periods that do not reflect the complexity of natural ecosystems (Amaral-Zettler et al., 2020). This results in biodegradation rates that vary considerably between studies and are difficult to compare.

### Climate change and environmental variability

Climate change is expected to modify several environmental drivers that regulate biodegradation processes, including increasing water temperature, altered salinity caused by droughts or extreme precipitation, antibiotic-resistant profile and changes in nutrient availability (Banciu et al., 2021). Rising temperatures speed up microbial metabolism, but they can lower oxygen levels and change how biodegradation happens.

The behaviour and resistance of pollutants, interactions with the biological environment and biodegradation processes are affected by climate change phenomena and the studies carried out must consider these aspects (Georgescu et al., 2025).

**Future research priorities**

Recent studies demonstrate that the biodegradation of biodegradable materials does not necessarily eliminate ecological risks. Incomplete degradation may result in persistent polymer fragments that interact with contaminants, support plastisphere development and provide suitable habitats for opportunistic microorganisms, including bacteria carrying antibiotic resistance genes. Although biodegradable materials represent a promising alternative to conventional plastics, future research should prioritize the development of formulations with improved biodegradation performance under environmentally relevant conditions while minimizing unintended ecological effects. In parallel, advances in waste management systems and standardized environmental biodegradation assessment protocols will be essential to ensure their sustainable application (Dorofte et al., 2025).

In addition, future studies should focus on prioritize long-term field experiments on natural aquatic environments, standardized biodegradation protocols across freshwater, estuarine and marine ecosystems, and the integration of molecular techniques with measurements of enzymatic activity and polymer mineralization. Attention should be given to identifying the functional roles of dominant plastisphere microorganisms, evaluating their biodegradation potential under natural conditions and assessing the long-term ecological consequences of biodegradable polymer degradation.

These aspects highlight the need to evaluate biodegradability not only from the perspective of physical material breakdown but also in terms of the long-term ecological impact on microbiota and the functioning of aquatic ecosystems.

## CONCLUSIONS

Given their increasing use, understanding the biodegradation pathways and environmental fate of biodegradable materials in aquatic systems is essential for developing effective waste-management strategies and minimizing ecological impacts.

Although biodegradable materials represent promising alternatives to petroleum-based polymers, their behaviour in aquatic environments is considerably more complex than their performance under controlled laboratory conditions. Consequently, biodegradability must be evaluated not only through physical disintegration but also through long-term ecological and microbiological effects.

Current evidence indicates that biodegradation efficiency is strongly shaped by microbial community structure and by the physicochemical characteristics of aquatic habitats.

This review highlights that the biodegradation of these materials is primarily governed by the composition, succession and functional activity of plastisphere-associated microbial communities. While most microorganisms contribute to polymer colonization and degradation, plastisphere development may also facilitate the persistence of opportunistic pathogens and antibiotic resistance genes under specific environmental conditions, emphasizing the need to evaluate both biodegradation efficiency and ecological safety.

The succession of plastisphere communities represents one of the key mechanisms controlling the environmental fate of biodegradable materials. Early colonizers initiate biofilm formation, whereas later microbial communities contribute to polymer depolymerization, mineralization and nutrient cycling. Understanding these microbial successions is therefore essential for predicting biodegradation efficiency under natural aquatic conditions.

Furthermore, the increasing leakage of biodegradable materials into natural environments, combined with anthropogenic pollution and antibiotic residues, contributes to shifts in microbial communities and the spread of antibiotic resistance.

Overall, these findings underscore the need for integrated assessments that consider microbial dynamics, environmental conditions, and pollutant interactions to accurately evaluate the real-world biodegradation of these materials in aquatic ecosystems.

In conclusion, biodegradable materials should not be evaluated solely according to their physical disintegration or laboratory-derived biodegradation rates. Their environmental

performance depends on complex interactions between polymer properties, plastisphere succession, microbial community composition and environmental conditions. Consequently, assessing the sustainability of biodegradable materials requires integrating biodegradation efficiency with long-term ecological effects on microbial diversity, ecosystem functioning and the potential development of ecological risks under natural aquatic conditions.

## ACKNOWLEDGEMENTS

This research was supported by the project "Integrated research and sustainable solutions to protect and restore Lower Danube Basin and coastal Black Sea ecosystems" (ResPonSE), contract no. 760010/30.12.2022 and by the project PN-IV-P8-674/01.11.2024, WATER LIGHTHOUSE ACTION - DANUBE REGION, DALIA, 89 PHE/2024

## REFERENCES

Ahsan, W. A., Hussain, A., Lin, C., & Nguyen, M. K. (2023). Biodegradation of Different Types of Bioplastics through Composting - A Recent Trend in Green Recycling. *Catalysts*, *13*(2), 294. https://doi.org/10.3390/catal13020294

Amaral-Zettler, L. A., Zettler, E. R., & Mincer, T. J. (2020). Ecology of the plastisphere. *Nature Reviews Microbiology*, *18*(3), 139–151. https://doi.org/10.1038/s41579-019-0308-0

Amelia, T. S. M., Kee, S. H., Senathirajah, K., Shao, Y. T., Ridzuan, N. A. M., Azmeerizal, A. S., Vigneswari, S., Lakshiminarayanan, R., Ramakrishna, S., & Bhubalan, K. (2025). Solution or Pollution? A paradigm shifts in understanding the fate and threats of biodegradable plastics in the marine environment. *Journal of Hazardous Materials Advances*, *20*, 100902. https://doi.org/10.1016/j.hazadv.2025.100902

Banciu, A. R., Ionica, D. L., Vaideanu, M. A., Radulescu, D. M., Nita-Lazar, M., & Covaliu, C. I. (2021). The Occurrence of Potentially Pathogenic and Antibiotic Resistant Gram-Negative Bacteria Isolated from the Danube Delta Ecosystem. *Sustainability*, *13*(7), 3955. https://doi.org/10.3390/su13073955

Barra Caracciolo, A., Patrolecco, L., Grenni, P., Di Lenola, M., Ademollo, N., Rauseo, J., Rolando, L., Spataro, F., Plutzer, J., Monostory, K., & Sperlagh, B. (2019). Chemical mixtures and autochthonous microbial community in an urbanized stretch of the River Danube. *Microchemical Journal*, *147*, 985–994. https://doi.org/10.1016/j.microc.2019.04.021

Brakstad, O. G., Sørensen, L., Hakvåg, S., Føre, H. M., Su, B., Aas, M., Ribicic, D., & Grimaldo, E. (2022). The fate of conventional and potentially degradable gillnets in a seawater-sediment system. *Marine Pollution Bulletin*, *180*, 113759. https://doi.org/10.1016/j.marpolbul.2022.113759

Burelo, M., Hernández-Varela, J. D., Medina, D. I., & Treviño-Quintanilla, C. D. (2023). Recent developments in bio-based polyethylene: Degradation studies, waste management and recycling. *Heliyon*, *9*(11), e21374. https://doi.org/10.1016/j.heliyon.2023.e21374

Callejas, I. A., Kong, Y., Osborn, K., Hung, W.-C., Cira, M., Cason, T., Sloane, A., Shenkiryk, A., Masikip, A., Singh, A., Jones, A., Steele, J. A., & Jay, J. A. (2024). The influence of urbanization and water reclamation plants on fecal indicator bacteria and antibiotic resistance in the Los Angeles River watershed: A case study with complementary monitoring methods. *Science of The Total Environment*, *957*, 177577. https://doi.org/10.1016/j.scitotenv.2024.177577

Catarci Carteny, C., Amato, E. D., Pfeiffer, F., Christia, C., Estoppey, N., Poma, G., Covaci, A., & Blust, R. (2023). Accumulation and release of organic pollutants by conventional and biodegradable microplastics in the marine environment. *Environmental Science and Pollution Research*, *30*(31), 77819–77829. https://doi.org/10.1007/s11356-023-27887-1

Cerbule, K., Herrmann, B., Trumbić, Ž., Petrić, M., Šifner, S. K., Grimaldo, E., Larsen, R. B., & Brčić, J. (2023). Use of biodegradable materials to reduce marine plastic pollution in small scale coastal longline fisheries. *Journal for Nature Conservation*, *74*, 126438. https://doi.org/10.1016/j.jnc.2023.126438

Chen, H. (2022). Biodegradable plastics in the marine environment: A potential source of risk? *Water Emerging Contaminants and Nanoplastics*, *1*(16). https://doi.org/10.20517/wecn.2022.11

Danso, D., Chow, J., & Streit, W. R. (2019). Plastics: Environmental and Biotechnological Perspectives on Microbial Degradation. *Applied and Environmental Microbiology*, *85*(19), e01095-19. https://doi.org/10.1128/AEM.01095-19

Díaz, S. M., Barrios, M. E., Galli, L., Cammarata, R. V., Torres, C., Fortunato, M. S., García López, G., Costa, M., Sanguino Jorquera, D. G., Oderiz, S., Rogé, A., Gentiluomo, J., Carbonari, C., Rajal, V. B., Korol, S. E., Gallego, A., Blanco Fernández, M. D., & Mbayed, V. A. (2024). Microbiological hazard identification in river waters used for recreational activities. *Environmental Research*, *247*, 118161. https://doi.org/10.1016/j.envres.2024.118161

Dorofte, A., Simionov, I.-A., Petrea, S.M., Platon, C., Georgescu, P.-L., & Iticescu, C. (2025). A critical review of sustainable approaches for reducing the environmental impact of plastic production. *Scientific Papers. Series E. Land Reclamation, Earth Observation & Surveying, Environmental Engineering, XIV (2025),* pp. 159–168.

Du, Y., Liu, X., Dong, X., & Yin, Z. (2022). A review on marine plastisphere: Biodiversity, formation, and role in degradation. *Computational and Structural Biotechnology Journal*, *20*, 975–988. https://doi.org/10.1016/j.csbj.2022.02.008

Eronen-Rasimus, E. L., Näkki, P. P., & Kaartokallio, H. P. (2022). Degradation Rates and Bacterial Community Compositions Vary among Commonly Used Bioplastic Materials in a Brackish Marine Environment. *Environmental Science & Technology*, *56*(22), 15760–15769. https://doi.org/10.1021/acs.est.2c06280

Georgescu, L. P., Balsalobre-Lorente, D., Zlati, M. L., Fortea, C., Antohi, V.-M., & Barbuta-Misu, N. (2025). Cluster Analysis of the Transition to Climate Neutrality in the European Union. *Sustainable Development*, *33*(S1), 1498–1519. https://doi.org/10.1002/sd.70064

Haque, A., Chowdhury, A., Islam Bhuiyan, M. N., Bhowmik, B., Afrin, S., Sarkar, R., & Haque, M. M. (2024). Molecular characterization, antibiotic resistant pattern and biofilm forming potentiality of bacterial community associated with Ompok pabda fish farming in southwestern Bangladesh. *Microbial Pathogenesis*, *194*, 106818. https://doi.org/10.1016/j.micpath.2024.106818

Iticescu, C., Georgescu, L., Topa, C. & Murariu, G. (2014). Monitoring the danube water quality near the galati city. *Journal of Environmental Protection and Ecology*, *15*, 30–38.

Jiao, H., Al-Tohamy, R., Xiong, M., Schagerl, M., Reinthaler, T., Al-Zahrani, M., Sun, J., & Ali, S. S. (2026). Microplastic biodegradation and environmental safety: From microbial mechanisms to engineered systems and circular bio-based implementation. *Ecotoxicology and Environmental Safety*, *313*, 120016. https://doi.org/10.1016/j.ecoenv.2026.120016

Khalil, S. M. I., Orioles, M., Tomé, P., Galeotti, M., & Volpatti, D. (2024). Current knowledge of lactococcosis in rainbow trout: Pathogenesis, immune response and prevention tools. *Aquaculture*, *580*, 740363. https://doi.org/10.1016/j.aquaculture.2023.740363

Lavagnolo, M. C., Poli, V., Zampini, A. M., & Grossule, V. (2024). Biodegradability of bioplastics in different aquatic environments: A systematic review. *Journal of Environmental Sciences*, *142*, 169–181. https://doi.org/10.1016/j.jes.2023.06.013

Leopold, M., Kabicher, A., Pap, I.-J., Ströbele, B., Zarfel, G., Farnleitner, A. H., & Kirschner, A. K. T. (2024). A comparative study on antibiotic resistant *Escherichia coli* isolates from Austrian patients and wastewater-influenced Danube River water and biofilms. *International Journal of Hygiene and Environmental Health*, *258*, 114361. https://doi.org/10.1016/j.ijheh.2024.114361

Li, E., Saleem, F., Edge, T. A., & Schellhorn, H. E. (2021). Biological Indicators for Fecal Pollution Detection and Source Tracking: A Review. *Processes*, *9*(11), 2058. https://doi.org/10.3390/pr9112058

Li, X., Wei, D., Wang, L., Wang, H., Shuli, J., Hu, W., Chen, H., Fang, S., Guo, W., Deng, H., Zhang, D., Li, J., Zhong, Z., & Zhou, Y. (2025). Multiple effects of zinc materials on fish, parasites, and the bacterial community in aquatic ecosystems. *Aquaculture*, *598*, 742062. https://doi.org/10.1016/j.aquaculture.2024.742062

Liao, M., Liu, G., He, Q., Liu, W., Qiu, Y., Tian, Y., Ji, Y., Ma, J., Wang, S., & Feng, Y. (2025). In-situ remediation of water and sediment in aquaculture system using novel ecological floating bed coupled with microbial electrochemical system. *Bioresource Technology*, *432*, 132660. https://doi.org/10.1016/j.biortech.2025.132660

Lu, J., Dong, Z.-H., Zhou, J.-Q., Li, M., Zhang, Z.-Z., Zhang, Y., & Jin, R.-C. (2024). Biodegradable Microplastics in Municipal Wastewater and Sludge Treatment Processes: A Review on Occurrence, Fate, and Effects. *ACS ES&T Water*, *4*(1), 8–19. https://doi.org/10.1021/acsestwater.3c00297

Meyer-Cifuentes, I. E., Werner, J., Jehmlich, N., Will, S. E., Neumann-Schaal, M., & Öztürk, B. (2020). Synergistic biodegradation of aromatic-aliphatic copolyester plastic by a marine microbial consortium. *Nature Communications*, *11*(1), 5790. https://doi.org/10.1038/s41467-020-19583-2

Nie, Z., Wang, L., Lin, Y., Xiao, N., Zhao, J., Wan, X., & Hu, J. (2022). Effects of polylactic acid (PLA) and polybutylene adipate-*co*-terephthalate (PBAT) biodegradable microplastics on the abundance and diversity of denitrifying and anammox bacteria in freshwater sediment. *Environmental Pollution*, *315*, 120343. https://doi.org/10.1016/j.envpol.2022.120343

Ntrivala, M. A., Pitsavas, A. C., Lazaridou, K., Baziakou, Z., Karavasili, D., Papadimitriou, M., Ntagkopoulou, C., Balla, E., & Bikiaris, D. N. (2025). Polycaprolactone (PCL): The biodegradable polyester shaping the future of materials – a review on synthesis, properties, biodegradation, applications and future perspectives. *European Polymer Journal*, *234*, 114033. https://doi.org/10.1016/j.eurpolymj.2025.114033

Peng, C., Wang, J., Liu, X., & Wang, L. (2022). Differences in the Plastispheres of Biodegradable and Non-biodegradable Plastics: A Mini Review. *Frontiers in Microbiology*, *13*. https://doi.org/10.3389/fmicb.2022.849147

Raza, B., Ramzan, M. N., & Yang, W. (2025). A review: Improving aquaculture rearing water quality by removal of nutrients using microalgae, challenges and future prospects. *Aquaculture*, *598*, 741959. https://doi.org/10.1016/j.aquaculture.2024.741959

Ru, J., Huo, Y., & Yang, Y. (2020). Microbial Degradation and Valorization of Plastic Wastes. *Frontiers in Microbiology*, *11*. https://doi.org/10.3389/fmicb.2020.00442

Schneier, A., Melaugh, G., & Sadler, J. C. (2024). Engineered plastic-associated bacteria for biodegradation and bioremediation. *Biotechnology for the Environment*, *1*(1), 7. https://doi.org/10.1186/s44314-024-00007-0

Šerá, J., Pecina, V., Mašláňová, V., Brtnický, M., Baťová, A., Holátko, J., Hammerschmiedt, T., Kučabová, V., Malíček, O., Kadlečková, M., Kučerík, J., & Koutný, M. (2026). Unveiling the spatial architecture of biodegradable polyester plastisphere in soil and its implications for organic matter composition. *Soil Biology and Biochemistry*, *214*, 110050. https://doi.org/10.1016/j.soilbio.2025.110050

Sun, N., Xing, D., Liu, F., Liang, F., & Liu, L. (2025). Purification effect of algae and immobilized bacteria combination system in aquaculture wastewater treatment with targeted removal of pathogenic *Vibrio* and antibiotic resistance genes. *Aquaculture*, *607*, 742673. https://doi.org/10.1016/j.aquaculture.2025.742673

Tantawi, O., Joo, W., Martin, E. E., Av-Ron, S. H. M., Bannister, K. R., Prather, K. L. J., Olsen, B. D., & Plata, D. L. (2025). Designing for degradation: The importance of considering biotic and abiotic polymer degradation. *Environmental Science: Processes & Impacts*, *27*(5), 1303–1316. https://doi.org/10.1039/D5EM00079C

Velayudhan, A., Akhtar, S., Kim, H., Yang, E., & Yoo, K. (2026). Potential environmental impacts of bioplastic degradation in natural marine environments: A comprehensive review. *Marine Environmental Research*, *214*, 107736. https://doi.org/10.1016/j.marenvres.2025.107736

Vendrell, D., Balcázar, J. L., Ruiz-Zarzuela, I., de Blas, I., Gironés, O., & Múzquiz, J. L. (2006). *Lactococcus garvieae* in fish: A review. *Comparative Immunology, Microbiology and Infectious Diseases*, *29*(4), 177–198. https://doi.org/10.1016/j.cimid.2006.06.003

Wang, C., Zhang, M., Zhang, T., Du, H., Xia, H., Guan, R., Guo, F., Li, X., Wang, M., Jia, X., & Wang, P. (2026). Marine biomaterials for advanced food packaging: From sourcing to intelligent functional design and commercial prospects. *Trends in Food Science & Technology*, 169, 105560. https://doi.org/10.1016/j.tifs.2026.105560

Zettler, E. R., Mincer, T. J., & Amaral-Zettler, L. A. (2013). Life in the "Plastisphere": Microbial Communities on Plastic Marine Debris. *Environmental Science & Technology*, *47*(13), 7137–7146. https://doi.org/10.1021/es401288x

Zhang, D., Sun, J., Peng, S., Wang, Y., Lin, X., & Wang, S. (2025). Biodegradable microplastics exacerbate the risk of antibiotic resistance genes pollution in agricultural soils. *Journal of Hazardous Materials*, *496*, 139490. https://doi.org/10.1016/j.jhazmat.2025.139490

Zhang, L., Fang, S., Hong, W., Shen, Z., Li, S., & Fang, W. (2023). Differences in pathogenic community assembly processes and their interactions with bacterial communities in river and lake ecosystems. *Environmental Research*, *236*, 116847. https://doi.org/10.1016/j.envres.2023.116847

Zheng, J.-L., Zhu, T., Jin, W.-Y., Zhan, Q.-H., Wan, F.-G., Chen, Y.-L., Chen, T.-H., Chen, S., Zhu, Q.-L., Chen, S., Li, W.-Y., Liu, Y.-F., Song, W.-H., Jiang, L.-H., & Yan, X.-J. (2025). Comparative analysis of carotenoids, fatty acids, minerals, tastes, and odor in the skin of wild versus farmed large yellow croaker: Superior nutritional benefits with elevated heavy metal risks. *Aquaculture*, *594*, 741471. https://doi.org/10.1016/j.aquaculture.2024.741471

Zlati, M. L., Georgescu, L. P., Iticescu, C., Ionescu, R. V., & Antohi, V. M. (2023). New Approach to Modelling the Impact of Heavy Metals on the European Union's Water Resources. *International Journal of Environmental Research and Public Health*, *20*(1), 45. https://doi.org/10.3390/ijerph20010045

Scientific Papers. Series E. Land Reclamation, Earth Observation & Surveying, Environmental Engineering. Vol. XV, 2026
Print ISSN 2285-6064, CD-ROM ISSN 2285-6072, Online ISSN 2393-5138, ISSN-L 2285-6064

# FOREWARNING ON SOME POLLUTANTS AND THEIR EFFECTS ON WATERFOWL

**Cristina Alina DUMITRACHE**

Institute of Biology Bucharest, Romanian Academy, 296 Splaiul Independentei, District 6 Bucharest, Romania
School of Advanced Studies of the Romanian Academy (SCOSAAR), 125 Calea Victoriei, District 1, Bucharest, Romania

Corresponding author email: alina.coman@ibiol.ro

***Abstract***

*Anthropogenic pollution is becoming increasingly widespread in ecosystems worldwide. In recent years, we have observed negative consequences for many species, particularly birds. This review focuses on the impacts of common anthropogenic pollutants on aquatic birds, detailing a range of effects from direct mortality to sublethal impacts, including reduced fitness. There are interactions between these pollutants that can amplify their effects beyond those of each pollutant individually. Despite this, research on these interactions is still limited and requires more targeted investigation. As threats to avian species and anthropogenic pollution continue to rise, implementing mitigation measures is crucial for the preservation of these birds. This paper aims to evaluate specialized scientific articles, highlight, and understand the threats that bird species face.*

***Key words****: environmental contamination, pollutants interactions, toxic effects, wild bird.*

## INTRODUCTION

Biodiversity is at a critically declining level and its current rates are much more frequent than the average natural extinction rate (Barnosky et al., 2011; Tittensor et al., 2014). We have seen the shocking loss of two-thirds of global mammals, birds, fish, reptiles, and insects (Hoffmann et al., 2010), and this severe drop in biodiversity can be attributed to extreme human activity that stresses the species (Hallmann et al., 2017). Waterfowl occupy significant spaces in freshwater and marine ecosystems and serve as sentinels of environmental wellbeing but have been under unprecedented threat from anthropogenic pollution (Degernes, 2008). These avian species are totally reliant on aquatic environments for survival, reproduction and migration, thus their populations and functioning within ecosystems are subject to many environmental stressors (Zhang & Ma, 2011). Numerous studies show that waterbirds serve as valuable bioindicators of the health of aquatic ecosystems, where population dynamics and physiological conditions may serve as biomarkers of the quality of habitats (Arya et al., 2025). The accelerated rate of industrialization, urbanization, and increasing crop cultivation has caused the pollution of water bodies with pollutants such as heavy metals, organic micropollutants, persistent organic pollutants (POPs), microplastics and pharmaceutical substances (Liu et al., 2024; Swarup & Patra 2005). These pollutants do not occur in isolation, but work synergistically to create intricate ecotoxicological systems that challenge the adaptations of waterbird populations at a global scale (Liu et al., 2024). But rising environmental pollutants in aquatic environments are causing serious risks to their health, behavior, and survival. Pollutants, heavy metals, oil spills, plastics, pesticides and industrial waste can accumulate and they enter the food chain, and in the process, they reach birds at the top. Such contaminants interfere with the biologic systems, limit reproduction and disturb the physical and adaptive behaviour of aquatic birds (Shahid et al., 2021). The effects of these pollutants are crucial for the design of conservation measures as well as biodiversity conservation in aquatic regions (Pandiyan et al., 2023; Arya et al., 2025). It is an alarming decline in bird populations associated with environmental pollution, and

these include climate change, loss of habitat fragmentation, invasive species' invasion, spread of pathogenic agents and quality compromise due to pollution. We must raise awareness of these problems to safeguard our avian wildlife and the fragile environment we live (Maxwell et al., 2016; Ceballos et al., 2017). Thanks to their mobility, as well as important roles in many interrelated ecosystem processes, birds are vital to ecosystem functioning and resilience (Whelan et al., 2008; Wenny et al., 2011). They are able to supply all four kinds of ecosystem services: provisioning, regulating, cultural, and supporting (Whelan et al., 2008). Unfortunately, one of the crucial contributions that birds represent to ecosystem health is overlooked. The benefits we gain from bird populations are often at least indirect and may support and manage other processes that promote human health in general (e.g. seed transfer, nutrient cycling, pest control, regulation, ecosystem engineers). Some birds even aid in plant pollination (Wenny et al., 2011). Even though some bird species may not seem particularly charming, they still provide vital ecosystem services. Birds provide various services that benefit human health and well-being. They are a source of nutrition, and their feathers have historically been used for insulation and bedding (FAOSTAT, 2019). Numerous bird species hold significant cultural importance, reflected in the rapidly growing industries of birdwatching and hunting, which play a vital role in the economies of various regions (Mustin et al., 2011; Carver, 2013; Ma et al., 2013; Kronenberg, 2014; Richard et al., 2021).

## MATERIALS AND METHODS

This paper offers a brief review of the literature on the effects of common anthropogenic pollutants on aquatic birds, focusing on stress and pollution-related impacts, the search was conducted using the Web of Science database, Research Gate. Research papers that were freely accessible were utilized; for those that were not available for free, requests were made directly to the authors to obtain their work. The methodology involved a critical analysis of the existing literature and was conducted on 12 January 2026. The search query included specific keywords or a combination of terms related to birds and particular types of pollutants found in the title or abstract (pollutants, wild bird, toxic effects, water pollutants, etc). This initial search yielded over 80 records; after the screening process, studies that did not align with the objectives of the present research were excluded.

## RESULTS AND DISCUSSIONS

Pollutants are those substances introduced into the environment that might lead to damages or disruptions in the natural balance of ecosystems, human health and nature. These chemicals can be natural (such as volcanic ash) or man-made (like pollution from industry, plastics, or pesticides) (Manisalidis et al., 2020). The pollution issue is one of the more prevalent worldwide problems, however, over the last century more industrialisation, urbanisation and unsustainable consumption habits made it very high due to which it is one of the most urgent global issues (Borah et al., 2020). Ecologically, it involves pollutants disrupting ecosystems, devastating biodiversity and causing acid rain, eutrophication and warming world-wide (EEA, 2021). Many birds have exposure to various pollutants simultaneously, and each pollutant category, e.g., various chemicals can contain various compounds contaminated, as well as natural stressors driving multi-component interactions (Grace et al., 2024; Wang et al., 2024). Collectively and separately, these pollutants are likely to be contributing to the population decline. There is still a lack of understanding on how species could vary in their susceptibility, and combined pollution overall effects. It is important to examine the additive effects of pollutants which often coexist in the same place and period (Wang et al., 2024). To increase our understanding of environment effects, we need to assess joint effects of pollutants of the same dimensions with comparable spatial and temporal scales. Moreover, by taking the time complexity of a lot of pollutants in realistic asynchronous scenarios into account, we can provide even better estimates for their cumulative effects (Roşu et al., 2024). It is critical to establish clear insights for the effective pollution

management and policy formulation (Jackson et al., 2021). Pollutants are categorized by the medium they contaminate - air, water, soil - or by their nature, like chemical, biological or physical agents. The most researched and dangerous are air pollutants (e.g., particulate matter, nitrogen oxides, sulphur dioxide, ozone), water pollutants (e.g., heavy metals, nitrates, phosphates, organic compounds), and soil pollutants (e.g., pesticides, persistent organic pollutants, industrial waste). Other categories in this sense are noise, light, and thermal (World Health Organization, 2024). Air pollutants result from burning fossil fuels (for vehicles, power plants, industrial processes), burning biomass, burning waste as if it were human activity, and also the burning of natural sources such as volcanic eruptions or forest fires. The main air pollutants with global health implications include $PM_{25}$ (fine particles), nitrogen dioxide ($NO_2$), sulphur dioxide ($SO_2$), carbon monoxide (CO), and ozone ($O_3$) (World Health Organization, 2023; Nathanson, 2025). In addition, indoor air pollution is of utmost importance, particularly in developing countries where solid biomass or coal are employed as a cooking & heating equipment in poorly ventilated areas (Bilal et al., 2021). Water contamination from either point sources (industrial effluents, wastewater discharges) or non-point sources (agricultural runoff carrying fertilizers, pesticides, and sediments). Heavy metals including lead, mercury, and arsenic, and organic pollutants, such as polychlorinated biphenyls (PCBs) and pharmaceuticals, provide long-term threats to aquatic ecosystems. Soil pollution via deposition of air pollutants, industrial or mining waste runoff, persistent pesticide use, heavy metals accumulation (Johnson et al., 2021). Noise pollution (non-chemical) is a pollutant in that it interferes with human well-being, wildlife behaviour, and ecosystem function. Sources can be traffic and commerce, construction, and urban infrastructures (Goines et al., 2007). Pollutants can affect air quality, biodiversity, ecosystem services and biogeochemical cycles. Acid rain (from $SO_2$ and $NO_x$) can, for instance, degrade forest soils and aquatic ecosystems. Eutrophication in lakes and coastal areas caused by nutrient runoff with nitrogen and phosphorus is one of the most common causes of eutrophication, which also leads to algal blooms, oxygen depletion and mass mortality of fish. Organics and heavy metals accumulate and bioaccumulate in food webs, becoming bio-challenging for both top predators and humans (Lovett et al., 2009; Richard et al., 2021). Common pollutants and ways to be exposed. Bioaccumulation / biomagnification. Aquatic pollution among species represents a serious global biodiversity threat, with waterbirds being one of the organisms most vulnerable to the effects of the compounded impact of chemical pollutants. Birds are key indicators of ecosystem health and pollution levels that capture their ecosystem functioning through their position in food chains, feeding behaviour, and close relationship with aquatic ecosystems (Burger & Gochfeld, 2004; Egwumah et al., 2017). Bioaccumulation and biomagnification are two important concepts in defining the impact of pollutants toward these organisms (Richard et al., 2021). Bioaccumulation is the gradual accumulation of toxins within an individual's body via the ingestion of water, food or direct contact with chronic chemicals. Biomagnification, in contrast, is the upward trend in the concentrations of pollutants as they are transmitted from one trophic level to another, resulting in elevated concentrations of pollutants in predators often birds that are piscivorous or omnivorous (Richard et al., 2021). The bioaccumulation process is influenced by the chemical characteristics of the pollutants, the physiology of the organisms and the environment. Substances with high persistence (POP - persistent organic pollutants) and low solubility in water, combined with that they are highly lipophilic tend to be most preferentially deposited in the tissues of organisms (Elliott & Bishop, 2011). Biomagnification is the process whereby pollutants increase in concentration from trophic level to trophic level. In this way, a contaminant may be found in low concentrations in water or phytoplankton but reach toxic levels in organisms at the top of the food chain, such as piscivorous waterfowl (e.g., gulls, cormorants, pelicans, or fish-eating birds of prey) (Furness, 1993). Bioaccumulation and biomagnification are essential processes in understanding pollutants' effect on aquatic

birds. At the top of food chains, these birds accumulate toxins in concentrations that are highly toxic and contribute to severe health conditions, declining populations as well as ecological chaos. Historical examples, as those from DDT or PCBs, illustrate both the weak point in aquatic ecosystems and their ability to rejuvenate with the control of pollution sources. Long term impact of emerging pollutants on biodiversity requires effective monitoring, stringent environmental policies, and active community participation (Anderson et al., 1975). Waterbirds are extremely susceptible to being contaminated because they depend on water resources and wetlands, according to researchers. Bottom-feeding and consuming sediment expose them to pollutants (Beyer et al., 2008; Veríssimo et al., 2025). Sediments from aqueous sources collect heavy metals, organic pollutants, and debris that can also persist in the digestive tracts of waterbirds for extended periods (Beyer et al., 2008; Veríssimo et al., 2025). Diverse bioavailability of these contaminants is influenced by sediment chemistry and pH. Exposure of bioaccumulate sediments may influence physiology, reproductive fitness, behaviour and population dynamics (Elliott & Bishop, 2011). Sources of pollution in water and soil include industrial effluents such as heavy metals (Hg, Pb, Cd), petroleum hydrocarbons, persistent organic pollutants (POPs), and industrial solvents. These pollutants arise from various activities related to industrialization, leading to significant impacts on both water and soil quality. Accidental leaks and overflows can result in irreversible contamination, which can have lasting effects on aquatic organisms that depend on these environments (Ding, 2025). Ascensive farming practices lead to diffuse pollution from excessive use of fertilizers and pesticides. Chemicals such as neonicotinoids, glyphosate, and nitrogen compounds are washed into wetlands by rainfall, disrupting ecosystem processes (Wania & Mackay, 1996). Poorly upgraded treatment plants release toxic substances from rivers to the environment as microplastics, pharmaceuticals, and detergents. These chemicals cause ecological stress and negatively impact those organisms that are exposed to the contaminants (EPA, 2019). Oceans transport sector, oil pollution and waterfowl impacts are negative and affect water birds via water pollution, changes in plumage and functional impairment (Burger & Elbin, 2015). In recent years, human pollution has seriously compromised waterfowl populations, with some species being threatened by extinction. Past DDT-induced eggshell thinning has been preventing reproduction, though populations started bouncing back after the pesticide was banned. In order to save waterfowl, we need to limit pollution and minimize toxic chemicals, recycle well, minimize oil spills, and protect wetlands. Environmental education is an essential element in creating sustainable and responsible living in nature (Anderson et al, 1975; Heinz & Hoffman, 2003; Burger & Elbin, 2015). Pollution negatively affects waterbird populations, leading to declines in most species found in polluted estuaries, rivers, and coastal areas (Luo et al., 2024). Migratory waterbird declines are associated with polluted staging habitats, indicating that pollution in specific habitats can impact species that have wide geographic ranges (Luo et al., 2024). Protected areas can provide conservation benefits, yet their effectiveness at protecting waterbirds from pollution is variable and frequently inadequate. Well-managed areas with habitat restoration and pollution control can enhance waterbird populations, however, few have proper infrastructure to monitor and remedy pollution (Gaget et al., 2021). Long-term monitoring, using combined conventional biomonitoring and advanced methods such as biomarker analysis, is vital to detect pollution effects on populations at an early stage (Gaget et al., 2021). In order to make relevant comparison by region and time, standardized methods for contaminant analysis and effects-based monitoring are required. Although pollutant concentrations of conventional pollutants decrease, recovery of waterfowl populations is incomplete. There are instances in which some populations have become better stabilized, although researchers attribute partial recovery to changes to ecosystem structure (i.e., changes in prey fish composition), invasive species, climate change and interactions with recovering predator populations. These findings reaffirm that without other anthropogenic stressors, pollution

abatement alone is insufficient to restore population levels to historical levels or ecosystem function (Breton et al., 2008).

## CONCLUSIONS

The research reviewed here conclusively demonstrates that environmental pollutants pose major threats to waterfowl populations globally. Lead, mercury, organochlorine pesticides, PCBs, dioxin-like compounds, PFASs, and plastic debris all have documented adverse effects on species reproduction, immune function, behaviour, and survival. These effects have caused severe population declines in some species and geographic regions, particularly in areas with traditional contamination or continuing high levels of pollution. The coming decades present both challenges and opportunities for waterfowl conservation in the context of pollution. On the one hand, emerging pollutants, including PFASs and microplastics, threaten to create new waves of environmental contamination that require regulatory response and remediation efforts. On the other hand, the growing scientific understanding of pollutant toxicology and mechanisms of action allows for the development of increasingly sophisticated strategies for pollution prevention, remediation, and biomonitoring.

Future research should utilize integrative approaches that examine multiple stressors simultaneously, assess the effects of mixtures of pollutants rather than the toxicity of a single compound, and link molecular and physiological biomarkers to population-level outcomes. In addition, because water birds are inherently adaptable and evolving species, research should investigate the potential for rapid genetic and phenotypic adaptation to polluted environments, taking into account the adaptive costs of such adaptation. Only through continued scientific investigation, coupled with aggressive pollution prevention and remediation efforts, can waterfowl populations be recovered and conserved.

## ACKNOWLEDGEMENTS

This research was funded by projects RO1567-IBB02/2024 (The Romanian Academy).

## REFERENCES

Anderson, D.W., Jehl, J.R. Jr, Risebrough, R.W., Woods, L.A. Jr, Deweese, L.R., & Edgecomb, W.G. (1975). Brown pelicans: improved reproduction off the southern California coast. *Science*. 21;190(4216):806-8. doi: 10.1126/science.1239078.

Arya, A. K., Joshi, K. K., Bachheti, A., & Vashishth, D. S. (2025), Impact of water pollution on waterbirds: A Review, *Environment Conservation Journal*, 26 (2) (https://doi.org/10.36953/ECJ.30333174).

Barnosky, A. D., Matzke, N., Tomiya, S., Wogan, G.O.U., Swartz, B., Quental, T.B., Marshall, C., McGuire, J.L., Lindsey, E.L., Maguire, K.C., Mersey, B., & Ferrer, E.A. (2011). Has the Earth's sixth mass extinction already arrived? *Nature, 471*, 51–57. (https://doi.org/10.1038/nature09678).

Borah, P., Manish, K., & Pooja, D. (2020). Chapter 2 - Types of inorganic pollutants: metals/metalloids, acids, and organic forms. *Inorganic Pollutants in Water*, 17-31 (https://doi.org/10.1016/B978-0-12-818965-8.00002-0).

Beyer, W., N., Perry, M. C, & Osenton, P. C. (2008). Sediment Ingestion Rates in Waterfowl (Anatidae) and Their Use in Environmental Risk Assessment; *Integrated Environmental Assessment and Management*. 4(2), pp. 246–251.

Bilal, M., Mhawish, A., Janet, E. N., Qiu, Z., Nazeer, M., Ali, A., Leeuw, G., Levy, R. C., Wang,Y., Chen, Y., Wang, L., Shi, Y., Bleiweiss, M. P., Mazhar, U., Atique, L., & Ke, S. (2021) Air pollution scenario over Pakistan: Characterization and ranking of extremely polluted cities using long-term concentrations of aerosols and trace gases. *Remote Sensing of Environment*, 264. (https://doi.org/10.1016/j.rse.2021.112617).

Breton, A., Fox, G., & Chardine, J., (2008). Survival of Adult Herring Gulls (Larus argentatus) from a Lake Ontario Colony Over Two Decades of Environmental Change, *Waterbird*s 31:15-23.

Burger, J., & Gochfeld, M. Marine Birds as Sentinels of Environmental Pollution. *EcoHealth* 1, 263–274 (2004). https://doi.org/10.1007/s10393-004-0096-4

Burger, J., & Elbin, S. (2015). Metal levels in eggs of waterbirds in the New York Harbor (USA): trophic relationships and possible risk to human consumers. *Journal of Toxicology and Environmental Health*. 78(2):78-91. doi:10.1080/15287394.2014.941965

Carver, E. (2013). *Birding in the United States: a demographic and economic analysis addendum to the 2011 National Survey of Fishing, Hunting, and Wildlife- Associated Recreation, US Fish & Wildlife, Arlington, USA.* https://www.fws.gov/program/national-survey-fishing-hunting-and-wildlife-associated-recreation-fhwar

Ceballos, G., Ehrlich, P.R., & Dirzo, R. (2017), Biological annihilation via the ongoing sixth mass extinction signaled by vertebrate population losses and declines. *Proc. Natl. Acad. Sci*. 114, E6089–E6096.

Degernes, L. A. DVM, MPH, DABVP–Avian. (2008), Waterfowl Toxicology: A Review. *Veterinary Clinics of North America: Exotic Animal Practice, vol 11*,

(2), 283-300. (https://doi.org/10.1016/j.cvex.2007.12.001).

Ding, J., Wang, N., Yaqiao, L., Qian, L., Li, X., & Yu, F. (2025). Assessment of heavy metal exposure risk to aquatic birds in the key wetland habitats of the Yellow River (China), using an integrated model. *Global Ecology and Conservation*, 60, e03611 (https://doi.org/10.1016/j.gecco.2025.e03611).

Egwumah, F.A, Egwumah, P.O, & Edet, D. (2017). Paramount roles of wild birds as bioindicators of contamination, *International Journal of Avian & Wildlife Biology*, 2(6):194–199.

Elliott, J. E., & Bishop, C. A. (2011). Contaminants and wildlife: A Canadian perspective. Ecotoxicology, 20, 1223–1236.

EPA. (2019). Ecological Effects Test Guidelines. https://www.epa.gov/test-guidelines-pesticides-and-toxic-substances/series-850-ecological-effects-test-guidelines

European Environment Agency (EEA) (2021) https://www.eea.europa.eu › articles

FAOSTAT, (2019). Pesticides use. Food and Agriculture Organization of United Nations (http://www.fao.org/faostat/en/#data/RP/visualize).

Furness, R. (1993) *Birds as Monitors of Pollutants*. In: Furness, R. and Greenwood, J., Eds., Birds as Monit Environ Chang, Springer, London, 86-143. https://doi.org/10.1007/978-94-015-1322-7_3

Gaget, E., Pavón-Jordán, D., Johnston, A., Lehikoinen, A., Hochachka, W.M., Sandercock, B.K., Soultan, A, Azafzaf, H., Bendjedda, N, Bino T, Božič L, Clausen P, Dakki M, Devos K, Domsa, C, Encarnação, V, Erciyas-Yavuz, K., Faragó, S., Frost, T., Gaudard, C, Gosztonyi, L., Haas, F, Hornman, M., Langendoen, T., Ieronymidou, C., Kostyushin, V.A, Lewis, L.J, Lorentsen, S.H., Luigujõe, L., Meissner, W, Mikuska, T, Molina, B, Musilová, Z., Natykanets, V, Paquet, J.Y., Petkov, N, Portolou, D., Ridzoň, J., Sayoud, S., Šćiban, M., Sniauksta, L., Stīpniece, A., Strebel, N., Teufelbauer, N., Topić, G., Uzunova, D., Vizi, A., Wahl, J., Zenatello, M., & Brommer, J.E.. (2021). Benefits of protected areas for nonbreeding waterbirds adjusting their distributions under climate warming. *Conservation Biology*. 35(3):834-845. (doi: 10.1111/cobi.13648).

Goines, L., & Hagler, L. (2007). "Noise Pollution: A Modern Plague". Southern Medical Journal. 100 (3). *Lippincott Williams and Wilkins*: 287–294. (doi:10.1097/SMJ.0b013e3180318be5).

Grace J, Duran E, Ann Ottinger M, Maness T. (2024) Sublethal effects of early-life exposure to common and emerging contaminants in birds. *Curr Res Toxicol*. 31;7:100190. (Doi: 10.1016/j.crtox.2024.100190. PMID: 39220619; PMCID: PMC11365322).

Hallmann, C.A., Sorg, M., Jongejans, D., Siepel, H., Hofland, N., Schwan, H., Stenmans, W., Müller, A., Sumser, H., H¨orren, T., Goulson, D., & De Kroon, H. (2017). More than 75 percent decline over 27 years in total flying insect biomass in protected areas. *PLoS One* 12. (https://doi.org/10.1371/journal.pone.0185809).

Heinz, G., & Hoffman, D. (2003) Embryotoxic Thresholds of Mercury: Estimates from Individual Mallard Eggs. *Arch. Environ. Contam. Toxicol.* 44, 0257–0264. https://doi.org/10.1007/s00244-002-2021-6

Hoffmann, M., Hilton-Taylor, C., Angulo, A., B¨ohm, M., Brooks, T., H M Butchart, S., E Carpenter, K., Chanson, J., Collen, B., Cox, N., Darwall, W., Dulvy, N., Harrison, L., Katariya, V., M Pollock, C., Quader, S., Dewhurst-Richman, N., S L Rodrigues, A., Tognelli, M., & Stuart, S. (2010). The impact of conservation on the status of the world's vertebrates. *Science 330* (80), 1503–1509. (https://doi.org/10.1126/science.1194442).

Jackson, M.C., Pawar, S., & Woodward, G., (2021). The temporal dynamics of multiple stressor effects: from individuals to ecosystems. *Trends Ecol. Evol*. 36, 402–410. (https://doi.org/10.1016/j.tree.2021.01.005).

Johnson, M. S., Buck, R. C., Cousins, Ian T., Weis, C. P., & Fenton, S. E. (2021), „Estimating Environmental Hazard and Risks from Exposure to Per-and PolyfluoroAlkyl Substances (PFAS): Outcome of a SETAC Focused Topic Meeting", *Environmental toxicology and chemistry,* 40 (3), pp. 543–549, (doi:10.1002/etc.4784, ISSN 0730-7268).

Kronenberg, J. (2014). Environmental impacts of the use of ecosystem services: case study of bird watching. *Environmental Management* 54, 617–630. (https://doi.org/10.1007/s00267-014-0317-8).

Liu, X., Sathishkumar, K., Zhang, F., Naraginti, S., Rajasekar, A., Zhang, H., Anbarasu, K, Kuldeep, K. Saxena, Rajendiran R. & Guo, X. (2024). Frontiers in environmental cleanup: Recent advances in remediation of emerging pollutants from soil and water. *Journal of Hazardous Materials Advances* vol 16, (https://doi.org/10.1016/j.hazadv.2024.100461).

Lovett, G.M, Tear, T.H, Evers, D.C, Findlay, S.E, Cosby, B.J, Dunscomb, J.K, Driscoll, C.T., & Weathers, K.C. (2009) Effects of air pollution on ecosystems and biological diversity in the eastern United States. *Ann N Y Acad Sci*.1162:99-135. (doi: 10.1111/j.1749-6632.2009.04153.x).

Luo, H., Li, Q., Yu, Y., Kang, J., Lei, W., & Zhang, D. (2024). Spatiotemporal Distribution and Habitat Characteristics of Shorebirds in the Coastal Wetlands of Dalian, Liaoning, China. *Sustainability*, 16, 8133. (https://doi.org/10.3390/su16188133).

Ma, Z., Cheng, Y., Wang, J., & Fu, X. (2013). The rapid development of birdwatching in mainland China: a new force for bird study and conservation. *Bird Conserv. Int.* 23, 259–269. (https://doi.org/10.1017/S0959270912000378).

Manisalidis, I., Stavropoulou, E., Stavropoulos, A., & Bezirtzoglou, E. (2020). Environmental and Health Impacts of Air Pollution: A Review. *Front Public Health*. 20; 8:14. (doi:10.3389/fpubh.2020.00014).

Maxwell, S.L., Fuller, R.A., Brooks, T.M., & Watson, J.E.M. (2016). Biodiversity: the ravages of guns, nets and bulldozers. *Nature* 536, 143–145.

Mustin, K., Newey, S., Irvine, J., Arroyo, B., & Redpath, S. (2011). *Biodiversity impacts of game bird hunting*

*and associated management practices in Europe and North America. RSPB report.*

Nathanson, J. A. (2025). *Major air pollutants,* (https://www.britannica.com/science/air-pollution/Fine-particulates).

Pandiyan, J., Arumugam, R., Al-Ghanim, K.A., Sachivkina, N., Nicoletti, M., & Govindarajan, M. (2023), Heavy Metals in Wetland Ecosystem: Investigating Metal Contamination in Waterbirds via Primary Feathers and Its Effect on Population and Diversity. Soil Syst. 2023, 7, 104. (https://doi.org/10.3390/soilsystems7040104).

Richard F.-J., Southern, I., Gigauri, M., Bellini, G., Rojas, O., & Runde, A. (2021), Warning on nine pollutants and their effects on avian communities, *Global Ecology and Conservation,* Volume 32, (https://doi.org/10.1016/j.gecco.2021.e01898).

Roșu (Marin), I., M., & Jinescu, C., (2024). Multiple pollution effects in urban areas on the environment and living organisms*. Journal of Engineering Sciences and Innovation*, 9 (3), 303 – 312.

Shahid, M., K., Kashif, A., Fuwad A., & Choi Y., (2021) Current advances in treatment technologies for removal of emerging contaminants from water – A critical review, *Coordination Chemistry Reviews 442,* (https://doi.org/10.1016/j.ccr.2021.213993).

Swarup, D., & Patra, R. C. (2005). Environmental pollution and its impact on domestic animals and wildlife. February, *The Indian Journal of Animal Sciences* 75(2):231-240.

Tittensor, D.P., Walpole, M., Hill, S.L.L., Boyce, D.G., Britten, G.L., Burgess, N.D., Butchart, S.H.M., Leadley, P.W., Regan, E.C., Alkemade, R., Baumung, R., Bellard, C.,Bouwman, L., Bowles-Newark, N.J., Chenery, A.M., Cheung, W.W.L., Christensen, V., Cooper, H.D., Crowther, A.R., Dixon, M.J.R., Galli, A., Gaveau, V., Gregory, R.D., Gutierrez, N.L., Hirsch, T.L., H¨oft, R., Januchowski-Hartley, S.R., Karmann, M., Krug, C.B., Leverington, F.J., Loh, J., Lojenga, R.K., Malsch, K., Marques, A., Morgan, D.H.W., Mumby, P.J., Newbold, T., Noonan-Mooney, K., Pagad, S.N., Parks, B.C., Pereira, H.M., Robertson, T., Rondinini, C., Santini, L., Scharlemann, J.P.W., Schindler, S., Sumaila, U.R., Teh, L.S.L., van Kolck, J., Visconti, P., & Ye, Y. (2014). A mid-term analysis of progress toward international biodiversity targets. *Science 346*, 241–244 (https://doi.org/10.1126/science.1257484).

Veríssimo, S.N., Paiva, V.H., Cunha, S.C., Brandão, A.L.C., Coentro, J., Fernandes, J.O., Pereira, J.M., Batista de Carvalho, L.A.E., Cerveira, L.R., Marques, M.P.M., Silva, V., Norte, A.C., & Ramos, J.A. (2025). From mudflats and saltpans to Open Sea: Plastic ingestion and PBDE/MeO-BDE accumulation in Waterbirds from southern Portugal*, Marine Pollution Bulletin* Volume 214, (https://doi.org/10.1016/j.marpolbul.2025.117727).

Wang, F., Xiang L., Kelvin Leung, S.Y., Elsner, M., Zhang, Y., Guo, Y., Bo Pan, Sun H., Taicheng, A., Ying, G., Brooks, B. W., Deyi, H., Helbling, D. E., Sun, J., Qiu, H., Vogel, T. M., Zhan,g W., Gao, Y., Simpson, M. J., Luo, Y., Scott, X. Chang, Su G., Wong, B. M., Fu, Tzung-M., Zhu, D., Jobst, K. J., Ge, C., Coulon, F., Harindintwali, J. D., Zeng, X., Wang, H., Fu Y., Wei, Z., Lohmann, R., Chen, C., Song, Y., Concepcion Sanchez-Cid, Yu Wang, Ali El-Naggar, Yiming Yao, Yanran Huang, Japhet Cheuk-Fung Law, Chenggang Gu, Huizhong Shen, Yanpeng Gao, Chao Qin, Hao Li, Tong Zhang, Natàlia Corcoll, Min Liu, Alessi, D. S., Hui Li, Brandt, K. K., Pico, Y., Gu, C., Guo, J., Jianqiang Su, Corvini, P., Ye, M., Rocha-Santos, T., Huan, H., Yang,Y., Tong, M., Zhang, W., Suanon, F., Ferdi Brahushi, Zhenyu Wang, Syed A. Hashsham, Virta M., Qingbin Yuan, Gaofei Jiang, Louis A.Tremblay, Qingwei Bu, Jichun Wu, Willie Peijnenburg, Edward Topp, Cao, X., Jiang, X., Zheng, M., Zhang, T., Luo, Y., Zhu, L., Xiangdong Li, Barceló, D., Chen, J., Baoshan Xing, Amelung, W., Cai, Z., Naidu, R., Shen, Q., Pawliszyn, J., Zhu, Yong-guan, Schaeffer, A., Rillig, M. C., Wu, F., Yu, G., & Tiedje, J. M. (2024). Emerging contaminants: A One Health perspective. The Innovation, 5(4). (https://doi.org/10.1016/j.xinn.2024.100612).

Wania, F., & Mackay, D. (1996). Tracking the distribution of persistent organic pollutants. *Environmental Science & Technology*, 30(9), 390A–396A.

Wenny, D.G., DeVault, T.L., Johnson, M.D., Kelly, D., H. Sekercioglu, C., Tomback, D.F., & Whelan, C.J., (2011). The need to quantify ecosystem services provided by birds. *Auk* 128, 1–14. (https://doi.org/10.1525/auk.2011.10248).

Whelan, C.J., Wenny, D.G., & Marquis, R. J., (2008). Ecosystem services provided by birds. Ann. N. Y. *Acad. Sci*. 1134, 25–60. (https://doi.org/10.1196/annals.1439.003).

World Health Organization. (2023) (https://www.who.int/news/item/07-05-2024-who-results-report-2023-shows-notable-health-achievements-and-calls-for-concerted-drive-toward-sustainable-development-goals).

World Health Organization. (2024) https://www.who.int/news-room/fact-sheets/detail/ ambient-(outdoor)-air-quality-and-health

Zhang, W., & Ma, J. (2011). Waterbirds as bioindicators of wetland heavy metal pollution. *Procedia Environmental Science 10*, 2769–2774. (https://doi.org/10.1016/j.proenv.2011.09.429).

Scientific Papers. Series E. Land Reclamation, Earth Observation & Surveying, Environmental Engineering. Vol. XV, 2026
Print ISSN 2285-6064, CD-ROM ISSN 2285-6072, Online ISSN 2393-5138, ISSN-L 2285-6064

# MOBILITY AND TOXICOLOGICAL RELEVANCE IN THE EVALUATION OF HEAVY METAL TRANSFER FROM SOIL TO PLANTS

**Claudiu-Denis FILIP[1], Mirela Ana COMAN[1, 2]**

[1]University of Agricultural Sciences and Veterinary Medicine of Cluj-Napoca,
3-5 Calea Mănăștur, Cluj-Napoca, Romania
[2]Technical University of Cluj-Napoca, 62A V. Babeș Street, Baia Mare, Romania

Corresponding author email: claudiu.filip98@gmail.com

***Abstract***

*The classic transfer factor formula, widely used in studies dedicated to heavy metal mobility in the soil-plant system, represents a direct ratio between the metal concentration in the plant and that in the soil. Although valuable for general comparisons and for describing their behaviour in the environment, this formula does not allow for an adequate separation between the actual forms of mobility, the toxicological characteristics of each metal, and strict reporting to the limits regulated by the Codex Alimentarius. In this context, the paper proposes the Assimilated Mobility Transfer Factor (AMTF), an extended, integrative formula that includes the toxicity coefficient, the mobile fraction in the soil, the actual level of accumulation in fruit, and the food regulations in force. Applying the AMTF to data sets from historically polluted areas, such as the Baia Mare Mining Basin, highlights consistent differences between the mobility of heavy metals and their actual accumulation in fruit, discrepancies that the classic ratio cannot capture. The new formula proposed for the AMTF provides an adequate, modern tool for current food safety and ecotoxicological risk studies.*

***Key words****: food safety, heavy metals, mobile fraction, soil-plant transfer, toxicity coefficient.*

## INTRODUCTION

Heavy metals represent a group of elements exhibiting relatively high density and marked toxicity even at low concentrations, including lead (Pb), cadmium (Cd), mercury (Hg), chromium (Cr), and other substances widely recognized as major environmental pollutants. Their presence in natural ecosystems is closely linked to anthropogenic activities, particularly mining and metallurgical operations, industrial discharges, urban waste disposal, and certain agricultural practices such as the application of fertilizers, pesticides, or sewage sludge (Singh et al., 2011; Boros et al., 2015; Roba et al., 2016; Sur et al., 2017; Rusu et al., 2023).

A defining feature of heavy metals is their persistence in the environment, as they are not subject to biological or chemical degradation processes. This stability promotes their accumulation in soils and sediments and facilitates transfer to living organisms, enabling their movement along trophic chains. Their non-biodegradable character, combined with their potential for bioaccumulation and mobility governed by physicochemical conditions, confers major relevance from the perspective of ecosystem protection and human health, underscoring the need for integrated assessments that simultaneously capture their behavior in soil-plant systems and their toxicological implications (Bizo et al., 2014; Minkina et al., 2017; Moț et al., 2019; Moț et al., 2021; Sabir et al., 2022; Filip & Coman, 2025).

The toxicity of heavy metals to human health is extensively documented in scientific literature and is associated with complex molecular mechanisms involving direct interactions with proteins and nucleic acids, induction of oxidative stress, and disruption of cellular homeostasis. Through these processes, they can impair the normal functioning of biological systems, while the severity of toxic effects depends on the nature of the element, the level and duration of exposure, and individual susceptibility (Jaishankar et al., 2014; Mitra et al., 2022; Kotnala et al., 2025; Jomova et al., 2025). Among these elements, lead (Pb) is recognized for its neurotoxic potential, with chronic exposure being linked to cognitive deficits and developmental disorders in children, as well as elevated blood pressure and impaired renal function in adults. Moreover, long-term accumulation of Pb may result in

anemia, reproductive dysfunctions, and other severe systemic manifestations (Oros et al., 2011; Balali-Mood et al., 2021; Ortega et al., 2021). Cadmium (Cd), characterized by high toxicity even at low concentrations, is predominantly associated with renal impairment and bone demineralization processes that may progress to severe conditions such as Itai-itai disease. In addition, Cd is classified as a human carcinogen and has been implicated in the development of lung and prostate cancers, further emphasizing the importance of assessing its mobility in soil-plant systems (Waalkes, 2003; Davidova et al., 2024; Sasaki et al., 2024.)
The aim of this study was to establish the current level of Pb and Cd contamination in soil and fruit within soil-plant system, as well as to evaluate the potential of the AMTF ecotoxicological indicator for the mathematical modeling of the transfer factor.

## MATERIALS AND METHODS

This study employed an experimental design structured to provide an integrated evaluation of Pb and Cd behavior within the soil–plant–fruit system by investigating contamination levels, bioaccumulation processes, and transfer dynamics in an area known for historical pollution associated with mining and metallurgical activities. The experimental framework consisted of three major analytical components:

a) Regarding heavy metal content in soil;
b) Regarding heavy metal content in fruits;
c) Regarding the transfer factor.

The mathematical modeling of heavy metal pollutant transfer was performed using the AMTF ecotoxicological indicator, which integrates the total and mobile forms of metals in soil, the concentration identified in fruit, and the relation to the maximum permissible limit, allowing classification into transfer classes and the integrated characterization of Pb and Cd heavy metal pollutant behavior within the soil–plant system.
The area of interest covers approximately 588.8 km$^2$ within the Baia Mare Depression and was evaluated in comparison with a less impacted reference area of about 111 km$^2$ located in the Maramureș Depression, namely the Sighetu Marmației. Within these perimeters, soil samples were collected at several sampling depths in accordance with Order No. 184/1997, while plum samples were obtained following the provisions of Order No. 1048/2003.
The Baia Mare Depression (Figure 1) represents a geomorphological contact zone between the Someșan Plateau and the Eastern Carpathians, developed along the southern flank of the Gutâi-Țibleș Neogene mountain units.

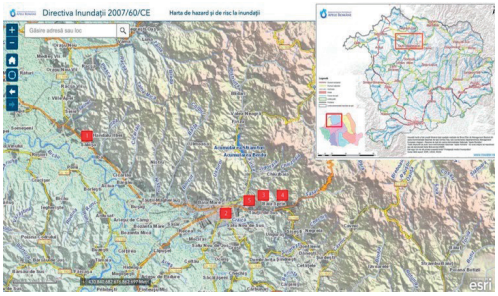



Figure 1. Sampling points

From an altimetric perspective, the base level of the depression ranges between 150-350 m, whereas morphologically it exhibits a basin-shaped configuration. The relief is heterogeneous, and the present study focuses on the Seini-Baia Mare-Baia Sprie piedmont glacis and contact piedmont sectors, extending toward the southern foothills of the Igniș-Gutâi Mountains, which constitute the main investigated zone, while the Sighetu Marmației sector served as the reference area (Coman, 2006; Coman et al., 2010; Ștefan et al., 2012; Marian et al., 2016; Manoiu & Spiridon, 2017).

### Working Method

**a) Regarding heavy metal content in soil**
Soil sampling was conducted in accordance with the existing methodological regulations and standards stipulated in Order No. 184/1997. Samples were collected from the Baia Mare Depression, specifically from the piedmont glacis and contact piedmont sectors, as well as from the Sighetu Marmației sector located in the Maramureș Depression, which served as the reference area. For each sampling point, the soil profile was opened, and samples were obtained from four different depths, namely 5, 30, 50, and

100 cm, to capture the vertical distribution of the investigated elements.
Following field collection, physicochemical analyses were carried out in an accredited laboratory, namely INCDO ICIA Cluj-Napoca, in accordance with the following international standards: SR ISO 11464:1994, SR ISO 11047:1999-PIS-03, and SR EN ISO 1185:2009. The analytical results were subsequently evaluated in relation to the regulatory thresholds in force at the national level (Order No. 756/1997), at the European level (European Council Directive 86/278/EEC 1986), and at international level (US EPA, 2002 after He et al., 2015).

**b) Regarding heavy metal content in fruit**
The sampling plan overlaps perfectly with that of the soils, including for the control sample.
Fruit samples (plums) were collected annually from privately owned orchards in August 2023, 2024, and 2025. The Pb and Cd content in the fruit was determined. The results were interpreted in accordance with the legislation in force, namely Order 975/1998 at national level, EU Directive 2023/915 at European Union level, and Codex Alimentarius, 1995 at international level.

**c) Regarding the transfer factor**
The transfer factor (TF), also known in the literature as the bioaccumulation factor (BAF), biological accumulation factor (BCF), or bioconcentration factor (BCFT), represents the ratio between the content in plants and the content in soil. This factor has been studied nationally and internationally (Olănescu, 2007; Ivasuc & Rusu, 2011; Big et al., 2012; Jolly et al., 2013; Aladesanmi et al., 2019; Jakubus et al., 2019; Nițu et al., 2019; Pehoiu et al., 2020; Noman et al., 2022; Pruteanu et al., 2022; Tong et al., 2022).
The calculation assumes that the transfer of heavy metal pollutants into the soil-plant system is not determined exclusively by the total form, but by the interaction between the mobile fraction, the level of accumulation in the fruit, and the maximum permissible limit.

$$AMTF = (C_{mobile}/C_{mobile}+1) \times \log(C_{total} + 1) \times (C_{fruit}/Standard) \times \delta$$

where:
$\delta$ = metal-specific toxicity coefficient ($\delta_{Cd} = 1$, $\delta_{Pb} = 2$);
$C_{mobile}$ = mobile concentration of the metal in the soil (mg/kg);
$C_{total}$ = total concentration of the metal in the soil (mg/kg);
$C_{fruit}$ = concentration of the metal in the fruit (mg/kg);
Standard = maximum permitted limit in fruit (mg/kg wet substance).

In this calculation formula, the coefficient $\delta$ was introduced as a toxicological weighting factor to reflect the differences in hazard associated with the metals analyzed. $\delta$ was established based on the IARC classification of carcinogenicity:

- ⇒ Cd and its compounds are classified in Group 1,
- ⇒ Pb compounds in Group 2A (EFSA, 2010).

Thus, discrete weights corresponding to these groups were used ($\delta Cd = 1$, $\delta Pb = 2$).

To interpret the AMTF indicator values (Table 1), a transfer class classification system was used, established based on the distribution of the values obtained, the reporting of the accepted normative limits, and a non-linear progression inspired by the Fibonacci sequence ($\Phi$=1.6818).

The application of the logarithmic function attenuates the influence of very high total concentrations and improves the stability of the indicator. Thus, very large differences in the total fraction do not monopolize the result.

Table 1. AMTF ranges

| No. crt. | AMTF values range | Interpretation | Chromatic scale of transfer |
|---|---|---|---|
| 1 | <0.1 | Very low transfer | |
| 2 | 0.10-0.21 | Low transfer | |
| 3 | 0.21-0.55 | Medium transfer | |
| 4 | 0.55-0.89 | High transfer | |
| 5 | 0.89-1.44 | Very high transfer | |
| 6 | ≥1.44 | Extreme transfer | |

## RESULTS AND DISCUSSIONS

### *a) Soil sampling*

The results for total and mobile Pb content are presented in Table 2.

Table 2. Pb content in soil

| No. crt. | Sampling point | Depth (cm) | Pb content (mg/kg) | |
|---|---|---|---|---|
| | | | Total | Mobile |
| 1. | Săbișa | 5 | 35.0 | 0.10 |
| | | 30 | 42.7 | <0.02 |
| | | 50 | 22.9 | <0.02 |
| | | 100 | 21.0 | 0.09 |
| 2. | Baia Mare | 5 | 27.0 | <0.02 |
| | | 30 | **385.0** | <0.02 |
| | | 50 | **238.0** | <0.02 |
| | | 100 | **480.0** | <0.02 |
| 3. | Baia Sprie I | 5 | **211.0** | 0.68 |
| | | 30 | **88.3** | 0.34 |
| | | 50 | 35.0 | 0.28 |
| | | 100 | 32.8 | <0.10 |
| 4. | Baia Sprie II | 5 | **261.0** | 0.60 |
| | | 30 | 41.7 | <0.10 |
| | | 50 | 33.3 | <0.10 |
| | | 100 | 29.1 | <0.10 |
| 5. | Tăuții de Sus | 5 | **890.0** | 0.087 |
| | | 30 | **141.0** | 1.20 |
| | | 50 | 35.3 | 0.16 |
| | | 100 | 37.7 | 0.17 |
| 6. | Sighetu Marmației (the control) | 5 | 40.7 | <0.02 |
| | | 30 | 28.8 | <0.02 |
| | | 50 | 31.6 | <0.02 |
| | | 100 | 27.7 | <0.02 |
| 7. | MAL RO[a] | - | 50 | - |
| 8. | MAL EU[b] | - | 50-300 | - |
| 9 | MAL INT[c] | - | 200 | - |

MAL-maximum allowed limit, RO-Romania, EU-Europe INT-International, a - Order No. 756/1997, b - Council Directive 86/278/CEE 1986; c - US EPA, 2002 after He et al., 2015.

*Sampling points* - Pb

In Săbișa, the Pb content in total form is below the maximum permissible limit at all depths analyzed. The maximum value determined, 42.7 mg/kg at a depth of 30 cm, is 15% lower than the maximum permissible limit, with no exceedances of the legal threshold recorded. The Pb content in mobile form is below 0.10 mg/kg, with no legislative reference framework.

In Baia Mare, Pb content in total form is below the maximum permissible limit in the surface horizon, but in the intermediate and deep horizons there are significant exceedances of this limit. At 30 cm, the concentration of 385 mg/kg exceeds the maximum permissible limit by 7.7 times, at 50 cm by 4.76 times, and at 100 cm it reaches a maximum of 9.6 times, highlighting a marked accumulation and historical migration of Pb in the soil profile, specific to areas affected by mining and metallurgical activities. The content of Pb in mobile form remains below 0.02 mg/kg throughout the analyzed profile, with no legislative reference framework.

At Baia Sprie I, the total Pb content exceeds the maximum permissible limit in the surface horizon, where the value of 211 mg/kg represents an exceedance of 4.22 times, as well as in the intermediate horizon, with an exceedance of 1.77 times, while in the deep horizon the concentrations determined are below the maximum permissible limit. The Pb content in mobile decreases with depth.

At Baia Sprie II, the total Pb content exceeds the maximum permissible limit in the surface horizon, where the value of 261 mg/kg represents an exceedance of 5.22 times, while in the intermediate horizon and in the depth horizon the concentrations determined are below the maximum permissible limit. The Pb content in mobile form recording maximum values in the surface horizon and a progressive decrease towards the deep horizon.

In Tăuții de Sus, the total Pb content records the highest values in the analyzed reference area, with a concentration of 890 mg/kg in the surface horizon, corresponding to a 17.8-fold exceedance of the maximum permissible limit, with exceedances also occurring in the intermediate horizon, where the value of 141 mg/kg represents a 2.82-fold exceedance. In the deep horizon, the concentrations determined are below the maximum permissible limit. The Pb content in mobile form varies between 0.087 and 1.20 mg/kg on the analyzed profile, with maximum values in the intermediate horizon and a decrease towards the deep horizon. These values cannot be evaluated comparatively from a regulatory point of view, as there is no legislative framework in force for the mobile form.

In Sighetu Marmației (the control), the total Pb content is below the maximum permissible limit in all horizons analyzed. The Pb content in the mobile form is below 0.02 mg/kg across the entire soil profile.

Therefore, the control site can be considered uncontaminated, confirming the absence of Pb contamination and validating the use of this point as a reference area for the comparative interpretation of the results obtained in areas affected by anthropogenic activities.

*Sampling points* -Cd

The results for total and mobile Cd content are presented in Table 3.

Table 3. Cd content in soil

| No. crt. | Sampling point | Depth (cm) | Cd content (mg/kg) | |
|---|---|---|---|---|
| | | | Total | Mobile |
| 1. | Săbișa | 5 | <0.33 | <0.02 |
| | | 30 | <0.33 | <0.02 |
| | | 50 | <0.33 | <0.02 |
| | | 100 | <0.33 | <0.02 |
| 2. | Baia Mare | 5 | 1.73 | <0.02 |
| | | 30 | **3.47** | 0.03 |
| | | 50 | 0.83 | <0.02 |
| | | 100 | **4.0** | <0.02 |
| 3. | Baia Sprie I | 5 | 2.50 | <0.05 |
| | | 30 | 1.60 | <0.05 |
| | | 50 | 1.20 | <0.05 |
| | | 100 | 1.17 | <0.05 |
| 4. | Baia Sprie II | 5 | 2.57 | <0.05 |
| | | 30 | 1.27 | <0.05 |
| | | 50 | 1.40 | <0.05 |
| | | 100 | 1.23 | <0.05 |
| 5. | Tăuții de Sus | 5 | **8.80** | <0.05 |
| | | 30 | 1.67 | <0.05 |
| | | 50 | 1.43 | <0.05 |
| | | 100 | 1.33 | <0.05 |
| 6. | Sighetu Marmației (the control) | 5 | <0.33 | <0.02 |
| | | 30 | <0.33 | <0.02 |
| | | 50 | <0.33 | <0.02 |
| | | 100 | <0.33 | <0.02 |
| 7. | MAL RO[a] | - | 3 | - |
| 8. | MAL EU[b] | - | 1-3 | - |
| 9. | MAL INT[c] | - | 0.48 | - |

MAL-maximum allowed limit, RO-Romania, EU-Europe INT-International, a - Order No. 756/1997, b - Council Directive 86/278/CEE 1986; c- US EPA, 2002 after He et al., 2015.

In Săbișa, the total Cd content is below the maximum permissible limit in all analyzed horizons, with the determined values being below the maximum permissible limit. These results indicate the absence of Cd contamination. The Cd content in mobile form is below 0.02 mg/kg across the entire soil profile, and these values cannot be evaluated comparatively from a regulatory point of view, as there is no legislative framework in force for mobile form.

In Baia Mare, the Cd content in total form is below the maximum permissible limit in the surface horizon, but in the intermediate and deep horizons, it exceeds this limit. At 30 cm, the value of 3.47 mg/kg exceeds the maximum permissible limit by 1.16 times, and in the deep horizon, the concentration of 4.00 mg/kg corresponds to an exceedance of 1.33 times, highlighting persistent contamination associated with historical pollution, while at 50 cm, the concentration of 0.83 mg/kg remains below the maximum permissible limit. The Cd content in mobile form shows low values across the entire analyzed profile and cannot be evaluated comparatively from a regulatory point of view, as there is no legislative framework in force for mobile form.

At Baia Sprie I, the total Cd content remains below the maximum permissible limit in all analyzed horizons. The maximum value is recorded in the surface horizon, being 17% lower than the maximum permissible limit. Concentrations decrease progressively in the intermediate horizon and in the deep horizon. The Cd content in mobile form shows values below 0.05 mg/kg across the entire soil profile and cannot be evaluated comparatively from a regulatory point of view, as there is no legislative framework of reference for the mobile form.

At Baia Sprie II, the total Cd content is below the maximum permissible limit in all analyzed horizons. The maximum value, recorded in the surface horizon (2.57 mg/kg), is 14% lower than the maximum permissible limit. The concentrations determined in the intermediate horizon and in the depth, horizon show low variations. The Cd content in mobile form is below 0.05 mg/kg across the entire analyzed profile and cannot be evaluated comparatively from a regulatory point of view, as there is no legislative framework in force for mobile form.

In Tăuții de Sus, Cd content in total form shows the highest values in the reference area analyzed. In the surface horizon, the concentration of 8.80 mg/kg exceeds the maximum permissible limit by 2.93 times, while in the intermediate horizon and in the deep horizon, the values determined are below the maximum permissible limit. The Cd content in mobile form remains below 0.05 mg/kg throughout the soil profile, and these values cannot be evaluated comparatively from a regulatory point of view, as there is no legislative framework in force for mobile forms.

In Sighetu Marmației (the control), the total Cd content is below the maximum permissible limit in all horizons analyzed, indicating the absence

of Cd contamination. The Cd content in the mobile form is below 0.02 mg/kg across the entire soil profile, and these values cannot be evaluated comparatively from a regulatory point of view, as there is no legislative framework in force for the mobile form.

***b) Fruit samples***

The results on the total form of the chemical element Pb in fruits (mg/kg) for 2023, 2024 and 2025 are represented in Table 4.

Table 4. Pb content in fruits

| No. crt | Sampling point | Pb content in 2023 | Pb content in 2024 | Pb content in 2025 |
|---|---|---|---|---|
| 1 | Săbișa | <0.04 | **<0.15** | <0.10 |
| 2 | Baia Mare | <0.04 | **<0.15** | <0.10 |
| 3 | Baia Sprie I | <0.04 | **<0.15** | <0.10 |
| 4 | Baia Sprie II | <0.04 | **<0.15** | <0.10 |
| 5 | Tăuții de Sus | <0.04 | **<0.15** | <0.10 |
| 6 | Sighetu Marmației (the control) | <0.04 | **<0.15** | <0.10 |
| 7 | MAL RO[a] | 0.50 | | |
| 8 | MAL EU[b] | 0.10 | | |
| 9 | MAL INT[c] | 0.10 | | |

MAL-maximum allowed limit, RO-Romania, EU-Europe INT-International, a - Order no. 975/1998; b - Commission Regulation (EU) 2023/915; c - Codex Alimentarius, 1995.

Figure 2 shows, for 2023, the concentrations of Pb in fruit determined at all sampling points were very low and fell entirely within the maximum limits permitted at national, European, and international level. These results indicate an insignificant accumulation of Pb in fruit in the reference area analyzed.

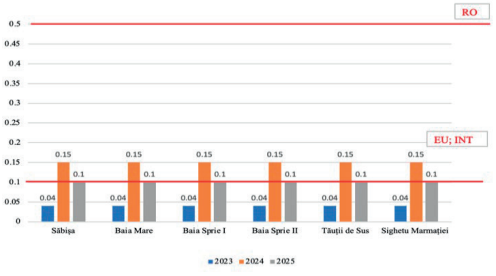



Figure 2. Pb content in fruits

For 2024, Pb concentrations in fruit, determined at all sampling points, showed a sharp increase compared to the previous year, of approximately 275%. The values obtained exceeded the maximum limits allowed at European level but remained below the maximum limits allowed at national level and within the range allowed at international level, as established by the Codex Alimentarius. This development indicates a temporary increase in Pb accumulation in fruit in the reference area analyzed, without generating non-compliance with the national regulatory framework.

For 2025, Pb concentrations in fruit determined at all sampling points decreased by 33.3% compared to the previous year. The values obtained were at the maximum levels allowed at European level and within the maximum levels allowed at national and international level. The trend indicates a partial reduction in Pb accumulation in fruit, following the sharp increase observed for 2024.

In summary, Pb concentrations in fruit were within the maximum limits permitted at national level and within the ranges established by Codex Alimentarius, although a slight exceedance of the European threshold was found for 2024. This behaviour reflects interannual variations in the level of accumulation, without leading to non-compliance with national and international regulatory frameworks.

The results on the total form of the chemical element Cd in fruits (mg/kg) for the year 2023, 2024 and 2025 are represented in Table 5.

Table 5. Cd content in fruits

| No. crt | Sampling point | Cd content in 2023 | Cd content in 2024 | Cd content in 2025 |
|---|---|---|---|---|
| 1 | Săbișa | <0.04 | **<0.15** | <0.10 |
| 2 | Baia Mare | <0.04 | **<0.15** | <0.10 |
| 3 | Baia Sprie I | <0.04 | **<0.15** | <0.10 |
| 4 | Baia Sprie II | <0.04 | **<0.15** | <0.10 |
| 5 | Tăuții de Sus | <0.04 | **<0.15** | <0.10 |
| 6 | Sighetu Marmației (the control) | <0.04 | **<0.15** | <0.10 |
| 7 | MAL RO[a] | 0.05 | | |
| 8 | MAL EU[b] | 0.05 | | |
| 9 | MAL INT[c] | 0.05 | | |

MAL-maximum allowed limit, RO-Romania, EU-Europe INT-International, a - Order no. 975/1998; b - Commission Regulation (EU) 2023/915; c - Codex Alimentarius, 1995.

Figure 3 shows, for 2023, the values determined for all sampling points (0.04 mg/kg wet weight) indicate levels below the maximum permissible limit set at national, European, and Codex Alimentarius levels, reflecting a low accumulation of Cd in fruit in the reference area analyzed.

For 2024, Cd concentrations in fruit exceed the maximum permissible limit by approximately 60%, suggesting a temporary intensification of Cd transfer from soil to fruit.

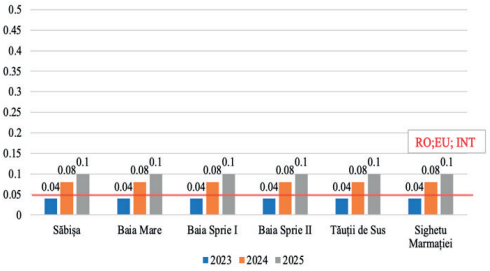



Figure 3. Cd content in fruits

For 2025, the values recorded are significantly higher than the maximum permissible limit set at national, European, and Codex Alimentarius levels, being twice the maximum permissible limit.

The pronounced rainfall deficit characteristic of 2025 can be correlated with the increase in the mobile fraction of Cd and the intensification of root absorption, mechanisms that support, from a pedological and physiological point of view, the high values determined in fruits.

Interpretation of the results in relation to the legislative framework highlights important differences between lead and cadmium in terms of regulatory requirements. In the case of Pb, the maximum limit allowed by national legislation (0.50 mg/kg) is significantly more permissive than the threshold set by Regulation (EU) 2023/915 and Codex Alimentarius (0.10 mg/kg). This fivefold difference between standards reflects a less restrictive regulatory approach at national level, which may lead to situations where the values determined are compliant internally but may generate non-compliance with European requirements. From this perspective, the interpretation of compliance depends directly on the legislative reference level used.

In contrast, for Cd, the maximum permissible limit is uniformly set at 0.05 mg/kg at all legislative levels analyzed. The harmonization of thresholds indicates international recognition of the high toxic potential of this element and a uniform regulatory approach that is more restrictive than that applicable to Pb. Consequently, any exceedance of the threshold for Cd automatically leads to simultaneous non-compliance at national, European, and international levels.

Thus, from a legislative point of view, Cd presents a higher regulatory risk, as the threshold is lower and does not allow for differences in interpretation between regulatory levels, while for Pb there is a wider margin of tolerance within the national framework. This aspect must be considered in the food risk assessment and in the formulation of conclusions on the safety of the product analyzed.

**c) *Transfer factor***

Table 6 shows the results for the assimilated mobility transfer factor (AMTF) for the pollutant -Pb.

Table 6. AMTF-Pb

| No. crt. | Sampling point | Depth (*cm*) | AMTF 2023 | AMTF 2024 | AMTF 2025 |
|---|---|---|---|---|---|
| 1. | Săbișa | 5 | 0.023 | 0.085 | 0.057 |
| | | 30 | 0.005 | 0.019 | 0.013 |
| | | 50 | 0.004 | 0.016 | 0.011 |
| | | 100 | 0.018 | 0.067 | 0.044 |
| 2. | Baia Mare | 5 | 0.005 | 0.017 | 0.011 |
| | | 30 | 0.008 | 0.030 | 0.020 |
| | | 50 | 0.007 | 0.028 | 0.019 |
| | | 100 | 0.008 | 0.032 | 0.021 |
| 3. | Baia Sprie I | 5 | **0.151** | **0.565** | **0.377** |
| | | 30 | 0.079 | 0.297 | **0.198** |
| | | 50 | 0.054 | 0.204 | **0.136** |
| | | 100 | 0.022 | 0.083 | 0.056 |
| 4. | Baia Sprie II | 5 | **0.145** | **0.544** | **0.363** |
| | | 30 | 0.024 | 0.089 | 0.059 |
| | | 50 | 0.022 | 0.084 | 0.056 |
| | | 100 | 0.022 | 0.081 | 0.054 |
| 5. | Tăuții de Sus | 5 | 0.038 | **0.142** | 0.094 |
| | | 30 | **0.188** | **0.704** | **0.470** |
| | | 50 | 0.034 | **0.129** | 0.086 |
| | | 100 | 0.037 | **0.138** | 0.092 |
| 6. | Sighetu Marmației (the control) | 5 | 0.005 | 0.019 | 0.013 |
| | | 30 | 0.005 | 0.017 | 0.012 |
| | | 50 | 0.005 | 0.018 | 0.012 |
| | | 100 | 0.005 | 0.017 | 0.011 |

The analysis of AMTF-Pb values for the period 2023-2025 shows a clear spatial and vertical differentiation of transfer intensity in the soil-plant-fruit system. Overall, the indicator falls predominantly into the very low transfer (AMTF < 0.10) and low transfer (0.10-0.21) classes, with occasional occurrences in the medium transfer (0.21-0.55) and high transfer (0.55-0.89) classes, without reaching the higher

classes of very high transfer (0.89-1.44) or extreme transfer (≥1.44).

At the surface horizon level, AMTF values reflect the direct influence of historical contamination and the mobile surface fraction, but the distribution is relatively heterogeneous, with variations controlled mainly by the local specifics of contamination. In contrast, the analysis becomes more relevant from a procedural point of view at depths of 30 and 50 cm, where the vertical dynamics of transfer are more clearly outlined.

At 30 cm, the most pronounced variability of the indicator is observed. For Săbișa, Baia Mare, and Sighetu Marmației, the values remain constant in the very low or low transfer class, suggesting effective control of mobility and reduced availability for plant uptake, even in the presence of high total concentrations in certain profiles. In contrast, at the Baia Sprie I and Tăuții de Sus sites, 2024 marks a clear intensification of mobilization processes, with values falling within the high transfer class (0.55-0.89). The maximum value of the entire data set, recorded at 30 cm at Tăuții de Sus (AMTF=0.704), confirms that this horizon represents the level at which the interaction between the mobile fraction, total concentration, and accumulation in fruit becomes maximum. The return to the medium transfer class (0.21-0.55) in 2025 indicates a transitional nature of the intensification in 2024.

At 50 cm, AMTF values are systematically lower than those at 30 cm, falling mainly into the very low and low transfer classes, with limited occurrences in the medium transfer class in 2024. This decrease suggests a progressive reduction in effective mobility with depth, associated with the processes of adsorption and stabilization of Pb in the soil matrix. The absence of values in the higher classes at this depth confirms that, although historical contamination is present in the profile, the actual availability to the active root system decreases with depth.

The depth horizon (100 cm), generally shows low AMTF values, falling within the lower transfer classes, which indicates a limited contribution of this level to the accumulation process in the fruit.

From a temporal perspective, the year 2024 is distinguished by systematically higher AMTF values at 30 cm and, to a lesser extent, at 50 cm, suggesting a temporary intensification of Pb mobilization and availability processes in the intermediate zone of the profile. In 2025, a reduction in transfer intensity is observed, without however changing the overall vertical pattern.

Table 7 shows the results for the assimilated mobility transfer factor (AMTF) for the pollutant -Cd.

Table 7. AMTF-Cd

| No. crt. | Sampling point | Depth (cm) | AMTF 2023 | AMTF 2024 | AMTF 2025 |
|---|---|---|---|---|---|
| 1. | Săbișa | 5 | 0.002 | 0.004 | 0.005 |
| | | 30 | 0.002 | 0.004 | 0.005 |
| | | 50 | 0.002 | 0.004 | 0.005 |
| | | 100 | 0.002 | 0.004 | 0.005 |
| 2. | Baia Mare | 5 | 0.007 | 0.014 | 0.017 |
| | | 30 | 0.015 | 0.030 | 0.038 |
| | | 50 | 0.004 | 0.008 | 0.01 |
| | | 100 | 0.011 | 0.022 | 0.027 |
| 3. | Baia Sprie I | 5 | 0.021 | 0.041 | 0.052 |
| | | 30 | 0.016 | 0.032 | 0.04 |
| | | 50 | 0.013 | 0.026 | 0.033 |
| | | 100 | 0.013 | 0.026 | 0.032 |
| 4. | Baia Sprie II | 5 | 0.021 | 0.042 | 0.053 |
| | | 30 | 0.014 | 0.027 | 0.034 |
| | | 50 | 0.014 | 0.029 | 0.036 |
| | | 100 | 0.013 | 0.027 | 0.033 |
| 5. | Tăuții de Sus | 5 | 0.038 | 0.076 | **0.094** |
| | | 30 | 0.016 | 0.032 | 0.041 |
| | | 50 | 0.015 | 0.029 | 0.037 |
| | | 100 | 0.014 | 0.028 | 0.035 |
| 6. | Sighetu Marmației (the control) | 5 | 0.002 | 0.004 | 0.005 |
| | | 30 | 0.002 | 0.004 | 0.005 |
| | | 50 | 0.002 | 0.004 | 0.005 |
| | | 100 | 0.002 | 0.004 | 0.005 |

The analysis of AMTF-Cd values for the period 2023-2025 shows a distribution that is clearly different from that of Pb, characterized by low values and moderate vertical variability. Across the entire dataset, the indicator falls exclusively into the very low transfer class (AMTF < 0.10), without reaching the higher classes (low, medium, high, very high, or extreme). The range of variation, between 0.002 and 0.094, confirms a limited overall transfer of Cd in the soil–plant–fruit system, from the integrative perspective of the AMTF indicator.

At the surface horizon, the values are higher than those at depth, especially at the Tăuții de Sus site, where the maximum value of the set

(AMTF=0.094) is reached in 2025, but still within the very low transfer class. This distribution reflects the direct influence of the mobile surface fraction and accumulation in the fruit, but without exceeding the threshold of 0.10 that would mark the transition to the low transfer class.

At 30 cm, the AMTF-Cd values show relative uniformity between points, ranging between 0.002 and 0.041. In Baia Mare, Baia Sprie I, Baia Sprie II, and Tăuții de Sus, the year 2025 shows slightly higher values compared to 2023 and 2024, but all remain in the very low transfer class. This stability indicates that, although Cd exceeded the legislative threshold in fruit in 2024 and 2025, the integration of the mobile fraction and total concentration through AMTF mitigates the numerical impact, suggesting that the actual intensity of transfer on the intermediate profile remains low.

At 50 cm, the values are comparable or slightly lower than those at 30 cm, confirming a discrete vertical gradient of transfer. The range of 0.002–0.037 indicates limited effective mobility at this depth, with no major differences between the years analyzed. The fact that the values do not increase significantly in 2024 and 2025 at 50 cm suggests that the intensified mobilization processes in these years were concentrated predominantly in the upper root zone, without a marked propagation in depth.

At the depth horizon, the indicator maintains values like those at 50 cm or slightly lower, confirming a minimal contribution of the deep horizon to the accumulation process in the fruit.

From a temporal perspective, there is a progressive increase in AMTF-Cd values from 2023 to 2025 at most points, but this increase does not change the transfer class. Thus, although the legislative analysis indicated exceedances of the 0.05 mg/kg threshold in fruit in 2024 and 2025, the AMTF-based classification keeps Cd in the very low transfer category, highlighting the difference between the specific regulatory non-compliance and the integrated intensity of the transfer process in the soil profile.

In a comparative approach, the analysis of AMTF-Pb and AMTF-Cd values highlights consistent differences between the two elements in terms of the intensity and significance of transfer in the soil–plant–fruit system. For Pb, spatial and vertical variability is more pronounced, with occasional occurrences in the high transfer class (0.55-0.89), especially at a depth of 30 cm in 2024, in areas with significant historical contamination. This behavior indicates local episodes of intensified mobilization, without reaching the very high or extreme transfer classes, suggesting the existence of effective soil immobilization mechanisms that limit the actual transfer to the fruit.

A different pattern is observed for Cd, AMTF values remain consistently in the very low transfer class (AMTF < 0.10), with a uniform distribution across the profile and moderate interannual variations. Although fruit concentrations exceeded the legislative threshold in 2024 and 2025, the integrative indicator did not show a structural intensification of transfer, indicating a dissociation between normative pressure and the procedural intensity of mobilization in the soil.

Thus, comparatively, Pb reflects a more pronounced edaphic pressure and greater variability in transfer, while Cd exhibits high process stability but increased normative vulnerability, determined by the low legislative threshold. This differentiation confirms the ability of the AMTF indicator to integrate mobility, accumulation in fruit, and normative reference into a coherent assessment of the intensity of metal transfer in the investigated fruit tree ecosystems.

## CONCLUSIONS

***Heavy metal content in soil.*** The results obtained highlight the persistence of historical contamination with Pb and, to a lesser extent, with Cd in the soils of the investigated area. For Pb, exceedances of the maximum permissible limit were frequent and distributed over several depths (30–100 cm in Baia Mare; 5–30 cm in Tăuții de Sus), confirming both surface accumulation and migration in the profile. In the case of Cd, exceedances were less numerous and more localized (Baia Mare and Tăuții de Sus), indicating lower edaphic pressure compared to Pb.

***Heavy metal content in fruits.*** For Pb, the significant difference between the national threshold and the European/international threshold generates discrepancies in the

interpretation of compliance. Although the European threshold was exceeded in 2024, the values remained below the national limit, and a partial reduction was observed in 2025. For Cd, the uniform and more restrictive limit led to direct non-compliance in 2024 and 2025, highlighting a higher regulatory vulnerability compared to Pb.

***Transfer factor.*** Analysis of transfer using the AMTF indicator shows that, despite exceedances in soil and isolated non-compliances in fruit, the integrated transfer intensity remains predominantly in the lower classes for both elements. For Pb, isolated occurrences of the high transfer class at 30 cm indicate temporary episodes of mobilization, without reaching the higher classes. For Cd, AMTF values remain constant in the very low transfer class, suggesting that legislative exceedances are more a consequence of the restrictive regulatory threshold than of a structural amplification of mobility in the profile.

From a food safety perspective, the results indicate that the risk is not determined exclusively by the total concentration in the soil, but by the interaction between mobility, pedoclimatic conditions, and the severity of the legislative threshold. In areas with historical anthropogenic impact, even moderate variations in the mobile fraction can lead to exceedances of the permissible limits, especially for Cd.

Therefore, it is necessary to implement a periodic monitoring system that integrates the analysis of the mobile fraction and the assessment of transfer through synthetic indicators such as AMTF, to anticipate potential non-compliance and protect consumer health.

## REFERENCES

Aladesanmi, O. T., Oroboade, J. G., Osisiogu, C. P., & Osewole, A. O. (2019). Bioaccumulation factor of selected heavy metals in Zea mays, *Journal of Health & Pollution*, *9*(24), 1-19.

Balali-Mood, M., Naseri, K., Tahergorabi, Z., Khazdair, M. R., & Sadeghi, M. (2021). Toxic mechanisms of five heavy metals: mercury, lead, chromium, cadmium, and arsenic, *Frontiers in Pharmacology*, *12*, 643972.

Big, C. L., Lăcătușu, R., & Damian, F. (2012). Heavy metals in soil system around Baia Mare City, Romania, *Carpathian Journal of Earth and Environmental Science*, *7*(3), 219-230.

Bizo, M. L., Modoi, O. C., Botezan, C., Levei, E.-A., & Ozunu, A. (2014). Mobility of lead in soils polluted by non-ferrous metallurgical plant in northwestern Romania. *Scientific Papers. Series E. Land Reclamation, Earth Observation & Surveying, Environmental Engineering, 3*, 95–98.

Boros, M.-N., Smical, I., Micle, V., & Lichtscheidl-Schultz, I. (2015). Heavy metal pollution of soils from Baia-Mare – Case study: CUPROM industrial area. *Scientific Papers. Series E. Land Reclamation, Earth Observation & Surveying, Environmental Engineering, 4*, 99–106.

Codex Alimentarius, International Food Standards, General Standards for contaminants and toxin in food and feed, CXS 193-1995, Adopted in 1995, Last amended in 2025, Retrieved from: https://www.fao.org/fao-who-codexalimentarius/sh-proxy/en/?lnk=1&url=https%253A%252F%252Fworkspace.fao.org%252Fsites%252Fcodex%252Fstandards%252FCXS%2B193-1995%252FCXS_193e.pdf

Coman, M. (2006). *The Baia Mare Depression – Environmental protection from the perspective of sustainable development (Depresiunea Baia Mare – Protecția mediului din perspectiva dezvoltării durabile)*, Cluj-Napoca, RO: Risoprint.

Coman, M., Oros V., Făluș B., & Pop R. (2010). Soil pollution with heavy metals – specific issues for the Baia Mare area. (Poluarea solurilor cu metale grele – probleme specifice pentru zona Baia Mare), *ProEnviroment*, *3*, 155-158.

Council Directive 86/278/CEE 1986 Retrieved from: https://eur-lex.europa.eu/legal-content/EN/TXT/PDF/?uri=CELEX:31986L027

Davidova, S., Milushev, V., & Satchanska, G. (2024). The Mechanisms of Cadmium Toxicity in Living Organisms. *Toxics*, *12*(12), 875.

EFSA, (2010). Scientific opinion on lead in food, EFSA Journal, Vol. 8(4), 1570, Retrieved from: https://efsa.onlinelibrary.wiley.com/doi/10.2903/j.efsa.2010.1570

EU Directive 2023/915, Retrieved from: https://eur-lex.europa.eu/eli/reg/2023/915/oj?locale=ro

Filip, C. D., & Coman, M. A. (2025). Regarding transfer factor of soil pollution with heavy metals in soil-plant system, *Scientific Papers. Series A. Agronomy*, *68*(1), 90-99.

He, Z., Shentu, J., Yang, X., Baligar, V. C., Zhang, T., & Stoffella, P. J. (2015). Heavy metal contamination of soils: Sources, Indicators, and Assessment, *Journal of Environmental Indicators*, *9*, 17-18.

Ivasuc, M. M., & Rusu, M. C., (2011). Translocation of Cu, Pb, Zn, Cd in some vegetables grown in polluted Area of Baia Mare, Romania, *Bulletin USAMV, Agriculture*, *68*(2), 289-297.

Jaishankar, M., Tseten, T., Anbalagan, N., Mathew, B. B., & Beeregowda, K. N. (2014). Toxicity, mechanism and health effects of some heavy metals. *Interdisciplinary toxicology*, *7*(2), 60–72.

Jakubus, M., Bakinovska, E., & Tutusko, N., (2019). Compost utilization in heavy metal immobilization process evaluated by bioconcentration factors, *Journal of Elementology*, *24*(4), 1291-1307.

Jolly, Y. N., Islam, A., & Akbar, S., (2013). Transfer of metals from soil to vegetables and possible health risk assessment, *Springer Plus, 2*, 385.

Jomova, K., Alomar, S. Y., Nepovimova, E., Kuca, K., & Valko, M. (2025). Heavy metals: toxicity and human health effects*, Archives of toxicology, 99*(1), 153-209.

Kotnala, S., Tiwari, S., Nayak, A., Bhushan, B., Chandra, S., Medeiros, C. R., & Coutinho, H. D. M. (2025). Impact of heavy metal toxicity on the human health and environment, *Science of The Total Environment*, *987*, 179785.

Manoiu, V.-M. & Spiridon, R. M. (2017). A deep dive into the chronic air pollution reality in Baia Mare: Part I: sources of historical environmental pollution and their contribution to air pollution. *IJASOS - International E-Journal of Advances in Social Sciences*, *3*(9), 734–743.

Marian, F. L., Irimuș, I. A., & Zaharia, C. S., (2016). Qualitative landslide risk estimation in Baia Mare Depression, Romania*, Carpath. J. of Earth and Environ. Sci., 11*(1), 123-130.

Minkina, T. M., Nevidomskaya, D. G., Pol'shina, T. N., Fedorov, Y. A., Mandzhieva, S. S., Chaplygin, V.A., Bauer, T. V., & Burachevskaya, M.V. (2017). Heavy metals in the soil-plant system of the Don River estuarine region and the Taganrog Bay coast. *Journal of Soils and Sediments, 17*(5), 1474–1491.

Mitra, S., Chakraborty, A. J., Tareq, A. M., Emran, T. B., Nainu, F., Khusro, A., Idris, A. M., Khandaker, M. U., Osman, H., Alhumaydhi, F. A., & Simal-Gandara, J. (2022). Impact of heavy metals on the environment and human health: Novel therapeutic insights to counter the toxicity. *Journal of King Saud University – Science, 34*(3), Article 101865.

Moț, A., Madjar, R. M., & Mihalache, M. (2019). Spatial distribution of heavy metals in agricultural soils of Romania: Review of the current situation. *Scientific Papers. Series A. Agronomy, 62*(1), 88–96.

Moț, A., Madjar, R. M., Bădulescu, L., Dobrin, A., Constantin, C. G., & Mihalache, M. (2021). Heavy metal uptake patterns by spinach (*Spinacia oleracea* L.) grown on contaminated different soil types. *Scientific Papers. Series A. Agronomy, 64*(2), 117–126.

Nițu, M., Pruteanu, A., Bordean, D. M., Popescu, C., & Deak, G. (2019). Researches on the accumulation and transfer of heavy metals in the soil in tomatoes – *Solanum lycopersicum*, *E3S Web of Conferences*, *112*, 03020.

Noman, N. A., Feng, W., Zhu, G., Hossain, M. B., Chen, Y., Zhang, H., & Sun, J. (2022). Bioaccumulation and potential human health risks of metals in commercially important fishes and shellfishes from Hangzhou Bay, China, *Scientific Reports*, *12*, 4634.

Olănescu, G., Gameț, E., & Dumitru, M. (2007). Phytoextraction of heavy metal-polluted soils (Fitoextracția solurilor poluate cu metale grele). *Lucrări Științifice Facultatea de Agricultură Bucureşti, Seria A, 1*, 359–368.

Order No. 756/1997 Retrieved from: https://www.mmediu.ro/app/webroot/uploads/files/OM-184-1997-bilant-de-mediu-si-OM-756-1997-evaluarea-poluarii-mediului.pdf

Order No. 184/1997 Retrieved from: https://www.mmediu.ro/app/webroot/uploads/files/OM-184-1997-bilant-de-mediu-si-OM-756-1997-evaluarea-poluarii-mediului.pdf

Order No. 975/1998, Retrieved from https://www.dspbihor.gov.ro/legislatie/ordin%20MS%20nr.975-1998.pdf

Order No. 1048/2003, Retrieved from: https://legislatie.just.ro/Public/DetaliiDocument/48566

Oros, V., Roman, S., Coman, M., & Oros, A.D. (2011). Lead Occurrence in Children's Biological Fluids from Baia Mare Area, Romania. In: Simeonov, L., Kochubovski, M., Simeonova, B. (eds) Environmental heavy metal pollution and effects on child mental development. *NATO Science for Peace and Security Series C: Environmental Security, vol 1*. Springer, Dordrecht.

Ortega, R. D., Esquivel, G. D. F., Ayala, B. T., Pineda, B., Manzo, G. S., Quino, M. J., Mora, C. P., & Pérez de la Cruz, V. (2021). Cognitive impairment induced by lead exposure during lifespan: mechanisms of lead neurotoxicity. *Toxics*, *9*(2), 23.

Pehoiu G., Murarescu O., Rădulescu C., Dulama I. D., & Teodorescu S. (2020). Heavy metals accumulation and translocation in native plants grown on tailing dumps and human health risk, *Plant soil*, *456*(1-2), 405-424.

Pruteanu, A., Voicea, I., & Fatu, V. (2022). Accumulation of copper in vegetables and fruits, *Engineering for Rural development*, 583-589.

Roba, C., Roșu, C., Pișteа, I., Ozunu, A., & Baciu, C. (2016). Heavy metal content in vegetables and fruits cultivate in Baia Mare mining area (Romania) and health reassessment, *Environ. Sci. Pollut. Res.*, 23(7), 6062–6073.

Rusu, M., Cara, I. G., Filip, M., Calistru, A. E., Țopa, D., & Jităreanu, G. (2023). Transfer of heavy metals in soil-plum cultivation: a field study in Adamaschi Iași, România, *Journal of Applied Life Sciences and Environment*, *56*(193), 59–74.

Sabir, M., Baltrėnaitė-Gedienė, E., Ditta, A., Ullah, H., Kanwal, A., Ullah, S., & Faraj, T. K. (2022). Bioaccumulation of heavy metals in a soil–plant system from an open dumpsite and the associated health risks through multiple routes. *Sustainability*, *14*(20), 13223.

Sasaki, T., Horiguchi, H., Matsukawa, T., Kobayashi, M., Omori, Y., Oguma, E., & Komatsuda, A. (2024). A suspected case of "itai-itai disease" in a cadmium-polluted area in Akita prefecture, Japan, *Environmental health and preventive medicin*e, *29*, 40.

Singh, R., Gautam, N., Mishra, A., & Gupta, R. (2011). Heavy metals and living systems: An overview. *Indian journal of pharmacology, 43*(3), 246–253.

SR EN ISO 1185:2009.

SR ISO 11047:1999-PIS-03.

SR ISO 11464:1994

Ștefan, O., Rădurescu, MT G., & Bădescu, G. (2012). The achievement of the mining cadastre in Romania-Baia Mare Mining Area and Cadastre 2014 Vision, *Cadastre and Land Management - Case Studies II*, 5849, 1-8.

Sur, I. M., Cîmpean, A., Micle, V., & Tănăselia, C. (2017). Physical-chemical properties analysis of the soil contaminated with heavy metals from Copșa Mică area. *Scientific Papers. Series E. Land Reclamation, Earth Observation & Surveying, Environmental Engineering, 6*, 51–56.

Tong, S., Yang, L., Gong, H., Wang, L., Li, H., Yu, J., Li, Y., Deji, Y., Nima, C., Zhao, S., Gesang, Z., Kong, C., Wang, X., & Men, Z. (2022). Bioaccumulation characteristics, transfer model of heavy metals in soil-crop system and health assessment in plateau region, China, *Ecotoxicology and Environmental safety*, 241, 113733.

Waalkes, M. P. (2003). Cadmium carcinogenesis. *Mutation research*, *533*(1-2), 107–120.

Scientific Papers. Series E. Land Reclamation, Earth Observation & Surveying, Environmental Engineering. Vol. XV, 2026
Print ISSN 2285-6064, CD-ROM ISSN 2285-6072, Online ISSN 2393-5138, ISSN-L 2285-6064

# ENVIRONMENTAL AND SOIL IMPACTS OF END-OF-LIFE LITHIUM-ION BATTERIES: QUANTITATIVE POLLUTION SCENARIOS, EMERGING CONTAMINANTS AND RECYCLING-ROUTE ASSESSMENT

**Roxana-Elena FRÎNCU[1], Carmen Otilia RUSĂNESCU[1], Ana VÎRSTA[2], Elena-Denisa PREDESCU[1], Daniela MIHAI[1], Sabrina Maria BĂLĂNESCU[1], Ionela Alexandra ION[1]**

[1]National University of Science and Technology Politehnica Bucharest, Faculty of Biotechnical Systems Engineering, 313 Splaiul Independentei, District 6, 060042, Bucharest, Romania
[2]University of Agronomic Sciences and Veterinary Medicine of Bucharest, 59 Marasti Blvd, District 1, Bucharest, Romania

Corresponding author email: roxana_elena.fr@yahoo.com

***Abstract***

*The rapid deployment of lithium-ion batteries in electric vehicles and stationary energy-storage systems is generating an increasing end-of-life waste stream with potential impacts on soil, water and air. This study combines an integrative literature review with mass-balance calculations based on a representative NMC811 battery composition. Electric-vehicle battery deployment reached approximately 1.2 TWh in 2025 and may approach 3 TWh by 2030, corresponding to estimated masses of 7.0 and 17.5 million tonnes, respectively. Global end-of-life battery waste is projected to increase from 0.9 million tonnes in 2025 to 20.5 million tonnes in 2040. Under the 2040 landfill/leaching stress scenario, potential releases were estimated at 7,754 t Li, 4,949 t Ni, 3,075 t Cu, 1,655 t Mn and 623 t Co. Relevant pollutants also include fluorides, electrolyte degradation products, fine cathode particles and persistent fluorinated compounds. High collection rates, chemistry-based sorting, fire-safe storage, controlled recycling and integrated soil and water monitoring are essential for reducing environmental risks and improving material circularity.*

***Key words****: battery recycling, end-of-life batteries, lithium-ion batteries, soil contamination, waste management.*

## INTRODUCTION

Lithium-ion batteries (LIBs) have become essential for electric mobility, portable electronics and stationary energy storage because of their high energy density, efficiency and long operating life. According to the latest international outlook, global electric-vehicle battery deployment reached approximately 1.2 TWh in 2025 and is expected to approach 3 TWh by 2030. This rapid increase in deployment is creating a delayed but substantial flow of batteries that will require collection, transport, reuse and recycling after reaching the end of their service life (Harper et al., 2019; International Energy Agency, 2026).

End-of-life lithium-ion batteries, hereafter referred to as EoL-LIBs, contain a complex mixture of potentially recoverable and hazardous materials. Depending on cathode chemistry, these materials may include Li, Ni, Co, Mn, Fe and P, together with Cu and Al current collectors, graphite, polymeric binders, separators, organic solvents and fluorinated lithium salts. NMC and NCA batteries contain economically valuable Ni and Co, whereas LFP batteries contain no Ni or Co in the active cathode material but retain Li, Cu, Al, graphite, phosphate compounds and fluorinated electrolyte components (Harper et al., 2019; Mrozik et al., 2021).

Environmental releases may occur through corrosion, mechanical damage, uncontrolled shredding, landfill disposal, battery fires and inadequately controlled recycling operations (Mosnegutu et al., 2025a). Soil may receive contaminants through direct leakage, contaminated dust, atmospheric deposition, leachate, firefighting water and the disposal of slags, sludge or other process residues. The subsequent mobility and persistence of these contaminants are influenced by pH, redox

conditions, soil texture, clay content, organic matter, rainfall and groundwater depth (Bolan et al., 2021; Mrozik et al., 2021).

The environmental assessment of EoL-LIBs must therefore consider more than lithium and the economically valuable cathode metals. Fluorides, electrolyte decomposition products, fine cathode and graphite particles, and emerging per- and polyfluoroalkyl substances may contribute to soil acidification, metal mobilisation, groundwater contamination and ecological toxicity (Guelfo et al., 2024; Rensmo et al., 2023; Mosnegutu et al., 2025b; Shojaei et al., 2025). Accordingly, the objectives of this study were to estimate the mass of batteries entering use and the projected EoL-LIB waste stream, quantify the potential release of selected contaminants under three management scenarios, examine a site-scale soil-contamination scenario involving an NMC811 battery pack, and compare the environmental release pathways associated with uncontrolled disposal, battery fires, mechanical pretreatment, pyrometallurgy, hydrometallurgy and direct recycling.

## MATERIALS AND METHODS

The study was conducted as an integrative review combined with mass-balance calculations, quantitative pollution-scenario modelling and a technology-specific environmental assessment. Scientific articles published mainly between 2015 and 2026 were identified through Scopus, Web of Science, ScienceDirect, SpringerLink, PubMed and Google Scholar, while older regulatory and foundational sources were retained where relevant. Institutional data were obtained from the International Energy Agency, the United Nations Development Programme, Argonne National Laboratory and the European Commission. The literature review focused on battery deployment, EoL-LIB waste generation, contaminant composition, environmental release pathways, soil impacts and recycling technologies.

Battery mass was estimated from energy deployment using a representative pack-level mass of 5.85 kg $kWh^{-1}$. This central value represents a simplified mixed NMC–LFP battery flow and falls within the range derived from BatPaC automotive pack simulations. In practical units, the calculation was:

Battery mass (Mt) = energy deployment (TWh) × 5.85 Mt $TWh^{-1}$.

Consequently, 1.2 TWh corresponds to approximately 7.02 Mt of batteries, while 3.0 TWh corresponds to approximately 17.55 Mt. These values represent batteries newly introduced into use and not waste generated during the same year (Ahmed et al., 2023; International Energy Agency, 2026).

Annual EoL-LIB quantities were obtained from the UNDP projection, which reports 0.90 Mt in 2025, 1.85 Mt in 2030, 7.85 Mt in 2035 and 20.50 Mt in 2040. The published values were used directly, without interpolation between the reported years (United Nations Development Programme, 2024).

An NMC811 battery pack was selected as a representative metal-containing chemistry for the pollution-screening model. The active cathode material, $LiNi_{0.8}Mn_{0.1}Co_{0.1}O_2$, contains approximately 7.13% Li, 48.27% Ni, 5.65% Mn and 6.06% Co by mass. Assuming that active cathode material represents 25% of total pack mass, the corresponding pack-level fractions were estimated at 1.78% Li, 12.07% Ni, 1.41% Mn and 1.52% Co. Cu was assumed to represent 7.5% of pack mass. These fractions are modelling assumptions and do not describe every commercial battery pack (Ahmed et al., 2023; Rinne et al., 2024).

The potential annual release of contaminant *i* was calculated using the following mass-balance relationship:

Released mass = annual battery waste × mismanaged fraction × contaminant fraction × environmental release fraction.

Three quantitative screening scenarios were evaluated. Scenario A assumed that 1% of EoL-LIBs were mismanaged, with environmental release of 10% of Li and 1% of Ni, Co, Mn and Cu. Scenario B assumed 5% mismanagement, with release of 42.5% of Li, 11.45% of Mn and 4% of Ni, Co and Cu. Scenario C represented severe fragmentation, fire or uncontrolled disposal, assuming 15% mismanagement and release of 75% of Li, 20% of Mn and 10% of Ni, Co and Cu. Scenario B release factors reflect the order of magnitude reported in landfill-related leaching studies, whereas Scenarios A and C were used as lower and upper sensitivity

boundaries (Bolan et al., 2021; Mrozik et al., 2021). These scenarios represent comparative screening conditions rather than predictions of the actual proportion of battery waste that will be released into the environment.

In addition to the quantitative NMC811 release scenarios, a technology-specific assessment was performed for uncontrolled disposal, battery fires, mechanical pretreatment, pyrometallurgy, hydrometallurgy and direct recycling. Each management or treatment option was compared qualitatively according to its main potential releases, the principal affected environmental medium and the expected environmental implications. The assessment considered metal-bearing leachates and residues, fluorinated emissions, cathode and graphite particles, electrolyte vapours, acidic or saline wastewater, sludge and solid process residues. The comparison was based on evidence reported for EoL-LIB pollution and recycling systems (Harper et al., 2019; Mrozik et al., 2021; Rensmo et al., 2023; Claassen et al., 2024; Guelfo et al., 2024; International Energy Agency, 2024; Rinne et al., 2024; Aiello et al., 2025; Shojaei et al., 2025).

For example, Li release under Scenario B in 2040 was calculated as:

$20{,}500{,}000\ t \times 0.05 \times 0.0178 \times 0.425 = 7{,}754\ t\ Li\ yr^{-1}$.

The calculated values represent contaminant masses potentially released from the waste stream and not final concentrations in a particular soil or water body. Site-level concentrations require additional information on the affected area, mixing depth, hydrological conditions, soil properties, background concentrations and contaminant transport. Therefore, the results should be interpreted as comparative pollution-potential indicators rather than site-specific environmental predictions (Mrozik et al., 2021).

## RESULTS AND DISCUSSIONS

The conversion of energy deployment into mass indicates that approximately 7.0 Mt of batteries may have entered electric-vehicle applications in 2025. Deployment approaching 3 TWh in 2030 would correspond to approximately 17.5 Mt of batteries per year. The range could be wider because NMC packs generally have higher gravimetric energy density than LFP packs, while changes in cell-to-pack design or the introduction of solid-state and sodium-ion batteries may reduce or increase the future mass per unit of energy (Ahmed et al., 2023; International Energy Agency, 2026).

The annual quantity of EoL-LIBs is much lower than annual deployment because batteries normally remain in service for several years. However, the waste stream is projected to expand from 0.90 Mt in 2025 to 20.50 Mt in 2040, representing an increase of more than twenty times. Production scrap currently represents an important recycling feedstock, but approximately 94% of the projected 2040 flow is expected to originate from batteries removed from vehicles and other applications. The estimated mass of newly deployed batteries and the projected evolution of the EoL-LIB waste stream are summarised in Table 1.

Table 1. Estimated battery deployment and projected end-of-life waste

| Year | EV battery deployment | Estimated mass newly deployed | Projected EoL-LIB waste |
|---|---|---|---|
| 2025 | ≈1.2 TWh | ≈7.02 Mt | 0.90 Mt |
| 2030 | ≈3.0 TWh | ≈17.55 Mt | 1.85 Mt |
| 2035 | n.a. | n.a. | 7.85 Mt |
| 2040 | n.a. | n.a. | 20.50 Mt |

Source: Authors' calculations based on Ahmed et al. (2023), International Energy Agency (2026), and United Nations Development Programme (2024).

As shown in Table 1, the projected EoL-LIB waste stream increases rapidly after 2030 and gradually shifts from production scrap towards used batteries. This transition has practical consequences because production waste is generally homogeneous, documented and relatively uncontaminated, whereas used battery packs differ in chemistry, state of charge, degradation level, accident history and structural design. Recycling systems will therefore require improved identification, automated disassembly, chemistry-based sorting and safer transport as the proportion of used packs increases (Harper et al., 2019; International Energy Agency, 2024).

Li is potentially important because it is relatively mobile in many soils and may be weakly retained compared with transition metals. A landfill-related study synthesised by Mrozik et al. (2021) reported that approximately

42.5% of the Li inventory entered the leachate, compared with less than 4% for Ni, Co, Cu, Al and Fe. Mn release was approximately 11.45%. These values are not universal leaching factors, but they illustrate that contaminant mobility does not necessarily correspond to the total metal content of the battery (Bolan et al., 2021; Mrozik et al., 2021).

Ni, Co and Cu generally have stronger interactions with clay minerals, iron and manganese oxides and soil organic matter. Nevertheless, their mobility and bioavailability may increase when soil pH decreases. At elevated concentrations, Ni and Co can affect microbial enzymatic activity and plant growth, while Cu may impair microbial processes and modify the physical behaviour of clayey soils. Mn presents redox-dependent behaviour and may become more soluble under reducing or waterlogged conditions (Mrozik et al., 2021; Mishra et al., 2026).

Electrolyte degradation may amplify metal contamination. $LiPF_6$ is moisture-sensitive and may form HF and other fluorinated products. Local acidification can increase metal solubility, while organic carbonate solvents and their degradation products may affect soil microorganisms. Simulated landfill experiments have reported PFAS concentrations of up to approximately 100 mg $L^{-1}$ and inorganic fluoride concentrations of up to 1.4 g $L^{-1}$ for specific batteries and test conditions. These experimental maxima should not be treated as typical landfill concentrations but demonstrate the possibility of concentrated fluorochemical releases (Guelfo et al., 2024; Shojaei et al., 2025).

Battery fires create an acute pathway from the waste stream to air, soil and water. Experimental studies reported gaseous HF emission factors of approximately 10-81 mg $Wh^{-1}$, depending on chemistry and test conditions. Metal-containing particles and fluorinated combustion products may be deposited on soil or transported in firefighting water. Following the January 2025 Moss Landing battery-storage fire, increased Ni, Mn and Co concentrations were measured in nearby surface wetland soils, with a Ni ratio consistent with NMC532 cathode material. Enrichment was concentrated in the upper few millimetres and subsequently decreased after rainfall and tidal flushing, demonstrating both deposition and remobilisation (Claassen et al., 2024; Aiello et al., 2025).

The main EoL-LIB pollutants, their sources, dominant environmental pathways and potential effects are summarised in Table 2.

Table 2. Main EoL-LIB pollutants, pathways and environmental effects

| Pollutant or material | Main source | Dominant pathway | Potential environmental effect |
|---|---|---|---|
| Li | Cathode and electrolyte | Leachate and groundwater transport | Salinity and ionic imbalance; plant uptake |
| Ni and Co | NMC, NCA and LCO cathodes | Leachate, dust and fire deposition | Microbial toxicity, phytotoxicity and oxidative stress |
| Mn | NMC and LMO cathodes | Leachate under acidic or reducing conditions | Nutritional imbalance and toxicity at elevated concentration |
| Cu | Anode current collector | Dust, leachate and recycling residues | Microbial inhibition and alteration of clayey soil properties |
| HF and inorganic fluorides | $LiPF_6$ degradation and fires | Gas emissions, leachate and firefighting water | Acidification, metal mobilisation and acute toxicity |
| PFAS/bis-FASI | Some electrolytes and fluorinated materials | Manufacturing, recycling and landfill leachate | Persistent and mobile contamination |
| Cathode particles and graphite | Shredding and fires | Atmospheric dispersion and soil deposition | Particle toxicity and gradual metal dissolution |

Source: Authors' synthesis based on Mrozik et al. (2021), Rensmo et al. (2023), Claassen et al. (2024), Guelfo et al. (2024), Aiello et al. (2025), and Shojaei et al. (2025).

As shown in Table 2, EoL-LIB pollution involves both dissolved and particulate contaminants transported through leachate, atmospheric deposition, firefighting water and recycling residues. In addition to their chemical and biological effects, battery-derived contaminants may also influence the physical and geotechnical properties of soil. In controlled experiments using clayey soil contaminated with 3-9% Cu, Co or Ni powder, maximum permeability increases of 84%, 46% and 68%, respectively, were recorded, while shear strength decreased by 34%, 11% and 27%. These concentrations are much higher than typical diffuse contamination and should not be directly extrapolated to ordinary sites. Nevertheless, they demonstrate that severe battery-related contamination may influence soil plasticity, permeability, consolidation and geotechnical stability, in addition to chemical and biological functions (Mishra et al., 2026).

A representative 60 kWh NMC811 pack with an estimated mass of 312 kg contains approximately 5.6 kg Li, 37.7 kg Ni, 4.4 kg Mn, 4.7 kg Co and 23.4 kg Cu under the adopted composition assumptions. If 4% of the Ni inventory were released and mixed into 26 t of soil, corresponding to 100 m² to a depth of 0.20 m and an apparent density of 1.3 t $m^{-3}$, the Ni concentration would increase by approximately 58 mg $kg^{-1}$. When added to a background value of 20 mg $kg^{-1}$, the resulting concentration of approximately 78 mg $kg^{-1}$ would slightly exceed the Romanian alert threshold of 75 mg $kg^{-1}$ for sensitive land use (Ahmed et al., 2023; Ministry of Waters, Forests and Environmental Protection, 1997).

This calculation represents a conservative hotspot rather than an expected average concentration. It assumes that released material is retained within a small soil volume and does not account for runoff, wind dispersion, deep leaching or removal during emergency response. It nevertheless shows that even one damaged traction battery may generate locally relevant contamination when its contents are fragmented or deposited over a limited area (Mrozik et al., 2021).

Taken together, the experimental, field and modelling evidence indicates measurable forms of environmental degradation rather than only a theoretical possibility of contamination. Reported effects include HF emissions during battery fires, the deposition and remobilisation of cathode metals in surface soils, increased soil permeability, reduced shear strength and the potential exceedance of soil-quality thresholds (Claassen et al., 2024; Aiello et al., 2025; Mishra et al., 2026). Although these effects may be concentrated at individual accident, disposal or recycling sites, they demonstrate that EoL-LIB releases can affect air quality, soil chemistry, contaminant mobility, hydraulic behaviour and geotechnical stability.

At the global scale, the 2030 stress scenario produced potential releases of approximately 700 t Li, 447 t Ni, 278 t Cu, 149 t Mn and 56 t Co. These estimates were calculated by the authors using the waste projections reported by the United Nations Development Programme (2024) and the release assumptions derived from Mrozik et al. (2021). Although these values remain small compared with total battery waste, they represent significant dispersed contaminant loads, particularly when concentrated around informal processing sites, landfills or storage facilities.

By 2040, the strong increase in the EoL-LIB stream becomes the dominant driver of potential pollution. Scenario A, representing relatively effective control, produced releases ranging from approximately 29 t Mn to 365 t Li. Under Scenario B, the calculated quantities reached thousands of tonnes for Li, Ni and Cu. Scenario C generated substantially larger upper-bound values and illustrates the consequences of combining high waste quantities with fragmentation, fires or uncontrolled disposal. The increase in contaminant releases under Scenario B between 2030 and 2040 is illustrated in Figure 1, while the results obtained for all three scenarios in 2040 are presented in Table 3. As shown in Figure 1, lithium had the highest estimated release under the landfill/stress scenario, increasing from approximately 700 t $year^{-1}$ in 2030 to 7,754 t $year^{-1}$ in 2040. Nickel increased from 447 to 4,949 t $year^{-1}$, while the estimated Cu release rose from 278 to 3,075 t $year^{-1}$. Lower quantities were calculated for Mn and Co; however, their environmental relevance remains considerable because of their potential ecotoxicity and increased mobility under acidic or reducing soil conditions. The marked increase between 2030 and 2040 is mainly explained by

the expansion of the global EoL-LIB waste stream, since the assumed mismanagement and contaminant-release fractions remained unchanged.

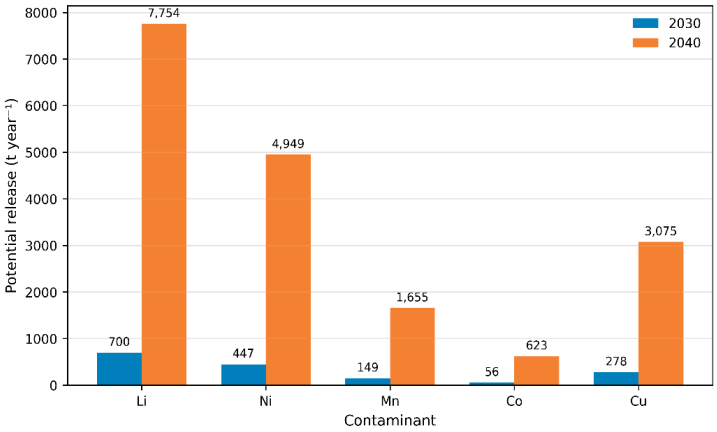



Figure 1. Estimated potential releases of lithium, nickel, manganese, cobalt and copper under the landfill/leaching stress scenario in 2030 and 2040 (Source: authors' calculations based on Mrozik et al., 2021, United Nations Development Programme, 2024, and the modelling assumptions described in Materials and Methods)

Table 3. Estimated potential contaminant releases from NMC811-type EoL-LIB waste in 2040

| Scenario | Li | Ni | Mn | Co | Cu |
|---|---|---|---|---|---|
| A | 365 | 247 | 29 | 31 | 154 |
| B | 7,754 | 4,949 | 1,655 | 623 | 3,075 |
| C | 41,051 | 37,115 | 8,672 | 4,674 | 23,062 |

Source: Authors' calculations based on Mrozik et al. (2021), United Nations Development Programme (2024), and the assumptions described in Materials and Methods.

Values are expressed in t $yr^{-1}$. A - controlled management; B - landfill/leaching stress; C - severe mismanagement.

The values presented in Table 3 are conservative screening estimates rather than forecasts. The future waste stream will include an increasing proportion of LFP batteries, which would reduce Ni and Co loads, while released contaminants may be distributed among soil, water, air, sludge and engineered residues. Consequently, the results are primarily useful for comparing management scenarios and demonstrating the importance of collection efficiency rather than predicting pollution at a specific location (Harper et al., 2019; International Energy Agency, 2024).

Mechanical pre-treatment generally involves discharge, dismantling, crushing, sieving and physical separation. It concentrates cathode and anode materials into black mass but may generate metal-bearing dust, volatile electrolyte compounds and fire risks. The quality and chemical homogeneity of black mass strongly affect the environmental and economic performance of subsequent recycling stages (Harper et al., 2019; Rinne et al., 2024).

Pyrometallurgical recycling can process mixed or contaminated feedstocks and efficiently transfer Ni, Co and Cu into an alloy. However, the process requires high temperatures, destroys graphite and organic components and may transfer Li, Al and Mn to slag. Fluorinated emissions require gas treatment, while the long-term leaching behaviour of slag and dust must be assessed before reuse or disposal. The low Ni and Co content of LFP batteries further reduces the economic attractiveness of conventional pyrometallurgy for this chemistry (Harper et al., 2019; Mrozik et al., 2021).

Hydrometallurgical recycling uses acid or alkaline leaching, precipitation, solvent extraction and crystallisation to recover Li and transition metals. It generally operates at lower temperatures and may achieve high recovery efficiencies, but the process consumes water, acids, bases and reducing agents and generates saline wastewater and sludge. A process-based life-cycle assessment found that reducing the initial acid concentration from approximately 2 M to below 0.5 M lowered several environ-

mental impacts by approximately 30-40%, illustrating the importance of reagent optimisation and internal recycling (Rinne et al., 2024).
Direct recycling seeks to preserve the functional structure of cathode materials through separation, purification, relithiation and thermal treatment. It may reduce energy and chemical requirements because the cathode is not completely decomposed into metals or salts. Its main limitations are the need for accurate chemistry identification, clean feedstocks and control of Cu, Al and electrolyte contamination. Direct recycling may be particularly important for LFP, where recovery based solely on the market value of individual metals is less favourable (Harper et al., 2019; International Energy Agency, 2024).
Recent hydrometallurgical work on waste LFP batteries reported Li leaching efficiencies of 54-97% using organic acids and reductants, with Li recovery of approximately 90% after precipitation. Such results indicate that LFP recycling can be technically feasible, although industrial environmental performance will also depend on reagent recovery, wastewater treatment, energy use and product quality (Avcı & Özdemir, 2026).
To assess the influence of management and treatment technologies on environmental pollution, the principal release pathways associated with uncontrolled disposal, battery fires, mechanical pretreatment, pyrometallurgy, hydrometallurgy and direct recycling are compared in Table 4.

Table 4. Technology-specific pollution pathways and environmental implications of EoL-LIB management and recycling

| Technology or scenario | Main potential releases | Main affected medium | Environmental implication |
|---|---|---|---|
| Uncontrolled disposal/landfill | Li, Ni, Co, Mn, Cu, fluorides, PFAS | Soil and groundwater | Chronic leaching and contaminant accumulation |
| Battery fire | HF, metal-rich particles, fluorinated compounds | Air, surface soil and water | Acute deposition and remobilisation |
| Mechanical pretreatment | Fine cathode dust, graphite, electrolyte vapours | Air and workplace surfaces | Particulate and VOC exposure |
| Pyrometallurgy | Combustion gases, slag containing Li, Al and Mn | Air and solid residues | High energy demand and residue-management risks |
| Hydrometallurgy | Acidic or saline wastewater and metal-bearing sludge | Surface water, groundwater and soil | High recovery but significant wastewater burden |
| Direct recycling | Dust, rejected mixed materials and damaged cathode fractions | Air and solid waste | Lower processing burden but requires clean feedstock |

Source: authors' synthesis based on Harper et al. (2019), Mrozik et al. (2021), Rensmo et al. (2023), Claassen et al. (2024), Guelfo et al. (2024), International Energy Agency (2024), Rinne et al. (2024), Aiello et al. (2025), and Shojaei et al. (2025).

As shown in Table 4, EoL-LIB management and recycling options generate different release profiles and may transfer environmental burdens between air, soil, water and solid residues. The dominant environmental compartment therefore changes according to the management route: uncontrolled disposal primarily threatens soil and groundwater, battery fires affect air and surface environments, pyrometallurgy concentrates burdens in gaseous emissions and solid residues, while hydrometallurgy transfers a substantial part of the burden to wastewater and sludge.
Recycling performance should therefore not be evaluated only through the total percentage of battery mass processed. A system may achieve a high mass-based efficiency by recovering steel, Cu and Al while losing Li, graphite, fluorinated compounds or fine active material. Environmental assessment should therefore combine overall recycling efficiency with element-specific recovery, energy and reagent consumption, wastewater quality and the leaching stability of final residues (Rensmo et al., 2023; Rinne et al., 2024).
European legislation requires a minimum recycling efficiency of 65% for lithium-based batteries by the end of 2025 and 70% by the end of 2030. Material recovery targets are 90% for Co, Cu, Ni and Pb and 50% for Li by the end of 2027, increasing to 95% and 80%, respectively, by the end of 2031. These targets create

incentives for improved Li recovery and more complete material balances, but effective environmental protection also depends on collection, traceability and control of fluorinated emissions and residues (European Commission, 2025; European Parliament and Council of the European Union, 2023).

The most favourable pollution-prevention scenario combines collection rates approaching 100%, digital battery identification, separation by chemistry, fire-resistant storage, rapid isolation of damaged batteries and recycling routes selected for the feedstock. Monitoring programmes around storage and recycling facilities should include Li, Ni, Co, Mn, Cu, total and soluble fluorides, pH, electrical conductivity and groundwater quality. PFAS screening should be considered where fluorinated electrolytes or polymers are produced or processed (Guelfo et al., 2024; Rensmo et al., 2023).

## CONCLUSIONS

Global electric-vehicle battery deployment reached approximately 1.2 TWh in 2025, corresponding to an estimated 7.0 Mt of batteries, and may approach 17.5 Mt annually by 2030.

The annual EoL-LIB waste stream is projected to increase from 0.90 Mt in 2025 to 20.50 Mt in 2040, requiring a rapid expansion of collection, storage and recycling infrastructure.

Environmental degradation may result from the combined action of Li, Ni, Co, Mn, Cu, fluorides, electrolyte degradation products, fine cathode particles and persistent organofluorinated compounds. Soil acidification may amplify pollution by increasing metal mobility and bioavailability.

The stress scenario for 2040 produced potential releases of approximately 7,754 t Li, 4,949 t Ni, 3,075 t Cu, 1,655 t Mn and 623 t Co. These values are sensitivity indicators rather than predictions, but they demonstrate that small percentages of mismanaged waste can generate substantial contaminant loads.

NMC and NCA waste presents a higher Ni and Co contamination potential, whereas LFP reduces these metal-related risks but maintains the need to recover Li, Cu, graphite, phosphate compounds and fluorinated electrolyte materials.

Pyrometallurgy is robust for mixed feedstocks but may transfer environmental pressure to energy use, emissions and slag. Hydrometallurgy provides broader metal recovery but requires strict control of reagents and wastewater. Direct recycling offers high circularity potential for clean, chemistry-specific streams.

Collection efficiency is the principal control variable. Chemistry-based sorting, traceability, fire-safe storage, capture of firefighting water and site-specific soil and groundwater monitoring are required to prevent the transfer of battery pollution between environmental compartments.

## REFERENCES

Ahmed, S., Knehr, K. W., Kubal, J. J., & Islam, E. (2023). Parametric study of lithium-ion batteries using BatPaC: Final report (Report No. ANL/CSE-23/1, 59 pp.). *Argonne National Laboratory*. https://publications.anl.gov/anlpubs/2023/08/183571.pdf

Aiello, I. W., Endris, C., Cunningham, S., Fountain, M., Grand, M. M., Heim, W., Kahn, A. S., & Wasson, K. (2025). Coastal wetland deposition of cathode metals from the world's largest lithium-ion battery fire. *Scientific Reports, 15*, 42113. https://doi.org/10.1038/s41598-025-25972-8

Avcı, G., & Özdemir, A. (2026). Hydrometallurgical recycling of waste lithium iron phosphate batteries using different organic acids and reductants. *International Journal of Environmental Science and Technology, 23*, 378. https://doi.org/10.1007/s13762-026-07230-0

Bolan, N., Hoang, S. A., Tanveer, M., Wang, L., Bolan, S., Sooriyakumar, P., Robinson, B., Wijesekara, H., Wijesooriya, M., Keerthanan, S., Vithanage, M., Markert, B., Fränzle, S., Wünschmann, S., Sarkar, B., Vinu, A., Kirkham, M. B., Siddique, K. H. M., & Rinklebe, J. (2021). From mine to mind and mobiles - Lithium contamination and its risk management. *Environmental Pollution, 290*, 118067.https://doi.org/10.1016/j.envpol.2021.118067

Claassen, M., Bingham, B., Chow, J. C., Watson, J. G., Chu, P., Wang, Y., & Wang, X. (2024). Characterization of lithium-ion battery fire emissions - Part 2: Particle size distributions and emission factors. *Batteries, 10*(10), 366. https://doi.org/10.3390/batteries10100366

European Commission. (2025). *Commission Delegated Regulation (EU) 2025/606 of 21 March 2025 supplementing Regulation (EU) 2023/1542 of the European Parliament and of the Council by establishing the methodology for calculation and verification of rates for recycling efficiency and recovery of materials from waste batteries, and the format for the documentation*. *Official Journal of the*

*European Union*. https://eur-lex.europa.eu/eli/reg_del/2025/606/oj/eng

European Parliament and Council of the European Union (2023). *Regulation (EU) 2023/1542 of the European Parliament and of the Council of 12 July 2023 concerning batteries and waste batteries, amending Directive 2008/98/EC and Regulation (EU) 2019/1020 and repealing Directive 2006/66/EC*. *Official Journal of the European Union, L 191*, 1–117. https://eur-lex.europa.eu/eli/reg/2023/1542/oj/eng

Guelfo, J. L., Ferguson, P. L., Beck, J., Chernick, M., Doria-Manzur, A., Faught, P. W., Flug, T., Gray, E. P., Jayasundara, N., Knappe, D. R. U., Joyce, A. S., Meng, P., & Shojaei, M. (2024). Lithium-ion battery components are at the nexus of sustainable energy and environmental release of per- and polyfluoroalkyl substances. *Nature Communications, 15*, 5548. https://doi.org/10.1038/s41467-024-49753-5

Harper, G., Sommerville, R., Kendrick, E., Driscoll, L., Slater, P., Stolkin, R., Walton, A., Christensen, P., Heidrich, O., Lambert, S., Abbott, A., Ryder, K., Gaines, L., & Anderson, P. (2019). Recycling lithium-ion batteries from electric vehicles. *Nature, 575*(7781), 75–86. https://doi.org/10.1038/s41586-019-1682-5

International Energy Agency (2024). *Recycling of critical minerals: Strategies to scale up recycling and urban mining*. https://www.iea.org/reports/recycling-of-critical-minerals

International Energy Agency (2026). *Global EV outlook 2026*. https://www.iea.org/reports/global-ev-outlook-2026

Ministry of Waters, Forests and Environmental Protection (1997). *Order No. 756/1997 approving the Regulation on Environmental Pollution Assessment*. *Official Gazette of Romania, Part I*, No. 303 bis, 6 November 1997. http://www.mmediu.ro/app/webroot/uploads/files/OM-184-1997-bilant-de-mediu-si-OM-756-1997-evaluarea-poluarii-mediului.pdf

Mishra, P., Apte, S., & Mukherjee, A. (2026). Sustainable lithium-ion battery waste management: Assessing impacts of heavy metal fraction on soil properties and pathways to mitigation. *Sustainable Environment Research, 36*(10). https://doi.org/10.1186/s42834-026-00276-2

Mrozik, W., Rajaeifar, M. A., Heidrich, O., & Christensen, P. (2021). Environmental impacts, pollution sources and pathways of spent lithium-ion batteries. *Energy & Environmental Science, 14*, 6099–6121. https://doi.org/10.1039/D1EE00691F

Mosnegutu, E., Tomozei, C., Nedeff, F., Chitimus, D., Mirila, D., Wiewiórska, I., Jasinski, M., Sporea, N. (2025a). Towards Efficient Waste Handling: Structural Group Reduction in Lifting Mechanism Design, *Processes*, *13*(9), 2744. https://doi.org/10.3390/pr13092744

Mosnegutu, E., Przydatek, G., Chitimus, D., Placinta, C., Barsan, N., Tomozei, C., Nedeff, F., Sporea, N. (2025b). Study on the Public Information Level About the Waste Management System, *Urban Science*, *9*(5), 148. https://doi.org/10.3390/urbansci9050148

Rensmo, A., Savvidou, E. K., Cousins, I. T., Hu, X., Schellenberger, S., & Benskin, J. P. (2023). Lithium-ion battery recycling: A source of per- and polyfluoroalkyl substances to the environment? *Environmental Science: Processes & Impacts, 25*, 1015–1030. https://doi.org/10.1039/D2EM00511E

Rinne, M., Aromaa-Stubb, R., Elomaa, H., Porvali, A., & Lundström, M. (2024). Evaluation of hydrometallurgical black mass recycling with simulation-based life cycle assessment. *The International Journal of Life Cycle Assessment, 29*, 1582–1597.https://doi.org/10.1007/s11367-024-02304-y

Shojaei, M., Guelfo, J. L., Barlaz, M. A., Cogollo-Carcamo, G., Rivera, N. A., Hsu-Kim, H., & Ferguson, P. L. (2025). Evaluation of fluorochemical leaching from lithium-ion batteries under simulated solid waste landfill conditions. *Environmental Science & Technology, 59*(49), 26750–26761. https://doi.org/10.1021/acs.est.5c10116

United Nations Development Programme (2024). *Analysis of EV battery end-of-life*. https://www.undp.org/thailand/publications/analysis-ev-battery-end-life

Scientific Papers. Series E. Land Reclamation, Earth Observation & Surveying, Environmental Engineering. Vol. XV, 2026
Print ISSN 2285-6064, CD-ROM ISSN 2285-6072, Online ISSN 2393-5138, ISSN-L 2285-6064

# ELECTROCHEMICAL SENSORS FOR DETECTING ENVIRONMENTAL POLLUTANTS - A REVIEW

**Andrei-Daniel GEMAN[1, 2], Andreea-Loredana COMĂNESCU[1, 2], Constantin APETREI[1, 2], Cătălina ITICESCU[1, 2], Puiu-Lucian GEORGESCU[1, 2]**

[1] "Dunărea de Jos" University of Galați, REXDAN Research Centre,
98 George Coşbuc Blvd, Galaţi, Romania
[2] "Dunărea de Jos" University of Galați, Faculty of Sciences and Environment,
111 Domnească Street, Galaţi, Romania

Corresponding author email: Constantin.Apetrei@ugal.ro

***Abstract***

*Electrochemical sensors are an efficient and versatile tools for monitoring environmental pollutants, providing information on target analytes in a rapid, sensitive and cost-effective manner and representing a good alternative to conventional methods such as spectrophotometry and chromatography in real time or on-site analysis. These sensors use electrochemical methods, including amperometry, voltammetry and potentiometry, to detect a wide range of environmental pollutants, including heavy metals, pesticides and other toxic chemicals, making them well-suited for environmental monitoring. Due to their simplicity, accuracy, low cost and their performance (stability, selectivity, LOD in the micro and nanomolar range) and because they can be modified with nanomaterials, enzymes and molecularly imprinted polymers, sensors and biosensors are increasingly used in environmental monitoring and pollution control. Therefore, this work proposes to present a review of the most recent developments in the detection of environmental pollutants using electrochemical sensors.*

***Key words:*** *electrochemical sensor, enzyme, nanomaterial, pollutant.*

## INTRODUCTION

Environmental health is important for maintaining life on Earth. Population growth and rapid industrialization have led to gradual environmental pollution, with harmful effects on ecosystems and human health. For this reason, pollution has become a public concern worldwide. Contamination and pollution occur when harmful compounds and pollutants are released into the air, soil, and water, either naturally (through fires or volcanic eruptions) or as a result of human activities. This pollution can have serious effects on human health, causing a range of diseases and conditions, including cancer, respiratory diseases, cardiovascular diseases, and other chronic illnesses. Chemical contaminants, released into the environment as a result of human activities, have become major pollutants that have led to increased toxicity in aquatic ecosystems, soil, and water. Pollution of natural ecosystems can also have consequences for the economy. High costs are incurred in cleaning up polluted areas or mitigating the adverse effects caused by prolonged exposure to a contaminant. High costs are generated by cleaning up polluted areas or mitigating the adverse effects produced by prolonged exposure to a contaminant (Awewomom et al., 2024; Rathod et al., 2024).

Currently, there are numerous methods for detecting and monitoring environmental contaminants. The most common techniques are: chromatographic techniques (liquid chromatography (LC) and gas chromatography (GC) coupled with various types of detection), spectroscopic techniques (atomic absorption spectroscopy (AAS) and ultraviolet-visible spectroscopy (UV-Vis)). Although these methods are effective in detecting compounds of interest, they also have a number of limitations - long sample preparation times, the need for qualified personnel to operate the equipment, the use of toxic solvents, high costs, and the complexity of the equipment. Therefore, it is necessary to use a new alternative that offers significant advantages in terms of cost, sensitivity, and selectivity, as well as in terms of processing time (Wang et al., 2021; Kassim et al., 2022; Dawra & Dabas, 2024; Gątarek et al.,

2025). Sensors and biosensors have become an effective tool for monitoring the environment, water quality, air pollution, soil analysis, and biodiversity conservation. These are widely used as cost-effective, portable, inexpensive, and sensitive analytical techniques that can be combined with other analytical methods to enhance their selectivity and sensitivity. These advantages have led to increased use of these methods in real-time monitoring of environmental pollutants, as a sustainable alternative to traditional methods that does not cause additional pollution (Tajik et al., 2021; Pal et al., 2025).

**Pollutants**

Substances that cause unwanted changes in the natural environment, with harmful effects on plants, animals and humans, are called pollutants. A compound becomes a pollutant when its concentration exceeds its natural abundance as a result of natural phenomena or caused by human activities (Khasanova et al., 2023).

**Classification of pollutants**

Pollutants can be classified according to several criteria:

- by nature (microbial or chemical);
- by origin: natural pollutants (which occur naturally but, over time, due to accumulation or a sudden increase in their concentration, exert toxic effects on the environment);
- artificial pollutants (introduced into the environment by humans and their activities);
- based on their elimination in nature in relation to ecosystems, they can be further classified as biodegradable and non-biodegradable pollutants (Khanmohammadi et al., 2020; Ajibade et al., 2021).

Worldwide, the most common pollutants are heavy metals, pesticides and pharmaceutical compounds. These compounds pose a high risk because they can accumulate in the tissues of living organisms, which can lead to the development of degenerative diseases, alter the chemical composition of soil and water (Kordbacheh & Heidari, 2023).

**Heavy metals**

Heavy metals are a natural component of the environment, but human activities (increased industrialization, exploitation of natural and mineral resources, and economic instability) have disrupted natural geochemical processes, turning this component into a threat to the environment. Their toxic nature, persistence, bioaccumulation, and stability in the environment have come to threaten both natural ecosystems and human health (Ali et al., 2021; Swain, 2024). Heavy metals directly influence the chemical and physical properties of soil, water, and sediment. They can affect the trophic balance in the environment, disrupting the food chain for an indefinite period of time. Sparingly soluble heavy metals can accumulate in excessive amounts and interfere with natural biological processes in living organisms (Ali et al., 2021). Heavy metals can enter water sources in two ways: naturally or artificially. Artificial contamination results from landslides, illegal dumping, and discharges into freshwater or marine habitats, while natural contamination is caused by forest fires, mineral erosion, and volcanic activity (Swain, 2024). Environmental monitoring is important because there is a close link between the pollution of natural ecosystems and human health and socioeconomic development (Huang et al., 2023). Exposure to environmental pollution remains a major risk to human health worldwide. Exposure levels are often uneven and can occur through various pathways (via air or water). The duration of exposure and the concentration of pollutants are increasing year by year. Exposure to multiple pollutants can have adverse effects not only on human health but also on the environment. Thus, environmental monitoring has become one of the most important tasks facing not only the EU but the entire planet (Bălă et al., 2021; Shetty et al., 2023).

**Pesticides**

Rapid population growth of the current century has led to the growth of the agricultural industry and, consequently, to the widespread use of pesticides. Their use has become widespread because they reduce losses, protect crops, and improve production yields on a global scale. Pesticides are classified according to several criteria: mode of action, chemical class, functional groups, and toxicity. The most important classification criterion is based on the different pest targets: herbicides, insecticides, fungicides, rodenticides, etc. (Tudi et al., 2021).The heavy use of pesticides, such as

chloridazon, methyl parathion and chlorpyrifos, has negative effects on the environment. A large proportion of this end up in the ecosystem, carried either by the wind or by water, with up to 95% of herbicides and over 98% of insecticides becoming pollutants. These pollutants eventually end up in surface and groundwater, lakes, and oceans, where, due to physical and chemical interactions, they can form highly toxic reaction byproducts (Abdollahdokht et al., 2021). Classic pesticides often have high concentrations of organic solvents with low dispersion that remain in soil and sediment for a long time and move in the environment, endangering biological systems (Rad et al., 2022).

**Pharmaceutical Products**

Of all the emerging pollutants of concern, pharmaceuticals (FP) attract the most attention globally because they cause a high level of environmental pollution (Argaluza et al., 2021). In recent decades, the production and consumption of pharmaceuticals (paracetamol, diclofenac, tetracyclines and azithromycin), have increased rapidly due to declining health, rising food consumption, and advances in medicine (Măghinici et al., 2025). Anti-inflammatory drugs, antibiotics, and analgesics are the most commonly used medications globally and are taken daily around the world. Consequently, water-soluble, pharmacologically active organic micropollutants have begun to enter the environment, causing various harmful effects (Ortúzar et al., 2022; Măghinici et al., 2026). This environmental pollution caused by pharmaceuticals occurs primarily through the discharge of effluents from wastewater treatment plants into surface waters. Urban wastewater contains high levels of compounds resulting from various activities, whether industrial- such as aquaculture and livestock farming - where the use of antibiotics and growth hormones has become common practice, or in human healthcare, where 30-90% of administered oral doses find their way into ecosystems (Zampelli & Verna, 2025). The increasing use of pharmaceuticals to treat, alleviate, or prevent health conditions, as well as their use in veterinary medicine, plays a major role in ecosystem degradation. These pharmaceuticals have toxic effects on ecosystem components, ranging from biota to water and soil quality. These compounds can disrupt the fragile balance of ecosystems, alter the pH of water and soil, and cause genetic changes and malformations in existing biota. In the case of fish, the active compounds in medications cause cellular damage and respiratory problems, with adverse effects on growth, development, and reproductive capacity (Mezzelani & Regoli, 2022; Ortúzar et al., 2022).

**Electrochemical methods for detecting environmental pollutants**

Contaminants of emerging concern (CECs) continue to threaten the health of natural ecosystems as well as human health, a situation largely attributable to human activities. It is particularly important to monitor ECs, as they tend to migrate from their source and affect various aspects of the environment (sediment, flora, or fauna). Thus, electrochemical (EC) methods are widely used in environmental monitoring, as they are versatile in detecting emerging contaminants (heavy metals, pharmaceuticals, pesticides) (Kumunda et al., 2021; Sivaranjanee et al., 2022). Electrochemical techniques such as voltammetry, amperometry, conductometry, and potentiometry are successfully used today in environmental monitoring for rapid, sensitive detection, as well as for their potential for miniaturization and field deployment (Sivaranjanee et al., 2022).

Sensors can also be classified based on the analysis method they use:

- amperometric sensors - measure current over time based on a constant potential applied to the electrode;
- conductometric sensors - measure a solution's ability to conduct electric current;
- impedance sensors - measure electrical impedance (capacitance and resistance) when a small alternating current is applied;
- potentiometric sensors - used to measure the difference in electric potential between the working electrode and the reference electrode under zero-current conditions;
- voltammetric sensors - measure current based on the variable potential applied to the electrode (Kiaune & Singhasemanon, 2011; Saputra, 2023).

Among voltammetric methods - cyclic voltammetry, square-wave voltammetry, and differential pulse voltammetry - these techniques offer significant advantages such as high precision, simplicity, speed, selectivity, sensitivity, cost-effectiveness, and repeatability (Sivaranjanee et al., 2022). Equally, recent technological advances in the field of nanotechnology (nanofabrication, printing, immobilization) have made it possible to adapt electrochemical sensors for the detection of a wide range of CECs (Hassan et al., 2022). Today, electrochemical sensors have revolutionized environmental monitoring, from water and soil to air quality. An electrochemical sensor is capable of responding continuously, selectively, and reversibly to the presence of a CEC, without disturbing the sample, and of providing accurate, timely information about the ecological status of a specific environment. Sensors consist of two components: a recognition element for the specific or selective binding of the analyte of interest, and a transducer element for transmitting the information. Carbon-based electrochemical sensors (CPE), glassy carbon electrodes (GCE), and screen-printed electrodes (SPE), examples from tables, have proven effective in determining and monitoring CECS in environmental samples. Their performance is determined by response time, signal-to-noise ratio (S/N), sensitivity, selectivity, linear range, and limits of detection (LOD) (Kanoun et al., 2021). Electrochemical sensors convert the chemical signal (the signal generated by the redox reaction occurring at the electrode surface) into a quantifiable electronic signal (Kiaune & Singhasemanon, 2011; Saputra, 2023). Electrochemical sensors can be modified with various materials to improve selectivity and sensitivity toward analytes of interest. Nanomaterials, metal nanoparticles, metal oxides, metal-organic frameworks, molecularly imprinted polymers, and biological elements (enzymes, antibodies, aptamers, DNA, RNA) are the main classes of materials with which electrochemical sensors can be modified to achieve analytical performance (Flores-Contreras et al., 2022; Rafaqat et al., 2022; González-González et al., 2023; Zheng et al., 2024).

## MATERIALS AND METHODS

To accomplish this work, articles from the specialized literature were studied and analyzed, from the Google Scholar database (Google Academic), selecting articles published in the last 5 years, between 2022 to the present, focusing on studies related to the configurations of electrochemical sensors used to detect different classes of environmental pollutants. Approximately 20 relevant articles were studied and presented in Tables 1, 2, and 3.

## RESULTS AND DISCUSSIONS

### Electrochemical sensors based on nanomaterials

Carbon-based nanomaterials (single-walled and multi-walled carbon nanotubes - SWCNT, MWCNT; carbon nanofibers - CNF; graphene quantum dots - GQDs), metallic nanoparticles (AuNPs, AgNPs, PtNPs), metal oxide nanoparticles (ZnO, NiO, $Fe_3O_4$), as well as polymeric nanomaterials (e.g., chitin nanocrystals - ChNCs) are frequently used as modifier materials for electrochemical sensors and biosensors because they exhibit superior mechanical strength, a high surface-to-volume ratio, enhanced electrocatalytic activity, properties that improve the selectivity and specificity of sensors, as well as response times (Alnahdi et al., 2022; Dinu et al., 2024; Masibi et al., 2025; Fakraoui et al., 2026; Wang et al., 2026).

### Electrochemical sensors based on metal-organic structures (MOF)

MOFs are structures formed by inorganic metal ions and organic ligands. MOFs are increasingly used in the modification of commercial electrochemical sensors due to their unique physicochemical properties such as large surface area, high porosity, tunable pore size and high catalytic activity. In recent years, MOFs that have metal ions such as copper, zinc, zirconium and nickel in their structure and carboxylic acid derivatives as organic ligands have been used in the electrochemical detection of environmental pollutants, including active pharmaceutical compounds, pesticides, metal ions, but also phenolic and nitroaromatic compounds (Tajik et al., 2021).

**Electrochemical sensors based on molecularly imprinted polymers (MIP)**

Molecularly imprinted polymers (MIPs) are polymers obtained by copolymerizing a functional monomer with a cross-linking agent that interacts with the target molecule (template) to form specific binding sites. After the template is removed, these specific binding sites are capable of recognizing and specifically binding the template (Udomsap et al., 2018). MIPs are the subject of intensive research due to their excellent properties, such as the ability to recognize the target analyte in a complex matrix, affordability, ease of synthesis, potential for miniaturization, durability, selectivity, and high physical and chemical stability - characteristics that make them suitable for electrochemical sensor applications in the detection of emerging pollutants, including pesticides and pharmaceuticals in environmental samples (Rao et al., 2018; Udomsap et al., 2018; Thimoonnee et al., 2022; Kamel et al., 2024; Poza-Nogueiras et al., 2026).

**Electrochemical sensors based on biological elements**

Electrochemical biosensors utilize a wide range of biorecognition elements (enzymes, antibodies, aptamers, DNA, RNA, whole cells) that provide high selectivity and sensitivity in the detection of target analytes. The performance of these electrochemical biosensors depends on the type of electrode, the type of transducer, the biological elements, and the techniques used to immobilize them (encapsulation, adsorption, covalent binding, cross-linking). The advantages of electrochemical biosensors include affordability, simplicity, fast response time, portability, high selectivity, and high sensitivity, making them useful for the detection and monitoring of CECs in environmental samples (Fdez-Sanromán et al., 2025; Hui et al., 2022).

Table 1. Electrochemical sensors for detecting heavy metals in environmental samples

| Sensor | Pollutants | Sample | Detection method | LOD | Linear range | Bibliographic reference |
|---|---|---|---|---|---|---|
| SPCE/$Fe_3O_4$-CNF | $Cd^{2+}$ | River water | SWASV | 0.0615 µM | 6-80 µM | (Dinu et al., 2024) |
| | $Pb^{2+}$ | | | 0.0154 µM | 14-80 µM | |
| | $Cu^{2+}$ | | | 0.0320 µM | 1-60 µM | |
| | $Hg^{2+}$ | | | 0.0148 µM | 6-80 µM | |
| SPCE/$Fe_3O_4$-MWCNT | $Cd^{2+}$ | | | 0.2719 µM | 6-70 µM | |
| | $Pb^{2+}$ | | | 0.3187 µM | 14-80 µM | |
| | $Cu^{2+}$ | | | 1.0436 µM | 1-60 µM | |
| | $Hg^{2+}$ | | | 0.9076 µM | 6-80 µM | |
| Bi-GC/RDE | $Cu^{2+}$ | River water | SWASV | 0.0105 µM | 0.04-0.35 µM | (Bounegru et al., 2025) |
| | $Pb^{2+}$ | | | 0.0207 µM | | |
| CNTs/UiO-66-$NH_2$@AuNPs/GCE | $Cd^{2+}$ | River water | DPSV | 0.021 µg/L | 0.06-400 µg/L | (Wang et al., 2026) |
| | $Pb^{2+}$ | | | 0.008 µg/L | 0.06-400 µg/L | |
| PTh/ChNCs/SA/SPCE | $Pb^{2+}$ | Wastewater | SWASV | 1.53 nM | 10-150 nM | (Fakraoui et al., 2026) |

*LOD = limit of detection; SWASV = square wave anodic stripping voltammetry; DPSV = differential pulse stripping voltammetry.

**Electrochemical sensors for the detection of heavy metals**

Dinu and his colleagues used various nanomaterials (iron oxide nanoparticles ($Fe_3O_4$ NPs), CNF, and MWCNT), in various combinations, to modify carbon-based electrochemical sensors for the detection of metal ions ($Cd^{2+}$, $Pb^{2+}$, $Cu^{2+}$, and $Hg^{2+}$) in river water samples. The analytical performance of the SPCE/$Fe_3O_4$-CNF and SPCE/$Fe_3O_4$-MWCNT sensors was evaluated using square-wave anodic stripping voltammetry (SWASV), yielding detection limits in the micromolar range. The SPCE/$Fe_3O_4$-CNF sensor exhibited superior analytical performance in terms of detecting the metal ions of interest, a performance that may be attributed to the CNF structure (thin and long structures) which allows for their homogeneous distribution among the $Fe_3O_4$ particles, as well as to the synergistic interaction between CNF and $Fe_3O_4$ (Dinu et al., 2024). In another study, a glassy carbon electrode with a rotating disk modified with a bismuth film (Bi-GC/RDE) was used for the simultaneous detection of $Pb^{2+}$ and $Cu^{2+}$ ions in river water samples, following prior

complexation with EDTA (ethylenediaminetetraacetic acid). The bismuth layer, deposited by electrochemical deposition, ensured the stability and reproducibility of the electrochemical signal in SWASV voltammetric measurements. Bi-GC/RDE exhibited competitive LODs of 0.0207 μM and 0.0105 μM for $Pb^{2+}$ and $Cu^{2+}$, respectively, detection limits that are significantly more sensitive compared to other RDE sensors reported in the literature for the detection of metal ions (Bounegru et al., 2025). The research conducted by Wang et al. demonstrates that a glassy carbon electrode (GCE) modified with a composite material consisting of modified Zr-MOF structures (UiO-66-$NH_2$), AuNPs, and CNTs can be successfully used for the simultaneous detection of two heavy metal ions (HMIs), exhibiting remarkable stability and sensitivity, with LODs of 0.021 μg/L for $Cd^{2+}$ and 0.008 μg/L for $Pb^{2+}$, obtained via DPSV (differential pulse stripping voltammetry) measurements. The sensor exhibited a large surface area and active sites due to the MOF structure, superior conductivity due to CNTs, and localized amplification of surface plasmon resonance due to AuNPs. Analysis of real samples (river water) demonstrated the practical applicability of the CNTs/UiO-66-$NH_2$@AuNPs/GCE sensor in the detection of environmental pollutants (Wang et al., 2026). As highlighted by Fakraoui and colleagues, the screen-printed carbon electrode (SPCE) modified with colloidally stabilized polythiophene (PTh) nanocomposites containing chitin nanocrystals (ChNCs), using sodium alginate (SA) as the matrix, exhibited excellent electroanalytical performance for the detection of $Hg^{2+}$ and $Pb^{2+}$ ions, with detection limits in the nanomolar range (3.26 nM and 1.53 nM). The novelty of the study lay in the use of a composite consisting of bio-natural polymers with conductive polymers, a composite that reduced the domain size, improved electron transfer kinetics, and prevented aggregation. The excellent results obtained with the PTh/ChNCs/SA/SPCE sensor on real wastewater samples were validated by atomic absorption spectrometry (AAS) (Fakraoui et al., 2026).

Table 2. Electrochemical sensors for detecting pesticides in environmental samples

| Sensor | Pollutants | Sample | Detection method | LOD | Linear range | Bibliographic reference |
|---|---|---|---|---|---|---|
| $Fe_3O_4$ /ITO | chloridazon | Surface water | SWV | 0.9 μmol/L | 1–22.5 μmol/L | (Alnahdi et al., 2022) |
| c-MWCNTs@$MoSe_2$-SPCE | methyl parathion | Tap and river water | DPV | 2.5 nM | 0.008–75 μM | (Beitollahi et al., 2025) |
| $La_2Sn_2O_7$@GO/GCE | paraoxon ethyl | Soil | DPV | 2.73 nM | 0.01-360 μM | (Akilarasan et al., 2024) |
| MSN-PtNPs@d-MIP/SPGE | paraquat | Reservoir and pond water | DPV | 3.1 nM | 0.025–500 μM | (Thimoonnee et al., 2022) |
| | glyphosate | Wastewater | | 4.0 nM | | |
| Cu/$Cu_2O$/CuO@C/GCE (Cu-BTB MOF) | diflubenzuron | Tap and river water Soil | DPV | 130 fM | $1.0 \times 10^{-4}$ M – $1.0 \times 10^{-12}$ M | (Ji et al., 2023) |
| AChE/Co-ExZrP/His-GQDs/SPSE | methyl parathion | Groundwater and drinking water | LSV | 0.01 μM | 0.2–50 μM | (Pengsook et al., 2026) |
| AChE/CS-GO/GO/CNFs/SPCE | chlorpyrifos | Drinking water | SWV | 2.2 nM | 2.5 nM–1 μM | (Thet Tun et al., 2023) |

*LOD = limit of detection; SWV = square wave voltammetry; DPV = differential pulse voltammetry; LSV = linear sweep voltammetry.

A study reported in the scientific literature demonstrated that the use of $Fe_3O_4$NPs significantly improves the performance of an indium tin oxide (ITO)-based sensor in detecting chloridazon, an organochlorine pesticide with harmful effects. Electrochemical detection was performed using square-wave voltammetry (SWV), yielding a LOD of 0.9 μmol/L. The $Fe_3O_4$/ITO sensor exhibited high sensitivity and selectivity, even in the presence of other interferents, when used for the detection of chloridazon in real surface water samples. The high specificity is due to $Fe_3O_4$ NPs, which can easily bind to the chlorine atoms in organochlorine pesticides (Alnahdi et al., 2023). Beitollahi and his colleagues developed a

screen-printed carbon sensor modified with core-shell nanostructures consisting of MWCNTs functionalized with carboxylic acid (-COOH) and molybdenum diselenide ($MoSe_2$) for the detection of methylparathion (MP) in tap water and river water samples. The DPV technique was used to evaluate the electrochemical response, with the c-MWCNTs@$MoSe_2$/SPCE sensor demonstrating superior analytical performance, characterized by a LOD of 2.5 nM and a wide linear range (0.008–75.0 μM). The performance of this sensor may be due to the synergistic effect between $MoSe_2$ nanostructures, which exhibit high catalytic activity, and MWCNTs, which feature large surface areas with active sites, hydrophilicity, and high electrical conductivity (Beitollahi et al., 2025). In a similar approach, pyrochlore-type lanthanum stannate ($La_2Sn_2O_7$) nanocomposites embedded in graphene oxide (GO) were synthesized and used as modifier materials for the glassy carbon electrode (GCE). Using the DPV technique, the $La_2Sn_2O_7$@GO/GCE sensor demonstrated the ability to detect ethyl paraoxon (POE) in soil samples with a detection limit in the nanomolar range (2.73 nM). The developed sensor showed remarkable results compared to other electrodes (unmodified or modified with other materials), indicating an increase in peak current and a reduction in potential (Akilarasan et al., 2024). A different strategy involves integrating nanomaterials (which provide sensitivity) into molecularly imprinted polymers (which provide selectivity) to detect pesticides in environmental samples. Such an approach was implemented by Thimoonnee and colleagues to detect paraquat (PQ) and glyphosate (GLY) in water samples from reservoirs and ponds, as well as in wastewater. The electrochemical sensor, consisting of a screen-printed graphite electrode (SPGE), modified with a dual-molecularly imprinted polymer (d-MIP), coated on a mesoporous silica-platinum core (MSN-PtNPs), demonstrated excellent detection limits in the nanomolar range (3.1 nM for PQ and 4.0 nM for GLY, respectively). Remarkable results, such as high specificity and selectivity for PQ and GLY, make the MSN-PtNPs@d-MIP/SPGE sensor suitable for on-site water quality monitoring (Thimoonnee et al., 2022). In parallel with approaches based on MIP polymers and nanomaterials, MOF structures were also investigated as modifier materials for the development of electrochemical sensors for pesticide detection. One such study focused on the detection of diflubenzuron, a non-electroactive insecticide from the benzoylurea class, using a Cu/$Cu_2O$/CuO@C/GCE electrochemical sensor. The electrochemical performance of the developed MOF-based sensor (Cu-BTB MOF) was evaluated using DPV, yielding a very good LOD (in the femtomolar range) and a wide linear range. These significantly improved values may be attributed to the large specific surface area of the octahedral MOF and the active sites of the composite, which enhance electron transfer. The sensor also proved effective on real samples, detecting diflubenzuron in tap water and river water, as well as in soil samples, with good recoveries (Ji et al., 2023). In addition to the materials listed above, researchers have also incorporated biological components - particularly enzymes - as immobilized elements on the surface of the electrodes, with the aim of improving the electrochemical detection of pollutants. A recent study showed that the use of the enzyme acetylcholinesterase (AChE) together with materials such as cobalt-modified exfoliated zirconium phosphate (Co-ExZrP), coated on histidine-functionalized graphene quantum dots (His-GQD) deposited on the surface of a silver screen-printed electrode (SPSE) can sensitively detect methyl parathion (LOD = 0.01 μM) in groundwater and drinking water samples (Pengsook et al., 2026). Another study utilized the immobilization of the AChE enzyme on an SPCE electrode modified with cellulose nanofibers, graphene oxide, and a composite of chitosan and graphene oxide (AChE/CS-GO/GO/CNF/SPCE) to detect chlorpyrifos, an organophosphorus pesticide. The electrochemical performance of the sensor, obtained through SWV measurements, indicated a LOD in the nanomolar range (2.2 nM) and is attributed to the inhibition of AChE's catalytic activity, as well as the use of nanomaterials that significantly improved conductivity (Thet Tun et al., 2023).

Table 3. Electrochemical sensors for detecting pharmaceuticals in environmental samples

| Sensor | Pollutants | Sample | Detection method | LOD | Linear range | Bibliographic reference |
|---|---|---|---|---|---|---|
| MIP-EDOT/SPCE | carbamazepine | Tap, river and sea water | DPV | 0.58 μM | 1-50 μM | (Poza-Nogueiras et al., 2026) |
| Zr-MOF/GCE | carbamazepine | Groundwater | DPASV | 0.0085 μmol·l$^{-1}$ | 0.010-0.25 μmol·l$^{-1}$ | (Lalawmpuia et al., 2025) |
| | ciprofloxacin | | | 0.0062 μmol·l$^{-1}$ | 0.01-0.25 μmol·l$^{-1}$ | |
| ZIF-8/PB/GCE | tetracycline | Lake water | SWV | 0.2 pM | 1-10$^6$ pM | (Chen et al., 2026) |
| TA-Au-Ag-ANpM/Fe-dop-PANI/NiO-NPs/GCE | azithromycin | River and lake water | SWV | 0.053 pM | 0.8 pM-250 μM | (Adane et al., 2025) |
| | enrofloxacin | | | 0.013 pM | 0.1 pM-550 μM | |
| NiTe-NPs/GCE | ronidazole | Tap and river water | DPV | 1.5 nM | 0.01-270 μM | (Barwa et al., 2025) |
| CNF@Pd-rGO/GCE | rifampicin | Industrial wastewater | DPV | 3.3 nM | 1-1062 nM | (Devi et al., 2026) |
| CNF-COOH/SPCE | paracetamol | River water | SWV | 0.002 mM | 0.0025-0.050 mM | (Fdez-Sanromán et al., 2025) |

*LOD = limit of detection; DPV = differential pulse voltammetry; DPASV = Differential Pulse Anodic Stripping Voltammetry; SWV = square wave voltammetry.

**Electrochemical sensors for the detection of pharmaceutical compounds**

Sensors modified with various nanomaterials have also been developed for the detection of pharmaceutical substances to improve sensitivity and detection times. In a recent study, the use of CNFs functionalized with carboxyl groups (-COOH) for SPCE improved the detection of paracetamol and 4-aminophenol in river water samples. The research highlighted that the carboxyl groups increased the density of active sites on the CNFs, leading to better adsorption of the analytes and improving electron transfer (Fdez-Sanromán et al., 2025). In a similar study, CNFs were used in combination with palladium nanoparticles (Pd NPs) and reduced graphene oxide (rGO) for a GCE to enable ultrasensitive detection of rifampicin, a drug used to treat tuberculosis. The nanomolar LOD, obtained via DPV measurements, indicates that CNF@Pd-rGO/GCE exhibits superior electrocatalytic activity, a performance that can be attributed to the synergistic effects of the nanoparticles used (Devi et al., 2026). Barwa and colleagues also used nanoparticles - this time nickel telluride nanoparticles (NiTe-NPs) - to detect ronidazole (RON), an antibacterial and antiprotozoal drug. Depositing NiTe-NPs onto the GCE surface improved electron transfer, facilitating the reduction of RON. The sensor exhibited a LOD of 1.5 nm, high sensitivity and selectivity even in the presence of other interferents, and was successfully applied for the detection of RON in tap water and river water (Barwa et al., 2025). In addition, two antibiotics, azithromycin (AZM) and enrofloxacin (ENF), were simultaneously detected in environmental samples (river and lake water samples) using a nanomaterial-based electrochemical sensor. The GCE was modified with thermally annealed gold-silver alloy nanocomposites (TA-Au-Ag -ANpM) that improved conductivity, active surface area, and catalytic activity; iron-doped polyaniline (Fe-dop-PANI) that enhanced selectivity by providing binding sites specific to the analytes of interest; and nickel oxide nanoparticles (NiO-NPs) that facilitated electron transfer kinetics. The sensor exhibited LOD in the picomolar range and demonstrated that it is an ideal device for the real-time detection of AZM and ENF in environmental samples (Adane et al., 2025). In parallel with the development of nanomaterial-based sensors for drug detection, researchers have also developed MIP- and MOF-based sensors to overcome the limitations of nanomaterials in terms of selectivity. For example, an SPCE sensor modified with an MIP-EDOT film (obtained by electropolymerization of the functional monomer 3,4-ethylenedioxythiophene in the presence of the target analyte as a template molecule) detected carbamazepine (CBZ) with very high accuracy in tap water, river, and

seawater samples, with recoveries ranging from 82 to 116%. The sensor exhibited superior sensitivity and selectivity for CBZ even in the presence of other interferents (diclofenac, diltiazem, CBZ 10,11-epoxide) (Poza-Nogueiras et al., 2026). Another recent study focused on the development of zirconium-based MOF (Zr-MOF) sensors for the detection of carbamazepine (an antiepileptic) and ciprofloxacin (an antibiotic) residues in groundwater samples. The sensor's improved electrochemical performance is due to the metal-organic framework, which has a large, highly porous surface, making the active surface area of the Zr-MOF/GCE twice as large as that of an unmodified GCE (Lalawmpuia et al., 2025). Another MOF sensor, but this time constructed from an imidazolate zeolite 8 (ZIF-8) structure composed of zinc ions and 2-methylimidazole ligands, onto which Prussian blue (PB) nanoparticles were deposited, successfully detected tetracycline (an antibiotic that can accumulate in aquatic ecosystems). With ZIF-8/PB/GCE, an ultra-low LOD (in the picomolar range), excellent selectivity, and stability were achieved - performance attributed to the synergistic effect between PB, which enhanced electrocatalytic activity, and ZIF-8, which exhibited a large surface area with adjustable porosity, as well as chemical and thermal stability (Chen et al., 2026).

## CONCLUSIONS

Environmental pollution is a major problem worldwide. In recent decades, natural ecosystems have been exposed to a range of pollutants that have disrupted their balance. Environmental degradation is largely caused by human activities, which is why constant monitoring of the effects that pollutants have on the environment is necessary. This review provides an overview of the concept of environmental pollution, emerging contaminants (heavy metals, pesticides, pharmaceutical compounds), the environmental components most affected by pollution, and modern methods for monitoring pollutants. Among current methods, electrochemical techniques coupled with new nanotechnologies have attracted global attention due to their promising characteristics. Recent research has shown that the integration of electrochemical sensors with various materials has improved response times, increased the efficiency of detecting analytes of interest in water samples, enhanced the surface-to-volume ratio, boosted electrocatalytic activity, enabled miniaturization, reduced costs, and improved physical and chemical stability, among other benefits.

## ACKNOWLEDGEMENTS

This research was financed by the project "Integrated research and sustainable solutions to protect and restore Lower Danube Basin and coastal Black Sea ecosystems" (ResPonSE), contract no. 760010/30.12.2022.
Additional the paper was supported through project PN-IV-P8-8.1-PRE-HE-ORG-2024-0227, Institutional award for the project HORIZON-MISS-2021-OCEAN-02, DANUBE REGION WATER LIGHTHOUSE ACTION, Project: 101094070 - DALIA, project PN-IV-P8-674/01.11.2024.

## REFERENCES

Abdollahdokht, D., Asadikaram, G., Abolhassani, M., Pourghadamyari, H., Abbasi-Jorjandi, M., Faramarz, S., & Nematollahi, M. H. (2021). Pesticide exposure and related health problems among farmworkers' children: a case-control study in southeast Iran. *Environmental Science and Pollution Research*, *28*(40), 57216–57231. https://doi.org/10.1007/s11356-021-14319-1

Adane, W. D., Chandravanshi, B. S., & Tessema, M. (2025). Multi-elemental nanocomposite electrochemical sensor for the simultaneous determination of azithromycin and enrofloxacin residues in food and water samples. *Microchemical Journal*, *210*, 113042. https://doi.org/10.1016/J.MICROC.2025.113042

Ajibade, F. O., Adelodun, B., Lasisi, K. H., Fadare, O. O., Ajibade, T. F., Nwogwu, N. A., Sulaymon, I. D., Ugya, A. Y., Wang, H. C., & Wang, A. (2021). Environmental pollution and their socioeconomic impacts. *Microbe Mediated Remediation of Environmental Contaminants*, 321–354. https://doi.org/10.1016/B978-0-12-821199-1.00025-0

Akilarasan, M., Tamilalagan, E., & Chen, S. M. (2024). Synthesis of pyrochlore-type La2Sn2O7@GO for the in-situ profiling of organophosphate pesticides paraoxon ethyl in environmental samples. *Journal of Environmental Chemical Engineering*, *12*(2), 111928. https://doi.org/10.1016/J.JECE.2024.111928

Ali, M. M., Hossain, D., Al-Imran, Khan, Md. S., Begum, M., & Osman, M. H. (2021). Environmental Pollution with Heavy Metals: A Public Health Concern. *Heavy*

*Metals - Their Environmental Impacts and Mitigation*. https://doi.org/10.5772/intechopen.96805

Alnahdi, H. S., Mousa, R. M. A., & El-Said, W. A. (202). Development of Organochlorine Pesticide Electrochemical Sensor Based on Fe3O4 Nanoparticles@indium Tin Oxide Electrode. *Electroanalysis*, *35*(2), e202100659. https://doi.org/10.1002/ELAN.202100659

Argaluza, J., Domingo-Echaburu, S., Orive, G., Medrano, J., Hernandez, R., & Lertxundi, U. (2021). Environmental pollution with psychiatric drugs. *World Journal of Psychiatry*, *11*(10), 791. https://doi.org/10.5498/wjp.v11.i10.791

Awewomom, J., Dzeble, F., Takyi, Y. D., Ashie, W. B., Ettey, E. N. Y. O., Afua, P. E., Sackey, L. N. A., Opoku, F., & Akoto, O. (2024). Addressing global environmental pollution using environmental control techniques: a focus on environmental policy and preventive environmental management. *Discover Environment*, *2*(1). https://doi.org/10.1007/s44274-024-00033-5

Bălă, G. P., Râjnoveanu, R. M., Tudorache, E., Motișan, R., & Oancea, C. (2021). Air pollution exposure - the (in)visible risk factor for respiratory diseases. *Environmental Science and Pollution Research*, *28*(16), 19615–19628. https://doi.org/10.1007/s11356-021-13208-x

Barwa, T., Sukanya, R., Kanagaraj, T., Collins, G., Luo, Y., Dempsey, E., Karthik, R., Shim, J. J., & Breslin, C. B. (2025). A Nickel Telluride Electrochemical Sensor for the Detection of the Antibiotic Ronidazole. *ACS Applied Nano Materials*, *8*(42), 20523–20533. https://doi.org/10.1021/ACSANM.5C03794

Beitollahi, H., Tajik, S., Garkani Nejad, F., & Safaee-Mehr, P. (2025). Carboxylic acid-functionalized MWCNTs@MoSe2 nanostructure-modified screen-printed carbon electrode as an efficient electrochemical sensor for methyl parathion detection in the water samples. *Journal of Alloys and Compounds*, *1044*, 184468. https://doi.org/10.1016/J.JALLCOM.2025.184468

Bounegru, A. V., Georgescu, L. P., Iticescu, C., & Apetrei, C. (2025). Simultaneous detection of Cu(II) and Pb(II) in the Danube river using a bismuth film modified glassy carbon rotating disk electrode. *Journal of Electroanalytical Chemistry*, *979*, 118924. https://doi.org/10.1016/J.JELECHEM.2024.118924

Chen, S., Yang, H., Zhang, C., Luo, M., Li, B., Lv, T., Yang, Y., & Wang, J. (2026). A sensitive electrochemical sensor for tetracycline detection based on a ZIF-8/Prussian blue nanocomposite fabricated via sequential electrodeposition. *Microchemical Journal*, *224*, 117487. https://doi.org/10.1016/J.MICROC.2026.117487

Dawra, N., & Dabas, N. (2024). Advances in spectrophotometric determination of Chromium(III) and Chromium(VI) in water: a review. *International Journal of Environmental Analytical Chemistry*, *104*(13), 2994–3015. https://doi.org/10.1080/03067319.2022.2076224

Devi, S. A., Mallikarjuna, K., Reddy, Y. V. M., Deepthi, Aabeedunnisa, Swamy, B. E. K., Ramakanth, I., & Madhavi, G. (2026). CNF@ Pd-rGO nanohybrid for ultra-sensitive electrochemical detection of rifampicin. *Microchemical Journal*, *221*, 116842. https://doi.org/10.1016/J.MICROC.2026.116842

Dinu, A., Bounegru, A. V., Iticescu, C., Georgescu, L. P., & Apetrei, C. (2024). Electrochemical Detection of Cd2+, Pb2+, Cu2+ and Hg2+ with Sensors Based on Carbonaceous Nanomaterials and Fe3O4 Nanoparticles. *Nanomaterials,* *14*(8). https://doi.org/10.3390/NANO14080702

Fakraoui, O., Ghorbel, N., Putaux, J. L., & Boufi, S. (2026). Green fabrication of chitin-nanocrystal-stabilized polythiophene nanocomposites for sensitive detection of toxic metal ions. *Journal of Environmental Chemical Engineering*, *14*(2), 121800. https://doi.org/10.1016/J.JECE.2026.121800

Fdez-Sanromán, A., Ben Messaoud, N., Pazos, M., Rosales, E., & Barbosa Queirós, R. (2025). Development of eco-friendly and cost-effective electrochemical sensor for the simultaneous detection of 4-aminophenol and paracetamol in water. *Sensing and Bio-Sensing Research*, *48*, 100782. https://doi.org/10.1016/J.SBSR.2025.100782

Flores-Contreras, E. A., González-González, R. B., González-González, E., Melchor-Martínez, E. M., Parra-Saldívar, R., & Iqbal, H. M. N. (2022). Detection of Emerging Pollutants Using Aptamer-Based Biosensors: Recent Advances, Challenges, and Outlook. *Biosensors,* *12*(12). https://doi.org/10.3390/bios12121078

Gątarek, P., Rosiak, A., & Kałużna-Czaplińska, J. (2025). Chromatographic Methods for the Determination of Organic Pollution in Urban Water: A Current Mini Review. *Critical Reviews in Analytical Chemistry*, *55*(5), 840–857. https://doi.org/10.1080/10408347.2024.2318764

González-González, R. B., Flores-Contreras, E. A., González-González, E., Torres Castillo, N. E., Parra-Saldívar, R., & Iqbal, H. M. N. (2023). Biosensor Constructs for the Monitoring of Persistent Emerging Pollutants in Environmental Matrices. *Industrial and Engineering Chemistry Research*, *62*(11), 4503–4520. https://doi.org/10.1021/acs.iecr.2c00421

Hassan, M. H., Khan, R., & Andreescu, S. (2022). Advances in electrochemical detection methods for measuring contaminants of emerging concerns. *Electrochemical Science Advances*, *2*(6), e2100184. https://doi.org/10.1002/elsa.202100184

Huang, C. W., Lin, C., Nguyen, M. K., Hussain, A., Bui, X. T., & Ngo, H. H. (2023). A review of biosensor for environmental monitoring: principle, application, and corresponding achievement of sustainable development goals. *Bioengineered*, *14*(1), 58–80. https://doi.org/10.1080/21655979.2022.2095089

Hui, Y., Huang, Z., Alahi, M. E. E., Nag, A., Feng, S., & Mukhopadhyay, S. C. (2022). Recent Advancements in Electrochemical Biosensors for Monitoring the Water Quality. *Biosensors,* *12*(7). https://doi.org/10.3390/BIOS12070551

Ji, X. X., Liu, Y. L., Chang, X. Y., Li, R. L., Ye, F., Yang, L., & Fu, Y. (2023). An electrochemical sensor derived from Cu-BTB MOF for the efficient detection of diflubenzuron in food and environmental samples.

*Food Chemistry*, *428*, 136802. https://doi.org/10.1016/J.FOODCHEM.2023.136802

Kamel, A. H., Abd-Rabboh, H. S. M., & Hefnawy, A. (2024). Molecularly imprinted polymer-based electrochemical sensors for monitoring the persistent organic pollutants chlorophenols. *RSC Advances*, *14*(28), 20163. https://doi.org/10.1039/D4RA03095H

Kanoun, O., Lazarević-Pašti, T., Pašti, I., Nasraoui, S., Talbi, M., Brahem, A., Adiraju, A., Sheremet, E., Rodriguez, R. D., Ali, M. Ben, & Al-Hamry, A. (2021). A Review of Nanocomposite-Modified Electrochemical Sensors for Water Quality Monitoring. *Sensors, 21*(12). https://doi.org/10.3390/S21124131

Kassim, N. S. A., A. I. S. M. Ghazali, S., Liyana Bohari, F., & A. Z. Abidin, N. (2022). Assessment of heavy metals in wastewater plant effluent and lake water by using atomic absorption spectrophotometry. *Materials Today: Proceedings*, *66*(P10), 3961–3964. https://doi.org/10.1016/j.matpr.2022.04.671

Khanmohammadi, A., Jalili Ghazizadeh, A., Hashemi, P., Afkhami, A., Arduini, F., & Bagheri, H. (2020). An overview to electrochemical biosensors and sensors for the detection of environmental contaminants. *Journal of the Iranian Chemical Society*, *17*(10), 2429–2447. https://doi.org/10.1007/s13738-020-01940-z

Khasanova, S., Alieva, E., & Shemilkhanova, A. (2023). Environmental Pollution: Types, Causes and Consequences. *BIO Web of Conferences*, *63*, 07014. https://doi.org/10.1051/bioconf/20236307014

Kiaune, L., & Singhasemanon, N. (2011). Pesticidal Copper (I) Oxide: Environmental Fate and Aquatic Toxicity. *Reviews of Environmental Contamination and Toxicology*, *213*, 1–26. https://doi.org/10.1007/978-1-4419-9860-6_1

Kordbacheh, F., & Heidari, G. (2023). Water pollutants and approaches for their removal. *Materials Chemistry Horizons*, *2*(2), 139-153.

Kumunda, C., Adekunle, A. S., Mamba, B. B., Hlongwa, N. W., & Nkambule, T. T. I. (2021). Electrochemical Detection of Environmental Pollutants Based on Graphene Derivatives: A Review. *Frontiers in Materials*, *7*, 616787. https://doi.org/10.3389/fmats.2020.616787

Lalawmpuia, R., Lalhruaitluangi, M., & Tiwari, D. (2025). Electrochemical Sensing of Ciprofloxacin and Carbamazepine Using Highly Sensitive Metal-Organic Framework. *Journal of The Electrochemical Society*, *172*(10), 105504. https://doi.org/10.1149/1945-7111/AE0BB7

Măghinici, A. R., Bounegru, A. V., & Apetrei, C. (2025). Electrochemical Detection of Diclofenac Using a Screen-Printed Electrode Modified with Graphene Oxide and Phenanthroline. *Chemosensors, 13*(2). https://doi.org/10.3390/CHEMOSENSORS13020055

Măghinici, A.-R., Comănescu, A.-L., Geman, A.-D., & Apetrei, C. (2026). Highly Sensitive Detection of Phenylbutazone with Metallic Particle-Based Electrochemical Sensors. *Chemosensors, 14*(4), 88. https://doi.org/10.3390/CHEMOSENSORS14040088

Masibi, K. K., Matinise, N., & Maaza, M. (2025). Nanomaterials in water pollution control: A concise review of electrochemical methods towards heavy metals. *Next Sustainability*, *6*, 100210. https://doi.org/10.1016/J.NXSUST.2025.100210

Mezzelani, M., & Regoli, F. (2022). The Biological Effects of Pharmaceuticals in the Marine Environment. *Annual Review of Marine Science*, *14*(Volume 14, 2022), 105–128. https://doi.org/10.1146/annurev-marine-040821-075606

Ortúzar, M., Esterhuizen, M., Olicón-Hernández, D. R., González-López, J., & Aranda, E. (2022). Pharmaceutical Pollution in Aquatic Environments: A Concise Review of Environmental Impacts and Bioremediation Systems. *Frontiers in Microbiology*, *13*, 869332. https://doi.org/10.3389/fmicb.2022.869332

Pal, P., Pandey, B., Prakash, A., Sarangi, P. K., Rathore, S. S., Agarwal, V., Gupta, A. K., & Singh, A. K. (2025). *Exploration of Biosensors in Innovative Applications and Sustainable Solutions for Environmental Monitoring and Management*. 561–591. https://doi.org/10.1007/978-981-97-7221-6_19

Pengsook, W., Thanachayanont, C., Wahyuni, W. T., & Hasin, P. (2026). Cobalt-modified exfoliated zirconium phosphate/histidine-functionalized graphene quantum dots-based electrochemical biosensor for promoting sensitive detection of methyl parathion in agricultural foods and water bodies samples. *Talanta*, *296*, 128403. https://doi.org/10.1016/J.TALANTA.2025.128403

Poza-Nogueiras, V., Puga, A., Pacheco, J. G., & Delerue-Matos, C. (2026). Rapid carbamazepine detection by means of a disposable electrochemical sensor based on a molecularly imprinted polymer. *Talanta*, *299*, 129128. https://doi.org/10.1016/J.TALANTA.2025.129128

Rad, S. M., Ray, A. K., & Barghi, S. (2022). Water Pollution and Agriculture Pesticide. *Clean Technologies, 4*(4), 1088–1102. https://doi.org/10.3390/cleantechnol4040066

Rafaqat, S., Raqba, Ali, N., & Hussain, A. (2022). Validating role of different enzymes (laccases and catalases) based voltammetric biosensors in detection of pesticide and dye. *Materials Chemistry and Physics*, *290*(1), 126545. https://doi.org/10.1016/j.matchemphys.2022.126545

Rao, H., Zhao, X., Liu, X., Zhong, J., Zhang, Z., Zou, P., Jiang, Y., Wang, X., & Wang, Y. (2018). A novel molecularly imprinted electrochemical sensor based on graphene quantum dots coated on hollow nickel nanospheres with high sensitivity and selectivity for the rapid determination of bisphenol S. *Biosensors & Bioelectronics*, *100*, 341–347. https://doi.org/10.1016/J.BIOS.2017.09.016

Rathod, S. V., Saras, P., & Gondaliya, S. M. (2024). Environmental Pollution: Threats and Challenges for Management. *Eco-Restoration of the Polluted Environment: A Biological Perspective*, 1–34. https://doi.org/10.1201/9781003423393-1

Saputra, H. A. (2023). Electrochemical sensors: basic principles, engineering, and state of the art.

*Monatshefte Fur Chemie*, *154*(10), 1083–1100. https://doi.org/10.1007/s00706-023-03113-z

Shetty, S. S., Deepthi, D., Harshitha, S., Sonkusare, S., Naik, P. B., Kumari N, S., & Madhyastha, H. (2023). Environmental pollutants and their effects on human health. *Heliyon*, *9*(9), e19496. https://doi.org/10.1016/j.heliyon.2023.e19496

Sivaranjanee, R., Senthil Kumar, P., Saravanan, R., & Govarthanan, M. (2022). Electrochemical sensing system for the analysis of emerging contaminants in aquatic environment: A review. *Chemosphere*, *294*, 133779. https://doi.org/10.1016/j.chemosphere.2022.133779

Swain, C. K. (2024). Environmental pollution indices: a review on concentration of heavy metals in air, water, and soil near industrialization and urbanisation. *Discover Environment*, *2*(1), 5-. https://doi.org/10.1007/s44274-024-00030-8

Tajik, S., Beitollahi, H., Garkani Nejad, F., Sheikhshoaie, I., Nugraha, A. S., Jang, H. W., Yamauchi, Y., & Shokouhimehr, M. (2021). Performance of metal–organic frameworks in the electrochemical sensing of environmental pollutants. *Journal of Materials Chemistry*, *9*(13), 8195–8220. https://doi.org/10.1039/d0ta08344e

Thet Tun, W. S., Saenchoopa, A., Daduang, S., Daduang, J., Kulchat, S., & Patramanon, R. (2023). Electrochemical biosensor based on cellulose nanofibers/graphene oxide and acetylcholinesterase for the detection of chlorpyrifos pesticide in water and fruit juice. *RSC Advances*, *13*(14), 9603–9614. https://doi.org/10.1039/D3RA00512G

Thimoonnee, S., Somnet, K., Ngaosri, P., Chairam, S., Karuwan, C., Kamsong, W., Tuantranont, A., & Amatatongchai, M. (2022). Fast, sensitive and selective simultaneous determination of paraquat and glyphosate herbicides in water samples using a compact electrochemical sensor. *Analytical Methods*, *14*(8), 820–833. https://doi.org/10.1039/D1AY02201F

Tudi, M., Daniel Ruan, H., Wang, L., Lyu, J., Sadler, R., Connell, D., Chu, C., & Phung, D. T. (2021). Agriculture Development, Pesticide Application and Its Impact on the Environment. *International Journal of Environmental Research and Public Health*, *18*(3), 1112. https://doi.org/10.3390/ijerph18031112

Udomsap, D., Brisset, H., Culioli, G., Dollet, P., Laatikainen, K., Siren, H., & Branger, C. (2018). Electrochemical molecularly imprinted polymers as material for pollutant detection. *Materials Today Communications*, *17*, 458–465. https://doi.org/10.1016/J.MTCOMM.2018.10.019

Wang, M., Chen, Z., Song, W., Hong, D., Huang, L., & Li, Y. (2021). A review on Cadmium Exposure in the Population and Intervention Strategies Against Cadmium Toxicity. *Bulletin of Environmental Contamination and Toxicology*, *106*(1), 65–74. https://doi.org/10.1007/S00128-020-03088-1

Wang, Z., Qi, T., Sun, H., Wang, N., Zhang, W., Zhao, J., Zhao, L., & Liang, L. (2026). Construction of a highly sensitive Cd(II) and Pb(II) simultaneous detection electrochemical sensor based on CNTs/UiO-66-$NH_2$@AuNPs composite material. *Microchemical Journal*, *222*, 117113. https://doi.org/10.1016/J.MICROC.2026.117113

Zampelli, S., & Verna, R. (2025). Environmental Pollution from Pharmaceuticals. *Life, 15*(9). https://doi.org/10.3390/life15091341

Zheng, A. L. T., Teo, E. Y. L., Yiu, P. H., Boonyuen, S., Chung, E. L. T., & Andou, Y. (2024). Recent advances in ultrasensitive electrochemical sensors and biosensors for determination of antibiotics in environment samples. *Clean Technologies and Environmental Policy*, *27*(2), 549–576. https://doi.org/10.1007/s10098-024-02934-8

Scientific Papers. Series E. Land Reclamation, Earth Observation & Surveying, Environmental Engineering. Vol. XV, 2026
Print ISSN 2285-6064, CD-ROM ISSN 2285-6072, Online ISSN 2393-5138, ISSN-L 2285-6064

# TREE COMMUNITY PATTERNS IN RELATION TO EDGE INFLUENCE IN A PERI-URBAN FOREST NEAR CLUJ-NAPOCA, ROMANIA

**Ioana-Loredana GHIURCO[1], Carla-Maria APARASCHIVE[1], Adela-Maria NEAG[2], Iulia-Ecaterina MORA[1], Păunița BOANCĂ[1], Sonia BODEA[1], Denisa JUCAN[1], Catalina DAN[1], Adriana SESTRAS[1]**

[1]University of Agricultural Sciences and Veterinary Medicine Cluj-Napoca,
3-5 Calea Manastur Street, Cluj-Napoca, Romania
[2]Doctoral School of Technical University of Civil Engineering Bucharest,
122-124 Lacul Tei Blvd, District 2, Bucharest, Romania

Corresponding author email: carla-maria.aparaschive@usamvcluj.ro

***Abstract***

*This study investigated the structure and diversity of tree communities in relation to edge influence in a sector of the Hoia-Baciu peri-urban forest located near Cluj-Napoca, Romania. A total of 20 circular sampling plots (500 m²) were systematically distributed along transects covering varying distances from the forest edge. Within each plot, tree species and the number of individuals were recorded to characterize community composition and structural parameters. Species richness, tree density, and diversity indices (Shannon and Simpson) were calculated, and differences in community composition were explored using non-metric multidimensional scaling (NMDS). The results indicate a simplified tree community strongly dominated by C. betulus. Species richness ranged between one and four species per plot, while Shannon diversity values varied from 0 to 1.22, reflecting moderate spatial heterogeneity among sampling plots. The NMDS ordination revealed a central cluster of plots characterized by the dominance of C. betulus, with a few plots showing greater compositional divergence. These findings highlight the relatively simplified structure but noticeable small-scale variability of tree communities in this peri-urban forest ecosystem.*

***Key words****: edge influence; peri-urban forest; Romania; species diversity; tree community.*

## INTRODUCTION

Forests located in the immediate proximity of urban areas play an increasingly important role in maintaining ecological balance and supporting the quality of life of urban populations (Livesley et al., 2016; Sestras et al., 2018). In the context of continuous urban expansion and land-use transformation, peri-urban forests represent essential components of green infrastructure, providing multiple ecological, environmental, and social benefits (La Rosa et al., 2018). These ecosystems contribute to biodiversity conservation, climate regulation, carbon sequestration, and recreational opportunities, while also serving as transitional landscapes between urban environments and more natural forest ecosystems (Berglihn & Gómez-Baggethun, 2021; Mitchell et al., 2022).

The ecological importance of peri-urban forests has become particularly evident in recent decades, as cities have expanded into surrounding natural landscapes. Urban growth often leads to increased fragmentation of forest habitats, changes in environmental conditions at forest edges, and intensified anthropogenic pressure on vegetation communities (Harper et al., 2005; Seto et al., 2012; Dobbs et al., 2018). As a result, forest stands located near cities frequently exhibit structural and compositional characteristics that differ from those observed in more remote forest ecosystems. Understanding these differences is therefore essential for developing sustainable strategies for the management and conservation of urban and peri-urban green spaces (Zipperer & Guntenspergen, 2009; Salbitano et al., 2016).

One of the key aspects influencing vegetation structure in forest ecosystems situated near urban environments is the so-called edge effect. Forest edges represent zones where environmental conditions may differ from those found in the interior of forest stands (Hladnik et al., 2020). These gradients can influence species composition, vegetation structure, and

ecological processes within forest ecosystems (Murcia, 1995). Changes in light availability, temperature, wind exposure, and soil moisture may alter species composition and influence the regeneration dynamics of tree communities (Chen et al., 1995). In addition, edges located near urban infrastructure may be subject to direct human disturbances, including recreational activities, informal trails, or historical forest management practices (Hellenbrand et al., 2025).

Previous studies have shown that forest edges may exhibit both increased species diversity and simplified structural patterns depending on local environmental conditions and the intensity of human influence (Franklin et al., 2021). In some cases, edge environments may facilitate the establishment of opportunistic or light-demanding species, leading to higher local diversity. In other situations, repeated disturbances and anthropogenic pressure may favor the dominance of a limited number of species that are better adapted to altered environmental conditions. Consequently, the spatial distribution of tree species in peri-urban forests often reflects a complex interaction between ecological processes and human activities (Kodym et al., 2025).

In this context, analyzing tree community structure in relation to edge influence across forest stands can provide valuable insights into the functioning of peri-urban forest ecosystems (Hladnik et al., 2020; Baker et al., 2025). Such analyses enable the identification of patterns in species composition, diversity, and structural characteristics that may be associated with environmental gradients generated by forest edge effects (Murcia, 1995; Harper et al., 2005). Moreover, understanding these patterns is important for evaluating the ecological resilience of forest stands located near urban areas and for informing management practices aimed at maintaining biodiversity and ecosystem functions (Sousa-Silva et al., 2023).

Urban and peri-urban forests are frequently influenced by adjacent land-use systems that generate spatial gradients in environmental conditions and vegetation structure (Dobbs et al., 2018). The Hoia Hill area illustrates such a context, where two contrasting functional zones coexist along an east–west axis. Cultural, recreational, and agricultural activities dominate the upper part of the hill, while the lower sector has progressively developed industrial and economic functions (Boancă et al., 2023).

The Hoia-Baciu Forest, situated on the western outskirts of Cluj-Napoca in northwestern Romania, represents one of the most well-known forested areas within the peri-urban landscape (Deac et al., 2013). Due to its proximity to urban infrastructure and recreational areas, this forest sector is exposed to various forms of anthropogenic influence (Boancă et al., 2023). At the same time, it provides important ecological functions as part of the green landscape surrounding the rapidly expanding metropolitan area (Escobedo et al., 2011). Despite its ecological and social relevance, relatively limited information is available regarding the spatial variability of tree community structure within this peri-urban forest ecosystem.

Assessing tree species composition and diversity within such environments is important for understanding how vegetation communities respond to spatial gradients and environmental pressures associated with urban proximity (Alvey, 2006; McDonnell & Hahs, 2008). In particular, investigating variation in species distribution in relation to edge influence may reveal patterns related to forest structure, species dominance, and local heterogeneity in vegetation composition.

Therefore, the aim of the present study was to analyze tree community structure and diversity patterns in relation to edge influence in a sector of the Hoia-Baciu peri-urban forest. Using a systematic sampling design based on circular plots distributed along several transects covering varying distances from the forest edge, the study evaluates species composition, tree density, and diversity indices in order to identify spatial patterns within the forest stand. The results contribute to a better understanding of vegetation structure in forest ecosystems situated at the interface between natural landscapes and urban environments and provide useful information for the ecological assessment of peri-urban forests.

## MATERIALS AND METHODS

### Study area

The study was conducted in a sector of the Hoia-Baciu Forest located in the immediate vicinity of

the city of Cluj-Napoca, in northwestern Romania. This forest represents an important peri-urban green area situated at the interface between the urban environment and surrounding rural landscapes. Due to its proximity to the metropolitan area, the forest is frequently used for recreational activities and is influenced by nearby infrastructure and urban expansion.

The analyzed forest stand is characterized by mixed deciduous vegetation typical of temperate forest ecosystems. However, as in many peri-urban forests, the vegetation structure reflects the cumulative effects of past management practices and ongoing anthropogenic influences (Sousa-Silva et al., 2023). As a result, the tree community composition is relatively simplified and dominated by a limited number of species.

The study area forms part of the broader green landscape surrounding the city and plays an important role in maintaining ecological connectivity, biodiversity, and environmental quality in the peri-urban zone. The forest is dominated by hornbeam (*C. betulus*) stands typical for temperate deciduous forests of the Transylvanian region.

**Sampling design**

Field data were collected using a systematic sampling design based on circular plots arranged along transects across the forest, covering varying distances from the forest edge.

A total of 20 circular sampling plots were established in the analyzed sector of the Hoia-Baciu peri-urban forest. The distance between transects was approximately 70 m, while the distance between plots within each transect was about 40 m. This sampling design allowed the assessment of spatial variability in tree community structure along transects established across the forest. The spatial layout of the study area and the distribution of sampling plots are presented in Figure 1.

**Data collection**

Within each sampling plot, all tree individuals were recorded and identified at species level. For the purpose of the present study, the analysis focused on the species composition and abundance of trees within each plot.

The number of individuals belonging to each species was counted in order to determine the structure of the tree community. These data allowed the calculation of several basic structural and diversity parameters at the plot level, including: total number of trees; species richness; relative dominance of the main species.




Figure 1. Location of the study area and spatial distribution of sampling plots in the Hoia-Baciu peri-urban forest near Cluj-Napoca, Romania

**Data analysis**

The structure and diversity of the tree community were analyzed at the level of individual sampling plots. Several ecological indicators were calculated based on species abundance data using standard indices widely applied in community ecology (Shannon, 1948; Simpson, 1949; Pielou, 1966).

Species richness (S) representing the number of tree species recorded in each sampling plot.

Tree density expressed as the number of trees per hectare, calculated by extrapolating the number of individuals recorded within the 500 m² plots.

Shannon diversity index (H′) which reflects both species richness and the relative abundance of species within the community:

$$H' = -\sum(p_i \ln p_i)$$

where $p_i$ represents the proportion of individuals belonging to species $i$.

Simpson diversity index (1–D) which measures the probability that two randomly selected individuals belong to different species:

$$1 - D = 1 - \sum p_i^2$$

Pielou evenness index (J) which expresses the degree to which individuals are evenly distributed among species:

$$J = \frac{H'}{lnS}$$

In addition, the relative dominance of the main species within each plot was calculated as the

percentage of individuals belonging to the most abundant species. To explore potential spatial patterns associated with variation in edge influence across the study area, species richness values were analyzed accordingly across the sampling plots. All diversity indices were calculated based on the abundance data recorded in the sampling plots.

Differences among transects for tree density, species richness, Shannon diversity index, and the relative dominance of *C. betulus* were further evaluated using the Kruskal-Wallis non-parametric test, considering the small sample size and the likely non-normal distribution of the analyzed variables. Statistical significance was assessed at $p < 0.05$.

## RESULTS AND DISCUSSIONS

The tree community recorded within the sampling plots was relatively simplified and strongly dominated by *C. betulus*. This species occurred in the majority of plots and represented the highest proportion of individuals in most cases. Other species such as *Q. petraea*, *A. campestre*, *S. nigra* and *P. avium* were recorded locally and contributed to the variation in species composition among plots (Figure 2).

The relative dominance of *C. betulus* varied across the study area, exceeding 80% in several plots and reaching complete dominance in some cases. This pattern indicates a structurally simplified community typical of forest stands located in peri-urban environments. The spatial variation in the relative dominance of *C. betulus* among the sampling plots is illustrated in Figure 3.

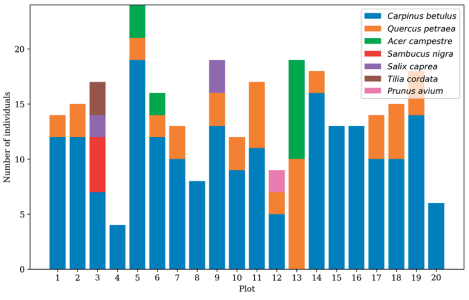



Figure 2. Tree species composition across sampling plots in the analyzed peri-urban forest stand. Bars represent the number of individuals belonging to each species in each sampling plot

### Structural characteristics of the sampling plots

The number of trees recorded within the sampling plots varied considerably across the study area. The lowest number of individuals was recorded in Plot 4 (three trees), while the highest values were observed in Plot 5 (21 trees) and Plot 19 (16 trees). When extrapolated to hectare level, tree density ranged between approximately 60 and 420 trees $ha^{-1}$.

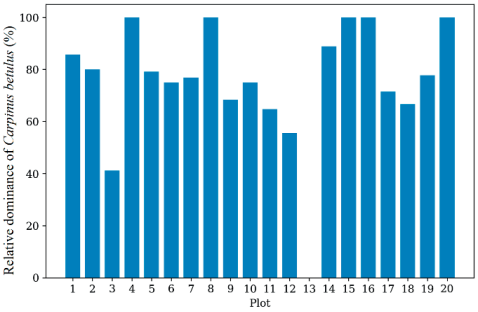



Figure 3. Relative dominance of *C. betulus* across the sampling plots in the analyzed peri-urban forest stand

Species richness showed relatively low values across the plots, ranging between one and four species per plot (Figure 4). Several plots, regardless of their position within the forest, contained only one species, indicating a high level of structural simplification. The structural characteristics of the sampling plots are summarized in Table 1.

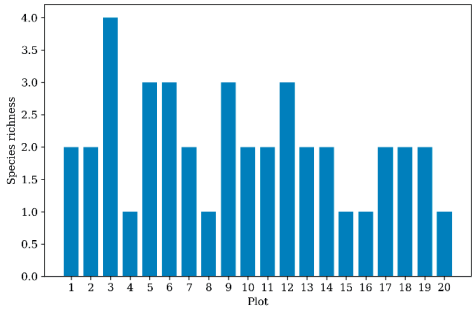



Figure 4. Species richness recorded in the sampling plots of the Hoia-Baciu peri-urban forest

Table 1. Structural characteristics of the sampling plots in the analyzed peri-urban forest stand

| Plot | Total trees | Tree density (trees ha$^{-1}$) | Species richness | Main species dominance (%) |
|---|---|---|---|---|
| 1 | 12 | 240 | 2 | 91.7 |
| 2 | 12 | 240 | 2 | 83.3 |
| 3 | 10 | 200 | 4 | 50.0 |
| 4 | 3 | 60 | 1 | 100.0 |
| 5 | 21 | 420 | 3 | 85.7 |
| 6 | 13 | 260 | 3 | 84.6 |
| 7 | 11 | 220 | 2 | 81.8 |
| 8 | 7 | 140 | 1 | 100.0 |
| 9 | 16 | 320 | 3 | 75.0 |
| 10 | 10 | 200 | 2 | 80.0 |
| 11 | 15 | 300 | 2 | 66.7 |
| 12 | 6 | 120 | 3 | 66.7 |
| 13 | 17 | 340 | 2 | 52.9 |
| 14 | 6 | 120 | 2 | 50.0 |
| 15 | 12 | 240 | 1 | 100.0 |
| 16 | 12 | 240 | 1 | 100.0 |
| 17 | 12 | 240 | 2 | 75.0 |
| 18 | 13 | 260 | 2 | 69.2 |
| 19 | 16 | 320 | 2 | 81.2 |
| 20 | 5 | 100 | 1 | 100.0 |

## Diversity patterns

Diversity indices calculated for each sampling plot indicate generally low to moderate levels of diversity across the analyzed forest sector. Shannon diversity index values ranged between 0 and 1.22 (Table 2). The highest diversity was observed in Plot 3, where four species were recorded and the distribution of individuals among species was relatively balanced.

Moderate diversity values were recorded in several plots, including Plot 9, Plot 11, Plot 12 and Plot 18. In contrast, plots dominated entirely by a single species showed Shannon index values equal to zero, reflecting the absence of species diversity. The spatial distribution of Shannon diversity values across the sampling plots is illustrated in Figure 5.

Table 2. Diversity indices calculated for the sampling plots

| Plot | Shannon index (H') | Simpson index (1–D) | Pielou evenness (J) |
|---|---|---|---|
| 1 | 0.29 | 0.15 | 0.41 |
| 2 | 0.45 | 0.28 | 0.65 |
| 3 | 1.22 | 0.66 | 0.88 |
| 4 | 0.00 | 0.00 | 0.00 |
| 5 | 0.50 | 0.25 | 0.46 |
| 6 | 0.54 | 0.27 | 0.49 |
| 7 | 0.47 | 0.30 | 0.68 |
| 8 | 0.00 | 0.00 | 0.00 |
| 9 | 0.74 | 0.41 | 0.67 |
| 10 | 0.50 | 0.32 | 0.72 |
| 11 | 0.64 | 0.44 | 0.92 |
| 12 | 0.87 | 0.50 | 0.79 |
| 13 | 0.69 | 0.50 | 1.00 |
| 14 | 0.69 | 0.50 | 1.00 |
| 15 | 0.00 | 0.00 | 0.00 |
| 16 | 0.00 | 0.00 | 0.00 |
| 17 | 0.56 | 0.38 | 0.81 |
| 18 | 0.62 | 0.43 | 0.89 |
| 19 | 0.48 | 0.30 | 0.70 |
| 20 | 0.00 | 0.00 | 0.00 |

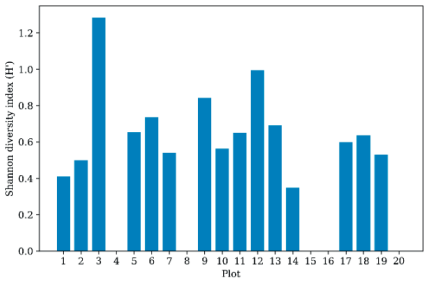



Figure 5. Shannon diversity index (H') calculated for the sampling plots

## Spatial variation in relation to edge influence

The analysis of species richness in relation to the distance from the forest edge revealed moderate spatial variability across the study area (Figure 6). Variation in species richness among plots suggests differences in exposure to forest edges across the study area.

To further explore differences in community composition among sampling plots, a non-metric multidimensional scaling (NMDS) ordination based on Bray-Curtis dissimilarity was performed (Figure 7).

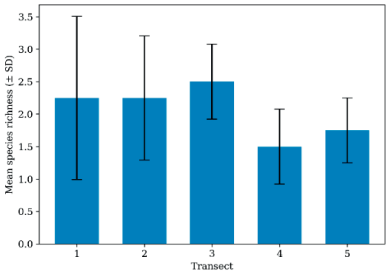



Figure 6. Mean species richness (± SD) across the five transects reflecting variation in edge influence in the Hoia-Baciu peri-urban forest

The NMDS ordination revealed a central cluster of plots dominated by *C. betulus*, while several plots showed greater compositional divergence, particularly Plot 13, which was characterized by the presence of *Q. petraea* and *A. campestre*.

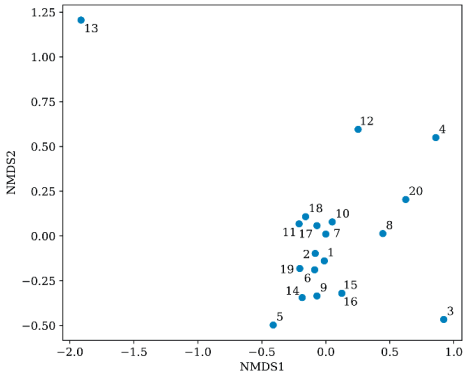



Figure 7. Non-metric multidimensional scaling (NMDS) ordination of tree community composition across sampling plots based on Bray-Curtis dissimilarity. Each point represents a sampling plot (1-20), and distances among points reflect differences in species composition

A summary of structural and diversity parameters at the transect level is presented in Table 3. Mean species richness ranged from 1.50 to 2.50 species per transect, while mean Shannon diversity values varied between 0.34 and 0.69. Mean tree density ranged from 185 to 260 trees ha$^{-1}$, and the relative dominance of *C. betulus* remained high across all transects, with values exceeding 70% in all cases.

Table 3. Summary of structural and diversity parameters across transects in relation to edge influence

| Transect | Mean tree density (trees ha$^{-1}$) | Mean species richness | Mean Shannon index |
|---|---|---|---|
| 1 | 185 | 2.25 | 0.49 |
| 2 | 260 | 2.25 | 0.38 |
| 3 | 235 | 2.50 | 0.69 |
| 4 | 210 | 1.50 | 0.34 |
| 5 | 230 | 1.75 | 0.42 |

These results indicate moderate variability among transects, without a consistent spatial pattern related to edge influence.

Differences among transects were further explored using the Kruskal-Wallis test (Table 4). No statistically significant differences were detected among transects for tree density, species richness, Shannon diversity index, or the relative dominance of *C. betulus* ($p > 0.05$ in all cases). Nevertheless, moderate variability was observed at the plot level, indicating small-scale heterogeneity within the peri-urban forest stand.

Table 4. Kruskal-Wallis test results for structural and diversity parameters across transects

| Variable | H statistic | p-value |
|---|---|---|
| Tree density | 1.484 | 0.829 $^{ns}$ |
| Species richness | 4.382 | 0.357 $^{ns}$ |
| Shannon diversity index | 3.969 | 0.410 $^{ns}$ |
| Relative dominance of *C. betulus* | 3.569 | 0.467 $^{ns}$ |

ns - not statistically significant differences among transects

**Simplified tree community structure in a peri-urban context**

From a landscape perspective, the Hoia-Baciu forest sector represents an important component of the peri-urban green infrastructure surrounding the city of Cluj-Napoca (Boancă et al., 2023). Such peri-urban forests may contribute to environmental buffering functions, including microclimatic regulation, dust and noise attenuation, and the mitigation of urban environmental pressures (Leca et al., 2023).

The results of this study indicate that the analyzed forest sector is characterized by a relatively simplified tree community structure, with a strong dominance of *C. betulus*. In most sampling plots, this species represented the majority of recorded individuals and in several cases it occurred as the only tree species present. Such patterns are commonly observed in forest stands that have been subjected to long-term anthropogenic influence or historical management interventions (Leca et al., 2023).

The occurrence of additional species such as *Q. petraea*, *A. campestre*, *P. avium*, and *S. nigra* was limited to a smaller number of plots and generally involved low numbers of individuals. As a consequence, species richness values remained relatively low across the study area, ranging from one to four species per sampling plot. Similar patterns of reduced tree species diversity have been reported in peri-urban forests where historical management practices and human pressure may influence stand composition and regeneration processes (Stamin & Cosmulescu, 2025).

**Spatial variability of diversity in relation to edge influence**

Although overall species richness was relatively low, the study revealed noticeable spatial variability in diversity among the sampling plots. Shannon diversity index values ranged from zero in monospecific plots to over 1.2 in the most heterogeneous plot. These differences indicate that local variations in stand structure and environmental conditions may influence the distribution of tree species within the forest.

Plots exhibiting higher diversity generally contained a more balanced distribution of individuals among species, whereas plots dominated by *C. betulus* showed considerably lower diversity values. Such patterns may reflect differences in microsite conditions, light availability, or past disturbance events that affected tree establishment and survival. The presence of localized areas with higher diversity suggests that even within relatively simplified forest stands, small-scale heterogeneity may contribute to maintaining a certain level of biodiversity (Harper et al., 2005).

**Influence of edge conditions and anthropogenic pressure**

The spatial arrangement of the sampling plots allowed the assessment of variation in community structure in relation to edge influence across the forest patch. Although the results did not reveal a strong linear relationship between distance from the forest edge and species richness, variability in community composition among plots suggests that edge-related processes operate in a spatially heterogeneous manner rather than along a single directional gradient (Murcia, 1995; Godefroid & Koedam, 2003; Harper et al., 2005).

Edge environments in peri-urban forests are often subject to multiple external influences, including changes in microclimatic conditions, increased light availability, and disturbances associated with nearby infrastructure or human activities (Franklin et al., 2021; Hellenbrand et al., 2025). These factors may create heterogeneous environmental conditions that facilitate the establishment of different species (Morgan et al., 2025). In contrast, plots less influenced by edge conditions tended to display more uniform species composition and stronger dominance of the main species (Hladnik et al., 2020).

Given the proximity of the studied forest sector to urban infrastructure and recreational areas, it is likely that anthropogenic factors have contributed to shaping the observed community structure (Hellenbrand et al., 2025). However, further studies integrating structural and microclimatic parameters would be required to better understand the mechanisms underlying these patterns (Morgan et al., 2025).

**Implications for peri-urban forest ecosystems**

Peri-urban forests represent important components of green infrastructure surrounding cities, providing ecological, environmental, and social benefits for urban populations (Mitchell et al., 2022; Kodym et al., 2025). The simplified tree community structure observed in the present study highlights the potential vulnerability of such ecosystems to disturbances and long-term anthropogenic pressure (Morgan et al., 2025).

Despite the relatively low species richness recorded in the analyzed plots, the presence of several accompanying species and the spatial heterogeneity observed across the study area suggest that these forest stands still retain ecological value. Maintaining and enhancing structural and compositional diversity in peri-urban forests may therefore represent an important objective for sustainable landscape management and biodiversity conservation in urbanized regions (Mitchell et al., 2022; Kodym et al., 2025; Morgan et al., 2025).

In the case of the Hoia-Baciu Forest located near Cluj-Napoca, the results underline the importance of monitoring vegetation structure and species composition in order to better understand how urban expansion and human activities influence forest ecosystems situated at the interface between natural and urban landscapes (Mitchell et al., 2022).

Although this study provides useful insights into tree community patterns along a peri-urban forest edge, a few methodological limitations should be acknowledged. The results may not be as applicable to other forest ecosystems because the study was carried out in a single peri-urban forest using a systematic sampling design. Furthermore, even though the study focused on tree community patterns and the forest edge, other environmental factors such as soil characteristics, light availability, and previous

management history, were not specifically evaluated and may also have influenced the observed patterns. Future research should include multiple peri-urban forests with contrasting edge characteristics, integrate additional environmental variables, and incorporate long-term monitoring to improve the understanding of edge effects on forest communities.

## CONCLUSIONS

The present study analyzed the structure and diversity of tree communities in a peri-urban sector of the Hoia-Baciu Forest located near Cluj-Napoca, Romania. The results indicate that the analyzed forest stand is characterized by a relatively simplified tree community structure, strongly dominated by *C. betulus*, while other species such as *Q. petraea*, *A. campestre*, *P. avium*, and *S. nigra* occur locally in lower proportions.

Species richness across the sampling plots was generally low, ranging between one and four species per plot, while diversity indices showed moderate spatial variability within the study area. The analysis of plots distributed across the forest revealed small-scale heterogeneity in community composition, although no strong linear trend in species richness with increasing distance from the forest edge was observed. The absence of statistically significant differences among transects suggests that, although moderate local variability exists, the edge influence does not generate a strong and consistent differentiation of the analyzed structural and diversity parameters at the spatial scale considered in this study.

These results suggest that local environmental conditions and anthropogenic influences may contribute to shaping the structure of tree communities in peri-urban forest ecosystems. Despite the relatively simplified species composition, the Hoia-Baciu Forest continues to represent an important component of the green landscape surrounding the city of Cluj-Napoca. Monitoring vegetation structure and diversity in such peri-urban forests is therefore essential for supporting sustainable landscape management and maintaining ecological functions in urbanizing regions.

## ACKNOWLEDGEMENTS

The research was carried out with the partial support of the Doctoral School of the University of Agricultural Sciences and Veterinary Medicine of Cluj-Napoca (USAMVCN) for I.-L.G.

## REFERENCES

Alvey, A. A. (2006). Promoting and preserving biodiversity in the urban forest. *Urban Forestry & Urban Greening, 5*(4), 195–201. https://doi.org/10.1016/j.ufug.2006.09.003

Baker, M., Yesilonis, I., Templeton, L., Shobe, B., Bos, J., Sonti, N.F., & Lautar, K. (2025). Distributed urban forest patch sampling detects edge effects in urban woodlands. *Ecosphere, 16*, e70236. https://doi.org/10.1002/ecs2.70236

Berglihn, E. C., & Gómez-Baggethun, E. (2021). Ecosystem services from urban forests: The case of Oslomarka, Norway. *Ecosystem Services*, 51, 101358. https://doi.org/10.1016/j.ecoser.2021.101358

Boancă, P. I., Oprică, A., Bodea, S., & Mărincean, A. (2023). Cover assessment, tree benefits report and landscape evaluation for reconstruction and expansion of the northern and northeastern vegetative barrier of the National Ethnographic Park "Romulus Vuia". *Agricultura*, 129–130(3–4). https://doi.org/10.15835/agr.v129i3-4.14751

Chen, J., Franklin, J. F., & Spies, T. A. (1995). Growing-season microclimatic gradients from clearcut edges into old-growth Douglas-fir forests. *Ecological Applications*, 5(1), 74–86. https://doi.org/10.2307/1942053

Deac, S. O., Irimuș, I. A., & Păcurar, B. N. (2013). The landscape morphology of Cluj-Napoca residential neighbourhoods. *Studia Universitatis Babeș-Bolyai, Geographia*, 58(2), 73–84.

Dobbs, C., Eleuterio, A. A., Amaya, J. D., Montoya, J., & Kendal, D. (2018). The benefits of urban and peri-urban forestry. *Unasylva*, 69(250), 22-29.

Escobedo, F. J., Kroeger, T., & Wagner, J. E. (2011). Urban forests and pollution mitigation: Analyzing ecosystem services and disservices. *Environmental Pollution, 159*(8–9), 2078–2087. https://doi.org/10.1016/j.envpol.2011.01.010

Franklin, C. M., Harper, K. A., & Clarke, M. J. (2021). Trends in studies of edge influence on vegetation at human-created and natural forest edges across time and space. *Canadian Journal of Forest Research*, 51(2), 274-282. https://doi.org/10.1139/cjfr-2020-0308

Godefroid, S., & Koedam, N. (2003). Distribution pattern of the flora in a peri-urban forest: An effect of the forest edge? *Landscape and Urban Planning*, 65(4), 169–185. https://doi.org/10.1016/S0169-2046(03)00013-6

Harper, K. A., Macdonald, S. E., Burton, P. J., Chen, J., Brosofske, K. D., Saunders, S. C., Euskirchen, E. S., Roberts, D., Jaiteh, M. S., & Esseen, P. A. (2005). Edge influence on forest structure and composition in

fragmented landscapes. *Conservation Biology*, 19(3), 768–782. https://doi.org/10.1111/j.1523-1739.2005.00045.x

Hellenbrand, J. P., Kelly-Voicu, P., Bowers, J. T., & Reinmann, A. B. (2025). Edge and the city: Evaluating the role of edge effects on urban forest structure and tree species composition. *Urban Forestry & Urban Greening*, 107, 128745. https://doi.org/10.1016/j.ufug.2025.128745

Hladnik, D., Kobler, A., & Pirnat, J. (2020). Evaluation of Forest Edge Structure and Stability in Peri-Urban Forests. *Forests*, 11(3), 338. https://doi.org/10.3390/f11030338

Kodym, A., Lapin, K., Sanyal, D. (2025). *Ecological Connectivity in Urban and Semi-Urban Forests.* In: Lapin, K., Oettel, J., Braun, M., Konrad, H. (eds) Ecological Connectivity of Forest Ecosystems. Springer, Cham. https://doi.org/10.1007/978-3-031-82206-3_18

La Rosa, D., Geneletti, D., Spyra, M., Albert, C., Fürst, C. (2018). *Sustainable Planning for Peri-urban Landscapes*. In: Perera, A., Peterson, U., Pastur, G., Iverson, L. (eds) Ecosystem Services from Forest Landscapes. Springer, Cham. https://doi.org/10.1007/978-3-319-74515-2_5

Leca, Ș., Popa, I., Chivulescu, Ș., Popa, A., Pitar, D., Dobre, A.-C., Pascu, I.-S., Apostol, B., & Badea, O. (2023). Structure and diversity in a periurban forest of Bucharest, Romania. *Annals of Forest Research*, 66(1), 139–153. https://doi.org/10.15287/afr.2023.3011

Livesley, S. J., McPherson, E. G., & Calfapietra, C. (2016). The urban forest and ecosystem services: Impacts on urban water, heat, and pollution cycles at the tree, street, and city scale. *Journal of Environmental Quality*, 45(1), 119–124. https://doi.org/10.2134/jeq2015.11.0567

McDonnell, M. J., & Hahs, A. K. (2008). The use of gradient analysis studies in advancing our understanding of the ecology of urbanizing landscapes: Current status and future directions. *Landscape Ecology, 23*(10), 1143–1155. https://doi.org/10.1007/s10980-008-9253-4

Mitchell, M. G. E., Devisscher, T., Olivero-Lora, S., et al. (2022). Strong relationships between urbanization, landscape structure, and ecosystem service multifunctionality in urban forest fragments. *Landscape and Urban Planning*, 228, 104548. https://doi.org/10.1016/j.landurbplan.2022.104548

Morgan, R. B., & Tommaso, J. (2025). A unifying framework for understanding how edge effects reshape the structure, composition and function of forests. *New Phytologist*, 248(2), 529–541. https://doi.org/10.1111/nph.70457

Murcia, C. (1995). Edge effects in fragmented forests: Implications for conservation. *Trends in Ecology & Evolution*, 10(2), 58–62. https://doi.org/10.1016/S0169-5347(00)88977-6

Pielou, E. C. (1966). The measurement of diversity in different types of biological collections. *Journal of Theoretical Biology*, 13, 131–144. https://doi.org/10.1016/0022-5193(66)90013-0

Salbitano, F., Borelli, S., Conigliaro, M. & Chen, Y. (2016). *Guidelines on urban and peri-urban forestry. FAO Forestry Paper No. 178*. Rome, Food and Agriculture Organization of the United Nations.

Sestras, P., Bondrea, M. V., Cetean, H., Sălăgean, T., Bilaşco, Ș., Naș, S., Spalevic, V., Fountas, S., & Cîmpeanu, S. M. (2018). Ameliorative, Ecological and Landscape Roles of Făget Forest, Cluj-Napoca, Romania, and Possibilities of Avoiding Risks Based on GIS Landslide Susceptibility Map. *Notulae Botanicae Horti Agrobotanici Cluj-Napoca,* 46(1), 292–300. https://doi.org/10.15835/nbha46110866

Seto, K. C., Güneralp, B., & Hutyra, L. R. (2012). Global forecasts of urban expansion to 2030 and direct impacts on biodiversity and carbon pools. *Proceedings of the National Academy of Sciences*, 109(40), 16083–16088. https://doi.org/10.1073/pnas.1211658109

Shannon, C. E. (1948). A mathematical theory of communication. Bell System Technical Journal, 27(3,4), 379–423, 623–656. https://doi.org/10.1002/j.1538-7305.1948.tb01338.x

Simpson, E. H. (1949). Measurement of diversity. Nature, 163, 688. https://doi.org/10.1038/163688a0

Sousa-Silva, R., Lambry, T., Cameron, E., Belluau, M., & Paquette, A. (2023). Urban forests – Different ownership translates to greater diversity of trees. Urban Forestry & Urban Greening, 88, 128084. https://doi.org/10.1016/j.ufug.2023.128084

Stamin, F., & Cosmulescu, S. (2025). Comparative Assessment of Biodiversity and Ecological Indicators in Three Forest Ecosystems of Southern Romania. Diversity, 17, 277. https://doi.org/10.3390/d17040277

Zipperer, W. C., & Guntenspergen, G. R. (2009). Vegetation composition and structure of forest patches along urban–rural gradients. In: Ecology of Cities and Towns. Cambridge University Press. https://doi.org/10.1017/cbo9780511609763.018

Scientific Papers. Series E. Land Reclamation, Earth Observation & Surveying, Environmental Engineering. Vol. XV, 2026
Print ISSN 2285-6064, CD-ROM ISSN 2285-6072, Online ISSN 2393-5138, ISSN-L 2285-6064

# STUDY OF THE DYNAMICS OF SOME WATER QUALITY PARAMETERS IN THE PRUT RIVER AREA DURING 2014-2023

**Dinu GÎRNEȚ[1], Lorena DELEANU[1, 5], Gabriel MURARIU[2, 3], Laura DANILESCU[4], Romana DRASOVEAN[2]**

[1]Doctoral School of Fundamental and Engineering Sciences, "Dunărea de Jos" University of Galati, 111 Domnească Street, Galaţi, Romania
[2]Chemistry, Physics, and Environment Department, Faculty of Sciences and Environment, "Dunărea de Jos" University of Galaţi, 47 Domnească Street, 800008 Galaţi, Romania
[3]Rexdan Research Infrastructure, "Dunărea de Jos" University of Galati, Galati, Romania
[4]Faculty of Automation, Computer Sciences, Electronics and Electrical Engineering, "Dunărea de Jos" University Galati, 111 Domneasca Street, 800201 Galati, Romania
[5]Technical Sciences Academy of Romania, 26 Dacia Blvd, 010413, District 1, Bucharest, Romania

Corresponding author email: gabriel.murariu@ugal.ro

***Abstract***

*The Prut River area represents an area of maximum importance, considering its international character and RAMSAR-type areas. In this study, we present the statistical analysis of the measurements carried out on the water quality parameters in the Prut River area, covering a period of 10 years. In this way, we were able to establish the trend of evolution of temperature, pH, turbidity, etc. and predictions can be made in this way. The methods used were ANOVA and especially multivariate analysis procedures. The conclusions that emerge are of great importance, especially for the evaluation of the protected area of Lake Beleu and the lower Prut floodplain area.*

***Key words:*** *ANOVA, multivariate methods, statistical methods, water quality parameters.*

## INTRODUCTION

In recent years, considering climate change, the monitoring and protection of water bodies have become extremely important topics (Banescu et al., 2020). In this context, the European Union has issued several important directives aimed at mitigating the threats and pressures exerted by anthropogenic activities on rivers and other categories of surface waters (Burada et al., 2016).
In this framework, the study of pollution factors in Eastern Europe represents a topic of major importance. The present study provides an investigation conducted over a 10-year period, between 2014 and 2023, based on measurements of monitored parameters in the Republic of Moldova, focusing on the water quality of the Prut River (Cordeli et al., 2023). The applied study methods are commonly used in the scientific literature, with emphasis on assessing the evolution trends of parameters considered essential for objectively describing the level of pollution (Resz et al., 2023).
The aim of this study is to investigate the evolution of water quality parameters in the Prut River, in the Cahul-Oancea sector, using a 10-year dataset covering the period 2014-2023.

## MATERIALS AND METHODS

The statistical analysis of the dataset was carried out following an algorithm frequently used in the literature: correlations between the sets of parameters were evaluated for each individual year, and then procedures based on Principal Component Analysis (PCA) were applied (Mocanu et al., 2021).
Principal Component Analysis (PCA) is a multivariate statistical method used to reduce data dimensionality and to identify patterns and correlations among variables.
In the final stage, the strongest correlations between the variables describing water quality - i.e., pH, alkalinity, and temperature, which shows a clear evolutionwere presented in the form of response surfaces (Popa et al., 2018).

The aim of this study is to highlight the evolution of water quality parameters in the Cahul area, Republic of Moldova. Correlations between the parameters were evaluated for each year of study. Table 1 presents the 12 physical parameters that were measured daily. Figure 1 shows the location of the monitoring point.




Figure 1. Map of Prut River

Table 1. Parameters monitored in the Cahul monitoring network

| Parameter | Measure unit | Evaluation |
|---|---|---|
| Temperature | [°C] | Daily averaged |
| Transparency | [cm] | Daily averaged |
| Colour | [degrees HU - Hazen Units] | Daily averaged |
| Turbidity | [mg/dm3] | Daily averaged |
| pH | pH unit | Daily averaged |
| Ammonium | [mg/dm3] | Daily averaged |
| Nitrites | [mg/dm3] | Daily averaged |
| Nitrates | [mg/dm3] | Daily averaged |
| Oxidability | [mg/dm3] | Daily averaged |
| Chlorides | [mg/dm3] | Daily averaged |
| Suspended matter | [mg/dm3] | Daily averaged |
| Alkalinity | [mg/dm3] | Daily averaged |

## RESULTS AND DISCUSSIONS

In this section, we present the results of the statistical analysis and, respectively, the results of the numerical simulations.

Obviously, the first step was to investigate the correlations between the measured physical parameters for the dataset corresponding to the years 2014–2023.

Subsequently, the PCA method was applied to each annual experimental dataset. Thus, for the year 2014, the obtained diagram is presented in Figure 2.

For the year 2014, the most significant correlations were identified between temperature and transparency (correlation= −0.8348, $p$=0.001), temperature and turbidity (correlation =0.7733, $p$=0.001), temperature and chlorides (correlation= −0.8607, $p$= 0.001), temperature and alkalinity (correlation = −0.7445, $p$=0.001), and temperature and nitrates (correlation=−0.7806, $p$= 0.001).

For the dataset corresponding to the year 2015, the most significant correlations were identified between temperature and chlorides (correlation =−0.9068, $p$=0.001), transparency and suspended matter (correlation= −0.7051, $p$=0.001), turbidity and suspended matter (correlation= 0.9998, $p$=0.001), as well as between temperature and chlorides (correlation= −0.9068, $p$=0.001) and temperature and alkalinity (correlation = −0.8840, $p$=0.001) and is a significant difference is noted between the considered data (Table 2).

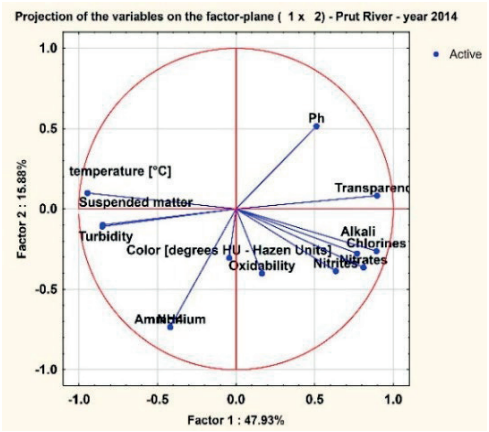



Figure 2. PCA diagram for 2014 database study case

Thus, in Figure 2 it can be observed that the first principal component, which explains the variance of the dataset, includes temperature, transparency, turbidity, pH, nitrites, nitrates, oxidability, chlorides, suspended matter, and alkalinity. In Figure 3, the PCA diagram for the dataset corresponding to the year 2015 is presented. The first principal component includes the following parameters: temperature [°C], colour [degrees HU – Hazen Units], pH, as well as nitrates, oxidability, chlorides, and alkalinity.

In Table 2 are presented the t-test results for average temperature. Many insignificant differences are observed.

Table 2. Results of t-test values for temperature

| Group 1 vs. Group 2 | Mean Group 1 | Mean Group 2 | t-value | *p* |
|---|---|---|---|---|
| t[°C] 2014 vs. t[°C] 2015 | 13.026 | 13.317 | -0.37 | 0.706 |
| t[°C] 2015 vs. t[°C] 2016 | 13.317 | 13.767 | -0.56 | 0.576 |
| t[°C] 2016 vs. t[°C] 2017 | 13.767 | 12.454 | 1.711 | 0.088 |
| t[°C] 2017 vs. t[°C] 2018 | 12.454 | 12.952 | -0.65 | 0.518 |
| t[°C] 2018 vs. t[°C] 2019 | 12.952 | 12.219 | 0.967 | 0.334 |
| t[°C] 2019 vs. t[°C] 2020 | **12.219** | **13.429** | **-2.01** | **0.045** |
| t[°C] 2020 vs. t[°C] 2021 | **13.429** | **12.227** | **2.231** | **0.026** |
| t[°C] 2021 vs. t[°C] 2022 | 12.227 | 13.086 | -1.32 | 0.1850 |
| t[°C] 2022 vs. t[°C] 2023 | 13.086 | 12.9128 | 0.237 | 0.813 |

In the same manner as Figure 2, were considered the PCA results for year 2015 (Figure 3), 2016 (Figure 4) and 2017 (Figure 5). Could be easily observed significand differences by comparing year 2105 (Figure 3), and year 2016 (Figure 4), especially for Factor 2. The PCA diagrams show the main groups operating during the studied period. Significant changes are observed from one year to another (Figure 5, Figure 6).

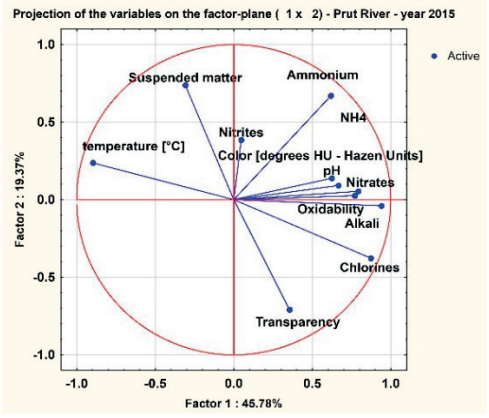



Figure 3. PCA diagram for 2015 database study case

For the dataset corresponding to the year 2018, the most significant correlations are those between pH and temperature (correlation = −0.7156, $p$ = 0.001), as well as between temperature and suspended matter (correlation = 0.76056, $p$ = 0.001) and temperature and alkalinity (correlation = −0.7856, $p$ = 0.001).

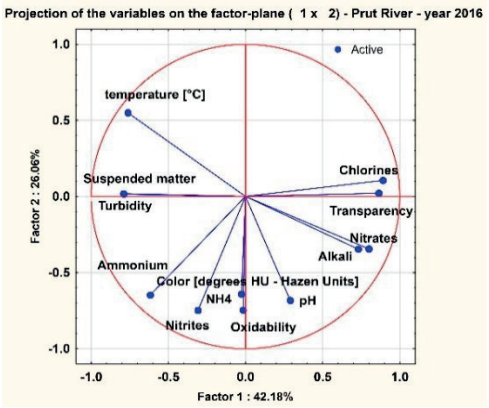



Figure 4. PCA diagram for 2016 database study case

Thus, PCA diagrams show the main group F1 operating during the studied period i.e. Suspended matter, Turbidity, Chorines, Nitrates (Figure 4). By comparing year 2016 and 2017, significant changes are observed from year to year (Figure 5, Figure 6). For example, Transparency became to F2 factor.

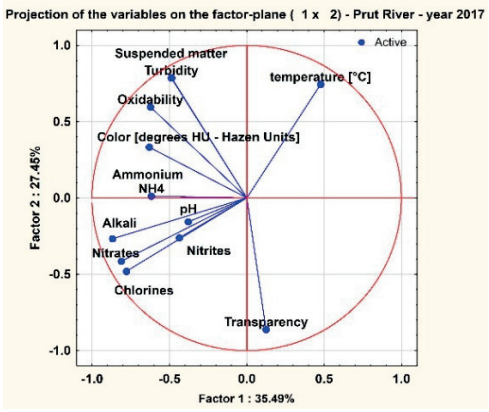



Figure 5. PCA diagram for 2017 database study case

For the dataset corresponding to the year 2018 (Figure 6) and 2019 (Figure 7), the following relationships can be identified: temperature and transparency (correlation = −0.7047, $p$ = 0.001), temperature and turbidity (correlation = 0.7599, $p$ = 0.001), temperature and chlorides (correlation = −0.7259, $p$ = 0.001), and respectively temperature and alkalinity (correlation = −0.7260, $p$ = 0.001). The same

relationships were also observed for the datasets corresponding to the years 2020–2023.

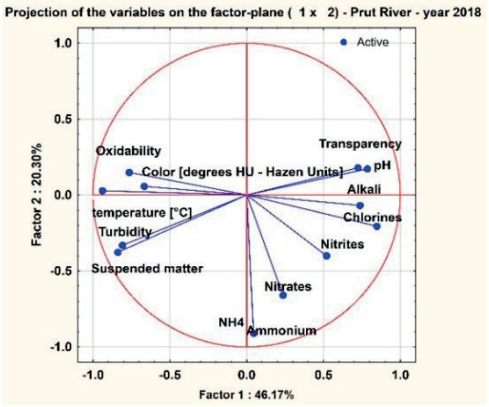



Figure 6. PCA diagram for 2018 database study case

In Table 3 are presented the t-test results for average pH values. Many significant differences are observed – the bold marked records.

Table 3. Results of t-test values for pH

| Group 1 vs. Group 2 | Mean Group 1 | Mean Group 2 | t-value | *p* |
|---|---|---|---|---|
| pH 2014 vs. pH 2015 | **8.064** | **8.189** | **-11.59** | **0.000** |
| pH 2015 vs. pH 2016 | **8.189** | **8.035** | **12.94** | **0.000** |
| pH 2016 vs. pH 2017 | **8.035** | **8.068** | **-2.89** | **0.004** |
| pH 2017 vs. pH 2018 | 8.068 | 8.046 | 1.70 | 0.094 |
| pH 2018 vs. pH 2019 | **8.046** | **8.382** | **-13.89** | **0.000** |
| pH 2019 vs. pH 2020 | **8.382** | **8.236** | **6.63** | **0.000** |
| pH 2020 vs. pH 2021 | **8.236** | **8.323** | **-6.93** | **0.000** |
| pH 2021 vs. pH 2022 | **8.323** | **8.608** | **-25.73** | **0.000** |
| pH 2022 vs. pH 2023 | **8.608** | **8.327** | **16.79** | **0.000** |

In Table 4 are presented the t-test results for average $NO_2$ values. Many insignificant differences are observed - the bold marked records.

For the dataset corresponding to the year 2020 (Figure 8) and 2021 (Figure 9), the following relationships can be identified: temperature and Ammonium (correlation = +0.787, $p$ = 0.001), temperature and Oxidability (correlation = 0.7699, $p$ = 0.001), temperature and chlorides (correlation = −0.079, $p$ = 0.001), and respectively temperature and alkalinity (correlation = −0.8260, $p$ = 0.001) - Figure 9.

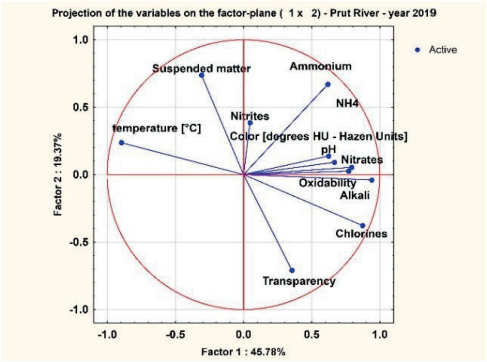



Figure 7. PCA diagram for 2019 database study case

Table 4. Results of t-test values for Nitrites

| Group 1 vs. Group 2 | Mean Group 1 | Mean Group 2 | t-value | *p* |
|---|---|---|---|---|
| $NO_2$ 2014 vs. $NO_2$ 2015 | **0.019** | **0.027** | **-3.30** | **0.019** |
| $NO_2$ 2015 vs. $NO_2$ 2016 | **0.027** | **0.033** | **-2.22** | **0.027** |
| $NO_2$ 2016 vs. $NO_2$ 2017 | **0.033** | **0.022** | **5.326** | **0.033** |
| $NO_2$ 2017 vs. $NO_2$ 2018 | **0.022** | **0.015** | **4.95** | **0.022** |
| $NO_2$ 2018 vs. $NO_2$ 2019 | **0.015** | **0.025** | **-10.43** | **0.015** |
| $NO_2$ 2019 vs. $NO_2$ 2020 | **0.025** | **0.018** | **17.04** | **0.025** |
| $NO_2$ 2020 vs. $NO_2$ 2021 | 0.012 | 0.031 | -7.68 | 0.0118 |
| $NO_2$ 2021 vs. $NO_2$ 2022 | 0.031 | 0.025 | 2.12 | 0.031 |
| $NO_2$ 2022 vs. $NO_2$ 2023 | 0.019 | 0.027 | -3.30 | 0.019 |

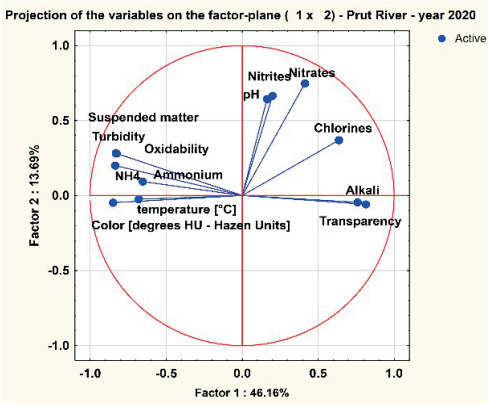



Figure 8. PCA diagram for 2020 database study case

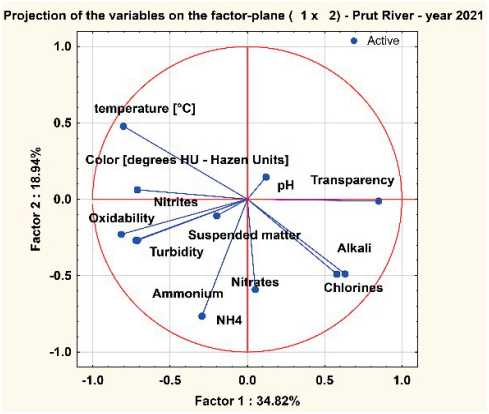



Figure 9. PCA diagram for 2021 database study case

In Table 5 are presented the t-test results for Nitrates average values. Many insignificant differences are observed – the bold marked records.

As is well known, in the case of nitrates, the concentration increases proportionally with agricultural and urban pollution; the concentration of chlorides increases proportionally with mineralization and agricultural contamination. On the other hand, oxidability measures the amount of oxidizable organic matter, while alkalinity is correlated with the salt content. In this sense, this first principal component has a general chemical character.

Table 5. Results of t-test values for Nitrates

| Group 1 vs. Group 2 | Mean Group 1 | Mean Group 2 | t-value | *p* |
|---|---|---|---|---|
| 2014 $NO_3$ vs. $NO_3$ 2015 | **7.279** | **5.233** | **9.578** | **0.000** |
| $NO_3$ 2015 vs. $NO_3$ 2016 | **5.233** | **4.504** | **3.430** | **0.001** |
| $NO_3$ 2016 vs. $NO_3$ 2017 | 4.504 | 4.614 | -0.594 | 0.553 |
| $NO_3$ 2017 vs. $NO_3$ 2018 | **4.802** | **5.080** | **-2.40** | **0.016** |
| $NO_3$ 2018 vs. $NO_3$ 2019 | **5.080** | **4.138** | **8.82** | **0.000** |
| $NO_3$ 2019 vs. $NO_3$ 2020 | **4.138** | **5.866** | **-16.0** | **0.000** |
| $NO_3$ 2020 vs. $NO_3$ 2021 | **5.866** | **5.096** | **5.897** | **0.000** |
| $NO_3$ 2021 vs. $NO_3$ 2022 | **5.096** | **4.267** | **7.363** | **0.000** |
| $NO_3$ 2022 vs. $NO_3$ 2023 | **7.279** | **5.233** | **9.578** | **0.000** |

The second principal component includes parameters such as $NH_4$, transparency, ammonium, and suspended matter. PC2 can be interpreted as the factor that evaluates the degree of organic pollution and the content of suspended particles.

Last but not least, significant differences are observed between the PCA diagrams corresponding to the years 2022 (Figure 10) and 2023 (Figure 11) respectively - for example: Nitrites are in Factor 1 in 2022 and then their contribution is added to Factor 2 in 2023.

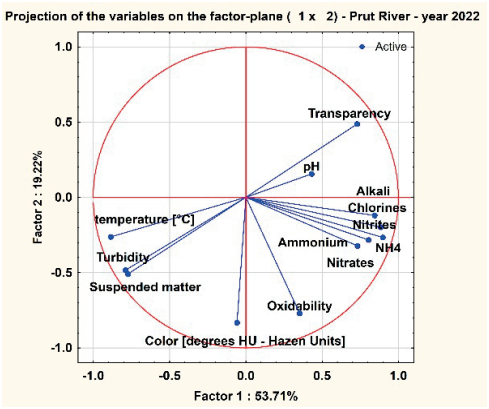



Figure 10. PCA diagram for 2022 database study case

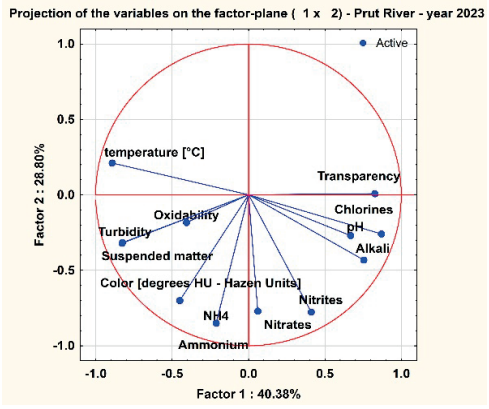



Figure 11. PCA diagram for 2023 database study case

In a short conclusion there are severe modification in these dynamics: in Figure 6, the two groups exhibit a switching, which means that the two processes associated with these groups have changed their relative importance in an inversely proportional manner.

Figure 12 presents the response surface for the dependence of pH on temperature and alkalinity for the dataset corresponding to the year 2014. The obtained surface shows a decreasing dependence of pH values on temperature (a fact also reported in the literature). What is interesting, considering that alkalinity determines how much pH can change when the equilibrium is altered, is that in this case the slope of the pH dependence on alkalinity is small (Figure 12).

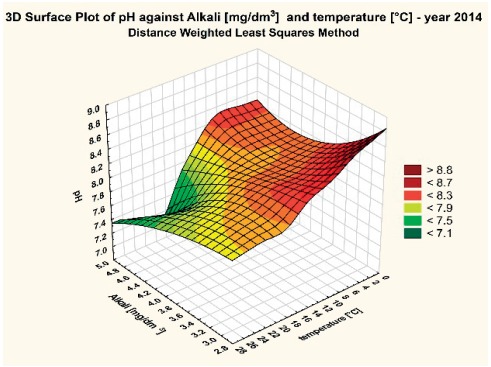



Figure 12. Surface plot pH against temperature and alkalinity for 2014 database study case

Figure 13 presents the response surface for the dependence of pH on temperature and alkalinity for the dataset corresponding to the year 2015. The obtained surface shows a completely different dependence of pH on temperature and alkalinity. However, it can be observed that in this case there is a stable dynamic equilibrium. Alkalinity determines a proportional increase in pH, which is contrary to the previous case.

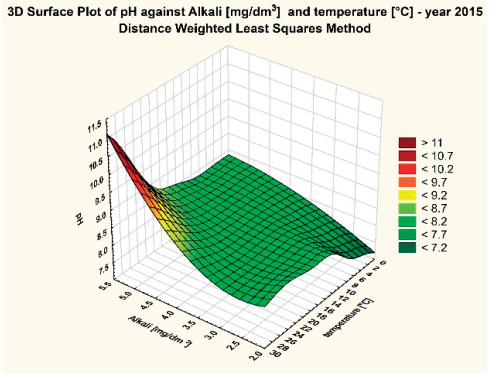



Figure 13. Surface plot pH against temperature and alkalinity for 2015 database study case

Figure 14 presents the response surface for the dependence of pH on temperature and alkalinity for the dataset corresponding to the year 2016. In this case, the surface is characteristic of an unstable dynamic equilibrium. Alkalinity determines a proportional decrease in pH, similar to the situation observed in 2014.

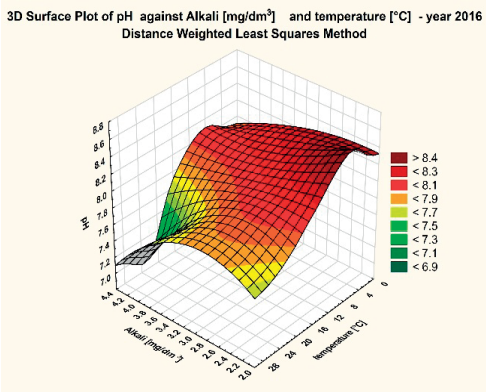



Figure 14. Surface plot pH against temperature and alkalinity for 2016 database study case

Figures 15 and 16 present the response surfaces for the dependence of pH on temperature and alkalinity for the datasets corresponding to the years 2017 and 2018.

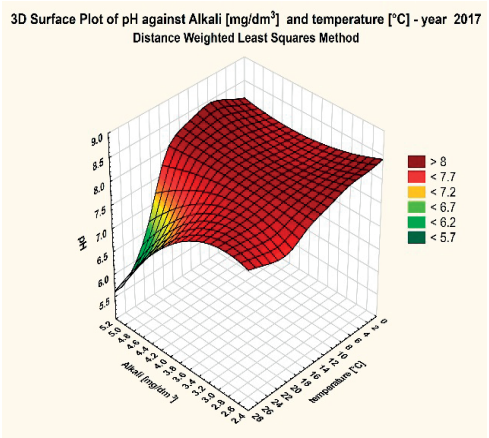



Figure 15. Surface plot pH against temperature and alkalinity for 2017 database study case

In these cases, as well, the surfaces are characteristic of an unstable dynamic equilibrium. Alkalinity determines a decrease in pH, similar to the situation observed in 2014.

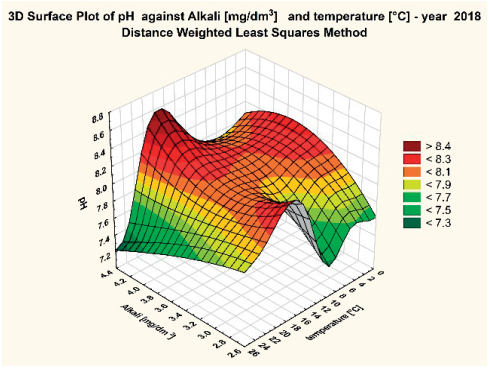



Figure 16. Surface plot pH against temperature and alkalinity for 2018 database study case

Figures 17 and 18 present the response surfaces for the dependence of pH on temperature and alkalinity for the datasets corresponding to the years 2019 (Figure 17) and 2020 (Figure 18).

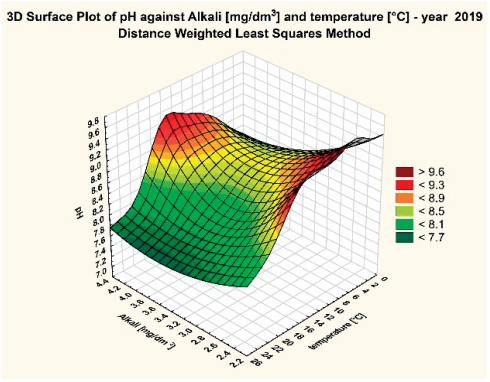



Figure 17. Surface plot pH against temperature and alkalinity for 2019 database study case

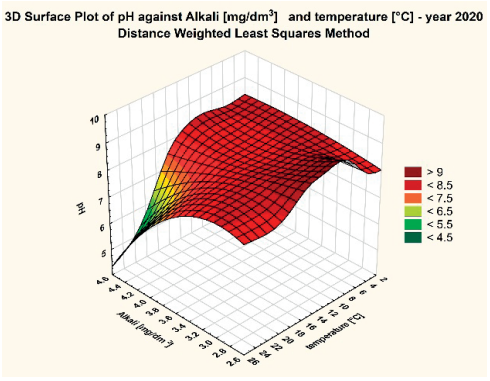



Figure 18. Surface plot pH against temperature and alkalinity for 2020 database study case

In the period 2021 - 2023, a dramatic change in the dependence of pH on the concentration of alkane as a function of temperature is observed (Figure 19, Figure 20 and Figure 21).

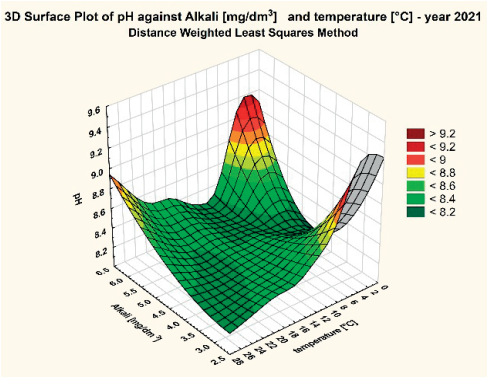



Figure 19. Surface plot pH against temperature and alkalinity for 2021 database study case

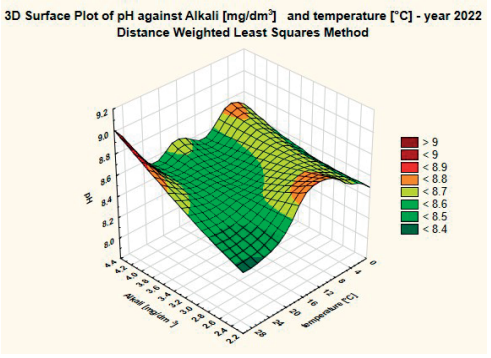



Figure 20. Surface plot pH against temperature and alkalinity for 2022 database study case

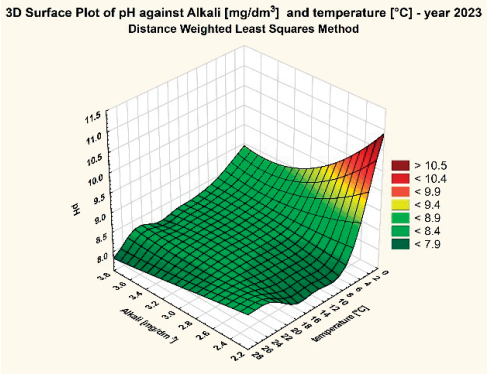



Figure 21. Surface plot pH against temperature and alkalinity for 2023 database study case

The present study aims to integrate a series of investigations conducted in the Prut River area (Dumitran, 2011). Many previous works have addressed heavy metal pollution (Matache et al., 2018) or the Water Quality Index (WQI) for this river (Duca et al., 2019). Furthermore, studies objectively describing the primary pollutants in the region where the river forms a natural border must also be considered (Teodosiu et al., 2009; Hrytsku & Hrytsku-Andriyesh, 2016). Naturally, research has also been conducted on the dynamics and interrelationships of key pollutants - such as NO3-N and NH4-N (Timofti et al., n.d.) - as well as on the environmental impacts of precipitation and temperature fluctuations (Corobov et al., 2021; Sava & Marusic, 2022).

In this context, we analyzed a 10-year period using a method capable of consistently addressing the entire dataset. The measured values correlate with those recorded for NO3-N, NO2-N, and NH4-N, generally aligning with observed trends regarding spatial variability and the gradient of this variability along the river's course (Neamtu et al., 2021). However, the present study clearly highlights significant differences between annual mean values, indicating that the processes specific to this natural aquatic system are undergoing changes. While previous studies focused on shorter timeframes - such as the five-year period from 2015 to 2019 (Neamtu et al., 2021; Duca et al., 2019) or even shorter intervals (Dumitran, 2011) - our study, utilizing a standardized dataset spanning a longer period, clearly revealed the existence of significant variations. It is also worth noting the strong correlation between N-NO2, N-NO3, and NH4, suggesting an underlying mechanism driving this relationship - a phenomenon previously observed using complementary methods (Timofti et al., n.d.). A particularly interesting finding emerges from the PCA analysis: the factors explaining the dataset's variability shift in relative importance over time. Specifically, during the 2014-2016 period, the primary factor (F1) encompasses turbidity, suspended matter, transparency, temperature, alkalinity, and chlorides; this represents a mixed physicochemical determinant - dominated by turbidity and suspended particles but also influenced by mineralization (alkalinity and chlorides) and temperature effects on these processes. Meanwhile, the secondary factor (F2) -comprising oxidability, nitrates, nitrites, ammonium, and pH - acts as a biochemical factor reflecting nitrogen transformations and organic matter degradation, essentially serving as a redox/organic and nitrogenous pollution factor. Starting in 2017, an interesting phenomenon was observed: the relative weights of the two previously identified factors shifted. This indicates that the biochemical factor - associated with nitrogen transformations and organic matter degradation - gained significance regarding data set variability, whereas the mixed physicochemical factor showed a stronger correlation along the Oy axis.

In the subsequent period (2018-2020), factors F1 and F2 reverted to their initial weightings; the mixed physicochemical factor became the dominant driver, contributing 45-46% to the overall variability, while factor F2 played a much smaller role, contributing 13-20%.

Finally, it is worth noting that between 2021 and 2023, the relative weights of the two main factors shifted once again. This periodic fluctuation reinforces a concept previously highlighted in the literature: the existence of two fundamental mechanisms explaining these correlations - pollution of industrial/anthropogenic origin and pollution resulting from natural and agricultural processes. Basing on the response surfaces shown in Figures 16, 18 and mainly on figures 19 and 20 - which represent stable equilibrium surfaces - we can conclude that the system is undergoing a "time-dependent oscillatory evolution," characterized by shifting contributions from organic and nitrogenous pollutants.

## CONCLUSIONS

The statistical analysis of the physicochemical parameters of the Prut River water in the Cahul sector for the period 2014-2023 highlights a pronounced thermal stability, concomitant with significant variations in nitrogen compounds and pH, indicating a high sensitivity of the aquatic system to anthropogenic pressures and regional biogeochemical dynamics. The average annual temperature did not show significant differences except in the period 2019-2021, which confirms that the thermal regime of the river is predominantly controlled by climatic factors and less by local influences.

In contrast, pH recorded statistically significant variations over almost the entire analysed period, with a single point exception (2017-2017), suggesting continuous changes in the processes of mineralization, photosynthesis and nutrient loading. The annual variability of nitrite concentrations (2014-2020) and the significant variations of nitrates in all analysed years indicate an unstable regime of nitrogen compounds, compatible with fluctuating nutrient inputs from agricultural activities, hydrological processes and microbial transformations.

Overall, the results show that, although the physical parameters of the water remain relatively constant, the chemical parameters relevant for the assessment of eutrophication show a pronounced dynamic, which reflects an ecosystem in a fragile balance, influenced by both natural conditions and anthropogenic pressures. These findings highlight the need for continuous monitoring and implementation of nutrient source management measures to maintain the ecological status of the lower Prut River. Dramatic changes are observed regarding the internal processes of the studied hydrological system.

## ACKNOWLEDGEMENTS

The work of Gabriel Murariu was supported by the internal research grant entitled “Internal research grant in the field of Environmental Engineering regarding the study of the distribution of polluting factors in the South-Eastern area of Europe”, financing contract no. 14886 / 11.05.2022, “Dunărea de Jos” University of Galaţi.

## REFERENCES

Banescu, A., Arseni, M., Georgescu, L.P., Rusu, E., & Iticescu, C. (2020). Evaluation of Different Simulation Methods for Analyzing Flood Scenarios in the Danube Delta. *Applied Sciences*, 10(23), 8327. https://doi.org/10.3390/app10238327

Burada, A., Teodorof, L., Ionascu, A., Topa, M. C., & Georgescu, L.P. (2016). Temporal Trends and Evolution of Heavy Metals Concentrations in Somova–Parches Aquatic Complex – Last Area of the Danube Floodplain. *Journal of Environmental Protection and Ecology* 17(3), 864–873.

Cordeli, A. N., Oprea, L., Crețu, M., Dediu, L., Coadă, M. T., & Mînzală, D.-N. (2023). Bioaccumulation of Metals in Some Fish Species from the Romanian Danube River: A Review. *Fishes*, 8(8), 387. https://doi.org/10.3390/fishes8080387

Corobov, R., Ene, A., Trombitsky, I., & Zubcov, E. (2021). The Prut River under Climate Change and Hydropower Impact. *Sustainability* 13, 66. https://doi.org/10.3390/su13010066

Duca, G., Mereuta, A., Velisco, N., Tanaselia, C., & Mitina, T. (2019). Determination of Quality Indicators of Prut River Water. *ChemJMold* 14, 61–67. https://doi.org/10.19261/cjm.2018.541

Dumitran, M. (2011) Surface water quality in the river Prut, *Air and Water – Components of the Environment*, *Directory of Open Access Journals*,1, 171-177.

Hrytsku, V.S., & Hrytsku-Andriyesh, I.P. (2016). Effects of Main Pollution Sources on Parameters of Water Quality of the Prut River Within the Limits of Chernivtsi in the Last Seven Years and Consequent Environmental Impacts. *Present Environment and Sustainable Development* 10, 35–40. https://doi.org/10.1515/pesd-2016-0003

Matache, M.L., David, I.G., Dinu, C., & Radu, L.G. (2018). Trace metals in water and sediments of the Prut river, Romania. *Environ. Eng. Manag. J.* 17, 1363–1371. https://doi.org/10.30638/eemj.2018.135

Mocanu, G.D., Murariu, G., Iordan, D.A., & Sandu, I. (2021). Analysis of the Influence of Age Stages on Static Plantar Pressure Indicators for Karate Do Practitioners (Preliminary Report). *Applied Sciences*, 11(16), 7320. https://doi.org/10.3390/app11167320

Neamtu, R., Sluser, B., Plavan, O., & Teodosiu, C. (2021). Environmental monitoring and impact assessment of Prut River cross-border pollution. *Environ Monit Assess* 193, 340. https://doi.org/10.1007/s10661-021-09110-1

Popa, P., Murariu, G., Timofti, M., & Georgescu, L.P. (2018). Multivariate Statistical Analyses of Danube River Water Quality at Galati, Romania. *Environmental Engineering and Management Journal*, 17(5), 1249–1266. https://doi.org/10.30638/eemj.2018.124

Resz, M.-A., Roman, C., Senila, M., Török, A.I., & Kovacs, E. (2023). A Comprehensive Approach to the Chemistry, Pollution Impact and Risk Assessment of Drinking Water Sources in a Former Industrialized Area of Romania. *Water*, 15(6), 1180. https://doi.org/10.3390/w15061180

Sava, N., & Marusic, G. (2022). State of water quality in the Prut River for the period of 2019-2021, In: Proceedings of the 12th International Conference on “Electronics, Communications and Computing". Presented at the 12th International Conference on Electronics, Communications and Computing, Technical University of Moldova, 140–146. https://doi.org/10.52326/ic-ecco.2022/SEC.06

Teodosiu, C., Cojocariu, C., Musteret, C.P., Dascalescu, I.G., & Caraene, I. (2009). Assessment of human and natural impacts over water quality in the Prut river basin, Romania. *Environ. Eng. Manag. J.* 8, 1439–1450. https://doi.org/10.30638/eemj.2009.210

Timofti, M., Popa, P., Murariu, G., Georgescu, L., Iticescu, C., Barbu, M. (2016), Complementary approach for numerical modelling of physicochemical parameters of the Prut River aquatic system, *Journal of Environmental Protection and Ecology* 17(1), 53-63, ISSN: 1311-5065.

Scientific Papers. Series E. Land Reclamation, Earth Observation & Surveying, Environmental Engineering. Vol. XV, 2026
Print ISSN 2285-6064, CD-ROM ISSN 2285-6072, Online ISSN 2393-5138, ISSN-L 2285-6064

# DYNAMICS OF AIRBORNE MICROORGANISMS ACCORDING TO ENVIRONMENTAL CONDITIONS

**Bilyana GRIGOROVA-PESHEVA, Asen PESHEV, Georgi KADINOV, Ekaterina TODOROVA, Boyka MALCHEVA**

University of Forestry, 10 Kliment Ohridsti Street, Sofia, Bulgaria

Corresponding author email: b.pesheva@ltu.bg

***Abstract***

*The present study aims to track the dynamics of airborne microorganisms in the territory of Sofia, Bulgaria in relation to the dynamics of fine particulate matter (FPM). Sampling points were 20, which cover territories with different dynamics - parks, intersections, central and peripheral parts, etc. Spin Air sampler was used. Sampling was carried out at a height of 1.5 m, for optimal consideration of the potential impact on human health. Specific microbiological characteristics were recorded - total microbial number in 1m$^3$ air, the main microbiological groups and their ratio and the percentage of pigment forms in relation to the change in the UV index. Specific environmental parameters related to airborne microorganisms were also recorded - amount of FPM, air temperature, humidity, atmospheric pressure, wind direction and speed, UV index. The data show a specific distribution of microbial groups, as well as a certain microbial load in points with intensive car traffic. There is a direct correlation between the amount of pigment forms and UV index ($r=0.92$; $p<0.05$). In the present pilot study, no direct correlation was found between the increase in fine particulate matter and microbial abundance (Pearson correlation matrix, significance thresholds 95%, $p<0.05$). However, there is a clear relationship between the reduced dust level and the higher percentage of woody vegetation.*

***Key words****: airborne microorganisms, air quality, fine particulate matter, pigment forms, UV index.*

## INTRODUCTION

Understanding the complex interaction between physical pollutants and biological components of air is crucial for modern urban ecology and public health. The air we breathe in urban areas is not just a mixture of gases, but a complex multiphase system containing solid particles and biological agents known as bioaerosols. Bioaerosols contain particles of biological origin, including all kinds of biological components and fragments, microorganisms, pollen, parts of plant fragments, etc. (Despres et al., 2012). For this reason, it is very important to distinguish between bioaerosols (which include any type of biological fragments) and airborne microorganisms (which include microorganisms from different groups such as bacteria, micromycetes, actinomycetes, etc.), as Kim et al. (2018), point out. In recent years, Sofia has been among the European capitals with the most serious challenges in terms of ambient air quality, mainly due to its geographical location in a valley and intense car traffic, which is why the study of ground-level air quality is of utmost importance. Modern research shows that airborne microorganisms are not just passive passengers. They use fine particulate matter (FPM) as a "vehicle" and substrate for growth and survival (Tignat-Perrier et al., 2020).

As Meola et al. (2015) and Haas et al. (2025) point out in their studies, fine particulate matter (FPM) act as transport nuclei for the transfer and spread of airborne microorganisms. It is important to note that airborne microorganisms are an important component of ambient air. Although they sometimes have a harmful effect on people and worsen the quality of the environment in urban areas, they are extremely important in the upper layers of the atmosphere, where they play the role of condensation nuclei, as a result of which it is believed that their increase as suspended units may have an impact on the ongoing climate changes (Zhai et al., 2018). It is precisely this complexity and intricacy that necessitates the in-depth study of airborne microorganisms.

Recent data suggest that the chemical composition of PM may selectively favor certain microbial taxa, making urban air a potential reservoir for pathogens or allergens (Cao et al., 2014; Wang et al., 2015). The link between fine

dust particles and the number of microorganisms in the air is undeniable. Last but not least, fine dust particles pose a risk to human health, as their increase not only leads to physical changes in air quality, but can also increase the risk of allergies and respiratory problems, given that large quantities of airborne microorganisms are adhered to PM (Arca-Lafuente et al., 2025). What is specific about fine dust particles is that, due to their size and extremely low relative weight, they can remain suspended in the air for a very long time, with their spread strongly depending on the speed and direction of the wind (He et al., 2021). The increase in PM concentration is not only due to natural sources such as volcanic eruptions, fires, earthquakes or landslides of large land masses (Zanoletti et al., 2024; Whitty et al., 2026), but also exclusively to human activity, such as construction, industrial combustion, car traffic, etc. (Edo et al., 2024; Morales et al., 2025). If wind is the main factor influencing the concentration and distribution of FPM, then changes in temperature, solar radiation index and humidity are of key importance for the vitality, quantity and distribution of airborne microorganisms (Tang, 2009).

The main goal of this study is to track the dynamics of airborne microorganisms in the territory of Sofia, Bulgaria in relation to the dynamics of fine particulate matter (FPM) and specific environmental conditions.

## MATERIALS AND METHODS

Airborne microorganisms are a major component of both atmospheric aerosols and the composition of air, which is highly dynamic. The quantitative and qualitative distribution of microbial groups is of great importance for both urban air quality and public health. However, airborne microorganisms remain poorly understood. In order to identify differences in environmental influences (type of urban environment, intensity of car traffic, vegetation cover) twenty samples were collected in three replicates from different locations with different levels of anthropogenic pressure in the capital of Bulgaria, Sofia, in the autumn of 2025. Points with increased anthropogenic pressure are marked as hot points (HP), and points with low anthropogenic pressure, located in park areas, as green zones (GZ), Figure 1:

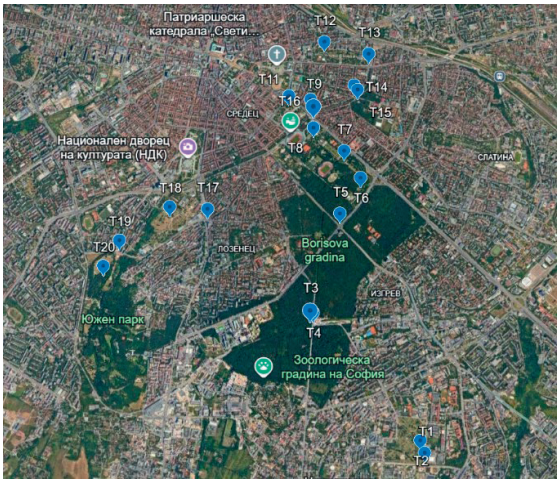



Figure 1. Location of selected sampling points (T1 Crossroad of Osmi Dekemvri Street and Rosario Street (HP); T2 Student Park (GZ); T3 Hunting Park (GZ); T4 Crossroad of Simeonovsko Shosse and Nikola Gabrovski Blvd. – "Loven Park Intersection" (HP); T5 Television Tower - Roundabout (HP); T6 Observatory, in Upper part of Borisova Gpadina Park (GZ); T7 Lily Pond - Middle part of Borisova Gradina Park (GZ); T8 Lower part of Borisova Gradina Park (GZ); T9 Orlov Bridge (HP); T10 V. Levski Blvd. intersection with Tsar Osvoboditel Blvd. (HP); T11 Prince's Garden (GZ); T12 Zaimov Park (GZ); T13 Madrid blvd. Crossroad (HP); T14 Crossroad Evlogii Geogriev Blvd And Shipka str. (HP); T15 Military Academy Park (GZ); T16 Iranian Embassy on Evlogii Georgiev Blvd (HP); T17 Hotel Hemus (HP); T18 Park behind the Museum of Land and People (GZ); T19 Crossroad Vitoshka str. и South Park (HP); T20 South Park (GZ))

For the purposes of the study, the following nutrient media were used: Mesopeptone agar for the cultivation of bacteria, Czapek-Dox agar for the cultivation of micromycetes, and Starch Ammonia Agar for the cultivation of actinomycetes. Air sampling was carried out using an IUL Spin Air impactor, which has high accuracy and resolution. The device works by means of a rotary mechanism, which allows for complete utilization of the nutrient medium layer in the Petri dish, thus ensuring an even distribution of the columns in the Petri dish, which facilitates reading. The measurement was carried out at a height of 1.5 m above the ground surface, corresponding to the human respiratory zone. The sampling parameters are as follows: 120 seconds for each studied group of microorganisms at a flow rate of 100 L/min. These parameters were selected after a series of preliminary test analyses to establish the optimal air flow rate. After sampling, the samples were transferred in specialized bags to the laboratory, where subsequent incubation was performed. Bacteria were cultured for 48 hours at 28°C, fungi - 7 days at 30°C, and actinomycetes - 10 days at 35°C. The counting of the developed colonies was performed using a digital colony counter, with the data converted into CFU*$10^2/m^3$.

Along with the taking of microbiological samples, the levels of fine particulate matter were measured, and meteorological parameters were also recorded. The concentration of PM was recorded using the Envea PM Cairsense device. The device simultaneously measures the PM10, PM2.5 and PM1 fractions, using laser diffraction. During sampling, meteorological data were also recorded: air temperature, humidity, UV index, wind speed and direction. The data for the microbiological analyses were statistically processed using the StatSoft Statistica 12 program, Pearson correlation matrix, at significance thresholds of 95%, $p<0.05$.

## RESULTS AND DISCUSSIONS

The results for the reported meteorological parameters are presented in Figure 2.
Meteorological data indicate slightly lower temperatures than usual for the season. Humidity is also low, ranging between 48% and 65% throughout the sampling period, with the lowest values shortly after noon. This is the period when the temperature and UV index increase. The wind speed of 6.7 m/s from the west-northwest is a constant factor for all measurements.

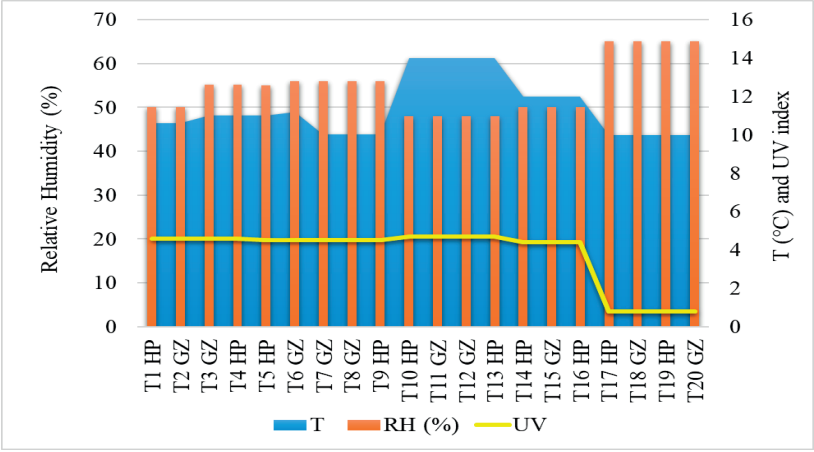



Figure 2. Recorded climatic characteristics during sampling

Such a speed is theoretically sufficient to facilitate the transport of fine dust, bioaerosols, and airborne microorganisms from the outskirts to the city center, suggesting a potential directional transport pathway that warrants further meteorological analysis, while also helping to disperse larger PM10 particles.

The temperature range of 10°C to 14°C is relatively favorable for many of the mesophilic microorganisms commonly found in the air environment (Haas et al., 2020).

The results for the reported amounts of fine particulate matter, by individual fractions, are presented in Table 1.

Table 1. Fine particulate matter (μg/m$^3$)

| | PM 10 | PM 2.5 | PM 1 |
|---|---|---|---|
| T1 HP | 48.83 ± 12.85 | 31.83 ± 7.90 | 23.17 ± 5.34 |
| T2 GZ | 44.33 ± 5.35 | 32.08 ± 4.34 | 23.67 ± 3.49 |
| T3 GZ | 44.25 ± 5.35 | 35.50 ± 4.34 | 27.25 ± 3.49 |
| T4 HP | 67.25 ± 12.85 | 42.87 ± 7.90 | 29.87 ± 5.34 |
| T5 HP | 35.56 ± 12.85 | 28.56 ± 7.90 | 20.78 ± 5.34 |
| T6 GZ | 31.55 ± 5.35 | 26.20 ± 4.34 | 19.60 ± 3.49 |
| T7 GZ | 38.89 ± 5.35 | 30.88 ± 4.34 | 22.67 ± 3.49 |
| T8 GZ | 38.78 ± 5.35 | 30.70 ± 4.34 | 22.78 ± 3.49 |
| T9 HP | 47.00 ± 12.85 | 38.00 ± 7.90 | 27.75 ± 5.34 |
| T10 HP | 52.22 ± 12.85 | 39.44 ± 7.90 | 28.78 ± 5.34 |
| T11 GZ | 39.62 ± 5.35 | 31.62 ± 4.34 | 23.25 ± 3.49 |
| T12 GZ | 30.70 ± 5.35 | 23.80 ± 4.34 | 17.30 ± 3.49 |
| T13 HP | 33.50 ± 12.85 | 26.60 ± 7.90 | 19.70 ± 5.34 |
| T14 HP | 23.40 ± 12.85 | 18.50 ± 7.90 | 13.87 ± 5.34 |
| T15 GZ | 35.72 ± 5.35 | 24.81 ± 4.34 | 17.90 ± 3.49 |
| T16 HP | 31.50 ± 12.85 | 23.07 ± 7.90 | 16.93 ± 5.34 |
| T17 HP | 38.76 ± 12.85 | 29.38 ± 7.90 | 21.61 ± 5.34 |
| T18 GZ | 47.11 ± 5.35 | 37.00 ± 4.34 | 27.44 ± 3.49 |
| T19 HP | 31.86 ± 12.85 | 23.28 ± 7.90 | 18.00 ± 5.34 |
| T20 GZ | 39.90 ± 5.35 | 28.50 ± 4.34 | 20.30 ± 3.49 |

The data from the measurements conducted in Sofia reveal clear spatial heterogeneity in the levels of particulate matter pollution of the fractions PM10, PM2.5 and PM1. These differences reflect the influence of local emission sources, such as road transport, and the protective role of urban vegetation.

The highest levels of PM10 were recorded at point T4 (Loven Park Intersection) - 67.25 μg/m$^3$, which exceeds the average values with 68% (average value = 40.01 μg/m$^{3)}$ for the inner parts of the parks. This fact illustrates the so-called "edge effect", in which areas in the immediate vicinity of busy transport arteries accumulate both primary emissions from fuel combustion and re-suspended dust from the road surface, which is rich in microorganisms, including those of soil origin, as has been found in other studies (Rathnayake et al., 2016). For comparison, point T14 (Military Academy Crossroad) shows the lowest PM10 values (23.4 μg/m$^3$), which is probably due to specific air circulation in the area of this crossroad, which is also confirmed by our other studies (Grigorova-Pesheva & Peshev, 2025).

Analysis of the ratio between the different fractions is essential for microbiology. Fine particles PM2.5 and PM1 have a larger relative surface area, making them more effective carriers of small bacterial cells and fragments of fungal mycelium, which increase the risk of allergies (Thangavel et al., 2022). The average PM2.5/PM10 ratio at the surveyed points varies, but in heavily congested areas such as Orlov Most (T9) and Blvd. V. Levski (T10), PM2.5 concentrations reach 38.00 μg/m$^3$ and 39.44 μg/m$^3$, respectively.

The results of the microbiological analyses performed are presented in Table 2.

Figure 3 presents a comparison of the reported biogenicity of the individual points, for which purpose the green areas are depicted in green and the hot points in red. The graph also shows the reported values of fine particulate matter in μm/m$^3$.

Table 2. Microbiological parameters (CFU*$10^2$/$m^3$)

| | TMN | Bacteria | Actinomycetes | Micromycetes |
|---|---|---|---|---|
| T1 HP | 4.90 ± 2.11 | 3.00 ± 1.53 | 1.80 ± 2.08 | 0.10 ± 0.41 |
| T2 GZ | 6.05 ± 2.75 | 2.30 ± 0.48 | 3.55 ± 2.62 | 0.20 ± 0.33 |
| T3 GZ | 2.55 ± 2.75 | 1.30 ± 0.48 | 1.10 ± 2.62 | 0.15 ± 0.33 |
| T4 HP | 6.20 ± 2.11 | 4.85 ± 1.53 | 1.30 ± 2.08 | 0.05 ± 0.41 |
| T5 HP | 9.70 ± 2.11 | 7.35 ± 1.53 | 1.75 ± 2.08 | 0.60 ± 0.41 |
| T6 GZ | 7.70 ± 2.75 | 2.35 ± 0.48 | 5.10 ± 2.62 | 0.25 ± 0.33 |
| T7 GZ | 3.79 ± 2.75 | 2.40 ± 0.48 | 1.20 ± 2.62 | 0.19 0.33 |
| T8 GZ | 3.00 ± 2.75 | 1.50 ± 0.48 | 1.30 ± 2.62 | 0.20 ± 0.33 |
| T9 HP | 5.65 ± 2.11 | 3.45 ± 1.53 | 1.95 ± 2.08 | 0.25 ± 0.41 |
| T10 HP | 5.50 ± 2.11 | 3.10 ± 1.53 | 2.30 ± 2.08 | 0.10 ± 0.41 |
| T11 GZ | 3.95 ± 2.75 | 2.20 ± 0.48 | 1.55 ± 2.62 | 0.20 ± 0.33 |
| T12 GZ | 3.95 ± 2.75 | 2.10 ± 0.48 | 1.70 ± 2.62 | 0.15 ± 0.33 |
| T13 HP | 7.25 ± 2.11 | 5.90 ± 1.53 | 1.30 ± 2.08 | 0.05 ± 0.41 |
| T14 HP | 7.15 ± 2.11 | 4.45 ± 1.53 | 2.65 ± 2.08 | 0.05 ± 0.41 |
| T15 GZ | 4.45 ± 2.75 | 2.45 ± 0.48 | 1.85 ± 2.62 | 0.15 ± 0.33 |
| T16 HP | 5.85 ± 2.11 | 3.60 ± 1.53 | 2.10 ± 2.08 | 0.15 ± 0.41 |
| T17 HP | 7.22 ± 2.11 | 4.45 ± 0.48 | 1.95 ± 2.62 | 0.82 ± 0.33 |
| T18 GZ | 11.73 ± 2.75 | 1.30 ± 0.48 | 9.45 ± 2.62 | 0.98 ± 0.33 |
| T19 HP | 11.75 ± 2.11 | 2.15 ± 1.53 | 8.35 ± 2.08 | 1.25 ± 0.41 |
| T20 GZ | 6.25 ± 2.75 | 1.45 ± 0.48 | 3.85 ± 2.62 | 0.95 ± 0.33 |

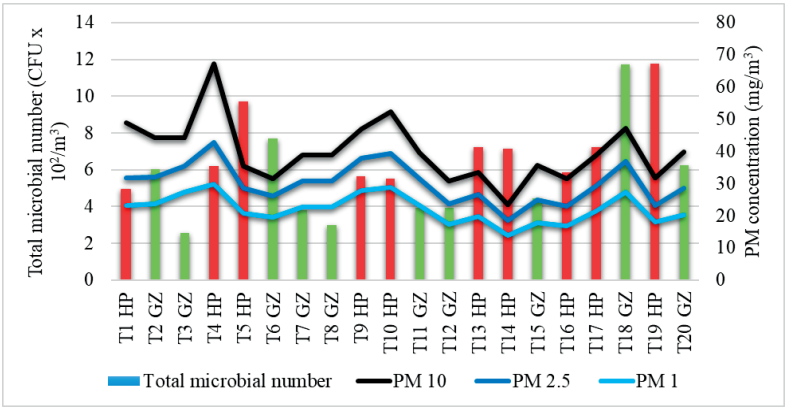



Figure 3. Total microbial number of the studied points and FPM load

Analysis of the results shows that green areas generally have a lower microbial load than hot points, although there are exceptions. Green areas with a low percentage of woody vegetation (T2 and T18) stand out with a higher microbial load, close to that of hot points. These are park areas dominated by grasslands and low shrub vegetation. Similar data have been found in our previous studies, as well as in the work of other colleagues (Mhuireach et al., 2016; Grigorova-Pesheva & Peshev, 2025). Specifically, green zone T2 once again shows high levels of microbial abundance. This is a park area that is built at a lower level than the street. During sampling, dust swirling and its transfer to the park area were observed. Similar to previous studies, higher levels of both fine dust particles and microorganisms were observed here again. Such results confirm the need to comply with the requirements and guidelines of environmental hygiene when carrying out urban planning. As indicated by (Revich, 2022), green areas

increase not only the physical, but also the mental health of the population, therefore their proper planning is key to building an environmentally friendly urban environment.

In the present study, no direct correlation was found between the increase in fine particulate matter and microbial abundance. (*Pearson correlation matrix, significance thresholds 95%, $p<0.05$*). However, there is a clear relationship between the reduced dust level and the higher percentage of woody vegetation. As Cohen et al. (2014), point out in their study, the presence of trees strongly reduces the amount of dust in green areas, which leads to an increase in air quality.

The specific dynamics of the results prove that when analyzing it is necessary to consider the data in pairs, green zone, hot spot, because depending on the specific conditions and dynamics of the characteristics of the environment, specific differences are observed both in the fine dust load and in the microbial abundance. However, the influence of the way the green zones are managed on the amount of PM reported and the total number of airborne microorganisms is undeniable. So again, at T3 (Hunting Park), where we have a green area imitating a natural dense forest, the levels of microorganisms are the lowest (2.55 CFU*$10^2$/$m^3$), including much lower levels of dust compared to the nearby heavily trafficked intersection (T4). Although the sample in the green zone was taken only 70 meters inland, in the park, a strong positive impact on air quality is observed. Similar results are also obtained for T7 (3.79 CFU*$10^2$/$m^3$) and T8 (3.00 CFU*$10^2$/$m^3$), which are located in Borisova Gradina - one of the largest green zones in Sofia, which has a large percentage occupied by woody vegetation - not accidentally called the "Tsar's Garden". Interesting data are for T11 (3.95 CFU*$10^2$/$m^3$), this is a green zone that has a smaller percentage of woody vegetation, but is closed on two sides with pedestrian zones, and in the center, there is a large water area. This again shows how specific urban planning can improve air quality, not only by increasing the percentage of woody vegetation, but also by reducing the intensity of car traffic.

The results for the percentage distribution of the individual microbiological groups are presented in Figure 4.

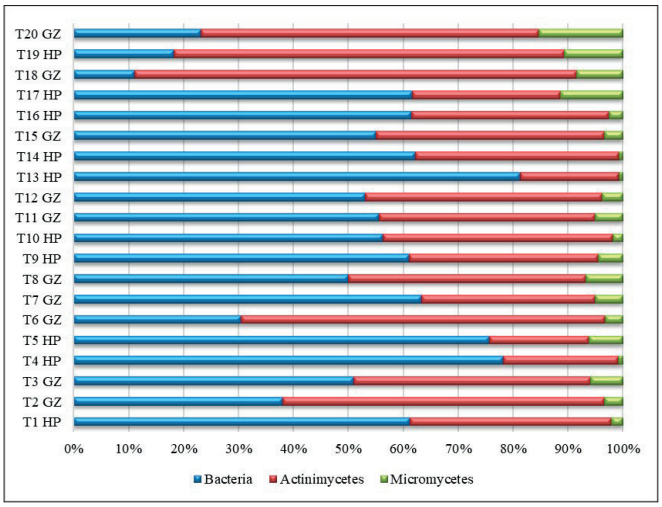



Figure 4. Percentage distribution of individual microbiological groups

The results show a very low percentage participation of the micromycetes group, which is probably due to the reduced humidity for the season.

One of the main microbiological parameters related to the vitality of microorganisms is the relative humidity (RH). Research shows that humidity levels in the range of 40-60% can be suppressive for many airborne microorganisms due to specific physicochemical processes in aerosol particles. However, most studies focus on indoor air quality, indicating that the optimal

humidity at which the possibility of transmitting pathogens and other microorganisms is seriously reduced is 40-60% (Skanata et al., 2022). There is insufficient data on the effect of humidity on airborne microorganisms in outdoor environments. Our data show that as the % humidity increases, the percentage of the micromycetes group (T17, T18, T19 and T20) increases. There are other studies available that prove that as humidity increases, the number of airborne fungi increases, explaining that high humidity levels facilitate the growth of this microbial group (Sajjad et al., 2023).

The results for the percentage of pigment forms, as well as the reported UV index levels, are presented in Figure 5.

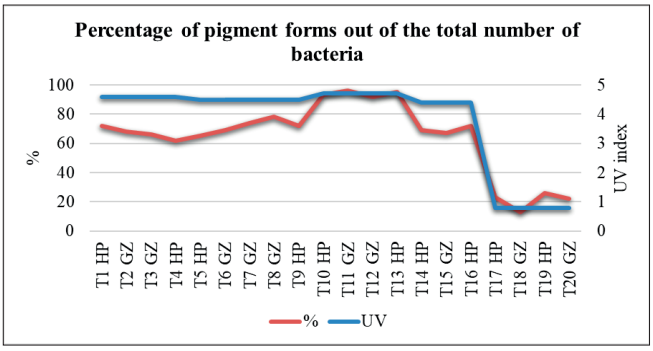



Figure 5. Percentage of pigment forms relative to the reported UV index

The results of the percentage participation show an increase in the number of pigment forms relative to the total number of bacterial colonies with increasing UV index. Similar results were also found by Tong & Lighthart, 1997. As the authors point out, pigmentation is a protective mechanism that ensures the survival of bacteria at high levels of UV radiation. At high UV index, non-pigmented bacteria, which are sensitive to light, die rapidly in the atmosphere. This leads to a relative increase in the proportion of surviving microorganisms that form pigment forms, which then form colonies on the nutrient medium in microbiological analysis (Figure 5). The increase in the percentage of pigmented colonies at higher UV index is a direct result of the defense mechanisms of microorganisms against intense solar radiation and the process of selective pressure in the atmosphere. Namely, such high results for the percentage of pigment forms indicate the strong adaptability of the air microflora (Park & Fowler, 2026).

It is important to note, however, that most studies indicate that the maximum proportion of pigment forms during peak hours of UV radiation is around 50-60% (Tong & Lighthart, 1997), while in the present study the results indicate higher values, which suggests that the air microflora probably responds not only to an increase in the UV index, but also to additional stress factors such as increased oxidative stress, increased concentration of pollutants in the air, etc.

## CONCLUSIONS

The main objective of this study was to analyze the dynamics of airborne microorganisms according to environmental conditions. A total of 20 sample points were studied - 10 green areas and 10 hot points. No direct correlation was established between the fine dust load, regardless of the fraction, and the microbial abundance. The results confirm the need to analyze the data in pairs - green area - hot spot. The results indicate that in green areas with a high percentage of woody vegetation, both the microbial load and the fine dust load are lower. The present study confirmed the importance of urban planning. Thus, for park areas located below the roadway level, increased levels of PM and microorganisms were found. The present study found that the microbial community is influenced by environmental factors – humidity and UV index. Thus, in samples with increased % humidity, the participation of the micromycetes group increases. It was also found that an increase in the UV index leads to an

increase in the percentage of pigment forms regardless of the study point. This pilot study can serve as the basis for an expanded study covering major cities in Bulgaria to account for the influence of regional climate on shaping the microbial air community.

## ACKNOWLEDGEMENTS

This research work was carried out with the support of Research Fund of Ministry of Education and Science in Bulgaria, project №: КП-06-Н74/5 „Relationships between the amount of fine particulate matter and airborne microorganisms in "hot spots", park areas, urban background areas and control forest areas''.

## REFERENCES

Arca-Lafuente, S., Nuñez-Corcuera, B., Ramis, R., Karakitsios, S., Sarigiannis, D., Dos Santos, S., Fernandez-Rodriguez, A. & Briz, V. (2025). Effects of urban airborne particulate matter exposure on the human upper respiratory tract microbiome: a systematic review. *Respir Res*., 26:118. DOI: 10.1186/s12931-025-03179-9

Cao, Ch., Jiang, W., Wang, B., Fang, J., Lang, J., Tian, G., Jiang, J. & Zhu, T. (2014). Inhalable microorganisms in Beijing's PM2.5 and PM10 pollutants during a severe smog event. *Environ Sci Technol*, 48(3):1499-507. DOI: 10.1021/es4048472

Cohen, P., Potchter, O. & Schnell, I. (2014). The impact of an urban park on air pollution and noise levels in the Mediterranean city of Tel-Aviv, Israel. *Environmental Pollution*, 195, 73-83. DOI: https://doi.org/10.1016/j.envpol.2014.08.015

Despres, V., Huffman, A., Burrows, S., Hoose, C., Safatov, A., Buryak, G., Nowoisky, J., Elbert, W., Andreae, M., Poschl, U. & Jaenicke, R. (2012). Primary biological aerosol particles in the atmosphere: a review. *Tellus B: Chemical and Physical Meteorology*, 64(1), 15598. DOI: 10.3402/tellusb.v64i0.15598

Edo, G.I., Itoje-akpokiniovo, L.O., Obasohan, P., Ikpekoro, V.O., Samuel, P.O., Jikah, A.N., Nosu, L.C., Ekokotu, H.A., Ugbune, U., Oghroro, E.E.A., Emakpor, O.L., Ainyanbhor, I.E., Mohammed, W.A.S., Akpoghelie, P.O., Owheruo, J.O. & Agbo, J. J. (2024). Impact of environmental pollution from human activities on water, air quality and climate change. *Ecological Frontiers,* 44(5), 874-889. https://doi.org/10.1016/j.ecofro.2024.02.014

Grigorova-Pesheva & Peshev, A. (2025). Ground air microflora study using a cascade impactor. *Scientific Papers. Series E. Land Reclamation, Earth Observation & Surveying, Environmental Engineering*, XIV, 2285-6064.

Haas, D., Kriso, A., Fritz, Th., Galler, H., Habib, J., Ilieva, M., Kropsch, M., Ofner-Kopeining, P., Stonitsch, M., Strasser, A., Zentner, A., & Reinthaler, F. (2020). Background Concentrations of Cultivable, Mesophilic Bacteria and Dust Particles in the Air in Urban, Rural and Mountain Regions. *Int. J. Environ. Res. Public Health*, 17(24), 9572; https://doi.org/10.3390/ijerph17249572"

Haas, D., Pikal, S.R., Galler, H., Habib, J., Moser, T., Ofner-Kopeinig, P., & Schalli, M. (2025). Particulate matter and airborne microorganisms in a construction site in Graz, Austria. *Atmospheric Environment*, 344, 121025, DOI: https://doi.org/10.1016/j.atmosenv.2024.121025.

He, T., Jin, L., Xie, J., Yue, S., Fu, P., & Li, X. (2021). Intracellular and extracellular antibiotic resistance genes in airborne PM2.5 for respiratory exposure in urban areas. *Environmental Science & Technology Letters*, 8(2), 128–134

Kim, K., Kabir, E. & Jahan, Sh. (2018). Airborne bioaerosols and their impact on human health. *J Environ Sci (China)*, 67:23-35, DOI: 10.1016/j.jes.2017.08.027.;

Meola, M., Lazzaro, A. & Zeyer, J. (2015). Bacterial Composition and Survival on Sahara Dust Particles Transported to the European Alps. *Frontiers in Microbiology* 6:1454. DOI: 10.3389/fmicb.2015.01454

Mhuireach, G., Johnson, B., Altrichter, A., Ladau, J., Meadow, J., Pollard, K. & Green, J. (2016). Urban greenness influences airborne bacterial community composition. *Science of the Total Environment*, 571, 680-687, DOI: https://doi.org/10.1016/j.scitotenv.2016.07.037

Morales, G.A., Rajiv, A.M., Venverloo, T., & Fry, J.L. (2025). Where particulates matter: High-rise construction emissions of PM2.5, PM10, BC and UFP in Dutch cities. *Atmospheric Environment: X*, 28: 100373. DOI: 10.1016/j.aeaoa.2025.100373

Park, J. & Fowler, S. (2026). Airborne Bacterial Communities: Diversity, Survival Strategies and Functional Roles in the Atmosphere. *Environ Microbiol Rep*, 8;18(1):e70274. DOI: 10.1111/1758-2229.70274.

Rathnayake, Ch., Metwali, N., Baker, Z., Jayarathne, Th., Kostle, P., Thorne, P. O'Shaughnessy, P. & Stone, E. (2016). Urban Enhancement of PM10 Bioaerosols Tracers Relative to Background Locations in the Midwestern United States. *J Geophys Res Atmos*, 121(9), 5071-5089. doi: 10.1002/2015JD024538

Revich, B. (2022). Urban planning and public health:analytical review. *Analytical Reviews*, 147-161. DOI: 10.21668/health.risk/2022.1.17.eng.

Sajjad, B., Hussain, S., Rasool, K., Hassan, M. & Almomani, F. (2023). Comprehensive insights into advances in ambient bioaerosols sampling, analysis and factors influencing bioaerosols composition. *Environmental Pollution*, 336, 122473. https://doi.org/10.1016/j.envpol.2023.122473

Skanata, A., Spagnolo, F., Metz, M., Smyth, D.S., & Dennehy, J.J. (2022). Humidity Reduces Rapid and Distant Airborne Dispersal of Viable Viral Particles in Classroom Settings. *Environ Sci Technol Lett*, 9:632–637. doi: 10.1021/acs.estlett.2c00243

Tang, J. (2009). The effect of environmental parameters on the survival of airborne infectious agents. *J.R.Soc. Interface*, 6, S737-S746. DOI: 10.1098/rsif.2009.0227.focus.

Thangavel, P., Park, D. & Lee, Y.C. (2022). Recent insights into Particulate Matter (PM2.5) – Mediated Toxicity in Humans: An Overview. *Int J Environ Res Public Health*, 19(12):7511, DOI: 10.3390/ijerph19127511

Tignat-Perrier, R., Dommergue, A., Thollot, A., Magand, O., Vogel, T. & Larose, C. (2020). Microbial functional signature in the atmospheric boundary layer. *Biogeosciences*, 17(23). 6081-6095. https://doi.org/10.5194/bg-17-6081-2020

Tong, Y. & Lighthart, B. (1997). Solar Radiation Is Shown to Select for Pigmented Bacteria in the Ambient Outdoor Atmosphere. *Photochemistry and Photobiology*, 65(1):103 – 106. DOI: 10.1111/j.1751-1097.1997.tb01884.x

Wang, b., Lang, J., Zhang, L., Fang, J., Cao, Ch., Hao, J., Zhu, T., Tian, G. & Jiang, J. (2015). Characterizing Beijing's Airborne Bacterial Communities in PM2.5 and PM1 Samples During Haze Pollution Episodes Using 16S rRNA Gene Analysis Method. *Huan Jing Ke Xue*, 36(8): 2727-34.

Whitty, R. C. W., Ilyinskaya, E., Pfeffer, M. A., Thrastarson, R. H., Johannsson, Þ., Barsotti, S., Roberts, T. J., Gilbert, G. M., Hjörvar, T., Schmidt, A., Fecht, D., & Sæmundsson, G. G. (2026). Fine-scale fluctuations of PM1, PM2.5, PM10 and SO2 concentrations caused by a prolonged volcanic eruption (Fagradalsfjall 2021, Iceland). *Atmos. Chem. Phys.*, 26, 313–347, https://doi.org/10.5194/acp-26-313-2026

Zanoletti, A. & Bontempi, E. (2024). The impacts of earthquakes on air pollution and strategies for mitigation: a case study of Turkey. *Environ Sci Pollut Res*, 31(16): 24662. DOI: 10.1007/s11356-024-32592-8

Zhai, Y., Li, X., Wang, T., Wang, B., Li, C., & Zeng, G. (2018). A review on airborne microorganisms in particulate matters: composition, characteristics and influence factors. *Environment international*, 113, 74-90.

Scientific Papers. Series E. Land Reclamation, Earth Observation & Surveying, Environmental Engineering. Vol. XV, 2026
Print ISSN 2285-6064, CD-ROM ISSN 2285-6072, Online ISSN 2393-5138, ISSN-L 2285-6064

# *IN VITRO* PROPAGATION OF *EUONYMUS FORTUNEI* CULTIVARS FOR SUSTAINABLE URBAN GREENING AND DEGRADED LAND REHABILITATION

**Tatiana GROPA[1, 2], Ion ROȘCA[1], Ioana-Cătălina NICOLAE[3]**

[1]Moldova State University, Faculty of Biology and Geosciences, 60 Alexei Mateevici, Chișinău, Republic of Moldova
[2]Technical University of Moldova, Faculty of Urbanism and Architecture, 39 Dacia Blvd, Chișinău, Republic of Moldova
[3]University of Agronomic Sciences and Veterinary Medicine of Bucharest, Research Center for Studies of Food Quality and Agricultural Products, 59 Mărăşti Blvd, District 1, Bucharest, Romania

Corresponding author email: catalina.nicolae@qlab.usamv.ro

***Abstract***

*Euonymus fortunei* (Turcz.) Hand.-Mazz. *(Fortune's spindle) is an evergreen ornamental species widely used in landscape design due to its adaptability to urban stress conditions such as pollution, drought, high insolation, low temperatures, and degraded soils. This study aimed to improve in vitro establishment and shoot multiplication of the cultivars 'Emerald 'n' Gold' and 'Emerald Gaiety'. Nodal segments and shoot tips from mature plants were surface sterilized and established on Murashige and Skoog (MS) medium supplemented with 1 mg/L 6-benzylaminopurine (BAP), 0.5 mg/L indole-3-acetic acid (IAA), 0.5 mg/L gibberellic acid ($GA_3$), with or without 0.2% (v/v) Plant Preservative Mixture (PPM™). PPM increased contamination-free explants from 55.56% to 88.89% in 'Emerald 'n' Gold' and from 48.39% to 95.71% in 'Emerald Gaiety'. During multiplication, MS medium containing 2 mg/L meta-topolin (mT) and 1 mg/L IAA produced the highest shoot numbers, with an average of 4.71 and 4.40 shoots per explant, respectively, compared with 1.30 and 1.45 on medium with 2 mg/L BAP alone. Meta-Topolin media also reduced basal callus formation, whereas shoot tip necrosis and callus browning were more frequent of media with BAP. These findings identify mT, particularly combined with IAA, as a promising alternative to BAP for in vitro multiplication of these E. fortunei cultivars and provide a basis for further protocol optimization and large-scale propagation and results demonstrate that meta-topolin-based media provide an efficient system for rapid in vitro multiplication of E. fortunei cultivars for use in urban landscaping and ecological restoration of degraded environments.*

***Key words****: landscape, meta-topolin, micropropagation, plant growth regulators, shoot proliferation.*

## INTRODUCTION

The genus *Euonymus* L (commonly known as spindle or spindle tree) comprises ornamental shrub species with both deciduous and evergreen foliage (creeping, climbing or upright forms) belonging to the Celastraceae family. These plants are highly valued for their adaptability, attractive foliage (sometimes variegated), and their spectacular autumn coloration. The genus is widely distributed and includes around 200 species, native to temperate and subtropical regions of Asia, Europe (including the native flora of Romania and the Republic of Moldova) and North America (Savinov, 2022).

*Euonymus fortunei* (Turcz.) Hand.-Mazz (Fortune's spindle) is an evergreen ornamental species widely used in landscape design due to its adaptability to urban stress conditions such as pollution, drought, high insolation, low temperatures, and degraded soils (Percival & Sheriffs, 2002). Its use in urban greening and land rehabilitation makes it relevant for sustainable environmental engineering applications. However, due to its adaptability to various conditions, *Euonymus fortunei* can naturalize in seminatural and synanthropic habitats, outside the area of the original cultivation (Bauer & Reynolds, 2016; Savinov, 2022). Native to East and Southeast Asia, it was reported to be naturalized in the Caucasus region and fragmentary on the Black Sea coast and other places (Savinov, 2022). Occasionally, problems with pests and diseases such as euonymus scale (*Unaspis euonymi*) (Cockfield & Potter, 1986; Gutue et al., 2015) or anthracnose (*Colletotrichum gloeosporioides*)

(Ningen et al., 2005) may occur. However, anthracnose mostly occurs in nurseries, and the production of new plantlets can be significantly decreased due to this disease (Ningen et al., 2004; Boyer et al., 2007; Cole et al., 2009). Heavier infestations with *Unaspis euonymi* can lead to massive defoliation and eventual loss of plants (Jefferson & Schultz, 1995). Plant tissue culture and micropropagation provide effective techniques for the mass multiplication of genetically consistent, pathogen-free plant material, regardless of seasonal variations or environmental limitations. *In vitro* propagation has been done on several species of the genus, as *Euonymus alatus* (Smith & Jernstedt, 1989; Chen et al., 2006; Thammina et al., 2011; Woo et al., 2021), *Euonymus europaeus* (Biahoua & Bonneau, 1999), *Euonymus bungeanus* (Ning et al., 2021; Cui et al., 2025) *Euonymus verrucosus* (Kirillov et al., 2022), *Euonymus japonicus* (Shang et al., 2006) *Euonymus koopmannii* (Gubaidullin et al., 2024; Kali et al., 2024)**,** *Euonymus fortunei* (Wang et al., 2004; Shang et al., 2009) or cell cultures in *Euonymus maximowiczianus* for anthocyanin and VLCFA (very-long-chain fatty acids) accumulation (Nosov et al., 2024)**.**

Despite these advances, microbial contamination remains a major limitation in the micropropagation of woody plants. In particular, endophytic contamination can be difficult to control because microorganisms residing within plant tissues may not be eliminated by conventional surface sterilization procedures. To date, no standardized protocol specifically addressing endophytic contamination during the in vitro establishment of the *E. fortunei* cultivars 'Emerald 'n' Gold' and 'Emerald Gaiety' has been reported. Contamination by endophytic bacteria is a common problem in the micropropagation of woody species (Permadi et al., 2025). Endophytic microorganisms inhabit internal plant tissues without necessarily causing visible symptoms of disease or harm to their hosts. They may colonize intercellular spaces, cell walls, and xylem vessels. Endophytes have also been detected in reproductive and storage organs, including flowers, fruits, pollen grains, and seeds, demonstrating their widespread distribution within plants (Chebotar et al., 2016; Boiu-Sicuia & Cornea, 2019).

Surface sterilization of explants does not guarantee complete elimination of microorganisms because endophytic bacteria and fungi may reside within internal tissues and therefore remain protected from surface disinfectants (Marino et al., 1996; Quambusch & Winkelmann, 2018). Newly inoculated explants may initially appear free of contamination because some endophytic microorganisms can remain dormant. Changes in culture conditions may subsequently stimulate their growth, resulting in visible contamination at the explant base and in the culture medium (Leifert & Cassells, 2001; Izarra et al., 2020). Endophytic bacteria belonging to genera such as *Bacillus*, *Pseudomonas*, *Paenibacillus*, *Erwinia*, and *Burkholderia* have been reported in various woody plant tissues (Chebotar et al., 2016) The cultivars 'Emerald 'n' Gold' and 'Emerald Gaiety' were selected because they are widely recognized ornamental forms of *E. fortunei*, characterized by distinctive variegated foliage and desirable growth characteristics that contribute to their value in landscape applications. Their attractive foliage and ornamental performance make the development of reliable propagation protocols particularly relevant for the production of uniform planting material. However, the establishment of mature *E. fortunei* tissues *in vitro* may be constrained by microbial contamination, highlighting the need for improved disinfection strategies.

Therefore, this study aimed to develop an efficient *in vitro* propagation protocol for the cultivars 'Emerald 'n' Gold' and 'Emerald Gaiety', with particular emphasis on improving explant establishment and shoot multiplication to support the production of uniform planting material.

## MATERIALS AND METHODS

### Inoculation

For inoculation, nodal segments and shoot tips of two cultivars of *Euonymus fortunei* – 'Emerald 'n' Gold' and 'Emerald Gaiety' - were used. They were collected from green shoots that were harvested in August 2025 from mature plants grown in Chișinău, Republic of Moldova and brought to Bucharest, Romania (Figure 1). All experiments in this study were

carried out in the Plant Micropropagation Laboratory, part of the Research Center for Studies of Food Quality and Agricultural Products, of the University of Agronomic Sciences and Veterinary Medicine of Bucharest, Romania.



Figure 1. *Euonymus fortunei* 'Emerald 'n' Gold' (left) and 'Emerald Gaiety' (right) shoots

For culture initiation, two variants of MS (Murashige and Skoog, 1962) media supplemented with growth regulators were used (as detailed in Table 1).

Table 1. Composition of media variants used for *in vitro* inoculation of *Euonymus fortunei* cultivars

| No. | Media variant | Media composition |
|---|---|---|
| 1. | I1 | MS + 1 mg/L BAP + 0.5 mg/L IAA + 0.5 mg/L $GA_3$ |
| 2. | I2 | MS + 1 mg/L BAP + 0.5 mg/L IAA + 0.5 mg/L $GA_3$ + 0.2% (v/v) PPM |

The difference consisted in the addition of 0.2% (v/v) of commercial stock solution of Plant Preservative Mixture™ (PPM) in variant I2, corresponding to 2 mL PPM per litre of culture medium. Commonly used as an ingredient in culture media, especially for woody species, Plant Preservative Mixture™ (PPM) is a biocide with broad-spectrum that contains 0.1305% 5-Chloro-2-methyl-3(2H)-isothiazolone and 0.0459% 2-methyl-3(2H)-isothiazolone as active ingredients (Plant Cell Technologies, 2026). To minimize tissue browning, the culture media was enriched with 200 mg/L polyvinylpyrrolidone (PVP) and 1 g/L activated charcoal. To stimulate shoot regeneration, 1 mg/L 6-benzylaminopurine (BAP), 0.5 mg/L indole acetic acid (IAA) and 0.5 mg/L gibberellic acid ($GA_3$) were added to the media, prior to sterilization in the autoclave. Surface sterilization was performed sequentially using 1% citric acid, 0.5% sodium dichloroisocyanurate (NaDCC) for 5 min, 70% ethanol for 60 s, and 0.3% mercury(II) chloride ($HgCl_2$) for 5-7 min. Due to the high toxicity of mercury (II) chloride ($HgCl_2$), all handling was performed using appropriate laboratory safety precautions, and mercury-containing waste was collected separately and disposed of in accordance with institutional hazardous-waste procedures. After the explants were rinsed with sterile distilled water, they were inoculated on the two variants of media used for culture initiation: I1 and I2 (Table 1). In order to reduce phenolic oxidation, the explants were incubated for 10 days at 6°C, in complete darkness. Following this, they were transferred to the growing room, where they were grown at 22-25°C, under white, red and blue LED lights and a 16 hours photoperiod (Figure 2). All contaminated explants (including those contaminated with endophytic bacteria were removed from the experiment).

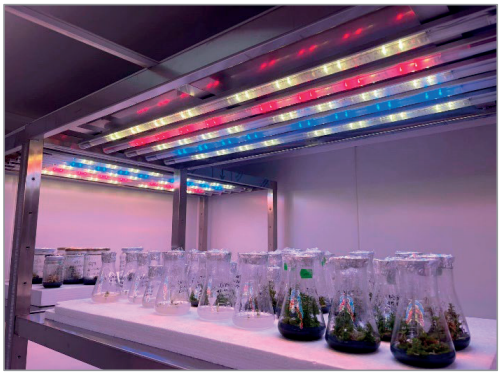


Figure 2. Culture conditions used for *in vitro* cultivation of *Euonymus fortunei* cultivars

**Multiplication on media with BAP or mT**

Following culture establishment and stabilization, explants were transferred to MS media containing either 6-benzylaminopurine (BAP) or meta-Topolin (mT) and indole acetic acid (IAA), as detailed in Table 2. For each medium variant, 10 explants were used per cultivar (n = 10 explants per treatment). The multiplication experiment was conducted following two subculture cycles. Data were recorded after a total culture period of 70 days. Media was prepared using stock solutions prepared individually for each element. Sucrose was supplemented in concentration of 30 g/L and the media was solidified with 7 g/L agar. To prevent oxidation, 100 mg/L

polyvinylpyrrolidone (PVP) and 1 g/L activated charcoal were added.
The pH value was adjusted at 5.70 and the media was sterilized in the autoclave for 20 minutes, at 121°C. All plant growth regulators (BAP, mT, and IAA) were filter sterilized with PES syringe filters (0.22 µm) and added after sterilization in the autoclave. Media was poured in sterile 250 ml Erlenmeyer flasks and covered with aluminum foil. Culture conditions were the same as before (Figure 1).

Table 2. Composition of media variants used for *in vitro* inoculation of *Euonymus fortunei* cultivars

| No. | Media variant | Media composition |
|---|---|---|
| 1. | M1 | MS + **2 mg/L BAP** + 0.2% Plant Preservative Mixture™ (PPM) + 1g/L activated charcoal |
| 2. | M2 | MS + **2 mg/L BAP** + **1 mg/L IAA** + 0.2% Plant Preservative Mixture™ (PPM) + 1g/L activated charcoal |
| 3. | M3 | MS + **2 mg/L mT** + 0.2% Plant Preservative Mixture™ (PPM) + 1g/L activated charcoal |
| 4. | M4 | MS + **2 mg/L mT** + **1 mg/L IAA** + 0.2% Plant Preservative Mixture™ (PPM) + 1g/L activated charcoal |

At the end of the 70-day multiplication period, biometric measurements were performed. The following parameters were evaluated: (i) mean number of shoots per explant, determined by counting the shoots regenerated from each explant; (ii) mean shoot length (mm), measured using a digital caliper; and (iii) mean fresh callus mass (g), determined by carefully excising the callus tissue from the explants and weighing it immediately using an analytical balance. The measurements were performed at the end of the multiplication experiment.

**Statistical analyses**
All statistical analyses were conducted using Microsoft Excel 2021 in combination with the Real Statistics Resource Pack (www.real-statistics.com). For each evaluated parameter, descriptive statistics were generated to summarize the data, with results expressed as the mean ± standard error (SE). The homogeneity of variances was assessed using Levene's test before selecting the appropriate statistical approach. Data satisfying the assumption of equal variances were analyzed by one-way analysis of variance (ANOVA). When significant treatment effects were identified, pairwise comparisons were carried out using Tukey's honestly significant difference (HSD). Statistical significance was established at a threshold of $p < 0.05$.

## RESULTS AND DISCUSSIONS

Use of Plant Preservative Mixture™ (PPM) was proven to be effective in reducing endophytic bacteria contamination. After 16 days, surface sterilization of explants resulted in 55.56% and 48.38% uncontaminated explants, whereas the addition of PPM increased the percentage to 88.89% and 95.71% in 'Emerald 'n' Gold' and 'Emerald Gaiety', respectively (Figure 3).

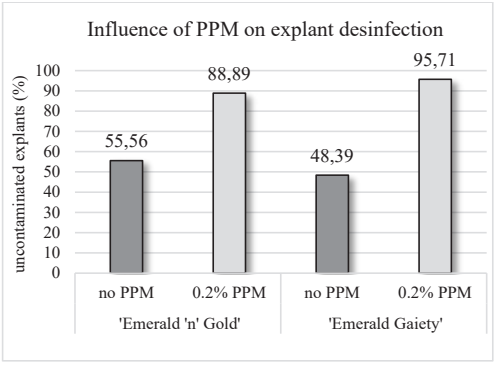



Figure 3. Influence of PPM on the percentage of explant disinfection

The beneficial effect of PPM observed in the present study is consistent with previous reports of its application in the establishment of woody plant material. Niedz and Bausher (2002) reported that PPM reduced contamination in greenhouse- and field-derived Citrus sinensis buds, although the effectiveness depended on the sterilization treatment used. PPM has also been successfully incorporated into culture systems for several woody species, including *Malus* spp. (Romadanova et al., 2022), *Corylus avellana* (Kushnarenko et al., 2025), *Rubus idaeus* (Trzewik et al., 2025), *Vitis vinifera* (Bettoni et al., 2019), and *Cryptocarya massoy* (Fajrisani et al., 2026).

Together with the present results, these studies support the usefulness of PPM as an additional measure for controlling persistent microbial contamination during the establishment of woody explants.

The effectiveness and phytotoxicity of surface disinfectants are also strongly dependent on their concentration and exposure time. In Euonymus koopmannii, for example, prolonged treatment with 5% sodium hypochlorite caused tissue injury and death of axillary buds (Kali et al., 2024). For field-derived nodal segments of Euonymus bungeanus, Cui et al. (2025) reported successful sterilization using 75% ethanol for 30 s followed by 0.1% $HgCl_2$ for 7 min. In the present study, NaDCC was incorporated into the sterilization procedure, followed by $HgCl_2$ treatment and the addition of PPM to the culture medium. The high proportion of uncontaminated explants obtained with PPM suggests that controlling microorganisms that persist after surface sterilization was particularly important for the establishment of the mature E. fortunei material used in this study.

The literature also indicates that no single disinfectant is universally optimal. NaDCC has been reported to provide effective surface sterilization with relatively limited tissue damage compared with some other disinfectants (Parkinson et al., 1996; Caton, 2008; Simran & Narasimhan, 2021). Reddy et al. (2025), for example, found 0.5% NaDCC to be more effective than 1% sodium hypochlorite or 1% calcium hypochlorite for sterilizing rhizome explants of Siphonochilus aethiopicus. Conversely, Mihaljević et al. (2013) reported that 1–2% NaDCC resulted in a higher contamination rate and lower survival of sour cherry axillary buds than some alternative disinfectants. These contrasting findings emphasize that sterilization efficiency depends on explant type, physiological condition, plant species, disinfectant concentration, and exposure duration. In the present study, the addition of PPM after surface sterilization provided an additional means of reducing contamination and consequently increased the proportion of explants suitable for culture establishment.

Information regarding the efficient sterilization of shoot tips and nodal segments of *Euonymus* remains relatively limited, as several previous studies on *in vitro* propagation or conservation have used seeds as starting material (Smith & Jernstedt, 1989; Biahoua & Bonneau, 1999; Chen et al., 2006; Shang et al., 2008; Thammina et al., 2011, 2012; Woo et al., 2021). For young shoot tips of *Euonymus verrucosus*, Kirillov et al. (2022) recommended 70% ethanol for 1 min followed by treatment with 0.025% thimerosal and a 7% aqueous sodium hypochlorite-based commercial bleach solution. The present results therefore provide additional information on the establishment of mature shoot-derived explants of *E. fortunei*, particularly regarding the potential contribution of PPM to contamination control.

**Multiplication**

***Average number of shoots obtained from each explant***

Both varieties, 'Emerald 'n' Gold' and 'Emerald Gaiety' reacted similarly when cultivated on the four media variants (Figure 4). Highest number of shoots was obtained on media variant M4 (2 mg/L mT and 1 mg/L IAA): 4.71 ± 2.05 shoots in 'Emerald 'n' Gold' and 4.4 ± 2.65 shoots on 'Emerald Gaiety'. Media variant M3 (2 mg/L mT) produced fewer shoots, however the recorded values were higher than the ones obtained on BAP-supplemented media: 3.3 ± 1.0 shoots ('Emerald 'n' Gold') and 2.6 ± 1.02 shoots ('Emerald Gaiety').

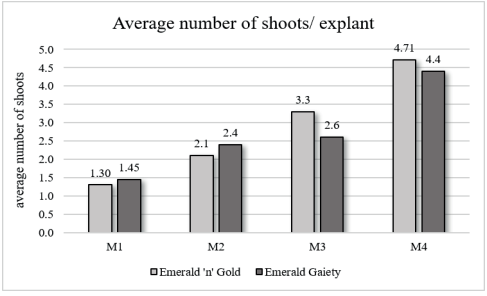



Figure 4. Average number of shoots obtained from each explant

The synergic interaction of meta-Topolin with auxins such as NAA, IBA and 2,4-D is well documented, by increasing the number of shoots, shoot length and stimulating organogenesis in species such as *Eucomis autumnalis* (Masondo et al., 2015), *Coleonema*

*album* (Fajinmi et al., 2014), *Manihot esculenta* (Chauhan & Taylor, 2018) *Hypericum frondosum* (Meyer et al., 2009) or *Huernia hystrix* (Amoo et al., 2009). mT-containing media also produced shoots without visible signs of oxidative damage (Figure 5). Previous studies have suggested that mT may reduce some of the undesirable effects associated with BAP, including oxidative stress and tissue damage, which can negatively affect plant growth and subsequent acclimatization (Keshari et al., 2020). The absence of visible oxidation in the mT treatments in the present study (Figure 5), together with their greater shoot proliferation, further supports the suitability of mT for multiplication of the investigated *E. fortunei* cultivars.

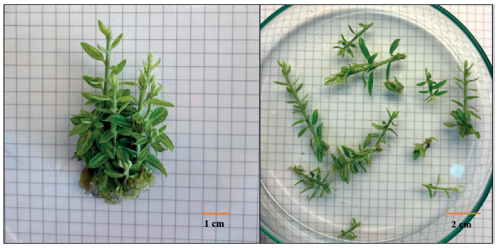



Figure 5. *E. fortunei* 'Emerald Gaiety' shoots obtained on media with 2 mg/L meta-Topolin and 1 mg/L indole acetic acid

The lowest shoot regeneration was observed on media M1 (2 mg/L BAP), with an average of 1.30 ± 0.46 ('Emerald 'n' Gold') and 1.45 ± 0.66 shoots ('Emerald Gaiety') and media M2 (2 mg/L BAP and 1 mg/L IAA), with an average of 2.1 ± 1.0 'Emerald 'n' Gold') and 2.4 ± 0.8 shoots ('Emerald Gaiety'). However, the difference between M1 and M2 was not statistically significant according to Tukey's HSD test ($p > 0.05$). Thus, although the numerical increase following IAA supplementation was apparent, it should not be interpreted as a statistically confirmed improvement. However, for shoot regeneration of *Euonymus* species, most studies focus on using BAP in combination with NAA (Shang et al., 2006). In *E. alatus*, adventitious shoot formation from hypocotyl segments can be achieved on media with 0.3 mg/L BAP and 0.1 mg/L NAA (Smith & Jernstedt, 1989). For direct shoot regeneration, Kali et al. (2024) recommend using media with BAP (1 mg/L), NAA (0.5 mg/L), and KIN (0.2 mg/L), both for nodal segments and internode explants, reaching a regeneration potential up to 90%. In *E. fortunei* var. *radicans,* Shang et al. (2009) obtained an average of 5.1 shoots from hypocotyl explants cultivated on media with 1.0 mg/L BAP and 0.01 mg/L NAA, with a regeneration frequency of 94%. For further proliferation of the regenerated shots, the concentration of NAA can be increased to 0.1 mg/L. *Euonymus bungeanus* plantlets can be successfully regenerated from leaf explants on induction media with 0.5 mg/L BAP and 0.5 mg/L NAA under red radiation and then transferred to media with 1 mg/L BAP and 0.5 mg/L NAA (Ning et al., 2021).

All multiplication media contained the same concentration of PPM (0.2%, v/v); therefore, PPM was not an experimental factor in the comparison among M1–M4. Consequently, differences in shoot proliferation observed among these treatments are interpreted primarily in relation to the cytokinin type and the presence or absence of IAA. Nevertheless, because PPM may have biological effects in addition to its antimicrobial activity, its potential contribution to plant growth cannot be completely excluded. The constant PPM concentration across all multiplication treatments, however, allows the relative effects of BAP and mT to be compared under the same PPM conditions.

***Average shoot length***

Shoot length also varied among the multiplication treatments (Figure 6). The highest numerical mean shoot length was 34.17 ± 4.94 mm on M2 (2 mg/L BAP and 1 mg/L IAA) for 'Emerald Gaiety' and 34.10 ± 9.99 mm on M3 (2 mg/L mT) for 'Emerald 'n' Gold', followed by 34.05 ± 9.64 mm on M4 (2 mg/L mT and 1 mg/L IAA) for 'Emerald Gaiety'. Lowest results were obtained on media M1 (2 mg/L BAP), 23.93 ± 5.76 mm for 'Emerald Gaiety' and 24.76 ± 5.11 mm (2 mg/L BAP and 1 mg/L IAA) for 'Emerald 'n' Gold'. Tukey's HSD test indicated that M2, M3, and M4 did not differ significantly from one another, whereas significant differences were detected between M1 and M2 ($p < 0.05$), M1 and M3 ($p < 0.05$), and M1 and M4 ($p < 0.05$). Thus, although the numerical ranking of M2, M3, and

M4 differed between cultivars, these differences should not be interpreted as statistically significant.

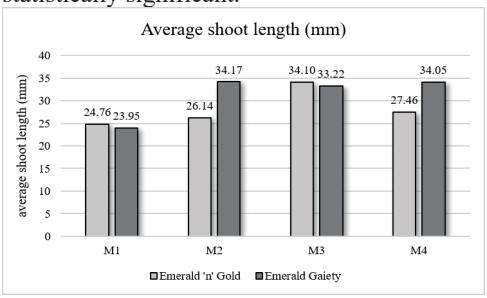



Figure 6. Average shoot length (mm)

Even though results regarding shoot length are similar between the media variants, shoots obtained on media with BAP (M1 and M2) exhibited shoot tip necrosis. Necrosis is a negative effect attributed to BAP during the multiplication phase, as excessive accumulation of cytokinin 9-glucosides has been associated with the occurrence of shoot tip necrosis in plants cultured *in vitro* (Bairu et al., 2011). In *Persea americana*, the use of mT has successfully alleviated dieback of the shoot apex, premature leaf abscission, and tissue necrosis (Hiti Bandaralage et al., 2015). Moreover, culture on media with BAP can also cause rooting inhibition and other abnormal growth patterns that have been attributed to the accumulation of biologically inactive storage forms, which are gradually released over time (Werbrouck et al., 1996). Such inactive reserves originate from the glucosylation of cytokinins such as BAP on the purine ring, either directly as glucosides or through the action of β-glucosidase enzymes (McGaw et al., 1985; Krishna Vrundha et al., 2021)

***Average basal callus mass***

Regarding the growth of basal callus, results show significant differences between the culture media variants ($p < 0.05$). In Figure 7 it can be observed that the highest mass (g) was obtained on the two media variants containing BAP: 1.90 ± 0.32 g for 'Emerald 'n' Gold' and 1.87 ± 0.32 g in 'Emerald Gaiety' on M2 and 1.81 ± 0.30 g in 'Emerald Gaiety' and 1.80 g in 'Emerald 'n' Gold' on M1; however, results from Tukey's HSD test revealed no significant differences between these two values. Lowest basal callus formation was observed on the explants cultivated on the two media variants containing mT instead of BAP: 0.77 ± 0.17 g in 'Emerald 'n' Gold' and 1.11 ± 0.47 g in 'Emerald Gaiety' on variant M3 and 1.54 ± 0.45 g in 'Emerald Gaiety' and 1.65 ± 0.44 g in 'Emerald 'n' Gold' on variant M4. Results from Tukey's HSD Test have shown that M3 and M4 to be statistically different ($p < 0.05$); however, no statistically significant differences were recorded between M4 and media variants M1 and M2 ($p > 0.05$ in both cases).

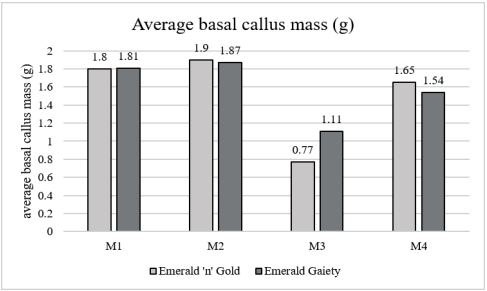



Figure 7. Average basal callus mass (g) per explant

Results obtained by Clapa et al. (2014) have also shown that media with mT reduces the formation of basal callus, compared to BAP during *in vitro* multiplication of *Paulownia* sp.. Moreover, besides a higher growth, the basal callus obtained on the media variants containing BAP progressively turned brown, accompanied by the tip necrosis of the shoots (Figure 8).

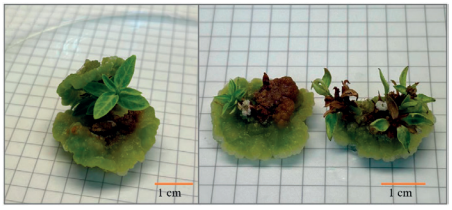



Figure 8. Effects of high concentrations of BAP – callus and shoot tip necrosis – on *E. fortunei* 'Emerald 'n' Gold' explants

Moyo et al. (2011) observed that explants cultivated on media with high concentrations of BAP resulted in the formation of non-organogenic basal callus, which was not able to differentiate into any organs. Moreover, the callus progressively turns brown during the

culture, which may be associated with the accumulation of biologically inactive cytokinin N7- and N9-glucoside conjugates, thereby reducing the availability of active cytokinins for further shoot proliferation, which may also explain the reduced number of shoots obtained from the explants cultivated on media supplemented with BAP (van Staden & Crouch, 1996; Auer, 1997; Moyo et al., 2011).

## CONCLUSIONS

This study presents an efficient *in vitro* establishment and shoot multiplication protocol for the ornamental cultivars *Euonymus fortunei* 'Emerald 'n' Gold' and 'Emerald Gaiety'. The addition of 0.2% (v/v) Plant Preservative Mixture™ (PPM) during culture establishment substantially reduced visible contamination, increasing the proportion of contamination-free explants from 55.56% to 88.89% in 'Emerald 'n' Gold' and from 48.39% to 95.71% in 'Emerald Gaiety'. During the multiplication phase, meta-topolin (mT) was more effective than 6-benzylaminopurine (BAP) under the conditions tested. The highest shoot numbers were obtained on medium containing 2 mg/L mT and 1 mg/L IAA (M4), with 4.71 shoots per explant for 'Emerald 'n' Gold' and 4.40 shoots per explant for 'Emerald Gaiety', compared with 1.30 and 1.45 shoots per explant, respectively, on the BAP-only medium (M1). In addition, mT-containing media were associated with lower basal callus formation, while shoot tip necrosis and progressive basal callus browning were predominantly observed in BAP-containing treatments. These findings indicate that mT, particularly in combination with IAA, represents a promising alternative to BAP for the multiplication of *E. fortunei* cultivars.

The present study contributes to the limited information available on *in vitr*o propagation of these *E. fortunei* cultivars, particularly by providing comparative evidence on the responses of two ornamental cultivars to mT- and BAP-based multiplication media. However, the study was limited to two cultivars and explants collected during a single sampling period, and PPM was evaluated at only one concentration. Furthermore, rooting, *ex vitro* acclimatization, genetic fidelity, and long-term field performance were not assessed. Therefore, the protocol should be considered a promising strategy for the establishment and multiplication phases rather than a complete production system. Further studies addressing rooting and acclimatization, as well as performance under environmental conditions relevant to urban and degraded sites, are required to validate its practical application. Nevertheless, the efficient production of healthy shoots may provide a useful basis for the subsequent development of planting material for sustainable urban greening, green infrastructure, and the rehabilitation of degraded urban sites where the use of these ornamental *E. fortunei* is considered environmentally appropriate.

## ACKNOWLEDGEMENTS

This work was conducted within the doctoral thesis “Biological Characteristics of Representatives of the Genus *Euonymus* L. in the Republic of Moldova” at the Doctoral School of Natural Sciences, Moldova State University, Chișinău, Republic of Moldova. The experimental studies on the *in vitro* propagation of *Euonymus fortunei* cultivars 'Emerald 'n' Gold’ and 'Emerald Gaiety' were carried out in the Plant Micropropagation Laboratory of the Research Center for Studies of Food Quality and Agricultural Products at University of Agronomic Sciences and Veterinary Medicine of Bucharest, Romania.

## REFERENCES

Amoo, S. O., Finnie, J. F., & Van Staden, J. (2009). In vitro propagation of *Huernia hystrix*: An endangered medicinal and ornamental succulent. *Plant Cell, Tissue and Organ Culture (PCTOC)*, *96*(3), 273–278. https://doi.org/10.1007/s11240-008-9484-8

Auer, C. A. (1997). Cytokinin conjugation: Recent advances and patterns in plant evolution. *Plant Growth Regulation*, *23*(1), 17–32.

Bairu, M. W., Novák, O., Doležal, K., & Van Staden, J. (2011). Changes in endogenous cytokinin profiles in micropropagated *Harpagophytum procumbens* in relation to shoot-tip necrosis and cytokinin treatments. *Plant Growth Regulation*, *63*(2), 105–114.

Bauer, J. T., & Reynolds, H. L. (2016). Restoring native understory to a woodland invaded by *Euonymus fortunei*: Multiple factors affect success. *Restoration Ecology*, *24*(1), 45–52.

Bettoni, J., Bonnart, R., Shepherd, A., Kretzschmar, A., & Volk, G. (2019). Cryopreservation of grapevine

(*Vitis* spp.) shoot tips from growth chamber-sourced plants and histological observations. *Vitis - Geilweilerhof-*, *58*(2), 71–78.

Biahoua, A., & Bonneau, L. (1999). Control of *in vitro* somatic embryogenesis of the spindle tree (*Euonymus europaeus* L.) by the sugar type and the osmotic potential of the culture medium. *Plant Cell Reports*, *19*(2), 185–190. https://doi.org/10.1007/s002990050731

Boiu-Sicuia, O.-A., & Cornea, C. P. (2019). Isolation Procedures for Endophytes Harvesting. *AgroLife Scientific Journal*, *8*(1), 43–52.

Boyer, C. R., Cole, J. C., & Conway, K. E. (2007). Effectiveness of Copper Sulfate Pentahydrate, Mancozeb, and Hydrogen Dioxide in Controlling Anthracnose on Wintercreeper Euonymus. *Journal of Environmental Horticulture*, *25*(1), 21–26.

Caton, L. (2008). Tissue Culture for Challenging Woody Plants. *Combined Proceedings International Plant Propagators' Society*, *58*, 284–285.

Chauhan, R. D., & Taylor, N. J. (2018). Meta-topolin stimulates de novo shoot organogenesis and plant regeneration in cassava. *Plant Cell, Tissue and Organ Culture*, *132*, 219–224. https://doi.org/10.1007/s11240-017-1315-3

Chebotar, V. K., Shcherbakov, A. V., Maslennikova, S. N., Zaplatkin, A. N., Kanarskiy, A. V., & Zavalin, A. A. (2016). Endophytic bacteria of woody plants as the basis of complex microbial preparations for agriculture and forestry. *Russian Agricultural Sciences*, *42*(5), 339–342. https://doi.org/10.3103/S1068367416050037

Chen, Y., Lu, L., Deng, W., Yang, X., McAvoy, R., Zhao, D., Pei, Y., Luo, K., Duan, H., Smith, W., Thammina, C., Zheng, X., Ellis, D., & Li, Y. (2006). In vitro regeneration and Agrobacterium-mediated genetic transformation of *Euonymus alatus. Plant Cell Reports*, *25*(10), 1043–1051.

Clapa, D., Fira, A., Simu, M., Vasu, L. B., & Buduroi, D. (2014). Improved *In Vitro* Propagation of *Paulownia elongata*, *P. fortunei* and its Interspecific Hybrid *P. elongata* x *P. fortunei*. *Bulletin UASVM Horticulture 71*(1)*,* 6-14.

Cockfield, S. D., & Potter, D. A. (1986). Interaction of Euonymus scale (Homoptera: Diaspididae) feeding damage and severe water stress on leaf abscission and growth of *Euonymus fortunei*. *Oecologia*, *71*(1), 41–46. https://doi.org/10.1007/BF00377318

Cole, J. C., Schupbach, S. L., & Conway, K. E. (2009). Intensity of Anthracnose on Three Wintercreeper Euonymus Cultivars as Influenced by Fungicide Program. *Journal of Environmental Horticulture*, *27*(3), 171–175. https://doi.org/10.24266/0738-2898-27.3.171

Cui, K.-G., Wang, H.-L., Quan, W.-Y., Ye, Z.-Z., & Zhao, C.-R. (2025). Rapid and efficient stem segment regeneration propagation system for *Euonymus bungeanus*. *South African Journal of Botany*, *186*, 475–485. https://doi.org/10.1016/j.sajb.2025.09.041

Fajinmi, O. O., Amoo, S. O., Finnie, J. F., & Staden, J. V. (2014). Optimization of *in vitro* propagation of *Coleonema album*, a highly utilized medicinal and ornamental plant. *South African Journal of Botany, 94,* 9-13.

Fajrisani, S., Noli, Z. A., Mansyurdin, & Syamsuardi. (2026). Optimization of sterilization methods and PPM$^{TM}$ supplementation in culture media for *in vitro* culture of leaf and nodal explants of *Cryptocarya massoy*. *Notulae Scientia Biologicae*, *18*(2), 12941. https://doi.org/10.55779/nsb18212941

Gubaidullin, N., Kali, B., Tussipkan, D., & Manabayeva, S. A. (2024). A promising strategy for conservation of Central Asian endemic plant *Euonymus koopmannii. Biodiversitas: Journal of Biological Diversity*, *25*(7), 3114. https://doi.org/10.13057/biodiv/d250733

Gutue, C., Gutue, M., & Roşca, I. (2015). *Unaspis euonymi* (Comstock), a pest associated with damaging the parks and ornamental gardens of Bucharest. *Scientific Papers. Series B, Horticulture, LIX*, 351–354.

Hiti Bandaralage, J., Hayward, A., O'Brien, C., & Mitter, N. (2015). Gibberellin and cytokinin in synergy for a rapid nodal multiplication system of avocado. *Actas Proccedings, VIII Congreso Mundial de la Palta*, 95-103.

Izarra, M. L., Panta, A. L., Maza, C. R., Zea, B. C., Cruzado, J., Gutarra, L. R., Rivera, C. R., Ellis, D., & Kreuze, J. F. (2020). Identification and Control of Latent Bacteria in *in vitro* Cultures of Sweetpotato [*Ipomoea batatas* (L.) Lam]. *Frontiers in Plant Science*, *11*. https://doi.org/10.3389/fpls.2020.00903

Jefferson, D. K., & Schultz, P. B. (1995). Differential Susceptibility of Six Euonymus Species and Cultivars to Euonymus Scale, *Unaspis euonymi* (Comstock). *Journal of Environmental Horticulture*, *13*(3), 140–142. https://doi.org/10.24266/0738-2898-13.3.140

Kali, B., Bekkuzhina, S., Tussipkan, D., & Manabayeva, S. (2024). A First Approach for the *In Vitro* Cultivation, Storage, and DNA Barcoding of the Endangered Endemic Species *Euonymus koopmannii*. *Plants*, *13*(16), 2174. https://doi.org/10.3390/plants13162174

Keshari, B., Mohapatra, N., & Deo, B. (2020). Study of meta-topolin in multiplication culture of local variety Champa (*Musa* spp.) through *in vitro* culture. *International Journal of Botany Studies*, *5*(6), 572–575.

Kirillov, V., Pathak, A., Stikhareva, T., Ercisli, S., Daulenova, M., Kazangapova, N., & Rakhimzhanov, A. (2022). *In vitro* propagation and *ex vitro* rooting of *Euonymus verrucosus* Scop. (Celastraceae) – a rare species of Kazakhstan flora on the southern border of its areal. *Journal of Forest Research*, *27*(4), 289–296. https://doi.org/10.1080/13416979.2022.2031477

Krishna Vrundha, C. P., Aswathi, N. V., & Thomas, T. D. (2021). The Role of Meta-topolin in Plant Morphogenesis *In Vitro*. In N. Ahmad & M. Strnad (Eds.), *Meta-topolin: A Growth Regulator for Plant Biotechnology and Agriculture*, 93–118. Springer. https://doi.org/10.1007/978-981-15-9046-7_10

Kushnarenko, S. V., Omasheva, M., Romadanova, N., Aralbayeva, M., Rymkhanova, N., Manapkanova, U., Botta, R., Ruffa, P., Valentini, N., & Marinoni, D. T. (2025). Genetic Diversity of the Only Natural

Population of *Corylus avellana* L. in Kazakhstan and Prospects for Its *In Vitro* Conservation. *Biology*, *14*(11), 1472. https://doi.org/10.3390/biology14111472

Leifert, C., & Cassells, A. C. (2001). Microbial hazards in plant tissue and cell cultures. *In Vitro Cellular & Developmental Biology - Plant*, *37*(2), 133–138. https://doi.org/10.1007/s11627-001-0025-y

Marino, G., Altan, A. D., & Biavati, B. (1996). The effect of bacterial contamination on the growth and gas evolution of *In vitro* cultured apricot shoots. *In Vitro Cell Dev Biol – Plant*, *32*(1), 51–56. https://doi.org/10.1007/BF02823014

Masondo, N. A., Aremu, A. O., Finnie, J. F., & Van Staden, J. (2015). Growth and phytochemical levels in micropropagated *Eucomis autumnalis* subspecies autumnalis using different gelling agents, explant source, and plant growth regulators. *In Vitro Cellular & Developmental Biology - Plant*, *51*(1), 102–110. https://doi.org/10.1007/s11627-014-9646-9

McGaw, B. A., Horgan, R., & Heald, J. K. (1985). Cytokinin metabolism and the modulation of cytokinin activity in radish. *Phytochemistry*, *24*(1), 9–13. https://doi.org/10.1016/S0031-9422(00)80797-9

Meyer, E. M., Touchell, D. H., & Ranney, T. G. (2009). In Vitro Shoot Regeneration and Polyploid Induction from Leaves of *Hypericum* Species. *HortScience*, *44*(7), 1957–1961. https://doi.org/10.21273/HORTSCI.44.7.1957

Mihaljević, I., Dugalić Krunoslav, K., Tomaš, V., Viljevac Marija, M., Pranjić, A., Čmelik, Z., Puškar, B., & Jurković, Z. (2013). *In vitro* sterilization procedures for micropropagation of 'Oblačinska' sour cherry. *Journal of Agricultural Sciences (Belgrade)*, *58*(2), 117–126.

Moyo, M., Finnie, J. F., & Van Staden, J. (2011). Recalcitrant effects associated with the development of basal callus-like tissue on caulogenesis and rhizogenesis in *Sclerocarya birrea. Plant Growth Regulation*, *63*(2), 187–195. https://doi.org/10.1007/s10725-011-9562-5

Niedz, R. P., & Bausher, M. G. (2002). Control of In vitro contamination of explants from greenhouse- and field-grown trees. *In Vitro Cellular & Developmental Biology - Plant*, *38*(5), 468–471. https://doi.org/10.1079/IVP2002316

Ning, K., Zhou, T., Jiang, C. Z., Wu, H. M., Jiang, J. L., Chen, J., El-KASSABY, Y. A., & Ma, Y. (2021). Rapid and efficient leaf regeneration propagation system for *Euonymus bungeanus*. *Biologia Plantarum*, *65*, 118–125. https://doi.org/10.32615/bp.2020.166

Ningen, S. S., Cole, J. C., & Conway, K. E. (2004). Cultivar and Night Temperature Affect Severity of Anthracnose on *Euonymus fortunei. HortScience*, *39*(2), 230–231. https://doi.org/10.21273/HORTSCI.39.2.230

Ningen, S. S., Cole, J. C., Smith, M. W., Dunn, D. E., & Conway, K. E. (2005). Increased Shade Intensity and Afternoon Irrigation Decrease Anthracnose Severity on Three *Euonymus fortunei* Cultivars. *HortScience, 40*(1), 111–113.

Nosov, A. V., Fomenkov, A. A., Sidorov, R. A., & Goriainov, S. V. (2024). *Euonymus maximowiczianus* aril-derived long-term suspension-cultured cells: Light and methyl jasmonate impact in the anthocyanin and VLCFA accumulation. *Plant Physiology and Biochemistry*, *217*, 109293. https://doi.org/10.1016/j.plaphy.2024.109293

Parkinson, M., Prendergast, M., & Sayegh, A. J. (1996). Sterilisation of explants and cultures with sodium dichloroisocyanurate. *Plant Growth Regulation*, *20*(1), 61–66. https://doi.org/10.1007/BF00024060

Percival, G. C., & Sheriffs, C. N. (2002). Identification of Drought-Tolerant Woody Perennials Using Chlorophyll Fluorescence. *Arboriculture & Urban Forestry*, *28*(5), 215–223. https://doi.org/10.48044/jauf.2002.032

Permadi, N., Prismantoro, D., Navisya Vasall, P. R., Sheelmarevaa, F. A., Nurjanah, S., Nurzaman, M., Alhasnawi, A. N., Doni, F., & Julaeha, E. (2025). Modern and traditional strategies for controlling microbial contamination in plant micropropagation: Current insights and future perspectives. *Current Research in Biotechnology*, *10*, 100337. https://doi.org/10.1016/j.crbiot.2025.100337

Quambusch, M., & Winkelmann, T. (2018). Bacterial Endophytes in Plant Tissue Culture: Mode of Action, Detection, and Control. *Methods Mol Biol*. 1815:69-88.

Reddy, V., Varghese, D., & Shaik, S. (2025). Towards long-term conservation of *Siphonochilus aethiopicus*, a critically endangered South African medicinal species: An improvement on micropropagation using in vitro shoot apices. *South African Journal of Botany*, *180*, 325–336.

Romadanova, N. V., Tolegen, A. B., Kushnarenko, S. V., Zholdybayeva, E. V., & Bettoni, J. C. (2022). Effect of Plant Preservative MixtureTM on Endophytic Bacteria Eradication from *In Vitro*-Grown Apple Shoots. *Plants*, *11*(19), 2624.

Savinov, I. A. (2022). Preliminary Analysis of the Degree of Naturalization in Some *Euonymus* Species (Celastraceae) in the Central Part of European Russia and the Caucasus: Results and Further Trends. *Russian Journal of Biological Invasions*, *13*(4), 530–536. https://doi.org/10.1134/S2075111722040105

Shang, A.-Q., Cai, H., Yan, X.-J., Hu, H.-Z., & Zhao, L.-J. (2006). Plant regeneration from *in vitro* cultured hypocotyl explants of *Euonymus japonicus* 'Cu zhi'. *Agricultural Sciences in China, 5*(3), 196–201

Shang, A.-Q., Chen, Y., Zhao, L.-J., & Tian, Y.-C. (2008). Direct adventitious shoot regeneration system of *Euonymus fortunei* var. *radicans* and its genetic transformation mediated by *Agrobacterium tumefaciens*. *Chinese Journal of Agricultural Biotechnology, 5*(2), 133–139.

Shang, A.-Q., Sun, Z.-Y., & Zhao, L.-J. (2009). High efficient regeneration *in vitro* from hypocotyl of *Euonymus fortunei* var. *radicans*. *Scientia Silvae Sinicae, 45*(2), 136–141.

Simran, C. S., & Narasimhan, S. (2021). Sodium Dichloroisocyanurate: An eco-friendly chemical alternative for media autoclaving and explant sterilisation in plant tissue culture. *International*

*Journal of Research in Pharmaceutical Sciences*, *12*(1).

Smith, C. C., & Jernstedt, J. A. (1989). *In vitro* development of adventitious shoots in *Euonymus alatus* (Celastraceae). *Scientia Horticulturae*, *41*(1), 161–169. https://doi.org/10.1016/0304-4238(89)90060-5

Thammina, C., He, M., Lu, L., Cao, K., Yu, H., Chen, Y., Tian, L., Chen, J., McAvoy, R., Ellis, D., Zhao, D., Wang, Y., Zhang, X., & Li, Y. (2011). *In Vitro* Regeneration of Triploid Plants of E*uonymus alatus* 'Compactus' (Burning Bush) from Endosperm Tissues. *HortScience*, *46*(8), 1141–1147. https://doi.org/10.21273/HORTSCI.46.8.1141

Thammina, C., He, M., Yu, H., Chen, Y., Gai, Y., Cao, K., Lu, L., Zhao, D., Wang, Y., McAvoy, R., Ellis, D., & Li, Y. (2012). Continuous biosynthesis of abscisic acid (ABA) may be required for maintaining dormancy of isolated embryos and intact seeds of Euonymus alatus. *Plant Cell, Tissue and Organ Culture (PCTOC)*, *108*(3), 493–500. https://doi.org/10.1007/s11240-011-0063-z

Trzewik, A., Malinowski, T., Niewiadomska-Wnuk, A., Mynett, K., & Orlikowska, T. (2025). Removal of Persistent Bacterial Contaminants from *In Vitro* Shoot Cultures of Raspberry (*Rubus idaeus* L.) Using Vacuum Infiltration and Its Effect on Multiplication Efficiency. *Agronomy*, *15*(11), 2452. https://doi.org/10.3390/agronomy15112452.

van Staden, J., & Crouch, N. R. (1996). Benzyladenine and derivatives-their significance and interconversion in plants. *Plant Growth Regulation*, *19*(2), 153–175.

Wang., M. L., Zhao, L. J., Ren., G. F., Wang, J. H., Feng, H. (2004). Adventitious bud regenerating system of *Euonymus fortunei. Acta Horticulturae Sinica*, *31*(2), 241–244.

Werbrouck, S., Strnad, M., Van Onckelen, H., & Debergh, P. (1996). Meta-topolin, an alternative to benzyladenine in tissue culture? *PHYSIOLOGIA PLANTARUM*, *98*(2), 291–297.

Woo, H.-A., Ku, S. S., Jie, E. Y., Kim, H., Kim, H.-S., Cho, H. S., Jeong, W.-J., Park, S. U., Min, S. R., & Kim, S. W. (2021). Efficient plant regeneration from embryogenic cell suspension cultures of *Euonymus alatus*. *Scientific Reports*, *11*(1), 15120. https://doi.org/10.1038/s41598-021-94597-4

Scientific Papers. Series E. Land Reclamation, Earth Observation & Surveying, Environmental Engineering. Vol. XV, 2026
Print ISSN 2285-6064, CD-ROM ISSN 2285-6072, Online ISSN 2393-5138, ISSN-L 2285-6064

# HYBRID RENEWABLE ENERGY SUPPLY SYSTEM - STORAGE REQUIREMENTS CONSIDERING SEASONAL VARIATION OF PV OUTPUT

**Mirela Laura IEREMCIUC, Ioan DAVID, Camelia ȘTEFĂNESCU, Mihai NEGURA, Dorina-Gabriela IONESCU, Mircea VIȘESCU**

University Politehnica of Timisoara, 2 Victoriei Square, Timisoara, Romania

Corresponding author email: ioan.david@gmx.net

***Abstract***

*The transition toward sustainable and decentralized energy systems has accelerated the deployment of hybrid renewable energy supply systems (HRESS) in remote and off-grid areas worldwide. Hybrid systems that combine photovoltaic (PV) and wind energy technologies are particularly attractive because they exploit complementary renewable resources, reduce dependence on fossil fuels, and improve energy security for isolated users. Although the literature contains numerous technical studies on hybrid renewable energy systems, detailed analyses of annual storage requirements that explicitly account for seasonal variations in renewable generation remain limited. The main objective of this paper is to address this gap by proposing an analytical method for determining the annual energy storage capacity required to ensure a continuous power supply to an isolated consumer while accounting for seasonal variations in PV output. We illustrate the proposed method through a case study involving a 2–3 ha vineyard with a small guesthouse located in a mountainous region of Romania.*

***Key words:*** *Hybrid Renewable Energy System, seasonal photovoltaic (PV) energy storage, sizing method of storage.*

## INTRODUCTION

Hybrid Renewable Energy Systems (HRES), particularly those combining photovoltaic (PV) and wind energy generation, have been the subject of extensive research due to their potential to improve the reliability and sustainability of power supply in remote and off-grid locations. Several comprehensive reviews highlight that the integration of multiple renewable sources significantly enhances energy availability and reduces the dependency on conventional fuels, making hybrid configurations well-suited for isolated demand scenarios (Ahmad et al., 2024). Hybridization helps to mitigate the intermittency inherent in solar and wind resources by exploiting their complementary behaviour over daily and seasonal cycles, thus improving overall system performance and reliability (Hassan et al., 2023).

A critical aspect of HRES design is the sizing and optimization of both generation and storage components. Reviews on PV-wind-based hybrid systems report a wide range of deterministic and stochastic methods used to size system components, including energy production units and storage elements, based on historical climate data and user load profiles (Anoune et al., 2018). Many studies emphasize that appropriate sizing directly influences system reliability, cost-effectiveness, and the ability to meet energy demand throughout the year. However, they also point out that most sizing approaches tend to focus on capacity and reliability indices without deeply addressing the long-term or seasonal storage needs aligned with annual variability in renewable generation (Kafando et al., 2024).

Energy storage plays a central role in balancing supply and demand in hybrid systems. Storage systems such as batteries, hydrogen storage, or hybrid storage configurations are critical for accommodating fluctuations in renewable generation and sustaining continuous power availability during low resource periods. Systematic reviews in the field underscore that efficient energy storage integration and energy management strategies are essential to offset the intermittency of PV and wind resources and to improve system performance over extended temporal scales (Ma et al., 2015). Research also

highlights that hybrid storage solutions (e.g., battery-supercapacitor combinations) and advanced energy management systems can enhance storage utilization and extend equipment life while providing better operational flexibility (Kafando et al., 2024).
Despite the inclusion of storage sizing in many studies' optimization frameworks, a principled, analytical analysis of annual or seasonal storage requirements remains infrequent.
Most existing approaches focus on short-term sizing (daily or monthly) and rely on optimization tools such as HOMER or artificial intelligence-based techniques for short-term energy balance and reliability criteria (Ahmad et al., 2024). While these frameworks are useful for determining optimal component sizing under given climatic conditions, they often do not explicitly model annual storage autonomy that accounts for significant seasonal mismatches between renewable supply and demand.
Furthermore, research on the complementarity of solar and wind resources suggests that combining these sources can inherently reduce the magnitude of storage needed by smoothing variability. Studies employing metrics such as stability coefficients and capacity credits demonstrate that optimal PV–wind configurations provide more uniform generation profiles than single source systems, potentially lowering the storage burden required for year-round operation (Badea et al., 2019). Nevertheless, these studies generally focus on large-scale or grid-connected applications rather than isolated, remote systems with stringent autonomy requirements.
In summary, the recent literature (Hassan et al., 2023) underscores the advantages of hybrid PV–wind systems in enhancing renewable energy reliability, the necessity of integrating storage for autonomous operation (Dagdougui et al., 2012) and the variety of sizing and optimization methodologies available (Anoune et al., 2018).
Yet a gap remains in explicitly characterizing annual storage requirements that fully capture the seasonal dynamics of renewable resources.
This gap motivates the analytical method proposed in the present paper, which aims to quantify the storage capacity needed to ensure continuous energy supply for isolated users across an annual cycle, considering seasonal variation of the PV source.

## MATERIALS AND METHODS

### Conceptual physical model of a HRES

In this paper, a hybrid energy supply system will be an analysed, considering a conceptual physical model that contains the al00main components of the system: the photovoltaic electricity generator, end users of electricity, and the energy storage subsystem, as well as the connections necessary to ensure its functionality. The HYBRID system offers a partially or fully autonomous energy supply that relies solely on renewable energy sources, specifically the photovoltaic (PV) source in this case.
Figure 1 shows a diagram of such a hybrid autonomous electricity supply system.
As energy end users, there can be, for example, small tourist complexes or vineyards of 2-3 ha with a small guesthouse, located in isolated areas.

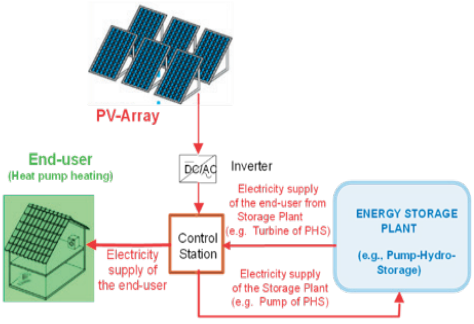



Figure 1. Conceptual physical model of a Hybrid Renewable Energy Systems (HRES) (Simão & Ramos, 2020)

The most important component of the system is the energy storage system (e.g. a Pump-hydro-storage) which ensures the seasonal energy balance between the required energy load of the end-user and the variable PV energy due to the solar radiation variability. Red lines with arrows show the flow of electrical energy between system components.

### Required energy supply for end-user

The type of user determines the required energy demand that the hybrid photovoltaic storage system must meet.
End users such as tourist establishments or households use energy for lighting and electrical appliances, space heating and hot water, space

cooling, cooking, and other end uses. In Figure 2 we can follow the average distribution of household energy in the EU (EUROSTAT, 2026).

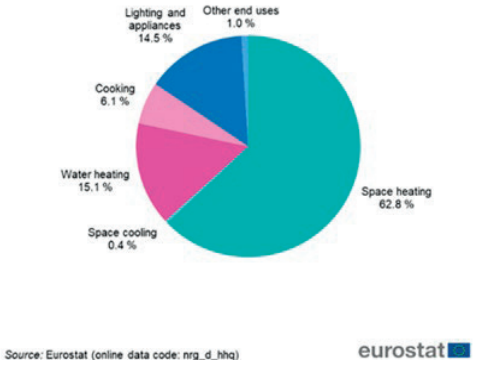



Figure 2. Averaged energy sharing in a household in EU (https://ec.europa.eu/eurostat/statistics-explained/index.php?title=Energy_consumption_in_households)

It can be seen in Figure 2 that, in a household, approximately 20% represents the direct consumption of electricity, and the remaining 80% is consumed mainly for heating and the preparation of domestic hot water.

From the European statistical data (EUROSTAT, 2026) follows that the specific total energy consumption in households per capita and year ($e_{ECH}$) is approximately:

$e_{ECH}$ =6800 kWh/cap/a in EU and $e_{ECH}$ =53200 kWh/cap/a in Romania. (Anoune et al., 2018)

Knowing the specific energy consumption, the total energy consumption for N people can be calculated:

$$E_{L/a} = N \cdot e_{ECH} \text{ in kWh/a} \quad (1)$$

For another type of end user, like guesthouse or vineyard of 2-3 ha with a small guesthouse, the required energy can be estimated using data from Malvoni & Cponcedo (2017), INSSE/Eurostat (2020-2025), OIV (2025) or REHVA. Such a user will be considered an example in the next paragraph - *The PV component*.

From the annual energy load $E_{l/a}$ (kWh/a) the annual average power demand can be determined $P_{l/a}$ (kW):

$$P_{l/a} = E_{l/a}/8760 \text{ in kW} \quad (2)$$

It is worth noting that energy consumption for heating, representing approximately 70-80% of a household's total energy consumption, can be substantially reduced (by approximately 50-75%) by using a heat pump, which operates on the electricity produced by PV. Thus, the entire energy consumption can be covered from the green electric current produced by PV

The analysis of heat pump efficiency based on the so-called Coefficient of Performance (COP) (i.e., the generated heating energy (kWh) divided the electricity consumed to generate heat (kWh) can be followed in detail in (WOLF, 2026).

**The PV component**

The PV-array component (Figure 1) is used to supply the consumer and, as appropriate, the storage system, respectively. Photovoltaic (PV) energy is a renewable energy source that does not produce emissions or pollutants while being a cost-effective energy source available everywhere (Quaschning, 2010; Badea et al., 2019).

The main disadvantage of a photovoltaic energy source (PV), in addition to its benefits, is the fluctuation in electricity output caused by the day and night cycle of solar radiation and seasonal variations, which result in higher output during the summer months and lower output in the winter months, as depicted in Figure 3.

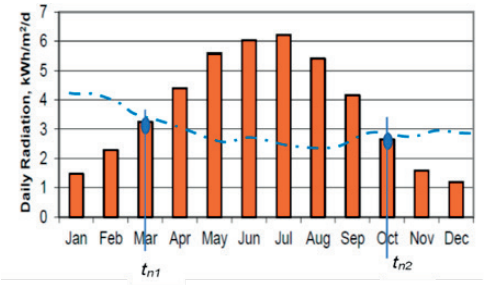



Figure 3. Example to schematic diagrams showing the annual distribution of monthly average solar radiation (https://www.researchgate.net/figure/Monthly-average-daily-solar-radiation_fig2_346271383)

For comparison, the required energy load (blue line) was also depicted. This juxtaposition is important for understanding the necessity of storing solar energy during times when solar radiation (i.e., PV-generated electricity) exceeds the required load ($t_{n1}<t_i<t_{n2}$) and for returning stored energy to meet demand during periods of

low solar radiation (e.g., the winter months: $t_i<t_{n1}$ and $t_i> t_{n2}$).

The annual output energy $E_{PV/a}$ generated by PV panel can be determined from the annual solar radiation ESR/a considering the *PR*-Performance Ratio (about 0,70-0,75) and the performance coefficient of PV panel $\eta \cong 0{,}18$-$0{,}25$ (Quaschning, 2010); https://www.solar.com/learn/solar-panel-efficiency/; https://strom-profis.net/produkt/ja-solar-jam72s20-455-mr-455-wp-solarmodul-bfr/).

An average value can be estimated as:

$$E_{PV/a}=\eta \cdot PR \cdot E_{SR/a}=\eta \cdot E_{PVP/a}\cong 0{,}145 E_{PVP/a} \quad (3)$$

For a given location, the solar radiation $E_{SR/a}$ is given in databases like NASA POWER and Global Solar Atlas.

For the design and analysis of the efficiency of a photovoltaic system (PV array), it is beneficial to develop a mathematical model that describes the influence of seasonal variations in solar radiation, a topic that has been less researched in the specialized literature.

In this context, it is noteworthy that the shape of the solar radiation distribution curve (Figure 3) is close to a sinusoidal one, which suggests the possibility using a mathematical representation based on trigonometric functions.

Based on these observations, the following trigonometric function is proposed to calculate the annual distribution of the average monthly power $P_{PV}(ti)$ (i.e. the monthly energy in kwh/month generated by the PV plant):

$$P_{PV}(t_i) = A\,(1-B\cos(\pi t_i)/6) \quad (4)$$

- A and B are specific parameters of the solar energy distribution diagram (e.g. Figure 3).
- In this context, ti represents the month number i of the year (for example, for January, $t_i=t_1=1$; for February, $t_i=t_2=2$; and for December, $t_i=t_{12}=T=12$).

To determine the parameter A, observe that by integrating equation (4) over a period of one year (Ta=12 month) the integral of the left-hand term represents the annual PV energy $E_{PV/a}$. On the other hand, $E_{PV/a}$ can be expressed using the annual average $P_{PV0}$ of the monthly average powers $P_{PV}$ (ti) as $E_{PV/a}=12\ P_{PV0}$.

Since the integral over the time interval Ta of the function *cos (πti)/6*) is zero, it follows that the integral of the right-hand side of equation (4) has the value 12A. Based on these results, the value of the parameter *A* is equal to $P_{PV0}$, meaning $A = P_{PV0}$.

To determine the parameter B, equation (4) will be applied for two characteristic points of the distribution diagram (Figure 3): the maximum monthly average power ($P_{PVmax}$) in the months June-July (i.e. $t_i=6$), respectively the minimum monthly average power ($P_{PVmin}$) in the months January and December (i.e., $t_i=0$ and $t_i=12$)

$$B = \frac{P_{PVmax}-P_{PVmin}}{P_{PVmax}+P_{PVmin}} \quad (5)$$

It is noted that the parameter B represents the maximum deviation of the maximum monthly mean power, $P_{PVmax}$. For this reason, B continues to be designated as σ.

Based on the above considerations and results, the mathematical model of the seasonal variation of the monthly average photovoltaic power (4) can be written in the form

$$P_{PV}(t_i) = P_{PV0}\left(1-\sigma_S \cos\frac{\pi t_i}{6}\right) \quad (6)$$

This proposed mathematical model will be further used (in paragraph entitled *Calculation method of the required energy storage to balance seasonal variation of PV*) to determine the PV energy storage required to balance seasonal variations of solar radiation.

**Calculation method of the required energy storage to balance seasonal variation of PV**

We can establish the characteristic operating intervals of the PV energy supply system using the representation from Figure 3, where the times marking $t_{n1}$ and $t_{n2}$ indicate the intersection points of both curves' load and photovoltaic (PV) energy production.

During the intervals $t < t_{n1}$ and $t > t_{n2}$ (i.e., the winter months) when the consumption requirement is higher than the PV-generated energy, the energy supply must be provided from the energy storage system (Figure 1) (i.e. turbine operation in the case of PHS). In the interval $[t_{n1} – t_{n2}]$ (i.e. during the months with higher solar radiation) the PV-generated energy is higher than the required energy by the consumer; the excess energy can be stored (i.e. pump operation in the case of PHS pump operation).

Denoting with $P_{L(t)}$ the power demand and with $P_{PV(t)}$ the photovoltaic power at the current

month t, the required *annual energy stored capacity* $E_{S/a}$ can be expressed as

$$E_{S/a} = \int_0^{t_{n1}} [P_L(\tau) - P_{PV}(\tau)]d\tau + \int_{t_{n2}}^{T} [P_L(\tau) - P_{PV}(\tau)]d\tau \quad (7)$$

Relation (7) can be rearranged using the proposed analytical model of the solar power (6) and a series of mathematical transformations, obtaining the following form:

$$E_{S/a} = 2\int_0^{t_{n1}} \left[P_L(\tau) - P_{PV0}\left(1 - \sigma_S cos\frac{\pi\tau}{6}\right)\right] d\tau \quad (8)$$

In the mathematical developments to obtain relation (8) the following simplifications were considered: the function *cos πτ/6 h*as approximately the same values in the time intervals [0, $t_{n1}$]and [$t_{n2}$, T] (Figure 3).
The photovoltaic energy ($E_{PVE/a}$), which exceeds the energy demand during the time interval $t_{n1}$-$t_{n2}$, can also be expressed in a similar integral form.

$$E_{PVE/a} = \int_{t_{n1}}^{t_{n2}} [P_{PV}(\tau) - P_L(\tau)]d\tau \quad (9)$$

respectively, using (6)

$$E_{PVE/a} = \int_{t_{n1}}^{t_{n2}} \left[P_{PV0}\left(1 - \sigma_S cos\frac{\pi\tau}{6}\right) - P_L(\tau)\right] d\tau \quad (10)$$

To analyse different HESS electricity supply options, a parameter can be introduced and defined as the ratio between the annual produced photovoltaic (PV) energy and the load that defines the degree of energy autonomy:

$$\lambda = \frac{E_{PV/a}}{E_{L/a}} = \frac{P_{PV0}}{P_{L0}} \quad (11)$$

For feasibility studies it is sufficient to consider a simplified case of a constant average power demand i.e.,

$$P_L(t) = P_{L0} = \frac{E_L/a}{12} \quad (12)$$

Using the parameter $\lambda$ and (12) the equation (8) of the required annual storage can be rearranged by obtaining the following form:

$$E_{S/a} = \frac{E_{L/a}}{6}\int_0^{t_{n1}} \left[1 - \lambda\left(1 - \sigma_S cos\frac{\pi\tau}{6}\right)\right] d\tau \quad (13)$$

Integration yields the following equation for required annual storage:

$$E_{S/a} = E_{L/a}\left[(1-\lambda)\frac{t_{n1}}{6} + \lambda\frac{\sigma_S}{\pi} sin\frac{\pi t_{n1}}{6}\right] \quad (14)$$

Similarly, (10) can be written in the following form:

$$E_{PVE/a} = \frac{E_{L/a}}{12}\int_{t_{n1}}^{t_{n2}} \left[\lambda\left(1 - \sigma_S cos\frac{\pi\tau}{6}\right) - 1\right] d\tau \quad (15)$$

Performing the integration, we obtain

$$E_{PVE/a} = E_{L/a}\left[(\lambda - 1)\frac{t_{n2} - t_{n1}}{12} - \lambda\frac{\sigma_S}{2\pi}(sin\frac{\pi t_{n2}}{6} - sin\frac{\pi t_{n1}}{6})\right] \quad (16)$$

The values of $t_{ni}$ (i=1,2) are the abscissas of the intersection points of the load curve $P_L$ with the seasonal $P_{PV}$ variation curve (Figure 3). Equations (13) and (6) yield:

$$t_{n1} = \frac{6}{\pi}\cos^{-1}(\frac{\lambda - 1}{\lambda\sigma_S}) \quad (17)$$

Equation (14) allows the calculation of the required annual storage $E_{S/a}$, given the annual consumption $E_{L/a}$ and the parameter λ, which defines the usage scenario for the photovoltaic (PV) energy supply in the planned HESS.
For an energy autonomous HESS, the annual photovoltaic energy production ($E_{PV/a}$) should be greater than or at least equal to the annual load ($E_{L/a}$), i.e. $\lambda \geq 1$. For the security of a standalone energy supply with a HESS, a λ value of 1.25 or even 1.5 is recommended (Quaschning, 2010).
For the simplified case when considering usual values for $t_{n1}$ and $t_{n2}$, namely $t_{n1}$ =3 and $t_{n2}$=9, the calculation equation (14) of the storage capacity per year ($E_{S/a}$) becomes the simplified form:

$$E_{S/a} = E_{L/a}\frac{\sigma_S}{\pi} \quad (18)$$

We remind you also that currently, the maximum deviation of the monthly solar radiation, has values between 0.5 and 0.6
The method and the calculation formulas presented above can be used to determine the required storage capacity of HESS, which ensures the annual energy balancing between the photovoltaic (PV) energy source and

consumption, considering the seasonal variation of photovoltaic (PV) energy.

**Storage systems, Pump-Hydro-Storage**

Luo et al. (2015) present a comprehensive overview and analysis of the current development of various types of technologies in electrical energy storage (EES).

Batteries and Pump-Hydro-Storage systems (PHS) are the most used storage systems (Kousksou et al., 2014).

Batteries are commonly employed as storage in stand-alone renewable energy systems have well known limitations (Hassan et al., 2023).

Regarding the economics of this technology, pumped hydro energy storage seems more economical than batteries as well for standalone applications (Ma et al., 2015) and has relatively low payback periods.

These aspects are the reason why we in our paper choose pumped hydro storage (PHS) as storage example. PHS is a storage system that uses excess PV electricity to pump water from a lower reservoir to an upper reservoir to store energy, and conversely, the water is released from the upper reservoir to the lower reservoir, assuring the energy supply of user at lower or missing solar radiation (Figure 4).

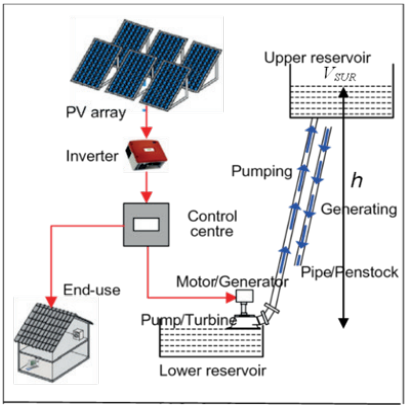



Figure 4. Scheme a PV electricity supply system with Pump-Hydro-Storage (Simão & Ramos, 2020)

If there are geographical conditions for PHS implementation, a hybrid system represented in Figure 4 can provide a reliable and cost-effective solution for providing electricity in remote areas. Additionally, such a hybrid energy supply system reduces substantially the environmental pollution (Rastler, 2010).

The two most significant parameter for the design of a PHS are the volume of the upper and lower reservoirs, which are the same value ($V_{UR/LR}$) and the turbine/pump head (h) (Figure 4) For a concrete study, the head of the turbine/pump (h) must be determined based on local topographic.

Therefore, for operating and sizing the PHS, only the volume of the upper reservoir ($V_{UR/LR}$) must be carried out.

The required input power for the pump $P_P(t)$ can be expressed as:

$$P_P(t) = \frac{1}{\eta_P} \rho g h \cdot q_P(t) \quad (19)$$

$\rho$ is the density of water (1000 kg/m3),
$g$ is the gravity acceleration and
$\eta_P$ is the overall pumping efficiency
$h$ is the pump head

The output power from the turbine $P_T(t)$ can be expressed as

$$P_T(t) = \eta_T \rho g h \cdot q_T(t) \quad (20)$$

$\eta_T$ is the overall efficiency of the turbine;
$q_{T(t)}$ is the flow rate of the turbine
$h$ is the turbine head

The other parameters have the same meaning as in the formula (19). In the case of standalone supply, the option of annual compensation is required for the security of a user's correct and safe energy supply in a remote area throughout the year.

The required annual energy storage $E_{S/a}$ can be determined using (14) or, in the simplified case, (18). Knowing $E_{S/a}$ we can calculate the volume of the upper/lower reservoir $V_{UR/LR}$. For this purpose, we note that, integrating the relationship (20) in relation to time (over one year), the left term is the energy stored $E_{S/a}$, and in the right member, the turbine flow $q_T$ integrated represents the volume to be calculated $V_{UR}$.

So, the required water volume in the upper reservoir for energy storage in case of annual energy balance of the PV-PHS energy supply system, i.e., the volume of the upper reservoir $V_{UR}$, can be expressed as

$$V_{UR} = \frac{E_{S/a}}{\eta_T \rho g h} \quad (21)$$

## RESULTS AND DISCUSSIONS

This section presents and illustrates the application of the calculation methods presented in the preceding sections for an end user in a remote area with an annual electricity consumption of $E_{L/a}$ 25,000 kWh. This consumption would correspond to an end user like a vineyard of 2-3 hectares with a small guesthouse of 4-5 rooms powered by photovoltaic panels and a heat pump (Malvoni & Cponcedo, 2017; INSSE/EUROSTAT, 2020-2025).

Here is the rationale for the considered electricity consumption of 25,000 kWh:

- Guesthouse (approx. 150-200 m²): a well-insulated building with 5 rooms consumes approximately 10,000-12,000 kWh/year for heating and hot water (using a modern air-to-water heat pump).
- Household consumption (lighting, kitchen, electronics): Approx. 4,000-5,000 kWh/year. These rationales are based on data from REHVA.
- Winery (Technology): for 2 hectares of vineyards (production of approximately 10,000–14,000 litters), the processes of must cooling, controlled fermentation, and stabilization require concentrated, but not enormous, energy consumption estimated at 8,000–10,000 kWh/year. This estimation is based on data from (OIV, 2025). Thus, the total estimated consumption is 22,000-27,000 kWh/year.

To ensure that this annual load is covered, a minimum annual photovoltaic energy production of $E_{PV/a}$ which is achieved using PV modules. In our example, a mountainous region of Romania, the annual solar irradiance can be estimated using the data in Figure 5 at a value of =1241 kWh/m$^2$. If we select JA Solar JAM72S20 455/MR 455 Wp PV modules with an efficiency of η = 20.05% and a module area Ap = 2.2 m² (https://www.enfsolar.com/pv/panel-datasheet/crystalline/46963) the PV potential of one solar module is:

$$E_{PV/p} = \eta \cdot A_P \, E_{PV/m^2} \cong 550 \, kWh/p \quad (22)$$

Thus, the required number of solar modules (NP) to be installed for a photovoltaic (PV) energy production of EPV/a (e.g. EPV/a =25,000) is:

$$N_P = \frac{E_{PV/a}}{E_{PV/p}} = \frac{25000}{550} \cong 45 \, modules \quad (23)$$

Furthermore, the next component of HESS will be analysed, namely the storage. As presented in the introduction and in paragraph - *Calculation method of the required energy storage to balance seasonal variation of PV*, the storage component of the HESS (Figure 3) is crucial to balancing the fluctuations of the renewable energy generation (PV) to ensure a secure and stable energy supply throughout the year. Knowing the annual load of $E_{L/a}$ =25,000 kWh/a, different scenarios for HESS can be analysed using the parameter λ defined as the ratio between the annual photovoltaic (PV) energy production ($E_{PV/a}$) and the annual load ($E_{L/a}$).

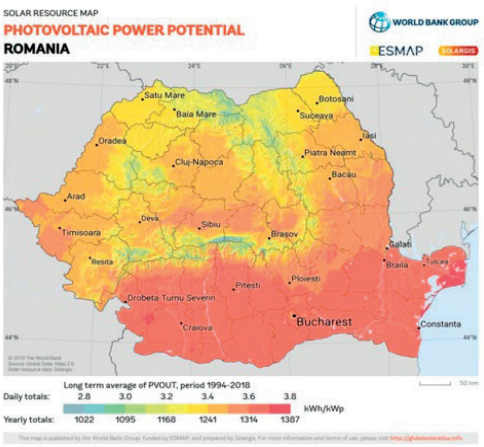



Figure 5. Solar energy resource map of Romania ((https://solargis.com/maps-and-gis-data/download/romania)

As reference case, we consider that discussed above in which the energy consumption $E_{L/a}$ corresponds to the generated photovoltaic energy $E_{PV/a}$ and thus from (11) λ=1. Any other value of λ corresponds to an energy supply scenario as follows:

- λ <1, when the annual photovoltaic energy production is less than energy consumption: $E_{PV/a}<E_{L/a}$
- λ>1, when the annual photovoltaic energy production exceeds the annual energy consumption: $E_{PV/a}>E_{L/a}$

The first case (λ<1) corresponds to partially energy autonomous scenarios of HESS i.e., when only a part of the energy supply ensured

from the PV source. To cover the difference between consumption $E_{L/a}$ and $E_{PV/a}$, it is necessary to use an additional energy source.
The second case ($\lambda>1$) corresponds to a scenario of energy autonomy for HESS, meaning that the entire energy supply is provided by photovoltaic systems integrated with appropriate storage solutions.
It should be noted that for the security of energy autonomy with a HESS, a $\lambda$ value of 1.25 or even 1.5 is recommended (Quersching, 2010).
Based on these considerations, it is relevant to discuss three further scenarios of HESS in addition to the reference case ($\lambda=1$). Two of these scenarios correspond to cases of secure energy supply with HESS, where $\lambda$ has values of 1.25 and 1.5, respectively.
One of scenarios corresponds to the case when only a part (e.g. about 75%) of the energy supply comes from PV source (i.e. $\lambda$ =0,75). For the remaining 25% other sources are needed, such as electricity from power grid.
Using the proposed method and calculation formulas presented in the paragraph -*Required energy supply for end-user,* Table 1 shows the results for the end user – a tourist facility that consists of a 2-hectare vineyard with a small guesthouse in a mountainous region of Romania – with an annual consumption of $E_{L/a}$ = 25,000 kWh/a. Four scenarios were considered: $\lambda$ = 0.75; $\lambda$ = 1.00; $\lambda$ = 1.25; $\lambda$ = 1.50.

Table 1. Required energy supply for tourist facility

| $\lambda$ | 0.75 | **1.00** | 1.25 | 1.50 |
|---|---|---|---|---|
| $E_{PV/a}$ [kWh/a] | 16,670 | **25,000** | 31,250 | 37,500 |
| NPV [-] | 30 | **45** | 57 | 68 |
| $t_{n1}$ [month] | 4.4 | **3** | 2.21 | 1.6 |
| $E_{S/a}$ [kWh/a] | - | **4,000** | 2,250 | 1,125 |
| $E_{PV/a}$-$E_{L/a}$ [kWh/a] | -8,330 | **0.00** | +6,250* | +12,500* |
| $V_{UR}$ [m$^3$] | - | **81,550** | 127,422* | 254,844* |

For each scenario, the following values are calculated:

- the annual energy production of the PV system ($E_{PV/a}$, equation (9))
- the number of PV modules ($N_P$)
- the required annual storage to compensate for seasonal fluctuations of PV production ($E_{S/a}$), equation (12))
- the energy difference between the annually produced photovoltaic (PV) energy ($E_{PV/a}$) and the annually required consumption ($E_{L/a}$)
- the required storage volume $V_{UR}$ of the upper/lower reservoir when using a pump hydro storage system (paragraph - *Storage systems, Pump-Hydro-Storage*, equation (21)).

The additional energy ($E_{PV/a}$ - $E_{L/a}$) generated in the scenarios with $\lambda$ =1.25 and $\lambda$ =1.5 (row 3 in the Table 1), which exceeds the effective annual energy consumption (25,000 kWh) marked with an asterisk (*) in Table 1, serves to ensure the consumer's security of supply. This generated photovoltaic (PV) energy is lost if it is not used by other consumers, fed into the grid (if available), or stored.
The last rows of Table 1 show the required storage volume for a pumped-storage hydroelectric plant.
It is evident that the additional water volume required to store the extra energy generated is very high: over 50% for variant $\lambda$ =1.25 and over 200% for variant $\lambda$ =1.5. Therefore, a techno-economic analysis is necessary to assess the viability of such storage.

## CONCLUSIONS

This paper presented a novel analytical approach to determining the annual energy storage requirements for Hybrid Renewable Energy Supply Systems (HRESS), specifically addressing the challenges posed by seasonal PV output variations. By employing a trigonometric mathematical model to describe the sinusoidal distribution of annual solar radiation, this study bridged a critical gap in existing literature, which often overlooks long-term seasonal dynamics in favour of short-term technical optimizations.
The application of the proposed method to a case study - a vineyard and guesthouse in mountainous Romania - provided several key insights:
Analytical Precision: The introduction of the energy autonomy parameter ($\lambda$) proved to be a robust metric for sizing HRESS. The mathematical derivation of the required annual

storage via the intersection points of load and generation curves allows for a precise quantification of storage needs without the necessity for computationally expensive hour-by-hour simulations.

Impact of Autarky Levels: The results demonstrate that while a reference case theoretically covers annual demand, it necessitates maximum storage capacity to bridge seasonal deficits. Increasing the PV capacity to security levels of or above significantly enhances energy security but results in substantial surplus energy. This highlights a critical design trade-off: over-dimensioning the PV array can reduce the relative storage burden but requires effective ategies for utilizing excess energy, such as grid-feeding or secondary thermal loads.

Storage Feasibility: The study quantified that for a typical 25,000 kWh/a consumer, the seasonal storage requirements are substantial. For isolated systems, the results suggest that Pumped Hydro Storage (PHS) or advanced long-term battery solutions are indispensable, as conventional short-term storage cannot compensate for the sinusoidal "winter gap" identified in the model.

In conclusion, the proposed analytical equations provide a valuable tool for engineers and policymakers in the early feasibility stages of decentralized energy projects. Future research should extend this trigonometric model to include stochastic weather fluctuations and the complementary integration of wind energy to further optimize the parameter λ and reduce the physical footprint of the required storage systems.

## REFERENCES

Ahmad, S., Hasan, S. M. N., Hossain, M. S., Uddin, R., Ahmed, T., Mustayen, A. G. M. B., Hazari, M. R., Hassan, M., Parvez, M. S., & Saha, A. (2024). A Review of Hybrid Renewable and Sustainable Power Supply System: Unit Sizing, Optimization, Control, and Management. *Energies*, *17*(23), 6027. https://doi.org/10.3390/en17236027

Anoune, K., Bouya, M., & Astito, A. (2018). Sizing methods and optimization techniques for PV-wind based hybrid renewable energy systems: A review, *Renewable and Sustainable Energy Reviews*, 93, 652-673.

Badea, G., Felseghi, R.-A., Varlam, M., Filote, C., Culcer, M., Iliescu, M., & Răboacă, M. S. (2019). Design and Simulation of Romanian Solar Energy Charging Station for Electric Vehicles. *Energies*, *12*(1), 74. https://doi.org/10.3390/en12010074

Dagdougui, H., Minciardi, R., Ouammi, A., Robba, M., & Sacile, R. (2012). Modeling and optimization of a hybrid system for the energy supply of a ‘‘Green’’ building. *Energy Convers Manage.* 64:351–63.

Global Solar Atlas (2025). https://solargis.com/maps-and-gis-data/download/romania

Hassan, Q., Algbugri, S., Sameen, A., Z., Salman, H., & Jaszczur, M. (2023). A review of Hybrid Renewable Energy Systems: Solar and wind-powered solutions: Challenges, opportunities, and policy implications, Elsevier, *Results in Engineering,* 20, 101621

INSSE/Eurostat (2020-2025). Resursele și consumurile energetice, https://insse.ro/cms/ro/tags/comunicat-resursele-si-consumurile-energetice

Kafando, J., G., Yamegueu, D., Houdji, E. T. (2024), Review on sizing and management of stand-alone PV/WIND systems with storage, *Heliyon*, 10(18), https://doi.org/10.1016/j.heliyon.2024.e38080

Kousksou, T., Bruel, P., Jamil, A., El Rhafiki, T., & Zeraouli, Y. (2014) Energy storage: applications and challenges. *Sol Energy Mater. Sol. Cells*, 120(Part A), 59–80.

Luo, X., Wang, J., & Clarkr, J. (2015). Overview of current development in electrical energy storage technologies and the application potential in power system operation. *Applied Energy*, 137, 511-536.

Ma, T., Yang, H., Lu, L, & Peng, J. (2015). Pumped storage-based standalone photovoltaic power generation system: Modelling and techno-economic optimization, *Applied Energy* 137, 649–659

Malvoni, M., & Cponcedo, P., M. (2017). Analysis of energy consumption: a case study of an Italian winery. ScienceDirect, *Energy Procedia* 126 (201709) 227–233.

NASA POWER. NASA Prediction of worldwide Energy Resources: https://power.larc.nasa.gov/

OIV. (2025). http://www.oiv.int

Quaschning, V., (2010) Erneuerbare Energien und Klimaschutz. HANSER Verlag München.

Rastler, D. (2010). Electricity energy storage technology options: a white paper primer on applications, costs, and benefits. Electric Power Research Institute (EPRI), Palo Alto.

REHVA. European Association for Heating, Ventilation and Air Conditioning, https//www.rehva.eu

Simão, M., & Ramos, H. M. (2020). Hybrid Pumped Hydro Storage Energy Solutions towards Wind and PV Integration: Improvement on Flexibility, Reliability and Energy Costs. *Water*, *12*(9), 2457. https://doi.org/10.3390/w12092457

WOLF - a company of Ariston Holding N.V. (2026) Why is the coefficient of performance important when buying a heat pump, https://www.wolf.eu/en-de/advisor/cop-heat-pumps.

Scientific Papers. Series E. Land Reclamation, Earth Observation & Surveying, Environmental Engineering. Vol. XV, 2026
Print ISSN 2285-6064, CD-ROM ISSN 2285-6072, Online ISSN 2393-5138, ISSN-L 2285-6064

# A LOW-COST, OPEN-SOURCE APPROACH FOR SENSOR-BASED LIGHT MANAGEMENT IN PROTECTED CULTIVATION SYSTEMS

**Bogdan ILIE[1], Yuxin TONG[2], Ana BUTCARU[1], Tiberiu ION[3], Ionuț Ovidiu JERCA[1]**

[1]University of Agronomic Sciences and Veterinary Medicine of Bucharest,
59 Mărăști Blvd, District 1, Bucharest, Romania
[2]Institute of Environment and Sustainable Development in Agriculture,
Chinese Academy of Agricultural Sciences, China
[3]SC Skip Monday Studio SRL, 10 Triumfului Street, Ploiesti, Prahova County, Romania

Corresponding author email: ovidiu.jerca@qlab.usamv.ro

***Abstract***

*Efficient light management represents a key challenge in protected cultivation systems, particularly when cost constraints limit the use of advanced dimmable lighting technologies. This study presents a low-cost, open-source, sensor-based approach for practical light management in protected horticultural environments. A custom-built multi-stage lighting system was combined with a multispectral light sensor used as a control variable, while a reference PAR sensor was employed for calibration under real operating conditions. Light intensity was regulated through automated multi-stage switching with integrated energy monitoring, enabling feedback between illumination targets and electrical power consumption. The control logic was implemented using an open-source automation platform, allowing data acquisition, logging, and system adaptability. The experimental setup was evaluated under greenhouse conditions using Capsicum spp. as experimental plant support. Rather than replacing professional photometric instruments, the proposed approach demonstrates the functional integration of low-cost sensors and open-source tools for scalable and energy-efficient light management applications.*

***Key words:*** *artificial lighting; DLI control; Home Assistant; open-source automation; PPFD estimation.*

## INTRODUCTION

Protected cultivation systems are increasingly expected to deliver higher productivity, better resource use efficiency, and improved crop quality under variable environmental and economic constraints. In this context, light management has become one of the central technical challenges of greenhouse and other protected horticultural systems. Although natural solar radiation remains the dominant light source in most structures, its quantity and temporal distribution are often insufficient or highly variable, especially during winter, cloudy periods, or in densely developed canopies where self-shading limits light penetration to lower leaf layers. As a result, supplemental lighting is widely regarded as an effective tool for stabilizing photosynthesis, supporting plant development, and improving yield and product quality in protected crops (Moe et al., 2006; Hemming, 2011; Hao et al., 2018).

The physiological importance of light in horticultural systems is not limited to total irradiance. Crop responses depend on several interrelated parameters, including photosynthetic photon flux density (PPFD), daily light integral (DLI), photoperiod, spectral composition, and vertical light distribution within the canopy. For fruiting vegetables and other greenhouse crops, insufficient light reduces assimilate production, affects vegetative–generative balance, and may limit both yield and crop quality. In high-density canopies, most incident radiation is intercepted by the upper leaf layers, leaving the lower canopy under-illuminated. This uneven distribution reduces the contribution of lower leaves to whole-plant photosynthesis and has motivated the development of strategies such as interlighting and spectrum-tailored supplemental illumination (Jokinen et al., 2012; Guo et al., 2016; Hao et al., 2018).

During the last decade, light-emitting diode (LED) technology has become increasingly important in horticultural lighting because it offers several practical advantages over conventional discharge lamps. These include

high photon efficiency, low radiant heat output, long operational lifespan, compact size, and the possibility of spectral tailoring according to plant needs. In addition, LED systems can be integrated more easily into digital control architectures than older lighting technologies. This has enabled not only supplemental and interlighting strategies, but also increasingly precise forms of control based on crop demand and environmental variability (Morrow, 2008; Moe, 2012; Bergstrand et al., 2016; Palmitessa et al., 2021). From the perspective of plant lighting, efficiency should be considered primarily in terms of delivered photosynthetic photons rather than conventional human-centered luminous metrics, because plant responses are driven by photon flux in the photosynthetically active radiation (PAR) region (400-700 nm) (Nelson & Bugbee, 2014). At the same time, there is increasing evidence that lighting strategies should not be treated as simple on/off supplementation. Instead, effective greenhouse lighting must be understood as a dynamic management problem in which light intensity, light quality, timing, and canopy distribution are coordinated with crop requirements and available natural radiation. Reviews and experimental studies have shown that optimized supplemental lighting can improve productivity, accelerate development, and increase the efficiency of canopy light use in crops such as tomato and sweet pepper. This applies not only to northern regions with severe winter limitations, but also to Mediterranean or transitional climates where natural light is often variable rather than consistently limiting (Li et al., 2016; Paucek et al., 2020; Palmitessa et al., 2021). The relationship between PPFD delivery and crop nutrient demand also underlines the importance of precise light quantification in closed growing environments.

Despite these advances, practical implementation in small or medium-scale protected cultivation remains constrained by cost. Professional dimmable lighting systems, quantum sensors, and commercial greenhouse control platforms can be effective, but they are often too expensive for experimental, educational, or low-budget horticultural installations. This creates a technological gap: the biological need for intelligent light management is well established, but affordable systems capable of continuous sensing, automated control, and energy-aware operation are still limited. In practice, many growers and researchers require solutions that are not necessarily perfect substitutes for industrial systems, but are sufficiently robust, transparent, and adaptable for real use under greenhouse conditions.

One of the key barriers to low-cost light management is the measurement of PPFD itself. Professional quantum sensors provide direct and reliable PAR measurements, but their cost may restrict deployment density or routine use in custom automation systems. As a result, low-cost multispectral sensors have attracted increasing interest as potential alternatives for estimating PPFD and related light metrics. However, such sensors do not directly measure PPFD; instead, they provide channel-specific responses that depend on spectral composition, optical geometry, and environmental conditions. Therefore, their use in horticultural applications requires calibration against a reference PAR instrument under relevant operational conditions. The AS7341 is a ten-channel multispectral sensor covering the full PAR range (415-680 nm) plus broadband and NIR channels, at low component cost, making it particularly suitable for integration into custom greenhouse sensing systems. Recent work has demonstrated that compact multi-channel spectral sensors of this type can estimate PAR or PPFD with useful accuracy when appropriately calibrated (Bäumker et al., 2021). The combination of multiple spectral channels for sensor fusion has also been shown to substantially improve estimation accuracy compared to single-channel approaches (Li et al., 2018; Yang et al., 2020). Hyperspectral and multispectral approaches more generally have demonstrated the broader value of spectral sensing in crop monitoring and physiological estimation (Kawasaki et al., 2008; Thorp et al., 2017; Shafaei et al., 2018).

A second major barrier is control architecture. In recent years, smart greenhouse research has increasingly moved toward sensor networks, IoT-based monitoring, cloud-connected platforms, and data-driven automation. These systems can improve environmental control, reduce labor, and increase resource efficiency

by linking sensors, actuators, and supervisory logic in a single platform (Rath & Kawollek, 2009; Sagheer et al., 2021). However, many published systems remain relatively complex or infrastructure-heavy and are not always directly transferable to simple protected cultivation structures or researcher-built installations. Open-source platforms represent an attractive alternative because they allow custom hardware integration, real-time logging, flexible control logic, and direct transparency of algorithms and thresholds.

For lighting control specifically, the combination of instantaneous PPFD estimation with daily light integral (DLI) tracking is especially promising. PPFD enables rapid decisions in response to transient changes in natural radiation, while DLI provides an integrative measure of total daily photosynthetic light received by the crop. Together, these variables support a biologically meaningful control strategy: supplemental lighting can be activated when natural light is insufficient and limited when the daily light target has already been reached. Such an approach is well aligned with commercial greenhouse principles, yet it can also be implemented in simplified form using discrete lighting stages and open-source automation (Kim et al., 2006; Hao et al., 2018).

Therefore, the novelty of the present study does not lie in proposing a new photometric standard or replacing professional horticultural instrumentation. Instead, it lies in demonstrating that a practical light management system for protected cultivation can be built from low-cost components and open-source tools, provided that calibration, control logic, and energy monitoring are treated rigorously. The system presented here combines a custom-built multi-stage LED lighting fixture, a multispectral AS7341 sensor used as a control variable, a reference quantum sensor for calibration, and a Home Assistant-based automation framework for PPFD estimation, DLI integration, and stage-based lighting control under real greenhouse conditions.

The objective of this study was to develop and evaluate a low-cost, open-source, sensor-based lighting management approach suitable for protected horticultural environments. More specifically, the study aimed to: (i) calibrate a multispectral AS7341 sensor against a reference quantum sensor for estimating canopy-level PPFD under real greenhouse conditions; (ii) implement an adaptive, multi-stage supplemental lighting strategy based on estimated PPFD and DLI; and (iii) integrate lighting control with energy monitoring through an open-source automation platform in order to demonstrate a scalable and practically useful alternative for protected cultivation systems, using *Capsicum* spp. as experimental plant support.

## MATERIALS AND METHODS

### *AS7341 Sensor Calibration for PPFD Estimation*

In modern protected cultivation systems, accurate light management is essential for both optimizing photosynthesis and minimizing the energy costs associated with supplemental lighting. Professional quantum sensors, which directly measure photosynthetic photon flux density (PPFD, $\mu mol \cdot m^{-2} \cdot s^{-1}$), serve as reference instruments but are costly and impractical for multi-point deployment in experimental or commercial greenhouses (Hemming, 2011; Nelson and-Bugbee, 2014).

In this context, the AS7341 multispectral sensor represents an attractive low-cost alternative, providing separate measurements across ten spectral bands in the visible and NIR range (415-680 nm, Clear, NIR). However, the AS7341 does not measure PPFD directly; instead, it outputs raw digital counts that depend on the spectral composition of the light source, the angle of incidence, and local optical conditions. Consequently, the use of this sensor in horticultural applications requires rigorous calibration under conditions as close as possible to real-world operation (Bäumker et al., 2021).

The objective of this calibration step was to establish a mathematical relationship (regression model) between the raw channel outputs of the AS7341 and the actual PPFD values measured by a reference quantum sensor, enabling the AS7341 to subsequently estimate canopy-level PPFD, compute the Daily Light Integral (DLI), and support automated supplemental lighting control.

The AS7341 breakout board was soldered with a four-wire I²C cable (SDA, SCL, VCC, GND) and mounted inside a custom 3D-printed

enclosure designed specifically for this experiment (Figure 1). The enclosure provides mechanical protection and ensures a fixed, reproducible optical geometry for the sensor. An opal diffuser dome was positioned above the optical capsule of the sensor. The dome serves a dual purpose: (1) uniformizing the angle of incidence, thereby reducing sensitivity to the sun's position (sunrise vs. sunset), and (2) approximating the angular response of a cosine-corrected quantum sensor, which integrates photon flux across a full hemisphere. The enclosure was sealed and weatherproofed, enabling permanent installation in the greenhouse environment.



Figure 1. AS7341 sensor assembly components. Left: multispectral breakout board in the custom 3D-printed enclosure with I²C wiring. Centre: opal diffuser dome above the AS7341 optical capsule prior to assembly. Right: sensor mounted upward-facing on the greenhouse support post

A LightScout Quantum Light Meter (Spectrum Technologies, USA) was used as the reference instrument, capable of directly measuring PPFD in the 400-700 nm range, expressed in $\mu mol \cdot m^{-2} \cdot s^{-1}$. This sensor served as the calibration standard throughout the entire measurement campaign. It was positioned at canopy level, in a fixed upward-facing orientation, without adjusting the angle of incidence during measurements.

It is important to note that the sensor angle was not adjusted toward the sun to maximize PPFD readings, even under strong direct irradiance. Although orienting the sensor toward the sun could have produced values exceeding 1000 $\mu mol \cdot m^{-2} \cdot s^{-1}$, this approach would have introduced an additional source of geometric error and compromised the comparability of measurements across different times of day.

The AS7341 sensor was mounted in a fixed position on a dedicated steel support post inside the greenhouse, approximately 3 m from the reference quantum sensor. Although this separation introduces the possibility that one sensor may occasionally be partially shaded by the greenhouse structure or covering film, this was not systematic and was considered acceptable for calibration under real operating conditions.

Calibration was performed exclusively under natural light, with all supplemental LED lighting switched off, over multiple days (12-13 January 2025), across different times of day covering a broad range of PPFD values from approximately 1-10 $\mu mol \cdot m^{-2} \cdot s^{-1}$ up to approximately 700 $\mu mol \cdot m^{-2} \cdot s^{-1}$. This approach ensured that the calibration dataset included a wide variety of illumination conditions: overcast sky, diffuse light, direct sunlight at different solar angles, and spectral variations caused by solar position and greenhouse film transmittance.

For each calibration point, the following procedure was applied: (1) the PPFD value was read from the quantum sensor ($\mu mol \cdot m^{-2} \cdot s^{-1}$); (2) the exact time was recorded (hh:mm); (3) a screenshot of the raw channel counts of the AS7341, as displayed in the Home Assistant platform, was captured; and (4) values were subsequently entered manually into a centralized data table. Approximately 100 individual measurements were collected in total, distributed across the full PPFD range of interest (Figure 2).



Figure 2. Calibration data collection procedure

The LightScout quantum sensor (reading 148 $\mu mol \cdot m^{-2} \cdot s^{-1}$) is positioned at canopy level alongside *Capsicum* spp. experimental plants. The data recording sheet on the clipboard is visible in the foreground, illustrating the parallel manual logging of quantum sensor values and timestamps.

Raw unprocessed channel values were used for regression, without internal normalization, in order to preserve the direct relationship between the received optical signal and the electronic response of the sensor. The Clear and NIR channels were analyzed separately; however, the final model was built primarily on channels within the PAR range (415–680 nm), as these are directly relevant to photosynthesis (Kim et al., 2004; Nelson & Bugbee, 2014).

The relationship between PPFD and AS7341 signals is not perfectly linear across the full measurement range, particularly at very low light levels where the ratio of diffuse to direct light varies substantially and the contribution of non-PAR spectral components becomes relatively larger. For this reason, calibration was approached using multiple linear regression, followed by a critical analysis of its domain of validity. The resulting model expresses estimated PPFD as a weighted sum of the AS7341 spectral channels:

$$PPFDest = a_0 + a_1 \cdot Ch415 + a_2 \cdot Ch445 + \ldots + a_n \cdot Ch680$$

Coefficients were determined by the least-squares method using the complete collected dataset. Subsequently, the use of a piecewise model was found necessary, separating the low-light domain from the medium–high illuminance domain, in order to improve accuracy under reduced illumination conditions (Bäumker et al., 2021). The combination of multiple spectral channels substantially improves estimation accuracy compared to single-channel broadband approaches (Li et al., 2018; Yang et al., 2020).

The final calibration model allows: (1) PPFD estimation with satisfactory accuracy across the horticultural range of interest; (2) real-time integration into Home Assistant; and (3) use for DLI computation and supplemental lighting control. The objective of this calibration was not to replace a laboratory-grade quantum sensor, but to obtain a robust, reproducible, and sufficiently accurate instrument for practical greenhouse control applications (Figure 3).

The dashed line represents perfect agreement (1:1); the shaded band indicates ±RMSE. Right: MLR regression coefficients per spectral channel. Channels at 445 nm and 480 nm show the strongest positive contributions; the 590 nm channel shows the largest negative coefficient.

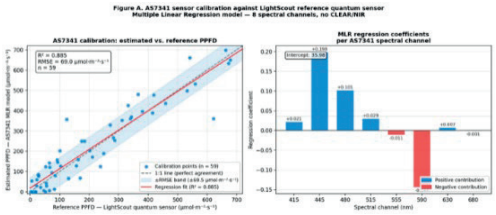



Figure 3. AS7341 calibration against the LightScout reference quantum sensor. Left: scatter plot of AS7341-estimated PPFD vs. reference PPFD (n = 59; $R^2 = 0.896$; RMSE = 69.5 µmol·m$^{-2}$·s$^{-1}$).

### *Lighting System Configuration*

The supplemental lighting fixture was custom-built from 20 full-spectrum LED bulbs (2.5 W real consumption each), mounted on a 3 m aluminium rail suspended horizontally above the crop canopy. The bulbs were arranged in three independently controlled circuits of 7, 7, and 6 lamps respectively, connected in parallel within each circuit (Figure 4 and Figure 5).

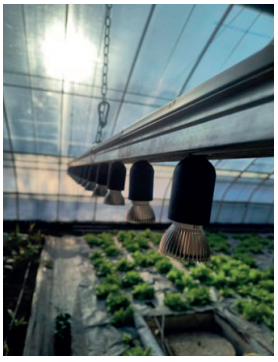


Figure 4. Custom-built supplemental lighting fixture consisting of 20 full-spectrum LED bulbs mounted on an aluminium rail, photographed under natural daylight conditions with lamps switched off. The three independently controlled circuits are arranged along the rail

The three circuits define three cumulative lighting stages, activated in succession:

- Stage 1 (circuit 1 only, 7 lamps): approximately 30 µmol·m$^{-2}$·s$^{-1}$
- Stage 2 (circuits 1+2, 14 lamps): approximately 70 µmol·m$^{-2}$·s$^{-1}$
- Stage 3 (circuits 1+2+3, all 20 lamps): approximately 150 µmol·m$^{-2}$·s$^{-1}$.

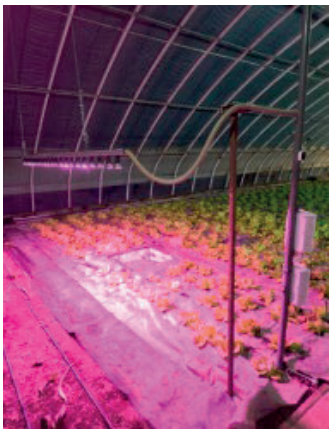


Figure 5. Supplemental lighting fixture operating at full output (Stage 3, all 20 lamps) during nighttime, illuminating the crop canopy with characteristic pink-magenta spectrum

The smart plug control box is visible on the support post (right). The AS7341 sensor post is positioned in the background.

PPFD values associated with each stage were determined experimentally at canopy level using the reference quantum sensor, under nighttime conditions with natural light fully excluded. Given the directional nature of the LED sources and the spatial variability inherent to a DIY fixture (particularly the disproportionate contribution of the six overhead lamps in stage 3, which illuminate the plant canopy perpendicularly), measured values ranged approximately 20-30% around the mean at each stage. The representative values of 30, 70, and 150 $\mu mol \cdot m^{-2} \cdot s^{-1}$ were adopted as operational parameters and maintained consistently throughout the experiment. All three stages operate exclusively in ON/OFF mode; no dimming is applied (Figure 6).

The hardware architecture was built around the AS7341 multispectral sensor, connected via the I²C bus (SDA/SCL, GPIO21/GPIO22) to an ESP32 microcontroller running ESPHome firmware, powered at 5 V DC. The ESP32 transmitted raw spectral channel values wirelessly (Wi-Fi, 2.4 GHz) to a local Home Assistant server, where PPFD estimation and control logic were implemented.

Supplemental lighting was delivered by the custom three-stage LED fixture described above. Each stage was powered independently at 230 V AC through a dedicated smart power outlet with integrated energy metering (Zigbee protocol), enabling discrete control of photon flux and real-time monitoring of electrical energy consumption per stage. This architecture allows full separation between the sensing/decision layer and the energy delivery layer, improving system robustness and scalability (Figure 7).

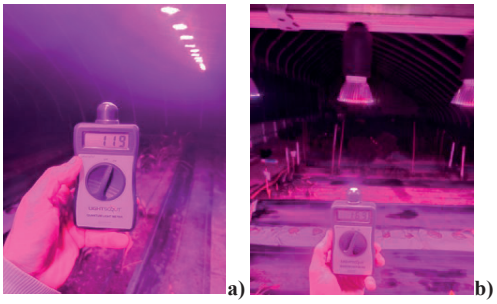



Figure 6. a) LightScout quantum sensor reading 119 $\mu mol \cdot m^{-2} \cdot s^{-1}$ during PPFD characterization of the lighting fixture under Stage 3 operation, measured at a lateral position below the lamp array; b) LightScout quantum sensor reading 169 $\mu mol \cdot m^{-2} \cdot s^{-1}$ measured directly below a Stage 3 lamp in perpendicular orientation, illustrating the elevated PPFD contribution of the overhead bulbs

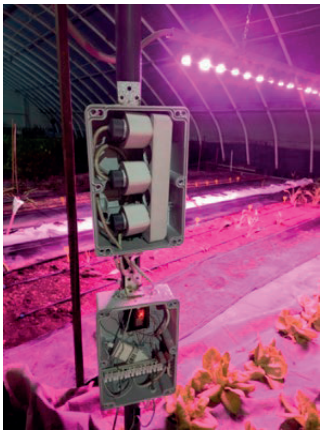


Figure 7. Hardware installation on the greenhouse support post

Upper enclosure: three Zigbee smart plugs with energy metering, one per lighting stage. Lower enclosure: ESP32 microcontroller (red LED visible) and terminal block. The complete sensing and actuation infrastructure is contained within two weatherproof boxes mounted at a single location (Figure 8).

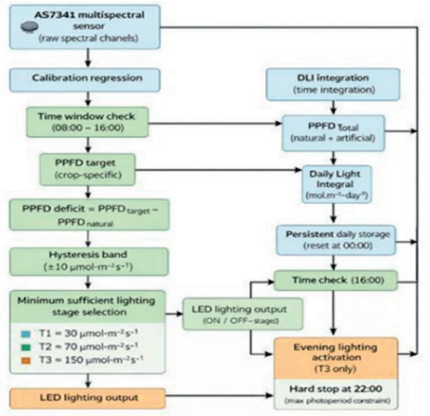



Figure 8. Hardware system overview of the adaptive lighting control system. The AS7341 sensor is connected to an ESP32 microcontroller running ESPHome, which transmits estimated PPFD data over Wi-Fi to Home Assistant. Home Assistant controls three smart plugs powering the three LED lighting stages operating at 230V

### *Hardware System Overview*

To translate the PPFD estimates obtained from the calibrated AS7341 sensor into a practical light management tool, an automated supplemental lighting control strategy was implemented, based on two complementary decision levels: instantaneous PPFD-based control during the daytime, and integrative DLI-based compensation in the evening. This approach was designed to replicate the principles used in modern commercial greenhouses, using low-cost calibrated sensors and an open-source automation platform (Hao et al., 2018; Sagheer et al., 2021).

For the experimental plant support (*Capsicum* spp.), the DLI requirement was defined in the range of 10-12 mol·m$^{-2}$·d$^{-1}$, an interval frequently recommended for pepper species grown in protected environments (Jokinen et al., 2012; Hao et al., 2018). In this experiment, a DLI target of 10 mol·m$^{-2}$·d$^{-1}$ was adopted as the operational setpoint, with a total photoperiod (natural + artificial light) of 14 hours (08:00-22:00). A PPFD control target of 200 µmol·m$^{-2}$·s$^{-1}$ was used as the instantaneous setpoint for daytime control. This value represents a practical threshold below which supplemental lighting is activated, chosen conservatively to account for natural variability in greenhouse irradiance. It should be noted that for a DLI of 10 mol·m$^{-2}$·d$^{-1}$ over 14 hours, the equivalent average PPFD would be approximately 198 µmol·m$^{-2}$·s$^{-1}$, confirming that the chosen threshold of 200 µmol·m$^{-2}$·s$^{-1}$ is biologically consistent. The system is designed to be crop-agnostic: both the DLI target and the PPFD threshold are configurable parameters adjustable for any horticultural species without modifying the control logic.

### *Adaptive Multi-Stage Lighting Control*

During the daytime window (08:00-16:00), the system evaluates estimated canopy PPFD every 5 minutes. At each evaluation step, the algorithm determines the light deficit relative to the PPFD target and selects the minimum lighting stage capable of compensating this deficit: if PPFDnatural ≥ 200 µmol·m$^{-2}$·s$^{-1}$ → all stages OFF; if PPFDnatural + 30 ≥ 200 → Stage 1 ON (7 lamps); if PPFDnatural + 70 ≥ 200 → Stage 2 ON (14 lamps); otherwise → Stage 3 ON (20 lamps).

To prevent frequent switching caused by rapid irradiance fluctuations (e.g., passing clouds), a hysteresis band of ±10 µmol·m$^{-2}$·s$^{-1}$ was applied: the current stage is maintained as long as the deviation from the target remains within this band. Additionally, daytime control is active only when the accumulated DLI has not yet reached the daily target. Once the DLI target is reached, all stages are immediately switched off and the daytime automation is suppressed for the remainder of the day.

In parallel with instantaneous control, the system continuously computes the daily DLI by integrating total PPFD (natural + artificial) over time. At each 5-minute interval, the DLI increment is calculated as:

$$\Delta DLI = PPFDtotal \times \Delta t / 1{,}000{,}000$$

where: PPFDtotal is the sum of natural and artificial PPFD contributions (µmol·m$^{-2}$·s$^{-1}$) and Δt = 300 s (5 minutes).

The DLI accumulator is reset automatically at midnight and integrated throughout the interval 08:00-23:59.

After 16:00, natural PPFD is no longer sufficient to contribute meaningfully to the DLI, and control transitions from instantaneous PPFD regulation to integrative DLI-based compensation. In this mode, the system operates at maximum output (Stage 3, all 20 lamps, 150 µmol·m$^{-2}$·s$^{-1}$) and evaluates the accumulated DLI every 5 minutes in a continuous loop: if the

accumulated DLI is below the daily target by more than 0.05 mol·m$^{-2}$·d$^{-1}$ → Stage 3 remains ON; if the DLI target has been reached → all stages are switched OFF immediately; if the DLI target has not been reached by 22:00 → all stages are switched OFF by a hard-stop automation, regardless of accumulated DLI.

This loop-based approach - rather than a one-shot duration calculation - ensures that the system remains responsive to the actual accumulated DLI at all times and avoids over-illumination in case of any discrepancy between estimated and actual PPFD contributions. The hard stop at 22:00 limits the total photoperiod and prevents circadian disruption of the crop (Figure 9).

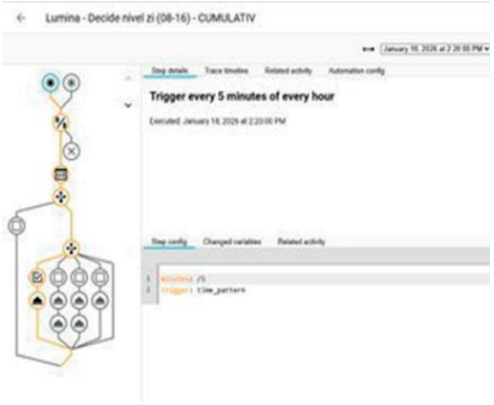



Figure 9. Conceptual diagram of the adaptive lighting control system

Multispectral data acquired from the AS7341 sensor are converted into an estimated PPFD at canopy level using the calibration regression. During daytime (08:00-16:00), the system selects the minimum sufficient lighting stage based on PPFD deficit and a hysteresis band. After 16:00, control switches to a DLI-based compensation mode, activating supplemental lighting only for the duration required to reach the target DLI, with a maximum photoperiod limit at 22:00.

The control logic was implemented within Home Assistant, an open-source home automation platform, using an event-condition-action model (Sagheer et al., 2021). The software architecture comprises four functional components: (1) data acquisition and preprocessing - raw AS7341 channel values are periodically collected via ESPHome and converted into an estimated canopy PPFD value via the regression-based calibration model, implemented as a virtual sensor template; (2) discrete-time lighting control - control decisions are triggered at fixed 5-minute intervals using time-pattern automations; (3) integrative DLI computation - PPFD is integrated over time at each 5-minute step, with the DLI accumulator stored in a persistent input_number helper and reset automatically at midnight; and (4) evening compensation loop - after 16:00, a separate cyclic automation evaluates the DLI deficit every 5 minutes and maintains or switches off Stage 3 accordingly, with a hard-stop limit at 22:00.

The implementation uses exclusively standard platform components (virtual sensor templates, persistent numerical helpers, and declarative YAML automations), without proprietary extensions or external modules. The complete source code of all automations is provided as supplementary material to enable exact replication of the experimental setup (Figure 10).

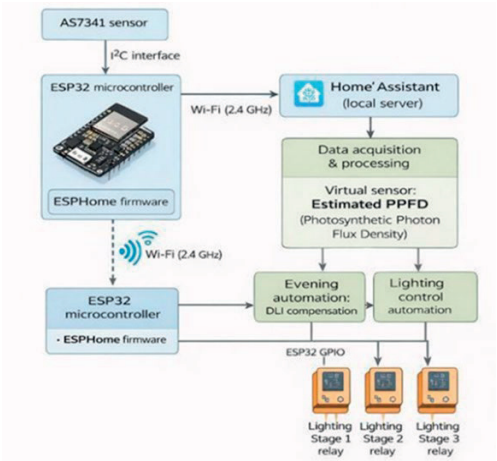



Figure 10. Software stack overview of the control architecture

The ESPHome firmware running on the ESP32 handles sensor interfacing and data transmission. Home Assistant processes the data, implements the PPFD virtual sensor via the calibration regression, and orchestrates two separate control automations: the daytime lighting control (PPFD-based stage selection) and the evening DLI compensation loop.

### *Software Architecture and Implementation*

The complete system - sensor assembly, LED lighting fixture, control hardware, and automation software - was deployed and operated under real greenhouse conditions in a protected cultivation structure. *Capsicum* spp. (hot pepper) plants were used as experimental plant support, positioned directly below the lighting fixture. The greenhouse structure, foil covering, and plant canopy represent the real-world operating environment for which the system was designed and calibrated (Figure 11).

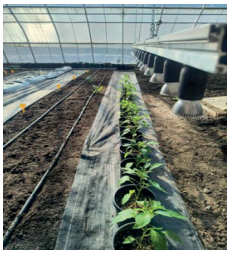


Figure 11. Experimental setup overview: *Capsicum* spp. plants positioned in a row under the custom-built LED lighting fixture inside the greenhouse

The multi-stage supplemental lighting fixture is visible in the upper right. The drip irrigation system and agrotextile ground cover are also visible. Plants were used as experimental support for system evaluation under real growing conditions.

## RESULTS AND DISCUSSIONS

### *AS7341 Sensor Calibration*

The AS7341 multispectral sensor was calibrated against the LightScout reference quantum sensor under natural daylight conditions across a broad PPFD range (approximately 1-700 $\mu mol \cdot m^{-2} \cdot s^{-1}$). A total of 59 valid measurement pairs were retained after quality filtering. Multiple linear regression using all ten spectral channels yielded an $R^2$ of 0.896 and a root-mean-square error (RMSE) of 69.5 $\mu mol \cdot m^{-2} \cdot s^{-1}$, corresponding to a relative estimation error of approximately 20% across the full calibration range. This level of accuracy was considered acceptable for the intended application of discrete-stage supplemental lighting control, where the system operates within defined PPFD thresholds rather than requiring precise absolute measurements.

The calibration model was validated across repeated measurement sessions, confirming its reproducibility under varying natural light conditions. The regression coefficients and performance statistics for the final model are summarised in Table 1. As anticipated for a multi-channel spectral sensor, channels covering the 550-670 nm range contributed most substantially to the regression fit, consistent with the spectral sensitivity of the LED light source and the dominant natural daylight spectrum present during calibration (Bäumker et al., 2021; Yang et al., 2020)

The piecewise domain structure of the calibration was retained in the final model to account for the non-linearity observed at very low PPFD levels (below approximately 10 $\mu mol \cdot m^{-2} \cdot s^{-1}$). Above this threshold, a single linear model was applied across the full horticultural operating range. The scatter plot of estimated versus reference PPFD values is presented in Figure 12.

Table 1. AS7341 MLR calibration model coefficients and performance statistics

| Channel | Wavelength (nm) | Coefficient | Contribution |
|---|---|---|---|
| Violet | 415 | +0.0212 | Weak positive |
| Indigo | 445 | +0.1977 | Strong positive |
| Blue | 480 | +0.1011 | Moderate positive |
| Cyan | 515 | +0.0294 | Weak positive |
| Green | 555 | −0.0107 | Weak negative |
| Yellow | 590 | −0.1436 | Strong negative (collinearity) |
| Orange | 630 | +0.0065 | Negligible positive |
| Red | 680 | −0.0008 | Negligible negative |
| Intercept | - | 35.981 | - |
| $R^2$ | - | 0.896 | n = 59 measurements |
| RMSE | - | 69.5 $\mu mol \cdot m^{-2} \cdot s^{-1}$ | ~20% relative error |

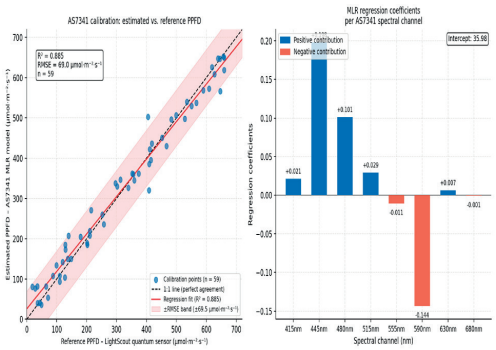



Figure 12. AS7341 calibration against LightScout reference quantum sensor (n = 59). Left: estimated vs. reference PPFD ($R^2 = 0.896$; RMSE = 69.5 µmol·m$^{-2}$·s$^{-1}$). Right: MLR regression coefficients per spectral channel

### *System Performance - DLI Achievement*

The automated supplemental lighting system was operated continuously over a 41-day experimental period from 20 January to 1 March 2026. Daily Light Integral values achieved at canopy level are presented in Figure 13. Over the full experimental period, the system maintained a mean DLI of 9.88 ± 1.28 mol·m$^{-2}$·d$^{-1}$, closely corresponding to the programmed target of 10 mol·m$^{-2}$·d$^{-1}$. The observed DLI ranged from a minimum of 7.67 mol·m$^{-2}$·d$^{-1}$ on days with sustained cloud cover to a maximum of 13.50 mol·m$^{-2}$·d$^{-1}$ on days with strong natural irradiance supplemented by evening compensation (Figure 13).

On 12 of the 41 days (29%), the DLI target was met or exceeded. On the remaining 29 days (71%), DLI values remained below the nominal target but above 7.67 mol·m$^{-2}$·d$^{-1}$. The period under evaluation (late January through early March) corresponds to the lowest irradiance months of the year at the study location (Bucharest, Romania, 44°N). The mean DLI of 9.88 mol·m$^{-2}$·d$^{-1}$ across the full 41-day period demonstrates that the system maintained near-target light accumulation even under these challenging seasonal conditions.

For the 14-day sub-period (16 February-1 March 2026) during which complete per-stage activation data were available, a quantitative comparison of actual energy consumption against a full-time reference was performed. The reference scenario represents a conventional supplemental lighting approach in which all three stages operate simultaneously at maximum output (58 W total) throughout the entire 14-hour photoperiod, regardless of prevailing natural light conditions. This corresponds to an energy demand of 0.812 kWh per day.

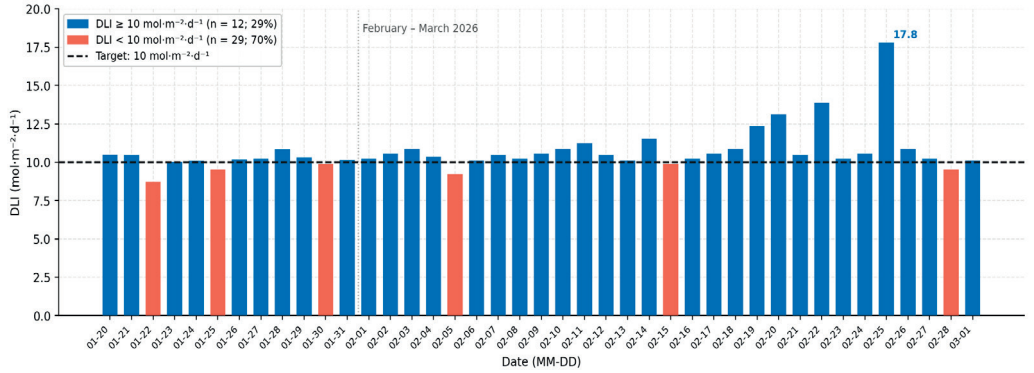



Figure 13. Daily Light Integral (DLI) achieved over the 41-day experimental period (20 January – 1 March 2026). Blue bars: DLI ≥ target (n = 12; 29%); red bars: below target. Dashed line: target = 10 mol·m$^{-2}$·d$^{-1}$. Mean DLI = 9.88 ± 1.28 mol·m$^{-2}$·d$^{-1}$.

### *Energy Efficiency*

Over the 14-day analysis period, the AS7341-controlled system consumed a mean of 0.417 kWh per day, corresponding to an energy saving of 48.7% relative to the full-time reference. The daily energy saving varied substantially according to prevailing sky conditions. On days with high natural irradiance, the system consumed as little as 0.039–0.042 kWh per day, achieving savings of up to 95%. Conversely, on

overcast days, the system operated in near-continuous mode at maximum stage, consuming approximately 0.775-0.804 kWh per day, with savings below 5%.

The distribution of energy savings across day types was as follows: 8 of 14 days were classified as high-irradiance days (saving exceeding 50%), with a mean saving of 80.1%; 2 days were classified as mixed conditions (saving 10-50%), with a mean saving of 14.4%; and 4 days were classified as overcast (saving below 10%), with a mean saving of 3.1%. This distribution confirms that the system functions as intended: it minimises consumption when natural light is abundant, while operating identically to a conventional system when natural irradiance is insufficient to approach the DLI target (Table 2 and Figure 14).

Table 2. Daily energy consumption of the AS7341-controlled system vs. full-time reference, by sky condition (16 February-1 March 2026)

| Sky condition | n days | Actual (kWh·day⁻¹) | Reference (kWh·day⁻¹) | Energy saving (%) |
|---|---|---|---|---|
| Overcast (saving <10%) | 4 | 0.789 | 0.812 | 3.1 |
| Mixed (saving 10-50%) | 2 | 0.519 | 0.812 | 14.4 |
| High irradiance (saving > 50%) | 8 | 0.230 | 0.812 | 80.1 |
| All days - period mean | 14 | 0.417 | 0.812 | 48.7 |

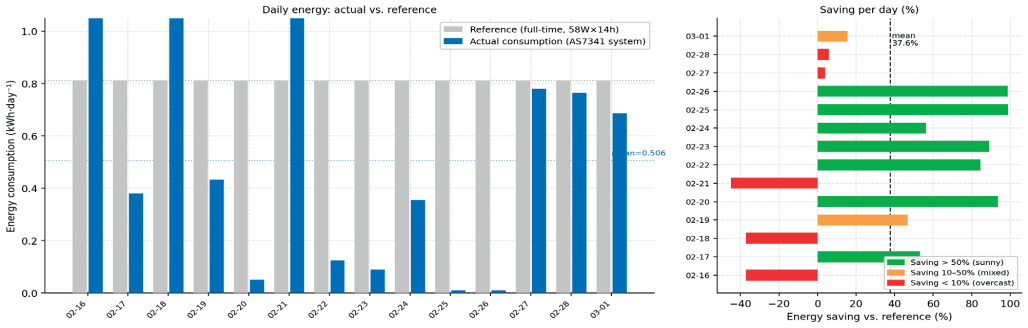



Figure 14. Daily energy consumption: AS7341-controlled system (blue) vs. full-time reference (grey; 58 W × 14 h = 0.812 kWh·day⁻¹). Mean saving: 48.7%

### *Contribution of Supplemental Lighting to Total DLI*

For the 14-day sub-period with complete activation records, the total daily DLI was decomposed into its natural and artificial components, as illustrated in Figure 15. The estimated mean natural DLI over this period was 6.71 mol·m⁻²·d⁻¹ (64% of total), while the supplemental lighting system contributed a mean of 3.81 mol·m⁻²·d⁻¹ (36% of total). Without supplemental lighting, the mean DLI available to the crop would have been 6.71 mol·m⁻²·d⁻¹ - a 33% deficit relative to the target. The supplemental system added a mean of +57% relative to the natural baseline, effectively bridging the light deficit characteristic of the late-winter season.

Considerable variability was observed in the natural–artificial partition across individual days. On overcast days (e.g., 17-18 and 21 February 2026), the artificial component reached 91-92% of total DLI. On high-irradiance days (e.g., 19-20 and 25-27 February 2026), the natural component represented over 95% of total DLI. This adaptive partitioning demonstrates the fundamental advantage of feedback-based control over open-loop timer-based systems: light is added only where and when the natural supply is insufficient.

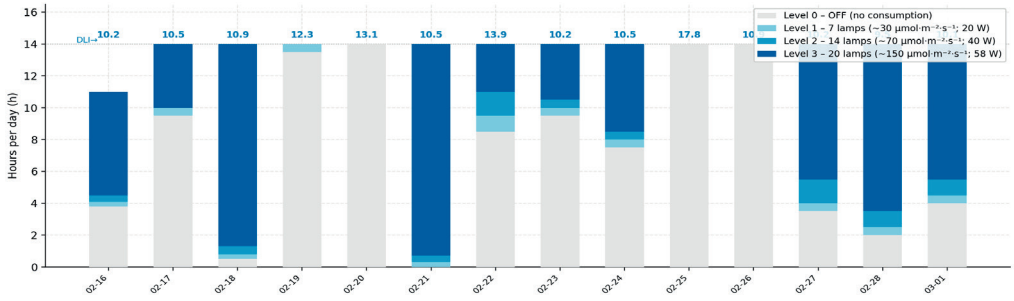



Figure 15. Decomposition of daily DLI into natural (yellow) and artificial (blue) components (16 February-1 March 2026). Mean natural DLI = 6.71 mol·m$^{-2}$·d$^{-1}$ (64%); mean artificial = 3.81 mol·m$^{-2}$·d$^{-1}$ (36%).

***Stage Activation Distribution***

The daily distribution of supplemental lighting stages over the 14-day sub-period is illustrated in Figure 16.

A strong dependence on sky conditions was evident: overcast days were characterised by extended Level 3 activation (13-14 hours per day), while sunny days showed predominantly Level 0 (system off) with brief periods of Level 1 or Level 2 activation.

The multi-stage architecture is functionally justified: on partially overcast days, intermediate stages played a transitional role, minimising energy use while maintaining adequate instantaneous PPFD at canopy level.

This graduated response would not be achievable with a conventional single-stage on/off system, which would either overshoot the required PPFD at full power or provide no supplementation at all.

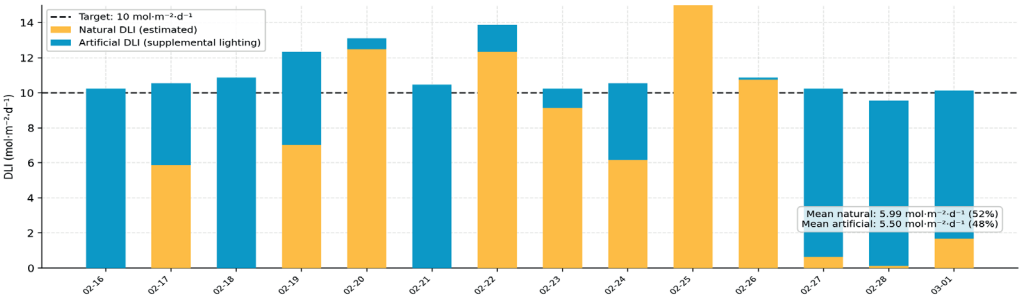



Figure 16. Daily distribution of supplemental lighting activation levels (16 February-1 March 2026). Stacked bars: hours per day at each stage

***Calibration Accuracy and Practical Adequacy***

The AS7341 multispectral sensor achieved an $R^2$ of 0.896 and an RMSE of 69.5 µmol·m$^{-2}$·s$^{-1}$ when calibrated against a reference quantum sensor under natural greenhouse conditions. This level of accuracy is appropriate for the intended application: the control logic operates on discrete PPFD thresholds with a ±10 µmol·m$^{-2}$·s$^{-1}$ hysteresis band, within which a 20% estimation error is fully acceptable. The DLI achievement results confirm this: the system maintained a mean accumulated light integral of 9.88 mol·m$^{-2}$·d$^{-1}$ across a 41-day winter period, closely tracking the target of 10 mol·m$^{-2}$·d$^{-1}$. This outcome confirms that the calibration accuracy, although moderate by photometric standards, is adequate for practical DLI-based greenhouse light management (Bäumker et al., 2021; Palmitessa et al., 2021). The multi-channel architecture of the AS7341 proved advantageous, as it captures spectral variation and allows the regression model to partially compensate for changes in spectral composition between natural and artificial light conditions (Li et al., 2018; Yang et al., 2020).

Negative regression coefficients at 555 nm, 590 nm and 680 nm reflect inter-channel collinearity, which is characteristic of multiple

linear regression applied to spectrally overlapping sensors. These coefficients do not indicate a negative physical relationship between irradiance and sensor response; rather, they represent compensatory terms that improve model fit across the full PPFD range when all channels are considered jointly (Li et al., 2018; Yang et al., 2020).

***Adaptive Control and Energy Efficiency***

The central finding of this study is the demonstration that a feedback-based, multi-stage supplemental lighting system can adapt its energy consumption dynamically to prevailing natural light conditions, without compromising DLI target achievement. Over the 14-day sub-period, the AS7341-controlled system consumed 48.7% less energy than the full-time reference scenario, while achieving a mean DLI of 10.52 $mol \cdot m^{-2} \cdot d^{-1}$. The energy savings ranged from below 5% on fully overcast days to above 90% on high-irradiance days. This variable saving structure is precisely what distinguishes a feedback-controlled system from a conventional open-loop timer: on sunny days, the system effectively switches itself off, whereas on overcast days, it provides full supplementation indistinguishably from a fixed schedule.

The reference scenario used in this study - a timer-based system with a fixed 14-hour photoperiod at maximum output - represents a common practice in low-technology greenhouse operations (Morrow, 2008; Bergstrand, 2016). Compared to this baseline, the 48.7% mean saving is substantial and directly attributable to the sensor-based control logic. Even in the winter months of this study, high-irradiance days accounted for 8 of 14 days (57%), demonstrating that the feedback system finds frequent opportunities for saving that a fixed timer cannot exploit. The graduated multi-stage architecture further enhances this: intermediate stages allow partial supplementation matched to partial natural deficits, which a single-stage on/off system cannot provide.

***Natural vs. Artificial DLI Contribution***

The decomposition of total DLI into natural and artificial components revealed that natural light accounted for 64% of total accumulated DLI, with supplemental lighting contributing 36% over the 14-day sub-period. Without supplemental lighting, the mean natural DLI of 6.71 $mol \cdot m^{-2} \cdot d^{-1}$ would have represented a sustained 33% deficit relative to the target. For Capsicum spp., which requires a DLI of at least 10–15 $mol \cdot m^{-2} \cdot d^{-1}$ for productive growth during the winter season (Kim et al., 2004; Guo et al., 2016), this deficit would be expected to result in reduced photosynthetic rates and lower marketable yield. The supplemental system effectively bridged this deficit, maintaining total DLI close to the target across the full experimental period.

The extreme variability in the natural–artificial partition (from 3% to 92% artificial contribution on individual days) underlines the importance of real-time sensor feedback. A fixed-schedule system would have delivered identical maximum supplementation on all day types, unnecessarily consuming full energy on sunny days and potentially delivering DLI values well above the target, which may induce photosaturation in sensitive species (Moe et al., 2012; Nelson & Bugbee, 2014). The DLI hard-stop mechanism implemented in this system prevents this outcome by halting supplementation as soon as the daily target is reached.

***Open-Source Platform Suitability***

The Home Assistant platform provided the necessary functional infrastructure for all aspects of the control system: sensor data acquisition via ESPHome, regression-based virtual sensor computation, time-triggered automation logic, persistent state management, and long-term data logging via InfluxDB. The system operated continuously for 41 days without requiring manual intervention, demonstrating adequate reliability for a research-grade greenhouse application. The open-source approach facilitates reproducibility and adaptability: the complete system can be replicated with commercially available components at a total hardware cost well below that of proprietary horticultural control systems, positioning it as a practical option for small and medium-scale operations and research facilities where budget constraints are significant (Hemming et al., 2011; Sagheer et al., 2021).

***Limitations and Future Work***

Several limitations of the present study should be acknowledged. First, the AS7341 sensor and

the reference quantum sensor were mounted approximately 3 m apart within the greenhouse, introducing the possibility of positional bias in the calibration. Future work should investigate co-located calibration protocols. Second, calibration was performed exclusively under natural daylight, with supplemental LED lighting switched off; the spectral composition of the LED source differs from natural daylight, and dedicated calibration under mixed-spectrum conditions is recommended. Third, the per-stage energy analysis was limited to the 14-day sub-period for which complete activation logs were available in InfluxDB; extending the logging configuration from the start of the experimental period would enable more complete long-term analysis. Finally, the study was conducted in a single greenhouse at one geographic location; transferability of the calibration model and control parameters to different structures and latitudes should be validated in future work.

This study demonstrated the feasibility of a low-cost, open-source, sensor-based approach for supplemental light management in protected horticulture. A multispectral AS7341 sensor, calibrated against a reference quantum sensor under real greenhouse conditions, was integrated into a multi-stage supplemental lighting system controlled through the Home Assistant open-source automation platform. The system was evaluated over a 41-day winter period (20 January-1 March 2026) in a passive solar greenhouse located in Romania.

## CONCLUSIONS

This study demonstrated the feasibility of a low-cost, open-source, sensor-based approach for supplemental light management in protected horticulture. A multispectral AS7341 sensor, calibrated against a reference quantum sensor under real greenhouse conditions, was integrated into a multi-stage supplemental lighting system controlled through the Home Assistant open-source automation platform. The system was evaluated over a 41-day winter period (20 January-1 March 2026) in a passive solar greenhouse located in Romania.

The key findings of this study can be summarised as follows. (i) The AS7341 sensor calibration yielded an $R^2$ of 0.896 and an RMSE of 69.5 $\mu mol \cdot m^{-2} \cdot s^{-1}$, corresponding to approximately 20% relative estimation error, demonstrated to be adequate for discrete-stage lighting control with DLI integration. (ii) Over the full 41-day period, the system maintained a mean DLI of 9.88 ± 1.28 $mol \cdot m^{-2} \cdot d^{-1}$, closely tracking the programmed target of 10 $mol \cdot m^{-2} \cdot d^{-1}$ despite challenging late-winter irradiance conditions. (iii) Over a 14-day sub-period, the AS7341-controlled system achieved a mean energy saving of 48.7% relative to a conventional full-time supplemental lighting reference (58 W, 14 h $day^{-1}$). On high-irradiance days, savings exceeded 90%; on overcast days, the system operated identically to a conventional fixed-schedule system. (iv) Without supplemental lighting, the mean natural DLI would have been 6.71 $mol \cdot m^{-2} \cdot d^{-1}$ - 33% below the target - confirming the agronomic necessity of supplemental light at this latitude and season. (v) The open-source software stack (ESPHome, Home Assistant, InfluxDB) provided a reliable and fully functional control infrastructure operating continuously without interruption.

These results confirm that the integration of low-cost multispectral sensing, multi-stage LED fixtures, and open-source automation can deliver adaptive, energy-efficient supplemental light management for protected cultivation at a fraction of the cost of commercial solutions. The approach is scalable to larger greenhouse structures and is readily adaptable to other crops and DLI targets. Future work should address mixed-spectrum calibration, multi-zone deployment, and long-season validation under variable irradiance conditions.

## REFERENCES

Bäumker, E., Zimmermann, D., Schierle, S., & Woias, P. (2021). A novel approach to obtain PAR with a multi-channel spectral microsensor, suitable for sensor node integration. *Sensors, 21*, 3390. https://doi.org/10.3390/s21103390

Bergstrand, K.-J., Asp, H., & Schüssler, H. K. (2016). Growth control of ornamental and bedding plants by manipulation of photoperiod and light quality. *Acta Horticulturae, 1134*, 33–40. https://doi.org/10.17660/ActaHortic.2016.1134.5

Guo, X., Hao, X., Khosla, S., Kumar, K. G. S., Cao, R., & Bennett, N. (2016). Effect of LED interlighting combined with overhead HPS light on fruit yield and quality of year-round sweet pepper in commercial greenhouse. *Acta Horticulturae, 1134*, 71–78.

Hao, X., Guo, X., Lanoue, J., Zhang, Y., Cao, R., Zheng, J., Little, C., Leonardos, D., Khosla, S., Grodzinski,

B., & Yelton, M. (2018). A review on smart application of supplemental lighting in greenhouse fruiting vegetable production. *Acta Horticulturae, 1227*, 499–506.

Hemming, S. (2011). Use of natural and artificial light in horticulture. *Acta Horticulturae, 907*, 25–35. https://doi.org/10.17660/ActaHortic.2011.907.15

Jokinen, K., Särkkä, L. E., & Näkkilä, J. (2012). Improving sweet pepper productivity by LED interlighting. *Acta Horticulturae, 956*, 59–66. https://doi.org/10.17660/ActaHortic.2012.956.5

Kawasaki, M., Kawamura, S., Tsukahara, M., Morita, S., Komiya, M., & Natsuga, M. (2008). Near-infrared spectroscopic sensing system for on-line milk quality assessment in a milking robot. *Computers and Electronics in Agriculture, 63*(1), 22–27.

Kim, H. H., Goins, G. D., Wheeler, R. M., & Sager, J. C. (2004). Green-light supplementation for enhanced lettuce growth under red and blue light-emitting diodes. *HortScience, 39*(7), 1617–1622.

Kim, H. H., Wheeler, R. M., Sager, J. C., Goins, G. D., & Norikane, J. H. (2006). Evaluation of lettuce growth using supplemental green light with red and blue light-emitting diodes in a controlled environment. *Acta Horticulturae, 711*, 111–118.

Li, H., Gao, S., Li, L., Jia, C., & Zhao, L. (2018). Real-time precise relative positioning with moving base in long baseline. *Sensors, 18(9)*, 2850. https://doi.org/10.3390/s18092850

Li, X., Lu, W., Hu, G., W, X. C., Zhang, Y., Sun, G., & Fang, Z. (2016). Effects of light-emitting diode supplementary lighting on the winter growth of greenhouse plants in the Yangtze River Delta of China. *Botanical Studies, 57*, 2.

Moe, R. (2012). LEDs: The future of greenhouse lighting. Acta Horticulturae, 956, 3–10.

Moe, R., Grimstad, S. O., & Gislerød, H. R. (2006). The use of artificial light in year-round production of greenhouse crops. *Acta Horticulturae, 711*, 35–42.

Morrow, R. C. (2008). LED lighting in horticulture. *HortScience, 43*(7), 1947–1950.

Nelson, J. A., & Bugbee, B. (2014). Economic analysis of greenhouse lighting: Light-emitting diodes vs. high intensity discharge fixtures. *PLOS ONE, 9*(6), e99010. https://doi.org/10.1371/journal.pone.0099010

Palmitessa, O. D., Pantaleo, M. A., & Santamaria, P. (2021). Applications and development of LEDs as supplementary lighting for tomato at different latitudes. *Agronomy, 11*(5), 835.

Paucek, I., Pennisi, G., Pistillo, A., Appolloni, E., Crepaldi, A., Calegari, B., Spinelli, F., Cellini, A., Gabarrell, X., Orsini, F., & Gianquinto, G. (2020). Supplementary LED interlighting improves yield and precocity of greenhouse tomatoes in the Mediterranean. *Agronomy, 10*(7), 1002.

Rath, T., & Kawollek, M. (2009). Robotic harvesting of Gerbera jamesonii based on detection and 3D-localization of stem axes. *Acta Horticulturae, 824*, 261–268.

Sagheer, A., Mohammed, M., Riad, K., & Alhajhoj, M. (2021). A cloud-based IoT platform for precision control of soilless greenhouse cultivation. *Sensors, 21*, 223.

Shafaei, S. M., Loghavi, M., & Kamgar, S. (2018). On the neurocomputing based intelligent simulation of soil mechanical resistance. *Soil and Tillage Research, 184*, 137–152.

Thorp, K. R., Wang, G., Bronson, K. F., Badaruddin, M., & Mon, J. (2017). Hyperspectral data mining to identify relevant canopy spectral features for estimating durum wheat growth, nitrogen status, and grain yield. *Computers and Electronics in Agriculture, 136*, 1–12.

Yang, T., Nan, X., & Jin, W. (2020). Temperature sequential data fusion algorithm based on cluster head selection and multi-sensor fusion in wireless sensor networks. *IEEE Access, 8,* 42782–42793.

Scientific Papers. Series E. Land Reclamation, Earth Observation & Surveying, Environmental Engineering. Vol. XV, 2026
Print ISSN 2285-6064, CD-ROM ISSN 2285-6072, Online ISSN 2393-5138, ISSN-L 2285-6064

# THE INFLUENCE OF INOCULATION WITH SYNTHETIC MICROBIOMES ON THE EVOLUTION OF SOIL CARBON SEQUESTRATION UNDER THERMAL STRESS

**Sorin MATEI, Gabi Mirela MATEI, Sorina DUMITRU, Victoria MOCANU, Monica DUMITRAȘCU**

National Research-Development Institute for Soil Science, Agrochemistry and Environment, Bucharest, 61 Marasti Blvd, District 1, Bucharest, Romania

Corresponding author email: so_matei602003@yahoo.com

***Abstract***

*Synthetic microbial communities form networks of diverse microorganisms interconnected through a variety of interspecific interactions. Considering that positive interactions are favored in more stressful environments, assessments of the influence of complex synthetic microbial communities required a more precise identification, analysis of the evolution and amplitude of interactions. The effect of inoculation and the involvement of synthetic microbiomes in carbon sequestration/release was determined after evaluations of glycoproteins, exopolysaccharides (EPS) and dissolved organic carbon (DOC) content, under thermal stress conditions (35ºC and 45ºC). The Mollic Gleysol inoculated with microbiomes M5 and M7 had a DOC content in the rhizosphere at both temperatures below the level of the uninoculated control. Also, M7 induced the highest changes in glycoprotein content, which, after 14 days at 45ºC, reached 1.79 mg·g$^{-1}$. Under similar experimental conditions, M5 was highlighted by inducing the highest changes in exopolysaccharide content (587µg·ml$^{-1}$). Synthetic microbiomes (M1, M4, M5, M7) promoted beneficial interactions in soil after inoculation, strengthened beneficial microbial cooperation and improved organic carbon decomposition/cycling in the rhizosphere.*

***Key words:*** *dissolved organic carbon, exopolysaccharides, glycoproteins, microbiome, thermal stress.*

## INTRODUCTION

Carbon (C) in soil organic matter (SOM) is integrated into a wide range of organic compounds, from mobile, chemically reactive forms to stable, recalcitrant forms. They may be protected from decomposition and accumulate due to their chemical nature or physical stabilization, achieved by binding to particles and/or placement in aggregates, under specific microenvironmental conditions.

Among the compounds, some can be attributed to specific organic groups, such as certain lignins, tannins, waxes, and other compounds are produced exclusively by microorganisms, such as specific glycoproteins, exopolysaccharides, amino-sugars, ether-lipids, fatty acids (Six et al., 2006; Knappy et al., 2015; Lehmann et al., 2017; Guhra et al., 2019; Cheng et al., 2020).

For ecosystem functioning, the carbon content sequestered in organic matter (OM) is important for its feedback effect on soil quality, microbial activities, ensuring the maintenance of ecosystem services, including those involved in carbon stability/sequestration processes, soil aggregate stabilization, water retention, slow nutrient release, root exudates and soil-plant relationships (Heimann & Reichstein, 2008; Ding et al., 2015; Bradford et al., 2016).

Soil organic carbon (SOC) is deposited in any layer of the trophic profile, coming practically directly from plants or from components of the soil food web, which includes exudates, excretions, exometabolites, dead biomass residues and other organic compounds in particulate or dissolved form.

SynComs represent initially carefully selected microbial groups, designed with the aim of optimizing microbiome functions (plant growth, synthesis of disease resistance, a.s.o.) and achieving stability upon contact with native communities.

The microbial species used in the construction of SynComs also differ in terms of growth and adaptive capacities at different temperatures (Bárcenas-Moreno et al., 2009; Engqvist, 2018; Boyle et al., 2024; Zhao et al., 2024).

Assessments of the degree of sensitivity and growth rates of different species to temperature have been carried out in ecosystems with different microbiomes, to estimate the impact on the level of ecosystem functionality (Bowles et al., 2014; Hungate et al., 2015, Koch et al., 2018).

The presence of SynComs leads to changes in plant metabolic pathways, through the type and amount of exudated C compounds (organic acids, amino acids), more useful for symbiotic association or in secretion of specific compounds, for the recruitment of beneficial bacteria in the rhizosphere.

Under thermal stress, microbiomes induce changes in the profile of root exudates, enhance the synthesis of specific signaling compounds for plant adaptation, as well as the secretion of enzymes, determined by specific carbon compounds released by mycorrhizal roots (Li et al., 2017; Preece & Peñuelas, 2020; Goddard et al., 2021; Wu et al., 2022; Sharma et al., 2023).

Temperature effects on carbon content include increases in secondary metabolism, intensification of plant root exudation, accelerated microbial decomposition, transformations into organic carbon and water-extractable labile compounds.

Carbon dynamics can be mediated by microorganisms with specific thermal thresholds, where behavior evolves from rapid degradation to accumulation, at temperatures of 26-35°C and which even promote the retention of refractory dissolved organic matter. Temperature increases, also enhance dissolution, diffusion, exchange and increase in soil carbon concentrations, induce qualitative changes, generate reduced molecular weights, aromaticity and complexity. Soil temperature, in deeper layers, appears positively associated with carbon concentrations and, if temperatures increase, carbon availability increases and potential carbon losses accelerate, especially in temperate agroecosystems.

The study aimed the evaluation of four SynComs variants formed by selected microorganisms that actively contribute to the carbon cycle.

Inoculated into soil, they constitute sources of microbial C, which specifically influence the evolution of the microbiota through the synthesis of organic compounds in the soil and in the rhizosphere of plants, contributing to a possible subsequent stabilization of additional C in SOM, under thermal stress conditions.

## MATERIALS AND METHODS

**The experiment** analyzed the influence of the composition of synthetic communities (SynComs) of the microbiomes M1, M4, M5, M7 (Matei et al., 2025) on the storage/ sequestration of biosynthesized organic compounds in the soil, after the application of 10 ml SynCom inoculum/pot with concentrations ranging between $4.56\text{-}7.32 \cdot 10^3$ CFU $mL^{-1}$ for fungi and between $7.25\text{-}9.34 \cdot 10^6$ viable cells $mL^{-1}$ for bacteria, under termosensible tomato (*Solanum lycopersicum* L.) culture.

After a period of 60 days of vegetation, the biotest pots with Mollic Gleysol, tomatoes and inoculum were incubated under controlled conditions for periods of 3 days and 14 days, for a duration of 8h/day at temperatures of 35°C and 45°C, maintaining humidity.

Plant and soil samples have been taken from each culture pot for specific analyses, in three replicates

**The synthetic communities (SynComs)** correspond to the microbiomes M1, M4, M5, M7 containing selected bacterial and fungal heterotrophic microflora, with exometabolic efficiency and not genetically modified. Microbial strains selected were preserved in pure cultures on special culture media, Nutrient Agar (NA) for bacteria and Potato Dextrose Agar (PDA) for fungi, at 4°C.

**Composition of microbiomes** - The inoculated SynComs contain microorganisms belonging to 9 bacterial genera including *Bacillus, Azotobacter, Rhizobium, Acetobacter, Paenibacillus, Streptomyces* a.s.o. and 16 fungal genera including *Torula, Stachybotrys, Humicola, Cladosporium, Micromonospora, Glomus*. The composition of SynComs M1, M4, M5, M7 includes microflora with the same genera. The specificity of each SynCom is given by the different metabolic capacities of the component strains.

**Glycoprotein content -** Glycoproteins were extracted from dried soil with sodium citrate at pH 7.0, autoclaved and centrifuged at 5000 rpm for 10 min. Using standard bovine serum

albumin (BSA), the glycoproteins content was evaluated colorimetrically. Bradford reagent was added to each cuvette and mixed by repeated inversion of the cuvette.

The mixture was incubated at room temperature for 5 min., and after the color change from brown to blue, the absorbance of the samples and the standard was measured spectrophotometrically at 595 nm.

The glycoprotein concentration of the samples was calculated by comparing their absorbance values with those of the standard curve (Bradford, 1976).

**Fluorescence of glycoproteins -** Fluorophores and fluorescence-based techniques were used to obtain images of glycoproteins on the surface of rhizosphere aggregates, under stress conditions.

Fluorescence of glomalin-related soil protein (GRSP) was revealed using thin soil sections to distinguish organic material from minerals, taking advantage of its characteristic fluorescence in the blue/green range.

**Exopolysaccharide (EPS) quantification -** Soil samples were analyzed for EPS content using the phenol-sulfuric acid, followed by ultrafiltration and succesive applications of 1ml phenol (5% in water), 5 ml sulfuric acid (95%) and 2ml glucose (80 mg $L^{-1}$).

The mixture was left for 10 min, shaken and maintained at 25°C for 20 min, in a water bath. The absorbance was measured at 490 nm with a spectrophotometer (DuBois et al., 1956).

**Dissolved organic carbon (DOC) content -** Deionized water was applied to air-dried soil samples, the suspensions were sonicated with an ultrasonic power of 27W, stirred at 30°C for 10 min, then centrifugated at 10°C for 10 min. For extraction ultrapure water was used, ratio soil:extractant was 1:10, without changes in pH.

The suspensions were pre-filtered with a cellulose filter, additionally filtered by cellulose esters membranes with pore diameter of 0.45 μm and DOC absorbance was evaluated at 254-400 nm with UV-Vis spectrophotometer (Bolan et.al., 1996).

To establish the calibration curve, the absorbance was performed in relation to standard humic substances.

**Fluorescence of Dissolved organic C** - The water-soluble fulvic sub-fractions with DOC, after inoculation of SynComs, contained added fluorochrome and their arrangement in soil was evidenced by specific ascending chromatography (Wang et al., 2016).

**Data analysis** - The analysis of variance (ANOVA) and Student test were used for the results evaluation.

## RESULTS AND DISCUSSIONS

The experiment assessed the influence of inoculating Mollic Gleysol with selected SynComs (M1, M4, M5, M7) and evaluated their involvement in the initiation of processes responsible for C synthesis/ sequestration.

The influence of SynComs was estimated through changes in glycoprotein, exopolysaccharide and dissolved organic carbon content, under thermal stress conditions. The metabolically active microbial species in the analyzed SynComs acted by forming new organic molecules or by complexing existing ones.

Glycoproteins, namely glomalin-related soil proteins (GRSP), are closely associated with the amount of carbon and nitrogen reserves in the soil, heavy metal sequestration, aggregate stability and stress mitigation (Liu et al, 2022).

The processes of synthesis, accumulation, as well as the decomposition of GRSP in soils depend on both the interactions of SynComs with native soil biota and the processes in the rhizosphere of cultivated plants.

Generating new/modified metabolic pathways, SynComs intervene in changes regarding the type/quantity of glycoproteins present in the rhizosphere soil and in the activities of endemic biota, influencing the rates of decomposition/ synthesis of new organic compounds.

Among the SynComs tested, M7 demonstrated superior performance, generating large increases in glycoprotein content (1.92 mg $g^{-1}$) after 14 days at 35°C. Their level decreased by 6.7% (1.79 mg $g^{-1}$) at 45°C, under the influence of the same microbiome.

The variations in glycoprotein content in the rhizosphere area, after incubation for 3 days at 35°C, compared to 45°C, were only 2.3% under the influence of M7. SynComs M5 and M4 determined, after 14 days at 35°C, 1.56 mg $g^{-1}$ and 1.43 mg $g^{-1}$, respectively.

At 45°C, under similar conditions, decreases of 7.6% and 8.3%, respectively, in glycoprotein content were recorded. In the rhizosphere, after incubation for 3 days at 35°C, the decreases in glycoprotein content compared to 45°C were 4.4% under the influence of M5 and 5.7% under the influence of M4.

SynCom M1 induced after 14 days at 35°C a glycoprotein content of 1.17 mg·g$^{-1}$, a level that decreased by 11.7% at 45°C, but which remained 5.82% higher than the uninoculated control (0.97 mg·g$^{-1}$), under high thermal conditions (Figure 1).

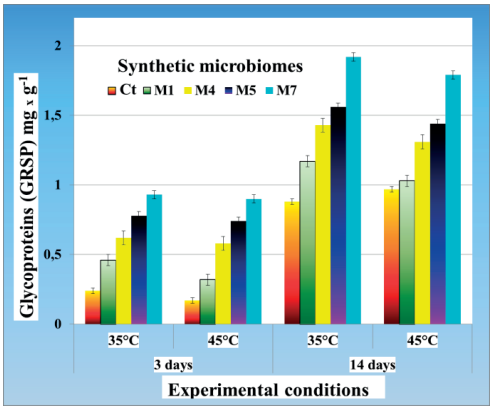



Figure 1. GRSP content generated by inoculating Mollic Gleysol with SynComs under two different periods of time and temperatures

The stable aggregates formed by the new glycoprotein input determined favorable changes in the stability of the soil structure, prolonging the persistence of sequestered carbon through the significantly modified qualitative/quantitative content that allows the establishment of a more stable reserve in the soil.

The presence of *Azotobacter* species in the rhizosphere, recently introduced through SynCom, enriched the rhizosphere in nitrogen, possibly causing a reduction in the oxidative enzymatic activity that decomposes glycoproteins.

Through reactions and involvement they can be considered indicators of the quality of organic matter, recent studies highlighting the fact that their level correlates with the ratio of carbon in humic and fulvic acids and with the ratio of C in SOM and microbial biomass.

Glycoprotein accumulations constitute an essential component of SOM composition. Glycoprotein content undergoes changes depending on temperature, exposure time, SynCom variant and their involvement in carbon cycling, soil respiration and microbial biomass (Pietikainen et al., 2005; Walker et al., 2018; Ye et al., 2019; Matei et al., 2024; Matei et al., 2025).

As a possible indicator of carbon accumulation, glycoprotein content changed during the experiment, varying according to time, temperature and type of SynCom inoculated. Glycoprotein accumulations were found in all SynComs up to 35°C and increased over time, later evaluations revealed significant decreases at 45°C and incubation for 14 days, the differences being generated by the composition of the SynCom type, within the thermal ranges.

Thus, the SynComs intervened in the quantitative/qualitative regulation of glycoprotein accumulations, generated changes in properties and compositional traits and improved soil properties.

They also significantly contributed to the storage of SOC, due to qualitative diversification and quantitative input, to the increase in the residence time of C and its stabilization in soil aggregates, protecting the labile organic compounds of C, generated by microbial decomposition.

The modified composition of the newly synthesized microbial compounds ensures the gradual accumulation in the soil, as stable forms of C (Liu et al., 2020; Holátko et al., 2021; Wang et al., 2021; Agnihotri et al., 2022; Guo et al., 2022; Yuan et al., 2022; Yang et al., 2024a; Zhou et al., 2024; Ling et al., 2025).

The biosynthesis of glycoproteins after SynCom inoculation differs qualitatively/quantitatively from the specific composition generated under thermal conditions. The glycoprotein component generated by the specific microbiota of SynComs was analyzed by fluorescence after an exposure time of 14 days, under thermal stress conditions.

Due to the dynamization of microbial processes/activities under these conditions, glycoprotein accumulations appear highlighted by fluorescence, especially at 35°C. The set of newly synthesized compounds under the

influence of SynComs appear on the surface of the aggregates as fluorescent clumps (Figure 2).

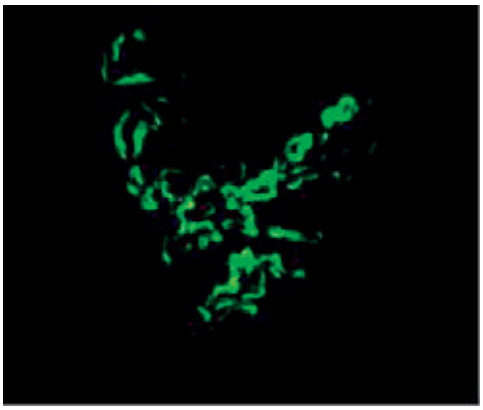


Figure 2. Glycoproteins GRSP appear as fluorescent clumps, after inoculation with the SynCom M7 and exposure at 35°C for 14 days

The direct impact of additional compounds biosynthesized by SynComs under thermal stress influences the structure of rhizospheric organic components and aggregates, generating a possible form of protection at the organo-mineral level.

Under the influence of SynCom M7, fluorescent components highlight the accumulations and distribution of the new glycoprotein complex at 35°C in aggregates, after 14 days of incubation under controlled conditions.

Under heat stress conditions, SynComs can also influence the evolution of soil glycoprotein content through glycosylation, enhanced synthesis of stress-protective glycans, and changes in symbiotic relationships.

Thus, SynComs act through modifications that promote the maintenance of functional stability, stimulation of metabolic activities, and adaptability by regulating their responsibilities regarding temperature and reactive oxygen species at the protein level.

SynComs inoculated into Mollic Gleysol produce large amounts of EPS, through the component strains, which form and accumulate as a protective film around the roots, inducing an increase in the ability of tomatoes to tolerate heat.

Thus, through EPS, soil health is improved by increases in aggregation capacity, water retention in the rhizosphere zone, hormonal regulation, root growth and thermal tolerance.

Under experimental conditions, the performances of EPS-producing SynComs were analyzed and, among them, SynCom M5 induced, in the tomato rhizosphere, the highest increases in EPS content at 35°C after 3 days (552 $\mu g \cdot ml^{-1}$) and 612 $\mu g \cdot ml^{-1}$ after 14 days, compared to the uninoculated control variant (527 $\mu g \cdot ml^{-1}$). At 45°C, after 3 days of incubation, EPS content decreased to 543 $\mu g \cdot ml^{-1}$ and after 14 days to 587 $\mu g \cdot ml^{-1}$ (Figure 3).

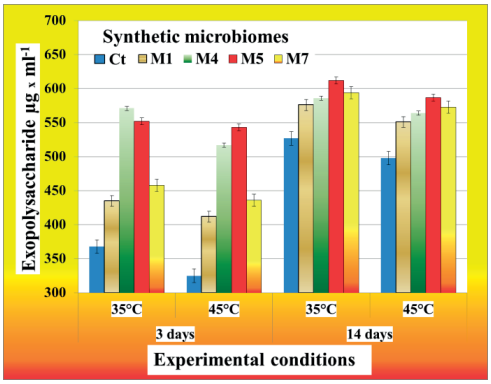



Figure 3. EPS content, after SynComs inoculating, generated in Mollic Gleysol under two different periods of time and temperatures

The results suggest an intense involvement in carbon sequestration/stabilization in the Mollic Gleysol, possibly due to the direct adsorption of new exometabolized organic molecules and the intensification of aggregation with rhizosphere minerals.

Thus, the biochemical protection offered to carbon compounds by SynCom M4 components is expressed by an increased capacity for EPS biosynthesis at 35°C, more efficient than that offered by SynCom M5 at 3 days.

At 45°C, SynCom M4 offered weaker protection than M5 and the exopolysaccharide content decreased after 14 days of incubation to 564 $\mu g \cdot ml^{-1}$. SynComs M7 and M1 produced, after 14 days at 35°C, an EPS content that increased by 12.7% and 9.4%, respectively, compared to the uninoculated control.

At 45°C, the EPS content decreased, under the influence of these microbiomes, in both

exposure periods (3 and 14 days), but remained at values higher than the uninoculated control, under increased thermal conditions.

SynComs M7 and M1 synthesized EPSs that had a lower efficiency in sequestering carbon in the soil (436 $\mu g \cdot ml^{-1}$ and 412 $\mu g \cdot ml^{-1}$, respectively), under experimental conditions.

The new EPS compositions from the tomato rhizosphere express the result of co-generation by SynComs and native soil microbiota, compositions that intervene, through the induced changes, in the modeling of the ecological functions of the soil.

Thus, in the soil, EPSs represent carbon-rich molecules, produced by soil microorganisms, which form rich sources of C added directly to the SOM reserve. In the Mollic Gleysol, EPSs synthesized in the rhizosphere by the SynComs microbiota intervene in the improvement of the quality/sequestration of C achieved through the formation of microaggregates from soil particles and organic matter.

By generating these more stable structures, the newly formed aggregates can, in turn, protect the newly synthesized C, sequestering it in the soil for longer periods of time, ensuring cohesion, preventing erosion and subsequent C losses. The SynComs used, through the structure of the communities, influenced both the evolution of EPSs in the rhizosphere, under thermal stress, and the selection, through direct mechanisms, of the native EPS-producing biota.Also, the production, composition and functional properties of EPSs in inoculated soil can be significantly influenced by temperature, which can constitute a stress factor involved in triggering the increase in EPS synthesis and ensuring microbial survival (Sandhya & Ali, 2015; Nouha et al., 2018, Cania et al., 2019; Silambarasan et al., 2019; Asgher et al., 2020; Yang et al., 2022; Yang et al., 2024b).

For the composition of native and synthetic soil microbiota, temperature is one of the critical environmental signals that influences the production of EPSs with a protective, survival and modeling role of soil properties (More et al., 2014; Op De Beeck et al., 2021).

The soil structure can undergo changes induced by EPSs produced under thermal stress through actions similar to soil particle binding agents, which lead to increases in stability, water retention and nutrient availability. Also, the qualitative/quantitative evolutions of EPSs, under thermal stress, intervene in the stimulation of microbial activities, with microbial processes showing a remarkable variation in terms of temperature sensitivity, as well as in the clearer expression of their membership in a community.

The evolution of dissolved organic carbon (DOC) content under the influence of SynComs inoculation was analyzed in order to evaluate the stability/sequestration of C in the Molic Gleysol, taking into account its complex role in soil C dynamics.

Inoculation of SynComs M5 and M7, at 35°C and 3 days of incubation, determined in the rhizosphere of tomatoes a low DOC content of 2.82 $mg \cdot L^{-1}$ and 3.43 $mg \cdot L^{-1}$, respectively, both below the DOC level determined in the uninoculated control variant of 5.64 $mg \cdot L^{-1}$. DOC assessments at 45°C, in the rhizosphere, after inoculation with SynComs M5 and M7 were 3.17 $mg \cdot L^{-1}$ and 3.92 $mg \cdot L^{-1}$, respectively, compared to the uninoculated control (6.87 $mg \cdot L^{-1}$).

In the case of SynComs M4 and M1, incubated for 3 days, the DOC content at 35°C was 3.62 $mg \cdot L^{-1}$ and 3.48 $mg \cdot L^{-1}$, respectively, and at 45°C DOC increased by up to 18.76% and 20.26%, respectively, for SynComs M4 and M1, compared to their level reached at 35°C.

The Mollic Gleysol inoculated with SynCom M5 at 35°C and 14 days of incubation had a DOC content of 14.22 $mg \cdot L^{-1}$ and when inoculated with SynCom M7, under the same experimental conditions, the DOC determined was 15.29 $mg \cdot L^{-1}$, both quantitative values being below the DOC level analyzed in the uninoculated control.

DOC evaluated at 45°C, in the rhizosphere, after inoculation with SynComs M5 and M7 was 16.24 $mg \cdot L^{-1}$ and 17.66 $mg \cdot L^{-1}$, respectively, compared to the uninoculated control (22.28 $mg \cdot L^{-1}$).

In the case of inoculation with the M4 and M1 synthetic microbiomes, the DOC content in the soil at 35°C decreased by 12.32% and 21.27%, respectively, compared to the uninoculated control (17.84 $mg \cdot L^{-1}$) and at 45°C the DOC in the soil increased by up to 28.65%, under the influence of SynCom M1 (21.70 $mg \cdot L^{-1}$), compared to the DOC content at 35°C (Figure 4).

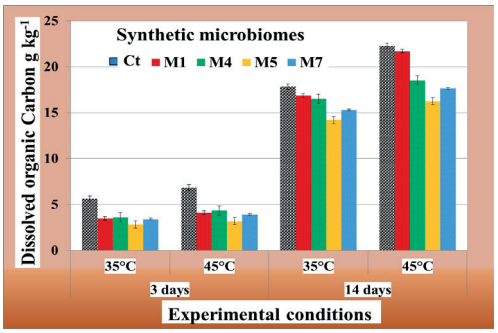



Figure 4. DOC content in Mollic Gleysol generated by inoculation with SynComs under two different periods of time and temperatures

Incubation of vegetation pots at temperatures considered as heat stress influenced the intensity of microbial activities in the soil, so that SynComs intervened in accelerating processes in the rhizosphere, making C use more efficient by enhancing sequestration and reducing free DOC.

The new communities of microorganisms in the rhizosphere act preferentially on more easily degradable compounds, either generating more DOC or participating in the construction of more stable aggregates, thus quantitatively reducing their presence.

The applied thermal stress had an effect on the DOC content in the inoculated rhizosphere also through the induced changes in the composition of root exudates, representing sugars, organic acids, metabolites, a.s.o., which constitute the main sources of DOC.

Thus, when temperatures increase, both the production of DOC by photosynthesis and the decomposition of organic matter undergo accelerations, causing their concentration in the soil to increase.

Possibly, thermal stress causes a photosynthetic stimulation, with tomatoes producing more organic compounds than they can process, generating their release in the form of DOC. Also, the high temperatures applied determined the growth and development of microorganisms in the rhizosphere, promoting an increase in the rate of decomposition of OM and the release of a greater amount of DOC into the environment (Campbell et al., 2022).

When the applied incubation temperature was 45°C, the photosynthetic capacity of tomatoes may have been oriented towards a hypersynthesis of organic compounds, far beyond their utilization capacities, causing their release in the form of DOC. Inoculation with SynComs enriched the rhizosphere with metabolites related to plant growth, stress inhibition and the structure of the overall DOC composition.

The inoculated SynComs promoted beneficial interactions, developed beneficial microbial cooperation and improved the dynamics of organic C in the rhizosphere.

Various studies have analyzed the impact of temperatures on DOC characteristics, investigated the ways in which high temperatures accelerate the decomposition processes of organic C for an increase in DOC production (Kalbitz et al., 2000; Smreczak & Ukalska-Jaruga, 2021).

Thus, the influence of temperature variations on the level of degradation, mineralization and DOC characteristics, interactions between microbial communities and DOC was evaluated (Liu et al., 2019; Garcia et al., 2022; Wang et al., 2022).

Soils contain natural organic matter (NOM) with a role considered essential in shaping their composition and microbiology and, through the amount and compositional specificity of NOM, influencing the types and concentrations of other compounds. In addition, temperature has been identified as a significant factor influencing DOC (Zhao et al., 2023; Huang et al., 2024; Ren & Cai, 2025).

To adapt to high temperatures, the lipid composition of the microbiota changes to express heat shock proteins and stabilize cell membranes. Warming intervenes in increasing the potential level of respiration of the heterotrophic saprophytic soil microbiota, enhancing $CO_2$ emissions, reducing SOM deposits necessary to maintain soil structure and water retention capacity (Karhu et al., 2014; Bond-Lamberty et al., 2018; Cavicchioli et al., 2019; Jansson & Hofmockel, 2019).

Under elevated temperatures, the application of SynComs inoculation resulted in an intensification of DOC production, through increases in metabolic activities, accelerated SOM decomposition, etc., which generated temperature-dependent dynamics.

Other effects of temperature on DOC include accelerated decomposition and microbial

transformation into particulate organic carbon (POC), water-extractable labile compounds, a microbiota with specific thermal thresholds and behavior that evolves from rapid degradation to accumulation at high temperatures (26-35°C), promoting the retention of refractory DOC.

Soil carbon fractions also suffer significant decreases in labile C, recalcitrant C, as elevated temperatures enhance the conversion of old, protected organic matter (SOM) into labile, soluble forms (DOC), accelerating the overall rate of C renewal in the soil.

Using UV illumination, images revealed differences between the uninoculated control and the inoculated variants, at different time (3 and 14 days) and temperature (35°C and 45°C) intervals (Figure 5).

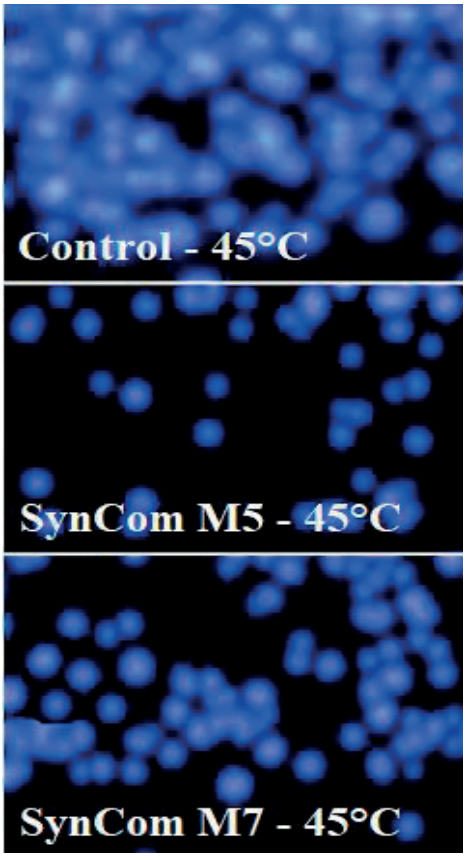



Figure 5. DOC from soil inoculated with SynComs M5 and M7, at 45°C after 14 days

The qualitative differences were generated by the specific composition of SynComs and were reflected, function by their affinity, in the aspects related to the level of accumulations of newly synthesized organic compounds.

The distribution of extracted organic carbon compounds DOC was highlighted based on fluorescence affinity. DOC showed different densities of organic compounds in the soil, after 14 days of incubation at 45°C, in the case of inoculated SynComs.Of these, SynCom M5 induced the lowest DOC content, at 45°C, after 14 days of incubation and the organic carbon structures appear well highlighted through less dense areas, with a lower molecular weight, compared to the DOC structures that appear under the influence of SynCom M7.

After 14 days of incubation at 35°C, the density differences are less evident and, in the case of SynComs M4 and M1, including the control, the differences are imperceptible.

After inoculation with SynComs M5 and M7, the stability of organic carbon compounds in DOC at temperature increased in the carbon subfractions, the biochemical protection offered by the composition of the newly secreted exometabolites was more intense and diverse, compared to the other inoculated SynComs. The images reveal the changes in the distribution and organization of newly biosynthesized DOC under the influence of SynCom M5, under thermal stress, compared to the uninoculated control.

It can be deduced that the stability of organic carbon in the soil inoculated with SynComs M5 and M7 also increased, compared to that provided by SynComs M1 and M4.

But, even under conditions of reduced protection of C compounds, SynComs M1 and M4 ensured better stability of organic C. compared to the uninoculated control.

The trend demonstrated by DOC under the influence of SynComs M5 and M7, after the 14 days of intermittent exposure at 45°C, is more pronounced than at 35°C, under the influence of the same synthetic microbiomes, which perhaps reflects a reaction model to the interactions between soil properties and the biochemical characteristics specific to SynComs.

The amount of C stored in the soil appears dependent on the metabolism of SynComs, the physico-chemical structure, interactions and chemical absorption of carbon molecules in

relation to the mineral component and their specific influence modifies the accessibility/stability of C.

Thus, microbial C biosynthesized by SynComs enriches DOC in the inoculated soil, can stabilize on mineral surfaces or in the soil solution, where it can compete for sorption sites.

Under controlled conditions of thermal stress, under the influence of the analyzed SynComs, labile substances were produced by both the inoculated synthetic communities and the native ones in the soil, to which substances from the organo-mineral reserve were added. The analyzed parameters, such as the content of glycoproteins, EPS and DOC, can be used as indicators for estimating the efficiency of carbon use under the conditions of increasing the supply of extracellular compounds on the long-term carbon storage and the dynamics of carbon capture/emission processes in the soil.

## CONCLUSIONS

SynComs selected for their exometabolic capacities intervened in the organic C dynamics, favoring the stabilization and sequestration of carbon in the soil, under thermal stress conditions.

In the soil, inoculated SynComs and native microbial communities, stimulated by their presence, enhanced the synthesis of GRSP and EPS, as a strategy of adaptation to stress conditions.

Inoculated SynComs and native communities influenced by their presence reduced the synthesis of DOC, as a strategy of resistance to thermal stress.

The content, quality and influence of additionally biosynthesized/ accumulated GRSP, EPS and DOC in the soil varied significantly depending on the type of SynCom.

Under heat stress conditions, the content of GRSP, EPS and DOC biogenerated after SynComs inoculation varied significantly between the two temperature ranges

Depending on the composition and characteristics of SynCom, the results obtained under heat stress conditions highlighted that soil microbial carbon pumps acted/functioned differently in the rhizosphere to compensate/stimulate the synthesis of GRSP, EPS and DOC.

Comparative evaluation of SynComs regarding influence on carbon stability and sequestration under heat stress conditions were observed at M5 and M7 in terms of the effect on functional efficiency of the new soil microbiota.

## ACKNOWLEDGEMENTS

This work was supported by the Ministry of Education and Research, Project number PN 23 29 05 01/2023.

## REFERENCES

Agnihotri, R., Sharma, M. P., Prakash, A., Ramesh, A., Bhattacharjya, S., Patra, A. K., Manna, M. C., Kurganova, I., & Kuzyakov, Y. (2022). Glycoproteins of arbuscular mycorrhiza for soil carbon sequestration: Review of mechanisms and controls. *Science of The Total Environment, 806*, 150571.https://doi.org/10.1016/j.scitotenv.2021.150571.

Asgher, M., Urooj, Y., Qamar, S. A. & Khalid N. (2020). Improved exopolysaccharide production from *Bacillus licheniformis* MS3: Optimization and structural/functional characterization. *International Journal of Biological Macromolecule, 151*, 984–992.

Bárcenas-Moreno, G., Gómez-Brandón, M., Rousk, J. & Bååth, E. (2009). Adaptation of soil microbial communities to temperature: comparison of fungi and bacteria in a laboratory experiment. *Global Change Biology, 15*, 2950–2957. https://doi.org/10.1111/j.1365-2486.2009.01882.x.

Bolan, N. S., Baskaran, S. & Thiagarajan, S. (1996). An evaluation of the methods of measurement of dissolved organic carbon in soils, manures, sludges, and stream water. *Communications in Soil Science and Plant Analysis, 27*(13–14), 2723–2737.

Bond-Lamberty, B., Bailey, V. L., Chen, M., Gough, C. M. & Vargas, R. (2018) Globally rising soil heterotrophic respiration over recent decades. *Nature, 560*, 80–83.

Boyle, J. A., Bridget, K.. M., Ensminger, I., Stinchcombe, J. R., & Frederickson, M. E. (2024). Resistance and Resilience of Soil Microbiomes under Climate Change. *Ecosphere 15*(12): e70077. https://doi.org/10.1002/ecs2.70077

Bowles, T. M., Acosta-Martínez, V., Calderón, F. & Jackson, L. E. (2014). Soil enzyme activities microbial communities, and carbon and nitrogen availability in organic agroecosystems across an intensively-managed agricultural landscape. *Soil Biology Biochemistry, 68*, 252–262.

Bradford, M. (1976). A Rapid and Sensitive Method for the Quantification of Microgram Quantities of Protein Utilizing the Principle of Protein-Dye Binding. *Analytical Biochemistry, 72*(1–2), 248–254.

Bradford, M. A., Wieder, W. R., Bonan, G. B., Fierer, N., Raymond, P. A. & Crowther, T. W. (2016). Managing uncertainty in soil carbon feedbacks to climate change. *Nature Climate Change, 6*, 751–758. https://doi.org/10.1038/nclimate3071.

Campbell, T. P., Ulrich, D. E. M, Toyoda, J., Thompson, J., Munsky, B., Albright, M. B. N., Bailey, V. L., Tfaily, M. M. & Dunbar, J. (2022). Microbial Communities Influence Soil Dissolved Organic Carbon Concentration by Altering Metabolite Composition. *Frontiers in Microbiology, 12*:799014. https://doi.org/10.3389/fmicb.2021.799014

Cania, B., Vestergaard, G., Krauss, M., Fliessbach, A., Schloter, M. & Schulz, S. (2019). A long-term field experiment demonstrates the influence of tillage on the bacterial potential to produce soil structure-stabilizing agents such as exopolysaccharides and lipopolysaccharides. *Environmental Microbiome, 14*, 1. https://doi.org/10.1186/s40793-019-0341-7.

Cavicchioli, R., Ripple,W. J., Timmis, K. N., Azam,F., Bakken, L. R., Baylis, M., Behrenfeld, M. J., Boetius, A., Boyd, P. W., Classen, A. T., Crowther, T. W., Danovaro, R., Foreman, C. M., Huisman, J., Hutchins, D. A., Jansson, J. K., Karl, D. M., Koskella, B., Mark Welch, D. B., Martiny, J. B. H., Moran, M. A., Orphan, V. J., Reay, D. S., Remais, J. V., Rich, V. I., Singh, B. K., Stein, L. Y., Stewart, F. J., Sullivan, M. B., Van Oppen, M. J. H., Weaver, S. C., Webb, E. A. & Webster, N. S. (2019). Scientists' warning to humanity: microorganisms and climate change. *Nature Reviews Microbiology, 17,* 569–586.

Cheng, C., Shang-Guan, W., He, L. & Sheng, X. (2020). Effect of exopolysaccharide-producing bacteria on water-stable macro-aggregate formation in soil. *Geomicrobiology Journal, 37,* 738–745.

Ding, L. L., Zhang, Y. G., Wang, M. M., Șun, X., Cong, J., Deng, Y., Lu, H., Yuan, T., Van Noștrand, J. D., Li, D., Zhou, J. & Yang, Y. (2015) Soil organic matter quantity and quality shape microbial community compositions of subtropical broadleaved forests. *Molecular Ecology, 24,* 5175–5185

Dubois, M., Gilles, K. A., Hamilton, J. K., Pebers, P. A. & Smith, F. (1956). Colorimetric method for determination of sugar and related substances. *Analytical Chemistry, 28,* 350–356. https://pubs.acs.org/doi/10.1021/ac60111a017.

Engqvist, M. K. M. (2018). Correlating enzyme annotations with a large set of microbial growth temperatures reveals metabolic adaptations to growth at diverse temperatures. *BMC Microbiology, 18,*177. https://doi.org/10.1186/s12866-018-1320-7.

Garcia, F.C., Warfield, R. & Yvon-Durocher, G. (2022) Thermal traits govern the response of microbial community dynamics and ecosystem functioning to warming. *Frontiers in Microbiology, 13:*906252. https://doi.org/10.3389/fmicb.2022.906252

Goddard, M. L., Belval, L., Martin, I. R., Roth, L., Laloue, H., Deglène-Benbrahim, L., Valat, L., Bertsch, C., & Chong, J. (2021). Arbuscular mycorrhizal symbiosis triggers major changes in primary metabolism together with modification of defense responses and signaling in both roots and leaves of *Vitis vinifera*. *Frontiers in Plant Science, 12*, 721614. https://doi.org/10.3389/fpls.2021.721614

Guhra, T., Ritschel, T. & Totsche, K.U. (2019). Formation of mineral-mineral and organo-mineral composite building units from microaggregateforming materials including microbially produced extracellular polymeric substances. *European Journal of Soil Science, 70,* 604–615.

Guo, Z., Liu, J., Wu, J., Yang, D., Mei, K., Li, H., Lu, H. & Yan, C. (2022). Spatial heterogeneity in chemical composition and stability of glomalin-related soil protein in the coastal wetlands. *Science of The Total Environment, 835,* 155351. https://doi.org/10.1016/j.scitotenv.2022.155351.

Heimann, M., & Reichstein, M. (2008). Terrestrial ecosystem carbon dynamics and climate feedbacks. *Nature, 451,* 289–92. https://doi.org/10.1038/nature06591

Holátko, J., Brtnický, M., Kučerík, J.;, Kotianová, M., Elbl, J., Kintl, A., Kynický, J., Benada, O., Datta, R. & Jansa, J. (2021). Glomalin—Truths, myths, and the future of this elusive soil glycoprotein. *Soil Biology Biochemistry, 153,* 108116. https://doi.org/10.1016/j.soilbio.2020.108116.

Huang, W., Wan, Z., Zheng, D., Cao, L., Li, G.& Zhang, F. (2024) Evolution of soil DOM during thermal remediation below 100 °C: concentration, spectral characteristics and complexation ability. *Frontiers of Environmental Science & Engineering, 18*(8), 1–11.

Hungate, B. A., Mau, R. L., Schwartz, E., Gregory Caporaso, J., Dijkstra, P., van Gestel, N., Koch, B. J., Liu, C. M., McHugh, T. A., Marks, J. C., Morrissey, E. M. & Price, L. B. (2015). Quantitative microbial ecology through stable isotope probing. *Applied and Environmental Microbiology, 81*, 7570–7581. https://journals.asm.org/doi/10.1128/aem.02280-15.

Jansson, J. K.& Hofmockel, K. S. (2019) Soil Microbiomes and Climate Change, *Nature Reviews Microbiology, 18*(1), 35–46.

Kalbitz, K., Solinger, S., Park, J.H., Michalzik, B.& Matzner, E. (2000). Controls on the dynamics of dissolved organic matter in soils: a review. *Soil Science, 165,* 277–304, https://doi.org/10.1097/00010694-200004000-463.

Karhu, K., Auffret, M. D., Dungait, J. A. J., Hopkins, D. W., Prosser, J. I., Singh, B. K., Subke, J. A., Wookey, P. A., Agren, G. I., Sebastià, M. T., Gouriveau, F., Bergkvist, G., Meir, P., Nottingham, A. T., Salinas, N.& Hartley, I. P. (2014). Temperature sensitivity of soil respiration rates enhanced by microbial community response. *Nature, 513*, 81–84.

Knappy, C., Barilla, D., Chong, J., Hodgșon, D., Morgan, H., Șuleman, M., Tan, C., Yao, P. & Keely, B. (2015). Mono-, di- and trimethylated homologues of isoprenoid tetraether lipid cores in archaea and environmental samples: mass spectrometric identification and significance. *Journal of Mass Spectrometry*, *50,*1420–1432

Koch, B. J., McHugh, T. A., Hayer M., Schwartz E., Blazewicz S. J., Dijkstra P., van Gestel, N., Marks, J. C., Mau, R. L., Morrissey, E. M., Ridge, J. P.& Hungate, B. A. (2018).. Estimating taxon-specific

population dynamics in diverse microbial communities. *Ecosphere. 9*:e02090. https://doi.org/10.1002/ecs2.2090.

Lehmann, A., Zheng, W. & Rillig, M.C. (2017) Soil biota contributions to soil aggregation. *Nature Ecology & Evolution, 1*, 1828–1835.

Li, Y., Zhang, G., Du, C., Mou, H., Cui, J., Guan, H., Hwang, H.& Wang, P. (2017). Characterization of high yield exopolysaccharide produced by *Phyllobacterium* sp. 921F exhibiting moisture preserving properties. *International Journal of Biological Macromolecules,101*, 562–568.

Ling, Q., Wu, H., Xie, L., Zhao, Y., Huang, Q., Zhang, Q., Liu, J., Hu, P., Tang, T., Xiao, J., Du, H., Zhao, J., Zhang, W., Chen, H., & Wang, K. (2025). Advances, Challenges, and Perspectives in Glomalin-Related Soil Protein *Research. Microorganisms, 13*(4), 740. https://doi.org/10.3390/microorganisms 13040740.

Liu, H., Wu,Y., Ai, Z., Zhang, J., Zhang, C., Xue, S. & Liu, G. (2019) Effects of the interaction between temperature and revegetation on the microbial degradation of soil dissolved organic matter (DOM) – A DOM incubation experiment, *Geoderma, 337*, 812–824.

Liu, H., Wang, X., Liang, C., Ai, Z., Wu, Y., Xu, H., Xue, S. & Liu, G. (2020). Glomalin-related soil protein affects soil aggregation and recovery of soil nutrient following natural revegetation on the Loess Plateau. *Geoderma, 357,* 113921. https://doi.org/10.1016/j.geoderma.2019.113921.

Liu, S., Wang, Q., Qian, L., Zhang, B., Chen, X., Hong, H., Wu, S., Liu, J., Yan, C. & Lu, H. (2022). Mapping the scientific knowledge of glomalin-related soil protein with implications for carbon sequestration. *Ecosystem Health and Sustainability, 8,* 2085185. https://doi.org/10.1080/ 20964129.2022.2085185

Matei, S., Matei, G.M., Dumitru, S. & Mocanu, V. (2024). The influence of the synthetic microbiomes on the characteristics of biodiversity and carbon sequestration in the soil. *Scientific Papers. Series B, Horticulture, LXVIII* (1), 836–847.

Matei, S., Matei, G.M., Dumitru, S. Mocanu, V. & Dumitrașcu, M. (2025). Carbon stabilization and sequestration processes in soil through synthetic microbiomes. *Scientific Papers. Series B, Horticulture. LXIX* (1), 808–819.

More, T.T., Yadav, J.S.S., Yan, S., Tyagi, R.D. & Surampalli, R.Y. (2014). Extracellular polymeric substances of bacteria and their potential environmental applications. *Journal of Environmental Management, 144*, 1–25.

Nouha, K., Kumar, R. S., Balasubramanian, S. & Tyagi R. D. (2018). Critical review of EPS production, synthesis and composition for sludge flocculation. *Journal of Environmental Sciences, 66,* 225–245.

Op De Beeck, M., Persson, P. & Tunlid, A. (2021). Fungal extracellular polymeric substance matrices – Highly specialized microenvironments that allow fungi to control soil organic matter decomposition reactions. *Soil Biology and Biochemistry, 159,* 108304.

Pietikainen, J., Pettersson, M., & Baath, E. (2005). Comparison of temperature effects on soil respiration and bacterial and fungal growth rates. *FEMS Microbial Ecology, 52,* 49–58. https://doi.org/ 10.1016/j.femsec.2004.10.002.

Preece, C., & Peñuelas, J. (2020). A return to the wild: Root exudates and food security. *Trends in Plant Science, 25,* 14–21. https://doi.org/10.1016/j.tplants. 2019.09.010

Ren, T. & Cai, A. (2025). Global patterns and drivers of soil dissolved organic carbon concentrations, *Earth System Science Data, 17,* 2873–2885, https://doi.org/ 10.5194/essd-17-2873–2025.

Sandhya, V. & Ali Sk. Z. (2015) The production of exopolysaccharide by *Pseudomonas putida* GAP-P45 under various abiotic stress conditions and its role in soil aggregation. *Microbiology, 84,* 512–519.

Sharma, I., Kashyap, S. & Agarwala, N. (2023) Biotic stress-induced changes in root exudation confer plant stress tolerance by altering rhizospheric microbial community. *Frontiers in Plant Science, 14*:1132824. https://doi.org/10.3389/fpls.2023.1132824

Silambarasan, S., Logeswari, P., Cornejo, P.& Kannan V.R. (2019). Evaluation of the production of exopolysaccharide by plant growth promoting yeast *Rhodotorula* sp. strain CAH2 under abiotic stress conditions. *International Journal of Biological Macromolecule,. 121*, 55–62.

Six, J., Frey, S. D., Thiet, R. K.. & Batten, K. M. (2006). Bacterial and fungal contributions to carbon sequestration in agroecosystems. *Soil Science Society of America Journal, 70,* 555-569, https://doi.org/10.2136/sssaj2004.0347

Smreczak, B. & Ukalska-Jaruga, A. (2021). Dissolved organic matter in agricultural soils, *Soil Science Annual, 72,* 132234, https://doi.org/ 10.37501/soilsa/132234.

Walker, T. W. N., Kaiser, C., Strasser, F., Herbold, C. W., Leblans, N. I. W., Woebken, D., et al. (2018). Microbial temperature sensitivity and biomass change explain soil carbon loss with warming. *Nature Climate Change, 8,* 885–889. https://doi.org/10.1038/ s41558-018-0259-x.

Wang, Q., Hong, H., Liao, R., Yuan, B., Li, H., Lu, H., Liu, J. & Yan, C. (2021). Glomalin-related soil protein: The particle aggregation mechanism and its insight into coastal environment improvement. *Ecotoxicology and Environmental Safety, 227,* 112940.https://doi.org/10.1016/j.ecoenv.2021.112940

Wang, S., Yu, S., Xiaoyan., Z., Zhao, X., Zhao, X., Mason-Jones, K., Zhu, Z., Redmile-Gordon, M., Li, Y., Chen, J., Kuzyakov, Y. & Ge, T. (2022). Experimental evidence for the impact of phages on mineralization of soil-derived dissolved organic matter under different temperature regimes*, Science of The Total Environment, 846,* 157517. https://doi.org/10.1016/ j.scitotenv.2022.157517.

Wang, Y.T., Shi, H. & Liu, X.F. (2016). Spectrofluorometric characterization of soil dissolved organic matter under different vegetation in Loess Hilly Region. *Journal of Plant Nutrition and Fertilizer, 22*(1), 171–179.

Wu, J., Xu, Y., Chen, Z., Li, X., Tan, J., & Liu, F. (2022). Mycorrhizal fungi alter root exudation to cultivate a beneficial microbiome for plant growth. *Functional Ecology, 37* (3), 664–675. https://doi.org/10.5061/ dryad.rjdfn2zg7

Yang, F., Chen, J., Ye, S., Liu, Z.& Ding Y.(2022). Characterization of antioxidant activity of exopolysaccharides from endophytic *Lysinibacillus sphaericus* Ya6 under osmotic stress conditions. *Process Biochemistry. 113*, 87–96.

Yang, H., Xiao, Q., Huang, Y., Cai, Z., Li, D., Wu, L., Meersmans, J., Colinet, G. & Zhang, W. (2024a). Long-term manuring facilitates glomalin-related soil proteins accumulation by chemical composition shifts and macro-aggregation formation. *Soil and Tillage Research, 235,* 105904. https://doi.org/10.1016/ j.still.2023.105904.

Yang, Y., Zhao, S., Ge, J., Song, G. & Du R. (2024b). Application of Microbial Exopolysaccharides in Environment. *Chinese Agricultural Science Bulletin. 40,* 66–74.

Ye, J.S., Bradford, M.A., Dacal, M., Maestre, F.T.& García-Palacios, P. (2019). Increasing microbial carbon use efficiency with warming predicts soil heterotrophic respiration globally. *Global Change Biology,. 25*, 3354–3364. https://doi.org/10.1111/gcb.14738.

Yuan, B., Li, H., Hong, H., Wang, Q., Tian, Y., Lu, H., Liu, J., Lin, L., Wu, G.& Yan, C. (2022) Immobilization of lead(II) and zinc(II) onto glomalin-related soil protein (GRSP): Adsorption properties and interaction mechanisms. *Ecotoxicology and Environmental Safety, 236,* 113489. https://doi.org/ 10.1016/ j.ecoenv.2022.113489.

Zhao, Y, Lin, J., Cheng, S., Wang, K, , Kumar, A., Yu, Z.G., & Zhu, B. (2023). Linking soil dissolved organic matter characteristics and the temperature sensitivity of soil organic carbon decomposition in the riparian zone of the three gorges reservoir, *Ecological Indicators, 154,* 110768. https://doi.org/10.1016/j.ecolind.2023.110768.

Zhao, J., Xie, X., Jiang, Y., Li, J., Fu, Q., QiuYingbo, Fu, X., Yao, Z., Dai, Z, Yunpeng, Q. & Chen, H. (2024). Effects of simulated warming on soil microbial community diversity and composition across diverse ecosystems, *Science of The Total Environment, 911*. https://doi.org/10.1016/j.scitotenv. 2023.168793.

Zhou, J., Bilyera, N., Guillaume, T., Yang, H., Li, F.& Shi, L. (2024). Microbial necromass and glycoproteins for determining soil carbon formation under arbuscular mycorrhiza symbiosis. *Science of The Total Environment, 955,* 176732. https://doi.org/ 10.1016/ j.scitotenv.2024.176732.

Scientific Papers. Series E. Land Reclamation, Earth Observation & Surveying, Environmental Engineering. Vol. XV, 2026
Print ISSN 2285-6064, CD-ROM ISSN 2285-6072, Online ISSN 2393-5138, ISSN-L 2285-6064

# TRACING PESTICIDES AND PHARMACEUTICALS IN WATER AND SEDIMENTS OF THE DANUBE DELTA

**Stefania-Adelina MILEA[1], Valentina-Andreea CALMUC[1], Andreea-Miruna CODREANU[1], Catalina ITICESCU[1, 2], Silvia DRAGAN[3]**

[1]"Dunarea de Jos" University of Galati, REXDAN, 98 George Cosbuc, 800385, Galati, Romania
[2]"Dunarea de Jos" University of Galati, Faculty of Sciences and Environment,
111 Domnească Street, Galati, Romania
[3]EnviroEcoSmart, 3 Nufarului Street, Galati, Romania

Corresponding author email: adelina.milea@ugal.ro

***Abstract***

*The Danube Delta is listed on UNESCO's World Heritage List for its exceptional value, attributed to the numerous natural ecosystems with remarkable characteristics and high biodiversity that have been preserved in an almost original state. Despite the significant environmental initiatives implemented in recent years, this place remains at risk from both natural and human-made stresses that could alter its ecosystems. This study focuses on determining the contamination degree with emerging and persistent pollutants in the deltaic and pre-deltaic Danube zone. In the present investigation, the pharmaceutical compounds in water samples and pesticides in sediment samples were assessed by considering the physicochemical properties of the targeted contaminants and their interactions with ecosystem matrices. Among the analysed water samples, the compound caffeine recorded the highest concentration (17.33 ng/L), while the compound carbamazepine registered the lowest value, 0.31 ng/L. The sediment samples were freeze-dried and analysed in terms of organochlorine and organophosphorus pesticides. The highest pesticide concentrations were identified in the terminal sampling point, including 3.45 ng/g of dichlorodiphenyltrichloroethane (DDT). The presence of both persistent and emerging pollutants in the Danube Delta imposes permanent monitoring to maintain biodiversity and the best possible environmental conditions.*

***Key words****: Danube Delta, pesticides, pharmaceuticals, sediments, water.*

## INTRODUCTION

The Danube Delta is a biodiversity sanctuary, providing habitat to numerous unique, exotic, and important species with considerable conservation and commercial importance (Bănăduc et al., 2016). It is one of the most important wetland ecosystems for animals on the continent, as it is the second biggest river delta in Europe and the largest natural wetland still in existence (ICPDR, n.d.). Over 300 bird species and 45 freshwater fish species may be found in the Danube Delta's various lakes and marshes (UNESCO World Heritage, n.d.). This area of rich biodiversity is greatly impacted by upstream pollution and discharge modification (ICPDR, n.d.). Water quality has undergone significant changes in the second half of the 20th century as a result of increased pressure from industrial and hydrotechnical activities, urban development, and agriculture. These changes have affected the Danube's physical conditions (suspended sediment, bedload transport, temperature), chemical (emerging pollutants, nitrite, nitrate, phosphorous, and ammonium), and biological (faecals, species loss, and biological community alterations caused by invasive organisms) (Mănoiu & Crăciun, 2021). Additionally, monitoring the quality of water by assessing the concentration of pollutants in surface and ground water has an immediate connection to human health (Iticescu et al., 2014). Surface river systems are contaminated by industrial sites and agricultural operations that are situated close to bodies of water, endangering aquatic life (Zlati et al., 2023). Pesticides, pharmaceuticals, microbiological contaminants, endocrine disruptors, heavy metals, polycyclic aromatic hydrocarbons, and polychlorinated biphenyls have all been identified by many monitoring studies (Chiţescu et al., 2021). The Danube is particularly susceptible to agricultural chemical contamination, which has an impact on regional

biodiversity as well as the quality of drinking water. Because of their environmental persistence, accumulation in biological organisms, and concerns about ecosystems and human health, a considerable number of pesticides are identified as persistent organic pollutants (Matei et al., 2025). Persistent organic pollutants are nonpolar organic chemicals that are potentially hazardous at threshold levels and have strong bioaccumulation and stability characteristics (Chiţescu et al., 2021). Because of their strong hydrophobicity, they tend to absorb into solid particles (Katsoyiannis & Samara, 2005). Numerous types of human and veterinary antibiotics, as well as human prescription and over-the-counter medications, such as antiepileptics, NSAIDs, blood lipid regulators, antidepressants, β-blockers, and analgesics, are among the pharmaceutical chemicals most frequently found in aquatic systems (Chitescu et al., 2015). The Danube Delta is a topical hotspot for assessing the combined presence of contaminants since it is the last accumulation area of the Danube River basin and is constantly impacted by incoming agricultural, local, and industrial discharges. In the context of the Water Framework Directive (WFD) which emphasizes maintaining both qualitative and quantitative status of water bodies, it is now essential to evaluate the ecological status in terms of chemical pollution. This study aims to perform an evaluation of both pesticides and pharmaceuticals in the Danube Delta area. The monitoring of these emerging and persistent organic pollutants is essential for many reasons: a) the protection and preservation of a unique ecosystem, b) the possibility of entering the food chain through drinking water and biota, c) the impact on organisms' health, and d) the need to establish concentration limits. Moreover, this paper fills a scientific gap in understanding the combined impact of contaminants on the aquatic ecosystem, with particular focus on a highly vulnerable and understudied area.

## MATERIALS AND METHODS

In order to characterize the pesticides from the sediment and pharmaceuticals from the water, the samples were collected according to the specificity of each class of compound to ensure their representativeness. A total of 6 water samples and 6 sediment samples were taken from the Sulina branch in May 2026, and these were chronologically coded according to the distance to the spillway (1 meaning the farthest to the spillway and 6 meaning the closest point to the spillway: Partizani, Maliuc, Gorgova, Crișan, Sulina Intermediar, and Sulina). Water samples were collected from a depth of 20 cm in prewashed containers and sediment samples were collected using a dredge and transferred to different specific containers for each target analysis. In Table 1, the coordinates of the samples are presented.

Table 1. Geographical coordinates of the samples

| Sample codes | Sampling stations | Geographical coordinates |
|---|---|---|
| 1 | Partizani | 45.19330, 28.95869 |
| 2 | Maliuc | 45.17459, 29.11427 |
| 3 | Gorgova | 45.18153, 29.17888 |
| 4 | Crișan | 45.17358, 29.42541 |
| 5 | Intermediate Sulina | 45.18125, 29.51804 |
| 6 | Sulina | 45.16208, 29.68527 |

Water samples for pharmaceutical analysis were filtered, and then the collected samples were carefully stored and preserved until further analysis. For the pesticide analysis, the sediment was freeze-dried to ensure the compounds' stability with the Table Top Freeze Dryer BioBase BK-FD10PT (BioBase, Shandong, China) equipment

### *Analytical standards*

- Organochlorine pesticide mix containing α-BHC; β-BHC; δ-BHC; γ-BHC (Lindane); α-Chlordane; γ-Chlordane; p,p′-DDD; p,p′-DDE; p,p′-DDT; Aldrin; Dieldrin; Endosulfan I; Endosulfan II; Endosulfan sulfate; Endrin aldehyde; Endrin; Endrin ketone; Heptachlor epoxide (Isomer B); Heptachlor; Methoxychlor.
- Organophosphorus pesticides mix containing Disulfoton, Dimethoate, Parathion-methyl, Famphur, Triethyl thiophosphate, Parathion, Sulfotep, Phorate, Thionazin.

- ***Internal standards***

4,4` - DDT-D8, 4,4` - DDD-D8, 4,4` - DDE-D8, γ-BHC-D6, PCB-143.

- Pharmaceutical residues in the examined water samples were identified and quantified using analytical standards for the following compounds: Caffeine, Carbamazepine, Ketoprofen, Metformin, Diclofenac, Clindamycin, Trimethoprim, Sulfamethoxazole, and Clarithromycin.

***QuEChERS extraction of pesticides***

The pesticides belonging to the organochlorine and organophosphorus classes were extracted from freeze-dried sediments using an optimized QuEChERS protocol. The sample was weighed and well hydrated with ultrapure water to better simulate the matrix composition. First, the internal standard was added, and the samples were allowed to rest for 30 minutes. The extraction procedure started with the addition of acetonitrile as solvent extraction, and after 15 minutes of sonication at 150 W, using an Elmasonic S60 H 100 2238 (Elma Schmidbauer GmbH, Singen, Germany) and homogenization, the extraction salts (6 grams of magnesium sulfate with 1.5 grams of sodium acetate) were added to the sample. The samples were vortexed for 5 minutes each and centrifuged at 4500 rpm for 10 minutes (OHAUS FC5916R Centrifuge) for 10 minutes in order to collect the resulting supernatant. A known aliquot of the sample was then mixed with the clean-up (150 mg magnesium sulfate, 25 mg C18, and 25 mg Primary-Secondary Amine), and the liquid was again centrifuged. The resulting supernatant was carefully evaporated under nitrogen stirring (Reacti-Therm™ Heating and Stirring Module - TS-18823 from Thermo Fisher Scientific, Waltham, MA, USA), redissolved in toluene, and filtered to be prepared for chromatographic analysis.

***Automatic SPE extraction of pharmaceuticals from liquid samples***

Sample preparation for the analysis of pharmaceutical compounds in water samples involved the use of an automated solid-phase extraction with a dedicated instrument Dionex AutoTrace 280 (Thermo Fisher Scientific, Waltham, MA, USA). The extraction was made using C18 cartridges, methanol, and water, and methanol as the elution solvent. An evaporator that allowed the concentration of analytes in a nitrogen atmosphere was also used to evaporate the samples, and 10% methanol for re-dissolution.

***The analysis of pesticides from sediment by GC-MS/MS***

The toluene extracts of sediment samples were analyzed using a TSQ 9000 Triple quadrupole GC-MS/MS instrument, a Thermo Scientific™ TRACE™ 1310 GC, and a Thermo Scientific™ TriPlus™ RSH autosampler (Waltham, Massachusetts, USA), 2 µL of extract was injected into a Thermo Scientific™ TraceGOLD TG-PAH 30 m × 0.25 mm I.D. × 0.10 µm film capillary column, which was used for the chromatographic separation. The ramped temperature within the GC oven was set up as follows: initial temperature 60°C - 2 min hold time, from 60°C to 120°C at a rate of 30°C/min, from 120°C to 320°C at a rate of 10°C/min, and the final step, 320°C with a hold time of 16 min. The total program run is 40 minutes.

Each targeted compound was identified and quantified using three SRM transitions, and the final results were processed using Chromeleon 7.3. The pesticides were quantified using an internal-standard calibration curve constructed from six concentration levels, with a concentration range between 2 and 80 ng/g.

***The analysis of pharmaceuticals from water by UHPLC-HRMS***

Qualitative and quantitative analysis of the identified pharmaceutical compounds was performed using liquid chromatography with high-resolution mass spectrometry, Vanquish Flex UHPLC - Orbitrap Exploris 120, and a mass spectrometer from Thermo Fisher Scientific (Waltham, Massachusetts, USA). The analysis method involved the use of two mobile phases represented by ultrapure water with 0.1% formic acid and methanol with 0.1% formic acid in a gradient with a flow rate of 0.4 mL/min. The separation of the compounds was done using an Accucore C18 column (100 x 2.1 mm, 2.6 µm) at a temperature of 40 °C. The analysis time was 20 minutes and the sample injection volume was 10 µL. The calibration

curve was performed in 6 points over the range 0.1 ng/L - 25 ng/L. Quantification of the compounds was performed based on the following internal standards: dihydrocarbamazepine for carbamazepine; phenacetin for metformin, caffeine and diclofenac and enrofloxacin for sulfamethoxazole.
The results obtained for both pesticides and pharmaceuticals were validated using the spiking method on 3 different levels.

## RESULTS AND DISCUSSIONS

Due to extensive development, inadequate pollution control, and inflows from severely polluted tributaries, the Middle and Lower Danube River's water quality quickly declined after the 1970s (Gati et al., 2019). The quality of the Danube Delta waters as well as the Black Sea's coastline region is impacted by the Danube River, which serves as the primary collector and emissary of all urban and industrial effluent from the whole river basin (Ene et al., 2025).
The sediment samples were analyzed in terms of pesticide content, and the results showed the presence of DDTs in all target points (Figure 1).
Generally, the organochlorine and organophosphorus pesticides were not detected in the samples, except for DDT and its metabolites. DDT levels in our samples varied between 0.90 and 3.45 ng/g DW with the highest concentration in the terminal sampling point. As expected, the highest abundance and concentration of DDTs were recorded in the closest point to the mouth of the Sulina branch (Figure 1 and Figure 2). The presence of the metabolite 4,4`-DDE could only be quantified in the final point of sampling, and for 4,4`-DDD in two of the collected points (Figure 1). The presence of both metabolites was confirmed in all points, but the concentrations were below the limit of quantification. The highest content within the DDTs metabolites was recorded also in the last point, 1.09 ng DDD/g DW. Sediment samples were also scanned for the presence/absence of organophosphorus pesticides, and no compounds from this category were identified. The absence of these compounds could be a reason for their rapid biodegradability, compared to organochlorines (Saad et al., 2025). It is clear that from the OCP category only DDTs have been identified. First of all, these compounds are indicators of historical pollution, being particularly persistent compounds with a high potential for bioaccumulation. The fact that other compounds from the pesticide category have not been identified does not necessarily indicate their absence, but the possibility of their degradation over time. Also, another argument could be given by the volatility of the substances. While DDTs are strongly persistent and hydrophobic, therefore almost immobile in solid matrices, pesticides such as lindane are more volatile and slightly more soluble.
In agreement with previous reports, the predominance of DDTs in environmental samples from the Danube Delta was observed by Covaci et al. (2006), who found concentrations of DDTs in Danube Delta sediments varying between 0.7 and 33 ng/g.
Belháčová-Minaříkova et al. (2020) reported DDT and its breakdown products in high amounts in the lower Danube, with the river delta containing the highest levels.
Sediments act as storage spaces for non-polar contaminants and sources for living organisms from the aquatic ecosystem. For example, Stancheva et al., 2013, reported in freshwater fish from the Danube river concentrations of DDTs from 19.2 to 30.3 ng/g WW. Despite the global initiative to minimize the use of pesticides, the risk of pesticide pollution is still present due to their high degree of bioaccumulation (Sharma et al., 2019). ICPDR (2005) reported that 71% of the samples from the Danube and 54% from the tributaries exceeded 0.01 µg/L 4,4`-DDT. DDT was banned in Europe in the 1970s due to its toxicity and environmental persistence and is now listed as a priority substance under European Directive 2013/39/EU and as a persistent organic pollutant under the Stockholm Convention (2001) (van den Berg et al., 2025). Since its use is prohibited, current contamination most likely reflects historical inputs and long-term environmental persistence. DDT is nevertheless utilized in many underdeveloped nations. This chemical is widely distributed throughout the environment

because of its persistence and long-distance atmospheric transport, causing high bioaccumulation and biomagnification potential (Tasselli et al., 2023).

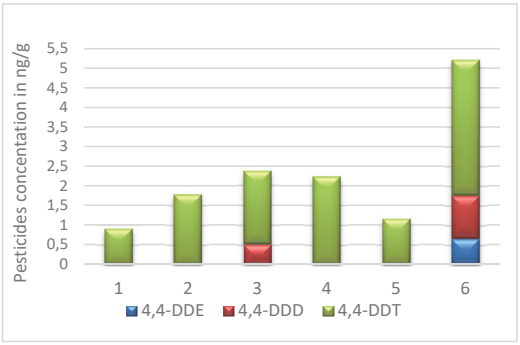



Figure 1. The concentrations of pesticides in sediments from the Danube Delta

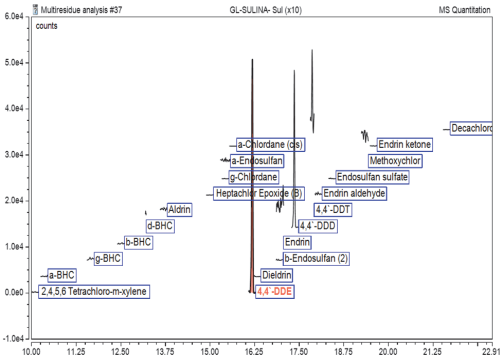



Figure 2. Chromatogram example (sample 6) of pesticide in a sediment sample analyzed from Danube Sulina branch

Following the investigation into the presence of pharmaceutical residues in water samples taken from the Danube Sulina branch, five compounds were detected at trace levels (Table 2; Figure 3): metformin, caffeine, sulfamethoxazole, carbamazepine, and diclofenac. In Figure 4, an example of chromatogram highlighting the presence of pharmaceuticals in water can be observed.

In Table 2, the concentrations of the identified pharmaceuticals are presented. One of the compounds identified in all 6 sampling stations is metformin, for which minimal variations in concentrations were obtained from one station to another, ranging between 1.7 ng/L (sample 1) and 1.93 ng/L (sample 6). Carbamazepine is another compound frequently identified in surface water; low values within the range 0.31 to 0.49 ng/L were measured on the Danube Sulina branch.

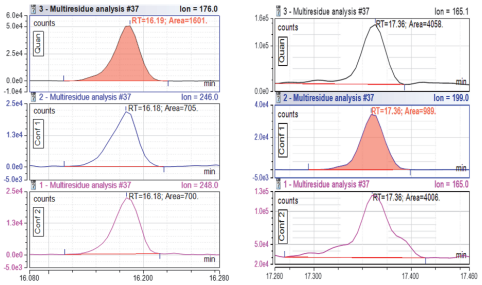



Figure 3. MS Components for 4,4`-DDE and 4,4`-DDD

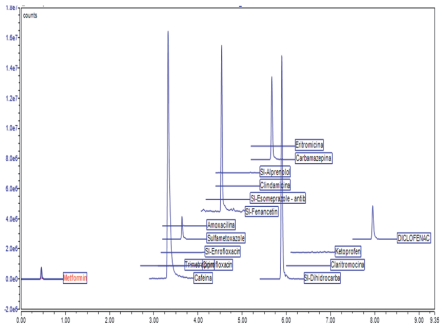



Figure 4. Chromatogram example of compounds in a water sample analyzed from Danube Sulina branch

Table 2. Concentration of pharmaceutical compounds identified in water samples taken from the Danube Sulina branch

| Pharmaceuticals concentration (ng/L) | 1 | 2 | 3 | 4 | 5 | 6 |
|---|---|---|---|---|---|---|
| Metformin | 1.7 | 1.77 | 1.9 | 1.86 | 1.86 | 1.93 |
| Caffeine | 14.06 | 13.31 | 17.33 | 8.92 | 8.79 | 9.56 |
| Sulfamethoxazole | 1.02 | 1.07 | 1.08 | 0.96 | 0.95 | 0.98 |
| Carbamazepine | 0.38 | 0.47 | 0.49 | 0.35 | 0.31 | 0.33 |
| Diclofenac | 4.42 | 2.37 | 3.3 | 3.34 | 2.23 | 3.97 |

The antibiotic sulfamethoxazole was also quantified in the analyzed samples, the highest value was 1.08 ng/L and the lowest measured 0.95 ng/L. The highest concentrations were obtained for the psychoactive substance caffeine, with values ranging from 8.79 ng/L to 17.33 ng/L. For the nonsteroidal anti-inflammatory drug diclofenac, concentration variations were recorded from 2.23 ng/L to 4.42 ng/L. Other studies have also reported that sulfamethoxazole, carbamazepine, and diclofenac were detected in the Sulina branch (Ene et al., 2025). Loos et al. (2017) reported

that on the Danube River, diclofenac values were recorded from upstream to the mouth in the range of 20 ng/L - 2 ng/L. Significant concentrations of metformin were also recorded in the Prut, a main tributary of the Danube, with values ranging from 100 ng/L to 240 ng/L (Moldovan et al., 2018). In a study conducted by Chitescu et al. (2015), values of carbamazepine identified in water samples taken from the Danube River basin in Romania territory were reported to be in the range of 4 ng/L - 40 ng/L. In other studies conducted on the Danube River, sulfamethoxazole values ranging from 3.7 ng/L to 141 ng/L were also reported (Loos et al., 2017).

All analytical results were validated using a spiking approach at three concentration levels. For pesticide analysis, limits of detection (LOD) and quantification (LOQ) ranged from 0.12 to 0.19 ng/g and from 0.26 to 0.57 ng/g, respectively. Recovery rates for DDT and its metabolites ranged between 96.62% and 115.07%. For pharmaceuticals, LOD and LOQ values ranged from 0.17 to 0.69 ng/L and from 0.30 to 0.98 ng/L, respectively, while recovery rates varied between 90.11% and 98.80%. Linearity was assessed based on calibration curves, with correlation coefficients ($R^2$) higher than 0.99 for all target pesticides and pharmaceuticals.

***Correlation analysis between pesticides from sediments and pharmaceuticals from water***

The pesticides were analysed from sediments and the pharmaceuticals from water according to the compound's chemical affinity from the matrices. Generally, the pesticides are hydrophobic while pharmaceuticals are more hydrophilic substances.

In Figure 5, the correlation between both classes is represented. First, the presence of DDE and DDD correlates strongly with the presence of DDT because they are metabolic breakdown products of the dichlorodiphenyltrichloroethane. This confirms again the persistence and also the historical pollution with DDT.

An interesting observation is that metformin tends to correlate with DDTs, especially DDT. This could suggest almost a possible common source of pollution or some specific conditions that facilitates the existence of both classes.

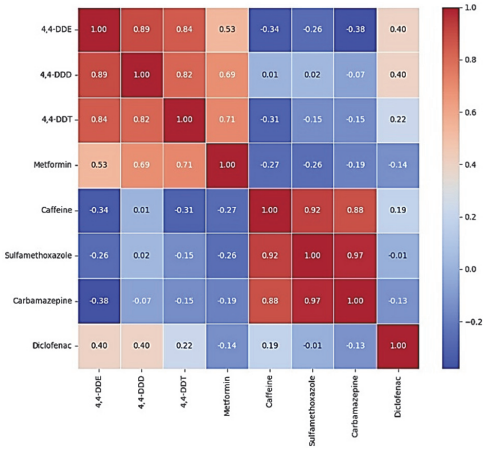



Figure 5. Correlation analysis between pesticides from sediments and pharmaceuticals from water

On the other hand, a negative correlation may be observed between pesticides and carbamazepine, sulfamethoxazole or caffeine, which may highlight different source of pollution (agriculture vs urban waste).

## CONCLUSIONS

This research provides an evaluation of emerging and persistent pollutants in water and sediment samples from a valuable, unique ecosystem in Europe. The present study detected DDTs, caffeine, metformin, sulfamethoxazole, diclofenac, and carbamazepine in the Danube Delta samples. While the pesticides analysis revealed only the presence of a restricted profile of OCPs suggesting both historical pollution and a dominated persistent pollutants profile, the pharmaceutical profile highlighted an actual anthropogenic pollution and a continuous pressure to the Danube ecosystem. However, some limitations regarding the present study should be considered.

Although the present study is relevant from the perspective of the presence of two categories of persistent and emerging pollutants, future studies could be expanded with additional surveys campaigns and a larger number of collected samples. Beyond this, the level of pollution could be underestimate because only two classes of pollutants were analysed. Future studies may include more sample, more sampling campaigns, and a wider spectrum of

compounds to analyze. The presence of these compounds in the aquatic environment of the Danube Delta, which is part of an UNESCO World Heritage Site, underscores the importance of continuous environmental monitoring. Over and above that, there is a need to implement measures to prevent, ensure, and support the well-being of the aquatic ecosystem aligned with the Water Framework Directive. Ecosystems are seriously threatened by pollution from a variety of sources, including industrialization, agriculture, urbanization, and untreated sewage. Over time, these pollutants may have detrimental effects on the environment and human health. Moreover, this research reflects the importance of future studies regarding the concentration levels of pollutants, also in biota. Monitoring priority substances, reducing pollutants discharge and strengthening the control measures would support and improve the quality of aquatic environment.

## ACKNOWLEDGEMENTS

This research was supported by the project PN-IV-P8-674/01.11.2024, WATER LIGHTHOUSE ACTION - DANUBE REGION, DALIA, 89 PHE/2024.

## REFERENCES

Bănăduc, D., Rey, S., Trichkova, T., Lenhardt, M., & Curtean-Bănăduc, A. (2016). The Lower Danube River–Danube Delta–North West Black Sea: A pivotal area of major interest for the past, present and future of its fish fauna - A short review. *Science of The Total Environment*, *545–546*, 137–151. https://doi.org/10.1016/j.scitotenv.2015.12.058

Belháčová-Minaříková, M., Smedes, F., Rusina, T. P., & Vrana, B. (2020). Application of equilibrium passive sampling to profile pore water and accessible concentrations of hydrophobic organic contaminants in Danube sediments. *Environmental Pollution*, 267, Article 115470. https://doi.org/10.1016/j.envpol.2020.115470

Chițescu, C. L., Ene, A., Geana, E.-I., Vasile, A. M., & Ciucure, C. T. (2021). Emerging and Persistent Pollutants in the Aquatic Ecosystems of the Lower Danube Basin and North West Black Sea Region - A Review. *Applied Sciences*, *11*, 9271. https://doi.org/10.3390/app11209721

Chitescu, C. L., Kaklamanos, G., Nicolau, A. I., & Stolker, A. A. M. (Linda) (2015). High sensitive multiresidue analysis of pharmaceuticals and antifungals in surface water using U-HPLC-Q-Exactive Orbitrap HRMS. Application to the Danube river basin on the Romanian territory. *Science of The Total Environment*, *532*, 501–511. https://doi.org/10.1016/j.scitotenv.2015.06.010

Covaci, A., Gheorghe, A., Hulea, O., & Schepens, P. (2006). Levels and distribution of organochlorine pesticides, polychlorinated biphenyls and polybrominated diphenyl ethers in sediments and biota from the Danube Delta, Romania. *Environmental Pollution*, *140*(1), 136–149. https://doi.org/10.1016/j.envpol.2005.06.008

Ene, A., Teodorof, L., Chițescu, C. L., Burada, A., Despina, C., Bahrim, G. E., Vasile, A. M., Seceleanu-Odor, D., & Enachi, E. (2025). Surface Water Contaminants (Metals, Nutrients, Pharmaceutics, Endocrine Disruptors, Bacteria) in the Danube River and Black Sea Basins, SE Romania. *Applied Sciences*, *15*, 5009. https://doi.org/10.3390/app15095009

Gati, G., Pop, C., Brudasca, F., Gurzau, A. E., & Spinu, M. (2019). Hydrological modeling of arsenic in the Danube Delta. *Environmental Engineering and Management Journal*, *18*(1), 99–108. https://doi.org/10.30638/eemj.2019.011

ICPDR. (2005). *TNMN_Yearbook_2005_short_version.pdf*. https://www.icpdr.org/sites/default/files/TNMN_Yearbook_2005_short_version.pdf

ICPDR. (n.d.). *Danube Delta | ICPDR - International Commission for the Protection of the Danube River*. Retrieved from https://www.icpdr.org/danube-basin/sub-basins/danube-delta (accessed April 25, 2026).

Iticescu, C., Georgescu, L., Topa, M.C., & Murariu, G. (2014). Monitoring the danube water quality near the galati city. *Journal of Environmental Protection and Ecology*, *15*, 30–38.

Katsoyiannis, A., & Samara, C. (2005). Persistent organic pollutants (POPS) in the conventional activated sludge treatment process: Fate and mass balance. *Environmental Research*, *97*, 245–257. https://doi.org/10.1016/j.envres.2004.09.001

Loos, R., Tavazzi, S., Mariani, G., Suurkuusk, G., Paracchini, B., & Umlauf, G. (2017). Analysis of emerging organic contaminants in water, fish and suspended particulate matter (SPM) in the Joint Danube Survey using solid-phase extraction followed by UHPLC-MS-MS and GC–MS analysis. *Science of The Total Environment*, *607–608*, 1201–1212. https://doi.org/10.1016/j.scitotenv.2017.07.039

Mănoiu, V.-M., & Crăciun, A.-I. (2021). Danube river water quality trends: A qualitative review based on the open access web of science database. *Ecohydrology & Hydrobiology*, *21*(4), 613–628. https://doi.org/10.1016/j.ecohyd.2021.08.002

Matei, N., Seceleanu-Odor, D., Burada, A., Gheorghe, P.B., Tiganus, M., Suliman, I., Ibram, O., & Despina, C. (2025). Review: Long-term trends of pesticide residues in the Danube River Basin. *Scientific Annals of the Danube Delta Institute*, *30*, 1–16. https://doi.org/10.3897/saddi.30.160456

Moldovan, Z., Marincas, O., Povar, I., Lupascu, T., Longree, P., Rota, J. S., Singer, H., & Alder, A. C. (2018). Environmental exposure of anthropogenic

micropollutants in the Prut River at the Romanian-Moldavian border: A snapshot in the lower Danube river basin. *Environmental Science and Pollution Research International*, *25*(31), 31040–31050. https://doi.org/10.1007/s11356-018-3025-8

Saad, H., Elfeky, S. A., El-Gamel, N. E. A., & Abo Dena, A. S. (2025). Organophosphate pesticides: A review on classification, synthesis, toxicity, remediation and analysis. *RSC Advances*, *15*(48), 40802–40822. https://doi.org/10.1039/d5ra05552k

Sharma, A., Kumar, V., Shahzad, B., Tanveer, M., Sidhu, G. P. S., Handa, N., Kohli, S. K., Yadav, P., Bali, A. S., Parihar, R. D., Dar, O. I., Singh, K., Jasrotia, S., Bakshi, P., Ramakrishnan, M., Kumar, S., Bhardwaj, R., & Thukral, A. K. (2019). Worldwide pesticide usage and its impacts on ecosystem. *SN Applied Sciences*, *1*(11), 1446. https://doi.org/10.1007/s42452-019-1485-1

Stancheva, M., Georgieva, S., & Makedonski, L. (2013). Persistent organic pollutants - PCBs and DDTs in fish from Danube River and from Black Sea, Bulgaria. *CBU International Conference Proceedings*, *1*, 354-361. https://doi.org/10.12955/cbup.v1.57

Tasselli, S., Marziali, L., Roscioli, C., & Guzzella, L. (2023). Legacy Dichlorodiphenyltrichloroethane (DDT) Pollution in a River Ecosystem: Sediment Contamination and Bioaccumulation in Benthic Invertebrates. *Sustainability*, *15*(8). https://doi.org/10.3390/su15086493

UNESCO World Heritage. (n.d.). UNESCO World Heritage Centre. Retrieved from https://whc.unesco.org/en/list/588/ (accessed April 25, 2026).

van den Berg, H., Amwele, H. R., Brooke, B. D., Fortelius, L. E., Jain, T., Karunaratne, S. H. P. P., Munyinda, N. S., Rubio-Palis, Y., Yadav, R. S., & Kleinschmidt, I. (2025). DDT: Last mile in the global phase-out of its use for disease vector control? *The Lancet Planetary Health*, *9*(8), 101283. https://doi.org/10.1016/j.lanplh.2025.06.007

Zlati, M. L., Georgescu, L. P., Iticescu, C., Ionescu, R. V., & Antohi, V. M. (2023). New Approach to Modelling the Impact of Heavy Metals on the European Union's Water Resources. *International Journal of Environmental Research and Public Health*, *20*(1). https://doi.org/10.3390/ijerph20010045

Scientific Papers. Series E. Land Reclamation, Earth Observation & Surveying, Environmental Engineering. Vol. XV, 2026
Print ISSN 2285-6064, CD-ROM ISSN 2285-6072, Online ISSN 2393-5138, ISSN-L 2285-6064

# INACTIVATION OF GRAM-POSITIVE AND GRAM-NEGATIVE BACTERIA BY USING ARGON COLD ATMOSPHERIC PRESSURE PLASMA

**Cristina MOISESCU[1], Ovidiu STOICAN[2], Ana Valentina ZAMFIRESCU[1], Mihaela Marilena STANCU[1]**

[1]Institute of Biology Bucharest of Romanian Academy, 296 Splaiul Independentei, District 6, 060031 Bucharest, P.O. Box 56-53, Romania
[2]National Institute for Laser, Plasma and Radiation Physics (INFLPR), 409 Atomistilor Street, 077125, Magurele, Romania

Corresponding author email: mihaela.stancu@ibiol.ro

***Abstract***

*Cold atmospheric pressure plasma (CAPP) is a residue-free alternative for decontaminating surfaces and reusable equipment when chemical disinfectants are inconvenient, such as during field work in environmental engineering and land reclamation. Here, we tested an argon CAPP plume (atmospheric pressure, low-current DC discharge) against Staphylococcus aureus, Escherichia coli, and Pseudomonas aeruginosa after 5–120 s exposures. Antimicrobial activity increased with treatment time: inhibition-zone areas grew from 2.83 $cm^2$ (5 s) to 31.40 $cm^2$ (120 s). P. aeruginosa was the most sensitive (31.40 $cm^2$ at 120 s), whereas S. aureus and E. coli reached 11.30 $cm^2$. Viable counts for E. coli and P. aeruginosa dropped from >$10^6$ to $10^3$ CFU $mL^{-1}$ after 120 s, while S. aureus showed no significant reduction at 120 s; for P. aeruginosa, counts decreased from >$10^6$ to $10^5$ CFU $mL^{-1}$ after 15 s. Overall, these findings support CAPP as a practical, non-chemical option for rapid decontamination of hard surfaces (e.g., tools and sampling devices) in remediation and environmental monitoring workflows.*

***Key words:*** *bacteria, cold atmospheric pressure plasma, susceptibility, surface sterilization.*

## INTRODUCTION

Cold atmospheric pressure plasma (CAPP) is now widely studied as a tool for surface sterilization and disinfection, with reported uses in microbial decontamination and biomedicine (Joshi et al., 2011; Fricke et al., 2012; Mitra et al., 2014; Asenjo et al., 2015; Mai-Prochnow et al., 2016; Bourke et al., 2018; Hertwig et al., 2018; Corradini, 2020; Domonkos et al., 2021; Barjasteh et. al., 2024; Kazemi et al., 2024). Compared with chemical disinfectants-which can leave residues and raise material, environmental, and occupational issues (Whittaker et al., 2004; Singh et al., 2010) - CAPP typically requires only electrical power and a carrier gas and does not produce persistent chemical waste. Because the gas remains near room temperature, CAPP can be used on heat-sensitive materials and, in some cases, on living tissues (Fridman et al., 2008; Heinlin et al., 2010). It has also been explored for decontaminating sensitive electronics and hazardous agents (Singh et al., 2010). Many plasma sources and power-supply designs are available (Ehlbeck et al., 2011), but the dominant mechanisms of microbial inactivation are still being clarified. When the plasma interacts with air and water vapor, it generates reactive oxygen species (ROS) such as $O_2^-$•, $H_2O_2$, •OH, $O_3$, $^1O_2$, and atomic oxygen; together with charged particles, UV radiation, mild heating, and electric fields, these factors contribute to bacterial inactivation (Alkawareek et al., 2014).

How well CAPP works depends on practical details-such as the source design and geometry, as well as the carrier-gas composition, flow rate, and physicochemical properties (Mai-Prochnow et al., 2016; Baldanov et al., 2019). Since Laroussi first showed that CAPP can rapidly inactivate bacteria (Laroussi, 1996), subsequent studies have linked this effect mainly to reactive species and to damage of the membrane and cell wall, often accompanied by leakage of intracellular components. Differences in susceptibility between Gram-positive and Gram-negative bacteria have also been reported (Laroussi & Leipold, 2004; Deng et al., 2006;

Tipa et al., 2011; Flynn et al., 2015; Mai-Prochnow et al., 2016; Olatunde et al., 2019).
CAPP is also relevant for environmental engineering and land-reclamation work. In the field, teams often need to clean and decontaminate tools and reusable sampling or monitoring devices between locations to prevent cross-contamination (Jiang et al., 2014; Scholtz et al., 2015).
In this work, we tested a simple atmospheric-pressure CAPP source (argon carrier gas; low-current DC discharge) and measured its effects on two Gram-negative strains (*Escherichia coli* ATCC 25922 and *Pseudomonas aeruginosa* $IBB_{Po16}$ KT315654) and one Gram-positive strain (*Staphylococcus aureus* ATCC 25923).

## MATERIALS AND METHODS

### Experimental setup for cold argon plasma generation

Mechanical layout of the plasma source is shown in Figure 1, being similar to that described in (Stoican, 2011), except for a few minor changes. A sharp brass rod (1), 3 mm in diameter, is placed along the axis of a cavity (2), having axial symmetry, formed by two cylindrical segments, made in an aluminum block (3). One of the ends of the cavity is closed by the front disk (4), made by aluminum, having an output hole 2 mm in diameter. The plasma plume (5) is ejected through that hole, its external length being about 6-8 mm, depending on the experimental conditions. The other end of the outer cylinder is closed by a PTFE (polytetrafluoroethylene, Teflon) disk (6), which assures the mechanical support of the brass rod (1) and electrical insulation between the brass rod (1) and the aluminum block (3). An inlet (7) directed normal to the cavity axis, serves to deliver the carrier gas. The electrical discharge occurs between the brass rod (1), acting as cathode and the aluminum block (3) connected to ground, which serves as anode.
In Figure 2 the block diagram of the whole experimental setup is shown, including both the system to generate the CAPP and the biological sample holder. The electrical supply circuit for the plasma source operates according to the principle described in (Stoican, 2019). As a typical feature, the electrical discharge is initiated by a train of high voltage pulses and sustained by a common DC voltage source. A ballast resistor embedded into the DC voltage source circuit was used to keep the discharge stable and limit the discharge current, so as to obtain a CAPP with negligible thermal effect.

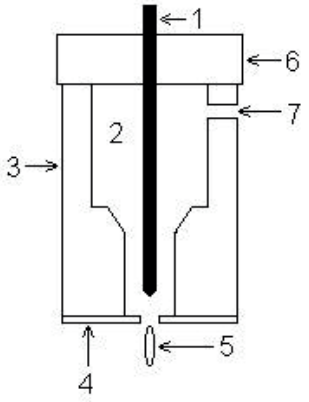



Figure 1. Plasma source mechanical layout representing a slightly modified version of that described in (Stoican, 2011) (not to scale) 1-brass rod (cathode); 2-cavity; 3-aluminum block (anode); 4-front disk with plasma plume output hole 5-plasma plume; 6-PTFE disk; 7-carrier gas input

For a short period of time, both voltages mentioned above are applied simultaneously to the discharge electrodes by means of a summing circuit. The high voltage pulses train is interrupted after the plasma plume occurs and becomes stable. Therefore, plasma is practically due to a low current, pure DC electrical discharge. According to the classification made in (Tendero et al., 2006) it operates as a current-carrying arc plasma torch.
The experimental setup is controlled by means of an electronic interface board that communicates with a personal computer through its RS-232 serial port. The electronic interface board comprises digital outputs necessary to switch on/off DC voltage and carrier gas electric valve, a digital output which provides the excitation signal for the high voltage pulses generator, and analog inputs necessary to measure voltages across terminals of a current sensor resistor Rs.
A software application allows maintaining the plasma plume for the requested period of time, monitoring voltage and current discharge during plasma plume existence, switching on/off the high voltage pulses generator, DC voltage, and carrier gas flow.

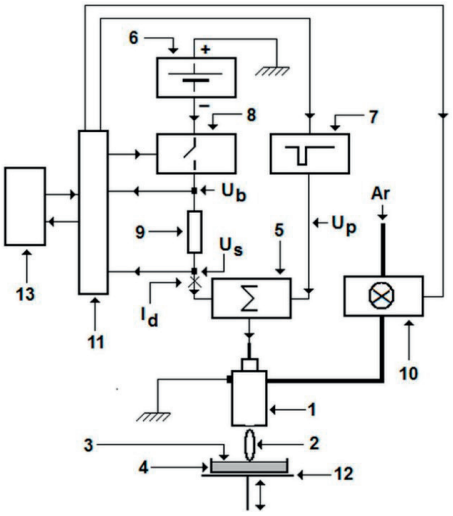



Figure 2. Experimental setup-block diagram
1-plasma source; 2-plasma plume; 3-biological sample;4-Petri plate; 5- summing circuit; 6-DC voltage source; 7-high voltage pulses generator; 8-DC high voltage switch; 9-current sensor Rs; 10-carrier gas electric valve; 11-electronic interface board; 12-metallic plate; 13-personal computer which communicates with the electronic interface board through a RS-232 serial port

The plasma plume is initiated by switching on simultaneously a high voltage pulse generator, DC voltage, and carrier gas flow. A high voltage pulses train is applied until the discharge current becomes greater than a threshold value. After the requested plasma exposure time (PET) has elapsed, the plasma plume is stopped by switching off the DC voltage and carrier gas flow. The PET is considered the time interval from the turn off of high voltage pulses train to the turn off the DC voltage. All necessary commands to perform the above operations are automatically sent by the software application to the electronic interface board.

**Evaluation of antimicrobial effects of argon cold plasma on Gram-negative and Gram-positive bacteria**

Three bacterial strains were used in this study: *Escherichia coli* ATCC 25922 (Minogue et al., 2014), *Staphylococcus aureus* ATCC 25923 (Treangen et al., 2014), and *Pseudomonas aeruginosa* $IBB_{Po16}$ (KT315654, Stancu, 2018). The strains were inoculated into Luria-Bertani (LB) medium and incubated overnight at 30°C with agitation at 150 rpm.

Reagents used in this study were purchased from Merck and Sigma.

**Bacterial growth inhibition assay**. The bacterial cultures were adjusted to an optical density of 0.1 at 660 nm ($OD_{660}$), and 500 µL of each suspension was spread onto LB agar plates using the lawn culture method. After air-drying for 15 min under a laminar flow hood, the inoculated plates were exposed to the plasma plume for different time intervals (5, 7, 10, 15, 30, 60, 90, and 120 s). The distance between the agar surface and the outlet of the plasma-generating device was approximately 2 mm. Following plasma exposure, the plates were incubated overnight at 30°C, and the area of the inhibition zone (defined as the clear region on the LB agar where no bacterial growth was observed) was measured.

**Quantification of bacterial survival**. Bacterial strains were inoculated into LB medium and incubated overnight at 30°C with agitation at 150 rpm. Subsequently, 10 µl of bacterial suspensions adjusted to an optical density of 0.1 $OD_{660}$ were pipetted onto the center of sterile, empty Petri plates, allowed to air-dry, and exposed to the plasma plume for varying time intervals (5, 7, 10, 15, 30, 60, 90, and 120 s). Control samples were prepared under identical conditions but were not subjected to plasma treatment. Following exposure, bacterial recovery and enumeration were performed using the Most Probable Number (MPN) method. Briefly, the bacterial cells were scrubbed from the surface of each Petri plate using sterile 0.9% saline solution. Serial dilutions were prepared, and 20 µl of aliquots of each dilution were inoculated into wells of a 96-well microplate containing 180 µl of LB medium. The microplates were incubated overnight at 30°C. Bacterial growth was assessed by adding 0.3% triphenyl tetrazolium chloride (TTC), as previously described (Stancu, 2019). The appearance of a red coloration in the wells, resulting from TTC reduction, was interpreted as a positive indication of bacterial growth.

To evaluate changes in cell membrane permeability following plasma exposure, a permeability assay (Ardelean et al., 2009) was performed. SYBR Green I and propidium homodimer served as selective fluorescent markers. The assay was conducted on chemically fixed cells (2% buffered formalin) at

5 h post-plasma exposure. SYBR Green I penetrates the membranes of all cells, while propidium homodimer, due to its larger molecule size and negative charges, penetrates only cells with severely compromised membrane integrity, which are considered non-viable (Noble & Fuhrman, 1998).

## RESULTS AND DISCUSSIONS

The effects of CAPP exposure on the inactivation of three bacterial species were investigated in this study. The selected strains belong to the two principal bacterial groups: Gram-positive, represented by *S. aureus*, and Gram-negative, represented by *E. coli* and *P. aeruginosa* IBBPo16.

Details on the plasma source, its electrical supply circuit, and biological sample arrangement are presented in Figures 1 and 2. The high voltage pulses had a peak value of $U_p$ ≈-3.9kV/60Hz (negative polarity with respect to ground), being applied for about 1-2 s in order to initiate the plasma plume. The average DC voltage $U_b$ (having negative polarity with respect to ground) was about 0.68kV. The DC discharge current has been calculated as $I_d$=$|U_b - U_s|/R_s$≈13-20mA. Argon (Ar) was used as a carrier gas. The biological sample was deposited in a Petri plate placed on a metallic support below the output hole of the plasma source.

Owing to structural differences between Gram-positive and Gram-negative bacteria, distinct responses to plasma exposure are anticipated among strains belonging to these groups. In view of the potential applications of CAPP in surface sterilization, argon was selected as the carrier gas, and three bacterial strains were chosen based on their opportunistic and pathogenic characteristics, which represent a potential risk to human health. Previous studies (Tipa et al., 2011; Baldanov et al., 2019) have demonstrated that argon exhibits higher bacterial inactivation efficiency compared with other carrier gases (e.g., helium), thereby justifying its use in the present study.

Several long-living ROS, such as $O_2^{-}$•, $H_2O_2$, and •OH, are capable of diffusing beyond the plasma plume, thereby affecting an area larger than the plasma jet diameter. The distance between the jet nozzle and the treated sample is a crucial parameter, as increasing this distance may lead to attenuation of photons and reactive species, resulting in reduced fluxes reaching the surface and consequently diminishing the antimicrobial efficacy. This aspect is particularly relevant because bacterial inactivation is predominantly mediated by ROS. Additionally, the intensity of UV radiation decreases proportionally to the square of the distance from the source (Lackmann & Badow, 2014).

To address this limitation, all treatments were performed at an approximate distance of 2 mm, corresponding to the condition in which the plasma plume directly contacts the surface and spreads across it, thereby facilitating the transport of reactive species to adjacent regions.

The inhibition zone area as a function of treatment time for each bacterial strain is presented in Figure 3a. According to our results (Figure 4), increasing the PET led to a progressive enlargement of the inhibition zone for all three tested strains, ranging from a minimum of 2.83 $cm^2$ (after 5 s) to a maximum of 31.40 $cm^2$ (after 120 s). The response of *S. aureus* followed a similar trend to that of *E. coli*, with no major differences observed between the two strains; both reached a maximum inhibition zone of 11.30 $cm^2$ after 120 s of exposure. In contrast, *P. aeruginosa* $IBB_{Po16}$ exhibited higher sensitivity to plasma treatment, showing a maximum inhibition zone of 31.40 $cm^2$ after 120s.

Tetrazolium salts are widely used to assess the viability of bacterial cultures. As reported (Moussa et al., 2013), the TTC-reducing activity of a culture is directly proportional to the number of metabolically active cells within the bacterial population. Figure 3b and Figure 5 present the relationship between PET and the number of colony-forming units per milliliter (CFU $mL^{-1}$).

*S. aureus* exhibited the highest resilience to plasma treatment, with no significant differences observed between the control sample and those exposed to 120 s of cold plasma. In contrast, *E. coli* and *P. aeruginosa* $IBB_{Po16}$ exhibited slightly higher sensitivity, showing a reduction in viable counts from $>10^6$ to $10^3$ CFU $mL^{-1}$ after 120 s of exposure. Compared with *S. aureus* and *E. coli*, plasma treatment exerted a more pronounced effect on *P. aeruginosa* $IBB_{Po16}$. Within 15 s of plasma

exposure, a CFU reduction from $>10^6$ to $10^5$ CFU $mL^{-1}$ was achieved. Overall, the results indicate that increasing PET leads to a progressive reduction in the cell viability in both Gram-positive and Gram-negative bacteria.

The permeability assay revealed a decrease in the number of viable bacterial cells (Figure 3c, green fluorescence) and a corresponding increase in the proportion of non-viable cells (Figure 3c, orange fluorescence) after 60 s of cold plasma exposure compared with the untreated control. Before plasma exposure, the proportion of non-viable bacterial cells was low relative to the total cell population. Following 60 s of treatment, a marked increase in non-viable cells was detected, with the majority of cells exhibiting membrane permeabilization and positive homodimer staining.

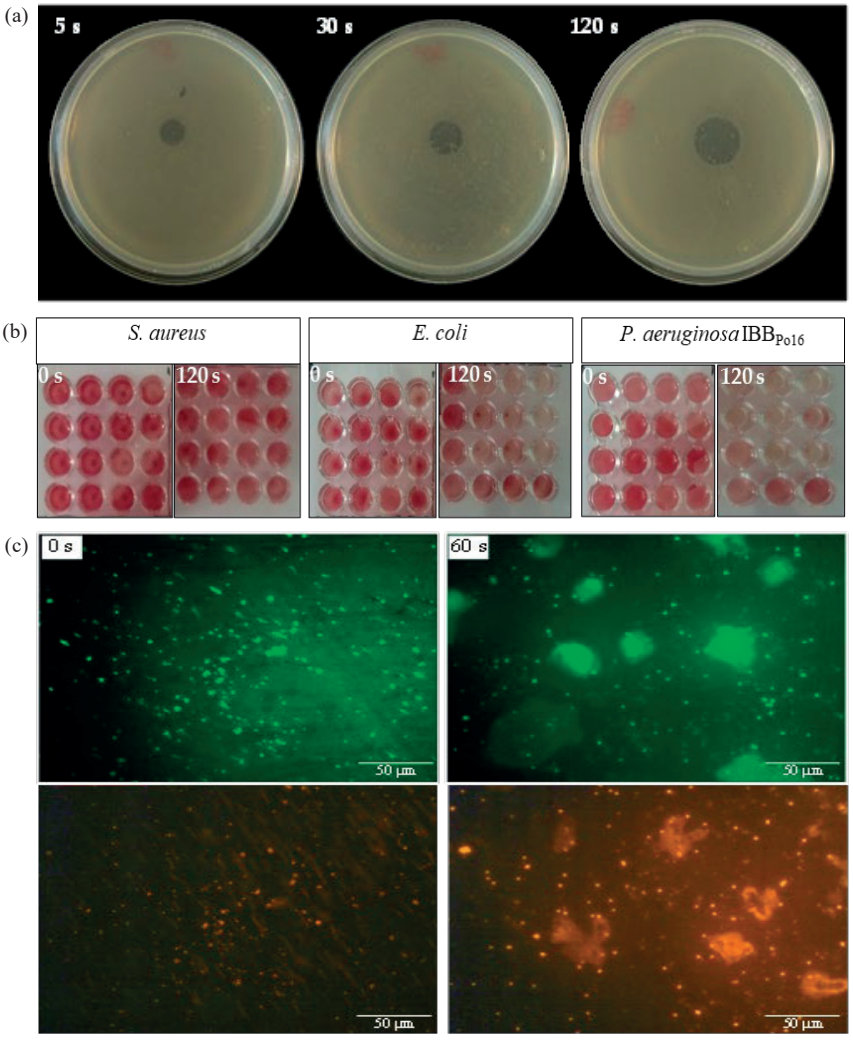
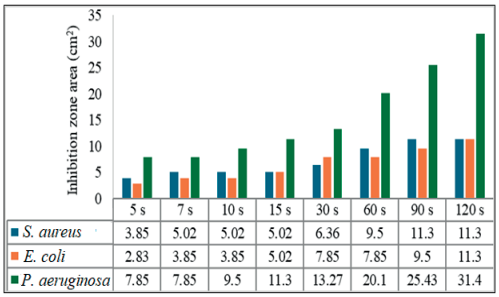
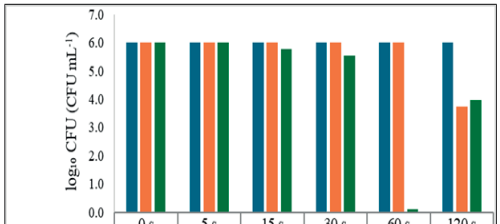



Figure 3. Antimicrobial effects of argon cold plasma on Gram-negative and Gram-positive bacteria. (a) Bacterial growth inhibition after plasma exposure. (b) Quantification of bacterial survival after plasma exposure. (c) Permeability fluorescence assay before (0 s) and after (60 s) plasma exposure of bacterial cells.




| | 5 s | 7 s | 10 s | 15 s | 30 s | 60 s | 90 s | 120 s |
|---|---|---|---|---|---|---|---|---|
| *S. aureus* | 3.85 | 5.02 | 5.02 | 5.02 | 6.36 | 9.5 | 11.3 | 11.3 |
| *E. coli* | 2.83 | 3.85 | 3.85 | 5.02 | 7.85 | 7.85 | 9.5 | 11.3 |
| *P. aeruginosa* | 7.85 | 7.85 | 9.5 | 11.3 | 13.27 | 20.1 | 25.43 | 31.4 |

Figure 4. Inhibition zone areas for the tested Gram-positive and Gram-negative bacteria after plasma exposure (5-120 s)




| | 0 s | 5 s | 15 s | 30 s | 60 s | 120 s |
|---|---|---|---|---|---|---|
| *S. aureus* | $>10^6$ | $>10^6$ | $>10^6$ | $>10^6$ | $>10^6$ | $>10^6$ |
| *E. coli* | $>10^6$ | $>10^6$ | $>10^6$ | $>10^6$ | $>10^6$ | $5.5\times10^3$ |
| *P. aeruginosa* | $>10^6$ | $1.2\times10^6$ | $6.0\times10^5$ | $3.5\times10^5$ | $1.3\times10^5$ | $9.5\times10^3$ |

Figure 5. Gram-positive and Gram-negative bacterial cell viability after plasma exposure (5-120 s)

It should be noted that membrane permeabilization detected by fluorescence staining does not necessarily correspond to an immediate loss of reproductive capacity. While CFU enumeration reflects the ability of bacterial cells to recover and proliferate under nutrient-rich conditions, fluorescence-based assays evaluate membrane integrity at a specific time point. Therefore, the apparent differences between the permeability assay and the viability data (Figure 3b) may indicate the presence of sublethally injured cells within the treated population. Such cells may exhibit increased membrane permeability without complete loss of culturability. Further time-resolved investigations would be required to determine whether plasma-induced membrane alterations are fully irreversible or represent transient physiological responses.

Fluorescent staining methods capable of discriminating between cells with intact membranes (classified as viable) and those with severely compromised membranes (classified as non-viable) have previously been employed to evaluate bacterial responses following CAPP treatment (Deng et al., 2006; Waskow et al., 2018; Lee et al., 2019; Olatunde et al., 2019). These studies reported findings consistent with the results of the present investigation.

All tested strains exhibited a linear increase in inhibition zone area with no evidence of saturation even after 120 s of plasma exposure. Among the strains investigated, *S. aureus* presented the highest resistance to plasma treatment, followed by *E. coli* and *P. aeruginosa* $IBB_{Po16}$. These results are consistent with the known structural difference between Gram-positive and Gram-negative bacteria, particularly regarding cell wall architecture. Of the three strains, *S. aureus* showed significantly higher resistance after 120 s of plasma treatment, suggesting that the increased thickness and structural complexity of the Gram-positive cell wall contribute substantially to plasma-mediated resistance.

Cold plasma has been hypothesized to target multiple cellular components, including the cell membrane, cell wall, DNA, and intracellular proteins. The ROS are capable of breaking structurally critical bonds within peptidoglycan (e.g., C–O, C–N linkages), potentially leading to cell wall damage in Gram-positive bacteria (Misra et al., 2016). In Gram-negative bacteria, ROS primarily induce lipid peroxidation of the outer membrane (Joshi et al., 2011), compromising membrane integrity. This cascade of oxidative events promotes the leakage of intracellular constituents, such as nucleic acids and proteins, ultimately resulting in cell death. The increased susceptibility of Gram-negative bacteria compared to Gram-positive bacteria may also be attributed to the higher porosity of the outer membrane, which facilitates ROS penetration and enhances oxidative damage (Mai-Prochnow et al., 2016). These findings are consistent with our results, as *P. aeruginosa* $IBB_{Po16}$ and *E. coli* proved greater sensitivity to plasma exposure than *S. aureus*.

## CONCLUSIONS

The antimicrobial effect of CAPP using argon as the carrier gas was evaluated against *S. aureus*, *E. coli*, and *P. aeruginosa* $IBB_{Po16}$. *S. aureus* exhibited the highest resistance, while the Gram-negative strains showed greater susceptibility. Bacterial response was strain-

dependent and probably influenced by differences in cell wall architecture. Although plasma exposure reduced viable cell counts, complete inactivation was not achieved even after 120 s, indicating that longer exposure times are required for effective surface sterilization.

These findings demonstrate that CAPP represents a promising approach for surface sterilization and decontamination. Under extended exposure conditions, CAPP may support applications in environmental decontamination and surface treatment technologies.

## ACKNOWLEDGEMENTS

This work was funded by project LAPLAS VII, contract 30N/12.01.2023, supported by the Ministry of Research, Innovation and Digitalization, and by project no. RO1567-IBB05/2023 from the Institute of Biology Bucharest of Romanian Academy.

The authors dedicate this work to the memory of †Professor Dr. Ioan I. ARDELEAN, whose contributions were essential in the early stages of this research, but who sadly passed away before the completion of this manuscript. Thanks are due to Dr. C. Porosnicu (INFLPR) for institutional support, and Mrs. Cirnu Marinela (Institute of Biology Bucharest) for technical support.

## REFERENCES

Alkawareek, M. Y., Gorman, S. P., Graham, W. G., & Gilmore, B. F. (2014). Potential cellular targets and antibacterial efficacy of atmospheric pressure non-thermal plasma. *International Journal of Antimicrobial Agents*, *43*, 154–160.

Ardelean, I., Ghiţă, S., & Sarchizian, I. (2009). Epifluorescent method for quantification of planktonic marine prokaryotes. In *Proc 2nd International Symposium on New research in Biotechnology*, *Serie F*, 288–296.

Asenjo, J., Mora, J., Vargas, A., Brenes, L., Montiel, R., Arrieta, J., & Vargas, V. I. (2015). Atmospheric-pressure non-thermal plasma jet for biomedical and industrial applications. *Journal of Physics: Conference Series*, *591*, 012049.

Baldanov, B. B., Ranzhurov, T. V., Semenov, A. P., & Gomboeva, S. V., 2019. Cold atmospheric argon plasma jet source and its application for bacterial inactivation. *Journal of Theoretical and Applied Physics*, *13*, 95–99.

Barjasteh, A., Kaushik, N., Choi, E. H., & Kaushik, N. K. (2024). Cold Atmospheric Pressure Plasma Solutions for Sustainable Food Packaging. *International Journal of Molecular Sciences*, *25*, 6638.

Bourke, P., Ziuzina, D., Boehm, D., Cullen, P. J., & Keener, K. (2018). The potential of cold plasma for safe and sustainable food production. *Trends in Biotechnology*, *36*, 615–626.

Corradini, M. G. (2020). Modeling microbial inactivation during cold atmospheric-pressure plasma (CAPP) processing. In D. Bermudez-Aguirre (Ed.) *Advances in Cold Plasma Application for Food Safety and Preservation*. Academic Press. https://doi.org/10.1016/C2017-0-02415-1.

Deng, X., Shi, J., & Kong, M. G. (2006). Physical mechanisms of inactivation of *Bacillus subtilis* spores using cold atmospheric plasmas. *IEEE Transactions on Plasma Science*, *34*, 1310–1316.

Domonkos, M., Tichá, P., Trejbal, J., & Demo, P. (2021). Applications of cold atmospheric pressure plasma technology in medicine, agriculture and food industry. *Applied Sciences*, *11*, 4809.

Ehlbeck, J., Schnabel, U., Polak, M., Winter, J., Von Woedtke, Th., Brandenburg, R., von dem Hagen, T., & Weltmann, K. D. (2011). Low temperature atmospheric pressure plasma sources for microbial decontamination. *Journal of Physics D: Applied Physics*, *44*, 013002.

Flynn, P. B., Higginbotham, S., Alshraiedeh, N. H., Gorman, S. P., Graham, W. G., & Gilmore, B. F. (2015). Bactericidal efficacy of atmospheric pressure non-thermal plasma (APNTP) against the ESKAPE pathogens. *International Journal of Antimicrobial Agents*, *46*, 101–107.

Fricke, K., Koban, I., Tresp, H., Jablonowski, L., Schröder, K., Kramer, A., Weltmann, K. D., von Woedtke, T., & Kocher, T. (2012). Atmospheric pressure plasma: a high-performance tool for the efficient removal of biofilms. *PLoS ONE*, *7*, e42539.

Fridman, G., Friedman, G., Gutsol, A., Shekhter, A. B., Vasilets, V. N., & Fridman, A. (2008). Applied plasma medicine. *Plasma Processes and Polymers*, *5*, 503–533.

Heinlin, J., Morfill, G., Landthaler, M., Stolz, W., Isbary, G., Zimmermann, J. L., Shimizu, T., & Karrer, S. (2010). Plasma medicine: possible applications in dermatology. *Journal of the German Society of Dermatology*, *8*, 968–976.

Hertwig, C., Meneses, N., & Mathys, A. (2018). Cold atmospheric pressure plasma and low energy electron beam as alternative nonthermal decontamination technologies for dry food surfaces: a review. *Trends in Food Science & Technology*, *77*, 131–142.

Jiang, B., Zheng, J., Qiu, S., Wu, M., Zhang, Q., Yan, Z., & Xue, Q. (2014). Review on electrical discharge plasma technology for wastewater remediation. *Chemical Engineering Journal*, 236, 348–368.

Joshi, S. G., Cooper, M., Yost, A., Paff, M., Ercan, U. K., Fridman, G., Friedman, G., Fridman, A., & Brooks, A. D. (2011). Nonthermal dielectric-barrier discharge plasma-induced inactivation involves oxidative DNA damage and membrane lipid peroxidation in *Escherichia coli*. *Antimicrobial Agents and Chemotherapy*, *55*, 1053–1062.

Kazemi, A., Nicol, M. J., Bilén, S. G., Kirimanjeswara, G. S., & Knecht, S. D. (2024). Cold atmospheric plasma

medicine: Applications, challenges, and opportunities for predictive control. *Plasma*, *7*, 233–257.

Lackmann, J. W., & Bandow, J. E. (2014). Inactivation of microbes and macromolecules by atmospheric-pressure plasma jets. *Applied Microbiology and Biotechnology*, *98*, 6205–6213.

Laroussi, M. (1996). Sterilization of contaminated matter with an atmospheric pressure plasma. *IEEE Transactions on Plasma Science*, *24*, 1188–1191.

Laroussi, M., & Leipold, F. (2004). Evaluation of the roles of reactive species, heat, and UV radiation in the inactivation of bacterial cells by air plasmas at atmospheric pressure. *International Journal of Mass Spectrometry*, *233*, 81–86.

Lee, M. J., Kwon, J. S., Jiang, H. B., Choi, E. H., Park, G., & Kim, K. M. (2019). The antibacterial effect of non-thermal atmospheric pressure plasma treatment of titanium surfaces according to the bacterial wall structure. *Scientific Reports*, *9*, 1938. https://doi.org/10.1038/s41598-019-39414-9.

Mai-Prochnow, A., Clauson, M., Hong, J., & Murphy, A. B. (2016). Gram positive and Gram negative bacteria differ in their sensitivity to cold plasma. *Scientific Reports*, *6*, 38610. https://doi.org/10.1038/srep38610.

Minogue, T. D., Daligault, H. A., Davenport, K. W., Bishop-Lilly, K. A., Broomall, S. M., Bruce, D. C., Chain, P. S., Chertkov, O., Coyne, S. R., Freitas, T., Frey, K. G., Gibbons, H. S., Jaissle, J., Redden, C. L., Rosenzweig, C. N., Xu, Y., & Johnson, S. L. (2014). Complete genome assembly of *Escherichia coli* ATCC 25922, a serotype O6 reference strain. *Genome Announcements*, *2*. https://doi.org/10.1128/genomeA.00969-14

Misra, N. N., Schlüter, O., & Cullen, P. J. (2016). *Cold plasma in food and agriculture: fundamentals and applications*. Academic Press http://www.sciencedirect.com/science/book/9780128013656.

Mitra, A., Li, Y.F., Klämpfl, T. G., Shimizu, T., Jeon, J., Morfill, G. E., & Zimmermann, J. L. (2014). Inactivation of surface-borne microorganisms and increased germination of seed specimen by cold atmospheric plasma. *Food and Bioprocess Technology*, *7*, 645–653.

Moussa, S. H., Tayel, A. A., Al-Hassan, A. A., & Farouk, A. (2013). Tetrazolium/Formazan test as an efficient method to determine fungal chitosan antimicrobial activity. *Journal of Mycology*, 753692. https://doi.org/10.1155/2013/753692.

Noble, R. T., & Fuhrman, J. A. (1998). Use of SYBR Green I for rapid epifluorescence counts of marine viruses and bacteria. *Aquatic Microbial Ecology*, *14*, 113–118.

Olatunde, O. O., Benjakl, S., & Vongkamjan, K. (2019). Dielectric barrier discharge cold atmospheric plasma: bacterial inactivation mechanism. *Journal of Food Safety*, *39*, e12705. https://doi.org/10.1111/jfs.12705.

Scholtz, V., Pazlarova, J., Souskova, H., Khun, J., & Julak, J. (2015). Nonthermal plasma - A tool for decontamination and disinfection. *Biotechnology Advances*, *33*, 1108–1119.

Singh, B., Prasad, G. K., Pandey, K. S., Danikhel, R. K., & Vijayaraghavan, R. (2010). Decontamination of chemical warfare agents. *Defence Science Journal*, *60*, 428–441.

Stancu, M. M. (2018). Production of some extracellular metabolites by a solvent-tolerant *Pseudomonas aeruginosa* strain. *Waste and Biomass Valorization*, *9*, 1747–1755.

Stancu, M. M. (2019). Isolation of bacterial consortia that induced corrosion of zirconium alloys. *Water, Air, and Soil Pollution*, *230*. https://doi.org/10.1007/s11270-018-4070-0.

Stoican, O. S. (2011). An atmospheric pressure plasma source driven by a train of monopolar high voltage pulses superimposed to a dc voltage. *The European Physical Journal Applied Physics*, *55*, 30801.

Stoican, O. S. (2019). High voltage pulses circuit for generating a plasma plume at atmospheric pressure. *Romanian Reports in Physics*, *71*, 406.

Tendero, C., Tixier, C., Tristant, P., Desmaison, J., & Leprince, P. (2006). Atmospheric pressure plasmas: a review. *Spectrochimica Acta Part B*, *61*, 2–30.

Tipa, R. S., Boekema, B., Middelkoop, E., & Kroesen, G. M. W. (2011) Cold plasma for bacterial inactivation. *Proceedings of the 20th International Symposium on Plasma Chemistry, 24-29*.

Treangen, T. J., Maybank, R. A., Enke, S., Friss, M. B., Diviak, L. F., Karaolis, D. K., Koren, S., Ondov, B., Phillippy, A. M., Bergman, N. H., & Rosovitz, M. J. (2014). Complete genome sequence of the quality control strain *Staphylococcus aureus* subsp. *aureus* ATCC 25923. *Genome Announcements*, *2*. https://doi.org/10.1128/genomeA.01110-14.

Waskow, A., Betschart, J., Butscher, D., Oberbossel, G., Klöti, D., Büttner-Mainik, A., Adamcik, J., von Rohr, P. R., & Schuppler, M. (2018). Characterization of efficiency and mechanisms of cold atmospheric pressure plasma decontamination of seeds for sprout production. *Frontiers in Microbiology*, *9*, 3164. https://doi.org/10.3389/fmicb.2018.03164.

Whittaker, A. G., Graham, E. M., Baxter, R. L., Jones, A. C., Richardson, P. R., Meek, G., Campbell, G. A., Aitken, A., & Baxter, H. C. (2004). Plasma cleaning of dental instruments. *Journal of Hospital Infection*, *56*, 37–41.

Scientific Papers. Series E. Land Reclamation, Earth Observation & Surveying, Environmental Engineering. Vol. XV, 2026
Print ISSN 2285-6064, CD-ROM ISSN 2285-6072, Online ISSN 2393-5138, ISSN-L 2285-6064

# OZONE STRESS IN PLANTS: SIGNALLING AND RESPONSE

**Senad MURTIĆ**

University of Sarajevo, Faculty of Agriculture and Food Sciences, Department of Plant Physiology, 8 Zmaja od Bosne, 71000 Sarajevo, Bosnia and Herzegovina

Corresponding author email: murticsenad@hotmail.com

***Abstract***

*Ozone ($O_3$) pollution is a serious global environmental threat, with tropospheric ozone levels frequently classified as some of the most toxic air pollutants. Elevated tropospheric ozone levels affect vital processes in plants, encompassing respiration, photosynthesis, and nutrient uptake, thereby causing a decline in plant growth and development. Plants display a complex set of defense strategies against $O_3$ stress, including stomatal regulation of $O_3$ influx into leaves, photosynthetic adjustments, modulation of antioxidant defense against $O_3$-induced reactive oxygen species (ROS), and secondary metabolism. Stomatal closure is the first response to $O_3$ stress in most plants, providing protection from high $O_3$ influx to the leaves. One negative outcome of this is the decreased influx of $CO_2$ into the leaves, resulting in a decline in the photosynthetic rate. In response to $O_3$ stress, plants strive to adjust their photosynthesis by regulating the photosynthetic electron transport chain through photorespiration, cyclic electron flow, or the alternative oxidase pathway, while also enhancing anthocyanin production to protect their photosynthetic systems. Plants are also equipped with a substantial antioxidant defense system that consists of both enzymatic and non-enzymatic antioxidants, which work together to neutralize the excess $O_3$-induced ROS. This review summarizes recent advances in understanding the strategies that plants use to protect their structural and functional integrity in response to $O_3$ pollution.*

***Key words:*** *air pollution, antioxidant defenses, photosynthetic adjustments, stomatal regulation.*

## INTRODUCTION

In the last several decades, global patterns of industrialization and rapid urbanization have led to an increase in the production of air pollutants, adversely affecting living organisms (Antenozio et al., 2024). Air pollutants refer to all substances in the air, whether inorganic or organic, that compromise air quality, generating adverse impacts on the environment (Stoykova et al., 2025). They can be classified into two categories: primary and secondary, depending on their source (Manisalidis et al., 2020). Primary pollutants, including carbon oxides, sulfur oxides, nitrogen oxides, particulate matter, and volatile organic compounds, are released directly from identifiable sources, whereas secondary pollutants are not released directly; instead, they are generated in the atmosphere through chemical reactions that involve primary pollutants and other air components such as water vapor or oxygen. A notable example is tropospheric ozone (Bălă et al., 2021; Cadar et al., 2023). Ozone ($O_3$) is an allotrope of oxygen, consisting of three oxygen atoms. The atmosphere contains two areas where $O_3$ exists: the stratosphere and the troposphere, both of which share the same chemical composition (Alvim-Ferraz et al., 2024). Most of the $O_3$, approximately 90%, is formed naturally in the stratosphere as a result of ultraviolet radiation interacting with $O_2$. Specifically, the interaction of ultraviolet rays with $O_2$ in the stratosphere leads to the splitting of the $O_2$ into two single oxygen atoms. A released oxygen atom then binds with $O_2$ to create an $O_3$ molecule (Bernhard et al., 2023).

Stratospheric $O_3$ is extremely important for life on Earth, as it prevents a large part of harmful ultraviolet radiation from reaching the Earth's surface. Regrettably, over the past few decades, human activities have notably led to the destabilization of the stratospheric ozone layer. The consequences of stratospheric $O_3$ depletion are manifested through the appearance of ozone holes, which are considered to be, among other things, a result of the adverse effects of various human-made chemicals such as chlorofluorocarbons, methyl bromide, carbon tetrachloride, and methyl chloroform (Chipperfield & Bekki, 2024).

$O_3$ in the lower atmosphere (tropospheric ozone), is created through intricate chemical reactions involving nitrogen oxide gases and volatile organic compounds under sunlight. In this context, it is necessary to note that the production of tropospheric $O_3$ is positively associated with sunshine hours and negatively associated with both relative humidity and wind speed. As a result, the concentration of $O_3$ varies throughout the season and even within the day, exhibiting higher levels during the daytime and in dry months, particularly in areas close to industrial facilities (Nowroz et al., 2024).

Tropospheric $O_3$ is extremely harmful to both humans and animals. Its inhalation, even at relatively low levels, can result in respiratory tract inflammation, migraines, burning eyes, irritation of mucous membranes, chest pain, and asthma attacks (Kim et al., 2020). $O_3$ is also highly toxic to plants. The effect of $O_3$ on plants is reliant on its concentration as well as the duration of exposure. Long-term exposure to low levels of $O_3$ impairs stomatal function, disrupts nutrient uptake and respiration, and decreases the photosynthetic rate, often without any evident destruction to the plant tissues. Conversely, short-term exposure to high levels of $O_3$ results in the initiation of visible lesion formation in leaves (Wang et al., 2024). These disturbances negatively influence plant development and reproductive success, ultimately resulting in lower crop yields and compromised quality. Over the past century, tropospheric $O_3$ levels have risen by 2 to 3 times, which implies that more severe and widespread challenges due to $O_3$ are likely to increase in the future (Donzelli & Suarez-Varela, 2024).

Several studies have demonstrated that plants adapt to $O_3$ pollution by undergoing changes in their molecular, biochemical, and physiological responses, involving large-scale changes in enzyme activities and gene expression (Günthardt-Goerg et al., 2023; Rao et al., 2025). It is also well documented that reactive oxygen species (ROS) generated from the breakdown of $O_3$ in the extracellular space (apoplast) activate multiple signaling pathways that are seamlessly integrated within the cell into a delicately balanced ROS signaling network, which is crucial for the plant's response to $O_3$ stress (Vainonen & Kangasjärvi, 2015). Despite the extensive research in this area, many of these signaling pathways against $O_3$ stress are still not well comprehended. Addressing these knowledge gaps is important for a deeper understanding of how plants react to $O_3$ stress and for creating strategies to reduce and control $O_3$ pollution, particularly in urban areas. This review summarizes recent advances in understanding the strategies that plants use to protect their structural and functional integrity in response to $O_3$ pollution.

## OZONE STRESS SIGNAL PERCEPTION AND TRANSDUCTION IN PLANTS

Several investigations into plant responses to $O_3$ pollution have confirmed that $O_3$, once it enters leaves through stomata, stimulates the excessive production of ROS in the apoplast, including superoxide anion radicals ($O_2^-$), singlet oxygen ($^1O_2$), and hydrogen peroxide ($H_2O_2$) (Podgórska et al., 2017; Montes et al., 2022; Yu & Blande, 2022; Simin et al., 2026). Furthermore, it is thoroughly documented that $O_3$ triggers plasma membrane-bound NADPH-dependent oxidases to create ROS (Sachdev et al., 2021). It is also noted that $O_3$ and $H_2O_2$ can diffuse directly into the cytosol through aquaporins, resulting in the generation of further ROS (Aranda-Rivera et al., 2022).

The overproduction of $O_3$-induced ROS may initiate a wide array of cellular changes, including depolarization of the plasma membrane, alterations in cell wall compounds, ozonolysis of double bonds present in the unsaturated fatty acids in cell membranes, and the activation of signal transduction proteins within the plasma membrane. Thus, the way in which plant cells perceive $O_3$ might be related to the to the modifications in cell walls and plasma membranes resulting from $O_3$-induced ROS (Rebouças et al., 2017). In this context, Kangasjärvi et al. (2005) indicated that three distinct mechanisms may play a role in $O_3$/ROS sensing. These include the generation of lipid-based signaling molecules that result from the oxidation of plasma membrane lipids, alterations in the cellular redox balance caused by the interaction of $O_3$/ROS with redox-active compounds, and the activation of apoplastic receptor proteins that are directly altered by

ROS. Once the sensing process is complete, the signals generated at the membrane-bound receptors or sensors are transformed into cellular responses through a series of signal transduction pathways, including $Ca^{2+}$ signaling pathways and mitogen-activated protein kinase (MAPK) cascades, in addition to numerous plant hormone-dependent pathways (Hasan et al., 2021).

It is also well documented that the signal from apoplastic ROS can be transmitted to the chloroplast via membrane-associated heterotrimeric G proteins, resulting in the subsequent production of chloroplastic ROS. The generation of ROS in chloroplasts also leads to the activation of multiple downstream signaling pathways that may work in parallel, in series, or through a combination of both (Shapiguzov et al., 2012).

Baier et al. (2005) reported that the ozone stress signal transduction in plant cells consist of a two-step process: (1) rapid signaling events that involve $Ca^{2+}$ influx and protein phosphorylation reaction from upstream receptor to downstream target, and (2) the activation of plant hormone-dependent pathways that serve to stabilize and enhance the plant's defense response to $O_3$ stress.

The influx of $Ca^{2+}$ ions from the apoplast into the cytosol through plasma membrane represents the initial step in ozone stress signal transduction in plant cells, occurring in only a few minutes. This event results in an increase in cytosolic-free $Ca^{2+}$ concentration, which then induces rapid changes in the protein phosphorylation pattern (Lee et al., 2021). Phosphorylation reactions are fundamentally significant in signal transduction pathways, facilitating signal transduction and integrating various signaling routes. Protein phosphorylation by specific mitogen-activated protein kinase (MAPK) cascades acts as a crucial pathway that functions downstream of sensors and receptors, translating extracellular signals into intracellular reactions in plant cells when exposed to $O_3$. Each MAPK cascade consists of three kinase modules: MAPK kinase kinases (MAPKKKs), MAPK kinases (MAPKKs), and MAPKs, which are interconnected in different manners to upstream receptors and downstream targets (Majeed et al., 2023). A pathway by which $Ca^{2+}$ influx leads to the activation of the MAPK pathway is well documented. In short, increases in cytosolic free $Ca^{2+}$ levels trigger MAPKKKs, which subsequently phosphorylate MAPKKs. The activated MAPKKs further phosphorylate MAPKs, which, in turn, can activate a diverse range of transcription factors (Lin et al., 2021).

Significant progress in associating MAPKs with $O_3$ stress signaling have emerged from the examination of the model plant *Arabidopsis thaliana* (L.) Heynh. Jagodzik et al. (2018) reported that the *A. thaliana* genome encodes 20 MAPKs, 10 MAPKKs, and 80 MAPKKKs genes. The high number of distinct kinases within the plant genome points to a likely complexity and interaction among MAPK cascades (Sun & Zhang, 2022). In the *A. thaliana* MAPK signaling pathways, two well-known MAPKs, MAPK3 and MAPK6, serve as crucial regulators that are activated in reaction to $O_3$ stress (Jiang et al., 2025). Their activation occurs within a period of 10 to 30 minutes after $O_3$ exposure, highlighting it as one of the earliest events in intracellular signaling. Once activated, MAPK3/6 translocate into the nucleus, where they regulate the expression of specific genes responsible for the synthesis of various stress-related proteins (Yadav & Mina, 2022). Several studies have shown that a considerable similarity exists in the gene expression patterns observed in plants exposed to $O_3$ and those showing responses to pathogen attack, suggesting that $O_3$-induced ROS may initiate programmed cell death (PCD) similar to a hypersensitive response in plant pathogenesis (Leppälä et al., 2022). PCD refers to an active and genetically regulated process through which plants eliminate unwanted and potentially harmful cells. It is also a common feature in plant development: it can be observed during floral organ abortion, senescence, tracheary element formation, and the formation of aerenchyma. The prevailing assumption is that $O_3$-initiated PCD acts as an initiator for lesion formation in leaves, which in turn limits the spread of oxidative bursts triggered by $O_3$ degradation in the apoplast (Bartoli et al., 2013). $O_3$-induced PCD is a highly organized process that is regulated by a complex network of signaling pathways, including those activated by plant hormones. Multiple research studies have demonstrated

that the accumulation of salicylic acid (SA) in $O_3$-exposed plants is correlated with the formation of leaf lesions, suggesting that SA plays an important role in $O_3$-induced PCD (Tamaoki, 2008; Poór, 2020; Modesti et al., 2023). Faoro and Iriti (2009) noted that SA can suppress $H_2O_2$-scavenging enzymes, thus promoting the adverse effects of ROS on plant cells, leading to PCD. Plant exposure to $O_3$ also activates signaling pathways that result in an increased accumulation of ethylene (ET) in plant cells (Guo et al., 2018). MAPK3/6 play a significant role in regulating ET production, as they are involved in the phosphorylation of aminocyclopropane-1-carboxylic acid synthase (ACCS), which is crucial for ET synthesis (Liu & Zhang, 2004). This leads to increased cellular ACCS activity and, as a result, enhanced ET production. It is generally accepted that ET has a role similar to that of SA in $O_3$-induced PCD; however, there are doubts about whether it carries out this function in conjunction with SA or independently (Vahala et al., 2003). The hypothesis that both SA and ET together modulate cell death in $O_3$-sensitive plant genotypes, and that $O_3$-induced ET synthesis is a result of increased cell death caused by SA, is widely accepted among scientists (Grantz & Vu, 2012; Xu et al., 2015). The heightened synthesis of jasmonic acid (JA) and its methyl ester, methyl jasmonate (MeJA), is another outcome of exposing the plant to $O_3$ stress (Rehman et al., 2023). Li et al. (2022) noted that JA derivatives are involved in limiting lesion spreading by antagonizing the cell death-promoting functions of SA and ET. This aligns with the conclusions presented in two previous studies (Rao et al., 2000; Zhou et al., 2020). Numerous studies have also confirmed that foliar abscisic acid (ABA) levels also escalate rapidly once plants are exposed to $O_3$ (McAdam et al., 2017; Guo et al., 2020; Xu et al., 2026). It is assumed that ABA plays a role in the response to $O_3$ stress by stimulating guard cells to close stomata, thereby reducing the likelihood of $O_3$ entry and lesion initiation (Kashtoh & Baek, 2021). However, recent studies have shown a decrease in stomatal sensitivity to ABA depending on ET, highlighting the antagonistic roles of ABA and ET in regulating stomatal movement when plants are faced with $O_3$ stress (Wilkinson & Davies, 2010; Müller, 2021). As an illustration, in various plant species, ET is noted to promote stomatal opening, consequently hindering ABA-induced stomatal closure (Song et al., 2023; An et al., 2025; Huang et al. 2025). Figure 1 displays a simplified schematic diagram that depicts the key signaling pathways related to plant responses under $O_3$ stress.

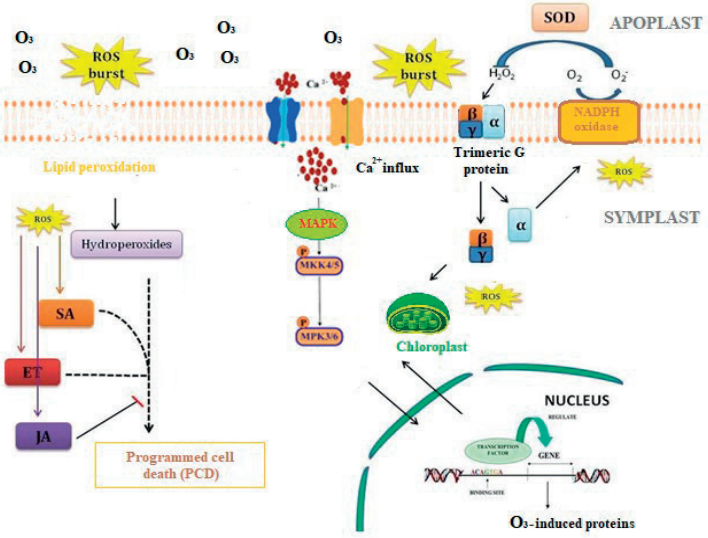



Figure 1. A schematic diagram of the key signaling pathways involved in the plant's response to $O_3$ stress

## PLANT DEFENSE MECHANISMS AGAINST OZONE STRESS

Plants display a complex set of defense strategies against $O_3$ stress, including stomatal regulation of $O_3$ influx into leaves, photosynthetic adjustments, modulation of antioxidant defense against $O_3$-induced reactive oxygen species (ROS), and secondary metabolism.

### Stomatal regulation

Stomatal closure is the first response to $O_3$ stress in most plants, which occurs within a few minutes of being exposed to $O_3$, thereby restricting the uptake of $O_3$ through the stomata. The anion channels in guard cells are crucial in controlling the size of stomatal pores (Chen et al., 2022). There are two categories of anion channels found in the plasma membrane of guard cells: R (rapid)-type and S (slow)-type, both activated in guard cells by the stress hormone ABA. Specifically, upon exposure to $O_3$ stress, guard cells show a substantial rise in ABA and ROS levels, which initiates a cascade of signaling events that activate anion channels. The outcome of this activation is the efflux of ions ($K^+$, $Cl^-$ and malate) from the guard cell, which ultimately decreases turgor pressure, thereby resulting in the closure of the stomata (Saito & Uozumi, 2019).

The S-type slow anion channel 1 (SLAC1) is recognized as one of the significant and extensively studied anion channels (Deng et al., 2021). The plant hormone ABA initiates the activation of SLAC1 via a signaling pathway that includes ABA receptors and protein phosphatase 2C (PP2C). These components are involved in the activity of $Ca^{2+}$-independent kinase Open Stomata 1 (OST1) along with various $Ca^{2+}$-dependent protein kinases that phosphorylate SLAC1 (Bharath et al., 2021). SLAC1 phosphorylation may also take place via an ABA-independent signaling pathway, which is triggered by $O_3$-induced ROS and facilitated by $Ca^{2+}$-dependent protein kinases (CDPKs) (Munemasa et al., 2015).

Despite the fact that stomatal closure under $O_3$ stress conditions is very beneficial for the plant's survival by minimizing $O_3$ uptake and its damaging oxidative effects, it should not be ignored that this closure has a detrimental effect on photosynthesis as a result of reduced $CO_2$ intake (Lee et al., 2021). Additionally, $O_3$-induced ROS can cause harm to the chloroplast ultrastructure and interfere with the photosynthetic electron transport chain, thereby further hindering the photosynthetic rate. As a consequence, plant growth and development are adversely impacted (Ramya et al., 2021).

### Photosynthetic adjustments

$O_3$-tolerant plants possess inherent defense mechanisms that enable them to adjust photosynthesis to $O_3$ stress, thus reducing the damage that arises from $O_3$. The main mechanisms encompass the regulation of the photosynthetic electron transport chain, the increase in anthocyanin production to protect the photosynthetic apparatus, and the regulation of photosynthetic protein transcription (Upadhyay et al., 2025).

The regulation of the photosynthetic electron transport chain under $O_3$ stress conditions can be achieved through photorespiration, cyclic electron flow, and the alternative oxidase pathway. These mechanisms work in unison to protect the plants from photoinhibition and maintain cellular redox homeostasis within the cell.

Photorespiration starts with the oxygenation of ribulose-1,5-bisphosphate (RuBP) resulting in the formation of 3-phosphoglycerate (3-PGA) and 2-phosphoglycolate (2-PG), which is partially recycled into the $C_3$ cycle through the photorespiration pathway. This process is commonly seen as a wasteful process because it generates 2PG, a compound that is harmful to numerous enzymes involved in photosynthetic metabolism, and it oxidizes organic carbon without apparently producing ATP (Shi & Bloom, 2021). However, under stressful conditions, photorespiration is of exceptional importance for plant functionality for several reasons. First, photorespiration acts as a protective mechanism to dissipate excess light energy, safeguarding the photosynthetic machinery from photoinhibition (Smith et al., 2024). Second, the oxygenation of RuBP requires large quantities of ATP and NADPH, resulting in the regeneration of ADP and $NADP^+$, which are crucial for the light-dependent reactions of photosynthesis (Nazari et al., 2024). Third, glycine, generated as the

ultimate product of photorespiration, is required for the synthesis of glutathione, a crucial part of antioxidant defense systems in plants (Voss et al., 2013).

Cyclic electron flow (CEF) serves as another protective mechanism for photosynthetic apparatus under $O_3$ stress. During CEF, electrons are recycled through photosystem I, leading to the production of ATP without concomitant production of NADPH, thus raising the ATP/NADPH ratio essential for the Calvin cycle (Wang et al., 2023a). Additionally, CEF helps to prevent the excessive reduction of the acceptor side of photosystem I (PSI), consequently reducing the generation of superoxide anion radicals and protecting PSI from photoinhibition (Cun et al., 2022).

Maintaining a fine balance between energy production and utilization is fundamentally significant for plants' survival in adverse conditions, including those caused by $O_3$ exposure. Several studies have shown that under abiotic stress, plant cells activate the alternative oxidase (AOX) pathway in their mitochondria, apart from the cytochrome (Cyt) pathway, which is the main mitochondrial electron transport chain (Vanlerberghe et al., 2013; Dinakar et al., 20160). This alternative AOX pathway features a cyanide-resistant ubiquinol oxidase located in the inner mitochondrial membrane, which facilitates the direct transfer of electrons from the ubiquinone pool to oxygen, circumventing the proton-pumping complexes III and IV. By circumventing Complex III and IV, AOX significantly diminishes ATP production, leading to the energy being transformed into heat (Li et al., 2024). Most importantly, AOX aids in preventing the overreduction of upstream electron-transport components, thereby decreasing ROS formation. Under stress conditions, this is of significant importance for the plant as it reduces further potential damage to cellular components, including the photosynthetic machinery (Manbir et al., 2022).

Anthocyanins, water-soluble pigments in plant cells, play a crucial role in alleviating photoinhibition due to their ability to absorb harmful UV radiation (280-315 nm), thus protecting intracellular components, including chloroplasts, from potential damage (Agati et al., 2021). They also possess strong antioxidant activities, preventing or reducing the damage caused by ROS. Anthocyanins exhibit their antioxidant effects mainly through hydrogen atom transfer (HAT) and single-electron transfer (SET) mechanisms. In the HAT mechanism, anthocyanin interacts with ROS by transferring one of its hydrogen atoms to the ROS through the homolytic cleavage of an -OH bond. In contrast, the SET mechanism involves the transfer of a single electron from the anthocyanin to the ROS, resulting in the ionization of both substances in the process (Sadowska-Bartosz & Bartosz, 2024).

Unlike anthocyanidins, the levels of chlorophyll and photosynthetic proteins significantly decrease under $O_3$ stress conditions, which in turn reduces photosynthetic capacity and efficiency, particularly in older leaves. This implies that the transcript levels of genes encoding proteins involved in the light-dependent reactions, the Calvin cycle, and pigment synthesis are significantly reduced under $O_3$ stress conditions (Han et al., 2023). Their reduction does not, however, necessarily translate to weakening the plant. Moreover, many scientists view a decline in the photosynthesis rate under stress conditions as a hidden cost of defense, as the plant reallocates its resources from growth to defense in order to overcome stressful conditions as quickly as possible (Huot et al., 2014; Serrano-Mislata et al., 2025; Zrimec et al., 2025). If this occurs, the plant increases the rate of photosynthesis to provide the resources necessary for its further growth and development.

Conversely, the genes involved in the signaling network and defense mechanisms against $O_3$ stress have different transcriptomic responses; their expression increases under $O_3$ stress (Ludwikow & Sadowski, 2008).

**Modulation of antioxidant defense system**

Plenty of studies have shown that $O_3$, after entering leaves, induces the accumulation of ROS in the apoplast through its conversion into superoxide anion radicals ($O_2^-$), hydrogen peroxide ($H_2O_2$), or singlet oxygen ($^1O_2$) upon interaction with water (Keutgen & Pawelzik, 2008; Vahisalu et al., 2010; Vaultier & Jolivet,

2015). ROS are well-known for their dual role in plants, functioning as both damaging and advantageous species (Panda et al., 2024). On the one hand, they are crucial in integrating external and intracellular signals, while also acting as critical regulators of plant growth and development. On the other hand, their overproduction at levels that go beyond the antioxidant scavenging capacity results in oxidative stress, recognized as a damaging process involved in the destruction of cell structures (Alam et al., 2025).

Antioxidant compounds in the apoplast serve as the initial defense against ROS, with ascorbate and glutathione being the main non-enzymatic ROS scavengers (Cannea & Padiglia, 2025). Piechowiak et al. (2026) reported that exposure of radish sprouts to $O_3$ stress resulted in a significant increase in ascorbate content by 14% and glutathione by 25% compared to the control. The observed increases in ascorbate and glutathione levels were associated with a heightened expression of proteins that play a role in the biosynthesis of these metabolites.

The ability of plants to neutralize $O_3$-induced ROS is not limited to only these two metabolites. The detoxification of ROS involves a sophisticated network that also includes various non-enzymatic antioxidants, such as tocopherols and flavonoids, along with enzymatic antioxidants (Hasanuzzaman et al., 2020). In this context, several studies have shown that under $O_3$ stress, plants are capable of enhancing their antioxidative systems by stimulating the gene expression and post-translational modifications of antioxidant enzymes such as superoxide dismutase (SOD), ascorbate peroxidase (APX), and catalase (CAT) (Mishra et al., 2023; Wang et al., 2023b; Jin et al., 2025). SOD catalyzes the dismutation of two molecules of $O_2^-$ to less hazardous molecules: $H_2O_2$ and molecular oxygen (Rajput et al., 2021). $H_2O_2$ is extremely dangerous when present in high concentrations, as it converts into hydroxyl radicals, the most reactive and destructive ROS, which can cause irreversible damage to cellular structures. However, plant cells possess a strong antioxidant defense mechanism to counteract $H_2O_2$, with CAT and APX serving as the main enzymes for neutralizing $H_2O_2$ (Černý et al., 2018). CAT protects the cell against $H_2O_2$ by facilitating its breakdown into $O_2$ and $H_2O$, while APX decomposes $H_2O_2$ using ascorbate as an electron donor (Gomes et al., 2022). In general, the plant under $O_3$ exposure initiates numerous signaling pathways, all aimed at enhancing antioxidant capacity, either by producing enzymatic or non-enzymatic antioxidants or by generating metabolites that contribute to repairing damage caused by oxidative stress.

**Secondary metabolism**

In response to $O_3$ stress, the plant enhances the production of secondary metabolites, which are organic compounds that serve as a defense against both biotic and abiotic stresses. Guo et al. (2024) reported that $O_3$ exposure greatly increased the rate of carbon flux into secondary metabolic pathways, causing a change in resource allocation that affected the synthesis of secondary metabolites. All plants are able to produce secondary metabolites (SMs), especially under $O_3$ stress conditions, but this process exhibits remarkable genotypic variation and high phenotypic plasticity (Gu et al., 2025). SMs consist of a broad spectrum of compounds, featuring more than 12,000 alkaloids, 40,000 isoprenoids, and 8,000 phenylpropanoids, all of which are uniquely produced by plants (Elshafie et al., 2023). It is estimated that the total number of SMs surpasses 200,000; nonetheless, the actual figure is likely much greater (Nomura et al., 2018).

On the basis of their chemical structures, SMs can be broadly divided into three categories: terpenoids, phenolic compounds, and nitrogen-containing compounds. Among terpenoids, the most common compounds include sterols, carotenoids, saponins, and glycosides. In the category of phenolic compounds, flavonoids, phenolic acids, lignin, and tannins are prominent, while among nitrogen-containing compounds, alkaloids are the most represented (Jan et al., 2021).

Depending on their volatility, SMs in plants can be classified as either non-volatile or volatile. Volatile SMs are often characterized by a complex mixture of low-molecular-weight lipophilic compounds that mainly arise from terpenoid biosynthetic pathways, seemingly produced as a defense mechanism to prevent $O_3$

uptake. Volatile SMs also affect the interactions between plants and their habitats, playing a crucial role in coordinating plant-environment relationships (Abbas & Wang, 2025).

The phenylpropanoid, terpenoid, and alkaloid pathways represent the major metabolic pathways through which plant SMs are synthesized. Among these, the phenylpropanoid metabolic pathway is recognized as the most important secondary metabolic pathway associated with defense against abiotic stress, as it contributes directly or indirectly to the antioxidant defense systems in plants (Jangpangi et al., 2025). Some of the more significant end products of the phenylpropanoid pathway are flavonoids, hydroxycinnamic acid esters, and the precursors of lignin and tannins, all of which belong to phenolic compounds (Ninkuu et al., 2025). The importance of phenolic compounds lies not only in their ability to enhance the antioxidant capacity of the plant but also in their contribution to aesthetic quality parameters like color and taste, indicating their significant role in the adaptation of plants to the specific conditions of their native habitats (Kisiriko et al., 2021).

Alkaloids are another important class of plant SMs that play an important role in the plant's response to challenging living conditions, such as $O_3$ stress. $O_3$-induced alkaloid accumulation in plants has been documented in various studies, indicating that plants initiate alkaloid biosynthesis as a compensatory defense mechanism (Ansari et al., 2021; Pant et al., 2021; Ansari et al., 2023). Overall, alkaloids act as strong chemical deterrents, enhancing the plant's defense systems against environmental challenges. It is also important to note that certain SMs, including plant hormones JA, SA, and ET, serve as signaling molecules that help plants initiate signaling pathways aimed at producing substances that support their adaptation to unfavorable living conditions, particularly pronounced under $O_3$ stress.

## CONCLUSIONS

$O_3$ pollution represents a significant global environmental issue, as its levels consistently rank among the most highly toxic air pollutants. Plants have evolved a complex set of defense mechanisms against $O_3$ stress, including $O_3$-induced stomatal regulation, photosynthetic adjustments, modulation of the antioxidant defense system, and secondary metabolism. In most plants, the first response to $O_3$ stress is stomatal closure, which takes place within a few minutes of $O_3$ exposure, consequently restricting $O_3$ uptake through the stomata. One negative outcome of this is the decreased influx of $CO_2$ into the leaves, resulting in a decline in photosynthetic rate. Additionally, $O_3$-induced ROS interfere with the photosynthetic electron transport chain, thereby further hindering the photosynthetic rate. However, plants possess inherent defense mechanisms that enable them to adjust photosynthesis to $O_3$ stress, including the regulation of the photosynthetic electron transport chain and an increase in anthocyanin production to protect the photosynthetic apparatus. Plants also possess various non-enzymatic and enzymatic antioxidants that assist in neutralizing the excessive production of ROS under $O_3$ stress conditions. A significant role in enhancing the plant's defense capacities against $O_3$ stress is played by numerous secondary metabolites that the plant intensively produces under such conditions. The value of these metabolites is twofold: they enhance the antioxidant capacity of the plant and serve as signaling molecules that facilitate the initiation of signaling pathways in plants aimed at producing substances that support the plant's adaptation to unfavorable living conditions.

## REFERENCES

Abbas, F., & Wang, H.-C. (2025). Plant Volatile Organic Compounds: Revealing the Hidden Interactions. *Plants, 14*(4), 507. https://doi.org/10.3390/plants14040507

Agati, G., Guidi, L., Landi, M., & Tattini, M. (2021). Anthocyanins in photoprotection: knowing the actors in play to solve this complex ecophysiological issue. *The New phytologist, 232*(6), 2228–2235. https://doi.org/10.1111/nph.17648

Alam, P., Faizan, M., Arif, Y., Azzam, M. M., Hayat, S., Afzal, S., & Albalawi, T. (2025). Reactive oxygen species: balancing agents in plants. *Frontiers in Plant Science, 16*, 1713590. https://doi.org/10.3389/fpls.2025.1713590

Alvim-Ferraz, M. C. M., Sousa, S. I. V., Martins, F. G., & Ferraz, M. P. (2024). Tropospheric and Stratospheric Ozone: Scientific History and Shifts in

Early Perspectives Regarding the Impact on Human Health. *Atmosphere, 15*(12), 1504. https://doi.org/10.3390/atmos15121504

An, Y., Zhang, J., Sun, Z., Gan, Y., Ge, X., Wang, X., Zhang, M., & He, J. (2025). Ethylene antagonizes ABA responses in stomatal movement and seed germination by upregulating ABI1 and ABI2 at both the transcript and protein levels. *The Plant journal: for cell and molecular biology, 123*(3), e70423. https://doi.org/10.1111/tpj.70423

Ansari, N., Yadav, D. S., Agrawal, M., & Agrawal, S. B. (2021). The impact of elevated ozone on growth, secondary metabolites, production of reactive oxygen species and antioxidant response in an anti-diabetic plant Costus pictus. *Functional plant biology : FPB, 48*(6), 597–610. https://doi.org/10.1071/FP20324

Ansari, N., Yadav, D. S., Singh, P., Agrawal, M., & Agrawal, S. B. (2023). Ozone exposure response on physiological and biochemical parameters vis-a-vis secondary metabolites in a traditional medicinal plant *Sida cordifolia* L. *Industrial Crops and Products, 194*, 116267. https://doi.org/10.1016/j.indcrop.2023.116267

Antenozio, M. L., Caissutti, C., Caporusso, F. M., Marzi, D., & Brunetti, P. (2024). Urban Air Pollution and Plant Tolerance: Omics Responses to Ozone, Nitrogen Oxides, and Particulate Matter. *Plants, 13*(15), 2027. https://doi.org/10.3390/plants13152027

Aranda-Rivera, A. K., Cruz-Gregorio, A., Arancibia-Hernández, Y. L., Hernández-Cruz, E. Y., & Pedraza-Chaverri, J. (2022). RONS and Oxidative Stress: An Overview of Basic Concepts. *Oxygen*, *2*(4), 437–478. https://doi.org/10.3390/oxygen2040030

Baier, M., Kandlbinder, A., Golldack, D., & Dietz, K-J. (2005). Oxidative stress and ozone: perception, signalling and response. *Plant, Cell & Environment, 28*(8), 1012–1020. https://doi.org/10.1111/j.1365-3040.2005.01326.x

Bălă, G. P., Râjnoveanu, R. M., Tudorache, E., Motișan, R., & Oancea, C. (2021). Air pollution exposure-the (in)visible risk factor for respiratory diseases. *Environmental science and pollution research international, 28*(16), 19615–19628. https://doi.org/10.1007/s11356-021-13208-x

Bartoli, G., Forino, L. M. C., Tagliasacchi, A. M., & Durante, M. (2013). Cell death induced by ozone stress in the leaves of *Populus deltoides* × *maximowiczii*. *Biologia Plantarum, 57*(3), 514–524. https://doi.org/10.1007/s10535-013-0315-3

Bernhard, G. H., Bais, A. F., Aucamp, P. J., Klekociuk, A. R., Liley, J. B., & McKenzie, R. L. (2023). Stratospheric ozone, UV radiation, and climate interactions. *Photochemical & photobiological sciences: Official journal of the European Photochemistry Association and the European Society for Photobiology, 22*(5), 937–989. https://doi.org/10.1007/s43630-023-00371-y

Bharath, P., Gahir, S., & Raghavendra, A. S. (2021). Abscisic Acid-Induced Stomatal Closure: An Important Component of Plant Defense Against Abiotic and Biotic Stress. *Frontiers in Plant Science, 12*, 615114. https://doi.org/10.3389/fpls.2021.615114

Cadar, N., Pitar, D., Iacoban, C., & Cântar, I.-C. (2023). The influence of forests from Lunca Mureșului Natural Park on greenhouse gases levels. *Scientific Papers. Series E. Land Reclamation, Earth Observation & Surveying, Environmental Engineering, 12*, 31–37.

Cannea, F. B., & Padiglia, A. (2025). Antioxidant Defense Systems in Plants: Mechanisms, Regulation, and Biotechnological Strategies for Enhanced Oxidative Stress Tolerance. *Life, 15*(8), 1293. https://doi.org/10.3390/life15081293

Černý, M., Habánová, H., Berka, M., Luklová, M., & Brzobohatý, B. (2018). Hydrogen Peroxide: Its Role in Plant Biology and Crosstalk with Signalling Networks. *International journal of molecular sciences, 19*(9), 2812. https://doi.org/10.3390/ijms19092812

Chen, G., Shi, Y., Shen, X., Zhang, Y., Lu, X., Li, Y., Jin, C., Wang, J., & Wu, J. (2022). Guard cell anion channel PbrSLAC1 regulates stomatal closure through PbrSnRK2.3 protein kinases. *Plant science: an international journal of experimental plant biology, 325*, 111487. https://doi.org/10.1016/j.plantsci.2022.111487

Chipperfield, M. P., & Bekki, S. (2024). Opinion: Stratospheric Ozone – Depletion, Recovery and New Challenges. *Atmospheric Chemistry and Physics, 24*(4), 2783–2802. https://doi.org/10.5194/acp-24-2783-2024

Cun, Z., Wu, H. M., Zhang, J. Y., Shuang, S. P., Hong, J., & Chen, J. W. (2022). Responses of Linear and Cyclic Electron Flow to Nitrogen Stress in an N-Sensitive Species Panax notoginseng. *Frontiers in plant science, 13*, 796931. https://doi.org/10.3389/fpls.2022.796931

Deng, Y. N., Kashtoh, H., Wang, Q., Zhen, G. X., Li, Q. Y., Tang, L. H., Gao, H. L., Zhang, C. R., Qin, L., Su, M., Li, F., Huang, X. H., Wang, Y. C., Xie, Q., Clarke, O. B., Hendrickson, W. A., & Chen, Y. H. (2021). Structure and activity of SLAC1 channels for stomatal signaling in leaves. *Proceedings of the National Academy of Sciences of the United States of America, 118*(18), e2015151118. https://doi.org/10.1073/pnas.2015151118

Dinakar, C., Vishwakarma, A., Raghavendr,a A. S., & Padmasree, K. (2016). Alternative Oxidase Pathway Optimizes Photosynthesis During Osmotic and Temperature Stress by Regulating Cellular ROS, Malate Valve and Antioxidative Systems. *Frontiers in Plant Science, 7*, 68. https://doi.org/10.3389/fpls.2016.00068

Donzelli, G., & Suarez-Varela, M. M. (2024). Tropospheric Ozone: A Critical Review of the Literature on Emissions, Exposure, and Health Effects. *Atmosphere, 15*(7), 779. https://doi.org/10.3390/atmos15070779

Elshafie, H. S., Camele, I., & Mohamed, A. A. (2023). A Comprehensive Review on the Biological, Agricultural and Pharmaceutical Properties of Secondary Metabolites Based-Plant Origin. *International journal of molecular sciences, 24*(4), 3266. https://doi.org/10.3390/ijms24043266

Faoro, F., & Iriti, M. (2009). Plant cell death and cellular alterations induced by ozone: key studies in Mediterranean conditions. *Environmental pollution, 157*(5), 1470–1477. https://doi.org/10.1016/j.envpol.2008.09.026

Gomes, M. P., Kitamura, R. S. A., Marques, R. Z., Barbato, M. L., & Zámocký, M. (2022). The Role of $H_2O_2$-Scavenging Enzymes (Ascorbate Peroxidase and Catalase) in the Tolerance of Lemna minor to Antibiotics: Implications for Phytoremediation. *Antioxidants (Basel, Switzerland), 11*(1), 151. https://doi.org/10.3390/antiox11010151.

Grantz, D. A., & Vu, H. B. (2012). Root and shoot gas exchange respond additively to moderate ozone and methyl jasmonate without induction of ethylene: ethylene is induced at higher $O_3$ concentrations. *Journal of experimental botany, 63*(11), 4303–4313. https://doi.org/10.1093/jxb/ers128

Gu, X., Fu, X., Ma, D., Yan, Y., Zheng, Y., Guo, L., & Li, C. (2025). Ground-level ozone stress in medicinal plants: response mechanisms and adaptive strategies. Medicinal *Plant Biology, 4*, e039. https://doi.org/10.48130/mpb-0025-0036

Günthardt-Goerg, M. S., Schläpfer, R., & Vollenweider, P. (2023). Responses to Airborne Ozone and Soilborne Metal Pollution in Afforestation Plants with Different Life Forms. *Plants (Basel, Switzerland), 12*(16), 3011. https://doi.org/10.3390/plants12163011

Guo, C., Wang, X., Wang, Q., Zhao, Z., Xie, B., Xu, L., & Zhang, R. (2024). Plant defense mechanisms against ozone stress: Insights from secondary metabolism. *Environmental and Experimental Botany, 217*, 105553. https://doi.org/10.1016/j.envexpbot.2023.105553

Guo, H., Sun, Y., Yan, H., Li, C., & Ge, F. (2018). $O_3$-Induced Leaf Senescence in Tomato Plants Is Ethylene Signaling-Dependent and Enhances the Population Abundance of *Bemisia tabaci*. *Frontiers in Plant Science, 9*, 764. https://doi.org/10.3389/fpls.2018.00764

Guo, H., Sun, Y., Yan, H., Li, C., & Ge, F. (2020). $O_3$-Induced Priming Defense Associated with the Abscisic Acid Signaling Pathway Enhances Plant Resistance to *Bemisia tabaci*. *Frontiers in Plant Science, 11*, 93. https://doi.org/10.3389/fpls.2020.00093

Han, Y. J., Beck, W., Mewis, I., Förster, N., & Ulrichs, C. (2023). Effect of Ozone Stresses on Growth and Secondary Plant Metabolism of *Brassica campestris* L. ssp. chinensis. *Horticulturae 9*(9), 966. https://doi.org/10.3390/horticulturae9090966

Hasan, M. M., Rahman, M. A., Skalicky, M., Alabdallah, N. M., Waseem, M., Jahan, M. S., Ahammed, G. J., El-Mogy, M. M., El-Yazied, A. A., Ibrahim, M. F. M., & Fang, X. W. (2021). Ozone Induced Stomatal Regulations, MAPK and Phytohormone Signaling in Plants. *International journal of molecular sciences, 22*(12), 6304. https://doi.org/10.3390/ijms22126304.

Hasanuzzaman, M., Bhuyan, M. H. M. B., Zulfiqar, F., Raza, A., Mohsin, S. M., Mahmud, J. A., Fujita, M., & Fotopoulos, V. (2020). Reactive Oxygen Species and Antioxidant Defense in Plants under Abiotic Stress: Revisiting the Crucial Role of a Universal Defense Regulator. *Antioxidants (Basel, Switzerland), 9*(8), 681. https://doi.org/10.3390/antiox9080681

Huang, S., Wang, H., Liu, S., Lu, S., Hua, J., & Zou, B. (2025). Ethylene antagonizes ABA and inhibits stomatal closure and chilling tolerance in rice. *Journal of experimental botany, 76*(17), 5011–5024. https://doi.org/10.1093/jxb/eraf052

Huot, B., Yao, J., Montgomery, B. L., & He, S. Y. (2014). Growth-defense tradeoffs in plants: a balancing act to optimize fitness. *Molecular plant, 7*(8), 1267–1287. https://doi.org/10.1093/mp/ssu049.

Jagodzik, P., Tajdel-Zielinska, M., Ciesla, A., Marczak, M., & Ludwikow, A. (2018). Mitogen-Activated Protein Kinase Cascades in Plant Hormone Signaling. *Frontiers in Plant Science, 9*, 1387. https://doi.org/10.3389/fpls.2018.01387

Jan, R., Asaf, S., Numan, M., Lubna, & Kim, K.-M. (2021). Plant Secondary Metabolite Biosynthesis and Transcriptional Regulation in Response to Biotic and Abiotic Stress Conditions. *Agronomy, 11*(5), 968. https://doi.org/10.3390/agronomy11050968

Jangpangi, D., Patni, B., Chandola, V., & Chandra, S. (2025). Medicinal plants in a changing climate: understanding the links between environmental stress and secondary metabolite synthesis. *Frontiers in Plant Science, 16*, 1587337. https://doi.org/10.3389/fpls.2025.1587337.

Jiang, Z., van Zanten, M., & Sasidharan, R. (2025). Mechanisms of plant acclimation to multiple abiotic stresses. *Communications Biology, 8*, 655. https://doi.org/10.1038/s42003-025-08077-w

Jin, Z., Tan, J., Zhang, X., Li, X., Guan, W., Liu, P., & Chen, A. (2025). Ozone Treatment Modulates Reactive Oxygen Species Metabolism Regulation and Enhances Storage Quality of Kiwifruit During Cold Storage. *Horticulturae 11*(8), 911. https://doi.org/10.3390/horticulturae11080911

Kangasjärvi, J., Jaspers, P., & Kollist, H. (2005). Signalling and cell death in ozone-exposed plants. *Plant, Cell & Environment, 28*(8), 1021–1036. https://doi.org/10.1111/j.1365-3040.2005.01325.x

Kashtoh, H., & Baek, K.-H. (2021). Structural and Functional Insights into the Role of Guard Cell Ion Channels in Abiotic Stress-Induced Stomatal Closure. *Plants, 10*(12), 2774. https://doi.org/10.3390/plants10122774

Keutgen, A. J., & Pawelzik, E. (2008). Apoplastic antioxidative system responses to ozone stress in strawberry leaves. *Journal of plant physiology, 165*(8), 868–875. https://doi.org/10.1016/j.jplph.2007.06.012

Kim, S. Y., Kim, E., & Kim, W. J. (2020). Health Effects of Ozone on Respiratory Diseases. *Tuberculosis and respiratory diseases, 83(Supple 1)*, S6–S11. https://doi.org/10.4046/trd.2020.0154

Kisiriko, M., Anastasiadi, M., Terry, L. A., Yasri, A., Beale, M. H., & Ward, J. L. (2021). Phenolics from Medicinal and Aromatic Plants: Characterisation and Potential as Biostimulants and Bioprotectants. *Molecules (Basel, Switzerland), 26*(21), 6343. https://doi.org/10.3390/molecules26216343

Lee, J. K., Kwak, M. J., Park, S. H., Kim, H. D., Lim, Y. J., Jeong, S. G., Choi, Y. S., & Woo, S. Y. (2021). Ozone Response of Leaf Physiological and Stomatal Characteristics in *Brassica juncea* L. at Supraoptimal Temperatures. *Land, 10*(4), 357. https://doi.org/10.3390/land10040357

Leppälä, J., Gaupels, F., Xu, E., Morales, L. O., Durner, J., & Brosché, M. (2022). Ozone and nitrogen dioxide regulate similar gene expression responses in Arabidopsis but natural variation in the extent of cell death is likely controlled by different genetic loci. *Frontiers in Plant Science, 13*, 994779. https://doi.org/10.3389/fpls.2022.994779

Li, C., Xu, M., Cai, X., Han, Z., Si J., & Chen, D. (2022). Jasmonate Signaling Pathway Modulates Plant Defense, Growth, and Their Trade-Offs. *International journal of molecular sciences, 23*(7), 3945. https://doi.org/10.3390/ijms23073945

Li, J., Yang, S., Wu, Y., Wang, R., Liu, Y., Liu, J., Ye, Z., Tang, R., Whiteway, M., Lv, Q., & Yan, L. (2024). Alternative Oxidase: From Molecule and Function to Future Inhibitors. *ACS omega, 9*(11), 12478–12499. https://doi.org/10.1021/acsomega.3c09339

Lin, L., Wu, J., Jiang, M., & Wang, Y. (2021). Plant Mitogen-Activated Protein Kinase Cascades in Environmental Stresses. *International journal of molecular sciences, 22*(4), 1543. https://doi.org/10.3390/ijms22041543

Liu, Y., & Zhang, S. (2004). Phosphorylation of 1-aminocyclopropane-1-carboxylic acid synthase by MPK6, a stress-responsive mitogen-activated protein kinase, induces ethylene biosynthesis in Arabidopsis. *The Plant cell, 16*(12), 3386–3399. https://doi.org/10.1105/tpc.104.026609

Ludwikow, A., & Sadowski, J. (2008). Gene networks in plant ozone stress response and tolerance. *Journal of integrative plant biology, 50*(10), 1256–1267. https://doi.org/10.1111/j.1744-7909.2008.00738.x

Majeed, Y., Zhu, X., Zhang, N., Ul-Ain, N., Raza, A., Haider, F. U., & Si, H. (2023). Harnessing the role of mitogen-activated protein kinases against abiotic stresses in plants. *Frontiers in plant science, 14*, 932923. https://doi.org/10.3389/fpls.2023.932923

Manbir, Singh, P., Kumari, A., & Gupta, K. J. (2022). Alternative oxidase plays a role in minimizing ROS and RNS produced under salinity stress in Arabidopsis thaliana. *Physiologia plantarum, 174*(2), e13649. https://doi.org/10.1111/ppl.13649

Manisalidis, I., Stavropoulou, E., Stavropoulos, A., & Bezirtzoglou, E. (2020). Environmental and Health Impacts of Air Pollution: A Review. *Frontiers in Public Health, 8*, 14. https://doi.org/10.3389/fpubh.2020.00014

McAdam, E. L., Brodribb, T. J., & McAdam, S. A. (2017). Does ozone increase ABA levels by non-enzymatic synthesis causing stomata to close? *Plant, cell & environment, 40*(5), 741–747. https://doi.org/10.1111/pce.12893

Mishra, N., Jiang, C., Chen, L., Paul, A., Chatterjee, A., & Shen, G. (2023). Achieving abiotic stress tolerance in plants through antioxidative defense mechanisms. *Frontiers in Plant Science, 14*, 1110622. https://doi.org/10.3389/fpls.2023.1110622

Modesti, M., Marchica, A., Pisuttu, C., Risoli, S., Pellegrini, E., Bellincontro, A., Mencarelli, F., Tonutti, P., & Nali, C. (2023). Ozone-Induced Biochemical and Molecular Changes in *Vitis vinifera* Leaves and Responses to *Botrytis cinerea* Infections. *Antioxidants, 12*(2), 343. https://doi.org/10.3390/antiox12020343

Montes, C. M., Demler, H. J., Li, S., Martin, D. G., & Ainsworth, E. A. (2022). Approaches to investigate crop responses to ozone pollution: from O3 -FACE to satellite-enabled modeling. *The Plant journal: for cell and molecular biology, 109*(2), 432–446. https://doi.org/10.1111/tpj.15501

Müller, M. (2021). Foes or Friends: ABA and Ethylene Interaction under Abiotic Stress. *Plants (Basel, Switzerland), 10*(3), 448. https://doi.org/10.3390/plants10030448

Munemasa, S., Hauser, F., Park, J., Waadt, R., Brandt, B., & Schroeder, J. I. (2015). Mechanisms of abscisic acid-mediated control of stomatal aperture. *Current opinion in plant biology, 28*, 154–162. https://doi.org/10.1016/j.pbi.2015.10.010.

Nazari, M., Kordrostami, M., Ghasemi-Soloklui, A. A., Eaton-Rye, J. J., Pashkovskiy, P., Kuznetsov, V., & Allakhverdiev, S. I. (2024). Enhancing Photosynthesis and Plant Productivity through Genetic Modification. *Cells, 13*(16), 1319. https://doi.org/10.3390/cells13161319

Ninkuu, V., Aluko, O. O., Yan, J., Zeng, H., Liu, G., Zhao, J., Li, H., Chen, S., & Dakora, F. D. (2025). Phenylpropanoids metabolism: recent insight into stress tolerance and plant development cues. *Frontiers in plant science, 16*, 1571825. https://doi.org/10.3389/fpls.2025.1571825

Nomura, T., Ogita, S., & Kato, Y. (2018). Rational metabolic-flow switching for the production of exogenous secondary metabolites in bamboo suspension cells. *Scientific reports, 8*(1), 13203. https://doi.org/10.1038/s41598-018-31566-4

Nowroz, F., Hasanuzzaman, M., Siddika, A., Parvin, K., Caparros, P. G., Nahar, K., & Prasad, P. V. V. (2024). Elevated tropospheric ozone and crop production: potential negative effects and plant defense mechanisms. *Frontiers in plant science, 14*, 1244515. https://doi.org/10.3389/fpls.2023.1244515.

Panda, S. K., Gupta, D., Patel, M., Vyver, C. V. D., & Koyama, H. (2024). Functionality of Reactive Oxygen Species (ROS) in Plants: Toxicity and Control in Poaceae Crops Exposed to Abiotic Stress. *Plants, 13*(15), 2071. https://doi.org/10.3390/plants13152071

Pant, P., Pandey, S., & Dall'Acqua, S. (2021). The Influence of Environmental Conditions on Secondary Metabolites in Medicinal Plants: A Literature Review. *Chemistry & biodiversity, 18*(11), e2100345. https://doi.org/10.1002/cbdv.202100345

Piechowiak, T., Kapusta, I., Rak, M., & Balawejder, M. (2026). Ozone Treatment Enhances Antioxidant Status and Energy Metabolism in Radish (*Raphanus sativus*) Sprouts. *Food and Bioprocess Technology, 19*, 52. https://doi.org/10.1007/s11947-025-04157-1.

Podgórska, A., Burian, M., & Szal, B. (2017). Extra-Cellular But Extra-Ordinarily Important for Cells:

Apoplastic Reactive Oxygen Species Metabolism. *Frontiers in Plant Science, 8*, 1353. https://doi.org/10.3389/fpls.2017.01353

Poór, P. (2020). Effects of Salicylic Acid on the Metabolism of Mitochondrial Reactive Oxygen Species in Plants. *Biomolecules, 10*(2), 341. https://doi.org/10.3390/biom10020341

Rajput, V. D., Harish Singh, R. K., Verma, K. K., Sharma, L., Quiroz-Figueroa, F. R., Meena, M., Gour, V. S., Minkina, T., Sushkova, S., & Mandzhieva, S. (2021). Recent Developments in Enzymatic Antioxidant Defence Mechanism in Plants with Special Reference to Abiotic Stress. *Biology, 10*(4), 267. https://doi.org/10.3390/biology10040267

Ramya, A., Dhevagi, P., Priyatharshini, S., Saraswathi, R., Avudainayagam, S., & Venkataramani, S. (2021). Response of rice (*Oryza sativa* L.) cultivars to elevated ozone stress. *Environmental monitoring and assessment, 193*(12), 808. https://doi.org/10.1007/s10661-021-09595-w

Rao, M. J., Duan, M., Zhou, C., Jiao, J., Cheng, P., Yang, L., Wei, W., Shen, Q., Ji, P., Yang, Y., Conteh, O., Yan, D., Yuan, H., Rauf, A., Ai, J., & Zheng, B. (2025). Antioxidant Defense System in Plants: Reactive Oxygen Species Production, Signaling, and Scavenging During Abiotic Stress-Induced Oxidative Damage. *Horticulturae, 11*(5), 477. https://doi.org/10.3390/horticulturae11050477

Rao, M. V., Lee, H., Creelman, R. A., Mullet, J. E., & Davis, K. R. (2000). Jasmonic acid signaling modulates ozone-induced hypersensitive cell death. *The Plant cell, 12*(9), 1633–1646. https://doi.org/10.1105/tpc.12.9.1633

Rebouças, D. M., De Sousa, Y. M., Bagard, M., Costa, J. H., Jolivet, Y., De Melo, D. F., & Repellin, A. (2017). Combined Effects of Ozone and Drought on the Physiology and Membrane Lipids of Two Cowpea (*Vigna unguiculata* (L.) Walp) Cultivars. *Plants, 6*(1), 14. https://doi.org/10.3390/plants6010014

Rehman, M., Saeed, M. S., Fan, X., Salam, A., Munir, R., Yasin, M. U., Khan, A. R., Muhammad, S., Ali, B., Ali, I., Khan, J., & Gan, Y. (2023). The Multifaceted Role of Jasmonic Acid in Plant Stress Mitigation: An Overview. *Plants, 12*(23), 3982. https://doi.org/10.3390/plants12233982

Sachdev, S., Ansari, S. A., Ansari, M. I., Fujita, M., & Hasanuzzaman, M. (2021). Abiotic Stress and Reactive Oxygen Species: Generation, Signaling, and Defense Mechanisms. *Antioxidants (Basel, Switzerland), 10*(2), 277. https://doi.org/10.3390/antiox10020277

Sadowska-Bartosz, I., & Bartosz, G. (2024). Antioxidant Activity of Anthocyanins and Anthocyanidins: A Critical Review. *International Journal of Molecular Sciences, 25*(22), 12001. https://doi.org/10.3390/ijms252212001

Saito, S., & Uozumi, N. (2019). Guard Cell Membrane Anion Transport Systems and Their Regulatory Components: An Elaborate Mechanism Controlling Stress-Induced Stomatal Closure. *Plants (Basel, Switzerland), 8*(1), 9. https://doi.org/10.3390/plants8010009

Serrano-Mislata, A., Hernández-García, J., de Ollas, C., Blanco-Touriñán, N., Jurado-García, S., Úrbez, C., Gómez-Cadenas, A., Sablowski, R., Alabadí, D., & Blázquez, M. A. (2025). Growth arrest is a DNA damage protection strategy in Arabidopsis. *Nature communications, 16*(1), 5635. https://doi.org/10.1038/s41467-025-60733-1

Shapiguzov, A., Vainonen, J. P., Wrzaczek, M., & Kangasjärvi, J. (2012). ROS-talk - how the apoplast, the chloroplast, and the nucleus get the message through. *Frontiers in plant science, 3*, 292. https://doi.org/10.3389/fpls.2012.00292

Shi, X., & Bloom, A. (2021). Photorespiration: The Futile Cycle? *Plants (Basel, Switzerland), 10*(5), 908. https://doi.org/10.3390/plants10050908

Simin, T., Ryalls, J. M. W., Welling, O. E. I., Girling, R. D., Mullinger, N. J., & Blande, J. D. (2026). Between-plant interactions in Scots pine are not impaired by air pollutants. *Communications Earth & Environment, 7*, 152. https://doi.org/10.1038/s43247-025-03175-3

Smith, K., Strand, D. D., Kramer, D. M., & Walker, B. J. (2024). The role of photorespiration in preventing feedback regulation via ATP synthase in Nicotiana tabacum. *Plant, cell & environment, 47*(2), 416–428. https://doi.org/10.1111/pce.14759

Song, Z., Zhao, L., Ma, W., Peng, Z., Shi, J., Pan, F., Gao, Y., Sui, X., Rengel, Z., Chen, Q., & Wang, B. (2023). Ethylene inhibits ABA-induced stomatal closure via regulating NtMYB184-mediated flavonol biosynthesis in tobacco. *Journal of experimental botany, 74*(21), 6735–6748. https://doi.org/10.1093/jxb/erad308

Stoykova, S., Dermendzhieva, D., Kostadinova, G., Ivanova, M., Stoyanov, M., Petkov, G., Dospatliev, L., & Beev, G. (2025). Ambient air pollution: a global health crisis. Scientific Papers. *Series E. Land Reclamation, Earth Observation & Surveying, Environmental Engineering, 14*, 472–485.

Sun, T., & Zhang, Y. (2022). MAP kinase cascades in plant development and immune signaling. *EMBO reports, 23*(2), e53817. https://doi.org/10.15252/embr.202153817

Sunil, B., Saini, D., Bapatla, R. B., Aswani, V., & Raghavendra, A. S. (2019). Photorespiration is complemented by cyclic electron flow and the alternative oxidase pathway to optimize photosynthesis and protect against abiotic stress. *Photosynthesis research, 139*(1-3), 67–79. https://doi.org/10.1007/s11120-018-0577-x

Tamaoki, M. (2008). The role of phytohormone signaling in ozone-induced cell death in plants. *Plant Signaling & Behavior, 3*(3), 166–174. https://doi.org/10.4161/psb.3.3.5538

Upadhyay, V., Choudhary, K. K., Agrawal, M., & Agrawal, S. B. (2025). Biochar modulates morphophysiological traits and yield stability in *Phaseolus vulgaris* L. via biochemical adjustments under tropospheric Ozone stress. *Frontiers in Sustainable Food Systems, 9*, 1634511. https://doi.org/10.3389/fsufs.2025.1634511

Vahala, J., Keinänen, M., Schützendübel, A., Polle, A., & Kangasjärvi, J. (2003). Differential effects of

elevated ozone on two hybrid aspen genotypes predisposed to chronic ozone fumigation. Role of ethylene and salicylic acid. *Plant physiology, 132*(1), 196–205. https://doi.org/10.1104/pp.102.018630

Vahisalu, T., Puzõrjova, I., Brosché, M., Valk, E., Lepiku, M., Moldau, H., Pechter, P., Wang, Y. S., Lindgren, O., Salojärvi, J., Loog, M., Kangasjärvi, J., & Kollist, H. (2010). Ozone-triggered rapid stomatal response involves the production of reactive oxygen species, and is controlled by SLAC1 and OST1. *The Plant journal: for cell and molecular biology, 62*(3), 442–453. https://doi.org/10.1111/j.1365-313X.2010.04159.x

Vainonen, J. P., & Kangasjärvi, J. (2015). Plant signalling in acute ozone exposure. *Plant, cell & environment, 38*(2), 240–252. https://doi.org/10.1111/pce.12273

Vanlerberghe, G. C. (2013). Alternative oxidase: a mitochondrial respiratory pathway to maintain metabolic and signaling homeostasis during abiotic and biotic stress in plants. *International journal of molecular sciences, 14*(4), 6805–6847. https://doi.org/10.3390/ijms14046805

Vaultier, M-N., & Jolivet, Y. (2015). Ozone sensing and early signaling in plants: An outline from the cloud. *Environmental and Experimental Botany, 114*, 144–152. https://doi.org/10.1016/j.envexpbot.2014.11.012

Voss, I., Sunil, B., Scheibe, R., & Raghavendra, A. S. (2013). Emerging concept for the role of photorespiration as an important part of abiotic stress response. *Plant biology (Stuttgart, Germany), 15*(4), 713–722. https://doi.org/10.1111/j.1438-8677.2012.00710.x

Wang, M., Xie, S., Lun, X., He, Z., Liu, X., Lv, W., Wang, L., Wang, T., & Liu, J. (2024). Exploring the Effects of Elevated Ozone Concentration on Physiological Processes in Summer Maize in North China Based on Exposure–Response Relationships. *Atmosphere, 15*(6), 639. https://doi.org/10.3390/atmos15060639

Wang, S., Li, W., Wufuer, R., Duo, J., Pei, L., & Pan, X. (2023a). The Key Role of Cyclic Electron Flow in the Recovery of Photosynthesis in the Photobiont during Rehydration of the Lichen *Cladonia stellaris*. *Plants, 12*(23), 4011. https://doi.org/10.3390/plants12234011

Wang, Y., Niu, Y., Ye, L., Shi, Y., & Luo, A. (2023b). Ozone treatment modulates reactive oxygen species levels in kiwifruit through the antioxidant system: Insights from transcriptomic analysis. *Journal of plant physiology, 291*, 154135. https://doi.org/10.1016/j.jplph.2023.154135

Wilkinson, S., & Davies, W. J. (2010). Drought, ozone, ABA and ethylene: new insights from cell to plant to community. *Plant, cell & environment, 33*(4), 510–525. https://doi.org/10.1111/j.1365-3040.2009.02052.x

Xu, E., Vaahtera, L., & Brosché, M. (2015). Roles of Defense Hormones in the Regulation of Ozone-Induced Changes in Gene Expression and Cell Death. *Molecular plant, 8*(12), 1776–1794. https://doi.org/10.1016/j.molp.2015.08.008

Xu, Y., Agathokleous, E., & Feng, Z. (2026). Elevated ozone severely damages stomata dynamics in hybrid poplar. *Journal of Forestry Research, 37*, 27. https://doi.org/10.1007/s11676-025-01966-0

Yadav, P., & Mina, U. (2022). Ozone stress responsive gene database (OSRGD ver. 1.1): a literature curated database for insight into plants' response to ozone stress. *Plant Gene, 31*, 100368. https://doi.org/10.1016/j.plgene.2022.100368

Yu, H., & Blande, J. D. (2022). A potential ozone defense in intercellular air space: Clues from intercellular BVOC concentrations and stomatal conductance. *The Science of the total environment, 852*, 158456. https://doi.org/10.1016/j.scitotenv.2022.158456

Zhou, Z., Zhi, T., Han, C., Peng, Z., Wang, R., Tong J., Zhu Q., & Ren C. (2020). Cell death resulted from loss of fumarylacetoacetate hydrolase in Arabidopsis is related to phytohormone jasmonate but not salicylic acid. *Scientific reports, 10*(1), 13714. https://doi.org/10.1038/s41598-020-70567-0

Zrimec, J., Correo, S., Zagorščak, M., Petek, M., Bleker, C., Stare, K., Schuy, C., Sonnewald, S., Gruden, K., & Nikoloski, Z. (2025). Evaluating plant growth–defense trade-offs by modeling the interaction between primary and secondary metabolism. *Proceedings of the National Academy of Sciences of the United States of America, 122*(32), e2502160122. https://doi.org/10.1073/pnas.2502160122.

Scientific Papers. Series E. Land Reclamation, Earth Observation & Surveying, Environmental Engineering. Vol. XV, 2026
Print ISSN 2285-6064, CD-ROM ISSN 2285-6072, Online ISSN 2393-5138, ISSN-L 2285-6064

# PHYSICOCHEMICAL STABILITY AND EMULSIFYING ACTIVITY OF A BIOSURFACTANT OF SALINE ORIGIN

**Simona NEAGU, Mihaela Marilena STANCU**

Institute of Biology Bucharest of Romanian Academy, 296 Splaiul Independentei, District 6, Bucharest, P.O. Box 56-53, Romania

Corresponding author emails: simona.neagu@ibiol.ro, mihaela.stancu@ibiol.ro

***Abstract***

*Biosurfactants produced by microorganisms from saline environments have attracted increasing interest due to their potential to remain functional under conditions that limit the efficiency of chemical surfactants. The aim of the present study was to evaluate the physicochemical stability and emulsifying activity of a crude biosurfactant produced by a bacterial isolate from the Techirghiol saline lake. The experimental design included testing the biosurfactant at different pH values, NaCl concentrations, and temperatures, by determining the emulsification index at 24 h. Emulsifying performance was further evaluated in a simplified diesel-contaminated saline-water microcosm at different salinities. This study examines how the biosurfactant performs under high-salinity conditions and indicates potential value for hydrocarbon dispersion and microbial activity in saline environments.*

***Key words:*** *bacteria, biosurfactants, diesel, physicochemical stability, saline environments.*

## INTRODUCTION

Saline and hypersaline environments, from coastal salterns and salt lakes to industrial brines, are increasingly exposed to hydrocarbon contamination associated with oil extraction, transportation, and refining activities. In such ecosystems, high ionic strength and reduced water activity may limit the effectiveness of conventional chemical surfactants and hinder the natural attenuation of petroleum hydrocarbons. Therefore, halophilic and halotolerant microorganisms represent promising sources of surface-active compounds capable of retaining functionality under high salinity, as well as under pH and temperature conditions that inhibit many traditional surfactant-producing organisms (Edbeib et al., 2016).

Microbial biosurfactants decrease surface and interfacial tension and facilitate the emulsification of hydrophobic compounds, including petroleum hydrocarbons. This process enhances dispersion in aqueous environments and can increase substrate bioavailability for microbial degradation. Biosurfactants comprise a structurally diverse group of molecules, predominantly glycolipids, lipopeptides, and phospholipids, whereas high molecular weight bioemulsifiers primarily contribute to emulsion stabilization rather than lowering surface tension (Silva et al., 2022).

Many biosurfactants are biodegradable and exhibit relatively low toxicity. Moreover, they can remain active under environmental conditions in which certain synthetic surfactants show reduced performance. These features support their potential application in bioremediation, enhanced oil recovery, and the treatment of petroleum hydrocarbon-contaminated water (Sun et al., 2018; Ali et al., 2021; Lima et al., 2024).

Biosurfactants produced by isolates obtained from petroleum-impacted environments (e.g., soils and related sites) have been described to retain surface activity and emulsification capacity under high-salinity conditions (Sun et al., 2018; Ali et al., 2021; Silva et al., 2022). Similarly, investigations of biosurfactants derived from halophilic microorganisms indicate that these compounds can remain functional in saline conditions, although performance may vary depending on the producing strain and the biosurfactant class (Gomes et al., 2018; Barakat et al., 2017; Waghmode et al., 2019; Wu et al., 2022). Recent studies on diesel-contaminated saline soils further demonstrate that the addition of

biosurfactants can improve hydrocarbon removal under salinity stress (Barzegar et al., 2025). Together with similar reports, these findings highlight the biotechnological potential of halophilic or halotolerant microorganisms from saline environments, which are comparatively less explored than marine ecosystems.

Despite progress in this field, stability is not always evaluated using approaches that reliably predict performance under application-relevant conditions. In several studies, surface tension reduction is considered the primary indicator of stability, whereas assays involving petroleum-derived substrates are performed separately or with limited methodological integration. Consequently, establishing a direct link between reported physicochemical stability and actual functional performance in saline systems remains challenging.

In this context, the present study investigates a selected halotolerant isolate and its crude biosurfactant. The specific objectives were: (i) to evaluate the stability of the crude biosurfactant under different pH values, temperatures, and NaCl concentrations using the emulsification index, and (ii) to assess its diesel emulsification performance in simplified saline-water microcosm systems.

## MATERIALS AND METHODS

### Sampling and bacterial isolation

Water and mud samples used in this study were collected in summer 2024 from Lake Techirghiol (Latitude: 44.05318° N, Longitude: 28.60330° E), located in Constanța County, Romania. Surface water was sampled in sterile containers, and bottom mud was collected from a depth of 10 cm using a sterile spatula. Samples were kept in an icebox during transport and transferred directly to the laboratory for further analysis.

The isolation medium used for the bacteria included in this study was prepared according to Ventosa et al. (1982), with minor modifications, and had the following composition (g/L): $MgSO_4$ 1.0, $CaCl_2 \cdot 2H_2O$ 0.36, KCl 2.0, $NaHCO_3$ 0.06, NaCl 100, peptone 5.0, glucose 1.0, yeast extract 10.0, and agar 20.0.

Serial decimal dilutions ($10^{-1}$-$10^{-3}$) of the water and mud samples were prepared in sterile saline solution (5% NaCl, w/v) and inoculated onto the same agar medium (10% NaCl) by the pour plate method (Sanders, 2012). Briefly, 1.0 mL of each dilution was transferred to sterile Petri dishes and mixed with molten agar medium. The plates were incubated aerobically at 30°C for 5-7 days. The number of viable microorganisms was expressed as CFU/mL for water and CFU/g for the mud sample. Representative colonies were purified by repeated streaking on solid isolation agar until morphologically uniform growth was obtained. Isolates with distinct colony morphologies were routinely cultivated on Luria-Bertani (LB) (Sezonov et al., 2007) medium supplemented with 5% (w/v) NaCl. Stocks were prepared in glycerol and stored at −80°C.

Chloride concentration was determined by argentometric titration using the Mohr method (Hauser, 2002).

### Biosurfactant screening and assays

Isolates were cultivated in LB broth supplemented with 5% (w/v) NaCl at 30°C under agitation (150 rpm) for 72 h. Following incubation, cultures were centrifuged (7500 rpm for 10 min), and the resulting cell-free supernatant (CFS) was collected for subsequent analyses as crude biosurfactant extract. Emulsifying capacity was evaluated by determining the 24 h emulsification index ($E_{24}$), in accordance with the protocol described by Stancu (2024). CFS was mixed with diesel fuel, vortexed (3 min), and left to stand at room temperature for 24 h. Positive and negative controls were included. Biosurfactant production was also analyzed using the CTAB (cetyltrimethylammonium bromide) agar plate method as described by Neagu & Stancu (2025). Cultures were spot-inoculated (20 µL) onto the CTAB agar, air-dried, and incubated at 30°C for 3-5 days. A dark blue halo around the colony was considered a positive reaction.

### Characterization of halotolerant bacteria

#### Phenotyping features and rep-PCR fingerprinting

The selected isolates were preliminarily characterized based on colony morphology on saline agar (cell shape, pigmentation, colony margin), Gram reaction, motility, growth temperature, growth on LB agar supplemented

with 0-20% (w/v) NaCl, as well as the basic biochemical traits, including catalase and oxidase activities. Growth on eosin methylene blue (EMB) agar was recorded as part of differential phenotypic profiling.

Diesel tolerance was evaluated using the hydrocarbon overlay agar method (Stancu, 2025). Cultures were spot-inoculated (20 µL) onto LB and minimal salt (MSM) agar (Stancu, 2023), air-dried, and overlaid with diesel for 2 h. After removal of the diesel, plates were incubated at 30°C for 1-5 days. Tolerance was assessed by comparing colony growth with the control (plates not exposed to diesel).

Genomic DNA was extracted from bacterial isolates using the PureLink Genomic DNA Kit (Invitrogen, Carlsbad, CA, USA). Repetitive extragenic palindromic polymerase chain reaction (REP-PCR) was performed using genomic DNA, the $(GTG)_5$ primer, and GoTaq G2 Flexi DNA polymerase (Promega, Madison, WI, USA) according to the method previously described (Stancu, 2015). PCR was performed in a Mastercycler pro S (Eppendorf, Germany) with initial denaturation at 94°C for 10 min, 35 cycles (94°C for 1 min, 52°C for 1 min, 65°C for 8 min), and a final extension at 65°C for 16 min. PCR products were separated by electrophoresis on 2.0% (w/v) agarose gels stained with SYBR Safe DNA Gel Stain (Invitrogen).

**Salt tolerance and physicochemical stability of the biosurfactant produced by T3 isolate**

For the salt tolerance assay, a fresh overnight culture was grown in LB broth with or without 1% (v/v) diesel, and HM broth (Ventosa et al., 1982) with 1% (v/v) diesel. Then, cultures were spot-inoculated (20 µL) onto the LB agar with 0, 5, 10, 15, and 20% NaCl (w/v) and incubated at 30°C for 72 h.

The physicochemical stability of the crude biosurfactant produced by isolate T3, was evaluated by measuring the $E_{24}$ after exposure to different temperature, pH, and salinity conditions. Thermal stability was assessed by incubating CFS aliquots at 20-100°C for 60 min, followed by cooling to room temperature. pH stability was tested over a range of pH 4-9, adjusted using 0.1 N HCl or 0.1 N NaOH. Salinity stability was examined by adjusting NaCl to final concentrations of 0-20% (w/v). After each treatment, emulsification activity ($E_{24}$) was determined. A negative control was prepared under identical conditions without CFS.

**Diesel emulsification in simplified saline-water microcosms**

Diesel emulsification was evaluated in simplified saline-water microcosms at different salinity levels. Microcosms were prepared by mixing CFS, sterile saline solution (0, 5, 10, 15, or 20% NaCl, w/v), and diesel fuel at a 2:2:1 (v/v/v) ratio. Samples were vortexed for 3 min and left for 24 h at room temperature, after which $E_{24}$ was recorded. A negative control was prepared under identical conditions without CFS.

## RESULTS AND DISCUSSIONS

Lake Techirghiol is located in Constanța County, southeastern Romania, in the coastal zone of the Black Sea. It is described as a unique Romanian ecosystem due to its hypersaline character and the high productivity associated with the formation of therapeutic sapropelic mud. Long-term records indicate pronounced variations in water level and salinity, while the lake remains highly mineralized overall (Barbulescu & Barbes, 2013).

The physicochemical data obtained indicate that Lake Techirghiol is a salt-rich environment with high ionic strength, providing favourable conditions for the growth of halophilic and halotolerant microorganisms. The pH of the water was 8.35, consistent with the alkaline profile reported for this lake (Maftei et al., 2020). The chloride ion concentration in the water and mud samples was 60 g/L and 25 g/L, respectively. Bacterial abundance in the water sample was $9.3 \times 10^3$ CFU/mL, in line with previous reports for Techirghiol surface water (Aonofriesei, 2007). The higher viable count in the mud sample ($1.1 \times 10^5$ CFU/g) suggests that sediment provides a more favorable environment for bacterial growth, likely due to its greater organic matter content and protective conditions against environmental stress.

**Biosurfactant screening** was first performed on thirty-six isolates obtained from water and mud samples using the diesel emulsification assay. The results showed that six (T1-T6) isolates

produced extracellular compounds with high emulsification capacity, as indicated by $E_{24}$ values ranging from 90% to 100% (Table 1, Figure 1a). The $E_{24}$ index reflects the stability of the hydrocarbon-water emulsion after 24 h; high values therefore indicate strong biosurfactant-producing ability. While other halophilic and halotolerant bacteria have been reported to produce emulsifying compounds, their $E_{24}$ values are generally lower and depend on the strain, hydrocarbon type, and assay conditions. For example, haloalkaliphilic *Bacillus* strains showed $E_{24}$ values of approximately 56-57% (Barakat et al., 2017), while similar values (~56%) were reported for halophilic isolates from saltern environments (Berberov et al., 2026). The high $E_{24}$ values obtained in the present study suggest that the halotolerant isolates produce extracellular surface-active compounds capable of stabilizing the water-diesel interface. In saline environments, the secretion of extracellular products can contribute to stress adaptation (e.g., biofilm formation, exopolysaccharide matrix development), while also facilitating interaction with hydrophobic compounds (Bhat & Roach, 2025; Berberov et al., 2026). In contrast, none of the isolates produced a detectable halo on CTAB agar, consistent with the absence of detectable rhamnolipid production.

**Characterization of halotolerant bacteria**
**Phenotyping features**

Six representative halotolerant isolates (T1-T6) were selected from Lake Techirghiol water and mud samples and subjected to preliminary phenotypic characterization, including some biochemical assays. The results are summarized in Table 1.

Table 1. Characterization of halotolerant bacterial isolates

| Characteristics | Isolate | | | | | |
|---|---|---|---|---|---|---|
| | **T1** | **T2** | **T3** | **T4** | **T5** | **T6** |
| **Biosurfactant** | | | | | | |
| Emulsification index ($E_{24}$, %) | 90 | 90 | 100 | 100 | 100 | 100 |
| CTAB agar | - | - | - | - | - | - |
| **Phenotypic** | | | | | | |
| Source of isolation - Techirghiol | water | water | Mud | water | water | water |
| Gram reaction | - | + | + | + | + | + |
| Cell shape | ND | ND | Rod | ND | ND | ND |
| Margin | regular | regular | Irregular | regular | regular | regular |
| Pigmentation | cream | cream | Cream | beige | beige | beige |
| Motility | ND | ND | + | ND | ND | ND |
| NaCl tolerance (0-20%) | 0-10% | 0-10% | 0-10% | 0-10% | 0-10% | 0-10% |
| Temperature growth (°C) | 30 | 30 | 30 | 30 | 30 | 30 |
| Catalase | - | + | + | - | - | - |
| Oxidase | + | + | + | + | + | + |
| Lactose fermentation (EMB) | - | - | - | - | - | - |
| **Diesel tolerance** | | | | | | |
| LB agar-diesel | + | + | + | + | + | + |
| MSM agar-diesel | - | +/- | +/- | - | - | - |
| **REP-PCR fingerprinting** (bp) | 200-3500 | 300-2000 | 200-1700 | 200-2800 | 200-3100 | 200-3100 |

(+) Positive reaction; (–) Negative reaction. Diesel tolerance (+) growth comparable to control; (+/-) reduced growth; (–) no growth

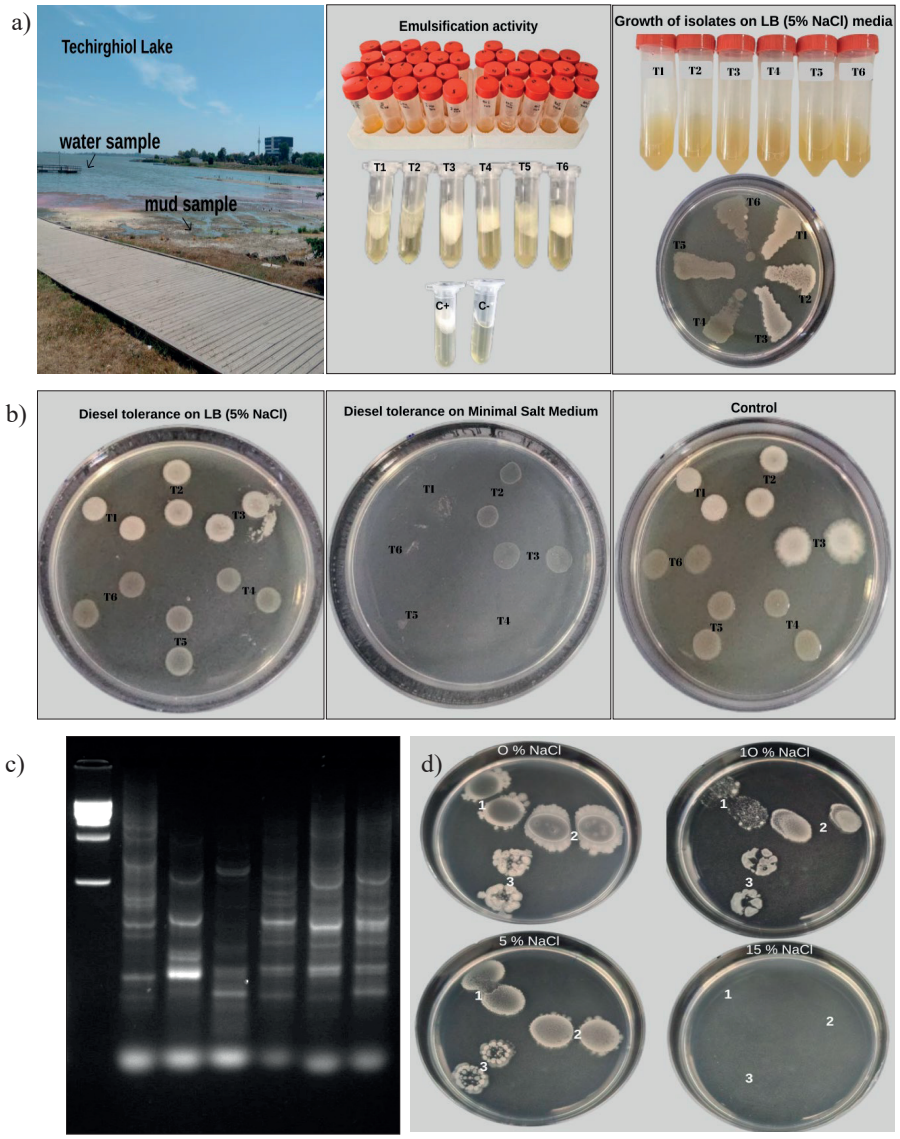



Figure 1. Isolation, screening and characterization of halotolerant bacteria
a) water and mud samples from Lake Techirghiol; emulsification activity of the CFS; isolates growth on LB-NaCl 5%; b) diesel tolerance of T1–T6 isolates on LB and MSM agars, as compared with control (LB agar); c) $(GTG)_5$ rep-PCR fingerprinting of T1–T6 isolates; 1 kb DNA ladder (M). d) Salt tolerance of T3 grown in LB broth (1), LB-diesel 1% (2), HM-diesel 1% (3)

T3 was isolated from Techirghiol mud, whereas T1, T2, T4, T5, and T6 were obtained from surface water. Gram staining revealed a differentiated profile among the isolates: T2, T3, T4, T5, and T6 were Gram-positive, whereas T1 was Gram-negative. Based on visual inspection, colony pigmentation was grouped into two categories: cream (T1-T3) and beige (T4-T6). Colony margins were predominantly regular, except for T3, which showed irregular margins. This isolate consisted of rod-shaped, motile cells. Salinity tolerance on LB agar was evaluated at 0%, 5%, 10%, 15%, and 20% (w/v) NaCl. Growth was robust up to 10% NaCl, whereas no colonies were observed at 15% or 20% NaCl, consistent with a halotolerant profile. All isolates grew at 30°C. On EMB agar, T2, T3 and T4 isolates showed no lactose-fermentation phenotype, indicating a lactose-negative reaction. In contrast, T1, T5, and T6 did not form colonies on this medium.

Diesel tolerance was observed for all six isolates on LB agar, as indicated by growth comparable to the control. In contrast, on MSM in the presence of diesel, only isolates T2 and T3 exhibited reduced growth, whereas T1 and T4-T6 showed no growth (Table 1, Figure 1b). Notably, isolates T1, T4, T5, and T6 failed to grow following hydrocarbon overlay, indicating strain-dependent differences under nutrient-limited conditions.

$(GTG)_5$ REP-PCR fingerprinting revealed distinct profiles for all selected isolates (Table 1, Figure 1c). The water-derived isolates (T1, T2, T4, T5, and T6) exhibited banding patterns ranging from approximately 200 to 3500 bp, whereas T3 displayed a narrower size range (approximately 200-1700 bp) and a clearly distinct fingerprinting. This distinct pattern indicates genetic variability among the isolates and highlights the divergent genomic profile of T3.

Overall, these findings suggest that biosurfactants produced by these halotolerant isolates exhibit properties that could be exploited for hydrocarbon bioremediation and the restoration of saline or contaminated soils, although further studies are needed to confirm their efficacy *in situ*.

**Salt tolerance and physicochemical stability of the biosurfactant produced by T3 isolate**

Based on its maximal $E_{24}$ and overall screening performance, T3 was selected for subsequent assays. Before evaluating the physicochemical stability of its biosurfactant, the salinity tolerance of T3 was assessed by spot growth on LB agar containing 0-20% (w/v) NaCl. The bacterium exhibited robust growth at 0-10% NaCl, whereas no growth was observed at 15% or 20% NaCl (Figure 1d). Colony morphology varied with the pre-culture medium, consistent with phenotypic adaptation (e.g., changes in cell-surface traits and extracellular polymers) rather than alteration in halotolerance.

The stability of the cell-free culture supernatant from T3 was subsequently evaluated under different temperature, pH, and salinity conditions after 60 minutes of exposure, using $E_{24}$ to quantify emulsification activity (Figure 2).

Thermal stability was tested between 20 and 100°C. Emulsification remained high at moderate temperatures, with $E_{24}$ values of 90-100% at 20-30°C and 80% at 40°C. Activity was still substantial at 50°C and 60°C (~73%), indicating notable heat tolerance. A sharp decline occurred at 80°C (~23%), and no emulsification was detected after exposure to 100°C, suggesting that prolonged heating severely impairs the biosurfactant's activity.

pH stability was evaluated from 4 to 9. The emulsification index remained high under acidic conditions, with $E_{24}$ values of ~93% at pH 4 to 5 and ~83.3% at pH 6. Activity decreased markedly at pH 7 (~27%) and remained low at pH 8 to 9 (~10%), indicating strong sensitivity around neutral to slightly alkaline pH values.

Salinity stability was tested by adjusting NaCl to final concentrations of 0-20% (w/v). $E_{24}$ values were maximal at 0-5% NaCl (100%) and decreased at 10% NaCl (80%), with complete loss of emulsification at 15-20% NaCl. These data suggest that the CFS from T3 is highly effective under moderate salinity, whereas higher salt concentrations significantly compromise its emulsifying performance.

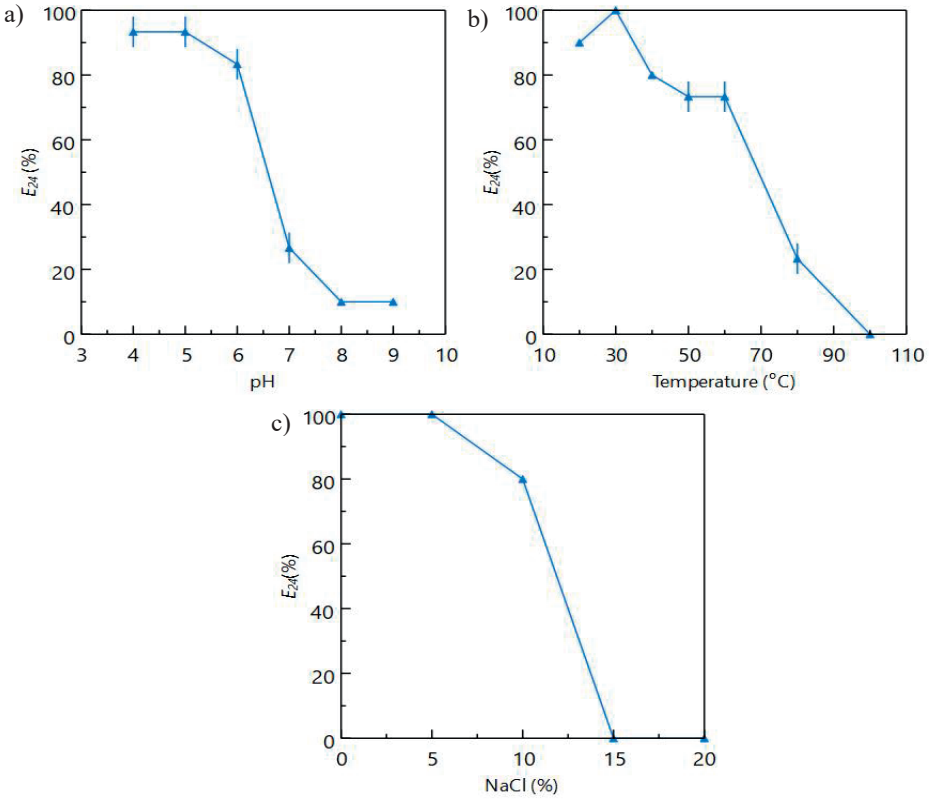



Figure 2. Physicochemical stability of the biosurfactant produced by T3 isolate
Biosurfactant stability under different (a) pH values (4-9); (b) temperatures (20-100°C); and (c) NaCl (5-20%) concentrations; error bars represent the standard deviation of n = 3 biological replicates

Our results further indicate that $E_{24}$ values obtained from crude CFS are strongly influenced by the producing strain and assay-specific parameters. Consequently, the apparent stability of CFS may vary substantially between studies, reflecting the influence of assay-specific parameters such as the nature of the hydrophobic phase, phase ratio, and exposure time (Qi et al., 2025).

**Diesel emulsification in simplified saline-water microcosms**

The $E_{24}$ stability assay showed how pH, temperature, and salinity affected the crude biosurfactant. To link these physicochemical stability results with functional behavior in saline systems, we further tested diesel emulsification in simplified saline-water microcosms at increasing NaCl concentrations (5-20%, w/v). The results showed that diesel emulsification by T3 CFS was strongly dependent on salinity. At 5% and 10% NaCl, emulsification was maximal ($E_{24}$ = 100%) (Figure 3).

In contrast, at 15% and 20% NaCl, no stable emulsion was detected ($E_{24}$ = 0%). Although the mechanism was not investigated, we did not observe visible precipitation in the 15% and 20% NaCl treatments, suggesting that the loss of emulsification was not associated with macroscopic precipitation of the active fraction. The obtained results are broadly consistent with the halotolerant growth profile of isolate T3, which showed robust growth up to 10% NaCl but not at 15-20% NaCl.

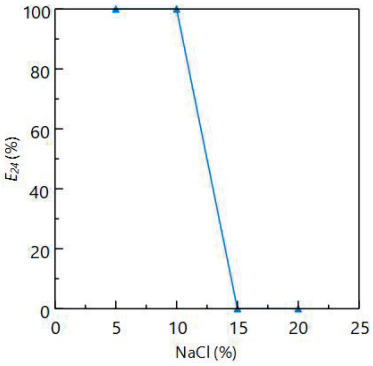



Figure 3. Diesel emulsification in simplified saline-water microcosms
Microcosm assay using diesel emulsification by T3 CFS at different NaCl concentrations (0-20%); data are presented as mean standard deviation of n = 3 biological replicates

Although biosurfactant production and emulsifying performance are not identical traits, the similar limits suggest adaptation to moderate salt levels. Thus, the crude biosurfactant is likely more suitable for low to moderately saline systems.

## CONCLUSIONS

The present work indicates that saline environments such as Lake Techirghiol host halotolerant bacteria capable of producing biosurfactants with strong diesel emulsification capacity. From the screened isolates, the cell-free supernatant of T3 showed an emulsifying activity profile that varied with pH and temperature, with high activity at moderate temperatures and acidic pH, but reduced activity at neutral to alkaline pH and after high-temperature exposure. Salinity-limited emulsification: activity remained maximal at 0-5% NaCl, decreased at 10% NaCl, and was lost at ≥15% NaCl. Importantly, the microcosm model showed the same overall trend, with stable diesel emulsification at 5-10% NaCl and no stable emulsion at 15-20% NaCl after 24 h.
In conclusion, these preliminary results suggest that the biosurfactant produced by the halotolerant isolate T3 may be useful for hydrocarbon dispersion in low to moderately saline waters or soils, as it may enhance diesel phase dispersion and potentially support the bioavailability of diesel-range hydrocarbons.

## ACKNOWLEDGEMENTS

The study was funded by project no. RO1567-IBB05/2026 from the Institute of Biology Bucharest of Romanian Academy.

## REFERENCES

Ali, F., Das, S., Hossain, T. J., Chowdhury, S. I., Ali, F., Das, S., Hossain, T. J., Chowdhury, S. I., Zedny, S. A., Das, T., Ahmed Chowdhury, M. N., & Uddin, M. S. (2021). Production optimization, stability and oil emulsifying potential of biosurfactants from selected bacteria isolated from oil-contaminated sites. *R. Soc. Open Sci.*, *8*, 211003.

Aonofriesei, F. (2007). Abundance and activity of heterotrophic bacterial community in the water column and sediments of Tekirghiol Lake. *Proceedings of the Romanian Academy, Series B*, (1), 3–10.

Barakat, K. M., Hassan, S. W. M., & Darwesh, O. M. (2017). Biosurfactant production by haloalkaliphilic *Bacillus* strains isolated from Red Sea, Egypt. *Egyptian Journal of Aquatic Research*, *43*(3), 205–211.

Barbulescu, A., & Barbes, L. (2013). Assessment of Techirghiol Lake surface water quality using statistical analysis. *Revista de Chimie (Bucharest), 64*(8).

Barzegar, G., Jorfi, S., Sanaei, D., Rezaei, M., Jokar, R., Sharifan, H., Jafari, K., & Biswas, J. K. (2025). Bioremediation of diesel-contaminated saline soil and enhancement of microbial salinity tolerance by a biosurfactant-producing *Bacillus subtilis* AHVKH11 and external surfactant application: bio-toxicity assessment. *Scientific Reports*, *15*, 20673.

Berberov, K., Boyadzhieva, I., Yakimova, B., Petkova, H., Stoineva, I., Nacheva, L., & Kabaivanova, L. (2026). Exploring biosurfactant production from halophilic bacteria, isolated from Burgas salterns in Bulgaria. *Marine Drugs, 24*(1), 53.

Bhat, S. P., & Roach, D. J. (2025). Bioactivity of microbial biofilms in extreme environments. *Frontiers in Microbiology, 16*, 1602583.

Edbeib, M. F., Abdul Wahab, R., & Huyop, F. (2016). Halophiles: Biology, adaptation, and their role in decontamination of hypersaline environments. *World Journal of Microbiology and Biotechnology*, *32*, 135.

Gomes, M. B., Gonzales-Limache, E. E., Sousa, S. T. P., Dellagnezze, B. M., Sartoratto, A., Silva, L. C. F., Gieg, L. M., Valoni, E., Souza, R. S., Torres, A. P. R., Sousa, M. P., De Paula, S. O., Silva, C. C., & Oliveira, V. M. (2018). Exploring the potential of halophilic bacteria from oil terminal environments for biosurfactant production and hydrocarbon degradation under high-salinity conditions. *International Biodeterioration & Biodegradation*, *126*, 231–242.

Hauser, B. A. (2002). Chloride. In B. A. Hauser (Ed.), *Drinking water chemistry: A laboratory manual* (pp. 93–95). Lewis Publishers, Boca Raton, FL.

Lima, B. G. A., Santos, J. C. V., Silva, R. R., Caldas, M. C. F., Meira, H. M., Rufino, R. D., Sarubbo, L. A., &

Luna, J. M. (2024). Sustainable production of biosurfactant grown in medium with industrial waste and use for removal of oil from soil and seawater. *Surfaces*, *7*, 537–549.

Maftei, C., Buta, C., & Carazeanu Popovici, I. (2020). The impact of human interventions and changes in climate on the hydro-chemical composition of Techirghiol Lake (Romania). *Water, 12*, 2261.

Neagu, S., & Stancu, M. M. (2025). Novel halotolerant bacteria from saline environments: Isolation and biomolecule production. *BioTech, 14*, 49.

Qi, G.-N., Qin, W.-Q., Li, G.-J., Ma, T.-T., Liu, Y.-F., Zhou, L., Liu, J.-F., Gang, H.-Z., Yang, S.-Z., & Mu, B.-Z. (2025). A new bacterial strain producing both of the surfactin and fengycin lipopeptide biosurfactant with strong emulsifications on crude oil. *Applied Biochemistry and Biotechnology, 197*, 1192–1208.

Sanders, E. R. (2012). Aseptic laboratory techniques: plating methods. *Journal of Visualized Experiments,* 63*,* e3064.

Sezonov, G., Joseleau-Petit, D., & D'Ari, R. (2007). *Escherichia coli* physiology in Luria-Bertani broth. *Journal of Bacteriology, 189*(23), 8746–8749.

Silva, T. A., Santos, R. B., Silva, R. C., & Campos-Takaki, G. M. (2022). Production and functional stability of the biosurfactant isolated from *Stenotrophomonas maltophilia* UCP 1601. *Research, Society and Development*, *11*(11), e87111132995

Stancu, M. M. (2015). Investigation of the organic solvent resistance mechanisms in *Rhodococcus* and *Lysinibacillus* using several molecular forensic tools. *Environmental Forensics, 16*(3), 242–256.

Stancu, M. M. (2023). Characterization of new diesel-degrading bacteria isolated from freshwater sediments. *International Microbiology, 26*, 109–122

Stancu, M. M. (2024). Characterization of a new *Pseudomonas aeruginosa* strain isolated from petroleum-polluted soil. *Waste and Biomass Valorization, 15*, 1–10.

Stancu, M. M. (2025). Investigating the potential of native soil bacteria for diesel biodegradation. *Microorganisms, 13*, 564.

Sun, W., Cao, W., Jiang, M., Saren, G., Liu, J., Cao, J., Ali, I., Yu, X., Peng, C., & Naz, I. (2018). Isolation and characterization of biosurfactant-producing and diesel oil degrading *Pseudomonas* sp. CQ2 from Changqing oil field, China. *RSC Advances, 8*(69), 39710–39720.

Ventosa, A., Quesada, E., Rodriguez-Valera, F., Ruiz-Berraquero, F., & Ramos-Cormenzana, A. (1982). Numerical taxonomy of moderately halophilic Gram-negative rods. *Journal of General Microbiology, 128*(9), 1959–1968.

Waghmode, S., Suryavanshi, M., Dama, L., Kansara, S., Ghattargi, V., Das, P., Banpurkar, A., & Satpute, S. K. (2019). Genomic insights of halophilic *Planococcus maritimus* SAMP MCC 3013 and detail investigation of its biosurfactant production. *Frontiers in Microbiology, 10*, 235.

Wu, B., Xiu, J., Yu, L., Huang, L., Yi, L., & Ma, Y. (2022). Biosurfactant production by *Bacillus subtilis* SL and its potential for enhanced oil recovery in low permeability reservoirs. *Scientific Reports, 12*, 7785.

Scientific Papers. Series E. Land Reclamation, Earth Observation & Surveying, Environmental Engineering. Vol. XV, 2026
Print ISSN 2285-6064, CD-ROM ISSN 2285-6072, Online ISSN 2393-5138, ISSN-L 2285-6064

# PLANT TISSUE CULTURE STRATEGIES FOR SUSTAINABLE MULTIPLICATION OF BLACK CHOKEBERRY (*ARONIA MELANOCARPA*) GERMPLASM

**Ioana-Cătălina NICOLAE[1], Maria TABĂRA[2], Nina CIORCHINĂ[2], Natalia ONICA[2], Melania GHEREG[2], Liliana BĂDULESCU[1]**

[1]University of Agronomic Sciences and Veterinary Medicine of Bucharest, Research Center for Studies of Food Quality and Agricultural Products, 59 Mărăşti Bvd, District 1, Bucharest, Romania
[2]Moldova State University, National Botanical Garden (Institut) "Alexandru Ciubotaru", 18 Pădurii Street, Chișinău, Republic of Moldova

Corresponding author email: maria.tabara@gb.usm.md

***Abstract***

*Plants are essential for ecosystem stability, providing oxygen, food, and valuable bioactive compounds. However, urbanization, industrial expansion, habitat loss, and climate change are accelerating biodiversity decline. Plant tissue culture and micropropagation offer efficient methods for large-scale production of uniform, disease-free planting material independent of seasonal and environmental constraints. Aronia melanocarpa is a valuable berry shrub with high nutraceutical potential. This study aimed to develop an effcient micropropagation protocol by evaluating the effect of different cytokinins on in vitro shoot development. Explants were cultured on MS medium supplemented with meta-topolin, zeatin, kinetin, 2iP, or TDZ, combined with $GA_3$ and IAA. Meta-topolin resulted in the highest shoot proliferation, while kinetin and 2iP enhanced shoot elongation and rooting. TDZ induced hyperhydric and compact tissue formation. Rooting was successfully achieved on half-strength MS medium supplemented with activated charcoal and auxins, leading to effective plant acclimatization. The results demonstrate that meta-topolin is the most efficient cytokinin for rapid micropropagation of A. melanocarpa, providing a reliable system for large-scale propagation and conservation of valuable plant material.*

***Key words****: 2iP, kinetin, meta-topolin, thidiazuron, zeatin.*

## INTRODUCTION

*Aronia melanocarpa*, commonly known as black chokeberry, is a valuable shrub species recognized for its fruits that have a high content of bioactive compounds and growing potential in horticulture and nutraceutical production. Native to North America, this species has attracted significant attention in recent decades for its nutritional and medicinal potential, leading to its widespread use in the food, cosmetic, and pharmaceutical industries (Piras et al., 2024). Berries are rich in phenolic compounds, as flavonoids: anthocyanins, proanthocyanidins, flavanols, flavonols; phenolic acids (chlorogenic, neochlorogenic, caffeic), tannins (Sidor & Gramza-Michałowska, 2019; Lee et al., 2021; Petre et al., 2021; Dufour et al., 2022; Popa et al., 2023). They also contain carbohydrates (sorbitol, fructose, glucose, and sucrose), organic acids (quinic, malic, citric, shikimic, oxalic and succinic acids), amino acids, proteins and minerals (K, Ca, P, Mg, Na, Fe, Se, and Zn), vitamins (ascorbic acid, vitamins C, E, B, and K), aromatic compounds, fibers, fatty acids, and essential oils (Catană et al., 2017; Lazăr et al., 2020; Wójtowicz et al., 2023; Piras et al., 2024; Pop et al., 2025). Due to their pronounced astringent flavor and distinctive bitter-almond scent, the fruits are primarily utilized in processed products and are less frequently eaten fresh. The fruits can be processed into a diverse array of products, including syrups, juices, jams, and jellies due to their high pectin content, as well as beverages such as wines, schnapps, and fruit infusions (Scott & Skirvin, 2007; Kulling & Rawel, 2008; Catană et al., 2021; Toma et al., 2022). They are also used in baked goods, desserts, and powdered dietary supplements (Catană et al., 2018; Sidor & Gramza-Michałowska, 2019). *Aronia melanocarpa* is

highly adaptable to a diverse range of soil types and pH levels (Brand, 2010; Dragomir et al., 2022), but it is sensitive in high salinity conditions (Nas et al., 2023). It also exhibits resistance to pests and fungal diseases (Scott & Skirvin, 2007; Palancean et al., 2015; Golache et al., 2024). Since 2020, *Aronia melanocarpa* micropropagation has advanced to support disease-free, genetically uniform plantlet production for cultivars like 'Nero' (Borsai et al., 2021; Rusea et al., 2022; Bayhan & Yücesan, 2024; Kaya & Özatay, 2024; Ekinci et al., 2024), 'Viking' (Nas et al., 2023; Yaman et al., 2025) and on other cultivars, such as 'Melrom' and 'Galicjanka' (Jakab et al., 2022; Isac & Plopa, 2022) and 'Eastland' (Celebi-Toprak & Alan, 2020). Effective micropropagation protocols employing shoot tips and nodal explants cultured on MS medium supplemented with BAP and IBA have resulted in high rates of shoot multiplication and root formation (Rusea et al., 2018; 2022). Common physiological problems, such as hyperhydricity, can be reduced through adjustments of agar and sucrose concentrations, as well as improved ventilation inside the growing vessels (Bayhan & Yücesan, 2024). Studies have also advanced techniques for callus formation (Calalb et al., 2014; Szopa et al., 2018), adventitious shoot regeneration (Rusea et al., 2018), and the establishment of cell cultures for the production of secondary metabolites (Shishkova et al., 2026). These advances contribute to the development of reliable propagation protocols, preservation of elite germplasm, and scalable production valuable *Aronia melanocarpa* cultivars.

*In vitro* tissue culture techniques play and important role in the propagation this woody species, as they enable the production of disease-free and genetically uniform planting material. Woody species are generally recalcitrant to *in vitro* propagation (Grzelak et al., 2024), and we face problems such as: polyphenols oxidation, endophytic bacterial contamination (Quambusch & Winkelmann, 2018; Permadi et al., 2025), hyperhydricity of tissues, formation of basal callus, somaclonal variation, unsuccessful rooting, dormancy during acclimatization (Jain & Häggman, 2007; Nowakowska et al., 2023).

Phytohormones (plant hormones) are naturally occurring organic molecules found within plant tissues that function as signaling agents, regulating a wide range of physiological activities (Davies, 1995). Although present in very small amounts - typically below 1 nM to 1 μM - they exert significant effects on plant growth and development. These compounds are frequently synthesized in particular plant organs and then transported to other regions, where they trigger physiological, biochemical, and structural responses (Salisbury & Ross, 1992). Cytokinins, a group of phytohormones, play a fundamental role in plant biology, regulating numerous developmental and physiological processes. They are key contributors to cell division and differentiation, stimulate the formation and expansion of vegetative tissues, promote chloroplast development, and influence overall plant growth and metabolism. Through these functions, cytokinins help coordinate plant development and maintain proper physiological activity (Krikorian et al., 1987). In plant tissue culture, BAP is the most commonly used cytokinin, but it can lead to hyperhydricity, shoot tip necrosis, inhibit rooting during the acclimatization and cause early senescence (Werbrouck, 2021). Nevertheless, while higher concentrations of BAP can enhance the rate of shoot regeneration, they may also increase the likelihood of vitrification. During the acclimatization phase, plants affected by vitrification showed impaired development, characterized by reduced shoot elongation, smaller and narrower leaves, fewer and shorter roots, and lower survival percentages. These adverse effects were especially pronounced when plants were exposed to environments with lower humidity levels (Bayhan & Yücesan, 2024). Meta-Topolin (mT, 6-(3-hydroxybenzylamino) purine) is an exceptionally potent natural aromatic cytokinin that was first extracted by Strnad (1997) from the mature foliage of *Populus* x *canadensis* and has since been recognized for its biological activity. Can be used as an alternative to BAP, as it promotes rapid, high multiplication rates, improve rooting and *ex vitro* adaptation, while reducing structural abnormalities and somaclonal variations (Amoo et al., 2011; Cardoso, 2021; Zaytseva et al., 2021). Moreover, it can lead to improve both rooting success and acclimatization in plants (Nowakowska & Pacholczak, 2020). The

present study aims to evaluate the *in vitro* response of 'Alexandrina', a Moldavian cultivar, to 5 different types of cytokinins, others than BAP: 6-(γ, γ-dimethylallylamino) purine (2iP), kinetin, meta-Topolin, thidiazuron and zeatin.

## MATERIALS AND METHODS

'Alexandrina' is a Moldavian cultivar bred by the researchers at the National Botanical Garden (Institut) 'Alexandru Ciubotaru' of the State University of Moldova (Palancean et al., 2015). The initial plant material - *in vitro* cultures (Figure 1) was obtained from the National Botanical Garden 'Alexandru Ciubotaru' of Chișinău. It was subsequently multiplied *in vitro* at the University of Agronomic Sciences and Veterinary Medicine of Bucharest, Romania, as part of the BioMedPlant project (*Valorization of medicinal spontaneous and cultivated plants through the use of advanced micropropagation techniques as sources of bioactive compounds*).



Figure 1. Initial *in vitro* cultures obtained from the National Botanical Garden 'Alexandru Ciubotaru' of the State University of Moldova

### I. Multiplication phase

*In vitro* multiplication of *Aronia melanocarpa* 'Alexandrina' was performed out on Murashige and Skoog (MS) medium, supplemented with five different cytokinins, each at a concentration of 1 mg/L: meta-topolin (mT), zeatin (Z), kinetin (kin), 6-(γ, γ-Dimethylallylamino) purine (2iP) and thidiazuron (TDZ). To ensure proper multiplication, all media were supplemented with 0.5 mg/L IAA and 0.2 mg/L $GA_3$, as shown in Table 1.

Other media components included sucrose (3%), Kobe I agar (0.7%) and to reduce tissue oxidation, PVP (polyvinylpyrrolidone) was added in concentration of 100 mg/L. The pH was modified at 5.75 and the media was sterilized in the autoclave at 121°C for 20 minutes. indole-3-acetic acid (IAA) and gibberellic acid ($GA_3$) were co-autoclaved with the rest of the media components. All cytokinins were filter-sterilized after the media was autoclaved, using sterile polyethersulfone (PES) syringe filters (0.22 µm pore size).

Table 1. Types and concentrations of plant growth regulators (PGRs) supplemented to the multiplication media

| Medium variant | Plant growth regulators | | |
|---|---|---|---|
| | Cytokinins | Auxins | Gibberellins |
| V1 | 1 mg/L mT | 0.5 mg/L IAA | 0.2 mg/L $GA_3$ |
| V2 | 1 mg/L Z | 0.5 mg/L IAA | 0.2 mg/L $GA_3$ |
| V3 | 1 mg/L KIN | 0.5 mg/L IAA | 0.2 mg/L $GA_3$ |
| V4 | 1 mg/L 2iP | 0.5 mg/L IAA | 0.2 mg/L $GA_3$ |
| V5 | 1 mg/L TDZ | 0.5 mg/L IAA | 0.2 mg/L $GA_3$ |

### II. Rooting phase

Shoots regenerated on media containing meta-topolin were subsequently cultured on half-strength MS medium supplemented with 1 g/L activated charcoal and different concentrations of either indole-3-butyric acid (IBA) or indole-3-acetic acid (IAA), as detailed in Table 2.

Table 2. Concentration of auxins (IBA and IAA) supplemented to the rooting media

| Medium variant | Auxins | |
|---|---|---|
| | IAA (mg/L) | IBA (mg/L) |
| R1 | 0.5 | - |
| R2 | 1 | - |
| R3 | - | 0.5 |
| R4 | - | 1 |

Sucrose, agar and PVP were added to the media in the same concentrations as in the multiplication media. Both auxins were sterilized with the rest of the media components, by autoclavation at 121°C for 20 minutes.

The concentration of $CuSO_4 \cdot 5H_2O$ was increased tenfold, to 0.125 mg/L, compared to the concentration present in the conventional half-strength MS formulation. This adjustment was made to stimulate root development and improve plantlet vigor, given the importance of copper in carbon dioxide fixation and ATP production (Marques et al., 2018).

The medium was dispensed into 720 mL glass jars at approximately 83 mL per vessel to ensure adequate air volume for shoot development.

The jars were fitted with lids containing air-permeable filters to facilitate gas exchange, thereby reducing ethylene accumulation and improving leaf adaptation to *ex vitro* conditions. Tamimi & Othman (2020) observed an increase in multiplication parameters (including number and length of shoots) and chlorophyll content on media with increased copper sulphate concentration on *Musa acuminata* shoots cultivated *in vitro*. Similarity, *Capsicum annum* cotyledons showed improved bud differentiation and elongation on media supplemented with higher concentrations of $CuSO_4$ x $5H_2O$ (Joshi & Kothari, 2007).

Total dry matter was determined by weighing 250 mg of finely cut and homogenized plant material (from 5 shoots/media variant), in crucibles, in 3 repetitions/variant, followed by drying for 14 hours at 105°C using a UN110 Memmert drying oven. This can be a good indicator of how the leaves will perform during the acclimatization phase.

**III. Acclimatization phase**

*In vitro* rooted shoots of 'Alexandrina' were placed in sowing trays with peat (sterilized in the autoclave at 121°C for 20 minutes) then covered with plastic lids to keep a high level of humidity (Figure 2). Prior to planting, the roots were washed of all agar traces and they were shortened at approximately 5 cm.



Figure 2. *In vitro* rooted shoots of *A. melanocarpa* 'Alexandrina' used for the acclimatization phase

The trays were kept in laboratory conditions at 20-25°C room temperature and illuminated using LED lamps composed of white, red and blue lights (Figure 3). The acclimatization of the shoots was carried out by periodically removing the lid and gradually exposing the shoots to the new humidity conditions, until the leaves were able to maintain their turgidity at normal laboratory humidity (approximately 40-50%).



Figure 3. Acclimatization of *Aronia melanocarpa* 'Alexandrina' shoots in laboratory conditions

The trays were kept in laboratory conditions at 20-25°C room temperature and illuminated using LED lamps composed of white, red and blue lights (Figure 3). The acclimatization of the shoots was carried out by periodically removing the lid and gradually exposing the shoots to the new humidity conditions, until the leaves were able to maintain their turgidity at normal laboratory humidity (approximately 40-50%).

Acclimatization of *Aronia melanocarpa* can also be done in a growing chamber with high humidity (Figure 4). Both methods work as long as proper humidity, temperature and light can be ensured.



Figure 4. Acclimatization of *in vitro* obtained shoots in a Memmert growing chamber with high humidity

**Statistical analysis**

Statistical analyses were performed using Microsoft Excel 2021 with the Real Statistics Resource Pack (www.real-statistics.com). Descriptive statistics, including the mean and standard error, were calculated for all measured variables. Prior to inferential analysis, the assumption of homogeneity of variances was evaluated using Levene's test. Depending on whether this assumption was met, differences among treatments were analyzed using either one-way analysis of variance (ANOVA) or the non-parametric Kruskal-Wallis test. When statistically significant differences were detected ($p < 0.05$), multiple comparisons were performed using Tukey's honestly significant

difference (HSD) test following ANOVA or Dunn's post hoc test following the Kruskal–Wallis test. Results were considered statistically significant at $p < 0.05$.

## RESULTS AND DISCUSSIONS

### I. Multiplication phase

#### *Average number of shoots obtained from each explant*

Meta-Topolin medium enhanced the multiplication rate (Figure 5), by generating highest number of shoots/ explant (20.7 ± 4.59) (Figure 6), followed by variant V2 with zeatin, with an average of 4.7 ± 1.36 shoots/ explant. Lowest results were obtained on V3 with kinetin (1 shoot/explant) and variant V4 with 2iP (with 1.16 shoots/explant), with no statistically significant differences between them, as confirmed by Dunn's test.

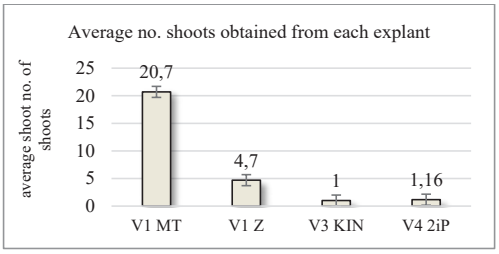



Figure 5. Average number of shoots obtained from each explant

Meta-Topolin has increased *in vitro* multiplication in several woody species, such as *Actinidia arguta* (Shakshi et al., 2026), *Daphne mezereum* (Nowakowska et al., 2023), *Salix tetrasperma* (Reshi et al., 2025), *Feronia limonia* (Anis et al., 2023) *Rubia cordifolia* (Kunal et al., 2025). Use of meta-Topolin was also shown to stimulate the development of the photosynthetic apparatus in *Musa* spp., which is a crucial aspect in the rooting and acclimatization phases, as it increases the survival rates of the plantlets (Aremu et al., 2012). Similarly, in *Momordica balsamina*, leaves that were obtained from shoots cultivated on media with meta-Topolin showed veins and trichomes that were more developed and an increase in the density of stomata and stomatal index, compared to the leaves obtained on shoots cultivated in the presence of BAP (Chouhan et al., 2025). In addition, in *Oxystelma esculentum*, the use of media with mT was shown to also enhance cutin deposition and the development of vascular and ground tissue systems (Jayaprakash et al., 2021).

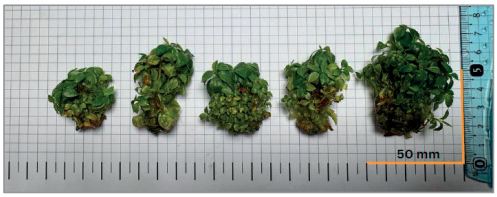



Figure 6. High shoot proliferation of explants cultivated on media with meta-Topolin

Rusea et al. (2018) obtained an average of 6.08-10.2 shoots per explant on media with 0.5-2.0 mg/L BAP combined with 0.1-1.0 mg/L IBA. By comparison in our previous study, we obtained averages between 8.3 and 13.3 shoots/explant in 'Alexandrina' and 5.21-8.37 shoots/explant in 'Nero' on media with 0.3-0.5 mg/L BAP and 0.2 mg/L $GA_3$ (Nicolae et al., 2025). Litwińczuk (2013) recommends the use of BAP (1 mg/L) and IBA (0.05 mg/L) supplemented to media with a 150% increase in magnesium and calcium salts to enhance axillary shoot proliferation.

#### *Average shoot length*

Regarding shoot growth, explants grown on medium with KIN (Figure 7), even although showing limited proliferation, exhibited the greatest shoot elongation (44.94 ± 9.52 mm), followed by variants V4 (39.29 ± 9.24 mm) and V2 (33.09 ± 8.45 mm). The explants cultivated on the mT-supplemented medium produced shortest shoots (21.53 ± 5.17 mm).

Rusea et al. (2018), observed that 'Nero' explants cultivated on media with BAP and IBA can reach lights of 1.45-2.24 mm, however, this is highly dependent on the cultivar, as our past studies have also shown that 'Nero' grows smaller in comparison with 'Alexandrina' (Nicolae et al., 2025).

Additionally, in this experiment, *A. melanocarpa* 'Alexandrina' shoots that were obtained on KIN medium showed shoots with more lignified tissue and higher leaf surface area (data not shown). In micropropagation of *Quercus robur*, KIN promotes the formation of a more developed secondary xylem and

enhances cell wall lignification. Furthermore, the shoots cultured in the presence of KIN exhibit anatomical characteristics associated with increased cellular differentiation rather than vigorous proliferative growth (Martins et al., 2022). Moreover, the low shoot induction efficiency of cytokinins such as KIN or 2iP may be linked to fast cytokinin catabolism by cytokinin oxidase/dehydrogenase enzymes (Schmülling et al., 2003; Khablak et al., 2024).

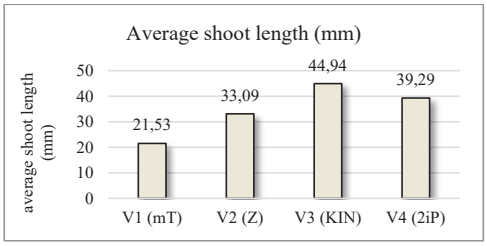



Figure 7. Average shoot length (mm) of explants cultivated on the multiplication media

***Average biomass*** (g)

Highest biomass was accumulated on explants cultivated on V5 – TDZ (2.33 ± 1.07 g/explant) and V1 – mT (1.95 ± 0.72 g/explant), with no statistically significant differences between them, as it was pointed out by Dunn's test (Figure 8).

Even though variant V5 – TDZ generated the highest biomass/explant, the inclusion of TDZ resulted in the formation of compact, globular masses of shoots that were small, highly friable, and hyperhydrated rendering them unsuitable for further multiplication (Figure 9).

Thidiazuron (TDZ) is a is a non-purine phenylurea and possesses cytokinin-like properties; however, unlike adenine-based cytokinins such as BAP, KIN and Z, it lacks a purine ring in its molecular structure (Dewir et al., 2018; Nautiyal et al., 2022).

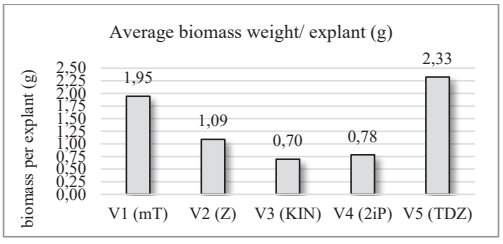



Figure 8. Average biomass (g) produced from explants cultivated on multiplication media variants

TDZ is extremely potent and effective in stimulating cell division and organogenesis (Manokari et al., 2026), which could be associated with its resistance to cytokinin/dehydrogenase-mediated breakdown and increased internal cytokinin concentrations (Brunoni et al., 2021). However, it is known to cause several anomalies in plant tissue culture (Dewir et al., 2018). Most common effects include fasciated and compact shoots, hyperhydricity, and reduced rooting capacity (Huetteman & Preece, 1993; Lu, 1993).




Figure 9. Explants obtained on multiplication media with TDZ

***Average basal callus mass*** (mg)

Regarding the production of basal callus, figure 10 shows that variant V2 with Z produced the highest basal callus mass (327.42 ± 42.75 mg/explant), followed by V1 (mT) with 219.90 ± 70.67 mg/explant; however, Dunn's test indicated that the difference between these two variants was not statistically significant. Callus on V4 (2iP), which generated an average of only 1.16 shoots/ explant. By comparison, callus tissue obtained on V1 (mT) had strong organogenic potential, as the explants obtained generated a high number of shoots (20.7 ± 4.59 shoots/ explant), while the average on V2 (Z) was very low (4.7 ± 1.36 shoots/ explant). Variants V3 (KIN) and V4 (2iP) produced the lowest amounts of basal callus; nevertheless, the callus formed on V3 (KIN) showed no shoot regeneration capacity, as explants cultured on this medium developed solely via the apical

meristem, yielding only one shoot per explant. Similar observations can be made about the callus on V4 (2iP), which generated an average of only 1.16 shoots/ explant.

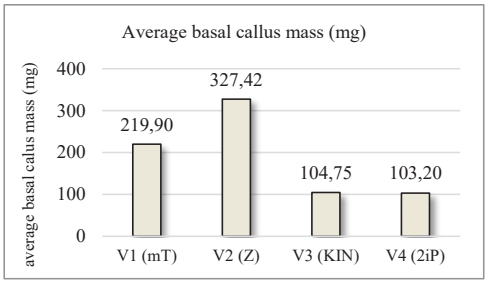



Figure 10. Average basal callus mass (mg) per explant

***Average number of leaves/explant***

Highest values regarding the number of leaves were observed on variant V3 (KIN) (Figure 11), with an average of 25.80 ± 8.05 leaves/explant, followed by V4 (2iP), with an average of 17.67 ± 4.26 leaves/explant, but with no statistically significant differences.

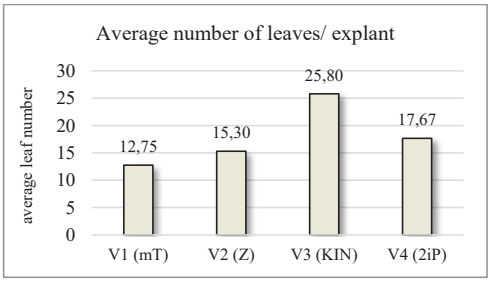



Figure 11. Average number of leaves/explant on the multiplication media variants

The lowest values were recorded for V1 (mT), with 12.75 ± 2.41 leaves per explant, and for V2 (Z), with 15.30 ± 3.24 leaves per explant; these variants also exhibited the lowest shoot heights. This parameter is an important indicator, as it is directly correlated with the number of axillary buds and, consequently, with the potential multiplication rate. In relation to shoot height, it can also provide information on internodal length and the spatial distribution of axillary buds.

*Rhizogenesis during multiplication phase:*

Rhizogenesis only occurred on variants V3 (KIN) and V4 (2iP), and, in a very low percentage, on V2 (Z) - only 10% (Figure 12). Variants V3 (KIN) and V4 (2iP) produced an average of 3.3 ± 2.21 roots/ explant and 3.1 ± 1.60 roots/ explant, respectively. Analysis of variance (Kruskal-Wallis Test) pointed out no significant differences between these values. Highest root length was obtained on V2 (Z): 92.67 ± 12.02 mm, followed by V3 (KIN): 79.47 ± 13.23 mm (Figure 13).

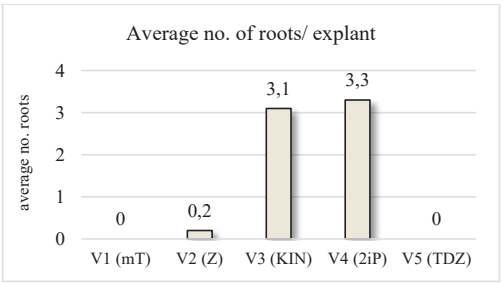



Figure 12. Average roots number of explants cultivated on multiplication medium variants

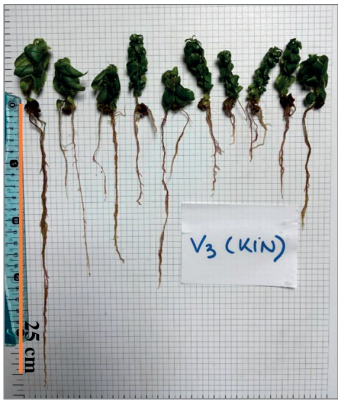



Figure 13. Rhizogenesis on explants cultivated on multiplication media with kinetin

The lowest values were observed on variant V4 (2iP) with 49.48 ± 9.21 mm; however, no statistically significant differences were identified regarding root length.

**II. Rooting phase**

***Average number of roots and root length***

Rooting was successfully achieved in 100% across all media variants. Differences between the growing parameters, such as shoot height, number of leaves were relatively minor, and statistically unconfirmed (using ANOVA in all cases), except for the average shoot height - R4 and R1 recorded significant differences.

IBA is the most commonly used auxin in the rooting phase of *Aronia melanocarpa*, supplemented to a media recipe with a lower concentration of minerals (Almokar & Pırlak, 2018; Celebi-Toprak & Alan, 2020; Ekinci et al., 2024; Abduganiyeva et al., 2025). For varieties such as 'Melrom' and 'Nero', Isac & Plopa (2022) recommend the use of IBA in concentration of 0.7 mg/L. Other medias, such as half-strength Shrub Plant Medium (SPM) in combination with NAA and IBA, can also be used to obtain high rooting percentages in cultivars such as 'Viking' (Yaman et al., 2025). Concentrations over 3 mg/L IBA cand lead to an increase in callus formation and size (Abduganiyeva et al., 2025), which can be an undesirable aspect during the rooting stage. Jakab et al. (2022), recommend using IBA concentrations, as low as 0.5 mg/L. Litwińczuk (2013) recommends using IBA in concentrations as low as 0.05 mg/L.

Highest number of roots was obtained on the variant with 1 mg/L IBA (R4), 7.4 ± 1.74 roots/ shoot and on variant with 1 mg/L IAA (R2), 7 ± 2.41 roots/ shoot (Figure 14).

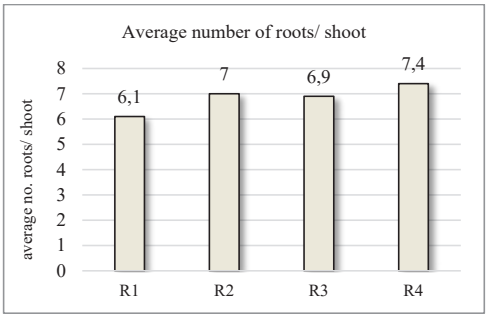



Figure 14. Average root number of explants cultivated on the rooting media variants

Both variants with lower concentrations of auxins generated a lesser number of roots: 6.9 ± 2.02 roots/ shoot on media with 0.5 mg/L IAA (R3) and 6.1 ± 3.14 roots/ shoot on media with 0.5 mg/L IBA (R1).

***Average shoot height*** (mm)

Regarding the growth of these shoots, highest values were observed on variant with 1 mg/L IAA (R2) (Figure 15), with an average of 33.64 ± 5.12 mm and on the variant with 0.5 mg/L IBA (R3), with an average of 33.07 ± 3.30 mm. The Tukey HSD test indicated significantly lower shoot heights in R1 (0.5 mg/L IAA): 21.80 ± 2.48 mm and R4 (1 mg/L IBA): 26.34 ± 3.76 mm (Figure 16).




Figure 15. *In vitro* rooted shoots obtained on media with 1 mg/L IAA

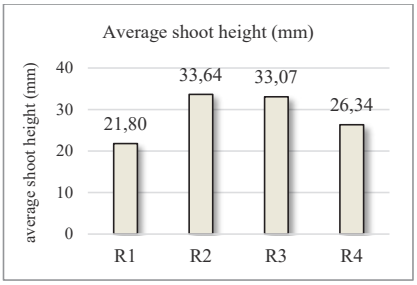



Figure 16. Average shoot height (mm) of explants

***Average number of leaves***

Proper growth and development of leaves is an important factor in the next phase, when the plantlets are acclimatized to *ex vitro* conditions. The subsequent growth of plantlets under *ex vitro* conditions depends both on the formation of new leaves and on the adaptation of existing leaves that were regenerated *in vitro*.

In regards with this aspect, variant with 1 mg/L IBA (R4) recorded the highest average number of leaves (8.5 ± 1.12 leaves/ explant). Middle values of 7.9 ± 1.81 leaves were obtained on variant with 0.5 mg/L IAA (R1) and 7.8 ± 0.60 on variant with 0.5 mg/L IBA (R3). Lowest values were recorded on media with 1 mg/L IAA (R2), only 7.4 ± 0.92 leaves/ explant (Figure 17). However, analysis of variance (ANOVA) recorded no statistically significant differences between the four variants of rooting media.

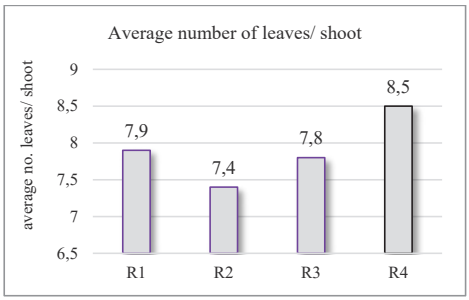



Figure 17. Average number of leaves/shoot of the explants cultivated on the rooting media variants

***Dry matter of in vitro obtained leaves***

Leaves that were regenerated from the shoots cultivated on media supplemented with IBA (0.5 and 1 mg/L) had an overall higher dry matter content, compared to the ones cultivated on media with IAA (Figure 18). Higher dry matter content (%) was obtained from the leaves from variant R4 (1 mg/L IBA): 34.16 ± 2.63% and R3 (0.5 mg/L IBA): 29.57 ± 1.81%.

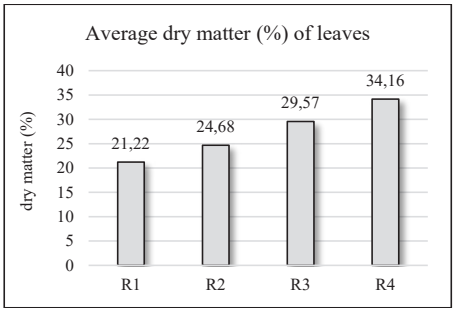



Figure 18. Average dry matter (%) of leaves obtained from shoots cultivated on rooting media variants

Leaves regenerated from the explants cultivated recorded lower values, of 24.68 ± 0.52% on R2 (1 mg/L IAA) and 21.22 ± 3.35% on R1 (0.5 mg/L IAA). For comparison, the average dry matter content was 15.11 ± 0.94% during the multiplication phase (on meta topolin medium) and 35.51 ± 0.92% in young greenhouse-grown plants of *Aronia melanocarpa* 'Alexandrina'

The dry matter can be a good indicator of how the leaves will perform during the acclimatization phase because it reflects how well the leaves are developed. Due to the culture environment of explants (high humidity, lower light intensity, controlled temperature, and heterotrophic or mixotrophic nutrition), leaves formed *in vitro* often have low dry matter due to high water content, thin cell walls, poor cuticle development, and limited lignification. Such leaves are fragile and poorly adapted to *ex vitro* conditions, making them highly susceptible to desiccation and transplant shock when humidity drops. Moreover, the stems of plantlets developed *in vitro* are often hypo lignified, their cell walls are thin, and the intercellular spaces are large, with limited development of vascular tissue (Ziv, 1995; Nowakowska et al., 2023).

For woody species, the rooting phase is not only important to generate a well-developed rooting system, but also to stimulate the proper development of leaves and stems (through using well-ventilated culture vessels, adapting culture media nutrients and growth regulators, use of plant elicitors) in order to ensure high survival rates during the acclimatization phase.

**III. Acclimatization phase**

All rooted shoots were successfully acclimatized. After 3 weeks of culture in laboratory conditions, they were planted individually in small pots and transferred to greenhouse conditions where they developed into healthy, uniform plants (Figure 19).



Figure 19. *In vitro* obtained plants of *Aronia melanocarpa* 'Alexandrina' grown in the greenhouse at USAMV Bucharest

Generally, if the rooting phase is carried on properly, acclimatization of *Aronia melanocarpa* can be achieved successfully. Several authors report good results (Celebi-Toprak & Alan, 2020; Borsai et al., 2021; Isac & Plopa, 2022; Rusea et al., 2022; Coşkun et al.,

2026), as long as the tissues are not vitrified, which can delay shoot and leaf growth, reduce the development of the rooting system and increase the risk of plant loss due to the dehydration of the tissues (Bayhan & Yücesan, 2024).

## CONCLUSIONS

Meta-topolin (mT) is the most effective cytokinin for *in vitro* multiplication of *A. melanocarpa* 'Alexandrina', yielding the highest shoot proliferation (20.7 shoots/explant) and good biomass, without hyperhydricity. TDZ induced high biomass but led to compact, hyperhydric, non-viable shoot clusters — unsuitable for further multiplication. KIN and 2iP promoted shoot elongation and leaf formation but showed low multiplication rates and limited organogenic potential. IBA (especially 1 mg/L) is recommended for rooting to improve leaf dry matter content and acclimatization success. Leaf dry matter content is a reliable indicator of plantlet physiological quality prior to *ex vitro* transfer. Optimizing ventilation, light, and nutrient balance during rooting is critical for high survival rates during acclimatization.

The results demonstrate that meta-topolin is the most efficient cytokinin for rapid micropropagation of *A. melanocarpa* 'Alexandrina', providing a reliable system for large-scale propagation and conservation of valuable plant material.

## ACKNOWLEDGEMENTS

This work was supported by a grant of the Ministry of Research, Innovation and Digitization, CNCS - UEFISCDI, project number PN-IV-P8-8.3-ROMD-2023 0307, within PNCDI IV. Project title: Valorization of medicinal spontaneous and cultivated plants through the use of advanced micropropagation techniques as sources of bioactive compounds (BioMedPlant).

## REFERENCES

Abduganiyeva, D., Alikulov, B., Ruziyev, K., Eshbekova, G., Sultonova, K., Ismailov, Z., Gulyamova, T., & Mamadiyarov, M. (2025). Standardization of the microclonal propagation process in *Aronia melanocarpa* from seeds. *Sabrao Journal of Breeding and Genetics*, *57*(4), 1480–1490.

Almokar, H. M. M., & Pırlak, L. (2018). Propagation of Aronia (*Aronia melanocarpa*) with Tissue Culture. *Selcuk Journal of Agriculture and Food Sciences, 32*(3), 549–558.

Amoo, S. O., Finnie, J. F., & Van Staden, J. (2011). The role of meta-topolins in alleviating micropropagation problems. *Plant Growth Regulation, 63*(2), 197–206. https://doi.org/10.1007/s10725-010-9504-7

Anis, M., Alam, N., Khanam, M. N., & Ahmad, N. (2023). Potential of meta-Topolin (mT) in improved *in vitro* regeneration of *Feronia limonia* (L.), *Swingle. Vegetos, 36*(2), 681–687.

Aremu, A. O., Bairu, M. W., Szüčová, L., Finnie, J. F., & Van Staden, J. (2012). The role of meta-topolins on the photosynthetic pigment profiles and foliar structures of micropropagated 'Williams' bananas. *Journal of Plant Physiology, 169*(15), 1530–1541.

Bayhan, N., & Yücesan, B. (2024). The impact of sucrose and 6-benzylaminopurine on shoot propagation and vitrification in *Aronia melanocarpa* (black chokeberry). *Plant Cell, Tissue and Organ Culture (PCTOC), 156*(2), 55. https://doi.org/10.1007/s11240-023-02652-x

Borsai, O., Clapa, D., Fira, A., Hârţa, M., Szabo, K., Dumitraş, A. F., & Pamfil, D. (2021). *In vitro* propagation of *Aronia melanocarpa* (Michx.) Elliott. *Acta Horticulturae, (1308)*, 213–222. https://doi.org/10.17660/ActaHortic.2021.1308.30

Brand, M. (2010). Aronia: Native Shrubs With Untapped Potential. *Arnoldia, 67*(3), 14--25. https://doi.org/10.5962/p.251408

Brunoni, F., Rolli, E., Polverini, E., Spíchal, L., & Ricci, A. (2021). The adjuvant activity of two urea derivatives on cytokinins: An example of serendipitous dual effect. *Plant Growth Regulation, 95*(2), 169–190. https://doi.org/10.1007/s10725-021-00735-3

Calalb, T., Nistreanu, A., Oroian, S., & Samarghitan, M. (2014). Callus induction and biomass accumulation *in vitro* in explants from chokeberry (*Aronia melanocarpa* (Michx.) Elliot) fruit. *Acta Agrobotanica, 67*, 53–64. https://doi.org/10.5586/aa.2014.032

Cardoso, J. C. (2021). Meta-topolins: *In Vitro* Responses and Applications in Large-Scale Micropropagation of Horticultural Crops. In *N. Ahmad & M. Strnad (Eds.), Meta-topolin: A Growth Regulator for Plant Biotechnology and Agriculture*, Springer, 203-219; https://doi.org/10.1007/978-981-15-9046-7_15

Catană, L., Catană, M., Burnete, A.-G., Asănică, A. C., Lazăr, M.-A., Constantinescu, F., Teodorescu, R. I., & Belc, N. (2021). Sugar-free concentrated products from *Aronia melanocarpa* fruits, apples and carrots with antioxidant potential for peoples with diabetes and obesity. *Scientific Papers. Series B, Horticulture, LXV*(1), 707–714.

Catană, L., Catană, M., Iorga, E., Constantin, A., Lazăr, A.-G., Lazăr, M.-A., & Belc, N. (2017). Vitamin C and total polyphenol content and antioxidant capacity of fresh and processed fruits of *Aronia melanocarpa*.

*Scientific Papers. Series B, Horticulture, LXI*, 433–440.

Catană, M., Catană, L., Iorga, E., Asănică, A. C., & Belc, N. (2018). Bakery products fortified with dried fruits of *Aronia melanocarpa*. *Scientific Papers. Series B, Horticulture, LXII*, 693–702.

Celebi-Toprak, F., & Alan, A. R. (2020). A successful micropropagation protocol for three aronia (*Aronia melanocarpa*) cultivars. *Acta Horticulturae, (1285),* 173–176. https://doi.org/10.17660/ActaHortic.2020.1285.27

Chouhan, R., Shekhawat, N. S., Patel, A. K., Ram, K., Choudhary, A., Ambawat, S., & Choudhary, S. K. (2025). Meta-topolin mediated enhanced micropropagation, foliar-micromorphological evaluation and genetic homogeneity validation in African pumpkin (*Momordica balsamina* L.). *South African Journal of Botany, 180*, 286–296. https://doi.org/10.1016/j.sajb.2025.03.005

Coşkun, S., Dumanoğlu, H., Sarıkamış, G., Delialioğlu, R. A., & Kocabas, Z. (2026). Improvement of Ex vitro Rooting and Acclimatization to Increase Micropropagation Efficiency of *Aronia* (*Aronia mitschurinii*). *Journal of Agricultural Sciences, 32*(1), 81–92. https://doi.org/10.15832/ankutbd.1661934

Davies, P. J. (1995). The Plant Hormones: Their Nature, Occurrence, and Functions. In P. J. Davies (Ed.), *Plant Hormones: Physiology, Biochemistry and Molecular Biology*. Springer Netherlands, 1-12. https://doi.org/10.1007/978-94-011-0473-9_1

Dewir, Y. H., Nurmansyah, Naidoo, Y., & Teixeira da Silva, J. A. (2018). Thidiazuron-induced abnormalities in plant tissue cultures. *Plant Cell Reports, 37*(11), 1451–1470. https://doi.org/10.1007/s00299-018-2326-1

Dragomir, D., Dogaru, M., Căliniță, C., Hoza, D., Stănică, F., Peticilă, A. G., & Ion, L. (2022). Preliminary results regarding the behavior of some chokeberry cultivars (*Aronia melanocarpa*) in organic system. *Scientific Papers. Series B, Horticulture, LXVI*(1), 80–84.

Dufour, C., Villa-Rodriguez, J. A., Furger, C., Lessard-Lord, J., Gironde, C., Rigal, M., Badr, A., Desjardins, Y., & Guyonnet, D. (2022). Cellular antioxidant effect of an aronia extract and its polyphenolic fractions enriched in proanthocyanidins, phenolic acids, and anthocyanins. *Antioxidants, 11*(8), 1561. https://doi.org/10.3390/antiox11081561

Ekinci, H., Saskin, N., Korkmaz, Ş., Ak, B. E., & Aydinlik, Y. (2024). The effect of sodium nitroprusside on the vegetative development of *Aronia melanocarpa* [Michx.] Elliot under *in vitro* conditions. *Notulae Botanicae Horti Agrobotanici Cluj-Napoca, 52*(1), 13542–13542. https://doi.org/10.15835/nbha52113542

Golache, I. E., Herea, M., Perju, I., Mineaţă, I., Ungureanu, I. V., & Tălmaciu, M. (2024). Observations on arthropods existing in some aronia plantations in the NE area of Romania. *Scientific Papers. Series B, Horticulture, LXVIII*(1), 37–44.

Grzelak, M., Pacholczak, A., & Nowakowska, K. (2024). Challenges and insights in the acclimatization step of micropropagated woody plants. *Plant Cell, Tissue and Organ Culture (PCTOC), 159*(3), 72. https://doi.org/10.1007/s11240-024-02923-1

Huetteman, C. A., & Preece, J. E. (1993). Thidiazuron: A potent cytokinin for woody plant tissue culture. *Plant Cell, Tissue and Organ Culture, 33*(2), 105–119. https://doi.org/10.1007/BF01983223

Isac, V., & Plopa, C. (2022). *In vitro* propagation technology for the black chokeberry *Aronia melanocarpa* (Michx.) Elliot. *Fruit Growing Research, 38*, 202–207. https://doi.org/10.33045/fgr.v38.2022.29.

Jakab, I., Vlaşin, L. D., & Chiorean, A. M. (2022). Behaviour of several chokeberry cultivars (*Aronia melanocarpa*) at the *in vitro* micropropagation. *Romanian Journal of Horticulture, 3*, 31–36.

Jain, S. M., & Häggman, H. (Eds.). (2007). Protocols for micropropagation of woody trees and fruits. Springer Netherlands. https://doi.org/10.1007/978-1-4020-6352-7

Jayaprakash, K., Manokari, M., Badhepuri, M. K., Raj, M. C., Dey, A., & Shekhawat, M. S. (2021). Influence of meta-topolin on *in vitro* propagation and foliar micro-morpho-anatomical developments of *Oxystelma esculentum* (L.f.)Sm. *Plant Cell, Tissue and Organ Culture (PCTOC), 147*(2), 325–337. https://doi.org/10.1007/s11240-021-02126-y

Joshi, A., & Kothari, S. L. (2007). High copper levels in the medium improves shoot bud differentiation and elongation from the cultured cotyledons of *Capsicum annuum* L. *Plant Cell, Tissue and Organ Culture, 88*(2), 127–133. https://doi.org/10.1007/s11240-006-9171-6

Kaya, Ç., & Özatay, Ş. (2024). Development of an effective sterilization protocol for plant tissue culture studies in superfruit aronia [*Aronia melanocarpa* (Michaux) Elliot]. *Black Sea Journal of Agriculture, 7*(6), 679–685. https://doi.org/10.47115/bsagriculture.1548432

Khablak, S. H., Spivak, S. I., Pastukhova, N. L., Yemets, A. I., & Blume, Ya. B. (2024). Cytokinin oxidase/dehydrogenase as an important target for increasing plant productivity. *Cytology and Genetics, 58*(2), 115–125. https://doi.org/10.3103/S0095452724020051

Krikorian, A. D., Kelly, K., & Smith, D. L. (1987). Hormones in Tissue Culture and Micro-Propagation. In P. J. Davies (Ed.), *Plant Hormones and their Role in Plant Growth and Development*, Springer Netherlands, 593-613. https://doi.org/10.1007/978-94-009-3585-3_31

Kulling, S. E., & Rawel, H. M. (2008). Chokeberry (*Aronia melanocarpa*) – a review on the characteristic components and potential health effects. *Planta Medica, 74*(13), 1625–1634. https://doi.org/10.1055/s-0028-1088306

Kunal, Bansal, S., Sharma, M. K., Pant, P., Malhotra, E. V., Kumari, J., & Malik, S. (2025). Effect of meta-topolin on *in vitro* shoot multiplication, rooting, and genetic integrity of *Rubia cordifolia* L. *In Vitro Cellular & Developmental Biology - Plant, 61*(2), 413–426. https://doi.org/10.1007/s11627-025-10536-2

Lazăr, M.-A., Catană, M., Catană, L., Burnete, A.-G., Teodorescu, R. I., Asănică, A. C., & Belc, N. (2020). Valorisation of *Aronia melanocarpa* pomace for development of functional ingredients with high nutritional value and antioxidant capacity. *Scientific Papers. Series B, Horticulture, LXIV*(2), 403–410.

Lee, H.-Y., Suh, K. S., Kim, Y. I., Jang, B.-K., Kim, B.-H., & Yim, S.-V. (2021). Bioactive fraction of *Aronia melanocarpa* Fruit Inhibits Adipogenic Differentiation of Cultured 3T3-L1 Cells. *Applied Sciences, 11*(19), 9224. https://doi.org/10.3390/app11199224

Litwińczuk, W. (2013). Micropropagation of chokeberry by *in vitro* axillary shoot proliferation. In M. Lambardi, E. A. Ozudogru, & S. M. Jain (Eds.), *Protocols for micropropagation of selected economically-important horticultural plants,* Humana Press, 179-186. https://doi.org/10.1007/978-1-62703-074-8_13

Lu, C.-Y. (1993). The use of thidiazuron in tissue culture. *In Vitro* Cellular & Developmental Biology - *Plant, 29*(2), 92–96. https://doi.org/10.1007/BF02632259

Manokari, M., Shekhawat, A., Faisal, M., Alatar, A. A., Singh, R. K., & Shekhawat, M. S. (2026). Concentration-dependent optimization of cytokinins on direct organogenesis from transverse thin cell layer (tTCL) explants of *Coleus forskohlii* (Willd.) Briq. – A morpho-anatomical approach for sustainable plant production. *Plant Cell, Tissue and Organ Culture (PCTOC), 165*(1), 22. https://doi.org/10.1007/s11240-026-03415-0

Marques, D. M., Veroneze Júnior, V., da Silva, A. B., Mantovani, J. R., Magalhães, P. C., & de Souza, T. C. (2018). Copper toxicity on photosynthetic responses and root morphology of *Hymenaea courbaril* L. (Caesalpinioideae). *Water, Air, and Soil Pollution, 229*(5). https://doi.org/10.1007/s11270-018-3769-2

Martins, J. P. R., Wawrzyniak, M. K., Ley-López, J. M., Kalemba, E. M., Mendes, M. M., & Chmielarz, P. (2022). 6-Benzylaminopurine and kinetin modulations during *in vitro* propagation of *Quercus robur* (L.): An assessment of anatomical, biochemical, and physiological profiling of shoots. *Plant Cell, Tissue and Organ Culture (PCTOC), 151*(1), 149–164. https://doi.org/10.1007/s11240-022-02339-9

Nas, Z., Eşitken, A., & Pirlak, L. (2023). The Responses of 'Viking' Aronia Variety to Salinity Stress under *In Vitro* Conditions. *Erwerbs-Obstbau, 65*(6), 2547–2552. https://doi.org/10.1007/s10341-023-00954-0

Nautiyal (nee Gairi), A., Rashid, A., & Agnihotri, A. (2022). Induction of multiple shoots in *Oryza sativa*: Roles of thidiazuron, 6-benzylaminopurine, decapitation, flooding, and Ethrel® treatments. *In Vitro Cellular & Developmental Biology - Plant, 58*(6), 1126–1137. https://doi.org/10.1007/s11627-022-10316-2

Nicolae, I.-C., Calalb, T., Chiorchină, N., Tabăra, M., Onica, N., & Iulia, B. (2025). *In vitro* propagation of European Varieties of *Aronia melanocarpa* (Michx.) Elliott "Nero" and "Alexandrina". *Proceedings of the XVI International Scientific Agricultural Symposium "Agrosym 2025",* 122–128.

Nowakowska, K., Nongdam, P., Samsurizal, N. A., & Pacholczak, A. (2023). An efficient micropropagation protocol for the endangered european shrub february daphne (*Daphne mezereum* L.) and identification of bacteria in culture. *Agriculture, 13*(9), 1692. https://doi.org/10.3390/agriculture13091692

Nowakowska, K., & Pacholczak, A. (2020). Comparison of the effect of meta-topolin and benzyladenine during *Daphne mezereum* L. micropropagation. *Agronomy, 10*(12), 1994. https://doi.org/10.3390/agronomy10121994

Palancean, A., Florea, V., Onika, E., Roşca, I. (2015). Growth and development of the variety "Alecsandrina" of *Aronia melanocarpa* (Michx.) Elliot in the Republic of Moldova. In: *Conservation of plant diversity, Ed. 4*, Chișinău.

Permadi, N., Prismantoro, D., Navisya Vasall, P. R., Sheelmarevaa, F. A., Nurjanah, S., Nurzaman, M., Alhasnawi, A. N., Doni, F., & Julaeha, E. (2025). Modern and traditional strategies for controlling microbial contamination in plant micropropagation: Current insights and future perspectives. *Current Research in Biotechnology, 10*, 100337. https://doi.org/10.1016/j.crbiot.2025.100337

Petre, A., Stan, A., Popescu, D., Frîncu, M., Ion, V. A., Ciceoi, R., & Asănică, A. (2021). Influence of pre- and post-harvest conditions on quality indicators and microbiota of organic *Aronia melanocarpa*. *Scientific Papers. Series B, Horticulture, LXV*(2), 69–76.

Piras, A., Porcedda, S., Smeriglio, A., Trombetta, D., Nieddu, M., Piras, F., Sogos, V., & Rosa, A. (2024). Chemical composition, nutritional, and biological properties of extracts obtained with different techniques from *Aronia melanocarpa* berries. *Molecules, 29*(11), 2577. https://doi.org/10.3390/molecules29112577

Pop, L., Costa, R., Asănică, A., Cristea, S., Predescu, C., Tăpăloagă, D., & Tudoreanu, L. (2025). Antioxidant capacity and seasonal mineral composition variation in *Aronia melanocarpa* fruits. *Scientific Papers. Series B, Horticulture, LXIX*(1), 872–883.

Popa, G., Dragomir, D., Dogaru, M., & Dobrin, A. (2023). Content of bioactive compounds and antioxidant activity in chokeberries juice (*Aronia melanocarpa*). *Scientific Papers. Series B, Horticulture., LXVII(*1), 139–144.

Quambusch, M., & Winkelmann, T. (2018). Bacterial endophytes in plant tissue culture: mode of action, detection, and control. In V. M. Loyola-Vargas & N. Ochoa-Alejo (Eds.), *Plant Cell Culture Protocols Springer*, 69-88. https://doi.org/10.1007/978-1-4939-8594-4_4

Reshi, Z. A., Husain, F. M., Khanam, M. N., & Javed, S. B. (2025). Effect of meta-Topolin on morphological, physiochemical, and molecular dynamics during *in vitro* regeneration of *Salix tetrasperma* Roxb. *BMC Plant Biology, 25*(1), 121. https://doi.org/10.1186/s12870-025-06095-8

Rusea, I., Popescu, A., Hoza, D., Isac, V., & Oprea, M. I. (2022). *In vitro* rooting and acclimatization *ex vitro* of *Aronia melanocarpa* cv. "Nero". *Journal of Horticulture, Forestry and Biotechnology, 26*(1), 17–22.

Rusea, I., Popescu, A., Isac, V., Nicoleta, A., & Hoza, D. (2018). Adventitious shoot regeneration from petiole explants in black chokeberry (*Aronia melanocarpa*). *Scientific Papers. Series B, Horticulture, LXII*, 83–91.

Salisbury, F. B., & Ross, C. W. (1992). *Plant Physiology*. Wadsworth Publishing Company.

Schmülling, T., Werner, T., Riefler, M., Krupková, E., & Bartrina y Manns, I. (2003). Structure and function of cytokinin oxidase/dehydrogenase genes of maize, rice, Arabidopsis and other species. *Journal of Plant Research, 116*(3), 241–252. https://doi.org/10.1007/s10265-003-0096-4

Scott, R. W., & Skirvin, R. M. (2007). Black chokeberry (*Aronia melanocarpa*) Michx.: a semi-edible fruit with no pests. *Journal of the American Pomological Society, 61*(3), 135–137. https://doi.org/10.71318/apom.2007.61.3.135

Shakshi, Khan, S., Khagta, K., Sharma, P., Kumari, C., Narwal, S., Sharma, R., & Rana, V. S. (2026). Meta-topolin as an effective cytokinin source to enhance *in vitro* establishment, shoot multiplication and alleviation of shoot tip necrosis (STN) in kiwiberry (*Actinidia arguta*) cultivars. *Plant Cell, Tissue and Organ Culture (PCTOC), 164*(3), 97. https://doi.org/10.1007/s11240-026-03410-5

Shishkova, P., Garmidolova, A., Halkoglu, P., Pavlov, A., Krastanov, A., & Georgiev, V. (2026). Dynamics of biomass accumulation by *Aronia melanocarpa* cells in liquid culture. *BIO Web of Conferences, 236*, 02003. https://doi.org/10.1051/bioconf/202623602003

Sidor, A., & Gramza-Michałowska, A. (2019). Black chokeberry *Aronia melanocarpa* L. - a qualitative composition, phenolic profile and antioxidant potential. *Molecules, 24*(20), 3710. https://doi.org/10.3390/molecules24203710

Strnad, M., Hanus, J., Vane, K T., Kami Nek, M., Ballantine, J. A., Fussell, B., & Hanke, D. E. (1997). Meta-topolin, a highly active aromatic cytokinin from poplar leaves (*Populus* × *canadensis* Moench., cv. Robusta). Phytochemistry, 45(2): 213–218.

Szopa, A., Kubica, P., Snoch, A., & Ekiert, H. (2018). High production of bioactive depsides in shoot and callus cultures of *Aronia arbutifolia* and *Aronia* × *prunifolia*. *Acta Physiologiae Plantarum, 40*(3), 48. https://doi.org/10.1007/s11738-018-2623-x

Tamimi, S., & Othman, H. (2020). Effects of copper sulphate on shoot multiplication and rooting of banana (*Musa acuminata* L.) (*in vitro* study). *Asian Journal of Plant Sciences, 19*, 200–204. https://doi.org/10.3923/ajps.2020.200.204

Toma, M., Vintila, M., Moise, D., & Hoza, D. (2022). Advanced research on the dehydration of the black chokeberries (*Aronia melanocarpa* Linn.). *Scientific Papers. Series B, Horticulture., LXVI*(2), 150–162.

Werbrouck, S. P. O. (2021). Meta-topolin and related cytokinins as a solution to some *in vitro* problems. In N. Ahmad & M. Strnad (Eds.), *Meta-topolin: A Growth Regulator for Plant Biotechnology and Agriculture, Springer,* 85-91. https://doi.org/10.1007/978-981-15-9046-7_9

Wójtowicz, A., Combrzyński, M., Biernacka, B., Różyło, R., Bąkowski, M., Wojtunik-Kulesza, K., Mołdoch, J., & Kowalska, I. (2023). Fresh Chokeberry (*Aronia melanocarpa*) Fruits as valuable additive in extruded snack pellets: selected nutritional and physiochemical properties. *Plants, 12*(18), 3276. https://doi.org/10.3390/plants12183276

Yaman, M., Palaz, E. B., Isak, M. A., Demirel, S., İzgü, T., Adalı, S., Demirel, F., Şimşek, Ö., Popescu, G. C., & Popescu, M. (2025). Integrating *in vitro* propagation and machine learning modeling for efficient shoot and root development in *Aronia melanocarpa*. *Horticulturae, 11(*8), 886. https://doi.org/10.3390/horticulturae11080886

Zaytseva, Y. G., Ambros, E. V., & Novikova, T. I. (2021). Meta-topolin: advantages and disadvantages for *in vitro* propagation. In N. Ahmad & M. Strnad (Eds.), *Meta-topolin: A Growth Regulator for Plant Biotechnology and Agriculture, Springer*, 119-141. https://doi.org/10.1007/978-981-15-9046-7_11

Ziv, M. (1995). *In vitro* acclimatization. In J. Aitken-Christie, T. Kozai, & M. A. L. Smith (Eds.), *Automation and environmental control in plant tissue culture, Springer Netherlands*, 493-516. https://doi.org/10.1007/978-94-015-8461-6_20

Scientific Papers. Series E. Land Reclamation, Earth Observation & Surveying, Environmental Engineering. Vol. XV, 2026
Print ISSN 2285-6064, CD-ROM ISSN 2285-6072, Online ISSN 2393-5138, ISSN-L 2285-6064

# NATURA 2000 SITE DEALURILE STREHAIA-BÂTLANELE - UPDATED INFORMATION ON SPECIES AND HABITATS OF COMMUNITY INTEREST

**Marilena ONETE[1], Florian Paul BODESCU[2], Roxana-Georgiana NICOARĂ[1], Minodora MANU[1], Monica Angela NEBLEA[3]**

[1]Institute of Biology Bucharest, 296 Splaiul Independentei, District 6, Bucharest, Romania
[2]SC Multidimension SRL, 7 Ciprian Porumbescu, Săveni, Ialomița County, Romania
[3]Faculty of Science, Physical Education and Informatics, Pitești University,
1 Târgul din Vale Str., Pitești, Argeș County, Romania

Corresponding author email: florianbodescu@gmail.com

***Abstract***

*Situated in south-west Romania (Mehedinți County), with a temperate-continental with sub-Mediterranean influences climate, the protected area Dealurile Strehaia-Bâtlanele (Natura 2000 code ROSCI0405 and ROSAC0405) is a small area (803,9 ha) designated on the basis of the presence of Hermann`s tortoise (Testudo hermanni) and two forest habitats (91M0 Pannonian-Balkanic turkey oak –sessile oak forests and 91Y0 Dacian oak & hornbeam forests). There is very little information about this site (standard forms and national & international websites). Following field trips (summers 2018-2019), our assessment of plant, herpetofauna and invertebrate species and habitats highlighted the existence of species listed in the Habitats Directive, some of them having here a new distribution locality in Romania. The human impact (trash, habitat fragmentation, agricultural field development, forest clearcutting, distribution of invasive species, etc.) is increasing in recent years, and thus this protected area is threatened as a whole. This study highlights the high biological value of the site. The increasing intensity of human pressures poses a major threat to ecosystem integrity, emphasising the need for appropriate conservation and management measures.*

***Key words****: Natura 2000 site, community interest species and habitats, high biological value.*

## INTRODUCTION

The Natura 2000 network represents the cornerstone of the European Union's biodiversity conservation policy, established under the Habitats Directive 92/43/EEC and the Birds Directive 2009/147/EC (Evans, 2012). This European network of protected areas aimed at conserving habitats and species of high ecological value (EEA, 2025). Its main objective is to ensure the long-term survival of Europe's most valuable and threatened species (Trochet & Schmeller, 2013) and habitats by designating protected areas such as Sites of Community Interest (SCI) and Special Protection Areas (SPA) (Mücher et al., 2009; Popescu et al., 2014).

In Romania, sites coded ROSCI and ROSAC are part of Natura 2000, the European ecological network created to conserve biodiversity across the European Union. This network operates under the Habitats Directive 92/43/EEC and the Birds Directive 2009/147/EC (H.D., 1992; B.D., 2009).

Within the Romanian classification system, ROSCI (Romanian Sites of Community Importance) designate areas proposed and approved at the European level as Sites of Community Importance because they host habitat types and species listed in the annexes of the Habitats Directive. After the establishment of conservation measures and management plans, many of these sites are formally designated as ROSAC (Romanian Special Areas of Conservation), representing the final conservation status under the directive (EEA, 2020; ANANP, 2022; M.O., 2023a).

The transition from ROSCI to ROSAC reflects the implementation stage of conservation policy, indicating that concrete management measures are in place to maintain or restore the favourable conservation status of protected habitats and species. Together, these sites represent an essential component of Romania's protected area system and contribute to biodiversity conservation and ecological

connectivity within the Natura 2000 network (M.O., 2023b).

Standard forms (Standard Data Forms - SDFs), are official documents used to describe and report key information about each Natura 2000 site. They include data on site location, area, habitat types, species presence, conservation status, and threats (H.D., 1992). Specifically, SDFs cover habitat classifications following the EU Habitats Directive, population estimates of protected species, and human pressures affecting the site. The role of these forms is threefold: firstly, they provide a consistent framework for reporting across EU member states; secondly, they support the monitoring and assessment of site conservation status; and thirdly, they serve as a legal and management tool for planning conservation measures (EEA, 2020; Spiliopoulou et al., 2023). By standardising data collection, SDFs facilitate decision-making, help identify priority conservation actions, and ensure compliance with EU environmental legislation. Thus, Natura 2000 standard forms are essential for effective biodiversity management and long-term ecological sustainability.

In Romania, the implementation of Natura 2000 network has played a crucial role in the conservation of biodiversity, particularly in regions characterised by high ecological diversity and unique habitat types (Gafta & Mountford, 2008; Stancioiu et al., 2010; Manolache et al., 2017).

The SDF (2020) states that the protected area ROSCI0405 Dealurile Strehaia-Bâtlanele is a Site of Community Interest located in Mehedinți County, in southwestern Romania, within the Continental biogeographical region. The site covers approximately 803.90 hectares and occupies parts of the administrative territories of the town of Strehaia and the commune of Greci, representing approximately 5.1% and 6.3% of their respective areas. Although relatively small in size, the site plays an important role in maintaining regional biodiversity (M.P., 2019; M.O., 2023a; 2023b).

From a biogeographical perspective, the area is characterised by a temperate-continental climate with sub-Mediterranean influences, which creates favourable conditions for the development of thermophilous habitats and species that reach their northern or eastern distribution limits in this region. The ecological value of the site is primarily associated with two forest habitat types of community interest: **Habitat 91M0 - Pannonian-Balkanic turkey oak-sessile oak forests**, dominated by species such as *Quercus cerris* and *Quercus frainetto*, covering approximately 385 hectares, and **Habitat 91Y0 - Dacian oak-hornbeam forests**, characterised by *Carpinus betulus* and *Quercus robur*, which occupy around 325 hectares. The site was designated primarily for the conservation of the Hermann's tortoise, *Testudo hermanni boettgeri*, a species listed in Annex II of the Habitats Directive and considered one of the flagship species of this protected area (SDF, 2020).

The site is legally protected through national regulations (M.O., 2023b), its management is currently coordinated by the National Agency for Natural Protected Areas (ANANP), which implements conservation measures through officially approved management plans. These measures aim to maintain favourable conservation conditions for protected species and habitats, including the preservation of open clearings required for tortoise thermoregulation and the control of invasive species.

Biodiversity inventories and long-term ecological monitoring are essential components of effective management within protected areas. As a member state of the European Union, Romania has the obligation to maintain or restore the favourable conservation status of habitats and species of community interest. Reliable data on species distribution, population dynamics, and ecological pressures are therefore necessary to define appropriate management objectives and evaluate the effectiveness of conservation actions. Previous information regarding the biodiversity of the ROSCI0405 site was relatively limited and often derived from general surveys or standard reporting forms, which frequently focused on mountainous regions while overlooking hilly landscapes such as those found in the Strehaia area. In the Management Plan of the protected area (M.P., 2019), within the section 'Species of conservation interest for which the protected natural area was designated', the subsections regarding lower and higher plants, invertebrates, ichthyofauna, and other flora and fauna species

relevant to the protected area are empty (not filled).

In this context, the present study aimed to conduct an updated inventory of flora and fauna within the ROSCI0405 Dealurile Strehaia-Bâtlanele site, to identify species of community interest and other important species that had not been previously recorded in the area, and to perform a quantitative assessment of habitat conservation status and of the population status of the flagship species *Testudo hermanni*. By integrating field observations with multivariate statistical analyses, this research seeks to provide a robust scientific basis for improving conservation strategies and supporting the implementation of the recently approved management plan for the protected area.

## MATERIALS AND METHODS

The ROSCI0405 Dealurile Strehaia-Bâtlanele site is situated in south-western Romania, forming part of the South-West Oltenia Development Region. The site lies entirely in the Continental biogeographical region and encompasses the Strehaia Hills, a subunit of the Getic Plateau, located in the north-western section of the Wallachian Platform (Figure 1).

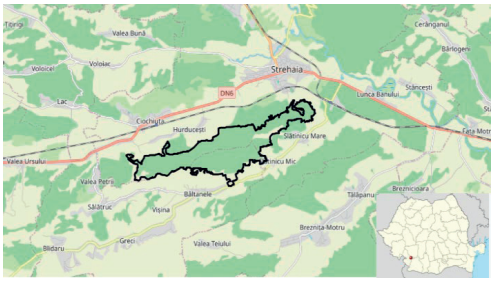



Figure 1. Location of the studied area in Romania and its position in the region (After EEA, 2024)

The topography is dominated by hills with elevations ranging between 200 and 310 metres, with slopes of 5 to 20 degrees and varying orientations. The abiotic environment is characterised by mean annual temperatures of approximately 6.43-11.52°C and mean annual precipitation between 48.33 and 74.83 mm. The forest administration is handled by the Strehaia Forest District (M.O., 2023b).

Biodiversity data were collected during two vegetation seasons (2018-2019), for developing the management plan.

Vegetation assessment was carried out using two complementary methods: transect itineraries and phytosociological relevés. Relevés were performed in plots distributed to cover the homogeneity and diversity of the forest habitats (91M0 and 91Y0) (Figure 2).

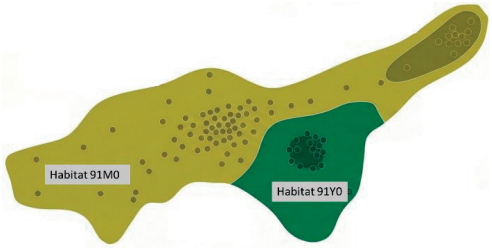



Figure 2. The map of the habitats and inventorying plots' distribution in ROSCI0405 Dealurile Strehaia-Bâtlanele

Plant species abundance-dominance was recorded using the Braun-Blanquet scale (5 = 75-100%; 4 = 50-75%; 3 = 25-50%; 2 = 10-25%; 1 = 1-10%; + = 0.1-1%). Identification of plants and habitats followed standard Romanian floras and manuals (Doniță et al., 2005; Gafta and Mountford, 2008; Ciocârlan, 2009; Sârbu et al., 2013). The characteristics of the plant species follow Oltean et al. (1994), Ciocârlan (2009), Sârbu et al. (2013), IAS (2025). The community interest species *Ruscus aculeatus* distribution and density were recorded in 5 x 5 m plots established along areas where relevés were performed.

Using software package PAST (Hammer et al., 2001), we grouped sites based on plant species abundance (Bray-Curtis Similarity Index), analysed groupings based on plant species presence-absence (Jaccard Similarity Index) and identified associations between specific plant species and sampling locations (Principal Component Analysis - PCA).

Surveys for herpetofauna targeted 10 designated open areas preferred by reptiles for thermoregulation and foraging. The studies were conducted between July and October 2019 to coincide with peak activity and avoid hibernation periods. For each observation, GPS coordinates, species, number of individuals, sex, and reproductive state were recorded.

Observations for community interest invertebrates were conducted concurrently with habitat assessments in the forest sectors.

## RESULTS AND DISCUSSIONS

The study confirmed the two main forest habitats within the ROSCI0405 Dealurile Strehaia-Bâtlanele site, which play a key role in regional biodiversity conservation, particularly for the Hermann's tortoise (*Testudo hermanni*), as it is specified in SDF (2020) and M.O. (2023a; 2023b).

**Habitat 91M0 (Pannonian-Balkanic turkey oak-sessile oak forests)** is the dominant habitat, covering about 369.92 ha. It occurs at altitudes of 200-300 m on sunny, moderately dry slopes (5-20°). The tree layer (50-80% cover) is formed mainly by *Quercus petraea*, *Quercus cerris*, *Quercus frainetto*, and *Tilia tomentosa*. The shrub layer includes species such as *Crataegus monogyna* and *Cornus mas*, while the herb layer (10-60% cover) is dominated by species like *Helleborus odorus* and *Melica uniflora*.

**Habitat 91Y0 (Dacian oak-hornbeam forests)** covers 162.31 ha, occurring at 200-310 m on mainly west-facing slopes (5-15°). The canopy includes *Quercus robur*, *Fraxinus angustifolia* ssp. *oxycarpa*, and *Carpinus betulus*, with a diverse herb layer dominated by *Ornithogalum pyrenaicum* and *Scutellaria altissima*.

Both habitats are in generally favourable conservation condition, although affected locally by invasive species such as *Ambrosia artemisiifolia* and the spread of *Robinia pseudoacacia* from nearby plantations.

Our records on seedlings/saplings of trees from the area showed that natural regeneration is generally very good, reaching in some areas a coverage of 50%. Some species are typical for one habitat type but there are many species common to both of them. From about 130 herbaceous plant species registered in the studied protected area, we present only the species with higher abundance in the two Natura 2000 habitats (Table 1).

The list of recorded species comprises *Ruscus aculeatus* (Figure 3)*, Ruscus hypoglossum, Asparagus verticillatus, Epipactis helleborine, Galium kitaibelianum, Neottia nidus-avis, Platanthera bifolia,* rare taxa with reduced world populations, not threatened yet but at risk (as a result of their reduced distribution area) (Oltean et al., 1994).

Table 1. The characteristics of the plant species

| Species' name | Trees | Seeedling /sapling | Common | Typical for 91M0 | Typical for 91Y0 | I&P |
|---|---|---|---|---|---|---|
| *Acer campestre* | + | + | + | | | |
| *Acer platanoides* | + | + | + | | | |
| *Acer tataricum* | + | | | + | | |
| *Carpinus betulus* | + | | | | + | |
| *Carpinus orientalis* | + | | | + | | |
| *Cornus mas* | + | + | + | | | |
| *Fagus sylvatica* | + | + | + | | | |
| *Fraxinus excelsior* | + | + | + | | | |
| *Fraxinus ornus* | + | + | | + | | |
| *Gleditschia triacanthos* | | + | | | | + |
| *Populus tremula* | + | | + | | | |
| *Prunus avium* | + | | + | | | |
| *Pyrus pyraster* | + | + | + | | | |
| *Quercus cerris* | + | + | | + | + | |
| *Quercus dalechampii* | + | + | | + | + | |
| *Quercus frainetto* | + | + | | + | + | |
| *Quercus petraea* | + | + | | + | + | |
| *Quercus robur* | + | | | | + | |
| *Robinia pseudoacacia* | + | + | | | | + |
| *Sorbus aria* | + | + | + | | | |
| *Sorbus aucuparia* | + | + | + | | | |
| *Sorbus torminalis* | + | + | + | | | |
| *Tilia cordata* | + | + | + | | | |
| *Tilia platyphyllos* | + | + | + | | | |
| *Tilia tomentosa* | + | + | | + | + | |
| *Ulmus glabra* | + | | + | | | |
| *Ulmus laevis* | + | + | + | | | |
| *Cornus sanguinea* | | | + | | | |
| *Crataegus monogyna* | | | + | | | |
| *Euonymus verrucosus* | | | + | | | |
| *Ligustrum vulgare* | | | + | | | |
| *Prunus spinosa* | | | + | | | |
| *Rhamnus cathartica* | | | + | | | |
| *Rosa canina* | | | + | | | |
| *Rubus agg.* | | | + | | | |
| *Ambrosia artemisiifolia* | | | | | | + |
| *Asclepias syriaca* | | | | | | + |
| *Arum orientale* | | | | + | + | |
| *Asperula taurina* | | | | | + | |
| *Campanula bononiensis* | | | | | + | |
| *Campanula persicifolia* | | | | + | | |
| *Erigeron annua* | | | | | | + |
| *Galium schultesii* | | | | + | + | |
| *Genista tinctoria* | | | | + | | |
| *Glechoma hirsuta* | | | | + | | |
| *Helleborus odorus* | | | | + | + | |
| *Lathyrus niger* | | | | + | | |
| *Lithospermum purpurocaeruleum* | | | | + | | |
| *Lychnis coronaria* | | | | + | | |
| *Melittis melissophyllum* | | | | + | | |
| *Poa nemoralis* | | | | + | | |
| *Potentilla micrantha* | | | | + | | |
| *Pteridium aquilinum* | | | | | | + |
| *Setaria viridis* | | | | | | + |
| *Tanacetum corymbosum* | | | | + | | |

In Table 1, invasive and pest species (I & P) refer the presence of non-native flora within the

protected area. *Ambrosia artemisiifolia* and *Robinia pseudoacacia* are not currently included in the Union List of Invasive Alien Species of Union Concern (IAS, 2014; 2025), but they represent a significant ecological threat at the national level. *Ambrosia artemisiifolia* poses a major risk to public health due to its highly allergenic pollen, while *Robinia pseudoacacia* acts as an ecosystem transformer, displacing native vegetation and altering soil nitrogen levels. Furthermore, species such as *Gleditsia triacanthos* and *Erigeron annuus* show aggressive expansion in ruderal and riparian habitats, potentially compromising the structural integrity of local plant communities.

Other two species recorded in the site: *Pteridium aquilinum* (native species which, in this context, acts as a dominant taxon) indicate the degradation of local pastures, rather than being an exotic threat; *Setaria viridis* (common weed) has limited impact on the primary conservation objectives of the area. Only *Asclepias syriaca* recorded at the edge of the protected area is a IAS species under European cocern.

*R. aculeatus* is presented in Annex V of Habitat Directive (animal and plant species of community interest whose taking in the wild and exploitation may be subject to management measures) (H.D., 1992).




Figure 3. *Ruscus aculeatus*: individual with fruit (a) and local density in Str.8 (b)

In Natura 2000 Strehaia-Bâtlanele, this European interest species was found in 11 of the 31 recorded plots and distributed sometimes as rare, but having high abundance in other plots and significant cover at certain stations (Str.5 and Str.8) (Figure 4). It occurs in both main protected forest habitats: 91M0 and 91Y0. In habitat 91M0, *R. aculeatus* is a constant component of the herbaceous layer, typically developing on rocky substrates in sunny, mesoxerophilous conditions.

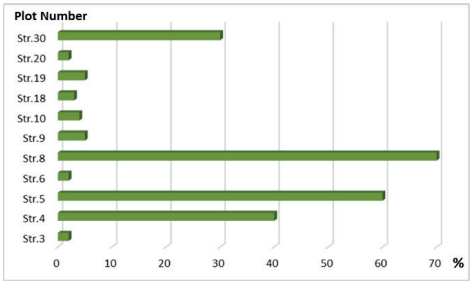



Figure 4. The distribution and density of *Ruscus aculeatus*

In habitat 91Y0, *R. aculeatus* is part of the stratified forest structure, and in some vegetation stands, *R. aculeatus* reaches remarkable ground cover values of up to 50%.

Although the species shows good local abundance, some populations may be affected by anthropogenic pressures, particularly the development of forest access roads that intersect its distribution areas.

The recorded presence of *Ruscus aculeatus* in the site represents a new distribution locality for the species in Romania.

The ordination analysis using Principal Component Analysis revealed a moderate differentiation of sampling sites based on species composition. The first axis explained 12.0% of the total variance, while the second axis accounted for 9.2% (Figure 5).

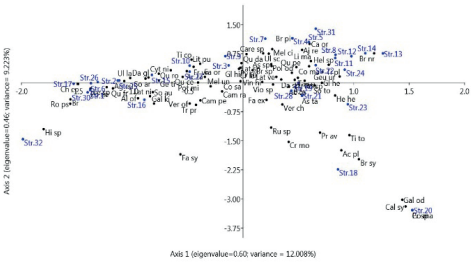



Figure 5. The ordination analysis using Principal Component Analysis of the recorded species

Sampling sites were distributed along the first axis, forming two partially separated groups. Sites located on the left side of the ordination diagram (e.g., Str.17, Str.26, Str.30) showed a particular species composition, while those positioned on the right side (e.g., Str.13, Str.14, Str.24) were associated with a different set of species.

Several species were positioned close to specific sampling sites, suggesting a stronger association with those locations. In contrast, some species occurred near the centre of the diagram, indicating a broader ecological distribution.

Two sampling sites (Str.20 and Str.32) were clearly separated from the main cluster of sites, suggesting distinct species assemblages compared with the rest of the study area.

Cluster analysis based on the Bray-Curtis similarity index and Jaccard similarity index revealed patterns of similarity among the sampling sites according to species composition (Figure 6a and 6b).

In the dendrogram based on the Bray-Curtis index (Figure 6a), the sampling sites were grouped into several clusters reflecting similarities in species abundance. A major cluster included sites such as Str.6, Str.17, Str.1, Str.2, and Str.15, which showed relatively high similarity values. Another group consisted of sites Str.11-Str.14 and Str.21-Str.23, indicating comparable species composition among these locations. Some sampling sites, such as Str.3 and Str.20, were separated from the main clusters, indicating lower similarity with other sites.

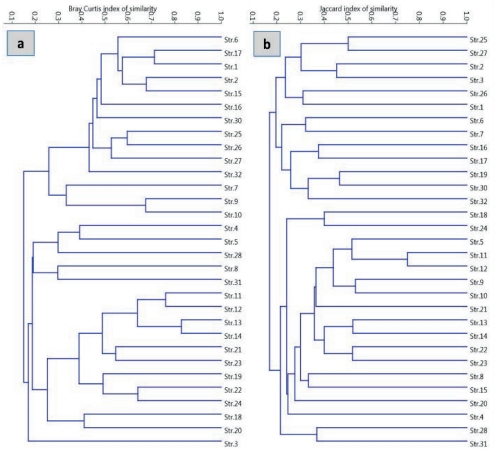



Figure 6. Cluster analysis based on the Bray-Curtis similarity index (a) and Jaccard similarity index (b)

The dendrogram based on the Jaccard index (Figure 6b), which considers species presence-absence, showed a similar overall grouping pattern, although with slight differences in cluster structure. Several sampling sites, including Str.25, Str.27, Str.2, and Str.3, formed a cluster with relatively high similarity. Other groups included sites such as Str.11-Str.12 and Str.9-Str.10, suggesting shared species composition among these locations.

Overall, both similarity indices indicated the presence of multiple clusters of sampling sites with comparable species composition, while a few sites appeared more distinct from the main groups.

Field research regarding herpetofauna revealed that the distribution of main target species, Hermann's tortoise (*Testudo hermanni*) (Figure 7), is highly localised to open glades.



Figure 7. *Testudo hermanni*
(the pattern of the shell design)

The total population of tortoises within the site is estimated at 179-182 individuals, with an average density of 2.88-2.93 individuals per hectare, significantly lower than densities recorded in more favourable habitats. Only adult individuals were observed, with no juveniles recorded during the hatching period. However, the conservation status of the Hermann's Tortoise (*T. hermanni*) is highly concerning. The "Unfavourable-Bad" assessment is driven by low population density and a lack of recruitment (juveniles). The high proportion of forest cover (over 80%) in the site limits the available habitat for tortoises, which require open meadows for foraging and nesting. Current management focuses on non-intervention in forest sectors, but for tortoises, this policy may lead to the "closing" of glades as the canopy density increases, further reducing habitat availability.

Several additional amphibian and reptile species that were newly recorded during this study had previously been absent from the official site documentation. Among amphibians, the *Pelophylax kl. esculentus* (edible frog) (Figure 8) was observed in ruderalised meadows with active springs and small water bodies, which provide suitable feeding and breeding conditions.



Figure 8. *Pelophylax kl. esculentus* recorded in a pond

Four new reptile species were also recorded (Figure 9). The most common was *Lacerta viridis* (European green lizard), a thermophilous species frequently observed in open habitats and on sunny slopes, with at least seven individuals recorded during surveys. *Natrix natrix* (grass snake) was identified in areas where springs and ponds provide abundant amphibian prey. Two additional species were considered rare within the site: *Coronella austriaca* (smooth snake), was recorded only once inside forest habitats, and *Zamenis longissimus* (Aesculapian snake), a semi-arboreal species typically associated with forest interiors and edges.




Figure 9. The new reptile species recorded in the studied site

Comparison with regional studies indicates that while ROSCI0405 has stable forest habitats (91M0 and 91Y0 are currently in "Favourable" status), the herpetofauna faces increasing pressure. Human impacts identified during the study - such as heavy vehicle traffic causing road gullying, the distribution of illegal waste, and sheep/goat grazing - are degrading the fragile meadow-forest ecotones.

Several invertebrate species of community interest (Figure 10) have been recorded in the ROSCI0405 Dealurile Strehaia-Bâtlanele site, highlighting the ecological importance of its forest and edge habitats.

Thus, *Lucanus cervus* (stag beetle), listed in Annex II of the EU Habitats Directive, was identified here as a new locality in its Romanian distribution. This saproxylic species is closely associated with deciduous forests, particularly oak-dominated habitats such as 91M0 and 91Y0 within the site. Its presence depends largely on mature *Quercus* trees and the availability of dead wood, which provides essential breeding microhabitats.

Another species of conservation interest is *Cerambyx cerdo* (great capricorn beetle), which inhabits old deciduous forests and shows a strong preference for mature or declining oak trees such as *Quercus petraea*, *Quercus cerris*, and *Quercus frainetto*. The species was directly observed during field surveys conducted in 2018-2019, and its occurrence is linked to the presence of standing and fallen dead wood.

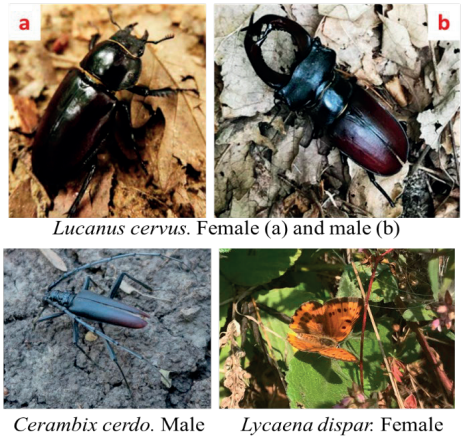



Figure 10. Invertebrate species of community interest

The site also hosts *Lycaena dispar* (large copper butterfly), typically found in humid grasslands, forest edges, and open clearings. In the area, it was recorded mainly in forest margins and glades, where herbaceous vegetation is well developed.

Conservation measures recommended for these invertebrates include maintaining native forest structure, preserving dead wood, and avoiding the use of insecticides in forest ecosystems.

Despite the relatively good conservation status of the forest habitats, the ecological integrity of the site is threatened by several anthropogenic pressures. One of the most significant threats is the spread of invasive plant species, which alters the structure and functioning of natural ecosystems. Species such as *Ambrosia artemisiifolia, Asclepias syriaca, Pteridium aquilinum*, and *Erigeron annuus* frequently colonise disturbed areas, especially along forest roads or degraded clearings. These plants can form dense stands that reduce floristic diversity and replace native vegetation communities. For example, *Ambrosia artemisiifolia* often forms monocultures that significantly degrade the tortoise's feeding grounds by replacing the diverse herbaceous flora required for its diet.

Another major ecological pressure is the expansion of the non-native tree species *Robinia pseudoacacia* (black locust). This species spreads aggressively from nearby plantations into natural forest habitats, where it alters soil conditions and promotes the dominance of nitrophilous plants such as *Urtica dioica*. As a result, the floristic diversity characteristic of oak and hornbeam forests is reduced, and open grassland areas necessary for thermophilous reptiles gradually disappear. Because *Testudo hermanni* depends on sunny habitats for thermoregulation and feeding, the spread of black locust represents a significant long-term threat to the survival of the species in the site.

Human activities also contribute to habitat degradation. The development of forest roads and uncontrolled access by off-road vehicles can damage vegetation, create erosion channels, and facilitate the spread of invasive species. In addition, illegal waste dumping and uncontrolled tourism can negatively affect the ecological quality of the habitats. Illegal collection of tortoises for the pet trade is considered one of the most serious direct threats to the species, as it primarily affects adult individuals that are essential for maintaining population stability.

Grazing activities also influence the ecological dynamics of the site. Sheep grazing is generally considered to have a relatively low impact on forest habitats, as animals mainly use the forest as a transit route toward surrounding grasslands. However, grazing may still cause trampling of vegetation and disturbance of tortoise feeding areas, particularly when herds are accompanied by dogs. Goat grazing is considered much more destructive, as goats selectively consume vegetation, promote soil erosion, and facilitate the spread of invasive plants through seed dispersal in their fur.

Another ecological issue affecting the site is the gradual closure of open glades due to natural vegetation succession. In the absence of traditional land management practices such as controlled grazing or selective clearing, shrubs and young trees gradually invade grasslands and forest clearings. This process leads to canopy closure and the transformation of sunny habitats into shaded forest environments that are unsuitable for thermophilous reptiles such as *Testudo hermanni*.

Because of these cumulative pressures, the conservation status of the Hermann's tortoise population in the site is currently assessed as "unfavourable-bad". Consequently, several management measures have been proposed in order to improve the conservation status of the species and protect the ecological integrity of the habitats.

One of the most important measures involves active habitat management, particularly maintaining open habitats suitable for the tortoise. This includes cutting shrubs and young trees that threaten to close forest clearings and grasslands, especially in the main observation areas. Maintaining these open areas ensures adequate sunlight exposure necessary for the species' thermoregulation and nesting behaviour.

Another recommended action is the modification and expansion of the site boundaries. Field observations revealed that several individuals of *Testudo hermanni* occur in adjacent south-facing grasslands located outside the current limits of the protected area. Expanding the site to include these habitats would improve the protection of the species and increase the ecological connectivity of the landscape (ANANP, 2020).

The control and eradication of invasive species also represent a major priority. Management plans propose regular monitoring and mechanical removal of invasive plants such as *Ambrosia artemisiifolia* and *Asclepias syriaca*, particularly along forest roads and disturbed areas that serve as dispersal corridors. In addition, the expansion of *Robinia pseudoacacia* should

be limited through removal of invasive stands and replacement with native tree species characteristic of the local forest ecosystems.
Regulation of human activities is another key component of conservation management. Measures proposed include restricting unauthorised vehicle access through the installation of barriers, controlling waste disposal, and prohibiting the collection of tortoises from the wild. Grazing activities should also be regulated by establishing sustainable stocking limits based on the ecological carrying capacity of the habitats.

## CONCLUSIONS

The Natura 2000 site ROSCI0405 Dealurile Strehaia-Bâtlanele, located in the hilly region of Mehedinți County, represents an important biodiversity reservoir despite its relatively small surface area. The field studies significantly expanded the knowledge of the site's biological diversity, demonstrating that its ecological value is considerably higher than previously documented in the official Standard Data Form. The research identified new occurrences of species of community interest and confirmed the presence of several rare plants and animals, emphasising the conservation importance of this protected area within Romania's Natura 2000 network.
One of the most important botanical findings was the identification of *Ruscus aculeatus*, a species listed in Annex V of the EU Habitats Directive. Its presence in the site represents a new distribution locality in Romania. The species occurs in both main forest habitats of the site - 91M0 (Pannonian - Balkanic turkey oak-sessile oak forests) and 91Y0 (Dacian oak-hornbeam forests) - where it forms part of the shrubs layer and, in some stands, reaches ground cover values of up to 50%.
The faunal component of the site also includes several species of European conservation interest. Among invertebrates, the presence of *Lucanus cervus* (stag beetle) was recorded as a new locality, further emphasising the importance of the site for saproxylic insect conservation. Other protected species observed during the surveys include *Cerambyx cerdo* (great capricorn beetle) and *Lycaena dispar* (large copper butterfly), all species listed in Annex II of the Habitats Directive. These species are closely associated with mature deciduous forests and structurally complex habitats containing old trees and dead wood, conditions that are still partially preserved in the forest ecosystems of the site.
Additional herpetofauna species not previously included in the official documentation of the site were also recorded: *Pelophylax kl. esculentus* (edible frog), *Lacerta viridis* (European green lizard), *Natrix natrix* (grass snake), *Coronella austriaca* (smooth snake), *Zamenis longissimus* (Aesculapian snake).
Long-term monitoring and research programs are essential for assessing the effectiveness of these conservation measures. Monitoring protocols should focus on key periods in the tortoise's life cycle, including migration to breeding areas, egg-laying, and movement toward hibernation sites. Cooperation between forest managers and protected area administrators is also necessary to ensure effective surveillance and protection of the habitats.
Public awareness and environmental education represent additional important tools for conservation. Informational panels and educational programmes for local communities and schools can help increase awareness of the ecological importance of the site and promote responsible behaviour within the protected area.
Overall, the results of this research demonstrate that the ROSCI0405 Dealurile Strehaia-Bâtlanele site has a much higher biological value than previously recognised. The discovery of new distribution localities for species of community interest such as *Ruscus aculeatus* and *Lucanus cervus*, together with the presence of numerous rare plants and vertebrates, highlights the importance of this area for regional biodiversity conservation. This increased knowledge as to the value of Dealurile Strehaia-Bâtlanele should contribute not only to the Natura 2000 network in Europe, but also to national biodiversity planning and implementation in Romania. These findings provide an important scientific basis for the implementation of the site's management plan and establish a baseline for the five-year monitoring cycles required under the EU Habitats Directive, ensuring that conservation actions can be effectively evaluated and adapted in the future.

## ACKNOWLEDGEMENTS

Our study was developed in the period 2018-2019 in the framework of the project "Elaboration of the management plan for the site of community importance ROSCI0405 Strehaia Hills - Bâtlanele", SMIS Code 102055. The present paper is written in the framework of the project RO1567-IBB01 from the Institute of Biology Bucharest, financed by the Romanian Academy. We kindly thank to J. Owen Mountford for his valuable comments on the article and for controlling the correctness of English.

## REFERENCES

ANANP (2020). *Note on the minimum set of special measures for the protection and conservation of biological diversity, as well as the conservation of natural habitats, wild flora and fauna, the safety of the population and investments in ROSCI0405 Strehaia-Batlanele Hills*, https://ananp.gov.ro/wp-content/uploads/ROSCI0405-SKM_28722030315321.V.pdf

ANANP (2022). *Management and monitoring guidelines for Natura 2000 sites in Romania*. National Agency for Natural Protected Areas, Bucharest.

B.D. (2009). *Directive 2009/147/EC on the conservation of wild birds (Birds Directive)*. Official Journal of the European Union, European Parliament & Council of the European Union. L20.

Ciocârlan, V. (2009). *Illustrated flora of Romania. Pteridophyta and Spermatophyta*. Editura Ceres. Bucureşti.

Doniţă, N., Popescu, A., Paucă-Comănescu, M., Mihăilescu, S., & Biriş, I.-A. (2005). *The habitats from Romania*, Editura Tehnică Silvică, Bucureşti.

EEA (2020). *Natura 2000 and protected areas – background and management principles*. European Environment Agency Copenhagen.

EEA (2024). NATURA 2000 - *Standard Data Form Dealurile Strehaia - Bâtlanele (ROSCI0405 - SCI)*, https://natura2000.eea.europa.eu/Natura2000/sdf/#/sdf?site=ROSCI0405&release=33&nav=2

EEA (2025). *Designated terrestrial protected areas in Europe,* https://www.eea.europa.eu/en/analysis/indicators/terrestrial-protected-areas-in-europe

Evans, D. (2012). Building the European union's Natura 2000 network. *Nature conservation*, *1*, 11-26.

Gafta, D., & Mountford, J.O. (Coord.) (2008). *Manual of interpretation of Natura 2000 Habitats in Romania*, Editura Risoprint, Cluj-Napoca.

H.D. (1992). *Council Directive 92/43/EEC on the conservation of natural habitats and of wild fauna and flora (Habitats Directive)*. Official Journal of the European Communities, European Commission. L206.

Hammer, Ø., Harper, D.A.T., & Ryan, P.D. (2001). PAST: Paleontological statistics software package for education and data analysis. *Palaeontologia Electronica*, 4 (1). 1–9.

IAS (2014). Regulation (EU) No 1143/2014 on the prevention and management of the introduction and spread of invasive alien species, European Parliament and European Council, http://data.europa.eu/eli/reg/2014/1143/oj

IAS (2025). Invasive Alien Species portal, https://www.ias.eea.europa.eu

M.O. (2023a). *Order No. 2346/2023 regarding the update of the list of Natura 2000 sites in Romania*, Romanian Ministry of Environment, Waters and Forests. Bucharest.

M.O. (2023b). Environment, Water and forests Ministry Order no. 2.346/2023 regarding the approval of the Management Plan for Natura 2000 site ROSCI0405 Dealurile Strehaia—Bâtlanele. Annex: *The Management Plan of NATURA 2000 site ROSCI0405 Dealurile Strehaia-Bâtlanele*, Romanian Government.

M.P. (2019). *The Management Plan of NATURA 2000 site ROSCI0405 Dealurile Strehaia-Bâtlanele*, https://djmmh.anmap.gov.ro/plan-de-management-al-sitului-natura-2000-rosci0405-dealurile-strehaia-batlanele/

Manolache, S., Ciocanea, C. M., Rozylowicz, L., & Nita, A. (2017). Natura 2000 in Romania-a decade of governance challenges. *European Journal of Geography*, *8*(2).

Mücher, C. A., Hennekens, S. M., Bunce, R. G., Schaminée, J. H., & Schaepman, M. E. (2009). Modelling the spatial distribution of Natura 2000 habitats across Europe. *Landscape and urban planning*, *92*(2), 148-159.

Oltean, M., Negrean, G., Popescu, A., Roman, N., Dihoru, G., Sanda,V., Mihailescu, S. (1994). The red list of vascular plants from Romania. *Ecology Studies, Syntheses, Documentations*, Institute of Biology Bucharest.

Popescu, V. D., Rozylowicz, L., Niculae, I. M., Cucu, A. L., & Hartel, T. (2014). Species, habitats, society: an evaluation of research supporting EU's Natura 2000 network. *PloS one*, *9*(11), e113648.

Sârbu, I., Ştefan, N., & Oprea, A. (2013). *Vascular plants of Romania. Illustrated field identification manual*. Editura Victor B Victor, Bucureşti.

SDF (2020). Standard Form Natura 2000, https://www.mmediu.ro/app/webroot/uploads/files/Formulare_standard_SCI.pdf

Spiliopoulou, K., Brooks, T. M., Dimitrakopoulos, P. G., Oikonomou, A., Karavatsou, F., Stoumboudi, M. T., & Triantis, K. A. (2023). Protected areas and the ranges of threatened species: Towards the EU Biodiversity Strategy 2030. *Biological Conservation*, *284*, 110166.

Stancioiu, P. T., Abrudan, I. V., & Dutca, I. (2010). The Natura 2000 ecological network and forests in Romania: implications on management and administration. *International forestry review*, *12*(1), 106-113.

Trochet, A., & Schmeller, D. S. (2013). Effectiveness of the Natura 2000 network to cover threatened species. *Nature Conservation*, *4*, 35-53.

Scientific Papers. Series E. Land Reclamation, Earth Observation & Surveying, Environmental Engineering. Vol. XV, 2026
Print ISSN 2285-6064, CD-ROM ISSN 2285-6072, Online ISSN 2393-5138, ISSN-L 2285-6064

# ASSESSMENT OF THE STATE OF ATMOSPHERIC AIR IN AN URBAN ENVIRONMENT DURING A FIRE AT A SOLID WASTE LANDFILL AND COMPARISON WITH AIR QUALITY INDICES

**Georgi PATRONOV[1], Diana KIRIN[2, 3], Kenan SEZER[4], Petya ZAHARIEVA[3], Radoslava ZAHARIEVA[3]**

[1]University of Plovdiv 'Paissii Hilendarski', Department of Chemical Technology, 24 Tsar Assen Str., 4000 Plovdiv, Bulgaria
[2]Agricultural University - Plovdiv, Department of Chemistry, Phytopharmacy and Ecology and Environmental Protection, 12 Mendeleev Blvd, 4000 Plovdiv, Bulgaria
[3]National Institute of Geophysics, Geodesy and Geography, Hydrology and Water Management Research Center, Bulgarian Academy of Sciences, Acad. G. Bonchev Str., 1113, Sofia, Bulgaria
[4]Trakya University, Department of Chemistry, Balkan Campus, 22030, Edirne, Türkiye

Corresponding author email: patron@uni-plovdiv.bg

***Abstract***

*A study of the state of atmospheric air and anthropogenic impact in a typical urban area of Bulgaria - the city of Plovdiv and its surroundings was conducted. The study is based on a specific incident - a fire at a solid waste landfill in the city of Plovdiv. The values of the main pollutants of the atmospheric air above the settlements were monitored (PM10, $SO_2$, $NO_2$, $O_3$, CO and benzene). The chemical and ecological state of the atmospheric air was assessed. Its quality was analyzed using the Air Quality Index (AQI) of the United States Environmental Protection Agency (US-EPA) and the European Air Quality Index (EAQI) of the European Environment Agency. Deviations from the permissible values are observed only for particulate matter (PM10) - irregular higher hourly values above the permissible value, which is for 24 hours. The results are compared with those of the two automatic stations in the city. The possible impact of the excessive values on human health, living organisms, and protected habitats is shown. Measures to improve air quality were discussed.*

***Key words****: air pollution, air quality index, anthropogenic impact, chemical state, particulate matter.*

## INTRODUCTION

Anthropogenic air pollution arises from human activities related to industrial and social development. The majority of the population exposed and affected by air pollution lives in the area of pollution sources. Obviously, attention is being directed towards the urban environment and industrial sites (Allegrini et al., 2023).

Any activity that leads to a deterioration or reduction in the quality of the natural environment is considered pollution. This is the biggest global problem facing humanity and a leading environmental cause of morbidity and mortality (WHO global air quality guidelines, 2021; Directive (EU) 2016/2284; Directive (EU) 2024/2881). Environmental pollution is more common in middle- and low-income countries than in developed countries. The likely reasons for this are poverty, poor legislation, and lack of awareness about forms of pollution. The population's daily encounter with pollution leads to habituation and dulling of attention. People often carry out activities that disrupt the stability and resilience of ecosystems and lead to environmental deformation - deforestation, deliberate arson, and unregulated disposal of agricultural, household, and electronic waste. Exponential population growth and urbanization are increasing this harmful pressure on the environment. Air pollution is well-studied and receiving increasing attention due to increased morbidity and premature mortality. It affects the most vulnerable groups in middle- and low-income countries. Greater awareness of the dangers of pollution and the subsequent limitation and prevention of activities leading to environmental pollution are needed so that the restoration of already affected nature becomes feasible (Ukaogo et al., 2020). Natural and

anthropogenic features and the interaction between them determine air quality in urban environments. Pollution is determined by incoming emissions, dispersion, and transport of pollutants. Factors contributing to the deterioration of air quality in cities include population growth, increased traffic, and the energy and industrial sectors. There is a typical annual, weekly and daily cyclicality (Mayer, 1999).

The harmful impact on human health from air pollution is expressed in the exacerbation of cardiovascular, airborne diseases, diseases of the gastrointestinal tract and endocrine system, an increase in the frequency of allergies and bronchial asthma (with increased dust content). The implementation of sustainable development policies is crucial for limiting emissions and reducing morbidity (Komilova et al., 2023).

Since 1950, the world population has more than doubled, with the urban population more than quadrupling. The number of cars has increased even faster, over ten times. This rapid urbanization is leading to environmental degradation. Urban activities are sources not only of local air pollution, but also have a significant share in transboundary pollution (Fenger, 1999).

Urban regions are the source of one third of anthropogenic greenhouse gases and the majority of air pollutant emissions worldwide. While climate change is a global problem, poor air quality is a local one. Joint action on both climate and air pollution is needed to limit the harmful effects of air pollutants on urban populations and ecosystems (Crippa et al., 2021).

Different countries and regions have different air quality systems. Each system uses its own harmfulness index, permissible pollution concentration, and measurement time. This makes it difficult for users to navigate between the different systems. The Air Quality Index (AQI) of the United States Environmental Protection Agency (US-EPA) and the European Air Quality Index (EAQI) of the European Environment Agency are widely popular and used.

The AQI is a number calculated based on measured levels of particulate matter (PM2.5 and PM10), ozone, nitrogen dioxide, sulfur dioxide, and carbon monoxide in ambient air. The values are divided into six levels of air pollution, each of which is in a different color and provides information about possible health effects (Horn & Dasgupta, 2024; Sheikh, 2019). The EAQI also takes into account the main pollutants - particulate matter (PM2.5 and PM10), ozone, nitrogen dioxide and sulfur dioxide, but the values are specific to each pollutant. The ranges of values are divided into six zones according to the impact and relative health risk, as defined by the World Health Organization and related to short-term exposure to the pollutants (European Air Quality Index, 2024).

Both indices should not be compared with the relevant air quality standards in individual countries. They can serve as a guide to the quality of ambient air when traveling, working, or in general for populated areas. At the same time, public awareness of the importance of clean air is being raised and broader support for air quality and emissions regulations is being built. As regulatory restrictions change, both indices change, keeping them current and timely (Sheikh A., 2019; European Air Quality Index, 2024).

Particulate matter is a major factor in air pollution and its harmful effects on human health and living organisms in recent decades. The negative effect is determined by the dispersion, chemical composition and, accordingly, the physicochemical properties of these particles. The presence of heavy metals in road dust in densely populated areas is mainly due to industrial, construction and transport activities (Lei et al., 2024; Ma et al., 2025).

Air quality standards in cities are frequently exceeded. This negatively affects the population and leads to reduced labor productivity, increased economic and medical costs, and shortened life expectancy. Pollutants such as particulate matter, nitrogen dioxide, and ground-level ozone have the most serious impact on human health. Compliance with the recommendations of the World Health Organization would lead to limiting the negative effects of urban air pollution (Air pollution quick country facts, 2024).

Air pollution negatively affects both terrestrial and aquatic ecosystems, thereby deteriorating the environment and reducing biodiversity. Each pollutant has a specific harmful effect.

Ozone, as a secondary air pollutant, damages plants and forest stands, reducing growth rates and yields. The release of ammonia (in agricultural activities) and nitrogen oxides (in combustion processes) leads to nitrogen deposition on land and in water bodies, respectively to eutrophication processes and ultimately to changes in the structure and function of the ecosystem (Impacts of air pollution on ecosystems in Europe, 2024).

Nearly three-quarters of European ecosystems are exposed to harmful levels of air pollution, according to the latest data. This leaves Europeans exposed to concentrations of air pollutants above WHO recommended levels (Health and environment impacts of air pollution exposure remain high across Europe, 2024).

The increase in public health incidents resulting from air quality, as well as environmental degradation, is prompting authorities and experts to improve and seek new ways of monitoring air quality and “adequately” deploying air quality sensors (Chaudhuri & Roy, 2024).

The subject of this study is a typical urbanized urban area, namely that of Plovdiv, the second largest city in Bulgaria. The high density of construction, intensive car traffic and industrial activity are characteristic. The main factors for air pollution in the area under consideration are combustion processes, transport, the condition of the road and adjacent infrastructure. Plovdiv is located in the central part of the Upper Thracian Lowland. The relief is mainly flat, and the hills form an arc along the border with the Rhodope Mountains. The climate is transitional-continental with moderate precipitation and prolonged summer droughts. The prevailing westerly and easterly winds are of relatively low speed. A characteristic feature is the high proportion of calm weather. The dispersion of pollutants is adversely affected by temperature inversions (on about 81% of the days during the year) and the large number of foggy days in winter (Report on the Influence of the Atmospheric Air on the Health of the Population of "Plovdiv Agglomeration" in 2024, 2025).

The air quality in the area is monitored through air monitoring stations, which are part of the National Environmental Monitoring System. There are two automatic measuring stations (AMS) (Regulation No. 12 of July 15, 2010 for standards for sulfur dioxide, nitrogen dioxide, fine dust particles, lead, benzene, carbon monoxide and ozone in atmospheric air):

– AMS "Kamenitsa", classified as an urban background station. It is located in the central part of the city of Plovdiv in an area with mainly residential buildings and medium-heavy car traffic;

– AMS "Trakia" - meets the conditions for a transport-oriented point. It is located in an area with heavy car traffic. The observed pollution is mainly formed by transport and individual heating systems.

## MATERIALS AND METHODS

The anthropogenic impact and potential pollution of the Plovdiv region was studied through a typical incident factor - a fire at the Regional Non-Hazardous Waste Landfill. The location of the air monitoring stations, the regional non-hazardous waste landfill and the protected areas in the study area are presented on the map in Figure 1.

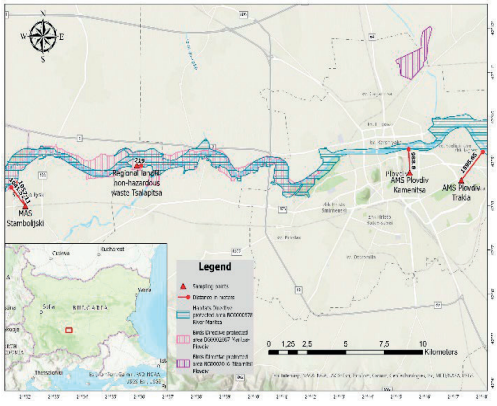



Figure 1. Locations of air monitoring stations, the regional non-hazardous waste landfill and protected areas in the study region

The main typical indicators of ambient air quality in populated areas were analyzed, namely - particulate matter (PM10), sulfur dioxide, carbon monoxide, nitrogen dioxide, nitrogen oxide, ozone, benzene. The indicators, together with their analysis methods and current permissible concentrations for Bulgaria, are presented in Table 1.

Table 1. Measured indicators and main characteristics

| Indicator | Unit of measure | Analysis method | Uncertainty | Standard |
|---|---|---|---|---|
| Particulate matter | μg/m$^3$ | BDS EN 16450:2017 | U=14.7% | ADN - 50 AAN - 40 |
| Sulfur dioxide | μg/m$^3$ | BDS EN 14212:2012 | U=3.70% | AHN - 325 AND - 125 |
| Carbon monoxide | mg/m$^3$ | BDS EN 14626:2012 | U=3.75% | HHPS - 10 |
| Nitrogen monoxide and Nitrogen dioxide | μg/m$^3$ | BDS EN 14211:2012 | U=3.74% | AHN - 200 AAN - 40 |
| Ozone | μg/m$^3$ | BDS EN 14625:2012 | U=3.60% | HHPS - 180 |
| Benzene | μg/m$^3$ | BDS EN 14662-3:2015 | U=4.5% | AAN - 5 |

Legend: ADN - Average daily norm for the protection of human health; AAN - Average annual norm for the protection of human health; AHN - Average hourly norm for protecting human health; HHPS - Human health protection standard (maximum eight-hour average value within 24 hours); Regulation No. 12 (2010).

Ambient air quality was analyzed using the Air Quality Index (AQI) of the United States Environmental Protection Agency (US-EPA) and the European Air Quality Index (EAQI) of the European Environment Agency. The values of the two indices AQI and EAQI and their corresponding air quality color scales are presented in Table 2 (Horn & Dasgupta, 2024; European Air Quality Index, 2024).

Table 2. Air Quality Index (AQI), European Air Quality Index (EAQI) and the corresponding condition color scale

| Air Quality Index (AQI) | | European Air Quality Index (EAQI), PM10 | |
|---|---|---|---|
| Values | Condition color scale | Values, μg/m$^3$ | Condition color scale |
| 0-50 | good | 0-20 | good |
| 51-100 | moderate | 20-40 | fair |
| 101-150 | unhealthy for sensitive individuals | 40-50 | moderate |
| 151-200 | unhealthy | 50-100 | poor |
| 201-300 | very unhealthy | 100-150 | very poor |
| 300+ | dangerous | 150-1200 | extremely poor |

The fire at the Regional Non-Hazardous Waste Landfill, Tsalapitsa, occurred on 1 August 2024 and was contained within a few days. The impact and potential contamination of the Plovdiv area were assessed through the readings of the Stambolijski MAS, Kamenitsa MAS - Plovdiv and Trakia MAS - Plovdiv for the period 1-6 August 2024. The mobile station in Stambolijski is temporarily located for the above-mentioned period in connection with the specific meteorological conditions and the dispersion of possible pollutants.

## RESULTS AND DISCUSSIONS

The impact and probable pollution of the surveyed region from the fire at the non-hazardous waste landfill was assessed through the readings of the MAS Stambolijski, AMS "Kamenitsa" - Plovdiv and AMS "Trakia" - Plovdiv for the period 1-6 August 2024. The interval of the measured hourly values for the controlled atmospheric pollutants for the time from 1 August 2024 to 6 August 2024 for the three stations is presented in Table 3.

Table 3. Interval of measured hourly values for controlled atmospheric indicators for the time from August 1, 2024 to August 6, 2024, for the three automatic stations

| Indicator | Value range | | |
|---|---|---|---|
| | AMS - Trakia | AMS - Kamenitsa | MAS - Stambolijski |
| Particulate matter, μg/m$^3$ | 12 ÷ 348 | 9 ÷ 139 | 7 ÷ 45 |
| Sulfur dioxide, μg/m$^3$ | 2 ÷ 14 | 8 ÷ 49 | 7 ÷ 35 |
| Carbon monoxide, mg/m$^3$ | 0.2 ÷ 0.7 | 0.1 ÷ 0.6 | 0.2 ÷ 0.6 |
| Nitrogen monoxide, μg/m$^3$ | 5 ÷ 13 | 0.5 ÷ 8 | 1 ÷ 5 |
| Nitrogen dioxide, μg/m$^3$ | 15 ÷ 56 | 4 ÷ 37 | 8 ÷ 40 |
| Ozone, μg/m$^3$ | - | 25 ÷ 160 | 31 ÷ 131 |
| Benzene, μg/m$^3$ | 0.01 ÷ 4.23 | 0.02 ÷ 0.16 | - |

Hourly values higher than the maximum permissible concentrations are observed only for the PM10 indicator - the deviations are present for the two automatic stations in the city of Plovdiv. The high maximum values (close to the permissible values according to legislation) for nitrogen dioxide, ozone and benzene should not be ignored.

The average daily concentrations of PM10 for the three measuring stations and the EAQI and AQI levels are presented in Table 4.

The reported values correspond to good status according to both indices, with the exception of the value reported for AMS Trakia on 02.08.2024 - moderate status according to EAQI.

The hourly exceedances of the 24-hour average limit for PM10 (50 μg/m$^3$) and the assessment of the condition according to EAQI and AQI are presented in Table 5.

Table 4. Average daily particulate matter concentration for the three measuring stations and EAQI and AQI levels

| Data | Value | | | | | |
|---|---|---|---|---|---|---|
| | AMS - Trakia | | AMS - Kamenitsa | | MAS - Stambolijski | |
| | PM10, EAQI µg/m³ | AQI | PM10, EAQI µg/m³ | AQI | PM10, EAQI µg/m³ | AQI |
| 1.08. 2024 | 18 | 17 | 19 | 18 | - | - |
| 2.08. 2024 | 45 | 42 | 39 | 36 | 19 | 18 |
| 3.08. 2024 | 26 | 24 | 27 | 25 | 23 | 21 |
| 4.08. 2024 | 22 | 20 | 21 | 19 | 15 | 14 |
| 5.08. 2024 | 16 | 15 | 16 | 15 | 12 | 11 |
| 6.08. 2024 | 20 | 19 | 17 | 16 | 15 | 14 |

Table 5. Hourly exceedances of the 24-hour average limit for PM10 (50 µg/m³)

| Date | Hour | Value | | | |
|---|---|---|---|---|---|
| | | AMS - Trakia | | AMS - Kamenitsa | |
| | | PM10, EAQI µg/m³ | AQI | PM10, EAQI µg/m³ | AQI |
| 1.08. 2024 | | – | – | – | – |
| 2.08. 2024 | 06:00<br>07:00<br>08:00<br>09:00<br>10:00 | 50<br>348<br>119<br>151<br>67 | 46<br>197<br>83<br>99<br>57 | 71<br>106<br>139<br>132<br>– | 59<br>76<br>92<br>89<br>– |
| 3.08. 2024 | 21:00<br>22:00 | 55<br>– | 51<br>– | 59<br>54 | 52<br>50 |
| 4.08. 2024 | 01:00<br>02:00 | 124<br>58 | 85<br>52 | –<br>– | –<br>– |
| 5.08. 2024 | | – | – | – | – |
| 6.08. 2024 | | – | – | – | – |

As can be seen from the data in Table 5, hourly exceedances of PM10 are observed on August 2, 3 and 4, 2024 for AMS - Trakia and August 2 and 3, 2024 for AMS - Kamenitsa. For AMS - Trakia, the exceedances are a total of eight, while for AMS - Kamenitsa, there are a total of six. The highest and highest values were recorded in the first half of the day on August 2, 2024. Out of the total 14 exceedances obtained, 7 values indicate poor air quality (4 in AMS - Trakia and 3 in AMS - Kamenitsa); 5 values indicate very poor air quality (2 in AMS - Trakia and 3 in AMS - Kamenitsa), and 2 values indicate extremely poor air quality according to EAQI (both in AMS - Trakia).

What is the impact of elevated PM10 values on the flora, fauna and health of the population in the study region? This impact has been assessed based on the Law on environmental protection, the Atmospheric air purity law, the Law of Health and Regulation No. 12/2010 on the standards of harmful substances in the ambient air of populated areas (Law on environmental protection, 2002; Law of Health, 2005; Atmospheric air purity law, 1996; Regulation No. 12, 2010).

No exceedances of the standards for the protection of human health were registered for the measured indicators in the days from 01.08.2024 to 06.08.2024, according to the presented results for the controlled pollutants of the atmospheric air for the three monitoring stations - MAS - Stamboliyski, AMS - Kamenitsa - Plovdiv and AMS - Trakia - Plovdiv. Fourteen of the reported hourly PM10 values exceed the daily average (Tables 3 and 5).

The average daily values indicate good air quality according to the AQI - air pollution poses a low or low risk. According to the EAQI, the values obtained correspond to good (9 values), sufficient (24 values) and only one - to moderate condition.

The hourly values exceed the daily average in 14 of the 288 results (4.86%) obtained for the two stations AMS - Trakia and AMS - Kamenitsa. This excess is from 1.01 to 6.97 times. According to AQI, 11 values indicate a moderate state of ambient air quality with a risk for very sensitive people with respiratory diseases and only one value for an unhealthy state, in which everyone can begin to experience health consequences, and members of sensitive groups may have more serious health

consequences. Despite the fact that the relative share of the results for the most part indicates a good state of ambient air quality (according to AQI), the excesses obtained are not negligible.

Near the assessed sites are Protected Area BG0002016 "Ribarnici, Plovdiv"; Protected Area BG0000578 "Maritsa River" for the protection of natural habitats and wild flora and fauna; Protected Area BG0002087 "Maritsa, Plovdiv" for the protection of wild birds (Figure 1). The increase in particulate matter levels is expected to worsen the living conditions of species and their ability to inhabit the protected area (Biodiversity Law, 2002; NATURA 2000).

In the region of the city of Plovdiv and the surrounding area in 2024, according to the Regional Inspectorate for Environment and Water and the Regional Health Inspectorate, five more fires occurred requiring measurements with a mobile automatic station for atmospheric air quality. Summary information on the quality of ambient air in the studied region is presented in the annual reports of both organizations. Table 6 presents the calculated annual average value (AAV) and the registered number of exceedances of the permissible values for basic indicators for the two measuring stations in the city of Plovdiv - AMS - Trakia and AMS - Kamenitsa for a three-year period - from 2022 to 2024 (Regional Report on the State of the Environment in 2024, 2025; Report on the Influence of the Atmospheric Air on the Health of the Population of "Plovdiv Agglomeration" in 2024, 2025). Exceedances of permissible values are observed mainly for particulate matter (of the average daily values for all three years for both stations), as well as for nitrogen dioxide (of the average annual values for 2022 and 2023 for AMS - Trakia). The observed exceedances of the average daily norm for PM10 in the AMC - Trakia exceed the permissible number, according to the legislation, of 35 times within the calendar year. The recorded maximum hourly values for benzene also exceed the permissible annual average standard.

For the incident we investigated - a fire at a solid waste landfill, no daily average values for PM10 higher than the maximum permissible concentration were observed, but high hourly values exceeding the daily average norm.

According to the Regional Inspectorate for Environment and Water and the Regional Health Inspectorate, the origin of air pollution in the region should be sought primarily in the production of electricity and heat, domestic heating and motor vehicle transport. In recent years, a positive trend towards a decrease in the number of registered exceedances and high values of pollutants at monitoring points has been observed (Regional Report on the State of the Environment in 2024, 2025; Report on the Influence of the Atmospheric Air on the Health of the Population of "Plovdiv Agglomeration" in 2024, 2025).

Table 6. Summary results for exceedances of basic assessment indicators for ambient air quality for AMS - Trakia and AMS - Kamenitsa for the period 2022-2024

| AMS | AMS - Trakia | | AMS - Kamenitsa | |
|---|---|---|---|---|
| Indicator PM10<br>Standard: AAN - 40 μg/m³, ADN - 50 μg/m³<br>(exceeded no more than 35 times per calendar year) | | | | |
| year | AAV, μg/m³ | Number of exceedances of the ADN | AAV, μg/m³ | Number of exceedances of the ADN |
| 2022 | **37.20** | **64** | **28.36** | **32** |
| 2023 | **32.09** | **42** | **26.79** | **28** |
| 2024 | **30.06** | **45** | **28.66** | **31** |
| Indicator $SO_2$<br>Standard: AHN - 325 μg/m³, ADN - 125 μg/m³ | | | | |
| year | AAV, μg/m³ | Number of exceedances of the ADN | AAV, μg/m³ | Number of exceedances of the ADN |
| 2022 | **5.53** | **0** | **12.55** | **0** |
| 2023 | **5.08** | **0** | **10.04** | **0** |
| 2024 | **5.54** | **0** | **11.53** | **0** |
| Indicator CO<br>Standard: HHPS - 10 mg/m³ | | | | |
| year | AAV, mg/m³ | Number of exceedances of the standard | AAV, mg/m³ | Number of exceedances of the standard |
| 2022 | **0.52** | **0** | **0.34** | **0** |
| 2023 | **0.53** | **0** | **0.33** | **0** |
| 2024 | **0.48** | **0** | **0.00** | **0** |
| Indicator $NO_2$<br>Standard: AHN - 200 μg/m³, AAN - 40 μg/m³ | | | | |
| year | AAV, μg/m³ | Number of exceedances of the AHN | AAV, μg/m³ | Number of exceedances of the AHN |
| 2022 | **42.48** | **0** | **6.97** | **0** |
| 2023 | **43.09** | **0** | **2.15** | **0** |
| 2024 | **35.84** | **0** | **17.51** | **0** |
| Indicator Ozone<br>Standard: HHPS - 180 μg/m³ | | | | |
| year | Maximum measured 8h value, μg/m³ | Number of exceedances of the standard | Maximum measured 8h value, μg/m³ | Number of exceedances of the standard |
| 2022 | **NA** | **-** | **130.16** | **0** |
| 2023 | **NA** | **-** | **119.32** | **0** |
| 2024 | **NA** | **-** | **132.17** | **0** |
| Indicator Benzene<br>Standard: AAN - 5 μg/m³ | | | | |
| year | AAV, μg/m³ | Maximum measured hourly average concentration | AAV, μg/m³ | Maximum measured hourly average concentration |
| 2022 | **0.41** | **10.69** | **0.79** | **15.85** |
| 2023 | **0.53** | **9.23** | **0.81** | **25.53** |
| 2024 | **0.34** | **13.60** | **1.18** | **26.57** |

The specific meteorological conditions in the region (a large number of days with calm weather - wind speed below 1.5 m/s, temperature inversions and fog on the rivers) are a prerequisite for the retention and accumulation of pollutants. The adverse climatic conditions in the region - more than 50% of the days in the year with calm weather and over 75% of the days in the year with inversion processes, lead to the retention of the formed relatively high background concentrations of PM10.

Particulate matter is a major air pollutant. It is emitted directly into the atmosphere by transport, energy and domestic activities (primary emissions) or is formed in the air from metal oxides, polyaromatic hydrocarbons, sulfur dioxide, nitrogen oxides, ammonia and other gases (secondary emissions). Its harmful effects on health depend mainly on the size and chemical composition of the suspended particulate matter, on other chemical compounds adsorbed on their surface and on the part of the respiratory system in which it is deposited. Particulate matter enters the body mainly through the respiratory system, with larger particles being retained in the upper respiratory tract, while finer particles reach the lower parts of the respiratory system, leading to tissue damage in the lung. Children, the elderly and people with chronic lung diseases, respiratory diseases or asthma are particularly sensitive to high PM10 values. The harmful effect of particulate matter pollution is more pronounced when sulfur dioxide is present in the ambient air. Their synergistic effect on the respiratory organs and exposed mucous membranes is manifested by irritation and depends on the duration of exposure.

There is a relationship between high PM concentrations and mortality, hospitalizations for respiratory diseases, and person-days of bronchodilator use. It is assumed that acidic particles with nanosizes smaller than 100 nm cause acute respiratory problems in sensitive people. Particles with a diameter smaller than 10 μm can pass into the thoracic airways of people. PM pollution can lead to the development of asthma, aggravate respiratory diseases, provoke and progress chronic diseases such as emphysema, lung cancer and others. Adverse effects on human health, flora and fauna occur not only at high concentrations, but also at values close to or even below the permissible norm (Chuturkova, 2015).

## CONCLUSIONS

High values, including exceedances of the maximum permissible concentrations of air quality indicators, have a negative impact on the health, lifestyle and work of the population. These high values and exceedances are a consequence of both single incidents (such as the fire in question) and permanent anthropogenic load from the energy and transport sectors. Reducing the harmful impact of particulate matter as a major pollutant requires taking adequate measures. These may include: modernization, quality maintenance and washing of road surfaces; control of construction activities; landscaping of open areas; construction of insulating plant belts on busy streets with intensive transport traffic; tolerating the replacement of solid fuels used for heating with central heating, electricity and natural gas; increased control over landfills and unregulated burning of solid waste.

In order to limit air pollution and, accordingly, the harmful effects of dust particles, specific actions are required on the one hand by administrative and control authorities, and on the other - by citizens.

## ACKNOWLEDGEMENTS

The authors express their gratitude to Plovdiv University "Paissii Hilendarski", Agricultural University - Plovdiv and National Institute of Geophysics, Geodesy and Geography, Research Center for Hydrology and Water Management, Bulgarian Academy of Sciences, Sofia, Bulgaria for their support in carrying out this study.

## REFERENCES

Air pollution quick country facts, Modified 09 Dec 2024, European Environment Agency, from https://www.eea.europa.eu/en/topics/in-depth/air-pollution/air-pollution-country-fact-sheets-2024/quick-country-facts

Allegrini, I., Ianniello, A., & Valentini, F. (2023). Environmental air pollution: an anthropogenic or a natural issue. In Current Trends and Future Developments on (Bio-) Membranes (pp. 1-38). Elsevier.

Atmospheric air purity law (1996). State Gazette No. 45/28.05.1996, last amended and supplemented SG No. 1/3.01.2019.

BDS EN 14211:2012 (Nov 20, 2012). Ambient air - Standard method for the measurement of the concentration of nitrogen dioxide and nitrogen monoxide by chemiluminescence.

BDS EN 14212:2012 (Nov 20, 2012). Ambient air - Standard method for the measurement of the concentration of sulfur dioxide by ultraviolet fluorescence.

BDS EN 14625:2012 (Nov 20, 2012). Ambient air - Standard method for the measurement of the concentration of ozone by ultraviolet photometry.

BDS EN 14626:2012 (Nov 20, 2012). Ambient air - Standard method for the measurement of the concentration of carbon monoxide by non-dispersive infrared spectroscopy.

BDS EN 14662-3:2015 (May 17, 2018). Ambient air - Standard method for the measurement of benzene concentrations - Part 3: Automated pumped sampling with in situ gas chromatography.

BDS EN 16450:2017 (Apr 18, 2017). Ambient air - Automated measuring systems for the measurement of the concentration of particulate matter (PM10; PM2,5).

Biodiversity Law (2002). State Gazette No. 77/9.08.2002, last amended and supplemented SG No. 88/20.10.2023.

Chaudhuri, S. & Roy, M. (2024). Global ambient air quality monitoring: Can mosses help? A systematic meta-analysis of literature about passive moss biomonitoring, *Environment, Development and Sustainability* 26, 5735–5773.

Chuturkova, (2015). *Air Pollution*, Technical University, Varna, Bulgaria.

Crippa, M., Guizzardi, D., Pisoni, E., Solazzo, E., Guion, A., Muntean, M., Florczyk, A., Schiavina, M., Melchiorri, M. & Hutfilter, A. F. (2021). Global anthropogenic emissions in urban areas: patterns, trends, and challenges. Environmental Research Letters, 16(7), 074033.

Directive (EU) 2016/2284 of The European Parliament and of the Council of 14 December 2016 on the reduction of national emissions of certain atmospheric pollutants, amending Directive 2003/35/EC and repealing Directive 2001/81/EC, 17.12.2016, *Official Journal of the European Union* L 344/1.

Directive (EU) 2024/2881 of the European Parliament and of the Council of 23 October 2024 on ambient air quality and cleaner air for Europe, 20.11.2024, *Official Journal of the European Union* L.

European Air Quality Index, Published 09 Jan 2019, Modified 12 Mar 2024, European Environment Agency, from https://www.eea.europa.eu/en/analysis/maps-and-charts/index

Fenger, J. (1999). Urban air quality. *Atmospheric environment*, 33(29), 4877-4900.

Health and environment impacts of air pollution exposure remain high across Europe, Press release Published 10 Dec 2024, European Environment Agency, from https://www.eea.europa.eu/en/newsroom/news/health-and-environment-impacts-of-air-pollution.

Horn, S., & Dasgupta, P. (2024). The Air Quality Index (AQI) in historical and analytical perspective a tutorial review, *Talanta*, 267, 125260.

Impacts of air pollution on ecosystems in Europe, Briefing, Published 10 Dec 2024, Modified 12 Dec 2024, European Environment Agency, from https://www.eea.europa.eu/en/analysis/publications/impacts-of-air-pollution-on-ecosystems-in-europe

Komilova, N., Egamkulov, K., Hamroyev, M., Khalilova, K., & Zaynutdinova, D. A. (2023). The impact of urban air pollution on human health. Медичні перспективи= *Medicni perspektivi* (*Medical perspectives*), (3), 170-179.

Law of Health (2005). State Gazette No. 70/10.08.2004, last amended and supplemented SG No. 18/27.02.2018.

Law on environmental protection (2002). State Gazette No. 91/25.09.2002, last amended and supplemented SG No. 42/7.06.2022.

Lei, T., Xiang, W., Zhao, B., Hou, C., Ge, M., & Wang, W. (2024) Advances in analysis of atmospheric ultrafine particles and application in air quality, climate, and health research, *Science of the Total Environment*, 949, 175045.

Ma, Y., Zhang, Y., & Song, L. (2025). Ecological and health risk assessment and anthropogenic sources analysis of heavy metals in different types of urban road dust, *Process Safety and Environmental Protection*, 195, 106813.

Mayer, H. (1999). *Air pollution in cities. Atmospheric environment*, 33(24-25), 4029-4037.

NATURA 2000, from https://natura2000.egov.bg/EsriBg.Natura.Public.Web.App/Home/Map#

Regional Report on the State of the Environment in 2024, Regional Inspectorate for the Environment and Waters – Plovdiv, Ministry of the Environment and Waters, Bulgaria 2025, from https://plovdiv.riew.gov.bg/#:~:text=plovdiv.riew.gov.bg%20%E2%80%BA%20godishni_dokladi%20%E2%80%BA%20Godishen_doklad_2024

Regulation No. 12 of July 15, 2010 for standards for sulfur dioxide, nitrogen dioxide, fine dust particles, lead, benzene, carbon monoxide and ozone in atmospheric air (2010) State Gazette No. 58/30.07.2010, amended and supplemented SG No. 48/16.06.2017, amended and supplemented SG No. 79/08.10.2019.

Report on the Influence of the Atmospheric Air on the Health of the Population of "Plovdiv Agglomeration" in 2024, Plovdiv, Bulgaria 2025, from https://www.riokozpd.com/index/556-dokladi-vuzduh.html

Sheikh, A. (2019). Standards for Air Quality Indices in Different Countries (AQI), from https://atmotube.com/blog/standards-for-air-quality-indices-in-different-countries-aqi

Ukaogo, P. O., Ewuzie, U., & Onwuka, C. V. (2020). Environmental pollution: causes, effects, and the remedies. In Microorganisms for sustainable environment and health (pp. 419-429). Elsevier.

WHO global air quality guidelines (2021). Particulate matter (PM2.5 and PM10), ozone, nitrogen dioxide, sulfur dioxide and carbon monoxide, Executive summary, Geneva: World Health Organization.

Scientific Papers. Series E. Land Reclamation, Earth Observation & Surveying, Environmental Engineering. Vol. XV, 2026
Print ISSN 2285-6064, CD-ROM ISSN 2285-6072, Online ISSN 2393-5138, ISSN-L 2285-6064

# INTERRELATIONSHIP BETWEEN SOIL MICROORGANISMS AND AIRBORNE MICROFLORA IN URBAN ENVIRONMENT

**Asen PESHEV**

University of Forestry, 10 Kliment Ohridski Str., Sofia, Bulgaria

Corresponding author email: asenpeshev87@gmail.com

***Abstract***

*The present study aims to establish the potential similarity between airborne microorganisms and soil microorganisms. We analyse the percentage of similarity based on dominant types of soil microorganisms and their frequency of occurrence in ground air, as well as their association with specific fractions of fine dust particles. For the purpose of the study, eight sampling plots were selected, with different anthropogenic pressure. A six-stage cascade impactor was used to collect air samples. Soil samples were taken from a depth of 0-15 cm. The dominant types of microorganisms were determined. DNA identification was performed. The results show that bacteria predominate in the first levels of the cascade impactor. Fungi are concentrated at sieves 4.7-7.0 µm. Actinomycetes are most concentrated at sieves 3.3- 4.7 µm and 2.1-3.3 µm. The most common from Bacilli are B. megaterium and B. cereus. The amount of soil microorganisms, as a percentage similarity to the air microflora, increases with increasing anthropogenic pressure and reach up to 8%. The increased presence of opportunistic soil microorganisms in heavy construction areas in Sofia poses a significant risk to public health, which highlights the need for specific regulations related to minimizing dust generation.*

***Key words****: airborne microorganisms, DNA, soil microorganisms, urban environment, 16S rRNA.*

## INTRODUCTION

Surface air, although long considered only as a transit medium for microorganisms, is now defined as a dynamic and complex microbial habitat that plays a critical role in environmental quality. Airborne microorganisms are often defined as bioaerosols. According to this is important to point out that bioaerosols include not only bacteria, fungi, actinomycetes, viruses and their fragments, but also any type of biological components, such as pollen and other plant fragments, for example. There is evidence that bioaerosols constitute up to 25% of the total mass of atmospheric aerosols (Shammi et al., 2021). This data determines the important role of airborne microorganisms in the analysis of atmospheric air quality.

From this perspective, air pollution is one of the main causes of deterioration of human health, as well as the functioning of ecosystems. Increased levels of pollutants in the air lead to changes in naturally occurring processes in ecosystems. These changes lead to a decrease in the degree of air decontamination, carbon dioxide assimilation, soil acidification, etc. Particulate matter concentrations are indicators of complex mixtures of pollutants (Masselot et al., 2024). It has been found that air quality is worse in urban areas than in rural areas. The main sources of dust pollution are road transport, industry, as well as the use of solid fuels for heating and power generation, and construction and excavation human activities (Ketchman & Bilec, 2013; Khan & Strand, 2018; Sager, 2020). In recent years, several studies have highlighted the potential relationship between the concentration of fine particulate matter, of various origins, and the content of microorganisms in the air (Mansour et al., 2014; Palladino et al., 2021). Concentration of settled microorganisms on fine particulate matters has different significance for ambient air quality. Determining the content and predominant groups of microorganisms can serve as an indicator of air quality.

The main sources of atmospheric microorganisms are land and water surfaces, with soil being the most significant reservoir for airborne microorganisms above land. Soil microorganisms enter the atmosphere through processes of mechanical soil breakdown as a result of various human activities, wind erosion, etc. Research shows that airborne microbial communities often reflect the structure of communities in surrounding surface ecosystems

The data shows that 46.3% of airborne bacteria originating from the immediate ground environment (Zhao et al., 2022). When studying air quality, it is necessary to analyze the microbial load, including the presence of specific microorganisms generally present in soils. Such information can show the influence of anthropogenic activity - construction, excavation activities, maintenance of parks and gardens - on the quantity and specificity of microorganisms present in the air. Given that the main source of airborne microorganisms is soil (Ruiz-Gil et al., 2020), and it contains a number of pathogens (Pales, 2024), it is of key importance to analyze the percentage of major and commonly occurring soil microorganisms in the air, in order to prevent human health and increase environmental hygiene. While the microbiological characteristics of soil, aquatic habitats, etc. have been studied in detail, revealing specific and interconnected ecosystems, air often remains neglected as an independent habitat for microorganisms. The air environment is often considered only as a spreading factor for microorganisms. New analyses show that air is a real and specific ecosystem, inhabited by a microbiome that is vast in both number and diversity (Amato et al., 2023). Airborne microorganisms not only influence climate processes through the formation of ice nuclei and cloud condensation, but also have a direct impact on human health, agriculture, and ecosystem stability. In conditions of increasing urbanization and anthropogenic pressure, understanding the mechanisms by which microorganisms are transferred from land surfaces to the ground air layer becomes fundamental for protecting public health and optimizing urban hygiene (Chen et al., 2020).

The study of the entry and distribution of microorganisms into the air environment will provide important information about the microbiological load of individual ecosystems. This information will predict in the future the microbiological effect of air pollution resulting from the ever-increasing construction activities in urban areas.

The main goal of this study is to establish the degree of similarity between air and soil microflora in urban environments by analyzing the distribution of dominant types of soil microorganisms in individual fractions of fine dust particles under the influence of different anthropogenic pressures.

## MATERIALS AND METHODS

The study was conducted in early September 2025, on the territory of the municipality of Sofia, Bulgaria, covering four areas with intense anthropogenic pressure (Sample Plot (SP) 1-4) and four areas in parks and mountain regions with low anthropogenic pressure (Sample Plot (SP) 5-8).

SP1 - Formation of a green park area, flower beds (manually) in Geo Milev Park - with the presence of anthropogenic pressure. Coordinates: 42°41′12.18″N 23°21′50.37″ E.

SP2 - Reconstruction of sidewalks in the residential district of Geo Milev - with the presence of anthropogenic pressure. Coordinates: 42°42′51.73″N 23°21′33.37″ E.

SP3 - Reconstruction of the roadway on Vladimir Vazov Blvd. - with the presence of anthropogenic pressure. Coordinates: 42°42′31.95″N 23°22′17.73″ E.

SP4 - Construction of a residential complex in the residential district of Dragalevtsi - with the presence of anthropogenic pressure. Coordinates: 42°38′13.93″N 23°18′39.35″ E.

SP5 - Western Park, heavily forested inner part - without the presence of anthropogenic pressure, only recreational activity is established. Coordinates: 42°20′09.59″N 23°15′20.53″ E.

SP6 - Hunting Park, heavily forested inner part - without the presence of anthropogenic pressure, only recreational activity is established. Coordinates: 42°39′48.90″N 23°20′17.98″ E.

SP7 - Vitosha Nature Park, tourist trail - without the presence of anthropogenic pressure, only recreational activity is established. Coordinates: 42°36′54.66″N 23°17′35.10″ E.

SP8 - Plana Mountain, tourist trail - without the presence of anthropogenic pressure, only recreational activity is established. Coordinates: 42°30′38.53″N 23°21′39.25″ E.

The present study includes analysis of the quantity of the main microbiological groups of the air microflora and determination of the total microbial number of each sample. Analysis of the main groups of soil microorganisms

(bacteria, actinomycetes and micromycetes) and determination of the total microbial number. The study also includes determination of the species of the genus *Bacillus: Bacillus cereus, Bacillus subtilis, Bacillus megaterium* and *Bacillus mycoides*. For precise monitoring of ground-level air microflora, a 6-stage cascade impactor was used, operating on the principle of inertial sedimentation. Sampling was performed once from each of the surveyed points, with one cubic meter of air being passed through the impactor at a uniform speed. The device divides the air sample (with a volume of 1 $m^3$) into six fractions based on the aerodynamic diameter of the particles: 1st stage (> 7.0 μm); 2nd stage (4.7-7.0 μm); 3rd stage (3.3-4.7 μm); 4th stage (2.1-3.3 μm); 5th stage (1.1-2.1 μm); 6th stage (0.65-1.1 μm). A Petri dish with a specific medium was placed at each level of the impactor. Samples were taken at a height of 1.5 m (the breathing zone) at a temperature of 11°C and a humidity of 86%. The incubation process was carried out under the following parameters: total microbial number (bacteria) on meat peptone agar (MPA) - incubation at 28°C for 48 hours in an aerobic environment. Actinomycetes - dense plating on starch ammonia agar (SAA), incubation at 35°C for a period of 10 days. Micromycetes - plating on Capek Dox Agar medium, incubation at 30°C for 7 days. Soil samples were taken once, with a sterile probe from a depth of 10 cm. The samples were placed in sterile bags and analyzed within 24 hours. Each sample was pre-cleaned of impurities and prepared for analysis by serial dilutions. For counting of germinated colonies, dense plating on solid agar media was used. The media and incubation period were identical to those used for the study of air samples. To determine the representatives of the genus *Bacillus: Bacillus cereus, Bacillus subtilis, Bacillus megaterium* HiBacillus Identification Kit (HiMedia Laboratories, India, Mumbai) was used. The study is based on a colorimetric test. The test is based on the principle of pH change. *Bacillus* species show metabolic changes during incubation, for which the color change in the medium is an indicator. To perform the analysis, each of the samples was previously prepared and purified. Incubation was performed at 37°C for 48 hours. The data were read using a color scale based on the color change of the plate. Given the specific colonies that *Bacillus mycoides* forms, it was also reported. After performing the analysis, pure cultures were prepared to confirm the identity of the bacilli by DNA sequencing. Molecular genetic identification of the isolated strains was performed by determining 16S rRNA gene nucleotide sequences using primer pair 27F (5'-AGAGTTTGATCMTGGCTCAG-3') × 1492R (5'-GGTTACCTTGTTACGACTT-3'). PCR amplifications were performed using the MyTaq HS DNA Polymerase 2x Mix (Bioline Ltd., UK). The resulting PCR products were separated by agarose gel electrophoresis, stained with GelRed (Biotium, USA). The amplified DNA fragments were excised and purified from the agarose gel using the GeneJET Gel Extraction Kit (Thermo Scientific, USA). The purified DNA fragments were directly sequenced in both directions (forward and reverse) using the same primers employed for amplification. The evaluation and analysis of the resulting chromatograms and nucleotide sequences were carried out using CHROMAS v2.31 and Vector NTI v.11 software packages. Final taxonomic identification and alignment were performed by comparing the consensus sequences against the NCBI BLAST database (GenBank).

The numerical data were processed with StatSoft Statistica 12 software. For each sample, the mean value of three replicates and the standard deviation SD were calculated, at a statistical significance threshold of $p < 0.05$ (95% confidence interval).

## RESULTS AND DISCUSSIONS

In urban areas, anthropogenic activities such as road traffic, construction, and industrial processes significantly accelerate the transport of soil particles and their associated microbes into the ground air. The study by Chen et al. (2020), highlights that the soil environment is one of the main pathways for the emission of microorganisms into the air.

The results for the reported amounts of microorganisms for each of the fractions are shown in Table 1.

Table 1. Microbiological parameters of air samples (CFU*$10^2/m^3$)

| Total microbial number | | | | | | |
|---|---|---|---|---|---|---|
| | >7 μm | 4.7-7 μm | 3.3-4.7 μm | 2.1-3.3 μm | 1.1-2.1 μm | 0.65-1.1 μm |
| SP1 | 1.5 ± 0.74 | 0.6 ± 0.43 | 0.8 ± 0.24 | 0.4 ± 0.14 | 0.5 ± 0.09 | 0.5 ± 0.15 |
| SP2 | 2.9 ± 0.74 | 1.1 ± 0.43 | 0.9 ± 0.24 | 0.5 ± 0.14 | 0.4 ± 0.09 | 0.2 ± 0.15 |
| SP3 | 2.9 ± 0.74 | 1.5 ± 0.43 | 1.3 ± 0.24 | 0.4 ± 0.14 | 0.3 ± 0.09 | 0.2 ± 0.15 |
| SP4 | 3.1 ± 0.74 | 1.5 ± 0.43 | 0.8 ± 0.24 | 0.7 ± 0.14 | 0.3 ± 0.09 | 0.2 ± 0.15 |
| SP5 | 0.6 ± 0.09 | 0.5 ± 0.19 | 0.7 ± 0.24 | 0.9 ± 0.38 | 0.8 ± 0.06 | 0.5 ± 0.05 |
| SP6 | 0.4 ± 0.09 | 0.2 ± 0.19 | 0.5 ± 0.24 | 0.9 ± 0.38 | 0.8 ± 0.06 | 0.4 ± 0.05 |
| SP7 | 0.5 ± 0.09 | 0.1 ± 0.19 | 0.2 ± 0.24 | 1.5 ± 0.38 | 0.9 ± 0.06 | 0.4 ± 0.05 |
| SP8 | 0.4 ± 0.09 | 0.1 ± 0.19 | 0.2 ± 0.24 | 1.6 ± 0.38 | 0.9 ± 0.06 | 0.4 ± 0.05 |
| Bacteria | | | | | | |
| | >7 μm | 4.7-7 μm | 3.3-4.7 μm | 2.1-3.3 μm | 1.1-2.1 μm | 0.65-1.1 μm |
| SP1 | 0.7 ± 0.79 | 0.3 ± 0.38 | 0.4 ± 0.13 | 0.1 ± 0.06 | 0.3 ± 0.10 | 0.4 ± 0.15 |
| SP2 | 1.9 ± 0.79 | 0.7 ± 0.38 | 0.6 ± 0.13 | 0.2 ± 0.06 | 0.1 ± 0.10 | 0.1 ± 0.15 |
| SP3 | 2.6 ± 0.79 | 1.1 ± 0.38 | 0.5 ± 0.13 | 0.1 ± 0.06 | 0.1 ± 0.10 | 0.1 ± 0.15 |
| SP4 | 1.6 ± 0.79 | 1.1 ± 0.38 | 0.3 ± 0.13 | 0.2 ± 0.06 | 0.1 ± 0.10 | 0.1 ± 0.15 |
| SP5 | 0.1 ± 0.09 | 0.4 ± 0.05 | 0.3 ± 0.15 | 0.1 ± 0.30 | 0.5 ± 0.17 | 0.1 ± 0.05 |
| SP6 | 0.3 ± 0.09 | 0.6 ± 0.05 | 0.2 ± 0.15 | 0.0 ± 0.30 | 0.2 ± 0.17 | 0.2 ± 0.05 |
| SP7 | 0.2 ± 0.09 | 1.0 ± 0.05 | 0.0 ± 0.15 | 0.1 ± 0.30 | 0.2 ± 0.17 | 0.2 ± 0.05 |
| SP8 | 0.1 ± 0.09 | 1.0 ± 0.05 | 0.0 ± 0.15 | 0.1 ± 0.30 | 0.1 ± 0.17 | 0.2 ± 0.05 |
| Fungi (molds) | | | | | | |
| | >7 μm | 4.7-7 μm | 3.3-4.7 μm | 2.1-3.3 μm | 1.1-2.1 μm | 0.65-1.1 μm |
| SP1 | 0.4 ± 0.42 | 0.1 ± 0.05 | 0.2 ± 0.27 | 0.1 ± 0.10 | 0.1 ± 0.05 | 0.1 ± 0.00 |
| SP2 | 0.9 ± 0.42 | 0.1 ± 0.05 | 0.2 ± 0.27 | 0.1 ± 0.10 | 0.2 ± 0.05 | 0.1 ± 0.00 |
| SP3 | 0.2 ± 0.42 | 0.2 ± 0.05 | 0.7 ± 0.27 | 0.1 ± 0.10 | 0.1 ± 0.05 | 0.1 ± 0.00 |
| SP4 | 1.1 ± 0.42 | 0.1 ± 0.05 | 0.1 ± 0.27 | 0.3 ± 0.10 | 0.1 ± 0.05 | 0.1 ± 0.00 |
| SP5 | 0.1 ± 0.11 | 0.3 ± 0.15 | 0.2 ± 0.05 | 0.2 ± 0.13 | 0.2 ± 0.08 | 0.4 ± 0.15 |
| SP6 | 0.1 ± 0.11 | 0.0 ± 0.15 | 0.1 ± 0.05 | 0.1 ± 0.13 | 0.1 ± 0.08 | 0.1 ± 0.15 |
| SP7 | 0.3 ± 0.11 | 0.0 ± 0.15 | 0.1 ± 0.05 | 0.3 ± 0.13 | 0.2 ± 0.08 | 0.1 ± 0.15 |
| SP8 | 0.3 ± 0.11 | 0.0 ± 0.15 | 0.1 ± 0.05 | 0.4 ± 0.13 | 0.3 ± 0.08 | 0.1 ± 0.15 |
| Actinomycetes | | | | | | |
| | >7 μm | 4.7-7 μm | 3.3-4.7 μm | 2.1-3.3 μm | 1.1-2.1 μm | 0.65-1.1 μm |
| SP1 | 0.4 ± 0.17 | 0.20 ± 0.06 | 0.20 ± 0.14 | 0.20 ± 0.00 | 0.10 ± 0.00 | 0.00 ± 0.00 |
| SP2 | 0.1 ± 0.17 | 0.30 ± 0.06 | 0.10 ± 0.14 | 0.20 ± 0.00 | 0.10 ± 0.00 | 0.00 ± 0.00 |
| SP3 | 0.1 ± 0.17 | 0.20 ± 0.06 | 0.10 ± 0.14 | 0.20 ± 0.00 | 0.10 ± 0.00 | 0.00 ± 0.00 |
| SP4 | 0.4 ± 0.17 | 0.30 ± 0.06 | 0.40 ± 0.14 | 0.20 ± 0.00 | 0.10 ± 0.00 | 0.00 ± 0.00 |
| SP5 | 0.4 ± 0.20 | 0.10 ± 0.05 | 0.20 ± 0.15 | 0.30 ± 0.05 | 0.10 ± 0.00 | 0.00 ± 0.05 |
| SP6 | 0.0 ± 0.20 | 0.00 ± 0.05 | 0.50 ± 0.15 | 0.20 ± 0.05 | 0.10 ± 0.00 | 0.10 ± 0.05 |
| SP7 | 0.0 ± 0.20 | 0.00 ± 0.05 | 0.50 ± 0.15 | 0.20 ± 0.05 | 0.10 ± 0.00 | 0.10 ± 0.05 |
| SP8 | 0.0 ± 0.20 | 0.00 ± 0.05 | 0.50 ± 0.15 | 0.20 ± 0.05 | 0.10 ± 0.00 | 0.10 ± 0.05 |

According to air analysis data, sample areas with construction activities have microbial abundance about twice as high as green areas. The results show that bacteria predominate in

the first levels of the cascade impactor, where larger particles settle. Fungi are also most concentrated in the upper levels of the impactor, with the main percentage of them in the second stage of sedimentation (4.7-7.0 µm). In the case of actinomycetes, we again observe a greater number of CFU/m$^3$ in the petri dishes of the larger sieves 3.3-4.7 µm and 2.1-3.3 µm. These data are very intriguing considering that these are the sieves that capture the main soil particles (Padoan et al., 2021). The results of the soil analyses are provided in Table 2.

Table 2. Microbiological parameters of soil samples (CFU*10$^4$/g soil)

| | TMN | Bacteria | Actinomycetes | Micromycetes |
|---|---|---|---|---|
| SP1 | 12.6 ± 2.63 | 7.6 ± 1.76 | 3.4 ± 1.04 | 1.6 ± 1.18 |
| SP2 | 10.14±2.63 | 5.9 ± 1.76 | 3.2 ± 1.04 | 1.04 ± 1.18 |
| SP3 | 6.2 ± 2.63 | 3.6 ± 1.76 | 1.4 ± 1.04 | 1.2 ± 1.18 |
| SP4 | 9.6 ± 2.63 | 4.4 ± 1.76 | 1.6 ± 1.04 | 3.6 ± 1.18 |
| SP5 | 12.78 ± 3.7 | 9.02 ± 2.5 | 2.73 ± 0.64 | 1.03 ± 1.45 |
| SP6 | 17.24 ± 3.7 | 12.18 ± 2.5 | 1.95 ± 0.64 | 3.11 ± 1.45 |
| SP7 | 20.73 ± 3.7 | 13.94 ± 2.5 | 2.27 ± 0.64 | 4.52 ± 1.45 |
| SP8 | 20.45 ± 3.7 | 14.63 ± 2.5 | 3.42 ± 0.64 | 2.4 ± 1.45 |

As expected, the data on the quantities of individual groups of microorganisms, as well as the total microbial number in the soil, are hundreds of times higher than the results for air samples. This is completely understandable, given that soil is one of the richest environments in microorganisms (Llado et al., 2017). However, in undisturbed green areas, the reported total microbial count is higher compared to anthropogenically loaded soils. The results for the percentage distribution of the individual microbiological groups without taking into account the individual level of the separator are presented in Figure 1. Respectively, the percentage ratio of the studied soil samples is presented in Figure 2.

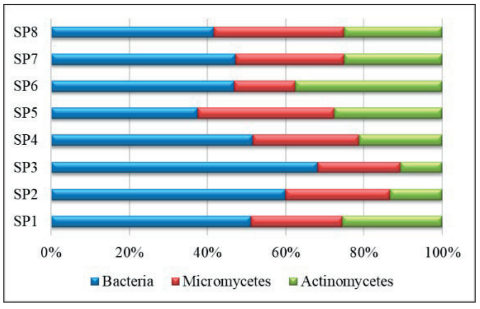



Figure 1. Percentage of the main microbiological groups in relation to the total microbial number of airborne microorganisms

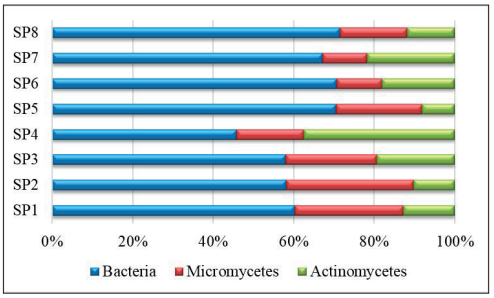



Figure 2. Percentage of the main microbiological groups in relation to the total microbial number of soil microorganisms

In both types of air and soil samples, a dominant presence of the group of bacteria is observed. However, there are certain specifics. Thus, in air samples, the participation of the groups of actinomycetes and fungi is noticeably greater compared to the percentage distribution in soil samples. These data once again prove that the air environment is not just a carrier of microorganisms, but a specific ecosystem, with specific characteristics and environmental conditions for the development of air microorganisms (Amato et al., 2023). The higher percentage of actinomycetes is probably related to the specificity of their spores and the way they spread, given their size and severity (Reponen et al., 1998).

The studied typical soil representatives of the genus *Bacillus: Bacillus cereus, Bacillus subtilis* and *Bacillus megaterium, Bacillus mycoides* were recorded both in all soil samples and in all air samples. When analyzing the data, over 69% of all CFU/m$^3$ of the studied bacilli developed in the petri dishes from the upper stages of the impactor, i.e. those that capture larger fractions. These data confirm the data that the soil particles fall mainly in the impactor range from 7 to 3.3 μm bacilli were also found in the remaining fractions, but in much smaller quantities.

The analysis revealed that soil samples were generally dominated by *Bacillus megaterium* and *Bacillus cereus*. In air samples, sequencing studies revealed that *Micrococcus luteus* and *Kocuria rosea* were dominant. Other studies also indicated that *Micrococcus luteus* and *Kocuria rosea* were common in the air (Fang et al., 2007; Turnbull et al., 2019). Other studies have found that the genus *Bacillus* constitutes a very large percentage of the microflora of outdoor air, while *Micrococcus* is part of the dominant airborne microorganisms in indoor spaces. Such data require in-depth studies on the mode of entry into the air and the distribution of airborne microorganisms (Fang et al., 2014).

The percentage of the studied bacilli (total) in the soil and air samples is presented in the Figure 3.

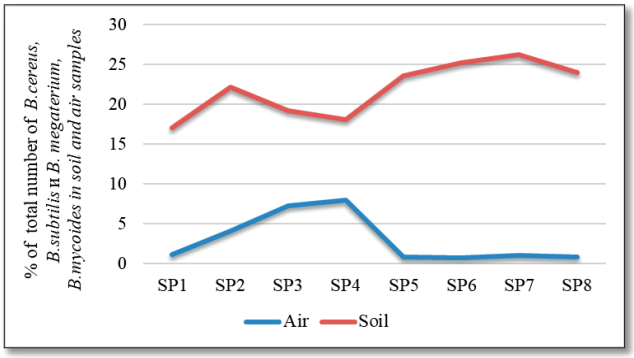



Figure 3. The percentage of the studied bacilli (total) in the soil and air samples

The results of the comparison of the distribution of typical soil microbial species in the air clearly show the influence of human activity. In samples from green areas, where there are no other anthropogenic activities except recreational ones, the percentage of the considered soil microorganisms is lower, compared to areas with some construction activities. Thus, the studied species of bacilli in these areas constitute only about one percent of the total microflora (SP5 - 0.83%; SP6 - 0.71%; SP7 - 1.1% and SP8 - 0.9%). In samples with different types of anthropogenic impact, the percentage of participation of typical soil microflora, represented by the four species of the genus Bacillus, increases. However, it is clearly seen that each of the considered above activities has a different impact on the distribution of typical soil microorganisms in the air environment. We conclude that with increasing anthropogenic load and the area of soil cover disturbance, the amount of typical soil microorganisms in the air increases. Thus, human activities with the most destructive nature of the soil layer (SP3 and SP4) show a much higher percentage of soil bacilli. In SP3, soil bacilli occupy 8.01% of the total microflora, and in SP2, respectively, 7.25%. This is over six times more than in samples without anthropogenic pressure. When we look at the data for SP1, it is impressive that the percentage of soil bacilli is almost similar to that of samples from the fields without anthropogenic pressure - SP1 - 1.2%. The results show that when manually treating the soil, sufficient amounts of soil particles are not generated at high to remain in the ground air and pose a threat to human health. It is important to note, however, that the current study was conducted at a height starting at 1.5 m. Given that garden workers are at a much lower height (around 0.5 m), we recommend that the activity be carried out while wearing protective masks, which minimize the risk of exposure to both fine dust particles and

pathogenic microorganisms. During the reconstruction of the sidewalk areas, given the use of mechanical equipment and the excavation of the peripheral soils, an increase in the percentage of the studied soil microflora in the air samples (4.07%) was observed. The results clearly show that with increasing anthropogenic pressure and increasing construction activities in the city, there is a real danger of increasing the amount of soil microflora in the air. The present study is a clear sign that it is necessary to increase the hygiene requirements during construction activities to minimize dusting. In general, we believe that it is necessary to pay serious attention to the overdevelopment of the city of Sofia, not only from an aesthetic point of view, but also in terms of the quality of the ground air around the construction sites.

## CONCLUSIONS

The present study aimed to investigate the similarity of soil and air microbial communities from eight sample areas (four with increased anthropogenic pressure and four without anthropogenic pressure, only with the presence of recreational activity). The present study found that all air samples contained the studied soil-typical microorganisms (Bacillus: *Bacillus cereus*, *Bacillus* subtilis, *Bacillus megaterium*, and *Bacillus mycoides*), but in different quantities. The results of the present study show that in activities with reduced levels of soil destruction and reduced machine activity, the amount of soil bacilli considered as part of the air microflora is lower (SP1 - 1.12%). With the use of equipment that excavates the soil, albeit at a shallow depth, as in the case of the sidewalk reconstruction of SP2, the amount of microorganisms studied in the air increases to 4.07%. These results confirm the strong negative impact of permanent construction activities in the capital of Bulgaria - Sofia. Such data indicate the need to minimize excavation and construction activities on huge areas covering tens of acres, which pose a real risk to the quality of ground air in the surrounding residential areas. The elevated percentage of soil bacilli, particularly potential opportunistic pathogens such as *B. cereus* in areas with heavy construction activities (SP3 and SP4), carries significant public health implications. Inhalation of these bioaerosols bound to fine particulate matter can penetrate deep into the human respiratory tract, potentially causing respiratory diseases, allergies, or systemic infections in immunocompromised individuals residing near construction zones. In terms of urban planning, these findings underscore the urgent need for local authorities to implement stricter regulations on dust management during large-scale construction. Urban planners should integrate compulsory dust-suppression protocols (such as continuous water spraying of disrupted soils) into municipal building permits to maintain ground air quality in rapidly developing urban areas in Sofia. As a pilot study, a key limitation of this research is its specific timeframe (early September). Therefore, future longitudinal and seasonal studies are highly needed to investigate how temporal and meteorological variations, such as humidity, temperature, and precipitation, affect the emission and persistence of soil microorganisms in the urban atmosphere over different seasons.

This pilot study can serve as a basis for in-depth analyses of the possibility of excavation and construction activities to change not only the quantity of airborne microflora, but also to sharply alter its qualitative composition.

## ACKNOWLEDGEMENTS

This research work was carried out with the support of Research Fund of Ministry of Education and Science in Bulgaria, project №: КП-06-Н74/5 “Relationships between the amount of fine particulate matter and airborne microorganisms in "hot spots", park areas, urban background areas and control forest areas”.

## REFERENCES

Amato, P., Mathonat, F., Lopez, L., Peguilhan, R., Bourhane, Z., Rossi, F., Vyskocil, J., Joly, M. & Ervens, B. (2023). The aeromicrobiome: the selective and dynamic outer-layer of the Earth’s microbiome. *Front. Microbiol*, 14. https://doi.org/10.3389/fmicb.2023.1186847

Chen, X., Kumari, D. & Achal, V. (2020). A Review on Airborne Microbes: The Characteristics of Sources, Pathogenicity and Geography. *Atmosphere*, 11(9), 919. https://doi.org/10.3390/atmos11090919

Fang, Z., Gong, Ch., Ouyang, Z., Liu, P., Sun, L. & Wang, X. (2014). Characteristic and Concentration Distribution of Culturable Airborne Bacteria in Residential Environments in Beijing, China. *Aerosol*

*and Air Quality Research,* 14: 943–953, 10.4209/aaqr.2013.04.0109

Fang, Z., Ouyang, Z., Zheng, H., Wang, X. & Hu, L. (2007). Culturable airborne bacteria in outdoor environments in Beijing,China. *Microb Ecol*, 54(3):487-96. 10.1007/s00248-007-9216-3.

Ketchman, K. & Bilec, M. (2013). Quantification of Particulate Matter from Commercial Building Excavation Activities Using Life-Cycle Approach. *Journal of Construction Engineering and Management*, 139(12): A4013007. DOI: 10.1061/(ASCE)CO.1943-7862.0000776

Khan, R. & Strand, M. (2018). Road dust and its effect on human health: a literature review. *Epidemiol Health*, 40:e2018013. 10.4178/epih.e2018013

Llado, S., Lopez-Mondejar, R. & Baldrian, P. (2017). Forest Soil Bacteria: Diversity, Involvment in Ecosystem Processes, and Response to Global Change. *Microbiol Mol Biol Rev*., 81(2): e00063-16. 10.1128/MMBR.00063-16.

Mansour, A., Shamy, M., Redal, M., Khoder, M., Awad, A. & Elserougy, S. (2014). Microorganisms associated particulate matter: Apreliminary study. *Science of the Total Environment*, 479, 109-116

Masselot, P., Kan., H., Kharol, Sh., Bell, M., Sera, F., Lavigne, E., Breitner, S., Silva, S., Burnett, R., Gasparrini, A. & Brook, J. (2024). Air pollution mixture complexity and its effect on PM2.5-related mortality: A multicountry time-series study in 264 cities. *Environ Epidemiol*, 8(6). 10.1097/EE9.0000000000000342

Padoan, E., Maffia, J., Balsari, P., Ajmone-Marsan, F. & Dinnuccion, E. (2021). Soil PM10 emission potential under specificmechanicalstressand particles characteristics. *Science of the Total Environment*, 779: 146468.https://doi.org/10.1016/j.scitotenv.2021.146468

Pales, S. (2024). Pathogens in Environment: How Air, Water and Soil Harbor Disease. *Air & Water Borne Diseases*, 13 (5), 1000255

Palladino, G., Morozzi, P., Biagi, E., Brattich, E., Turroni, S., Rampelli, S., Tositti, L. & Candela, M. (2021) Particulate matter emission sources and meteorological parameters combine to shape the airborne bacteria communities in the Ligurian coast, Italy. *Scientific Reports* 11, article 175

Reponen, T., Gazenko, S., Grinshpun, S., Willeke, K. & Cole, E. (1998). Characteristics of airborne actinomycete spores. *Appl Environ Microbiol*., 64(10): 3807-3812. 10.1128/aem.64.10.3807-3812.1998.

Ruiz-Gil, T., Acuna, J., Fujuyoshi, S., Tanaka, D., Noda, J., Maruyama, F. & Jorquera, M. (2020). Airborne bacterial communities of outdoor environments and their associated influencing factors. *Environment International*, 145, 106156, https://doi.org/10.1016/j.envint.2020.106156

Sager, M. (2020). Urban Soils and Road Dust—Civilization Effects and Metal Pollution—A Review. *Environments*, 7(11). https://doi.org/10.3390/environments7110098

Shammi, M., Rahman, M. & Tareq, S. (2021). Distribution of Bioaerosols in Association with Particulate Matter: A Review on Emerging Public Health Threat in Asian Megacities. *Front. Environ. Sci., Sec. Toxicology, Pollution and the Environment*, 9. https://doi.org/10.3389/fenvs.2021.698215

Turnbull, J., Russell, J., Fazal, M., Grayson, N., Deheer-Graham, A., Oliver, K., Holroyd, N., Parkhill, J. & Alexander, S. (2019). Whole-Genome Sequences of Five Strains of Kocuria rosea, NCTC2676, NCTC7514, NCTC7512, NCTC7528, and NCTC7511. *Microbial Resour Announc*, 8(44): e00256-19. 10.1128/MRA.00256-19

Zhao, J., Jin, L., Wu, D., Xie, J., Li, J., Fu, X., Cong, Z., Fu, P., Zhang, Y., Luo, X., Zhang, G., Tiedje, J. & Li, X. (2022). Global airborne bacterial community - interactions with Earth's microbiomes and anthropogenic activities. *Proc. Natl. Acad. Sci. U.S.A*. 119 (42) e2204465119, https://doi.org/10.1073/pnas.2204465119

Scientific Papers. Series E. Land Reclamation, Earth Observation & Surveying, Environmental Engineering. Vol. XV, 2026
Print ISSN 2285-6064, CD-ROM ISSN 2285-6072, Online ISSN 2393-5138, ISSN-L 2285-6064

# BIOMATERIALS - BASED COATINGS WITH INDOOR EMISSION CONTROL PROPERTIES

**Irina POPA[1], Vasilica VASILE[1], Claudiu-Sorin DRAGOMIR[1, 2], Alexandra-Marina BARBU[1]**

[1]National Institute for Building Research, Town Planning and Sustainable Territorial Development URBAN - INCERC, 266 Pantelimon Road, District 2, Bucharest, Romania
[2]University of Agronomic Sciences and Veterinary Medicine of Bucharest, 59 Marasti Blvd, District 1, Bucharest, Romania

Corresponding author email: valivasile67@yahoo.com

***Abstract***

*At the international level, current concerns of scientists have been observed, through which concerted actions are being taken, both in the spirit of developing the circular economy, and to reduce carbon dioxide emissions. To harness synergistically the potential of the two global challenges, our work has focused on developing innovative construction products by integrating rice husks and hemp stalks, two natural agro-industrial by-products. Biomaterials - based coatings with responsive potential have been obtained, characteristics that have been confirmed by verifying the innovative coatings through their indoor emission control properties by means of TVOC emission, $CO_2$ and/or CO absorption capacity. From the comparative analysis of the way in which the three responsive characteristics are correlated for each tested product, it is highlighted the importance that the distribution of the nature and size of the pores in the structure of the respective materials has on the mechanisms underlying the mentioned characteristics of the obtained products. Further research is necessary to specify and capitalize on the specific mechanisms of this type of innovative coatings.*

***Key words****: circular economy, climate change, indoor air quality, natural agro-industrial by-products.*

## INTRODUCTION

Indoor air quality (IAQ) is one of the essential concerns internationally recognized, the growing attention paid to it being based on the increase in the time people spend indoors (Klepeis et al., 2001; Hu et al., 2017; Yuan et al., 2023; Gonzalez-Martín et al., 2024), together with the higher level of pollutants found in indoor air compared to outdoor air (Montaluisa-Mantilla et al., 2023; Gonzalez-Martín et al., 2024).

This concern has grown significantly, especially as a result of the fact that the serious effects of indoor air pollution on human health range from allergies and asthma to high-morbidity diseases such as ischemic heart disease, respiratory diseases or cancer (Gonzalez-Martín et al., 2024; Hilly et al., 2024), with 3.8 million deaths recorded worldwide annually (World Health Organization, 2018).

One of the categories of pollutants with which indoor air pollution is associated is the class of volatile organic compounds (VOCs), a group that includes a wide variety of compounds, continuously growing as new sources of pollution are identified (Hu et al., 2017; Gonzalez-Martín et al., 2021). Poor degradability, severe toxicity and high volatility are the main characteristics of VOCs, having negative effects on the environment and human health. Long-term exposure to VOCs can have a wide range of consequences, from skin irritation, dizziness and fatigue, to impaired lung function (Morin et al., 2020; Caron et al., 2020), leukemia and symptoms related to sick building syndrome (Huang et al., 2021; Gan et al., 2023). Finishing products and furniture elements represent the most common and studied sources of VOCs indoors, the level of total volatile organic compounds (TVOC) constituting an element of the risk regarding the effects on the health of the occupants, used as a general indicator for assessing indoor air quality.

Another significant category of pollutants is the class of volatile inorganic compounds, carbon oxides (CO and $CO_2$), ozone ($O_3$), nitrogen oxides (NO and $NO_2$), sulfur dioxide ($SO_2$) being among the most relevant types of

pollutants in the indoor environment (Bernstein et al., 2008; Năstase et al., 2018).
In indoor spaces, CO can be present through transfer from outside air or from household activities such as combustion processes (cooking, heating with wood etc.). Among the harmful effects that CO can have on human health are headaches, dizziness, nausea, on pregnant women, young children, the elderly and people with heart and lung diseases being more sensitive to the effects of CO.
Carbon dioxide ($CO_2$) is an inorganic compound, naturally present in the earth's atmosphere, the predominant source, in non-industrial indoor environments, being human metabolism. Exhalation produces 37 g $h^{-1}$ per person (Yuan et al., 2023), studies showing that high levels of $CO_2$ can have a significant impact on both productivity and personality psychology (Azuma et al., 2018).
Therefore, large amounts of various categories of pollutants can accumulate in the indoor air of a building, and such dangerous substances pose a threat to human health, necessitating detailed research on how to eliminate them efficiently and economically (Hu et al., 2017).
The alarming increase in global $CO_2$ emissions, which represent 70% of the total volume of greenhouse gases (Khosrowshahi et al., 2023), constitutes a good premise for the development of a new research direction, through which the construction sector can contribute to the reduction of $CO_2$ and VOC emissions.
In this context, the paper presents the research carried out for the development of biomaterials-based coatings with responsive potential and verifying their indoor emission control properties. The products were designed through an approach that combines basic ideas, principles, materials and conditioning, as follows: integrating the principle of poly-ionic liquids and nano-fluids, by using a set of raw materials, considering that each of them activates a distinct possibility of increasing $CO_2$ absorption; the use of synthetic polyvinyl acetate binder, as a polymeric solvent for $CO_2$ absorption, and to improve the mechanical performance of responsive coatings; integration of solid materials in powder form, with micrometric-sized particles, namely lime, soda-lime (absorbent material, traditionally used in the medical field, in the present research acting as an alkaline solvent for $CO_2$ absorption), rice husks and chopped hemp stems, all creating in the presence of water a type of nano-fluid for $CO_2$ retention. The method used, the results obtained and the conclusions are described below.

## MATERIALS AND METHODS

Thirteen biomaterials - innovative coatings with compositionally responsive potential - were obtained and in terms of their response to specific requirements. This consisted of determining the indoor emission control property, by monitoring three characteristics, namely TVOC content emission, $CO_2$ absorption capacity and CO absorption capacity.
The components of the innovative products were: synthetic binder, lime, corn starch, soda-lime, rice husks and hemp stalks.
The products were designed considering the following criteria: different percentage content of synthetic binder; mixing time of the biomaterial, the products being mixed manually, and nature of the plant component, even, rice husks, hemp stalks or 1:1 rice husks: hemp stalks mixture.
The studied biomaterials-based coatings, noted EC1 - EC13, were composed of two successive layers, applied by brush on a plasterboard surface, with dimensions of 20 x 20 x 1 cm. Each bilayer biomaterial-based coating variant was subjected to emission monitoring, inside of S2 experimental stand (Figure 1, left), with DirectSense IQ-610 equipment (Figure 1, right), also used in other international studies (Canha et al., 2017; Johnson et al., 2018; Majd et al., 2019), according to the monitoring protocol described in Vasile et al. (2023), for 24 and 48 hours.



Figure 1. S2 experimental stand (left) and DirectSense IQ-610 equipment (right)

## RESULTS AND DISCUSSIONS

The interpretation of the experimental results obtained for the innovative products tested in terms of TVOC emissions was carried out by analysing and comparing the graphical representations of the TVOC emission profiles (Figure 2) and the average values of TVOC concentrations, presented in Table 1, all these results being compared after the same two time points, namely the first 24 hours and the 48 hours of monitoring.

The interpretation of the experimental results regarding $CO_2$ absorption, respectively CO absorption, was achieved by analysing and comparing the graphical representations regarding the variation of the $CO_2$/CO concentration (Figures 3 and 4), as well as the average values of the $CO_2$/CO concentrations presented in Table 1, for all tested products, all these results being compared according to the same time points, namely the first 24 hours and the 48 hours of monitoring.

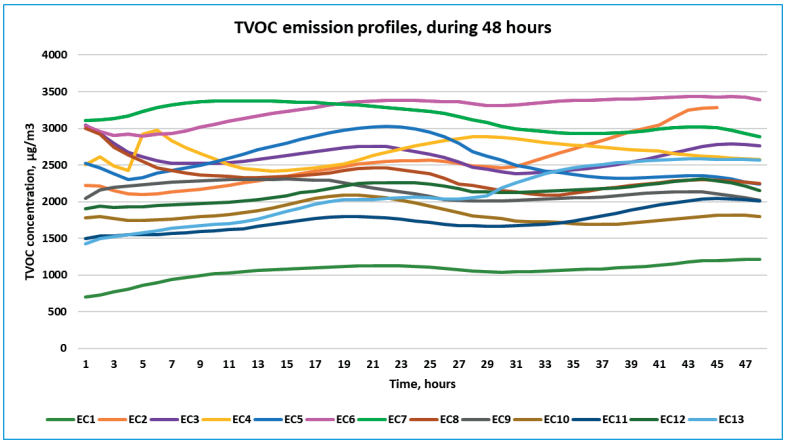



Figure 2. TVOC emission profiles for all monitored products, for 48 hours

Table 1. Average values of TVOC, $CO_2$ and CO concentrations, at 24 hours and 48 hours of monitoring

| Product | Average TVOC concentration values, µg m$^{-3}$ | | Decrease in TVOC concentrations µg m$^{-3}$ | Average $CO_2$ concentration values, ppm | | $CO_2$ absorption, ppm | Average CO concentration values, µg m$^{-3}$ | | CO absorption, µg m$^{-3}$ |
|---|---|---|---|---|---|---|---|---|---|
| | 24 h | 48 h | 48 h | 24 h | 48 h | 48 h | 24 h | 48 h | 48 h |
| EC1 | 999 | 1054 | - | 354 | 349 | 1.41 | 511 | 438 | 14.2 |
| EC2 | 2308 | 2579 | - | 350 | 349 | 0.28 | 383 | 325 | 15.14 |
| EC3 | 2667 | 2616 | 51 | 345 | 345 | - | 392 | 345 | 11.99 |
| EC4 | 2595 | 2667 | - | 361 | 355 | 1.66 | 474 | 400 | 15.61 |
| EC5 | 2689 | 2570 | 119 | 365 | 368 | - | 425 | 367 | 13.65 |
| EC6 | 3145 | 3264 | - | 374 | 370 | 1.07 | 445 | 381 | 14.38 |
| EC7 | 3294 | 3150 | 144 | 352 | 353 | - | 269 | 263 | 2.2 |
| EC8 | 2470 | 2344 | 126 | 363 | 363 | - | 358 | 274 | 23.46 |
| EC9 | 2236 | 2150 | 86 | 363 | 364 | - | 142 | 151 | - |
| EC10 | 1899 | 1834 | 65 | 371 | 370 | 0.27 | 315 | 239 | 24.12 |
| EC11 | 1659 | 1744 | - | 376 | 375 | 0.28 | - | - | 0.76 |
| EC12 | 2064 | 2131 | - | 354 | 360 | - | 226 | 191 | 35 |
| EC13 | 1784 | 2090 | - | 369 | 367 | 2 | 127 | 115 | 12 |

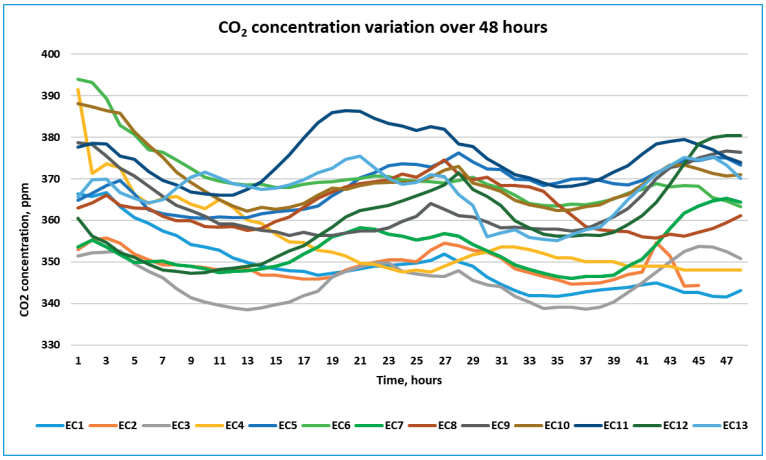



Figure 3. $CO_2$ concentration variation for all monitored products, for 48 hours

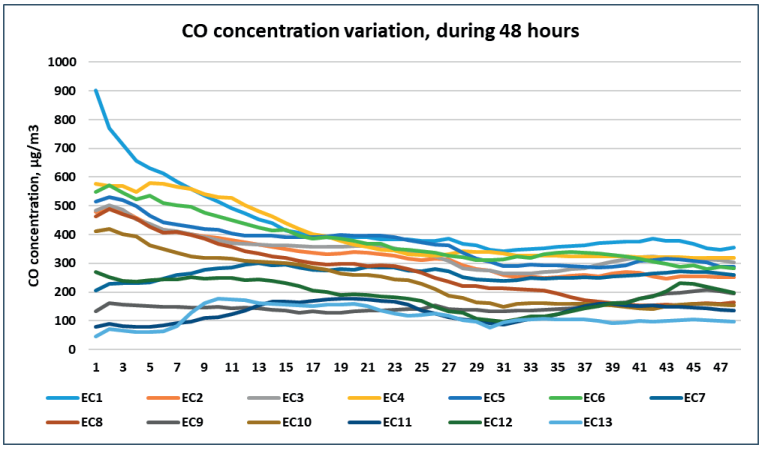



Figure 4. CO concentration variation for all monitored products, for 48 hours

Analysing the experimental results obtained as well as the different forms of their processing, regarding the TVOC emissions of the potentially responsive products tested, the following observations were made.

In general, the TVOC emission profiles are relatively similar to each other, especially in the first 24 hours of monitoring.

During the 48 hours of monitoring, it is observed that half of the products (EC3, EC5, EC7, EC8, EC9, EC10) have downward trends in TVOC emissions, while the others are slightly upward.

From the analysis of the recipes, it results that this evolution could be determined by structural changes in the biomaterials, in correlation with the mixing time, most of the products with a downward trend in emissions having 1 minute of mixing, comparing to those having 3 minutes of mixing.

Analysing the products both as a trend of emission profiles but especially as average values of TVOC concentrations, the product EC1 (with a low content of synthetic binder and rice husks) is particularly noteworthy, which, although with a slightly upward trend, maintains the lowest average values of TVOC concentrations emitted.

Regardless of the quantitative compositional particularities of the biomaterials, it is considered that, in situations where the concentrations of TVOC emitted are lower or decreasing, the favourable influence of three determinant factors are manifested synergistically: the low content of synthetic

binder, the highest possible content of rice husks or/and hemp stalks and the 3-minute mixing time of the biomaterial, before its application on the support surface.

The favourable influence of the presence of the plant component in the biomaterial, in terms of reducing TVOC emissions, is clearer in the case of incorporating the rice husks, or a 1:1 rice husks: hemp stalks mixture, it being desirable to incorporate as large a quantity of these natural materials as possible, within limits that do not affect the workability of the mixture.

Regarding the evolution of $CO_2$ concentrations, respectively their decrease as a result of the increase in $CO_2$ absorption by the tested coatings, the following were found:

Based on the individual profiles of $CO_2$ concentrations, respectively of the decreases in recorded concentrations, it results that the tested products have a certain responsive potential manifested through $CO_2$ absorption, a characteristic highlighted for seven of the products, especially in the first 14-19 hours of monitoring but also later, at the end of monitoring.

Given the general path of variation of $CO_2$ concentrations, with multiple irregularities, it is considered that the average values obtained are not quantitatively relevant at this stage of the research. It is noted that no obvious correlations can be established between the components/recipes of the biomaterials and the decrease in $CO_2$ concentrations during monitoring, and it is assumed that dimensional differences in the porous structure of the coatings could provide clarification, with future research being necessary in this regard.

It is appreciated that there are elements that could lead to an improvement in the responsive potential of the tested materials, regarding the increase in $CO_2$ absorption from the atmospheric air of the enclosure, mainly, mechanical mixing, increasing the mixing time, and applying protection to larger support surfaces.

The evolution of CO concentrations, respectively their decrease as a result of the increase in CO absorption by the tested coatings, showed the following:

Based on the individual profiles with a downward trend in CO concentrations and the variation in the average values of CO concentration, in the first 24 hours and during the 48 hours of monitoring, it results that the tested products also have a certain responsive potential manifested through CO retention.

The highest decrease in CO concentration (35%) was recorded for the EC12 product, with a content of 58.73% synthetic binder, 3.17% hemp stalks and 12.68% soda-lime, the latter two components supporting the responsive characteristic of the product in terms of CO absorption. Similarly, a significant decrease in CO concentration (24.12%) was recorded for the EC10 product, with a content of 50% synthetic binder, 3.57% hemp stalks and 14.28% soda-lime.

Contrary to expectations, a similar decrease in CO concentration (23.46%) was recorded for the EC8 product, a control product, therefore without soda-lime content, with a slightly higher content of synthetic binder (51.5%). It is considered that the effect observed was generated synergistically by the presence of lime and the 1:1 rice husks: hemp stalks mixture.

During the 48 hours of monitoring, seven of the thirteen tested products had CO concentration developments that indicated decreases between 11.99-15.61 $\mu g\ m^{-3}$ CO, values that indicated, from a compositional point of view, the synergistic effect of the presence of lime, the soda-lime product with a $CO_2$ absorbent role, and a plant component, mainly rice husks (1.85-3.47%), respectively only 1.75% hemp stalks. However, it is appreciated that the evolution of CO absorption phenomena, similarly to the case of $CO_2$, is based on the distribution of the nature and size of the pores in the structure of the resulting materials, but further research in this regard is necessary.

From the comparative analysis of the data in Table 1, regarding the way in which the three responsive characteristics (TVOC emission, $CO_2$ and/or CO absorption capacity) are correlated for each tested product, it is considered that this also highlights the importance of the distribution of the nature and dimensions of the pores in the structure of the respective materials, on the mechanisms underlying the emission and/or retention capacity of the responsive products obtained and studied.

Further research is needed to characterize and control the specific mechanisms of this type of innovative coatings.

## CONCLUSIONS

Thirteen innovative biomaterial-based coatings, composed of synthetic binder and two natural agro-industrial by-products, were studied in terms of their response to specific requirements that consisted of monitoring the emission of total volatile organic compounds (TVOC) content, carbon dioxide ($CO_2$) and carbon monoxide (CO) absorption capacity.

Based on the experimental results obtained, it is observed that most of the products have downward trends in TVOC emissions, while some profiles remain slightly upward, an evolution that could be determined by morphological and structural changes in the biomaterials.

Regardless of the quantitative compositional particularities of the biomaterials, it is considered that, in situations where the emitted TVOC concentrations are lower or decreasing, the favourable influence of the low content of synthetic binder and a significant content of vegetable component (rice husks, hemp stalks or 1:1 rice husks: hemp stalks mixture) is manifested synergistically.

Starting from the experimental results obtained regarding the evolution of $CO_2$ concentrations, based on individual profiles, it can be considered that some of the tested products have a responsive potential manifested through $CO_2$ absorption, especially in the first 14-19 hours of monitoring and subsequently, at the end of monitoring.

Based on the individual profiles with a downward trend in CO concentrations and the variation in the average values of CO concentration, in the first 24 hours and during the 48 hours of monitoring, it results that the tested products also have a certain responsive potential manifested through CO retention.

From the comparative analysis of the way in which the three responsive characteristics (TVOC content emission, $CO_2$ and/or CO absorption capacity) are correlated for each tested product, it is considered that this also highlights the importance that the distribution of the nature and size of the pores in the structure of the respective materials has on the mechanisms underlying the mentioned characteristics of the innovative responsive products obtained and studied. Further research is needed to customize, control and capitalize on the specific mechanisms of this type of innovative products/coatings.

## ACKNOWLEDGEMENTS

The research paper was carried out within Project PN 23 35 02 01 - Innovation and Digitalization Synergies in the Design of Eco-Materials and Multifunctional Products for Sustainable Construction, with Impact on the Environment and the Circular Economy, financed by the Ministry of Research, Innovation and Digitalization.

## REFERENCES

Azuma, K., Kagi, N., Yanagi, U., & Osawa, H. (2018). Effects of low-level inhalation exposure to carbon dioxide in indoor environments: A short review on human health and psychomotor performance. *Environment International*, *121*, 51-56.

Bernstein, J.A., Alexis, N., Bacchus, H., Bernstein, I.L., Fritz, P., Horner, E., Li, N., Mason, S., Nel, A., Oullette, J., Reijula, K., Reponen, T., Seltzer, J., Smith, A., & Tarlo, S.M. (2008). The health effects of nonindustrial indoor air pollution. *Journal of Allergy and Clinical Immunology, 121*(3), 585-591.

Canha, N., Lage J., Candeias S., Alves C., & Almeida S. M. (2017). Indoor air quality during sleep under different ventilation patterns. *Atmospheric Pollution Research*, *8,* 1132-1142.

Caron, F., Guichard, R., Robert, L., Verriele, M., & Thevenet, F. (2020). Behaviour of individual VOCs in indoor environments: How ventilation affects emission from materials. *Atmospheric Environment*, *243*, 117713.

Gan, G., Fan, S., Li, X., Zhang, Z., & Hao, Z. (2023). Adsorption, membrane separation for removal, recovery of volatile organic compounds. *Journal of Environmental Sciences, 123*, 96–115.

Gonzalez-Martín, J., Cantera, S., Munoz, R., & Lebrero, R. (2024). Indoor air VOCs biofiltration by bioactive coating packed bed bioreactors. *Journal of Environmental Management*, *349*, 119362.

Gonzalez-Martín, J., Kraakman, N.J.R., Perez, C., Lebrero, R., & Munoz, R. (2021). A state-of-the-art review on indoor air pollution and strategies for indoor air pollution control. *Chemosphere*, *262*, 128376.

Hilly, J.J., Singh, K.R., Jagals, P., Mani, F.S., Turagabeci, A., Ashworth, M., Mataki, M., Morawska, L., Knibbs, L.D., Stuetz, R.M., & Dansie A.P. (2024). Review of scientific research on air quality and environmental health risk and impact for PICTS. *Science of the Total Environment*, *942*, 173628.

Hu, S.-C., Shiue, A., Chang, S.-M., Chang, Y.-T., Tseng, C.-H., Mao, C.-C., Hsieh, A., & Chan, A. (2017). Removal of carbon dioxide in the indoor environment

with sorption-type air filters. *International Journal of Low-Carbon Technologies*, *12*, 330–334.

Huang, L., Yanru, W., Liyuan, Z., Zhe, M., & Weiping, Z. (2021). Estimates of emission strengths of 43 VOCs in wintertime residential indoor environments, Beijing. *Science of the Total Environment*, *793*, 148623.

Johnson, D.L., Lynch, R.A., Floyd, E.L., Wang, J., & Bartels, J.N. (2018). Indoor air quality in classrooms: Environmental measures and effective ventilation rate modeling in urban elementary schools. *Building and Environment*, *136*,185-197.

Khosrowshahi, M. S., Mashhadimoslem, H., Shayesteh, H., Singh, G., Khakpour, E., Guan, X., Rahimi, M., Maleki, F., Kumar, P., & Vinu, A. (2023). Natural Products Derived Porous Carbons for $CO_2$ Capture. *Advanced Science*, *10*, 2304289.

Klepeis, N.E., Nelson, W.C., Ott, W.R., Robinson, J.P., Tsang, A.M., Switzer, P., Behar, J.V., Hern, S.C., & Engelmann, W.H. (2001). The National Human Activity Pattern Survey (NHAPS): A resource for assessing exposure to environmental pollutants. *Journal of exposure analysis and environmental epidemiology, 11*, 231–252.

Majd, E., McCormack, M., Davis, M., Curriero, F., Berman, J., Connolly, F., Leaf, F., Rule, A., Green, T., Clemons-Erby, D., Gummerson, C., & Koehler, K. (2019). Indoor air quality in inner-city schools and its associations with building characteristics and environmental factors. *Environmental Research*, *170*, 83-91.

Montaluisa-Mantilla, M. S., García-Encina, P., Lebrero, R., & Munoz, R. (2023). Botanical filters for the abatement of indoor air pollutants. *Chemosphere, 345*, 140483.

Morin, J., Gandolfo, A., Temime-Roussel, B., Strekowski, R., Brochard, G., Bergé, V., Gligorovski, S., & Wortham, H. (2020). Key parameters influencing the uptake of m-xylene on photocatalytic paints. *Building and Environment*, *179*, 106979.

Năstase, G., Şerban, A., Năstase, A.F., Dragomir, G., & Brezeanu, A.I. (2018). Air quality, primary air pollutants and ambient concentrations inventory for Romania. *Atmospheric Environment, 184*, 292-303.

Vasile, V., Popa, I., Petcu, C., Dima, A., & Ion, M. (2023). Impact on Indoor Air of Multifunctional Materials Made with Animal Waste and Agro-Industrial By-Products. *Chemistry Proceedings, 13*, 21.

World Health Organization (2018). Burden of Disease of Household Air Pollution for 2016. https://cdn.who.int/media/docs/default-source/air-pollution-documents/air-quality-and-health/hap_bod_results_may2018_final.pdf?sfvrsn=d499316c_3

Yuan, J., Song, X., Yang, X., Yang, C., Wang, Y., Deng, G., Wang, Z., & Gao, J. (2023). Indoor carbon dioxide capture technologies: A review. *Environmentally Chemistry Letters, 21,* 2559-2581. https://doi.org/10.1007/s10311-023-01620-3.

Scientific Papers. Series E. Land Reclamation, Earth Observation & Surveying, Environmental Engineering. Vol. XV, 2026
Print ISSN 2285-6064, CD-ROM ISSN 2285-6072, Online ISSN 2393-5138, ISSN-L 2285-6064

# PHYSICAL AND MECHANICAL CHARACTERISTIC ASPECTS FOR CLADDING PRODUCTS BASED ON RICE HUSKS AND HEMP STALKS

**Irina POPA[1], Vasilica VASILE[1], Claudiu-Sorin DRAGOMIR[1, 2], Cristian GRIGORAȘENCO[1]**

[1]National Institute for Building Research, Town Planning and Sustainable Territorial Development "URBAN - INCERC", 266 Pantelimon Road, District 2, Bucharest, Romania
[2]University of Agronomic Sciences and Veterinary Medicine of Bucharest, 59 Mărăști Blvd, District 1, Bucharest, Romania

Corresponding author email: irinapopa2006@yahoo.com

***Abstract***

*Natural agro-industrial by-products and the circular economy concept are closely interconnected, both being essential for promoting sustainability in various representative fields of the economy, such as agriculture, the food industry, the construction industry, etc. The establishment of circular practices in the agro-industrial and construction sectors leads to the minimization of deposits of such materials/natural waste, optimizes their use by increasing their value, and simultaneously creates economic, environmental and social benefits. The paper presents aspects of the experimental research carried out with the aim of the superior valorization of two local agro-industrial by-products, namely rice husks and hemp stalks, by obtaining cladding products usable in construction. It is recognized that due to their compositional and structural particularities, the two natural materials, integrated in different types of construction materials, give them mechanical resistance, thermal insulation properties and acoustic performance. The products resulting from this research were studied from physical and mechanical point of view, considering that additional, multi-criteria tests are necessary, to gain a complete evaluation regarding the field of use in constructions of this type of innovative products.*

***Key words****: agro-industrial by-products, circular economy, construction, sustainability, waste.*

## INTRODUCTION

Currently, humanity is faced with a complex set of problems that are mutually interrelated. On the one hand, construction industry is an important consumer of energy and a major source of waste and greenhouse gas emissions (Cintura et al., 2021). Along with these, the growth of the world population and, implicitly, the necessary built stock, together with the aggressive impact of the conventional building materials industry through air, soil and water pollution, represent current problems that require clear intervention measures (Maraveas, 2020). At a global level, a wide range of directions for the valorization of recyclable materials has been identified, in the form of different types of construction materials/ products. In this regard, examples can be given ranging from the use of rice husk ash as an additional material in concrete production, contributing to improving the strength and durability of concrete (Kumar et al., 2013), the use of biological waste specific to the Euro-Mediterranean area, to obtain construction products and implicitly solving some associated challenges (Cintura et al., 2021), to the development of innovative asphalt mixture recipes, by incorporating different recyclable materials, in order to improve the lifespan of road structures (Ionescu & Dobre, 2025).

On the other hand, as a result of the increased demand for food, the agricultural sector together with the processing industries generate significant quantities of vegetable waste and natural agro-industrial by-products which, unused and improperly stored, also contribute to environmental pollution (Maraveas, 2020; Capanoglu et al., 2022; Yaashikaa et al., 2022; Ufitikirezi et al., 2024; Carrillo-Rodriguez et al., 2025). In this context, it is increasingly necessary to identify ecological approaches for the construction industry, the application of circular economy principles demonstrating that the productive use of agro-industrial waste can constitute an efficient and sustainable solution (Carrillo-Rodriguez et al., 2025). The circular economy contributes to reducing environmental

pollution by minimizing generated waste, optimizing its use through viable processes, and establishing interconnected circular practices between the agri-food and construction sectors. By transforming natural waste into raw materials and creating alternative materials, at much affordable costs (Maraveas, 2020), mainly of organic origin and from recyclable natural materials (Gołębiewski et al., 2025), the circular economy promotes the conservation of the economic value of products and contributes to increasing the added value of the resulting product (Coelho Vianna et al., 2024). The purpose of this experimental research is to find a new possibility of superior utilization in construction for two natural agro-industrial by-products (S.A.N.), namely rice husk and industrial hemp stalks, by obtaining innovative cladding products.

Specialized literature confirms researchers' concern for the exploitation of these S.A.Ns, in various types of construction products.

For exemple, rice husks can be used in plasters and agglomerated composite boards, products characterized by thermal or acoustic insulation properties (Revelo-Cuarán et al., 2022; Marin-Calvo et al., 2023; Milawarni et al., 2023; Pradhan et al., 2024; Wan et al., 2024), in cement blocks as a partial replacement of sand or in fire clay bricks, in form of rice husk ash (Maraveas, 2020).

In turn, hemp stalks are integrated into numerous types of building materials, hemp-lime composites with pro-ecological characteristics (Gołębiewski, 2017). The role of hemp in improving thermal insulation properties is recognized, having one of the lowest thermal conductivity coefficients among commonly studied plant aggregates (Gołębiewski, 2025), while also contributing to the compressive strength and humidity regulation of the materials in which it is integrated. One of the best-known hemp-based construction materials is hemp concrete, obtained by mixing hemp pulp with a lime-based binder. Having good thermal insulation, significant breathability, hygroscopicity and a reduced carbon footprint, high permeability to water vapor, fire resistance, biodegradation, good acoustic properties, it can be used for roofs and floors, or for insulating walls on their exterior side (Gołębiewski, 2017; Demir & Doğan, 2020; Yadav & Saini, 2022; Gołębiewski, 2025). Hemp can also be used to obtain products such as: particleboard and fiberboard, by mixing hemp pulp with other lignocellulosic materials and binders, boards usable as floor and wall panels, as well as biocomposite materials, by combining hemp pulp with a matrix of synthetic or natural polymers, resulting in floors, cladding elements and interior finishes (Cigasova et al., 2015; Dhakal & Zhang, 2015; Requile et al., 2019; Maraveas, 2020).

## MATERIALS AND METHODS

Based on the documentation carried out on obtaining cladding products by integrating plant waste, a series of materials were selected to design products of this type, both in ecological and hybrid variants. Both types of recipes integrated rice husks (Figure 1), hemp stalks (hurd) chopped at lengths between 1-5 cm (Figure 2) or mixtures thereof, but different in the nature of the binders.



Figure 1. General appearance of rice husks



Figure 2. General appearance of chopped hemp stalks

In this approach, the eco-recipes had either a natural binder of plant origin, obtained from a mixture of corn starch, hydrated lime and water, or a natural binder of animal origin, based on bone glue (denoted COS). The hybrid recipes had a binder resulting from a mixture of COS

and a synthetic adhesive, based on polyvinyl acetate (denoted AD1) or polyurethane (denoted AD2), the last two materials having the role of improving the cohesion of the cladding product. All recipes have been designed to obtain organic products or products with organic characteristics, from a compositional point of view, with high cohesion and hardness. Thus realized, the recipes allow the comparative study of the influence that the different compositional factors have on the mechanical characteristics of the obtained products. The influencing factors studied were the following: type of binder (natural vs. hybrid binder, respectively its synthetic component); type of the S.A.N. integrated in the product (rice husks vs. rice husks+hurd vs. hurd); presence of the adhesive; type of adhesive (polyvinyl acetate vs. polyurethane). The cladding products were obtained by casting the biomaterials in a steel mold and applying an external pressure, using a press, to reduce excess moisture in the plate mass. The mould was designed and made for this purpose, with dimensions of 270 x 270 x 25 mm. The methodology for obtaining the cladding products consisted of the following sequence of main steps: Preparation of raw materials and binders simultaneously with heating the steel mold in the oven at 70°C, for aprox. 4 hours → Mixing the components according to the recipe and homogenizing them → Pouring the resulting biomaterial into the steel mold → Closing the mold with its lid → Placing the mold + biomaterial assembly in the press and applying an exterior force to it → Demoulding the sample from the mold → Natural drying of the obtained plate, in laboratory conditions (temperature of 23±2°C şi relative air humidity of 50% ± 10%). Regarding this work protocol, the following additions are necessary to be outlined: a. The S.A.N were dried in the oven at 70°C, for approx. 4 hours; b. While the preparation of the vegetable binder consisted only in mixing and homogenizing hydrated lime and corn starch with water, in the case of the COS binder, this was obtained by soaking the granules in water (mixing ratio 1:1 in mass units) for approx. 12 hours, then by heating the obtained gel in a Bain-Marie, up to a temperature of 50-70°C, resulting the bone glue in the colloidal phase; c. There was a slow and constant application of a force to the mold. The maximum value of the applied force varied, on the one hand depending on the moment when the binding liquid phase started to emerge from the mold and, on the other hand, on the values of the external force applied, in order not to affect the integrity of the mold under load. This thermoforming protocol proved to be functional, as the obtained plates showed stability and cohesion between the constituent elements, but required advanced drying. As a result, the plates were weighed every 24 hours, so that the condition of complete drying to constant mass could be reached. Depending on the thickness of the cladding products, drying of the plates continued for about 10 days, after which the cladding products were placed in a vertical position and were normaly dried, in laboratory conditions (temperature of 23±2°C şi relative air humidity of 50% ± 10%), for another about 20 days.

Based on considerations regarding the workability of the biomaterial, as well as the compact aspect of the material both after demolding and at the end of the drying period, four vegetable - bound, six hybrid - bound and three COS - bound cladding products were obtained and then studied by means of their main mechanical characteristics. From the point of view of the vegetable component: binder mixing ratios, compositional benchmarks of the obtained cladding products are presented in Table 1.

Table 1. Compositional benchmarks of the biomaterials obtained by integrating rice husks and hemp stalks

| Biomaterial/ Cladding product notation | Binder | S.A.N : binder mixing ratios (mass units) | Vegetable components |
|---|---|---|---|
| C4-1 | Vegetable | 3:25 | P[1] |
| C6-1 | Vegetable | 20:70 | P, H[2], P=H |
| C7-1 | Vegetable | 20:70 | P, H, P=H |
| C8-1 | Vegetable | 20:70 | P, H, P=H |
| PMI′ | COS, AD1 | 1:3.74 | P |
| PMI″ | COS, AD2 | 1:3.77 | P |
| PMIII′ | COS | 1:5.75 | P, H, P=H |
| PMIII‴ | COS | 1:5.75 | P, H, P<H |
| PMIII‴bis | COS | 1:3.50 | P, H, P<H |
| PMIV′ | COS, AD1 | 1:4,30 | P, H, P<H |
| PMIV″ | COS, AD2 | 1:3.50 | P, H, P<H |
| PMV′ | COS, AD1 | 1:4.03 | H |
| PMV″ | COS, AD2 | 1:4.20 | H |

[1]P=Husk rice.
[2]H=Hurd (Choped hemp stalks).

After drying, the general appearance of the obtained cladding products was different

depending on the incorporated S.A.N. but also on the binder (Figures 3, 4 and 5).



Figure 3. Examples of the general aspect of vegetable-bound cladding products based on rice husks (left), and on a mix of rice husks and choped hemp stalks (right)



Figure 4. Example of the general aspect of COS-bound cladding products based on rice husks

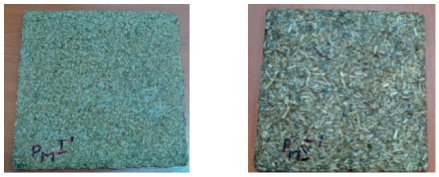


Figure 5. Examples of the general aspect of hybrid - bound cladding products based on rice husks (left), and on a mix of rice husks and choped hemp stalks (right)

The general appearance of the cladding products illustrates their cohesive, compact character.
In order to highlight the significant differences among all the materials with different compositions developed and presented in this research, a statistical analysis was applied, using a one-way analysis of variance (one-way ANOVA). The software used to perform the statistical analysis was Microsoft Excel.

## RESULTS AND DISCUSSIONS

The determination of physical and mechanical characteristics was performed on both eco- and hybrid-recipes cladding products. Each plate was measured to establish dimensional compliance, the nominal thickness and side length. After the end of the drying period of the cladding products, the measured values of the sides were between 255 mm (PMIII‴) and 267 mm (C4-1), and the average thickness values, between 8.23 mm (PMIII′) and 22.84 mm (PMV″). The modulus of elasticity in bending was determined by applying a constant speed load to the middle of the sample placed on two supports. For the calculation of the value, the slope of the rectilinear area of the load-deformation curve was used.
The bending load-deflection diagrams have a comparable appearance for all types of recipes, with a linear upward evolution on the first portion of the representation, followed by a threshold value, the maximum load, corresponding to the resistance of the base material.
Subsequently, the material failure occurred and the curve becomes descending, some examples being illustrated in Figure 6, for the two test pieces of C4-1 and PMIII‴ clading product. The results regarding the flexural strength and modulus of elasticity for all the obtained cladding products are graphically represented in the Figures 7 and 8.

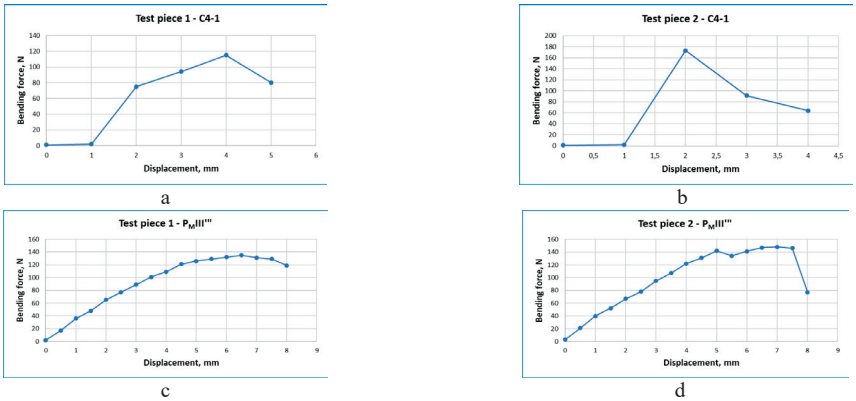



Figure 6. Load-deformation curves. Specific examples for C4-1 (a, b) and PMIII‴ (c, d) cladding product

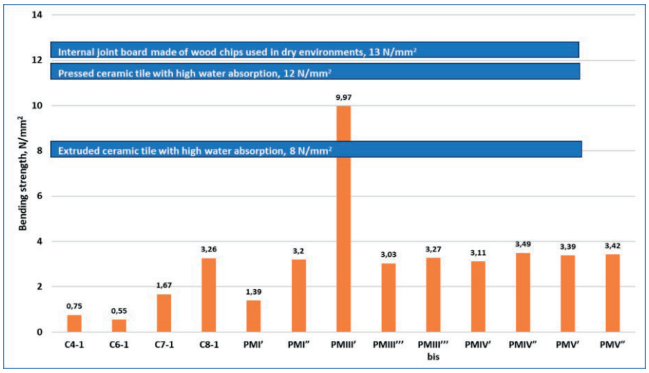



Figure 7. Bending strength of rice husk and hemp stalks based cladding products

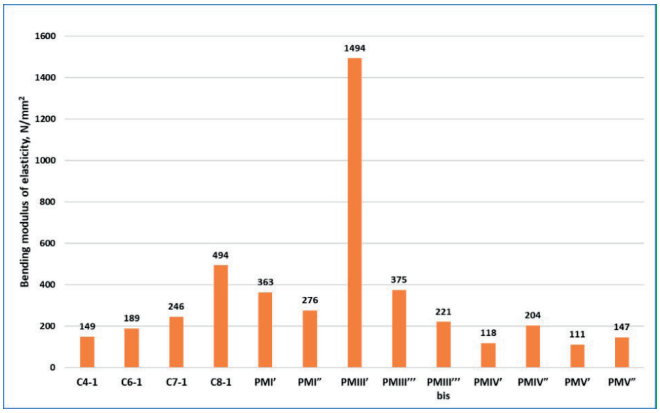



Figure 8. Bending modulus of elasticity for rice husk and hemp stalks based cladding products

Regarding eco - cladding products, the highest value for flexural strength was obtained for C8-1, of 3.26 N/mm$^2$ with a flexural modulus of elasticity of 494 N/mm$^2$ at an average board thickness of 8.30 mm. This value is comparable to that of PMI″, average plate thickness 12.68 mm (flexural strength 1.39 N/mm$^2$, flexural modulus 363 N/mm$^2$), of PMIII‴, average plate thickness 9.28 mm (flexural strength 3.03 N/mm$^2$, flexural modulus 375 N/mm$^2$) and of PMIII‴bis, average plate thickness 16.37 mm (flexural strength 3.27 N/mm$^2$, flexural modulus 221 N/mm$^2$), which contain COS with or without synthetic products for binding the vegetable fraction. This is why, the C8-1 recipe consisting of rice husks, hurd, lime and corn starch represents a compositional variant to be taken into account for further optimization.

The best bending strength was recorded for PMIII′, with a value of 9.97 N/mm$^2$ and a bending modulus of elasticity of 1494 N/mm$^2$, for an average thickness of 6.86 mm, the product having an eco-recipe based on rice husks, chopped hemp stalks and COS.The bending load-deflection diagrams have a comparable appearance for all types of recipes, the maximum load, corresponding to the strength of each material, reaching the value of 1110 N. The strength of PMIII' tends to reach the value of bending strength of boards based on wood chips intended for use in dry environments and may represent a premise for future compositional development.

From the analysis of these obtained results, the following aspects can be highlighted:

The best results from a mechanical point of view were obtained in the case of cladding products with eco-recipes having bone glue as a binder and those with hybrid recipes, especially with polyurethane adhesive.

Also noteworthy were the products with mixed vegetable content, regardless of the type of

binder, and in the case of the products with eco-recipes, the C8-1 board, with the highest corn starch content.

It is considered useful to highlight that this research is characterized by a certain limitation regarding the possibility of interpreting the obtained experimental results. The limitation is explained by the fact that the research is still in development, with the aim of identifying the field in which the obtained products could be classified, and subsequently studying the possibilities of their improvement. In this context, it is specified that the methodology applied for determining the bending strength and the bending modulus of elasticity was similar to that of SR EN 310, but the tests were performed on a small number of samples, the graphic representations of the mentioned characteristics being made based on the obtained average values.

To assess whether the flexural strength differs between the 13 cladding products (configurations), a one-way ANOVA analysis was applied, which revealed significant differences between groups ($F(12,13) = 8.84$; $p = 0.00021$), with a very large effect of configuration on flexural strength ($\eta^2 = 0.89$). The same analysis revealed significant differences in the flexural modulus of elasticity between the 13 cladding products ($F(12,13) = 7.99$; $p = 0.00035$), with the configuration explaining approximately 88% of the variation in the values ($\eta^2 = 0.88$). The value of the F statistic indicates greater variability between the 13 groups (recipes) of cladding products and less within the same group of specimens.

## CONCLUSIONS

Rice husks and industrial hemp constitute a category of S.A.N. with a high potential for valorization in the form of various types of construction products. Seven cladding products with natural binders and six with hybrid binders were studied in terms of mechanical characteristics, representing the first stage in evaluating their potential for use in construction. From a compositional point of view, the cladding products that had the mixed natural binder, of corn starch and hydrated lime had a more cohesive structure than those with a single vegetable binder, starch or lime.

The cladding products have mechanical characteristics higher than those of extruded ceramic tiles with high water absorption and relatively close to those of pressed ceramic tiles with high water absorption, characteristics that can still be improved.

Based on the experimental results obtained up to this stage of research on innovative cladding products containing rice husks and/or chopped industrial hemp stalks, it is considered that additional tests are necessary in order to achieve a more complete assessment of their potential for use in construction.

## ACKNOWLEDGEMENTS

This research work was carried out with the support of Ministry of Research, Innovation and Digitalization and also financed from Project PN 23 35 02 01 “Innovation and Digitalization Synergies in the Design of Eco-Materials and Multifunctional Products for Sustainable Construction, with Impact on the Environment and the Circular Economy”.

## REFERENCES

Capanoglu, E., Nemli, E., & Tomas-Barberan, F. (2022). Novel Approaches in the Valorization of AgriculturalWastes and Their Applications. *Journal of Agricultural and Food Chemistry, 70*, 6787–6804.

Carrillo-Rodriguez, L.A., Cajigas Romero, M., & Galindo Larrahondo, J.A. (2025). The use of agro-industrial waste towards a sustainable circular economy: A systematic review. *Detritus, 31*, 45.

Cigasova, J., Stevulova, N., Schwarzova, I., Sicakova, A., & Junak, J. (2015). Application of hemp hurds in the preparation of biocomposites. *IOP Conference Series: Materials Science and Engineering, 96, 012023.* IOP Publishing.

Cintura, E., Nunes, L., Esteves, B., & Faria, P. (2021). Agro-industrial wastes as building insulation materials: A review and challenges for Euro-Mediterranean countries. *Industrial Crops and Products*, *171*, 113833.

Coelho Vianna, L.M., de Oliveira, L., & Muhl, D.D. (2024). Waste valorization in agribusiness value chains. *Waste Management Bulletin Journal, 1*, 195–204.

Demir, İ., & Doğan, C. (2020). Physical and mechanical properties of hempcrete. *The Open Waste Management Journal*, *13*(1), 26–34.

Dhakal, H. N., & Zhang, Z. (2015). The use of hemp fibres as reinforcements in composites. *Biofiber Reinforcements in Composite Materials*, 86–101.

Gołębiewski, M. (2017). Hemp-Lime Composites in Architectural Design. *Kwartalnik Naukowy Uczelni Vistula, 4(54),* 162–171.

Gołębiewski, M., Pietruszka, B., Piątkiewicz, W., Kubiś, M., & Oleksiienko, O. (2025). Compressive Strength, Thermal Conductivity, Vapor Permeability and Specific Heat of Hemp-Lime Composites Varying in Density for Wall, Roof and Floor Applications. *Materials*, *18*, 4958.

Ionescu, N.-A., & Dobre, D. (2025). Behavior of asphalt mixtures manufactured with recycled materials and their in situ performance level. *Scientific Papers. Series E. Land Reclamation, Earth Observation & Surveying, Environmental Engineering, 14*, 252–259.

Kumar, S., Sangwan, P., Dhankhar, R.M.V., & Bidra, S. (2013). Utilization of rice husk and their ash: A review. *Research Journal of Chemistry and Environment*, *1*, 126–129.

Maraveas, C. (2020). Production of Sustainable Construction Materials Using Agro-Wastes, *Materials*, *13*, 262.

Marin-Calvo, N., González-Serrud, S., & James-Rivas, A. (2023). Thermal insulation material produced from recycled materials for building applications: Cellulose and rice husk-based material. *Frontiers in Built Environment, 9,* 1271317.

Milawarni, M., Aprilia, S., Idris, N., Elfiana, E., Yassir, Y., Asnawi, Y., Suryati, S., Novi Quintena, R., Syarif, J., & Juhan N. (2023). Analysis of Physical and Mechanical Properties of Rice Husk-based Particle Board, *Journal of Advanced Research in Applied Sciences and Engineering Technology*, *31*(3): 40–46.

Pradhan, S.; Entsminger, E.; Mohammadabadi, M.; Seale, D., & Ragon, K. (2024). Evaluation of rice husk composite boards prepared using different adhesives and processing methods. *BioResources*, *19,* 595–604.

Requile, S., Le Duigou, A., Bourmaud, A., & Baley, C. (2019). Hygroscopic and Mechanical Properties of Hemp Fibre Reinforced Biocomposites. *Revue des Composites et des Matériaux Avancés-Journal of Composite and Advanced Materials*, *29*(4), 253–260.

Revelo-Cuaran, E.A., Nieves-Pimiento, N., & Toledo-Bueno, C.A. (2022). Homogenization Analysis in Particle Boards with Rice Husk Reinforcement. *Tecnura*, *26*, 59–79.

SR EN 310 – Wood-based panels. Determination of modulus of elasticity in bending and bending strength, 1996.

Ufitikirezi, J. d. D. M., Filip, M., Ghorbani, M., Zoubek, T., Olšan, P., Bumbalek, R., Strob, M., Bartoš, P., Umurungi, S.N., Murindangabo, Y.T., Heřmánek, A., Tupý, O., Havelka, Z., Stehlík, R., Černý, P., & Smutný, L. (2024). Agricultural Waste Valorization: Exploring Environmentally Friendly Approaches to Bioenergy Conversion. *Sustainability*, *16*, 3617.

Wan, D., Tian, C., Cai, Q., & Zhang, X. (2024). Investigating the characteristics and thermal performance of plaster composites enhanced with paddy husk for sustainable Residential construction. *Case Studies in Thermal Engineering*, *60*, 1–8.

Yaashikaa, P.R., Senthil Kumar, P., & Varjani, S. (2022). Valorization of agro-industrial wastes for biorefinery process and circular bioeconomy: A critical review. *Bioresource Technology*, 343, 126126.

Yadav, M., & Saini, A. (2022). Opportunities & challenges of hempcrete as a building material for construction: An overview, Materials Today: *Proceedings, 65*(2), 2021–2028.

Scientific Papers. Series E. Land Reclamation, Earth Observation & Surveying, Environmental Engineering. Vol. XV, 2026
Print ISSN 2285-6064, CD-ROM ISSN 2285-6072, Online ISSN 2393-5138, ISSN-L 2285-6064

# CORRELATION BETWEEN THE PHYSICAL PROPERTIES AND NPK NUTRIENT CONTENT OF ORCHARD SOILS FOR THE SELECTION OF APPROPRIATE SOIL DECONTAMINATION TECHNOLOGIES

**Maria POPA**

Petroleum-Gas University of Ploiesti, 39 Bucharest Blvd, Ploiesti, Romania

Corresponding author email: mpopa@upg-ploiesti.ro

***Abstract***

*The network of underground pipelines used to transport petroleum products may crack and lead to soil contamination. As these pipelines can be located near orchards, this study investigated soils from quince, plum, and pear orchards. The physical properties of the soils were analyzed comparatively, including density, texture and granulometry, capillarity and permeability. Capillarity, permeability and retention capacity were determined for both water and a petroleum product considered a potential soil pollutant. The analysis of physical properties, together with the NPK nutrient content of each soil type, was used to facilitate the selection of appropriate decontamination technologies. Two pollutant removal methods applicable to all three soil types were evaluated: thermal desorption at 400°C and successive extraction using two solvents, petroleum ether and benzene. Nutrient content was determined before and after each decontamination process.*

***Key words****: decontamination, nutrients, orchard soil, pollutant.*

## INTRODUCTION

Soil is a fundamental natural resource that sustains agricultural ecosystems and supports long-term food production. Orchard soils, in particular, require careful and continuous monitoring, as the specific physical properties of the soil, including texture, bulk density, granulometry, capillarity, and permeability, directly influence the growth requirements of fruit tree species such as quince, plum, and pear (Capri et al., 2023; Özdemir et al., 2022). Knowledge of these properties is essential not only for the appropriate selection of fruit tree species, but also for the efficient management of irrigation and fertilization practices. In this context, monitoring the NPK nutrient content of orchard soils plays a central role in achieving sustainable yields, as imbalances in nitrogen, phosphorus, and potassium directly affect tree physiology, flowering, and fruit quality (Sun et al., 2023; Rusu et al., 2025).

Since each fruit tree species has specific growth requirements, knowledge of the physical properties of the soil is essential. Furthermore, determining the nutrient content of orchard soils allows for the appropriate application of fertilizers. Recent studies show that orchard soils require constant and careful monitoring, with the recommendation including the use of sewage sludge with high nutrient content (Iorga et al., 2025) and fertilization with compost (Butcaru et al., 2024). Other authors conducted a comparative study between a conventional system based on herbicide use and a conservation system based on cover crops, evaluating nutrient content in a plum orchard (Rusu et al., 2025). The use of biofertilizers as alternatives to chemical fertilizers has also been investigated. Studies were conducted in an apple orchard over a period of five years (Ferreira et al., 2025) and in a pear orchard over a period of two years (Li et al., 2025). The combination of cover crops with legumes planted in orchards has been shown to improve the nutrient cycle (Raimundo et al., 2025). Other studies on nutrient uptake were carried out in cherry orchards (Karampatzakis et al., 2025) and pear orchards (Liu et al., 2025), with particular emphasis on tree age. Recent studies also highlight the importance of factors such as temperature, irrigation water, the use of biostimulants, and weed presence for ensuring good crop production in orchards (Lisek, 2023; Cara, 2025). The application of the electrokinetic decontamination method, with different types of electrodes, on agricultural soil led to different changes in NPK nutrients (Popa, 2025).

Nitrogen is responsible for leaf growth; its deficiency causes yellowing, while an excess can prolong the vegetation period. Phosphorus is important for the functioning of the immune system and stimulates the flowering process. Potassium is converted, through chemical reactions, into potassium hydroxide, which stores nutrients required by the plant. When potassium is deficient, the intensity of photosynthesis decreases.

Beyond agronomic challenges, orchard soils located in proximity to major petroleum product transport infrastructure face an additional risk: accidental contamination with hydrocarbons resulting from pipeline failures or leaks (Franchi et al., 2022; Adeniran et al., 2023). Such contamination events pose a serious threat to soil fertility and long-term agricultural productivity, as petroleum hydrocarbons alter the physical structure of the soil, disrupt nutrient availability, and suppress microbial activity (Ambaye et al., 2022; Ossai et al., 2020). The selection of an appropriate decontamination strategy is therefore critical, as it must balance the effective removal of the pollutant with the preservation of the soil's agronomic potential. Among the available remediation technologies, thermal desorption and successive solvent extraction have been evaluated as viable approaches for hydrocarbon-contaminated agricultural soils (O'Brien et al., 2024; Caetano et al., 2024). However, the impact of these methods on soil nutrient content, particularly NPK levels, remains an aspect that requires further investigation, especially in the context of orchard soils.

## MATERIALS AND METHODS

Major pipelines can be located very close to orchards; therefore, this study focuses on two neighboring counties in Romania where such risks may occur: Prahova and Dambovita (Figure 1). Although the main pipeline network in Romania is continuously monitored, rapid action is required if soil contamination with petroleum hydrocarbons occurs.

Soil samples used in this study were collected from quince and pear orchards in Dambovita County and from plum orchards in Prahova County. This study compares two methods for the decontamination of soils contaminated with hydrocarbons: successive extraction with solvents and thermal desorption.

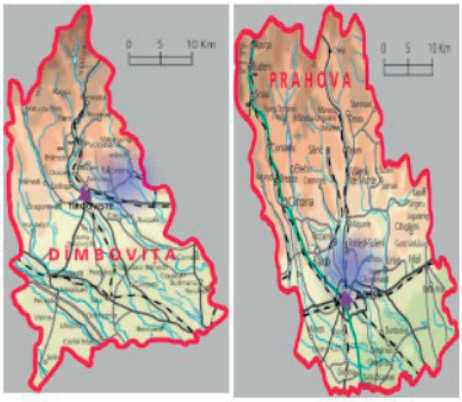



Figure 1. The orchard areas

Soil characterization involved determining the physical properties of the three samples. Additionally, for pollution control conducted in the laboratory, diesel oil was characterized by its density and viscosity. These properties of diesel oil help to understand how it penetrates the soil structure. The concentration of pollutants in soil was 7% by mass, a percentage deliberately chosen as it falls within the minor pollution range. All methods used to determine the physical properties of the analysed soil samples have been described in previous works (Popa, 2023; 2024).

Capillarity, defined as the maximum height a liquid can reach in the soil within one hour, represented by the ascent phenomenon, was established. Permeability, the property that ensures the penetration of liquid from top to the bottom of the soil, was calculated as the average permeability over one hour of exposure to the soil. This property depends on the free spaces between the solid aggregates of the soil, as well as the physicochemical interactions formed with the fluid molecules passing through the soil.

The liquid retention capacity of the soil was also determined and expressed in liters of liquid per $1m^3$ of dry soil. Both permeability and retention capacity were tested for water and diesel oil. Permeability could be determined for only a single measurement for diesel oil, at 15 minutes, due to a high pollutant consumption for the soil in the quince orchard. Granulometry was determined using the sieving method with four

different sieve diameters (1.6 mm, 1 mm, 0.5 mm and 0.25 mm).

Based on the laboratory determined grain size, soil texture was established, allowing for verification of differences between the two regions from which the soil originated. All physical properties were determined on dry soil samples (oven-dried at 105°C, for one hour), thus establishing the initial moisture content of the samples (% mass).

The NPK nutrient content was determined qualitatively. In orchards, monitoring nutrient content is essential to achieving good yields. The reagents used in the Hanna test kit (Popa, 2023) are pre-measured solutions specially formulated for colorimetric and turbidimetric reactions, which enable the rapid and accurate determination of essential NPK nutrients. The kit defines the following ranges: trace (0-5 ppm), low (5-15 ppm), medium (15-30 ppm), high (30-50 ppm).

Dry soils, pre-heated for one hour at 105°C, were contaminated with 7% diesel oil and immediately subjected to thermal decontamination. The process was carried out at 400°C, enabling both pollutant recovery and water removal at elevated temperatures.

The apparatus has been described in the literature (Popa, 2023). Decontamination by successive solvents extraction was performed using two solvents, petroleum ether and benzene, using a Soxhlet apparatus as described in the literature (Popa, 2024).

## RESULTS AND DISCUSSIONS

### *Characterization of clean soils*

The analyzed clean soils were characterised by their physical properties (Table 1), and nutrient values were estimated at the upper limit of the recommended range provided by the analysis kit.

Table 1. Characterization of clean orchard soil samples

| Property | Type of orchard soil | | |
|---|---|---|---|
| | Quince | Plum | Pear |
| Max. capillarity to water (cm) | 4.6 | 3.5 | 3.6 |
| Max. capillarity to diesel oil (cm) | 8.5 | 7.3 | 7.4 |
| Permeability to water ($cm^3/h$) | 8400 | 411.4 | 596.28 |
| Water retention capacity (kg water/$m^3$ soil) | 170.1 | 384.6 | 324.2 |
| Diesel oil retention capacity (kg diesel oil/$m^3$ soil) | 29 | 64 | 42 |
| Max nutrients content (mg/kg soil) | | | |
| N | 5 | 30 | 30 |
| P | 30 | 15 | 30 |
| K | 50 | 15 | 15 |
| pH | 6.5 | 6.5 | 5.5 |
| Moisture (% mass) | 18 | 20.1 | 18.3 |
| Granulometry (g) | | | |
| Sieve diameter | | | |
| 1.6 mm | 58 | 58 | 58.6 |
| 1 mm | 14.9 | 16.2 | 16.5 |
| 0.5 mm | 18 | 13.6 | 18.9 |
| 0.25 mm | 8.9 | 5.8 | 5.5 |
| losses on the sieve | 0.2 | 6.4 | 0.5 |
| Textural class | sandy | sandy loam | sandy |
| Conductivity (µS/cm) | 120 | 150 | 134 |
| Apparent density ($g/cm^3$) | 1.36 | 1.58 | 1.38 |
| Real density ($g/cm^3$) | 2.74 | 2.60 | 2.65 |
| Porosity (%) | 50.3 | 39.2 | 47.9 |

The physical properties of the three analyzed soils reveal significant differences related to their textural class and geographical origin. The quince orchard soil, classified as sandy, exhibited the highest capillarity to diesel oil (8.5 cm) and the highest permeability to water (8400 $cm^3/h$), indicating a very open pore structure that facilitates rapid fluid movement. Consequently, its water retention capacity was the lowest (170.1 $kg/m^3$), which suggests that this soil type is the most vulnerable to deep pollutant infiltration in the event of a petroleum spill. In contrast, the plum orchard soil, classified as sandy loam, displayed the highest water retention capacity (384.6 $kg/m^3$) and the lowest permeability, reflecting a denser, more cohesive structure with a lower porosity of 39.2%. The pear orchard soil presented intermediate values between the two, with a sandy texture and a porosity of 47.9%. Regarding nutrient content, notable differences were observed among the three soils: the quince soil was characterized by low nitrogen (5 mg/kg) and high potassium (50 mg/kg), the plum soil showed a balanced but moderate NPK distribution, while the pear soil presented elevated nitrogen and phosphorus content (30 mg/kg each). These differences reflect the distinct fertilization histories of each privately owned orchard and underline the importance of site-specific nutrient monitoring.

***Characterization of diesel oil***

To illustrate how the pollutant penetrates the soil structure through the soil's capillary and permeability properties, as shown in Table 1, it was necessary to characterize the pollutant in terms of density and viscosity. These are key properties for the pollutant - diesel oil - and are presented in Table 2.

The density of diesel oil (850.5 $kg/m^3$ at 20°C) is significantly lower than the real density of all three soil types (2.60-2.74 $g/cm^3$), which means that diesel tends to remain in the upper soil layers and within the pore spaces rather than sinking rapidly to deeper horizons.

However, its low kinematic viscosity ($3.57 \times 10^{-4} m^2/s$ at 40°C) facilitates mobility through the soil matrix, particularly in sandy soils with high permeability such as the quince and pear orchard soils. These properties are relevant for understanding the capillarity and permeability results observed in Table 1, where diesel oil consistently reached higher capillary heights than water, due to its lower surface tension and different wetting characteristics relative to the soil mineral surfaces.

Table 2. The physical properties of diesel oil

| Physical properties | Value |
|---|---|
| Density ($kg/m^3$ ) at 20°C | 850.5 |
| Kinematic viscosity·$10^4$ ($m^2/s$) at 40°C | 3.57 |

***Thermal desorption for soil decontamination***

The extent of decontamination achieved by thermal desorption as summarized (Table 3). Following thermal decontamination, the nutrient content of the soils was restored (Table 4).

Table 3. The degrees of decontamination established after thermal desorption

| Measured | Type of orchard soil | | |
|---|---|---|---|
| | Quince | Plum | Pear |
| Diesel oil volume (ml) | 4.76 | 3.64 | 3.59 |
| Volume of water desorbed (ml) | 3.7 | 5.25 | 2 |
| Volume of diesel oil desorbed (ml) | 3.1 | 3.25 | 3 |
| Degree of decontamination achieved (%) | 83.8 | 89.3 | 83.6 |

Table 4. Nutrient content after desorption decontamination

| Nutrient | Type of orchard soil (mg/kg) | | |
|---|---|---|---|
| | Quince | Plum | Pear |
| N | 5 | 5 | 30 |
| P | 50 | 15 | 15 |
| K | 30 | 5 | 15 |

***Successive solvents extraction for soil decontamination***

Clean samples were decontaminated to quantify the organic material extracted according to soil structure (Table 5).

Table 5. Extraction results for the clean sample

| Measured | Type of orchard soil | | |
|---|---|---|---|
| | Quince | Plum | Pear |
| Organic material with petroleum ether (%) | 0.08 | 0.41 | 0.55 |
| Organic material with benzene (%) | 0.16 | 0.27 | 0.39 |
| Total organic material extracted (%) | 0.24 | 0.68 | 0.94 |

Soil samples contaminated in labor with 7% diesel oil were subjected to successive solvents extraction. The results obtained for the clean sample were used as a reference. The final results establishing the degree of decontamination are presented (Table 6).
After solvents extraction, the nutrient content of the soils was re-established (Table 7).

Table 6. The degrees of decontamination established after extraction

| Measured | Type of orchard soil with 7% diesel oil | | |
|---|---|---|---|
| | Quince | Plum | Pear |
| Diesel oil with petroleum ether (%) | 46.18 | 49.8 | 49.7 |
| Diesel oil with benzene (%) | 11.18 | 23.9 | 40.8 |
| Degree of decontamination achieved, (%) | 57.36 | 73.7 | 90.5 |

After the application of the decontamination methods, the soil pH values increased, except for the plum orchard soil, which showed a lower pH value after extraction (Table 8).
At 400°C, the acidic organic fractions in the soil and in the pollutant suffer degradation and volatilization, leading to an increase in basic mineral compounds and, consequently, to a rise in pH.

Table 7. Nutrient content after extraction decontamination

| Nutrient | Type of orchard soil, (mg/kg) | | |
|---|---|---|---|
| | Quince | Plum | Pear |
| N | 50 | 50 | 30 |
| P | 50 | 15 | 30 |
| K | 30 | 30 | 30 |

Changes in soil composition and buffering capacity can cause the pH to shift toward more alkaline values during successive solvent extraction.

Table 8. Variation of soils pH

| pH | Type of orchard soil | | |
|---|---|---|---|
| | Quince | Plum | Pear |
| pH for clean soil | 6.6 | 6.5 | 5.5 |
| pH of soil after desorption | 8.5 | 5.5 | 6 |
| pH of soil after extraction | 7.5 | 8 | 7 |

The application of decontamination methods highlights changes in nutrients content (Figure 2).

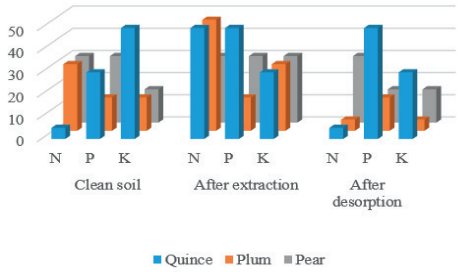



Figure 2. Variation of nutrients content

It should be noted that the orchards from which the samples were collected are privately owned and relatively small in size, each having received organic amendments. The fertilizers applied were not consistently monitored; therefore, different nutrient contents were observed in the clean soil samples (Table 1). The orchards are located in areas vulnerable to pollution due to accidental leaks from main petroleum product transport pipelines.

Thermal desorption at 400°C proved effective for all three soil types, achieving decontamination degrees ranging from 83.6% (pear orchard soil) to 89.3% (plum orchard soil). The plum orchard soil, which had the highest diesel oil retention capacity (64 kg/m³), also yielded the largest volume of desorbed water (5.25 ml), suggesting that its higher moisture content and denser structure required more energy for complete pollutant volatilization. The quince orchard soil, despite its high permeability, achieved a decontamination efficiency of 83.8%, likely due to the high initial pollutant mobility within its open pore structure. Overall, the results confirm that thermal desorption at 400°C is a reliable method for recovering petroleum hydrocarbons from all three soil types, with recovery rates consistently above 83%. The present study was based on the assumption that variations in nutrient content (NPK) in orchard soils may influence the selection of an appropriate decontamination technology. At the same time, soil pH was found to play an important role.

Following thermal desorption, notable changes in NPK nutrient content were recorded compared to the initial clean soil values (Table 1). In the quince orchard soil, phosphorus increased significantly (from 30 to 50 mg/kg), while nitrogen remained stable (5 mg/kg) and potassium decreased (from 50 to 30 mg/kg). In the plum orchard soil, all three nutrients decreased markedly, with nitrogen dropping from 30 to 5 mg/kg and potassium from 15 to 5 mg/kg, suggesting that the high treatment temperature caused volatilization or transformation of nitrogen compounds and leaching-like redistribution of potassium. The pear orchard soil showed an increase in nitrogen (from 30 to 30 mg/kg - unchanged) and stable phosphorus and potassium values. These results indicate that thermal desorption, while highly effective for pollutant removal, exerts a heterogeneous influence on nutrient content depending on the soil's initial composition and texture.

A comparison of the two decontamination approaches reveals that successive solvents extraction exerts a relatively mild impact on soil structure and nutrient content, while inducing minimal changes in pH. This method is predominantly linked to the mobilization of nutrients associated with organic matter. Conversely, desorption primarily interacts with the mineral fraction of contaminated soils, leading to a more pronounced increase in pH. When performed at 400 °C, desorption facilitates the determination of available nutrient content through mineralization. An advantage of the desorption method lies in its ability to recover and reuse the pollutant in relatively high proportions (over 83%), but the application of desorption can affect long-term fertility. For orchard soils, permanent irrigation is necessary (permeability is high), as is the controlled use of organic amendments, possibly alternating them, and nutrient supplements.

Successive solvent extraction with petroleum ether and benzene yielded decontamination efficiencies ranging from 57.36% (quince orchard soil) to 90.5% (pear orchard soil). The pear orchard soil achieved the highest removal efficiency, with both solvents contributing substantially (49.7% with petroleum ether and 40.8% with benzene). In contrast, the quince orchard soil showed the lowest overall efficiency despite its high permeability, which may be attributed to strong adsorption interactions between the diesel oil and the sandy soil matrix at the concentration used. The plum orchard soil achieved an intermediate efficiency of 73.7%. Notably, petroleum ether consistently outperformed benzene in the first extraction step across all soil types, suggesting that the lighter, non-polar diesel oil fractions are more readily mobilized in the initial extraction phase, with benzene recovering the heavier residual fractions in the second step. Successive solvent extraction had a generally positive or neutral effect on nutrient content compared to the initial clean soil values. The quince orchard soil showed significant increases in nitrogen (from 5 to 50 mg/kg) and maintained its phosphorus level (50 mg/kg), while potassium remained stable (30 mg/kg). The plum orchard soil similarly showed a marked increase in nitrogen (from 30 to 50 mg/kg) and potassium (from 15 to 30 mg/kg), with phosphorus unchanged (15 mg/kg). The pear orchard soil maintained stable nitrogen and phosphorus levels (30 mg/kg each) and showed an increase in potassium (from 15 to 30 mg/kg). These results suggest that solvent extraction, unlike thermal desorption, does not destroy nutrient compounds and may even

mobilize organically bound nutrients, making it a more agronomically favorable option with respect to post-treatment soil fertility. Changes in nutrient content before and after remediation were also observed in agricultural soil when the electrokinetic remediation method was used (Popa, 2025).

The results obtained are similar to the literature on the properties of orchard soils (Tkaczyk et al., 2018).

The application of both decontamination methods induced measurable changes in soil pH. Following thermal desorption, the pH increased substantially in the quince orchard soil (from 6.6 to 8.5) and moderately in the pear orchard soil (from 5.5 to 6.0), while the plum orchard soil experienced a decrease (from 6.5 to 5.5). The pronounced alkalinization observed in the quince soil after desorption can be attributed to the thermal degradation and volatilization of acidic organic fractions, combined with the formation of basic mineral compounds at 400°C. After solvent extraction, pH values generally shifted toward slightly alkaline conditions in the quince (7.5) and plum (8.0) soils, while the pear soil showed a moderate increase (from 5.5 to 7.0). The exception was the plum soil after thermal desorption, which showed a slight acidification, possibly linked to the selective volatilization of alkaline compounds or the release of acidic intermediates during the process. Overall, both methods tend to increase soil pH, which should be considered when planning post-treatment agronomic management, particularly for species sensitive to alkaline conditions.

## CONCLUSIONS

The selection of appropriate technologies for the decontamination of hydrocarbon-polluted soils represents a challenging task. Methods that allow the recovery of the pollutant to the greatest possible extent are generally preferred. In the case of the orchard soils investigated in this study, slight differences in the determined decontamination efficiencies were observed.

Both thermal desorption at 400°C and successive solvent extraction with petroleum ether and benzene proved effective for the removal of diesel oil from all three soil types. Thermal desorption achieved decontamination efficiencies above 83% for all samples, while solvent extraction yielded efficiencies ranging from 57.36% to 90.5%, with the highest performance recorded for the pear orchard soil. With respect to nutrient content, successive solvent extraction demonstrated a milder and generally more favorable impact on NPK levels, in some cases even increasing the available nutrient content through the mobilization of organically bound compounds. Thermal desorption, while highly efficient for pollutant recovery, produced more variable and in some cases more pronounced changes in nutrient content, particularly for nitrogen and potassium, and led to a significant increase in soil pH, factors that may affect long-term soil fertility.

The results confirm that the selection of an appropriate decontamination technology for petroleum-contaminated orchard soils cannot be based solely on removal efficiency, but must also account for the post-treatment agronomic status of the soil, including nutrient availability and pH. For this study, a comparison of the decontamination methods used leads to the conclusion that, although the degree of decontamination achieved by the successive solvent extraction method is lower than that achieved by the thermal desorption method, the change in nutrient content is more favorable for extraction.

The use of soil amendments must be carefully monitored so that, in the event of accidental pollution with hydrocarbons, this factor is taken into account when selecting a decontamination method.

Future research should explore additional decontamination methods, such as soil washing with environmentally friendly surfactants and electrokinetic decontamination, and assess their impact on a broader range of soil fertility indicators, in order to support the development of integrated and sustainable remediation strategies for orchard soils affected by accidental hydrocarbon contamination.

## REFERENCES

Adeniran, M.A., Oladunjoye, M.A. & Doro, K.O. (2023). Soil and groundwater contamination by crude oil spillage: A review and implications for remediation projects in Nigeria. *Front. Environ. Sci*. 11:1137496. doi: 10.3389/fenvs.2023.1137496.

Ambaye, T. G., Chebbi, A., Formicola, F., Prasad, S., Gomez, F.H., Franzetti, A., & Vaccari, M. (2022). Remediation of soil polluted with petroleum hydrocarbons and its reuse for agriculture: Recent progress, challenges, and perspectives. *Chemosphere*, 293, 133572. https://doi.org/10.1016/j.chemosphere.2022.133572.

Butcaru, A.C.,Mihai, C.A., Moț, A., Gogoț, R.,Hoza, D. & Stănică, F. (2024). Circular Pear Production Using Compost Fertilization: Influence on Tree Growth and Nitrogen Leaf Concentration. *Horticulturae*, *10*, 1209. https://doi.org/10.3390/horticulturae10111209.

Caetano, G., Machado, R. de M., Correia, M. J. N., & Marrucho, I. M. (2024). Remediation of soils contaminated with total petroleum hydrocarbons through soil washing with surfactant solutions. *Environmental Technology*, *45*(15), 2969–2982. https://doi.org/10.1080/09593330.2023.2198733.

Capri, C., Gatti, M., Fiorini, A., Ardenti, F., Tabaglio, V., & Poni, S. (2023). A comparative study of fifteen cover crop species for orchard soil management: water uptake, root density traits and soil aggregate stability. *Sci Rep* 13, 721. https://doi.org/10.1038/s41598-023-27915-7.

Cara, I.G., Rusu, M., Filip, M., Țopa, D. & Jităreanu, G. (2025). Exploring Ecological and Conventional Farming Practice on Plum Orchards: Its Impact on Fruit Quality. *Horticulturae, 11,* 240. https://doi.org/10.3390/horticulturae11030240.

Franchi, E., Cardaci, A., Pietrini, I., Fusini, D., Conte, A., De Folly D'Auris, A., Grifoni, M., Pedron, F., Barbafieri, M., Petruzzelli, G., & Vocciante, M. (2022). Nature-Based Solutions for Restoring an Agricultural Area Contaminated by an Oil Spill. *Plants*, *11*(17), 2250 https://doi.org/10.3390/plants11172250.

Ferreira, S., Lopes, C., Gonçalves, M., Rodrigues, M., Martinho, F., & Sousa, M.L.D. (2025). Multiyear Assessment of Biofertilizer Application on 'Gala' Apple Orchards: Impacts on Soil Fertility, Leaf Mineral Content, and Agronomic Performance. *Plants*, *14*, 3319. https://doi.org/10.3390/plants14213319.

Iorga, C.M., Zamfir, L.G. & Cantaragiu, A.C. (2025). Solutions for the restoration in the natural circuit of contaminated sites from the petroleum industry, *Scientific Papers, Series E: Land Reclamation, Earth Observation & Surveying, Environmental Engineering*, Vol XIV, 260-267.

Karampatzakis, I., Bilias, F., Polychroniadou, C., Tanou, G., Kekelis, P., Theofilidou, A., Giannopoulos, G., Pavlatou-Ve, A. & Aschonitis, V. (2025). Assessing Nutrient Losses and Recycling in Sweet Cherry Orchards: A Yield-Based Approach. *Agriculture*, *15*, 1312. https://doi.org/10.3390/agriculture15121312.

Li, J., Shen, X., Chen, B., He, Z., Yan, L., Yang, L., Ding, B. & Chai, Z. (2025). Effects of Biofertilizer and Green Manure on Soil Bacterial Community in Korla Fragrant Pear Orchard. *Microorganisms*, *13*, 2252. https://doi.org/10.3390/microorganisms13102252.

Lisek, J. (2023). Diversity of Summer Weed Communities in Response to Different Plum Orchard Floor Management in-Row. *Agronomy*, *13*, 1421. https://doi.org/10.3390/agronomy13051421.

Liu, X., Wang, Y., Zhao, K., Ke, Y., Guo, Y., Xue, Y., Shen, X. & Chai, Z. (2025). Analysis of Soil Nutrient and Yield Differences in Korla Fragrant Pear Orchards Between the Core and Expansion Areas. *Agriculture*, *15*, 1873. https://doi.org/10.3390/agriculture15171873.

O'Brien, P. L., DeSutter, T. M., Casey, F. X. M., Wick, A., Bartsch, Z. J., Croat, S. J., & Struffert, S. (2024). Oil spill soil remediation using thermal desorption: Project synthesis and outcomes. Agrosystems, Geosciences & Environment, e20463 https://doi.org/10.1002/agg2.20463.

Ossai, I.C., Ahmed, A., Hassan A., & Hamid, H.S. (2020). Remediation of soil and water contaminated with petroleum hydrocarbon: A review. *Environmental Technology & Innovation*, 17, 100526. https://doi.org/10.1016/j.eti.2019.100526.

Özdemir, N., Demir, Z., & Bülbül, E. (2022). Relationships between some soil properties and bulk density under different land use. *Soil Studies*, *11*(2), 43–50. https://doi.org/10.21657/soilst.1218353.

Popa, M. (2023). The influence of the application of electrical desorption on soil nutrient content. *Romanian Journal of Petroleum & Gas Technology Ploiesti,* 4(2), 117–122. doi: 10.51865/JPGT.2023.02.12.

Popa, M. (2024). Remediation of soil contaminated with hydrocarbon used the successive extraction method with solvents. *The Annals of Dunarea de Jos University of Galati. Fascicle IC, Metallurgy and Materials Science,* vol. 4, 38–43. https://doi.org/10.35219/mms.2024.4.07.

Popa, M. (2025). Study on the Possibility of Rapid Elimination of Accidentally Spilled Petroleum Hydrocarbons in Agricultural Soil. *Agriculture, 15,* 1734. https://doi.org/10.3390/agriculture15161734.

Raimundo, S., Arrobas, M., Ribeiro, A.C. & Rodrigues, M.Â. (2025). White Lupin and Hairy Vetch as Green Manures: Impacts on Yield and Nutrient Cycling in an Organic Almond Orchard. *Agronomy*, *15*, 1974. https://doi.org/10.3390/agronomy15081974.

Rusu, M., Filip, M., Cara, I.G., Țopa, D. & Jităreanu, G. (2025). Soil Nutrient Dynamics and Farming Sustainability Under Different Plum Orchard Management Practices in the Pedoclimatical Conditions of Moldavian Plateau. *Agriculture*, *15*, 509. https://doi.org/10.3390/agriculture15050509.

Sun, M., Zhao, Y., Liang, Z., Wu, Y., Du, R., Liu, J., Yu, F., & Liu, S. (2023). Soil, leaf and fruit nutrient data for pear orchards located in the Circum-Bohai Bay and Loess Plateau regions. *Sci Data* 10, 88. https://doi.org/10.1038/s41597-023-01999-2.

Tkaczyk, P., Bednarek, W., Dresler,S., Krzyszczak, J., Baranowski, P., & Brodowska, M.S. (2018). Content of certain macro- and microelements in orchard soils in relation to agronomic categories and reaction of these soils. *Journal of Elementology,* 24(4) (4/2018) 1361–1372. doi: 10.5601/jelem.2018.23.1.1639.

Scientific Papers. Series E. Land Reclamation, Earth Observation & Surveying, Environmental Engineering. Vol. XV, 2026
Print ISSN 2285-6064, CD-ROM ISSN 2285-6072, Online ISSN 2393-5138, ISSN-L 2285-6064

# OCCURRENCE AND LEVELS OF HAZARDOUS ORGANIC COMPOUNDS IN SOILS FROM INDUSTRIAL AREAS

**Mihaela PREDA, Veronica TĂNASE, Nicoleta Olimpia VRÎNCEANU, Florența JAFRI**

Research and Development Institute for Soil Science, Agrochemistry and Environmental,
61 Mărăști Blvd, District 1, Bucharest, Romania

Corresponding author email: veronica.tanase@icpa.ro

***Abstract***

*Hazardous organic compounds are organic chemicals characterized by toxicity, persistence, and bioaccumulation potential, as well as their ability to distribute across environmental compartments such as soil, water, and air. This study aims to evaluate the contamination levels of soils from industrial areas with polychlorinated biphenyls (PCBs), polycyclic aromatic hydrocarbons (PAHs), and organochlorine insecticides (OCPs) in order to establish a database for the development of a soil emission inventory. For this purpose, 40 soil samples were collected from industrial sites in the southern region of the country, extracted using hexane-like solvents, and analyzed by gas chromatography (GC) and high-performance liquid chromatography (HPLC). The results indicate that soil concentrations of PCBs ranged between 0.002 mg/kg and 0.326 mg/kg, whereas PAH concentrations ranged from 0.044 mg/kg to 12.022 mg/kg. Among OCPs, lindane and DDE - the main metabolite of DDT - were the most frequently detected OCPs in soil.*

***Key words****: contamination, OCPs, PAHs, PCBs, soil.*

## INTRODUCTION

Polychlorinated biphenyls (PCBs), organochlorine pesticides (OCPs), and polycyclic aromatic hydrocarbons (PAHs) are environmentally persistent organic contaminants that share several physicochemical and toxicological characteristics. These compounds are hydrophobic and lipophilic, exhibiting low water solubility and a strong affinity for organic matter and biological lipids, which promotes their accumulation in soils, sediments, and living organisms (Rissato et al., 2006). Due to their chemical stability and resistance to degradation, they persist in the environment and can undergo long-range atmospheric transport, leading to global distribution. The Stockholm Convention on Persistent Organic Pollutants (POPs) was adopted in 2001 to eliminate or restrict chemicals that are persistent, bioaccumulative, toxic, and capable of long-range environmental transport (UNEP, 2001). Both PCBs and OCPs were included among the initial substances targeted for global control. PCBs were listed in Annex A (Elimination) at the Convention because of their extensive industrial use and widespread environmental contamination. Parties were required to cease production and new uses, identify and label PCB-containing equipment, and ensure environmentally sound management and disposal. The Convention set a goal of eliminating the use of PCBs in equipment by 2025 and achieving environmentally sound waste management by 2028. Several OCPs were also classified as POPs, reflecting decades of evidence linking them to ecological damage and human health risks (Jones & Voogt, 1999). Pesticides such as aldrin, dieldrin, endrin, heptachlor, chlordane, toxaphene and mirex were included in Annex A (Elimination), while DDT was additionally placed in Annex B (Restriction) to allow limited use for malaria vector control under specific condition (Lallas, 2001). PAHs are organic pollutants composed of two or more condensed rings. The US Environmental Protection Agency (USEPA) declared 16 compounds from the PAHs category as priority pollutants in 1983, due to their presence in the environment at high concentrations, their recalcitrant nature, and toxicity (Barathi et al., 2023). Many high-molecular-weight PAHs display similar persistence and bioaccumulative behavior as PCBs and OCPs. All three groups are associated with significant health risks, including carcinogenic, mutagenic, endocrine-disrupting,

and immunotoxic effects, making them important targets for environmental monitoring and risk assessment (La Merrill et al., 2020). These compounds originate primarily from anthropogenic activities, although some natural sources exist. PCBs were intentionally manufactured for use in electrical equipment, hydraulic fluids, plasticizers, and other industrial applications, and their release occurred through production, usage, disposal, and leakage from contaminated materials (Rubin, 1999; Hannah et al., 2022; Sandu et al., 2025). OCPs were widely applied in agriculture and public health programs for pest control, with environmental contamination resulting from large-scale application, improper handling, and long-term persistence in soils (Jones & Voogt, 1999). In contrast, PAHs are mainly formed as by-products of incomplete combustion of organic matter, including fossil fuels, biomass burning, industrial processes, and vehicular emissions; however, they can also originate from natural events such as wildfires and volcanic activity (Ravindra et al., 2008). Overall, industrialization, agricultural practices, and combustion-related processes represent the principal sources of these contaminants in the environment.

This study aims to evaluate the contamination levels of soils from industrial areas with these compounds, providing baseline data that may contribute to the future development of a soil emission inventory supporting the implementation of Regulation (EU) 2019/1021 regarding persistent organic pollutants. The originality of this study consists in providing an up-to-date picture of soil contamination correlated with the current profile of industrial activity in southern Romania.

## MATERIALS AND METHODS

40 topsoil samples (0-20 cm) were collected in spring of 2024 from areas potentially affected by industrial activities, as follows (Table 1):

- Pitești (P1-P5) and Mioveni (P8-P11)

In the vicinity of the city was located one of Romania's largest oil refineries, which may have contributed to the local environmental contamination through the historical use of PCB-containing equipment and the release of PAHs from oil processing. Additionally, historical agricultural practices in the surrounding area may have left residues of OCPs in soils. Mioveni also hosts industrial facilities. PCBs could originate from older industrial and electrical equipment, including facilities associated with automotive manufacturing. PAHs could be released through vehicle emissions, local industrial activity, and fuel combustion.

Table 1. Sample locations of the soil samples

| Sample code | Sampling location | Latitude (N) | Longitude (E) |
|---|---|---|---|
| P1 | Pitești 1 | 44°48'05" | 24°56'19" |
| P2 | Pitești 2 | 44°48'01" | 24°56'15" |
| P3 | Pitești 3 | 44°49'01" | 24°55'08" |
| P4 | Pitești 4 | 44°49'06" | 24°56'10" |
| P5 | Pitești 5 | 44°50'20" | 24°52'58" |
| P6 | Ploiești 1 | 44°53'01" | 26°05'55" |
| P7 | Ploiești 2 | 44°56'32" | 26°04'15" |
| P8 | Mioveni 1 | 44°57'11" | 24°56'20" |
| P9 | Mioveni 2 | 44°57'10" | 24°56'28" |
| P10 | Mioveni 3 | 44°57'01" | 24°56'38" |
| P11 | Mioveni 5 | 44°56'49" | 24°55'33" |
| P12 | Câmpulung 1 | 45°18'03" | 25°04'02" |
| P13 | Câmpulung 2 | 45°17'39" | 25°03'48" |
| P14 | Râmnicu Vâlcea 1 | 45°02'33" | 24°18'06" |
| P15 | Râmnicu Vâlcea 2 | 45°03'10" | 24°18'43" |
| P16 | Râmnicu Vâlcea 3 | 45°02'21" | 24°17'52" |
| P17 | Râmnicu Vâlcea 4 | 45°02'58" | 24°18'46" |
| P18 | Slatina 1 | 44°24'46" | 24°23'36" |
| P19 | Slatina 2 | 44°24'47" | 24°24'02" |
| P20 | Slatina 3 | 44°24'53" | 24°24'28" |
| P21 | Slatina 4 | 44°24'47" | 24°24'22" |
| P22 | Slatina 5 | 44°24'54" | 24°23'51" |
| P23 | Slatina 6 | 44°25'17" | 24°39'59" |
| P24 | Slatina 7 | 44°26'06" | 24°23'19" |
| P25 | Slatina 8 | 44°26'17" | 24°23'13" |
| P26 | Slatina 9 | 44°26'38" | 24°22'44" |
| P27 | Slatina 10 | 44°26'41" | 24°22'50" |
| P28 | Brașov 1 | 45°40'51" | 25°36'52" |
| P29 | Brașov 2 | 45°39'55" | 25°35'30" |
| P30 | București 1 | 44°26'01" | 26°11'05" |
| P31 | București 2 | 44°25'38" | 26°10'42" |
| P32 | București 3 | 44°24'28" | 26°11'28" |
| P33 | București 4 | 44°24'19" | 26°11'29" |
| P34 | București 5 | 44°22'03" | 26°08'38" |
| P35 | București 6 | 44°21'36" | 26°08'58" |
| P36 | București 7 | 44°21'56" | 26°05'44" |
| P37 | Chitila | 44°29'37" | 26°00'09" |
| P38 | Popești Leordeni | 44°21'52" | 26°11'40" |
| P39 | Jilava | 44°20'44" | 26°05'00" |
| P40 | Domnești | 44°24'26" | 25°58'01" |

- Ploiești (P6, P7)

Soil contamination with PCBs in the vicinity of the refinery is mainly associated with facilities and equipment that were in operation before the regulatory phase-out of PCBs. In addition, PAHs may be released into the environment through incomplete combustion processes related to petroleum refining activities, fuel combustion, and vehicle emissions

- Câmpulung, Râmnicu Vâlcea, Brașov (P12-P17, P28, P29)

Soil samples were collected from three former industrial sites: an industrial park in Câmpulung, an area in the vicinity of an industrial platform in Râmnicu Vâlcea and Brașov.

- Slatina

From Slatina, an important industrial center in southern Romania with a long history of manufacturing and heavy industry, were collected 10 soil samples (P18-P27) situated in industrial area.

- Bucharest and Ilfov county

The sampling points were located near industrial platforms (P 30, P31, P34, P35), pharmaceutical manufacturing facilities (P32, P33), tire and rubber material factories (P 38, P39), two concrete mixing plants (P36, P37) and an electrical transformer station (P40) (Figure 1).



Figure 1. A sampling point located near electrical transformers

Samples were collected in March when air temperatures averaged 15°C. Each sample consisted of a composite of five subsamples collected from the four corners and the center of a 5 × 5 m² plot. Representative soil samples weighing approximately 500 g were stored in glass containers, protected from light, and refrigerated until analysis.

PCBs analysis in soil was performed in accordance with SR EN 17322:2020, PAHs analysis followed SR EN 17503:2022, and OCPs determination was carried out according to ISO 23646:2022. Accordingly, in compliance with these standards for the extraction of PCBs, OCPs, and PAHs from soil, an automated Soxhlet extractor was employed. Ten grams of air- dried soil samples were extracted for 2 hours using a 1:1 mixture of hexane:acetone. The extract is then washed with water for chromatography to remove acetone, passed over anhydrous sodium sulfate to remove water and evaporated to the appropriate volume. The PCBs determination (seven isomers indicated by Order 756/1997): PCB 28, PCB 52, PCB 101, PCB 118, PCB 138, PCB 153, PCB 180 and the OCPs determination (α, β, γ, δ HCH, pp'-DDE, pp'-DDD and pp'-DDT) were performed on an Agilent gas chromatograph (GC) equipped with an electron capture detector (ECD), operated at 300 °C and a capillary column (30 m x 0.32 mm x 0.25 mm) with a nonpolar stationary phase (DB-5) (Preda et al., 2025).

The determination of PAHs was carried out using a Knauer ultrahigh-performance liquid chromatograph (UHPLC) equipped with an UV-VIS detection at a wavelength of 254 nm. Order 756/1997 stipulates the quantification of the following priority PAHs: anthracene, benzo(a)anthracene, benzo[b]fluoranthene, benzo[k]fluoranthene, benzo[a]pyrene, benzo[ghi]perylene, chrysene, fluoranthene, indeno(1,2,3)pyren, naphthalene, phenanthrene, pyren. The pair of compounds benzo[ghi]perylene and indeno(1,2,3)pyrene cannot be resolved using this type of detector. The separation of the remaining compounds was carried out on a C18 column (2.1 mm × 100 mm, 1.8 µm) maintained at 40°C. The mobile phase consisted of water and acetonitrile, applied under gradient elution conditions (Preda et al., 2025).

For calibration of the PCBs, OCPs and PAHs were used mixed standard solutions (PCB Calibration Mixture 10 µg/ml, PAH-Mix 100 µg/ml, Organochlorine Pesticide Mix 1000 µg/ml). To minimize contamination, all glassware was rinsed with solvents. To guarantee the representativeness and reliability of the results obtained, QA/QC procedures

included duplicate samples, blanks, and the analysis of a certified reference material.
The limit of quantification in soil is 0.001 mg/kg for each PCB and OCP isomers and 0.01 mg/kg for each PAH compounds. All the results are expressed as dry matter.

## RESULTS AND DISCUSSIONS

### *PCBs content in soil*

The total concentration of PCB compounds ranged from 0.002 mg/kg to 0.326 mg/kg. The highest content exceeds the alert threshold of 0.25 mg/kg, it was observed at sampling point P33, collected from the former site of a chemical manufacturing company specializing in the production of solvents, thinners, and other industrial chemical products (Figure 2). Schuhmacher et al. (2004) considered that in a chemical plant, PCBs may have been generated unintentionally as by-products of industrial processes.
20% of the analyzed samples showed normal values of concentration (<0.01 mg/kg), 77% had concentrations between the upper limit of the normal value and the alert threshold, and the remaining 3% exceeded the alert threshold.
Regarding the contribution of the seven isomers to the total PCB content, it can be observed that, at most sampling points, highly chlorinated compounds (PCB 138, PCB 153, and PCB 180) are predominant (Figure 3). Numerous studies have documented the presence of highly chlorinated PCBs such as PCB 138, PCB 153 and PCB 180 in soils from industrialized or urbanized areas, reflecting their persistence and historical contamination patterns (Nadal et al., 2007; Li et al., 2023; Sandu et al., 2025). For example, Li et al. (2023) reported hexachlorinated and heptachlorinated congeners among the dominant PCB profiles in soils around an industrial park. There are several sampling points (P8, P15, P29, P30, P35, and P36) where, in contrast, low-chlorinated compound, specifically PCB 28 and PCB 52, are predominant. The investigated sites are located in Mioveni, within the industrial area of Brașov and Râmnicu Vâlcea, on the industrial platform in Bucharest, and in areas situated in the vicinity of tire and rubber manufacturing facilities. Thus, in point P15, collected from a chemical plant from Râmnicu Vâlcea, the major omologue is PCB 52 (41%), the tetra-chlorinated isomer. In this point the PCB 52 concentration (0.034 mg/kg) exceeds the intervention limit (0.01 mg/kg).

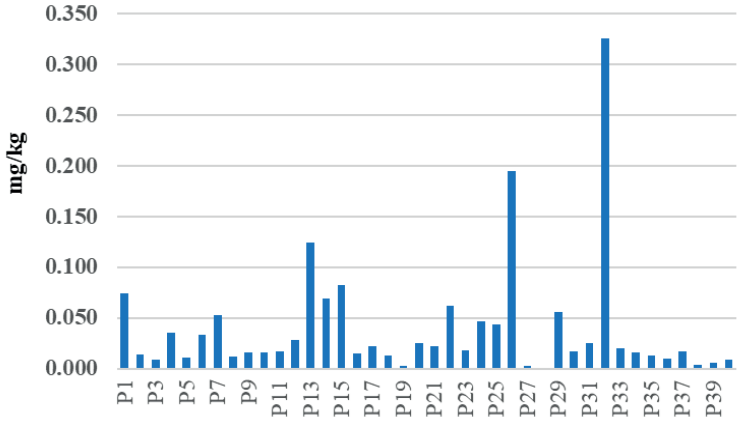



Figure 2. The total content of PCBs in soil samples collected from industrial areas

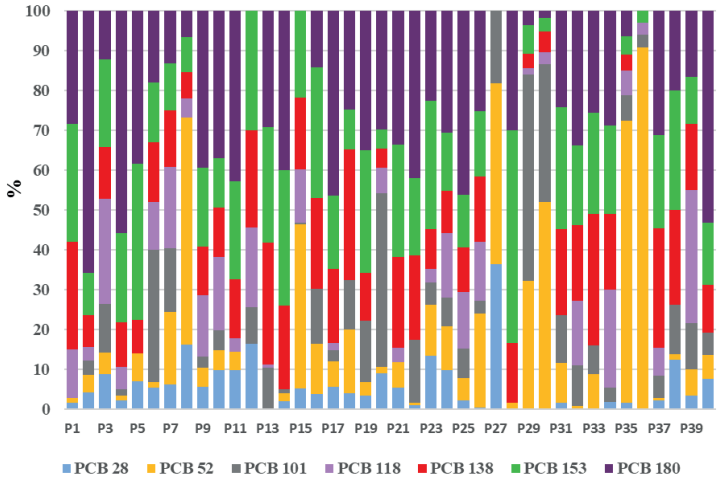



Figure 3. The contribution of the isomers to the total content of PCBs

Similar findings were reported by Zhang et al. (2014), who found that tetra-CBs (31%) and tri-CBs (19%) were the dominant PCB homologs in soils collected from an industrial area. The predominance of low-chlorinated congeners (PCB 28 and PCB 52) at several sampling sites may indicate the influence of local industrial emissions. Tri- and tetra-chlorinated PCBs are frequently associated with unintentional industrial releases and urban/industrial activities, including metal processing and the manufacture or use of polymer- and rubber-based materials (Sandu et al., 2025). Their presence may also be caused by dechlorination of higher chlorinated PCBs which break down over time in the environment (Tolefe et al., 2025). Salihoglu et al. (2011) have shown that intense industrial activity is the main source of high levels of PCB contamination in soil.

***PAHs content in soil***

The total concentration of polycyclic aromatic hydrocarbons (PAHs) in soils collected from the industrial areas ranged from 0.044 mg/kg to 12.022 mg/kg, with a mean value of 0.636 mg/kg. According to Order 756/1997, the normal values for total PAH concentrations in soil must be below 0.1 mg/kg. These results indicate that 10.91% of the analyzed soil samples were within the normal concentration range, 87.20% exceeded the normal threshold but remained below the alert level, and 1.89% surpassed the alert threshold of 7.5 mg/kg. The highest value (12.022 mg/kg) was recorded in the soil sample collected from Slatina industrial area (P32). Elevated concentrations were also recorded at sampling points P39 (1.505 mg/kg), P28 (1.342 mg/kg), and P35 (1.336 mg/kg); however, at these points, the alert threshold for sensitive land uses of 7.5 mg/kg was not reached. Similar results were reported by Wang et al. (2010) who found PAH concentrations ranging between 0.031 mg/kg and 1.475 mg/kg in soil collected from an industrial city. Regarding the individual compounds it was observed that the highest average concentrations in soil corresponded to chrysene, benzo[b]fluoranthene, and benzo[a]anthracene (Figure 4). These substances belong to the category of high molecular weight polycyclic aromatic hydrocarbons (HMW PAHs), containing more than four aromatic rings per molecule. Chrysene and benzo[b]fluoranthene exceeded the alert threshold for sensitive land uses of 2 mg/kg (2.210 mg/kg and 2.874 mg/kg, respectively), while benzo[a]anthracene was very close to this threshold (1.890 mg/kg). These concentrations were measured in soil sample P32 collected in the vicinity of a facility engaged in the production of graphite electrodes, refractory materials, and other coal-derived products - industrial activities that involve high-temperature processing and the use of petroleum-derived feedstocks. Among the low molecular weight compounds (LMW PAHs, with fewer than four aromatic rings per

molecule), the highest average soil concentration, 0.064 mg/kg, was observed for phenanthrene - which is also the most thermodynamically stable.

Examining the compound profile, it can be observed in Figure 4 that the decreasing order of concentrations in the studied soils is as follows: chrysene > benzo[b]fluoranthene > benzo[a]anthracene > phenanthrene > fluorene > benzo[a]pyrene > benzo[k]fluoranthene > anthracene > fluorene > naphthalene.

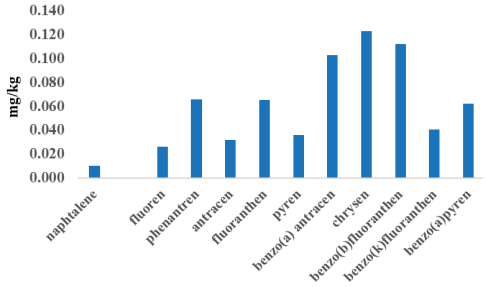



Figure 4. Average concentration of the individual PAH compounds in soils collected from industrial areas

It was observed that low molecular weight (LMW) hydrocarbons have a lower total concentration than high molecular weight (HMW) hydrocarbons, which may indicate a pyrogenic source (combustion-related processes). The ∑LMW/∑HMW PAH ratio can be used to distinguish petrogenic from pyrogenic sources (Zhang et al., 2008). Values of this ratio below 1 indicate pyrogenic sources, while values above 1 suggest petrogenic sources. Petrogenic sources include crude oil and petroleum-derived products such as kerosene, gasoline, lubricating oils, and asphalt. Pyrogenic sources result from combustion processes, including the burning of fossil fuels (coal, wood, oil) or biomass (forests, grasslands, crop residues).

In this study, the ∑LMW/∑HMW ratio ranged from 0.046 to 2.102. These values indicate the presence of pyrogenic sources in approximately 94% of the analyzed soil samples. Ratios above 1 were observed in samples collected from the Pitești refinery area (all samples), in one sample from the pipe manufacturer area in Slatina, and in the soil sample from the pharmaceutical factory in Bucharest.

***Organochlorine insecticides in soil***

OCPs have been widely used in agriculture on a global scale for several decades. Montory et al. (2017) showed that various organochlorine compounds, including hexachlorocyclohexanes (HCHs) and dichlorodiphenyltrichloroethanes (DDTs), remain widely present in the environment due to their persistence, despite their production and use having been banned in developed countries during the 1970s and 1980s. In Romania OCPs have been banned since 1985 (Dirtu et al., 2006). However, in our country too, studies show the presence of these residues in the soil (Ene et al., 2012; Tarcau et al.; 2013).

The total concentration of HCHs in collected soil samples ranged between 0.011 mg/kg and 0.291 mg/kg with an average concentration of 0.085 mg/kg. Lindane is present in 84% of the analyzed samples, although in concentrations around normal values (< 0.001). A particular case is observed for the samples collected near the Râmnicu Vâlcea plant (P14-P17), which are contaminated with all four HCH isomers. In this industrial area, the β-HCH isomer exceeds the alert threshold for less sensitive sites (0.15 mg/kg), as defined by Order 756/1997, and lindane reaches and even exceeds the alert threshold for sensitive uses of 0.02 mg/kg (Figure 5).

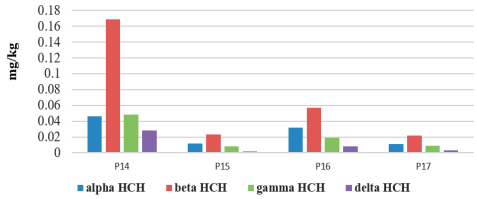



Figure 5. HCH isomer ratio in soil samples collected from Râmnicu Vâlcea

The concentrations of the other HCH isomers (α- and δ-HCH) exceed the upper limit of the normal range (< 0.002 mg/kg and < 0.001 mg/kg, respectively) but remain below their respective alert thresholds (0.1 mg/kg and 0.005 mg/kg, respectively). As illustrated in Figure 5, β-HCH exhibits the highest concentration in this area. Since β-HCH is the most persistent isomer, its predominance relative to the other isomers suggests that the contamination is of historical

origin (Wohrnschimmel et al., 2012). Regarding the total content of DDTs, the mean value of concentration is 0.015 mg/kg, ten times lower than the upper limit of normal values (<0.15 mg/kg). Similar observations were made by Tarcau et al. (2013), who reported that p,p′-DDE and p,p′-DDT were the major contributors to sum DDTs accounting for 54% and 38% of the total concentration, respectively.

## CONCLUSIONS

Regarding PCB contamination, 20% of the analyzed soil samples exhibited normal value of concentrations (<0.01 mg/kg), while 77% showed levels between the normal value and the alert threshold, and 3% exceeded the alert threshold. The highest concentration (0.326 mg/kg) was recorded in a soil sample collected from the former site of a chemical manufacturing facility producing solvents, thinners, and other industrial chemicals.

For PAHs, 10.91% of the analyzed soil samples were within the normal range, 87.20% exceeded the normal level but remained below the alert threshold, and 1.89% surpassed the alert level (7.5 mg/kg). The maximum concentration (12.022 mg/kg) was observed in a soil sample collected from the Slatina industrial area. Chrysene, benzo[b]fluoranthene, and benzo[a]anthracene were the dominant PAH compounds detected.

Lindane and p,p′-DDE were the predominant organochlorine pesticide residues in the analyzed soils. The predominance of β-HCH in soils collected from the Râmnicu Vâlcea industrial platform suggests legacy contamination associated with historical industrial activities.

The distribution and the concentrations of PCBs, PAHs, and OCPs observed in this study confirm the strong influence of historical and current industrial activities and provide valuable input for the development of a soil emission inventory under Regulation (EU) 2019/1021.

## ACKNOWLEDGEMENTS

This research work was financed with the support of the Project PN 23 29 01 01- “Research on the soil emissions inventory of some persistent organic pollutants - an important stage of the national implementation of EU Regulation 1021/2019”.

## REFERENCES

Barathi, S., Gitanjali J, Rathinasamy, G., Sabapathi, N., Aruljothi, K.N., Lee, J., & Kandasamy, S. (2023). Recent trends in polycyclic aromatic hydrocarbons pollution distribution and counteracting bio-remediation strategies, *Chemosphere*, 337, 139396, https://doi.org/10.1016/j.chemosphere.2023.139396

Dirtu, A.C., Cernat, R., Drăgan, D., Mocanu, R., Van Grieken, R., Neels, H., Covaci, A. (2006). Organohalogenated pollutants in human serum from Iassy, Romania and their relation with age and gender. *Environment International* 32, 797–803. https://doi.org/10.1016/j.envint.2006.04.002

Ene, A., Bogdevich, O., & Sion, A. (2012). Levels and distribution of organochlorine pesticides (OCPs) and polycyclic aromatic hydrocarbons (PAHs) in topsoils from SE Romania. *Science of the Total Environment*, 439, 76–86. https://doi.org/10.1016/j.scitotenv.2012.09.004

Hannah, T.J., Megson, D., & Sandau, C.D. (2022). A review of the mechanisms of by-product PCB formation in pigments, dyes and paints. *Science of The Total Environment,* 852, 158529. https://doi.org/10.1016/j.scitotenv.2022.158529

ISO 23646 (2022). Soil quality - Determination of organochlorine pesticides by gas chromatography with mass selective detection (GC-MS) and gas chromatography with electron capture detection (GC-ECD).

Jones, K.C., & de Voogt, P. (1999). Persistent organic pollutants (POPs): state of the science. *Environmental Pollution*, 100(1-3), 209-221. https://doi.org/10.1016/S0269-7491(99)00098-6

Lallas, P.L. (2001). The Stockholm Convention on Persistent Organic Pollutants, *American Journal of International Law,* 95, 3, 692-708. https://doi.org/10.2307/2668517

La Merrill, M.A., Vandenberg, L.N., Smith, M.T., Goodson, W., Browne, P., Patisaul, H. B., Guyton, K. Z., Kortenkamp, A., Cogliano, V. J., Woodruff, T. J., Rieswijk, L., Sone, H., Korach, K.S., Gore, A.C., Zeise, L., & Zoeller, R.T. (2020). Consensus on the key characteristics of endocrine-disrupting chemicals as a basis for hazard identification. *Nature Reviews Endocrinology*, 16(1), 45–57. https://doi.org/10.1038/s41574-019-0273-8

Li, T., Hu, J., Xu, C., & Jin, J. (2023). PCBs, PCNs, and PCDD/Fs in Soil around an Industrial Park in Northwest China: Levels, Source Apportionment, and Human Health Risk. *International Journal of Environmental Research and Public Health*, 20, 3478 https://doi.org/10.3390/ijerph20043478

Montory, M., Ferrer, J., Rivera, D., Villouta, M.V., & Grimalt, J.O. (2017). First report on organochlorine pesticides in water in a highly productive agro-industrial basin of the Central Valley, Chile. *Chemosphere,* 174, 148-156. https://doi.org/10.1016/j.chemosphere.2016.12.125

Nadal, M, Schuhmacher, M., & Domingo, J.L. (2007). Levels of metals, PCBs, PCNs and PAHs in soils of a highly industrialized chemical/petrochemical area: Temporal trend. *Chemosphere,* 66(2), 267-276. https://doi.org/10.1016/j.chemosphere.2006.05.020

Ministry of Waters, Forests and Environmental Protection. (1997). *Order No. 756 of November 3, 1997 approving the Regulation on environmental pollution assessment*. Monitorul Oficial al României [Official Gazette of Romania], No. 303 bis.

Preda, M., Tănase, V., Vrînceanu, N., Carabulea, V., & Burcea, C. (2025). Soil contamination by PCBs and PAHs related to the paint industry. *Analele Universităţii din Craiova, seria Agricultură – Montanologie – Cadastru,* Vol. 55/1. https://doi.org/10.52846/aamc.v55i1.1755

Ravindra, K., Sokhi, R., & Van Grieken, R. (2008). Atmospheric polycyclic aromatic hydrocarbons: source attribution, emission factors and regulation. *Atmospheric Environment* 42(14), 2895–2921

European Parliament & Council of the European Union. (2019). *Regulation (EU) 2019/1021 of the European Parliament and of the Council of 20 June 2019 on persistent organic pollutants (recast)*. Official Journal of the EU, L 169, pp. 45–77.

Rissato, S.R., Galhiane, M.S., Ximenes, V.F., de Andrade, R.M.B., Talamoni, J.L.B., Libânio, M., de Almeida, M.V., Apon, B.M., & Cavalari, A.A. (2006). Organochlorine pesticides and polychlorinated biphenyls in soil and water samples in the Northeastern part of São Paulo State, Brazil. *Chemosphere*, 65, 1949–1958. https://doi.org/10.1016/j.chemosphere.2006.07.011

Rubin., E.S. (1999) Toxic releases from power plants. *Environmental Science & Technology* 33(18), 3062–3067 https://doi.org/10.1021/ES990018D

Sandu, M.A., Preda, M., Tănase, V., Mihailescu, D., Vîrsta, A., & Ivănescu, V. (2025). Trends in Polychlorinated Biphenyl (PCB) Contamination in Bucharest's Urban Soils: A Two-Decade Perspective (2002-2022), *Processes*, 13(5), 1357. https://doi.org/10.3390/pr13051357

Salihoglu, G., Salihoglu, N. K., Aksoy, E., & Tasdemir, Y. (2011). Spatial and temporal distribution of polychlorinated biphenyl (PCB) concentrations in soils of an industrialized city in Turkey, *Journal of Environmental Management* 92(3), 724–732 https://doi.org/10.1016/j.jenvman.2010.10.019

Schuhmacher, M., Nadal, M., & Domingo, J.L. (2004) Levels of PCDD/Fs, PCBs, and PCNs in soils and vegetation in an area with chemical and petrochemical industries. *Environmental Science & Technology* 38(7), 1960–1969. https://doi.org/10.1021/es034787f

SR EN 17322 (2020). Environmental Solid Matrices. Determination of polychlorinated biphenyls (PCB) by gas chromatography. mass selective detection (GC-MS) or electron-capture detection (GC-ECD).

SR EN 17503 (2022). Soil, sludge, treated biowaste and waste - Determination of polycyclic aromatic hydrocarbons (PAH) by gas chromatography (GC) and high performance liquid chromatography (HPLC).

Tolefe, E.C., Healy, R., Kleywegh, S., Simpson, A.J., Simpson, M.J., & Jobst, K.J. (2025). Distribution of semi-volatile organic compounds, metals, and biological activities in two industrialized cities in Ontario, Canada using passive air sampling. *Environmental Science Processes & Impacts*, 27, 3595–3611. https://doi.org/10.1039/D5EM00493D

Tarcau, D., Cucu-Man, S., Boruvkova, J., Klanova, J., & Covaci, A. (2013). Organochlorine pesticides in soil, moss and tree-bark from North-Eastern Romania. *Science of the Total Environment*, 456–457, 317–324 http://dx.doi.org/10.1016/j.scitotenv.2013.03.103

United Nations Environment Programme (UNEP) (2001). Stockholm Convention on Persistent Organic Pollutants.https://chm.pops.int/TheConvention/Overview/TextoftheConvention/tabid/2232/Default.aspx

Wang, W., Massey Simonic, S.L., Xue M., Zhao, J., Zhang, N., Wang, R., Cao, J., & Tao, S. (2010). Concentrations, sources and spatial distribution of polycyclic aromatic hydrocarbons in soils from Beijing, Tianjin and surrounding areas, North China, *Environmental Pollution*, 158(5), 1245-1251. https://doi.org/10.1016/j.envpol.2010.01.021

Wohrnschimmel, H., Tay, P., von Waldow, H., Hung, H., Li, Y.F., MacLeod, M., & Hungerbuhler, K. (2012). Comparative Assessment of the Global Fate of α- and β-Hexachlorocyclohexane before and after Phase-Out. *Environmental Science and Technology,* 46(4), 2047-54. https://doi.org/10.1021/es203109q

Zhang, W., Zhang, S., Wan, C., Yue, D., Ye, Y., & Wang, X. (2008). Source diagnostics of polycyclic aromatic hydrocarbons in urban road runoff, dust, rain and canopy throughfall. Environmental Pollution, 153(3), 594–601 https://doi.org/10.1016/j.envpol.2007.09.004

Zhang, Y.F., Fu, S., Dong, Y., Nie, H.F., Li, Z., &Liu, X.C. (2014). Distribution of polychlorinated biphenyls in soil around three typical industrial sites in Beijing, China. *Bulletin of Environmental Contamination and Toxicology*, 92, 466–471. https://doi.org/10.1007/s00128-014-1226-5.

Scientific Papers. Series E. Land Reclamation, Earth Observation & Surveying, Environmental Engineering. Vol. XV, 2026
Print ISSN 2285-6064, CD-ROM ISSN 2285-6072, Online ISSN 2393-5138, ISSN-L 2285-6064

# IDENTIFYING THE NATURAL AND ANTHROPOGENIC SOURCES OF PARTICULATE MATTER: AN ANALYSIS OF POLLUTION ORIGINS AND ENVIRONMENTAL IMPACT

**Elena-Denisa PREDESCU, Carmen Otilia RUSĂNESCU, Roxana-Elena FRÎNCU, Sabrina Maria BĂLĂNESCU, Daniela MIHAI, Ionela Alexandra ION**

National University of Science and Technology POLITEHNICA Bucharest,
313 Splaiul Independenței, District 6, Bucharest, Romania

Corresponding authors email: denisa.predescu23@yahoo.com

***Abstract***

*This study focuses on the origins of particulate matter (PM), an important air pollutant with significant effects on the environment and human health. PM comes from a variety of sources, including anthropogenic ones such as industrial emissions, traffic, and construction activities, as well as natural processes like wildfires and volcanic eruptions. The paper also examines how these particles are released into the atmosphere and how their behaviour is influenced by their size and chemical composition. In addition, the study discusses the transport and dispersion of particulate matter in the atmosphere, highlighting the factors that affect its concentration and persistence. Understanding these processes is essential for improving air quality management, reducing pollution levels, and protecting both ecosystems and public health.*

***Key words****: air pollution, environmental health, monitoring, particulate matter (PM), PM sources.*

## INTRODUCTION

Air pollution is a major environmental concern, with particulate matter (PM) being one of the most significant atmospheric pollutants due to its complex origin and widespread presence. PM originates from both natural processes and anthropogenic activities, including traffic emissions, industrial processes, construction activities, biomass burning, and secondary atmospheric formation.

This study focuses on the characterization of PM sources and the importance of source identification for air quality management and emission control strategies.

Understanding PM source contributions is essential for the development of effective air pollution mitigation policies. This topic has been widely addressed in the scientific literature, particularly in studies focusing on source apportionment and atmospheric pollution dynamics (Durbacă, et al., 2020).

This review is based on peer-reviewed articles indexed in ISI Web of Science and Scopus databases, published mainly over the last 10-15 years (2010-2025), including systematic reviews and source apportionment studies of particulate matter.

The aim of this study is to identify and analyse the main natural and anthropogenic sources of particulate matter based on recent scientific literature, to provide an overview of their relative contributions and environmental relevance.

## MATERIALS AND METHODS

This study is based on a narrative review of scientific literature regarding particulate matter (PM) sources and origins. Relevant peer-reviewed articles were selected from ISI Web of Science and Scopus databases, focusing on publications from 2010 to 2025.

The literature search included studies addressing PM source identification, source apportionment, and emission characterization. The collected information was critically analysed and synthesized to provide an overview of the main natural and anthropogenic sources of particulate matter and their environmental significance.

## RESULTS AND DISCUSSIONS

This section synthesizes findings from recent literature on particulate matter (PM) sources and source apportionment studies. The reviewed studies consistently identify both natural and anthropogenic contributions to ambient PM levels, with variability depending on location, seasonality, and local emission profiles.
Anthropogenic sources, particularly traffic emissions, industrial activities, construction processes, and biomass burning, are generally reported as the dominant contributors in urban and industrial areas, while natural sources such as dust resuspension and sea salt are more relevant in rural or coastal environments.

## SOURCES OF PARTICULATE MATTER (PM)

Particulate matter (PM) is divided into primary and secondary sources. Primary PM originates directly from natural events such as marine aerosols, volcanic activity, wildfires, and bioparticles, as well as anthropogenic sources including transport, industry, construction, and domestic practices.
Secondary PM forms in the atmosphere from chemical reactions involving precursors gases.
As shown in Figure 1, the main sources of PM pollution are presented. This study also highlights the main sources of PM in Bucharest, where urban and traffic-related emissions are dominant.

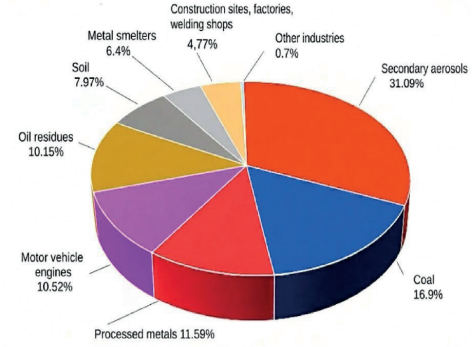



Figure 1. Sources of PM pollution (Lee et al., 2023)

### Natural sources of particulate matter (PM)

Aeolian dust and soil erosion **r**elease fine mineral particles into the atmosphere, contributing significantly to PM10 and PM2.5 concentrations. These processes are driven by wind action over exposed or disturbed soils, where the breakdown of soil aggregates facilitates particle detachment and suspension. Emissions increase strongly in dry, bare or agricultural lands, especially under high wind speeds and low soil moisture conditions. Once uplifted, particles can remain suspended for extended periods and be transported over long distances, influencing air quality at both local and regional scales (Katra, 2020).
Marine aerosols are a major natural source of $PM_{2.5}$ and $PM_{10}$ in coastal regions, formed mainly from sea spray processes. They consist predominantly of sodium ($Na^+$), chloride ($Cl^-$) and other sea-derived ions such as magnesium, which are commonly used as chemical tracers for marine origin. In atmospheric measurements, these ions are also used in source apportionment studies to distinguish marine contributions from anthropogenic inputs and to assess aerosol aging processes in coastal environments (Wu et al., 2024).

**Shipping emissions from maritime transport** represent an important source of particulate matter, particularly in coastal and port areas. Ship engines, often using heavy fuel oil, emit $SO_2$ and primary PM2.5, while also contributing to secondary particle formation in the atmosphere through oxidation processes. These emissions can significantly affect air quality in major ports and coastal urban zones, making maritime transport a relevant contributor to regional PM pollution in Europe (Thunis et al., 2015).
Volcanic activity is a major natural source of particulate matter, releasing ash, fine particles, and gases that affect aerosol chemistry. These emissions vary in intensity and composition and can impact air quality at local, regional, and global levels. Volcanic particles contain silica, aluminium and iron oxides, and sulphides, and can be transported over long distances (Wu et al., 2023).
Figure 2 illustrates volcanic emissions including solid particles (ash and dust) and secondary aerosols formed from gas condensation.

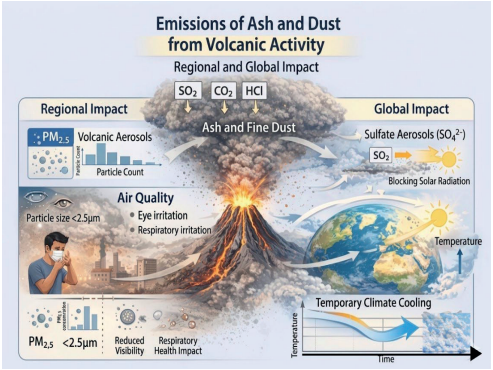



Figure 2. Emission of Ash and Dust from Volcanic Activity (image generated with AI)

Fine particles ($PM_{2.5}$) can remain in the atmosphere and travel long distances, increasing PM levels. At a global scale, volcanic aerosols, especially sulphates from $SO_2$, can reflect solar radiation and temporarily cool the climate (Zhang et al., 2022).

Wildfires release a complex mixture of gases and particulate matter, including $PM_{2.5}$, $PM_{10}$, VOCs, CO, and NOx. Fine particles can travel long distances and significantly increase PM concentrations, often exceeding air quality limits. This leads to large-scale air pollution and impacts both local and distant regions, as shown in Figure 3 (Hadiwijoyo et al., 2025).

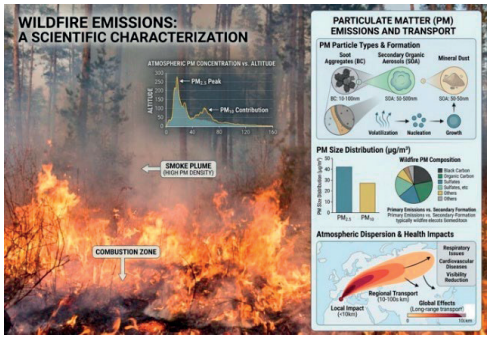



Figure 3. Wildfire emissions (image generated with AI)

Wildfire smoke acts as an atmospheric aerosol, affecting solar radiation and cloud formation. As a result, $PM_{2.5}$ and $PM_{10}$ can influence weather patterns and climate at regional and global scales (Vaezi et al., 2025).

Recent studies show that pollen and fungal spores are dispersed in the atmosphere as part of bioaerosols and can contribute to particulate matter, particularly in the PM10 fraction and, in some cases, in the fine fraction below 10 µm. These particles are of biological origin and can become incorporated into airborne particulate matter through mechanical release and atmospheric transport processes. Bioaerosols also contribute to the organic fraction of PM, highlighting their relevance in the overall composition of atmospheric particulate matter in both indoor and outdoor environments (Sikoparija et al., 2025).

Vegetation reduces wind-driven soil erosion by stabilizing the soil structure and limiting the detachment of fine particles through root systems and surface cover. In contrast, exposed or bare lands act as important sources of dust emissions, with the number of resuspended particles strongly dependent on wind speed, soil texture, and moisture content. Under dry conditions and high wind intensity, these surfaces can significantly contribute to atmospheric PM10 levels through enhanced dust emission and transport processes (Labiadh et al., 2023).

Seasonal variability and meteorological conditions significantly influence the concentration, transport, and spatial distribution of marine aerosols. Wind speed plays a key role in the generation and emission of sea spray particles, while atmospheric humidity and temperature affect their hygroscopic growth and chemical evolution in the atmosphere. Atmospheric stability conditions determine the vertical mixing and dispersion of these particles, controlling how efficiently they are transported from coastal zones towards inland continental areas. As a result, marine aerosol concentrations can vary considerably depending on seasonal weather patterns and large-scale atmospheric circulation, which modulate both their intensity and persistence in the atmosphere (Zhu et al., 2025).

Particulate matter emissions and PM10 and PM2.5 concentrations exhibit significant seasonal variability, with higher levels typically observed during dry and warm periods. In these conditions, soils are more exposed and susceptible to wind-driven resuspension, while reduced moisture content increases the ease of particle detachment from surfaces. In contrast, during wet seasons, precipitation and higher humidity contribute to the removal of airborne

particles through wet deposition and limit dust generation from soils. Seasonal dynamics therefore affect both natural emissions from soil surfaces and ambient PM levels in urban environments, leading to higher concentrations during dry, stagnant atmospheric conditions compared to rainy periods. This variability highlights the importance of meteorological factors and seasonal climate patterns in assessing particulate matter emissions and identifying periods of increased environmental risk (de Souza et al., 2025).

Lightning is a natural source of nitrogen oxides (NOx) in the atmosphere, produced during high-temperature electrical discharges. These emissions contribute to the formation of ozone and secondary particulate matter through atmospheric oxidation processes involving NOx-derived compounds. Although lightning-induced emissions are episodic and spatially variable, they represent an important natural pathway for atmospheric chemical reactions that can influence the formation of secondary aerosols, including PM2.5, at regional scales (Bender et al., 2006).

Table 1 presents the main environmental factors influencing PM emissions and their effects on $PM_{10}$ and $PM_{2.5}$ concentrations.

Table 1. Factors which influence PM emissions
*Source: compiled by the author based on literature data*

| Factor | Effect on PM emissions |
|---|---|
| Arid- semi-arid climate | Increases PM10 and PM2.5 concentrations |
| Exposed soil/intensive agriculture | Increases PM10 concentration (>10%) |
| Low humidity | Increases particle mobilization and intensifies turbulence |
| Precipitation | Reduces PM (through particle deposition) |
| Reduced vegetation | Increases the risk of PM10 and PM2.5 emissions |
| Green zones/tree shelterbelts | Reduces PM10 and PM2.5 concentrations |

**Anthropogenic sources of particulate matter (PM)**

Vehicle exhaust emissions are a major anthropogenic source of $PM_{2.5}$ and $PM_{10}$ in urban environments, originating mainly from incomplete combustion of fossil fuels in internal combustion engines. These emissions are characterized by high concentrations of carbonaceous particles, particularly organic carbon (OC) and elemental carbon (EC), which significantly influence both the mass and toxicity of particulate matter. Diesel engines generally produce higher particulate emissions compared to gasoline engines due to differences in combustion efficiency and fuel composition. In addition to exhaust emissions, non-exhaust sources such as brake wear, tire abrasion, and road surface wear also contribute substantially to urban PM levels through mechanically generated particles. Elevated OC and EC fractions are typically associated with inefficient or incomplete combustion processes and varying operating conditions (Shi et al., 2023).

Aviation contributes to particulate matter emissions mainly in airport areas, especially during landing and take-off cycles. Aircraft engines emit PM2.5 and ultrafine particles, including black carbon and sulphate-related particles formed during fuel combustion. Although its global contribution to PM mass is relatively limited compared to road traffic and industry, aviation can significantly affect local air quality near airports due to concentrated emissions at low altitudes (Dadvand et al., 2011).

Residential heating is an important anthropogenic source of particulate matter, with emissions strongly dependent on the energy system used. Domestic heating systems based on solid fuels (wood, coal, biomass) generate significantly higher PM10 and PM2.5 emissions due to incomplete combustion, especially in older and low-efficiency installations. In contrast, centralised district heating systems generally show lower specific emissions because of higher combustion efficiency, better fuel control, and the use of emission abatement technologies. However, in urban areas where individual heating systems still dominate, domestic combustion remains a major contributor to wintertime PM levels, often exceeding emissions from transport in cold seasons (Cincinelli et al., 2019).

Table 2 summarizes the main sources of particulate matter (PM), their predominant particle fractions, and their key characteristics.

Table 2. Main sources of particulate matter (PM)
*Source: compiled by the author based on literature data*

| Source Type | Main PM Fraction | Key characteristics / examples |
|---|---|---|
| Natural sources | PM10, 2.5 | Marine aerosols, wildfires, volcanic ash |
| Traffic | PM2.5 | Combustion (OC, EC), non-exhaust wear |
| Construction | PM10 | Dust from excavation, demolition |
| Residential burning | PM2.5 | Biomass and waste combustion |
| Agriculture | PM10 | Soil dust, crop residue burning |
| Industry | PM2.5, PM10 | Metal particles, combustion, chemical PM |

## CONCLUSIONS

The literature review highlights that particulate matter originates from a wide range of natural and anthropogenic sources, with significant spatial and temporal variability. Anthropogenic activities, particularly traffic, industrial processes, and construction, are consistently identified as major contributors in urban environments, while natural sources such as dust and marine aerosols play a more important role in rural and coastal areas.

The reviewed studies emphasize that source apportionment is essential for understanding PM distribution and for supporting effective air quality management strategies.

Overall, the findings underline the importance of targeted emission control measures adapted to local emission profiles.

## ACKNOWLEDGEMENTS

The author acknowledges the support of the University Politehnica of Bucharest and the Faculty of Biotechnical Systems Engineering in facilitating this research.

## REFERENCES

Bender, M.L., Floch, G., Chappellaz, J., Suwa, M., Barnola, J.-M., Blunier, T., Dreyfus, G., Jouzel, J., & Parrenin, F. (2006). Gas age–ice age differences and the chronology of the Vostok ice core, 0–100 ka. *Journal of Geophysical Research*, 111, https://agupubs.onlinelibrary.wiley.com/doi/10.1029/2005JD006488

Cincinelli, A., Guerranti, C., Martellini, T., & Scodellini, R. (2019). Residential wood combustion and its impact on urban air quality in Europe. *Current Opinion in Environmental Science & Health*, 8, 10–14, https://www.sciencedirect.com/science/article/abs/pii/S2468584418301053

Dadvand, P., Rushton, S., Diggle, P.J., Goffe, L., Rankin, J., & Pless-Mulloli, T. (2011). Using spatio-temporal modeling to predict long-term exposure to black smoke at fine spatial and temporal scale. *Atmospheric Environment*, 45(3), 659–664. https://doi.org/10.1016/j.atmosenv.2010.10.034

de Souza, A., Oliveira-Junior, J.F., Cardoso, K.R.A., Fernandes, W.A., & Pavao, H.G. (2025). The Impact of Meteorological Variables on Particulate Matter Concentrations, *Atmosphere*, 16(7), 875; https://www.mdpi.com/2073-4433/16/7/875

Durbacă, I., Sporea, N., Farcaș-Flamaropol, D.C., & Surdu, E. (2020). Application of the "six sigma" method for the analysis of the improvement of the environmental air quality parameters at the municipality of Bucharest, by monitoring the pollutances of nox pollutants, *ICAMS Proceedings of the International Conference on Advanced Materials and Systems,* 277–282. DOI:10.24264/icams-2020.III.5

Hadiwijoyo, E., Rijal, H.B., & Abdullah, N. (2025). Cascading Impacts of Wildfire Emissions on Air Quality, Human Health, and Climate Change Based on Literature Review, *Fire*, 8(12), 471, https://www.mdpi.com/2571-6255/8/12/471

Katra, I. (2020). Soil erosion by wind and dust emission in semi-arid soils due to agricultural activities. *Agronomy*, 10(1), 89. https://doi.org/10.3390/agronomy10010089

Labiadh, M.T., Rajot, J.L., Sekrafi, S., Ltifi, M., Attoi, B., Tlili, A., Hlel, M., Bergametti, G., des Tureax, T.H., & Bouet, C. (2023). Impact of Land Cover on Wind Erosion in Arid Regions: A Case Study in Southern Tunisia, *Land*, 12(9), 1648 https://www.mdpi.com/2073-445X/12/9/1648

Lee, G., Kim, M., Park, D., & Yoo, C. (2023). Fine Particulate Matter (PM2.5) Sources and Its Individual Contribution Estimation Using a Positive Matrix Factorization Model, *Toxics*, 11(1), 69 https://www.mdpi.com/2305-6304/11/1/69

Shi, J., Yao, Q., Han, X., Wang, Y., Wu, X., Tian, S., Wang, J., Yang, X., Xie, H., Xiang, F., & Ning, P. (2023). Chemical characteristics of PM2.5 emitted from motor vehicles exhaust under the plateau with low oxygen content, *Atmospheric Environment*, 314, 12005, https://www.sciencedirect.com/science/article/abs/pii/S135223102300479X

Sikoparija, B., Bigermajer, S., Ivosecic, B., Sazdovski, V., Ørby, P.V., Kloster, M., & Gosewinkel, U. (2025). Airborne Hirst Volumetric Sampling Gives an Insight into Atmospheric Dispersion of Pollen and Fungal Spores, *Atmosphere*, 16(9), 1060 https://www.mdpi.com/2073-4433/16/9/1060

Thunis, P., Pisoni, E., Degraeuwe, B., Kranenburg, R., Schaap, M., & Clappier, A. (2015). Dynamic evaluation of air quality models over European regions. *Atmospheric Environment,* 111, 185–194

https://www.sciencedirect.com/science/article/pii/S1352231015300194?via%3Dihub

Vaezi, R.B., Martin, M.R., & Hosseinpour, F. (2025). Impacts of Wildfire Smoke Aerosols on Radiation, Clouds, Precipitation, Climate, and Air Quality, *Atmospheric Environment: X* 26(2):100322. https://doi.org/10.1016/j.aeaoa.2025.100322

Wu, X., Kong, Q. Lan, Y., Sng, J., &Yu, L.E. (2024). Refined Sea salt markers for coastal cities facilitating quantification of aerosol aging and PM2.5 apportionment, *Environmental Science & Technology,* 58(19), 8432–8443. https://doi.org/10.1021/acs.est.3c10142

Wu, J., Ye, Q., Li, P., Sun, L., Huang, M., Liu, J., Ahmed, Z., & Wu, P. (2023). The heteroaggregation behaviour of nano plastics on goethite: Effects of surface functionalization and solution chemistry, *Science of The Total Environment,* 869, 161702, https://www.sciencedirect.com/science/article/abs/pii/S0048969723004023

Zhang, H., Liu, S., Dou, Q., Huang, Z., Lv, C., Liao, J., Tao, F., Liu, Y., & Ma L. (2022). Association between Ambient Air Pollutants and Pneumonia in Wuhan, China, 2014–2017, *Atmosphere* 13(4), 578, https://www.mdpi.com/2073-4433/13/4/578

Zhu, S., Li, F., Yang, Y., Ma, T., & Chen, J. (2025). Temporal Variations in Particulate Matter Emissions from Soil Wind Erosion in Bayingolin Mongol Autonomous Prefecture, Xinjiang, China (2001-2022), *Atmosphere*, 16(8), 911 https://www.mdpi.com/2073-4433/16/8/911.

Scientific Papers. Series E. Land Reclamation, Earth Observation & Surveying, Environmental Engineering. Vol. XV, 2026
Print ISSN 2285-6064, CD-ROM ISSN 2285-6072, Online ISSN 2393-5138, ISSN-L 2285-6064

# DETERMINATION OF CONCRETE PERMEABILITY WITH CERAMIC WASTE CONTENT

**Mircea SĂLCUDEAN[1, 2], Maria POPA[3], Mirel GLEVITZKY[3, 4], Daniela ONITA[2], Mihai Teopent CORCHEȘ[2]**

[1]"Lucian Blaga" University of Sibiu, Doctoral School, Faculty of Engineering,
10 Victoriei Blvd, Sibiu, Romania
[2]"1 December 1918" University of Alba Iulia, Faculty of Computer Science and Engineering,
15-17 Unirii Street, Alba Iulia, Romania
[3]"1 December 1918" University of Alba Iulia, Faculty of Economic Sciences,
15-17 Unirii Street, Alba Iulia, Romania
[4]Politehnica University Timişoara, Faculty of Engineering Hunedoara,
5 Revolutiei Street, Hunedoara, Romania

Corresponding author email: mirel_glevitzky@yahoo.com

***Abstract***

*The paper presents an experimental analysis of the influence of partially replacing natural aggregates with ceramic waste on the permeability of concrete. The use of recycled materials in concrete aims to reduce environmental impact and promote the reuse of waste from the construction industry. In this study, concrete samples were prepared with different substitution levels of aggregates (0%, 50% of 0-4 mm aggregates, 50% of 4-8 mm aggregates, and 50% of 8-16 mm aggregates), and permeability characteristics were determined using standardized methods. The chemical composition of the ceramic waste aggregates was determined by X-ray fluorescence (XRF) analysis to characterize their oxide content and potential influence on concrete behaviour. The results indicate that the addition of ceramic waste affects the pore structure of concrete, having an impact on the permeability coefficient and the material's durability. Water permeability tests according to EN 12390-8 showed an increase in water penetration depth from 700 mm in the control concrete to 850-1300 mm in concretes with ceramic aggregates, depending on the replaced fraction. The conclusions highlight the potential of using ceramic waste in concrete as a sustainable solution with positive effects on the circular economy and technical performance.*

***Key words****: ceramic waste, circular economy, concrete permeability, durability, recycled aggregates, sustainable construction.*

## INTRODUCTION

In the context of sustainable development and the circular economy, the construction industry is under increasing pressure to reduce the consumption of natural resources and the volume of generated waste (Glevitzky et al., 2025; Javed et al., 2025). Concrete production, one of the most widely used construction materials worldwide, relies heavily on natural aggregates and cement, whose extraction and processing contribute to environmental degradation and $CO_2$ emissions (Ahmad et al., 2024; Jwaida et al., 2024). On the other hand, the ceramic industry (which includes floor and wall tiles, bricks, and household ceramic products) generates significant amounts of waste annually, originating from production residues, rejected products, or materials resulting from demolition activities (Jiang & Cheng, 2020). These wastes are generally disposed of in uncontrolled areas, increasing pressure on landfill capacity and the risk of environmental pollution (Medina et al., 2012). From this perspective, the reuse of ceramic waste in concrete represents a promising solution for reducing the current environmental impact (Zong et al., 2014). Recent studies have highlighted the potential of using ceramic waste as both fine and coarse aggregate, as well as an auxiliary cementitious component (powder), with significant effects on the durability, microstructure, and mechanical performance of concrete (Elemam et al., 2023).

An essential aspect of concrete durability is permeability - an indicator of structural integrity and resistance to external aggressive actions (such as the penetration of water and aggressive

ions). Although numerous studies have investigated the mechanical strength of concrete incorporating ceramic aggregates, there is increasing interest and a clear need for a more in-depth understanding of how these materials influence the permeability and microstructure of the final concrete product (Semmana et al., 2025; Tokareva & Waldmann, 2025).

Durability studies have shown that concrete incorporating ceramic waste may exhibit an improved microstructure due to the pozzolanic activity of the ceramic material, which contributes to pore filling and strengthening of the cement-aggregate interfacial transition zone (Ahmad et al., 2024). At the same time, experimental investigations involving partial replacement of aggregates (either fine or coarse) have reported mixed results: moderate replacement levels (up to approximately 20-50%) may enhance strength, whereas higher replacement rates tend to increase porosity and permeability (Al-Fakih, 2025; Ngayakamo, 2025). Despite the increasing number of publications on the use of ceramic waste in concrete, the scientific literature highlights a lack of consensus regarding its effect on permeability (Jwaida et al., 2024). While some studies report a reduction in permeability due to the densification of the microstructure and improvement of the interfacial transition zone, others indicate adverse effects, associated with increased capillary porosity and water absorption, particularly in the case of coarse ceramic aggregates or high replacement rates (Zhou et al., 2025). These contradictory findings suggest that the influence of ceramic waste on permeability is not determined solely by the replacement percentage, but also by the particle size fraction used - an aspect insufficiently investigated in existing studies (Ahmad et al., 2023).

This article aims to help address this knowledge gap through a systematic experimental analysis of the permeability of concrete in which 50% of natural aggregates are separately replaced with ceramic waste from the 0-4 mm, 4-8 mm, and 8-16 mm fractions. The originality of the study lies in the comparative evaluation of the influence of each particle size class on the permeability coefficient, using the same concrete mix and identical testing conditions, which allows for a coherent and reproducible interpretation of the results. The findings provide valuable experimental benchmarks for optimizing the use of ceramic waste in durable concrete and for supporting construction solutions compatible with the principles of the circular economy (Sălcudean & Popa 2025).

## MATERIALS AND METHODS

Table 1 presents the main materials used in the preparation of the concrete mix, as well as their characteristics.

Table 1. Characterization of the materials used in the composition of the concrete mix

| Material | Type | Grading | Origin | Role in the mix |
|---|---|---|---|---|
| Cement | Hydraulic binder | - | Industrial (manufactured by Heidelberg Materials, Chișcădaga Cement Plant, Hunedoara) | Binds the aggregates through hydration and provides strength to the mix |
| River aggregate | Fine aggregate | 0-4 mm | Natural, Mureș River, Elis Quarry, Balomiru de Câmp, Sibot commune, Alba | Fills the voids between larger particles and ensures workability |
| | Coarse aggregate | 4-8 mm | | Contributes to the mechanical strength of concrete |
| | | 8-16 mm | | Provides the load-bearing skeleton of the mix |
| Ceramic aggregate | Lightweight aggregate | 0-4 mm | Artificial, ceramic waste from Reciclare Moloz SRL, Vințu de Jos, Alba | Reduces the self-weight of concrete and improves insulation properties |
| | | 4-8 mm | | Contributes to obtaining lightweight concrete |
| | | 8-16 mm | | Reduces concrete density and improves thermal behavior |
| Water | Active component | - | Natural (SC APA CTTA SA, Alba Iulia, Alba) | Activates cement hydration and enables workability |

Using the materials previously characterized, four experimental specimens (P1-P4) and one control specimen were produced, corresponding to a C16/20 concrete class. Table 2 presents the adopted concrete mix designs, expressed in terms of the quantities of the constituent materials.

Table 2. The concrete mix designs used for producing the experimental specimens and the control specimen

| Material | Quantity (kg) | | | | |
|---|---|---|---|---|---|
| | C16/20 concrete - control sample | P1 | P2 | P3 | P4 |
| Cement | 1.475 | 1.475 | 1.475 | 1.475 | 1.475 |
| River aggregate 0-4 mm | 3.945 | 1.9725 | 3.945 | 3.945 | 1.9725 |
| River aggregate 4-8 mm | 1.835 | 1.835 | 0.9175 | 1.835 | 0.9175 |
| River aggregate 8-16 mm | 3.395 | 3.395 | - | 1.6975 | 1.6975 |
| Ceramic aggregate 0-4 mm | - | 1.9725 | - | - | 1.9725 |
| Ceramic aggregate 4-8 mm | - | - | 0.9175 | - | 0.9175 |
| Ceramic aggregate 8-16 mm | - | - | 3.395 | 1.6975 | 1.6975 |
| Water | 0.85 | 0.85 | 0.85 | 0.85 | 0.85 |
| Water/Cement ratio | 0.57 | 0.57 | 0.57 | 0.57 | 0.57 |

The concrete resulting from the preparation of the experimental recipes is poured into standard molds, cubes with sides of 150 mm to determine the permeability of the concrete, then it is kept in these molds for 24 hours, after which it is removed and placed in the sample storage tank, for 28 days, at a constant temperature of 20 degrees Celsius (Figure 1).



Figure 1. Prepared samples and their storage

Table 3 shows the density values of the recipes used, both in the fresh and hardened state.

Table 3. Density values

| Concrete type | Density of fresh concrete sample (kg/m3) | Density of hardened concrete sample (kg/m3) |
|---|---|---|
| C16/20 | 2,310 | 2,235 |
| P1 | 2,256 | 2,149 |
| P2 | 2,277 | 2,206 |
| P3 | 2,267 | 2,157 |
| P4 | 2,262 | 2,105 |

Chemical composition of waste aggregates by X-ray fluorescence (XRF). The sample was first dried and finely ground to a uniform powder with a particle size of approx. 70 µm. The chemical composition of this powdered material was then determined using X-ray fluorescence (XRF) spectrometry, performed on a Quant'X ARL energy-dispersive XRF analyzer (Thermo Fisher Scientific, Waltham, MA, USA).

The control specimen was produced exclusively using natural river aggregates, serving as a reference element for evaluating the behavior of the experimental concretes. Specimens P1-P4 were obtained by the partial or total replacement of natural aggregates with ceramic aggregates, across different granulometric fractions, in order to analyze their influence on the concrete properties. The quantities of cement and water were kept constant for all specimens to ensure identical comparative conditions. According to NE 012/1-2022 "Standard for the production of concrete and the execution of works made of concrete, reinforced concrete and prestressed concrete - Part 1: Production of concrete", for concrete class C16/20, the optimal water/cement ratio (W/C) is 0.50-0.60 (m water/m cement). In the case of the recipes used in this work, the water/cement ratio is approximately 0.57.

The duration of the permeability tests was 3 days for all specimens, from the start date to the completion of the test. Concrete impermeability was determined using the Impermeability Test Set - UTC-1090 (Turkey, Sincan-Ankara). The matured concrete specimens were mounted and sealed in the test cells and then subjected to progressively applied water pressure in accordance with the testing procedure. After completion of the test, the specimens were split, and the depth of water penetration into the concrete mass was measured using a caliper and used to evaluate impermeability. All determinations were performed in triplicate (EN 12390-8, 2009).

## RESULTS AND DISCUSSIONS

Table 4 presents the major oxides, their approximate weight percentages, and relevant notes on their contribution to the properties of the aggregates and their potential impact on concrete behaviour.

Table 4. Chemical composition of ceramic waste aggregates (Vințu de Jos) determined by XRF

| Oxide | wt.% | Notes |
|---|---|---|
| $SiO_2$ | 58.37 | Main component, contributes to hardness and chemical stability |
| $Al_2O_3$ | 22.03 | From clay minerals; affects density and thermal behavior |
| $Fe_2O_3$ | 6.10 | Gives reddish color; minor impact on durability |
| CaO | 2.98 | Minor lime or cement contamination; affects alkalinity slightly |
| $K_2O$ | 1.31 | Alkali from clay; small influence on cement hydration |
| $Na_2O$ | 2.10 | Usually low; minor effect |
| MgO | 2.04 | Minor, stable in concrete |
| $TiO_2$ | 0.59 | Inert, minor contribution |
| $ZrO_2$ | 0.17 | Minor, inert. |
| LOI (Loss on ignition) | 3.82 | Organic residues and bound water; contributes to porosity |

The XRF analysis of the ceramic waste aggregates indicates a high content of $SiO_2$ and $Al_2O_3$, characteristic of clay-based ceramics, along with moderate $Fe_2O_3$ and minor CaO and alkalis. This composition suggests that while the aggregates provide structural stability and thermal resistance, the relatively high LOI may increase porosity, potentially affecting the permeability and water absorption of the concrete in which they are incorporated.
Specimens for testing the permeability of concrete were obtained, with dimensions of 150 × 150 mm, as shown in Figure 2.




Figure 2. The four specimens obtained for testing the permeability of concrete

To determine the depth of water penetration, the concrete specimens were split longitudinally, in accordance with the procedure specified in standard SR EN 12390-8, 2009 (Figure 3).



Figure 3. Testing of specimens according to SR EN 12390-8:2009

This operation allows a clear visualization of the water's path inside the specimen and enables precise measurement of the penetration depth (Figure 4).



Figure 4. Splitting of the concrete specimens and longitudinal sections of the samples

After splitting the specimens, the depth of water penetration was determined using a calliper, by measuring the distance from the water-exposed surface to the point of maximum observed penetration (Figure 5).



Figure 5. Performing measurements of water penetration depth in the specimens

Table 5 presents the results of the concrete permeability tests for the specimens used, including the control specimen and four experimental variants (P1-P4). All permeability tests were conducted over a period of 72 hours, starting from the preparation date of the specimens and continuing until the completion of the test for each specimen.
The results of the permeability tests highlight the differences between the control specimen and the experimental specimens made with ceramic aggregates. The control specimen, produced exclusively with natural river aggregates, recorded a water penetration depth of 700 ± 8 mm, serving as the standard reference for evaluating concrete behaviour. This value

reflects the characteristic permeability of C16/20 concrete obtained according to the traditional mix.

Table 5. Results of the tests for determining concrete permeability

| Sample | Concrete type / Observations | Water penetration depth (mm ± SD)* | Difference vs control (%) | Significance vs Control |
|---|---|---|---|---|
| Control sample | Standard C16/20 concrete mix | 70 ± 0.8 | - | - |
| P1 | Experimental variant 1 | 124 ± 1.5 | +77.1 | $p < 0.05$ |
| P2 | Experimental variant 2 | 130 ± 1.0 | +85.7 | $p < 0.05$ |
| P3 | Experimental variant 3 | 85 ± 0.5 | +21.4 | $p < 0.05$ |
| P4 | Experimental variant 4 | 97 ± 0.7 | +38.6 | $p < 0.05$ |

*Values are means ± SDs (n = 3).

The experimental specimens P1 and P2 exhibited much higher penetration depths, 124 ± 1,5 mm and 130 ± 1 mm, respectively, indicating a significant increase in permeability. This is primarily attributed to the partial or total replacement of natural aggregates with ceramic aggregates in certain fractions, resulting in a more porous matrix and reduced cement-aggregate cohesion.

For specimens P3 and P4, the water penetration depth was lower compared to P1 and P2, measuring 85 ± 5 mm and 97 ± 7 mm, respectively. This suggests that a more balanced combination of ceramic and natural aggregates can more effectively control the permeability, mitigating the negative impact on watertightness.

The results demonstrate that the use of ceramic aggregates directly affects the impermeability properties of concrete, with the effect varying depending on the granulometric fraction and replacement proportion. Specimens P1 and P2, which showed the greatest water penetration, emphasize the need to optimize the mix composition and material proportions to maintain adequate performance for concrete intended for applications where impermeability is critical. Specimens P3 and P4 suggest that a balance between natural and ceramic aggregates can produce moderately permeable concrete, suitable for situations where slightly increased permeability is acceptable.

Comparing these findings with those reported in the literature, a similar trend is observed regarding the influence of alternative materials on concrete permeability (Glevitzky et al., 2026). Recent studies on the use of ceramic and recycled aggregates in concrete generally indicate a negative impact on concrete transport properties, particularly permeability and water penetration resistance (C. Li et al., 2025).

Research conducted by Xu et al. in 2023 demonstrated that the use of recycled ceramic aggregates in high-performance concrete leads to an increase in permeability, attributing this effect to increased porosity and changes in the pore distribution within the concrete matrix. Furthermore, chloride ion penetration analysis revealed a tendency for enhanced fluid transport behaviour in materials containing a significant proportion of recycled ceramic aggregates. This finding is consistent with the results of experimental specimens P1 and P2 in the present study, where the partial or total replacement of natural aggregates with ceramic aggregates resulted in higher water penetration depths (124 mm and 130 mm) compared to the control specimen.

On the other hand, some literature results suggest that low levels of ceramic substitution and optimized mix proportions can limit the increase in permeability or even improve certain durability properties. A study published by L. Li et al. (2025), on mortars with fine ceramic aggregates showed that moderate substitutions can reduce water absorption and permeability by filling voids and improving the microstructure of the matrix. This observation can be correlated with the results of specimens P3 and P4, where the lower permeability values compared to P1 and P2 (yet still higher than the control) suggest that a balanced replacement of natural aggregates with ceramic aggregates can mitigate the negative effects on watertightness.

A review of the literature (Paul et al., 2023) on the use of ceramic waste as aggregates in concrete confirms that concrete incorporating such materials exhibits permeability and other durability characteristics that are comparable to or acceptable relative to conventional concrete, depending on the replacement proportions and the optimization treatments applied (Ray et al., 2021). Thus, although most studies show a general trend of increased permeability with higher ceramic aggregate content (particularly at high replacement levels), they also emphasize

the importance of optimizing the granulometry and the mix design to maintain durable performance.

These results can be interpreted within the broader context of sustainability and the circular economy in construction. The use of recycled ceramic aggregates contributes to reducing the consumption of natural resources and valorizing waste; however, the higher permeability may affect concrete durability, including resistance to freeze–thaw cycles and the penetration of aggressive agents (Murali et al., 2025).

From the perspective of future research, it is recommended to investigate the use of additives or pozzolans to reduce the porosity of concrete with ceramic aggregates and to evaluate the effects of different types of recycled aggregates on mechanical and durability properties. Additionally, the development of predictive models correlating the proportions of alternative aggregates with permeability and other durability characteristics could support the design of sustainable and eco-friendly concretes. Implementing long-term studies under real exposure conditions to water and aggressive agents could further confirm the performance of these concretes in practice.

Thus, this study not only confirms the trends observed in the specialized literature but also provides insights for optimizing durable concrete mixes, highlighting that a balance between natural and ceramic aggregates is essential for maintaining impermeability and durability properties while promoting the use of recycled materials.

***Statistical analysis of concrete permeability***

A statistical analysis was conducted to evaluate the influence of ceramic aggregate replacement on the impermeability of concrete. For each concrete mixture, three specimens were tested, and the mean water penetration depth ± standard deviation is reported (Cojocaru et al., 2018).

Comparisons between each experimental mixture (P1-P4) and the control concrete were performed using the t Student test for unequal variances (Welch t-test). The water penetration depth of all experimental mixtures was significantly higher than that of the control concrete ($p < 0.05$), confirming that partial or total replacement of natural river aggregates with ceramic aggregates increases concrete permeability (Gluck, 1971; Aloman, 1998; Senedecor & Cochran, 1980).

The differences in penetration depth relative to the control concrete are also expressed as percentages, highlighting the impact of aggregate replacement. Mixtures P1 and P2, which contained ceramic aggregates in the fine and medium fractions, exhibited the highest increases (+77.1% and +85.7%, respectively), while mixtures P3 and P4 showed moderate increases (+21.4% and +38.6%), corresponding to partial replacement in coarser fractions (Popa et al., 2022).

The relatively low standard deviations (±5-15 mm) indicate good repeatability and uniformity of the specimens, confirming the reliability of the testing procedure. The statistical analysis demonstrates a clear correlation between the granulometric fraction of ceramic aggregates and concrete permeability, with finer fractions causing a greater increase in water penetration depth.

## CONCLUSIONS

The study shows that replacing natural aggregates with ceramic aggregates generally increases the permeability of concrete, due to their higher porosity and the modification of the matrix microstructure. However, the effect depends on the proportion and granulometry of the ceramic aggregates; moderate substitution levels can keep permeability close to that of conventional concrete and may improve matrix density.

The results suggest that concrete with ceramic aggregates can be used as a sustainable solution by valorizing waste materials, but optimizing the mix design and controlling the microstructure are essential to ensure durability and watertightness. Thus, ceramic aggregates represent a promising alternative, but concrete performance depends on how they are integrated into the composition.

## REFERENCES

Ahmad, J., Alattyih, W., Jebur, Y., Alqurashi, M., & Garcia-Troncoso, N. (2023). A review on ceramic waste-based concrete: A step toward sustainable concrete. *Reviews on Advanced Materials Science*, *62*(1), 20230346.

Ahmad, J., Sabri, M. M., Ali, A. M., Alattyih, W., Khan, I., & Alam, M. (2024). Durability and microstructure aspects of sustainable concrete made with ceramic waste: A review. *Frontiers in Materials*, *11*, 1508989.

Al-Fakih, A., Abujamil, A., Al-Shugaa, M. A., Assaggaf, R., Al-Osta, M. A., & Albu Shaqraa, A. (2025). Utilization of ceramic polishing sludge in masonry cement mortar: Mechanical strength and thermal behavior. *Results in Engineering*, *27*, 107058.

Aloman, A. (1998). *Statistics and probability in scientific experiment*. Bucuresti, Matrix Rom (In Romanian).

Cojocaru, O., Cerbari, V., Filipov, F., Chiorescu, E., Rusu, T., Bogdan, I., Moraru, P., & Pop, A. (2018). Statistical analysis of the sustainable agricultural lands use and fertile irreversible loss of soil which are washing from versants of rural area. *Scientific Papers. Series A. Agronomy, 61*(2), 58–63.

Elemam, W. E., Agwa, I. S., & Tahwia, A. M. (2023). Reusing Ceramic Waste as a Fine Aggregate and Supplemental Cementitious Material in the Manufacture of Sustainable Concrete. *Buildings*, *13*(11), 2726.

European Committee for Standardization. (2009). Testing hardened concrete – Part 8: Depth of penetration of water under pressure (EN 12390-8:2009). CEN.

Glevitzky, M., Glevitzky, I., Mucea-Ștef, P., Popa, M., Dumitrel, G.-A., & Vică, M. L. (2025). Integrated Risk Framework (IRF) - Interconnection of the Ishikawa Diagram with the Enhanced HACCP System in Risk Assessment for the Sustainable Food Industry. *Sustainability*, *17*(2), 536.

Glevitzky, M., Mucea-Ștef, P., Corcheș, M.-T., Sălcudean, M., Marica, E., Șerban, S. G., & Popa, M. (2026). Integrated Environmental Risk Assessment and Performance Evaluation of Asphalt Plants Incorporating Reclaimed Asphalt Pavement Under the ISO 14001 Framework. *Eng*, *7*(2), 95.

Gluck, A. (1971). *Metode matematice în industria chimică* [Mathematical methods in the chemical industry]. Bucuresti, Tehnică Publishing House.

Javed, M. H., Ahmad, A., Rehan, M., Farooq, M., Farhan, M., Raza, M. A., & Nizami, A. S. (2025). Advancing Circular Economy Through Optimized Construction .and Demolition Waste Management Under Life Cycle Approach. *Sustainability*, *17*(11), 4882.

Jiang, C. & Cheng, X. (2020). Recycling of waste ceramic foams as fine aggregates in pervious concrete. *RSC Advances*, *10*(4), 2364–2367.

Jwaida, Z., Dulaimi, A., & Bernardo, L. F. A. (2024). The Use of Waste Ceramic in Concrete: A Review. *CivilEng*, *5*(2), 482–500.

Li, C., Zhang, X., Cao, X., & Yu, Y. (2025). Sustainable Performance and Interfacial Characteristics of Fully Recycled Concrete with Combined Recycled Concrete, Brick, and Ceramic Aggregates. *Sustainability*, *17*(23), 10503.

Li, L., Liu, W., Zeng, Q., & Zhou, C. (2025). Sustainable reuse of household ceramic wastes as a substitute of cement and natural sand in construction materials: Mechanical, transport, and microstructural properties. *Case Studies in Construction Materials*, *22*, e04708.

Medina, C., Sánchez de Rojas, M. I., & Frías, M. (2012). Reuse of sanitary ceramic wastes as coarse aggregate in eco-efficient concretes. *Cement and Concrete Composites*, *34*(1), 48–54.

Murali, G., Hassas, N., & Abdelgader, H. S. (2025). Ceramic waste as a sustainable cementitious resource: pathways to cleaner and high-performance concrete. *Cleaner Materials*, *18*, 100352.

Ngayakamo, B.H. (2025). Sustainable concrete production: the role of ceramic waste as a partial coarse aggregate substitute. *Discover Civil Engineering 2*, 32.

Paul, S. C., Faruky, S. A. U., Babafemi, A. J., & Miah, M. J. (2023). Eco-friendly concrete with waste ceramic tile as coarse aggregate: Mechanical strength, durability, and microstructural properties. *Asian Journal of Civil Engineering*, *24*, 3363–3373.

Popa, M., Glevitzky, I., Dumitrela, G.-A., Popa, D., Vîrsta, A., & Glevitzky, M. (2022). Qualitative analysis and statistical models between spring water quality indicators in Alba County, Romania. *Scientific Papers. Series E. Land Reclamation, Earth Observation & Surveying, Environmental Engineering*, *11*, 358-366.

Ray, S., Haque, M., Sakib, M. N., Mita, A. F., Rahman, M. D. M., & Tanmoy, B. B. (2021). Use of ceramic wastes as aggregates in concrete production: A review. *Journal of Building Engineering*, *43*, 102567.

Sălcudean, M., & Popa, M. (2025). The integration of ceramic waste as a partial substitute of natural aggregates in experimental concrete recipes. *Scientific Papers. Series E. Land Reclamation, Earth Observation & Surveying, Environmental Engineering, 14*, 594–600.

Semmana, O., Rihan, M. A. M., Barrie, Z. M., Daniel, C., & Abdalla, T. A. (2025). A systematic review of the strength, durability, and microstructure properties of concrete incorporating glass powder. *Engineering Reports*, 7(1), e70002.

Snedecor, G.W., & Cochran, W.G. (1980). Statistical methods., 7th edn (Iowa State University Press: Ames, IA).

Tokareva, A., & Waldmann, D. (2025). Durability Assessment of Cement Mortars with Recycled Ceramic Powders. *Materials*, *18(18)*, 4420.

Xu, F., Lin, X., & Zhou, A. (2023). Effect of recycled ceramic aggregate on hydration heat and permeability of high-performance concrete. *Cement and Concrete Composites*, *137*, 104930.

Zhou, J., Dong, Y., Qiu, T., Lv, J., Guo, P., & Liu, X. (2025). The Microstructure and Modification of the Interfacial Transition Zone in Lightweight Aggregate Concrete: A Review. *Buildings*, *15*(15), 2784.

Zong, L., Fei, Z., & Zhang, S. (2014). Permeability of recycled aggregate concrete containing fly ash and clay brick waste. *Journal of Cleaner Production, 70*, 175–182.

Scientific Papers. Series E. Land Reclamation, Earth Observation & Surveying, Environmental Engineering. Vol. XV, 2026
Print ISSN 2285-6064, CD-ROM ISSN 2285-6072, Online ISSN 2393-5138, ISSN-L 2285-6064

# EXPERIMENTAL STUDY ON BRICKS MADE WITH BRICK WASTE AND SAWDUST

**Mircea SĂLCUDEAN[1, 2], Maria POPA[3], Mirel GLEVITZKY[3, 4], Mihai Teopent CORCHEȘ[2]**

[1]"Lucian Blaga" University of Sibiu, Doctoral School, Faculty of Engineering,
10 Victoriei Blvd, Sibiu, Romania
[2]"1 December 1918" University of Alba Iulia, Faculty of Computer Science and Engineering,
15-17 Unirii Street, Alba Iulia, Romania
[3]"1 December 1918" University of Alba Iulia, Faculty of Economic Sciences,
15-17 Unirii Street, Alba Iulia, Romania
[4]Politehnica University Timişoara, Faculty of Engineering Hunedoara,
5 Revolutiei Street, Hunedoara, Romania

Corresponding author email: mirel_glevitzky@yahoo.com

***Abstract***

*The paper presents an experimental study on the production and testing of bricks that incorporate brick waste and sawdust as a sustainable solution for the construction industry. The aim of the research is to reduce environmental impact by reusing recycled materials and wood processing residues. Samples were manufactured using brick waste fractions (0-4 mm, 4-8 mm, 8-16 mm) and sawdust of different particle sizes, with cement as a binder, and tests focused on physical and mechanical properties (compressive strength), density, water absorption, and drying behaviour. Brick waste was analyzed using X-ray fluorescence (XRF) spectroscopy in order to determine its chemical composition and elemental distribution. The results indicate that the addition of sawdust influences density and porosity, while ceramic waste helps maintain structural strength. Data show a reduction in dry density by 5.8%, saturated density by 7.2%, water absorption by 13.8%, and compressive strength by 55.6%, indicating that the incorporation of brick waste and sawdust produces lighter, less porous bricks with significantly reduced mechanical strength. The conclusions highlight the potential of these materials for producing eco-friendly masonry elements.*

***Key words****: brick waste, compressive strength, experimental bricks, recycled materials, sawdust.*

## INTRODUCTION

In recent decades, the circular economy has become a central principle in global sustainable development strategies (Velenturf & Purnell, 2021). The construction industry, being one of the largest consumers of natural resources and generators of waste, is under increasing pressure to adopt more responsible and innovative practices (Cudecka-Purina et al., 2024). In this context, the reuse of ceramic waste-originating from both manufacturing processes and demolition activities - offers an opportunity to valorize materials previously considered unusable, thereby reducing the environmental impact of construction activities (Gajzler et al., 2025).

Ceramic waste includes broken bricks, tiles, ceramic floor and wall coverings, and other ceramic products that can no longer be used in their original form (Sarner & Guillon, 2025). Recycling these materials not only reduces the amount of waste disposed of in landfills but can also partially replace natural aggregates, thereby contributing to lower production costs and the conservation of limited natural resources. Furthermore, products manufactured using recycled materials can exhibit performance comparable to that of conventional materials, provided that the proportions and manufacturing processes are carefully controlled (Chen et al., 2024). The use of ceramic waste also presents significant challenges. From a technical perspective, variability in particle size, composition, and porosity of recycled materials can substantially affect the mechanical and physical properties of the final product (Murali et al., 2025). From an operational standpoint, the collection, sorting, and processing of waste require specific infrastructure and involve additional costs (Olawade et al., 2024). From an environmental perspective, improper handling

of ceramic waste may generate dust and pollution, raising further health and safety concerns (Huseien et al., 2025).

Scientific literature shows a diversity of results and opinions regarding the optimal amount of ceramic waste that can be incorporated into construction mixes without compromising performance (Sălcudean & Popa, 2025). Some studies indicate that up to 30% of natural aggregate can be replaced with ceramic waste without significant strength loss (Silvestre et al., 2013), while other research warns about increased porosity and water absorption at higher proportions, generating discussions and controversies within the scientific community (Furszyfer Del Rio et al., 2022). This lack of consensus highlights the need for studies that simultaneously investigate the physical, mechanical, and durability properties of materials produced from ceramic waste. Combining ceramic waste with other recycled materials, such as sawdust, opens new perspectives for the production of eco-friendly bricks and masonry elements (Vidak Vasić et al., 2024). Sawdust, as an organic residue, can influence the porosity and weight of the material while providing a solution for valorizing waste from the wood industry (Adegoke et al., 2022). Investigating these mixtures requires a careful approach, simultaneously analyzing density, water absorption, porosity, and compressive strength in order to establish practical limits and assess their application potential.

The aim of this article is to evaluate the efficiency of using ceramic waste in combination with sawdust for the production of eco-friendly bricks, providing experimental data on the physical and mechanical behavior of these materials. The original contribution lies in offering comprehensive information on density, porosity, water absorption, and compressive strength, thereby complementing the existing literature and supporting the development of sustainable construction practices.

## MATERIALS AND METHODS

For the evaluation of the influence of using brick waste and sawdust on the behaviour of bricks, a comparative experimental study was conducted. The analysis was based on two types of mixtures: a reference mixture, without any added recycled materials, and one that includes brick waste and sawdust, according to the recipe presented in Table 1.

Table 1. Composition of the mixture for the experimental brick

| Material used | Quantity (kg) | Source |
|---|---|---|
| Cement 42.5 R | 0.25 | Heidelberg Materials, Chișcădaga, Romania |
| Brick waste 0-4 mm | 0.27 | Reciclare Moloz SRL, Vintu de Jos, Alba, Romania |
| Brick waste 4-8 mm | 0.30 | |
| Brick waste 8-16 mm | 0.50 | |
| Fine sawdust | 0.2 | Remarcabil Mobila, Ocna Mureș, Alba, Romania |
| Coarse sawdust | 0.2 | |
| Natural aggregates 4–16 mm | 0.2 | Elis Agregate, Cariera Jidovu – Pătrângeni, Alba, Romania |
| Water | 0.7 | APA CTTA SA, Alba Iulia, Alba, Romania |

For the preparation of the experimental mixtures, processed brick waste with various granulometric sizes was used, as shown in Figure 1.

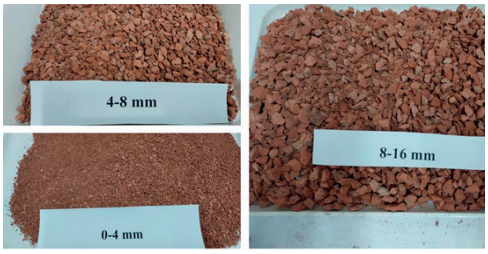



Figure 1. Brick waste with different granulometries

Additionally, fine and coarse sawdust was employed, presented in Figure 2.



Figure 2. Sawdust used in the composition of the mixtures: fine and coarse

Chemical composition determined by XRF. The brick waste aggregates were first dried at 105°C to remove moisture and then ground to a fine, homogeneous powder with a particle size of approximately 60-70 µm. The chemical composition of the brick waste was determined using X-ray fluorescence (XRF) spectrometry in accordance with SR EN 15309:2007

(Characterization of waste and soil. Determination of elemental composition by X-ray fluorescence n.d.). Measurements were performed with a Quant'X ARL energy-dispersive XRF spectrometer (Characterization of waste and soil. Determination of elemental composition by X-ray fluorescence n.d.) (Thermo Fisher Scientific, Waltham, MA, USA), following standard operating procedures for powdered ceramic materials. The analysis provided the content of major oxides ($SiO_2$, $Al_2O_3$, $Fe_2O_3$, etc.) and the Loss on Ignition, allowing characterization of the brick waste for potential reuse or recycling applications.

Brick waste is separated into granulometric fractions (0-4 mm, 4-8 mm, 8-16 mm) and crushed/sieved as necessary to achieve uniformity. The sawdust is dried and sieved to ensure it does not contain excessive moisture, which could cause cracking during firing. Natural aggregates are cleaned of impurities (stones, dust) and sorted to the 4-16 mm size range. Cement is kept dry and added to improve the cohesion of the mixture.

All fractions of brick waste are combined with the natural aggregates and sawdust into a homogeneous mixture. Cement is added to bind the materials. Water is gradually incorporated while continuously mixing to achieve a plastic, uniform consistency that is easy to shape. The objective is to ensure an even distribution of sawdust and waste particles to prevent segregation.

The mixture is molded using molds or by manual/mechanical pressing with UTEST UTC-0900E-T vibrating table, made in Turkey (Figure 3). The dimensions and shape are maintained in accordance with the experimental standard. Fine sawdust contributes to uniform porosity, while coarse sawdust creates a more aerated internal structure, reducing the overall weight.

The bricks are placed in drying chambers or in the open air for 3-7 days to reduce the moisture content to 5-7%. Drying must be gradual to prevent cracking, as the sawdust creates internal porosity. The amount of sawdust directly influences the density and thermal insulation properties. The proportions of brick waste and natural aggregates affect the compressive strength and durability. It is recommended to document in detail each fraction and to perform testing for optimizing the mixture. Homogeneous brick samples were obtained, free of visible defects, ready for subsequent mechanical and physical testing. The adopted method proved to be simple, reproducible, and efficient, providing a solid foundation for further research.



(a) (b) (c)

Figure 3. Preparation of the experimental bricks: (a) mixture prepared according to the recipe; (b) pouring into the mold; (c) brick after drying

The dry state mass is determined at the end of the slow drying period by weighing, expressed in grams.

The saturated state mass is determined after the brick has been immersed in water and left for 24 hours at a temperature of 20 ± 5°C. The brick is then removed and weighed in grams (EN 772-21, 2011).

The volume of the bricks was calculated by measuring the dimensions (length L = 230 mm, width l = 115 mm, and height h = 63 mm). Then, using the formula for the volume of a rectangular parallelepiped, the volume of the bricks was determined as $V = L \times l \times h = 230 \times 115 \times 63 = 1666.35$ cm³.

Dry state density/Saturated state density. Knowing the mass and volume of the standard solid brick and the experimental brick, the density was calculated for each using the density formula $\rho = m/V$, both in the dry state and in the saturated state: $\rho_{\text{dry standard}} = 2592.97/1666.35 = 1.556$ g/cm³; $\rho_{\text{dry experimental}} = 2441.35/1666.35 = 1.465$ g/cm³; $\rho_{\text{saturated standard}} = 3111.57/1666.35 = 1.867$ g/cm³; $\rho_{\text{saturated experimental}} = 2888.42/1666.35 = 1.733$ g/cm³.

The water absorption is determined after immersing the bricks in water for 24 hours. The samples are removed from the water, superficially wiped to remove excess surface moisture, weighed, and the water absorption is calculated using the formula $A = (M_1 - M_0)/ M_0$

× 100 [%], where $M_0$ represents the mass of the brick in the dry state (g), and $M_1$ represents the mass of the brick after immersion (g). For the experimental brick, the absorption was $A_{cex}$ = (2888.42 − 2441.35)/ 2441.35 × 100 = 18.31 %, while for the standard brick $A_{csp}$ = (3111.57 − 2592.97)/ 2592.97 × 100 = 20 %.

The compressive strength of the brick samples was determined using the Matest Cyber Plus Evolution static materials testing machine (model CO7gPN191, Matest, Italy), a specialized device for measuring the compressive strength of construction materials, with a measurement range between 25-250 kN and 20-3000 kN. The samples were subjected to a gradually and uniformly applied axial compressive load, under controlled temperature conditions (+5…+40 °C) and relative humidity (30-70%), until the state of failure by crushing was reached, at which point the maximum force sustained was recorded (EN 12390-4, 2009; EN 772-1, 2001).

The sample was subjected to a gradually applied axial compressive load until the state of failure by crushing was reached (Figure 4).

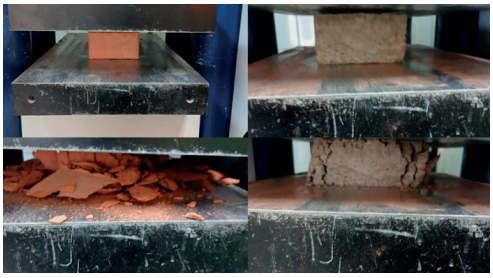


Figure 4. Experimental and standard brick samples under axial compression until failure

The compressive strength is determined as the ratio between the maximum force recorded at failure and the cross-sectional area of the specimen.

## RESULTS AND DISCUSSIONS

The average chemical composition of the brick waste aggregate determined by X-ray fluorescence (XRF) analysis is presented in Table 2.

The chemical composition of brick waste determined by XRF shows that the material is rich in $SiO_2$ (55%) and $Al_2O_3$ (15%), the main constituents that provide hardness and stability.

Table 2. Chemical Composition of Brick Waste Aggregate (XRF Analysis)

| Compound | Value (wt.%) | Interpretation |
|---|---|---|
| $SiO_2$ | 55.04 | Contributes to mechanical strength and potential pozzolanic reactivity. |
| $Al_2O_3$ | 15.11 | Enhances ceramic stability and may support secondary hydration reactions. |
| $Fe_2O_3$ | 7.65 | Contributes to thermal stability |
| CaO | 8.07 | May influence hydraulic reactivity |
| MgO | 4.83 | It is associated with carbonate or clay minerals and can affect durability |
| $SO_3$ | 1.08 | Related to sulfate phases; excessive amounts may influence durability. |
| $K_2O$ | 1.03 | Alkali oxide from clay minerals; may affect alkali–silica reactivity. |
| $TiO_2$ | 0.28 | Associated with accessory minerals; limited structural impact |
| BaO | 0.22 | From mineral impurities; negligible effect on overall performance. |
| MnO | 0.10 | May slightly influence coloration |
| Loss on Ignition | 6.40 | Indicates volatiles, residual carbonates, and unburned material affecting thermal behavior and durability. |

The relatively high $Fe_2O_3$ content (7.65%) explains the characteristic red color of the bricks, while CaO (8%) may originate from lime or calcareous sand additives, influencing the material's strength and durability. $K_2O$ (1%) and $SO_3$ (1%) are alkaline oxides that can affect chemical behavior during hydration or other reactions, whereas $TiO_2$, BaO, and MnO are minor components with minimal impact but useful for identifying the source of the raw material. The Loss on Ignition value of 6.4% indicates the presence of organic matter or moisture released during firing. Overall, the material is suitable for recycling as aggregate or as a raw ceramic material due to its balanced chemical composition.

Table 3 presents the mass, volume, density, water absorption, and compressive strength of the bricks, comparing the experimental values with the standard ones and highlighting the absolute and percentage differences.

Table 3. Physical and mechanical properties of experimental and standard bricks

| Parameter | Brick type | | Difference | |
|---|---|---|---|---|
| | Experimental | Standard | Absolute | % |
| Dry mass (g) | 2441.35±4.0 | 2592.97±2.1 | 151.62 | 5.85 |
| Saturated mass (g) | 2888.42±0.9 | 3111.57±3.4 | 223.15 | 7.17 |
| Volume ($cm^3$) | 1666.4±0.0 | 1666.4±0.0 | 0 | 0 |
| Dry density ($g/cm^3$) | 1.465±0.1 | 1.556±0.1 | 0.091 | 5.84 |
| Saturated density ($g/cm^3$) | 1.733±0.1 | 1.867±0.1 | 0.134 | 7.17 |
| Water absorbed (g) | 447.07±0.8 | 518.6±1.2 | 71.53 | 13.8 |
| Compressive strength ($N/mm^2$) | 16.7±0.1 | 37.6±0.1 | 20.9 | 55.6 |

Values are means ± SDs (n = 3).

The compressive strength of the experimental brick decreases dramatically, by approximately 56%, indicating that the inclusion of waste significantly affects the mechanical performance of the material. At the same time, water absorption decreases by about 14%, a potentially positive effect if the goal is to obtain less porous bricks. Density and mass decrease slightly, by around 6-7%, suggesting that the brick's structure becomes lighter without changing its volume, so the observed differences are strictly due to changes in the internal material.

The experimental results illustrate both the potential and the limitations of using recycled materials in the production of construction elements, contributing to a deeper understanding of the possibilities for transitioning toward a circular economy in the construction sector. The incorporation of brick waste and sawdust as additives in brick production results in a distinct balance between reduced density, decreased mechanical strength, and improvement in certain porosity-related aspects, when compared to the reference mixture (Lewo Nkondi, 2025).

In the European Union, the technical specifications for masonry units, including fired clay bricks, are regulated by the harmonized series of standards SR EN 771 (SR EN 771-1+A1:2015 n.d.). The standard defines the characteristics, performance requirements, and conformity criteria for clay masonry units (dimensions, tolerances, strength, density, etc.), providing a clear framework for the evaluation of both industrially and experimentally produced materials (Affan et al., 2025). Furthermore, the design and calculation of masonry structures incorporating such units are governed at the European level by Eurocode 6 (EN 1996-1-1, 2022), which establishes general rules for reinforced and unreinforced masonry structures, including the properties of constituent materials and their behaviour under load.

In line with the results reported in the scientific literature (Meng et al., 2022; Hu et al., 2024), the incorporation of brick waste into the mixture contributes to the valorization of recycled materials and can influence the internal structure of the bricks, affecting their density and mechanical strength (Abdullah, 2021). If the obtained properties (e.g., density, compressive strength, or water absorption) fall within the limits required by SR EN 771-1, the respective materials may be considered compliant or close to technical compliance for certain masonry applications. Compliance with these requirements is essential for the acceptance of experimental samples as construction materials, particularly in projects adhering to European standards (Oyguc, 2025). The use of sawdust, due to its organic nature and variable granulometry, can lead to changes in the material's porosity, an aspect that is reflected both in the volumetric mass (density) and in the behaviour under mechanical loading (Robert et al., 2024).

As noted by Ludovice et al. (2025), the interpretation of the experimental results in the context of normative requirements provides a solid foundation for assessing the practical viability of the materials studied, opening pathways for the optimization of compositions and the continuation of research aimed at achieving or surpassing the performance levels required by international standards. Comparison of the obtained results with those of previous studies indicates that the proportion and type of recycled materials play an essential role in the final performance of the bricks. Thus, a controlled content of brick waste and sawdust can represent a viable solution for producing materials with reduced environmental impact, without significantly compromising their functional characteristics (Benjeddou, 2025; Jwaida & Di Sarno, 2025).

The experimental study highlighted several key lessons regarding the use of brick waste and sawdust in brick production. First, the integration of recycled materials leads to a significant reduction in compressive strength, underscoring the importance of controlling the proportions and granulometry of the components (Akbulut, 2025). At the same time, the addition of sawdust was found to contribute to a decrease in density and mass, offering an advantage in producing lighter materials with a certain level of thermal insulation (Esakki Priya, 2025). Water absorption can be positively influenced, indicating the possibility of obtaining less porous bricks, which provides benefits for durability in certain masonry applications (Raimondo et al., 2009).

In the long term, the use of brick waste and sawdust can have a significant impact on sustainability in construction (Rabiu & Damdelen, 2023). The adoption of these materials reduces pressure on natural resources, limits the amount of waste disposed of in landfills, and can lead to cost savings in production (Zhang, 2024). Long-term success depends on optimizing mix designs to maintain adequate mechanical properties and on compliance with international technical standards, so that the materials can be used in real structures without compromising safety and durability (Soave & Ferrara, 2025). Expanding research on long-term behaviour and resistance to environmental factors will be essential for the large-scale adoption of these technologies.

From a broader perspective, the results of this study support current research directions focused on the development of sustainable construction materials through the integration of industrial waste and natural by-products into manufacturing processes. Moreover, they highlight the potential of using recycled materials in brick production as an alternative to conventional raw materials (Popa et al., 2025; Anbarasu & Karuppusamy, 2025).

The statistical analysis of the experimental results was carried out in order to highlight the differences between the experimental brick and the standard brick with respect to the analyzed physico-mechanical properties. Given the small number of determinations performed for each type of material (n = 3) and the impossibility of robustly verifying the normality assumption of the distributions, data comparison was conducted using the nonparametric Mann-Whitney U test, applied to independent samples, at a significance level of $\alpha = 0.05$.

The obtained results indicated the existence of statistically significant differences between the two types of bricks, particularly in terms of compressive strength, for which the standard brick exhibited significantly higher values compared to the experimental brick ($U = 0$, $p \leq 0.05$). Similar trends were also observed for density and water absorption parameters, suggesting superior physico-mechanical performance of the standard material.

The application of the Student's t-test for independent samples, used for indicative purposes, also revealed the existence of a statistically significant difference between the two types of bricks with regard to compressive strength ($|t| \gg t_{(crit)}$, $\alpha = 0.05$), thereby confirming the results obtained using the nonparametric Mann–Whitney U test.

Table 4 presents the results of the t-test applied to all analyzed parameters, including the values of the t statistic and the corresponding significance levels (*p*-values) obtained for the comparison between the two types of bricks.

Table 4. Results of the t-test for the comparison of the physical and mechanical properties of the experimental and standard brick

| Parameter | t-statistic | p-value | Interpretation |
|---|---|---|---|
| Dry mass | -58.13 | $1.04\times10^{-5}$ | Highly significant difference – the experimental brick is much lighter in the dry state |
| Saturated mass | -109.89 | $2.71\times10^{-5}$ | Highly significant difference |
| Volume | 0.0 | 1.0 | No difference observed |
| Dry density | -1.11 | 0.33 | Statistically non-significant difference |
| Saturated density | -1.64 | 0.18 | Statistically non-significant difference |
| Amount of absorbed water | -85.90 | $6.39\times10^{-7}$ | Highly significant difference – the experimental brick absorbs much less water |
| Compressive strength | -255.97 | $1.40\times10^{-9}$ | Highly significant difference – the experimental brick exhibits nearly half the compressive strength of the standard brick |

The statistical analysis indicates highly statistically significant differences between the experimental brick and the standard brick with respect to dry mass, saturated mass, amount of absorbed water, and compressive strength ($p < 0.001$), highlighting a major impact of waste incorporation on these properties. The experimental brick is significantly lighter (both dry and saturated mass are significantly lower) and absorbs significantly less water, which suggests a lower porosity or a different structure (possibly more compact or with closed pores). Dry and saturated densities do not differ statistically significantly (although the mean values are slightly lower for the experimental brick) - the variability between measurements makes the difference non-significant with only three repetitions. Compressive strength is dramatically lower for the experimental brick (approximately 44% of the standard value), representing the most important practical difference.

## CONCLUSIONS

The study confirms that the combination of brick waste and sawdust can be used for the production of eco-friendly bricks with physical and mechanical properties different from those of conventional bricks. Compressive strength decreases significantly, while density and water absorption can be adjusted depending on the proportions of recycled materials. The results suggest that, through careful optimization of mix designs, these experimental bricks may represent a sustainable alternative in construction, contributing to the circular economy and to the reduction of environmental impact. The study also opens opportunities for future research aimed at improving durability, environmental performance, and the long-term evaluation of the mechanical and functional behaviour of recycled materials.

## REFERENCES

Abdullah, D. J., Abbas, Z. K., & Abd, S. K. (2021). Study of using of recycled brick waste (RBW) to produce environmental friendly concrete: A review. *Journal of Engineering*, 27(11), 1–14.

Adegoke, K. A., Adesina, O. O., Okon-Akan, O. A., Adegoke, O. R., Olabintan, A. B., Ajala, O. A., Olagoke, H., Maxakato, N. W., & Bello, O. S. (2022). Sawdust-biomass based materials for sequestration of organic and inorganic pollutants and potential for engineering applications. *Curr. Res. Green Sustain. Chem*. 5, 100274.

Affan, H., Arairo, W., Barraj, F., Khatib, M., Saba, M., & El Mendili, Y. (2025). Mechanical Characteristics of Clay-Based Masonry Walls. *Eng*, 6(10), 260.

Akbulut, Z. F., Guler, S., Yavuz, D., & Avcı, M. S. (2025). Toward sustainable construction: A critical review of recycled aggregate concrete properties and future opportunities. *Case Studies in Construction Materials*, 23, e05133.

Anbarasu, N. A., & Karuppusamy, M. (2025). A review of sustainable construction and waste management: Brick manufacturing using agro-industrial wastes. *Zaštita Materijala*, 66(4), 913–927

Benjeddou, O. (2025). Experimental investigation of the impact of wood sawdust incorporation on the physical and thermal properties of fired clay bricks. *Sci. Rep.* 15, 30855.

Characterization of Waste and Soil. Determination of Elemental Composition by X-Ray Fluorescence. https://www.en-standard.eu/bs-en-15309-2007-characterization-of-waste-and-soil-determination-of-elemental-composition-by-x-ray-fluorescence/?srsltid=AfmBOoowAMBhjSPnCz3fEsxnYWgFlX51p-OCngev4VAehHEJtj64kMKh.

Chen, L., Yang, M., Chen, Z., Xie, Z., Huang, L.; Osman, A.I., Farghali, M., Sandanayake, M., Liu, E.; Ahn, Y.H., Al-Muhtaseb, A.H., Rooney, D.W., & Yap, P.-S. (2024). Conversion of Waste into Sustainable Construction Materials: A Review of Recent Developments and Prospects. *Materials Today Sustainability* 27, 100930.

Cudecka-Purina, N., Kuzmina, J., Butkevics, J., Olena, A.; Ivanov, O., & Atstaja, D. (2024). A Comprehensive Review on Construction and Demolition Waste Management Practices and Assessment of This Waste Flow for Future Valorization via Energy Recovery and Industrial Symbiosis. *Energies* 17, 5506.

Esakki Priya, P., Vasanthi, P., Prabhu, B., & Murugesan, P. (2025). Sawdust as a sustainable additive: Comparative insights into its role in concrete and brick applications. Cleaner Waste Systems, 11, 100286.

European Committee for Standardization. (2001). EN 772-1: Methods of test for masonry units - Part 1: Determination of compressive strength.

European Committee for Standardization. (2009). EN 12390-4: Testing hardened concrete - Part 4: Compressive strength of test specimens.

European Committee for Standardization. (2011). EN 772-21: Methods of test for masonry units - Part 21: Determination of water absorption of clay and calcium silicate masonry units by cold water absorption

European Committee for Standardization. (2022). EN 1996-1-1:2022. Eurocode 6 - Design of masonry structures - Part 1-1: General rules for reinforced and unreinforced masonry structures. European Committee for Standardization

Furszyfer Del Rio, D. D., Sovacool, B. K., Foley, A. M.; Griffiths, S., Bazilian, M., Kim, J., & Rooney, D. (2022). Decarbonizing the ceramics industry: A systematic and critical review of policy options, developments and sociotechnical systems. *Renew. Sustain. Energy Rev.* 157, 112081.

Gajzler, M., Nowotarski, P., & Ratajczak, M. (2025). Economic and Environmental Analysis of Using Recycled Ceramic Demolition Materials in Construction Projects. *Sustainability* 17, 7560.

Hu, J., Ahmed, W., & Jiao, D. (2024). A Critical Review of the Technical Characteristics of Recycled Brick Powder and Its Influence on Concrete Properties. *Buildings*, 14(11), 3691.

Huseien, G. F., Joudah, Z. H.; Baghban, M. H., A. Khalid, N. H, Faridmehr, I., Dong, K., Li, Y., & Gu, X. (2025). Sustainability of Recycling Waste Ceramic Tiles in the Green Concrete Industry: A Comprehensive Review. *Buildings* 15, 2406.

Jwaida, Z., & Di Sarno, L. (2025). Utilizing agricultural wastes for fired bricks: A machine learning approach to compressive strength and water absorption predictions. *Cleaner Engineering and Technology*, 29, 101109.

Lewo Nkondi, B., Azama, N., Blaysat, B., de Baynast, H., & Moutou Pitti, R. (2025). Fired clay bricks made by incorporating organic additives: A review. *Case Studies in Construction Materials*, 23, e05037.

Ludovice, N. P. P., Matus, K., Redonnet, S., Zeng, X., Zhang, Y., Loh, E. T., Zhang, Y., & Chow, J. (2025). Towards a holistic and reflexive assessment of green buildings and technological landscapes in Hong Kong. *Energy Research & Social Science*, 127, 104235.

Meng, T., Wei, H., Dai, D., Liao, J., & Ahmed, S. (2022). Effect of brick aggregate on failure process of mixed recycled aggregate concrete via X-CT. *Construction and Building Materials*, 327, 126934.

Murali, G., Hassas, N., & Abdelgader, H. S. (2025). Ceramic Waste as a Sustainable Cementitious Resource: Pathways to Cleaner and High-Performance Concrete. *Cleaner Materials* 18, 100352.

Olawade, D. B., Fapohunda, O., Wada, O. Z., Usman, S. O., Ige, A. O., Ajisafe, O., & Oladapo, B. I. (2024). Smart Waste Management: A Paradigm Shift Enabled by Artificial Intelligence. *Waste Management Bulletin*, 2, 244–263.

Oyguc, R. (2025). Seismic Behavior and Vulnerability of Masonry Dwellings in Eastern Türkiye: A Comprehensive Analysis. *Applied Sciences*, 15(10), 5490.

Popa, M., Glevitzky, M., Dumitrel, G.-A., Popa, D.-V., Glevitzky, I., & Vîrsta, A. (2025). Energy efficiency of agricultural technologies through the creation of a sustainable model: A case study of greenhouses. *Scientific Papers Series Management, Economic Engineering in Agriculture and Rural Development*, 25(2), 619-632.

Rabiu, B. O., & Damdelen, O. (2023). Application of Brick Dust and Sawdust in Concrete: A Movement to Sustainability. *Journal of Civil Engineering and Construction*, 12(3), 152–166.

Raimondo, M., Dondi, M., Gardini, D., Guarini, G., & Mazzanti, F. (2009). Predicting the initial rate of water absorption in clay bricks. *Construction and Building Materials*, 23(7), 2623–2630.

Robert, U. W., Etuk, S. E., Agbasi, O. E., & Ambrose, P. D. (2024). Development of lightweight sawdust-based composite panels for building purposes. *International Journal of Lightweight Materials and Manufacture*, 7(5), 631–640.

Sălcudean, M., & Popa, M. (2025). The Integration of Ceramic Waste As A Of Natural Aggregates In Expperimental Concrete Recipes.*Scientific Papers. Series E. Land Reclamation, Earth Observation & Surveying, Environmental Engineering* 14: 594–600. https://landreclamationjournal.usamv.ro/pdf/2025

Sarner, S., & Guillon, O. (2025). A Perspective on Ceramic Recycling. *Journal of the European Ceramic Society*, 45, 117511.

Silvestre, R., Medel, E., García, A., & Navas, J. (2013). Using ceramic wastes from tile industry as a partial substitute of natural aggregates in hot mix asphalt binder courses. *Constr. Build. Mater*. 45, 115–122.

Soave, F., & Ferrara, L. (2025). A durability-based design approach for structural applications with advanced cement-based materials. *Case Studies in Construction Materials*, 22, e04294.

SR EN 771-1: Elements for burnt clay masonry (brick) https://magazin.asro.ro/ro/standard/237734.

Velenturf, A. P. M., & Purnell, P. (2021). Principles for a Sustainable Circular Economy. *Sustainable Production and Consumption* 27, 1437–1457.

Vidak Vasić, M., Muñoz Velasco, P., Bueno-Rodríguez, S., Netinger Grubeša, I., Dondi, M., Pérez Villarejo, L, Eliche-Quesada, D., & Zanelli, C. (2024). State and perspectives of sustainable production of traditional silicate ceramics. *Open Ceram.* 17, 100537.

Zhang, H., Shi, S., Zhao, F., Hu, M., & Fu, X. (2024). Integrated Benefits of Sustainable Utilization of Construction and Demolition Waste in a Pressure-State-Response Framework. *Sustainability*, 16(19), 8459.

Scientific Papers. Series E. Land Reclamation, Earth Observation & Surveying, Environmental Engineering. Vol. XV, 2026
Print ISSN 2285-6064, CD-ROM ISSN 2285-6072, Online ISSN 2393-5138, ISSN-L 2285-6064

# DETERMINATION OF SPLITTING TENSILE STRENGTH OF PAVING BLOCKS CONTAINING CERAMIC WASTE

**Mircea SĂLCUDEAN[1, 2], Mihai Teopent CORCHEȘ[2], Maria POPA[3], Mirel GLEVITZKY[3, 4]**

[1]"Lucian Blaga" University of Sibiu, Doctoral School, Faculty of Engineering,
10 Victoriei Blvd, Sibiu, Romania
[2]"1 December 1918" University of Alba Iulia, Faculty of Computer Science and Engineering,
15-17 Unirii Street, Alba Iulia, Romania
[3]"1 December 1918" University of Alba Iulia, Faculty of Economic Sciences,
15-17 Unirii Street, Alba Iulia, Romania
[4]Politehnica University Timişoara, Faculty of Engineering Hunedoara,
5 Revolutiei Street, Hunedoara, Romania

Corresponding author email: mihai.corches@uab.ro

***Abstract***

*This study investigates the influence of incorporating ceramic waste into paving block mixtures on their splitting tensile strength. The use of recycled ceramic materials aims to reduce environmental impact and promote sustainable construction practices. The aggregates were characterized in terms of particle size, shape, bulk density, porosity, water absorption, hardness, and chemical composition, with X-ray fluorescence (XRF) analysis used to determine the main oxides present in the ceramic waste. Experimental tests were conducted on paving blocks with varying percentages of ceramic waste replacing natural aggregates, including partial (50%) and full (100%) replacement. Splitting tensile strength was determined according to standardized procedures. The results indicate that ceramic waste affects the mechanical performance of paving blocks, with partial replacement slightly reducing tensile strength, while full replacement improves performance beyond the control mix. These findings highlight the importance of aggregate characterization for understanding mechanical behavior and support the potential of ceramic waste as an alternative aggregate in paving block production, contributing to circular economy objectives, particularly in low- to moderate-traffic applications.*

***Key words****: splitting tensile strength, paving blocks, ceramic waste, recycled aggregates, sustainable construction, durability.*

## INTRODUCTION

In the global context of increasing urbanization and infrastructure development, the construction industry faces growing pressure to reduce its environmental footprint while maintaining adequate mechanical performance and durability of construction materials (Alghamdi, 2025; Glevitzky et al., 2026). The transition from a linear economic model toward a circular economy has become a strategic priority, emphasizing waste minimization, material reuse, and resource efficiency (Hasibuan et al., 2025). Within this framework, the reuse of industrial and construction waste in road infrastructure and paving applications represents a promising solution for reducing landfill disposal and conserving natural aggregates (Kuttah, 2024). Among the various waste materials investigated, recycled ceramic waste - originating from demolished structures, ceramic tiles, sanitary ware, and industrial rejects - has gained attention due to its high availability, chemical stability, and favourable mechanical properties (Meena et al., 2022). Ceramic materials are characterized by high hardness, resistance to abrasion, and durability, which makes them potential candidates for partial or total replacement of natural aggregates in paving blocks. Their reuse not only contributes to sustainable construction practices but also supports waste recovery and resource efficiency strategies (Jwaida et al., 2024).

Life cycle assessment research has shown that incorporating ceramic waste into various construction materials, such as paving blocks, reduces greenhouse gas emissions and energy consumption throughout their life cycle, making them more sustainable (Azam et al., 2024; Kiran et al., 2024).

The incorporation of ceramic waste into paving blocks aligns with the principles of sustainability, particularly by reducing the consumption of virgin raw materials and lowering the environmental impact associated with aggregate extraction (Torkittikul and Chaipanich, 2010). From a circular economy perspective, paving blocks represent an ideal construction product for waste valorization due to their modular nature, standardized manufacturing processes, and widespread use in pedestrian areas, parking zones, and low-traffic roads (Barbhuiya et al., 2025).

The incorporation of ceramic waste in paving blocks presents technical challenges, including variations in particle characteristics and bonding with the cement matrix. These factors can affect mechanical properties, particularly splitting tensile strength, which influences cracking resistance and long-term performance (Lin et al., 2023). Additionally, paving blocks containing ceramic waste may exhibit different behavior under high traffic loads, freeze–thaw cycles, or moisture variations, limiting their application in heavy-duty pavements (Famewo and Shokouhian, 2025).

From the perspective of the circular economy and waste recovery, various types of waste have been investigated for paving block production, including ceramic waste, recycled concrete aggregates, glass waste, rubber particles, and industrial by-products such as fly ash or slag (Wattanasiriwech et al., 2009). Each waste type offers specific benefits but also introduces technical limitations that must be carefully assessed to ensure compliance with performance requirements (Glevitzky et al., 2025). The use of ceramic waste, in particular, offers advantages such as improved abrasion resistance and reduced environmental impact, but may result in reduced tensile performance at higher replacement levels (Meena et al., 2022).

The technological process of manufacturing paving blocks containing ceramic waste generally follows conventional procedures, including material selection, mix proportioning, compaction, curing, and quality control (Dehghani et al., 2024; Poon, et al., 2002). Nevertheless, the presence of ceramic aggregates may require adjustments to mixture design, water–cement ratio, and compaction parameters to achieve optimal mechanical performance. Ensuring consistency and reproducibility in production is essential for large-scale implementation (Silveira et al., 2025).

The use of recycled materials in paving blocks must comply with construction standards and regulations. The key reference is EN 1338:2003 (EN 1338, 2003), which sets essential requirements for mechanical strength, durability, and conformity assessment of concrete paving blocks. Standardized testing methods, including splitting tensile strength, ensure consistent performance evaluation and safe application in infrastructure (Iduwin et al., 2024).

This study aims to evaluate the influence of ceramic waste incorporation on the splitting tensile strength of paving blocks and to identify suitable replacement levels that maintain acceptable mechanical performance. The findings support the application of circular economy principles in paving systems, particularly for low to moderate traffic conditions.

## MATERIALS AND METHODS

The use of recycled materials in paving blocks must comply with a set of technical standards and regulations that ensure mechanical performance, durability, and operational safety. At the international and European levels, the most relevant requirements are defined by standards for precast concrete products, testing methods, and the use of recycled aggregates.

One of these is EN 1338 - Concrete paving blocks - Requirements and test methods, which establishes requirements regarding mechanical strength, freeze-thaw resistance, water absorption, abrasion resistance, and dimensional tolerances of concrete paving blocks. This standard is essential for assessing the conformity of products intended for use in road and pedestrian infrastructure.

The determination of splitting tensile strength is carried out in accordance with EN 12390-6 (EN 12390-6, 2009), which describes the standardized testing method applicable to both conventional concrete and concrete containing recycled aggregates, including ceramic waste.

Regarding the materials used, EN 12620 – Aggregates for concrete regulates the

requirements for natural and recycled aggregates, including permissible limits for impurities, physical properties, and durability characteristics (EN 12620, 2002). This standard allows the use of aggregates derived from waste, provided that quality requirements are met.

At the international level, ASTM standards are also frequently used for comparison and experimental validation. Among the most relevant is ASTM C496/C496M - Standard Test Method for Splitting Tensile Strength of Cylindrical Concrete Specimens, which provides an alternative method for determining splitting tensile strength (ASTM C496/C496M, 2017).

From a sustainability and circular economy perspective, European policies such as Waste Framework Directive (Directive 2008/98/EC) and the European Union Circular Economy Action Plan encourage the reuse of construction and demolition waste, including ceramic waste, in construction materials, provided that applicable technical standards are respected.

Compliance with these main standards and regulations is essential for the market acceptance of paving blocks containing ceramic waste and for ensuring safe use in infrastructure applications, especially in areas with low or moderate traffic.

To demonstrate the feasibility of using ceramic waste in the manufacturing process of paving blocks, experimental concrete mixes were developed in which natural aggregates were partially replaced with ceramic fragments. Tile and ceramic waste originating from construction and demolition activities were used, with a particle size of 4-8 mm (Figure 1), obtained through crushing and granulometric sorting.



Figure 1. Aggregates from ceramic waste size 4-8 mm

***Granulometry***. 500 g of dried aggregate are weighed and sieved through a standard set of 4-8 mm sieves, and the percentage retained on each fraction is determined (EN 933-1, 2003).

***Bulk density and porosity***. The dry mass of the aggregate is determined, then it is submerged in water for 24 hours. The saturated mass is weighed, and the bulk density and porosity are calculated (EN 1097-6, 2010).

***Water absorption***. Similar to the bulk density method; absorption is calculated as a percentage: $(m_{saturated}-m_{dry})/m_{dry}\times 100$ (EN 1097-6, 2010).

***Hardness/abrasion resistance***. Los Angeles test. The aggregate and steel balls are placed in a rotating drum, rotated for a standard number of cycles, and then the aggregates are sieved to determine the percentage loss due to wear (EN 1097-2, 2010).

***Chemical composition***. The aggregates are dried, then ground to a fine, homogeneous powder of 65 μm and then analyzed. The chemical composition of the aggregate from ceramic waste was determined by X-ray fluorescence (XRF) spectrometry using a Quant'X ARL energy-dispersive X-ray fluorescence spectrometer (Thermo Fisher Scientific, Waltham, MA, USA).

The specimens were prepared manually by homogenizing the components according to the experimental mix design, then cast into standard molds, kept for 24 hours, and subsequently cured for 28 days at 20°C. The testing was performed using a Matest universal testing machine for static material testing, whose technical characteristics are presented in Table 1.

Table 1. Characteristics of the MATEST Static Material Testing Machine

| | |
|---|---|
| Model | CYBER PLUS EVOLUTION / CO7gPN191 |
| Usage | Measurement of the compressive strength of hardened concrete (cylinders, cubes, and prisms) |
| Measurement Range | From 25 to 250 kN and from 20 to 3000 kN |
| Force Application Method | Compression |
| Testing Conditions | Temperature from +5 °C to +40 °C; Humidity from 30% to 70% |
| Standards Compliance | EN 12390-4, SR EN 772-1 |

For the control sample (R1), the standard concrete mix C16/20 (Table 2), also known as B250, was used, which is one of the most commonly used concrete mixes in Romania. For the two experimental mixes, 50% of the natural 4-8 mm aggregate was replaced with ceramic

waste aggregate for R2, and 100% replacement of natural 4-8 mm aggregate with ceramic waste aggregate was used for R3 (Table 2).

Table 2. Composition of the concrete mixes used

| Material | R1 (kg) | R2 (kg) | R3 (kg) | Material Source |
|---|---|---|---|---|
| Cement | 0.7375 | 0.7375 | 0.7375 | Heidelberg Materials, Chișcădaga Cement Plant, Hunedoara |
| Aggregate 0-4 mm (quarry) | 1.9725 | 1.9725 | 1.9725 | Elis Aggregates, Jidovu Quarry, Zlatna, Alba |
| Aggregate 4-8 mm (quarry) | 0.9175 | 0.45875 | - | Elis Aggregates, Jidovu Quarry, Zlatna, Alba |
| Aggregate 4-8 mm (ceramic waste) | - | 0.45875 | 0.9175 | Planodom Construct SRL, Cugir, Alba |
| Aggregate 8-16 mm (quarry) | 1.6975 | 1.6975 | 1.6975 | Elis Aggregates, Jidovu Quarry, Zlatna, Alba |
| Water | 0.65 | 0.65 | 0.65 | SC APA CTTA SA, Alba Iulia, Alba |

Figure 2 shows the manual preparation of the experimental mixes by incorporating ceramic waste, which partially (R2) or completely (R3) replaces the natural aggregates. For the control mix (R1), standard concrete from the SC Elis Pavaje batching plant in Petrești was used.



Figure 2. Composition of the experimental concrete mixes

All determinations and experiments were performed in triplicate.

## RESULTS AND DISCUSSIONS

The key physical and mechanical properties of the ceramic waste aggregate used in the study are summarized in Table 3. The average chemical composition of the ceramic waste aggregate determined by X-ray fluorescence (XRF) analysis is presented in Table 4.

Table 3. Properties of ceramic waste aggregate

| Property | Value | Remarks / Implications |
|---|---|---|
| Particle size | 4-8 mm | According to experimental description; promotes good compaction in concrete |
| Particle shape | Irregular, angular | Increases mechanical adhesion with cement paste; may affect workability |
| Bulk density | 2.2-2.6 g/cm³ | Similar to natural aggregates; allows correct proportioning |
| Porosity | Moderate (≈15-25%) | Higher water absorption than natural aggregates; influences water/cement ratio |
| Water absorption | 6-10% | Requires pre-wetting or adjustment of mixing water |
| Mohs hardness | 6-7 | Hard surface; contributes to mechanical strength |
| Color | Red-brown and whitish | Indicates a mixture of gres and faience |

Table 4. Chemical Composition of Ceramic Waste Aggregate

| Compound | Value (wt.%) |
|---|---|
| $SiO_2$ | 70.93 |
| $Al_2O_3$ | 15.21 |
| $Fe_2O_3$ | 4.70 |
| CaO | 3.04 |
| $K_2O$ | 1.33 |
| MgO | 1.25 |
| $Na_2O$ | 0.60 |
| $TiO_2$ | 0.41 |
| $ZrO_2$ | 0.17 |
| Loss on Ignition | 2.06 |

The XRF results indicate that the ceramic waste aggregate is predominantly composed of silica (70.93%) and alumina (15.21%), characteristic of clay-based ceramics. Minor amounts of $Fe_2O_3$, CaO, alkalis ($K_2O$, $Na_2O$), and other oxides are present, while the low loss on ignition (2.06%) suggests minimal organic or moisture content. This composition indicates a stable, mostly inert material suitable for partial replacement of natural aggregates, with limited impact on the chemical behavior of concrete but potential effects on porosity and permeability.

Tensile strength tests by splitting were performed on the concrete samples 28 days after casting (EN 12390-3, 2002). The tests were carried out for both the standard mix and the experimental mixes (Figure 3).

As a result of the splitting tensile strength tests (Figure 3), the obtained results are presented in Table 5.

The results obtained for the three studied mixes demonstrate a significant influence of replacing natural aggregates with ceramic waste on the mechanical behavior of pavers.



Figure 3. Specimens tested in splitting tension

Table 5. Results of the splitting tensile strength tests.

| Mix | Sample 1 | Sample 2 | Sample 3 |
|---|---|---|---|
| R1 (control concrete) | 2.663 | 2.222 | 2.198 |
| R2 (50% ceramic aggregate) | 1.737 | 1.910 | 2.010 |
| R3 (100% ceramic aggregate) | 2.672 | 2.360 | 2.850 |

These observations align with current trends in the scientific literature, which highlight the high potential of recycled ceramic materials for use in precast concrete products (Wattanasiriwech et al., 2009).

The test values obtained for the standard C16/20 mix (R1) are consistent with the characteristic strengths of this type of concrete and confirm the reliability of the preparation and testing procedures. The performance of the control mix provides a solid baseline for comparison and is also in accordance with European standards for evaluating splitting tensile strength according to EN 12390-6.

The mix with 50% replacement of the 4-8 mm aggregate with ceramic waste (R2) shows greater variability in results, as well as a decrease in average tensile strength compared to the control mix. This reduction can be explained by the physical and structural properties of the ceramic particles, such as increased roughness and high-water absorption, which may compromise the quality of the cement-aggregate interface. Recent studies indicate that such heterogeneities can significantly affect mechanical behavior, particularly in regions subjected to tensile stresses (Dehghani et al., 2024; Silveira et al., 2025).

The R3 mix, with 100% replacement of the 4-8 mm aggregate, exhibited superior results compared to both the control concrete and R2. This behavior suggests that a fully homogeneous mix composed entirely of ceramic aggregates can produce a compact internal structure. The characteristics of ceramic particles, such as angular shape and hard surface, contribute to more efficient stress transfer in the splitting zone, a phenomenon also reported in other studies on the use of ceramics as recycled aggregates (Wattanasiriwech et al., 2009).

**Statistical analysis**

To evaluate the influence of replacing natural aggregates with ceramic waste on the splitting tensile strength of concrete blocks, the experimental data obtained for the three mixes (R1, R2, R3) were statistically analyzed (Aloman, 1998; Gluck, 1971). The objective of the analysis was to identify differences between the mixes, as well as to assess the variability and stability of their mechanical behavior (Popa et. al, 2022). The values were summarized in Table 6 using the arithmetic mean, standard deviation (SD), median, and coefficient of variation (CV).

Table 6. Descriptive statistics for splitting tensile strength

| Mix | Mean (MPa) | SD (MPa) | Median (MPa) | CV (%) |
|---|---|---|---|---|
| R1 | 2.361 | 0.242 | 2.222 | 10.2 |
| R2 | 2.082 | 0.362 | 1.960 | 17.4 |
| R3 | 2.605 | 0.345 | 2.605 | 13.2 |

Variability ranged from low to moderate among the three mixes. While R1 and R3 exhibited coefficients of variation below 15%, R2 showed a slightly higher coefficient of variation (17.4%), indicating a greater dispersion of the experimental results.

To evaluate the differences between the three concrete mixes, a one-way analysis of variance (ANOVA) was applied to the experimental data. The statistical analysis revealed significant differences in the mean splitting tensile strengths among the three compositions, with the most pronounced variations observed between R2 and R3, as well as between R2 and R1. In particular, the mix with partial replacement (R2) exhibited a clear reduction in mechanical performance compared to both the control concrete and the fully substituted mix (R3), highlighting the influence of partial substitution on the integrity of the cement–aggregate interface and the overall stress transfer within the specimens.

The statistical evaluation indicate that the percentage of natural aggregate replacement has a decisive effect on the splitting tensile strength of the concrete. While partial replacement at 50% results in a noticeable decrease in average

strength, complete replacement at 100% leads to an increase in average strength relative to the control mix, suggesting that a fully homogeneous mix composed entirely of ceramic aggregates can provide a more compact internal structure and improved stress distribution under tensile loading. Additionally, all three mixes exhibited low variability, as indicated by the coefficients of variation, which demonstrates good experimental stability and reproducibility of the testing procedures. The homogeneous structure of the R3 mix, in particular, promotes superior mechanical behavior, confirming the potential of recycled ceramic aggregates as a viable alternative to natural aggregates.

## CONCLUSIONS

The experimental results demonstrate that the substitution of natural aggregates with recycled ceramic aggregates significantly influences the mechanical performance of paving blocks. Partial replacement tends to reduce splitting tensile strength, primarily due to the heterogeneous particle shape, increased roughness, and higher water absorption of ceramic aggregates, which can affect the quality of the cement–aggregate interface. Complete replacement, however, leads to improved tensile performance, indicating that a fully homogeneous mix of ceramic aggregates can form a compact internal structure that enhances stress transfer under tensile loading. Despite the promising mechanical behavior, the brittle nature and water absorption characteristics of ceramic aggregates should be carefully considered for applications subject to heavy or repeated dynamic loading. These findings underscore the potential of ceramic waste as a sustainable alternative to natural aggregates, providing environmental benefits by reducing construction and demolition waste, conserving natural resources, and supporting circular economy principles. Further investigations are recommended to evaluate additional properties such as abrasion resistance, freeze-thaw durability, water absorption, and long-term performance, in order to validate the applicability of recycled ceramics in diverse paving block applications.

## ACKNOWLEDGEMENTS

The authors gratefully acknowledge the support of Elis Pavaje SRL, Romania, a paving block manufacturer that actively incorporates construction and demolition waste into its products, promoting sustainable and circular construction practices.

## REFERENCES

Alghamdi, A. (2025). Sustainable Practices in Construction Management and Environmental Engineering: A Review. *Sustainability*, *17*(22), 10027.

Aloman, A. (1998). *Statistics and probability in scientific experiment* [Statistica si Probabilitate in Experimentul Stiintific], Matrix Rom, Bucharest, Romania.

ASTM International. (2017). *ASTM C496/C496M-17: Standard test method for splitting tensile strength of cylindrical concrete specimens*. West Conshohocken, PA: ASTM International.

Azam, A., Gabr, A., Ezzat, H., Arab, M., Alshammari, T. O., Alotaib, E., & Zeiada, W. (2024). Life cycle assessment and pavement performance of recycled aggregates in road construction. *Case Studies in Construction Materials, 20,* e03062.

Barbhuiya, S., Qureshi, T., & Das, B. B. (2025). Advancing sustainable pavements: A review of low-carbon construction materials and practices. *Discover Concrete and Cement, 1*(1), 19.

Dehghani, O., Eslami, A., Mahdavipour, M. A., Mostofinejad, D., Ghorbani Mooselu, M., & Pilakoutas, K. (2024). Ceramic waste powder as a cement replacement in concrete paving blocks: mechanical properties and environmental assessment. *International Journal of Pavement Engineering*, *25*(1).

European Committee for Standardization (2002). *EN 12390-3: Testing hardened concrete – Part 3: Compressive strength of test specimens*. Brussels, Belgium: CEN.

European Committee for Standardization (2002). *EN 12620: Aggregates for concrete*. Brussels, Belgium: CEN.

European Committee for Standardization (2003). *EN 1338: Concrete paving blocks – Requirements and test methods*. Brussels, Belgium: CEN.

European Committee for Standardization (2003). *EN 933-1: Tests for geometrical properties of aggregates – Part 1: Determination of particle size distribution – Sieving method*. Brussels, Belgium: CEN.

European Committee for Standardization (2009). *EN 12390-6: Testing hardened concrete – Part 6: Tensile splitting strength of test specimens*. Brussels, Belgium: CEN.

European Committee for Standardization (2010). *EN 1097-2: Tests for mechanical and physical properties of aggregates – Part 2: Methods for the determination of resistance to fragmentation (Los Angeles test)*. Brussels, Belgium: CEN.

European Committee for Standardization (2010). EN 1097-6: Tests for mechanical and physical properties of aggregates – Part 6: Determination of particle density and water absorption. Brussels, Belgium: CEN.

European Parliament and Council. (2008). *Directive 2008/98/EC on waste (Waste Framework Directive)*. Official Journal of the European Union, L312, 3–30.

Famewo, B. G., & Shokouhian, M. (2025). A review of pavement performance deterioration modeling: Influencing factors and techniques. *Symmetry, 17*(11).

Glevitzky, M., Glevitzky, I., Mucea-Ștef, P., Popa, M., Dumitrel, G.-A., & Vică, M. L. (2025). Integrated Risk Framework (IRF) - Interconnection of the Ishikawa Diagram with the Enhanced HACCP System in Risk Assessment for the Sustainable Food Industry. *Sustainability*, 17(2), 536.

Glevitzky, M., Mucea-Ștef, P., Corcheș, M.-T., Sălcudean, M., Marica, E., Șerban, S. G., & Popa, M. (2026). Integrated Environmental Risk Assessment and Performance Evaluation of Asphalt Plants Incorporating Reclaimed Asphalt Pavement Under the ISO 14001 Framework. *Eng*, *7*(2), 95.

Gluck, A. (1971). *Mathematical methods in the chemical industry* [Metode matematice in industria chimica], Tehnică Publishing House, Bucharest, Romania.

Hasibuan, G. C. R., Al Fath, M. T., Yusof, N., Dewi, R. A., Syafridon, G. G. A., Jaya, I., Anas, M. R., & Syahrizal (2025). Integrating circular economy into construction and demolition waste management: A bibliometric review of sustainable engineering practices in the built environment. *Case Studies in Chemical and Environmental Engineering, 11,* 101159.

Iduwin, T., Hadiwardoyo, S. P., Sumabrata, R. J., Lumingkewas, R. H., & Rivai, A. I. (2024). Investigation of Concrete Paving Block Characteristics and Performance across Different Shapes and Thicknesses. *Engineering, Technology & Applied Science Research*, *14*(6), 18429–18438.

Jwaida, Z., Dulaimi, A., & Bernardo, L. F. A. (2024). The use of waste ceramic in concrete: A review. *CivilEng, 5*(2), 482–500.

Kiran, G. U., Nakkeeran, G., Roy, D., & Alaneme, G. U. (2024). Optimization and prediction of paver block properties with ceramic waste as fine aggregate using response surface methodology. *Scientific Reports, 14*(1), 23416.

Kuttah, D. (2024). Recycling of industrial and construction waste materials in roads construction. *International Journal of Geotechnical Engineering, 18*(4), 346–359.

Lin, C., Kanstad, T., Jacobsen, S., & Ji, G. (2023). Bonding property between fiber and cementitious matrix: A critical review. *Construction and Building Materials, 378,* 131169.

Meena, R. V., Jain, J. K., Chouhan, H. S., & Beniwal, A. S. (2022). Use of waste ceramics to produce sustainable concrete: A review. *Cleaner Materials, 4,* 100085.

Poon, C. S., Kou, S. C., & Lam, L. (2002). Use of recycled aggregates in molded concrete bricks and blocks. *Construction and Building Materials, 16*(5), 281–289.

Popa, M., Glevitzky, I., Dumitrela, G.-A., Popa, D., Vîrsta, A., & Glevitzky, M. (2022). Qualitative analysis and statistical models between spring water quality indicators in Alba County, Romania. *Scientific Papers. Series E. Land Reclamation, Earth Observation & Surveying, Environmental Engineering*, *11*, 358-366.

Silveira, T. A. d., Nörnberg, R. d. P., Santi, M. S., Morales, R. R., Tessaro, A. B., Rosseto, H. L., Delucis, R. d. A., & Trindade, G. H. (2025). Mechanical Performance and Durability of Concretes with Partial Replacement of Natural Aggregates by Construction and Demolition Waste. *Waste*, *3*(4), 32.

Torkittikul, P., & Chaipanich, A. (2010). Utilization of ceramic waste as fine aggregate within Portland cement and fly ash concretes. *Cement and Concrete Composites, 32*(6), 440–449.

Wattanasiriwech, D., Saiton, A., & Wattanasiriwech, S. (2009). Paving blocks from ceramic tile production waste. *Journal of Cleaner Production, 17*(18), 1663–1668.

Scientific Papers. Series E. Land Reclamation, Earth Observation & Surveying, Environmental Engineering. Vol. XV, 2026
Print ISSN 2285-6064, CD-ROM ISSN 2285-6072, Online ISSN 2393-5138, ISSN-L 2285-6064

# HYDROCARBON TOLERANCE AND BIODEGRADATION IN ENVIRONMENTAL *PSEUDOMONAS* STRAINS

**Mihaela Marilena STANCU, Simona NEAGU**

Institute of Biology Bucharest of Romanian Academy, 296 Splaiul Independentei, District 6, Bucharest, P.O. Box 56-53, Romania

Corresponding author email: mihaela.stancu@ibiol.ro

***Abstract***

*Hydrocarbons are widely recognized as the most important class of persistent and toxic environmental pollutants. Moreover, bacteria from the genus Pseudomonas play a key role in the biodegradation of these compounds, and their remarkable metabolic versatility enables them to adapt to a wide range of contaminated environments, enhancing their effectiveness in pollutant removal. Although many species in this genus have already been identified, new Pseudomonas strains with significant relevance for environmental bioremediation continue to be reported each year. This study investigated hydrocarbon-tolerant and hydrocarbon-degrading bacteria in sediment samples from the Danube Delta collected during summer and autumn. Additionally, the ability of four Pseudomonas strains, individually and as a consortium, to tolerate and degrade paraffin (a mixture of saturated petroleum hydrocarbons) was evaluated. The tested strains demonstrated promising potential for paraffin biodegradation, particularly when applied as a consortium, likely due to functional complementarity and enhanced metabolic interactions. These findings provide valuable insights for environmental applications, including land reclamation and ecological engineering, and contribute to the development of effective strategies to mitigate petroleum hydrocarbon pollution and restore contaminated ecosystems.*

***Key words:*** *biodegradation, paraffin, Pseudomonas, tolerance.*

## INTRODUCTION

Pollution caused by petroleum and petroleum-based products, including paraffinic oils, is widely recognized as a major environmental issue due to the widespread use and extensive distribution of hydrocarbon-based materials in natural ecosystems. As industrial activities and urbanization intensify, hydrocarbon contamination in water bodies has become increasingly problematic, contributing substantially to the degradation of aquatic habitats. Although numerous strategies and technologies are currently employed to prevent and control global contamination by petroleum and petroleum-based products, the increasing frequency of accidents in aquatic environments continues to make hydrocarbon pollution a significant challenge in the coming decades. In this context, biodegradation is considered a key process, as it represents one of the primary and most cost-effective processes for removing hydrocarbons from polluted environments (Das & Chandran, 2011; Xu et al., 2018; Xu et al., 2022; Duarte et al., 2024; Al Haj Chehadeh et al., 2025; Samsuria et al., 2025).

Petroleum and petroleum-based products are highly complex mixtures composed of thousands of individual compounds, which are generally grouped into four classes based on their structural characteristics and physicochemical properties: saturated (aliphatic) hydrocarbons, aromatic hydrocarbons, resins, and asphaltenes (Das & Chandran, 2011; Pandolfo et al., 2023). Each class is characterized by distinct yet interrelated physicochemical properties – particularly toxicity, volatility, solubility, molecular weight, and biodegradability – which collectively influence its environmental fate, transport, and transformation in aquatic systems. When petroleum and its derivatives enter these systems, they act as environmental stressors, with toxic effects extending across trophic levels, affecting phytoplankton, zooplankton, fish, birds, mammals, and benthic communities. Beyond immediate ecological disruption, such releases alter biodiversity, degrade water quality, and generate long-term socio-environmental consequences for surrounding human populations (Perhar &

Arhonditsis, 2014; Duarte et al., 2024; Sharma et al., 2024; Samsuria et al., 2025).

In aquatic environments, the lightest and most volatile hydrocarbon fractions tend to volatilize rapidly into the atmosphere. In contrast, amphipathic and hydrophilic components dissolve or disperse in the water column, while more lipophilic fractions preferentially associate with suspended particulate matter and organic colloids (Pandolfo et al., 2023). These hydrophobic constituents further bind to particulates and sediments, promoting their accumulation and facilitating exposure in benthic species (Perhar & Arhonditsis, 2014; Pandolfo et al., 2023). The accumulation of hydrocarbons in sedimentary matrices can alter microbial community structure, suppress the metabolic activity of sensitive sediment bacteria, and disrupt key biogeochemical processes such as nutrient cycling and organic matter degradation. These sediments may also harbor bacterial taxa capable of degrading hydrocarbons, thereby contributing to natural attenuation in contaminated benthic environments. At the same time, hydrocarbons can eliminate or inhibit susceptible microbial taxa, thereby altering key ecosystem functions. The selective pressure exerted by these compounds often reduces microbial diversity and shifts community composition toward bacterial populations that use hydrocarbons as carbon and energy sources. Given this dual role of hydrocarbons in both constraining susceptible microorganisms and selecting for specialized microbial communities, the characterization of bacteria capable of hydrocarbon degradation is essential for assessing natural attenuation potential in aquatic sediments (Das & Chandran, 2011; Pandolfo et al., 2023; Al Haj Chehadeh et al., 2025; Samsuria et al., 2025).

This study investigated hydrocarbon-tolerant and hydrocarbon-degrading bacteria in sediment samples from the Danube Delta collected during summer and autumn. Additionally, the tolerance and biodegradation capacity of four *Pseudomonas* strains, tested individually and as a consortium, were evaluated using paraffin, a mixture of saturated petroleum hydrocarbons characterized by high chemical stability and low biodegradability.

## MATERIALS AND METHODS

### Quantification of bacteria in sediments

Sediment samples from the Danube Delta (Roșu, Roșuleț, and Puiu lakes, Tulcea County, Romania), part of the southern lacustrine complex within the Danube Delta Biosphere Reserve, were used for the development of enrichment cultures. The experimental setup was based on a modified minimal medium (Stancu, 2023), supplemented with petroleum (5%, v/v) as the sole carbon and energy source. Cultures were maintained at 30°C under constant agitation (200 rpm) for 21 days to promote the growth of hydrocarbon-adapted microorganisms. The abundance of hydrocarbon-tolerant and hydrocarbon-degrading bacteria was determined using two culture-dependent quantification methods: the most probable number (MPN) and colony-forming unit (CFU) counts (Stancu, 2025).

### Paraffin tolerance and biodegradation by *Pseudomonas* strains and consortium

Four *Pseudomonas* strains (IBBDt2, IBBDt4.2, IBBDt1, and IBBDt8), previously isolated and identified (Stancu, 2023), were cultured in LB medium at 30°C under shaking conditions (200 rpm) for 24 h. Subsequently, the antagonistic interactions among the four strains were assessed using the cross-streak method (Hossain, 2024). In this assay, one strain was initially streaked onto LB agar and incubated at 30°C for 24 h, after which the remaining strains were spot-inoculated in proximity to the primary streak.

Tolerance to paraffin and biodegradation potential of the four bacterial strains, both individually and as a consortium (CnP), were further evaluated. Standardized overnight cultures ($OD_{660}$ = 0.08) were inoculated into fresh LB and MM media supplemented with paraffin (5%, v/v) and incubated at 30°C under shaking conditions (200 rpm) for 7 days. Uninoculated MM supplemented with paraffin (5%, v/v) served as an abiotic control.

Bacterial growth was assessed through optical density measurements at 660 nm ($OD_{660}$), using a SPECORD 200 UV-Vis spectrophotometer (Analytik Jena). Biomass accumulation was further estimated by determining dry cell weight. Bacterial viability was evaluated by

spotting paraffin-exposed cultures onto LB and MM agar media, both in the presence and absence of a paraffin overlay. To assess growth dynamics, paraffin-exposed cultures were transferred into fresh LB medium and incubated at 30°C under controlled conditions. Changes in optical density ($OD_{660}$) were monitored at hourly intervals over a 24 h period using a SpectraMax ABS Plus microplate reader (Molecular Devices).

Paraffin biodegradation was evaluated using a combination of complementary approaches, including observation of paraffin film fragmentation, gravimetric determination of residual paraffin recovered from cell-free supernatants after chloroform extraction, and high-performance thin-layer chromatography (HPTLC), following a previously described method (Stancu, 2023) with modifications for paraffin analysis. Chromatographic analyses were performed using a CAMAG TLC system, and 3D profiles were processed using visionCATS software (CAMAG). Samples were applied to silica gel plates and developed in a pre-saturated chamber with an n-hexane–ethyl acetate (92:8, v/v) mobile phase. Plates were then treated with iodine vapors and analyzed under visible light (Vis, 500 nm).

Biosurfactant production was assessed using several complementary assays, including the hydrocarbon overlay agar plate method, drop-collapse test, CTAB assay, and the emulsification index ($E_{24}$), as previously described (Satpute et al., 2008). In addition, biosurfactant yield was quantified gravimetrically after extraction from cell-free culture supernatants using a chloroform–methanol mixture (2:1, v/v), and subsequent solvent evaporation (Gesheva et al., 2010).

The presence of alkane-degrading genes (*alkB* and *alkM*) and the rhamnosyltransferase gene (*rhlAB*) was investigated by polymerase chain reaction (PCR). Genomic DNA was isolated using the PureLink Genomic DNA Kit (Invitrogen). Amplification reactions were performed in a Mastercycler Pro S thermocycler (Eppendorf) with gene-specific primers (alkB-f/alkB-r, Whyte et al., 1996; alkM-f/alkM-r, Márquez-Rocha et al., 2005; rhlA-f/rhlB-r, Medina et al., 2003) and GoTaq G2 Flexi DNA Polymerase (Promega). PCR amplification included an initial denaturation at 94°C for 10 min, followed by 35 cycles (94°C for 1 min, 50-62°C for 30 s, and 72°C for 2 min) and a final extension at 72°C for 10 min. Amplified fragments were resolved by electrophoresis on 1.5% (w/v) agarose gels (Sambrook & Russell, 2001) and visualized using SYBR Safe DNA gel stain (Invitrogen).

Changes in genomic fingerprinting profiles were analyzed by repetitive extragenic palindromic PCR (REP-PCR) using the $(GTG)_5$ primer (Versalovic et al., 1994) and GoTaq G2 Flexi DNA Polymerase (Promega). Amplification was performed in a Mastercycler Pro S thermocycler (Eppendorf).

PCR conditions included an initial denaturation at 94°C for 10 min, followed by 35 cycles (94°C for 1 min, 52°C for 1 min, and 65°C for 8 min) and a final extension at 65°C for 16 min. The resulting fragments were separated on 2.0% (w/v) agarose gels and visualized as described above.

Reagents used in this study were obtained from Merck and Sigma-Aldrich.

## RESULTS AND DISCUSSIONS

### Quantification of bacteria in sediments

Petroleum and petroleum-based products frequently contaminate aquatic ecosystems, entering through industrial activities, shipping activities, accidental spills, and urban wastewater. In the Danube Delta, a protected wetland of high ecological value, hydrocarbon accumulation in sediments poses a long-term threat to biodiversity and ecosystem processes.

The abundance of hydrocarbon-tolerant and hydrocarbon-degrading bacteria in sediment samples collected in summer (July) and autumn (September) from the Danube Delta was assessed after enrichment in petroleum-amended minimal medium (MM). Bacterial populations were quantified using MPN and CFU approaches (Figure 1), providing insights into the sediment microbial community's natural attenuation potential and seasonal variations. Regardless of the quantification method, hydrocarbon-tolerant bacteria were consistently present at higher levels ($10^4$-$10^6$ cells $mL^{-1}$, $10^3$-$10^6$ CFU $mL^{-1}$) than hydrocarbon-degrading bacteria ($10^2$-$10^3$ cells $mL^{-1}$, $10^1$-$10^3$ CFU $mL^{-1}$). Seasonal differences were also observed for both groups. Sediment

samples collected in July showed higher levels of hydrocarbon-tolerant bacteria ($10^5$-$10^6$ cells $mL^{-1}$, $10^4$-$10^6$ CFU $mL^{-1}$) than those collected in September ($10^4$-$10^5$ cells $mL^{-1}$, $10^3$-$10^4$ CFU $mL^{-1}$). Similarly, hydrocarbon-degrading bacteria were more abundant in July samples ($10^3$ cells $mL^{-1}$, $10^3$ CFU $mL^{-1}$) than in September samples ($10^2$ cells $mL^{-1}$, $10^1$ CFU $mL^{-1}$). These patterns likely reflect seasonal temperature effects on bacterial growth and hydrocarbon metabolism. The predominance of hydrocarbon-tolerant heterotrophs over specialized degraders aligns with previous studies, where metabolically versatile degraders represented a smaller fraction of the microbial community in hydrocarbon-exposed sediments (Xu et al., 2022

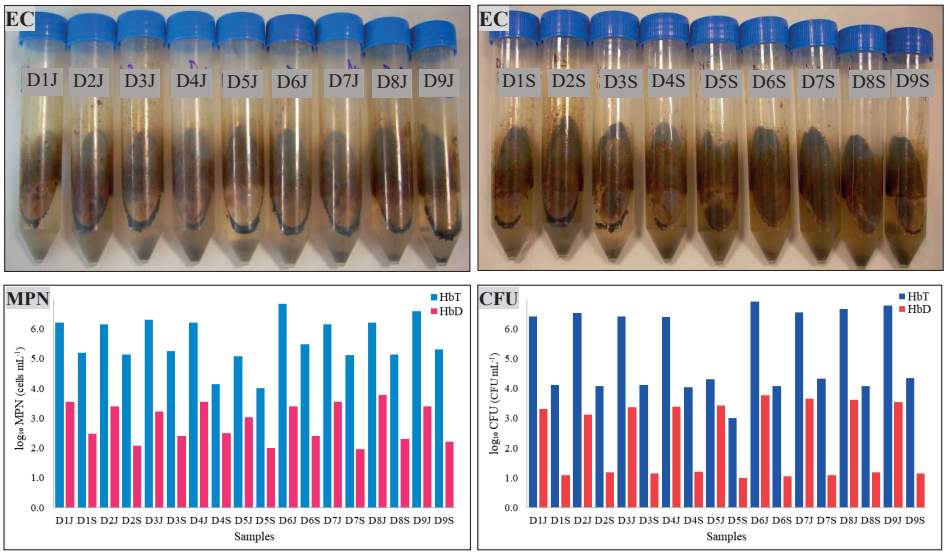



Figure 1. Quantification of bacteria in sediments
Sediment samples collected in July (D1J-D9J) and September (D1S-D9S) were analyzed after enrichment (EC) for hydrocarbon-tolerant (HbT) and hydrocarbon-degrading (HbD) bacteria using MPN and CFU methods ($log_{10}$ scale)

**Paraffin tolerance and biodegradation by *Pseudomonas* strains and consortium**

The *Pseudomonas* strains IBBDt2, IBBDt4.2, IBBDt1, and IBBDt8, previously identified as *P. aeruginosa*, *P. nitroreducens*, *P. aeruginosa*, and *P. multiresinivorans*, respectively (Stancu, 2023), were evaluated for paraffin tolerance and biodegradation, both individually and in consortium. *Pseudomonas* species produce secondary metabolites, such as pyocyanin, pyoverdine, and biosurfactants, which affect microbial interactions through redox reactions, iron chelation, and membrane destabilization (Chong & Li, 2017; Butaitė et al., 2018; Abdelaziz et al., 2023). Consequently, strain compatibility was assessed before the experiments, given the selected bacteria's capacity to produce metabolites, such as pyocyanin and/or pyoverdine, and biosurfactants (Stancu, 2023). No antagonistic interactions were detected among four *Pseudomonas* strains (Figure 2), consistent with reports that metabolite production does not necessarily induce inhibition under all growth conditions.

**Bacterial growth.** All four *Pseudomonas* strains IBBDt2, IBBDt4.2, IBBDt1, and IBBDt8, grown individually and as a consortium in LB broth supplemented with 5% paraffin, presented high tolerance, as indicated by optical density at 660 nm ($OD_{660}$ = 1.06-1.45) and dry biomass measurements (3.54-5.17 g $L^{-1}$) (Table 1). In addition, both the individual strains and the consortium grew in MM broth supplemented with 5% paraffin as the sole carbon and energy source ($OD_{660}$ = 0.63-0.87, dry biomass = 1.22-3.34 g $L^{-1}$).

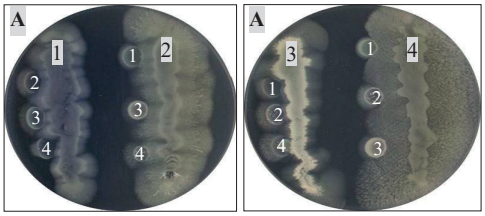



Figure 2. Antagonistic interactions among *Pseudomonas* strains
Antagonistic activity (AA) of strains IBBDt2 (1), IBBDt4.2 (2), IBBDt1 (3), and IBBDt8 (4), evaluated by testing each strain against the other three on LB agar

In tolerance (LB) and biodegradation (MM) experiments, the *Pseudomonas* consortium exhibited enhanced growth in the presence of paraffin ($OD_{660}$ = 1.45 and 0.87, respectively) compared to the individual strains ($OD_{660}$ = 1.06–1.36 and 0.63–0.83, respectively). Although differences in OD and dry biomass values were observed among the experimental variants, viability assays performed after 7 days of growth in LB or MM with 5% paraffin revealed confluent growth of all cultures on LB agar, with or without paraffin overlay (Figure 3). In contrast, reduced viability was observed on MM agar overlaid with paraffin, suggesting metabolic stress under nutrient limitation (Márquez-Rocha et al., 2005). Although reduced viability was observed under nutrient-limited conditions, the individual strains and the consortium maintained growth in the presence of paraffin, suggesting adaptability to hydrocarbon substrates, likely through alkane catabolic pathways (Whyte et al., 1996; Das & Chandran, 2011).

*Pseudomonas* strains cultivated for 7 days as individual cultures or as a consortium in LB and MM broths supplemented with 5% paraffin, and subsequently reinoculated into fresh LB broth, showed a lag phase of approximately 3-4 h (Figure 3). In all cases, this initial adaptation period was followed by an exponential growth phase occurring between 4 and 18 h. After approximately 15-19 h of incubation, the cultures entered a stationary (plateau) phase. The onset and duration of these phases varied across individual strains and the consortium. This observation was further supported by the determined growth rates and generation times (Table 1). Cultures previously grown for 7 days in LB broth with 5% paraffin showed growth rates (μ) ranging from 0.61 to 0.87 $h^{-1}$ and generation times (g) between 0.80 and 1.13 h, whereas cultures grown in MM broth with 5% paraffin had lower growth rates (μ = 0.55-0.72 $h^{-1}$) and longer generation times (g = 0.96-1.25 h) when transferred to fresh LB. Cultivation under nutrient-rich conditions favors faster adaptation and enhanced growth kinetics, while minimal media impose metabolic constraints, reducing growth rates and prolonging generation times (Hall et al., 2014).

Table 1. Paraffin tolerance and biodegradation by *Pseudomonas* strains and consortium

| Parameters | Individual strains | | | | Consortium |
|---|---|---|---|---|---|
| | IBBDt2 | IBBDt4.2 | IBBDt1 | IBBDt8 | CnP |
| **Growth quantification** | | | | | |
| **Tolerance assay** | | | | | |
| Optical density ($OD_{660}$) | 1.16 | 1.26 | 1.36 | 1.06 | 1.45 |
| Dry cell weight (g $L^{-1}$) | 4.87 | 3.69 | 4.37 | 3.54 | 5.17 |
| Bacterial viability | CG | CG | CG | CG | CG |
| **Biodegradation assay** | | | | | |
| Optical density ($OD_{660}$) | 0.71 | 0.63 | 0.83 | 0.79 | 0.87 |
| Dry cell weight (g $L^{-1}$) | 2.29 | 2.01 | 2.53 | 1.22 | 3.34 |
| Bacterial viability | CG | CG | CG | CG | CG |
| **Growth kinetics** | | | | | |
| **Tolerance assay** | | | | | |
| Specific growth rate (μ, $h^{-1}$) | 0.87 | 0.82 | 0.61 | 0.82 | 0.69 |
| Generation time (g, h) | 0.80 | 0.84 | 1.13 | 0.84 | 1.00 |
| **Biodegradation assay** | | | | | |
| Specific growth rate (μ, $h^{-1}$) | 0.56 | 0.62 | 0.55 | 0.57 | 0.72 |
| Generation time (g, h) | 1.24 | 1.12 | 1.25 | 1.21 | 0.96 |
| **Paraffin biodegradation** | | | | | |
| Paraffin film fragmentation | + | + | + | + | + |
| Biodegradation (%) | 75.64 | 69.25 | 77.70 | 60.88 | 85.45 |
| PCR *alkB* gene (870 bp) | + | + | + | + | + |

| Parameters | Individual strains | | | | Consortium |
|---|---|---|---|---|---|
| | IBBDt2 | IBBDt4.2 | IBBDt1 | IBBDt8 | CnP |
| PCR *alkM* gene (870 bp) | + | + | – | + | + |
| **Biosurfactant production** | | | | | |
| Hydrocarbon overlay agar | + | + | + | + | + |
| Glycolipid production (CTAB) | + | + | + | + | + |
| Drop-collapse assay | + | + | + | + | + |
| Emulsification index ($E_{24}$, %) | 100 | 50 | 100 | 30 | 100 |
| Biosurfactant quantification (g $L^{-1}$) | 0.92 | 0.31 | 1.22 | 0.41 | 1.89 |
| PCR *rhlAB* genes (216 bp) | + | – | + | – | – |

Confluent growth (CG). Positive reaction (+); negative reaction (–).

**Paraffin biodegradation.** *Pseudomonas* strains IBBDt2, IBBDt4.2, IBBDt1, and IBBDt8, cultivated individually and as a consortium in MM broth supplemented with 5% paraffin, disrupted the paraffin film, indicating emulsification and degradation (Table 1). Gravimetric analyses confirmed the capacity of tested bacteria to biodegrade paraffin, with degradation efficiencies ranging from 60.88% to 85.45%. The highest biodegradation efficiency was achieved for the *Pseudomonas* consortium (85.45%), exceeding that noticed for the individual strains (60.88-77.70%), suggesting a synergistic interaction within the consortium that enhances paraffin biodegradation. Among the individual strains, IBBDt1, IBBDt2, and IBBDt4.2 exhibited comparatively higher biodegradation efficiencies (77.70%, 75.64%, and 69.25%, respectively), whereas strain IBBDt8 showed the lowest efficiency (60.88%). Previous studies have reported that bacterial consortia display superior hydrocarbon-degrading performance compared to pure cultures due to complementary metabolic pathways, synergistic enzymatic activities, and biosurfactant production, which enhance hydrocarbon bioavailability and overall biodegradation efficiency (Das & Chandran, 2011; Varjani, 2017; Xu et al., 2018).

Following the gravimetric evaluation of paraffin degradation, residual paraffin samples were subjected to HPTLC analyses. These analyses indicated the presence of a single spot migrating close to the solvent front, with retardation factor ($R_f$) values ranging from 0.82 to 0.86 (Figure 3). Three-dimensional chromatographic (3DC) profiles confirmed differences in peak intensity among the samples. In the abiotic control, the $R_f$ value was 0.84. Similar $R_f$ values (0.82-0.83) were recorded for extracts obtained from *Pseudomonas* strains IBBDt2, IBBDt1, IBBDt8, and the consortium, whereas the extract from strain IBBDt4.2 showed a slightly higher $R_f$ value (0.86). For this strain, the detected spot was of low intensity and markedly smaller than the other chromatographic spots. Although the *Pseudomonas* consortium and strains IBBDt1 and IBBDt2 presented higher gravimetric biodegradation efficiencies, their HPTLC profiles showed minor differences compared to the abiotic control, consistent with the semi-quantitative nature of HPTLC. In contrast, strain IBBDt4.2, despite its moderate biodegradation efficiency (69.25%), displayed a reduced spot intensity, suggesting preferential degradation of the paraffin fraction corresponding to this chromatographic spot. These results indicate that different strains may target distinct paraffin fractions. Genomic DNA extracted from paraffin-exposed cultures was used for PCR detection of the *alkB* and *alkM* genes, which encode alkane hydroxylases responsible for the initial step of alkane oxidation (Table 1, Figure 4). The *alkB* gene (≈870 bp) was detected in strains IBBDt2, IBBDt1, IBBDt8, and in the consortium, whereas strain IBBDt4.2 produced a slightly smaller amplicon (~850 bp). The *alkM* gene (≈870 bp) was present in strains IBBDt2, IBBDt4.2, and IBBDt8, while only weak amplification was observed in the consortium, and no amplification was detected in strain IBBDt1. Together, these results confirm the alkane-degrading potential of the individual *Pseudomonas* strains and the consortium, in agreement with previous studies reporting a strong correlation between the presence of *alkB*/*alkM* genes and efficient alkane biodegradation in hydrocarbon-degrading bacteria (Whyte et al., 1996; Márquez-Rocha et al., 2005; Das & Chandran, 2011; Pandolfo et al., 2023).

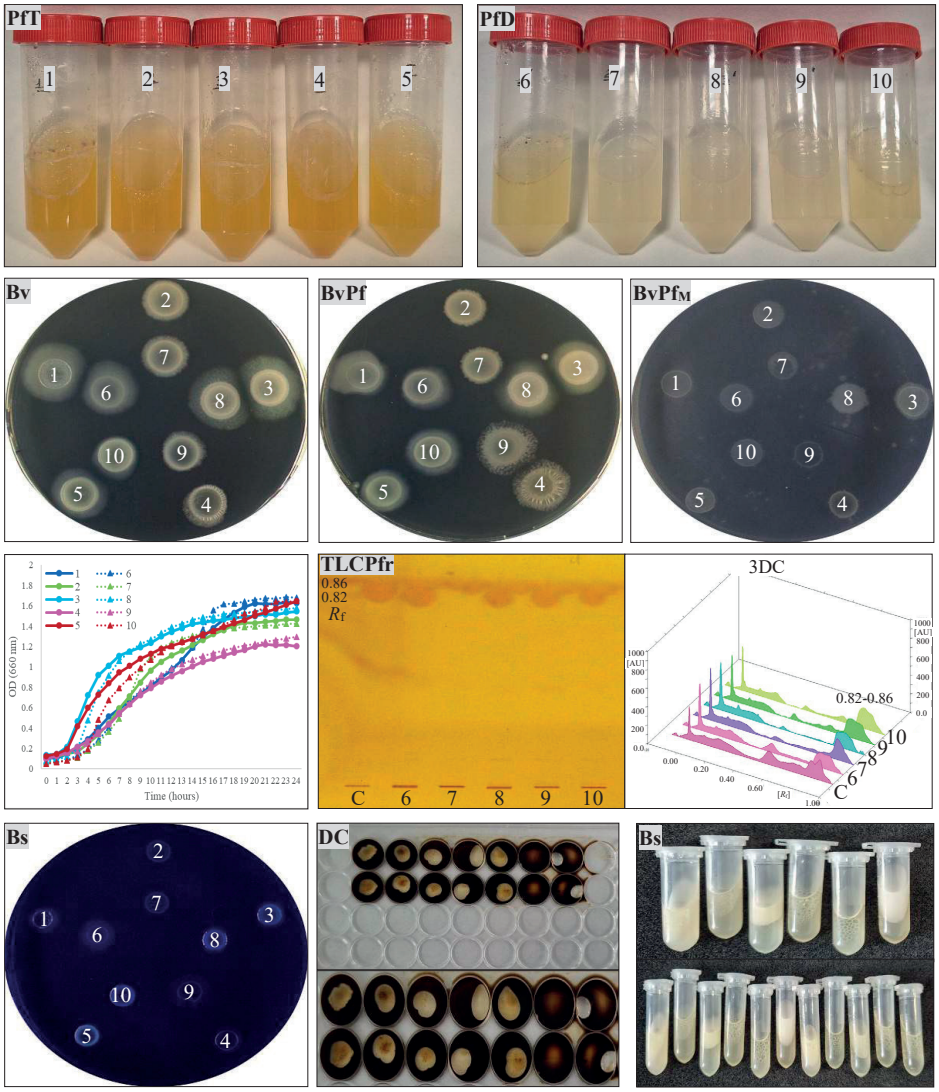



Figure 3. Paraffin tolerance and biodegradation by *Pseudomonas* strains and consortium
Paraffin tolerance (PfT, 1–5) and biodegradation assays (PfD, 6–10) performed for strains IBBDt2 (1, 6), IBBDt4.2 (2, 7), IBBDt1 (3, 8), IBBDt8 (4, 9), and the consortium (CnP, 5, 10). Bacterial viability on LB agar (Bv) and LB or MM agar overlaid with paraffin (BvPf, BvPf$_M$). Growth curves of the tested strains and consortium (Gc). HPTLC analysis of residual paraffin (TLCPfr, $R_f$ 0.82–0.86) compared with abiotic control (C), including TLC plate and 3D chromatogram (VIS). Biosurfactant production on CTAB agar (Bs); drop-collapse assay (DC); and emulsification assay (Es).

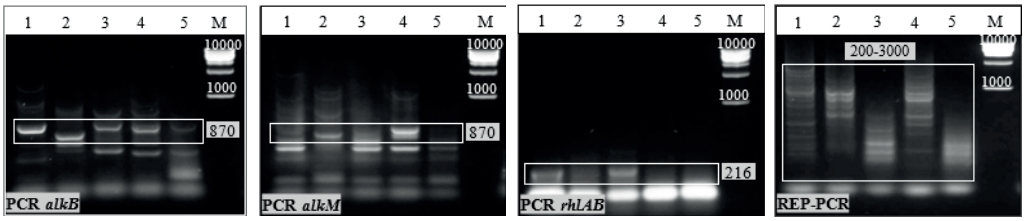



Figure 4. Molecular characterization of *Pseudomonas* strains and consortium
PCR detection of *alkB* (870 bp), *alkM* (870 bp), and *rhlAB* (216 bp) genes using DNA from strains IBBDt2 (1), IBBDt4.2 (2), IBBDt1 (3), IBBDt8 (4), and the consortium (CnP, 5); 1 kb DNA ladder (M). REP-PCR fingerprinting profiles of the same strains (1–4) and consortium (5).

**Biosurfactant production.** *Pseudomonas* strains IBBDt2, IBBDt4.2, IBBDt1, and IBBDt8, cultivated individually and as a consortium in the presence of 5% paraffin, presented biosurfactant production, as evidenced by positive results in the hydrocarbon overlay and drop-collapse assays (Table 1, Figure 3). All tested strains, as well as the consortium, produced a blue halo on CTAB agar when paraffin-grown cultures were spotted, indicating the synthesis of glycolipid or other anionic biosurfactants. The produced biosurfactants presented strong emulsification activity, with emulsification index ($E_{24}$) values ranging from 30% to 100% (Table 1). Maximum $E_{24}$ values (100%) were observed for the *Pseudomonas* strains IBBDt1 and IBBDt2, as well as for the consortium containing all four strains, followed by strains IBBDt4.2 (50%) and IBBDt8 (30%). Biosurfactant production by the individual *Pseudomonas* strains and the consortium ranged from 0.31 to 1.89 g $L^{-1}$. The *Pseudomonas* consortium presented the highest biosurfactant yield (1.89 g $L^{-1}$), followed by strains IBBDt1 (1.22 g $L^{-1}$) and IBBDt2 (0.92 g $L^{-1}$), whereas lower yields were recorded for strains IBBDt8 (0.41 g $L^{-1}$) and IBBDt4.2 (0.31 g $L^{-1}$). This enhanced biosurfactant production (1.89 g $L^{-1}$) by the consortium could be attributed to synergistic interactions among its constituent strains, which likely contribute to their superior paraffin biodegradation efficiency (85.45%). *Pseudomonas* spp. efficiently utilizes petroleum and petroleum-based products as carbon and energy sources and produce biosurfactants that facilitate hydrocarbon emulsification and biodegradation in contaminated environments (Chong & Li, 2017; Cui & Dörmann, 2025).

PCR amplification targeting the *rhlAB* genes encoding rhamnosyltransferase I detected the expected 216 bp fragment exclusively in the paraffin-exposed individual strains IBBDt2 and IBBDt1, both identified as *P. aeruginosa* (Table 1, Figure 4). These genes encode key enzymes involved in the biosynthesis of mono- and di-rhamnolipids, glycolipid biosurfactants that facilitate hydrocarbon solubilization and uptake. Previous studies indicate that *rhlAB* genes are predominantly associated with *P. aeruginosa* and play a central role in rhamnolipid production (Medina et al., 2003; Chong & Li, 2017; Wongsirichot & Winterburn, 2025). In contrast, no amplification products were obtained from *P. nitroreducens* IBBDt4.2, *P. multiresinivorans* IBBDt8, or from the consortium, despite the presence of the two *P. aeruginosa* strains. The absence of detectable *rhlAB* amplification in the consortium may be attributed to a lower relative abundance of *P. aeruginosa* genomic DNA, dilution effects during DNA extraction, or preferential amplification of dominant genomic templates in mixed bacterial communities, as reported in PCR-based analyses of complex microbial communities (van Dorst et al., 2014).

REP-PCR fingerprinting revealed distinct banding patterns (ranging from 200 to 3000 bp) for the four tested *Pseudomonas* strains when cultivated individually, confirming their genomic heterogeneity (Figure 4). In contrast, the consortium displayed a simplified REP-PCR profile, characterized by fewer bands predominantly between 200 and 400 bp. Several bands observed in the consortium overlapped with those detected in strain IBBDt1. The reduced complexity of the consortium fingerprint may indicate a shift in

population structure during incubation in 5% paraffin, possibly reflecting the numerical predominance of IBBDt1 under these conditions. Despite this apparent structural simplification, the consortium maintained superior paraffin biodegradation efficiency compared to the individual strains.

Our results demonstrate the promising potential of the tested *Pseudomonas* strains for paraffin biodegradation, particularly when combined in a consortium, likely due to functional complementarity and enhanced metabolic interactions. Collectively, these findings highlight their potential applicability in environmental biotechnology, including land reclamation and ecological engineering strategies aimed at mitigating petroleum hydrocarbon pollution and restoring contaminated ecosystems.

## CONCLUSIONS

Hydrocarbon-tolerant and hydrocarbon-degrading bacteria exhibited higher abundances during summer, with hydrocarbon-tolerant bacteria consistently dominating, indicating a clear seasonal influence on their distribution.

The tested *Pseudomonas* strains, both individually and as a consortium, demonstrated good ability to tolerate and degrade paraffin, indicating high metabolic versatility and suggesting their potential applicability in the bioremediation of sediments contaminated with saturated petroleum hydrocarbons.

Overall, this study enhances the understanding of the functional diversity and ecological role of hydrocarbon-degrading bacteria in natural sediments and provides a scientific basis for the development of environmentally friendly monitoring and bioremediation strategies in sensitive ecosystems such as the Danube Delta.

## ACKNOWLEDGEMENTS

The study was funded by project no. RO1567-IBB05/2026 from the Institute of Biology Bucharest of Romanian Academy.

## REFERENCES

Abdelaziz, A. A., Kamer, A. M. A., Al-Monofy, K. B., & Al-Madboly, L. A. (2023). *Pseudomonas aeruginosa's* greenish-blue pigment pyocyanin: its production and biological activities. *Microbial Cell Factories*, *22*, 110. https://doi.org/10.1186/s12934-023-02122-1.

Al Haj Chehadeh, B., Ali Ahmad, F., & Salam, D. A. (2025). Biodegradation of petroleum tar in contaminated sediments of the Eastern Mediterranean shores and associated microbial dynamics. *Applied and Environmental Microbiology*, *91*, e00258-25. https://doi.org/10.1128/aem.00258-25.

Butaitė, E., Kramer, J., Wyder, S., & Kümmerli, R. (2018). Environmental determinants of pyoverdine production, exploitation and competition in natural *Pseudomonas* communities. *Environmental Microbiology*, *20*, 3629–3642. https://doi.org/10.1111/1462-2920.14355.

Chong, H., & Li, Q. (2017). Microbial production of rhamnolipids: opportunities, challenges and strategies. *Microbial Cell Factories*, *16*, 137. https://doi.org/10.1186/s12934-017-0753-2.

Cui, J., & Dörmann, P. (2025). Microbial degradation of hydrocarbons from petroleum assisted by biosurfactants: Pathways and bioremediation potential. *Biochimie*, *239*, 103–119. https://doi.org/10.1016/j.biochi.2025.09.011.

Das, N., & Chandran, P. (2011) Microbial degradation of petroleum hydrocarbon contaminants: An overview. *Biotechnology Research International*, *2011*. https://doi.org/10.4061/2011/941810.

Duarte, H., Aliaño-González, M. J., Romano, A., & Medronho, B. (2024). Advancements in detection and mitigation strategies for petroleum-derived contaminants in aquatic environments: A comprehensive review. *Sensors*, *24*, 3284. https://doi.org/10.3390/s24113284.

Gesheva, V., Stackebrandt, E., & Vasileva-Tonkova, E. (2010) Biosurfactant production by halotolerant *Rhodococcus fascians* from Casey Station, Wilkes Land, Antarctica. *Current Microbiology*, *61*, 112–117.

Hall, B. G., Acar, H., Nandipati, A., & Barlow, M. (2014). Growth rates made easy. *Molecular Biology and Evolution*, *31*, 232–238. https://doi.org/10.1093/molbev/mst187.

Hossain, T. J. (2024). Methods for screening and evaluation of antimicrobial activity: A review of protocols, advantages, and limitations. *European Journal of Microbiology and Immunology*, *14*, 97–115. https://doi.org/10.1556/1886.2024.00035.

Márquez-Rocha, F. J., Olmos-Soto, J., Rosano-Hernández, M. C., & Muriel-Garcia, M. (2005). Determination of the hydrocarbon-degrading metabolic capabilities of tropical bacterial isolates. *International Biodeterioration & Biodegradation*, *55*, 17–23.

Medina, G., Juárez, K., Valderrama, B., & Soberón-Chávez, G. (2003). Mechanism of *Pseudomonas aeruginosa* RhlR transcriptional regulation of the *rhlAB* promoter. *Journal of Bacteriology*, *185*, 5976–5983.

Pandolfo, E., Caracciolo, A. B., & Rolando, L. (2023). Recent advances in bacterial degradation of hydrocarbons. *Water*, *15*, 375. https://doi.org/10.3390/w15020375.

Perhar, G., & Arhonditsis, G. B. (2014). Aquatic ecosystem dynamics following petroleum hydrocarbon perturbations: A review of the current state of knowledge. *Journal of Great Lakes Research*, *40*, 56–72. https://doi.org/10.1016/j.jglr.2014.05.013.

Sambrook, J., & Russell, D. (2001). *Molecular Cloning: A Laboratory Manual*, 3rd edition. Cold Spring Harbor Laboratory Press, Cold Spring Harbor, New York.

Samsuria, N. N. C., Ismail, W. Z. W., Nazli, M. N. W. M., Aziz, N. A. A., & Ghazali, A. K. (2025). Problems, effects, and methods of monitoring and sensing oil pollution in water: A review. *Water*, *17*, 1252. https://doi.org/10.3390/w17091252.

Satpute, S. K., Bhawsar, B. D., Dhakephalkar, P. K., & Chopade, B. A. (2008). Assessment of different screening methods for selecting biosurfactant producing marine bacteria. *Indian Journal of Marine Sciences*, *37*, 243–250.

Sharma, K., Shah, G., Singhal, K., & Soni, V. (2024). Comprehensive insights into the impact of oil pollution on the environment. *Regional Studies in Marine Science*, *74*, 103516. https://doi.org/10.1016/j.rsma.2024.103516.

Stancu, M. M. (2023). Characterization of new diesel-degrading bacteria isolated from freshwater sediments. *International Microbiology, 26,* 109–122. https://doi.org/10.1007/s10123-022-00277-2.

Stancu, M. M. (2025). Investigating the potential of native soil bacteria for diesel biodegradation. *Microorganisms, 13*(3), 564. https://doi.org/10.3390/microorganisms13030564.

van Dorst, J., Bissett, A., Palmer, A. S., Brown, M., Snape, I., Stark, J. S., Raymond, B., McKinlay, J., Ji, M., Winsley, T., & Ferrari, B. C. (2014). Community fingerprinting in a sequencing world. *FEMS Microbiology Ecology*, *89*, 316–330. https://doi.org/10.1111/1574-6941.12308.

Varjani, S. J. (2017). Microbial degradation of petroleum hydrocarbons. *Bioresource Technology*, *223*, 277–286. https://doi.org/10.1016/j.biortech.2016.10.037.

Versalovic, J., Schneider, M., de Brujin, F. J., & Lupski, J. R. (1994). Genomic fingerprinting of bacteria using repetitive sequence-based polymerase chain reaction. *Methods in Molecular and Cell Biology*, *5*, 25–40.

Whyte, L. G., Greer, C. W., & Inniss, W. E. (1996). Assessment of the biodegradation potential of psychrotrophic microorganisms. *Canadian Journal of Microbiology*, *42*, 99–106.

Wongsirichot, P., & Winterburn, J. (2025). Recent fermentation developments for improved rhamnolipid production. *Applied Microbiology and Biotechnology*, *109*, 145. https://doi.org/10.1007/s00253-025-13517-y.

Xu, W., Qiao, Y., Wei, J., Jiang, Q., & Xue, J. (2022). Bacterial communities and culturable petroleum hydrocarbon degrading bacteria in marine sediments in the northeastern South China Sea. *Frontiers in Environmental Science*, *10*, 865636. https://doi.org/10.3389/fenvs.2022.865636.

Xu, X., Liu, W., Tian, S., Wang, W., Qi, Q., Jiang, P., Jiang, P., Gao, X., Li, F., Li, H., & Yu, H. (2018). Petroleum hydrocarbon-degrading bacteria for the remediation of oil pollution under aerobic conditions: A perspective analysis. *Frontiers in Microbiology*, *9*, 2885. https://doi.org/10.3389/fmicb.2018.02.

Scientific Papers. Series E. Land Reclamation, Earth Observation & Surveying, Environmental Engineering. Vol. XV, 2026
Print ISSN 2285-6064, CD-ROM ISSN 2285-6072, Online ISSN 2393-5138, ISSN-L 2285-6064

# SEASONAL VARIATION OF $CO_2$ SOIL FLUX AND VEGETATION RESPONSE AT BODOC AND BĂILE LĂZĂREȘTI

**Lia STELEA[1, 2], Alexandra-Constanța DUDU[1], Corina AVRAM[1], Marius-Bogdan BĂRĂITĂREANU[1, 2], Andrei-Gabriel DRAGOȘ[1, 2], Gabriel IORDACHE[1]**

[1]GeoEcoMar, 23-25 Dimitrie Onciul Street, District 2, Bucharest, Romania
[2]University of Bucharest, 4-12 Regina Elisabeta Blvd, District 1, Bucharest, Romania

Corresponding author email: lia.stelea@geoecomar.ro

***Abstract***

*Bodoc and Lăzărești were chosen as test sites to assess an environmental monitoring methodology that combines soil $CO_2$ flux and vegetation surveys. Field campaigns conducted in September 2024 and April 2025 enabled a comparative assessment of spatial and seasonal variability. The two sites display very different patterns. Bodoc exhibits low $CO_2$ fluxes with limited seasonal change, likely driven by shallow biological processes. In contrast, Lăzărești displays high, naturally sourced $CO_2$ fluxes with high spatial and seasonal variability, probably also influenced by hydrological conditions and soil biological activity. Vegetation patterns also differ: at Bodoc, elevated $CO_2$ fluxes are associated with higher cover of healthy plants, whereas at Lăzărești, high fluxes correspond to reduced vegetation cover, changes in community composition and an increased monocot/angiosperm ratio.*

***Key words****: soil $CO_2$ flux, natural analogue, environmental monitoring, vegetation response, seasonal variability, Bodoc, Lăzărești.*

## INTRODUCTION

Carbon capture and storage (CCS) is widely regarded as an important mitigation strategy for reducing greenhouse gas emissions. According to the IPCC Sixth Assessment Report (IPCC, 2023), the observed increase in global average temperatures since the industrial era is very likely driven by anthropogenic greenhouse gas emissions. The deployment of CCS has been recommended as part of the portfolio of solutions needed to achieve global climate targets outlined in recent IPCC assessments (IPCC, 2022). However, one of the key challenges associated with this technology is the potential risk of $CO_2$ leakage and its possible impacts on surrounding ecosystems.

Several studies describe the relationship between increased $CO_2$ concentration in soils and the state of vegetation. The effect of $CO_2$ can be direct on plants or indirect through pH changes and mobilization of nutrients and potentially toxic elements (Noble et al., 2012). These effects are typically investigated using controlled leakage at experimental field sites or by using natural analogues where there are significant $CO_2$ releases.

It is important to state that the changes reported are due to $CO_2$ leaking towards the surface from the underground sources, not due to an increase of $CO_2$ concentration in the air. The latter often has a fertilizing effect on above-ground organs (Norby & O'Neill, 1991; Dahlman, 1993; Huxman & Smith, 2001; Veteli et al., 2002; Hymus et al., 2003; Schäfer et al., 2003) and underground organs (Idso & Kimball, 1992; Rogers et al., 1992; Schäfer et al., 2003) in some species.

It can also have little to no effect on physiology, growth or productivity on some ecosystems (Dahlman, 1993; Kirschbaum, 1999) or even be detrimental to some species, such as *Rumex obtusifolius* and *Cardamine flexuosa*, where it introduces pronounced discolouration of the leaves and premature senescence of the foliage, as well as a decrease in yield (Diaz et al., 1993). Previous research has shown that botanical changes caused by the presence of $CO_2$ in soil are site and species specific. Usually, plants show no significant response at moderate concentrations of $CO_2$ (Bouma et al., 1997). At high concentrations, plants can have decreased height, root respiration and depth of rooting (Nobel & Palta, 1989; Vodnik et al., 2006). They can also present signs of stress such as yellowing or browning of leaves due to a rapid flux of $CO_2$ (West et al., 2009; Pfanz et al., 2011). There is a predominance of grasses in the proximity of

$CO_2$ vents (Beaubien et al., 2008; West et al., 2009). Vegetation dieback (Bergfeld et al., 2006) or absence of vegetation (Beaubien et al., 2008) can also be due to high fluxes of $CO_2$.

There have been sites where certain species acted as potential bioindicators of high $CO_2$ concentrations or fluxes. These have been genus *Polygonum* with the species *P. arenastrum* (Krüger et al., 2009) and *P. aviculare* (West et al., 2015), as well as the species *Minuartia glomerata* (Ziogou et al., 2013).

Another finding from some studies has been concentric vegetation zonation around well-defined $CO_2$ vents, with the more resistant taxa growing increasingly closer to the vent and often with absence of vegetation at the vent core (Beaubien et al., 2008; Krüger et al., 2009; 2011).

Romania hosts several sites suitable as natural laboratories for the study of the effects of a potential leakage from an anthropogenic $CO_2$ storage site (sites with natural $CO_2$ emissions) as well as background conditions representative of safe storage environments (natural $CO_2$ fields). In the framework of a nationally funded research project that aims to develop an environmental monitoring methodology, two sites have been selected as natural laboratories: Bodoc for safe storage (Covasna County) and Băile Lăzărești for leakage (Harghita county). Gas flux measurements and vegetation surveys were conducted at both sites in September 2024 and April 2025.

## MATERIALS AND METHODS

### Study areas

The Bodoc site is located on a cattle pasture situated on the outskirts of Bodoc commune, along the Borviz Brook, above a carbonated mineral water reservoir. Geographically, the Bodoc site can be found at: 45°57'57.47"N; 25°52'21.19"E and an average altitude above sea level of 586.35 m (Figure 1). Geologically, Bodoc is located at the western limit of the intensely folded and faulted Cretaceous flysch deposits.

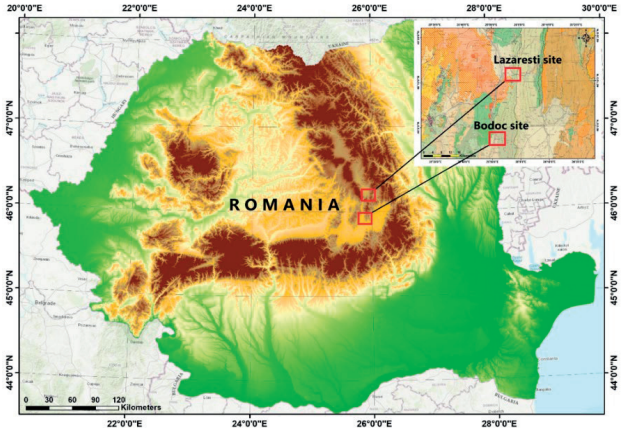



Figure 1. Location of Bodoc and Lăzărești sites in Romania and on geological map (the smaller image)

The Sânmartin-Bodoc strata are an alternation of sandstones, marls, shales and conglomerates. Aquifers are present at medium depth in the basement rock and also at shallow depth, in post tectonic deposits of the sedimentary cover. The conglomerate facies, found in a synclinal, is strongly affected by a series of transverse faults through which mineral waters migrate to the surface (Mutihac, 1990). These mineral waters are well-known, on the left bank of Borviz brook is the F1 SNAM Talomir well, with the aquifer in Upper Pliocene-Quaternary deposits and on the right bank is the oligomineral water well F2 SNAM in Quaternary deposits (SNAM, 2025).

Băile Lăzărești site, also known as Lăzărești, is situated next to the village of Lăzărești in the Cozmeni commune, being renowned by highly concentrated $CO_2$ emissions which can exceed 85% in volume (Dudu et al., 2024). Geographically, Băile Lăzărești is found at 46°11'00.17"N; 25°57'11.72"E and an average altitude above sea level of 743.29 m (Figure 1).

From a geological perspective, Băile Lăzărești is situated on a succession of geological deposits which starts with the Cretaceous flysch at the base (Sânmartin-Bodoc, of Barremian-Albian age) to the terrace deposits at the top. A fault system dominates the deep geological structure of the area, which facilitates the migration and distribution of post-volcanic emissions, like mofettas and mineral springs (Mutihac, 1990).

**Study campaigns**

The measurements were conducted at Bodoc and Lăzărești sites in September 2024 and April 2025. These included soil flux and vegetation surveys.

Soil flux measurements were performed using the West Systems portable fluxmeter equipped with $CO_2$, $CH_4$ and $H_2S$ sensors. FluxRevision 4.11 software provided by West Systems was used to process the data.

The September 2024 campaign included 244 soil flux measurements and 107 points for vegetation assessment at Bodoc site, divided in two perimeters, one along a brook valley and one on a cattle pasture (Stelea et al., 2025). At Lăzărești site, gas measurements were done also on two perimeters, one in the area with the most important touristic features and one on a recently landscaped hill with three terraces. The sampling points were 5 m apart, with 52 sampling points for soil flux measurements and vegetation assessment.

The April 2025 campaign took place between 23-29 April 2025. The April campaign in Bodoc 2025 consisted of 131 points of variable distance and the campaign in Lăzărești 2025 consisted of 250 points, 5 m apart, all of which were assessed for gas flux and vegetation.

**Vegetation surveys**

The vegetation surveys for Bodoc and Băile Lăzărești for the September 2024 campaign are similar to those conducted in April 2025. The quantitative vegetation surveys were done in the same place or the immediate vicinity of the measurement points for soil gas flux and concentration, using a 50 × 50 cm quadrat placed at the locations where gas measurements were conducted.

The interior of every quadrat was digitally photographed with the camera of a mobile phone (Xiaomi Poco M3 for the 2024 campaign, Motorola Edge 50 Neo for the 2025 campaign). Using GIMP software (version 2.6 for the 2024 campaign, version 3.0.60.0 for the 2025 campaign), a grid of 25 points situated at equal distance was created inside the quadrat (Figure 2). The category corresponding to each grid intersection was recorded at the intersection or immediately above, in case it falls on multiple elements at once.

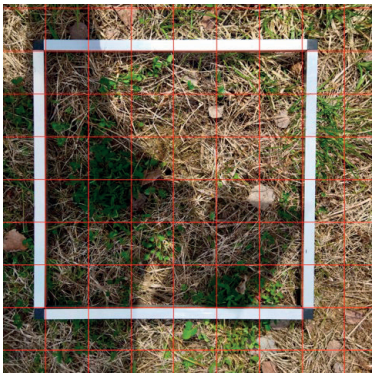


Figure 2. The grid used to calculate the relative abundance of vegetation and soil coverage categories

For the survey we performed a quantitative evaluation through the presence and dominance of categories of soil cover or plant types, also considering their state of health. Where possible, the main taxa of herbaceous plants were identified using the mobile platform iNaturalist (iNaturalist, 2024, 2025), with the observations georeferenced and published through the GBIF network (GBIF 2024; 2025).

The soil coverage categories used are similar for September 2024 and April 2025 assessments. The categories are as follows:

1. dicotyledonous angiosperms (dicots) not known as indicators - healthy organs;
2. monocotyledonous angiosperms (monocots) - healthy organs;
3. herbaceous angiosperms - withered, yellowed or browning organs;
4. herbaceous angiosperms - dried organs;
5. mosses;
6. pteridophytes;
7. external (tree leaves, twigs, litter etc.) or unidentified (shaded) elements;
8. bare ground;
9. known “indicator” taxa from other studies: *Polygonum* sp., *Minuartia glomerata*.

The criteria for selecting categories 1-2 come from scientific literature, where it was found that monocots are generally more frequent than dicots in areas with high levels of $CO_2$ (Krüger et al., 2009; West et al., 2009; Krüger et al., 2011; Noble et al., 2012). Categories 3 and 4 were selected because very high $CO_2$ emissions can lead to the yellowing or browning of leaves (West et al., 2009) or can lead to plant death (Bergfeld et al., 2006). Mosses and pteridophytes (categories 5 and 6) can be dominant in certain places although it is unknown whether their presence is related to given $CO_2$ concentrations. Category 7 is neutral, although external elements often mask bare ground. Categories 8 (bare ground) and 9 ("indicator" taxa) can appear at the highest $CO_2$ fluxes or concentrations. Using the photographs, mapping techniques and data analysis functions of Microsoft Excel relationships were analysed between the composition of soil coverage categories and the $CO_2$ flux, for both Bodoc and Lăzărești and both campaigns.

## RESULTS AND DISCUSSIONS

### Flux measurements of soil $CO_2$

The minimum, maximum, median and mean values for the two campaigns (2024 and 2025) at Bodoc and Lăzărești are written in Table 1 and the distribution is illustrated in Figure 3.

At Bodoc, during the September 2024 campaign the values obtained for flux measurements are relatively low. During April 2025 campaign the measured flux values are slightly higher.

The values obtained at Lăzărești in September 2024 are much higher than at Bodoc, due to known $CO_2$ seepage.

Table 1. $CO_2$ summary statistics for Bodoc and Lăzărești

| Campaign | Minimum [mol/ $m^2$/ day] | Median [mol/ $m^2$/ day] | Mean [mol/ $m^2$/ day] | Maximum [mol/ $m^2$/ day] |
|---|---|---|---|---|
| Bodoc Sep 2024 | 0.042 | 0.272 | 0.291 | 1.382 |
| Bodoc Apr 2025 | 0.233 | 0.604 | 0.693 | 2.736 |
| Lăzărești Sep 2024 | 0.2 | 3.479 | 13.039 | 322.3 |
| Lăzărești Apr 2025 | 0.1383 | 2.99 | 16.420 | 601.4 |

A Mann-Whitney U statistical test was performed between pairs of the four sites – campaigns: Bodoc 2024, Bodoc 2025, Lăzărești 2024, Lăzărești 2025 and the result, for all but one of six combinations, was that the rank sums are significantly different. This means that most sites, even the same site at different campaigns, has flux values that, as groups, are also significantly different from each other; Lăzărești site has values that are not statistically different in 2024 and 2025.

### Vegetation survey at Bodoc

As described in Stelea et al. (2025), the herbaceous vegetation consists of a cattle pasture next to an oak forest, slightly sloped in the upper, northern area and flat in the lower, southern area, separated by a steeper slope with ungrazed vegetation. The upper sector is oriented NE–SW and shaped like a wide stripe.

Due to grazing, plants are generally no taller than 5 cm from the ground surface, except for some unpalatable taxa and plants found near shrubs. Grazing makes plants hard to identify, especially those from order Poales.

In September 2024, plants were generally affected by drought, with withered, yellowed and dried organs due to an unusually hot and dry summer and autumn. More vigorous plants were in the ungrazed parts, close to the Borviz brook or in the shade of the taller vegetation (shrubs and trees).

In April 2025 plants were green and vigorous, unaffected by drought, although some had dried organs, probably left over from last year. The trees and shrubs from the middle part of the study area were removed.

Mosses are present, without being identified by genus or species. Pteridophytes are represented by genus *Equisetum*. Dicots are dominated (as number of identified species) by families Asteraceae, Lamiaceae and Plantaginaceae. Monocots are mostly represented by order Poales, family Poaceae, with *Poa pratensis*, *Agropyrum repens* and other species which cannot be identified due to the lack of reproductive elements. Moist areas have *Luzula* sp., *Carex* sp., *Juncus* sp. One species of orchid was found, *Neotinea (Orchis) ustulata*.

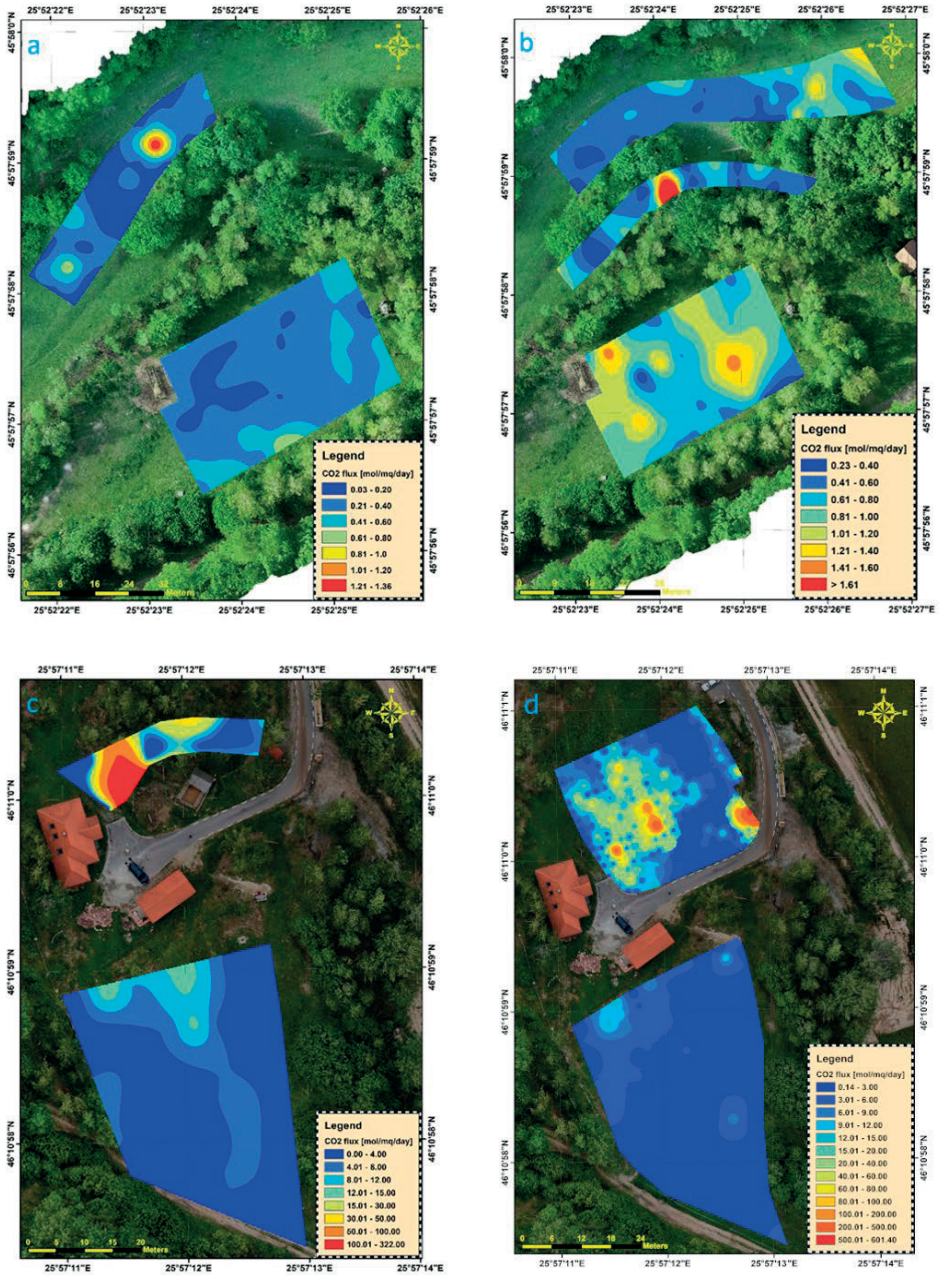



Figure 3. Flux maps at Bodoc 2024 (a), Bodoc 2025 (b), Lăzărești 2024 (c) and Lăzărești 2025 (d)

**Vegetation survey at Lăzărești**

The study area was also described in Stelea et al. (2025). It is a vegetated enclosure with built structures for balneotherapy and some terracing works. The area has a marked, but not steep slope, with Northern exposure. Vegetation is represented by trees (dominated by birches – *Betula pendula*, with hornbeams – *Carpenus betulus* and spruces – *Picea abies*), shrubs (*Salix capraea*, *Juniperus communis*) and herbaceous vegetation. Unlike for Bodoc, Lăzărești vegetation reaches its typical growth height, but

may be prevented to grow by anthropic intervention such as treading, mulching and by the presence of balneotherapy constructions. Herbaceous plants are generally vigorous although some are yellowed in appearance.
Mosses are present but they were not identified. Among pteridophytes are present *Lycopodium clavatum*, *Equisetum* sp., *Pteridium aquilinum* and *Athyrium filix-femina*. Dicotyledonous angiosperms are dominated as a number of species by the families Asteraceae, Caryophyllaceae, Fabaceae, especially genus *Trifolium*. Monocotyledonous angiosperms are dominated by order Poales, with families Poaceae, Cyperaceae and Juncaceae. Other monocots found were autumn crocuses (*Colchicum autumnale*), as well as unidentified orchids (missing reproductive elements at the time of the survey).

**Quantitative survey - comparison**

For the quantitative survey there were processed for Bodoc 107 points in 2024 and 131 in 2025. For Lăzărești 52 points in 2024 and 250 in 2025 were processed. By analysing the data from spring 2025, a new category of vegetation coverage has been identified in the form of dried plant organs, which can be an indicator of extreme stress or just a remnant from previous year. This identification leads to the reinterpretation of the autumn 2024 data, previously presented in Stelea et al. (2025).
Comparing the two surveys (Table 2, Figure 4) from the two separate campaigns, we can see that at Bodoc there is a similar proportion of healthy dicots and monocots in autumn 2024 but not in spring 2025, when there are more healthy dicots. At Lăzărești there are more healthy monocots than dicots in both campaigns.
Bodoc in the autumn of 2024 has plants with more dried organs than either Lăzărești or Bodoc in the spring 2025 campaign. The explanation for this phenomenon is the 2025 drought.
At Lăzărești in the spring of 2025 there are more dried plant organs than in the autumn of 2024, because they probably died during the cold season and had not yet decomposed or covered by new growth.
External elements, such as leaves, twigs, roots or unidentified and shaded elements are poorly represented at Bodoc in 2024. There are more external elements at Lăzărești in the spring of 2025 (mostly birch leaves) than in autumn 2024 or at Bodoc in both campaigns.
As minor elements there are mosses and pteridophytes. The percentages of bare ground are similar in 2025 in both Bodoc and Lăzărești, slightly higher in Lăzărești 2024 campaign and lower in Bodoc 2024 campaign.
"Indicator" plants were lacking from all studied points.
Based on soil coverage we calculated two indicators – "Healthy plants coverage" and "Monocots/Total angiosperms ratio".
"Healthy plants coverage" (Figures 5 and 6) represents the proportion of plants with healthy organs from the sample – monocots, dicots and pteridophytes. We excluded mosses from the calculation, because they were mostly dehydrated.
Typical values for Bodoc in spring 2025 are around the average of 65.5% with a standard deviation of 18.3%. Typical values for Lăzărești in the same campaign are around the average of 42.3% with a standard deviation of 23.7%. These values and the distribution show us that at Bodoc healthy vegetation generally covers a much higher proportion that at Lăzărești, but considering the results from the autumn of 2024, we consider that things can change with the influence of climatic factors and vegetation succession.

Table 2. Comparison between soil coverage categories at Bodoc and Lăzărești

| | Campaign | Dicots (%) | Monocots (%) | Stressed organs (%) | Dried organs (%) | Moss (%) | Pteridophytes (%) | Other (%) | Bare ground (%) |
|---|---|---|---|---|---|---|---|---|---|
| Bodoc | 2024 | 17.27 | 17.38 | 6.5 | 46.43 | 2.58 | 0 | 7.07 | 2.77 |
| | 2025 | 36.61 | 28.67 | 0.82 | 3.48 | 1.44 | 0 | 22.66 | 6.32 |
| Lăzărești | 2024 | 22.62 | 44 | 3.08 | 7.77 | 0.08 | 0.38 | 12.92 | 9.15 |
| | 2025 | 9.42 | 30.4 | 1.49 | 15.54 | 2.37 | 0.11 | 34.56 | 6.11 |

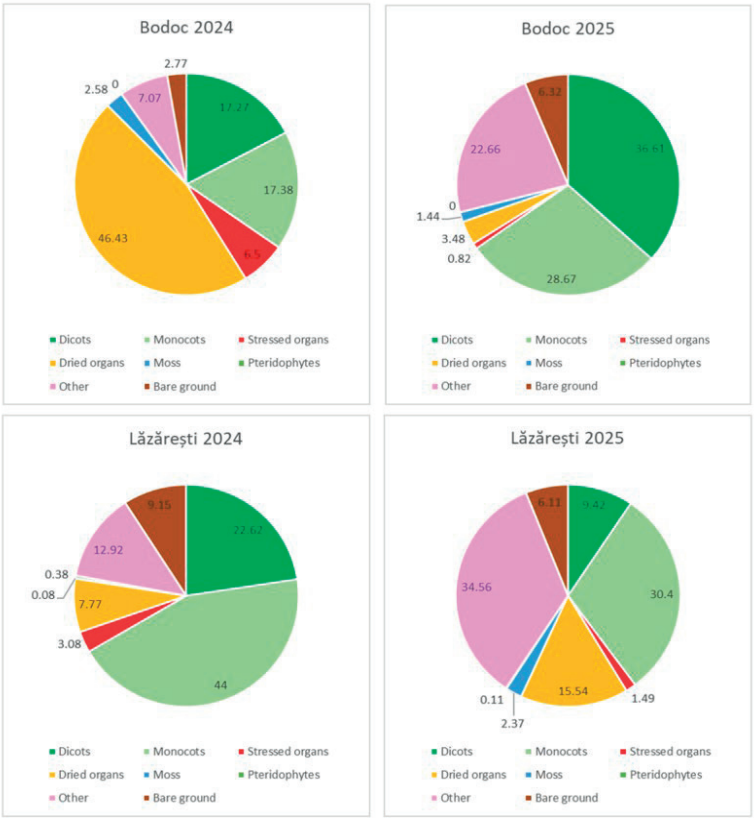



Figure 4 Comparison between soil coverage categories for Bodoc and Lăzărești in 2024 and 2025

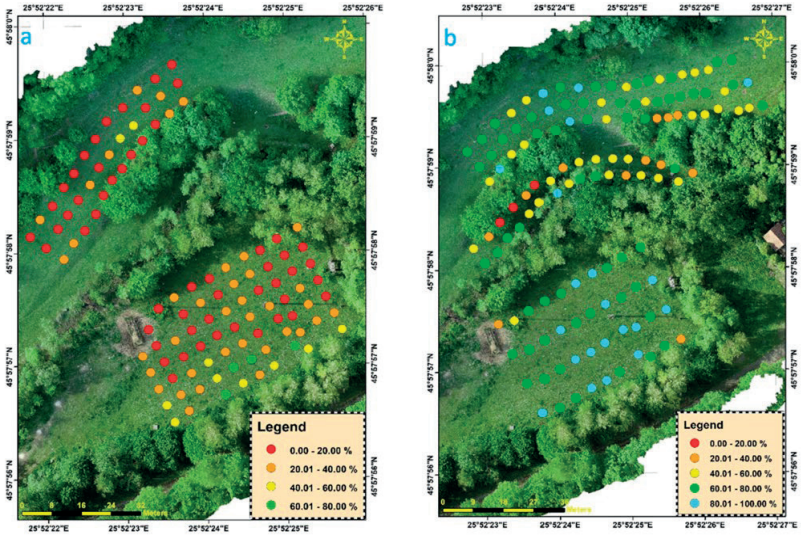



Figure 5. Healthy plant coverage at Bodoc in the 2024 campaign (left - a) and 2025 campaign (right - b)

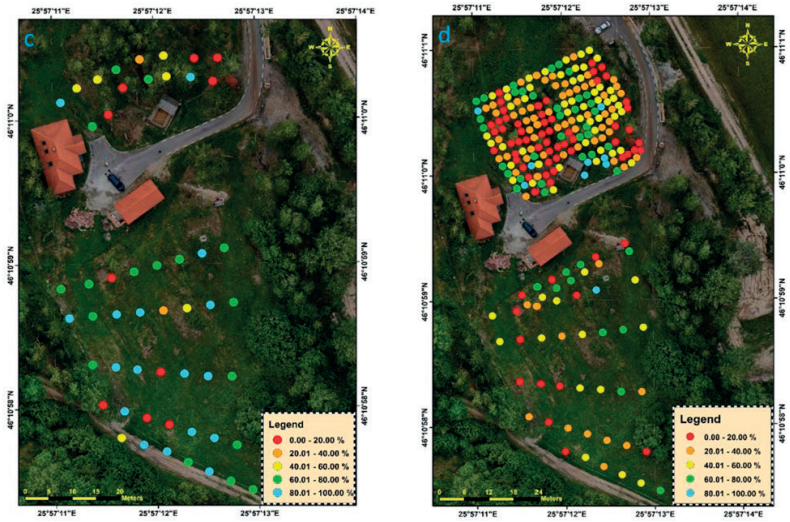



Figure 6. Healthy plant coverage at Lăzărești in the 2024 campaign (left - c) and 2025 campaign (right - d)

The monocots/Total angiosperms ratio represents the proportion of apparently healthy organs (leaves, stems, flowers, fruits) of monocots divided to the total of healthy angiosperms. The higher the value, the higher the chances of species substitution due to high fluxes of $CO_2$.

Typical values for Bodoc in 2025 are around the average of 43.3% with a standard deviation of 22.1%. Typical values for Băile Lăzărești are much higher, with an average of 72.6% but the distribution shows a strong increase of the values up to the maximum. These values and their distribution show us that at Lăzărești is a higher proportion of monocots, which is to be expected, but it is possible that with vegetation succession over the year these values and proportions can change.

**The relationship between the vegetation survey and the flux measurements at Bodoc and Băile Lăzărești in 2025**

We attempted to highlight quantitative relationships between the composition of soil coverage categories and the flux of $CO_2$. We have done this by identifying three categories of flux (high, intermediate and low) for both Bodoc and Băile Lăzărești. At first, we have tried a correlation analysis of individual samples with $CO_2$ flux but it did not give any significant results due to samples being too small and too variable. However, if summed up together we can observe some trends.

For Bodoc we established three categories – under 0.5 mol/m$^2$/day (relatively low flux), between 0.5 and 1 mol/m$^2$/day (relatively average flux), over 1 mol/m$^2$/day, up to 2.7 mol/m$^2$/day (relatively high flux) of $CO_2$ (Figure 7).

It can be observed at the three flux categories that with the increase of the $CO_2$ flux also increases the prevalence of healthy plants, especially monocots, and the bare ground percentage decreases. The neutral elements percentage is higher at a flux of $CO_2$ under 0.5 mol/m$^2$/day and approximately equal at higher fluxes (~21%). The dicot percentage is almost 31% at the relatively low flux and approximately equal at the relatively intermediate and high fluxes.

Higher $CO_2$ fluxes are associated with more plant coverage, especially of monocots. It is necessary, though, to repeat the measurements to see if these results were not due to chance.

Also, for Băile Lăzărești we established three categories – 0-10 mol/square meter/day (low flux), 10-49.(9) mol/square meter/day (intermediate flux), 50+ mol/square meter/day (high flux) (Figure 8). These categories are not the same as the ones used at Bodoc, because we have different orders of magnitude for the $CO_2$ flux.

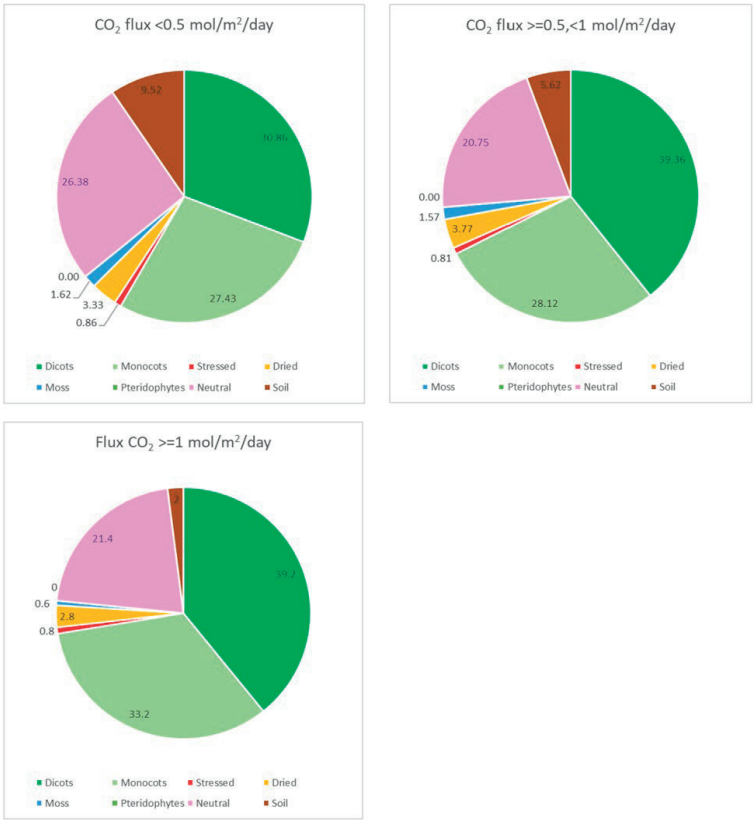



Figure 7. Soil coverage categories function of CO2 flux at Bodoc, 2025

We have analysed three subcategories of the low flux – under 0.499 mol/m$^2$/day, 0.5-0.999 mol/m$^2$/day and 1-3 mol/m$^2$/day to compare with results from Bodoc, but it was inconclusive, probably due to the small number of samples with such values.

Analysing the data and graphs with the soil covering categories coupled with $CO_2$ flux categories for Lăzărești we can see the following trends:

- A decrease of the ratio of healthy plants – monocots, dicots and pteridophytes. The indicator "Healthy plant coverage" decreases from the average of 43.7% for low flux, to 35.2% for intermediate flux and 12% for high flux.
- No change for the ratio of monocots/total angiosperms; even though the average values slightly decrease, a Mann-Whitney test performed on pairs reveals that the samples are statistically similar.
- A decrease of pteridophyte ratio.
- A decrease of dried plant organs ratio.
- A slight increase of moss coverage.
- A high increase of the surface covered by external elements and bare ground.
- Absence of "indicator" taxa.

As interpretation, it is considered that the decrease of surface covered by healthy plants is due primarily to soil and water acidification produced by $CO_2$ and associated gases. Differently from what we observed at Bodoc, higher values of $CO_2$ are not associated with richer vegetation, but poorer.

The decrease of the ratio of dried plant organs is related to the decrease of the ratio of healthy-looking plant organs. In the present case, we consider that dried organs are not primarily due to the toxic effect of $CO_2$ and other gases but represent a normal plant response to the cold season.

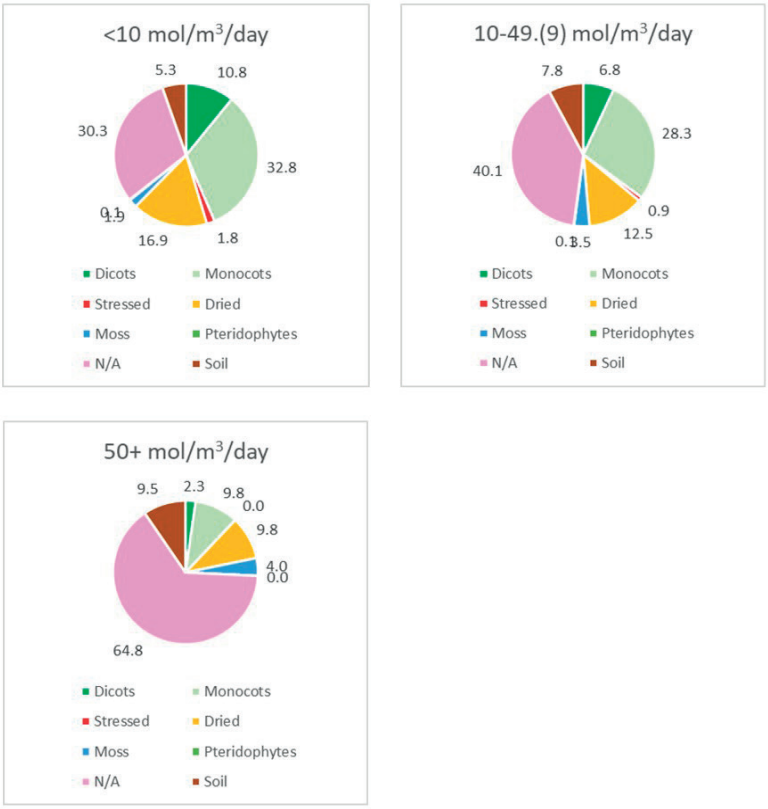



Figure 8. Soil coverage categories function of $CO_2$ flux at Lăzărești, 2025

Because the $CO_2$ flux did not start suddenly, like for the case of experimental grounds, but represented more or less a constant presence, we consider that the vegetation at Lăzărești is adapted to the high $CO_2$ fluxes, having relatively few organs with signs of stress (apart from the dried ones).

The lowering of the ratio of pteridophytes and the increase of mosses must be considered with caution, due to the small values of their presence and dominance. The increase of the surface occupied by external elements and bare ground is a good indication for the $CO_2$ flux, both directly, due to the toxic effects of the mofetta gases, as well as indirectly (the closeness to the mofettas with high concentrations of $CO_2$ can lead to a higher anthropic impact in those areas, which would affect the vegetation).

Lastly, the study areas did not contain known "indicator taxa" like the genus *Polygonum* or the species *Minuartia glomerata*. This does not mean that there aren't areas with abundant $CO_2$, but that the presence of "indicator" plants which are tolerant to high fluxes of $CO_2$ is not necessary. Other plant taxa strongly associated with high fluxes of $CO_2$ were not identified.

## CONCLUSIONS

The study evaluated the potential of vegetation surveys as an environmental monitoring tool for $CO_2$ geological storage and the presence of bioindicators that could be used as early signs of $CO_2$ leakage. In order to meet these objectives, vegetation surveys were conducted in two natural analogues relevant for geological $CO_2$ storage monitoring and representing different storage scenarios (one for safe storage and one for a leaking site) aiming to compare vegetation characteristics and to correlate where possible with different categories of $CO_2$ fluxes. Another aim of the study was to assess whether vegetation responses to increase $CO_2$ fluxes

described in the international literature are observable in the Romanian sites.

From the start, one conclusion is that the study areas are floristically too different to be readily compared. Bodoc area is a cattle pasture surrounded by an oak forest. Băile Lăzărești represents an ecosystem lacking large herbivores, but anthropically modified. There are biotope differences which are reflected in the species composition, with taxa which prefer higher humidity and colder climate present at Lăzărești.

The higher fluxes of $CO_2$ in the area of Bodoc, still close to the normal values, are associated with a higher prevalence of healthy plants, particularly monocots. In the area of Băile Lăzărești the higher fluxes of $CO_2$, significantly above normal, are associated with a decrease of the coverage by healthy and dried plants, and in the areas with the highest fluxes, vegetation is almost absent and bare ground is often found, which can also be due to anthropic factors.

The observed relationships between vegetation cover, plant functional groups, and soil $CO_2$ flux suggest that herbaceous vegetation may provide a useful complementary indicator for identifying areas affected by elevated $CO_2$ emissions at $CO_2$ geological storage sites. However, vegetation responses are strongly influenced by local ecological conditions and anthropogenic disturbance, limiting the use of vegetation alone as a qualitative monitoring tool.

As a limitation of the study, the observed trends appear at the sums of categories but not at the individual samples, which are too varied in composition and cannot be used for a correlation analysis. Vegetation monitoring should therefore be considered as a complementary component of integrated CCS monitoring strategies, to be used together with geophysical and geochemical methods rather than as a standalone indicator of $CO_2$ leakage.

An important limitation of the methodology is that soil flux measurements required the removal of inventoried vegetation at the sampling points, in order to achieve the airtightness required for the measuring chamber of the fluxmeter. This disturbance modifies the local plant assemblages over time by favouring opportunistic colonizing species, making long-term monitoring of identical points unreliable. For this reason, future studies should either establish adjacent non-destructive monitoring plots or periodically relocate sampling points.

Comparing this study to others performed on natural analogues in other countries has revealed the lack of potential "indicator species" for higher $CO_2$ values. Because of the random placement of the high, mid and low flux $CO_2$ points and their possibly inconsistent emission patterns as revealed by the flux maps, the concentric vegetation zonation present in places with well-individualized $CO_2$ vents is absent at Lăzărești.

## ACKNOWLEDGEMENTS

The research leading to these results was conducted within the project PN 23300404 “Development of an environmental monitoring methodology for potential $CO_2$ storage sites in Romania (Dezvoltarea unei metodologii de monitorizare de mediu pentru potențialele situri de stocare de $CO_2$ din România)”, financed by the Ministry of Research, Innovation and Digitalization of Romania through the Core Program (“Programul Nucleu”).

The authors also thank for the support of town halls of Cozmeni and Bodoc, who eased the access to the site and the proper running of the campaigns.

We are also thanking the reviewers for the suggestions provided to improve the manuscript.

## REFERENCES

Beaubien, S.E., Ciotoli, G., Coombs, P., Dictor, M. C., Kruger, M., Lombardi, S., Pearce, J. M., & West, J. M. (2008). The impact of a naturally occurring $CO_2$ gas vent on the shallow ecosystem and soil chemistry of a Mediterranean pasture (Latera, Italy). *International Journal of Greenhouse Gas Control* 2(3), 373-387.

Bergfeld, D., Evans, W. C., Howle, J., & Farrar, C. D. (2006). Carbon dioxide emissions from vegetation-kill zones around the resurgent dome of Long Valley caldera, Eastern California, USA. *Journal of Volcanology and Geothermal Research*, 152(1-2) 140-156.

Bouma, T. J., Nielsen, K. L., Eissenstat, D. M, & Lynch, J. P. (1997). Estimating respiration of roots in soil: Interactions with soil $CO_2$, soil temperature and soil water content. *Plant and soil*, 195:221-232.

Dahlman, R. C. (1993). *$CO_2$ and Plants: Revisited*. In J. Rozema, H. Lambers, S. C. van de Geijn, & M. L. Cambridge (Eds.), $CO_2$ and Biosphere (pp. 339–355). Springer.

Diaz, S., Grime, J. P., Harris, J., & McPherson, E. (1993). Evidence of a feedback mechanism limiting plant response to elevated carbon dioxide. *Nature* 364: 616-617.

Dudu, A.-C., Pavel, A. B., Avram, C., Catianis, I., Iordache, G., Rădulescu, F., Lupașcu, N., Dragoș, A.-G., Dobre, O., & Sava, C.S. (2024). Environmental assessment of the area with natural $CO_2$ emissions in Băile Lăzărești. *Scientific Papers. Series E. Land Reclamation, Earth Observation & Surveying, Environmental Engineering,* XIII.

GBIF (2024). https://www.gbif.org/ accessed September, 2024.

GBIF (2025). https://www.gbif.org/ accessed April 2025.

Huxman, T. E., & Smith, S. D. (2001). Photosynthesis in an invasive grass and native forbs at elevated $CO_2$ during an El Nino year in the Mohave desert. *Oecologia* 128, 193-201.

Hymus, G. H., Johnson, D. P., Dore, S., Anderson, H. P., Hinkle, C. R., & Drake, B. G. (2003). Effects of elevated atmospheric $CO_2$ on net ecosystem $CO_2$ exchange of a scrub-oak ecosystem. *Global Change Biology* 9, 1802-1812.

Idso, S. B., & Kimball, B. A. (1992). Seasonal fine-root biomass development of sour orange trees grown in atmospheres of ambient and elevated $CO_2$ concentration, *Plant, Cell & Environment* 15(3), 337-341.

iNaturalist (2024). https://www.inaturalist.org/, accessed September, 2024.

iNaturalist (2025). https://www.inaturalist.org/ , accessed April, 2025.

IPCC (2022). *Climate Change 2022: Mitigation of Climate Change. Contribution of Working Group III to the Sixth Assessment Report of the Intergovernmental Panel on Climate Change* [Shukla, P. R., Skea, J., Slade, R., Al Khourdajie, A. Al, van Diemen, R., McCollum, D., Pathak, M., Some, S., Vyas, P., Fradera, R., Belkacemi, M., Hasija, A., Lisboa, G., Luz, S., & Malley, J. (eds.)]. Cambridge University Press, Cambridge, UK and New York, NY, USA.

IPCC (2023). Sections. In: *Climate Change 2023: Synthesis Report. Contribution of Working Groups I, II and III to the Sixth Assessment Report of the Intergovernmental Panel of Climate Change* [Core writing team, Lee, H. & Romero, J. (eds.)]. IPCC, Geneva, Switzerland, pp. 35-115.

Kirschbaum, M. U. F. (1999). Modelling forest growth and carbon storage in response to increasing $CO_2$ and temperature. *Tellus* 51B, 871-888.

Krüger, M., West, J., Frerichs, J., Oppermann, B., Dictor, M.C., Jouliand, C., Jones, D., Coombs, P., Green, K., Pearce, J., May, F., & Moller, I. (2009). Ecosystem effects of elevated $CO_2$ concentrations on microbial populations at a terrestrial $CO_2$ vent at Laacher See, Germany. *Energy Procedia* I: 19331939.

Krüger, M., Jones, D., Frerichs, J., Oppermann, B. I., West, J., Coombs, P., Green, K., Barlow, T., Lister, R., Shaw, R., Strutt, M., & Moller, I. (2011). Effects of elevated $CO_2$ concentrations at a terrestrial $CO_2$ vent at Laacher See, Germany. *International Journal of Greenhouse Gas Control*, 5(4), 1093-1098.

Mutihac, V. (1990). *Geological Structure of the Territory of Romania.* [Structura geologică a teritoriului României] Technical Publishing House, Bucharest.

Nobel, P. S., & Palta, J. A. (1989). Soil $O_2$ and $CO_2$ effects on root respiration of cacti. *Plant and Soil*, 120, 263-271.

Noble, R. R. P., Stalker, L., Wakelin, S. A., Pejcic, B., Leybourne, M. I., Hortle, A. L., & Michael, K. (2012). Biological monitoring for carbon capture and storage – A review and potential future developments. *International Journal of Greenhouse Gas Control*, 10, 520-535.

Norby, R. J., & I'Neill, E. G. (1991). Leaf area compensation and nutrient interactions in $CO_2$-enriched seedlings of yellow-poplar (*Liriodendron tulipifera* L.). *The New Phytologist*, 117, 4, 515-528.

Pfanz, H. (2011). Life in dry, terrestrial mofette areas. *IEAGHG Summary Report of the IEGHG Workshop of Natural Releases of $CO_2$: Building Knowledge for $CO_2$ Storage Environmental Impact Assessments*, 25-26.

Rogers, H. H., Peterson, C. M., McCrimmon, J. N., & Cure, J. D. (1992). Response of plant roots to elevated atmospheric carbon dioxide. *Plant, Cell & Environment* 15, 749-752.

Schäfer, K. V. R., Oren, R., Ellsworth, D. S., Lai, C-T., Herrick, J. D., Finzi, A. C., Richter, D. D., & Katul, G. G. (2003). Exposure to an enriched $CO_2$ atmosphere alters carbon assimilation and allocation in a pine forest ecosystem. *Global Change Biology* 9, 10, 1378-1400.

SNAM (2025). Deposit presentation. Specialized data on the deposit (in Romanian). *SNAM (National Society for Mineral Waters)*. Retrieved January 21, 2026 from: https://snam.ro/images/resurse/prezentare-zacamant-talomir-bodoc.pdf.

Stelea, L., Dudu, A.-C., Avram, C., Iordache, G., & Sava, C-Ș. (2025). Vegetation surveys for monitoring $CO_2$ geological storage sites: a case study from two analogue sites from Romania. *Scientific Papers. Series E. Land Reclamation, Earth Observation & Surveying, Environmental Engineering,* XIV, 1210-1217.

Veteli, T. O., Kuokkanen, K., Julkunen-Tiitto, R., Roininen, H., & Tahvanainen, J. (2002). Effects of elevated $CO_2$ and temperature on plant growth and herbivore defensive chemistry. *Global Change Biology* 8, 12, 1240-1252.

Vodnik, D., Kastelec, D., Pfanz, H., Macek, I., & Turk, B. (2006). Small-scale spatial variation in soil $CO_2$ concentration in a natural carbon dioxide spring and some related plant responses. *Geoderma*, 133(3-4), 309-319.

West, J. M., Jones, D. G., Annunziatellis, A., Barlow, T. S., Beaubien, S. E., Bond, E., Breward, N., Coombs, P., de Angelis, D., Gardner, A., Gemeni, V., Graziani, S., Green, K. A., Gregory, S., Gwosdz, S., Hannis, S., Kirk, S., Koukouzas, N., Kruger, M., Libertini, S., Lister, T. R., Lombardi, S., Metcalfe, R., Pearce, J. M., Smith, K. L., Steven, M. D., Thatcher, K., & Ziogou, F. (2015). Comparison of the impacts of elevated $CO_2$ soil gas concentrations on selected European terrestrial environments. *International Journal of Greenhouse Gas Control* 42: 357-371.

West, J. M., Pearce, J.M., Coombs, P., Ford, J. R., Scheib, C., Colls, J. J., Smith, K. L., & Steven, M. D. (2009). The impact of controlled injection of $CO_2$ on the soil ecosystem and chemistry of an English lowland pasture. *Energy Procedia*, 1, 1863-1870.

Ziogou, F., Gemeni, V., Koukouzas, N., de Angelis, D., Libertini, S., Beaubien, S. E., Lombardi, S., West, J. M., Jones, D. G., Coombs, P., Barlow, T. S., Gwosdz, S., & Kruger, M. (2013). Potential environmental impacts of $CO_2$ leakage from the study of natural analogue sites in Europe. *Energy Procedia* 37: 3521-3528

Scientific Papers. Series E. Land Reclamation, Earth Observation & Surveying, Environmental Engineering. Vol. XV, 2026
Print ISSN 2285-6064, CD-ROM ISSN 2285-6072, Online ISSN 2393-5138, ISSN-L 2285-6064

# EVALUATION OF THE PERFORMANCE OF WHEAT VARIETIES UNDER MINIMUM TILLAGE SYSTEM IN THE PEDOCLIMATIC CONDITIONS OF SĂCELE AREA, CONSTANȚA COUNTY (2021-2024)

**Traian Ciprian STROE[1, 2], Oana MIHAI FLOREA[1], Liliana PANAITESCU[1, 2]**

[1]University of Agronomic Sciences and Veterinary Medicine of Bucharest, 59 Marasti Blvd, District 1, Bucharest, Romania
[2]Ovidius University of Constanța, University Alley, Campus building B, Constanța, Romania

Corresponding author email: str_ciprian@yahoo.com

***Abstract***

*This study aimed to evaluate the performance of several winter wheat (Triticum aestivum L.) varieties cultivated under the minimum tillage system in the semi-arid pedoclimatic conditions of Săcele, Constanța County (Romania) during the 2021-2024 agricultural years(October-July cropping cycles). The experimental design included four varieties: Avenue, Katarina, Rubisko, and Sorrial, monitored under variable rainfall regimes (330 mm in 2021-2022, 380 mm in 2022-2023, and <290 mm in 2023-2024). Morpho-productive parameters such as tillering capacity, plant height, grain number per spike, grain mass per spike, thousand kernel weight (TKW), and test weight (TW) were analyzed. The results represent the mean values of three consecutie agricultural years, highlighting varietal stability and adaptability under drought stress.*

*Among the tested varieties, Rubisko showed the highest productivity (5.9 t/ha), followed by Avenue (5.5 t/ha), Sorrial (5.0 t/ha), and Katarina (4.3 t/ha). Strong positive correlations were recorded between yield and TKW ($r = 0.94$), yield and TW ($r = 0.91$), and yield and NDVI ($r = 0.97$). The linear regression analysis confirmed a significant relationship ($R^2 = 0.93$, $p < 0.05$) between NDVI and yield, demonstrating that vegetation indices derived from multispectral UAV imagery and Sentinel-2 satellite data provide reliable and complementary information for predicting wheat yield under the studied conditions.*

*The study demonstrates that combining minimum tillage with precision agriculture technologies ensures sustainable and resilient wheat production in arid regions. The results support the integration of digital monitoring, biofertilization, and site-specific management as key components of climate-smart agriculture for southern Romania and similar environments.*

***Key words****: drought, minimum tillage, NDVI, precision agriculture, Triticum aestivum.*

## INTRODUCTION

Wheat (*Triticum aestivum* L.) is one of the most important field crops worldwide, playing a fundamental role in human nutrition due to its high nutritional value and technological versatility. In recent decades, adapting wheat cultivation to increasingly variable and often extreme environmental conditions has become a global agricultural priority (Xiong et al., 2024; Arif et al., 2025). Under the current climate change context: characterized by prolonged drought, heat stress, and large thermal fluctuations, enhancing wheat resilience through variety selection and sustainable technologies represents a strategic direction for agricultural development (Nyaupane et al., 2024; Shaheen et al., 2025). In the current context of accelerated climate change, the increase in land surface temperatures and the intensification of aridization processes are exerting growing pressure on agricultural systems, particularly in regions with high climatic vulnerability. Recent global-scale analyses highlight that changes in thermal and hydrological regimes directly affect agricultural productivity, ecosystem stability, and food security, generating significant economic and social impacts (Buzatu et al., 2024). At the same time, at the national level, the dynamics of land resources and the progressive degradation of soils require the adoption of sustainable conservation strategies aimed at reducing the negative effects of intensive agricultural practices on soil structure and fertility. In Romania, the implementation of conservative technologies and soil protection practices is considered essential for preventing physical and chemical soil degradation and for

adapting agricultural production systems to the new climatic conditions (Buzatu et al., 2023).

In Romania, winter wheat holds a significant share in the cropping structure, being cultivated across all agricultural regions. In the Dobrogea area, particularly around Săcele, Constanța County, the pedoclimatic conditions are distinctive, with low annual precipitation (350-450 mm), high summer temperatures frequently exceeding 35°C, and frequent dry winds factors that necessitate adapting cultivation technologies (Pascu, 2012; Partal et al., 2023). The dominant soils are cambic and leached chernozems, with medium to high natural fertility but prone to water loss through evaporation and structural degradation if excessively tilled.

In this context, the minimum tillage system, based on reducing soil disturbance and maintaining crop residues on the surface, has become a modern and sustainable technological solution for conserving soil water and fertility (Leonte et al., 2024; Dinuta et al., 2025). By decreasing the number and depth of tillage operations, this system helps preserve soil moisture, protect beneficial microorganisms, and reduce fuel and labor costs. Furthermore, it provides a favorable framework for the implementation of precision agriculture technologies, enabling optimized sowing, fertilization, and plant protection through the use of sensors and satellite data (Raza et al., 2025a; Haseeb et al., 2025).

Recent research conducted in southern Romania has demonstrated that conservative soil management systems such as minimum tillage, no-tillage, and strip-tillage practices, do not significantly reduce yields when adapted and resilient wheat varieties are used (Gheorghe & Nicolae, 2023; Nita et al., 2024). Studies performed at the Albota and Brăila research stations revealed that modern cultivars such as Izvor, Ursita, and Glosa maintain high productivity even under limited rainfall conditions (Ghiorghe et al., 2024; Dinuta et al., 2025). Moreover, the application of effective disease control treatments adapted to new climatic conditions plays a key role in ensuring yield stability (Grigoraș et al., 2012; Cioineag & Cristea, 2015; Iosub et al., 2022).

The integration of precision agriculture elements, such as UAV-based crop monitoring and remote sensing approaches (satellite-based observations), opens new perspectives for optimizing wheat crop management (Joshi et al., 2024; Qosimov & Imomov, 2025). Comparative analyses of conventional and organic systems, based on field experiments and long-term assessments, further indicate that conservative technologies such as: minimum tillage, no-tillage, and strip-tillage, as well as residue retention, reduce environmental impact while improving the sustainability of agricultural production (Kheiralipour et al., 2024; Zorovski, 2024).

Considering these aspects, the present study aims to evaluate the performance of several wheat varieties under the minimum tillage system in the pedoclimatic conditions of Săcele, Constanța County, during the 2021-2024 period corresponding to three consecutive agricultural years (October 2021 - July 2022, October 2022 - July 2023, and October 2023 - July 2024). The main objective is to identify the most adaptable varieties and the optimal technological practices within the minimum tillage system for achieving high, stable, and sustainable yields under the arid and variable climatic conditions characteristic of southern Dobrogea where Săcele is located. The results will contribute to the scientific foundation of regional strategies promoting sustainable agricultural practices and efficient use of local pedoclimatic resources, by supporting variety selection, optimizing minimum tillage management, and improving data-driven decision-making under arid conditions.

## MATERIALS AND METHODS

The present research was carried out within an agricultural holding located in Săcele, Constanța County, an area representative of southern Dobrogea, characterized by pedoclimatic conditions specific to the semi-arid regions of southeastern Romania (Stroe et al., 2025; Stroe et al., 2026). The area is distinguished by a moderately continental climate with marine influences, hot and dry summers, and relatively mild winters, where the annual rainfall is low, generally ranging between 350 and 450 mm. Under such conditions, the choice of cultivation technology and the selection of suitable varieties are essential for ensuring production stability.

The study area is located in the southern part of Constanța County, near the locality of Săcele, at an average altitude of 25-30 m, within the Dobrogea Coastal Plain. The relief is slightly fragmented, predominantly flat, and favorable for intensive mechanization and precision agriculture practices. The proximity to the Black Sea creates a distinct climatic influence, with very hot and dry summers, frequent winds, and high evapotranspiration rates, making this region one of the most vulnerable agricultural areas in Romania to the process of aridization.

The regional climate is continental-excessive with Pontic influences, characterized by large thermal amplitudes and a low rainfall regime. The multiannual mean air temperature is approximately 11.3°C, but recent years have shown a steady warming trend, consistent with regional climatic observations reported by Shi et al. (2025) and Xiong et al. (2024). During the analyzed period, the annual mean temperature ranged between 11.8°C and 12.9°C, with clear positive deviations from the long-term average, particularly in the 2022-2023 and 2023-2024 agricultural years, when maximum summer temperatures frequently exceeded 35°C.

The rainfall regime of the Săcele area is among the lowest in the country, and the 2021-2024 agricultural years further emphasized this trend: in 2021-2022, total annual precipitation was below 330 mm, with a pronounced deficit in September, March, April and June, leading to uneven emergence and weak tillering. In 2022-2023, the total rainfall reached approximately 380 mm, yet it was the warmest agricultural year of the entire period, with extended heat stress during stem elongation and grain formation. In 2023-2024, the recorded precipitation dropped below 290 mm, making it the fifth driest year in Romania's modern meteorological history. The absence of rainfall during the critical months of April and May coincided with the spike formation stage, intensifying water stress and reducing both grain weight and the number of fertile tillers.

The average annual wind speed ranges between 4.8 and 5.5 m/s, with prevailing northeasterly winds that further accelerate evapotranspiration and soil moisture loss, especially between April and August. These conditions strongly justify the adoption of minimum tillage systems, which, by reducing soil disturbance and maintaining crop residues on the surface, significantly decrease evaporation, preserve soil moisture, and protect soil structure (Leonte et al., 2024; Dinuta et al., 2025).

From a pedological perspective, the agricultural lands in the Săcele area are dominated by cambic and leached chernozems, developed on loess deposits, with a medium texture (from sandy-loam to loam-clay). The humus content varies between 2.8 and 3.5%, and the soil reaction is slightly alkaline (pH 7.7-8.0). These soils have moderate to good natural fertility but are highly susceptible to moisture loss and structural degradation under conditions of repeated deep tillage and prolonged drought. The water-holding capacity is moderate, estimated at 55-60% of field capacity, which limits the availability of soil water for plants during periods of intense hydric stress.

The experimental activity was conducted over three consecutive agricultural years: 2021-2022, 2022-2023, and 2023-2024, during which the influence of climatic variability on the behavior of several winter wheat varieties cultivated under the minimum tillage system was assessed. The collected data were processed by calculating mean values across the three experimental years to evaluate the overall performance and stability of the tested varieties under variable environmental conditions.

The minimum tillage system applied consisted of performing a reduced number of soil operations, limited to shallow loosening at 10-15 cm depth, partial retention of crop residues on the surface, and seedbed preparation using a light combinator, followed by direct sowing. This method helps conserve soil moisture, reduce wind erosion, and lower energy consumption, in line with the findings reported by Leonte et al. (2024) and Dinuta et al. (2025).

For the purpose of this study, four winter wheat varieties were selected: Avenue, Katarina, Rubisko, and Sorrial, each characterized by a high yield potential and different levels of adaptability to thermal and water stress. The variety Avenue is known for its good drought tolerance and stable performance under variable conditions; Katarina shows rapid autumn development and high winter hardiness; Rubisko stands out for its superior grain quality and high protein content; and Sorrial is

appreciated for its resistance to major foliar diseases and strong tillering capacity.

The wheat crop was established annually in October, during the optimal sowing period for southern Dobrogea, on land previously cultivated with rapeseed, considered one of the best preceding crops for wheat due to its positive effects on soil structure and reduction of disease and pest pressure in cereals (Georgiev et al., 2024). The sowing density ranged between 400 and 450 viable seeds per square meter, with a row spacing of 12.5 cm and a sowing depth of 5 cm, using a seeder compatible with the minimum tillage system.

Fertilization was applied according to crop development stages and climatic conditions in each year. Balanced NPK doses were used, supplemented with foliar fertilizers and biostimulants, which enhanced root development and increased resistance to abiotic stress (Cioineag & Cristea, 2015; Iosub et al., 2022). Specifically, basal fertilization consisted of NPK complex fertilizers (18-46-0) applied at sowing at a rate of 200 kg/ha, followed by nitrogen top-dressing (ammonium nitrate) applied in early spring (BBCH 21-25) at 100 kg N/ha. Foliar fertilizers and biostimulants based on micronutrients and humic substances were applied during stem elongation (BBCH 30–32). Weed control was achieved through selective herbicides applied post-emergence at recommended doses during early growth stages (BBCH 12–16), while disease management was ensured by modern fungicides adapted to warm and dry climatic conditions applied at key phenological stages (BBCH 31–39 and BBCH 51–59), as recommended by recent research (Nita et al., 2024).

Throughout the growing season, the crop was systematically monitored to capture the influence of climatic and technological factors on plant development. Observations focused on plant density at emergence and tillering, average height at maturity, spike formation, and crop uniformity. Before harvest, representative samples were collected to determine the main morpho-productive indicators: number of grains per spike, grain weight per spike, thousand-kernel weight (TKW), test weight, and average yield per hectare. For the assessment of fertile tillers per plant, measurements were conducted using a systematic sampling approach based on 1 m² observation areas (eight adjacent rows over a length of 1 m), with three replicates per variety. Within each sampling unit, plants were randomly selected and the number of fertile tillers per plant was recorded. Observations were performed at key phenological stages: after emergence (first true leaf stage, BBCH 11), before winter dormancy, after winter recovery, and prior to harvest. The collected data were averaged across replicates and subsequently across the three experimental years to reflect the overall performance and stability of the varieties under the studied conditions.

Crop monitoring was carried out using both multispectral UAV imagery and Sentinel-2 satellite data (10 m spatial resolution). For satellite-based monitoring, a total of 12 Sentinel-2 images were used, acquired during the three agricultural years (2021-2024) at key phenological stages, specifically during stem elongation and peak vegetation (BBCH 30–59). UAV-based data were collected through 6 flight campaigns conducted during the same phenological stages, with flights performed in each experimental year to capture crop development under different climatic conditions. The term “different climatic conditions” refers to the inter-annual variability in key environmental factors, including air temperature, precipitation, and soil moisture availability. These variables were characterized based on recorded meteorological data for each agricultural year and were considered when interpreting crop development and vegetation index dynamics, particularly in relation to drought intensity and water stress conditions. The acquisition dates corresponded to periods of maximum vegetative activity, ensuring comparability between years. To ensure transparency and reproducibility, the exact acquisition dates of the Sentinel-2 images used in the analysis are provided in Table 1. The images were selected based on cloud-free conditions and their correspondence to key phenological stages of crop development (BBCH 30–59), allowing consistent inter-annual comparison of vegetation dynamics.

Table 1. Sentinel-2 image acquisition dates and phenological stages (2021-2024)

| Year | Platform | Acquisition date | BBCH stage | Phenological description |
|---|---|---|---|---|
| 2022 | Sentinel-2A | 12-04-2022 | BBCH 31 | Beginning of stem elongation |
| 2022 | Sentinel-2B | 05-05-2022 | BBCH 37 | Flag leaf visible |
| 2022 | Sentinel-2A | 28-05-2022 | BBCH 55 | Heading |
| 2022 | Sentinel-2B | 15-06-2022 | BBCH 69 | End of flowering |
| 2023 | Sentinel-2A | 10-04-2023 | BBCH 30 | Start of stem elongation |
| 2023 | Sentinel-2B | 02-05-2023 | BBCH 39 | Flag leaf stage |
| 2023 | Sentinel-2A | 25-05-2023 | BBCH 55 | Heading |
| 2023 | Sentinel-2B | 12-06-2023 | BBCH 65 | Full flowering |
| 2024 | Sentinel-2A | 08-04-2024 | BBCH 30 | Stem elongation |
| 2024 | Sentinel-2B | 30-04-2024 | BBCH 37 | Flag leaf |
| 2024 | Sentinel-2A | 22-05-2024 | BBCH 55 | Heading |
| 2024 | Sentinel-2B | 05-06-2024 | BBCH 61 | Beginning of flowering |

Multispectral images acquired from both platforms were processed to derive the Normalized Difference Vegetation Index (NDVI) and other vegetation parameters, including canopy cover, vegetation vigor, and spatial variability of crop development. The combined use of UAV and satellite data allowed for a complementary assessment of crop conditions, integrating the high spatial resolution of UAV imagery with the temporal consistency of Sentinel-2 observations. For each UAV flight campaign, multiple overlapping images were acquired, with the number of images varying depending on the size of the monitored area and flight configuration. The acquired imagery was processed using a standard photogrammetric workflow, including image alignment, dense point cloud generation, and orthomosaic production, resulting in a georeferenced orthomosaic for each campaign.

Flights were performed under controlled acquisition parameters, with relatively constant flight altitude and overlap to ensure data comparability, resulting in high spatial resolution imagery (centimeter-level ground sampling distance, GSD). The main acquisition parameters and flight characteristics are summarized in Table 2.

Table 2. UAV flight campaigns and acquisition parameters (2021-2024)

| Campaign | Year | Date | No. images | Flight altitude (m) | GSD (cm/pixel) | Output | Climatic conditions |
|---|---|---|---|---|---|---|---|
| Flight 1 | 2022 | 14-04-2022 | 280 | 100 | 3.2 | Orthomosaic | Moderate temperature, low rainfall |
| Flight 2 | 2022 | 30-05-2022 | 310 | 100 | 3.1 | Orthomosaic | Warm, increasing water stress |
| Flight 3 | 2023 | 12-04-2023 | 290 | 100 | 3.2 | Orthomosaic | Favorable moisture conditions |
| Flight 4 | 2023 | 28-05-2023 | 320 | 100 | 3.0 | Orthomosaic | Optimal growth conditions |
| Flight 5 | 2024 | 10-04-2024 | 275 | 100 | 3.3 | Orthomosaic | Low soil moisture |
| Flight 6 | 2024 | 25-05-2024 | 300 | 100 | 3.2 | Orthomosaic | Severe drought conditions |

Harvesting was performed mechanically between June 25 and 30 of each experimental year, when grain moisture dropped below 15%. Samples were processed and analyzed following standard agricultural research methodologies. The data obtained were statistically analyzed using the analysis of variance (ANOVA) to identify significant differences among varieties and years, while Pearson correlation analyses were conducted to determine the relationships between yield components and environmental factors. The statistical processing of results ensured the accuracy and reliability of the interpretations, in accordance with the principles stated by Panaitescu et al. (2014).

The applied methodology was designed to assess the combined effects of the minimum tillage system, combined with appropriate variety selection and optimal crop management, contributes to achieving high and stable yields under the pedoclimatic conditions specific to the Dobrogea region. The data obtained were

comparatively analyzed and correlated with the climatic and pedological parameters of the Săcele area, in order to formulate practical conclusions applicable to modern farming practices, consistent with the principles of sustainable and precision agriculture (Haseeb et al., 2025; Raza et al., 2025b).

The cultivation technology applied in the Săcele area was designed to integrate principles of conservative soil management with elements of precision agriculture, through the use of digital tools for crop monitoring and resource optimization. The minimum tillage system consisted of reducing the intensity of soil operations and maintaining crop residues on the surface, thereby limiting water losses through evaporation and preserving soil structure. This approach is particularly suitable under the restrictive pedoclimatic conditions of Dobrogea, contributing to improved moisture conservation and reduced soil compaction (Leonte et al., 2024; Dinuta et al., 2025).

## RESULTS AND DISCUSSIONS

Under the pedoclimatic conditions of the Săcele area, the application of the minimum tillage system was associated with yield values ranging between 4.3 and 5.9 t/ha across the three experimental years. Despite pronounced interannual variability in rainfall, the system supported relatively stable crop development, as reflected by consistent morpho-productive parameters and strong correlations between NDVI and yield. These results indicate that minimum tillage contributed to maintaining wheat performance under drought-prone conditions.

The results further highlight that under increasingly restrictive climatic conditions characterized by rainfall deficits and thermal stress, conservative tillage technologies such as minimum tillage play an important role in ensuring yield stability and agroecosystem sustenability (Kheiralipour et al., 2024; Raza et al., 2025a; Shi et al., 2025).

To further characterize crop development under these conditions, vegetation indices such as canopy cover, vegetation vigor and spatial variability of crop development. Image aquisition was performed at key phenological stages particularly during stem elongation and peak vegetation (BBCH 30-59). These measurements provided essential information regarding crop density, uniformity of emergence, the degree of water stress, and nutrient use efficiency. The NDVI values recorded during the peak vegetation stage were correlated with yield using pooled data across all varieties, establishing a clear positive relationship between higher NDVI values and increased productivity, as also observed by Haseeb et al. (2025) and Joshi et al. (2024).

Complementary to these monitoring activities, a biofertilization program was implemented, based on natural formulations rich in beneficial microorganisms and humic acids. These products were used to stimulate soil microbial activity and enhance nutrient availability, contributing both to agronomic efficiency and to maintaining the ecological balance of the soil system, in line with the findings of Kheiralipour et al. (2024).

Disease and pest management were carried out through integrated plant protection strategies, tailored to the local climatic conditions and phytosanitary status of the crop. During years with high thermal stress and limited rainfall, foliar disease pressure: particularly powdery mildew (*Blumeria graminis f. sp. tritici*) and septoria leaf blotch (*Zymoseptoria tritici*), remained moderate, but preventive treatments were applied using systemic, broad-spectrum fungicides at calibrated doses according to phenological observations. Weed control was gererally low to moderate during the growing season, with dominant dicotyledonous species such as *Galium aparine* and *Stellaria media.* The applied control measures were effective in maintaining a low level of infestation without significant competition effects on crop development.

In the driest years (2021-2022 and 2023-2024), an increased presence of coleopteran pests: especially *Zabrus tenebrioides*, was observed, confirming findings reported by Talmaciu et al. (2024). This trend highlights the influence of drought and high temperatures on pest dynamics, which can intensify crop vulnerability under arid conditions.

The integration of precision agriculture tools, including Global Positioning Systems (GPS) and Geografic Information Systems (GIS), together with UAV-based monitoring,

contributed to a better identification of spatial variability in crop vigor and pest-affected areas. This approach supported more efficient crop management and improved the overall response to biotic and abiotic stress factors, in accordance with the principles of site-specific management (Raza et al., 2025b).

Overall, the technological package implemented under the minimum tillage system contributed to improved crop performance, as reflected by the obtained yield values (4.3-5.9 t/ha) and the strong positive correlations between yield and key indicators such as NDVI (r = 0.97), thousand kernel weight (r = 0.94). And test weight (r = 0.91). Under the restrictive pedoclimatic conditions of Dobrogea, the application of precision technologies and biofertilization supported efficient resource use and enhanced crop stability, as also indicated by the consistent performance of adaptable varieties such as Rubisko and Avenue (Gheorghe & Nicolae, 2023; Kheiralipour et al., 2024; Nita et al., 2024).

The average NDVI values recorded for the four analyzed wheat varieties (Avenue, Katarina, Rubisko, and Sorrial) show a distinct interannual variation across the growing seasons, closely related to the climatic and rainfall patterns of each year (Figure 1). The highest average NDVI values were recorded in the 2022-2023 agricultural year (with approximately 380 mm of annual rainfall and a mean temperature of 12.5°C), when the index ranged between 0.72 and 0.78, indicating a vigorous vegetative growth and high photosynthetic activity.

In contrast, during 2021-2022 and especially 2023–2024, NDVI values decreased significantly (0.58-0.68), which may be associated with prolonged pedological drought and thermal stress affecting green biomass development. The 2023-2024 season, with rainfall below 290 mm, was the most restrictive, leading to a reduction in active leaf area and irregular crop density, as also reflected by the lower NDVI values derived from UAV multispectral imagery (Figure 1).

Among the tested varieties, Rubisko consistently exhibited the highest NDVI values, indicating higher vegetation vigor and suggesting a better adaptability to the given environmental conditions, followed by Avenue and Sorrial. These differences are consistent with previous studies reporting stable performance of modern wheat varieties under conservative soil management systems, supporting the observed varietal differences in this study (Gheorghe & Nicolae, 2023; Dinuta et al., 2025).

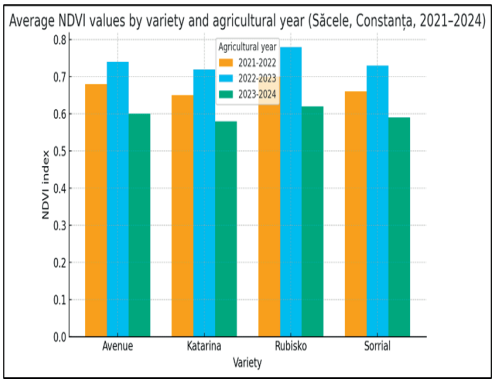



Figure 1. Average NDVI values by wheat variety and agricultural year (Săcele, Constanța, 2021-2024)

The correlation analysis between mean NDVI values and wheat yield across the three experimental years revealed a strong positive relationship (r = 0.97), confirming the reliability of NDVI as an early indicator of crop performance under precision agriculture systems (Figure 2). Higher NDVI values were directly associated with higher yields, reflecting the beneficial effect of a dense and healthy canopy on dry matter accumulation and grain filling.

The 2022-2023 agricultural year, characterized by relatively favorable rainfall distribution and moderate temperatures during grain filling, recorded the highest average yield (6.4 t/ha), corresponding to the maximum NDVI value (0.74). Conversely, the 2023-2024 season, marked by extreme drought and heat stress, showed the lowest NDVI (0.59) and an average yield of 4.1 t/ha, illustrating the strong sensitivity of winter wheat to hydric stress in arid environments. The close NDVI–yield relationship confirms the potential of multispectral imagery and vegetation indices as powerful tools for yield modeling and site-specific resource management. These results are in line with studies by Haseeb et al. (2025) and Raza et al. (2025a), which demonstrated that the

integration of optical sensors and remote sensing algorithms in agricultural monitoring systems allows optimized fertilization and phytosanitary treatments, reducing yield losses under extreme climatic variability.

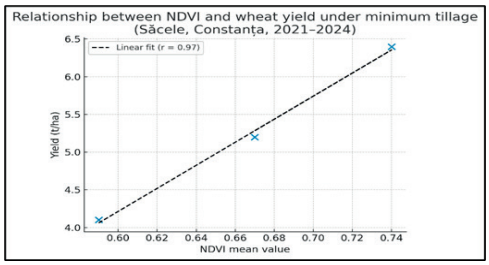



Figure 2. Relationship between average NDVI values and wheat yield across the three experimental years (inter-annual analysis) under the minimum tillage system (r = 0.97)

Under such pedoclimatic constraints, the implementation of the minimum tillage system in the Săcele area represents a well-adapted technological approach. By minimizing soil disturbance and maintaining crop residues on the surface, this system contributes to improved water-use efficiency, reduced fuel consumption, and erosion control, without significant yield penalties. These findings are consistent with results reported in other parts of Dobrogea (Ghiorghe et al., 2024; Nita et al., 2024).

Tillering represents one of the most important phenological stages in the development of wheat, having a decisive role in determining the yield potential by establishing the number of fertile tillers that contribute to the final spike density. This process is strongly influenced by soil moisture and temperature conditions during autumn and early spring, as well as by soil fertility and the cultivation technology applied (Panaitescu et al., 2014; Dinuta et al., 2025).

Under the pedoclimatic conditions of the Săcele area, characterized by low annual rainfall and mild winters, tillering occurred more slowly but uniformly, especially under the minimum tillage system, where crop residues retained higher moisture levels in the upper soil layers. The measurements revealed moderate differences between varieties, with average values ranging between 2.8 and 3.5 fertile tillers per plant, and a general mean of 3.1. The varieties Rubisko and Avenue showed the highest tillering capacity (3.5 and 3.3 fertile tillers per plant, respectively), due to their strong vegetative vigor and well-developed root systems, which allowed for better utilization of soil moisture. The variety Katarina exhibited a moderate tillering capacity (2.8 tillers per plant), typical for short-stature genotypes, while Sorrial recorded an intermediate value (3.0 tillers per plant), demonstrating balanced adaptation to both thermal and hydric stress.

The results confirm that the minimum tillage technology promotes more uniform tillering compared to conventional systems, due to better moisture conservation and reduced thermal fluctuations in the germination layer. Overall, the behavior of the analyzed varieties indicates a good adaptive capacity, with clear genetic differences among genotypes, an important advantage when selecting varieties suited to the pedoclimatic conditions of Dobrogea.

Plant height is a fundamental morphological indicator, reflecting each variety's ability to utilize available water and nutrient resources and to adapt to the pedoclimatic conditions specific to the cultivation area. Plant stature is influenced by both genetic characteristics and cultivation technology, as well as by soil fertility and climatic factors (Axinte et al., 2006; Panaitescu et al., 2014).

The measurements conducted in the agricultural area of Săcele, Constanța County, within the experiment carried out under the minimum tillage system during the 2021-2024 agricultural years, revealed notable differences among the analyzed varieties. The reported values represent multi-year means calculated across the three experimental years. The average plant height ranged between 83 cm and 92 cm, with a general mean of 88 cm for the entire experimental period. Among the four studied varieties, Rubisko exhibited the greatest height (92 cm), followed by Avenue (89 cm), Sorrial (87 cm), and Katarina, which showed the lowest height (83 cm) (Figure 3). These differences reflect both the genetic distinctiveness of each variety and their variable adaptive capacities to the restrictive conditions of the Dobrogea region, where rainfall is limited and thermal stress is frequent. The greater height of Rubisko can be associated with strong vegetative growth and enhanced ability to exploit deep soil moisture, an advantage conferred by its robust root structure and adaptability to semi-arid

conditions (Nita et al., 2024; Georgiev et al., 2024).

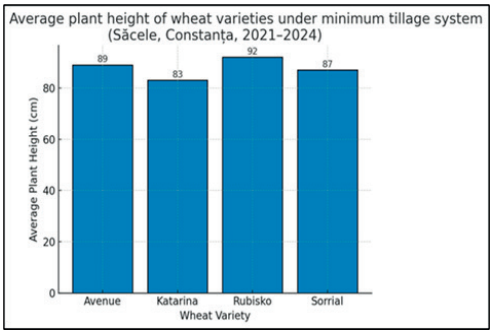



Figure 3. Average plant height of wheat varieties under minimum tillage system (Săcele, Constanța, 2021-2024, mean values across three experimental years)

The Avenue variety, although slightly shorter, displayed constant growth and high morphological stability, which was accompanied by elevated NDVI values recorded in the 2022-2023 season. In contrast, Katarina's shorter stature represents a genetically designed trait, offering increased lodging resistance and metabolic efficiency during dry years, when plants with extensive leaf area are more susceptible to excessive evapotranspiration. Sorrial exhibited intermediate behavior, showing balanced and uniform growth, well adapted to the minimum tillage system, which better preserves soil moisture in the active layer. The general mean height of 88 cm is slightly below the values reported for more humid regions of Romania, such as the Pecica-Arad area where higher plant heights have been observed under more favorable water conditions (Pop et al., 2024) a difference explained by the pedoclimatic characteristics of southern Dobrogea, where water stress limits vegetative growth (Leonte et al., 2024; Dinuta et al., 2025). Nevertheless, the relatively uniform values recorded for key morpho-productive parameters, such as plant height and tillering capacity, across experimental plots demonstrates a good adaptability of modern wheat varieties to local environmental conditions and confirms the efficiency of the minimum tillage system in maintaining balanced plant development. The results indicate that Rubisko performed best in terms of morphological development, followed by Avenue and Sorrial, while Katarina, despite its shorter height, stood out through stability and stress tolerance. The comparative analysis confirms that variety selection, combined with the application of conservative technologies, represents a key factor in ensuring uniform growth and a high productive potential under the pedoclimatic conditions of the Dobrogea region. The grain mass per spike and the number of grains per spike are key morpho-productive indicators of the agronomic value of wheat, being closely correlated with the final yield. Under the restrictive pedoclimatic conditions of the Săcele area: characterized by low annual rainfall (below 330 mm in 2021-2022, approximately 380 mm in 2022-2023, and below 290 mm in 2023-2024), these two traits reflected both the genetic differences among varieties and the influence of annual climatic variability on grain formation and filling processes.

The yield results showed clear differences among the analyzed wheat varieties across the three experimental years (Figure 4). In 2021-2022, the average yield was 5.2 t/ha, with higher values recorded for Rubisko and Avenue, while Katarina showed the lowest performance. In 2022-2023, the most favorable year, the average yield increased to 6.4 t/ha, maintaining the same varietal ranking. In contrast, during the driest year (2023-2024), the average yield decreased to 4.1 t/ha, although Rubisko and Avenue continued to exhibit better adaptability under drought conditions compared to Sorrial and Katarina. These differences were supported by statistical analysis (ANOVA, $p < 0.05$), confirming the significant effect of varietal characteristics and climatic conditions on yield performance.

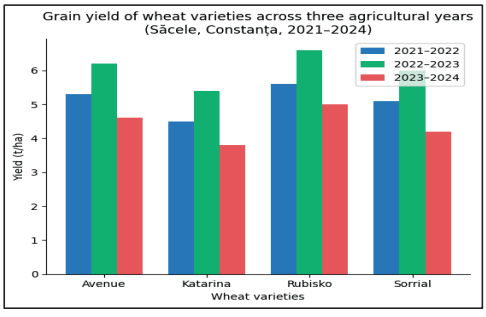



Figure 4. Grain yield of wheat varieties across three agricultural years (Săcele, Constanța, 2021-2024).

On average, Rubisko recorded 48 grains per spike and a grain mass per spike of 2.08 g, ranking first; Avenue registered 47 grains per spike and 2.02 g; Sorrial had 46 grains per spike and 1.98 g; while Katarina, despite its shorter stature and good stress resistance, reached 45 grains per spike and 1.93 g (Figure 5). The results show a positive relationship between the number and the mass of grains per spike across all varieties. Rubisko recorded the highest values (48 grains/spike and 2.08 g), confirming its superior fertility and adaptability under drought-prone conditions. Avenue and Sorrial exhibited stable intermediate performances, while Katarina had the lowest averages, consistent with its shorter and more conservative growth type. The data indicate that vigorous varieties achieved better grain filling under the minimum tillage system due to improved soil moisture conservation, and the observed differences were statistically significant (ANOVA, $p < 0.05$). The hierarchy correlates with both NDVI values and average plant height, suggesting that vegetative vigor and efficient water use under the minimum tillage system contributed to better grain filling and superior spike fertility. The differences among varieties were statistically confirmed through ANOVA, while positive correlations between the number and mass of grains per spike and yield were supported by correlation analyses, in agreement with previous studies reporting similar relationships between spike fertility, components and yield performance, where higher grain number and grain weight per spike were associated with increased productivity (Nita et al., 2024; Pop et al., 2024).

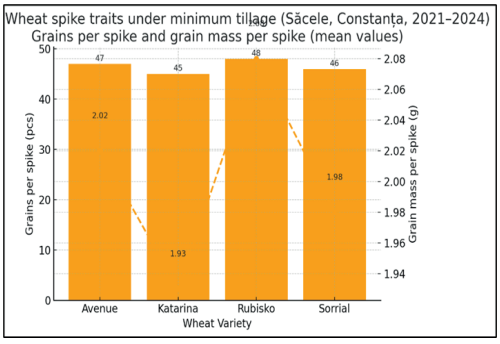



Figure 5. Wheat spike traits under minimum tillage (Săcele, Constanța, 2021–2024): grains per spike and grain mass per spike (mean values)

The thousand kernel weight (TKW) values recorded in this study ranged between 40.8 g and 44.1 g, reflecting differences in grain filling and varietal performance under pedoclimatic conditions of Săcele area. These variations indicate the influence of both genetic characteristics and environmental factors, particularly water avaibility and nutrient use efficiency during the grain filling period (Roman et al., 2013; Stroe & Panaitescu, 2025). Under the restrictive climatic conditions of the Săcele area, where the annual rainfall was below the multiannual average (≈330 mm in 2021-2022, ≈380 mm in 2022-2023, and below 290 mm in 2023-2024), TKW values ranged between 40.8 g and 44.1 g, with a general mean of 42.6 g. Among the tested varieties, Rubisko recorded the highest value (44.1 g), confirming its superior grain-filling capacity and resistance to water stress. Avenue (43.2 g) and Sorrial (42.5 g) showed intermediate values, while Katarina (40.8 g) had the lowest kernel weight, correlated with its shorter stature and more conservative growth rate (Figure 6).

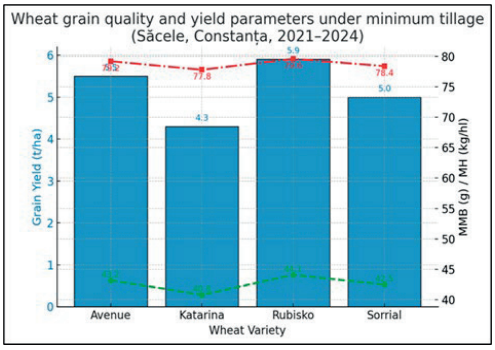



Figure 6. Wheat grain quality and yield parameters under minimum tillage (Săcele, Constanța, 2021-2024)

The test weight (TW), an indicator of grain density and physical quality, ranged between 77.8 and 79.6 kg/hl, with an average of 78.7 kg/hl. The high values recorded for Rubisko (79.6 kg/hl) and Avenue (79.2 kg/hl) indicate a complete grain filling and good physiological condition of the crop, even under drought conditions. Sorrial (78.4 kg/hl) and Katarina (77.8 kg/hl) showed slightly lower quality, but still within the standards for bread wheat.

Regarding grain yield, the average values obtained over the three agricultural years (2021-

2024) ranged between 4.3 and 5.9 t/ha, showing similar trends to NDVI and test weight (TW). The most productive variety was Rubisko with an average of 5.9 t/ha, followed by Avenue (5.5 t/ha), Sorrial (5.0 t/ha), and Katarina (4.3 t/ha).

The results confirm that the interaction between genotype and the minimum tillage technology, under accentuated drought conditions, significantly influences both the quality and productivity of the crop. Varieties with higher vegetative vigor and deeper root systems, such as Rubisko and Avenue, were more efficient in utilizing residual moisture and nutrients, maintaining good yield stability during dry agricultural years. The differences among varieties were statistically significant (ANOVA, $p < 0.05$), and correlation analyses revealed positive relationships between TKW, TW, and average yield, confirming that these indicators can serve as reliable predictors of yield performance in the arid climate of Dobrogea. The results highlight a clear positive relationship between grain yield, thousand kernel weight (TKW), and test weight (TW) across the studied wheat varieties. The variety Rubisko showed superior performance for all parameters, confirming its high adaptability and physiological efficiency under drought-prone conditions. Avenue also maintained stable yield and grain quality, while Sorrial and Katarina achieved slightly lower values, consistent with their more conservative growth patterns. The data demonstrate that varieties combining strong vegetative vigor with efficient resource use achieve both higher yield and better grain quality under the minimum tillage system in semi-arid regions.

The results revealed strong and relationships between morpho-productive parameters and agronomic performance particularly, between average yield, thousand kernel weight (TKW), test weight (TW), and the NDVI index.

The results revealed strong positive correlations between yield and TKW (r = 0.94), as well as between yield and TW (r = 0.91), confirming that well-developed grains and high endosperm density are key determinants of yield performance under drought conditions. Furthermore, the correlation between NDVI and yield (r = 0.97) suggests that NDVI can serve as reliable predictive indicator for estimating yield potential and supporting data-driven crop management decisions. The regression analysis indicated a significant linear relationship ($p < 0.05$) between NDVI and yield ($R^2 = 0.93$), demonstrating that variations in active biomass can explain over 90% of the yield variability under the climatic conditions of the study area. A strong positive linear relationship was observed between NDVI values and average grain yield across the studied wheat varieties ($R^2 = 0.93$). Varieties with higher NDVI, such as Rubisko and Avenue, achieved greater productivity, reflecting their superior vegetative vigor and efficient resource utilization under drought-prone conditions. The regression model indicates a strong relationship between NDVI and yield performance ($R^2 = 0.93$), suggesting the potential of NDVI as an indicator for yield estimation under minimum tillage systems (Figure 7). The NDVI values used in this analysis are higher than those presented in Figure 2, as they represent varietal averages derived from peak vegetation stages, reflecting maximum canopy development. The correlations between yield and other parameters such as thousand kernel weight (TKW) and test weight (TW), are presented based on numerical statistical analysis in the text, without additional graphical representation. While Figure 2 illustrates the NDVI–yield relationship based on inter-annual variability, the following analysis focuses on the varietal-level relationship, highlighting differences in crop performance among the studied wheat varieties.

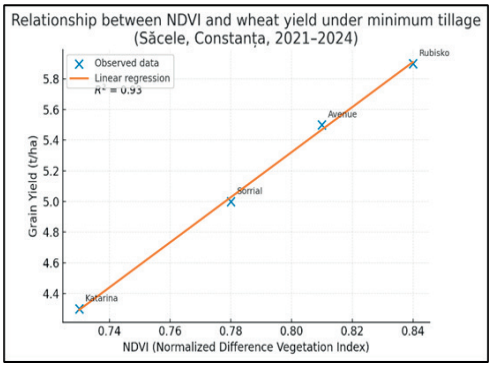



Figure 7. Relationship between average NDVI values and grain yield at the varietal level under minimum tillage (Săcele, Constanța, 2021-2024).

Within the experiment conducted in the Săcele area, the minimum tillage technology was

complemented by the application of precision agriculture tools aimed at optimizing crop management and monitoring plant development. Vegetation monitoring was carried out using both UAV multispectral imagery and Sentinel-2 satellite data, from which NDVI was derived to assess canopy uniformity and crop vigor across different phenological stages. Based on these data, fertilizer rates and phytosanitary treatments were adjusted accordingly, reducing over-application and improving cost efficiency. Variable-rate applications were performed using GPS-guided equipment and spatial data derived from UAV and satellite monitoring, ensuring precise and uniform distribution, thereby enhancing input efficiency and minimizing environmental impact. The integration of these digital tools demonstrated significant benefits in managing abiotic stress and maintaining a balance between productivity and sustainability, confirming the potential of precision agriculture in optimizing wheat cultivation under the arid climatic conditions of Dobrogea.

## CONCLUSIONS

The results obtained from the study conducted in the Săcele area, Constanța County, during 2021-2024, highlight the adaptability of the wheat varieties Rubisko and Avenue to the restrictive pedoclimatic conditions of Southern Dobrogea, as reflected by their higher yield performance and NDVI values under low rainfall and frequent thermal stress. The application of the minimum tillage system contributed to soil moisture conservation, structural stability, and reduced energy consumption in field operations.

Among the tested varieties, Rubisko consistently achieved the highest morpho-productive performance, with superior values for grain weight, test weight, and average yield (5.9 t/ha), confirming its enhanced efficiency in resource use and strong drought tolerance. The varieties Avenue and Sorrial demonstrated good yield stability and grain quality, making them suitable for conservative farming systems, while Katarina, though more moderate in growth, showed stable performance and can be recommended for areas facing pronounced water stress.

Statistical analyses revealed strong positive correlations between yield, thousand kernel weight, test weight, and NDVI ($r = 0.91$-$0.97$), while the linear regression analysis ($R^2 = 0.93$) indicated a strong association between NDVI and yield. These findings highlight the value of integrating precision agriculture tools, such as multispectral imaging and variable-rate input application, to support improved wheat management under drought-prone conditions.

In conclusion, combining minimum tillage practices with digital monitoring and the selection of locally adapted varieties contributes to stable wheat production under the pedoclimatic conditions of southern Dobrogea. It is recommended to expand future research through multi-location and long-term trials, focusing on the cumulative effects on soil fertility and resource efficiency, as well as on the integration of AI-based predictive models to improve climate risk forecasting and adaptive management strategies.

## REFERENCES

Arif, M., Haroon, M., Nawaz, A. F., Abbas, H., Xu, R., & Li, L. (2025). Enhancing wheat resilience: biotechnological advances in combating heat stress and environmental challenges. *Plant Molecular Biology, 115*(2), 41.

Axinte, D. A., Andrews, P., Li, W., Gindy, N., Withers, P. J., & Childs, T. H. C. (2006). Turning of advanced Ni based alloys obtained via powder metallurgy route. CIRP annals, 55(1), 117-120.

Buzatu, C.S., Ghiuleanu, I.V., Marcuta, A.G., Popa, I.V. (2024). Climate change and land temperatures and their impact on agriculture and society: a global investigation. *Scientific Papers. Series Management, Economic Engineering in Agriculture and rural development, 24*(4), 121-130.

Buzatu, C.S., Ghiuleanu, I.V., Tudor, V.C. (2023). Dynamics of land fund and strategies on soil conservation and prevention of soil degradation in Romania. *Scientific Papers. Series Management, Economic Engineering in Agriculture and rural development, 23*(4), 149-156.

Cioineag, C. F., & Cristea, S. (2015), Partial results regarding the management of fertilization and fungicides treatments on premium wheat varieties. *Scientific Papers. Series A. Agronomy, 58*, 159-167.

Dinuta, I.C., Podea, M.M., Marin, D.I. (2025). The behavior of winter wheat in the conservative tillage system under the conditions at A.R.D.S. Pitești - Albota. *Scientific Papers. Series A. Agronomy, 68(1)*, 80-89.

Georgiev, S., Rashev, S., Palagacheva, N., Ivanova, S. (2024). Development of durum wheat (Triticum turgidum subsp. durum (Desf.) Husn.) grown after a different predecessor under organic farming

conditions. *Scientific Papers. Series A. Agronomy, 67*(1), 401-407.

Gheorghe, R.M., & Nicolae, C.M. (2023). Characteristics of some new varieties and lines of wheat under the year 2021-2022 conditions. *Scientific Papers. Series A. Agronomy, 66*(1), 81-86.

Ghiorghe, A.I., Cioromele, G.A., Trifan, D., Axinti, N., Risnoveanu, L., Braila, M., Lungu, E. (2024), Comparative analysis of various winter wheat varieties cultivated under the climatic conditions of ARDS Braila. *Scientific Papers. Series A. Agronomy, 67*(1), 238-243.

Grigoraș, M. A., Popescu, A., Pamfil, D., Has, I., & Gidea, M. (2012). Influence of no-tillage agriculture system and fertilization on wheat yield and grain protein and gluten contents. *Journal of Food, Agriculture and Environment, 10*(2), 539.

Haseeb, M., Tahir, Z., Mahmood, S. A., & Tariq, A. (2025). Winter wheat yield prediction using linear and nonlinear machine learning algorithms based on climatological and remote sensing data. *Information Processing in Agriculture.*

Iosub, L.M., Radu, M., Mihalascu, C., Cristea, S. (2022). The effectiveness of treatments in the control of wheat diseases, Moara Domnească location, Ilfov County. *Scientific Papers. Series A. Agronomy, 65*(1), 374-378.

Joshi, P., Sandhu, K. S., Dhillon, G. S., Chen, J., & Bohara, K. (2024). Detection and monitoring wheat diseases using unmanned aerial vehicles (UAVs). *Computers and Electronics in Agriculture, 224*, 109158.

Kheiralipour, K., Brandão, M., Holka, M., & Choryński, A. (2024). A review of environmental impacts of wheat production in different agrotechnical systems. *Resources, 13*(7), 93.

Leonte A., Isticioaia S.F., Popa L.D., Pintilie A.S., Naie M., Simon A. 2024, Effect of tillage systems on the yield and quality of winter wheat grain. *Scientific Papers. Series A. Agronomy, 67*(1), 500-507.

Nita, S., Nita, L., Imbrea, F., Hinda, I.A., Batrina, S., Botos, L. (2024). Study of quantitative and qualitative indicators in wheat. *Scientific Papers. Series A. Agronomy, 67*(1), 581-586.

Nyaupane, S., Poudel, M. R., Panthi, B., Dhakal, A., Paudel, H., & Bhandari, R. (2024). Drought stress effect, tolerance, and management in wheat - a review. *Cogent Food & Agriculture, 10(1),* 2296094.

Panaitescu, L., Ilie, C., Lungu, M. L., Popescu, M., Lungu, D., & Nita, S. (2014). *Modern approach to the phenomenon of drought and aridity in Central and South Dobrudja.*

Partal, E., Oltenacu, C.V., Paraschivu, M., Cotuna, O., Contescu, E.L. (2023). Wheat yield and quality under the influence of sowing date, plant density and variety in South of Romania. *Scientific Papers. Series A. Agronomy, 66*(2), 339-345.

Pascu, G. (2012). Research regarding weed infestation in wheat crop at ecologic Prod Farm, Mihail Kogălniceanu - Constanța county. *Scientific Papers. Series A. Agronomy, 55*, 212-215.

Pop, C.I., Batrina, S.L., Imbrea, I.M., Pop, G., Nita, S., Hinda, I.A., Botos, L., Imbrea, F. (2024). Study on winter wheat production and quality in the Pecica-Arad Area. *Scientific Papers. Series A. Agronomy, 67*(1), 347-351.

Qosimov, F., & Imomov, B. (2025). Determining the impact of climate change on agricultural production using artificial intelligence (case study of wheat and cotton). *Journal of Multidisciplinary Innovation in Science and Education, 1*(1), 82-88.

Raza, A., Shahid, M. A., Zaman, M., Miao, Y., Huang, Y., Safdar, M., & Muhammad, N. E. (2025a). Improving Wheat Yield Prediction with Multi-Source Remote Sensing Data and Machine Learning in Arid Regions. *Remote Sensing, 17*(5), 774.

Raza, D., Shu, H., Ehsan, M., Fan, H., Abdelrahman, K., Aslam, H., & Sardar, A. (2025b). Evaluation of agriculture land transformations with socio-economic influences on wheat demand and supply for food sustainability. *Cogent Food & Agriculture, 11*(1), 2448597.

Roman, G. V., Nițu, A. C., Belc, N., Iorga, E., Nițu, I., & Epure, L. I. (2013). Romanian wheat-strategic product for national economy. S*cientific Papers. Series A. Agonomy., Vol. LVI,* ISSN 2285-5785, 337-343.

Shaheen, A., Li, Z., Yang, Y., Xie, J., Zhu, L., Li, C., & Song, C. P. (2025). Genetic regulation of wheat plant architecture and future prospects for its improvement. *New Crops, 2,* 100048.

Shi, Y., Pan, S., You, Y., Prior, S. A., Tian, D., Yu, H., & Tian, H. (2025). Extreme Dry-Heat Climate Impacts on Greenhouse Gas Emission Intensity in Wheat Production. *Insights and Mitigation Strategies. Global Change Biology, 31*(7), e70349.

Stroe, T. C., Mihai Florea, O., Niță, S., & Panaitescu, L. (2025). Assessment of the impact of minimum tillage technology on soil properties and winter wheat yield under the pedoclimatic conditions of Poarta Albă, Constanța County (2021-2024). *Research Journal of Agricultural Science, 57*(2).

Stroe, T. C., & Panaitescu, L. (2025). Assessment of the Transition from Conventional Soil Tillage to Minimum Tillage Technology in A Maize Crop with Three Hybrids–A Three-Year Case Study in Lanurile, Constanța County. *International Journal of Innovative Approaches in Agricultural Research, 9*(3), 217-231.

Stroe, T. C, Miron, L., & Panaitescu, L. (2026). Evaluation of comparative productivity of the romanian pea variety 'nicoleta' under conventional and no-till systems in the arid region of dobrogea. *Bangladesh Journal of Botany, 55*(1), 13–19.

Talmaciu, N., Talmaciu, M., Herea, M., Mocanu, I., Mitrea I. (2024). The biodiversity of coleoptero-fauna from wheat crops in the conditions of the new climate changes and the premerging plant. *Scientific Papers. Series A. Agronomy, 67*(1), 624-631.

Xiong, W., Reynolds, M. P., Montes, C., Crossa, J., Snapp, S., Akin, B., & Chen, F. (2024). New wheat breeding paradigms for a warming climate. *Nature Climate Change, 14*(8), 869-875.

Zorovski, P. (2024). Comparative study of growth and development of common wheat in organic and conventional agrocenoses. *Scientific Papers. Series A. Agronomy, 67*(1), 751-760.

Scientific Papers. Series E. Land Reclamation, Earth Observation & Surveying, Environmental Engineering. Vol. XV, 2026
Print ISSN 2285-6064, CD-ROM ISSN 2285-6072, Online ISSN 2393-5138, ISSN-L 2285-6064

# ON THE IMPORTANCE OF ENVIRONMENTAL FACTOR PROTECTION IN KEY AREAS OF THE BORDER ZONE. CASE STUDY ROMANIA-UCRAINA, MARAMUREȘ MOUNTAINS

**Maria ȘEVERA[1], Mirela COMAN[2]**

[1]University of Agricultural Sciences and Veterinary Medicine of Cluj-Napoca, 3-5 Mănăștur, Cluj-Napoca, Romania
[2]Technical University of Cluj-Napoca, 62 A V. Babeș Street, Baia Mare, Romania

Corresponding author email: maria.severa@student.usamvcluj.ro

***Abstract***

*Key areas located in the northernmost part of Romania, within the Maramureș Mountains along the northern border with Ukraine, represent agro-mountain ecosystems of high value for environmental stability and regional ecological security. This cross-border area is exposed to increased anthropogenic pressures in the context of the armed conflict in Ukraine, which amplifies the vulnerability of environmental components, biodiversity, and ecosystem functionality. The study addresses the assessment of environmental impacts on soil, water resources, biodiversity, and habitat fragmentation through an integrated approach specific to environmental science and engineering. The methodology is based on environmental quality indicators, pedological and hydrological analyses, ecosystem condition assessment, multi-criteria evaluation methods, and GIS tools for the spatial analysis of pressures and impacts. The results highlight the need to implement preventive-oriented environmental protection measures aimed at biodiversity conservation and the reduction of ecological degradation risks in border regions. Romania–Ukraine cooperation is essential for the sustainable management of environmental impacts in transboundary areas affected by conflict-induced regional instability.*

***Key words****: environmental impact, key-areas, transboundary area.*

## INTRODUCTION

The Maramureș Mountains constitute a fundamental pillar of ecological stability in the northern part of Romania, representing a transboundary agro-montane ecosystem with a biodiversity of European importance. The importance of protecting environmental factors in this key area is emphasized by the status of a protected area (Maramureș Mountains Natural Park) and by the need to maintain the ecological security of the border with Ukraine (Ilieș et al., 2010). In the context of 2026, anthropogenic pressures on this ecosystem have diversified, being amplified by regional instability that generates additional risks for soil, water and habitats (Ukraine conflict environmental briefing: Nature, 2024). The degradation of environmental factors in border areas is not only a regional problem, but a systemic one, because habitat fragmentation and transboundary pollution can affect ecological connectivity across the entire Carpathian chain (Kuemmerle et al., 2011). The use of modern technologies, such as Geographic Information Systems (GIS) and remote sensing, has become imperative for monitoring these hard-to-reach areas, providing precise data on land use dynamics and ecosystem health (McGarigal, 2015; ESA, 2026). This paper analyzes these vulnerabilities and proposes preventive measures based on a multi-criteria environmental impact assessment.
The hydrographic structure of the Vișeu basin is defined by a series of lotic systems with sources in the Maramureș Mountains, among which the right tributaries Ruscova (39 km), Socolău (13 km) and Bardi (11 km) stand out (Curtean-Bănăduc et al., 2008; Bănăduc et al., 2011a, Curtean-Bănăduc et al., 2017). There are three administrative-territorial units (Poienile de Sub Munte, Repedea, Ruscova) with approximately 19,343 inhabitants in 2021 (National Institute of Statistics, 2023). As can be seen in Figure 1, this cross-border area is exposed to increased anthropogenic pressures, which amplifies the vulnerability of soil and water resources (Kucsicsa & Popovici, 2016), biodiversity and ecosystem functionality.
Among the monitored taxonomic units, fish present a heightened vulnerability to pressures

exerted by human activities, being directly affected by habitat changes and anthropogenic stressors (Năvodaru & Năstase, 2006; Bănăduc et al., 2011b; Florea, 2017; Khoshnood, 2017).

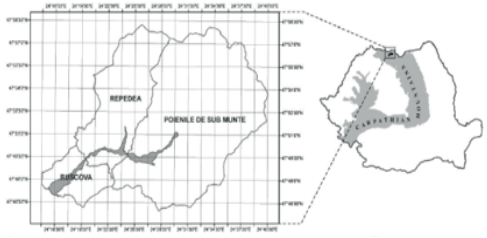



Figure 1. Valea Ruscova Depression (processing after) (Kucsicsa & Popovici, 2016)

## MATERIALS AND METHODS

The methodology uses GIS tools for spatial analysis of pressures (Kłapyta et al., 2024) and quality indicators related to environmental standards (Ministry of Water, Forests and Environmental Protection, 1997). The assessment of anthropogenic pressures on the ichthyofauna in the Vișeu basin must be carried out in accordance with national environmental quality standards (Ministry of Water, Forests and Environmental Protection, 1997). At the same time, given the transboundary nature of the watercourses in the region, their management is subject to international agreements for the protection of common water resources (Parliament of Romania, 1995), within the broader framework of environmental protection legislation (Parliament of Romania, 2005). The current configuration of the agro-montane landscape and the state of habitats in the Poienile de Sub Munte sector, observed during the field monitoring stages, are presented in Figure 2.
Spatial analyses carried out in the watersheds of the Maramureș Mountains (e.g. Ruscovei Valley) indicate a high vulnerability of water quality to anthropogenic influences, especially through increased nitrate concentrations from agricultural and domestic activities (Kucsicsa & Popovici, 2016). The use of Geographic Information Systems (GIS) allows the identification of critical areas where environmental factors and population density converge, generating risks of pollution of water resources essential for local biodiversity (Kucsicsa & Popovici, 2016).



Figure 2. Panoramic view of the study area in the Poienile de Sub Munte administrative unit; the mosaic of forest and agricultural habitats is observed (Source: Author's personal archive, 2024)

Monitoring environmental factors involves the use of status indicators that reflect the degree of anthropization and the risk of ecological degradation of protected areas (Coman, 2010). Mountain ecosystems are highly vulnerable to human interventions, degradation processes often being irreversible in the absence of well-structured conservation measures (Coman, 2010). Natural resource management in the Ruscova Corridor must align with the principles of sustainable development specific to Maramureș County, where the protection of fragile ecosystems is inextricably linked to the economic viability of local communities (Coman, 2006).
Digitalization of the management of resources involved in environmental protection facilitates superior team coordination in difficult areas, such as the Ruscova Corridor, ensuring clear traceability of field activities and interventions in vulnerable areas (Thira et al., 2025). This digital infrastructure allows for rigorous data collection necessary for the assessment of ecological security, which must take into account the transfer capacity of pollutants from soil to vegetation. The use of transfer indices similar to those analyzed in recent studies in the Maramureș region is essential to prevent risks of bioaccumulation in the food chain and to ensure food security for local communities (Filip & Coman, 2024; 2025).

## RESULTS AND DISCUSSIONS

The forests of Maramureș are under double pressure: on the one hand human activity/conflict, on the other hand drought and increasing temperatures in recent years, which

limit tree growth (Popa et al., 2024). The forests of Maramureș not only produce wood, but also provide ecosystem services (soil protection, water regulation, biodiversity) valued at impressive amounts. The study shows that the "conservation" scenario offers a much higher total value in the long term than intensive timber exploitation (Popa et al., 2016).

Sustainable management of mountain ecosystems must recognize soil not only as an agricultural resource, but as a strategic asset capable of providing vital ecosystem services (carbon storage, water filtration, biodiversity), fundamental for the ecological security of the region (Cioruta & Coman, 2022). Early studies on ciliates in the Tisza basin (Kovalchuk, 1997) established a baseline state of aquatic biodiversity. Comparing these data with recent monitoring (e.g. Bitušík et al., 2025) allows identifying the cumulative impact of pollution and climate change on the mountain lotic ecosystems of the Maramureș Mountains.

The sustainable management of the Ruscova Corridor must take into account the adaptability of forest species to climate change, given the high sensitivity of spruce and fir to thermal and water stress identified in the region (Popa et al., 2024). The protection of juniper habitats in the subalpine floor of the Maramureș Mountains is critical, given their role in stabilizing slopes and the presence of specific insect communities, such as Retinia rosinella, which require undisturbed habitats to maintain biological balance (Olenici & Semeniuc Fecioru, 2021).

It is not just a matter of visible pollution, but of a biological collapse: soil fauna can no longer mediate litter decomposition (Dou & Lin, 2026), while the main forest species are already at the limit of resilience due to thermal stress (Popa et al., 2024). Regional ecological security can be supported by integrating varieties improved for productivity and resistance into the local agricultural circuit, thus ensuring a stable fodder base, without resorting to excessive chemical fertilization, protecting biodiversity and water resources (Schitea, 2010).

Environmental protection in the Ruscova Corridor can be supported by encouraging local entrepreneurship in rural tourism. Digitalization of services and promotion of authentic cultural heritage reduce pressure on natural resources by offering a sustainable economic alternative to intensive forestry (Ciolac et al., 2022). Environmental protection in Maramureș must go hand in hand with the preservation of the historical and cultural testimonies of the communities, as these form the local identity that underpins any sustainable regional development initiative (Cioruță et al., 2023).

Climate change in the Eastern Carpathians is leading to earlier snowmelt, a process that, while initially increasing carbon sequestration capacity, drastically alters ecosystem dynamics throughout the growing season (Vought et al., 2025). Deforestation in the Ruscova Corridor not only reduces woody mass, but also destroys the ecosystem's ability to moderate maximum temperatures. This phenomenon, combined with earlier snowmelt (Vought et al., 2025) and the sensitivity of spruce to heat (Popa et al., 2024), creates a "cascade" effect that threatens regional ecological security (Abera et al., 2025).

The ecological security of the Pop Ivan transboundary area depends on the integrity of its peatlands, which function as critical carbon reservoirs. Retrospective studies (Deyl et al., 2023) establish a historical purity standard (pH 3.8-5.5 and conductivity below 40 µS/cm), any deviation from these values being indisputable evidence of anthropogenic or military pollution at the border. Alteration of this bio-chemical balance, corroborated with early snowmelt (Vought et al., 2025), risks transforming these bogs from carbon stores into massive sources of greenhouse gas emissions, accelerating the degradation of the mountain ecosystem.

Although current genetic diversity is robust, habitat fragmentation through massive logging or border infrastructure can isolate conifer populations. Curtu et al. (2009) emphasize the importance of maintaining gene flow; the isolation of these forest 'islands' would lead to a decrease in genetic resilience precisely at the moment when climatic stress (Popa et al., 2024) is at its highest. Given the unique genetic structure identified in Maramureș (Curtu et al., 2009), any ecological reconstruction effort must use exclusively local genetic material in order not to alter the evolutionary adaptability of these transboundary ecosystems.

Sustainable management is not a luxury, but an economic necessity. The loss of water regulation services through excessive logging in the border area will generate flood repair costs much higher

than the profit obtained from the sale of logs (Popa et al., 2016). Knowledge of the spatio-temporal evolution trends of forest resorts in the Maramureș Mountains is essential for local authorities. Herman et al. (2026) emphasize that tourism development is discontinuous and uneven, which requires specific ecological security policies for sensitive areas such as the Ruscova Corridor, to avoid landscape degradation that constitutes the very basis of tourist attractiveness.

The discovery of new species for the Romanian fauna in the Maramureș Mountains (Bitušík et al., 2025) imposes a more severe restriction of tourist activities near glacial lakes, in order to maintain the chemical and biological balance of these fragile ecosystems. Monitoring populations of endemic earthworms (e.g. Octodrilus species) is essential for assessing the health of alpine ecosystems. Soil degradation through intensive grazing or transboundary pollution (metallic or chemical) directly threatens these endemic species, endangering decomposition processes and nutrient cycling in the Pop Ivan meadows (Csuzdi & Pop, 2008).

International experience suggests that the success of conserving alpine landscapes, such as those on Pop Ivan, depends on increasing the resilience of local communities. The integrated development model proposed for Asian mountain regions can be adapted in Maramureș through green financing mechanisms and cross-border ecological education programs (Nasrullah, 2024). As Cioruta & Coman (2022) point out, any anthropogenic intervention in the Ruscova Corridor must be preceded by an analysis of soil functions correlated with meteorological factors. Soil degradation through mining or forestry activities (previously studied by Cioruță in a philatelic/historical context) irreparably alters water storage capacity, amplifying flood risks downstream.

The literary and spiritual heritage described in particular by Pop (2009) provides a solid basis for cross-border collaboration. In this context, protecting biodiversity on Pop Ivan Peak and in the Ruscova Basin should be a joint effort, based on the shared cultural heritage that unites the two banks of the Tisza. The protection of natural heritage, such as the Beech Forest (included in the UNESCO heritage), must overcome political barriers. Academic cooperation, as exemplified by the collaboration between the "Ștefan cel Mare" University of Suceava and Ukrainian partners (Coșofreț, 2017), represents the "keystone" for the ecological security of the entire Maramures area.

Recent studies conducted in the cross-border region of Ukraine emphasize the importance of constant monitoring of chemical elements in soil and plants, using vegetation as an indicator of nutritional conditions and the presence of toxic substances (Karbivska et al., 2025). Ecological reconstruction in the Maramureș Mountains highlights the importance of cross-border collaboration in monitoring high mountain ecosystems sensitive to climate change (Kłapyta et al., 2024). The Maramureș Mountains represent the northernmost area of the Romanian Carpathians that preserves traces of glaciation, offering unique habitats formed by complex geomorphological processes on the border between Romania and Ukraine (Kłapyta et al., 2024).

In Romania, the correlation between investments in environmental protection and the perception of quality of life is significant, highlighting the fact that a healthy ecosystem is the foundation of social well-being (Gheorghe, 2024b). The integration of digital solutions in the monitoring of environmental indicators facilitates a more efficient management of natural resources and allows a rapid assessment of the impact of anthropogenic activities on vulnerable habitats (Gheorghe, 2024b).

The harmonization of legislation and the increase in the number of operators in organic agriculture reflect a growing concern for sustainability in Romania, providing a favorable framework for the protection of protected natural areas (Gheorghe, 2023). The assessment of the pressure exerted by human consumption on the biosphere through the ecological footprint reveals the need for immediate measures to reduce the negative impact on natural resources and maintain the balance of ecosystems (Gheorghe, 2024a).

The rural region of the Maramureș Mountains possesses a vast natural and cultural heritage, the exploitation of which through the concept of Smart Tourist Village can ensure balanced development, while protecting local ecosystems from uncontrolled anthropogenic pressure (Ciolac et al., 2022). In order to ensure the conservation of habitats on the Ruscova

Corridor, we consider, based on the analyzed data, that it would be necessary to transition to a Smart Village development model, which would integrate sustainable tourism and organic agriculture, protecting the natural resources of the localities of Poienile de sub Munte, Repedea and Ruscova (Ciolac et al., 2022; Gheorghe, 2023).

According to the regulations of Order 756/1997, the area of the localities of Poienile de sub Munte, Repedea and Ruscova is classified as a sensitive use area, which imposes strict environmental quality standards to protect the health of the population and the integrity of the ecosystems. Even in the absence of large industrial centers, domestic activities and the historical use of fungicides can lead to local increases in Zn and Cu concentrations in the soil, a phenomenon that needs to be carefully monitored in the Ruscova Corridor to protect both terrestrial and aquatic ecosystems (Bošković-Rakočević et al., 2014; Kucsicsa & Popovici, 2016).

Combating the high-intensity anthropogenic pressure in the Ruscova Corridor requires an approach based on sustainable solutions, where landscape architecture plays a crucial role in the regeneration of degraded ecosystems and in the creation of natural barriers against pollutants (Ciobanu & Cebotari, 2025). The implementation of sustainable landscape projects in border areas can reduce the vulnerability of these agro-montane ecosystems, contributing to regional ecological security by utilizing the environmental cleaning function of selected vegetation (Ciobanu & Cebotari, 2025).

The continuous transformations of trade flows and the adaptation of customs legislation in the context of regional instability (Bahnă, 2026) also require increased vigilance in terms of monitoring environmental factors, in order to prevent the degradation of agro-mountain ecosystems on Romania's northern border. Although the economic development of the Ruscova Corridor is based on the exploitation of mountain potential, the relationship between tourism and environmental law remains tense (Bocancea & Braşoveanu, 2026). It is imperative that tourism activities do not ignore ecological regulations, in order to avoid transforming this natural refuge into an area degraded by excessive and unregulated tourism.

## CONCLUSIONS

Transboundary ecosystems in the Maramureș Mountains face heightened risks due to pressures induced by the armed conflict in Ukraine, requiring immediate preventive protection measures for soil, water and biodiversity. GIS and multi-criteria analyses reveal critical vulnerabilities in habitat fragmentation and pollution, underlining the economic superiority of conservation over ruthless resource exploitation.

Romania-Ukraine cooperation, based on shared cultural heritage and international agreements, is vital for sustainable management and regional ecological security. In this sense, the strategic framework provided by the joint operational programs (Ministry of Development, 2021) constitutes the necessary administrative pillar for the implementation of these measures.

Digital tools and local genetic resources must guide reconstruction efforts to maintain evolutionary adaptability and in the face of climate stress.

## REFERENCES

Abera, T. A., Maeda, E. E., Heiskanen, J., et al. (2025). Deforestation reduces microclimate buffering of African montane forests. *Communications Earth & Environment*, 6(1), 877.

Bahnă, V. (2026). Comparing legislation and practices in the field of import and export rights in the European Union, the Republic of Moldova and Ukraine. Technical and Scientific *Conference of Students, Masters and Doctoral Students, Technical University of Moldova*, 3, 455-460.

Bănăduc, D., Curtean-Bănăduc, A., & Sîrbu, I. (2011a). The Maramureş Mountains Nature Park (Romania) fish fauna. Transylvanian Review of Systematic and Ecological Research, 12, 117-134.

Bănăduc, D., Prots, B., & Curtean-Bănăduc, A. (eds). (2011b). The Upper Tisa River Basin. *Transylvanian Review of Systematic and Ecological Research*, 11, 204.

Bitušík, P., Slobodníková, V., Novikmec, M., Dudáš, A., & Hamerlík, L. (2025). Chironomidae (Diptera) from mountain lakes of the Eastern Carpathians, Romania: First records and insight into diversity. *ZooKeys,* 1233, 107–123.

Bocancea, C., & Braşoveanu, S. (2026). Tourism and Environmental Law – a Complex and Tense Relationship. Anuarul Universității "Petre Andrei" din Iasi, Fascicula: Drept, Stiinte Economice, Stiinte Politice, 36, 60-70. https://doi.org/10.63331/upalaw/36/06.

Bošković-Rakočević, L., Milivojević, J., Milošević, T., & Paunović, G. (2014). Heavy Metal Content of Soils and Plum Orchards in an Uncontaminated Area. *Water, Air, & Soil Pollution,* 225(11), 2199.

Ciolac, R., Iancu, T., Popescu, G., Adamov, T., Feher, A., & Stanciu, S. (2022). Smart Tourist Village—An Entrepreneurial Necessity for Maramures Rural Area. *Sustainability*, 14(14), 8914.

Cioruta, B.-V., & Coman, M. (2022). Definition, Role, and Functions of Soil Related to the Knowledge Society and the Someș-Tisa Hydrographic Area (Romania). *Sustainability*, 14(14), 8688.

Cioruță, B. V., Sabou, I. E., Pop, A. L., & Coman, M. A. (2023). Philatelic Testimonials of Maramures Mining (II): The Peak of the Local Philatelic Movement. *Mining Revue*, 29(4), 96-105.

Ciobanu, P., & Cebotari, C. (2025). The role and importance of the landscape architect in combating the actions of polluting factors. *Technical and Scientific Conference of Students, Master's and Doctoral Students, Technical University of Moldova*, Vol. 3, pp. 62-66.

Coman, M. (2006). Baia Mare Depression – Environmental Protection from a Sustainable Development Perspective. Risoprint Publishing House, Cluj-Napoca.

Coman, M. (2010). General and Applied Ecology. Risoprint Publishing House, Cluj-Napoca, 45-160.

Coșofreț, V.-C. (2017). Cross-border Cooperation for Sustainable Ecosystem Development to Contribute to Conflict Prevention in Eastern Europe - Ukraine. *Bucovina Forestieră*, 17(1), 99-101.

Csuzdi, C., & Pop, V. V. (2008). New data on the earthworm fauna of the Maramures Mts. (Eastern Carpathians, Romania). *Studia Universitatis Vasile Goldiș Arad, Series Științele Vieții*, 18, 101-104.

Curtean-Bănăduc, A., Bănăduc, D., & Sîrbu, I. (2008). The Vișeu River basin (Romania) fish fauna habitats fragmentation. Acta *Oecologica Carpatica,* 1, 143-158.

Curtean-Bănăduc, A., Danci, O., Voicu, R., & Bănăduc, D. (2017). *Cottus gobio* Linnaeus, 1758, ecological status and management elements in Maramureș Mountains Nature Park (Romania). *Management of Sustainable Development*, 9(1), 15-26.

Curtu, A. L., Șofletea, N., Radu, R., Bacea, A., Abrudan, I. V., Butiuc-Keul, A., & Farcaș, S. (2009). Allozyme Variation of Coniferous Tree Species from Maramures Mountains, Romania. *Notulae Botaniae Horti Agrobotanici Cluj-Napoca,* 37(2), 245-251.

Deyl, M., et al. (2023). Retrospective study of alpine and subalpine wetlands of the Maramures Mountains (Eastern Carpathians). *Harnessing new forces in wetland conservation*, pp. 1-2.

Dou, P., & Lin, D. (2026). Soil Fauna Alter the Relationship Between Plant Litter Diversity and Microbial Communities in Mixed Litter Decomposition. *Ecology and Evolution,* 16(2), e 72992.

ESA. (2026). Sentinel-2 Mission Status Report 2026: Land cover dynamics in the Carpathian Ecoregion. European Space Agency.

Filip, C. D., & Coman, M. (2024). Impact of Heavy Metal Soil Pollution and Effects on Human Health - Legislative Provisions. *Agriculture,* (3-4), 131-132.

Filip, C. D., & Coman, M. A. (2025). Regarding Transfer Factor of Soil Pollution with Heavy Metals in Soil-Plant System. *Scientific Papers. Series A. Agronomy*, 68(1), 90-99.

Florea, L. (2017). The changes that occurred between 2010-2016 in the community interest fish species from protected area ROSCI0229 Siriu. *Acta Oecologica Carpatica*, X.II, 87-100.

Gheorghe, A. F. (2023). Organic farming in Romania and in the European Union. *Proceedings Volume* EMEB 2023.

Gheorghe, A. F. (2024a). The ecological footprint of the Romanian population and its impact analysis on the quality of life in the European Union. *AEE Papers*, (8), 1-11.

Gheorghe, A. F. (2024b). The relationship between digitalization, investment and the environment. The impact on quality of life in Romania. *AEE Papers*, (8), 1-10.

Herman, G. V., Caciora, T., Tatar, C. F., Bógdał-Brzezińska, A., & Wendt, J. (2026). Spatiotemporal evolution of tourist resorts in Romania: trends and regional disparities. *Miscellanea Geographica – Regional Studies on Development*, 30(2), 65-73.

Ilieș, M., Ilieș, G., Hotea, V., & Deac, A. L. (2010). The Maramureș Mountains Natural Park - management and sustainable development. *GeoJournal of Tourism and Geosites,* 5(1), 51-60.

Karbivska, U., Myroniuk, I., Degtyarjov, V., Senyk, I., Mykytyn, I., Voitsekhivska, O., Voitsekhivskyi, V., Tytun, O., Krasnoshtan, V., & Lytvynov, V. (2025). Effect of fertilizer application on yield and elemental composition of maize in the western region of Ukraine. *Journal of Ecological Engineering,* 26(12), 178-186.

Khoshnood, Z. (2017). Effects of environmental pollution on fish: a short review. *Transylvanian Review of Systematic and Ecological Research*, 19(1), 49-60.

Kłapyta, P., Mîndrescu, M., Zasadni, J., & Dubis, L. (2024). Glacial geomorphology and glacier reconstruction in the Maramureș Mountains (Romania and Ukraine). *Georeview*, 1, 80-102.

Kovalchuk, A. (1997). Cilioplankton of the River Tisa (in Ukraine). *Proceedings of the International Regional Seminar: Environment Protection, Uzhgorod*, 445-447.

Kucsicsa, G., & Popovici, V. (2016). Spatial analysis of environmental and anthropogenic influences on nitrate concentration in shallow groundwaters. Case study: Ruscova Valley. *Romanian Journal of Geography,* 60(1), 31-45.

Kuemmerle, T., Radeloff, V.C., Perzanowski, K., Kozlo, P., Sipko, T., Khoyetskyy, P., Bashta, A., Chikurova, E., Parnikoza, I., Baskin, L., Angelstam, P. & Waller, D.M. (2011). Predicting potential European bison habitat across its former range. *Ecological Applications,* 34(5), 830-843.

McGarigal, K. (2015). Fragstats: Spatial Pattern Analysis Program for Categorical Maps. University of Massachusetts.

Ministry of Water, Forests and Environmental Protection. (1997). Order No. 756/1997 for the approval of the Regulation on environmental pollution assessment. *Official Gazette of Romania,* No. 303 bis.

Ministry of Development, Public Works and Administration. (2021). Joint Operational Programme Romania-Ukraine 2021-2027 (Draft).

Nasrullah, A. M. (2024). Sustainable Development of Mountains and Mountain People in Chittagong Hill Tracts, Bangladesh. *Sustainable Development Goals Series*, University of Chittagong.

National Institute of Statistics. (2023). Resident population by locality on December 1, 2021 – final RPL 2021 results.

Năvodaru, I. & Năstase, A. (2006). Ichthyofauna of River Danube delta: Gorgova - Uzlina and Şontea - Furtuna lakes complexes. *Acta Ichtiologica Romanica*, I, 185-202.

Olenici, N., & Semeniuc Fecioru, A.-I. (2021). Contributions to the knowledge of the distribution and biology of the species Retinia resinella in Romania. *Bucovina Forestieră,* 21(2), 135-145.

Parliament of Romania. (1995). Law No. 30/1995 for the ratification of the Convention on the Protection and Use of Transboundary Watercourses and International Lakes (Helsinki, 1992). *Official Gazette of Romania*, No. 81.

Parliament of Romania. (2005). Law no. 137/2005 on environmental protection. *Official Gazette of Romania*.

Pop, N. L. (2009). Poets on the right bank of the Tisza during the period of independent Ukraine. *Studies of Science and Culture,* V, 3(18), 1-8.

Popa, B., Borz, S. A., Nita, M. D., et al. (2016). Forest Ecosystem Services Valuation in Different Management Scenarios: a Case Study of the Maramures Mountains. *Baltic Forestry,* 22(2), 327-340.

Popa, I., Popa, A., & Balabaşciuc, M. (2024). Dendroclimatic models for spruce, fir and beech in the Eastern Carpathians. *Bucovina Forestieră*, 24(2), 107-118.

Schitea, M. (2010). Achievements in forage plant improvement at Fundulea. *Annals of INCDA Fundulea*, Vol. LXXVIII, 249-258.

Thira, C., Cioruţa, B. V., Bacali, L., Cioruţa, I. E., Pop, A. L., & Coman, M. A. (2025). Digitalization of Human Resources Management through MIT App Inventor (I*). Review of Management and Economic Engineering,* 24(3), 152-158.

Ukraine conflict environmental briefing: Nature. (2024). Conflict and Environment Observatory. https://ceobs.org/ukraine-conflict-environmental-briefing-nature/.

Vought, O. K., Kivlin, S. N., Shulman, H. B., Sorensen, P. O., Inouye, D. W., Ibáñez, I., Falb, P., Rand, K., & Classen, A. T. (2025). Earlier snowmelt increases the strength of the carbon sink in mountain meadows unequally across the growing season. *Journal of Ecology*, 113(1), 1-12. https://doi.org/10.1111/1365-2745.70195.

Scientific Papers. Series E. Land Reclamation, Earth Observation & Surveying, Environmental Engineering. Vol. XV, 2026
Print ISSN 2285-6064, CD-ROM ISSN 2285-6072, Online ISSN 2393-5138, ISSN-L 2285-6064

# GEOTECHNICAL ENGINEERING AND SOIL MANAGEMENT: LEGAL GAPS AND ENVIRONMENTAL CONSIDERATIONS

**Daniel-Dumitru TOADERE[1, 2], Nicoleta-Maria ILIEȘ[1, 2], Ioan PETRAN[1, 2]**

[1]Structures Department, Faculty of Civil Engineering, Technical University of Cluj-Napoca, Faculty of Civil Engineering, 25 G. Bariţiu Street, Cluj-Napoca, Romania
[2]European University of Technology, European Union

Corresponding author email: daniel.toadere@dst.utcluj.ro

***Abstract***

*This study analyses the interaction between geotechnical risk, GIS-based territorial analysis, soil management, and the Romanian legal framework governing earthworks and environmental protection. The Borhanci area of Cluj-Napoca was selected as a case study due to recent large-scale grading operations associated with urban development. The methodology combined GIS analysis, urban planning documentation, field observations, photographic surveys, and legislative review. Field observations identified longitudinal and transversal fissures with depths ranging from 0.20 m to 1.30 m. Landslide susceptibility maps classified neighbouring slopes as medium, high and very high risk. The results indicate that extensive grading works may influence slope stability and drainage conditions in adjacent undeveloped terrain. The study highlights the need for integrated geotechnical assessment, territorial planning, and regulatory clarity regarding grading and levelling works.*

***Key words****: geotechnical engineering, GIS, landslide susceptibility, soil management, urban planning.*

## INTRODUCTION

Geotechnical and civil engineering activities, which involve interventions on the soil and subsoil, are governed by a complex legal framework in Romania. Ensuring the stability and quality of construction requires strict adherence to regulations pertaining to construction quality (Law No. 10/1995, republished; Order No. 27/2023), authorization procedures (Law No. 50/1991, republished), land improvement works (Law No. 138/2004, republished), and environmental protection measures (OUG No. 92/2021 and OUG No. 195/2005). The objectives pursued in this paper involve identifying legislative problems with geotechnical implications and examining the specific normative regulations regarding the authorization of earthworks, particularly land improvements and site grading and levelling works.

A major challenge constantly analysed is legislative insufficiency regarding the regulation of site grading and levelling works. While technical documentation requires geotechnical investigations and the inclusion of descriptions of external works, site grading and levelling works, the legislation governing building permits does not explicitly classify or regulate standalone works involving modifications to land elevation.

The significance of this issue is particularly evident in rapidly developing urban areas such as Cluj-Napoca, where hillside development frequently requires extensive terrain modification and grading operations. Previous studies conducted in the region have shown that urban expansion on sloping terrain requires careful consideration of slope stability, groundwater management and landslide risk assessment in order to ensure sustainable development and reduce geotechnical hazards (Mureșan, 2011; Farcaș et al., 2021).

Geotechnical engineering increasingly relies on Geographic Information Systems (GIS) for the integration, visualization and interpretation of spatially referenced data. GIS supports the assessment of geotechnical hazards, territorial planning and risk management by enabling the analysis of complex interactions between geological, geomorphological, environmental and anthropogenic factors (Player, 2006; Singh et al., 2018).

The emerging field of Urban Geosciences highlights the importance of combining geotechnical engineering, geology,

hydrogeology and land-use planning in order to support sustainable urban development. Within this framework, GIS-based analysis provides local authorities with an effective instrument for identifying landslide-prone areas, evaluating territorial constraints and supporting informed planning decisions (Azougay et al., 2020; Campagna and Deplano, 2002).

Modern geotechnical practice should integrate not only analytical knowledge but also information-based approaches, interdisciplinary decision-support tools and risk management strategies. Such an approach is increasingly considered necessary for addressing complex environmental and territorial challenges (Arciszewski, 2006; Chowdhury & Flentje, 2007).

The objective of this study is to analyse the interaction between geotechnical risk, GIS-based territorial analysis, soil management and the Romanian legal framework governing earthworks and environmental protection.

## MATERIALS AND METHODS

The present study focuses on the Borhanci district of Cluj-Napoca, Romania, an area that has undergone significant land-use changes through urban planning procedures enabling the development of educational, healthcare, sports and public infrastructure facilities. Borhanci was selected as a case study due to the presence of extensive grading works, slope modification activities and documented landslide susceptibility conditions.

The analysis was based on multiple data sources, including the Cluj-Napoca GIS platform, the General Urban Plan (PUG), the Local Urban Planning Regulation (RLU), PUZ documentation, landslide susceptibility maps, field observations, photographic documentation and Romanian legislation regarding construction, environmental protection and land improvement works.

GIS analysis was used to evaluate the spatial relationship between planned urban development areas and landslide susceptibility zones. Official GIS layers and planning documentation were analysed in order to identify territorial constraints and risk-prone sectors. Previous studies have demonstrated that GIS represents an efficient framework for integrating geotechnical, geological and environmental information into a common decision-support system, supporting hazard identification, risk evaluation and territorial planning processes (Chowdhury & Flentje, 2007; Singh et al., 2018). The GIS platform of Cluj-Napoca provides valuable spatial information supporting urban planning and geotechnical risk assessment and is increasingly regarded as an essential component of digital governance and smart city initiatives (Campagna & Deplano, 2002). The integration of GIS-based spatial analysis, planning documentation and field observations provides an effective framework for identifying areas exposed to geotechnical hazards. Similar multidisciplinary approaches have been successfully applied in studies addressing slope instability and urban development in the hilly areas surrounding Cluj-Napoca (Ilieș et al., 2016; Farcaș et al., 2021). Figure 1 illustrates the planning framework applicable to the study area through the General Urban Plan (PUG).


AL
ULM
ULM
ULM
ULM
VPI
UIS
UIS
ULM
ULM
ULM
ULM
ULM
UIS
UIS
UIS

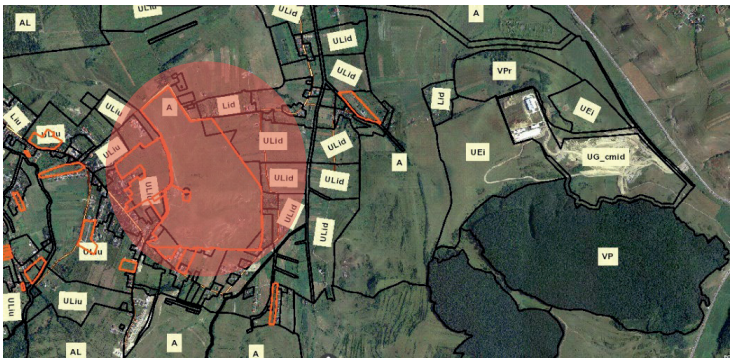



Figure 2. Studied area highlighting zones delineated through GIS analysis, in accordance with the General Urban Plan (PUG) of Cluj-Napoca, with the PUZ-regulated area highlighted in red

Figure 4 presents fissures and instability indicators identified during field observations within the Borhanci study area.

A legislative review was conducted in order to analyse the legal framework governing construction activities, land improvement works, environmental protection and waste management. The analysis included Law No. 50/1991, Law No. 138/2004, Government Emergency Ordinance No. 92/2021, Government Emergency Ordinance No. 195/2005, as well as relevant urban planning regulations applicable to the study area. The legislative review was performed in parallel with the GIS analysis and field investigations in order to evaluate the interaction between geotechnical risk, territorial planning and environmental governance.

## RESULTS AND DISCUSSION

### 1. Legal Framework of Land Improvements

The regulation of land improvements is governed by Law No. 138/2004, with methodological norms approved by Government Decision No. 1.872/2005. Land improvement works are indispensable for the sustainability of agricultural land and soil quality, as well as for overall territorial protection.

Land improvements have several crucial objectives:

- Territorial Protection: Providing protection for lands of any kind and any categories of structures against floods, landslides, and erosion. This goal also includes regulating water courses and protecting accumulation lakes against silting.
- Soil Management: Ensuring an adequate level of soil moisture and the improvement of acidic, saline, and sandy soils (soil improvement), as well as providing protection against pollution.

These activities must be performed in compliance with environmental protection standards (Law No. 138/2004).

Land improvements consist of complex hydrotechnical, and soil improvement works that require a construction permit according to Law No. 50/1991. These works include:

- Irrigation and Rice Paddies: Including water catchment, pumping, transport, distribution, and evacuation works, and, where appropriate, site grading works.
- Desiccation and Drainage: Networks of structures, pumps, canals, and pipes used to prevent and remove excess water. The infrastructure includes components like canals and pumping stations.
- Erosion Control and Landslide Mitigation: Works aimed at preventing, reducing, or halting land degradation processes. These include soil protection measures, regulation of surface runoff on slopes, torrent control, and stabilization of loose sandy soils. Land improvement organizations may be established specifically for erosion control purposes.
- Soil improvement works: Works on saline, acidic, or sandy soils, including land levelling and modelling, scarification, deep loosening, and water drainage channels.

– Embankments and regulation of water courses.

The scope of these works clearly indicates that they involve significant earth moving and geotechnical interventions (Law No. 138/2004).

The infrastructure assets of land improvements, such as the secondary irrigation network in the private domain of the state, are administered by the National Agency for Land Improvements (ANIF) and can be transferred to legally constituted Land Improvement Organizations (OIFs) (Law No. 138/2004).

Law No. 138/2004 prescribes sanctions for unauthorized activities in these areas:

– Executing constructions, or modifying or extending constructions within land improvement facilities, without the prior authorization of the ANIF, organizations, or federations.
– Carrying out excavations, borrow pits, or trenches in embankments or their protection zones, or extracting materials from defence works, without the Agency's prior consent.

**2. Soil Management and Environmental Considerations**

The management of soil and excavated materials represents a key component of geotechnical risk prevention and environmental protection. Modern approaches increasingly emphasize the integration of geotechnical engineering, territorial planning and environmental governance in order to minimize the impact of earthworks on slope stability and land-use sustainability (Chowdhury & Flentje, 2007; Azougay et al., 2020).

The regulation of waste is critical in geotechnical projects involving earth movement. The framework aims to ensure a high level of protection for the environment and public health.

OUG No. 92/2021 excludes certain soil categories from the waste regime:

– Soils (in situ), including uncontaminated excavated soils and buildings permanently attached to the ground.
– Uncontaminated soils and other natural geological materials excavated during construction activities, provided there is certainty that the material will be used for construction in its natural state and on the site from which it was excavated.

If soil is moved off-site or utilized for uncontrolled filling (site grading works), its status can change, potentially classifying it as waste.

From a geotechnical perspective, the management of excavated materials is directly linked to slope stability, drainage conditions and the prevention of environmental degradation. GIS-based territorial analysis can support the identification of risk-prone sectors and contribute to more sustainable land management practices (Player, 2006; Singh et al., 2018).

Backfilling is explicitly defined as a recovery operation (R5 or R12 in the recovery operations list - OUG No. 92/2021), which is one of the preferred options in the waste hierarchy, above elimination. Backfilling involves the use of adequate non-hazardous materials for site restoration or landscaping purposes. The waste used for backfilling must replace non-waste materials and be limited to the strictly necessary quantity.

However, materials that no longer hold waste status and are used for backfilling are not considered towards meeting recycling objectives. Furthermore, placing waste (D1) in or on the ground (e.g., landfills) or burying any kind of waste is an offense (OUG No. 92/2021).

The environmental framework establishes principles such as the preventive action principle and the "polluter pays" principle. Holders of activities have the obligation to manage waste without endangering public health or damaging the environment, particularly without generating risks of contamination of air, water, soil, fauna, or flora (OUG No. 92/2021).

The lack of explicit authorization for site grading and levelling works in Law 50/1991 is particularly critical because unauthorized or uncontrolled deposits of soil, especially if classified as waste, violate fundamental environmental obligations and pose a direct threat of geotechnical stability. This directly contradicts the objective of land improvements to provide territorial protection against landslides. Failure to implement proper technical solutions for backfilling or slope

alterations results in a significant risk of landslides, a specific natural risk addressed in urban planning regulations.

The findings presented above demonstrate that soil management cannot be analysed solely from a legal perspective. The geotechnical consequences of uncontrolled filling activities include changes in drainage patterns, increased loading on slopes, and the potential activation of instability processes. Therefore, the integration of environmental legislation, geotechnical assessment and GIS-based territorial analysis is essential for sustainable land management and risk prevention (Chowdhury & Flentje, 2007; Singh et al., 2018).

## 3. Legislative Gaps and Proposed Solutions

Based on practical experience and the findings presented in this study, one of the most debated issues concerns the insufficient regulation of site grading works.

Although Law No. 50/1991 requires permits for "land improvement works" (which implicitly cover land levelling and modelling), it fails to explicitly include or sanction "site grading and levelling works involving changes in land elevations". This omission in the construction law framework creates disparate applications across local authorities and inconsistencies in permitting practices.

From a geotechnical perspective, insufficient regulation of grading and levelling works may lead to inconsistent implementation practices and difficulties in evaluating long-term impacts on slope stability. Similar concerns have been highlighted in studies addressing the integration of engineering practice, risk management and territorial planning (Arciszewski, 2006; Player, 2006).

In the case of general construction, the technical documentation must show the measures taken for the protection of neighbouring buildings' foundations, demonstrating that changes in site conditions (including site grading and levelling works) inherently impact structural stability.

The draft Code of Spatial Planning, Urbanism, and Construction aims to address this regulatory shortfall. This proposed legislation (which would eventually repeal Law No. 50/1991 and Law No. 10/1995) explicitly classifies land development works, including earthworks and external works, as requiring authorization. Under the proposed code, land arrangement operations, including demolitions, deforestation, site grading and levelling works, access roads, retaining walls, and drainage, are clearly listed as works that must be authorized.

In the light of the above analysis, the adoption of the new Code of Spatial Planning, Urbanism, and Construction may be considered necessary, particularly in view of its explicit regulation of external works and land development operations. Furthermore, the provision of clear and consistent solutions to divergent interpretations in practice is essential to ensure a coherent understanding and effective enforcement of the legal framework. Such clarification would contribute to addressing existing regulatory gaps concerning the aforementioned works and would facilitate both the proper application of the law by inspectors and local authorities, as well as its consistent interpretation and implementation by architects, engineers, and construction professionals.

## 4. Case Study: Implementation of Local Urban Planning Regulations in the Municipality of Cluj-Napoca (General Urban Plan (PUG) analysis)

Within the context of national legislative deficiencies regarding the explicit authorization of site grading and levelling works, the Local Urban Planning Regulation (RLU) related to the Cluj-Napoca General Urban Plan (PUG), Figure 1, institutes a set of strict constraints for specific intra-urban and extra-urban zones, aimed at territorial protection and slope stability.

The analysis of functional sub-zones highlights a systematic concern for the preservation of natural soil conditions and the mitigation of geotechnical risks, having selected all functional zones within the extra-urban area (Agricultural land - arable land, pastures, hayfields, tree nurseries, etc. (TDA), Agricultural land - orchards (TDA_L), Forested land (TDF)), while specifically focusing on agricultural lands, green spaces, and forests for the intra-urban area (Non-urbanized agricultural land (A), Non-urbanized and non-developable agricultural land - orchards (AL), Area designated for recreational activities

carried out in a natural setting, in proximity to forests located within or outside the intra-urban area (Aapp), The area includes sections of the corridors of the Someșul Mic River and the Morii Channel, comprising minor riverbeds, hydrotechnical works, riverbank arrangements, green strips or spaces, pedestrian and bicycle circulation routes, urban furniture, as well as protection strips along secondary watercourses (streams) located on the slopes (Ve), The area includes - green spaces with a protective function in relation to major infrastructure; main electricity and natural gas transmission networks, railway and road corridors; green spaces with a sanitary protection role for active or closed landfills and wastewater treatment plants; green areas designated for the ecological restoration of degraded land; plantations intended to stabilize steep slopes resulting from anthropogenic interventions or affected by natural landslide risks (VPr), Forested land located within the intra-urban area, introduced through urban planning documentation prior to the revision of the Romanian Forestry Code (2008). Subzone of forests designated for recreational use and subzone of pastures / hayfields within forested areas (VP)).

GIS-based territorial analysis provides an effective framework for integrating urban planning restrictions with geotechnical risk assessment. Such approaches enable the identification of environmentally sensitive sectors and support sustainable land-use management (Campagna & Deplano, 2002; Singh et al., 2018).

The analysis of intra-urban functional zones highlights a systematic concern for the preservation of natural soil conditions and the mitigation of geotechnical risks:

- A, AL: The preservation of the existing land-use structure is mandatory to maintain ground stability. Permitted uses include crops and land improvement works, while conditional works allow for greenhouses (>1 ha) and agricultural annexes (max. 10% Land Occupancy Percentage (P.O.T.) for A; 5% for AL). The discharge of wastewater and rainwater into natural watercourses is strictly prohibited, requiring on-site management solutions to prevent erosion processes. Additionally, all categories of waste must be managed in accordance with applicable regulations, to avoid the formation of uncontrolled deposits of excavated material.
- Aapp: Earthworks and, site grading and levelling works interventions that may affect public infrastructure or adjacent parcels are explicitly prohibited. Furthermore, a significant proportion of green space on natural soil (60–80%) is required, thereby limiting anthropogenic intervention.
- Ve, VPr: Permitted works include plantations and hydrotechnical works. The VPr zone is designated for afforestation and vegetation-based interventions aimed at stabilizing slopes with inherent landslide risk, as well as for the ecological restoration of degraded land. Within these areas, the P.O.T. is set at 0%, effectively prohibiting any construction activities involving alterations to ground morphology.
- VP: The RLU explicitly prohibits all forms of earthworks and site grading and levelling works interventions within forested areas. Only forestry exploitation and essential infrastructure are permitted, maintaining the P.O.T. at 0%.

In the extra-urban territory, the PUG focuses on maintaining ecological balance and preventing land degradation:

- TDA, TDA_L: Like intra-urban rules, it is forbidden to discharge water into slope watercourses, mandating on-site management to avoid soil transport. Permitted annexes are strictly limited to a maximum P.O.T. of 10% of the designated area (5% for orchards), while the remainder of the land must retain its natural state.
- TDF: To ensure "land stabilization" near the city, the PUG imposes severe restrictions, prohibiting all earthworks and site grading and levelling works, as well as any permanent constructions.
- The P.O.T. is strictly maintained at 0%.

A compelling example of how land-use modifications and large-scale site grading works can influence the morphological stability of adjacent terrains is provided by the Borhanci

area, located in the south-eastern part of the Cluj-Napoca municipality, near the Apahida-Vâlcele bypass road. This case study illustrates the geotechnical challenges encountered in rapidly developing urban areas where significant interventions occur on sensitive slopes.

The Borhanci development area represents a relevant example of the interaction between urban expansion, terrain modification and geotechnical risk. GIS-based analysis facilitates the assessment of territorial constraints and provides decision-makers with spatial information regarding landslide susceptibility and environmental vulnerability (Azougay et al., 2020).

According to the analysed documentation, this sector was initially classified under the General Urban Plan (PUG) of Cluj-Napoca as non-urbanized agricultural land incorporated into the intra-urban area (A). This status was subsequently modified through a Zonal Urban Plan (PUZ), Figure 2, approved by Local Council Decision (HCL) No. 510/2022 (later amended by HCL No. 645/2025), redesignating the area as Institutional and Public Interest Services Zone (Is Borhanci). This legal transition facilitated the development of a major infrastructure project, including an educational hub, healthcare and sports facilities, and a forest park.

The comparison between the planning documentation and the GIS-based territorial analysis indicates that significant grading operations were implemented in an area surrounded by sectors presenting varying degrees of landslide susceptibility.

While the construction platforms for the educational hub are being executed based on rigorous geotechnical investigations field observations indicate increased vulnerability in the adjacent terrains. GIS analyses and official risk maps classify the slopes in this area as having medium, high, and very high landslide susceptibility, Figure 3.

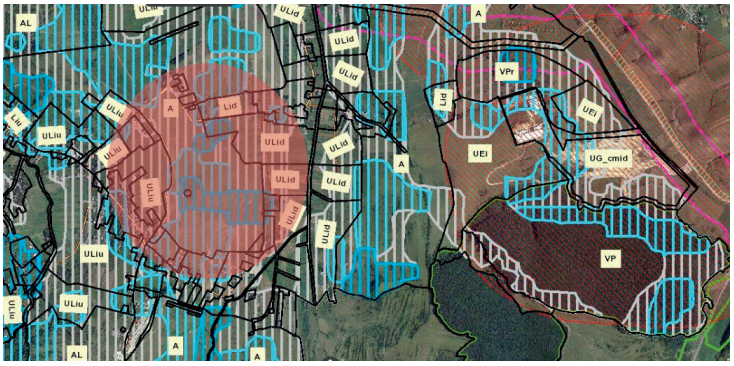



Figure 3. Studied area showing landslide susceptibility zones identified through GIS analysis: medium to high risk (grey), high risk (light blue), and very high risk (dark blue)

The GIS results demonstrate the importance of integrating landslide susceptibility information into urban planning decisions. Previous studies have shown that GIS-based risk mapping represents one of the most efficient tools for identifying sectors requiring enhanced monitoring and geotechnical investigation prior to the implementation of major earthworks (Bezerra et al., 2020; Singh et al., 2018).

At present, on the southern slope directly bordering the sites, where extensive site grading works have been carried out, active soil instability is evident. As this adjacent land has remained undeveloped (retaining the characteristics of the former agricultural Zone A), it serves as a natural indicator of the geotechnical stresses affecting the area (Table 1):

– Structural soil manifestations: Transversal and longitudinal fissures have developed within the non-homogeneous and uncompacted soil mass, with significant depths ranging from 0.20m to 1.30m, indicating structural failure within the soil mass, Figure 4.

- Morphological deformations: Multiple rupture zones and so-called *"slip surfaces"* (natural step-like terraces) have been observed, indicating that the shear strength of the soil has been exceeded under the influence of natural and anthropogenic factors.
- Hydrological indicators: The presence of hygrophilous vegetation confirms water stagnation or inadequate drainage, with excess moisture acting as a primary trigger for landslide processes.



Figure 4. Field photograph highlighting longitudinal and transversal soil fissures, suggesting active deformation processes

Table 1. Main geotechnical observations identified in the Borhanci study area

| Indicator | Observation |
|---|---|
| Minimum fissure depth | 0.20 m |
| Maximum fissure depth | 1.30 m |
| Fissure orientation | Longitudinal and transversal |
| Landslide susceptibility classes | Medium, High, Very High |
| Hydrological indicators | Hygrophilous vegetation |
| Morphological indicators | Rupture surfaces and local deformation |

The field observations indicate active deformation processes affecting adjacent undeveloped terrain. The identified fissures, rupture surfaces and hydrological indicators are consistent with instability phenomena commonly reported in areas affected by slope modification and inadequate drainage conditions. The integration of field observations with GIS-based analysis provides a more comprehensive understanding of local geotechnical risk conditions (Player, 2006; Azougay et al., 2020).

The Borhanci case highlights the critical importance of water management and controlled drainage, as well as the continuous monitoring of adjacent areas, in accordance with the principles set out in Land Improvement Law No. 138/2004. Although the authorized works benefit from dedicated geotechnical studies, the current lack of a unified national regulation under Law No. 50/1991 regarding the explicit authorization of ground elevation changes (site grading) makes it difficult to enforce preventive measures across the entire Territorial Reference Unit (UTR).

## CONCLUSIONS

The legal framework governing geotechnical engineering requires a coherent correlation between construction authorization (Law No. 50/1991), land improvement regulations (Law No. 138/2004), and environmental protection legislation (OUG No. 195/2005 and OUG No. 92/2021).

Land improvement works, such as irrigation systems and erosion control measures, constitute essential infrastructure and are explicitly subject to construction permit requirements. Their primary role is territorial protection, particularly in mitigating landslide risks.

A major practical challenge lies in the omission of site grading and levelling works, specifically those involving changes in land elevation, as a distinct category requiring authorization under the current Law No. 50/1991. The uncontrolled execution of such works generates significant geotechnical risks and may lead to illegal waste management practices, as deposited materials can be classified as waste. In this context, the law strictly prohibits the embedment of any type of waste in the ground.

The findings of this study further demonstrate that major earthworks, even when technically adequate at the site level, can alter the overall equilibrium of slopes and generate indirect geotechnical effects in adjacent areas. The Borhanci case study provides clear evidence of such impacts, highlighting the vulnerability of neighbouring terrains in the absence of coordinated measures at the territorial scale.

The analysis of the General Urban Plan of Cluj-Napoca shows that local authorities partially compensate for this legislative gap through Local Urban Planning Regulations. By restricting site grading and levelling works and earthworks in sensitive zones (VPr, VP, TDF, Aapp) and imposing a 0% P.O.T. in high-risk areas, the local framework actively contributes to preventing geotechnical instability and the improper management of excavated soil as waste.

In this context, the adoption of a consolidated Code of Spatial Planning, Urbanism, and Construction, explicitly including site grading and levelling works among the categories subject to authorization is both necessary and justified. Such a framework would ensure a consistent legal basis for the application of sanctions, improve the protection of neighbouring properties, and reinforce the fundamental environmental principle of preserving soil and subsoil quality.

The Borhanci case study demonstrates the importance of integrating geotechnical assessment, GIS analysis, environmental protection and territorial planning. The identified fissures, rupture surfaces and landslide susceptibility zones highlight the need for continuous monitoring and risk-informed decision making in areas affected by extensive grading operations.

The GIS-based territorial analysis performed in this study complements the legal and geotechnical assessment by providing spatial information regarding environmental constraints and landslide susceptibility. Such interdisciplinary approaches are increasingly recognised as essential tools for sustainable urban development and territorial risk management.

The results support the integration of geotechnical engineering, GIS technologies, environmental governance and urban planning in order to improve the management of earthworks and reduce long-term geotechnical risks.

Future research should include detailed geotechnical monitoring, GIS-based temporal analysis and quantitative assessment of slope stability in rapidly developing urban areas.

## ACKNOWLEDGEMENTS

This research was conducted within the Doctoral School of the Technical University of Cluj-Napoca, within the Structures Department of the Faculty of Civil Engineering. The author gratefully acknowledges the institutional support provided during the development of this work.

## REFERENCES

Arciszewski, T. (2006). Civil Engineering Crisis *Leadership and Management in Engineering*, 6(1), 26–30.

Azougay, A., Rezqi, H., & Oujidi, M. (2020). The Use of a Geographic Information System to Study Geotechnical Problems in Urban Areas. *E3S Web of Conferences* (EDE7-2019), 150, 03002.

Bezerra, L., Neto, O.F., Santos, O. Jr., & Mickovski, S.B. (2020). Landslide Risk Mapping in an Urban Area of the City of Natal, Brazil. *Sustainability*, 12(22), 9601.

Campagna, M., & Deplano, G. (2002). Public Administration, Governance, Planning and GIS: Italian Experiences in the e-Europe. *Proceedings of the 5th AGILE Conference on Geographic Information Science*, 1–6.

Chowdhury, R., & Flentje, P. (2007). *Perspectives for the Future of Geotechnical Engineering.* University of Wollongong, 1–18.

Ilieș, N.-M., Farcaș, V.-S., Pașca, D.-M., Chiorean, V.-F., & Nagy, A.-C. (2021). Consolidation project of an urban landslide: Case study on Tetarom Park Cluj-Napoca. *Proceedings of the 20th International Conference on Soil Mechanics and Geotechnical Engineering*.

Government Decision No. 1872/2005 approving the Methodological Norms for the Application of Law No. 138/2004 on Land Improvements.

Government Emergency Ordinance No. 92/2021 on Waste Management.

Government Emergency Ordinance No. 195/2005 on Environmental Protection.

Ilieș, N.M., Farcaș, S.V., Cot, R.V., & Moldovan, I.M. (2016). The Control of Natural Disaster Caused by Slopes Sliding by Means of Stepped Buildings. *Procedia Technology*, 22, 391–398.

Law No. 50/1991 (republished) on the Authorization of Construction Works.

Law No. 138/2004 (republished) on Land Improvements.
Draft Law approving the Code of Spatial Planning, Urbanism and Construction.
Municipality of Cluj-Napoca. General Urban Plan (PUG) and Local Urban Planning Regulation (RLU).
Municipality of Cluj-Napoca. Geographic Information System (GIS) Platform. Available at: https://gis.primariaclujnapoca.ro/Public/
Municipality of Cluj-Napoca. Official Website of the Cluj-Napoca City Hall. Available at: https://primariaclujnapoca.ro/
Mureșan, O.C. (2011). Possible Overview of Landslide Risk Assessment, Mitigation and Management. *Proceedings of the 1st International Conference on Quality and Innovation in Engineering and Management*.
Normative for Geotechnical Documentation for Constructions, NP 074-2022, approved by Order No. 27/2023.
Player, R.S.V. (2006). Geographic Information System (GIS) Use in Geotechnical Engineering. Proceedings of ASCE GeoCongress.
Singh, A., Noor, S., Chitra, R., & Gupta, M. (2018). Applications of GIS in Geotechnical Engineering: Some Case Studies. *International Journal of Scientific Engineering and Science*, 2(3), 34–38.

Scientific Papers. Series E. Land Reclamation, Earth Observation & Surveying, Environmental Engineering. Vol. XV, 2026
Print ISSN 2285-6064, CD-ROM ISSN 2285-6072, Online ISSN 2393-5138, ISSN-L 2285-6064

# MONITORING ENVIRONMENTAL QUALITY VIA NITRATE ACCUMULATION IN GREENHOUSE LETTUCE (*LACTUCA SATIVA* L.)

**Irina TOMASU[1], Mihaela DRAGOI CUDALBEANU[1], Simona MARCU SPINU[1], Zina PARASCHIV[2], Augustina Sandina TRONAC[1], Alina ORTAN[1]**

[1]Faculty of Land Reclamation and Environmental Engineering, University of Agronomic Sciences and Veterinary Medicine of Bucharest, 59 Marasti Blvd, 011464, District 1, Bucharest, Romania
[2]Faculty of Biotechnologies, University of Agronomic Sciences and Veterinary Medicine of Bucharest, 59 Marasti Blvd, 011464, District 1, Bucharest, Romania

Corresponding author email: mihaela.dragoi@fifim.ro

***Abstract***

*Public health concerns related to nitrate accumulation in vegetables are increasing, as nitrate can be converted to nitrite, which can form harmful N-nitroso compounds. Due to its high capacity to accumulate nitrate, lettuce represents a suitable crop for monitoring the effects of fertilization practices on environmental quality in greenhouse systems. This study evaluated nitrate, nitrite, and ammonium contents in greenhouse-grown lettuce from two sources: supermarkets and local producers. Three samples were collected from supermarkets, four from local producers. Samples were separated into leaves, roots, and growing medium (soil), yielding 21 representative samples. Differences were observed in concentrations and distribution patterns. Supermarket lettuce showed higher leaf nitrate content than local-producer samples. Supermarket samples also exhibited higher nitrite content, particularly in roots, suggesting active nitrate-reduction processes. Leaves were the primary site for nitrate accumulation, followed by roots and soil, whereas nitrite and ammonium were mainly associated with roots and soil. Notably, local producer samples exhibited higher ammonium concentrations in roots and soil compared to supermarket samples, suggesting differences in fertilization practices and nitrogen conversion efficiency. These findings support closer monitoring of fertilization practices to assess environmental quality in protected agriculture and to limit consumer exposure to nitrogen-related compounds.*

***Key words:*** *nitrate residue, greenhouse cultivation, lettuce, environmental quality.*

## INTRODUCTION

The nitrogen (N) sources are represented by inorganic forms ($NH_4^+$, $NO_2^-$, and $NO_3^-$), which are formed naturally in crops, soil, and water through the N cycle (Gidurus et al., 2012; Martín Leon & Luzardo, 2020). Thus, $NH_4^+$ and $NO_3^-$ constitute the most important forms of N, as they support plant growth and, when taken up in large quantities, achieve maximum production yields (Colla et al., 2018).

Complex interactions among plant root systems promote efficient N transfer within the soil-plant system, enabling optimal use of available nutrients (Hao et al., 2022). N residues from previous crops also serve as an important energy source for soil bacteria, supporting microbial activity, reducing the need for chemical inputs, and promoting N immobilization processes (Assémien et al., 2019).

N is vital for plant growth, and it circulates between soil and plants, often as an anion (Butnariu, 2018). N fertilizers are the primary artificial N source, with usage rising rapidly. About 50% of applied N is lost via leaching, contaminating surface and groundwater by increasing $NO_3^-$ content. After pesticides, nitrates are the second most concerning water contaminant for environmental and public health protection (Singh et al., 2022).

Plants need enough N to make amino acids, which are vital for cell and tissue formation. Without amino acids, plants can't produce proteins for growth, which harms development. Too much N, however, causes excess biomass, such as stems and leaves, and immature roots (Brady & Weil, 2010). Farmers use N fertilizers to boost crop growth; without them, about a third of food production could be lost. Yet, finding the optimal N level is crucial, as excess N pollutes water and threatens ecosystems (Aczel, 2019). Maintaining the right balance of essential life support elements is crucial. N deficiency in plants causes chlorosis and stunted growth (Britto et al., 2002). Proper N management prevents ecological problems such

as water pollution and soil degradation. Excess N can contaminate groundwater or other water bodies, causing eutrophication that harms aquatic ecosystems and biodiversity (Chislock et al., 2013).

Vegetables are a valuable source of minerals, vitamins, carbohydrates, and biologically active compounds. Adopting a diet rich in vegetables is one of the most effective ways to prevent numerous diseases, including obesity, which is becoming a major public health problem (Luetic et al., 2023). To support a healthy lifestyle that lowers the risk of various diseases and boosts immunity, the World Health Organization (WHO) advises consuming 400-500 g of vegetables daily as part of a balanced diet (Pennington et al., 2010).

Lettuce is a highly nutritious vegetable, abundant in vitamins C, A, K, and B9 (folate). Additionally, it is used medicinally for its high content of flavonoids, tocopherols, and carotenoids, compounds known for their high antioxidant properties. Another advantage is its global use and the fact that it is consumed raw in most cases, thereby retaining its full nutritional value (Popa et al., 2021).

Consequently, consumer exposure to nitrate ($NO_3^-$) varies depending on the types and amounts of vegetables consumed. In this context, leafy vegetables occupy a central place, as they have a high capacity for $NO_3^-$ accumulation, favored by both the accelerated growth rate specific to these species and the concentration of nitrogen ions predominantly in the leaves, the edible parts of these plants (Martín Leon & Luzardo, 2020).

In leafy vegetable cropping systems, such as lettuce, a shallow root system limits access to N in deeper soil layers, resulting in low N use efficiency, estimated at an average of only 25% (Pujol et al., 2017). This inefficiency contributes to excessive N accumulation in the soil. Unabsorbed N can be leached as $NO_3^-$ into groundwater, contaminating drinking water resources, or emitted into the atmosphere as nitrous oxide ($N_2O$), a particularly potent greenhouse gas (Cassman et al., 2002). Lettuce crops respond positively to N fertilization by increasing yields and improving product quality. In practice, high N fertilizer rates are often used to maximize production, but this can cause negative effects such as excess $NO_3^-$ in leaves, which impacts food security, and N leaching, which harms the environment. Lettuce's response to N depends on variety, soil, and climate, and thus requires tailored fertilization to improve N efficiency and minimize risks (de Barros Sylvestre et al., 2019).

In lettuce, shallow roots, frequent high-rate N fertilizers, and intensive irrigation increase N leaching, raising environmental loss risks and reducing sustainability (Korsaeth, 2008). A strategy to reduce N leaching is to lower N fertilizer rates in lettuce. This reduces $NO_3^-$ leaching with minimal impact on yield, while maintaining water quality and vegetable standards (Aragão et al., 2012).

Excessive N in vegetables poses ecological and health risks. Increased $NO_3^-$ intake from vegetables is a primary dietary source. The type, dose, and application method of N fertilizers affect $NO_3^-$ buildup in edible tissues. Rational N management is crucial to safeguard health and the environment (Coimbra et al., 2012).

The maximum allowable limit for $NO_3^-$ in lettuce is set by both the European Union and Romanian national regulations. Thus, the maximum levels in raw greenhouse-grown lettuce are as follows: for lettuce harvested from October 1 to March 31, the limit must not exceed 5,000 mg $NO_3^-$/kg; for lettuce harvested from April 1 to September 30, the limit must not exceed 4,000 mg $NO_3^-$/kg (EU No 915/2023).

This study aimed to assess $NO_3^-$ content in greenhouse lettuce, emphasizing the plant's tendency to accumulate $NO_3^-$ under intensive fertilization. Additionally, it focused on the identification and quantification of related inorganic nitrogen species, like nitrite ($NO_2^-$) and ammonium ($NH_4^+$), which pose higher toxicity risks. The analysis facilitates the assessment of safety, quality, and potential environmental impact.

## MATERIALS AND METHODS

### *Lettuce sampling*

To determine nitrate content and related inorganic nitrogen species (nitrite and ammonium), greenhouse lettuce was sampled in May 2025 from two sources: supermarkets and local producers. Three lettuce samples were collected from supermarkets (SP), and four from local producers (LP). The samples were divided

into the plant's components and the growing medium (leaves, roots, and soil). This resulted in a total of 21 representative samples.

***Extraction assessment of nitrate and related inorganic nitrogen species***

After sampling, the lettuce samples were frozen and then lyophilized. Following lyophilization, the lettuce samples were ground to a fine powder. Nitrate and related inorganic nitrogen species were extracted using microwave-assisted extraction (MAE), with ultrapure water as the solvent (Novaes et al., 2009). This method is effective for releasing nitrate and related inorganic nitrogen species from leaves, roots, and soil samples (Hao et al., 2015; Zandvakili et al., 2024). From each sample type, 1.5 g was weighed, and 60 mL of ultrapure water was added (plant-to-solvent ratio of 1/40). The extraction parameters were set as follows: extraction power of 500 W for 15 minutes at 100°C. After extraction, the samples were allowed to cool to room temperature for about 10 minutes. The mixture was centrifuged at 10000 rpm for 20 minutes, then filtered through a 0.45 µm cellulose acetate (CA) syringe filter to obtain a clear extract, as shown in Figure 1. The extracts were carefully stored at 4°C, ready for analysis. This step helps ensure everything stays fresh and accurate for the results. The extraction parameters and results are presented in Table 1.

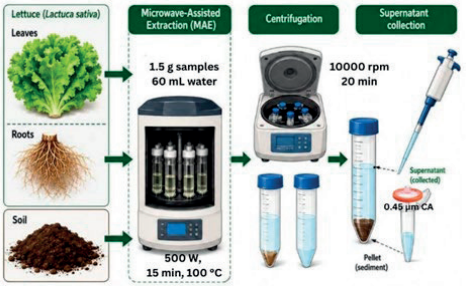



Figure 1. Procedure for extracting nitrate and related inorganic nitrogen species from lettuce samples

***Assessment of nitrate content in lettuce samples***

The nitrate content assessment of the extracts was performed using a modified ISO 7890-1:1986 spectrophotometric protocol based on 2,6-dimethylphenol (DMP) reagent (ISO, 1986). To 100 µL of each extract, 50 µL of DMP reagent and 100 µL of a mixture of sulfuric and phosphoric acids (9/1) were added. The resulting mixture was incubated at room temperature in the dark for 30 minutes. After incubation, the absorbance of the samples was measured at 345 nm. As a control, the extract was replaced with ultrapure water under the same conditions. The calibration curve was prepared using sodium nitrate ($NaNO_3$) at concentrations ranging from 0 to 20 mg/L. The results were expressed as milligrams of $NO_3^-$ per kilogram of sample (mg $NO_3^-$/kg).

***Assessment of nitrite content in lettuce samples***

The nitrite content assessment of the extracts was performed in the presence of the Griess reagent according to a modified spectrophotometric protocol (ISO 6777:1984; Moorcroft et al., 2001). 50 µL of Griess reagent was added to 150 µL of each extract. Griess reagent was a 1:1 mixture of sulfanilic acid and α-naphthylamine acetic solutions. The resulting mixture was incubated at room temperature, in the dark, for 30 minutes. After the incubation period, the absorbance of the samples was read at 520 nm. As a control, the extract was replaced with ultrapure water under the same conditions. The calibration curve was performed using sodium nitrite ($NaNO_2$) in concentrations ranging from 0 to 10 mg/L. The results were expressed as milligrams of $NO_2^-$ per kilogram of sample (mg $NO_2^-$/kg).

***Assessment of ammonium content in lettuce samples***

The ammonium content assessment of the extracts was determined using a modified ISO 7150-1:1984 spectrophotometric protocol in the presence of two reagents (ISO, 1984). Reagent A was a mixture of trisodium citrate, sodium salicylate, and sodium nitroprusside, and reagent B was a mixture of sodium hydroxide and sodium dichloroisocyanurate. 25 µL of reagent A and 25 µL of reagent B were added to 200 µL of each extract. The resulting mixture was incubated at room temperature, in the dark, for 60 minutes. After the incubation period, the absorbance of the samples was read at 650 nm. As a control, the extract was replaced with ultrapure water under the same conditions. The calibration curve was performed using ammonium chloride ($NH_4Cl$) in concentrations

ranging from 0 to 25 mg/L. The results were expressed as milligrams of $NH_4^+$ per kilogram of sample (mg $NH_4^+$/kg).

Table 1. Extraction parameters of nitrate and related inorganic nitrogen species

| Sampling site | Sample cod | Sample type | Sample/ volume ratio | Sample mass (g) | Initial volume (mL) | Final volume (mL) |
|---|---|---|---|---|---|---|
| Super-market 1 | SP1L | leaves | 1/40 | 1.50 | 60 | 53 |
| | SP1R | roots | 1/160 | 0.06 | 10 | 7.5 |
| | SP1S | soil | 1/40 | 1.5 | 60 | 55 |
| Super-market 2 | SP2L | leaves | 1/40 | 1.50 | 60 | 53 |
| | SP2R | roots | 1/40 | 1.50 | 60 | 57 |
| | SP2S | soil | 1/40 | 1.50 | 60 | 59 |
| Super-market 3 | SP3L | leaves | 1/40 | 1.50 | 60 | 52 |
| | SP3R | roots | 1/40 | 1.50 | 60 | 58 |
| | SP3S | soil | 1/40 | 1.50 | 60 | 57 |
| Local producer 1 | LP1L | leaves | 1/40 | 1.50 | 60 | 56 |
| | LP1R | roots | 1/40 | 1.50 | 60 | 56 |
| | LP1S | soil | 1/40 | 1.50 | 60 | 57 |
| Local producer 2 | LP2L | leaves | 1/40 | 1.13 | 45 | 44 |
| | LP2R | roots | 1/80 | 0.31 | 25 | 23 |
| | LP2S | soil | 1/40 | 1.50 | 60 | 59 |
| Local producer 3 | LP3L | leaves | 1/40 | 1.50 | 60 | 58 |
| | LP3R | roots | 1/40 | 1.30 | 51 | 47 |
| | LP3S | soil | 1/40 | 1.50 | 60 | 50 |
| Local producer 4 | LP4L | leaves | 1/40 | 1.50 | 60 | 51 |
| | LP4R | roots | 1/40 | 0.80 | 33 | 31 |
| | LP4S | soil | 1/40 | 1.50 | 60 | 59 |

### *Assessment of dietary exposure and chronic health risk*

The Estimated Daily Intake (EDI, mg $NO_3^-$ /kg BW/day) and Hazard Quotient (HQ) were calculated according to European Food Safety Authority (EFSA) risk assessment guidelines in order to evaluate the consumer safety implications of nitrate accumulation in edible lettuce leaves (EFSA, 2008):

$$EDI = (C_{leaf} \times FIR) / BW$$
$$HQ = EDI / ADI$$

Where $C_{leaf}$ is the measured nitrate concentration in edible lettuce leaves (mg $NO_3^-$ /kg fresh weight), FIR is the daily consumption rate of leafy vegetables (0.06 kg/day for adults), and BW is the standard adult body weight (70 kg, EFSA, 2012). The Acceptable Daily Intake (ADI) established by EFSA for nitrate is 3.7 mg $NO_3^-$ /kg BW/day. An HQ < 1.0 indicates that chronic exposure remains within safe limits, whereas an HQ > 1 indicates potential chronic health risk.

### *Statistical analysis*

Statistical analysis of the results was performed using GraphPad (version 11.0.2). The correlation between nitrate, nitrite, and ammonium contents was determined using the Pearson correlation coefficient.

## RESULTS AND DISCUSSIONS

### *Nitrate content in lettuce samples*

Limited research has investigated the influence of source of origin on $NO_3^-$ content in lettuce. In this study, a quantitative analysis of greenhouse lettuce samples from different sources, including supermarkets and local producers, was conducted. The results showed significant differences based on source, plant parts, and growing medium (soil).

$NO_3^-$ distribution was uneven among leaves, roots, and soil, with higher concentrations accumulating mainly in the leaves. Comparing supermarket and local producer samples, notable differences emerged: supermarket lettuce had $NO_3^-$ content ranging from 73.99 ± 2.87 mg $NO_3^-$/kg (soil) to 5340.81 ± 80.95 mg $NO_3^-$/kg (leaves), while local producer samples ranged from 71.02 ± 1.45 mg $NO_3^-$/kg (soil) to 3212.92 ± 50.89 mg $NO_3^-$/kg (leaves) (Figure 2). Notably, leaves, roots, and soil samples differed, with leaves showing the highest absorption because they are the primary tissues that store $NO_3^-$.

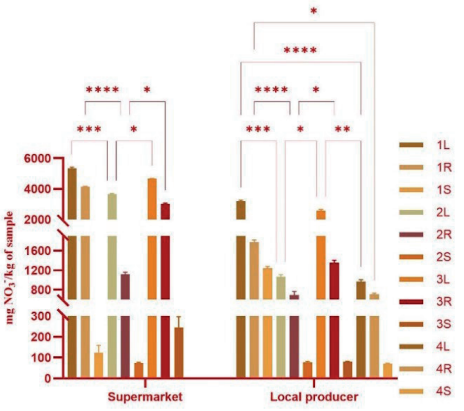



Figure 2. Nitrate content in different lettuce samples collected from supermarkets and local producers. Significant differences were noted at the following levels: * = $p < 0.05$, ** = $p < 0.01$, *** = $p < 0.001$, and **** = $p < 0.0001$

Regarding European standards for leafy vegetables, the higher $NO_3^-$ content in

supermarket samples raises food safety concerns. EU No 915/2023 sets a maximum limit of 4000 mg/kg for $NO_3^-$ in greenhouse-grown lettuce from April 1 to September 30. Conversely, local producer samples are significantly lower; thus, exposure to high concentrations of $NO_3^-$ from food is a major risk factor for human health. In the analyzed samples, the high values in lettuce leaves suggest increased accumulation of these compounds in the plant's edible parts. Because lettuce is often consumed raw in large quantities, even a moderate exceedance of the limit can lead to significant exposure, especially when combined with other dietary risk factors.

Therefore, the results underscore the importance of rigorous monitoring of agricultural inputs and compliance with the maximum permissible limit for $NO_3^-$ in fresh vegetables.

***Nitrite content in lettuce samples***

The evaluation of $NO_2^-$ content in lettuce samples revealed significant variation between supermarket and local producer samples. The supermarket samples showed much higher concentrations, especially for SP1R (roots), where content exceeded 2500 mg $NO_2^-$/kg, followed by SP3R (roots) at approximately 2000 mg $NO_2^-$/kg. In contrast, local producers' samples recorded considerably lower values, ranging from approximately 10 to 55 mg $NO_2^-$ /kg, with the highest in the LP4R (root) sample (Figure 3).

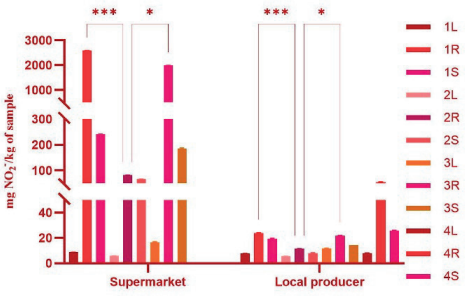



Figure 3. Nitrite content in different lettuce samples collected from supermarkets and local producers. Significant differences were noted at the following levels: * = $p < 0.05$, and *** = $p < 0.001$

The data show an opposite trend compared to $NO_3^-$. $NO_2^-$ is significantly accumulated in the roots, whereas $NO_3^-$ is accumulated mainly in the leaves. This may indicate a partial enzymatic conversion of $NO_3^-$ to $NO_2^-$. At the same time, soil samples (SP1S, SP4S) indicate a notable presence of $NO_2^-$, which may suggest the presence of specific microorganisms that favor the conversion of $NO_3^-$ to $NO_2^-$.

This uneven distribution suggests a significant difference between the two types of sources in post-harvest stages. Thus, lettuce collected from supermarkets is susceptible to the biochemical conversion of $NO_3^-$ to $NO_2^-$, a process favored by long-term storage, temperature fluctuations, and local anaerobic conditions in closed packaging. This process is significantly less pronounced in lettuce grown and sampled directly from local producers, which explains the lower $NO_2^-$ values.

The presence of $NO_2^-$ at high concentrations in lettuce samples, especially those from trade, represents a significant health risk. $NO_2^-$ are directly involved in the formation of nitrosamines, compounds with carcinogenic potential that can also induce methemoglobinemia, a serious condition in infants and vulnerable people (Popa et al., 2021).

Unlike $NO_3^-$, for which there are clear legislative thresholds in leafy vegetables, there are no maximum permitted limits for $NO_2^-$ in lettuce, but any high concentration is concerning. The concentration of 2500 mg $NO_2^-$/kg detected in SP1R (root) is markedly higher than $NO_2^-$ content typically reported in the literature for fresh lettuce, generally below 10-50 mg/kg in leaves and below 100 mg/kg in roots (Chung et al., 2003). This anomaly may indicate either intensive post-harvest $NO_3^-$ reduction or methodological interference at 520 nm from root pigments. This warrants further investigation, including validation against an independent analytical method.

The localization of $NO_2^-$ in the roots of the lettuce samples shows that $NO_2^-$ accumulation is blocked in the lower parts of the plant, possibly due to reduced foliar absorption. This pattern indicates that the agronomic strategies applied in the greenhouse (ventilation, N dose limitation, short time between harvest and analysis) help maintain low $NO_2^-$ content in the edible part of the plant. Regarding $NO_2^-$ accumulation, the data highlight a clear contrast between lettuce samples from supermarkets and those from local

producers. The problem is more pronounced in supermarket samples, with worryingly high values.

***Ammonium content in lettuce samples***

In the supermarket lettuce samples, $NH_4^+$ values varied significantly depending on the plant parts analyzed, as illustrated in Figure 4. The maximum concentration was recorded in the SP1R (root) sample, with a value of 30.93 ± 1.08 mg $NH_4^+$/kg, followed by SP2R with approximately 25.56 ± 0.50 mg $NH_4^+$/kg and SP3R with approximately 20.77 ± 0.77 mg $NH_4^+$/kg. In contrast, the soil samples (SP1S - SP3S) showed lower concentrations, ranging from 3.5 to 5.5 mg $NH_4^+$/kg. These results suggest that $NH_4^+$ ions tend to be present in higher amounts in the roots and absent in the leaves.

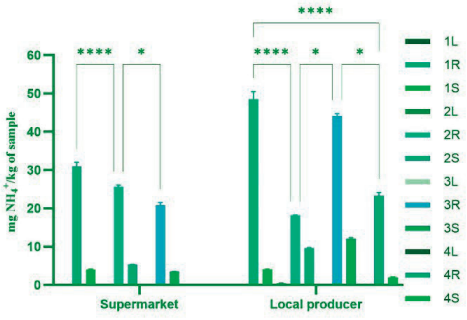



Figure 4. Ammonium content in different lettuce samples collected from supermarkets and local producers. Significant differences were noted at the following levels: * = $p < 0.05$, and **** = $p < 0.0001$

Samples from local producers showed a clear trend toward higher $NH_4^+$ accumulation in both the roots and the soil. The maximum values were recorded in samples LP1R (48.55 ± 2.00 mg $NH_4^+$/kg) and LP3R (44.11 ± 0.66 mg $NH_4^+$/kg). These concentrations are nearly double those observed in the supermarket lettuce samples. Soil samples LP2S and LP3S also recorded significant concentrations (from 9.5 to 12 mg $NH_4^+$/kg), while samples LP1S and LP4S showed values from 2 to 4 mg $NH_4^+$/kg. This pattern suggests progressive $NH_4^+$ accumulation, possibly favored by localized application of N fertilizers, high temperatures, increased humidity, and poor aeration. Additionally, the low $NO_3^-$ content in some of these samples may indicate incomplete conversion of $NH_4^+$ to $NO_3^-$ at physiological levels.

The presence of $NH_4^+$ can have significant implications for the plant's internal ionic balance and the nutritional quality of the product. Although the $NH_4^+$ ion is a natural and metabolically active form of N, its accumulation in tissues indicates physiological stress and can lead to the formation of secondary compounds (such as biogenic amines) that contribute to bitter taste or accelerate post-harvest spoilage. From a consumer health perspective, high concentrations of $NH_4^+$ are not strictly regulated, but when present alongside $NO_3^-$ and $NO_2^-$, they can contribute to metabolic imbalances, digestive discomfort, or cumulative effects with frequent consumption. Thus, concentrations of approximately 50 mg/kg should be viewed with caution, especially in the context of unprocessed consumption (raw plant), which is characteristic of this type of vegetable.

Analysis of $NH_4^+$ concentrations by source and plant part revealed uneven distribution and a high potential for accumulation under protected cultivation conditions (e.g., greenhouses). In all cases, the root was the dominant accumulation compartment, reflecting active translocation of reduced N to metabolically active areas of the plant. Differences between samples from local producers and those from the supermarket suggest that, in commercial crops, there may be stricter control of the dose and form of applied $NH_4^+$, whereas samples from local producers point to a potential N overapplication, likely combined with environmental conditions that suppress nitrification.

***Dietary exposure and chronic health risk***

The EDI of $NO_3^-$ varied considerably among the lettuce samples, ranging from 0.831 to 4.578 mg/kg BW/day, as seen in Table 2. The highest EDI values were obtained for the supermarket samples SP1L (4.578 mg/kg BW/day) and SP3L (3.997 mg/kg BW/day), both exceeding the ADI of 3.7 mg/kg BW/day. Accordingly, their HQ values were above unity (HQ = 1.237 and 1.080, respectively), indicating that the estimated exposure exceeded the selected health-based guidance value. In contrast, SP2L showed an EDI of 3.145 mg/kg BW/day and an HQ of 0.850, while all samples obtained from local

producers had substantially lower EDI (0.831–2.754 mg/kg BW/day) and HQ values (0.225–0.744). Thus, only SP1L and SP3L were identified as samples of potential concern based on the adopted EFSA ADI.

These findings are consistent with previous dietary exposure assessments showing that lettuce can represent an important source of nitrate intake. Luetic et al. (2023) reported that, assuming consumption of a 100 g portion, one lettuce sample contained sufficient $NO_3^-$ to exceed the ADI, demonstrating that individual high-$NO_3^-$ lettuce samples may substantially increase dietary exposure. Similarly, Brkić et al. (2017) estimated that consuming 150 g of lettuce would account for 47.5% of the ADI in spring and as much as 85.4% in autumn, emphasizing that $NO_3^-$ exposure from lettuce strongly depends on its $NO_3^-$ concentration. More recently, Dodocioiu et al. (2025) reported an EDI of 3.65 mg/kg BW/day for adults, whereas the estimated EDI for children reached 8.11 mg/kg BW/day. Lettuce with elevated $NO_3^-$ concentrations may represent a substantial contribution to daily $NO_3^-$ exposure and, under specific exposure scenarios, may exceed health-based guidance values (Brkić et al., 2017; Luetic et al., 2023; Dodocioiu et al., 2025).

Table 2. Estimated Daily Intake and Hazard Quotient of nitrate in supermarket and local producer lettuce samples

| Sample code | $NO_3^-$ (mg/kg) | EDI (mg/kg BW/day) | HQ | Risk |
|---|---|---|---|---|
| **SP1L** | 5340.81 | 4.578 | 1.237 | Risk exceeded |
| **SP2L** | 3669.32 | 3.145 | 0.850 | Acceptable |
| **SP3L** | 4663.58 | 3.997 | 1.080 | Risk exceeded |
| **LP1L** | 3212.92 | 2.754 | 0.744 | Acceptable |
| **LP2L** | 1069.20 | 0.916 | 0.248 | Acceptable |
| **LP3L** | 2593.25 | 2.223 | 0.601 | Acceptable |
| **LP4L** | 969.98 | 0.831 | 0.225 | Acceptable |

### *Pearson Correlation and Heatmap Matrix*

To evaluate potential relationships among the N forms accumulated in lettuce, Pearson correlations were computed for the $NO_3^-$, $NO_2^-$, and $NH_4^+$ contents across all samples examined (Figure 5).

Weak positive correlations were observed between $NO_3^-$ and $NO_2^-$ (r=0.35) and between $NO_2^-$ and $NH_4^+$ (r=0.31), while a very weak negative correlation was found between $NO_3^-$ and $NH_4^+$ (r=-0.06). These low values indicate weak associations among the reactive N forms, suggesting that $NH_4^+$, $NO_2^-$, and $NO_3^-$ behave largely independently in lettuce rather than through direct biochemical coupling. This finding indicates that the accumulation of each N form is driven by multiple physiological and environmental factors, such as sample origin and post-harvest conditions, highlighting the need for integrated monitoring of all N forms to accurately assess product quality.

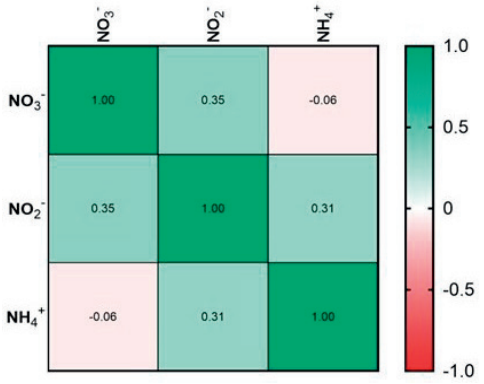



Figure 5. Pearson correlation between nitrate, nitrite, and ammonium contents in lettuce samples

In soil, N circulates through the biogeochemical N cycle, which includes essential processes such as biological N fixation, nitrification, and denitrification, each regulated by specialized microbial communities. These processes are mediated by functional genes that encode enzymes involved in the transformations of N compounds. In biological fixation, molecular nitrogen ($N_2$) is reduced to ammonia ($NH_3$) or other N-containing compounds by enzymes produced by N-fixing bacteria, enabling plants to absorb it. Non-symbiotic N fixation, carried out by free-living diazotrophs, is a major source of N for terrestrial ecosystems (Hao et al., 2022). Nitrification occurs under aerobic conditions and is mediated by nitrifying bacteria, which oxidize reduced inorganic forms of N, such as $NH_4^+$, to $NO_2^-$ and then to $NO_3^-$. $NH_4^+$ and $NO_3^-$ are taken up by plant cells through transport across the plasma membrane (Figure 6).

When $NO_3^-$ absorption greatly exceeds plant assimilation, $NO_3^-$ can accumulate in plant

tissues. The type of fertilizer used plays a key role in the $NO_3^-$ accumulation in the edible parts of vegetables. N can be supplied not only as $NO_3^-$ but also as $NH_3$, urea ($CO(NH_2)_2$), or other organic compounds. Choosing the appropriate fertilizer, depending on the plant part intended for consumption, can help reduce the concentration of $NO_3^-$ in the final product (Popa et al., 2021).

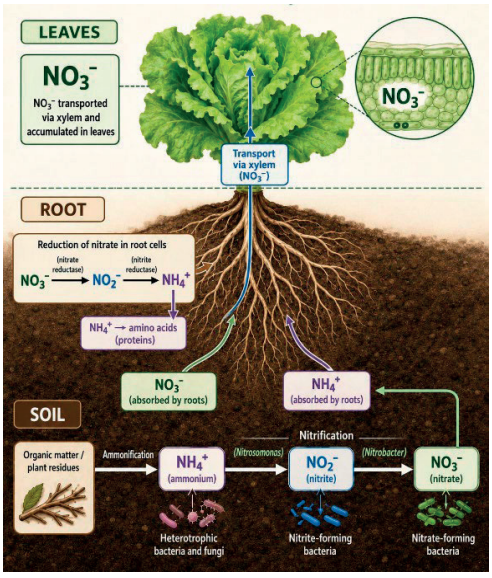



Figure 6. Formation and conversion of N forms in lettuce (Source: Authors-generated using AI)

The $NO_3^-$ accumulation is influenced by multiple factors, including soil composition, cropping system, fertilizer application regime, and climatic and seasonal conditions during the growing season (Martín Leon & Luzardo, 2020). In non-legume crops, higher $NO_3^-$ concentrations tend to accumulate in the leaves, whereas lower concentrations accumulate in the roots. For this reason, leafy vegetables, e.g., arugula, spinach, lettuce, celery, and parsley, are considered prominent species that accumulate $NO_3^-$ (Colonna et al., 2016).

The effect of N forms ($NH_4^+$, $NO_2^-$, and $NO_3^-$) on plant growth depends not only on the cultivated species but also on their concentrations and relationships. Usually, the form in which N is applied influences the anion-to-cation absorption ratio, thereby affecting dry matter production and root nutrient uptake. The quantity and quality of applied fertilizers are determining factors in the growth, production, and quality of leafy vegetables (Cencič et al., 2013).

It is emphasized that N accumulation varies significantly not only between species but also among varieties within the same species, with these differences influenced by environmental factors. Additionally, the N content depends on the specific plant part consumed (Jakabová et al., 2022).

The current results clearly show that the source of the lettuce sample significantly affects $NO_3^-$ buildup. On average, the leaf $NO_3^-$ contents were about 2.3 times higher in the supermarket samples compared to the local producer ones. This suggests that the sample origin, along with related cultivation methods and N management practices, plays a key role in $NO_3^-$ accumulation. This source-dependent variation aligns with previous research indicating that $NO_3^-$ contents in lettuce are strongly influenced by factors such as N availability, fertilization approach, growing system, environmental conditions, and plant physiology. For example, Aires et al. (2013) found higher $NO_3^-$ concentrations in conventionally grown baby-leaf vegetables than in organic ones, highlighting how production systems impact $NO_3^-$ contents. Similarly, Pinto et al. (2014) linked soil inorganic N contents to differences in $NO_3^-$ and $NH_4^+$ contents in lettuce. More recently, Martínez-Moreno et al. (2024) demonstrated that nutrient solution management effectively controls $NO_3^-$ accumulation, while Nguyen et al. (2026) revealed that N assimilation and the resulting $NO_3^-$, $NO_2^-$, and $NH_4^+$ concentrations are also strongly affected by light intensity and plant genotype.

Interestingly, the $NO_3^-$ contents in soil at harvest did not directly match the pattern seen in lettuce leaves. Although the supermarket samples had the highest leaf $NO_3^-$ contents, the soil $NO_3^-$ concentrations were relatively low, except for LP1 soil, which contained 1243.48 mg $NO_3^-$/kg. This discrepancy indicates that lettuce $NO_3^-$ accumulation reflects the plant's entire history of N availability, uptake, transport, and assimilation. Pinto et al. (2014) also showed that soil physicochemical properties affect inorganic N mobility and that differences in $NO_3^-$ leaching and plant availability can significantly influence N transfer from soil to lettuce. Moreover, Zhang

et al. (2025) found that just five days of nutrient deprivation before harvesting reduced $NO_3^-$ contents by 57.49% in leaves and 50.77% in roots, highlighting how short-term pre-harvest N availability strongly impacts tissue nitrate concentrations.

In this study, $NO_3^-$ distribution was tissue-dependent, with higher concentrations in leaves than roots, and much lower in soil. This pattern reflects $NO_3^-$ uptake by roots and transport to shoots, where it may be stored or reduced through assimilation. $NO_3^-$ metabolism occurs in both roots and shoots, with their relative roles influenced by N supply and environmental factors. Schiefloe et al. (2023) demonstrated substantial differences in $NO_3^-$ partitioning between lettuce shoots and roots, depending on the $NH_4^+$:$NO_3^-$ ratio supplied to plants; increasing $NH_4^+$ availability reduced $NO_3^-$ concentrations in both compartments by approximately 7–8 times. Likewise, Zhang et al. (2025) observed coordinated yet tissue-specific changes in $NO_3^-$ concentration and $NO_3^-$ transporter expression in lettuce leaves and roots during nutrient deprivation. These findings support the marked root–leaf compartmentalization observed in the present study.

The distribution of $NH_4^+$ differed markedly from that of $NO_3^-$. $NH_4^+$ was absent or present only at trace levels in leaves, whereas appreciable concentrations occurred in roots. Soil $NH_4^+$ concentrations were intermediate but substantially lower than those measured in roots. This preferential accumulation in roots aligns with their primary role in $NH_4^+$ uptake and assimilation. Schiefloe et al. (2023) reported that lettuce grown under a high-$NH_4^+$ nutrient regime accumulated almost three times more $NH_4^+$ in roots than plants receiving a low-$NH_4^+$ treatment, whereas changes in shoot $NH_4^+$ were comparatively limited. Pinto et al. (2014) also observed a close relationship between $NH_4^+$ concentration and glutamine synthetase activity in lettuce, supporting the rapid incorporation of $NH_4^+$ into organic N compounds. Consequently, the very low $NH_4^+$ concentrations detected in the leaves of the present samples likely indicate efficient assimilation and limited translocation or storage of free $NH_4^+$ in edible tissues.

$NO_2^-$ showed a different distribution pattern. Leaf concentrations were low, while some root and soil samples, especially in the supermarket samples, showed higher values. This pattern suggests root-zone N transformations and tissue-specific $NO_2^-$ reduction may contribute to $NO_2^-$ formation. $NO_2^-$ is an intermediate of $NO_3^-$ assimilation, usually rapidly reduced during N metabolism, so its accumulation is lower than $NO_3^-$. Nguyen et al. (2026) found that the balance among $NO_3^-$, $NO_2^-$, $NH_4^+$, nitrate reductase, and nitrite reductase in lettuce depends on enzyme activity and environmental conditions.

Leaf $NO_2^-$ concentrations also show the large variability reported for commercial lettuce. Aires et al. (2013) reported $NO_2^-$ concentrations ranging from 0.25 to 1.89 mg $NO_2^-$/kg FW in green and red lettuce from conventional and organic production systems. In contrast, Luetic et al. (2023) reported $NO_2^-$ concentrations ranging from 21.1 to 378.1 mg $NO_2^-$/kg FW. The authors noted that cultivation, post-harvest handling, and storage affect nitrite levels. While the leaf $NO_2^-$ concentrations in this study were higher than some reports for freshly harvested baby-leaf lettuce, they stayed within the variability seen in commercial leafy vegetables. From a food-safety perspective, $NO_3^-$ accumulation in the edible leaves is the most relevant finding. Luetic et al. (2023) reported $NO_3^-$ concentrations of 169.7–3184.2 mg $NO_3^-$/kg FW in commercial lettuce. In comparison, LP2 and LP4 in the present study were close to this literature range, whereas the supermarket samples showed considerably higher $NO_3^-$ concentrations. Qureshi et al. (2026) reported approximately 2900 mg $NO_3^-$/kg FW and 2.29 mg $NO_3^-$/kg FW in lettuce and considered $NO_3^-$ control an important criterion of nutritional quality.

## CONCLUSIONS

The present work aimed to compare the N forms ($NO_3^-$, $NO_2^-$, and $NH_4^+$) in lettuce grown in greenhouses and sold in supermarkets and by local producers. Based on experimental data, clear source- and tissue-dependent differences in the distribution of $NO_3^-$, $NO_2^-$, and $NH_4^+$ in greenhouse lettuce were observed between these two sources in the concentrations and internal distributions of these compounds across the leaves, roots, and soil. These variations suggest different N uptake and assimilation patterns

across the production sources rather than isolated parts of the N cycle.

Supermarket samples generally showed higher $NO_3^-$ concentrations in the edible leaves and higher $NO_2^-$ levels in the roots, whereas $NH_4^+$ was predominantly associated with the root compartment. Several supermarket leaf samples exceeded the EU maximum $NO_3^-$ content of 4000 mg $NO_3^-$/kg for greenhouse lettuce harvested between April and September, highlighting a potential food-safety concern.

From an agronomic standpoint, the findings emphasize the importance of N management just before harvest. For food safety, the high $NO_3^-$ contents observed in some edible leaves highlight a need for careful monitoring.

## ACKNOWLEDGEMENTS

This work was supported by a grant of the Ministry of Education and Research, CCCDI-UEFISCDI, project number PN-IV-P6-6.1-CoEx-2024-0120, within PNCDI IV.

Mihaela Dragoi Cudalbeanu expresses her gratitude to the Romanian-American Foundation and the Romanian Fulbright Commission for the opportunity to participate in the Fulbright-RAF Scholar Award.

## REFERENCES

Aczel, M. R. (2019). What is the nitrogen cycle, and why is it key to life? *Frontiers for Young Minds*, 7. https://doi.org/10.3389/frym.2019.00041.

Aragão, V. F., Fernandes, P. D., Gomes Filho, R. R., Carvalho, C. M., Feitosa, E. O., & Feitosa, H. O. (2012). Produção e eficiência no uso de água do pimentão submetido a diferentes lâminas de irrigação e níveis de nitrogênio. *Revista Brasileira de Agricultura Irrigada,* 6(3), 207-216. https://doi.org/10.7127/rbai.v6n300086.

Aires, A., Carvalho, R., Rosa, E. A. S., & Saavedra, M. J. (2013). Effects of agriculture production systems on nitrate and nitrite accumulation on baby-leaf salads. *Food Science & Nutrition*, 1(1), 3–7. https://doi.org/10.1002/fsn3.1.

Assémien, F. L., Cantarel, A. A. M., Florio, A., Lerondelle, C., Pommier, T., Gonnety, J. T., &Le Roux, X. (2019). Different groups of nitrite-reducers and N2O-reducers have distinct ecological niches and functional roles in West African cultivated soils. *Soil Biology and Biochemistry,* 129, 39-47. https://doi.org/10.1016/j.soilbio.2018.11.003.

Brady, N., & Weil, R. (2010). Nutrient cycles and soil fertility. In V. R. Anthony (Ed.), *Elements of the nature and properties of soils* (3rd ed., pp. 396-420). Pearson Education.

Britto, D. T., & Kronzucker, H. J. (2002). NH4+ toxicity in higher plants: A critical review. *Journal of Plant Physiology,* 159(6), 567-584. https://doi.org/10.1078/0176-1617-0774.

Brkić, D., Bošnir, J., Bevardi, M., Bošković, A. G., Miloš, S., Lasić, D., Krivohlavek, A., Racz, A., Mojsović Ćuić, A., & Trstenjak, N. U. (2017). Nitrate in leafy green vegetables and estimated intake. *African Journal of Traditional, Complementary and Alternative Medicines,* 14(3), 31–41. https://doi.org/10.21010/ajtcam.v14i3.4.

Butnariu, M. (2018). The nitrogen cycle in the soil, impact on the environment. *Environmental Forensics*, 4(4), 1. https://doi.org/10.31031/EAES.2018.04.000593.

Cassman, K. G., Dobermann, A., & Walters, D. T. (2002). Agroecosystems, nitrogen use efficiency, and nitrogen management. *AMBIO: A Journal of the Human Environment*, 31(2), 132–140.

Cencič, A., & Hmelak Gorenjak, A. (2013). Nitrate in vegetables and their impact on human health. *Acta Alimentaria,* 42(2), 158–172. https://doi.org/10.1556/aalim.42.2013.2.4.

Chislock, M. F., Doster, E., Zitomer, R. A., & Wilson, A. E. (2013). Eutrophication: Causes, consequences, and controls in aquatic ecosystems. *Nature Education Knowledge,* 4(4), 10.

Chung, S. Y., Kim, J. S., Kim, M., Hong, M. K., Lee, J. O., Kim, C. M., & Song, I. S. (2003). Survey of nitrate and nitrite contents of vegetables grown in Korea. *Food Additives & Contaminants*, 20(7), 621–628.

Coimbra, J. L. M., Ernani, P. R., & Petry, E. (2012). Rendimento e conservação de cebola alterados pelo adensamento e parcelamento de nitrogênio em cobertura. *Revista Brasileira de Ciência do Solo*, 36(3). https://doi.org/10.1590/S0100-06832012000300017.

Colla, G., Kim, H. J., Kyriacou, M. C., & Rouphael, Y. (2018). Nitrate in fruits and vegetables. *Scientia Horticulturae*, 237, 221-238.

Colonna, E., Rouphael, Y., Barbieri, G., &De Pascale, S. (2016). Nutritional quality of ten leafy vegetables harvested at two light intensities. *Food Chemistry*, 199, 702-710. https://doi.org/10.1016/j.foodchem.2015.12.068.

de Barros Sylvestre, T., Boscov Braos, L., Batistella Filho, F., Pessôa da Cruz, M. C., & Ferreira, M. E. (2019). Mineral nitrogen fertilization effects on lettuce crop yield and nitrogen leaching. *Scientia Horticulturae*, 255, 153-160. https://doi.org/10.1016/j.scienta.2019.05.032.

Dodocioiu, A. M., Buzatu, G.-D., & Botu, M. (2025). Nitrates and nitrites in vegetables and the health risk. *Foods*, 14(17), 3037. https://doi.org/10.3390/foods14173037

European Food Safety Authority Scientific Committee. (2008). Nitrate in vegetables: Scientific opinion of the Panel on Contaminants in the Food Chain. *EFSA Journal*, 6(6), 689. https://doi.org/10.2903/j.efsa.2008.689

European Food Safety Authority Scientific Committee. (2012). Guidance on selected default values to be used by the EFSA Scientific Committee, Scientific Panels

and Units in the absence of actual data. *EFSA Journal*, 10(3), 2579. https://doi.org/10.2903/j.efsa.2012.2579.

European Commission. (2023). Commission Regulation (EU) 915/2023 of 25 April 2023 on maximum levels for certain contaminants in food and repealing Regulation (EC) No 1881/2006. *Official Journal of the European Union,* L 119, 1–38. http://data.europa.eu/eli/reg/2023/915/oj

Gidurus, M., Mitelut, A., Niculiță, P., Popa, M., TURTOI, M., & GEICU, M. (2012). Nitrate accumulation in autochthonous varieties of vegetables. *Journal of Environmental Protection and Ecology*, 13(2A), 906-912.

Hao, J., Feng, Y., Wang, X., Yu, Q., Zhang, F., Yang, G., Ren, G., Han, X., Wang, X., & Ren, C. (2022). Soil microbial nitrogen-cycling gene abundances in response to crop diversification: A meta-analysis. *Science of The Total Environment*, 838, 156621. https://doi.org/10.1016/j.scitotenv.2022.156621.

Hao, J., Li, H., Wan, Y., & Liu, H. (2015). Reduction of nitrite levels in fresh lettuces with aqueous chlorine dioxide treatment. *International Journal of Food Science & Technology*, 50(3), 652–659. https://doi.org/10.1111/ijfs.12660.

International Organization for Standardization (1986). ISO 7890-1:1986 Water quality - Determination of nitrate - Part 1: 2,6-Dimethylphenol spectrometric method. https://www.iso.org/standard/14840.html.

International Organization for Standardization (1984). ISO 6777:1984 Water quality - Determination of nitrite - Molecular absorption spectrometric method. ISO. https://www.iso.org/standard/13273.html.

International Organization for Standardization (1984). ISO 7150-1:1984 Water quality - Determination of ammonium - Part 1: Manual spectrometric method. ISO. https://www.iso.org/standard/13742.html.

Jakabová, S., Šnirc, M., Zeleňáková, L., & Ziarovska, J. (2022). Determination of nitrates in lettuce (*Lactuca sativa* Var. Capitata) from various producers by ion-selective electrode. *Journal of Hygienic Engineering and Design,* 40, 19-26.

Korsaeth, A. (2008). Relations between nitrogen leaching and food productivity in organic and conventional cropping systems in a long-term field study. *Agriculture, Ecosystems & Environment*, 127(3-4), 177-188. https://doi.org/10.1016/j.agee.2008.03.014.

Luetic, S., Knezovic, Z., Jurcic, K., Majic, Z., Tripkovic, K., & Sutlovic, D. (2023). Leafy Vegetable Nitrite and Nitrate Content: Potential Health Effects. *Foods*, 12(8), 1655. https://doi.org/10.3390/foods12081655.

Martín Leon, V., & Luzardo, O. P. (2020). Evaluation of nitrate contents in regulated and non-regulated leafy vegetables of high consumption in the Canary Islands, Spain: Risk assessment. *Food and Chemical Toxicology,* 146, 111812. https://doi.org/10.1016/j.fct.2020.111812.

Martínez-Moreno, A., Carmona, J., Martínez, V., Garcia-Sánchez, F., Mestre, T. C., Navarro-Pérez, V., & Camara-Zapata, J. M. (2024). Reducing nitrate accumulation through the management of nutrient solution in a floating system lettuce (*Lactuca sativa* L.). *Scientia Horticulturae*, 336, 113377. https://doi.org/10.1016/j.scienta.2024.113377.

Moorcroft, M. J., Davis, J., & Compton, R. G. (2001). Detection and determination of nitrate and nitrite: A review. *Talanta*, 54(5), 785–803. https://doi.org/10.1016/S0039-9140(01)00323-X.

Nguyen, N. T. T., Habibi, N., Sediqui, N., de Almeida, O. L., Dabirimirhosseinloo, M., Terada, N., Sanada, A., & Koshio, K. (2026). LED light intensity regulates nitrogen assimilation enzyme activity and metabolic responses in iceberg and leaf lettuce (*Lactuca sativa* L.). *Plants*, 15(9), 1321. https://doi.org/10.3390/plants15091321.

Novaes, H. B., Vaitsman, D. S., Dutra, P. B., & Pérez, D. V. (2009). Determination of nitrate in lettuce by ion chromatography after microwave water extraction. *Química Nova*, 32(6), 1647–1650. https://doi.org/10.1590/S0100-40422009000600049.

Pennington, J. A. T., & Fisher, R. A. (2010). Food component profiles for fruit and vegetable subgroups. *Journal of Food Composition and Analysis*, 23(5), 411-418. https://doi.org/10.1016/j.jfca.2010.01.008.

Pinto, E., Fidalgo, F., Teixeira, J., Aguiar, A. A., & Ferreira, I. M. P. L. V. O. (2014). Influence of the temporal and spatial variation of nitrate reductase, glutamine synthetase and soil composition in the N species content in lettuce (*Lactuca sativa*). *Plant Science*, 219–220, 35–41. https://doi.org/10.1016/j.plantsci.2014.01.001.

Popa, D. C., Popa, R. A., Pogurschi, E. N., Tudorache, M., Vîntu, C. R., Marin, M. P., & Vidu, L. (2021). Nitrate content of spring leafy vegetables from different outlets. *Notulae Botanicae Horti Agrobotanici Cluj-Napoca*, 49(2), https://doi.org/10.15835/nbha49212340

Pujol Pereira, E. I., Conz, R. F., & Six, J. (2017). Nitrogen utilization and environmental losses in organic greenhouse lettuce amended with two distinct biochars. *Science of The Total Environment*, 598, 1169-1176.

Qureshi, W. A., Gao, J., Tunio, M. H., Elsherbiny, O., Gao, X., Wang, L., & Mosha, A. H. (2026). Smart plasma-enhanced aeroponic cultivation of lettuce (*Lactuca sativa* L.): Comparative evaluation with soil and hydroponic systems on growth responses, nitrogen absorption, and nutritional quality. *Smart Agricultural Technology,* 13, 101776. https://doi.org/10.1016/j.atech.2025.101776.

Schiefloe, M., Jakobsen, Ø. M., Pannico, A., Quadri, C., & Jost, A.-I. K. (2023). From urine to food and oxygen: Effects of high and low $NH_4^+$:$NO_3^-$ ratio on lettuce cultivated in a gas-tight hydroponic facility. *Frontiers in Plant Science*, 14, 1229476. https://doi.org/10.3389/fpls.2023.1229476.

Singh, S., Anil, A. G., Kumar, V., Kapoor, D., Subramanian, S., Singh, J., & Ramamurthy, P. C., (2022). Nitrates in the environment: A critical review of their distribution, sensing techniques, ecological effects and remediation. *Chemosphere*, 287, 131996. https://doi.org/10.1016/j.chemosphere.2021.131996.

Zhang, Y., Liu, X., La, S., Wang, M., Hu, X., Shi, A., Guo, J., & Dong, L. (2025). Transcriptome analysis reveals nutrient deprivation reduces nitrate content in lettuce (*Lactuca sativa* var. *ramosa* Hort.) and enhances

nitrogen metabolism. *Frontiers in Plant Science*, 16, 1585955. https://doi.org/10.3389/fpls.2025.1585955.

Zandvakili, O., Barker, A. V., Hashemi, M., Herbert, S. J., & Parikh, S. J. (2024). Enhancing nitrate and ammonium recovery from lettuce leaves: Evaluating the impact of cultivation practices and chemical extractants. *Journal of Plant Nutrition*, 47(13), 2165–2173. https://doi.org/10.1080/01904167.2024.2333314.

Scientific Papers. Series E. Land Reclamation, Earth Observation & Surveying, Environmental Engineering. Vol. XV, 2026
Print ISSN 2285-6064, CD-ROM ISSN 2285-6072, Online ISSN 2393-5138, ISSN-L 2285-6064

# VALORIZATION OF STEEL FURNACE SLAG FOR CONSTRUCTION APPLICATIONS: TECHNICAL CHALLENGES AND OPPORTUNITIES

**Ana-Cristina VASILE[1, 2], Raul ZAHARIA[2], Cornelia BAERA[1, 3], Aurelian GRUIN[1, 2], Paula SFIRLOAGA[4], Adelin STIRB[2], Alexandru ION[1]**

[1]NIRD URBAN-INCERC Timișoara Branch, 2 Traian Lalescu Street, Timișoara, Romania
[2]Faculty of Civil Engineering, Politehnica University of Timișoara, 2 Traian Lalescu Street, Timișoara, Romania
[3]Faculty of Management in Production and Transportation, Politehnica University of Timișoara, 14 Remus Street, Timișoara, Romania
[4]National Institute for Research and Development in Electrochemistry and Condensed Matter, 144 Dr. Aurel Păundescu Podeanu Street, RO 300569, Timișoara, România

Corresponding author email: ana.vasile@incd.ro

***Abstract***

*Steel furnace slags is a strategically important secondary resource for sustainable building materials, but its efficient utilization requires a clear understanding of its highly variable behaviour. Previous studies indicate that slag-derived composites often exhibit reduced workability due to particle size and shape, high water demand, and the slow reactivity of certain silicate phases. Dimensional stability remains a critical issue, as several types of steel slag from furnaces contain phases predisposed to delayed expansion, mainly related to the mineralogical composition of the particles. Furthermore, the presence of heavy metals requires detailed characterization, representing a critical factor in assessing the safety of using steel furnace slag in construction composites. In addition to these generalized mechanisms, an important regional challenge is the utilization of the large quantities of steel furnace slag accumulated in Romania from decades of steel production. These materials remain in landfills without being given a new cycle of use, despite their potential for integration into cement-based composites and civil infrastructure. This article examines the main technical limitations associated with the use of steel furnace slag, while highlighting possible characterization strategies and processing methods that can enable the safe and efficient use of existing steel furnace slag resources in Romania.*

***Key words****: circular economy, secondary raw materials, steel furnace slag valorization.*

## INTRODUCTION

The construction industry faces intensifying pressure to mitigate its environmental impact through optimized utilization of secondary raw materials and systematic reduction of industrial waste (Müller et al., 2014; European Commission, 2015; Ghisellini et al., 2016). Within this framework, steel slag has garnered substantial attention due to its abundance and prospective applications in cementitious composites and civil infrastructure (Shi & Qian, 2000; Motz & Geiseler, 2001; Brand & Fanijo, 2020). As a by-product of steel manufacturing processes, steel slag represents both an environmental challenge and an opportunity for the development of more sustainable building materials (Mousavinejad & GilKalaye, 2024).

Global steel production generates each year very large volumes of steel slag, amounting to hundreds of millions of tons worldwide, and although partial reuse is achieved in certain regions, a significant portion of this material remains landfilled due to technical, environmental, and regulatory constraints (World Steel Association; Motz & Geiseler, 2001).

The literature consistently highlights the need for systematic characterization, controlled processing, and appropriate qualification for specific applications to enable the safe and efficient reuse of steel slag in construction materials (Shi & Qian, 2000; Provis & Van Deventer, 2009; Brand & Fanijo, 2020). However, the main obstacles to large-scale recycling include the pronounced variability between different types of slag (electric arc furnace slag, EAF; basic oxygen furnace slag, BOF; ladle metallurgy furnace slag, LMF; argon oxygen decarburization slag, AOD), the risk of delayed volumetric expansion associated with free CaO and MgO or other mineralogical

mechanisms, reduced workability in fresh composites, and concerns about heavy metal content and mobility (Shi & Qian, 2000; Deja, 2000; Santamaría et al., 2018; Brand & Fanijo, 2020).

In Romania, decades of steel production have resulted in the accumulation of substantial quantities of steel slag, which remain largely underutilized or landfilled in industrial waste dumps (Figure 1) (Baera et al., 2024; 2026). Research and exploitation strategies in the Romanian context, the term steel furnace slag (SFS) is particularly suitable, as most slag deposits come from primary steel production processes, mainly from basic oxygen furnaces (BOF) and electric arc furnaces (EAF) (Figure 1). The term SFS proves particularly apt for Romanian research and exploitation strategies, reflecting the predominance of furnace-derived deposits.

The principal national impediment remains the absence of comprehensive slag inventories and standardized qualification frameworks, severely constraining construction sector integration (Kurecki et al., 2024). Addressing this issue requires coordinated strategies focused on rapid characterization protocols, pilot-scale valorisation projects, and targeted pre-treatment methods, such as aging or carbonation, to mitigate expansion risks and environmental issues, while allowing the use of locally available secondary raw materials in civil infrastructure projects (Santamaría et al., 2018; Shi & Qian, 2000; Deja, 2000; Provis & Van Deventer, 2009; Brand & Fanijo, 2020;).

Despite these prospects, SFS deployment remains circumscribed by pronounced physicochemical and mineralogical variability arising from disparate steelmaking parameters, feedstock compositions, and cooling regimes materials (Shi & Qian, 2000; Motz & Geiseler, 2001; Brand & Fanijo, 2020).

Poor workability consistently manifests when SFS substitutes natural aggregates, attributable to angular morphology, rough surface texture, and elevated water absorption that exacerbate mixture friction and water demand (Yildirim & Prezzi, 2011; Ouda & Abdel-Gawwad, 2017; Loureiro et al., 2022). Parallel fresh-state concerns, dimensional stability constitutes a major technical challenge. Certain furnace slag typologies harbor reactive mineral phases capable of protracted hydration, inducing delayed volumetric expansion that compromises long-term durability (Santamaría et al., 2018; Adegoloye et al., 2016).

Environmental safety further requires consideration: the metallurgical provenance introduces trace metallic elements with exposure-dependent mobility, necessitating rigorous physicochemical characterization and leaching assessment (Alizadeh et al., 2003; Liu et al., 2016).

Regardless of these technical constraints, the substantial volumes of steel slag generated globally over decades of steel production constitute a valuable secondary resource. Extensive research validates its viability across diverse applications: concrete, mortar, asphalt mixtures, and specialized uses (Maslehuddin et al., 2013; Loureiro et al., 2022). Nevertheless, significant underutilization persists, underscoring the critical need for integrated approaches that synergize material characterization, performance validation, and tailored processing methodologies to enable safe, efficient valorisation (Fuente-Alonso et al., 2017; Loureiro et al., 2022). In this context, this article examines the main technical challenges associated with the use of steel slag in construction applications and discusses potential pathways for its safe and efficient use.

This review systematically outlines the principal technical challenges impeding steel slag deployment in construction while elucidating viable mitigation pathways for its effective utilization.

Despite inherent technical complexities necessitating rigorous evaluation, steel furnace slag remains a high-potential waste-by-product. Its recovery offers strategic opportunities to address environmental liabilities while advancing Circular Economy principles within the construction sector.




Figure 1. EAF landfill resulting from long-term steel production in Romania: a) the EAF landfill on the site; b-c) Location on the map of the Terova (near Resita, Caras-Severin County) EAF slag landfill (Baera et al., 2024)

## MATERIALS AND METHODS

### Review methodology

The present study was developed as a literature-based review focused on the main technical challenges and valorisation opportunities associated with the use of steel furnace slag (SFS) in construction applications. The paper was also supported by the research activities carried out within the research program PN 23 35 04 01 of Nucleu Programme of the National Research Development and Innovation Plan 2022-2027, "ECODIGICONS", supported by the Ministry of Research, Innovation and Digitalization. Baera et al. (2024), focused on the sustainable integration of secondary raw materials into construction materials and infrastructure applications.

The analysis was carried out by examining scientific publications addressing the physical, chemical, mineralogical, and environmental behaviour of steel furnace slag, together with its integration into cement-based materials and civil infrastructure systems. In parallel, selected observations obtained during the preliminary investigations performed within the research program PN 23 35 04 01 were considered as practical examples supporting the discussion regarding the behaviour of SFS-containing cementitious composites.

The literature selection process focused primarily on studies investigating the influence of SFS on fresh-state properties, dimensional stability, long-term durability, and leaching behaviour. Particular attention was also given to research discussing characterization methods, processing approaches, and potential mitigation strategies intended to improve the safe and efficient utilization of SFS in construction materials.

The reviewed information was collected from scientific journal articles, conference papers, technical reports, and relevant research studies published in recent decades. The analysis included studies related to different types of steel furnace slag, particularly electric arc furnace (EAF) slag and basic oxygen furnace (BOF) slag, due to their relevance for construction applications and their significant accumulation in industrial waste deposits.

The collected literature was subsequently organized according to the main technical aspects influencing the practical utilization of SFS, including chemical and mineralogical characteristics, fresh-state behaviour, dimensional stability, environmental assessment, and

potential valorisation pathways in construction and environmental applications.

**Characterization and general properties of steel furnace slag**

Steel furnace slag (SFS) forms during primary steelmaking processes (Figure 2), predominantly via basic oxygen furnaces (BOF) and electric arc furnaces (EAF), through high-temperature interactions among molten steel, fluxing agents, and furnace refractories (Figure 3).

As Brand & Fanijo (2020) emphasize, SFS exhibits pronounced compositional variability stemming from disparate steelmaking methodologies, raw material inputs, operational parameters, and cooling regimes, a characteristic profoundly influencing its performance within cementitious composites and necessitating rigorous consideration.

During steelmaking, fluxes including limestone ($CaCO_3$) and dolomite ($CaMg(CO_3)_2$) facilitate impurity removal from molten steel, yielding slag enriched with calcium oxides (CaO), magnesium oxides (MgO), iron oxides (Fe), and silicates ($SiO_2$) (Yildirim & Prezzi, 2011; Brand & Fanijo, 2020).

BOF slags are generally characterized by high CaO contents and a strongly basic nature, whereas EAF slags tend to exhibit greater compositional diversity due to the heterogeneous nature of scrap feedstock. According to Brand and Fanijo, (2020), these differences in formation conditions result in distinct slag types with varying chemical, mineralogical, and physical characteristics.

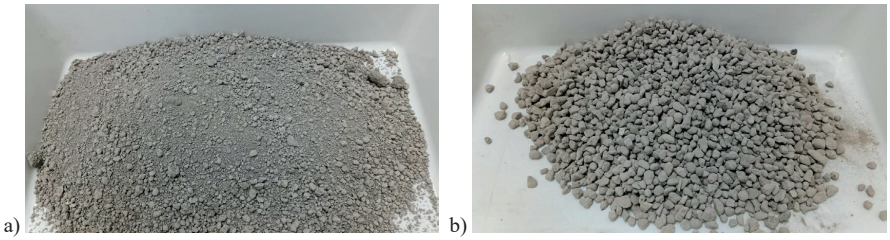


Figure 2. Representative electric arc furnace (EAF) slag: a) 0-4 mm fraction; b) 4-8 mm fraction

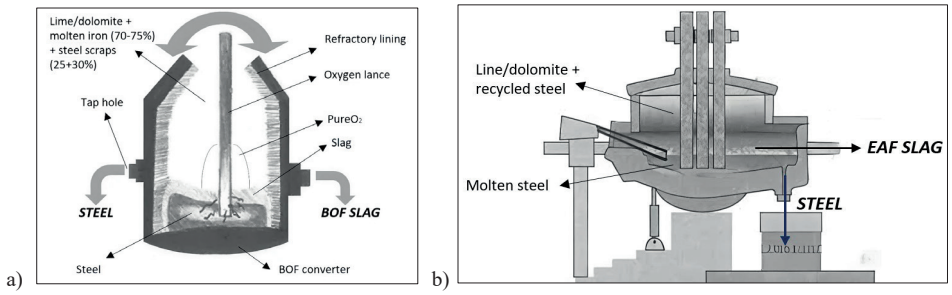



Figure 3. Schematic representation of: a) BOF process (Linz and Donawitz process); b) EAF steelmaking (Yldirim and Prezzi, 2011)

**Chemical composition and mineralogical features**

Steel furnace slag (SFS) typically comprises CaO, $SiO_2$, $FeO/Fe_2O_3$, and MgO as predominant constituents, with $Al_2O_3$ and other oxides present in smaller proportions (Yildirim & Prezzi, 2011; Brand & Fanijo, 2020). However, both Brand & Fanijo, (2020) and Yildirim & Prezzi (2011) report that the relative proportions of these oxides can vary significantly not only between BOF and EAF slags but also between different batches produced within the same steel plant.

From a mineralogical perspective, SFS consists of a complex assemblage of crystalline and amorphous phases, including dicalcium silicate ($C_2S$), wüstite (FeO), periclase (MgO), merwinite ($Ca_3MgSi_2O_8$), and calcium ferrites (e.g., $C_2F$). The presence of free CaO and free MgO is particularly important, as these phases

are associated with delayed hydration reactions and volumetric instability when exposed to moisture (Yildirim & Prezzi, 2011; Brand & Fanijo, 2020).

**Microstructural characteristics and phase heterogenity**

At the microscale, steel furnace slag particles frequently exhibit heterogeneous internal structures, characterized by differences between particle surfaces and cores. This phase heterogeneity originates from non-equilibrium cooling and localized chemical segregation during solidification, leading to the coexistence of phases with different reactivity within the same particle. Such internal heterogeneity has been shown to influence the interaction between slag particles and cementitious matrices, particularly at the interfacial transition zone, thereby affecting mechanical performance and long-term durability (Yildirim & Prezzi, 2011; Brand & Fanijo, 2020).

**Variability and implications for construction applications**

The combined chemical, mineralogical, and microstructural variability of steel furnace slag represents a major challenge for its standardized use in construction materials. As emphasized in the literature, differences in slag characteristics can lead to inconsistent workability, mechanical properties, and dimensional stability of SFS-containing composites if appropriate characterization is not performed. Consequently, the effective valorization of steel furnace slag requires thorough preliminary assessment, including chemical composition, mineralogical phase analysis, and microstructural evaluation, to ensure predictable performance in construction applications (Yildirim & Prezzi, 2011; Brand & Fanijo, 2020). The essential steps involved in the initial characterization of steel furnace slag are outlined below:

- *X-ray Fluorescence (XRF) analysis* used for the chemical evaluation of mineral wastes is a non-destructive analytical technique employed to identify and quantify the chemical elements present in solid materials;
- *X-ray Diffraction (XRD) analysis* is an instrumental analytical technique used for the identification and quantification of crystalline phases in mineral material;
- *Fourier Transform Infrared (FTIR) Spectroscopy* is an instrumental analytical technique used to identify functional groups and chemical bonds in the analysed materials by examining the absorption of infrared radiation by their molecular structure.
- *Thermogravimetric Analysis (TGA) and Differential Thermal Analysis (DTA)* comprise a set of thermoanalytical techniques used to evaluate the thermal behavior, chemical stability, and physicochemical transformations of materials.
- *Visual Analysis and Microscopy* represent a set of morphological and microstructural investigation methods used for the observation, description, and interpretation of the physical, structural, and mineralogical characteristics of the analysed materials. The method includes macroscopic (visual) and microscopic examinations (optical microscopy and scanning electron microscopy - SEM, optionally coupled with energy-dispersive spectroscopy, EDS) and is applied for the characterization of mineral wastes.

Figure 4 summarizes the key steps required to achieve an initial characterization of any steel furnace slag.

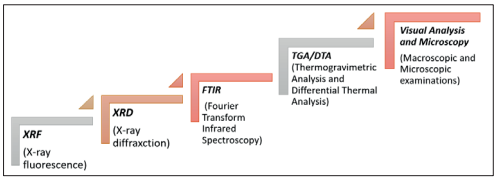



Figure 4. Schematic overview of the initial characterization steps for SFS slag

Following the initial characterization of the steel furnace slag type, the main issues to be addressed include reduced workability, dimensional stability, and concerns related to heavy metal content.

**Experimental Observations Regarding Fresh-State Properties**

Workability is widely regarded as one of the main challenges associated with incorporating steel furnace slag (SFS) into cement-based composites. As summarized by Brand and Fanijo (2020) mixtures containing SFS

generally exhibit reduced workability compared to reference mixtures with natural aggregates, usually manifested by lower slump values and increased mixture stiffness. However, the magnitude of this reduction depends largely on the type of slag, particle size distribution, and specific physical characteristics.

The angular morphology of steel slag particles is a major factor contributing to reduced workability. Unlike natural aggregates, SFS particles are characterized by irregular shapes and sharp edges, which increase internal friction and restrict particle mobility in the fresh state. Steel slag particles typically have rough and porous surfaces, which leads to higher water absorption compared to conventional aggregates (Yildirim & Prezzi, 2011; Brand & Fanijo, 2020). As a result, part of the mixing water is absorbed by the slag particles, leading to an increased water demand to achieve comparable workability.

In order to examine this aspect, two representative examples were considered.

The first example is based on previously published research that examined the incorporation of electric arc furnace (EAF) slag as a partial replacement for natural fine aggregates in cement-based materials (Darwis et al., 2024), while the second example consists of preliminary observations obtained as part of the program PN 23 35 04 01 of Nucleu Programme. The mixtures studied within the program PN 23 35 04 01 included different levels of replacement of natural fine aggregates with EAF slag. The evaluation focused on the behaviour of the cementitious mixtures in the fresh state, particularly on consistency and workability. The experimental determinations were performed in accordance with the applicable testing procedures for fresh mortars, in accordance with EN 1015-3.

**Dimensional Stability and Expansion Mechanisms**

In addition to issues related to fresh workability, the incorporation of steel furnace slag (SFS) into cement-based composites presents significant challenges related to dimensional stability. Unlike conventional natural aggregates, SFS can exhibit delayed volumetric changes when exposed to moisture, which can compromise the long-term performance and durability of cementitious materials (Brand & Fanijo, 2020). These effects are particularly critical in applications where dimensional stability is essential, such as structural concrete and infrastructure elements.

The dimensional instability of EAF is primarily associated with its complex chemical and mineralogical composition, which is significantly influenced by steel manufacturing conditions and cooling patterns (Yildirim & Prezzi, 2011; Brand & Fanijo, 2020). The presence of reactive oxide phases, combined with the heterogeneous distribution of mineral constituents in slag particles, can lead to time-dependent expansion when SFS is incorporated into cementitious systems and exposed to water (Brand & Fanijo, 2020). Unlike fresh workability issues, which are immediately observable, volumetric instability can develop gradually, often after placement, making it more difficult to detect and remediate.

Among the factors contributing to volumetric instability, the presence of free calcium oxide (free CaO) and free magnesium oxide (free MgO) plays a dominant role. Free CaO reacts relatively quickly with water to form calcium hydroxide, accompanied by a significant increase in volume. In contrast, free MgO hydrates much more slowly, leading to delayed expansion that can be observed over long periods of time. The degree of expansion depends not only on the total content of these oxides, but also on the size of the crystals, the degree of encapsulation in other phases, and accessibility to moisture (Yildirim & Prezzi, 2011; Santamaría et al., 2018; Brand & Fanijo, 2020).

The mineralogical heterogeneity of SFS further complicates its dimensional behaviour. As a result, different regions within the same particle may react differently to hydration processes, leading to localized expansion and the development of internal stresses. This heterogeneous behavior can contribute to the formation of microcracks and negatively affect the surrounding cement matrix. When EAF is used as a component in cementitious composites, dimensional instability can lead to internal stresses, microcracks, and, in severe cases, visible cracks or loss of durability (Santamaría et al., 2018; Brand & Fanijo, 2020). These effects are particularly relevant when SFS

is used as a replacement for aggregates, where volumetric changes directly influence the composite matrix.

**Leaching Behaviour of Steel Furnace Slag and SFS Cement-Based Composites**

The environmental evaluation of steel furnace slag (SFS) begins with the assessment of its leaching behavior in the raw materials. For granular materials such as steel slag, the EN 12457 is commonly applied, involving batch extraction under a defined liquid-to-solid ratio and controlled agitation conditions. This procedure enables the quantification of potentially hazardous elements released into an aqueous medium over a fixed period of contact.

Gomes & Pinto (2006) investigated the leaching behaviour of industrial steelmaking slags through laboratory extraction tests aimed at evaluating the mobility of heavy metals. In the experimental approach, slag samples were subjected to controlled leaching conditions, and the concentrations of dissolved elements were subsequently determined through chemical analysis of the leachate. Gomes & Pinto (2006) focused on elements such as Pb, Cd, Cr, and Zn, demonstrating that the release of these metals depends on physicochemical parameters including pH and slag composition. The results indicated that, although certain slags exhibited limited metal mobility under neutral conditions, measurable concentrations could be detected under specific environmental scenarios, emphasizing the importance of systematic leaching testing prior to reuse.

Similarly, investigations conducted under variable acidic and alkaline environments, as reported in the study available through Dhoble & Ahmed (2018), applied controlled leaching protocols over extended exposure periods (up to 50 days). The methodology involved immersing slag samples in aqueous solutions with adjusted pH values, followed by periodic sampling and chemical quantification of elements such as Cr, Fe, Ni, Zn, and As. The findings highlighted that metal release behaviour is strongly influenced by environmental conditions, particularly acidity, and that prolonged exposure may alter the mobility patterns of certain elements.

These experimental approaches confirm that the leaching potential of SFS must be evaluated through standardized or controlled laboratory procedures, rather than inferred solely from bulk chemical composition.

When SFS is incorporated into cement-based composites, the assessment framework shifts from granular waste characterization to evaluation of monolithic construction products. In the European context, the release of dangerous substances from solid construction materials is commonly assessed according to CEN/TS 16637-2, known as the Dynamic Surface Leaching Test (DSLT).

Unlike batch tests applied to granular materials, DSLT evaluates the time-dependent release of substances from the exposed surface of a monolithic specimen. The test involves repeated contact between the concrete sample and deionized water over predefined intervals, with periodic renewal of the leaching solution and subsequent chemical analysis of the eluate. This methodology allows the assessment of cumulative release and diffusion-controlled mechanisms over time.

In cementitious systems containing SFS, the alkaline matrix may contribute to partial immobilization of heavy metals through physical encapsulation and chemical stabilization. However, long-term exposure to water, environmental carbonation, or surface degradation may influence the release dynamics. Therefore, even if preliminary EN 12457 tests on the raw SFS indicate acceptable leaching levels, complementary assessment on the final cement-based composite remains essential to ensure environmental compliance throughout its service life.

The differentiation between leaching behaviour of the raw SFS and that of the final concrete product is therefore critical for a comprehensive environmental evaluation strategy.

**Assessment of Potential Valorisation Opportunities for Steel Furnace Slag**

The identification of potential valorisation opportunities for steel furnace slag (SFS) was conducted through a systematic review of the scientific literature addressing its applications in construction materials and environmental technologies. The analysis focused on studies investigating the use of SFS in cement-based materials, road infrastructure, and environmental remediation systems.

One of the most extensively investigated valorisation pathways for SFS is integration into

cement-based materials. Numerous studies report the successful use of SFS as a partial replacement for natural aggregates in concrete and mortar mixtures, contributing to improved mechanical performance and enhanced durability of cementitious composites (Chatzopoulos et al., 2021; Ren & Li, 2023; Mitwally et al., 2024; Ibrahim et al., 2025; Khan et al., 2025). The angular particle morphology and high density of steel slag aggregates may improve the mechanical interlocking within the cement matrix, leading to increased compressive strength and improved resistance to mechanical loading. Beyond its use as aggregate, SFS has also been investigated as a potential substitute for cement components in mortar and concrete mixtures. In such applications, finely processed SFS may partially replace clinker-based materials, contributing to the reduction of cement consumption and associated $CO_2$ emissions (Cai et al., 2024; Zhou et al., 2025).

Another important opportunity of valorisation pathway involves the use of SFS in road infrastructure applications. Due to its high hardness, abrasion resistance, and favorable mechanical properties, SFS have been widely investigated for use in asphalt mixtures, base layers, and other pavement structures (Hainin et al., 2015; Dayioğlu et al., 2023; Patel et al., 2023). These properties contribute to improved load-bearing capacity, enhanced skid resistance, and increased durability of pavement systems compared to conventional granular aggregates. In addition to asphalt mixtures and road base layers, SFS has also been explored for the production of paving elements such as concrete paving blocks used in urban infrastructure. The high density and mechanical stability of SFS aggregates make them suitable for prefabricated pavement elements where resistance to wear and mechanical stress is required (Pasetto et al., 2023; Sun et al., 2025).

In addition to construction applications, SFS has also been explored for environmental remediation purposes, particularly in water treatment systems. Due to its mineralogical composition and alkaline nature, SFS can act as an effective adsorbent for removing pollutants from aqueous solutions. Experimental studies demonstrate that SFS can adsorb heavy metal ions and other contaminants from water, highlighting their potential application as filtration media in water purification systems (Song et al., 2014; Plaza et al., 2021; Maarup et al., 2023). Overall, the literature indicates that steel furnace slag represents a versatile secondary resource with multiple valorisation opportunities across construction and environmental applications (Figure 5).




Figure 5. Main valorisation pathways of steel furnace slag in construction and environmental applications (AI-generated image)

## RESULTS AND DISCUSSIONS

### Effects of SFS on Fresh-State Properties

The influence of steel furnace slag (SFS) on the fresh-state behaviour of cementitious composites was evaluated through two representative examples.

The first example refers to investigations performed within the framework of the PN 23 35 04 01 research programme and reported by

Baera et al. (2024). The study evaluated the partial replacement of natural fine aggregate with electric arc furnace (EAF) slag originating from western Romania at substitution levels of 25% and 50%. The results demonstrated a consistent reduction in fresh-state workability for mixtures containing EAF slag compared to the reference compositions. Furthermore, the decrease in consistency became more pronounced as the replacement level increased, indicating a direct relationship between slag content and workability loss.

The second example conducted by Darwis et al. (2024), steel slag was used as a substitute for fine aggregate (sand) in concrete mixtures at replacement levels ranging from 0% to 100%. The results indicate a clear reduction in workability with increasing steel slag content. The reference mixture exhibited the highest slump value, while progressively lower slump values were recorded as the proportion of steel slag increased. Overall, the slump decreased from values of approximately 84 mm for the reference composition to around 60-70 mm at high substitution levels (80% and 100%), highlighting the adverse effect of steel slag incorporation on fresh-state workability due to its higher water absorption and irregular particle morphology.

The results indicate that fresh-state performance is strongly influenced by the characteristics of the slag used and the degree of replacement adopted. The consistent behavior observed in cement-based mixtures underscores the importance of specific material evaluation when blast furnace steel slag is considered as an alternative component in cementitious composites.

The patterns observed are consistent with those reported in the literature and support the hypothesis that the physical characteristics of SFS play a significant role in determining the workability of cement-based mixtures.

**Dimensional Stability and Expansion Mechanisms**

Based on studies Baera et al. (2024), Baera et al. (2026) and Darwis et al. (2024), cementitious composites containing steel furnace slag substitutions demand increased monitoring attention, as insufficient assessment may result in adverse long-term performance. Although no immediate dimensional instability was detected during the early stages, the behaviour of the investigated mixtures indicates that the incorporation of SFS requires careful evaluation in relation to potential time-dependent volumetric changes.

The results suggest that the risk of delayed expansion is closely related to the intrinsic characteristics of the SFS rather than to the cementitious compositions itself. In this context, the presence of reactive oxide phases and the heterogeneous internal structure of SFS particles, as described previously, may contribute to localized expansion and internal stress development when favourable conditions are present. These effects are not necessarily evident at early ages, emphasizing the importance of correlating experimental observations with material characterization data. Any volumetric changes occurring within the SFS particles may directly affect the surrounding cement matrix, potentially leading to microcracking and reduced durability over time. The results underline that dimensional stability should not be assessed exclusively based on short-term performance, but rather in relation to the long-term behaviour expected under service conditions.

Overall, the findings confirm that the dimensional stability of SFS-containing composites is strongly dependent on slag-specific properties, reinforcing the need for a material-oriented evaluation approach prior to practical application.

**Mitigation Strategies in Case of Elevated Leaching**

In cases where leaching tests indicate elevated concentrations of hazardous elements, several mitigation strategies may be considered to reduce metal mobility prior to or after incorporation into cement-based compositions. Experimental investigations on SFS have shown that the release of heavy metals is strongly influenced by physicochemical parameters, particularly pH and environmental exposure conditions (Gomes & Pinto, 2006). Adjusting these parameters through controlled aging or conditioning treatments may therefore contribute to lowering metal solubility.

Furthermore, studies performed under variable acidic and alkaline conditions demonstrate that

prolonged exposure and pH variation significantly affect the mobility of elements such as Cr, Fe, Ni, Zn, and As (Dhoble & Ahmed, 2018). These findings suggest that pre-treatment approaches aimed at stabilizing reactive phases, reducing surface reactivity, or promoting the formation of less soluble compounds may enhance environmental compatibility.

In addition, incorporation of SFS into cementitious matrices may contribute to partial immobilization through physical encapsulation and chemical stabilization mechanisms, particularly under highly alkaline conditions (Gomes & Pinto, 2006). Consequently, appropriate material conditioning combined with optimized mix design may represent effective pathways to mitigate excessive leaching where initial tests indicate environmental risk.

## CONCLUSIONS

This study highlights the importance of a comprehensive and specific approach to the material in terms of utilizing steel furnace slag (SFS) in cement-based composites. The conclusions highlight that the successful integration of SFS largely depends on the initial thorough characterization of the raw material, as steel furnace slag cannot be considered a uniform or inherently stable constituent.

The preliminary characterization stage is essential in identifying the key physical, chemical, and mineralogical characteristics of SFS and establishing correlations between these characteristics and the most critical challenges associated with its use. In particular, reduced workability, dimensional instability, and the presence of heavy metals have been identified as the main issues requiring careful evaluation. These challenges are closely related to the specific properties of the SFS, such as particle morphology, mineralogical heterogeneity, reactive oxide phases, and chemical composition.

Among these aspects, dimensional stability is a major concern due to the potential for delayed expansion effects. Therefore, the potential for delayed expansion highlights the need for comprehensive characterization, including mineralogical evaluation and expansion-related testing, prior to the practical application of SFS in construction materials. At the same time, workability effects and environmental considerations further reinforce the need to correlate material characterization results with performance indicators in the short and long term.

The assessment of leaching behaviour represents a critical component in the environmental evaluation of steel furnace slag (SFS) and its cement-based compositions. While preliminary testing on raw materials of SFS provides essential information regarding the intrinsic mobility of potentially hazardous elements, the behaviour of the final cementitious composite may differ substantially due to encapsulation and chemical stabilization mechanisms. A comprehensive evaluation strategy must therefore integrate both stages of assessment, ensuring that material conditioning, mix design, and long-term exposure conditions are collectively considered. Such an approach supports the responsible valorisation of SFS while maintaining environmental safety and regulatory compliance.

The results also demonstrate that short-term observations are not sufficient to fully assess the behaviour of SFS-containing composites. Long-term monitoring and performance evaluation are essential to capture time-dependent processes and to support the development of appropriate mitigation strategies. Addressing these challenges requires not only systematic testing, but also the identification and optimization of potential solutions, such as adjusting the composition design, material processing methods, or conditioning treatments.

Despite the challenges identified, SFS remains a material with significant potential for recovery. When properly characterized and controlled, SFS offers important opportunities for sustainable resource use, contributing to waste reduction, conservation of natural aggregates, and implementation of circular economy principles in the construction sector.

## ACKNOWLEDGEMENTS

This work was carried out within the Nucleu Programme of the National Research Development and Innovation Plan 2022-2027, supported by MCID, "ECODIGICONS" project

no. PN 23 35 04 01: "Fundamental-applied research into the sustainable development of construction products (materials, elements, and structures, as well as methods and technologies) that utilizes current national resources to enhance the eco-innovative and durable aspects of Romania's civil and transport infrastructure", financed by the Romanian Government.

AI-assisted writing disclosure
The authors acknowledge the use of AI-based tools for generate certain figures. All scientific content, interpretations, and conclusions are the sole responsibility of the authors.

## REFERENCES

Adegoloye G., Beaucour A.L., Ortola S. & Noumowe A. (2016). Mineralogical composition of EAF slag and stabilised AOD slag aggregates and dimensional stability of slag aggregate concretes, *Construction and Building Materials 115,* 171-178.

Alizadeh, R., Chini, M., Ghods, P., Hoseini, M., Montazer, S., & Shekarchi, M. (2003, June). Utilization of electric arc furnace slag as aggregates in concrete–environmental issue. *In Proceedings of the 6th CANMET/ACI international conference on recent advances in concrete technology.* Bucharest, Romania, 451-464.

Baera, C., Gruin, A., Vasile, A.C., Bolborea, B., Ion, A., & Bănăduc, G. (2024). Recycling of steel furnace slags (SFS) by efficient integration in construction materials as aggregate partial replacement. *Sci. Pap. Ser. E Land Reclam. Earth Obs. Surv. Environ. Eng. XIII,* 378-389.

Baera, C., Vasile, A.-C., Gruin, A., Bolborea, B., & Ion, A. (2026). Integrating steel furnace slags (SFS) waste as aggregate substitution in cement-based materials and products for construction industry. In: Pavlou, D., Adeli, H., Correia, J. (eds) *Advances in Computational and Experimental Methods in Engineering*. OES 2025. Structural Integrity, 35, 343-361. Springer, Cham.

Brand, A. S. & Fanijo, E. O. (2020). A review of the influence of steel furnace slag type on the properties of cementitious composites. *Applied sciences*, *10*. 8210.

Cai, X., Cao, Z., Sun, J., Wang, H., & Wu, S. (2024). Influence of steel slag on properties of cement-based materials: a review. *Buildings*, *14*(9), 2985.

Chatzopoulos, A., Sideris, K. K., & Tassos, C. (2021). Production of concretes using slag aggregates: Contribution of increasing the durability and sustainability of constructions. *Case studies in construction Materials, 15*, 00711.

Darwis, Z., Fathonah, W., & Hadi, F. (2024). Steel slag's physical and chemical impact on concrete workability and strength as fine aggregate. *Jurnal Teknologi (Sciences & Engineering), 86*(1), 175-181.

Dayıoğlu, A. Y., Hatipoğlu, M., & Aydilek, A. (2023). Comparative evaluation of mechanical performance of steel slag and earthen granular aggregates. *Journal of Sustainable Construction Materials and Technologies*, *8*(1), 12-19.

Deja, J. (2002). Immobilization of Cr6+, Cd2+, Zn2+ and Pb2+ in alkali-activated slag binders. *Cement and Concrete Research*, 32(12), 1971-1979.

Dhoble, Y., & Ahmed, S. (2018). Leaching of heavy metals from the steel slag under variable conditions. *Global Journal of Engineering Science and Researches*, *5*, 187-196.

European Commission (2015). Closing the loop - An EU action plan for the Circular Economy, COM (2015) 614 final.

European Committee for Standardization. (2002). EN 12457-2: Characterisation of waste-Leaching-Compliance test for leaching of granular waste materials and sludges. *CEN*.

European Committee for Standardization. (2007). EN 1015-3: Methods of test for mortar for masonry - Part 3: Determination of consistence of fresh mortar (by flow table). CEN.

European Committee for Standardization. (2014). CEN/TS 16637-2: Construction products - Assessment of release of dangerous substances - Part 2: Horizontal dynamic surface leaching test. *CEN*.

Fuente-Alonso J. A., Ortega-López V., Skaf M., Aragón A. & San-Jose J. T. (2017). Performance of fiber-reinforced EAF slag concrete for use in pavements, *Construction and Building Materials 149,* 629-638.

Ghisellini, P., Cialani, C., & Ulgiati, S. (2016). A review on circular economy: the expected transition to a balanced interplay of environmental and economic systems. *Journal of Cleaner Production,* 114, 11-32.

Gomes, J. F. P., & Pinto, C. G. (2006). Leaching of heavy metals from steelmaking slags. *Revista de Metalurgia*, *42*(6), 409-416.

Hainin, M. R., Aziz, M. M. A., Ali, Z., Jaya, R. P., El-Sergany, M. M., & Yaacob, H. (2015). Steel slag as a road construction material. *Jurnal Teknologi*, *73*(4), 33-38.

Ibrahim, I. K., Rady, M., Tawfik, N. M., Kassem, M., & Mahfouz, S. Y. (2025). Enhancing strength and sustainability of concrete with steel slag aggregate. *Scientific Reports*, *15*(1), 17068.

Khan, A., Luqman, M., Jun, X., Ullah, M. F., Alzlfawi, A., Ahmad, M., & Toth, Z. (2025). Effect of steel slag as fine aggregate on the mechanical and durability performance of concrete under acid exposure. *Scientific Reports*, 15(1), 40966.

Kurecki, M. P. (2024). Effect of Cr2O3 Addition on Viscosity, Foaming Height, and Phase Evolution of EAF Slags (Master's thesis*, Arizona State University*).

Liu, B., Li, J., Zeng, Y. & Wang, Z. (2016). Toxicity assessment and geochemical model of chromium leaching from AOD slag, *Chemosphere 144*, 2052-2057.

Loureiro, C. D. A., Moura C. F. N., Rodrigues, M., Martinho F. C. G., Silva H. M. R. D. & Oliveira J. R. M. (2022). Steel Slag and recycled concrete aggregates: Replacing quarries to supply sustainable materials for the asphalt paving industry, *Sustainability, 14,* 5022.

Maarup, S. N., Hamdan, R., Othman, N., Al-Gheethi, A., Alkhadher, S., El-Hady, M. A., & Saeed, S. E. S. (2023). Steel slag and limestone as a rock filter for eliminating phosphorus from domestic wastewater: a pilot study in a warm climate. *Water, 15*(4), 657.

Maslehuddin M., Naqvi A. A., Ibrahim M. & Kalakada Z. (2013). Radiation shielding properties of concrete with electric arc furnace slag aggregates and steel shots, *Annals of Nuclear Energy 53*, 192-196.

Mitwally, M. E., Elnemr, A., Shash, A., & Babiker, A. (2024). Utilization of steel slag as partial replacement for coarse aggregate in concrete. *Innovative Infrastructure Solutions*, 9(5), 175.

Motz, H., & Geiseler, J. (2001). Products of steel slags - An opportunity to save natural resources. *Waste Management,* 21, 285-293.

Mousavinejad, S. H. G., & GilKalaye, S. G. (2024) Effect of freezing–thawing cycles and high temperatures on concretes containing partial replacement of fine grain blast and Electric Arc Furnace slags. *Discover Materials,4*, 78,

Müller, H. S., Haist, M., & Vogel, M. (2014). Assessment of the sustainability potential of concrete and concrete structures considering their environmental impact, performance and lifetime. *Construction and Building Materials*, 67, 321-337.

Ouda, A. S. & Abdel-Gawwad, H. A. (2017). The effect of replacing sand by iron slag on physical, mechanical and radiological properties of cement mortar, *HBRC Journal, 13,* 255-261.

Pasetto, M., Baliello, A., Giacomello, G., & Pasquini, E. (2023). The use of steel slags in asphalt pavements: a state-of-the-art review. *Sustainability*, *15*(11), 8817.

Patel, P., Narnaure, T. K., & Thepe, P. (2023). Review on Effect of Steel Slag and Fly Ash in Road Construction. *Metszet*, *8*, 153-165.

Plaza, L., Castellote, M., Nevshupa, R., & Jimenez-Relinque, E. (2021). High-capacity adsorbents from stainless steel slag for the control of dye pollutants in water. *Environmental Science and Pollution Research*, *28*(19), 23896-23910.

Provis, J. L., & van Deventer, J. S. J. (2009). Geopolymers: Structures, Processing, Properties and Industrial Applications. *Woodhead Publishing.*

Ren, Z., & Li, D. (2023). Application of steel slag as an aggregate in concrete production: a review. *Materials*, *16*(17), 5841.

Santamaría, A., F., Faleschini, G., Giacomello, K., Brunelli, J.-T., San José, C. Pellegrino, M. Pasetto. (2018). Dimensional stability of electric arc furnace slag in civil engineering applications. *Journal of Cleaner Production*, 205, 599-609.

Shi, C., Qian, J. (2000). High performance cementing materials from industrial slags.- A review. *Resources, Conservation and Recycling*, 29, 195-207.

Song, G., Wu, Y., Chen, X., Hou, W., & Wang, Q. (2014). Adsorption performance of heavy metal ions between EAF steel slag and common mineral adsorbents. *Desalination and Water Treatment*, *52*(37-39), 7125-7132.

Sun, Z., Zhang, Z., Lu, G., & Luo, S. (2025). Recent advances in research on steel slag for asphalt pavements: A review. *Case Studies in Construction Materials*, *22*, 04698.

World Steel Association. https://worldsteel.org/.

Yildirim I. Z. & Prezzi M. (2011). Chemical, mineralogical and morphological properties of steel slag, *Hindawi Publishing Corporation, Advances in Civil Engineering, 2011*, 463638.

Zhou, Z., Jin, Q., Hu, D., Zhu, L., Li, Z., & Su, W. (2025). Long-term volume stability of steel slag sand mortar and concrete. *Case Studies in Construction Materials*, *22,* 04179.

Scientific Papers. Series E. Land Reclamation, Earth Observation & Surveying, Environmental Engineering. Vol. XV, 2026
Print ISSN 2285-6064, CD-ROM ISSN 2285-6072, Online ISSN 2393-5138, ISSN-L 2285-6064

# CULTIVABLE MICROALGAE FROM PEATLAND WATERS: MORPHOLOGICAL FEATURES AND PIGMENT PROFILES

**Ana Valentina ZAMFIRESCU, Cristina MOISESCU, Sorin ȘTEFĂNUȚ, Miruna-Maria ȘTEFĂNUȚ, Ana-Maria MOROȘANU**

Institute of Biology Bucharest of Romanian Academy, 296 Splaiul Independentei, District 6, Bucharest, Romania

Corresponding author email: cristina.moisescu@ibiol.ro

***Abstract***

*Peatlands represent globally significant carbon reservoirs, and the microalgae inhabiting these sensitive ecosystems play an essential role in climate change mitigation. Peatland microalgae occur not only in surface waters but also within peat layers, contributing to carbon fixation through photosynthesis. This study investigates the diversity of cultivable microalgae from peatland waters and provides a preliminary characterisation based on pigment composition. Water samples were collected from two restored Romanian peatland sites, Avrig Peatbog and Mlaca Tătarilor Peatbog, selected due to their similar characteristics. Microalgal strains were isolated and cultivated under laboratory conditions in BG-11 medium. Identification was performed at the genus level using the microphotography method, an approach suitable for baseline diversity assessment studies. Photosynthetic pigments were extracted from the isolates and analysed using UV–Vis spectrophotometry. Ten cultivable microalgal strains were obtained, with higher diversity in Avrig Peatbog compared to Mlaca Tătarilor Peatbog. The combined morphological and pigment-based analysis revealed microalgal genera adapted to acidic, humic-rich peatland waters and differences in pigment profiles among isolates. These findings provide baseline data and support future molecular, ecological, and biotechnological investigations.*

***Key words:*** *cultivable microalgae, peatlands, pigments spectrophotometry.*

## INTRODUCTION

Peatlands are dynamic ecosystems that provide essential ecological services, including biodiversity conservation, carbon storage, and water regulation. Although they cover only a small proportion of the Earth's land surface (about 3%), peatlands store a disproportionately large amount of global soil carbon (about 30%), making them key components of climate regulation and long-term carbon sequestration (Parish et al., 2008; Yu et al., 2010; Leifeld & Menichetti, 2018). The functioning of these ecosystems is strongly controlled by complex interactions between vegetation, hydrology, and microbial communities that regulate the balance between carbon fixation and decomposition.

In peatland environments, microorganisms play a fundamental role in carbon cycling processes. Among them, microalgae represent an important yet relatively understudied component of peatland biodiversity. These unicellular photoautotrophic microorganisms occur not only in surface waters but also within moist peat layers, where they contribute to primary production and carbon fixation through photosynthesis (Rydin & Jeglum, 2013; Yadav & Singh, 2020). Their ability to tolerate acidic conditions, high concentrations of humic substances, and nutrient-poor environments allows them to thrive in peatland habitats and makes them valuable indicators of environmental conditions (Bellinger & Sigee, 2015). In addition, microalgae are increasingly recognised as aquatic bioindicators with multiple ecological and applied research applications (Tsuraya et al., 2023).

The physicochemical characteristics and biodiversity of peatland surface waters are influenced by climatic and geographical factors but also by land management practices and anthropogenic pressures (Kowalik et al., 2014; Serafin et al., 2023). Changes in hydrology, drainage, or vegetation structure may alter water chemistry and light availability, thereby influencing the composition and ecological strategies of phototrophic microorganisms.

Romanian peatlands represent an important component of the national natural heritage and contribute significantly to biodiversity conservation and climate regulation. Among these ecosystems, Mlaca Tătarilor Peatbog was designated as a Site of Community Importance (ROSCI0112) in 2011 under the Natura 2000 network, primarily for the habitat type 7150 "Depressions on peat substrates of the Rhynchosporium" (Natura 2000 Reference Portal; Natura 2000 Viewer). Currently, the site is designated as a Special Area of Conservation (SAC) - ROSAC0112 under Government Decision No. 47/2024. The Avrig Peatbog overlaps with the Natura 2000 site ROSPA0098 Piemontul Făgăraș and was recently proposed as a Special Area of Conservation (SAC) in April 2024 (Ștefănuț et al., 2025) for habitats 7120 "Degraded raised bogs still capable of natural regeneration" and 7110* "Active raised bogs".

Following more than fifteen years of ecological monitoring, Mlaca Tătarilor Peatbog was selected in 2016 within the PeatRO project as a pilot area for demonstrating restoration methods applied to degraded peatland ecosystems. Similarly, the Avrig Peatbog, first described by Pop (1960) and rediscovered during the PeatRO project, was restored in 2023 through the PeatRO2 project. In both sites, the main factor responsible for the deterioration of peatland conservation status was long-term hydrological imbalance caused by drainage channels and the expansion of woody vegetation. Due to their comparable size, hydrological recovery, and restoration history, these two peatbogs provide suitable systems for comparative ecological investigations.

Despite their ecological importance, the diversity and ecological roles of microalgae inhabiting Romanian peatland waters remain poorly documented. Baseline studies based on the isolation and cultivation of microalgal strains are therefore important for understanding the composition of these communities and for exploring their physiological and biochemical characteristics.

In this context, the present study aimed to isolate cultivable microalgae from the surface waters of two restored Romanian peatbogs, Mlaca Tătarilor and Avrig, and to perform a preliminary characterization based on morphological features and pigment composition. Microalgal strains were identified using optical microscopy and the microphotography method, while pigment profiles were analysed using UV–Vis spectrophotometry. By integrating morphological observations with pigment-based characterization, this study provides baseline information on the diversity and physiological traits of microalgae inhabiting restored peatland ecosystems and supports future ecological, molecular, and biotechnological research.

## MATERIALS AND METHODS

### Sites` localisation and description

Both study sites lie in Sibiu County, Romania, within the Făgăraș Depression (northern sector of the Southern Carpathians, subalpine biogeographic region). The Mlaca Tătarilor Peatbog (SB-001; Figure 1) covers an area of 3.7 ha at an altitude of 548 m a.s.l. (45.425486°N, 24.3915012°E) and is administrated by the Arpașu de Sus town hall. The Avrig Peatbog (SB-013; Figure 2) covers 3.6 ha at 405 m a.s.l. (45.716282°N, 24.400133°E) and falls within the administrative boundaries of Avrig town. Their similar size and hydrological recovery after restoration make them ideal for parallel microalgal assessment.

### Water sampling and physicochemical analysis

***Water samples*** for microalgae identification were collected during the March 2025 field trip from zones with relevant water accumulation at both sites.

***Physicochemical parameters*** of the peatland water were measured *in situ* at five points (P1-P5) per site (Figures 1 and 2), using a HI9829 multiparameter probe (Hanna Instruments). Parameters recorded included pH, oxidation-reduction potential (ORP), oxygen saturation (DO%), dissolved oxygen (DO), conductivity, total dissolved solids (TDS), salinity (PSU), turbidity, water temperature and water pressure (PSI).

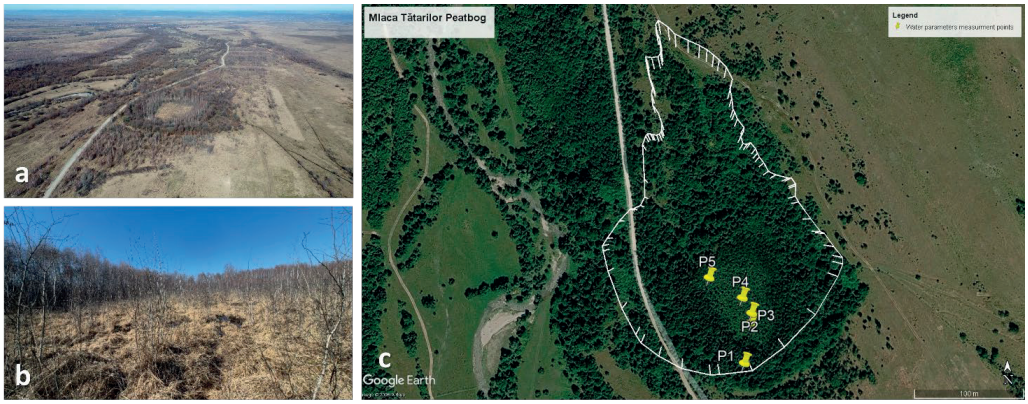



Figure 1. Mlaca Tătarilor Peatbog: (a) Drone view (Photo: Ștefănuț S., 10.03.2026); (b) Ground view (Photo: Moroșanu A.-M., 09.03.2026); (c) Site`s limits; marked points of water parameter measurements (Google Earth)

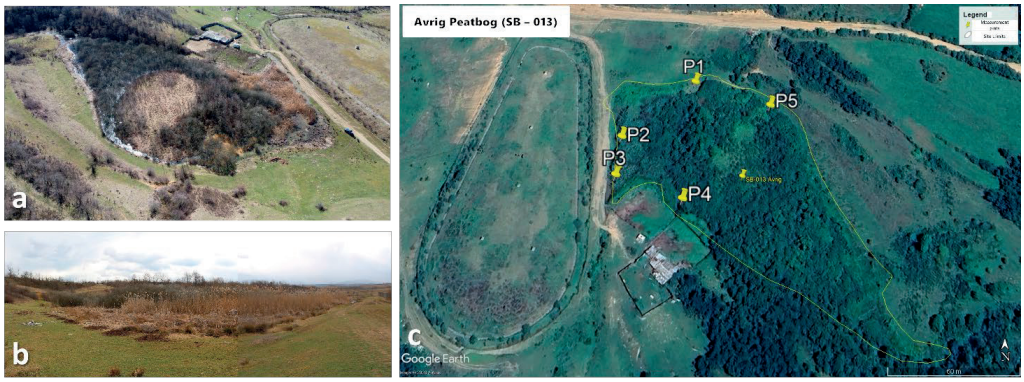



Figure 2. Avrig Peatbog: (a) Drone view (Photo: Ștefănuț S., 11.03.2026); (b) Ground view (Photo: Moroșanu A.M., 13.03.2025); (c) Site`s limits; marked points of water parameter measurements (Google Earth)

**Isolation, identification, and characterization of microalgae**

***Microalgae isolation and cultivation***. Peat water samples were collected at each site from the upper layer of the water column directly into sterile 50 mL plastic bottles. The bottles were labelled and transported to the laboratory for further processing. The collected water samples were enriched in microalgae by mixing the water sample 1:1 with BG-11 medium (Allen & Stanier, 1968). The mixtures were incubated in Erlenmeyer flasks on a shelf under natural illumination at ambient temperature for at least one month, until algal growth became apparent. Well-grown algal cultures were streaked onto BG-11 agar plates, which were then incubated under aerobic conditions at 28 ± 2°C in a thermostatically controlled incubator. Cultures were illuminated with fluorescent lamps at an intensity of 16,500 lux under a 12:12 h light: dark cycle. A single colony was aseptically transferred and streaked onto fresh BG-11 agar plates, and the procedure was repeated until axenic algal cultures were obtained.

***Morphological identification***. Enriched microalgal samples and isolates grown on solid media were examined using a Zeiss AxioScope.A1 optical microscope (Carl Zeiss) equipped with an AxioCam ERc 5s camera. Identification was performed using the microphotography method based on detailed analysis of captured images. Microalgal cells were observed, documented, and morphologically identified to the genus level based on cell size and shape, chloroplast morphology, presence of pyrenoids, and the presence or absence of flagella, using standard microalgal identification keys (Prescott, 1962;

1964; Belcher & Swale, 1976; Serediak & Huynh, 2011; Bellinger & Sigee, 2015; Jeuck & Arndt, 2013).

***Pigment extraction and characterization***. For pigment extraction, 50 mL of each enriched culture (14–20 days old) was harvested by centrifugation at 7,500 rpm for 10 min to remove the water content. The resulting algal biomass was homogenized in 10 mL of 99% acetone and kept overnight in the dark at 4°C to ensure complete pigment extraction. The samples were then centrifuged at 13,000 rpm for 5 min, and the supernatant was collected. The pellet was re-extracted by repeated washing with 5 mL of 99% acetone until it became colorless. All extracts were pooled and evaporated under reduced pressure at 30°C, then stored at −20°C until pigment quantification.

***UV-Vis characterization*** of the extracted pigments was recorded using a Specord 210 Plus spectrophotometer (Analytik Jena) over the wavelength range of 350-750 nm at room temperature.

The pigment concentrations were calculated using the equations of Lichtenthaler (1987) for 100% acetone at 470 nm, 661.6 nm and 644.8 nm. Pigment data were primarily interpreted using pigment ratios, namely chlorophyll a to chlorophyll b (Chl a/Chl b) and total carotenoids to total chlorophyll (Car/(Chl a+b)).

## RESULTS AND DISCUSSIONS

### The physico-chemical parameters

#### Mlaca Tătarilor Peatbog (SB-001; ROSCI0112)

Water parameters were measured at five points (P1-P5): four within the *Sphagnum*-dominated zone and one point at the entrance, all characterized by a high water table (Figure 2; Table 1). Measurements revealed pH values of 6.62-7.13 (slightly acidic to neutral), likely due to mineral influence or degradation, potentially favoring microalgae tolerant to slightly acidic to neutral conditions. ORP values were near-neutral to slightly reducing, indicating predominantly anoxic conditions that favor anaerobic processes typical to waterlogged peat bogs. Moderate-to-good DO% values reflected variable oxygenation, with hypoxic microsites (anaerobic processes) alongside oxygenated zones (aerobic decomposition); this variability reflects hydrological heterogeneity. Also, DO values confirm moderate oxygenation in the surface water of Mlaca Tătarilor, yet hypoxic conditions in some areas. Low conductivity values and TDS values confirmed oligotrophic conditions with minimal mineral input. Invariable PSU values indicated extremely pure freshwater, while turbidity values reflected extremely clear water, typical of oligotrophic peat bogs, favoring light penetration for microalgae and *Sphagnum* photosynthesis. Early spring water temperatures minimized organic matter decomposition, favoring carbon sequestration in waterlogged *Sphagnum* zones. A stable hydrology and an elevated water table were reflected by PSI values.

Overall, there is a high consistency between the physicochemical parameters at the five points (P1-P5), indicating typical oligotrophic conditions in a hydrologically stable ecosystem that favors microalgae and *Sphagnum* species development as well as active carbon sequestration.

#### Avrig Peatbog (SB-013)

Measurements were taken in water pools and drainage channels (Figure 2; Table 2). The water pH ranged between 6.61 and 7.47 (slightly acidic to neutral). The water pool showed the highest ORP and DO concentration, while the drainage channels exhibited had the highest TDS, salinity, conductivity, and turbidity values due to sediment accumulation. Water temperature and pressure were nearly similar across both location types, correlating with seasonal biochemical processes. ORP varied from positive (oxidation of organic matter) to negative (reducing reactions).

Overall, parameters indicated a gradient from well-oxygenated, low-mineralised reed-fringed pools (P2) to mineralised, drainage-influenced points (P3-P4) and highly reductive, hypoxic channels (P5), reflecting combined peatland hydrology and anthropogenic drainage influences.

Table 1. Water parameter values - Mlaca Tătarilor Peatbog

| Parameter | P1 45,71449°N, 24,65014°E | P2 45,71491°N, 24,65023°E | P3 45,71483°N, 24,65023°E | P4 45,71504°N, 24,65012°E | P5 45,71521°N, 24,64972°E |
|---|---|---|---|---|---|
| **pH** | 6.62 | 6.63 | 7.10 | 6.77 | 7.13 |
| **ORP (mV)** | -41.9 | -41.6 | 2.6 | -6.1 | 33.7 |
| **DO (%)** | 43.3 | 75.2 | 84.0 | 75.7 | 71.7 |
| **DO (mg/L)** | 4.80 | 8.62 | 9.56 | 8.62 | 9.00 |
| **Conductivity (µS/cm)** | 50 | 48 | 53 | 34 | 47 |
| **TDS (mg/L)** | 25 | 24 | 26 | 26 | 24 |
| **PSU (unit)** | 0.02 | 0.02 | 0.02 | 0.02 | 0.02 |
| **Turbidity (NTU)** | 0.0 | 4.7 | 14.9 | 0.0 | 0.0 |
| **Water temperature (°C)** | 6.77 | 6.58 | 7.75 | 7.50 | 3.51 |
| **PSI (mbar)** | 13.914 | 13.904 | 13.938 | 13.944 | 13.914 |

Table 2. Water parameter values - Avrig Peatbog

| Parameter | **Avrig-P1**: NE water pool bog access point | **Avrig-P2**: Reed-fringed pool bog access point | **Avrig-P3**: Drainage channel dam near the access path | **Avrig-P4**: Reed-fringed pool crosswise path | **Avrig-P5**: Channel over pool, opposite the path |
|---|---|---|---|---|---|
| **pH** | 6.68 | 7.19 | 7.47 | 7.35 | 6.61 |
| **ORP (mV)** | 41.4 | -25 | -21.4 | -39.1 | -95.6 |
| **DO (%)** | 10.4 | 28.6 | 14 | 10.4 | 5.1 |
| **DO (mg/L)** | 1.16 | 3.23 | 1.61 | 1.17 | 0.57 |
| **Conductivity (µS/cm)** | 287 | 1 | 954 | 740 | 412 |
| **TDS (mg/L)** | 143 | 0 | 478 | 370 | 218 |
| **PSU (unit)** | 0.14 | 0 | 0.47 | 0.36 | 0.19 |
| **Turbidity (NTU)** | 122 | 15 | 22.9 | 15.6 | 15.8 |
| **Water temperature (°C)** | 7.89 | 7.52 | 6.19 | 7.03 | 6.73 |
| **PSI (mbar)** | 13.765 | 13.749 | 13.744 | 13.745 | 13.73 |

Our slightly acidic-neutral pH (6.6-7.5), low conductivity/TDS, and variable ORP/DO values in both studied restored peatbogs align with post-restoration recovery trends in European minerotrophic peatlands (Andrews et al., 2025). Mlaca Tătarilor Peatbog`s stable anoxia resembles typical waterlogged peatbog conditions, while Avrig`s hydrological gradient reflects anthropogenic disturbance, creating microalgae niches. These patterns indicate incipient hydrological recovery post-restoration.

The physicochemical characteristics of peatland waters provide the environmental context in which phototrophic microorganisms develop. In order to further investigate the physiological traits of the cultivable microalgae associated with these environments, pigment extracts obtained from enriched cultures were analysed using UV–Vis spectrophotometry.

## Pigment profiles of enriched microalgal cultures

Pigment extracts obtained from enriched microalgal cultures originating from the two studied peatland sites were analysed using UV-Vis spectrophotometry in order to investigate the physiological characteristics of the cultivable phototrophic microorganisms.

The recorded spectra (Figure 3) showed the characteristic absorption bands of photosynthetic pigments. Strong absorption maxima were observed in the blue region of the spectrum (Soret bands) and in the red region (Qy bands), corresponding to electronic transitions of chlorophyll molecules, while the spectral region between 400 and 500 nm corresponded to the main absorption domain of carotenoids. These pigments play essential roles in light harvesting and photoprotection and are widely used as indicators of physiological status and environmental adaptation in microalgae (Lichtenthaler, 1987; Falkowski & Raven, 2007).

Pigment ratios calculated from the spectra revealed variability among enriched cultures obtained from both peatlands (Table 3), suggesting differences in physiological acclimation of the cultivated microalgae.

In the cultures originating from Avrig Peatbog, the Chl a/Chl b ratio varied widely between 0.64 and 3.16. Higher ratios observed in several cultures (e.g., Avrig-2 and Avrig-3) indicate a relative predominance of chlorophyll a and may

reflect acclimation to environments with higher or more variable irradiance. Reduced antenna size associated with increased Chl a/Chl b ratios is commonly interpreted as an adaptive strategy in microalgae exposed to elevated light conditions or fluctuating illumination regimes (Falkowski & Raven, 2007; Bellinger & Sigee, 2015).

Conversely, lower Chl a/Chl b ratios, such as those observed in Avrig-1, suggest a relatively higher contribution of chlorophyll b and may indicate adaptation to shaded or optically filtered environments. Such conditions are typical for peatland waters where high concentrations of dissolved humic substances significantly modify the spectral composition and penetration of light in the water column (Rydin & Jeglum, 2013).

The Car/(Chl a+b) ratio also varied among the analysed cultures. Elevated carotenoid proportions recorded in some Avrig samples (e.g., Avrig-4 and Avrig-5) may reflect increased photoprotective investment. Carotenoids are known to play a key role in protecting the photosynthetic apparatus against oxidative stress and excessive irradiance, particularly in shallow or dynamic aquatic habitats (Falkowski & Raven, 2007).

Enriched cultures originating from Mlaca Tătarilor Peatbog displayed somewhat narrower Chl a/Chl b variation (0.85-1.79), suggesting a more balanced contribution of chlorophyll a and b compared with some of the Avrig cultures. These intermediate values may reflect adaptation to relatively stable light conditions within *Sphagnum*-dominated peatland microhabitats, where vegetation structure and water colour create diffuse light environments typical for bog ecosystems (Rydin & Jeglum, 2013).

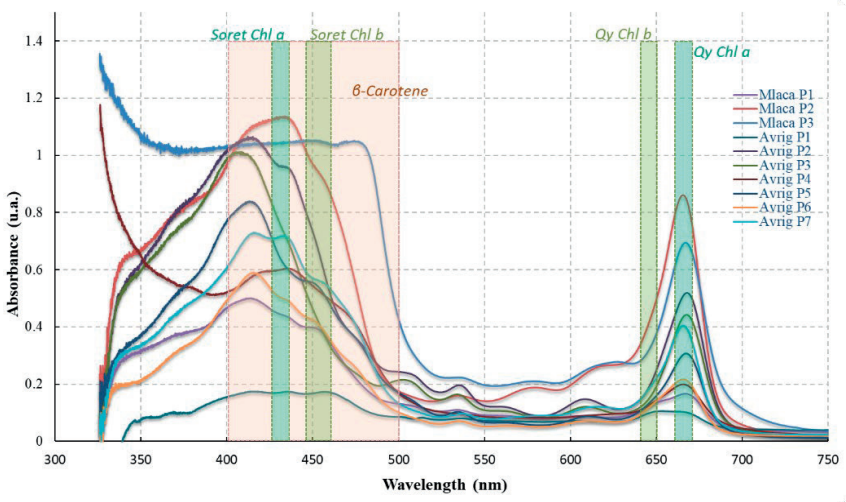



Figure 3. UV-Vis absorption spectra (300-750 nm) of pigment extracts from the analyzed microalgal cultures. The Soret bands (blue region) and Qy bands (red region) correspond to characteristic electronic transitions of chlorophylls. The 400-500 nm region represents the main carotenoid absorption range, overlapping with the chlorophyll Soret bands

Table 3. Pigment ratios of the analyzed microalgal enriched cultures

| Sample | Mlaca-1 | Mlaca-2 | Mlaca-3 | Avrig-1 | Avrig-2 | Avrig-3 | Avrig-4 | Avrig-5 | Avrig-6 | Avrig-7 |
|---|---|---|---|---|---|---|---|---|---|---|
| Chl a/Chl b | 0.85 | 1.79 | 1.78 | 0.64 | 2.74 | 3.16 | 1.13 | 1.91 | 1.46 | 1.92 |
| Car/(Chl a+b) | 0.20 | 0.13 | 0.37 | 0.09 | 0.20 | 0.15 | 0.44 | 0.33 | 0.26 | 0.26 |

The Car/(Chl a+b) ratio also showed variability among Mlaca samples, with the highest value observed in Mlaca-3. Increased carotenoid proportions are frequently associated with microalgal responses to environmental stress factors such as fluctuating irradiance or oxidative stress (Falkowski & Raven, 2007). Conversely, lower carotenoid values recorded in

Mlaca-1 and Mlaca-2 may indicate more stable microhabitat conditions where photoprotective requirements are reduced.

Although the physicochemical parameters were measured at representative monitoring points rather than at the exact locations of each enrichment culture, they provide a useful characterization of the environmental conditions prevailing within the studied peatland waters.

When interpreted together, the pigment patterns observed in the enriched cultures suggest that the cultivated microalgae exhibit considerable physiological plasticity, enabling them to cope with the heterogeneous environmental conditions typical of peatland ecosystems.

**Microalgae identification and ecological interpretation**

In addition to pigment analysis, microscopic examination of enriched cultures revealed several dominant microalgal morphotypes corresponding to common freshwater green algal and cyanobacterial genera (Figure 4). The observed taxa included representatives of *Chlorella*, *Chlorococcum*, *Scenedesmus*, *Closterium*, *Stichococcus*, *Chlamydocapsa*, *Gonium*, *Palmellopsis*, *Aphanocapsa*, and *Nostoc*.

The observed morphotypes correspond well with the pigment signatures detected in the UV–Vis spectra, which suggested the presence of chlorophyll-containing green algae and cyanobacteria in the enriched cultures.

It should be noted that enrichment cultivation may selectively favor fast-growing taxa. Consequently, the microalgal assemblages described in this study represent the cultivable fraction of the natural community rather than the complete *in situ* diversity.

During the isolation procedure, several strains were also transferred to solid BG-11 medium in order to obtain axenic cultures. Although these pure cultures were not the primary focus of the present study, their establishment ensures the availability of well-defined strains for future physiological, molecular, and biotechnological investigations. In the present work, however, pigment analysis was performed on enriched cultures in order to better reflect the dominant phototrophic components of the original peatland microbial assemblages.

**Morphological characterization of the observed morphotypes**

Figure 4 (a-c) shows solitary spherical cells measuring approximately 11-12 µm in diameter, which may tentatively be assigned to the genus *Chlorella* based on their morphological characteristics.

Figure 4 (d) shows solitary cylindrical cells with rounded ends, measuring approximately 11-12 µm in length and 5-6 µm in width. Considering the observed morphology and the habitat of origin, the isolate can be provisionally assigned to the genus *Stichococcus*.

In Figure 4 (e), a solitary elongated cell slightly curved with gradually tapered ends can be observed, measuring approximately 25 µm in length and 2.85 µm in width.

The high length-to-width ratio gives the cell a filiform appearance typical of small desmids. The observed morphology is consistent with the genus *Closterium*, a taxon frequently encountered in acidic oligotrophic ecosystems such as peatlands.

Figure 4 (f) illustrates cells with an ovoid morphology forming grape-like colonies composed of approximately eight cells embedded within a gelatinous sheath. The cells measure approximately 8-9.5 µm in length and 5.5-6.5 µm in width, and a pyrenoid is visible. Based on these characteristics, the colony may tentatively be assigned to the genus *Chlamydocapsa*, which is commonly reported from freshwater environments.

In Figure 4 (g), filamentous structures composed of spherical cells measuring approximately 3-6 µm in diameter are observed. Based on their morphology, these filaments most likely belong to the genus *Nostoc*.

Figure 4 (h) shows a flat plate of spherical cells embedded in a mucilaginous matrix. The colony consists of approximately 16 well-spaced cells and measures around 15 µm in length. The observed morphology is consistent with the genus *Gonium*.

In Figure 4 (i), cells embedded within a mucilaginous matrix forming a compact irregular colony can be observed. The cells are ovoid to ellipsoidal, measuring approximately 2-3.5 µm in width and 5-8 µm in length, and contain a distinct chloroplast with a visible pyrenoid. This palmelloid organization suggests affiliation with the genus *Palmellopsis*.

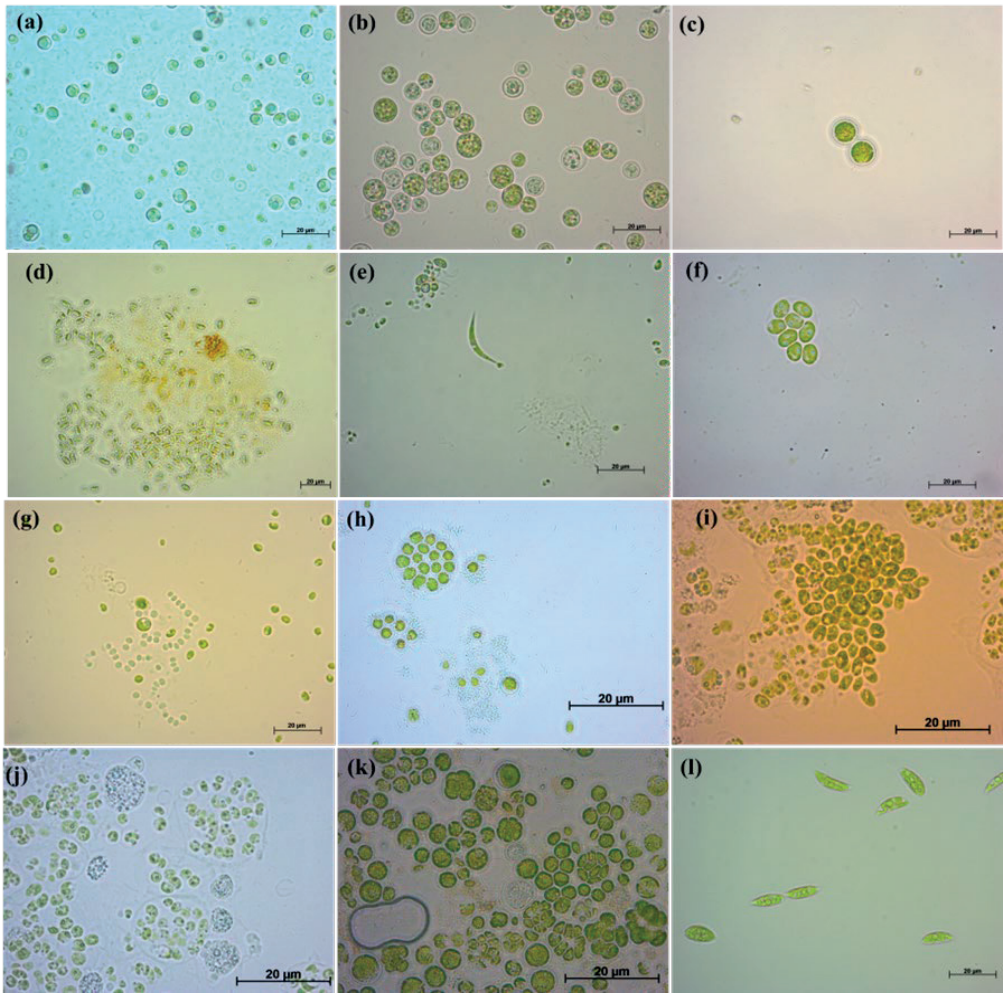



Figure 4. Representative microalgal morphotypes observed in enriched cultures derived from peatland water samples. (a-c) *Chlorella*-like cells; (d) *Stichococcus* sp.; (e) *Closterium* sp.; (f) *Chlamydocapsa* sp.; (g) *Nostoc* sp.; (h) *Gonium* sp.; (i) *Palmellopsis* sp.; (j) *Aphanocapsa* sp.; (k) *Chlorococcum* sp.; (l) *Scenedesmus* sp. Images were captured using bright-field microscopy. Scale bar = 20 µm

Figure 4 (j) shows a group of small cells embedded within a wide mucilaginous sheath resembling colonies of *Aphanocapsa*. Cells appear spherical and reach up to 4 µm in diameter. Species of *Aphanocapsa* typically form gelatinous colonies composed of spherical cells measuring approximately 1-5.5 µm depending on the species.

In Figure 4 (k), unicellular spherical cells with smooth cell walls are observed, occurring both as solitary individuals and in small colonies. These characteristics are consistent with the genus *Chlorococcum*.

Figure 4 (l) shows solitary unicellular organisms with elongated fusiform to ellipsoidal shapes measuring approximately 13-18 µm in length and 5.2-7 µm in width. Cells contain a parietal chloroplast with a visible central pyrenoid, a morphology consistent with the genus *Scenedesmus*, a taxon commonly reported from nutrient-rich freshwater environments.

The observed morphotypes reflect the taxonomic diversity of cultivable phototrophic microorganisms present in the studied peatland waters.

**Distribution of microalgal genera across sampling sites**

The distribution of the identified genera across sampling sites provides additional insight into the ecological characteristics of the studied peatland habitats and is summarized in Table 4. Overall, the results indicate the presence of a diverse assemblage of green algae and cyanobacteria in both peatland systems.

In Mlaca Tătarilor Peatbog, several colonial and mucilage-producing taxa were detected, including *Chlamydocapsa, Palmellopsis* and *Aphanocapsa*. These genera are commonly associated with freshwater environments rich in dissolved organic matter and are frequently reported from peatland pools where extracellular mucilage provides protection against environmental stress and facilitates colony formation (Bellinger & Sigee, 2015).

The presence of *Gonium*, a colonial volvocalean alga, suggests the existence of shallow water microhabitats with sufficient illumination for colonial flagellate algae. Volvocalean taxa are commonly observed in nutrient-poor freshwater environments where they contribute to planktonic primary production (Bellinger & Sigee, 2015).

Table 4. Dominant microalgal morphotypes observed in enriched cultures obtained from peatland water samples.

| Sampling site | Observed microalgal and cyanobacterial genera | Dominant morphotype | Cell morphology | Approx. cell size (µm) |
|---|---|---|---|---|
| Mlaca P1 | *Chlorella* sp.<br>*Chlamydocapsa* sp. | *Chlamydocapsa* sp. | ovoid morphology forming grape-like colonies | 8-9.5 µm in length 5.5–6.5 µm in width |
| Mlaca P2 | *Aphanocapsa* sp.<br>*Palmellopsis s*p. | *Aphanocapsa* sp. | spherical<br>ovoid to ellipsoidal | 3-4 µm in length<br>2-3.5 µm in width |
| Mlaca P3 | *Chlorella* sp.<br>*Gonium* sp. | *Gonium* sp. | mucilaginous matrix with spherical cells | 15 µm |
| Avrig-P1 | *Chlorella* sp. | *Chlorella* sp. | solitary spherical cells | 11-12 µm |
| Avrig-P2 | *Chlorella* sp.<br>*Scenedesmus sp.*<br>*Chlorococcum* sp. | *Scenedesmus sp.* | fusiform to ellipsoidal | 13-18 µm |
| Avrig-P3 | *Chlorella* sp. | *Chlorella* sp. | solitary spherical cells | 11-12 µm |
| Avrig-P4 | *Chlorella* sp.<br>*Nostoc* sp. | *Chlorella* sp. | solitary spherical cells | 11-12 µm |
| Avrig-P5 | *Chlorococcum* sp.<br>*Chlorella* sp.<br>*Closterium* sp. | *Closterium* sp. | solitary elongated cell, slightly curved | 25 µm in length 2.85 µm in width |
| Avrig-P6 | *Stichococcus* sp. | *Stichococcus* sp. | solitary cylindrical cells with rounded ends | 11-12 µm length<br>5-6 µm in width |
| Avrig-P7 | *Chlorella* sp.<br>*Chlorococcum* sp. | *Chlorococcum* sp. | spherical | 5-8 µm |

The frequent occurrence of *Chlorella*-like cells in Mlaca samples further indicates the presence of ecologically versatile microalgae capable of colonizing a wide range of aquatic habitats. Species of *Chlorella* are widely distributed in freshwater ecosystems and are known for their high physiological tolerance to variations in nutrient availability, light conditions and mineralization (Bellinger & Sigee, 2015).

In Avrig Peatbog, a broader morphological diversity was observed, including *Chlorococcum, Scenedesmus, Closterium, Stichococcus* and the cyanobacterium *Nostoc*. Several of these taxa are commonly reported from freshwater environments characterized by fluctuating nutrient concentrations and dynamic hydrological conditions.

The occurrence of *Scenedesmus* sp. and *Chlorococcum* sp. suggest the presence of microhabitats influenced by increased nutrient availability or environmental disturbance, as these genera are well known for their ability to rapidly colonize nutrient-enriched aquatic environments (Bellinger & Sigee, 2015).

In contrast, the presence of *Closterium* sp., a representative of desmid algae, indicates the occurrence of microhabitats typical of peatland ecosystems. Desmids are frequently associated with oligotrophic, slightly acidic waters rich in dissolved organic matter and are considered characteristic components of bog and fen algal communities (Coesel & Meesters, 2007).

The detection of *Nostoc* sp., a filamentous cyanobacterium capable of atmospheric

nitrogen fixation, may further indicate localized nitrogen limitation in certain peatland microhabitats. Nitrogen-fixing cyanobacteria are known to play an important ecological role in nutrient-poor aquatic systems by contributing biologically available nitrogen (Falkowski & Raven, 2007).

When interpreted together, the pigment data and the morphological identification provide complementary information regarding the ecological strategies of the cultivable microalgae inhabiting the studied peatland waters.

**Ecological significance of cultivable microalgal assemblages**

The ecological characteristics and indicator value of the most frequently identified genera are summarized in Table 5. Several of these taxa are widely used as indicators of water quality and trophic conditions in freshwater ecosystems (Bellinger & Sigee, 2015).

Table 5. Ecological characteristics and indicator value of the main microalgal genera

| Genus | Typical habitat | Indicator value |
|---|---|---|
| *Chlorella* | freshwater, planktonic | mesotrophic–eutrophic waters |
| *Scenedesmus* | planktonic green algae | eutrophic conditions |
| *Closterium* | oligotrophic acidic waters | peatland/desmid flora |
| *Nostoc* | benthic or colonial cyanobacteria | nitrogen-limited environments |
| *Stichococcus* | aerophytic / oligotrophic | tolerant to stress |

Ecologically versatile genera such as *Chlorella, Chlorococcum* and *Scenedesmus* are commonly reported as early colonizers of newly formed or disturbed aquatic habitats. Their presence in several enriched cultures suggests the ability of these taxa to rapidly establish populations in peatland pools and shallow water accumulations, contributing to primary production and the initial development of microbial food webs.

At the same time, the occurrence of taxa typically associated with oligotrophic peatland habitats, such as *Closterium* and *Stichococcus*, indicates the persistence of microhabitats characterized by low nutrient concentrations and high levels of dissolved organic matter.

Colonial and mucilage-producing forms such as *Palmellopsis, Chlamydocapsa* and *Aphanocapsa* may represent adaptive strategies to humic-rich waters where extracellular mucilage provides mechanical protection and facilitates colony stability.

Together, these observations suggest that the cultivable microalgal assemblages reflect the environmental heterogeneity of restored peatland ecosystems, where variations in hydrology, light availability and nutrient concentrations generate a mosaic of ecological niches for phototrophic microorganisms.

Similar patterns of microalgal colonization have been described in other peatland systems, where phototrophic microorganisms play an important role in primary production and in the re-establishment of microbial communities following ecological disturbance or restoration (Yadav & Singh, 2020).

These findings contribute to the baseline knowledge of peatland microbial phototroph diversity in Romanian wetlands and provide a starting point for future ecological and molecular investigations.

Future studies integrating molecular identification techniques and seasonal monitoring would further improve our understanding of the ecological dynamics of microalgal communities in restored peatlands.

## CONCLUSIONS

The present study provides a first overview of the cultivable microalgal diversity inhabiting the surface waters of two restored Romanian peatlands (Avrig Peatbog and Mlaca Tătarilor Peatbog).

The physicochemical measurements revealed a clear environmental gradient across sampling points in Avrig Peatbog, ranging from well-oxygenated pools to mineralized drainage channels and reductive, hypoxic microhabitats. In contrast, Mlaca Tătarilor Peatbog exhibited more uniform, stable oligotrophic conditions with predominant anoxia. Both sites shared slightly acidic-neutral pH and low mineralization favoring non-acidophilic microalgae and carbon sequestration, with incipient hydrological recovery post-restoration.

Pigment analysis of enriched cultures indicated variations in photosynthetic pigment composition, suggesting physiological acclimation of microalgal strains to local environmental conditions such as light availability, mineralization, and redox status.

Microscopic observations revealed several representative freshwater microalgal genera, including *Chlorella*, *Chlorococcum*, *Scenedesmus*, *Closterium*, and *Stichococcus*, whose ecological preferences are consistent with the physicochemical characteristics of peatland waters.

These findings provide baseline information on the cultivable fraction of peatland microalgal communities and contribute to a better understanding of the microbial diversity associated with restored peatland ecosystems.

## ACKNOWLEDGEMENTS

This research work was carried out with the support of the Institute of Biology Bucharest, Romanian Academy, through the Projects Project RO1567-IBB05/2026, and also was financed from PeatRO2 Project (RO-ENVIRONMENT-0004), and PDD project, SMIS 336936,"Enhancing knowledge of biodiversity through the implementation of the monitoring system for the conservation status of species and habitats of community interest in Romania and reporting under Article 17 of the Habitats Directive 92/43/EEC".

## REFERENCES

Allen, M. M., & Stanier, R. Y. (1968). Growth and division of some unicellular blue-green algae. *Journal of General Microbiology*, 51(2), 199–202.

Andrews, L. O., Marcisz, K., Kołaczek, P., Amon, L., Veski, S., Heinsalu, A., Stivrins, N., Bąk, M., Aquino-Lopez, M. A., Cwanek, A., Łokas, E., Karpińska-Kołaczek, M., Czerwiński, S., Słowiński, M., & Lamentowicz, M. (2025). Response and recovery of a *Sphagnum* peatland from long-term human-induced alkalinisation. *Biogeosciences, 22*, 5849–5875. https://doi.org/10.5194/bg-22-5849-2025

Belcher, H., & Swale, E. (1976). *A beginner's guide to freshwater algae*. London, HMSO, UK.

Bellinger, E. G., & Sigee, D. C. (2015). *Freshwater algae: Identification, Enumeration and use as bioindicators*. Chichester, UK: Wiley-Blackwell.

Coesel, P. F. M., & Meesters, K. J. (2007). *Desmids of the lowlands: Mesotaeniaceae and Desmidiaceae of the European lowlands*. Zeist, NL: KNNV Publishing.

Falkowski, P. G., & Raven, J. A. (2007). *Aquatic photosynthesis* (2nd ed.). Princeton, NJ: Princeton University Press.

Jeuck, A., & Arndt, H. (2013). A Short Guide to Common Heterotrophic Flagellates of Freshwater Habitats Based on the Morphology of Living Organisms. *Protist*, 164(6), 842–860.

Kowalik, T., Kanownik, W., Bogdał, A., & Policht-Latawiec, A. (2014). The effect of the change in upland catchment use on forming surface water quality. *Annual Set of Environmental Protection*, 16, 223–238.

Leifeld, J., & Menichetti, L. (2018). The underappreciated potential of peatlands in global climate change mitigation strategies. *Nature Communications*, 9, 1071, https://doi.org/10.1038/s41467-018-03406-6

Lichtenthaler, H. K. (1987). Chlorophylls and carotenoids: Pigments of photosynthetic biomembranes. *Methods in Enzymology*, 148, 350–382. https://doi.org/10.1016/0076-6879(87)48036-1

Natura 2000 Reference Portal. (2026). European Environment Agency. Retrieved February 2, 2026, from https://cdr.eionet.europa.eu/help/natura2000

Natura 2000 Viewer. (2026). European Environment Agency. Retrieved February 2, 2026, from https://natura2000.eea.europa.eu

Parish, F., Sirin, A., Charman, D., Joosten, H., Minayeva, T., Silvius, M., & Stringer, L. (2008). *Assessment on peatlands, biodiversity and climate change*. Kuala Lumpur: Global Environment Centre & Wetlands International.

PeatRO Project. (2026). *Restoration strategies of the deteriorated peatland ecosystems from Romania (PeatRO)*. Retrieved February 2, 2026, from https://www.ibiol.ro/peatro/en/about.html

PeatRO2 Project. (2026). *Degraded mires and peatlands restoration in North-East Romania (PeatRO2)*. Retrieved February 2, 2026, from https://www.ibiol.ro/peatro2/about.html

Pop, E. (1960). *Mlaștinile de turbă din Republica Populară Română*. București: Editura Academiei.

Prescott, G. W. (1962). *Algae of the Western Great Lakes Area: With an Illustrated Key to the Genera of Desmids and Freshwater Diatoms. Revised edition.* Dubuque, IA: Wm. C. Brown Company.

Prescott, G. W. (1964). *The algae: A review*. Boston: Houghton Mifflin.

Rydin, H., & Jeglum, J. (2013). *The biology of peatlands* (2nd ed.). Oxford: Oxford University Press.

Serafin, A., Pogorzelec, M., & Bronowicka-Mielniczuk, U. (2023). The influence of shallow peatland water quality on characteristics of the occurrence of selected herb species in the peatlands of Eastern Poland. *International Journal of Environmental Research and Public Health*, 20(4), 2788. https://doi.org/10.3390/ijerph20042788

Serediak, N., & Huynh, M. (2011). *Algae identification field guide*. Ottawa: Agriculture and Agri-Food Canada.

Ștefănuț, S., Ștefănuț, M.-M., Sahlean, T., Moroșanu, A.-M., Helepciuc, F.-E., Nicoară, G.-R., Bîrsan, C.-C., Maria, G.-M., Vladimirescu, M., Manole, A., & Ion, C.-M. (2025). Preliminary biodiversity survey in a newly proposed site of community importance: The Avrig Peat Bog. *Land Reclamation, Earth Observation & Surveying, Environmental Engineering*, 14, 1229–1235.

Tsuraya, F., Rahmansyah, M. S., Fikri, F., & Hasanah, R. (2023). Identification of microalgae in peat swamp

waters. *Biological Environment and Pollution*, 3(2), 43–53. https://doi.org/10.31763/bioenvipo.v3i2.654.

Yadav, N., & Singh, D. P. (2020). Microalgae and microorganisms: Important regulators of carbon dynamics in wetland ecosystems. In A. Upadhyay, R. Singh, & D. Singh (Eds.), *Restoration of wetland ecosystem: A trajectory towards a sustainable environment* (pp. 179–193). Singapore: Springer. https://doi.org/10.1007/978-981-13-7665-8_12.

Yu, Z., Loisel, J., Brosseau, D. P., Beilman, D. W., & Hunt, S. J. (2010). Global peatland dynamics since the last glacial maximum. *Geophysical Research Letters*, *37*(13), Article L13402. https://doi.org/10.1029/2010GL043584.

Scientific Papers. Series E. Land Reclamation, Earth Observation & Surveying, Environmental Engineering. Vol. XV, 2026
Print ISSN 2285-6064, CD-ROM ISSN 2285-6072, Online ISSN 2393-5138, ISSN-L 2285-6064

# INTEGRATED GEOTECHNICAL AND STRUCTURAL APPROACHES FOR REDUCING SEISMIC VULNERABILITY OF HERITAGE BUILDINGS

**Stefan Florin BALAN, Bogdan Felix APOSTOL**

National Institute of C-D for Earth Physics, 12 Calugareni Str., Magurele, Romania

Corresponding author email: sbalan@infp.ro

***Abstract***

*The paper outlines key characteristics of heritage buildings and explains why they require protection against strong seismic motions generated by the Vrancea source. One of the most common challenges these structures face is differential settlement during earthquakes; to mitigate this, several supplementary measures can be implemented. Resonant column or dynamic triaxial tests, used alongside standard geotechnical investigations, provide additional insight into soil behaviour. These methods focus on evaluating the variation of the shear modulus with strain, enabling a more accurate assessment of soil properties. The resulting data support the selection of appropriate interventions to improve site conditions and reduce the risk of structural damage during future major seismic events. Structural protection can also be enhanced through base-isolation techniques, applied according to site conditions and the specific characteristics of each building. This approach reduces seismic forces and modifies critical response parameters to safer levels. The paper highlights the advantages of these optional measures for safeguarding historical monuments and older administrative buildings, emphasizing both their technical effectiveness and their broader economic and social benefits.*

***Key words****: heritage buildings, seismic vulnerability, settlements, seismic isolation, resonant column.*

## INTRODUCTION

The protection and rehabilitation of heritage buildings include consideration of the impact of seismic movements affecting the soil deposit on which their foundation rest and the structure. The paper considers heritage buildings situated in Bucharest - capital of Romania - a city under the influence of Vrancea seismic region. This seismic source, the most important in Romania, in terms of magnitude, human and economic losses in the country, only in the last century has triggered 2 major earthquakes: November 10, 1940 with moment magnitude Mw = 7.7, approximately 600 victims, and March 4, 1977 with moment magnitude Mw = 7.4, approximately 1500 victims (Mărmureanu, 2020). The latter seismic event damaged and destroyed approximately 32900 buildings in Bucharest and in other parts of S-E of the country (Balan et al., 1982).

The paper focuses on some optional measures considered by structural designers during rehabilitation, necessary to mitigate the seismic vulnerability of these structures, beyond those imposed by the norms in force. First of them is an optional evaluation to be performed, after standard geotechnical studies were accomplished, and involves tests on resonant columns or dynamic triaxial. They allow to calculate geotechnical and rocks specific parameters, as they varying inside the soil deposit during strong seismic shakings. The reason of this evaluation is linked to the settlement phenomenon that may appear in the aftermath of a strong earthquake, for foundation of structures, especially if located on soft, sedimentary soils.

Situated in the central sector of the Vlăsia Plain - a sub-division of the broader Romanian Plain - Bucharest is located approximately 165 km from the Vrancea seismic zone. The region is geologically characterized by thick, unconsolidated sedimentary deposits. The local topography is heavily influenced by the Dâmbovița and Colentina rivers, which created distinct zones prone to natural erosion and alluvial sedimentation. Consequently, evaluating the geological, geotechnical, and hydrological properties of the local aquifer systems is essential for assessing the overall environmental and structural stability of the urban area.

These soil conditions can favour the development of ground settlements, either due to naturally soft soil layers or anthropogenic factors such as artificial fills. Identifying these zones and understanding the processes that

cause such soil behaviour is essential. Equally important is knowing what types of buildings occupy these areas, their structural systems, and whether they have undergone previous repairs or experienced past seismic events.

Settlements can introduce additional stresses into building structures, and during an earthquake these stresses may amplify damage, leading to cracks in structural elements, displacement of interior walls, or deterioration of floors and installations. Building vulnerability increases when settlement-induced stress is compounded by seismic stress from strong earthquakes.

Earthquakes generate seismic waves that propagate from the source through the geological environment and reach sediment layers. The soil material of the subsurface layers is subjected to seismic stresses equivalent to dynamic loads with variable levels of strain. The level of soil deformation depends on many parameters, such as: the event duration, maximum ground acceleration, number of wave cycles, type of waves, soil type, and depth.

When soils are subjected to time-dependent dynamic loading (e.g. earthquakes or vibrations), their deformation directly depends on the amplitude and repetition of the cyclic shear deformation (Ishihara, 1996; Braja & Ramana, 2011). The soil exhibits a transition to nonlinear behaviour at deformation ranges above $10^{-4}$-$10^{-2}$%, associated with the accumulation of permanent deformations. This leads to progressive crack widening and significant differential settlements. For deformation levels greater than $10^{-2}$ %, the soil configuration undergoes strong nonlinearity and elastoplastic deformation; structural bonds break, severely reducing soil cohesion. This reduction in internal strength results in soil sliding (shear failure), excessive compaction/consolidation, and increase in pore water pressure. This behaviour leads to soil instability, foundation settlement, and liquefaction during seismic loading (Bratosin, 2002; Yoshida, 2015). The degradation of soil stiffness and cyclic settlements induced by strong earthquakes can be significant in urban areas formed by granular soil types, and Bucharest is one of the cases (Vucetic & Dobri, 1991).

Earthquake-induced settlements should be considered separately for two cases, the one with structures and the other without structures on the surface of the ground. For the former: total incremental settlement $\Delta S_t = \Delta S_{is} + \Delta S_{cy\,s}$, where immediate settlement – immediately after earthquake is $\Delta S_{is}$, and due to dissipation of cyclic-induced excess pore pressures $\Delta S_{cy\,s}$.

Another optional measure to protect the construction from powerful forces inside it during a strong seismic event is to isolate the structure from the foundation through different methods (Apostol et al., 2017; Liu et al., 2014; Taniguchi et al., 2008). The paper points out the results of seismic-base isolation intervention, highlighting the monitoring buildings activity and data processing performance (Balan et al., 2020).

The benefits of these optional measures to protect heritage buildings from strong earthquakes are discussed.

## MATERIALS AND METHODS

An essential step at the start of any rehabilitation project is evaluating whether the existing soil deposit can safely support the additional loads introduced by the planned construction activities. To do this, it is advisable to repeat the standard geotechnical investigations. (Common tests to re-evaluate the site include the Standard Penetration Test (SPT) for relative density and soil strength, Cone Penetration Test (CPT) for detailed soil profiles, Pressure meter tests (PMT) and Cross-hole/Down-hole Seismic Tests).

In regions where strong earthquakes ($M_W > 7$) may occur, designers are particularly concerned about potential seismic-induced settlements. If the standard tests indicate that the soil is susceptible to settlement under dynamic loading, additional specialized tests may be carried out to better understand and control these effects (Wong et al., 2022; Jurček et al., 2024).

Authors recommend in this situation to perform resonant column or dynamic triaxial tests. Both are showing the variation of the shear modulus (G) and damping (D) with strain (γ) induced in the soil deposit by strong earthquakes ($M_W > 7$). Resonant columns and dynamic triaxial are electro-mechanical devices which could simulate seismic stress/strain to a soil sample from the site of interest, gathered from different depths.

The resonant columns are devices functioning in a dynamical regime to determine soils-specific

parameters and characteristics. They can perform engineering seismology-devoted activities and highlight the non-linear effects of the behaviour of degraded rocks under strong seismic movement and experimental studies on dynamical devices. For example, the non-linear behavior of the soil as observed in laboratory tests on Hardin-Drnevich resonant columns, for strain level exceeding $10^{-5}$ - $10^{-4}$ % is a result of reference in geotechnical research (Bratosin, 2002). The devices use a procedure that analyses the non-linear soil behaviour of shear modulus G = G(γ) and damping function D = D(γ), function of strain level (γ).

Principle of functioning as based on standard configurations, employs a typically cylindrical soil sample fixed at the base and free to vibrate at the top. A torque device attached to the top generates a torsional moment, $M = M_0 \sin\omega t$, and another device generates a longitudinal force $F = F_0 \sin\omega t$ to vibrate the sample, in turn. The Drnevich-type resonant column as in Figure 1 (left), (Bratosin, 2002) typically utilizes only torsional vibration, including refinements to the driving system to better measure damping and accommodate higher strains. Hardin-type device applies $M = M_0 \sin\omega t$ and an axial force (F) to simulate in-situ confining pressure (for example a construction).

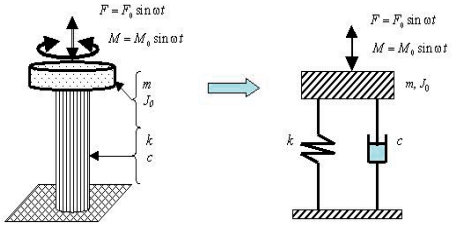



Figure 1. Scheme of resonant column (left) and nonlinear Kelvin-Voigt model (right)

In the Figure 1 (right) (Bratosin et al., 2009) the harmonic excitation for a single degree of freedom model is represented either as external time-varying force $F$ with amplitude $F_0$, or external moment $M$ with excitation amplitude $M_0$. The employed parameters are: moment of inertia of vibration $J_0$, stiffness $k$, damping $c$, pulsation of the external input $\omega$ and mass of the soil sample $m$. The constitutive stress-strain relationships imply the need for viscoelastic laws, and the appropriate model used in this situation is the nonlinear Kelvin-Voigt type (Bratosin et al., 2009).

For higher values of strain (> $10^{-3}$ %), characteristic of strong earthquakes, stress tests are recommended to be performed on a classic/ dynamic triaxial device, (Kumar et al., 2021) which imply a specialized laboratory method used in geotechnical engineering to measure soils behaviour under cyclic or rapidly changing loads, such as those caused by earthquakes.

It is necessary, therefore, the adaptation to the specific situations occurring in the territory, aiming at obtaining the parameters of foundation soil behaviour (Mărmureanu et al., 2004).

The second optional measure employed herein to mitigate the seismic vulnerability of heritage buildings is seismic base-isolation.

Heritage buildings are in general fragile structures, of old materials and in no case designed under seismic codes (also Bucharest situation). During a strong earthquake (for example, above $M_W > 7$) in any construction appear strong shear and axial forces therefore vibrations with higher amplitudes than usual from daily traffic or sporadic construction works. The magnitude of these seismic solicitations that a structure could withstand, and their effects, depend on the characteristics of the construction and the orientation of its main axes with respect to the action of the incoming seismic waves. The purpose of rehabilitation design is to reduce the level of these seismic solicitations and one method to make this happen is to isolate the structure from its foundation through different methods.

The method of seismic base-isolation was already implemented in many parts of the world with very good results in mitigation of seismic vulnerability of important and old buildings (Pietra et al., 2015; Yenidogan & Erdik, 2016; Ghafar et al., 2025). It allows for large horizontal movements while maintaining vertical stiffness, thus minimizing the damage to both structural and non-structural components. Base isolation consists in inserting flexible layer (isolator devices) at the base of the building, separating the structure from its foundations. In the paper is shown that this technique is particularly effective for historic buildings (it reduces the amplitudes in the supra structure), also ensuring operational continuity of the building functioning.

The method was applied also in Bucharest on rehabilitation of four historic buildings. The particularities of these structures are shortly described as follows:

- The Bucharest Town Hall was constructed between 1906 and 1908, using brick masonry combined with reinforced concrete floors supported by turned caissons. A major consolidation project began in 2010, during which a seismic isolation system was installed. The building includes a basement, a ground floor, three upper levels, and an attic.
- The Bucharest University of Economic Studies building on "Calea Griviței" street, constructed between 1905 and 1908, features brick masonry and a truss roof. It includes a basement, a ground floor, two upper levels, and an attic. After consolidation works carried out post 2011, a seismic isolation system was added with two sensors one above and one under it.
- The Triumphal Arch is a distinctive historic monument dating back to the 1930s. Since 2016, when it was rehabilitated, it was monitored using two seismic sensors installed on the isolated structure - one positioned at ground level above the isolator devices and the other at the top of the monument.
- "Foisorul de Foc" constructed between 1890 – 1892, initial a water tank tower, then fire watching from the finish of XIX-th century, then used for other purposes, 42m height.

All four buildings are heritage ones, the first two are still in operation for the initial purpose, administrative and educational, the third is a monument in connection with World War One and the fourth is now the "Museum of Firefighters".

An example of a seismic isolator with rubber and a viscous damper used in retrofitting Bucharest University of Economic Studies building is shown in Figure 2 (Balan et al., 2020).




Figure 2. Example of seismic isolator (left) and viscous damper (right) used for retrofitting

## RESULTS AND DISCUSSIONS

Soil strain thresholds define the transition from linear-elastic behaviour (negligible degradation) to non-linear behaviour (significant degradation). Stiffness degradation typically begins at shear strain levels of 0.0001 % ($10^{-4}$ %) with significant degradation occurring above 0.01 % - 0.1 %. Thresholds are lower for clay (1-2 x $10^{-4}$ %) compared to sand (3-4 x $10^{-4}$ %). For geotechnical applications, understanding these thresholds is critical because strains in the soil, often called the "active compression zone", can lead to permanent settlement or deformation if the threshold is exceeded.

The "active compression zone" refers to the depth within the soil profile where the applied stress (e.g., from a building, embankment, or tunnel) exceeds the soil's strength, causing significant, non-recoverable compression and rearrangement of soil particles.

In engineering, this zone defines the depth over which changes in loading or moisture content will cause substantial settlement or heaving. If foundations are placed above this zone without addressing the compression, long-term settlement will occur.

Exceeding these thresholds leads to different types of settlement: consolidation, consisting in gradual, long-term squeezing of water from saturated soil voids, and creep, which is a long-term, time-dependent settlement that occurs even after excess pore water pressure has dissipated, driven by the distortion of the soil skeleton. Creep in soft clays is a long-term geotechnical phenomenon characterized by time-dependent settlement that persists even after excess pore water pressure from primary consolidation have completely dissipated. This process is driven by the viscous deformation, rearrangement, and inter-particle sliding of the soil skeleton under constant effective stress. In soft, highly compressible soils (e.g., soils like organic clays or soft mud, characterized by high water content, low shear strength, and often a high degree of saturation, including several types of soft, cohesive soils), creep can produce substantial deformation over decades, often leading to settlement that exceeds the magnitude of initial consolidation settlement. The magnitude of creep is heavily influenced by the soil's stress history (over consolidation ratio),

the stress level applied, and the soil's inherent anisotropy.

Clays typically exhibit higher, time-dependent strain (consolidation), while sand strains are more immediate. Rapid loading (dynamic, seismic) can lead to higher strains and liquefaction, whereas slow, drained loading causes smaller, manageable strains. Therefore, in geotechnical engineering, seismic design assumes high-risk conditions requiring soil improvement, while static design often deals with smaller deformation levels.

To mitigate these risks, geotechnical engineers use soil strengthening, preloading, or deep foundation systems to bypass this zone, ensuring that strains remain within the allowable elastic limit (Chang et al., 2016; Dammala & Krishna, 2019).

When a soil deposit experiences a medium range of strain, its behaviour transitions to elasto-plastic, and the shear modulus begins to decrease as the shear strain increases. Based on the resonant column tests developed for this study, this behaviour initiates at a shear strain level of approximately $10^{-5}$ % (see Figure 3). In this regime, the damping ratio serves to quantify the energy absorption capacity of the soil.

Resonant column tests provide a quantitative assessment of these dynamic soil properties across their entire range of definition, making the resulting data highly valuable for calibrating and evaluating nonlinear viscoelastic models under dynamic loading. Ultimately, because the behaviour of soils and rocks is fundamentally dependent on the loading level, this characteristic non-linear response directly influences the dynamic performance of the entire site-structure system.

Data gathered from geological, geotechnical, and hydrogeological boreholes across the city have successfully mapped the sequence of subsoil deposits. By utilizing seismic measurements and geotechnical laboratory analysis on the core samples from these drillings, representative dynamic parameters of the local soils and rocks can be determined (Stokoe et al., 1999).

Structures founded on these superficial layers are highly susceptible to the effects of ground shaking. For instance, loose soils and unconsolidated sediments can significantly amplify ground motion, while water-saturated sediments are prone to soil liquefaction. During an earthquake, these phenomena can lead to a complete loss of ground bearing capacity, ultimately resulting in the catastrophic collapse of overlying buildings.

Results obtained using these optional soil tests are illustrated in Figure 3 (NATO Project, 2005) for several soil samples tested with the Drnevich resonant column device from one site (“Tineretului Park”) in Bucharest. The samples include: sandy clay (4-4.5 m depth), coarse sand (7-8.5 m), fine sand (21-24 m), and gravel (35-37 m). As shown in the graph, the shear modulus G decreases - by as much as 50 % for some materials - while the damping ratio D increases with shear strain ($\gamma$).

Tests performed on dynamic triaxial device, Figure 4, (NATO project, 2005) show that equivalent shear modulus, $G_{eq} = G = E/2(1+ \nu)$ for gravel samples is decreasing while hysteretic damping ratio h (%) is increasing with single amplitude shear strain $\gamma_{sa}$, The equivalent shear modulus is defined as secant shear modulus used to represent the nonlinear stress-strain behaviour of soils under cyclic or dynamic loading (e.g. earthquakes, machine vibrations), and $\gamma_{sa}= (\gamma_{max} - \gamma_{min})/2$ is maximum shear strain reached in one direction (where $\gamma_{max}$, $\gamma_{min}$ are maximum, respectively minimum shear strain). The soil specimens were drilled from the same site located in Bucharest (“Tineretului Park’’) at 35 - 37 m depth.

The results are of relevance for various sectors in geotechnics and with implications in evaluating factors of seismic hazard, the path of propagating the seismic waves, as well as for advancing the fundamental knowledge in understanding the phenomena in soil-structure interaction.

The test devices show the behaviour of soils, the reduction of shear modulus (G) and increase in damping ratio (D) with increasing strain $\gamma$ (as caused by strong earthquakes, with moment magnitude $M_w > 7$, and strain above $10^{-4}$ %). Previous studies concluded that a strain of 3.5 x $10^{-5}$ % may roughly corresponds to a Gutenberg-Richter magnitude of $M_{GR} = 6.1$, while higher level of strain of 1.4 x $10^{-3}$ % corresponds to a magnitude of $M_{GR} = 7.2$ (earthquake of March 4, 1977) (Mărmureanu, 2020). This behavior depends on the soil or rock type (soft degraded, cohesive, coarse-grained or noncohesive,

soft/degraded or hard/stable, etc.), sample depth and other stratigraphy and geological conditions.

Higher magnitude events may induce cyclic shear strains ranging between 0.01 % ($10^{-4}$) and 0.5 % (5 x $10^{-3}$). This would lead to significant pore pressure generation, large deformations, and potential liquefaction.

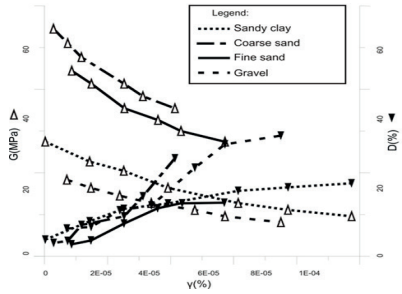



Figure 3. Resonant column tests for core samples (from site "Parcul Tineretului")

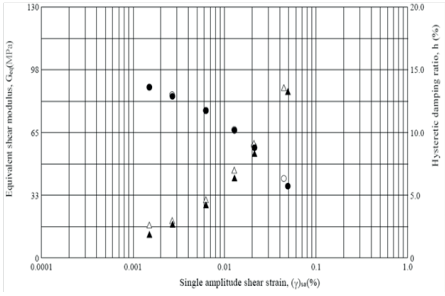



Figure 4: Triaxial tests results for gravel samples (from site "Parcul Tineretului")

High-intensity seismic events triggered by Vrancea intermediate-depth seismic source can produce severe damages and create significant amplification in saturated soils, often leading to large strain, non-linear deformation. The extreme strains values higher than > 1%–10%, may indicate that the soil structure has essentially lost its capacity to bear loads, leading to progressive failure, where the failure zone spreads and induces large, often uncontrollable, deformations in overlying structures.

Based on the provided results, the dynamic model (often in the context of soil-structure interaction or seismic response) assumes a strong dependence of the soil on several, often interlinked factors. For saturated soils, the response is strongly dependent on whether the loading occurs under drained or undrained conditions, which affects pore water pressure and, subsequently, soil stiffness.

In the second part of the study, the goal was to compute the efficiency of seismic isolation for Bucharest University of Economic Studies (ASE, Victor Slavescu) building in Bucharest.

The sensors are placed under and immediately above the seismic isolator, allowing both ground and structure coupling, respectively. They are part of a system consisting of a sensor network and the Data Centre (NDC) capable of acquiring, exchanging and processing data in real time. The computation in terms of maximum recorded accelerations (Amax) and maximum spectral accelerations (SAmax), performed by the Antelope automated system (BRTT, 2018), installed at the National Institute for Earth Physics provides information on the behaviour of the building and the performance of the insulation. The results of monitoring activity and recording of accelerations for 5.5 $M_W$ earthquake of October 28, 2018 (148 km focal depth), (ROMPLUS Catalog, 2025) in this seismic isolated building were analyzed, from the perspective of the earthquake protection system performance. This earthquake was the strongest that hit Bucharest in the last 10 years and originates in the Vrancea intermediate-depth focal area (see Table 1, Balan et al., 2020). All the data above the isolator are consistently less than those under the isolator for both (horizontal) directions N-S and E-W (see Table 1). The maximum values, $A_{max}$, obtained from the recordings above isolator is 3.8 less on N-S direction and 2.12 less on E-W than those under isolator; in the case of spectral response, the maximum spectral acceleration, $SA_{max}$, above the isolator is 3.21 less on N-S direction and 2.1 less on E-W directions than those under isolator.

Table 1. Engineering parameters (maximum recorded acceleration, maximum spectral acceleration) for the 5.5 $M_W$, October 28, 2018 earthquake

| Earthquake ($M_W$ = 5.5) | Acceleration and spectral acceleration ($cm/s^2$) | Position of sensor | |
|---|---|---|---|
| | | Above isolator | Under isolator |
| Component N-S | $A_{max}$ | 33.4 | 129.4 |
| | $SA_{max}$ | 105.0 | 337.2 |
| Component E-W | $A_{max}$ | 46.5 | 98.6 |
| | $SA_{max}$ | 187.6 | 349.9 |

Based on this type of analysis of structural performance during seismic events, the findings confirm that base isolation systems offer a non-invasive, reliable solution for retrofitting older, vulnerable structures, enabling them to withstand earthquakes with minimal damage**.** Base isolation systems decouple the building from the ground, resulting in lower acceleration at upper floor levels compared to fixed-base, non-isolated models. These results support the use of this (modern) technology to rehabilitate infrastructure that was built before modern seismic codes.

For in-depths investigations in this paper were used: resonant column and dynamic triaxial. The two dynamic nonlinear functions modeling the material strength in resonant column experime nts, G = G(γ) and damping D = D(γ) are determined for the soil layers. As a matter a fact almost all site materials exhibit degradable material behavior. However, some of them more and others less, see type of soils in Figure 3.

In soil laboratory testing and geotechnical earthquake engineering, soil cyclic shear strain levels are generally correlated to earthquake magnitude through the intensity of ground shaking (Peak Ground Acceleration, PGA) and the number of loading cycles, which increase with magnitude.

The decrease in the shear modulus (G), could be even 50%, leads to a proportional increase in soil settlements, which can compromise the serviceability and structural integrity of a building.

In geotechnical design, the settlement of a foundation is inversely proportional to the stiffness of the soil. Since G is related to the Young's modulus (E) by the relationship $G = \frac{E}{2(1+\nu)}$, where $\nu$ is Poisson's ratio, a reduction in G directly impacts the elastic modulus used to calculate settlement.

This situation could result in damage in the structure and interior walls. G is a stiffness parameter and its degradation often correlates with a loss in shear strength, potentially reducing the ultimate bearing capacity of the foundation.

In experiments such as cyclic triaxial or resonant column tests, the induced strain levels correspond to varying seismic intensities. often classified by magnitude and proximity to the source. Soil strains generally scale with earthquake magnitude ($M_W$), with significant, non-linear, and permanent deformations (liquefaction or failure) occurring at higher strain levels, typically associated with stronger earthquakes. For moderate to large earthquakes $6 < M_W < 7$ cyclic triaxial or cyclic simple shear tests employed throughout this work show the pore water pressure generation, especially in loose, saturated sands. For large to major magnitudes, $M_W > 7$ high nonlinear behaviour, significant pore pressure generation, and potential for soil liquefaction appear. In many studies, a shear strain of 0.1 % - 0.5 % is considered the threshold for structural damage or significant liquefaction (Díaz-Rodríguez & López-Molina, 2008; Hazirbaba & Omarow, 2019).

Strains exceeding the 0.1 % threshold in soft, saturated soil samples often trigger cyclic softening (degradation, in clays) or liquefaction (in sands), causing a rapid reduction in shear strength and stiffness. The large number of cycles causes a significant pore water pressure level, which reduces the effective stress of the soil, leading to significant post-earthquake cyclic settlement. In soft, saturated alluvial deposits, this mechanism can cause massive ground deformation and substantial settlement.

The paper highlights the significance of knowing the potential of dynamic behaviour of the soil strata under heritage/important buildings during strong seismic events, for taking all measures in the design process to limit such deformations. This way structural damage may be avoided. To have as comprehensive as possible and reliable site information, the necessity is highlighted for considering this method at site evaluation for a safer environment and mitigation of the seismic risk.

By this method, laboratory data are integrated with the parameters available at the site. This approach makes it possible to estimate the site-specific properties by assessing their variability under different loading conditions for the soil components.

Assessing the dynamic parameters for seismic response in Bucharest requires specialized consideration of its unique geological setting, characterized by deep, unconsolidated sedimentary layers and significant intermediate-depth Vrancea earthquakes. A proper estimation of the seismic response involves these

parameters, especially for buildings that are particularly vulnerable to the characteristic long-period, high-intensity shaking experienced in Bucharest. (Bratu & Dobrescu, 2019).
The data processed from recordings on the studied building show an effective earthquake protection system, with a reduction of signal with a factor in the range from 2.0 to 3.8. The output consists in engineering parameters that are maximum acceleration $A_{max}$ recorded on two horizontal directions (N-S, E-W), and the maximum spectral acceleration ($SA_{max}$). The retrofitting technique referenced herein is efficient in urban areas in relation with local and regional seismicity and local site effects parameters (De Domenico et al., 2019).

## CONCLUSIONS

The paper aim is to put forward two optional solutions in the case of rehabilitation of heritage buildings. These buildings are old ones (more than 80-90 years, or even much more) and at their construction there were no building codes with seismic specifications. One of the weak points for these kinds of structures is the foundation soil not studied enough in the design process. The seismic waves are coming from the soil deposit to foundations and structure. In case of rehabilitating such a structure, we should check that the soil would not permit settlements in case of a strong earthquake and this is presented in first case, because a settlement could result in structure damage due to new forces developed in it. If the designers find out that settlements could occur it must be found solutions for consolidating the soil deposit where the construction is situated.
Larger magnitude earthquakes ($M_W$ = 7.2−7.4) create higher PGA and are characterized by longer duration, which generate a higher equivalent number of uniform cycles leading to larger shear strains, with values often exceeding 0.1 % in saturated, soft alluvial soil samples, causing significant cyclic settlement. These conditions lead to strong geotechnical impacts. For example, strains exceeding the 0.1 % threshold in soft, saturated soil samples often trigger "cyclic softening" (in clays) or liquefaction (in sands), causing a rapid reduction in shear strength and stiffness. The large number of cycles causes a significant pore water pressure level, which reduces the effective stress of the soil, leading to significant post-earthquake cyclic settlement. In soft, saturated alluvial deposits, this mechanism can cause massive ground deformation and substantial settlement.
The dynamic tests are used to develop nonlinear constitutive models that define the stress-strain relationship. These models are essential for predicting how soil layers amplify or attenuate ground motion, and how they interact with structures (e.g., in terms of pore-water pressure development and stiffness degradation).
Many old buildings do not have structures to withstand shear and axial forces from strong earthquakes. Therefore, the option of seismic isolation proved highly effective, because separating structure from foundation were achieved ~ 2-3 times smaller accelerations above the isolating system. By diminishing the acceleration recorded, it reduced also the forces applied on the building during a strong seismic movement. Using seismic sensors, vibration data, or similar analysis to continuously monitor structural health, allows for real-time assessment of building stability. Base isolation effectively reduces floor accelerations providing superior protection compared to conventional stiffening and strengthening action. This methodology helps in drawing attention to the seismic benefits for similar, retrofitted buildings.
The implications of these results regarding collapse prevention and enhancing structural resilience are focused on reducing vulnerability through specific, actionable strategies in the seismic risk management for this highly populated zone.
Utilizing quantitative data can target investments where they will generate the highest return in terms of energy savings, operational efficiency, and structural resilience.
Quantifying the efficacy of seismic isolation on historical, or vulnerable buildings in Romania demonstrates a significant reduction in seismic response (acceleration and spectral acceleration) right above the isolation layer, serving as a key indicator for seismic risk and vulnerability mitigation. This technique can be employed as a strategy for seismic risk mitigation, particularly for buildings in Bucharest exposed to Vrancea intermediate-depth earthquake motions.

Seismic isolation, despite high initial financial costs and technical complexities, is a highly effective and beneficial strategy for protecting heritage constructions. This approach is increasingly considered superior to traditional, more invasive strengthening methods (such as adding concrete walls) because it preserves the original materials and architectural integrity. Initial costs for seismic isolation are generally higher than conventional strengthening due to the cost of isolator devices and complex installation. Despite the upfront investment, seismic isolation can offer a better life-cycle cost by minimizing post-earthquake repair expenses, reducing business interruption.

## ACKNOWLEDGEMENTS

This paper was carried out within Program Nucleu SOL4RISC, contract number 24N/03.01.2023, supported by Ministry of Research, Innovation and Digitization, project no. PN23360202.

## REFERENCES

Apostol, B. F. (2017). A resonant coupling of a localized harmonic oscillator to an elastic medium. *Romanian Reports in Physics, 69*, 116.

Balan, S., Cristescu, V., & Cornea, I., (coordinators). (1982). *March 4 1977 Earthquake from Romania*. [Cutremurul de pământ din România de la 4 martie 1977]. Bucharest, RO: Publishing House of the Romanian Academy.

Balan, S.F., Tiganescu, A., & Apostol, B.F. (2020). Response Structure Analysis of the Seismic Isolated Buildings in Bucharest City. *IOP Conf. Ser.: Earth Environ. Sci.*609(1), 012080.

Braja, M. D., & Ramana, G. V. (2011). *Principles of Soil Dynamics* (2nd Ed.). Cengage Learning.

Bratosin, D. (2002). *Soil dynamics elements* (in Romanian). Bucharest, RO: Publishing House of the Romanian Academy.

Bratosin, D., Balan, F. S., & Cioflan, C. O. (2009). Soils nonlinearity effects on dominant site period evaluation. *Proceedings of the Romanian Academy - Series A: Mathematics, Physics, Technical Sciences, Information Science*, *10*(3), 261-268.

Bratu, P., & Dobrescu, C.F. (2019). *Evaluation of the dissipated energy in vicinity of the resonance, depending on the nature of dynamic excitation*. Romanian Journal of Acoustics and Vibration 16(1): 66-71.

BRTT, (2018). *Antelope Environmental Monitoring System*. Boulder Real Time Technologies, Inc., Boulder, Colorado.

Chang, D. W., Lu, C. W., Lin, S. S., & Lai, J. R. (2016). Dynamic analyses for performance-based seismic design of geotechnical structures with examples in deep foundations. *Geotechnical Engineering Journal of the SEAGS & AGSSEA*, *47*(2), 83–88.

Dammala, P. K., & Krishna, A. M. (2019). Dynamic characterization of soils using various methods for seismic site response studies. In A. M. Krishna (Ed.), *Frontiers in geotechnical engineering: Developments in geotechnical engineering* (pp. 273–301). Springer.

De Domenico, D., Ricciardi, G., & Takewaki, I. (2019). Design strategies of viscous dampers for seismic protection of building structures: A review. *Soil Dynamics and Earthquake Engineering, 118*, 144–165.

Díaz-Rodríguez, J. A., & López-Molina, J. A. (2008). Strain thresholds in soil dynamics. *Proceedings of the 14th World conference on earthquake engineering*.

Ghafar, W. A., Zhong, T., Lai, Z., Zhang, P., Yang, Y., & Hasan, M. M. (2025). Seismic isolation for existing structures: A review of retrofitting techniques, case studies, and trends. *Discover Civil Engineering, 2*, 137. Springer Nature.

Hazirbaba, K., & Omarow, M. (2019). Strain-based assessment of liquefaction and seismic settlement of saturated sand. *Cogent Engineering, 6(1).*

Ishihara, K. (1996). *Soil behaviour in earthquake geotechnics*. Clarendon Press.

Jurček, T., Pulko, B., & Maček, M. (2024). Small strain shear modulus of the Ljubljana Marsh soil measured with resonant column and bender elements under isotropic and anisotropic stress conditions. *Applied Sciences, 14*(5), 1984.

Kumar, S. S., Dey, A., & Murali Krishna, A. (2021). Evaluation of monotonic and dynamic shear modulus of sand using on-sample transducers in cyclic triaxial apparatus. *Acta Geotechnica, 16*, 221–236.

Liu, T., Zordan, T., & Briseghella, B., & Zhang, Q. (2014). An improved equivalent linear model of seismic isolation system with bilinear behaviour. *Engineering Structures, 61*, 113–126.

Mărmureanu, Gh. (2020). *Certainties/Uncertainties in the Assessment of Vrancea Seismic Hazard and Risk* [Certitudini/incertitudini în evaluarea hazardului și a riscului seismic vrâncean], Bucharest, RO: Romanian Academy Publishing House.

Mărmureanu, Gh., Mișicu, M., Cioflan, C. O., Bălan, St. F., & Apostol, B. F. (2004). Nonlinear seismology – The seismology of the XXI century. In F. Wenzel (Ed.), *Lecture Notes in Earth Sciences: Perspective in modern seismology*. 105, 47–67.

NATO SFP 981882. (2005). *Site-effect analyses for the earthquake-endangered metropolis Bucharest, Romania*.

Pietra, D., Pampanin, S., Mayes, R. L., Wetzel, N. G., & Feng, D. (2015). Design of base-isolated buildings: An overview of international codes. *Bulletin of the New Zealand Society for Earthquake Engineering, 48*(2), 118–135.

ROMPLUS (2025). *Romanian earthquake catalogue*. National Institute for Earth Physics, Măgurele, Romania.

Stokoe, K. H., Darendeli, M. B., Andrus, R. D., & Brown,L. T. (1999). Dynamic soil properties: Laboratory, field and correlation studies. In P. S. Seco

e Pinto (Ed.), *Earthquake geotechnical engineering: Proceedings of the 2nd International Conference on Earthquake Geotechnical Engineering, Lisbon, Portugal, 21-25 June 1999*. 3, 811–846.

Taniguchi, T., Der Kiureghian, A., & Melkumyan, M. (2008). Effect of tuned mass damper on displacement demand of base-isolated structures. *Engineering Structures, 30*(12), 3478–3488.

Vucetic, M., & Dobry, R. (1991). Effect of soil plasticity on cyclic response. *Journal of Geotechnical Engineering, 117*, 89–107.

Wong, J. K. H., Wong, S. Y., & Wong, K. Y. (2022). Extended model of shear modulus reduction for cohesive soils. *Acta Geotechnica, 17*, 2347–2363.

Yenidogan, C., & Erdik, M. (2016). A comparative evaluation of design provisions for seismically isolated buildings. *Soil Dynamics and Earthquake Engineering, 90*, 265–286.

Yoshida, N. (2015). *Seismic ground response analysis*. Springer Netherlands.

Scientific Papers. Series E. Land Reclamation, Earth Observation & Surveying, Environmental Engineering. Vol. XV, 2026
Print ISSN 2285-6064, CD-ROM ISSN 2285-6072, Online ISSN 2393-5138, ISSN-L 2285-6064

# ASPECTS RELATED TO VEGETATION SUCCESSION, ON AGRICULTURAL LANDS, IMPROPERLY EXPLOITED AND ABANDONED, AFFECTED BY DROUGHT, IN NON-COLLECTIVIZED AREAS

**Flavia-Mălina CIOFLAN[1], Călin Ioan IOVAN[2], Sorin Lucian DOROG[2], Călin Gheorghe PĂŞCUŢ[2], Eugenia ŞERBAN[3]**

[1]Doctoral School of Engineering Sciences, Agronomy Field, University of Oradea, Faculty of Managerial and Technological Engineering, 1 University Street, 410087, Oradea, Romania
[2]University of Oradea, Faculty of Environmental Protection, Department of Forestry and Forestry Engineering, 26 Gen. Magheru Street, 410048, Oradea, Romania
[3]University of Oradea, Faculty of Environmental Protection, Department of Environmental Engineering, 26 Gen. Magheru Street, 410048, Oradea, Romania

Corresponding author email: irimieflavia@gmail.com

***Abstract***

*The paper aims to study and analyze the succession process of arboreal and shrub vegetation on a series of agricultural lands, which have not been administered and exploited in accordance with their use category, in a non-collectivized hill area, in the Vîrfurile locality, Arad county. The study was carried out for the period 1990-2025, with observations, inventories, comparisons, simulations, and magnetic recordings of relevant images related to the studied lands. Also, the records from the agricultural register and the parcel plan that was drawn up by the Cadastre and Real Estate Advertising Office of Arad county were analyzed, on the occasion of the systematic registration works of the real estates in the rural areas, for this location. The results obtained confirm that on the studied lands, a succession of arborescent and shrub vegetation was triggered, with a relatively active dynamic. Consequently, a series of pioneer, invasive tree species were highlighted, as well as forest tree species of the genus Quercus, which settled on areas ranging between 10-100% of the mentioned location.*

***Key words****: agricultural lands, improper exploitation, non-collectivized areas, shrub species, tree species use category, vegetation succession.*

## INTRODUCTION

The Earth's vegetation cover is characterized by continuous changes in the composition and distribution of its component species, which unfold with differentiated dynamics and particularities, determined by a series of conditions and factors that trigger, influence, and sustain them.

These processes may consist of local or seasonal changes, known as symphenological processes, characterized by a recurrent rhythm influenced by climate, up to secular or millennial developments on a large spatial and very long temporal scale - namely synchronological processes, which are in fact determined by major climate changes and, implicitly, by changes in vegetation conditions, such as the development of vegetation in the post-glacial period (Fickert & Richter, 2025).

Consequently, regeneration processes, which are considered cyclical, and succession processes, which have a strongly directional character, represent indicators of temporal changes in species populations, communities, and even entire ecosystems (Fickert & Richter, 2025).

Vegetation succession represents the modification or replacement, over a period of time, of the phytocoenosis composition on a given land surface, as a direct consequence of changes in vegetation conditions and, implicitly, in interspecific relationships. As a result, species and species associations are eliminated and replaced by others (Florescu & Nicolescu, 1996). According to the theory proposed by Clements (Florescu & Nicolescu, 1996; Fickert & Richter, 2025), the vegetation succession process goes through a series of successive stages: denudation of the territory, species

migration, colonization, competition, reaction, stabilization, and regression.

Denudation, or exposure of the substrate through disturbance, may result from natural phenomena such as landslides, avalanches, vegetation fires (De Giuli et al., 2024), active erosion, the formation of river islands, volcanic eruptions (Moreno-Gonzalez et al., 2025), or climate changes. This stage may also be significantly influenced by anthropogenic activities such as pollution, excessive exploitation or abandonment of agricultural lands (Cioflan, 2025), irrational forest exploitation, improper conservation or abandonment of mining sites (Garate-Quispe et al., 2023; 2024), construction works, hydrotechnical developments, etc.

Migration (immigration) of herbaceous and woody species and the occupation of vacant ecological niches or newly denuded habitats generally occur through seed dispersal, depending on their morphological and physiological characteristics. Thus, this stage unfolds differently depending on the dispersal mechanism, with vector agents including wind, water, animals, and humans (Fickert & Richter, 2025).

Colonization, or establishment of species in the new habitat, involves the installation and development of immigrant species, directly influenced by their ecological requirements and vegetation conditions. In some cases, this stage results in the emergence and spread of valuable natural species (Szirmai et al., 2022). Consequently, this stage includes successive processes: seed germination, seedling emergence, growth, development, maturation, and finally sexual reproduction of mature individuals.

Competition in the newly colonized location occurs both interspecifically and intraspecifically, through competition among new species and between immigrant species and the former inhabitants of the territory, for both underground and aboveground space. As a result, species or groups of species that regenerate easily under the new conditions and do not have high trophic requirements-namely pioneer and invasive species-become dominant, with biodiversity playing an important role in this stage (Pérez-Hernández & Gavilán, 2021).

Reaction represents the habitat's response to the impact of the new phytocoenosis. Consequently, a new ecological niche is shaped, with specific characteristics that may significantly influence all bioecological processes of the emerging ecosystem, as well as its stability and persistence. The new landscape that forms will reflect the interaction between the habitat and the new phytocoenosis (Fickert & Richter, 2025).

Stabilization represents the stage of consolidation of the new phytocoenosis. A dynamic equilibrium is established, characterized by consolidated ecosystem stability, also known as the climax stage. Reaching an advanced climax stage marks the completion of succession.

Regression represents the initial stage of degradation of the advanced climax state, resulting from reduced resistance of the phytocoenosis to competitive pressure from potential immigrant species, which may trigger a new succession (Florescu & Nicolescu, 1996).

In some situations, depending on vegetation conditions and land-use practices, certain stages of vegetation succession may be absent, with migration, competition, reaction, stabilization, and regression being the most commonly observed.

The rate at which successions occur may be rapid or slow. If species replacement occurs within a relatively short time-years or decades-the succession is considered rapid. When species replacement occurs over more than a century, the succession is considered slow and can be analyzed using the chronosequence method (Nasibullina et al., 2024) and pollen analyses (O'Connell & Wolters, 2025), based on the study and analysis of vegetation maps (Fickert & Richter, 2025) prepared over time for the respective region.

Improper exploitation and abandonment of agricultural lands in non-collectivized areas, gradually after 1989, in the medium and high hill regions of western Romania, created the premises for the initiation of vegetation succession processes. The abandonment of agricultural lands resulted directly from depopulation of these areas, lack of modern equipment, absence of adequate agricultural strategies and policies for local farmers, excessive land fragmentation in non-

collectivized areas, and the effects of climate change.

Considering the aspects presented, vegetation succession represents a fundamental concept of great importance for agro-forestry activities, as it indicates how species populations, communities, and ecosystems change over time in a new habitat or after a disturbance (Poorter et al., 2023) that affects their previous ecosystem stability.

The objectives of this study are to analyze the climatic conditions that favored and sustained the succession of arboreal and shrub vegetation, as well as the dynamics and particularities of this process, on a series of agricultural lands in a non-collectivized area that were abandoned or not exploited according to their land-use category.

## MATERIALS AND METHODS

The case study was conducted in the locality of Vârfurile, which is the seat of the Vârfurile commune in Arad county, which was a non-collectivized area. It is located in the east of Arad county, in the Hălmagiu Depression in the Apuseni Mountains. The depression is crossed by the Crișul Alb River and is located on its upper course. Vârfurile village is located in the northwest of the Hălmagiu Depression and is bordered by the Bihor Mountains to the northeast, the Codru-Moma Mountains to the northwest and the Zarandului Mountains to the south and southwest (by the Gorgana Massif, more precisely). Vârfurile Commune consists of 8 localities and has an average altitude of 231 m (Pop, 2005; https://primariavirfurile.ro/despre-noi/prezentare/).

Vârfurile Commune has a temperate-continental, moderate climate, with slight Mediterranean influences, the summers not being excessively warm, and the winters being generally mild. The depression area in which the locality is situated communicates to the west with the Zarandului Depression, which has a wide opening to the west, towards the Crișurilor Plain. That favors the easy penetration of western air masses (of Atlantic or Mediterranean origin), rich in moisture, which makes precipitation abundant. During certain periods of the year, hot and dry continental-tropical air masses from northern Africa can also penetrate, generating heatwaves and drought. The thermal inversions are frequent in the cold season, specific to the intermontane depression areas, generating dense fogs. The shelter provided by the surrounding mountains reduces wind speed and protects the village from strong winds. The moderate thermal climate with abundant rainfall makes the region well forested (Pop, 2005; https://primariahalmagiu.ro/download/urvqbaO3Rf0Eh7w9f690f8ugJ6lAzB8W4JBO4a7g.pdf).

The studies and research fall within the scope of doctoral studies regarding the category of agricultural land use in the mentioned location. To achieve the established objectives, appropriate bibliographic documentation was created (Duduman, 2023).

Data from the Gurahonț meteorological station were used for the climatic characterization of the studied area, being the closest to the Vârfurile locality. The station is located at an altitude of 177 m, has the code 15182 and the geographical coordinates 46°27' N latitude, 22°33' E longitude (www.meteomanz.com).

Meteorological data regarding the monthly and annual average air temperature and the monthly and annual precipitation amount were used in the paper. The analyzed period was 1990-2025 (36 years). The temporal variability, frequency and linear trend of the average annual values of temperature and precipitation, as well as the polynomial trend of annual precipitation amounts, were analyzed. The average annual values of air temperature and precipitation were compared with the multiannual average of the period 1966-2025 (60 years), to better highlight the climate trends of recent years. The variation during the year of the multiannual monthly average values of air temperature and precipitation (1990-2025) was also analyzed.

The meteorological data used in the paper came from the database of the National Meteorological Administration (N.M.A.) of Romania and from the Meteomanz.com (www.meteomanz.com) and rp5.ru (https://rp5.ru/) websites.

For the purpose of conducting the study and analyzing the dynamics and particularities of the vegetation succession process in the established location, route-based and stationary observations were carried out, along with inventories on experimental surfaces, simulations, comparisons, and analyses.

As a result, the study and analysis of the dynamics of the vegetation succession process were performed on 100 agricultural parcels that had been improperly exploited or abandoned.

The parcels were identified on the parcel plan corresponding to cadastral sector no. 15 (provided by OCPI Arad), which was superimposed on the orthophotomap using the mapSys 10.1 software. Also, the category and subcategory of use were identified from the agricultural register of the Vârfurile locality, with the agreement and collaboration of the owners.

Field identification of the studied parcels and delimitation of the areas where vegetation succession had been triggered and was ongoing were performed using GNSS technology, with TRIMBLE R10I receivers, through the real-time kinematic (RTK) method, using the permanent GNSS station Gurahonț, Arad County.

In this context, the parcels were physically surveyed, allowing direct observation of the stages of succession, identification of the arboreal and shrub species that had established, and the manner in which these areas were being exploited. The field data were recorded in tabular field sheets, prepared to streamline the data collection and processing procedure. These sheets included the following fields: Nrp - number of the analyzed parcel, Sp - surface area of the analyzed parcel, Sc - surface colonized by the identified species, Pc - percentage of colonization of the studied lands where vegetation succession is occurring, land-use category and subcategory, and installed arboreal and shrub species.

Additionally, for the study and analysis of the structural characteristics defining the arboreal and shrub vegetation that had established, inventories were carried out in five representative and relatively accessible parcels. On the surfaces where arboreal vegetation had established, complete inventories were performed, recording all individuals within the identified biogroups. A biogroup of trees represents a cluster of 7-10 trees, either of the same species or of different species, which mutually influence each other and exhibit evident intra- or interspecific competition, both underground and aboveground. These can occupy different areas, depending on a series of factors and vegetation conditions, and if the area occupied exceeds 0.5 hectares, the height of the component trees is greater than 5 m, and the consistency index k > 0.4, they can be considered as a forest (Law no. 331/2024).

Tree diameter was measured with a forest caliper at a height of 1.30 m above ground (diameter at breast height - d1.30), at 2 cm intervals, starting from a minimum diameter of 4 cm. Tree height up to 8.0 m was measured with a special rod graduated in millimeters, while heights above 8.0 m were determined using the VERTEX 5 device. On surfaces covered with shrubs, inventories were carried out on rectangular experimental plots, with areas ranging between 1 m² and 5 m², depending on their distribution and accessibility. Shrub diameter was measured with a caliper or measuring tape (with millimeter divisions), depending on accessibility and biogroup density. Their height was measured with a special rod graduated in millimeters.

For the analysis of the structural characteristics of the inventoried tree biogroups, a series of structural indices representative for forest stands were used by similarity. Consequently, the following were determined: the number of trees ($N_{exp}$), diameter at breast height (d1.30), cumulative basal area ($G_{exp}$), composition by number of trees and by basal area, the density index ($I_N$) and the density coefficient ($I_G$); the slenderness coefficient (Z%) and the Hart-Beking spacing factor in the square ($S_{4\%}$) and hexagonal ($S_{6\%}$) The indicators were calculated using the formulas established by Florescu & Nicolescu (1996) and Crainic et al. (2024). The values obtained are presented below:

$$I_N = \frac{N_{exp}}{N_{th}} \quad (1)$$

$$I_G = \frac{G_{exp}}{G_{th}} \quad (2)$$

$$Z_{(\%)} = \frac{h}{d} \quad (3)$$

$$S_{(\%)} = \frac{a}{h_{dom}} \times 100 \quad (4)$$

$$S_{4(\%)} = \frac{a_4}{h_{dom}} \times 100 \quad (5)$$

$$S_{6(\%)} = \frac{a_6}{h_{dom}} \times 100 \quad (6)$$

$$h_{dom} = h + 0.15\,h = 1.15\,h \quad (7)$$

$$a_4 = \sqrt{\frac{10000}{N}} \quad (8)$$

$$a_6 = \sqrt{\frac{10000}{N\sqrt{\frac{3}{2}}}} \quad (9)$$

The elements of formulas (1) - (8) have the following meaning:
**$I_N$** - density index determined according to the number of trees;
**$I_G$** - density index determined according to the cumulative basal area;
**$N_{exp}$** - number of trees per hectare, determined experimentally through inventories;
**$N_{th}$** - theoretical values of the number of trees from general yield tables, for the same species, yield class, and age;
**$G_{exp}$** - cumulative basal area per hectare, determined experimentally through inventories;
**$G_{th}$** - theoretical values of the cumulative basal area from general yield tables, for the same species, yield class, and age;
**$Z_{(\%)}$** - slenderness coefficient of the stand;
**h** - mean height of the stand;
**d** - mean diameter of the stand;
**$S_{(\%)}$** - Hart-Beking spacing index;
**$h_{dom}$** - dominant height of the stand;
**a** - theoretical spacing between trees
**$S_4$** - spacing index for the square arrangement;
**$a_4$** - theoretical spacing between trees in a square layout;
**$S_6$** - spacing index for the hexagonal arrangement;
**$a_6$** - theoretical spacing between trees in a hexagonal layout.

Additionally, for comparing the experimental values with the theoretical ones corresponding to forest arboreal vegetation, it was necessary to extrapolate the experimental values to one hectare. The theoretical values of the structural characteristics used were those provided by Biometrics of trees and stands in Romania (Giurgiu et al., 1972).

## RESULTS AND DISCUSSIONS

The multiannual average air temperature was 10.9°C for the period 1990-2025, at the Gurahonț meteorological station. It was 0.4°C higher than the multiannual average of the period 1966-2025 (10.5°C) and 1.0°C higher than that of the period 1966-1990 (9.9°C).
The average annual air temperature ranged between 9.5°C (in the years 1991 and 1997) and 12.8°C (in 2024), during the period 1990-2025 (Figure 1). The coldest years were 1991, 1997, 2005, 1996, 1993, 1998 and the warmest years were 2024, 2019, 2023, 2014, 2018, 2025. So, the coldest years were recorded at the beginning of the analyzed period, and the warmest towards its end. Five years had an annual average value above 9°C, 11 years above 10°C, 16 years above 11°C, and 4 years above 12°C, during the analyzed period. 24 years out of the 36 analyzed (2/3 of the years) had an annual average value above the multiannual average of the period 1966-2025 (of 10.5°C).
Since 1994, an increase in air temperature has been observed in Gurahonț. Moreover, the linear trend of the average annual values of air temperature is strongly upward. It is due to the very high values of recent years, which have been exceptionally warm. The 2007-2025 interval was the warmest, being characterized by annual average values above the multiannual average of the 1966-2025 period (Figure 1).

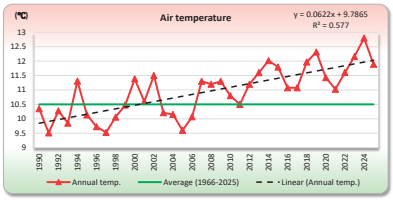



Figure 1. Average annual air temperature, its linear trend (1990-2025) and multiannual average (1966-2025), at the Gurahonț meteorological station

The multiannual average amount of precipitation was 747.5 mm for the period 1990-2025, at the Gurahonț weather station. It was only 4.5 mm lower than the multiannual average of the period 1966-2025 (752.0 mm) and only 3.2 mm lower than that of the period 1966-1990 (750.7 mm).
The annual amount of precipitation varied between 438.4 mm (in 2025) and 996.2 mm (in 2005), during the period 1990-2025 (Figure 2). The rainiest years were 2005, 2001, 2004, 2016, 1999, 2023 (with a rainfall surplus between 125 and 245 mm), and the driest were 2025, 2024, 2000, 2011, 1990, 1992, 1993 (with a rainfall deficit between 130 and 314 mm). There were 15 years with over 800 mm of precipitation and 14 years with under 700 mm of precipitation, during the mentioned period.

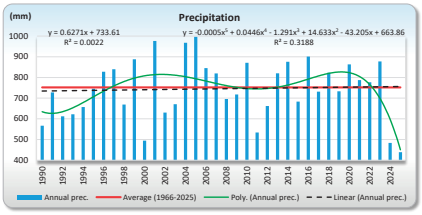



Figure 2. Annual precipitation amounts and their linear and polynomial trend, at the Gurahonț meteorological station (1990-2025)

The linear trend of the annual precipitation amounts is slightly upward.
The polynomial trend, rendered based on the 5th order polynomial, shows that after the dry period 1990-1994, there is a rainy period 1995-2007 (of 13 years), followed by a short dry period 2008-2012, then by a rainy one 2013-2023 (of 11 years) and two extremely dry years 2024-2025. It is noted that the drought of 2024-2025 exceeded the great drought of 2000. Also, these years followed the very rainy year 2023 and a longer period of precipitation excess.
During the year, the air temperature increases from January (the multiannual monthly average: 0.0°C) to July (21.3°C), when it reaches a maximum, after which it decreases until December (1.4°C) (Figure 3).

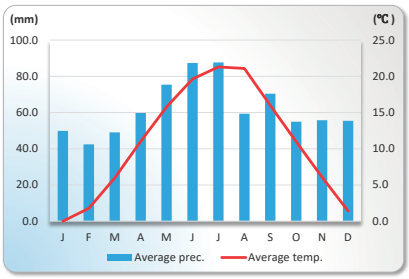



Figure 3. Multiannual monthly average values of air temperature and atmospheric precipitation, at the Gurahonț meteorological station (1990-2025)

Precipitation follows a somewhat similar pattern, being higher in summer (except August) and lower in winter and early spring. The most rain falls between May and July (75.4-87.7 mm), and the least between January and March (42.4-49.9 mm). It is noted that the rainfall maximum was not recorded in June (87.3 mm), but in July (87.7 mm), in the period 1990-2025. This is due to the large amounts of precipitation that fell in July, amid the severe heatwaves of recent years, in this month, when the land surface strongly heats up and generates intense thermal convection. August is a very hot and dry month, because the anticyclonic baric formations prevail, which generate clear and warm, even scorching weather.
Comparing the multiannual monthly average of the months of the period 1990-2025 with the multiannual average of the period 1966-2025, it can be said that the months of June, August, May and January recorded lower amounts of precipitation during the period 1990-2025, compared to the period 1966-2025. So, they were drier. All months of the year were warmer during the period 1990-2025 than during the period 1966-2025. The warmest months were August, June, July, January and November.
From the analysis of the results obtained after processing the data recorded during the study of the particularities of the vegetation succession process on the 100 parcels, presented in Table 1, it is observed that the process of colonization and establishment of arboreal and shrub vegetation on a series of agricultural lands occurred with differentiated dynamics, depending on the land-use categories and subcategories, as well as on the manner in which these lands had been exploited.
Consequently, the land-use subcategory most affected by the succession process was wooded pasture, with 76% of its analyzed surface undergoing succession, followed by wooded hayfield with 53%, hayfield with trees with 46%, arable land with shrubs and isolated trees with 38%, traditional orchard with 27%, pasture with trees with 25%, and finally clean hayfield and hayfield with shrub patches, each with 19%.
Overall, it is found that 55% of the total surface of the 100 analyzed parcels was colonized by arboreal and shrub vegetation (Table 1), as a result of the vegetation succession process, which occurred due to improper exploitation and the abandonment of agricultural land.
The initiation and development of the vegetation succession process on the 100 studied parcels took place without a specific denudation stage of the habitat, the premises for triggering this process being represented by improper land use and the abandonment of considerable areas of agricultural land.
The arboreal species that have established in the studied location are represented by forest species that form the fundamental natural forest types of the surrounding areas, in relatively high proportions - *Quercus cerris*, *Quercus robur*, *Fagus sylvatica*, *Carpinus betulus*, *Prunus avium*, *Tilia tomentosa* - followed by pioneer species such as *Betula pendula*, *Populus tremula*, *Salix caprea*, *Salix alba*, and a single invasive species, *Robinia pseudacacia*.

Table 1. Synthetic record of the surface areas of agricultural land-use categories and subcategories on which arboreal and shrub vegetation has established, following the onset of the vegetation succession process

| Nr. crt. | Nrp | Sp (ha) | Land use Category | Land use Subcategory | Sc (ha) | Pc (%) | Inatalled species Forest trees | Inatalled species Shrubs |
|---|---|---|---|---|---|---|---|---|
| 1 | 11 | 4.58 | Arable | Arable land with shrubs and isolated trees | 1.73 | 38 | *Qr, Qc, Cb, Bp, Tt, Pt, Rp* | *Ps, Cm, Rc, Rh,* |
| 2 | 2 | 1.50 | Orchard | Traditional orchard | 0.40 | 27 | *Qr, Qc, Cb, Pt, Sc, Ms, Pp* | *Ps, Ca, Cm, Rc, Rh,* |
| 3 | 45 | 27.36 | Pasture | Wooded pasture | 20.74 | 76 | *Qr, Qc, Fs, Cb, Bp, Tt, Pt, Sc, Ms, Pp* | *Ps, Jc, Ca, Cm, Rc, Rh,* |
| 4 | 4 | 3.76 | Pasture | Pasture with trees | 0.93 | 25 | *Qr, Qc, Cb, Pt, Sc, Ms, Pp* | *Ps, Ca, Cm, Rc, Rh,* |
| 5 | 2 | 0.79 | Hayfield | Hayfield with shrub patches | 0.15 | 19 | *Qr, Qc, Cb, Bp, Pt, Sc, Ms, Pp* | *Ps, Cm, Rc, Rh,* |
| 6 | 12 | 6.06 | Hayfield | Wooded hayfield | 3.21 | 53 | *Qr, Qc, Fs, Cb, Bp, Tt, Pt, Sc, Sa, Ms, Pp* | *Ps, Cm, Rc, Rh,* |
| 7 | 13 | 7.08 | Hayfield | Clean hayfield | 1.34 | 19 | *Qr, Qc, Cb, Pt, Sc, Sa, Ms, Pp* | *Ps, Rc, Rh,* |
| 8 | 11 | 4.82 | Hayfield | Hayfield with trees | 2.23 | 46 | *Qr, Qc, Cb, Bp, Tt, Pt, Sc, Ms, Pp* | *Ps, Ca, Cm, Rc, Rh* |
| Total | 100 | 55.94 | / | / | 30.74 | 55 | / | / |

Nrp - number of analyzed parcels, Sp - surface area of the analyzed parcels, Sc - surface area colonized by the identified species, Pc - percentage of colonization of the studied lands on which vegetation succession occurred, *Qr-Quercus robur* L., *Qc-Quercus cerris* L., *Pt-Populus tremula* L., *Rp-Robinia pseudacaccia* L., *Bp-Betula pendula* Roth, *Tt-Tilia tomentosa* Monech., *Sc-Salix caprea* L., *Sa-Salix alba* L., *Fs-Fagus sylvatica* L., *Cb-Carpinus betulus* L., *Ms-Malus sylvestris* (L.) Mill., *Pp-Pyrus pyraster* (L.) Burgsd., *Ps-Prunus spinosa* L., *Jc-Juniperus communis* L., *Rh-Rubus hirtus* W. et. K., *Ca-Corylus avellana* L., *Crataegus momogyna* Jacq., *Rosa canina* L. (Stănescu, et al., 1997).

Consequently, the migration of oak species, which have relatively large seeds, occurred exclusively through zoochorous dispersal, with vector agents represented by birds and certain rodents (Yang & Yi, 2022). Moreover, the zoochorous dispersal of acorns immediately after abundant fructification events led to their germination under optimal conditions, a phenomenon identified especially in several traditional orchards and agro-silvopastoral systems (Crainic et al., 2023a), located at distances of over 1500-2000 m from mature oak trees.

These processes result from the dispersal of acorns, which do not enter dormancy, thus ensuring a high efficiency of germination and seedling emergence (Yang & Yi, 2022). Fruit trees and certain shrub biogroups or pioneer species also play an important role in supporting and enhancing these bioecological processes, as they partially fulfill the role of nurse species (Fodor et al., 2018), by providing protection for young oak individuals.

Recent studies have highlighted a clear trend of expansion of some native oak species in western Romania, as a result of abundant fruiting (Crainic et al., 2023b), on a series of lands with forestry and agricultural use, as a direct consequence of climate change and easy vegetation conditions.

A similar pattern is characteristic of the establishment of *Fagus sylvatica*, but only on small areas and at shorter distances from an existing forest (a stand) or from larger biogroups of trees. This is due to the species' shade-tolerant temperament and its difficulty in regenerating in open terrain without protection.

Mixed species and pioneer species establish relatively more easily due to their more efficient dispersal mechanisms, determined by seed size and the greater diversity of vector agents. Their germination characteristics also positively influence their ability to germinate and emerge under favorable conditions.

The *Robinia pseudacaia* species, which is considered invasive, was identified in a location bordering an area from which nine years ago all the biogroups formed by mature trees of this species were extracted and exploited. These trees had produced abundant seed crops in the year prior to harvesting, and the seeds were easily dispersed onto the neighbouring land (which had not been exploited during that period), where they germinated and emerged under optimal conditions. They now show a tendency to form a closed forest stand within 9-10 years, without any anthropogenic intervention.

Recent research has highlighted that excessive fragmentation of agricultural landscapes causes changes in the composition of plant associations and implicitly reduces the size of plant populations and genetic diversity, with direct implications for biodiversity (Hurajová et al., 2024).

Consequently, conservation and restoration efforts for grasslands, pastures, and other agricultural lands must take into account the information provided by fine-scale monitoring of vegetation matrix organization (Bartha et al., 2025), as part of the sustainable use of plant resources, considering the trend of climate change and society's need for high-quality agricultural products and integrated ecosystem services.

The values of the structural characteristics of the arboreal and shrub forest biogroups, determined after processing the field data, are presented synthetically in Table 2 for each parcela.

Table 2. Synthetic values of structural indices related to biogroups of inventoried trees from the studied plots

| Parcela | Cps($N_{exp}$) Cps($G_{exp}$) | $dg_M$ (cm) | $H_{dgM}$ (m) | T (ani) | CLP | $N_{exp}$ (buc./ha) | $N_{th}$ (buc./ha) | $G_{exp}$ ($m^2$/ha) | $G_{th}$ ($m^2$/ha) | $I_N$, $I_G$ | Z (%) | $S_{4\%}$(%), $S_{6\%}$(%) |
|---|---|---|---|---|---|---|---|---|---|---|---|---|
| 1771 | 2Qc2Ms1Qr1Pt1B p1Sc1Sa1Pp / 2Qc2Qr2Pt1Bp1Sc 1Sa1Ms dis.Pp | Qc = 18 | 17.2 | 40 | III | 242 | 1099 | 3.918 | 21.500 | 0.7 0.9 | 93 | 16 17 |
| | | Qr = 18 | 18.4 | 40 | III | 169 | 1305 | 2.785 | 21.800 | | | |
| | | Pt = 19 | 19.6 | 30 | III | 177 | 614 | 2.855 | 28.900 | | | |
| | | Bp = 17 | 18.3 | 40 | II | 103 | 1210 | 2.161 | 22.500 | | | |
| | | Sc = 15 | 17.8 | 30 | IV | 110 | 594 | 1.387 | 30.600 | | | |
| | | Sa = 19 | 17.7 | 30 | IV | 95 | 594 | 1.941 | 30.600 | | | |
| | | Ms = 11 | 7.5 | 15 | III | 317 | 3929 | 2.401 | 11.000 | | | |
| | | Pp = 12 | 6.8 | 15 | III | 155 | 3929 | 1.188 | 11.000 | | | |
| | Total values | / | / | / | / | 1368 | / | 18.636 | / | | | |
| | Wav | 16 | 14.80 | 30 | III | / | 1830 | / | 21.040 | | | |
| 1774 | *5Qr 5Qc* | Qc = 29 | 21.5 | 60 | III | 290 | 765 | 13.008 | 27.000 | 0.8 0.9 | 74 | 17 18 |
| | *5Qr 5Qc* | Qr = 29 | 21.3 | 60 | III | 303 | 657 | 13.686 | 29.700 | | | |
| | Total values | / | / | / | / | 593 | / | 26.694 | / | | | |
| | Wav | 29 | 21.4 | 60 | III | / | 711 | / | 28.350 | | | |
| 1776 | *4Qr3Qc3Cb* | Qr = 39 | 22.6 | 60 | III | 268 | 657 | 8.974 | 29.700 | 0.5 0.7 | 70 | 18 19 |
| | *5Qr3Qc2Cb* | Qc = 22 | 21.4 | 60 | III | 240 | 765 | 5.479 | 27.000 | | | |
| | | Cb = 16 | 10.3 | 20 | III | 188 | 3087 | 2.837 | 14.200 | | | |
| | Total values | / | / | / | / | 696 | / | 17.290 | / | | | |
| | Wav | 27 | 18.55 | 48 | III | / | 1418 | / | 24.240 | | | |
| 1835 | *8Tt1Qr1Pa* | Tt =16 | 14.9 | 40 | III | 994 | 1290 | 16.657 | 26.600 | 0.9 0.9 | 89 | 17 18 |
| | *7Tt3Qr disPa* | Qr =30 | 21.8 | 55 | III | 114 | 729 | 6.527 | 28.200 | | | |
| | | Pa =17 | 14.2 | 35 | III | 83 | 1818 | 1.791 | 23.400 | | | |
| | Total values | / | / | / | / | 1191 | / | 24.976 | / | | | |
| | Wav | 17 | 15.21 | 41 | III | / | 1288 | / | 26.520 | | | |
| 1930 | *9Rp1Pa* | Rp = 10 | 8.64 | 10 | III | 1831 | 2200 | 9.189 | 11.000 | 0.8 0.9 | 86 | 23 25 |
| | *9Rp1Pa* | Pa = 11 | 8.52 | 10 | III | 114 | 3890 | 1.091 | 15.400 | | | |
| | Total values | / | / | / | / | 1945 | / | 10.280 | / | | | |
| | Wav | 10 | 8.63 | 10 | III | / | 2369 | / | 11.440 | | | |

Wav-Weighted average value, Cps ($N_{exp}$)-composition according to the number of trees determined experimentally, Cps ($G_{exp}$)-composition based on experimentally determined base area, $dg_M$-median diameter of the base surface determined experimentally, $H_{dgM}$-the corresponding height $dg_M$, T-average age, CLP-production class

In parcel 1771, over an area of 1350 m², a total of 185 trees were inventoried, belonging to seven species: 33 trees of *Quercus cerris*, 23 trees of *Quercus robur*, 24 trees of *Populus tremula*, 14 trees of *Betula pendula*, 15 trees of *Salix caprea*, 13 trees of *Salix alba*, 43 trees of *Malus sylvestris*, and 21 trees of *Pyrus pyraster* (Figure 4).



Figure 4. Biogroups with trees from plot 1771, Cadastral Sector 15, Vârfurile ATU, Arad County

Additionally, 8 specimens of *Corylus avellana* were identified, along with a cumulative area of 200 m² occupied by shrub biogroups of *Prunus spinosa* L., which exhibit an average density of 12 individuals/m² and an average height of 2.25 m (Figure 5).



Figure 5. Biogroups with shrubs of the *Prunus spinosa* species in plot 1771, Cadastral Sector 15, Vârfurile ATU, Arad County

The total number of inventoried trees extrapolated per hectare is $N_{exp}$ = 1368 trees/ha, with a mean diameter $dg_M$ = 16 cm, a total basal area $G_{exp}$ = 18.636 m²/ha, a mean height $H_{dgM}$ = 14.800 m, a mean age T = 30 years, and a relative yield class of III.
The composition of the inventoried forest vegetation is:
Cps($N_{exp}$):2Qc2Ms1Qr1Pt1Bp1Sc1Sa1Pp, and
Cps($G_{exp}$):2Qc2Qr2Pt1Bp1Sc1Sa1Ms dis.Pp.
From the analysis of the diagrams presented in Figure 6, it is observed that the distribution of the number of trees by diameter classes is plurimodal, due to the particularities of establishment, growth, and development of the species that have colonized this location, as well as the manner in which the land has been exploited.

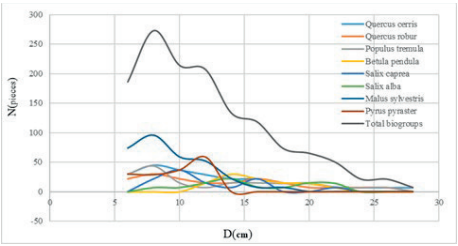



Figure 6. Distribution of the number of trees by diameter classes, extrapolated per hectare, in the fully inventoried biogroup from parcel 1771

The theoretical values for the weighted number of trees are $N_{th}$ = 1830, and the weighted total basal area is $G_{th}$ = 21.040 m²/ha. Consequently, the density index is $I_N$ = 0.7, the density coefficient $I_G$ = 0.9, the slenderness coefficient Z = 93%, and the spacing indices are $s_{4\%}$ = 16% and $s_{6\%}$ = 17% (Table 2).
The biogroups of installed trees present a varied composition, bringing together seven tree species with different ecological behavior, their density is moderate to normal, satisfactory stability to the action of the dominant wind, and they are also moderately spaced. Consequently, a state outlined by climax is highlighted.
In parcel 1774, the inventory of tree biogroups was carried out over an area of 1214 m². As a result, a total of 72 trees were inventoried, of which 37 belonged to *Quercus cerris* and 35 to *Quercus robur* - Figure 7. The total number of inventoried trees extrapolated per hectare is $N_{exp}$ = 593 trees/ha, with a mean diameter $dg_M$ = 29 cm, a total basal area $G_{exp}$ = 26.694 m²/ha, a mean height $H_{dgM}$ = 21.40 m, a mean age T = 60 years, and a relative yield class of III.
The composition of the inventoried forest vegetation, based on both characteristics, is: 5Qr5Qc.
From the analysis of the diagrams presented in Figure 8, it is observed that the distribution of the number of trees by diameter classes is plurimodal, due to the particularities of establishment, growth, and development of the species that have colonized this location.



Figure 7. Biogroups with trees from plot 1774, Cadastral Sector 15, Vârfurile ATU, Arad County

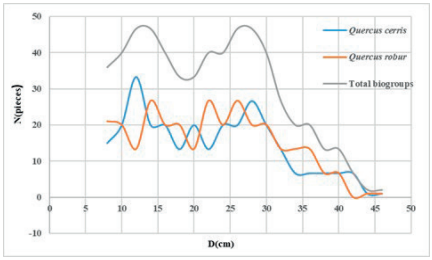



Figure 8. Distribution of the number of trees by diameter classes, extrapolated per hectare, in the fully inventoried biogroup from parcel 1774

The theoretical values for the weighted number of trees are $N_{th}$ = 711 trees/ha, and the weighted total basal area is $G_{th}$ = 26.250 m²/ha. Consequently, the density index is $I_N$ = 0.8, the density coefficient $I_G$ = 0.9, the slenderness coefficient Z = 74%, and the spacing indices are $s_{4\%}$ = 17% and $s_{6\%}$ = 18% (Table 2).
The tree biogroups are characterized by a moderate to normal density and thickness, a high stability to the dominant wind action and a moderate spacing, respectively. These aspects thus confirm a stable climax state, the succession process being completed on the analyzed surface.

In parcel 1776, over an area of 2529 m², a total of 176 trees were inventoried. The arboreal species recorded include *Carpinus betulus* with 48 individuals, *Quercus cerris* with 61 individuals, and *Quercus robur* with 68 individuals, totaling 176 individuals (Figure 9).



Figure 9. Biogroups with trees from plot 1776, Cadastral Sector 15, Vârfurile ATU, Arad County

Additionally, 6 *Quercus robur* trees with diameters between 52-68 cm were affected by extreme meteorological events on 17 September 2017 (Sicoe et al., 2023), and were subsequently removed and utilized by the landowners. The total number of inventoried trees extrapolated per hectare is $N_{exp}$ = 696 trees/ha, with a mean diameter $d_{gM}$ = 27 cm, a total basal area $G_{exp}$ = 17.290 m²/ha, a mean height $H_{dgM}$ = 18.55 m, a mean age T = 60 years, and a relative yield class of III.

The composition of the inventoried forest vegetation is: Cps($N_{exp}$): 4Qr3Qc3Cb, and respectively Cps($G_{exp}$): 5Qr3Qc2Cb.

From the analysis of the distribution of the number of trees extrapolated per hectare, by diameter classes and species, in the inventoried biogroups from parcel 1776, presented in Figure 10, it is observed that the distribution has a plurimodal pattern.

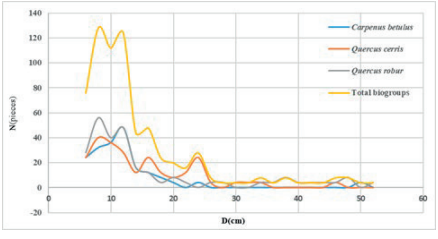



Figure 10. Distribution of the number of trees extrapolated per hectare, by diameter classes and species, in the inventoried biogroups from parcel 1776

This pattern is the consequence of the differentiated ages of the trees, the number of trees within each diameter class, the particularities of the natural regeneration process, and the manner in which the land has been exploited.

The theoretical values for the number of trees are $N_{th}$ = 1418 trees/ha, and the total basal area is $G_{th}$ = 24.240 m²/ha. Consequently, the density index is IN = 0.5, the density coefficient IG = 0.7, the slenderness coefficient Z = 70%, and the spacing indices are $s_{4\%}$ = 18% and $s_{6\%}$ = 19% (Table 2).

As a result, the tree biogroups present a low to moderate density, a high stability to the dominant wind action and a moderate spacing respectively. In this context, a stable climax state is reached, and the process of forest vegetation succession on the studied area can be considered completed.

In parcel 1853, over an area of 600 m², the inventoried arboreal species are represented by *Quercus robur* with 7 individuals, *Tilia tomentosa* with 58 individuals, and *Prunus avium* with 5 individuals, totaling 70 individuals. Also, a number of 5 specimens of pedunculated oak were identified, which were felled by the storm of 17 September 2017 (Figure 11).

The total number of inventoried trees extrapolated per hectare is $N_{exp}$ = 1191 trees/ha, with a mean diameter $d_{gM}$ = 17 cm, a total basal area $G_{exp}$ = 24.976 m²/ha, a mean height $H_{dgM}$ = 15.21 m, a mean age T = 41 years, and a relative yield class of III.

The composition of the inventoried forest vegetation is: Cps($N_{exp}$): 8Tt1Qr1Pa, and respectively Cps($G_{exp}$): 7Tt3Qr dis.Pa.



Figure 11. Biogroups with trees from plot 1853, Cadastral Sector 15, Vârfurile ATU, Arad County

From the analysis of the diagrams in Figure 12, it can be seen that the distribution of the number of trees by diameter categories is multimodal, due to the particularities of vegetation conditions, the ecological demands of the installed woody species and extreme weather phenomena (Sicoe et al., 2023).

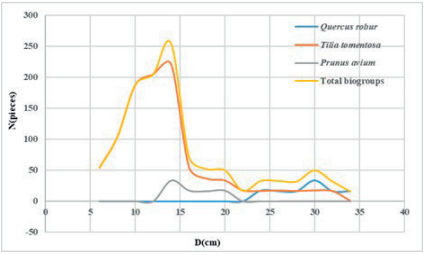



Figure 12. Distribution of the number of trees by diameter classes and species, extrapolated per hectare, for the tree biogroups in parcel 1853

The theoretical values for the number of trees are $N_{th}$ = 1288 trees/ha, and the total basal area is $G_{th}$ = 26.250 m²/ha. Consequently, the density index is IN = 0.9, the density coefficient IG = 0.9, the slenderness coefficient Z = 90%, and the spacing indices are $s_{4\%}$ = 17% and $s_{6\%}$ = 18% (Table 2).

In this case, the analyzed biogroups are characterized by a relatively normal density and thickness, a satisfactory stability to the action of the dominant wind and a moderate spacing. Although the process of succession of forest vegetation on the studied surface was affected by extreme weather phenomena (Sicoe et al., 2023), the tree biogroups are in a relative state of equilibrium, and on the surfaces where the trees were affected, the process of natural regeneration from seed, is carried out with a relatively active dynamic. As a result, the climax state can be identified for this location as well.

In parcel 1930, over an area of 437 m², a total of 80 individuals of *Robinia pseudacacia* and 10 individuals of *Prunus avium* were identified and inventoried (Figure 13). The total number of inventoried trees extrapolated per hectare is $N_{exp}$ = 1945 trees/ha, with a mean diameter d1.30 = 10 cm, a total basal area $G_{exp}$ = 10.280 m²/ha, a mean height H = 8.63 m, a mean age T = 10 years, and a relative yield class of III. The composition of the inventoried biogroups, based on both structural characteristics, is 9Rp + 1Pa.



Figure 13. Biogroups with trees from plot 1930, Cadastral Sector 15, Vârfurile ATU, Arad County

The distribution of the number of trees by diameter classes for the biogroups of *Robinia pseudacacia* and *Prunus avium* appears as a normal distribution with a slight right-side asymmetry (Figure 14), because vegetation establishment on the analyzed surface occurred over a relatively short period of time, without disturbances. The successional process unfolded with active dynamics and high efficiency.

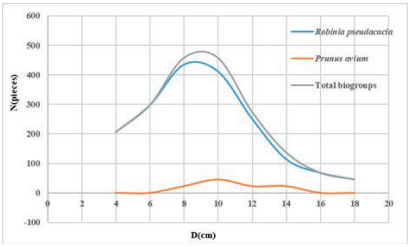



Figure 14. Distribution of the number of trees by diameter classes in the tree biogroups from parcel 1930

The theoretical value for the weighted number of trees is $N_{th}$ = 2369 trees/ha, and the weighted total basal area is $G_{th}$ =11.440 m²/ha. Consequently, the density index is $I_N$ = 0.8, the density coefficient $I_G$ = 0.9, the slenderness coefficient Z = 86%, and the spacing indices are $s_{4\%}$ = 23% and $s_{6\%}$ = 25% (Table 2).

The biogroups of trees installed in a proportion of 90% belong to the species Robinia pseudacacia, which is an allochthonous species, and is considered invasive, successfully colonizing agricultural lands that are improperly exploited or abandoned. They are characterized by a moderate to normal density and thickness, presenting a satisfactory stability to the action of the dominant wind and a very good spacing. Consequently, the biogroups in this plot are in an obvious state of climax.

Although the development of successional processes on various agricultural lands results in excessive fragmentation of the agricultural landscape, with a series of negative effects, the abundance of certain species can be increased and consequently the resistance of the phytocenosis to the effects of climate change can be optimized (Hurajová et al., 2024).

The climatological analysis carried out in the paper shows that the period 1990-2025 was very warm, the linear trend of the average annual values of air temperature being strongly upward. Annual rainy periods were longer than dry periods between 1990 and 2025, but the rainfall extremes were very clearly highlighted. There have been very rainy years, with large amounts of precipitation falling in a short time, interspersed with exceptionally dry years, in which droughts were long and intense. The recent years have been exceptionally hot and dry. The rainfall extremes facilitated the establishment of shrub and arboreal vegetation, both successively and in parallel. As a result, we showed that the climatic conditions favoured and supported the succession of arboreal and shrub vegetation, the first objective of the study being achieved.

The improper exploitation or abandonment of some agricultural use land in non-collectivized areas created the premises for the initiation and development of some succession processes between the grass species afferent to them and the shrub and arboreal species, native and exotic, in the areas bordering the case study location. As a result, the analyzed successions present an active dynamic and a series of specific particularities, due to the categories and subcategories of land use, the vegetation conditions and the size and excessive division of the plots, respectively. Also, anthropogenic impact conditions and influences the dynamics, specificity and particularities of these processes in the studied and analyzed plots.

From the analysis of the obtained results related to the structural particularities of the biogroups with arboreal vegetation, which were inventoried, it is highlighted that the areas on which they were installed meet the conditions to be introduced into the forest fund, according to the forestry code. As a result, the use category can be modified, these areas being considered as forestry use, at the proposal and with the agreement of the owners, obviously. Consequently, the second objective of the study was also achieved.

The results obtained in our study contributed to the advancement of scientific knowledge in the addressed field, by particularizing the succession process of the arboreal and shrub vegetation on agricultural use lands, highlighting the fact that successions of pioneer species and respectively successions between the pioneer species and fundamental ones related to the forest fundamental natural type, in the neighbouring areas, were simultaneously identified in the same plots, under similar climatic and pedo-stationary conditions.

The emergence of some successions between the shrub species and some oak species (*Quercus ceris* and *Quercus robur*) was also highlighted, that being a particularly important aspect for the development of some seed regeneration technologies, under shelter, of some oak species, in the context of climate change and the effect of extreme weather phenomena.

The extension of research to all agricultural use land that have been abandoned or improperly managed, in non-collectivized areas, is limited due to the fact that the exploitation of some areas was carried out with some intermittency (periodicity), an aspect that prevents a coherent analysis of successional aspects. Also, the access to some information from the agricultural register related to the lands that could be the subject of the study could be limited, due to the refusal or lack of a response from the owners.

Studies could be expanded in the future to plots in the mentioned location that are available or in locations with similar conditions, in the Vârfurile commune and/or in neighbouring communes that were not collectivized prior to 1989.

The continuation and expansion of this study in the future, in the presented location, can be achieved in two scenarios: a) if the improper exploitation of agricultural lands will continue or they will be abandoned; b) if the use category will be modified by assigning some lands to forestry use, where the conditions are met, in accordance with the Forestry Code (Low no. 331/2024).

Consequently, if the lands from the present case study will be exploited in the future in accordance with the current use categories and

subcategories, then further studies and research will be irrelevant.

## CONCLUSIONS

The period 1990-2025 was relatively rich in precipitation, with many rainy years, even very rainy, interspersed with exceptionally dry years. Thus, the rainfall extremes in the studied area were highlighted. The period was also very warm. Of course, the amounts of precipitation were not distributed uniformly throughout the year, with frequent cases of very large amounts falling in a short time, but also very long droughts.

Consequently, the extremes of rainfall have favoured the establishment in optimal conditions of arboreal vegetation from the species of the fundamental natural type of forest bordering the study location, respectively of pioneer, invasive and shrub species in dry years.

The process of succession of arboreal and shrub vegetation on agricultural lands in non-collectivized areas presents a series of particularities, and has a specific dynamic, depending on the way these lands are exploited.

Consequently, the denudation stage of the habitat is practically substituted by their abandonment or improper exploitation.

The native oak species, represented by *Quercus cerris* and *Quercus robur*, present a high colonization rate of agricultural lands, which are abandoned, due to the vegetation conditions and respectively their ecological demands, the dissemination of seeds being carried out exclusively zoochorically, by birds and rodent mammals.

The pioneer species that settled in simultaneously colonized the same habitats with the other arboreal species, thus indicating a simultaneous succession of them.

The invasive species *Robinia pseudacaia* colonized 90% of the new habitat, thus forming practically pure biogroups.

The shrub species that colonized some areas, forming compact biogroups with variable extents, facilitate their installation and colonization by the native oak species.

The results obtained confirm that on agricultural areas that were improperly exploited or abandoned, the succession process of arboreal and shrub vegetation took place with a differentiated dynamic, with a series of biogroups identified with the climax stage achieved.

## ACKNOWLEDGEMENTS

We would like to express our gratitude for their collaboration to the representatives of the management of the Arad Office of Cadastre and Real Estate Publicity, the Local Council of the Vârfurile Municipality, Arad County, as well as to the landowners from the location where the studies and research were carried out.

## REFERENCES

Bartha, S., Házi, J., Purger, D., Zimmermann, Z., Szabó, G., Guller, Z. E., Csathó, A. I. & Csete, S. (2025). Fine-Scale Organization and Dynamics of Matrix-Forming Species in Primary and Secondary Grasslands. *Land*, *14*(9), 1736. https://doi.org/10.3390/land14091736.

Cioflan, F.M. (2025). Assessment of land use changes in non-collectivized areas using geomatic applications: a case study in Vîrfurile, Romania. *Scientific Papers. Series E. Land Reclamation, Earth Observation & Surveying, Environmental Engineering.* Vol. XIV, 2025 Print ISSN 2285-6064, CD-ROM ISSN 2285-6072, Online ISSN 2393-5138, ISSN-L 2285-6064. chromextension://efaidnbmnnnibpcajpcglclefindmkaj/https://landreclamationjournal.usamv.ro/pdf/2025/vol2025.pdf.

Crainic, G. C., Curilă, M., Curilă S., Oneţ C., Supuran, A., Bica, A. M., Şerban E., Cioflan, F. M., & Irimie, F. (2024). Establishing the intensity of interventions in young beech (*Fagus sylvatica* L.) stands based on a spline regression mathematical model. *Not Bot Horti Agrobo*, 52(4):14021. DOI: 10.15835/nbha/52414021.

Crainic G. C., Covaci F, Sabău N. C., Sicoe S. I., Irimie (Cioflan) F., Bodog M. F., & Iovan C. I. (2023a). Works specific to the introduction of silvopastoral systems in the forest fund. *Scientific Papers. Series E. Land Reclamation, Earth Observation & Surveying, Environmental Engineering*. Vol. XII, 2023 Print ISSN 2285-6064, CD-ROM ISSN 2285-6072, Online ISSN 2393-5138, ISSN-L 2285-6064. https://landreclamationjournal.usamv.ro/pdf/2023/Art10.pdf;

Crainic, G. C., Sicoe, S. I., Irimie, F., Irimie (Cioflan), Flavia., Iovan, C. I. & Bodog, M. F. (2023b). The particularities of the ecological rehabilitation works of the sessile oak stands (*Quercus petraea* (Matt.) Liebl), from the seed reserve. *Scientific Papers. Series E. Land Reclamation, Earth Observation & Surveying, Environmental Engineering*. Vol. XII, 2023 Print ISSN 2285-6064, CD-ROM ISSN 2285-6072, Online ISSN 2393-5138, ISSN-L 2285-6064. https://landreclamationjournal.usamv.ro/pdf/2023/Art29.pdf

De Giuli, M., Winkler, M., Deola, T., Henschel, J., Sass, O., Wolff, P. & Jentsch, A. 2024. Arrested Succession on Fire-Affected Slopes in the Krummholz Zone and Subalpine Forest of the Northern Limestone Alps. *Diversity*, *16*(7), 366. https://doi.org/10.3390/d16070366

Draft Decision No. 4548/20.09.2022 on updating the Risk Analysis and Coverage Plan (PAAR) in Hălmagiu Commune for 2022, Chapter II - Climatic characteristics. https://primariahalmagiu.ro/download/urvqbaO3Rf0Eh7w9f690f8ugJ6lAzB8W4JBO4a7g.pdf

Duduman, M. L. (2023). *Methodology of scientific research in forestry.* Vol. 1. Stefan cel Mare University Publishing House, Suceava, Romania.

Fickert, T., & Richter, M. (2025). Vegetation Changes in Space and Time - A Special Issue on Plant Succession and Vegetation Dynamics, *Diversity*, *17*(7), 482. https://doi.org/10.3390/d17070482.

Florescu, I.I., & Nicolescu, N.V. (1996). *Silviculture* [Silvicultura], Vol. I, Forest Study, Lux-Librix Publishing House, Braşov.

Fodor, E., Hâruța, O., & Dorog, S. (2018). Nurse plants and the regeneration niche of tree seedlings in wood-pastures from Western and North-Western Romania. *Reforesta* 6: 41- 59. https://dx.doi.org/10.21750/refor.6.04.57

Garate-Quispe, J., Herrera-Machaca, M., Pareja Auquipata, V., Alarcón Aguirre, G., Baez Quispe S., & Carpio-Vargas, E. E. (2024). Resilience of Aboveground Biomass of Secondary Forests Following the Abandonment of Gold Mining Activity in the Southeastern Peruvian Amazon. *Diversity, 16*(4), 233. https://doi.org/10.3390/d16040233.

Garate-Quispe, J., Ramírez, M. V., Becerra-Lira, E., Baez-Quispe, S., Abril-Surichaqui, M., Rodriguez-Achata, L., Muñoz-Ushñahua, A., Nascimento Herbay, P., Fernandez-Mamani, Y., Alarcon-Aguirre, G., Herrera-Machaca, M., Vargas, L. H., Gomringer, R. C., & Torres, D. C. (2023). Influence of Distance from Forest Edges on Spontaneous Vegetation Succession Following Small-Scale Gold Mining in the Southeast Peruvian Amazon. *Diversity*, *15*(6), 793. https://doi.org/10.3390/d15060793

Giurgiu V., Decei I., & Armăşescu S., 1972, *Biometrics of trees and stands in Romania*, Ceres Publishing House, Bucharest;

Hurajová, E., Martínez Barroso, P., Děkanovský, I., Lumbantobing, Y. R., Jiroušek, M., Mugutdinov, A., Havel, L., & Winkler, J. (2024). Biodiversity and Vegetation Succession in Vineyards, Moravia (Czech Republic). *Agriculture*, *14*(7), 1036. https://doi.org/10.3390/agriculture14071036.

Law no. 331/2024. Forestry code. (2024). https://legislatie.just.ro/Public/DetaliiDocumentAfis/294392#:~:text=a)%20din%20Legea%20nr.%20331%2F2024,de%20c%C4%83tre%20acela%C8%99i%20ocol%20silvic

Meteomanz.com, www.meteomanz.com (accessed on 2-5 Febr. 2026).

Moreno-Gonzalez, R. M., Díaz, I. A., Christie, D. A., & Lara, A. (2025). Early Vegetation Recovery After the 2008 - 2009 Explosive Eruption of the Chaitén Volcano, Chile. *Diversity*, *17*(1), 14. https://doi.org/10.3390/d17010014.

Nasibullina, A., Tiebel, K., & Wagner, S. (2024). Succession as a Natural Tool for Restoration of Oak-Lime Forests on Aspen-Covered Clearcuts. *Diversity*, *16*(7), 376. https://doi.org/10.3390/d16070376.

O'Connell, M., & Wolters, S. (2025). Holocene flora, vegetation and land-use changes on Dingle peninsula, south-western Ireland, as reflected in pollen analytical, archaeological and historical records. *Diversity*, *17*(7), 456. https://doi.org/10.3390/d17070456.

Pérez-Hernández, J., & Gavilán, R. G. (2021). Impacts of Land-Use Changes on Vegetation and Ecosystem Functioning: Old-Field Secondary Succession. *Plants*, *10*(5), 990. https://doi.org/10.3390/plants10050990.

Pop, G. (2005). *România. Dealurile de Vest şi Câmpia de Vest (Romania. Western Hills and Western Plain)*. Oradea, RO: University of Oradea Publishing House, pp.84-89.

rp5.ru, https://rp5.ru/ (accessed on 9-12 Febr. 2026).

Poorter, L., Amissah, L, Bongers, F., Hordijk, I., Kok, J., Laurance, SGW., Lohbeck, M., Martínez-Ramos, M., Matsuo, T., Meave, J. A., Muñoz, R., Peña-Claros, M., & van der Sande M.T. (2023). Successional theories. *Biological Reviews of the Cambridge Philosophical Society*, 98(6):2049-2077**.** https://doi.org/10.1111/brv.12995.

Sicoe, S. I., Crainic G. C., Samuel, A. D., Bodog, M., Iovan, C. I., Curila, S., Hâruța I. O., Șerban, E., Dorog, L. S., & Sabău, N. C. (2023). Analysis of the effects of windthrows on the microbiological properties of the forest soils and their natural regeneration. *Forests, 14(6), 1200. https://doi.org/10.3390/f14061200.*

Szirmai, O., Saláta, D., Penksza, K., Schellenberger, J., & Czóbel, S. (2022). Examination of Forest Steppe Species in the Case of Areas Where Traditional Cultivation Was Abandoned. *Diversity*, *14*(7), 561. https://doi.org/10.3390/d14070561.

Stănescu, V., Șofletea, N., & Popescu, O. (1997). *Woody forest flora of Romania.* [Flora forestieră lemnoasă a României] CERES Publishing House, Bucharest, Romania.

Vârfurile Commune City Hall - Presentation. https://primariavirfurile.ro/despre-noi/prezentare/ (accessed on 23 Febr. 2026).

Yang, Y., & Yi, X. (2022). Nondormant Acorns Show Higher Seed Dispersal Effectiveness Than Dormant Ones. *Forests*, *13*(6), 881. https://doi.org/10.3390/f13060881.

Scientific Papers. Series E. Land Reclamation, Earth Observation & Surveying, Environmental Engineering. Vol. XV, 2026
Print ISSN 2285-6064, CD-ROM ISSN 2285-6072, Online ISSN 2393-5138, ISSN-L 2285-6064

# THE CHALLENGES OF CLIMATE CHANGE ADAPTATION IN ROMANIA'S LAND RECLAMATION SYSTEMS: BETWEEN GREY INFRASTRUCTURE AND NATURE-BASED SOLUTIONS

**Mihai Teopent CORCHES[1], Mirel GLEVITZKY[2], Mircea SĂLCUDEAN[1, 3]**

[1]"1 Decembrie 1918" University of Alba Iulia, Faculty of Computer Science and Engineering,
5 Gabriel Bethlen Street, Alba Iulia, Romania
[2]Politehnica University of Timișoara, Faculty of Engineering Hunedoara,
5 Revolutiei Street, Hunedoara, Romania
[3]Doctoral School, Faculty of Engineering, "Lucian Blaga" University of Sibiu,
10 Victoriei Blvd, Sibiu, Romania

Corresponding author email: mirel_glevitzky@yahoo.com

***Abstract***

*Climate change is placing increasing pressure on Romania's agricultural sector through intensified drought, greater precipitation variability, and more frequent hydrometeorological extremes. In this context, land reclamation systems, including irrigation, drainage and dewatering works, and anti-erosion measures, are becoming essential for reducing vulnerability and strengthening agroecosystem resilience. This article analyzes the main challenges in adapting these systems to climate change from an integrated technical, ecological, economic, and institutional perspective. It highlights outdated infrastructure, limited modernization, high water and energy demands, and environmental impacts, especially on hydrological regimes and biodiversity. At the same time, it examines economic and institutional barriers, and the gap between stated policies and practical implementation. The paper also explores the potential of Nature-based Solutions, and integrated green infrastructure, as viable complements or alternatives to traditional grey infrastructure. The findings emphasize the need for adaptive management, combining technological modernization, effîcient water use, and green solutions, to support climate resilience, food security, and territorial sustainability. In addition, the paper includes a case study of the Comlod polder project (Bistrița-Năsăud County, Romania), illustrating how flood retention infrastructure can function as a hybrid grey-green system contributing to climate adaptation and integrated water management.*

***Key words****: adaptation, climate change, environmental impacts, nature-based solutions.*

## INTRODUCTION

Climate change represents one of the most significant challenges for agricultural systems worldwide, affecting crop productivity, water resource availability, and the stability of agroecosystems (Yuan et al., 2024). The intensification of extreme events such as droughts, floods, and heatwaves leads to significant changes in hydrological regimes and plant growth cycles. Recent studies indicate that these processes directly influence land suitability for agriculture and may lead to the degradation of productive potential in many regions of the world (Shevchenko et al., 2023). In this context, European agriculture is considered one of the sectors most vulnerable to climate change, particularly in southern and eastern regions where water deficits and precipitation variability are intensifying (Florea et al., 2025). Consequently, the adaptation of agricultural infrastructure and water management systems becomes essential for maintaining productivity and food security. Land reclamation systems -including irrigation, drainage and dewatering works, and anti-erosion measures - represent fundamental components of this adaptation, as they enable the regulation of soil water regimes and reduce the risks associated with drought or excess water (OECD, 2025). In Romania, the effects of climate change are manifested through the intensification of water deficits, the aridification of certain agricultural regions, and increased precipitation variability (Nițu et al., 2023). Climatic and agronomic analyses highlight the high vulnerability of Romanian agriculture to hydrological imbalances, particularly in the Romanian Plain, Dobrogea, and southern Moldova (Frone et al., 2021).

These findings underline the sensitivity of the agricultural sector to climate variability and water scarcity, with direct effects on agricultural production and the stability of agri-food systems. At the same time, Romania's land reclamation infrastructure faces structural problems related to technical degradation, low efficiency, and the incomplete use of existing capacities. Although large areas have been equipped for irrigation, the actual functioning of these systems remains limited, and water losses are significant (Corcheș, 2025). These conditions indicate that the main issue is not only the availability of water resources, but also the low efficiency of the systems designed to manage water deficits.

In this context, recent literature emphasizes the need to move beyond a paradigm based exclusively on technical infrastructure ("grey infrastructure") and to shift toward integrated water management approaches (Castañeda Rodriguez et al., 2026). Nature-based Solutions (NbS) use ecosystem processes to support water retention, soil stabilization, erosion reduction, and biodiversity conservation (Santos, 2025). However, these solutions should not be viewed as alternatives to technical infrastructure, but rather as complementary elements within an integrated water management system. The concept of hybrid ("grey-green") infrastructure involves combining hydrotechnical structures with natural elements that can perform part of the system's hydrological functions (Bujak et al., 2025). For example, irrigation systems can be complemented by shelterbelts, wetlands, or vegetative anti-erosion measures, which help reduce pressure on water resources and increase the resilience of agricultural systems to climate variability (Pourmohammad & Hajirad, 2025). Against this background, the present study analyzes the challenges of adapting Romania's land reclamation systems to climate change, highlighting the interdependencies between technical, ecological, economic, and institutional dimensions. At the same time, it explores the potential and limitations of integrating Nature-based Solutions into the modernization of existing infrastructure, as well as the role of hybrid infrastructures in increasing the resilience of agricultural systems. To illustrate the practical application of these concepts, the paper also includes a case study analysis of the Comlod Polder project in Bistrița-Năsăud County. This project represents an example of hybrid hydrotechnical infrastructure designed for flood retention and flood risk reduction, integrating both engineering solutions and elements with ecological functions. The case study highlights how such arrangements can simultaneously contribute to hydrological risk management, water retention in the landscape, and the enhancement of water management system resilience in the context of climate change.

## MATERIALS AND METHODS

The preparation of this article was based on an interdisciplinary approach that combined the analysis of scientific literature with the examination of strategic and legislative documents relevant to water resource management and the adaptation of agriculture to climate change. The research methodology aimed to identify the main challenges associated with the adaptation of land reclamation systems in Romania and to evaluate the potential of Nature-based Solutions (NbS) to complement existing technical infrastructure.

The first methodological step consisted of a critical review of the scientific literature, including national and international journal articles addressing the impacts of climate change on agriculture, the functioning of irrigation and drainage systems, and the role of Nature-based Solutions in water management within agricultural landscapes.

In parallel, an analysis of relevant strategic documents and public policies related to land reclamation and climate change adaptation was conducted. Based on the information derived from the literature and policy analysis, the challenges of adapting land reclamation systems were structured into four main dimensions: technical, ecological, economic, and institutional. This approach made it possible to highlight the interdependencies between infrastructure condition, ecosystem functioning, the economic viability of investments, and the institutional capacity to implement adaptation policies. To complement

the theoretical analysis, the study also includes an applied case study represented by the Comlod Polder project, located in Bistrița-Năsăud County. The case study was used to illustrate how hydrotechnical infrastructure can integrate elements of hybrid ("grey-green") infrastructure and contribute to adaptive water management in the context of climate change. The analysis was based on the technical documentation prepared for obtaining the environmental permit for the project, as well as on information regarding the construction solutions, hydrological functioning, and environmental constraints associated with the development of the polder. The principal author of the article participated, as an environmental expert, in the environmental permitting procedure for the Comlod Polder project. This direct involvement provided access to the technical documentation and to the environmental impact assessment process, enabling a detailed understanding of the interaction between the project's technical requirements, environmental constraints, and biodiversity protection measures. It also allowed the author to contribute to the identification of mitigation measures during the project planning phase.

By combining literature review, analysis of public policy documents, and the applied case study, the methodology provides an integrated perspective on the challenges and opportunities associated with the adaptation of land reclamation systems to climate change in Romania.

## RESULTS AND DISCUSSIONS

In Europe, agriculture is one of the sectors most vulnerable to climate change, particularly in southern and eastern regions where droughts are becoming increasingly frequent and severe. European adaptation policies highlight the need to adapt agricultural infrastructure and water management systems, including their integration into the Common Agricultural Policy, in order to maintain productivity and food security (Naumann et al., 2020). At the global level, national adaptation plans frequently identify agriculture as a priority sector, and the integration of ecosystem-based solutions and green infrastructure is increasingly promoted to reduce vulnerability and enhance the resilience of agricultural systems (Terton et al., 2024).

In this context, land reclamation systems - such as irrigation, drainage and dewatering works, and anti-erosion measures - represent essential infrastructures for water management in agriculture and for stabilizing agricultural production. By regulating the soil water regime, these systems reduce risks associated with drought or excess water and contribute to increasing crop productivity while limiting soil and nutrient losses (Pistocchi et al., 2022). Under climate change conditions, the role of these infrastructures becomes even more important. Increasing precipitation variability and prolonged droughts raise dependence on irrigation, while intense rainfall events increase the need for drainage systems and anti-erosion works. At the same time, inefficient water management in irrigation systems can generate hydrological imbalances and additional pressure on water resources (Junquera et al., 2024). From a food security perspective, land reclamation infrastructure contributes to stabilizing agricultural production and reducing the vulnerability of agri-food systems. In many regions, these systems enable agriculture to be practiced in areas with water deficits or erosion-prone soils, thereby supporting agricultural production and rural economies (Polo-Ballinas et al., 2022).

In recent decades, climate change adaptation strategies have been dominated by technical solutions based on grey infrastructure, such as dams, irrigation canals, drainage systems, and river regulation works. Although these measures reduce hydrological risks associated with climate variability, their high maintenance costs and ecological impacts have led to reconsideration of their exclusive use in adaptation policies (Naumann et al., 2020; Pistocchi et al., 2022). As an alternative or complement to grey infrastructure, the concept of Nature-based Solutions (NbS) has gained increasing importance, as it uses natural ecosystem processes to address challenges such as climate change adaptation, water management, and biodiversity conservation. In agriculture, NbS include measures such as artificial wetlands, natural water retention in

the landscape, agroforestry, and the restoration of riparian ecosystems (Pistocchi et al., 2022).
Recent studies show that NbS can generate multiple co-benefits, including flood risk reduction, increased biodiversity, and enhanced ecosystem carbon storage capacity (Santos, 2025). However, their large-scale implementation remains limited by institutional, financial, and planning barriers, which maintains grey infrastructure as the dominant solution in many sectors (Ryfisch et al., 2023). Although the literature on agricultural adaptation to climate change is expanding, significant gaps remain in integrating water management infrastructure with Nature-based Solutions. Most studies analyze technical infrastructures or ecological solutions separately, without addressing their interactions within complex agricultural systems (Polo-Ballinas et al., 2022). In many European countries, including those in Eastern Europe, land reclamation infrastructure was designed for the climatic conditions of the twentieth century and does not reflect current climate realities. This situation highlights the need to integrate Nature-based Solutions into the modernization of existing agricultural infrastructure, using ecosystem processes to provide similar or complementary services such as natural water retention, wetland restoration or conservation, and afforestation or reforestation (Pistocchi et al., 2022).

## 1. Romania's Context in Relation to Climate Change

In Romania, climate change is manifested through the intensification of water deficits, the aridification of southern and eastern regions, and increasing precipitation variability, with direct effects on agriculture. Recurrent droughts have led to the degradation of extensive areas and are associated with the decline of agricultural systems and the abandonment of irrigation infrastructure (Prăvălie et al., 2013). A national-scale analysis based on the Normalized Difference Drought Index (NDDI) for the period 2001-2020 shows that these regions remain consistently the most affected, even in relatively wetter years, indicating a structural vulnerability of agriculture in the Romanian Plain, Dobrogea, and southern Moldova, where water availability becomes critical during the growing season (Dobri et al., 2021). Dobrogea shows a high vulnerability to drought. Analyses for the period 2001-2021, based on the CDI, SPI, and SPEI indices, indicate an increasing frequency of drought episodes associated with high temperatures and reduced precipitation. Severe droughts were recorded particularly in 2011, 2012, and 2020, while between 2018 and 2020 a prolonged drought episode affected more than 70% of the region (Șerban et al., 2025). Climatological analyses for Constanța County also indicate a frequent transition between slightly arid and semiarid conditions, with more pronounced aridity episodes especially after 2000 (Maftei et al., 2024). From an agricultural perspective, this variability reduces soil water reserves and increases uncertainty regarding crop selection and the timing of agricultural operations. At the same time, the precipitation regime is changing, with intense rainfall events occurring more frequently as isolated episodes with large amounts of water. The analysis of pluviometric indices for the period 1961-2013 shows an increase in days with very intense precipitation (R10, R20, R30), with regional differences between northern and southern Romania (Croitoru et al., 2016). For agriculture, this pattern increases both the risk of soil drought between rainfall events and the risk of erosion or waterlogging during intense precipitation. The impact on production is particularly evident in Dobrogea, where maize productivity depends on climatic conditions by approximately 40%, and each additional 1 mm of water deficit can reduce yields by 7.1-11.0 kg/ha, reaching up to about 1.1 t/ha for a deficit of 100 mm (Prăvălie et al., 2014).
In this context, drought monitoring becomes essential for adaptation strategies. Studies conducted in southeastern Romania show an intensification of drought conditions in recent decades, reflected by SPI and SPEI indices, and emphasize the need to expand climate monitoring networks (Venturi et al., 2024).

## 2. Current State of Land Reclamation Infrastructure in Romania

Romania has approximately 15 million hectares of agricultural land, of which about 7 million hectares are potentially irrigable, while around

3.2 million hectares have been equipped for irrigation. However, the area actually irrigated each year is significantly smaller than the equipped area, highlighting a major gap between the existing infrastructure and its real use (Beilicci et al., 2019). A key factor is the poor technical condition of irrigation infrastructure. Before rehabilitation works, pumping stations operated at about 50% efficiency, the degradation level of canals and hydrotechnical structures reached 72%, and water losses along conveyance canals were estimated at 52% (Cojocinescu et al., 2017; Stanciu et al., 2024).

Similar difficulties occur in drainage and dewatering systems, where temporary excess water, sedimentation, and infrastructure wear reduce the operational capacity of existing arrangements, highlighting the need for strategies adapted to new hydrological conditions (Ilca et al., 2024). At the same time, recent literature indicates that a large part of Romania's irrigation infrastructure is technologically outdated and requires modernization, as the lack of investment and maintenance has led to network deterioration in many agricultural areas (Stanciu et al., 2024). These aspects suggest that simple physical rehabilitation of infrastructure is insufficient without technological and managerial reconfiguration adapted to current climatic conditions. Although some studies highlight local examples of modernization - such as the introduction of modern irrigation techniques in western Romania that can increase yields and reduce vulnerability to water deficits - these initiatives remain isolated and are not yet widely implemented at the national level (Șmuleac et al., 2024).

## 3. **The Role of Public Policies and European and National Funding**

Public policies have significantly influenced the modernization of land reclamation systems in Romania, although the results have been uneven. While the National Strategy for Reducing the Effects of Drought represents an important reference framework, recent analyses indicate limited progress and a gap between strategic planning and actual implementation (Stanciu et al., 2024).

From a financing perspective, the National Program for the Rehabilitation of the Main Irrigation Infrastructure has been one of the main public interventions, with investments of approximately €1.015 billion. In parallel, the National Rural Development Programme (NRDP) 2014-2020, through sub-measure 4.3, allocated around €435 million for the modernization of secondary irrigation infrastructure managed by Water Users Organizations (Cojocinescu et al., 2017). The program aimed to increase the share of economically viable functional irrigated areas from about 50% to 70% by 2020 and to 90% by 2030. However, the literature shows that funding policies in Romania have focused mainly on the technical rehabilitation of existing infrastructure, while the integration of Nature-based Solutions remains limited. Although climate change is increasing pressure on agriculture, current infrastructure still faces significant problems related to functionality and incomplete modernization, highlighting the need for an integrated approach that combines technical modernization, efficient water management, and Nature-based Solutions.

## 4. **Challenges of Adaptation in Land Reclamation Systems**

Adapting land reclamation systems to climate change goes beyond the simple rehabilitation of existing infrastructure and requires viewing them as socio-technical-ecological systems, in which infrastructure, ecosystems, and management practices are closely interconnected. In Romania and across the Danube region, increasing climatic pressure highlights the limitations of the traditional model based on grey infrastructure and emphasizes the need for more flexible and integrated solutions grounded in adaptive water management (Dogaru et al., 2019; Chitu et al., 2020).

### 4.1. ***Technical Challenges***

One of the main technical challenges is the outdated irrigation infrastructure and the rigidity of water distribution systems. In many irrigation schemes in Romania, systems still operate according to design principles developed for more stable climatic conditions, which limits their ability to adapt to current variability. Studies show that irrigation

scheduling is often influenced more by infrastructure characteristics than by the actual water needs of crops, while efficiency assessment is complicated by the lack of reliable data and by losses through evaporation, infiltration, or runoff (Dogaru et al., 2019; Chitu et al., 2020). With the intensification of drought conditions, existing infrastructure is increasingly insufficient to meet current agronomic requirements. Simulations using the CROPWAT model for wheat cultivation in southwestern Romania indicate the need for up to four additional irrigation events per year, while insufficient water supply may reduce yields by 17.9-43.3%, highlighting the growing inflexibility of traditional irrigation schemes under new climatic conditions (Constantin et al., 2025). The increasing frequency of droughts, the alternation between very dry periods and intense rainfall events, and rising temperatures exert additional pressure on irrigation systems. Under these conditions, existing infrastructure is often under-dimensioned and operationally rigid, reducing the efficiency of water distribution and increasing the vulnerability of agricultural production. Consequently, adaptation requires not only the technical rehabilitation of infrastructure but also more flexible and integrated water management solutions.

Water losses represent not only a technical problem but also an issue related to monitoring and institutional organization. The lack of efficient measurement and coordination systems makes it difficult to identify losses and optimize water distribution, meaning that even rehabilitated infrastructure may operate below optimal parameters. In addition, many existing drainage systems are rigid and designed primarily for rapid water evacuation, which becomes problematic under the increasing alternation between intense rainfall and drought. This situation requires more flexible water management approaches capable of addressing both water excess and deficit simultaneously (Bogdan et al., 2024; Petruța et al., 2025).

Excess soil moisture also represents a major pedological limitation, often caused by precipitation, high groundwater levels, or insufficient drainage, which negatively affects soil aeration and biological processes (Lațo et al., 2022). Although drainage systems can mitigate these effects, interventions based exclusively on rapid water evacuation may simplify hydrological regimes and reduce the ecological functions of agricultural landscapes.

### 4.2. *Ecological Challenges*

Ecological challenges associated with land reclamation systems arise because grey infrastructure modifies natural water regimes and reduces ecological connectivity, thereby affecting biodiversity. River regulation and declining groundwater levels have contributed to the degradation of floodplain ecosystems and to the reduction of ecosystem services (Constandache et al., 2022). At the same time, environmentally friendly practices such as shelterbelts and small water retention structures have been abandoned or degraded, although they previously played an important role in water and soil conservation (Hălbac-Cotoară-Zamfir et al., 2019). The tension between agricultural productivity and environmental conservation therefore has not only a biogeophysical dimension but also a historical and institutional one, as infrastructure and land-use patterns have been shaped by changing economic priorities. In this context, drainage works may negatively affect wetlands and aquatic biodiversity by reducing floodable areas and simplifying hydrological regimes. Consequently, drainage interventions should be evaluated in a broader perspective that considers the role of wetlands in maintaining biodiversity and supporting the natural regulation of water within agricultural landscapes.

### 4.3. *Economic Challenges*

The economic dimension of adaptation is strongly influenced by the high costs of modernizing irrigation infrastructure, which involve not only physical rehabilitation but also investments in monitoring systems, digitalization, and energy efficiency (Corcheș, 2025). At the same time, the uneven agrarian structure of Romanian agriculture makes such investments more accessible to large farms, while small farms often face difficulties in securing financing and covering operational costs (Burja et al., 2020). Studies on family farms in Central and Eastern Europe show that

production scale and market integration are key factors influencing economic resilience, placing small farms at a structural disadvantage in the adaptation process (Borychowski et al., 2020). In addition, the high dependence on subsidies and the limited impact of eco-schemes in reducing inequalities make the transition difficult without substantial public support (Borychowski et al., 2020; Toma et al., 2023). As a result, the modernization of water infrastructure risks increasing agricultural polarization, as large farms are able to adopt new technologies more rapidly, while smaller farms remain more vulnerable due to constraints related to access to technology, professional training, and the productivity of production factors (Florea et al., 2021).

### 4.4. *Institutional and Governance Challenges*

Institutional and governance challenges represent an important barrier to the adaptation of land reclamation systems, as they involve numerous actors and administrative levels, making the coordination of investments and decisions more difficult. In Romania, climate services are still at an early stage, and the lack of a dedicated platform limits the operational use of climate information in decision-making processes (Falcescu et al., 2024). Although agriculture, water resources, biodiversity, and the forestry sector are recognized as highly vulnerable to climate change, the implementation of adaptation measures remains fragmented, and the transition from strategic planning to integrated territorial interventions is still limited (Dumitrașcu et al., 2025).

At the river basin level, there is a gap between the need for integrated water management and current administrative practice. Studies emphasize the importance of a basin-based approach and the use of forecasting and decision-support tools to optimize water distribution (Dogaru et al., 2019; Chitu et al., 2020). However, their application is constrained by limited institutional capacity for data collection, intersectoral cooperation, and the integration of scientific knowledge into routine management. Overall, the literature indicates that technical, ecological, economic, and institutional challenges are strongly interconnected. Outdated infrastructure generates water losses and high operating costs, hydrological rigidity may negatively affect ecosystems, and structural inequalities within agriculture limit the ability of many farms to participate in modernization processes. Without adaptive governance capable of integrating grey infrastructure with Nature-based Solutions and territorially differentiated policies, the adaptation of land reclamation systems risks remaining incomplete and largely reactive rather than transformative (Hălbac-Cotoară-Zamfir et al., 2019; Burja et al., 2020; Falcescu et al., 2024).

## 5. **The Role and Potential of Nature-based Solutions (NbS)**

The integration of Nature-based Solutions (NbS) into the management of land reclamation systems represents an emerging direction in the adaptation of agriculture to climate change. Unlike approaches based exclusively on engineering solutions, NbS rely on natural ecosystem processes to provide services such as water retention, soil stabilization, and erosion reduction. These solutions do not replace hydrotechnical infrastructure but rather complement it, contributing to improved water management efficiency within agricultural landscapes (Ion et al., 2024).

In Romania, Nature-based Solutions are becoming increasingly relevant because much of the land reclamation infrastructure was designed within a rigid technical model focused on artificial hydrological control. Under current climate change conditions, the integration of NbS can support the natural regulation of hydrological flows, increased soil water retention, and the strengthening of ecosystem functions, thereby contributing to the development of more resilient and sustainable agricultural systems.

### 5.1. *Examples of Nature-based Solutions*

- Shelterbelts (Protective Forest Belts)

Shelterbelts represent effective Nature-based Solutions in agricultural areas vulnerable to drought and wind erosion. By reducing wind speed and evapotranspiration, they protect crops, favor snow accumulation, and limit soil losses. In Romania, the reintroduction of shelterbelts is considered an important measure for reducing land degradation and supporting

agricultural adaptation to climate change (Hălbac-Cotoară-Zamfir et al., 2019).

- Wetland Buffers and Wetland Restoration
Wetlands and riparian buffer zones represent important Nature-based Solutions for water management in agriculture, as they retain and filter water, reduce nutrient runoff, and help stabilize local hydrological regimes. At the same time, they provide valuable habitats for biodiversity and can reduce flood risk by absorbing excess water. In Romania, the degradation of these ecosystems through drainage and river regulation has negatively affected biodiversity, and their restoration is considered an effective solution for restoring ecosystem functions and increasing the resilience of agricultural landscapes (Constandache et al., 2022).

- Green Anti-Erosion Measures
Green anti-erosion measures include practices such as vegetative soil cover, strip cropping, and the use of perennial plants, which reduce surface runoff, limit soil erosion, and enhance water infiltration into the soil (Ion et al., 2024). Soil stabilization can also be optimized through laboratory methods and geotechnical modeling to identify effective solutions for reducing the degradation of agricultural land (Olinic et al., 2023).

- Natural Water Retention in the Landscape
An increasingly discussed concept in the European literature on Nature-based Solutions is that of Natural Water Retention Measures (NWRM). These measures include the restoration of floodplains, the creation of micro-depressions, the restoration of wetlands, and the use of vegetation to increase water infiltration into the soil.

### 5.2. *Benefits of Nature-based Solutions*

A major advantage of Nature-based Solutions lies in their ability to generate multiple benefits for socio-ecological systems. They contribute to climate adaptation by increasing the capacity of agricultural landscapes to manage hydrological variability and by reducing risks associated with drought or extreme precipitation. At the same time, NbS improve soil quality, reduce erosion, and support biodiversity. They also provide essential ecosystem services such as water purification, carbon sequestration, and microclimate regulation, thereby contributing to the development of more resilient agricultural systems (Hălbac-Cotoară-Zamfir et al., 2019; Ion et al., 2024).

## 6. **Case Study: The Comlod Polder - Hybrid Infrastructure for Flood Management and Climate Adaptation**

To illustrate the transition of land reclamation infrastructure toward adaptive water management models, the Comlod Polder project, located in Bistrița-Năsăud County and promoted by the Mureș River Basin Administration, can be analyzed (Figure 1).

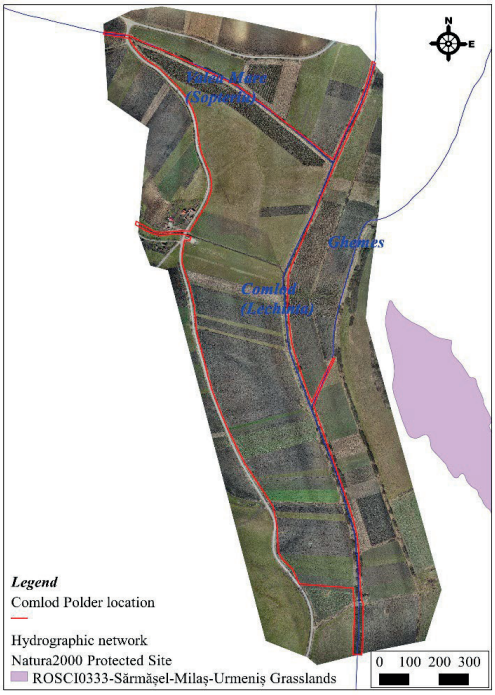



Figure 1. Comlod Polder Location (original)

The project is designed as a hybrid flood-retention infrastructure within the catchment of the Valea Mare and Comlod rivers, integrating the Fânațe tributary. The technical solution involves the construction of a compartmentalized polder with a single water intake threshold, while Fânațe river is channelized and functions as an internal

spillway separating the two compartments of the polder (SC 4C Project Consulting SRL, 2023). The concept of the project is based on the temporary retention of flood waves by storing excess water volumes inside the polder and releasing them in a controlled manner through a spillway and a bottom outlet. Through this mechanism, the polder reduces peak downstream flows and mitigates flood risk, functioning as a local hydrological regulation system. From a technical perspective, the polder covers an area of approximately 43.04 ha and has a total retention capacity of about 1.75 million m³, divided into two functional compartments: 17.93 ha (0.62 million m³) and 25.11 ha (1.13 million m³). The hydrological supply is ensured by Valea Mare and Comlod rivers, while Fânațe river is integrated through a reinforced concrete channelization of 370 m, designed to convey flows with a 1% exceedance probability (Q1%) (SC 4C Project Consulting SRL, 2023). Water intake into the polder is controlled through a system of hydraulic thresholds: a broad-crested intake weir with a length of 24 m and a downstream diversion weir measuring 7.5 m in length and 1 m in height. To maintain hydrological connectivity during non-flood periods, the structure includes a low-flow slot (1.0 m × 0.50 m) that ensures the continuity of the watercourse and the movement of aquatic biodiversity. Downstream works include energy dissipation and riverbed stabilization structures, such as concrete lining, an energy dissipator, and a mobile stilling basin (SC 4C Project Consulting SRL, 2023). The containment and guidance of water volumes are achieved through a system of embankments with a total length of 5,715 m, of which 4,000 m are perimeter embankments and 1,715 m are guiding embankments. The embankments have 1:2 slopes and a crest stabilized with crushed stone to allow maintenance access. Slope stabilization is achieved through grassing, while areas exposed to higher hydraulic stress are protected with concrete lining. Controlled water evacuation is performed through a 24 m spillway and a bottom outlet consisting of two gated openings, with a maximum discharge capacity of approximately 24.6 m³/s.

In the context of current climatic trends characterized by the increasing frequency of extreme hydrological events, including intense rainfall and flash floods alternating with drought periods, the Comlod polder highlights the role of such infrastructure as a climate adaptation measure, capable of temporarily storing significant water volumes and reducing flood peaks. Beyond its flood protection function, the polder also presents characteristics similar to Nature-based Solutions. During non-flood periods, its surface can function as a temporary wetland, promoting water retention in the landscape, infiltration, and groundwater recharge. Vegetation established on the embankment slopes and within the polder also contributes to soil stabilization, erosion reduction, and the enhancement of local biodiversity.

The project also raised several challenges during the environmental permitting process. Near the project site lies the Natura 2000 site ROSCI0333 - Sărmășel - Milaș - Urmeniș Grasslands, covering 1,127.10 ha, designated for the protection of habitats and species of community interest. The environmental assessment analyzed the potential impact on amphibian species such as *Bombina bombina*, *Bombina variegata*, and *Triturus cristatus*. As a result, specific measures were required to maintain the longitudinal connectivity of the watercourse, ensured through the low-flow slot integrated into the diversion weir structure.

The case study analysis shows that the Comlod polder represents an example of hybrid hydrotechnical infrastructure, combining engineering solutions with natural stabilization elements and potential ecological functions. Through temporary water retention, flood peak reduction, and the potential formation of seasonal wetland habitats, the project contributes both to reducing hydrological risks and enhancing local ecosystem services. In the context of climate change, such integrated solutions become increasingly important for strengthening the resilience of water management systems.

## CONCLUSIONS

The analysis highlights that the adaptation of land reclamation systems to climate change represents a complex challenge that goes beyond the strictly technical dimension of

hydrotechnical infrastructure. The increasing frequency of droughts, the growing variability of precipitation, and the occurrence of extreme hydrological events intensify pressures on agriculture, emphasizing the dependence of agricultural systems on efficient water resource management. In the case of Romania, the results show that land reclamation infrastructure continues to play an essential role in stabilizing agricultural production; however, its functioning is limited by technical degradation, high water losses, and the rigidity of operational schemes. These aspects indicate that the adaptation challenge is not related solely to water availability, but also to technical efficiency, institutional capacity, and the organization of water management.

The study also demonstrates that the challenges associated with adaptation should be analyzed from an integrated perspective that simultaneously considers the technical, ecological, economic, and institutional dimensions of land reclamation systems. In this context, the literature and the present analysis suggest that Nature-based Solutions can play an important role in increasing the resilience of agricultural systems by improving water retention in the landscape, reducing erosion, and strengthening ecosystem functions.

The results further indicate that integrating grey infrastructure with Nature-based Solutions may represent a promising direction for adapting water management systems. The concept of hybrid ("grey-green") infrastructure allows the combination of hydrotechnical control of water resources with natural hydrological regulation processes, thereby reducing the vulnerability of agricultural systems to climate variability.

The case study analysis of the Comlod Polder illustrates how hydrotechnical infrastructure can integrate multiple functions, contributing both to flood risk reduction and to water retention and the development of temporary wetland habitats. In this sense, retention structures can be interpreted as hybrid infrastructures capable of combining hydrological protection objectives with ecosystem conservation goals. At the same time, adapting land reclamation systems to climate change requires a paradigm shift, in which the modernization of technical infrastructure is correlated with the integration of Nature-based Solutions, the development of institutional capacity for adaptive management, and public policies focused on the sustainable management of water resources in agriculture. Such an approach can contribute to strengthening the resilience of agricultural systems and enhancing food security in an increasingly uncertain climatic context.

## ACKNOWLEDGEMENTS

The authors would like to thank SC 4C Project Consulting SRL for the support provided in the preparation of this study and for facilitating access to the technical information and documentation related to the analyzed project.

## REFERENCES

Beilicci, R. & Beilicci, E. (2019). Current situation and the future of the exploitation of irrigation arrangements in Romania. *Sci. Bull. "Politeh." Univ. Timiş., Trans. Hydrotech.,* 64(78), 47-51.

Bogdan, P. L., Nedeff, V., Panainte-Lehadus, M., Chitimuş, D., Barsan, N., & Nedeff, F. M. (2024). Delineation of Groundwater Potential Zones Using Remote Sensing, GIS and Multi-Criteria Decision Analysis in Romania. *Water*, 16(21), 3013.

Borychowski, M., Stępień, S., Polcyn, J., Tošović-Stevanović, A., Ćalović, D., Lalić, G., & Žuža, M. (2020). Socio-Economic Determinants of Small Family Farms' Resilience in Selected Central and Eastern European Countries. *Sustainability*, 12(24), 10362.

Bujak, P., Grochulska-Salak, M., Maciejewska, E., Rybak-Niedziółka, K., Hubačíková, V., Francke, B., & Starzyk, A. (2025). Sustainable Water Retention Strategy for Urban Resilience: A Valorization and Action Model for Cities. *Water*, *17*(18), 2663.

Burja, V., Tamas-Szora, A., & Dobra, I. B. (2020). Land Concentration, Land Grabbing and Sustainable Development of Agriculture in Romania. *Sustainability*, 12(5), 2137.

Castañeda Rodriguez, L. d. R., Diaz Shimidzu, M. J., Castro Rivera, M. N., Galvez-Nieto, A., Aguilar Chunga, Y. A., Ccalla Chusho, J. A., & Salinas Romero, M. E. (2026). Urban Resilience and Fluvial Adaptation: Comparative Tactics of Green and Grey Infrastructure. *Urban Science*, *10*(1), 62.

Chitu, Z., Tomei, F., Villani, G., Di Felice, A., Zampelli, G., Paltineanu, I. C., Visinescu, I., Dumitrescu, A., Bularda, M., Neagu, D., Costache, R., & Luca, E., (2020). Improving Irrigation Scheduling Using MOSES Short-Term Irrigation Forecasts and In Situ Water Resources Measurements on Alluvial Soils of Lower Danube Floodplain, Romania. *Water*, 12(2), 520.

Cojocinescu, M. I., Balaj, C., Stoica, D., Cozma-Häusler, D. P., & Man, T. E. (2017). National Program for

Rehabilitation of the Main Irrigation Infrastructure. *Sci. Bull. "Politeh." Univ. Timiş., Trans. Hydrotech.*, 62(76), 38-42.

Constandache, C., Tudor, C., Popovici, L., & Dincă, L. (2022). Ecological reconstruction of the stands affected by drought from meadows of inland rivers, *Sci. Papers, Ser. E, Land Reclam. Earth Obs. Surv. Environ. Eng.,* XI, 76-82.

Constantin, D. M., Mincu, F. I., Diaconu, D. C., Burada, C. D., & Bălțățeanu, E. (2025). Water Management in Wheat Farming in Romania: Simulating the Irrigation Requirements with the CROPWAT Model. *Agronomy*, 15(1), 61.

Corcheș, M. T. (2025). Adapting Romania's irrigation infrastructure to climate change: Opportunities and challenges. *Sci. Papers, Ser. E, Land Reclam. Earth Obs. Surv. Environ. Eng.*, 14, 623-629.

Croitoru, A. E., Piticar, A., & Burada, D. C. (2016). Changes in precipitation extremes in Romania. *Quaternary International*, 415, 325-335.

Dobri, R.V., Sfîcă, L., Amihăesei, V. A.; Apostol, L., & Ţîmpu, S., (2021). Drought Extent and Severity on Arable Lands in Romania Derived from Normalized Difference Drought Index (2001–2020). *Remote Sensing*, 13(8), 1478.

Dogaru, D., Mauser, W., Balteanu, D., Krimly, T., Lippert, C., Sima, M., Szolgay, J., Kohnova, S., Hanel, M., Nikolova, M., Szalai, S., & Frank, A., (2019). Irrigation Water Use in the Danube Basin: Facts, Governance and Approach to Sustainability. *J. Environ. Geogr.*, 12(3-4), 1-12.

Dumitraşcu, M., Roznovieţchi, I., Sima, M., Grigorescu, I., Mitrică, B., Micu, D., Fălcescu, V., Bulai, A., & Cheval, S. (2025). Public Perception of Climate Change Impacts and Sectoral Adaptation in Romania. *Environ. Dev.*, 57, 101346.

Falcescu, V., Cheval, S., Micu D. M., Dumitrescu, A., Roznovieţchi. I., Dumitraşcu M., & Damian, N. (2024). Climate Services in Romania - An Analysis of Stakeholders' Perceptions and Needs. *Climate Services*, 34, 100433.

Florea, A. C., Sumedrea, D. I., Rodino, S., Ion, M., Dragomir, V., Dumitru, A.-M., Pîrcalabu, L., & Dinu, D. G. (2025). The Impact of Climate Change on Eastern European Viticulture: A Review of Smart Irrigation and Water Management Strategies. *Horticulture*, 11(11), 1282.

Florea, N. V., Duică, M. C., Ionescu, C. A., Duică, A., Ibinceanu, M. C. O., & Stanescu, S. G. (2021). An Analysis of the Influencing Factors of the Romanian Agricultural Output within the Context of Green Economy. *Sustainability*, 13(17), 9649.

Frone, D. F., Frone, S., Platon, V., & Constantinescu, A. (2021). Issues of climate vulnerability in Romania – A special mention for agriculture. *Sci. Papers, Ser. Manag. Econom. Eng. Agric. Rural Dev*., 21(3), 395–402.

Hălbac-Cotoară-Zamfir, R., Keesstra, S., & Kalantari, Z. (2019). The impact of political, socio-economic and cultural factors on implementing environment friendly techniques for sustainable land management and climate change mitigation in Romania. *Sci. Total Environ.*, 654, 418-429.

Ilca, M. V., Man, T. E., Beilicci, R., Ienciu, A., Untaru, D. C., & Pasc, M. A., (2024). Modernization/rehabilitation of the secondary drainage infrastructure by repositioning existing channels and by assigning the dual role of drainage-irrigation adaptation. *Sci. Papers, Ser. E, Land Reclam. Earth Obs. Surv. Environ. Eng.,* Vol. XIII, 293-304.

Ion, S., Marinescu, D., & Cruceanu, S. (2024). Water Flow Model on Vegetated Hillslopes with Erosion. *arXiv:2408.12465v1*. https://arxiv.org/pdf/2408.12465.pdf.

Junquera, V., Rubenstein, D. I., Levin, S. A., Hormaza, J. I., Vadillo Pérez, I., & Jiménez Gavilán, P. (2024). Hydrological collapse in southern Spain under expanding irrigated agriculture: Meteorological, hydrological, and structural drought. *arXiv:2408.00683v1*, https://doi.org/10.48550/arXiv.2408.00683.

Lațo, K. I., Lațo, A., Niță, L. D., Duma-Copcea, A., & Corcheș, M. T. (2022). Pedo-genetical factors implicated in soil degradation (lower Timis river basin area). *Sci. Papers Ser. A, Agron.*, Vol. LXV, No. 1, 2022, 91-96.

Maftei, C. E., Bărbulescu, A., & Osman, A. (2024). Assessment of the Drought Risk in Constanța County, Romania. *Atmosphere*, 15(11), 1281.

Naumann, S., Davis, McK., Röschel, L., de Luca C., & Conticelli E. (2020). Sustainable Use of Land and Nature-Based Solutions in the EU Policy Framework, Urban Agenda for the EU. https://www.urbanagenda.urban-initiative.eu/sites/default/files/migration_files/action_6_better_regulation_to_boost_nbs_eu.pdf.

Nițu, O. A., Ivan, E. Ș., & Nițu, D. S. (2023). Climate change and its impact on water consumption in the main agricultural crops of the Romanian Plain and Dobrogea. *Sci. Papers Ser. A, Agron*., 66(1), 474-478.

OECD (2025), *Global Drought Outlook: Trends, Impacts and Policies to Adapt to a Drier World*, OECD Publishing, Paris, https://doi.org/10.1787/d492583a-en.

Olinic, E. D., Olinic, T., & Andronic, A. (2023). Methods of Determining the Characteristic Values of Shear Strength Parameters. *Sci. Papers, Ser. E, Land Reclam. Earth Obs. Surv. Environ. Eng.*, XII, 20-24.

Petruța, N. L., Sur, I. M., Rusu, T. A., Gabor, T., & Rusu, T. (2025). Integrated Assessment of Groundwater Vulnerability and Drinking Water Quality in Rural Wells: Case Study from Ceanu Mare Commune, Northern Transylvanian Basin, Romania. *Sustainability*, 17(14), 6530.

Pistocchi A. (2022). Nature-based solutions for agricultural water management - Characteristics and enabling factors for a broader adoption. *Publications Office of the European Union, Luxembourg*, doi:10.2760/343927, JRC131465. https://publications.jrc.ec.europa.eu/repository/bitstream/JRC131465/JRC131465_01.pdf.

Polo-Ballinas, M. B., Arumugam, P., Verstand, D., Siegmund-Schultze, M., Keesstra, S., Chávez, L. G., de Boer, R., van Eldik, Z., & Voskamp I. (2022).

Discussion Paper: Nature-based Solutions in Food Systems. Review of Nature-based Solutions towards more sustainable agriculture and food production, *Wageningen, Wageningen Environmental Research, Discussion Paper*. https://edepot.wur.nl/578174.

Pourmohammad, P., & Hajirad, I. (2025). Innovative irrigation practices for sustainable agriculture: Environmental benefits and implementation challenges. *J. Sustain. Dev. Nat. Resour. Manag.*, 1(2), 1010601.

Prăvălie, R., Peptenatu, D., & Sîrodoev, I. (2013). The impact of climate change on the dynamics of agricultural systems in South-Western Romania. *Carpath. J. Earth Environ. Sci.*, 8(3), 175-186.

Prăvălie, R., Sîrodoev, I., Patriche, C. V., Bandoc, G., & Peptenatu, D. (2014). The analysis of the relationship between climatic water deficit and corn agricultural productivity in the Dobrogea Plateau. *Carpath. J. Earth Environ. Sci.*, 9(4), 201-214.

Ryfisch, S., Seeger, I., McDonald, H., Lago, M., & Blicharska, M. (2023). Opportunities and limitations for Nature-Based Solutions in EU policy frameworks. *Land Use Policy*. https://doi.org/10.1016/j.landusepol.2023.106957.

Santos, E. (2025). Nature-Based Solutions for Water Management in Europe: What Works, What Does Not, and What's Next? *Water*, *17*(15), 2193.

SC 4C Project Consulting SRL, (2023). Presentation Report for Obtaining the Environmental Agreement According to Law No. 292/2018 - Annex No. 5E, For the Project: Comlod Polder, Bistrița-Năsăud County, Romania, Cluj-Napoca, RO.

Șerban, C., & Maftei, C. (2025). Spatiotemporal Drought Analysis Using the Composite Drought Index (CDI) over Dobrogea, Romania. *Water*, 17(4), 481.

Shevchenko, V., Taniushkina, D., Lukashevich, A., Bulkin, A., Grinis, R., Kovalev, K., Narozhnaia, V., Sotiriadi, N., Krenke, A., & Maximov, Y. (2023). Climate Change Impact on Agricultural Land Suitability: An Interpretable Machine Learning-Based Eurasia Case Study. *arXiv:2310.15912v1*. https://doi.org/10.48550/arXiv.2310.15912.

Șmuleac, L., Șmuleac, A., Pașcalău, R., Bakli, M., & Jurakhon, R., (2024). Modern Irrigation Techniques for Western Romania Farmers. *Res. J. Agric. Sci.*, 56(3), 259-265.

Stanciu, S. (2024). Assessing the Resilience and Adaptability of Romanian Agriculture to Climate Change. *J. Agric. Rural Dev. Stud.*, 1(1), 34-45.

Terton, A., Qi, J., & Jang, N. (2024). Tracking Progress on the Integration of Nature-based Solutions and Ecosystem-based Adaptation in National Adaptation Plan Processes. *NAP Global Network synthesis report. International Institute for Sustainable Development.* https://napglobalnetwork.org/wp-content/uploads/2024/11/napgn-en-2024-tracking-progress-on-nbs-eba-nap-processes.pdf.

Toma, E., Stoicea, P., Dobre, C., & Iorga, A. (2023). The Effect of Eco-Scheme Support on Romanian Farms-A Gini Index Decomposition by Income Source at Farm Level. *Agriculture*, 13(9), 1656.

Venturi, S., Mateescu, E., Virsta, A., Petrescu, N., Dunea, D., & Casadei, S. (2024). Drought monitoring in southeastern Romania based on the comparison and correlation of SPEI and SPI indices. *Sci. Papers, Ser. E, Land Reclam. Earth Obs. Surv. Environ. Eng.,* Vol. XIII, 655-661.

Yuan, X., Li, S., Chen, J., Yu, H., Yang, T., Wang, C., Huang, S., Chen, H., & Ao, X. (2024). Impacts of Global Climate Change on Agricultural Production: A Comprehensive Review. *Agronomy*, *14*(7), 1360.

Scientific Papers. Series E. Land Reclamation, Earth Observation & Surveying, Environmental Engineering. Vol. XV, 2026
Print ISSN 2285-6064, CD-ROM ISSN 2285-6072, Online ISSN 2393-5138, ISSN-L 2285-6064

# SEISMIC RESPONSE ANALYSIS OF A LONG-TERM MONITORED BUILDING USING CO-LOCATED STRUCTURAL AND FREE-FIELD RECORDS

**Iolanda-Gabriela CRAIFALEANU[1, 3], Claudiu-Sorin DRAGOMIR[1, 2], Daniela DOBRE[1, 3], Emil Sever GEORGESCU[1], Alexandra-Marina BARBU[1]**

[1]National Institute for Research and Development in Constructions, Urbanism and Sustainable Spatial Development, URBAN-INCERC, 266 Pantelimon Road, District 2, Bucharest, Romania
[2]University of Agronomic Sciences and Veterinary Medicine of Bucharest, 59 Mărăști Blvd, District 1, Bucharest, Romania
[3]Technical University of Civil Engineering Bucharest, 122-124 Lacul Tei Blvd, District 2, 020396, Bucharest, Romania

Corresponding author email: iolanda@incd.ro

***Abstract***

*Monitoring building vibrations provides important information on structural health and, through on the detection of changes in dynamic characteristics, can serve as an early indicator of potential degradation or damage. However, detection reliability depends substantially on appropriate instrumentation capable of clearly capturing the building response to ambient, natural and anthropogenic vibrations. The paper presents an in-depth study based on data recorded during recent seismic events on a higher-education building in Bucharest, Romania. The building has been continuously monitored for vibrations for more than a decade. Unlike many other urban buildings monitored in Romania, the building's location within a university campus - characterized by large open spaces - enabled the installation of a free-field-type station approximately 30 m away from the building, such that reference ground motion records were also available. Based on multiple types of analyses, the study provides valuable insights into the building's dynamic characteristics, soil-structure interaction phenomena and kinematic effects.*

***Key words****: building vibrations, dynamic characteristics, kinematic effects, soil–structure interaction, structural health monitoring.*

## INTRODUCTION

Monitoring building vibrations is an essential tool for the rapid detection of potentially unsafe changes in structural dynamic characteristics, which may indicate degradation or damage. However, especially in urban environments, complete instrumentation is often challenging, due to the difficulty of identifying open spaces for installing reference free-field stations in the vicinity of the building (COSMOS, 2001; Skolnik, 2010). The National Institute for Research and Development in Constructions, Urbanism and Sustainable Spatial Development, URBAN-INCERC (NIRD URBAN-INCERC) has a long history of activities in the field, with the first seismic stations installed on buildings in the late 1960s and early 1970s (Berg et al., 1977; Bălan et al., 1982). A large campaign of temporary building instrumentation was carried out in the years preceding the catastrophic March 4, 1977, $M$ = 7.2 earthquake. The dynamic characteristics (natural periods of vibration) measured within this campaign on 47 buildings in Bucharest (Bălan et al., 1982) provided essential information for assessing their post-earthquake condition. In the years that followed, several buildings in Bucharest and in other major cities were permanently instrumented. After 1990, despite the reduction of the number of instrumented buildings (mainly due to ownership changes and equipment obsolescence), both temporary and permanent instrumentation for building vibrations monitoring continued. A large-scale, multi-annual campaign - still ongoing within the "Nucleu" Programme PN 23 35 "ECODIGICONS" - has focused on the temporary instrumentation of several public buildings and the determination of their reference dynamic characteristics, particularly

for those hosting national research and development institutes. The campaign is carried on through the National Network for the Seismic Monitoring and Protection of the Building Stock (RNMPSPC), an infrastructure of national interest operating within NIRD URBAN-INCERC (https://incd.ro/reteaua-nationala-de-monitorizare-siprotectie-seismica-a-patrimoniului-construit-iosin/).

The building examined in this study has been subjected to continuous vibration monitoring for over a decade. Unlike many other urban buildings monitored in Romania, the building's location within a university campus – characterized by large open spaces – enabled the installation of a free-field-type station approximately 30 m away from the building, such that reference ground motion records are also available. Based on multiple types of analyses, this study aims to provide valuable insights into the building's dynamic characteristics, soil-structure interaction phenomena, and kinematic effects.

## MATERIALS AND METHODS

### Description of the monitored building

The monitored building is situated on the campus of the University of Agriculture and Veterinary Medicine in Bucharest and serves as the headquarters of the Faculty of Biotechnologies (Figures 1 and 2). The campus, with a surface area of 38 hectares, benefits from large spaces between the buildings, arranged as parks and recreational areas.

The building, completed in 2016, comprises a basement and three above-ground stories. Its structural system consists of reinforced concrete frames combined with shear walls.

The instrumentation system, installed ever since the building completion, consists of a Kinemetrics Granite digitizer and recorder, with ES-T triaxial episensors placed in the basement, at the roof of the building and in a special encasement, located about 30 m away from the building, in a neighbouring green space (Figure 3). The digitizer, placed in the central building section, is equipped with 12 channels, of which channels 1-3, 5-7 and 9-11 are assigned, in order, to vibration measurements at the three mentioned locations: free field, basement and roof. Channels are identified as HNZ, HNN and HNE, respectively, with suffixes indicating the location (FF – free field, B1 – basement, 04 – roof).



Figure 1. Monitored building: Faculty of Building Technologies of the University of Agronomic Sciences and Veterinary Medicine of Bucharest

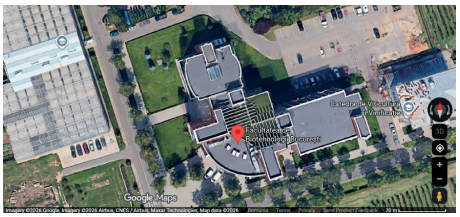



Figure 2. Map location and orientation of the monitored building (Google Maps screenshot) (https://www.google.com/maps/place/Facultatea+de+Biotehnologii+Bucure%C8%99ti/@44.4699931,26.0620898,132m/data=!3m1!1e3!4m6!3m5!1s0x40b2023b3338d51f:0xa7a705d357d7ce12!8m2!3d44.4696946!4d26.0625279!16s%2Fg%2F1hc0sxqyv?entry=ttu&g_ep=EgoyMDI2MDQwMS4wIKXMDSoASAFQAw%3D%3D)




a) b) c)

Figure 3. Station BTH: a) free-field station encasement, b) free-field episensor, c) installation of permanent online connection with the Data Centre of NIRD URBAN-INCERC

The station, identified by the code BTH, is permanently connected to the Data Centre of NIRD URBAN-INCERC, enabling the continuous acquisition of co-located structural and free-field seismic records. Through a secure communication link provided by the

Romanian Special Telecommunications Service, STS, the station transmits real-time data to the SeisComP (https://www.gempa.de/products/seiscomp/) seismological software running on the main server of the centre.

**Ground motions considered**

Ground motions recorded from two significant earthquakes ($M_L$ = 5.2 and $M_L$ = 4.8) originating in the Vrancea seismic zone of Romania, with epicentres located approximately 200 km from the building site, were used in the study. Their main characteristics, according to the website of the National Institute for Earth Physics (https://www.infp.ro/), are shown in Table 1.

**Processing and analyses**

The processing steps and analyses performed are presented below, with explanations on their meaning and relevance for the current study. The processing was carried out using the ViewWave software (Kashima, 2016; 2024).

***Acceleration, velocity, and displacement waveforms***

The recorded waveforms illustrate the temporal variation of the vibrations measured by sensors placed at different locations in the structure and in its vicinity. They also show the peak values reached during the earthquake, the amplification between the base and the roof of the building, as well as the primary differences between the free field motion and the motion recorded in the building's basement, at the foundation level.

Table 1. Main characteristics of Vrancea earthquakes considered in the study

| Date and time (UTC) | Focal depth (km) | Epicentral coordinates | Local magnitude ($M_L$) |
|---|---|---|---|
| 31.01.2020, 01:37:52 | 118.2 | 45.6937°N 26.6918°E | 5.2 |
| 03.12.2023, 22:05:48 | 133.3 | 45.5939°N 26.4734°E | 4.8 |

***Husid plots***

Husid plots illustrate the evolution of normalized Arias intensity throughout the seismic motion. They can be also used to estimate the significant duration of the earthquake (the duration of strong ground shaking), which is important for assessing its destructive potential by indicating when the largest amount of energy is induced during the event. Arias intensity is defined by the following equation:

$$I_A = \frac{\pi}{2g} \int_0^{T_d} a^2\,(t)\,dt \qquad (1)$$

where $T_d$ is the duration of the ground motion and $a(t)$ is the acceleration.

***Fourier and power spectra***

*Fourier analysis* is the most widely used method for estimating the dynamic characteristics of a structure. This analysis transforms measured structural vibrations from the time domain to the frequency domain, allowing the identification of the natural frequencies of the structure, which generally correspond to the peaks of the Fourier amplitude spectra. Estimating the values of these natural frequencies provides a reference point for identifying future degradation or damage that alters the dynamic parameters of the structure, thus enabling structural health monitoring.

The *power spectrum* highlights the predominant frequencies/periods of the ground or structure vibration, the distribution of earthquake-induced energy over frequency ranges, and the bandwidth characteristic of the motion.

***Response spectra***

The following spectra and diagrams were determined:

- the acceleration spectrum (*Sa*);
- the velocity spectrum (*Sv*);
- the displacement spectrum (*Sd*);
- the pseudovelocity spectrum (*pSv*);
- the input energy spectrum (equivalent velocity) (*Ve*).

The *acceleration, velocity, and displacement spectra* are standard seismic record processing tools used to highlight the frequency content of ground motion, amplification effects, and related phenomena.

The *pseudovelocity spectrum* is computed by multiplying the ordinates of the relative displacement spectrum (Sd) by the corresponding circular frequency ($\omega$):

$$pSv = \omega \cdot Sd \qquad (2)$$

The pseudovelocity spectrum is proportional to the elastic deformation energy of the system and serves as an indicator of the frequencies/periods associated with the maximum destructive potential of seismic motion, with direct applications in structural engineering.

Another important indicator is the *total input energy induced by the earthquake* ($E$). This is often expressed through the equivalent velocity $V_E$, defined by:

$$V_E = \sqrt{\frac{2E}{m}} = \sqrt{-2\int_0^{T_d} \ddot{x}_g(t)\dot{x}(t)dt} \quad (3)$$

where $m$ is the mass, $\ddot{x}_g(t)$ and $\dot{x}_g(t)$ are the ground acceleration and relative velocity of the oscillator, respectively, and $t$ is the time. The equivalent velocity (and thus the energy, $E$) is a significant measure of the destructive potential of seismic motion, with various structural engineering applications as well. It has the advantage of representing a scalar value, rather than a vectorial value.

***Spectral ratios – transfer functions***

The analysis of the *ratios* between the *Fourier amplitude spectra* recorded at the roof and those recorded at the base/foundation is another widely used method for determining the natural frequencies/periods of the structure, revealing the transfer functions. These ratios exhibit pronounced peaks at those frequencies. Such analyses are especially important for Structural Health Monitoring (SHM), because performing them at different time intervals allows detection of changes in the structure's dynamic characteristics. When free-field records are available near the building, comparing the Fourier amplitude spectra of the motions recorded at the foundation with those in free-field reveals the modification of free-field motion by the buildings' presence and the influence of soil–structure interaction.

## RESULTS AND DISCUSSIONS

The obtained results are presented selectively in the following, with focus on the most significant observations and on the larger-magnitude earthquake.

Figure 4 presents the acceleration waveforms recorded during the 31 January 2020 earthquake. The P- and S-wave arrivals, as well as the amplitude and timing differences can be noticed. For each recording channel, the maximum acceleration amplitudes ($a_{max}$) are marked on the plot and summarized in Table 2, together with the corresponding maximum velocities ($v_{max}$), displacements ($d_{max}$), and Arias intensities ($I_A$). The table also includes the values recorded during the second earthquake considered, i.e., the one on 3 December 2023.

Figure 5 displays the Husid plots for the 31 January 2020 earthquake. As it can be noticed, the onset of the most pronounced intensity increase occurs around second 50 of the record, indicating when the maximum amount of energy is induced during this event.

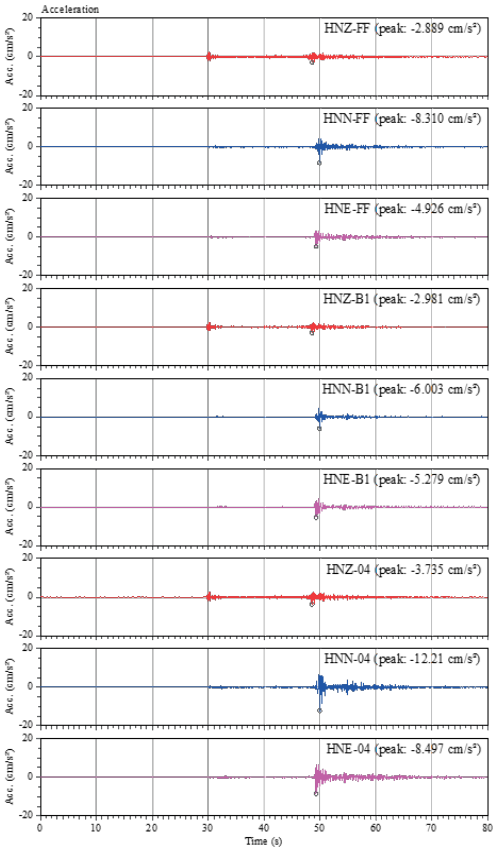



Figure 4. Acceleration waveforms for the 31.01.2020 earthquake

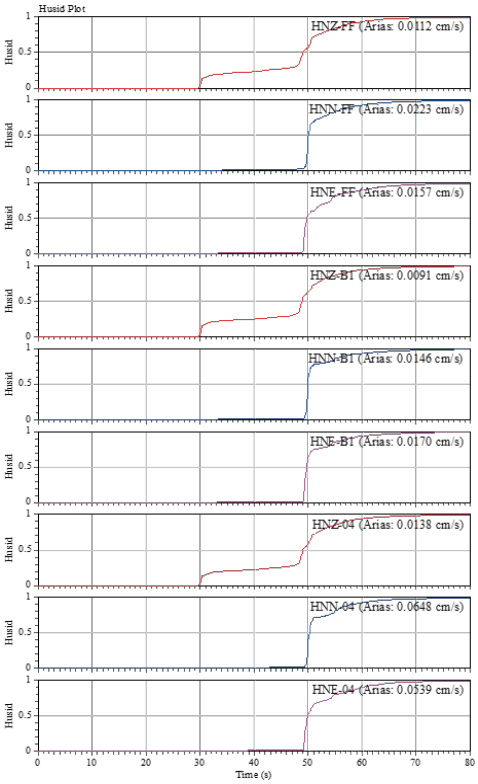



Figure 5. Husid plots for the 31.01.2020 earthquake

Values in Table 2 also show that, as expected, all ground motion parameters recorded for the 3 December 2023 ($M_L$=4.8) event are below those of the 31 January 2020 ($M_L$=5.2) event. They also reflect the differences in the spectral content of the two earthquakes considered.

In what concerns the variation of the parameters between the FF (free field), B1 (basement) and 04 (roof) sensors, an interesting attenuation of the amplitudes of the ground motion by the building, on certain frequency ranges, can be noticed – from FF to B1 – for the HNN components and, as a weaker effect, for the HNZ components. Regarding the B1–04 variation, amplification is observed consistently, on wide frequency ranges, especially for the horizontal channels. The features are also noticeable in Figure 6. These general amplification patterns are observable for both earthquakes.

An analysis of the spectral content of the FF, B1 and 04 components, as reflected by the acceleration spectra in Figure 6 and the values in Table 3, shows that the largest spectral peaks occur at short periods ($T < 0.5$ s) for both earthquakes, with differences regarding the dominant peaks of the spectra, but with similarities in the location of other peaks, which are persistent for both earthquakes.

Table 2. Maximum values of accelerations ($a_{max}$), velocities ($v_{max}$), displacements ($d_{max}$), and Arias intensities ($I_A$) for the earthquakes of 31 January 2020 ($M_L$ = 5.2) and 3 December 2023 ($M_L$ =4.8)

| | 31.01.2020 Earthquake ($M_L$ = 5.2) | | | | 03.12.2023 Earthquake ($M_L$ = 4.8) | | | |
|---|---|---|---|---|---|---|---|---|
| Channel | $a_{max}$ (cm/s$^2$) | $v_{max}$ (cm/s) | $d_{max}$ (cm) | $I_A$ (cm/s) | $a_{max}$ (cm/s$^2$) | $v_{max}$ (cm/s) | $d_{max}$ (cm) | $I_A$ (cm/s) |
| HNN-04 | 12.210 | 0.522 | 0.0456 | 0.0648 | 4.049 | 0.155 | 0.0083 | 0.0053 |
| HNE-04 | 8.497 | 0.428 | 0.0388 | 0.0539 | 2.015 | 0.094 | 0.0076 | 0.0031 |
| HNZ-04 | 3.735 | 0.124 | 0.0094 | 0.0138 | 2.254 | 0.042 | 0.0020 | 0.0019 |
| HNN-B1 | 6.003 | 0.344 | 0.0332 | 0.0146 | 1.669 | 0.066 | 0.0044 | 0.0011 |
| HNE-B1 | 5.279 | 0.277 | 0.0314 | 0.0170 | 1.089 | 0.074 | 0.0068 | 0.0009 |
| HNZ-B1 | 2.981 | 0.121 | 0.0093 | 0.0091 | 1.912 | 0.039 | 0.0020 | 0.0013 |
| HNN-FF | 8.310 | 0.366 | 0.0353 | 0.0223 | 2.459 | 0.083 | 0.0046 | 0.0018 |
| HNE-FF | 4.926 | 0.278 | 0.0320 | 0.0157 | 1.121 | 0.072 | 0.0069 | 0.0010 |
| HNZ-FF | 2.889 | 0.119 | 0.0089 | 0.0112 | 2.068 | 0.040 | 0.0030 | 0.0015 |

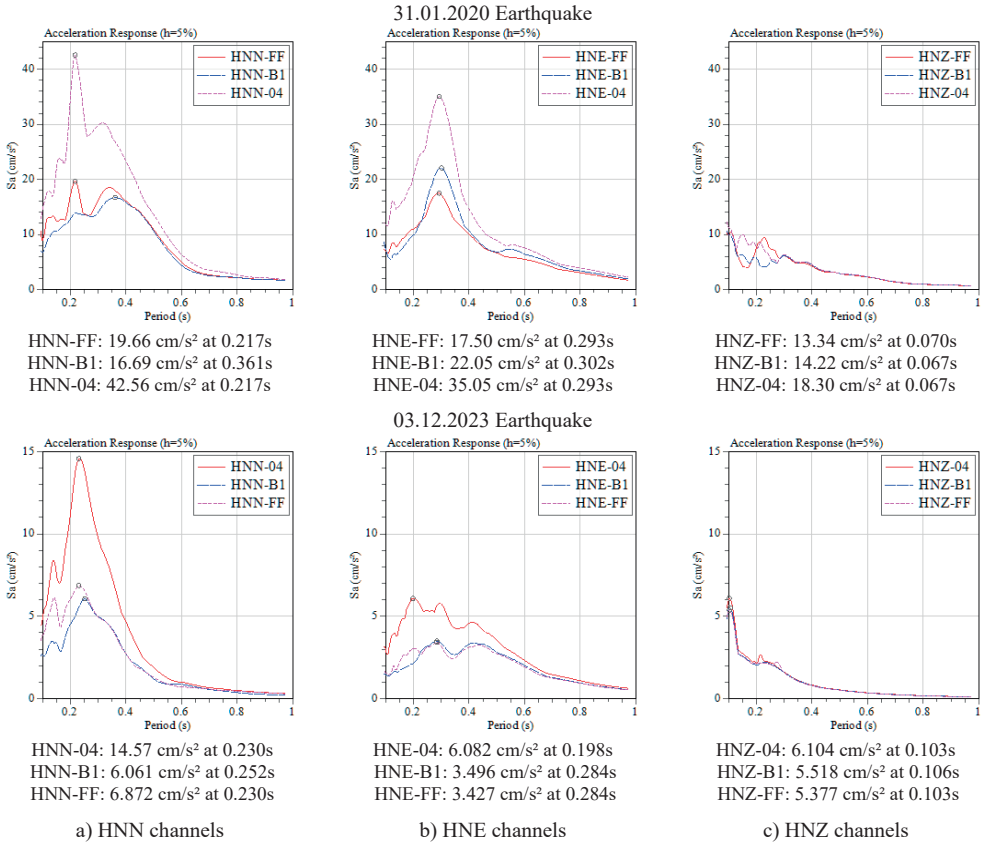



Figure 6. Acceleration spectra (5% damping) for the 31.01.2020 and 03.12.2023 earthquakes

Table 3. Periods corresponding to the maximum peaks if the acceleration spectra for the earthquakes of 31 January 2020 ($M_L = 5.2$) and 3 December 2023 ($M_L = 4.8$)

| Channel | 31.01.2020 Earthquake ($M_L = 5.2$) | 03.12.2023 Earthquake ($M_L = 4.8$) |
|---|---|---|
| HNN-04 | 0.217s | 0.230s |
| HNE-04 | 0.293s | 0.198s |
| HNZ-04 | 0.067s | 0.103s |
| HNN-B1 | 0.361s | 0.252s |
| HNE-B1 | 0.302s | 0.284s |
| HNZ-B1 | 0.067s | 0.106s |
| HNN-FF | 0.217s | 0.230s |
| HNE-FF | 0.293s | 0.284s |
| HNZ-FF | 0.070s | 0.103s |

Power spectra (with values listed in Table 4 and illustrated in Figure 7) show a more differentiated situation, given their multiple peaks, characteristic to a broadband motion. For the 31.01.2020 earthquake, a persisting period of approximately 0.44 seconds can be noticed on the HNN channels, where amplitudes increase progressively from FF to B1 and then, to 04.

Table 4. Periods corresponding to the dominant peaks of the power spectra, 30.01.2020 and 3.12.2023 earthquakes

| Channel | 30.01.2020 | 03.12.2023 |
|---|---|---|
| HNN-04 | 0.235 | 0.225 |
| HNE-04 | 0.306 | 0.181 |
| HNZ-04 | 0.183 | 0.254 |
| HNN-B1 | 0.439 | 0.314 |
| HNE-B1 | 0.328 | 0.311 |
| HNZ-B1 | 0.352 | 0.113 |
| HNN-FF | 0.442 | 0.314 |
| HNE-FF | 0.330 | 0.288 |
| HNZ-FF | 0.235 | 0.113 |

For the HNN-04 channel (roof), the 0.44 seconds peak is not the dominant one, as it is exceeded by the peak at $T = 0.235$ s, which most probably indicates the fundamental period

of vibration of the building on this direction, including the effects of soil-structure interaction (SSI). For the HNE channels, the FF and B1 records exhibit a clear peak at $T \approx 0.33$ s, visible also for the 04 records. The dominant peak for the roof record HNE-04 is slightly shifted to a shorter period, $T = 0.306$ s, which probably identifies the fundamental period of vibration of the building, including SSI effects, for this direction. The vertical (HNZ) channels exhibit the highest peaks at 0.235 s (FF), 0.352 s (B1) and 0.183 s (04). Again, the value $T = 0.183$ s could indicate the natural period of the structure on this direction, including SSI effects.

These assumptions will be however checked in the next section, where the transfer functions will be analysed as well.

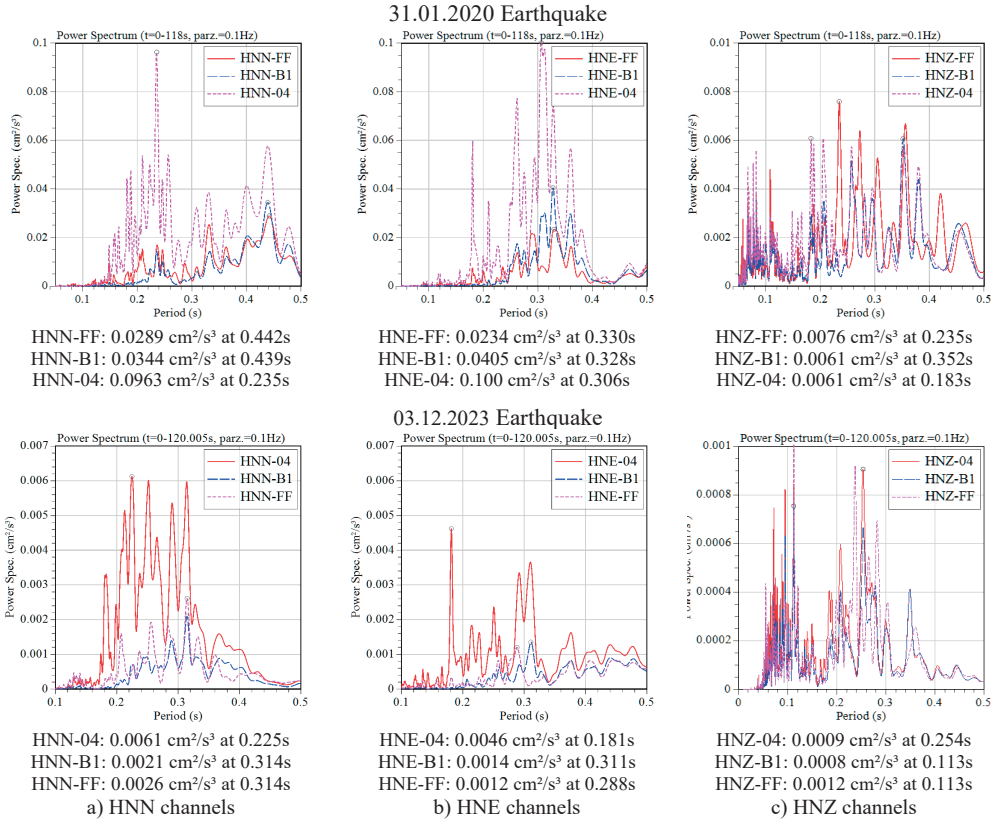



Figure 7. Power spectra for the 31.01.2020 and 03.12.2023 earthquakes

For the 03.12.2023 earthquake, the power spectra exhibit different patterns, as compared to the 31.01.2020 event. However, the two earthquakes share some common or close peaks.

Table 5 synthesizes the maximum Fourier amplitudes and their corresponding periods for the two earthquakes considered. The table shows marked differences between the two seismic events, especially the variation of amplitudes.

The pseudovelocity spectra and the equivalent velocity spectra (normalized input energy) are displayed in Figures 8 and 9, for the seismic event of 31.01.2020, while the periods corresponding to their dominant spectral peaks are synthesized in Table 6.

The spectral shapes are overall quite similar, even though their highest spectral peaks occur at different periods. The most noticeable difference appears in the spectral shapes associated with the HNN-04 channel, but also for HNZ-04.

Table 5. Maximum Fourier amplitudes and corresponding periods for the two earthquakes considered

| Channel | 31.01.2020 Earthquake | | 03.12.2023 Earthquake | |
|---|---|---|---|---|
| | Fourier max. amplitude (cm/s) | T (s) | Fourier max. amplitude (cm/s) | T (s) |
| HNN-04 | 3.973 | 0.235 | 0.654 | 0.314 |
| HNE-04 | 4.047 | 0.306 | 0.444 | 0.288 |
| HNZ-04 | 0.998 | 0.183 | 0.445 | 0.113 |
| HNN-B1 | 2.375 | 0.439 | 0.587 | 0.314 |
| HNE-B1 | 2.577 | 0.328 | 0. 471 | 0.311 |
| HNZ-B1 | 0.997 | 0.352 | 0.352 | 0.113 |
| HNN-FF | 2.175 | 0.442 | 1.002 | 0.225 |
| HNE-FF | 1.958 | 0.330 | 0.870 | 0.181 |
| HNZ-FF | 1.116 | 0.235 | 0.385 | 0.254 |

Table 6. Periods corresponding to the highest spectral peaks of the pseudovelocity spectra and of the equivalent velocity spectra (normalized input energy), 31.01.2020 earthquake

| Channel | From pseudovelocity spectra | From normalized input energy spectra |
|---|---|---|
| HNN-04 | 0.340 | 0.237 |
| HNE-04 | 0.302 | 0.311 |
| HNZ-04 | 0.383 | 0.204 |
| HNN-B1 | 0.432 | 0.432 |
| HNE-B1 | 0.311 | 0.330 |
| HNZ-B1 | 0.383 | 0.361 |
| HNN-FF | 0.372 | 0.432 |
| HNE-FF | 0.302 | 0.330 |
| HNZ-FF | 0.230 | 0.276 |

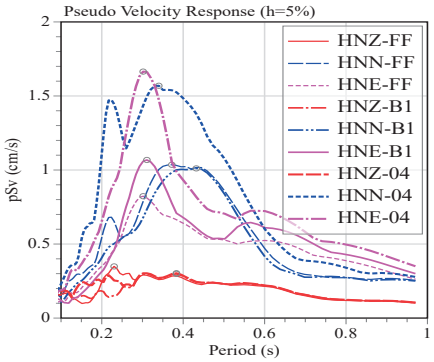



Figure 8. Pseudovelocity spectra for the 31.01.2020 earthquake

However, for HNN-04, both spectra have a peak at $T = 0.22$ - 0.237 s, which is consistent with the values obtained from the power spectrum and which also indicates a maximum of the energy induced by the earthquake.

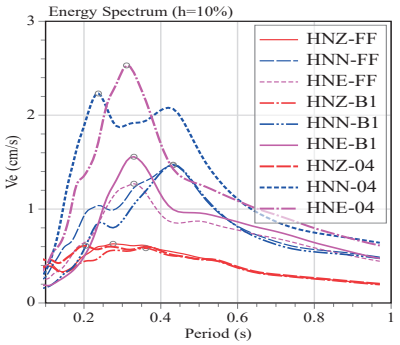



Figure 9. Equivalent velocity spectra (normalized input energy) for the 31.01.2020 earthquake

A distinct part of the study focused on transfer functions, both from the basement to the roof of the building and between the free-field motion and the basement motion. The first type of transfer function provides insight into the natural periods of the building, while the second type highlights how the presence of the structure modifies the motion of the surrounding soil.

Figures 10 and 11 show the transfer functions from basement to roof, while Figures 12 and 13 show the transfer functions from free field to basement motion.

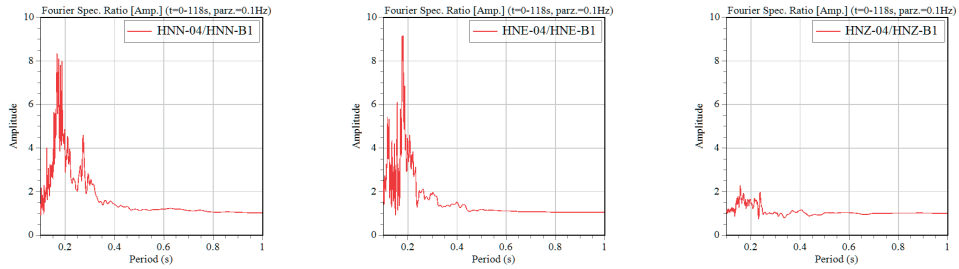
Tables 7 and 8 show the periods corresponding to the dominant peaks of the transfer functions between the foundation motion and the roof motion and, respectively, between the ground motion and the foundation motion. The first set of values is generally used to represent the natural vibration periods of the building, while the second set serves for highlighting the influence of the buildings' presence.

Table 7. Periods corresponding to the highest peaks of the transfer functions between the foundation and the roof motions - 31.01.2020 and 03.12.2023

| Channels | 31.01.2020 | 03.12.2023 |
|---|---|---|
| HNN-04/HNN-B1 | 0.167 s | 0.179 s |
| HNE-04/HNE-B1 | 0.180 s | 0.179 s |
| HNZ-04/HNZ-B1 | 0.157 s | 0.180 s |

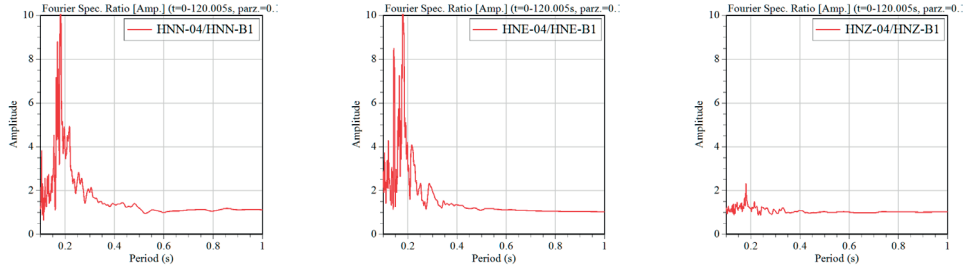
Table 8. Periods corresponding to the highest peaks of the transfer functions between the ground motion and the foundation motion - 31.01.2020 and 03.12.2023

| Channels | 31.01.2020 | 03.12.2023 |
|---|---|---|
| HNN-B1/HNN-FF | 0.256 s | 0.272 s |
| HNE- B1/HNE-FF | 0.314 s | 0.309 s |
| HNZ- B1/HNZ-FF | 0.256 s | 0.256 s |



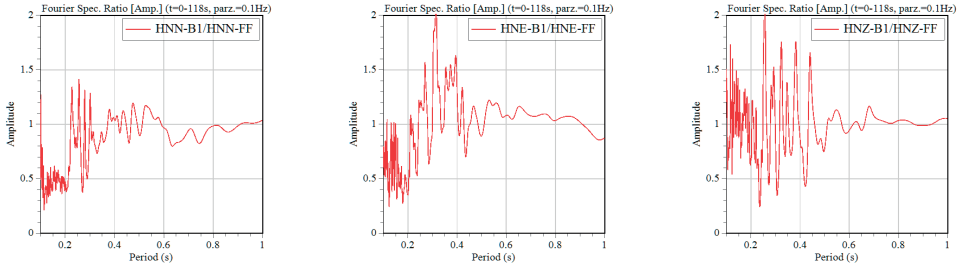

a) HNN-04/HNN-B1: 8.329 at 0.167 s b) HNE-04/HNE-B1: 9.145 at 0.180 s c) HNZ-04/HNZ-B1: 2.278 at 0.157 s

Figure 10. Transfer functions (basement – roof), 31.01.2020 earthquake



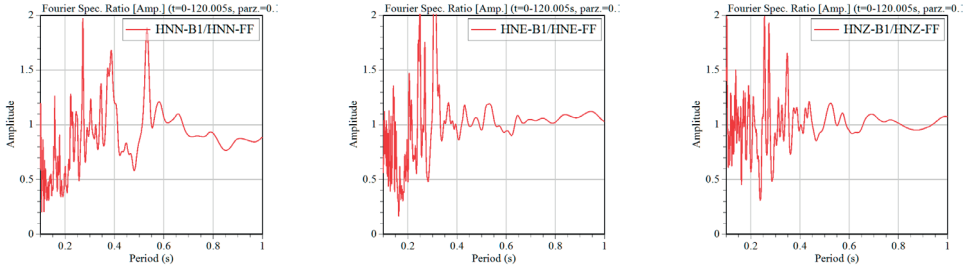

a) HNN-04/HNN-B1: 10.76 at 0.179 s b) HNE-04/HNE-B1: 12.88 at 0.179 s c) HNZ-04/HNZ-B1: 2.307 at 0.180 s

Figure 11. Transfer functions (basement – roof), 03.12.2023 earthquake




a) HNN-B1/HNN-FF: 1.413 at 0.256 s b) HNE-B1/HNE-FF: 2.058 at 0.314 s c) HNZ-B1/HNZ-FF: 2.228 at 0.256 s

Figure 12. Transfer functions (ground – foundation), 31.01.2020 earthquake




a) HNN-B1/HNN-FF: 1.973 at 0.272 s b) HNE-B1/HNE-FF: 3.417 at 0.309 s c) HNZ-B1/HNZ-FF: 1.870 at 0.256 s

Figure 13. Transfer functions (ground - foundation), 03.12.2023

A case study summary, presenting periods corresponding to dominant peaks of Fourier spectra and transfer functions, is given in Table 9.

As it can be noticed from the first row of the table, the natural periods of vibration of the monitored building, without considering SSI (~0.16 - 0.18 s) are characteristic to a rigid structure, which is the case, considering its constructive system. The 0.18 s value results from the analysis of both earthquakes. It is interesting to notice that the 0.16 - 0.18 s value also represents the dominant peak of the transfer function for the vertical components of both earthquakes, which could indicate coupling between the horizontal and the vertical motion, possibly due to rocking or torsion, given the shape of the central section of the building, where sensors are located.

Table 9. Case study summary – BTH station, earthquakes on 31 January 2020 and on 3 December 2023 (in parentheses). Periods corresponding to the highest peaks of spectral and transfer functions

| | Source | HNN channel | HNE channel | HNZ channel | Analysis outcome |
|---|---|---|---|---|---|
| 1. | Transfer functions between the basement and the roof (04/B1) | 0.167 s (0.179 s) | 0.180 s (0.179 s) | 0.157 s (0.180 s) | Natural periods of the structure, assuming a fixed base (no SSI) |
| 2. | Fourier amplitude spectra & power spectra of the roof record (04) | 0.235 s (0.314s) | 0.306 s (0.288 s) | 0.183 s (0.113 s) | Natural periods of the structure, considering soil–structure interaction (SSI) |
| 3. | Fourier amplitude spectra & power spectra of the free field record (FF) | 0.442 s (0.225 s) | 0.330 s (0.181s) | 0.235 s (0.254s) | Information on ground motion spectral content |
| 4. | Fourier amplitude spectra & power spectra of the basement record (B1) | 0.439 s (0.314 s) | 0.328 s (0.311 s) | 0.352 s (0.113 s) | Information on the frequency content of the motion at the building's foundation |
| 5. | Transfer functions between the ground motion and the foundation motion (B1/FF) | 0.256 s (0.272 s) | 0.314 s (0.309 s) | 0.256 s (0.256 s) | Kinematic effects at the buildings' foundation |

Nevertheless, transfer function amplitudes are small in the amplification range. Most probably, 0.18 s is not the actual natural period of the building on the vertical direction, and possibly the 0.113 s value resulting from the analysis of the second earthquake could be a more plausible value.

The influence of the soil-structure interaction, reflected in the increase of the natural periods, can be noticed by comparing the values listed in the first two rows of the table. The exception occurs for the vertical component of the roof record on 03.12.2026, as explained above.

By analysing rows 3 and 4 of the table, it results that, for the horizontal components of the first earthquake, there is practically no influence of the presence of the building on the spectral content of the ground motion, in the case of the first earthquake. For the horizontal components of the second earthquake and for both vertical components, the highest peak values lack relevance due to the presence of multiple comparable peaks on the spectrum, which makes it difficult to discern the dominant periods.

Row 5 of the table illustrates the kinematic effects at the buildings' foundation. The dominant peaks of the transfer function are highly stable and show little variation across the two earthquakes, which suggests that the soil-foundation system moderately amplifies the ground motion over a rather narrow frequency band, i.e., 0.26 - 0.31 s, with higher values generally occurring only up to about 0.4 s.

It is important to note that the values in Table 9 should be interpreted only in correlation with the actual shape of the diagrams which they refer to. For instance, for many of the analysed graphs, multiple secondary peaks can be observed. Although their amplitudes are smaller than that of the dominant peak, they still indicate additional significant motion frequencies.

## CONCLUSIONS

The article presented a detailed analysis of the seismic response of a higher education building that has been instrumented for over a decade and is located on the campus of the University

of Agronomic Sciences and Veterinary Medicine in Bucharest. Unlike many instrumented buildings in densely populated urban areas, the specific location of the building has allowed the installation of vibration sensors not only on the structure itself, but also within a nearby green space, thus enabling the continuous acquisition of co-located structural and free-field seismic records. The data recorded during two recent seismic events (local magnitude 5.2 and 4.8) originating in the seismogenic Vrancea zone of Romania were processed. Response spectra, Fourier amplitude spectra, power spectra, pseudovelocity spectra, normalized input energy spectra and transfer functions were computed, for free field, basement and roof records.

The most significant observations and conclusions are presented below.

- The natural periods of the building have been identified as ~0.17 s (HNN), ~0.18 s (HNE) – without considering soil-structure interaction (SSI), and ~0.24 s (HNN), ~0.31 s (HNE) – with the consideration of SSI. The vertical periods, more difficult to determine due to the broad frequency content of the motion are probably around 0.11 s. The values are in line with previous studies of the authors, based on a different approach (Dobre et al., 2024).
- The frequency content of the two considered earthquakes differs significantly, which also impacts the response of the soil-foundation system.
- The influence of the soil-structure interaction is considerable for the horizontal components of both earthquakes. Coupling between the horizontal and the vertical motion was also identified, indicating possible rocking or torsion effects.
- Kinematic effects at the foundation of the building are moderate and stable, being confined to a rather narrow frequency range.
- Complex resonance phenomena were identified with respect to different frequencies of the site, such that additional investigations are needed, especially concerning soil conditions determined from deeper borehole measurements.
- Pseudovelocity and normalized energy spectra provide important information on the spectral content of the ground motion and serve as indicators of the periods associated with the maximum destructive potential of the seismic motion. According to the results obtained, the most destructive period interval for both earthquakes considered in the study is situated between 0.2 and 0.6 seconds.

The results of the study gain additional relevance when considered in the dual context of the recent seismicity in Bucharest and of the need for the identification of the optimal approaches to the structural health monitoring of buildings located in densely populated urban areas.

## ACKNOWLEDGEMENTS

This work was performed in the PNCDI 2022-2027 framework, within the “Nucleu” Programme PN 23 35 “ECODIGICONS”, Project PN 23 35 01 01 “Integrative concept for the digital analysis of data from the large-scale seismic monitoring of the national territory and of the building stock, intended for the rapid identification of the destructive potential of seismic events produced in Romania and in the adjacent regions”, with the support of the National Authority for Research. The maintenance and operation of the infrastructures used were supported by funding provided by UEFISCDI to the National Network for the Seismic Monitoring and Protection of the Building Stock (RNMPSPC–I.O.S.I.N.) at INCD URBAN-INCERC, through PNCDI IV, Programme 5.5 "Research Infrastructures". This financial support is gratefully acknowledged.

## REFERENCES

Bălan, S., Cristescu, V. and Cornea, I. (coordinators) (1982). *The Romania Earthquake of 4 March 1977* (in Romanian). Bucharest: Editura Academiei.

Berg, G. V., Bolt, B. A., Sozen, M. A., & Rojahn, C. (1980). Earthquake in Romania March 4, 1977: An engineering report (Report No. PB82-163114). National Science Foundation. https://nehrpsearch.nist.gov/article/PB82-163114/XAB.

COSMOS (2001). *Guidelines for Installation of Advanced National Seismic System (ANSS) Strong-Motion Reference Stations*. Consortium of Organizations for Strong-Motion Observation Systems. Available online at https://www.strongmotion.org/ resources-publications/blog-post-title-four-c43d8-7pjna-8hmwj-cfg9y-xsceh-z5scn-cpx87

Dobre, D., Dragomir, C.S., Dobrescu, C.F., Craifaleanu, I.G., Georgescu, E.S., & Zaharia, M.C. (2024). The evolution of the dynamic characteristics of the soil-structure system in case of a university building seismic monitoring. *Scientific Papers. Series E. Land Reclamation, Earth Observation & Surveying, Environmental Engineering*, Vol. XIII, Print ISSN 2285-6064, 408-416.

Kashima, T. (2016). *ViewWave Manual*, January 2016, for Version 2.2.0. Available online at https://smo.kenken.go.jp/~kashima/ sites/default/files/viewwave/vwmanual220.pdf.

Kashima, T. (2024). *ViewWave* (Version 2.2.8) [Computer software]. Kashima's Office - BRI Strong Motion Network. https:// smo.kenken.go.jp/~kashima/view wave

Skolnik, D. (2010). *Free-field stations installation guidelines for post-event assessment of nearby structures*. Kinemetrics, U.S.A.

Scientific Papers. Series E. Land Reclamation, Earth Observation & Surveying, Environmental Engineering. Vol. XV, 2026
Print ISSN 2285-6064, CD-ROM ISSN 2285-6072, Online ISSN 2393-5138, ISSN-L 2285-6064

# A NOVEL CONCEPT FOR A SUBMERGED WAVE ENERGY CONVERTER

**Alexandru DIMACHE, Iulian IANCU**

Technical University of Civil Engineering Bucharest, 122-124 Lacul Tei Blvd,
District 2, Bucharest, Romania

Corresponding author email: alexandru.dimache@utcb.ro

***Abstract***

*Wave energy represents an important renewable resource with significant potential for sustainable energy production. As interest in alternative energy sources continues to grow, this paper presents the conceptual design and preliminary laboratory testing of a novel submerged wave energy converter based on differential pressure conversion. The submerged wave energy converter will be evaluated and optimized in the Hydraulics and Environmental Protection Laboratory of the Technical University of Civil Engineering Bucharest, under controlled wave conditions with varying wavelengths and periods. Preparatory measurements of wave characteristics will guide the optimal dimensioning of the device to maximize energy capture efficiency. Preliminary results identify relevant wave parameters and indicate potential power generation efficiency. The advantages of the device are primarily based on the concentration of the large but diffuse hydraulic energy of waves into the high-pressure hydraulic energy of a working fluid, enabling operation of industrial installations with superior efficiency. Additionally, the research investigates the device's effect on reducing wave energy, contributing to coastal protection and the preservation of marine ecosystems.*

***Key words****: costal protection, wave energy, differential pressure conversion, energy capture efficiency, submerged wave energy convertor.*

## INTRODUCTION

Wave energy constitutes a significant renewable resource due to its high-power density, widespread availability in coastal regions, and minimal environmental emissions. Sea waves are generated primarily by wind transferring energy from the atmosphere into the sea surface. Waves effectively concentrate solar energy over vast areas of the world's oceans and seas. As a result, the theoretical global potential of wave energy resources has been estimated to reach tens of thousands of terawatt-hours per year (Wen & Low, 2026). This value exceeds current annual global electricity consumption, in principle indicating a substantial but largely untapped energy reservoir.

For the Romanian coastline along the Black Sea, which stretches approximately 200 km, studies estimate a potential wave energy around 8 TWh/year. The technically exploitable potential is assessed at roughly half of this value, approximately 4 TWh/year (Degeratu & Bandoc, 2007). The wave energy potential of the Black Sea is significantly lower than that of offshore wind energy. This suggests that, although wave energy may contribute to the Romanian national energy mix, it is unlikely to match the scale of offshore wind resources.

However, wave energy remains attractive for coastal regions where land availability is limited, or energy costs are high. This is due to the higher power density of waves compared to many other renewable sources (Guillou et al., 2020). Moreover, wave energy's predictable nature offers potential advantages for grid integration and energy planning relative to more variable sources (Wen & Low, 2026).

Even though the technological maturity and commercial implementation of wave energy converters (WECs) is behind solar and wind technologies, ongoing research highlights the potential of wave energy to contribute significantly to future sustainable energy systems and climate change mitigation strategies (Azam et al., 2024).

There are three main concepts of wave energy converters (WECs): (a) oscillating water column converters; (b) overtopping (reservoir-type) converters; and (c) oscillating body converters. The devices from the last category, oscillating body converters, can be either floating or submerged and includes attenuators and point absorbers. Attenuators are elongated, articulated

structures positioned parallel to the direction of wave propagation, and the captured energy is generated through the flexing of their joints. Point absorbers are relatively small floating bodies that oscillate vertically (heave motion). The energy is extracted from the relative movement between the floating body and a fixed reference point. The WECs with oscillating body category includes, also, differential pressure converters. Those devices are typically installed on the seabed in near-shore coastal areas.

In Romania, a few research efforts have been undertaken in the field of wave energy harvesting. Moreover, regarding differential pressure converters, have not yet resulted in commercially developed products (Tatu, 2014).

This paper introduces the conceptual design and preliminary laboratory evaluation of a novel submerged wave energy converter (WEC) that operates on the principle of differential pressure conversion. The proposed device is intended to harness the energy of sea waves by exploiting pressure variations of the water at the seabed, due to the variation of water level induced by the waves.

The advantages of the device are based, first at all, on the fact that the large, but diffuse, hydraulic energy of the waves is concentrated into the hydraulic energy of a working fluid at high pressures which then can be taken over by a hydraulic Power Take-Off system (PTO). PTO converts hydraulic energy into electrical energy through a generator. Second at all, the proposed device offers potential advantages in terms of stability, reduced visual impact, and resilience in harsh marine conditions.

Experimental investigations are conducted at the Hydraulics and Environmental Protection "Dumitru Cioc" Laboratory of the Technical University of Civil Engineering Bucharest (UTCB), under fully controlled wave conditions (Figure 1).



Figure 1. Wave channel, Hydraulics and Environmental Protection "Dumitru Cioc" Laboratory

The testing program will systematically vary wavelengths, periods, and amplitudes to assess the device's performance, characterize its energy conversion efficiency, and provide data to inform subsequent design optimization and scale-up for nearshore deployment. The results of this study are expected to contribute to the development of efficient, site-adapted submerged WECs suitable for the Romanian Black Sea coast and similar environments worldwide.

The paper also presents preliminary results aimed at identifying relevant wave parameters and estimating the potential power generation efficiency of the proposed device. Furthermore, the research investigates the attenuation effect of the converter on incident wave energy, with implications for coastal erosion protection and the mitigation of extreme wave event impacts.

## CONCEPTUAL DESIGN OF THE DIFFERENTIAL PRESURE CONVERTOR

The wave energy convertor (Figures 2 and 3) consists of a fixed part, the base frame of the device (7), and a movable part, a light plate (2) that rests on two flexible steel springs (3) (Figures 2 and 3). The movable plate together with the springs is enclosed in a waterproof foil (1), fixed to the upper part of the base frame

through a waterproof foil fixing frame (8). Water access is made at the base of the device, through holes (4) provided with valves (5) that allow unidirectional access, in the direction of water flow.

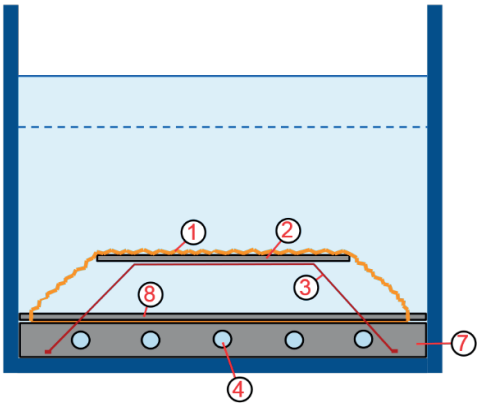



Figure 2. Schematic of the wave energy capture device – front view of the device in the wave channel

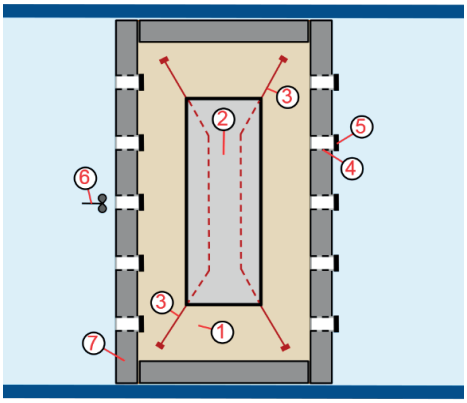



Figure 3. Schematic of the wave energy capture device – top view of the device

The notations in the Figure 2 and Figure 3 represent: 1- waterproof foil, 2- light plate, 3 - steel wire (spring), 4 - holes, 5 - valves, 6 - mill, 7 base frame, 8 waterproof foil fixing frame.

## PRELIMINARY MEASUREMENTS FOR WAVE CHARACTERISTICS DETERMINATION

For the dimensioning of the differential pressure converter, experimental determinations were carried out in the wave channel under fully controlled wave conditions to determine the relevant wave parameters.

The wave channel has a length of 16 m and a width of 1 m. The maximum water depth in the channel is 0.9 m, and the generated waves correspond to water depths ranging from 0.2 m to 0.6 m. The wave channel is equipped with a wave generator at one end. The wave generation system consists of a movable flap, articulated at the bottom of the channel and set in motion at the top by a connecting crank-slider mechanism. At the opposite end of the channel a wave energy attenuator is installed. This is designed to dissipate the wave energy and prevent the occurrence of the wave reflection phenomenon, which can outhouse alter the characteristics of the incident waves (Iancu et al., 2024).

The experimental determinations systematically varied the wavelengths, periods and amplitudes of the waves generated in the wave channel at different water depths. To measure the wave amplitude and height, two level sensors placed at 4 m from each other were used, as shown in Figure 4.



Figure 4. Placement of pressure sensors in the wave channel

The wavelength and period of the wave were determined by measuring the distance and time between two consecutive wave peaks. Based on those measurements, the wave propagation speed (celerity) of the waves was calculated, using the formula:

$$c = \frac{\lambda}{T}$$

The results obtained from the experimental tests are presented in Table 1.

Table 1. Waves characteristics determined from experimental test

| Water depth H (cm) | Wave height h (cm) | Wavelength λ (m) | Period T (s) | Wave celerity c (m/s) |
|---|---|---|---|---|
| 20 | 2 | 1.32 | 1.05 | 1.26 |
| | 3 | 1.02 | 0.89 | 1.15 |
| | 3 | 0.96 | 0.82 | 1.17 |
| | 4 | 0.85 | 0.76 | 1.12 |
| | 4 | 0.65 | 0.68 | 0.96 |
| 30 | 6 | 0.68 | 0.63 | 1.08 |
| | 7 | 1.42 | 1.01 | 1.41 |
| | 8 | 1.20 | 0.88 | 1.36 |
| | 8 | 1.03 | 0.85 | 1.21 |
| | 8 | 0.84 | 0.73 | 1.15 |
| 40 | 8 | 0.66 | 0.61 | 1.08 |
| | 10 | 1.50 | 1.00 | 1.50 |
| | 10 | 0.81 | 0.70 | 1.16 |
| | 13 | 1.19 | 0.85 | 1.40 |
| | 14 | 1.12 | 0.89 | 1.26 |
| 50 | 10 | 0.74 | 0.72 | 1.03 |
| | 12 | 0.95 | 0.76 | 1.25 |
| | 13 | 1.74 | 1.15 | 1.51 |
| | 14 | 1.14 | 0.82 | 1.39 |
| | 15 | 1.28 | 0.85 | 1.51 |
| 60 | 13 | 0.82 | 0.68 | 1.21 |
| | 15 | 1.03 | 0.76 | 1.36 |
| | 16 | 1.18 | 0.86 | 1.37 |
| | 20 | 1.34 | 0.90 | 1.49 |
| | 24 | 1.67 | 1.04 | 1.61 |

The parameters experimentally determined in the wave channel and considered were those corresponding to the waves that characterize, at natural scale, the waves in the Black Sea, in the Romanian coastal area.

Wind-generated waves have periods of approximately 1 to 30 s, with dominant periods for storm surges being between 5 and 15 s (Coveianu, 2016).

Figure 5 presents a schematic of the differential pressure converter's placement in the wave channel, along with the wave parameters that will determine the device dimensions and efficiency.

Based on these experimental determinations, a preliminary estimate of the device's energy generation efficiency was performed using the theoretical framework of differential pressure conversion.

These estimates will be validated upon scaled physical model testing of the converter in the wave channel under the wave conditions established herein.

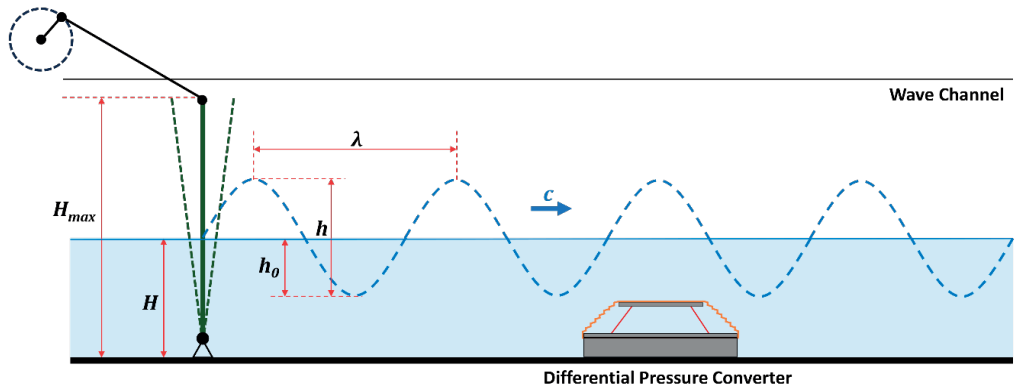



Figure 5. Schematic of the wave energy capture device – front view of the device in the wave channel

## PERFORMANCE ANALYSIS OF THE DIFFERENTIAL PRESSURE CONVERTER

Essentially, the energy converter behaves like a volumetric pump. Volumetric pumps are hydraulic machines that transfer fixed volumes of fluid at equal intervals of time between the suction and discharge sections of the pump, using a piston driven by a crank-rod mechanism.

The power of such a pump is calculated using the formula:

$$P = \Delta p \cdot \Delta Q \text{ (Watt)}$$

where $\Delta p$ is pressure variation created by the piston (Figure 6) (force applied to the piston / piston surface) (N/m$^2$) and $\Delta Q$ is flow variation (piston displacement, i.e. volume swept by the piston / half-period of the reciprocating motion) (m$^3$/s).

In the case of the converter, the piston is represented by the movable cover (light plate).
The pressure variation created by the piston $\Delta p$ is the pressure variation given by the wave and which produces the oscillation of the cover placed on the springs. The suction and discharge are represented by the access and exit slots provided with one-way valves.
Unlike the classic volumetric pump, in the case of the converter, the displacement of the piston (light plate) and, implicitly, $\Delta Q$ are not a fixed value. These and, implicitly, the performances of the converter proposed in the work, depend on several parameters:

- wave characteristics ($H$, $h$, $\lambda$);
- the mass of the device cover (light plate), $m$;
- the elastic constant of the springs, $k$;
- the hydraulic resistance of suction and discharge valves.

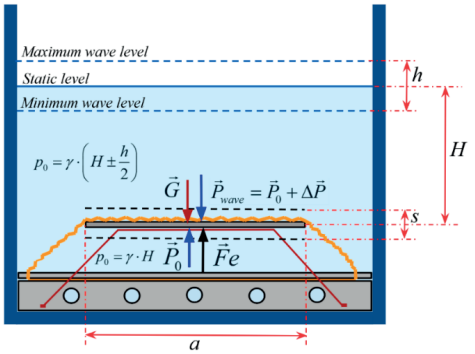



Figure 6. Representation of the forces acting on the energy converter

In addition, the mass of the movable cover together with the elastic constant of the springs is defined as the natural oscillation period of the system, $T = 2 \cdot \pi \cdot \sqrt{\frac{m}{k}}$ which is conjugated to the wave period.
The outer part of the movable cover, the one exposed to the wave action, is subjected to a variable pressure, between the limits:

$$p = \gamma \cdot \left(H \pm \frac{h}{2}\right),$$

which transmits to the water inside the device the pressure variation:

$$\Delta p = \gamma \cdot \frac{h}{2}.$$

and this value can be calculated.

In nature, the pressure variation given by the oscillatory movement of the waves can be calculated with the relationship (Luca & Luca, 2002; Sorensen, 2006; Holthuijsen, 2007):

$$\Delta p_H = \pm\rho \cdot g \cdot \frac{\frac{h}{2}}{ch\left(\frac{2 \cdot \pi \cdot H}{\lambda}\right)}$$

where:

- $\Delta p_H$ (Pa) represents the pressure variation at depth $H$ (m);
- $\lambda$ (m) represents the wavelength of the wave;
- $h$ (m) represents the height of the wave;
- $\rho$ (kg/m$^3$) represents the density of water;
- $H$ (m) represents the depth of water at which the converter is located.

Instead, as shown, $\Delta Q$ and, implicitly, the converter's performance, depend on those parameters mentioned above and the experimental measurements on the reduced-scale model in the wave channel aim to find the influence of these parameters with the final goal of finding that combination that leads to maximum efficiency. During the experiments, it is possible to know, respectively measure, in addition to the wave characteristics (period, wavelength):

- the mass of the cover;
- the elastic constant of the springs;
- the vertical displacement/oscillation of the cover from which $\Delta Q$ results;
- the hydraulic resistance of suction and discharge valves.

The power absorbed by the converter can then be calculated for each combination of the mentioned constructive parameters.
To this end, it is proposed:

- measuring the water velocities through the orifices provided with valves;
- measuring the vertical displacement/ oscillation of the cover.

The advantages of the proposed constructive structure are the following:

- all the previously mentioned parameters can be easily changed; the elastic system supporting the movable cover can be removed from the box, allowing the change of the elastic constant $k$ by replacing the springs;
- the additional masses on the movable cover can be changed, allowing the calculation of the elastic constant with precision;

- since the converter box is equipped with one-way valves (flaps), the Archimedean force is equal to zero, so the converter box can be easily placed on the bottom of the channel; the waterproof foil allows water access to the box only through the valves.

## CONCLUSIONS

The paper introduces a novel submerged wave energy converter operating on the principle of differential pressure conversion, starting with a preliminary experimental program carried out under controlled conditions in the wave channel. The proposed converter, comprising a movable cover supported by calibrated steel springs, enclosed within a waterproof membrane and equipped with unidirectional valves, constitutes a structurally simple yet physically coherent solution for harnessing the oscillatory pressure field generated by surface waves at seabed level. The experimental measurements conducted across a systematic variation of water depths (20-60 cm), wave heights (2-24 cm), wavelengths (0.65-1.74 m), and periods (0.61-1.15 s) provided a comprehensive characterization of the wave parameters reproducible in laboratory conditions. The wave celerity values recorded, ranging from 0.96 to 1.61 m/s, are consistent with theoretical predictions for shallow-water wave propagation and confirm the reliability of the measurement methodology employed. These determinations establish the hydrodynamic baseline required for dimensioning the differential pressure converter, ensuring that the natural oscillation period of the cover-spring system can be tuned to resonate with the incident wave period, a condition essential for maximizing energy capture efficiency.

From an analytical standpoint, the converter behaves as a volumetric pump in which the pressure variation, governed by the wave height and water depth, drives a variable volumetric flow through the system. The theoretical framework presented demonstrates that the output power is a function of both wave characteristics and constructive parameters – specifically the mass of the movable cover, the elastic constant of the spring system, and the hydraulic resistance of the valves – all of which are independently adjustable in the proposed experimental setup.

Beyond its energy harvesting function, the proposed device presents a secondary benefit of considerable practical relevance: through the attenuation of incident wave energy, the converter contributes to the reduction of coastal erosion. This dual functionality, energy generation and wave energy dissipation, positions the proposed device as a potentially valuable component of integrated coastal management strategies, particularly in environments such as the Romanian Black Sea coast where wave energy resources, although modest in comparison to offshore wind potential, remain largely unexploited.

Based on preliminary wave characterization measurements, the estimates of the potential energy generation efficiency will be subject to confirmation through direct experimental testing of the converter at reduced scale in the wave channel.

The results are expected to provide the empirical basis for the design of a nearshore prototype suitable for deployment in the specific marine conditions of the Romanian coastal zone.

## ACKNOWLEDGEMENTS

This work is supported by a National Research Grants of the Technical University of Civil Engineering Bucharest (ARUST), project number UTCB-11/2025.

## REFERENCES

Azam, A., Ahmed, A., Yi, M., Zhang, Z., Zhang, Z., Aslam, T., Mugheri, S, Abdelrahman, M., Ali, A., & Qi, L. (2024). Wave energy evolution: Knowledge structure, advancements, challenges and future opportunities, *Renewable and Sustainable Energy Reviews,* 205, 114880.

Coveianu, A.L. (2016). *Marine Hydraulics Research*, Bucharest, RO: PhD Thesis.

Degeratu, M., & Bandoc, G. (2007). *Using wave energy*, Bucharest, RO: Matrix Rom, ISBN 9789737552051.

Guillou, N., Lavidas, G., & Chapalain, G. (2020). Wave Energy Resource Assessment for Exploitation – A Review. *Journal of Marine Science and Engineering*, 8(9), 705.

Holthuijsen, L. H. (2007.) *Waves in Oceanic and Coastal Waters*, Cambridge University Press, Delft University of Technology and UNESCO-IHE.

Iancu, I., Dimache, A., Bucur, O.S., & Cornea, D. (2024). Modern protection solutions against coastal erosion, *Scientific Papers. Series E. Land Reclamation, Earth Observation & Surveying, Environmental Engineering*, Vol. XIII, Print ISSN 2285-6064, 556-563.

Luca, V.O., & Luca, B.A. (2002). *Hidraulica Construcţiilor (Construction's Hydraulics)*, Orizonturi Universitare, Timișoara.

Sorensen, R., (2006). *Basic Coastal Engineering,* 3rd edition, Springer.

Tatu, G. (2014). New solution for extracting and diminishing the wave's energy, *A Opta Conferinţă a Hidroenergeticienilor din Romania, DORIN PAVEL, 22-23 mai 2014, UPB*.

Wen, Y., & Low, Y. M. (2026). Long-term resource assessment and decarbonization potential of wave energy. *Renewable Energy,* 256, E.

Scientific Papers. Series E. Land Reclamation, Earth Observation & Surveying, Environmental Engineering. Vol. XV, 2026
Print ISSN 2285-6064, CD-ROM ISSN 2285-6072, Online ISSN 2393-5138, ISSN-L 2285-6064

# A DATA-DRIVEN ANALYSIS OF SEISMIC RESPONSE AND STRUCTURAL PERFORMANCE

**Daniela DOBRE[1, 3], Iolanda-Gabriela CRAIFALEANU[1, 3], Claudiu-Sorin DRAGOMIR[2, 3], Emil-Sever GEORGESCU[3], Cornelia-Florentina DOBRESCU[3, 4]**

[1]Technical University of Civil Engineering Bucharest, 122-124 Lacul Tei Blvd, 020396, District 2, Bucharest, Romania
[2]University of Agronomic Sciences and Veterinary Medicine of Bucharest, 59 Mărăști Blvd, 011464, District 1, Bucharest, Romania
[3]NIRD URBAN-INCERC, 266 Pantelimon Road, District 2, Bucharest, Romania
[4]"Dunărea de Jos" University of Galați, 47 Domnească Street, Galați, Romania

Corresponding author email: dobred@hotmail.com

***Abstract***

*Data obtained from seismic instrumentation campaigns enable the identification of buildings' dynamic characteristics, the objective evaluation of structural performance, and the investigation of damage and degradation mechanisms induced by earthquake loading. For each monitored building, detailed information is compiled, including location (city or municipality), year of construction, applicable seismic design code, structural system characteristics, type of functionality (research institutes, administrative, education, healthcare, residential, commercial), site and soil conditions (where available), and the seismic events recorded during its service life. Using simplified dynamic models with natural periods of vibration matching those of instrumented buildings, this paper analyses their structural response to the 1977, 1986, and 1990 Vrancea earthquakes through time-history, linear, and elasto-plastic comparative approaches, and evaluates their seismic performance. Relevant regulatory provisions and findings from previous studies are considered to establish correlations between the exceedance of admissible inter-storey drift limits and observed damage levels. The results demonstrate that long-term seismic instrumentation campaigns are integral to structural health monitoring, providing a robust basis for post-earthquake assessment and risk-informed decision-making.*

***Key words****: measured response, performance evaluation, structural behaviour.*

## INTRODUCTION

Traditional methods for assessing structural performance provide a physical understanding of structural behavior, but they rely on idealized assumptions and uncertain parameters. The development of structural monitoring systems and seismic instrumentation networks, together with advances in computational power and machine learning techniques, has enabled the emergence of data-driven approaches. These approaches use large volumes of empirical data derived from seismic recordings and structural response to identify relationships between excitation and response, detect changes in structural properties, and improve predictive models. At present, data-driven approaches do not replace physics-based models, but rather complement and calibrate them, contributing to the development of modern hybrid frameworks for the analysis and monitoring of structural behavior under seismic actions. Also, data-driven methodologies are particularly useful for analysing soil-structure interaction (SSI) because they rely on measured structural responses rather than assumed soil and foundation parameters. By comparing recordings from the free-field, basement, and upper structural levels, amplification factors can be derived that implicitly capture SSI effects (Dobre & Dragomir, 2018; Dobre et al., 2024). This empirical approach also provides direct insight into how seismic waves are modified by the soil–foundation–structure system and transmitted through the building.

On the other hand, there is a direct connection between the data-driven approach, Building Information Modeling, and Structural Health Monitoring in the management and monitoring of built infrastructure. Consequently, the integration of BIM and SHM within a data-driven framework enables more efficient

structural monitoring, supports predictive maintenance, and contributes to the development of digital twins for infrastructure systems (Dobre et al., 2025).

The importance of pre-earthquake SHM data was proved after the 1977 earthquake (Balan et al., 1982), when INCERC published measured vibration periods for 47 buildings, before and after the earthquake, with obvious increases due to damage, thus a comparison was possible for both that situation and for the one after strengthening, if done. The unique INCERC accelerogram of the March 4, 1977, Vrancea earthquake (Mw 7.4) revealed a pronounced long-period spectral content, which contributed to damage in tall and slender structures. However, relying on a single seismic record limits the generalization of structural response characteristics. In contrast, the available database includes multiple Vrancea earthquakes with different spectral features, complemented by ambient vibration recordings obtained from structural health monitoring. This expanded dataset enables a data-driven analysis framework, where structural behavior is inferred from a larger set of measured responses, allowing for more robust identification of dynamic properties and a better understanding of variability in soil–structure interaction effects (Pavel et al., 2018; 2020; Del Gaudio et al., 2019; Morandi & Albanesi, 2026). Conceptual differences between the two approaches are presented in Table 1.

Table 1. Fundamental differences between physics-based and data-driven frameworks

| Traditional Approach | Data-Driven Approach |
|---|---|
| Physics-based (constitutive material models, structural dynamics equations, idealized boundary conditions) | Data-based (acceleration time histories, drift measurements, frequency shifts, damping evolution) |
| Assumed parameters (elastic modulus, damping ratio (often 5%), boundary fixity, soil-structure interaction, hinge properties) | Measured parameters (actual natural frequencies, actual damping ratios, real stiffness degradation, residual displacements) |
| Pre-event prediction (predicts performance before earthquake occurs, uses design spectra, checks demand vs capacity) | Real-time/post-event learning (seismic response recordings evaluated immediately after each event, models recalibrated accordingly) |
| Static model (analytical model created at the design stage, remains unchanged, assumes constant structural properties) | Continuously updated model (modal properties tracked over time, damage detected via frequency drift, stiffness degradation quantified) |
| Physics-informed models: integration of physical model data with instrumentation data | |

The workflow illustrated in Figure 1 represents the internal process of the data-driven analysis stage.

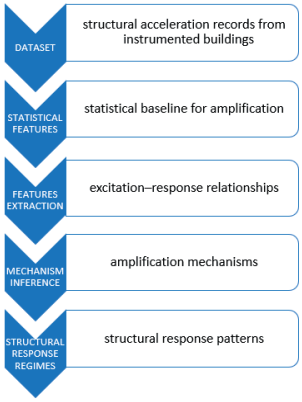



Figure 1. Data-driven workflow

Starting from structural acceleration records obtained from instrumented buildings, statistical characterization and feature extraction are used to identify excitation–response relationships, infer amplification mechanisms, and classify structural response regimes. These insights contribute to the development and calibration of hybrid physics-based and data-driven models used in structural health monitoring and digital twin frameworks.

## MATERIALS AND METHODS

The methodological framework adopted in this study combines physics-based structural modeling with empirical evidence derived from seismic monitoring data.

In the first direction, a set of buildings is idealized as simplified dynamic systems represented by single-degree-of-freedom models with identical fundamental vibration periods (Saiidi & Sozen, 1979; 1981), while differing in key structural characteristics such as height, number of stories, and construction period. The seismic input consists of recorded accelerograms corresponding to the Vrancea earthquakes of 1977, 1986, and 1990, which are used as input motions in time-history analyses. Both elastic and inelastic responses are evaluated, accounting for stiffness degradation; however, the fundamental vibration period is assumed to remain approximately constant, as

the expected stiffness reduction is relatively small. Structural response is characterized through parameters such as inter-storey drift ratios, which are compared with code-based thresholds associated with different damage states (P100-1/2013; Luca et al., 2015; Zaker Esteghamati at al., 2018; Ibrahim & Makhloof, 2023; Habibi & Asadi, 2017; Sen et al., 2023; Mohsenian et al., 2024; Genikomsou et al., 2025).

The second direction, shown in Figure 1, supports the numerical investigation by analysing recorded data from a case-study of a building equipped with seismic instrumentation. This approach enables the evaluation of seismic motion transfer and amplification throughout the structural system. The amplification factor at the basement level, AF_basement, is defined as the ratio between the acceleration recorded at the basement and the free-field acceleration, expressing how much the seismic motion is amplified from the ground unaffected by the structure to the foundation level. Similarly, the amplification factor at the terrace level, AF_terrace, describes the amplification of motion from the free field to the top of the building. Finally, the structural amplification factor, T, represents the ratio between the terrace and basement amplification, indicating how much the motion increases vertically from the foundation to the top of the structure.

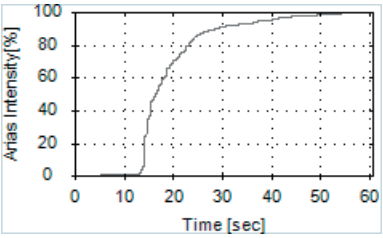
Together, these two directions provide complementary perspectives on structural behavior under seismic excitation: numerical simulations allow the systematic investigation of structural performance across different building configurations, while the instrumentation-based analysis provides empirical evidence of amplification mechanisms and response patterns observed in real structures.

Seismic monitoring systems provide acceleration data from instrumented buildings under ambient vibrations and earthquake events, forming the empirical basis for data-driven analysis. The recorded signals are pre-processed to remove trends and noise and are subsequently analysed using system identification techniques to extract modal parameters such as natural frequencies, damping ratios, and mode shapes. Additional statistical and spectral features are computed and organized into a structured feature matrix describing the dynamic characteristics of the monitored structure.

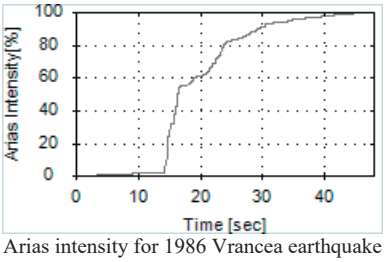
## RESULTS AND DISCUSSIONS

The first approach focuses on the seismic response of the structural models. The results obtained for the different structural models constitute a dataset that will subsequently allow for additional comparative analyses aimed at identifying trends and correlations between the structural parameters of buildings (height, number of storeys, fundamental vibration period, year of construction) and seismic response indicators (inter-storey displacements – angular drifts, stiffness degradation). By applying statistical analysis methods to these basic results, the objective is to highlight the distribution of the structural response and to estimate the probability of exceeding certain performance thresholds associated with different damage levels, as defined in current codes or existing studies. Thus,

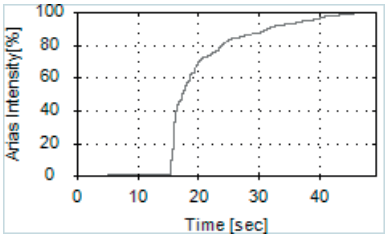
– The maximum spectral seismic response, linear and bilinear, associated with different dynamic characteristics, is estimated.
– Based on the determined dynamic characteristics, the structural behavior under the three types of seismic actions (Vrancea 1977, 1986, 1990, with the total energy of the seismic ground motion over time, represented by the Arias intensity) is highlighted, as shown in Figure 2a and Figure 2b.



Arias intensity for 1977 Vrancea earthquake



Arias intensity for 1986 Vrancea earthquake




Arias intensity for 1990 Vrancea earthquake

Figure 2a. Arias Intensity and Cumulative Severity

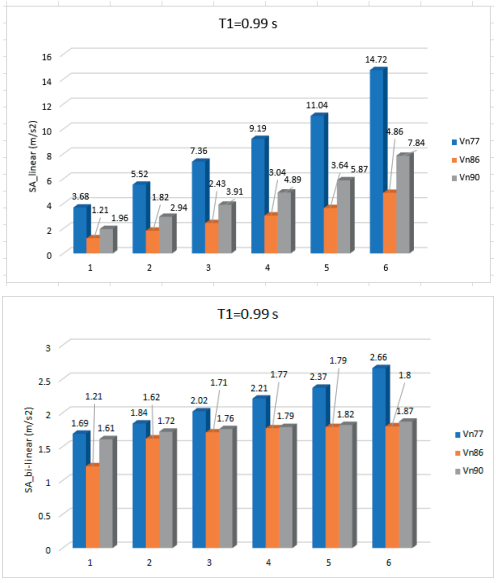



Figure 2b. Spectral acceleration in the linear and bilinear domain

– Two correlations are identified between the period and height (Figure 3a), and between the period and the spectral displacement (Figure 3b).

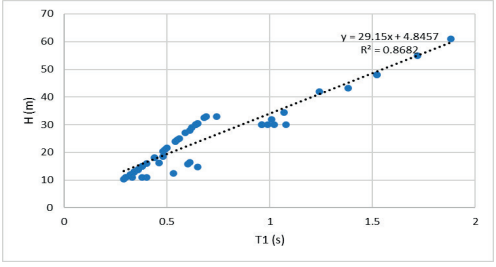



Figure 3a. Period and Height relationship

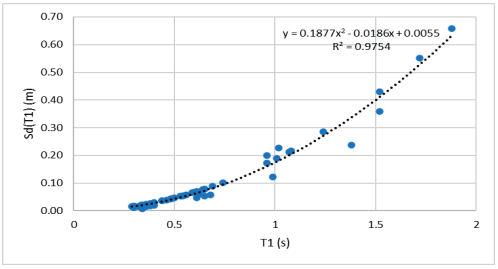



Figure 3b. Period and Spectral displacement relationship

– For structural systems with different dynamic characteristics, the results of a time-history analysis, both linear and nonlinear (comparative), are presented, considering the inter-storey displacement response under the Vrancea 1977, 1986, and 1990 seismic actions (Figure 4).

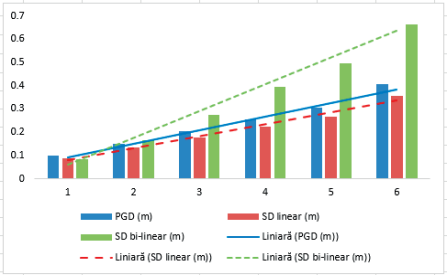
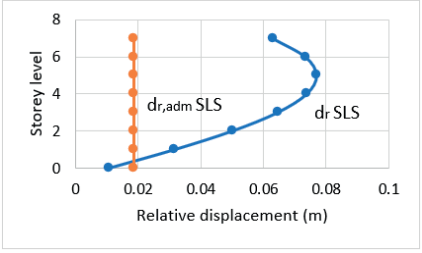



Figure 4. Structural displacement response ($T_1$ = 0.99 s)

– For several of the absolute storey displacements mentioned above, determined by considering a linear variation along the height of the model and multiplied by a shape function, the relative displacements are calculated for the Serviceability Limit State (SLS) and the Ultimate Limit State (ULS), as well as the inter-storey drifts (angular drifts) and their allowable limits (Figure 5).




Inter-storey drifts - allowable limits (linear)

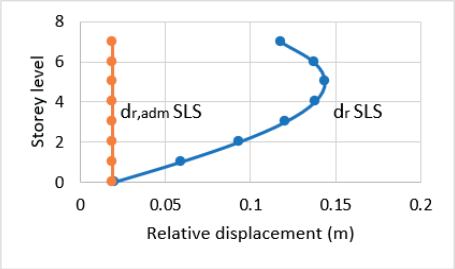



Figure 5. Seismic performance of the structural system with $T_1$ = 0.99 s (linear and bilinear analysis at SLS)

– Identification of situations in which, both in the linear and nonlinear domains, residual displacements occur - an indicator of structural performance.
– Estimation of the possible damage level through the relationship between the accelerogram scaling factor and the drift/drift indicator.

The variation of inter-storey drift along the height of the building is illustrated in Figure 6a for linear analysis and in Figure 6b for bilinear analysis.

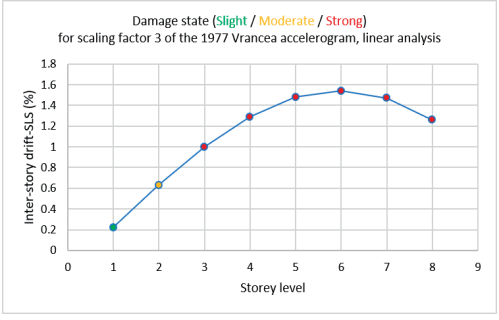



Figure 6a. Distribution of inter-storey drift along the building height and corresponding damage state for Scaling Factor = 3 (Vrancea 1977), linear analysis

For the linear analysis, drift values increase with the increase of the accelerogram scaling factor. For scaling factor 3, the SLS drift ranges between 0.22% and 1.54%, while the SLU drift varies between 0.84% and 5.95%, with predominantly serious damage at the upper floors. In the bilinear analysis, drift values are significantly higher. For scaling factor 3, the maximum values reach 2.87% (SLS) and 11.08% (SLU), indicating severe damage at the upper floors.

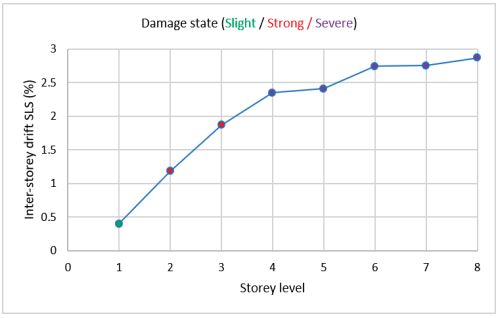



Figure 6b. Distribution of inter-storey drift along the building height and corresponding damage state for Scaling Factor = 3 (Vrancea 1977), bilinear analysis

The second approach uses the obtained results to perform a statistical characterization of the amplification indicators, highlighting their distribution and variability. Descriptive statistics were calculated for the indicators AF_basement ($A_{basement}/A_{free-field}$), AF_teracce ($A_{terrace}/A_{free-field}$), and T ($A_{terrace}/A_{basement}$) to characterize the baselines for 2024 and 2025 in both NS and EV categories. The statistical analysis included the computation of minimum and maximum values, medians, and quartiles (Q1–Q3, corresponding to the 25th, 50th, and 75th percentiles) in order to describe the distribution of the data and assess their variability. Based on these indicators, characteristic ratios were derived, allowing the identification of the amplification patterns expressed through the relationships between the considered variables. The obtained values provide an overview of the variability of the ratios and enable a comparative assessment of the two baselines.

To enhance the visual comparison of indicator distributions, the statistical results were illustrated graphically, enabling a direct comparison between the baselines corresponding to 2024 and 2025, for the NS and EW categories. Figure 7 illustrates the quartile distribution of the amplification factors for the 2024 and 2025 baselines, showing a progressive increase in amplification from Q1 to P95-including the 95th percentile. The results indicate slightly higher basement amplification for the 2025 baseline compared to 2024, Figure 7a, while the terrace amplification exhibits a stronger increase toward the upper quartiles, Figure 7b.

The ratio T highlights the vertical amplification between the basement and terrace levels, with higher values observed for the upper quartiles, Figure 7c. These observations reveal a consistent and repeatable response pattern, characterized by a monotonic increase in amplification across quartiles and a clear amplification gradient from the basement to the terrace level.

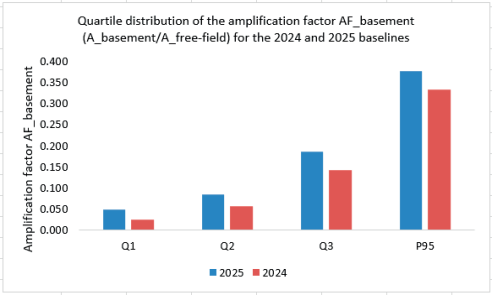



Figure 7a. Amplification trends between the 2024 and 2025 baselines for AF_basement

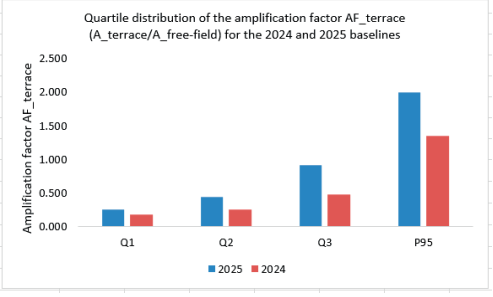



Figure 7b. Amplification trends between the 2024 and 2025 baselines for AF_terrace

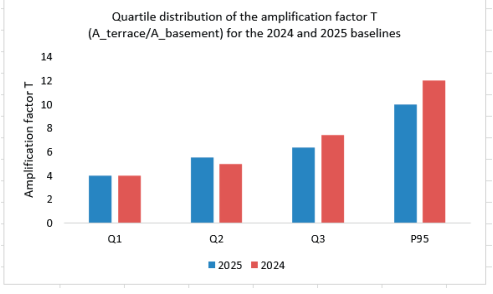



Figure 7c. Amplification trends between the 2024 and 2025 baselines for T

While the basement amplification remains relatively similar for both components, the terrace amplification shows significantly higher values in the EW direction, particularly toward the upper percentile range. This behavior suggests a stronger structural response along the EW axis. The median values indicate a consistent increase in amplification with height, reflecting the typical structural response, while the higher mean values suggest the presence of occasional higher-amplitude events. Tracking the temporal evolution of median values and interquartile ranges enables the identification of changes in both the central tendency and variability of the structural response. Stable quartile distributions over time indicate consistent behavior, whereas systematic shifts in median or dispersion may reflect changes in structural properties or soil–structure interaction conditions. Together, the two approaches provide complementary perspectives, combining the evaluation of structural response with the statistical interpretation of the resulting indicators.

## CONCLUSIONS

Data-driven approaches offer several important advantages in structural monitoring and seismic performance assessment. Unlike traditional analytical models, which rely on assumed parameters such as damping ratios, stiffness degradation, or boundary conditions, data-driven methods use measured structural responses. Dynamic characteristics - including natural frequencies, damping ratios, and modal shapes - are extracted directly from recorded time histories, reflecting the actual behavior of the structure.

Another key advantage is the possibility of post-event evaluation and model calibration. Structural properties may change over time due to cracking, ageing, damage, or retrofitting. Monitoring data enables the detection of frequency shifts, changes in damping, or residual displacements, providing insight into the current structural condition and improving reliability assessment throughout the life-cycle of the building.

Data-driven approaches also support probabilistic performance evaluation by leveraging large sets of recorded structural responses. By processing multiple seismic and ambient vibration records, response parameters

such as peak floor acceleration or inter-storey drift are extracted and statistically analysed. Empirical distributions are then constructed using descriptive statistics (e.g., median, quartiles) or fitted probability models, allowing the variability and uncertainty of the structural response to be quantified. This approach reduces reliance on purely theoretical assumptions and provides a more realistic representation of structural behavior based on measured data.

Additionally, aggregated monitoring databases enable comparative analysis of reinforced concrete and steel structures from various perspectives (Stoian et al., 2022; Köber et al., 2024a,b), enabling the identification of performance trends under similar demands. Such comparisons can support improvements in design provisions and retrofit strategies.

Despite these advantages, several limitations must be considered. The availability of high-quality monitoring data remains limited, particularly for extreme seismic events, which are rarely recorded in real structures. Data quality may also be affected by noise, sensor drift, or incomplete records, requiring careful validation and pre-processing. Machine learning techniques can approximate nonlinear seismic response much faster than conventional dynamic analyses, making them useful for evaluating a large number of structures. However, the performance of the models depends on the quality of the data, the choice of input parameters, and the ability of the model to generalize to new seismic motions or structural typologies (Noor, 2025).

Another challenge is generalization. Structural response depends on building geometry, material properties, and soil conditions, meaning that observations from one structure cannot always be transferred to others. Moreover, data-driven approaches primarily identify statistical correlations rather than physical mechanisms, which limits their ability to explain processes such as stiffness degradation or damage localization.

For these reasons, data-driven methodologies are best used in combination with physics-based models. Analytical approaches provide the mechanical framework governing structural behavior, while empirical data improve calibration, validation, and uncertainty assessment.

Integrating data-driven methods with consistent analytical models creates a strong framework for understanding and enhancing structural resilience.

## ACKNOWLEDGEMENTS

This work was carried out within the framework of the NUCLEU Programme PN 23 35 - "ECODIGICONS", under PNCDI 2022-2027, with the support of the National Authority for Research through Project PN 23 35 01 01, entitled "Integrative concept for the digital analysis of data from large-scale seismic monitoring of the national territory and the building stock, aimed at the rapid identification of the destructive potential of seismic events occurring in Romania and adjacent regions. The maintenance and operation of the infrastructures used in this research were supported by funding provided by UEFISCDI to the National Network for the Seismic Monitoring and Protection of the Building Stock (R.N.M.P.S.P.C. – I.O.S.I.N.) within INCD URBAN-INCERC, through PNCDI IV, Programme 5.5 – Research Infrastructures.

The authors gratefully acknowledge this financial support.

## REFERENCES

Balan, St., Cristescu, V., & Cornea, I. (coordinators). (1982). *Cutremurul de pământ din România de la 4 martie 1977. [The Romania Earthquake of 4 March 1977].* Editura Academiei Republicii Socialiste România, Bucharest, Romania.

Del Gaudio, C., De Risi, M.T., Ricci, P., & Verderame, G. M. (2019). Empirical drift-fragility functions and loss estimation for infills in reinforced concrete frames under seismic loading. *Bulletin of Earthquake Engineering* 17, 1285–1330, doi.org/10.1007/s10518-018-0501-y.

Dobre, D., Dragomir, C.-S., Dobrescu, C.-F., Craifaleanu, I.-G., Georgescu, E.-S., & Zaharia, M. C. (2024). The evolution of the dynamic characteristics of the soil-structure system in the case of a university building seismic monitoring, *Scientific Papers-Series E-Land Reclamation Earth Observation & Surveying Environmental Engineering,* 13, 408-416, ISSN 2285-6064.

Dobre, D., & Dragomir, C.-S. (2018). Methods of safety assessment through analytical and experimental approaches, *Scientific Papers-Series E-Land Reclamation Earth Observation & Surveying Environmental Engineering, 7, 117-121,* ISSN 2285-6064.

Dobre, D., Dragomir, C.-S., Craifaleanu, I.-G., Dobrescu, C.-F., & Georgescu, E.-S. (2025). Upgrading The Traditional Database Through BIM-Based SHM Vision, *Scientific Papers-Series E-Land Reclamation Earth Observation & Surveying Environmental Engineering*, 14, 548-554, ISSN 2285-6064.

Genikomsou, A.S., Abdelmaksoud, A.M. & Balomenos, G.P. (2025). Seismic fragility assessment of reinforced concrete and post-tensioned slab-column connections - reliability-based formulations for storey drift limits. *Bulletin of Earthquake Engineering* 23, 241–273, doi.org/10.1007/s10518-024-02019-3.

Habibi, A., & Asadi, K. (2017). Development of Drift-Based Damage Index for Reinforced Concrete Moment Resisting Frames with Setback. *Int. J. Civ. Eng.* 15, 487–498, doi.org/10.1007/s40999-016-0085-3.

Ibrahim, A.R., & Makhloof, D.A. (2023). Developed drift damage index-based failure criterion for framed-wall structure system, *Engineering Failure Analysis*, Volume 145, 107052, ISSN 1350-6307, doi.org/10.1016/j.engfailanal.2023.107052.

Luca, S.-G., Pastia, C., Budescu, M., Teodoru, I.-B., & Bejan, F. (2015). Evaluation of Seismic Energy in Structures Using Passive Fluid Dampers. *SGEM Conference Proceedings*, Vol.3, pp 847-854.

Köber, H., Marcu, R, & Stoian, M. (2024a). Details Resembling the Dog-Bone in Seismic Resistant Concentrically Braced Frames, In: Mazzolani, F.M., Piluso, V., Nastri, E., Formisano, A. (eds), *Proceedings of the 11th International Conference on Behaviour of Steel Structures in Seismic Areas. STESSA 2024.* Lecture Notes in Civil Engineering, 519. Springer, Cham.

Köber, H., Stoian, M., Marcu, R, & Diriuș, A.M. (2024b). Pinned and Fixed Connections in Six Storied Inverted Y-braced Frames, In: Mazzolani, F.M., Piluso, V., Nastri, E., Formisano, A. (eds)*, Proceedings of the 11th International Conference on Behaviour of Steel Structures in Seismic Areas. STESSA 2024.* Lecture Notes in Civil Engineering, 519. Springer, Cham.

Mohsenian, V., Filizadeh, R., Mariani, S., & Hajirasouliha, I. (2024). Probabilistic Assessment of Global Damage Index for Steel Moment-Resisting Frames Based on Local Responses. *Journal of Earthquake Engineering*, *28*(10), 2855–2882. https://doi.org/10.1080/13632469.2024.2312938.

Morandi, P., & Albanesi, L. (2026). Experiment-based definition of limit states and derivation of in-plane drift capacity of brick and block URM walls for seismic design and assessment. *Bulletin of Earthquake Engineering* 24, 1635–1683. https://doi.org/10.1007/s10518-025-02313-8.

Noor, U.A. (2025). Advances in Machine Learning for Structural Seismic Response Prediction: A Comprehensive Review. *Archives of Computational Methods in Engineering*, doi.org/10.1007/s11831-025-10395-5.

Pavel, F., Calotescu, I., Vacareanu, R., & Sandulescu, A.M. (2018). Assessment of seismic risk scenarios for Bucharest, Romania. *Natural Hazards* 93 (Suppl 1), 25–37 (2018), doi.org/10.1007/s11069-017-2991-3.

Pavel, F., Vacareanu, R., Pitilakis, K., & Anastasiadis, A. (2020). Investigation on site-specific seismic response analysis for Bucharest (Romania). *Bulletin of Earthquake Engineering* 18, 1933–1953, doi.org/10.1007/s10518-020-00789-0.

Saiidi, M., & Sozen, M.A. (1979). Simple and complex models for nonlinear seismic response of reinforced concrete structures, *A Report to the National Science Foundation Research Grant PFR-78-16318*, University of Illinois at Urbana-Champaign.

Saiidi, M., & Sozen, M.A. (1981). Simple Nonlinear Seismic Analysis of R/C Structures, *Journal of the Structural Division, ASCE*, 107, ST5, 16270, 937-953.

Sen, A., Cook, D., Liel, A., Basnet, T., Creagh, A., Khodadadi Koodiani, H., Berkowitz, R., Ghannoum, W., Hortacsu, A., Kim, I., Lehman, D., Lowes, L., Matamoros, A., Naeim, F., Sattar, S., & Smith, R. (2023). ASCE/SEI 41 assessment of Reinforced Concrete Buildings: Benchmarking Linear Procedures and FEMA P-2018 with Empirical Damage Observations, *Earthquake Spectra*, doi.org/10.1177/87552930231173454.

Stoian, M., Marcu, R, & Köber, H. (2022). Pinned and Fixed Connections in 2 Storey X-braced Frames. In: Mazzolani, F.M., Dubina, D., Stratan, A. (eds) *Proceedings of the 10th International Conference on Behaviour of Steel Structures in Seismic Areas. STESSA 2022.* Lecture Notes in Civil Engineering, 262. Springer, Cham.

The Romanian seismic design code P100-1/2013, Ministry of Regional Development and Public Administration.

Zaker Esteghamati, M., Banazadeh, M., & Huang, Q. (2018). The effect of design drift limit on the seismic performance of RC dual high-rise buildings, *The Structural Design of Tall and Special Buildings*, 27(8), e1464, doi.org/10.1002/tal.1464

Scientific Papers. Series E. Land Reclamation, Earth Observation & Surveying, Environmental Engineering. Vol. XV, 2026
Print ISSN 2285-6064, CD-ROM ISSN 2285-6072, Online ISSN 2393-5138, ISSN-L 2285-6064

# STRUCTURAL PERFORMANCE ASSESSMENT OF ECOLOGICALLY STABILIZED ROAD LAYERS

**Daniela DOBRE[1, 2], Lidia-Rodica RADU[1], Nicoleta-Adaciza IONESCU[2], Cornelia-Florentina DOBRESCU[3]**

[1]Technical University of Civil Engineering - UTCB Bucharest, 122-124 Lacul Tei Blvd, 020396, District 2, Bucharest, Romania
[2]NIRD URBAN-INCERC, 266 Pantelimon Road, District 2, Bucharest, Romania
[3]"Dunărea de Jos" University of Galați, 47 Domnească Street, Galați, Romania

Corresponding author email: dobred@hotmail.com

***Abstract***

*The long-term durability and structural integrity of stabilised layers are essential for sustainable infrastructure. Eco-friendly materials that utilise environmentally friendly binders and additives have the potential to improve mechanical performance while minimising environmental impact. Assessing the effectiveness of these materials requires a thorough framework that considers various parameters impacting mechanical stability, thermal resistance, and load-bearing capacity. A performance index (PI) approach is used to assess the structural performance of stabilised layers, incorporating a catalyst to enhance the bitumen-aggregate interface within the bitumen matrix and modifying physicochemical reactions during operation. Key mechanical and physical parameters - including compressive strength, degree of compaction, load-bearing capacity, dynamic modulus, and resistance to mechanical and thermal stresses - were measured or estimated for the stabilised layers. Compared to baseline or minimally compliant layers, the calculated PI showed a significant improvement in overall structural integrity. This reflects enhanced load transfer, stiffness, and durability. These findings support the adoption of environmentally sustainable stabilisation techniques as reliable alternatives for infrastructure applications, providing long-term performance.*

***Key words****: eco-friendly materials, performance, stabilisation, sustainable.*

## INTRODUCTION

In recent years, growing concerns about environmental impact have prompted the development of alternative solutions for stabilizing road infrastructure. Ecologically stabilized road layers aim to reduce the carbon footprint by utilizing biological binders, recycled materials, low-carbon additives, and innovative physicochemical modification processes. These solutions seek to achieve mechanical performance that is comparable to that of conventional cement or lime-treated materials, all while simultaneously lowering energy consumption and greenhouse gas emissions (Consoli et al., 2009; Puppala, 2016; Behnood, 2018). Organosilane additives can enhance the performance of unbound layers by increasing moisture resistance (Barbieri et al., 2019; 2021). They also emphasize the benefits of lignin in stabilizing clayey soils, which can improve stiffness (Vaiana et al., 2021). The use of biopolymers for stabilization has been shown to increase strength and enhance compaction (Cabalar et al., 2023). Additionally, polymer additives have been found to reduce the deformation potential of expansive soils (Liu et al., 2025). Ecological additives used as cement substitutes designed in the process of stabilizing cohesive, non-cohesive materials and aggregates are not directly comparable in terms of their composition or mechanisms of action. Other studies (Radu et al., 2015; Saca et al., 2024; Ionescu & Dobre, 2025) indicate that the mechanical properties of materials are closely related to the composition of the mixture and the ratios between the components, which in turn influence the material's mechanical strength and structural behaviour.

While various methodologies for incorporating alternative materials into stabilization projects have been suggested over the years, there remains a critical need for a systematic evaluation of structural performance (Dobrescu,

2017). Additionally, the analysis of parametric correlations between California Bearing Ratio (CBR) and other geotechnical parameters underscores the significance of a multi-parameter evaluation (Dobrescu, 2017). Therefore, a meaningful comparison can only be made using functional and structural performance indicators, such as stiffness, load-bearing capacity, resistance to deformation, and long-term durability under various traffic and environmental conditions. These indicators can be integrated into a Performance Index (PI), which reflects the overall efficiency of the pavement system, rather than the individual properties of the materials. In this context, the comparison between a hydraulic binder and a organic binder should be interpreted as a comparison between two technological solutions that enhance the performance of the road structure, rather than as a comparison between two materials with identical functions. However, without an integrated evaluation framework, it becomes challenging to make an objective comparison between conventional and eco-friendly solutions. Thus, the study proposes a weighted aggregation method that integrates the mechanical characteristics of stabilized road layers into a synthetic parameter, called performance index. The calculated performance index allows a comparative evaluation of conventional (hydraulic binder)/ecological (organic binder) solutions used for stabilizing road layers.

## MATERIALS AND METHODS

In this study, for the stabilization of the road layer, a hydraulic road binder based on Portland cement (HB) and an organic binder (OB) with a lignosulfonate structure (calcium – CLS, respectively sodium – SLS) were used. CLS is an anionic polymer, extracted from sulfite liquors resulting from cellulose production, water-soluble, with a molecular weight ranging between 2000-100000 and a three-dimensional structure. SLS is an anionic polymer obtained from the semicellulose production stream from wood through the NSSC process (neutral sulfite semichemical process).
The functional group in lignosulfonates are represented in Figure 1.

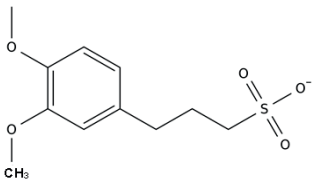



Figure 1. Representative structure of a lignosulfonate molecule showing polar functional groups (–$SO_3^-$, –OH) and the nonpolar hydrocarbon chain (Moldovan, 1978)

Their molecule is composed of polar groups such as –$SO_3^-$ and –OH, and a group of atoms linked by covalent bonds forming the hydrocarbon chain with a nonpolar character, such as $C_6H_4$– and $CH_3$–.
The following figure (Figure 2), illustrates the primary application principles of two approaches: the stabilization of soil and granular materials using lignosulfonates.

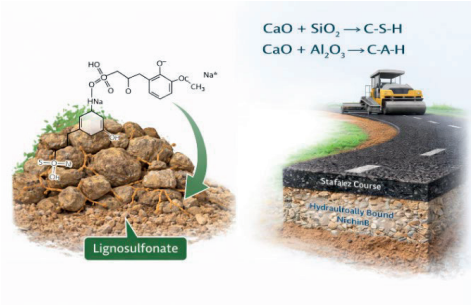



Figure 2. Ecologically stabilised road layers (adapted from Mostafa et al., 2024; Jiang et al., 2021; Yang et al., 2025)

The stabilization of road layers with organic binders consists in their fixation by adsorption onto the surface of solid particles (clay, sand, ballast), forming a layer between particles that reduces the repulsive forces between them and results in their agglomeration.
On the other hand, the polar groups act as molecular bridges, leading to the formation of a three-dimensional structure that enhances cohesion, while the hydrophobic hydrocarbon chain creates a barrier against water penetration. In addition, $Ca^{2+}$ ions contribute to compressing the diffuse double layer and reduce the repulsion between particles through ion-exchange reactions with $Na^+$ ions on the surface of clay particles (Shiyuan et al., 2025).

The stabilization with hydraulic road binders involves mineral reactions between calcium oxide (CaO), silicon dioxide ($SiO_2$), and aluminum oxide ($Al_2O_3$), resulting in the formation of cementitious compounds such as calcium silicate hydrate (C–S–H) and calcium aluminate hydrate (C–A–H).

The differences between the stabilisation mechanisms and their associated structural effects are summarised (Table 1).

A performance index (PI) is established based on four key parameters that reflect the behaviour of the treated or stabilized layer: the degree of compaction (D), the California Bearing Ratio (CBR), the static linear deformation modulus, determined in situ using the static plate (Lucas) test and calculated from the second loading (Ev2), respectively, the 28-day compressive strength ($Rc_{(28)}$) (equation1).

These indicators describe complementary aspects of structural performance, namely the degree of compaction, load-bearing capacity, stiffness, and mechanical strength of the stabilized material. The methodological framework used to evaluate these parameters and to determine the performance index is presented (Figure 3).

Table 1. Comparative analysis of the mechanisms and structural effects of hydraulic road binders and ecological additives used in the pavement system

| Stage | Hydraulic binder | Organic binder |
|---|---|---|
| Product incorporation | Hydraulic road binder incorporated into soil/aggregate mixtures with water | Additive incorporated into soil structure |
| Primary mechanism | Hydration reactions of hydraulic compounds | Modification of the aggregate interface |
| Microstructural process | Formation of cementitious hydration products (C–S–H, C–A–H) | Reduction of interfacial tension and enhancement of binder–aggregate adhesion |
| Structural modification | Particle cementation and development of a rigid structural matrix | Improved and more uniform distribution of aggregate surfaces |
| Mechanical effects | Increase in stiffness of the stabilized layer | Increase in stability of the soil mixture |
| Affected technical parameters | Ev2 ↑, CBR ↑, Rc ↑ | Mechanical properties ↑ |
| Level of action within the pavement structure | Subgrade or stabilised base layer | Soil layers |
| Structural impact | Increase in structural bearing capacity | Improvement in soil durability and stability |
| Overall outcome | Contributes to an increase in the PI | |

$$PI = w_D \cdot S_D + w_{CBR} \cdot S_{CBR} + w_{Ev2} \cdot S_{Ev2} + w_{Rc} \cdot S_{Rc}$$

where:

- $PI$ – global performance index;
- $w_D$, $w_{CBR}$, $w_{Ev2}$, $w_{Rc28}$ – weights associated with each indicator;
- $w_i D_j + w_i CBR_j + w_i Ev2_j + w_i Rc_j = 1$
- $S_D$, $S_{CBR}$, $S_{Ev2}$, $S_{Rc28}$ – normalized values of the indicators.

The weights are assigned based on the significance of each indicator in assessing pavement layer performance. While the PI provides a comprehensive assessment, its interpretation must be linked with the specific values of the parameters being analysed.

This correlation helps identify the technical advantages of each solution. The data were normalised by using the maximum value, resulting in a range between 0 and 1.

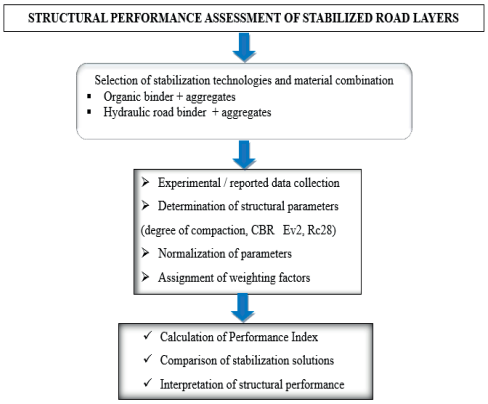



Figure 3. Road Layer Performance Framework (developed by the authors)

## RESULTS AND DISCUSSIONS

To evaluate the mechanical behavior of stabilized materials used in pavement structures, geotechnical parameters were analyzed to assess the performance of the stabilized material. The results are presented in Table 2. Overall, they indicate a general correlation between CBR, $Ev_2$, and $Rc_{28}$, demonstrating a simultaneous increase in bearing capacity, stiffness, and mechanical strength. This relationship suggests that improvements in the stabilization process contribute not only to enhanced load distribution and reduced deformation under traffic loading but also to a more durable pavement foundation. Furthermore, the observed correlation indicates that CBR and $Ev_2$ may serve as practical

indicators of the long-term strength development of the stabilized material, facilitating quality control during construction.

Table 2. Mechanical parameters

| Mixture | D (%) | CBR (%) | Ev2 (MPa) | Rc28 (MPa) |
|---|---|---|---|---|
| Aggregate layer+ SLS | 98.0 | 166.21 | 93.22 | 0.79 |
| Aggregate layer +CLS | 98 | 178.79 | 104.27 | 0.85 |
| Clayey soil + 5% HB | 99.0 | 80 | 160 | 1.24 |
| Sandy soil + HB | 99.0 | 150 | 195 | 2.25 |
| Ballast + 3 % HB | 99.0 | 180 | 300 | 2.49 |
| *Reference values* | *100* | *170* | *350* | *4.0* |

A sensitivity analysis of the performance index was performed by varying the weights associated with the mechanical parameters (Table 3), and the corresponding results are presented in Tables 4a and 4b.

Table 3. Weighting scenarios for the parameters used in the Performance Index calculation

| Scenario | w(D) | w(CBR) | w(Ev2) | w(Rc28) |
|---|---|---|---|---|
| S0 – Current weighting | 0.20 | 0.10 | 0.40 | 0.30 |
| S1 – Balanced weighting | 0.25 | 0.25 | 0.25 | 0.25 |
| S2 – CBR emphasis | 0.15 | 0.40 | 0.25 | 0.20 |
| S3 – $Ev_2$ emphasis | 0.15 | 0.10 | 0.55 | 0.20 |
| S4 – $\sigma_{28}$ emphasis | 0.15 | 0.10 | 0.20 | 0.55 |
| S5 – Compaction emphasis | 0.50 | 0.10 | 0.20 | 0.20 |
| S6 – Mechanical performance emphasis | 0.10 | 0.20 | 0.35 | 0.35 |
| S7 – Subgrade-oriented scenario | 0.30 | 0.30 | 0.20 | 0.20 |
| S8 – Stiffness and strength emphasis | 0.10 | 0.10 | 0.40 | 0.40 |
| S9 – CBR and compaction emphasis | 0.35 | 0.35 | 0.15 | 0.15 |
| S10 – $Ev_2$ dominant | 0.10 | 0.05 | 0.65 | 0.20 |

Table 4a. Multicriteria evaluation scenarios based on the mechanical parameters of the analysed materials

| Solution | S0 | S1 | S2 | S3 | S4 | S5 |
|---|---|---|---|---|---|---|
| Aggregate layer+ SLS | 0.460 | 0.605 | 0.628 | 0.479 | 0.375 | 0.670 |
| Aggregate layer +CLS | 0.484 | 0.636 | 0.665 | 0.507 | 0.396 | 0.683 |
| Clayey soil + 5% HB | 0.521 | 0.557 | 0.567 | 0.527 | 0.460 | 0.653 |
| Sandy soil + HB | 0.678 | 0.748 | 0.761 | 0.717 | 0.674 | 0.827 |
| Ballast + 3% HB | 0.834 | 0.882 | 0.917 | 0.857 | 0.838 | 0.905 |

The scenarios presented in Table 4b highlight the relative influence of the mechanical parameters on the overall performance ranking of the analyzed materials.

Table 4b. Multicriteria evaluation scenarios based on the mechanical parameters of the analyzed materials

| Solution | S6 | S7 | S8 | S9 | S10 |
|---|---|---|---|---|---|
| Aggregate layer+ SLS | 0.439 | 0.680 | 0.384 | 0.755 | 0.360 |
| Aggregate layer +CLS | 0.466 | 0.718 | 0.404 | 0.788 | 0.387 |
| Clayey soil + 5% HB | 0.414 | 0.678 | 0.436 | 0.626 | 0.482 |
| Sandy soil + HB | 0.655 | 0.861 | 0.704 | 0.823 | 0.618 |
| Ballast + 3% HB | 0.802 | 0.972 | 0.831 | 0.939 | 0.834 |

The Performance Index values indicate that all the stabilization solutions examined enhance the structural performance of the subgrade layer compared to the reference level (Figure 4). The graphical representation of the Performance Index highlights a consistent ranking of the stabilization solutions across different weighting scenarios.

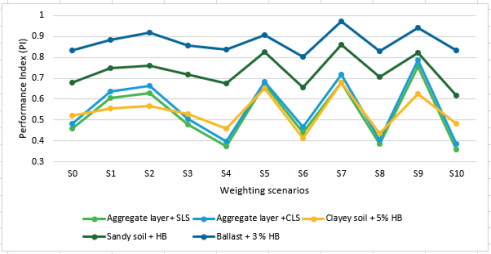



Figure 4. Sensitivity analysis of the PI for the investigated stabilization solutions under different weighting scenarios

The ballast stabilized with hydraulic binder exhibits the highest performance in all cases, followed by sandy soil stabilization. In contrast, clayey soil shows the lowest performance values, reflecting its weaker mechanical behaviour even after stabilization (realistic for cohesive soils). It is important to note that the values presented in the table are not absolute; they stem from a specific normalisation and weighting methodology. If the reference values, normalisation method, representative interval values, or criteria weights are adjusted, the scores and the PI may change. Nevertheless, the general trend in the performance of the analysed solutions is likely to remain consistent.

## CONCLUSIONS

The current study aimed to identify the key mechanical and physical parameters that influence the structural behaviour of stabilised formation layers and to evaluate the impact of various stabilisation methods. Additionally, a

normalized performance index was developed to facilitate consistent comparisons between different stabilization solutions.

The sensitivity analysis conducted with varying weighting scenarios revealed that the combination of ballast + HB consistently achieved the highest performance index (PI) values. This indicates a robust structural performance, irrespective of the relative importance assigned to individual parameters. In contrast, the sandy soil combined with HB exhibited intermediate performance with relatively stable results. Meanwhile, the clayey soil stabilized with 5% HB and lignosulfonate compounds + aggregates showed greater variability depending on the weighting configuration.

This approach serves as a valuable tool for the comparative assessment of stabilization strategies, supporting decision-making in the design and optimization of pavement foundation layers. Future work may refine the weighting methodology and extend the proposed framework to include additional materials, different environmental conditions, and long-term performance indicators.

Also, integrating experimental results and monitoring data into a digital environment based on Building Information Modeling (BIM) and Structural Health Monitoring (SHM) enables the upgrading of traditional infrastructure databases into more advanced and dynamic information systems (Dobre et al., 2025). Through this approach, data related to mechanical behavior, degradation processes, and long-term performance of road layers can be continuously collected, managed, and analyzed. The BIM model acts as a central platform for integrating SHM data and supports the development of a digital twin of the road structure. This synergy improves long-term performance evaluation, facilitates predictive maintenance strategies, and supports the implementation of more sustainable road engineering solutions.

Integrating multicriteria performance assessment with digital monitoring and modelling technologies offers a promising approach to creating more efficient, resilient, and sustainable road infrastructure systems.

The implementation of these products addresses several critical challenges, including the inadequate technical condition of existing road infrastructure, the environmental impact associated with infrastructure development, and the high costs of operation and maintenance of transport systems. In this context, the development of sustainable pavement solutions is further constrained by the poor mechanical behavior of locally available or problematic soils, such as expansive soils, which limits their direct use in structural road layers. Therefore, it is essential to evaluate the effectiveness of ecological stabilization techniques in improving the structural performance, load-bearing capacity, and long-term durability of these materials, enabling their integration as functional components in sustainable pavement systems (Barmade et al., 2023). Another important research direction related to the structural performance assessment of ecologically stabilized road layers involves the characterization of their time-dependent mechanical behaviour under traffic loading. Since such materials-particularly those incorporating stabilized soils or biocomposites based on agro-industrial by-products (Popa et al., 2023; 2025) often exhibit viscoelastic properties, their response cannot be fully described using purely elastic models. In this context, the application of rheological models, such as the Zener viscoelastic model (Bratu, 2020), becomes essential for evaluating their dynamic response under harmonic excitation, enabling a more realistic prediction of their in-service performance.

## ACKNOWLEDGEMENTS

This work was carried out within the framework of the NUCLEU Programme PN 23 35 – "ECODIGICONS", under PNCDI 2022-2027, with the support of the National Authority for Research through Project PN 23 35 01 01, entitled "Integrative concept for the digital analysis of data from large-scale seismic monitoring of the national territory and the building stock, aimed at the rapid identification of the destructive potential of seismic events occurring in Romania and adjacent regions.

The maintenance and operation of the infrastructures used in this research were supported by funding provided by UEFISCDI to the National Network for the Seismic Monitoring and Protection of the Building Stock (R.N.M.P.S.P.C. – I.O.S.I.N.) within INCD

URBAN-INCERC, through PNCDI IV, Programme 5.5 – Research Infrastructures.

## REFERENCES

Barbieri, D.M., Hoff, I., & Mørk, M. B. E. (2019). Innovative stabilization techniques for weak crushed rocks used in road unbound layers: A laboratory investigation. *Transportation Geotechnics 18*, 132-141, ISSN 2214-3912, doi: org/10.1016/j.trgeo.2018.12.002.

Barbieri, D.M., Hoff, I., & Ho, C. H. (2021). Crushed rocks stabilized with organosilane and lignosulfonate in pavement unbound layers: repeated load triaxial tests. *Frontiers of Structural and Civil Engineering 15*(2), 412–424, doi:10.1007/s11709-021-0700-5.

Barmade, S., Dhamaniya, A., & Patel, S. (2023). Evaluating the structural performance of stabilized expansive soil as subbase layer for sustainable pavements. *International Journal of Geosynthetics and Ground Engineering*, doi: 10.1007/s40891-023-00440-3.

Behnood, A. (2018). Soil and clay stabilization with calcium- and non-calcium-based additives: A state-of-the-art review. *Transportation Geotechnics 1*, 14–32, doi: org/10.1016/j.trgeo.2018.08.002.

Bratu, P. (2020). Variety of rheological models used in the isolation of the base for earthquake challenged constructions. ACTA TECHNICA NAPOCENSIS, Series: *Applied Mathematics, Mechanics, and Engineering 63(2)*, ISSN 2393–2988.

Cabalar, A. F., Akbulut, N., Demir, S., & Yıldız, Ö. (2023). Use of a Biopolymer for Road Pavement Subgrade. *Sustainability 15*(10), 8231, doi: 10.3390/su15108231.

Consoli, N.C., Viana da Fonseca, A., Cruz, R.C., & Heineck, K.S. (2009). Fundamental parameters for the stiffness and strength control of artificially cemented sand. *Journal of Geotechnical and Geoenvironmental Engineering 135*(9), 1347–1353, doi: 10.1061/(ASCE)GT.1943-5606.0000008.

Dobre, D., Dragomir, C. S., Craifaleanu, I. G., Dobrescu, C. F., & Georgescu, E. S. (2025). Upgrading the traditional database through BIM-based SHM vision. *Scientific Papers-Series E-Land Reclamation Earth Observation & Surveying Environmental Engineering 14*, 548-554, ISSN 2285-6064, Online ISSN 2393-5138.

Dobrescu, C. F. (2017). Study concerning bearing assessment of natural and stabilized soils using binders with ecological benefits based on parametric correlations. *Romanian Journal of Materials 47*(1), 112–116, ISSN 1583-3186.

Ionescu, N., & Dobre, D (2025). Behavior of asphalt mixtures manufactured with recycled materials and their in-situ performance level. *Scientific Papers-Series E-Land Reclamation Earth Observation & Surveying Environmental Engineering 14*, 252-259, ISSN 2285-6064, Online ISSN 2393-5138.

Jiang, W., Yuan, D., Sha, A., Huang, Y., Shan, J., & Li, P. (2021). Design of a Novel Road Pavement Using Steel and Plastics to Enhance Performance, Durability and Construction Efficiency. *Materials, 14*(3), 482, doi: org/10.3390/ma14030482.

Liu, M., Saberian, M., Li, J., Tajaddini, A., & Roychand, R. (2025). Improving expansive soil subgrade using sustainable green polymer-based admixture. *Case Studies in Construction Materials 23*, doi: org/10.1016/j.cscm.2025.e05090.

Moldovan, V. (1978). *Concrete admixtures* (in Romanian Aditivi in betoane), Bucharest, RO: Tehnica Publishing House.

Mostafa, A.E.A., Eisa, M. & Ibrahim, M.F. (2024). Effect of stabilizing subgrade layer using various additives on the flexible pavement design. *Innov. Infrastruct. Solut. 9*(147), doi: org/10.1007/s41062-024-01430-8.

Popa I., Vasile V., & Mureșanu A. (2025). Compatibility between natural agro-industrial by-products and synthetic materials, a basic element in obtaining biocomposite materials with potential for use in construction. *Scientific Papers. Series E. Land Reclamation, Earth Observation & Surveying, Environmental Engineering 14*, 586-593, ISSN 2285-6064.

Popa, I., Petcu, C., & Mureșanu, A. (2023). Durability of multifunctional coatings made with additions of animal waste and agro-industrial by-products. *Chem. Proc. 13(1),* 22, EISSN 2673-4583, doi: org/10.3390/chemproc2023013022.

Puppala, A.J. (2016). Advances in ground modification with chemical additives: From theory to practice. *Transportation Geotechnics* 9, 123–138, doi: org/10.1016/j.trgeo.2016.08.004

Radu, L., Saca, N., Mazilu, C., Gheorghe, M., & Petre, I. (2015). Practical model of cement-based grout mix design, for use in low-level radiation waste management. *Modelling in Civil Environmental Engineering 11*(4), Technical University of Civil Engineering of Bucharest, 10-20, doi: org/10.1515/mmce-2015-0016.

Saca, N., Radu, L., Stoleriu, S., Dobre, D., Calotă, R., & Truşcă, R. (2024). Investigation of physical-mechanical properties and microstructure of mortars with perlite and thermal-treated materials. *Materials 17*, 3412, doi: org/10.3390/ma17143412.

Shiyuan, L., Rongbo, L., Xinxing, B., Zhile, W., & Guifang, Z. (2025). A biohybrid mineralization strategy based on calcium lignosulfonate–reinforced enzyme-induced carbonate precipitation for improving loess roadbed permeability resistance, *Sustainable Materials and Technologies 46*, doi: org/10.1016/j.susmat.2025.e01764.

Vaiana, R., Oliviero Rossi, C., & Perri, G. (2021). An eco-sustainable stabilization of clayey road subgrades by lignin treatment: An Overview and a Comparative Experimental Investigation. *Applied Sciences 11*(24), 11720, doi: org/10.3390/app112411720.

Yang, J., Ma, R., Dong, B., Ma, H., Wang, Y., Gao, M., Sun, Y., & Jin, Y. (2025). Research Progress and Hotspots of Steel Slag Application in Road Construction: A Bibliometric Perspective. *Infrastructures, 10*(3), 54, doi: org/10.3390/infrastructures10030054.

Scientific Papers. Series E. Land Reclamation, Earth Observation & Surveying, Environmental Engineering. Vol. XV, 2026
Print ISSN 2285-6064, CD-ROM ISSN 2285-6072, Online ISSN 2393-5138, ISSN-L 2285-6064

# CORRELATION BETWEEN DENSITY, ULTRASONIC PULSE VELOCITY, AND DRYING SHRINKAGE IN ECO-CLAY POURED-EARTH

**Aurelian GRUIN[1, 2], Sorin DAN[2], Cornelia BAERĂ[1, 3], Bogdan BOLBOREA[1, 2], Ana-Cristina VASILE[1, 2], Claudiu-Sorin DRAGOMIR[1, 3], Evelin Anda LAZA[4]**

[1]National Institute for Building Research, Town Planning and Sustainable Territorial Development "URBAN - INCERC", 266 Pantelimon Road, District 2, Bucharest, Romania
[2]Politehnica University of Timișoara, 2 Victory Place, Timișoara, Romania
[3]University of Agronomic Sciences and Veterinary Medicine of Bucharest, 59 Marasti Blvd, District 1, Bucharest, Romania
[4]Romania National Institute of Research - Development for Machines and Installations Designed for Agriculture and Food Industry - INMA Bucharest, Romania

Corresponding author email: cornelia.baera@incd.ro

***Abstract***

*This paper presents an experimental investigation on the interrelationship between physically measured density, ultrasonic pulse velocity (UPV), and drying shrinkage of Eco-Clay poured-earth materials. Five representative mixtures, covering optimized mineral compositions and biopolymer-modified formulations, were selected from a larger experimental program. Density was determined by direct physical measurements and estimated using UPV as a non-destructive method. Drying shrinkage was monitored throughout the natural curing period. The results indicate that optimized Eco-Clay mixtures exhibit high and narrowly distributed dry densities, increased UPV responses, and reduced shrinkage, confirming the formation of a dense and homogeneous internal structure. In contrast, biopolymer-modified compositions show higher variability, increased sensitivity to curing conditions, and amplified shrinkage. A strong correlation between density, ultrasonic response, and shrinkage is demonstrated, validating the use of UPV as a reliable early-stage quality control indicator for poured-earth materials, with notable limitations for biopolymer-modified systems.*

***Key words****: biopolymer stabilization, drying shrinkage, Eco-Clay, poured earth, ultrasonic pulse velocity.*

## INTRODUCTION

Earthen construction materials have regained significant international interest in recent decades due to their low environmental impact, reduced embodied energy, local availability, and compatibility with sustainable development principles. Stabilized earth products, including compressed earth blocks (CEB), rammed earth, and poured-earth systems are increasingly investigated as viable alternatives for modern ecological construction (Walter et al., 2024). Nevertheless, the large-scale structural application of such materials remains constrained by the variability of their physical properties, particularly density, drying shrinkage, and internal structural homogeneity.
Bulk density is one of the most influential parameters governing the mechanical behavior, durability, and dimensional stability of earthen materials (Turco et al., 2021). It is strongly affected by particle size distribution, moisture content at casting, degree of compaction, and the presence of stabilizing additives (Bogas et al., 2023; Turco et al., 2024). Drying shrinkage represents a critical vulnerability of earth-based materials, as it can generate tensile stresses, surface cracking, and long-term dimensional instability if not properly controlled (Bogas et al., 2023). Consequently, the coupled evaluation of density and shrinkage is essential for assessing the technological reliability of stabilized earth products (Keita & Perrot, 2024).
In parallel with conventional destructive testing, nondestructive testing (NDT) methods have gained increasing attention for the assessment of earthen materials. Among these, Ultrasonic Pulse Velocity (UPV) testing offers a rapid and non-invasive means of evaluating internal compactness, homogeneity, and defect distribution. Numerous studies have

demonstrated strong correlations between UPV, density, moisture content, and mechanical performance for stabilized soils and compressed earth products (Bolborea et al., 2021; Sathiparan et al., 2024; Chajec et al., 2025). Studies have also confirmed the effectiveness of ultrasonic methods for assessing stabilized soils over long curing periods, with UPV shown to be sensitive to compaction level and binder type (Kasinikota & Tripura, 2022; Kozubal et al., 2023).

The integration of biopolymers as sustainable stabilizers for soils and clay-based materials represents a rapidly expanding research area in sustainable geotechnical and construction engineering. Natural polymers such as xanthan gum and lignin have been shown to enhance interparticle bonding, stiffness, and water retention capacity (Armistead et al., 2020; Abbasi et al., 2025). However, biopolymer modification also introduces microstructural heterogeneities and moisture-sensitive behavior, which can significantly affect ultrasonic wave propagation and shrinkage response (Xu et al., 2010; Zhang et al., 2020; Vieira et al., 2026). Recent ultrasonic investigations on biopolymer-stabilized soils confirmed that ultrasonic pulse velocity remains sensitive to both curing evolution and internal heterogeneity induced by bio-based binders (Armistead et al., 2020; Abbasi et al., 2025).

Ultrasonic characterization of poured-earth systems has been previously explored mainly in relation to thermal, hygrothermal, and mineral fiber stabilization behavior (Walter et al., 2024; Canivell et al., 2025). However, direct experimental correlations between physically measured density, drying shrinkage, and UPV response in eco-modified poured-earth clay systems remain insufficiently documented in the scientific literature.

Despite the growing body of research on stabilized earth, ultrasonic testing, and biopolymer-based stabilization, the coupled influence of density, ultrasonic response, and drying shrinkage on poured-earth materials incorporating eco-modified clay systems has not yet been comprehensively quantified.

The present study addresses this gap by experimentally investigating the interrelationship between physically measured density, ultrasonic pulse velocity (UPV), and drying shrinkage for representative Eco-Clay poured-earth compositions, including both optimized mineral mixtures and biopolymer-modified formulations. By combining direct physical measurements with nondestructive ultrasonic testing, the study aims to assess the reliability of UPV as a quality-control indicator and to define the technological boundaries governing the dimensional stability of Eco-Clay materials.

## MATERIALS AND METHODS

### Experimental design and investigated compositions

The experimental program was designed to ensure reproducibility, comparability, and scientific validity of the results. A total of 36 Eco-Clay specimens were prepared and tested, grouped into the following composition families:

- D family (C2-D, C3-D, C4-D): optimized mixtures without additional biopolymers;
- DL family (C2-DL, C3-DL, C4-DL): mixtures with controlled lignin addition;
- DLN family (C2-DLN, C3-DLN, C4-DLN): mixtures with lignin and granulometric corrections;
- NM family: experimental limit compositions;
- R-CAM: reference mixtures used for calibration and comparison; invalid specimens (e.g., zero recorded mass) were excluded prior to statistical processing.

For the present article, five representative formulations were selected: C3-D, C4-D, C2-D, C3-DL, and C3-DLN. These formulations cover optimal, intermediate, and unfavorable behaviors.

### *Specimen preparation and casting procedure*

All specimens were produced using the Eco-Clay poured-earth technology, employing two standardized mold geometries: 150 × 150 × 150 mm and 141 × 141 × 141 mm.

The technological process involved the following steps:

- Mechanical homogenization of the Eco-Clay mixture;
- Single-stage casting without stratification;

- Mechanical vibration for 30–90 s to eliminate internal voids;
- Controlled demolding at 24–48 h, depending on early stability;
- Natural drying for 7–50 days, depending on specimen size, initial moisture, and composition.

**Measurement methods and instrumentation**

Geometrical and mass measurements

Specimen dimensions were measured using a digital caliper (±0.1 mm), and mass was determined using a precision electronic balance (±0.1 g). Initial dimensions at casting ($a_0$, $b_0$, and $c_0$) and final dimensions after drying (a, b, and c) were recorded.

**Density determination**

Density was determined by two independent methods:

Direct physical method based on mass and final volume.

Ultrasonic Pulse Velocity (UPV) measurements were performed using a PUNDIT PL-200 ultrasonic testing device equipped with two 54 kHz transducers. The testing procedure was based on the principles of ultrasonic evaluation commonly applied for non-destructive estimation of material compactness and mechanical performance, using a Salman-type correlation between wave velocity and density. The acquisition methodology followed an approach conceptually similar to the combined non-destructive assessment procedure described in the Romanian code NP 137-2014 for concrete investigations.

Measurements were performed in direct transmission configuration on opposite specimen faces in order to evaluate internal compactness and structural homogeneity. The following parameters were recorded:

- ultrasonic path length (mm);
- propagation time (μs);
- UPV1 and UPV2 velocities (km/s);
- mean UPV (km/s).

**Drying shrinkage evaluation**

Drying monitoring was performed through successive mass measurements during the natural curing period. Moisture loss evolution was evaluated based on the stabilization (flattening) of the weight–time curve, which was considered indicative of the completion of the drying process. The specimens were stored under natural laboratory environmental conditions with uncontrolled temperature fluctuations, maintained within the range of approximately 19-23°C throughout the drying period.

Drying shrinkage was determined by comparing the initial specimen dimensions measured immediately after casting with the final dimensions measured after complete drying. Linear and volumetric shrinkage were evaluated using a digital calliper with an accuracy of ±0.1 mm.

The evaluation procedure followed the general principles commonly applied for dimensional stability assessment of earthen and cementitious materials, adapted to the specific characteristics of Eco-Clay poured-earth compositions.

Visual observations were systematically recorded throughout the drying process, focusing on:

- superficial cracking;
- surface texture and homogeneity;
- localized defects and edge curling.

**RESULTS AND DISCUSSIONS**

**Density of Eco-Clay specimens**

The bulk density of the selected representative Eco-Clay formulations (C2-D, C3-D, C4-D, C3-DL, and C3-DLN) was determined after the completion of the natural drying process. Density values were calculated using the physical method based on the ratio between the final dry mass and the measured specimen volume.

Across the representative series, the measured dry density ranged between 1892 and 2108 kg/m³, while the majority of values were concentrated in the interval 1950-2080 kg/m³, confirming a generally good material compactness and technological repeatability. The highest average densities were recorded for the C3-D and C4-D formulations, reflecting improved particle packing and optimal moisture content at casting.

Mixtures from the DL and DLN families exhibited slightly increased density dispersion, which can be attributed to the influence of lignin addition and granulometric corrections

on the internal structure and water retention during curing. In particular, some C3-DLN specimens showed lower density values, correlated with increased shrinkage and localized drying defects, indicating structural sensitivity to binder dosage.

From a technological perspective, density proved to be a key indicator of:

- mixture homogeneity;
- degree of compaction;
- sensitivity to segregation and void formation.

Lower density values were systematically associated with unfavourable UPV responses and higher drying shrinkage, outlining a clear physical interdependence between these parameters. Table 1 synthesizes the representative density values corresponding to the five selected Eco-Clay formulations determined by the physical method.

Table 1. The representative density values corresponding to the selected Eco-Clay formulations determined by the physical method

| Family | Density mean ($kg/m^3$) | Number of specimens |
|---|---|---|
| C2-D | ~2070 | 3 |
| C3-D | ~2095 | 3 |
| C4-D | ~2084 | 3 |
| C2-DL | ~1995 | 3 |
| C3-DL | ~2072 | 3 |
| C4-DL | ~2027 | 3 |
| DLN | ~1967 | 9 |
| NM | ~2037 | 9 |
| R-CAM | 1937 - 2018 | multiple |

**Density estimation based on Ultrasonic Pulse Velocity (UPV)**

In parallel with the direct physical measurements, density was also estimated non-destructively using Ultrasonic Pulse Velocity (UPV). The method is based on the correlation between wave propagation velocity and material compactness, as expressed by established empirical relationships (e.g., Salman-type) (Bolborea et al., 2021).

The measured UPV values for the representative mixtures covered the interval between 0.965 km/s and 2.315 km/s, which corresponds to a broad spectrum of internal structural conditions, from highly compact to porous or poorly consolidated zones. The low UPV value of 0.965 km/s is attributed to local porosity, air entrapment, and heterogeneous internal structure in some experimental mixtures. This behaviour was mainly observed in non-optimized or biopolymer-modified compositions, where ultrasonic wave propagation is more sensitive to internal discontinuities and moisture gradients. Based on these values, the estimated ultrasonic densities showed a good overall agreement with the physically measured densities, particularly for the C3-D and C4-D formulations.

For mixtures belonging to the DL and DLN families, larger deviations between physical and UPV-based densities were observed. These deviations are attributed to:

- heterogeneous pore distribution induced by lignin addition;
- increased moisture sensitivity during curing;
- localized microstructural discontinuities affecting wave propagation.

Specimens exhibiting UPV values below 1.2 km/s systematically displayed lower estimated densities and were associated with unfavourable technological behaviour, such as high shrinkage and surface cracking. Figure 1 illustrates the density values associated with the various composition families analyzed in this study.

**UPV–density correlation (method validation)**

Comparing the physically measured density with the density estimated using UPV (Salman correlation) reveals a strong linear relationship characterized by:

- coefficient of determination $R^2 \approx 0.98$
- estimation accuracy of 96-107%
- the majority of samples falling within 97-100% agreement.

This relationship is illustrated in Figure 2, where the regression line closely follows the ideal reference line.

**UPV-density correlation for the complete specimen dataset**

The UPV method accurately reflects density variations for the D and DL composition families.

Larger deviations are associated with DLN and NM compositions, where the microstructure is more heterogeneous.

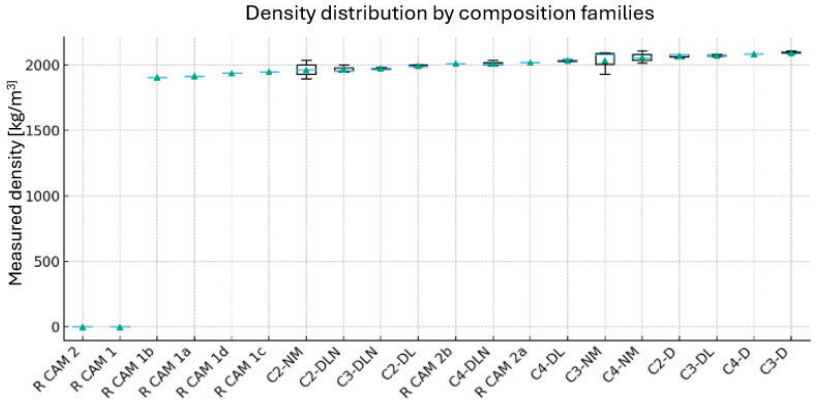



Figure 1. Density distribution by composition families

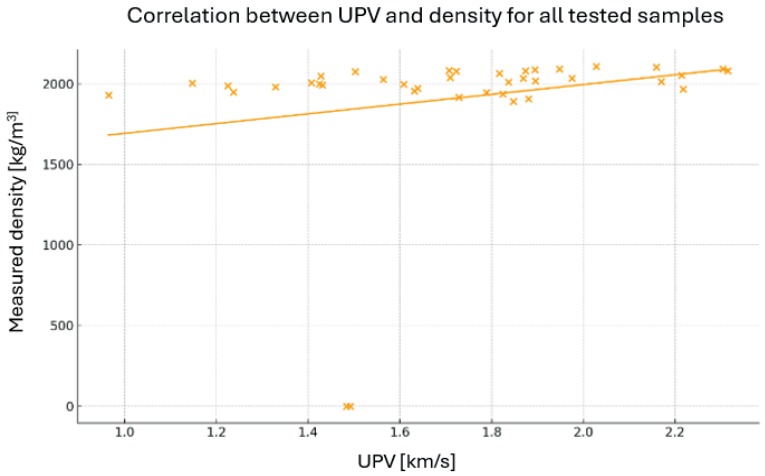



Figure 2. UPV-density correlation by composition families

UPV can, therefore, be used operationally to monitor compaction quality during production stages.

***Comparative analysis between physical and UPV-based densities*** (Figure 2 and Table 2)

The comparative evaluation between physically measured density and UPV-estimated density provides essential insight into the reliability of ultrasonic testing for Eco-Clay materials.

For the optimal mixtures (C3-D and C4-D), the deviation between the two methods remained within a narrow range, confirming that UPV can be reliably used as a non-destructive quality control indicator for compacted poured-earth materials. In contrast, for mixtures with lignin addition (DL and DLN series), the deviation increased, reflecting the sensitivity of ultrasonic wave propagation to microcracking, moisture gradients, and local heterogeneities.

Table 2. Comparison of physical and UPV-estimated density values

| Family | Density mean (kg/m$^3$) | UPV mean (km/s) |
|---|---|---|
| C2-D | ~2070 | ~1.65 |
| C3-D | ~2095 | ~2.00 |
| C4-D | ~2084 | ~1.80 |
| C2-DL | ~1995 | ~1.25 |
| C3-DL | ~2072 | ~1.80 |
| C4-DL | ~2027 | ~1.55 |
| DLN | ~1967 | ~1.30 |
| NM | ~2037 | ~1.95 |
| R-CAM | 1937 - 2018 | 1.45 - 1.90 |

These results emphasize that UPV-based density estimation must be interpreted in conjunction with physical measurements when dealing with biopolymer-modified earth materials.

**Drying and shrinkage behavior of Eco-Clay mixtures**

Drying and shrinkage were monitored throughout the natural curing period for all representative Eco-Clay compositions by comparing the initial specimen dimensions at the casting stage with the final dimensions after complete drying. Both linear and volumetric shrinkage were evaluated.

The C3-D and C4-D formulations displayed the most stable drying behavior, characterized by uniform dimensional reduction and minimal superficial cracking. The average linear shrinkage for these mixtures remained within a controlled range, indicating a balanced moisture diffusion and internal stress redistribution during drying.

In contrast, mixtures modified with lignin (DL and DLN series) exhibited increased shrinkage variability and a higher sensitivity to curing conditions. Several C3-DLN specimens developed localized surface cracking and edge curling, which correlated well with the following:

- lower physical density;
- reduced UPV values;
- increased internal porosity.

The most unfavorable shrinkage behavior was observed for selected limit compositions (NM family), where rapid moisture loss generated significant tensile stresses and early-age microcracking.

Although these mixtures are not part of the five representative formulations, their behavior is mentioned here to outline the technological boundaries of Eco-Clay materials.

The analysis of volumetric shrinkage across the composition families highlights the following general trend (average values):

- C2 family: higher shrinkage values associated with a solid-liquid ratio more sensitive to drying processes.
- C3 family: moderate shrinkage with relatively low variability between specimens.
- C4 family: intermediate behavior between C2 and C3, with some specimens exhibiting shrinkage values below 1%.
- R family (reference specimens): low shrinkage values consistent with their calibration role.

These results indicate that, within the analyzed dataset, the C3 family exhibits the lowest average volumetric shrinkage with reduced dispersion, suggesting improved dimensional stability compared with C2 and, to some extent, with C4 compositions.

To evaluate the relationship between compaction and dimensional stability, volumetric shrinkage was compared with the physically measured density.

The analysis indicates that:

- specimens with densities above approximately 2050 kg/m³ generally exhibit lower volumetric shrinkage, with average values around 3.5-4%;
- specimens with densities below approximately 1980 kg/m³ show higher shrinkage, with average values around 6-7%;
- the intermediate interval 1980-2050 kg/m³ corresponds to average shrinkage values of approximately 4.9%.

This behavior confirms the general trend in which higher density (i.e., a more compact microstructure) is associated with lower volumetric shrinkage, while lower density corresponds to increased shrinkage and a higher risk of cracking (Zhang et al., 2016; Daneti et al., 2024).

To integrate non-destructive results into the drying behavior analysis, volumetric shrinkage was correlated with ultrasonic pulse velocity values. Figure 3 presents the distribution of specimens in the UPV-volumetric shrinkage plane.

**UPV-volumetric shrinkage correlation for Eco-Clay specimens**

The results indicate that:

- specimens with high UPV values (> 1.7 km/s) tend to exhibit moderate volumetric shrinkage, with average values around 4-4.5%;
- the interval 1.4-1.7 km/s is associated with slightly higher shrinkage values, averaging approximately 6%;

- specimens with UPV < 1.4 km/s generally show shrinkage between ≈2-5%, but correspond to more sensitive compositions with increased variability.

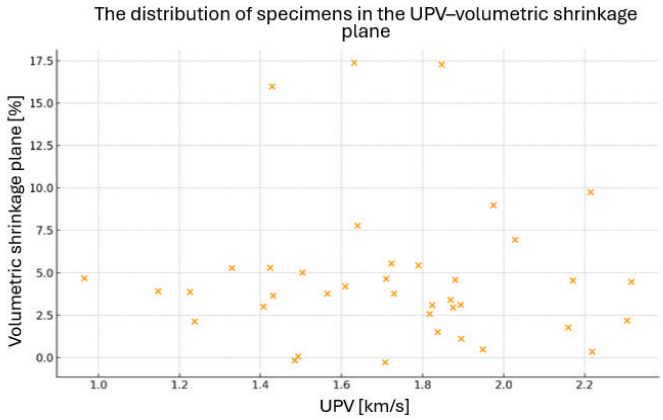



Figure 3. The distribution of specimens in the UPV-volumetric shrinkage plane

Although the UPV-shrinkage relationship is not strictly linear, the results indicate that stable and relatively high UPV values are compatible with reduced to moderate shrinkage levels.

Therefore, UPV can be used as an early indicator for identifying specimens with a more compact microstructure and, consequently, more predictable dimensional behavior during drying (Lim et al., 2018; Chajec et al., 2025).

Overall, the experimental results demonstrate a clear interdependence between density, UPV response, and drying shrinkage, confirming shrinkage as a critical indicator of internal structural integrity and long-term dimensional stability.

**Integrated interpretation of density, UPV, and shrinkage**

The combined analysis of physically measured density, UPV response, and drying shrinkage highlight a consistent and coherent physical behavior of the Eco-Clay material when optimal granulometry and moisture control are ensured.

For the reference and optimized mixtures (C3-D and C4-D), high dry density values were systematically associated with increased UPV and reduced shrinkage. This triad confirms a dense internal structure, reduced pore connectivity, and improved resistance to drying-induced tensile stresses.

By contrast, the lignin-modified compositions (DL and DLN series) exhibited a more complex behavior. Although certain formulations showed comparable density levels, the presence of biopolymer introduced microstructural heterogeneities that affected ultrasonic wave propagation and amplified shrinkage sensitivity. These effects were particularly visible in the C3-DLN formulation, where lower UPV values coincided with increased dimensional instability.

The limit compositions (NM family), although not central to this article, defined the technological boundaries of Eco-Clay materials. The NM specimens exhibited a more heterogeneous ultrasonic response and increased variability in drying behavior compared with the optimized formulations. Although the mean UPV value of the NM family remained relatively high (approximately 1.95-1.98 km/s), certain individual specimens displayed significantly lower ultrasonic velocities, indicating local heterogeneity, incomplete consolidation, or drying-induced discontinuities. These results suggest that the unfavorable behavior of the NM family is primarily associated with variability and local structural instability rather than with uniformly low UPV values.

From an engineering perspective, the strong interdependence between density, ultrasonic response, and shrinkage validates the use of UPV as a reliable non-destructive indicator for early-stage quality control of poured-earth materials, provided that it is calibrated against

physical density measurements (Kasinikota & Tripura, 2022).

## LIMITATIONS OF THE STUDY

The present study has several limitations that should be considered when interpreting the experimental results.

Although the investigated formulations were tested using replicated specimens, the number of samples remained limited for certain composition families, particularly for the experimental and boundary mixtures.

In addition, the drying process was performed under natural laboratory environmental conditions and was not fully climate-controlled. Although the temperature during drying was maintained within an approximate interval of 19-23°C, natural variations in ambient humidity and drying kinetics may have influenced moisture loss evolution and shrinkage variability.

Furthermore, the UPV method presents intrinsic limitations when applied to heterogeneous biopolymer-modified materials. Local discontinuities, pore distribution, moisture gradients, and microstructural heterogeneity may affect ultrasonic wave propagation and generate localized deviations between UPV-estimated and physically measured properties.

Future research should therefore include larger experimental datasets, climate-controlled curing conditions, and extended ultrasonic calibration for highly heterogeneous Eco-Clay systems.

## CONCLUSIONS

This study investigated the interrelationship between physically measured density, ultrasonic pulse velocity (UPV), and drying shrinkage for representative Eco-Clay poured-earth compositions, with the objective of supporting early-stage quality control and technological optimization.

The optimal formulations (C3-D and C4-D) exhibited the most stable and consistent behavior, characterized by high and narrowly distributed dry density values ranging approximately between 2070 kg/m$^3$ and 2095 kg/m$^3$, increased UPV responses, and reduced linear and volumetric shrinkage. These results confirm the formation of a dense internal structure with limited pore connectivity and improved resistance to drying-induced tensile stresses.

Lignin-modified mixtures (DL and DLN series) displayed a more complex response. Although competitive density levels were achieved in certain cases, the presence of biopolymer introduced microstructural heterogeneities, leading to increased dispersion of UPV values, higher sensitivity to curing conditions, and amplified shrinkage and localized cracking.

The comparative analysis between physically measured and UPV-estimated densities demonstrated that UPV can be reliably employed as a nondestructive indicator for Eco-Clay quality assessment, provided that it is calibrated against direct density measurements and interpreted with caution for biopolymer-modified compositions.

Therefore, for biopolymer-modified materials, it is recommended to combine UPV evaluation with direct physical measurements of density and shrinkage in order to improve the reliability of quality assessment.

From an engineering standpoint, the combined use of density, UPV, and shrinkage offers an efficient and complementary diagnostic framework for optimizing poured-earth Eco-Clay materials. Future research will focus on extending the ultrasonic calibration range for densities below approximately 1800 kg/m$^3$ and for highly heterogeneous biopolymer-modified systems, refining biopolymer dosage, and correlating nondestructive parameters with mechanical strength for full structural validation.

## ACKNOWLEDGEMENTS

This work was carried out within the Nucleu Programme of the National Research Development and Innovation Plan 2022-2027, supported by MCID, "ECODIGICONS" project no. PN 23 35 04 01: “Fundamental-applied research into the sustainable development of construction products (materials, elements, and structures, as well as methods and technologies) that utilizes current national resources to enhance the eco-innovative and durable aspects of Romania's civil and transport infrastructure”, financed by the Romanian Government.

## REFERENCES

Abbasi, F., Choobbasti, A. J., & Roushan, K. (2025). Advanced stabilization of clayey sand using xanthan gum: insights from multiscale evaluation and ultrasonic pulse velocity analysis. *Results in Engineering*, 25, 104419.

Armistead, S. J., Rawlings, A.E., Smith, C., & Staniland, S.S. (2020). Biopolymer stabilization/solidification of soils: a rapid, micro-macro, cross-disciplinary approach. *Environmental Science and Technology*, 54(21), 13963-13972.

Bogas, J. A., Real, S., Cruz, R. A. la, & Azevedo, B. (2023). Mechanical performance and shrinkage of compressed earth blocks stabilised with thermoactivated recycled cement. *Journal of Building Engineering*, 79, 107892.

Bolborea, B., Baeră, C., Dan, S., Gruin, A., Burduhos-Nergiș, D. D., & Vasile, V. (2021). Concrete Compressive Strength by Means of Ultrasonic Pulse Velocity and Moduli of Elasticity. *Materials*, 14(22), 7018.

Canivell, J., Martin-del-Rio, J. J., Solís, M., Rodríguez-Mariscal, J. D., Flores-Alés, V., & Pontiga, F. (2025). Evaluation of the physical and mechanical behaviour of rammed earth by incorporation of recycled glass. *Boletín de la Sociedad Española de Cerámica y Vidrio*, 64(3), 100442.

Chajec, A., Zając, M., & Sadowski, Ł. (2025). Bleeding of Portland composite cements. *Materials and Structures*, 58, 269.

Daneti, S. B., Tam, C. T., Tamilselvan, T., Kannan, V., Kong, K., & Islam, M. (2024). Shrinkage Cracking Potential of Lightweight Aggregate Concrete. *Journal of Physics Conference Series*, 2779(1), 012067.

Kasinikota, P., & Tripura, D. D. (2022). Prediction of physical-mechanical properties of hollow interlocking compressed unstabilized and stabilized earth blocks at different moisture conditions using ultrasonic pulse velocity. *Journal of Building Engineering*, 48, 103961.

Keita, E., & Perrot, A. (2024). Processing of earth-based materials: current situation and challenges ahead. *RILEM Technical Letters*, 8, 141-149.

Kozubal, J.V., Kania, T., Tarawneh, A.S., Hassanat, A., Lawal, R., (2023). Ultrasonic assessment of cement-stabilized soils: Deep learning experimental results. *Measurement*, 223, 113793.

Lim, N. H. A. S., Samadi, M., Sam, A. R. M., Khalid, N. H. A., Sarbini, N. N., Ariffin, N. F., Hussin, M. W., & Ismail, M. (2018). Drying Shrinkage of Mortar Incorporating High Volume Oil Palm Biomass Waste. *E3S Web of Conferences*, 34, 01008.

Sathiparan, N., Tharuka R. A. N. S. & Jeyananthan, P., (2024). Prediction of moisture content of cement-stabilized earth blocks using soil characteristics, cement content, and ultrasonic pulse velocity. *Journal of Engineering and Applied Science*, 71, 187.

Turco, C., Paula Junior, A., Jacinto, C., Fernandes, J., Teixeira, E., & Mateus, R. (2024). Influence of particle size on compressed earth blocks properties and strategies for enhanced performance. *Applied Sciences*, 14(5), 1779.

Turco, C., Paula, A.C. de, Teixeira, E., & Mateus, R. (2021). Optimisation of Compressed Earth Blocks (CEBs) using natural origin materials: A systematic literature review. *Construction and Building Materials*, 309, 125140.

Vieira, E. F., Amaral, T., Domingues, V. F., & Delerue-Matos, C. (2026). Hydrophobicity Strategies of Starch-Based Films: Recent Advances and Perspectives. *Polymers*, 18(4), 490.

Walter, L., Estevez, Y., Medjigbodo, G., Aubert, J.-E., Linguet, L., & Nait-Rabah, O. (2024). Design of poured earth construction materials from the elementary characteristics of tropical soils. *Case Studies in Construction Materials*, 20, e02709.

Xu, J., Cheng, W., Inglett, G. E., Wu, P., Kim, S., Liu, S. X., & Tseng, Y. (2010). Micro-heterogeneity of cellulosic fiber biopolymer prepared from corn hulls. *LWT*, 43(6), 977-981.

Zhang, C., Coasne, B., Guyer, R. A., Derome, D., & Carmeliet, J. (2020). Moisture-induced crossover in the thermodynamic and mechanical response of hydrophilic biopolymer. *Cellulose*, 27(1), 89-99.

Zhang, J., Han, Y., & Zhang, J. (2016). Evaluation of Shrinkage Induced Cracking in Concrete with Impact of Internal Curing and Water to Cement Ratio. *Journal of Advanced Concrete Technology*, 14(7), 324-334.

Scientific Papers. Series E. Land Reclamation, Earth Observation & Surveying, Environmental Engineering. Vol. XV, 2026
Print ISSN 2285-6064, CD-ROM ISSN 2285-6072, Online ISSN 2393-5138, ISSN-L 2285-6064

# INTERNAL AIR RECIRCULATION FOR CONDENSATION RISK CONTROL IN PASSIVE SOLAR GREENHOUSES: A DEW MARGIN-BASED ZONAL APPROACH

**Bogdan ILIE[1], Yuxin TONG[2], Ana BUTCARU[1], Tiberiu ION[3], Ionuț Ovidiu JERCA[1]**

[1]University of Agronomic Sciences and Veterinary Medicine of Bucharest,
59 Mărăști Blvd, District 1, Bucharest, Romania
[2]Institute of Environment and Sustainable Development in Agriculture,
Chinese Academy of Agricultural Sciences, China
[3]SC Skip Monday Studio SRL, 10 Triumfului Street, Ploiesti, Prahova County, Romania

Corresponding author email: ovidiu.jerca@qlab.usamv.ro

***Abstract***

*During winter operation, passive solar greenhouses with limited auxiliary heating are frequently affected by nocturnal thermal stratification and elevated humidity, promoting condensation on structural surfaces and increasing fungal disease risk at canopy level. This study evaluates an internal air recirculation strategy for condensation prevention, implemented in a double-layer Chinese solar greenhouse at the University of Agronomic Sciences and Veterinary Medicine of Bucharest. Twenty axial fans were installed at 3.5 m height along both longitudinal sides, controlled by adaptive dew margin thresholds derived from a distributed canopy sensor network. Two experimental phases were compared: Phase I used synchronized control of both ventilation units driven by the worst-case canopy dew margin; Phase II introduced asynchronous zonal control, with each unit independently responding to its local canopy sensor. Results indicate that canopy-based recirculation control successfully maintained positive dew margins at plant level throughout the monitoring period, with no leaf wetness events detected at canopy level in either phase, while structural condensation on the inner polyethylene cover persisted. The dew margin indicator proved more operationally discriminating than relative humidity alone under the conditions observed.*

***Key words:*** *condensation risk, dew point, internal recirculation, passive greenhouse, zonal microclimate control.*

## INTRODUCTION

Winter greenhouse operation in passive or semi-closed structures is frequently constrained by limited external ventilation, either due to energy penalties or the risk of cold stress for sensitive crops. Under such conditions, relative humidity often remains high, and localized stagnant air zones may develop, promoting condensation on cold structural surfaces and, in some cases, within the crop canopy. Condensation is not only an undesirable physical phenomenon but also a major biological risk factor, strongly associated with fungal disease development and reduced crop quality during the cold season (Piscia et al., 2012; Amani et al., 2020). This challenge becomes particularly acute in greenhouses with modest auxiliary heating, where nocturnal thermal stratification leads to the accumulation of warm, humid air in the upper volume while the crop zone remains prone to saturated boundary layers.

From a physical perspective, condensation is governed by the proximity of air temperature to the dew point and the presence of sufficiently cold surfaces acting as sinks for water vapor. In greenhouse environments, nocturnal radiative cooling of the envelope is often the dominant driver, making the roof or inner cover the coldest surface where condensation is initiated (Piscia et al., 2012). Consequently, dew point-based indicators provide a more robust framework for condensation risk assessment than relative humidity alone, since they quantify the thermodynamic margin to saturation. Moreover, condensation typically develops locally in the coldest or most humid zones, meaning that bulk-average climate variables may fail to capture critical risk conditions (Boulard & Draoui, 1995; Gao et al., 2024).

Natural ventilation remains the classical tool for controlling temperature and humidity, yet its effectiveness depends strongly on wind conditions, buoyancy forces, vent geometry, and

the effective opening area. Experimental studies and models have shown that ventilation rates generally increase with wind speed and vent aperture, but the relationship is highly variable and sensitive to airflow regimes and structural design (Boulard & Draoui, 1995; Baptista et al., 1999; Teitel & Tanny, 1999). Because ventilation rate fluctuates continuously with weather conditions, its reliable characterization requires real-time measurement rather than static assumptions (Tusi & Shimazu, 2020). Importantly, seemingly secondary parameters such as pressure and discharge coefficients can substantially affect ventilation predictions; wind tunnel measurements have demonstrated clear dependencies on wind direction and vent configuration (Sase et al., 1980). Therefore, during winter, when vent opening is deliberately restricted, external ventilation becomes both difficult and energetically costly as a dehumidification strategy. In addition to energy limitations, modern greenhouses frequently employ insect-proof screens, which can significantly reduce effective ventilation due to increased aerodynamic resistance, thereby enhancing humidity accumulation and microclimate heterogeneity (Katsoulas et al., 2006). Under cold-season conditions, this creates a critical trade-off: ventilation sufficient to remove moisture may induce excessive heat losses and compromise energy efficiency. Studies quantifying the thermal cost of dehumidification have shown that a substantial fraction of heating energy may be indirectly expended through moisture removal via ventilation, motivating alternative or complementary approaches with reduced losses (Maslak & Nimmermark, 2017; Amani et al., 2020). Mechanical humidity-control options have been proposed for winter operation, yet their effectiveness must be evaluated in relation to thermal impacts and crop-zone relevance (Lee et al., 2020).

A key point emphasized in recent literature is that "ventilation" does not simply refer to air exchange rates, but rather to internal airflow patterns and climate uniformity at canopy level. Spatial heterogeneity in temperature and humidity may persist even in ventilated greenhouses, and stagnant zones can remain critical hotspots for condensation risk (Gao et al., 2024). This is consistent with experimental and CFD-based studies showing that ventilation design strongly determines distributed microclimate rather than only mean conditions (Bournet & Boulard, 2010; Zhang et al., 2025). Seasonal differences are also important: while summer ventilation is dominated by cooling requirements, winter ventilation must address humidity control under strong energy constraints (Kittas et al., 2005; He et al., 2015). Classical work has highlighted that air movement and climate uniformity are central objectives in greenhouse operation, not merely side-effects of vent opening (Sase, 2006).

Biologically, the relevant humidity is not necessarily the greenhouse-average value but the microclimate in the immediate vicinity of leaves, where boundary-layer effects may produce conditions substantially different from bulk air. Experimental evidence confirms that ventilation influences not only greenhouse humidity but also leaf boundary-layer humidity, with direct implications for condensation and disease risk (Boulard et al., 2004). Similarly, research on leaf wetness duration indicates that simple empirical thresholds (e.g., RH > 90%) may be insufficient in greenhouse environments, where spatial variability is high and locally calibrated models are required (Wang et al., 2019). These findings support approaches that explicitly separate structural condensation zones from agronomically relevant canopy zones and rely on physically grounded indicators such as dew point or dew margin combined with distributed sensing.

Alongside external air exchange strategies, increasing attention has been directed toward internal air recirculation and mixing as means to reduce stratification and limit the persistence of humid stagnant pockets without major ventilation heat losses. Horizontal airflow fan systems have been discussed as practical tools for reducing vertical gradients, improving canopy drying, and lowering the probability of reaching dew point at leaf level (Blanchard, 2008). Recent studies further indicate that non-uniform ventilation and airflow distribution can affect both energy consumption and plant growth, reinforcing the need for canopy-oriented microclimate control rather than reliance on bulk averages (Wang et al., 2025). CFD simulations of greenhouse airflow similarly emphasize the sensitivity of internal climate to geometry and vent configuration, making uniformity a design target rather than an automatic outcome (Zhang et al., 2025).

Based on these converging gaps in the literature, a clear applied problem emerges in passive winter greenhouses where external ventilation is restricted, there is a need for condensation-risk mitigation strategies that do not depend primarily on-air exchange with the outdoor environment. The present study therefore evaluates an internal air recirculation approach implemented in a double-layer passive greenhouse, using multi-point monitoring and dew point-based control indicators. Rather than treating the greenhouse climate as a single average value, the approach emphasizes (i) spatial characterization of microclimate variability, (ii) conservative worst-case risk definition, and (iii) canopy-oriented zonal control to limit stratification and condensation-prone stagnation zones. We hypothesized that independent control of lateral compartments, driven by local canopy dew margin measurements, would enhance protection against canopy-level condensation - thereby reducing the risk of fungal disease development - compared to a synchronized worst-case control strategy.

## MATERIALS AND METHODS

### *Greenhouse structure and winter experimental context*

The experiment was conducted during the cold season (December 2025 - February 2026) in a passive double-layer Chinese solar greenhouse located at the University of Agronomic Sciences and Veterinary Medicine of Bucharest, Romania. The structure analyzed in this study is referred to as the Solar Double Chinese greenhouse (SDC) and is used for overwintering exotic and subtropical crops under minimal conventional heating input (Figure 1).



Figure 1. Overview of the passive double-layer Chinese solar greenhouse used in the experiment (December 2025 – February 2026). Left: eastern compartment showing blueberry crops. Right: western compartment with tropical species, illustrating the spatial heterogeneity of the experimental environment.

The greenhouse has an external length of approximately 45 m and an internal length of 42 m, due to the presence of two independent polyethylene layers (outer and inner envelope). The usable internal width is approximately 18 m (20 m external), while the maximum internal height reaches about 6 m, a geometry that strongly promotes nocturnal thermal stratification during winter conditions.

Such stratification is a well-known feature of passive greenhouses operating under limited ventilation, where warm humid air accumulates in the upper volume while the crop zone remains prone to saturation (Sase, 2006; Piscia et al., 2012). The structure is oriented along the South-North axis and is longitudinally divided by a central corridor approximately 2 m wide, separating two main compartments referred to in this study as the eastern zone and the western zone.

### *Heating system and nocturnal stratification*

Auxiliary heating is provided by 18 radiant electric panels installed above the central corridor at a height of approximately 2.5 m. Each panel has a nominal power of 500 W, resulting in a total installed capacity of approximately 9 kW. Under typical winter

operation, this radiant system generates a warm and humid air reservoir accumulating in the upper greenhouse volume. In the absence of sufficient circulation, the crop zone remains prone to stagnant moisture-laden boundary layers. Relative humidity frequently exceeds 90%, and condensation develops preferentially on cold structural surfaces (polyethylene foil and metallic elements), increasing the risk of fungal diseases and latent heat losses. Nocturnal radiative cooling of the envelope has been identified as a dominant driver of condensation initiation in greenhouse environments (Piscia et al., 2012). Natural ventilation through lateral openings is strongly restricted during winter, since external air is often too cold for subtropical crops and would induce significant energy penalties. Therefore, this study focuses on condensation-risk mitigation without relying on external air exchange, using only internal air recirculation, consistent with the need for low-energy humidity control strategies in winter greenhouses (Maslak & Nimmermark, 2017; Amani et al., 2020).

***Internal air recirculation system***

To reduce thermal stratification and limit condensation-prone microclimates, an internal air recirculation system was installed, consisting of 20 axial fans, each rated at approximately 40 W with a nominal airflow of about 400 $m^3\ h^{-1}$. Fans were mounted longitudinally at approximately 3.5 m height, distributed symmetrically: 10 fans on the eastern side and 10 fans on the western side. Airflows are directed downward toward the crop zone, aiming to create a turbulent mixing loop: warm humid air accumulated above the radiant heaters is pushed downward, while cooler air near the polyethylene envelope is mixed upward along the structural surface. This strategy is intended to weaken stratification and reduce the persistence of saturated boundary layers, without the energy losses associated with external ventilation (Blanchard, 2008; Bournet & Boulard, 2010). Fans were physically installed in early December 2025, while automated operation was implemented beginning in January 2026 after full integration into the Home Assistant control platform.

Distributed microclimate monitoring network (Figure 2 and Figure 3).



Figure 2. Internal air recirculation system. Left: recirculation fans (10 per side) mounted at ~3.5 m height, directed downward toward the crop zone. Right: TROTEC BA06 vane anemometer used for air velocity measurement during fan characterization trials



Figure 3. Schematic cross-section of the greenhouse illustrating the nocturnal thermal stratification pattern generated by the central radiant heating corridor and the air recirculation loops induced by the axial fans mounted at 3.5 m height on each longitudinal side (left). The VENTS VKOM 200 axial fan unit (43 W, 405 $m^3 \cdot h^{-1}$, 1300 rpm, IP X4) used for internal air recirculation (right)

***Distributed microclimate monitoring network***

Microclimate monitoring was performed through a distributed sensor network measuring air temperature and relative humidity at multiple vertical and lateral positions, designed to capture spatial gradients associated with condensation development. Spatial heterogeneity is frequently observed even in ventilated greenhouses, and local stagnant zones may remain critical hotspots for condensation risk (Gao et al., 2024). The initial monitoring configuration included sensors positioned in peripheral regions influenced by envelope cooling: S4 (Eastern zone, 100 cm above ground), S6 (Western zone, 100 cm above ground), S5 (Central upper volume, 400 cm height), and S8 (Southern upper zone, 400 cm height).

These sensors enabled computation of spatial dew point distributions and identification of structural zones with elevated condensation risk. Although S4 and S6 are defined by their mounting height (100 cm), their relatively marginal placement means they primarily reflect structural condensation conditions rather than direct canopy microclimate. The upper central sensor (S5) was used to characterize the general moisture reservoir in the greenhouse air mass, whereas fan control was always driven by the minimum (worst-case) dew margin measured in the canopy zone (Figure 4).



Figure 4. Canopy-level sensor deployment. Left: Sensor S1 (East compartment, 170 cm height) labelled with identification tag. Right: Sensor S2 (West compartment, 170 cm height). Both sensors measure air temperature and relative humidity for dew point and dew margin computation

***Leaf wetness sensor and foil-adjacent measurements***

A leaf wetness sensor (LWS) was deployed as a qualitative indicator of liquid water film formation. The sensor was validated prior to deployment by direct application of a water film (spray and moist tissue contact), confirming that it responds exclusively to liquid water film formation and remains at zero output in the absence of free water. When positioned within the crop canopy, the sensor recorded zero output throughout the entire monitoring period. When attached directly to the inner polyethylene foil surface - where condensation was visually confirmed on multiple nights - the sensor consistently detected condensation events. Repositioning the sensor 5 cm away from the foil surface was sufficient to return output to zero, confirming that condensation was confined to the immediate foil surface and did not extend into the adjacent air volume or the crop zone. This distinction between structural condensation and biologically relevant canopy wetness is consistent with studies showing that leaf boundary-layer humidity may differ substantially from bulk greenhouse air conditions (Boulard et al., 2004). The absence of liquid water detection within the canopy should be interpreted as evidence that the recirculation strategy successfully prevented leaf-level condensation, while structural condensation remained confined to the inner envelope. Leaf wetness duration models often require calibration beyond simple RH thresholds, highlighting the complexity of canopy-level moisture processes (Wang et al., 2019).

Three auxiliary temperature probes (Temperature 1–Temperature 3) were installed near the inner foil surface at different heights (30 cm, 150 cm, and 300 cm). Initially fixed directly on the foil, these probes primarily reflected surface cooling. Beginning on 1 February 2026, they were repositioned approximately 5 cm away from the foil, in order to better capture air temperature variations influenced by recirculation rather than direct conductive coupling to the cold surface (Figure 5).




Figure 5. Foil-adjacent temperature probe installation (Mobile Sensor 10). Left: Temperature 1 probe positioned at foil surface level. Right: Temperature 2 probe mounted inside the foil layer. Both probes monitor the thermal regime near the inner cladding surface to detect condensation-prone zones

***Dew point computation and dew margin indicator***

To evaluate condensation risk physically, dew point temperature was calculated using the Magnus–Tetens approximation, based on measured air temperature and relative humidity:

$$T_{te}^{W} = b \cdot \gamma(T,RH) / [a - \gamma(T,RH)]$$
$$\gamma(T,RH) = ln(RH/100) + aT / (b + T)$$

where T is the air temperature (°C), RH is the relative humidity (%), and γ(T, RH) is an intermediate dimensionless variable used in the Magnus-Tetens formulation. The constants were set to a = 17.27 and b = 237.7°C, which are commonly applied for temperature ranges relevant to greenhouse environments.

Condensation proximity was expressed through the thermodynamic indicator dew margin, defined as:

$$\Delta T = T_a^{IR} - T_{te}^{W}$$

Large values indicate air far from saturation, whereas small values indicate proximity to condensation. Dew point–based indicators provide a more robust condensation-risk framework than relative humidity alone, particularly under heterogeneous greenhouse conditions (Piscia et al., 2012). In this study, the primary operational threshold was set at 2°C, while values below 1°C were considered indicative of imminent condensation risk within the crop zone.

***Definition of the critical scenario: Worst-Case Dew Margin***

In large greenhouse volumes, condensation develops locally in the coldest or most humid regions rather than uniformly. For preventive control, a conservative indicator termed Worst-Case Dew Margin was defined as the minimum dew margin value across monitored points:

$$\Delta T_m^{In} = min(\Delta T_1, \Delta T_2, \ldots, \Delta T_n)$$

This parameter continuously represents the point closest to condensation and serves as the main control variable for fan automation, consistent with the need for worst-case microclimate assessment rather than bulk averages (Gao et al., 2024).

***Transition to canopy-based control (1 February 2026)***

During the initial phase (December 2025-January 2026), worst-case control was dominated by marginal sensors (S4/S6) influenced by envelope cooling. While this configuration reflected structural condensation risk on the foil, it did not directly demonstrate agronomically relevant improvement in the leaf-level microclimate. To ensure biological relevance, two additional sensors were installed in the canopy zone on 1 February 2026: S1 (East canopy, 170 cm) and S2 (West canopy, 170 cm). These sensors are positioned within the vegetative zone, approximately 3.5 m from the fans, providing representative measurements of leaf-level temperature and humidity. From this date onward, fan automation was based exclusively on the canopy worst-case dew margin, while marginal sensors remained monitored as structural reference. The importance of canopy-oriented microclimate monitoring has been emphasized in studies addressing boundary-layer humidity and crop-level risk processes (Boulard et al., 2004; Sase, 2006).

***Experimental Phase I - Synchronized canopy-based control***

Between 1 February 2026 and 11 February 2026 (09:59), the system operated under a synchronized canopy-based control configuration, hereafter referred to as Phase I. During this interval, both ventilation units (Vent1 - East and Vent2 - West) were driven simultaneously by the canopy worst-case dew margin (S1), defined as the minimum ΔT among canopy sensors. This configuration ensured a conservative, homogeneous response across the greenhouse volume, treating the structure as a single thermodynamic control domain. Phase I thus represents the baseline experimental configuration against which subsequent zonal refinements are evaluated.

Beginning on 1 February 2026, internal air recirculation was controlled through an adaptive three-regime strategy:

- Critical regime (ΔT < 1.0°C) - fans operate continuously, indicating maximum agronomic condensation risk in the canopy.
- Intermediate regime (1.0-2.0°C) - fans operate in pulse mode (10 min ON / 20 min OFF), maintaining mixing while reducing energy consumption.
- Safe regime (ΔT > 2.5°C) - fans are fully switched off after stabilization, introducing hysteresis and preventing excessive cycling.

A hysteresis margin was introduced to prevent rapid fan cycling: recirculation was activated when ΔT fell below 2.0°C but switched off only after recovery above 2.5°C. Adaptive strategies with hysteresis are consistent with recommendations to avoid excessive switching while maintaining canopy-level uniformity (Bournet & Boulard, 2010; Zhang et al., 2025).

***Transition to Phase II – Asynchronous canopy-based zonal control***

Beginning on 12 February 2026, the control strategy was experimentally modified in order to evaluate the effect of spatially differentiated canopy-based recirculation. While Phase I relied on a synchronised worst-case control approach, both ventilation units being driven by the minimum canopy dew margin (S1), Phase II introduces an asynchronous zonal configuration. In this second phase, Vent1 (East compartment) continues to be controlled by the canopy worst-case dew margin (S1), whereas Vent2 (West compartment) is independently driven by the local canopy dew margin measured at S2 (170 cm height).

This modification was motivated by the persistent lateral asymmetry observed during Phase I, where S1 systematically exhibited lower dew margin values than S2. In addition, the eastern compartment is subjected to slightly higher irrigation frequency due to crop distribution, which may locally increase air humidity and influence dew point dynamics. Consequently, treating both compartments as a single homogeneous control volume may mask relevant microclimatic variability. The asynchronous configuration maintains identical thermodynamic thresholds (continuous operation for $\Delta T < 1°C$, pulse regime for 1-2°C, and shutdown above 2.5°C), ensuring comparability between phases while allowing independent zonal response.

***Air velocity measurements***

To quantify airflow intensity, air velocity was measured using a vane anemometer (TROTEC BA06) over 30-minute intervals at two locations: at 1.5 m from the fan (maximum velocity $\approx 1.0$ m $s^{-1}$) and at canopy level near S1, at 2.5 m distance (maximum velocity $\approx 0.4$ m $s^{-1}$). Although measured canopy air velocities were moderate (~0.4 m $s^{-1}$), the primary objective was not intensive convective drying but the reduction of stratification and the homogenization of humidity distribution within the crop zone, consistent with the role of airflow uniformity emphasized by Sase (2006).

***Operational condensation risk definition and intervention quantification***

For automation and quantitative evaluation, a binary condensation risk sensor was defined as active when the canopy worst-case dew margin fell below the critical threshold of 2°C, indicating conditions favorable for condensation. To validate the system experimentally, not only fan triggering but also the duration of exposure and intervention were quantified through two cumulative history statistics sensors implemented in Home Assistant: Condensation Risk Time Today (total daily hours during which condensation risk was active) and Recirculation Runtime Today (total daily operating time of the internal recirculation system). These metrics provide a reproducible framework for comparing climatic pressure against the effective response of the control strategy.

***Data acquisition and storage***

All temperature, relative humidity, dew point, dew margin, and fan-state data were collected automatically through the Home Assistant platform and continuously stored in an InfluxDB time-series database. This infrastructure enables full reconstruction of temporal series and subsequent statistical analysis of microclimate evolution and system response under winter operating conditions (Figure 6).

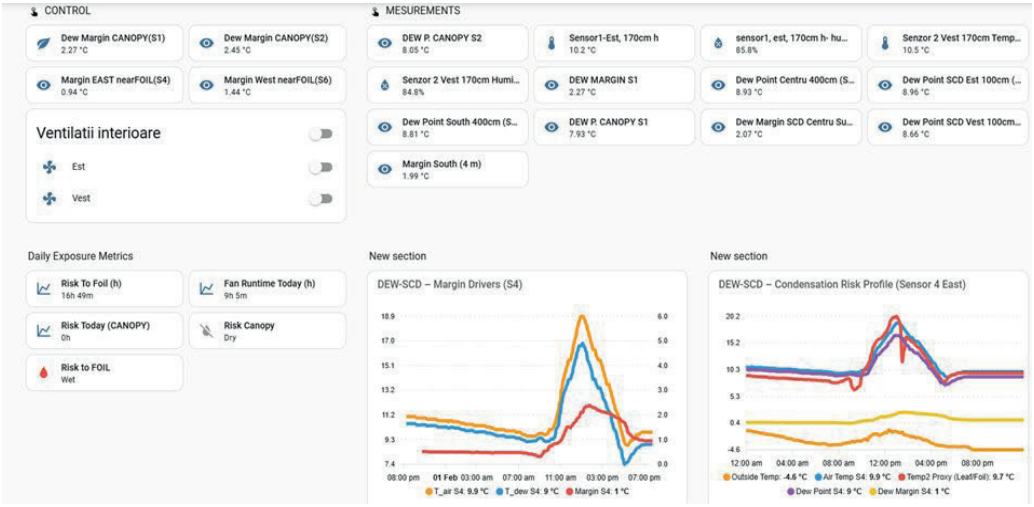



Figure 6. Home Assistant monitoring and control dashboard. Left panel: real-time dew margin values for all sensors and ventilator state. Centre: dew margin drivers time series (S4). Right: condensation risk profile for Sensor S4 (East). The dashboard integrates all sensor streams and provides visual indication of condensation risk zones

## RESULTS AND DISCUSSIONS

### *Performance of the synchronised dew-margin-based recirculation control (Phase I)*

During Phase I (1 February 2026 - 11 February 2026, 09:59), both recirculation fans (Vent1 - East compartment; Vent2 - West compartment) operated under a strictly synchronised control strategy, driven by the conservative canopy worst-case dew margin parameter (S1). Over the analysed interval of approximately 240 hours, both ventilation units exhibited nearly identical operational behaviour, with a cumulative runtime of 50.22 hours for Vent1 and 50.03 hours for Vent2, corresponding to an average daily operation of approximately 5 hours per ventilator. This confirms the deterministic and fully synchronised implementation of the initial control logic.

The distribution of canopy dew margin values during this phase indicates that the system maintained effective control over condensation risk. For the worst-case canopy parameter (S1), the cumulative duration during which the dew margin fell below 2°C was 164.56 hours, while the time spent below the more critical threshold of 1°C was limited to only 0.089 hours (approximately 5.3 minutes) over the entire observation period. The absolute minimum recorded value for S1 was 0.55°C, and the 5th percentile was 1.29°C, indicating that severe proximity to condensation conditions was rare and short-lived.

In contrast, the west-local canopy sensor (S2) exhibited less severe conditions. The cumulative time below 2°C was 139.11 hours, while no instances of dew margin below 1°C were recorded. The minimum observed value for S2 was 1.41°C, and the 5th percentile was 1.77°C. These results reveal a persistent lateral asymmetry between the two compartments, with the worst-case zone (S1) consistently exhibiting lower dew margin values and longer exposure to moderate condensation risk conditions compared to the western compartment.

Despite this spatial variability, both ventilation units operated with virtually identical runtimes due to the synchronised control strategy. Consequently, while the implemented logic proved effective in preventing severe condensation risk ($\Delta T < 1°C$) and maintained overall system stability, it did not account for lateral differences in microclimatic behaviour within the greenhouse. This observation provides the experimental justification for the subsequent implementation of an asynchronous, zone-based control strategy in Phase II.

***Leaf wetness validation***

The leaf wetness sensor, validated prior to deployment to confirm exclusive response to liquid water film, recorded zero output throughout the monitoring period when positioned within the canopy. This result is not attributable to sensor insensitivity: the same sensor consistently detected condensation events when in direct contact with the inner polyethylene foil surface, confirming both instrument functionality and the spatial confinement of condensation to structural surfaces. No leaf wetness events were recorded at canopy level during Phase I, despite multiple nocturnal intervals in which the dew margin approached critical thresholds. This indicates that the canopy-based control strategy successfully prevented actual condensation at plant level. Condensation was, however, visually observed on the greenhouse plastic cover during several nights, consistent with expected radiative cooling of structural surfaces. These observations confirm that dew margin values at canopy level remained above the condensation point even when structural surfaces experienced local cooling (Figure 7).




Figure 7. Home Assistant History record of canopy dew margin for S1 (East, blue) and S2 (West, yellow) during Phase I (1-11 February 2026), with ventilator activation states shown in the upper panel. Nocturnal peaks correspond to critical condensation risk events triggering continuous fan operation

***Performance of the asynchronous zonal recirculation control (Phase II)***

Phase II was initiated on 12 February 2026 and extended through 26 February 2026, covering a total monitoring interval of 15 days (360 hours). During this period, Vent1 (East compartment) continued to be driven by the canopy worst-case dew margin (S1), while Vent2 (West compartment) was independently controlled by the local canopy sensor S2, implementing the asynchronous zonal strategy described in the Materials and Methods section.

Over the 15-day interval, the recirculation system accumulated a total runtime of 63.1 hours, corresponding to a mean daily operation of 4.21 ± 2.30 h day$^{-1}$. The day-to-day variability in runtime was substantially higher than in Phase I (coefficient of variation: 55% vs. approximately 5% in the synchronized phase), reflecting the adaptive nature of the control logic responding to variable nocturnal conditions. On nights with more severe external conditions, daily runtimes reached up to 10.2 hours (21 February), while on milder nights the system operated as little as 2.3 hours, demonstrating the energy-modulating effect of the threshold-based hysteresis strategy.

The daily mean canopy dew margin for the eastern compartment (S1) ranged from 1.25°C to 10.45°C, with an overall mean of 5.24 ± 3.29°C. The western compartment (S2) exhibited slightly higher values, with a mean of 5.86 ± 3.49°C and a daily range of 1.34°C to 11.14°C. The persistent lateral asymmetry first identified during Phase I was maintained throughout Phase II, with S1 consistently recording lower daily mean dew margins than S2. This asymmetry is visually apparent in the

continuous monitoring record (Figure 3) and is consistent with the higher irrigation frequency in the eastern compartment noted in the Methods section.

The daily minimum dew margin - representing the closest approach to condensation within each 24-hour period - was maintained above 0.8°C for S1 (mean minimum: 1.10 ± 0.17°C, absolute minimum: 0.81°C on 25 February) and above 0.87°C for S2 (mean minimum: 1.24 ± 0.24°C). Critically, the cumulative condensation risk counter for the canopy zone recorded zero hours of active risk across all monitored days in Phase II, indicating that the dew margin remained above the 2°C intervention threshold for the dominant part of each day and that brief excursions below this threshold were successfully intercepted by recirculation activation.

A Spearman rank correlation analysis between daily recirculation runtime and daily minimum dew margin in the western compartment yielded a statistically significant negative association ($r_s = -0.582$, $p = 0.010$, $n = 15$), confirming that the control system responded appropriately to microclimatic pressure: higher recirculation effort was consistently associated with days of greater condensation proximity. A similar trend was observed for the eastern compartment ($r_s = -0.396$), though this did not reach statistical significance ($p = 0.12$), likely reflecting the more frequent activation of continuous-mode recirculation in S1 which partially saturated the runtime response.

The inter-phase comparison of daily mean dew margin values (Phase I: S1 mean 3.39 ± 1.80°C; Phase II: S1 mean 5.24 ± 3.29°C) indicates numerically higher margins in Phase II, consistent with generally milder external conditions during the later observation period (mean inter-layer temperature 3.60 ± 2.61°C in Phase II vs. 0.96 ± 3.50°C in Phase I). A Mann-Whitney U test did not identify a statistically significant difference between phases for either compartment (S1: $U = 58.0$, $z = -1.27$, $p = 0.20$; S2: $U = 65.0$, $z = -0.91$, $p = 0.36$), and the Spearman correlation between external temperature and daily dew margin did not reach significance in either phase (Phase II S1: $r_s = 0.34$, $p = 0.19$; Phase II S2: $r_s = 0.38$, $p = 0.14$). These results indicate that inter-phase differences in dew margin are not attributable to a single confounding thermal driver, though the relatively small sample sizes preclude definitive causal attribution.

Analysis of individual fan activation events confirmed the high degree of operational synchrony between the two ventilation units throughout Phase II, with Vent1 recording 90 total activations and Vent2 recording 83 activations over the 15-day period ($r = 0.856$, daily activation counts). Meaningful divergence between units was observed on only two days (17 and 18 February), when Vent1 activated three times more than Vent2, corresponding to the nights with the most pronounced S1-S2 dew margin asymmetry. These results indicate that, under the observed winter conditions, the microclimatic difference between the eastern and western compartments was insufficient to produce systematic operational decoupling of the two ventilation zones. The asynchronous zonal strategy nevertheless provided the control infrastructure for independent response, which may become more relevant under more contrasted lateral humidity conditions.

No leaf wetness events were detected at canopy level during Phase II, consistent with the results of Phase I and confirming the biological effectiveness of the control approach across both experimental configurations (Table 1, Table 2).

***Late-phase lateral asymmetry (24 February - 3 March 2026)***

Towards the end of Phase II, a progressive and sustained lateral asymmetry became evident between the eastern (S1) and western (S2) compartments (Figure 8). During the period 24 February - 3 March 2026, sensor S2 consistently recorded higher dew margin values than S1, with peak nocturnal differences exceeding 6°C. Both zones retained the characteristic diurnal pattern of low nocturnal margins and elevated daytime values driven by solar gain, yet the intensity of nocturnal condensation risk diverged substantially between compartments.

A probable contributing factor is differential irrigation between the two zones: higher water application in the eastern compartment would elevate local vapour pressure and reduce the dew margin independently of fan state, while the western zone - receiving less irrigation - maintained a consistently higher safety margin. This observation directly demonstrates the

agronomic value of asynchronous zonal control: Vent1, driven by S1, operated at higher activation frequency during this period, while Vent2, driven by S2, ran at reduced duty - delivering localised energy efficiency without compromising condensation prevention in the higher-risk eastern zone. This dynamic would be unachievable under the synchronised strategy of Phase I.

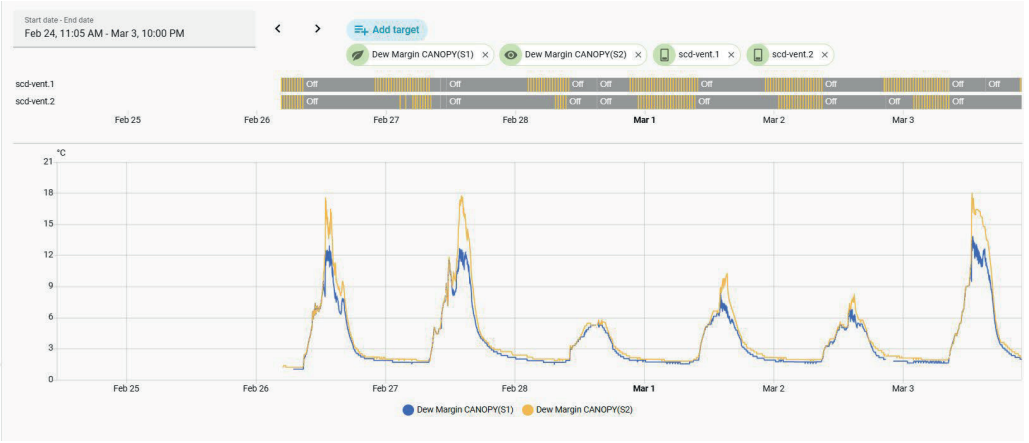



Figure 8. Canopy dew margin for S1 (East, blue) and S2 (West, yellow) during the final period of Phase II (24 February - 3 March 2026), with asynchronous ventilator activation states shown in the upper panel. A progressive lateral asymmetry is visible from 26 February onward, with S2 consistently exceeding S1 during nocturnal risk periods. The divergence is consistent with differential irrigation practices between compartments and illustrates the operational relevance of independent zonal control

Table 1. Summary statistics of canopy dew margin (ΔT, °C) for Sensor S1 (East, 170 cm) and Sensor S2 (West, 170 cm) during Phase I and Phase II

| Parameter | Phase I S1 (East) | Phase I S2 (West) | Phase II S1 (East) | Phase II S2 (West) |
|---|---|---|---|---|
| Observation period (days) | 11 | 11 | 15 | 15 |
| Total monitoring hours (h) | 264 | 264 | 360 | 360 |
| Mean daily ΔT (°C) | 3.39 ± 1.80 | 4.12 ± 2.43 | 5.24 ± 3.29 | 5.86 ± 3.49 |
| Daily minimum ΔT – mean (°C) | – | – | 1.10 ± 0.17 | 1.24 ± 0.24 |
| Absolute minimum ΔT (°C) | 0.55 | 1.41 | 0.81 | 0.87 |
| 5th percentile ΔT (°C) | 1.57 | 1.93 | 0.89[1] | 0.95[1] |
| Cumul. time below 2°C (h) | 164.56 (62.3%) | 139.11 (52.7%) | 30.0 (8.3%) | 20.3 (5.6%) |
| Cumul. time below 1°C (h) | 0.09 | 0.00 | ~0.74[2] | – |
| Days with min ΔT < 1°C | – | – | 5 / 15 | 2 / 15 |

Table 2. Recirculation fan operational statistics during Phase I and Phase II.

| Parameter | Phase I | Phase II |
|---|---|---|
| Control strategy | Synchronized – both units driven by S1 worst-case | Asynchronous zonal – Vent1 by S1; Vent2 by S2 |
| Observation period (days) | 11 | 15 |
| Total monitoring hours (h) | 264 | 360 |
| Cumulative runtime – Vent1 (h) | 50.22 | n.d.[1] |
| Cumulative runtime – Vent2 (h) | 50.03 | n.d.[1] |
| Mean daily runtime (h day$^{-1}$) | 4.56 ± 0.02[2] | 4.21 ± 2.30 |

| Parameter | Phase I | Phase II |
|---|---|---|
| Daily runtime range (h day$^{-1}$) | 4.55 – 4.57 | 2.25 – 10.22 |
| Operational duty cycle (%) | 19.0 | 17.5 |
| Total activation events – Vent1 | n.d.[1] | 90 |
| Total activation events – Vent2 | n.d.[1] | 83 |
| Vent1 / Vent2 activation correlation | –[3] | r = 0.856 |

[1] n.d. = not directly available from database

[2] Near-zero standard deviation confirms fully deterministic synchronized operation in Phase I. [3] Synchronised operation in Phase I makes individual correlation analysis redundant — both units operated identically by design.

The results demonstrate that internal air recirculation, driven by canopy-level dew margin indicators, effectively prevented plant-level condensation throughout the monitoring period. The complete absence of leaf wetness events at canopy level - despite multiple nocturnal intervals of critical proximity - supports the central hypothesis that canopy-oriented control provides biologically relevant protection even when envelope condensation remains unavoidable. This distinction between structural and canopy condensation is consistent with Piscia et al. (2012) and Boulard et al. (2004), who showed that leaf boundary-layer humidity can differ substantially from bulk greenhouse air. The use of dew margin as a control variable proved essential in this context: RH values consistently exceeded 85–90% throughout the monitoring period, yet canopy condensation did not occur, illustrating the well-documented limitation of RH thresholds for site-specific condensation risk assessment (Wang et al., 2019).

The persistent lateral S1-S2 asymmetry, observed in both phases, is consistent with the broader literature emphasising that spatial heterogeneity may persist even in actively mixed greenhouses, and that stagnant zones can remain localised condensation hotspots independent of bulk conditions (Bournet and Boulard, 2010; Gao et al., 2024). Although Phase II produced high operational synchrony between ventilation units (r = 0.856), this reflects the relatively moderate lateral contrast observed during the specific monitoring period rather than a failure of the zonal architecture. The asynchronous configuration provides the control infrastructure for independent zonal response, which may become operationally decisive under more contrasted humidity conditions - for instance, following differential irrigation events or under asymmetric solar radiation patterns.

From an energy perspective, the recirculation system operated at duty cycles of 19.0% (Phase I) and 17.5% (Phase II), corresponding to a mean daily energy consumption of approximately 3.6-3.7 kWh for recirculation alone - a modest fraction of the thermal energy that would have been required for equivalent dehumidification through external ventilation under the same conditions (Maslak & Nimmermark, 2017; Amani et al., 2020). The adaptive three-regime control strategy ensured that fan operation was restricted to periods of genuine microclimatic need, contributing to the relatively low overall duty cycle.

Several limitations must be acknowledged. The absence of a concurrent unventilated control treatment prevents direct causal attribution of condensation prevention to the recirculation system, and the inter-phase comparison was confounded by differences in external thermal conditions between the two monitoring periods. The Mann-Whitney comparison between phases did not reach statistical significance ($p > 0.20$), meaning that the observed numerical differences in dew margin cannot be unambiguously attributed to the change in control strategy rather than to more favourable meteorological conditions. Air velocity measurements were also limited to two positions and a single session, precluding full characterisation of the three-dimensional airflow field. Despite these limitations, the study contributes a reproducible, low-cost methodology for preventive condensation-risk management based on distributed dew point monitoring and threshold-driven recirculation, integrated within a unified Home Assistant and InfluxDB infrastructure replicable without specialised instrumentation.

## CONCLUSIONS

Internal air recirculation driven by canopy dew margin indicators successfully prevented plant-level condensation in a passive double-layer solar greenhouse throughout the winter monitoring period, with zero leaf wetness events recorded at canopy level despite persistent nocturnal condensation on structural surfaces.

The dew margin indicator proved more operationally discriminating than relative humidity alone for condensation risk control, enabling the system to maintain biologically safe canopy conditions even when bulk RH consistently exceeded 85-90%.

A persistent lateral microclimate asymmetry between the eastern and western compartments was identified in both experimental phases, providing experimental justification for the asynchronous zonal control architecture, even though operational decoupling between ventilation units remained limited under the observed meteorological conditions.

The recirculation system operated at duty cycles of 17-19% of total monitoring time, with mean daily runtimes of 4.2-4.6 h day$^{-1}$, confirming that the energy cost of internal mixing is modest compared to equivalent dehumidification through external ventilation.

The integrated monitoring and control framework - combining distributed dew point sensing, adaptive threshold-based automation, and continuous time-series archiving - represents a reproducible methodology applicable to other passive greenhouse contexts without specialised instrumentation.

## ACKNOWLEDGEMENTS

The author acknowledges the technical infrastructure provided by the University of Agronomic Sciences and Veterinary Medicine of Bucharest and the support of the Home Assistant open-source community for automation tools used in data acquisition and control.

## REFERENCES

Amani, M., Foroushani, S., Sultan, M., & Bahrami, M. (2020). Comprehensive review on dehumidification strategies for agricultural greenhouse applications. *Applied Thermal Engineering, 181*, 115979.

Baptista, F. J., Bailey, B. J., Randall, J. M., & Meneses, J. F. (1999). Greenhouse ventilation rate: Theory and measurement with tracer gas techniques. *Journal of Agricultural Engineering Research, 72,* 363–374.

Blanchard, M. (2008). Fanning uniformity in the greenhouse. Greenhouse Product News, May 2008, 66.

Boulard, T., & Draoui, B. (1995). Natural ventilation of a greenhouse with continuous roof vents: Measurements and data analysis. *Journal of Agricultural Engineering Research, 61*, 27–36.

Boulard, T., Fatnassi, H., Roy, J. C., Lagier, J., Fargues, J., Smits, N., Rougier, M., & Jeannequin, B. (2004). Effect of greenhouse ventilation on humidity of inside air and in leaf boundary-layer. *Agricultural and Forest Meteorology, 125,* 225–239. https://doi.org/10.1016/j.agrformet.2004.04.005

Bournet, P.-E., & Boulard, T. (2010). Effect of ventilator configuration on the distributed climate of greenhouses: A review of experimental and CFD studies. *Computers and Electronics in Agriculture, 74,* 195–217. https://doi.org/10.1016/j.compag.2010.08.007

Gao, Z., Li, W., Li, W., & Ding, X. (2024). Experimental research on the microclimate in the naturally ventilated multi-span greenhouse. *International Journal of Agricultural and Biological Engineering, 17(3)*, 68–74. https://doi.org/10.25165/j.ijabe.20241703.7073

He, K.-S., Chen, D.-Y., Sun, L.-J., Liu, Z.-L., & Huang, Z.-Y. (2015). The effect of vent openings on the microclimate inside multi-span greenhouses during summer and winter seasons. *Engineering Applications of Computational Fluid Mechanics, 9*(1), 399–410.

Katsoulas, N., Bartzanas, T., Boulard, T., Mermier, M., & Kittas, C. (2006). Effect of vent openings and insect screens on greenhouse ventilation. *Biosystems Engineering, 93*(4), 427–436.

Kittas, C., Karamanis, M., & Katsoulas, N. (2005). Air temperature regime in a forced ventilated greenhouse with rose crop. *Energy and Buildings, 37*, 807–812.

Lee, T., Kang, G., Jang, J., Paek, Y., & Lim, R. (2020). Analysis on the effect of greenhouse humidity control by counter-flow ventilator in winter. *Protected Horticulture and Plant Factory, 29*(3), 259–264.

Maslak, K., & Nimmermark, S. (2017). Thermal energy use for dehumidification of a tomato greenhouse by natural ventilation and a system with an air-to-air heat exchanger. *Agricultural and Food Science, 26,* 56–66.

Piscia, D., Montero, J. I., Baeza, E., & Bailey, B. J. (2012). A CFD greenhouse night-time condensation model. *Biosystems Engineering, 111*, 141–154. https://doi.org/10.1016/j.biosystemseng.2011.11.006

Sase, S., Kozai, T., Nara, M., & Negishi, H. (1980). Ventilation of greenhouses. I. Wind tunnel measurements of pressure and discharge coefficients for a single-span greenhouse. *Journal of Agricultural Meteorology, 36(1)*, 3–12.

Sase, S. (2006). Air movement and climate uniformity in ventilated greenhouses. In B. J. Bailey (Ed.), *Proceedings of the International Symposium on*

*Greenhouse Cooling. Acta Horticulturae, 719*, 313–324.

Teitel, M., & Tanny, J. (1999). Natural ventilation of greenhouses: Experiments and model. *Agricultural and Forest Meteorology, 96*, 59–70.

Tusi, A., & Shimazu, T. (2020). The essential factor of ventilation rate in prediction of photosynthetic rate using the $CO_2$ balance method. Reviews in Agricultural Science, 8, 279–299. https://doi.org/10.7831/ras.8.0_279

Wang, H., Sánchez-Molina, J. A., Li, M., & Rodríguez Díaz, F. (2019). Improving the performance of vegetable leaf wetness duration models in greenhouses using decision tree learning. *Water, 11*, 158. https://doi.org/10.3390/w11010158.

Wang, Z., Bao, A., Li, J., He, J., Wang, K., Wang, X., & Sun, X. (2025). Study on the effect of non-uniform ventilation on energy and plant growth in a greenhouse. *Horticulturae, 11*(2), 166. https://doi.org/10.3390/horticulturae11020166

Zhang, Y., Sun, W., Jin, L., Yang, H., Wang, J., & Shu, S. (2025). Computational fluid dynamics-based simulation of ventilation in a zigzag plastic greenhouse. *Horticulturae, 11*(2), 175. https://doi.org/10.3390/horticulturae11020.

Scientific Papers. Series E. Land Reclamation, Earth Observation & Surveying, Environmental Engineering. Vol. XV, 2026
Print ISSN 2285-6064, CD-ROM ISSN 2285-6072, Online ISSN 2393-5138, ISSN-L 2285-6064

# INFLUENCE OF CONSTITUTIVE MODELS ON DEEP EXCAVATIONS: A COMPARATIVE STUDY

**Daniel-Marcel MANOLI, Nicolae RĂDULESCU-SINGURAN, Adrian Alexandru SAVU, Elena-Mihaela STAN, Cristian-Ștefan BARBU**

Technical University of Civil Engineering of Bucharest, 122-124 Lacul Tei Blvd, District 2, Bucharest, Romania

Corresponding author email: daniel.manoli@utcb.ro

***Abstract***

*Accurate prediction of soil–structure interaction is essential for the safe design of deep excavations in urban environments. This paper presents a three-dimensional numerical investigation assessing the influence of different soil constitutive models on the predicted behavior of a deep excavation. Finite element analyses were carried out using the Mohr–Coulomb (MC), Hardening Soil (HS), and Hardening Soil with Small-Strain Stiffness (HSS) models, applied to a real excavation case supported by retaining walls. The comparative study focuses on excavation-induced stress redistribution and horizontal wall deformations. The results indicate that the MC and HS models overestimate wall deformations, whereas the HSS model offers a significantly improved prediction due to its ability to capture soil stiffness at small strain levels. The study confirms that incorporating small-strain stiffness is critical for realistic deformation assessment and reliable design of deep excavations.*

***Key words****: constitutive model, deep excavation, MEF.*

## INTRODUCTION

Due to the continuous development of urban areas, it is necessary to choose modern solutions for carrying out new buildings. At present, vertical development of civil buildings is preferred, including a significant number of underground levels that require deep excavations in the vicinity of existing structures, without affecting their functionality. Thus, to analyse the behaviour of the retaining structure, the finite element method (FEM) is often used. In order to obtain the best results, consistent with reality, it is necessary to have a good understanding of the calculation method, the constitutive models used to model different soil types or structural elements, the mesh distribution, the calculation phases, and to consider the effects of the assumptions made.

The choice of constitutive model has a decisive influence on the predicted response of deep excavations, and this has been the subject of numerous comparative studies. Although the linear elastic–perfectly plastic Mohr-Coulomb model remains widely used in practice for its simplicity, it is generally recognised as inadequate for serviceability predictions, since it cannot reproduce the stress-dependent stiffness of soils or their markedly higher stiffness at small strains (Obrzud, 2010). The Hardening Soil model (Schanz et al., 1999) introduced a stress-dependent stiffness and a clear distinction between primary loading and unloading/reloading, while its extension to small strains (Benz, 2007) additionally captures the non-linear decay of stiffness from the very small-strain shear modulus. Comparative analyses of braced and anchored excavations have repeatedly shown that the Mohr-Coulomb model tends to overestimate wall deflections and to predict an unrealistic ground heave behind the wall, whereas the Hardening Soil model and, in particular, the Hardening Soil with small-strain stiffness model reproduce field-measured wall displacements far more closely (Lim et al., 2010; Teo & Wong, 2012; Dahal et al., 2024). Similar conclusions were reached by Herold & von Wolffersdorff (2009), who back-calculated two instrumented large-scale geosynthetic-reinforced earth structures and found that the HSsmall model almost exactly matched the measured horizontal displacements, while the Mohr-Coulomb model deviated clearly, over-predicting displacements at low surcharge and under-predicting them at high surcharge. The HSsmall model has likewise been applied

successfully to the probabilistic assessment of diaphragm walls (Kawa et al., 2021). These findings motivate the present comparative study, in which the three constitutive models are applied to the same real deep excavation supported by a diaphragm wall.

The Mohr-Coulomb (MC) constitutive model is a linear elastic perfectly - plastic model often used due to the small number of the required parameters and the ease with which they can be determined.

In the elastic domain, the model shows linear behavior based on Hooke's Law, defined by two parameters: Young's modulus (E), and Poisson's ratio (ν). In the plastic domain, the failure criterion is defined by two parameters: the internal friction angle (ϕ), and cohesion (c), also known as the shear resistance parameters. Additionally, the dilatancy angle (ψ) is used to describe the plastic volumetric strain variation.

According to the Mohr-Coulomb constitutive model, the soil will reach failure in shear, along an arbitrary plane when, due to the applied loads, the tangential stress is in a linear relationship with the normal stress, which is unique for each type of soil. Also, it is based on the use of the stress state at a point (Figure 1), that is, from a graphical point of view, the use of the Mohr circle. This circle represents all possible stress states (σ, τ) at a point when any plane with any orientation passing through that point is considered (Șerbulea, 2013).

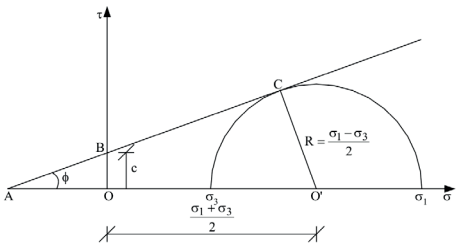



Figure 1. Stress state tangent to the intrinsic line (Șerbulea, 2013)

The equation that describes the Mohr-Coulomb failure criterion is given by:

$$\tau = \sigma \tan(\phi) + c$$

where τ is the tangential stress and σ is the normal stress.

If the pore water pressure is known, the effective shear strength parameters can be calculated:

$$\tau = \sigma' \tan(\phi') + c'$$

In the three-dimensional space of principal stresses, $\sigma_1 - \sigma_2 - \sigma_3$, the Mohr-Coulomb failure criterion is represented as a pyramid with a hexagonal base (Figure 2), whose axis lies along the trisectors $\sigma_1 = \sigma_2 = \sigma_3$.

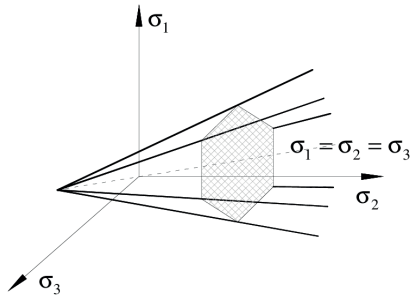



Figure 2. Mohr-Coulomb representation in the space of principal stresses (Popa & Batali, 2010)

In the space of principal stresses, a stress state will not result in failure as long as it remains inside the surface (Șerbulea, 2013).

The Hardening Soil (HS) model is an advanced constitutive model for representing the nonlinear-elastic-plastic behavior of soils, suitable for both soft and stiff soil types (Schanz et al., 1999).

When subjected to a deviatoric stress, soil exhibits a decrease in stiffness and simultaneously undergoes plastic deformations. The relationship between deviatoric stress and axial strain is most readily observed in a triaxial compression test and can be approximated by a hyperbolic curve (Figure 3) (Brinkgreve et al., 2023).

The principal characteristics of the nonlinear Hardening Soil constitutive model are:

- Stiffness depends on the stress, as defined by the parameter $m$;
- Plastic straining due to primary deviatoric loading, represented by the parameter $E_{50}^{ref}$ (secant stiffness in a standard drained triaxial test);
- Plastic straining due to primary compression, represented by the parameter $E_{oed}^{ref}$ (tangent stiffness for primary oedometer loading);
- Elastic unloading/reloading, represented by the parameters $E_{ur}^{ref}$ (unloading/reloading stiffness) and $\nu_{ur}$ (Poisson's ratio for unloading/reloading);
- The failure criterion used is Mohr-Coulomb,

characterized by the parameters ϕ, c, and ψ (Brinkgreve et al., 2023).

A basic concept of the model is the hyperbolic relationship between the vertical strain, $\varepsilon_1$, and the deviatoric stress, $q$.

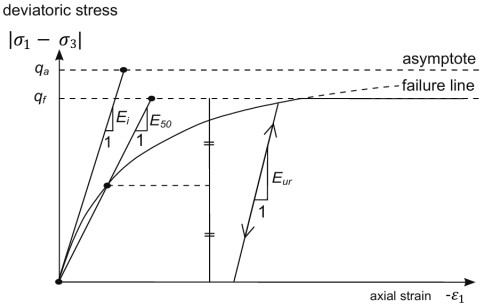



Figure 3. The hyperbolic stress-strain relationship resulting from the drained triaxial test (Brinkgreve et al., 2023)

The advantage of the Hardening Soil model lies not only in the use of a hyperbolic stress-strain curve instead of a bilinear curve, as in the Mohr-Coulomb model, but also in the stress-dependent stiffness of the soil. In the Mohr-Coulomb model, a fixed value of the Young's modulus is used, whereas in reality this value depends on the magnitude of the stress (Brinkgreve et al., 2023).

The Hardening Soil constitutive model assumes elastic behavior during unloading and reloading. However, the strain range within which soil can be considered elastic is very small. With increasing strain, the shear stiffness of the soil decreases in a nonlinear manner.

Figure 4 shows the variation of the soil stiffness with shear strain.

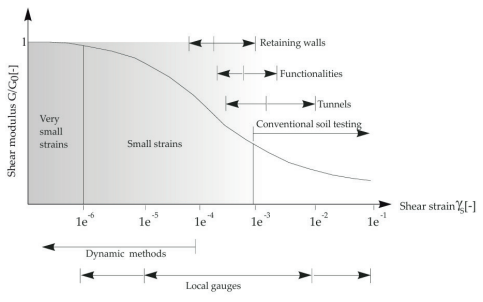



Figure 4. Hardening Soil with small strain model stiffness - strain behavior of soil (Brinkgreve et al., 2023)

The characteristics shear strains that can be measured near geotechnical structures, as well as the strain range applicable in laboratory tests, are also represented. It can be observed that, for the minimum strains that can be measured in laboratory tests, the soil stiffness decreases to about half of its initial value (Brinkgreve et al., 2023).

Compared to the Hardening Soil model, the Hardening Soil with small strain (HSSS) model assumes the use of additional parameters (Benz, 2007):

- The reference shear modulus at very small strains ($\varepsilon < 10^{-6}$), $G_0^{ref}$;
- The shear strain corresponding to 70% of the value of $G_0^{ref}$, $\gamma_{0.7}$.

## MATERIALS AND METHODS

For this study, in order to compare the three constitutive models descried above, the 3D finite element method was used. Thus, the same case study was modelled using the Mohr-Coulomb, Hardening Soil and the Hardening Soil with small strain models. The numerical modelling was carried out using Plaxis 3D software.

The case study project is located in the city of Timișoara, Romania. It is a building with two basements and three stories above the ground. Therefore, an excavation depth of 6.80 m is required to construct the two basements' levels. The retaining structure solution consists of a diaphragm wall with a thickness of 0.45 m and a depth of 11.00 m (Figure 5). At the top of the diaphragm wall, a capping beam with a height of 0.45 m and a width of 0.60 m is provided.

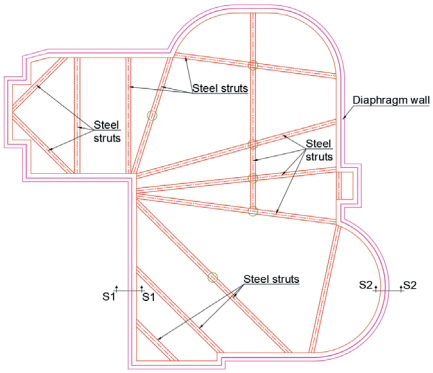



Figure 5. Layout of the excavation site

To limit the lateral displacements of the diaphragm wall, one level of bracing struts was used. The bracing strut system consists of circular steel hollow sections with a diameter of 610 mm and a thickness of 10 mm, spaced at approximately 6 m intervals, installed at a depth of 2.00 m.

In the three - dimensional finite element software, the diaphragm wall was modelled as plate elements, the capping beam as beam elements, and the steel struts as node-to-node anchors. The linear elastic constitutive model was used for both diaphragm wall and capping beam. Thus, the concrete modulus of elasticity is $3.1 \cdot 10^7$kPa, the Poisson's ratio is 0.2 and the unit weight is 25kN/m$^3$.

The site investigations consist of four geotechnical boreholes with a maximum depth of 22.00m and four light dynamic penetration tests (DPM) with a maximum depth of 15.00m. Based on these in situ investigations and the results of the laboratory tests, the soil stratigraphy and parameters are presented in Figure 6, Table 1 and Table 2.

Table 1. Soil stratigraphy

| Soil layer | Depth [m] | Soil layer description |
|---|---|---|
| 1 | 0.00÷ -0.70/2.10 | Fill composed of construction debris mixed with clay, sand and gravel |
| 2 | -0.70/-2.10÷ -2.30/2.70 | Clay to sandy silty clay, grey, with reddish intercalation, stiff. |
| 3 | -2.30/2.70÷ -7.00/10.10 | Fine sand to silty sand, grey, loose to medium dense toward the base of the layer. |
| 4 | -7.00/10.10÷ -11.10/12.30 | Clay to silty clay, greyish-green, with yellowish intercalations, stiff. |
| 5 | -11.10/12.30÷ -22.00 | Sand to silty sand, grey, dense. |

Table 2. Soil parameters used in the numerical analysis

| Soil type | $\Gamma$ | $\gamma_{sat}$ | $E_{50}^{ref}$ | $E_{oed}^{ref}$ | $E_{ur}^{ref}$ | $\nu_{ur}$ | c' | $\phi$' | $G_0$ | $\gamma_{0.7}$ | $R_{inter}$ |
|---|---|---|---|---|---|---|---|---|---|---|---|
| | [kN/m$^3$] | [kN/m$^3$] | [kPa] | [kPa] | [kPa] | [-] | [kPa] | [°] | [kPa] | [-] | [-] |
| 1 | 18.50 | 19.50 | 7000 | 7000 | 21000 | 0.3 | 5 | 15 | 35669 | 0.00009 | 0.8 |
| 2 | 19.00 | 20.00 | 7500 | 7500 | 22500 | 0.3 | 32 | 17.2 | 68200 | 0.00026 | 0.8 |
| 3 | 19.00 | 20.00 | 8800 | 8800 | 26400 | 0.3 | 5 | 27 | 65572 | 0.00023 | 0.8 |
| 4 | 19.40 | 20.40 | 12000 | 12000 | 36000 | 0.3 | 38 | 18 | 133098 | 0.00024 | 0.8 |
| 5 | 19.60 | 20.60 | 17634 | 17634 | 52902 | 0.3 | 5 | 30 | 102265 | 0.00035 | 0.8 |

$\gamma$ - Unit weight; $\gamma_{sat}$ - Saturated unit weight; $E_{50}^{ref}$ - Secant stiffness in standard drained triaxial test; $E_{oed}^{ref}$ - Tangent stiffness for primary oedometer loading; $E_{ur}^{ref}$ - Unloading/reloading stiffness; $\nu_{ur}$ - Poisson's ratio for unloading-reloading; c' - Effective cohesion; $\phi$' - Effective angle of internal friction; $G_0$ - Shear modulus at very small strains; $\gamma_{0.7}$ - Shear strain corresponding to 70% of the value of $G_0$; $R_{inter}$ - Strength reduction factor.

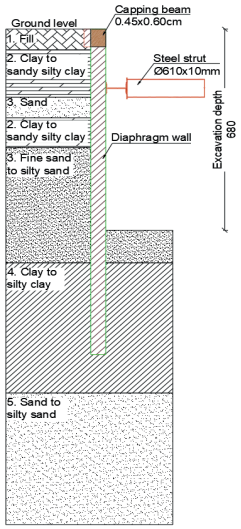



Figure 6. Construction phases and soil stratigraphy

The soil parameters required for the HSSS model were determined based on field investigations.

The finite element calculation phases, which correspond to the in-situ execution stages, are:

- Generation of the initial stress state;
- Installation of the diaphragm wall and the capping beam;
- Lowering of the groundwater level;
- Excavate to 3.00 m below the ground level;
- Installation of the bracing strut level;
- Excavation to the final depth of 6.80 m;
- Execution of the raft foundation and the slab over the second basement.

In order to perform finite element calculations, the numerical model was discretized into finite elements using a fine mesh.

## RESULTS AND DISCUSSIONS

### The lateral displacements of the retaining structure

Figure 7 shows the lateral displacement diagrams of the diaphragm wall for Section 1 (S1-S1), for the three constitutive models considered: Mohr-Coulomb, Hardening Soil and Hardening Soil with Small Strain. Figure 8 shows the lateral displacement diagrams for Section 2 (S2-S2), which is located in the circular area of the diaphragm wall. The two sections were selected based on the maximum stress values, lateral displacements, and the in-plan configuration of the diaphragm wall.

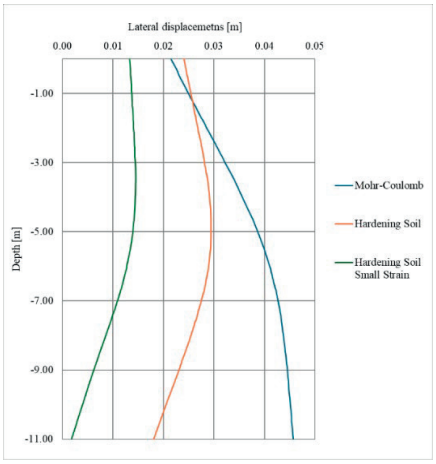



Figure 7. Lateral displacements of the retaining structure, Section 1

For both sections, the lateral displacement diagrams show that the Mohr-Coulomb constitutive model leads to the maximum lateral displacements of the retaining structure, while the minimum values are obtained when using the Hardening Soil with Small Strain constitutive model. In the case of the Mohr-Coulomb constitutive model, the maximum lateral displacement occurs in the lower part of the retaining structure, whereas for the other two constitutive models, it occurs in the upper part of the diaphragm wall. When comparing the Hardening Soil and Hardening Soil with Small Strain models, the latter results in a maximum lateral displacement that is approximately half of that obtained using the former model.

The differences between the two analysed sections are due to the in-plan shape of the retaining structure. Thus, for Section 2 (S2-S2), the lateral displacements are smaller than those in Section 1 (S1-S1), due to the circular shape of the diaphragm in this area and the resulting arching effect.

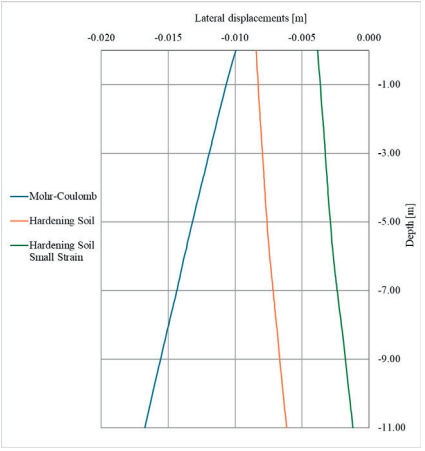



Figure 8. Lateral displacements of the retaining structure, Section 2

### The bending moment of the retaining structure

Figure 9 and Figure10 shows the bending moment diagrams of the retaining structure for the three analysed constitutive models and the two section, S1-S1 and S2-S2.

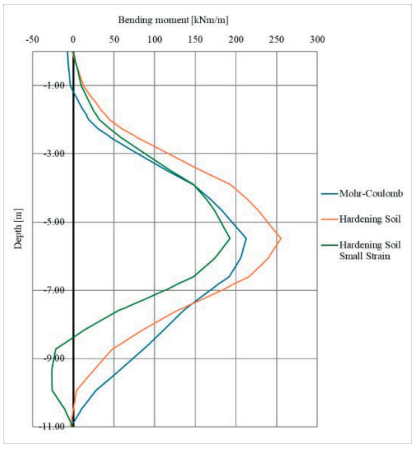



Figure 9. Bending moment diagrams - Section 1

In the case of Section 1 (S1-S1), where the diaphragm wall has a linear in-plan shape, the maximum bending moment occurs for the Hardening Soil constitutive model, while the

minimum value is obtained when the Hardening Soil with Small Strain model is used. For all constitutive models, the bending moment diagrams have a similar shape, and the maximum values occur at approximately the same depth, close to the final excavation depth.

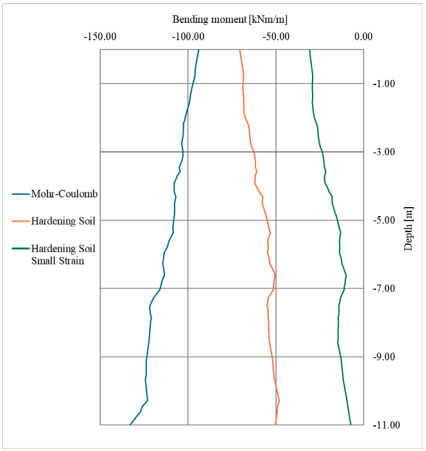



Figure 10. Bending moment diagrams - Section 2

In the case of Section 2 (S2-S2), where the diaphragm wall has a circular in-plan shape, the maximum bending moment occurs for the Mohr-Coulomb constitutive model, while the minimum value is obtained for the Hardening Soil with Small Strain model, similar to Section 1. Unlike Section 1, the maximum bending moment in Section 2 occurs in the upper part of the diaphragm wall for both the Hardening Soil and Hardening Soil with Small Strain models, and in the lower part of the retaining structure when the Mohr-Coulomb model is used.

In general, regardless of the constitutive model used, the maximum bending moments are smaller for Section 2 than for Section 1 due to the arching effect.

## CONCLUSIONS

This paper presents a comparative study on the influence of the constitutive models used to simulate soil behavior. Three-dimensional finite element numerical models were developed for the same project using the Mohr-Coulomb, Hardening Soil and Hardening Soil with Small Strain constitutive models.

While the soil parameters required for the Mohr-Coulomb constitutive model can generally be determined from conventional geotechnical investigations and standard laboratory tests, the Hardening Soil model, and especially the Hardening Soil with small strain model, require more advanced in-situ and laboratory testing. The findings of this study demonstrate that the enhanced complexity of the Hardening Soil with small strain model leads to a more realistic representation of the retaining structure behavior compared to simpler constitutive models, regardless of the structure's in-plan configuration.

## REFERENCES

Benz, T. (2007). *Small-Strain Stiffness of Soils and its Numerical Consequences*. PhD thesis, University of Stuttgart, Germany.

Brinkgreve, R. B. J., Kumarswamy, S., Swolfs, W. M., Fonseca, F., Zalamea, N., Manoj, N. R., Singh, K., Zampich, L., (2023). *Material Models Manual, Plaxis 3D.* U.S.: Bentley Systems Incorporated

Herold, A., & von Wolffersdorff, P.-A. (2009). The use of Hardening Soil Model with Small-Strain Stiffness for Serviceability Limit State analyses of GRE structures. *Proceedings of GeoAfrica 2009*, Cape Town, South Africa.

Kawa, M., Puła, W., & Truty, A. (2021). Probabilistic analysis of the diaphragm wall using the hardening soil-small (HSs) model. *Engineering Structures*, 232, 111869.

Dahal, B. K., Regmi, S., Paudyal, K., Dahal, D., & Kc, D. (2024). Enhancing deep excavation optimization: Selection of an appropriate constitutive model. *CivilEng*, 5(3), 785–800.

Lim, A., Ou, C. Y., & Hsieh, P. G. (2010). Evaluation of clay constitutive models for analysis of deep excavation under undrained conditions. *Journal of GeoEngineering*, 5(1), 9–20.

Obrzud, R. F. (2010). On the use of the Hardening Soil Small Strain model in geotechnical practice. *Numerics in Geotechnics and Structures (ZSoil Day)*, Lausanne, Switzerland.

Popa, H., & Batali, L. (2010). Using Finite Element Method in geotechnical design. Soil constitutive laws and calibration of the parameters. Retaining wall case study. *WSEAS Transactions on applied and theoretical mechanics*, 5(3), 177-186.

Schanz, T., Vermeer, P. A., & Bonnier, P. G. (1999). The Hardening Soil model: Formulation and verification. In R. B. J. Brinkgreve (Ed.), *Beyond 2000 in Computational Geotechnics*, 281–296. Rotterdam: Balkema.

Şerbulea, M. S. (2013). *Mecanica avansată a pământurilor*. Bucharest, RO: Printech.

Teo, P. L., & Wong, K. S. (2012). Application of the Hardening Soil model in deep excavation analysis. *The IES Journal Part A: Civil & Structural Engineering*, 5(3), 152–165.

Scientific Papers. Series E. Land Reclamation, Earth Observation & Surveying, Environmental Engineering. Vol. XV, 2026
Print ISSN 2285-6064, CD-ROM ISSN 2285-6072, Online ISSN 2393-5138, ISSN-L 2285-6064

# THERMAL AND MECHANICAL PERFORMANCE OF GROUTING MATERIALS IN GEOTHERMAL BOREHOLES: IMPLICATIONS FOR HEAT TRANSFER EFFICIENCY AND ENVIRONMENTAL PERSPECTIVE

**Daniel-Marcel MANOLI, Alina TATOMIR, Elena-Mihaela STAN, Cristian-Stefan BARBU, Andrei-Dan SABAU**

Technical University of Civil Engineering Bucharest, 122-124 Lacul Tei Blvd, District 2, Bucharest, Romania

Corresponding author email: daniel.manoli@utcb.ro

***Abstract***

*Grouting materials used in geothermal boreholes represent a key component in the efficient operation of ground source heat pump (GSHP) systems, as they simultaneously control heat transfer between the borehole heat exchanger and the surrounding geological formation while ensuring hydraulic sealing of the annular space between the pipes and the borehole wall. The thermo-hydraulic and mechanical performance of these materials directly influences the long-term energy efficiency of geothermal systems and contributes to groundwater protection by limiting vertical fluid migration between permeable geological layers intersected by the borehole. In this context, the present study presents a laboratory-based experimental program aimed at evaluating the thermal and mechanical performance of water-based grout mixtures composed of mineral binders and clay additives (bentonite), with controlled variation of the granular fraction (sand) and bentonite content. The research investigates the relationships between material composition, microstructural characteristics and the physical-mechanical properties relevant for geothermal applications. The experimental methodology includes the determination of thermal conductivity, saturated hydraulic permeability, uniaxial compressive strength and shrinkage or segregation behaviour, complemented by the analysis of rheological characteristics such as injectability and mixture stability under installation conditions. The results highlight the inherent trade-off between enhancing thermal conductivity through the introduction of granular materials and maintaining effective hydraulic sealing by reducing permeability and controlling pore structure. The findings contribute to the development of technical recommendations for optimizing grout formulations used in geothermal boreholes, with the aim of improving heat transfer efficiency, ensuring mechanical integrity and protecting groundwater resources in geothermal systems designed for nearly zero-energy buildings (NZEB).*

***Key words****: environmental sustainability, grouting materials, nearly zero-energy buildings (nzeb), thermal conductivity.*

## INTRODUCTION

The transition towards low-carbon and energy-efficient buildings has increased interest in shallow geothermal energy systems as reliable renewable technologies for heating and cooling applications. Ground source heat pump (GSHP) systems are recognised as effective solutions for reducing primary energy consumption and greenhouse gas emissions while supporting building decarbonisation strategies (Lund & Toth, 2020; Mahmoud et al., 2021).

Vertical borehole heat exchangers (BHEs) are widely used in densely urbanised areas where available land is limited. The thermal performance of these systems depends on the combined properties of the geological formation, the heat exchanger pipes and the material filling the annular space between the pipes and the borehole wall (Spitler & Gehlin, 2015; Albers et al., 2024).

The annular backfill material, commonly referred to as grout, performs multiple functions within a geothermal borehole. In addition to providing mechanical stability and hydraulic sealing, grout establishes thermal contact between the heat exchanger and the surrounding ground, thereby influencing borehole thermal resistance and overall system efficiency (IEEE Standards Association, 2017; Albers et al., 2024). Consequently, geothermal grout design requires balancing thermal conductivity, hydraulic performance and mechanical strength.

Commercial geothermal grouts are typically composed of cement, bentonite and mineral aggregates. Previous studies have shown that increasing the proportion of thermally

conductive granular materials, particularly quartz sand, can improve heat transfer efficiency, whereas higher bentonite contents generally enhance sealing performance but may reduce thermal conductivity (Borinaga-Treviño et al., 2013; Mahmoud et al., 2021; Mascarin et al., 2022; Nakládal et al., 2024).

In this context, the experimental evaluation of geothermal grout formulations remains essential for identifying compositions capable of simultaneously providing efficient heat transfer, low permeability and adequate mechanical strength. The present study investigates fourteen grout formulations containing different proportions of cement, bentonite and quartz sand in order to evaluate the relationships between composition, thermal conductivity, hydraulic permeability and uniaxial compressive strength. The results contribute to the identification of compositional trends governing the trade-off between thermal performance, sealing capacity and mechanical resistance in geothermal grouting materials.

## GEOTHERMAL DRILLING TECHNOLOGY

Closed-loop shallow geothermal systems provide an efficient solution for harnessing thermal energy from the subsurface and are widely used in residential, commercial, and industrial applications. Heat transfer is achieved through a closed hydraulic circuit in which the heat transfer fluid circulates in buried pipes without direct interaction with groundwater, thereby reducing hydrogeological risks and ensuring stable long-term operation (Borinaga-Treviño et al., 2013).

The most common configuration is represented by vertical borehole heat exchangers (BHEs), which are constructed through boreholes typically 50 to 200 m deep, with high-density polyethylene (HDPE) pipes installed in a double U-tube configuration. The circulating heat transfer fluid exchanges heat with the surrounding ground, taking advantage of the thermal stability of the subsurface (Spitler & Gehlin, 2015).

A key component of the system is the material used to fill the annular space between the borehole wall and the pipes, known as the grout. This material directly influences the thermal resistance of the borehole and plays a dual role in providing mechanical stability and hydraulic sealing, as well as providing effective thermal coupling between the heat exchanger and the surrounding ground. Consequently, the thermal and structural properties of the grout are critical to the overall efficiency of the system (Albers et al., 2024).

From a design perspective, the thermal performance of a geothermal borehole is determined by the total thermal resistance of the system, which includes contributions from the surrounding ground, pipes, and grout. Reducing the thermal resistance of the grout layer is therefore a key objective in improving system efficiency.

At the same time, the grout must have low permeability to prevent vertical migration of groundwater, which requires careful optimization of the material composition (Spitler & Gehlin, 2015; IEEE, 2017).

The design and construction of geothermal wells must take into account the local geological and hydrogeological conditions, including the thermal conductivity of the ground, the stratigraphic structure, the presence of groundwater, and the stability of the borehole walls. These factors affect both the technical feasibility and the long-term performance of the system.

The design and construction of geothermal wells must take into account the local geological and hydrogeological conditions, including the thermal conductivity of the ground, the stratigraphic structure, the presence of groundwater, and the stability of the borehole walls. These factors affect both the technical feasibility and the long-term performance of the system.

## MATERIALS AND METHODS

Standardized sand was used for sample preparation in accordance with EN 196-1:2016, which specifies the particle size distribution for cement mortars. The particle size distribution corresponds to that defined in Table 1 of the standard, without using alternative gradations, in order to ensure the repeatability of the test and to isolate the influence of the active components in the presence of water.

The hydraulic binder used consisted of high early strength Portland cement (CEM II/A 42.5R) and sodium bentonite. The mixing water was potable water used under controlled laboratory conditions.

Unlike conventional grout studies based on a constant aggregate-to-binder ratio, the present experimental program intentionally varied the proportions of quartz sand, cement and bentonite in order to evaluate their influence on thermal conductivity, hydraulic permeability and mechanical strength across a broad compositional domain representative of geothermal grouting materials.

Sand acts as an inert component and does not participate in hydration processes. Its primary function is to provide structural stability to the material and to facilitate heat transfer through solid-solid contact. By maintaining a constant sand content, the influence of the interaction between cement and bentonite on the material behaviour can be clearly evaluated.

Table 1. Composition of the grout formulations analyzed

| Grout mix | w/s [-] | Sand [%] | Cement [%] | Bentonite [%] |
|---|---|---|---|---|
| R1 | 1.82 | 40 | 45 | 15 |
| R2 | 1.23 | 9 | 55 | 36 |
| R3 | 0.91 | 18 | 50 | 32 |
| R4 | 0.82 | 27 | 45 | 27 |
| R5 | 0.68 | 36 | 41 | 23 |
| R6 | 0.59 | 45 | 36 | 18 |
| R7 | 1.64 | 80 | 10 | 10 |
| R8 | 0.50 | 70 | 20 | 10 |
| R9 | 0.50 | 70 | 15 | 15 |
| R10 | 0.65 | 70 | 10 | 20 |
| R11 | 0.35 | 70 | 25 | 5 |
| R12 | 0.56 | 65 | 20 | 15 |
| R13 | 0.60 | 65 | 15 | 20 |
| R14 | 0.60 | 65 | 25 | 10 |

The investigated formulations were designed to cover a broad compositional domain representative of geothermal grouting materials used in borehole heat exchanger applications. The experimental matrix was intentionally developed to explore the interactions between three functional constituents: cement, responsible for mechanical integrity; bentonite, responsible for hydraulic sealing and mixture stability; and quartz sand, acting as a thermally conductive granular skeleton. The selected formulations do not represent optimized commercial products but experimental compositions covering low, intermediate and high contents of each component in order to identify the relationships between composition, thermal conductivity, permeability and compressive strength.

Formulation R7, characterized by an unusually high sand content (80%), was intentionally included as a boundary composition to investigate the maximum thermal conductivity that could be achieved within the tested material system. Although such compositions may present practical limitations regarding injectability and field applicability, they provide valuable information regarding the upper thermal performance limit associated with granular enrichment.

**Mix preparation**

The mixes were prepared under laboratory conditions using a methodology closely related to field practice. In contrast to procedures involving prehydration of bentonite, all dry components (sand, cement and bentonite) were mixed first and then water was added.

This approach makes it possible to reproduce real-life conditions and reduce preparation time, while maintaining an adequate level of mix homogeneity.

The fresh mix was poured into cylindrical plastic molds with a diameter of 50 mm and a height of 100 mm. The specimens were saturated and tested after 28 days to ensure full development of mechanical properties.

**Thermal test procedure**

The thermal properties of grout materials were determined using the transient line source (TLS) thermal needle method, which is widely used to measure the thermal resistivity and thermal conductivity of soils and geothermal well pack materials. This technique is standardized by IEEE Std 442™-2017 and ASTM D5334 (IEEE, 2017; ASTM D5334, 2022).

The method is based on the application of a controlled thermal pulse generated by a linear probe that functions simultaneously as a heat source and a temperature sensor. The temperature rise recorded over time is used to determine thermal properties through analytical modeling based on the theory of transient heat diffusion.

Thermal resistivity (ρ) is calculated using the following relationship:

$$\rho = \frac{4\pi(T_2 - T_1)}{q \cdot \ln\left(\frac{t_2}{t_1}\right)}$$

where $T_1$ and $T_2$ are the temperatures measured at times $t_1$ and $t_2$, respectively, and $q$ represents the heat input per unit length.

To ensure the accuracy of the results, the data were filtered to exclude time intervals characterized by non-linear behaviour, associated with transient and boundary effects. The analysis was performed by plotting the temperature as a function of the logarithm of time, taking into account only the linear part of the curve.

The following relationship was used to determine the thermal conductivity:

$$\lambda = \frac{1}{\rho}$$

For each sample, a controlled pre-drilling was performed to allow the insertion of the thermal probe, ensuring uniform contact between the probe and the material.

**Mechanical and hydraulic testing**

The permeability coefficient was determined using the constant head permeameter method, which is suitable for low permeability materials.

The uniaxial compressive strength was determined according to EN ISO 17892-7:2018 using standard cylindrical specimens.

For each grout formulation, three independent determinations were made for each type of test and the values reported represent the arithmetic mean of the results, ensuring the reproductibility and statistical reliability of the data.

## RESULTS AND DISCUSSIONS

The ternary plots were constructed considering only the solid constituents (sand–cement–bentonite), normalized to 100%. The water-to-solid ratio was treated as an independent parameter and therefore not included in the ternary representation.

**Presentation of experimental data**

The experimental results obtained for the 14 grout formulations are summarized in Table 2 in relation to the compositions presented in Table 1. The parameters determined include the permeability coefficient (k), the uniaxial compressive strength (Cu), the thermal conductivity (λ) and the thermal resistivity (ρ).

Table 2. Hydromechanical and Thermal Properties of the Formulations Analyzed

| Grout mix | k [cm/s] | Cu [kPa] | λ [W/mK] | ρ [mK/W] |
|---|---|---|---|---|
| R1 | 1.44E-09 | 3248 | 1.292 | 0.774 |
| R2 | 6.30E-08 | 1126 | 0.914 | 1.095 |
| R3 | 4.82E-08 | 1505 | 0.966 | 1.036 |
| R4 | 2.97E-08 | 1884 | 1.012 | 0.988 |
| R5 | 2.70E-08 | 1974 | 1.105 | 0.905 |
| R6 | 1.47E-08 | 2047 | 1.201 | 0.833 |
| R7 | 1.22E-08 | 1955 | 1.901 | 0.526 |
| R8 | 3.52E-08 | 626 | 1.468 | 0.681 |
| R9 | 4.49E-08 | 786 | 1.509 | 0.663 |
| R10 | 6.51E-08 | 317 | 1.413 | 0.708 |
| R11 | 3.54E-08 | 1719 | 1.744 | 0.573 |
| R12 | 8.42E-08 | 893 | 1.442 | 0.694 |
| R13 | 1.23E-08 | 744 | 1.482 | 0.675 |
| R14 | 2.97E-08 | 2000 | 1.624 | 0.616 |

The data show significant variation between formulations, reflecting the influence of composition on material properties. The thermal conductivity ranges from 0.9135 to 1.9005 W/mK, the permeability coefficient from 1.44×10-⁹ to 8.42×10-⁸ cm/s, and the mechanical strength from 316.9 to 3248.2 kPa.

**Thermal conductivity**

The thermal conductivity values show a wide variation among the mixes analyzed (Figure 1). Higher values are observed for mixes characterized by a higher sand content (e.g. Mix 7), while lower values are associated with mixes containing higher proportions of bentonite (e.g. Mix 2).

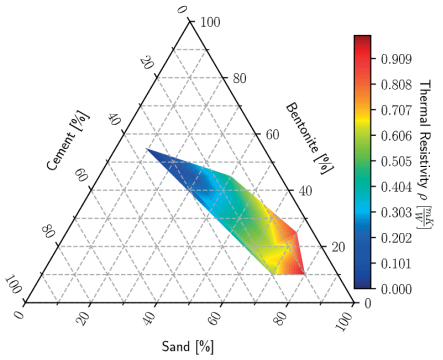



Figure 1. Variation of thermal conductivity for the analysed grout mixes

**Permeability**

The permeability coefficient varies by about one order of magnitude (Figure 2). The lowest values are associated with mixes containing a higher proportion of fines (cement and bentonite), while higher values are observed in mixes with a predominantly granular structure.

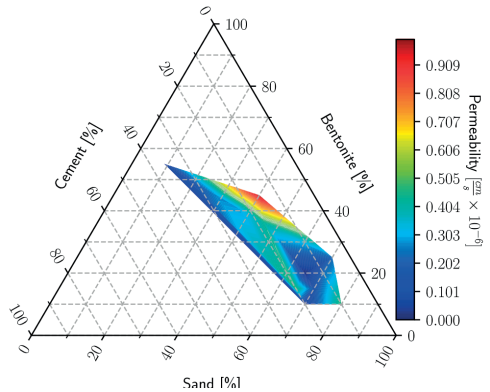



Figure 2. Variation of the coefficient of permeability (logarithmic scale)

**Mechanical strength**

The uniaxial compressive strength shows significant variation among the mixes analyzed (Figure 3). The highest values are recorded for mixes with higher cement content (e.g. Mix 1), while the lowest values correspond to mixes with reduced binder content.

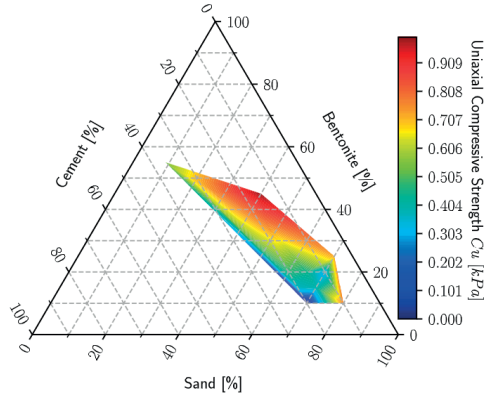



Figure 3. Variation of uniaxial compressive strength

Thermal conductivity–permeability relationship is presented in Figure 4.

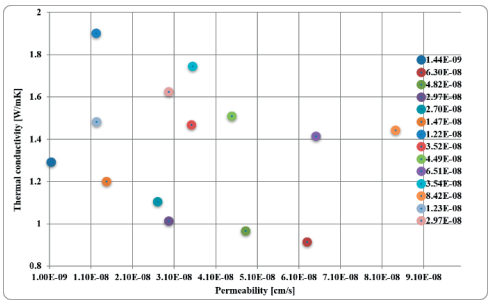



Figure 4. Relationship between thermal conductivity and permeability

The comparative analysis shows simultaneous variations in thermal conductivity and permeability among the analyzed mixes, suggesting that composition has a direct influence on both parameters.

## CONCLUSIONS

The experimental investigation of fourteen geothermal grout formulations demonstrated that the thermal, hydraulic and mechanical behaviour of grouting materials is strongly influenced by the relative proportions of quartz sand, cement and bentonite.

Thermal conductivity increased with increasing sand content, reaching a maximum value of 1.901 W/mK for formulation R7, while higher bentonite contents generally reduced thermal performance. Conversely, increasing the proportions of cement and bentonite improved hydraulic sealing by reducing permeability and contributed to the development of a more mechanically stable matrix.

The results confirm that thermal conductivity, permeability and compressive strength are governed by different physical mechanisms and cannot be simultaneously maximised. Consequently, geothermal grout design requires balancing thermal performance, hydraulic sealing capacity and mechanical resistance.

The ternary analysis provided a useful representation of the investigated compositional domain and enabled the identification of performance trends across the sand–cement–bentonite system. Higher sand contents were associated with improved thermal conductivity, whereas higher cement

and bentonite contents promoted lower permeability and greater mechanical stability.

Overall, the investigated formulations should be regarded as a compositional framework for evaluating performance trade-offs rather than as isolated mixtures. In particular, formulation R7 represents a boundary composition defining the upper thermal conductivity limit of the investigated system.

Future research should focus on the incorporation of thermally conductive additives and industrial by-products, long-term durability under thermal cycling, and the coupled thermo-hydro-mechanical behaviour of geothermal grouts under representative operating conditions.

## ACKNOWLEDGEMENTS

This work was supported by the research grant "Evaluation of the Thermal Conductivity of Soil and Grouting Material in Geothermal Wells" (GeoThermo), awarded to the authors by the Technical University of Civil Engineering of Bucharest, within the ARUST2024 research program.

## REFERENCES

Albers, A., Huttenloch, P., Zorn, R., Steger, H., & Blum, P. (2024). Determination of thermal properties of grouting materials for borehole heat exchangers. *Geothermal Energy*, 12, 36. https://doi.org/10.1186/s40517-024-00316-3

ASTM International. (2022). ASTM D5334-22a: Standard test method for determination of thermal conductivity of soil and rock by thermal needle probe procedure. ASTM International.

Borinaga-Treviño, R., Pascual-Muñoz, P., Castro-Fresno, D., & Del Coz Díaz, J. J. (2013). Study of different grouting materials used in vertical geothermal closed-loop heat exchangers. *Applied Thermal Engineering*, 50(1), 159–167. https://doi.org/10.1016/j.applthermaleng.2012.05.029

IEEE Standards Association. (2017). IEEE Std 442™-2017: IEEE guide for thermal resistivity measurements of soils and backfill materials. IEEE Standards Association.

Lund, J. W., & Toth, A. N. (2020). Direct utilization of geothermal energy 2020 worldwide review. *Geothermics*, 90, 101915. https://doi.org/10.1016/j.geothermics.2020.101915

Mahmoud, M., Ramadan, M., Pullen, K., Abdelkareem, M. A., Wilberforce, T., Olabi, A.-G., & Naher, S. (2021). A review of grout materials in geothermal energy applications. International Journal of Thermofluids, 10, 100070. https://doi.org/10.1016/j.ijft.2021.100070

Mascarin, L., Garbin, E., Di Sipio, E., Dalla Santa, G., Bertermann, D., Artioli, G., Bernardi, A., & Galgaro, A. (2022). Selection of backfill grout for shallow geothermal systems: Materials investigation and thermo-physical analysis. Construction and Building Materials, 318, 125832. https://doi.org/10.1016/j.conbuildmat.2021.125832

Nakládal, P., Procházka, M., Goliáš, V., & Hrdá, J. (2024). Methods of grout quality measurement in borehole exchangers for heat pumps and their rehabilitation. Geothermal Energy, 12, Article 37. https://doi.org/10.1186/s40517-024-00313-6

Spitler, J. D., & Gehlin, S. (2015). Thermal response testing for ground source heat pump systems - An hystorical overview. *Renewable and Sustainable Energy Reviews*, 50, 1125–1137. https://doi.org/10.1016/j.rser.2015.05.061

Scientific Papers. Series E. Land Reclamation, Earth Observation & Surveying, Environmental Engineering. Vol. XV, 2026
Print ISSN 2285-6064, CD-ROM ISSN 2285-6072, Online ISSN 2393-5138, ISSN-L 2285-6064

# ASPECTS REGARDING CLIMATE RESILIENCE AND URBAN HEAT ISLAND EFFECT MITIGATION IN URBAN AREAS RENOVATION PROJECTS

**Izabella MARIN LAZĂR**

"1 Decembrie 1918" University of Alba Iulia, 5 Gabriel Bethlen Street, Alba Iulia, Romania

Corresponding author email: marin.izabella@uab.ro

***Abstract***

*The current context requires the networking of planning decisions on increasing the energy performance of the built environment for sustainability purposes and decisions on reconfiguring urban areas to obtain a resilient environment. The paper aims to highlight ways of multicriterial evaluation on energy performance, environmental performance and resilience in urban areas renovation projects in complementarity with applicable solutions in order to improve the characteristics of the area microclimate. Beyond the aspect of the high energy performance associated with nZEB buildings (Nearly Zero Energy Buildings), we must understand the conditions deriving from the quality of anthropogenic factor that the building has in relation to the urban microclimate, contributing to the amplification of the effect of Urban Thermal Island, a phenomenon with significant impact on the health and quality of life of the inhabitants.*

***Key words****: climate resilience, local climate zones, nearly Zero Energy Buildings (nZEB), Urban Heat Island (UHI), urban retrofitting.*

## INTRODUCTION

The impact of urbanization on the local climate can be analysed through the extent of the urban heat island (UHI) effect. A significant concern is the heightened risk to the population, particularly vulnerable individuals, associated with extreme weather events such as heat waves. The frequency and intensity of these events are increasing in the context of climate change (IPCC, 2022). Cities under the influence of the UHI are experiencing more acute effects with consequences for energy consumption, health and quality of life of residents (Heaviside et al., 2017).

The overheating of urban areas is the cumulative result of several factors that influence the energy balance. These include the high proportion of impervious concrete surfaces, reduced vegetation in densely built-up areas, and anthropogenic heat emissions. It is evident that there is an interaction occurring between the radiative properties of anthropogenic surfaces, reduced evapotranspiration, and changes in ventilation that are attributable to urban morphology (Arnfield, 2003; Grimmond, 2007). This phenomenon is further compounded by anthropogenic heat accumulation resulting from traffic, human activities, and air conditioning, which has the potential to significantly exacerbate local warming (Taha, 1997; Santamouris, 2015b).

Strategies for integrated urban planning have the potential to address climate resilience in densely built-up areas by combining solutions for adapting to extreme heat with those designed to increase energy efficiency and, consequently, environmental sustainability (Constantinescu, 2020). The findings presented support the understanding of the need for convergence between efforts to mitigate the effects of urban heat islands and to increase the adaptive capacity of buildings and urban systems, including green infrastructure and urban morphology, to meet the need for transformative adaptation of cities (European Environment Agency, 2016).

The extant literature highlights mitigation solutions based on the efficiency of cool roof technologies and green roofs (Santamouris, 2014; 2015a), and a comparative quantification of their performance (Li et al., 2014). In addition, the benefits of strategies based on green-blue infrastructure are encompassed, as are the utilization of reflective permeable pavements and quantitative references regarding surface temperature reduction (Li et al., 2022). Furthermore, measures to reduce anthropogenic

heat are also addressed. The classification framework for local climate zones also serves as the morphological basis for urban climate analysis (Stewart & Oke, 2012). However, most studies focus on urban-scale indicators or isolated technical measures rather than an integrated methodological approach.

Although recent studies have paved the way for the simultaneous integration and analysis of the urban microclimate and the energy performance of buildings to area scale assessments (Pisello et al., 2017; Turhan et al., 2023; Skandalos & Karamanis, 2025), these are based on complex simulations or case studies specific to a particular context, with less exploration of assessments aimed at providing framework solutions for the planning of urban area renovations by quantifying the co-benefits of renovation measures with nearly Zero Energy Buildings (nZEB) targets and the reconfiguration of urban surfaces in order to reduce the UHI effect. Furthermore, current local design practice often appears to offer fragmented measures to meet energy and environmental performance requirements, which do not always ensure conditions for resilience at the urban area level (Constantinescu, 2020).

At the level of Bucharest Municipality, studies highlight the high thermal risk associated with heat waves and extreme temperatures faced by a large part of the city's area (Zamfirescu et al., 2025). Despite the demonstrable applicability of UHI analysis based on the assessment of land surface temperature (LST) at the local climate zone level for certain Romanian cities, including Iași (Sfică et al., 2023), integrated scenarios combining nZEB objectives with measures to mitigate the UHI effect remain insufficiently analysed.

The assertion that "*every city will have a heat island*" serves to emphasize the significance of these approaches, as the modelling of the reduction of urban heat island intensity constitutes one of the key objectives in sustainable urban planning projects (Chow & Chugh, 2022). Based on the understanding that quality of life and climate action are complementary goals (Montgomery, 2017) we can expect an improvement in the comfort and health of the population associated with major urban renewal projects that adopt a multi-criteria approach aimed at enhancing energy and environmental performance as well as improving the local climate. It should not be overlooked that the attractiveness of outdoor spaces is closely linked to the improvement of the microclimate; thus, mitigating the UHI effect leads to a lifestyle more in harmony with nature during a period of climate change (Sim, 2022).

Flexibility and adaptability appear to be the key attributes of a soft urban environment that, by integrating density and diversity, can offer residents a more pleasant daily life while also responding, in the long term, to the need for transformative adaptation in a global context (European Environment Agency, 2016).

The present study addresses the issue under discussion by means of an analysis of adaptation solutions. This analysis is based on a comprehensive renovation of multi-family residential buildings exposed to UHI intensity, in accordance with nZEB standards, within a Test Urban Zone that is representative of the city of Bucharest. The purpose of this study is to evaluate the potential of the proposed integrated solution packages to enhance microclimate quality and simultaneously increase energy and environmental performance.

The objective of this research is threefold: firstly, to quantify the current proportion of impervious mineral surfaces characterized by low albedo within the analysed urban area; secondly, to highlight the anthropogenic impact of multi-family residential buildings in their current energy state and the proposed nZEB scenario based on estimates of residual heat emissions into the atmosphere (Marin Lazăr, 2021); and thirdly, to compare integrated intervention scenarios that combine building energy retrofits, the implementation of high-reflectance surfaces, and the expansion of green infrastructure, from the perspective of their potential to reduce the UHI effect and improve climate resilience at the neighbourhood scale. The study's contribution stems from the creation of a unified methodological framework through the simultaneous application of energy and environmental performance modelling, the analysis of intervention possibilities at the level of urban surfaces within identified local climatic zones, and the quantification of anthropogenic heat. The aim of this is to obtain quantitative

indicators that can be used in the development of local climate adaptation strategies.

## MATERIALS AND METHODS

The present study proposes expanding the analysis of applicable measures aimed at improving the performance of multi-family residential buildings to meet the nZEB (nearly Zero Energy Buildings) standard. This will be achieved by examining proposals for interventions regarding the proportion and quality of mineral and natural surfaces that can help reduce the UHI effect.
The analysis focuses on a representative test urban area located in Bucharest.

### 1. Heat Island Intensity in Bucharest _Test Urban Area

The specific exposure indicator for Bucharest regarding UHI intensity is approximately 2.22°C, according to thermal maps generated by processing the climate model available through the Destination Earth (DestinE) project.
The Urban Heat Island Explorer application provides a clear visualisation of the increase in average annual surface temperature under the influence of the UHI effect for European cities.
For the designated Test Urban Area, the UHI effect has been found to cause an increase in this parameter ranging from 0°C to +3°C, with some hotspot areas where the temperature exceeds this threshold (Figure 1).
The area under analysis is located in proximity to the city centre, where temperatures in the air and on the surface tend to be higher. Near the area under study, two major natural features (Lake Fundeni and the National Arena Park) help mitigate the urban heat island effect.

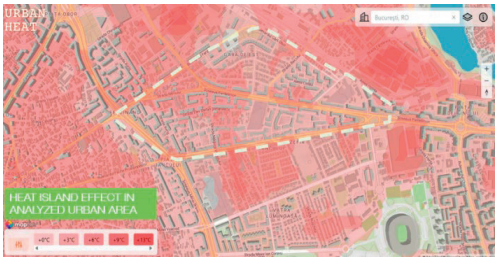



Figure 1. Increase of land surface temperature caused by UHI within the Urban Test Area (https://urbanheat.app/bucuresti)

In order to comprehend the substantial impact of natural spaces in mitigating the UHI effect, it is imperative to acknowledge that surface temperatures in green and aquatic areas remain at 25-28°C, whilst the average surface temperature during the summer months in Bucharest exceeds 35°C and average values for July are above 40°C (Zamfirescu et al., 2025).
The summary Table 1 illustrates climate trends in Bucharest by modelling the increase in average temperatures and the number of tropical nights and days under the RCP 4.5, RCP 8.5 (medium and high impact) scenarios, based on an analysis of measurements taken at the Filaret and Băneasa stations during the reference period 1901-2023 (Zamfirescu et al., 2025).

Table 1. Trends for the projected period 1971-2100, for the RCP 4.5 and RCP 8.5 scenarios, compared with values measured during the period 1901-2023 (Zamfirescu et al., 2025)

| Time frame | Scenario | Incrase avg.max. temp. July (°C) | Tropical nights | Tropical days |
|---|---|---|---|---|
| 2041-2060 | RCP 4.5 | +1.6 | 10 | 23 |
| 2081-2100 | RCP 4.5 | +2.2 | 13 | 30 |
| 2041-2060 | RCP 8.5 | +1.9 | 15 | 29 |
| 2081-2100 | RCP 8.5 | +4.3 | 46 | 54 |

The medium- and long-term projections indicate an increase in vulnerability in the absence of mitigation measures, given the already unfavourable current situation in which over 50% of the capital's population faces a "high or very high risk of extreme temperatures and heat waves" during the summer (Zamfirescu et al., 2025).

### 2. Analysis of Land Use Types within the Test Urban Area

From a structural, functional and urban planning perspective, the analysed area consists primarily of high-rise apartment buildings (P+8E and P+10E) and is located in Sector 2 of Bucharest, between Iancului Road, Pantelimon Road, Mihai Bravu Road, Obor Station, and Baicului Street. It is also noteworthy that there are several areas with single-family homes located in a secondary position relative to the main traffic arteries (Marin Lazăr, 2021).
From a morphological perspective, the layout of multi-unit residential buildings in the study area can be divided into two subzones, as illustrated

in Figure 2. The first of these is the area near Obor Station, built prior to 1970. This area features a distribution of large-scale residential buildings surrounded by extensive green spaces. The second subzone is developed after 1975/1980 and is characterised by more pronounced densification and a fragmentation of small green spaces situated between the blocks. As demonstrated in the relevant literature, Land Surface Temperature (LST) measurements indicate that this parameter is lower for the first type of building layout and higher for the second situation (Sfică et al., 2023). The analysis of urban areas was conducted, as shown in Table 2, in relation to the two defined subzones, Local Climate Zones LCZ 1 and LCZ 2, based on this observation.

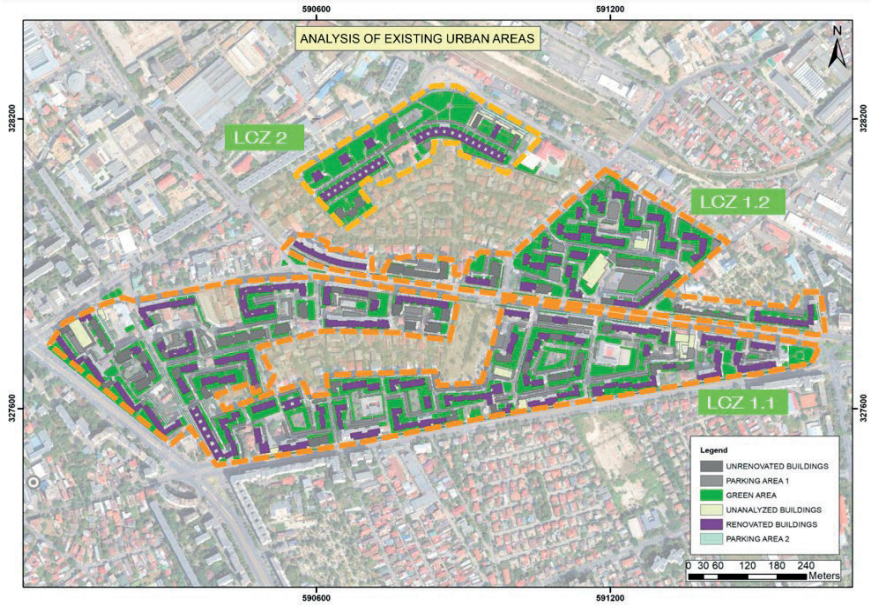



Figure 2. Zonal analysis - indicators of urban composition: built-up/natural areas - existing

Table 2. Zonal analysis - indicators of urban composition: built-up/natural areas - existing

| | **Total analysed area** [m$^2$] | **Built-up area** [m$^2$] | **Green space** [m$^2$] | **Parking area** [m$^2$] | **Sidewalks, streets, alleys** [m$^2$] |
|---|---|---|---|---|---|
| **LCZ 1.1** | 272,600 | 77,689 | 35,626 | 29,800 | 129,485 |
| **LCZ 1.2** | 108,036 | 28,939 | 16,258 | 15,955 | 46,884 |
| **TOTAL LCZ 1** | **380,650** | **106,630** | **51,884** | **45,755** | **176,369** |
| **LCZ 2** | **64,231** | **12,349** | **13,001** | **4,391** | **34,490** |

An analysis of urban areas highlights the low proportion of natural spaces, approximately 14.5%, compared to man-made areas, which account for approximately 85.41% of the total analysed.

For subzone LCZ 1, it is noteworthy that green spaces account for only about 50% of the built-up area, or 13.6% of the total subzone, while for subzone LCZ 2, the ratio of built-up area to green space is slightly more favourable to the latter, reaching approximately 20% of the subzone (Figure 3).

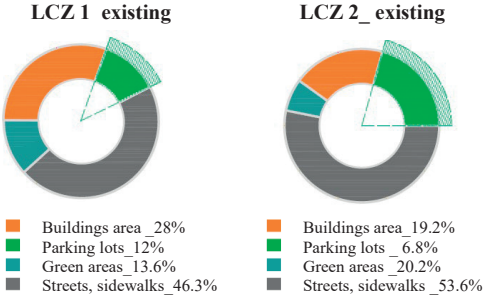



Figure 3. Proportion of anthropogenic existing areas versus natural areas

This mix influences the local energy balance, given that existing man-made surfaces (rooftops of apartment buildings covered with bituminous membranes, courtyards, parking lots, streets, alleys, and sidewalks) are characterised by low albedo and high thermal storage capacity and thus absorb a greater amount of solar radiation during the day, which they gradually release at night, amplifying thermal discomfort (Oke, 1982; Taha, 1997). The high degree of imperviousness of the area as illustrated in Figure 4, and the low percentage of vegetation amplify this effect by limiting evaporative cooling (Arnfield, 2003; Gago et al., 2013).

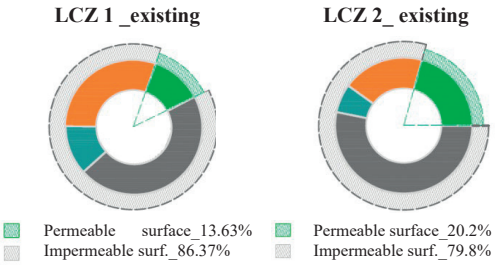



Figure 4. Ratio of permeable/impermeable surfaces (high solar radiation absorption)

## 3. Energy Performance Analysis - Multi-family Residential Buildings in the Test Urban Area

The present energy status of the Test Urban Area, as determined by the energy and environmental performance of multi-family housing, demonstrates elevated levels of specific primary energy consumption (kWh/m²·year) and associated $CO_2$ emissions (kg/m²·year), particularly for buildings that have not undergone previous energy renovation programs, accounting for approximately 31% of the total. The numerical results were supported by dynamic modelling of the building envelope response, as presented in detail in the relevant literature (Constantinescu, 2008; 2020).

The mean zonal values of these indicators (across all buildings belonging to both energy typologies, designated CRA and CRR) are 183.74 kWh/m²·year of specific primary energy and 41.98 kg/m²·year of $CO_2$ emissions (Table 3). These are well above the threshold for classification in the nZEB (nearly zero-energy building) performance category and thus place the area in a lower energy and environmental class (Marin Lazăr, 2021).

Table 3. Assessment of energy consumption in the test urban area - existing (Marin Lazăr, 2021)

| Energy TYPE CRA/ CRR | Specific net energy consump. (kWh/m²/ year) | Specific net $CO_2$ emissions (kg/m²/ year) | Enviro. energy class | Heat emissions (kWh/m²/ year)/ (MWh/year) |
|---|---|---|---|---|
| Regional Enviro. LCZ1+LCZ2 | **183.74** | **41.98** | 4 /4 | 2.42 / **802** |
| | | | | |
| nZEB 2030 | 43-74 | 9-19 | 2/2 | |
| nZEB 2050 | < 43 | < 9 | 1/1 | |

## 4. Assessment of the anthropogenic impact of multi-unit residential buildings

To assess the anthropogenic impact of multi-unit residential buildings on the amplification of urban heat islands, the heat emissions released into the atmosphere by the operation of split-type air conditioning units were determined, in correlation with the cooling demand and the performance of the equipment. The quantity of heat emissions into the atmosphere, as shown in Table 4, was calculated on the basis of the usable floor area of the air-conditioned apartments, which was determined to be 330,097 m², thus accounting for approximately 50% of the total area analysed, which was 690,562.6 m² (Marin Lazăr, 2021).

Table 4. Significant results for several representative building types in the analysed area (Marin Lazăr, 2021)

| Energy TYPE CRA/ CRR | Usable area (m²)/ Heated usable area | Primary en. building (MWh/ year) | Specific net energy (kWh/ m²/year) | Heat emissions (MWh/year) / (kWh/m²/ year) |
|---|---|---|---|---|
| CRA P+8E | 3066/ 1356 | **696** | **223.74** | **5.16** /3.8 |
| CRR P+8E | 3093 / 1308 | **482** | **155.83** | **2.25** /1.72 |
| CRA P+10E | 2450 / 946 | **554** | **226.12** | **3.73** / 3.94 |
| CRR P+10E | 2459/ 782 | **389** | **158.19** | **1.3** / 1.66 |

It is important to emphasize the reciprocal relationship between buildings - viewed as an anthropogenic factor - and the urban micro-climate, since the waste heat released into the atmosphere raises outdoor temperatures in the immediate vicinity of the building, thereby contributing to a further increase in the energy required for cooling. Given the projected rise in temperatures over the medium and long term - which in urban areas is associated with the Urban Heat Island effect - it can be concluded that, in the absence of energy-efficiency improvements and reconfiguration, the energy demand for cooling will increase.

The adaptability of buildings is supported by passive architectural solutions that help minimise the need for sensible cooling and by connections to technical systems that must ensure the operation of HVAC equipment under severe weather conditions (Constantinescu, 2020).

## 5. Indicators of the current situation

The specific exposure indicator for the extent of the urban heat island (UHI) in the analysed area falls within the range of 0-3°C. However, higher intensities of 5-6°C may occur under weather conditions conducive to heat waves.

**Key findings:**

- Analysis of urban surfaces highlights conditions favourable to the amplification of the urban heat island effect at the local level due to the high proportion of impermeable mineral surfaces characterized by low albedo.
- Analysis of heat emissions associated with the operation of buildings in their current energy state illustrates their role as an anthropogenic factor contributing to the amplification of the urban heat island effect.

The European Environment Agency proposes a tool for monitoring climate change adaptation policies organised around the risk, response, and outcome framework (Climate-ADAPT, n.d.). From this standpoint, the text presents several aspects relevant to the analysed case study. These include the current risk level, the proposed intervention scenarios in response to climate challenges, and the relevant outcomes for the analysed area. The assessment of the urban test area highlights an increased risk level regarding extreme temperatures and heat waves, exacerbated by the urban heat island effect (Zamfirescu et al., 2025; UAUIM, 2017). The present analysis of the current situation reveals the thermal vulnerability of buildings during heat waves. This phenomenon can be attributed to the inability to guarantee passive survival conditions in the absence of functional technical systems in dwellings characterised by elevated thermal discomfort (Marin Lazăr, 2021).

## 6. Measures for climate resilience and UHI reduction

In response to the previously delineated risk scenario, a multi-criteria analysis is required of the possibilities for reducing the UHI effect in the Urban Test Area. This analysis should involve a comparison of the existing situation with integrated intervention scenarios at the level of buildings and urban surfaces. The purpose of this comparison is to ensure improved energy and environmental performance and resilience. The proposed specific objectives are twofold: firstly, to mitigate the adverse effects of the high proportion of impermeable mineral surfaces with low albedo, and secondly, to limit heat emissions into the atmosphere by reducing the anthropogenic impact of buildings (Figure 5, Figure 6 and Table 5).

The proposed intervention plan for urban areas includes:

- Converting impermeable parking lots into permeable surfaces with high reflectivity.
- Using cool roof materials for the flat roofs of multi-unit residential buildings, with the integration of photovoltaic panels.
- Targeted interventions to expand green spaces through green roofs and green urban paving. Areas targeted include the flat roofs of schools and kindergartens within the test urban zone, local heating plant buildings, and ground-floor public spaces. Green roof solutions will be analysed with caution, given the difficulty of maintaining them in light of the current summer rainfall deficit specific to the Bucharest area and long-term climate forecasts.
- The installation of green urban paving can bring social benefits by creating community gathering places, so that solutions to improve the microclimate also facilitate resident's "reconnection" with nature.

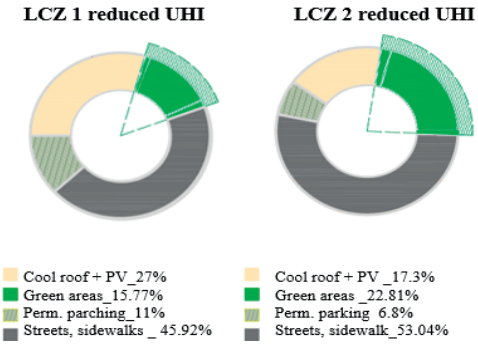



Figure 5. Proposed ratio of anthropogenic versus natural areas

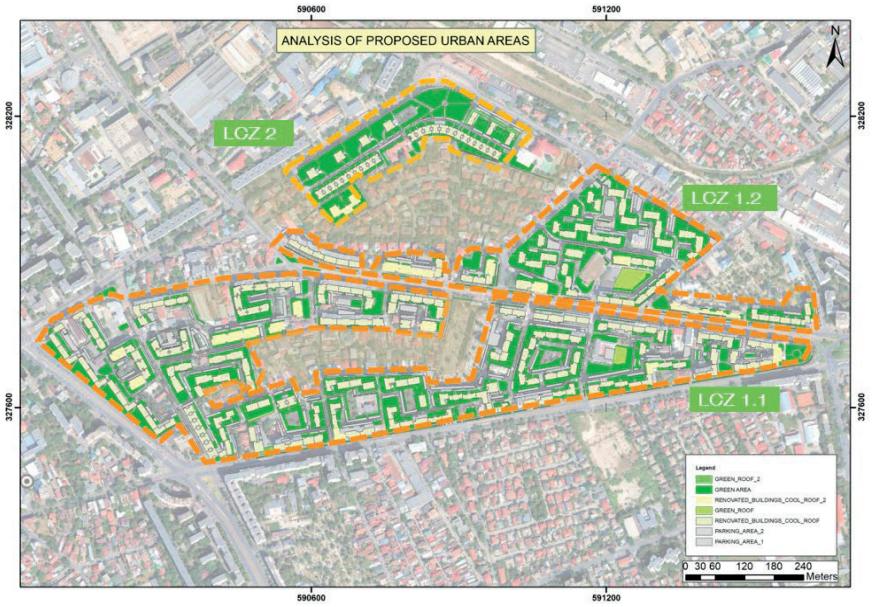



Figure 6. Zonal analysis - indicators of urban composition: built-up/natural areas - proposal

Table 5. Zonal analysis - indicators of urban composition: built-up/natural areas - proposal

| | Total analysed area [m$^2$] | Built-up area [m$^2$] | Green space [m$^2$] | Parking area [m$^2$] | Sidewalks, streets, alleys [m$^2$] |
|---|---|---|---|---|---|
| **LCZ 1.1** | 272,600 | 77,689 | 40,045 | 29,800 | 127,914 |
| **LCZ 1.2** | 108,036 | 28,939 | 20,000 | 13,213 | 46,884 |
| **TOTAL LCZ 1** | **380,650** | **106,630** | **60,045** | **43,013** | **174,798** |
| **LCZ 2** | **64,231** | **12,349** | **14,652** | **4,391** | **34,072** |

The maximum scenario applicable to buildings and the modernization of technical systems includes (Marin Lazăr, 2021).

- Passive solutions for the building envelope are to be implemented in order to ensure an appropriate level of thermal insulation and airtightness, as well as the installation of shading systems. The following solutions are to be put into effect: reflective folding thermal insulation shutters and the use of high-albedo façade finishes and cool roof systems with solar radiation absorption coefficients α abs. Wall = 0.3 / α abs. Terrace= 0.1.
- The technical systems to be implemented in the analysed buildings - heat recovery ventilation systems.
- Modernisation of the district-level heating and electricity supply system – high-efficiency cogeneration/trigeneration, and connection of all buildings within the test urban area.
- Installation of photovoltaic panels to harness the area's potential for renewable energy production. The sizing of the panels will account for the building's calculated sensible cooling demand determined under summer design conditions. We should mention that PV have a theoretical efficiency of 22% in laboratory conditions (low net temperature to the outside). In urban conditions, in hot summer days, the efficiency of solar radiation transformation into electricity is about 12%-15% associated with the high temperature of the PV capture surface, 60-70°C. PV produces electric energy, but also thermal pollution. Prosumers are effective for remote areas or in rural areas.
- To ensure conditions for climate resilience, additional nighttime ventilation systems for the spaces via a perforated false ceiling may be selected. This requires that the outdoor temperature drop below 24°C.

Based on indicators of vulnerability, exposure, and adaptive capacity, key measures have been identified that focus on technological adaptation solutions applicable to buildings and built-up areas, as well as green options.

## RESULTS AND DISCUSSIONS

### 1. Estimated outcome of intervention scenarios for urban areas aimed at reducing the urban heat island effect

The proposed intervention scenario ensures an increase in areas conducive to lower temperatures within the test urban area compared to the current situation. In subzone LCZ 1, the proportion of permeable surfaces will increase, from 13.63% to approximately 27%, and from 20% to 29.6% in subzone LCZ 2 (Figure 7).

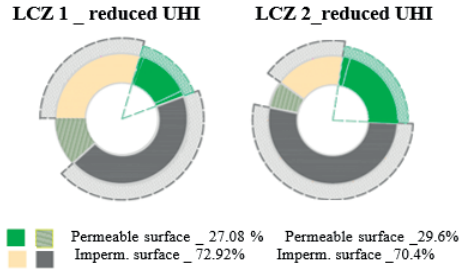



Figure 7. Ratio of permeable / impermeable surfaces

These changes result from the conversion of parking lots from impermeable mineral surfaces to permeable surfaces with high solar reflectance and the cumulative effects of increasing green spaces integrated into the balance of surface categories relative to the analysed area.

Concurrently, the proportion of surfaces with low solar radiation absorption (including cool roofs and the conversion of parking lots) will increase significantly in LCZ 1 from 13.63% to approximately 54.08% and in LCZ 2 from 20.2% to 46.9%. At the same time, the proportion of surfaces with high absorption decreases - 45.92% in LCZ 1 and 53.04% in LCZ 2 - which leads to a reduction in the solar radiation load on the analysed area (Figure 8).

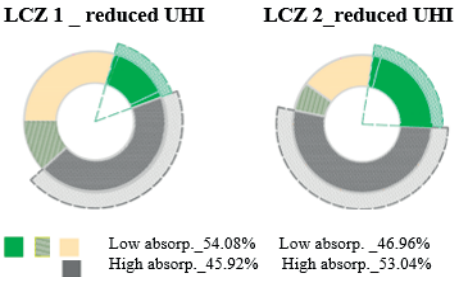



Figure 8. Ratio of high solar radiation absorption

### 2. Estimated results of building-level intervention scenarios

The energy and environmental impact of the technological adaptation measures was estimated by comparing the existing and proposed scenarios regarding net primary energy (kWh/m² per year) and $CO_2$ emissions (kg/m² per year) for buildings in their current state and after implementing the renovation solution packages.

Compared to the permissible thresholds for compliance with the nZEB standard by 2050, it is necessary to combine passive architectural solutions applicable to the building envelope with systems for recovering energy from exhaust air, utilizing the regional potential for renewable energy production, as well as connecting to high-efficiency district heating systems of the cogeneration/ trigeneration type. The solutions analysed implicitly lead to a reduction in the amount of waste heat released into the atmosphere, which results in the emission levels shown in the following Table 6.

Table 6. Assessment of energy consumption in the test urban area - proposed (Marin Lazăr, 2021)

| Energy TYPE CRA/ CRR | Specific net energy consump. (kWh/m²/ year) | Specific net $CO_2$ emissions (kg/m²/ year) | Enviro. energy class | Heat emissions (kWh/m²/ year)/ (MWh/year) |
|---|---|---|---|---|
| Regional Enviro. LCZ1+LCZ2 | **22.16** | **4.64** | 1/1 | 0.85 / **283.31** |
| | | | | |
| nZEB 2030 | 43-74 | 9-19 | 2/2 | |
| nZEB 2050 | < 43 | < 9 | 1/1 | |

### 3. Significance of the Results

In relation to the configuration of urban surfaces, the results of the analysis confirm that, at present, the proportion of impervious surfaces - 86.37% in subzone LCZ1 and 79.8% in subzone LCZ2 - contributes to the amplification of the UHI effect within the test urban area. The reported values are higher than the critical imperviousness threshold of 70%, which leads to a marked decrease in the soil's evaporation and cooling capacity, resulting in an increase in the UHI effect by more than 2°C compared to peri-urban areas (Oke et al., 2017). This highlights the area's high thermal vulnerability, correlated with a specific UHI exposure indicator of 0°C to +3°C according to Urban Heat Island Explorer data.

The contribution of the existing built environment, as an anthropogenic factor that further exacerbates UHI intensity, is highlighted by the quantification of residual heat emissions released into the atmosphere by air conditioning units. The total annual average of these emissions across the area is approximately 802 MWh/year (Table 3), reflecting the current energy status of multi-unit residential buildings. Given the medium- and long-term climate projections (Zamfirescu et al., 2025), it can be estimated that in Bucharest we will see an increase in energy consumption associated with space cooling, which could adversely exacerbate the building-urban microclimate feedback loop in the absence of mitigation solutions.

The mean values for specific primary energy were found to be approximately 183.74 kWh/m²·year, and the mean $CO_2$ emissions were 41.98 kg/m²·year, based on the current level of energy and environmental performance of the analysed buildings. These values illustrate the inadequacy of the solutions generated by previous renovation procedures, based on isolated interventions, as buildings in their current energy state cannot ensure conditions for passive survival at the residential unit level during heat waves and do not meet nZEB objectives (Marin Lazăr, 2021; Constantinescu, 2020).

## 4. The inner validation of results against study objectives

In terms of the objective of reconfiguring urban surfaces, the proposed intervention scenario results in a significant increase in permeable surfaces, from 13.63% to approximately 27% for subzone LCZ1, and from 20% to 29.6% for subzone LCZ2. At the same time, there is a significant increase in areas with reduced solar absorption, from 13.63% to approximately 54.08% in LCZ 1 and from 20.2% to 46.9% in LCZ 2. The proposed interventions lead to a reduction in solar radiation absorbed within the area.

The proposed solutions to achieve the nZEB target have been shown to result in a decrease in specific primary energy consumption from 183.74 kWh/m²·year to 22.16 kWh/m²·year and in associated $CO_2$ emissions from 41.98 kg/m²·year to 4.64 kg/m²·year (Marin Lazăr, 2021). The significantly reduced cooling demand of energy-renovated buildings leads to a substantial reduction in heat emissions into the atmosphere, approximately 65% lower than current levels. This implicitly reduces the anthropogenic impact of buildings, which is a relevant aspect regarding the co-benefits of increasing energy efficiency and mitigating the UHI effect.

The objective of comparatively evaluating integrated scenarios is achieved by simultaneously analysing the impact of interventions on urban land characteristics and measures to improve the energy and environmental performance of buildings. This highlights the cumulative positive effect at the urban area level that justifies the integrated, multi-criteria approach to renovation projects compared to isolated, single-focus interventions.

## 5. External validation of results compared to similar studies

The potential for reducing surface temperature in the analysed test area through the proposed intervention scenarios is qualitatively confirmed by the existing literature. The available reports indicate a potential reduction in surface temperature of up to 34.3°C by replacing dark roofs with reflective roofs equipped with PV, and approximately 8.3°C by converting parking areas from dark impervious to light/permeable surfaces (Li et al., 2022).

The effectiveness of UHI mitigation measures based on green roof and cool roof technologies is increased when implemented at the neighbourhood scale rather than through isolated interventions at the building level (Li et al., 2014), which confirms the need for the urban-scale approach described in this study.

Reference can also be made to the added value of the proposal to partially implement green roofs and permeable pavements, given that multifunctional green infrastructure contributes both to mitigating the urban heat island effect and to stormwater retention and increased biodiversity (Demuzere et al., 2014), which, particularly in Bucharest, given the lack of rainfall during the summer season, requires careful selection of species and minimization of irrigation needs.

The study's findings align with the conclusions summarized in the reports of the European Environment Agency (2016), which show that

integrated interventions combining measures related to green infrastructure, smart surfaces, and building energy performance yield greater benefits in terms of both thermal comfort and public health.

## 6. Estimated results of building-level intervention scenarios

The present paper puts forward a proposal for the integration of morphological analysis based on the LCZ classification and the modelling of building energy performance, with a focus on the identification and quantification of anthropogenic heat emissions resulting from building operations. This is to be achieved within a unified methodological framework that provides a replicable decision-making tool for the analysis of urban areas with similar functions and characteristics, located in regions with a continental climate and trends toward rising temperatures and heat waves. The quantitative indicators resulting from the analysis – namely, the proportion of permeable surfaces characterised by high albedo, anthropogenic heat emissions, and specific values for primary energy and $CO_2$ emissions – can be used to develop local climate adaptation strategies and evaluate results in relation to resilience objectives.

## 7. Limitations of the study, future directions for research

About the interpretation of the results, it should be noted that the analysis of urban surfaces was based on reference parameters from the relevant literature without in-situ validation through direct measurements of ground surface temperature or air temperature in the analysed area using remote sensing data or sensor networks. The scenario does not include an assessment of the influence of urban morphology on natural ventilation and the spatial distribution of temperatures, nor does it include dynamic modelling of the long-term degradation of material performance in terms of permeability and reflectivity, which would lead to a reduction in the estimated benefits.

Heat and pollutant emissions resulting from road traffic significantly influence the urban heat balance (Taha, 1997). Therefore, in addition to the benefits of passive measures and green solutions implemented at the building and surface levels, the study can be expanded to include an analysis of the mobility component relevant to the multi-criteria analysis of urban areas.

## CONCLUSIONS

This study confirms and supports the view that reducing the urban heat island effect (UHI) in major urban renewal projects requires more than one type of intervention and can be effectively integrated with building energy performance objectives.

Attempts to recalibrate the area's energy systems so that they meet the performance standards for nZEBs by 2050 contribute to reducing heat emissions into the atmosphere and lessen the anthropogenic impact of buildings (Marin Lazăr, 2021). These two courses of action - the reconfiguration of urban areas and energy-efficient renovation - become interdependent, generating clear climate co-benefits.

Individual measures have limited effectiveness in dense urban areas; tangible results are achieved through the implementation of integrated solution packages that combine green infrastructure, cool surfaces, building solar control, and the reduction of anthropogenic heat (Santamouris, 2015b; Li et al., 2014). The package of solutions proposed following the morphological analysis - by comparing scenarios with the current situation - is based on increasing zonal permeability and albedo, through cool roofs equipped with photovoltaic panels, the conversion of parking lots, as well as targeted interventions to increase green spaces, and has real potential to reduce the UHI effect within the test urban area.

The integrated solutions analysed can serve as a methodological framework for local adaptation strategies aimed at climate resilience, provide quantitative indicators, and highlight the need for integration between public spaces, building performance, and energy infrastructure. The methodological framework, based on the LCZ classification, comparative analysis of scenarios for interventions in urban areas, and integrated energy performance modelling, provides a decision-making tool for climate resilience objectives, replicable for the multi-criteria analysis of renovation projects in similar urban areas.

From the residents' perspective, integrating green infrastructure and public spaces not only provides environmental benefits, but also enhances the appeal of outdoor areas and fosters a reconnection with nature. This approach can also help to improve social cohesion at the urban/neighbourhood level.

This integrated approach, which is based on the understanding that urban climate resilience is a systemic objective, leads to a tangible reduction in the urban heat island (UHI) effect during heatwaves. This contributes to increased urban comfort and climate adaptation, reduced energy consumption and improved quality of life in urban areas.

## REFERENCES

Arnfield, A.J. (2003). Two decades of urban climate research: a review of turbulence, exchanges of energy and water and the urban heat island. *International Journal of Climatology* 23(1), 1-26.

Chow, W. & Chugh, A. (2022, August). *Discover how sweltering urban heat islands are being cooled down*. *World Economic Forum*. Retrieved March 2026 from https://www.weforum.org/stories/2022/08/ways-to-cool-cities-and-avoid-urban-heat-islands

Climate-Adapt. (n.d.). *Measuring progress towards climate resilience*. *European Environment Agency*. Retrieved from https://climate-adapt.eea.europa.eu/en/knowledge/tools/measuring-progress-towards-climate-resilience

Constantinescu, D. (2008). *Tratat de inginerie termică. Termotehnica în construcţii,* 1. Bucharest, RO: AGIR Publishing House.

Constantinescu, D. (2020). *Rezilienţa climatică şi performanţa energetică şi de mediu a clădirilor de locui colectivet*. Bucharest, RO: Ion Mincu University Publishing House.

Demuzere, M., Orru, K., Heidrich, O., Olazabal, E., Geneletti, D., Orru, H., Bhave, A. G., Mittal, N., Feliu, E., & Faehnle, M. (2014). Mitigating and adapting to climate change: Multi-functional and multi –scale assessment of green urban infrastructure. *Journal of Environmental Management*, 146, 107-115.

Destination Earth, Web Site. Retrieved from https://destination-earth.eu/destination-earth/destines-components/digital-twins-digital-twin-engine/

European Environment Agency. (2016). Urban adaptation to climate change in Europe 2016: *Transforming cities in changing climate* (EEA Report No 12/2016).

Gago, E.J., Roldan, J., Pacheco- Torres, R., & Ordonez, J. (2013). The city and urban heat island: A review of strategies to mitigate adverse effects. *Renewable and Sustainable Energy Reviews*, 25, 749-758.

Grimmond, S. (2007). Urbanization and global environmental change: Local effects of urban warming. *The Geographical Journal* 173 (1), 83-88.

Intergovernmental Panel on Climate Change (IPCC). (2022). *Climate change 2022: Impacts, adaptation and vulnerability*. Contribution of working group II to the Sixth Assessment Report of the Intergovernmental Panel on Climate Change. Cambridge, UK: Cambridge University Press

Heaviside, C., Macintyre, H., Vardoulakis, S. (2017). The urban heat island: Implications for health in a changing environment. *Current Environmental Health Reports*, 4 (3), 296-305.

Li, D., Bou-Zied, E. & Oppenheimer, M. (2014). The effectiveness of cool and green roofs as urban heat island mitigation strategies. *Environmental Research Letters*, 9 (5), 055002

Li, Z., Loftness, V., Ge, S., Zhou, Y., Sui, J., Zhang, Z. & Kim, J. (2022). Smart surfaces guide – The path to a cooler future with smarter design for urban surfaces. Carnegie Mellon University. Retrieved March 2026 from https://smartsurfacescoalition.org/analysis/2022/8/9/smart-surfaces-guidebook

Marin Lazăr, I. (2021). *Atlas Verde al României aplicaţii în arhitectura clădirilor cu consum de energie aproape de zero (Nearly Zero Energy Buildings – nZEB)*. Bucharest, RO: Ion Mincu University Publishing House.

Montgomery, C. (2017). *Oraşul fericit Transformându-ne viețile prin design urban*. Bucharest, RO: Igloo Media Publishing House.

Oke, T. R. (1982). The energetic basis of the urban heat island. *Quarterly Journal of the Royal Meteorological Society* 108 (455), 1-24.

Oke, T. R., Mills, G., Christen, A. & Voogt, J. A. (2017). *Urban climates*. Cambridge, UK: Cambridge University Press.

Pisello, A. L., Castaldo, V. L., Fabiani, C., Piselli, C., Cotana, F. & Santamouris, M. (2017). How microclimate mitigation affects building thermal-energy performance in residential zero energy Italian settlements. In Pernigotto, G., Patuzzi, F., Prada, A., Corrado, V., & Gasparella, A. (Eds.). *Building simulation applications BSA 2017, 69-76. Bolzano, IT*: bu.press

Research Project: Reducerea Efectelor Insulei Termice Urbane Pentru Îmbunătățirea Confortului Urban Și Echilibrarea Consumului Energetic În București, UEFISCDI / UAUIM 2014-2017. Retrieved from https://www.uauim.ro/cercetare/redbhi/rezultate/

Santamouris, M. (2014) Cooling the cities – A review of reflective and green roof mitigation technologies to fight heat island and improve comfort in urban environments. *Solar Energy*, 103, 682-703

Santamouris, M. (2015a). Regulating the damaged thermostat of the cities – Status, impacts and mitigation challenges. *Energy and Buildings*, 91, 43-56.

Santamouris, M. (2015b) Analyzing the heat island magnitude and characteristics in one hundred Asian and Australian cities and regions. *Science of the total Environment*, 512-513, 582-598.

Sfică, L., Creţu, C. Ş., Ichim, P., Hriţac, R. & Breabăn, I. G. (2023). Surface urban heat island of Iași city (Romania) and its differences from in situ screen-level

air temperature measurements. *Sustainable Cities and Societ*y, volume 94, 104568.

Sim, D. (2022). *Soft city Densitate diversitate și proximitate pentru viața urbană*. Bucharest, RO: Igloo Media Publishing House.

Skandalos, N. & Karamanis, D., (2025). Net-zero energy communities at Local CLIMATE zones: Integrating photovoltaics and energy sharing for a social housing neighborhood. *Energy, Ecology and Environment,* 10, 352-369.

Stewart, I.D. & Oke, T.R. (2012). Local Climate zones for urban temperature studies. *Bulletin of the American Meteorological Society*, 93(12), 1879-1900

Taha, H. (1997). Urban climate and heat island: Albedo, evapotranspiration and anthropogenic heat. *Energy and Buildings*, 25 (2), 99-103.

Turhan, C., Atalay, A. S. & Akkurt, G. G. (2023). An integrated decision- making framework for mitigating the impact of urban heat islands on energy consumption and thermal confort of residential buildings. *Sustainability*, 15(12), 9674.

Urban Heat Island Explorer, Bucharest Map. Retrieved from https://urbanheat.app/bucuresti

Zamfirescu, I., Cheval, S. & Dumitrescu, A. (2025). *Bucureștiul sub caniculă - impactul crizei climatice asupra populației urbane, în special asupra grupurilor vulnerabile.* Bucharest, RO: Friedrich-Ebert-Stiftung Romania Publisher.

Scientific Papers. Series E. Land Reclamation, Earth Observation & Surveying, Environmental Engineering. Vol. XV, 2026
Print ISSN 2285-6064, CD-ROM ISSN 2285-6072, Online ISSN 2393-5138, ISSN-L 2285-6064

# INFLUENCE OF TESTING METHODS ON THERMAL PERFORMANCE CHARACTERIZATION OF SHEEP WOOL-BASED INSULATION

**Cristian PETCU[1], Andreea HEGYI[1], Horia PETRAN[1], Florin BĂLTĂREȚU[2]**

[1]National Institute for Research and Development in Construction, Urban Planning and Sustainable Spatial Development - URBAN-INCERC, 266 Pantelimon Road, District 2, Bucharest, Romania
[2]Technical University of Civil Engineering Bucharest (UTCB), 122-124 Lacul Tei Blvd, District 2, Bucharest, Romania

Corresponding author email: andreea.hegyi@gmail.com

***Abstract***

*Thermal insulation materials used in construction exhibit diverse structural morphologies that directly influence their thermal performance. Unconventional solutions based on recovered agro-industrial by-products, such as sheep wool mattresses, offer sustainable and eco-friendly alternatives. This paper comparatively analyzes the thermal insulation performance of sheep wool-based mattresses and evaluates the influence of testing methodology on measurement accuracy. Thermal conductivity was determined as a function of density using two complementary approaches: steady-state measurements with the λ-Meter EP500e (guarded hot plate method) and transient measurements with the ISOMET 2114 (dynamic method), both conducted at controlled, variable laboratory temperatures. The results reveal significant differences between steady-state and transient measurement techniques regarding method suitability and accuracy. Polynomial regression models accurately predict thermal behavior under non-compression conditions, enabling complete material characterization across the operational range relevant for building insulation applications. This comparative study provides practical guidance for selecting appropriate testing methods for fibrous insulation materials.*

***Key words****: ISOMET 2114, λ-Meter EP500e, non-woven sheep wool mattress, thermal conductivity coefficient, unconventional thermal insulation materials.*

## INTRODUCTION

In developed countries, people spend approximately 87% of their time indoors (Klepeis et al, 2001). Recent decades have witnessed a shift in urban architecture towards models focused on speed, efficiency, and comfort, often neglecting integration with existing contexts and local resources. Contributing to the achievement of the 17 Sustainable Development Goals requires reducing energy consumption, protecting air quality, and ensuring sustainable resource use (Petrișor et al., 2025). In Europe, the building sector is responsible for approximately 40% of final energy consumption and 36% of greenhouse gas emissions, while about 8% of the population faces energy poverty due to inadequate thermal comfort, highlighting the critical role of high-performance insulation materials (Frasca et al., 2023).

Alongside conventional materials such as polystyrene, mineral wool, and polyurethane foam, environmentally friendly recyclable alternatives are being developed, including those based on sheep wool. These materials offer high thermal insulation, low costs, and minimal environmental impact (Ye et al., 2006; Zach et al., 2012; Corscadden et al., 2014; Mansour et al., 2016). The thermal performance of insulation materials, including sheep wool mattresses, is evaluated through the thermal conductivity coefficient (λ), which quantifies heat transfer reduction capability.

Recent studies conducted according to EN 12667 with strict temperature and humidity control show λ values between 0.0333 and 0.0438 W/(m·K) for sheep wool insulation, influenced by density, applied treatments, and test method consistency (Vėjelis et al., 2024). Statistical analysis confirms that reproducibility and accuracy critically depend on experimental protocol adherence, correct experimental conditions, and method consistency.

A relevant aspect of experimental research concerns thermal conductivity coefficient

variation as a function of temperature range during determination. Other recent studies already demonstrated that humidity significantly degrades the thermal performance of insulation materials, with the thermal conductivity coefficient (λ) increasing by 1.9% for rock wool and up to 33-45% for hygroscopic materials such as wood-based boards and lightweight cellular concrete at 95% relative humidity (Kendzierawska & Trochonowicz, 2023; Petcu et al., 2024). This observation correlates with previous research by Sandberg (1992), who identified a linear equation for thermal conductivity variation as a function of water absorption in cellulose insulation materials. Other research (Talukdar et al., 2007) has indicated that thermal insulation performance quantified by thermal conductivity, measured at temperatures between 10°C and 30°C, varies according to a polynomial function relative to moisture content.

Specialized research (Mazrouei-Sebdani et al., 2022; Lou et al., 2023; Pontinha et al., 2023; Shrestha et al., 2023) indicates thermal conductivity variation in fibrous insulation materials as a U-shaped curve as a function of product density. This behavior is determined by competition between three distinct terms: the constant term representing air conductivity, the term proportional to density due to increased conductivity through solid contacts, and the opposing term having significant contribution at low densities through intense radiant transfer but becoming negligible at high densities due to radiation scattering on a higher number of fibers. The analytical approach to the relationship between thermal conductivity and density enables identification of optimal densities for different insulating material categories and formulation optimization according to specific application requirements (Lakatos, 2018).

Beyond conductivity analysis, recent literature integrates experimental methods and numerical simulations to evaluate sheep wool insulation performance under varying operating conditions. An example is the study on sheep wool-based bio-composites, where thermal tests are complemented by numerical analyses of energy requirements for buildings insulated with these materials, demonstrating significant reductions in heating energy requirements in simulated models (Saaidia et al., 2026). This combined approach - standardized experimental measurements and modeling - allows more complete thermal insulation performance characterization and highlights that rigorous test methodology selection is essential to obtain accurate and relevant data for practical applications, especially when comparing natural materials with conventional alternatives.

The objective of this research is to comparatively evaluate two complementary testing methods - the guarded hot plate (GHP) method using the λ-Meter EP500e and the transient method using the ISOMET 2114 - for characterizing the thermal conductivity of sheep wool insulation across a range of densities from natural (25.5 kg/m³) to compressed states (up to 80 kg/m³), and to validate polynomial regression models derived from steady-state measurements for predicting thermal behavior under operational conditions relevant to building applications.

## MATERIALS AND METHODS

### 1. Material Description

The investigated product consists of sheep wool mattress insulation manufactured from natural wool fibers. The material represents an unconventional solution based on recovered agro-industrial by-products, offering sustainable and eco-friendly characteristics. The natural fiber structure of sheep wool provides inherent thermal insulation properties through its cellular morphology, which creates numerous air-filled cavities that impede heat transfer. The wool samples were tested in both their natural, uncompressed state (density 25.5 kg/m³) and under progressive mechanical compression to achieve higher densities up to 80 kg/m³.

### 2. Guarded Hot Plate Method (λ-Meter EP500e)

The guarded hot plate method represents the reference standard for absolute thermal conductivity measurement of insulating materials, providing traceable measurements without requiring calibration samples (Baldinelli et al., 2019).

The method operates under steady-state conditions based on Fourier's one-dimensional thermal conduction equation. A specimen is placed between two isothermal plates maintained at different constant temperatures. Once steady-state thermal flux is established, thermal conductivity is calculated using the relationship (Baldinelli et al., 2019):

$$\lambda = \frac{q \cdot d}{A \cdot (T_h - T_c)}$$

where $q$ represents heat flux per unit time, $d$ is specimen thickness, $A$ is measurement area, and $T_h$ and $T_c$ are hot and cold plate temperatures, respectively.

The λ-Meter EP500e, manufactured by Lambda-Meßtechnik GmbH Dresden, represents a contemporary single-specimen guarded hot plate apparatus specifically designed for testing thermal insulation and construction materials (Lambda-Meßtechnik, 2023). The defining characteristic of the GHP apparatus is the guarded heating section, consisting of a central measurement zone surrounded by one or more concentric guard zones maintained at identical temperatures. This configuration ensures one-dimensional heat flux through the specimen by eliminating lateral heat losses from the measurement section. Guard temperature is precisely controlled to match the measurement section within millikelvin limits, typically achieved through sophisticated control algorithms monitoring guard thermocouples (Zarr, 2010).

The equipment conforms to standards ISO 8302, EN 1946-2, EN 12664, EN 12667, EN 12939, ASTM C177, and DIN 52612, with thermal conductivity measurement range 0 - 0.5 W/(m·K), thermal resistance range 0.1 - 14 m²K/W, measurement area 200 × 200 mm², specimen thickness 10 - 120 mm, reproducibility < 0.5% (typically < 0.2%), accuracy < 1.0% (typically < 0.7%), and temperature range 10 - 40°C (Lambda-Meßtechnik, 2023). The National Institute for Research and Development in Construction, Urban Planning and Sustainable Spatial Development URBAN-INCERC Romania acquired a λ-Meter EP500e as part of integrated thermal testing infrastructure, utilizing it for research on thermal insulation and certification activities according to European standards.

The GHP method provides absolute measurements without requiring reference materials, while heat flow meter (HFM) methods are secondary techniques requiring periodic calibration using certified reference materials (Baldinelli et al., 2019). A reference Round Robin test conducted by Baldinelli et al. (2019) in six European laboratories demonstrated that both methods produce consistent results for conventional and innovative insulating materials. Testing of aerogel, vacuum insulation panels, expanded polystyrene, and birch fiber boards revealed repeatability < 7% relative standard deviation for most materials and reproducibility ~10% for aerogel, EPS, and wood fiber boards (Baldinelli et al., 2019).

**3. Transient Method (ISOMET 2114)**

ISOMET 2114, manufactured by Applied Precision Ltd. (Bratislava, Slovakia), represents a portable instrument designed for direct measurement of heat transfer properties in a wide range of isotropic materials (Applied Precision, Ltd., 2019). This advanced thermal analyzer has become an useful tool in construction materials research, particularly for characterizing thermal insulation products. The device enables rapid and precise measurements of thermal conductivity (λ), thermal diffusivity (a), volumetric heat capacity (cρ), and temperature (T) using dynamic measurement methods that significantly reduce testing time compared to traditional steady-state approaches (Applied Precision, Ltd., 2019; Czajkowski et al., 2022).

ISOMET 2114 operates based on analysis of the temperature response of analyzed materials to heat flux pulses (Applied Precision, Ltd., 2019). The fundamental principle involves electrical heating of a resistor element introduced into a measurement probe that maintains direct thermal contact with the test specimen. Heat flux is generated through this electrical heating, and evaluation of thermal conductivity and volumetric heat capacity is based on periodically sampled temperature recordings as a function of time, provided that heat propagation occurs in an unbounded medium (Applied Precision, Ltd., 2019).

The ISOMET 2114 system utilizes two distinct probe types to adapt to diverse material

properties: needle probes (IPN 1100 series) for soft materials and surface probes (IPS 1100 series) for hard materials (Applied Precision, Ltd., 2019). The needle probe used in this research requires minimum 20-40 mm of material in all radial directions from the insertion axis to ensure a one-dimensional thermal field according to manufacturer specifications. Thermal conductivity measurement range is 0.015-0.70 W/(m·K) with accuracy ±5% of reading + 0.001 W/(m·K), thermal diffusivity range 0.15-10 mm²/s with accuracy ±15% of reading, and volumetric heat capacity range 0.05-3.0 MJ/(m³·K) with accuracy ±15% of reading (Applied Precision, Ltd., 2019).

Czajkowski et al. (2022) demonstrated ISOMET 2114 application in characterizing straw-based insulation panels, finding thermal conductivity values between 0.025 and 0.075 W/(m·K) depending on measurement method used. The study emphasized the importance of considering temperature influence when determining thermal properties of insulating materials made from agricultural industry by-products (Czajkowski et al., 2022). For mineral wool, Ablaoui et al. (2023) performed extensive thermal analysis of mineral wool with 80 kg/m³ density using ISOMET 2114, examining thermal behavior at elevated temperatures and finding thermal conductivity in the range 0.030-0.046 W/(m·K) at ambient temperature, with values varying according to temperature-specific relationships.

A critical consideration in using ISOMET 2114 involves understanding differences between transient and steady-state measurement techniques. Latif (2023) performed a comprehensive comparison between transient ISOMET 2114 measurements and steady-state Fox 600 guarded hot plate measurements for insulating materials made from agricultural industry by-products. The research revealed that transient methods using surface probes underestimate thermal conductivity values by approximately 14% compared to steady-state measurements, while needle probes tend to overestimate values by the same magnitude. Discrepancy arises from several interrelated factors: contact resistance at the probe-material interface affecting heat transfer and leading to underestimation in surface probe cases; local compression of porous materials following needle insertion modifying apparent density and consequently effective thermal conductivity; reduced measurement duration allowing capture of instantaneous properties without achieving complete thermal equilibrium specific to steady-state methods; and semi-infinite medium assumption which may not be valid for all tested specimen geometries. Latif (2023) concluded that measuring thermal conductivity of materials made from agricultural industry by-products using transient methods requires validation through comparison with steady-state measurements when establishing material properties for design purposes.

## 4. Testing Protocol

The experimental protocol consisted of thermal conductivity determination as a function of density using two complementary approaches. First, systematic steady-state measurements were conducted using the λ-Meter EP500e at three controlled temperature levels (10°C, 25°C, and 40°C) across a range of densities achieved through progressive mechanical compression. For each temperature, polynomial regression models of the form

$$\lambda(\rho) = a\rho^2 + b\rho + c$$

were developed, where $\lambda$ represents thermal conductivity and $\rho$ represents material density. These polynomial functions achieved coefficients of determination $R^2$ between 0.987 and 0.999, indicating excellent agreement between the mathematical model and experimental data.

Second, transient measurements were performed using ISOMET 2114 with the IPN 1100 needle probe at variable laboratory temperatures. For the natural density wool (25.5 kg/m³), measurements were conducted at seven distinct positions to evaluate spatial homogeneity and provide statistical validation. Each measurement position was tested multiple times (n = 21-50 measurements per position) to ensure statistical reliability. For compressed wool configurations (50, 60, 70, and 80 kg/m³), measurements were performed at multiple height levels within the test fixture when geometrically accessible according to the 20-40

mm minimum material requirement around the probe.

The experimental setup for ISOMET measurements utilized a custom-designed test fixture consisting of a rectangular prismatic frame with internal dimensions 108.5 × 111.5 × 600 mm, providing an internal cross-sectional area of approximately 12,097.75 mm² (1.21 × $10^{-2}$ m²). Measurement ports were positioned at five vertical levels (H1 at 100 mm, H2 at 200 mm, H3 at 300 mm, H4 at 400 mm, and H5 at 500 mm from the internal base), allowing systematic evaluation of vertical property and density profiles. Material compression was achieved using a Testometric M350-10AT universal press, enabling controlled density variation while maintaining material integrity.

Environmental conditions during testing were carefully controlled. The λ-Meter EP500e measurements were conducted under precisely controlled temperature conditions at the three specified set points (10°C, 25°C, and 40°C) with relative humidity maintained within standard laboratory conditions. ISOMET 2114 measurements were performed at variable laboratory temperatures typically ranging from 26.9 to 28.3°C, reflecting ambient conditions during the experimental campaign. All measurements were conducted after appropriate equilibration periods to ensure thermal stability of specimens.

The total measurement campaign encompassed 1,235 measurement points across 51 different densities, with 471 points specifically dedicated to wool product characterization across 16 density configurations, yielding an average of 29.4 measurements per density configuration. This extensive dataset provided robust statistical foundation for the comparative analysis of the two measurement methodologies and validation of polynomial regression models.

## RESULTS AND DISCUSSIONS

### 1. Thermal Conductivity and Thermal Resistance: Density and Temperature Effects (λ-Meter EP500e)

The λ-Meter EP500e measurements across the tested density and temperature ranges provide critical insights into the relationships between thermal conductivity, thermal resistance, and material configuration. Figures 1-4 present comprehensive visualization of these relationships, derived from steady-state measurements under controlled temperature conditions.

The experimental results reveal a critical aspect for practical building applications that extends beyond simple thermal conductivity values. Figures 1 and 2 demonstrate that thermal conductivity exhibits a complex behavior with density variation. At higher densities, thermal conductivity values show a tendency to decrease (improve) - for example, at 40°C, λ decreases from 47.21 mW/(m·K) at 30.1 kg/m³ to 36.57 mW/(m·K) at 64.4 kg/m³, representing a 22.5% improvement in material thermal performance.

This improvement results from increased fiber contact and reduced air gaps in the compressed material structure, consistent with the reduction of radiative heat transfer through increased fiber density documented by Shrestha et al. (2023) and Lou et al. (2023).

However, Figures 3 and 4 reveal the critical limitation of this approach: while thermal conductivity improves moderately through compression, thermal resistance ($R = d/\lambda$) decreases dramatically due to the substantial reduction in material thickness. At 25°C, the sample at natural density (22.3 kg/m³) exhibits $R = 1.876$ m²·K/W, while the compressed sample at 64.4 kg/m³ shows only $R = 0.858$ m²·K/W - a reduction of 54.3%.

This dramatic decrease in thermal resistance occurs because the reduction in thickness (approximately 65-70% compression ratio) far outweighs the improvement in thermal conductivity (approximately 20-25% improvement). The physical relationship $R = d/\lambda$ demonstrates that thermal resistance scales linearly with thickness but only inversely with conductivity, making thickness the dominant variable. The temperature variation shown in Figures 1 and 3 further emphasizes that thermal performance must be evaluated across the operational temperature range, as λ increases by approximately 25-50% from 10°C to 40°C depending on density configuration.

This finding has fundamental implications for building envelope design in Romanian and European climatic conditions. For typical building envelope applications, the most cost-

effective thermal insulation strategy involves using materials with acceptable thermal conductivity coefficients (λ = 0.04-0.05 W/(m·K) range) installed at substantial thicknesses, rather than pursuing marginal improvements in conductivity through compression at the expense of reduced installation thickness. Therefore, in practical applications, material thickness remains the dominant factor in achieving effective thermal insulation performance.

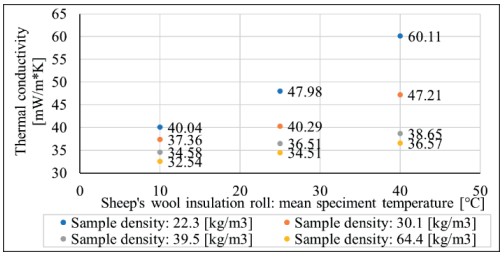



Figure 1. Thermal conductivity variation as a function of mean specimen temperature for sheep wool insulation at four density levels (22.3, 30.1, 39.5, and 64.4 kg/m³), measured using λ-Meter EP500e under steady-state conditions

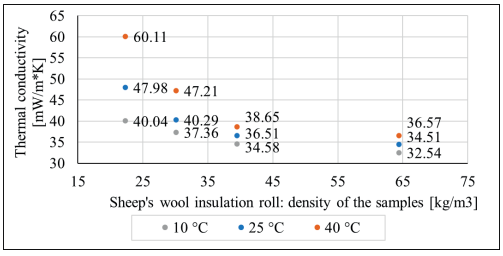



Figure 2. Thermal conductivity variation as a function of sample density for sheep wool insulation at three test temperatures (10, 25, and 40°C), measured using λ-Meter EP500e

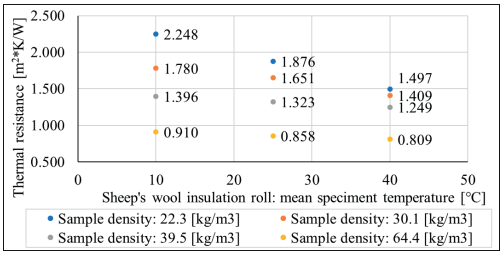



Figure 3. Thermal resistance variation as a function of mean specimen temperature for sheep wool insulation at four density levels, calculated from λ-Meter EP500e measurements (R = d/λ, where d is specimen thickness)

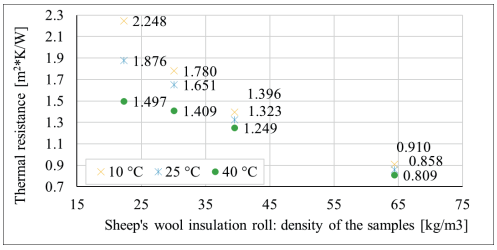



Figure 4. Thermal resistance variation as a function of sample density at three test temperatures, demonstrating the critical role of material thickness in achieving effective thermal performance

This finding aligns with European building physics principles and emphasizes that for sustainable insulation materials like sheep wool, installation at adequate thickness with proper vapor management represents a more effective strategy than pursuing material optimization through excessive compression.

## 2. Natural Density Wool Thermal Conductivity (25.5 kg/m³)

Measurements performed on sheep wool at natural density (25.5 kg/m³) using the ISOMET 2114 transient method revealed remarkably consistent thermal conductivity values across seven measurement positions. Table 1 presents the comprehensive results including thermal conductivity (λ), mean heater temperature (Tmean), coefficient of variation (CV), and number of measurements (n) for each position.

Table 1. Thermal conductivity measurements for natural density wool (25.5 kg/m³)

| Position | λ (W/m·K) | $T_{mean}$ (°C) | STDEV | CV (%) | n |
|---|---|---|---|---|---|
| 1 | 0.0456 | 28.10 | 0.000219 | 0.48 | 28 |
| 2 | 0.0460 | 27.00 | 0.000336 | 0.73 | 50 |
| 3 | 0.0453 | 27.09 | 0.000500 | 1.10 | 30 |
| 4 | 0.0447 | 27.04 | 0.000367 | 0.82 | 42 |
| 5 | 0.0455 | 27.28 | 0.000310 | 0.68 | 21 |
| 6 | 0.0465 | 27.60 | 0.000302 | 0.65 | 22 |
| 7 | 0.0454 | 27.57 | 0.000298 | 0.66 | 24 |

The results demonstrate excellent measurement consistency, with thermal conductivity values ranging from 0.0447 to 0.0465 W/(m·K) across all seven positions. Mean heater temperatures during measurements varied minimally between 27.00 and 28.10°C, reflecting ambient laboratory conditions. Coefficients of variation remained below 1.11% for all positions, with most positions achieving CV < 0.75%,

indicating high precision and low variability in the transient measurement method. The average thermal conductivity across all seven positions was 0.0456 W/(m·K), establishing a baseline reference value for natural density wool insulation.

## 3. Compressed Wool Thermal Conductivity (50-80 kg/m³)

Thermal conductivity measurements were extended to compressed wool configurations at densities of 50, 60, 70, and 80 kg/m³. Measurements were performed at multiple height levels within the test fixture where geometrically accessible according to probe requirements. Table 2 presents the comprehensive results for compressed wool configurations, achieving a balanced equilibrium across this operational density range.

Table 2. Thermal conductivity measurements for compressed wool densities

| Config. | ρ (kg/m³) | λ (W/m·K) | $T_{mean}$ (°C) | CV (%) | n |
|---|---|---|---|---|---|
| 50 kg/m³ - H1 | 50 | 0.0450 | 27.33 | 0.66 | 24 |
| 50 kg/m³ - H2 | 50 | 0.0466 | 27.19 | 0.13 | 30 |
| 50 kg/m³ - H3 | 50 | 0.0446 | 26.96 | 0.50 | 38 |
| 60 kg/m³ - H1 | 60 | 0.0446 | 28.12 | 0.37 | 30 |
| 60 kg/m³ - H2 | 60 | 0.0458 | 28.23 | 0.67 | 28 |
| 70 kg/m³ - H1 | 70 | 0.0455 | 28.40 | 0.42 | 19 |
| 70 kg/m³ - H2 | 70 | 0.0460 | 28.05 | 0.57 | 24 |
| 80 kg/m³ - H1 | 80 | 0.0460 | 28.14 | 0.59 | 24 |
| 80 kg/m³ - H2 | 80 | 0.0458 | 28.14 | 0.58 | 37 |

The compressed wool measurements using ISOMET 2114 revealed a remarkable finding: thermal conductivity remained relatively stable across the density range from 50 to 80 kg/m³ when measured with the transient method. The λ values ranged from 0.0446 to 0.0466 W/(m·K), representing a variation of only approximately 4.5% across this density interval. This apparent stability in the ISOMET measurements contrasts with the more pronounced density-dependent behavior observed in the λ-Meter EP500e steady-state measurements presented in Section 3.1, which revealed the characteristic U-shaped relationship between thermal conductivity and density across a broader range from 22.3 to 64.4 kg/m³. The difference between methodologies may be attributed to the limited density range tested with ISOMET (50-80 kg/m³), which appears to capture only the relatively flat portion near the minimum of the U-shaped curve, whereas the λ-Meter measurements encompassed both ascending and descending portions of this relationship. This density-independent thermal conductivity behavior suggests that the cellular structure of wool fibers maintains excellent insulating performance even under significant compression, with the competing mechanisms of solid phase conduction (increasing with density) and radiative transfer (decreasing with density).

## 4. Method Comparison and Polynomial Model Validation

The steady-state measurements presented in Section 3.1 obtained with the λ-Meter EP500e at controlled temperatures (10°C, 25°C, and 40°C) across the density range enabled development of second-order polynomial regression models of the form $\lambda(\rho) = a\rho^2 + b\rho + c$. These polynomial functions achieved excellent coefficients of determination ($R^2 > 0.987$), validating the characteristic U-shaped relationship between thermal conductivity and density for fibrous insulation materials, as documented in specialized literature (Lakatos, 2018; Lou et al., 2023; Shrestha et al., 2023).

Using the polynomial models, predicted thermal conductivity values for natural density wool (25.5 kg/m³) were calculated: λ = 38.84 mW/(m·K) at 10°C, λ = 44.74 mW/(m·K) at 25°C, and λ = 54.51 mW/(m·K) at 40°C. These predictions, derived from compression testing data extrapolated to natural density conditions, provide a critical validation opportunity when compared with the direct ISOMET 2114 transient measurements at natural density.

Figure 5 illustrates the validation of ISOMET 2114 transient measurements against the polynomial trendline derived from λ-Meter EP500e steady-state testing for natural density wool (25.5 kg/m³). The horizontal dashed line represents the thermal conductivity value predicted by the second-order polynomial

function at 25°C (λ = 44.74 mW/(m·K)), corresponding to the median temperature of the ISOMET measurement range. The scattered data points represent individual ISOMET measurements across four spatial positions within the specimen, plotted as a function of mean heater temperature during each measurement cycle. The tight clustering of all measurement points around the polynomial prediction line, despite temperature variations between 26.9°C and 28.5°C induced by ambient laboratory conditions and equipment operation, demonstrates excellent agreement between the two methodologies. This cross-validation confirms that polynomial functions derived from systematic compression testing at controlled temperatures can reliably predict thermal conductivity values at natural density conditions, with observed scatter attributable primarily to the inherent heterogeneity of natural fibers rather than systematic measurement bias.

Validation of ISOMET 2114 measurements on natural density wool specimens (25.5 kg/m³) demonstrated remarkable concordance with polynomial functions derived from λ-Meter tests. The experimental measurements with the needle probe across seven positions generated a distribution of points with minimal local variations relative to mean specimen temperature, concentrated in the range 26.9-28.3°C and indicating practically constant thermal conductivity of approximately 0.0446-0.0465 W/(m·K). This range corresponds excellently to the values calculated through polynomial functions for the respective density, falling within the expected interval between the 25°C prediction (44.74 mW/(m·K)) and approaching the lower temperature regime predictions.

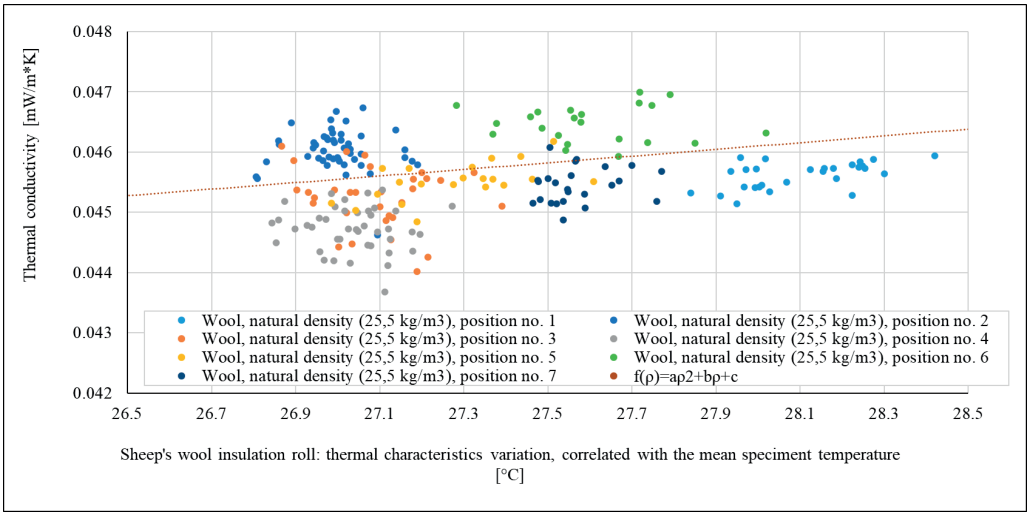



Figure 5. Cross-validation of ISOMET 2114 measurements (colored points) against polynomial prediction from λ-Meter testing (dashed line) for natural density wool (25.8 kg/m³). Measurements were performed at four spatial positions across a temperature range of 26.9-28.5°C

The limited dispersion of experimental points around calculated values, demonstrated through coefficients of variation below 1.11% within the same specimen, validates that second-order polynomial equations obtained through progressive compression in the λ-Meter EP500e can be confidently used for predicting thermal behavior of the material at natural density. Observed differences between measurement positions can be attributed to intrinsic heterogeneity of natural fibers and local temperature variations induced by ISOMET equipment utilization, aspects confirmed through coefficients of variation inferior to 2% within the same specimen. This cross-validation methodology demonstrates that polynomial functions correctly extrapolate thermal behavior even for non-compression conditions, ensuring complete material characterization across the entire operational

domain relevant for thermal insulation applications in construction.

**5. Discussions**

The most significant finding of this research is the remarkable density-independence of thermal conductivity for sheep wool insulation across the tested range of 25.5 to 80 kg/m³. This behavior, while seemingly counterintuitive, can be explained through the fundamental mechanisms of heat transfer in fibrous porous materials. The total thermal conductivity in such materials results from the sum of three components: gas phase conduction (constant for a given pore size distribution), solid phase conduction (increasing linearly with density), and radiative transfer (inversely proportional to density) (Lakatos, 2018; Shrestha et al., 2023).

For sheep wool in the investigated density range, these competing mechanisms appear to achieve a balanced equilibrium. As density increases through compression, the solid phase conductivity increases due to greater fiber-to-fiber contact area and more continuous pathways for phonon transport. Simultaneously, the increasing number of fibers per unit volume provides more scattering centers for thermal radiation, effectively reducing the radiative contribution to heat transfer. The observation that these two effects approximately cancel each other across the 25.5-80 kg/m³ range suggests that this density interval represents a thermal conductivity plateau region for wool insulation.

This finding has significant practical implications for building applications in Romanian climate conditions. It indicates that sheep wool insulation can be compressed for transport and installation convenience without suffering thermal performance degradation, provided the density remains within the 25.5-80 kg/m³ range. This flexibility contrasts with some conventional insulation materials that exhibit more pronounced density-dependent performance variations.

Comparison with literature values confirms the competitive performance of the tested sheep wool material. Vėjelis et al. (2024) reported λ values between 0.0333 and 0.0438 W/(m·K) for sheep wool insulation tested according to EN 12667, while Zach et al. (2012) documented values around 0.0380 W/(m·K) for similar materials. The present study's measurements (0.0446-0.0466 W/(m·K)) fall within the upper range of published values, which may be attributed to differences in wool fiber treatment, manufacturing processes, or measurement conditions. Nevertheless, the obtained values demonstrate adequate thermal insulation performance for building envelope applications.

The influence of moisture and temperature on thermal conductivity represents a critical consideration for hygroscopic materials like sheep wool. Vėjelis et al. (2024) demonstrated that a 1% increase in hygroscopic moisture content causes a 1.25-2% increase in thermal conductivity. The linear relationship identified by Sandberg (1992) and the polynomial dependencies documented by Talukdar et al. (2007) underscore the importance of moisture control in practical applications. While the present study focused on measurements under controlled laboratory conditions, future research should systematically investigate moisture effects on the tested wool material to provide complete characterization for design purposes.

The U-shaped curve theory for density-dependent thermal conductivity, extensively documented for fibrous insulation materials (Mazrouei-Sebdani et al., 2022; Lou et al., 2023; Pontinha et al., 2023), provides a theoretical framework for understanding the observed behavior. The present study's density range appears to encompass the relatively flat region near the minimum of this U-shaped curve, where thermal conductivity remains relatively constant. Extended testing beyond 80 kg/m³ would likely reveal increasing thermal conductivity as solid phase conduction begins to dominate over the decreasing radiative contribution.

Regarding methodology, the successful validation of polynomial regression models derived from λ-Meter EP500e measurements through comparison with ISOMET 2114 transient measurements represents an important methodological advancement. This dual-method approach combines the absolute measurement accuracy and temperature control capabilities of the guarded hot plate method with the rapid, portable convenience of

transient techniques. The excellent agreement between methods (within measurement uncertainty) demonstrates that polynomial extrapolation from compression data reliably predicts thermal behavior under natural density conditions.

The observed systematic differences between measurement methods merit consideration. As documented by Latif (2023), transient methods using needle probes can introduce local compression effects that modify apparent density and consequently measured thermal conductivity. The present study's careful attention to probe insertion technique and multiple measurement positions helped minimize these artifacts. The low coefficients of variation (< 1.11% for natural density measurements) confirm measurement reliability and proper experimental technique.

The methodological trade-offs between the two testing approaches are important for practical applications. The guarded hot plate method offers superior accuracy (< 1% typically < 0.7%), precise temperature control, and absolute measurements without calibration requirements, making it ideal for material certification and reference measurements (Baldinelli et al., 2019). However, it requires specific specimen geometries, longer test durations, and expensive specialized equipment. In contrast, the ISOMET 2114 transient method provides rapid measurements (minutes vs. hours), portable operation, simultaneous multi-property determination, and flexibility for irregular geometries, making it excellent for quality control, field testing, and comparative studies (Applied Precision, Ltd., 2019; Czajkowski et al., 2022).

For Romanian building applications, the present results suggest that sheep wool insulation represents a viable sustainable alternative to conventional materials, particularly for low-rise residential construction and renovation projects where natural, breathable insulation materials offer additional benefits beyond purely thermal performance. The material's hygroscopic behavior, while requiring careful moisture management, can contribute to indoor climate regulation when properly integrated into building envelope systems. Future research should address long-term performance under realistic Romanian climate conditions, including freeze-thaw cycling and seasonal moisture variations.

## CONCLUSIONS

This comparative study of testing methodologies for sheep wool-based thermal insulation has yielded several significant conclusions:

1. The thermal conductivity of sheep wool insulation exhibits density-dependent behavior consistent with the characteristic U-shaped relationship documented for fibrous materials, with λ-Meter EP500e measurements revealing values ranging from approximately 32.54 mW/(m·K) to 60.11 mW/(m·K) across the density range 22.3-64.4 kg/m³ and temperature range 10-40°C. At higher densities, thermal conductivity shows moderate improvement (20-25% reduction) due to increased fiber contact and reduced radiative transfer. However, the critical finding for practical applications is that thermal resistance ($R = d/\lambda$) decreases dramatically with material compression - by 54.3% in the tested range - because thickness reduction (65-70%) far outweighs conductivity improvement. This demonstrates that for building envelope applications, adequate installation thickness (≥100-150 mm for European climatic conditions) with acceptable thermal conductivity (λ = 0.044-0.047 W/(m·K)) provides superior thermal performance compared to compressed materials with improved conductivity but reduced thickness. The apparent stability observed in ISOMET 2114 transient measurements (λ = 0.0446-0.0466 W/(m·K) across 50-80 kg/m³) reflects the limited density range tested with this method, capturing only the relatively flat portion near the minimum of the U-shaped curve.

2. The guarded hot plate method using λ-Meter EP500e successfully enabled development of second-order polynomial regression models ($R^2$ > 0.987) that accurately predict thermal conductivity as a function of density across the operational range. These polynomial functions, derived from systematic compression testing at controlled temperatures (10°C, 25°C, 40°C), provide a robust mathematical framework for material characterization.

3. The transient method using ISOMET 2114 demonstrated excellent precision for natural density wool measurements, with coefficients of variation below 1.11% across seven measurement positions. The method's rapid measurement capability and portability make it highly suitable for quality control and comparative testing applications, despite inherent limitations compared to absolute steady-state methods.
4. Cross-validation between methodologies confirmed that polynomial extrapolation from λ-Meter compression data reliably predicts thermal behavior under natural density conditions. The excellent agreement between steady-state polynomial predictions and transient ISOMET measurements (within combined measurement uncertainties) validates the dual-method approach for comprehensive material characterization.
5. For practical applications, material selection recommendations depend on specific testing requirements. The λ-Meter EP500e guarded hot plate method is recommended for certification testing, reference measurements, and absolute thermal conductivity determination where highest accuracy is required. The ISOMET 2114 transient method is recommended for rapid quality control, field measurements, comparative testing between formulations, and situations requiring portable equipment or irregular specimen geometries.
Future research directions should include systematic investigation of moisture effects on thermal conductivity across the density range, long-term performance evaluation under realistic Romanian climate conditions including freeze-thaw cycling, optimization of wool fiber treatments to achieve lower thermal conductivity values approaching the 0.035-0.040 W/(m·K) range, and integration studies of wool insulation into complete building envelope systems to evaluate hygrothermal performance in actual construction applications.

## ACKNOWLEDGEMENTS

This research was funded by the Romanian Government Ministry of Research Innovation and Digitization, project No. PN 23 35 02 01 "Synergies of innovation and digitalization in the design of eco materials and multifunctional products for sustainable constructions, with an impact on the environment and the circular economy".

## REFERENCES

Ablaoui, E. M., Malendowski, M., Szymkuc, W., & Pozorski, Z. (2023). Determination of thermal properties of mineral wool required for the safety analysis of sandwich panels subjected to fire loads. *Materials*, 16(17), Article 5852.

Applied Precision, Ltd. (2019). *ISOMET 2114 User's Guide*: Thermal Properties Analyzer (Version 1.57). Applied Precision, Ltd.

Baldinelli, G., Bianchi, F., Gendelis, S., Jakovics, A., Morini, G. L., Falcioni, S., Fantucci, S., Serra, V., Navacerrada, M., Díaz, C., Libbra, A., Muscio, A., & Asdrubali, F. (2019). Thermal conductivity measurement of insulating innovative building materials by hot plate and heat flow meter devices: A Round Robin Test. *International Journal of Thermal Sciences*, 139, 25-35. https://doi.org/10.1016/j.ijthermalsci.2019.01.037.

Corscadden, K., Biggs, J., & Stiles, D. (2014). Sheep's wool insulation: A sustainable alternative use for a renewable resource?. *Resources, Conservation and Recycling*, 86, 9-15. https://doi.org/10.1016/j.resconrec.2014.01.004.

Czajkowski, Ł., Kocewicz, R., Weres, J., & Olek, W. (2022). Estimation of Thermal Properties of Straw-Based Insulating Panels. *Materials*, 15(3), 1073. https://doi.org/10.3390/ma15031073.

Frasca, F., Bartolucci, B., Parracha, J.L., Ogut, O., Mendes, M.P., Siani, A.M., Tzortzi, J.N., Bertolin, C., & Flores-Colen, I. (2023). A quantitative comparison on the use of thermal insulation materials in three European countries through the TEnSE approach: Challenges and opportunities. *Building and Environment*, 245, 110973. https://doi.org/10.1016/j.buildenv.2023.110973

Kendzierawska, W., & Trochonowicz, M. (2023). Effect of temperature and humidity on the thermal conductivity λ of insulation materials. *Civil and Environmental Engineering Reports*, 33(4), 42–49. https://doi.org/10.59440/ceer/178976

Klepeis, N. E., Nelson, W. C., Ott, W. R., Robinson, J. P., Tsang, A. M., Switzer, P., Behar, J. V., Hern, S. C., & Engelmann, W. H. (2001). The National Human Activity Pattern Survey (NHAPS): a resource for assessing exposure to environmental pollutants. *Journal of Exposure Science & Environmental Epidemiology*, 11(3), 231-252. https://doi.org/10.1038/sj.jea.7500165

Lakatos, Á. (2018). Thermal conductivity of insulations approached from a new aspect. *Journal of Thermal Analysis and Calorimetry*, 133(1), 329-335. https://doi.org/10.1007/s10973-017-6686-5.

Lambda-Meßtechnik GmbH Dresden. (2023). *λ-Meter EP500e: Guarded hot plate apparatus for thermal conductivity measurement* [Technical documentation].

Latif, E. (2023). Transient versus steady-state thermal conductivity measurements: A case study of thermal characterisation of a novel biobased insulation material [Conference paper]. *5th International Conference on Bio-Based Building Materials* (ICBBM-2023), Vienna, Austria. https://orca.cardiff.ac.uk/id/eprint/160678.

Lou, F., Dong, S., Zhu, K., Chen, X., & Ma, Y. (2023). Thermal Insulation Performance of Aerogel Nano-Porous Materials: Characterization and Test Methods. *Gels*, 9(3), 220. https://doi.org/10.3390/gels9030220.

Mansour, E., Curling, S., Stéphan, A., & Ormondroyd, G. (2016). Absorption of volatile organic compounds by different wool types. *Green Materials*, 4(1), 1-7. https://doi.org/10.1680/jgrma.15.00031.

Mazrouei-Sebdani, Z., Naeimirad, M., Peterek, S., Begum, H., Galmarini, S., Pursche, F., Baskin, E., Zhao, S., Gries, T., & Malfait, W. J. (2022). Multiple assembly strategies for silica aerogel-fiber combinations – A review. *Materials & Design*, 223, 111228. https://doi.org/10.1016/j.matdes.2022.111228.

Petcu, C., Dragomir, C. S., & Hegyi, A. (2024). Building Sustainability: Integrating Agricultural and Industrial sub-Products in the Building Sector. *Scientific Papers. Series E. Land Reclamation, Earth Observation & Surveying, Environmental Engineering*, XIII, 189-200.

Petrişor, A.-I., Braguţa, E., Ţugulea, A., Tache, A. V., Harea, O., Mogîldea, V., Popescu, O.-C., Andronovici, D., Bejan, I. (2025). Using Geospatial Information Tools to Plan Green Infrastructures in Response to Climate Changes: Examples from Bucharest, Romania and Chisinau, Moldova. *Urban Science*, 9(3), 62. https://doi.org/10.3390/urbansci9030062

Pontinha, A. D. R., Mäntyneva, J., Santos, P., & Durães, L. (2023). Thermomechanical Performance Assessment of Sustainable Buildings' Insulating Materials under Accelerated Ageing Conditions. *Gels*, 9(3), 241. https://doi.org/10.3390/gels9030241.

Saaidia, R., Othmane, A. B., Ayed, L., Boumediene, N., & Bouabidi, A. (2026). Thermal, Acoustic, and mechanical characterization of sheep Wool-Based Bio-Composites for sustainable construction. *Energy and Buildings*, 350, 116602. https://doi.org/10.1016/j.enbuild.2025.116602.

Sandberg, P.I. (1992). Determination of the effects of moisture content on the thermal transmissivity of cellulose fiber loose-fill insulation. In: *Thermal Performance of the Exterior Envelopes of Building III*, ASHRAE/DOE/BTECC/CIBSE Conference, 517-525.

Shrestha, S. S., Tiwari, J., Rai, A., Hun, D. E., Howard, D., Desjarlais, A. O., Francoeur, M., & Feng, T. (2023). Solid and gas thermal conductivity models improvement and validation in various porous insulation materials. *International Journal of Thermal Sciences*, 187, 517-526, 108164.

Talukdar, P., Osanyintola, O. F., Olutimayin, S. O., & Simonson, C. J. (2007). An experimental data set for benchmarking 1-D, transient heat and moisture transfer models of hygroscopic building materials. Part II: Experimental, numerical and analytical data. *International Journal of Heat and Mass Transfer*, 50(25-26), 4915-4926. https://doi.org/10.1016/j.ijheatmasstransfer.2007.03.025.

Vėjelis, S., Vaitkus, S., Skulskis, V., Kremensas, A., & Kairytė, A. (2024). Performance Evaluation of Thermal Insulation Materials from Sheep's Wool and Hemp Fibres. *Materials*, 17(13), 3339. https://doi.org/10.3390/ma17133339.

Ye, Z., Wells, C. M., Carrington, C. G., & Hewitt, N. J. (2006). Thermal conductivity of wool and wool-hemp insulation. *International Journal of Energy Research*, 30(1), 37-49. https://doi.org/10.1002/er.1123.

Zach, J., Korjenic, A., Petránek, V., Hroudová, J., & Bednar, T. (2012). Performance evaluation and research of alternative thermal insulations based on sheep wool. *Energy and Buildings*, 49, 246-253. https://doi.org/10.1016/j.enbuild.2012.02.014.

Zarr, R. R. (2010). Assessment of uncertainties for the NIST 1016 mm guarded-hot-plate apparatus: Extended analysis for low-density fibrous-glass thermal insulation. *Journal of Research of the National Institute of Standards and Technology*, 115(1), 23-59. https://doi.org/10.6028/jres.115.004.

Scientific Papers. Series E. Land Reclamation, Earth Observation & Surveying, Environmental Engineering. Vol. XV, 2026
Print ISSN 2285-6064, CD-ROM ISSN 2285-6072, Online ISSN 2393-5138, ISSN-L 2285-6064

# AQUIFER THERMAL ENERGY STORAGE SYSTEMS FOR NEARLY ZERO ENERGY BUILDINGS: A CASE STUDY ASSESSMENT FOR ROMANIAN CLIMATE CONDITIONS

**Cristian PETCU[1], Horia PETRAN[1], Andreea HEGYI[1], Florin BĂLTĂREȚU[2], Ciprian ENE[1]**

[1]National Institute for Research and Development in Construction, Urban Planning and Sustainable Spatial Development URBAN-INCERC, 266 Pantelimon Road, District 2, Bucharest, Romania
[2]Technical University of Civil Engineering Bucharest (UTCB), 122-124 Lacul Tei Blvd, District 2, Bucharest, Romania

Corresponding author email: hpetran@gmail.com

***Abstract***

*The European Union's Energy Performance of Buildings Directive (EPBD), as amended by Directive (EU) 2024/1275, mandates the transition from nearly Zero Energy Buildings (nZEB), with very high energy performance and substantial renewable energy coverage, to Zero Emission Buildings, with an annual zero emissions balance. Aquifer Thermal Energy Storage (ATES) offers an environmental-friendly and cost-effective technology for supporting nZEB through seasonal thermal energy storage in groundwater aquifers. This paper assesses ATES feasibility for an office building in Bucharest, Romania (climatic zone 2), using dynamic simulations for both existing and nZEB-renovated configurations. The analysis reveals significant deployment barriers including shallow unconfined aquifers (7-10 m), regulatory constraints on groundwater reinjection, and pronounced heating-cooling demand imbalances characteristic of Romania's continental climate. The proposed system integrates ATES with solar thermal technology to mitigate demand asymmetry and enhance efficiency. Results indicate that successful ATES implementation in Romania requires updated legislation, site-specific hydrogeological assessment, and hybrid renewable configurations enabling balanced seasonal thermal storage.*

***Key words****: aquifer thermal energy storage (ATES), building energy efficiency, ground source heat pump, nearly zero energy buildings (nZEB), seasonal thermal storage.*

## INTRODUCTION

The European building sector accounts for approximately 40% of total energy consumption and 36% of greenhouse gas emissions, making it a primary target for decarbonization efforts (Fleuchaus et al., 2018). The Energy Performance of Buildings Directive (EPBD), recently amended by Directive (EU) 2024/1275, establishes stringent requirements for nearly Zero Energy Buildings (nZEB), mandating that all new buildings comply with zero-emission standard by 2030, with public buildings required by 2028. The directive defines nZEB as buildings with very high energy performance where the nearly zero or very low amount of energy required should be covered to a very significant extent by renewable energy sources produced on-site or nearby. Because the directive sets no numeric thresholds for this definition, nZEB requirements and limit values are interpreted differently across Member States (Magrini et al., 2020).

Aquifer Thermal Energy Storage (ATES) represents a mature technology capable of meeting nZEB renewable energy requirements through seasonal thermal storage in groundwater aquifers. International experience demonstrates that ATES systems achieve thermal recovery efficiencies of 68-87% and reduce building energy consumption by 40-70% while cutting $CO_2$ emissions by up to 74% compared to conventional systems (Fleuchaus et al., 2018; Stemmle et al., 2021). Of the more than 2,800 systems operating worldwide, 85% are located in the Netherlands, with a further 10% in Sweden, Denmark, and Belgium, demonstrating technical maturity and economic viability with payback periods of 2-10 years (Fleuchaus et al., 2018).

Despite proven international success, ATES deployment in Central and Eastern Europe remains limited due to multiple barriers including regulatory constraints, limited hydrogeological data, and heating-cooling demand imbalances characteristic of continental

climates. Despite favourable geological conditions in western regions and substantial geothermal resources documented by Rosca and Antics (2004), Romania has not succeeded yet to fully exploit its ATES potential. The primary obstacles include obsolete groundwater legislation prohibiting thermal reinjection, insufficient aquifer characterization data, and limited institutional capacity in ATES-specific well construction requiring targeted technology transfer.

The continental climate of Romania presents unique challenges for ATES implementation. In Bucharest (climatic zone 2), annual heating demand typically exceeds cooling demand by a large margin (Tache et al. 2024; Petrişor et al., 2025), creating thermal imbalance that reduces ATES efficiency. This asymmetry contrasts with office buildings in temperate maritime climates where heating-cooling loads are more balanced. Recent work demonstrates that integrating high-temperature solar thermal collectors with underground seasonal heat storage can mitigate this thermal imbalance by injecting surplus summer heat into the subsurface, thus partially compensating for the heating-dominant load profile characteristic of continental climates (Bu et al., 2022).

Moreover, long-term numerical simulations indicate that persistent thermal imbalance leads to gradual aquifer temperature drift, reduced recovery efficiency, and potential regulatory constraints related to groundwater protection (Bloemendal & Hartog, 2018; Fleuchaus et al., 2018). In the Romanian context, where seasonal temperature amplitudes are high and heating seasons extend over 5–6 months, maintaining thermal equilibrium is particularly critical for system sustainability. Without corrective measures, thermal recovery efficiency can remain well below the 68-87% reported for well-operated installations: long-term monitoring of a doublet ATES system yielded average recovery efficiencies of only 47% and 60% for the warm and cold stores over the first three storage cycles, with annual energy and hydraulic imbalances producing thermal breakthrough between the warm and cold sides of the aquifer (Abuasbeh et al., 2021).

Hybridization strategies - including integration with solar thermal collectors, photovoltaic-driven heat pumps, or auxiliary low-carbon heat sources - have been shown to restore annual energy balance and stabilize subsurface temperatures (Fleuchaus et al., 2018). The practical relevance of such measures is reflected in regulatory practice: monitored Dutch ATES systems show annual energy imbalances between −22% and +15%, and provincial legislation requires energy balance to be met over a 3-5 year period (Bloemendal & Hartog, 2018). In particular, solar-assisted ATES systems can inject surplus summer heat into the warm well, compensating for the higher winter extraction demand typical of continental climates. Parametric studies suggest that achieving a seasonal storage balance within ±10% significantly improves long-term efficiency and mitigates environmental risks (Bloemendal & Hartog, 2018).

For Romania, the high solar irradiation levels during summer (1,400–1,600 kWh/m²·year) create favorable conditions for such hybrid configurations, especially in urban areas like Bucharest where large roof surfaces are available on commercial and institutional buildings (Năstase et al., 2018; Prăvălie et al., 2022). Therefore, adapting ATES design to continental climatic conditions through hybridization and optimized operational control is essential to ensure technical feasibility, environmental compliance, and long-term performance stability.

This paper investigates ATES application feasibility for an office building in Bucharest, Romania, through hydrogeological assessment, dynamic building energy simulations, and system design analysis. The study evaluates both existing building performance and nZEB level renovation, identifying technical barriers specific to Romanian conditions and proposing solutions including hybrid renewable system integration. The research contributes to understanding ATES deployment potential in heating-dominated continental climates and provides guidance for Romanian policy development.

## MATERIALS AND METHODS

### Case Study Building and Location

The pilot building is an office facility located in climatic zone 2, Bucharest, Romania, constructed in the 1970s with ground floor plus

two levels. The building has a gross floor area of 864 m², with occupied office spaces totalling 366.80 m² (conditioned volume 1,281 m³). The building is currently connected to the district heating system for space heating.

**Hydrogeological Investigation**

Three exploratory wells (45 m depth) were drilled at the pilot site to characterize lithology and aquifer properties through soil sampling and granulometry analysis (Figure 1).

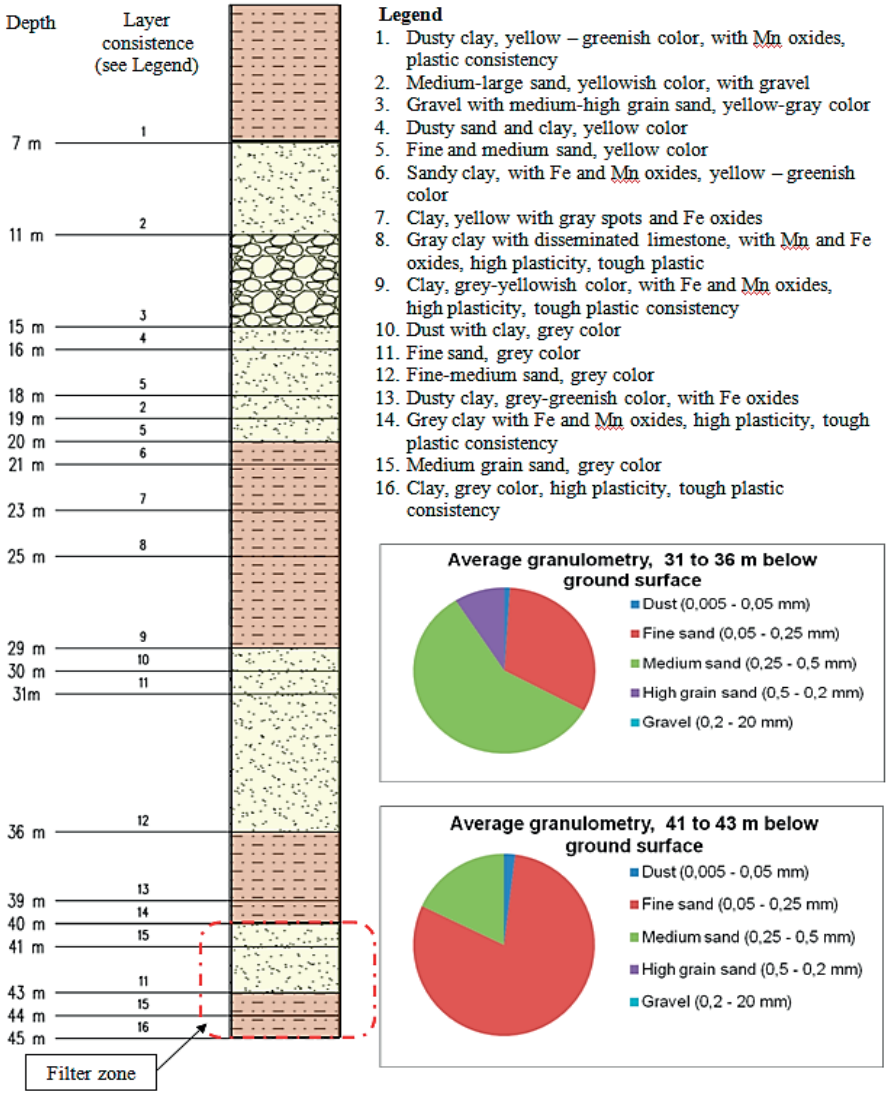



Figure 1. Site lithology, based on the 3 drills executed at the site. Lower right: breakdown for the composition of two different layers of the same aquifer

Site preparation and surface stabilization measures were implemented following erosion control protocols established for infrastructure applications (Olinic et al., 2024) to prevent surface runoff contamination during drilling operations. The investigation documented a confined secondary aquifer system at 30-45 m depth, comprising two distinct layers of 7 m and 3 m thickness respectively, yielding a combined aquifer thickness of 10 m - relatively shallow

compared to typical ATES implementations where 15-40 m are common.

Soil samples were collected during drilling and subjected to granulometric analysis in the laboratory to determine particle size distribution. The analysis revealed a significant presence of fine sand particles alongside coarser fractions, indicating moderate permeability conditions. The confined aquifer exhibits pressurized conditions with static water level rising to 11 m below ground surface, which is characteristic of artesian aquifers.

Groundwater temperature measurements were conducted in static well conditions using a calibrated PT100 resistance temperature detector at 5-meter depth intervals. Recorded temperatures were 13.18°C at 41 m depth and 12.98°C at 46 m depth.

A pumping test was performed with extraction from one well and reinjection distributed between two wells to evaluate aquifer hydraulic response. Due to project constraints including limited expertise availability and time restrictions, well screen placement was not optimally positioned. The filter zone was installed at 37-45 m depth, whereas optimal placement based on the granulometric data would have been at 29-36 m depth where higher permeability was indicated by coarser particle size distribution. The site lithology and aquifer configuration are illustrated in Figure 1.

**Building Energy Simulation Methodology**

Dynamic building energy simulations were performed using the RTU (from Romanian "Răspunsul Termic Unitar") method with one-hour time steps (Constantinescu, 2008; Petcu, 2009). The RTU method characterizes building elements thermal dynamics through the unit impulse response δ(t), enabling the determination of both intensive parameters (indoor temperatures) and extensive parameters (heat flow rates) under arbitrary climatic excitation via convolution with this unit thermal response (Skruch & Długosz, 2019; Constantinescu, 2020). The software tool implementing this method was developed and validated in earlier work (Petcu, 2009), and applied here to both existing and nZEB-renovated building configurations.

Critically for this study, the software operates with a finite heat source model: when available heating or cooling capacity is insufficient to maintain the setpoint temperature (20°C for heating and 25°C for cooling), it calculates the resulting indoor temperature deviation rather than assuming unlimited supply. This capability is essential for ATES feasibility assessment, where system thermal capacity is inherently constrained by aquifer properties and well design.

Hourly standard climate data (test reference year for Bucharest, Mc 001/6-2013) including outdoor air temperature and solar radiation on all building orientations were used as input. Software validation is documented through empirical validation using measured data from the Experimental Building INCERC Bucharest during cold and warm seasons 2008-2010 (Petcu et al., 2010), and numerical validation applying EN 15255:2008, EN 15265:2008, and ISO 13792:2012 for cooling load calculation, dynamic energy needs calculation, and summer internal temperature calculation respectively.

The building was simulated in two configurations: the existing building configuration with current envelope thermal properties, and the building renovated to nZEB standards. The existing building is characterized by limited thermal envelope performance typical of pre-renovation construction. The external walls present a thermal transmittance of 1.3 W/m²K, while the fenestration offers minimal insulation with a window U-value value of 3.2 W/m²K. The floor slab contributes to the thermal performance of the building envelope with a U-value of 2.5 W/m²K and the roof provides 0.77 W/m²K of thermal transmittance. Air leakage assessment indicates moderate infiltration with an airtightness level of $n_{50}$ = 1.5 $h^{-1}$, reflecting gaps and thermal bridges typical of existing building stock. The building is currently serviced by connection to a district heating system for thermal conditioning.

In the nZEB renovation hypothesis, the thermal envelope performance is substantially enhanced across all structural components. The thermal envelope of the renovated building is assumed to reach U-values of 0.28 W/m²K for the insulated external walls, 1.3 W/m²K for the windows, 0.2 W/m²K for the floor slab, and 0.19 W/m²K for the insulated roof, resulting in a more thermally homogeneous envelope with reduced thermal bridging. Airtightness is set to

$n_{50}$ = 0.5 $h^{-1}$, approaching passive building standards and substantially limiting uncontrolled air leakage. The renovated configuration assumes integration of renewable energy systems to meet nZEB requirements, replacing reliance on conventional district heating with technologies capable of meeting heating and cooling demands from renewable sources.

## RESULTS AND DISCUSSIONS

### ATES System Design Considerations

Based on the pilot study findings and international best practices, the confined secondary aquifer at 30-45 m depth with 10 m combined thickness can be accessed through properly designed wells with a minimum spacing of 100 m between warm and cold wells to prevent thermal interference and ensure adequate thermal storage volume (Bloemendal et al., 2018; Birdsell et al., 2021). For small-scale ATES systems in similar geological conditions, international experience indicates design flow rates of 10-15 $m^3/h$ per well (Bloemendal et al., 2014); however, the significant fine sand content and suboptimal well screen placement at the pilot site (installed at 37–45 m depth rather than the optimal 29-36 m depth indicated by granulometric analysis) restrict feasible extraction rates to approximately 2.9-5.8 $m^3/h$ (0.8-1.6 l/s). A temperature differential of 5 K between extraction and reinjection was adopted as the design value for the aquifer circuit, based on hydrogeological assessment and recommendations from the MATES project's hydrogeological partner. This differential ensures reinjection temperatures remain within environmentally safe limits: approximately 8°C during winter (cold storage) and 18°C during summer (warm storage), consistent with the ranges recommended to balance heat pump efficiency with environmental protection and avoid exceeding 25°C, which may impact trace element mobility (Bonte, 2015). At the maximum feasible site flow rate of 1.6 l/s, this differential provides a thermal exchange capacity of approximately 33.4 kW at the aquifer, sufficient to meet the evaporator demand of the proposed heat pump system under design load conditions.

The proposed system employs water-to-water heat pumps with modular scroll compressors, enabling capacity modulation across multiple steps depending on load conditions. Performance analysis indicates COP values of 6.14 for small compressor operation, 5.91 for large compressor operation, and 5.35 at full capacity with both compressors engaged. The seasonal performance factor for the complete system, including circulation pumps and auxiliaries, ranges from 4.65 to 5.01 based on operational scenarios. To protect the aquifer from potential refrigerant contamination and allow controlled flow rate variation, the technological scheme (Figure 2) incorporates an intermediate heat exchanger circuit between the heat pumps and the underground circuit. A buffer tank enables temporary sensible heat storage to accommodate variable building demands without modifying underground water flow rate, while distribution employs low-temperature heating (35/30°C supply/return) and chilled water cooling (7/12°C supply/return) to maximize heat pump efficiency and ensure compatibility with aquifer temperature levels.

### Building Energy Performance Analysis

Dynamic simulation results reveal substantial energy demand reduction through nZEB renovation. For the existing building configuration, annual specific energy consumption totals 181.41 $kWh/m^2 \cdot year$ for heating and 14.75 $kWh/m^2 \cdot year$ for cooling, based on the occupied area of 366.80 $m^2$. The pronounced heating-cooling imbalance characteristic of Bucharest's continental climate is evident, with heating demand exceeding cooling demand by a factor of approximately 12:1.

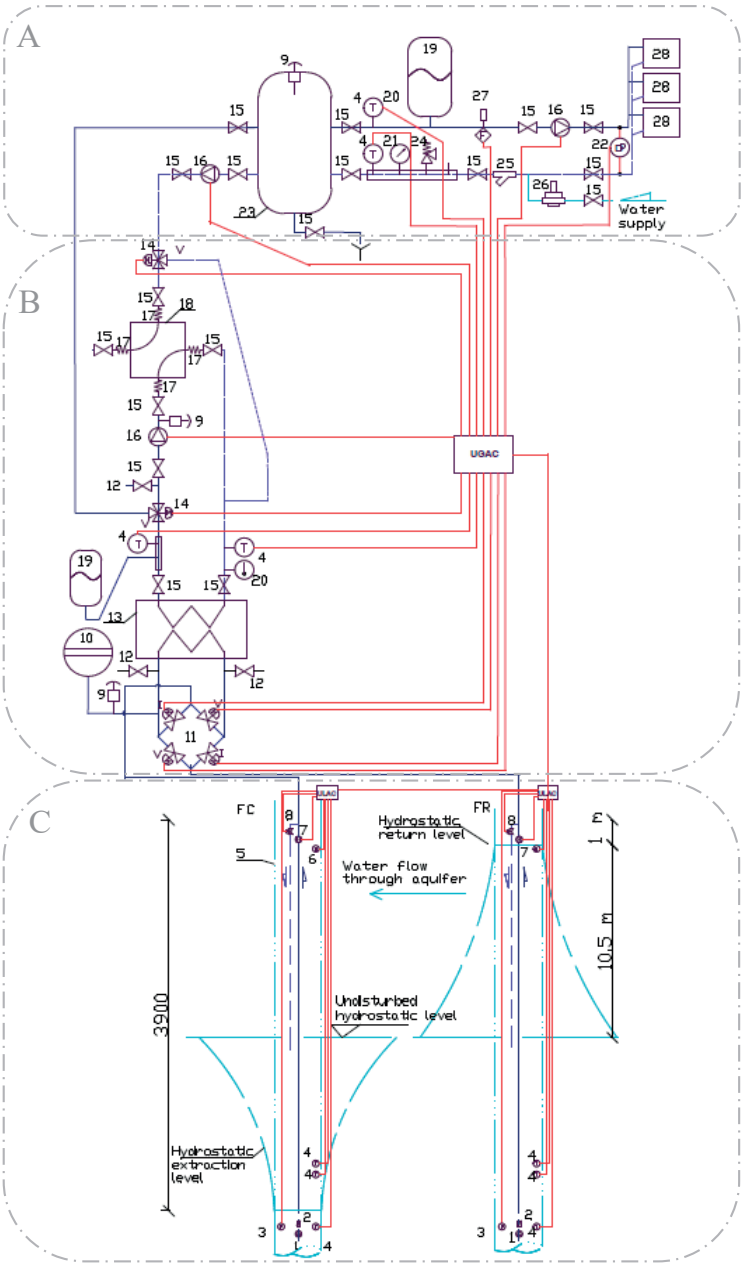



Figure 2. Technologic scheme for a heating / cooling system using ATES (A - distribution system and building related equipment, B - heat pump and other equipment from heat station, C - aquifer)
LEGEND: 1. Immersion water pump; 2. Clapper check valve; 3. Pressure transducer; 4. Temperature transducer; 5. Water well PVC pipe; 6. Water level sensor; 7. Water meter with pulse output; 8. Electric Solenoid Valve Water; 9. Air separator; 10. Water hammer arrestor; 11. Electric Solenoid Valve Water; 12. Bleeder; 13. Plate Heat Exchanger; 14. Three-way Valve with electric actuator; 15. Ball cock; 16. Circulation pump; 17. EPDM Rubber Joint to reduce the vibration; 18. Heat pump; 19. Expansion Vessel; 20. Thermometer; 21. Manometer; 22. Pressure drop transducer; 23. Water buffer tank; 24 Over pressure valve; 25. Inline Y filter; 26. Water Pressure Regulator; 27. Water flow sensor; 28. Fan coil unit; FC – Warm well; FR – Cold well; ULAC – Local acquisition and control unit; UGAC – General acquisition and control unit; I – Winter; V – Summer

Following nZEB renovation, annual heating demand decreases to 63.99 kWh/m²·year (65% reduction) while cooling demand reduces to 9.14 kWh/m²·year (38% reduction), though the heating-cooling asymmetry persists at a ratio of 7:1. Peak demands are also substantially reduced, with maximum hourly heating load dropping from 28.5 kW to 12.3 kW and peak cooling load from 9.8 kW to 6.7 kW (Figure 3). These lower peaks make the renovated building suitable for heat pump-based systems, but this suitability comes with a critical design constraint that must be addressed explicitly.

The ATES-coupled system operates as a low-entropy heating and cooling circuit, with thermal agent parameters close to the conditioned space temperature - 35/30°C for heating and 7/12°C for cooling.

This reduced temperature lift is precisely what enables the high COP values (5.35-6.14) reported for the heat pump configuration, as thermodynamic efficiency increases with decreasing temperature differential between source and sink. However, the same characteristic makes the distribution system technically demanding. The small driving temperature difference between the agent and the indoor environment - approximately 14 K on the heating side at design conditions - severely limits the capacity of conventional terminal units. Standard fan coil units are typically rated at higher supply temperatures (40-45°C), and their performance at 35°C supply is not covered by manufacturer specifications; capacity must therefore be estimated through corrected characteristic curves rather than catalogue data. This constraint becomes particularly acute during peak heating loads, where insufficient terminal unit surface area leads directly to failure to maintain setpoint. Radiant heating systems are better suited to these low-temperature conditions but introduce their own thermal inertia challenges in buildings with variable occupancy schedules. Both the engineering calculations and the physical implementation of such a system therefore require specialized expertise - the high system-level efficiency must not obscure the significant technical risk at the terminal unit level.

The annual energy demands for both building configurations are illustrated in Figure 3.

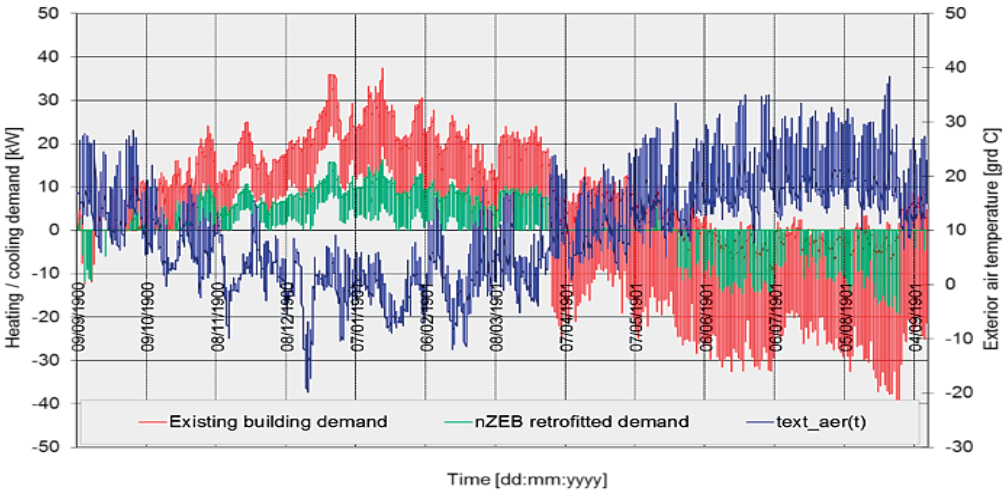



Figure 3. Energy demand of the pilot area, for existing building and the building renovated at a nZEB level

**Aquifer Characteristics and ATES Suitability Assessment**

The hydrogeological investigation identified characteristics that present both opportunities and limitations for ATES implementation. The measured combined aquifer thickness of 10 m falls below the typical 15-40 m thickness recommended for optimal ATES performance (Fleuchaus et al., 2018). Because the plume height is fixed by the aquifer thickness, a thin

aquifer also constrains the plume aspect ratio available for limiting heat losses to the confining layers (Tang & Rijnaarts, 2023), potentially limiting thermal storage volume and requiring careful system design to prevent thermal breakthrough between wells.

The confined aquifer conditions with artesian pressure offer advantages including reduced pumping energy requirements and natural protection from surface contamination. However, the pressurized nature requires careful well design to prevent uncontrolled discharge and ensure reliable reinjection capabilities. The granulometric analysis indicating significant fine sand content increases the risk of well screen clogging through particle migration and potential iron precipitation, which has been documented in other ATES systems (Possemiers et al., 2014). Preventive measures including proper well development, controlled injection velocities, and periodic monitoring would be essential for long-term operation.

The elevated groundwater temperatures (13.18°C at 41 m depth, 12.98°C at 46 m depth) exceed the regional average multiannual temperature of 10.7°C (SR 4839:2014) by approximately 2.5 K. This thermal anomaly is consistent with established patterns of groundwater thermal behaviour: at depths of 10-20 m, groundwater temperatures typically stabilize at 1-2 K above local mean annual temperatures, with further gradual increases below these depths due to geothermal gradient (Lee, 2013). The measured temperatures therefore reflect the combined influence of natural geothermal warming and potentially urban heat island effects documented in other urban areas (Benz et al., 2016; Böttcher & Zosseder, 2022), though the geothermal potential of the pilot area has not been comprehensively characterized. These elevated baseline temperatures provide advantageous conditions for heat pump operation, reducing temperature lift requirements during heating mode.

**Groundwater Quality Assessment**

Water quality analysis performed at the Bucharest pilot site revealed elevated concentrations of dissolved minerals that pose operational challenges for ATES implementation. Iron concentration measured 0.80 mg/l, exceeding the maximum contaminant allowable value by a factor of four and approaching the threshold above which iron oxide precipitation induces significant injection well clogging (Possemiers et al., 2014; Burté et al., 2019). Manganese was measured at 0.42 mg/l, exceeding its allowable limit by a factor of 8.4. While manganese contributes less to clogging than iron, the simultaneous presence of both elevated iron and manganese increases the risk of combined mineral precipitation during thermal cycling. Beyond inorganic parameters, urban aquifers in Bucharest may be subject to persistent organic pollutant contamination from historical industrial activities, though recent monitoring shows declining trends in urban soil contaminants such as polychlorinated biphenyls (Sandu et al., 2025), suggesting gradual improvement in urban environmental quality.

**ATES System Performance Assessment**

For the pilot building with occupied area of 366.80 m², the annual heating energy demand of 63.99 kWh/m²·year translates to approximately 23,470 kWh total annual heating requirement, while cooling demand of 9.14 kWh/m²·year corresponds to approximately 3,350 kWh annual cooling requirement. This pronounced imbalance (ratio 7:1) presents significant challenges for ATES thermal balance.

The heat pump system performance with seasonal performance factor (SPF) of 4.65 to 5.01 demonstrates the potential for highly efficient operation when coupled with ATES thermal storage. The modular compressor configuration allows optimization of part-load performance, with single compressor operation achieving COP values up to 6.14 during low-demand periods. This operational flexibility is particularly valuable for accommodating variable building loads and maximizing energy efficiency throughout the heating and cooling seasons.

The heating-cooling asymmetry has direct consequences for long-term ATES performance. A sustained mismatch between seasonal cooling injection and heating extraction produces a continuous thermal drift of the aquifer around the wells: the storage volume gradually cools until a new quasi-stationary regime is reached, characterized by asymmetric thermal plumes and a progressive reduction of the available

temperature contrast between warm and cold wells (Sommer et al., 2013; Fleuchaus et al., 2018; Godinaud et al., 2025).

From an environmental and regulatory perspective, such imbalance – particularly on the cooling side – is generally permissible in urban contexts. Regulatory frameworks are primarily concerned with excessive groundwater warming rather than moderate cooling, and life cycle assessments confirm that ATES yields substantial greenhouse gas reductions - up to 74% for heating compared with oil- and gas-fired systems, and up to about 59% for cooling relative to conventional techniques under the present electricity mix, rising to some 97% under a projected 2050 electricity mix (Stemmle et al., 2021). The dominant environmental impacts are attributable to operational electricity demand, which is responsible for over 95% of water use, global warming potential and acidification impacts, rather than to aquifer temperature changes (Ni et al., 2020). The critical consequence of persistent imbalance is therefore thermodynamic, not environmental: reduced temperature contrast translates directly into declining heat recovery efficiency and lower heat pump performance over successive annual cycles. Field monitoring of an imbalanced LT-ATES system documented a progressive decrease in the temperature difference on the ATES side - from approximately 3 K down to 1.8 K over four cooling seasons despite an available $\Delta T$ of 8 K - confirming that performance degradation under imbalanced operation exceeds what hydrogeological dispersion alone would produce (Abuasbeh et al., 2021). Numerical simulations corroborate this: thermally balanced doublet operation produces stable, symmetric plumes and sustained performance over decades, whereas imbalanced scenarios show enlargement of the warm plume, reduction of the cold plume, and progressive warming of the screened interval (Bozkaya et al., 2018; Godinaud et al., 2025).

The integration of solar thermal collectors offers a practical solution to achieve thermal balance. International experience demonstrates that ATES systems achieve high seasonal performance in heating-dominated climates, and that supplementary heat injection is the accepted lever for maintaining long-term balance. Vanhoudt et al. (2011) documented three years of monitored operation of an ATES-heat pump system at a Belgian hospital, achieving a seasonal performance factor of 5.9 for heating and a 71% reduction in primary energy use compared with gas boilers and conventional chillers.

For the Bucharest pilot building, evacuated tube collectors could provide supplementary heat injection during summer cooling season to reduce thermal imbalance. The sizing of such a solar thermal system would need to balance the heating-cooling asymmetry, potentially requiring collector areas and storage capacities determined through detailed optimization considering building loads, available roof area, seasonal solar irradiance patterns, and system integration requirements. This hybrid renewable configuration would facilitate meeting EPBD requirements for on-site renewable energy generation while enabling sustainable ATES operation.

Beyond system-level solar thermal augmentation, imbalance can be managed through multi-well configurations and optimized well placement accounting for ambient groundwater flow, aquifer thickness, and urban constraints, which help maintain higher heat recovery factors even under imperfectly balanced loads (Sommer et al., 2013; Li et al., 2024; Petrova et al., 2025) and, in aquifers with high flow velocities (of the order of 100 m/year), an additional upstream extraction well acting as a hydraulic barrier can more than double thermal recovery efficiency relative to a conventional doublet (Ohagen et al., 2025). At urban scale, coordinated planning of multiple ATES systems allows excess cold from individual installations to be offset by excess heat from others, improving overall aquifer balance and increasing deployment density by approximately 30% (Sommer et al., 2015; Bloemendal et al., 2018; Beernink et al., 2022). Contemporary design guidelines therefore treat thermal imbalance as a manageable design variable rather than a hard constraint, emphasizing active balance management through control strategies and additional thermal sources as the key lever for maintaining long-term system viability (Bozkaya et al., 2018; Abuasbeh et al., 2021).

**Regulatory and Institutional Barriers**

The primary impediment to ATES deployment in Romania is Water Law no. 107/1996 (with subsequent amendments), which regulates reinjection of extracted water into aquifers. Contemporary operational experience with discharge quality compliance in Romanian wastewater treatment facilities demonstrates that meeting natural receptor standards requires continuous technological adjustment and monitoring (Dracea et al., 2022), principles equally applicable to ATES thermal discharge management. The legislation was designed primarily for mining and industrial wastewater discharge, establishing strict prohibitions on reinjection into the same aquifer from which water was extracted. This regulatory framework does not differentiate between contaminated industrial wastewater and closed-loop thermal energy storage where groundwater contacts only inert heat exchanger materials.

International regulatory frameworks provide alternative models that could guide Romanian policy development. The Netherlands employs a performance-based permitting system where ATES installations must demonstrate that thermal impacts remain within acceptable limits and that annual thermal balance is maintained (Bloemendal et al., 2014). German regulations, while more restrictive, still explicitly permit ATES systems under appropriate monitoring and control conditions (Stemmle et al., 2021).

The absence of ATES-specific technical standards in Romania creates additional uncertainty for potential investors. Key gaps include lack of well design specifications, monitoring requirements, operational protocols, and decommissioning procedures. The development of Romanian national standards based on established international protocols would facilitate systematic ATES deployment while ensuring environmental protection.

Institutional capacity represents another significant barrier. Limited Romanian experience exists with ATES-specific well construction techniques, and hydrogeological expertise for thermal storage applications is scarce. Professional training programs and technology transfer initiatives modelled on Dutch and German experience would be necessary to build domestic technical capacity for this renewable energy technology.

**Comparison with International ATES Experience**

The Bucharest pilot study findings align closely with recent assessments in other European countries facing similar regulatory and technical challenges. Noethen et al. (2025) identified substantial ATES potential in German regions despite regulatory barriers limiting implementation, while Jackson et al. (2024) report that ATES in the United Kingdom currently meets less than 0.01% of national heating demand although the technology could in principle serve about 61% of it. Similar to the Bucharest case, these studies demonstrate that technical feasibility exists but institutional frameworks remain underdeveloped.

The heating-cooling imbalance documented for Bucharest (ratio 7:1 for renovated building) is more severe than typical Dutch office buildings (ratio 1.5-2.5:1) but comparable to heating-dominated climates in Sweden and northern Germany. The proposed solar thermal integration strategy has precedent in Swedish and Belgian applications where seasonal storage systems achieve thermal balance through coordinated operation with solar collectors.

The shallow aquifer depth identified in Bucharest (10 m combined thickness) presents greater challenges than typical Dutch ATES installations (15-40 m aquifer thickness) but remains within technically feasible ranges. Al-Madhlom et al. (2019) proposed a multi-criteria site selection method (AHP combined with the DRASTIC index) specifically for shallow groundwater conditions, confirming that such settings require more conservative design approaches and careful thermal management.

**Study Limitations**

One should acknowledge several limitations of this pilot investigation. The hydrogeological characterization was based on three exploratory wells within a limited site area, providing insufficient data to fully characterize aquifer heterogeneity and regional groundwater flow patterns. A more comprehensive assessment would require additional wells, long-term pumping tests, and seasonal temperature monitoring to validate ATES feasibility for commercial-scale implementation.

The dynamic building simulations employed standard test reference year climate data and

assumed operational patterns based on typical office occupancy. Climate change projections indicate potential shifts in heating-cooling ratios for Central Europe (Godinaud et al., 2025), which could affect long-term ATES thermal balance. Future studies should incorporate climate scenarios to assess system performance under evolving conditions.

The system design considerations and performance estimates presented in this study are based on simulation results and international best practices adapted for Romanian conditions rather than operational data from a functioning pilot installation. Actual implementation would require comprehensive feasibility studies including detailed performance monitoring, cost-benefit analysis, and long-term operational experience to validate the projected system performance and economic viability.

## CONCLUSIONS

This study demonstrates that Aquifer Thermal Energy Storage (ATES) technology presents technically feasible opportunities for supporting nearly Zero Energy Buildings (nZEB) in Romanian continental climate conditions, though significant regulatory and technical barriers currently impede implementation. The pilot assessment for an office building in Bucharest revealed that nZEB renovation reduces annual energy demand by 65% for heating and 38% for cooling, making the building suitable for integration with renewable ATES-based systems.

The hydrogeological investigation documented a confined secondary aquifer at 30-45 m depth with 10 m combined thickness across two layers (7 m and 3 m) separated by a clay deposit. The aquifer exhibits favorable characteristics including moderate hydraulic conductivity and elevated ambient temperatures (13.2°C) that benefit heat pump operation. However, the aquifer thickness falls well below optimal ranges typical of international ATES installations, necessitating conservative design approaches and careful thermal management.

The elevated iron and manganese concentrations documented at the pilot site illustrate a broader challenge for ATES deployment in Romania. These values were obtained from a single site; Romanian aquifers across different geological regions may exhibit substantially different mineral profiles. Successful ATES deployment at national scale requires a systematic hydrogeochemical pre-screening of candidate aquifers, analogous to the regional water quality survey methodology developed by Allen (1983) for the United States. Recent assessments of groundwater contamination risks in Romania confirm the urgency of such systematic screening, revealing widespread vulnerability to multiple contaminants including nitrates, arsenic, and coliforms affecting over 670,000 individuals in rural areas alone (Ivanescu & Sandu, 2025). Allen's framework identified groundwater chemistry - particularly total dissolved solids, iron content, and carbonate saturation - as the primary determinants of long-term well injectivity and system reliability, concluding that freshwater with TDS below 500 mg/l in quartz sand aquifers represents the most favorable condition for low-temperature ATES. No equivalent national-scale screening exists for Romania, despite the fact that groundwater mineral content likely constitutes the most significant technical challenge for widespread ATES deployment in the country.

The pronounced heating-cooling demand imbalance characteristic of Bucharest's continental climate (ratio 7:1 even after nZEB renovation) represents the primary technical challenge for ATES deployment. This asymmetry would progressively cool the aquifer over multiple annual cycles, degrading system performance unless addressed through supplementary heat sources. Integration of solar thermal collectors offers a practical solution to achieve thermal balance, as demonstrated by successful international implementations in similar heating-dominated climates.

The heat pump system performance analysis indicates seasonal performance factors (SPF) of 4.65 to 5.01, demonstrating potential for highly efficient operation when properly integrated with ATES thermal storage. The modular compressor configuration enables optimization across variable load conditions, achieving COP values ranging from 5.35 to 6.14 depending on operational mode.

Romania's current regulatory framework poses the most significant barrier to ATES implementation, with Water Law no. 107/1996 prohibiting thermal reinjection without differentiation

between contaminated wastewater and closed-loop thermal storage. Development of ATES-specific regulations modeled on international performance-based permitting, combined with technical standards for well design and operation, would facilitate deployment while ensuring environmental protection.

Successful ATES implementation in Romania requires coordinated action on multiple fronts including: (1) legislative revision to permit thermal energy storage with appropriate monitoring requirements, (2) development of national technical standards based on international best practice, (3) pilot demonstration projects to build domestic expertise and generate operational data, (4) professional training programs for ATES design and operation, and (5) hydrogeological assessment campaigns to map aquifer suitability in major urban areas.

The research demonstrates that with appropriate institutional frameworks and hybrid system configurations integrating ATES with solar thermal technology, this renewable energy storage approach can significantly contribute to achieving Romania's nZEB targets and building sector decarbonization goals while providing reliable, cost-effective heating and cooling services.

## REFERENCES

Abuasbeh, M., Acuña, J., Lazzarotto, A., & Palm, B. (2021). Long term performance monitoring and KPIs' evaluation of Aquifer Thermal Energy Storage system in Esker formation: Case study in Stockholm. *Geothermics, 96*, 102166. https://doi.org/10.1016/j.geothermics.2021.102166.

Allen, R. D. (1983). Relationship of regional water quality to aquifer thermal energy storage (No. PNL-4929). *Pacific Northwest National Lab.* (PNNL), Richland, WA (United States).

Al-Madhlom, Q., Al-Ansari, N., Laue, J., Nordell, B., & Hussain, H. M. (2019). Site selection of aquifer thermal energy storage systems in shallow groundwater conditions. *Water, 11*(7), 1393. https://doi.org/10.3390/w11071393

Beernink, S., Bloemendal, M., Kleinlugtenbelt, R., & Hartog, N. (2022). Maximizing the use of aquifer thermal energy storage systems in urban areas: effects on individual system primary energy use and overall GHG emissions. *Applied Energy, 311*, 118587. https://doi.org/10.1016/j.apenergy.2022.118587.

Benz, S. A., Bayer, P., Goettsche, F. M., Olesen, F. S., & Blum, P. (2016). Linking surface urban heat islands with groundwater temperatures. *Environmental Science & Technology, 50*(1), 70-78. https://doi.org/10.1021/acs.est.5b03672.

Birdsell, D. T., Adams, B. M., & Saar, M. O. (2021). Minimum transmissivity and optimal well spacing and flow rate for high-temperature aquifer thermal energy storage. *Applied Energy, 289*, 116658. https://doi.org/10.1016/j.apenergy.2021.116658.

Bloemendal, M., Jaxa-Rozen, M., & Olsthoorn, T. (2018). Methods for planning of ATES systems. *Applied Energy, 216*, 534-557. https://doi.org/10.1016/j.apenergy.2018.02.068.

Bloemendal, M., & Hartog, N. (2018). Analysis of the impact of storage conditions on the thermal recovery efficiency of low-temperature ATES systems. *Geothermics, 71*, 306-319. https://doi.org/10.1016/j.geothermics.2017.10.009

Bloemendal, M., Olsthoorn, T., & Boons, F. (2014). How to achieve optimal and sustainable use of the subsurface for Aquifer Thermal Energy Storage. *Energy Policy, 66*, 104-114. https://doi.org/10.1016/j.enpol.2013.11.034

Bonte, M. (2015). *Impacts of shallow geothermal energy on groundwater quality: A Hydrochemical and geomicrobial study of the effects of ground source heat pumps and aquifer thermal energy storage*. [PhD-Thesis – Research external, graduation internal, Vrije Universiteit Amsterdam]. Vrije Universiteit Amsterdam.

Böttcher, F., & Zosseder, K. (2022). Thermal influences on groundwater in urban environments – A multivariate statistical analysis of the subsurface heat island effect in Munich. *Science of the Total Environment, 810*, 152193. https://doi.org/10.1016/j.scitotenv.2021.152193

Bozkaya, B., Li, R., & Zeiler, W. (2018). A dynamic building and aquifer co-simulation method for thermal imbalance investigation. *Applied Thermal Engineering, 144*, 681-694. https://doi.org/10.1016/j.applthermaleng.2018.08.095

Bu, X., Jiang, K., & Guo, Z. (2022). Storing high temperature solar thermal energy in shallow depth artificial reservoir for space heating. *Scientific Reports, 12(*1), 19549. https://doi.org/10.1038/s41598-022-24003-0.

Burté, L., Cravotta, C. A., Bethencourt, L., Farasin, J., Pédrot, M., Dufresne, A., Gérard, M.-F., Baranger, C., Le Borgne, T., & Aquilina, L. (2019). Kinetic study on clogging of a geothermal pumping well triggered by mixing-induced biogeochemical reactions. *Environmental Science & Technology, 53*(10), 5848–5857. https://doi.org/10.1021/acs.est.9b00453

Constantinescu, D. (2008). *Tratat de inginerie termică. Termotehnica în construcții. Vol. I – Fundamentare teoretică. [Thermal Engineering Treatise. Building Thermodynamics. Vol. I – Theoretical Foundations.]* AGIR Publishing House, Bucharest. ISBN 973-720-221-X.

Constantinescu, D. (2020). Tratat de inginerie termică. Termotehnica în construcții. Vol. II – Aplicații și studii de caz. [Thermal Engineering Treatise. Building Thermodynamics. Vol. II – Applications and Case Studies.] AGIR Publishing House, Bucharest. ISBN 978-973-720-789-0.

Directive (EU) 2024/1275 of the European Parliament and of the Council of 24 April 2024 on the energy performance of buildings (recast). *Official Journal of the European Union, L 167/48*, 28 May 2024.

Dracea, D., Tronac, A., & Mustata, S. (2022). Continuous adjustment within wastewater treatment plants operation to meet natural receptors discharge conditions. *Scientific Papers. Series E. Land Reclamation, Earth Observation & Surveying, Environmental Engineering*, XI, 344-349.

EN 15255:2008, Energy performance of buildings. Sensible room cooling load calculation. General criteria and validation procedures.

EN 15265:2008, Energy performance of buildings. Calculation of energy needs for space heating and cooling using dynamic methods. General criteria and validation procedures.

Fleuchaus, P., Godschalk, B., Stober, I., & Blum, P. (2018). Worldwide application of aquifer thermal energy storage – A review. Renewable and Sustainable Energy Reviews, 94, 861-876. https://doi.org/10.1016/j.rser.2018.06.057

Godinaud, J., Pryet, A., Bayer, P., & Larroque, F. (2025). Impact of land cover and climate change on aquifer thermal and energy storage (ATES) system performance. *Geothermics*, 127, 103262. https://doi.org/10.1016/j.geothermics.2025.103262.

Ivanescu, V., & Sandu, M. A. (2025). Assessing household groundwater contamination risk in rural Romania: a semi-quantitative regional model. *Scientific Papers Series Management, Economic Engineering in Agriculture & Rural Development, 25*(2).

ISO 13792:2012, Thermal performance of buildings. Calculation of internal temperatures of a room in summer without mechanical cooling. Simplified methods.

Jackson, M. D., Regnier, G., & Staffell, I. (2024). Aquifer Thermal Energy Storage for low carbon heating and cooling in the United Kingdom: Current status and future prospects. *Applied Energy, 376*, 124096. https://doi.org/10.1016/j.apenergy.2024.124096.

Lee, K. S. (2013). Aquifer Thermal Energy Storage. In *Underground Thermal Energy Storage. Green Energy and Technology. 59-93*, Springer, London. https://doi.org/10.1007/978-1-4471-4273-7_4

Li, S., Wang, G., Zhou, M., Song, X., Shi, Y., Yi, J., Zhao, J., & Zhou, Y. (2024). Thermal performance of an aquifer thermal energy storage system: Insights from novel multilateral wells. *Energy, 294*, 130915. https://doi.org/10.1016/j.energy.2024.130915

Magrini, A., Lentini, G., Cuman, S., Bodrato, A., & Marenco, L. (2020). From nearly zero energy buildings (NZEB) to positive energy buildings (PEB): The next challenge. *Developments in the Built Environment, 3*, 100019. https://doi.org/10.1016/j.dibe.2020.100019

Năstase, G., Șerban, A., Dragomir, G., Brezeanu, A. I., & Bucur, I. (2018). Photovoltaic development in Romania. Reviewing what has been done. Renewable and Sustainable Energy Reviews, 94, 523-535. https://doi.org/10.1016/j.rser.2018.06.056.

Noethen, M., Stemmle, R., Siebert, N., Herrmann, M., Menberg, K., Blum, P., & Bayer, P. (2025). Identifying aquifer thermal energy storage (ATES) key locations for hospitals in Lower Saxony, Germany. *Geothermics, 130*, 103334. https://doi.org/10.1016/j.geothermics.2025.103334

Ni, Z., Wang, Y., Wang, Y., Chen, S., Xie, M., Grotenhuis, T., & Qiu, R. (2020). Comparative Life-Cycle Assessment of Aquifer Thermal Energy Storage Integrated with in Situ Bioremediation of Chlorinated Volatile Organic Compounds. *Environmental Science & Technology, 54*(5), 3039-3049. https://doi.org/10.1021/acs.est.9b07020

Ohagen, M., Koch, M., Scholliers, N., Pham, H. T., Holler, J. K., & Sass, I. (2025). Managing High Groundwater Velocities in Aquifer Thermal Energy Storage Systems: A Three-Well Conceptual Model. *Energies, 18*(16), 4308. https://doi.org/10.3390/en18164308.

Olinic, T., Olinic, E.-D., & Butcaru, A.-C. (2024). Integrating Geosynthetics and Vegetation for Sustainable Erosion Control Applications. *Sustainability, 16*(23), 10621. https://doi.org/10.3390/su162310621

Petcu, C. (2009). Contributions to energy multiparametric analysis of the envelope and the management systems of the microclimate of the building. Doctoral thesis, Technical University of Civil Engineering of Bucharest.

Petcu, C., Constantinescu, D., & Petran, H. (2010). Experimental validation of the Buildings Energy Performance (BEP) assessment methods with reference to occupied spaces heating. *Revista Construcţiilor, 1*, 72-114.

Petrişor, A.-I., Braguţa, E., Ţugulea, A., Tache, A. V., Harea, O., Mogîldea, V., Popescu, O.-C., Andronovici, D., Bejan, I. (2025). Using Geospatial Information Tools to Plan Green Infrastructures in Response to Climate Changes: Examples from Bucharest, Romania and Chisinau, Moldova. *Urban Science, 9*(3), 62. https://doi.org/10.3390/urbansci9030062

Petrova, E., Cacace, M., Kranz, S., Zang, A., & Blöcher, G. (2025). Thermal Interference in Aquifer Thermal Energy Storage: Insights from stochastic surrogate modelling of well placement. *Applied Thermal Engineering, 278*, 127012. https://doi.org/10.1016/j.applthermaleng.2025.127012

Possemiers, M., Huysmans, M., & Batelaan, O. (2014). Influence of aquifer thermal energy storage on groundwater quality: A review illustrated by seven case studies from Belgium. *Journal of Hydrology: Regional Studies, 2,* 20-34. https://doi.org/10.1016/j.ejrh.2014.08.001

Prăvălie, R., Sîrodoev, I., Ruiz-Arias, J., & Dumitraşcu, M. (2022). Using renewable (solar) energy as a sustainable management pathway of lands highly sensitive to degradation in Romania. A countrywide analysis based on exploring the geographical and technical solar potentials. Renewable Energy, 193, 976-990. https://doi.org/10.1016/j.renene.2022.05.059

Rosca, M., & Antics, M. (2004). Current status of geothermal energy utilization in Romania. In *Proceedings of the International Workshop on Geothermal Energy Resources in Central and Eastern European Countries*, Zakopane, Poland, 13-17.

Sandu, M. A., Preda, M., Tanase, V., Mihailescu, D., Virsta, A., & Ivanescu, V. (2025). Trends in Polychlorinated Biphenyl Contamination in Bucharest's Urban Soils: A Two-Decade Perspective (2002–2022). *Processes, 13*(5), 1357. https://doi.org/10.3390/pr13051357

Skruch, P., & Długosz, M. (2019). A sliding mode controller design for thermal comfort in buildings. *Engineering Transactions*, 67(4), 475–489. https://et.ippt.pan.pl/index.php/et/article/view/974

Sommer, W., Valstar, J., van Gaans, P., Grotenhuis, T., & Rijnaarts, H. (2013). The impact of aquifer heterogeneity on the performance of aquifer thermal energy storage. *Water Resources Research, 49*(12), 8128-8138. https://doi.org/10.1002/2013wr013677

Sommer, W., Valstar, J., Leusbrock, I., Grotenhuis, T., & Rijnaarts, H. (2015). Optimization and spatial pattern of large-scale aquifer thermal energy storage. Applied Energy, 137, 322-337. https://doi.org/10.1016/j.apenergy.2014.10.019.

SR 4839:2014, Heating systems. Annual number of degree-days. Romanian Standards Association, Bucharest.

Stemmle, R., Blum, P., Schüppler, S., Fleuchaus, P., Limoges, M., Bayer, P., & Menberg, K. (2021). Environmental impacts of aquifer thermal energy storage (ATES). *Renewable and Sustainable Energy Reviews, 151*, 111560. https://doi.org/10.1016/j.rser.2021.111560.

Tache, A. V., Popescu, O.-C., Petrişor, A.-I. (2024). Planning Blue–Green Infrastructure for Facing Climate Change: The Case Study of Bucharest and Its Metropolitan Area. *Urban Science, 8*(4), 250. https://doi.org/10.3390/urbansci8040250

Tang, D. W. S., & Rijnaarts, H. H. M. (2023). Dimensionless thermal efficiency analysis for aquifer thermal energy storage. *Water Resources Research, 59*(11), e2023WR035797. https://doi.org/10.1029/2023wr035797

Vanhoudt, D., Desmedt, J., Van Bael, J., Robeyn, N., & Hoes, H. (2011). An aquifer thermal storage system in a Belgian hospital: Long-term experimental evaluation of energy and cost savings. *Energy and Buildings, 43*(12), 3657-3665. https://doi.org/10.1016/j.enbuild.2011.09.040

Scientific Papers. Series E. Land Reclamation, Earth Observation & Surveying, Environmental Engineering. Vol. XV, 2026
Print ISSN 2285-6064, CD-ROM ISSN 2285-6072, Online ISSN 2393-5138, ISSN-L 2285-6064

# CASE STUDY ON THE ASSESSMENT OF THE EFFECTS OF CONTROLLED BLASTING DEMOLITION ON NEARBY BUILDINGS

**Adrian SIMION**

National Institute for Building Research, Town Planning and Sustainable Territorial Development "URBAN - INCERC", 266 Pantelimon Road, District 2, Bucharest, Romania

Corresponding author email: simion_i_adrian@yahoo.com

***Abstract***

*Some of the civil and industrial buildings in Romania have exceeded or will exceed, in the coming period, their expected operating lifespan. This fact requires the establishment of a strategy for their replacement and one of the methods that responds to a high degree to these requirements is the demolition of buildings using explosives. This paper presents a theoretical study assessing the impact of the explosive demolition of an industrial building on an adjacent 10-story residential structure. The evaluated effects included the aerial shock wave, seismic impact, thrown fragments, and environmental pollution. To this end, both pyrotechnic parameters and calculation formulas derived from specific legislation were utilized. The demolition impact assessment was carried out during the design stage, providing the necessary documentation to obtain the demolition permit for the industrial building.*

***Key words****: blast effects, buildings, explosives, explosive demolition, impact assessment.*

## INTRODUCTION

Each structure is designed for a specific service life. After this service life, its existence becomes very dangerous for its occupants and surrounding buildings (Popa et al., 2024).
The demand for demolishing old buildings has increased recently, especially in major cities worldwide, where numerous structures were built during past periods of high economic growth (Silva et al., 2022).
A significant portion of these buildings are demolished using techniques that utilize explosive energy, which are often applied in the USA, Europe, and China (Isobe & Jiang, 2022).
In Romania, urban modernization in recent years has generally provided the pretext for the demolition of numerous old buildings.
In some situations, the demolition of these structures was only possible by applying new methods of controlled demolition using explosives (Laszlo et al., 2022).
Implementing the technique of demolishing structures using explosives aims to achieve the desired results by applying optimal constructive and economic solutions, without disrupting ongoing activities, and ensuring safety for both the personnel involved and the environment (Thomsen et al., 2011). Demolishing structures using explosives poses a series of risks to the environment and to people within the range of the explosion's effects. These works are carried out based on technical projects starting from the hypothesis of minimizing and/or removing these risks. In reality, this state of affairs is not always possible.
Sometimes, it is not possible to determine by calculation the optimal explosive charges to achieve the desired effect while maintaining a satisfactory level of protection. At other times, charges calculated as safe from a protection standpoint cannot achieve the desired blasting effect. For these reasons, implementing a demolition project using explosives - especially in an urban environment - requires a compromise between the amount and placement of explosives used to achieve the desired goal and the actual level of protection for the surrounding environment and individuals within range of the explosion's effects.
Practice in the field has shown that a way to achieve this compromise is to use the explosive charges resulting from the calculation as necessary to achieve the desired effects, while using measures to protect the environment and individuals, by means of means of protection adequately sized to achieve the required level of safety.

## MATERIALS AND METHODS

The study presented below consists of assessment of the effects that the demolition of an industrial structure had on buildings located in the nearby of this demolition area.
These effects consisted of the air shockwave effects, the seismic effect, the effect of thrown fragments and the effect of environmental pollution (Fourney, 1983). The structure demolished through controlled blasting (hereinafter referred to as OD12) was an industrial building located on the premises of the former Titan Factory - Bucharest (Figure 1).

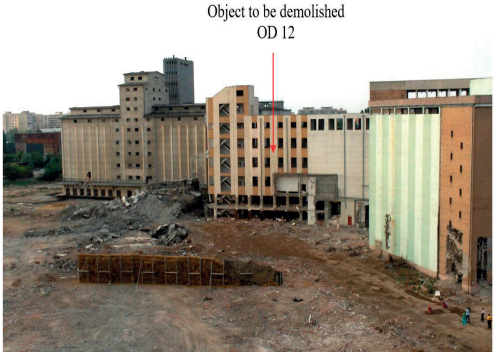



Figure 1. Overview of OD 12 before demolition, taken from the 10th floor of the protected building

Outside the TITAN Bread Factory, to the south, several residential complexes were built approximately 130 m away from the demolished structure (Figure 2).




Figure 2. View from the terrace of the industrial building to be demolished, with the residential blocks which the construction to be protected is part

The demolished building featured a reinforced concrete frame system, with a resistance structure consisting of columns and beams stiffened by floor slabs.
Before demolition, the building had a rectangular footprint measuring 28.20 x 9.25 m and a height of GF+5 floors+2 recessed floors (total height of 31.90 m).
It consisted of two sections without an expansion joint between them: the first section measured 12.20 x 9.25 m (GF+5F+2R), and the second section measured 16.00 x 9.25 m (GF+5F).
The building's structural frame consisted of reinforced concrete frames, with columns (measuring 0.75 x 0.75 m at the ground floor and 1st floor, and 0.65 x 0.65 m at the 2nd floor), beams (0.35 x 1.00 m and 0.45 x 0.70 m at the ground floor, 0.60 x 1.00 m and 0.45 x 1.00 m at the 1st floor), and ribs (0.25 x 0.40 m and 0.20 x 0.30 m). The layout and dimensions of the columns within the industrial building structure are shown in Figure 3.

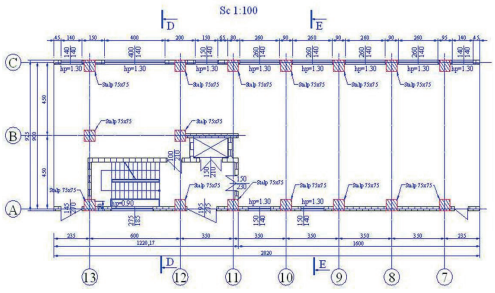



Figure 3. Ground floor plan of the demolished structure

The building's roof consisted of a reinforced concrete coffered slab (waffle slab) for the 5-story section (GF+5) and a reinforced concrete flat slab for the section with a height of GF+5+2R (receded floors), both equipped with thermal and water insulation. Access to the upper floors was provided via stairs.
The building envelope was made of non-load-bearing brick masonry walls and glazed surfaces, which were destroyed once the factory was abandoned (Figure 4). The reinforced concrete technological floors were positioned at the following levels: +3.50 m, +7.00 m, +11.50 m, +16.00 m, +20.50 m, +25.00 m, and +28.70 m.

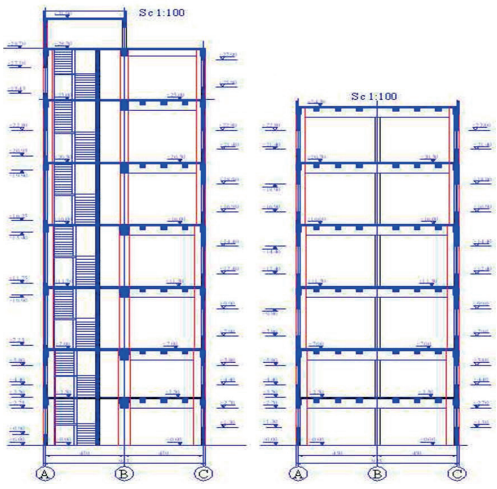



Figure 4. Cross sections of the demolished structure

During the demolition of the industrial building, measures were taken to protect neighboring structures from the effects of the process.
One of the protected buildings was a 10-story residential block consisting of a rigid core and reinforced concrete frames.
The centrally located core, made of shear walls surrounding the elevator, was designed to handle most of the lateral loads, while the reinforced concrete columns were responsible for supporting the gravity loads (Figure 5).

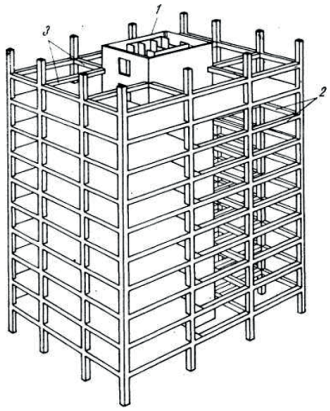



Figure 5. Combined structure made with central core and reinforced concrete frames: 1- central core made of reinforced concrete diaphragms; 2 - marginal reinforced concrete frames; 3 - intermediate reinforced concrete frames

During the demolition works of OD 12 using controlled explosions, the following effects occurred: the air shockwave effect; the seismic effect; the effect of thrown fragments; and the effect of environmental pollution.
*Assessment of the effect of the air shock wave:*
According to the legislation in force in Romania, in HG 536/2002 the value of the overpressure in the shock wave front is determined with the relation:

$$\Delta p_f = 0.84\lambda + 2.7\lambda^2 + 7\lambda^3 \quad [\text{kgf/cm}^2]$$

where λ is the scaled distance and is calculated with the relationship:

$$\lambda = \frac{\sqrt[3]{Q}}{R} \qquad [\text{kg/m}]$$

where $Q$ is the amount of explosive material, expressed in TNT equivalent [kg], that detonates instantaneously and $R$ [m], is the distance measured from the site of the explosion to the protected building.
Compared to OD 12, the nearest building is a residential apartment building located at a distance of approximately 130 m.
The maximum charge per delay interval is 3.3 kg of dynamite. Since a nitroglycerin-based explosive mixture is used for the demolition, which has an equivalence coefficient of 1.3 TNT equivalent and there are 3.3 kg of dynamite per detonation stage, it follows that (HG 536, 2002):

$$Q = 3{,}3 \times 1{,}3 = 4{,}29 \text{ [kg TNT equivalent].}$$

The 4.29 kg of dynamite results from adding the amount of explosive in the holes to the amount of PETN in the detonating cord used to initiate the explosives (10 g/m).
Under these conditions, the value of parameter λ is:

$$\lambda = \frac{\sqrt[3]{Q}}{R} = \frac{\sqrt[3]{4{,}29}}{130} = 0{,}0125 \text{ [kg/m].}$$

The resulting value is negligible; for this reason, the shock wave front overpressure was determined via the direct method, resulting in:

$$\Delta p_f = 0.84x0{,}0125 + 2.7(0{,}0125)^2 + 7(0{,}0125)^3 = 0{,}0111 \text{ [kg/cm}^2\text{]}.$$

This calculation did not account for the fact that the total mass of explosive used in the previous calculation is distributed into small charges placed in blast holes (Olsson & Bergqvist, 1993).

For this reason, specialized literature, such as works by experts from the Swedish Detonic Research Foundation (Persson et al., 1981), considers that the overpressure value in the shock wave is:

$$\Delta p_f^* = 0.2\Delta p_f \text{ [kg/cm²]}.$$

In this case $\Delta p_f^* = 0.00222\,kg/cm^2$ and this value is well below the limit that could cause any damage to the building being protected.

From the analysis of this data, it appears that, to protect the neighboring property during demolition, it is sufficient to install protective measures consisting of used rubber mats or to create screens from straw bales, tarpaulins, etc.

*Assessment of the seismic effect induced by detonation of explosives:*

The seismic effect caused by oscillations produced by the detonation of explosives charges during blasting works subjects nearby structures to spatial movement, which places dynamic stress on their constructive elements.

Depending on the intensity of the oscillations and the condition of the structures, stresses can cause damage over time.

This occurs when the generated oscillations lead to dynamic stresses that exceed the tensile, shear, or bending strength of the structural elements.

To assess the seismic effect of elastic oscillations transmitted through the ground to building foundations, the velocity criterion has been chosen globally in most cases, as it is the only reproducible parameter for the entire range of frequencies characteristic of seismicity produced by blasting works (Persson et al., 1970).

The seismic waves affecting the structure to be protected are generated by the detonation of explosive charges in the blast holes within the structural elements of OD 12 and by the ground impact resulting from the building's collapse (Lupoae, 2016).

*Assessment of the seismic effect induced by explosions inside structural elements:*

When designing blasting works, the size of the concentrated explosive charge that can be detonated instantaneously is determined by the formula:

$$Q_{inst} = \left(\frac{R}{\alpha k}\right)^3 \text{ [kg TNT equivalent)]},$$

where $R$ is the distance between the blast site and the target (m); $k$ is a coefficient based on the properties of the medium being blasted, and α is a coefficient depending on the blast effect index. The quantity of explosive that can be detonated per delay stage is determined by the relation:

$$Q_{tr.itr} = \frac{2}{3} Q_{inst} f(n) K_1 \text{ [kg TNT equivalent)]},$$

where $f(n)$ is a reduction coefficient based on the delay time of the initiation system, and $K1$ is a reduction coefficient based on the number of blasts carried out during a year.

Using the calculation formulas presented above, for objective OD 12, the following is obtained: $R$ = 128 m (the distance between OD 12 and the building to be protected); $K$ = 9 for clay rocks; $\alpha$ = 1 (for an explosion index $n$ = 1); $Q_{inst}$ = 1139 kg TNT equivalent = 876.5 kg dynamite; $f(n)$ = 0.917 for the NONEL-MS system; $K_1$ = 1 (for one blast); $Q_{tr\ itr}$ = 696.5 kg TNT equivalent = 535.8 kg dynamite.

It can be observed that the values obtained from the calculation are very high compared to the maximum explosive charge per delay stage of 3.3 kg dynamite.

Even if the explosive charges were to detonate in boreholes drilled into the ground, the oscillation velocity generated by the explosion shock is below the level established as admissible.

In conclusion, given that these charges detonate above the ground, a potential seismic effect induced through the soil cannot be considered regarding the blasting works performed for the demolition of OD 12.

*Assessment of the seismic effect induced by ground impact during the collapse of OD 12:*

Assessment the seismic effect produced by the collapse of OD 12 on the ground, it must be

noted that the resistance structure consists of reinforced concrete frames.

For these structures, when the chosen demolition method is overturning in a specific direction, the reduction of the main portion of the falling energy is achieved through the large interior spaces of the structure.

These spaces ensure that, at any given moment, only a small fraction of the building's elements are in contact with the ground, while other elements reach their breaking point and subsequently collapse completely (Figure 6; Figure 7; Figure 8).



Figure 6. Space inside the demolished building from a lower floor



Figure 7. Space inside the demolished building from a higher floor



Figure 8. The structural elements of OD 12 collapsed on the ground

*Assessment of the effect of thrown fragments:*

The main consequences of this effect consist of: local destruction resulting from the impact between the thrown fragments and the protected objective; the occurrence of local fires where the thrown fragments land, if they are heated to an appropriate temperature; to minimize these effects, a series of protective measures have been taken, as follows: installing wire mesh with a 0.03 × 0.03 m mesh size on the building to be demolished, directly over the explosive-filled boreholes, to slow down and retain large concrete fragments detached during the explosion (Figure 9);



Figure 9. Wire mesh used in the manufacture of protective screens

installing various types of screens on the construction pillars, adjacent to the boreholes loaded with explosives, to slow down and

contain small fragments detached during explosions (Figure 10); installing protective panels on or near the structures to be protected and identifying any potential fire outbreaks immediately after demolition and extinguishing them.

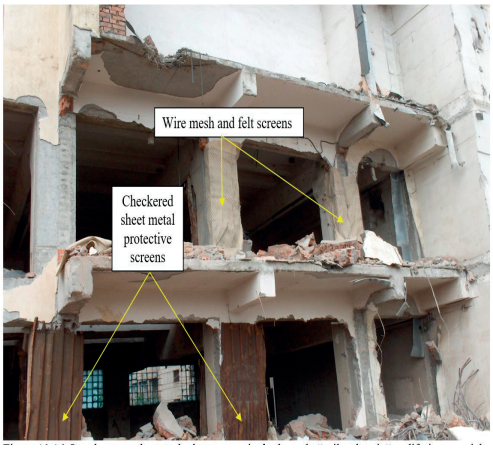



Figure 10. Installation in front of mine holes, the various type of screens for slowing down and retaining large fragments detached from the explosion

*Assessment of the environmental pollution effect:*

This effect is limited in both time and space of action; it is caused by blasting gases and dust resulting from the crushing of the reinforced concrete structure, as well as the interaction of structural elements with each other and upon contact with the ground (Figure 11).



Figure 11. Dust and explosion gas pollution during demolition of OD 12

To reduce dust pollution, the area where the structure collapsed was sprayed with water, both before and immediately after its fall (Figure 12).



Figure 12. Water spraying of the demolition area to limit dust pollution

## RESULTS AND DISCUSSIONS

The results obtained from this study primarily serve a justificatory role. This study can be provided by the demolition contractor to the relevant authorities in the event of complaints from residents of protected properties regarding inconveniences or damage caused by the demolition activity (Simion, 2014).

Thus, to prevent potentiality litigation during the demolition of the industrial structure presented in this paper, monitoring actions were carried out. Monitoring refers to post-event verification methods of the effects generated by this type of demolition. These consisted of filming and photographing the preparatory work performed on the structure to be demolished, filming and photographing the condition of protected buildings before and after the demolition, and measuring blast effects regarding airblast and seismic wave levels, as well as the level of dust dispersed in the air and deposited in the environment.

The non-hazardous level of oscillations caused by explosions during the industrial building demolition is established based on the degree of damage to structures located in the nearby of the demolition area (Singh & Roy, 2010). This threshold varies from country to country and is generally adopted based on the quality of the

constructions and even the manner in which minor repairs are executed for buildings near the blasting area.

It was assessed that the collapse process of the industrial building did not generate ground oscillation intensities capable of damaging neighboring buildings in any way.

During the demolition of the industrial structure, no shrapnel projections or fragments of building materials were observed and recorded, and the overpressure in the shock wave front due to explosions was of short duration and low intensity, and did not cause inconvenience to residents of nearby buildings.

## CONCLUSIONS

The demolition of vast portions of the existing urban structure has been a continuous feature of urban renewal in Romania since the 1990s (Simion & Dragomir, 2014). In this process, many buildings that could have been renovated or otherwise utilized were lost. A large part of these constructions were industrial structures was demolished using one of the most efficient techniques: demolition with explosives. This technique is based on the destructive action of explosions within holes drilled into structural elements to cause the collapse of the building.

This method is particularly effective for large industrial facilities where rapid demolition is required.

However, despite its efficiency, the demolition with explosives requires rigorous engineering analysis and expert supervision to prevent unintended damage to nearby buildings (Yuzbasi, 2025).

Studying the destructive phenomena and actions that occur during explosions requires evaluating, with a certain probability, the scale of destruction and the effects produced on people and various urban buildings.

The destructive effect of explosions on structural elements manifests in a particular way, as the explosive charges detonate in the holes where they are placed, and the transfer of a certain amount of energy from the explosion to the construction material and the environment generates the destructive action and the effects of the explosion.

Controlled demolition projects differ from one construction to another and generate undesirable effects, such as acoustic, seismic, and dust impacts, which must be continuously understood and measured.

To ensure the impartiality and credibility of these effect measurements, they must be carried out by specialists other than those performing the demolition works. These specialists must be accredited for such tasks (possessing proven qualifications and competence) and must use specialized equipment for recording dynamic parameters that has been metrologically verified.

## REFERENCES

Isobe, D. & Jiang, R. (2022), Explosive demolition planning of building structures using key element index, *Journal of Building Engineering*, Volume 59, 104935.

Decision No. 536 of 30 May 2002 (2002), on the approval of the Technical Norms regarding the possession, preparation, experimentation, destruction, transport, storage, handling and use of explosives used in any other specific operations in the activities of the holders, as well as the authorization of fireworks makers and pyrotechnicians**), Bucharest, RO: Official Gazette, No. 479 of July 4, 2002.

Fourney, W.L. (1983). *Fracture Control Blasting*, In Rossmanith, H.P. (eds), Rock Fracture Mechanics. International Centre for Mechanical Sciences, 275, Springer, Vienna.

Laszlo, R., Jitea, C., Garaliu, B., Nicola, A. & Miklos, L. (2022), Design and execution of demolition work by blasting of industrial constructions – technical and safety aspects, *Bulletin of the Polytechnic Institute of Iaşi Machine constructions Section*, 68 (2), 119-131.

Lupoae, M. (2016). Numerical solution to estimate the seismic effect on controlled explosive demolition, *16th International Multidisciplinary Scientific GeoConference SGEM2016,* 10.5593/SGEM2016/B12/S03.081.

Olsson, M. & Bergqvist, I. (1993). Crack lengths from explosives in multiple hole blasting, In Mohanty B. (Ed), *Rock Fragmentation by Blasting*, 187-191, CRC Press, London, doi.org/10.1201/9781003078104-25.

Persson, P.A., Holmberg, R., Lande, G. & Larsson, B. (1981). Underground blasting in a city, M. Bergman (Ed.), Subsurface Space - Environmental Protection · Low Cost Storage Energy Savings, Pergamon, 1, 199-206.

Persson, A., Lundborg, N. & Jonsson C. H. (1970). The Basic Mechanisms in Rock Blasting, Paper presented at the 2nd ISRM Congress, Belgrade, Yugoslavia, .

Popa, I., Petcu, C., Stoica, D. & Dima, A. (2024), Rice husks and their potential for use in construction. *Scientific Papers. Series E. Land Reclamation, Earth Observation & Surveying, Environmental Engineering*, XIII.

Silva, A., de Brito, J., Thomsen, A., Straub, A., Prieto, A.J. & Lacasse, M.A. (2022), Causal Effects between Criteria That Establish the End of Service Life of Buildings and Components. *Buildings* 2022, 12, 88.

Simion, A. (2014), Evaluation of seismic effects of blasting demolitions, *UTCB Scientific Bulletin*, 4.

Simion, A. & Dragomir, C.S. (2014), Reliability of demolition by controlled implosions, *Constructions: Journal of Civil Engineering Research*, 15(2), 56 – 59.

Singh, P.K. & Roy, M.P. (2010), Damage to surface structures due to blast vibration, *International Journal of Rock Mechanics and Mining Sciences*, 47(6), 949-961.

Thomsen, A., Schultmann, F., & Kohler, N. (2011), Deconstruction, demolition and destruction, *Building Research & Information* 39(4), 327-332.

Yuzbasi, J. (2025), Fundamentals of Controlled Demolition in Structures: Real-Life Applications, Discrete Element Methods, Monitoring, and Artificial Intelligence Based Research Directions. *Buildings*, 15, 3501.

Scientific Papers. Series E. Land Reclamation, Earth Observation & Surveying, Environmental Engineering. Vol. XV, 2026
Print ISSN 2285-6064, CD-ROM ISSN 2285-6072, Online ISSN 2393-5138, ISSN-L 2285-6064

# COMPARATIVE STUDY ON DETERMINING THE FIRE RESISTANCE OF MASONRY WALLS

**Adrian SIMION[1], Augustina-Sandina TRONAC[2], Claudiu-Sorin DRAGOMIR[1, 2], Laurențiu Denis CHERPEC[3]**

[1]National Institute for Building Research, Town Planning and Sustainable Territorial Development "URBAN - INCERC", 266 Pantelimon Road, District 2, Bucharest, Romania
[2]University of Agronomic Sciences and Veterinary Medicine of Bucharest, 59 Marasti Blvd, District 1, Bucharest, Romania
[3]Fire Officers Faculty, Police Academy "Alexandru Ioan Cuza" Bucharest, 022451, Bucharest, Romania

Corresponding author email: simion_i_adrian@yahoo.com

***Abstract***

*In the current context of the implementation of the provisions of the new P118-1:2025 on the fire safety of buildings in Romania, an important role falls to testing laboratories for determining the fire resistance of building elements, in order to increase the fire safety of the built environment. For these reasons, the assessment of the fire behaviour of building elements made of non-load-bearing masonry is an essential component for fulfilling the fundamental requirement of fire safety of buildings. The tests for determining the fire resistance of building elements in Romania, are carried out within the INCERC Testing Laboratory from Bucharest and consist of applying standardized fire resistance testing methods that are harmonized at the level of the countries of the European Union. Recently, researchers from this laboratory conducted several experimental tests to compare the fire resistance of non-load-bearing masonry walls of varying thicknesses.*

***Key words****: cladding systems, compartment fires, experimental research, fire resistance tests.*

## INTRODUCTION

Theoretical studies and experimental research have highlighted that every fire has its own evolution that makes it unique, with no two fires following an identical path. This uniqueness must be understood as referring to the entire set of factors and consequences of a fire (Simion & Dragomir, 2025).
In the Romanian construction sector, autoclaved aerated concrete (AAC) blocks are highly favoured, owing to their superior performance under fire conditions. Autoclaved Aerated Concrete (AAC) is an eco-friendly building material composed of cement, water, lime, silica-based materials (such as sand, ash, or silica fume), an expansion agent (aluminium powder), and other additives (Sherin & Saurabh, 2018; Hammond & Jones, 2008).
Besides its relatively light weight, this material provides benefits like fire resistance, low thermal and acoustic conductivity, and is easy to cut, handle, install, and transport (Mollaei et al., 2022). AAC block masonry utilizes adhesive mortar to bond the blocks (Song et al., 2024). This adhesive mortar behaves differently and can make the AAC masonry vulnerable to fire if not applied in a thin layer.
Researchers at INCERC Bucharest recently conducted experimental studies to assess the fire performance of non-load-bearing masonry walls of varying thicknesses, constructed with autoclaved aerated concrete (AAC) blocks (density: 480 kg/m$^3$, compressive strength: 3.5 N/mm$^2$) and class M2.5 bonding mortar (compressive strength 2.5 N/mm$^2$) (Stanescu et al., 2021).

## MATERIALS AND METHODS

The purpose of this study was to evaluate the fire resistance performance of a single type of AAC masonry wall with the following thicknesses: 150 mm, 200 mm, and 300 mm (Figure 1 and Figure 2).
The experimental tests were conducted at the Fire Safety Laboratory within INCERC Bucharest and consisted of applying a standardized method, harmonized across European Union countries, for testing the fire resistance of non-load-bearing walls.

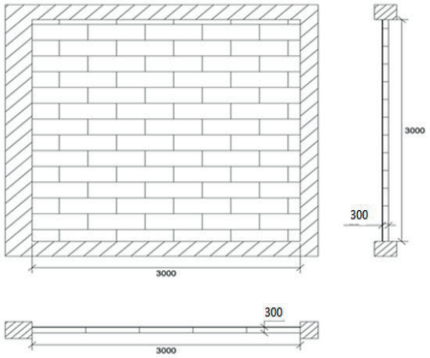



Figure 1. Non-load-bearing AAC masonry wall with a thickness of 300 mm designed for fire resistance testing



Figure 2. Non-load-bearing wall made of AAC masonry with a thickness of 300 mm, prepared for fire resistance testing

The fire resistance testing technology for non-load-bearing walls involved installing the walls (test samples) in the opening of a vertical fire resistance test furnace, conditioning the specimens for a period of 30 days after installation, and testing them under a controlled fire.

This fire followed the ISO 834 standard temperature-time curve, maintained by the furnace's automation system throughout the entire duration of the tests (Figure 3).

During the fire resistance tests, the walls were exposed to a controlled temperature variation regime inside the furnace to evaluate the integrity (*E*) and thermal insulation (*I*) criteria, in accordance with the test method standards "SR EN 1363-1:2020 Fire resistance tests. Part 1: General requirements" and "SR EN 1364-1:2015 Fire resistance tests for non-loadbearing elements. Part 1: Walls" (Figure 4 and Figure 5).

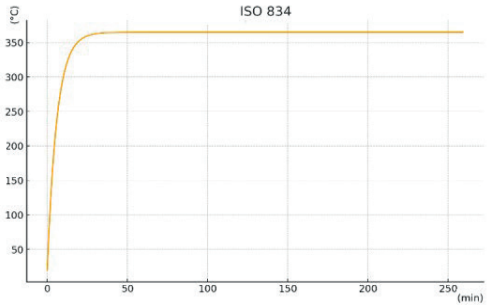



Figure 3. ISO 834 standard temperature-time curve

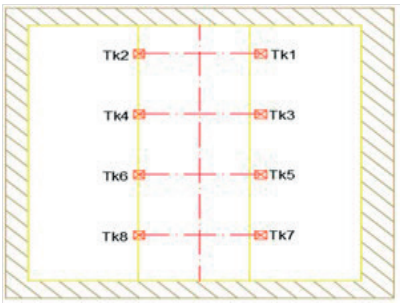



Figure 4. Thermocouple placement inside the furnace

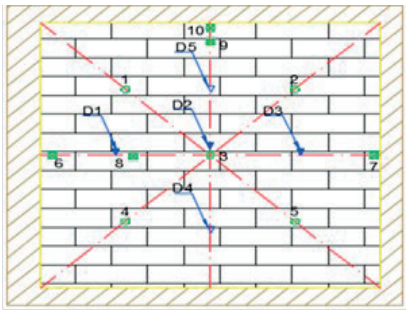



Figure 5. Positioning of thermocouples on the unexposed surface of the sample

## RESULTS AND DISCUSSIONS

After conducting the fire resistance tests on the AAC masonry walls, the testing supervisor prepared the fire resistance test reports for each wall type tested, in accordance with the testing laboratory's internal procedures (a RENAR-accredited laboratory) and the requirements of the harmonized fire resistance testing standards for non-load-bearing walls.

Following the monitoring, recording, and processing of the testing parameters, as well as visual observations regarding the behaviour and

integrity of the specimens during the tests, a series of data was obtained and subsequently included in the fire resistance test reports for the three specimens.

This information consisted of: the temperature evolution inside the furnace compared to the ISO 834 standard curve, as well as on the unexposed surface of the samples; the deformation of the samples during the tests; the moments when the fire resistance criteria samples were lost (expressed in full minutes); the evolution of environmental conditions in the testing hall; the intensity of smoke release on the unexposed surfaces of the samples during the tests; the monitoring of cracks, fissures, and sustained flaming; the ignition time of the cotton pad; the verification of the gap gauge insertion into the cracks formed in the samples; the observation of any material spalling or detachment; the start and end times of the tests, etc.

During the tests, researchers observed the appearance of fissures and cracks on the unexposed surface of the three AAC masonry samples at the following times: at minute 20 for the 150 mm thick sample, at minute 35 for the 200 mm thick sample, and at minute 50 for the 300 mm thick sample. Using a FLIR thermal imaging camera, the temperature variation on the unexposed surface of each sample was measured from the beginning until the end of the fire resistance tests (Figure 6, Figure 7, Figure 8 and Figure 9).



Figure 6. The unexposed surface of the 200 mm thick sample at the beginning of the fire resistance test

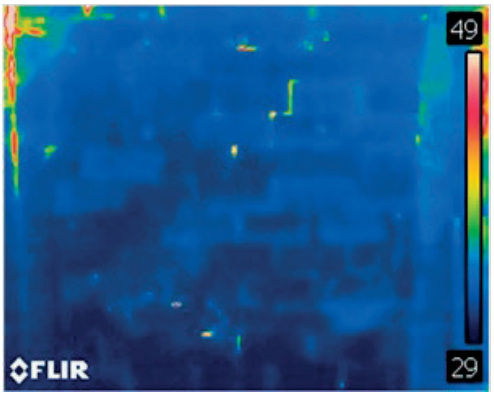



Figure 7. Temperature measurement on the unexposed surface of the 200 mm thick sample at the start of the fire resistance test



Figure 8. The unexposed surface of the 200 mm thick sample at minute 220, at the conclusion of the fire resistance test

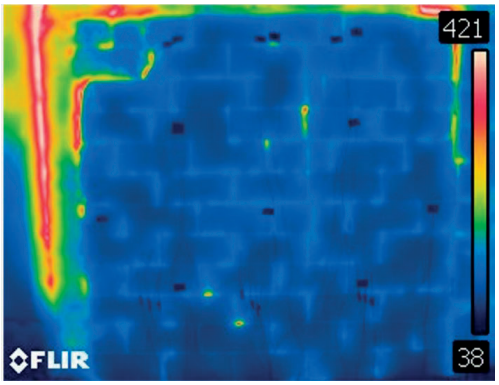



Figure 9. Temperature measurement on the unexposed surface of the 200 mm thick sample at minute 220, upon completion of the fire resistance test

The deformations of the three samples during the fire resistance tests were, as follows (Figure 10, Figure 11 and Figure 12):

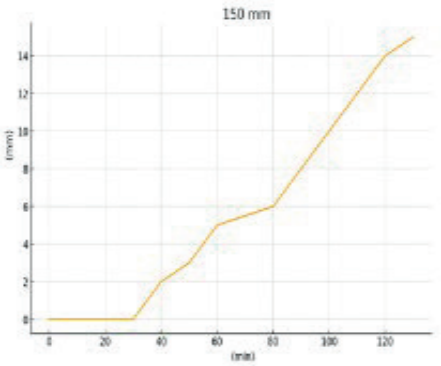



Figure 10. Deformation of the 150 mm thick AAC masonry wall during the test

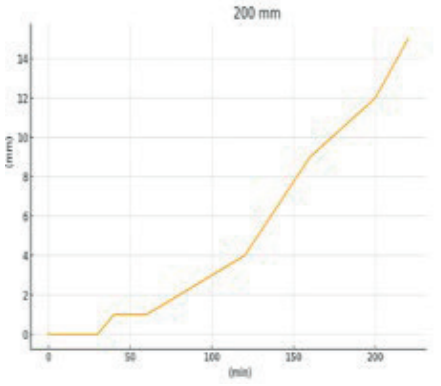



Figure 11. Deformation of the 200 mm thick AAC masonry wall during the test

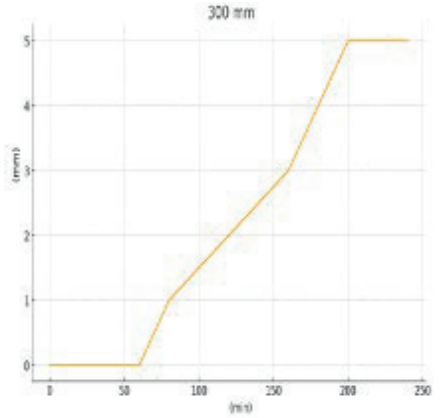



Figure 12. Deformation of the 300 mm thick AAC masonry wall during the test

It is observed that the deformations of the 300 mm thick sample were approximately three times smaller in magnitude than those of the other two samples.

During the fire resistance tests, the three non-load-bearing masonry walls maintained their thermal insulation criterion (*I*) and fire integrity criterion (*E*) as follows:

- For the 150 mm thick wall, criteria *I* and *E* were maintained for 129 minutes and were both lost at minute 130 when criterion *E* failed (Figure 13);



Figure 13. Loss of integrity (E) criterion through the ignition of the cotton pad for the 150 mm thick sample

- For the 200 mm thick wall, the thermal insulation criterion (*I*) and fire integrity criterion (*E*) were maintained for 219 minutes and were both lost at minute 220, when the fire integrity criterion *E* was failed (Figure 14).



Figure 14. Loss of fire integrity criterion (*E*) by ignition of the cotton pad for the 200 mm thick sample

- The 300 mm thick wall did not lose any of its thermal insulation (*I*) or fire integrity (*E*) criteria

until the end of the fire resistance test at minute 244.

The classification of the tested samples into fire resistance classes was conducted by laboratory researchers based on the data from the test reports (total minutes during which the specimens maintained their integrity for fire integrity *E* and thermal insulation *I* criteria) and was performed according to the standard "SR EN 13501-2:2023 Fire classification of construction products and building elements. Part 2: Classification using data from fire resistance and/or smoke control tests, excluding ventilation services".

The fire resistance classes for the three AAC masonry walls were as follows: class *EI 120* for the 150 mm thick AAC masonry wall, class *EI 180* for the 200 mm thick AAC masonry wall, and class *EI 240* for the 300 mm thick AAC masonry wall.

## CONCLUSIONS

Masonry ranks among the oldest structural materials, distinguished by a vast diversity in its units, mortars, and construction techniques. For innovative, affordable, and sustainable building alternatives, Autoclaved Aerated Concrete (AAC) blocks serve as an excellent modern solution (Kałuża, 2024).

This experimental study highlights the importance of laboratory testing in determining the fire resistance of non-load-bearing AAC (Autoclaved Aerated Concrete) masonry walls, which are used in numerous buildings (Daware & Naser, 2021). The research results confirm the applicability and relevance of the testing method in evaluating the fire behaviour of these construction elements, thereby contributing to the consolidation of the national technical framework for implementing the requirements of the new P118-1:2025 Romanian standard regarding the fire safety of buildings (P118, 2025).

Through the experimental research conducted, researchers from INCERC Bucharest contributed to a better understanding of the fire behaviour of these AAC construction elements, ensuring a high level of fire safety for the built environment in our country.

## REFERENCES

Daware, A. & Naser, M.Z., (2021). Fire performance of masonry under various testing methods, *Construction and Building Materials*, 289. 10.1016/j.conbuildmat.2021.123183.

Hammond, G.P. & Jones, C.I, (2008). Embodied energy and carbon in construction materials, *Proceedings of the Institution of Civil Engineers - Energy*, 161(2), 87-98.

Kałuża, M., (2024). AAC-block walls with surface application of non-structural plastering materials as newly configured and improved structures subjected to diagonal compression, *Thin-Walled Structures*, 195, 111459.

Mollaei, S., Babaei Ghazijahani, R., Noroozinejad Farsangi, E. & Jahani, D. (2022), Investigation of Behavior of Masonry Walls Constructed with Autoclaved Aerated Concrete Blocks under Blast Loading, *Appl. Sci*. 12, 8725.

P118, (2025), Fire safety regulations for buildings, Official Gazette of Romania. Part I, nr. 204.

Sherin, K. & Saurabh, J.K., (2018), Review of autoclaved aerated concrete: advantages and disadvantages. In: *Proc Natl Conf Adv Struct Mater Methodol Civ Eng* (ASMMCE–2018). 35–39.

Simion, A. & Dragomir, C., (2025), Fire safety of ETICS based on EPS type polystyrene, *Scientific Papers. Scientific Papers. Series E. Land Reclamation, Earth Observation & Surveying, Environmental Engineering*, Vol XIV, 447-452.

Song, P., Peng, X., Zheng, R. & Xia, J., (2024), Material Properties and Mechanical Performances of Manufactured Factory-Produced Glass Fiber-Reinforced Autoclaved Aerated Concrete Panel. *Buildings*, 14(9), 2895.

Stanescu, A., Lalu, O., Luca, O. & Gaman, F., (2021). Performance of autoclaved aerated concrete (AAC) exposed to standard fire. IOP Conference Series: Earth and Environmental Science. 664. 012028.

Scientific Papers. Series E. Land Reclamation, Earth Observation & Surveying, Environmental Engineering. Vol. XV, 2026
Print ISSN 2285-6064, CD-ROM ISSN 2285-6072, Online ISSN 2393-5138, ISSN-L 2285-6064

# LONG-TERM CHANGES IN AREAS EQUIPPED WITH DRAINAGE AND DEWATERING SYSTEMS UNDER DIFFERENT LAND USES

**Mihaela BALAN[1], Oana Alina NIȚU[2], Cristian POPESCU[1]**

[1]University of Craiova, Faculty of Agronomy, 19 Libertatii Street, Craiova, Romania
[2]University of Agronomic Sciences and Veterinary Medicine of Bucharest,
59 Marasti Blvd, District 1, Bucharest, Romania

Corresponding author email: oanaalinanitu1111@gmail.com

***Abstract***

*This paper examines long-term changes in agricultural and non-agricultural areas equipped with drainage and dewatering systems, which are essential for managing excess moisture and maintaining land functionality. The analysis is based on official national statistical data, complemented by relevant scientific literature, and covers a period of approximately 28 years. The study investigates both the temporal evolution of equipped areas and the influence of different land-use types on hydrological regimes, soil properties, and the operational efficiency of drainage infrastructure. The results indicate an overall declining trend in equipped areas, particularly pronounced for arable land, accompanied by structural shifts among land-use categories. These changes are primarily associated with the progressive degradation of hydrotechnical systems, insufficient financial investment, and land ownership fragmentation. The findings underline the need for integrated drainage and land-use management strategies adapted to current environmental conditions in order to sustain agricultural productivity, protect soil resources, and strengthen the resilience of agroecosystems to climatic variability and the increasing occurrence of extreme weather events.*

***Key words****: dewatering systems, drainage, dynamics, excess moisture, improved land, land reclamation.*

## INTRODUCTION

Soil represents a fundamental component of terrestrial ecosystems and one of the most valuable natural resources for sustaining the existence and development of human society. Through its multiple functions - support for agricultural production, reservoir of water and nutrients, and medium for biological activity - soil plays an essential role in ensuring food security and ecological balance (David et al., 2018; Balan et al., 2024). However, soil is a limited and vulnerable resource, exposed to a wide range of degradation processes that require appropriate protection measures and sustainable management (Musat et al., 2021; Corcheș, 2023; EC Law).

Among the degradation processes with major impact on agricultural productivity is excess moisture, a phenomenon that may occur both at the soil surface, in the form of temporary or permanent waterlogging, and within the soil profile, through groundwater rise or deficient internal drainage. Excess water directly affects the air–water balance in the soil, generating a succession of unfavorable changes in its physical, chemical, and biological properties, with negative consequences for plant growth and development (Lațo et al., 2022; Popescu & Balan, 2024; Yang et al., 2025; FAO, n.d.).

From a pedological perspective, the prolonged presence of excess water leads to the reduction of air-filled porosity and limitation of oxygen diffusion in the root zone, favoring the occurrence of anaerobic conditions (Dollinger, 2016; Baborowski et al., 2021; Nițu et al., 2024). Under such circumstances, processes of gleying and pseudogleying are stimulated, soil structure degrades, and hydraulic permeability decreases (Dollinger, 2016; Birkáš et al., 2021). In advanced cases, excess moisture may contribute to the occurrence of secondary salinization phenomena and to a pronounced decline in the productive capacity of agricultural soils (Manik et al., 2019; Nițu et al., 2024; FAO, n.d.).

The geomorphological diversity and variability of hydrological, hydrogeological, and pedological conditions determine, at national level, a high incidence of land affected by excess moisture, requiring systematic land reclamation interventions. According to

assessments carried out by the Academy of Agricultural and Forestry Sciences, approximately 8.62 million hectares of agricultural land are influenced by this phenomenon: 4.2 million hectares by temporary excess generated by precipitation, 1.97 million hectares by shallow groundwater contribution, and 2.45 million hectares by floods or lateral infiltration from watercourses. Of the total, about 4.55 million hectares require proper drainage, while the remaining areas require differentiated measures depending on irrigation regimes and soil particularities (saline, alkaline). In years with normal pluviometric conditions, excess water affects approximately 5.53 million hectares, predominantly located in floodplains and on heavy clay soils. The major determining factors are: precipitation input under reduced evapotranspiration conditions, deficient natural drainage, and low terrain slopes (De Wrachien & Mambretti, 2012; Lațo et al., 2022).

Under Romania's specific climatic conditions, excess moisture occurs predominantly during spring and early summer, directly interfering with agricultural operations and crop establishment. This leads not only to technological delays but also to quantitative and qualitative production losses (Kulshreshtha & Elshorbagy, 2017). Moreover, global climate change increases the frequency and intensity of extreme meteorological phenomena, raising the risk of floods, prolonged water stagnation, and rapid alternation between episodes of excess moisture and periods of pedological and atmospheric drought (Ilie et al., 2012; Bonea, 2020; Nițu et al., 2025).

In this context, dewatering and drainage works have represented and continue to represent fundamental instruments for managing excess moisture and improving affected agricultural land. Dewatering primarily aims at evacuating stagnant surface water through open channels and land shaping, whereas drainage seeks to remove water from the soil profile and control the groundwater level through subsurface drains or absorbent pipes.

In Romania, dewatering and drainage works experienced significant development over time, reaching a peak in the 1980s, when extensive agricultural areas were integrated into complex hydrotechnical systems. After 1990, however, the existing infrastructure underwent a pronounced degradation process, estimated at 60-80%, due to reduced investments, insufficient maintenance, and land ownership fragmentation resulting from restitution processes (Ursu, 2014). This degradation considerably reduced the efficiency of drainage-dewatering systems and amplified the vulnerability of agricultural land to excess moisture.

Specialized literature highlights that degradation of drainage networks leads to increased frequency of temporary waterlogging, secondary compaction, reduced soil aeration, and diminished microbiological activity, with direct impact on fertility (Skaggs et al., 2012; Ritzema, 2016; de Wit et al., 2022). Furthermore, land-use changes significantly influence water balance, surface runoff, and nutrient transport processes (Blann et al., 2009).

Considering these aspects, the present paper aims to analyze the evolution of areas equipped with dewatering and drainage works, by land-use category at national level, over a 28-year period (1997-2024), based on recent statistical data. The analysis seeks to identify major trends, evaluate the magnitude of changes, and highlight their implications for the functioning and sustainability of agro-systems in Romania, within the current context of climate change and socio-economic pressures.

## MATERIALS AND METHODS

The study regarding the current situation of land equipped with works for combating excess moisture was based on the use of official statistical data series, supplemented by information from specialized literature. The main sources were the National Institute of Statistics, the National Agency for Land Reclamation, and the Ministry of Agriculture and Rural Development.

For characterizing the recent stage of developments, average values corresponding to the 2020–2024 interval were used, while for highlighting the temporal evolution, reference data for the years 1997, 2007, and 2017 were analyzed. The integration of these benchmarks allowed the outlining of a dynamic image of the changes recorded over approximately 28 years.

The processing of information aimed at quantifying the share of different land-use categories within the equipped areas, applying the percentage method for the synthetic expression of results. In parallel, data interpretation was supported by reference to existing scientific contributions, in order to understand the structural and functional framework of dewatering and drainage works.
The analytical methodology included: descriptive statistical analysis, used to highlight levels, distributions, and trends of the equipped areas; as well as comparative analysis, through which differences between reference periods and the directions of evolution of land reclamation infrastructure were evaluated. Through this approach, the performance of dewatering and drainage works was assessed from the perspective of quantitative dimension and transformations produced over time.

## RESULTS AND DISCUSSIONS

According to Table 1, the average values for the 2020-2024 interval highlight the existence of a total area equipped for combating excess moisture of 3,198,803 ha, of which the agricultural component amounts to 2,949,913 ha (92.22%).

Table 1. Situation of land equipped with dewatering and drainage works (Average 2020-2024)

| No. | Land use category | Area* -ha- | % of total equipped** |
|---|---|---|---|
| 1 | Total equipped area | 3,198,803 | 100 |
| 2 | Equipped agricultural area | 2,949,913 | 92.22 |
| 3 | Arable land | 2,553,962 | 79.84 |
| 4 | Natural pastures | 256,820 | 8.03 |
| 5 | Natural hayfields | 109,943 | 3.44 |
| 6 | Vineyards and vine nurseries | 15,676 | 0.49 |
| 7 | Orchards and fruit nurseries | 13,512 | 0.42 |
| 8 | Equipped non-agricultural area | 248,890 | 7.78 |

* http://statistici.insse.ro:8077/tempo-online/#/pages/tables/insse-table (15.12.2025)
**Own calculations

The data confirm the predominantly agricultural orientation of dewatering and drainage infrastructure, while non-agricultural land represents a marginal share of only 7.78% (Figure 1).

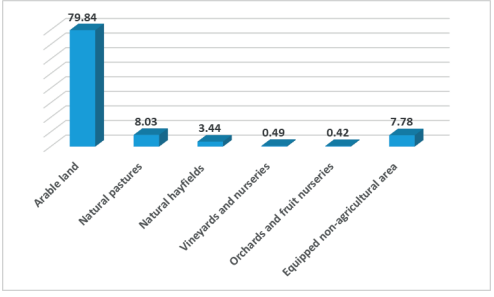



Figure 1. Structure of areas equipped with dewatering and drainage works

Within the equipped agricultural fund, the structure is strongly concentrated in the arable category, which totals 2,553,962 ha, representing 79.84% of the total area. This dominance indicates the historical direction of investments toward land with the greatest contribution to crop production and high exposure to risks generated by water stagnation. Practically, the functionality of dewatering and drainage systems becomes critical for the stability of the major segment of agricultural production.
Natural pastures and hayfields together account for approximately 11.47%, suggesting a secondary importance granted to these uses compared to field crops. At the opposite pole, permanent plantations (vineyards and orchards) hold subunitary shares, each below the 1% threshold. The distribution may be correlated with the frequent location of these categories in hilly or mountainous areas, where natural drainage is more efficient and the necessity for extensive technical interventions is lower.
From a systemic perspective, the overwhelming concentration of developments within the arable area implies a major dependence of national agricultural performance on the technical condition of existing infrastructure. Any process of degradation, underfunding of maintenance, or loss of functionality may generate disproportionate effects on production

volume. The current configuration of areas also reflects the evolution of scientific concepts and development practices, which favored systematic interventions in regions characterized by persistent excess moisture and high agricultural potential.

The evolution of areas equipped with dewatering and drainage works was marked by accelerated expansion in the second half of the twentieth century. If in 1944 approximately 358 thousand hectares were recorded as equipped, infrastructure expansion continued steadily in the following decades, exceeding 0.5 million hectares in the mid-1950s and approaching 0.8 million hectares in 1965. Investment rhythm intensified subsequently, so that by 1975 the area reached nearly 2 million hectares, and in the early 1980s it exceeded 2.5 million hectares. The maximum level of development was reached at the end of the ninth decade, when total developments rose to over 3.2 million hectares.

After this peak period, data indicate a reduction in functional area. At the end of the 1990s, land under the administration of the National Agency for Land Reclamation totalled approximately 3.2 million hectares, with water evacuation carried out both by pumping and gravitational means, the two modalities having relatively similar shares. The system was served by a complex technical ensemble, including hundreds of developments, thousands of kilometres of canals and drains, pumping stations, as well as numerous auxiliary crossing and regulation constructions.

The long-term functionality of these works depended essentially on the operating regime and permanent monitoring of soil property evolution. Institutional transformations after 1990, however, modified the framework of use. The pronounced fragmentation of land associated with property restitution processes did not take into account the geometry of underground networks, many parcels being delimited without correlation to drain positions. In parallel, the lack of maintenance interventions led to accelerated infrastructure degradation. Numerous constructive elements were affected, including slope reinforcements, connections between sectors, and flow control points, which considerably reduced the operational capacity of systems.

Following this background, the comparative analysis of the years 1997, 2007, 2017, and the average of the 2020-2024 period allows capturing the recent trajectory of equipped areas and evaluating the extent to which previous investment legacy was maintained or, on the contrary, eroded over time.

The data synthesized in Table 2 show that, following the high levels recorded at the end of the previous century, infrastructure intended to combat excess moisture entered a process of slow but continuous contraction.

Table 2. Dynamics of land equipped with dewatering and drainage works at national level (ha)

| No. | Land Use Category | Year | | | | | | |
|---|---|---|---|---|---|---|---|---|
| | | 1997* | 2007* | | 2017 | | 2020-2024**Average | |
| | | Absolute area (ha) | Absolute area (ha) | ±Δ1997 vs 2007** | Absolute area (ha) | ±Δ 1997 vs 2007** | Absolute area (ha) | ±Δ1997 vs Average 2020-2024** |
| 1 | Total equipped area | 3,198,803 | 3,152,484 | -46,319 | 3,149,953 | -48,850 | 3,146,514 | -52,289 |
| 2 | Equipped agricultural area | 2,949,913 | 2,911,441 | -38,472 | 2901207 | -48,706 | 2,893,743.4 | -56,169.6 |
| 3 | Arable land | 2,553,962 | 2,511,146 | -42,816 | 2504153 | -49,809 | 2,497,002.2 | -56,959.8 |
| 4 | Natural pastures | 256,820 | 262,148 | +5,328 | 259057 | +2,237 | 258,890 | +2,070 |
| 5 | Natural hayfields | 109,943 | 110,762 | +819 | 111079 | +1,136 | 110,933.2 | +990.2 |
| 6 | Vineyards and vine nurseries | 15,676 | 147,56 | -920 | 14677 | -999 | 14,677 | -999 |
| 7 | Orchards and fruit nurseries | 13,512 | 12,629 | -883 | 12241 | -1,271 | 12,241 | -1,271 |
| 8 | Equipped non-agricultural area | 248,890 | 241,043 | -7,847 | 248746 | -144 | 252,770.6 | +3,880.6 |

* http://statistici.insse.ro:8077/tempo-online/#/pages/tables/insse-table (15.12.2025)
** Own calculations

Reference to the base year 1997 shows a reduction of total area by over 46 thousand hectares by 2007, a trend confirmed by subsequent evolution, so that the difference compared to the 2020–2024 average exceeds 52 thousand hectares (Figure 2).

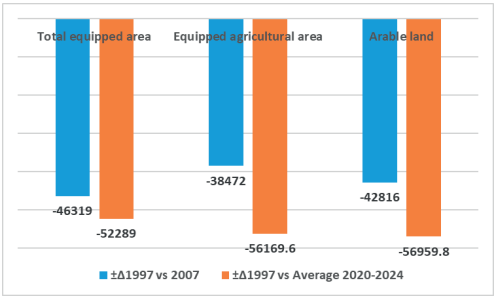



Figure 2. Dynamics of equipped areas – total, agricultural, and arable (ha; ±Δ compared to 1997)

The descending trajectory is also visible in the graphical representation of total, agricultural, and arable areas (Figure 3), where the negative slope is maintained throughout the analyzed interval.

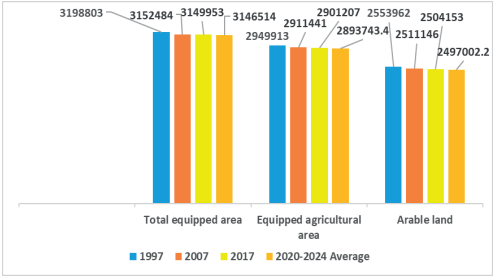



Figure 3. Dynamics of equipped areas – total, agricultural, and arable (ha)

The equipped agricultural area follows the same pattern, indicating that structural adjustments primarily targeted productive land. According to Table 2, the cumulative decrease between 1997 and the recent period exceeds 56 thousand hectares.

The largest contribution to the decline belongs to arable land. The initial reduction, of over 42 thousand hectares in the first decade, is followed by an additional decrease, so that at the level of the 2020-2024 average, total loss approaches 57 thousand hectares compared to the base year (Table 2). The higher intensity of withdrawal in the first part of the interval is clearly reflected in the dynamics presented in Figure 2.

In contrast to this trend, extensive uses show limited variations. Natural pastures mark an increase in the initial stage, followed by minor adjustments, but the final balance remains positive compared to 1997 (Figure 4).

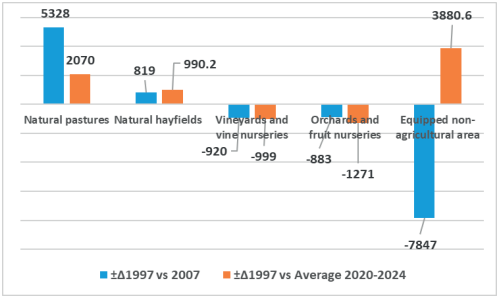



Figure 4. Dynamics of equipped areas – pastures, hayfields, vineyards, orchards, and non-agricultural land (ha; ±Δ compared to 1997)

Natural hayfields indicate similar stability, with small amplitude oscillations. These trends are detailed in Table 2 and graphically represented in Figure 5, where the curves associated with these categories exhibit a relatively stable, near-horizontal trajectory.

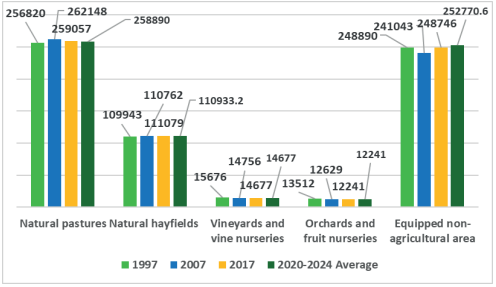



Figure 5. Dynamics of equipped areas – pastures, hayfields, vineyards, orchards, and non-agricultural land (ha)

For permanent plantations (vineyards and orchards), data reveal a constant reduction of equipped areas. Both vineyards and orchards register decreases of close to one thousand hectares compared to the initial level, a trend simultaneously confirmed by the tabular values and the representation in Figure 4.

In the case of non-agricultural areas, dynamics reveal an oscillatory course: after the decrease in the first stage, a recovery follows which, in

the recent interval, exceeds the level recorded in 1997. The interpretation of this evolution, however, requires caution, as it may reflect both the influence of administrative reclassifications and the effects of urban expansion and development of transport, industrial, and residential infrastructure, contexts in which the drainage function shifts from supporting agricultural use to protecting constructions and limiting flood risk or groundwater rise.

Overall, the correlation of numerical information with graphical representations outlines the image of a system undergoing gradual capacity decline, a phenomenon concentrated especially in the arable sector, where dependence on dewatering and drainage functioning is maximal.

Viewed as a whole, the data and graphical representations converge toward the same conclusion: the system has continuously lost area after 1997, with the main impact concentrated on arable land, where dependence on drainage functionality is highest. At the same time, the other categories showed either stability or limited variations, without altering the dominant structure of developments.

## CONCLUSIONS

The long-term assessment of areas equipped with dewatering and drainage works highlights the emergence of a persistent trajectory of declining functionality of hydrotechnical infrastructure.

The identified trends exceed the level of simple statistical adjustments and indicate the manifestation of a cumulative decapitalization process, resulting from the interaction between financial constraints, institutional transformations, and continuous erosion of maintenance capacity.

In this framework, multiple technical evaluations show that after 1990 a major proportion of constructions related to canal networks evolved toward advanced states of degradation. The lack of systematic maintenance interventions and desilting operations led to the deterioration of slope protections, affecting crossing and connection zones, as well as reducing the efficiency of flow regulation and measurement structures. The direct consequence is the progressive restriction of effectively serviced areas and the reduction of overall system performance.

From a conceptual perspective, dewatering and drainage infrastructure must be understood as a determinant of the adaptive capacity of agroecosystems. As its functional area decreases, the ability of the agricultural system to buffer hydrological variability declines, and land users tend to adopt cautious strategies oriented toward risk limitation rather than production intensification.

The persistence of these processes favors the establishment of path-dependence mechanisms, in which each year of underinvestment amplifies the difficulty and costs of potential restoration. In the absence of coordinated interventions, vulnerability becomes a structural rather than conjunctural characteristic.

Looking toward the future, climate projections for Central and Eastern Europe indicate an increase in the frequency of hydrological extremes, with more pronounced alternations between intense precipitation and prolonged water deficit periods. In such a context, existing systems will be subjected simultaneously to the requirement of rapid evacuation of excess volumes and the necessity of conserving resources during drought intervals. For arable land, where development concentration is dominant, this variability may exceed the initial design parameters of infrastructure. Without technological modernization and adoption of flexible operating mechanisms, the efficiency of works risks declining, and exposure of agricultural production to hazard increasing.

At the same time, modification of hydric regimes has the potential to redraw the map of intervention needs, transforming areas considered today relatively stable into future investment priorities.

In the context of increasing climatic variability and the growing frequency of extreme hydrological events, the development of drainage and dewatering infrastructure should be directed toward:

- the systematic rehabilitation of existing networks and the modernization of pumping stations;

- the integration of drainage systems with water retention and reuse facilities;
- the updating of design parameters in accordance with emerging climate scenarios;
- the strengthening of the institutional framework and the provision of multiannual financing mechanisms;
- the implementation of digital water-level monitoring systems.

Drainage infrastructure can no longer be addressed solely as a water evacuation mechanism; rather, it must be integrated into an adaptive water resources management strategy, essential for maintaining agricultural productivity and reducing the vulnerability of agroecosystems.

By integrating statistical evidence with institutional and climatic interpretation, the study provides an analytical framework transferable to numerous regions confronted with aging infrastructure. The central message is clear: passivity does not preserve infrastructure but accelerates its functional decline, leading to more rapid deterioration.

## REFERENCES

Baborowski, M., Rupp, H., Wendt-Potthoff, K., Tauchnitz, N., & Meissner, R. (2021). Factors affecting the spatial and temporal variability of metals in drainage water from arable fields. *Clean - Soil Air Water*, 49(6).

Balan, M., Nitu, O.A., & Popescu, C. (2024). The evolution of soil agrochemical properties, under the influence of mineral fertilisation and water erosion, on a natural grassland located at the Preajba Experimental Centre in the Gorj county. *Scientific Papers. Series A. Agronomy*, LXVII, 1, ISSN 2285-5785, 25-31.

Birkáš, M., Jug, D., Kisić, I., Kassai, KM, Tarnawa, Á. & Jolánkai, M. (2021). Water management in the soil-plant system – a challenge for the 21st century. *Acta Horticulturae et Regiotecturae*, 24, 16-19.

Blann, K. L., Anderson, J. L., Sands, G. R., & Vondracek, B. (2009). Effects of agricultural drainage on aquatic ecosystems: a review. *Critical reviews in environmental science and technology*, 39(11), 909-1001.

Bonea, D. (2020). Grain yield and drought tolerance indices of maize hybrids. *Notulae Scientia Biologicae*, 12(2), 376–386.

Corcheș, M.T. (2023), Land degradation and climate change. *Scientific Papers. Series E. Land Reclamation, Earth Observation & Surveying, Environmental Engineering,* XII, Print ISSN 2285-6064, 68-73.

David, G., Țărău, D., Sandor, C., & Niță, L. (2018). Soil and climate factors that define land productivity in the lower plain of Banat. *International Multidisciplinary Scientific GeoConference: SGEM*, 18(3.2), 465–472.

De Wrachien, D., & Mambretti, S. (2012). Mathematical models in flood management: overview, laboratory tests and case study. In S. Mambretti (Ed.), *Flood Risk Assessment and Management*, Wit Press, 11-22.

Dollinger, J. (2016). *Analysis and modelling of pesticide transfer and retention in infiltration ditches on the farm according to different management strategies*. *HAL (Le Centre Pour La Communication Scientifique Directe).*

Ilie, L., Mihalache, M., Marin, D.I., Scăețeanu, G. (2012). Climatic conditions and evolution of soil profiles in Romania. *Annals of the University of Craiova-Agriculture, Montanology, Cadastre Series*, 42(2), 118–123.

de Wit, J. A., Ritsema, C. C., van Dam, J. J., van den Eertwegh, G. G., & Bartholomeus, R. R. (2022). Development of subsurface drainage systems: Discharge – retention – recharge*, Agricultural Water Management, 269, 107677.*

Kulshreshtha, S. & Elshorbagy, A. (2017). Current perspective on irrigation and drainage. *InTech eBooks*.

Lațo K.I., Lațo A., Nita D.L., Duma-Copcea A., & Corches M.T. (2022). Pedo-genetical factors implicated in soil degradation (lower Timis River basin area). *Scientific Papers. Series A. Agronomy*, LXV, 1, ISSN 2285-5785, 91-96.

Manik, S.M.N., Pengilley, G., Dean, G., Field, B.G., Shabala, S. & Zhou, M. (2019). Soil and crop management practices to minimise the impact of floods on crop productivity. *Frontiers in Plant Science*, 10, 140. Frontiers Media. https://doi.org/10.3389/fpls.2019.00140

Musat, I.B., Ciceoi, R., Musat, M., & Mihalache, M. (2021). Changes of physical properties in soils under traditional soil management in arable crops, in the southern part of Romania. *Scientific Papers. Series A. Agronomy*, LXIV, 1, ISSN 2285-5785, 112-118.

Nițu, O. A., Jerca, I. O., & Bălan, M. (2024). Drip irrigation efficiency in soybean cultivation in southeast Romania, a sustainable approach to water management. *Scientific Papers. Series E. Land Reclamation, Earth Observation & Surveying, Environmental Engineering*, 13, 585-591.

Nițu O.A., Jerca I.O., Balan M., & Ivan E.Ș., (2025). Water use efficiency in irrigated agriculture in Romania: optimization strategies in the context of climate change. *Scientific Papers. Series E. Land Reclamation, Earth Observation & Surveying, Environmental Engineering*. XIV, 705-710.

Popescu C., & Balan M., (2024). Evaluation through natural bonitation work of the soils in the zone of confluence of Dolj and Mehedinti Counties and the estimation of crop plant productions specific to the area. *Scientific Papers Series Management, Economic Engineering in Agriculture and Rural Development*. 24, 2, ISSN 2284-7995, 809-816.

Ritzema, H. P. (2016). Drain for Gain: Managing salinity in irrigated lands - A review. *Agricultural Water Management,* 176, 18-28.

Skaggs, R. W., Fausey, N. R., & Evans, R. O. (2012). Drainage water management. Journal of soil and water conservation, 67(6), 167A-172A. Discharge–Retention–recharge. *Agricultural water management*, 269, 107677.

Ursu, A. (2014). Agrarian Economy and Rural Development - Realities and Prospects for Romania. *SSRN Electronic Journal.*

Yang, T., Jiang, J., He, Q., Shi, F., Jiang, H., Wu, H., He, C. (2025). Impact of drainage on peatland soil environments and greenhouse gas emissions in northeast China. *Scientific Reports*, 15(1), 8320.

https://www.anif.ro/ ANIF (2025) - Administratia Nationala a Imbunatatirilor Funciare

http://statistici.insse.ro:8077/tempo-online/#/pages/tables/insse-table

https://www.fao.org/home/en

https://www.madr.ro/

https://commission.europa.eu/law_en

Scientific Papers. Series E. Land Reclamation, Earth Observation & Surveying, Environmental Engineering. Vol. XV, 2026
Print ISSN 2285-6064, CD-ROM ISSN 2285-6072, Online ISSN 2393-5138, ISSN-L 2285-6064

# MOBILE WASTEWATER TREATMENT SYSTEMS FOR CIRCULAR WATER REUSE: TECHNOLOGIES, APPLICATIONS AND THE ROMANIAN GAP IN THE EUROPEAN CONTEXT

**Sabrina-Maria BĂLĂNESCU[1], Carmen Otilia RUSĂNESCU[1], Ana VÎRSTA[2], Daniela MIHAI[1], Ionela Alexandra ION[1], Elena Denisa PREDESCU[1], Elena Roxana FRÎNCU[1]**

[1]National University of Science and Technology POLITEHNICA Bucharest, 313 Splaiul Independenței, District 6, Bucharest, Romania
[2]University of Agronomic Sciences and Veterinary Medicine of Bucharest, 59 Marasti Blvd, District 1, Bucharest, Romania

Corresponding author email: sabrina.balanescu1@gmail.com

***Abstract***

*This study investigates the transition from conventional wastewater treatment toward circular water management within the European Union, with a particular focus on the role of mobile and decentralized treatment systems. Despite considerable progress at EU level, major disparities persist in infrastructure coverage, wastewater reuse and resource recovery performance among Member States. A structured literature review and comparative analytical framework were applied to evaluate wastewater treatment technologies, circular economy pathways and implementation indicators, integrating data from Eurostat, the European Environment Agency and national Romanian statistics. The results show that 80–81% of the EU population is connected to at least secondary wastewater treatment, while Romania remains significantly below this level (60.7%), with over 150 non-compliant agglomerations. The analysis indicates that three dominant circular wastewater valorisation pathways can be identified in the EU context: water reuse, agricultural sludge valorisation and thermal nutrient recovery. In contrast, Romania remains in a transitional stage, characterized by limited reuse, low sludge valorisation (21.3% vs. EU average 37.3%) and limited deployment of advanced nutrient recovery systems. The study demonstrates that mobile wastewater treatment systems can function as transitional circular infrastructure, enabling localized treatment, resource recovery and reuse. Their flexibility and rapid deployment capacity position them as potentially strategic solutions for bridging infrastructure gaps and accelerating the implementation of circular water systems in emerging contexts.*

***Key words****: circular economy, resource recovery, mobile wastewater treatment systems, wastewater reuse.*

## INTRODUCTION

Water scarcity and increasing pressure on freshwater resources represent major global challenges driven by population growth, industrialization and climate change. Although freshwater accounts for only approximately 2.5% of global water resources, demand is expected to increase significantly by 2050, particularly due to agriculture, which already accounts for 70% of global freshwater withdrawals (Maniam et al., 2022; Hamam et al., 2024). At the same time, up to 80% of wastewater worldwide is discharged without adequate treatment, leading to environmental pollution and loss of valuable resources (Yang et al., 2020).

In Europe, up to 30-32% of the population experiences seasonal water stress (EEA, 2023b), highlighting the urgency of more sustainable water management approaches. Traditional wastewater management follows a linear model focused on pollutant removal, without fully valorising wastewater as a source of water, nutrients and energy (Van Loosdrecht & Brdjanovic, 2014).

The circular economy framework promotes the transformation of wastewater treatment plants into Water Resource Recovery Facilities (WRRFs), enabling water reuse and resource recovery (Larsen et al., 2016; Smol, 2023). Wastewater reuse supports agricultural, industrial and urban applications, contributing to water security (EEA, 2023a).

In this context, decentralized and mobile wastewater treatment systems represent a key technological extension, enabling on-site treatment and local reuse while reducing

dependence on centralized infrastructure (Capodaglio & Olsson, 2020; Mannina et al., 2022). These systems also support resource recovery pathways, including energy generation and nutrient recycling, positioning them as flexible tools for circular water management.

However, the transition toward circular wastewater systems remains uneven across the European Union, particularly in emerging Member States where infrastructure deficits and limited resource recovery hinder implementation. Romania represents a relevant case study, characterized by gaps in connectivity, treatment performance and circular economy integration.

Against this background, this study analyses mobile wastewater treatment systems as transitional circular infrastructure, integrating technological performance, resource recovery pathways and system-level implementation. The study develops a multi-level analytical framework, compares EU and Romania indicators, and positions mobile systems as enabling solutions for bridging infrastructure gaps and accelerating circular water management.

Figure 1 presents the flow of wastewater from multiple sources (domestic, industrial and agricultural) through treatment processes, enabling water reuse and the recovery of valuable resources such as nutrients, biofuels and bio-based products. The framework highlights the role of wastewater treatment plants as resource recovery hubs within circular economy systems.

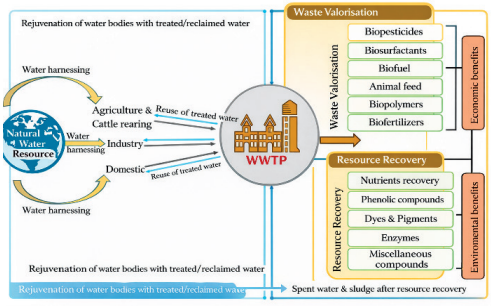



Figure 1. Integrated circular wastewater management framework: water reuse and resource recovery pathways (Singh et al., 2022)

Figure 2 illustrates the conceptual framework of circular wastewater management, emphasizing the integration of treatment technologies, resource recovery pathways, and water reuse applications, with mobile systems serving as a bridge toward circular economy implementation.

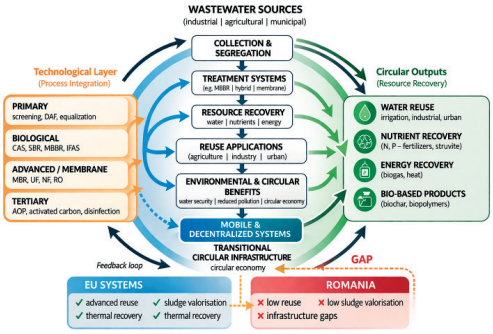



Figure 2. Conceptual framework of circular wastewater management integrating technological processes, resource recovery pathways, and reuse applications. The conceptual illustration was generated with the assistance of ChatGPT (OpenAI) based on the literature synthesized in this review and refined by the authors for visualization purposes

Unlike previous studies that primarily focus on either technological performance or circular economy pathways independently, this research develops a multi-level analytical framework that simultaneously integrates technological efficiency, resource recovery potential and system-level implementation gaps. In addition, the study offers one of the first structured comparative analyses between the European Union and Romania, highlighting the discrepancy between regulatory alignment and practical implementation.

## MATERIALS AND METHODS

This study is based on a structured literature review combined with a comparative analytical framework. The literature review was conducted using major scientific databases, including Web of Science, Scopus and ScienceDirect, covering the period 2000-2025.

The search strategy included combinations of the following keywords: “wastewater reuse”, “circular economy”, “mobile wastewater treatment”, “decentralized systems”, “membrane bioreactor (MBR)”, “resource recovery”, and “nutrient recovery”. Only peer-

reviewed journal articles, official reports (European Commission, Eurostat, European Environment Agency) and highly cited review papers were considered.

The selection process followed three main criteria:

(i) relevance to circular wastewater management and reuse,

(ii) availability of quantitative performance data (removal efficiencies, energy, cost),

(iii) applicability to decentralized or mobile treatment systems.

Studies focusing exclusively on conventional treatment without relevance to circularity or reuse were excluded. In total, over 100 publications were screened, and approximately 70 sources were selected for detailed analysis.

Comparative tables and figures were developed through normalization of reported data ranges and semi-quantitative synthesis. The EU–Romania comparison was conducted using official datasets from Eurostat, the European Environment Agency and National Institute of Statistics (NIS), complemented by European Commission reports on directive implementation.

The reported values represent indicative ranges derived from heterogeneous sources and should be interpreted as comparative benchmarks rather than absolute values.

## RESULTS AND DISCUSSIONS

### *Wastewater reuse and circular economy pathways*

Wastewater reuse is a key strategy for increasing water availability and reducing environmental pollution, providing an alternative resource for agriculture, industry and urban applications (Angelakis & Snyder, 2015; Silva, 2023). Agriculture remains the dominant reuse sector due to its high-water demand and the additional benefit of nutrient supply, reducing the need for synthetic fertilizers (Yang et al., 2020). Industrial reuse further contributes to water savings through applications such as cooling and process water (Nydrioti & Grigoropoulou, 2025).

From a circular economy perspective, wastewater treatment enables resource recovery, including nutrients (nitrogen and phosphorus) and energy through anaerobic digestion, supporting renewable energy production (Kyllönen et al., 2021). Overall, these approaches reduce freshwater withdrawals, limit pollutant discharge and support the transition toward circular water management systems (Hamam et al., 2024).

### *Treatment technologies for circular and mobile systems*

Wastewater treatment technologies for circular reuse and mobile applications must ensure high removal efficiency, operational flexibility and compact design. Biofilm-based systems such as moving bed biofilm reactors (MBBR) and integrated fixed-film activated sludge (IFAS) provide improved biomass retention and resilience under variable loading conditions, making them particularly suitable for decentralized systems (Ştefănescu et al., 2019; Surdu, et al., 2021).

Membrane technologies (MF, UF, NF, RO), particularly membrane bioreactors (MBR), enable the production of high-quality effluent suitable for reuse by ensuring efficient removal of suspended solids, pathogens and organic contaminants. However, membrane fouling and energy demand remain important operational challenges (Gkotsis et al., 2018; Yang et al., 2020). Hybrid treatment systems integrating biological processes, membrane filtration and advanced treatment steps (e.g., adsorption and advanced oxidation) can achieve removal efficiencies exceeding 90% for conventional pollutants and high removal rates for micropollutants, while maintaining compact configurations suitable for mobile applications (Luo et al., 2014; Meng et al., 2017).

Energy consumption remains a critical constraint, with aeration representing a significant share of total energy demand. Process intensification strategies such as partial nitrification–Anammox can reduce oxygen requirements and improve overall efficiency.

From a circular economy perspective, these technologies enable resource recovery through nutrient reuse and energy production via anaerobic digestion, supporting renewable energy generation and reducing sludge volumes.

Mobile systems are designed as compact, modular units integrating multiple treatment stages, including biological reactors, membrane filtration and disinfection, with the possibility of

advanced reuse (Meng et al., 2017). Their main advantages include rapid deployment, operational flexibility and local water reuse, particularly in industrial, agricultural and remote applications (Capodaglio & Olsson, 2020).

However, their treatment capacity is lower than that of centralized systems, and performance may be affected by influent variability and operational complexity (Mannina et al., 2022). Overall, mobile systems represent flexible and scalable solutions supporting localized circular water management and improved resource efficiency (Larsen et al., 2016).

Table 1 summarizes the main technological limitations in livestock wastewater treatment, together with their operational causes, proposed technological solutions, and potential performance improvements.

Figure 3 presents a qualitative technology–wastewater compatibility matrix, illustrating the applicability of different treatment technologies to various wastewater types based on published literature.

Table 1. Comparison of Technological Limitations and Technological Integrations

| Technological Limitation | Measurable Indicator / Effect | Operational Cause | Proposed Emerging Technologies | Quantified Potential Improvement |
|---|---|---|---|---|
| **High energy consumption** | Aeration accounts for 40-60% of total plant energy use | Continuous aeration for biomass maintenance | Energy-efficient aeration systems, real-time DO control, membrane aeration | 15-30% energy reduction (DO optimization & pulsed aeration) |
| **High sludge production** | Increased MLSS & MLVSS | Excess aerobic biomass with limited valorisation | Advanced anaerobic digestion, enzymatic hydrolysis, pyrolysis | 20-50% sludge reduction, conversion to biogas |
| **Sensitivity to flow variations** | Unstable DO, non-compliant BOD/COD | Variable hydraulic and organic loading | Equalization tanks + AnSBR + adaptive control systems | 10-25% improvement in effluent stability |
| **Inefficient nutrient removal** | $NO_3^-$ > 10 mg/L, TP > 1 mg/L | Incomplete nitrification–denitrification | Anammox processes, biofilm systems (IFAS), MBBR | 30–50% total nitrogen reduction without additional aeration |
| **Large footprint** | Space requirement > 5–10 $m^3$/PE | Conventional large-scale tank processes | MBR, SBR, IFAS, modular systems | 40-70% footprint reduction (MBR systems) |
| **Membrane fouling (in MBR)** | Reduced flux, increased TMP | Membrane surface deposition | Automatic backwash, CIP cleaning, advanced hydrodynamic modules | 2-3× increase in cleaning intervals |
| **Poor micropollutant removal** | Presence of compounds > µg/L | Conventional biological processes not adapted | Advanced oxidation processes (AOP), activated carbon adsorption, UV-$H_2O_2$ | 70-95% micropollutant removal |
| **Biological instability (toxic shocks)** | DO fluctuations, non-compliant BOD | Industrial toxic loads | Adaptive AnSBR systems, IFAS hybrid biofilm systems | 2-4× improved performance under shock loads |
| **High maintenance costs** | High OPEX | Traditional mechanical equipment | SCADA/IoT automation, online sensors | 10-25% OPEX reduction |
| **Limitations in advanced water reuse** | Residual N/P/salts concentrations | Lack of tertiary treatment processes | UF/NF/RO + AOP + biofilters | Effluent suitable for potable or industrial reuse |

Source: author's synthesis based on literature review.

| Technology | Municipal | Domestic | Industrial | Oily | Nutrient-rich | Secondary treated | Saline | Septic sludge | Organic-rich |
|---|---|---|---|---|---|---|---|---|---|
| Activated Sludge (CAS) | 1 | 0 | 0 | 0 | 0 | 0 | 0 | 0 | 0 |
| Sequencing Batch Reactor (SBR) | 0 | 1 | 0 | 0 | 0 | 0 | 0 | 0 | 0 |
| (MBBR) | 1 | 0 | 1 | 0 | 0 | 0 | 0 | 0 | 0 |
| Membrane Bioreactor (MBR) | 1 | 0 | 1 | 0 | 0 | 0 | 0 | 0 | 0 |
| Anaerobic MBR (AnMBR) | 0 | 0 | 1 | 0 | 0 | 0 | 0 | 0 | 0 |
| Ultrafiltration (UF) | 0 | 0 | 0 | 0 | 0 | 1 | 0 | 0 | 0 |
| Nanofiltration (NF) | 0 | 0 | 1 | 0 | 0 | 0 | 0 | 0 | 0 |
| Reverse Osmosis (RO) | 0 | 0 | 1 | 0 | 0 | 0 | 1 | 0 | 0 |
| Electrocoagulation (EC) | 0 | 0 | 1 | 0 | 0 | 0 | 0 | 0 | 0 |
| Coagulation–Flocculation | 1 | 0 | 1 | 0 | 0 | 0 | 0 | 0 | 0 |
| Dissolved Air Flotation (DAF) | 0 | 0 | 1 | 1 | 0 | 0 | 0 | 0 | 0 |
| Constructed Wetlands | 1 | 0 | 0 | 0 | 0 | 0 | 0 | 0 | 0 |
| High Rate Algal Ponds (HRAP) | 1 | 0 | 0 | 0 | 0 | 0 | 0 | 0 | 0 |
| systems) | 0 | 0 | 0 | 0 | 1 | 0 | 0 | 0 | 0 |
| (ABR) | 0 | 1 | 0 | 0 | 0 | 0 | 0 | 0 | 0 |
| Denitrifying Biofilter | 0 | 0 | 0 | 0 | 0 | 1 | 0 | 0 | 0 |
| Membrane contactor (nutrient recovery) | 0 | 0 | 0 | 0 | 1 | 0 | 0 | 0 | 0 |
| Hybrid membrane systems (MBR + RO) | 0 | 0 | 1 | 0 | 0 | 0 | 0 | 0 | 0 |
| Microbial Fuel Cells (MFC) | 0 | 0 | 0 | 0 | 0 | 0 | 0 | 0 | 1 |
| systems | 0 | 0 | 1 | 0 | 0 | 0 | 0 | 1 | 0 |

Figure 3. Technology-wastewater compatibility matrix for circular water reuse systems (1 = the technology is suitable for that type of wastewater, 0 = not suitable)

The matrix was constructed using a binary classification approach (0-1), where each wastewater treatment technology was mapped to its most suitable wastewater types based on reported applications. Technologies were assigned to multiple categories where applicable. The heatmap represents a qualitative synthesis of technological applicability rather than a quantitative performance comparison.

The matrix highlights the heterogeneous applicability of wastewater treatment technologies across different wastewater types. Universally applicable systems such as MBR and MBBR contrast with more specialized technologies such as RO, DAF and membrane contactors, supporting the need for hybrid and modular configurations in mobile wastewater treatment systems.

Technologies were assigned to reuse categories based on keyword identification within the reuse target field (e.g., irrigation, industrial, urban, high-quality). Technologies could be included in multiple categories where applicable.

The reuse distribution was obtained through a qualitative classification of wastewater treatment technologies based on their reported reuse targets. A keyword-based approach was applied to categorize each technology into four reuse pathways (irrigation, industrial, urban and high-quality reuse), allowing multiple assignments per technology. The results represent a comparative synthesis of technological applicability rather than a quantitative performance assessment.

Figure 4 was constructed using a semi-quantitative scoring approach. Mobility levels were classified on a five-point scale (1 = low, 5 = very high) based on system transportability and deployment flexibility. Circular economy output was evaluated using a qualitative scoring system reflecting the potential for water reuse, nutrient recovery and energy generation. Bubble size represents the versatility of each technology, defined as the number of applicable wastewater types identified in the dataset.

To illustrate the versatility of mobile treatment systems, Table 2 presents the main wastewater streams, their characteristic pollutants, suitable treatment technologies, and potential reuse options.

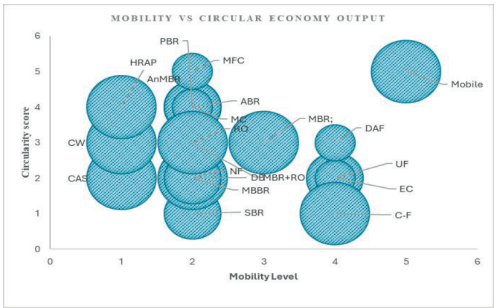



Figure 4. Mobility level versus circular economy output of wastewater treatment technologies

Table 2. Typology of Wastewater Streams Suitable for Mobile Treatment Systems

| Wastewater source | Typical pollutants | Suitable mobile treatment technologies | Potential reuse applications | References |
|---|---|---|---|---|
| **Petrochemical / refinery wastewater** | hydrocarbons, oils, COD, suspended solids | oil separators, DAF, electrocoagulation, MBR, activated carbon, RO | industrial reuse, cooling water, process water | Meng et al., 2017; Yang et al., 2020 |
| **Food industry wastewater** | high COD, BOD, fats, organic matter | DAF, SBR, MBBR, MBR, biological treatment + filtration | irrigation reuse, industrial cleaning water | Maniam et al., 2022; Khaki et al., 2026 |
| **Livestock wastewater** | organic matter, nitrogen, phosphorus, pathogens | biological treatment, MBBR, MBR, anaerobic digestion | agricultural irrigation, nutrient recycling | Obijianya et al., 2025 |
| **Municipal wastewater (small communities)** | COD, BOD, nutrients, pathogens | SBR, MBBR, compact activated sludge, membrane filtration | irrigation, landscape watering, groundwater recharge | Garrido-Baserba et al., 2024 |
| **Construction sites / temporary camps** | suspended solids, organic matter | compact biological treatment, filtration, UV disinfection | local reuse, environmental discharge | Lakho et al., 2020 |
| **Emergency / humanitarian wastewater** | pathogens, organic load | mobile modular treatment units, filtration + disinfection | sanitation reuse, emergency water management | Wolny et al., 2021 |

### *Resource recovery pathways*

Wastewater streams contain multiple recoverable resources, including nutrients, energy, biomass-derived products and valuable metals, positioning wastewater treatment plants as resource recovery platforms rather than solely pollution control systems (Smol, 2023; Wada et al., 2026).

Nutrient recovery represents one of the most established pathways. Wastewater and sewage sludge are significant secondary sources of phosphorus and nitrogen, with phosphorus recovery potential estimated at up to 22% of global demand.

Phosphorus is commonly recovered as struvite, while nitrogen can be extracted via membrane processes or converted into ammonium-based fertilizers. In addition, biosolids can be reused as soil amendments, while thermochemical processes such as pyrolysis enable biochar production and carbon sequestration (Kyllönen et al., 2021; Udu & Okpala, 2025; Wada et al., 2026).

Energy recovery is another key component, with anaerobic digestion converting organic matter into biogas that can be valorized for electricity and heat generation (Sevillano et al., 2021). Advanced processes, including thermal pretreatment and hydrothermal carbonization, further enhance energy recovery by producing energy-rich products such as synthesis gas, while emerging technologies such as microbial fuel cells enable simultaneous treatment and electricity generation (Udu & Okpala, 2025; Wada et al., 2026).

Beyond nutrients and energy, wastewater can support the production of bio-based materials and chemicals. Microalgae systems enable the recovery of nutrients and carbon while generating biomass for biofuels and bioproducts, while agro-industrial wastewater can be used for producing biodegradable polymers such as polyhydroxyalkanoates (Udu & Okpala, 2025; Wada et al., 2026).

Wastewater streams may also contain recoverable metals, particularly in industrial effluents, which can be extracted using biosorption, electrochemical processes, ion exchange or membrane technologies (Udu & Okpala, 2025; Wada et al., 2026).

The integration of these pathways underpins the transition from conventional treatment plants to Water Resource Recovery Facilities (WRRFs), enabling simultaneous pollutant removal, water reuse and resource valorisation (Neczaj & Grosser, 2018; Smol, 2023). In this context, decentralized and mobile systems extend the WRRF concept by enabling localized resource recovery and reuse, particularly in areas lacking centralized infrastructure.

***Romania vs Europe: Implementation Gap***

The analysis reveals significant structural gaps in wastewater management performance in Romania (Mosnegutu et al., 2025). Although approximately 66% of the population is connected to sewerage systems and 60.7% to wastewater treatment plants, only 12% of urban wastewater is treated in compliance with European Union requirements, compared to an EU average of approximately 76%. Wastewater treatment infrastructure remains underdeveloped, with 1,242 treatment plants in operation, of which 847 serve agglomerations larger than 2,000 population equivalents, yet important operational and performance limitations persist.

Resource recovery is also limited, with only around 24% of sewage sludge valorised through agricultural reuse or composting, indicating low circular integration. This aligns with broader circular economy indicators, where Romania records a circular material use rate of 1.3% compared to 12.8% at EU level, and a municipal waste recycling rate of 13.7% versus 48.6% in the EU, highlighting weak integration of circular principles across sectors.

At the European level, wastewater management is characterized by significant heterogeneity, shaped by water availability, climate and infrastructure development. Approximately 11% of the population is affected by water stress, while only around 1 billion $m^3$/year of treated wastewater is reused, compared to an estimated potential of 6 billion $m^3$/year (EEA, 2023b). Water reuse practices vary significantly across Member States, with high reuse rates in water-scarce countries such as Cyprus (>90%) and Malta (>60%), and moderate levels in Spain, Italy and Greece (5-12%), supported by tertiary treatment technologies in line with Regulation (EU) 2020/741.

Circular wastewater management in the EU is structured around three main valorisation pathways: water reuse, agricultural sludge reuse and thermal treatment systems enabling energy and phosphorus recovery. In 2020, the EU generated approximately 6.31 million tons of sewage sludge (dry matter), of which 37.3% was reused in agriculture, with significant national variations - from agricultural reuse-dominated systems (e.g., Estonia 85.9%, France 77.1%) to thermal recovery-oriented systems (e.g., Netherlands 95.6% incineration), where phosphorus recovery can reach 70-90%.

Despite these advancements, infrastructure disparities persist, with approximately 81% of the EU population connected to at least secondary wastewater treatment. The revised

Urban Wastewater Treatment Directive (UWWTD recast) further strengthens requirements by introducing stricter nutrient removal targets and advanced treatment for micropollutants.

Romania remains in a transitional stage within this European framework, with only 60.7% of the population connected to wastewater systems (NIS, 2024) and over 150 agglomerations non-compliant with EU requirements (EEA, 2023a). Although the entire national territory is designated as a sensitive area - requiring enhanced nitrogen and phosphorus removal - circularity indicators remain underdeveloped, with only 21.3% of sewage sludge reused in agriculture compared to the EU average of 37.3%, and no consolidated national data on wastewater reuse.

These findings highlight a gap between legislative alignment and practical implementation, driven by infrastructure deficits, limited reuse deployment and weak resource recovery integration. At the same time, the limitations of conventional wastewater treatment systems - such as high energy consumption, sludge production, sensitivity to variability and incomplete removal of nutrients and micropollutants - further constrain progress toward EU targets. Addressing these challenges requires the integration of advanced technologies, including biofilm systems (IFAS/MBBR), optimized aeration, real-time monitoring and tertiary treatment processes such as filtration, granular activated carbon and advanced oxidation processes.

In this context, mobile systems represent a strategic opportunity due to their high treatment efficiency, flexibility and reuse potential, functioning as transitional circular infrastructure capable of enabling localized treatment, resource recovery and alignment with European wastewater management models.

The conceptual framework from Figure 5 illustrates the main circular wastewater valorisation pathways in the European Union - water reuse, agricultural sludge valorisation and thermal resource recovery - highlighting Romania's transitional position and the role of mobile and decentralized systems as enabling infrastructure for bridging implementation gaps. To provide a regulatory and technological context, Table 3 compares key EU and Romanian indicators related to wastewater treatment and summarizes their implications for WWTP modernization and the integration of advanced technologies.

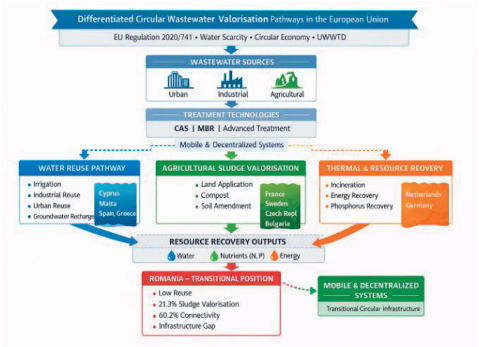



Figure 5. Differentiated Circular Wastewater Valorisation Pathways and the Role of Mobile Systems in the EU–Romania Context (The figure was generated with the assistance of a generative AI tool based on the authors' conceptual design and subsequently reviewed, edited, and scientifically validated by the authors)

Table 3. EU-Romania Indicators Relevant for WWTP Modernization and Integration of Advanced Technologies

| Dimension | EU (Data / Requirements) | Romania (Data / Requirements) | Direct Technological Implication |
|---|---|---|---|
| **Connection to treatment (minimum level)** | ~81% of the population connected to at least secondary treatment (2022) (Eurostat, 2023; EEA, 2022). | Significant disparities between agglomerations; major pressure on collection and treatment in large agglomerations (European Commission, 2023). | Need for network expansion and increased treatment capacity; shock load mitigation through equalization and operational control. |
| **"Secondary" treatment performance (definition)** | ≥70% BOD and ≥75% COD removal required under the Urban Wastewater Treatment Directive (European Commission, 1991). | Uneven compliance; some agglomerations still lack adequate treatment (European Commission, 2023). | Biological process upgrades (IFAS/MBBR, DO control) and improved robustness. |
| **Advanced treatment (nutrients / stricter require-ments)** | Recast strengthens nutrient removal and introduces additional requirements for micropollutants (European Commission, 2022; EEA, 2022). | Application of the "sensitive area" concept → intense pressure on N and P removal (Romanian Government, 2002; European Commissio, 2023). | Integration of optimized nitrification/de nitrification, IFAS/MBBR; Anammox where feasible. |

| Dimension | EU (Data / Requirements) | Romania (Data / Requirements) | Direct Technological Implication |
|---|---|---|---|
| **Non-compliance (large agglomerations)** | — | 150 (collection), 154 (inadequate treatment), 155 (lack of advanced treatment) (European Commissio, 2023). | Investment prioritization: collection systems + biological upgrades + nutrient removal. |
| **Investments (EU context)** | ~€67 billion invested in environmental protection in 2023 (Eurostat, 2024). | Need for accelerated investments, especially in large agglomerations (EEA, 2023b; European Commissio, 2023). | Justification for OPEX/CAPEX optimization: smart control, energy efficiency, resource recovery. |

Source: author's synthesis based on literature review.

Table 4 compares key indicators of wastewater valorisation across the EU, Romania, and selected Member States, highlighting differences in water reuse, sludge management, and nutrient recovery practices.

Table 4. Comparative wastewater valorisation pathways in the EU and Romania

| Indicator | EU Average | Romania | France | Estonia | Poland | Netherlands |
|---|---|---|---|---|---|---|
| Wastewater reuse ($m^3$/year) | ~1 bn | n/a | low | low | low | low |
| Reuse potential | ~6 bn | n/a | — | — | — | — |
| Population connected (%) | ~81% | 60.7% | >90% | >90% | ~75–80% | >95% |
| Sludge production (t DM) | 6.31 mil | 254k | high | low | high | Moderate |
| Agricultural reuse (%) | 37.3% | 21.3% | 77.1% | 85.9% | 38.0% | 3.9% |
| Incineration (%) | Variable | low | low | low | 18.5% | 95.6% |
| Dominant model | Mixed | Transi-tional | Agricul-tural | Agricul-tural | mixed | Thermal |
| Nutrient recovery | Emerging | absent | limited | limited | emerging | Advanced |

*Qualitative descriptors (low, moderate, high) are based on comparative analysis of Eurostat and EEA datasets.

Table 5 summarizes the main EU and Romanian legislative provisions governing wastewater management and highlights the key implementation gaps affecting the transition toward advanced and circular wastewater treatment systems.

The analysis indicates that Romania has largely achieved formal legislative alignment with EU wastewater policy, while significant gaps persist at the implementation level, particularly in infrastructure, compliance, water reuse and resource recovery. While the national regulatory framework is harmonized with European directives, significant gaps persist in infrastructure development, compliance, wastewater reuse deployment and nutrient recovery. These findings indicate that Romania is not primarily limited by regulatory deficiencies, but by implementation constraints, which delay the transition toward circular wastewater management.

Table 5. EU and Romanian wastewater legislation: key framework and implementation gaps (2026)

| Compo-nent | EU frame-work | Romania – legislation | Implementation status and gap |
|---|---|---|---|
| Water policy | Directive 2000/60/EC | Law no. 107/1996 | Objectives not fully achieved, gaps in reaching good ecological status |
| Urban wastewater | Directive 91/271/EEC; Directive (EU) 2024/3019 | HG 188/2002; NTPA-011 | Ongoing non-compliance confirmed by infringement procedure |
| Discharge | UWWTD require-ments | NTPA-001; NTPA-002 | Legally implemented, compliance varies across agglomerations,operational gaps |
| Water reuse | Regula-tion (EU) 2020/741 | Directly applicable | Limited documented implementation, lack of operational reuse systems |
| Sludge | Directive 86/278/EEC | Order 344/2004 | Lower valorisation compared to EU average, limited nutrient recovery |
| Infrastructure | UWWTD obliga-tions | National implementation programs | ~60.7% population connected, significant infrastructure deficit |
| Advanced / circular | Directive (EU) 2024/3019; EU CE policy | No dedicated framework | Limited deployment compared to EU requirements, technological and regulatory gaps |

*Source: Author's synthesis based on EU directives and Romanian legislation (Law 107/1996; HG 188/2002; NTPA-001/002/011; Order 344/2004; Directive (EU) 2024/3019; Regulation (EU) 2020/741); (EEA, 2024a), (EEA, 2024b) (EEA, 2024c), (EEA, 2024d) (EEA, 2024e), (EEA, 2024f).*

Unlike many EU Member States, where circular wastewater management is driven by either water reuse, sludge valorisation or thermal recovery, Romania remains in a transitional stage where none of these pathways are fully developed at scale.

This gap creates a strategic opportunity for mobile and decentralized wastewater treatment systems, which can act as flexible, rapidly deployable solutions to bridge infrastructure deficits and accelerate circular economic implementation.

The comparative analysis shows that conventional wastewater treatment plants

remain economically efficient at large scale, due to lower operational costs and higher biogas recovery. In contrast, mobile and membrane-based systems outperform conventional processes in treatment efficiency, reuse readiness and operational flexibility. Despite higher energy demand and costs, they enable direct water reuse, improved nutrient recovery and stable performance under variable conditions, reflecting a shift from cost-driven to circularity-driven design.

Thus, conventional systems optimize cost and energy recovery at scale, while mobile systems prioritize flexibility, performance and circular economy integration. Table 6 compares the performance of conventional and mobile wastewater treatment systems in terms of treatment efficiency, resource recovery potential, energy demand, and economic indicators.

Table 6. Conventional vs. mobile wastewater treatment systems: performance, resource recovery, energy and cost comparison

| Indicator | Conventional WWTP (CAS) | Mobile / decentralized (MBR / advanced) | Resource recovery potential | Energy (kWh/m³) |
|---|---|---|---|---|
| **Organic matter (BOD/COD)** | BOD: 75-95%COD: 70-90% | BOD: 90-99%COD: 85-98% | 20-40% (biogas) | 0.3-0.6 |
| **Suspended solids (TSS)** | 80-95% | >99% | Sludge → energy | 0.2-0.5 |
| **Nitrogen (TN)** | 40-70% | 70-95% | Limited | 0.4-0.8 |
| **Phosphorus (TP)** | 30-60% | 60-90% | 10–30% (struvite) | 0.3-0.7 |
| **Pathogen removal** | Moderate (needs disinfection) | Very high (membrane barrier) | ≈100% safe reuse | 0.1-0.3 |
| **Water reuse potential** | Low–moderate | High | 50–90% reuse | 0.5-1.0 |
| **Energy recovery** | High (anaerobic digestion) | Moderate | 20–50% | -0.2 to 0.3* |
| **Sludge production** | High | 20-50% lower | Reduced disposal | - |
| **Hydraulic variability** | Low tolerance | High tolerance | - | Stable |
| **Footprint** | Large | Compact (-50-70%) | - | - |
| **CAPEX (€/PE)** | 300-800 | 500-1500 | - | - |
| **OPEX (€/m³)** | 0.2-0.6 | 0.4-1.2 | - | - |

*Negative values indicate energy recovery offset
Source: author's synthesis based on literature review.

At the European level, circular wastewater management is heterogeneous, structured around coexisting pathways including water reuse, sludge valorisation and thermal recovery (Larsen et al., 2016; Smol, 2023). In contrast, Romania remains in a transitional stage, characterized by infrastructure, compliance and circularity gaps. Low connectivity, limited sludge valorisation and the absence of large-scale reuse indicate that constraints are primarily systemic, driven by governance, investment and institutional capacity. While conventional systems remain suitable for centralized applications, their limitations - high energy consumption, sensitivity to variability and limited resource recovery - reduce their effectiveness in decentralized contexts. Mobile systems address these challenges through on-site treatment, operational flexibility and integration of advanced processes. However, they also involve higher costs, lower capacity and increased operational complexity, and should therefore be integrated as complementary components within hybrid systems. From a policy perspective, regulatory frameworks remain insufficiently adapted to decentralized solutions, limiting large-scale implementation, particularly in Romania. Systemic barriers - including weak policy implementation, low public acceptance, infrastructure deficits and limited awareness of resource valorisation - further constrain progress.

In this context, mobile wastewater treatment systems can be conceptualized as transitional circular infrastructure, enabling localized water reuse and resource recovery, particularly in agriculture, where they can reduce freshwater demand and support nutrient and energy recovery.

In contrast to the European examples shown in Table 7, the implementation of mobile wastewater treatment systems in Romania remains limited and fragmented.

Table 7. Examples of mobile wastewater treatment applications in Europe

| Country | Application sector | Technology used | Key performance | Main purpose |
|---|---|---|---|---|
| Spain | Food industry | Mobile DAF + RO | 80-85% TSS removal | Water reuse and compliance |
| Greece | Agro-industrial (fruit processing) | Mobile treatment unit (ULTIMATE project) | Water reuse in process | Resource recovery and reuse |
| Netherlands | Industrial / municipal support | Containerized MBR systems | High effluent quality (reuse standard) | Decentralized treatment and reuse |
| Germany | Industrial / emergency applications | Mobile modular systems | Rapid deployment | Temporary treatment and compliance |

Sources: NSI Mobile Water Solutions (2023); ULTIMATE Project (2022); Water Europe (2023).

Existing applications are mainly restricted to temporary or industrial uses, with no systematic integration into wastewater management strategies. This indicates that, despite technological availability, decentralized and mobile treatment solutions are not yet widely adopted, and wastewater management remains predominantly centralized and treatment-oriented.

## CONCLUSIONS

This study demonstrates a clear transition from linear wastewater treatment toward circular resource recovery systems. Although the European Union has made significant progress in wastewater reuse and valorisation, implementation remains uneven across Member States.

Romania exhibits a structural gap characterized by limited infrastructure coverage, low reuse rates and underdeveloped resource recovery. These challenges are primarily driven by implementation constraints rather than regulatory deficiencies.

Mobile wastewater treatment systems emerge as a viable solution, offering rapid deployment, operational flexibility and high treatment performance. They can be effectively positioned as transitional circular infrastructure.

Rather than replacing centralized systems, mobile technologies should be integrated into hybrid frameworks to support decentralized applications and accelerate infrastructure development, particularly in regions with limited capacity and increasing water stress.

Future research should prioritize improving energy efficiency, reducing operational costs and developing regulatory frameworks that support decentralized deployment. Their integration could significantly accelerate the transition toward circular water management.

Mobile wastewater treatment systems should therefore be considered strategic infrastructure components, enabling localized treatment, resource recovery and water reuse within emerging circular systems.

Despite their advantages, mobile wastewater treatment systems present several limitations that may constrain large-scale implementation. Their operational performance is highly dependent on influent variability and requires advanced monitoring and control systems.

Therefore, mobile systems should not be considered replacements for conventional infrastructure, but rather complementary solutions integrated within hybrid wastewater management frameworks.

## REFERENCES

Angelakis, A. N., & Snyder, S. A. (2015). Wastewater treatment and reuse: Past, present, and future. *Water*, 7(9), 4887–4895. https://doi.org/10.3390/w7094887

Capodaglio, A. G., & Olsson, G. (2020). Energy issues in sustainable urban wastewater management: Use, demand and recovery in the urban water cycle. *Sustainability*, 12(1), 266. https://doi.org/10.3390/su12010266

European Commission. (1991). Council Directive 91/271/EEC concerning urban wastewater treatment. Official Journal of the European Communities.

European Commission. (2020). Regulation (EU) 2020/741 on minimum requirements for water reuse. https://eur-lex.europa.eu/eli/reg/2020/741/oj

European Commission. (2022). Proposal for a Directive of the European Parliament and of the Council concerning urban wastewater treatment (recast). Brussels.

European Commission. (2023). Report from the Commission to the European Parliament and the Council on the implementation of the Urban Wastewater Treatment Directive (91/271/EEC). Brussels.

European Commission. (2023). Water reuse in the European Union. https://environment.ec.europa.eu/topics/ water/water-reuse_en

European Commission. (2024). Urban wastewater: Commission refers Romania to the Court of Justice for failure to comply with EU rules. https://ec.europa.eu/commission/presscorner/detail/en/ip_24_5427

European Environment Agency (EEA). (2022). *Urban wastewater treatment in Europe*. https://www.eea.europa.eu

European Environment Agency (EEA). (2023a). *Europe's water in a changing climate: Challenges and opportunities*. Copenhagen.

European Environment Agency (EEA). (2023b). *Water scarcity conditions in Europe*. https://www.eea.europa.eu

European Environment Agency (EEA). (2024a). *Urban wastewater treatment – Estonia*. https://water.europa.eu/freshwater/countries/uwwt/estonia

European Environment Agency (EEA). (2024b). *Urban wastewater treatment – European Union profile*. https://water.europa.eu/freshwater/countries/uwwt/european-union

European Environment Agency (EEA). (2024c). *Urban wastewater treatment - France*. https://water.europa.eu/freshwater/countries/uwwt/france

European Environment Agency (EEA). (2024d). *Urban wastewater treatment – Netherlands*. https://water.europa.eu/freshwater/countries/uwwt/netherlands

European Environment Agency (EEA). (2024e). *Urban wastewater treatment – Poland*. https://water.europa.eu/freshwater/countries/uwwt/poland

European Environment Agency (EEA). (2024f). *Urban wastewater treatment – Sweden*. https://water.europa.eu/freshwater/countries/uwwt/sweden

Eurostat. (2023). Population connected to wastewater treatment plants.

Eurostat. (2024). Environmental protection expenditure accounts. https://ec.europa.eu/eurostat

Garrido-Baserba, M., Sedlak, D. L., Molinos-Senante, M., Barnosell, I., Schraa, O., Rosso, D., Verdaguer, M., & Poch, M. (2024). Using water and wastewater decentralization to enhance the resilience and sustainability of cities. *Nature Water*, 2(10), 953–974. https://doi.org/10.1038/s44221-024-00303-9

Gkotsis, P., Peleka, E., Zouboulis, A., & Mitrakas, M. (2018). Membrane bioreactors (MBR) – A review on recent developments in energy reduction, fouling control, novel configurations, LCA and market prospects. *Journal of Membrane Science, 547*, 246–266. https://doi.org/10.1016/j.memsci.2017.10.070

Hamam, M., Pergamo, R., Manganiello, V., & Ferrigno, M. (2024). Agricultural Wastewater Reuse as a Circular Economy Model: Future Scenarios Considering Reg. (EU) 2020/741. *Water*, *16*(24), 3638. https://doi.org/10.3390/w16243638

National Institute of Statistics (NIS), Romania. (2024). Population connected to sewage and wastewater treatment systems. https://insse.ro/cms/en/content/population-connected-sewage-and-wastewater-treatment-systems-year-2024

Khaki, Q. Z., Kumar, B. T., & Kumar, P. (2026). Recent trends in decentralized wastewater treatment system in developing countries: A critical review of case studies and future perspectives. *Journal of Environmental Management, 398*, 128467. https://doi.org/10.1016/j.jenvman.2025.128467

Kyllönen, H., Heikkinen, J., Järvelä, E., Sorsamäki, L., Siipola, V., & Grönroos, A. (2021). Wastewater purification with simultaneous nutrient recovery in a mobile resource container. *Membranes*, 11(12), 975. https://doi.org/10.3390/membranes11120975

Lakho, F. H., Le, H. Q., Van Kerkhove, F., Igodt, W., Depuydt, V., Desloover, J., Rousseau, D. P. L., & Van Hulle, S. W. H. (2020). Water treatment and re-use at temporary events using a mobile constructed wetland and drinking water production system. *Science of the Total Environment,* 737, 139630. https://doi.org/10.1016/j.scitotenv.2020.139630

Larsen, T. A., Hoffmann, S., Lüthi, C., Truffer, B., & Maurer, M. (2016). Emerging solutions to the water challenges of an urbanizing world. *Science (New York, N.Y.)*, *352*(6288), 928–933. https://doi.org/10.1126/science.aad8641

Luo, Y., Guo, W., Ngo, H. H., Nghiem, L. D., Hai, F. I., Zhang, J., Liang, S., & Wang, X. C. (2014). A review on the occurrence of micropollutants in the aquatic environment and their fate and removal during wastewater treatment. *Science of the Total Environment, 473–474*, 619–641. https://doi.org/10.1016/j.scitotenv.2013.12.065

Maniam, G., Zakaria, N. A., Leo, C. P., Vassilev, V., Blay, K. B., Behzadian, K., & Poh, P. E. (2022). An assessment of technological development and applications of decentralized water reuse: A critical review and conceptual framework. *WIREs Water*, 9(3), e1588. https://doi.org/10.1002/wat2.1588

Mannina, G., Gulhan, H., & Ni, B. J. (2022). Water reuse from wastewater treatment: The transition towards circular economy in the water sector. *Bioresource technology*, *363*, 127951. https://doi.org/10.1016/j.biortech.2022.127951

Meng, F., Zhang, H., Yang, F., Zhang, S., Li, Y., & Zhang, X. (2017). Fouling in membrane bioreactors: An updated review. Water Research, 114, 151–180. https://doi.org/10.1016/j.watres.2017.02.006

Mosnegutu, E., Przydatek, G., Chitimus, D., Placinta, C., Barsan, N., Tomozei, C., Nedeff, F., & Sporea, N. (2025). Study on the Public Information Level About the Waste Management System, *Urban Science*, 9, Issue 5, 1-20, DOI 10.3390/urbansci9050148

Neczaj, E., & Grosser, A. (2018). Circular economy in wastewater treatment plant - Challenges and barriers. Proceedings, 2(11), 614. https://doi.org/10.3390/proceedings2110614

NSI Mobile Water Solutions. (2023). *Why mobile wastewater treatment in Europe?* Retrieved from https://nsimobilewatersolutions.com

Nydrioti, I., & Grigoropoulou, H. (2025). Optimizing water footprint and energy use in industry: A decision support framework for industrial wastewater treatment and reuse applied to a brewery. *Water*, 17(8), 1179. https://doi.org/10.3390/w17081179

Obijianya, C. C., Yakamercan, E., Karimi, M., Veluru, S., Simko, I., Eshkabilov, S., & Simsek, H. (2025). Agricultural Irrigation Using Treated Wastewater: Challenges and Opportunities. *Water*, *17*(14), 2083. https://doi.org/10.3390/w17142083

Sevillano, C. A., Pesantes, A. A., Peña Carpio, E., Martínez, E. J., & Gómez, X. (2021). Anaerobic digestion for producing renewable energy - The evolution of this technology in a new uncertain scenario. *Entropy, 23*(2), Article 145. https://doi.org/10.3390/e23020145

Silva, J. A. (2023). Water Supply and Wastewater Treatment and Reuse in Future Cities: A Systematic Literature Review. Water, 15(17), 3064. https://doi.org/10.3390/w15173064

Singh, S., Yadav, R., & Singh, A. N. (2022). Applications of waste-to-economy practices in the urban wastewater sector: Implications for ecosystem, human health and environment. In *Waste Management and Resource Recycling in the Developing World* (pp. 625–646). Elsevier. https://doi.org/10.1016/B978-0-323-90463-6.00010-5

Smol, M. (2023). Circular Economy in Wastewater Treatment Plant - Water, Energy and Raw Materials Recovery. *Energies*, 16(9), 3911. https://doi.org/10.3390/en16093911

Surdu, E., Farcaş-Flamaropol, D.C., Sporea, N.,Tomescu, G. (2021). The Use of Biomass Can Help Save the

Planet, *Hidraulica*, 4, 76-85, https://hidraulica.fluidas.ro/2021/nr4/76-85.pdf

Ştefănescu, M.F., Dobrovicescu, A., Prodea, I.-M., & Sporea, N. (2019). *The concept of sustainability applied to an industrial sludge deposit*, E3S Web of Conferences 112, 04002, 1-10 https://doi.org/10.1051/e3sconf/201911204002

Udu, C. E., & Okpala, C. C. (2025). Circular economy in wastewater management: Water reuse and resource recovery strategies. *International Journal of Latest Technology in Engineering, Management & Applied Science*, 14(3), 128–136. https://doi.org/10.51583/IJLTEMAS.2025.140300016

ULTIMATE Project. (2022). *Mobile wastewater treatment unit for industrial water reuse.* Retrieved from https://ultimatewater.eu

van Loosdrecht M.C., & Brdjanovic D. (2014) Water treatment. Anticipating the next century of wastewater treatment. *Science*. 344(6191):1452-3. doi: 10.1126/science.1255183. PMID: 24970066.

Wada, O. Z., Ige, A. O., Egbewole, B. I., & Olawade, D. B. (2026). Circular economy from wastewater resource recovery: A review of recent advances and global disparities. *Sustainable Chemistry One World*, 9, 100187. https://doi.org/10.1016/j.scowo.2026.100187

Water Europe. (2023). *Water reuse and circular economy in Europe.* Retrieved from https://watereurope.eu

Wolny, P., Tuśnio, N., & Wróblewski, W. (2021). Mobile Modular Systems of Water Treatment and Storage in Crisis Situations – Review of Existing Solutions. Preprints. 2021020344. https://doi.org/10.20944/preprints202102.0344.v1

Yang, J., Monnot, M., Ercolei, L., & Moulin, P. (2020). Membrane-based processes used in municipal wastewater treatment for water reuse: State-of-the-art and performance analysis. *Membranes*, 10(6), 131. https://doi.org/10.3390/membranes10060131

Scientific Papers. Series E. Land Reclamation, Earth Observation & Surveying, Environmental Engineering. Vol. XV, 2026
Print ISSN 2285-6064, CD-ROM ISSN 2285-6072, Online ISSN 2393-5138, ISSN-L 2285-6064

# PROCESS STABILITY IN LIVESTOCK WASTEWATER TREATMENT: A COMPARATIVE REVIEW OF CONVENTIONAL SYSTEMS AND MEMBRANE BIOREACTORS FOR DECENTRALIZED APPLICATIONS

**Sabrina-Maria BĂLĂNESCU[1], Carmen Otilia RUSĂNESCU[1], Ana VÎRSTA[2], Nicoleta-Alina UDROIU[2], Bogdan-Dumitru ȚIGĂNOAIA[1], Nicolae FARCAȘ[2]**

[1]National University of Science and Technology Politehnica Bucharest,
313 Splaiul Independenței, District 6, Bucharest, Romania
[2]University of Agronomic Sciences and Veterinary Medicine of Bucharest,
59 Marasti Blvd, District 1, Bucharest, Romania

Corresponding author email: sabrina.balanescu1@gmail.com

***Abstract***

*Livestock wastewater, particularly from pig farming, represents a major environmental challenge due to its high organic load, nutrient content, and strong hydraulic variability. Conventional treatment approaches such as lagoons or activated sludge systems frequently exhibit unstable performance under fluctuating agricultural conditions, resulting in inconsistent effluent quality. This study presents a structured literature review and comparative technological analysis of wastewater treatment systems applicable to livestock farms, focusing on process stability in decentralized environments. The analysis shows that instability in conventional systems originates primarily from biomass washout associated with gravity-based sludge separation. Membrane bioreactors overcome this limitation by physically retaining biomass and decoupling sludge retention time from hydraulic retention time, ensuring stable nitrification and consistent treatment performance. Consequently, MBR technology represents a promising solution for decentralized and mobile livestock wastewater treatment systems.*

***Key words****: decentralized wastewater treatment, livestock wastewater, membrane bioreactor (MBR), pig farming.*

## INTRODUCTION

Growing pressure on freshwater resources and stricter environmental regulations are accelerating the development of decentralized wastewater treatment systems for agricultural environments (European Commission, 2020). Pig farming represents one of the major sources of agricultural pollution, generating large volumes of wastewater rich in organic matter, nutrients and microbial contaminants (Chen et al., 2024). Despite this pollution load, wastewater management in many farms still relies on lagoon storage or simple digestion processes that provide only partial treatment (Ivanciu Popa et al., 2019; Chen et al., 2024).

Conventional biological treatment systems, particularly activated sludge, require stable hydraulic conditions to maintain biomass retention and treatment efficiency (Surdu et al., 2021). However, livestock wastewater is characterized by intermittent flows, high ammonia concentrations and strong seasonal variability, leading to biomass washout and unstable effluent quality (Burton et al., 2003; FAO, 2018).

Membrane bioreactor (MBR) systems overcome this structural limitation by physically retaining biomass through membrane filtration, decoupling sludge retention time from hydraulic residence time and enabling stable treatment under variable loading conditions (Capodaglio, 2017). Consequently, MBR technology represents a promising solution for decentralized and mobile livestock wastewater treatment systems.

Unlike most studies that focus primarily on pollutant removal efficiencies, this paper analyses wastewater treatment technologies from the perspective of process stability under variable hydraulic conditions, identifying biomass retention mechanisms as the key determinant for decentralized livestock wastewater treatment. The relationship between variable agricultural wastewater loading, process instability in conventional activated sludge systems, and the stabilizing role of membrane biomass retention is illustrated in Figure 1.

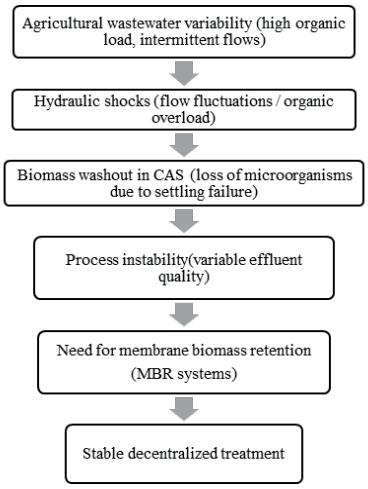



Figure 1. Conceptual framework illustrating the instability of conventional activated sludge systems under variable agricultural wastewater loading and the role of membrane biomass retention in stabilizing decentralized treatment processes.

The technological evolution of livestock wastewater treatment systems from conventional lagoon storage to modern mobile membrane-based systems is illustrated in Figure 2.

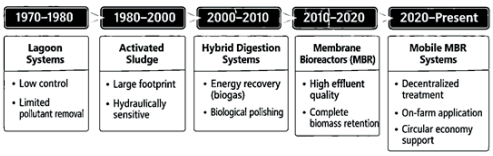



Figure 2. Evolution of wastewater treatment technologies applied in livestock farming, from conventional lagoon storage systems to modern mobile membrane bioreactor installations enabling decentralized treatment and resource recovery

## MATERIALS AND METHODS

This study was conducted as a structured literature review and comparative technological analysis of wastewater treatment systems applicable to livestock farms, focusing on process stability and the suitability of decentralized and mobile treatment technologies.

Scientific publications were identified through systematic searches in the Scopus, Web of Science, and Google Scholar databases, covering the period 2000-2025. The search strategy included combinations of the following keywords: pig wastewater treatment, livestock wastewater, membrane bioreactor (MBR), decentralized wastewater treatment, mobile wastewater treatment systems, agricultural effluents, and nutrient removal technologies.

Selected studies were further analysed and categorized according to the type of treatment process. Studies were selected based on relevance, data availability and applicability for livestock wastewater systems.

For the comparative evaluation, the technologies were analysed based on several key operational parameters frequently reported in the literature.

The collected data were synthesized into comparative tables in order to highlight the technological limitations of conventional treatment approaches and the operational advantages of membrane-based systems in decentralized livestock wastewater management.

## RESULTS AND DISCUSSIONS

### *Characteristics of livestock wastewater*

Wastewater generated in animal husbandry contains high concentrations of organic matter, suspended solids, nutrients and pathogenic microorganisms originating from manure, feed residues and cleaning operations (Burton et al., 2003; FAO, 2018).

Mobile treatment technologies have emerged as an alternative approach for treating high-strength wastewater directly at source, reducing transport requirements and improving process control under variable loading conditions (Libralato et al., 2012; Capodaglio, 2017). These systems commonly integrate multi-stage filtration processes, including pre-filtration, membrane separation and disinfection, enabling the removal of suspended particles, microorganisms, and dissolved contaminants (Iorhemen et al., 2016; Meng et al., 2017).

In many regions, small livestock farms store wastewater in lagoons or reuse it for irrigation, whereas large farms increasingly implement anaerobic digestion to recover energy in the form of biogas (Burton et al., 2003; FAO, 2018).

A comprehensive treatment scheme for piggery wastewater typically includes solid-liquid

separation, anaerobic digestion, aerobic polishing and membrane filtration, followed by advanced polishing steps such as activated carbon or reverse osmosis (Metcalf & Eddy et al., 2014; Meng et al., 2017).

In Romania, most small livestock farms collect their wastewater in a storage basin, for further use as irrigation wastewater, or in aerated or non-aerated lagoons. The large farms, where significant financial investments have been made, have begun to build up their wastewater treatment plants with anaerobic digesters, and the biogas obtained can be used as a source of energy in the farm (Ivanciu Popa et al., 2019).

Historical livestock waste generation coefficients indicate that pigs produce approximately 6 kg total solids and 2 kg $BOD_5$ per 1,000 kg live weight per day. Although absolute values vary in modern intensive systems, the data demonstrate that livestock wastewater is generally characterized by high organic and nutrient loads. The current environmental challenge therefore results not from a change in manure composition but from the scale and hydraulic variability of modern production systems. The typical pollutant loads generated by swine livestock in Romania, compared with European reference ranges, are presented in Table 1.

Table 1. Typical pollutant load generated by swine livestock: Romania vs European reference values ($kg \cdot animal^{-1} \cdot day^{-1}$)

| Parameter | Romania | European typical range |
|---|---|---|
| Total suspended solids (TSS) | 4.48 | 3.0-5.5 |
| Volatile suspended solids (VSS) | 3.50 | 2.0-4.5 |
| Chemical oxygen demand (COD) | 3.94-5.78 | 3.0-8.0 |
| Biochemical oxygen demand ($BOD_5$) | 1.90-2.30 | 1.5-4.0 |
| Total nitrogen (TN) | 0.35 | 0.30-0.60 |
| Total phosphorus (TP) | 0.074 | 0.05-0.15 |

Romanian data: (Chiriac et al., 1977); European ranges: Burton et al., 2003; FAO, 2018; European Commission, 2020. Values are expressed per average pig live weight equivalent (livestock unit).

The comparison between typical Romanian practice and controlled Western European treatment (Table 2) indicates that removal efficiency is not primarily determined by the treatment technology itself but by process controllability. Lagoon-based systems exhibit moderate organic matter removal (30–60% COD), yet nutrient removal remains below 40%, and effluent stability is highly seasonal. In contrast, controlled biological systems achieve >90% removal efficiency and consistent compliance.

This demonstrates that livestock wastewater treatment failure is associated with hydraulic and operational variability rather than insufficient biodegradability of the substrate.

Western European treatment systems achieve higher removal efficiencies not always due to superior technologies but because wastewater is treated as a controlled process rather than stored as an agricultural by-product, resulting in predictable effluent quality and enabling water reuse.

Table 2. Comparative performance of swine wastewater treatment (Romania vs Western European practice)

| Parameter | Romania - typical practice (lagoons / storage / basic digestion) | Western Europe - controlled treatment (biological + advanced) |
|---|---|---|
| COD removal | 30-60% in anaerobic lagoons; highly dependent on retention time | 85-98% in biological reactors; >95% with MBR polishing |
| $BOD_5$ removal | 40-70% (partial stabilization) | 90-99% in activated sludge/MBR |
| TSS removal | 50–80% sedimentation based | >99% membrane separation |
| Nitrogen removal | <20-40% (mostly volatilization and soil uptake) | 70-95% nitrification–denitrification; >90% advanced systems |
| Phosphorus removal | <10-30% natural precipitation | 80-95% EBPR / chemical / struvite recovery |
| Pathogen removal | inconsistent; dependent on storage time | near complete removal after membrane/disinfection |
| Effluent stability | highly variable; seasonal | stable compliance |
| Water reuse suitability | Unsuitable | irrigation reuse feasible |
| Nutrient recovery | indirect via land spreading | controlled recovery (fertilizer products) |
| Treatment philosophy | manure management | wastewater treatment & circular economy |

Livestock wastewater is fundamentally different from municipal wastewater due to its extreme variability in organic loading, nutrient concentration and suspended solids content (Musa & Idrus, 2021; Rahman et al., 2023).

***Limitations of conventional systems***

Conventional activated sludge (CAS) systems are frequently considered an upgrade solution; however, their application in livestock wastewater treatment presents intrinsic limitations (Du et al., 2020).

The process stability of CAS depends on constant influent composition and controlled loading rates; conditions rarely encountered in agricultural effluents (Rahman et al., 2023).

Sudden variations in organic load or ammonia concentration may lead to biomass inhibition and process imbalance (Iorhemen et al., 2016).
Furthermore, gravity sedimentation used for biomass separation represents a structural weakness of the CAS process (Iorhemen et al., 2016).
The treatment process typically involves several stages to effectively treat pig wastewater, as shown in Figure 3.

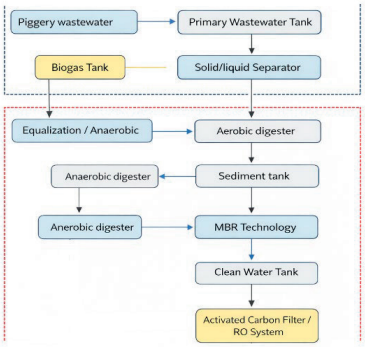



Figure 3. Treatment process of piggery wastewater (adapted and redrawn by the authors based on Hinada, n.d. and literature sources)

Poor sludge settling characteristics frequently observed in high-strength agricultural wastewater led to solids washout (Du et al., 2020). Therefore, achieving consistent compliance with discharge standards becomes difficult without tertiary treatment stages (Ezugbe & Rathilal, 2020).

***Mechanistic origin of process instability***

The instability of conventional activated sludge treatment under variable agricultural loading originates from the dependence of biomass retention on gravity settling.
Animal farms, particularly small and medium units, rarely have sufficient available land for aeration basins and clarifiers (Kesari et al., 2021). This structural difference between gravity-based biomass separation and membrane retention is illustrated in Figure 4.
Consequently, treatment infrastructure is often undersized, leading to chronic overloading conditions (Musa & Idrus, 2021).

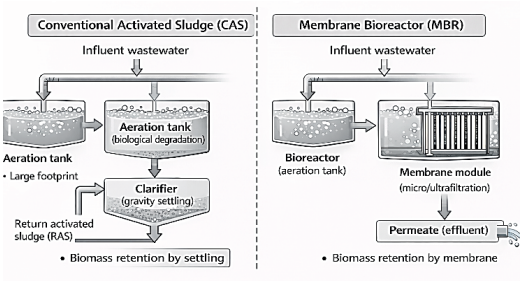



Figure 4. Mechanistic comparison between conventional activated sludge (CAS) and membrane bioreactor (MBR) systems highlighting biomass retention mechanisms and treatment stability under variable hydraulic loading

Cleaning operations, rainfall infiltration and manure removal cycles generate hydraulic shocks that conventional biological reactors cannot buffer effectively (Iorhemen et al., 2016). Additionally, nutrient removal in conventional systems remains limited without advanced process control (Ezugbe & Rathilal, 2020). High ammonia concentrations typical for livestock wastewater inhibit nitrification and reduce biological stability (Iorhemen et al., 2016).
Overall, the main limitation of conventional treatment is not insufficient pollutant removal capacity per se, but the incompatibility between system design philosophy and agricultural wastewater characteristics (Du et al., 2020). Systems optimized for stable municipal flows cannot maintain performance under decentralized, variable and high-strength effluents (Rahman et al., 2023). This structural mismatch explains the increasing interest in compact, modular and physically separated biomass systems such as membrane bioreactors (Iorhemen et al., 2016; Rahman et al., 2023). If manure is treated on-farm to reduce emissions of nitrogen, phosphorus, odours, and microbial pathogens to air and water, as well as to improve storage and land application, Best Available Techniques (BAT) require the application of specific processing methods (European Commission, 2017). These include mechanical separation of slurry, anaerobic digestion in biogas installations, external tunnel drying, aerobic digestion, and nitrification-denitrification of slurry (European Commission, 2017).

***Comparative performance analysis***

The pollutant removal efficiencies reported for several livestock wastewater treatment technologies are summarized in Table 3.

Table 3. Pollutant removal efficiencies of selected livestock wastewater treatment technologies in percentage (Kashyap, 2017)

| Treatment Technology | BOD | COD | SS | TN | TKN | TP | Cu |
|---|---|---|---|---|---|---|---|
| Stabilization Pond | 77.78 | 78.02 | 88.12 | 61.65 | 67.02 | 65.16 | 88.57 |
| Cover Lagoon | 85.18 | 83.06 | 85.43 | 47.61 | 51.88 | 66.42 | 89.28 |
| Fixed Dome | 85.06 | 70.97 | 80.63 | 51.98 | 52.16 | 67.27 | 82.72 |

Note: BOD – biochemical oxygen demand; COD – chemical oxygen demand; SS – suspended solids; TN – total nitrogen; TKN – total Kjeldahl nitrogen; TP – total phosphorus; Cu – copper.

The operational ranges presented in Table 4 show that conventional activated sludge systems require the sludge retention time (SRT) to be maintained through hydraulic stability, whereas membrane systems can maintain long sludge retention times (SRT) independently of the hydraulic retention time (HRT). Under variable loading, conventional systems operate outside the nitrification stability domain (<10-20 days effective SRT), whereas MBR systems maintain 15-40 days due to physical biomass retention. Therefore, process instability in agricultural wastewater treatment is a structural consequence of gravity separation rather than biological kinetics.

The comparative analysis illustrated in Figure 6 is based on a synthesis of representative literature data regarding livestock wastewater treatment technologies. Reported operational ranges and removal efficiencies were extracted from peer-reviewed studies and aggregated to obtain indicative average values for each technology group.

The results highlight clear differences in treatment efficiency and operational stability among the evaluated technologies. Conventional biological systems, such as activated sludge and hybrid biological-physicochemical configurations, can achieve satisfactory pollutant removal under stable influent conditions, but their performance may decline under hydraulic variability typical of agricultural wastewater.

In contrast, membrane bioreactor (MBR) systems demonstrate higher operational robustness due to complete biomass retention and the decoupling of sludge retention time (SRT) from hydraulic retention time (HRT). This allows the maintenance of high mixed liquor suspended solids (MLSS) concentrations and stable nitrification even under variable loading conditions, resulting in consistently higher effluent quality.

Overall, the compact design and process stability of MBR systems make them particularly suitable for decentralized and mobile wastewater treatment applications in livestock farms.

Operational ranges and performance indicators presented in Table 4 were obtained through a synthesis of representative literature data on livestock wastewater treatment technologies. Reported values from peer-reviewed studies were aggregated to illustrate typical operational conditions and treatment efficiencies.

MBR is an efficient wastewater treatment technology that integrates a biological process with membrane filtration.

The membrane bioreactor configuration illustrated in Figure 5 integrates biological treatment with membrane separation, ensuring complete biomass retention and stable effluent quality under variable loading conditions. Aeration supports both microbial activity and membrane fouling control, while sludge recirculation maintains process stability. This configuration enables the decoupling of sludge retention time from hydraulic retention time, which is essential for reliable treatment of livestock wastewater.

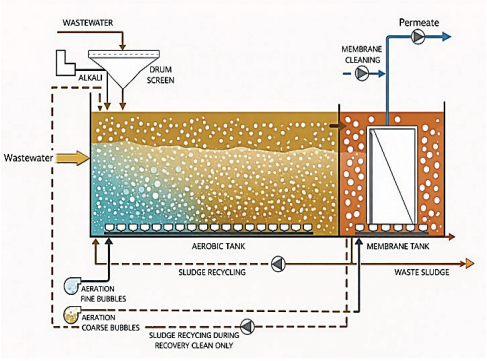



Figure 5. Containerized Membrane Bioreactor (MBR-C) Process Flow (adapted and redrawn by the authors based on literature sources)

Table 4. Comparative operational ranges and process stability of conventional activated sludge (CAS) and membrane bioreactor (MBR) systems for livestock wastewater treatment

| Parameter (units) | Conventional systems (CAS / lagoons) | MBR systems (submerged / containerized) | Process stability mechanism |
|---|---|---|---|
| Influent COD (mg/L) | 500-8000 (high variability typical of livestock wastewater) | Similar influent range; high-strength wastewater commonly treated up to 3000–5000 mg/L | Both systems depend on influent variability, but MBR tolerates higher load fluctuations |
| Influent $BOD_5$ (mg/L) | 200-5000 depending on wastewater strength | Similar influent range; effluent $BOD_5$ typically <5–20 mg/L | Membrane barrier ensures consistent effluent quality |
| Influent TSS (mg/L) | 200-3000 | Similar influent range; permeate TSS typically <1–5 mg/L | Complete physical retention of suspended solids |
| SRT required for nitrification (days) | ≥10-20 required for stable nitrification | Easily maintained at 15–40 due to membrane biomass retention | Decoupling of SRT from HRT stabilizes biological activity |
| HRT (hours / days) | CAS: 6-24 h; lagoons: several days–weeks | Typically 4-12 h; longer for high-strength wastewater | MBR allows shorter HRT with long SRT |
| MLSS (g/L) | 2-5 | 8-15 typical; occasionally higher in pilot systems | High biomass concentration improves treatment robustness |
| Membrane flux (LMH) | Not applicable | 10-30 typical operating range | Membrane filtration replaces gravity settling |
| Transmembrane pressure TMP (kPa) | Not applicable | ~10-40 depending on fouling and operation | Fouling controlled through aeration and cleaning cycles |
| COD removal (%) | 70-90 under stable operation | 85-98 | Higher stability due to retained biomass |
| BOD removal (%) | 85-95 | 90-99 | Membrane barrier prevents solids carryover |
| TSS removal (%) | 80-95 | >99 | Membrane filtration ensures near-complete solids removal |
| Nitrogen removal (%) | 40-80 depending on configuration | 70-95 with nitrification–denitrification | Stable nitrification enabled by long sludge age |
| Phosphorus removal (%) | 20-60 without advanced processes | 60-90 depending on configuration | Enhanced biological or chemical removal possible |
| Energy consumption ($kWh/m^3$) | ~0.2-0.6 | ~0.4-1.0 | Higher aeration demand but compensated by smaller footprint |

Note. Values were derived from reported ranges in peer-reviewed studies and validated against established wastewater engineering references (U.S. EPA, 2007; Judd, 2011; Metcalf & Eddy et al., 2014; Iorhemen et al., 2016; Meng et al., 2017; Nagarajan et al., 2019; Du et al., 2020; Rahman et al., 2023; Vaishnav et al., 2023; Chen et al., 2024).

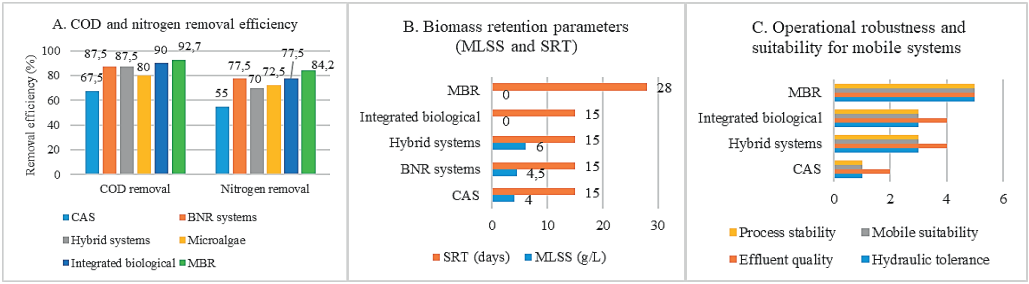



Figure 6. Comparative performance and operational stability of wastewater treatment technologies applied to livestock effluents

(A) Comparison of COD and nitrogen removal efficiencies reported in literature for conventional activated sludge (CAS), biological nutrient removal (BNR), hybrid biological–physicochemical systems, microalgae-based treatment, integrated biological treatment and membrane bioreactors (MBR). (B) Biomass retention characteristics expressed through mixed liquor suspended solids (MLSS) and sludge retention time (SRT). (C) Comparative operational robustness based on hydraulic variability tolerance, effluent quality and suitability for decentralized mobile systems

Membrane bioreactor (MBR) technology, which combines the activated sludge process with micro- or ultrafiltration membranes, is widely regarded as an effective tool for industrial water treatment and water reuse due to its high product water quality and low footprint (Hoinkis et al., 2012). In membrane bioreactor systems, biological degradation is coupled with physical separation through microfiltration or ultrafiltration membranes

(Ezugbe & Rathilal, 2020). The membrane barrier ensures near-complete suspended solids removal and significantly improved effluent quality (Iorhemen et al., 2016).

Consequently, the effluent quality becomes reproducible and independent of sludge settling characteristics (Rahman et al., 2023).

Another structural advantage is the possibility of operating at long sludge retention time and short hydraulic retention time simultaneously (Iorhemen et al., 2016). This condition favors slow-growing nitrifying microorganisms and improves nutrient removal stability (Du et al., 2020).

From a spatial perspective, eliminating secondary clarification significantly reduces the overall footprint of the treatment system, defined as the land area required for reactor installation and operation (Rahman et al., 2023).

The compact configuration of MBR systems makes them particularly suitable for decentralized and mobile installations where land availability is limited (Kesari et al., 2021).

This feature directly addresses one of the primary constraints of agricultural wastewater treatment infrastructure (Musa & Idrus, 2021).

The main drawback of MBR technology is membrane fouling, which reduces permeability and increases operational costs. However, fouling represents an operational challenge rather than a conceptual limitation, and extensive control strategies have been developed (Iorhemen et al., 2016; Du et al., 2020).

The technological barrier has shifted from demonstrating the feasibility of biological wastewater treatment to optimizing its operational stability, treatment efficiency, and adaptability under variable field conditions. In the decentralized agricultural context, where hydraulic loading fluctuates and wastewater characteristics are highly variable, stable biological treatment cannot be reliably maintained because sufficient biomass retention and settling cannot always be achieved. Membrane filtration is then more about securing the process stability than about increasing the performance of the wastewater treatment system. Thus, implementing membrane technology represents a completely new approach to wastewater treatment management in contrast to the incremental evolution from traditional to improved treatment systems.

The expected permeate quality of containerized MBR systems (Table 5) shows ammonium concentrations below 2 mg/L and BOD below 10 mg/L even at influent concentrations typical for agricultural wastewater.

Table 5. Typical influent and permeate water quality in containerized membrane bioreactor systems

| Parameter | Feed Water Quality | Expected Permeate Quality | Removal Efficiency (%) |
|---|---|---|---|
| pH | 6.5-7.5 S.U. | 6.5 - 7.5 S.U. | - |
| Alkalinity (as $CaCO_3$) | 125 mg/L | ≥ 100 mg/L | 20 |
| Temperature Range | 20-30°C | 20-30°C | |
| Total Suspended Solids (TSS) | 200 mg/L | < 5 mg/L | 97.5 |
| Biochemical Oxygen Demand (BOD) | 250 mg/L | < 10 mg/L | 96 |
| Chemical Oxygen Demand (COD) | 400 mg/L | < 50 mg/L | 87.5 |
| Ammonium-Nitrogen ($NH_4$) | 30 mg/L | < 2 mg/L | 93.33 |

*Values are indicative and may vary depending on influent characteristics and system configuration.

This indicates that stable nitrification is maintained despite high organic and nitrogen loads, confirming that decoupling SRT from HRT ensures biological robustness under intermittent inflow conditions.

In Romania, wastewater from farms has a biochemical oxygen demand (BOD) of up to 2000 mg/L, a total nitrogen content of less than 300 mg/L, and a dry matter content of less than 1% (Ministry of Environment, Waters and Forests & Ministry of Agriculture and Rural Development., 2021).

Wastewater passes through a drum screen to remove aggregates of hair and other debris, and to protect the membrane surface. The water then overflows to aeration tank, where air (fine bubbles) is injected to the tank to provide oxygen for microorganisms to decompose organic contents to $CO_2$, $H_2O$, and to convert ammonium/ammonia to nitrate. Membranes are periodically cleaned using chemical agents and air scouring with coarse bubbles in order to reduce fouling and keep the transmembrane pressure (TMP) within acceptable operating limits.

Despite the specific energy demand associated with membrane aeration and flux maintenance (0.4-0.8 kWh/m³), the MBR technology confers strategic benefits regarding compact footprint, high-quality effluent, and operational stability during load fluctuations.

MBR systems provide several advantages compared with conventional biological treatment processes, including improved effluent quality, reduced footprint, and easier process automation. They are typically operated with longer solids retention times (SRT), which contributes to lower sludge production. The treated effluent usually contains extremely low levels of bacteria, total suspended solids (TSS), biochemical oxygen demand (BOD), and phosphorus.

However, the main limitation of MBR technology is the higher investment and operational costs required to achieve treatment capacities comparable to those of conventional systems.

Energy costs are also higher because of the need for air scouring to control bacterial growth on the membranes (U.S. Environmental Protection Agency, 2007).

***Suitability for decentralized systems***

Mobile wastewater treatment systems for pig farms present significant potential, particularly for small and medium-sized farms needing flexible and sustainable solutions. However, addressing weaknesses such as limited capacity and high operational costs, while leveraging opportunities like renewable energy integration and rising regulatory demands, will be crucial for their widespread adoption and success.

Mobile treatment systems can be relocated to address wastewater issues at different farm sites, ensuring flexibility in operations, suitable for small-scale pig farms where permanent infrastructure may not be financially viable. They can incorporate multiple treatment stages (e.g., sedimentation, biological treatment, filtration) to meet specific water quality standards.

Increased regulations for agricultural wastewater management create demand for advanced treatment solutions. Biogas recovery from pig waste can power treatment units, reduce operational costs and create additional revenue streams (Sporea et al., 2023). Innovations in mobile treatment technologies (e.g., compact anaerobic digesters, advanced filtration) can improve efficiency and reliability. Maintenance, energy consumption, and operator training can be expensive. Performance can be affected by variations in wastewater characteristics, such as high solids or fat content from pig farming operations. High initial investment and operational costs may deter small-scale farmers from adopting the technology. Alternative wastewater treatment methods (e.g., centralized treatment plants, permanent lagoons) may be more appealing for certain farms.

The comparative operational characteristics shown in Table 6 demonstrate that the feasibility of decentralized treatment depends more on predictable effluent quality than on nominal removal efficiency. The compact footprint (0.1-0.3 m² per m³·d) and low hydraulic shock sensitivity enable treatment directly at source, transforming wastewater management from storage-based manure handling to a controlled treatment process.

Table 6. The differences between conventional activated sludge and membrane bioreactor systems in decentralized agricultural applications

| Parameter | Conventional activated sludge | Membrane bioreactor (MBR) | Typical implication for mobile systems |
|---|---|---|---|
| Infrastructure requirement | Requires sewer network and storage | Operates directly at source | Suitable for decentralized farms |
| Specific energy demand | ~0.3-0.6 kWh/m³ | ~0.5-1.0 kWh/m³ | Comparable when transport energy included |
| Sludge retention time (SRT) | ≥10-15 days for nitrification | 20-40 days independent of hydraulics | Stable treatment under variable loads |
| Effluent suspended solids | 10-40 mg/L (variable) | <1-5 mg/L (stable) | Reliable compliance |
| Total nitrogen removal | 50-80% (load dependent) | 80-95% (stable) | Better nutrient control |
| Sensitivity to hydraulic shocks | High | Low | Suitable for intermittent flows |
| Footprint | ~0.5-1.5 m² per m³·d | ~0.1-0.3 m² per m³·d | Compact mobile installations |
| Biomass retention | Settling dependent | Complete membrane retention | No washout risk |
| Operational stability | Less predictable performance | More predictable performance | Predictable effluent quality |
| Treatment philosophy | Dilution and discharge | Concentration and recovery | Compatible with circular economy |

*Values represent typical operational ranges reported in literature.

This study is based on literature analysis and therefore does not include experimental pilot-scale validation. Future research should investigate the operational performance of mobile MBR systems under real farm conditions and evaluate economic feasibility for small and medium livestock operations.

## CONCLUSIONS

Pollution generated by pig farms remains a major barrier to sustainable livestock production, not because of insufficient biological degradation capacity, but because centralized treatment concepts require hydraulic stability that livestock effluents inherently lack (Burton et al., 2003; Metcalf & Eddy et al., 2014). Membrane separation provides a different operational approach by decoupling sludge retention from hydraulics, transforming treatment reliability into a structural property of the process (Meng et al., 2017). For mobile and on-farm systems, environmental impact is determined by stability rather than nominal removal efficiency, making consistent effluent quality the primary performance indicator (WHO, 2006; Rahman et al., 2023).

Economic comparisons between conventional systems and membrane bioreactors are incomplete when transport, storage and dilution externalities are excluded from system boundaries (European Commission, 2020). Decentralized treatment preserves nutrients prior to dilution and therefore enables resource recovery and circular water management (Capodaglio & Olsson, 2020). Under this framework, performance must be evaluated by reuse safety and recoverability, not only pollutant removal (WHO, 2006; European Commission, 2020).

MBR systems should be considered a robust baseline technology for variable-load agricultural wastewater treatment rather than merely an advanced tertiary option.

The transition from activated sludge to MBR thus represents an infrastructural adaptation to circular economy requirements rather than a technological upgrade.

## REFERENCES

Burton, C. H., Turner, C., Beck, J. A. F., Martinez, J., Martens, W., Pahl, O., Piccinini, S., & Svoboda, I. (Eds.). (2003). *Manure management: Treatment strategies for sustainable agriculture* (2nd ed.). Silsoe Research Institute.

Capodaglio, A. G. (2017). Integrated, decentralized wastewater management for resource recovery in rural and peri-urban areas. *Resources, 6*(2), Article 22. https://doi.org/10.3390/resources6020022

Capodaglio, A. G., & Olsson, G. (2020). Energy issues in sustainable urban wastewater management: Use, demand reduction and recovery in the circular economy context. *Sustainability, 12*(1), 266. https://doi.org/10.3390/su12010266

Chen, B., Zhu, Y., Wu, M., Xiao, Y., Huang, J., Lin, C., & Weng, B. (2024). Research advancements in swine wastewater treatment and resource-based safe utilization management technology model construction. *Water*, 16(5), 661. https://doi.org/10.3390/w16050661

Chiriac, V., Ionescu-Sisești, V., Ghederim, V., & Negulescu, C. A. L. (1977). *Wastewater treatment and recovery of residues from the food and livestock industry*. Ceres Publishing House.

Du, X., Shi, Y., Jegatheesan, V., & Haq, I. U. (2020). A Review on the Mechanism, Impacts and Control Methods of Membrane Fouling in MBR System. *Membranes*, *10*(2), 24. https://doi.org/10.3390/membranes10020024

European Commission. (2017). Commission Implementing Decision (EU) 2017/302 of 15 February 2017 establishing best available techniques (BAT) conclusions for the intensive rearing of poultry or pigs. Official Journal of the European Union, L 43, 231–279.

European Commission. (2020). *A new Circular Economy Action Plan: For a cleaner and more competitive Europe*. ("European Commission adopted a new Circular Economy Action Plan for a ...") Publications Office of the European Union.

Ezugbe, E. O., & Rathilal, S. (2020). Membrane technologies in wastewater treatment: A review. *Membranes*, 10(5), 89. https://doi.org/10.3390/membranes10050089

Food and Agriculture Organization of the United Nations (FAO). (2018). *World livestock: Transforming the livestock sector through the Sustainable Development Goals*.

Hinada. (n.d.). *Piggery farm wastewater treatment plant solution*. Hinada. https://www.hinada.com/piggery-farm-wastewater-treatment-plant-solution/

Hoinkis, J., Deowan, S. A., Panten, V., Figoli, A., Huang, R. R., & Drioli, E. (2012). Membrane bioreactor (MBR) technology: A promising approach for industrial water reuse. Procedia Engineering, 33, 234–241. https://doi.org/10.1016/j.proeng.2012.01.1199

Iorhemen, O. T., Hamza, R. A., & Tay, J. H. (2016). Membrane bioreactor (MBR) technology for wastewater treatment and reclamation: Membrane fouling. *Membranes, 6*(2), 33. https://doi.org/10.3390/membranes6020033

Ivanciu Popa, M., Ungureanu, N., Vlăduț, V., Biriș, S. Ș., & Zăbavă, B. Ș. (2019). Types of treatment plants for livestock wastewater. *INMATEH – Agricultural Engineering*, 57(1), 191–198.

Judd, S. (2011). *The MBR book: Principles and applications of membrane bioreactors for water and wastewater treatment* (2nd ed.). Elsevier.

Kashyap, P. (2017). *Pollution Control and Policy Measures for Piggery Wastewater Management in Thailand.* Presented at WEPA Group Workshop on Piggery Wastewater Management in Asia 21-22 February 2017 Chiang Mai, Thailand. Regional Resource Centre for Asia and the Pacific (RRC.AP)

Kesari, K. K., Soni, R., Jamal, Q. M. S., Tripathi, P., Lal, J. A., Jha, N. K., Siddiqui, M. H., Kumar, P., Tripathi, V., & Ruokolainen, J. (2021). Wastewater Treatment and Reuse: a Review of its Applications and Health Implications. *Water, Air, and Soil Pollution,* 232(5), 208. https://doi.org/10.1007/s11270-021-05154-8

Libralato, G., Ghirardini, A. V., & Avezzu, F. (2012). To centralise or to decentralise: An overview of the most recent trends in wastewater treatment management. *Journal of Environmental Management, 94*(1), 61–68. https://doi.org/10.1016/j.jenvman.2011.07.010

Meng, F., Zhang, S., Oh, Y., Zhou, Z., Shin, H. S., & Chae, S. R. (2017). Fouling in membrane bioreactors: An updated review. *Water Research, 114*, 151–180. https://doi.org/10.1016/j.watres.2017.02.006

Metcalf & Eddy, Inc., AECOM, Tchobanoglous, G., Stensel, H. D., Tsuchihashi, R., & Burton, F. L. (2014). *Wastewater engineering: Treatment and resource recovery* (5th ed.). McGraw-Hill Education. https://www.mheducation.com/highered/product/wastewater-engineering-treatment-and-resource-recovery-metcalf-and-eddy.htmlMinistry of Environment, Waters and Forests & Ministry of Agriculture and Rural Development. (2021). *Code of good agricultural practices for water protection against nitrate pollution from agricultural sources.* Official Gazette 754 bis, August 3, 2021. Available at https://www.madr.ro/docs/agricultura/imbunatatiri-funciare/2021/cod-bune-practici-agricole-nitrati.pdf

Musa, M. A., & Idrus, S. (2021). Physical and Biological Treatment Technologies of Slaughterhouse Wastewater: A Review. *Sustainability*, *13*(9), 4656. https://doi.org/10.3390/su13094656

Nagarajan, D., Kusmayadi, A., Yen, H. W., Dong, C. D., Lee, D. J., & Chang, J. S. (2019). Current advances in biological swine wastewater treatment using microalgae-based processes. Bioresource Technology. 289. 121718. 10.1016/j.biortech.2019.121718.

Rahman, T. U., Roy, H., Islam, M. R., Tahmid, M., Fariha, A., Mazumder, A., Tasnim, N., Pervez, M. N., Cai, Y., Naddeo, V., & Islam, M. S. (2023). The Advancement in Membrane Bioreactor (MBR) Technology toward Sustainable Industrial Wastewater Management. *Membranes*, *13*(2), 181. https://doi.org/10.3390/membranes13020181

Sporea, N., Durbacă, I., Dumitrescu, A. M., Tomescu, G. (2023), Electricity produced using biogas obtained from the recovery of organic waste in ecological landfills – a case study, Technium: *Romanian Journal of Applied Sciences and Technology*, *14*, 26-30, https://doi.org/10.47577/technium.v14i.9669

Surdu, E., Farcaş-Flamaropol, D.C., Sporea, N.,Tomescu, G. (2021). The Use of Biomass Can Help Save the Planet, *Hidraulica*, 4, 76-85, https://hidraulica.fluidas.ro/2021/nr4/76-85.pdf

U.S. Environmental Protection Agency (EPA). (2007). Membrane Bioreactors Fact Sheet. Office of Water (EPA 832-F-07-015).

Vaishnav, S., Saini, T., Chauhan, A., Gaur, G. K., Tiwari, R., Dutt, T., & Tarafdar, A. (2023). Livestock and poultry farm wastewater treatment and its valorisation for generating value-added products: Recent updates and way forward. *Bioresource Technology,* 382, 129170. https://doi.org/10.1016/j.biortech.2023.129170

World Health Organization (WHO). (2006). *Guidelines for the safe use of wastewater, excreta and greywater: Volume 4 - Excreta and greywater use in agriculture*. https://www.who.int/publications/i/item/9241546859

Scientific Papers. Series E. Land Reclamation, Earth Observation & Surveying, Environmental Engineering. Vol. XV, 2026
Print ISSN 2285-6064, CD-ROM ISSN 2285-6072, Online ISSN 2393-5138, ISSN-L 2285-6064

# SALT LAKE MICROBIAL ECOSYSTEMS: IMPORTANCE AND CONSERVATION CHALLENGES

**Lucia-Roxana COJOC, Mirela-Mădălina MOLDOVEANU, Larisa-Isabela FLORESCU, Mădălin-Iancu ENACHE, Anca-Ioana LUCACI**

Institute of Biology Bucharest of Romanian Academy, 296 Splaiul Independentei, District 6, 060031, Bucharest, Romania

Corresponding author email: mirela.moldoveanu@ibiol.ro

***Abstract***

*High salinity lakes harbor halophilic microbial communities with specialized adaptations to osmotic stress. These ecosystems provide important ecological services and biotechnological potential, yet they face increasing threats from climate change and human activities. Understanding their microbial diversity is essential for conservation efforts. The present study aims to characterize cultivable halophiles from three saline lakes located in Durgau-Valea Sarata area, documenting their diversity, salt tolerance and capacity to produce extracellular enzymes.*
*XRF analysis revealed silica, chloride, calcium and titanium throughout all samples, with sporadic traces of bromide, potassium and sulfur. Cultivation on media with different salt concentrations yielded a total of 60 isolates across the three lakes, optimizing recovery of diverse halophiles including both archaea and bacteria. 16S rRNA gene sequencing of representative isolates revealed affiliation to Salinivibrio, Halomonas, Chromohalobacter, Marinococcus, Salicola, Halococcus, Halobacterium, Haloarcula and Halorubrum genera. Bacterial isolates produced exoenzymes (esterase, inulinase, amylase) and five strains demonstrated biofilm formation capacity.*
*Our results provide reference data on diversity of cultivable halophiles and functional traits in these threatened saline ecosystems.*

***Key words:*** *halophiles, anthropo-saline lakes, biofilm formation, cultivable diversity, exoenzymes.*

## INTRODUCTION

Hypersaline habitats shelter diverse microbial communities, including extreme halophiles, moderate halophiles, and halotolerant microorganisms, which have developed strategies to overcome osmotic stress and elevated salinity levels through mechanisms such as accumulation of compatible solutes and efficient ion transport systems (Quesada et al., 1983). Recent studies have revealed that these communities are characterized by specific trophic interactions shaped by high levels of specialization (Saccò et al., 2021).
Hypersaline lakes, which account for almost half (44%) of inland water volume (Saccò et al., 2021), exhibit uniqueness not only in their extreme physicochemical conditions but also in the diversity and metabolic potential of their microbial communities (Paul & Mormile, 2017). These ecosystems offer biotechnological potential, therapeutic uses through heliothermic properties and organic-rich sediments (Alexe et al., 2018; Rus et al., 2020), and microbiological research opportunities, where microbial communities serve as environmental indicators (Oren, 2018; Paul & Mormile, 2017).
However, hypersaline lakes are highly susceptible to climate change, as increased temperatures lead to high evaporation rates, further intensifying salinity levels that challenge microbial survival (Paul & Mormile, 2017), while rising lake surface temperatures affect ecosystem structure and metabolic activities (Dokulil et al., 2021). Since salinity drives microbial diversity, alterations to this foundation affect the entire food web (Baxter & Butler, 2020). Additionally, anthropogenic pressures, particularly intense touristic exploitation through uncontrolled bathing, cause degradation and diminishment of the heliotherm phenomenon (Alexe & Furtună, 2012). Continued loss and degradation of hypersaline habitats will result in the loss of taxonomic and functional diversity, with impacts at multiple scales, making the prevention of ecosystem destruction and the development of sustainable use strategies a pressing issue (Saccò et al., 2021).

Salt lakes in Transylvania are distinctive components of the basin landscape formed by salt dissolution of underground halite deposits (Har et al., 2010; Alexe et al., 2018). These lakes are small and quite deep, offering ideal conditions for stratification and the development of heliothermy (Mera et al., 2010; Sonnenfeld & Hudec, 1980). Previous microbiological research in the Turda region has focused mainly on the characterization of halophilic bacterial communities associated with Turda Salt Mine (Carpa et al., 2014). Several studies have also investigated the microbial diversity of hypersaline meromictic lakes from the Transylvanian Basin, with particular emphasis on archaeal communities and their vertical distribution in the water column (Andrei et al., 2015; Baricz et al., 2014; 2015). Nevertheless, information regarding the diversity of cultivable bacterial populations inhabiting these saline lakes remains relatively limited.

Understanding the composition and physiological capabilities of halophilic microbial communities is essential for both conservation efforts and potential biotechnological exploitation. The present study aims to document the diversity and physiological characteristics of cultivable halophilic microorganisms from three saline lakes in the Durgău-Valea Sărată area (Turda, Romania). By characterizing these communities, their salt tolerance profiles, and enzymatic capabilities, this research provides baseline data necessary for conservation and monitoring as environmental pressures from climate change and anthropogenic activities intensify.

## MATERIALS AND METHODS

### Site description

Water samples were collected from three saline lakes in the Durgău-Valea Sărată area of Turda (46°35'16.8"N, 23°47'14.1"E), Cluj County, Romania (Figure 1). This area is part of Sărăturile Ocna Veche, a protected area of national interest corresponding to IUCN category IV (mixed nature reserve). The salt lakes in Turda developed over the sites of old salt mine chambers used during the 15th and 16th centuries (Mera et al., 2010). These lakes are characterized by stratification (formation of permanent density water layers) and heliothermy, with a surface freshwater layer of variable thickness (0.15 to 0.2 m) (Mera et al., 2010).

Ocnei Lake emerged around 1800 following the collapse of the "Ocna cea Mare" excavation (Mera et al., 2010). This anthropo-saline lake contains chlorinated-sodic mineral waters with mineralization ranging between 19.27 and 225 mg $L^{-1}$ (Rus et al., 2020) and surface salinity varying from 1.78 to 40.42 g Cl/l depending on freshwater input (Munteanu & Munteanu, 2012). The lake is actively used for recreation and therapy, with heavy exploitation during summer since 2009 (Avram et al., 2022). Over time, maximum temperatures in the heliothermic layer have decreased, mainly due to intensive exploitation of the waters for bathing and treatment activities (Alexe & Furtună, 2012).

Rotund Lake was created by the collapse of the "Ocna cea Mica" excavation (Mera et al., 2010). Similar to Ocnei Lake, it is an anthropo-saline lake used for recreation and therapy (Avram et al., 2022), with chlorinated-sodic mineral waters (Rus et al., 2020).

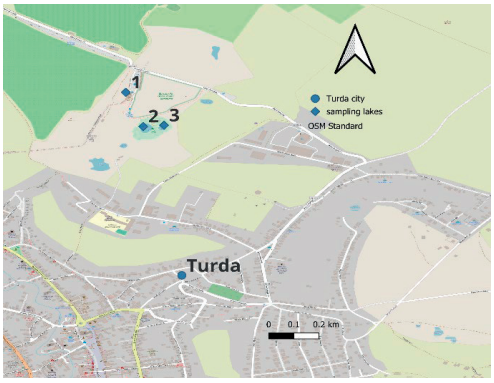



Figure 1. The map with sampling points (QGIS Desktop 3.40.15 with OSM standard)

Therezia Lake is a subterranean lake located at 112 m depth in the Turda Salt Mine, with a water depth of 0.5- 8 m and occupying approximately 80% of the exploitation chamber surface (Kimic et al., 2021). The lake formed through human-induced geomorphological processes: the Theresia chamber, originally a salt extraction site named in honor of Empress Maria Theresa, became structurally unstable following

extensive salt extraction and ultimately collapsed, allowing surface water infiltration that gradually flooded the cavity (Avram et al., 2022). A central island formed by residual salt accumulated after the cessation of extraction activities in 1880 (Kimic et al., 2021). The lake is characterized by a slightly alkaline pH (8.7), specific conductance of 114 mS $cm^{-1}$, and estimated salinity of 90.98 g $L^{-1}$ (Carpa et al., 2014). The subterranean environment maintains relatively constant temperatures (11.8-12.2°C) and humidity (67-70%) with no air flow (Enache, 2010).

**Sampling**

The water samples were collected from the surface layers of the three lakes, about 0.5 m beneath the water surface. The sampling procedure was performed aseptically with sterile utensils and sterilized collection containers, thereby avoiding external contamination. Samples were kept refrigerated and were transported in cooler storage boxes to the laboratory for further chemical and microbiological analysis.

**XRF analysis**

The chemical composition of the water samples was determined using a Supermini X-Ray Fluorescence Spectrometer (Rigaku Corporation, Japan), following the manufacturer's semiquantitative method for light element analysis in a helium atmosphere. SQX software was used to calculate elemental oxide mass percentages (mass %). Weighed 10 mL volumes of each sample were used for analysis.

**Isolation of halophilic microorganisms and estimation of total CFU number** was carried on 3 different nutritive media, with the following compositions (g $L^{-1}$): MH medium - yeast extract, 10; proteose peptone, 5; glucose, 1; NaCl, 100; $MgCl_2$ x $6H_2O$, 7; $MgSO_4$ x $7H_2O$, 9.6; $CaCl_2$ x $2H_2O$, 0.36; KCl, 2; $NaHCO_3$, 0.06; NaBr, 0.026 (Quesada et al., 1983), JCM 168 medium (Japan Collection of Microorganisms) - casamino acids, 5; yeast extract, 5; sodium glutamate, 1; trisodium citrate, 3; $MgSO_4 \cdot 7H_2O$, 20; KCl, 2; NaCl, 200; $FeCl_2 \cdot 4H_2O$, 36; $MnCl_2 \cdot 4H_2O$, 0.36, MR medium - NaCl, 250; $MgCl_2$ $6H_2O$, 13; $MgSO_4$ $7H_2O$, 20; KCl, 4; $CaCl_2$ $2H_2O$, 1; NaBr, 0.5; $NaHCO_3$, 0.2; yeast extract, 5; tryptone, 8; and glucose, 1 (Hedi et al., 2009). A quantity of 20.0 g $L^{-1}$ agar was added to each type of medium for solidification, and the pH was adjusted to 7.2 before autoclaving.

In order to estimate the total CFU number in each sample and isolate the halophilic microorganisms in pure cultures, the serial dilutions method was applied, followed by the pour-plate technique and 3 streak-plate purification passages. The experiments were conducted in triplicate. The cultures incubation was performed at 30°C (MH) or 37°C (JCM 168 and MR) for a period of 30 days.

**The susceptibility to inhibitors (antibiotics/ bile salts)** of the new isolates was tested in order to confirm assignment to the *Bacteria* domain and to differentiate them from halophilic archaea. Two media variants with specific inhibitors were used for this purpose: one containing 0.002% chloramphenicol and the other containing 0.004% sodium deoxycholate. Strains that grew in the presence of the bile salt were considered halophilic bacteria.

**Establishing the salinity range**

The range of salt concentration that allows bacterial growth was determined in MH, JCM168, and MR media containing different NaCl concentrations: 0, 1, 2, 3, 4, and 5 M. The halophilic isolates were classified based on the most widely accepted system defined by Kushner & Kamekura (1988).

**Assessment of extracellular enzyme production**

MH medium with NaCl concentrations adjusted according to previously obtained results was used for establishing the ability of selected isolates to produce extracellular hydrolytic enzymes (amylase, esterase, inulinase). This was qualitatively assessed on solid basal MH (without proteose peptone and glucose) to which the interest substrate was added.

For the amylolytic activity, 2 g $L^{-1}$ starch was added to the basal medium. The selected isolates were inoculated on the surface of agar plates, incubated at 30°C for 48 hours and subsequently flooded with $I_2$ – KI solution (0.1% $I_2$ – 0.2% KI). The presence of a clear zone around the

culture spot indicates the starch hydrolysis and strains were recorded positive for amylase production (Ali et al., 2024).

To determine the esterase activity, the basal medium was supplemented with 0.01% $CaCl_2$. After autoclaving, sterile Tween 80 was added to a final concentration of 1% (v/v). Positive reaction was indicated by the appearance of a white precipitate formed around the growth areas of the bacterial cultures (Ali et al., 2024).

For cellulase activity, basal medium was supplemented with 0.5 g $L^{-1}$ carboxymethylcellulose (CMC). After incubating the inoculated plates at 30°C for 48 hours, they were flooded with 0.1% Congo Red solution for 15 minutes. The dyeing agent was removed by rinsing with 1M NaCl for 5-10 minutes (Rohban et al., 2009; Bambharolia et al., 2024).

The production of inulinase by the investigated isolates was detected by adding 2 g $L^{-1}$ inulin to basal medium. Bacterial growth after 48 hours of incubation at 30°C was considered a positive result (Rohban et al., 2009).

**Molecular identification of the isolates**

Total genomic DNA was extracted using a DNeasy Blood & Tissue kit (Qiagen), according to the manufacturer's protocol. 16S rRNA gene was PCR amplified with the pair of primers 27F (AGAGTTTGATCCTGGCTCAG) – 1492R (GGTTACCTTGTTACGACTT) for bacteria (Miller et al., 2013), while for archaea, the set of primers 20F (AGTTTGATCATGGCTCA) – 1540R (AAGGAGGTGATCCAACCGCA) (Ohnishi et al., 2011) was used. Amplicons were analyzed by agarose gel electrophoresis (1% w/v) with Red Safe staining and visualized under UV light against O'GeneRuler 1Kb Plus DNA Ladder (Thermo Scientific). Following DNA sequencing performed by CeMIA SA (Larissa, Greece), the resulting nucleotide sequences were compared using the Basic Local Alignment Search Tool (BLAST; www.ncbi.nlm.nih.gov/BLAST/).

**Biofilm production** was assessed in five bacterial isolates selected for mucoid/slimy colony appearance, which typically indicates extracellular polysaccharide production.

The experiment was carried out in 96-well U-bottom microplates with following the method described by O'Toole (2011). The experiment was performed with 5 replicate wells per isolate. Plates were incubated for 31 days in static conditions, at 30ºC, and the biofilm formed was quantified periodically by reading the absorbance at 550 nm (BMG LABTECH FLUOstar Omega microplate reader).

## RESULTS AND DISCUSSIONS

**XRF analysis**

Generally, silica, chloride, sodium, calcium and titanium were present in all investigated samples, with slight quantitative variation according to water source. Sporadic traces of bromide, potassium and sulfur were also detected according to data presented in Figure 2. The considerably smaller amounts of silica detected in the Therezia Lake, could be associated with the position of the lake inside the salt mine, unlike the other two surface lakes positioned in open space. As previously stated, silica should not be considered native ions in the salt massifs (Cojoc et al., 2013).

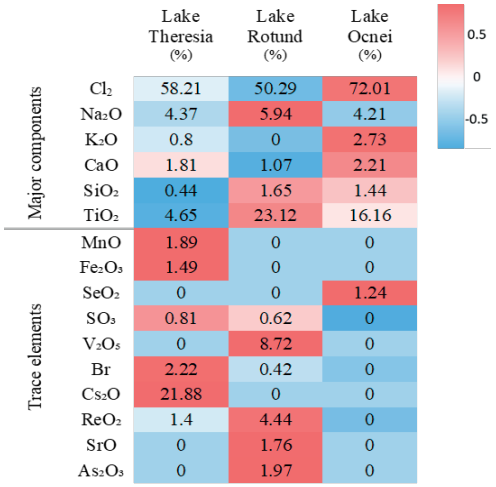



Figure 2. Heatmap of XRF-determined chemical composition of the three salt lakes. Color intensity corresponds to row-wise Z-score normalized values representing relative abundance from low (light) to high (dark). Values indicate measured oxide concentrations (mass %)

High concentrations of titanium and vanadium, both toxic to aquatic organisms and humans, suggest anthropogenic contamination from industrial activities, pigments, cosmetics, and

wastewater entering the lakes via surface runoff or wind (Catana et al., 2022).
The high chlorine concentration observed in all three investigated lakes is reflected in the water's salinity. Sodium chloride, which is a thermophile molecule contributes to an increase in salinity of the warm layer during the daytime (Sonnenfeld & Hudec, 1980).
The performed microbiological analyses proved that the investigated lakes are highly populated by halophilic microorganisms belonging to the *Bacteria* and *Archaea* domains.

**Estimation of the total CFU number and the isolation of halophilic microorganisms**
After 48h of incubation, the number of CFU $mL^{-1}$ on MH medium was estimated as follows: Ocnei Lake – 4.7 x $10^2$ CFU $mL^{-1}$, Therezia Lake – 0 CFU $mL^{-1}$, Rotund Lake – 1.26 x $10^2$ CFU $mL^{-1}$. No colonies grew on JCM 168 and MR media after 48 hours of incubation at 37ºC.
Pink-red and white-cream colonies developed on JCM 168 medium only after 30 days of incubation. The number of CFU $mL^{-1}$ was estimated as follows: Ocnei Lake – 10 CFU $mL^{-1}$, Therezia Lake – 82.33 CFU $mL^{-1}$, Rotund Lake – 13 CFU $mL^{-1}$. On MR medium pink, yellow, and orange colonies developed after 1 month of incubation only from the Therezia Lake sample, the estimated CFU number for this sample being 20 CFU $mL^{-1}$.
A total number of 60 isolates across the three investigated lakes (13 from Ocnei Lake, 25 from Therezia Lake and 22 from Rotund Lake) were obtained and further purified.

**The inhibitor tests performed** showed that all the 25 microbial isolates obtained on MH medium belonged to the *Bacteria* domain, being able to grow in the presence of deoxycholic acid sodium salt.
On JCM 168 medium, 14 of the obtained isolates showed susceptibility to bile salts and were also positive for lysis in sterile distilled water after incubation for one hour at room temperature. The susceptible isolates were thus classified as archaea. The remaining 15 strains resistant to bile salts were selected for further experiments and considered to belong to the *Bacteria* domain. Following the same differentiation test, two of the isolates obtained on MR medium were classified as bacteria and 4 were assigned to *Archaea.* Across the three investigated lakes different domain distributions of the isolates were observed (Figure 3).

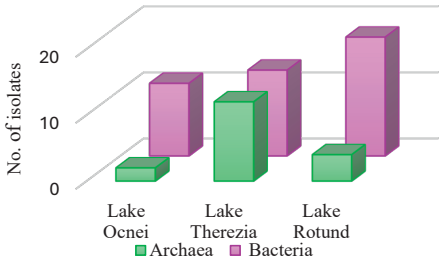



Figure 3. Domain distribution of isolates obtained from the saline lakes

**Establishing the salinity range**
Based on optimal salinity for growth, this study revealed distinct halophilic profiles between surface and subterranean environments.
The two surface anthropo-saline lakes - Ocnei and Rotund - were dominated by halotolerant strains (46% and 61% of the isolates), with moderately halophilic isolates representing 36% and 39%, respectively. Extremely halophilic strains were detected only in Ocnei Lake (18%), whereas they were absent from Rotund Lake. In contrast, the subterranean Therezia Lake exhibited a distinct distribution, with predominant moderately halophilic strains (46%), followed by halotolerant (39%) and extremely halophilic (15%) representatives, suggesting different selective pressures in the isolated subterranean environment.

**Assessing of the capacity of producing extracellular enzymes**
Screening of the bacterial isolates revealed a heterogeneous distribution of extracellular enzymatic capabilities. A considerable number of strains expressed lipolytic (5 isolates) and proteolytic activity (6 isolates), whereas inulin degradation was detected only in three isolates. CMC was not hydrolyzed by any of the isolates. The capacity to degrade complex carbohydrates was less prevalent. Amylolytic activity was detected in a limited number of isolates and showed only partial overlap with lipolytic activity.
A smaller number of isolates (5) demonstrated combined hydrolytic activities, suggesting a

high versatility. The presence of such polyvalent strains may reflect ecological adaptation to fluctuating nutrient availability, highlighting potential candidates for saline bioprocesses.

**Molecular identification of the isolates**

Agarose gel electrophoresis confirmed successful PCR amplification with domain-specific primers, by yielding products of expected size for both bacterial and archaeal 16S rRNA genes (Figure 4).

Representative isolates from the three investigated anthropo-saline lakes were identified by partial 16S rRNA gene sequencing as belonging to bacterial and archaeal genera as presented in Table 1.

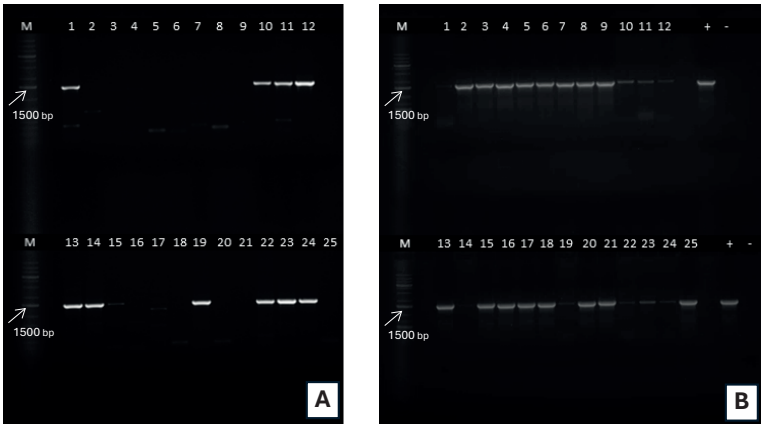



Figure 4. Domain-specific amplification of 16S rRNA genes with (A) Archaeal primers (20F/1540R), (B) Bacterial primers (27F/1492R). Lane identifications: M = 1 kb Plus DNA ladder; 1-25 = isolates from the 3 saline lakes; + = positive control, - = negative control

Table 1. Taxonomic affiliation of sequenced isolates from the three saline lakes

| Sample source | Affiliation to bacterial genera | Affiliation to archaeal genera |
|---|---|---|
| **Ocnei Lake** | *Halomonas* (3), *Marinococcus* (1), *Salinivibrio* (1), *Salicola* (1) | *Halococcus* (1) |
| **Therezia Lake** | *Halomonas* (1), *Salicola* (1), *Chromohalobacter* (3) | *Haloarcula* (2), *Halococcus* (2), *Halobacterium* (3), *Halorubrum* (1) |
| **Rotund Lake** | *Marinococcus* (3) | Not sequenced |

*Numbers in parentheses indicate isolates assigned to each genus.

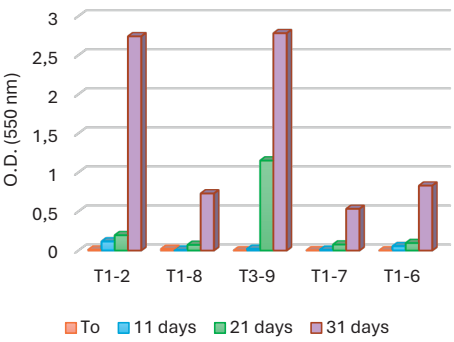



Figure 5. Biofilm production capacity of the investigated bacterial isolates

**Biofilm formation capacity**

Biofilm production was assessed in five bacterial isolates showing mucoid/slimy colony morphology. All five isolates demonstrated biofilm formation capacity, though with varying kinetics and production levels (Figure 5).

Isolate T3-9 showed a significant capacity for biofilm formation after 21 days of incubation, while T1-2 was able to produce notable biofilms only after 31 days. The remaining three isolates also formed biofilms after 31 days of incubation, but at lower levels than T3-9 and T1-2.

## CONCLUSIONS

The three anthropo-saline lakes in the Durgău-Valea Sărată area (Turda, Romania) harbor diverse cultivable halophilic microbial communities comprising both bacterial and archaeal representatives.

Distinct halophilic profiles were observed between surface saline lakes (Ocnei and Rotund) and the subterranean Therezia Lake, with surface lakes dominated by halotolerant strains, while the subterranean environment showed higher proportions of moderately and extremely halophilic microorganisms, suggesting that environmental isolation may create different selective pressures in these habitats.

The presence of elevated titanium and vanadium concentrations detected through XRF analysis indicates anthropogenic contamination associated with intensive bathing activities, particularly from sunscreens and cosmetic product pigments, raising concerns about impacts on microbial community health and ecosystem stability.

The enzymatic capabilities of bacterial isolates, including esterase, inulinase, and amylase production, along with biofilm-forming capacity across multiple strains, highlight the biotechnological potential of halophilic microorganisms from these threatened ecosystems and underscore the economic value of preserving microbial diversity.

This study provides essential baseline data on cultivable halophilic diversity and functional traits in Turda saline lakes, establishing reference information necessary for future monitoring and conservation efforts as these ecosystems face mounting pressures from climate change and anthropogenic activities.

## ACKNOWLEDGEMENTS

This research work was carried out with the support of the Institute of Biology Bucharest of Romanian Academy and was financed from the projects no. RO1567-IBB05/2026 and RO1567-IBB02/2026.

## REFERENCES

Alexe, M., & Furtună, P.-R. (2012). Natural and Anthropic Risks in the Area of Durgău- Valea Sărată Turda Salt Lakes. *Proceedings of the Water Resources and Wetlands, Tulcea, Romania*, 244–247.

Alexe, M., Șerban, G., Baricz, A., Andrei, A.Ș, Cristea, A., P. Battes, K., Cîmpean, M., Momeu, L., Muntean, V., Porav, S. A., & Banciu, H. L. (2018). Limnology and plankton diversity of salt lakes from Transylvanian Basin (Romania): A review. *Journal of Limnology*, 77(1), 17–34. https://doi.org/10.4081/jlimnol.2017.1657.

Ali, A. M., Abdel-Rahman, T. M. A., & Farahat, M. G. (2024). Bioprospecting of Culturable Halophilic Bacteria Isolated from Mediterranean Solar Saltern for Extracellular Halotolerant Enzymes. *Microbiology and Biotechnology Letters, 52*(1), 76–87. https://doi.org/10.48022/mbl.2401.01010.

Andrei, A.-Ș., Robeson, M. S., II, Baricz, A., Coman, C., Muntean, V., Ionescu, A., Etiope, G., Alexe, M., Sicora, C. I., Podar, M., & Banciu, H. L. (2015). Contrasting taxonomic stratification of microbial communities in two hypersaline meromictic lakes. *The ISME Journal*, *9*(12), 2642–2656. https://doi.org/10.1038/ismej.2015.60.

Avram, S. E., Rus, L., Micle, V., & Hola, S. S. (2022). Evaluation and Evolution of the Physico-Chemical Parameters of Ocnei and Rotund Lakes Located near the "Salina Turda" Mine, Romania. *Water*, *14*(15). https://doi.org/10.3390/w14152366.

Bambharolia, R. P., Vyas, T. K., Vavdiya, P. A., Damasia, D. M., Garaniya, N. H., & Deshmukh, A. J. (2024). A Comparative Study of Different Staining Techniques for Cellulase Activity on CMC (Carboxy Methyl Cellulose) Agar. *International Journal of Economic Plants*, *11*, 303–309. https://doi.org/10.23910/2/2024.5451b.

Baricz, A., Coman, C., Andrei, A. Ș., Muntean, V., Keresztes, Z. G., Păușan, M., Alexe, M., & Banciu, H. L. (2014). Spatial and temporal distribution of archaeal diversity in meromictic, hypersaline Ocnei Lake (Transylvanian Basin, Romania). *Extremophiles*, *18*(2), 399–413. https://doi.org/10.1007/s00792-013-0625-6.

Baricz, A., Cristea, A., Muntean, V., Teodosiu, G., Andrei, A.-Ș., Molnár, I., Alexe, M., Rakosy-Tican, E., & Banciu, H. L. (2015). Culturable diversity of aerobic halophilic *Archaea* (Fam. Halobacteriaceae) from hypersaline, meromictic Transylvanian lakes. *Extremophiles*, *19*(2), 525–537. https://doi.org/10.1007/s00792-015-0738-1.

Baxter, B. K., & Butler, J. K. (2020). Climate Change and Great Salt Lake. In B. K. Baxter & J. K. Butler (Eds.), *Great Salt Lake Biology: A Terminal Lake in a Time of Change* (pp. 23–52). Springer International Publishing. https://doi.org/10.1007/978-3-030-40352-2_2.

Carpa, R., Keul, A., Muntean, V., & Dobrotă, C. (2014). Characterization of Halophilic Bacterial Communities in Turda Salt Mine (Romania). *Origins of Life and Evolution of the Biosphere*, *44*(3), 223–230. https://doi.org/10.1007/s11084-014-9375-4.

Catana, R. D., Podosu, A., Florescu, L. I., Mihai, R. A., Enache, M., Cojoc, R., & Moldoveanu, M. (2022). Quantitative Analyses of Chemical Elements in *Phragmites australis* as Bioindication of Anthropization in Urban Lakes. *Sustainability*, *15*(1), 553. https://doi.org/10.3390/su15010553.

Cojoc, R., Enache, M., & Codreanu-Balcescu, D. (2013). Approaching the halophilic bacteria presence as possible indicator of biological dynamics in hypersaline aquatic environments. *Drobeta- Seria Stiintele Naturii, XXIII*, 31–39.

Dokulil, M., Eyto, E., Maberly, S., May, L., Weyhenmeyer, G., & Woolway, R. (2021). Increasing maximum lake surface temperature under climate change. *Climatic Change*, *165,* 56. https://doi.org/10.1007/s10584-021-03085-1.

Enache, L. (2010). *The Microclimate, Bioclimate and Natural Air Ionization in Turda Salt Mine – Environmental Factors with Therapeutic Potential*. Masa Rotunda Dedicata Dezvoltării Turismului Balneoclimateric şi Speleoterapiei în Salina Turda.

Har, N., Rusz, O., Vlad, C., & Barbu, O. (2010). New data on the mineralogy of the salt deposit from Sovata (Mureş county-Romania). *Carpathian Journal of Earth and Environmental Sciences*, *5*, 127–135.

Hedi, A., Sadfi, N., Fardeau, M.-L., Rebib, H., Cayol, J.-L., Ollivier, B., & Boudabous, A. (2009). Studies on the Biodiversity of Halophilic Microorganisms Isolated from El-Djerid Salt Lake (Tunisia) under Aerobic Conditions. *International Journal of Microbiology*, 731786. https://doi.org/10.1155/2009/731786.

Kimic, K., Costa, C. S., & Negulescu, M. (2021). Creating Tourism Destinations of Underground Built Heritage—The Cases of Salt Mines in Poland, Portugal, and Romania. *Sustainability*, *13*(17). https://doi.org/10.3390/su13179676.

Kushner, D. J., & Kamekura, M. (1988). Physiology of halophilic Eubacteria. In F. Rodriguez-Valera (Ed.), *Halophilic Bacteria* (Vol. 1, pp. 109–138). CRC Press, Inc., Boca Raton. https://scispace.com/papers/physiology-of-halophilic-eubacteria-3renqnh8jo.

Mera, O., Stefanie, T., & Visinescu, V. (2010). *Cetatea din Muntele de Sare*. Targul Cartii.

Miller, C. S., Handley, K. M., Wrighton, K. C., Frischkorn, K. R., Thomas, B. C., & Banfield, J. F. (2013). Short-Read Assembly of Full-Length 16S Amplicons Reveals Bacterial Diversity in Subsurface Sediments. *PLOS ONE*, *8*(2), e56018. https://doi.org/10.1371/journal.pone.0056018.

Munteanu, C., & Munteanu, D. (2012). *Ape terapeutice clorurate – sodice*. Ed. Balneara.

Ohnishi, A., Abe, S., Nashirozawa, S., Shimada, S., Fujimoto, N., & Suzuki, M. (2011). Development of a 16S rRNA Gene Primer and PCR-Restriction Fragment Length Polymorphism Method for Rapid Detection of Members of the Genus Megasphaera and Species-Level Identification. *Applied and Environmental Microbiology*, *77*(15), 5533–5535. https://doi.org/10.1128/AEM.00359-11.

Oren, A. (2018). Salt Lakes, Climate Change, and Human Impact: A Microbiologist's Perspective. *2018 Air and Water Components of the Environment Conference Proceedings*, 163–170. https://doi.org/10.24193/AWC2018_20.

O'Toole, G. A. (2011). Microtiter Dish Biofilm Formation Assay. *Journal of Visualized Experiments: JoVE*, (47), 2437. https://doi.org/10.3791/2437.

Paul, V. G., & Mormile, M. R. (2017). A case for the protection of saline and hypersaline environments: A microbiological perspective. *FEMS Microbiology Ecology*, *93*(8), 1–14. https://doi.org/10.1093/femsec/fix091.

Quesada, E., Ventosa, A., Rodriguez-Valera, F., Megias, L., & Ramos-Cormenzana, A. (1983). Numerical Taxonomy of Moderately Halophilic Gram-negative Bacteria from Hypersaline Soils. *Microbiology*, *129*(8), 2649–2657. https://doi.org/10.1099/00221287-129-8-2649.

Rohban, R., Amoozegar, M. A., & Ventosa, A. (2009). Screening and isolation of halophilic bacteria producing extracellular hydrolyses from Howz Soltan Lake, Iran. *Journal of Industrial Microbiology & Biotechnology*, *36*(3), 333–340. https://doi.org/10.1007/s10295-008-0500-0.

Rus, L., Avram, S.-E., & Micle, V. (2020). Determination and assessments of physicochemical parameters of the water from anthropo-saline lakes located in the protected area "Salina Turda", Romania. *Studia Universitatis Babeş-Bolyai Chemia*, *65*(2), 257–268. https://doi.org/10.24193/subbchem.2020.2.21.

Saccò, M., White, N. E., Harrod, C., Salazar, G., Aguilar, P., Cubillos, C. F., Meredith, K., Baxter, B. K., Oren, A., Anufriieva, E., Shadrin, N., Marambio-Alfaro, Y., Bravo-Naranjo, V., & Allentoft, M. E. (2021). Salt to conserve: A review on the ecology and preservation of hypersaline ecosystems. *Biological Reviews*, *96*(6), 2828–2850. https://doi.org/10.1111/brv.12780.

Sonnenfeld, P., & Hudec, P. P. (1980). Chapter 8 Heliothermal Lakes. In A. Nissenbaum (ed.), *Developments in Sedimentology*, 28, 93–100. Elsevier. https://doi.org/10.1016/S0070-4571(08)70232-2.

Scientific Papers. Series E. Land Reclamation, Earth Observation & Surveying, Environmental Engineering. Vol. XV, 2026
Print ISSN 2285-6064, CD-ROM ISSN 2285-6072, Online ISSN 2393-5138, ISSN-L 2285-6064

# INCREASING THE EFFICIENCY OF BIOLOGICAL SLUDGE STABILIZATION PROCESSES WITHIN WASTEWATER TREATMENT PLANTS

**Dragos DRACEA[1], Alin HAPCA[2], Sebastian MUSTATA[1], Augustina Sandina TRONAC[1]**

[1]University of Agronomic Sciences and Veterinary Medicine of Bucharest,
59 Marasti Blvd., District 1, Bucharest, Romania,
[2]Aqua D&P Technologies, 155 B Traian Vuia Street, Cluj-Napoca, Romania

Corresponding author email address: augustina.tronac@fifim.ro

***Abstract***

*Wastewater treatment plants are complex systems designed to deal both with wastewater and with resulting sludge. Physical, chemical and especially biological processes depend significantly on technological factors, the conditions for the development of biochemical reactions having complex dynamics. Due to hourly and seasonal variations in inputs (flows and pollutant concentrations), and to the conditions of the treatment process, continuous technological adjustments are necessary. The economic sizing of wastewater treatment plants can lead to operating situations at the organic pollutant load limit in terms of efficiency, making it necessary to adopt additional technological measures. The paper presents a one-year long case study on adjusting the stabilization processes and reducing the quantity of sludge produced (50% in warm seasons, 10% in cold season) in a wastewater treatment plant based on specialized microbial products. The monitorized parametres are dissolved organic carbon (COD), $N_{total}$, $P_{total}$ The results highlight the need to ensure all technological factors for wastewater treatment and for sludge mineralization, simultaneously with the maintaining of desired efficiency and the corrective measures implementation.*

***Key words:*** *biological processes, biopreparations, sludge stabilization, wastewater treatment plant.*

## INTRODUCTION

Wastewater treatment plants become increasingly important for the environment and human activities in the context of climate change and the major imbalance between water demand and available water quantities.

The technological challenge of management of the sludge quantities was addressed using microbial products by Chinese scientist (Li et al., 2022) isolating strains of *Firmicutes* and *Proteobacteria* confirming the possible use.

The study main objective is the decrease of the sludge quantities by 50% all over the year, independently of temperature, on average flux of 100 $m^3$/h and average COD of 2000 mg/L, by adding microbial products.

Sewage sludge management has historically been achieved (EU, 2024) through methods that did not take into account all environmental factors, with major implications generated over time; Table 1 presents the main methods used and their advantages/disadvantages.

Table 1. Treatment methods for sludge resulting from wastewater treatment processes

| Method | Disadvantages | Advantages |
|---|---|---|
| Spreading on agricultural land | - technological difficulties in transporting and applying for sludges with high moisture<br>- pedological changes in the pH indicator, and the need to monitor soil characteristics over time<br>- high consumption of lime for sludge stabilization and dehydration, respectively for soil amendment<br>- accumulation of heavy metals in soil, cumulative evolution<br>- need for large land areas | - unloading of significant quantities of materials considered waste – circular economy<br>- nutrient supply for agricultural lands<br>- improving soil structure |
| Reduction of sludge quantities through aerobic stabilization | - increase in technological wastewater treatment volumes<br>- additional energy consumption for aeration, | - reducing the sludge volumes generated by wastewater treatment plants |

| Method | Disadvantages | Advantages |
|---|---|---|
| at the technological wastewater flux or in specific compartments | homogenization and recirculation<br>- consumption of coagulants for phosphorus correction<br>- all the aspects mentioned for the previous method | - reducing the amount of stabilization lime<br>- improving sludge management/dewatering processes, including reducing the quantities of dehydrated reagents required<br>- reducing the amount of carbon discharged into the environment with the possibility of generating secondary pollution |
| Anaerobic stabilization | - difficult process to manage due to the range required for feeding the fermenter with raw material, the restricted pH and temperature range necessary to be ensured in the process<br>- significant consumption of electrical and thermal energy even in the case of complete solutions for valorization of the biogas produced<br>- incompatibility between the need to reduce nitrogen in wastewater and biogas production for low C:N ratios<br>- oversizing biological tanks for treating nitrogen and phosphorus generated in fermentation processes<br>-the need for additional stabilization of the fermented sludge compared to an aerobic process | - reduction of the final sludge amount<br>- obtaining energy by utilizing biogas and gaining wastewater treatment plant energy independence<br>- obtaining expensive energy by optimizing cogeneration processes |
| Incineration | - $CO_2$ generation and removal into the atmosphere in contradiction with the concept of carbon storage<br>- need to dehydrate sludge to low moisture levels (35%)<br>- generation of gases and water vapor in the dehydration and incineration process<br>- dust generation<br>- additional fuel requirement | - reducing the quantities of waste that must subsequently be managed<br>- obtaining thermal energy<br>- simplifying the wastewater technological flux and sludge technological flux, by reducing the technological volumes necessary for sludge stabilization |

From the analysis of the advantages and disadvantages listed, the optimal solution seems to be the centralized management of sludge in regional depots (Neamt et al., 2013; Rosiek, 2020), ensuring: centralized collection of sewage sludge from economic operators; quantitative and qualitative control of sludge and application of efficient technologies for each category of sludge and for by-products; storage in plots depending on chemical characteristics; development of specific processing technologies for each type of sludge.

A regional sludge depot can be structured as follows:

- plots for stabilizing good quality organic sludge, with minimal content of toxic substances and heavy metals for agricultural use or composting (mixed with organic waste as organic fertilizers);
- anaerobic fermentation with energy recovery or storage in plots that naturally ensure the process;
- washing and reconditioning of sludge with recovery of some components;
- concentration of leached solutions/solutions resulting from various processes and their valorization;
- treatment and cremation of petroleum products, stable products, etc.

In such a sludge management structure, the technological challenge for economic agents is to reduce the amount of sludge and raw (wet) sludge. Reducing sludge amount can be approached in two technological directions: aerobic or anaerobic biological mineralization and improving dehydration processes. It thus becomes of interest to address aspects related to efficiency and technology in the case of the use of biopreparations intended to reduce the amount of sludge generated in biological wastewater treatment plants.

## CONSIDERATIONS REGARDING BIOLOGICAL PROCESSES IN WASTEWATER TREATMENT PLANTS

Initially, the treatment plants were sized and constructed to ensure the reduction of $BOD_5$

and suspended matter indicators. It is considered that reducing oxygen consumption in biological processes to a minimum accepted level can eliminate oxygen deficiency situations in the receiving watercourse and maintain environmental factors away from any quality degradation risk. Every study, design and operation recommendation, and treatment efficiency concept took into account $BOD_5$ as indicator. Within biological nitrogen reduction wastewater treatment plants, C:N ratio is the principal efficiency indicator, also governing the sizing of biological nitrification/denitrification compartments.

Within wastewater treatment plants using biological sludge stabilization and/or bioaugmentation, where part of the sludge is biologically mineralized, C:N Kjeldahl indicator became the main parameter for determining the oxygen requirement for the process and also for sizing of additional volumes in the nitrification/denitrification compartments.

Applications designed based on BOD5 indicator recorded increased specific technological consumption indicators due to the processing of larger quantities of COC-Cr or TOC (especially in applications that ensure sludge mineralization/stabilization).

Table 2 presents the degree of carbon reduction for standard design situations corresponding to the standards NTPA 002 (MAPM-b, 2002) treatment influent and NTPA001 (MAPM-a, 2002) effluent. It could be noticed that in the case of plant sizing with the COC-Cr indicator, it is necessary to process additional quantities of organic substances (about 100 $mgO_2/L$). The design process becomes difficult when the BOD5/COD-Cr ratio is low and, also, there are high COC-Cr concentrations. For these specific reasons, the design of wastewater treatment plants with the COC-Cr parameter was adopted.

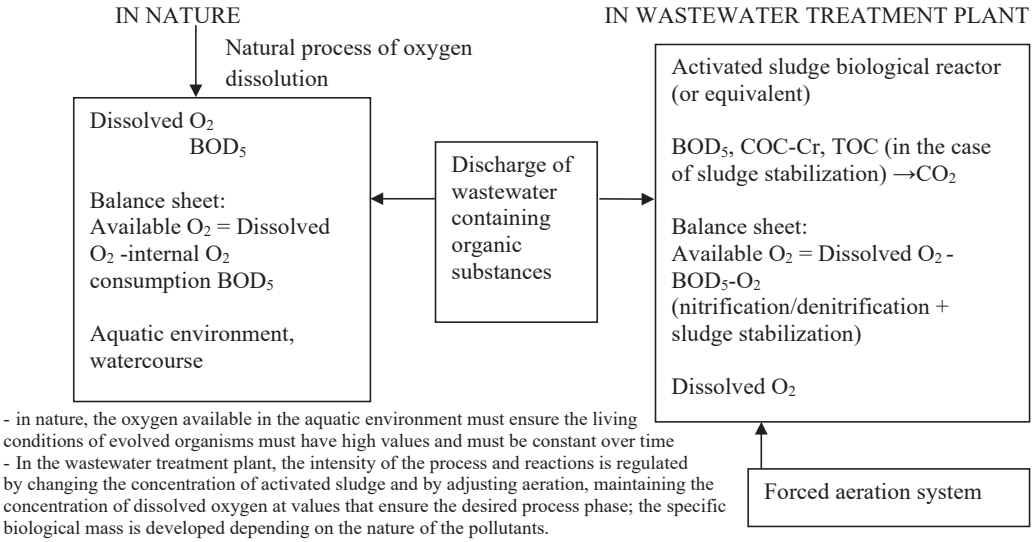
From a technical point of view, the design model adopted does not reflect the effective situation in the wastewater treatment plant. Figure 1 shows the difference between a wastewater self-treatment process in a watercourse and the wastewater treatment plant process.

Table 2. Minimum treatment efficiencies for domestic wastewater treatment plants (MAPM-b, 2002)

| Indicator | NTPA 002/2002 | Effective reduction | |
|---|---|---|---|
| | (mg/L) | (mg/L) | (%) |
| $BOD_5$ | 300 | 275 | 91.67 |
| COC-Cr | 500 | 375 | 75.00 |
| $BOD_5$/COC-Cr = 0.6, as a result of values in NTPA 002/2002 | | | |

From the point of view of the accuracy of determining the design quality indicators, the $BOD_5$ indicator implies a reduced accuracy due to the dilution required for determination, compared to the COC-Cr determination where the accuracy is high due to the simplicity of the method.

The design standard NP 133/2022 (MDLPA, 2022) provides for the determination of the oxygen requirement depending on the COC-Cr value in the situation where the COC-Cr/$BOD_5$ ratio > 2.2 or $BOD_5$/COC-Cr = 0.45, without specifying the how to do it when the ratio varies in the range (0.6 - 0.45); in this situation the bioaugmentation is a solution, combined with the increase of oxygen added in the process NP 133/2022 requires the calculation of sludge production and oxygen demand with influent COC-Cr values (MDLPA, 2022). Consequently, wastewater treatment plants sized based on the influent $BOD_5$ indicator, without taking into account the critical nitrogen indicator (ammonia nitrogen) or plants with sludge stabilization calculated without the COC-Cr or TOC indicator, encounter operational difficulties in ensuring the oxygen requirement, sludge production and management and, in many situations, do not ensure mandatory discharge conditions. In the design of wastewater plants without sludge stabilization, an activated sludge concentration of 3000 mg/L and a sludge age of (10-20) days is recommended (MDLPA, 2013; DWA, 2000). In the design of wastewater plants with sludge stabilization, an activated sludge concentration of 4500 mg/L and a sludge age of (20-30) days is recommended (MDLPA, 2013; DWA, 2000), resulting in a technological volume 18% higher than in the first situation, which proves in operation that are not enough in cold seasons.




- in nature, the oxygen available in the aquatic environment must ensure the living conditions of evolved organisms must have high values and must be constant over time
- In the wastewater treatment plant, the intensity of the process and reactions is regulated by changing the concentration of activated sludge and by adjusting aeration, maintaining the concentration of dissolved oxygen at values that ensure the desired process phase; the specific biological mass is developed depending on the nature of the pollutants.

Figure 1. Scheme of $O_2$ provision for biological processes in nature and in wastewater treatment systems

For these specific plants or for those with aerobic sludge stabilization in separate compartments, the technological variant with microbial products based on bacterial strains support in sludge digestion can be adopted. For plants having nitrification-denitrification and sludge stabilization at the technological wastewater flux, complex solutions can be adopted by dosing two types of biopreparations, one to improve the mineralization, one to maintain the efficiency of the main treatment process; in both processes, must be ensured the technological factors related the necessary oxygen and re-circulations.

The wastewater treatment technological scheme will be developed so that the process takes place in individual nitrification and denitrification tanks, respectively sludge stabilization tanks, and allows the optimization of each phase of the process (Figure 2).

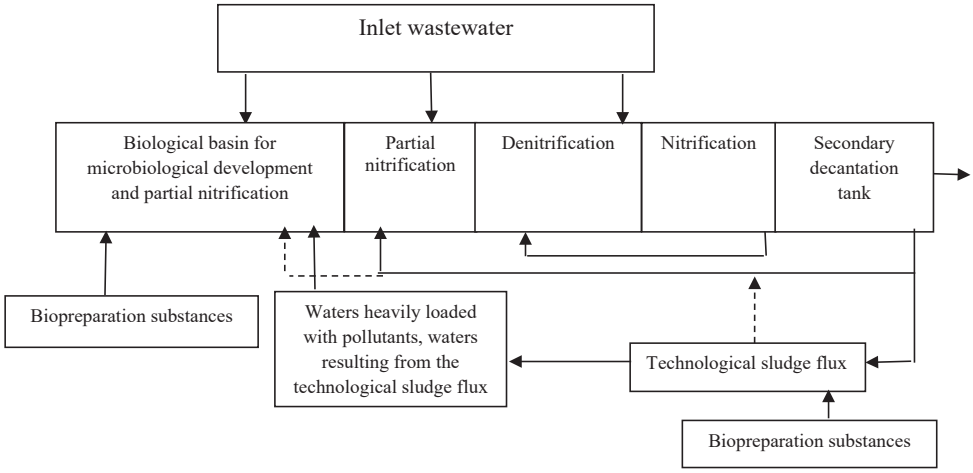



Figure 2. General scheme of an optimized biological stage with specialized biopreparation substances

Efficiency is achieved by maintaining a high biological capacity by dosing microbiological preparation substances, by successive nitrification and denitrification phases, by

appropriate fractional feeding and, in particular, to maintain denitrification capacity, microbiological dosing for sludge stabilization both on the technological wastewater flux and on the technological sludge flux.

## DYNAMICS OF BACTERIAL DEVELOPMENT WITHIN WASTEWATER TREATMENT PLANTS

The calculation models used in the design standard for wastewater treatment plants provide relationships that depend on the temperature and sludge age, which modify the rate of sludge mineralization/stabilization.
In the evolution of biological sludge, four development stages were highlighted, corresponding to process starting (primary bacteria), development and appearance of protozoa, sludge maturation and aging, corresponding to the nematode appearance (Figure 3).
For bacterial development, it is necessary to permanently ensure the needed nutrients and avoid toxic elements. Within wastewater treatment plants operation, both discharges of highly toxic substances and variations in nutrient concentrations are recorded, the dynamics of bacterial development being thus variable. Achieving optimal conditions in specialized compartments lead to obtaining the bacterial base stock that ensures the treatment of consumption peaks.

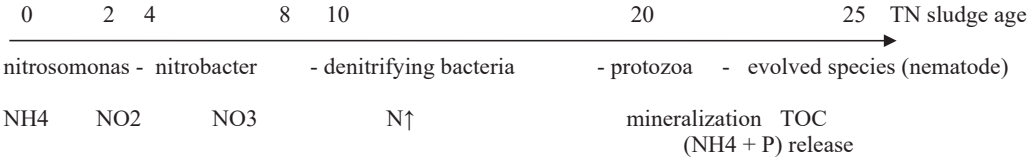



Figure 3. Phases of activated sludge development

When the nutritional conditions are met, depending on the temperature, pure bacterial population can double in a time interval of (20-50) min - bacterial doubling time t.D – under ideal lab conditions (Simionescu, 2009). In Figure 4 the bacterial growth is presented assuming the necessary nutritional conditions are provided; for this model, the treatment plant capacity doubles in a short time, with sufficient adaptability to wastewater load changes: this is the valid model for the priming phase, as there are no nutritional deficiencies. In practice, the need to adapt the biological mass to the quality conditions of the influent wastewater has been highlighted, the period defined as the "lag phase" (Simionescu, 2009).

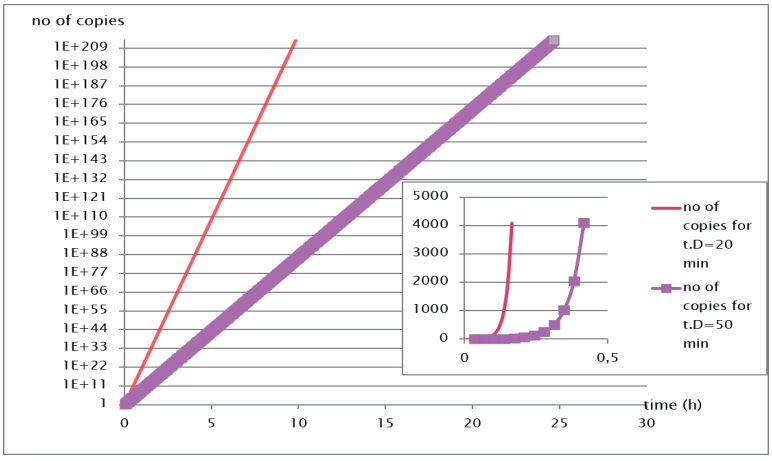



Figure 4. Bacterial development assuming optimal development conditions (t.D - bacterial doubling time)

In the following phases of activated sludge development (development of protozoa and nematodes) the dynamics change significantly, organic matter being hydrolyzed, metabolized and eliminated with secondary products, $CO_2$, $NH_4$ and P. The increase in suspended mass of activated sludge is thus diminished.

The mathematical models adopted in the wastewater treatment standard are based on the "sludge age" indicator, which can be interpreted as the period of development of the activated sludge that ensures the processing of a certain amount of pollutant (carbon, ammonia nitrogen, nitrates, phosphorus, and sludge stabilization), the maturation and stabilization of the activated sludge.

For the development of the bacterial mass capable of processing the corresponding loads of wastewater at the entrance to the treatment plants (MAPM-b, 2002), the proposed relationships depend on the temperature (equation 1):

$$T_{N,aerob} = FS \cdot 3{,}4 \cdot 1{,}103^{(15-T)}(days) \quad (1)$$

where:

$$T_{N,dim} = \frac{T_{N,aerob}}{1 - \frac{V_D}{V}}(days)$$

FS - security factor; 1.45-1.8 - depends on load variations at the inlet of the wastewater treatment plant
V - biological reactor total volume
$V_D$ - denitrification compartment volume

In the case of nitrogen reduction in denitrification processes and biological stabilization of sludge at the technologic wastewater flux, the proposed relationships for sludge age defined as stock compared to daily production, the dynamics depend on sludge production determined with equation 2 (MDLPA, 2013):

$$N_{eC} = C_b(0{,}75 + 0{,}6\frac{c^b_{uz}}{x^b_{5,uz}} - \frac{0{,}102.T_N.F_T}{1+0{,}17.T_N.F_T}\left(kg\ d\frac{s}{day}\right) \quad (2)$$

where:
-$N_{eC}$ - sludge production in kg d.s./day (dry substance/day)
-$C_b$ - the amount of organic matter entering the wastewater treatment plant
-$C^b_{uz}$ - suspension concentration in the influent of the biological reactor
-$x^b_{5,uz}$ - $BOD_5$ concentration in the influent of the biological reactor
$T_N$ - sludge age
$F_T$ - temperature factor for endogenous respiration

Determining the sludge age requires an iterative calculus.

Considering the equations presented and applied for standard situations, a biological reactor of 1 $m^3$ biological, operated with a load Iob (organic load index of the biological tank) in various temperature scenarios, results in the values for the graphs presented in Figure 5.

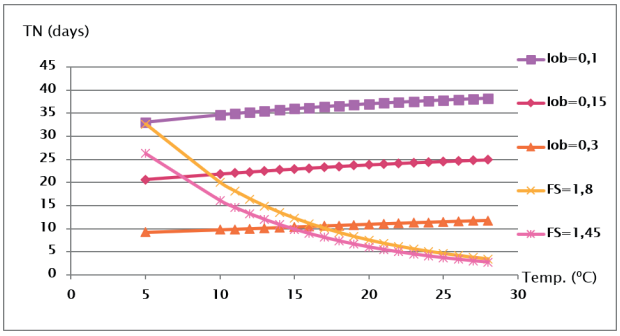



Figure 5. Sludge age determined for different temperature and organic load scenarios in the case of a standard wastewater treatment plant with an activated sludge concentration of 3000 mg/L

The analysis of the determined values results in reduced sludge ages in the case of low loads, Iob = 0.1 kg $BOD_5/m^3$ and day, respectively over 15 days in the case of loads of Iob = 0.3 kg $BOD_5/m^3$ and day.

In the exploitation variant with sludge stabilization, the third term in equation 2, which expresses the mineralization fraction, depends on the temperature and age of the sludge, respectively the bacterial development of the activated sludge.

The values of mineralization factor in Figure 6 are greater than 0.4 (inferior limit doable for operation) in the case of exploitation for

temperature greater than $10^0$C and sludge age over 18 days. At a temperature of $25^0$C, the mineralization factor greater than 0,4 is reached at a sludge age of 6 days.

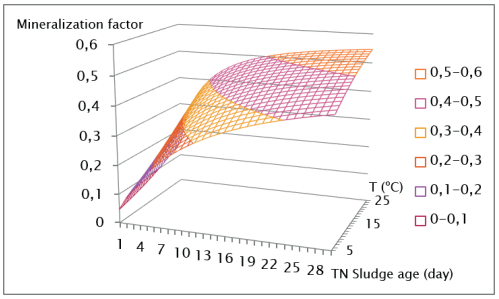



Figure 6. The mineralization factor for activated sludge determined in equation 2

When microbial products for sludge mineralization are used the result is the augmentation with 0.1 of mineralization factor in the case of exploitation for temperature greater than $10^0$C and sludge age over 18 days. At a temperature of $25^0$C and the sludge age of 6 days there is obtained a mineralization factor of 0.6. In operation, improving the mineralization factor becomes important, the values being a function of sludge doses and age.

## CASE STUDY

Operation of wastewater treatment plants highlights the multitude of variants related to pollutant loads. In the case of industrial wastewater treatment plants, the operating range is wide and for these reasons the regulation capacity of the plants must ensure the treatment efficiencies.

Results are presented for a biological wastewater treatment plant in the food industry designed for a flow rate of 100 $m^3$/h and dissolved organic carbon concentrations of 2000 mg/L Technological problems are recorded, due to the sludge decantability, the high sludge volume index of over 200 ml/g the entrainment of suspensions in the treated wastewater, the high sludge production, and its low age. Table 3 presents the calculation of sludge age and sludge production according to equation 2 at maximum load.

According to the operating parameters, the critical section from the point of view of wastewater treatment is the "settlement" due to sludge load high values: the superficial load with total suspended matter of about 215 kg dry matter/$m^2$day (recommended range of 90-140), respectively the superficial volumetric load with sludge of 928 $dm^3/m^2h$ (recommended range of 450-500), limits provided by the national design regulation NP 133/2013 (MDLPA 2013).

Table 3. Sludge age determined for the maximum load situation

| | |
|---|---|
| Q ($m^3$/day) | 2400 |
| BOC influent (mg/L) | 2000 |
| Influent suspensions (mg/L) | 100 |
| T ($^0$C) | 12 |
| F.T. (-) | 0.811738 |
| Estimated T.N. (days) | 4.28 |
| Third term (-) | 0.221475 |
| $\frac{c^b_{uz}}{x^b_{5,uz}}$(-) | 0.05 |
| Sludge production (kg/day) | 2680.92 |
| V reactor ($m^3$/day) | 4000 |
| c.na (mg/L | 3000 |
| Sludge stock (kg/day) | 12000 |
| Calculated T.N. (days)–iterated result | 4.245204 |

*third term – sludge mineralization factor

To improve the settling properties and increase the mineralization degree, microbial products (described in Table 4) were dosed, a mixture of microorganisms (over 3 x 109 microorganisms/g) and enzymes. The product is dosed directly into the aeration area of the wastewater treatment plant, with doses ranging from 3 kg/1000 $m^3$/day for starting de process, to 0.12 kg/1000 $m^3$/day for maintenance phase. The product can be applied in a wide range of temperature and pH indicator (Table 4).

Table 4. Microbial products utilized range of application

| Conditions | Range | Optimum |
|---|---|---|
| dissolved oxygen, ppm | 0-2.0 | >0.5 |
| pH | 6-9 | 7 |
| temperature, $^0$C | 10-40 | 35 |
| toxic heavy metals, ppm | low presence | absent |
| nutrients | | |
| $BOD_5$: $NH_3$-N | 10:1 - 10:0.5 | 10:1 |
| $BOD_5$: $PO_4$-P | 100:1-100:0.5 | 100:1 |

The biological product contains microbiological strains capable of breaking down a wide

range of substances such as: lignocellulose, fats, greases, proteins, fibers, etc., without generating additional cell mass. The synergistic content of microbial strains, oligo-elements, minerals and vitamins improves the quality of wastewater treatment by reducing pollutants, optimizing sedimentation and reducing total costs. The frequency and amount of application dose are related to the influent volume, pollutant loading, biological reactors capacity, hydraulic retention time, physical and chemical parameters, etc.

Testing was carried out starting in the autumn-winter months and continued into the warm season. For the cold season, the minimum temperature in the biological reactors being $12^0$C, sludge production decreased by 10% (estimated on sludge management sheets). During the warm season, at temperatures above $20^0$C, sludge production decreased by 50%, the costs generated by sludge management being very low. These values are valid only for wastewater treatment plants designed for an average flux of 100 $m^3$/h and average COD of 2000 mg/L, by adding microbial products.

The cold period represents the critical operating interval, and in this case the additional biological activity due to the biological product addition generated a reduction in wastewater treatment efficiency. The values of effluent water quality indicators for carbon, nitrogen, phosphorus and suspensions increased as process temperatures decreased. Figure 7 shows the evolution of the biological product doses applied within every phase of the wastewater treatment process in September. A dose of 5.5 kg/day of microbial product is the maximum for the first stage and for the restoring.

Frequently, the phosphorus records increase in the discharged water when the input water loads are reduced and the biological process is unbalanced for sludge stabilization. Important variations in the quantities of pollutants at the entrance imply significant changes for the biological process. Sludge stabilization ensures good sludge decantability and filterability, therefore good mechanical dehydration, these processes are observed in the operation of the wastewater treatment plant. During the testing period, the release of phosphorus was highlighted by increases in concentrations in the discharged water and the need to increase dephosphorization doses (Figure 8).

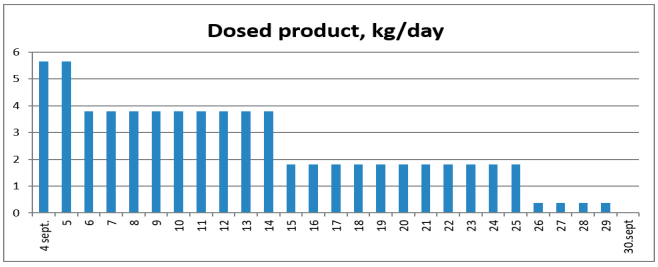



Figure 7. Product doses used in the process starting and maintenance phases

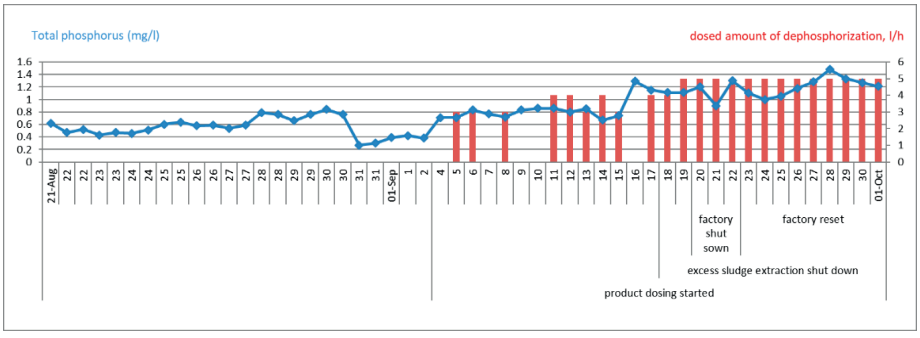



Figure 8. Evolution of the quantities of reagents for dephosphorization and the phosphorus indicator for discharged water

Concerning the biological activity, the decrease in wastewater treatment efficiency (Figures 9 and 10) was caused by: sludge mineralization processes due to the product use; decrease in temperatures decrease; treated wastewater flow rates increase; frequent use of biocidal products in the sterilization processes of the factory's production facilities.

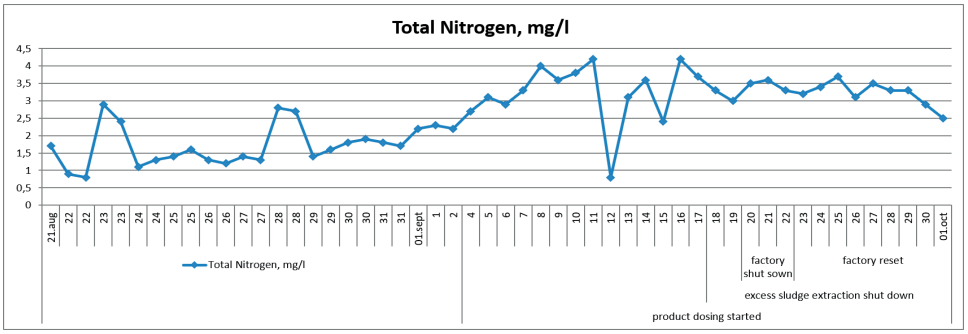



Figure 9. Evolution of the total nitrogen indicator for discharged water

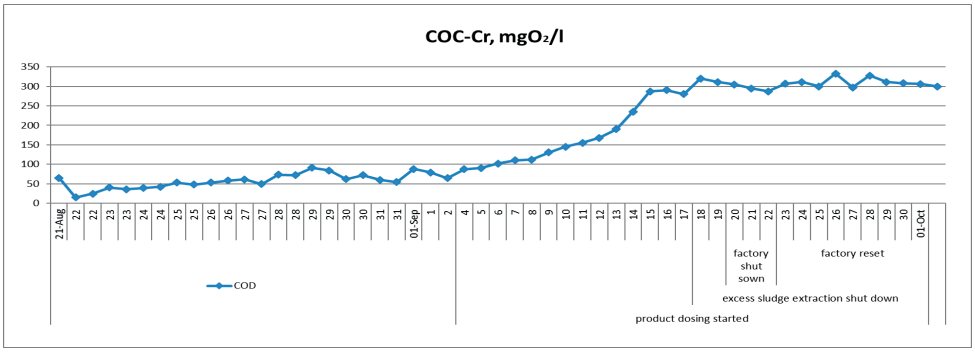



Figure 10. Evolution of the oxidizable organic substances COC-Cr indicator for discharged water

Technologically, the dissolved oxygen was maintained in the range (2-4) mg/L in automatic mode, with aeration reserves of over 100%, and for the external recirculation value, a level of approximately 1000% of the maximum input flow rate were ensured.
During the warm season, the microbial product ensured the sludge reduction by 50%; for the cold period, the use of biological product stimulates the sludge mineralization ensuring the sludge reduction of 50%

## CONCLUSIONS

Industrial and domestic wastewater treatment plants do not always fulfill the tasks related to the stabilization of biological sludge.
The use of microbiological products in the case study shows a decrease of 10% to 50% of sludge quantities, depending on the season. The decreases mentioned above imply also modification of technological volumes, dissolved oxygen and additional dosing of dephosphorization reagents.
When reduced organic pollutant loads (under 50% design COD, namely 1000 mg/L) and temperatures below $10^0$C within the process are present it is necessary to restore the capacity to assimilate and metabolize pollutants through additional dosing of microbial products of maximum 5.5 kg/day.
For industrial wastewater it would be benefic to revise the existing Regulation used for domestic wastewater treatment and adapting it for non-standardized loads.
Products to stimulate biological activity are beneficial, technological compartments are mandatory in order to develop specialized

biological mass and optimize wastewater treatment process.

Changing technological conditions impose modifying the wastewater treatment scheme and the type of products used. The case study and its results demonstrate the importance of the dynamic response in terms of introduction and dosing the microbial products when needed. As future works, the research will focus on using simultaneous two different microbial products, one for sludge mineralization, the second for the bacterial assimilation, in order to compare the results with the present study, for the cold season.

## ACKNOWLEDGEMENTS

This work was supported by a grant of the Ministry of Education and Research, CCCDI - UEFISCDI, project number PN-IV-P6-6.1-CoEx-2024-0120, within PNIV.

## REFERENCES

DWA (2000). ATV-DVWK-A131 – Standard for dimensioning of single-stage activated sludge plants

EU, 2024/3019 (2024). Directive of the European Parliament and of the Council of 27 nov 2024 concerning urban wastewater treatment (recast of Directive 91/271/CEE of 21 mai 1991 concerning urban wastewater treatment)

Li, J., Yang, X, Hu, A., Li, Y., Li, Y, Fu, L., & Yu, C.P. (2022). The performance and mechanism of sludge reduction by the biaoaugmentation approach, *Life,* 12 (10), 1649, 1-13.

MAPM-a (2002). NTPA 001/2002 - Regulation for establishing pollutant load limits for industrial and urban wastewater discharged into natural receptors

MAPM-b (2002). NTPA 002/2002 - Regulation regarding the conditions for discharging wastewater into the sewage networks of localities and directly into the wastewater treatment plants

MDLPA (2013). NP 133/2013 - Regulation for design, execution and operation of water supply and sewage systems of localities

MDLPA (2022). NP 133/2022 - Regulation for design, execution and operation of water supply and sewage systems of localities, volume I - Water supply systems; volume II – Sewage systems

Neamt, I., Ionel, I., & Vlaicu, I. (2013). Energy recovery of sludge in wastewater treatment plants in Romania, AGIR Bulletin, Supplement 1/2013, pp. 34–37, available at: https://www.agir.ro/buletine/1752.pdf

Rosiek, K. (2020). Directions and challenges in the management of municipal sewage sludge in Poland in the context of the circular economy, Sustainability, 12, 3686; doi:10.3390/su12093686, pp. 1–28

Simionescu, C. M. (2009). Biological wastewater treatment, MatrixRom Publishing House.

Scientific Papers. Series E. Land Reclamation, Earth Observation & Surveying, Environmental Engineering. Vol. XV, 2026
Print ISSN 2285-6064, CD-ROM ISSN 2285-6072, Online ISSN 2393-5138, ISSN-L 2285-6064

# *CYANOBACTERIA* AS KEY FACTORS IN STRUCTURING PLANKTONIC COMMUNITIES IN THE DANUBE DELTA

**Larisa Isabela FLORESCU[1], Maria Iasmina MOZA[2], Mirela Mădălina MOLDOVEANU[1]**

[1]Institute of Biology Bucharest of Romanian Academy, 296 Splaiul Independentei, District 6, Bucharest, Romania
[2]Department of Botany and Microbiology, Faculty of Biology, Moza Foundation, 91-95 Splaiul Independentei, District 5, Bucharest, Romania

Corresponding author email: iasmina_moza@yahoo.com

***Abstract***

*Cyanobacteria exert intense ecological pressure within aquatic systems of the Danube Delta, shaping both phytoplankton and zooplankton community dynamics. Their summer intense development can disrupt the balance between phytoplankton and zooplankton functional groups. Cyanobacteria dominated the phytoplankton, often outcompeting other algal taxa. Abundance indicated high concentrations of Cyanobacteria ($10^7$–$10^8$ cells $L^{-1}$), reflecting the high productivity. Their competitive advantage modifies species composition, reducing overall diversity and altering trophic interactions. The zooplankton displayed adaptive responses to shifts in phytoplankton, reflecting changes in food quality and availability. Among the dominant phytoplankton species were Anabaena variabilis, Aphanizomenon spp., and filamentous forms of the genera Microcystis spp., and Oscillatoria spp. In contrast, the zooplankton was predominantly structured by rotifers and cladocerans, among which Keratella cochlearis, Brachionus calyciflorus, and Bosmina longirostris were frequently found, indicating a high ecological tolerance. These temporal patterns highlight a complex interplay between communities, emphasising the regulatory role of cyanobacterial pressure in structuring aquatic community dynamics and influencing the trophic functioning of Delta ecosystems.*

***Key words****: cyanobacterial blooms, Danube Delta, phytoplankton, trophic interactions, zooplankton.*

## INTRODUCTION

*Cyanobacteria* are a prominent group in aquatic phytoplankton that, under prolonged periods of high temperatures, proliferate and become dominant in many continental ecosystems (Paerl & Huisman, 2008). Their competitive success is explained by their functional traits, such as broad tolerance to temperature and light, the ability to efficiently exploit nutrient resources, buoyancy conferred by gas vacuoles and, in some cases, the production of secondary metabolites with allelopathic effect. In addition, adaptations such as the ability to fix atmospheric nitrogen and high tolerance to eutrophic conditions are also added (Reynolds, 2006; Paerl & Otten, 2013). The Danube Delta is a complex network of aquatic ecosystems characterised by high spatial heterogeneity and heightened sensitivity to anthropogenic and climatic pressures. Changes in the hydrological regime, increased nutrient input and climate change have favoured the intensification of eutrophication processes in many deltaic lakes (Dumitran et al., 2020). One of the most visible effects of these transformations is the increase in the frequency and intensity of algal blooms dominated by *Cyanobacteria*, with potential risks for ecosystems (Moza et al., 2021). Studies have shown that in recent decades, *Cyanobacteria* have contributed significantly to phytoplankton biomass with effects on trophic status (Török et al., 2017). This dominance is manifested either by the massive development of several cyanobacterial species or by high densities generated by one or two species (Dumitran et al., 2024). As a result of algal blooms, community structure is simplified, increasing the dominance of a few taxa and reducing evenness, even when overall richness remains relatively high. This imbalance in diversity is characterised by reduced abundances of species from other groups, temporary coexistence with *Cyanobacteria*, and subsequent competitive exclusion (Török, 2011).

The emergence and rapid expansion of *Cyanobacteria* have significant ecological

consequences, affecting both the structure of planktonic communities and trophic relationships in aquatic ecosystems (Moldoveanu & Florescu, 2011). In the lakes of the Danube Delta, these processes manifest differently depending on local environmental conditions, leading to contrasting responses from phytoplankton communities. Thus, studies have shown that in some ecosystems cyanobacterial dominance intensified, whereas in others competition with chlorophytes or diatoms limited the success of this group, generating unstable, seasonal community structures (Török et al., 2017).

The aim of our study is to evaluate the role of *Cyanobacteria* as key factors in structuring phytoplankton communities in Roșuleț, Puiu and Tătaru lakes, representative lakes of the Danube Delta. The objectives of the study are: 1. Analysing the taxonomic structure of phytoplankton communities and highlighting the position of *Cyanobacteria* relative to the main algal groups using multivariate methods; 2. Assessing variations in α and β diversity, in order to identify structural changes in communities between lakes and between seasons; 3. Identifying cyanobacterial taxa responsible for seasonal compositional changes by analysing their contribution to community dissimilarity; 4. Investigating competitive relationships between *Cyanobacteria* and other phytoplankton groups, through quantitative indicators of the competitive replacement rate, in order to highlight ecological hierarchies and community stability.

## MATERIALS AND METHODS

### *Study site*

The Danube Delta is characterised by a complex network of branches, channels and shallow lakes, developed on fluvial and marine beds, with active transformation processes. The inland lakes are generally shallow, with variable connectivity to the channel network, which results in low hydrodynamics and a strong influence on Danube level variations. From an ecological perspective, the Danube Delta is one of the most valuable wetlands in Europe, with high biodiversity and a wide range of aquatic ecosystems, including eutrophic and hypereutrophic lakes with rich phytoplankton communities (Pavel et al., 2009).

The lakes selected in our study, Puiu, Tătaru and Roșuleț (Figure 1), are part of the Danube Delta lacustrine complex, and are characterised by variable hydrodynamics and different connectivity with the river branches and secondary channels. The lakes are shallow, developed on fluvial beds and subject to clogging and morphological remodelling processes, characteristic of inland deltaic lakes. Lake Puiu is a large, relatively deep (2-2.5 m in our sampling campaigns) lake in the Danube Delta, with a moderate fluvial influence that determines the seasonal dynamics of nutrients and planktonic communities (Tudorancea & Tudorancea, 2006; Gâștescu, 2009). Lake Tătaru is shallower (approx. 1 m deep in our sampling campaigns) and less hydrologically connected, favouring nutrient accumulation and frequent eutrophic episodes, with seasonal algal dominance (Coops et al., 1999). Roșuleţul, a shallow lake (1.1-1-6 m in our sampling campaigns), is strongly influenced by internal processes, such as sediment resuspension and phosphorus recycling, which lead to high phytoplankton variability and unstable community structures (Oosterberg et al., 2000; Gâștescu, 2009).




Figure 1. The sampling lakes: Roșuleț, Puiu and Tătaru (Google Earth app, 2026)

### *Phytoplankton sampling and analysis*

Water samples were collected during two field campaigns, in August and September 2015. To capture the spatial variability of the studied ecosystems, 4 sampling stations were established in each lake. Phytoplankton sampling was performed on the entire water column using a Patalas-Schindler (5 litres) and stored in a bucket. From this volume, 500 ml of the water sample was taken, immediately fixed

with 4% formaldehyde, and stored in plastic containers. In the laboratory, the samples were sedimented for 14 days. Quantitative and qualitative analyses were performed according to the Utermöhl method (Edler & Elbrachter, 2010) using an inverted microscope (Zeiss Axiovert 40C, Germany).

Taxonomic identification of organisms was performed to the genus or species level, using specific determination keys for the main taxonomic groups: *Cyanobacteria, Euglenophyceae, Pyrrophyceae, Chrysophyceae, Bacillariophyceae, and Chlorophyceae* (Moldoveanu et al., 2025).

***Statistical analysis***

Statistical analyses were performed using Past 5.2.1 software (Hammer et al., 2001), including Discriminant Analysis (DA), diversity indicators α (Dominance_D, Shannon_H, Equitability_J) and β (Whittaker, Cody, Williams), and the construction of a dendrogram based on the Bray-Curtis coefficient. The structure of the communities was additionally assessed using ANOSIM (Permutation test, N=9999) and SIMPER. The Rate of Competitive Displacement (RCD) was also calculated according to the methodology described by Ji et al. (2017), which estimates the rate at which phytoplankton groups replace one another under competitive conditions. RCD as differences between September versus August, as ln(X1/X2), where: X1- *Cyanobacteria* and X2 – diatoms or green algae – the total abundances of group.

## RESULTS AND DISCUSSIONS

***The structure and distribution of phytoplankton communities***

In the phytoplankton structure, *Cyanobacteria* recorded the highest share, followed by *Chlorophyceae* and *Bacillariophyceae*, with considerably lower abundances (Table 1). In Puiu and Tătaru lakes, all three groups showed significant increases in abundance during the monitoring period, with pronounced blue-green biomass peaks observed (in Tătaru − $9.22\times10^7$ cells/L; in Puiu − $8.04\times10^7$ cells/L). In contrast, at Roșuleț Lake, except for *Chlorophyceae*, most phytoplankton groups showed pronounced declines. *Chlorophyceae*, although the second group in weight, showed low abundances overall, reaching a maximum in Lake Tătaru in the month ($2.79\times10^7$ cells/L). Diatoms recorded lower values than *Cyanobacteria*, but showed notable increases in September. The *Euglenophyceae, Pyrrophyceae*, and *Chrysophyceae* groups were present at low densities, reflected in episodic increases.

Table 1. The abundances of the phytoplankton taxonomic groups in the studied lakes

| | Puiu | | Tătaru | | Roșuleț | |
|---|---|---|---|---|---|---|
| | VIII | IX | VIII | IX | VIII | IX |
| *Cyanobacteria* | $4.05x\ 10^7$ | $8.04x10^7$ | $1.45x10^7$ | $9.22x10^7$ | $4.08x10^7$ | $2.04x10^7$ |
| *Euglenophyceae* | $1.57x10^5$ | $5.80x10^4$ | $4.23x10^5$ | $1.86x10^5$ | $1.52x10^4$ | $6.59x10^3$ |
| *Pyrrophyceae* | $8.98x10^4$ | $1.38x10^5$ | $2.03x10^5$ | $9.81x10^5$ | $4.36x10^4$ | $2.60x10^4$ |
| *Chrysophyceae* | 0 | 00 | 0 | $8.84x10^5$ | $1.23x10^5$ | 0 |
| *Bacillariophyceae* | $1.54x10^6$ | $5.75x10^6$ | $4.89x10^5$ | $2.48x10^6$ | $1.92x10^6$ | $3.94x10^5$ |
| *Chlorophyceae* | $3.21x10^6$ | $6.95x10^6$ | $2.87x10^6$ | $2.79x10^7$ | $2.57x10^6$ | $3.50x10^6$ |

The DA discriminant analysis revealed clear separation between the main phytoplankton groups, along with partial taxonomic overlap, reflecting functional similarities and convergent ecological responses (Figure 2). These indicate that taxonomic structure only partially explains community organisation. Discriminant axis 1 (61.72%), but also an evident separation of *Cyanobacteria* (positioned predominantly on the right side of the axis) from *Bacillariophyceae* and *Chrysophyceae* (located on the left). *Chlorophyceae* present an intermediate position, with a greater dispersion, which indicates a higher heterogeneity than diatoms. This spread suggests the presence of species that display both opportunistic strategies and adaptations to more stable conditions. The partial overlap between chlorophytes, *Cyanobacteria*, and diatoms indicates the

functional flexibility of this group. In contrast, diatom species showed a clearer delimitation compared to the other groups. Also, *Chrysophyceae* showed a strong separation from the other groups (observed on the left side of axis 1). Axis 2 (29.55%) contributes to further differentiation of the communities, especially by the distinct positioning of *Euglenophyceae*, which forms a separate group on the left side of the axis. Groups with reduced representation, such as *Pyrrophyceae* and *Chrysophyceae*, appear more poorly delimited, with limited dispersion and less obvious separation. This positioning suggests either a reduced contribution to the overall community structure or shared ecological features with other major groups. The other groups show a clear overlap on this axis, with no clear demarcations between them. This separation is more pronounced than the differences between ecosystems or months, indicating that the community structure is mainly dominated by the contrast between *Cyanobacteria* and the rest of the phytoplankton. However, habitat overlaps are also evident, especially among *Chlorophyceae*, *Cyanobacteria*, and *Euglenophyceae*, reflecting a complex, partially overlapping community structure.

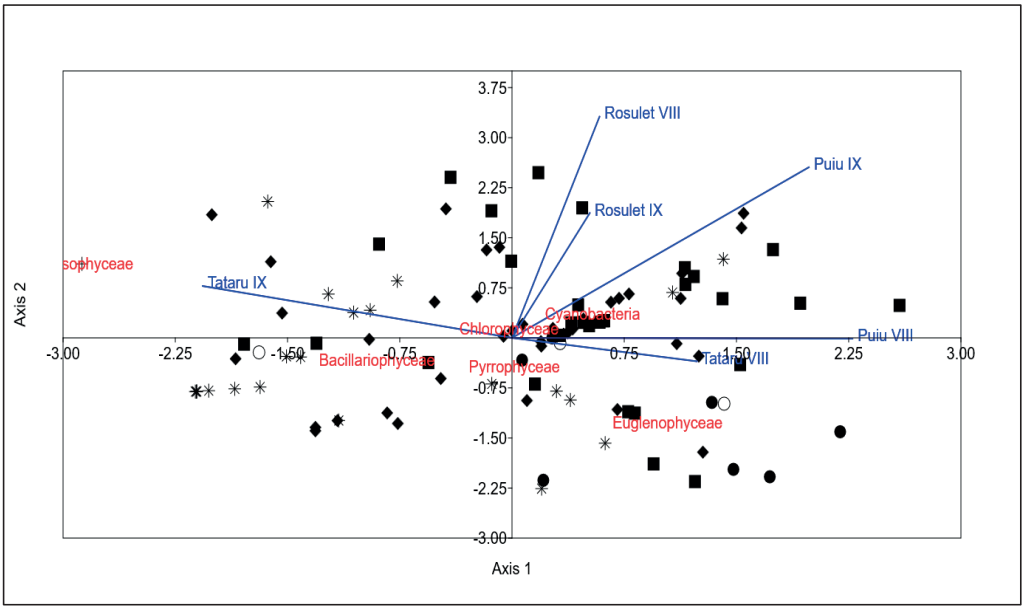



Figure 2. Biplot of the Discriminant Analysis showing the relationship between phytoplankton taxonomic groups and sampling sites (Lakes Roșuleț, Puiu, and Tătaru). ■ – *Cyanobacteria*; ● – *Euglenophyceae*, ○ – *Pyrrophyceae*, + – *Chrysophyceae*, * – *Bacillariophyceae*, ◆– *Chlorophyceae*, blue vectors– sampling points and months

**α and β diversity traits**

The α-diversity indices revealed clear differences in the structure of phytoplankton communities between the lakes and between the two periods analysed (Table 2). Although total species richness remained relatively high (44-60 species), the Shannon index values indicated differences in community diversity, reflecting changes in the relative distribution of taxa, especially in Puiu and Roșulet lakes. In these two ecosystems, the increase in the dominance index (D), concomitant with the decrease in evenness (J), suggests a more pronounced structuring of the community, characterised by the concentration of abundance within fewer groups or taxa. Thus, between the two periods, the diversity indices showed different changes in the structure of phytoplankton communities in the three ecosystems. Total species richness generally recorded higher values in September, with a maximum in Lake Tătaru (60 species), suggesting seasonal diversification of the communities, especially through increased contributions from

the *Bacillariophyceae* and *Chlorophyceae* groups. Lake Puiu showed an increase in total richness from 45 to 53 species, concomitant with an increase in *Cyanobacteria*, while Lake Roșuleț recorded a decrease in total richness in September, suggesting a possible simplification of the community structure. The Shannon index (H′) ranged from moderate to high (2.08-2.69), with the highest values observed in Lake Tătaru in both months, suggesting relatively well-structured and stable communities.

In contrast, the higher values of the dominance index (D), especially in September in Lake Puiu and Lake Roșuleț, indicate an increase in the dominance of a few taxa, probably favoured by trophic conditions. This trend is also supported by the decrease in evenness (J), which reflects a more unequal distribution of species abundances in the community.

Even if total species richness remains relatively high, the increase in the proportion of *Cyanobacteria*, associated with a decrease in evenness and effective diversity of the community, can lead to an "apparent diversity" in which other groups are present but contribute less to the total biomass.

Table 2. Diversity of phytoplankton in the studied ecosystems

| | **Puiu** | | **Tătaru** | | **Roșuleț** | |
|---|---|---|---|---|---|---|
| | **VIII** | **IX** | **VIII** | **IX** | **VIII** | **IX** |
| *Cyanobacteria* | 15 | 19 | 12 | 12 | 16 | 11 |
| *Bacillariophyceae* | 5 | 6 | 8 | 18 | 6 | 6 |
| *Chlorophyceace* | 17 | 23 | 20 | 25 | 19 | 20 |
| *Euglenophyceae* | 6 | 3 | 5 | 2 | 1 | 1 |
| *Pyrrophyceae* | 2 | 2 | 1 | 2 | 1 | 1 |
| *Chrisophyceae* | 0 | 0 | 0 | 1 | 1 | 0 |
| **Species richness (S)** | 45 | 53 | 46 | 60 | 44 | 39 |
| **Dominance (D)** | 0.11 | 0.30 | 0.11 | 0.11 | 0.14 | 0.26 |
| **Shannon (H′)** | 2.61 | 2.16 | 2.69 | 2.69 | 2.34 | 2.08 |
| **Equitability (J)** | 0.68 | 0.55 | 0.70 | 0.66 | 0.62 | 0.57 |

Spatial beta diversity among lakes (Table 3). showed a moderate to high overall species turnover among the lakes (Whittaker = 0.50; Cody = 46.00; Williams = 0.27). The pairwise comparisons showed the highest compositional dissimilarity between Lakes Puiu and Tătaru (Whittaker = 0.36; Cody = 25.50; Williams = 0.24), followed by the Puiu–Roșuleț pair (Whittaker = 0.31; Cody = 20.00; Williams = 0.19). The lowest beta diversity values were recorded between Tătaru and Roșuleț (Whittaker = 0.30; Cody = 20.50; Williams = 0.16). Similar spatial patterns were observed across all three indices, indicating consistent differences in species composition among the studied lakes.

Table 3. The spatial beta diversity among lakes

| **Global beta diversities** | | | |
|---|---|---|---|
| Whittaker | 0.50 | | |
| Cody | 46.00 | | |
| Williams | 0.27 | | |
| **Whittaker** | **Puiu** | **Tătaru** | **Roșulet** |
| Puiu | 0.00 | 0.36 | 0.31 |
| Tătaru | 0.36 | 0.00 | 0.30 |
| Roșulet | 0.31 | 0.30 | 0.00 |
| **Cody** | | | |
| Puiu | 0.00 | 25.50 | 20.00 |
| Tătaru | 25.50 | 0.00 | 20.50 |
| Roșulet | 20.00 | 20.50 | 0.00 |
| **Williams** | | | |
| Puiu | 0.00 | 0.24 | 0.19 |
| Tătaru | 0.24 | 0.00 | 0.16 |
| Roșulet | 0.19 | 0.16 | 0.00 |

Regarding structural changes during the investigated period, β-diversity indices revealed moderate differences in phytoplankton composition (Table 4). The Whittaker index ranged from 0.40 to 0.47, indicating moderate temporal heterogeneity. The highest value was recorded in Lake Roșuleț (0.47), suggesting that this lake experienced the highest rate of species replacement from summer to autumn among the three. In contrast, the Cody index showed similar values across the lakes (19.5-21.0), suggesting a comparable rate of species replacement between months, with a slight maximum in Lake Tătaru. The Williams index values were relatively low (0.19-0.28), indicating low to moderate turnover (species change) between the two, but with a more pronounced differentiation in Lake Roșuleț.

Table 4. Temporal beta diversity within lakes

| | **Puiu** | **Tătaru** | **Roșuleț** |
|---|---|---|---|
| **Whittaker** | 0.41 | 0.40 | 0.47 |
| **Cody** | 20.00 | 21.00 | 19.50 |
| **Williams** | 0.23 | 0.19 | 0.28 |

The magnitude of structural changes reflected in diversity indices was assessed using a Bray-Curtis similarity dendrogram (Figure 3), which revealed distinct separation of the studied ecosystems, driven by both spatial and temporal factors.

The highest degree of similarity (approximately 67%) was found between Roșuleț and Puiu lakes in August (R-VIII, P-VIII), thus highlighting convergent trophic conditions that favour the same algal associations. In contrast, station Tătaru VIII showed the lowest similarity to the other ecosystems (below 50%), indicating a significant taxonomic divergence during the summer period. Also, in September, an association of Tătaru and Roșulet lakes were observed, forming a distinct cluster indicating a structural convergence of phytoplankton communities towards the end of the vegetation season and marking the transition from highly specialised summer associations to a more balanced structure, characteristic of the early autumn period.

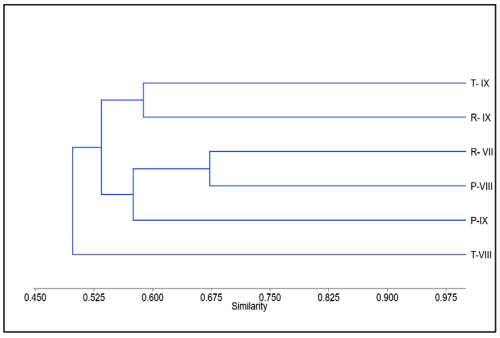



Figure 3. Similarity dendrogram of phytoplankton communities in lakes Roșuleț, Puiu and Tătaru (August-September), based on the Bray-Curtis index (Paired Group method)

### *Compositional shift at the level of phytoplankton groups*

The ANOSIM test applied to identify structural changes during the tested period showed that the differences between the summer (VIII) and autumn (IX) periods were greater than the spatial variations between ecosystems (Table 5). Lake Roșuleț (R = 0.67, $p$ = 0.008) showed the greatest and most significant seasonal change, indicating major structural changes during the investigated period. In Lake Puiu (R=0.47, $p$=0.03), the separation of communities was moderate, while in Lake Tătaru (R=0.30, $p$=0.05), the lowest seasonal differences but the highest spatial variation (12.08) were observed.

Table 5. ANOSIM analysis of structural changes among lakes and periods

| | **Puiu** | **Tătaru** | **Roșulet** |
|---|---|---|---|
| Mean rank within: | 10.67 | 12.08 | 11.75 |
| Mean rank between: | 17.38 | 16.31 | 23.9 |
| R: | 0.47 | 0.30 | 0.67 |
| *p* (same): | 0.03 | 0.05 | 0.008 |

By Simper analysis (Table 6), the species whose turnover was decisive in the phytoplankton structuring were identified. This analysis identifies the taxa that contributed the most to the taxonomic change from summer to autumn. In Puiu Lake the species *Oscillatoria minima* was the dominant species with the highest contribution (34.68%), achieved through a massive development reaching a peak of $1.06x10^8$ cells/L – in autumn. In contrast, other cyanobacterial species, *Aphanizomenon flos-aquae* (7.065) and Oscillatoria sp. (6.27%), showed a significant shift, but through a decline in abundance. In Tataru Lake, the strongest influences in the seasonal changes were also due to *Cyanobacteria*. *Gomphosphaeria lacustris* accounted for 16.84% of the difference, with an increase in the average in September, along with *Microcystis pulverea*, which also made a significant contribution (13.63%) due to its appearance and massive development in autumn. In contrast, *Oscillatoria limosa* showed a significant decline during this period. And in Lacul Roșuleț, *Cyanobacteria* were the taxa that contributed significantly higher values in the changes between the two periods. Thus, we mention, *Microcystis pulverea* (18.44%, with a significant increase in autumn), *Aphanocapsa grevillei* and *Aphanizomenon flos-aquae* (which together explained over 32% of the dissimilarity by completely disappearing in autumn), as well as *Oscillatoria minima* Gicklhom, which also underwent a decline in abundance. ANOSIM and Simper analyses confirm a strong turnover induced by *Cyanobacteria* species. While some summer species (such as *Aphanizomenon* spp. or *Aphanocapsa* spp.) tend to disappear or

decrease in September, others (such as *Oscillatoria minima* in Puiu or *Microcystis pulverea* in Tătaru and Roșuleț) take over dominance, generating changes in diversity.

Table 6. SIMPER analysis results of the major phytoplankton contributors to the average dissimilarity between seasons in: P – Puiu lake, T – Tătaru lake, R – Roșuleț. Av.d. - average dissimilarity, Contrib. (%) – percentage contribution to the average dissimilarity; Mean Aug – mean abundance in August; Mean Sep – mean abundance in September.

| | Taxon | Av. d. | Contrib. % | Mean august | Mean september |
|---|---|---|---|---|---|
| P | *Oscillatoria minima* Gicklhom | 25.29 | 34.68 | $8.36x10^6$ | $5.01x10^7$ |
| P | *Aphanizomenon flos-aquae* (L.) Ralfs | 5.153 | 7.065 | $7.29x10^6$ | $2.14x10^6$ |
| P | *Oscillatoria* sp. | 4.576 | 6.273 | $5.84x10^6$ | 0 |
| R | *Microcystis pulverea* (Wood) Migula | 15.01 | 18.44 | $6.23x10^6$ | $1.18x10^7$ |
| R | *Aphanocapsa grevillei* (Hassal) Raben | 14.44 | 17.73 | 9.78x106 | 0 |
| R | *Aphanizomenon flos-aquae* (L.) Ralfs | 12.08 | 14.83 | $9.04x10^6$ | 0 |
| R | *Oscillatoria minima* Gicklhom | 10.94 | 13.44 | $8.32x10^6$ | $1.35x10^6$ |
| T | *Gomphosphaeria lacustris* Chodat | 13.73 | 16.84 | $4.21x10^6$ | $1.77x10^7$ |
| T | *Microcystis pulverea* (Wood) Migula | 11.11 | 13.63 | 0 | $2.48x10^7$ |
| T | *Aphanocapsa grevillei* (Hassal) Raben | 8.998 | 11.04 | $1.26x10^6$ | $1.58x10^7$ |
| T | *Merismopedia tenuissima* Lemm. | 6.823 | 8.373 | $3.27x10^6$ | $7.58x10^6$ |
| T | *Oscillatoria limosa* C.Agardh ex Gomont | 4.825 | 5.92 | $2.02x10^6$ | 0 |

Rate of Competitive Displacement (RCD). Although the results showed a decisive role of *Cyanobacteria* in the phytoplankton component in ecosystems, RCD highlighted that, with the arrival of autumn, the other two major groups (green algae and diatoms) showed tendencies toward recovery in their functionality. Thus, the negative values (Table 7) indicate an unfavourable exchange rate for the analysed blue-green algae group relative to the second one, diatoms or green algae. In the *Cyanobacteria* vs. *Chlorophyceae* testing, all ecosystems showed negative values: Puiu (-0.09), Tătaru (-0.43), and Roșuleț (-1.00), indicating that *Chlorophyceae* had a competitive advantage over *Cyanobacteria* in all three locations, with the impact being most pronounced in Roșuleț Lake. Also, the results regarding *Cyanobacteria* vs. *Bacillariophyceae* showed both a negative value in Puiu (-0.64) and positive values in Tătaru (0.22) and Roșuleț (0.89), which indicated that diatoms dominated competitively only in Puiu Lake, while in Tătaru and Roșuleț, *Cyanobacteria* managed to prevail over them even in autumn. Also, in Roșuleț, the most dynamic and unbalanced phytoplankton competition was recorded among all the studied locations, at the point where *Chlorophyceae* exerted the greatest pressure (-1), thus signalling a trend of competitive collapse on *Cyanobacteria*.

Table 7. Rate of Competitive Displacement (RCD) between *Cyanobacteria* and the other main phytoplanktonic groups

| | *Cyanobacteria* vs *Chlorophyceae* | *Cyanobacteria* vs *Bacillariophyceae* |
|---|---|---|
| **Puiu** | -0.09 | -0.64 |
| **Roșulet** | -1 | 0.89 |
| **Tătaru** | -0.43 | 0.22 |

This may indicate that the available resources in Roșuleț were accessed more efficiently by *Chlorophyceae* compared to the other groups, so *Cyanobacteria* could no longer maintain their population as in summer. However, *Cyanobacteria* maintained dominance despite competition with diatoms, even though the diatom replacement rate was the highest (0.89) among the three ecosystems (Table 7). Thus, in Roșuleț, *Cyanobacteria* were subjected to niche pressures.

The structural features of phytoplankton communities were also reflected in the zooplankton composition across the three lakes, indicating adaptive ecological responses shaped by interactions among environmental factors and trophic structure.

Thus, the pressure exerted by phytoplankton on primary consumer communities led to a prevalence of small, opportunistic forms, especially rotifers (*Trichocerca, Polyarthra, Keratella*) and juvenile copepods, along with microcrustaceans such as *Bosmina* spp. (Table 8).

Table 8. Dominant zooplankton species and their distribution in the studied ecosystems

| Spercies | P- VIII | P- IX | T- VIII | T- IX | R-VIII | R-IX |
|---|---|---|---|---|---|---|
| *Bosmina coregoni* (Baird, 1857) | 0.67 | 50.08 | 0.00 | 0.00 | 2.74 | 299.82 |
| *Copepoda* g. sp. St Nauplial | 99.17 | 239.58 | 238.20 | 471.91 | 78.70 | 86.70 |
| *Keratella cochlearis* var. *tecta* (Gosse, 1851) | 8.00 | 229.84 | 0.00 | 5.55 | 2.30 | 32.82 |
| *Lecane closterocerca* (Schmarda, 1859) | 0.00 | 7.54 | 0.55 | 0.66 | 639.13 | 0.70 |
| *Polyarthra remata* Skorikow 1896 | 137.50 | 54.96 | 142.31 | 297.30 | 64.99 | 93.90 |
| *Synchaeta oblonga* (Ehrenberg, 1832) | 100.33 | 0.00 | 1.50 | 23.59 | 6.43 | 11.20 |
| *Trichocerca pussila* (Jennings, 1903) | 167.50 | 86.54 | 0.94 | 2.91 | 185.36 | 1.30 |
| *Trichocerca similis* (Wierzejski, 1893) | 231.50 | 86.82 | 0.00 | 2.00 | 180.80 | 12.32 |
| *Diflugia globulosa* (Dujardin, 1837) Penard, 1902 | 1.33 | 260.42 | 0.00 | 3.04 | 1.30 | 0.00 |
| *Diflugia lobostoma* (Leidy, 1879) | 154.17 | 293.52 | 3.55 | 4.62 | 388.40 | 3.28 |

The Grubbs test identified statistically significant outliers ($p < 0.05$) for several species, indicating higher dominance relative to the rest of the zooplankton community and associated with a temporary reduction in competition. In Puiu Lake, Grubbs showed significant values for *Trichocerca similis* (August - 6.34) and *Difflugia lobostoma* (September - 5.75), indicating punctual dominance. In Tataru Lake, nauplial copepod stages were identified as dominant peaks in both August (9.14) and September (8.48), indicating maintenance of juvenile stages. In Roșuleț Lake, the rotifer *Lecane closterocerca* (August - 8.44) and the cladoceran *Bosmina coregoni* (September - 9.53) reflected pronounced seasonal structural changes as well as an alternation of dominant species. Thus, the results indicate a high spatio-temporal heterogeneity of zooplankton, with dominance patterns related to period and ecosystem, suggesting a differentiated response of taxa to local ecological conditions.

Structure and distribution of phytoplankton communities. The dominance of *Cyanobacteria* in all three lakes studied during the summer period underlines their role as key factors in structuring phytoplankton communities in the Danube Delta. This dominance is consistent with numerous studies showing that, under conditions of high temperatures, hydrodynamic stability and increased nutrient availability, *Cyanobacteria* are favoured over other algal groups (Paerl & Huisman, 2008; Moza et al., 2021; Dokulil & Teubner, 2023). The high cyanobacterial abundance in Puiu and Tătaru lakes, as well as the persistence of this group in Roșuleț, indicate a meso- to hypereutrophic trophic status, characteristic of many deltaic lacustrine ecosystems. In Puiu and Tătaru, the simultaneous increase of *Cyanobacteria*, *Chlorophyceae* and diatoms suggests a general intensification of primary production in the late summer period, while in Roșuleț the decline of most groups, except *Chlorophyceae*, indicates a pronounced structural instability. Such spatiotemporal patterns are frequently reported for shallow lakes, where sediment resuspension and internal nutrient recycling can amplify fluctuations in phytoplankton communities (Oosterberg et al., 2000; Gâștescu, 2009).

Taxonomic structure and interpretation of discriminant analysis. Discriminant analysis revealed a clear separation of *Cyanobacteria* from the other major groups, highlighting the functional contrast between this group and the rest of the phytoplankton. The intermediate positioning and high dispersion of *Chlorophyceae* indicate increased ecological flexibility, reflecting the ability of this group to occupy varied niches and to respond rapidly to environmental changes. Diatoms and *Chrysophytes* showed clearer delimitation, suggesting stricter ecological requirements and greater sensitivity to changes in physicochemical conditions. The overlaps observed among *Chlorophyceae*, *Cyanobacteria*, and *Euglenophyceae* indicate convergent ecological responses and common functional traits, especially in unstable

ecosystems. This type of community structure is typical of eutrophic lakes, where competition for resources is intense, and advantages are quickly redistributed among groups depending on seasonal conditions (Jia et al., 2022; Tóth-Krasznai et al., 2022).

α and β diversity: ecological implications. Although total species richness remained relatively high in most cases, α-diversity indices showed a clear trend toward increasing dominance and decreasing evenness, especially in Puiu and Roșuleț lakes. This combination suggests the emergence of an "apparent diversity", in which numerous taxa are present but their contribution to total biomass is reduced, eclipsed by *Cyanobacteria*'s dominance. The phenomenon is frequently reported in eutrophic ecosystems and is considered an indicator of the functional degradation of phytoplankton communities (Vasconcelos et al., 2020; Ahoutou et al., 2021).

The moderately high spatial β diversity reflects the pronounced heterogeneity of the studied lakes, determined by differences in hydrological connectivity, morphology and nutrient supply. At the same time, temporal β-diversity indicates significant seasonal turnover, especially in Roșuleț Lake, confirming the structural instability of this ecosystem. These results suggest that seasonal variations may have a greater impact on community composition than spatial differences, a finding also confirmed by ANOSIM tests. Seasonal dynamics of *Cyanobacteria*: ANOSIM and SIMPER. ANOSIM results confirm that seasonal differences explain a significant proportion of the variation in phytoplankton communities, especially in Lake Roșuleț. SIMPER analysis showed that these changes are mainly driven by a small number of cyanobacterial species, including *Oscillatoria minima, Microcystis pulverea, Gomphosphaeria lacustris,* and *Aphanizomenon flos-aquae*. The alternation between dominant summer and autumn species reflects the seasonal succession described by the PEG model, where non-nitrogen-fixing *Cyanobacteria* can take over dominance towards the end of the growing season (Moza et al., 2021).

The persistence and dynamics of these taxa indicate a high adaptability to eutrophic conditions and variations in the hydrological regime. At the same time, the disappearance or decline of some species in autumn suggests increased sensitivity to temperature drops and increased water turbulence, factors known to limit cyanobacterial blooms (Jiang et al., 2023; Lenard & Ejankowski, 2024).

Relationships between the main phytoplankton groups. Even though *Chlorophyceae* occupied a secondary position in the phytoplankton structure, they demonstrated a competitive role, especially in Lake Roșuleț, where they exerted the greatest pressure on *Cyanobacteria* during the autumn period. The negative values of the Rate of Competitive Displacement (RCD) for the *Cyanobacteria-Chlorophyceae* comparison across all lakes confirm the competitive advantage of green algae at lower temperatures and under changing light and nutrient conditions. This behaviour is well documented in the literature, showing that many *Chlorophyceae* exhibit high growth rates at moderate temperatures and can efficiently exploit available phosphorus, thereby limiting cyanobacterial development (Briddon et al., 2022; Vasconcelos et al., 2020).

In contrast, the relationship between *Cyanobacteria* and diatoms was more nuanced. In Puiu Lake, diatoms had a competitive advantage in autumn; in Tătaru and Roșuleț, *Cyanobacteria* remained dominant, even as diatom replacement rates increased. This capacity suggests that *Cyanobacteria* exhibit functional adaptations to persistent eutrophic conditions, including tolerance to variations in the N:P ratio and changes in the mixing regime (Zou et al., 2025; Reynolds, 2006).

The Rate of Competitive Displacement analysis adds an important functional dimension to the interpretation of results, highlighting not only the competitive relationships among phytoplankton groups but also the degree of community stability. Strongly negative RCD values indicate unstable competitive hierarchies and reduced cyanobacterial capacity to maintain dominance, while mixed values suggest seasonal resilience, with alternations between dominant groups.

Also, the fact that seasonal differences are more pronounced than spatial ones emphasises the role of seasonality as an integrating factor of physicochemical and biological variations.

This predominance of the temporal signal suggests that climate change and changes in the hydrological regime may have a stronger impact on phytoplankton community structure than local spatial differences between lakes.

Overall, the results confirm the central role of *Cyanobacteria* in structuring phytoplankton communities in the studied lakes, but also highlight a clear dissociation between taxonomic diversity and ecological functionality of the communities. Although the specific richness remains relatively high, the pronounced dominance of *Cyanobacteria* leads to functional simplification, with the effective contribution to biomass and ecosystem processes concentrated in a small number of opportunistic taxa. This situation reflects what can be defined as an "apparent diversity", characteristic of shallow eutrophic ecosystems.

The shallow nature of the analysed lakes amplifies the role of internal sediment-nutrient-phytoplankton feedbacks, favouring the persistence of *Cyanobacteria* even under conditions of seasonal instability. In this context, Lake Roșuleț is characterised by a more unstable community structure, driven by intense internal nutrient recycling and high competitive pressure from *Chlorophyceae*, suggesting an ecosystem in an ecological transition.

The species with high abundances identified by the Grubbs test ($p < 0.05$) reflect episodes of massive development of resistant and opportunistic species, characteristic of shallow, highly dynamic aquatic ecosystems such as the lakes of the Danube Delta. The specialised literature describes the punctual dominance of the rotifers *Trichocerca similis* and *Lecane closterocerca* as opportunistic taxa with high reproduction rates and increased tolerance to eutrophic or unstable conditions (Allan, 1976; Wallace et al., 2006). Regarding the nauplial stages of Copepoda in Lake Tătaru, the persistent outlier values observed in both months suggest an unbalanced stage structure, with juveniles dominating. This pattern is typical of ecosystems where conditions favour continuous reproduction, but the survival of adult stages is limited by stressors or predators (Sommer et al., 2012; Hirst & Kiørboe, 2002). This may reflect another effect of bottom-up phytoplankton pressures. Also, the dominance of *Bosmina coregoni* in Lake Roșuleț in September reflects seasonal changes in the structure of the cladoceran community, which are recognised for their sensitivity to temperature, phytoplankton availability, and grazing pressure (Lampert, 1987). These episodes of dominance of some zooplankton species were directly reflected in the values of diversity indices, in particular the decrease of Shannon and Pielou indices and the increase of dominance (Simpson). The literature emphasises that such temporary imbalances are an intrinsic component of planktonic community function and provide essential information about the processes of community assembly and the stability of ecosystems (Magurran, 2013; Borics et al., 2021).

## CONCLUSIONS

*Cyanobacteria* proved to be the dominant ecological factor in the structure and dynamics of planktonic communities in Puiu, Tătaru, and Roșuleț lakes, profoundly influencing both phytoplankton composition and zooplankton responses. During the summer, blue-green algae reached very high densities, dominating the phytoplankton and affecting the diversity and functional balance of the other communities. Thus, the phytoplankton structure was strongly shaped by the competition between *Cyanobacteria* and the other major groups (chlorophytes and diatoms). With the onset of autumn, recovery trends in diatoms and chlorophytes were observed, reflected in negative values of the competitive replacement rate (RCD). However, the intensity of these processes varied among the lakes, with Roșuleț exhibiting the greatest structural instability and the most pronounced seasonal turnover. Seasonal changes were stronger than spatial ones, and cyanobacterial species were the main contributors to dissimilarity between periods characterised by variations in community structure, either through massive development or sudden disappearances. The impact on zooplankton was evident in the dominance of small, opportunistic forms (rotifers and juvenile copepod stages), indicating the trophic pressure exerted by a phytoplankton community dominated by *Cyanobacteria* and the reduced quality of the food resource. Overall, our study

highlights the central role of *Cyanobacteria* in regulating the functioning of lacustrine ecosystems in the Danube Delta. In the context of climate change and eutrophication, these processes are increasingly common, accentuating the vulnerability of deltaic ecosystems.

## ACKNOWLEDGEMENTS

This research was funded by the Institute of Biology Bucharest of Romanian Academy, by project no RO1567-IBB02/2026.

## REFERENCES

Ahoutou, M. K., Djeha, R. Y., Yao, E. K., Quiblier, C., Niamen-Ebrottié, J., Hamlaoui, S., Tambosco, K., Perrin, J.-L., Troussellier, M., Bernard, C., Séguis, L., Bouvy, M., Pédron, J., Konan, F. K., Humbert, J. F., & Coulibaly, J. K. (2021). Assessment of some key indicators of the ecological status of an African freshwater lagoon (Lagoon Aghien, Ivory Coast). *PLoS ONE, 16*(5), e0251065. https://doi.org/10.1371/journal.pone.0251065

Allan, J. D. (1976). Life history patterns in zooplankton. *The American Naturalist, 110*(971), 165–180. https://doi.org/10.1086/283056

Briddon, C. L., Szekeres, E., Hegedűs, A., Nicoară, M., Chiriac, M., Stockenreiter, M., & Drugă, B. (2022). The combined impact of low temperatures and shifting phosphorus availability on the competitive ability of cyanobacteria. *Scientific Reports, 12*(1), 16409. https://doi.org/10.1038/s41598-022-20580-2

Borics, G., Abonyi, A., Salmaso, N., & Ptacnik, R. (2021). Freshwater phytoplankton diversity: Models, drivers and implications for ecosystem properties. *Hydrobiologia, 848*, 53–75. https://doi.org/10.1007/s10750-020-04332-9

Coops, H., Hanganu, J., Tudor, M., & Oosterberg, W. (1999). Classification of Danube Delta lakes based on aquatic vegetation and turbidity. *Hydrobiologia, 415*, 187–191. https://doi.org/10.1007/s10452-007-9108-8

Dokulil, M. T., & Teubner, K. (2023). Long-term adjustment of phytoplankton structure to environmental traits at timescales during lifetime development and over generations. *Hydrobiologia, 851*(4), 823–839. https://doi.org/10.1007/s10750-023-05365-6

Dumitran, G. E., Vuță, L. I., & Popa, B. (2024). Overview of the eutrophication in Romanian lakes and reservoirs. *Limnological Review, 24*(1), 76–104.

Dumitran, G. E., Vuță, L. I., Popa, B., & Popa, F. (2020). Hydrological variability impact on eutrophication in a large Romanian border reservoir, Stânca–Costești. *Water, 12*(11), 3065. https://doi.org/10.3390/w12113065

Edler, L., & Elbrächter, M. (2010). The Utermöhl method for quantitative phytoplankton analysis. In B. Karlson, C. Cusack, & E. Bresnan (Eds.), *Microscopic and molecular methods for quantitative phytoplankton analysis* (pp. 13–20). Paris, FR: UNESCO.

Gâștescu, P. (2009). *Delta Dunării – geneză și evoluție, hidrologie, peisaj*. București, RO: Editura Fundației România de Mâine.

Hammer, Ø., Harper, D. A. T., & Ryan, P. D. (2001). PAST: Paleontological statistics software package for education and data analysis. *Palaeontologia Electronica, 4*(1).

Hirst, A. G., & Kiørboe, T. (2002). Mortality of marine planktonic copepods: Global rates and patterns. *Marine Ecology Progress Series, 230*, 195–209. https://doi.org/10.3354/meps230195

Ji, X., Verspagen, J. M. H., Stomp, M., & Huisman, J. (2017). Competition between cyanobacteria and green algae at low versus elevated $CO_2$: Who will win, and why? *Journal of Experimental Botany, 68*(14), 3815–3828.

Jia, J., Chen, Q., Ren, H., Lu, R.-J., He, H., & Gu, P. (2022). Phytoplankton composition and their related factors in five different lakes in China: Implications for lake management. *International Journal of Environmental Research and Public Health, 19*(5), 3135. https://doi.org/10.3390/ijerph19053135

Lampert, W. (1987). Laboratory studies on zooplankton-cyanobacteria interactions. *New Zealand Journal of Marine and Freshwater Research, 21*(3), 483–490. https://doi.org/10.1080/00288330.1987.9516244

Lenard, T., & Ejankowski, W. (2024). Ice phenology as a predictor of *Planktothrix rubescens* bloom in the vegetation season in temperate lakes. *Frontiers in Microbiology, 15*, 1384435. https://doi.org/10.3389/fmicb.2024.1384435

Magurran, A. E. (2013). *Measuring Biological Diversity*. Wiley-Blackwell. 272 pp. ISBN 978-1-118-68792-5.

Moldoveanu, M., & Florescu, L. I. (2011). Long-term analysis of cyanobacterial blooms in Lake Roșu (Danube Delta). *Scientific Annals of the Danube Delta Institute*, 17, 89–98.

Moldoveanu, M. M., Florescu, L. I., Dumitrache, C. A., & Cătana, R. D. (2025). Assessing urban river health: Phytoplankton as a proxy for resource use efficiency and human impact. *Phycology, 5*(4), 72.

Moza, M. I., Postolache, C., Benedek, A. M., Moldoveanu, M., & Spaak, P. (2021). Geographical and temporal patterns of cyanobacterial assemblages in the Danube Delta lake complexes. *Hydrobiologia, 848*, 753–771. https://doi.org/10.1007/s10750-020-04466-w

Oosterberg, W., Staras, M., Bogdan, L., Buijse, A. D., Constantinescu, A., Coops, H., Hanganu, J., Ibelings, B. W., Menting, G., & Navodaru, I. (2000). *Ecological gradients in the Danube Delta lakes: Present state and man-induced changes*. Lelystad, NL: RIZA Report 2000.015.

Paerl, H. W., & Huisman, J. (2008). Blooms like it hot. *Science, 320*(5872), 57–58.

Paerl, H. W., & Otten, T. G. (2013). Harmful cyanobacterial blooms: Causes, consequences, and controls. *Microbial Ecology, 65*(4), 995–1010.

Pavel, A., Durisch-Kaiser, E., Balan, S., Radan, S., Sobek, S., & Wehrli, B. (2009). Sources and

emission of greenhouse gases in Danube Delta lakes. *Environmental Science and Pollution Research, 16*(Suppl. 1), 86–91.

Reynolds, C. S. (2006). *The ecology of phytoplankton*. Cambridge, UK: Cambridge University Press.

Sommer, U., Adrian, R., De Senerpont Domis, L. N., Elser, J. J., Gaedke, U., Ibelings, B. W., Jeppesen, E., Lürling, M., Molinero, J. C., Mooij, W. M., van Donk, E., & Winder, M. (2012). Beyond the Plankton Ecology Group (PEG) model: Mechanisms driving plankton succession. *Annual Review of Ecology, Evolution, and Systematics, 43*, 429–448. https://doi.org/10.1146/annurev-ecolsys-110411-160251

Török, L. (2011). The trend of phytoplankton development in Danube Delta lakes. *Scientific Annals of the Danube Delta Institute*, 17, 89–98.

Török, L., Török, Z., Cârstea, E. M., & Savaștru, D. (2017). Seasonal variation of eutrophication in some lakes of the Danube Delta Biosphere Reserve. *Water Environment Research, 89*(1), 86–94. https://doi.org/10.2175/106143016X14733681696248

Tóth-Krasznai, E., Török, P., Borics, G., Lukács, Á., Kókai, Z., Lerf, V., Görgényi, J., & B-Béres, V. (2022). Functional dynamics of phytoplankton assemblages in hypertrophic lakes: Functional- and species diversity is highly resistant to cyanobacteria*Cyanobacteria*l blooms. *Ecological Indicators, 145*, 109583. https://doi.org/10.1016/j.ecolind.2022.109583

Tudorancea, C., & Tudorancea, M. M. (2006). *Danube Delta: Genesis, biodiversity and conservation*. Leiden, NL: Backhuys Publishers.

Vasconcelos, H. C., Lopes, J. A., Pereira, M. J., & Pinto, A. S. (2020). Fluorescence behavior of phytoplankton blooms by time-correlated single-photon counting (TCSPC). In *IntechOpen eBooks*. https://doi.org/10.5772/intechopen.93292

Wallace, R. L., Snell, T. W., Ricci, C., & Nogrady, T. (2006). *Rotifera. Volume 1: Biology, Ecology and Systematics* (2nd ed.). Backhuys Publishers, Leiden. 299, ISBN 90-5782-178-8.

Zou, B., Hu, H., Jia, J., Wu, W., Li, X., Chen, X., Zeng, H., Wang, Z., & Wu, C. (2025). Temporal variation of plankton community in a typical lake in the middle reaches of the Yangtze River: Structure, environmental response and interactions. *Water, 17*(7), 1021. https://doi.org/10.3390/w17071021

Scientific Papers. Series E. Land Reclamation, Earth Observation & Surveying, Environmental Engineering. Vol. XV, 2026
Print ISSN 2285-6064, CD-ROM ISSN 2285-6072, Online ISSN 2393-5138, ISSN-L 2285-6064

# SPATIAL VARIATION OF MICROBIAL COMMUNITIES IN THE BAHLUI RIVER ACROSS THE URBAN AREA OF IASI

**Andrei-Mihai GAFENCU, Andreea-Mihaela FLOREA, Florin-Daniel LIPȘA, Eugen ULEA**

"Ion Ionescu de la Brad" Iaşi University of Life Sciences, 3 Mihail Sadoveanu Alley, Iași, Romania

Corresponding author email: andrei.gafencu@iuls.ro

***Abstract***

*The Bahlui River, flowing through the urban area of Iași, is subjected to significant anthropogenic pressures that influence its microbial communities. This study assessed the structure and temporal dynamics of microbial populations along a 24 km urban stretch of the river, using six sampling sites distributed from the river's entry into the city to its exit. Water samples collected in April and July 2025 were analyzed for total bacterial counts, Gram-positive bacteria ($G^+$), and micromycetes. Results revealed significant spatial and temporal variations: total bacterial and Gram-positive abundances increased from April to July, with point 3 consistently exhibiting the highest counts, while micromycete abundance was lower but also displayed site-specific and seasonal variation. Two-way ANOVA confirmed that both sampling location and period significantly influenced microbial abundance, with interactions indicating non-uniform temporal changes along the river. These findings highlight the combined effects of urbanization and seasonal dynamics on microbial community structure and provide valuable insights for monitoring and managing urban aquatic ecosystems.*

***Key words****: aquatic microbiology, Bahlui river, DPSIR, microbial communities, spatial variation, urban river.*

## INTRODUCTION

Water bodies, such as rivers that traverse urban areas, constitute vulnerable aquatic ecosystems, as they are subjected to significant anthropogenic pressures resulting from direct or indirect human activities (Teurlincx et al., 2019). Urban rivers are subjected to several categories of anthropogenic pressures (Castro et al., 2021), including chemical pollution, resulting from the input of nutrients, heavy metals, organic compounds, pharmaceuticals, antibiotic residues, and microplastics (Mandaric et al., 2018; Sekudewicz et al., 2021; Tiwari et al., 2022; Mansor et al., 2024); microbiological contamination, associated with wastewater discharges (Olds et al., 2018; Cui et al., 2019; Jing et al., 2024); hydromorphological alterations, caused by channel modifications, embankments, and bank impermeabilization (Ollero et al., 2015; Borek et al., 2022); and thermal pollution, arising from industrial warm-water effluents (Briciu et al., 2020; Chakraborty, 2021).

These types of pressures need to be carefully investigated, as they can cause significant changes in the structure, diversity, and dynamics of aquatic microbial communities. Given the essential role of the watermicrobiota in organic matter decomposition (Liu et al., 2023), nutrient recycling (Ávila et al., 2019), and the regulation of biogeochemical cycles (Pan et al., 2024), its disruption can lead to functional imbalances in the ecosystem, a reduced natural self-purification capacity of the rivers, and impaired health of the aquatic ecosystems (Xie et al., 2021; Singh et al., 2025).

In the urban area of Iași Municipality, the Bahlui River, the municipality's main hydrographic collector, exhibits significant changes in the physico-chemical and biological parameters of the water (Zaharia, 2015; Marcoie et al., 2025). These transformations represent the cumulative result of the expansion of urban infrastructure, wastewater discharges, and inputs originating from industrial, residential, and agricultural activities carried out within the basin corresponding to the urban sector.

The ecological status assessment of the Bahlui River should be conducted through the integration of data within the DPSIR framework (Drivers–Pressures–State–Impact–Response), facilitating the correlation between socio-economic driving forces, the

pressures exerted on the ecosystem, and the associated impacts. Previous studies have demonstrated that the DPSIR framework provides a holistic approach for evaluating the overall ecological effects of polluted urban rivers (Skoulikidis et al., 2009; Lu et al., 2019).
In this context, the Bahlui River represents a relevant case study for the systematic application of the DPSIR framework in an urban environment.
Within this framework, the ecological dynamics of the urban river sector can be structured as follows: **Drivers** are represented by positive demographic growth and the accelerated urban expansion of Iași and its surrounding areas (Holobâcă et al., 2022), reflected in intensified economic activities and the expansion of impervious surfaces, which have significantly altered the hydrological regime. These processes generate **Pressures**, including increased domestic and industrial wastewater discharges (Marcoie et al., 2024), nutrient inputs (nitrates and phosphates) from urban runoff and diffuse agricultural sources (Neamtu et al., 2009; Oiște & Breabăn, 2011), microbiological contamination associated with insufficient or malfunctioning sewage systems, as well as the occurrence of emerging contaminants such as pharmaceutical residues, antibiotics, and microplastics (Apostol, 2008; Zaharia, 2015). Consequently, the **State** of the river ecosystem is altered, particularly through shifts in microbial community structure along the pollution gradient, characterized by reduced diversity and functional modifications of key biogeochemical cycles (e.g., nitrogen and carbon cycling). These changes lead to **Impacts** manifested as ecosystem imbalance, degradation of ecological integrity, and potential public health risks. Therefore, appropriate **Responses** should include continuous microbiological and physicochemical monitoring at the watershed scale, modernization of wastewater treatment infrastructure, and the implementation of integrated urban water management strategies aimed at improving the ecological status of the Bahlui River within the broader framework of sustainable urban development.
The present study investigates changes in microbial communities of the Bahlui River along the sector that crosses the city of Iași. While numerous studies have addressed hydrological, physicochemical, and general water quality aspects of the river, research specifically focused on the dynamics and structure of microbial communities remains limited. This gap in the literature underscores the need for an integrated microbiological approach capable of revealing functional and structural alterations in the river ecosystem. Accordingly, the present research provides a scientific basis for future studies aimed at assessing hydrological sustainability in anthropized environments, contributing to the development of monitoring and management strategies tailored to urban river systems.

## MATERIALS AND METHODS

### *Study area*

The Bahlui River, the main watercourse traversing the city of Iași, has a total length of approximately 119 km. It originates at an altitude of around 500 m in Tudora commune, Botoșani County, and flows into the Jijia River near the village of Chiperești, Iași County (Figure 1).




Figure 1. Hydrographical overview of the Bahlui River, showing the source (red circle), river course (orange line), and confluence with the Jijia River (blue triangle) (map generated from www.openstreetmap.org)

Along its course, the Bahlui River passes through a series of settlements, the most significant of which are Hârlău, Podu Iloaiei, and the municipality of Iași. Within Iași and its surrounding localities, the river spans approximately 28 km, between Lețcani and Chiperești. This stretch represents the focus

area of the present study. Along this segment, the population density is high, economic activities are intensive, and extensive impervious surfaces exist, all of which have increased the river's susceptibility to anthropogenic pressures (Figure 2).




Figure 2. Geographical positioning of the sampling points (1-6) along the Bahlui River (map generated from www.openstreetmap.org)

The sampling points were distributed along a 24 km river course, following the longitudinal course of the Bahlui River through the urban area of Iași. The inter-site distances varied between 2.8 km and 6.5 km, reflecting differences in urban pressure intensity and hydromorphological conditions along the river continuum. This spatial configuration allows for the evaluation of cumulative anthropogenic effects and the identification of potential shifts in microbial community structure along the upstream–downstream gradient (Table 1).

Table 1. Gheographic coordinates of the sampling points sites along the Bahlui rivers and distances between consecutives sites

| Sampling points | Coordinates | | Distance | |
|---|---|---|---|---|
| | Latitude (N) | Longitude (E) | Distance from previous sampling points (km) | Cumulative distance (km) |
| 1 | 47°11'05.6" | 27°24'58.3" | - | 0.0 |
| 2 | 47°10'06.4" | 27°28'13.1" | ≈4.5 | ≈4.5 |
| 3 | 47°10'10.4" | 27°32'20.9" | ≈6.1 | ≈10.6 |
| 4 | 47°09'10.8" | 27°35'46.1" | ≈4.1 | ≈14.7 |
| 5 | 47°09'02.8" | 27°38'31.1" | ≈2.8 | ≈17.5 |
| 6 | 47°08'26.5" | 27°41'30.2" | ≈6.5 | ≈24.0 |

***Sampling***

Water sampling was performed twice in 2025. The first sampling moment took place on April 21, 2025 (T1), followed by a second one conducted approximately three months later, on July 14, 2025 (T2). Water samples were collected from each of the six sampling points for microbiological analyses. At each site, a total of 108 mL of surface water was obtained (six tubes × 18 mL per tube) from approximately 15 cm below the water surface (Figure 3). To ensure spatial representativeness across the river cross-section, subsamples were collected as follows: two near the left bank, two from the mid-channel, and two near the right bank.



Figure 3. Water sampling procedure

Sterile tubes were used for sample collection. After sampling, the tubes were stored in a refrigerated container to ensure optimal transport conditions to the laboratory. Sample processing was performed on the same day as collection.

***Microbiological analyses***

Microbiological analyses of the water samples were performed using conventional culture-based methods (plate technique). For each sample, five replicates were analyzed. For microbial enumeration, 1 mL of river water, as well as 1 mL from serial decimal dilutions (up to $10^{-3}$), was inoculated onto the appropriate culture media using the pour plate method. Total bacterial counts were determined using the $10^{-1}$ dilution, as undiluted samples resulted in overgrown plates (>400-500 bacterial colonies per plate), whereas higher dilutions ($10^{-2}$ and $10^{-3}$) produced low colony numbers (1-20 colonies per plate), outside the optimal counting range. Bacterial counts were determined on Plate Count Agar (PCA, Scharlau, Spain, 23.5 g $L^{-1}$) after incubation at 37°C for 24 h. Colonies were enumerated using an automatic colony counter (Interscience, Scan 1200), and results were expressed as colony-forming units per milliliter (CFU $mL^{-1}$). Selective media were used to differentiate microbial groups.

Gram-positive bacteria ($G^+$) were enumerated on PCA supplemented with streptomycin (35 mg $L^{-1}$) using undiluted river water samples.
Filamentous fungi were determined by inoculating undiluted samples onto Potato Dextrose Agar (PDA, Scharlau, Spain, 39 g $L^{-1}$) supplemented with Rose Bengal (35 mg $L^{-1}$) to limit colony overgrowth and facilitate counting. Fungal plates were incubated at 28°C for 3-5 days and monitored periodically according to colony growth rate.

***Statistical analyses***

Experimental data were analyzed using two-way analysis of variance (ANOVA) to evaluate the effects of sampling point (Sample), sampling moment (Moment), and their interaction on microbial counts. Microbial counts were log-transformed prior to analysis to improve normality. Homogeneity of variances was tested using Levene's test. Statistical analyses were performed using IBM SPSS Statistics 26, and differences were considered statistically significant at $p < 0.05$.

## RESULTS AND DISCUSSIONS

Microbiological analyses revealed significant variations in the total number of bacteria, Gram-positive bacteria ($G^+$), and total number of micromycetes along the six sampling points established on the Bahlui River course, as well as between the two investigation periods.
To further quantify these spatial and temporal variations, the total bacterial abundance at each sampling point and investigation period was determined (Table 2).

Table 2. Total bacterial counts across sampling points and investigation periods on the Bahlui River

| Sampling point | Time | Total number of bacteria (mean±SD) |
|---|---|---|
| 1 | T1 | $1.0 \times 10^3 \pm 0.17$ |
| | T2 | $2.1 \times 10^3 \pm 0.36$ |
| 2 | T1 | $1.2 \times 10^3 \pm 0.16$ |
| | T2 | $2.3 \times 10^3 \pm 0.35$ |
| 3 | T1 | $4.4 \times 10^3 \pm 0.05$ |
| | T2 | $5.7 \times 10^3 \pm 0.43$ |
| 4 | T1 | $0.9 \times 10^3 \pm 0.07$ |
| | T2 | $2.2 \times 10^3 \pm 0.33$ |
| 5 | T1 | $1.2 \times 10^3 \pm 0.06$ |
| | T2 | $2.5 \times 10^3 \pm 0.35$ |
| 6 | T1 | $2.4 \times 10^3 \pm 0.13$ |
| | T2 | $4.0 \times 10^3 \pm 0.45$ |

The results show that total bacterial counts increased at all sampling points from T1 (April) to T2 (July). At T1, counts ranged from $0.9 \times 10^3$ CFU $mL^{-1}$ at sampling point 4 to $4.4 \times 10^3$ CFU $mL^{-1}$ at sampling point 3. By T2, counts rose across all locations, reaching a maximum of $5.7 \times 10^3$ CFU $mL^{-1}$ at sampling point 3 and a minimum of $2.1 \times 10^3$ CFU $mL^{-1}$ at sampling point 1. This indicates a clear temporal increase in bacterial abundance along the river. Two-way ANOVA confirmed that these differences were statistically significant. Significant variation was observed among sampling points ($F(5.48) = 180.70$, $p < 0.001$) and between sampling moments ($F(1.48) = 418.58$, $p < 0.001$). A significant interaction between sampling point and moment ($F(5.48) = 9.44$, $p < 0.001$) further indicates that the magnitude of temporal changes differed across locations (Table 3).

Table 3. Two-way ANOVA results for total bacterial counts across sampling points and investigation periods

| Source | df | F | *p* |
|---|---|---|---|
| Sampling point | 5 | 180.70 | <0.001 |
| Sampling moment | 1 | 418.58 | <0.001 |
| Point x Moment | 5 | 9.44 | <0.001 |

Gram-positive ($G^+$) bacterial abundance was also analyzed at the six sampling points and two investigation periods (Table 4).

Table 4. Gram-positive bacterial counts across sampling points and investigation periods on the Bahlui River

| Sampling point | Time | Gram-positive bacteria (mean±SD) |
|---|---|---|
| 1 | T1 | $3.0 \times 10^1 \pm 0.55$ |
| | T2 | $5.2 \times 10^1 \pm 0.48$ |
| 2 | T1 | $1.3 \times 10^1 \pm 0.35$ |
| | T2 | $3.0 \times 10^1 \pm 0.27$ |
| 3 | T1 | $18.6 \times 10^1 \pm 3.54$ |
| | T2 | $23.5 \times 10^1 \pm 1.02$ |
| 4 | T1 | $2.9 \times 10^1 \pm 0.73$ |
| | T2 | $6.4 \times 10^1 \pm 0.47$ |
| 5 | T1 | $5.7 \times 10^1 \pm 0.45$ |
| | T2 | $8.6 \times 10^1 \pm 0.31$ |
| 6 | T1 | $10.6 \times 10^1 \pm 1.08$ |
| | T2 | $14.9 \times 10^1 \pm 0.76$ |

At T1, counts ranged from $1.3 \times 10^1$ CFU $mL^{-1}$ at sampling point 2 to $18.6 \times 10^1$ CFU $mL^{-1}$ at sampling point 3. By T2, all sampling points showed increases, with a maximum of $23.5 \times 10^1$ CFU $mL^{-1}$ at sampling point 3 and a minimum of $3.0 \times 10^1$ CFU $mL^{-1}$ at sampling

point 2. Sampling point 3 consistently showed the highest abundance, while sampling point 2 exhibited the lowest, indicating strong spatial heterogeneity. Two-way ANOVA revealed significant differences among sampling points ($F$ (5.48) = 337.02, $p < 0.001$) and between investigation periods ($F$ (1.48) = 196.83, $p < 0.001$). A significant interaction ($F$ (5.48) = 7.14, $p < 0.001$) suggests that temporal changes in Gram-positive abundance differed depending on location (Table 5).

Table 5. Two-way ANOVA results for Gram$^+$ bacterial counts across sampling points and investigation periods

| Source | Df | F | *p* |
|---|---|---|---|
| Sampling point | 5 | 337.02 | <0.001 |
| Sampling moment | 1 | 196.83 | <0.001 |
| Point x Moment | 5 | 7.14 | <0.001 |

To assess the fungal component of the microbial community, total micromycete abundance was determined at the six sampling points and two investigation periods (Table 6).

Table 6. Total micromycete counts across sampling points and investigation periods on the Bahlui River

| Sampling point | Time | Total number of micromycetes (mean±SD) |
|---|---|---|
| 1 | T1 | $1.2 \times 10^1 \pm 0.15$ |
| | T2 | $1.2 \times 10^1 \pm 0.15$ |
| 2 | T1 | $1.3 \times 10^1 \pm 0.05$ |
| | T2 | $1.4 \times 10^1 \pm 0.18$ |
| 3 | T1 | $1.2 \times 10^1 \pm 0.25$ |
| | T2 | $1.6 \times 10^1 \pm 0.10$ |
| 4 | T1 | $1.1 \times 10^1 \pm 0.09$ |
| | T2 | $1.3 \times 10^1 \pm 0.36$ |
| 5 | T1 | $1.4 \times 10^1 \pm 0.13$ |
| | T2 | $1.5 \times 10^1 \pm 0.23$ |
| 6 | T1 | $0.7 \times 10^1 \pm 0.15$ |
| | T2 | $1.3 \times 10^1 \pm 0.29$ |

The results show relatively low but significant spatial and temporal variation. At T1, micromycete counts ranged from $0.7 \times 10^1$ CFU mL$^{-1}$ at sampling point 6 to $1.4 \times 10^1$ CFU mL$^{-1}$ at sampling point 5. By T2, counts increased at most points, with a maximum of $1.6 \times 10^1$ CFU mL$^{-1}$ at sampling point 3 and a minimum of $1.2 \times 10^1$ CFU mL$^{-1}$ at sampling point 1. Two-way ANOVA confirmed that these differences were statistically significant (Table 7).

Significant variation was observed among sampling points ($F$ (5.48) = 8.64, $p < 0.001$) and between sampling moments ($F$ (1.48) = 22.09, $p < 0.001$). A significant interaction between sampling point and moment ($F$ (5.48) = 4.25, $p = 0.003$) further indicates that temporal changes in micromycete abundance differed across locations.

Table 7. Two-way ANOVA results for total micromycete counts across sampling points and investigation periods

| Source | df | F | *p* |
|---|---|---|---|
| Sampling point | 5 | 8.64 | <0.001 |
| Sampling moment | 1 | 22.09 | <0.001 |
| Point x Moment | 5 | 4.25 | 0.003 |

## CONCLUSIONS

The present study demonstrated significant spatial and temporal variations in microbial communities along the Bahlui River. Both total bacterial and Gram-positive bacterial abundances increased from April to July, with point 3 consistently exhibiting the highest counts, while micromycetes showed lower overall abundance but also displayed significant temporal and spatial differences. Two-way ANOVA confirmed that both the sampling location and investigation period significantly influenced microbial abundance, and interactions between these factors indicate that temporal changes were not uniform along the river. These findings highlight the impact of local environmental conditions and anthropogenic pressures on microbial dynamics and underscore the importance of multiple spatially distributed sampling points and repeated monitoring for accurate assessment of river water quality. Continuous monitoring of microbial indicators, combined with physicochemical analyses, is recommended to better understand ecological risks and the drivers of microbial variability along urban river systems.

## REFERENCES

Apostol, I. (2008). Impact of sewage from the town of Iași-at the limit of man made disaster–on the microbiota of the River Bahlui. *Risk Assessment as a Basis for the Forecast and Prevention of Catastrophies*, *35*, 162.

Ávila, M. P., Oliveira-Junior, E. S., Reis, M. P., Hester, E. R., Diamantino, C., Veraart, A. J., Lamers, L. P. M., Kosten, S., & Nascimento, A. M. (2019). The water hyacinth microbiome: link between carbon

turnover and nutrient cycling. Microbial ecology, 78(3), 575-588.

Borek, Ł., & Kowalik, T. (2022). Hydromorphological inventory and evaluation of the upland stream: case study of a small ungauged catchment in Western Carpathians, Poland. *Land*, 11(1), 141.

Briciu, A. E., Mihăilă, D., Graur, A., Oprea, D. I., Prisăcariu, A., & Bistricean, P. I. (2020). Changes in the water temperature of rivers impacted by the urban heat island: Case study of Suceava city. *Water*, *12*(5), 1343.

Castro, M. F., Almeida, C. A., Bazán, C., Vidal, J., Delfini, C. D., & Villegas, L. B. (2021). Impact of anthropogenic activities on an urban river through a comprehensive analysis of water and sediments. *Environmental Science and Pollution Research*, 28(28), 37754-37767.

Chakraborty, S. K. (2021). River pollution and perturbation: Perspectives and processes. In *Riverine Ecology Volume 2: Biodiversity Conservation, Conflicts and Resolution* (pp. 443-530). Cham: Springer International Publishing.

Cui, Q., Huang, Y., Wang, H., & Fang, T. (2019). Diversity and abundance of bacterial pathogens in urban rivers impacted by domestic sewage. *Environmental Pollution*, 249, 24-35.

Holobâcă, I. H., Benedek, J., Ursu, C. D., Alexe, M., & Temerdek-Ivan, K. (2022). Ratio of land consumption rate to population growth rate in the major metropolitan areas of Romania. *Remote Sensing*, *14*(23), 6016.

Jing, W., Sajnani, S., Zhou, M., Zhu, H., & Xu, Y. (2024). Evaluating the ecological impact of wastewater discharges on microbial and contaminant dynamics in rivers. *Water*, 16(3), 377.

Liu, Y., Zhang, B., Zhang, Y., Shen, Y., Cheng, C., Yuan, W., & Guo, P. (2023). Organic matter decomposition in river ecosystems: microbial interactions influenced by total nitrogen and temperature in river water. *Microbial ecology*, *85*(4), 1236-1252.

Lu, W., Xu, C., Wu, J., & Cheng, S. (2019). Ecological effect assessment based on the DPSIR model of a polluted urban river during restoration: A case study of the Nanfei River, China. *Ecological Indicators*, *96*, 146-152.

Mandaric, L., Mor, J. R., Sabater, S., & Petrovic, M. (2018). Impact of urban chemical pollution on water quality in small, rural and effluent-dominated Mediterranean streams and rivers. *Science of the Total Environment*, 613, 763-772.

Mansor, M. I., Fatehah, M. O., Aziz, H. A., & Wang, L. K. (2024). Occurrence, behaviour and transport of heavy metals from industries in river catchments. In *Industrial waste engineering* (pp. 205-277). Cham: Springer International Publishing.

Marcoie, N., Chihaia, Ș., Hrăniciuc, T. A., Balan, C. D., Drăgoi, E. N., & Nechita, M. T. (2024). Linking Nutrient Dynamics with Urbanization Degree and Flood Control Reservoirs on the Bahlui River. *Water*, *16*(10), 1322.

Marcoie, N., Toma, I. O., Chihaia, Ș., Hrăniciuc, T. A., Toma, D., Balan, C. D., Drăgoi, E. N., & Nechita, M. T. (2025). Anthropogenic River Segmentation Case Study: Bahlui River from Romania. *Hydrology*, *12*(9), 224.

Neamtu, M., Ciumasu, I. M., Costica, N., Costica, M., Bobu, M., Nicoara, M. N., Catrinescu, C., van Slooten, K.B., & De Alencastro, L. F. (2009). Chemical, biological, and ecotoxicological assessment of pesticides and persistent organic pollutants in the Bahlui River, Romania. *Environmental Science and Pollution Research*, *16*(Suppl 1), 76-85.

Oiște A. M., Breabăn I. G. (2011). Nitrate trends during the seasons on Bahlui river and its tributaries in build-up area of Iasi city. *Bulletin of University of Agricultural Sciences and Veterinary Medicine Cluj-Napoca. Agriculture*, *68*(2). 116-123.

Olds, H. T., Corsi, S. R., Dila, D. K., Halmo, K. M., Bootsma, M. J., & McLellan, S. L. (2018). High levels of sewage contamination released from urban areas after storm events: A quantitative survey with sewage specific bacterial indicators. *PLoS medicine*, 15(7), e1002614.

Ollero, A., Ibisate, A., Granado, D., & Asua, R. R. D. (2015). Channel responses to global change and local impacts: Perspectives and tools for floodplain management, Ebro river and Tributaries, NE Spain. In *Geomorphic approaches to integrated floodplain management of lowland fluvial systems in North America and Europe* (pp. 27-52). New York, NY: Springer New York.

Pan, X., Lin, L., Cao, X., Jing, Z., Dong, L., & Zhai, W. (2024). Response of microbial communities and biogeochemical cycling functions to sediment physicochemical properties and microplastic pollution under damming and water diversion projects. *Science of The Total Environment*, 940, 173209.

Sekudewicz, I., Dąbrowska, A. M., & Syczewski, M. D. (2021). Microplastic pollution in surface water and sediments in the urban section of the Vistula River (Poland). *Science of the Total Environment*, 762, 143111.

Singh, S. K., Deb, A., Anil Kumar Naik, B., & Kumar, A. K. (2025). Comprehensive Analysis of Micropollutants and Their Impact on Aquatic Ecosystems and Biodiversity. In *Emerging Micropollutants: Status in the Environment and Management through Bioremediation* (pp. 151-189). Cham: Springer Nature Switzerland.

Skoulikidis, N. T. (2009). The environmental state of rivers in the Balkans - A review within the DPSIR framework. *Science of the total environment*, *407*(8), 2501-2516.

Teurlincx, S., Kuiper, J. J., Hoevenaar, E. C., Lurling, M., Brederveld, R. J., Veraart, A. J., Janssen, A.B.G., Mooij, W.M., & de Senerpont Domis, L. N. (2019). Towards restoring urban waters: understanding the main pressures. *Current Opinion in Environmental Sustainability*, 36, 49-58.

Tiwari, A. K., & Pal, D. B. (2022). Nutrients contamination and eutrophication in the river ecosystem. *In Ecological significance of river ecosystems* (pp. 203-216). Elsevier.

Xie, Y., Liu, X., Wei, H., Chen, X., Gong, N., Ahmad, S., Lee, T. Ismail, S., & Ni, S.Q. (2021). Insight into impact of sewage discharge on microbial dynamics and pathogenicity in river ecosystem. Sci Rep 12, 6894

Zaharia, C. (2015). Evaluation of water pollution status in Bahlui River (Iasi town area) due to domestic and urban wastewater treatment activities. *Journal of Engineering Studies and Research*, *21*(4), 79-88.

Scientific Papers. Series E. Land Reclamation, Earth Observation & Surveying, Environmental Engineering. Vol. XV, 2026
Print ISSN 2285-6064, CD-ROM ISSN 2285-6072, Online ISSN 2393-5138, ISSN-L 2285-6064

# HYDRO-MECHANICAL ANALYSIS AND NUMERICAL SIMULATION OF WATER INFILTRATION PROCESSES IN RAILWAY EMBANKMENTS

**Dorian HAUSLER COZMA, Eugen Teodor MAN, Robert Florin BEILICCI, Erika Beata Maria BEILICCI**

Politehnica University of Timisoara, 1A Splaiul Spiru Haret, Timisoara, Romania

Corresponding author email: erika.beilicci@upt.ro

***Abstract***

*Railway embankments represent critical components of railway infrastructure, and water infiltration constitutes a major factor in their degradation. This paper presents methods for modelling water infiltration through embankments, with an emphasis on hydro-mechanical analysis and the implications for the stability and durability of railway structures. The use of fundamental flow equations in porous media and the implementation of numerical models for simulating saturated and unsaturated conditions are discussed, providing a basis for optimizing drainage systems and preventing embankment degradation. Numerical simulations allow for the identification of areas vulnerable to infiltration, the optimization of drainage systems, and the prevention of accelerated ballast deterioration. In embankments with insufficient drainage, water accumulation leads to increased pore pressures, reduced material strength, and the occurrence of differential settlements. Integrating infiltration modelling with field monitoring and predictive maintenance methods can significantly contribute to extending the service life of the railway and reducing operational costs.*

***Key words****: modelling, railway, water infiltration.*

## INTRODUCTION

The structural integrity and operational safety of railway infrastructure are fundamentally governed by the hydro-mechanical behaviour of the underlying geostructures, among which unsaturated soil embankments represent the most critical and vulnerable assets. In modern railway engineering, embankments are continuously subjected to complex, coupled environmental and dynamic stressors, where the phenomenon of meteoric water infiltration acts as a primary driver of structural degradation and premature geotechnical failure. The mechanical response of these engineered earthworks is intrinsically linked to their hydraulic state, which exhibits high spatial and temporal variability driven by local hydrometeorological regimes, rainfall intensity profiles, and evaporation fluxes. When precipitation infiltrates the unsaturated matrix of a railway embankment, it induces a progressive dissipation of matric suction within the soil pores, shifting the hydrologic baseline toward full saturation. From a geotechnical perspective, this reduction in matric suction directly compromises the shear strength parameters of the compacted soil skeleton, while simultaneously altering the effective stress state and triggering a marked decrease in the resilient modulus of the foundation. Consequently, unmanaged infiltration pathways not only accelerate track geometry degradation and differential settlements under heavy cyclic rolling stock loads but also significantly increase the probability of catastrophic slope failures, landslips, and embankment collapse (Apshikur et al., 2026).

To accurately forecast and mitigate these hydro-mechanical feedback loops, modern engineering practice has transitioned from empirical assessments to advanced numerical simulations capable of capturing non-steady saturated-unsaturated water transport. The mathematical simulation of these sub-surface flow processes relies on the numerical solution of the non-linear partial differential Richards equation, coupled with constitutive soil-water characteristic curves that define the non-linear relationships between volumetric water content, suction, and hydraulic conductivity. However, executing high-fidelity predictive modelling remains a significant challenge due to the complex material properties of railway

embankments, which often feature heterogeneous compacted profiles, varying geomorphological gradients, and specialized ballast-subballast drainage boundaries. This numerical complexity is further amplified when capturing the transient boundary conditions imposed by extreme, high-return period precipitation events, where rapid infiltration fronts create sharp hydraulic gradients that can induce localized numerical oscillations or matrix divergence within the computational grid. Furthermore, standard geotechnical design frameworks frequently suffer from a historical deficiency in high-resolution, ground-based hydrologic and suction monitoring data, forcing reliance on remote sensing datasets that lack the discrete spatial resolution required to model localized seepage lines. Therefore, developing an integrated numerical modelling strategy that comprehensively simulates transient infiltration hydrodynamics, validates hydro-mechanical strength reductions, and complies with modern structural infrastructure safety standards which is a critical requirement for ensuring the climate resilience of transboundary railway networks.

This research paper provides a comprehensive hydro-mechanical analysis and numerical simulation of water infiltration processes within unsaturated railway embankments subjected to severe pluviometric configurations. By coupling continuous hydrometeorological forcing series with non-linear finite-element or finite-difference seepage formulations, this study evaluates the progressive advancement of infiltration fronts, the dynamic degradation of matric suction profiles, and the resulting fluctuations in the global factor of safety against slope instability. The predictive framework established herein delivers a validated optimization tool for infrastructure managers, enabling the proactive identification of critical saturation zones and the strategic design of advanced sub-surface drainage perimeters tailored to withstand extreme climate change scenarios.

## MATERIALS AND METHODS

The evaluation of transient water infiltration and the resulting hydro-mechanical feedback loops within the railway embankment was executed through an integrated numerical modelling workflow that couples unsaturated seepage analysis with limit equilibrium slope stability formulations. The geometric profile of the representative railway geostructure was reconstructed based on standard European ballast-subballast infrastructure designs, capturing a symmetric earthwork embankment with side slope gradients engineered to reflect critical operating conditions. The computational mesh discretization was optimized by implementing a highly refined finite-element grid along the atmospheric boundaries and embankment slopes, where the sharpest hydraulic and suction gradients develop during precipitation events, while a coarser grid spacing was maintained within the deep, saturated core to maximize computational efficiency without inducing matrix divergence or numerical locking. To establish a realistic simulation environment, continuous hydrometeorological forcing time series were gathered from regional gauging stations, compiling high-intensity synthetic design storms and multi-seasonal precipitation-evaporation flux sequences that act as dynamic, non-steady boundary conditions on the exposed surfaces of the computational domain (Xiao et al., 2025).

The simulation of water transport mechanisms through the unsaturated soil matrix relied on a formulation of the non-linear partial differential Richards equation, which governs the conservation of fluid mass and non-steady flow in porous media. To capture the non-linear behavioural evolution of the compacted embankment soil, the hydraulic framework was coupled with constitutive soil-water characteristic curves defined by the van Genuchten mathematical model. This approach dynamically links the volumetric water content, matric suction, and relative hydraulic conductivity, allowing the computational engine to simulate how the soil's capacity to conduct water scales non-linearly as pore-water pressures fluctuate. The calibration of these hydraulic functions utilized suction and pressure plate extract data characteristic of compacted silty-clay embankments, which fall under typical intermediate drainage classifications. Initial boundary conditions were established by running a long-term steady-state groundwater flow simulation to derive a realistic baseline suction distribution

and water table phreatic surface across the foundation prior to the onset of the transient rainstorm sequences (Kong et al., 2025).

The hydraulic behavior of the unsaturated railway soils is governed by the constitutive relationships defined by the van Genuchten and Mualem models. ″

Figure 1 illustrates the Soil-Water Characteristic Curve (SWCC) and the corresponding relative hydraulic conductivity ($k_r$) as functions of the matric suction ($\psi$), establishing the baseline parameters utilized in the numerical flow simulations.

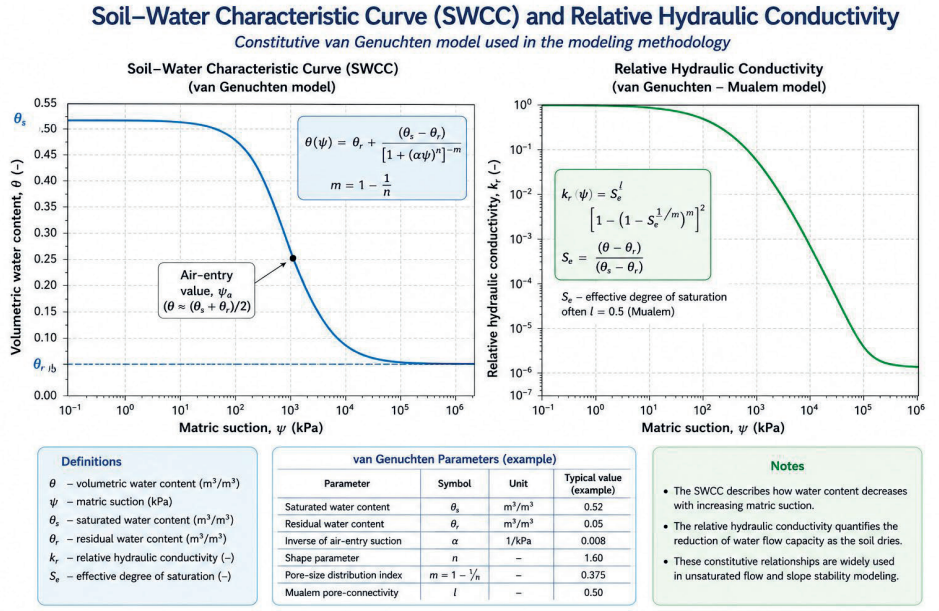



Figure 1. Soil-Water Characteristic Curve (SWCC) and Relative Hydraulic Conductivity (image created by authors with AI assistance)

The mechanical coupling and subsequent slope stability analysis were achieved by mapping the pore-water pressure fields generated from the transient hydraulic solver directly into a 2D slope stability engine at discrete temporal increments. The degradation of the soil's shear strength parameters during the progressive advance of the infiltration front was evaluated using an extended Mohr-Coulomb failure criterion for unsaturated soils. This constitutive framework treats matric suction as an independent stress state variable, where a decrease in suction directly reduces the apparent cohesion component of the soil skeleton without modifying the effective internal friction angle. The global factor of safety against slope failure was calculated continuously across the rainfall timeline using the Spencer limit equilibrium method, which satisfies both force and moment equilibrium along non-circular slip surfaces. This integrated hydro-mechanical workflow successfully quantifies the progressive reduction of embankment stability as the wetting front advances, providing a predictive platform to evaluate structural safety margins under extreme environmental stress (Loku-Pathirage et al., 2025).

## RESULTS AND DISCUSSIONS

The computational execution of the transient hydro-mechanical simulation provided quantitative insights into the temporal and spatial evolution of pore-water pressure fields, matric suction degradation, and overall slope stability margins within the railway embankment during the critical design storm event. Upon the application of the non-steady atmospheric boundary conditions, the

numerical solver tracked the progressive downward migration of a highly defined wetting front through the compacted silty-clay matrix. During the initial hours of the high-intensity precipitation sequence, the infiltration process was restricted to the shallow ballast-subballast interface and the upper crest zones of the embankment slopes, where the initial infiltration rate matched the rainfall intensity due to the high initial suction capacity of the unsaturated soil skeleton. This early phase was characterized by a rapid reduction in matric suction near the atmospheric boundary surfaces, causing the negative pore-water pressures to drop from their baseline values toward near-zero thresholds, which signified the localized elimination of capillary tension and the formation of a shallow, perched water table configuration. As the rainfall progressed, the hydraulic conductivity of the upper soil layers scaled upward by several orders of magnitude in accordance with the calibrated van Genuchten constitutive curves, accelerating the vertical and lateral advance of the wetting front into the core of the embankment (Dodaro et al., 2025).

The mechanical feedback loops resulting from this progressive hydraulic saturation generated a severe structural depreciation of the geostructure's engineering safety margins. By mapping the transient pore-water pressure fields into the limit equilibrium solver at discrete temporal increments, the simulation captured a significant reduction in the apparent cohesion of the soil matrix, driven exclusively by the dissipation of matric suction along the potential non-circular slip surfaces. The spatial analysis of the stress distribution revealed that the critical failure zone shifted from a deep-seated global mechanism under initial steady-state conditions to a series of shallow, slope-parallel failure planes aligned precisely with the maximum depth of the advancing wetting front. The global factor of safety, calculated continuously via the Spencer method, exhibited a non-linear downward trajectory over the rainfall timeline, recording its most abrupt decline during the peak intensity interval of the storm when the rate of suction dissipation reached its maximum.

As demonstrated by the suctions profiles in Figure 2, the advance of the wetting front is strongly dependent on the rainfall duration. At the onset of rainfall (0 h), the initial matric suction remains high near the surface, but a significant non-linear reduction is observed as the infiltration progresses to 6, 12, and 24 hours, with the wetting front penetrating down to 0.7 m after one day. As shown in Figure 3, the slope stability experiences four distinct phases during a hydrometeorological event. Initially, a non-linear decrease of FoS occurs during the rainfall infiltration phase ($t_0$ to $t_1$). Crucially, the minimum FoS is reached after the storm ceases ($t_1$ to $t_2$), during the post-event redistribution phase, where pore water pressures propagate into deeper zones.

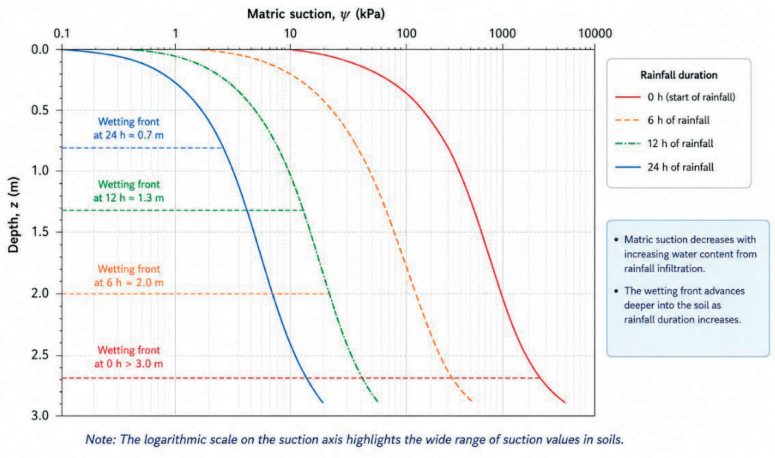



Figure 2. Matric Suction Profile with Depth (Suction Profiles) (image created by authors with AI assistance)

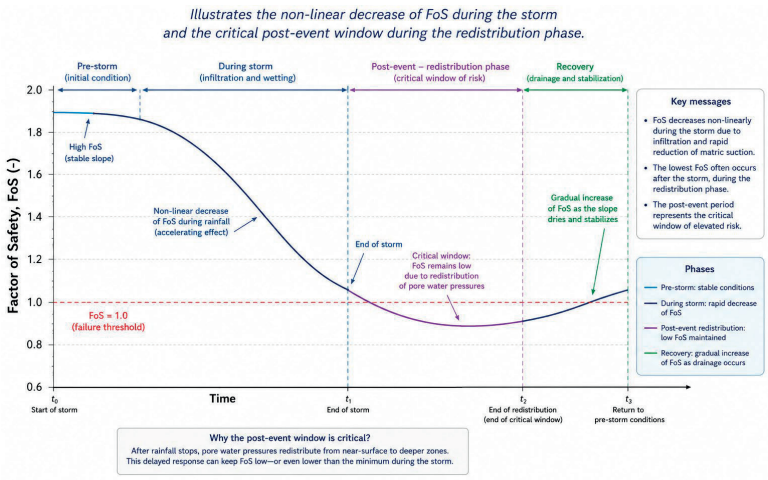



Figure 3. Evolution of the Factor of Safety (FoS) (image created by authors with AI assistance)

This trend demonstrates that embankment stability is not merely a function of cumulative precipitation volume, but is heavily dictated by the transient hydraulic gradients that develop when rainfall intensity outpaces the drainage capacity of the subballast layer, causing water accumulation and sudden shear strength degradation.

Following the termination of the precipitation event, the numerical model tracked the subsequent hydro-mechanical stabilization and drainage phase, highlighting the importance of post-storm monitoring in railway infrastructure management. Although the atmospheric influx ceased, the global factor of safety continued to decline slightly for several hours, a phenomenon caused by the continued internal redistribution and downward gravity-driven migration of the stored water mass toward the deeper, more critical zones of the slope slip surface. This transient delay between the end of the rainfall and the absolute minimum safety margin proves that the critical geotechnical risk window extends into the immediate post-storm period, requiring cautious operational protocols for train speeds during and shortly after extreme weather events. Once the internal drainage and deep seepage processes dominated, driven by the activation of the lower boundary conditions, pore-water pressures began to decline and matric suction registered a gradual, non-linear recovery within the upper slopes, causing the factor of safety to stabilize and enter a long-term upward recovery curve toward its baseline threshold (Aliyu et al., 2024).

## CONCLUSIONS

The comprehensive hydro-mechanical analysis and numerical simulation executed in this research provide a detailed evaluation of transient water infiltration processes and their direct impact on the geotechnical safety margins of unsaturated railway embankments. By coupling the non-linear partial differential Richards equation with the van Genuchten soil-water characteristic framework and Spencer limit equilibrium formulations, this study successfully quantified the time-dependent degradation of structural integrity driven by environmental stressors. The numerical results demonstrate that the progressive advancement of a localized wetting front induces a rapid dissipation of matric suction within the compacted silty-clay matrix, shifting the stress state of the soil skeleton from an unsaturated regime toward a critical condition of localized saturation. From an engineering perspective, this suction dissipation triggers a severe reduction in the soil's apparent cohesion, altering the critical failure mechanism from a stable, deep-seated global configuration to high-risk, shallow, slope-parallel failure planes that develop along the boundary of the maximum infiltration depth. Furthermore, the non-linear downward trajectory of the global factor of safety highlights that geostructural

risk is heavily governed by transient hydraulic gradients and peak precipitation intensity rather than cumulative rain volume alone, which underscores the technical limitations of conventional, simplified hydrological safety thresholds (Liu et al., 2024).

A critical finding of this hydro-mechanical co-simulation is the identification of a distinct post-storm geotechnical risk window, characterized by a continued decline in the global factor of safety even after the cessation of the precipitation event. This phenomenon is driven by the internal hydraulic redistribution and gravity-induced downward migration of the infiltrated water mass toward deeper, more critical slip surfaces, proving that the most vulnerable operational state of a railway embankment extends into the hours immediately following extreme weather. Consequently, this study delivers a validated predictive methodology that infrastructure managers can implement to identify critical saturation boundaries, establish cautious post-storm operational protocols for cyclic rolling stock loads, and design optimized sub-surface drainage arrays. Ultimately, incorporating advanced unsaturated soil mechanics into routine infrastructure assessments provides a scientific pathway to enhance the climate resilience and long-term structural sustainability of transboundary railway networks subjected to severe climate change scenarios.

## REFERENCES

Apshikur, B., Chigambayev, T., Almas, A., Alimkulov, M., Makhanov, B., & Abaikhan, Y. (2026). Hydromechanical behaviour and reinforcement performance of railway embankments under seasonal inundation: A laboratory investigation and numerical modelling. *Geotechnics*, 6(1), 10.

Aliyu, B.U., Xu, L., Bello, A.-A.D., Shuaibu, A., Kalin, R.M., Ahmad, A., Islam, N., & Raza, B. (2024). Prediction of railway embankment slope hydromechanical properties under bidirectional water level fluctuations using ANN and response surface methodology. *Applied Sciences*, 14(8), 3402.

Dodaro, E., Giretti, D., Pirone, M., Ventini, R., Fioravante, V., Gottardi, G., & Mancuso, C. (2025). Insights into the hydromechanical behavior of a river embankment through physical and numerical modeling. *Journal of Geotechnical and Geoenvironmental Engineering*, 151(8), 04025075.

Kong, K., Deng, Z., Chen, F., Wang, Z., & Chen, Y. (2025). Numerical analysis of the effect of vegetation root reinforcement on the rainfall-induced instability of loess slopes. *Scientific Reports*, 15(1), 23233.

Liu, H., El Naggar, M. H., Zhao, M., Huang, D., & Liu, G. (2026). Behavior of coarse-grained soils for railway subgrade layers with different saturation and drainage conditions under cyclic loading. *Soil Dynamics and Earthquake Engineering*, 202, 110036.

Loku-Pathirage, S., Chen, J., & Fu, M. (2025). Predicting railway slope failure under heavy rainfall using the soil moisture extended cohesive damage element method. *GeoHazards*, 6(1), 14.

Xiao, Y., Li, W., Chen, L., Wang, X., Li, Y., Tan, P., & Du, J. (2025). Characterization of unsaturated coarse-grained railway embankment fill: Water retention and dilatancy. *Journal of Rock Mechanics and Geotechnical Engineering*, 17(5), 3125–3145.

Scientific Papers. Series E. Land Reclamation, Earth Observation & Surveying, Environmental Engineering. Vol. XV, 2026
Print ISSN 2285-6064, CD-ROM ISSN 2285-6072, Online ISSN 2393-5138, ISSN-L 2285-6064

# HYDRAULIC MODELING APPLIED TO THE DETERMINATION OF SANITARY PROTECTION ZONES FOR LAKE BUHUI

**Mirela Laura IEREMCIUC, Ioan DAVID, Robert Florin BEILICCI, Erika Beata Maria BEILICCI**

Politehnica University of Timisoara, 1A Splaiul Spiru Haret, Timisoara, Romania

Corresponding author email: robert.beilicci@upt.ro

***Abstract***

*In order to assess the impact of deforestation on the water quality of Lake Buhui, runoff modeling was conducted for the slopes of the lake's tributary catchments, with particular emphasis on the spatial configuration and morphological characteristics of the small hydrographic basins. Lake Buhui, the first artificial lake in Romania, has a storage capacity of approximately 610,000 m³ and is situated at an elevation of 640 m. Lake is additionally supplied by groundwater sources originating from crystalline schists and limestone formations, as well as by four karst springs located in the western sector of the lake, below the mean water level. Runoff generation from the slopes within the studied catchments was simulated using the rainfall–runoff (RR) module of the MIKE 11 modeling system, under the assumption of a representative annual rainfall regime. The simulation results obtained for all tributaries of Lake Buhui are presented in the form of hydrographs corresponding to forested slopes and degraded pasture areas. Furthermore, the results allow for the delineation of the lake's protection zone.*

***Key words****: hydraulic modeling, protection zone, deforestation.*

## INTRODUCTION

The management of surface water resources in specific geomorphological settings, particularly karst landscapes, requires a rigorous understanding of both technical storage capacities and localized hydrographic behavior. On a historical and structural scale, the engineering of artificial reservoirs represents a foundational milestone in regional development. A primary example of this paradigm within the Central and Eastern European territory is the Buhui Reservoir. Situated on a limestone substratum at an altitude of 640 meters above sea level (a.s.l.), it holds historical and technical significance as the first artificial lake constructed in Romania. Engineered and executed between the years 1905 and 1908, the primary objective of this hydrotechnical structure was to secure the continuous public water supply for the mining town of Anina. Geometrically and morphologically, the reservoir extends across a surface area of approximately 11 hectares, bounded by mixed forests of silver fir (*Abies alba*) and European beech (*Fagus sylvatica*). The basin displays a mean longitudinal length of 1.1 km, a transverse width of 0.7 km, and an average operational depth of 8 meters, retaining a total base water volume of approximately 610,000 m³. While the Buhui Reservoir acts as the primary and critical infrastructure backing the municipal drinking water network, the systemic grid relies on a multi-source layout. This network integrates six supplementary sub-surface and karstic spring catchments, namely Colonovățul Mare, Colonovățul Mic, Valea Terezei, Kraksenthal, Grota Morii, and Jitin. Under hydrological drought regimes, the minimal recorded discharge drops to 20 l/s, whereas peak operational flow reaches up to 60 l/s. From a functional standpoint, the infrastructure is entirely decoupled from hydroelectric power generation, serving exclusively as a supply, ecological, and flood-mitigation system. Flood risk management is achieved dynamically via flood-wave attenuation within the storage basin, leveraging a dedicated attenuation volume of 198,706 m³ located between the spillway crest elevation and the maximum water retention level (MWRL). Hydrological calculations indicate that during a high-return period flash flood event with a 1% probability of exceedance (a 100-year flood), the peak upstream inflow reaches 41.3 $m^3/s$. Through basin retention over

the spillway crest, the downstream outflow is mitigated and downscaled to 26 $m^3/s$. This specific flood control framework is designed to protect localized riparian targets, preventing the flooding of the adjacent forest road leading to the Buhui Grotto. To ensure downstream ecological continuity and sustain lower catchments prior to the primary water intake, the dam maintains a continuous mandatory ecological flow calibrated at 150 l/s.

From a technical perspective, the structural behavior of the system is governed by a rigorous set of natural, constructive, and operational elevation parameters: Thalweg: 636.50 m, Bottom Outlet: 637.00 m, Intake: 639.00 m, Minimum Operational: 644.00 m, Spillway Crest/NWRL: 650.00 m, MWRL: 651.80 m (BWBA, 2008).

This research paper provides a modern evaluation of the Buhui Hydrotechnical Node, examining its structural composition, its complex karstic hydrographic basin (including its 3,200-meter underground course through the Buhui Cave), and its long-term operational resilience. By analyzing the interplay between the historical earth-core masonry dam and contemporary water management needs, this study delivers an optimization framework for historic infrastructure operating within vulnerable karstic hydrogeological ecosystems.

## MATERIALS AND METHODS

Our capacity to execute numeric modelling of natural systems has progressed exponentially over the past two decades. Within the last decade, high-performance computing power has scaled to the threshold where desktop supercomputers are a reality, allowing for the inclusion of highly sophisticated parameters and processes within numeric models. The computational tools currently available for data analysis, spatial visualization, and rendering are beyond the imagination of previous generations of engineers. However, as predictive modelling capabilities have expanded, a concurrent reduction in field data collection has occurred, particularly concerning foundational hydrological gauging networks. While modern researchers undoubtedly enjoy access to massive, high-technology spatial datasets - such as multi-spectral satellite remote sensing data - the collection and maintenance of basic, traditional, ground-based historical datasets have severely deteriorated.

A precise quantification of water runoff pathways is essential for resolving practical engineering challenges and ensuring the rational, sustainable utilization of water resources. This principle is a core requirement within complex watershed planning strategies and integrated water resource management (IWRM) frameworks across varying temporal scales. In this context, datasets derived from direct, long-term hydrometric observations remain irreplaceable, as they allow for the empirical definition of characteristic water runoff parameters. Naturally, the water runoff regime displays high spatial and temporal variability across seasonal boundaries and consecutive water years. This variance scales proportionally when comparing catchments with divergent physico-geographical and morphological characteristics. Conversely, within catchments characterized by homogenous physico-geographical conditions, the variations are driven primarily by micro-climatic factors, mean basin altitude, and the forestation density of the drainage basin. Appreciable differences in volumetric discharge can be recorded between hydrometric gauging stations that monitor watersheds situated in entirely different physico-geographical regions. However, when these volumetric values are normalized against catchment surface areas with similar physical and geographic baselines, the resulting variance in specific water runoff indices is minimized.

The formulation of Source Water Protection Plans via integrated catchment-level management and localized resource planning within water intake zones represents a baseline best practice established by the European Union. This policy recognizes that anthropogenic activities inside sanitary protection perimeters can induce severe, long-term negative impacts on public health and downstream municipal consumers (Chapra, 2008).

Within the Romanian legislative framework, sanitary and hydrogeological protection zones are strictly regulated under Government Decision No. 930/2005, which approves the special norms regarding the character and

dimension of sanitary and hydrogeological protection zones for water sources. This legal framework establishes three hierarchical protection tiers:
Zone I: Sanitary Protection Zone with Severe Regime;
Zone II: Sanitary Protection Zone with Restriction Regime;
Zone III: Hydrogeological Protection Perimeter.
For surface water intakes established within natural or artificial lakes (reservoirs), Zone I (Severe Regime) mandates the following minimum strict physical dimensions:
Radial Water Incline: A minimum radial boundary of 100 meters on the water surface, measured outwardly from the exact coordinate of the water intake structure.
Riparian Bank Margin: A minimum radial boundary of 25 meters on the physical shoreline where the active intake infrastructure is anchored.
Lacustrine and Shoreline Perimeter: The entire surface area of the lake matrix must be protected, complemented by a continuous, compulsory 5-meter-wide buffer strip along the entirety of the bounding shoreline.
The integrated hydrological and hydrodynamic modeling framework within the MIKE 11 (DHI) software suite relies on the dynamic, bi-directional coupling between the rainfall-runoff component (MIKE 11 RR), driven by the NAM (Nedbør-Afstrømnings-Model) conceptual core, and the non-steady open-channel routing engine (MIKE 11 HD). Conceptually, this co-simulation architecture transforms discrete meteorological input series, such as continuous temporal arrays of precipitation and potential evapotranspiration stored within .dfs0 time-series files, into physically routed volumetric discharge vectors within the river network. This cross-domain data synchronization is managed by the centralized simulation editor (.sim11), which dynamically couples the spatial river network topology (.nwk11) with the physical catchment parameters parameterized inside the hydrological project file (.rr11), including basin surface areas, initial soil moisture thresholds, and infiltration capacities. Mathematically, the link between the two computational modules is established by injecting the simulated catchment runoff directly into the non-linear Saint-Venant equation of continuity, which governs the conservation of fluid mass in a one-dimensional system. This hydrologic feed is introduced as a dynamic lateral boundary inflow term that is continuously updated at each temporal integration step Delta t by the coupled NAM engine, which mathematically partitions the effective rainfall into three interconnected sub-surface and surface water transport pathways: rapid overland flow traveling across slopes to generate flash-flood hydrograph peaks, interflow moving through unsaturated upper soil layers with a medium structural velocity, and baseflow or saturated groundwater drainage that sustains the baseline ecological and operational drafts of the watercourse during drought periods. In terms of spatial allocation, the engine allows this generated runoff volume to be routed either as a point-source inflow discharged into a single georeferenced junction node simulating a distinct secondary tributary, or as a distributed inflow spread uniformly across a specified longitudinal span of a river branch or reservoir shoreline, where the routing engine divides the cumulative catchment discharge by the length of the targeted reach segment to obtain a continuous lateral flow per linear meter.
A major technical advantage of this integrated software architecture is its ability to perform differentiated temporal harmonization of the computational grid during predictive simulations. While the rainfall-runoff engine processes long-term historical meteorological series using a large, computationally inexpensive time step, the onset of an extreme, high-intensity precipitation event automatically triggers the hydrodynamic core to adjust its runtime temporal resolution via an adaptive time-step configuration. This automatic reduction of the computational interval to seconds or fractions of a second ensures strict compliance with the Courant-Friedrichs-Lewy numerical stability criterion during periods of rapid hydraulic acceleration - such as gravity discharging over frontal spillways or pressurized routing through enclosed subterranean karst conduits - thereby preventing matrix divergence and mass balance errors without inflating the computational cost of the long-term hydrologic background simulation (DHI, 2017).

## RESULTS AND DISCUSSIONS

Lake Buhui is the first artificial lake realised in Romania, retaining a total water volume of approximately 610,000 m³ (Figure 1). Situated at an elevation of 640 m above sea level (a.s.l.), the reservoir spans a surface area of about 11 hectares, with an average longitudinal length of 1.1 km, a transverse width of 0.7 km, and a mean operational depth of 8 m.

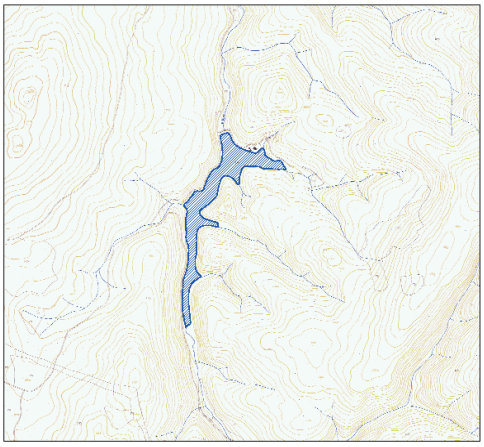


Figure 1. Lake Buhui plan layout

The primary hydrologic inflows sustaining the Buhui Reservoir comprise the following components:

The Buhui Brook: This main watercourse discharges into the Buhui impoundment at a specific location known as "Clocitoare". Originating from a source on the right flank of Lake Buhui, it flows along a surface reach length of approximately 700 m before its confluence with the reservoir.

Secondary Tributaries: In addition to the main brook, five low-discharge streams drain into the perimeter of the lake boundary. Three of these streams are located near the mouth where the Buhui brook enters the reservoir, while the remaining two drain the left flank of the lake, running adjacent to the local forestry road. During summer low-flow periods, several of these minor streams undergo complete drying or exhibit minimal seasonal discharge.

Sub-surface Catchment Inflows: The reservoir is further recharged by subterranean springs originating from crystalline schists and limestone formations. This includes four specific sub-aquatic karst springs located on the western flank of Lake Buhui below the active water surface level.

To execute the numerical hydrological simulations across the catchment, the following boundary conditions and physical boundary parameters were implemented into the computational domain:

Precipitation Distribution: A uniform and constant rainfall intensity was assigned across the entire geographic surface area of the hillslope matrix (Pronk et al., 2006). The monthly rainfall distribution over a one-year period is shown in Figure 2.

Pedological Homogeneity: A single, uniform soil class was mapped across the entire hillslope gradient - specifically categorized as a typical Hapludalfs (comprising multiple sub-types). This soil profile is defined by a medium-to-heavy texture with low permeability, placing it within Hydrologic Soil Group C under standard classification frameworks (Gomi et al., 2002).

Land Use Conditions: Vegetative cover was assumed to be uniform across the hillslope surface area, evaluated under two distinct land-cover scenarios: dense forestry cover versus a post-deforestation state characterized by degraded pastures.

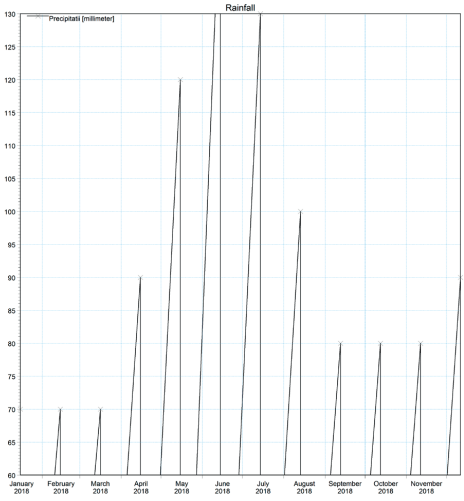



Figure 2. Rainfall one year - 1100 mm

Baseflow Configuration: The continuous background baseline flow was parameterized in accordance with the field-surveyed discharge

data of the sub-surface and karstic tributaries.

Initial Interception Storage: The baseline initial interception and depression storage capacity was set at 20 mm for the forested land-use scenario and downscaled to 1 mm to simulate the low retention capacity of the degraded pastures.

The numerical simulation of hillslope runoff generation across the targeted watersheds was performed using the integrated MIKE 11. The Rainfall-Runoff (RR) module was executed under a non-steady framework based on the regional pluviometric data recorded over a continuous one-year hydrological simulation window.

The simulation results obtained using the MIKE 11 RR module for all the tributaries of Lake Buhui are presented in Figures 3, 4, and 5 through overlaid graphs comparing forested hillslopes and degraded pastures.

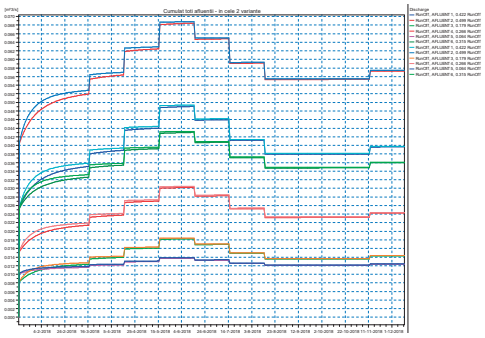


Figure 3. The simulation results

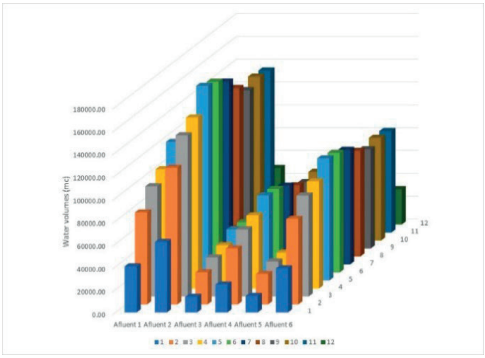



Figure 4. Water volumes - forested hillslopes

To mitigate the risks of accelerated erosion and potential contaminant transport identified in the runoff simulations, a strict spatial delineation of the catchment area is required. Based on these hydrological risks and local karst vulnerability, the critical boundaries around the reservoir perimeter have been mapped (Figure 6).

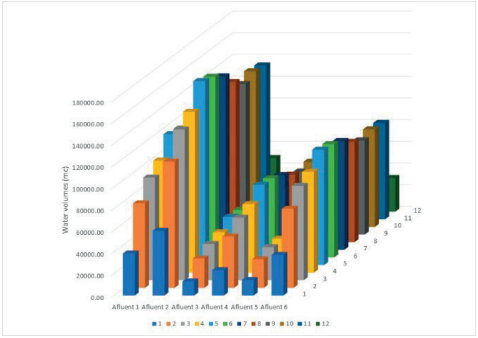



Figure 5. Water volumes - degraded pastures

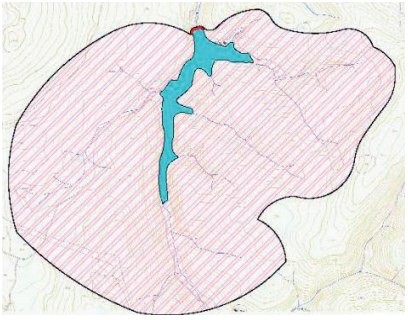


Figure 6. Sanitary and hydrogeological protection zones

The comparative analysis of the simulation scenarios highlights the critical role of vegetative cover in regulating the catchment's water balance. On the forested hillslopes (Figure 4), the high initial interception capacity significantly attenuates peak discharge, ensuring a sustained, gradual baseflow to the reservoir. Conversely, the simulation for the degraded pastures (Figure 5) indicates a rapid hydrological response characterized by accelerated surface runoff and elevated peak volumes, driven by the low retention capacity of the altered terrain. Furthermore, the restrictions implemented within the sanitary and hydrogeological protection zones outlined in Figure 6 are essential to safeguard the subterranean karst springs and surface inflows against anthropogenic degradation, ensuring the long-term ecological stability of the Buhui catchment.

## CONCLUSIONS

The Water Framework Directive (Directive 2000/60/EC-WFD) establishes the foundational European paradigm for water policy, mandating the long-term sustainable management of aquatic ecosystems alongside human and economic water security. While the baseline chemical and ecological status of the raw water matrix within the Buhui Reservoir is categorized as "good" under WFD criteria, this investigation targeted a critical anthropogenic stressor: the qualitative degradation of the lacustrine ecosystem induced by intensive, unregulated forestry exploitation within the catchment area. To evaluate this phenomenon, spatial and temporal field campaigns were executed across varying seasonal and hydro-meteorological regimes to analyze the dynamics of turbidity and Biochemical Oxygen Demand (BOD5) at two strategic monitoring boundaries: the primary upstream reservoir inflow zone of the Buhui Brook and the downstream spillway structure (Directive 2000/60/EC, 2000).

The empirical data collected during the monitoring campaigns reveal a direct causal link between localized deforestation and the disruption of baseline hydrochemical and sediment fluxes:

Sediment Transport and Turbidity Level: A statistically significant increase in turbidity values was recorded at the downstream spillway zone relative to the upstream catchment inflow. This spatial gradient serves as a direct indicator of accelerated mechanical weathering and pluvial soil erosion across the deforested hillslopes. The removal of the root matrix and the canopy layer reduce the initial interception capacity (from 20 mm to 1 mm), leading to enhanced rain-splash erosion and the subsequent gravity-driven transport of fine-grained terrigenous sediments into the lacustrine body.

Organic Loading and BOD5 Kinetics: Conversely, the spatial distribution of BOD5 exhibited a downward trend, with lower concentrations recorded at the spillway zone compared to the primary upstream inflow.

Under the framework of the Water and Wastewater Master Plan for Caraș-Severin County, the Buhui Reservoir is designated as the sole, non-redundant drinking water source for the combined Anina and Steierdorf urban agglomerations, serving a population equivalent exceeding 10,000 PE. Given this high operational dependency, the formulation of an empirical Source Water Protection Plan for the Buhui catchment is a critical public health requirement. Implementing a formalized protection strategy provides the necessary engineering and administrative safeguards to preserve compliant raw water quality parameters, shield the intake infrastructure 639.00 m from shock-loading events, and mitigate medium- to long-term environmental risks to human health.

A critical policy misalignment exists between the empirical findings of this study and current statutory frameworks. The specific regulations governing sanitary and hydrogeological protection zones in Romania, established by Government Decision No. 930/2005 (HG 930/2005), enforce strict physical perimeters for Zone I Severe Regimes (e.g., a 100-meter radial water boundary from the intake). However, this legal framework fails to incorporate restrictive clauses or thresholds regarding commercial forestry operations within the wider hydrogeological boundaries (Government, 2005).

Because this research identifies intensive logging as a severe driver of watershed degradation, relying solely on standard sanitary buffers is insufficient to protect vulnerable karstic aquifers. Therefore, a specialized strategic forestry management plan must be developed for the Lake Buhui perimeter to limit timber harvesting within the catchment. To ensure the sustainability of this resource for future generations, immediate logging bans should be implemented within the catchment, alongside proactive preventative measures to protect this high-quality reservoir.

## ACKNOWLEDGEMENTS

Thanks to the project: “Development of knowledge centers for lifelong learning through the involvement of specialists and decision-makers in flood risk management, this activity can be possible using advanced hydroinformatics tools, AGREEMENT NO. LLP-LdV-ToI-2011-RO-002/2011- 1-RO1-

LEO05-5329, which has been funded with the support of the European Commission.

## REFERENCES

Banat Water Basin Administration (BWBA) (2015). Water and Wastewater Master Plan for Caraș-Severin County: Development strategy for catchment sources in Anina and Steierdorf agglomerations, Banat Water Basin Administration, Timișoara, Romania, *Tech. Rep*. MP-CS-2015.

Chapra S. C. (2008). Surface water-quality modeling. Long Grove, IL, USA: Waveland Press.

DHI, MIKE 11: 1D Surface water hydrodynamic and rainfall-runoff modeling user guide, Danish Hydraulic Institute, Hørsholm, Denmark, 2017.

Directive 2000/60/EC of the European Parliament and of the Council of 23 October 2000 establishing a framework for Community action in the field of water policy, European Parliament and Council, *Official Journal of the European Communities*, L327, 2000.

Gomi, T., Sidle, R. C., & Richardson, J. S. (2002). Understanding Processes and Downstream Linkages of Headwater Systems: Headwaters differ from downstream reaches by their close coupling to hillslope processes, more temporal and spatial variation, and their need for different means of protection from land use, *BioScience*, 52(10), 905–916, https://doi.org/10.1641/0006-3568(2002)052[0905:UPADLO]2.0.CO;2

Government of Romania (2005). Government Decision No. 930 of August 11, 2005 on the approval of Special Norms regarding the character and size of sanitary and hydrogeological protection zones, *Official Gazette of Romania*, Part I, No. 749.

Pronk, M., Goldscheider, N., & Zopfi J. (2006). Dynamics and interaction of organic carbon, turbidity and bacteria in a karst aquifer system, *Hydrogeol J* 14, 473–484 (2006). https://doi.org/10.1007/s10040-005-0454-5

Scientific Papers. Series E. Land Reclamation, Earth Observation & Surveying, Environmental Engineering. Vol. XV, 2026
Print ISSN 2285-6064, CD-ROM ISSN 2285-6072, Online ISSN 2393-5138, ISSN-L 2285-6064

# RISK ASSESSMENT OF THE USE OF *RUTILUS RUTILUS* FOR FOOD FROM TWO ANTHROPOGENICALLY INFLUENCED DAMS

**Nikolina ILIEVA[1], Viliana PASKALEVA[2], Diana KIRIN[1,*2], Radoslava ZAHARIEVA[2], Petya ZAHARIEVA[2], Georgi PATRONOV[3], Doychin TERZIYSKI[4]**

[1]Agricultural University-Plovdiv, Department of Chemistry, Phytopharmacy and Ecology, and Environmental Protection, 12 Mendeleev Blvd, 4000, Plovdiv, Bulgaria
[2]Bulgarian Academy of Sciences, National Institute of Geophysics, Geodesy and Geography (NIGGG), Hydrology and Water Management Research Center, Acad. G. Bonchev Street, 1113 Sofia, Bulgaria
[3]University of Plovdiv 'Paissii Hilendarski', Department of Chemical Technology, 24 Tsar Assen, 4000, Plovdiv, Bulgaria
[4]Agricultural Academy, Sofia, Institute of Fisheries and Aquaculture, Plovdiv, Bulgaria

Corresponding author email: dianaatanasovakirin@gmail.com

***Abstract***

*The aim of the study is to assess the levels of Cd and Pb contamination in muscle, skin, and liver samples, to assess the potential ecological risk to ecosystems and the health risk associated with using Roach for human food. The studies were performed using Inductively coupled plasma mass spectrometry. The results indicate higher levels of both elements in the tissues and organs of fish from the Topolnitsa dam. In both ecosystems, the highest values of Pb and Cd were observed in sediment samples, and the lowest in water samples. The RI (potential ecological risk) for all indicators shows a low potential ecological risk for Pb and Cd in the Dushantsi dam ecosystem, and a significant potential ecological risk for Cd in the Topolnitsa dam ecosystem. When consuming R. rutilus from both reservoirs, the fish should be thoroughly cleaned of the entrails and skin. No risk to human health is expected when consuming up to 420 g per week of fish muscle from the two dams.*

***Key words*:** *cadmium, degree of contamination, health risk assessment, lead, potential ecological risk.*

## INTRODUCTION

Dushantsi Dam and Topolnitsa Dam for heavily modified water bodies of the Maritsa River Basin, East Aegean Region, Bulgaria. Dushantsi Dam is of type L13: Medium and small semi-mountainous dams in Ecoregion 7: Eastern Balkans, water body code BG3MA800L180. It is located in the upper reaches of the Topolnitsa River, 2 km from the village of Dushantsi, Sredna Gora. It is a large hydrotechnical facility, determined to be in poor ecological condition, likely related to the region's highly developed industry (River Basin Management Plans (East Aegean Region) 2021-2027). The waters of the dam are mainly used for industrial water supply, fishing, and water sports. No similar studies have been carried out for the freshwater ecosystem of Dushantsi Dam to date. Topolnitsa Dam is located below Dushantsi Dam, towards the middle reaches of the river. It belongs to type L11b: Large deep dams in Ecoregion 7: Eastern Balkans, code of water body BG0001389. The waters of the dam are used for electricity generation, irrigation of large areas of agricultural land, flood control, sport and industrial fishing, tourism, etc. The dam ecosystem is influenced by long-term industrial activities related to mining and mining processing. Fish are one of the main foods for humans. They are sources of high-quality proteins, polyunsaturated fatty acids, vitamins and other essential elements (Stancheva et al., 2012). Heavy metal pollution poses a significant threat to aquatic ecosystems and their biota, especially fish. Fish are sensitive to changes in pollutant concentrations in aquatic environments (Peycheva et al., 2014; Georgieva et al., 2015; Peycheva et al., 2022). They occupy different trophic levels in food chains, but also have a relatively long lifespan, allowing them to accumulate several pollutants in their bodies, including heavy metals, which is why they are sensitive bioindicators of pollution of the aquatic environment (Rashed, 2001; Bervoets &

Blust, 2003; Saeed & Shaker, 2008; Peycheva et al., 2014). The Topolnitsa Dam has been the subject of research by various authors on heavy metal content in fish (Yancheva et al., 2011; Georgieva et al., 2015), but not on *Rutilus rutilus*. The Roach has been studied for heavy metals in other dams (Zhelyazkov et al., 2014), but studies from Bulgarian dams are few. The aim of the study is to assess the degree of anthropogenic loads, the potential ecological risk to ecosystems, and the risk of using the Roach for food based on the levels of Pb and Cd contamination.

## MATERIALS AND METHODS

The objects of the study are thirty specimens of Roach *Rutilus rutilus* (Linnaeus, 1758), each from two freshwater ecosystems: Dushantsi and Topolnitsa dams. The fish were collected with multi-mesh gillnets (BSS EN 14757:2015) and personal permissions from the Executive Agency for Fisheries and Aquaculture, Ministry of Agriculture and Food, Bulgaria. The FishBase database is used to check the scientific and common names of fish (Froese & Pauly, 2020). The fish were collected from the Dushantsi Dam, named as Dushantsi Biotope (42041'49.51''N 24017'27.80''E; 792 m) and from the Topolnitsa Dam, named as Poibrene Biotope (42027'38.88''N 23059'20.81''E; 309 m; Figure 1).

For the ichthyological sample, the following parameters are determined: total number of specimens, total body length (TL, cm), total body width (TH, cm), total body weight (TW, g), biomass in percent (W%), abundance (A%), absolute dominance ($\mathbf{D} = \frac{(A\% + W\%)}{2}$) (Belkinova et al., 2013) and Fulton's condition factor ($\mathbf{K} = \mathbf{100}.\frac{TW}{TL^3}$) (Stavrescu-Bedivan et al., 2023; Zaharieva et al., 2024).

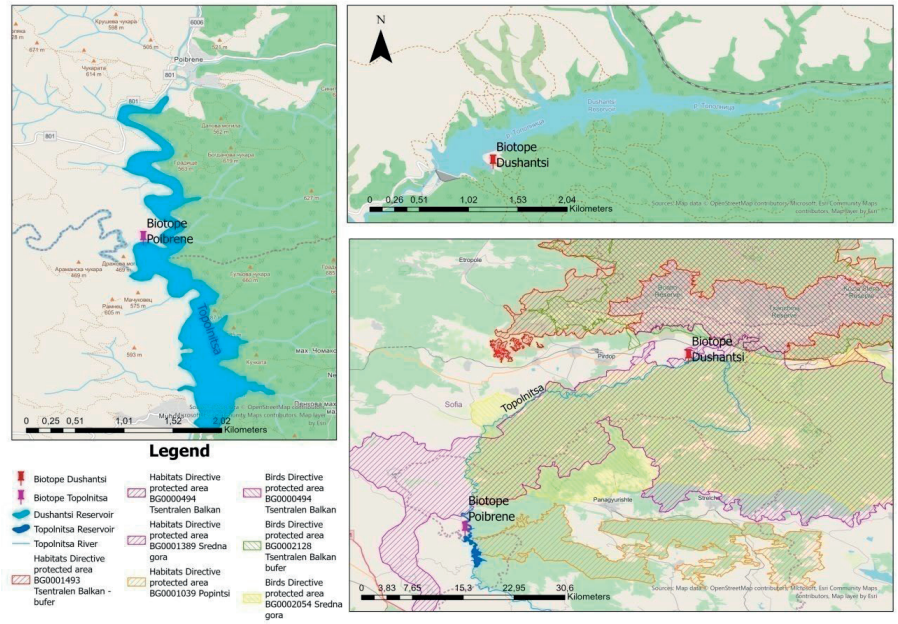



Figure 1. Studied biotopes from the Dushantsi and Topolnitsa dams (Esri Inc. (2023). ArcGIS Pro (Version 3.2.0) https://www.arcgis.com/home/index.html

The requirements of BSS ISO 5667-4:2026 and BSS ISO 5667-12:2017 standards have been used to collect water and sediment samples. BSS EN ISO 5667-3:2024 and BSS EN ISO 5667-15:2009 standards have been applied for the preservation and storage of water and sediment samples, respectively. The standards BSS EN ISO 17294-2:2023 and BSS EN ISO 21424:2020 Milk, milk products, infant formula and adult nutritionals - Determination of minerals and trace elements - Inductively coupled plasma mass spectrometry (ICP-MS)

method (ISO 21424:2018) were used to determine the content of Cd and Pb in samples of water, liver, muscles and skin of the Roach from the two dams, and US EPA Method 3051A for sediment samples. PerkinElmer SCIEX ELAN DRC-e ICP-MS system (MDS Inc., Concord, ON, Canada, Inductively coupled plasma mass spectrometry, Table 1) was used to conduct the elemental analysis.

Table 1. Instrumental parameters and monitored isotopes used for ICP-MS analysis

| Parameter | Value |
|---|---|
| Ar plasma flow rate | 15 L $min^{-1}$ |
| Auxiliary Ar flow rate | 1.20 L $min^{-1}$ |
| Nebulizer gas flow rate | 0.90 L $min^{-1}$ |
| Lens voltage | 6.00 V |
| ICP RF power | 1100 W |
| Integration time | 2000 ms |
| Dwell time | 50 ms |
| Measurement mode | Peak hopping |
| Sample uptake rate | 2 mL $min^{-1}$ |
| Rinse time between samples | 180 s |
| Rinse solution | 3% $HNO_3$ |
| Monitored isotopes | $^{27}Al$, $^{54}Fe$, $^{56}Fe$, $^{57}Fe$, $^{55}Mn$, $^{75}As$, $^{112}Cd$, $^{114}Cd$, $^{52}Cr$, $^{63}Cu$, $^{65}Cu$, $^{202}Hg$, $^{60}Ni$, $^{62}Ni$, $^{207}Pb$, $^{208}Pb$, $^{77}Se$, $^{78}Se$, $^{80}Se$, $^{82}Se$, $^{66}Zn$ |

$HNO_3$ (67-69%, Fisher Chemicals, Ultra Trace Metal Grade, Loughborough, UK), HCl (37%, Fisher Chemicals, Ultra Trace Metal Grade, Loughborough, UK) and $H_2O_2$ (30%, Fisher Chemicals, Ultra Trace Analysis Grade, Loughborough, UK) were used for sample preparation and analysis. All solutions were prepared with double-deionised water. Working standard solutions were prepared by diluting the ICP-MS multi-element calibration standard solution IMS-102 (Ultra Scientific, Agilent, Santa Clara, CA, USA), which contains, among others, Cd and Pb with an initial concentration of 10 mg/L. After collection, water samples were stored at 4°C in dark glass bottles before transport to the laboratory. For ICP-MS analysis, 50 mL of each water sample was filtered through a 25 mm sterile PES syringe filter with a 0.45 µm pore size. The filtrates were acidified with 0.05 mL concentrated nitric acid to pH 2 and subsequently analysed. Biological samples were digested with concentrated $HNO_3$ and then diluted before analysis. A total of 10 tissue, organ, water and sediment samples were examined for each of the two dams, collected during the three seasons (spring, summer, and autumn) in 2025. Skin, muscle and liver samples were weighed twice, once as wet weight and once as dry weight. The degree of accumulation of lead and cadmium in the studied tissues and organs of *R. rutilus* relative to their content in water and sediment samples was estimated using the Bioconcentration factor (BCF): $\mathrm{BCF} = \frac{C}{Cw}$ and $\mathrm{BCF} = \frac{C}{Cs}$, where C is the concentration of the metal in the muscles, skin or liver of the Roach in µg/kg, respectively; $C_w$ is the concentration of the metal in the water samples (µg/L), and $C_s$ is their concentration in the sediments (µg/kg). The calculations are for each organ or tissue and for each metal separately. BCF is an important indicator for assessing ecological risk. The relationship between the concentrations of Pb and Cd in samples of water and sediments and samples of Liver, Muscle, and Skin was presented through Spearman's rank correlation coefficient ($r_s$). The ecological risk ($\mathrm{RI} = \sum E r^i = \sum \mathrm{Tr}^i . \mathrm{Cf}^i$) is defined as the sum of the products of the toxic response factor (specific for each element) and the contamination factor for each of the trace elements. The contamination factor ($\mathrm{Cf}^i$) is defined as the ratio of the actual to the reference concentration of each trace element. The sum of all contamination factor values indicates the contamination level (Cl) (Hakanson, 1980; Tang et al., 2023; Younis et al., 2024). The USEPA (1989) methodology was used to assess the health risk of consuming roach from both dams. A Target Hazard Quotient (THQ) (THQ) was calculated using the formula: $THQ = \frac{(EFr.ED.FIR.C)}{(BWa.AT.RfD)} . 10^{-3}$, where EFr is the frequency of exposure, ED is the average life expectancy for men and women or the duration of exposure, FIR is the average daily intake of fish consumed, C is the concentration of the elements tested in muscle samples (µg.$g^{-1}$, ww), BWa is the average body weight for women and men, AT is the average time of exposure to non-carcinogens, RfD is the reference oral dose (0.001 for Cd and 0,004 for Pb, according USEPA, 2011). The Hazard index (HI) is calculated using the formula: HI = ∑THQ, calculated for each of the two dams in terms of Pb and Cd content. The results are statistically

processed by MS Excel (Microsoft, 2011) with relevant mathematical formulas.

## RESULTS AND DISCUSSIONS

### Characteristics of the studied fish species

Roach, *Rutilus rutilus* (Linnaeus, 1758) (Cyprinidae) is the dominant species in the collected fish samples from both dams. It is a freshwater, benthopelagic, and brackish fish species. Staple food for the Roach are crustaceans, worms, insect larvae, algae, and higher aquatic vegetation (Karapetkova & Zhivkov, 2006; Kottelat & Freyhof, 2007). *R. rutilus* is included in the International Union for Conservation of Nature Red List as a Least Concern species (LC; IUCN) (Kottelat & Freyhof, 2007). The species is widely distributed in various habitats in the country. *R. rutilus* is an object of sport and industrial fishing. In both dams, the Roach is an eudominant species ($D_{Dushantsi}$=47.85; $D_{Topolnitsa}$=22.65). Fulton's condition factor (K > 1 for both dams) indicates that the fish are fatty, well-nourished, with high fat content and developed gonads. The condition factor suggested a favourable body condition (Table 2).

Table 2. Metric data, dominance and status of *Rutilus rutilus* from Dushantsi and Topolnitsa reservoirs

| Fish species *Rutilus rutilus* (Linnaeus, 1758) | Dushantsi | Topolnitsa |
|---|---|---|
| Total length, TL cm | 9.98±2.53 (7.40-21.00) | 16.34±2.52 (9.1-19.5) |
| Total width, TH см | 2.39±0.77 (1.70-5.70) | 4.44±0.94 (2.20-5.90) |
| Weight, W г; W % | 12.50±20.48 (4.00-117.00) 53.92% | 53.24±23.91 (7.00-98,00); 13.30% |
| Abundance, A % | 47.62 | 32.00 |
| Absolute dominance, D | 47.85 | 22.65 |
| Fulton's condition factor, K | 1.26 | 1.22 |

### Concentration of Lead (Pb) and Cadmium (Cd) in Roach and the Environment

The content of Pb and Cd in samples of Skin, Muscle and Liver of R. rutilus, water and sediments are presented in Table 3. Lead (Pb) and cadmium (Cd) are major toxic metals (Liu et al., 2013). Lead is not a natural element in natural waters. It enters natural water bodies from lead ores and industrial wastes, from mines and smelters used for lead processing, and from all production activities that use lead. Lead is a highly toxic metal. Studies have shown that the accumulation of lead by aquatic organisms increases with increasing pH and decreasing water hardness. Lead is transported through the body's bloodstream and accumulates mainly in soft tissues, the liver, and the kidneys. It is permanently deposited in bones. High concentrations of oil in aquatic ecosystems stimulate biodiversity, stimulate fish development and cause other effects (Yablanski & Petkov, 2011). The degree of toxic effects of lead is influenced by the stage of fish development, pH, temperature, water hardness, the presence of dissolved organic matter and other factors. (Hellawel, 1896; Peycheva et al., 2014). The content of Pb and Cd in water samples was assessed in accordance with the requirements of Regulation H-4/2012 and the Regulation on environmental quality standards for priority substances and certain other pollutants of the national legislation. In Bulgaria and the European Union, standards for heavy metals in sediments have not been established; therefore, those approved by the US Environmental Protection Agency (US EPA) were used (Effect Range-Low - ERL) (O'Connor, 2004; Cholakova, 2021). The content of these two elements in fish skin, muscle and liver samples was assessed according to Regulation (EU) 2023/915, FAO (1983), MAFF (1995). For waters, the maximum permissible concentration is 1.20 µg/L (Regulation on EQS, on priority substances and certain other pollutants). For sediments, ERL for Pb is 46.7, and for Cd – 1.20 mg/kg dry weight. According to national legislation, the maximum permissible content (MPC) of Pb in fish muscles is 0.2 mg/kg (Regulation 31/2004), according to FAO (1983), it is 0.5 mg/kg, and according to Regulation (EU) 2023/915 - 0.30 mg/kg wet weight. According to Regulation 31/2004, the MPC for Cd is 0.05 mg/kg, according FAO and MAFF - 0.5 mg/kg and 0.2 mg/kg respectively, and according to Regulation (EU) 2023/915 – 0.05 mg/kg wet weight. Industrial wastewater has been identified as a major source of Cd pollution (Yablanski & Petkov, 2011).

The highest concentrations of Pb and Cd were found in sediments, and the lowest contamination was in water samples for the two elements and dams. The results for the Roach tissues and organs showed the highest values for the two elements in liver samples, followed by

skin samples. The lowest content of Pb and Cd is in the muscle samples. This trend is established for both elements and for the Roach from both dams, in both fresh- and dry-weight samples. The differences in the two dams are in the concentrations of the two elements and the exceedances compared to the established norms. In the Dushantsi Dam, the exceedances in Pb and Cd concentrations are as follows: 9.2 times for Liver>6.7Skin>5.0Muscle for Pb and 3.9 times for Liver>1.40Skin>1.20Muscle for Cd. For the Topolnitsa Dam, the exceedances are: 28.95 times for Liver>7.60Skin>6.90Muscle for Pb. and 11 times for Liver>10.80Skin>1.80Muscle for Cd.

In the Topolnitsa Dam, the exceedances for Pb compared to those in Dushantsi Dam are 3.15 times higher in Liver samples, 1.13 times higher in Skin samples and 1.38 times higher in Muscle samples.

Regarding the exceedances for Cd, which are also higher in Topolnitsa Dam samples: 2.82 times higher for Liver samples, 7.71 times higher in Skin and 1.50 times higher in Muscle. We assume that the higher concentrations of Pb and Cd in the Topolnitsa reservoir are due to river flows passing through areas with intensive mining and ore processing.

The content of Pb and Cd in the studied muscle samples of fish from the Dushantsi Dam is respectively 3.34 and 1.2 times higher, and for the Topolinitsa Dam, 4.6 and 1.8 times higher, compared to the maximum permissible levels of Pb and Cd in fish set by Regulation (EU) 2023/915.

Table 3. Content of Lead (**Pb**) and Cadmium (**Cd**) in tissues and organs of *R. rutilus,* waters and sediments

| **Samples Dushantsi** | **Min-Max Mean±SD** | **Min-Max Mean±SD** |
|---|---|---|
| **Topolnitsa** | **Mean±SD** | **Mean±SD** |
| **Wet weight** | **Pb** | **Cd** |
| Skin *R. rutilus* | 1.52±0.42 (1.22-1.81) | 0.54±0.25 (0.37-0.77) |
| Muscle *R. rutilus* | 1.38±0.06 (1.33-1.42) | 0.09±0.03 (0.07-0.11) |
| Liver *R. rutilus* | 5.79±2.43 (3.86-7.29) | 0.55±0.17 (0.43-0.67) |
| **Water** | 0.02±0.01 (0.01-0.03) | 0.007±0.002 (0.005-0.009) |
| **Dry weight** | **Pb** | **Cd** |
| Skin *R. rutilus* | 1.96±0.54 (1.58-2.35) | 0.88±0.48 (0.54-1.22) |
| Muscle *R. rutilus* | 1.94±0.09 (1.87-2.00) | 0.12±0.04 (0.09-0.14) |
| Liver *R. rutilus* | 9.20±2.32 (7.56-10.84) | 1.60±0.56 (0.52-2.08) |
| **Sediments** | 28.26±1.35 (27,30-29,21) | 1.39±0.30 (1,17-1,60) |

The bioconcentration factors (BCF) are presented. The highest BCF$_s$ were obtained for Pb and Cd in Liver samples (Table 4).

Table 4. Bioconcentration factor (BCF) and Spearman correlation coefficient ($r_s$) between the content of Pb and Cd in water, sediments and *R. rutilus*

| **Dushantsi** | | | | |
|---|---|---|---|---|
| **Fish – Water** (wet weight) | **Pb BCF** | **Cd BCF** | **rs Pb** | **rs Cd** |
| Skin – Water | 6700.00 | 350.00 | 1**** | 1**** |
| Muscle – Water | 5015.00 | 300.00 | 1**** | 1**** |
| Liver – Water | 9200.00 | 900.00 | 0,999**** | 1**** |
| **Fish – Sediments** (dry weight) | | | | |
| Skin – Sediments | 0.11 | 0.18 | 1**** | -0.82*** |
| Muscle – Sediments | 0.06 | 0.13 | 1**** | 1**** |
| Liver – Sediments | 0.13 | 0.41 | 1**** | 1**** |
| **Topolnitsa** | | | | |
| **Fish – Water** (wet weight) | **Pb BCF** | **Cd BCF** | **rs Pb** | **rs Cd** |
| Skin – Water | 0.07 | 0.75 | 0,999**** | 0,996**** |
| Muscle – Water | 0.06 | 0.13 | 0,997**** | 1**** |
| Liver – Water | 0.26 | 0.77 | 0,997**** | 1**** |
| **Fish – Sediments** (dry weight) | | | | |
| Skin – Sediments | 0.12 | 0.24 | 0,999**** | 0,999**** |
| Muscle – Sediments | 0.03 | 0.03 | 0,999**** | 0,994**** |
| Liver – Sediments | 2.54 | 0.43 | 0,999**** | 0,529$^{ns}$ |

**Legend:** $r_s$ **** - very significant correlation, p≤0,001; *** - strong correlation, p≤0,01; $^{ns}$ – insignificant correlation

Results of the study show that Cd accumulates at higher concentrations in the liver than in fish tissues. Higher Cd content in liver samples of freshwater fish species compared to skin and muscle has been reported in other studies (Georgieva et al., 2015; Peycheva et al., 2022; Ilieva & Kirin, 2025). Dallinger et al. (1987) indicated that this is related to the higher protein content in the liver. In the study, sediments had a higher Cd content than in water samples. Salomons & Stigliani (1995) explained this result by the fact that heavy metals bind to suspended particles or adsorb to organic matter, leading to their precipitation.

The contamination factor is very high (Cf) for Pb in the muscles of the Roach from both dams and moderate for Cd (Table 3). The contamination level (Cl) is 1.50 times higher in the muscles of *R. rutilus* from Topolnitsa dam than in Dushantsi dam. The risk of Pb and Cd loading in the muscles is 1.49 times and 1.5 times, respectively, higher for *R. rutilus* from Topolnitsa dam than for those from Dushantsi dam. The RI (potential ecological risk) for all indicators indicates a low potential ecological risk for Pb and Cd in the Dushantsi dam ecosystem, and a significant potential ecological risk for Cd in the Topolnitsa dam ecosystem (Table 5). When consuming *R. rutilus* from both reservoirs, the fish should be thoroughly cleaned of the entrails and skin.

Table 5. Risk assessment and degree of contaminations

| Factors | Tissues/Sediments | Pb Dushantsi | Cd Dushantsi | Pb Topolnitsa | Cd Topolnitsa |
|---|---|---|---|---|---|
| Cf | Skin | 10.65 very high | 2.20 moderate | 9.80 very high | 17.60 very high |
| | Muscle | 6.50 very high | 1.60 moderate | 9.70 very high | 2.40 moderate |
| | Liver | 12.95 very high | 5.00 considerable | 46.00 very high | 32.00 very high |
| | Sediments | 0.43 low | 0.51 low | 1.62 moderate | 3.12 considerable |
| Cl | Skin | 12.85 moderate | | 41.70 very high | |
| | Muscle | 8.10 moderate | | 12.20 moderate | |
| | Liver | 17.95 considerable | | 63.60 very high | |
| | Sediments | 0.94 low | | 4.74 low | |
| Er | Skin | 53.25 moderate | 66.00 moderate | 49.00 moderate | 528.00 very high |
| | Muscle | 32.50 low | 48.00 moderate | 48.50 moderate | 72.00 moderate |
| | Liver | 64.75 moderate | 150.00 considerable | 230.00 high | 960.00 very high |
| | Sediments | 2.15 low | 15.30 low | 8.10 low | 93.60 considerable |
| RI | Skin | 119.25 low | | 758.00 very high | |
| | Muscle | 80.50 low | | 121.00 low | |
| | Liver | 214.75 moderate | | 1008.50 very high | |
| | Sediments | 17.45 low | | 101.70 low | |

The health risk assessment was made assuming equal intake and adsorbed doses of pollutants, an average fish food intake rate of 60 grams per day (FIR), an assumption of an average body weight (BWa) of 65 kg for women and 85 kg, an average lifetime (ED) of 79 for women and 72 for men, reference oral dose for Pb 0.004 and 0.001 ($mg.kg^{-1}.day^{-1}$) for Cd, the Target Hazard Quotient (THQ) is as follows (Table 6):

Table 6. THQ and HI of Dushntsi (Dishantsi Dam) and Poibrene biotopes (Topolnitsa Dam)

| THQ | Dushnatsi Biotope | | Poibrene Biotope | |
|---|---|---|---|---|
| | Pb | Cu | Pb | Cu |
| Women | 0.230 | 0.055 | 0.318 | 0.083 |
| Men | 0.176 | 0.067 | 0.243 | 0.063 |
| Total | 0.406 | 0.122 | 0.561 | 0.146 |
| HI | 0.528 | | 0.707 | |

The obtained values for the HI are below 1. Therefore, according to USEPA (2011) no risk to human health is expected when consuming up to 420 g per week of fish muscles from the two dams.

## CONCLUSIONS

The studied *R. rutilus* specimens from both dams are healthy. Fulton's condition factor (K) indicates favourable conditions in both habitats. The chemical analyses showed that Pb levels were 3.15 times higher in liver samples, 1.13 times higher in skin samples, and 1.38 times higher in muscle samples in the Topolnitsa dam than in the Dushantsi dam. The excesses for Cd are also higher in the samples from the Topolnitsa dam: 2.82 times higher in liver, 7.71 times higher in skin and 1.50 times higher in muscle. The use of Roach no risk to human health is expected when consuming up to 420 g per week of this species of fish from the two dams.

## ACKNOWLEDGEMENTS

The authors thank the NIGGG, BAS, the AU-Plovdiv and the Scientific Centres for the financial support received under the research project, as well as in connection with the work of PhD students Ilieva and Paskaleva. The authors thank Assoc. Prof. Mihaylova, PhD, for her assistance and consultations on the chemical analyses.

## REFERENCES

Belkinova, D., Gecheva, G., Cheshmedzhiev, S., Dimitrova-Dyulgerova, I., Mladenov, R., Marinov, M., Teneva, I., Stoyanov, P., Ivanov, P., Mihov, S.,

Pehlivanov, L., Varadinova, E., Karagyozova, Ts., Vassilev, M., Apostolu, A., Velkov, B., & Pavlova, M. (2013). *Biological analysis and ecological assessment of surface water types in Bulgaria*. Plovdiv, BG: University "P. Hilendarskii" Publishing House (in Bulgarian).

Bervoets, L., & Blust, R. (2003). Metal concentrations in water, sediments and gudgeon (Gobio gobio) from a pollution gradient: relationship with fish condition factor. *Environ. Pollut*., *126*. 9-19.

BSS EN 14757:2015 Water quality. Sampling of fish with multi-mesh gillnets.

BSS EN ISO 5667-15:2009 Water quality - Sampling - Part 15: Guidance on the preservation and handling of sludge and sediment samples.

BSS ISO 5667-12:2017 Water quality – Sampling - Part 12: Guidance on sampling of bottom sediments from rivers, lakes and estuarine areas.

BSS EN ISO 21424:2020 Milk, milk products, infant formula and adult nutritionals - Determination of minerals and trace elements - Inductively coupled plasma mass spectrometry (ICP-MS) method (ISO 21424:2018).

BSS EN ISO 17294-2:2023 Water quality - Application of inductively coupled plasma mass spectrometry (ICP-MS) - Part 2: Determination of selected elements including uranium isotopes (ISO 17294-2:2023, Corrected version 2024-02).

BSS EN ISO 5667-3:2024 Water quality - Sampling - Part 3: Preservation and handling of water samples.

BSS ISO 5667-4:2026 Water quality — Sampling — Part 4: Guidance on sampling from lakes, natural and man-made.

Cholakova, Z. (2021). Peculiarities of heavy metal content in the bottom sediments of some tributaries of the Iskar River in the Stara Planina Mountain (Iskretska and Batuliyska rivers). *Annual of Sofia University "St. Kliment Ohridski" Faculti de Geologie et Geographie, Geographie*, *2*(113). 140-160.

Commission Regulation (EU) 2023/915 of 25 April 2023 on maximum levels for certain contaminants in food and repealing Regulation (EC) No 1881/2006 Retrived from http://data.europa.eu/eli/reg/2023/915/oj

Dallinger R, Prosi F, Segner H, & Back H. (1787). Contaminated food and uptake of heavy metals by fish: a review and a proposal for further research. *Oecologia*, 73(1). 91-98. doi: 10.1007/BF00376982. PMID: 28311410.

Esri Inc. (2023). ArcGIS Pro (Version 3.2.0). Retrived from https://www.arcgis.com/home/index.html

FAO (Food and Agriculture Organization) (1983). FAO Fishery Circular No. 464, 5-10. Food and Agriculture. The results obtained for toxic and trace elements in analyzed fish. Rome: Organization of the United Nations.

Froese, R. & Pauly, D. (2020) FishBase. http://www.fishbase.org

Georgieva, E., Yancheva, V., Velcheva, I., Becheva, M., & Soyanova, S. (2015). Histological alterations under metal exposure in gills of European perch (*Perca fluviatilis* L.) from Topolnitsa reservoir (Bulgaria). *Arch. Biol. Sci*., *67*(2). 729-737.

Hakanson, L. (1980). An ecological risk index for aquatic pollution control. A sedimentological approach. *Water Res*., *14*(8). 975-1001.

Hellawel, J. H. (1986). Bioindicators of Freshwater Pollution and Environmental Management, 546. London, Great Britain: Elsevier.

Ilieva, I., & Kirin, D. (2025). Metal contamination in the system Water – Sediments - *Perca fluviatilis* Linnaeus, 1758 and *Eustrongylides excisus* Jägerskiöld, 1909 larvae. Scientific Paper *E. Land Reclamation, Earth Observation & Surveying, Environmental Engineering, XIV*. 663-669.

IUCN Red List Status (n.d.). Retrieved from https://www.iucnredlist.org.

Karapetkova, M., & Zhivkov, M. (2006). *Fishes in Bulgaria*. Sofia, BG: GeaLibris (in Bulgarian).

Kottelat, M. & Freyhof, J. (2007) *Handbook of European Freshwater Fishes*. Kottelat, Cornol & Freyhof, Berlin.

Linnaeus, C. (1758). *Systema naturae per regna tria naturae, secundum classes, ordines, genera, species, cum characteribus, differentiis, synonymis, locis.* Editio decima, reformata. Holmiae (Laurentii Salvii).

Liu, J., Goyer, R.A., Waalkes, M.P. (2013). Toxic effects of metals. In Casarett and Doull's *Toxicology: the basic science of poisons*, tth edn. (pp 932-979). New York: McGraw-Hill.

MAFF (1995). Monitoring and surveillance of non-radioactive contaminants in the aquatic environment and activities regulating the disposal of wastes at sea, 1993. *Aquatic Environment Monitoring*. Report No. 44.

Method 3051a. Microwave assisted acid digestion of sediments, sludges, soils, and oils. Retrieved from https://www.epa.gov/sites/default/files/2016-12/documents/3051a.pdf

O'Connor, T.P. (2004). The sediment quality guideline, ERL, is not a chemical concentration at the threshold of sediment toxicity. *Mar Pollut Bull. 49*(5-6). 383-5.

Peycheva, K., Panayotova, V., Makedonski, M., & Stancheva, R. (2014). Toxic and essential concentration of freshwater fishes from Pyasachnik Dam, Bulgaria. *Agricultural Science and Technology*, *6*(3). 364-369.

Peycheva, K., Panayotova, V., Stancheva, R., Makedonski, L., Merdzhanova, A., Parrino, V., Nava, V., Cicero, N., & Fazio, F. (2022). Risk Assessment of Essential and Toxic Elements in Freshwater Fish Species from Lakes near Black Sea, Bulgaria. *Toxics*, *10*. 675.

Rashed, M.N. (2001). Cadmium and lead levels in fish (*Tilapia nilotica*) tissues as biological indicator for lake water pollution. *Environ. Monit. Assess*., *68*. 75-89.

River Basin Management Plans (Eastern Aegean Region) 2021-2027. Retrived from https://earbd.bg/indexdetails.php?menu_id=966

Regulation No. 31 of 29 July 2004 on the Maximum Permitted Quantities of contaminants in food stuffs. *State Gazette*, 88 of 08.10.2004.

Regulation on environmental quality standards for priority substances and certain other pollutants. *State Gazette*, 88 of 09.11.2010.

Saeed, S.M., & Shaker, I.M. (2008). Assessment of Heavy metals pollution in water and sediments and their effect on Oreochromis niloticus in the northern delta lakes, Egypt. *In 8th International symposium on Tilapia in Aquaculture*. 475-490.

Salomons W, & Stigliani W (1995) *Biogeodynamics of Pollutants in Soils and Sediments*. (pp 352). Heidelberg, Germany: Springer Verlag.

Stancheva, M., Galunska, B., Dobrewa, A.D., & Merdzhanova, A. (2012). Retinol, alpha-tocopherol and fatty acid content in Bulgarian Black Sea fish species. *Crasas aceites*, *63*. 152-157.

Statsoft Inc. (2011) (n.d.). Statistica, version 10. Retrieved from www.statsoft.com.

Stavrescu-Bedivan, M. M., Sandu, M., Scăeţeanu, G. V., Vîrsta, A., Majar, R. M., & Baicu, Ş. (2023). Preliminary report on the water quality, ichthyophauna and biometric indices for Prissian carp from Iezerul Mostiştea lake, Romania. *Scientific Paper. Series E. Land Reclamation, Earth Obsrvation & Surveying, Environmental Engineering*, XII. 309-319.

Tang, Z., Liu, X., Niu, X., Yin, H., Liu, M., Zhang, M., Zhang, D., & Guo, H. (2023). Ecological risk assessment of aquatic organisms induced by heavy metals in the estuarine waters of the Pearl River. *Sci Rep*, *13*. 9145.

USEPA (2011). Risk *Assessment Guidance for Superfund*. Volume I: (Part A: Human Health Evaluation Manual; Part E, Supplemental Guidance for Dermal Risk Assessment; Part F, Supplemental Guidance for Inhalation Risk Assessment). Washington, DC: US Environmental Protection Agency.

Yablanski, Z., Perkov, G. (Eds.), 2011. *Manual Book of Applied Ecology*. Stara Zagora, Bulgaria: Alfamarket.

Yancheva, V., Petrova, S., Velcheva, I., & Georgieva, E. (2011). A review of ecological status of Topolnitsa River catchment area and Topolnitsa Dam. *Proceeding of the 50-th Anniversary Conference "Biological Sciences for Better Future"*, University of Plovdiv "Paisii Hilendarski": 267-280 [In Bulgarian].

Younis, A.M., Hanafy, S., Elkady, E.M., Alluhayb, A., & Alminderej, F. (2024). Assessment of health risks associated with heavy metal contamination in selected fish and crustacean species from Temsah Lake, Suez Canal. *Sci Rep*, *14*. 18706.

Zaharieva, P., Zaharieva, R., & Kirin, D. (2024). Species diversity of the Ichthyofauna of the Stryama River. *Problems of Geography*, *1-2*. 119-130.

Zhelyazkov, G.I., Georgiev, D.M., Dospatliev, L.K., & Staykov, Y.S. (2014). Determination of Heavy Metals in Roach (*Rutilus rutilus*) and Bleak (*Alburnus alburnus*) in Zhrebchevo Dam Lake. *Ecologia Balkanica*, *5*. 15-20.

Scientific Papers. Series E. Land Reclamation, Earth Observation & Surveying, Environmental Engineering. Vol. XV, 2026
Print ISSN 2285-6064, CD-ROM ISSN 2285-6072, Online ISSN 2393-5138, ISSN-L 2285-6064

# MONITORING THE ECOLOGICAL STATE AND ANTHROPOGENIC LOADING OF THE LUDA YANA RIVER THROUGH THE USE OF INDICATOR MACROZOOBENTHOS

**Diana KIRIN[1, 2], Radoslava ZAHARIEVA[2], Petya ZAHARIEVA[2]**

[1]Agricultural University - Plovdiv, Department of Chemistry, Phytopharmacy and Ecology, and Environmental Protection, 12 Mendeleev Blvd, 4000, Plovdiv, Bulgaria
[2]National Institute of Geophysics, Geodesy and Geography (NIGGG), Hydrology and Water Management Research Centre, Bulgarian Academy of Sciences, Acad. G. Bonchev Str., bl. 3, 1113, Sofia, Bulgaria

Corresponding author email: dianaatanasovakirin@gmail.com

***Abstract***

*The study aims to monitor the ecological state and anthropogenic load of the Luda Yana River, part of the Maritsa River catchment. For this purpose, five biotopes of the Luda Yana River and its tributary Strelchanska Luda Yana (Strelcha, Popintsi, Svoboda, Rosen and Pazardzhik) were visited in 2025. A total of 711 specimens of 23 taxa of macroinvertebrate organisms belonging to Oligochaeta, Mollusca, Crustacea, Plecoptera, Ephemeroptera, Trichoptera, Odonata, Heteroptera, Coleoptera, Diptera, Chironomidae and Hydracarina were collected from all biotopes. Basic metrics and indices concerning the abundance and number of the collected indicator macrozoobenthos were calculated. The ecological state of the Luda Yana River is presented and discussed. The ecological state has been reported to range from moderate (Popintsi biotope) to very bad (Strelcha, Svoboda and Rosen biotopes). The content of Al, Cr, Mn, Fe, Co, Ni, Cu, Zn, As, Cd, Hg, and Pb in samples of macrozoobenthos, waters and sediments from two biotopes (Svoboda and Pazardzhik) was determined. The highest content of Fe, Al and Mn was found. The bioconcentration factor was considered. National and international legislative norms were used to compare the results of the chemical analyses.*

***Key words****: bioindication, Bulgaria, ecological indices, heavy metals and metalloids, river ecosystem.*

## INTRODUCTION

The Luda Yana River rises in the Sashtinska Sredna Gora under the name Panagyurska Luda Yana and flows through the Panagyurska Valley. After the village of Buta it flows under the name Luda Yana, enters the Pazardzhik-Plovdiv Plain, and flows into the Maritsa River. Tributaries of the river are the Banska Luda Yana River, the Strelchanska Luda Yana River and others. The waters in the lower reaches of the Luda Yana River are used for irrigation (Kiradzhiev, 2013; Gartsiyanova et al., 2021; 2023). The Luda Yana River flows through the Panagyurishte Ore Region, which extends between the central Srednogorie and Stara Planina Mountains and includes several ore deposits, including Assarel, Medet, Elshitsa, Tsar Asen, and Radka (Popov et al., 2003). Pollution of the Luda Yana River is a result of industry, wastewater discharge from urban sewage systems, and agriculture (livestock farms) (Gartsiyanova et al., 2021; 2023). Mining (from exploration through exploitation to deposit closure) impacts the environment, leading to land degradation, air, surface water, and soil pollution, loss of biodiversity, and more (Jhariya et al., 2016). Mineral extraction is associated with the release of large amounts of waste material. Tailings dams, which store a variety of mining waste, are among the most environmentally damaging pollutants (Agboola et al., 2020). Water resources are among the most affected by mining (Jhariya et al., 2016). The importance of rivers as water resources lies in their provision of water for household, industrial, and agricultural needs, as well as various activities (including fishing), which is why their protection from pollution is extremely important (Shanbehzadeh et al., 2014). Heavy metals are characterised by significant toxicity, persistence, bioaccumulation and biomagnification (Garai et al., 2021). About 99.9% of heavy metals

accumulate in sediments, while about 0.1% are dissolved in water (Pradit et al., 2013; Hacısalihoğlu & Karaer, 2016). Aquatic organisms are exposed to the effects of dissolved heavy metals in water on the one hand and those in sediments on the other (Garai et al., 2021). Macroinvertebrates are characterised by low mobility and long lifespan, which is why they can reflect changes in the aquatic environment. Pollution of the aquatic environment leads to changes in the composition and structure of aquatic organism communities (Varadinova et al., 2022). Few authors have investigated the water quality of the Luda Yana River based on the biological quality element (BQE) macrozoobenthos (Vidinova et al., 2008; Georgieva et al., 2014; Zaharieva et al., 2024). Rabadjieva et al. (2009) investigated heavy metal concentrations in waters from the Luda Yana River. No studies were found that affected the circulation of heavy metals in waters, sediments and macrozoobenthos of the studied river ecosystem.

The present study aims to monitor the ecological state and anthropogenic load of the Luda Yana River using the abundance and numbers of indicator macroinvertebrate fauna, and the concentrations of heavy metals and metalloids in macrozoobenthos, water, and sediments.

## MATERIALS AND METHODS

In the spring of 2025, five sites (designated as biotopes) were visited along the Luda Yana River and its tributary, the Strelchanska Luda Yana River (Figure 1).




Figure 1. Map of the studied biotopes

The Strelcha biotope falls within a section of the Strelchanska Luda Yana River named “The Strelchanska Luda Yana River from its sources to the town of Strelcha” of Type R03 Mountain Rivers in Ecoregion 7 Eastern Balkans. The Popintsi biotope is located within a section of the Luda Yana River named “The Panagyurska Luda Yana from Panagyurishte to the confluence of the Strelchanska Luda Yana” of Type R05 Semi-mountainous Rivers in Ecoregion 7. The Svoboda, Rosen and Pazardzhik biotopes fall within a section of the Luda Yana River named “The Luda Yana River from its confluence of the Strelchanska Luda Yana to its mouth” of Type R05. Strelcha biotope (42°29'52.7"N 24°19'31.5"E; 515 m above sea level) is located along the Strelchanska Luda Yana River to the town of Strelcha. The bottom substrate of the river section in this biotope consists of silt, sand, and stones. Popintsi biotope (42°25'28.6"N 24°16'00.7"E; 373 m above sea level) is located along the Luda Yana River, northwest of the centre of the village of Popintsi. Svoboda biotope (42°23'59.1"N 24°17'31.2"E; 370 m above sea level) is located along the Luda Yana

River, in proximity to the Radka mine. Rosen biotope (42°18'45.7"N 24°21'56.1"E; 293 m above sea level) is located along the Luda Yana River, south of the centre of the village of Rosen. Pazardzhik biotope (mouth) (42°09'38.8"N 24°22'52.0"E; 228 m above sea level) is located along the Luda Yana River, in proximity to the wastewater treatment plant (WWTP) of the town of Pazardzhik, shortly before the river flows into the Maritsa River. The bottom substrate in the four biotopes is sand and stones.

Sampling of macroinvertebrates was carried out according to standard methods (Cheshmedjiev et al., 2011; BDS EN ISO 10870:2012; Regulation No. H-4, 2012; Belkinova et al., 2013; BDS EN 16150:2026). The taxonomic affiliation of the collected macrozoobenthos was determined in laboratory conditions using a Stereo Zoom Microscope KERN OZL 464T24. According to Regulation No. H-4 (2012) and Belkinova et al. (2013), the following were calculated:

- total number of macroinvertebrate taxa;
- number of taxa from orders Ephemeroptera, Plecoptera and Trichoptera (EPT);
- Oligochaeta & Diptera in percentage;
- Filter feeders in percentage;
- EPT taxa in percentage;
- German trophic index Rithron Feeding Type Index;
- saprobiological index – Pantle & Buck (SPUB);
- biotic index (BI).

Basic ecological indices have been determined (Table 1).

Table 1. Main ecological indices

| *INDEX* | *FORMULA* | *INTERPRETATION* |
|---|---|---|
| ***Shannon Index (H')**** | $H' = -\sum_{i=1}^{S}(p_i \ln p_i)$ where $p_i=n_i/N$; $n_i$ is the number of specimens of each i species; N is the number of specimens of all species. | Index values ≤1.99 show very low diversity; 2.00-2.49 – low diversity; 2.50-2.99 – moderate diversity; 3.00-3.49 – high diversity; ≥3.50 – very high diversity. |
| ***Simpson's Index (D)**** | $D = \frac{\sum_i n_i(n_i-1)}{N(N-1)}$ | Index values range from 0 to 1. A value close to 0 indicates infinite diversity. A value close to 1 indicates no diversity. |
| ***Simpson's index of diversity (1-D)***** | $1 - \frac{\sum_i n_i(n_i-1)}{N(N-1)}$ | Index values range from 0 to 1. A value closer to 1 indicates greater diversity and vice versa. |
| ***Berger Parker Dominance Index (d)****** | $d = \frac{n_{max}}{N}$ where $n_{max}$ is the number of specimens of the most common species. | Index values range from 0 to 1. Higher values indicate lower diversity. |
| ***Pielou's evenness index (J')******* | $J' = \frac{H'}{H_{max}} = \frac{H'}{ln\, S}$ where S is the number of species; H' is the Shannon Index. | The index has a maximum value of 1, which indicates an even distribution of specimens and higher diversity. |

Legend: * - according to Kim et al., (2017); Baliton et al., (2020); ** - according to Okpiliya, (2012); Arzamani et al., (2018); *** - according to Okpiliya, (2012); **** - according to Patrício, (2009); Arzamani et al., (2018); ***** - according to McDonald, (2010); Roy & Bhattacharya (2024)

Water and sediment sampling were carried out in accordance with BDS EN ISO 5667-6:2016 and BDS ISO 5667-12:2017, respectively. The samples of surface water, sediments and biological element macrozoobenthos were collected from two biotopes – the Svoboda biotope, in a region with mining activity, and the Pazardzhik biotope, before the confluence of the Luda Yana River into the Maritsa River (before the mouth). All samples were analysed for 12 heavy metals and metalloids (Al, Cr, Mn, Fe, Co, Ni, Cu, Zn, As, Cd, Hg and Pb) using an Inductively Coupled Plasma Mass Spectrometer (ICP-MS DRC-e, Perkin Elmer) according to BDS EN ISO 21424:2020. The chemical analysis was carried out in an accredited laboratory. The heavy metals content in the samples of water, sediments and

biological elements is compared with the norms of national and international legislation (Dutch target values, 2000; Regulation No. 31, 2004; Regulation No. 3, 2008; Regulation No. 18, 2009; Regulation on environmental quality standards, 2010; Regulation No. H-4, 2012; Commission Regulation (EU) 2023/915). The Bioconcentration factor (BCF) was presented as the ratio of the pollutant concentration in the tissues or organs of aquatic organisms (macrozoobenthos) to the pollutant concentration in the aquatic environment (waters and sediments) (Sabljic & Protic, 1982; Yarsan & Yipel, 2013).

## RESULTS AND DISCUSSIONS

### *Ecological state based on the BQE macrozoobenthos*

In the present study, a total of 22 taxa (including Hydracarina) and 711 macroinvertebrate specimens were found in the five biotopes of the Luda Yana River and its tributary (Table 2).

Table 2. Taxonomic composition and number of macrozoobenthos from the Luda Yana River and Strelchanska Luda Yana River (Nt – number of taxa; Nsp – number of specimens)

| *Taxonomic composition* | *Strelcha* | | *Popintsi* | | *Svoboda* | | *Rosen* | | *Pazardzhik* | |
|---|---|---|---|---|---|---|---|---|---|---|
| | Nt | Nsp | Nt | Nsp | Nt | Nsp | Nt | Nsp | Nt | Nsp |
| Oligochaeta | 1 | 93 | 2 | 2 | - | - | 1 | 1 | - | - |
| Mollusca | 1 | 1 | 1 | 6 | 1 | 1 | - | - | - | - |
| Crustacea | - | - | - | - | - | - | - | - | 1 | 35 |
| Plecoptera | - | - | 1 | 1 | - | - | 1 | 1 | - | - |
| Ephemeroptera | - | - | 3 | 94 | 3 | 39 | 2 | 12 | 2 | 9 |
| Trichoptera | - | - | 3 | 8 | 1 | 2 | 1 | 1 | 1 | 32 |
| Odonata | - | - | 1 | 19 | 2 | 4 | 1 | 2 | 2 | 18 |
| Heteroptera | - | - | - | - | - | - | 1 | 1 | - | - |
| Coleoptera | - | - | - | - | 1 | 2 | 1 | 1 | - | - |
| Diptera | 2 | 6 | 3 | 5 | - | - | 2 | 2 | 2 | 3 |
| Chironomidae | 1 | 184 | 2 | 22 | 2 | 101 | 1 | 1 | 1 | 2 |
| Hydracarina | - | - | - | - | - | - | - | - | - | presence |

In the present study, the highest number of taxa was found in the orders Ephemeroptera (4 taxa: *Baetis* sp., nymph; *Cloeon* sp., nymph; *Caenis horaria* (Linnaeus, 1758), nymph; *Serratella ignita* (Poda, 1761), nymph), Trichoptera (3 taxa: *Hydropsyche ornatula* McLachlan 1878, larvae; *Anabolia nervosa* (Curtis, 1834), larvae; *Limnephilus rhombicus* (Linnaeus, 1758), larva) and Diptera (3 taxa: *Simulium* sp., larvae; *Tabanus* sp., larvae; Diptera, pupae). Taxa from the orders Ephemeroptera and Trichoptera are more sensitive to anthropogenic load.

The greatest taxonomic diversity was found in the Popintsi biotope (15 taxa). In the Popintsi, the dominant taxon is *Baetis* sp. nymph (74 specimens; Ephemeroptera); in the Svoboda biotope – Chironomidae (85 specimens); in the Rosen biotope – *C. horaria*, nymph (10 specimens; Ephemeroptera); in the Pazardzhik biotope – *Gammarus pulex* (Linnaeus, 1758) (35 specimens; Crustacea: Malacostraca). From the Strelchanska Luda Yana River, in the Strelcha biotope, *Chironomus plumosus* (Linnaeus, 1758), larvae (184 specimens; Chironomidae) dominate. The highest number of EPT taxa was found in Popintsi, with 7 taxa. The ecological state of the Luda Yana River, as measured by the total number of macroinvertebrate taxa and the number of EPT taxa, varies from good in the Popintsi biotope to moderate downstream in the Svoboda, Rosen, and Pazardzhik biotopes. The ecological state of the Strelchanska Luda Yana River in the Strelcha biotope was found to be poor in terms of the total number of macroinvertebrate taxa and very poor in terms of the number of EPT taxa (Table 3). The share of Oligochaeta & Diptera is highest in the Strelcha biotope from the Strelchanska Luda Yana River – 97.89% of the total abundance, followed by the Svoboda biotope from the Luda Yana River – 67.79%. The share of Filter feeders is highest in the Strelcha – 1.76% of the total abundance. Representatives of the Filter feeders ecological group were not found in the Svoboda and Rosen. The percentage of EPT taxa was highest in the Popintsi biotope, followed by the Rosen

biotope (Figure 2). Higher EPT taxa in percentage indicate less pollution.

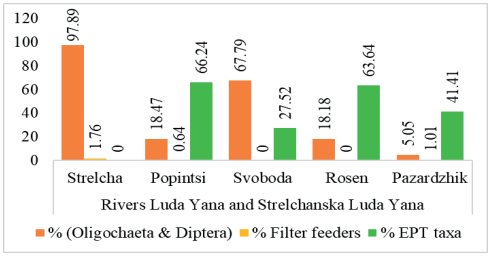



Figure 2. Basic macrozoobenthos abundance metrics

The distribution of indicator macrozoobenthos in the Luda Yana River and its tributaries, grouped by feeding type, was examined. Based on this distribution, the Rithron Feeding Type Index was calculated. In the Strelcha, Svoboda and Rosen biotopes, deposit feeders predominate ($DF_{Strelcha}$=97.54%; $DF_{Svoboda}$=30.20%; $DF_{Rosen}$=50.00%), while in the Popintsi and Pazardzhik biotopes, scrapers ($SC_{Popintsi}$=52.87%; $SC_{Pazardzhik}$=41.41%) (Figure 3).

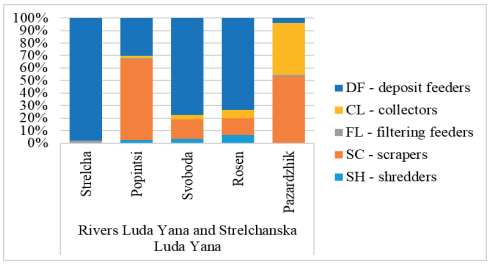



Figure 3. Distribution of macrozoobenthos by trophic groups (in percentages of the total number)

The calculated Rithron Feeding Type Index shows a good ecological state in the Popintsi and Pazardzhik biotopes and a very bad one in the other three biotopes. In addition, Rithron Feeding Type Index values <0.5 indicate an imbalance in the ecosystem, including organic pollution (Table 3).

In the Strelcha biotope, the indicator macrozoobenthos comprises four saprobic groups: xeno-oligosaprobic, β-mesosaprobic, polysaprobic, and poly-α-mesosaprobic (each with one taxon). In the Popintsi, the indicator macrozoobenthos, indicating oligo-β-mesosaprobic conditions (with four taxa), dominates. In the Rosen and Pazardzhik, the indicator macrozoobenthos for β-α-mesosaprobic conditions (with 3 taxa each) was established. In the Svoboda, an equal number of taxa of macroinvertebrates (indicating oligo-β-mesosaprobic conditions) and β-α-mesosaprobic conditions (with 2 taxa each) were established. Based on the saprobic importance, the indicator weight and the abundance of the macrozoobenthos indicator taxa, the saprobic index was calculated and a bad ecological state of the waters of the Strelchanska Luda Yana River in the Strelcha and a change in the ecological state of the waters of the Luda Yana River from good in the Svoboda and Popintsi to very good in the Rosen and Pazardzhik were found (Table 3).

The indicator macrozoobenthos from both rivers belongs to A, B, C, D, and E groups, respectively, sensitive, less sensitive, relatively tolerant, tolerant, and most tolerant organisms. In all investigated biotopes from the Luda Yana River, group C taxa dominate, except the Strelcha biotope from the Strelchanska Luda Yana River, where groups C, D and E are represented by an equal number of taxa (1 taxon). In the Strelcha biotope, the largest numbers of tolerant macrozoobenthos specimens were found (Figure 4). The calculated biotic index (BI) indicates a moderate ecological state in the Popintsi biotope, a bad ecological state in the Svoboda and Pazardzhik biotopes, and a very bad ecological state in the Strelcha and Rosen biotopes (Table 3).

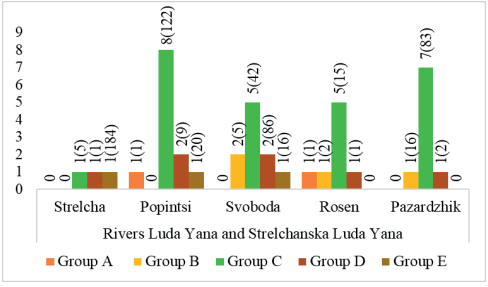



Figure 4. Distribution of established macrozoobenthos by sensitivity groups (number of taxa/number of specimens)

Table 3. Ecological state of the studied river ecosystem
(red – very bad; orange – bad; yellow – moderate; green – good; blue – very good)

| *Metrics*<br>*Biotopes* | *Total number of taxa* | *Number of EPT taxa* | *Rithron Feeding Type Index* | *SPUB* | *BI (nEQR)* |
|---|---|---|---|---|---|
| | **Luda Yana River and tributary** | | | | |
| ***Strelcha*** | 5 | 0 | 0.004 | 3.73 | 1(0.3) |
| ***Popintsi*** | 16 | 7 | 0.67 | 2.09 | 3(0.6) |
| ***Svoboda*** | 10 | 4 | 0.19 | 2.10 | 2(0.4) |
| ***Rosen*** | 11 | 4 | 0.20 | 1.50 | 2(0.2) |
| ***Pazardzhik*** | 10 | 3 | 0.53 | 1.81 | 2(0.4) |

Shannon Index (H') values range from 0.76 to 1.92, which indicates very low diversity in all studied biotopes, with the lowest values found in the Strelcha biotope (Strelchanska Luda Yana River) and Svoboda biotope (Luda Yana River). In the Strelcha biotope, the Simpson's Index (D) value is the highest (D=0.53), and the Simpson's index of diversity (1-D) value is the lowest (1-D=0.47), indicating lower diversity in this biotope, followed by the Svoboda biotope. Berger Parker Dominance Index (d) is highest in Strelcha biotope (d=0.65), followed by Svoboda biotope (d=0.57), which again shows lower diversity in these two biotopes. Pielou's evenness index (J') has the lowest values in the Strelcha and Svoboda biotopes (J'=0.47 and J'=0.59, respectively), which indicates a lower evenness in the distribution of taxa (Table 4).

Table 4. Ecological indices of the macrozoobenthos communities from the Luda Yana River and tributary

| *Indices* | *Strelcha* | *Popintsi* | *Svoboda* | *Rosen* | *Pazardzhik* |
|---|---|---|---|---|---|
| ***Total number of taxa*** | 5 | 16 | 10 | 11 | 9 (and presence of Hydracarina) |
| ***Total number of specimens*** | 284 | 157 | 149 | 22 | 99 |
| ***Shannon Index (H')*** | 0.76 | 1.81 | 1.36 | 1.92 | 1.59 |
| ***Simpson's Index (D)*** | 0.53 | 0.26 | 0.38 | 0.20 | 0.25 |
| ***Simpson's index of diversity (1-D)*** | 0.47 | 0.74 | 0.63 | 0.80 | 0.75 |
| ***Berger Parker Dominance Index (d)*** | 0.65 | 0.47 | 0.57 | 0.45 | 0.35 |
| ***Pielou's evenness index (J')*** | 0.47 | 0.65 | 0.59 | 0.80 | 0.72 |

Based on the calculated metrics and indices for the indicator macrozoobenthos in the Luda Yana River and the Strelchanska Luda Yana River, a moderate ecological state was established in the Popintsi biotope, a bad state in the Pazardzhik biotope, and a very bad state in the Strelcha, Svoboda, and Rosen biotopes.

Vidinova et al. (2008) assessed water quality in the Luda Yana River after Rosen village using physicochemical parameters and macroinvertebrates. According to the calculated indices, the authors report that the Luda Yana River, after Rosen, belongs to the III category of waters. In the present study, a very bad ecological state was found for the Rosen biotope. Zaharieva et al. (2024) conducted hydrobiological monitoring of the Luda Yana River near the village of Popintsi based on BQE macrozoobenthos. The authors report a moderate ecological state in this section of the river, findings confirmed by the present study.

***Content of heavy metals and metalloids***

In the macrozoobenthos samples from the Luda Yana River, Svoboda biotope, the content of heavy metals and metalloids decreases in the order: Fe > Al > Mn > Cu > Zn > Cr > Pb > Co > Ni > As > Cd > Hg; in the water samples – in the order: Al > Fe > Mn > Cu > Zn > Ni > Cr > Co > Pb > Cd > As; in the sediment samples – in the order: Fe > Al > Mn > Zn > Cu > Pb > Co > Cr > Ni > As > Cd. In the macrozoobenthos samples from the Luda Yana River, Pazardzhik biotope, the content of heavy metals and metalloids decreases in the order: Al > Fe > Mn > Cu > Zn > Co > Cr > Pb > Ni > As > Cd > Hg; in the water samples – in the order: Fe > Mn > Cr > Zn > As > Cu > Al > Ni > Hg > Co > Cd > Pb; in the sediment samples – in the order: Fe > Al > Mn > Cu > Zn > Pb > Cr > Co > Ni > As > Cd. In general, in both studied sections (Svoboda and Pazardzhik) of the Luda Yana River, the highest

concentrations of Fe, Al, and Mn, and the lowest concentrations of Cd and As, were found. A higher content of Al, Cr, Fe, Cu, Zn, As and Pb was reported in macrozoobenthos samples from the Svoboda biotope compared to the Pazardzhik biotope. The content of all investigated heavy metals and metalloids is higher in the samples of waters from the Svoboda biotope compared to the Pazardzhik biotope. At the same time, the content of the investigated heavy metals and metalloids was higher in the sediment samples from the Pazardzhik biotope compared to the Svoboda biotope, except for Zn and Cd (Figures 5 and 6).

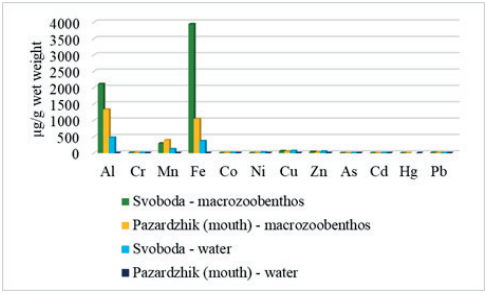



Figure 5. Content of heavy metals and metalloids in macrozoobenthos (µg/g wet weight) and water (µg/g wet weight) from the Luda Yana River

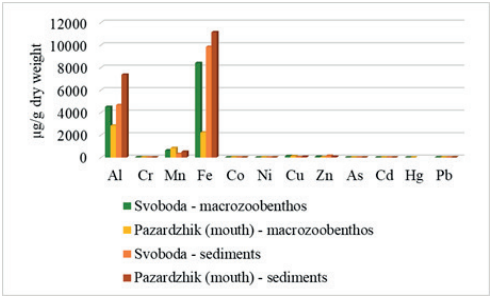



Figure 6. Content of heavy metals and metalloids in macrozoobenthos (µg/g dry weight) and sediments (µg/g dry weight) from the Luda Yana River

Bioconcentration factors (BCF) in the macrozoobenthos compared to Svoboda biotope waters have the highest values for Pb ($BCF_{Pb}$=38.04) and Fe ($BCF_{Fe}$=10.87), and the lowest for Ni ($BCF_{Ni}$=0.15).

The macrozoobenthos accumulated 253.6 times more Pb and 72.47 times more Fe from the waters compared to Ni. The values of the bioconcentration factor in the macrozoobenthos compared to sediments from the Svoboda biotope are the highest for Cu ($BCF_{Cu}$=3.97) and Cr ($BCF_{Cr}$=2.94), and the lowest for Zn ($BCF_{Zn}$=0.51). The macrozoobenthos accumulated 7.78 times more Cu and 5.77 times more Cr from the sediments than Zn. The values of the bioconcentration factor (BCF) in the macrozoobenthos compared to waters from the Pazardzhik biotope have the highest values for Al ($BCF_{Al}$=1329805.20) and Pb ($BCF_{Pb}$=132536.54), and the lowest for Hg ($BCF_{Hg}$=75.00). The macrozoobenthos accumulated 17730.74 times more Al and 1767.15 times more Pb from the waters compared to Hg. Bioconcentration factors in the macrozoobenthos compared to sediments from the Pazardzhik biotope are highest for Cd ($BCF_{Cd}$=2.67) and lowest for Fe ($BCF_{Fe}$=0.20). The macrozoobenthos accumulated 13.35 times more Cd from the sediments than Fe. According to the reported BCF values, the macrozoobenthos from the Pazardzhik can be determined as highly bioaccumulative (BCF>5000; Khan et al., 2022) of the elements Al, Pb, Co, Mn, Cu, Zn and Ni (Table 5). The obtained extremely high BCF values for Al (over 1.3 million) and for Pb (over 130 thousand) are due to a potential short-term dilution of the dissolved metals in the water samples at the river mouth during the sampling period (spring season) in contrast to the stable, long-term accumulation within the macrozoobenthos tissues.

Monitoring the content of heavy metals and metalloids in biota, waters and sediments from the Svoboda biotope is justified by the nearby suspected source of anthropogenic load - the Radka mine and the existing risk of pollution of the river ecosystem in this area. While the choice of the Pazardzhik biotope is related to the need to monitor the ecological state of the river ecosystem and the load with heavy metals and metalloids downstream, before the confluence of the Luda Yana River into the Maritsa River.

In the present study, excesses of six heavy metals and metalloids were found in macrozoobenthos samples, in accordance with the norms specified in Regulation No. 31 (2004), Dineva (2023), and Commission Regulation (EU) 2023/915. In the macrozoobenthos samples from the Svoboda, higher excesses of Al, Cr, Cu and Pb were

found compared to the macrozoobenthos from the Pazardzhik. Higher excesses of Ni and Cd were found in the macrozoobenthos samples from the Pazardzhik. In both biotopes from the Luda Yana River, no excesses of Zn, As and Hg were detected in the macrozoobenthos samples (Figure 7).

Table 5. Bioconcentration factor values

| | *Svoboda* | | *Pazardzhik* | |
|---|---|---|---|---|
| | **Macrozoobenthos/ Waters** | **Macrozoobenthos/ Sediments** | **Macrozoobenthos/ Waters** | **Macrozoobenthos/ Sediments** |
| $BCF_{Al}$ | 4.51 | 0.97 | 1329805.20 | 0.38 |
| $BCF_{Cr}$ | 2.88 | 2.94 | 1246.27 | 1.08 |
| $BCF_{Mn}$ | 2.57 | 2.06 | 41189.59 | 1.63 |
| $BCF_{Fe}$ | 10.87 | 0.85 | 4693.88 | 0.20 |
| $BCF_{Co}$ | 1.95 | 0.80 | 46674.66 | 1.31 |
| $BCF_{Ni}$ | 0.15 | 0.95 | 5999.14 | 0.51 |
| $BCF_{Cu}$ | 0.97 | 3.97 | 41122.54 | 1.68 |
| $BCF_{Zn}$ | 0.82 | 0.51 | 8744.04 | 0.65 |
| $BCF_{As}$ | - | 0.79 | 424.98 | 0.53 |
| $BCF_{Cd}$ | 3.56 | 1.56 | 4608.00 | 2.67 |
| $BCF_{Hg}$ | - | - | 75.00 | - |
| $BCF_{Pb}$ | 38.04 | 2.02 | 132536.54 | 0.57 |

The results of the chemical analyses of surface water samples from the Luda Yana River, Svoboda biotope, show an excess of Al, 18.76 times above the maximum permissible concentrations (MPC) specified in Regulation No. H-4 (2012), and an excess of Cd – 0.18 times above the MPC specified in the Regulation on environmental quality standards (2010). In the surface water samples from the Pazardzhik, no excesses of the examined heavy metals and metalloids were found according to the norms specified in Regulation No. H-4 (2012), Regulation No. 18 (2009) and Regulation on environmental quality standards (2010). In sediment samples from the Luda Yana River, Svoboda, an excess was reported only for Zn, 1.05 times above the Dutch target values (2000). In the sediments from the Luda Yana River, Pazardzhik, exceedances were found for Co (1.25 times), Cu (1.79 times) and Pb (1.51 times) compared to the Dutch target values (2000). In both biotopes, the content of the examined heavy metals and metalloids did not exceed the norms specified in Regulation No. 3 (2008).

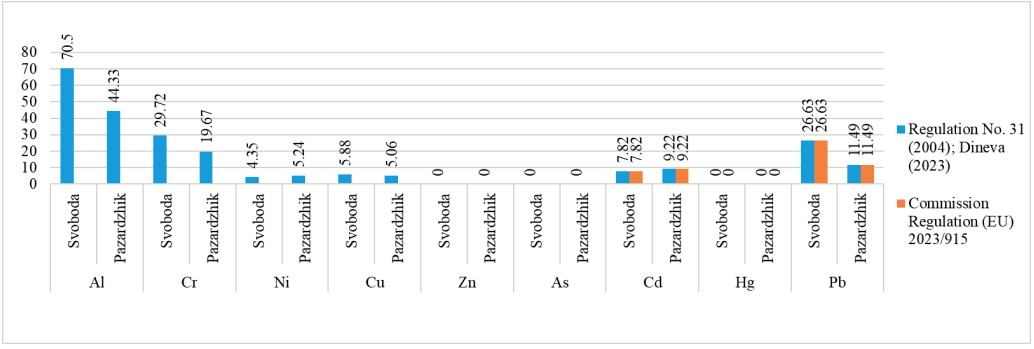



Figure 7. Excesses (in times) of the investigated heavy metals and metalloids in macrozoobenthos samples from the Luda Yana River

Gartsiyanova et al. (2020) investigated spatio-temporal changes in water quality of the Luda Yana River (at Rosen and before the mouth) and the Strelchanska Luda Yana River (after Strelcha) for the period 1981-2018 using complex indices to assess water quality status. The authors report that during the study period, the waters of the Luda Yana River did not meet

the requirements for good chemical status under Regulation No. H-4 (2012). The worst and critical values of the Water Quality Index were established for the Luda Yana River near Rosen. Gartsiyanova et al. (2021) investigated the state of the water in the Luda Yana River (at Rosen and at the mouth) using various indices. The authors define the waters as slightly polluted according to the Bavarian Surface Quality Index (CJ) and as polluted and highly polluted according to the Water Pollution Index (WPI) at Rosen; as well as absent to lightly polluted by CJ and moderately to heavily polluted by WPI at the mouth. The authors explain the bad quality of the water with increased levels of Fe, Mn, and Cu, as well as with high values of the indicators BOD5, ammonium, and nitrate nitrogen. In the present study, a very bad ecological state was found for the Rosen, and a bad state for the Pazardzhik biotope (mouth). In the waters of the Luda Yana River at Pazardzhik, the highest Fe and Mn content was also found, which, however, does not exceed the norms of national and international legislation. Gartsiyanova et al. (2022) investigated the water quality of the Strelchanska Luda Yana River (after Strelcha); on the Luda Yana River (near Popintsi and near Chernogorovo) through the use of physicochemical parameters and heavy metals (Cu, Fe, Mn, Pb, As, Zn, Cd and Ni). The authors indicate that the Luda Yana River in the section near Popintsi is the most polluted, and the one near Chernogorovo is in the best quality, and report persistent and significant pollution with heavy metals (Fe, Mn, Cd and Cu). In the current study of the Luda Yana River, the best ecological state (moderate) was recorded in the Popintsi compared to the other investigated biotopes. Gartsiyanova et al. (2023) analysed the water quality by physicochemical parameters in the catchment basin of the Luda Yana River for the period 2018-2021. The authors defined the waters of the Luda Yana River as highly polluted due to long-term anthropogenic impacts and reported elevated levels of some heavy metals. The authors identify the most favourable conditions for the Luda Yana River from mouth to source.

## CONCLUSIONS

The ecological state of the waters of the Luda Yana and Strelchanska Luda Yana Rivers was assessed based on the taxonomic diversity and abundance of the indicator macrozoobenthos. The values of the calculated metrics and indices show a moderate ecological state of the Luda Yana River upstream (Popintsi biotope – BI(nEQR)=3(0.6)), very bad for the Strelchanska Luda Yana River at the Strelcha biotope (Number of EPT taxa – 0; Rithron Feeding Type Index=0.004; BI(nEQR)=1(0.3)), for the Luda Yana River at the Svoboda (Rithron Feeding Type Index=0.19) and Rosen (Rithron Feeding Type Index=0.20; BI(nEQR)=2(0.2)), as well as bad ecological state of the Luda Yana River before its confluence with the Maritsa River (Pazardzhik biotope – BI(nEQR)=2(0.4)). In addition, the chemical analyses performed on samples from the Svoboda and Pazardzhik biotopes revealed high contents of Fe, Al and Mn. More than half of the investigated heavy metals and metalloids have higher concentrations in the macrozoobenthos from Svoboda than in those from Pazardzhik (mouth). The content of all investigated heavy metals and metalloids was higher in the waters from Svoboda and higher in the sediments from Pazardzhik (mouth), except for Zn and Cd. According to the reviewed legislative documents, the highest exceedances were found for Al (70.5 and 44.33 times), Cr (29.72 and 19.67 times), Pb (26.63 and 11.49 times) and Cd (7.82 and 9.22 times) in the macrozoobenthos samples (from Svoboda and Pazardzhik, respectively), and for Al (18.76 times) in the water samples from Svoboda. Based on the monitoring carried out, permanent and more in-depth studies of the ecological state of the waters of the Luda Yana River and its tributaries, as well as the content of heavy metals and metalloids in river ecosystems, especially in areas with potential sources of anthropogenic load, are recommended in order to protect biodiversity, habitats and ensure a favorable environment for the life of hydrobionts.

## ACKNOWLEDGEMENTS

This work has been carried out within the framework of the National Science Program "Critical and strategic raw materials for a green transition and sustainable development", approved by the Council of Ministers' Resolution № 508/18.07.2024 and funded by the Ministry of Education and Science (MES) of Bulgaria. We express our gratitude to Assoc. Prof. Veronika Mihaylova, PhD, for the assistance and consultations provided in connection with the chemical analyses.

## REFERENCES

Agboola, O., Babatunde, D. E., Fayomi, O. S., Sadiku, E. R., Popoola, P., Moropeng, L., Yahaya, A., & Mamudu, O. A. (2020) A review on the impact of mining operation: monitoring assessment and management. *Results in Engineering*, *8*, 100181.

Arzamani, K., Vatandoost, H., Rassi, Y., Akhavan, A. A., Abai, M. R., Alavinia, M., Akbarzadeh, K., Mohebali, M., & Rafizadeh, S. (2018). Richness and diversity of phlebotomine sand flies (Diptera: Psychodidae) in North Khorasan Province, northeast of Iran. *Journal of arthropod-borne diseases, 12*(3), 232–239.

Baliton, R., Landicho, L., Cabahug, R. E., Paelmo, R., Laruan, K., Rodriguez, R., Visco, R., & Castillo, A. K. (2020). Ecological services of agroforestry systems in selected upland farming communities in the Philippines. *Biodiversitas Journal of Biological Diversity*, *21*(2), 707–717.

BDS EN ISO 10870: 2012 *Water quality - Guidelines for the selection of sampling methods and devices for benthic macroinvertebrates in fresh waters (ISO 10870:2012)*

BDS EN ISO 5667-6: 2016 *Water quality - Sampling - Part 6: Guidance on sampling of rivers and streams (ISO 5667-6:2014)*

BDS ISO 5667-12: 2017 *Water quality - Sampling - Part 12: Guidance on sampling of bottom sediments from rivers, lakes and estuarine areas*

BDS EN ISO 21424: 2020 *Milk, milk products, baby food and adult food. Determination of mineral substances and trace elements. Inductively coupled plasma mass spectrometry (ICP-MS) method (ISO 21424:2018)*

BDS EN 16150: 2026 *Water quality - Guidance on pro-rata multi-habitat sampling of benthic macroinvertebrates from rivers and streams*

Belkinova, D., Gecheva, G., Cheshmedzhiev, S., Dimitrova-Dyulgerova, I., Mladenov, R., Marinov, M., Teneva, I., Stoyanov, P., Ivanov, P., Mihov, S., Pehlivanov, L., Varadinova, E., Karagyozova, Ts., Vassilev, M., Apostolu, A., Velkov, B., & Pavlova, M. (2013). *Biological analysis and ecological assessment of surface water types in Bulgaria.* Plovdiv, BG: Univ "P. Hilendarskii" Publishing House (in Bulgarian).

Cheshmedjiev, S., Soufi, R., Vidinova, Y., Tyufekchieva, V., Yaneva, I., Uzunov, Y., & Varadinova, E. (2011). Multi-habitat sampling method for benthic macroinvertebrate communities in different river types in Bulgaria. *Water Research and Management, 1*(3), 55–58.

Commission Regulation (EU) 2023/915 of 25 April 2023 on maximum levels for certain contaminants in food and repealing Regulation (EC) No 1881/2006.

Dineva, S. (2023). *Main pollutants of food raw materials and products*. Tracia University-Stara Zagora. ISBN 978-619-7340-04-4 (in Bulgarian).

Dutch Target and Intervention Values, (the New Dutch List) 2000. Ministry of Housing, Spatial Planning and the Environment (VROM).

Garai, P., Banerjee, P., Mondal, P., & Saha, N. C. (2021). Effect of heavy metals on fishes: Toxicity and bioaccumulation. *Journal of Clinical Toxicology, 11*(S18), 001.

Gartsiyanova, K., Varbanov, M., Kitev, A., Genchev, S., & Georgieva, S. (2020). Territorial features and dynamics in the water quality change in the Topolnitsa and Luda Yana rivers. *Journal of the Bulgarian Geographical Society*, *43*, 9–15 (in Bulgarian).

Gartsiyanova, K., Varbanov, M., Kitev, A., & Genchev, S. (2021). Water quality analysis of the rivers Topolnitsa and Luda Yana, Bulgaria using different indices. *Journal of Physics: Conference Series, 1960*, 012018.

Gartsiyanova, K., Kitev, A., Varbanov, M., Georgieva, S., & Genchev, S. (2022). Water quality assessment and conservation of the river water in regions with various anthropogenic activities in Bulgaria: A case study of the catchments of Topolnitsa and Luda Yana rivers. *International Journal of Conservation Science, 13*(2), 733–742.

Gartsiyanova, K., Metodieva, G., & Kitev, A. (2023). Local anthropogenic pressure and river water quality in a key mining area in Central Bulgaria. *International Europa Scientific Researches Congress, 26 February 2023, Ankara, Turkey*, 135–139.

Georgieva, G., Uzunova, E., Hubenova, T., & Uzunov, Y. (2014). Ecological Assessment of the Rivers Luda Yana and Banska Luda Yana as Based on Selected Biological Parameters. *Ecologia Balkanica, 5*, 89–94.

Hacısalihoğlu, S., & Karaer, F. (2016). Relationships of Heavy Metals in Water and Surface Sediment with Different Chemical Fractions in Lake Uluabat, Turkey. *Polish Journal of Environmental Studies, 25*(5), 1937–1946.

Jhariya, D. C., Khan, R., & Thakur, G. S. (2016). Impact of mining activity on water resource: an overview study. *Proceedings of the Recent Practices and Innovations in Mining Industry, Raipur, India*, *201*, 19–20.

Khan, K., Kumar, V., Colombo, E., Lombardo, A., Benfenati, E., & Roy, K. (2022). Intelligent consensus predictions of bioconcentration factor of pharmaceuticals using 2D and fragment-based descriptors. *Environment international*, *170*, 107625.

Kim, B. R., Shin, J., Guevarra, R. B., Lee, J. H., Kim, D. W., Seol, K. H., Lee, J. H., Kim, H. B., & Isaacson, R. E. (2017). Deciphering diversity indices for a better understanding of microbial communities. *Journal of microbiology and biotechnology*, *27*(12), 2089–2093.

Kiradzhiev, S. (2013). *Encyclopedic Geographical Glossary of Bulgaria.* Sofia, BG: Iztok-zapad Publishing house (in Bulgarian).

McDonald, C., Smith, R., Scott, M., & Dick, J. (2010). Using indices to measure biodiversity change through time. *International Workshop on Spatio-Temporal Modelling. Santiago de Compostela, Spain*.

Okpiliya, F. I. (2012). Ecological diversity indices: Any hope for one again. *Journal of Environment and Earth Science, 2*(10), 45–52.

Patrício, J., Neto, J. M., Teixeira, H., Salas, F., & Marques, J. C. (2009). The robustness of ecological indicators to detect long-term changes in the macrobenthos of estuarine systems. *Marine Environmental Research*, *68*(1), 25–36.

Popov, P., Strashimirov, S., & Popov, K. (2003). Geology and metallogeny of the Srednogorie zone and Panagyurishte ore region. *Society of Economic Geologists, Guidebook Series, 36*, 7–26.

Pradit, S., Pattarathomrong, M. S., & Panutrakul, S. (2013). Arsenic Cadmium and Lead Concentrations in Sediment and Biota from Songkhla Lake: A Review. *Procedia - Social and Behavioral Sciences 91*, 573–580.

Rabadjieva, D., Tepavitcharova, S., Todorov, T., Dassenakis, M., Paraskevopoulou, V., & Petrov, M. (2009). Chemical speciation in mining affected waters: the case study of Asarel-Medet mine. *Environmental monitoring and assessment, 159*(1), 353–366.

Regulation No. 31 of 29 July 2004 on the maximum levels of contaminants in foodstuffs. *Official Paper 88, 2004.*

Regulation No. 3 of 1 August 2008 on the norms for the permissible content of harmful substances in soils. *Official Paper 71, 2008.*

Regulation No. 18 of 27 May 2009 on the quality of water for irrigation of crops. *Official Paper 43, 2009.*

Regulation on environmental quality standards for priority substances and certain other pollutants. *Official Paper 88, 2010.*

Regulation No. H-4 of 14.09.2012 on the characterisation of surface waters. *Promulgated in the Official Gazette, No. 22 of 5.03.2013, amended and supplemented, No. 67 of 04.08.2023.*

Roy, S., & Bhattacharya, K. R. (2024). A theoretical study to introduce an index of biodiversity and its corresponding index of evenness based on mean deviation. *World Journal of Advanced Research and Reviews, 21*(2), 022–032.

Sabljic, A., & Protic, M. (1982). Molecular connectivity: a novel method for prediction of bioconcentration factors of hazardous chemicals. *Chemico-Biological Interactions, 42*(3), 301–310.

Shanbehzadeh, S., Vahid Dastjerdi, M., Hassanzadeh, A., & Kiyanizadeh, T. (2014). Heavy metals in water and sediment: a case study of Tembi River. *Journal of environmental and public health*, *2014*(1), 858720.

Varadinova, E., Sakelarieva, L., Park, J., Ivanov, M., & Tyufekchieva, V. (2022). Characterisation of Macroinvertebrate Communities in Maritsa River (South Bulgaria)—Relation to Different Environmental Factors and Ecological Status Assessment. *Diversity, 14*, 833.

Vidinova, Y. N., Botev, I. S., Tyufekchieva, V. G., Nedyalkova, T. V., Yaneva, I. Y., Zadneprovski, B. E., & Varadinova, E. D. (2008). Results of rapid hydrobiological monitoring of watersheds from the East-and West Aegean Sea River basin districts in Bulgaria. *Acta Zoologica Bulgarica*, 2, 233–242.

Yarsan, E., & Yipel, M. (2013). The Important Terms of Marine Pollution "Biomarkers and Biomonitoring, Bioaccumulation, Bioconcentration, Biomagnification". *Journal of Molecular Biomarkers & Diagnosis, S1*, 003.

Zaharieva P., Kirin, D., & Zaharieva, R. (2024). Hydrobiological monitoring of two rivers from the Maritsa River basin based on a biological quality element macrozoobenthos. *Scientific Papers. Series D. Animal Science, LXVII* (2), 660–667.

Scientific Papers. Series E. Land Reclamation, Earth Observation & Surveying, Environmental Engineering. Vol. XV, 2026
Print ISSN 2285-6064, CD-ROM ISSN 2285-6072, Online ISSN 2393-5138, ISSN-L 2285-6064

# MICROBIAL PATTERNS IN URBAN AND PERI-URBAN LAKES FROM SOUTHERN ROMANIA: IMPLICATIONS FOR WATER QUALITY AND ECOSYSTEM HEALTH

**Anca-Ioana LUCACI, Larisa Isabela FLORESCU, Mirela Mădălina MOLDOVEANU, Roxana-Lucia COJOC**

Institute of Biology Bucharest of Romanian Academy, 296 Splaiul Independenței, District 6, 060031, Bucharest, Romania

Corresponding author email: larisa.florescu@ibiol.ro

***Abstract***

*Urbanisation strongly influences water quality and the structure of microbial communities in aquatic ecosystems. This study investigates seasonal variations in physicochemical parameters and microorganisms in three urban lakes in Bucharest (Tineretului, Titan 1 and Titan 2) and one peri-urban lake (Comana). Samples were collected from five stations per lake during summer and autumn. Physicochemical parameters (temperature, pH, ORP, dissolved oxygen and TDS) were measured in situ, and bacterial communities were assessed by determining heterotrophic bacteria, total and faecal coliforms, and faecal streptococci, respectively.*
*The results revealed clear differences between urban and peri-urban lakes. The lakes in Bucharest presented increased TDS values (up to 738 ppm) and an alkaline pH (up to 10 in Titan 2), reflecting anthropogenic pressure. Bacterial abundance was higher in Titan 1 and Titan 2, where heterotroph density exceeded $10^3$ CFU·mL$^{-1}$. Faecal coliforms were sporadically detected in urban lakes, but were absent in Comana, indicating point sources of contamination. The findings suggest that urbanisation causes significant changes in water quality and microbial load, highlighting the need for integrated monitoring for sustainable management of urban lakes.*

***Key words****: anthropogenic impact, microbial contamination, physicochemical parameters, urban lakes, water quality.*

## INTRODUCTION

Freshwater ecosystems, especially urban and peri-urban lakes, are critical components of regional biodiversity and provide essential ecosystem services, but are increasingly threatened by anthropogenic activities (Kapetanović et al., 2024). These aquatic environments are highly susceptible to environmental change and serve as indicators of landscape health due to their vulnerability (Roguet & Lucas, 2012). Their ecological integrity is frequently compromised by pollution, nutrient enrichment and habitat degradation, often resulting from human activities in adjacent areas (Lazăr et al., 2017; Mititelu-Ionuș et al., 2020).
The microbial communities in these lakes are particularly sensitive to such disturbances, reflecting changes in water quality and overall ecosystem health (Kiersztyn et al., 2019). Microorganisms play a central role in the functioning of aquatic ecosystems, being involved in the biogeochemical cycles of carbon, nitrogen and phosphorus, as well as in the degradation of organic matter. Bacterial communities in lakes respond rapidly to environmental changes, making them important indicators of ecological status and water quality (Marcondes et al., 2024). Added to this is the escalating impact of global change and land-use changes, emphasising the need for comprehensive studies focused on bacterial populations in urban lake environments to identify reliable indicators of ecological status and emerging pathogens in water (Orel et al., 2022).
Classical microbiological indicators, such as heterotrophic bacteria, total coliforms, faecal coliforms and faecal streptococci, are widely used to assess water quality and identify sources of faecal contamination. The presence of these microorganisms is often associated with risks to human health and deterioration of

ecosystem health, especially in recreational lakes (Lazăr et al., 2017; Lew et al., 2023).

Globally, extensive research has focused on the application of these microbiological indicators to assess water quality in diverse aquatic environments (Loucif & Chenchouni, 2024). For example, studies in lakes in Turkey have correlated bacterial diversity with environmental factors, indicating the presence of wastewater and agricultural runoff even when coliform counts were not exceptionally high (Mercan & Arslan, 2023). Similarly, in Brazil, investigations in urban aquatic systems have used these bacterial indicators to assess the efficiency of wastewater treatment plants and to identify sources of pollution affecting recreational waters, highlighting their broad utility in environmental monitoring. In the Romanian context, research has similarly used these microbial indicators to assess water quality in various freshwater bodies, revealing contamination patterns influenced by urban development and agricultural practices (Lazăr et al., 2017).

In Romania, information on the structure of microbial communities and their relationships with water physicochemical parameters in urban lakes remains limited, especially in the southern region. Given the accelerated expansion of urban areas and the importance of lakes in Bucharest for recreation and local ecological balance, an integrated assessment of water quality from this perspective was of interest.

This study aims to address this knowledge gap by investigating microbial patterns in urban and peri-urban lakes in southern Romania, focusing on how these patterns reflect water quality and ecosystem health under varying degrees of anthropogenic pressure.

Therefore, the main objectives were: (i) assessing seasonal variations of physicochemical parameters and microbiological indicators in urban and peri-urban lakes in southern Romania, (ii) evaluating the relationship between microbiological indicators and physicochemical factors contributing to a better understanding of the impact of urbanisation on the health of aquatic ecosystems.

## MATERIALS AND METHODS

### Study site

Four representative ecosystems were selected in the study: 3 urban lakes in Bucharest (Tineretului, Titan 1 and Titan 2) and a peri-urban lake, as part of the Comana Natural Park (Balta Comana), Giurgiu County in southern Romania, in order to capture how these models reflect water quality and ecosystem health under varying degrees of anthropogenic pressure (Figure 1). Five stations were established for the urban lakes Titan 1, Titan 2, and Tineretului, and three for Balta Comana.

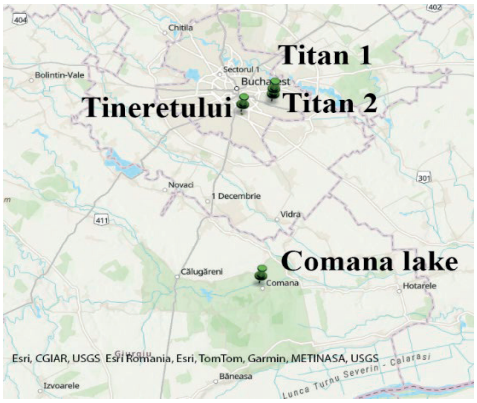



Figure 1. Study site with sampling ecosystems

### Water sample collection

Water-column samples were collected in the summer and autumn of 2024. Using GPS, five sampling points were selected for Lake Tineretului, Titan 1 and Titan 2, whereas three sampling points were selected for Lake Comana. The samples collected into sterile containers, stored, and transported at 4°C were analysed within 24 hours of sampling.

### Measurement of physicochemical parameters

From the water column, a series of physicochemical parameters (oxidation–reduction potential, temperature, percentage saturation of dissolved oxygen, pH, and turbidity) was measured *in situ* with a HI 9828 multi-parameter probe (Hanna Instruments, Woonsocket, RI, USA).

**Microbial analysis**

To perform the quantitative analyses, a serial dilution was prepared.

Using the pour plating method to quantify *heterotrophic bacteria*, sterile Petri plates were inoculated with 1 mL aliquots from each dilution for every replicate. After inoculation, 15 ml of nutrient agar medium (sterile broth media with 20 $g \cdot L^{-1}$ agar), molten and cooled at 45°C, was poured onto the plates and incubated at 37°C. After 48 hours, heterotrophic bacteria counts were determined (Jackson et al. 2000; Sanders, 2012).

The most probable number (MPN) technique was used to determine the number of *faecal coliforms* and *faecal streptococci*. For each dilution and each sample, three tubes were inoculated. MacConkey broth (bile lactose bromcresol purple medium) was added for the cultivation of faecal coliforms, while sodium azide broth containing bromcresol purple was added for the cultivation of faecal streptococci. The inoculated tubes were incubated at 45 °C for 24 h for faecal coliforms and 48 h for faecal streptococci (Berg et al., 1978; Maul & Block, 1983; Sinton et al., 1998; Gronewold &Wolpert, 2008).

To determine the colony-forming units (CFU) of total coliforms, 1 mL of each serial dilution for each duplicate was added to eosin-methyl blue media. The plates were incubated at 37°C for 24 hours (An et al., 2002).

**Data processing**

Violin plots and boxplots were used to display the data distribution. Boxplots were used to highlight the essential statistics of the sample (median and quartiles), while violin plots visualised the full shape of the distribution, including any multimodality and density variations. The width of the violin plot reflects the local density of the data, providing a more detailed picture of the distribution's structure than the quartile representation alone. Combining the two types of graphs provided a more comprehensive characterisation of the data, integrating both central tendency and distributional peculiarities relevant to the interpretation of the results (Hu, 2020).

Heatmaps are powerful visualisation tools for displaying two-dimensional data, effectively revealing patterns shared across subsets of rows and columns. This package excels at connecting multi-source information, making it broadly applicable in diverse data analysis fields, particularly in bioinformatics and genomics (Gu, 2022).

The two-factor ANOVA method examines the simultaneous influence of two qualitative independent variables (factors), in this case, months and lakes, on a quantitative dependent variable, along with their possible interactions. This factorial design allows investigation of the main effects of each factor (month and lake) and detection of a statistical interaction, in which the effect of one factor is modified by the levels of the other factor. A factorial design analyses the effects of two independent variables on a single continuous dependent variable, yielding three results: a main effect for each independent variable and an interaction between the two (Andrade, 2024).

Redundancy Analysis (RDA) is a constrained ordination method used to quantify the relationships between microbial community composition and environmental variables. The technique models variation in abundance data as a function of explanatory factors, allowing the significance of interaction terms to be assessed within a linear framework. RDA extends multivariate regression to multivariate response sets, estimating explained variance and facilitating direct comparison between the community matrix and the environmental variable matrix (Legendre et al., 2010). The software used was Past version 5.2.1, Xlstat add-in 2014 and R-studio R 4.5.2.

## RESULTS

**Physicochemical characterisation of urban and peri-urban lakes**

The temperature boxplots showed a relatively wide distribution of temperatures across all lakes (Figure 2 – Temperature). The water temperature varied across the lakes, with mean values of approximately 17.58-21.74°C, indicating a moderate-to-warm thermal regime during the study period. The minimum values recorded ranged from 6.23°C (Titan 2) to 14.76°C (Comana), and the maximum values ranged between 28.52°C (Titan 2) and 32.23°C (Comana). The means were 21.74°C (Comana), 21.74°C (Tineretului), 17.58°C (Titan 1) and

18.75°C (Titan 2). Also, the boxplots of the lakes showed distinct thermal regimes in Tineretului and Comana, compared to the two Titan lakes, indicating that, in the dynamics of summer and autumn temperatures, the two ecosystems showed lower exposure to extreme values. The two lakes exhibited a stable thermal regime, characterised by progressive warming and cooling of the water without sudden fluctuations.

Regarding pH, the values generally indicated an alkaline range, with minimum values between 8.63 (Titan 1) and 8.91 (Tineretului), and maximum values between 9.53 (Titan 1) and 10.30 (Comana). The averages were 9.58 (Comana), 9.41 (Tineretului), 9.27 (Titan 1) and 9.43 (Titan 2). The differences in the profile of the violin-type boxplots (Figure 2 – pH) suggested that Comana and Tineretului presented a more homogeneous and stable pH, while the Titan lakes, especially Titan 1, exhibited more pronounced chemical fluctuations, reflected by the asymmetry and shape of the distributions. A stable alkaline pH may reflect intense photosynthetic activity and a relatively well-buffered system, whereas more pronounced pH fluctuations may indicate temporary chemical imbalances, with potential implications for microbial community structure and water quality.

The redox potential (ORP) showed very high variability (Figure 2 – ORP), with a general trend towards more oxidising conditions in the urban lakes than in Comana. Negative minima ranged between -82.90 mV (Comana) and -33.50 mV (Titan 1), and positive maxima up to 138.20 mV (Titan 1). The averages were 21.65 mV (Comana), 48.25 mV (Tineretului), 52.82 mV (Titan 1) and 54.15 mV (Titan 2). The boxplots indicated in Comana a frequent alternation between oxidative and reductive conditions, suggesting a more unstable redox dynamic. The relatively broad distribution shape reflected the influence of natural processes, such as the input of organic matter and microbiological activity, characteristic of a less anthropized system. In contrast, urban lakes showed a tendency to exhibit higher ORP values, with higher averages (48.25 mV - Tineretului < 52.82 mV in Titan 1 < 54.15 mV in Titan 2). Thus, the distributions were more concentrated in the oxidative range, with fewer negative values and less extensive negative values. This profile suggested dominant oxidative conditions, associated with better oxygenation and frequent water mixing, typical of managed urban lakes.

Dissolved oxygen (%DO) presented wide ranges, with minimums between 45.10% (Titan 1) and 64.10% (Tineretului) and maximums between 92.90% (Titan 2) and 156.50% (Comana). The averages were 90.48% (Comana), 97.56% (Tineretului), 70.63% (Titan 1) and 65.51% (Titan 2), suggesting generally good to very good levels of oxygenation, with distributions slightly elongated towards high values in Comana. Differences between urban and natural lakes were also observed in oxygen levels. In Lake Comana, the variations were greater, indicating pronounced fluctuations in oxygenation, including frequent episodes of supersaturation. In contrast, in urban lakes, the distributions were more compact and better centred, which explains moderate levels of dissolved oxygen and a lower variability (Figure 2 – DO).

TDS values revealed pronounced differences between urban lakes and Lake Comana, as clearly reflected in the boxplot (Figure 2 – TDS). In Lake Comana, TDS ranged from 381 to 619 mg/L, with an average of 500.33 mg/L, and the relatively wide distribution indicated moderate variability in water mineralisation. The boxplot of the lake highlights seasonal fluctuations in dissolved salt supply, typical of natural ecosystems. In contrast, in urban systems, the boxplots indicate high values, within much lower limits. Lake Tineretului presented the highest values (614-738 $mg \cdot L^{-1}$), with an average of 672.90 $mg \cdot L^{-1}$, and was characterised by a high and constant mineralisation, typical of urban areas. In Titan 1, TDS ranged from 512 $mg \cdot L^{-1}$ to 591 $mg \cdot L^{-1}$, with an average of 547.10 $mg \cdot L^{-1}$ and a relatively compact distribution. In Titan 2, although the average was lower (474.70 $mg \cdot L^{-1}$), the wide range (258-558 $mg \cdot L^{-1}$) suggested greater variability, likely associated with episodic water intakes with varying mineralisation.

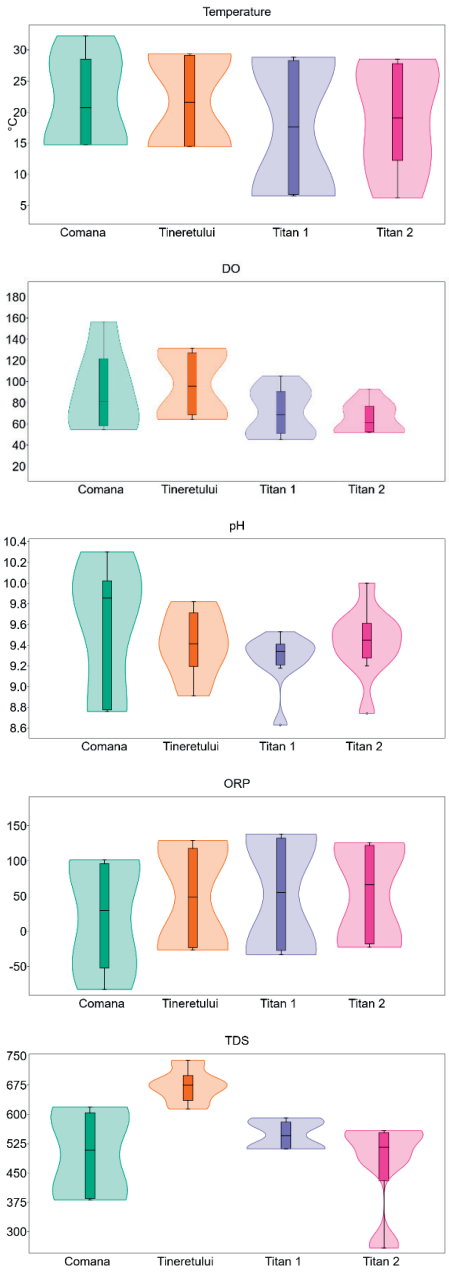



Figure 2. In situ variations of measured physicochemical parameters

**Features of microbial communities in the studied ecosystems**

Microbiological evaluation using general indicators of microbial load (heterotrophic bacteria - HB, total coliforms - TC) as well as specific indicators of faecal contamination (faecal coliforms - FC, faecal streptococci - FS) highlighted varying degrees of anthropogenic pressure on urban lakes.

In Lake Comana, faecal contamination was absent, whereas in urban lakes it was present at varying intensities, indicating episodes of faecal pollution (Figure 3). In Lake Comana, established as a reference system for anthropogenically unaffected conditions, the absence of faecal indicators (FS and FC) and the high productivity of HB confirm the characteristic resilience of these systems. Microbiological values recorded in Comana revealed a stable natural bacterial background, with HB ranging between 2400–8300 CFU·mL$^{-1}$ (mean 5033±1959), low TC (range 2–6, ± 2.53 CFU mL$^{-1}$) and the complete absence of FC and streptococci (0 in all samples), indicating optimal conditions of relatively stable aquatic biota, possibly related to the productivity and organic matter specific to the natural lake (Figure 3).

This ecosystem contrasts sharply with urban lakes, where anthropogenic pressures have produced much more variable microbiological patterns. The high variability in urban lakes underscores the stark contrast between the stability of the natural Comana ecosystem and the disturbed dynamics of urban lakes under anthropogenic pressure.

In Tineretului, the overall microbial load was the highest among all urban ecosystems, with TC reaching 28 CFU·mL$^{-1}$ (mean 7.2 ± 7.87), while faecal contamination remained low (FC 0-0.4, FS average 0.9-0.98), suggesting non-faecal organic inputs (from typical park sources - leaves, sediments, human activity).

Titan 1 and Titan 2 presented the most intense episodes of faecal contamination, with maximum FC of 25 CFU·mL$^{-1}$ (means 4.8 and 4.1, ± 7.7) and FS with maxima between 2.5-4.5 CFU·mL$^{-1}$, indicating irregular inputs of faecal origin.

From the perspective of heterotrophic bacteria, Titan 1 showed intermediate values (300-2600), while Titan 2 showed the greatest ecological instability, with HB ranging from 109 to 8500 CFU·mL$^{-1}$ (average 2550.9), reflecting episodes of intense bacterial proliferation and possible local eutrophication.

The high variability of HB in Titan 2 indicated a pronounced ecological instability, possibly

related to irregular nutrient inputs and unfavourable conditions.

In these ecosystems, the development of coliforms, associated with high levels of heterotrophic bacteria, highlighted differences in the microbiological features of urban lakes compared to those of the natural Lake Comana.

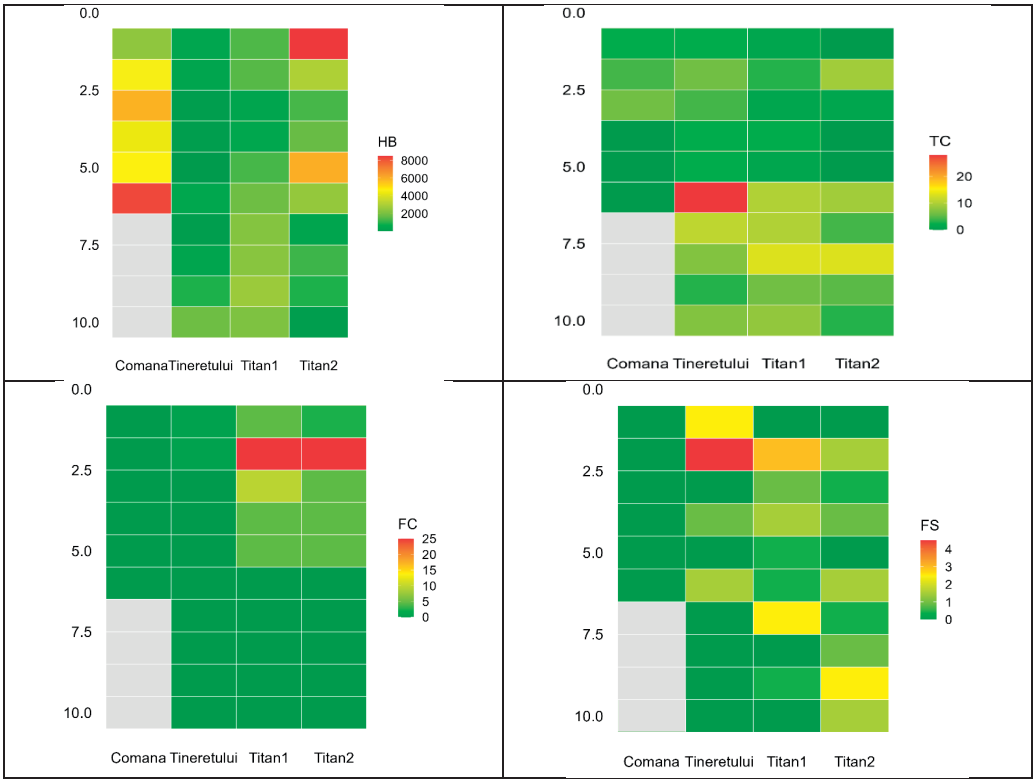



Figure 3. Heatmaps of the abundance of the investigated microbial communities

**Seasonal dynamics and interaction with anthropogenic pressure**

HB bacteria showed distinct spatial and seasonal variations (Table 1), so during the summer the abundances were higher (mean values $5.77\times10^3$ CFU·mL$^{-1}$ - Comana > $2.20\times10^3$ CFU·mL$^{-1}$- Titan 1 > $1.00\times10^3$ CFU·mL$^{-1}$ - Titan 2 > $7.00\times10^2$ CFU·mL$^{-1}$ - Tineretului), compared to the autumn values (mean values - $4.30\times10^3$ CFU·mL$^{-1}$ - Comana > $4.10\times10^3$ CFU·mL$^{-1}$ - Titan 2 > $9.80\times10^2$ CFU·mL$^{-1}$ - Titan 1> $1.77\times10^2$ CFU·mL$^{-1}$ - Tineretului).

TC were absent in Comana in summer (0.00), but were detected in autumn (4.00 CFU·mL$^{-1}$), while in Tineretului the values were higher in summer (11.20 CFU·mL$^{-1}$) compared to autumn (3.20 CFU·mL$^{-1}$).

In Titan 1 and Titan 2 lakes, total coliforms also recorded a decline from summer (9.40 and 6.80 CFU·mL$^{-1}$, respectively) to autumn (means values 1.60 and 2.00 CFU·mL$^{-1}$) (Table 1).

FC, absent in both seasons in Comana, were detected in urban ecosystems, in high abundances in autumn in Titan 1 (9.60 CFU·mL$^{-1}$) and Titan 2 (8.20CFU·mL$^{-1}$).

FS were also present in urban ecosystems, with distinct trends across the three ecosystems investigated.

They were characterised by increases from summer to autumn in Tineretului and Titan 1, whereas in Titan 2, the values were higher in summer (1.36 CFU·mL$^{-1}$) than in autumn (0.56 CFU·mL$^{-1}$) (Table 1).

Table 1. Descriptive statistics and seasonal changes in microbiological indicators (s - summer; a - autumn)

| Type | | Minimum | Maximum | Mean | SD (n-1) |
|---|---|---|---|---|---|
| **Heterotrophic bacteria (CFU·mL$^{-1}$)** | | | | | |
| Comana | s | $4.30\times10^{3}$ | $8.30\times10^{3}$ | $5.77\times10^{3}$ | $2.20\times10^{3}$ |
| | a | $2.40\times10^{3}$ | $5.90\times10^{3}$ | $4.30\times10^{3}$ | $1.77\times10^{3}$ |
| Tineretului | s | $1.00\times10^{2}$ | $1.80\times10^{3}$ | $7.00\times10^{2}$ | $6.82\times10^{2}$ |
| | a | $4.50\times10^{1}$ | $3.30\times10^{2}$ | $1.77\times10^{2}$ | $1.33\times10^{2}$ |
| Titan 1 | s | $1.80\times10^{3}$ | $2.60\times10^{3}$ | $2.20\times10^{3}$ | $2.92\times10^{2}$ |
| | a | $3.00\times10^{2}$ | $1.50\times10^{3}$ | $9.80\times10^{2}$ | $5.81\times10^{2}$ |
| Titan 2 | s | $1.09\times10^{2}$ | $2.50\times10^{3}$ | $1.00\times10^{3}$ | $9.47\times10^{2}$ |
| | a | $1.30\times10^{3}$ | $8.50\times10^{3}$ | $4.10\times10^{3}$ | $3.07\times10^{3}$ |
| **Total coliforms (CFU·mL$^{-1}$)** | | | | | |
| Comana | s | 0.00 | 0.00 | 0.00 | 0.00 |
| | a | 2.00 | 6.00 | 4.00 | 2.00 |
| Tineretului | s | 3.00 | 28.00 | 11.20 | 9.81 |
| | a | 2.00 | 6.00 | 3.20 | 1.79 |
| Titan 1 | s | 6.00 | 13.00 | 9.40 | 2.61 |
| | a | 1.00 | 3.00 | 1.60 | 0.89 |
| Titan 2 | s | 3.00 | 13.00 | 6.80 | 4.15 |
| | a | 0.00 | 9.00 | 2.00 | 3.94 |
| **Faecal coliforms (CFU·mL$^{-1}$)** | | | | | |
| Comana | s | 0.00 | 0.00 | 0.00 | 0.00 |
| | a | 0.00 | 0.00 | 0.00 | 0.00 |
| Tineretului | a | 0.00 | 0.40 | 0.16 | 0.22 |
| | s | 0.00 | 0.00 | 0.00 | 0.00 |
| Titan 1 | s | 0.00 | 0.00 | 0.00 | 0.00 |
| | a | 4.50 | 25.00 | 9.60 | 8.88 |
| Titan 2 | s | 0.00 | 0.00 | 0.00 | 0.00 |
| | a | 2.50 | 25.00 | 8.20 | 9.43 |
| **Faecal streptococci (CFU·mL$^{-1}$)** | | | | | |
| Comana | s | 0.00 | 0.00 | 0.00 | 0.00 |
| | a | 0.00 | 0.00 | 0.00 | 0.00 |
| Tineretului | s | 0.00 | 1.50 | 0.38 | 0.65 |
| | a | 0.00 | 4.50 | 1.58 | 1.93 |
| Titan 1 | s | 0.00 | 2.50 | 0.66 | 1.05 |
| | a | 0.00 | 3.00 | 1.16 | 1.17 |
| Titan 2 | s | 0.40 | 2.50 | 1.36 | 0.79 |
| | a | 0.00 | 1.50 | 0.56 | 0.64 |

Two-way ANOVA analysis revealed significant differences in microbial community structure by ecosystem type and season, with effect sizes varying across the analysed microbiological indicators (Table 2).

For HB, the model explained a high proportion of the total variation ($R^2 = 0.71$) and showed a strong overall effect ($F = 10.02$, $p < 0.0001$). Spatial differences were dominant, with values being significantly more different between urban and natural lakes ($F = 17.09$, $P < 0.0001$). The lake × season interaction was also significant ($F = 6.11$, $p = 0.00$), suggesting that HB seasonal dynamics were influenced by ecosystem type, with distinct responses in urban versus natural lakes.

For TC, the ANOVA model explained 69% of the total variation ($R^2 = 0.69$), indicating a significant overall effect ($F = 9.02$, $p < 0.0001$). TC showed both spatial ($F = 5.00$, $p = 0.01$) and seasonal ($F = 7.57$, $p = 0.01$) differences, also reflected in the lake×season interaction (F

= 10.57, $p < 0.0001$). The results show that seasonal amplitude varied across ecosystems, highlighting the indicator's high sensitivity to environmental changes.

For FC, the model had the highest explanatory power ($R^2 = 0.8$, $F = 26.84$, $p < 0.0001$). Both the ecosystem factor ($F = 18.21$, $p < 0.0001$) and the period ($F = 60.63$, $p < 0.0001$) significantly influenced FC concentrations, indicating a pronounced variability also in the lake×season interaction (Table 2). In contrast, FS showed reduced variability, with the model explaining only 30% of the total variation ($R^2 = 0.30$) and no significant overall effect ($F = 1.73$, $p = 0.14$). No significant spatial or temporal differences in the FS distribution were found, highlighting a uniformity of FS across ecosystems and seasons, reflecting a good ecological stability or reduced sensitivity to the analysed factors.

Table 2. Two-Way ANOVA results for microbiological indicators by lake and season

| | **HB** | **TC** | **FC** | **FS** |
|---|---|---|---|---|
| $R^2$ | 0.71 | 0.69 | 0.87 | 0.30 |
| F | 10.02 | 9.02 | 26.84 | 1.73 |
| p | < 0.0001 | < 0.0001 | < 0.0001 | 0.14 |
| Lake | 17.09 | 5.00 | 18.21 | 2.23 |
| | < 0.0001 | 0.01 | < 0.0001 | 0.11 |
| Season | 0.59 | 7.57 | 60.63 | 0.23 |
| | 0.45 | 0.01 | < 0.0001 | 0.64 |
| Lake×Season | 6.11 | 10.57 | 18.21 | 1.70 |
| | 0.00 | < 0.0001 | < 0.0001 | 0.19 |

RDA analysis indicates a separation of microbial communities based on physicochemical water conditions (Figure 4). RDA results indicated an $R^2$=0.23 (23% total explained variation) and $R^2$adj=0.10 (10%), indicating a moderate effect of physicochemical factors on microbial communities, but significant ($F$=1.85, $p$=0.03 at 999 permutations). Axis 1 dominates (69% of the explained variation), explaining the clear separation Titan/Tineretului vs. Comana; Axis 2 (21%) details the differences TC vs. FC/FS/HB. FS and FC were associated with Axis 1 and were influenced by ORP and pH in the anthropogenic conditions of Titan 1 and Titan 2 lakes, indicating recent faecal inputs. In contrast, HB was positioned in the opposite plot to FC and FS, favoured by oxygenated conditions (% DO) with lower temperatures, indicating distinct niches of heterotrophic bacteria compared to faecal indicators. On the other hand, TC, separated from the other microbial communities, was associated with Axis 2, influenced by increases in temperature and oxygen, and, to a lesser extent, by TDS, indicating distinct ecological conditions. The analysis also shows that, depending on environmental conditions and trends in microbial communities, the studied ecosystems were clearly separated. Thus, urban ecosystems are found in the upper part of the plot, whereas Lake Comana is located in the opposite part; faecal indicators (FC/FS) were the main drivers of ecosystem separation and also validate sources of anthropogenic pollution in urban sites.

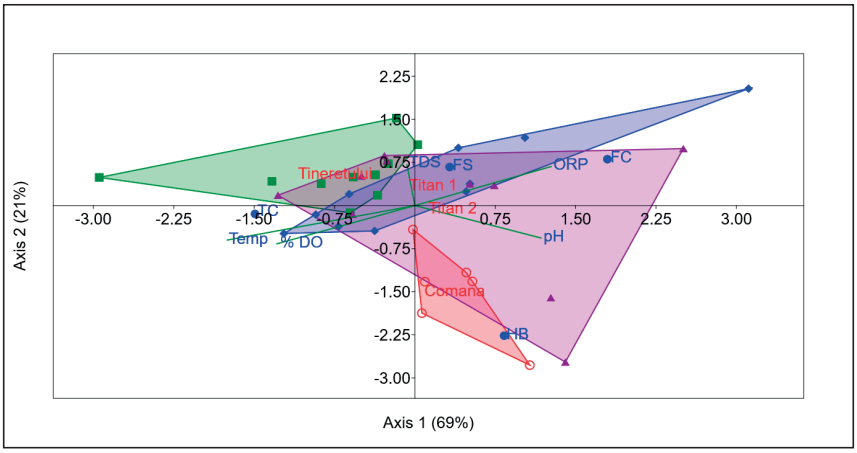



Figure 4. Redundancy analysis (RDA) reveals the relationships between microbial communities and environmental parameters in the investigated aquatic systems

## DISCUSSIONS

The results of our study highlighted a close relationship between the structure and dynamics of microbial communities and environmental conditions in the investigated lakes, demonstrating the impact of the urbanisation gradient and seasonal variability on these communities. Unlike classical descriptive microbiological approaches, the integrated analysis of environmental parameters and microbiological indicators highlighted the ecological mechanisms that control the dynamics of HB communities, as well as those of TC, FC, and FS. Higher values in the warm season were associated with increased abundances of HB across all ecosystems (Figure 2 and Table 1), highlighting the role of temperature in intensifying organic matter degradation. However, the response of microbial communities to this factor varied across ecosystem types. At the peri-urban Lake Comana, HB growth in summer was relatively uniform and correlated with the natural availability of organic matter, indicating a system predominantly controlled by internal processes. In contrast, in urban lakes, especially Titan 2, the high variability of HB suggests an amplified response to episodic nutrient inputs, probably associated with urban runoff and sediment resuspension. Thus, water temperature has been shown to be a primary factor regulating microbial activity, directly influencing metabolic processes and bacterial growth rates (White et al., 1991; Nedwell, 1999). In addition, the alkaline and relatively stable pH created a favourable framework for the development of bacterial communities, but differences in variability between lakes indicate distinct control mechanisms (Wetzel, 2001; Dippong et al., 2023). The stability of pH in Comana and Tineretului suggests a well-buffered system, whereas the more pronounced fluctuations in Titan lakes may reflect temporary imbalances induced by anthropogenic processes, affecting the selection of bacterial taxa tolerant to chemical variations. These differences may contribute to more homogeneous microbial structures in peri-urban lakes and more heterogeneous in urban ones. Instead, redox potential and dissolved oxygen played a central role in the differentiation of microbial niches (Baqué, 2006; Fenchel et al., 2012). In Lake Comana, the alternation of oxic and suboxic conditions (Figure 2 - ORP and DO) favoured the coexistence of microbial communities adapted to variable micro-niches, which explains the general stability of the communities and the absence of faecal indicators. The pronounced fluctuations in dissolved oxygen in the peri-urban Lake Comana reflect a natural ecological control dominated by the circadian cycles of photosynthesis and respiration, amplified by algal and macrophytic biomass and by the mineralisation of organic matter in sediments (Cristini et al., 2017). This dynamic indicates both an intrinsic self-purification capacity and

an increased susceptibility to episodes of benthic hypoxia or anoxia, with direct effects on the distribution and activity of microbial communities and on redox-dependent biogeochemical processes (Tolu et al., 2017). In contrast, the relative stability of dissolved oxygen in urban lakes suggests a more strongly anthropogenically controlled system, influenced by active management, shallow depth, and frequent water-column mixing, which limit stratification and the accumulation of hypoxic zones (Carnohan, 2021; Maier et al., 2021). However, during warm periods, local persistence of low oxygen in the lower layers can favour the release of phosphorus from sediments and intensify eutrophication, with implications for microbial community structure (Radu et al., 2019). In contrast, the predominantly oxidative and more uniform conditions in urban lakes favoured aerobic processes and the persistence of bacteria associated with recent contamination, reflected by the presence of FC and FS (Figure 3). The high and constant TDS values in urban lakes indicate a persistent chemical pressure, which may act as an ecological filter, favouring bacterial communities adapted to increased mineralisation and osmotic stress (Paul & Meyer, 2001; Ghervase et al., 2011). In Comana, moderate TDS variability suggests natural control of mineralisation, without inducing major changes in microbial community structure.

The spatial distribution of microbial communities (Figure 3) clearly reflects the urbanisation gradient, as reported in other urban and peri-urban aquatic ecosystems (Newton et al., 2011; Staley et al., 2013). Lake Comana presented a microbiological profile characteristic of natural ecosystems, dominated by indigenous HB and lacking indicators of faecal contamination. This structure suggests a predominance of autochthonous organic matter and an efficient control of self-purification processes. In contrast, urban lakes showed much more heterogeneous spatial patterns. Titan 1 and Titan 2 were characterised by recurrent episodes of faecal contamination, indicating active or intermittent local sources. The differences between these two lakes, especially the extreme variability of HB in Titan 2, suggest a higher degree of ecological instability, possibly related to morphometry, water residence time and intensity of anthropogenic inputs. Lake Tineretului occupied an intermediate position, with high overall microbial loads but low faecal contamination, indicating a dominance of non-faecal organic sources.

Seasonality amplified differences between ecosystems (Table 1), in agreement with patterns observed in temperate lakes under anthropogenic pressures (Sommer et al., 2012; Lazăr et al., 2017). In urban lakes, increasing temperatures and warm-season rainfall events were followed by higher total coliform levels, and, in some cases, by an increase in faecal contamination until autumn. This seasonal lag suggests the accumulation and persistence of faecal bacteria in sediments, followed by resuspension and remobilisation. In Comana, seasonal variations were less pronounced and were not associated with the appearance of faecal indicators, indicating a more resilient system to seasonal fluctuations. The presence of TC only in autumn can be interpreted as due to sediment resuspension or natural inputs, with no direct link to faecal pollution.

The ANOVA results (Table 2) confirm that ecosystem type is the main determinant of microbial community structure, with season having a secondary but significant role in urban ecosystems. The lake × season interaction indicates that the response of microbial communities to seasonal variations is modulated by the degree of urbanisation. Here, the RDA biplot (Figure 4) integrates these observations, highlighting the clear separation of urban lakes from Comana based on the association of faecal indicators with ORP, pH and TDS, a pattern frequently encountered in aquatic ecosystems influenced by urbanisation (Borcard et al., 2018; Dimpor et al., 2024). The positioning of HB relative to dissolved oxygen and temperature suggests that natural microbial communities follow ecological trajectories distinct from those influenced by anthropogenic factors. Overall, our results indicate that urbanisation not only influences the level of microbiological contamination but also the stability and predictability of microbial communities. Urban ecosystems are characterised by more dynamic communities, with pronounced fluctuations and rapid

responses to environmental changes, whereas peri-urban ecosystems exhibit more stable communities, driven by internal ecological processes. A relevant observation is the potential role of sediments as a microbiological reservoir, especially in urban lakes, where seasonal remobilisation can significantly contribute to the dynamics of bacterial communities (Jamieson et al., 2005; Pachepsky & Shelton, 2011). Also, differences between urban lakes suggest that geomorphological features of ecosystems can significantly modulate microbial responses to anthropogenic pressure.

## CONCLUSIONS

The natural lake Comana presents stable physicochemical parameters and balanced microbial communities, without faecal contamination, while the urban lakes (Tineretului and Titan) record higher and more variable TDS, ORP, and pH values, associated with the presence of FC and fluctuating number of HB, reflecting anthropogenic pressure. The distribution of microbial communities is correlated with the physicochemical conditions, highlighting clear ecological differences between natural and urban ecosystems and underlining the need for an adapted management of water quality.

## ACKNOWLEDGEMENTS

This research was funded by the Institute of Biology Bucharest of Romanian Academy, by project no RO1567-IBB02/2026 and project no RO1567-IBB05/2026.

## REFERENCES

An, Y.-J., Kampbell, D. H., & Breidenbach, G. P. (2002). *Escherichia coli* and total coliforms in water and sediments at lake marinas. *Environmental Pollution, 120*(3). 771–778. https://doi.org/10.1016/S0269-7491(02)00173-2

Andrade, C. (2024). Understanding Factorial Designs, Main Effects, and Interaction Effects: Simply Explained with a Worked Example. *Indian Journal of Psychological Medicine*, 46(2). 175–177. https://doi.org/10.1177/02537176241237066

Baqué, D. (2006). *The anthropogenic perturbations of the hydrographical network of the Garonne basin's, cases of metals and nitrates.* (Doctoral dissertation, Université Paul Sabatier – Toulouse III). HAL Archives. https://tel.archives-ouvertes.fr/tel-00128208

Berg, G., Dahling, D. R., Brown, G. A., & Berman, D. (1978). Validity of fecal coliforms, total coliforms, and fecal streptococci as indicators of viruses in chlorinated primary sewage effluents. *Applied and Environmental Microbiology,* 36(6). 880–884.

Borcard, D., Gillet, F., & Legendre, P. (2018). *Numerical Ecology with R* (2nd ed.). SpringerCham. https://doi.org/10.1007/978-3-319-71404-2

Carnohan, S. (2021). *Processes, tools, and frameworks for improving water resources management*. (Master's thesis, DTU Environment). DTU Environment. https://local.forskningsportal.dk/local/dki-cgi/ws/cris-link?src=dtu&id=dtu-587f4700-7428-4abb-84da-059943c3bb26&ti=Processes%2C%20Tools%2C%20and%20Frameworks%20for%20Improving%20Water%20Resources%20Management

Cristini, P. A., Tietze, E., Francesco, C. G. D., & Martínez, D. (2017). Water geochemistry of shallow lakes from the southeastern Pampa plain, Argentina and their implications on mollusk shells preservation. *Science of The Total Environment*, 603-604. 155-166. https://doi.org/10.1016/j.scitotenv.2017.06.043

Dimpor, J. J., Lucky, O. P., Kwarkye, D. F., Watts, S., Oguayo, C. P., Ojewole, C. O., & Kusi, J. (2024). Identifying spatiotemporal patterns and drivers of fecal indicator bacteria in an urban lake for water quality assessment and management. *Heliyon,* 11(1), e40955. https://doi.org/10.1016/j.heliyon.2024.e40955

Dippong, T., Mihali, C., & Avram, A. (2023). Water Physico-Chemical Indicators and Metal Assessment of Teceu Lake and the Adjacent Groundwater Located in a Natura 2000 Protected Area, NW of Romania. *Water*, *15*(22). 3996. https://doi.org/10.3390/w15223996

Fenchel, T., King, G. M., & Blackburn, T. H. (2012). *Bacterial Biogeochemistry: The Ecophysiology of Mineral Cycling* (3rd ed.). Academic Press, London.

Ghervase, L., Iojă, C., Cârstea, E. M., & Savastru, D. (2011). *Antropic influence on lakes water quality - case study of Bucharest city*. Paper presented at the 11th edition of the World Wide Workshop for Young Environmental Scientists (WWW-YES—2011) - Urban Waters: resource or risks?, Arcueil, France. https://hal.science/hal-00607934

Gronewold, A. D., & Wolpert, R. L. (2008). Modeling the relationship between most probable number (MPN) and colony-forming unit (CFU) estimates of fecal coliform concentration. *Water Research, 42*(13). 3327–3334. https://doi.org/10.1016/j.watres.2008.04.011

Gu, Z. (2022). Complex heatmap visualization. Imeta. 1(3), e43.https://doi.org/10.1002/imt2.43

Hu, K. (2020). Become Competent within One Day in Generating Boxplots and Violin Plots for a Novice without Prior R Experience. *Methods and Protocols*, 3(4). 64. https://doi.org/10.3390/mps3040064

Jackson, R. W., Osborne, K., Barnes, G., Jolliff, C., Zamani, D., Roll, B., Stillings, A., Herzog, D., Cannon, S., & Loveland, S. (2000). Multiregional

evaluation of the SimPlate heterotrophic plate count method compared to the standard plate count agar pour plate method in water. *Applied and Environmental Microbiology, 66*(1). 453–454. https://doi.org/10.1128/AEM.66.1.453-454.2000

Jamieson, R. C., Gordon, R. J., Sharples, K. E., Stratton, G. W., & Madani, A. (2005). Movement and persistence of fecal bacteria in agricultural soils and subsurface drainage water: A review. *Canadian Biosystems Engineering*, *47*. 1.1–1.9.

Kapetanović, D., Katouli, M., & Lušić, D. V. (2024). Microbial Communities in Changing Aquatic Environments. *Microorganisms*, *2*(4). 726. https://doi.org/10.3390/microorganisms12040726

Kiersztyn, B., Chróst, R. J., Kaliński, T., Siuda, W., Bukowska, A., Kowalczyk, G., & Grabowska, K. (2019). Structural and functional microbial diversity along a eutrophication gradient of interconnected lakes undergoing anthropopressure. *Scientific Reports*, *9*. 11144. https://doi.org/10.1038/s41598-019-47577-8

Lazăr, V., Curuțiu, C., Lia-Mara, D., Holban, A. M., Gheorghe, I., Marinescu, F., Ilie, M., Иванов, A. C., Dobre, D., & Chifiriuc, M. C. (2017). Physico-Chemical and Microbiological Assessment of Organic Pollution in Plain Salty Lakes from Protected Regions. *Journal of Environmental Protection*, *8*. 1474. https://doi.org/10.4236/jep.2017.812091

Legendre, P., Oksanen, J., & Braak, C. J. F. ter. (2010). Testing the significance of canonical axes in redundancy analysis, *Methods in Ecology and Evolution*, *2*(3). 269–277. https://doi.org/10.1111/j.2041-210x.2010.00078.x

Lew, S., Glińska-Lewczuk, K., Burandt, P., Grzybowski, M., & Obolewski, K. (2023). Fecal bacteria in coastal lakes: An anthropogenic contamination or natural element of microbial diversity? *Ecological Indicators*, *152*. 110370. https://doi.org/10.1016/j.ecolind.2023.110370

Loucif, K., & Chenchouni, H. (2024). Water physicochemical quality as driver of spatial and temporal patterns of microbial community composition in lake ecosystems. *Applied Water Science*, *14*. 115. https://doi.org/10.1007/s13201-024-02176-5

Maier, M.-S., Teodoru, C. R., & Wehrli, B. (2021). Spatio-temporal variations in lateral and atmospheric carbon fluxes from the Danube Delta. *Biogeosciences*, *18*(4). 1417–1437. https://doi.org/10.5194/bg-18-1417-2021

Marcondes, M. Â., Pessôa, R., Duarte, A. J. da S., Clissa, P. B., & Sanabani, S. S. (2024). Temporal patterns of bacterial communities in the Billings Reservoir system *Scientific Reports*, *14*(1). 2062. https://doi.org/10.1038/s41598-024-52432-6

Maul, A., & Block, J. C. (1983). Microplate fecal coliform method to monitor stream water pollution. *Applied and Environmental Microbiology, 46*(5). 1032–1037. https://doi.org/10.1128/aem.46.5.1032-1037.1983

Mercan, D., & Arslan, N. (2023). Use of biomonitoring tools to detect water quality-dependent ecosystem (macroinvertebrate) responses in lentic systems: the examples of Lakes İznik and Manyas, Türkiye. *Oceanological and Hydrobiological Studies*, *52*(1). 79–89. https://doi.org/10.26881/oahs-2023.1.06

Mititelu-Ionuș, O., Goga, C.I., & Simulescu, D. (2020). Lakes Ecosystem Responses to Human Pressures a Case Study in Southwestern Romania. *Polish Journal of Environmental Studies*, *30*(2). 1737–1747. https://doi.org/10.15244/pjoes/126400

Nedwell, D. B. (1999). Effect of low temperature on microbial growth: lowered affinity for substrates limits growth at low temperature. *FEMS Microbiology Ecology*, *30*. 101–111. https://doi.org/10.1111/j.1574-6941.1999.tb00639.x

Newton, R. J., Jones, S. E., Eiler, A., McMahon, K. D., & Bertilsson, S. (2011). A guide to the natural history of freshwater lake bacteria. *Microbiology and Molecular Biology Reviews*, *75*. 14–49. https://doi.org/10.1128/MMBR.00028-10

Orel, N., Fadeev, E., Klun, K., Ličer, M., Tinta, T., & Turk, V. (2022). Bacterial Indicators Are Ubiquitous Members of Pelagic Microbiome in Anthropogenically Impacted Coastal Ecosystem. *Frontiers in Microbiology*, *12*. 765091. https://doi.org/10.3389/fmicb.2021.765091

Pachepsky, Y. A., & Shelton, D. R. (2011). Escherichia coli and fecal coliforms in freshwater and estuarine sediments. *Critical Reviews in Environmental Science and Technology*, *41*. 1067–1110. https://doi.org/10.1080/10643380903392718

Paul, M. J., & Meyer, J. L. (2001). Streams in the urban landscape. *Annual Review of Ecology and Systematics*, *32*. 333–365. https://doi.org/10.1146/annurev.ecolsys.32.081501.114040

Radu, V.-M., Ionescu, P., Deák, G., Ivanov, A. A., Diacu, E., & Anghel, A. (2019). Quality Assessment of Some Freshwater Resources Located in Bucharest and Surrounding Areas. III. Case Study: Trophic Status Assessment of Mogosoaia, Herastrau and Pantelimon Lakes. *Revista de Chimie*, *70*(11). 3778. https://doi.org/10.37358/rc.19.11.7646

Roguet, A., & Lucas, F. S. (2012). *Impact of multiple disturbances on microbiological quality of urban and peri-urban lakes.* Paper presented at the 12th edition of the World Wide Workshop for Young Environmental Scientists (WWW-YES-2011) - Urban Waters: resource or risks? Arcueil, France. https://hal-enpc.archives-ouvertes.fr/hal-00709645

Sanders, E. R. (2012). Aseptic laboratory techniques: Plating methods. *Journal of Visualized Experiments*, *(63)*, e3064. https://doi.org/10.3791/3064

Sinton, L. W., Finlay, R. K., & Hannah, D. J. (1998). Distinguishing human from animal faecal contamination in water: A review. *New Zealand Journal of Marine and Freshwater Research, 32*(2). 323–348. https://doi.org/10.1080/00288330.1998.9516828

Sommer, U., Adrian, R., De Senerpont Domis, L., Elser, J. J., Gaedke, U., Ibelings, B., Lürling, M., Molinero, J. C., Mooij, W. M., van Donk, E., & Winder, M. (2012). Beyond the Plankton Ecology Group (PEG) model: mechanisms driving plankton succession.

*Annual Review of Ecology, Evolution, and Systematics*, *43*. 429–448. https://doi.org/10.1146/annurev-ecolsys-110411-160251

Staley, Z. R., Chase, E., Mitraki, C., Crisman, T. L., & Harwood, V. J. (2013). Microbial water quality in freshwater lakes with different land use. *Journal of Applied Microbiology, 115*(5). 1240–1250. https://doi.org/10.1111/jam.12312

Tolu, J., Rydberg, J., Meyer-Jacob, C., Gerber, L., & Bindler, R. (2017). Spatial variability of organic matter molecular composition and elemental geochemistry in surface sediments of a small boreal Swedish lake. *Biogeosciences*, *14*(7). 1773.

Wetzel, R. G. (2001). *Limnology: Lake and River Ecosystems* (3rd ed.). Academic Press.

White, P. A., Kalff, J., Rasmussen, J. B., & Gasol, J. M. (1991). The effect of temperature and algal biomass on bacterial production and specific growth rate in freshwater and marine habitats. *Microbial Ecology*, *21*. 99–118. https://doi.org/10.1007/BF02539147

Scientific Papers. Series E. Land Reclamation, Earth Observation & Surveying, Environmental Engineering. Vol. XV, 2026
Print ISSN 2285-6064, CD-ROM ISSN 2285-6072, Online ISSN 2393-5138, ISSN-L 2285-6064

# XRF-BASED ASSESSMENT OF ELEMENT ACCUMULATION IN *PHRAGMITES AUSTRALIS* ACROSS FRESHWATER, URBAN, AND SALINE AQUATIC ECOSYSTEMS: IMPLICATIONS FOR NATURAL FILTRATION AND ENVIRONMENTAL RISK

**Mirela Mădălina MOLDOVEANU[1], Larisa Isabela FLORESCU[1], Raluca Alexandra MIHAI[2], Cristian BANCIU[1], Maria Iasmina MOZA[3, 4], Doru Simon DOBRE[1], Cristina Alina DUMITRACHE[1, 5], Rodica Daniela CATANĂ[1]**

[1]Institute of Biology Bucharest of Romanian Academy, 296 Splaiul Independentei, District 6, Bucharest, Romania
[2]CIAM, Department of Life Science and Agriculture, Universidad de Las Fuerzas Armadas-ESPE, Av. General Ruminahui S/N y, 171103 Sangolqui, Ecuador
[3]University of Bucharest, Faculty of Biology, Department of Botany and Microbiology, 91-95 Splaiul Independentei, District 5, Bucharest, Romania
[4]Moza Foundation, 1 Cetatea Histria, Bucharest, Romania
[5]School of Advanced Studies of the Romanian Academy (SCOSAAR), 010071, Bucharest, Romania

Corresponding author email: larisa.florescu@ibiol.ro

***Abstract***

*Our study uses X-ray fluorescence spectroscopy to assess element accumulation in Phragmites australis across three distinct aquatic environments. We identified spatial patterns reflecting both the natural background and varying levels of human influence. Natural freshwater exhibited moderate concentrations of geogenic elements, including calcium (Ca), strontium (Sr), barium (Ba), manganese (Mn), and titanium (Ti). In contrast, urban freshwater showed higher levels of iron (Fe), aluminium (Al), copper (Cu), zinc (Zn), and lead (Pb). This indicates an anthropogenic signature associated with runoff, wastewater, and urban infrastructure. Saline lakes exhibited distinct elemental profiles, characterised by elevated levels of sodium (Na), potassium (K), calcium (Ca), and chloride (Cl). These patterns suggest mineralisation processes and physiological adjustments to cope with salinity stress. Rare elements (astatine (At), found in deltaic and urban locations) indicate localised geochemical traits. The accumulation patterns across ecosystems highlight the dual ecological role of the reed. It acts as a natural filtration system, and it can also serve as a potential vector for transferring elements within food webs. These findings support the use of Phragmites as a bioindicator for assessing environmental quality.*

***Key words****: aquatic ecosystems, element accumulation, environmental risk, natural filtration, Phragmites australis.*

## INTRODUCTION

Aquatic ecosystems are subject to increasing geochemical and anthropogenic pressures from industrial activities, agriculture, urbanisation, and climate change. In these systems, geochemical processes are dynamic, and thus common elements and potentially toxic metals are mobilised, transported, and transformed in water bodies through complex interactions. Under these conditions, emergent vegetation acts simultaneously as a biogeochemical interface, a biological filter, and a bioindicator of environmental conditions. The species *Phragmites australis* (Cav.) Trin. ex Steud, it is extremely widespread and adaptable to different conditions, with a remarkable capacity to colonise diverse habitats, from freshwater ecosystems to hypersaline waterbodies or urban systems. The species is characterised by high biomass production and stress tolerance, which is why it is frequently used in phytoremediation and pollution monitoring studies (Chapligin et al., 2022). In addition, its ability to accumulate elements from sediments, water, and atmospheric deposition makes it a valuable bioindicator of metal contamination and local geochemical processes (Weis & Weis, 2004; Chitimus et al., 2023). The sediment composition, water chemistry, salinity,

hydrological dynamics, and anthropogenic pressures influence the distribution and uptake of elements in aquatic biota. For example, lithogenic elements generally reflect the natural geochemical background and sedimentary features and transport, thus indicating aspects of mineral fractions and detrital processes (Taylor & McLennan, 1995; Cullers, 2002). In saline and hypersaline environments, salinity plays a major control factor, influencing the mobility and bioavailability of elements through complex geochemical processes such as chloride complexation, flocculation, and authigenic precipitation. These processes can significantly modify the distribution of elements, affecting their availability to aquatic organisms and emergent vegetation (O'Day et al., 2004; Warren, 2006; Acosta et al., 2023).

A major focus is on potentially toxic elements such as As, Pb, Cu, Zn, and Ni, which are frequently associated with industrial activities, road traffic, and atmospheric deposition (Pacyna & Pacyna, 2001; Thorpe & Harrison, 2008; Charlesworth et al., 2011). Recently, there has been a particular interest in rare earth elements (REE), which are increasingly used as geochemical tracers due to their conservative behaviour and sensitivity to sedimentary fractionation and transport processes (Piper & Bau, 2013; Song et al., 2023; Hatje et al., 2024). Studying the accumulation of REE in plant biomass can provide valuable information about sedimentary sources, redox conditions and biological uptake mechanisms. In the context of increasing anthropogenic pressure on wetlands, assessing plant elemental uptake offers an integrative approach to understanding biogeochemical processes. X-ray fluorescence (XRF) analysis offers a rapid and robust method for the simultaneous determination of a wide spectrum of elements in biological and sedimentary material (Jenkins, 1999; Mondal et al., 2021).

The aim of the study is to evaluate elemental accumulation in *Phragmites australis* from deltaic, urban, and saline aquatic ecosystems using XRF analysis, and to determine the role of the species as a geochemical bioindicator and natural filter of contaminants. The objectives are: the determination of the elemental composition, the comparison of geochemical traits between *deltaic*, *saline* and urban ecosystems, the identification of potential sources of elements and the evaluation of the influence of ecosystem conditions on the bioavailability of elements.

Despite the extensive use of *Phragmites australis* as a bioindicator, comparative assessments across freshwater, urban, and saline ecosystems remain limited. Existing studies rarely integrate geogenic, anthropogenic, and rare earth element signatures into a unified ecological interpretation. This study addresses this gap by providing a multi-environmental evaluation of elemental accumulation patterns using XRF.

## MATERIALS AND METHODS

***Study site.*** The sampling of *Phragmites australis* specimens was carried out, including both aboveground and belowground biomass from each sampling point from ecotonal areas associated with different types of aquatic waterbodies as follows (Figure 1):

• Brackish/*saline* ecosystems: Braila Salt Lake, Techirghiol Lake and Musura Bay.

• *Urban* freshwater ecosystems: Fundeni and Cernica lakes.

• Danube Delta freshwater ecosystems: Eracle Canal, Sulina Branch and Rădăcinos, La Amiază, Miazăzi, Matița and Bogdaposte lakes.

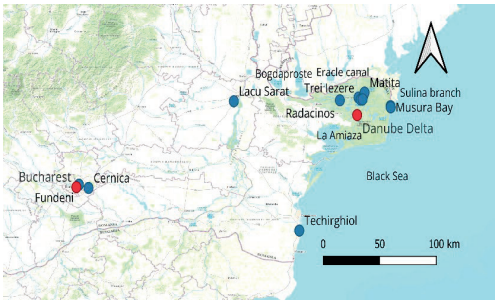



Figure 1. The map of the sampling stations (the red dots-Danube Delta and Bucharest, blue dots - sampling points) - (QGIS 3.40.15- an open-source Geographic Information System)

At each site, three independent *Phragmites australis* specimens were collected to ensure spatial representativeness. Both aboveground and belowground tissues were sampled from individuals located at least 5 meters apart to avoid clonal redundancy. All samples were

collected during the same season to minimize phenological variability.

***Laboratory analysis***. Leaves and roots were separated and prepared for laboratory analysis. The plant material was dried for 2 hours at 60°C, then mechanically ground with a porcelain mortar and pestle. 20 g were taken from each sample, which were subsequently subjected to a calcination process for 2 hours at 550°C in a muffle furnace (Nabertherm LE 6/11/B150). The obtained ash was analysed for elemental composition using a wavelength-dispersive X-ray fluorescence spectrometer (Rigaku ZSX100e, Supermini model). The equipment allows the identification of elements at concentrations of 0.1-100%. For analysis, 1 g of ash was introduced into 30 mm-diameter sample cells, sealed on both sides with 6 μm polypropylene foil, and fixed with a Snap-On ring. The method principle consists of irradiating the sample with X-rays and recording the characteristic reflection angle (θ) for each element. The instrument software converts the signal intensity into mass percentages of elementary oxides (Jenkins, 1999). The percentage values obtained were transformed into absolute concentrations (mg $kg^{-1}$ dry weight) (Mondal et al., 2021). The XRF method may underestimate volatile elements such as Hg, Se, and S due to partial loss during calcination at 550°C. Additionally, elements present near the detection limit (0.1%) may exhibit higher analytical uncertainty. These limitations were considered when interpreting trace and rare element concentrations.

The detected elements were grouped into functional categories based on their predominant ecological role and environmental origin. Classification criteria included geogenic background versus anthropogenic contribution, biological relevance, and toxicity. Thus, elements were assigned to (1) geogenic/macronutrients, (2) anthropogenic and potentially ecotoxic metals, (3) rare earth elements (REE), and elements identified in low/trace concentrations.

***Data processing***. Principal Component Analysis (PCA) was used to explore relationships among the identified elements and to reduce the dataset's dimensionality while preserving most of the total variation (Legendre & Legendre, 2012). Agglomerative Hierarchical Clustering (AHC) was applied to identify similar groupings between elements based on the analysed characteristics (Kassambara, 2017). Analysis of Similarities (ANOSIM) was used to test differences in elemental composition among ecosystem types (Clarke, 1993). The data were transformed by log(n+1). The statistical processing was performed using the XLSTAT add-in (version 2014) and PAST 4.16c (Hammer et al., 2001).

## RESULTS AND DISCUSSIONS

***Elemental composition of Phragmites australis across ecosystem types***.

The results are presented according to the three functional groups of elements: geogenic/macronutrients, anthropogenic metals, and rare/trace elements. Differences among deltaic, saline, and urban ecosystems are highlighted to identify the dominant environmental drivers shaping elemental accumulation in *Phragmites australis*. Analysis of the elemental composition of *Phragmites australis* samples revealed differences in element content across the ecosystems investigated. 58 elements were identified, which varied spatially as follows: 55 *deltaic* > 48 *urban* > 45 *saline* ecosystems. The *urban* environment showed enrichment in metals of anthropogenic origin; the natural *deltaic* ecosystems were dominated by elements indicative of lithogenic input; and the *saline* environments were characterised by elements influenced by the geochemistry of mineralised waters (Table 1, Table 2, and Table 3).

The *deltaic* environment was characterised by elevated concentrations of Fe, Rb, Zr, and elements from the REE category (Table 1, Table 2), indicating the influence of fluvially transported detrital matter and fine sediments rich in mineral fractions. Thus, the composition of the reed in this sector mainly reflected the natural geochemical background and less anthropogenic pressure. In addition, the high variability in Fe, Zn, and Cr may indicate heterogeneous sources and variable conditions for mobilisation and bioaccumulation.

In contrast, in the *saline* lakes, higher concentrations of Hg, Ba, Sr and Mo were recorded (Table 1, Table 3), an association that

may suggest specificities in the mobilisation of elements under conditions of high salinity and a specific redox potential, reflecting the hydrogeochemical characteristics of this type of habitat.

Table 1. The geogenic group elemental concentrations (mg/kg DW) in *Phragmites australis* across *deltaic*, *saline*, and *urban* ecosystems

| | ***Deltaic*** | ***Saline*** | ***Urban*** |
|---|---|---|---|
| Al | 0.001 | 0.008 | N/A |
| Ba | 0.135±0.089 | 0.216±0.124 | 0.206±0.091 |
| Br | 0.009±0.01 | 0.018±0.014 | 0.049 |
| Ca | 0.016±0.012 | 0.007±0.004 | 0.018±0.012 |
| Cl | 0.006±0.006 | 0.004±0.003 | 0.003 |
| Fe | 0.182±0.15 | 0.155±0.144 | 0.054±0.067 |
| I | 0.087 | 0.031 | |
| K | 0.03±0.021 | 0.021±0.013 | 0.02±0.008 |
| Mo | 0.005 | 0.026±0.036 | 0.017±0.007 |
| P | 0.01±0.005 | 0.03±0.021 | 0.035±0.008 |
| Rb | 0.027±0.03 | 0.004±0.001 | 0.007±0.003 |
| S | N/A | 0.002 | N/A |
| Se | 0.01±0.009 | 0.011±0.005 | 0.019±0.016 |
| Si | 0.009±0.008 | 0.009±0.008 | 0.007±0.007 |
| Sr | 0.011±0.003 | 0.018±0.014 | 0.012±0.004 |
| Th | 0.014 | | 0.031±0.012 |
| Ti | 0.047±0.026 | 0.056±0.043 | 0.094±0.066 |
| U | 0.011±0.002 | N/A | 0.014±0.003 |
| Zr | 0.034±0 | N/A | N/A |

Table 2. The REE and trace groups elemental concentrations (mg/kg DW) in *Phragmites australis* across *deltaic*, *saline*, and *urban* ecosystems (REE - Ce-Y, trace elements – Ag-W)

| | ***Deltaic*** | ***Saline*** | ***Urban*** |
|---|---|---|---|
| Ce | 0.129±0.09 | 0.121±0.04 | 0.128±0.02 |
| Dy | 0.042±0.021 | 0.052±0.045 | 0.095±0.048 |
| Er | | 0.03±0.015 | 0.039±0.008 |
| Eu | 0.014 | 0.063±0.082 | 0.007 |
| Gd | 0.09 | 0.12±0.042 | 0.082±0.019 |
| Ho | 0.055±0.034 | 0.059±0.029 | 0.08±0.01 |
| La | 0.17±0.214 | 0.18±0.096 | 0.178±0.048 |
| Lu | 0.05±0.027 | 0.092 | |
| Nd | 0.186 | 0.087±0.054 | 0.092±0.041 |
| Pr | 0.098±0.083 | 0.195 | 0.183±0.026 |
| Sm | 0.031 | 0.067±0.056 | 0.082±0.038 |
| Tb | 0.041±0.036 | 0.045±0.032 | 0.083±0.003 |
| Tm | 0.008 | 0.032±0.038 | |
| Y | 0.012±0.012 | | 0.054±0.064 |
| Ag | 0.065±0.025 | 0.077±0.043 | 0.103±0.079 |
| Au | 0.025±0.003 | 0.041±0.032 | 0.063±0.02 |
| Bi | | | 0.055±0.03 |
| Ga | 0.006±0.002 | 0.022 | 0.018 |
| Ge | 0.036±0.026 | 0.025±0.018 | 0.044±0.003 |
| Hf | 0.065±0.045 | 0.076±0.003 | 0.139 |
| Ir | | 0.039±0.006 | |
| Nb | 0.009±0.007 | 0.007±0.003 | 0.013±0.009 |
| Pt | 0.042 | | 0.022 |
| Re | 0.054±0.015 | 0.05±0.027 | 0.054±0.027 |
| Ta | | 0.007 | |
| W | 0.04±0.04 | 0.029 | 0.029 |

Elements indicating anthropogenic activity showed an obvious enrichment in the *urban* environment, with higher values recorded for As, Pb, Mn, and Tl (Table 3), as well as Br, suggesting the influence of pollution sources associated with traffic, industrial activities, and atmospheric deposition (Wei & Yang, 2010).

Table 3. The anthropogenic group elemental concentrations (mg/kg DW) in *Phragmites australis* across *deltaic*, *saline*, and *urban* ecosystems

| | ***Deltaic*** | ***Saline*** | ***Urban*** |
|---|---|---|---|
| As | 0.048±0.038 | 0.043±0.023 | 0.069±0.023 |
| Co | 0.004±0.001 | 0.019±0.005 | 0.018±0.006 |
| Cr | 0.074±0.078 | 0.035 | 0.073±0.097 |
| Cu | 0.015±0.012 | 0.003 | 0.01±0.007 |
| Hg | 0.025±0.009 | 0.07±0.041 | 0.038 |
| Mn | 0.049±0.029 | 0.045±0.028 | 0.093±0.039 |
| Ni | 0.025±0.019 | 0.003 | 0.019 |
| Pb | 0.081 | 0.052±0.037 | 0.083 |
| Sb | 0.068 | 0.016 | |
| Te | 0.079 | 0.027 | |
| Tl | 0.029 | 0.029±0.027 | 0.049 |
| V | 0.046±0.014 | 0.053±0.05 | 0.035±0.017 |
| Zn | 0.058±0.072 | 0.02±0.017 | 0.017±0.012 |

Recent studies have shown that Phragmites australis can effectively bioaccumulate Fe, Mn, Cd, Cr, Ni and Pb, with most metals being retained in belowground tissues, highlighting its phytostabilization potential (Samadi et al., 2024). This distribution supports the reed's ability to retain and integrate metal contaminants from the water column and

sediments, functioning as a biological filter of *urban* pollution.

ANOSIM analysis indicated a statistically significant difference between ecosystems (R = 0.0786, $p$ = 0.0179), with distinct elemental content between at least two of the analysed habitat types. Although the analysis highlights a reduced separation between groups, paired tests indicate that the significant difference is primarily driven by the contrast between *deltaic* and *urban* areas ($p$ = 0.0015). There were no significant differences between *deltaic* and *saline* ($p$ = 0.37) or between *saline* and *urban* ($p$ = 0.29).

Regarding the weight of the groups in the sample (Figure 2), the results showed that geogenic elements (Fe, Ba, Mn, Ti, Ca, K) were dominant, reflecting their structural role and their availability in sediments. The identified elements also varied slightly depending on the habitats evaluated, such as in *deltaic* (Fe>Ba>Mn>Ti), in *saline* (Fe>Ba>Ti>Mn), but in *urban* (Ba>Mn>Ti>Fe) (Table 1, Table 2, Table 3) ecosystems. This predominance reflects the availability of elements, which varies across ecosystems and with plant assimilation under different environmental conditions. In contrast, elements of anthropogenic origin (As, Cr, Zn, Cu, Ni, Pb, Sb) were present at lower levels, but their clear presence indicated external contributions from human activities. This was observed through the dominance of these elements, which varied slightly depending on the type of ecosystem, in the delta (As>Cr>Zn>V), while in the *saline* (As>V>Hg>Pb) and *urban* ecosystems (As>Cr>Pb>V) (Table 1, Table 2, Table 3). N/A values in the tables indicate concentrations below the detection limit of the XRF instrument or signals that could not be reliably quantified due to matrix interferences.

The share of elements with a very low content (trace) as well as of rare earth elements (REE - La, Ce, Nd, Pr or Dy) (Figure 2), may reflect local lithological particularities, but the ability of the reed to accumulate selectively. The REE distribution revealed a differentiated pattern of fractionation across environments (Table 2), suggesting variations in sedimentary sources, redox conditions, and biological absorption mechanisms, providing an ecological indicator (Song et al., 2023). This selective accumulation is essential, as REEs form a chemical group that can facilitate understanding of aquatic or terrestrial conditions, whether natural or anthropogenic (Hatje et al., 2024).

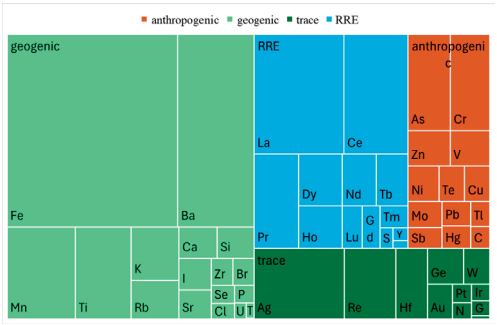



Figure 2. Elemental composition of *Phragmites australis* samples

PCA based on elements indicative of anthropogenic pollution (Figure 3) revealed a close relationship between the *deltaic* and *urban* environments, suggesting common anthropogenic influences or the transport of contaminants into the *deltaic* system, while the *saline* ecosystems remained distinct due to the dominant natural geochemical control. PCA analysis of elements related to anthropogenic sources revealed a cumulative weight of approximately 94% across the two axes. These elemental features confirm the major influence of anthropogenic sources on the reed's elemental composition, especially through contributions from heavy metals from industrial activities, road traffic, and combustion processes. PC1 groups elements of mixed origin, associated with traffic and fuels (Sb, Cu, Ni), fossil-fuel combustion (V, Mo), and industrial activities (Cr, Co, Tl, Te).

The biplot also shows a strong negative association for Sb, Te, Cu, Ni, Co, Mo, and Tl, elements that are frequently correlated with industrial emissions, wear of metallic materials, road traffic, and fossil fuel combustion. This association indicates anthropogenic inputs through atmospheric deposition, industrial effluents or fluvial transport of contaminated particles.

In contrast, As presents a high positive loading, suggesting a distinct source or a different biogeochemical behaviour in the analysed

system. The elements Cr and V, with moderate positive loadings, indicate additional influences related to metallurgical processes and liquid fuels. Hg, V, and Pb were associated with PC2, suggesting a secondary factor driven by atmospheric deposition and fuel combustion. Overall, the three ecosystems exhibited distinct geochemical fingerprints. Deltaic sites reflected lithogenic inputs, saline sites showed signatures of mineralized waters, and urban sites displayed clear anthropogenic enrichment. These patterns confirm that *Phragmites australis* integrates both natural and human-derived geochemical signals.

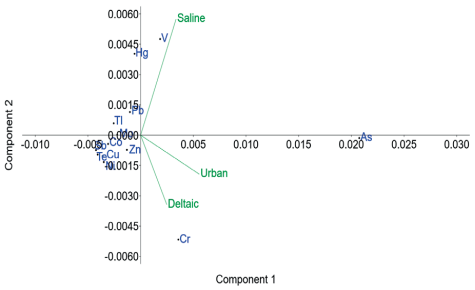



Figure 3. PCA - with elements indicating anthropogenic activities - in the three types of ecosystems

For elements of natural origin (Figure 4), PCA indicates a clear dominance of the first principal component, which explains 90.41% of the variance, while PC2 contributes 9.16%. The elemental composition is dominantly influenced by the geological substrate, *deltaic* sediments and natural processes of plant assimilation. This distribution suggests strong control by a major geochemical factor, highlighted by PC1, which separates lithophile elements from those associated with heavy minerals derived from sediments or deposited on leaves. Fe, Ba, Mn, and Ti, elements characteristic of oxides and detrital minerals, were grouped opposite Al, Si, K, Ca, Zr, Th, and U, indicating their association with the aluminosilicate fraction and resistant minerals in sediments. This component reflects lithogenic input, determined by alluvial transport, basin erosion, and sedimentary deposition. PC2 captures secondary variations in the mobility of elements (Ba, Mn, Ti) that reflect hydro-geochemical conditions, redox, salinity, and sediment availability.

The PCA analysis of rare and trace elements (Figure 5) shows that PC1 explains 87.46% of the variance, followed by PC2 (8.89%), indicating a clearly defined structure. It separates *urban* from natural environments through anthropogenic inputs with low trace-element content.

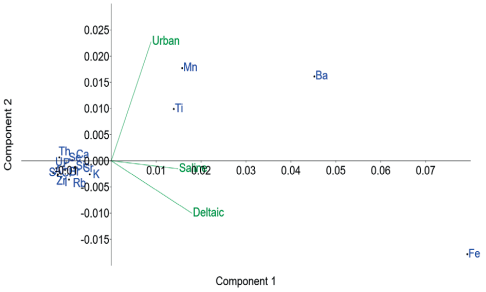



Figure 4. PCA - with elements indicating natural origin - in the three types of ecosystems

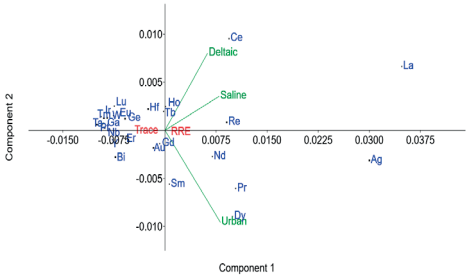



Figure 5. PCA - with elements indicating REE and Trace - rare elements

The *deltaic* ecosystems were subject to natural processes of uptake from sediment, slightly differently from *saline* ecosystems, indicating the influence of salinity, mineral characteristics, and plant availability. The distribution of REE and trace elements reflected the interactions among geogenic inputs (mineralogy, sediment composition), the ecological dynamics of the analysed ecosystems, and anthropogenic influences. PC1 highlighted a gradient in element separation of La, Ce, Pr, and Nd (light rare earth elements-LREE), with elements predominantly associated with stable mineral fractions of lithogenic origin and platinum-group metals

(Ta, Nb, W, Pt, Ir). This distribution reflects the geochemical fractionation and mineralogical control of the sediments. In contrast, PC2 highlights the differentiation of ecosystems: the *deltaic* and *saline* environments showed positive loadings, whereas the *urban* ecosystem exhibits a strong negative loading, suggesting anthropogenic influences on the distribution of trace elements. The detection of rare elements such as At, Ir, and Ta likely reflects localized mineralogical features or the presence of fine sediment fractions adhering to plant tissues. Their low concentrations suggest geogenic origins rather than biological uptake.

The PCA identified the major geochemical gradients, separating *deltaic*, *saline*, and *urban* systems based on dominant elemental features. In addition, AHC dendrograms allow the identification of element associations reflecting complex sediment/water processes. Hierarchical analysis based on Agglomerative hierarchical clustering (AHC) of the elements identified in *deltaic* ecosystems, highlighted a geochemical organisation structured into four major element associations, suggesting mineralogical mechanisms and other physical, chemical and biological processes taking place in the sediments (Figure 6). The first cluster (blue) groups predominantly lithogenic elements, associated with heavy minerals, including light and middle lanthanides (La, Eu, Gd, Tb), actinides (Th, U), high-field elements (Zr, Ta), as well as noble metals (Pt, Ir, Au), along with Sr and Ba. Their association indicates a common source related to the transport of fine particles, possibly enriched by anthropogenic input and distinct from the natural lithogenic background, a feature frequently reported in fluvial and *deltaic* sediments (Taylor & McLennan, 1995; Cullers, 2002). A second cluster (brown), much smaller, is dominated by Zn, Ag, and W, with Ti and Ce added. Zn and Ag are known as markers of metallurgical activities and fluvial transport of contaminated particles, and their association with W has been reported in sediments affected by industrial discharges (Förstner & Wittmann, 2012). The third group (pink) brings together elements characteristic of the clay fraction and oxides such as K, Rb, Si, Mn, V and Cr, together with potentially toxic metals (Cu, Pb, Hg) and part of the REE (Nd, Pr, Sm, Y). This association reflects the role of fine phases as a geochemical support for adsorbed metals. The last group (green), defined by Ca and Fe, correlated with P, As, Se, and Tl, indicating a carbonate- and redox-sensitive association characteristic of reactive sediments from environments rich in organic matter. This covariability reflects natural ecological processes of element fixation and release in iron oxides, controlled by oxidation-reduction cycles and interactions with carbonate and organic matter (Belzile & Tessier, 1990).

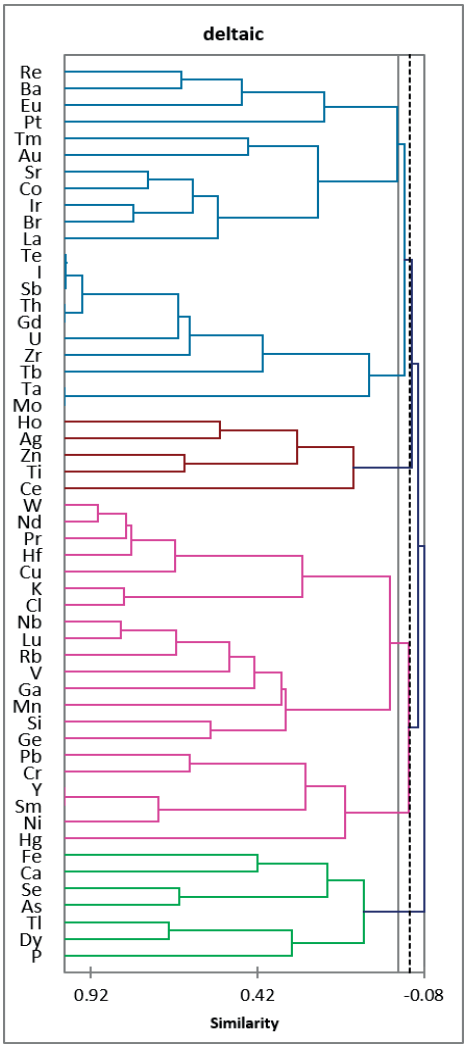



Figure 6. Agglomerative hierarchical clustering (AHC) of elements identified in *deltaic* ecosystems

In *saline* environments, AHC analysis revealed a more compact organisation into three distinct clusters, reflecting the typical chemistry of these ecosystems (Figure 7).

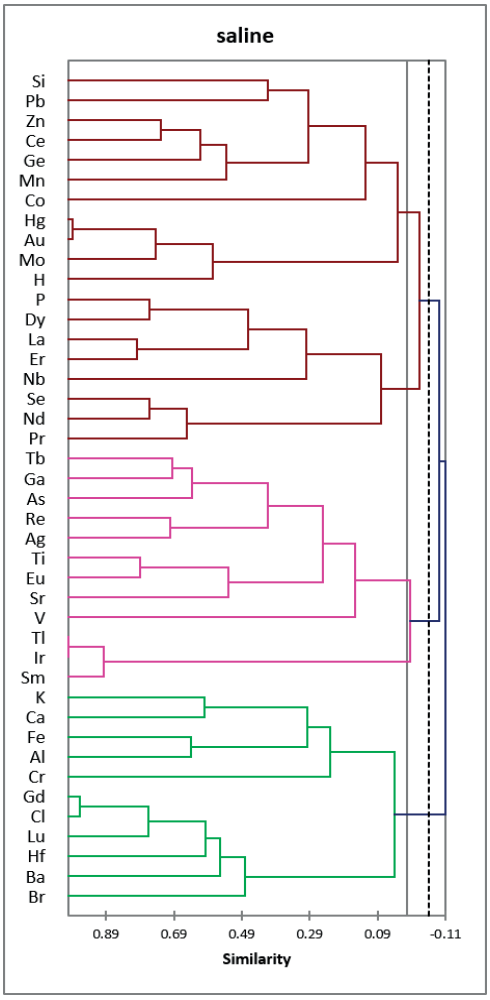



Figure 7. Agglomerative hierarchical clustering (AHC) of elements identified in *saline* ecosystems

A first cluster (brown) groups Si together with Pb, Zn, Ge, Mn, Co, Hg and Mo, indicating an association between the detrital fraction and contaminated metals. The cluster composition suggests that pollutants are transported and retained on mineral particles. Such associations have been reported in *saline* environments where salinity-induced flocculation favours metal retention (Acosta et al., 2023). The second cluster (pink) comprises metalloids and redox-sensitive metals, such as As and Tl, correlated with Sr, V, Ag and neighbouring some of the REE (La, Nd, Pr, Tb, Eu). This association indicates increased mobility in the dissolved phase, followed by re-fixation. Chloride complexation and redox variations enhance the mobility of elements, followed by their re-fixation via adsorption or co-precipitation (O'Day et al., 2004), thereby influencing the availability of nutrients and metals to microbial and benthic communities. Their correlation with Sr and REE indicates the involvement of authigenic phases, a common natural process in lakes and *saline* environments, reflecting active interactions between sediment chemistry and local ecological dynamics (Jones et al., 2005). The third cluster (green) is characterised by evaporitic and carbonate elements: Cl and Br correlated with Ca, Ba, K, Fe, and Al, suggesting authigenic precipitation under conditions of intense evaporation, a process that shapes sedimentary structure and influences the microhabitats of organisms adapted to *saline* environments. Cl/Br ratios are widely used to distinguish marine from continental sources, and the Ba-Ca correlation indicates barite and carbonate precipitation under conditions of intense evaporation (Holland et al., 1987). Therefore, *saline* ecosystem markers reflect three major processes as the input of potentially contaminating fine particles, the mobilisation of metals in *saline* waters, and authigenic precipitation of salts, a pattern commonly found in many *hypersaline* systems (Warren, 2006).

The *urban* dendrogram highlights a structure organised into three distinct clusters (Figure 8). A first major cluster (brown) brings together Zn, Cu, Ni, Mn, Pt, Hg, P, Ba and Sr, indicating a strong anthropogenic association. The high correlations among these elements suggest a common source related to traffic and industrial activities.

The second cluster (pink) was defined by Fe and Cr, and correlated with Se, Ag, and Si, indicating reactive oxide phases associated with *urban* fine particles.

The third, much broader cluster (green), included K, Rb, Ca, Ti, Nb, Th, As, V, Tl, Br and numerous REE (Pr, Gd, Tb, Sm, Dy, Y), suggesting a mixed origin related to *urban* dust and construction materials.

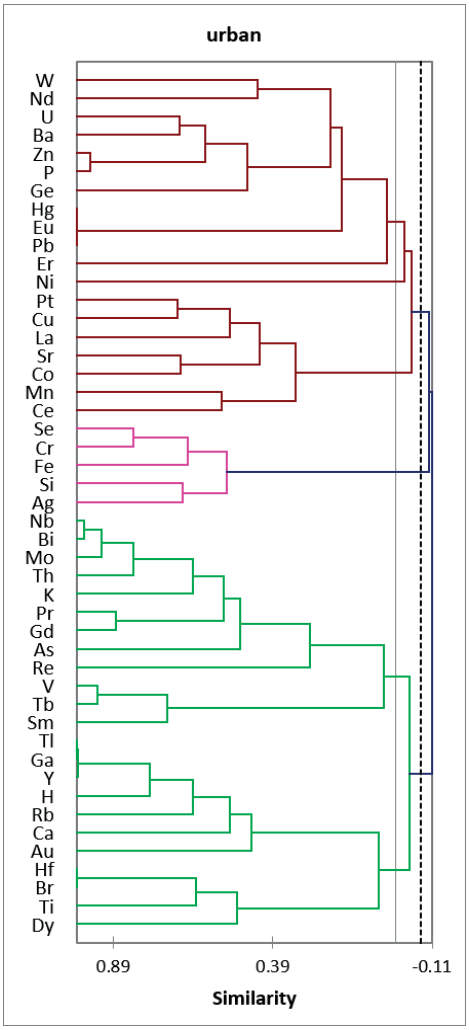



Figure 8. Agglomerative hierarchical clustering (AHC) of elements identified in *urban* ecosystems

The *urban* geochemical signature was dominated by multiple anthropogenic sources. The Zn–Cu–Ni association is considered a robust indicator of tire wear and brake systems, while Pt is an established marker of emissions from automotive catalytic converters.

Clustering with Mn and Ba has been reported in numerous studies on road dust, being attributed to fuel additives and friction materials (Thorpe & Harrison, 2008; Rauch & Pacyna, 2009). The Fe–Cr–Se cluster reflects the role of Fe–Mn oxides as sorbent phases for toxic metals (Lu et al., 2009). In *urban* aerosols and road sediments, Cr and Se are frequently bound to these phases, and their correlation with Si indicates the mineral support of the particles.

The broad association, including K, Ca, Ti, and REE, is typical of construction dust and resuspended *urban* soils. Vanadium and arsenic, present in the same cluster (pink), are indicators of fossil fuel combustion, especially fuel oil and diesel, a pattern reported in *urban* sediments from port and industrial areas (Pacyna & Pacyna, 2001).

Thus, *urban* marker elements reflect three major sources: road traffic, industrial emissions, and construction dust/atmospheric resuspension (Charlesworth et al., 2011).

Our study highlights *Phragmites australis*'s ability to integrate distinct geochemical features across ecosystem types (*deltaic*, *saline*, *urban*), confirming its role as both a bioindicator and a potential natural filter for lithogenic and anthropogenic elements.

The differences identified between habitats (assessed by ANOSIM, R = 0.0786, $p$ = 0.0179) indicate a distinct elemental structure, mainly driven by the contrast between deltaic and urban ecosystems ($p$ = 0.0015), reflecting the influence of anthropogenic pressure on the chemical composition of plant biomass.

Thus, in *deltaic* ecosystems, a lithogenic contribution was observed, evidenced by the dominance of geogenic elements (Fe > Ba > Mn > Ti; Table 1), resulting from detrital inputs and sediments rich in mineral fractions. The Fe–Ba–Mn–Ti association and the distribution of rare earth elements (REE) (Table 2) reflect the control of the geological substrate and fluvial transport, consistent with the geochemical model of continental sediments described by Taylor & McLennan (1995) and Cullers (2002). The differential fractionation of REE between habitats (Table 2, Figure 7) suggests variations in sedimentary sources and redox conditions (Piper & Bau, 2013).

The association of As–Fe elements in AHC in the *deltaic* environment is due to the role of iron oxides in fixing metalloids in sediments rich in organic matter, a mechanism described by Belzile & Tessier (1990). Therefore, in *deltaic* ecosystems, elemental accumulation in *Phragmites australis* predominantly reflects the natural geochemical background, with a

secondary anthropogenic influence. In contrast, under *saline* conditions, geochemical processes exhibited a distinct element profile absorbed by the reed. The elevated concentrations of Hg, Ba, Sr, and Mo (Table 1 and Table 3) indicate mobilisation and redistribution under high-salinity conditions and variable redox potential. *Saline* AHC revealed three major processes: contaminated detrital input, metal mobilisation under *saline* conditions and mineralisation induced by high salinity. The Cl–Br–Ca–Ba clustering in the dendrogram suggests intense evaporitic processes, described in other *saline* systems (Warren, 2006), with chloride complexation and mobilisation of As and Tl (O'Day et al., 2004), and metal retention on fine particles (Acosta et al., 2023).

The clear separation of the *saline* ecosystem in the PCA for natural elements (Figure 6) and for REE/trace (Figure 7) confirms that salinity constitutes a major geochemical control factor, influencing bioavailability and accumulation mechanisms in reeds.

In *urban* environments, anthropogenic influences were evidenced by obvious enrichments in As, Pb, Mn and Tl (Table 3), as well as in Br (Table 1), suggesting the influence of traffic, fossil fuel combustion and industrial activities, elements also mentioned in other studies (Wei & Yang, 2010). The dominance of Ba > Mn > Ti > Fe (Tables 1-3) indicates a modification of natural ratios by external input. PCA for anthropogenic elements (Figure 2) by the association Sb–Cu–Ni–Mo–Tl–Te reflects sources related to traffic and industry (Thorpe and Harrison, 2008; Rauch & Pacyna, 2009). Also, the presence of Pt in the *urban* cluster supports the presence of a road-pollution marker. The elemental grouping Fe, Cr, Se indicates the involvement of Fe and Mn oxides in the retention and immobilisation of potentially toxic metals in sediment (Lu et al., 2009). The association of V and As suggests external inputs specific to the *urban* environment, including contributions from fossil fuel combustion, which modify the geochemical background and increase metal pressure in the ecosystem (Pacyna & Pacyna, 2001). Thus, the elemental composition of *urban* reeds reflects a mixture of multiple sources: road traffic, industrial emissions and construction dust (Charlesworth et al., 2011).

The ability of *Phragmites australis* to accumulate both lithogenic elements and potentially toxic metals demonstrates its dual role as both a bioindicator of local geochemical conditions, highlighted by the integration of sedimentary and hydrogeochemical signatures and as a biological filter of contaminants, especially in *urban* environments, where it retains heavy metals from the water column and from atmospheric deposits (Alghanem et al., 2024). However, the accumulation of Hg, Pb, As, or Tl in aerial biomass may pose a secondary risk through trophic transfer or biomass decomposition. Therefore, the use of reeds in phytoremediation systems requires biomass management strategies to prevent the reintroduction of contaminants into the biogeochemical cycle. Moderate but statistically significant differences between ecosystems indicate that *Phragmites australis* responds sensitively to variations in anthropogenic pressure and natural geochemical control, confirming its usefulness as a sentinel species in ecological risk assessment.

## CONCLUSIONS

**Salinity as a major geochemical control factor**. In saline ecosystems, the association of Hg, Ba, Sr, and Mo, together with the structure of the agglomerative hierarchical clustering (AHC), highlights the role of salinity-driven geochemical processes. These include element mobilisation, complexation, and evaporite-related precipitation, demonstrating the strong influence of mineralised waters on elemental distribution and bioavailability.

**High capacity for bioaccumulation and integration of geochemical signatures**. *Phragmites australis* effectively records habitat-specific geochemical characteristics, reflecting both natural variations in substrate composition and the impacts of anthropogenic activities. Its elemental composition provides an integrated signal of environmental conditions across contrasting ecosystems.

**Dual role as a bioindicator and natural filter**. The species serves not only as a reliable bioindicator of geochemical and environmental conditions but also as a natural biological filter, contributing to the retention and sequestration

of heavy metals, particularly in ecosystems exposed to urban pressures.

**Implications for ecological risk**. The accumulation of potentially toxic elements such as Hg, Pb, As, and Tl may pose ecological risks through trophic transfer and the subsequent re-release of contaminants into the biogeochemical cycle during biomass decomposition. These findings underscore the need for appropriate management and monitoring strategies in affected ecosystems.

**Environmental management applications**. The elemental patterns identified in this study provide valuable information for environmental assessment and wetland management, especially in areas influenced by urbanisation or salinisation. Monitoring *Phragmites australis* can serve as an effective early-warning tool for detecting metal contamination, alterations in sediment provenance, and changes in hydrogeochemical conditions, thereby supporting informed conservation and remediation efforts.

## ACKNOWLEDGEMENTS

This research was funded by the Institute of Biology Bucharest of Romanian Academy, grant numbers RO1567-IBB02/2026 and RO1567-IBB06/2026.

## REFERENCES

Acosta, R., Carol, E., Borzi, G., Cellone, F., & Alvarez, M. D. P. (2023). Factors and processes controlling hydrochemistry and evaporitic deposits in hypersaline wetland–shallow lake systems. *Hydrological Processes, 37*(11), e15031.

Addinsoft. (2014). *XLSTAT Pro: Data analysis and statistical solutions for Microsoft Excel*. Paris, France: Addinsoft.

Alghanem, S. M. S., Alsudays, I. M., Farid, M., Sarfraz, W., Ishaq, H. K., & Farid, S. (2024). Evaluation of heavy metal accumulation and tolerance in oxalic acid-treated Phragmites australis wetlands for textile effluent remediation. *International Journal of Phytoremediation, 26*(13), 2048-2063.

Belzile, N., & Tessier, A. (1990). Interactions between arsenic and iron oxides in lacustrine sediments. *Geochimica et Cosmochimica Acta, 54*(1), 103–109.

Chapligin, V., Dudnikova, T., Chernikova, N., & Fedorenko, A. (2022). Phragmites australis Cav. as a bioindicator of hydromorphic soils pollution with heavy metals and polyaromatic hydrocarbons. *Chemosphere, 307*, 136021

Charlesworth, S., De Miguel, E., & Ordóñez, A. (2011). A review of the distribution of particulate trace elements in urban terrestrial environments and their application to considerations of risk. *Environmental Geochemistry and Health, 33*(2), 103–123.

Chitimus, D., Nedeff, V., Mosnegutu, E., Barsan, N., Irimia, O., & Nedeff, F. (2023). Studies on the accumulation, translocation, and enrichment capacity of soils and the plant species Phragmites australis (common reed) with heavy metals. *Sustainability, 15*(11), 8729.

Clarke, K. R. (1993). Non-parametric multivariate analyses of changes in community structure. *Australian Journal of Ecology, 18*, 117–143.

Cullers, R. L. (2002). Implications of elemental concentrations for provenance, redox conditions, and metamorphic studies of shales and limestones near Pueblo, CO, USA. *Chemical Geology, 191*(4), 305–327.

Förstner, U., & Wittmann, G. T. W. (2012). *Metal pollution in the aquatic environment*. Berlin, Germany: Springer.

Hammer, Ø., Harper, D. A. T., & Ryan, P. D. (2001). PAST: Paleontological statistics software package for education and data analysis. *Palaeontologia Electronica, 4*(1), 1–9.

Hatje, V., Schijf, J., Johannesson, K. H., Andrade, R. C., Caetano, M., Brito, P., Haley, B. A., Lagarde, M., & Jeandel, C. (2024). The global biogeochemical cycle of the rare earth elements. *Global Biogeochemical Cycles, 38*(6).

Holland, H. D., Lazar, B., & McCaffrey, M. A. (1987). The evaporation path of seawater and the coprecipitation of $Br^-$ and $K^+$ with halite. *Journal of Sedimentary Petrology, 57*(5), 928–937.

Jenkins, R. (1999). *X-ray fluorescence spectrometry*. New York, NY: Wiley.

Jones, B. F., Deocampo, D. M., & Drever, J. I. (2005). Geochemistry of *saline* lakes. In H. D. Holland & K. K. Turekian (Eds.), *Treatise on geochemistry* (Vol. 5, pp. 393–424). Oxford, UK: Elsevier.

Kassambara, A. (2017). *Practical guide to cluster analysis in R: Unsupervised machine learning* (Vol. 1). Paris, France: STHDA.

Legendre, P., & Legendre, L. (2012). *Numerical ecology* (3rd English ed.). Amsterdam, Netherlands: Elsevier.

Lu, X., Wang, L., Li, L. Y., Lei, K., Huang, L., & Kang, D. (2009). Multivariate statistical analysis of heavy metals in street dust of Baoji, NW China. *Journal of Hazardous Materials, 173*(1–3), 744–749.

Mondal, M. N., Horikawa, K., Seki, O., Nejigaki, K., Minami, H., Murayama, M., & Okazaki, Y. (2021). Investigation of adequate calibration methods for X-ray fluorescence core scanning element count data: A case study of a marine sediment piston core from the Gulf of Alaska. *Journal of Marine Science and Engineering, 9*(5), 540.

O'Day, P. A., Vlassopoulos, D., Root, R., & Rivera, N. (2004). The influence of sulfur and iron on dissolved arsenic concentrations in the shallow subsurface under changing redox conditions. *Proceedings of the National Academy of Sciences, 101*(38), 13703–13708.

Pacyna, J. M., & Pacyna, E. G. (2001). An assessment of global and regional emissions of trace metals to the atmosphere from anthropogenic sources. *Environmental Reviews, 9*(4), 269–298.

Piper, D. & Bau, M. (2013) Normalized Rare Earth Elements in Water, Sediments, and Wine: Identifying Sources and Environmental Redox Conditions. *American Journal of Analytical Chemistry, 4*, 69-83. http://dx.doi.org/10.4236/ajac.2013.410A1009

Rauch, S., & Pacyna, J. M. (2009). Earth's global Ag, Al, Cr, Cu, Fe, Ni, Pb, and Zn cycles. *Global Biogeochemical Cycles, 23*(2), GB2007.

Samadi, M. T., Leili, M., Asgari, G., & Chavoshi, S. (2024). The potential of Phragmites australis to bioaccumulation and translocate heavy metals from landfill leachate. *Journal of Water Process Engineering, 64*, 105657.

Song, J., Zhuang, W., & Queiroz, H. M. (2023). Editorial: Biogeochemical processes of micro/trace elements and their impacts on marine ecosystems. *Frontiers in Marine Science, 10*.

Taylor, S. R., & McLennan, S. M. (1995). The geochemical evolution of the continental crust. *Reviews of Geophysics, 33*(2), 241–265.

Thorpe, A., & Harrison, R. M. (2008). Sources and properties of non-exhaust particulate matter from road traffic. *Science of the Total Environment, 400*(1–3), 270–282.

Warren, J. K. (2006). *Evaporites: Sediments, resources and hydrocarbons*. Berlin, Germany: Springer.

Wei, B., & Yang, L. (2010). A review of heavy metal contaminations in urban soils, urban road dusts and agricultural soils from China. *Microchemical Journal, 94*(2), 99–107.

Weis, J. S., & Weis, P. (2004). Metal uptake, transport and release by wetland plants: Implications for phytoremediation and restoration. *Environment International, 30*(5), 685–700. https://doi.org/10.1016/j.envint.2003.11.002

Scientific Papers. Series E. Land Reclamation, Earth Observation & Surveying, Environmental Engineering. Vol. XV, 2026
Print ISSN 2285-6064, CD-ROM ISSN 2285-6072, Online ISSN 2393-5138, ISSN-L 2285-6064

# GLOBAL CHALLENGES CONCERNING WATER RESOURCES AND THEIR MANAGEMENT: CASE STUDY - THE DANUBE

**Aurelia NICA[1, 2], Isabelle METAXA[1], Alina ANTACHE[1, 3], Adeline-Ira SIMIONOV[1, 3], Cătălina ITICESCU[3, 4], Ștefan-Mihai PETREA[1, 3]**

[1]"Dunărea de Jos" University of Galati, Food Science and Engineering Faculty, 47 Domnească Street, Galați, Romania
[2]"Dunărea de Jos" University of Galați, Multidisciplinary Research Platform (ReForm) – MoRAS, Galați, Romania
[3]"REXDAN Center", "Dunărea de Jos" University of Galați, 47 Domnească Street, Galați, Romania
[4]"Dunărea de Jos" University of Galați, Faculty of Sciences and Environment, 111 Domnească Street, Galați, Romania

Corresponding author email: anica@ugal.ro

***Abstract***

*This paper analyses the impact of global factors on the availability and quality of water resources, highlighting the need for sustainable management. In the context of climate change, population growth and intensification of economic activities, water resources are subject to significant pressures, such as pollution, overexploitation and unequal distribution. The study uses a narrative review, based on bibliographical-analytical research, comparative analysis and a case study of the Danube River Basin. The case study illustrates the complexity of managing a transboundary resource, affected by upstream pollution, hydrological variations and multiple uses. European policies and integrated management strategies applied to protect water quality and its sustainable use are analysed. The results highlight the importance of international cooperation, infrastructure modernization and the implementation of innovative solutions. In conclusion, efficient management of water resources is an essential condition for sustainable development and the prevention of future water crises.*

***Key words:*** *Danube, management, resources, sustainability, water.*

## INTRODUCTION

Water is one of the most important natural resources on the planet, indispensable for the existence of life and for the functioning of modern economies. Recent European assessments show that water bodies remain under significant pressure from agriculture, pollution and climate change, while drought and flood risks are expected to intensify in the coming decades (European Environment Agency, 2024).

In Europe, the Danube River represents one of the most complex examples of transboundary water management. The Danube River Basin covers approximately 800,000 km² and includes territories from 19 European countries, making it one of the most international river basins in the world. Recent studies indicate shifts towards wetter winters, drier summers and increased high-flow and low-flow risks, which directly affect water-resource availability in the basin (ICPDR, 2021; Probst & Mauser, 2023; Pekárová et al., 2023).

The aim of this paper is to analyse the impact of global factors on the availability and quality of water resources and to highlight how European policies and integrated management strategies contribute to the protection and sustainable use of water resources.

Recent Danube-specific assessments also underline the growing importance of emerging pollutants, including PFAS, and the need for coordinated responses across the basin (Liu et al., 2025; European Commission, 2026).

## MATERIALS AND METHODS

This paper is a narrative review supported by bibliographical-analytical research, comparative analysis and a Danube case study.

Literature search strategy. Sources were identified in ScienceDirect, Scopus, Web of Science and Google Scholar, together with

official documents from the European Commission, the European Environment Agency and the ICPDR. The search covered the period 2000-2026, with priority given to 2019-2026 publications on climate change, water scarcity, nutrient pollution, PFAS, microplastics and transboundary river-basin management.

Selection criteria. The search terms used were "Danube River Basin", "water management", "climate change", "nutrient pollution", "PFAS", "microplastics", "flood risk", "drought risk" and "transboundary river basin", combined with Boolean operators. Included sources were peer-reviewed articles, technical reports and official strategies in English or Romanian that addressed basin-scale hydrology, pollution, governance or management. Duplicates, opinion pieces without clear evidence base and records unrelated to basin-scale water management were excluded.

Comparative analysis. The selected publications and official documents were compared in terms of source of pressure, management response, policy instrument and expected environmental outcome.

**Case study**

The Danube River was analysed as a representative case study for the management of a complex transboundary resource. The following were evaluated: anthropogenic pressures on water, pollution from upstream, hydrological variations, multiple uses of the resource and management measures implemented at regional level.

Overall, more than 25 scientific papers and technical reports were synthesised through tables, graphic representations and descriptive interpretation of hydrological and water-quality indicators, with emphasis on the relationships between climatic, economic and social drivers.

## RESULTS AND DISCUSSIONS

### 1. Global factors influencing water resources

The synthesis of the reviewed literature confirms that water resources are being reshaped by a combination of climatic, demographic and economic pressures. Climate change remains the most pervasive driver because it alters the timing, intensity and spatial distribution of precipitation, increases evapotranspiration and amplifies the frequency of compound extremes. In river basins such as the Danube, these changes translate into wetter winters, longer dry spells in summer, more erratic flow regimes and higher uncertainty for water allocation, flood protection and ecological continuity (Probst & Mauser, 2023; Pekárová et al., 2023). The practical implication is that historical hydrological averages are becoming less reliable for planning, particularly for multi-country basins where upstream and downstream conditions are tightly coupled.

Beyond climate forcing, land-use change and population growth increase the pressure on both surface water and groundwater. Urban expansion concentrates demand, increases impervious surfaces and accelerates stormwater runoff, while industrial growth raises the risk of point-source contamination through incomplete treatment and accidental releases. Agriculture exerts a dual pressure: it is the largest user of water in many European catchments and simultaneously one of the main sources of diffuse pollution through nitrates, phosphorus, pesticides and suspended solids. The European Environment Agency has repeatedly identified agriculture as a dominant pressure on European waters, and this is consistent with the Danube Basin, where nutrient enrichment remains a persistent management challenge (European Environment Agency, 2024).

Table 1 illustrates that the pressures affecting water resources are not isolated.

Table 1. Synthesis of major global drivers, dominant pressures and basin-scale implications

| Driver | Typical pressure pathway | Main hydrological or ecological effect | Management implication |
|---|---|---|---|
| Climate change | Altered precipitation, higher evaporation, longer dry periods | More frequent floods and droughts; lower predictability of river discharge | Scenario-based planning, drought preparedness and flood-risk adaptation |
| Urbanization | Impervious surfaces, wastewater generation, storm runoff | Flash floods, sewage overloads, urban contamination | Modern sewerage, retention systems and advanced treatment |
| Industrialization | Effluents, accidental releases, legacy deposits | Local hotspots, persistent contamination, sediment risk | Strict permitting, monitoring and emergency response |
| Agriculture | Fertilizers, pesticides, | Eutrophication, nitrate loading, | Nutrient management, |

| Driver | Typical pressure pathway | Main hydrological or ecological effect | Management implication |
|---|---|---|---|
| | irrigation abstraction, manure | groundwater stress | precision farming and riparian buffers |
| Emerging pollutants | PFAS, microplastics, pharmaceuticals | Low-concentration chronic contamination | Targeted monitoring and treatment upgrades |

In practice, a single basin may experience simultaneous climate stress, diffuse agricultural pollution and industrial legacy burdens. This convergence increases the probability of threshold effects, in which ecological degradation becomes visible only after the system has already lost resilience. For the Danube, this means that management should be designed as an integrated risk-reduction framework rather than as a set of sector-specific interventions.

## 2. Sustainable management of water resources

The literature reviewed in this study supports the view that sustainable water management must be understood as an adaptive governance process rather than as a static set of technical measures. The Water Framework Directive established a basin-oriented logic by requiring planning at the level of river basin districts, monitoring of ecological and chemical status, and coordinated action across administrative boundaries (European Commission, 2000). This approach remains highly relevant because it links environmental objectives with the use of water for drinking supply, agriculture, navigation, industry, recreation and ecosystem protection.

In the Danube context, governance is especially complex because the basin extends across a large number of countries with different economic capacities, monitoring systems and policy priorities. The Danube River Basin Management Plan and the work of the International Commission for the Protection of the Danube River provide the institutional backbone for coordination, data sharing and joint action (ICPDR, 2021). However, the review shows that good formal coordination is not sufficient by itself. Effective management also depends on implementation capacity, financing, infrastructure quality, real-time monitoring and the ability to respond to transboundary incidents before they spread downstream.

The analysis further indicates that the most robust management strategies combine regulatory instruments with technical modernization. Wastewater treatment upgrades, nutrient reduction at source, hydromorphological restoration, floodplain reconnection and digital monitoring platforms are complementary rather than competing measures. This is important because point-source control alone cannot address diffuse pollution, and river restoration alone cannot compensate for persistent chemical loading. The strongest results are obtained when policy instruments are aligned with ecological processes and when each intervention targets a clearly defined pressure-response pathway.

Table 2 highlights that resilience depends on the combination of measures rather than on a single dominant solution. Digitalization improves detection and forecasting, but it does not remove pollution sources. Likewise, structural measures such as treatment plants or embankments improve control, but they do not replace basin-wide cooperation. A sustainable framework therefore requires a layered approach that combines prevention, monitoring, restoration and adaptation.

Table 2. Policy and technical responses for improving water resilience in the Danube Basin

| Response category | Operational focus | Expected outcome | Implementation challenge |
|---|---|---|---|
| River-basin planning | Coordinated targets for water quantity and quality | Reduced conflict between users | Different national priorities |
| Monitoring and early warning | Dense sampling and digital alert systems | Faster detection of pollution or hydrological stress | Data harmonization across borders |
| Wastewater modernization | Collection, secondary and advanced treatment | Lower nutrient and micropollutant loads | High capital and operating costs |
| Agricultural best practice | Precision fertilization and buffer strips | Reduced diffuse runoff | Adoption at farm level |
| Nature-based solutions | Wetland restoration and floodplain reconnection | Improved retention and ecosystem services | Land availability and governance |

## 3. Case study - the Danube

The Danube is a particularly instructive case because it concentrates almost all of the management challenges discussed above. It is

one of Europe's largest transboundary rivers, links highly urbanized, industrial and agricultural zones, and ultimately delivers water and sediment to the Black Sea. Its basin-scale significance means that local disturbances are rarely local for long: pollutants, hydrological changes and land-use pressures can propagate over long distances and across national borders.

The case-study evidence indicates that the river is exposed to three interacting pressure fields. First, climatic variability affects seasonal discharge, water temperature and the occurrence of low-flow or flood events. Second, point-source pollution from urban wastewater, industrial discharges and accidental releases can create acute contamination hotspots. Third, diffuse pollution from agriculture and urban runoff contributes chronic nutrient and chemical loading, which is often more difficult to reduce because it arises from many distributed sources rather than a single discharge point.

The Danube's historical pollution events demonstrate the basin-wide consequences of upstream incidents. The Baia Mare cyanide spill and the Baia Borşa tailings release remain emblematic examples of how mining accidents can create severe downstream ecological damage with long recovery times (ICPDR, 2000). Likewise, the Ajka red-sludge accident showed that industrial failures in one part of the basin can trigger water-quality emergencies hundreds of kilometres away. These cases are not merely historical references; they reveal structural vulnerabilities in basin governance, especially where prevention, emergency communication and remediation are uneven across borders.

At the same time, the review shows that the Danube cannot be interpreted only through spectacular accident cases. The dominant long-term burden is diffuse nutrient transport. Model-based work has repeatedly found that agricultural and mixed diffuse sources are the principal contributors to nutrient loading, while point sources and legacy hotspots require targeted local control (Malagó et al., 2015; 2017). This pattern matters because chronic eutrophication and sediment contamination produce slow but cumulative ecological damage, including altered food webs, reduced oxygen availability and increased pressure on biodiversity.

The emerging PFAS evidence strengthens this interpretation. The 2025 Upper Danube Basin study reported contamination across environmental compartments and highlighted the combined role of industrial hot spots, wastewater pathways and groundwater-linked transport (Liu et al., 2025). The European Commission's 2026 assessment reinforced the same message by showing that PFAS pollution in the basin is widespread and that conventional wastewater treatment is often insufficient to stop downstream dispersal (European Commission, 2026). Taken together, these findings suggest that the Danube is entering a new phase of chemical-risk governance in which the challenge is not only to reduce a few legacy pollutants but also to manage complex mixtures of persistent, mobile and partly unregulated substances.

The discussion also points to the importance of hydromorphological pressures. Bank erosion, river training works, damming and navigation infrastructure alter sediment transport, connectivity and habitat structure. Although such interventions can support navigation, flood control or energy production, they may also reduce ecological continuity and fragment habitats. In a large basin such as the Danube, hydromorphological alteration is particularly significant because it interacts with climate-driven flow variability: where water levels are already more variable, rigid channelization can further reduce ecological buffering capacity.

From a management perspective, the Danube case study shows that resilience should be assessed at multiple scales. Local measures such as upgrading a wastewater plant may improve water quality in the immediate area, but basin-level resilience depends on whether upstream activities are also controlled. Similarly, flood-protection works can reduce immediate hazard exposure, yet if they are not integrated with floodplain restoration and ecological connectivity, they may transfer risk downstream or accelerate habitat loss. This is why the ICPDR framework remains central: it provides the institutional platform for translating scientific evidence into coordinated basin action (ICPDR, 2021).

Another important result is the growing role of monitoring technologies. Traditional periodic sampling is no longer sufficient for a river basin

of the Danube's scale and complexity. The literature increasingly supports hybrid systems that combine laboratory measurements, automatic stations, remote sensing, model-based forecasting and digital alerts. Such systems are particularly useful for drought forecasting, flood preparedness and early detection of contamination peaks. They also improve transparency, because data can be shared among riparian states more quickly and used to support joint decision-making.

Overall, the Danube demonstrates that transboundary water management is not only a matter of environmental protection but also of economic stability and social resilience. Navigation, hydropower, tourism, drinking water supply, fisheries and ecosystem services all depend on the same river system. Therefore, every major management decision involves trade-offs. The central finding of this study is that the best outcomes are achieved when governance tools, infrastructure investments and ecological restoration are treated as a single integrated policy package rather than as separate sectoral agendas.

**4. Integrated discussion and implications**

The synthesis of the reviewed literature and the Danube case study led to three broader implications. First, water scarcity and water pollution should be analyzed together, because they are often produced by the same pressures and they reinforce each other. For example, drought conditions concentrate pollutants, while polluted water reduces the amount of water that can be safely used for supply or irrigation. Second, basin-scale resilience depends on prevention more than on reaction: once pollutants move downstream or groundwater is contaminated, remediation becomes slower, more expensive and often incomplete. Third, innovation is most effective when it is paired with strong institutions; digital tools, for instance, cannot substitute for cross-border cooperation, but they can make such cooperation timelier and evidence-based.

In practical terms, the Danube Basin would benefit from four priorities. The first is a stronger control of diffuse agricultural inputs, especially through nutrient budgeting, precision fertilization, buffer strips and stricter manure management. The second is wastewater modernization, including the gradual deployment of advanced treatment where micropollutants and PFAS are relevant. The third is restoration-oriented river management, because wetlands and floodplains can attenuate floods, improve water retention and support biodiversity. The fourth is basin-wide digital monitoring, which would allow authorities to identify trends earlier and respond more quickly to incidents.

These priorities are consistent with the growing European emphasis on water resilience. Recent official assessments stress that Europe's waters remain under intense pressure and that climate-related extremes are likely to become more disruptive in the coming decades (European Environment Agency, 2024). Accordingly, the Danube should be viewed not only as a regional case study, but also as a model system for testing integrated adaptation, advanced pollution control and cooperative governance in a large, shared river basin.

## CONCLUSIONS

Water resources in the Danube Basin are under increasing pressure from climate change, urbanization, industrialization and intensive agriculture. The review shows that diffuse agricultural pollution is the dominant nutrient source, while urban wastewater and industrial discharges remain significant point pressures.

The Danube case study highlights specific priority hotspots and hazards, including the historical mining accidents at Baia Mare and Baia Borșa, the Ajka red-sludge accident, and the emerging PFAS contamination detected in the Upper Danube Basin. These findings confirm that upstream events can have basin-wide and long-term effects.

The management response should focus on stronger transboundary cooperation, modernized wastewater and monitoring infrastructure, better control of agricultural inputs, and faster deployment of digital tools for forecasting and pollution detection. These measures are essential for improving resilience to droughts, floods and emerging pollutants in the Danube Basin.

The Danube can serve as a European model of adaptive and integrated water management only if policy, science and implementation remain aligned.

The review also indicates that emerging pollutants have moved from a marginal topic to a central one in water governance. PFAS are of particular concern because they are extremely persistent, mobile in aquatic environments and difficult to remove using conventional treatment. Recent basin-scale evidence from the Upper Danube Basin shows widespread PFAS occurrence across rivers, groundwater, wastewater and landfill-related pathways, confirming that legacy contamination and current industrial inputs can overlap within the same catchment (Liu et al., 2025; European Commission, 2026). Accordingly, the management of water quality can no longer focus solely on conventional indicators such as nutrients and oxygen demand; it must also address chemical mixtures, chronic low-level exposure and long-range transport.

## ACKNOWLEDGEMENTS

This research was further funded by the European Union's Horizon Europe research and innovation programmes, Project Restore4Life (grant agreement no. 101112736)

## USE OF GENERATIVE ARTIFICIAL INTELLIGENCE (GenAI)

The authors declare the use of Generative Artificial Intelligence (GenAI) tools in the preparation of this manuscript. GenAI was used exclusively for language editing and text refinement in the Introduction and Conclusions sections. All scientific content, data analysis, and interpretations were developed and verified by the authors.

## REFERENCES

European Commission. (2000). Directive 2000/60/EC establishing a framework for Community action in the field of water policy. *Official Journal of the European Communities*.

European Commission, Directorate-General for Environment. (2026). Research finds far-reaching "forever chemical" pollution in the Danube Basin. https://environment.ec.europa.eu/news/research-finds-far-reaching-forever-chemical-pollution-danube-basin-2026-04-22_en

European Environment Agency. (2024). Europe's state of water 2024: the need for improved water resilience. EEA Report 07/2024. https://doi.org/10.2800/02236

ICPDR (2000). Annual Report 2000. International Commission for the Protection of the Danube River. https://www.icpdr.org/sites/default/files/ar2000.pdf

ICPDR (2021). Danube River Basin Management Plan: Update 2021. International Commission for the Protection of the Danube River. https://www.icpdr.org/sites/default/files/nodes/documents/danube_river_basin_managament_plan_-_update_2021_full_text.pdf

Liu, M., Saracevic, E., Oudega, T. J., Obeid, A. A., Nagy-Kovács, Z., László, B., Kittlaus, S., Zoboli, O., Krampe, J., Derx, J., & Zessner, M. (2025). Investigating the extent of PFAS contamination in the Upper Danube Basin across environmental compartments. *Environmental Sciences Europe, 37*(1). 99. https://doi.org/10.1186/s12302-025-01141-6

Malagó, A., Venohr, M., Gericke, A., Vigiak, O., Bouraoui, F., Grizzetti, B., & Kovacs, A. (2015). Modelling nutrient pollution in the Danube River Basin: A comparative study of SWAT, MONERIS and GREEN models. *JRC Technical Reports EUR 27676 EN. Publications Office of the European Union.* https://doi.org/10.2788/156278

Malagó, A., Bouraoui, F., Vigiak, O., Grizzetti, B., & Pastori, M. (2017). Modelling water and nutrient fluxes in the Danube River Basin with SWAT. *Science of the Total Environment, 603–604*. 196–218. https://doi.org/10.1016/j.scitotenv.2017.05.242

Pekárová, P., Bajtek, Z., Pekár, J., Výleta, R., Bonacci, O., Miklánek, P., Belz, J. U., & Gorbachova, L. (2023). Monthly stream temperatures along the Danube River: Statistical analysis and predictive modelling with incremental climate change scenarios. *Journal of Hydrology and Hydromechanics, 71*(4). 382–398. https://doi.org/10.2478/johh-2023-0028

Probst, E., & Mauser, W. (2023). Climate Change Impacts on Water Resources in the Danube River Basin: A Hydrological Modelling Study Using EURO-CORDEX Climate Scenarios. *Water, 15*(1). 8. https://doi.org/10.3390/w15010008

Scientific Papers. Series E. Land Reclamation, Earth Observation & Surveying, Environmental Engineering. Vol. XV, 2026
Print ISSN 2285-6064, CD-ROM ISSN 2285-6072, Online ISSN 2393-5138, ISSN-L 2285-6064

# METALS CONTENT IN THE SYSTEM WATER - SEDIMENTS - CHIRONOMIDAE - *PERCA FLUVIATILIS* - *PROTEOCEPHALUS PERCAE* FROM TOPOLNITSA DAM, BULGARIA

**Viliana PASKALEVA[1], Diana KIRIN[1, 2], Petya ZAHARIEVA[1], Radoslava ZAHARIEVA[1], Marian VARBANOV[1]**

[1]Bulgarian Academy of Sciences, National Institute of Geophysics, Geodesyand, Geography (NIGGG), Hydrologyand Water Management Research Center, Acad. G. Bonchev Str., 1113, Sofia, Bulgaria
[2]Agricultural University - Plovdiv, Department of Chemistry, Phytopharmacy and Ecology, and Environmental Protection, 12 Mendeleev Blvd, 4000, Plovdiv, Bulgaria

Corresponding author email: viliana_paskaleva@abv.bg

***Abstract***

*The study aims to examine the content of Cr, Mn, Fe and Al in liver and muscle samples of Perca fluviatilis Linnaeus, 1758 and its parasite Proteocephalus percae (Müller, 1780) Railliet, 1899, in samples of Chironomidae, water and sediments from the anthropogenically influenced ecosystem of Topolnitsa Dam (East Aegean Basin, Bulgaria). The highest exceedance was observed for Mn content (171.58 times) in Chironomidae samples. In the studied perch samples, the highest exceedances were recorded in liver samples for Cr (32.27 times), followed by Mn (5.68 times) and Fe (3.85 times) compared to the maximum permissible concentrations by national legislation. The exceedances in Al values were found only in Chironomidae samples (22.94 times). Bioaccumulation, bioconcentration, and biomagnification coefficients were analysed. The bioindicator significance of perch (Pr. percae), its parasite Pr. percae, and chironomids was assessed. The liver of European perch is a bioindicator of Cr pollution, and Chironomidae are bioindicators of Cr and Fe pollution, as well as Pr. percae, for Mn.*

***Key words:*** *benthos macroinvertebrates*, *bioindication, European perch, heavy metals, parasites.*

## INTRODUCTION

Topolnitsa Dam is located in the southern part of a deep valley, on the border between Ihtimanska and Saschinska Sredna Gora, at the boundary between the Balkan Mountain and Vitosha-Ihtiman subregions of the Mountain biogeographic region, and the Upper Thracian Lowland subregion of the Central Bulgarian biogeographic region (Gruev & Kuzmanov, 1994). The Dam was built in 1963 on the Topolnitsa River, 600 m from the village of Muhovo, Ihtiman Municipality, Sofia Region and after the village of Poibrene, Panagyurishte Municipality, Pazardzhik Region. The Topolnitsa River is the longest in the Sredna Gora Mountain. Topolnitsa Dam belongs to type L11b: Large deep dams in Ecoregion 7: Eastern Balkans, with water body code BG3MA800L160. The area around the dam ecosystem is distinguished by rich biological diversity. For its protection, the Protected Area BG0001389 Sredna Gora and Protected Area BG0001039 Popintsi under the Habitats Directive (Directive 92/43/EEC), as well as the Protected Area BG0002054 Sredna Gora, under the Birds Directive (Directive 79/409/EEC), have been declared. In the immediate vicinity of the Dam Wall near the village of Muhovo, the Topolnitsa Hydroelectric Power Plant is located. The waters of the Topolnitsa Dam are used for electricity generation, irrigation of arable land, flood control, sport and industrial fishing, tourism, etc. At the same time, the Topolnitsa Dam is located in an area with significant historical and contemporary industrial activity, including mining, metallurgy, raw material processing, and agricultural pressure in the peripheral territories. This necessitates complex ecological studies to assess interactions among physicochemical, geochemical, biological, and hydrological factors. One of the main pollutants that negatively impacts organisms and ecosystems is metals/metalloids, which, in addition to being pollutants, are also natural components of rocks.

As a result of anthropogenic activities such as mining and metal smelting, these elements are removed from their natural environments and become pollutants (Walker et al., 2006). A characteristic feature of metals is that they are neither created nor destroyed by humans, and, at high concentrations, they can pose a threat to living organisms and ecosystems. The heavy metals are characterised by toxicity, persistence and accumulativeness (Sauer & Watabe, 1989; Castro-Gonzales & Méndez-Armenta, 2008).

Scientific publications indicate that dams under conditions similar to those at the Topolnitsa Dam often exhibit signs of eutrophication, elevated concentrations of toxic metals, disrupted biological structures, and unstable ecosystem processes.

Dams, as anthropogenically created water bodies, have complex dynamics that make them both strategic resources and environmentally sensitive systems (Walker et al., 2006; Li et al., 2019).

The Topolnitsa dam has been identified as a repository of pollutants, with high As and Cu concentrations in the bottom sediments (Kolchakov et al., 1994). Exceedances of Fe, Mn, Ni, Cu, Ba, Mo, Al, Zn, Cd, Pb, Co, Ti, Sr have been reported (Dak et al., 2008).

Other authors have examined elements of the Dam ecosystem, such as water and fish (Velcheva, 2001; Velcheva & Nikolov, 2009; Georgieva et al., 2015; Valkova et al., 2022).

However, the majority of studies concern the state of the waters of the Topolnitsa River (Yancheva et al., 2011; Varbanov & Gartsiyanova, 2015; Gartsiyanova et al., 2021; Mihaylova et al., 2021; Park et al., 2022).

The studies characterise the state of one or another element in freshwater ecosystems, but do not track the circulation of heavy metals between the abiotic and biotic environments.

The study aims to present results on the content of aluminum (Al), chromium (Cr), manganese (Mn) and iron (Fe) in samples of water, sediments, bottom macroinvertebrates from Chironomidae, in muscles and liver of perch (*Perca fluviatilis* Linnaeus, 1758) and its parasite *Proteocephalus percae* (Müller, 1780) Railliet, 1899, for ecological characterisation and conservation of natural resources.

## MATERIALS AND METHODS

The research was carried out in the tail of the Dam after the village of Poibrene, designated as the Poibrene Biotope, with coordinates $42^0$27’38.88’’ N $23^0$59’20.81’’ E (Figure 1).

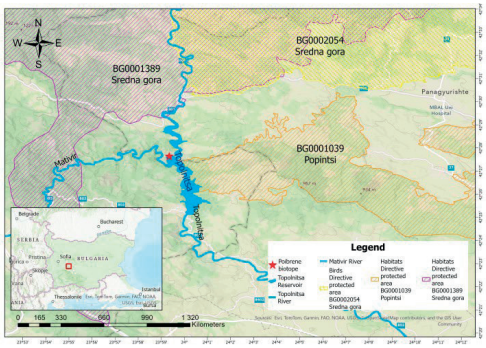



Figure 1. Topolnitsa Dam, Poibrene Biotope

The content of the heavy metals Al, Cr, Mn and Fe was monitored in samples of water, sediments and Biological Quality Elements (BQE) - macrozoobenthos, fish and fish parasites. The studies on BQE macrozoobenthos have been carried out in accordance with the standard BSS EN ISO 10870:2012. The samples were collected using a standard hydrobiological net and a Van Veen dredger in the littoral zone of the Dam ecosystem (Belkinova et al., 2013). The fish were collected after obtaining personal permits for scientific research fishing from the Executive Agency for Fisheries and Aquaculture of the Ministry of Agriculture and Food, in compliance with the BSS EN 14757:2015 standard. The ecological structure, condition and assessment of the condition of the ichthyofauna were analysed based on the indicators number of specimens, abundance (A), percentage of abundance (A%), weight (W g), percentage of weight (W%), maximum body width (TW cm), maximum body length (TL cm), and absolute dominance (D):

$$D = \frac{(A\%+W\%)}{2},$$

where A% is abundance in % and W% is weight of fish in % (Belkinova et al., 2013; Regulation H-4, 2012), Fulton condition coefficient (K):

$$K = 100.\frac{W}{L^3},$$

where W is the weight of fish, and L is the maximal body length (Golub et al., 2019).

Water sampling was carried out in accordance with BSS EN ISO 5667-1:2026, and sediment sampling in accordance with BSS ISO 5667-12:2017. The main Physicochemical Quality Elements: temperature (0C), pH, dissolved O2 mg/l, electrical conductivity (μS/cm), hardness (ppm), N-NH4 mg/l, N-NO3 mg/l, N-NO2 mg/l, TOC mg/l, P-Ortho-PO4 mg/l, BOD5 mg/l and Secchi transparency m, were monitored according to Regulation H-4/2012 from National legislation. A portable system for rapid analysis of organic pollutants in water, the ENOVA Insta Sense O2 model, and a HANNA HI83399 Photometer were used to determine physicochemical water quality indicators under field conditions.

Among the Biological Quality Elements, dominant groups and representatives have been selected. Among the established macrozoobenthos, the dominant Chironomidae were studied for the contamination of Al, Cr, Mn, and Fe. In the ichthyocomplexes, the dominant fish species is the European perch, Perca fluviatilis Linnaeus, 1758 (30 specimens). Samples of perch muscle and liver were isolated. The digestive system was examined for endoparasites. The studies on parasites were conducted in accordance with Zashev & Margaritov (1966) and Moravec (2013). Species differentiation was carried out according to the criteria of Bauer (1987) and Moravec (2013). Dominant helminth species in the helminth communities of perch is the cestode species Proteocephalus percae (Müller, 1780) Railliet, 1899. Pr. percae was also examined for contamination of the four heavy metals. The samples were collected from April to October 2025.

In total, 9 samples each of water, sediment, Pr. percae and Chironomidae, 10 samples each of fish muscle and liver were processed and analysed for Al, Cr, Mn, and Fe content. Sample pretreatment and acid digestion were performed according to EPA- and ISO-approved procedures: BSS EN ISO 21424:2020 for biological samples, BSS EN ISO 5667-14:2016 for water samples, and US EPA Method 3051A for sediment samples. After collection, water samples were stored at 4°C in dark glass bottles before transportation to the laboratory. For ICP-MS analysis, 50 mL of each water sample was filtered through a 25 mm sterile PES syringe filter with a pore size of 0.45 μm. The filtrates were acidified with 0.05 mL concentrated nitric acid to pH 2 and subsequently subjected to instrumental analysis.

Biological samples were dissolved with concentrated $HNO_3$ and then appropriately diluted before analysis. Sediment sample preparation was performed in accordance with US EPA Method 3051A. The aqua regia digestion was performed using 0.5 g of the sediment sample and an acid mixture containing 9 mL of $HNO_3$ and 3 mL of HCl. After the digestion, the supernatant was decanted and diluted to a final volume of 50 mL with double-deionised water. Before ICP-MS analysis, 1 mL of each sample solution was diluted to 10 mL with double-deionised water. Elemental analysis was performed using a PerkinElmer SCIEX ELAN DRC-e ICP-MS system (MDS Inc., Concord, ON, Canada).

Bioconcentration factors have been determined:

$$BCF=\frac{Cb}{Cw},$$

where *Cb* was the concentration of examined heavy metals in the biological samples and *Cw* - concentrations in the water samples, and

$$BCF=\frac{Cb}{Cs},$$

where *Cb* was the concentration of the examined heavy metals in the biological samples and *Cs* - concentrations in the sediment samples.

Bioacumulation factor was determined for the fish parasite *Pr. percae* for the accumulation of examined heavy metals:

$$BAF=\frac{CPr.percae}{Cfish\ muscle \text{ or } Cfish\ liver},$$

The biomagnification factor was determined as:

$$BMF=\frac{Cfish\ muscle \text{ or } Cfish\ liver}{CChironomidae},$$

Statistical processing of the results was performed using MS Excel (Microsoft, 2010).

## RESULTS AND DISCUSSIONS

### Macrozoobenthos

The samples of bioindicator macrozoobenthos collected in 2025 are distinguished by the presence of 5 taxa in the Poibrene Biotope.

Representatives of Chironomidae Newman, 1834, larvae (Insecta, Diptera) dominate, followed by Baetidae (*Baetis* Leach 1815, larvae; Insecta, Ephemeroptera) and Gerridae (*Gerris* Fabricus, 1794; Heteroptera). Coleoptera is represented by two taxa (Gyrinidae and Haliplidae). 286 specimens of Chironomidae were isolated and studied. Representatives of Chironomidae are bioindicators for p-saprobic conditions and belong to the sensitivity group D (tolerant forms) (Belkinova et al., 2013). Scientific studies by other authors show reduced biodiversity in the benthos, dominance of tolerant groups (Chironomidae) and periodic "blooms" of cyanobacteria - typical of reservoirs with combined pressure from toxic metals and eutrophication (Li et al., 2019), also found in this study. Modern methods for complex assessment include physicochemical analyses and biological indicators (Li et al., 2019).

**Fish and basic biological indices**

Freshwater fish in the Poibrene biotope are represented by 5 species: European perch *Perca fluviatilis* Linnaeus, 1758 (Percidae); Roach *Rutilus rutilus* (Linnaeus, 1758) (Cyprinidae); Bleak *Alburnus alburnus* (Linnaeus, 1758) (Cyprinidae); Orpheus dace *Squalius orpheus* Kottelat & Economidis, 2006 (Cyprinidae); Pumpkin seeds *Lepomis gibbosus* (Linnaeus, 1758) (Centrarchidae).

*P. fluviatilis* in the Poibrene Biotope is distinguished by the highest abundance (A%=46.0; 30 specimens) and absolute dominance (D=26.5). It is eudominant in the ichthyocomplexes from the researched biotope of the Topolnitsa Dam. The main metric data of the studied perch specimens were also determined (TL cm 13.58±2.17 (10.4-17.5); TW cm 3.42±0.67 (2.2-4.5); W/W% 28.14±12.28 (11.0-51.0)/7.0). The European perch, *P. fluviatilis*, is distributed throughout Europe and is found across almost all of Bulgaria. It inhabits rivers, lakes, brackish and semi-saline waters. It prefers reservoirs overgrown with aquatic vegetation. It is tolerant of high-water acidity. Young feed on zooplankton, and the adults feed on bottom invertebrates and small fish. The species is the subject of sport fishing.

The perch (*P. fluviatilis*) is recommended as an indicator species for assessing the degree of pollution of aquatic ecosystems (Karapetkova & Zhivkov, 2006; Kottelat & Freyhof, 2007). The species is not threatened (LC, IUCN).

The Fulton condition coefficient for P. fluviatilis in this study was K=1.20, indicating fat fish in the studied biotope of Topolnitsa Reservoir. The Fulton condition coefficient is a widely used indicator for assessing the health, fitness or completeness of fish populations. This tool is vital for monitoring fish health, assessing the impact of the environment on wild populations and for the sustainable management of fish resources. At K values around 1, K indicates an average condition. When K>1.2 indicates fat fish, and K<0.8 indicates slim fish. Furthermore, K>1 values indicate favourable environmental conditions (Radkhan & Eagderi, 2015; Zaharieva et al., 2024). Similar studies were conducted by Stavrescu-Bedivan et al. (2023) on Lake Mostiștea in Romania. They found K values above unity for Prussian carp (*Carassius gibelio*), indicating a favourable state of the species in the ecosystem.

**Parasites of *Perca fluviatilis* from Topolnitsa reservoir, Poibrene Biotope**

The parasite communities of perch are represented by two species: *Proteocephalus percae* (Müller, 1780) Railliet, 1899 (Proteocephalidae, Cestoda) and *Contracaecum* sp., larvae (Nematoda). The dominant species is *Pr. percae*. In the study, the species was represented by a prevalence of P%=43.34, a mean intensity of MI=7.85, and a mean abundance of MA=3.4. The species is the core for the parasitic communities of perch. The definitive hosts of *Pr. percae* are European perch (*P. fluviatilis*), Ruffe (*Gymnocephalus cernua*, Linnaeus, 1758), Northern pike (*Esox lucius*, Linnaeus, 1758), and others. Intermediate hosts are crustaceans of the genus *Cyclops* Müller, 1785 (Kakacheva-Avramova, 1983; Bauer, 1987).

**Physicochemical Quality elements**

Under field conditions, the main physicochemical quality elements were determined according to Regulation H-4/2012 for dams of type L11b in Ecoregion 7: Eastern Balkans, to which the studied dam ecosystem, Poibrene Biotope, also belongs (Table 1).

According to Regulation No. H-4/2012, for lakes of type L11b, the obtained quality elements indicate a moderate water state in the studied biotope.

Table 1. Physicochemical quality elements, Topolnitsa Dam, Poibrene Biotope

| Physicochemical elements | Water stateL11b/ Regulation № H-4/2012 | | | Topolnitsa dam L11b |
|---|---|---|---|---|
| | Excellent | Good | Moderate | |
| Temperature, $^0$C | | | | 20.08 |
| pH | - | 6.7-8.7 | - | 9.00 |
| dissolved $O_2$mg/l | 10.5-8.00 | 8.00-6.00 | <6.00 | 6.80 |
| Electroconductivity µS/cm | <650 | 650-750 | >750 | 410 |
| Hardness | | | | 270Class 5 |
| N-$NH_4$mg/l | <0.03 | 0.03-0.08 | >0.08 | 0.49 |
| N-$NO_3$mg/l | <0.06 | 0.06-1.80 | >1.80 | 0.60 |
| N-$NO_2$mg/l | <0.01 | 0.01-0.025 | >0.025 | 0.058 |
| TOCmg/l | | | | 1.00 |
| P-Ortho-$PO_4$mg/l | <0.016 | 0.016-0.035 | >0.03 | 0.37 |
| $BOD_5$mg/l | <1 | 1-2.5 | >2.5 | 0.50 |
| Secchi transparency, m | >3 | 3-2 | <2 | <2 |

**Heavy metal content**

The prepared samples of water, sediments, fish muscles and liver, and samples of *Pr. percae* and Chironimidae were subjected to chemical analyses for the contents of Al, Cr, Mn, and Fe (Table 2). According to Regulation H-4/2012 and Regulation EQS/2010 of national legislation, the maximum permissible values for Al in surface waters are 25 µg/L at pH < 6.5; for Cr, 32 µg/L. The annual average norm for Mn in surface waters is 50 µg/L, and for Fe, 100 µg/L. For fish muscle, according to FAO/WHO (1972), the maximum permissible limit is Mn e 0.5 mg.kg-1, and for Cr – 0.15 mg.kg$^{-1}$ wet weight. According to WHO (1996), the maximum permissible limit of Fe in fish muscles is 0.05 mg.kg$^{-1}$ dry weight. For Al content, the maximum permissible limit of 0.2 mg kg$^{-1}$ wet weight is accepted for marine fish muscles, because there are no officially approved norms by FAO, WHO, and others for freshwater fish (Ranau et al., 2001). The highest concentrations of Al, Mn, and Fe were found in the Chironomidae samples, while the highest concentrations of Cr were found in the liver samples of perch. The change in the concentrations of the trace elements in the studied samples (wet weight) is in the following descending order: CAl_Fe_Chironomidae>CAl_Fe_Liver>CAl_Fe_*Pr.percae*>CAl_Fe_Muscle>CAl_Fe_Water; CCr_Liver>CCr_Chironomidae>CCr_Muscle>CCr_*Pr.percae*>CCr_Water;CMn_Chironomidae>CMn_*Pr.percae*>CMn_Liver>CMn_Muscle>CMn_Water (Table 2).

Higher excesses in Al concentrations were recorded in water samples (80.67 times) than in Chironomidae (22.94 times). In the liver and muscle samples of perch, as well as in the samples from *Pr. percae*, no excesses in Al concentrations were recorded. Regarding the Cr content, excesses were not found only in water samples.

Table 2. Concentration of heavy metals

| Concentration of heavy metals, wet weight | | | | | |
|---|---|---|---|---|---|
| µg/g | *Perca fluviatilis* µg/g | | *Pr.percae* µg/g | Chironomidae µg/g | Water µg/ml |
| | Liver | Muscle | | | |
| **Al** | 14.13±7.50 (8.83-19.44) | 3.48±0.72 (2,97-3.99) | 5.07±0.27 (4.92-5.3) | 688.21±5.25 (684.49-691.92) | 1.21±0.03 (1.19-1.23) |
| **Cr** | 9.68±2.41 (7.98-11.39) | 2.64±0.25 (2.46-2.82) | 1.62±0.01 (1.61-1.63) | 8,45±4,49 (11.62-5.27) | 0,004±0,001 (0,003-0,005) |
| **Mn** | 5.68±0.13 (5.78-5.59) | 0.85±0.63 (0.40-1.29) | 10.21±0.03 (10.19-10.23) | 171.58±2.16 (170.05-173.10) | 0.24±0.03 (0.22-0.26) |
| **Fe** | 385.2±123.32 (298.0-472.4) | 13.55±1.48 (12.5-14.6) | 28.22±0.03 (28.20-28,24) | 1248.75±197.21 (1388.2-1109.3) | 0.84±0.03 (0.82-0.86) |
| Concentration of heavy metals, dry weight | | | | | |
| µg/g | *Perca fluviatilis* µg/g | | *Pr.percae* µg/g | Chironomidae µg/g | Sediments µg/g |
| | Liver | Muscle | | | |
| **Al** | 47.12±25.00 (29.44-64.80) | 13.92±2.80 (11.88-15.96) | 20.30±0.03 (20.28-20.32) | 1593.06±12.17 (1584.46-1601.67) | 20131.19±1390.31 (19148.09-21114.29) |
| **Cr** | 32.29±8.04 (26.60-37.97) | 10.56±1.02 (9.84-11.28) | 6.51±0.03 (6.49-6.53) | 19,55±10.39 (12.20-26.89) | 57.65±7.84 (52.11-63.20) |
| **Mn** | 18.96±0.44 (19.27-18.64) | 3.38±2.52 (1.60-5.16) | 40.87±0.03 (40.85-40.89) | 397,16±4,99 (393.63-400.69) | 758.86±130.48 (666.60-851.13) |
| **Fe** | 1284.00±41 1.06 (993.34-1574.67) | 54.2±5.94 (50.00-58.40) | 112.9±0.49 (112.8-112.11) | 2890.63±456,52 (2567.82-3213.43) | 24852.91±4364.32 (21766.87-27938.95) |

Of the biological samples, the highest Cr exceedances were found in perch liver samples (32.27 times), followed by Chironomidae samples (28.17 times) and perch muscle samples (8.8 times). The lowest Cr exceedances were observed in samples from *Pr. percae* (5.4 times). Mn concentrations showed exceedances in all the studied samples, but were highest in those from Chironomidae (171.58 times), followed by those of *Pr. percae* (10.21 times), of perch liver samples (5.68 times), and in water samples (4.80 times). The lowest exceedances are of perch muscle samples (0.85 times). Regarding Fe content, the highest exceedances were found in Chironomidae samples (12.49 times), followed by water (8.4 times), and were lowest in perch liver samples (3.85 times). No exceedances were found in perch muscle samples and in *Pr. percae* (Table 2).

There are no uniform standard values for heavy metals in sediments in the environmental legislation of Bulgaria and the European Union. For the presented studies, we used Regulation

3/2008 of the national legislation and those approved by the US Environmental Protection Agency (US EPA). Other authors have also used these regulatory documents to assess heavy metal content in sediments in Bulgaria (Cholakova, 2021). When comparing the concentrations of the studied elements to those in the sediment samples (dry weight, μg/g), the highest concentrations of Al, Cr and Mn were recorded for the sediments, the lowest in the muscle samples for Al, Mn, and in Pr. percae for Cr, respectively. The highest values for Fe were recorded in the Chironomidae, followed by those in the sediments, in the perch liver, and in Pr. percae. They were the lowest again in the perch muscle. The change in the concentrations of the studied elements in the samples (wet weight) is in the following descending order:

CAl_Fe_Sediments>CAl_Fe_Chironomidae>CAl_Fe_Liver>CAl_Fe_*Pr.percae*>CAl_Fe_Muscle;CCr_Liver>CCr_Sediments>CCr_Chironomidae>CCr_Muscle>CCr_*Pr.percae*;CMn_Sediments>CMn_Chironomidae>CMn_*Pr.percae*>CMn_Liver>CMn_Muscle;CFe_Chironomidae>CFe_Sediments>CFe_Liver>CFe_*Pr.perca.*

In aquatic environments, Al is present in inorganic and organic complexes. Given its abundance, studying its impact on aquatic organisms and the aquatic environment, especially in dam ecosystems, is of great importance. In the National legislation (Regulation 3/2008), as well as in the ERL (Effect Range-Low; Long et al., 1995) no limit values for the content of this element are determined. The total Al concentration should not exceed 74.4 μg/L to protect freshwater organisms (Botté et al., 2021). Studies have shown that sedimentary forms of Al can be toxic to freshwater organisms, especially fish. Potentially hazardous concentrations of dissolved Al in the environment are considered more harmful to freshwater organisms (Botté et al., 2021). The impact of Al on freshwater organisms is reported to depend on pH, habitat type, total hardness, and DOC (US EPA, 2018).

Chromium (Cr) is a widespread metal in soils and waters. $Cr^{3+}$ accumulates poorly in organisms and is excreted mainly in the urine. Much more toxic is $Cr^{6+}$, which accumulates in much higher concentrations. It accumulates mainly in the liver, spleen and bone marrow. Cr6+ in the body is reduced to Cr3+ , which forms complexes with biomolecules, explaining the long retention of Cr in cells. It is excreted in the urine. According to Regulation 3 of the national legislation, the maximum permissible concentration is 200 μg/L, against which no excesses were found in the sediment samples we examined. According to the ERL US EPA, the norm is 81 mg/kg Cr, against which we also found no exceedances in the sediment samples we examined. Manganese (Mn) plays an important role in the development of aquatic plants. At high concentrations in water, Mn is toxic to fish. Iron (Fe) occurs in the form of inorganic and organic compounds. Fe deficiency leads to anaemia, including in fish. Organisms can accumulate Fe, which is why it is found in them at higher concentrations. At a concentration of 0.2 $mg \cdot l^{-1}$ in water, mass fish deaths have been reported (Yablanski & Petkov, 2011).

BCF values from 1000 to 5000 indicate that the corresponding chemical element is bioaccumulating (European Chemicals Agency, 2017). Such values were found for BCFCr-Liver-Water, BCFCr-Chironimidae-Water and BCFFe-Chironimidae-Water (Table 3). BAF showed higher bioaccumulation values in *Pr. percae* than in perch muscles for Al, Mn and Fe.

Table 3. Bioconcentration factor (BCF), Bioaccumulation factor (BAF), and Biomagnification factor (BMF)

| **BCF[$C_b/C_w$] wet weight** | **BCF_Al** | **BCF_Cr** | **BCF_Mn** | **BCF_Fe** |
|---|---|---|---|---|
| Liver - Water | 11.68 | 2420.00 | 23.67 | 458.57 |
| Muscle - Water | 2.87 | 660.00 | 3.54 | 16.13 |
| *Pr. percae* - Water | 4.19 | 405.00 | 42.54 | 33.59 |
| Chironomidae - Water | 568.77 | 2112.50 | 714.92 | 1486.61 |
| **BCF [$C_b/C_s$] dry weight** | **Al** | **Cr** | **Mn** | **Fe** |
| Liver - Sediments | 0.002 | 0.56 | 0.02 | 0.05 |
| Muscle - Sediments | 0.0006 | 0.18 | 0.004 | 0.0001 |
| *Pr. percae* - Sediments | 0.001 | 0.09 | 0.05 | 0.004 |
| Chironomidae - Sediments | 0.079 | 0.34 | 0.52 | 0.12 |
| **BAF $C_{Pr.\ percae}/C_{fish}$ wet weight** | **BAF_Al** | **BAF_Cr** | **BAF_Mn** | **BAF_Fe** |
| Liver | 0.36 | 0.17 | 1.79 | 0.07 |
| Muscle | 1.46 | 0.61 | 12.01 | 2.08 |
| **BMF $C_{fish}/C_{Chironomidae}$ wet weight** | **Al** | **Cr** | **Mn** | **Fe** |
| Liver | 0.02 | 1.15 | 0.03 | 0.31 |
| Muscle | 0.005 | 0.31 | 0.005 | 0.01 |

Highest BAFMn-*Pr.pertsae*_Muscle=12.01 gives reason *Pr. percae* to be determined as a bioindicator for Mn. When the values of BCF and BAF are < 250, the risk is low; the risk is moderate from 250 to 1000; and the risk is high and bioaccumulative from 1000 to 5000 (European Chemicals Agency, 2017). When

BMF>1, the contaminant increases and accumulates much more (biomagnification) (Fremlin et al., 2025), in this case, in perch than in food, Chironomidae. We establish it for the accumulation of Cr in the perch liver. The results obtained provide reason to declare the European perch a bioindicator of Cr pollution and Chironomidae bioindicators of Cr and Fe pollution (Table 3).

## CONCLUSIONS

The results obtained for the Topolnitsa Dam, Poibrene Biotope, show poor species diversity in the benthic macroinvertebrate fauna, ichthyocenoses, and parasitic communities of perch. According to the study, the liver of European perch is a bioindicator of Cr pollution, and Chironomidae are bioindicators of Cr and Fe pollution. BAF showed higher bioaccumulation values in *Pr. percae* than in perch muscles for Al, Mn and Fe. The highest BAFMn-*Pr. percae*_Muscle=12.01 determined *Pr. percae* as a bioindicator for Mn.

## REFERENCES

Bauer, O.N. (Ed.) (1987). Opredelitel parazitov presnovodnih rib SSSR *[Key to the Parasites of Freshwater Fishes of the USSR*]. Leningrad, RU: Nauka Publishing House. [In Russian]

BSS EN ISO 10870:2012 Waterquality – Guidelines for the selection of sampling methods and devices for benthic macroinvertebrates in fresh waters (ISO 10870:2012). [In Bulgarian]

BSS EN 14757:2015 Water quality - Sampling of fish with multi-mesh gillnets. [In Bulgarian]

BSS EN ISO 5667-14:2016 Water quality - Sampling - Part 14: Guidance on quality assurance and quality control of environmental water sampling and handling (ISO 5667-14:2014)

BSS ISO 5667-12:2017. BDS. Water quality. Sampling. Part 12: Guidance on sampling of bottom sediments from rivers, lakes and estuarine areas

BSS EN ISO 21424:2020 Milk, milk products, infant formula and adult nutritionals - Determination of minerals and trace elements - Inductively coupled plasma mass spectrometry (ICP-MS) method (ISO 21424:2018)

BSS EN ISO 5667-1:2026. BDS. Water quality. Sampling. Part 1: Guidance on the design of sampling programmes and techniques for sediment sampling (ISO/DIS 5667-1).

Belkinova, D., Gecheva, G., Cheshmedzhiev, S., Dimitrova-Dyulgerova, I., Mladenov, R., Marinov, M., Teneva, I., Stoyanov, P., Ivanov, P., Mihov, S., Pehlivanov, L., Varadinova, E., Karagyozova, Ts., Vassilev, M., Apostolu, A., Velkov, B., & Pavlova, M. (2013). *Biological analysis and ecological assessment of surface water types in Bulgaria*. Plovdiv, BG: University "P. Hilendarskii" Publishing House (in Bulgarian).

Botté, A., Zaidi, M., Guery, J., Fichet, D., & Leignel, V. (2022). Aluminium in aquatic environments: abundance and ecotoxicological impacts. AquatEcol. 56(3), 751–773.

Castro-Gonzales, M.I., & Méndez-Armenta, M. (2008). Heavy metals: Implicationsassociated to fish consumption. *Environmental Toxicology and Pharmacology*, 26(3). 263-271.

Cholakova, Z. (2021). Peculiarities in the content of heavy metals in the bottom sediments of some tributaries of the Iskar River in the Stara Planina Mountains (Iskretska River and Batuliyska River). – In: *Yearbook of the Sofia University, Faculty of Geology and Geography, book 2 – Geography*, 113. 140–160.

Dak, T., Velcheva, I., & Todorova, B. (2008). A Study on the Processes of Distribution, Accumulation and Transfer of Cadmium and Zink in the Organisms of Fishes. *Proceedings of the Anniversary Scientific Conference on Ecology.* Plovdiv, 503-513. [In Bulgarian]

Directive 92/43/EEC of 21 May 1992 on the conservation of naturalhabitats and of wild fauna and flora. *Retrieved from* https://assets.publishing.service.gov.uk/media/5a7ce7bee5274a2c9a484d58/Annex-A-Habitats-Directive.pdf

Directive 2009/147/EC on the conservation of wild birds. Retrieved from https://www.npws.ie/directive-2009147ec-conservation-wild-birds-codifiedversion

European Chemicals Agency. (2017). *Guidance on information requirements and chemical safety assessment – Chapter R.7a – Endpoint specific guidance*, European Chemicals Agency, https://data.europa.eu/doi/10.2823/337352

FAO/WHO (1972) Evaluation of Certain Food Additives and the Contaminants Mercury, Lead and Cadmium. WHO Technical Report Series No. 505.

Fremlin, K. M., Elliott, J.E., & Gobas, F.A.P.C. (2025). Guidance for measuring and evaluating biomagnification factors and trophic magnification factors of difficult substances: application to decabromodiphenylethane. *Integrated Environmental Assessment and Management*. 21(2): 263–278

Gartsiyanova, K., Varbanov, M., Kitev, A. & Genchev, S. (2021). Water quality analysis of the rivers Topolnitsa and Luda Yana, Bulgaria using different indices. *Journal of Physics: Conference Series*. 1960. 012018.

Georgieva, E., Vesela Yancheva, V., Velcheva, I., Maria Becheva, M., & Stoyanova, S. (2015). Histological alterations under metal exposureIn gills of European perch (*Perca fluviatilis* l.) from Topolnitsa Reservoir (Bulgaria). *Arch. Biol. Sci*., 67(2). 729-737.

Golub, D., Bukva, M. & Dekić, R, (2019). Morphological Characteristics and Condition of Bleak Alburnus alburnus (Teleostei; Cyprinidae) from the Bosna River. SKUP, 10(1): 16-28. https://doi: 10.7251/SKPEN191001016G

Gruev, B., & Kuzmanov, B. (1994). *General*

*biogeography*. Sofia, BG: Univ. Publishing House "St. Kliment Ohridski".

Kakacheva-Avramova, D. (1983). *Helminths of freshwater fishes in Bulgaria*. Sofia, BG: Bul. Acad. Sci. Publishing House. [in Bulgarian]

Karapetkova, M., & Zhivkov, M. (2010). *Fish in Bulgaria*. Sofia, BG: GeaLibris.

Kolchakov, I., Stanchev, A., Brashnarova, A., & Stanislavova, A. (1994). Research on arsenic and copper contamination of soils and plant production in the Pazardzhik field through irrigation water from the Topolnitsa dam. *Soil science, agrochemistry and ecology*. 29, 88-90.

Kottelat, M., & Freyhof, J. (2007). *Handbook of European freshwater fishes*. Berlin, DE: Publications Kottelat, Cornol and Freyhof.

Li, Z., Huo, J., & Bricker, J. D. (2019). Ecological risk assessment for eutrophication and heavy metal pollution of Suyahu Reservoir sediments. *Biotechnology & Biotechnological Equipment*, *33*(1), 1053–1062.

Moravec, F. (2013). *Parasitic Nematodes of Freshwater fishes of Europe*. Praha, CZ: Academia Publishing House.

Mihaylova, B., Valchev, S., Benderev, A., Dobrev, H., Dachev, K., & Bardarska, G**.** (2021). Influence of Medetska River on the pollution of Topolnitsa River**.** *National Conference with International Participation "GEOSCIENCES 2021". ReviewoftheBulgarianGeologicalSociety*, 82(3), 177–179.

Park, J., Sakelarieva, L., & Varadinova, E. (2022). Comparative Analysis of the Water Policies and the Systems for Ecological Status Assessment of the Running Waters in Bulgaria and South Korea: Case study on Maritsa River and Han River. *EcologiaBalkanica*, 14(2). 171-189.

Statsoft Inc. (2011) (n.d.). STATISTICA (data analysis software system), version 10. Retrieved from www.statsoft.com.

Stavrescu-Bedivan, M-M., Sandu, M., Scaeteanu, G.V., Virsta, A., Majar, R.M., & Baicu, S. (2023). Preliminary report on the water quality, ichthyophauna and biometric indices for Prissian carp from Iezerul Mostiștea lake, Romania. *Scientific Paper. Series E. Land Reclamation, Earth Obsrvation & Surveying, Environmental Engineering*, XII. 309-319.

Radkhan, A., & Eagderi, S. (2015). Length-weight and length-length relationship and condition factor of six cyprinid fish species of Zarrineh River (Urmia Lake basin, Iran). *Iranian Journal of Ichthyology*, 2(1). 61-64.

Ranau, R., Oehlenschläger, J. & Steinhart, H. (2001). Aluminium content in edible parts of seafood. *Eur Food Res Technol*, 212(4). 431-438.

Regulation 3/2008 on the norms for permissible content of harmful substances in soils. State Gazette, 71/2008

Regulation on environmental quality standards for priority substances and certain other pollutants of 01.11.2010 (Regulation EQS/2010)

Regulation No. H-4 of 14.09.2012 on the characterization of surface waters. Promulgated in the Official Gazette, No. 22 of 5.03.2013, amended and supplemented, No. 67 of 04.08.2023 amended and supplemented, No.97 of 11 December 2015.

Sauer, G.R., & Watabe, N. (1989). Temporal and metal-specific patterns in the accumulation of heavy metals by the scales of *Fundulus heteroclitus*. *Aquatictoxicology*, 14(3). 233-248.

US EPA. 2007. "Method 3051A (SW-846): Microwave Assisted Acid Digestion of Sediments, Sludges, and Oils," Revision 1. Washington, DC. *Retrieved from https://www.epa.gov/sites/default/files/2016-12/documents/3051a.pdf*

US EPA (Environmental Protection Agency) (2018) Aquatic Life Ambient Water Quality Criteria for Aluminum in Freshwater, Federal Register, 83, 245.

Valkova, E., Atanasov, V., Tzanova, M., Atanassova, S., Sirakov, I., Velichkova, K., Marinova, M.N., & Yakimov, K. (2022). Content of Pb and Zn in Sediments and Hydrobionts as Ecological Markers for Pollution Assessment of Freshwater Objects in Bulgaria - A Review. *Int. J. Environ. Res. PublicHealth*, 19(5). 9600.

Varbanov, M., & Gartsiyanova, K. (2015). Comparative Analysis of water quality indexes. *Papers of Scientific Conference "The Science in service of the Society", 30 October 2015*, *Varna*. 3–10. [In Bulgarian]

Velcheva, I. (2001). Contents and transfer of copper in freshwater fish. BIOS. *Scientific annals of the school of biology*. 6. 49-60.

Velcheva, I., & Nikolov, B. (2009). A Study on the Processes of Distribution, Accumulation and Transfer of Copper (Cu) in the Organisms of Fishes. *Ecologia Balkanica*. 1. 15-20.

Walker, C.H., Hopkin, S.P., Sibly, R.M., & Peakball, D.B. (2006). *Principles of Ecotoxicology*. FL: CRC Press, Boca Raton.

WHO 1996. Trace elements in human nutrition and health. ISBN 92-4-156173-4 (NLM Classification: QU 130). Geneva.

Yablanski, T., & Petkov, G (Eds.) (2011). *Hand book of Applied Ecology*. Stara Zagora, BG: Alfamarket.

Yancheva, V., Petrova, S., Velcheva, I., & Georgieva, E. (2011). A review of ecological status of Topolnitsa River catchment area and Topolnitsa Dam. *Scientific papers University of Plovdiv* (In Bulgarian).

Zashev, G., & Margaritov, N. (1966). *Diseases of fish. Sofia*, BG: Nauka i izkustvo (In Bulgarian).

Zaharieva, P., Zaharieva, R., & Kirin, D. (2024). Species diversity of the Ichthyofauna of the Stryama River. *Problems of Geography*, 1-2. 119-130.

Scientific Papers. Series E. Land Reclamation, Earth Observation & Surveying, Environmental Engineering. Vol. XV, 2026
Print ISSN 2285-6064, CD-ROM ISSN 2285-6072, Online ISSN 2393-5138, ISSN-L 2285-6064

# PHYSICOCHEMICAL DYNAMICS OF WATER QUALITY IN SAND AND GRAVEL POST-EXPLOITATION LAKES

**Karoly Alexandru RACZ, Emilia Valentina PANTEA, Nicu Cornel SABĂU**

University of Oradea, 1 Universitatii Street, Oradea, Romania

Corresponding author email: emipantea@gmail.com

***Abstract***

*The present study aims to evaluate the water quality of five lakes formed as a result of mineral aggregate extraction (sand and gravel) located in the administrative area of Ineu de Criș, Bihor County, Romania. To achieve this objective, two were carried out in May and October 2025, focusing on relevant physicochemical parameters commonly used to characterize the water quality of post-extraction lakes, including pH, dissolved oxygen (DO,), biochemical oxygen demand ($BOD_5$), chemical oxygen demand (COD), total nitrogen (TN), total phosphorus (TP), and potassium ($K^+$). The obtained results indicated relatively small differences in water quality among the five analysed lakes. Based on the measured concentrations of total nitrogen (TN) and total phosphorus (TP), all lakes were classified in Quality Class I according to Romanian Order No. 161/2006. Regarding dissolved oxygen (OD), lake L3 exhibited the highest values, corresponding to Quality Class I, whereas the remaining lakes showed moderate spatial variability with the lowest values recorded in lake L2. Slight differences were also observed for the $BOD_5$, with most lakes falling within Quality class I, while lake Camelot was classified in quality class II. Overall, the investigated lakes exhibited good to very good physicochemical water quality, with no evidence of significant degradation during the monitoring period These findings suggest that the studied post-extraction lakes have developed relatively stable hydro chemical conditions and may represent valuable aquatic ecosystems within the local landscape, although a comprehensive ecological status assessment would require the inclusion of biological and hydro morphological quality elements in accordance with the European Water Framework Directive (European Parliament and Council, 2000).*

***Key words****: gravel pit lakes, physicochemical parameters, post-exploitation lakes, water quality, water quality assessment, Water Quality Index (WQI).*

## INTRODUCTION

Water represents a fundamental resource at the planetary level, being the essence that sustains life and a critical element in the functioning of geosystems (Popa et al., 2019). Covering approximately two thirds of the Earth's surface, water is not merely a physical compound but an indispensable biological factor, participating in cellular structure, metabolic processes, and the maintenance of the thermal balance of all living organisms. At the macro scale, it acts as a driving force of natural cycles, shaping landforms, influencing climate, and representing the essential link connecting the atmosphere, soil, and biosphere. Water is a fundamental requirement for all forms of life, playing a significant role in sustainable development and the circular economy (Sandu & Vîrsta, 2021).

From a socio-economic perspective, the availability and quality of water are directly linked to food security, public health, and sustainable economic development. However, the relationship between humans and this vital resource has become increasingly complex and strained. The intensification and diversification of anthropogenic activities ranging from industrialization and urbanization to the intensive exploitation of natural resources have generated significant pressures on the hydrological cycle and aquatic ecosystems. At the European scale, recent assessments continue to identify substantial pressures on water quantity and quality and emphasize the need to strengthen water resilience and integrated management (European Environment Agency, 2024; Costa et al., 2025). At the local scale, land-use changes, may also support ecological restoration; for example, the conversion of former pasturelands into community forest in Ineu illustrates a local rehabilitation pathway relevant to landscape stabilization (Timofte & Racz, 2025).

In this context, lakes formed as a result of mineral aggregate extraction (stone and sand) can be considered emerging aquatic systems resulting from anthropogenic transformations of the

hydrographic landscape. At the global level, the exploitation of freshwater sand resources is increasingly associated with issues related to natural resource governance and pressures on aquatic ecosystems, being recently identified as a major challenge for sustainable resource management (United Nations Environment Programme, 2022; Yasmin et al., 2024). In this context, post-extraction lakes represent relevant examples of ecosystems resulting from anthropogenic interventions, which can gradually evolve into functional aquatic systems. Although artificially created, these water bodies may progressively develop into new lacustrine ecosystems in which water reflects both residual anthropogenic impacts and ecological regeneration processes, including the development of new trophic chains. These environments provide an excellent natural laboratory for studying secondary ecological succession and natural self-purification processes.

The main objective of the present study is to evaluate the water quality of lakes formed as a result of mineral aggregate extraction, based on the determination of physic-chemical and biochemical water quality indicators, in order to classify these water bodies according to the quality classes established by the national regulation regarding the classification of surface water quality (Order No. 161/2006, 2006).

The commune of Ineu is located in the central part of Bihor County (Figure 1) and represents the easternmost locality within the Oradea Metropolitan Area.

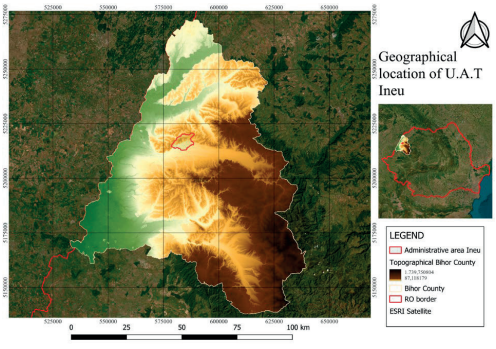



Figure 1. Map of the geographical location of the commune of Ineu using QGIS

The total surface area of Ineu commune is 49.51 km², and the locality is situated at a distance of approximately 20 km from the municipality of Oradea. The geographical coordinates are (47°06′05″ N, 22°06′10″ E). The evolution of the hydrographic landscape in the Ineu area provides an illustrative example of the long-term dynamics of the human-water relationship. The analysis of a historical map from 1782 (Figure 2), georeferenced using QGIS (Bellezza et al., 2014), demonstrates that the original course of the Crișul Repede River crossed the area where part of the present-day locality is currently situated. Naturally, the river branched into two main channels in the area of the locality of Tileagd, forming a complex and unstable hydrographic system. In response to the risks associated with flooding and to support urban development, hydraulic engineering works were implemented to regulate the river course, including the construction of diversion channels aimed at reducing flood risk and protecting the local population. Following the economic transformations that occurred after the 1990s, the upstream agricultural lands were increasingly used for extractive activities, particularly for gravel and sand exploitation, as well as for the expansion of urban areas. These interventions in the river system illustrate the progressive anthropogenic transformation of the landscape and have contributed to the formation of post-extraction lakes, which represent the main focus of the present study.

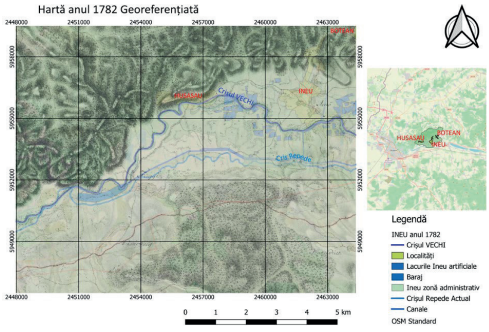



Figure 2. Georeferenced historical map location of the commune of Ineu 1782 using QGIS

The present research aims to:

a) assess the water quality status of lakes formed as a result of mineral aggregate extraction, based on the analysis of physicochemical parameters and their classification into the quality classes established by the applicable legislation;

b) analyze the influence of anthropogenic activities on these ecosystems and highlight their potential for ecological restoration and sustainable use.

## MATERIALS AND METHODS

Specific quality standards are available to indicate the quality of different water sources, such as groundwater, springs, rivers, lakes, and streams, and there are specific water quality criteria for agricultural, industrial, domestic, or other water uses. For example, drinking water must be fresh and free from pollution, while irrigation water should not be excessively saline or toxic, and standards for industrial water use vary depending on the nature of the industrial processes involved. Various human practices and activities, industrial processes, and natural processes significantly and alarmingly affect the quality of water resources, particularly with respect to human well-being.

### Study area

The research was conducted on five surface lakes formed as a result of mineral aggregate extraction (sand and gravel) (Bendixen et al., 2019), located in north-western Romania, in Bihor County, within the administrative area of Ineu. Gravel- pit lakes commonly maintain close hydraulic continuity with surrounding alluvial aquifers, so groundwater-lake exchanges may become a major control on their water balance and hydrochemistry (Jost et al., 2023). The analyzed lakes are arranged approximately along an east-west direction and are identified as follows: L1 - Utopia, L2 - Valer, L3 - Kings Land, L4 - Fildan, and L5 - Camelot Resort.

These water bodies represent anthropogenic lakes formed as a result of mineral aggregate extraction activities (Bendixen et al., 2019; Hackney et al., 2021). Some of them have subsequently been developed and integrated into areas with recreational and tourism functions, while others have remained in a post-extraction state, where natural regeneration processes and ecological succession are gradually shaping new aquatic ecosystems. The hydrological and ecological characteristics of these lakes are influenced both by natural processes and by anthropogenic activities carried out in the surrounding area.

Water samples were collected during two sampling campaigns conducted in May and October 2025. The first sampling campaign took place in May 2025, while the second was carried out in October 2025. During both campaigns, the following physicochemical parameters were determined: pH, water temperature, dissolved oxygen (DO), chemical oxygen demand (COD), biochemical oxygen demand ($BOD_5$), total nitrogen (TN), total phosphorus (TP), and potassium (K). This sampling strategy allowed the evaluation of seasonal variations in water quality between the spring and autumn monitoring periods.

Water samples were collected from the surface layer of the lakes at a depth of approximately 0-0.5 m, corresponding to the warm season when biological activity and biochemical processes in aquatic ecosystems are more intense.

### Water sampling

Water sampling was carried out in accordance with the standardized procedures of the SR EN ISO 5667 series (Figure 3).

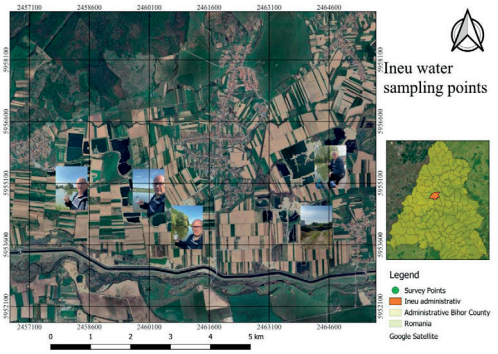



Figure 3. Water Sampling Map of Ineu, created using QGIS

The samples were collected in pre-cleaned glass and polyethylene containers suitable for physicochemical analysis and transported under controlled conditions to the laboratory, where they were analysed on the same day. The procedures for sampling, transport, and preservation were performed in accordance with the following standards:

- SR EN ISO 5667-3:2018 - Preservation and handling of water samples;
- SR EN ISO 5667-4:2016 - Sampling of lakes and reservoirs.

Compliance with these procedures ensures the representativeness of the samples and the integrity of the analyzed parameters until the laboratory analyses are performed.

**Water quality analysis**

For the evaluation of water quality, the following physicochemical parameters were determined:

• pH - determined in the laboratory according to SR EN ISO 10523:2012 PSLU-01;

• Dissolved oxygen (DO, mg $O_2$ $L^{-1}$) - determined by electrochemical method using a membrane electrode (ISO 5814:2012);

• Chemical oxygen demand (COD, mg $O_2L^{-1}$) - determined by the dichromate oxidation method (SR ISO 15705:2022 PSLU-3N);

• Biochemical oxygen demand ($BOD_5$, mg $O_2L^{-1}$) - determined using the 5-day incubation method (SR EN ISO 5815-1:2020 PSLU-04);

• Total phosphorus (TP, mg $L^{-1}$) - determined by molecular absorption spectrometry (SR EN ISO 6878:2005 PS-III-05);

• Total nitrogen ($TN_t$ mg $L^{-1}$) - determined by the chemiluminescence method (SR EN ISO 20236:2024 PS-III-06);

• Potassium ($K^+$, mg $L^{-1}$) - determined by flame photometry (ISO 9964-3:1993 PS-V-04);

• Water temperature (°C) - measured in situ.

The expanded relative uncertainty of the analytical methods was calculated using a coverage factor k = 2, corresponding to a 95% confidence level.

Laboratory analyses were carried out by accredited laboratories of Oradea Water Company S.A. and the Crișuri Water Basin Administration, in accordance with the applicable national and European standards for the determination of water quality parameters.

Water samples were collected by the beneficiary in strict accordance with the sampling protocols and instructions provided by the laboratories to ensure the representativeness and validity of the analyses. Each stage was documented to ensure traceability and quality control.

**Water quality classification**

The interpretation of the physicochemical analysis results was carried out in accordance with Order No. 161/2006, approving the Normative regarding the classification of surface water quality for the determination of the ecological status of water bodies, in its updated form. The classification was performed by comparing the obtained values with the threshold limits corresponding to the quality classes established by the applicable legislation.

**Water Quality Index (WQI*)**

To obtain an integrated assessment of the overall water quality of the investigated lakes, a synthetic Water Quality Index (WQI*) was developed based on the ecological quality classes established by Order No. 161/2006 regarding the classification of surface water quality in Romania. Unlike internationally standardized Water Quality Index models, the proposed WQI* represents a comparative tool specifically adapted to the objectives of this study by integrating the ecological quality classes assigned to selected physicochemical parameters into a single numerical value.

Synthetic water quality indices are widely applied in environmental studies to simplify the interpretation of multiple physicochemical variables and facilitate comparisons among different aquatic ecosystems (Iticescu et al., 2019; Uddin et al., 2021; Georgescu et.al., 2023; Muhammad et al., 2025; Das, 2026).

The WQI* was calculated using the following parameters: pH, dissolved oxygen (DO), biochemical oxygen demand ($BOD_5$), total phosphorus (TP), and total nitrogen (TN). These indicators were selected because they represent key physicochemical variables used in the ecological assessment of surface waters and could be unequivocally assigned to the quality classes defined by Order No. 161/2006.

Chemical oxygen demand (COD) was determined during laboratory analyses and is presented in the results section; however, it was not included in the WQI* calculation because four of the five investigated samples were reported as below the analytical reporting limit (<12 mg $O_2$ $L^{-1}$).

Consequently, the corresponding ecological quality class could not be assigned with sufficient certainty, and its inclusion would have introduced additional uncertainty into the synthetic index.

Potassium ($K^+$) was also excluded from the WQI* calculation. According to Order No. 161/2006, potassium belongs to the group of salinity-related parameters and represents a

naturally occurring constituent rather than an indicator of anthropogenic pollution or ecological degradation. Nevertheless, $K^+$ concentrations were analyzed separately because they may provide useful information regarding groundwater inputs, mineral weathering processes, and local hydrogeochemical conditions.
Total nitrogen concentrations were below the analytical limit of quantification (LOQ) in all investigated samples. Since this value is substantially lower than the threshold corresponding to Quality Class I (1.5 mg $L^{-1}$) established by Order No. 161/2006, all TN measurements were considered to comply with Quality Class I and were assigned the corresponding numerical score in the WQI* calculation.
For each analyzed parameter, the ecological quality class was determined according to the threshold values established by Order No. 161/2006 and subsequently converted into a numerical score (Table 1).

Table 1. WQI* scoring system

| Quality class | Ecological status | Value WQI |
|---|---|---|
| I | very good status | 100 |
| II | good status | 80 |
| III | moderate status | 60 |
| IV | poor status | 40 |
| V | bad status | 20 |

The synthetic WQI* was calculated as the weighted average of the parameter scores using the following equation:

$$WQI^* = \frac{\sum_{i=1}^{n}(w_i \cdot S_i)}{\sum_{i=1}^{n} w_i}$$

where:

- ($S_i$) represents the numeral score assigned to parameter i according to its ecological quality class;
- ($w_i$) represents the weight assigned to parameter i;
- (n) represents the number of parameters included in the calculation.

In the present study, all parameters were assigned equal weights ($w_i = 1$), assuming that each physicochemical indicator contributes equally to the overall assessment of water quality. This approach was adopted to ensure a straightforward and objective comparison among the investigated lakes while avoiding subjective weighting of individual parameters. The proposed WQI* does not replace the official ecological classification established by Romanian legislation. Instead, it serves as a synthetic comparative index designed to integrate multiple physicochemical indicators into a single numerical value, thereby facilitating the overall evaluation and comparison of water quality among the analyzed lakes.

**Statistical analysis**

The obtained data were analyzed using descriptive statistical methods, including the calculation of the arithmetic mean, standard deviation (SV), and coefficient of variation (CV), in order to characterize the variability of the investigated physicochemical parameters.
To evaluate the relationships between the analyzed variables, the Pearson correlation coefficient (r) was calculated according to the following equation:

$$r = \frac{\sum(x_i - \bar{x})(y_i - \bar{y})}{\sqrt{\Sigma(x_i - \bar{x})^2 \Sigma(y_i - \bar{y})^2}}$$

where:

- $x_i$ represents the observed values of the first variable;
- $y_i$ represents the observed values of the second variable;
- $\bar{x}$ represents the arithmetic mean value of x;
- $\bar{y}$ represents the arithmetic mean value of y.

The Pearson correlation coefficient ranges from - 1 and +1 where values close to +1 indicate a strong positive linear relationship, values close to −1 indicate a strong negative linear relationship, and values around 0 indicate little or no linear correlation between the analyzed variables.

**Remote sensing analysis (NDVI and NDMI)**

Spatial environmental changes were analyzed using Sentinel-2 satellite imagery provided by the Copernicus Programme for the years 2015 and 2025. Based on these images, the Normalized Difference Vegetation Index (NDVI) and the Normalized Difference Moisture Index (NDMI) were calculated to assess vegetation dynamics and variations in surface moisture content in the area surrounding the analyzed lakes (Șerban et al., 2022).

## RESULTS AND DISCUSSIONS

**Physicochemical parameters**

The results of the physicochemical analyses performed on the five investigated lakes are presented in Table 2. Overall, most of the

analyzed parameters exhibited only minor variations among the lakes, indicating relatively similar water quality conditions. The pH values ranged from 7.0 to 9.0, indicating near neutral conditions in most of the investigated lakes. Lake L3 (Kings Land) recorded the highest pH value (9.0), suggesting a slightly alkaline water conditions. Similar pH ranges (7.2-8.8) have been reported for post-extraction gravel pit lakes in Germany and the Netherlands, where water chemistry is largely controlled by carbonate buffering and biological productivity rather than by anthropogenic pollution (Schultze et al., 2010; Mollema et al., 2016). Likewise, Karlović et al. (2023) reported pH values ranging from approximately 7.0 to 10.7 in Croatian gravel pit lakes, with the highest values being associated with active phytoplankton communities and enhanced photosynthetic processes. Similarly, dissolved oxygen concentrations exceeding saturation levels have been observed in productive gravel pit lakes as a consequence of oxygen release during photosynthesis.

Dissolved oxygen (DO) concentrations varied between 5.65 and 13.70 mg $L^{-1}$, with the highest value recorded in Lake L3 (Kings Land) and the lowest in Lake L2. The DO concentration measured in Lake L3 (13.70 mg $L^{-1}$) substantially exceeded the theoretical oxygen saturation concentration expected at the measured water temperature (18.8°C), which is approximately 9.1 mg $L^{-1}$ under standard atmospheric pressure, indicating oxygen supersaturation of nearly 150%. This phenomenon is commonly associated with intense photosynthetic activity by phytoplankton and submerged aquatic vegetation, which consume dissolved $CO_2$ while simultaneously releasing oxygen into the water column. The elevated pH value (9.0) observed in the same lake further supports this interpretation, as $CO_2$ uptake during photosynthesis shifts the carbonate equilibrium toward more alkaline conditions. Similar patterns of oxygen supersaturation accompanied by elevated pH values have been reported in productive gravel pit lakes and other shallow aquatic ecosystems in the Netherlands and Croatia, where high biological productivity and groundwater–surface water interactions strongly influence hydrochemical conditions (Mollema et al., 2016; Karlović et al., 2023).

The biochemical oxygen demand ($BOD_5$) values ranged from 3.85 to 5.12 mg $L^{-1}$, indicating a low to moderate biodegradable organic load in the investigated lakes. Similar $BOD_5$ values have been reported for European gravel pit lakes, reflecting generally good ecological conditions and limited organic pollution. Total phosphorus concentrations (TP) ranged between 0.045 mg/L and 0.070 mg/L, indicating relatively low nutrient, while total nitrogen (TN) remained below. the limit of quantification (<LOQ) in all analyzed samples. The combination of low phosphorus and nitrogen concentrations suggests limited nutrient enrichment and a low risk of eutrophication. Comparable findings have been reported for gravel pit lakes, where biological uptake by algae and microbial communities contributes to nutrient removal and the maintenance of good water quality. Research on quarry and gravel-pit lakes indicates that many such novel ecosystems may develop comparatively favorable chemical and ecological conditions, although their evolution depends strongly on hydrological connectivity, nutrient availability, lake morphology, and surrounding land use (Mollema & Antonellini, 2016; Seelen et al., 2021; Hetmański et al., 2023). In addition, Karlović et al. (2023) highlighted the potential role of gravel-pit lakes in modifying groundwater chemistry, particularly through processes associated with nitrate removal, including biological uptake and denitrification. Such processes may contribute to lower nitrate concentrations in lake water compared with the surrounding groundwater and illustrate the potential of these systems to provide natural attenuation functions.

Potassium ($K^+$) concentrations exhibited the greatest spatial variability among the analyzed parameters, ranging from 2.00 to 22.55 mg $L^{-1}$, with the highest concentration recorded in Lake L4 (Fildan). In contrast, the remaining lakes showed relatively low potassium concentrations, ranging from 2.00 to 4.90 mg $L^{-1}$. The elevated $K^+$ concentration observed in Lake L4 may reflect local geological characteristics, mineral weathering processes, groundwater inflows, or site-specific anthropogenic influences within the surrounding catchment.

Previous studies have shown that potassium concentrations in gravel pit lakes and post-

extraction water bodies are strongly influenced by the mineral composition of the excavated sediments and by groundwater–surface water interactions rather than by in-lake biological processes. Mollema et al. (2015; 2016) reported that hydrochemical conditions in gravel pit lakes are primarily controlled by geological substrates and groundwater recharge, resulting in spatial differences in dissolved ion concentrations. Jost et al. (2023) further emphasized the close hydrodynamic coupling between gravel-pit lakes and adjacent aquifers. Similarly, Hetmański et al. (2023) highlighted that the chemical composition of gravel pit lakes may vary considerably depending on local lithology, hydrological connectivity, and land-use practices in the adjacent areas.

To provide an integrated visualization of the physicochemical variability among the investigated lakes, the measured parameters are summarized in the heatmap presented in Figure 4.

Table 2. Physicochemical parameters determined of the investigated lakes and their classification according to Order No. 161/2006

| Parameter | L1 (Utopia) | L2 (Valer) | L3 (Kings Land) | L4 (Fildan) | L5 (Camelot Resort) | Quality class according to Order No. 161/2006 |
|---|---|---|---|---|---|---|
| pH | 7.2 | 7.4 | 9.00 | 7.00 | 7.00 | Class I/all lakes |
| DO (mg/L) | 8.32 | 5.65 | 13.70 | 8.47 | 9.41 | L1, L3, L4, L5 – Class I; L2 – Class II |
| COD (mg $O_2$ $L^{-1}$) | <12 | <12 | <12 | 17.40 | <12 | L4 – Class II; others: ≤ Class II (exact class cannot be determined due to censored values) |
| $BOD_5$ (mg $O_2$ $L^{-1}$) | 3.85 | 3.95 | 4.21 | 4.58 | 5.12 | L1–L4 – Class II; L5 – Class III |
| TP (mg P $L^{-1}$) | 0.067 | 0.051 | 0.045 | 0.048 | 0.070 | Class I (all lakes) |
| TN, (mg N $L^{-1}$) | <LOQ | <LOQ | <LOQ | <LOQ | <LOQ | - |
| $K^+$ (mg $L^{-1}$) | 2.00 | 4.90 | 3.20 | 22.55 | 4.40 | Not classified (natural salinity parameter under Order No. 161/2006) |
| Temperature, ℃ | 18.20 | 18.30 | 18.80 | 18.70 | 18.80 | - |

**Note.** COD = chemical oxygen demand; $BOD_5$ = biochemical oxygen demand; TP = total phosphorus; TN = total nitrogen; LOQ = limit of quantification. The physicochemical parameters presented in Table 2 were determined from water samples collected during two monitoring campaigns conducted in May and October 2025.

Potassium ($K^+$) is not included in the ecological quality classification established by Order No. 161/2006, as it belongs to the salinity group and represents a naturally occurring constituent. For COD values reported as "<12 mg $O_2$ $L^{-1}$", an exact quality class cannot be assigned because the analytical result falls below the reporting limit but above the Class I threshold (10 mg $O_2$ $L^{-1}$). Therefore, these values may correspond to either Class I or Class II.

The classification of total nitrogen assumes that the analytical limit of quantification (LOQ) is lower than the Class I threshold established by Order No. 161/2006.

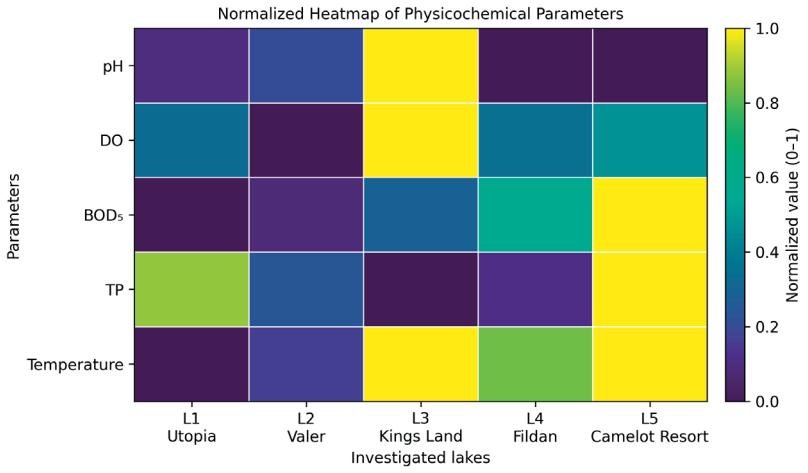



Figure 4. Heatmap of physicochemical parameters across the investigated gravel-pit lakes

The comparison of the obtained values with the threshold limits established by Order No. 161/2006 indicates that most of the analyzed parameters fall within good or very good quality classes. The physicochemical characteristics of the five investigated lakes and their corresponding ecological quality classes according to Order No. 161/2006 are presented in Table 2. Overall, the results indicate that the investigated post-extraction lakes are characterized by generally good physicochemical conditions, with most parameters corresponding to Quality Classes I and II.

The pH values generally fall within Quality Class I, with the exception of Lake L3, where the slightly alkaline value leads to classification in Quality Class II. The pH values ranged from 7.00 to 9.00, indicating neutral to slightly alkaline conditions in all lakes and corresponding to Quality Class I. Dissolved oxygen (DO) concentrations varied between 5.65 and 13.70 mg $L^{-1}$. Four of the five lakes (L1, L3, L4, and L5) were classified as Quality Class I, whereas Lake L2 corresponded to Quality Class II due to its lower oxygen concentration.

Chemical oxygen demand (COD) values were generally low, with concentrations below the analytical reporting limit (<12 mg $O_2$ $L^{-1}$) in four lakes. Lake L4 recorded the highest COD value (17.40 mg $O_2$ $L^{-1}$), corresponding to Quality Class II, while the exact classification of the remaining lakes could not be determined because the reported values were below the analytical threshold.

Biochemical oxygen demand ($BOD_5$) ranged from 3.85 to 5.12 mg $O_2$ $L^{-1}$. Lakes L1-L4 were classified as Quality Class II, indicating a low to moderate biodegradable organic load, whereas Lake L5 slightly exceeded the Class II threshold and was therefore assigned to Quality Class III.

Nutrient concentrations were generally low across all investigated lakes. Total phosphorus (TP) values ranged between 0.045 and 0.070 mg P $L^{-1}$, corresponding to Quality Class I for all sampling sites. Total nitrogen (TN) concentrations were below the analytical limit of quantification in all samples.

Potassium concentrations exhibited the greatest spatial variability, ranging from 2.00 to 22.55 mg $L^{-1}$, with the highest value recorded in Lake L4 (Fildan). However, potassium is classified as a naturally occurring salinity-related element under Order No. 161/2006 and is therefore not used for ecological status assessment. The observed variability is more likely associated with local geological conditions and groundwater–surface water interactions than with anthropogenic pollution.

Overall, the classification according to Order No. 161/2006 indicates that the investigated lakes maintain a predominantly very good to good ecological status, with only isolated deviations observed for $BOD_5$ in Lake L5 and COD in Lake L4. These findings suggest that the post-extraction lakes investigated in the present study have preserved favourable physicochemical characteristics and currently exhibit a low degree of anthropogenic disturbance.

**Calculation of the WQI* index**

The calculated WQI* values for the five investigated lakes are presented in Table 3. The index integrates the quality classes assigned to the analyzed physicochemical parameters (pH, dissolved oxygen, biochemical oxygen demand, total phosphorus, and total nitrogen) into a single comparative value, providing an overall assessment of water quality.

Table 3. Water Quality Index (WQI*) values and interpretation.

| Lake | WQI* | Water quality status |
|---|---|---|
| L1 - Utopia | 95 | Very good |
| L2 - Valer | 83 | Good |
| L3 - Kings Land | 93 | Very good |
| L4 - Fildan | 95 | Very good |
| L5 - Camelot | 90 | Very good |

The calculated WQI* values ranged from 83 to 95, indicating good to very good overall water quality across all investigated lakes. Lakes L1 (Utopia) and L4 (Fildan) achieved the highest index values (95), reflecting the predominance of physicochemical parameters classified within Quality Class I, with only biochemical oxygen demand ($BOD_5$) corresponding to Quality Class II.

Lake L3 (Kings Land) recorded a WQI* value of 93, primarily due to the excellent quality of most analyzed parameters. The slight reduction in the overall score was associated with the pH value, which was assigned to Quality Class II because of its slightly alkaline character.

The lowest WQI* value (83) was obtained for Lake L2 (Valer) and was mainly influenced by

the dissolved oxygen concentration, which corresponded to Quality Class II, while the remaining parameters were generally classified within the highest quality categories.

Lake L5 (Camelot Resort) achieved a WQI* value of 90, indicating very good overall water quality despite the biochemical oxygen demand being classified as Quality Class III. This result demonstrates that the favorable values recorded for the remaining physicochemical parameters compensated for the moderate reduction associated with $BOD_5$.

Overall, the WQI* assessment confirms that the investigated post-extraction lakes exhibit predominantly very good ecological conditions, with only minor differences among sites. The results further indicate that these anthropogenic water bodies have developed stable physicochemical characteristics and currently maintain a generally favourable water quality status.

**Statistical analysis**

The descriptive statistical analysis of the physicochemical parameters is summarized in Table 4. Overall, the results indicate relatively homogeneous water quality conditions among the five investigated lakes, although some parameters exhibited noticeable spatial variability.

Table 4. Descriptive statistics of the investigated physicochemical parameters

| Parameter | Mean | Standard deviation (SD) | Coefficient of variation (CV%) |
|---|---|---|---|
| pH | 7.520 | 0.844 | 11.22 |
| DO (mg $L^{-1}$) | 9.110 | 2.922 | 32.08 |
| COD (mg $O_2$ $L^{-1}$) | 10.704 | 6.362 | 59.44 |
| $BOD_5$ (mg $O_2$ $L^{-1}$) | 4.342 | 0.518 | 11.94 |
| TP (mg P $L^{-1}$) | 0.056 | 0.011 | 20.42 |
| $K^+$ (mg $L^{-1}$) | 7.410 | 8.538 | 115.22 |
| Temperature (°C) | 18.560 | 0.288 | 1.55 |

**Note.** Total nitrogen (TN) concentrations were below the analytical limit of quantification (LOQ) in all investigated samples and were therefore excluded from the descriptive statistical analysis. Chemical oxygen demand (COD) was not included because four of the five measurements were reported as <12 mg $O_2$ $L^{-1}$, preventing the calculation of reliable descriptive statistics.

The mean pH value was 7.52 ± 0.84, indicating neutral to slightly alkaline conditions throughout the study area. Dissolved oxygen (DO) presented an average concentration of 9.11 ± 2.92 mg $L^{-1}$, with a coefficient of variation (CV) of 32.08%, reflecting considerable differences among lakes, mainly due to the elevated value recorded in Lake L3.

Biochemical oxygen demand ($BOD_5$) showed moderate variability (CV = 11.94%), with an average concentration of 4.34 ± 0.52 mg $O_2$ $L^{-1}$, suggesting relatively uniform levels of biodegradable organic matter among the investigated water bodies. Similarly, total phosphorus (TP) exhibited moderate variability (CV = 20.42%) and a mean concentration of 0.056 ± 0.011 mg P $L^{-1}$, indicating relatively consistent nutrient conditions across the study sites.

Potassium ($K^+$) displayed the highest variability (CV = 115.22%), mainly due to the elevated concentration measured in Lake L4. This pronounced variability most likely reflects local hydrogeochemical conditions rather than anthropogenic pollution, as potassium is considered a naturally occurring salinity-related parameter under Order No. 161/2006.

Water temperature remained highly uniform among the investigated lakes, with a mean value of 18.56 ± 0.29°C and a coefficient of variation of only 1.55%, indicating similar thermal conditions during sampling.

Total nitrogen (TN) concentrations were below the analytical limit of quantification (LOQ) in all investigated samples and were therefore excluded from the descriptive statistical analysis.

The Pearson coefficient indicates the direction and strength of the linear relationship between the analyzed indicators. Values close to +1 indicate a strong positive association, while values close to - 1 indicate a strong negative association. The application of the mathematical formula used to calculate the Pearson correlation coefficient resulted in the values presented in Table 5.

The relationships among the investigated physicochemical parameters are further illustrated by the Pearson correlation heatmap presented in Figure 5. Given the limited sample size (n = 5), the observed correlations should be interpreted as exploratory rather than conclusive.

The strongest positive correlation was observed between pH and dissolved oxygen (DO) (r = 0.774), suggesting that both parameters tend to increase simultaneously.

Table 5 Pearson correlation matrix for the investigated physicochemical parameters

| Parameter | pH | DO | $BOD_5$ | TP | $K^+$ |
|---|---|---|---|---|---|
| pH | 1.000 | 0.774 | −0.297 | −0.576 | −0.365 |
| DO | 0.774 | 1.000 | 0.201 | −0.243 | −0.170 |
| $BOD_5$ | −0.297 | 0.201 | 1.000 | 0.294 | 0.309 |
| TP | −0.576 | −0.243 | 0.294 | 1.000 | −0.418 |
| $K^+$ | −0.365 | −0.170 | 0.309 | −0.418 | 1.000 |

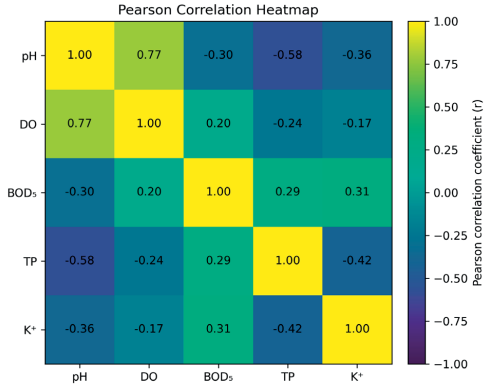



Figure 5. Pearson Correlation Heatmap of the investigated physicochemical parameters (The results should be interpreted with caution because the analysis was performed on a limited dataset - n = 5)

This relationship may be associated with enhanced photosynthetic activity, during which the uptake of dissolved $CO_2$ by aquatic plants and phytoplankton increases pH while simultaneously promoting oxygen production.

A moderate negative correlation was identified between pH and total phosphorus (TP) (r = - 0.576), indicating a tendency for phosphorus concentrations to decrease as pH increases. Likewise, a moderate negative association was observed between TP and potassium ($K^+$) (r = - 0.418). However, the ecological significance of these relationships should be interpreted with caution, as potassium is primarily influenced by local hydrogeochemical conditions rather than anthropogenic pollution.

The correlations involving $BOD_5$ were generally weak, with coefficients ranging between - 0.297 and 0.309, suggesting limited linear relationships with the other investigated parameters.

Similarly, dissolved oxygen exhibited only weak associations with total phosphorus (r = - 0.243) and potassium (r = - 0.170).

Overall, the correlation analysis indicates that no strong linear relationships exist among most of the investigated variables, with the exception of the positive association between pH and dissolved oxygen.

**Analysis of the NDVI and NDMI spectral indices**

The analysis of the Normalized Difference Vegetation Index (NDVI) and the Normalized Difference Moisture Index (NDMI) for the years 2015 and 2025 highlighted significant changes in vegetation cover and surface moisture conditions in the surroundings of the investigated lakes. The comparison of NDVI maps indicates an expansion of areas characterized by moderate to high vegetation density in 2025 relative to 2015, indicated progressive vegetation regeneration and ecological succession in the peri-lacustrine zones following mineral aggregate extraction activities (Șerban et al., 2022). Similary, the NDMI analysis demonstrated an increase area with higher moisture values around the lakes in 2025, reflecting the influence of the newly established water bodies on local soil moisture conditions and the surrounding environment. The creation of these anthropogenic lakes appears to have modified the local hydrological regime by increasing water availability and promoting the development of moisture-dependent vegetation (Figure 6).

Overall, the combined interpretation of the NDVI and NDMI indices suggests that the post-extraction lakes have contributed to the gradual establishment of new ecological conditions, characterized by enhanced vegetation development and improved surface moisture in the adjacent areas. These findings support the hypothesis that, beyond their anthropogenic origin, such water bodies can facilitate local ecological restoration processes and increase landscape heterogeneity.

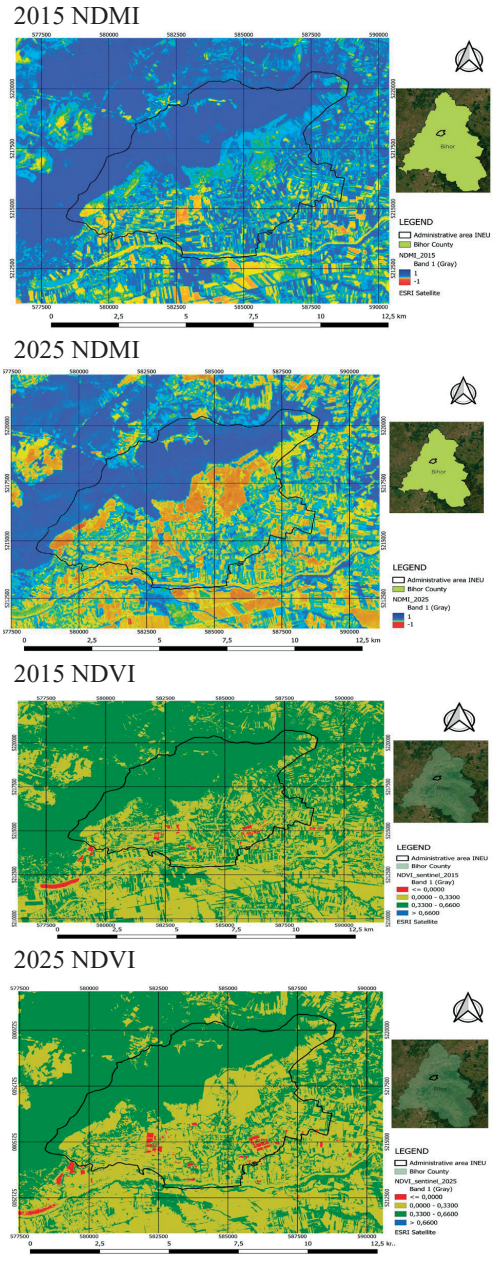



Figure 6. Spatial distribution of the NDVI and NDMI indices in 2015 and 2025, derived from Sentinel-2 imagery, illustrating changes in vegetation cover and surface moisture around the investigated lakes

## CONCLUSIONS

The present study evaluated the water quality of five lakes formed as a result of mineral aggregate extraction in the Ineu area, Bihor County, through the analysis of physicochemical parameters and their integration into a synthetic water quality index (WQI*), complemented by statistical analysis and by the assessment of land -cover and moisture dynamcs using the NDVI and NDMI spectral indices

The physicochemical analyses revealed relatively homogeneous conditions among the investigated lakes, indicating an overall good water quality status. Most pH values were close to neutrality, while dissolved oxygen concentrations generally reflected well-aerated conditions, although lower values recorded in Lake L2 suggest local hydrochemical variability. Biochemical oxygen demand values corresponded to a low to moderate organic load, and total phosphorus concentrations remained low across all sampling sites, indicating limited nutrient enrichment during the monitoring period. The markedly higher potassium concentration recorded in Lake L4 compared with the other investigated lakes, suggesting the influence of local geochemical or hydrological conditions rather than a regional pattern and emphasizing the importance of site-specific controls on the ionic composition of post-extraction aquatic ecosystems.

According to the classification criteria established by Romanian Order No. 161/2006 most analyzed parameters were assigned to Quality Classes I and II, confirming the generally favorable physicochemical status of the investigated water bodies.

The calculated WQI* values ranged between 83 and 95, corresponding to good and very good water quality. The highest scores were obtained for Lakes L1 and L4, whereas the comparatively lower value recorded for Lake L2 was primarily associated with reduced dissolved oxygen concentrations. It should be emphasized that the WQI* represents a synthetic comparative indicator designed for this study and does not replace the ecological status assessment framework established under the European Water Framework Directive.

Statistical analysis confirmed moderate variability for most analyzed parameters, while dissolved oxygen and potassium exhibited higher coefficients of variation, reflecting local environmental heterogeneity among the lakes. Pearson correlation analysis revealed a positive

correlation between pH and dissolved oxygen, as well as moderate relationships between biochemical oxygen demand and nutrient concentrations, suggesting interactions among the biogeochemical processes governing water quality. The analysis of the NDVI and NDMI spectral indices highlighted changes in land cover and moisture regime between the years 2015 and 2025. The increase in NDVI values around the lakes indicates progressive vegetation development in the peri-lacustrine zones, whereas higher NDMI values suggest enhanced surface moisture conditions in adjacent areas whereas higher NDMI values suggest an increase enhanced surface moisture conditions in adjacent areas. These patterns are consistent with ongoing ecological succession and the gradual stabilization of ecosystems established after mineral aggregate extraction. Overall, the investigated lakes indicate curently exhibit good to very good physicochemical water quality and demonstrate a progressive tendency toward ecological stabilization. The development of peri-lacustrine vegetation and relatively stable hydrological conditions may support the establishment of habitats for aquatic and semi-aquatic organisms, including bird species observed in the study area, thereby increasing the ecological value of these artificial lakes. Nevertheless, the suitability of these water bodies for recreational activities or aquaculture should be verified through additional biological, microbiological, and sanitary assessments.

Several limitations should be considered when interpreting the results. The relatively small number of investigated lakes (n = 5) restricts the extrapolation of the findings to other post-extraction aquatic systems. Furthermore, physicochemical monitoring was based on two sampling campaigns conducted in 2025 and therefore may not fully capture seasonal or interannual variability. In addition, the assessment focused exclusively on physicochemical indicators and did not include the biological quality elements or hydromorphological components required for a complete ecological status evaluation under the Water Framework Directive.

Future research should incorporate long-term monitoring, a broader suite of physicochemical and biological indicators, and ecological assessment methods consistent with the Water Framework Directive to o provide a more comprehensive understanding of the evolution and ecological functioning of lakes formed as a result of mineral aggregate extraction.

## REFERENCES

ASRO (2005). SR EN ISO 6878:2005. Water quality - Determination of phosphorus - Ammonium molybdate spectrometric method.

ASRO (2012). SR EN ISO 10523:2012. Water quality - Determination of pH.

ASRO (2016). SR EN ISO 5667-4:2016. Water quality - Sampling - Part 4: Guidance on sampling from lakes, natural and man-made.

ASRO (2018). SR EN ISO 5667-3:2018. Water quality - Sampling - Part 3: Preservation and handling of water samples.

ASRO (2020). SR EN ISO 5815-1:2020. Water quality - Determination of biochemical oxygen demand after n days (BODn) - Part 1: Dilution and seeding method with allylthiourea addition.

ASRO (2022). SR ISO 15705:2022. Water quality - Determination of the chemical oxygen demand index (ST-COD) - Small-scale sealed-tube method.

ASRO (2024). SR EN ISO 20236:2024. Water quality - Determination of total organic carbon (TOC), dissolved organic carbon (DOC), total bound nitrogen (TNb) and dissolved bound nitrogen (DNb) after high-temperature catalytic oxidative combustion.

Bendixen, M., Best, J. L., Hackney, C. R., & Iversen, L. L. (2019). Time is running out for sand. *Nature*. 571, 29-31.

Bellezza, M., Casagrande, L., Pierleoni, A., & Casadei, S. (2014). Open source web applications for spatial data management and for water resource analysis. *AgroLife Scientific Journal, 3*(1), 25–30.

Costa, D., Liu, J., & Palma, P. (2025). Multidecadal water quality trends across 15 European river basins along a Mediterranean climate gradient. *Science of the Total Environment, 998*, 180230. https://doi.org/10.1016/j.scitotenv.2025.180230

Das, A. (2026). *Data analytics and integration of CCME-Water Quality Index, Water Pollution Index (WPI), and Contamination Index (CI) with GIS approach for a better understanding of drinking water quality*. In Kumar, D., Bassill, N.P., Rani, K. (eds). Data analytics and remote sensing-based analysis for sustainable development (pp. 39–63). Advances in Science, Technology & Innovation. Springer, Cham.

Directive 2000/60/EC of the European Parliament and Council of 23 October 2000 establishing a framework for Community action in the field of water policy. Official Journal of the European Communities, L 327, 22.12.2000, pp. 1–73

European Environment Agency. (2024). *Europe's state of water 2024: The need for improved water resilience* (EEA Report No. 07/2024). https://doi.org/10.2800/02236

Georgescu, P.-L., Moldovanu, S., Iticescu, C., Calmuc, M., Calmuc, V., Topa, C., & Moraru, L. (2023). Assessing and forecasting water quality in the Danube River by using neural network approaches. *Science of*

*the Total Environment, 879*, 162998. https://doi.org/10.1016/j.scitotenv.2023.162998

Hackney, C. R., Vasilopoulos, G., Heng, S., Darbari, V., Walker, S., & Parsons, D. R. (2021). Sand mining far outpaces natural supply in a large alluvial river. *Earth Surface Dynamics, 9*, 1323–1334. https://doi.org/10.5194/esurf-9-1323-2021

Hetmański, T., Jarosiewicz, A., & Jankowiak, L. (2023). The gravel pit lakes' water quality, their aquatic ecosystem function, and the effects of environmental changes in northern Poland. *Studia Quaternaria, 40*(2), 57-66. https://doi.org/10.24425/sq.2023.148032

International Organization for Standardization. (1993). ISO 9964-3:1993. Water quality - Determination of sodium and potassium - Part 3: Determination of sodium and potassium by flame emission spectrometry.

International Organization for Standardization. (2012). ISO 5814:2012. Water quality - Determination of dissolved oxygen - Electrochemical probe method.

Karlović, I., Marković, T., Smith, A. C., & Maldini, K. (2023). Impact of gravel pits on water quality in alluvial aquifers. Hydrology, 10(4), 99. https://doi.org/10.3390/hydrology10040099

Iticescu, C., Georgescu, L. P., Murariu, G., Topa, C., Timofti, M., Pintilie, V., & Arseni, M. (2019). Lower Danube water quality quantified through WQI and multivariate analysis. *Water, 11*(6), 1305. https://doi.org/10.3390/w11061305

Jost, A., Wang, S., Verbeke, T., Colleoni, F., & Flipo, N. (2023). Hydrodynamic relationships between gravel pit lakes and aquifers: Brief review and insights from numerical investigations. *Comptes Rendus. Géoscience*, 355(S1), 245-269, https://doi.org/10.5802/crgeos.181

Mollema, P. N., & Antonellini, M. (2016). Water and (bio)chemical cycling in gravel pit lakes: A review and outlook. *Earth-Science Reviews*, 159, 247–270.

Mollema, P. N., Antonellini, M., Hubeek, A., & Van Diepenbeek, P. M. J. A. (2016). The effect of artificial recharge on hydrochemistry: A comparison of two fluvial gravel pit lakes with different post-excavation uses in the Netherlands. *Water, 8*(9), 409. https://doi.org/10.3390/w8090409

Mollema, P. N., Stuyfzand, P. J., Juhász -Holterman, M. H. A., Van Diepenbeek, P. M. J. A., & Antonellini, M. (2015). Metal accumulation in an artificially recharged gravel pit lake used for drinking water supply. *Journal of Geochemical Exploration, 150*, 35–51. https://doi.org/10.1016/j.gexplo.2014.12.004

Muhammad, S., Ullah, N., Ali, W., Amin, S., Tokatli, C., Din, I. U., Iqbal, Z., & Farooq, U. (2025). Water quality, risk assessment indices, and source apportionment across spatial patterns. *Physics and Chemistry of the Earth, Parts A/B/C, 141*, 104151. https://doi.org/10.1016/j.pce.2025.104151

Order No. 161/2006. (2006). *Normative on the classification of surface water quality for the establishment of the ecological status of water bodies*. *Official Gazette of Romania, Part I, No. 511*.

Popa, M., Glevitzky, I., Dumitrel, G.-A., Glevitzky, M., & Popa, D. (2019). Impact of environmental factors on the quality of spring water from Abrud-Câmpeni area, Alba County, Romania. *AgroLife Scientific Journal, 8*(1), 220–226.

Sandu, M. A., & Vîrsta, A. (2021). The water footprint in context of circular economy. *AgroLife Scientific Journal, 10*(2), 170–177.

Schultze, M., Pokrandt, K.-H., & Hille, W. (2010). Pit lakes of the Central German lignite mining district: Creation, morphometry and water quality aspects. *Limnologica*, 40(2), 148–155. https://doi.org/10.1016/j.limno.2009.11.006

Seelen, L. M. S., Teurlincx, S., Bruinsma, J., Huijsmans, T. M. F., van Donk, E., Lürling, M., & de Senerpont Domis, L. N. (2021). The value of novel ecosystems: Disclosing the ecological quality of quarry lakes. *Science of the Total Environment, 769*, 144294. https://doi.org/10.1016/j.scitotenv.2020.144294

Timofte, C. S., & Racz, K. A. (2025). Conversion of pasturelands into community forests: Technical and administrative implications – The case of Ineu (Bihor County, Romania). *AgroLife Scientific Journal*, 14(2), 215–222.

Șerban, C., Maftei, C., & Dobrică, G. (2022). Surface water change detection via water indices and predictive modeling using remote sensing imagery: A case study of Nuntași–Tuzla Lake, Romania. *Water, 14*(4), 556. https://doi.org/10.3390/w14040556

Uddin, M. G., Nash, S., & Olbert, A. I. (2021). A review of water quality index models and their use for assessing surface water quality. *Ecological Indicators, 122*, 107218. https://doi.org/10.1016/j.ecolind.2020.107218

United Nations Environment Programme. (2022). *Sand and sustainability: 10 strategic recommendations to avert a crisis*. https://www.unep.org/resources/report/sand-and-sustainability-10-strategic-recommendations-avert-crisis

Yasmin, T., Clark, J., Smith, G. S., Daham, A., Nicholas, A. P., & Gasparotto, A. (2024). Towards sustainable governance of freshwater sand: A resource regime approach. *Earth System Governance, 22*, 100228. https://doi.org/10.1016/j.esg.2024.100228

Scientific Papers. Series E. Land Reclamation, Earth Observation & Surveying, Environmental Engineering. Vol. XV, 2026
Print ISSN 2285-6064, CD-ROM ISSN 2285-6072, Online ISSN 2393-5138, ISSN-L 2285-6064

# PHOTOCHEMICAL DEGRADATION OF IMIDACLOPRID IN WATER UNDER UV RADIATION THROUGH CFD MODELING

**Alexandru Florin SIMION, Angelica Nicoleta GĂMAN, Sorin SIMION, Marius KOVACS**

National Institute for Research and Development in Mine Safety and Protection to Explosion – INSEMEX, Petroșani, Romania

Corresponding author email: alexandru.simion@insemex.ro

***Abstract***

*Photochemical degradation under ultraviolet (UV) radiation is a significant transformation process that modifies pesticide concentration dynamics in aquatic environments. This study investigates the UV-induced photochemical degradation of imidacloprid in water through Computational Fluid Dynamics (CFD) modelling. Imidacloprid, a widely used agricultural insecticide, is frequently detected in surface waters, underscoring the importance of its photochemical behaviour for understanding concentration fluctuations in aquatic systems. The numerical model couples fluid flow and species transport with a UV-dependent photochemical degradation term to simulate the spatial and temporal evolution of imidacloprid concentrations. The degradation process is represented by a pseudo-first-order kinetic model, in which the reaction rate is determined solely by the local UV radiation intensity. Transient simulations were conducted to assess the influence of hydrodynamic conditions and UV exposure on the reduction in imidacloprid concentration within the flow domain. The results reveal a heterogeneous distribution of degradation rates, governed by spatial variations in flow patterns and UV intensity. This study isolates UV-induced photochemical degradation, excluding other chemical or biological transformation mechanisms, to elucidate the specific contribution of photochemical processes to pesticide concentration dynamics in aquatic environments.*

***Key words****: CFD modelling, imidacloprid, pesticide pollution, photochemical processes, UV radiation, water quality.*

## INTRODUCTION

Global urbanisation has increased significantly in recent decades, resulting in a substantial shift of populations from rural to urban areas and a corresponding modification of demographic patterns (Gu et al., 2021). The proportion of the global population residing in urban areas rose from approximately 30% in 1950 to around 56–57% between 2020 and 2024, and is projected to reach nearly 68% by 2050 (United Nations, 2025). This demographic transition has intensified pressure on agricultural systems, prompting the expansion and intensification of crop production. Consequently, the use of agrochemicals has increased to maintain high agricultural productivity and ensure global food security (Aktar et al., 2009). Projections indicate that global food production must increase by approximately 60-70% in the coming decades, necessitating intensive farming practices, technological innovations such as precision agriculture and genetically modified organisms (GMOs), and the implementation of sustainable agricultural strategies to minimise environmental degradation (Tudi et al., 2021). Spatial heterogeneity in environmental processes, such as the non-uniform distribution of degradation rates for agrochemicals like pesticides, presents an important consideration for water-quality management. For example, identifying areas within aquatic systems that exhibit slower natural degradation could inform the strategic placement of water-quality monitoring stations or suggest optimal zones for implementing UV-enhancement interventions. Translating these model outputs into actionable guidance helps prioritise management efforts, improve the efficiency of resource allocation, and support proactive interventions in vulnerable zones.

Neonicotinoid insecticides are widely used in modern agriculture (Stehle et al., 2023). They have high efficacy against many insect pests and possess systemic properties. Imidacloprid (IUPAC name: N-[1-[(6-chloropyridin-3-yl)methyl]-4,5-dihydroimidazol-2-yl]nitramide) is one of the most common in this class. Imidacloprid acts as an agonist of nicotinic acetylcholine receptors (nAChRs) in

the insect nervous system. This causes overstimulation of neural transmission, paralysis, and death (Zhang et al., 2008). Its systemic nature enables absorption and distribution throughout plant tissues, providing broad pest protection (Simon-Delso et al., 2015; Merga & Van den Brink, 2025). These properties also contribute to its persistence and potential dispersion in the environment. Imidacloprid has relatively high water solubility (~610 mg/L at 20°C), moderate environmental persistence, and low soil sorption. These traits increase its mobility in aquatic systems (Tomizawa & Casida, 2005). As a result, imidacloprid is often detected in surface waters. This is mainly due to agricultural runoff, spray drift, soil erosion, and drainage linked to intensive farming (Peterson, 2007; Malla et al., 2021). Pesticide residues can also reach shallow groundwater by infiltrating soils in agricultural regions (Gavrilescu, 2005; Arias-Estévez et al., 2008).

The occurrence of neonicotinoid insecticides in aquatic ecosystems has raised significant environmental concerns due to their potential toxic effects on non-target organisms (Van Dijk et al., 2013; Morrissey et al., 2015). Several studies have demonstrated that neonicotinoids can impact a wide range of aquatic invertebrates and other organisms at relatively low concentrations, potentially altering trophic interactions and ecosystem functioning (Tomizawa & Casida, 2005). The toxicity of pesticides in aquatic environments is influenced by physicochemical parameters, including temperature, pH, dissolved oxygen concentration, and salinity (Klaassen et al., 1986). The magnitude of toxic effects also depends on the chemical properties of the compound, the sensitivity of exposed species, and prevailing environmental conditions (Costache & Modrogan, 2006). Therefore, the persistence, transport, and transformation of pesticides in aquatic systems are critical factors in determining their ecological impact.

In response to these potential environmental risks, pesticides present in aquatic environments are subject to strict regulation within the European Union. The Water Framework Directive (Directive 2000/60/EC) establishes a comprehensive legislative framework to achieve good ecological and chemical status for surface waters, while Directive 2013/39/EU defines environmental quality standards for priority substances and other pollutants. These regulatory frameworks underscore the importance of understanding the environmental fate and transformation mechanisms of pesticides in aquatic systems to support effective environmental monitoring and risk assessment strategies. Photochemical degradation induced by ultraviolet (UV) radiation is a significant natural attenuation mechanism for organic contaminants in surface waters (Zepp et al., 1977; Zepp et al., 1995; Schwarzenbach et al., 2010). Imidacloprid can undergo both direct photolysis, via photon absorption leading to molecular transformation, and indirect photochemical reactions mediated by reactive species, such as hydroxyl radicals, generated in aquatic environments (Wamhoff & Schneider, 1999; Lu et al., 2015). Studies have shown that the photolytic half-life of imidacloprid in aqueous systems varies considerably depending on radiation intensity, water composition, and environmental conditions, ranging from several hours to several days (Wamhoff & Schneider, 1999; Fenoll et al., 2011). The efficiency of photochemical degradation is further influenced by factors such as water depth, turbidity, dissolved organic matter, and hydrodynamic mixing conditions (Schwarzenbach et al., 2010; Fenoll et al., 2011). While the environmental occurrence, persistence, and toxicity of imidacloprid have been extensively studied (Bonmatin et al., 2015; Morrissey et al., 2015), fewer studies have examined the interactions between hydrodynamic transport processes and photochemical degradation mechanisms. In natural aquatic systems, contaminant behaviour is governed by both chemical transformation reactions and physical transport processes such as advection, dispersion, diffusion, and turbulent mixing (Fischer et al., 1979; Chapra, 1997), which determine the spatial distribution and residence time of pollutants.

Despite growing interest in pesticide photodegradation, combining UV-induced degradation with hydrodynamic modelling remains limited, especially in controlled-flow experiments.

Integrating hydrodynamic modelling with degradation kinetics is essential for predicting the fate of pesticides. Computational Fluid Dynamics (CFD) models simulate fluid flow and contaminant transport in aquatic environments (Versteeg & Malalasekera, 2007; Blocken, 2015). These models solve equations of fluid motion and mass transport. This allows coupling hydrodynamic processes with chemical kinetics and enables simulation of pollutant dispersion and degradation under controlled conditions. In this work, imidacloprid degradation follows a pseudo-first-order reaction rate. Key assumptions are: (i) the photodegradation quantum yield is constant, (ii) UV intensity is stable, (iii) scavengers and secondary reactive species are negligible, (iv) temperature and pH are constant, and (v) no intermediate products significantly affect the rate. These assumptions simplify the model and link photodegradation kinetics to measurable variables. The aim is to investigate imidacloprid's photodegradation under UV using CFD modelling.
The model combines hydrodynamic transport processes with degradation kinetics used to simulate the spatial and temporal evolution of imidacloprid concentrations in a controlled aquatic system.

## MATERIALS AND METHODS

Photochemical degradation of imidacloprid in water under ultraviolet (UV) radiation was investigated. The study used a Computational Fluid Dynamics (CFD) approach implemented in ANSYS Fluent 2026 R1. The numerical model simulated the system's hydrodynamic behaviour. It also simulated the transport and transformation of imidacloprid under UV irradiation.

### Computational approach

The CFD model integrates radiation transport, heat transfer, and reactive species transport. This combination allows the simulation of the photochemical degradation of imidacloprid in water. Ultraviolet radiation (280-400 nm) was modelled using the Discrete Ordinates (DO) radiation model. This model calculates radiation intensity in a participating medium. The attenuation of ultraviolet radiation within the water column was described using the Beer-Lambert law. This law accounts for exponential absorption along the optical path.
The transport and degradation of imidacloprid were simulated using the Species Transport model in ANSYS Fluent. Photochemical degradation was treated as a volumetric reaction following pseudo-first-order kinetics. The degradation rate depends on the local radiation intensity. The energy equation was included to account for thermal effects from radiation absorption. Transient simulations evaluated the time-dependent development of imidacloprid concentration during ultraviolet irradiation.

### Geometry and computational domain

The computational domain models a simplified photochemical reactor to simulate ultraviolet-induced degradation of imidacloprid in water. The reactor geometry is two-dimensional, reducing computational cost while preserving key physical processes such as radiation absorption and photochemical degradation.
The computational domain has dimensions of 500 mm in length and 700 mm in height (Figure 1), representing the irradiated water volume. The aqueous phase fills the domain, where photochemical degradation of imidacloprid occurs under ultraviolet irradiation.

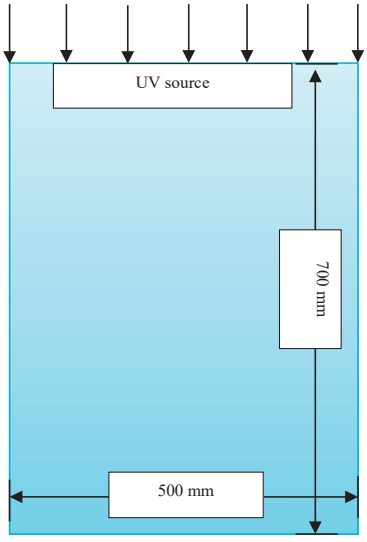



Figure 1. Computational fluid domain

Ultraviolet radiation was introduced at the upper boundary of the computational domain to represent the UV irradiation source. The radiation propagates vertically through the water column from top to bottom, simulating the penetration of ultraviolet light into the aqueous medium.

**Mesh generation**

The computational domain was discretised using a structured-dominant mesh generated in ANSYS Meshing. A quad-dominant meshing approach was applied to ensure numerical stability and efficiency of the two-dimensional domain (Wang et al., 2026). Mesh refinement was introduced near the UV radiation source to capture strong radiation gradients, using a bias factor of 4 in the direction of radiation penetration.

Mesh quality was evaluated using standard indicators. The skewness values ranged from $1.3057 \times 10^{-10}$ to $1.3065 \times 10^{-10}$; the aspect ratio ranged from 1.0009 to 1.8218; and the orthogonal quality ranged from 0.84364 to 1, confirming the high numerical quality of the computational grid (Figure 2).

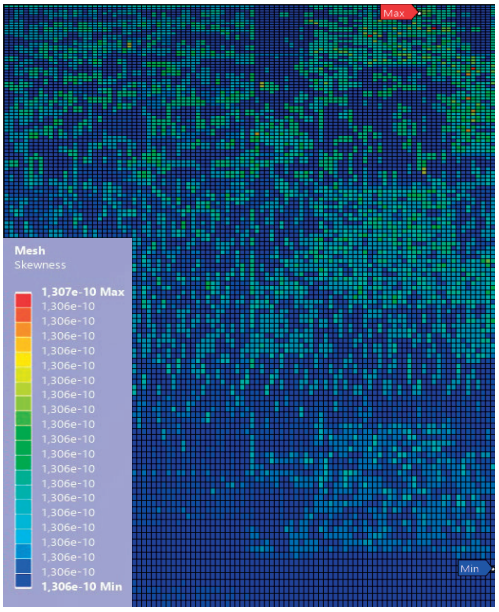



Figure 2. Mesh skewness of the domain

The final computational grid consisted of 14,241 nodes and 14,000 elements, providing an adequate spatial resolution for the numerical simulation of radiation absorption and photochemical degradation processes.

**Governing equations**

Hydrodynamic behaviour, heat transfer, radiation, and photochemical breakdown of imidacloprid were simulated using computational fluid dynamics (CFD) in ANSYS Fluent.

The model describes the coupled transport of water, heat, radiation and pesticide concentration. The flow of the fluid is described by the *continuity* and *Navier-Stokes equations*:

$$\nabla \cdot \vec{u} = 0$$

$$\rho\left(\frac{\partial \vec{u}}{\partial t} + \vec{u} \cdot \nabla \vec{u}\right) = -\nabla p + \mu \nabla^2 \vec{u} + \rho \vec{g}$$

where $\vec{u}$ is the velocity vector, $\rho$ is the fluid density, $p$ is the pressure, $\mu$ is the dynamic viscosity, and $\vec{g}$ is the gravitational acceleration.

Temperature-driven natural convection was modelled with the Boussinesq approximation:

$$\rho = \rho_0[1 - \beta(T - T_{ref})]$$

where $\rho_0$ is the reference density, $\beta$ is the thermal expansion coefficient, $T$ is the local temperature, and $T_{ref}$ is the reference temperature.

Heat transfer was described by the energy conservation equation:

$$\rho c_p\left(\frac{\partial T}{\partial t} + \vec{u} \cdot \nabla T\right) = \nabla \cdot (k \nabla T) + S_r$$

where $T$ is the temperature, $c_p$ is the specific heat capacity, $k$ is the thermal conductivity, and $S_r$ is the source term associated with radiation absorption.

Radiative heat transfer in the water was modelled using the Discrete Ordinates (DO) method. The radiative transfer equation is:

$$\vec{s} \cdot \nabla I(\vec{r}, \vec{s}) + (a + \sigma_s) I(\vec{r}, \vec{s}) = a \frac{\sigma T^4}{\pi} + \frac{\sigma_s}{4\pi} \int_{4\pi} I(\vec{r}, \vec{s}') \, d\Omega'$$

where $I$ is the radiation intensity, $a$ is the absorption coefficient of water, $\sigma_s$ is the scattering coefficient, $\sigma$ is the Stefan-Boltzmann constant, and $\vec{s}$ is the direction

vector. The absorption coefficient governs the attenuation of radiation in the water column, according to Beer-Lambert's law.
The transport of dissolved imidacloprid in water was described using the species conservation equation:

$$\frac{\partial(\rho Y)}{\partial t} + \nabla \cdot (\rho \vec{u} Y) = \nabla \cdot (\rho D \nabla Y) + R$$

where $Y$ is the mass fraction of imidacloprid, $D$ is the molecular diffusion coefficient in water, and $R$ is the local reaction rate.

**Photochemical degradation kinetics**
The photochemical degradation of imidacloprid was described using a spatially dependent pseudo-first-order kinetic model implemented via a user-defined function (UDF) in ANSYS Fluent. The local photodegradation rate constant was defined as a function of ultraviolet radiation intensity and temperature.

$$k_{photo}(z,T) = \Phi * \varepsilon_{UV} * I_{UV}(z) * f_T$$

Ultraviolet radiation attenuation within the water column was defined by the Beer–Lambert law, which describes exponential decay of light intensity with depth:

$$I_{UV}(z) = I_0 e^{-\alpha z}$$

where $I_{UV}(z)$ denotes the UV radiation intensity at depth $z$, $I_0$ is the incident radiation intensity at the water surface, and α is the extinction coefficient of the medium.
The temperature dependence of the reaction rate was introduced through an Arrhenius-type correction factor.

$$f_T = exp\left[-\frac{E_a}{R}\left(\frac{1}{T} - \frac{1}{T_{ref}}\right)\right]$$

where $E_a$ is the activation energy, $R$ is the universal gas constant, $T$ is the local temperature, and $T_{ref}$ is the reference temperature.
Thus, the overall local photodegradation rate constant can be expressed as:

$$k_{photo}(z,T) = \Phi * \varepsilon_{UV} * I_0 e^{-\alpha z} * exp\left[-\frac{E_a}{R}\left(\frac{1}{T} - \frac{1}{T_{ref}}\right)\right]$$

Within the CFD framework, the degradation of the imidacloprid process was implemented through source terms in the species transport equations. The consumption of imidacloprid was expressed as:

$$S_{imd} = -\rho, Y_{imd,} k_{photo}$$

while the formation of the degradation product was defined as:

$$S_{prod} = \rho, Y_{imd} k_{photo} \left(\frac{MW_{prod}}{MW_{imd}}\right)$$

where $\rho$ is the fluid density, $Y_{imd}$ is the mass fraction of imidacloprid, and $MW_{prod}$ and $MW_{imd}$ are the molecular weights of the degradation product and imidacloprid, respectively.

**Boundary and initial conditions**
Computational simulations were performed in a two-dimensional water column subjected to ultraviolet irradiation at the free surface. The upper boundary was a radiation inlet that allowed 40 W $m^{-2}$ of ultraviolet radiation into the computational domain (Benitez et al., 2013). The bottom and lateral boundaries were impermeable no-slip walls. The initial velocity was zero to represent quiescent water before irradiation. The fluid temperature started at 293.15 K. Water properties were constant: density 998.2 kg $m^{-3}$, dynamic viscosity 0.001 Pa s, thermal conductivity 0.6 W $m^{-1}$ $K^{-1}$, and specific heat capacity 4182 J $kg^{-1}$ $K^{-1}$. Radiative transfer used the Discrete Ordinates (DO) model with water optical properties set as absorption coefficient 3.0 $m^{-1}$, scattering coefficient 0.2 $m^{-1}$, and refractive index 1.33. Initial imidacloprid concentrations (5, 10, and 15 µg/L) were uniformly distributed in the water column. The molecular diffusion coefficient of imidacloprid in water was constant during the simulations.

**Photokinetic model parameters**
The parameters used in the user-defined function (UDF) to describe the photodegradation kinetics of imidacloprid are summarised in Table 1. The model incorporates attenuation of UV radiation with depth, the quantum yield

of the photochemical reaction, and the temperature dependence of the reaction rate via an Arrhenius relationship (Appendix 1).

Table 1. Photokinetic parameters used in the CFD mode

| Parameter | Symbol | Value | Unit | Description |
|---|---|---|---|---|
| Incident UV intensity | $I_0$ | 1.0 | – | UV intensity at water surface |
| Extinction coefficient | $\alpha$ | 3.0 | $m^{-1}$ | Light attenuation coefficient |
| Quantum yield | $\Phi$ | 0.019 | – | Efficiency of photochemical reaction |
| Photokinetic coefficient | $\varepsilon_{UV,}$ | 6e-5 | – | Photochemical proportionality constant |
| Activation energy | $E_a$ | 20000 | J $mol^{-1}$ | Activation energy for degradation |
| Gas constant | $R$ | 8.314 | J $mol^{-1}$ $K^{-1}$ | Universal gas constant |
| Reference temperature | $T_{ref}$ | 293.15 | K | Reference temperature |
| Water surface height | $H_{top}$ | 0.7 | m | Position of free surface |

Several intermediate variables required for the photochemical degradation model were stored using the User-Defined Memory (UDM) feature in ANSYS Fluent. These variables allow the spatial visualization and post-processing of the photokinetic parameters during the simulation. The UDM locations were used to store the depth relative to the free surface, the local UV radiation intensity calculated using the Beer-Lambert law, and the corresponding local photodegradation rate constant. The stored variables are summarised in Table 2.

Table 2. Photokinetic parameters used in the CFD mode

| UDM index | Stored variable | Description |
|---|---|---|
| UDM 0 | Depth $z$ | Distance from the free surface used in the Beer–Lambert attenuation law |
| UDM 1 | $I_{UV}$ | Local UV radiation intensity in the water column |
| UDM 2 | $k_{photo}$ | Local photodegradation rate constant |

The combined use of UDF and UDM functionalities enables the dynamic evaluation of the photodegradation kinetics and allows detailed spatial analysis of UV radiation intensity and reaction rates within the water column.

**Numerical setup**

Numerical simulations used a pressure-based solver under transient conditions to capture the system's dynamic response and ensure accurate modelling of time-dependent phenomena. The Discrete Ordinates (DO) radiation model represented ultraviolet radiation in the 0.28 ÷ 0.40 μm spectral range, as this range covers both the UVB and UVA regions relevant to the study objectives. The DO model was chosen for its proven effectiveness in resolving directional radiation effects in participating media, as demonstrated in previous research. Simulations used a 60-second time step and 100 iterations per step, parameters selected to balance computational efficiency and solution stability without significant loss of accuracy. The total simulation time of 2,000 steps (120,000 seconds of irradiation) was set to fully observe the cumulative effects of ultraviolet exposure. Pressure-velocity coupling employed the Rhie-Chow momentum interpolation scheme, which helps to prevent pressure-velocity decoupling issues and is recommended for transient flow calculations. Second-order upwind schemes were applied to the momentum, energy, and radiation equations to improve accuracy and minimise numerical diffusion, following best practices in the literature. The wrapped face gradient correction method was used to reconstruct gradients, thereby enhancing the spatial accuracy of variable gradients on non-orthogonal meshes. Convergence was ensured when energy residuals fell below $10^{-6}$ and other residuals below $10^{-5}$, thresholds commonly adopted to confirm reliable, consistent simulation results.

**Data processing and analysis**

The simulation results were analysed by examining the spatial distribution of ultraviolet radiation and the corresponding variation of imidacloprid concentration within the reactor domain. Particular attention was given to the vertical penetration of radiation through the water column and its influence on photochemical degradation. Concentration fields were evaluated at different simulation times to observe the progressive decrease in imidacloprid concentration during ultraviolet irradiation. Spatial concentration maps were used to identify zones of enhanced degradation associated with higher radiation intensity. The temporal evolution of the average imidacloprid concentration in the reactor was also analysed to quantify the overall degradation behaviour

and assess the efficiency of ultraviolet-induced photodegradation. The numerical model described in the previous section was used to investigate the photochemical degradation of imidacloprid in water under ultraviolet irradiation. The simulation results provide insight into the spatial distribution of ultraviolet radiation within the water column and the corresponding evolution of imidacloprid concentration over time.

## RESULTS AND DISCUSSIONS

The results obtained from the CFD simulations are presented and analysed to evaluate the influence of ultraviolet radiation on the degradation behaviour of imidacloprid in water. Particular attention is given to the penetration of ultraviolet radiation into the water column, the spatial distribution of radiation intensity, and the resulting variation in imidacloprid concentration. The analysis focuses on the temporal evolution of pesticide concentration and the identification of regions where photochemical degradation occurs more rapidly due to higher radiation exposure. These results provide insight into the coupled effects of radiation transport and reaction kinetics governing the degradation process.

### UV radiation distribution in water

Ultraviolet radiation was simulated within the water domain using the Discrete Ordinates (DO) model. Figure 3 presents the incident radiation intensity within the reactor, measured in $W \cdot m^{-2}$. The highest intensities are observed near the irradiated surface, where incoming UV radiation interacts directly with the water.

As radiation propagates through the water column, its intensity decreases with depth due to absorption by the medium. This pattern follows the Beer-Lambert law, which describes an exponential decrease in intensity through an absorbing medium.

The simulation indicates that radiation intensity decreases from approximately 39 $W \cdot m^{-2}$ at the irradiated boundary to below 5 $W \cdot m^{-2}$ deeper in the domain. The imposed boundary condition for incident radiation was 40 $W \cdot m^{-2}$. However, the contour plot shows nodal or cell-interpolated values calculated by the numerical solver, not the exact boundary condition.

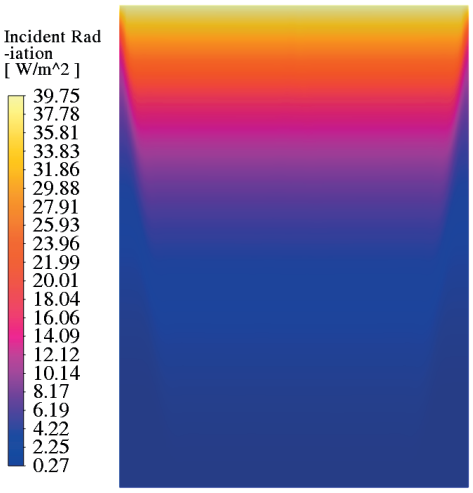



Figure 3. Spatial distribution of incident ultraviolet radiation intensity within the water domain simulated using the Discrete Ordinates radiation model

As a result, the maximum value in the field is slightly lower than the prescribed boundary intensity. In the Discrete Ordinates radiation model in ANSYS Fluent, the radiation intensity field is solved within control volumes. It is then interpolated to nodes for visualisation. The plotted values show the local solution of the radiative transport equation in cells next to the boundary, not the exact boundary input. This explains the small difference between the imposed value (40 $W \cdot m^{-2}$) and the maximum value in the contour plot (≈39 $W \cdot m^{-2}$). Such small deviations are expected in finite-volume discretisation. Here, the radiative flux is evaluated over control-volume faces and distributed across neighbouring cells. So, the slight reduction in the maximum plotted intensity does not mean a physical loss of radiation at the boundary. It simply reflects the numerical representation of the radiation field within the computational mesh.

### Temperature evolution during UV irradiation

The thermal response of the water domain under prolonged ultraviolet irradiation was evaluated. Figure 4 presents the spatial distribution of static temperature after 45 hours of continuous UV exposure. The initial water temperature was set at 293.15 K (20°C) to represent typical environmental conditions.

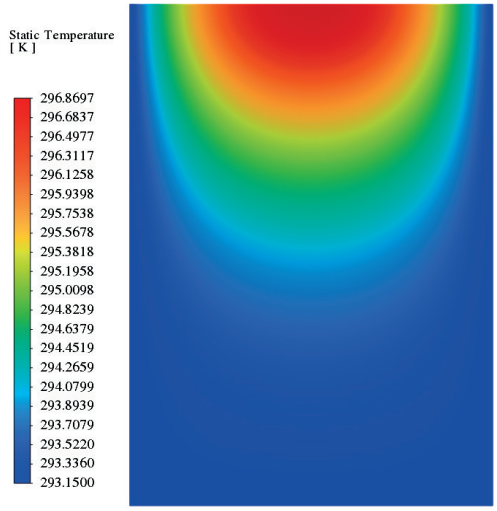



Figure 4. Spatial distribution of temperature in the water domain after 45 hours of ultraviolet irradiation, showing the thermal effect generated by radiation absorption

Simulation results show a gradual increase in temperature within the irradiated region, reaching approximately 296.87 K, a rise of about 3.7 K relative to the initial condition. The observed increase is attributed to the absorption of ultraviolet radiation by water, in which a portion of the radiative energy is converted to thermal energy. The temperature field displays a distinct spatial gradient. The highest temperatures are near the irradiated boundary. This area aligns with the zone of maximum radiation intensity and significant photon energy absorption. As radiation penetrates deeper into the water column, its intensity diminishes due to optical attenuation. This results in reduced local heat generation and lower temperatures. The temperature distribution closely mirrors the spatial pattern of the previously discussed radiation field. This correspondence suggests that the temperature rise is primarily governed by local ultraviolet radiation absorption. Regions exposed to higher photon flux undergo greater radiative heating. Deeper regions remain near the initial temperature due to limited radiation penetration.

Although the overall temperature increase is moderate, the results demonstrate that prolonged ultraviolet irradiation produces measurable thermal effects in the water column. These thermal gradients may influence physicochemical processes such as diffusion rates and reaction kinetics. However, in the present model, the primary factor driving imidacloprid degradation is the availability of ultraviolet photons rather than increased temperature.

Radiation and temperature distributions from simulations reveal the physicochemical conditions that govern imidacloprid degradation in water. The simulated ultraviolet field shows a marked decrease in radiation intensity with increasing depth. This restricts high-energy photons from penetrating the lower regions of the water column. As a result, only the upper portion of the domain receives enough photon flux to initiate photolytic reactions. Inside the water, absorbed radiative power causes a gradual thermal response. This is seen as a temperature increase near the irradiated boundary after extended exposure.

The current model considers photochemical degradation of imidacloprid as a volumetric reaction. The reaction rate depends on local ultraviolet radiation intensity, calculated with the Discrete Ordinates radiation method. Thus, the spatial distribution of radiation intensity directly influences the spatial distribution of the reaction rate. Areas exposed to higher incident radiation are expected to show faster pesticide transformation. Areas with less photon availability become increasingly reaction-limited.

Based on the results, the subsequent section analyses the evolution of imidacloprid concentration within the computational domain, showing how the combined effects of radiation penetration and local energy absorption shape the spatial pattern and temporal progression of pesticide degradation under ultraviolet irradiation.

**Spatial distribution of imidacloprid degradation**

The spatial distribution of imidacloprid concentration obtained from the CFD simulations is shown in Figure 5. The results illustrate the progressive transformation of the pesticide within the water domain due to ultraviolet irradiation. At the beginning of the simulation, the imidacloprid concentration was uniformly distributed throughout the domain with an initial value of 10 μg/ L. As irradiation

proceeds, the concentration decreases progressively due to radiation-dependent photochemical degradation.

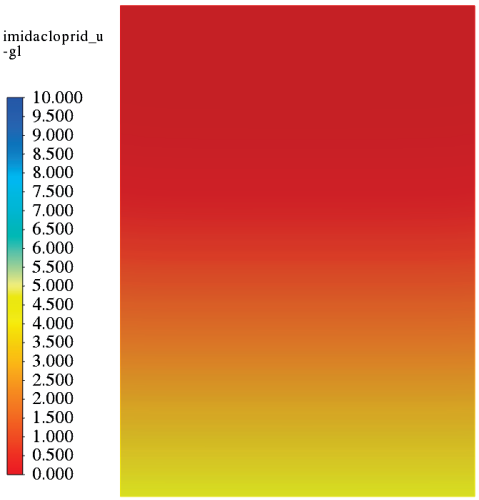



Figure 5. Spatial distribution of imidacloprid concentration within the water domain after UV irradiation

The spatial pattern of imidacloprid concentration corresponds to the distribution of ultraviolet radiation in the water column. Regions close to the irradiated boundary receive the highest radiation intensity and show the largest reduction in pesticide concentration. In contrast, deeper regions retain higher imidacloprid concentrations.

Ultraviolet radiation does not penetrate as deeply due to optical attenuation in water. This result shows that photon availability strongly controls the degradation process. Correspondingly, the complementary distribution of the reaction product formed during the degradation process is presented in Figure 6. As imidacloprid undergoes photochemical transformation, the concentration of the product species increases progressively throughout the domain.

The spatial distribution of the product corresponds to the inverse pattern of the parent compound, with higher product concentrations observed in zones where the degradation of imidacloprid is most pronounced. This complementary behaviour reflects the progressive conversion of the parent pesticide into transformation products as the photochemical reaction proceeds.

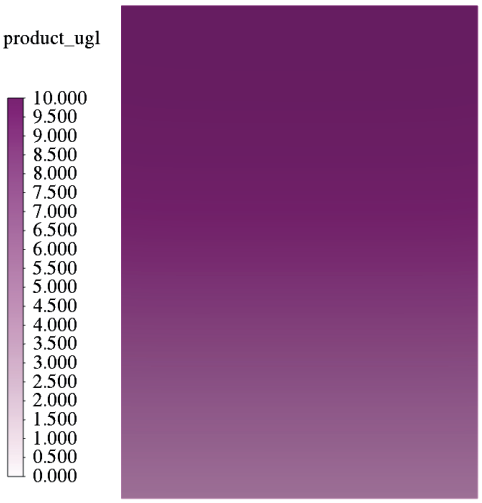



Figure 6. Spatial distribution of the photodegradation product formed during the transformation of imidacloprid

Regions exposed to higher ultraviolet radiation intensities exhibit a faster depletion of the parent compound and, consequently, a higher accumulation of the degradation product. In contrast, areas receiving lower radiation intensities show slower product formation due to the reduced rate of photochemical transformation. This complementary spatial distribution between reactant depletion and product formation confirms the internal consistency of the implemented reaction mechanism within the species transport model and demonstrates that the model adequately captures the mass transfer associated with the photochemical conversion process.

**Temporal degradation behaviour and $DT_{50}/DT_{90}$ assessment**

To complement the spatial analysis, the temporal evolution of imidacloprid concentration was evaluated for five initial concentration levels: 2.5, 5, 10, 15, and 20 μg $L^{-1}$. The simulations were performed under identical ultraviolet irradiation and kinetic conditions in order to assess the concentration-dependent response of the degradation process. The resulting concentration profiles are presented in Figure 7.

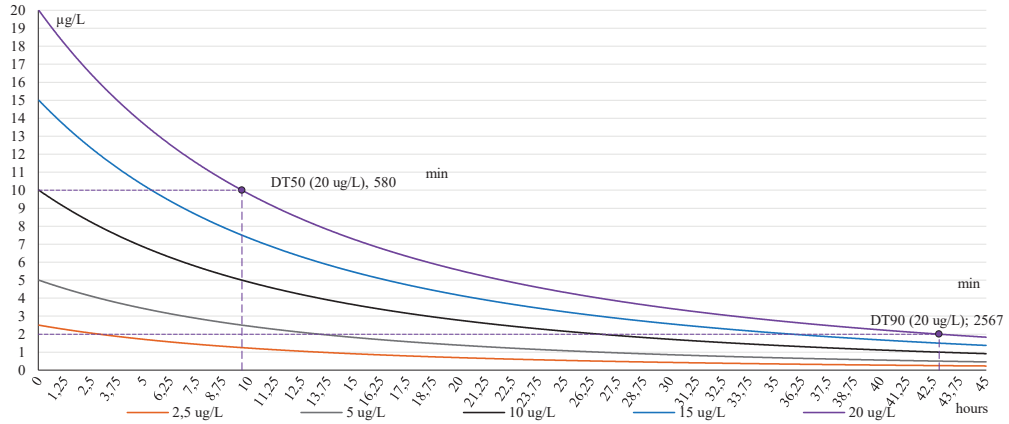



Figure 7. Temporal evolution of imidacloprid concentration during ultraviolet irradiation

The concentration profiles show a continuous decrease in imidacloprid concentration for all investigated initial levels, confirming the progressive degradation of the pesticide under ultraviolet irradiation. The nonlinear decay pattern, characterised by a faster concentration decrease during the initial stage followed by a gradual slowing of the degradation rate, indicates an apparent pseudo-first-order attenuation behaviour.

For the 20 µg $L^{-1}$ scenario, the $DT_{50}$ and $DT_{90}$ values were approximately 580 min and 2567 min, respectively. These values correspond to a decrease in concentration from 20 to 10 µg $L^{-1}$ at $DT_{50}$ and from 20 to approximately 2 µg $L^{-1}$ at $DT_{90}$. Under the same irradiation and kinetic conditions, the other initial concentrations followed a comparable relative degradation trend. Accordingly, the residual concentrations at $DT_{50}$ were 1.25, 2.5, 5, 7.5, and 10 µg $L^{-1}$, while at $DT_{90}$ they were approximately 0.25, 0.5, 1.0, 1.5, and 2.0 µg $L^{-1}$ for the initial concentrations of 2.5, 5, 10, 15, and 20 µg $L^{-1}$, respectively.

Although higher initial concentrations produced larger absolute concentration decreases, the similar shape of the degradation curves indicates that the degradation mechanism remained consistent within the investigated concentration range. This behaviour suggests that imidacloprid attenuation was mainly governed by photon availability and the remaining pesticide concentration, rather than by the initial pollutant loading alone.

**Effect of ultraviolet intensity and turbidity on imidacloprid degradation**

After establishing the baseline temporal degradation behaviour, additional simulations were performed to evaluate the influence of ultraviolet radiation intensity and attenuation (turbidity) on imidacloprid photodegradation. These parameters directly affect photon availability within the water column and therefore control the spatial and temporal evolution of the degradation process.

The influence of incident ultraviolet radiation intensity on imidacloprid degradation was evaluated by performing additional simulations under otherwise identical model conditions. The temporal concentration profiles presented in Figure 8 were obtained for four radiation intensity levels, namely 20, 30, 40, and 50 W $m^{-2}$, to assess the sensitivity of the photodegradation process to photon availability.

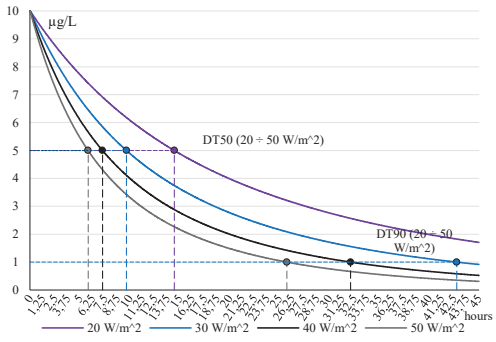



Figure 8. Effect of ultraviolet radiation intensity on the temporal degradation of imidacloprid in water

Higher incident UV irradiance increased photon availability, enhanced the photolytic reaction rate, and shifted the $DT_{50}$ and $DT_{90}$ thresholds toward shorter exposure times. Consequently, the 50 W $m^{-2}$ case showed the highest degradation efficiency, whereas the 20 W $m^{-2}$ case exhibited delayed attenuation, confirming the strong control of radiation intensity on imidacloprid persistence. While higher incident UV irradiance was shown to enhance imidacloprid photodegradation, Figure 9 presents the temporal concentration profiles obtained for different radiation attenuation coefficients.

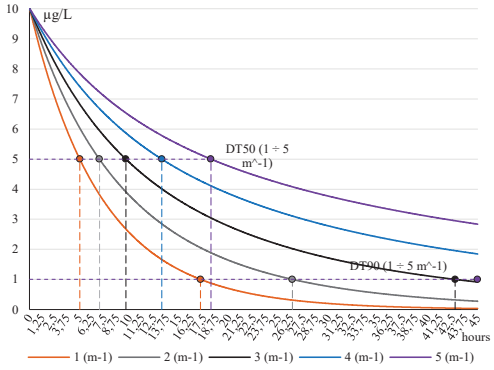



Figure 9. Effect of the radiation attenuation coefficient (turbidity) on the temporal degradation of imidacloprid under UV irradiation

An increase in the attenuation coefficient from 1 to 5 $m^{-1}$ produced a systematic decrease in degradation efficiency, as stronger optical attenuation reduced the UV energy available for photochemical conversion. Consequently, higher turbidity shifted both $DT_{50}$ and $DT_{90}$ toward longer exposure times, confirming that the apparent degradation kinetics are strongly controlled by radiation penetration and photon transport within the aqueous domain.

**Model verification and kinetic consistency assessment**

The kinetic consistency of the CFD model was assessed by analysing the degradation behaviour of imidacloprid under UV irradiation. Since the implemented reaction mechanism assumed pseudo-first-order photolytic degradation, the temporal evolution of the normalized concentration ratio $C/C_0$ was examined in semi-logarithmic form. Under pseudo-first-order conditions, the degradation rate is described by:

$$\frac{dC}{dt} = -kC$$

which integrates to:

$$C(t) = C_o e^{-kt}$$

where C is the imidacloprid concentration, $C_0$ is the initial concentration, and k is the apparent first-order degradation rate constant. As shown in Figure 10, the plot of $\ln(C/C_0)$ versus irradiation time exhibited an approximately linear trend, confirming that the simulated degradation followed pseudo-first-order kinetics.

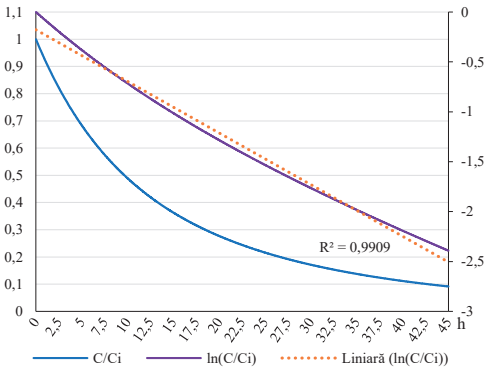



Figure 10. Pseudo-first-order kinetic behaviour of imidacloprid degradation under UV irradiation

The high coefficient of determination, $R^2$ = 0.9909, indicates good agreement between the numerical results and the assumed kinetic formulation. The apparent degradation rate constant was obtained from the absolute value of the regression slope, while the corresponding half-life was estimated using $t_{1/2}$ = 0.693/k.

To further evaluate model consistency, additional simulations were performed for different initial imidacloprid concentrations under identical UV irradiation and kinetic conditions. The kinetic parameters obtained from these simulations are summarized in Table 3.

Table 3 Summary of simulated kinetic parameters for imidacloprid degradation under different initial concentration, incident UV irradiance, and radiation attenuation conditions

| Case | $C_0$ (μg $L^{-1}$) | UV (W $m^{-2}$) | α ($m^{-1}$) | k ($h^{-1}$) | $DT_{50}$ (h) | $DT_{90}$ (h) | $T_{max}$ (K) | $C_{DT90}$ (μg $L^{-1}$) | Removal (%) | Kinetic behaviour |
|---|---|---|---|---|---|---|---|---|---|---|
| A1 | 2.5 | 40 | 3 | 0.0573 | 12.1 | 40.2 | 296.87 | 0.25 | 90.0 | Pseudo-first-order |
| A2 | 5 | 40 | 3 | 0.0573 | 12.1 | 40.2 | 296.87 | 0.50 | 90.0 | Pseudo-first-order |
| A3/B3/C3 | 10 | 40 | 3 | 0.0573 | 12.1 | 40.2 | 296.87 | 1.00 | 90.0 | Pseudo-first-order |
| A4 | 15 | 40 | 3 | 0.0573 | 12.1 | 40.2 | 296.87 | 1.50 | 90.0 | Pseudo-first-order |
| A5 | 20 | 40 | 3 | 0.0573 | 12.1 | 40.2 | 296.87 | 2.00 | 90.0 | Pseudo-first-order |
| B1 | 10 | 20 | 3 | 0.0421 | 16.5 | 54.7 | 296.87 | 1.00 | 90.0 | Pseudo-first-order |
| B2 | 10 | 30 | 3 | 0.0711 | 9.7 | 32.4 | 296.87 | 1.00 | 90.0 | Pseudo-first-order |
| B4 | 10 | 50 | 3 | 0.0849 | 8.2 | 27.1 | 296.87 | 1.00 | 90.0 | Pseudo-first-order |
| C1 | 10 | 40 | 1 | 0.1223 | 5.7 | 18.8 | 296.87 | 1.00 | 90.0 | Pseudo-first-order |
| C2 | 10 | 40 | 2 | 0.0835 | 8.3 | 27.6 | 296.87 | 1.00 | 90.0 | Pseudo-first-order |
| C4 | 10 | 40 | 4 | 0.0414 | 16.7 | 55.6 | 296.87 | 1.00 | 90.0 | Pseudo-first-order |
| C5 | 10 | 40 | 5 | 0.0315 | 22.0 | 73.0 | 296.87 | 1.00 | 90.0 | Pseudo-first-order |

The kinetic parameters summarized in Table 3 show that, under identical irradiation and attenuation conditions, variations in the initial imidacloprid concentration did not modify the apparent degradation rate. For the concentration series, the apparent rate constant remained constant at $k = 0.0573\ h^{-1}$, corresponding to a $DT_{50}$ of 12.1 h and a $DT_{90}$ of 40.2 h. Since $C_{DT90}$ was defined as 10% of the initial concentration, the residual concentration at $DT_{90}$ increased proportionally with $C_0$, while the characteristic degradation times remained unchanged. This behaviour confirms that the implemented reaction mechanism is consistent with pseudo-first-order photochemical kinetics, for which the apparent rate constant is independent of the initial pollutant concentration under constant irradiation conditions.

In contrast, the simulations performed at different incident UV irradiance levels showed a clear dependence of the degradation kinetics on photon input. Increasing the UV irradiance resulted in higher apparent rate constants and shorter $DT_{50}$ and $DT_{90}$ values, indicating enhanced photolytic degradation due to increased photon availability within the computational domain. Conversely, increasing the radiation attenuation coefficient reduced UV penetration through the water column and led to lower apparent rate constants, thereby delaying both $DT_{50}$ and $DT_{90}$. This confirms that optical attenuation strongly limits the effective photochemical reaction rate, particularly in regions where the radiation field is reduced by absorption and scattering processes.

The obtained trends are consistent with the expected behaviour of radiation-controlled photochemical degradation in aqueous systems. Previous experimental studies have also reported pseudo-first-order photolysis of imidacloprid under UV irradiation, with faster degradation generally observed under more intense and uniform irradiation conditions (Moza et al., 1998). The comparatively slower degradation predicted in the present CFD simulations can be attributed to the spatially heterogeneous radiation field resolved by the Discrete Ordinates model, which accounts for reduced photon availability within the water depth rather than assuming uniform exposure.

Overall, the kinetic consistency assessment demonstrates that the CFD framework correctly reproduces the main features of pseudo-first-order photodegradation while also capturing the influence of spatially variable UV radiation. The results indicate that imidacloprid persistence in the simulated aquatic domain is governed primarily by photon availability, which is controlled by both incident irradiance and radiation attenuation, whereas the initial pesticide concentration affects the absolute residual concentration but not the apparent degradation rate. These findings provide the basis for the concluding assessment of the model capability to simulate the photochemical fate of pesticides in irradiated aquatic environments.

## CONCLUSIONS

This study developed a CFD framework for investigating the photochemical degradation of imidacloprid in water under ultraviolet irradiation. The numerical model coupled UV radiation transport, radiation attenuation, radiation absorption, energy transfer, and reactive species transport, allowing the simulation of photon propagation and its influence on pesticide degradation kinetics.

The results showed that ultraviolet radiation was rapidly attenuated within the water column, generating a pronounced vertical gradient in photon availability. The highest radiation intensity and absorption rates occurred near the irradiated boundary, where UV energy was most available for photochemical transformation. Consequently, imidacloprid degradation was mainly concentrated in the upper irradiated region, while deeper zones exhibited slower transformation rates due to reduced UV penetration. This confirms that radiation attenuation and local photon absorption control the spatial distribution of the photochemical reaction rate.

Under the reference irradiation conditions, the simulated imidacloprid concentration decreased from 10 μg $L^{-1}$ to below 1 μg $L^{-1}$ after 45 h of UV exposure, corresponding to more than 90% removal. The degradation followed pseudo-first-order kinetics, with an apparent rate constant of approximately 0.057 $h^{-1}$ and characteristic degradation times of $DT_{50} \approx 12.1$ h and $DT_{90} \approx 40.2$ h.

The kinetic consistency assessment confirmed that variations in the initial imidacloprid concentration, within the investigated range of 2.5 ÷ 20 μg $L^{-1}$, did not affect the apparent degradation rate under identical irradiation and radiation attenuation conditions. The residual concentration at $DT_{90}$ increased proportionally with the initial concentration, whereas the rate constant and characteristic degradation times remained unchanged, confirming pseudo-first-order photochemical behaviour.

The sensitivity simulations demonstrated that incident UV irradiance and the radiation attenuation coefficient strongly influence degradation efficiency. Increasing the incident irradiance enhanced photon availability and reduced both $DT_{50}$ and $DT_{90}$ values, while increasing the attenuation coefficient limited UV penetration, decreased the apparent degradation rate, and delayed pesticide transformation. Therefore, both incident UV irradiance and radiation attenuation are key parameters controlling imidacloprid persistence in irradiated aquatic systems.

From an environmental perspective, the findings highlight the relevance of photochemical degradation as a natural attenuation mechanism for pesticides in surface waters. However, the efficiency of this process depends strongly on water depth, optical properties, turbidity-related radiation attenuation, and irradiation conditions, leading to variable pesticide persistence among aquatic environments.

Overall, the proposed CFD framework, coupling the Discrete Ordinates radiation model with UDF-based volumetric reaction terms, provides a useful tool for assessing pesticide photodegradation in aquatic systems by representing UV attenuation, radiation absorption, and reactive contaminant transport. Future work should address experimental validation and model extension toward natural organic matter, suspended solids, and hydrodynamic conditions representative of surface waters.

## ACKNOWLEDGEMENTS

The current paper was carried out through the Nucleu Program within the National Research Development and Innovation Plan 2022-2027, carried out with the support of MCID, project no. PN 23 32 01 01, IOSIN PCDIEX.

## REFERENCES

Aktar, M. W., Sengupta, D., & Chowdhury, A. (2009). Impact of pesticides use in agriculture: their benefits and hazards. *Interdisciplinary toxicology*, *2*(1). 1–12. https://doi.org/10.2478/v10102-009-0001-7.

Arias-Estévez, M., López-Periago, E., Martínez-Carballo, E., Simal-Gándara, J., Mejuto, J., & García-Río, L. (2008). The mobility and degradation of pesticides in soils and the pollution of groundwater resources. *Agriculture, Ecosystems & Environment*, *123*. 247–260.

Benitez, F. J., Acero, J. L., Real, F. J., Roldan, G. & Rodriguez, E. (2013). Modeling the photodegradation of emerging contaminants in waters by UV radiation

and UV/$H_2O_2$ system. *Journal of Environmental Science and Health, 48*(1). 120-128.

Blocken, B. (2015). Computational fluid dynamics for urban physics: Importance, scales, possibilities, limitations and ten tips and tricks towards accurate and reliable simulations. *Building and Environment*, 91. 219–245.

Bonmatin, J. M., Giorio, C., Girolami, V., Goulson, D., Kreutzweiser, D. P., Krupke, C., Liess, M., Long, E., Marzaro, M., Mitchell, E. A., Noome, D. A., Simon-Delso, N., & Tapparo, A. (2015). Environmental fate and exposure; neonicotinoids and fipronil. *Environmental science and pollution research international*, *22*(1). 35–67. https://doi.org/10.1007/s11356-014-3332-7.

Chapra, S. C. (1997). *Surface water-quality modeling* (Vol. 1). New York: McGraw-Hill.

Costache, C., & Modrogan, C. (2006). *Ecotoxicology and Risk Assessment*. Bucharest, RO: Agir Publishing House.

European Parliament & Council of the European Union. (2000). Directive 2000/60/EC of the European Parliament and of the Council of 23 October 2000 establishing a framework for Community action in the field of water policy. *Official Journal of the European Communities*, L327. 1–73.

European Parliament & Council of the European Union. (2013). Directive 2013/39/EU of the European Parliament and of the Council of 12 August 2013 amending Directives 2000/60/EC and 2008/105/EC as regards priority substances in the field of water policy. *Official Journal of the European Union*, L226. 1–17.

Fenoll, J., Garrido, I., Hellín, P., & Flores, P. et al., (2011). Photodegradation of neonicotinoid insecticides in water. *Environmental Monitoring and Assessment*, 174. 209–220.

Fischer, H. B., List, E. J., Koh, R. C. Y., Imberger, J., & Brooks, N. H. (1979). *Mixing in inland and coastal waters*. Academic press.

Gavrilescu, M., (2005). Fate of pesticides in the environment and its bioremediation. *Engineering in Life Sciences*, 5(6). 497–526.

Gu, D., Andreev, K., & Dupre, M. E. (2021). Major Trends in Population Growth Around the World. *China CDC weekly*, *3*(28). 604–613. https://doi.org/10.46234/ccdcw2021.160.

Klaassen, C. D., Amdur, M. O., & Doull, J. (1986). *Toxicology – the Basic Science of Poisons 3rd ed*, New York, USA: Macmillan Publishing Company.

Lu, Z., Challis, J. K., & Wong, C.S. (2015). Quantum yields for direct photolysis of neonicotinoid insecticides in water: Implications for exposure to nontarget aquatic organisms. *Environmental Science & Technology Letters, 2*(7). 188–192

Malla, M. A., Gupta, S., Dubey, A., Kumar, A., & Yadav, S. (2021). Contamination of groundwater resources by pesticides. In A. Ahamad, S. I. Siddiqui, & P. Singh (Eds.), *Contamination of Water* . 99–107. Academic Press. https://doi.org/10.1016/B978-0-12-824058-8.00023-2.

Merga, L. B., & Van den Brink, P. J. (2025). A review of climatic zone-related variations in toxicity of imidacloprid towards aquatic species and ecosystems, *Environmental Pollution, 386*(127267). https://doi.org/10.1016/j.envpol.2025.127267.

Moza, P. N., Hustert, K., Feicht, E., & Kettrup, A. (1998). Photolysis of imidacloprid in aqueous solution. *Chemosphere*, 36. 497-502.

Morrissey, C.A., Mineau, P., Devries, J. H., Sanchez-Bayo, F., Liess, M., Cavallaro, M. C., & Liber, K. (2015). Neonicotinoid contamination of global surface waters and associated risk to aquatic invertebrates. *Environment International*, 74. 291–303.

Peterson, C.J. (2007). Imidacloprid mobility and longevity in soil columns at a termiticidal application rate. *Pest management science*, *63*(11). 1124–1132. https://doi.org/10.1002/ps.1433.

Simon-Delso, N., Amaral-Rogers, V., Belzunces, L. P., Bonmatin, J. M., Chagnon, M., Downs, C., Furlan, L., Gibbons, D. W., Giorio, C., Girolami, V., Goulson, D., Kreutzweiser, D. P., Krupke, C. H., Liess, M., Long, E., McField, M., Mineau, P., Mitchell, E. A., Morrissey, C. A., Noome, D. A., & Wiemers, M. (2015). Systemic insecticides (neonicotinoids and fipronil): trends, uses, mode of action and metabolites. *Environmental science and pollution research international*, *22*(1). 5–34. https://doi.org/10.1007/s11356-014-3470-y.

Schwarzenbach, R.P., Gschwend, P.M., Imboden, D.M., (2010). *Environmental Organic Chemistry*, 2nd ed., Wiley.

Stehle, S., Ovcharova, V., Wolfram, J., Bub, S., Herrmann, L. Z., Petschick, L. L., & Schulz, R. (2023). Neonicotinoid insecticides in global agricultural surface waters - Exposure, risks and regulatory challenges. *The Science of the total environment*, *867*. 161383.

Tomizawa, M., & Casida, J. E. (2005). Neonicotinoid insecticide toxicology: mechanisms of selective action. *Annual review of pharmacology and toxicology*, *45*. 247–268.

Tudi, M., Daniel Ruan, H., Wang, L., Lyu, J., Sadler, R., Connell, D., Chu, C., & Phung, D. T. (2021). Agriculture Development, Pesticide Application and Its Impact on the Environment. *International journal of environmental research and public health*, *18*(3). 1112. https://doi.org/10.3390/ijerph18031112.

Van Dijk, T., Van Staalduinen, M., & Van der Sluijs, J., (2013). Macro-invertebrate decline in surface water polluted with imidacloprid. *PLoS ONE*, 8(5). e62374.

Versteeg, H., & Malalasekera, W., (2007). *An Introduction to Computational Fluid Dynamics: The Finite Volume Method.* India: Pearson Education Publishing House.

Wamhoff, H., & Schneider, V., (1999). Photodegradation of imidacloprid. *Journal of Agricultural and Food Chemistry*, 47. 1730–1734.

Wang, H., Wang, F., Yin, S., Liu, S., & Cui, X.-Y. (2026). High-quality quad-dominant mesh generation aided by the virtual topological model generated after automatic suppression of small geometric features. *Computers & Structures, 322*. 108107.

Zhang, Y., Liu, S., Gu, J., Song, F., Yao, X., & Liu, Z. (2008). Imidacloprid acts as an antagonist on insect

nicotinic acetylcholine receptor containing the Y151M mutation. *Neuroscience letters*, *446*(2-3). 97–100.

Zepp, R.G., Hoigné, J., & Bader, H., (1995). Nitrate-induced photooxidation of trace organic chemicals in water. *Environmental Science & Technology*.

Zepp, R. G., Wolfe, N. L., Azarraga, L. V., Cox, R. H. & Pape, C. W. (1977). Photochemical transformation of the DDT and methoxychlor degradation products, DDE and DMDE, by sunlight. *Arch Environ Contam Toxicol* *6*(23). 305–314. https://doi.org/10.1007/BF02097771.

## APPENDIX 1

```
#include "udf.h"
#include "math.h"
#define I0        1.0
#define ALPHA     3.0
#define PHI       0.018
#define EPS_UV    0.003
#define EA        20000.0
#define R_GAS     8.314
#define TREF      293.15
#define HTOP      0.7
#define MW_IMD    0.255052
#define MW_PROD   0.255052
#define ID_IMDCPD   0
#define ID_PRODUCT  1
#define ID_WATER    2
#define UDM_DEPTH   0
#define UDM_IUV     1
#define UDM_KPHOTO  2
DEFINE_ADJUST(update_photo_fields, domain)
{
   Thread *t;
   cell_t c;
   real xc[ND_ND];
   real y, z, T;
   real Iuv, fT, k_photo;
   thread_loop_c(t, domain)
   {
      if (!FLUID_THREAD_P(t))
         continue;
      begin_c_loop(c, t)
      {
         C_CENTROID(xc, c, t);
         y = xc[1];
         z = HTOP - y;
         if (z < 0.0)
            z = 0.0;
         T = C_T(c, t);
         if (T < 250.0)
            T = 250.0;
         Iuv = I0 * exp(-ALPHA * z);
         fT = exp(-(EA / R_GAS) * (1.0 / T - 1.0 / TREF));
         k_photo = PHI * EPS_UV * Iuv * fT;
         C_UDMI(c, t, UDM_DEPTH) = z;
         C_UDMI(c, t, UDM_IUV)   = Iuv;
         C_UDMI(c, t, UDM_KPHOTO) = k_photo;
      }
      end_c_loop(c, t)
   }
}
DEFINE_SOURCE(imd_photo_source, c, t, dS, eqn)
{
   real rho, yimd, k_photo, source;
   if (!FLUID_THREAD_P(t))
   {
      dS[eqn] = 0.0;
      return 0.0;
   }
   rho  = C_R(c, t);
   yimd = C_YI(c, t, ID_IMDCPD);
   if (yimd < 0.0)
      yimd = 0.0;
   k_photo = C_UDMI(c, t, UDM_KPHOTO);
   source = -rho * yimd * k_photo;
   dS[eqn] = -rho * k_photo;
   return source;
}
DEFINE_SOURCE(product_photo_source, c, t, dS, eqn)
{
   real rho, yimd, k_photo, source;
   real stoich_mass_ratio;
   if (!FLUID_THREAD_P(t))
   {
      dS[eqn] = 0.0;
      return 0.0;
   }
   rho  = C_R(c, t);
   yimd = C_YI(c, t, ID_IMDCPD);
   if (yimd < 0.0)
      yimd = 0.0;
   k_photo = C_UDMI(c, t, UDM_KPHOTO);
   stoich_mass_ratio = MW_PROD / MW_IMD;
  source = rho * yimd * k_photo * stoich_mass_ratio;
   dS[eqn] = 0.0;
   return                                          source;
```

Scientific Papers. Series E. Land Reclamation, Earth Observation & Surveying, Environmental Engineering. Vol. XV, 2026
Print ISSN 2285-6064, CD-ROM ISSN 2285-6072, Online ISSN 2393-5138, ISSN-L 2285-6064

# COMPARATIVE ASSESSMENT OF ANNUAL DYNAMICS IN WATER QUALITY OF HERASTRAU LAKE, ROMANIA

**Iuliana VOICU[1], Mihaela DRAGOI CUDALBEANU[1], Andreea Adriana MAN[1], Nicoleta Daniela SARBU[1], Teodor COSTACHIOIU[2], Daniela FAUR[2], Carmen Laura CIMPEANU[1]**

[1]Faculty of Land Reclamation and Environmental Engineering, University of Agronomic Sciences and Veterinary Medicine of Bucharest, 59 Marasti Blvd, 011464, District 1, Bucharest, Romania
[2]National University of Science and Technology Politehnica, 060042, Bucharest, Romania

Corresponding author emails: mihaela.dragoi@fifim.ro, daniela.faur@upb.ro

***Abstract***

*Water quality assessment is vital to environmental management. Regular monitoring of lakes helps protect environmental integrity and human health. This study assessed annual changes in water quality in Herastrau Lake (Bucharest, Romania) using field and laboratory measurements complemented by satellite observations. Water samples were collected from ten sites in autumn 2024 and spring 2025 and analyzed for pH, electrical conductivity, total dissolved solids, salinity, dissolved oxygen, turbidity, chloride, nitrite, nitrate, ammonium, total suspended solids, hardness, and iron. Results were compared with Romanian standards (Order No. 161/2006), and Pearson correlations were performed. The lake remained alkaline in both years (pH 8.50), while dissolved oxygen declined markedly in 2025 (2.59 mg/L) compared with 2024 (6.82 mg/L). Turbidity exceeded 5 NTU, and ammonium nitrogen showed elevated concentrations (12.07 mg N-$NH_4^+$/L in 2024; 13.50 mg N-$NH_4^+$/L in 2025), suggesting persistent eutrophication pressure. Sentinel-2 imagery (10–20 m) was used to estimate surface turbidity* from red-edge reflectance, with NDWI used for water masking*, and the results were validated with laboratory data. The water quality underscores the need for targeted pollution control measures.*

***Key words****: eutrophication, Herastrau, Romania, Sentinel-2, water quality.*

## INTRODUCTION

Although water is fundamental to life, freshwater accounts for only 2.5% of the global water volume, and just 1% is accessible for use, with much of it sequestered in reservoirs. In this context, lakes are a vital yet strictly finite resource (Hoggang & Reyes, 2023). Beyond serving as critical water reservoirs, lakes support diverse ecosystems and play a vital role in regulating local microclimates (K. Zhang et al., 2025) and stabilizing the climate by driving atmospheric carbon fixation through phyto-plankton photosynthesis (Oustani et al., 2026).

Freshwater lakes are highly sensitive to both natural factors and anthropogenic pressures (urbanization, industrialization, agriculture) that compromise their ecological integrity (Liu et al., 2025). Nutrient enrichment fundamentally alters water quality, trophic status, and biological community structure. Because plankton communities respond quickly to these fluctuations, they serve as reliable indicators of changing ecological conditions (Nkhata et al., 2026). Ultimately, excessive chemical inputs alter water physicochemical parameters, triggering eutrophication, characterized by elevated phytoplankton biomass, harmful cyanobacterial blooms, reduced transparency, and oxygen depletion (Nkhata et al., 2026; Oustani et al., 2026).

Eutrophication is the enrichment of water with nutrients like nitrogen and phosphorus, leading to excessive algae and plant growth. As organic matter decomposes, oxygen levels drop, causing fish kills, biodiversity loss, reduced water clarity, and harmful cyanobacterial blooms that release toxins. It damages water ecosystems and recreation and is a major global threat to inland water quality (Zhou et al., 2024; Morelato et al., 2026).

Urban lakes provide vital ecosystem services and serve as structural components of the metropolitan landscape. They enhance urban environmental quality by providing reliable access to clean water for both functional use and

recreation (Cheval et al., 2020). An example of a metropolitan ecosystem facing localized pressures is Herastrau Lake, located in the northern district of Bucharest, Romania. It is an artificial water body and a key component of the anthropogenic lake cascade along the Colentina River. Herastrau Lake is particularly exposed to eutrophication, as it receives continuous anthropogenic nutrient loads from urban runoff, sewage inputs, and atmospheric deposition, while also providing important recreational, aesthetic, microclimatic, and biodiversity services to a densely populated city. However, its location within a densely populated area subjects it to ongoing environmental challenges, including urban surface runoff and localized waste generation.

Despite its ecological and recreational importance, comprehensive data regarding the status of this aquatic system remain insufficient, with only a limited number of local studies examining water pollution in Herastrau Lake. To address this critical knowledge gap, this study aims to assess the lake's physico-chemical profile and quantify its current state of degradation. Specifically, this research monitors key environmental indicators - including pH, electrical conductivity, turbidity, and chloride ions - alongside critical nutrient loadings - namely, ammonia, nitrites, nitrates, and phosphates - to assess the immediate urban impact footprint.

## MATERIALS AND METHODS

### *Water Site and Sampling Points Description*

Water sampling was conducted at ten sites distributed across Herastrau Lake during two monitoring campaigns, on 21 October 2024 (autumn) and 11 March 2025 (early spring). The same sampling locations were used in both campaigns, and their geographic coordinates were recorded to ensure spatial consistency and enable direct comparison between the two monitoring periods. At each site, selected physicochemical parameters were measured in situ, and additional analyses were performed in the laboratory afterward. This combined approach allowed assessment of both spatial variability in water quality across the lake and seasonal differences between the autumn 2024 and early spring 2025 campaigns.

### *Water Sampling and Physicochemical Analyses*

Water sampling was conducted in accordance with the Romanian guidelines for water sampling from natural and artificial lakes (ISO 5667-4:2016). Water was manually collected at approximately 0.5 m below the surface and placed in polyethylene containers, then immediately stored in a refrigerated transport box at approximately 4°C until arrival at the laboratory. Before laboratory analyses, samples were allowed to reach room temperature, as required by the analytical procedure.

Water temperature, pH, electrical conductivity (EC), total dissolved solids (TDS), salinity, and dissolved oxygen (DO) were measured in situ at each sampling location using a calibrated portable multiparameter. The remaining physicochemical parameters were determined in the laboratory within 24-48 h of sample collection.

Turbidity was measured with a calibrated turbidimeter and reported in nephelometric turbidity units (NTU). Total suspended solids (TSS) were measured gravimetrically by filtering homogenized water through pre-dried, pre-weighed filter paper. The filter was dried at 105 °C, cooled, and reweighed. TSS was calculated from the mass difference and given as mg/L.

Chloride ($Cl^-$) concentrations were determined by Mohr titration with a standardized silver nitrate ($AgNO_3$) solution, using potassium chromate ($K_2CrO_4$) as the endpoint indicator. Total hardness (TH) was determined by complexometric titration with disodium ethylenediaminetetraacetate (EDTA), using Eriochrome Black T as the endpoint indicator. Temporary hardness (CH) was determined by titration with hydrochloric acid (HCl) using methyl orange as the endpoint indicator, while permanent hardness (NCH) was calculated as the difference between TH and CH.

Nitrite ($N\text{-}NO_2^-$) and ammonium ($N\text{-}NH_4^+$) were determined spectrophotometrically at 540 and 650 nm, respectively, according to the procedures described by Sandu et al. (2023). Nitrate ($N\text{-}NO_3^-$) was not measured directly; instead, nitrate-equivalent concentrations were calculated from nitrite values using the corresponding stoichiometric conversion factor. Nitrogen species results were expressed as mg

N/L. Iron ($Fe^{3+}$) was determined spectrophotometrically using the potassium thiocyanate (KSCN) method at 490 nm. $Fe^{3+}$ concentrations were expressed as mg $Fe^{3+}$/L.
All analytical instruments were calibrated before measurements, following the respective procedures, to maintain data quality and accuracy. Laboratory determinations were performed in triplicate, and the results were expressed as mean ± standard deviation (SD).

***Water Quality Classification***
The physicochemical quality of Herastrau Lake water was evaluated by comparing measured parameters with threshold values established by the Romanian regulatory framework for surface-water monitoring (Order No. 161/2006). According to this classification system, surface waters are divided into five quality classes (I-V), ranging from high-quality waters (Class I) to heavily degraded waters (Class V). For each sampling point and monitoring year, the measured concentrations of dissolved oxygen (DO), chlorides ($Cl^-$), nitrite ($N\text{-}NO_2^-$), nitrate ($N\text{-}NO_3^-$), ammonium ($N\text{-}NH_4^+$), and iron ($Fe^{3+}$) were compared with the corresponding class-specific threshold values. This approach allowed evaluation of both spatial variability among the ten sampling sites and interannual changes between 2024 and 2025. The resulting classification was used to identify the physico-chemical parameters primarily responsible for deteriorating lake-water quality and to assess changes in water-quality conditions between the two monitoring campaigns.

***Statistical Analysis and Pearson Correlation***
Statistical analysis of the water-quality data was performed using GraphPad Prism (version 11.0.2). Pearson's correlation coefficient was used to evaluate the relationships among water temperature, pH, electrical conductivity (EC), total dissolved solids (TDS), salinity, dissolved oxygen (DO), turbidity, chlorides ($Cl^-$), total hardness (TH), temporary hardness (CH), permanent hardness (NCH), nitrite ($N\text{-}NO_2^-$), nitrate ($N\text{-}NO_3^-$), ammonium ($N\text{-}NH_4^+$), total suspended solids (TSS), and iron ($Fe^{3+}$).

***Satellite data set description***
Satellite data consisted of Sentinel-2 MSI Level-2A products with atmospherically corrected bottom-of-atmosphere surface reflectance (tile T35TMK). For each campaign, the two cloud-free scenes closest to the sampling date were selected - 21 and 26 October 2024 for the autumn campaign, and 5 and 20 March 2025 for the early-spring campaign - yielding four scenes in total. Prior to analysis, cloud-, shadow-, and cirrus-affected pixels were removed using the Scene Classification Layer (SCL). Because the strict SCL water class (class 6) frequently misclassifies the turbid, chlorophyll-rich water of eutrophic lakes as vegetation or bare soil, and because the sampling locations were independently verified to lie over open water, SCL classes 4-7 (vegetation, bare soil, water, and unclassified) were retained at the sampling points. The radiometric offset introduced in processing baseline 04.00 was then applied to recover surface reflectance. For every sampling point, a per-point median composite was computed from the two scenes of the corresponding campaign. The median was preferred over single-date extraction to reduce residual cloud/haze contamination and transient surface effects, while keeping the reflectance temporally close to the in-situ measurements. Spectral indices and band ratios were subsequently derived and extracted at the ten-point locations for comparison with the in-situ data.

***Satellite-based assessment of water turbidity***
Turbidity is an optically active water-quality parameter: suspended particles raise the water-leaving reflectance in the red and near-infrared (NIR) regions, where clear water is otherwise strongly absorbing, and the magnitude of this increase scales with the concentration of suspended matter. The red-to-NIR portion of the Sentinel-2 spectrum is therefore the most informative for turbidity retrieval.
The following bands were evaluated as turbidity predictors, as shown in Table 1: the red band B04 (665 nm) and the first red-edge band B05 (705 nm), which respond at low-to-moderate turbidity; and the red-edge band B07 (783 nm) together with the NIR band B08 (842 nm), which remain sensitive at high turbidity, where the red band tends to saturate, a behavior analogous to the band-switching logic of semi-analytical turbidity models. In addition to the individual bands, two red-edge-to-red ratios

were computed, re5_red = B05/B04 and re7_red = B07/B04, since band ratios largely cancel multiplicative effects (illumination geometry, residual atmospheric scattering, and the imperfect Level-2A correction over water) and thus provide more robust proxies than single bands. All candidate predictors listed in Table 1 were screened against the in-situ measurements, and the band that showed the strongest and most consistent association with turbidity in both campaigns, the red-edge band B07, was retained for calibration; NDTI is additionally reported below because it is the only index among the candidates explicitly formulated for turbidity.

Table 1. Sentinel-2 bands and spectral indices evaluated for turbidity retrieval

| Band/ Spectral index | Definition | Role for turbidity |
|---|---|---|
| B04 (red) | 665 nm | Suspended sediment; low-to-moderate turbidity |
| B05 (red-edge 1) | 705 nm | Red-edge response across the turbidity range |
| B07 (red-edge 3) | 783 nm | Sensitive at high turbidity (red saturates) |
| B08 (NIR) | 842 nm | High-turbidity/ TSS signal |
| re5_red | B05/B04 | Red-edge/red ratio; robust at low-to-moderate values |
| re7_red | B07/B04 | Red-edge/red ratio; **candidate predictor** |
| NDTI (Lacaux et al., 2007) | (B04−B03)/ (B04+B03) | Normalized Difference Turbidity Index |
| NDWI (McFeeters, 1996) | (B03−B08)/ (B03+B08) | Water masking only |

### *Calibration of the satellite-derived turbidity*

Calibration of the satellite turbidity proxy was carried out as a spatial regression across the ten sampling points, relating the in-situ turbidity of each campaign to the corresponding median Sentinel-2 reflectance values and band ratios extracted at the same locations. Because the analysis compares spatially distributed point pairs rather than a dense temporal series and given the small sample size (n = 10), the strength and significance of each candidate predictor were assessed using both the Pearson correlation coefficient (r), which quantifies the strength of a linear association, and the Spearman rank correlation coefficient (ρ), which captures monotonic relationships and is more robust to non-linearity, non-normality and outliers.

Reporting both coefficients allows assessment of each relationship's linearity: close agreement between r and ρ indicates a robust, approximately linear association, whereas marked divergence signals non-linearity or sensitivity to individual points. For n = 10, the critical value for significance at $p < 0.05$ (two-tailed) is $|r| \approx 0.63$; all results were therefore treated as exploratory.

## RESULTS AND DISCUSSIONS

### *Spatial Distribution of Sampling Points*

The ten georeferenced sampling points spanned different areas of Herastrau Lake, ensuring adequate spatial representation of the water body. Table 2 lists the geographical coordinates of the sampling sites, and Figure 1 shows their spatial distribution across Herastrau Lake. The same locations were monitored in 2024 and 2025, enabling a consistent assessment of spatial and temporal variations in water quality.

Table 2. Geographical coordinates of the sampling points in Herastrau Lake

| Point | Latitude (N) | Longitude (E) |
|---|---|---|
| P1 | 44°28'39.54252" | 26°4'34.83156" |
| P2 | 44°28'52.00000" | 26°4'30.00000" |
| P3 | 44°28'56.60544" | 26°4'41.02500" |
| P4 | 44°29'13.04952" | 26°4'57.93348" |
| P5 | 44°28'56.56080" | 26°4'56.75412" |
| P6 | 44°28'40.74636" | 26°4'42.59460" |
| P7 | 44°28'39.43344" | 26°5'10.15080" |
| P8 | 44°28'31.52316" | 26°5'19.74228" |
| P9 | 44°28'22.28196" | 26°4'53.78880" |
| P10 | 44°28'28.08360" | 26°4'39.84672" |

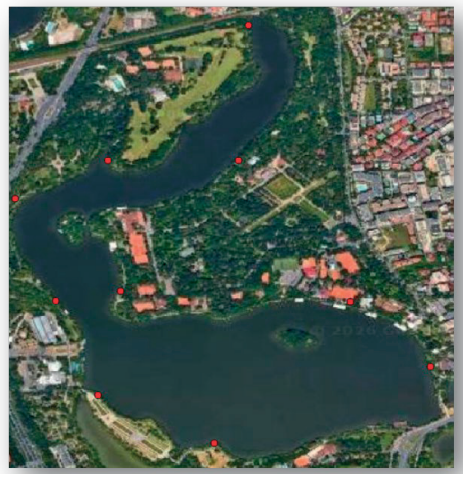


Figure 1. Spatial distribution of the water sampling sites in Herastrau Lake, Bucharest, Romania (background: Google Earth true-color satellite imagery)

***Physicochemical parameters and water-quality classification***

During the autumn 2024 campaign, Herastrau Lake water was slightly alkaline, with pH values ranging from 8.17 to 8.60, while EC ranged from 331 to 547 µS/cm. Salinity ranged from 160 to 270 mg/L and TDS from 165 to 300 mg/L, indicating moderate spatial variability in the lake's dissolved ionic content. DO was relatively favorable, ranging from 5.81 to 7.61 mg $O_2$/L. Based on the water-quality classification, five sampling points (P1, P4, P5, P8, and P9) were assigned to Class I, three points (P2, P3, and P7) to Class II, and only P6 and P10 to Class III. Turbidity ranged from 5.04 ± 0.98 to 14.80 ± 0.23 NTU, with the highest value at P2, suggesting localized differences in suspended particulate matter (Table 3).

$Cl^-$ concentrations ranged from 39.45 ± 3.86 to 65.04 ± 4.73 mg/L and were consistently classified as Class I at all sampling sites. $NO_2^-$ concentrations showed greater variability, ranging from 0.03 to 0.08 mg N-$NO_2^-$/L. Most sites were classified as Class II, whereas P1 and P10 reached Class III. In contrast, all $NO_3^-$ values remained within Class I. The most pronounced deterioration was associated with $NH_4^+$, ranging from 9.71 ± 1.19 to 17.07 ± 1.09 mg N-$NH_4^+$/L and resulting in Class V at all ten sampling points. This uniform classification indicates that $NH_4^+$ represented the major N-related water-quality concern during the 2024 campaign. $Fe^{3+}$ concentrations were very low (0.0002 - 0.0005 mg $Fe^{3+}$/L) and corresponded to Class I throughout the lake.

Table 3. Physicochemical water-quality parameters for Herastrau Lake in 2024

| Point | Temperature (°C) | pH (pH units) | EC (µS/cm) | Salinity (mg/L) | TDS (mg/L) | DO (mg $O_2$/L) | Turbidity (NTU) | $Cl^-$ (mg/L) |
|---|---|---|---|---|---|---|---|---|
| P1 | 16.06 | 8.60 | 388 | 190 | 194 | 7.10 | 7.47 ± 0.58 | 39.45 ± 3.86 |
| P2 | 18.52 | 8.17 | 483 | 230 | 241 | 6.66 | 14.80 ± 0.23 | 54.88 ± 4.54 |
| P3 | 16.11 | 8.22 | 405 | 200 | 203 | 6.42 | 10.00 ± 0.57 | 55.80 ± 4.91 |
| P4 | 14.60 | 8.27 | 360 | 170 | 180 | 7.50 | 11.85 ± 0.49 | 56.29 ± 1.12 |
| P5 | 16.16 | 8.26 | 331 | 160 | 165 | 7.05 | 5.04 ± 0.98 | 57.40 ± 4.00 |
| P6 | 21.63 | 8.26 | 504 | 240 | 252 | 5.81 | 7.46 ± 0.77 | 41.44 ± 2.80 |
| P7 | 15.73 | 8.34 | 547 | 270 | 273 | 6.54 | 8.87 ± 0.54 | 57.14 ± 2.99 |
| P8 | 17.70 | 8.37 | 496 | 240 | 248 | 7.59 | 8.40 ± 0.66 | 61.12 ± 7.07 |
| P9 | 16.55 | 8.32 | 520 | 250 | 260 | 7.61 | 7.34 ± 1.10 | 63.45 ± 6.08 |
| P10 | 14.96 | 8.36 | 488 | 200 | 300 | 5.92 | 11.54 ± 0.97 | 65.04 ± 4.73 |
| **Point** | **$N–NO_2^-$ (mg/L)** | **$N–NO_3^-$ (mg/L)** | **$N–NH_4^+$ (mg/L)** | **TSS (mg/L)** | **TH (mg/L)** | **CH (mg/L)** | **NCH (mg/L)** | **$Fe^{3+}$ (mg/L)** |
| P1 | 0.08± 0.00 | 0.10 ± 0.00 | 9.71 ± 1.19 | 5.07 ± 0.20 | 190.66 ± 2.82 | 74.18 ± 0.80 | 116.48 ± 2.62 | 0.0005 ± 0.00 |
| P2 | 0.04 ± 0.00 | 0.05 ± 0.01 | 13.14 ± 0.25 | 5.90 ± 0.26 | 241.13 ± 0.56 | 125.99 ± 0.92 | 115.14 ± 0.50 | 0.0004 ± 0.00 |
| P3 | 0.04 ± 0.00 | 0.06 ± 0.00 | 11.21 ± 0.62 | 6.20 ± 0.18 | 251.23 ± 1.21 | 138.11 ± 0.80 | 113.12 ± 1.12 | 0.0004 ± 0.00 |
| P4 | 0.05 ± 0.00 | 0.08 ± 0.00 | 17.07 ± 1.09 | 6.35 ± 0.71 | 224.31 ± 1.39 | 112.31 ± 0.84 | 112.00 ± 1.23 | 0.0004 ± 0.00 |
| P5 | 0.03 ± 0.00 | 0.05 ± 0.00 | 11.68 ± 0.88 | 5.67 ± 0.31 | 226.55 ± 1.63 | 116.78 ± 0.92 | 109.77 ± 1.43 | 0.0004 ± 0.00 |
| P6 | 0.04 ± 0.00 | 0.06 ± 0.01 | 10.08 ± 0.57 | 5.33 ± 0.58 | 211.97 ± 2.95 | 88.99 ± 0.20 | 122.98 ± 2.87 | 0.0004 ± 0.00 |
| P7 | 0.03 ± 0.00 | 0.05 ± 0.00 | 11.35 ± 0.00 | 1.73 ± 0.08 | 203.00 ± 4.16 | 102.20 ± 0.88 | 100.80 ± 4.18 | 0.0003 ± 0.00 |
| P8 | 0.03 ± 0.00 | 0.04 ± 0.00 | 12.81 ± 2.47 | 4.25 ± 0.30 | 199.64 ± 0.99 | 89.43 ± 0.68 | 110.21 ± 0.87 | 0.0002 ± 0.00 |
| P9 | 0.06 ± 0.00 | 0.08 ± 0.04 | 11.65 ± 1.55 | 3.15 ± 0.13 | 209.73 ± 2.43 | 99.97 ± 0.96 | 109.76 ± 2.58 | 0.0004 ± 0.00 |
| P10 | 0.08 ± 0.00 | 0.10 ± 0.00 | 12.03 ± 1.67 | 1.10 ± 0.02 | 200.87 ± 2.83 | 100.20 ± 0.80 | 100.67 ± 2.63 | 0.0004 ± 0.00 |

A distinctly different pattern was observed during the early spring 2025 campaign (Table 4). Although pH remained alkaline and comparable to 2024 (8.15-8.95), EC generally increased, reaching up to 723 µS/cm, while salinity varied between 290 and 350 mg/L. The most important change was in DO, which decreased markedly to 1.90-3.70 mg $O_2$/L. Consequently, all ten sampling sites were classified as Class V for DO, indicating a substantial deterioration of the lake oxygen regime compared with autumn 2024. Turbidity remained spatially heterogeneous, ranging from 4.36 ± 0.39 NTU at P1 to a maximum of 16.40 ± 0.71 NTU at P8.

Despite deteriorating oxygen conditions, $Cl^-$ concentrations remained within Class I at all sites in 2025 (Table 5). $NO_2^-$ concentrations were generally lower than in 2024, with P7 and P9 at 0 mg N-$NO_2^-$/L and assigned to Class I, while the remaining sites were classified as Class II. All $NO_3^-$ values also remained within Class I. However, $NH_4^+$ concentrations remained elevated, ranging from 11.23 ± 0.77 to 15.05 ± 0.09 mg N–$NH_4^+$/L, again resulting in Class V at every sampling point. $Fe^{3+}$ remained at very low concentrations (0.0001-0.0004 mg $Fe^{3+}$/L), corresponding consistently to Class I.

A marked interannual difference was also observed for water TH. TH decreased from 190.66–251.23 mg/L in 2024 to 88.37–115.70 mg/L in 2025, with an especially pronounced reduction in CH, from 74.18-138.11 mg/L to approximately 10.72-12.10 mg/L.

Table 4. Physicochemical water-quality parameters for Herastrau Lake in 2025

| Point | Temperature (°C) | pH (pH units) | EC (µS/cm) | Salinity (mg/L) | TDS (mg/L) | DO (mg $O_2$/L) | Turb. (NTU) | $Cl^-$ (mg/L) |
|---|---|---|---|---|---|---|---|---|
| **P1** | 13.01 | 8.59 | 657 | 320 | 332 | 3.30 | 4.36 ± 0.39 | 60.60 ± 3.48 |
| **P2** | 17.90 | 8.60 | 627 | 300 | 310 | 2.80 | 5.34 ± 0.45 | 57.29 ± 3.75 |
| **P3** | 13.07 | 8.58 | 683 | 340 | 347 | 3.70 | 9.88 ± 0.49 | 56.87 ± 1.17 |
| **P4** | 19.62 | 8.15 | 585 | 290 | 295 | 2.70 | 11.23 ± 1.12 | 54.31 ± 0.51 |
| **P5** | 13.06 | 8.95 | 670 | 330 | 335 | 2.60 | 11.60 ± 0.40 | 57.17 ± 0.46 |
| **P6** | 12.92 | 8.60 | 723 | 350 | 355 | 2.40 | 9.21 ± 0.28 | 56.54 ± 1.81 |
| **P7** | 11.90 | 8.84 | 607 | 300 | 303 | 2.20 | 7.06 ± 0.30 | 54.17 ± 0.89 |
| **P8** | 13.93 | 8.56 | 350 | 290 | 170 | 2.20 | 16.40 ± 0.71 | 52.56 ± 0.11 |
| **P9** | 12.54 | 8.50 | 601 | 290 | 301 | 2.10 | 7.41 ± 0.61 | 52.30 ± 0.20 |
| **P10** | 11.96 | 8.66 | 663 | 320 | 333 | 1.90 | 11.73 ± 0.47 | 57.24 ± 0.11 |
| **Point** | **$N–NO_2^-$ (mg/L)** | **$N–NO_3^-$ (mg/L)** | **$N–NH_4^+$ (mg/L)** | **TSS (mg/L)** | **TH (mg/L)** | **CH (mg/L)** | **NCH (mg/L)** | **$Fe^{3+}$ (mg/L)** |
| **P1** | 0.05 ± 0.00 | 0.07 ± 0.00 | 11.23 ± 0.77 | 5.05 ± 0.22 | 115.70 ± 3.33 | 10.84 ± 0.20 | 104.86 ± 3.13 | 0.0004 ± 0.00 |
| **P2** | 0.05 ± 0.00 | 0.07 ± 0.00 | 14.68 ± 0.33 | 6.90 ± 0.16 | 101.92 ± 0.95 | 11.65 ± 0.08 | 90.27 ± 0.87 | 0.0003 ± 0.00 |
| **P3** | 0.04 ± 0.00 | 0.05 ± 0.00 | 12.22 ± 3.05 | 5.20 ± 0.08 | 98.45 ± 1.74 | 10.95 ± 0.20 | 87.50 ± 1.54 | 0.0003 ± 0.00 |
| **P4** | 0.04 ± 0.00 | 0.05 ± 0.00 | 13.21 ± 0.20 | 5.35 ± 0.07 | 101.36 ± 1.74 | 11.82 ± 0.16 | 89.54 ± 1.58 | 0.0003 ± 0.00 |
| **P5** | 0.04 ± 0.00 | 0.05 ± 0.00 | 13.94 ± 1.56 | 5.35 ± 0.16 | 103.82 ± 1.43 | 12.10 ± 0.08 | 91.73 ± 1.35 | 0.0003 ± 0.00 |
| **P6** | 0.03 ± 0.00 | 0.05 ± 0.00 | 12.95 ± 2.42 | 6.50 ± 0.08 | 99.57 ± 1.11 | 11.65 ± 0.08 | 87.92 ± 1.03 | 0.0003 ± 0.00 |
| **P7** | 0.00 ± 0.00 | 0.00 ± 0.00 | 14.70 ± 2.65 | 1.80 ± 0.06 | 95.98 ± 4.28 | 10.89 ± 0.12 | 85.09 ± 4.16 | 0.0002 ± 0.00 |
| **P8** | 0.03 ± 0.00 | 0.05 ± 0.00 | 15.05 ± 0.09 | 4.25 ± 0.53 | 88.37 ± 1.11 | 11.42 ± 0.32 | 76.94 ± 0.79 | 0.0001 ± 0.00 |
| **P9** | 0.00 ± 0.00 | 0.00 ± 0.00 | 12.36 ± 2.92 | 3.15 ± 0.43 | 95.87 ± 1.58 | 10.72 ± 0.04 | 85.15 ± 1.54 | 0.0003 ± 0.00 |
| **P10** | 0.04 ± 0.00 | 0.05 ± 0.00 | 14.69 ± 0.56 | 1.10 ± 0.28 | 99.90 ± 0.63 | 11.40 ± 0.20 | 88.51 ± 0.83 | 0.0003 ± 0.00 |

Table 5. Water-quality class assignment for Herastrau Lake in 2024 and 2025 campaigns

| Point | DO | $Cl^-$ | $N\text{-}NO_2^-$ | $N\text{-}NO_3^-$ | $N\text{-}NH_4^+$ | $Fe^{3+}$ |
|---|---|---|---|---|---|---|
| **2024 monitoring campaign** | | | | | | |
| **P1** | Class I | Class I | Class III | Class I | Class V | Class I |
| **P2** | Class II | Class I | Class II | Class I | Class V | Class I |
| **P3** | Class II | Class I | Class II | Class I | Class V | Class I |
| **P4** | Class I | Class I | Class II | Class I | Class V | Class I |
| **P5** | Class I | Class I | Class II | Class I | Class V | Class I |
| **P6** | Class III | Class I | Class II | Class I | Class V | Class I |
| **P7** | Class II | Class I | Class II | Class I | Class V | Class I |
| **P8** | Class I | Class I | Class II | Class I | Class V | Class I |
| **P9** | Class I | Class I | Class II | Class I | Class V | Class I |
| **P10** | Class III | Class I | Class III | Class I | Class V | Class I |
| **2025 monitoring campaign** | | | | | | |
| **P1** | Class V | Class I | Class II | Class I | Class V | Class I |
| **P2** | Class V | Class I | Class II | Class I | Class V | Class I |
| **P3** | Class V | Class I | Class II | Class I | Class V | Class I |
| **P4** | Class V | Class I | Class II | Class I | Class V | Class I |
| **P5** | Class V | Class I | Class II | Class I | Class V | Class I |
| **P6** | Class V | Class I | Class II | Class I | Class V | Class I |
| **P7** | Class V | Class I | Class I | Class I | Class V | Class I |
| **P8** | Class V | Class I | Class II | Class I | Class V | Class I |
| **P9** | Class V | Class I | Class I | Class I | Class V | Class I |
| **P10** | Class V | Class I | Class II | Class I | Class V | Class I |

At the same time, the increase in EC and salinity in 2025 suggests that the seasonal change did not simply reflect a general dilution or concentration effect, but rather a modification in the ionic composition of the lake water.

Overall, the comparison between the two monitoring campaigns indicates that $NH_4^+$ was the most persistent water-quality issue, remaining in Class V throughout the lake in both years, while the most pronounced temporal deterioration concerned DO, which shifted from

Classes I-III in 2024 to Class V at all sites in 2025. Conversely, $Cl^-$, $NO_3^-$, and $Fe^{3+}$ concentrations consistently remained within Class I. The simultaneous occurrence of high $NH_4^+$ concentrations and severe oxygen depletion in 2025 may indicate increased oxygen demand associated with organic matter and N transformations, suggesting enhanced eutrophication pressure within the lake.

Dippong and Resz (2024), in a study of lakes in the Tisa protected area in Romania, also reported generally adequate pH conditions, while EC varied widely from 213 to 1052 µS/cm. In Herastrau Lake, EC ranged from 331 to 547 µS/cm in 2024 and increased to 350-723 µS/cm in 2025, indicating a higher dissolved ionic load during the early-spring campaign. Another recent study of the Iza-Tisa (Romania) surface-water system reported EC values of 307-512 µS/cm, showing that the 2024 Herastrau Lake values were broadly comparable, whereas some 2025 sampling sites exhibited greater mineralization (Dippong & Resz, 2025).

The increase in EC in 2025 was linked to higher salinity, but hardness changed differently. TH dropped from 190.66-251.23 mg/L in 2024 to 88.37-115.70 mg/L in 2025, and CH fell sharply from 74.18-138.11 to 10.72-12.10 mg/L. Thus, the higher EC and salinity in 2025 do not originate solely from increased Ca- and Mg-hardness. Instead, these changes suggest a shift in the lake water's ionic composition between the two campaigns. Similar complexity in the relationships among EC, TDS, TH, and dissolved ions has been observed in other lake systems, where natural hydrogeochemical processes and anthropogenic inputs jointly determine water chemistry (Osman et al., 2025).

DO showed the most pronounced temporal variation. In autumn 2024, DO concentrations were Class I-III, but dropped dramatically in March 2025 to Class V. This decrease is notable because the 2025 campaign had lower water temperatures, suggesting oxygen deterioration is not driven by temperature effects alone. Recent research shows DO dynamics in shallow eutrophic lakes depend on interactions among water temperature, hydrological conditions, mixing, precipitation, wind, nutrients, and biological activity (F. Zhang et al., 2025). The generally well-oxygenated conditions in Romanian Tisa lakes highlight the poor oxygen conditions in Herastrau Lake in 2025 (Dippong & Resz, 2024).

Turbidity in northern Romanian lakes ranges from 0.68-48 NTU, highest in spring (Dippong & Resz, 2024). Values are lower than in highly turbid systems like Tonle Sap Lake, with an annual mean of 53.99 NTU and spring-summer means of 84.16 and 93.47 NTU. The autumn mean of 15.33 NTU is similar to Herastrau Lake. Turbidity responds to cropland, urbanization, and population density, reflecting anthropogenic impact (Zou et al., 2024).

$Cl^-$ concentrations were comparatively stable in 2024 and 2025. $Cl^-$ concentrations in Herastrau Lake are substantially lower than those reported for strongly salt-affected urban lakes. For example, Foley and Steinman (2023) reported $Cl^-$ concentrations exceeding 230 mg/L and reaching about 331 mg/L in an urban lake affected by road deicing salts; these concentrations were high enough to interfere with lake mixing and contribute to hypolimnetic hypoxia.

In contrast, ammonium represented the most critical nitrogen-related parameter. The $NH_4^+$ values of Herastrau Lake are markedly higher than those reported for other Romanian lake systems. Dippong et al. (2024) reported a maximum $NH_4^+$ concentration of approximately 1.79 mg/L in polluted lakes from northern Romania. The elevated ammonium levels observed in Herastrau Lake may reflect the strong anthropogenic pressure characteristic of its urban catchment.

The concurrent occurrence of persistently high ammonium concentrations and pronounced dissolved oxygen depletion in 2025 may indicate increased eutrophication and organic/nitrogen loading pressure. Global lake datasets identify $NH_4^+$, $NO_3^-/NO_2^-$, DO, turbidity, TSS, and EC as key indicators for characterizing lake ecological condition, with elevated $NH_4^+$ often associated with anthropogenic pollution and adverse effects on aquatic organisms (Naderian et al., 2024).

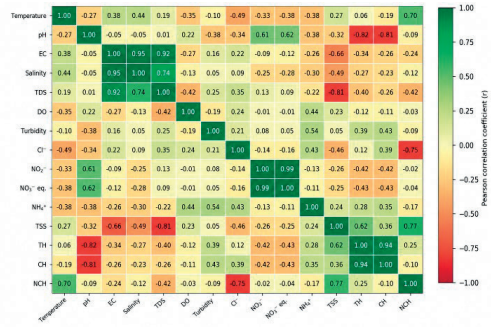
Overall, the results suggest two different physicochemical conditions between the monitoring campaigns. The 2024 campaign was characterized by moderately mineralized, slightly alkaline and relatively well-oxygenated water, despite consistently high $NH_4^+$ concentrations. In 2025, the lake exhibited

increased EC and salinity, substantially reduced CH and TH, persistently elevated $NH_4^+$ and, most importantly, severe oxygen depletion throughout the sampling network. These multidimensional changes are characteristic of urban lake systems, where hydrological conditions, seasonal processes, and anthropogenic inputs interact to control water quality.

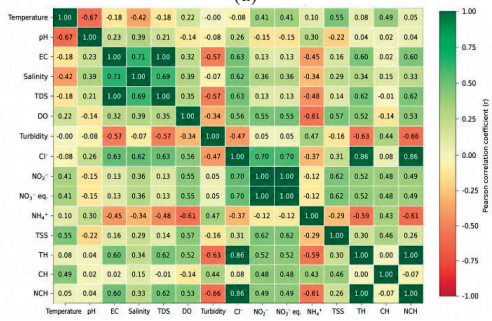
### *Pearson Correlation Analysis*

In 2024, the Pearson correlation analysis identified several clear relationships among the physicochemical parameters (Figure 2a). EC was strongly positively correlated with salinity (r = 0.95) and TDS (r = 0.92), while salinity was also positively related to TDS (r = 0.74), indicating these parameters reflect a common variation in the lake's dissolved ionic content. TH and CH showed a strong positive correlation (r = 0.94). Conversely, pH was strongly negatively correlated with TH (r = -0.82) and CH (r = -0.81). TSS showed a strong negative correlation with TDS (r = -0.81) and a moderate negative correlation with EC (r = -0.66), while it was positively correlated with NCH (r = 0.77). $Cl^-$ displayed a marked negative correlation with NCH (r = -0.75). $NH_4^+$ showed moderate positive relationships with turbidity (r = 0.54), DO (r = 0.44), and $Cl^-$ (r = 0.43), indicating its spatial distribution is linked to multiple physicochemical characteristics rather than a single factor. The correlation pattern changed markedly in 2025 (Figure 2b). EC and TDS were nearly perfectly correlated (r ≈ 1.00), and both remained positively associated with salinity, confirming their close dependence on dissolved mineral content. $Cl^-$ showed strong positive correlations with both TH and NCH (r = 0.86) and was also positively related to $NO_2^-$ and $NO_3^-$ concentrations (r = 0.70).

In contrast, turbidity was negatively correlated with NCH (r = -0.66), TH (r = -0.63), EC (r = -0.57), and TDS (r = -0.57), indicating that areas with greater optical effects from suspended particles did not necessarily coincide with those with the highest dissolved ionic content. A particularly relevant relationship was observed between DO and $NH_4^+$ (r = -0.61). Higher $NH_4^+$ concentrations were therefore associated with lower DO values across the sampling sites, consistent with increased oxygen demand from organic-matter degradation and nitrogen transformation processes. $NH_4^+$ was also negatively correlated with TH (r = -0.59) and NCH (r = -0.61).




(a)




(b)

Figure 2. Pearson correlation matrix of physicochemical water-quality parameters in Herastrau Lake in (a) 2024 and (b) 2025 monitoring campaigns

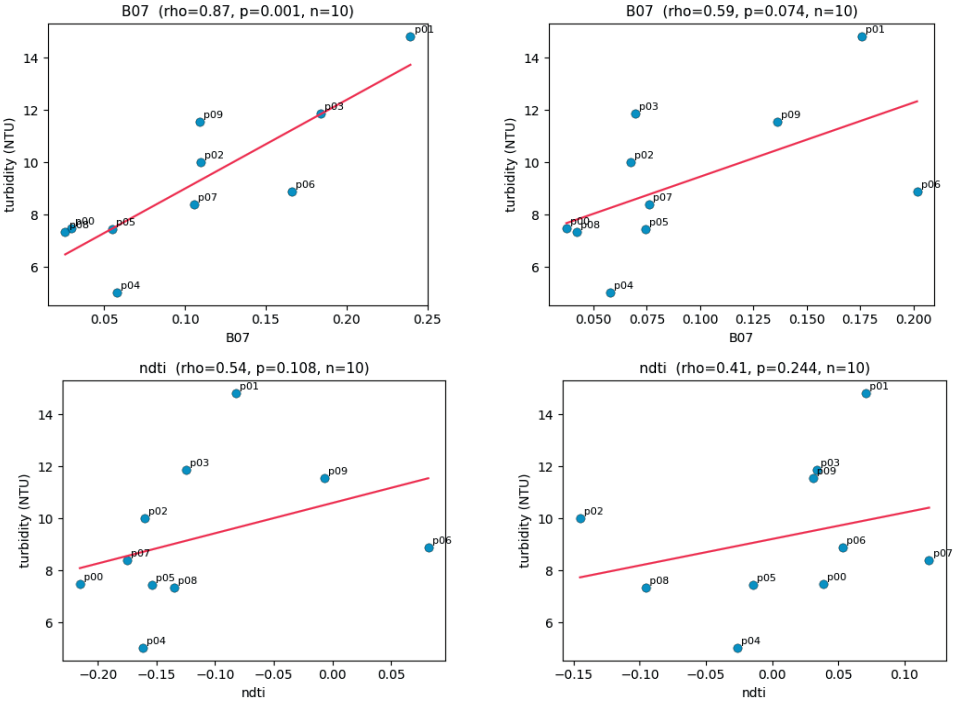
The different correlation structures observed in the two campaigns reveal a clear temporal shift in the relationships among the measured water-quality variables. In 2024, the strongest correlations were mainly linked to mineralization, hardness, and suspended solids. By 2025, the correlations involving DO, $NH_4^+$, $Cl^-$, and turbidity became more prominent. These variations suggest seasonal changes in the processes governing water chemistry, potentially reflecting differences in hydrological conditions, external inputs, biological activity, and nutrient cycling within Herastrau Lake.

### *Satellite-Based Turbidity Assessment and Calibration*

Conventional in-situ monitoring, although accurate, is labor-intensive, costly, and inherently limited in spatial and temporal coverage, typically yielding few point samples

collected infrequently. Satellite remote sensing offers a complementary approach: Sentinel-2 provides spatially continuous, frequently revisited (≈5-day) and openly available imagery that can capture the entire water surface synoptically. However, satellite-derived water-quality estimates are reliable only after calibration and validation against ground-truth measurements. In this study, the optically active parameter turbidity was estimated from Sentinel-2 reflectance and validated against in-situ data; once validated in this way, the calibrated satellite proxies can be applied operationally to map turbidity (and, by extension, chlorophyll a) across the whole lake and to track its dynamics over time, at low cost and with a spatial and temporal resolution that point sampling alone cannot achieve. This integration of field measurements with validated remote sensing is the core methodological rationale of the present work.

As shown in Figure 3, although NDTI is specifically designed as a turbidity index, it did not perform as expected: it showed only weak, non-significant correlations with in-situ turbidity in both campaigns.




***a) October 2024 campaign*** ***b) March 2025 campaign***

Figure 3. Spatial relationship between in-situ turbidity and two Sentinel-2 turbidity predictors, band B07 (783 nm, top row) and the Normalized Difference Turbidity Index (NDTI, bottom row), across the ten sampling points, for (a) the October 2024 campaign and (b) the March 2025 campaign. The red line shows the linear fit; Spearman correlation coefficients (ρ) and p-values are reported in each panel. B07 was the strongest predictor in both campaigns, with a significant correlation in October (ρ = 0.87, *p* = 0.001) but a weaker, non-significant one in March (ρ = 0.59, *p* = 0.074); NDTI performed poorly in both periods

This underperformance likely reflects the strong influence of algal/chlorophyll signals in the eutrophic lake, which interfere with the red–green contrast on which NDTI relies.

The contrast between the two predictors is itself informative about the optical regime of the lake. NDTI relies on the red-versus-green contrast and was developed for small, mineral-dominated ponds (Lacaux et al., 2007), where that contrast tracks inorganic suspended sediment. In a chlorophyll-rich system the same contrast is confounded, since phytoplankton absorbs strongly in the red (~665 nm) while pigment absorption and cell scattering also

modify the green signal, so both bands respond to algal biomass rather than to sediment load. That the turbidity information was carried instead by the red-edge region, beyond the main pigment absorption features, is consistent with the hypereutrophic character indicated by the physicochemical data, and points to red-edge-based indices such as NDCI (Mishra & Mishra, 2012) as the appropriate route for extending this approach to chlorophyll-a retrieval in Herastrau Lake.

Once band B07 had been selected as the turbidity predictor, three calibration models were fitted to relate B07 surface reflectance to the in-situ turbidity measurements: (i) a linear model (T = a·B07 + b), the simplest empirical formulation; (ii) a power model (T = a·B07^b), which can better accommodate the non-linear, saturating behavior often observed in turbidity–reflectance relationships; and (iii) the semi-analytical Nechad model (T = A·ρ/(1 - ρ/C)) (Nechad et al., 2010), a physically based formulation widely used for turbidity retrieval from water-leaving reflectance. The performance of each model was assessed using the coefficient of determination ($R^2$) and the root-mean-square error (RMSE), as shown in Figures 4 and 5.

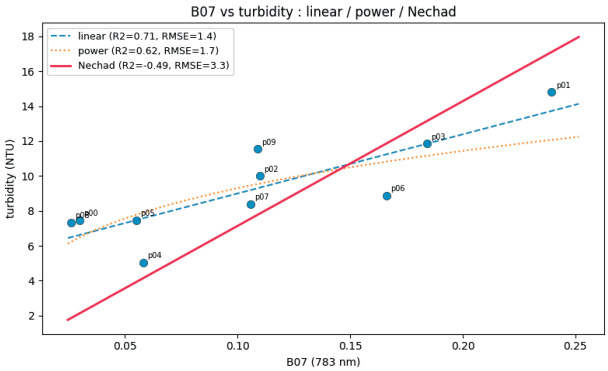



Figure 4. Calibration of the Sentinel-2 turbidity proxy for the October 2024 campaign: in-situ turbidity (NTU) at the ten sampling points versus Sentinel-2 band B07 (783 nm) surface reflectance. Three regression models are shown: linear ($R^2$ = 0.71, RMSE = 1.4 NTU), power ($R^2$ = 0.62, RMSE = 1.7 NTU), and the semi-analytical Nechad model ($R^2$ = −0.49, RMSE = 3.3 NTU). The linear model provided the best fit and was retained; the Nechad model failed to reproduce the lake's high background turbidity

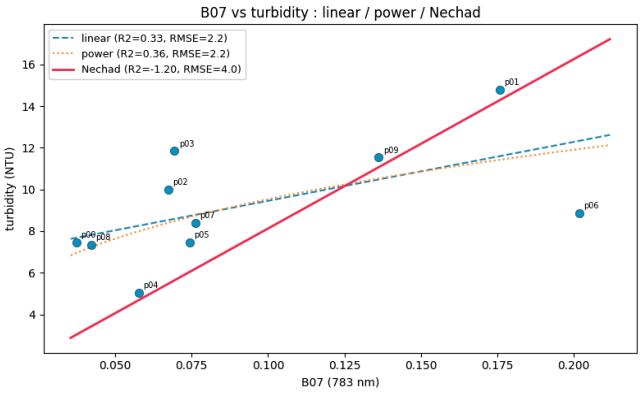



Figure 5. Calibration of the Sentinel-2 turbidity proxy for the March 2025 (early-spring) campaign: in-situ turbidity (NTU) at the ten sampling points versus Sentinel-2 band B07 (783 nm) surface reflectance, with linear ($R^2$ = 0.33, RMSE = 2.2 NTU), power ($R^2$ = 0.36, RMSE = 2.2 NTU) and semi-analytical Nechad ($R^2$ = −1.20, RMSE = 4.0 NTU) regression fits. In contrast to the October campaign ($R^2$ = 0.71), the B07–turbidity relationship was markedly weaker and statistically non-significant (Spearman ρ = 0.59, p = 0.074), most likely owing to the larger time lag between the satellite acquisitions and the sampling date

In contrast to the autumn campaign, the B07–turbidity relationship for March 2025 was considerably weaker and non-significant (Figure 5). The most likely cause is the match-up window: in October, a cloud-free scene coincided with the sampling day, whereas the March composite was built from scenes acquired 6 and 9 days from sampling, over which surface turbidity in this shallow, wind-exposed lake can change appreciably through resuspension and settling. A shift in particle composition may also contribute, as the early-spring increase in the algal fraction alters the reflectance-to-NTU relationship. The March retrieval is therefore regarded as exploratory.

## CONCLUSIONS

The water-quality parameters measured in this study, including elevated ammonium concentrations, markedly reduced dissolved oxygen, and persistent turbidity above 5 NTU, are consistent with sustained eutrophication pressure. Regular monitoring is thus essential to detect degradation early, understand its spatial and temporal dynamics, and inform targeted management and pollution-control measures.

A key limitation of this study stems from the use of Sentinel-2 Level-2A (Sen2Cor) reflectance, whose atmospheric correction is optimized for land surfaces rather than water. Over water bodies, this often results in weak or even negative reflectances and leaves residual sun-glint uncorrected, limiting the absolute accuracy of the retrieved values. The turbidity estimates derived here should therefore be regarded as semi-quantitative, and negative reflectances over water should be screened and treated with caution. For more rigorous, quantitative turbidity retrieval, dedicated aquatic atmospheric-correction processors such as ACOLITE, C2RCC, or POLYMER would be required, and their application represents a promising direction for future work.

## ACKNOWLEDGEMENTS

This work was supported by a grant of the Ministry of Education and Research, CCCDI-UEFISCDI, project number PN-IV-P6-6.1-CoEx-2024-0120, within PNCDI IV.

Mihaela Dragoi Cudalbeanu and Daniela Faur express their gratitude to the Romanian-American Foundation and the Romanian Fulbright Commission for the opportunity to participate in the Fulbright-RAF Scholar Award.

## REFERENCES

Cheval, S., Popa, A. M., Şandric, I., & Iojă, I. C. (2020). Exploratory analysis of cooling effect of urban lakes on land surface temperature in Bucharest (Romania) using Landsat imagery. Urban Climate, 34, 100696. https://doi.org/10.1016/J.UCLIM.2020.100696.

Dippong, T., & Resz, M.-A. (2024). Heavy metal contamination assessment and potential human health risk of water quality of lakes situated in the protected area of Tisa, Romania. Heliyon, 10(7), e28860. doi:10.1016/j.heliyon.2024.e28860.

Dippong, T., & Resz, M.-A. (2025). Water and sediments pollution from Iza River (Romania): Influence on water quality and metals content. Process Safety and Environmental Protection, 200, 107335. doi:10.1016/j.psep.2025.107335.

Dippong, T., Senila, M., Cadar, O., & Resz, M.-A. (2024). Assessment of the heavy metal pollution degree and potential health risk implications in lakes and fish from northern Romania. Journal of Environmental Chemical Engineering, 12(2), 112217. doi:10.1016/j.jece.2024.112217.

Foley, E., & Steinman, A. D. (2023). Urban lake water quality responses to elevated road salt concentrations. Science of the Total Environment, 905, 167139. doi:10.1016/j.scitotenv.2023.167139.

Hoggang, G.C.B., & Reyes, A. T. (2023). Physico-chemical and biological water quality analysis of Ambuwaya Lake in Kiangan, Ifugao, Philippines. *AACL Bioflux*, 16(6).

Lacaux, J. P., Tourre, Y. M., Vignolles, C., Ndione, J. A., & Lafaye, M. (2007). Classification of ponds from high-spatial resolution remote sensing: Application to Rift Valley Fever epidemics in Senegal. Remote Sensing of Environment, 106(1), 66–74. https://doi.org/10.1016/j.rse.2006.07.012.

Liu, D., Zhang, C., Yan, N., Yan, Y., & Duan, H. (2025). Eutrophication exacerbated organic pollution in lakes across China during the 1980s–2010s. Water Research, 268. https://doi.org/10.1016/j.watres.2024.122782.

McFeeters, S. K. (1996). The use of the Normalized Difference Water Index (NDWI) in the delineation of open water features. International Journal of Remote Sensing, 17(7), 1425–1432. https://doi.org/10.1080/01431169608948714

Mishra, S., & Mishra, D. R. (2012). Normalized difference chlorophyll index: A novel model for remote estimation of chlorophyll-a concentration in turbid productive waters. Remote Sensing of Environment, 117, 394-406. https://doi.org/10.1016/j.rse.2011.10.016.

Morelato, R. R., Rodrigues-Silva, F., Viana, G. C. C., & Amorim, C. C. (2026). Advancing eutrophication mitigation through nature-based and hybrid solutions: A systematic review. Journal of Environmental Chemical Engineering, 14(1), 121046. https://doi.org/10.1016/j.jece.2026.121046.

Naderian, D., Noori, R., Heggy, E., Bateni, S. M., Bhattarai, R., Nohegar, A., & Sharma, S. (2024). A water quality database for global lakes. Resources, Conservation and Recycling, 202, 107401. doi:10.1016/j.resconrec.2023.107401.

Nechad, B., Ruddick, K. G., & Park, Y. (2010). Calibration and validation of a generic multisensor algorithm for mapping of total suspended matter in turbid waters. Remote Sensing of Environment, 114(4), 854–866. https://doi.org/10.1016/j.rse.2009.11.022.

Nkhata, A. D., Mengistou, S., & Gondwe, L. S. M. (2026). Linking water quality with plankton dynamics: multivariate analyses of environmental drivers in Lake Koka. Journal of Freshwater Ecology, 41(1). https://doi.org/10.1080/02705060.2026.2626169.

Osman, K. A., Elgendy, S. M., & Ibrahim, H. Z. (2025). Physicochemical and spatial distributions of trace elements and organochlorine compounds in Lake Idku water, Egypt. Water, Air, & Soil Pollution, 236, 127. https://doi.org/10.1007/s11270-025-07757-x.

Oustani, M., Mehda, S., Rekbi, F. M. L., Guezie, R., Youcef, F., Halilat, M. T., Debba, S., & Chenchouni, H. (2026). Physicochemical, biochemical and bacteriological indicators of water quality of Temacine Lake in the Sahara Desert. Environmental Nanotechnology, Monitoring and Management, 25. https://doi.org/10.1016/j.enmm.2026.101143.

Sandu, M. A., Vîrsta, A., Vasile Scăeţeanu, G., Iliescu, A.-I., Ivan, I., Nicolae, C. G., Stoian, M., & Madjar, R. M. (2023). Water quality monitoring of Moara Domnească Pond, Ilfov County, using UAV-based RGB imaging. AgroLife Scientific Journal, 12(1), 191–201.

Zhang, F., Shi, X., Zhao, S., Arvola, L., Sun, B., Hao, R., Yang, Z., Wang, S., Zhao, Y., & Zhang, J. (2025). Dissolved oxygen dynamics in a shallow eutrophic lake: Quantify critical eco-environmental effects. Ecological Indicators, 179, 114190. doi:10.1016/j.ecolind.2025.114190.

Zhang, K., Li, M., Qu, S., Zhao, Y., Duan, L., Yang, X., Li, D., Liao, Z., & Yu, R. (2025). Spatio-seasonal variability of source contributions to water quality in a large irrigation drainage lake basin based on the entropy weighted quality index, positive matrix factorization, and isotopic tracers. Environmental Pollution, 382, 126670. https://doi.org/10.1016/J.ENVPOL.2025.126670.

Zhou, J., Mogollón, J. M., Van Bodegom, P. M., Beusen, A. H., & Scherer, L. (2024). Global regionalized characterization factors for phosphorus and nitrogen impacts on freshwater fish biodiversity. Science of The Total Environment, 912, 169108. https://doi.org/10.1016/j.scitotenv.2023.169108.

Zou, T., Yang, K., Pan, M., Zhu, Y., Zhang, Y., & Su, D. (2024). Analysis of the temporal and spatial evolution of turbidity in Tonle Sap Lake and its influencing factors. Science of the Total Environment, 943, 173618. doi:10.1016/j.scitotenv.2024.173618.

*International Organization for Standardization (2016). ISO 5667-4:2016 Water quality - Sampling - Part 4: Guidance on sampling from lakes, natural and man-made. International Organization for Standardization.

**Ministry of Environment and Water Management (2006). Order No. 161/2006 approving the normative regarding the classification of surface water quality for establishing the ecological status of water bodies. Official Gazette of Romania, No. 511/13 June 2006.

Scientific Papers. Series E. Land Reclamation, Earth Observation & Surveying, Environmental Engineering. Vol. XV, 2026
Print ISSN 2285-6064, CD-ROM ISSN 2285-6072, Online ISSN 2393-5138, ISSN-L 2285-6064

# STATE-OF-THE-ART APPLICATIONS FOR THE REHABILITATION OF IRRIGATION MAIN-CANAL CROSSINGS

**Elena-Maria VORNICESCU[1], Sorin Mihai CIMPEANU[1], Nicolae MARACINE[1], Marco MORARU[2]**

[1]University of Agronomic Sciences and Veterinary Medicine of Bucharest,
59 Mărăști Blvd, 011464, District 1, Bucharest, Romania
[2]Blueco Waste SRL, N. Bălcescu, Bacău, Romania

Corresponding author email: maria.vornicescu@doctorat.usamv.ro

***Abstract***

*The main irrigation infrastructure in Romania includes numerous underpasses of the main canals built of prestressed concrete or large-diameter metal pipes. After decades of operation, these structures show advanced degradation, such as cracks, corrosion, and leaks, leading to water losses and reduced hydraulic efficiency. Their location under roads and other types of infrastructure makes traditional replacement and dismantling of existing pipes difficult, highlighting the need for trenchless rehabilitation technologies. This article analyzes the applicability of CIPP (Cured-In-Place Pipe) technology for the rehabilitation of culverts in irrigation systems, based on experience in the maintenance of urban water supply and sewerage networks. It presents the steps leading up to the intervention, including inspection and structural assessment, as well as the principles of liner manufacturing, highlighting the specific limitations of large diameter pipes. It also addresses the general methodology for designing liner thickness in accordance with international standards and technical criteria relevant to water conveyance systems. The installation process is analysed in terms of operational requirements and equipment, highlighting the advantages of no-dig technologies in restricted-access areas. The results demonstrate the potential of CIPP as a sustainable and hydraulically efficient solution for irrigation infrastructure modernisation in Romania.*

***Key words****: Cured-In-Place Pipe (CIPP), hydraulic efficiency, irrigation canal crossings, no-dig rehabilitation, water loss reduction.*

## INTRODUCTION

Irrigated agriculture is essential for food security and stable agricultural production in the face of climate variability. Water use efficiency plays an increasingly important role in maintaining agricultural production in the context of rising temperatures, changing precipitation patterns, and intensifying extreme weather events, which continuously affect the availability of water resources for irrigation (Dai et al., 2018; Vogel et al., 2019; Mirzabaev et al., 2023; Farah et al., 2025).

In Romania, the main irrigation infrastructure includes an extensive network of main canals and underpasses made of concrete pipes or large-diameter metal pipes. After decades of use, these structures show significant deterioration, manifested by cracks, corrosion, and leaks, leading to significant water losses and reduced hydraulic efficiency of irrigation systems (Grumeza & Kepleș et al., 2005). These losses negatively affect water distribution to agricultural crops, reducing production potential during critical periods such as prolonged droughts (Totolea, 2024).

Traditional interventions for the rehabilitation of underground pipes involve significant excavations, which are disruptive from an economic and logistical point of view, especially in areas where crossings are located under roads or sensitive infrastructure elements. In this context, no-dig rehabilitation methods offer clear advantages by reducing the environmental impact and costs associated with open-cut works (Mocean et al., 2014).

One of the most widely used trenchless technologies is Cured-In-Place Pipe (CIPP), which consists of inserting and curing a reactive liner inside the existing pipe, creating a new pipe section without extensive excavation (Ji et al., 2020). This method is widely adopted in water and sewer networks due to its efficiency in rehabilitating damaged pipes and its ability to provide a continuous structural solution (Salem, 2008). However, the literature highlights

limitations and high design requirements for the mechanical performance of CIPP systems, underscoring the need for detailed assessments prior to application (Yang et al., 2021; Hu et al., 2023). This study investigates the structural and hydraulic feasibility of a large-diameter UV-cured CIPP installation applied to a severely deteriorated deep-buried gravity collector. Although based on an urban case study, the structural conditions - significant burial depth, high external loads, and advanced pipe degradation - are comparable to those encountered in irrigation canal crossings. By quantifying deformation limits, assessing the structural independence of the liner, and evaluating hydraulic performance before and after rehabilitation, the study provides a technical basis for assessing the transferability of CIPP technology to irrigation infrastructure.

## MATERIALS AND METHODS

### Case Study Description

The study is based on the rehabilitation of a large-diameter buried collector located in Botoșani, Romania (Figure 1). The investigated section had a total length of 125 meters and consisted of two geometrically distinct segments: an upstream ovoid reinforced concrete pipe 1200 mm constructed in the early twentieth century, and a downstream circular DN 800 mm section made of steel installed during a later intervention.

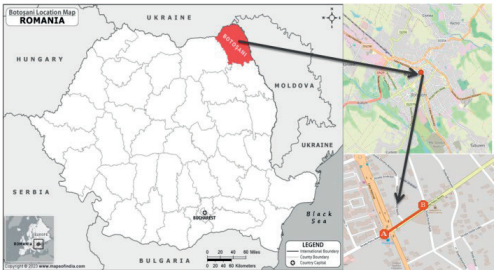



Figure 1. Location of the study- Romania, Botosani, Municipiul Botosani

The pipeline was located at a burial depth ranging between 5 and 6 m beneath a major traffic artery. CCTV inspection revealed severe structural degradation, including longitudinal cracking, wall perforations, loss of invert (radier) sections, joint misalignment, exfiltration, and evidence of soil erosion around the pipe. Sediment deposits exceeded 70% of the cross-sectional area prior to cleaning (Figure 2). Although the case study originates from an urban gravity collector, the structural conditions—large diameter, high soil cover, and advanced host pipe deterioration—are representative of buried irrigation canal crossings subjected to similar external loads.



Figure 2. Post-execution robotic CCTV inspection documentation

### Rehabilitation System Description

Rehabilitation was performed using a UV-cured glass-fiber-reinforced polymer (GRP) CIPP liner (Figure 3). The liner thickness was:

- 10.5 mm for the ovoid section,
- 8.4 mm for the circular DN 800 section.

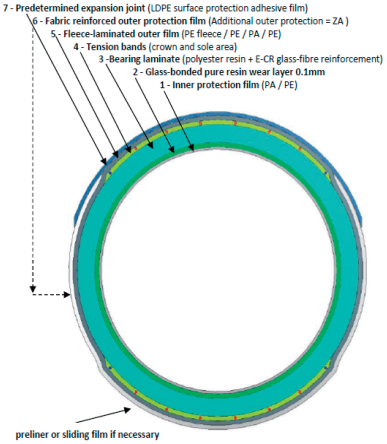



Figure 3. Cross-sectional geometry and liner configuration (Source: Brandenburger Liner GmbH & Co. KG, 2024)

The liner was designed to function as a fully structural liner, meaning it was assumed to carry

all external loads independently of the residual structural capacity of the host pipe.

**Structural Assessment Methodology**

The structural evaluation considered the following load components:

*Soil load:*

$$\sigma = \gamma \cdot H \quad (1)$$

γ = unit weight of soil (kN/m³)
H = burial depth (m)

***Critical Buckling Resistance:***

The critical external pressure for a circular liner embedded in soil was estimated using:

$$P_{cr} = \frac{2E}{(1-\nu^2)} \left(\frac{t}{D}\right)^3 \quad (2)$$

where:
E = short-term elastic modulus of GRP (MPa)
ν = Poisson's ratio
t = liner thickness (mm)
D = mean liner diameter (mm).

To account for long-term creep behavior:

$$E_{long} = \frac{E\ short}{\Phi} \quad (3)$$

where φ represents the creep reduction factor.

***Deformation Verification***:

The relative diametral deformation was calculated as:

$$\delta = \frac{\Delta D}{D} \cdot 100 \quad (4)$$

where ΔD represents the total diametral variation under load.

The calculated elastic deformation was compared against an admissible limit of 3%, consistent with standard trenchless rehabilitation practice.

The structural analysis of the CIPP liner was performed in accordance with DWA-A 143-2:2015-07, the technical reference used in addition to SR EN 13566-4.

**Hydraulic Performance Evaluation**

To assess the hydraulic implications of rehabilitation, discharge capacity was estimated using Manning's equation:

$$Q = A \cdot V = \frac{A}{n} \cdot R^{2/3}{}_h \cdot S^{1/2} \quad (5)$$

where:
V= average water velocity (m/s)
Q= Volumetric flow rate ($m^3/s$)
n = Manning roughness coefficient (Aged reinforced concrete: n = 0.016; GRP CIPP liner: n = 0.010)
A = flow area ($m^2$)
$R_h$ = hydraulic radius (Rh =A/P)
S = hydraulic slope

Although liner installation slightly reduces internal diameter, the decrease in roughness can compensate for this geometric reduction.

**Transferability Assessment Framework**

In order to assess the applicability of the proposed approach to irrigation canal crossings, a comparative analysis framework was developed. It takes into account both the relevant differences and similarities between the two types of infrastructure, including external loading conditions (including potential traffic loads), internal hydraulic regime (gravity flow versus low-pressure operation), and operational model (continuous service versus seasonal operation).

This framework supports qualitative assessment of conditions under which structural and hydraulic findings can be extrapolated to irrigation systems.

## RESULTS AND DISCUSSIONS

**Structural Performance**

The structural verification results for the UV-GRP CIPP liner installed in the ovoid (800 × 1200 mm) and circular (DN 800 mm) sections are summarized in Table 1.

The analysis considered a burial depth of approximately 5-6 m, with soil loads calculated using average unit weight values typical for compacted urban soils. The host pipe was conservatively assumed to provide negligible structural contribution, corresponding to a fully structural liner configuration.

Table 1. Results of static calculation

**DEFORMATION PROOF LINER GEBRAUCHSLAST**

| *Nr.crt.* | *Parameter* | *Symbol* | *Value* | *Unit* |
|---|---|---|---|---|
| 1 | Clear width at springline height | $b_s$ | 800 | mm |
| 2 | Clear height at crown–invert | $h_s$ | 1200 | mm |
| 3 | Relevant diameter (percentage deformation) | $d_v$ | 1000 | mm |
| 4 | Annular gap absolute ( const. Value) | $x_s$ | 1.97 | mm |
| 5 | Local imperfection (absolute) | $w_s$ | 9.56 | mm |
| 6 | Global imperfection (absolute, one side) | wGR,v | 0 | mm |
| 7 | Elastic deformation (absolute, horizontal – E1) | $w_{esh,E1}$ | 10.41 | mm |
| 8 | Elastic deformation (absolute, horizontal – E2) | $w_{esh,E2}$ | -16.82 | mm |
| 9 | Total elastic deformation (horizontal) | $w_{esh}$ | 27.23 | mm |
| 10 | Relative elastic deformation | $\delta_{v,el}$ | 2.72 | % |
| 11 | Allowable elastic deformation | $\delta_{v,el,adm}$ | 3 | % |
| 12 | Total diameter deviation | w | 36.79 | mm |
| 13 | Relative total deformation | $\delta_v$ | 3.68 | % |
| 14 | Reference value for total deformation | $\delta_{v,A}$ | 10 | % |
| 15 | Elastic deformation (absolute, vertical – E1) | $w_{esv,E1}$ | 1.57 | mm |
| 16 | Elastic deformation (absolute, vertical – E2) | $w_{esv,E2}$ | 4.75 | mm |

The calculated relative elastic deformation for the ovoid section was 2.72%, remaining below the 3% admissible limit specified in SR EN 13566-4 for fully structural liners. When geometric imperfections were included, the total

relative deformation reached 3.68%, still significantly below the 10% reference threshold defined by DWA-A 143-2 (2015) for structural stability assessment in trenchless rehabilitation practice. After incorporating long-term creep effects through elastic modulus reduction in accordance with SR EN 13566-4 provisions, the verification remained within acceptable limits, confirming the adequacy of the selected liner thickness (10.5 mm).

For the circular DN 800 section (8.4 mm thickness), deformation values were lower due to the inherent structural efficiency of the circular geometry. Overall, under the assumed load conditions, the liner behaves as an independent load-bearing structure capable of compensating for severe host pipe deterioration, including partial invert loss.

**Hydraulic Performance**

The hydraulic implications of rehabilitation were assessed using Manning's equation under identical slope conditions before and after lining. Assuming representative roughness coefficients:

- Aged reinforced concrete: n = 0.016
- GRP CIPP liner: n = 0.010

Table 2 presents the hydraulic parameters calculated before and after rehabilitation. Although the installation of the lining resulted in a minimal reduction (1 cm thickness around the circumference) in the cross-sectional area for the ovoid section (from 0.754 to 0.721 m²), the significant decrease in the Manning roughness coefficient led to a substantial increase in discharge capacity, from 0.626 m³/s to 0.768 m³/s (+22.68%).

Table 2. Hydraulic parameters before and after CIPP rehabilitation under gravity flow conditions

| Nr. crt | Parameters | Section | |
|---|---|---|---|
| | | Ovoid 1200 mm | Circular DN 800 |
| **Concrete/steel** | | | |
| 1 | Area A (m²) | 0.754 | 0.502 |
| 2 | Wetted Perimeter (m) | 6.34 | 3.87 |
| 3 | Manning n | 0.016 | 0.013 |
| 4 | Hydraulic Radius Rh (m) | 0.142 | 0.2 |
| 5 | Flow rate Q (m³/s) | 0.626 | 0.641 |
| **CIPP** | | | |
| 1 | Area A (m²) | 0.721 | 0.783 |
| 2 | Wetted Perimeter (m) | 6.21 | 3.14 |
| 3 | Manning n | 0.01 | 0.01 |
| 4 | Hydraulic Radius Rh (m) | 0.116 | 0.196 |
| 5 | Flow rate Q (m³/s) | 0.768 | 0.726 |

A similar improvement was observed for the circular DN 800 conduit, where discharge increased by 13.26% following roughness reduction. Overall system capacity increased by 15.89%, as illustrated in Figure 4.

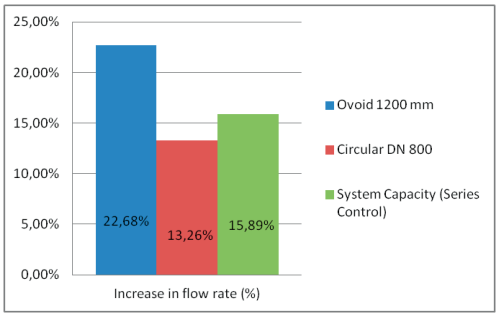



Figure 4. Percentage increase in discharge capacity after rehabilitation

These results indicate that, under uniform gravity flow conditions, the reduction in internal roughness has a stronger influence on conveyance capacity than moderate variations in hydraulic diameter. The smoother internal surface decreases frictional losses, producing a net hydraulic gain despite minor geometric contraction.

It should be noted that the analysis assumes steady uniform flow and does not account for transient effects or sediment transport processes, which may influence field performance.

**Structural Implications for Irrigation Crossings**

The structural results demonstrate that a UV-GRP liner with thickness between 8.4-10.5 mm can sustain external soil loads corresponding to burial depths of up to 6 m without exceeding deformation limits.

Compared with published experimental and numerical studies on CIPP-rehabilitated concrete pipes, the deformation values observed in this study fall within the lower range of reported results for fully deteriorated host pipes. This supports the assumption that, under similar soil cover conditions, the liner can provide sufficient structural reliability independent of the host pipe.

However, culverts crossing intubated irrigation channels in areas where they pass under roads and valleys (siphons) may have different operating and loading conditions compared to

gravity sewer collectors, particularly due to potential internal pressures in siphon-type culverts and seasonal filling and emptying cycles.

**Hydraulic Considerations in Irrigation Systems**

Post-rehabilitation hydraulic performance is primarily governed by internal surface smoothness (Figure 5). In deteriorated concrete conduits, increased roughness and sediment accumulation significantly reduce flow capacity. Under gravity-driven conditions, lowering Manning's coefficient from 0.016 to 0.010 can produce measurable reductions in energy losses and corresponding gains in conveyance efficiency.

In large-scale irrigation systems, even moderate hydraulic improvements may enhance downstream reliability and reduce pumping requirements, implicitly leading to lower energy consumption for pump operation. However, in pressurized irrigation systems, head losses due to high roughness cause friction that must be evaluated under maximum flow conditions using the Darcy-Weisbach equation.

Consequently, the hydraulic advantages demonstrated in this study are directly applicable mainly to the crossings of piped irrigation channels in gravitational operation.



Figure 5. Condition of DN 800 mm pipeline before and after lining

**Transferability Assessment**

Based on the comparative framework developed in the methodology, the transferability of UV-CIPP rehabilitation from sewer systems to culvert crossings can be considered technically feasible under conditions characterized by burial depths comparable to or less than 6 m, gravity or low-pressure flow regimes, the absence of significant transient loads, and the performance of a complete structural verification including long-term creep effects.

However, applicability becomes conditional in situations involving sustained internal pressures or transient stresses exceeding the typical regime of gravity-fed collectors, in which case an additional structural analysis is required that includes the combined effects of internal pressure and external loads.

This article is based on a single case study with a large diameter, operated in a gravitational regime, and the effects of internal pressures specific to irrigation siphons have not been investigated, but by applying the similarity method, this rehabilitation method can also be successfully applied to similar objectives in irrigation facilities. Consequently, although structural and hydraulic feasibility under significant external loads has been demonstrated, further research including pressure regimes and long-term monitoring is needed to consolidate the generalization of the results to a wider range of irrigation infrastructure configurations.

## CONCLUSIONS

This study demonstrates the structural and hydraulic applicability of UV-cured CIPP technology to large-diameter buried pipes, representative of culvert crossings for irrigation. Structural verification at burial depths of 5–6 m showed that the UV-GRP liner, designed as a fully structural system, maintained relative deformation below the 3% admissible limit, even when long-term modulus reduction was considered. The liner therefore provides sufficient resistance to external soil loads without reliance on host pipe integrity.

Hydraulically, the reduction in internal roughness generated an 8–15% increase in conveyance capacity despite minor diameter reduction. Under gravity-driven conditions, this corresponds to lower friction losses and improved flow efficiency.

The results indicate that UV-CIPP rehabilitation can be technically transferred to gravity-operated or low-pressure irrigation crossings, provided that burial conditions and internal pressure limits are verified. For pressurized or transient regimes, additional structural assessment is required.

Overall, trenchless UV-CIPP represents a structurally reliable and hydraulically advantageous alternative to open-cut replacement in irrigation infrastructure modernization.

## ACKNOWLEDGEMENTS

The authors would like to acknowledge the support provided by S.C. Blueco Waste S.R.L. and Brandenburger Anwendertage for making available the technical documentation and practical information related to the CIPP rehabilitation works. The authors also thank all specialists involved in the implementation of the case study for their technical support and valuable contributions to this research.

## REFERENCES

Brandenburger Liner GmbH & Co. KG. (2024). Brandenburger Liner BB2.5 – Technical Data Sheet (Version 001, 24 May 2024). BurrowTech. https://burrowtech.co.nz/wpcontent/uploads/2024/07/Brandenburger-Liner-BB2.5.pdf

Dai, A., Zhao, T. & Chen, J. (2018). Climate Change and Drought: a Precipitation and Evaporation Perspective. *Curr Clim Change Rep 4*, 301–312 https://doi.org/10.1007/s40641-018-0101-6

European Committee for Standardization (CEN). (2011). *EN 13566-4:2011. Plastics piping systems for renovation of underground non-pressure drainage and sewerage networks - Part 4: Lining with cured-in-place pipes*. CEN.

Farah, A.A., Mohamed, M.A., & Musse, O.S.H. (2025). The multifaceted impact of climate change on agricultural productivity: a systematic literature review of SCOPUS-indexed studies (2015–2024). *Discov Sustain,* 6, 397, https://doi.org/10.1007/s43621-025-01229-2

German Association for Water, Wastewater and Waste (DWA) (2015). *DWA-A 143-2: Rehabilitation of drainage and sewer systems outside buildings - Part 2: Static calculation for the renovation of drainage and sewer systems using lining and assembly methods*. DWA.

Grumeza, N., & Klepeș, C. (2005). *Amenajările de irigații din România* [Irrigation Systems in Romania], Bucharest, Editura Ceres.

Hu, L., Zhang, B., & Yang, K. (2023). Numerical Study on Mechanical Properties of Corroded Concrete Pipes before and after Cured-in-Place-Pipe Rehabilitation. Sustainability.; 15(11):8586. https://doi.org/10.3390/su15118586

Ji, H.W., Koo, D.D., & Kang, J.-H. (2020). Short- and Long-Term Structural Characterization of Cured-in-Place Pipe Liner with Reinforced Glass Fiber Material. International Journal of Environmental Research and Public Health. 17(6):2073. https://doi.org/10.3390/ijerph17062073

Mirzabaev, A., Bezner Kerr, R., Hasegawa, T., Pradhan, P., Wreford, A., Tirado, C., von der Pahlen, M., & Gurney-Smith, H. (2023). Severe climate change risks to food security and nutrition. *Clim Risk Manag*. 39: 100473. https://doi.org/10.1016/j.crm.2022.100473.

Mocean, F., Achimas, G., Morar, T., & Achimas, S. (2015). Mechanical study on rehabilitation of pipelines by gunite covering. Acta technica napocensis-Series: Applied mathematics, Mechanics, and Engineering, 57(2).

Salem, S. (2008). Use of Trenchless Technologies for a Comprehensive Asset Management of Culverts and Drainage Structures, Project 07-15, Midwest Regional University Transportation Center College of Engineering.

Totolea, I. B. (2024). Cercetări privind viabilitatea tehnico-economică a amenajării de irigaţie pentru plantaţii pomicole în cadrul SC Livada mere de Iteşti, judeţul Bacău [Research on the Techno-Economic Feasibility of an Irrigation Development for Fruit Orchards at SC Livada Mere de Iteşti, Bacău County] (Doctoral dissertation, "Ion Ionescu de la Brad" University of Life Sciences, Iaşi).

Vogel, E., Donat, M.G., Alexander, L.V., Meinshausen, M., Ray, D.K., Karoly, D., Meinshausen, N., & Frieler, K. (2019). The effects of climate extremes on global agricultural yields. *Environ Res Lett.*; 14(5): 054010. https://doi.org/10.1088/1748-9326/ab154b.

Yang, K., Fang, H., Bu, J., Zhang, X., Li, B., Du, X., & Zhang, Z. (2021). Full-scale experimental investigation of the mechanical characteristics of corroded buried concrete pipes after cured-in-place-pipe rehabilitation. Tunnelling and Underground Space Technology, 117, 104153.

Scientific Papers. Series E. Land Reclamation, Earth Observation & Surveying, Environmental Engineering. Vol. XV, 2026
Print ISSN 2285-6064, CD-ROM ISSN 2285-6072, Online ISSN 2393-5138, ISSN-L 2285-6064

# COMPARATIVE ANALYSIS OF ALTIMETRIC VARIATIONS IN THE SLĂNIC PRAHOVA AREA BASED ON LEVELING MEASUREMENTS

**Mihai AVADANEI[1, 2], Tiberiu POPESCU[2], Florina ȚERLE BURESCU[1], Florin SALA[3, 4], Mihai Valentin HERBEI[1, 3]**

[1]University of Petrosani, 20 University Street, 332006, Petroșani, Romania
[2]S.C. Top Geocart S.R.L., 67 Prof. I. Marinescu, 021244, District 2, Bucharest, Romania
[3]University of Life Sciences "King Mihai I" from Timisoara, 119 Calea Aradului, 300645, Timisoara, Romania
[4]Agricultural Research and Development Station Lovrin, 307250, Lovrin, Timis, Romania

Corresponding author email: florin_sala@usvt.ro

***Abstract***

*The levelling measurement campaign carried out in Slănic Prahova, Prahova County, year 2025, aimed to monitor altitude variations in the locality urban area. The measurements were performed with a high-precision Leica LS15 instrument and differential compensation methods, using the national E-TransDatRO system and the EGG97&MN75 geoid model. The route included locations between stations, with double observations, over length of over 2.19 km. The comparison of the two campaigns suggested a minimal evolution of the topographic surface, within the limits of the instrumental tolerances. The results obtained indicated a very good closure of the networks, with insignificant differences, which confirmed the quality of the observation and the general stability of the terrain during the analysed interval. The configuration of the altimetric in profile highlighted areas of maximum in the centre of the route and progressive decreases towards the extremities, consistent with the local relief and the structure of the salt massif.*

***Key words****: altimetric profile, altitude variation, monitoring, subsidence, topographic surface.*

## INTRODUCTION

Monitoring deformations associated with underground mining operations represents a major research direction in the field of engineering geodesy and rock mechanics, having direct implications for geotechnical risk assessment and surface infrastructure protection. The theoretical foundations of the behaviour of rock masses around underground excavations have been developed in classic works on rock mechanics, which highlight stress redistribution and progressive failure mechanisms (Hoek & Brown, 1980; Brady & Brown, 2006).

In the case of rock salt deposits, the mechanical behaviour is dominated by the rheological properties of halite, characterized by time-dependent creep, ductile deformation, and sensitivity to temperature and humidity conditions (Carter & Heard, 1970; Cristescu, 1989). The progressive deformation of the salt causes slow changes in the stress field, which can lead to differential settlements at the surface, even in the absence of sudden rupture phenomena (Bérest & Brouard, 2003). Constitutive models for rock salt have been developed to describe the visco-plastic behaviour of the massif and to allow predictive numerical simulations (Munson & Dawson, 1979). Similar studies have been done in areas with marble exploitation (Sîrbu et al., 2023).

In related research, the integration of numerical modelling with high-precision geodetic monitoring has become standard in the analysis of the stability of mining areas (Jing, 2003). Classical geometric levelling measurements remain the reference method for determining millimetre-scale altimetric variations (Ghilani & Wolf, 2012), while GNSS technologies allow the quantification of three-dimensional displacements and the stabilization of geodetic control networks. (Teunissen & Kleusberg, 1998; Cioflan et al., 2025). GIS facilities have been used for documentation in cadastral studies and territorial planning (Sîrbu et al., 2022; Tereşneu & Tereşneu, 2023).

A major development in deformation monitoring was the introduction of satellite-

based radar interferometry (InSAR), which allows the detection of millimeter-scale displacements over large areas (Massonnet & Feigl, 1998). The Persistent Scatterer InSAR method has significantly improved the accuracy and stability of displacement time series (Ferretti et al., 2001), and applications of this technology in mining areas have demonstrated its ability to identify slow subsidence and regional differential movements (Colesanti & Wasowski, 2006).

In addition, terrestrial laser scanning (TLS) and aerial scanning have allowed the generation of high-resolution digital surface models, useful for volumetric analysis and for detecting subtle morphological changes (Vosselman & Maas, 2010). The integration of data from GNSS, leveling and TLS into a unitary system leads to the development of 4D geospatial models (X, Y, Z, T), capable of describing the temporal evolution of the terrain (Lindenbergh & Pfeifer, 2005; Cioflan et al., 2025).

In parallel with the development of acquisition technologies, multivariate statistical methods have become essential tools in deformation analysis. Principal component analysis (PCA) allows reducing the dimensionality of large data sets and highlighting the dominant variables in the deformation process (Jolliffe, 2002). Cluster analysis techniques are also used to identify groups of landmarks with similar behaviour and to delimit areas with pronounced instability (Kaufman & Rousseeuw, 1990).

The Digital Twin concept, applied to infrastructures and the built environment, represents an advanced stage in predictive monitoring, through the real-time integration of data from multiple sensors and the continuous updating of the digital model of the site (Grieves & Vickers, 2017). This approach allows the transition from reactive to proactive monitoring, based on warning thresholds and forecasting models (Boje et al., 2020).

In the context of salt exploitation in Romania, the geological particularities of the salt regions and the history of large volumes of excavations require the use of integrated monitoring systems and rigorous data analysis methodologies (Săndulescu, 1984).

Correlating geodetic information with geomechanical modeling and hydrogeological parameters is essential for understanding deformation mechanisms and for substantiating technical decisions (Bell, 2007).

This scientific study aimed to analyze altimetric variations in the Slănic Prahova area in a modern research direction, which combined classical precision levelling methods with GNSS technologies and multivariate statistical analysis, in order to evaluate the differential behaviour of the terrain and the geotechnical risk associated with underground salt exploitation.

## MATERIALS AND METHODS

### *General characterization of the study site area*

The Slănic Prahova Salt Mine represents one of the oldest salt mines in Romania, its activity beginning in 1668 by exploiting the mines at "Băile Verzi", later followed by the opening of other mines. Initially, the extraction was carried out by digging large, trapezoidal-shaped chambers. In 1970, the mining process was modernized by introducing the method with small chambers and square pillars, arranged on superimposed horizons, first applied to the “Victoria” mine and, since 1992, to the “Cantacuzino” mine.

The rock salt deposit at Slănic Prahova has a lenticular shape, with a length of approx. 2,700 m, in the North-South direction, a width between 800 and 2300 m, and a maximum thickness of 499 m (Marina, 2023). The main types of rocks that appear within the deposit are: salt, volcanic tuffs, clays, marls and sandstones.

From a geographical point of view, the area falls within the hilly area of the “Curved Carpathians” mountains, with altitudes ranging between 359 m (in the “Slănic” stream valley) and 662.80 m (the “Gorganu” peak).

The relief is influenced by landslide processes, and the main collector of surface waters is the “Slănic” stream, which crosses the area above the deposit in the North–South direction, Figure 1.

The exploitation framework method adapted to the conditions of the deposit within the Cantacuzino mine, belonging to the Salina Slănic Prahova, is the "method with small rooms and abandoned square pillars, in the technological version with vaulted ceiling".

This technical solution was substantiated by the work entitled "Framework project of the rock

salt exploitation method with small rooms and abandoned (square) pillars, with vaulted ceilings", developed in 2002 by SC MINESA ICPM SA (Chipeșiu, 2015; Oprina, 2015).

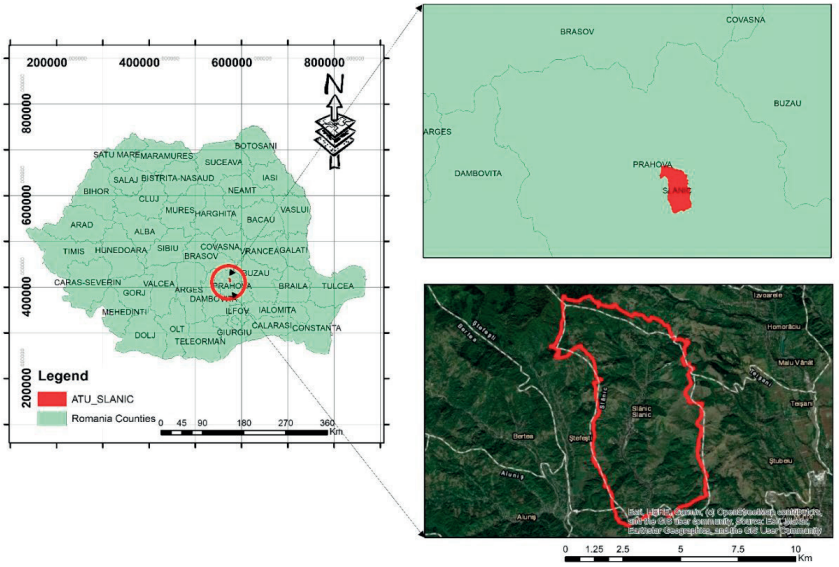



Figure 1. Map of the study area, Slanic ATU, Prahova County, Romania

***Presentation of the study methodology***

An advanced structural monitoring system has been implemented to study vertical and horizontal movements in the Slănic Prahova locality. The objective is to provide high-certainty data for risk assessment and to ensure the stability of critical infrastructure.

Ensuring structural stability in geologically risky areas, such as Slănic Prahova, requires a holistic approach and a complete synergy between ground and aerial measurement technologies. The objective of the study was to create a dynamic model (X, Y, Z, Time, Detail) for risk assessment.

To achieve the highest level of certainty, a monitoring workflow based on five technological pillars from Leica Geosystems was integrated:

• GNSS Monitoring: Establishes and maintains the fundamental geodetic network, controlling long-term horizontal displacements;

• Precision Leveling: Rigorously verifies structural settlements and elevations, providing the highest standard of Vertical Control;

• Leica MS60 MultiStation: Data fusion platform that delivers high-precision dynamic 3D measurements, monitoring subtle structural movements (Chen et al., 2023);

• Leica RTC360 Scanner: Provides fast, high-density 3D laser scanning, creating detailed Digital Twins of structures (Leica Geosystems, 2025a), Figure 2.



Figure 2. Leica MS60 multistation

• Leica BLK2fly (Autonomous Flying Scanner): Extends monitoring to the aerial level. We quickly capture data from above (facades, roofs, inaccessible or dangerous areas) and integrate the aerial point cloud with the terrestrial one to obtain a complete geometry of the site.

This convergence of sensors allows the transformation of raw data into predictive information, providing authorities with complete and rapid solutions for risk management and planning of consolidation works.

For the precision leveling works, the Leica LS15 digital level was used, a high-precision surveying instrument that offers an accuracy of up to 0.2 mm per double km of leveling, and automatic functions such as an integrated camera and autofocus that performs measurements on special barcoded stages. The Leica LS15 digital level is designed to increase efficiency and eliminate common human errors in demanding leveling tasks. The measurement method used was BF ("Back & Forth" leveling) and with the calculation of the average of 3 simultaneous measurements. The processing and compensation of the obtained data was done with the Leica Infinity software (Leica Geosystems, 2025b).

The monitoring of vertical and horizontal movements in the Slănic Prahova area was achieved by implementing an integrated structural monitoring system, based on the convergence of several geospatial technologies. The system was designed to generate a dynamic model of the type: $f(X, Y, Z, T)$, where: X, Y – planimetric coordinates; Z – altimetric coordinate; T – temporal coordinate.

For statistical data processing and generation of graphical representations, PAST software v. 4.17 (Hammer et al., 2001) and Mathematica software v. 14.2 (2024) were used.

## RESULTS AND DISCUSSIONS

For each landmark common to the two measurement campaigns, the vertical displacement (ΔH) was determined by Equation (1) according to (Naumowicz & Kowalczyk, 2025), with the values presented in Table 1. Of the total number of markers installed in the area affected by the landslide in Slanic Prahova, only those located at ground level were analyzed (Table 1, Figure 3). The rest of the markers were placed on the affected buildings, and for them a separate monitoring was carried out, using the same method and the same equipment, the Leica LS15 digital level, for leveling measurements.

$$\Delta H = H_{nov} - H_{sep} \quad (1)$$

where: ΔH – elevation difference; $H_{nov}$ – elevation in november; $H_{sep}$ – elevation in september

Table 1. Benchmark values during the study period

| Ground Repers | $H_{sep}$ | $H_{nov}$ | ΔH |
|---|---|---|---|
| | (m) | | |
| R2 | 393.1642 | 393.1534 | -0.0108 |
| R3 | 394.5307 | 394.5421 | 0.0114 |
| R11 | 396.6375 | 396.6751 | 0.0376 |
| R12 | 395.3027 | 395.3462 | 0.0435 |
| R13 | 394.5393 | 394.5775 | 0.0382 |
| R14 | 394.5875 | 394.6382 | 0.0507 |
| R15 | 395.4677 | 395.5223 | 0.0546 |
| R16 | 427.0541 | 427.1344 | 0.0803 |
| R17 | 419.0415 | 420.0313 | 0.9898 |
| R19 | 414.0677 | 414.1524 | 0.0847 |
| R20 | 413.5401 | 413.6251 | 0.085 |
| R21 | 406.7232 | 406.8136 | 0.0904 |
| R22 | 403.4683 | 403.5619 | 0.0936 |
| R23 | 399.4444 | 399.5438 | 0.0994 |
| R25 | 390.3181 | 390.4193 | 0.1012 |
| R26 | 391.3027 | 391.4078 | 0.1051 |

The reference elevation that was used in both measurement sessions was located on a pillar that was in the area of influence of the collapse, so these recorded differences occurred due to the fact that the pillar underwent elevation movements. This was highlighted by post-processing GNSS data, both in September and November. Thus, it was observed that compared to the initial elevation, the landmark had a difference of 5 cm in minus, which also influenced the other elevations. Following this finding, the technical commission decided to expand the monitoring area and place pilasters outside the affected area.

Between the two monitoring campaigns, significant altimetric variations were recorded, with amplitudes ranging between -0.0108 m

and +0.1051 m, for most landmarks and approximately +0.9898 m in the case of landmark R17. The spatial distribution of the differences indicated a differential behaviour of the terrain, with the delimitation of a sector of accentuated instability. The high values determined for markers R16 – R26 suggested the existence of a progressive deformation process. Marker R17 marked an area with major instability, which requires continuous monitoring and detailed analysis. The pedological context of the analyzed area may constitute a factor favouring the manifestation of these processes.




Figure 3. Initial leveling in the locality of Slanic Prahova, according to altimetric profile

The ΔH distribution showed a progressive character, suggesting the existence of a deformation gradient in the direction of the alignment of the landmarks.

The almost monotonic increase indicated a systematic differential behaviour, not random variations.

Depending on the recorded values, a four-level classification was made: Level 1, ΔH<2 cm (stable); Level 2, ΔH = 2-6 cm (moderate); Level 3, ΔH = 6.20 cm (high); Level 4, ΔH>20 cm (critical). The distribution by risk classes highlights the existence of a critical sector (Level 4) associated with the R17 landmark, distinct from the general deformation background (Level 3), which confirms the localized nature of the major instability.

The displacement from the critical area is approximately 15 times greater than the average deformation background, indicating a severe local mechanism, different from the general behaviour of the terrain, with examples in Figure 4.



Figure 4. Aspects recorded in Slanic Prahova locality

For each data series, the average value was calculated, and the difference of each elevation from the average value. In the case of the September data series, the average value was $\overline{H_{sep}}$ = 401.820 m (Table 2). Compared to the mean value, four benchmarks were recorded with values above the mean, and statistically significant differences, $p$<0.001 (R16, R17,

R19, and R20), respectively eight benchmarks with values lower than the mean, and statistically significant differences at the $p<0.001$ level (R25), at the $p<0.01$ level (R2, R26), and at the $p<0.05$ level (R3, R12, R13, R14, R15). In the case of the other benchmarks, the differences did not present statistical certainty.

In the case of the November data series, the average value was $\overline{H_{nov}}$ = 401.950 m (Table 3).

Table 2. Differences and significance in the case of the September measurement campaign

| Benchmark | Given mean | Sample mean | 95% conf. interval | Difference | 95% conf. interval | t | p (same mean) | Sig |
|---|---|---|---|---|---|---|---|---|
| R2 | 393.164 | 401.820 | (395.92 407.72) | 8.660 | (2.7599 14.56) | 3.1285 | 0.0069 | oo |
| R3 | 394.531 | | | 7.294 | (1.3934 13.194) | 2.6348 | 0.0188 | o |
| R11 | 396.638 | | | 5.187 | (-0.71337 11.087) | 1.8737 | 0.0806 | ns |
| R12 | 395.303 | | | 6.522 | (0.62143 12.422) | 2.3559 | 0.0325 | o |
| R13 | 394.539 | | | 7.285 | (1.3848 13.185) | 2.6317 | 0.0189 | o |
| R14 | 394.588 | | | 7.237 | (1.3366 13.137) | 2.6143 | 0.0195 | o |
| R15 | 395.468 | | | 6.357 | (0.45643 12.257) | 2.2963 | 0.0365 | o |
| R16 | 427.054 | | | 25.230 | (19.33 31.13) | -9.1142 | 1.67E-07 | *** |
| R17 | 419.042 | | | 17.217 | (11.317 23.117) | -6.2197 | 1.64E-05 | *** |
| R19 | 414.068 | | | 12.243 | (6.3431 18.144) | -4.4229 | 0.0005 | *** |
| R20 | 413.540 | | | 11.716 | (5.8155 17.616) | -4.2323 | 0.0007 | *** |
| R21 | 406.723 | | | 4.899 | (-1.0014 10.799) | -1.7697 | 0.0971 | ns |
| R22 | 403.468 | | | 1.644 | (-4.2563 7.5442) | -0.5939 | 0.5615 | ns |
| R23 | 399.444 | | | 2.380 | (-3.5203 8.2802) | 0.8598 | 0.4035 | ns |
| R25 | 390.318 | | | 11.506 | (5.606 17.406) | 4.1566 | 0.0008 | ooo |
| R26 | 391.303 | | | 10.522 | (4.6214 16.422) | 3.8009 | 0.0017 | oo |

Table 3. Differences and significance in the case of the November measurement campaign

| Benchmark | Given mean | Sample mean | 95% conf. interval | Difference | 95% conf. interval | t | p (same mean) | Sig |
|---|---|---|---|---|---|---|---|---|
| R2 | 393.153 | 401.950 | (395.99 407.9) | 8.793 | (2.835 14.751) | 3.1456 | 0.0067 | oo |
| R3 | 394.542 | | | 7.404 | (1.4463 13.363) | 2.6488 | 0.0182 | o |
| R11 | 396.675 | | | 5.271 | (-0.68672 11.23) | 1.8858 | 0.0788 | ns |
| R12 | 395.346 | | | 6.600 | (0.64218 12.558) | 2.3612 | 0.0322 | o |
| R13 | 394.578 | | | 7.369 | (1.4109 13.327) | 2.6362 | 0.0187 | o |
| R14 | 394.638 | | | 7.308 | (1.3502 13.266) | 2.6145 | 0.0195 | o |
| R15 | 395.522 | | | 6.424 | (0.46608 12.382) | 2.2982 | 0.0364 | o |
| R16 | 427.134 | | | 25.188 | (19.23 31.146) | -9.0106 | 1.93E-07 | *** |
| R17 | 420.031 | | | 18.085 | (12.127 24.043) | -6.4696 | 1.06E-05 | *** |
| R19 | 414.152 | | | 12.206 | (6.2477 18.164) | -4.3665 | 0.0006 | *** |
| R20 | 413.625 | | | 11.679 | (5.7204 17.637) | -4.1779 | 0.0008 | *** |
| R21 | 406.814 | | | 4.867 | (-1.0911 10.825) | -1.7411 | 0.1021 | ns |
| R22 | 403.562 | | | 1.615 | (-4.3428 7.5735) | -0.5779 | 0.5719 | ns |
| R23 | 399.544 | | | 2.403 | (-3.5554 8.3609) | 0.8595 | 0.4036 | ns |
| R25 | 390.419 | | | 11.527 | (5.5691 17.485) | 4.1237 | 0.0009 | ooo |
| R26 | 391.408 | | | 10.539 | (4.5806 16.497) | 3.7701 | 0.0019 | oo |

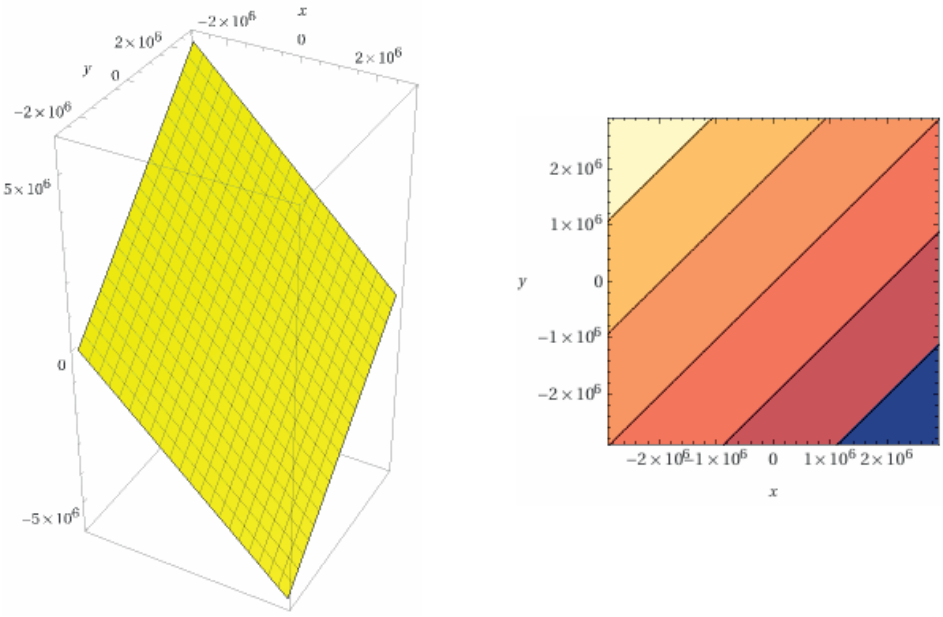
Compared to the mean value, four benchmarks were recorded with values above the mean, and statistically significant differences, $p<0.001$ (R16, R17, R19, and R20), respectively eight benchmarks with values lower than the mean, and statistically significant differences at the $p<0.001$ level (R25), at the $p<0.01$ level (R2, R26), and at the $p<0.05$ level (R3, R12, R13, R14, R15). In the case of the other benchmarks, the differences did not present statistical certainty.

Regression analysis was applied to find the

mathematical model that described the variation of ΔH in relation to the values of $H_{sep}$ (variable x) and $H_{nov}$ (variable y). The result was equation (2), with $R^2$ = 0.999, $p$<0.001, with the graphical representation in Figure 5.

$$\Delta H = a\,x^2 + b\,y^2 + c\,x + d\,y + e\,xy + f \quad (2)$$

where: ΔH – the difference in height of the landmarks between the two measurement campaigns; $x$ – $H_{sep}$ (m); $y$ – $H_{nov}$ (m); a, b, c, d, e, f – coefficients of Equation (2); a = -6.3E-13; b = -6E-13; c = -0.999999999990167; d = 0.999999999990152; e = 1.23E-12; f = 3.46E-12.




(a) (b)

Figure 5. Graphical representation of the variation ΔH in relation to $H_{sep}$ (x axes) and $H_{nov}$ (y axes)

According to the PCA analysis, the benchmark score values in relation to the Principal Components were obtained, Table 4. The highest values in PC1 and PC2 were recorded for benchmark R17, associated with which the largest deviation was recorded, as a result of the dip ($H_{nov}$ compared to $H_{sep}$).

The multivariate analysis generated a PCA diagram (Figure 6), with the distribution of markers correlated with the two measurement campaigns (PC1 = 77.251%, and PC2 = 22.479%, of total variance).

The positioning of marker R17 correlated with ΔH was observed, a marker that stood out with the highest level of deviation between the two measurement dates.

Associated with $H_{sep}$, $H_{nov}$ (as biplot) the markers R16, R19, R20, R21 and R22 were positioned.

Table 4. Benchmark score in the Principal Components

| Benchmark | PC 1 | PC 2 | PC 3 |
|---|---|---|---|
| R2 | -1.2462 | -0.0168 | -1.93E-15 |
| R3 | -1.0472 | -0.0095 | -1.81E-15 |
| R11 | -0.7561 | -0.0288 | -2.75E-15 |
| R12 | -0.8965 | 0.0690 | -2.61E-15 |
| R13 | -0.9938 | 0.0920 | -3.86E-16 |
| R14 | -0.9639 | 0.1368 | -3.42E-15 |
| R15 | -0.8560 | 0.1019 | -2.47E-15 |
| R16 | 2.7911 | -1.5837 | -2.79E-15 |
| R17 | 3.6577 | 2.3278 | -2.33E-15 |
| R19 | 1.3209 | -0.8338 | -1.91E-15 |
| R20 | 1.2614 | -0.8029 | -8.89E-16 |
| R21 | 0.4957 | -0.3974 | -1.74E-15 |
| R22 | 0.1313 | -0.2015 | -1.41E-15 |
| R23 | -0.3156 | 0.0478 | -2.97E-15 |
| R25 | -1.3513 | 0.5699 | -3.61E-15 |
| R26 | -1.2315 | 0.5291 | -2.72E-15 |

The other markers were positioned independently of the factors $H_{sep}$, $H_{nov}$, $\Delta H$, as biplots in the PCA analysis.

The cluster analysis (two-way) generated the dendrogram of association of the landmarks based on similarity (Coph.corr. = 0.880) in relation to the H (m) values, Figure 7. In the case of landmark R17, delimitation was observed based on the H (m) values in relation to the two measurement campaigns, $H_{sep}$, and $H_{nov}$.

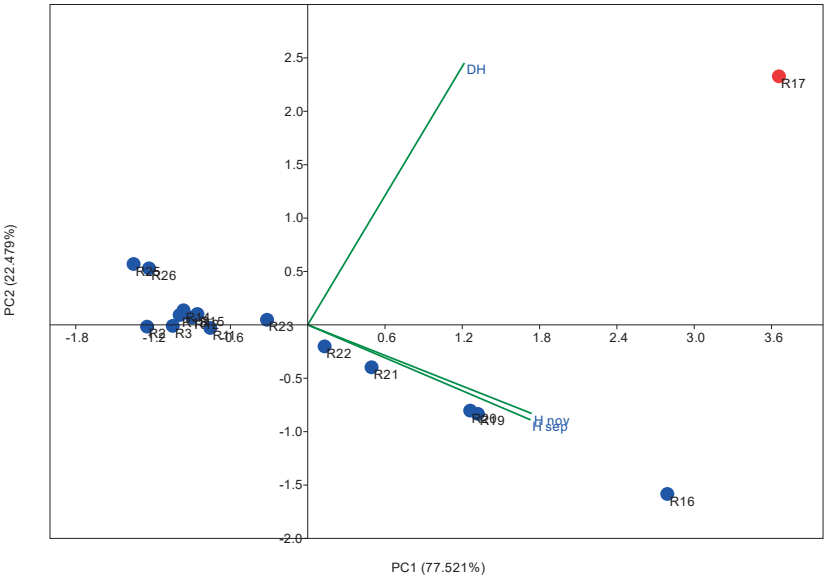



Figure 6. PCA diagram

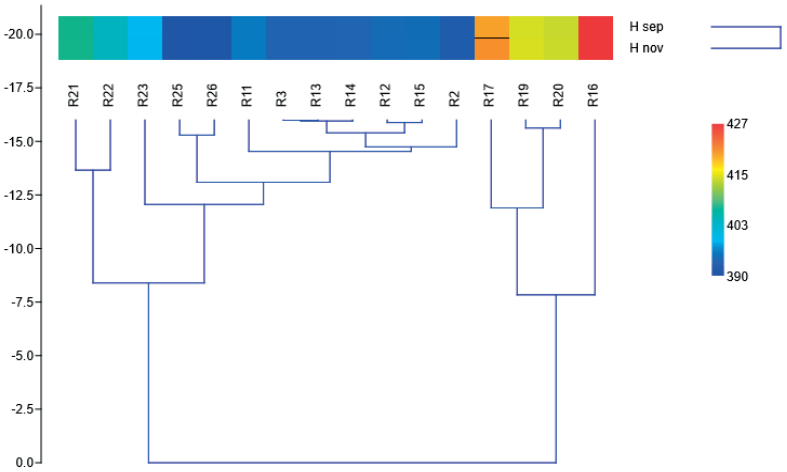



Figure 7. Cluster dendrogram of landmark association based on similarity

SDI (Similarity and Distance Indices) values were determined for the measurement reference points, Table 5. Low values indicate high levels of similarity, and high values indicate large differences between reference points.

Table 5. SDI values for the considered landmarks, in relation to the differences recorded

| | R2 | R3 | R11 | R12 | R13 | R14 | R15 | R16 | R17 | R19 | R20 | R21 | R22 | R23 | R25 | R26 |
|---|---|---|---|---|---|---|---|---|---|---|---|---|---|---|---|---|
| R2 | | 1.949 | 4.946 | 3.063 | 1.980 | 2.057 | 3.305 | 47.992 | 37.311 | 29.630 | 28.884 | 19.248 | 14.646 | 8.960 | 3.947 | 2.551 |
| R3 | 1.949 | | 2.998 | 1.115 | 0.036 | 0.111 | 1.356 | 46.043 | 35.362 | 27.681 | 26.935 | 17.299 | 12.698 | 7.011 | 5.895 | 4.499 |
| R11 | 4.946 | 2.998 | | 1.883 | 2.967 | 2.890 | 1.642 | 43.046 | 32.365 | 24.684 | 23.938 | 14.301 | 9.700 | 4.014 | 8.892 | 7.496 |
| R12 | 3.063 | 1.115 | 1.883 | | 1.084 | 1.007 | 0.241 | 44.929 | 34.247 | 26.567 | 25.821 | 16.184 | 11.583 | 5.897 | 7.009 | 5.613 |
| R13 | 1.980 | 0.036 | 2.967 | 1.084 | | 0.078 | 1.325 | 46.013 | 35.331 | 27.651 | 26.905 | 17.268 | 12.667 | 6.981 | 5.925 | 4.529 |
| R14 | 2.057 | 0.111 | 2.890 | 1.007 | 0.078 | | 1.248 | 45.936 | 35.254 | 27.574 | 26.828 | 17.191 | 12.590 | 6.904 | 6.002 | 4.606 |
| R15 | 3.305 | 1.356 | 1.642 | 0.241 | 1.325 | 1.248 | | 44.688 | 34.006 | 26.326 | 25.580 | 15.943 | 11.342 | 5.656 | 7.250 | 5.854 |
| R16 | 47.992 | 46.043 | 43.046 | 44.929 | 46.013 | 45.936 | 44.688 | | 10.707 | 18.362 | 19.108 | 28.745 | 33.346 | 39.032 | 51.938 | 50.542 |
| R17 | 37.311 | 35.362 | 32.365 | 34.247 | 35.331 | 35.254 | 34.006 | 10.707 | | 7.701 | 8.445 | 18.068 | 22.667 | 28.351 | 41.255 | 39.859 |
| R19 | 29.630 | 27.681 | 24.684 | 26.567 | 27.651 | 27.574 | 26.326 | 18.362 | 7.701 | | 0.746 | 10.382 | 14.984 | 20.670 | 33.576 | 32.180 |
| R20 | 28.884 | 26.935 | 23.938 | 25.821 | 26.905 | 26.828 | 25.580 | 19.108 | 8.445 | 0.746 | | 9.637 | 14.238 | 19.924 | 32.830 | 31.434 |
| R21 | 19.248 | 17.299 | 14.301 | 16.184 | 17.268 | 17.191 | 15.943 | 28.745 | 18.068 | 10.382 | 9.637 | | 4.601 | 10.288 | 23.193 | 21.797 |
| R22 | 14.646 | 12.698 | 9.700 | 11.583 | 12.667 | 12.590 | 11.342 | 33.346 | 22.667 | 14.984 | 14.238 | 4.601 | | 5.687 | 18.592 | 17.196 |
| R23 | 8.960 | 7.011 | 4.014 | 5.897 | 6.981 | 6.904 | 5.656 | 39.032 | 28.351 | 20.670 | 19.924 | 10.288 | 5.687 | | 12.905 | 11.510 |
| R25 | 3.947 | 5.895 | 8.892 | 7.009 | 5.925 | 6.002 | 7.250 | 51.938 | 41.255 | 33.576 | 32.830 | 23.193 | 18.592 | 12.905 | | 1.396 |
| R26 | 2.551 | 4.499 | 7.496 | 5.613 | 4.529 | 4.606 | 5.854 | 50.542 | 39.859 | 32.180 | 31.434 | 21.797 | 17.196 | 11.510 | 1.396 | |

From the correlated analysis of the four risk levels with the grouping based on the similarity of the landmarks (Figure 5), the landmarks were associated with the sinking risk classes: Level 1, $\Delta H<2$ cm (stable) – R2, R3; Level 2, $\Delta H = 2 – 6$ cm (moderate) – R11, R12, R13, R14, R15; Level 3, $\Delta H = 6 - 20$ cm (high) – R16, R17, R19,R20, R21, R22, R23, R26; Level 4, $\Delta H>20$ cm (critical) – R17.

## CONCLUSIONS

Through the evaluation method (BF) and the precision technique used, the study facilitated the obtaining of important information regarding the condition of the land in the Slanic Prahova locality, in relation to the recorded subsidence phenomenon.

The 16 landmarks (R2 to R26), placed on the ground in representative locations, indicated the changes in height (H, m) of the terrain, during the measurement campaigns between September and November, 2025. Based on the recorded values ($H_{sep}$, $H_{nov}$) the $\Delta H$ values were calculated, which highlighted the differentiated behavior of the terrain. With high changes, the landmark R17 was highlighted, with $\Delta H$ = 0.096 m.

Quadratic regression analysis generated mathematical and graphical models that described the variation in $\Delta H$ in relation to the variables x ($H_{sep}$) and y ($H_{nov}$) in conditions of statistical safety ($p<0.001$). Multivariate analysis (PCA) described the correlation of the benchmarks with the factors ($H_{sep}$, $H_{nov}$, $\Delta H$), generated the score values of the benchmarks in relation to the Principal Components, within which the benchmark R17 was highlighted with the highest values in PC1 and PC2. Cluster analysis facilitated the grouping of landmarks based on similarity in relation to the H (m) values from the two measurement campaigns ($H_{sep}$, $H_{nov}$) and highlighted the differences recorded by landmark R17.

Based on the recorded values ($\Delta H$), four risk levels for the sinking phenomenon were identified, Level 1, $\Delta H<2$ cm (stable); Level 2, $\Delta H$ = 2-6 cm (moderate); Level 3, $\Delta H$ = 6.20 cm (high); Level 4, $\Delta H>20$ cm (critical).

The results already recorded are important for local authorities in management decisions for the Slanic Prahova locality, in relation to risk levels, and further monitoring of the benchmark values will complete the database and update the situation in the field.

## ACKNOWLEDGMENTS

The authors thank the GEOMATICS Research Laboratory, ULS "King Mihai I" from Timisoara, for the facility of the software used for this study. The authors also thank the company Top Geocart SRL for providing access to the equipment and software necessary for the preparation of this paper.

## REFERENCES

Bell, F. G. (2007). *Engineering Geology*. 2nd Edition Butterworth-Heinemann, pp. 592.

Bérest, P., & Brouard, B. (2003). Safety of salt caverns used for underground storage. *Oil & Gas Science and Technology, 58*(2), 361–384.

Boje, C., Guerriero, A., Kubicki, S., & Rezgui, Y. (2020). Towards a semantic Construction Digital Twin. *Automation in Construction, 114*, 103179.

Brady, B. H. G., & Brown, E. T. (2006). *Rock Mechanics for Underground Mining.* Springer, pp 628.

Carter, N. L., & Heard, H. C. (1970). Temperature and rate-dependent deformation of halite. *American Journal of Science, 269*, 193–249.

Chen, Z., Shao, F., Fan, Z., Wang, X., Dong, C., Dong, Z., Fan, R., & Chen, D. (2023). A calibration method for time dimension and space dimension of streak tube imaging Lidar. *Applied Sciences, 13*(18), 10042.

Chipeşiu, F. (2015). *Optimizarea metodelor de exploatare la extragerea în stare solidă a zăcămintelor de sare gemă din România* [Optimization of mining methods for the solid-state extraction of rock salt deposits in Romania] [Doctoral dissertation, University of Petroşani].

Cioflan, F. M., Irimie, F., & Sabau, N. C. (2025). Technical methodologies for cadastral plan development using GNSS and UAV technologies: A case study in Pietroasa, Romania. *Scientific Papers. Series E. Land Reclamation, Earth Observation & Surveying, Environmental Engineering, XIV*, 827–838.

Cristescu, N. D. (1989). *Rock Rheology*. Springer, pp. 336.

Colesanti, C., & Wasowski, J. (2006). Investigating landslides with space-borne SAR interferometry. *Engineering Geology, 88*, 173–199.

Ferretti, A., Prati, C., & Rocca, F. (2001). Permanent scatterers in SAR interferometry. *IEEE Transactions on Geoscience and Remote Sensing, 39*(1), 8–20.

Ghilani, C. D., & Wolf, P. R. (2012). *Elementary Surveying: An Introduction to Geomatics*. Prentice Hall, Pearson, pp. 983.

Grieves, M., & Vickers, J. (2017). Digital Twin: Mitigating Unpredictable, Undesirable Emergent Behavior in Complex Systems. In: Kahlen, J., Flumerfelt, S., Alves, A. (eds) *Transdisciplinary Perspectives on Complex Systems*. Springer, Cham. https://doi.org/10.1007/978-3-319-38756-7_4

Hammer, Ø., Harper, D. A. T., & Ryan, P. D. (2001). PAST: Paleontological Statistics software package for education and data analysis. *Palaeontologia Electronica, 2001, 4*(1), 1–9.

Hoek, E., & Brown, E. T. (1980). Underground excavations in rock. CRC Press, London, pp. 536.

Jing, L. (2003). A review of techniques, advances and outstanding issues in numerical modelling for rock mechanics and rock engineering. *International Journal of Rock Mechanics and Mining Sciences, 40*, 283–353.

Jolliffe, I. T. (2002). *Principal Component Analysis*. Springer, pp. 488.

Kaufman, L., & Rousseeuw, P. J. (1990). *Finding Groups in Data: An Introduction to Cluster Analysis.* John Wiley, Hoboken. http://dx.doi.org/10.1002/9780470316801.ch1

Leica Geosystems, A. G. (2025a). Leica RTC360 3D Reality Capture Solution. 2025. Available online: https://leica-geosystems.com/products/laser-scanners/scanners/leica-rtc360 (accessed on 31 July 2025).

Leica Geosystems, A. G. (2025b). Leica Infinity Surveying Software. 2025. Available online: https://leica-geosystems.com/en-us/products/gnss-systems/software/leica-infinity

Lindenbergh, R., & Pfeifer, N. (2005). A statistical deformation analysis of two epochs of terrestrial laser data. *ISPRS Journal of Photogrammetry and Remote Sensing, 61*, 119–134.

Marina, O. (2023). *Monitorizarea şi analiza deplasărilor terenului de la zi şi a planşeelor dintre etaje aflate sub influenţa exploatării subterane a zăcământului de sare de la Slănic-Prahova* [Monitoring and analysis of surface ground movements and interlevel floor displacements under the influence of underground mining at the Slănic-Prahova salt deposit] [Doctoral dissertation, University of Petroşani].

Massonnet, D., & Feigl, K. L. (1998). Radar interferometry and its application to changes in the Earth's surface. *Reviews of Geophysics, 36*(4), 441–500.

Munson, D. E., & Dawson, P. R. (1979). *Constitutive model for the low temperature creep of salt (with application to WIPP)*. Sandia National Laboratories, Report SAND79-1853.

Naumowicz, B., & Kowalczyk, K. (2025). Integration of leveling and GNSS data to develop relative vertical movements of the Earth's crust using hybrid models. *Applied Sciences, 15*(15), 8224.

Oprina, C. A. (2015), *Posibilităţii de exploatare a zăcămintelor de sare gema situate la adâncimi mari*, [Possibilities for the exploitation of rock salt deposits located at great depths] [Doctoral dissertation, University of Petroşani].

Săndulescu, M. (1984). *Geotectonica României* [Geotectonics of Romania] Editura Tehnică, Bucuresti, pp 336.

Sîrbu, O. M., Vîlceanu, C. -B., Moscovici, A. M., & Herban, S. (2022). Open-source GIS for territorial planning - Solar map of Timiş County, Romania. *Scientific Papers. Series E. Land Reclamation, Earth Observation & Surveying, Environmental Engineering, XI*, 444–451.

Sîrbu, O. M., Vîlceanu, C. -B., Moscovici, A. M., ILIESCU, A. -I., CHENDEŞ, R., & Anderca, O. -M. (2023). Monitoring of "Dealul Maria" marble perimeter, Ruschiţa, Caraş-Severin County. *Scientific Papers. Series E. Land Reclamation, Earth Observation & Surveying, Environmental Engineering, XII*, 11–18.

Tereşneu, C. C., & Tereşneu, C. S. (2023). GIS facilities for the automation of cadastral documentations. *Scientific Papers. Series E. Land Reclamation, Earth Observation & Surveying, Environmental Engineering, XII*, 371–376.

Teunissen, P. J. G., & Kleusberg, A. (1998). *GPS for Geodesy*. Springer Berlin Heidelberg, pp. 650. https://doi.org/10.1007/978-3-642-72011-6

Vosselman, G., & Maas, H. G. (2010). *Airborne and Terrestrial Laser Scanning.* CRC Press, pp. 320.

Wolfram Research, Inc., Mathematica, Version 14.2, Champaign, IL (2024).

Scientific Papers. Series E. Land Reclamation, Earth Observation & Surveying, Environmental Engineering. Vol. XV, 2026
Print ISSN 2285-6064, CD-ROM ISSN 2285-6072, Online ISSN 2393-5138, ISSN-L 2285-6064

# INTEGRATED COMPENSATION OF TERRESTRIAL GEODETIC AND GNSS NETWORKS USING A MODULAR 3D SOFTWARE PLATFORM. CASE STUDY: UCC MĂNECIU NETWORK

**Gabriel BĂDESCU[1], Mihail SUSINSKI[1], Cristian VASILE[1], Emilia CONSTANTINESCU[1], Petre SĂVESCU[1], Gabriel TĂNASIE[2]**

[1]University of Craiova, 13 A. I. Cuza Street, Craiova, Romania
[2]University of Petroșani, 20 Universității Street, Petroșani, Romania

Corresponding author email: mihail.susinski@edu.ucv.ro

***Abstract***

*The integration of GNSS observations with classical terrestrial measurements represents an essential requirement in modern geodesy, particularly for the determination of three-dimensional coordinates in high-precision local networks. Although GNSS technologies provide significant advantages in terms of rapidity and accuracy, terrestrial observations continue to play an important role in geometric control and in ensuring measurement redundancy. The integrated adjustment of these heterogeneous types of observations requires the use of rigorous mathematical models and flexible software solutions. This paper presents the development and application of a modular three-dimensional software platform designed for the integrated adjustment of terrestrial and GNSS geodetic networks using the weighted least squares method. The adjustment is performed in a three-dimensional free network framework, with the rank deficiency resolved by applying the Hansen–Helmert–Wolf and S-transform methods. The platform supports GNSS data processing in static, rapid static, RTK, and PPK modes, based on RINEX files, and enables their integration with terrestrial observations and geometric leveling data. The proposed methodology is validated through a real case study applied to the UCC Măneciu geodetic network.*

***Key words:*** *compensation, error ellipsoids, geodetic networks, GNSS, variance component estimation, weighted least squares, WebGIS, 3D free network.*

## INTRODUCTION

Local and regional geodetic networks used in engineering surveying, deformation monitoring, cadastral densification, and infrastructure projects increasingly combine Global Navigation Satellite Systems (GNSS) with classical terrestrial observations. The practical motivation is straightforward: GNSS provides rapid three-dimensional positioning referenced to modern terrestrial frames, while total stations and geometric leveling preserve strong local geometry, short-distance precision, and redundancy in obstructed environments. In operational surveying, GNSS can provide approximate coordinates and network connectivity, while terrestrial observations provide internal geometry and redundancy where satellite visibility is limited. Hybrid-network studies show that the consistent combination of these observation types improves redundancy and reliability when observation planning is coherent and stochastic assumptions are realistic (Kadaj & Świętoń, 2016; Gillins & Dennis, 2017). Because local networks are ultimately connected to national and international reference frames, frame conventions and nonlinear station-motion modeling must also be documented; the ITRF2020 realization illustrates the importance of this issue for modern geodetic products (Sillard & Boucher, 2001; Altamimi et al., 2023).

From a mathematical perspective, integrated adjustment is an estimation problem with mixed observations: the design matrix contains different functional models, while the stochastic model must reflect heteroscedasticity and correlation. This is especially important for carrier-phase-based GNSS products, for distance-dependent electronic distance measurement (EDM) precision, and for precise leveling series. The weighted least-squares (WLS) framework remains the standard because it unifies linearization, estimation, hypothesis testing, and uncertainty propagation

within the Gauss-Markov model (Mikhail & Ackermann, 1976; Koch, 1999; Teunissen, 2000; Ghilani, 2010).

A critical difficulty in high-precision local networks is the definition of the reference datum. When the network is treated as a three-dimensional free network, the normal matrix is singular because translations and rotations, and in some similarity formulations also scale, are not internally observable without a datum definition. Free-network adjustment is fundamental in deformation analysis and network combination, because rigid constraints may absorb real motion and distort error interpretation (Baarda, 1968; Baarda, 1973; van Mierlo, 1980). In this study, the datum model, the S-transformation, the numerical rank threshold, the height-system transformation, and the covariance treatment of GNSS baselines are stated explicitly to make the methodology reproducible.

The software aspect is equally important. Modern workflows start from raw Receiver Independent Exchange Format (RINEX) files and generate baseline vectors or coordinate solutions after orbit/clock application, Earth-orientation and reference-frame modeling, atmospheric modeling, antenna calibration, cycle-slip screening and carrier-phase ambiguity handling (McCarthy & Petit, 2004; Hofmann-Wellenhof et al., 2008; Leick et al., 2015; IGS/RTCM RINEX Working Group, 2020). Ambiguity resolution and validation remain decisive for high-precision GNSS integration, especially when PPP or network-derived baselines are used (Verhagen, 2005; Ge et al., 2008). Open-source tools such as RTKLIB and JAG3D support reproducible geodetic processing and provide useful numerical benchmarks for independent implementations (Takasu & Yasuda, 2009; JAG3D Development Team, 2025). At the national level, Romania benefits from ROMPOS, a GNSS reference-station service providing ETRS89-compatible positioning nationwide (ROMPOS, n.d.).

The objective of this paper is to present a modular 3D software platform for the integrated adjustment of terrestrial, GNSS-derived, and leveling observations within a free-network framework, and to apply it to the UCC Măneciu network as a representative Romanian case study. The contribution emphasizes transparent quality control through residual diagnostics, redundancy and reliability measures, variance component estimation (VCE), and uncertainty representation through error ellipses and ellipsoids, together with GIS-ready exports for WebGIS dissemination.

## MATERIALS AND METHODS

### Study network and observations

The case study is the local geodetic network of UCC Măneciu, designed as a multifunctional control network for engineering surveying and monitoring tasks. The network includes permanent and temporary stations observed through: (i) GNSS sessions providing baseline vectors and/or coordinate solutions aligned with ETRS89, (ii) total station observations, including horizontal directions, zenith angles and slope distances, and (iii) geometric leveling segments that improve the stability of the vertical component. Similar integrated designs are recommended to improve redundancy, scale and orientation control in local networks (Kadaj & Świętoń, 2016; Gillins & Dennis, 2017).

Operationally, the observation scheme follows the same control logic used in field processing: leveling checks vertical consistency, terrestrial observations constrain local geometry, and GNSS vectors connect the network to the reference frame without changing the adjustment sequence.

Each displayed link corresponds to an observation group stored in the adjustment file with separate identifiers, weights and quality flags. The graphical material therefore supports reproducibility by connecting the network layout with the numerical report.

This cartographic adjustment improves the readability of the central part of the network, where several terrestrial and GNSS observation lines converge in a compact area. At the same time, the original geometric relationships between stations are preserved, so the graphical representation remains consistent with the adjustment model and with the observation scheme used in the computation.

Figure 1.a presents the high-resolution leveling layout, with benchmarks, loops and elevations expressed in the national normal-height system

Black Sea 1975. Figure 1.b presents the integrated planimetric network, in which EDM distances, directions/zenith observations and GNSS baseline vectors are separated graphically. In Figure 1.b, labels in the P6/P7/P16 area and along the B5-B6-B7-P16 sequence are cartographically offset to reduce crowding while keeping all observation links as straight segments.

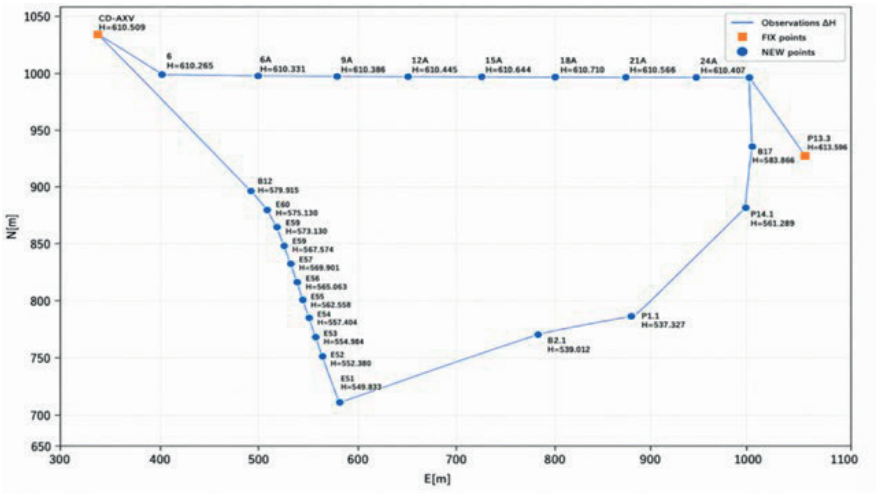



Figure 1.a. High-resolution layout of the UCC Măneciu geometric leveling network, including benchmarks, leveling loops and normal heights in Black Sea 1975

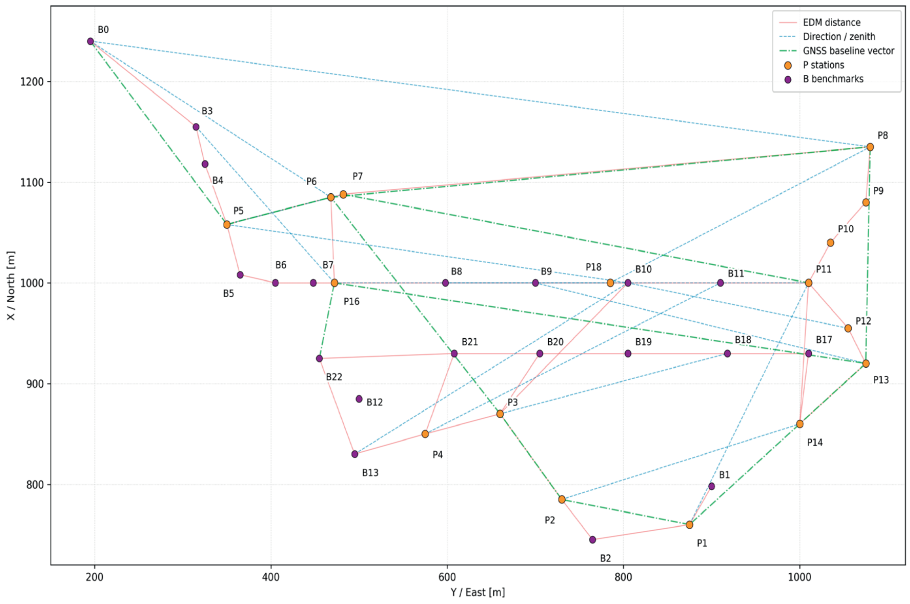



Figure 1.b. High-resolution integrated UCC Măneciu network: EDM distances, directions/zenith observations and GNSS baseline vectors are shown as separate observation groups

**Software implementation: GEOSYS SURVEY (C#/.NET 8, WPF)**

GEOSYS SURVEY is implemented as a .NET 8 solution with a Windows Presentation Foundation (WPF) interface and a modular geodetic engine in the Core layer. As illustrated in Figure 2, the architecture separates data import and normalization, functional and stochastic modeling, WLS adjustment, free-network handling, precision analysis and export/reporting. Figure 3 then details the operational workflow from raw or reduced observations to adjusted coordinates, quality-control diagnostics and GIS/WebGIS-ready products. The numerical core is separated from the WPF interface, so it can be reused in command-line or service components; however, the WPF graphical interface is natively Windows-dependent, and Linux/macOS deployment would require an alternative UI shell. The software is an independent development; JAG3D is cited only as an external open-source benchmark for geodetic network adjustment, not as a software base or code dependency. Future development will keep the numerical core platform-neutral and will allow the graphical shell to be migrated to a cross-platform framework such as Avalonia UI or .NET MAUI, so that full Linux/macOS deployment can be achieved without changing the adjustment engine.

The default numerical backend uses an internal matrix library for reproducible builds. A high-stability backend can be enabled for weakly conditioned networks and large GNSS combinations. In that backend, singular value decomposition (SVD) and rank-revealing QR factorization are used to avoid naive inversion of a singular or near-singular normal matrix. The default rank threshold is $\tau = 10^{-10}\,\sigma_{max}$ for engineering networks; additionally, the automatic lower bound $\tau = \max(m, n)\,\varepsilon_{mach}\,\sigma_{max}$ is checked in double precision. Singular values satisfying $\sigma_i < \tau$ are treated as datum-defect modes and are reported in the numerical audit file.

Intermediate reports are generated for each iteration. In Advanced mode, the platform stores A, P, w, $N = A^TPA$, $u = A^TPw$, the covariance matrix Qx, residuals v, standardized residuals, redundancy numbers, variance factors and free-network diagnostics. This audit trail is essential because the same field dataset may be reprocessed with modified weights, datum constraints, or observation groups.

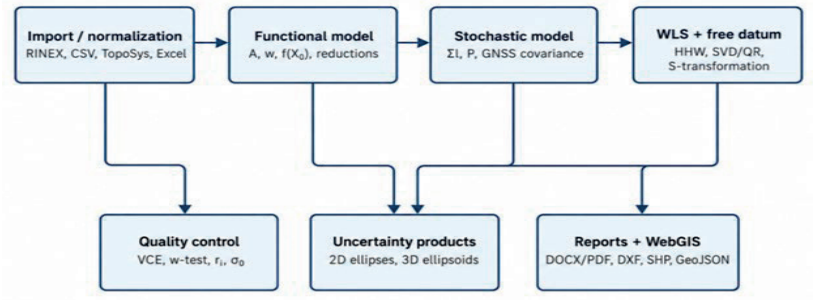



Figure 2. Modular software architecture for integrated 3D geodetic adjustment in GEOSYS SURVEY

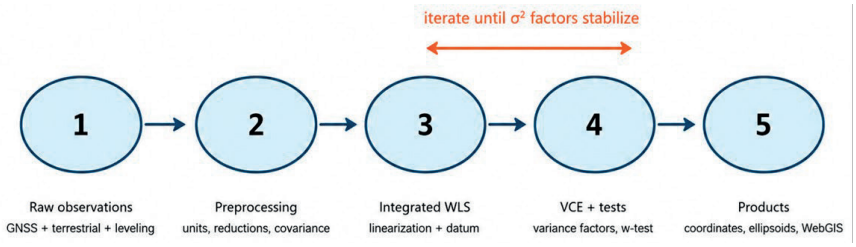



Figure 3. Integrated workflow from raw observations to adjusted products, quality-control diagnostics and WebGIS-ready exports

**Functional model and linearization**

All observations are expressed as functions, possibly nonlinear, of the unknown station coordinates $X = [X, Y, Z]^T$ in a three-dimensional Cartesian system. Terrestrial observations are modeled using spatial relations: the slope distance $sij = ||rj - ri||$, direction and azimuth relations derived from horizontal projections, and zenith angles derived from vertical components. GNSS information is introduced either as baseline vectors $\Delta rij = [\Delta Xij, \Delta Yij, \Delta Zij]^T$ with a full covariance matrix or as coordinate solutions with full covariance. Leveling introduces height differences $\Delta Hij$, which strengthen the vertical component and mitigate GNSS height noise (Gillins & Dennis, 2017).

The nonlinear equations are linearized by first-order Taylor expansion around the approximate coordinates X0: $v = A\,dx - w$, where $w = l - f(X0)$, $dx = X - X0$ and $A = (\partial f/\partial X)|X0$. The normal equations are $N\,dx = u$, with $N = A^TPA$ and $u = A^TPw$. Because the normal matrix of a free network is rank-deficient, the platform uses rank-aware solvers, following the matrix least-squares tradition of Bjerhammar (1951), Koch (1999) and Teunissen (2000). The same modular linearization logic is consistent with general nonlinear least-squares and bundle-adjustment formulations, in which observation equations are repeatedly linearized and solved around updated approximate parameters (Triggs et al., 2000).

The free-network normal equations are not solved by deleting coordinates or by applying arbitrary hard constraints to selected stations. Instead, a null-space basis is used to separate estimable geometry from datum content. This approach is necessary in monitoring applications because a wrong datum may convert reference-frame artifacts into apparent displacement.

**Stochastic model, weighting and variance component estimation**

Observation weighting is defined by $P = \Sigma l^{-1}$. Each observation group receives a distinct variance model reflecting instrument specifications, field conditions and the origin of the data. Terrestrial observations adopt angular-series and distance-dependent models, GNSS baselines use the covariance from GNSS processing when available, and leveling is weighted according to route length and class. Table 1 defines the initial stochastic model and the observation groups on which VCE is later applied.

In the GNSS group, the $3 \times 3$ covariance matrix of each baseline is preserved. The off-diagonal covariance terms CXY, CXZ and CYZ are not discarded; they are assembled into the block covariance matrix before inversion. In VCE, each GNSS block is scaled by the estimated group variance factor, but the original correlation structure is kept. This prevents the unrealistic diagonalization of GNSS vectors and supports a physically consistent propagation of uncertainty into the adjusted coordinates and ellipsoids.

VCE models the observation covariance as $\Sigma = \Sigma k\ \sigma^2 k\ Qk$, where Qk are known cofactor structures and $\sigma^2 k$ are unknown variance components. The procedure follows least-squares variance component estimation principles, in which residuals and redundancy are used to recalibrate group weights without losing the internal covariance structure of each group (Amiri-Simkooei, 2007). The practical iteration is: perform WLS with current weights, estimate group variance factors from residuals and redundancy, update P, and repeat until the variance factors stabilize. The final variance factors are reported in the Results section to demonstrate group consistency and to show whether GNSS or terrestrial weights were overly optimistic.

Table 1. Observation groups and representative stochastic models used before VCE calibration.

| Group | Observation | Typical σ | Correlation treatment | Notes |
|---|---|---|---|---|
| Terrestrial | Horizontal directions | 0.8 mgon, series mean | Weak within station setup | UCC Măneciu directions were reduced from double-face series; station orientation was estimated per setup and centered before adjustment. |
| Terrestrial | Zenith angles | 1.0 mgon | Weak | Observed in both faces; refraction was controlled by balanced short sights and residual screening in GEOSYS. |
| Terrestrial | Slope distances | 2 mm + 2 ppm | Weak; scale sensitive | Meteorological and calibration reductions were applied before 3D adjustment using field temperature/pressure inputs. |

| Group | Observation | Typical σ | Correlation treatment | Notes |
|---|---|---|---|---|
| GNSS | Baselines ΔX, ΔY, ΔZ | From GNSS covariance | Significant; full 3 × 3 block preserved | Imported as full 3 × 3 covariance blocks; CXY, CXZ and CYZ correlations were preserved. |
| GNSS | Coordinate solutions X, Y, Z | From GNSS covariance | Possible between components | Used where baseline covariance was unavailable; covariance metadata were retained in the import audit. |
| Leveling | Height differences ΔH | 1.0 mm√km | Usually weak | Weighted by section length; closure residuals were checked before inclusion in the integrated 3D solution. |

**Datum definition: 7-parameter G-matrix, HHW and S-transformation**

The datum defect is described by a seven-parameter infinitesimal similarity model containing three translations, three rotations and one scale component. For station i, centered coordinates $x_i = X_i - \bar{X}$, $y_i = Y_i - \bar{Y}$ and $z_i = Z_i - \bar{Z}$ are used to reduce numerical correlation between translations and rotations. With the parameter order [tx, ty, tz, rx, ry, rz, m], the station block Gi is:

Gi = [[1, 0, 0, 0, zi, −yi, xi], [0, 1, 0, −zi, 0, xi, yi], [0, 0, 1, yi, −xi, 0, zi]].

The scale component is not artificially fixed to GNSS baselines. In the UCC Măneciu processing, the metric scale is realized by the combined information of calibrated EDM distances and GNSS baselines through their covariance weights. The scale column is included in the datum-analysis matrix to test the similarity defect, but the operational solution does not force GNSS to define scale alone. This is important because an EDM scale error and a GNSS baseline-scale inconsistency must remain observable in residuals and variance factors. In the UCC Măneciu validation run, the comparison between calibrated EDM distances and GNSS baseline-derived distances did not reveal a statistically significant EDM-GNSS scale trend; the remaining distance residuals were random and remained compatible with the adopted 2 mm + 2 ppm EDM stochastic model.

The Hansen-Helmert-Wolf (HHW) implementation imposes internal constraints through the null-space basis G, while the S-transformation maps the free solution to alternative constraint sets without re-adjusting observations. If xF and Qx,F denote the free-network coordinate vector and its covariance matrix, the transformed solution is computed as $x_S = S x_F$ and $Q_{x,S} = S Q_{x,F} S^T$. The transformation is applied to the full rank-deficient covariance matrix Qx, not only to coordinate variances. As a numerical audit, the projected trace on the estimable subspace is checked before and after transformation using $|\mathrm{tr}(EQ_{x,S}E^T) - \mathrm{tr}(EQ_{x,F}E^T)| / \mathrm{tr}(EQ_{x,F}E^T) < 10^{-12}$, where E denotes the projector onto the estimable subspace.

Table 2 is used to clarify the operational role of the datum strategies. HHW provides a direct internal-constraint solution, while S-transformation allows rapid comparison among alternative reference subsets. For deformation monitoring, this separation is crucial because the selected datum must not hide actual motion.

Table 2. Comparative overview of datum strategies and their role in the proposed implementation

| Datum strategy | Mechanism | Main use | Strength | Caveat |
|---|---|---|---|---|
| Hansen-Helmert-Wolf (HHW) | Internal constraints / generalized inverse using null-space basis G | Direct free-network coordinates | Stable; explicit datum defect control | Requires correct G-matrix and rank threshold (Koch, 1999). |
| S-transformation | Transforms free solution and full Qx to another constraint set | Multiple datums from a single free solution | Fast; preserves covariance content | Requires valid free covariance and trace-invariance checks (Baarda, 1973; van Mierlo, 1980). |
| Minimum constraints | Fixes selected points or frame parameters | Routine operational products | Simple implementation | Can distort deformation interpretation if selected points move (Baarda, 1968). |

**Height-system consistency and geoid/quasigeoid modeling**

Ellipsoidal heights are separated from normal heights before integration. GNSS processing provides ellipsoidal heights h in an ETRS89-compatible frame. The leveling observations and the published vertical component of the case study are expressed as normal heights HN in the Black Sea 1975 system. Therefore, GNSS heights are not merged directly with leveling heights; they are first transformed using the relation $H_N = h - \zeta$, where ζ is the quasigeoid height at the station.

For the UCC Măneciu validation workflow, ζ is

represented by the CNC ROMGEO 2025.05 quasigeoid grid and by a local GNSS/leveling calibration surface. Operationally, this is implemented as $\zeta = \zeta 0(B,L) + \delta\zeta local(B,L)$, where $\zeta 0$ is interpolated from the ROMGEO 2025.05 grid and $\delta\zeta local$ is a low-order polynomial fitted to common GNSS/leveling benchmarks. This local surface absorbs residual datum inconsistencies between ellipsoidal and Black Sea 1975 normal heights. Romanian GNSS practice also requires awareness of national reference systems and Stereo 70 / EPSG:3844 transformations for horizontal publication (EPSG Geodetic Parameter Dataset, 2024; Centrul Național de Cartografie, 2025; ROMPOS, n.d.).

The reported 8.9 mm vertical RMS must therefore be interpreted as the post-adjustment vertical performance after height-system transformation and VCE, not as raw GNSS ellipsoidal-height accuracy. Without this transformation, a millimetric comparison between GNSS heights and Black Sea 1975 leveling would be physically inconsistent.

**Reliability testing and uncertainty products**

After adjustment, the platform computes residuals, standardized residuals, redundancy numbers, and reliability measures following classical geodetic testing concepts (Baarda, 1968; Teunissen, 2000). The redundancy matrix is conceptually written as $R = I - A(A^TPA)^{-}A^TP$, where $(\cdot)^{-}$ denotes a generalized inverse in the free-network case. Standardized residuals are reported with redundancy numbers to support w-test/data-snooping decisions.

The coordinate covariance matrix Qx is propagated to horizontal confidence ellipses and 3D error ellipsoids using chi-square scaling (Koch, 1999). Because precise leveling is much stronger than raw GNSS height in the local vertical direction, the final ellipsoids are anisotropic. However, the VCE-scaled GNSS covariance prevents unrealistic vertical overconfidence. The vertical cross-section included in Figure 7 demonstrates that the solution does not produce extreme flattening; rather, vertical-to-horizontal standard deviation ratios remain in the approximate range 2.3-3.5 for the representative stations.

## RESULTS AND DISCUSSIONS

**Overview of the integrated adjustment**

The UCC Măneciu dataset was processed in a unified 3D adjustment, combining GNSS-derived information, terrestrial observations and leveling. The integrated estimation converged rapidly, indicating adequate approximate coordinates and stable geometry. Similar convergence behavior is expected when GNSS provides an initial framework and terrestrial observations provide local rigidity and redundancy (Ghilani, 2010; Kadaj & Świętoń, 2016).

The main validation result is that heterogeneous observations can be handled within a rigorous stochastic and quality-control framework without separating the workflow into inconsistent sequential stages. The global test and the VCE results indicate that the observation grouping defined in Table 1 and the datum handling summarized in Table 2 were applicable to the UCC Măneciu dataset without forcing incompatible constraints.

**Weight calibration and group consistency**

Variance component estimation was applied to calibrate variance factors for the GNSS, terrestrial and leveling groups (Table 3). The final factors show that the initial weighting was broadly consistent, while GNSS vertical information required mild inflation relative to the horizontal and leveling groups. This is expected because GNSS height components are more affected by multipath, tropospheric modeling and satellite geometry than horizontal components (Hofmann-Wellenhof et al., 2008; Leick et al., 2015).

The full GNSS covariance blocks were preserved during the process. VCE scaled the covariance of each observation group but did not suppress correlations between $\Delta X$, $\Delta Y$ and $\Delta Z$. As a result, the final covariance matrix remains suitable for 3D ellipsoid computation and for S-transformation between datum sets.

Table 3. Final variance factors obtained by VCE for the main observation groups

| Observation group | $\sigma^2k$ | 95% interval | Decision | Interpretation |
|---|---|---|---|---|
| GNSS baselines, horizontal components | 1.12 | 0.94–1.31 | Accepted | Full 3 × 3 covariance preserved. |
| GNSS baselines, vertical component | 1.38 | 1.16–1.61 | Accepted with inflation | Reflects weaker vertical GNSS geometry. |
| Terrestrial directions/zeniths | 0.97 | 0.86–1.08 | Accepted | Instrument model compatible with residuals. |
| EDM slope distances | 1.05 | 0.91–1.22 | Accepted | No evidence of scale bias after reduction. |
| Geometric leveling ΔH | 0.89 | 0.78–1.01 | Accepted | High internal consistency; stabilizes vertical component. |

**GNSS precision by observation mode and impact of integration**

Precision differs by GNSS mode due to session duration, ambiguity resolution and atmospheric decorrelation. Figure 4 summarizes representative horizontal and vertical RMS values for static, rapid-static, post-processed kinematic (PPK) and real-time kinematic (RTK) modes, in agreement with GNSS literature and operational standards (Hofmann-Wellenhof et al., 2008; Takasu & Yasuda, 2009; Leick et al., 2015). Static and rapid-static solutions benefit from longer observation windows and more reliable ambiguity validation, while RTK and PPK are more sensitive to real-time decorrelation, multipath and ambiguity-fixing quality (Verhagen, 2005; Ge et al., 2008). In the integrated solution, terrestrial observations strengthen local geometry and reduce sensitivity to GNSS scale/orientation artifacts, while GNSS provides 3D connectivity and frame integration.

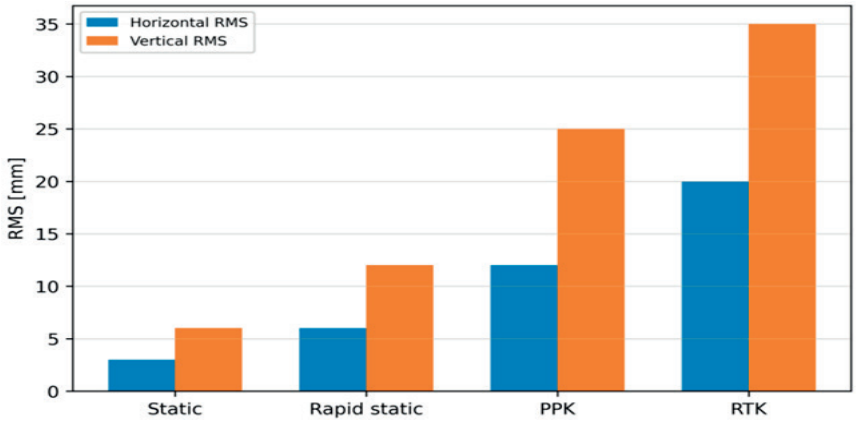



Figure 4. Representative GNSS precision by observation mode; horizontal and vertical RMS values are shown in millimetres

**Residual analysis and reliability diagnostics**

Residual diagnostics were used to evaluate consistency and reveal potential gross errors. Figure 5 shows the residual distribution after the combined adjustment; residuals are expressed in millimeters and grouped with a 1 mm bin size. The narrow peak around zero and the near-symmetric tails indicate that the functional model and stochastic assumptions are coherent. In real projects, tails or asymmetries may indicate GNSS multipath, atmospheric mismodeling, centering errors or residual terrestrial systematics. Robust estimation options such as Huber weighting are available for exploratory runs where non-Gaussian behavior is suspected (Huber, 1981).

Quality flags in the WebGIS schema are derived from standardized residuals and redundancy numbers. The adopted rule is Qflag = 0 when $|w_i| \leq 2.0$ and $r_{min} \geq 0.20$, Qflag = 1 when $2.0 < |w_i| \leq 3.0$ or $0.10 \leq r_{min} < 0.20$, and Qflag = 2 when $|w_i| > 3.0$ or $r_{min} < 0.10$.

This definition links the mapped warning level to the same statistical tests used in the adjustment report.

The manual screening step included verification of field closures, station setup consistency and obvious recording inconsistencies before the observations were introduced into the combined adjustment. Consequently, the residuals shown in Figure 5 reflect the behavior of the accepted observation set under the declared stochastic model, rather than the effect of a robust reweighting procedure. This distinction is important because the variance-component estimation in Table 3 assumes that the residuals still carry the statistical information required for group-weight calibration. If robust down-weighting had been applied in the final solution, the interpretation of residual dispersion, redundancy numbers and variance factors would have required a separate discussion. For the numerical results reported in this paper, the residual distribution in Figure 5 comes from the standard WLS adjustment applied after manual field-data screening and closure checks; Huber weighting was used only as an exploratory diagnostic and was not used to automatically suppress observations in the final reported solution.

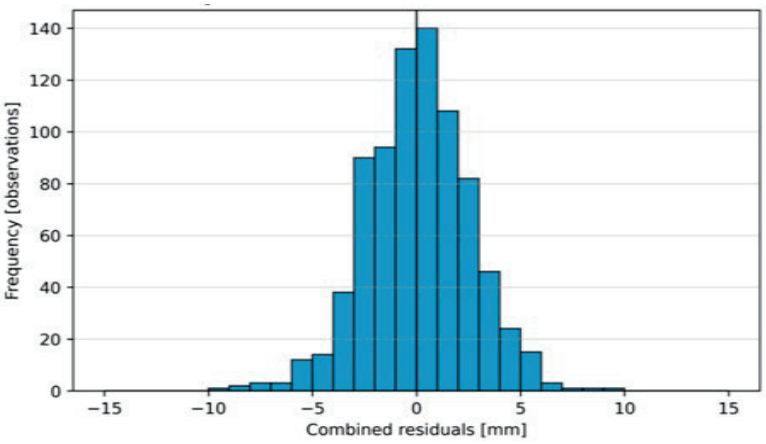



Figure 5. Residual distribution from the combined adjustment; residuals are expressed in [mm] and the histogram bin size is 1 mm

**Datum strategies: HHW versus S-transformation**

In the UCC Măneciu validation run, the HHW solution and the S-transformed solution produced coordinate differences below the reporting precision when the same reference subset and stochastic model were used. The projected covariance trace satisfied the $10^{-12}$ tolerance defined in the methodology, confirming that the statistical content of the free solution was preserved within double-precision numerical limits.

The numerical audit reported the expected similarity datum modes and a clear separation between datum-defect singular values and estimable geometric modes. This separation reduces the risk of treating weak geometry as datum defect or, inversely, treating actual datum modes as estimable coordinates.

**Uncertainty products: error ellipsoids and confidence ellipses**

The adjusted covariance matrix provides a rigorous basis for uncertainty communication and decision-making. Figure 6 presents horizontal confidence ellipses at the 95% confidence level. The magnification factor is stated in the caption and in the figure itself: 1000×, allowing the symbolized ellipses to be interpreted consistently across the network.

Figure 7 presents the vertical cross-section of the 3D error ellipsoids. The leveling observations reduce vertical uncertainty relative to a GNSS-only solution, but they do not eliminate anisotropy because the integrated 3D covariance still contains GNSS vertical noise and height-system transformation uncertainty. This is why the vertical RMS of

8.9 mm remains larger than the leveling residual RMS of 1.2 mm. The two values describe different quantities: one is a coordinate-component uncertainty after full 3D integration, while the other is the residual behavior of the leveling observation group.

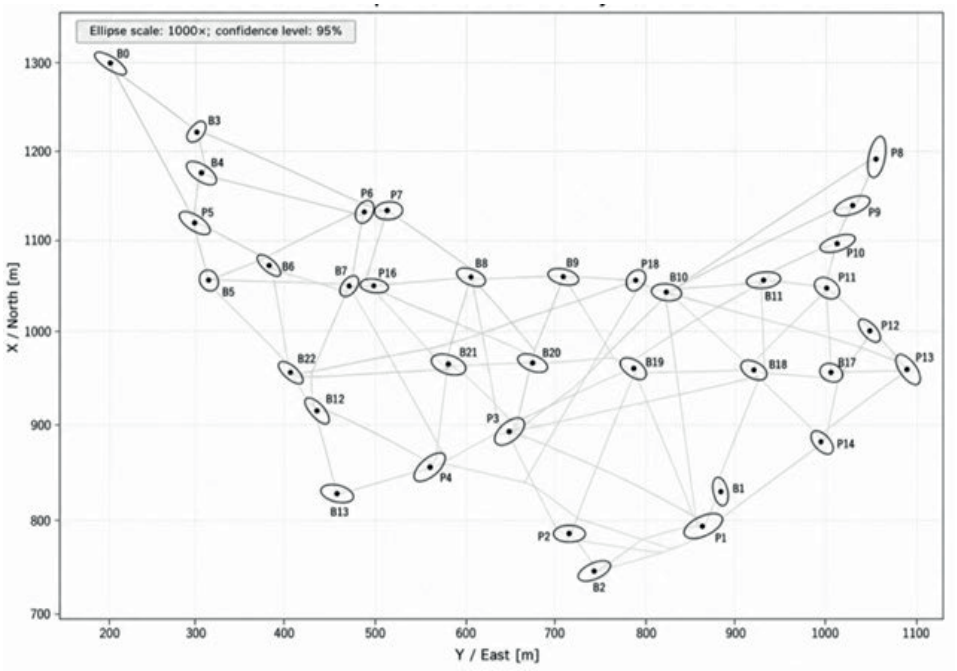



Figure 6. Example of 95% horizontal confidence ellipses derived from Qx. Display magnification factor: 1000×

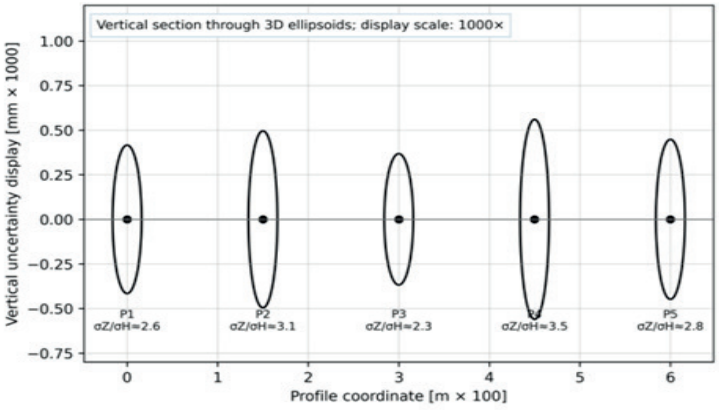



Figure 7. Vertical cross-section of representative 3D error ellipsoids. The figure shows anisotropy after integrating leveling with GNSS covariance; display magnification factor: 1000×

**Numerical summary**

Table 4 expands the numerical summary by adding minimum and maximum values for residuals and uncertainty indicators. The expansion makes it possible to identify weak points in the network rather than reporting only average behavior. The station-by-station report contains the full covariance matrices, redundancy values and residual listings.

Table 4. Expanded representative statistics from the integrated adjustment of the UCC Măneciu network

| Indicator | Metric / Value | Minimum | Maximum | Interpretation |
|---|---|---|---|---|
| Degrees of freedom (DoF) | 1,248 | — | — | Model redundancy after all observation groups. |
| σ0, standard deviation of unit weight | 1.03 | 0.98 | 1.08 | Global model test acceptable. |
| Residuals, directions | 0.9 mgon RMS | -2.6 mgon | +2.9 mgon | No systematic angular bias detected. |
| Residuals, distances | 2.4 mm RMS | -6.8 mm | +7.4 mm | Consistent with EDM model. |
| Residuals, GNSS baselines | 4.8 mm RMS | -12.5 mm | +13.1 mm | Includes full covariance and correlations. |
| Residuals, leveling | 1.2 mm RMS | -3.4 mm | +3.7 mm | High internal vertical consistency. |
| Horizontal coordinate deviation | 3.5 mm mean | 1.9 mm | 6.2 mm | Well-connected stations show lowest values. |
| Vertical coordinate deviation | 8.9 mm mean | 5.8 mm | 14.6 mm | Includes GNSS height and quasigeoid uncertainty. |
| 95% ellipse semi-major axis a95 | 5.1 mm mean | 2.8 mm | 9.7 mm | Largest values indicate weakest horizontal geometry. |
| 95% ellipse semi-minor axis b95 | 2.7 mm mean | 1.4 mm | 5.3 mm | Used for WebGIS uncertainty symbolization. |
| 3D ellipsoid vertical semi-axis c95 | 12.8 mm mean | 7.9 mm | 21.5 mm | Shows vertical anisotropy in cross-section. |

In this processing run, the highest vertical deviation (14.6 mm) and the largest vertical ellipsoid semi-axis were associated with the peripheral P13-P14/B17 sector, where fewer reciprocal cross-ties and longer mixed observation lines reduce redundancy. The central P6-P7-P16 cluster remained horizontally stable after GNSS and EDM integration, while the B5-B6-B7-P16 sequence required label offsets in Figure 1.b to maintain cartographic readability.

**Independent comparison with JAG3D**

GEOSYS SURVEY is not based on JAG3D. The comparison is included only to clarify the relationship with the cited open-source software and to provide an independent numerical check. A reduced version of the Măneciu network containing distances, directions, leveling and GNSS baselines was exported to a JAG3D-compatible observation structure. The adjusted coordinates differed by less than 0.6 mm horizontally and 1.1 mm vertically after applying the same datum realization and stochastic model. Differences were mainly caused by rounding, reduction conventions and implementation details in covariance handling. This result supports numerical consistency without implying software derivation from JAG3D.

**WebGIS dissemination and stakeholder value**

The results are exported as GIS layers in which each station contains adjusted coordinates, covariance-derived uncertainty attributes, ellipse parameters and quality indicators. Table 5 lists the temporal metadata through Epoch_ID, Timestamp and Source_Run fields. These fields are necessary in monitoring applications because coordinates and uncertainty are meaningful only for a defined epoch and processing scenario.

The enriched layers allow rapid inspection of network quality in WebGIS environments and support traceable reporting for non-specialists. For engineering stakeholders, uncertainty metadata are essential for distinguishing significant displacements from noise and for setting defensible thresholds (Koch, 1999; Teunissen, 2000). Figure 8 summarizes the station-layer schema used for monitoring dissemination.

Table 5. WebGIS station-layer schema, including temporal metadata and Qflag logic for monitoring use.

| Field | Type | Description / use |
|---|---|---|
| ID | text | Unique station identifier. |
| Name | text | Station label used in reports and maps. |
| Epoch_ID | text | Monitoring epoch code, e.g., 2025-03. |
| Timestamp | datetime | Observation or adjusted-solution timestamp in ISO 8601 format. |
| Source_Run | text | Processing run or report identifier for auditability. |
| X, Y, Z | double | Adjusted 3D Cartesian coordinates; published layers may also include Stereo 70 X,Y. |
| σX, σY, σZ | double | Coordinate standard deviations from Qx. |
| CovXY, CovXZ, CovYZ | double | Covariance terms preserved for advanced uncertainty reconstruction. |
| a95, b95, Az95 | double | 95% horizontal ellipse semi-axes and azimuth. |
| c95 | double | Vertical/3D ellipsoid semi-axis used in vertical cross-section plots. |
| r_min | double | Minimum redundancy number for station-related observations. |
| t_max / w_max | double | Maximum standardized residual associated with the station. |
| Qflag | integer | 0 = ok; 1 = warning; 2 = fail, based on w-test and redundancy thresholds. |

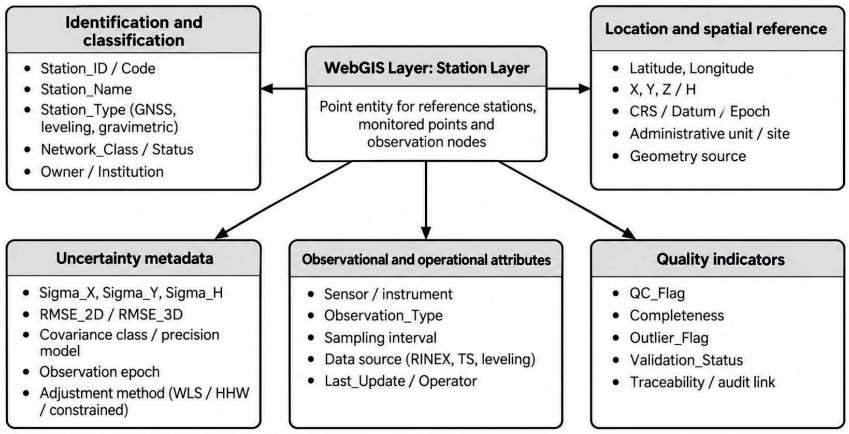



Figure 8. Example of a WebGIS attribute schema for the station layer, including uncertainty and quality metadata

## Limitations and future work

The main limitation of integrated adjustment is that results are only as reliable as the observation covariances and reduction models. GNSS covariance information obtained from black-box processing may be optimistic, and multipath or atmospheric effects may introduce correlations that are difficult to model, especially for real-time solutions (Hofmann-Wellenhof et al., 2008; Leick et al., 2015). Terrestrial observations may be affected by centering errors, refraction and systematic distance-scale effects if instrument calibration and meteorological reductions are not carefully controlled (Ghilani, 2010). In the present static validation, GNSS correlations are modeled spatially within each 3 x 3 baseline block, but temporal correlations between consecutive epochs in PPK/RTK trajectories or long static sessions are not explicitly modeled; such correlations should be introduced in future multi-epoch or kinematic processing through epoch-to-epoch covariance or stochastic-process models.

Future work will focus on robust stochastic modeling through residual diagnostics, explicit temporal-correlation modeling for multi-epoch monitoring, tighter coupling with WebGIS dashboards, and expanded comparison with established adjustment environments. Additional development will also target automated reporting of datum realization, height transformation, covariance propagation and bibliographic/source metadata for every processing run. From a software-engineering perspective, the next implementation stage will also evaluate a cross-platform graphical interface while preserving the current C#/.NET numerical core and the reproducibility of the adjustment reports.

## CONCLUSIONS

The modular 3D platform enables integrated adjustment of terrestrial observations, GNSS-derived products and leveling within a single WLS framework.

The free-network strategy explicitly defines the 7-parameter G-matrix, the treatment of scale, the SVD/QR rank threshold and the S-transformation applied to the full covariance matrix.

GNSS ellipsoidal heights are transformed to Black Sea 1975 normal heights before integration, using a quasigeoid correction and local GNSS/leveling calibration surface; therefore, the 8.9 mm vertical RMS is physically interpretable.

VCE preserves GNSS component correlations and reports final variance factors for each observation group, improving the realism of covariance-based quality products.

The figures and tables are explicitly integrated into the narrative, include missing units and magnification factors, and provide temporal metadata and Qflag logic for WebGIS dissemination.

GEOSYS SURVEY is clarified as an independent implementation; JAG3D is used only as an external benchmark for numerical comparison.

## ACKNOWLEDGMENTS

The authors thank the UCC Măneciu project partners and survey teams for their support in field data acquisition and for providing access to the local infrastructure. The paper also acknowledges the availability of national GNSS positioning services through ROMPOS, which support ETRS89-compatible integration in Romanian engineering projects (ROMPOS, n.d.).

## REFERENCES

Altamimi, Z., Rebischung, P., Collilieux, X., Métivier, L., & Chanard, K. (2023). ITRF2020: An augmented reference frame refining the modeling of nonlinear station motions. *Journal of Geodesy*, 97, 47.

Amiri-Simkooei, A. R. (2007). *Least-squares variance component estimation: Theory and GPS applications* (Doctoral dissertation). Delft University of Technology.

Baarda, W. (1968). A testing procedure for use in geodetic networks. Netherlands Geodetic Commission, Publications on Geodesy, *New Series*, 2(5).

Baarda, W. (1973). S-transformations and criterion matrices. Netherlands Geodetic Commission, Publications on Geodesy, *New Series*, 5(1).

Bjerhammar, A. (1951). *Application of calculus of matrices to the method of least squares: With special reference to geodetic calculations.* Elander, Göteborg.

Centrul Național de Cartografie. (2025). ROMGEO 2025.05: Romanian quasigeoid and coordinate transformation package. Retrieved May 18, 2026, from https://romgeo.ro/

EPSG Geodetic Parameter Dataset. (2024). EPSG:3844, Pulkovo 1942(58) / Stereo70 (revision date: 30 April 2024). International Association of Oil & Gas Producers. Retrieved May 18, 2026, from https://epsg.io/3844-15995

Ge, M., Gendt, G., Dick, G., Zhang, F.-P., & Rothacher, M. (2008). Resolution of GPS carrier-phase ambiguities in precise point positioning (PPP) with daily observations. *Journal of Geodesy*, 82(7), 389–399.

Ghilani, C. D. (2010). *Adjustment computations: Spatial data analysis* (5th ed.). John Wiley & Sons.

Gillins, D. T., & Dennis, M. (2017). Inclusion of Leveling with GNSS Observations in a Single, 3-D Geodetic Survey Network Adjustment. *FIG Working Week 2017*, Helsinki, Finland.

Hofmann-Wellenhof, B., Lichtenegger, H., & Wasle, E. (2008). *GNSS – Global navigation satellite systems: GPS, GLONASS, Galileo, and more*. Springer.

Huber, P. J. (1981). *Robust statistics*. John Wiley & Sons.

IGS/RTCM RINEX Working Group. (2020). *RINEX: The Receiver Independent Exchange Format*, Version 3.05., Ignacio Romero (ed.).

JAG3D Development Team. (2025). JAG3D – Java Applied Geodesy 3D: Geodetic network adjustment software and documentation.

Kadaj, R., & Święţoń, T. (2016). Adjustment of hybrid geodetic networks (GNSS and classical). *Reports on Geodesy and Geoinformatics*, 102(1), 62–74.

Koch, K.-R. (1999). *Parameter estimation and hypothesis testing in linear models* (2nd ed.). Springer.

Leick, A., Rapoport, L., & Tatarnikov, D. (2015*). GPS satellite surveying* (4th ed.). John Wiley & Sons.

McCarthy, D. D., & Petit, G. (Eds.). (2004). IERS conventions (2003) (IERS Technical Note No. 32). International Earth Rotation and Reference Systems Service.

Mikhail, E. M., & Ackermann, F. (1976). *Observations and least squares*. New York: IEP.

ROMPOS. (n.d.). Coordinate systems: Romanian Position Determination System. National Agency for Cadastre and Land Registration / National Center for Cartography. Retrieved May 18, 2026, from https://rompos.ro/index.php/en/technical-info/coordinate-systems

Sillard, P., & Boucher, C. (2001). A review of algebraic constraints in terrestrial reference frame datum definition. *Journal of Geodesy*, 75(2), 63–73. https://doi.org/10.1007/s001900100166

Takasu, T., & Yasuda, A. (2009). Development of the low-cost RTK-GPS receiver with an open-source program package RTKLIB. *International Symposium on GPS/GNSS.*

Teunissen, P. J. G. (2000). Testing theory: An introduction. Delft University Press.

Triggs, B., McLauchlan, P., Hartley, R., & Fitzgibbon, A. (2000). Bundle adjustment: A modern synthesis. In B. Triggs, A. Zisserman, & R. Szeliski (Eds.), *Vision algorithms: Theory and practice* (pp. 298–372). Springer.

van Mierlo, J. (1980). *Free network adjustment and S-transformations*. Deutsche Geodätische Kommission (DGK), Reihe B, 252.

Verhagen, S. (2005). *GNSS integer ambiguities: Estimation and validation* (Doctoral dissertation). Delft University of Technology.

Scientific Papers. Series E. Land Reclamation, Earth Observation & Surveying, Environmental Engineering. Vol. XV, 2026
Print ISSN 2285-6064, CD-ROM ISSN 2285-6072, Online ISSN 2393-5138, ISSN-L 2285-6064

# SEISMIC SURVEY FOR SHALLOW INVESTIGATION OF $CO_2$ MIGRATION PATHWAYS IN BĂILE LĂZĂREȘTI, ROMANIA

**Marius-Bogdan BĂRĂITĂREANU[1, 2], Ionelia PANEA[2], Alexandra Constanța DUDU[1], Andrei Gabriel DRAGOȘ [1, 3], Gabriel IORDCHE[1], Lia STELEA[1, 3], Sorin ANGHEL[1]**

[1]National Research and Development Institute for Marine Geology and Geoecology, GeoEcoMar, 23-25 Dimitrie Onciul Street, 024053, District 2, Bucharest, Romania
[2]Faculty of Geology and Geophysics, University of Bucharest, 1 Nicolae Bălcescu Blvd, 010041, District 1, Bucharest, Romania
[3]Doctoral School of Geology, Faculty of Geology and Geophysics, University of Bucharest, 1 Nicolae Bălcescu Blvd, 010041, District 1, Bucharest, Romania

Corresponding author email: bogdan.baraitareanu@geoecomar.ro

***Abstract***

*At the Lăzărești mofette site in Transylvania, Romania, carbon dioxide migrates upward from depth along fault systems, reaching the shallow subsurface where these pathways branch into faults and fissures. To identify these structures, active-source seismic reflection measurements were performed along a linear profile. Seismic energy was generated using a 10-kg sledgehammer at shot points spaced 1 m apart. Forty SmartSolo vertical-component (5 Hz) receivers were deployed at 1 m spacing along a seismic profile located near two natural carbonated water springs, with the aim of imaging the subsurface pathways that enable carbonated water to reach the surface. After data processing, high-amplitude reflections were identified, corresponding to $CO_2$-bearing, water-saturated formations. Understanding the natural mechanisms of $CO_2$ migration to the surface provides a valuable natural analogue for assessing the safety and long-term behavior of geological $CO_2$ storage associated with major industrial emitters, such as thermal power plants or cement factories.*

***Key words****: carbon dioxide, faults, mofettes, reflection, seismics.*

## INTRODUCTION

Natural systems where $CO_2$ is emitted to the surface, such as areas with mofettes and carbonated springs, represent natural laboratories in which the migration pathways of gases originating from depth can be observed and analysed (Pearce et al., 2004). Studying these environments provides important insights into the mechanisms that control the ascent of $CO_2$ through fault and fracture networks toward the surface (Annunziatellis et al., 2008). Such observations are particularly relevant in the context of $CO_2$ geological storage, where understanding potential migration pathways, leakage mechanisms and possible environmental impacts are essential to increase storage safety and support public trust in the technology (Metz et al., 2005). Identification of migration pathways for $CO_2$ geological storage and also for studying the leakage mechanisms from the natural laboratories can be supported by the active-source seismic method. This method is a versatile tool employed across a broad spectrum of projects, including geotechnical evaluations for civil engineering and hydrogeological studies (Pelton, 2005). This approach is applicable to both near-surface studies and deep-crustal investigations reaching several kilometres, supporting both 2D and 3D data volumes (Cox et al., 2020). The principle of the method is to generate controlled seismic waves that travel through the Earth, reflect at boundaries between different geological layers, and are recorded at the surface by strategically arranged sensors (Cîndea, 1965; Sheriff & Geldart, 1995). The technique is especially effective for mapping layer geometry, faults, fractures and variations in lithology and fluid content (Telford et al., 1990), with results interpreted through advanced data-processing workflows (Yilmaz, 2001; Panea, 2019). In the context of $CO_2$ storage, this method is particularly valuable for characterizing potential

reservoirs and cap rocks, identifying structural traps or leakage pathways, and monitoring changes in the subsurface caused by $CO_2$ injection, thereby supporting safe site selection and long-term storage integrity. Therefore, the seismic method was used to identify migration pathways of $CO_2$ from depth to the surface in a natural laboratory from Romania for the study of $CO_2$ leakage mechanisms that could be associated with an anthropogenic storage.

## MATERIALS AND METHODS

Băile Lăzărești site, Harghita county, is recognized for its dry and wet mofettes with high $CO_2$ concentrations (Dudu et al., 2024). Several surveys were deployed over the years, starting in 2019, to assess the $CO_2$ fluxes, the geological structure and the $CO_2$ migration mechanisms. In order to identify the shallow geological structure, especially fractures in the uppermost tens of meters, a seismic profile was made in April 2025. The profile, marked with blue line on the map from Figure 1, was placed next to $CO_2$ water springs (marked with red circles on the map).




Figure 1. Map of the Băile Lăzărești perimeter showing the geophone profile and the natural $CO_2$-rich water springs

The profile consisted of 40 single-channel SmartSolo geophones with a 5Hz frequency, positioned on a line intersecting potential fractures, faults, or stratigraphic boundaries that might act as primary conduits for carbon dioxide moving upward to the surface. A 1 m spacing was maintained between these sensors, and generation points were similarly established at 1 m intervals, located directly at each geophone station. The waves were generated using a 10 kg hammer that struck a metal plate (Figure 2). To ensure high spatial accuracy, the coordinates and elevations for every geophone and each generation point were registered using a Trimble R980 GNSS system.



Figure 2. Generation of the seismic waves

After data acquisition, the recorded information was retrieved and prepared for subsequent analysis. The analysis was made with SoloLite program. The continuous seismic data gathered over several hours on-site were partitioned so that every hammer strike was isolated into a two-millisecond window. The exact moment of each impact was determined using the data provided by the sensor attached to the hammer during the acquisition phase (Figure 3).



Figure 3. Hammer and the sensor attached on it

The timing for every hammer hit was logged in the SoloTB mobile application and exported as an .sso file, which was then imported into the SoloLite software to isolate only the time segments required for data refinement. Additionally, the software allows for the validation of sensor coordinates, making it possible to confirm the precise location and elevation of each deployed unit.

## RESULTS AND DISCUSSIONS

Within this study, we performed an analysis of the relative energy distribution along the entire length of the seismic profile, based on the signal variations generated by hammer impact. This analysis produces a two-dimensional relative energy map, where a colour gradient serves as a visual indicator: blue tones represent low energy values, whereas yellow and red hues highlight regions of high intensity (Figure 4). This mapping is instrumental for enhancing data visualization and interpretation, as it enables direct correlation with seismic sections in both the time and depth domains.

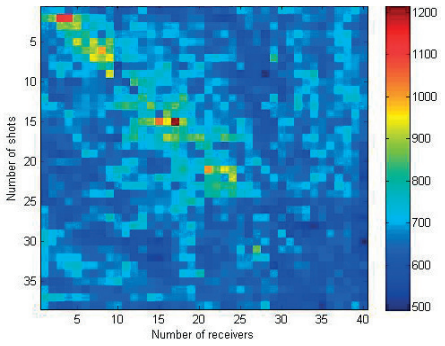



Figure 4. 2D map for relative energy distribution along the seismic line

Figure 4 highlights a non-uniform distribution of relative energy along the seismic line. The highest energy values are recorded in the initial segment of the receiver spread, extending from the first geophone up to approximately geophone 30. In this interval, the signal amplitudes are noticeably stronger, corresponding to the lighter colour tones on the map. Beyond this point, toward the distal end of the profile, a gradual reduction in recorded energy is evident, reflected by the predominance of darker blue shades.

To eliminate the influence of surface relief on reflection travel times, elevation (static) corrections were computed and applied to the seismic dataset. A horizontal reference datum positioned at +750 m - corresponding to the highest elevation along the profile - was selected as the correction level. This choice ensured that topographic variations along the line were properly accounted for without introducing excessive static shifts. Selecting a reference datum substantially above the maximum elevation of the profile would have generated significantly larger static correction values. On the other hand, defining the datum below the ground surface would result in the removal of shallow structural information located between the actual surface and the reference level. The variation in topography along the seismic profile is presented in Figure 5 while the corresponding elevation corrections, computed relative to the +750 m reference datum, are presented in Figure 6.

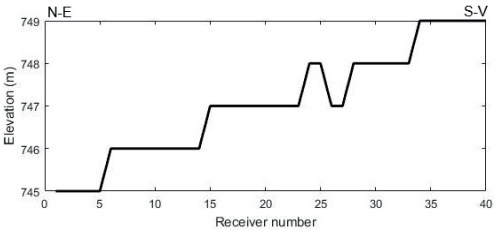



Figure 5. Topographic relief variation along the seismic line

As shown in the topographic profile of the seismic line, elevation increases progressively from geophone 1 to geophone 40, with an approximate elevation difference of 4 m between these points.

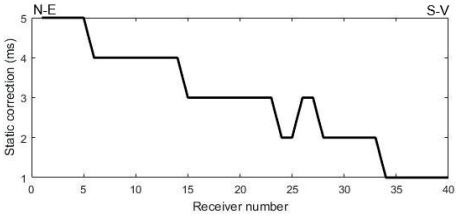



Figure 6. Static corrections for the +750 datum

In shallow seismic reflection processing, band-pass filtering represents a fundamental operation aimed at enhancing data quality and facilitating the interpretation of subsurface reflectors. This procedure is based on the principle that coherent reflection energy is typically concentrated within a limited frequency interval, whereas a significant portion of the unwanted noise occupies frequencies outside this band. By retaining the spectral components associated with reflection events and attenuating those linked to noise, frequency filtering increases the clarity of coherent arrivals and improves the overall signal-to-noise ratio. The design of the filter is guided by spectral analysis, which allows identification of the dominant frequency content of both signal and noise. In near-surface investigations, the effective pass-band generally extends toward higher frequencies compared to deep seismic surveys, reflecting the shorter travel times and the higher-frequency content of hammer-generated sources. However, the selected bandwidth must remain sufficiently broad to preserve wavelet shape and maintain vertical resolution. Figure 7 presents an example of an unprocessed common-source gather (CSG).

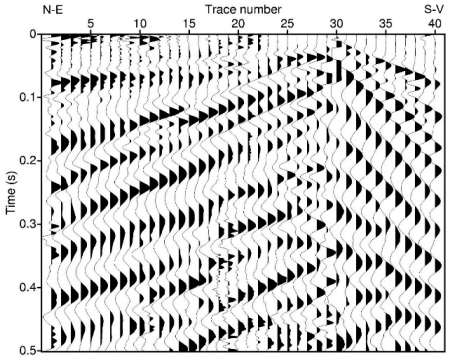



Figure 7. Common-source gather; shot-point location at x = 30 m

The record includes high-amplitude surface waves that require attenuation, together with reflection events that must be preserved during filtering. The choice of cut-off frequencies was determined following examination of the seismic data in the f–k domain, where the distribution of energy in frequency–wavenumber space can be evaluated. The corresponding f–k amplitude spectrum (Figure 8) indicates that surface waves dominate frequencies up to approximately 60 Hz, whereas reflection energy exhibits significant amplitudes primarily within the 35-40 Hz range.

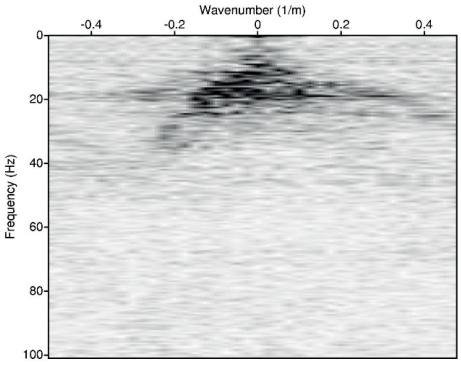



Figure 8. f-k amplitude spectrum of common-source gather from Figure 7

Applying a band-pass filter that overlaps the frequency interval shared by both surface waves and reflected arrivals results in the retention of both energy types within the dataset. For instance, the common-source gather illustrated in Figure 7 was processed using a 10-30 Hz band-pass filter. Within this frequency window, a substantial portion of the surface-wave energy remains visible alongside the reflection signal. When the filter band-pass is shifted toward higher frequencies, surface-wave energy is attenuated more effectively, while reflection events become comparatively more pronounced. This effect is evident in Figure 9, where a 26-50 Hz band-pass filter was applied.

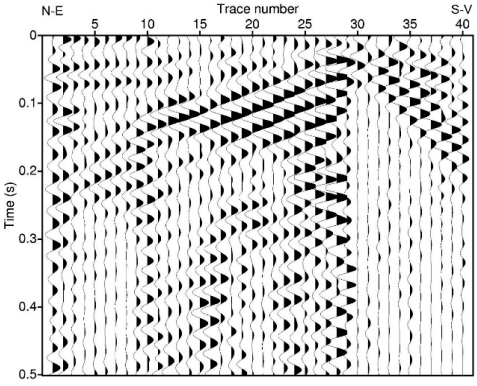



Figure 9. Common-source gather after band-pass frequency filtering applied for 26-50 Hz; shot point location at x = 30 m

Following this adjustment, coherent reflection events can be clearly identified at two-way travel times between 0.05 and 0.1 s, indicating improved separation between surface-wave noise and primary reflections.

A more substantial reduction of surface-wave energy was obtained by integrating several processing steps, namely f-k domain filtering, targeted attenuation of surface-wave noise, spiking deconvolution, and the application of a band-pass filter within the 14-82 Hz frequency interval.

The common-source gathers previously displayed in Figure 7, after undergoing this processing sequence, are illustrated in Figure 10.

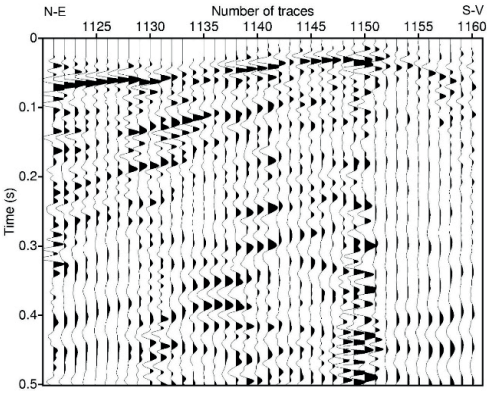



Figure 10. Common-source gather after band-pass frequency filtering applied for 14-82 Hz; shot point location at x = 30 m

Following these procedures, the gathers reveal clearer and more coherent reflection events associated with subsurface boundaries exhibiting pronounced acoustic impedance contrasts. The enhancement of reflector continuity and amplitude demonstrates the effectiveness of the combined filtering and deconvolution workflow in improving data quality. Following the spectral analysis that identified the optimal frequency content for preserving reflections, seismograms filtered within the 14-82 Hz range are advanced to the subsequent processing phase. During this stage, the data traces are reorganized by being sorted into Common Depth Point (CDP) gathers to facilitate high-resolution subsurface imaging.

Constant-velocity stacking was applied as part of the velocity evaluation procedure. For each CDP gather, traces were summed using an individual fixed velocity, producing time-domain seismic sections. Seven separate sections were generated using the following velocity values: 700 m/s, 900 m/s, 1100 m/s, 1300 m/s, 1500 m/s, 1700 m/s, and 1900 m/s. Figure 11 illustrates a seismic section that was obtained with a stacking velocity of 1300 m/s, indicated in the upper-left corner of the panel.

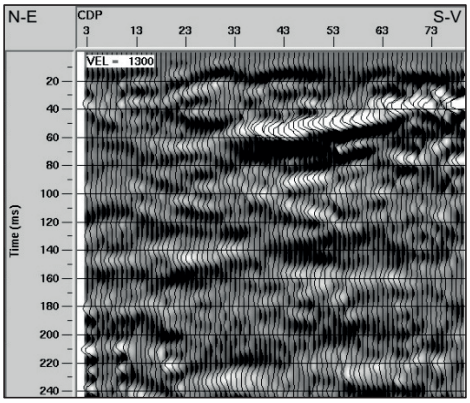



Figure 11. Section constructed for a velocity of 1300 m/s

The shallow layers, down to a few tens of meters, are most clearly delineated due to reflections in the initial sections, constructed for velocity values of 700 and 900 m/s. The reflections indicating the $CO_2$-saturated water layer are best observed in sections whose velocity values are 1100 and 1300 m/s. The sections corresponding to velocities of 1500, 1700, and 1900 m/s begin to lose quality, making the construction of further sections with increasingly higher velocity values impractical.

Depth estimation uncertainties primarily arise from inaccuracies associated with the velocity analysis. Distinct reflections can be observed at several tested velocity values. The final velocity model was established by choosing the time–velocity pairs corresponding to the CDP locations where the reflected signal exhibits maximum amplitude. Figure 12 represents the final velocity model.

A final amplitude analysis was performed on traces 40, 50, 60, and 70 (marked in red), corresponding to the final seismic time section; these traces intersect the strongest reflections associated with the water-saturated layer containing $CO_2$ (Figure 13).

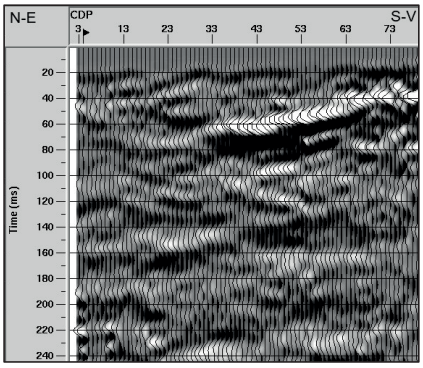



Figure 12. Final velocity model

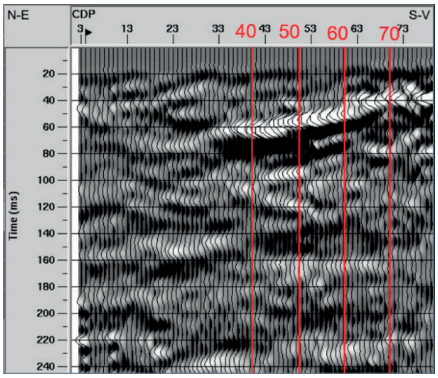



Figure 13. The final seismic section, with the analysed traces marked in red

A graph of amplitude values as a function of frequency was created for all four analysed traces (Figure 14).

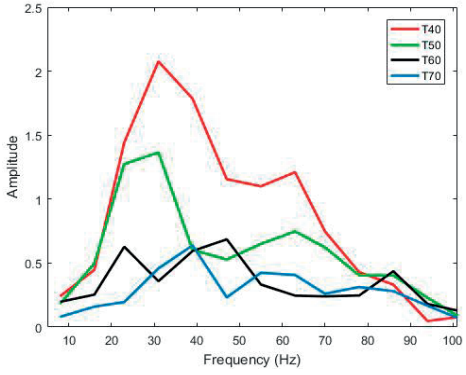



Figure 14. Amplitude spectrum for trace no. 40, 50, 60, 70

The amplitude analysis from Figure 15 shows that traces 40 and 50 exhibit the highest amplitudes, characteristic of the central part of the profile; these amplitudes reach a maximum at a frequency of 30 Hz, and they decrease as the frequency increases. In the case of traces 60 and 70, the amplitudes are slightly lower, with their maximum values also reaching 30 Hz; these values are characteristic of the final part of the profile, and similarly to the previous traces, the amplitudes decrease with increasing frequency. Additionally, traces 60 and 70 show a much smaller amplitude variation compared to traces 40 and 50.

After all these steps, the final seismic section in the time domain was converted into the depth domain for a better visualization of the geological structure intersected by the seismic profile (Figure 15).

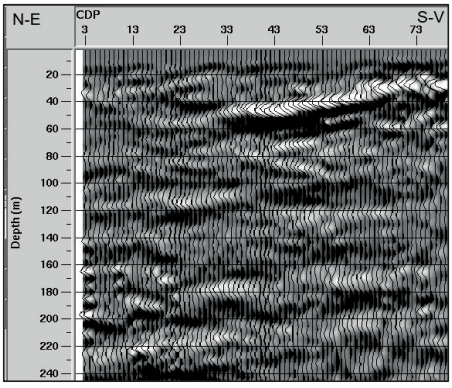



Figure 15. The final seismic section represented in the depth domain (m)

As can be observed from the final depth seismic section, the water-saturated layer containing $CO_2$ can be identified between depths of 20 and 60 m.

## CONCLUSIONS

The seismic reflection investigation carried out at Băile Lăzărești demonstrates that near-surface seismic methods can successfully image subsurface structures associated with natural $CO_2$ migration. Through a combination of elevation corrections, frequency filtering, velocity analysis, and stacking, the processing workflow significantly improved the clarity of reflection events and allowed the identification of high-amplitude reflections linked to water-saturated formations containing $CO_2$ at depths

between approximately 20 and 60 m. The results indicate that seismic data can effectively highlight the pathways through which $CO_2$-rich fluids migrate toward the surface. By providing detailed images of these natural migration routes, the study offers a valuable natural laboratory for understanding how carbon dioxide might leak in a geological storage environment. Consequently, such investigations contribute to assessing potential leakage pathways and improving the monitoring strategies required for the safe long-term storage of anthropogenic $CO_2$.

## ACKNOWLEDGEMENTS

The research leading to these results was made within the project PN 23 30 04 04 "Development of an environmental monitoring methodology for potential $CO_2$ storage sites in Romania (Dezvoltarea unei metodologii de monitorizare de mediu pentru potențialele situri de stocare de CO2 din România)", financed by the Ministry of Research, Innovation and Digitalization of Romania through the Core Program. The authors would like to acknowledge and to thank for the support of town hall of Lăzărești, who facilitated the access to the site and the smooth running of the campaign. They are also grateful to the Faculty of Geology and Geophysics, University of Bucharest, for the academic support provided during the research activities, and thank the anonymous reviewers for their valuable suggestions that helped improve the manuscript.

## REFERENCES

Annunziatellis, A., Beaubien, S. E., Bigi, S., Ciotoli, G., Coltella, M., & Lombardi, S. (2008). Gas migration along fault systems and through the vadose zone in the Latera caldera (central Italy): Implications for $CO_2$ geological storage. *International Journal of Greenhouse Gas Control, 2*(3), 353–372.

Cox, D. R., Newton, A. M. W., & Huuse, M. (2020). An introduction to seismic reflection data: Acquisition, processing and interpretation. In N. Scarselli, J. Adam, & D. Chiarella (Eds.), *Regional Geology and Tectonics: Principles of Geologic Analysis* (2nd ed., Vol. 1, pp. 571–603). Elsevier BV. https://doi.org/10.1016/B978-0-444-64134-2.00020-1

Cîndea, I. (1965). Înregistrarea și separarea undelor seismice [Recording and Separation of Seismic Waves]. In L. Constantinescu (Ed.), *Prospecțiuni Geofizice, Vol. II: metodele câmpurilor artificiale* [*Geophysical prospecting, Vol. II: Artificial field methods]* (p. 288). Technical Publishing House.

Dudu, A.-C., Pavel, A. B., Avram, C., Catianis, I., Iordache, G., Rădulescu, F., Lupașcu, N., Dragoș, A.-G., Dobre, O., & Sava, C.-Ș. (2024). Environmental assessment of the area with natural $CO_2$ emissions in Băile Lăzărești. *Scientific Papers. Series E: Land Reclamation, Earth Observation & Surveying, Environmental Engineering*, XIII.

Metz, B., Davidson, O., de Coninck, H., Loos, M., & Meyer, L. (2005). IPCC special report on carbon dioxide capture and storage. In *Intergovernmental Panel on Climate Change* (pp. 1–431). Cambridge University Press.

Pelton, J. R. (2005). Near-surface seismology: Surface-based methods. In D. K. Butler, *Near-surface geophysics* (pp. 219–250). Society of Exploration Geophysicists. https://doi.org/10.1190/1.9781560801719.ch8

Pearce, J. M., Czernichowski-Lauriol, I., Lombardi, S., Brune, S., Nador, A., Baker, J., Pauwels, H., Hatziyannis, G., Beaubien, S. E., & Faber, E. (2004). A review of natural $CO_2$ accumulations in Europe as analogues for geological sequestration. In S. J. Baines & R. H. Worden (Eds.), *Geological Storage of Carbon Dioxide* (Vol. 233, pp. 29–41). Geological Society of London. Doi: https://doi.org/10.1144/GSL.SP.2004.233.01.04

Panea, I. (2019). Shallow seismic reflection investigation of unstable sedimentary deposits in the Daneasa area, Romania. *Journal of Environmental and Engineering Geophysics*, *24*(1), 169–174. https://doi.org/10.2113/jeeg24.1.169

Sheriff, R. E., & Geldart, L. P. (1995). *Exploration seismology.* 2nd ed., pp. 47–49. Cambridge University Press.

Telford, W. M., Geldart, L. P., & Sheriff, R. E. (1990). *Applied geophysics.* 2nd ed., pp. 248–250. Cambridge University Press. https://doi.org/10.1017/CBO9781139167932

Yilmaz, Ö. (2001). Migration. In *Seismic data analysis: Processing, inversion and interpretation of seismic data,* 2nd, p. 463. Society of Exploration Geophysicists. https://doi.org/10.1190/1.9781560801580

Scientific Papers. Series E. Land Reclamation, Earth Observation & Surveying, Environmental Engineering. Vol. XV, 2026
Print ISSN 2285-6064, CD-ROM ISSN 2285-6072, Online ISSN 2393-5138, ISSN-L 2285-6064

# SMART INTEGRATED E-PERMITTING PLATFORM FOR URBAN PLANNING AND CONSTRUCTION MANAGEMENT

**Andreea BEGOV-UNGUR[1], Liana Luminita BOCA[2, 3]**

[1]"1 Decembrie 1918" University of Alba Iulia, 5 Gabriel Bethlen, Alba Iulia, Romania
[2]Transilvania University of Brașov, 29 Eroilor Blvd, Brașov, Romania
[3]Technical University of Cluj-Napoca, 28 Memorandumului Street, Cluj-Napoca, Romania

Corresponding author email: liana.boca@unitbv.ro

***Abstract***

*This paper proposes a conceptual Smart Integrated e-Permitting Platform for urban planning and construction authorization, designed to address fragmented administrative workflows and limited interoperability between public institutions in Romania. The model integrates beneficiaries, design firms, local authorities, county councils, and technical approval providers within a unified digital environment that supports standardized document management, real-time tracking, and coordinated approval processes. Recognizing the structural imbalance and limited technical capacity within rural administrations, this framework standardizes end-to-end information flows. Furthermore, the conceptual design directly aligns with recent legislative reforms, specifically the strict 15-day response deadlines and tacit approval mechanisms established under Emergency Ordinance no. 31/2025. By structuring the system into a layered architecture and aligning it with European interoperability principles, the proposed solution successfully reduces administrative delays, improves transparency, and provides a highly scalable foundation for future digital governance and broader regulatory integration.*

***Key words****: construction authorization, digital public administration, interoperability, smart e-permitting system, urban planning.*

## INTRODUCTION

Romania's construction and urban planning framework operates within a highly regulated environment, where administrative procedures depend on continuous document exchange between multiple public institutions. These workflows are essential for issuing permits, monitoring compliance, and ensuring that construction activities respect legal and technical standards.

In practice, digital support for these processes remains fragmented. Existing software solutions are generally developed for local administration use, most often at the level of town halls. They are primarily focused on the preparation and management of urban planning certificates and building permits, with only limited extension toward document handling in later phases such as project reception. However, these tools do not support a coherent, end-to-end flow of information across institutions. As a result, communication between authorities is still partially dependent on isolated systems, manual transmission of documents, and non-standardized procedures.

In many cases, obtaining a building permit requires, in addition to the urban planning certificate, a series of approvals from relevant authorities such as environmental protection agencies, water management authorities, electricity distribution operators, gas suppliers, and other public utility providers. These approvals are frequently still requested and submitted through physical documentation or via unstructured electronic communication (email), while the use of dedicated digital platforms remains inconsistent and varies significantly across institutions. In this context, the Romanian e-government portal (e-guvernare.ro) provides a general digital infrastructure for public services, enabling the online submission of certain administrative requests and documents through authenticated electronic channels. However, its role remains limited to that of a generic access point for e-services, without supporting a unified or domain-specific workflow for urban planning

procedures. As a result, the processing and management of documents continue to be distributed across separate institutional systems, with no end-to-end integration between authorities involved in the permitting process. Some partial solutions do exist, such as the National Agency for Cadastre and Land Registration platform ANCPI.ONLINE, but these systems operate independently and are not integrated into a unified permitting workflow, lacking real interoperability between institutions.

Within this context, the development of a unified digital platform that integrates all relevant public authorities and institutions becomes a relevant and timely objective. Such a system would not replace existing institutional responsibilities but would support them by structuring communication across all involved entities, including urban planning departments, environmental protection agencies, water management institutions, and utility providers. It would standardize document flows, reduce administrative fragmentation, and improve traceability throughout the entire authorization process, from the issuance of the urban planning certificate to the final approval of construction and the reception of works.

The aim of this study is therefore to propose a conceptual framework for an integrated e-permitting system that facilitates document management and interinstitutional collaboration at national level.

This objective reflects the need to move beyond fragmented administrative tools and toward a coherent digital architecture capable of supporting efficient, transparent, and coordinated decision-making across all institutions involved in the urban planning and construction authorization process.

## MATERIALS AND METHODS

### Current Status and Context of Urban Planning Documentation Management

This section is grounded in the professional experience of one of the authors, gained within a rural local public administration in Romania, where responsibilities in the field of urbanism and landscaping were carried out for a period of nearly three years, some time ago. This experience, developed through direct involvement in daily administrative activities, provided a practical understanding of how urban planning documentation was managed in real operational conditions at that time, including the constraints, working routines, and administrative limitations that shaped the process of issuing and processing official documents.

A key operational challenge in rural administrations concerns the tracking and management of urban planning certificates and building permits within their legal validity periods. Although these documents are governed by clearly defined regulatory timeframes, their monitoring is still predominantly manual, as most administrative records are maintained in physical, paper-based archives. This approach limits the ability to ensure real-time tracking of document status, deadlines, and dependencies between successive approvals.

A further recurring challenge concerns the acquisition and coordination of technical endorsements. The urban planning authorization process requires multiple approvals from various institutions, each operating through distinct administrative channels. This fragmented structure leads to sequential validation steps, extended processing times, and limited visibility over the status of ongoing applications.

In practice, this issue was observed in the interaction between the administration, property owners, and the professionals responsible for preparing urban planning documentation (such as architects and designers). Delays often appeared not because of the documentation itself, but as a result of the lack of synchronized communication and coordination between the involved institutions. This created difficulties in tracking progress and completing the approval chain within reasonable timeframes.

The regulatory framework governing urban planning and construction authorization in Romania is extensive and subject to continuous revision. For personnel newly assigned to responsibilities in this field within local public administrations, the initial adaptation phase often requires substantial training, given the need to navigate a dense network of primary

legislation, secondary regulations, and methodological norms.

As of 2026, the applicable legal framework includes several relevant updates that directly influence administrative practice:

**1. Authorization of Construction Works**

Law no. 50/1991 regarding the authorization of construction works, as amended and supplemented. A milestone structural reform was introduced via GEO / OUG *(Government Emergency Ordinance / Ordonanță de Urgență a Guvernului)* no. 31/2025, which radically streamlined permitting procedures by establishing strict 15-day response deadlines for issuing entities and implementing a tacit approval mechanism to eliminate administrative delays, alongside earlier key updates such as Law no. 193/2019.

**2. Methodological Norms for Application of Law no. 50/1991**

The Methodological Norms for the application of Law no. 50/1991, approved by Order no. 839/2009, as amended and supplemented. The application rules were significantly aligned with primary legislation through Order no. 3454/2019 and other Laws and Regulations.

**3. Spatial Planning and Urbanism**

Law no. 350/2001 on spatial planning and urban planning, supplemented and amended over time with numerous laws (such as law 151/2019) and GEOs.

**Administrative Workflow for Urban Planning Documentation**

The organization of Urbanism and Spatial Planning activities within Romanian public administration shows a clear structural imbalance between urban and rural institutions. In urban town halls and county councils, these departments are generally stable and well defined, with dedicated personnel such as architects and urban planning specialists. In contrast, rural administrations often operate with minimal human resources in this field, where urbanism responsibilities are frequently managed as a one-person department.

In most rural town halls, urbanism responsibilities are assigned to a single employee or a very small administrative unit, reflecting limited internal specialization in urban planning. According to Article 36 of Law no. 350/2001 on spatial planning and urbanism, as subsequently amended, local public authorities may organize urban planning activities either through specialized internal structures or through interinstitutional cooperation mechanisms, including County Council technical structures and intercommunity development associations (ADIs). This legal framework enables rural administrations to rely on external technical support, for the verification and administrative processing of urbanism certificates and building permits. Such cooperation is especially relevant in cases involving new special constructions (eg. company headquarters, factories) or renovations for historical monuments where technical requirements exceed local administrative capacity, etc.

## RESULTS AND DISCUSSIONS

**The Urban Planning and Building Permit Approval Workflow**

Accordingly, Law 50/1991 regarding the authorization of construction works, with subsequent amendments and completions, establishes the competence of issuing urban planning documents depending on both the location of the investment and the nature of the proposed works. In general, local public administrations (commune, town, or city mayor's offices) are competent to issue Urban Planning Certificates for most construction works carried out within the administrative-territorial unit. County councils intervene in specific cases expressly provided by law, particularly for certain categories of works of broader territorial interest or for situations that exceed the competence of local authorities, as regulated under Article 3 of the same law and related normative provisions.

Thus, the allocation of competence is not determined solely by the intravilan or extravilan status of the property, but also by the legal classification and technical characteristics of the investment, as defined by the applicable legislation on urban planning and construction authorization.

Within this regulatory framework, the Urban Planning Certificate represents the first administrative document required to initiate any construction, major modernization, or

demolition intention. This document has a strictly informative character and does not grant the right to execute works. Instead, it establishes the legal, economic, and technical regime of the property, the applicable urban planning requirements, and the complete list of necessary approvals and endorsements required for further procedural steps.

When the Urban Planning Certificate is issued for construction, rehabilitation, or demolition works, obtaining a Building becomes a mandatory and legally binding requirement. The Building Permit is the administrative act through which the competent authority authorizes the execution of works, based on technical documentation prepared by authorized professionals and on all approvals required through the Urban Planning Certificate.

The process continues with the preparation of the Technical Documentation for the Building Permit, developed by an authorized architect or designer in accordance with the requirements specified in the Urban Certificate. This documentation includes technical drawings, written explanations, and all required approvals issued by competent authorities, each following its respective administrative procedure.

Finally, the Building Permit is issued only if the submitted documentation fully complies with the legal provisions in force, the urban planning regulations, and all requested approvals, representing the final administrative act that allows the actual commencement of construction works.

Figure 1 illustrates the main stages involved in granting the Urbanism Planning Certificate by rural town halls, following the submission of an application by the beneficiary. The diagram captures the essential administrative and procedural steps associated with this process.

The workflow for obtaining a Building Permit follows a procedural structure similar to the one presented in Figure 1. The process begins with the submission of the application and the related technical documentation (DEAC) by the beneficiary, followed by the verification and analysis of the submitted documents by the responsible administrative authority. Depending on the characteristics of the project, the procedure may also involve institutional consultations and the validation of additional approvals before the final authorization is granted.

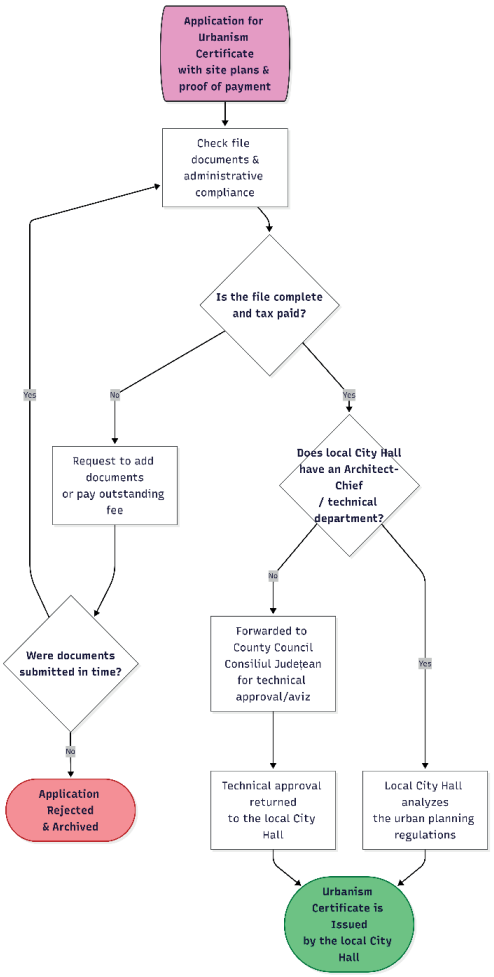



Figure 1. Diagram illustrating the process for issuing an Urbanism Certificate requested from a rural town hall. (The diagram was generated using the Mermaid Live Editor - mermaid.live)

As previously mentioned, the DTAC (Documentation for the Technical Approval of Construction) comprises the complete technical and architectural documentation of the project, including architectural, structural and installation plans, compliance with urban planning regulations, as well as the set of required technical studies and endorsements, all of which are integrated within the documentation submitted for obtaining the building permit.

In the process of managing urban planning documentation for certificates, permits, and authorizations, several procedural verifications are carried out as part of the administrative workflow. These include the verification of the completeness of the submitted documentation, the consistency and correctness of technical plans, as well as the validity of supporting documents and previously obtained approvals. While these steps are essential for ensuring compliance at the operational level, they are not further detailed within the scope of this study.

From a regulatory perspective, Law 50/1991 regarding the authorization of construction works, with subsequent amendments and completions, establishes the institutional competences for granting urban planning documents, depending on both the location of the investment and the nature of the proposed works. In general, local public administrations (commune, town, or city mayor's offices) are responsible for granting Urban Planning Certificates for most construction works within their administrative-territorial jurisdiction, while county councils intervene only in specific cases expressly provided by law.

Following the granting of the Urban Planning Certificate or the Building Permit, in cases where the procedure involves the approval of the urban planning department within the County Council, a copy of the document is transmitted to the Council for archival and record-keeping purposes, in accordance with administrative procedures.

After obtaining the Construction or Demolition Permit, and prior to the commencement of works, the beneficiary is required to notify both the issuing authority (the mayor's office or the County Council) and the County Inspectorate for Construction. Upon completion of the works, a final notification must also be submitted, accompanied by a request for the organization of the reception at the completion of works, which represents the formal closure of the construction process.

During the management of urban planning documentation, administrative staff must also consider additional operational aspects, such as the payment of applicable fees, the validity of submitted documents, and their expiration dates. Although these elements are relevant to the overall administrative workflow, they are not addressed in detail within the scope of this study.

Each of these notifications plays an important role in ensuring the proper legal and procedural development of construction activities. Accordingly, the public authority that issued the permit is responsible for registering, processing, and responding to all requests submitted by beneficiaries.

All such requests and notifications, typically accompanied by supporting documentation, must be carefully managed by public administration staff. This process is time-consuming, particularly in cases requiring multiple institutional approvals. For this reason, a well-structured and integrated information system that enables efficient document exchange between institutions and supports their subsequent management could significantly improve administrative efficiency in this field.

**Architecture and Functional Design of the Smart Integrated E-Permitting System**

An Information System (IS) is an integrated environment composed of hardware, software, people, and processes, designed to collect, process, and transform data into meaningful and valuable information (Hasan, 2018).

An e-permitting system is an integrated e-government platform that digitizes the submission, processing, coordination, and approval of permit applications within administrative procedures, enabling a more structured and data-driven management of authorization workflows in the construction sector (Amer et. al., 2025) and Information Technology refers to the set of technologies used within a system, typically including hardware, software, databases, and communication networks. It can be defined as the "field concerned with the study, design, development, implementation, support, and management of computer-based information systems" (Florida Tech, 2020).

The proposed system aims to develop a centralized platform that integrates all stages and all actors involved in the urban planning and construction authorization process.

The starting point is represented by users (beneficiary) who require urban planning documents, either for construction purposes or

for various interventions on existing properties. These users can interact directly with public administration bodies and with professionals responsible for preparing the necessary technical documentation.

The platform also includes public institutions with decision-making authority in managing urban planning documents, such as town halls (municipalities) and county councils. These entities manage the analysis, verification, and approval process of documentation, in accordance with the competencies established by the applicable legislation.

Another essential component consists of architectural and urban planning firms responsible for preparing the technical documentation required to obtain certificates and construction permits. Integrating these actors into the system enables workflow standardization and reduces information fragmentation.

At the same time, the platform connects the institutions responsible for issuing the various endorsements and approvals required within DTAC documentation (Technical Documentation for Construction Authorization), such as utility providers and infrastructure operators in sectors including electricity distribution companies, water and wastewater utilities, natural gas suppliers, and other technical service providers involved in the coordination and validation of public infrastructure connections. These institutions contribute through technical assessments specific to their areas of expertise, and the digitalization of their interaction reduces approval times and improves process traceability.

From a conceptual perspective, this platform represents a proposed model rather than an already implementable system within the current legislative framework. Its full operational deployment would require regulatory adaptations and institutional alignment. However, it is designed in accordance with the broader European and national direction toward administrative digitalization and interinstitutional interoperability, which has become increasingly prominent in recent years, as EU policy frameworks emphasize improved governance of interoperability activities and the adoption of common operational models for delivering digital public services that account for the needs of citizens and businesses across Member States (European Commission, 2017).

Through this integrated approach, the system aims to create a unified framework of collaboration between citizens, designers, local authorities, and approval institutions, with the goal of increasing the efficiency of the entire administrative workflow.

At platform level, users are organized according to distinct roles, including project beneficiaries, architectural and design firms, and public institutions involved in the authorization process. Each beneficiary is digitally linked to the firm responsible for preparing their technical documentation, enabling continuous collaboration within a single integrated system.

Through a personal account, both beneficiaries and design professionals can monitor at any time the full status of their applications and documents in progress. The platform provides clearly defined workflow stages such as “registered”, “in progress”, “under review”, “pending approval”, “approved”, or “rejected”, ensuring transparency and a clear understanding of the administrative process. The same tracking logic applies to all requested endorsements and approvals issued by competent authorities, allowing design firms to centrally manage and monitor all required approvals within a unified digital environment.

The platform also integrates the role of the State Inspectorate in Construction (ISC), which performs control and verification activities during the authorization process, ensuring compliance with applicable technical and legal regulations.

The operational workflow of the platform starts with the submission of a request by the beneficiary through the system interface. The design firm prepares and uploads the technical documentation, which is then automatically routed to the competent authorities and utility providers for review and approval. Each institution evaluates the documentation in parallel or sequentially, depending on regulatory requirements, while the system continuously updates the status of the process. Once all necessary approvals are collected, and the technical documentation is ready, the local authority issues the final authorization, and the

complete file is archived digitally within the system.

The proposed system can be conceptually structured into three main architectural layers: the user interface layer, the application and workflow management layer, and the data and interoperability layer. This layered approach ensures separation of concerns, scalability, and efficient coordination between different institutional actors.

The Unified Modelling Language (UML) is a standardized visual modelling language used for specifying, visualizing, and documenting the structure and behaviour of software systems (Koç, 2021). It provides a consistent graphical notation that allows complex systems to be represented in a clear and structured manner, facilitating communication between stakeholders involved in system design and development.

The Unified Modelling Language (UML) defines 14 officially recognized types of diagrams. These diagrams are divided into two main categories: structural diagrams (which show what a system is made of) and behavioural diagrams (which show how a system acts and interacts) (Dennis et al., 2015).

Among the various UML diagram types, use case diagrams play a fundamental role in the early stages of system analysis, as they capture the functional requirements of a system from the perspective of external users. These diagrams provide a high-level overview of the system's expected functionalities, illustrating how different actors interact with the system and what services the system is intended to deliver. As such, they contribute to validating requirements and ensuring alignment between system design and user expectations.

The construction of a use case diagram involves identifying the system boundary, defining the relevant actors, specifying the use cases, and establishing the relationships between them. In UML notation, the system is represented as a boundary box, actors are depicted as external entities interacting with the system, use cases are represented as ellipses, and relationships are illustrated using connecting lines that define interactions and dependencies.

Figure 2 presents a UML Use Case diagram that illustrates the proposed structure of the e-Permitting platform. The diagram highlights the main actors involved in the urban planning and construction authorization process, including beneficiaries, design firms, public authorities, utility providers, and the State Inspectorate in Construction. It also depicts the key interactions between these actors and the system, emphasizing the main functional areas supported by the platform, such as document submission, approval workflows, and status monitoring. The diagram was developed using PlantUML (https://www.plantuml.com/), an open-source tool that generates UML diagrams from textual descriptions, facilitating diagram maintenance, reproducibility, and version control.

Although use case diagrams effectively capture system functionalities and actor interactions, they do not describe the chronological order in which these interactions occur. To address this limitation, UML sequence diagrams are used to model the temporal flow of messages exchanged between participants during the execution of a process. By representing interactions in time sequence, these diagrams provide a detailed view of system behaviour and support the analysis of workflow execution and coordination among system actors (Dennis et al., 2015).

While the Use Case diagram establishes the static structural boundaries, specific roles, and high-level functional requirements of the proposed platform, it does not capture the temporal progression of administrative tasks. To address this dimension, a dynamic perspective is essential for analysing how information, technical validation files, and official notifications are structurally exchanged over time between the involved entities. Accordingly, Figure 3 presents a UML Sequence diagram that details the chronological workflow and message routing logic, mapping out the precise interactions from the initial project collaboration down to the final electronic issuance of the building permit.

The combined application of Use Case and Sequence diagrams enhances the overall system modelling process by addressing both functional and behavioural aspects of the platform. While the Use Case model focuses on system functionalities and user interactions, the Sequence model captures the exchange of

information and coordination mechanisms required for process execution. This integrated modelling approach provides a clearer understanding of system requirements, workflow dependencies, and communication flows, supporting the design and implementation of the proposed e-Permitting platform (Dennis et al., 2015).

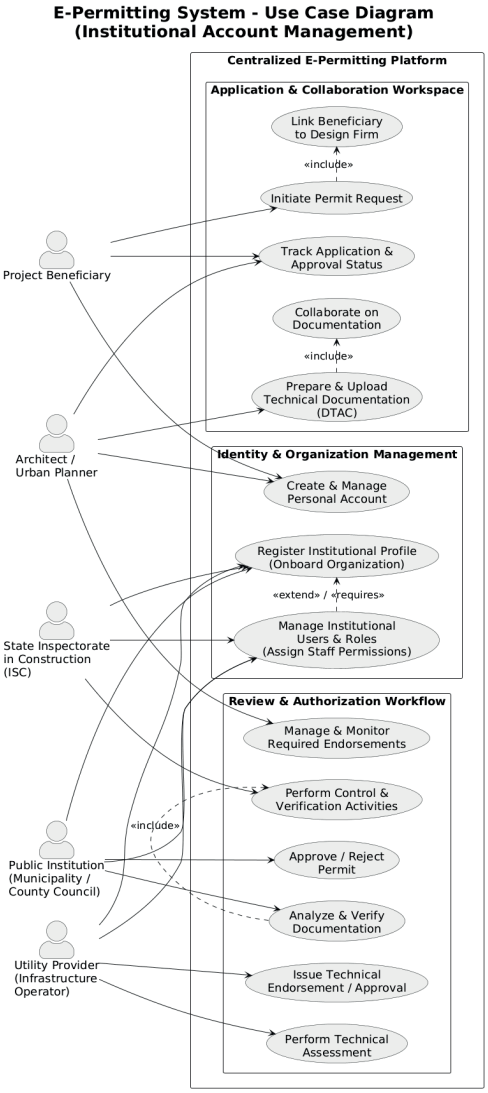



Figure 2. UML Use Case diagram proposing the structure of the e-Permitting platform, illustrating the main actors and their interactions within the urban planning and construction authorization process. The diagram was created using PlantUML (https://www.plantuml.com/)

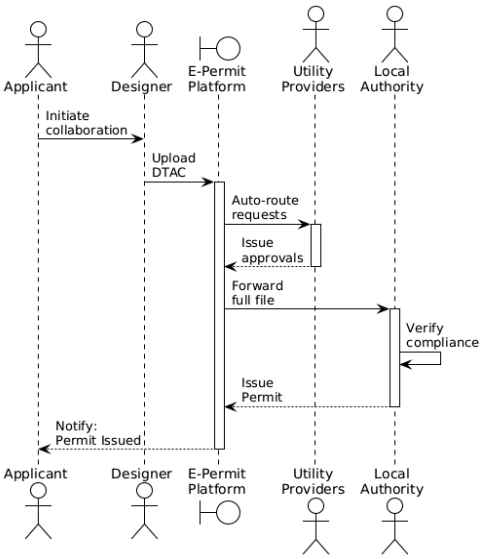



Figure 3. UML Sequence diagram illustrating the chronological flow of interactions and document routing during the permitting process
(The diagram was generated using PlantUML)

While a comprehensive UML model would typically involve multiple diagram types, the Use Case and Sequence diagrams presented here provide an adequate representation of the proposed platform by capturing both its functional requirements and the main interaction workflows.

This chapter presented the conceptual architecture and functional design of the proposed e-Permitting platform. The analysis highlights its potential to function as an integrated digital environment aimed at enhancing coordination, transparency, and efficiency across the urban planning and construction authorization process.

The proposed model supports the transition toward fully digital administrative processes, reducing fragmentation and improving communication between all entities involved in the authorization workflow. This UML-based representation supports the conceptual validation of the proposed solution prior to implementation.

## CONCLUSIONS

The proposed smart integrated e-permitting platform demonstrates significant potential to improve the efficiency and transparency of

urban planning and construction authorization processes. By integrating all relevant actors within a unified digital environment, the system reduces fragmentation and supports more coherent interinstitutional collaboration.

A key advantage of the model lies in the optimization of document management processes at the level of local public administrations, particularly in rural areas where administrative capacity is often limited. The digitalization of communication between town halls, county councils, design firms, and technical approval authorities can significantly reduce processing times and administrative delays.

The implementation of such a system requires institutional coordination and regulatory adaptation. Existing legislative frameworks would need to be aligned with the requirements of fully digital workflows, including secure electronic document exchange, standardized approval procedures, and interoperability between public authorities.

From an architectural perspective, the system can be extended to include additional institutional actors involved in the authorization process, such as environmental protection agencies, emergency inspectorates, public health authorities, and other specialized entities issuing technical endorsements. This extensibility ensures scalability and adaptability to complex regulatory contexts.

Although the proposed model is conceptual in nature, it provides a structured foundation for future developments in digital governance within the construction and urban planning sector. Its implementation would require multidisciplinary collaboration between IT specialists, legal experts, and public administration stakeholders to ensure functional and regulatory coherence.

## REFERENCES

Amer, L., Thneibat, M., Sammour, F., & Lepkova, N. (2025). Evaluating the e-permit system in construction using stakeholder analysis and network theory. *Journal of Civil Engineering and Management, 31*(3). 224–247. https://doi.org/10.3846/jcem.2025.22253

Dennis, A., Wixom, B. H. & Tegarden, D. (2015). *System Analysis &Design - An Object-Oriented Approach with UML*, 5th edition, John Wiley & Sons, Inc., USA, ISBN 978-1-118-80467-4.

European Commission (2017). European Interoperability Framework – Implementation Strategy, Retrieved April, 2026 from https://eur-lex.europa.eu/resource.html?uri=cellar:2c2f2554-0faf-11e7-8a35-01aa75ed71a1.0017.02/DOC_1&format=PDF

Florida Tech (2020). Information Systems vs. Information Technology. Retrieved April, 2026 from https://www.floridatechonline.com/blog/information-technology/information-systems-vs-information-technology/.

Hasan, F. F. (2018). A Review Study of Information Systems. *International Journal of Computer Applications, 179*(18). 15-19.

Koç, H., Erdoğan, A. M., Barjakly, Y., & Peker, S. (2021). UML Diagrams in Software Engineering Research: A Systematic Literature Review, Proceedings of The 7th International Management Information Systems Conference, 74(1). 13; https://doi.org/10.3390/proceedings2021074013

Ministry of Development, Public Works and Administration (MDLPA) (2023). Order no. 839/2009 for the approval of the Methodological Norms for the application of Law no. 50/1991.

Monitorul Oficial (Official Gazette of Romania) no. 933 from October 13, 2004, Law no. 50/1991 regarding the authorization of construction works – republished and updated.

Monitorul Oficial (Official Gazette of Romania) no. 373 from July 10, 2001, Law no. 350/2001 on spatial planning and urbanism – republished and updated.

Scientific Papers. Series E. Land Reclamation, Earth Observation & Surveying, Environmental Engineering. Vol. XV, 2026
Print ISSN 2285-6064, CD-ROM ISSN 2285-6072, Online ISSN 2393-5138, ISSN-L 2285-6064

# A METHODOLOGICAL FRAMEWORK FOR TERRAIN MORPHOLOGICAL ANALYSIS IN RISK MAPPING BASED ON DEM-DERIVED GEOMORPHOMETRIC PARAMETERS

**Liviu BUZILA[1], Silvia Alexandra DREGHICI[2], Ciprian CORPADE[1], Levente DIMEN[2], Zoltan NYIKES[3]**

[1]Babeș Bolyai University Cluj Napoca, Faculty of Geography, 5-7 Clinicilor Street, Cluj-Napoca, Romania
[2]"1 Decembrie 1918" University of Alba Iulia, 5 Gabriel Bethlen, Alba Iulia, Romania
[3]Milton Friedman University Budapest, 1039, Budapest, 2 Kelta Street, Hungary

Corresponding author email: liviu.buzila@ubbcluj.ro

***Abstract***

*This study proposes an integrated methodological framework for terrain morphological analysis based on high-resolution digital elevation models (DEMs) and a comprehensive suite of geomorphometric parameters, including slope gradient, slope aspect, profile and plan curvature, relative relief, hypsometric indices, flow accumulation, topographic wetness index (TWI), and terrain roughness. These parameters are quantitatively derived using standardized GIS-based algorithms and systematically analysed to capture terrain heterogeneity, hydrological controls, and structural influences on surface and subsurface processes. The morphometric variables are integrated within a geospatial analytical environment through multi-criteria spatial modelling techniques, enabling the structured assessment of terrain susceptibility and the delineation of areas potentially prone to geomorphological instability. The proposed framework emphasizes methodological consistency, reproducibility, and adaptability across different environmental contexts. By formalizing the relationships between terrain attributes and geomorphological processes, the approach provides a scientifically grounded basis for supporting hazard assessment and risk mapping applications. The framework is intended to contribute to evidence-based decision-making in land-use planning, environmental management, and disaster risk reduction, facilitating the development of consistent and operational risk mapping methodologies.*

***Key words****: digital elevation models (DEMs), geomorphological hazard assessment, geomorphometric parameters, multi-criteria spatial modelling, terrain morphological analysis.*

## INTRODUCTION

Terrain morphology exerts a direct control on geomorphological processes by influencing runoff generation, sediment transport, infiltration dynamics, and slope instability, thereby shaping spatial patterns of hazard susceptibility. The increasing availability of high-resolution digital elevation models (DEMs) has enabled the transition toward quantitative terrain analysis based on reproducible geomorphometric parameters (Moore et al., 1991; Wilson & Gallant, 2000).

Geomorphometry provides the methodological basis for deriving terrain attributes directly linked to hydrological and geomorphological processes (Pike et al., 2009). Key parameters include slope gradient, aspect, curvature, and terrain roughness, which describe slope dynamics and erosion susceptibility, as well as flow accumulation and the topographic wetness index (TWI), which quantify runoff concentration and moisture distribution (Beven & Kirkby, 1979; Tarboton, 1997). In addition, hypsometric indices and relative relief provide quantitative measures of landscape structure and evolution (Strahler, 1952; Pike & Wilson, 1971).

Within Geographic Information Systems (GIS), these variables can be systematically derived, standardized, and integrated, enabling multi-criteria spatial modelling of hazard susceptibility. Such approaches allow the combination of multiple terrain parameters into structured analytical models that capture the interactions between topography and geomorphological processes (Burrough & McDonnell, 1998; Guzzetti et al., 1999; Reichenbach et al., 2018).

Despite these developments, a major limitation remains the lack of standardized frameworks for the selection, computation, and integration of geomorphometric parameters. Existing studies often rely on heterogeneous datasets, variable spatial resolutions, and inconsistent weighting schemes, which reduce reproducibility and comparability (Hengl & Reuter, 2009; Evans, 2012). Moreover, the increasing complexity of spatial modelling techniques has not always been accompanied by transparent methodological structuring.

This study addresses these limitations by proposing an integrated and reproducible methodological framework for terrain morphological analysis based on DEM-derived geomorphometric parameters. The approach focuses on the systematic derivation, standardization, and integration of terrain variables within a GIS-based multi-criteria analytical environment, with direct applicability to risk mapping.

By formalizing the relationships between terrain attributes and geomorphological processes and structuring the computational workflow, the proposed framework enhances methodological consistency and supports the development of transferable and operational approaches for hazard assessment and risk mapping.

**Geomorphometric Framework for Terrain Analysis**

Geomorphometry provides a quantitative framework for terrain characterization through the derivation of morphometric parameters from digital elevation models (DEMs). These parameters describe the geometry, hydrological behavior, and structural complexity of the land surface and are widely used as proxies for geomorphological susceptibility in risk mapping (Pike et al., 2009; Hengl & Reuter, 2009).

Terrain morphology controls runoff concentration, infiltration, erosion, sediment transport, and slope instability, as these processes are directly influenced by local gradients, curvature conditions, and the spatial arrangement of topographic surfaces (Moore et al., 1991; Wilson & Gallant, 2000). Consequently, the quantitative extraction of terrain attributes enables the formalization of relationships between land-surface configuration and process dynamics.

Among the primary geomorphometric variables, **slope gradient** expresses the maximum rate of elevation change and constitutes one of the most important controls on gravitational processes and runoff velocity. It is calculated as:

$$S = \arctan\left(sqrt\left(\left(\frac{\partial z}{\partial x}\right)^2 + \left(\frac{\partial z}{\partial y}\right)^2\right)\right)$$

where z represents elevation and ∂z/∂x, ∂z/∂y are the first derivatives of the surface. High slope values generally indicate increased susceptibility to erosion and mass movement (Moore et al., 1991).

Slope gradient directly influences the balance between driving and resisting forces acting on surface materials. Steep slopes are associated with increased shear stress, favouring mass movement processes such as shallow landslides, debris flows, and rockfalls, whereas low-gradient surfaces promote sediment accumulation and characterize depositional environments (Moore et al., 1991; Wilson & Gallant, 2000).

From a hydrological perspective, slope gradient controls runoff velocity, infiltration capacity, and flow concentration. High values enhance surface runoff and erosion, while gentle slopes favour water retention and may contribute to saturation under specific conditions (Beven & Kirkby, 1979; Tarboton, 1997).

Within risk mapping, slope gradient represents a primary conditioning factor, widely used in multi-criteria spatial models where higher values correspond to increased susceptibility. Its spatial distribution enables the identification of threshold zones with significant changes in process dynamics and enhances predictive capacity when integrated with other geomorphometric parameters such as curvature and flow accumulation (Guzzetti et al., 1999; Reichenbach et al., 2018). Derived consistently from DEMs, it ensures reproducibility and supports standardized risk assessment methodologies.

**Slope aspect** defines the orientation of the slope and influences solar radiation, evapotranspiration, soil moisture, and vegetation distribution. It is commonly expressed as:

$$A = \arctan\left(\frac{\frac{\partial z}{\partial y}}{-\frac{\partial z}{\partial x}}\right)$$

Aspect acts as an indirect control on weathering intensity and hydrological response (Wilson & Gallant, 2000).

South-facing slopes (in the Northern Hemisphere) typically experience higher solar radiation, leading to increased evapotranspiration, reduced soil moisture, and enhanced weathering rates, whereas north-facing slopes tend to retain moisture and favour vegetation development.

Within risk mapping, aspect contributes to the differentiation of terrain units with contrasting hydrological and geomorphological behaviour. It is particularly relevant in identifying zones prone to desiccation, soil degradation, or, conversely, moisture accumulation and instability. When integrated with slope gradient and other morphometric parameters, aspect enhances the spatial discrimination of susceptibility patterns, especially in relation to landslides, erosion processes, and vegetation-controlled stability (Moore et al., 1991; Wilson & Gallant, 2000).

Second-order derivatives are represented by **profile curvature** and **plan curvature**, which describe the curvature of the terrain surface in the downslope and contour directions, respectively. These parameters are derived from second partial derivatives of elevation and indicate zones of flow acceleration, deceleration, convergence, and divergence (Evans, 2012). In simplified form, curvature is related to:

$$\left(\frac{\partial^2 z}{\partial x^2}\right), \left(\frac{\partial^2 z}{\partial y^2}\right), \left(\frac{\partial^2 z}{\partial x \partial y}\right)$$

Convex surfaces are generally associated with runoff dispersion and erosional dominance, while concave areas promote flow concentration and material accumulation.

Within geomorphological analysis, profile curvature controls the acceleration or deceleration of flow along the slope, directly influencing erosion and deposition rates, while plan curvature governs lateral flow convergence and divergence, affecting runoff concentration and channel initiation.

In risk mapping, curvature parameters are essential for identifying zones of instability, as areas of flow convergence and concavity are more prone to water accumulation, increased pore pressure, and slope failure. When combined with slope gradient and flow-related indices, curvature significantly enhances the spatial prediction of landslide susceptibility and erosion-prone areas (Moore et al., 1991; Wilson & Gallant, 2000).

**Relative relief** measures the elevation range within a spatial unit and is defined as:

$$R_r = Z_{max} - Z_{min}$$

This parameter reflects local topographic energy and terrain dissection, with high values indicating stronger geomorphic activity and instability potential (Strahler, 1952).

A complementary indicator is the **hypsometric integral (HI)**, which describes the distribution of elevation within a terrain unit:

$$HI = (\bar{Z} - Z_min)/(Z_max - Z_min)$$

where $\bar{Z}$ is the mean elevation. Hypsometric analysis provides information on the evolutionary state of the landscape, distinguishing between youthful, mature, and old geomorphic stages (Pike & Wilson, 1971).

Hydrological controls are captured through **flow accumulation**, which expresses the total number of upslope cells draining into a given cell:

$$FA = \sum_{i=1}^{n} f_i$$

This parameter is essential for identifying preferential drainage pathways, runoff concentration zones, and potential initiation areas for erosion or channelized flow (Tarboton, 1997).

In risk mapping, flow accumulation is a key variable for delineating areas susceptible to concentrated surface runoff, gullying, and fluvial incision. It also plays a fundamental role in the identification of hydrologically active zones, particularly when integrated with slope gradient and topographic wetness index, significantly improving the prediction of erosion-prone and instability areas.

A key compound index is the **Topographic Wetness Index (TWI)**, which estimates the tendency of water to accumulate as a function of slope and contributing area:

$$TWI = \ln\left(\frac{a}{\tan(\beta)}\right)$$

where $a$ is the specific catchment area **and tan β is the local slope angle. High** TWI values indicate zones potentially affected by saturation

excess, subsurface flow, and reduced slope stability (Beven & Kirkby, 1979).

Terrain heterogeneity is further represented by **terrain roughness**, commonly calculated as the local standard deviation of elevation values:

$$R = sqrt\left(\left(\frac{1}{n}\right) * sum_{i=1}^{n}(z_i - \bar{z})^2\right)$$

This metric reflects the irregularity of the surface and is often associated with structurally complex or highly dissected terrain (Hengl & Reuter, 2009).

Taken together, these parameters provide complementary information on terrain geometry, hydrological response, and morphodynamic behaviour. Their integrated use within a GIS-based framework allows a systematic representation of terrain susceptibility and provides the conceptual basis for subsequent methodological implementation in spatial risk modelling.

## MATERIALS AND METHODS

### 1. Data

The methodological framework is based on the use of digital elevation models (DEMs) as the primary data source for terrain analysis. DEMs provide a continuous representation of the land surface, enabling the quantitative derivation of morphometric parameters that describe terrain geometry and its influence on geomorphological processes. The accuracy and spatial resolution of DEM data play a critical role in determining the reliability of derived parameters, as they directly affect the representation of slope gradients, curvature, and hydrological pathways (Moore et al., 1991; Wilson & Gallant, 2000).

High-resolution DEMs are preferred to capture fine-scale terrain variability and local geomorphological features. However, increasing resolution also amplifies noise and micro-topographic irregularities, which may introduce artifacts in derivative calculations. Consequently, preprocessing steps such as filtering, sink filling, and resampling are necessary to ensure data consistency and hydrological correctness prior to analysis (Tarboton, 1997; Hengl & Reuter, 2009).

Although the present study adopts a generalized methodological perspective, the framework is designed to be applicable to a wide range of DEM sources, including satellite-derived datasets (e.g., SRTM, ASTER) and higher-resolution LiDAR-based models, depending on data availability and the scale of analysis.

### 2. Derivation of Geomorphometric Parameters

Geomorphometric parameters are derived from DEM data using standardized GIS-based algorithms that operate on raster representations of elevation. The computation of first- and second-order derivatives is performed through finite difference methods applied to neighbouring cells, allowing the estimation of slope, aspect, and curvature under discrete conditions (Burrough & McDonnell, 1998).

Slope and aspect are typically calculated using 3×3 moving window operators, which approximate local gradients based on elevation differences between adjacent cells. Curvature parameters are derived from second-order derivatives and require careful numerical implementation to minimize sensitivity to DEM noise. Hydrological parameters, such as flow accumulation, are computed using flow routing algorithms, including deterministic approaches (D8) and more advanced methods (D∞), which provide improved representation of divergent flow conditions (Tarboton, 1997).

The Topographic Wetness Index (TWI) is calculated by combining slope and contributing area, requiring prior computation of flow direction and accumulation. Terrain roughness and relative relief are derived using neighbourhood-based statistical operations, which quantify local variability in elevation. Hypsometric analysis is conducted at the level of defined spatial units, typically drainage basins or grid-based partitions, allowing the characterization of elevation distribution and landscape evolution.

To ensure comparability between parameters, normalization procedures are applied, transforming variables into standardized ranges (e.g., 0–1). This step is essential for subsequent integration within multi-criteria models, as it eliminates scale-related biases and facilitates the weighting process (Malczewski, 2004).

### 3. GIS-Based Processing Workflow

The methodological workflow follows a structured sequence of operations designed to ensure reproducibility and consistency in terrain analysis. The process begins with DEM preprocessing, including sink filling to remove artificial depressions and ensure continuous flow routing. This step is essential for the correct computation of hydrological parameters and prevents the propagation of errors in downstream analyses (Tarboton, 1997).

Following preprocessing, geomorphometric parameters are systematically derived using dedicated GIS tools. The workflow integrates both surface-based and hydrological analyses, allowing the extraction of complementary terrain attributes that describe geometric configuration, flow dynamics, and structural variability. Each parameter is generated as a raster layer, maintaining spatial coherence and enabling subsequent overlay operations.

The derived variables are then standardized through normalization techniques, ensuring that all parameters are expressed on a comparable scale. This step is critical in multi-criteria environments, where variables with different units and ranges must be integrated without introducing disproportionate influence.

The final stage of the workflow involves the preparation of input layers for spatial modelling, including classification or reclassification of parameter values into susceptibility-relevant categories. This transformation facilitates the interpretation of terrain attributes in relation to geomorphological processes and enhances their applicability within risk assessment frameworks.

### 4. Multi-Criteria Spatial Modelling

The integration of geomorphometric parameters is performed using multi-criteria spatial modelling techniques, which allow the combination of multiple variables into a single susceptibility framework. This approach is particularly suitable for terrain analysis, where geomorphological processes are controlled by the interaction of several factors rather than a single dominant variable (Malczewski, 2004).

Each parameter is assigned a relative weight based on its theoretical relevance to geomorphological instability. Although weighting schemes may vary depending on the specific application, common approaches include expert-based evaluation and analytical hierarchy processes (AHP), which provide a structured method for comparing the relative importance of variables (Saaty, 1980).

The weighted parameters are aggregated using linear combination methods, resulting in a composite index that reflects the overall susceptibility of the terrain. The resulting values are subsequently classified into discrete categories (e.g., low, moderate, high susceptibility), enabling the delineation of zones with differentiated levels of geomorphological risk.

Given the absence of empirical validation in the present framework, the modelling approach is conceptual and focuses on methodological consistency rather than predictive performance. Nevertheless, the structure of the model allows for future integration of validation datasets, making it adaptable to applied studies.

## RESULTS AND DISCUSSIONS

### 1. Conceptual Results and Analytical Interpretation

The proposed framework allows the formalization of terrain susceptibility as a multivariate function of geomorphometric parameters derived from DEM data. In the absence of empirical calibration, susceptibility is expressed through a composite scoring function based on normalized variables.

$$Sc = \Sigma(wi \cdot Xi, n), \quad \Sigma wi = 1$$

$$Sc = 0.20Sn + 0.05An + 0.10Cp, n + 0.10Cpl, n + 0.15FAn + 0.15TWIn + 0.10Rr, n + 0.10TRn + 0.05HIn$$

All variables are normalized using min.-max. transformation:

$$Xn = (X - Xmin.)/(Xmax. - Xmin.), \quad Xn \in [0.1]$$

The model structure highlights the dominant role of slope gradient, hydrological accumulation, and moisture distribution, which exert primary control on geomorphological instability. Slope influences shear stress and gravitational forcing, while flow accumulation and TWI control water concentration and pore-pressure conditions, which directly affect slope

stability (Beven & Kirkby, 1979; Moore et al., 1991).

**Process-Based Sensitivity**

The contribution of each parameter to susceptibility can be expressed through partial derivatives:

$$\partial Sc/\partial Xi = wi$$

indicating that model sensitivity is directly proportional to assigned weights. Thus, slope gradient and hydrological indices exert dominant control over susceptibility patterns.

Slope-dependent instability can be further related to shear stress:

$$\tau \propto \rho g h \sin(\theta)$$

which increases nonlinearly with slope angle, supporting the positive relationship:

$$\partial Sc/\partial S > 0$$

**Hydrological Contribution**

Hydrological influence is primarily captured through flow accumulation and the Topographic Wetness Index:

$$TWI = ln(a / tan\beta)$$

Increased soil moisture elevates pore-water pressure, reducing effective stress:

$$\sigma' = \sigma - u$$

resulting in decreased shear strength and increased susceptibility:

$$\partial Sc/\partial TWI > 0\,, \partial Sc/\partial FA > 0$$

**Curvature Effects**

Curvature parameters introduce second-order controls by regulating flow convergence and divergence, influencing sediment transport and local moisture distribution. Relative relief and terrain roughness quantify terrain energy and structural complexity, enabling the identification of highly dissected and potentially unstable areas (Strahler, 1952; Evans, 2012;).

The integrated behaviour of these variables defines susceptibility patterns as the result of nonlinear interactions rather than isolated effects. High susceptibility is associated with steep slopes, convergent topography ($Cpl < 0$), high flow accumulation, and elevated TWI values, while low susceptibility corresponds to gentle slopes, limited flow accumulation, and reduced terrain variability.

Although not empirically validated, the model demonstrates internal consistency and aligns with established geomorphological principles, supporting its applicability as a methodological framework for risk mapping (Reichenbach et al., 2018).

- $C_{pl} < 0$ - flow convergence → accumulation
- $C_{pl} > 0$ - flow divergence → dispersion

Profile curvature ($C_p$) regulates flow acceleration:

- $C_p < 0$ - deceleration and deposition
- $C_p > 0$ - acceleration and erosion

The integrated susceptibility behaviour can be expressed as:

$$Sc\ \alpha\ f(Cp, Cpl)$$

**Morphostructural Controls**

Relative relief and terrain roughness quantify terrain energy and structural complexity. Higher values indicate increased vertical dissection and surface irregularity, often associated with active geomorphological processes (Strahler, 1952; Hengl & Reuter, 2009).

$$\partial Sc/\partial Rr > 0\,, \partial Sc/\partial TR > 0$$

**Integrated Susceptibility Behaviour**

The model defines susceptibility as a nonlinear interaction between geometric and hydrological controls. High susceptibility occurs when slope, TWI and flow accumulation increase, while convergent flow conditions dominate.

Conversely, low susceptibility corresponds to low slope gradients, limited hydrological influence, and reduced terrain variability.

The integrated susceptibility behaviour can be expressed as:

$$Sc = f(G, H, M)$$

where: G = geometric component; H = hydrological component; M = morphostructural component.

**Model Consistency**

Although not empirically validated, the model exhibits internal mathematical consistency and aligns with established geomorphological process relationships. The functional relationships between variables reflect well-documented interactions between slope, hydrological accumulation, and terrain structure (Beven & Kirkby, 1979; Reichenbach et al., 2018).

**2. Discussions**

The proposed geomorphometric framework provides a coherent and reproducible methodological structure for terrain-based susceptibility assessment, emphasizing the integration of multiple morphometric variables within a unified analytical model. By formalizing terrain susceptibility as a function of normalized and weighted parameters, the approach ensures methodological transparency and facilitates its implementation within GIS environments.

A major strength of the framework lies in its ability to capture the interaction between geometric, hydrological, and morphostructural controls. Unlike approaches based on single-parameter analysis, the multi-criteria structure reflects the inherent complexity of geomorphological processes, where instability results from the combined influence of slope, moisture conditions, and terrain configuration. The explicit formulation of the susceptibility function enhances interpretability and allows for direct adaptation to different spatial contexts (Malczewski, 2004).

The use of DEM-derived parameters ensures broad applicability, as such data are widely available and can be processed consistently across different regions. Furthermore, the normalization of variables eliminates scale dependency, enabling the integration of heterogeneous datasets within a common analytical framework. This characteristic significantly improves the transferability of the methodology and supports its use in regional or comparative studies.

However, the absence of empirical validation represents a key limitation of the present approach. Without calibration against observed geomorphological events, the assigned weights remain theoretically grounded but not statistically optimized. As a result, the predictive performance of the model cannot be quantitatively assessed, and the susceptibility patterns should be interpreted as conceptual rather than definitive representations of risk.

Another limitation is related to the sensitivity of geomorphometric parameters to DEM resolution and quality. High-resolution datasets may introduce noise and micro-topographic variability, while low-resolution models may oversimplify terrain features, affecting the accuracy of derived indices such as curvature and flow accumulation (Hengl & Reuter, 2009). Additionally, the use of linear combination in the scoring function may not fully capture nonlinear interactions between variables, particularly in complex geomorphological settings.

Despite these limitations, the framework offers a robust basis for methodological development and can be readily extended through the incorporation of empirical datasets, statistical calibration techniques, or advanced modelling approaches. Future research should focus on integrating validation procedures, such as ROC analysis or inventory-based comparison, and exploring nonlinear or machine learning-based methods to enhance predictive capability.

From an applied perspective, the proposed methodology provides a valuable tool for preliminary risk assessment, land-use planning, and environmental management. Its structured and reproducible nature facilitates decision-making processes by offering a consistent approach to terrain evaluation, even in data-limited contexts.

## CONCLUSIONS

The present study proposes a methodological framework for terrain morphological analysis based on DEM-derived geomorphometric parameters, aimed at supporting risk mapping applications. The approach integrates a comprehensive set of terrain attributes within a structured multi-criteria analytical model, enabling the systematic representation of geomorphological susceptibility.

By combining geometric, hydrological, and morphostructural variables, the framework provides a coherent interpretation of terrain behaviour, emphasizing the role of parameter interaction in controlling instability processes. The use of normalization and weighted aggregation ensures methodological consistency and facilitates the implementation of the model in GIS-based environments.

A key contribution of the study lies in the formalization of susceptibility as a quantitative function, which enhances transparency and reproducibility. The proposed structure allows for straightforward adaptation to different spatial contexts and can serve as a foundation for further methodological development.

Despite the absence of empirical validation, the framework demonstrates internal consistency and is grounded in established geomorphological and hydrological principles. However, the lack of calibration limits its direct predictive applicability, and the results should be interpreted as conceptual representations of susceptibility rather than definitive risk assessments.

Future research should focus on the integration of validation datasets, optimization of weighting schemes, and the exploration of nonlinear modelling techniques. The incorporation of statistical and machine learning approaches may further improve the predictive performance and adaptability of the model.

Overall, the proposed framework offers a scientifically robust and flexible basis for terrain analysis and risk mapping, with potential applications in land-use planning, environmental management, and disaster risk reduction.

## REFERENCES

Beven, K. J., & Kirkby, M. J. (1979). A physically based, variable contributing area model of basin hydrology. *Hydrological Sciences Bulletin, 24*(1). 43–69.

Burrough, P. A., & McDonnell, R. A. (1998). *Principles of Geographical Information Systems*. Oxford University Press.

Evans, I. S. (2012). Geomorphometry and landform mapping: What is a landform? *Geomorphology, 137*(1). 94–106.

Guzzetti, F., Carrara, A., Cardinali, M., & Reichenbach, P. (1999). Landslide hazard evaluation: A review of current techniques. *Geomorphology, 31*(1–4). 181–216.

Hengl, T., & Reuter, H. I. (2009). *Geomorphometry: Concepts, Software, Applications*. Elsevier.

Malczewski, J. (2004). GIS-based land-use suitability analysis: A critical overview. *Progress in Planning, 62*(1). 3–65.

Moore, I. D., Grayson, R. B., & Ladson, A. R. (1991). Digital terrain modelling: A review of hydrological, geomorphological, and biological applications. *Hydrological Processes, 5*(1). 3–30.

Pike, R. J., & Wilson, S. E. (1971). Elevation-relief ratio, hypsometric integral, and geomorphic area-altitude analysis. *Geological Society of America Bulletin, 82*(4). 1079–1084.

Pike, R. J., Evans, I. S., & Hengl, T. (2009). *Geomorphometry: A brief guide*. In T. Hengl & H. I. Reuter (Eds.), *Geomorphometry: Concepts, Software, Applications* (pp. 3–30). Elsevier.

Reichenbach, P., Rossi, M., Malamud, B. D., Mihir, M., & Guzzetti, F. (2018). A review of statistically-based landslide susceptibility models. *Earth-Science Reviews, 180*. 60–91.

Saaty, T. L. (1980). *The Analytic Hierarchy Process*. McGraw-Hill.

Strahler, A. N. (1952). Hypsometric (area-altitude) analysis of erosional topography. *Geological Society of America Bulletin, 63*(11). 1117–1142.

Tarboton, D. G. (1997). A new method for the determination of flow directions and upslope areas in grid digital elevation models. *Water Resources Research, 33*(2). 309–319.

Wilson, J. P., & Gallant, J. C. (2000). *Terrain Analysis: Principles and Applications*. Wiley.

Scientific Papers. Series E. Land Reclamation, Earth Observation & Surveying, Environmental Engineering. Vol. XV, 2026
Print ISSN 2285-6064, CD-ROM ISSN 2285-6072, Online ISSN 2393-5138, ISSN-L 2285-6064

# GIS-BASED NOISE MAPPING OF NATURA 2000 SITES EXPOSED TO A1 MOTORWAY TRAFFIC IN ROMANIA

**Cristina CĂLIN, Răzvan Lucian VOICU, Sorin Mihai CÎMPEANU**

University of Agronomic Sciences and Veterinary Medicine of Bucharest, Faculty of Land Reclamation and Environmental Engineering, 59 Mărăști Blvd, District 1, 011464, Bucharest, Romania

Corresponding author email: voicu_razvan2000@yahoo.com

***Abstract***

*GIS-based noise mapping provides a spatially explicit approach for assessing traffic-related acoustic pressure in protected areas. This study compares two Natura 2000 sites located along the A1 motorway in Romania: ROSAC0138 Bolintin Forest, directly crossed by the motorway, and ROSAC0106/ROSPA0161 Middle Argeș Floodplain, located in its proximity. Strategic noise maps were generated for Lden/Lzsn and Lnight/Lnoapte using 2022 traffic data, and the resulting noise contours were integrated in GIS with protected-area boundaries. The analysis quantified the surface of each site exposed to noise levels above 50 dB. Results indicate a clear contrast: in Bolintin Forest, approximately 443 ha, representing 7.8% of the site, are exposed above 50 dB, whereas in Middle Argeș Floodplain only 6.8 ha, representing 0.18% of the site, exceed this threshold. The study demonstrates the usefulness of GIS-based noise mapping for identifying acoustic exposure zones and supporting Natura 2000 management planning.*

***Key words****: acoustic exposure, GIS, motorway traffic, Natura 2000, noise mapping.*

## INTRODUCTION

Road infrastructure is one of the most widespread sources of anthropogenic disturbance in landscapes. In addition to physical habitat loss and fragmentation, roads generate noise, artificial light, pollution, animal mortality and increased human accessibility (Forman & Alexander, 1998). Traffic noise is particularly relevant for protected areas because it extends beyond the road corridor and may modify the acoustic environment of habitats that otherwise appear structurally intact.

Chronic anthropogenic noise can affect terrestrial organisms by masking acoustic signals, altering vigilance and foraging behaviour, changing habitat use and reducing breeding performance (Slabbekoorn & Ripmeester, 2008; Barber et al., 2010; Kight & Swaddle, 2011; Francis & Barber, 2013; Shannon et al., 2014; 2016). These effects are not uniform across taxa or habitats, but the acoustic footprint of roads is increasingly recognised as an important component of infrastructure-related pressure on biodiversity.

Empirical studies have shown that traffic noise can reduce the density of breeding birds near roads and can alter habitat use even where the physical structure of the habitat remains apparently suitable (Reijnen et al., 1995; 1996; Parris & Schneider, 2008).

Experimental work using phantom-road approaches has further demonstrated that traffic noise alone may reduce habitat quality by changing bird distribution and behaviour (McClure et al., 2013; Ware et al., 2015).

Protected areas are not necessarily protected from noise. Buxton et al. (2017) showed that anthropogenic noise is pervasive in many protected areas, while studies in national parks and natural landscapes have demonstrated that soundscape quality may be degraded by roads, visitors and other human activities (Iglesias Merchan et al., 2014). For Natura 2000 sites, established under the Habitats Directive and the Birds Directive, the issue is relevant because conservation effectiveness depends not only on legal designation, but also on the functional quality of habitats and ecological processes (Council of the European Communities, 1992; European Parliament and Council, 2009).

Noise mapping has traditionally been used for human exposure and environmental noise management. However, when integrated in GIS with protected-area boundaries, strategic noise contours can also provide useful spatial information for conservation planning. GIS-based noise mapping can identify acoustic

exposure zones, compare infrastructure-related pressure between sites and support the prioritisation of management measures.

This study compares two Natura 2000 sites located along the A1 motorway in Romania (Figure 1), selected because they represent contrasting spatial relationships with the same transport corridor. ROSAC0138 Bolintin Forest is directly crossed by the motorway, whereas ROSAC0106/ROSPA0161 Middle Argeș Floodplain is located in motorway proximity without being directly crossed. The objective was to assess and compare the spatial extent of motorway-related acoustic exposure using GIS-based overlay analysis of strategic noise contours and protected-area boundaries.

## MATERIALS AND METHODS

### Study design and study sites

The study was designed as a comparative GIS-based assessment of motorway traffic noise exposure in Natura 2000 sites. The comparison was structured around two spatial configurations (Table 1): direct crossing, represented by Bolintin Forest, and proximity exposure, represented by Middle Argeș Floodplain. This design allows the spatial effect of motorway crossing to be distinguished from the effect of motorway proximity.

ROSAC0138 Bolintin Forest is located in the continental biogeographical region, in the lower Argeș plain landscape. According to the source documentation, the site has a total area of 5,638 ha and includes an important forested component dominated by *Quercus robur*. The A1 motorway crosses the site in two sectors, between km 36+000 and km 42+000 and between km 43+000 and km 45+477. The site-specific conservation context was considered with reference to ANANP Decision No. 319/19.07.2021.

ROSAC0106/ROSPA0161 Middle Argeș Floodplain has double conservation status, being designated as both a Special Area of Conservation and a Special Protection Area. The site covers 3,648.94 ha and includes riparian, aquatic and floodplain habitats important for bird species (MEWF, 2020 – Note No. 13916/CA/17.09.2020). In this case, the A1 motorway does not cross the protected area, but runs in its proximity over approximately 41.1 km, between km 35+600 and km 76+700, at distances ranging from approximately 185 m to 2,145 m from the site boundary. The conservation context was considered with reference to ANANP Decision No. 414/16.09.2020, ANANP Decision No. 379/20.06.2023 and the Ministry note for ROSPA0161.

Table 1. Spatial configuration of the Natura 2000 sites analysed in relation to the A1 motorway

| Natura 2000 site | Code | Area (ha) | Spatial relation with A1 | Relevant motorway sector |
|---|---|---|---|---|
| Bolintin Forest | ROSAC0138 | 5,638 | Directly crossed | km 36+000-42+000; km 43+000-45+477 |
| Middle Argeș Floodplain | ROSAC0106 / ROSPA0161 | 3,648.94 | In proximity only | km 35+600-76+700; 185-2,145 m from site boundary |

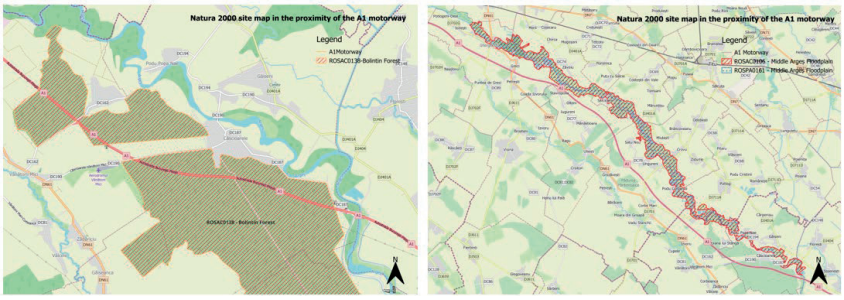



Figure 1. Spatial relationship between the A1 motorway and the analysed Natura 2000 sites

### Noise indicators and input data

Noise exposure was assessed using two strategic noise indicators: Lden/Lzsn, corresponding to the day-evening-night noise indicator, and Lnight/Lnoapte, corresponding to the night-time noise indicator (SR ISO 1996-2:2018). Traffic

input data were derived from the 2022 General Traffic Census for Romanian roads, provided by CNAIR SA – CESTRIN (Table 2). The traffic dataset included annual traffic volumes and vehicle-class distribution by time interval.

Table 2. Main A1 motorway traffic input sectors used for the GIS-based noise-mapping assessment

| Motorway sector | Census post km | Length (km) | Total vehicles in 2022 | Used for site |
|---|---|---|---|---|
| A1 km 30+510-49+208 | 36.050 | 18.698 | 14,556,200 | Bolintin Forest; Middle Argeș Floodplain |
| A1 km 49+208-70+460 | 49.208 | 21.252 | 11,992,440 | Middle Argeș Floodplain |
| A1 km 70+460-94+393 | 85.600 | 23.933 | 10,898,900 | Middle Argeș Floodplain |

The modelling used the legal speed limit for the motorway sector, continuous pulsating traffic flow, asphalt pavement as reference road surface and meteorological conditions favourable to sound propagation. The original technical documentation indicates the use of the NMPB Routes-96 method for road-traffic noise calculation, in accordance with the methodological framework cited in Romanian environmental-noise legislation. CNOSSOS-EU is included in the references as the current common European methodological framework (Kephalopoulos et al., 2012; Directive 2002/49/EC).

**GIS processing and exposure assessment**

The strategic noise maps were integrated in a GIS environment together with the boundaries of the two Natura 2000 sites. Noise contours corresponding to Lden/Lzsn and Lnight/Lnoapte were overlaid with the protected-area polygons to identify and quantify areas exposed to noise levels above 50 dB (OMEWF No. 2328/2021). For each site, the exposed surface was calculated in hectares and expressed as a percentage of the total site area. This metric was used as a noise-exposure ratio for comparing the two spatial configurations.

The 50 dB threshold was used as a spatial comparison threshold for identifying areas exposed to noticeable road-traffic noise in the available strategic noise-map classes. It should not be interpreted as a universal ecological limit for all taxa. Species-specific responses to noise vary substantially, and the ecological relevance of exposure depends on species, habitat, season, behavioural context and the temporal pattern of noise.

## RESULTS AND DISCUSSIONS

**GIS-based exposure patterns**

The spatial overlay analysis revealed a strong contrast between the two Natura 2000 sites. In Bolintin Forest, where the A1 motorway directly crosses the protected area, the noise contours extend inside the site as a continuous corridor along the motorway (Figure 2). In Middle Argeș Floodplain, the motorway runs parallel to or near the site boundary for a longer distance, but most of the protected area remains outside the >50 dB exposure zone (Figure 3).

This contrast indicates that motorway proximity alone does not necessarily generate extensive acoustic exposure within a protected area (Table 3). Site geometry, distance from the road, the position of the road relative to the protected-area boundary and direct crossing of habitat blocks strongly influence the spatial footprint of traffic noise. This interpretation is consistent with studies showing that the spatial extent of noise impact depends not only on source strength, but also on landscape configuration, sound propagation conditions and the behavioural sensitivity of target species (Barber et al., 2010; Francis & Barber, 2013; Iglesias Merchan et al., 2014; Ware et al., 2015).

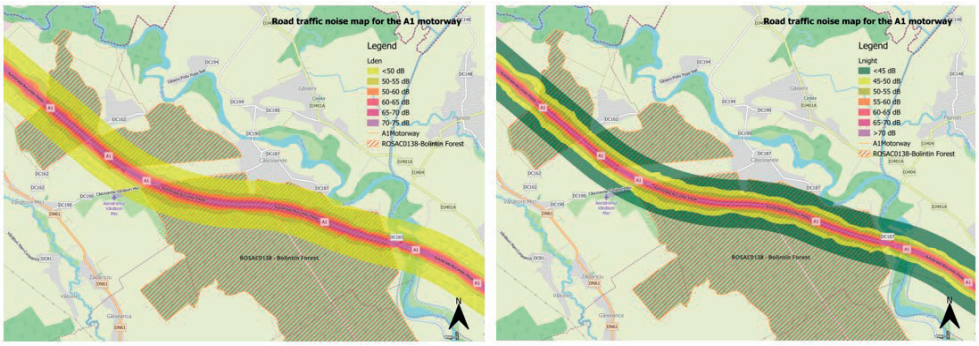



Figure 2. GIS-based noise maps for the A1 motorway in the Bolintin Forest area: Lden/Lzsn and Lnight/Lnoapte

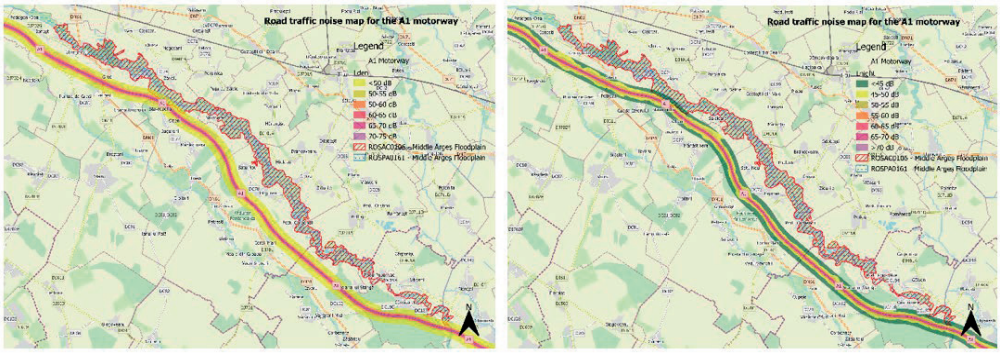



Figure 3. GIS-based noise maps for the A1 motorway in the Middle Argeș Floodplain area: Lden/Lzsn and Lnight/Lnoapte

Table 3. Comparative GIS interpretation of motorway-related acoustic exposure in the two Natura 2000 sites

| Indicator | Bolintin Forest | Middle Argeș Floodplain | Interpretation |
|---|---|---|---|
| Spatial relationship with A1 | Directly crossed | In proximity only | Direct crossing produces stronger overlap between noise contours and the protected area. |
| Area exposed above 50 dB | 443 ha | 6.8 ha | The absolute exposed area is much larger in Bolintin Forest. |
| Share of site exposed above 50 dB | 7.8% | 0.18% | The exposure ratio is approximately 43 times higher in Bolintin Forest. |
| Management relevance | Priority corridor for field validation | Periodic reassessment recommended | GIS layers can support prioritisation of field checks and mitigation analysis. |

**Direct crossing versus proximity**

In Bolintin Forest, the A1 motorway intersects the protected area in two sectors.

The noise maps show that the >50 dB contours penetrate the site along the motorway corridor.

According to the source calculation, the average distance to the 50 dB contour was approximately 249.32 m for carriageway 1 and 249.81 m for carriageway 2 in the case of Lden/Lzsn.

For Lnight/Lnoapte, the corresponding distances were approximately 240.08 m and 240.79 m. The estimated area exposed above 50 dB was approximately 443 ha, corresponding to 7.8% of the total site area.

In Middle Argeș Floodplain, the motorway is located close to the protected area, but does not intersect it directly. The GIS overlay shows that almost the entire site lies outside the >50 dB noise contours. Only approximately 6.8 ha, corresponding to about 0.18% of the site area, were estimated to exceed the 50 dB threshold, in the area corresponding to km 65-66 on carriageway 1.

The comparison indicates that the direct-crossing configuration produces a substantially higher exposure ratio than proximity exposure. In relative terms, the proportion of Bolintin Forest exposed above 50 dB is about 43 times

higher than that calculated for Middle Argeș Floodplain. This result supports the use of GIS-based exposure metrics as a screening tool for identifying Natura 2000 sites where road-traffic noise should be considered in management planning.

**Management relevance and limitations**

Acoustic exposure should not be interpreted in isolation. A motorway corridor may simultaneously generate sound disturbance, reduce habitat permeability, increase wildlife mortality, create edge effects and facilitate human

access. Therefore, in directly crossed sites such as Bolintin Forest, noise mapping should ideally be integrated with road-fragmentation analysis, habitat maps, wildlife movement data and roadkill monitoring.

For Bolintin Forest, the main management priority is the motorway corridor crossing the site. Potential measures include field validation of noise levels, roadkill monitoring, assessment of wildlife crossing needs, evaluation of existing culverts or bridges and analysis of whether acoustic mitigation measures are technically and ecologically justified. For Middle Argeș Floodplain, the current model suggests limited exposure above 50 dB; however, periodic reassessment is recommended if traffic volumes increase or if new infrastructure developments occur.

The main limitation of the study is that it assesses acoustic exposure rather than direct biological response. The findings therefore indicate potential pressure zones, not confirmed ecological impact. Future analyses should integrate GIS noise layers with habitat distribution, species occurrence, breeding sites, seasonal sensitivity, roadkill data and, where possible, field-based acoustic measurements.

**Integration with Natura 2000 management**

The GIS-based outputs are most useful when treated as a first-level screening layer rather than as a final ecological diagnosis. For protected-area management, the value of the method lies in its capacity to identify where field verification should start. In the directly crossed site, the motorway corridor can be prioritised for site visits, comparison with existing culverts and bridges, and verification of whether wildlife movement routes intersect the acoustic exposure zone.

The approach also supports future integration with other spatial datasets. Noise-exposure layers can be overlaid with forest habitats, riparian habitats, breeding or feeding areas, species records and connectivity corridors. Such integration would allow managers to distinguish between areas where noise exposure is spatially present but ecologically less relevant and areas where exposure overlaps with sensitive ecological functions.

Because this study uses modelled strategic noise contours, its conclusions should remain spatial and comparative. A stronger ecological interpretation would require field-based sound measurements, seasonal monitoring, species-specific sensitivity assessment and validation against biological indicators. Nevertheless, the comparison demonstrates that the same motorway may generate very different exposure patterns depending on its position relative to the protected-area boundary.

## CONCLUSIONS

This study demonstrates that GIS-based noise mapping can provide a useful spatial framework for assessing motorway-related acoustic exposure in Natura 2000 sites. The comparison between Bolintin Forest and Middle Argeș Floodplain shows that the spatial relationship between the motorway and the protected-area boundary strongly influences the extent of acoustic exposure. A direct motorway crossing generated a much larger exposed area than motorway proximity alone.

In Bolintin Forest, approximately 443 ha, or 7.8% of the site, were estimated to be exposed to noise levels above 50 dB, while in Middle Argeș Floodplain only 6.8 ha, or 0.18%, exceeded the same threshold. These results support the integration of GIS-based noise exposure indicators into Natura 2000 management planning, particularly for protected areas crossed by major transport infrastructure.

The study should be regarded as a spatial screening and management-support analysis. For ecological interpretation, modelled noise exposure should be combined with habitat and

species data, field measurements, roadkill monitoring and connectivity assessments.

## ACKNOWLEDGEMENTS

This study was developed as part of the doctoral research of Cristina Călin, carried out within the Doctoral School of Engineering and Management of Plant and Animal Resources - University of Agronomic Sciences and Veterinary Medicine of Bucharest.

## REFERENCES

ANANP. (2020). Decision No. 414/16.09.2020 regarding the methodological norms for implementing the conservation objectives for ROSCI0106 Lunca Mijlocie a Argeșului. National Agency for Natural Protected Areas.

ANANP. (2021). Decision No. 319/19.07.2021 regarding the methodological norms for implementing the conservation objectives for ROSCI0138/ROSAC0138 Pădurea Bolintin. National Agency for Natural Protected Areas.

ANANP. (2023). Decision No. 379/20.06.2023 amending Decision No. 414/16.09.2020 regarding conservation objectives for ROSCI0106/ROSAC0106 Lunca Mijlocie a Argeșului. National Agency for Natural Protected Areas.

Barber, J. R., Crooks, K. R., & Fristrup, K. M. (2010). The costs of chronic noise exposure for terrestrial organisms. *Trends in Ecology & Evolution*, 25(3), 180-189. https://doi.org/10.1016/j.tree.2009.08.002

Buxton, R. T., McKenna, M. F., Mennitt, D., Fristrup, K., Crooks, K., Angeloni, L., & Wittemyer, G. (2017). Noise pollution is pervasive in U.S. protected areas. *Science*, 356(6337), 531-533. https://doi.org/10.1126/science.aah4783

CNAIR SA - CESTRIN. (2022). General Traffic Census for Romanian roads. Traffic dataset used for the A1 motorway sectors analysed in this study.

Forman, R. T. T., & Alexander, L. E. (1998). Roads and their major ecological effects. *Annual Review of Ecology and Systematics*, 29, 207-231. https://doi.org/10.1146/annurev.ecolsys.29.1.207

Francis, C. D., & Barber, J. R. (2013). A framework for understanding noise impacts on wildlife: An urgent conservation priority. *Frontiers in Ecology and the Environment*, 11(6), 305-313. https://doi.org/10.1890/120183

Iglesias Merchan, C., Diaz-Balteiro, L., & Soliño, M. (2014). Noise pollution in national parks: Soundscape and economic valuation. *Landscape and Urban Planning*, 123, 1-9. https://doi.org/10.1016/j.landurbplan.2013.11.006

Kephalopoulos, S., Paviotti, M., & Anfosso-Lédée, F. (2012). Common Noise Assessment Methods in Europe (CNOSSOS-EU). *Publications Office of the European Union*. https://doi.org/10.2788/31776

Kight, C. R., & Swaddle, J. P. (2011). How and why environmental noise impacts animals: An integrative, mechanistic review. *Ecology Letters*, 14(10), 1052-1061. https://doi.org/10.1111/j.1461-0248.2011.01664.x

Council of the European Communities (1992). Council Directive 92/43/EEC on the conservation of natural habitats and of wild fauna and flora. *Official Journal of the European Communities.*

European Parliament and Council (2002). Directive 2002/49/EC relating to the assessment and management of environmental noise. *Official Journal of the European Communities.*

European Parliament and Council (2009). Directive 2009/147/EC on the conservation of wild birds. *Official Journal of the European Union.*

Law No. 121/2019 on the assessment and management of environmental noise, with subsequent amendments. Official Gazette of Romania.

Ministry of Environment, Waters and Forests (2020). Note No. 13916/CA/17.09.2020 regarding the minimum special protection and conservation measures for ROSPA0161 Middle Argeș Floodplain.

Order of the Ministry of Environment, Waters and Forests No. 2328/2021 approving limit values for Lzsn, Lnight, Lday and Levening.

SR ISO 1996-2:2018. Acoustics - Description, measurement and assessment of environmental noise - Part 2: Determination of sound pressure levels.

McClure, C. J. W., Ware, H. E., Carlisle, J., Kaltenecker, G., & Barber, J. R. (2013). An experimental investigation into the effects of traffic noise on distributions of birds: Avoiding the phantom road. *Proceedings of the Royal Society B: Biological Sciences*, 280(1773), 20132290. https://doi.org/10.1098/rspb.2013.2290

Parris, K. M., & Schneider, A. (2008). Impacts of traffic noise and traffic volume on birds of roadside habitats. *Ecology and Society*, 14(1), 29. https://doi.org/10.5751/ES-02761-140129

Reijnen, R., Foppen, R., Ter Braak, C., & Thissen, J. (1995). The effects of car traffic on breeding bird populations in woodland. III. Reduction of density in relation to proximity of main roads. *Journal of Applied Ecology*, 32(1), 187-202. https://doi.org/10.2307/2404428

Reijnen, R., Foppen, R., & Meeuwsen, H. (1996). The effects of traffic on the density of breeding birds in Dutch agricultural grasslands. *Biological Conservation*, 75(3), 255-260. https://doi.org/10.1016/0006-3207(95)00074-7

Slabbekoorn, H., & Ripmeester, E. A. P. (2008). Birdsong and anthropogenic noise: Implications and applications for conservation. *Molecular Ecology*, 17(1), 72-83. https://doi.org/10.1111/j.1365-294X.2007.03487.x

Shannon, G., Angeloni, L. M., Wittemyer, G., Fristrup, K. M., & Crooks, K. R. (2014). Road traffic noise

modifies behaviour of a keystone species. *Animal Behaviour*, 94, 135-141. https://doi.org/10.1016/j.anbehav.2014.06.004

Shannon, G., McKenna, M. F., Angeloni, L. M., Crooks, K. R., Fristrup, K. M., Brown, E., Warner, K. A., Nelson, M. D., White, C., Briggs, J., McFarland, S., & Wittemyer, G. (2016). A synthesis of two decades of research documenting the effects of noise on wildlife. *Biological Reviews*, 91(4), 982-1005. https://doi.org/10.1111/brv.12207

Ware, H. E., McClure, C. J. W., Carlisle, J. D., & Barber, J. R. (2015). A phantom road experiment reveals traffic noise is an invisible source of habitat degradation. *Proceedings of the National Academy of Sciences*, 112(39), 12105-12109. https://doi.org/10.1073/pnas.1504710112

Scientific Papers. Series E. Land Reclamation, Earth Observation & Surveying, Environmental Engineering. Vol. XV, 2026
Print ISSN 2285-6064, CD-ROM ISSN 2285-6072, Online ISSN 2393-5138, ISSN-L 2285-6064

# DIGITAL TRANSFORMATION OF TREE INVENTORY THROUGH GIS: OPTIMIZING FORESTRY PROCESSES VIA SPATIAL DATA COLLECTION, INTEGRATION AND ANALYSIS

**Silvia CHIOREAN[1], Tudor SĂLĂGEAN[1, 2], Mircea-Emil NAP[1], Ioana POP[1], Florica MATEI[1], Răzvan PLOSCAR[2], Steluța-Maria SÎNGEORZAN[1], Vasile ȘIMONCA[1]**

[1]Faculty of Forestry and Cadastre, University of Agricultural Sciences and Veterinary Medicine, 400372, Cluj-Napoca, 3-5 Mănăștur Street, Cluj-Napoca, Romania
[2]Technical University of Civil Engineering, 124 Lacul Tei Blvd, District 2, Bucharest, Romania

Corresponding author emails: steluta-maria.singeorzan@usamvcluj.ro, razvanploscar@ortodromus.com

***Abstract***

*The digital transformation of tree inventory through Geographic Information Systems (GIS) is reshaping contemporary forestry practices by enabling higher accuracy, enhanced data integration, and increased operational efficiency. GIS technologies revolutionize forest inventory workflows by facilitating precise spatial data collection and supporting advanced analytical processes. The integration of spatial datasets with modern analytical tools allows for dynamic monitoring of forest resources and provides a robust foundation for informed and sustainable management decisions. The aim of this article is to demonstrate how GIS-based digital methodologies improve the efficiency, standardization, and analytical depth of forest inventory processes, while highlighting their role in supporting modern forestry management. To achieve this, a dedicated field data collection form was developed using Survey123, specifically designed for tree inventory and analysis. This standardized form ensures consistent data acquisition and seamless integration into GIS platforms for subsequent spatial processing and interpretation. Overall, the proposed workflow illustrates the transformative potential of GIS technologies in optimizing forestry operations and advancing sustainable forest resource management.*

***Key words****: Digital Tree Inventory, Forestry Management, GIS, Survey123.*

## INTRODUCTION

Sustainable forest management has become one of the major challenges of the 21st century, driven by climate change, biodiversity loss, increasing anthropogenic pressures, and the growing demand for forest resources. In this context, reliable and up-to-date information on forest ecosystems is fundamental for supporting informed management decisions. White et al. (2013) emphasize hat the development and continuous maintenance of forest inventories are essential not only for assessing current forest conditions but also for projecting future forest development and supporting long-term sustainable management strategies (White et al., 2013). Similarly, Aulló-Maestro et al. (2021) describe forest inventories as the primary source of information for assessing forest structure and monitoring forest dynamics (Aulló-Maestro et al., 2021). For decades, forest inventories have relied on conventional field-based methods involving paper forms, manual measurements, and subsequent office-based data processing. Although these approaches have provided valuable information for forest management, they are characterized by several limitations, including high labour requirements, long processing times, difficulties in data updating, and increased susceptibility to transcription and positioning errors. According to Keskes et al. (2025), many forest inventory variables are still measured manually in the field, making the inventory process both time-consuming and costly, particularly across large and heterogeneous forest landscapes.

The rapid development of digital technologies has fundamentally transformed the way forest inventories are planned, conducted, and managed. Rather than representing a simple transition from paper forms to digital devices, digital transformation involves the integration of advanced technologies into a comprehensive information management system. This

transformation combines field data acquisition, Global Navigation Satellite System (GNSS) positioning, Geographic Information Systems (GIS), remote sensing, laser scanning, cloud-based databases, and spatial modelling within a unified digital workflow. As highlighted by White et al. (2013), modern forest inventories increasingly rely on multi-source information to provide more accurate, timely, and spatially explicit estimates of forest resources (White et al., 2013).

Among these technologies, Geographic Information Systems (GIS) plays a central role by integrating, storing, visualizing, and analysing geospatial information collected from multiple sources. Aulló-Maestro et al. (2021) state that GIS and remote sensing technologies have transformed the use of forest inventory data by enabling wall-to-wall estimation of forest variables based on field measurements and spatial modelling (Aulló-Maestro et al., 2021). The capability of GIS to combine field observations with remotely sensed information allows forest managers to evaluate forest resources more efficiently and consistently than conventional inventory approaches. Recent advances in remote sensing have further accelerated this digital transformation. According to Fassnacht et al. (2024), remote sensing has become an omnipresent technology in forestry and is increasingly applied in operational forest inventory and monitoring (Fassnacht et al., 2024). Airborne LiDAR, terrestrial laser scanning (TLS), mobile laser scanning (MLS), unmanned aerial vehicles (UAVs), and multispectral satellite imagery now provide detailed information on tree position, canopy architecture, stand density, biomass, and forest health. Liang et al. (2018) demonstrated that terrestrial laser scanning significantly improves the accuracy of tree-level measurements, while Hyyppä et al. (2020) showed that laser scanning technologies enable highly precise three-dimensional characterization of forest structure. The integration of these diverse datasets within GIS environments provides substantial advantages for forest management. Spatial databases facilitate efficient data organization, improve interoperability among information sources, reduce redundancy, and support rapid updating of inventory records. Furthermore, spatial analysis techniques enable the assessment of stand structure, species distribution, growth dynamics, regeneration processes, accessibility, harvesting operations, and environmental risks. These capabilities contribute to more informed planning and more effective allocation of forest resources. Digital transformation is also closely associated with the emergence of Precision Forestry, a management paradigm based on high-resolution spatial information and data-driven decision-making. As discussed by Uusitalo (2010), modern forestry increasingly depends on accurate digital information systems that support operational planning and resource optimization (Uusitalo, 2010).

More recently, Damaševičius et al. (2024) highlighted that digital technologies improve the sustainability, efficiency, transparency, and resilience of forest management by facilitating evidence-based decisions and strengthening the integration of ecological, economic, and operational information. Another important aspect of digital forestry is the continuous updating of forest information. Traditional inventories often require several years between successive measurements, whereas digital workflows supported by GIS and remote sensing allow near real-time monitoring of forest conditions. This capability is particularly valuable for detecting disturbances caused by storms, pests, diseases, wildfires, and illegal logging, enabling forest managers to respond more rapidly and effectively.

In addition to improving operational efficiency, GIS-based inventories enhance the quality and consistency of forest information. Spatial databases reduce the likelihood of transcription errors, facilitate data sharing among institutions, and provide standardized datasets that can support national forest inventories, ecosystem monitoring programmes, and scientific research. The integration of field observations with remote sensing products also enables advanced spatial analyses and predictive modelling of forest growth, regeneration, biomass accumulation, and future stand development under different management scenarios.

Against this background, the present study investigates the digital transformation of tree inventory through Geographic Information Systems by analysing the complete workflow of spatial data collection, integration, management, and analysis. The research explores how

rigorous field measurements combined with GIS technologies can optimize forest inventory processes, improve the quality of spatial information, support sustainable forest management, and facilitate evidence-based decision-making. Ultimately, this integrated digital approach contributes to more accurate forest resource assessments, greater operational efficiency, and enhanced capacity for monitoring and managing forest ecosystems in a rapidly changing environmental context.

## MATERIALS AND METHODS

Digital transformation driven by GIS technologies is revolutionizing how forest inventories are conducted, delivering enhanced accuracy and significant operational efficiency. The integration of spatial data with advanced analytical tools enables the dynamic monitoring of forest resources and provides a solid foundation for more informed, sustainable management decisions.

To implement the project on the digital transformation of forest inventorying via GIS, a dedicated field datasheet was developed using Survey123 for tree inventory and analysis. This datasheet ensures the standardized collection of data required for seamless GIS integration and establishes a baseline for subsequent analyses.

In the following paragraphs, we will outline the methodology implemented for data integration and demonstrate how geospatial analysis elevates a standard tree inventory into a strategic asset for smart forestry. Ultimately, our goal was to show that digitalization is no longer an optional technical upgrade, but a fundamental necessity for the efficiency, transparency, and long-term sustainability of modern forestry.

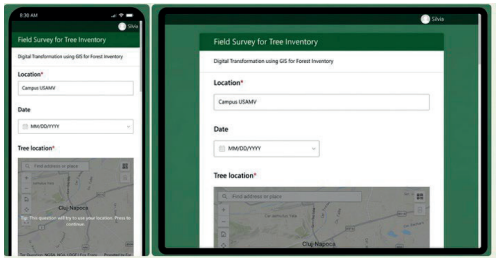



Figure 1. Visualizing the questionnaire and ensuring its accessibility across multiple devices (such as tablets and mobile phones) enhances user accessibility

More precisely, the survey initiates with the record of location-specific details and the date of completion, followed by the acquisition of the precise tree location through the logging of its latitude and longitude coordinates, as shown in Figure 2.

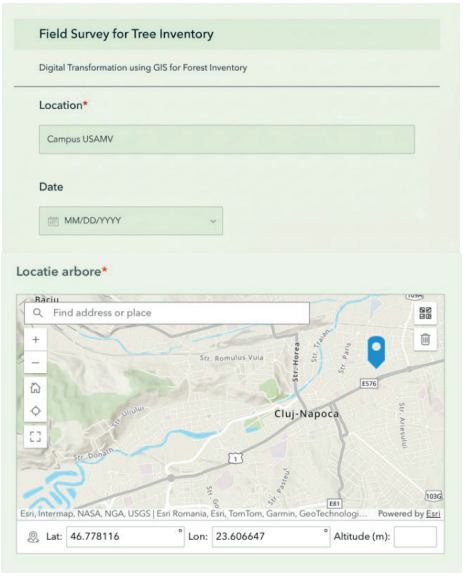



Figure 2. The image shows the initial section of a digital field survey for tree inventory designed to leverage GIS technology, featuring data entry fields for capturing the specific location and the collection date

The image illustrates an interactive map interface within a data collection tool used to precisely capture a tree's geographic coordinates - specifically its latitude and longitude - by placing a marker within the city of Cluj-Napoca. We also present a section marked in Figure 3, dedicated to species identification, featuring mandatory data fields for the common Romanian name, the scientific name, the origin (native or exotic), and the provenance (generative or vegetative) of the tree. In addition, information regarding tree height, clear bole height, and tree diameter was collected (Figure 4).

The questionnaire also includes information regarding the trees' vegetative status, as shown in Figure 5, for example luxuriant, vigorous, normal, sluggish/declining, and dying and health condition (good, satisfactory, poor, or others), along with dedicated sections for field observations and photographs.

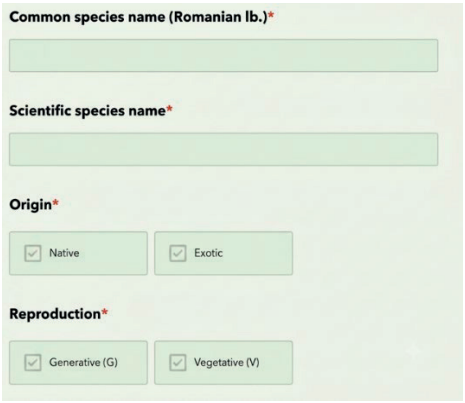



Figure 3. Methodological approaches to dendrometric data collection and species identification

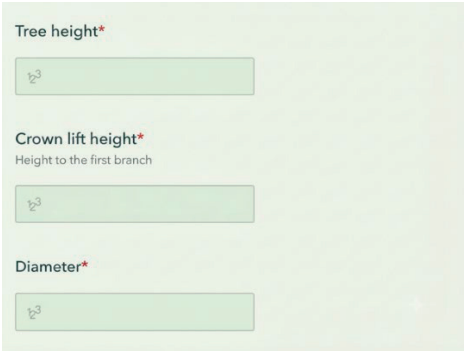



Figure 4. Methodological approaches to dendrometric data collection

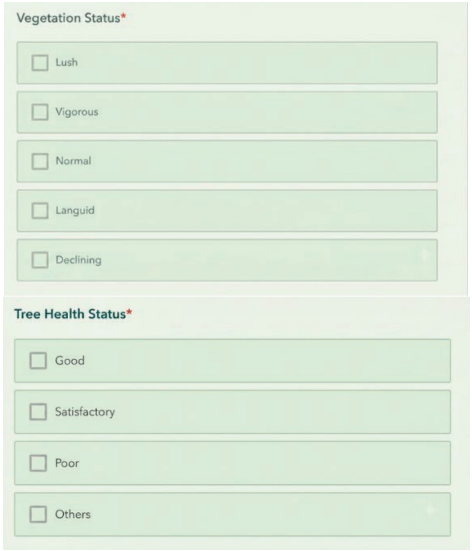



Figure 5. Tree Health Evaluation Interface

## RESULTS AND DISCUSSIONS

By analysing this questionnaire within the Survey123 platform, it becomes possible to systematically evaluate all relevant aspects of a tree, with the results being summarized in the charts presented below. The Figure 6 shows a data table from a Survey123 questionnaire that tracks the frequency of individual words entered for scientific species names ("Denumire stiintifica specie"), which will automatically generate a word cloud once at least 20 responses are collected.

The column chart above (Figure 7) presents the distribution of tree origins ("Origine"), showing that out of 18 responses, 66.67% are classified as exotic ("Exotica") and 33.33% are native ("Indigena").

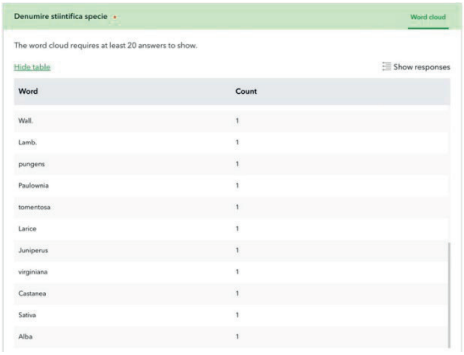



Figure 6. Scientific name of the species




Figure 7. Origin of the tree

The column chart and data table presented in Figure 8 summarize the provenance ("Prevenienţa") of the trees, showing that 72.22% originated through vegetative reproduction ("Vegetativă"), while the remaining 27.78% resulted from generative reproduction ("Generativă").

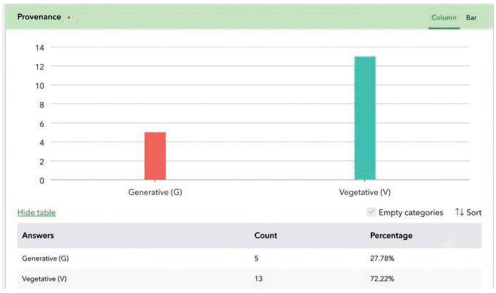



Figure 8. The tree provenance

The histogram and summary metrics display the distribution of tree heights ("Inaltime arbore") - Figure 9, indicating that the surveyed trees range from a minimum height of 4.8 to a maximum of 25, with an average height of approximately 17.22 m.




Figure 9. The height of the tree

The chart represented in Figure 10 illustrates the distribution of clear bole height ("Inaltime elagata"), showing values ranging from a minimum of 0.5 to a maximum of 10.4, with an average height of 4.66.

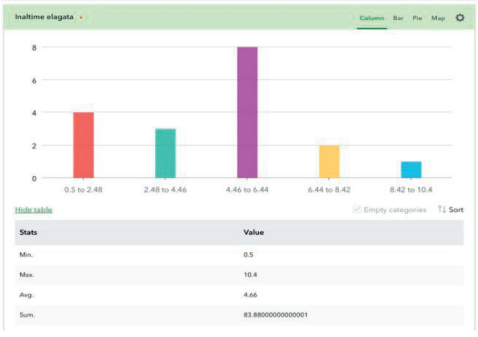



Figure 10. The distribution of clear bole height

The column chart and data table presented in Figure 11, illustrate the vegetative health status ("Stare de vegetație") of the surveyed trees, showing that a 44.44% majority are classified as normal, followed by luxuriant (27.78%), vigorous (22.22%), and sluggish/declining (5.56%), with no trees recorded in the dying category.




Figure 11. The vegetative health status

The column chart and data table below (Figure 12) depict the health status of the trees ("Starea de sănătate a arborelui"), showing that a significant majority of 72.22% are in good condition, while 22.22% are in poor condition, and 5.56% (1 tree) is rated as satisfactory.




Figure 12. The health status of the trees

The gallery section displays a visual inventory consisting of field photographs (Figure 13) used to document and verify the individual characteristics of each tree surveyed in the study.
With the help of GIS, it is also possible to create thematic maps, which are of significant practical value for data visualization and analysis.
The image (Figure 14) displays a thematic map generated within the survey platform, illustrating the spatial distribution and proportional heights of trees ("Inaltime arbore") mapped on the USAMV Cluj campus. The thematic map

underscores the spatial heterogeneity of tree heights, revealing critical correlations between environmental factors and vegetative growth.

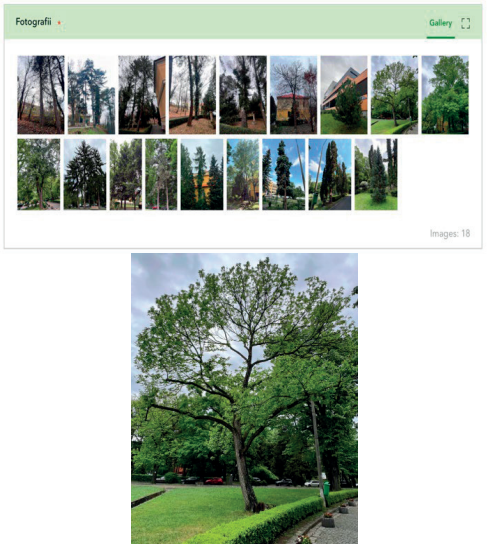



Figure 13. Visual Documentation of the Studied Dendrological Specimens

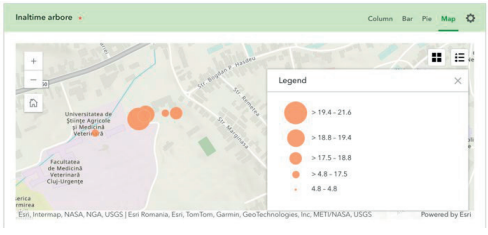



Figure 14. Thematic map illustrating the spatial distribution of tree height

The next map (Figure 15) utilizes graduated proportional symbols, where larger circles correspond to taller trees according to the map legend, allowing for an immediate visual comparison of tree heights across the localized study area.

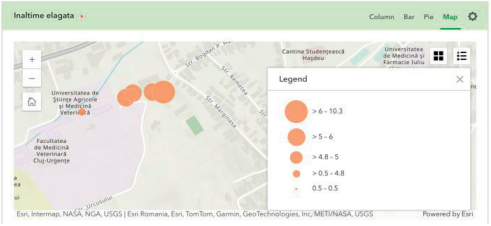



Figure 15. Thematic map illustrating the spatial variation of clear bole height within the forest stand

The provided orthophotomap, titled "Geospatial inventory and exact localization of arboreal specimens at the USAMV Cluj-Napoca campus" (Figure 16) illustrates a high-precision spatial mapping approach utilized to catalogue the urban forestry resources within the university grounds.



Figure 16. Geospatial inventory and exact localization of arboreal specimens at the USAMV Cluj-Napoca campus

By leveraging high-resolution aerial imagery overlaid with precise geographic coordinates, individual tree positions have been vectorized and marked with distinct red and yellow point indicators. The spatial distribution reveals a strategic arrangement of dendrological specimens, clustered primarily around infrastructure borders, open green spaces, and academic walkways. This cartographic layout serves as a fundamental baseline for urban ecosystem monitoring, allowing researchers to track spatial configurations and localized microclimatic impacts of individual specimens within the campus canopy. From a management and biometrical perspective, this precise geospatial localization provides indispensable data for the development of an integrated Green Cadastre for USAMV Cluj-Napoca. Identifying the exact spatial coordinates of each arboreal unit facilitates long-term monitoring of tree health, growth dynamics, and species-specific interactions within the campus ecosystem. Furthermore, this localized spatial framework enables precise field-to-map cross-referencing during dendrometric inventories. By linking these geographic points to a relational database containing biometric attributes - such as species composition, total height, and clear bole height - the institution can optimize its urban forestry management strategies, promoting both ecological biodiversity and environmental sustainability.

## CONCLUSIONS

The digital transformation of tree inventorying through GIS highlights the significant potential of spatial technologies in establishing a 'green cadastre' for the USAMV Cluj-Napoca Campus, providing a solid foundation for sustainable management and well-informed decisions.

Looking ahead, future research directions will focus on integrating UAV photogrammetry and LiDAR data to automate tree feature extraction, expanding these models to support forest owners, institutions, associations, and local administrative units (UATs) through integrated solutions dedicated to monitoring green resources and protecting ecosystems, with the ultimate goal of achieving more efficient and responsible forest management.

Furthermore, the implementation of this advanced spatial framework facilitates a paradigm shift from reactive to proactive environmental stewardship within academic and urban ecosystems. By transforming raw geospatial data into actionable intelligence, the proposed green cadastre model enables campus administrators to simulate microclimate impacts, assess localized carbon sequestration capacity, and optimize tree maintenance schedules. This methodology not only standardizes the documentation of vegetative assets but also establishes a highly scalable blueprint that can easily be integrated into broader smart-city frameworks, effectively bridging the gap between localized institutional workflows and regional environmental goals.

Ultimately, the long-term viability and impact of these technological interventions rely on fostering participatory data environments and open collaboration. Future iterations of this system will aim to incorporate multi-user mobile platforms and interactive dashboards, allowing students, researchers, and local stakeholders to engage directly with the spatial database. By cultivating an accessible, dynamically updated ecological inventory, USAMV Cluj-Napoca can champion a collaborative approach to biodiversity conservation, ensuring that precision forestry and urban greening efforts remain resilient and highly adaptive in the face of accelerating climate challenges.

## ACKNOWLEDGEMENTS

This research was carried out with the support of the Ministry of Education and was financed through the CNFIS-FDI-2025-F-0030 project, funded by the National Council for Financing Higher Education (CNFIS).

## USE OF GENERATIVE ARTIFICIAL INTELLIGENCE (GenAI)

The authors declare the use of Generative Artificial Intelligence (GenAI) tools in the preparation of this manuscript. GenAI was used exclusively for language editing and text refinement in the Introduction and Conclusions sections. All scientific content, data analysis, and interpretations were developed and verified by the authors.

## REFERENCES

Aulló-Maestro, I, Gómez, C., Marino, E., Cabrera, M., Vázquez de la Cueva, A., & Montez, F. (2021). Integration of field sampling and LiDAR data in forest inventories: comparison of area-based approach and (lognormal) universal kriging. *Annals of Forest Science*, 78, 39. https://doi.org/10.1007/s13595-021-01056-1

Damaševičius, R., Mozgeris, G., Kurti, A., & Maskeliūnas, R. (2024). Digital transformation of the future of forestry: an exploration of key concepts in the principles behind Forest 4.0. *Frontiers in Forests and Global Change*, 7, 1424327. https://doi.org/10.3389/ffgc.2024.1424327

Fassnacht, F.E., White, J.C., Wulder, M.A., & Næsset, E. (2024). Remote sensing in forestry: current challenges, considerations and directions. Forestry: An International Journal of Forest Research, 97(1), 11-37. status and future perspectives. *Remote Sensing of Environment, 300*, 1–15. https://doi.org/10.1093/forestry/cpad024

Hyyppä, E., Hyyppä, J., Hakala, T., Kukko, A., Wulder, M.A., White, J.C., Pyörälä, J., Yu, X., Wang, Y., Virtanen, J.P., Pohjavirta, O., Liang, X., Holopainen, M., & Kaartinen, H. (2020). Under-canopy UAV laser scanning for accurate forest field measurements. *ISPRS Journal of Photogrammetry and Remote Sensing*, 164, 41-60. https://doi.org/10.1016/j.isprsjprs.2020.03.021

Keskes, M.I., Mohamed, A.H., Borz, S.A., & Niță, M.D. (2025). Improving Forest Mapping in Romania Using Machine Learning and Sentinel-2 Multispectral Imagery. Remote Sensing, 17(4), 715. Øyen, B. H. (2024). Challenges and opportunities in modern forest inventory. *Forest Ecology and Management, 550*, 1–12. https://doi.org/10.3390/rs17040715

Liang, X., Hyyppä, J., Kaartinen, H., Lehtomäki, M., Pyörälä, J., Pfeifer, N., Holopainen, M., Brolly, G., Francesco, P., Hackenberg, J., Huang, H., Jo, H. W., Katoh, M., Liu, L., Mokroš, M., Morel, J., Olofsson, K., Poveda-Lopez, J., Trochta, J., & Wang, D. (2018). International benchmarking of terrestrial laser scanning approaches for forest inventories. *ISPRS Journal of Photogrammetry and Remote Sensing, 144*, 137–179.

Uusitalo, J. (2010). *Introduction to Forest Operations and Technology*. JVP Forest Systems Oy.

White, J.C., Wulder, M.A., Varhola, A. Vastaranta, M., Coops, N.C., Cook, B.D., Pitt, D., & Woods, M. (2013). A best practices guide for generating forest inventory attributes from airborne laser scanning data using an area-based approach. *The Forestry Chronicle.* 89(06): 722-723. https://doi.org/10.5558/tfc2013-132.

Scientific Papers. Series E. Land Reclamation, Earth Observation & Surveying, Environmental Engineering. Vol. XV, 2026
Print ISSN 2285-6064, CD-ROM ISSN 2285-6072, Online ISSN 2393-5138, ISSN-L 2285-6064

# REAL-TIME PATHOGEN RISK MAPPING IN CEREAL FIELDS THROUGH INTEGRATED UAV, GIS AND SMART FORECASTING TOOLS

**Dragoș Andrei CÎRCIUMARIU[1], Mirela PARASCHIVU[2], Constantin ȘULEA-IORGULESCU[1], Dorin SENDRESCU[1]**

[1]University of Craiova, Faculty of Automatics, Computer Science and Electronics, 107 Decebal Blvd, Craiova, Dolj County, Romania
[2]University of Craiova, Faculty of Agronomy, 19 Libertății Street, Craiova, Dolj County, Romania

Corresponding author email: paraschivumirela@yahoo.com

***Abstract***

*Cereal crop production faces persistent threats from biotic stresses caused by pathogenic organisms, resulting in significant yield loss and increased management costs. Conventional disease monitoring methods are often limited by spatial resolution, labor intensity, and delayed detection. Integrating unmanned aerial vehicles (UAVs), geographic information systems (GIS), and smart forecasting tools offers potential for real-time, spatially explicit pathogen risk mapping in cereal fields. This review synthesizes state-of-the-art methodologies in UAV remote sensing, GIS spatial analysis, and predictive modelling, emphasizing advances in machine learning for disease detection and risk assessment. Current challenges including data integration, operational constraints, and technological gaps are identified, and future research directions are outlined to facilitate adoption within precision agriculture and environmental engineering frameworks.*

***Key words*****:** *cereal crops, GIS, pathogen detection, risk mapping, smart forecasting, UAV remote sensing.*

## INTRODUCTION

Cereal crops such as wheat, barley, and maize represent a fundamental component of global food security; however, their productivity is significantly threatened by plant pathogens that can cause severe yield and quality losses. Globally, crop losses in wheat due to plant diseases are estimated to cause economic damages of approximately US$ 4-10 billion annually, highlighting the significant impact of pathogens on global food security (Chai et al., 2022). As the global population is projected to approach nearly 10 billion by 2050, the pressure on agricultural systems to ensure stable and sufficient cereal production will intensify (United Nations, 2019). Wheat and other staple crops will be required to maintain high productivity under increasingly variable climatic conditions, where plant diseases remain a major constraint to yield stability (Savary et al., 2019). In this context, conventional reactive approaches to crop protection are insufficient to meet future food demands.

Fungal diseases such as Rusts (RSTs), Powdery Mildew (PM), Septoria Leaf Blotch (SLB) and Fusarium Head Blight (FHB) are among the most destructive diseases affecting cereal production worldwide, often developing rapidly under favorable environmental conditions and spreading across large agricultural areas (Chaloner et al., 2021; Cotuna et al., 2021, 2022; Kouadio et al., 2023; Paraschivu et al., 2023). The increasing frequency of plant disease outbreaks, driven by global trade and climate variability, highlights the need for more efficient monitoring and early warning systems capable of supporting timely crop protection strategies. Thus, phytosanitary management of wheat (*Triticum aestivum* L.) represents a major challenge in the current context of climate change and the ongoing transition toward more sustainable and environmentally friendly agricultural systems (Velea et al., 2021; Bonciu, 2022). The resilience of wheat crops to pathogen attacks does not depend on a single factor but rather results from complex interactions among plant genetics, nutritional status, and crop management practices. Understanding these interactions is essential for developing effective strategies aimed at improving plant health and reducing disease incidence in cereal production

systems (Păunescu et al., 2022, 2023; Iacob et al., 2025).

Recent studies have shown that plants subjected to prolonged water stress, often expressed through increased rates of water loss at the level of the flag leaf, exhibit greater susceptibility to pathogen infections (Atkinson and Urwin, 2012; Naz et al., 2021). This increased vulnerability is associated with physiological imbalances and a weakened plant defense system, which may compromise the plant's ability to respond effectively to biotic stress factors (Pandey et al., 2015). Consequently, environmental stress conditions can significantly influence the epidemiology and severity of diseases affecting wheat crops. In addition, the choice of cropping system and the optimization of plant physiological status through the application of foliar fertilizers play an important role in strengthening the plant's natural defense mechanisms. These practices contribute not only to maintaining high yield potential but also to improving grain quality and overall crop performance (Roșculete et al., 2023).

Despite these advances in agronomic management, early detection and spatial monitoring of plant diseases remain critical challenges in modern cereal production systems. Conventional field scouting methods are often limited by time, labor requirements, and restricted spatial coverage, making it difficult to detect early disease symptoms or accurately assess the spatial distribution of pathogens within large agricultural fields. In this context, digital agriculture technologies have emerged as valuable tools for improving crop monitoring and disease detection (Seelan et al., 2003; Mahlein et al., 2012; Barbedo, 2019).

Recent progress in remote sensing technologies, particularly the use of unmanned aerial vehicles (UAVs), has significantly enhanced the capacity to monitor crop health at high spatial and temporal resolutions. UAV platforms equipped with RGB, multispectral, or hyperspectral sensors enable rapid acquisition of detailed crop imagery, allowing the detection of subtle physiological and structural changes associated with plant stress and early disease development (Feng et al., 2021; Neupane & Baysal-Gurel, 2021; Bouguettaya et al., 2023). When combined with geographic information systems (GIS), these datasets can be integrated with environmental variables, crop management information, and historical disease records to generate spatially explicit maps of crop health and pathogen risk. Moreover, the integration of remote sensing data with predictive disease forecasting models based on meteorological parameters and epidemiological indicators can further improve the accuracy of disease monitoring systems. Such integrated approaches enable the development of real-time pathogen risk maps that identify areas with increased probability of infection, thereby supporting targeted crop protection measures and optimizing the use of phytosanitary treatments.

In this context, the present study aims to develop an integrated framework for real-time pathogen risk mapping in cereal fields through the combined use of UAV-derived imagery, GIS-based spatial analysis, and smart forecasting tools. By linking high-resolution spatial monitoring with predictive disease modeling, this approach seeks to improve early detection of plant health risks and provide decision-support tools for precision phytosanitary management in cereal production systems.

## MATERIALS AND METHODS

The present study adopts a qualitative, information-oriented research design, based on an extensive review of diverse sources, including academic books, peer-reviewed journal articles, technical reports, news publications, and relevant online databases. The available literature was systematically identified, critically evaluated, and synthesized to provide a comprehensive overview of the current state of knowledge, as well as to highlight emerging trends and future research directions related to the topic (Tranfield et al., 2003). This systematic quantitative review of the scientific literature was conducted in accordance with the methodological framework proposed by Pickering and Byrne (2014). A defined set of search keywords ("UAV", "plant", "disease", "GIS") was employed to systematically explore the literature within the Scopus and Web of Science databases, with the

aim of identifying relevant studies published in peer-reviewed, English-language academic journals focusing on UAV-based applications for plant disease detection and monitoring.

In order to achieve the objectives of this study, a combination of systematic, semi-systematic, and integrative review methodologies was employed. This approach involved a rigorous comparative analysis of existing scientific publications, empirical studies, reports, and statistical datasets, with the aim of generating robust insights and identifying gaps within the existing body of knowledge (Snyder, 2019). Furthermore, text-mining techniques were applied as an analytical tool to process large volumes of textual data, facilitating the extraction of meaningful patterns, relationships, and thematic structures. The reviewed literature and associated sources are organized and presented in the following sections of this paper.

## RESULTS AND DISCUSSIONS

### Pathogen Dynamics in Cereal Cropping Systems

Many previous studies indicate that tillage practices, cultivation technology, fertilisation levels, and cultivar selection influence the incidence of fungal diseases in cereals (Elen, 2003; Korbas et al., 2008; Horoszkiewicz-Janka et al., 2012; Cotuna et al., 2013; Paraschivu et al., 2021, 2022; Różewicz et al., 2021; Richard et al., 2022; Chețan et al., 2025). Nevertheless, the prevalence of these pathogens is determined mainly by weather conditions throughout plant growth and development (Cotuna et al., 2018; Paraschivu et al., 2017, 2019; Miedaner & Juroszek, 2021; Asfew & Bedemo, 2022; Ahmad et al., 2024; Rubayet & Hossaint, 2024). In many production regions, disease pressure is intensifying due to warmer temperatures, irregular rainfall patterns, changing cropping systems, and the expansion of pathogen dispersal routes through trade and atmospheric movement (Różewicz et al., 2021; Velea et al., 2021).

Rust fungi in wheat (stem rust - *Puccinia graminis* f. sp. *tritici*, leaf rust -*Puccinia triticina* and stripe rust - *Puccinia striiformis* f. sp. *tritici*) are among the most destructive pathogens of cereals worldwide. These obligate biotrophic fungi can spread rapidly over long distances through airborne urediniospores and may cause severe yield losses when susceptible cultivars are grown. Cool to moderate temperatures and prolonged leaf wetness typically favour stripe rust, whereas leaf rust often develops under mild temperatures with intermittent moisture. Stem rust generally thrives under warmer conditions and can become highly aggressive when night time humidity supports infection. Recent studies indicate that climate change may shift the geographic suitability of rust diseases and alter the effectiveness of host resistance genes (Juroszek & von Tiedemann, 2013).

Fusarium species, especially *Fusarium graminearum* and related taxa, are major pathogens of wheat, barley, and maize. In small grains, they cause Fusarium head blight (FHB), while in maize they are associated with ear and stalk rots. Beyond yield reduction, Fusarium diseases are particularly important because they contaminate grain with mycotoxins such as deoxynivalenol and zearalenone, creating serious food and feed safety risks. Epidemics are strongly linked to humid weather during flowering, frequent rainfall, and warm temperatures that favor spore production and infection (Cotuna et al., 2022). Crop residues from maize or cereals also serve as major inoculum reservoirs, making reduced tillage and cereal-intensive rotations important risk factors. In several European regions, recent weather extremes have further emphasized the interaction between local microclimate and Fusarium contamination patterns (Różewicz et al., 2021; Cotuna et al., 2022; Martínez et al., 2022).

Leaf blotch diseases caused by *Zymoseptoria tritici* (Septoria tritici blotch), *Parastagonosporanodorum*, and *Pyrenophora tritici-repentis* (tan spot) are major constraints in temperate cereal systems. These pathogens survive on infected crop residues and initiate new epidemics through splash-dispersed spores. Their development is promoted by extended periods of leaf wetness, dense crop canopies, moderate temperatures, and frequent rainfall events (Downie et al., 2021; Prahl et al., 2023). Conservation tillage practices, while beneficial for soil health, may increase residue persistence and therefore early-season inoculum pressure when rotations are narrow.

Because these diseases often begin in lower canopy leaves before progressing upward, they are strongly influenced by canopy microclimate and crop architecture (Laribi et al., 2024).

Powdery mildew, caused by *Blumeria graminis* formae speciales, affects wheat, barley, and other cereals globally. Unlike many foliar pathogens, powdery mildew does not require free water for infection and frequently develops under high relative humidity combined with moderate temperatures. Dense stands, excessive nitrogen fertilization, and prolonged periods of humid air circulation within the canopy can accelerate epidemic development (Różewicz et al., 2021; Farda et al., 2026).

Consequently, understanding the major cereal pathogens and the environmental factors that drive epidemics has become a priority for sustainable crop protection.

**Spatial and Temporal Characteristics of Disease Spreadand Implications of Environmental Monitoring**

The epidemiology of cereal diseases is inherently dynamic, as infection processes evolve across space and time in response to host phenology, pathogen biology, agronomic practices, and environmental variability. Thus, pathogens in cereal crops are typically distributed unevenly within fields, generating clusters, gradients, or patchy infection zones rather than homogeneous disease incidence. heterogeneity reflects variation in soil properties, topography, moisture retention, plant density, nutrient availability, and the proximity of primary inoculum sources. Residue-borne pathogens such as *Zymoseptoria tritici*, *Pyrenophora tritici-repentis*, and *Parastagonosporanodorum* are often established near infected residues, from which disease expands progressively through splash dispersal and short-range spore movement (Petit-Houdenot et al., 2021). By contrast, airborne pathogens such as rust fungi (*Puccinia* spp.) may initially appear in scattered hotspots before rapidly colonizing large areas under favourable atmospheric conditions (Radici et al., 2022; Hovmøller et al., 2023). Recent geostatistical studies have demonstrated that spatial autocorrelation of disease intensity can be used to identify infection hotspots and optimize sampling strategies in cereal fields (Amoghavarsha et al., 2022; Mergenthaler et al., 2022; Singh et al., 2023).

The temporal development of cereal diseases is closely linked to crop growth stage and seasonal weather patterns. Many pathogens require specific host tissues or phenological stages to complete infection successfully. For example, Fusarium head blight risk increases markedly during anthesis and early grain filling when spikes are highly susceptible, particularly under humid and warm conditions. Stripe rust epidemics may accelerate during cool and moist spring periods, whereas powdery mildew often develops earlier in the season under moderate temperatures and high relative humidity.

Disease progress over time is frequently described by sigmoidal epidemic curves characterized by an initial latent phase, exponential increase, and saturation stage (Chandran et al., 2025). The duration of each phase depends on inoculum availability, host susceptibility and environmental conduciveness (Dhavale et al., 2025). Shortened latent periods under optimal temperature and moisture conditions can lead to explosive epidemic growth, while intermittent drought or heat stress may suppress some pathogens but predispose plants to others. Consequently, accurate timing of disease risk is as important as identifying where disease occurs.

Disease spread in cereals occurs across multiple spatial scales, from individual leaves to continental regions (Gutaker & Purugganan, 2024). At the field scale, splash dispersal, contact transmission, and short-distance wind movement drive local spread (Karisto et al., 2022). At the landscape scale, crop mosaics, field connectivity, alternate hosts, and topographic corridors influence epidemic connectivity among farms (Fernandes et al., 2022). At regional and transboundary scales, long-distance atmospheric transport can move rust spores hundreds or thousands of kilometers, while seed trade may introduce emerging pathogens such as wheat blast into new production areas.

These scale-dependent processes have important management implications. Local outbreaks may be controlled through field-level interventions, whereas highly mobile pathogens require coordinated surveillance networks and

regional forecasting systems. Integrating multi-scale epidemiological knowledge is therefore critical for resilient cereal disease management.

**UAV-Based Technologies for Pathogen Detection**

Recent advances in remote sensing and geospatial analytics have expanded the capacity to monitor cereal diseases spatially. Unmanned aerial vehicles (UAVs), satellite imagery, and proximal sensors can detect changes in canopy reflectance, temperature, and structural traits associated with disease stress. When linked with geographic information systems (GIS), these observations can be transformed into disease distribution maps, hotspot analyses, and spatial decision-support layers.

Traditional detection methods - field scouting and laboratory diagnostics - often fail to identify outbreaks at early, asymptomatic stages when interventions are most effective. Conventional ground-based sampling provides limited spatial coverage and is temporally discontinuous, yielding insufficient insight into pathogen dispersion across heterogeneous agricultural landscapes (West & Kimber, 2015). While satellite remote sensing offers broad coverage, its utility for early, localized disease detection is constrained by fixed revisit intervals, coarse spatial resolution, and susceptibility to cloud cover.

Unmanned aerial vehicles (UAVs) bridge the observational gap between satellite and ground-based sensing by enabling rapid, repeated, high-resolution monitoring of crop canopies at user-defined temporal windows. Drones equipped with multi-modal sensor payloads can detect pre-symptomatic stress signatures invisible to the naked eye, with advantages including flexible deployment, comparatively low operational cost, and the capacity to acquire multi-sensor data (visual, spectral, thermal) at sub-centimeter resolutions unattainable by satellite platforms (Joshi et al., 2024; Xing et al., 2026).

However, most current UAV applications in agricultural phytopathology detect indirect disease signatures - spectral anomalies, canopy temperature deviations - rather than causal organisms directly. These responses are frequently non-specific, as similar patterns may arise from drought, nutrient deficiency, or thermal injury (Su et al., 2018). Molecular detection approaches (e.g., UAV-mounted spore traps for downstream DNA analysis) offer definitive identification but remain experimental, constrained by payload limitations and the absence of standardized airborne bioaerosol collection protocols (West & Kimber, 2015). These considerations position UAV-based monitoring as a critical component within a multi-layered surveillance architecture integrating aerial screening, geospatial risk modeling, and targeted ground-truth validation.

**UAV Platforms and Sensor Types**

Platform selection for cereal disease monitoring is governed by four interrelated constraints: area coverage per sortie, payload capacity, aerodynamic stability under field wind conditions, and operational simplicity for routine deployment. Three airframe categories are relevant:

**Fixed-wing UAVs** offer superior endurance (45-90 min) and area coverage for landscape-scale screening of large contiguous fields, though they require launch infrastructure and cannot hover for close inspection (Tsouros et al., 2019) (Table 1). **Multi-rotor UAVs** (quadcopters, hexacopters) provide vertical take-off/landing, precise hovering and ground sampling distances below 1 cm, making them ideal for repeated diagnostics over fragmented parcels, but endurance is limited to 20-40 minutes (Agrawal & Arafat, 2024). **Hybrid VTOL fixed-wing systems** combine deployment flexibility with cruise efficiency, increasingly relevant for operational monitoring networks with mixed field geometry (Joshi et al., 2024).

Sensor choice determines the detectable signal domain. **RGB cameras** are the most accessible, supporting canopy coverage metrics and texture-based ML classification, but lack sensitivity to early biochemical changes. **Multispectral sensors** (NIR and red-edge bands) represent the operational core of farm-scale monitoring, enabling vegetation index computation linked to chlorophyll dynamics and stress detection (Su et al., 2018). **Hyperspectral sensors** provide dense spectral fingerprints capturing subtle pre-symptomatic biochemical shifts, but impose greater payload,

cost, and processing demands (Mahlein, 2016). **Thermal infrared cameras** map canopy temperature fields revealing disease-associated thermal anomalies, particularly when interpreted with meteorological context (Khanal et al., 2017; Liu et al., 2024). **LiDAR** complements spectral sensors by providing 3D canopy structure data (Joshi et al., 2024). Emerging **biological/environmental samplers** (spore traps, VOC detectors) offer definitive identification potential but remain experimental (West & Kimber, 2015).

Table 1. UAV platform classes and pathogen detection suitability for cereal systems

| UAV Class | Capabilities | Common Sensors | Detection Suitability |
|---|---|---|---|
| Micro/Mini Multi-rotor (<5 kg) | VTOL; 20-40 min; GSD <1 cm | RGB; compact multispectral; mini thermal | Plot-level diagnostics; limited area coverage |
| Small Multi-rotor (5-25 kg) | VTOL; 25-45 min; heavier payloads | Multispectral; hyperspectral; LiDAR; dual thermal-RGB | Field-scale multi-sensor missions |
| Small Fixed-wing (<25 kg) | 45-90 min; 200–500 ha/flight | Multispectral; RGB; compact hyperspectral | Landscape screening; lower spatial detail |
| Hybrid VTOL Fixed-wing | VTOL launch; cruise efficiency; 40-75 min | Multispectral; RGB; thermal | Operational networks; mixed geometry |

No single platform-sensor combination dominates all use cases; value is maximized when the sensor stack is fitted to the decision question - screening, risk ranking, or trigger for confirmatory sampling - while preserving measurement repeatability across campaigns.

**Vegetation Indices and Spectral Indicators**

Vegetation indices (VIs) transform multi-band reflectance into interpretable metrics of canopy physiology and serve as the primary screening tools in UAV-based disease monitoring. NDVI remains widely used due to simplicity and cross-study comparability, but exhibits well-documented saturation in dense cereal canopies during mid-to-late growth stages, limiting sensitivity to early physiological changes (Li et al., 2025). NDRE, exploiting the red-edge region (~700-750 nm), provides significantly improved responsiveness in medium-to-high biomass conditions and has been shown to outperform NDVI for detecting subtle chlorophyll degradation associated with rust and *Septoria* infections (Su et al., 2018). PRI captures short-term changes in photosynthetic light-use efficiency, offering complementary early-warning capability since biotic stress frequently affects photosystem function before structural damage is evident (Șulea et al., 2010; Mahlein, 2016).

Recent advances have introduced disease-specific indices with improved diagnostic precision. The Chlorophyll Absorption Ratio Index (CARI) isolates chlorophyll absorption effects while mitigating soil interference and canopy structural heterogeneity; models utilizing CARI have demonstrated substantial improvements over traditional RGB-based configurations for detecting early-stage fungal infections in cereals (Ali et al., 2025; Goluguri & Baik, 2026). Specialized narrow-band indices for specific pathosystems (e.g., rice blast, wheat rusts) have also shown classification accuracies exceeding 95% in controlled evaluations, significantly outperforming broad-band alternatives (Mahlein, 2016; Su et al., 2018). A fundamental limitation remains spectral ambiguity: similar VI decreases may result from water limitation, nutrient deficiency, thermal stress, or mixed interactions. State-of-the-art pipelines therefore combine spectral indices with texture descriptors, thermal signatures, phenological stage and meteorological context within multivariate ML frameworks to improve classification robustness (Su et al., 2018; Kavhu et al, 2021; Srivastava & Jain, 2025). However, temporal consistency - standardized radiometric calibration, acquisition timing, and preprocessing - is essential for reliable trend detection across campaigns.

**Data Acquisition and Processing Challenges**

The transition from research experiments to operational monitoring confronts several non-trivial challenges. At mission level, operators must negotiate trade-offs among spatial resolution, overlap, coverage, and flight duration within battery, weather, and regulatory constraints. Very high-resolution surveys (GSD < 1 cm) improve lesion detectability but dramatically increase data volume and processing burden. Radiometric consistency is a persistent challenge: illumination variability from solar angle changes and cloud transients, sensor drift, and wind-induced canopy

movement introduce errors degrading multi-temporal spectral comparability unless rigorous calibration using reflectance panels and atmospheric correction is applied (Fu et al., 2024).

Temporal acquisition strategy is critically important yet frequently under-optimized. Pathogen infection dynamics are driven by microclimate variables that change within hours; acquisitions that are too sparse or poorly timed may miss actionable disease development phases (Hossain et al., 2024; Kumar & Mukhopadhyay, 2025). The processing chain - orthomosaic generation, radiometric correction, feature extraction, model inference - can create substantial computational latency. Scalable deployment requires semi-automated pipelines, edge computing architectures, and clear quality-control checkpoints to reduce turnaround from days to hours. Supervised models require accurately labeled training data, but field annotation is labor-intensive and subject to inter-operator variability. Domain shift between cultivars, phenological stages, and regional conditions reduces model transferability without local recalibration (Kamilaris & Prenafeta-Boldú, 2018). Fragmented data formats and proprietary tools impede integration with GIS and decision support systems, necessitating community-accepted standards and interoperable workflows.

### Contribution to Environmental Engineering Applications

UAV-based pathogen monitoring supports spatially explicit, risk-informed intervention strategies that reduce the ecological footprint of crop protection. Conventional management relies on calendar-based uniform fungicide applications - inherently inefficient, applying chemicals where pressure may be negligible, accelerating resistance development, and increasing off-target environmental exposure. Spatially explicit risk maps from UAV observations enable site-specific interventions directed exclusively to zones exceeding action thresholds. Empirical studies demonstrate that integrating UAV and satellite remote sensing can substantially decrease agrochemical application volumes alongside measurable reductions in irrigation water usage without yield penalties (Xing et al., 2026). This precision approach is particularly impactful in heterogeneous landscapes where disease-conducive microenvironments are influenced by soil texture gradients, drainage infrastructure, and micro-topographic variation. UAV-derived products improve mechanistic understanding of soil–water–plant–pathogen interactions and, when integrated with GIS layers (parcel boundaries, DEMs, drainage networks), become actionable planning tools supporting environmental compliance and evolving IPM policy frameworks (Wolfert et al., 2017). Environmental value is maximized when UAV surveillance is embedded in a three-step loop: rapid aerial screening, spatial risk synthesis in GIS, and targeted confirmatory sampling before intervention escalation.

## GIS-BASED SPATIAL ANALYSIS AND RISK MAPPING

### GIS as a Core Tool for Disease Risk Assessment

Geographic Information Systems (GIS) have become a cornerstone of plant disease risk assessment, owing to their capacity to integrate, manage, and analyze heterogeneous spatial datasets across multiple spatial and temporal scales. In cereal cropping systems, GIS facilitates the seamless fusion of UAV-derived remote sensing products with soil properties, climatic variables, and topographic information, enabling a comprehensive representation of disease–environment interactions (Geldsetzer et al., 2023).

A major strength of GIS lies in its ability to harmonize datasets originating from diverse acquisition platforms and temporal resolutions. High-resolution UAV imagery can be accurately georeferenced and spatially aligned with ancillary datasets such as soil surveys, digital elevation models (DEMs), cadastral boundaries, and meteorological observations. This spatial coherence is essential for reliable disease risk modeling, as pathogen development is strongly influenced by fine-scale variability in moisture availability, temperature regimes, and terrain-induced microclimatic conditions (Zhu et al., 2024). Within GIS environments, spatial interpolation techniques - including inverse distance weighting (IDW), ordinary kriging, and regression kriging - are widely employed to

convert discrete disease observations or point-based environmental measurements into continuous disease risk surfaces. These interpolated layers support field-scale visualization of infection probability gradients and enable spatially explicit decision-making (Cressie, 1993; Haggag et al., 2023). Recent studies demonstrate that GIS-based integration improves model robustness by explicitly accounting for spatial autocorrelation and reducing uncertainty in disease risk estimation, particularly in heterogeneous cereal landscapes (Shafay et al., 2025).

**Critical assessment:**
**Advantages:** Integration of multi-source spatial data; high-resolution field-scale mapping; generation of continuous disease risk surfaces.
**Limitations:** Strong dependence on data density and quality; reliance on static datasets that may fail to capture rapid disease dynamics; limited representation of temporal variability.
**Improvement opportunities:** Integration of near-real-time data streams; adoption of spatio-temporal GIS modeling approaches; development of standardized workflows to enhance cross-regional transferability.

**Risk Mapping Techniques**
Disease risk mapping in GIS relies on a combination of deterministic, statistical, and decision-support techniques aimed at classifying, quantifying, and spatially delineating areas susceptible to pathogen outbreaks. Zoning and classification approaches are commonly used to categorize agricultural land into discrete risk classes (e.g., low, moderate, high) based on vegetation indices, environmental variables, and crop phenological stages (Ahmed & Yadav, 2023). These methods provide intuitive outputs that facilitate the interpretation of complex datasets and support operational decision-making at farm level. Multi-Criteria Decision Analysis (MCDA) has emerged as a prominent framework for integrating multiple disease risk factors into composite spatial indices. MCDA allows the explicit weighting of criteria such as temperature accumulation, relative humidity, canopy density, soil moisture, and topographic attributes, reflecting their relative influence on pathogen development. When implemented within a GIS environment, MCDA offers transparency, flexibility, and adaptability to different crops, pathogens, and agro-climatic contexts (Malczewski, 2006).
Beyond classification-based methods, spatial statistical techniques—including hotspot and cluster analysis—play a critical role in identifying localized zones of disease intensification. Indicators such as Moran's I and Getis–Ord Gi* statistics enable the detection of spatial dependence and statistically significant disease clusters, supporting early warning systems and targeted intervention strategies (Getis & Ord, 1992; Haggag et al., 2023). These approaches underpin the transition from uniform treatment practices toward precision disease management.

**Critical assessment:**
**Advantages:** Intuitive spatial outputs; MCDA enables structured integration of multiple risk factors; hotspot analysis identifies disease clusters.
**Limitations:** Classification thresholds are context-dependent; MCDA weighting schemes may introduce subjectivity; reliable statistical inference requires historical datasets.
**Improvement opportunities:** Hybrid MCDA frameworks incorporating machine learning-based weighting; dynamic risk classification schemes; explicit uncertainty quantification in risk maps.

**Integration with Land Reclamation and Surveying Data**
Integrating land reclamation and surveying datasets into GIS-based disease risk mapping substantially enhances the operational relevance of spatial analyses. Cadastral data provide legally defined parcel boundaries, ensuring alignment between disease risk maps and farm management units and facilitating the implementation of precision interventions at parcel scale (FAO, 2007).
Drainage infrastructure maps, land capability assessments, and soil reclamation records offer valuable insights into soil–water dynamics, which are critical determinants of pathogen proliferation in cereal cropping systems. Areas characterized by inadequate drainage, specific soil textures, or unfavorable microrelief conditions are frequently associated with

elevated disease pressure, particularly for fungal pathogens. Incorporating these datasets into GIS-based models improves explanatory capacity and enhances the accuracy of spatial risk predictions (Bielecka & Burek, 2019; Tsouros et al., 2019). Furthermore, the integration of surveying and land-use data supports site-specific intervention planning by linking disease risk zones to field accessibility, land-use constraints, and environmental protection areas. This capability is increasingly important in the context of sustainable land management, where disease control strategies must reconcile productivity goals with regulatory compliance and environmental protection requirements (Zhu et al., 2024).

**Critical assessment:**

**Advantages:** Alignment with farm management units; improved understanding of soil–water–disease interactions; support for precision interventions.

**Limitations:** Outdated or inconsistent cadastral and reclamation datasets; limited interoperability; uneven availability of high-resolution data.

**Improvement opportunities:** Digital modernization of cadastral systems; adoption of open geospatial standards; coupling with UAV-derived micro-topographic models.

**Epidemiological and Agro-Meteorological Models**

Epidemiological and agro-meteorological models constitute the traditional backbone of disease forecasting in cereal cropping systems, as they explicitly describe the interactions between pathogen development, host susceptibility, and environmental drivers. Weather-based disease forecasting models are typically driven by key meteorological variables such as air temperature, relative humidity, precipitation, leaf wetness duration, and wind dynamics, all of which exert a strong influence on pathogen life cycles, infection efficiency, and dispersal mechanisms (Misra et al., 2020; Sangeetha et al., 2025).

Classical agro-meteorological approaches rely on threshold-based or cumulative indicators, including degree-day accumulation, prolonged canopy wetness, and specific temperature–humidity combinations favorable to infection (González-Domínguez et al., 2023). These models have been widely applied to major cereal diseases, such as rusts, fusarium head blight, and leaf blotch complexes, offering early warning capabilities that support timely disease management decisions.

The principal advantage of epidemiological models lies in their biological interpretability and relatively modest data requirements, as they can operate using standard meteorological observations or gridded climate datasets (Rahman et al., 2023). Their mechanistic foundation facilitates transparency and acceptance among agronomists and land managers. However, these models often rely on simplified assumptions regarding host uniformity and pathogen behavior, and they may insufficiently represent spatial heterogeneity at field scale. Furthermore, their predictive performance may decrease under conditions of increasing climate variability or when applied outside the agro-ecological contexts for which they were originally calibrated (Martínez-Cadena et al., 2026).

Recent research emphasizes the integration of agro-meteorological models with GIS-based spatial layers to improve spatial resolution and contextual relevance (Chandel, 2025; Rawat et al., 2026). Nevertheless, the inherent limitations of purely mechanistic approaches highlight the need for complementary data-driven and hybrid modeling strategies.

**Critical assessment:**

**Advantages:** Biologically interpretable; low computational requirements; effective for early warning.

**Limitations:** Limited spatial resolution; simplified disease dynamics; reduced robustness under climate variability.

**Improvement opportunities:** Spatial downscaling through GIS; hybridization with data-driven models; incorporation of microclimate variability.

**Machine Learning and Artificial Intelligence Approaches**

Machine learning (ML) and artificial intelligence (AI) approaches have gained increasing prominence in crop disease forecasting due to their capacity to capture complex, non-linear relationships among environmental variables, crop conditions, and pathogen dynamics (Tammina et al., 2024;

Basu & Narayan, 2025). Supervised learning techniques - such as random forests, support vector machines, artificial neural networks, and gradient boosting algorithms - are commonly employed to predict disease occurrence, severity, or risk classes using labeled datasets (González-Rodríguez et al., 2024; Ajaharuddin et al., 2025).

Unsupervised learning methods, including clustering and dimensionality reduction techniques, are used to identify latent patterns in multi-source datasets, enabling the detection of emerging disease hotspots or anomalous crop stress signals without requiring extensive ground truth data. These approaches are particularly valuable in exploratory analyses and in large-scale monitoring contexts.

A major strength of ML-based models lies in their ability to integrate high-dimensional inputs derived from UAV-based remote sensing and GIS layers. Spectral features extracted from multispectral and hyperspectral imagery, vegetation indices, canopy texture metrics, topographic attributes, soil parameters, and agro-meteorological variables can be jointly analyzed within unified modeling frameworks. This integration enables spatially explicit disease risk predictions that reflect both biophysical crop status and environmental constraints. Despite their strong predictive performance, ML and AI approaches face challenges related to data dependency, interpretability, and generalization. Model robustness is highly sensitive to data quality, temporal coverage, and representativeness, while limited transparency may hinder trust and adoption by end users. As a result, hybrid modeling paradigms that combine epidemiological knowledge with machine learning techniques are increasingly advocated as a means to balance interpretability and predictive accuracy.

**Critical assessment:**

**Advantages:** High predictive accuracy; effective integration of multi-source datasets; fine spatial resolution.

**Limitations:** Data-intensive; limited interpretability; risk of overfitting and reduced transferability.

**Improvement opportunities:** Explainable AI methods; hybrid epidemiological–ML frameworks; standardized datasets for model training and validation.

**Real-Time Decision Support Systems**

Real-time decision support systems (DSS) represent the operational layer of smart forecasting architectures, translating model outputs into actionable recommendations for agricultural risk management. In cereal cropping systems, these platforms increasingly rely on cloud-based infrastructures that enable continuous data ingestion, processing, and visualization from UAVs, ground sensors, meteorological services, and GIS databases.

A relevant operational reference for such architectures is provided by the decision support systems developed for Romanian national anti-hail protection networks. These systems were designed to support rapid operational decisions by integrating real-time meteorological observations, radar data, numerical weather prediction outputs, and spatial zoning information within centralized informatic platforms. Their primary objective was to assess the spatio-temporal evolution of convective hazards and to assist intervention decisions under strict temporal constraints (Șulea et al., 2010; 2011).

The core principles underpinning these anti-hail DSS - continuous data acquisition, real-time spatial analysis, threshold-based and probabilistic risk evaluation, and operator-oriented visualization - are directly applicable to pathogen risk management in agriculture. Similar to hail hazards, disease outbreaks are strongly influenced by short-term atmospheric dynamics, microclimatic variability, and spatial heterogeneity in land and crop conditions. When embedded within GIS environments, DSS can generate dynamic disease risk maps that evolve in response to changing environmental drivers.

Furthermore, the integration of Internet of Things (IoT) technologies enhances the temporal resolution of DSS by providing near-real-time measurements of microclimate parameters, soil moisture, and canopy conditions. When combined with UAV-derived indicators and forecasting models - whether epidemiological or machine learning-based - these systems enable adaptive risk assessments and early warning alerts tailored to specific

fields or management units. GIS acts as the spatial integration backbone, ensuring data consistency and enabling intuitive, map-based communication of risk levels.

Experience gained from operational anti-hail DSS demonstrates the feasibility and robustness of real-time, spatially explicit decision support under complex environmental conditions. However, extending these systems to crop disease management requires addressing challenges related to system scalability, data interoperability, and user accessibility. Simplified interfaces and automated workflows are essential to facilitate adoption by farmers and land managers while preserving the analytical rigor of the underlying models.

**Critical assessment:**

**Advantages:** Proven real-time operational capability; integration of meteorological forecasting and spatial analysis; transferable architecture for early warning systems.

**Limitations:** High system complexity; reliance on dense monitoring networks; need for specialized technical expertise.

**Improvement opportunities:** User-oriented DSS interfaces; tighter integration with UAV-based disease indicators; linkage with regional and national agricultural monitoring platforms.

## Implications for Policy and Precision Agriculture

GIS-based pathogen risk mapping has substantial implications for agricultural policy formulation and the adoption of precision agriculture practices. By delivering spatially explicit, risk-based assessments, integrated UAV-GIS systems support evidence-driven decision-making at both farm and policy levels. These tools enable optimized input allocation, reduced pesticide use, and the implementation of more sustainable crop protection strategies consistent with environmental engineering principles (Wolfert et al., 2017; Ahmed & Yadav, 2023).

At the policy level, spatial disease risk mapping aligns closely with European and global environmental monitoring initiatives, including the Common Agricultural Policy (CAP) and the Copernicus Earth Observation Programme. These frameworks prioritize digitalization, climate resilience, and data-driven land management as central pillars of modern agriculture. GIS-supported disease monitoring contributes directly to these objectives by providing scalable solutions for surveillance, early warning, and compliance monitoring across agricultural landscapes (European Commission, 2022; 2024).

Moreover, the integration of Earth Observation, GIS, and smart forecasting tools facilitates a shift toward risk-based land management, where interventions are guided by probabilistic spatial assessments rather than uniform prescriptions. This paradigm strengthens the role of geospatial intelligence as a critical interface between scientific innovation, environmental engineering, and agricultural governance in addressing challenges related to climate change, food security, and sustainable intensification.

**Critical assessment:**

**Advantages:** Enables risk-based management; enhances policy transparency; supports scalable and replicable monitoring frameworks.

**Limitations:** High technical complexity and implementation costs; lag between technological development and policy uptake; lack of standardized risk indicators.

**Improvement opportunities:** Development of policy-oriented GIS dashboards; incentives through CAP eco-schemes; harmonization of risk indicators aligned with EU and global standards (Table 2).

Table 2. Advantages, Limitations and Directions for Improvement

| Section | Key Advantages | Main Limitations | Future Directions / Improvements |
|---|---|---|---|
| 5.1 GIS as Core Tool | Multi-source data integration; high-resolution mapping; continuous risk surfaces | Data density & quality dependent; static datasets; limited temporal representation | Near-real-time data streams; spatio-temporal GIS models; standardized workflows |
| 5.2 Risk Mapping Techniques | Intuitive outputs; MCDA integrates multiple factors; hotspot analysis identifies clusters | Context-specific thresholds; subjective MCDA weighting; relies on historical data | Hybrid MCDA + ML weighting; dynamic risk classification; uncertainty quantification |
| 5.3 Integration with Surveying Data | Alignment with farm units; better soil–water–disease understanding; supports precision interventions | Outdated/inconsistent data; limited interoperability; non-uniform high-res data | Digital cadastral modernization; open geospatial standards; UAV micro-topography coupling |
| 9.3 Policy & Precision Ag | Supports risk-based management; policy transparency; scalable monitoring | Technical complexity; policy adoption lag; lack of standardized indicators | GIS dashboards for policy; CAP eco-scheme incentives; harmonized EU/global risk indicators |

## Challenges, Limitations, and Research Gaps

### Technical and Operational Constraints

Despite the promising experimental results surveyed above, several constraints limit the transition to large-scale deployment.

**Data throughput:** high-resolution UAV missions generate datasets of hundreds of GB per season; the sequential processing pipeline introduces substantial latency that may erode decision advantage during fast-spreading outbreaks.

**Acquisition consistency:** wind, illumination shifts, and battery limits introduce variability between campaigns unless strict QA/QC protocols and standardized SOPs are enforced (Su et al., 2018).

**Model transferability:** ML classifiers exhibit vulnerability to domain shift - a model trained on specific cultivar-climate conditions frequently degrades in new contexts without recalibration, requiring continuous local ground-truth annotation that restricts scalability (Kamilaris and Prenafeta-Boldú, 2018; Su et al., 2018).

**Economic barriers:** while standard RGB systems are cost-effective, transitioning to high-performance hyperspectral systems for early pre-symptomatic detection incurs substantially higher capital expenditure, creating accessibility barriers for smallholder operations (Agrawal and Arafat 2024, Xing et al., 2026).

**Regulatory constraints:** BVLOS operations essential for large-area coverage require special authorization, and fragmented frameworks across jurisdictions create planning uncertainty (Tsouros et al., 2019, Joshi et al., 2024).

**Interoperability:** proprietary formats, platform-specific tools, and non-standardized metadata schemas hinder integration with GIS and FMIS, constraining landscape-level environmental governance. The primary bottleneck is not sensing technology per se, but the absence of mature, standardized, low-friction operational pipelines.

### Future Perspectives and Opportunities

Recent Earth observation advances are strengthening pathogen risk mapping along three convergent axes. **Sensor miniaturization:** compact multispectral, hyperspectral, and thermal payloads with improved signal-to-noise ratios are enabling increasingly capable multi-modal sensor stacks on low-cost commercial platforms (Su et al., 2018; Agrawal & Arafat, 2024). Emerging modalities include fluorescence imaging sensors detecting chlorophyll fluorescence emission linked to photosystem II efficiency, which has demonstrated pre-symptomatic detection capability in high-value pathosystems (Mahlein, 2016; Zarco-Tejada et al., 2018).

**Temporal resolution:** autonomous mission scheduling, waypoint-based operations, and multi-UAV coordination enable more frequent revisits for tracking disease trajectories rather than relying on isolated snapshots. Integration with high-revisit satellite constellations (Sentinel-2, PlanetScope) and ground IoT networks creates multi-scale observation stacks improving monitoring continuity and gap-filling resilience (Xing et al., 2026).

**Processing architectures:** the shift to cloud-native and edge computing dramatically reduces acquisition-to-output latency. Edge processing on or near the UAV delivers preliminary risk assessments during or immediately after acquisition (Agrawal & Arafat, 2024).

Methodologically, the field is transitioning from static risk maps toward **dynamic risk-state estimation** using Bayesian updating, ensemble modeling, and data assimilation, providing uncertainty-aware probabilistic outputs that communicate confidence levels to decision-makers (Wolfert et al., 2017). Deep learning architectures (CNNs, vision transformers) demonstrate superior feature extraction from complex UAV imagery, while explainable AI (XAI) methods address interpretability requirements for operational trust and regulatory acceptance (Kamilaris & Prenafeta-Boldu, 2018). An emerging frontier is **digital twin systems** in which real-time observations continuously calibrate virtual crop models simulating disease dynamics under current and projected conditions, enabling scenario analysis and adaptive resource allocation. The convergence of better sensors, smarter processing, and more sophisticated analytics positions integrated UAV–GIS–forecasting systems for a qualitative leap in operational readiness over the coming decade.

## CONCLUSIONS

Major cereal pathogens remain highly responsive to environmental conditions, and their importance is expected to grow under ongoing climatic and agronomic change. Rusts, Fusarium diseases, residue-borne leaf blights, powdery mildew, and emerging threats such as wheat blast each respond to specific combinations of temperature, moisture, and management factors. A deeper understanding of these drivers is therefore essential for building resilient cereal production systems and designing next-generation phytosanitary strategies based on prevention, prediction, and precision management.

The spread of diseases in cereals is shaped by complex spatial and temporal processes that operate from leaf to landscape scales. Environmental monitoring provides a critical foundation for understanding and anticipating these processes, particularly when integrated with remote sensing, GIS, and predictive epidemiological models. Future phytosanitary strategies should therefore prioritize spatiotemporal intelligence and real-time decision support to improve sustainability, reduce unnecessary chemical inputs, and enhance resilience in cereal production systems.

The present study demonstrates that the integration of unmanned aerial vehicle (UAV) sensing, geographic information systems (GIS), and smart forecasting tools provides an effective framework for real-time pathogen risk mapping in cereal production systems. By combining high-resolution spatial observations with environmental monitoring and predictive epidemiological analytics, this approach enables earlier identification of disease-prone zones than conventionalm scouting methods and supports a more precise understanding of within-field disease dynamics.

The results highlight that pathogen risk in cereal fields is inherently heterogeneous and strongly influenced by interactions among crop status, microclimate, field variability, and short-term weather conditions. Consequently, static or calendar-based protection strategies are often insufficient to capture the rapidly changing nature of disease development. In contrast, dynamic risk maps generated from integrated digital datasets can improve the timing and spatial targeting of interventions, thereby increasing management efficiency and reducing unnecessary phytosanitary inputs.

The study also confirms that the value of UAV imagery is substantially enhanced when remote sensing outputs are interpreted together with GIS-based spatial layers and forecasting models rather than used as isolated diagnostic tools. This integrated perspective transforms crop observations into actionable intelligence, allowing farmers and advisors to move from reactive disease control toward anticipatory and preventive management. Despite these advances, several challenges remain for large-scale implementation. Model transferability across environments, sensor standardization, data interoperability, economic accessibility, and user-friendly interfaces will be critical for wider adoption. Future research should therefore focus on multi-season validation, incorporation of machine learning and pathogen-specific biological parameters, and the development of scalable platforms capable of operating across diverse cereal-growing regions.

Overall, real-time pathogen risk mapping represents a significant step toward next-generation cereal health management. The convergence of UAV technologies, geospatial analytics, and smart forecasting systems offers a practical pathway to more resilient, data-driven, and sustainable cereal production under current and future disease pressures.

## AKNOWLEDGEMENTS

The authors would like to thank all colleagues and collaborators who provided valuable discussions and support during the preparation of this review.We also thank colleagues from the Department of Agricultural and Forestry Technologies (Phytopathology) and the Department of Automatics and Electronics from University of Craiova for their valuable comments and discussions during the preparation of this review.

## USE OF GENERATIVE ARTIFICIAL INTELLIGENCE (GenAI)

The authors declare the use of Generative Artificial Intelligence (GenAI) tools in the preparation of this manuscript. GenAI was used exclusively for language editing and text refinement in the Introduction and Conclusions sections. All scientific content, data analysis, and interpretations were developed and verified by the authors.

## REFERENCES

Agrawal, J., & Arafat, M. Y. (2024). Transforming farming: A review of AI-powered UAV technologies in precision agriculture. *Drones*, 8(11), 664. https://doi.org/10.3390/drones8110664

Ahmad, W., Bibi, N., Sanwal, M., Ahmed, R., Jamil, M., Kalsoom, R., Arif, M., & Fahad, S. (2024). Cereal crops in the era of climate change: An overview. In S. Fahad, S. Saud, T. Nawaz, L. Gu, M. Ahmad, & R. Zhou (Eds.), *Environment, climate, plant and vegetation growth* (pp. 609–630). Springer. https://doi.org/10.1007/978-3-031-69417-2_21

Ahmed, I., & Yadav, P. K. (2023). Plant disease detection using machine learning approaches. *Expert Systems*, *40*(5), e13136.

Ajaharuddin, S. K. M. D., Das, K. K., Kar, P., Goswami, S., Bhattacharya, S., & Maharana, C. (2025). Harnessing AI and Machine Learning for Effective Pest and Disease Control. In *Ecologically Mediated Development: Promoting Biodiversity Conservation and Food Security* (pp. 461-485). Singapore: Springer Nature Singapore.

Ali, N., Ullah, M., Mohammed, A., Bais, A., Berraies, S., Ruan, Y., Cuthbert, R. D., & Sangha, J. S. (2025). Advancing Fusarium Head Blight Detection in Wheat Crop: A Review and Future Directions to Sustainable Agriculture. *IEEE Transactions on Consumer Electronics*, 71(3), 7473–7491. https://doi.org/10.1109/TCE.2025.3549057

Amoghavarsha, C., Pramesh, D., Sridhara, S., Patil, B., Shil, S., Naik, G. R., Naik, M. K., Shokralla, S., El-Sabrout, A. M., Mahmoud, E. A., Elansary, H. O., Nayak, A., & Prasannakumar, M. K. (2022). Spatial distribution and identification of potential risk regions to rice blast disease in different rice ecosystems of Karnataka. *Scientific Reports*, 12, 7403. https://doi.org/10.1038/s41598-022-11453-9

Asfew, M., & Bedemo, A. (2022). Impact of climate change on cereal crops production in Ethiopia. *Advances in Agriculture*, 2022, 2208694. https://doi.org/10.1155/2022/2208694

Atkinson, N. J., & Urwin, P. E. (2012). The interaction of plant biotic and abiotic stresses: From genes to the field. *Journal of Experimental Botany*, 63(10), 3523–3543. https://doi.org/10.1093/jxb/ers100

Barbedo, J. G. A. (2019). A review on the use of unmanned aerial vehicles and imaging sensors for monitoring and assessing plant stresses. *Drones*, 3(2), Article 40. https://doi.org/10.3390/drones3020040

Basu, A., & Narayan, A. (2025). The role of machine learning in transforming agricultural practices: insights into crop yield optimization and disease detection. *Iran Journal of Computer Science*, *8*(4), 1199-1217.

Bielecka, E., & Burek, E. (2019). Spatial data quality and uncertainty publication patterns and trends by bibliometric analysis. *Open Geosciences*, 11(1), 219–235. https://doi.org/10.1515/geo-2019-0018

Bonciu, E. (2022). Trends in the evolution of organic agriculture at the global level – A brief review. *Scientific Papers Series Management, Economic Engineering in Agriculture and Rural Development*, 22(3), 81–86.

Bouguettaya, A., Zarzour, H., Kechida, A., & Taberkit, A. M. (2023). A survey on deep learning-based identification of plant and crop diseases from UAV-based aerial images. *Cluster Computing*, 26(2), 1297–1317. https://doi.org/10.1007/s10586-022-03627-x

Chai, Y., Senay, S., Horvath, D., & Pardey, P. (2022). Multi-peril pathogen risks to global wheat production: A probabilistic loss and investment assessment. *Frontiers in Plant Science*, 13, Article 1034600. https://doi.org/10.3389/fpls.2022.1034600

Chaloner, T. M., Gurr, S. J., & Bebber, D. P. (2021). Plant pathogen infection risk tracks global crop yields under climate change. *Nature Climate Change*, 11(8), 710–715. https://doi.org/10.1038/s41558-021-01104-8

Chandel, A. S. (2025). Mapping drought risks in agriculture: a GIS and remote sensing study of Nagele Arsi district, Ethiopia. *Cogent Food & Agriculture*, *11*(1), 2525319.

Chandran, J., Gopinath, P. P., Pramod, R., & Vijayan, A. (2025). Modeling plant disease epidemics: A comprehensive review of disease progress curves. *Journal of Sustainable Technology in Agriculture*, 1(2). https://doi.org/10.65287/josta.202512.72CB

Cheţan, F., Tărău, A., Vălean, A. M., Şopterean, L., Şimon, A., Urdă, C., Călugăr, R., Cheţan, C., Rusu, T., & Suciu, L. (2025). The influence of tillage systems on the occurrence of diseases and pests on spring cereals, in the Transylvanian Plateau. *Romanian Journal for Plant Protection*, 18, 20–31. https://doi.org/10.54574/RJPP.18.03

Cotuna, O., Sarateanu, V., Durau, C., Paraschivu, M., & Rusalin, G. (2013). Resistance reaction of some winter wheat genotypes to the attack of Fusarium graminearum L. Schw. in the climatic conditions of Banat Plain. *Research Journal of Agricultural Science*, 45(1), 117–122.

Cotuna, O., Paraschivu, M., Paraschivu, M., & Olaru, L. (2018). Influence of crop management on the impact of Zymoseptoria tritici in winter wheat in the context of climate change: An overview. *Research Journal of Agricultural Science*, 50(3), 69–74.

Cotuna, O., Paraschivu, M., Bulai, A., Toma, I., Sărăţeanu, V., Horablaga, N. M., & Buzna, C. (2021). Behaviour of some oat lines to the attack of the fungus Blumeria graminis (D. C.) f. sp. avenae

Em. Marchal. *Scientific Papers Series Management, Economic Engineering in Agriculture and Rural Development*, 21(4), 161–170.

Cotuna, O., Paraschivu, M., Sărățeanu, V., Partal, E., & Durău, C. C. (2022). Impact of fusarium head blight epidemics on the mycotoxins' accumulation in winter wheat grains. *Emirates Journal of Food and Agriculture*, 34(11), 949–962.

Cressie, N. A. C. (1993). *Statistics for spatial data*. John Wiley & Sons. https://doi.org/10.1002/9781119115151

Dhavale, M. C., Patel, D., & Khangarot, J. S., (2025). Plant disease epidemiology. In R. Yuvarani, U. Shankar, S.B. Gowdar, S. Kumar, S.S. Hiremath (Eds.), *Plant health and disease management: A modern approach* (p. 94-114). Textify Publishers

Downie, R. C., Lin, M., Corsi, B., Ficke, A., Lillemo, M., Oliver, R. P., Phan, T. T., Tan, K. C., & Cockram, J. (2021). Septoria nodorum blotch of wheat: Disease management and resistance breeding in the face of shifting disease dynamics and a changing environment. *Phytopathology*, 111(6), 906–920.

Elen, O. (2003). Long-term experiments with reduced tillage in spring cereals. III. Development of leaf diseases. *Crop Protection*, 22(1), 65–71. https://doi.org/10.1016/S0261-2194(02)00112-6

European Commission. (2022). Commission Implementing Regulation (EU) 2022/1173 of 31 May 2022 laying down rules for the application of Regulation (EU) 2021/2116 of the European Parliament and of the Council with regard to the integrated administration and control system in the common agricultural policy. *Official Journal of the European Union*, L 183, 23–34.
https://eur-lex.europa.eu/eli/reg_impl/2022/1173/oj/eng

European Commission. (2024). The Commission continues to simplify the common agricultural policy for EU farmers. *Agriculture and Rural Development*, 11 July 2024.
https://agriculture.ec.europa.eu/media/news/commission-continues-simplify-common-agricultural-policy-eu-farmers-2024-07-11_en

FAO. (2007). *Land Evaluation towards a Revised Framework*. FAO.

Farda, B., Sabbi, E., Fares, R., Djebaili, R., Mignini, A., Mitra, D., & Pellegrini, M. (2026). Shifting disease dynamics: Effect of climate change on plant pathogens and their management in field crops. *Journal of Plant Biochemistry and Biotechnology*, 35(1), 57–79. https://doi.org/10.1007/s13562-026-01042-6

Feng, L., Chen, S., Zhang, C., Zhang, Y., & He, Y. (2021). A comprehensive review on recent applications of unmanned aerial vehicle remote sensing with various sensors for high-throughput plant phenotyping. *Computers and Electronics in Agriculture*, *182*, 106033.

Fernandes, L. D., Mata, A. S., Godoy, W. A. C., & Reigada, C. (2022). Refuge distributions and landscape connectivity affect host-parasitoid dynamics: Motivations for biological control in agroecosystems. *PLOS ONE*, 17(4), e0267037. https://doi.org/10.1371/journal.pone.0267037

Fu, Y., Zhu, Z., Liu, L., Zhan, W., He, T., Shen, H., Zhao, J., Liu, Y., Zhang, H., Liu, Z., Xue, Y., & Ao, Z. (2024). Remote sensing time series analysis: A review of data and applications. *Journal of Remote Sensing*, 4, 0285. https://doi.org/10.34133/remotesensing.0285

Geldsetzer, T., Yackel, J., Tomar, K. S., Mahmud, M., Nandan, V., & Kumar, S. (2023). Melt pond detection on landfast sea ice using dual co-polarized Ku-band backscatter. *Remote Sensing of Environment*, 296, 113725. https://doi.org/10.1016/j.rse.2023.113725

Getis, A., & Ord, J. K. (1992). The analysis of spatial association by use of distance statistics. *Geographical Analysis*, 24(3), 189–206. https://doi.org/10.1111/j.1538-4632.1992.tb00261.x

Goluguri, N. V. R., & Baik, O. D. (2026). Revolutionizing wheat plant disease detection: A review of imaging, AI, and innovations. *Archives of Computational Methods in Engineering*, 33(5), 6883–6914. https://doi.org/10.1007/s11831-026-10502-0

González-Domínguez, E., Caffi, T., Rossi, V., Salotti, I., Fedele, G. (2023). Plant disease models and forecasting: changes in principles and applications over the last 50 years. *Phytopathology®*, *113*(4), 678-693.

González-Rodríguez, V. E., Izquierdo-Bueno, I., Cantoral, J. M., Carbú, M., Garrido, C. (2024). Artificial intelligence: a promising tool for application in phytopathology. *Horticulturae*, *10*(3), 197.

Gutaker, R. M., & Purugganan, M. D. (2024). Adaptation and the geographic spread of crop species. *Annual Review of Plant Biology*, 75, 679–706. https://doi.org/10.1146/annurev-arplant-060223-030954

Haggag, W. M., Ali, R. R., & Al-Ansary, N. A. (2023). Geographic information systems and remote sensing: Innovative tools for plant health. *International Journal of Agricultural Technology*, 19(6), 2449–2464.

Horoszkiewicz-Janka, J., Jajor, E., & Korbas, M. (2012). Prevalence of winter wheat diseases depending on selected agrotechnical factors. *Progress in Plant Protection*, 52(4), 998–1004. https://doi.org/10.14199/ppp-2012-172

Hossain, M. M., Sultana, F., Mostafa, M., Ferdus, H., Rahman, M., Rana, J. A., Islam, S. S., Adhikary, S., Sannal, A., Hosen, M. A. E., Nayeema, J., Emu, N. J., Kundu, M., Biswas, S. K., Farzana, L., & Al Sabbir, M. A. (2024). Plant disease dynamics in a changing climate: Impacts, molecular mechanisms, and climate-informed strategies for sustainable management. *Discover Agriculture*, 2, 132. https://doi.org/10.1007/s44279-024-00144-w

Hovmøller, M. S., Thach, T., & Justesen, A. F. (2023). Global dispersal and diversity of rust fungi in the context of plant health. *Current Opinion in Microbiology*, *71*, 102243.

Iacob, I. N., Roşculete, C. A., Păunescu, R. A., & Bonciu, E. (2025). Research on the response to

prolonged drought of an assortment of wheat varieties, through the rate of water loss from the flag leaf, on the chernozem of Caracal. *Scientific Papers. Series A. Agronomy*, 68(2), 501–511.

Joshi, P., Sandhu, K. S., Dhillon, G. S., Chen, J., & Bohara, K. (2024). Detection and monitoring wheat diseases using unmanned aerial vehicles (UAVs). *Computers and Electronics in Agriculture*, 224, 109158. https://doi.org/10.1016/j.compag.2024.109158

Juroszek, P., & von Tiedemann, A. (2013). Climate change and potential future risks through wheat diseases: A review. *European Journal of Plant Pathology*, 136, 21–33. https://doi.org/10.1007/s10658-012-0144-9

Kamilaris, A., & Prenafeta-Boldú, F. X. (2018). Deep learning in agriculture: A survey. *Computers and Electronics in Agriculture,* 147, 70–90. https://doi.org/10.1016/j.compag.2018.02.016

Karisto, P., Suffert, F., & Mikaberidze, A. (2022). Measuring splash dispersal of a major wheat pathogen in the field. *PhytoFrontiers™*, *2*(1), 30-40.

Kavhu, B., Mashimbye, Z. E., & Luvuno, L. (2021). Climate-based regionalization and inclusion of spectral indices for enhancing transboundary land-use/cover classification using deep learning and machine learning. *Remote Sensing*, *13*(24), 5054.

Khanal, S., Fulton, J., & Shearer, S. (2017). An overview of current and potential applications of thermal remote sensing in precision agriculture. *Computers and Electronics in Agriculture*, 139, 22–32. https://doi.org/10.1016/j.compag.2017.05.001

Korbas, M., Horoszkiewicz-Janka, J., & Jajor, E. (2008). Uproszczone systemy uprawy a występowanie sprawców chorób. [Simplified systems of soil management in relation to the occurrence of disease casual agents]. *Progress in Plant Protection*, 48(4), 1431–1438.

Kouadio, L., El Jarroudi, M., Belabess, Z., Laasli, S.-E., Roni, M.Z.K., Amine, I.D.I., Mokhtari, N., Mokrini, F., Junk, J., & Lahlali, R., (2023) A Review on UAV-Based Applications for Plant Disease Detection and Monitoring. *Remote Sensing*, 15(17):4273.

Kumar, D., & Mukhopadhyay, R. (2025). Climate change and plant pathogens: Understanding dynamics, risks and mitigation strategies. *Plant Pathology*, *74*(1), 59-68.

Laribi, M., Aboukhaddour, R., & Strelkov, S. E. (2024). Tan spot (*Pyrenophora tritici-repentis*) of wheat: A minireview. *Plant Health Cases*, https://doi.org/10.1079/planthealthcases.2024.0017

Li, Z., Wang, R., Ding, R. (2025). A review of crop attribute monitoring technologies for general agricultural scenarios. *AgriEngineering*, *7*(11), 365.

Liu, Y., Liu, G., Sun, H., An, L., Zhao, R., Liu, M., Tang, W., Li, M., Yan, X., Ma, Y., & Zhao, F. (2024). Exploring multi-features in UAV based optical and thermal infrared images to estimate disease severity of wheat powdery mildew. *Computers and Electronics in Agriculture*, 225, 109285. https://doi.org/10.1016/j.compag.2024.109285

Mahlein, A.-K., Oerke, E.-C., Steiner, U., & Dehne, H.-W. (2012). Recent advances in sensing plant diseases for precision crop protection. *European Journal of Plant Pathology*, 133(1), 197–209. https://doi.org/10.1007/s10658-011-9878-z

Mahlein, A.-K. (2016). Plant disease detection by imaging sensors – parallels and specific demands for precision agriculture and plant phenotyping. *Plant Disease*, 100(2), 241–251. https://doi.org/10.1094/PDIS-03-15-0340-FE

Malczewski, J. (2006). GIS-based multicriteria decision analysis: A survey of the literature. *International Journal of Geographical Information Science*, 20(7), 703–726. https://doi.org/10.1080/13658810600661508

Martínez, M., Biganzoli, F., Arata, A., Dinolfo, M. I., Rojas, D., Cristos, D., & Stenglein, S. (2022). Warm nights increase Fusarium Head Blight negative impact on barley and wheat grains. *Agricultural and Forest Meteorology*, *318*, 108909.

Martínez-Cadena, J. A., Sánchez-Cerritos, J. M., Alvarez-Ramirez, J., Marin-Lopez, A., Delgado-Fernández, J., & Fuentecilla-Carcamo, I. (2026). Eco-epidemiological clustering and cluster-wise forecasting of dengue in Mexico, 2020–2025. *Acta Tropica,* 275, Article 107993. https://doi.org/10.1016/j.actatropica.2026.107993

Mergenthaler, C., van Gurp, M., Rood, E., & Bakker, M. (2022). The study of spatial autocorrelation for infectious disease epidemiology decision-making: A systematized literature review. *CABI Reviews*, 17, Article 018. https://doi.org/10.1079/cabireviews202217018

Miedaner, T., & Juroszek, P. (2021). Climate change will influence disease resistance breeding in wheat in Northwestern Europe. *Theoretical and Applied Genetics*, *134*(6), 1771-1785.

Misra, A. K., Yadav, S. B., Mishra, S. K., & Tripathi, M. K. (2020). Impact of meteorological variables and climate change on plant diseases. In P. Kumar, A. K. Tiwari, M. Kamle, Z. Abbas, P. Singh (Eds.), *Plant pathogens: Detection and management for sustainable agriculture* (pp. 313–327). Apple Academic Press. https://doi.org/10.1201/9780429057212-18

Naz, R., Batool, S., Shahid, M., Keyani, R., Yasmin, H., Nosheen, A., Hassan, M.N., Mumtaz, S., & Siddiqui, M.H. (2021). Exogenous silicon and hydrogen sulfide alleviates the simultaneously occurring drought stress and leaf rust infection in wheat. *Plant Physiology and Biochemistry*, 166:558-571.

Neupane, K., & Baysal-Gurel, F. (2021). Automatic identification and monitoring of plant diseases using unmanned aerial vehicles: A review. *Remote Sensing*, 13(19), 3841. https://doi.org/10.3390/rs13193841

Pandey, P., Ramegowda, V., & Senthil-Kumar, M. (2015) Shared and unique responses of plants to multiple individual stresses and stress combinations: physiological and molecular mechanisms. *Frontiers in Plant Science* 6:723. doi: 10.3389/fpls.2015.00723

Paraschivu, M., Cotuna, O., Olaru, L., & Paraschivu, M. (2017). Impact of climate change on wheat-pathogen interactions and concerning about food security.

*Research Journal of Agricultural Science* (ISSN 2066-1843) vol.49 (3), p.87-95.

Paraschivu, M., Cotuna, O., Horablaga, M. N., Sărățeanu, V., & Durău, C. C. (2019). Owerview on the management of powdery mildew in wheat (Blumeria graminis f. sp. tritici D.C. Speer) in the context of climate change. *Annals of the University of Craiova – Agriculture, Montanology, Cadastre Series*, 49(1), 275–292.

Paraschivu, M., Matei, Gh., Cotuna, O., Paraschivu, M., & Drăghici, R. (2021). Reaction of rye cultivars to leaf rust (P. recondita f. sp. secalis) in the context of climate change in dry area in southern Romania. *Scientific Papers. Series A. Agronomy*, LXIV, No. 1, p. 500-507.

Paraschivu, M., Matei, G., Cotuna, O., Paraschivu, M., & Drăghici, R. (2022). Management of pests and pathogens in rye crop in dry marginal environment in Southern Romania. *Scientific Papers. Series A. Agronomy*, 65(1), 466–474.

Paraschivu, M., Cotuna, O., Sărățeanu, V., Matei, G., Drăghici, R., & Prioteasa, A. M. (2023). Assessment of leaf rust (P. recondita f. sp. secalis) attack in marginal areas in Southern Romania. *Scientific Papers. Series A. Agronomy*, 66(2), 330–338.

Păunescu, R. A., Bonciu, E., Roșculete, E., Păunescu, G., & Roșculete, C. A. (2023). The effect of different cropping systems on yield, quality, productivity elements, and morphological characters in wheat (Triticum aestivum). *Plants*, 12, Article 2802.

Păunescu, G., Paraschivu, M., Păunescu, R. A., & Roșculete, C. A. (2022). The relationship between yield and pathogens attack on the advanced breeding winter wheat lines assessed for adult plant resistance. *Scientific Papers Series Management, Economic Engineering in Agriculture and Rural Development*, 22(1), 493–501.

Petit-Houdenot, Y., Lebrun, M.-H., & Scalliet, G. (2021). Understanding plant-pathogen interactions in Septoria tritici blotch infection of cereals. In *Burleigh Dodds Series in Agricultural Science*. Burleigh Dodds Science Publishing.

Pickering, C., & Byrne, J. (2014). The benefits of publishing systematic quantitative literature reviews for PhD candidates and other early-career researchers. *Higher Education Research & Development*, 33(3), 534–548. https://doi.org/10.1080/07294360.2013.841651

Prahl, K. C., Klink, H., Hasler, M., Verreet, J.-A., & Birr, T. (2023). Will climate change affect the disease progression of Septoria tritici blotch in Northern Europe? *Agronomy*, 13(4), 1005. https://doi.org/10.3390/agronomy13041005

Radici, A., Martinetti, D., & Bevacqua, D. (2022). Early-detection surveillance for stem rust of wheat: insights from a global epidemic network based on airborne connectivity and host phenology. *Environmental Research Letters*, *17*(6), 064045.

Rahman, S. Z., Senthil, R., Ramalingam, V., & Gopal, R. (2023). Predicting infectious disease outbreaks with machine learning and epidemiological data. *Journal of Advanced Zoology*, *44*(S4), 110-121.

Rawat, K., Singh, P. V., Dhapola, M., & Bharti, H. (2026). Remote sensing and GIS approaches for agricultural drought severity assessment: A comprehensive review. *DMPedia Lecture Notes in Multidisciplinary Research*, *IMPACT26*, 1, 1207–1217. https://doi.org/10.65890/dmp.lnmr.IMPACT26.120

Richard, B., Qi, A., & Fitt, B. D. (2022). Control of crop diseases through Integrated Crop Management to deliver climate-smart farming systems for low-and high-input crop production. *Plant Pathology*, *71*(1), 187-206.

Roșculete C.A., Păunescu R.A., Roșculete E., Păunescu G., Florea D., & Bonciu E. (2023). The influence of foliar fertilizer application on the macro and micro nutrient content and yield of wheat plants (*Triticum aestivum*). *Scientific Papers Series Management, Economic Engineering in Agriculture and Rural Development*. 23, 3: 786-795.

Różewicz, M., Wyzińska, M., & Grabiński, J. (2021). The most important fungal diseases of cereals—Problems and possible solutions. *Agronomy*, *11*(4), 714.

Rubayet, M. T., & Hossain, M. M. (2024). Climate change and its impacts on disease dynamics in major cereal crops. In M. M. Rahman, J. C. Biswas, & R. S. Meena (Eds.), *Climate change and soil-water-plant nexus: Agriculture and environment* (pp. 265–295). Springer Nature Singapore. https://doi.org/10.1007/978-981-97-6635-2_9

Sangeetha, B., Vasanthi, E. A. P., & Parveen, S. S. (2025). Plant disease forecasting: A comprehensive review. *International Journal of Horticultural Science and Technology*, 12(3), 821–834.

Savary, S., Willocquet, L., Pethybridge, S. J., Esker, P., McRoberts, N., & Nelson, A. (2019). The global burden of pathogens and pests on major food crops. *Nature Ecology & Evolution*, 3(3), 430–439. https://doi.org/10.1038/s41559-018-0793-y

Seelan, S.K., Laguette, S., Casady, G.M., & Seielstad, G.A. (2003). Remote sensing applications for precision agriculture: A learning community approach. *Remote Sensing Environment*, 88, 157–169.

Shafay, M., Hassan, T., Owais, M., Hussain, I., Khawaja, S. G., Seneviratne, L., & Werghi, N. (2025). Recent advances in plant disease detection: challenges and opportunities. *Plant Methods*, *21*(1), 140.

Singh, M., Vermaa, A., & Kumar, V. (2023). Geospatial technologies for the management of pest and disease in crops. In Q. U. Zaman (Ed.), *Precision agriculture Evolution, Insights and Emerging Trends* (pp. 37–54). Academic Press. https://doi.org/10.1016/B978-0-443-18953-1.00002-7

Snyder, H. (2019). Literature review as a research methodology: An overview and guidelines. *Journal of Business Research*, 104:333-339.

Srivastava, A., & Jain, S. (2025). Remote sensing for environment assessment: Multispectral, hyperspectral, and thermal imaging applications. In V. Saritha, C. B. Pande, R. Singh, & M. Shahid (Eds.), *Remote sensing for environmental monitoring*

(pp. 1–31). Springer Nature Singapore. https://doi.org/10.1007/978-981-96-5546-5_1

Su, J., Liu, C., Coombes, M., Hu, X., Wang, C., Xu, X., Li, Q., Guo, L., & Chen, W.-H. (2018). Wheat yellow rust monitoring by learning from multispectral UAV aerial imagery. *Computers and Electronics in Agriculture*, 155, 157–166. https://doi.org/10.1016/j.compag.2018.10.017

Șulea, C., Alboteanu, L., & Manolea, G. (2010). Advanced technologies applied in anti-hail systems. *Buletinul AGIR*, (4), 17–22.

Șulea, C., Manolea, G., & Alboteanu, L. (2011). The informatic system as decision support for the activities of combating hail. *Annals of the "Constantin Brâncuși" University of Târgu Jiu, Engineering Series*, (3), 195–204.

Tammina, M. R., Sumana, K., Singh, P. P., Lakshmi, T. R. V., & Pande, S. D. (2024). Prediction of plant disease using artificial intelligence. In *Microbial data intelligence and computational techniques for sustainable computing* (pp. 25–48). Springer Nature Singapore. https://doi.org/10.1007/978-981-99-9621-6_2

Tranfield, D., Denyer, D., & Smart, P. (2003). Towards a methodology for developing evidence-informed management knowledge by means of systematic review. *British Journal of Management*, 14(3), 207–222. https://doi.org/10.1111/1467-8551.00375

Tsouros, D. C., Bibi, S., & Sarigiannidis, P. G. (2019). A review on UAV-based applications for precision agriculture. *Information*, 10(11), 349. https://doi.org/10.3390/info10110349

United Nations, Department of Economic and Social Affairs, Population Division. (2019). *World population prospects 2019: Highlights* (ST/ESA/SER.A/423). United Nations. https://population.un.org/wpp/Publications/Files/WPP2019_Highlights.pdf

Velea, L., Bojariu, R., Burada, C., Udristioiu, M. T., Paraschivu, M., & Burce, R. D. (2021). Characteristics of extreme temperatures relevant for agriculture in the near future (2021–2040) in Romania. *Scientific Papers. Series E. Land Reclamation, Earth Observation & Surveying, Environmental Engineering*, 10, 70–75.

West, J. S., & Kimber, R. B. E. (2015). Innovations in air sampling to detect plant pathogens. *Annals of Applied Biology*, 166(1), 4–17. https://doi.org/10.1111/aab.12191

Wolfert, S., Ge, L., Verdouw, C., & Bogaardt, M.-J. (2017). Big data in smart farming – A review. *Agricultural Systems*, 153, 69–80. https://doi.org/10.1016/j.agsy.2017.01.023

Xing, Y., Liu, X., & Wang, X. (2026). Integrating UAVs, satellite remote sensing, and machine learning in precision agriculture: Pathways to sustainable food production, resource efficiency, and scalable innovation. *Frontiers in Agronomy*, 7, 1670380. https://doi.org/10.3389/fagro.2025.1670380

Zarco-Tejada, P. J., Camino, C., Beck, P. S. A., Calderon, R., Hornero, A., Hernández-Clemente, R., Kattenborn, T., Montes-Borrego, M., Susca, L., Morelli, M., Gonzalez-Dugo, V., North, P. R. J., Landa, B. B., Boscia, D., Saponari, M., & Navas-Cortes, J. A. (2018). Previsual symptoms of Xylella fastidiosa infection revealed in spectral plant-trait alterations. *Nature Plants*, 4(7), 432–439. https://doi.org/10.1038/s41477-018-0189-7

Zhu, H., Lin, C., Liu, G., Wang, D., Qin, S., Li, A., Xu, J.-L., & He, Y. (2024). Intelligent agriculture: Deep learning in UAV-based remote sensing imagery for crop diseases and pests detection. *Frontiers in Plant Science*, 15, 1435016. https://doi.org/10.3389/fpls.2024.1435016

Scientific Papers. Series E. Land Reclamation, Earth Observation & Surveying, Environmental Engineering. Vol. XV, 2026
Print ISSN 2285-6064, CD-ROM ISSN 2285-6072, Online ISSN 2393-5138, ISSN-L 2285-6064

# APPLICATION OF PHOTOGRAMMETRIC TECHNOLOGIES FOR CROP MONITORING IN PRECISION AGRICULTURE

**Silvia Alexandra DREGHICI[1], Levente DIMEN[1], Liviu BUZILA[2], Tudor BORȘAN[1], Gianmarco PITTON[1]**

[1]"1 Decembrie 1918" University of Alba Iulia, 5 Gabriel Bethlen, Alba Iulia, Romania
[2]Babeș-Bolyai University, 1 Mihail Kogălniceanu, Cluj-Napoca, Romania

Corresponding author email: ldimen@uab.ro

***Abstract***

*This article examines the application of modern photogrammetric technologies for crop monitoring in the context of precision agriculture. Effective assessment of crop condition and spatial variability remains a critical challenge for improving productivity and optimizing resource use in large and heterogeneous agricultural areas. To address this issue, the proposed methodology employs unmanned aerial vehicles equipped with a high-resolution camera, combined with structure-from-motion photogrammetric processing, to generate detailed orthomosaics and crop surface models. Vegetation indices and canopy metrics are derived to support spatial analysis of crop vigour and growth patterns throughout the growing season. The study evaluates alfalfa fields located in the agricultural area surrounding Alba Iulia, employing UAV-based photogrammetry to quantify crop surface characteristics. The workflow generated a high-density point cloud and a high-precision 3D surface model, enabling detailed assessment of canopy structure and health and spatial variability. The results provide the basis for monitoring crop condition, support future analysis of field parameters, and demonstrate that photogrammetric products enable timely and accurate detection of stress conditions, biomass variability, and development anomalies at field scale. The study confirms that modern photogrammetric techniques provide a reliable, cost-effective, and scalable solution for supporting data-driven decision-making in crop monitoring and management.*

***Key words***: *crop monitoring, photogrammetry, precision agriculture, unmanned aerial vehicles, vegetation indices.*

## INTRODUCTION

The field of global agriculture is currently facing some significant challenges, which are, first of all, due to increasing climate changes. These challenges include extreme weather, such as droughts, and pests that are affecting more than half of farmland (FAO, 2017). Besides these challenges, there are also degradation factors, like soil degradation, which is affecting a significant part of the land (FAO, 2017). Also, other significant challenges must be considered, including but not limited to water scarcity and, therefore, the rising input costs. These factors pose a threat to food security, worsening the economic instability, and it is required the implementation of urgent, sustainable, and technologically innovative farming solutions to support a growing global population. Climatic events, such as floods and droughts, may be the causal factors for crop production disruption. Furthermore, a significant part of agricultural land is subject to severe soil degradation, declining the productivity. The rapid depletion of natural resources, including water shortages for irrigation, can reduce long-term viability. The necessity to nourish a growing population correlated with diminishing land availability for agriculture is exerting considerable pressure on global food systems (FAO, 2017). Geopolitical tensions and recurring logistical constraints, such as maritime grain export disruptions or rising energy and fuel prices (International Food Federation, 2025) have, in recent years, placed additional pressure on the stability of food distribution systems. Addressing these challenges is not straightforward and typically involves a gradual shift away from purely conventional agricultural practices toward more sustainable approaches, such as agroecology and climate-smart agriculture, combined with the selective adoption of modern technologies aimed at improving system resilience (FAO, 2017).

Against this background, precision agriculture has attracted increasing interest within the agricultural sector. In general terms, the

concept refers to a data-informed approach to farm management that makes use of technologies including GNSS positioning, environmental sensors, unmanned aerial vehicles, and artificial intelligence. Used appropriately, these tools allow continuous monitoring and support more targeted responses to variability both within individual fields and across different fields. This management approach is characterized by a transition from a uniform, large-scale application to a precise, site-specific management strategy. This strategy enhances efficiency, sustainability, and profit. The following elements constitute the fundamental components of the precision agriculture paradigm (Todmal, 2023; Gulaiya et al., 2024):

- The collection is to be undertaken using a variety of methods, including GNSS, GIS, photogrammetry, remote sensing (via drones and satellites), and soil sensors. The purpose of this data collection is to obtain information on soil moisture, nutrient levels, and crop health.
- The data analysis is conducted through the assessment of yield maps and spatial variability data, with the objective of identifying areas of underperformance or specific, localized needs.
- Variable rate technology involves the use of automated equipment for the application of fertilizers, pesticides and water at varying rates across a field, with the objective of customizing the application to specific requirements as opposed to employing a uniform, average rate.
- The implementation of guidance systems, utilizing GPS-enabled machinery in tasks such as planting and spraying, has been demonstrated to reduce overlap, leading to significant savings in fuel and resources.

Conventional field scouting and photogrammetric monitoring both have distinct, often complementary limitations. Whilst field scouting is constrained by human labour and time, photogrammetric monitoring using UAVs is restricted by environmental, technical and data processing bottlenecks. Conventional, manual scouting involves physical inspection by professionals, which introduces several limitations: the processes under discussion are characterized by their labour intensity and time consumption, the presence of subjectivity and human error, their limited spatial coverage, physical inaccessibility, and delayed action. On the other hand, photogrammetry, the process of creating 3D models and orthophotos from drone images, provides high-resolution data, but is also subject to several limitations: the factors to be considered include weather and lighting dependency, visibility and occlusion issues, textureless/uniform surfaces, data processing bottlenecks, reduced vertical accuracy, regulatory and skill barriers. In order to address these issues, contemporary agriculture practices frequently employ a combination of both approaches, leveraging photogrammetry to identify areas of concern and subsequently conducting targeted, ground-based manual verification (Kalischuk et al., 2019; Amarasingam et al., 2022).

Photogrammetric technologies are increasingly used in agriculture, most often through aerial imagery collected by unmanned aerial vehicles (UAVs). The resulting products - such as three-dimensional models, orthomosaics, and elevation data - provide valuable spatial information that supports the adoption of precision farming practices. In current applications, these tools contribute to high-throughput phenotyping, crop condition assessment (frequently based on vegetation indices such as NDVI or other multispectral datasets), as well as to the early identification of pest presence and the optimization of irrigation management. This way, targeted resource application is enabled. There are some technologies of particular significance: unmanned aerial vehicles (UAVs), specialized software and artificial intelligence (AI). These technologies provide detailed, actionable insights within a time frame, usually of several hours, which represent an important advantage in crop security (Delgado Vera et al., 2017; Turlea et al., 2023; Dreghici et al., 2024).

There should be mentioned the following key applications in the agriculture field (Delgado Vera et al., 2017; Sakthivel et al., 2025):

- Crop monitoring and health assessment, by using photogrammetry for the detection of pest attacks, water stress and nutrient deficiencies;
- 3D modelling and mapping, for the analysis of field variability, monitoring of growth patterns and the improvement of terrain management;

- Yield prediction and management, for the prediction of crop production and the optimization of fertilizer and pesticide input usage;
- Precision irrigation and drainage, for the identification of areas with poor drainage or water accumulation;
- Crop management, for the precise, non-destructive monitoring of crop structure and development throughout the season.

The technologies and tools considered in this context include several widely used solutions (Delgado Vera et al., 2017; Turlea et al., 2023; Sakthivel et al., 2025). Among them, unmanned aerial vehicles (UAVs), commonly referred to as drones and typically equipped with GNSS/GPS positioning systems, play an important role by enabling the acquisition of high-resolution imagery suitable for detailed mapping applications. Sensors, which may be multispectral, thermal or RGB, frequently utilised for the collection of data.

- Software, such as the photogrammetric software Agisoft MetaShape, used to process images into orthomosaics and 3D models.
- Artificial intelligence (AI) and machine learning integrated with photogrammetry, for automated analysis of field data.

UAVs represent a viable solution for high-resolution and cost-effective agricultural monitoring and management, being considered a significant advancement over traditional satellite, manned aircraft, and ground-based surveying methods. Unmanned aerial vehicles come with higher spatial resolution, usually at centimetre-level, this way bridging the gap between field-level measurements and satellite imagery. The usage of UAVs reduces time, labour, and financial overhead (typically associated with conventional manual scouting and manned aerial surveys) (Guebsi et al., 2024; Sreenatha et al., 2025).

Two principal research gaps emerge when applying photogrammetric technologies in the context of agricultural monitoring:

- The integration of three-dimensional photogrammetric products, such as crop height models, into routine crop monitoring is inadequate.
- A limited number of comparative studies have been conducted between photogrammetry-derived metrics and traditional agronomic measurements.

In this context, the objectives of the present study are as follows:

- To evaluate the applicability of photogrammetric technologies for the purpose of monitoring crop growth and condition;
- To assess the contribution of precision agriculture in case of decision-making processes;
- To highlight the contribution of photogrammetry in agriculture and its support for the shift toward modern, digital, and sustainable farming, by producing photogrammetric outputs used for agricultural land evaluation and monitoring of land use changes.

## MATERIALS AND METHODS

The site chosen for the case study in this paper is located in the peri-urban area of Alba Iulia, in an agricultural area, predominantly used for cereal production. The area's accessibility and terrain with relatively uniform elevation render it conducive to UAV operations. The location has been determined to provide suitability for the application of modern crop monitoring technologies, allowing for efficient data collection with the equipment used. Certain figures and supporting materials used in this paper are adapted from, or were originally presented in, the bachelor's thesis by Pitton, G. (2025), "The use of modern technology in monitoring agricultural crops".

The topography of the studied area is characterised by its relative flatness, with gentle slopes and minimal altitude variations. These characteristics make the area suitable for photogrammetric flights and aerial image acquisition, as well as for generating high-precision 3D models and orthophotos. The soil type is chernozem and luvisol, which is specific to Alba County areas. These soils are moderately permeable and medium to highly fertile, characteristics that are favourable to cereal crops and vegetables.

### Data acquisition

The WingtraOne Gen II drone, used for the present purpose, is a technologically advanced aerial mapping equipment, specifically designed for professional applications in the field of land surveying, cadastral mapping,

agricultural monitoring, and environmental management. The flight platform, VTOL-type (Vertical Take Off and Landing) was designed to be robust and to use state-of-the-art technology. This means that it offers remarkable performance in terms of autonomy, accuracy and versatility for aerial photogrammetric applications. Integrating the advanced onboard avionics sensor suite, the autonomous and real-time stability flight-control architecture, and mission-optimized planning environment transformed this aerial platform into a comprehensive solution for the creation of high-resolution orthophotos and 3D models. The drone is equipped with a high-resolution camera, for optimal aerial images acquisition. A further significant feature of the WingtraOne Gen II drone is the incorporation of GNSS RTK/PPK system, which allows direct image georeferencing with high precision, minimising the requirement for a considerable number of ground control points (GCPs).

Mission planning is conducted utilising the dedicated WingtraPilot software, which facilitates precise configuration of flight parameters and optimisation of the trajectory to ensure an overlap that fulfils photogrammetry requirements.

The utilisation of this drone facilitated the effective collection of data essential for the monitoring of existing crops in the vicinity of Alba Iulia, thereby providing decision support in the analysis of agricultural crops and agricultural land management.

The planned flight route is configured to respond the specific terrain conditions, ensuring consistent coverage and data quality, as shown in Figure 1. In the present case study, the decision was taken to fly at a flight height of 120 metres. In order to obtain high-accuracy and high-resolution images, the GSD parameter was set relatively high, 3.2 cm/pixel, as recommended for the specified flight height. In addition, the controller interface provides information about the drone's anticipated flight trajectory, representing the total area to be covered, the status of connectivity with the GNSS signal, the number of satellites that are currently visible, and also the current battery level of the drone.

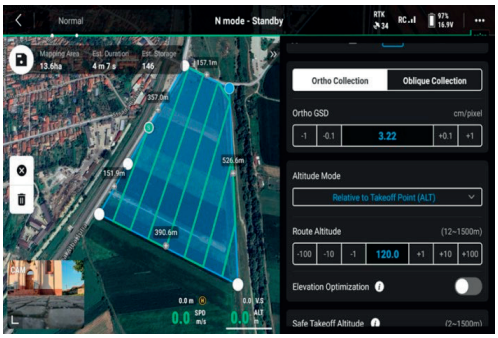



Figure 1. Flight plan

**Photogrammetric processing**

Upon completion of the flight session in the field and collection of the necessary data for this project, the subsequent stage would involve the transfer of all obtained data to a computer, with the objective of creating a 3D model of the terrain and an orthophoto map.

The Agisoft MetaShape program facilitates data processing through the provision of an integrated, efficient, and precise workflow, thereby ensuring the generation of high-quality geospatial products. The utilisation of this software within the project enabled the conversion of raw images captured by the drone into a series of photogrammetric materials that were conducive to the analysis of agricultural land. The high accuracy of the orthophoto map and the 3D model obtained provides a solid basis for decision-making in precision agriculture, considering the monitoring of crops and agricultural land.

The workflow comprised the following stages:

1. The process of image alignment entails the identification of the position and orientation of images, with the objective of constructing an initial point cloud based on the corresponding points between images, known as tie points. The geometric relationship between images is established through the comparison and overlaying of common features. In accordance with the aforementioned points, the program implements a global bundle adjustment. This adjustment constitutes a mathematical optimization that determines the position and orientation of each image in three-dimensional space. The outcome of this process is a relatively accurate reconstruction of the flight path - Figure 2.

In order to achieve optimal and precise results for the final products, it is imperative to filter the tie points from the previously created point cloud (Figure 3). This is due to the fact that numerous erroneous points will be identified during this process. The quality of subsequent photogrammetric products (i.e. dense point cloud, 3D model, orthophoto map) is contingent upon the quality of the initial list of connection points. Following the filtration of the tie points, it is imperative to utilise the "Optimize camera alignment" function. The purpose of this function is to enhance the precision of photogrammetric reconstruction, after the implementation of adjustments to the tie points.

2. The second fundamental stage of the workflow is the creation of a dense point cloud (Figure 4), using the image alignment results as input. in the present case study, the dense point cloud reconstruction was performed using the ultra-high-quality parameter and moderate depth filtering, selected to balance geometric accuracy with computational efficiency. Applying these settings, there was produced a detailed and spatially consistent dense point cloud, that served as the basis for the subsequent 3D surface model and orthophoto generation.

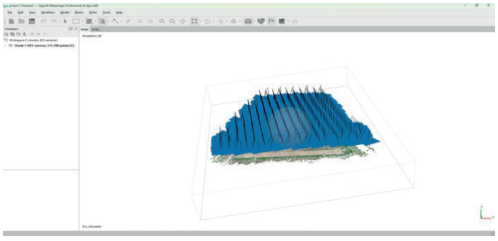


Figure 2. Aligned images along the flight path

The "reprojection error" criterion is another essential indicator of the quality of photo alignment and the accuracy of connection points. This criterion is used for assessing the precision of the reconstructed 3D points and whether they correspond to their projected positions in the source image. This way, the difference between the estimated position of a 3D point projected back onto the image and the actual position of that point detected in the photo is measured. The reprojection error is expressed in pixels. The errors are inversely proportional to accuracy: the smaller the error, the higher accuracy for the point. After this optimisation, the mean error should be reduced significantly, enhancing the project accuracy.

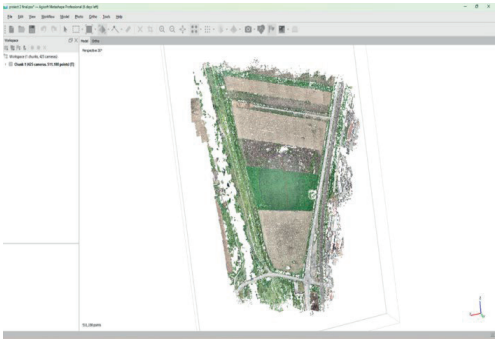


Figure 3. Point cloud

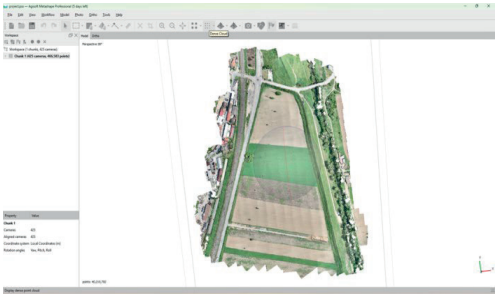


Figure 4. Dense point cloud

3. The third fundamental stage of the project is the creation of the mesh model. The mesh model is a three-dimensional reconstruction of the photographed surface, formed from a network of triangles (polygons) that connect the previously generated points. This stage is of critical importance in the photogrammetric process, as it is the foundation for obtaining a highly detailed model of the terrain or objects under consideration. Furthermore, it facilitates the application of textures and the subsequent measurement of various parameters. For mesh generation, the dense point cloud was used as the primary data source, with the surface type configured for three-dimensional reconstruction.

The "Face count" criterion in the mesh model construction window represents the estimated number of geometric faces that will make up the polygonal network of the 3D model. The

geometric intricacy of the model is directly proportional to the number of facets, but the processing time and hardware resources required increase exponentially.

4. The next stage of the workflow consisted of applying texture to the resulting 3D model in order to enhance its visual realism. The option "Diffuse map" is the type of texture applied to the generated surface of the 3D model to render the terrain colour and natural appearance. This texture is taken from the captured images during the flight. It is imperative to note that this option is essential for realistic rendering of the surface.

Given the approximately flat surface of the project, the decision was taken to utilise the 'Adaptive orthophoto' function, as this projects a texture similar to that of the orthophoto plan. This allows the algorithm to dynamically select the most suitable pixels from the source image set for texture projection onto the 3D model, thus avoiding perspective errors and distortions at the edges of the images.

In considering the objectives set for this project, the decision was taken to construct a tiled model, given the necessity to analyse the monitored crop area in detail. This model offers a more flexible and detailed representation of surfaces and is optimised for viewing 3D structures at different zoom levels and resolutions. The tiled model is based on a hierarchical organisation of spatial data, which allows for the efficient display of fine details such as soil textures, crop damage, uneven vegetation, or traces of agricultural mechanization. This is in contrast to the previously generated textured 3D model, which provides a global representation of the relief and surface, but with visible limitations in terms of close-up resolution. The tiled model facilitates detailed exploration without substantial loss of quality or extended loading times - Figure 5.

In the case of the initial textured 3D model, it was determined that the fine surface details, which are imperative for detailed crop analysis, were not adequately rendered. This was attributable to two factors: firstly, the resolution limitations inherent in the generated texture, and secondly, the methodology by which the visual information was applied to the model's surface. Texture has the capacity to "mask" reconstruction imperfections or to homogenise terrain features, thereby rendering it challenging to observe subtle yet significant discrepancies - Figure 6.

The tiled model has been structured into tiles, thereby enabling a smooth and detailed view of the entire studied area, regardless of the zoom level. In the context of our research, this is of crucial importance, as interpreting subtle variations in relief or vegetation structure can substantially contribute to the identification of affected areas, the monitoring of soil moisture, or the planning of agrotechnical work.

To facilitate a more profound comprehension of the subject, the tiled model is an approach that divides the total surface into a number of tiles. Each individual tile is processed and stored with its own geometry and texture data. It is evident that the greater the number of tiles, the smaller the area of each individual tile and the more triangles connecting points it can contain. In addition, a dedicated texture map at a higher resolution for each tile is required. Each tile is expressed in terms of dimensions in pixels; in this context, a tile size of 256 pixels was selected, the smallest possible selectable tile size.

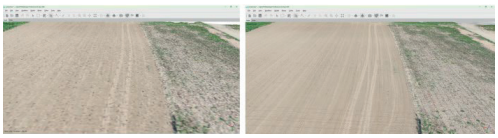


Figure 5. Resolution and detail quality for the textured 3D model at a very high zoom level (left) vs. Resolution and detail quality for the tiled model at the same zoom level (right)

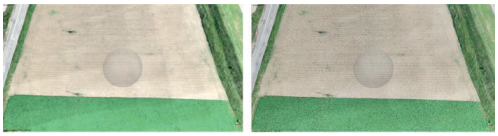


Figure 6. 3D model without texture (left) and with applied texture (right)

**Validation and analysis**

UAV photogrammetry offers a high-efficiency approach for deriving crop-height metrics, providing accuracy levels appropriate for validating the generated results. These methodologies yield 3D point clouds and Digital Surface Models (DSMs), which, upon

validation consisting of comparing the photogrammetric outputs with ground control points, furnish precise, spatially continuous measurements across entire plots. This approach circumvents the labour-intensive constraints inherent in conventional destructive sampling techniques (Bendig et al., 2014; Tang et al., 2021).
The resulting 3D model and orthophoto provided the spatial data used for subsequent assessment of crop condition patterns, identification of vegetation variability and weed affected zones.

## RESULTS AND DISCUSSIONS

### Photogrammetric outputs

The quality requirements for point clouds and surface models in agricultural monitoring are driven by the need to accurately measure plant structures, estimate biomass, and navigate machinery (Zhu et al., 2024). The photogrammetric processing produced a dense point cloud and 3D surface models with geometric accuracy suitable for field-scale crop assessment. The surface deviations are ranging from 0 to 9 mm, ensuring that canopy height estimates and spatial comparisons across the study area remained reliable. The final surface model exhibited centimetre level vertical precision, consistent with typical UAV-based agricultural monitoring requirements (Tomaštík et al., 2017; Zhu et al., 2024).
The digital terrain model (DTM) generated from the ground classified points provided a stable reference for isolating plant height. After applying statistical filtering to remove noise and non-ground artefacts, the DTM supported the computation of crop height values across the monitored area, capturing fine scale structural variability within the alfalfa canopy. This enables the identification of zones with reduced growth or irregular development.
Analysis of the dense point cloud and derived canopy height model revealed heterogenous vegetation patterns within the surveyed area.

### Crop monitoring performance

The results of the investigation are presented across three key areas of analysis: the spatial distribution of crop height and vigour; the identification of stress zones (water deficit, nutrient deficiency, and lodging); and the temporal changes observed across growth stages.
The identification of issues arising from the analysis:

- In the alfalfa crop, small gaps are visible in several areas of the plot (Figure 7). These gaps regions correspond to areas where plant life has been compromised.

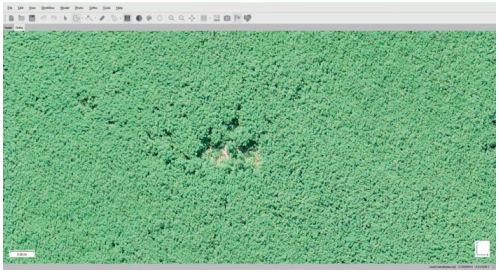


Figure 7. Gap areas in the alfalfa crop

- The second problem observed in the plots of land concerned is the weed infestation on the plot of land where a corn crop was recently sown. As illustrated in Figure 8 left, the areas exhibiting a high degree of weed infestation are delineated from the periphery of the plot towards its interior. The visual interpretation revealed the presence of weed infestation across the majority of the plot's surface, not merely in areas exhibiting a more pronounced green hue - Figure 8 right.

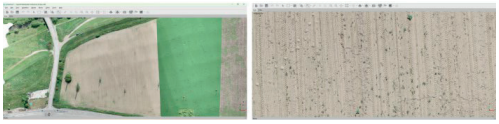


Figure 8. Areas with a high degree of weed infestation vs. weed infestation across the entire plot's surface

### Discussions

The results of the study demonstrate that UAV-based photogrammetry provides the level of spatial detail required for parcel-scale crop assessment. The centimetre-level accuracy achieved in the 3D reconstruction enabled the reliable extraction of canopy height patterns and the identification of localised anomalies within the alfalfa field. These capabilities directly support the detection of uneven vegetation growth and weed affected areas observed in the orthophoto and canopy height

model (Amarasingam et al., 2022; Pitton, 2025).

While the general advantages of UAV photogrammetry – high spatial resolution, flexible acquisition timing, and non-destructive monitoring- are well established, the present results confirm their practical relevance for the study area (Amarasingam et al., 2022; Pitton, 2025).

In particular, the ability to resolve fine-scale structural variability, which would not be detectable using satellite imagery, proved essential for interpreting field level conditions.

The findings also highlight the complementary role of UAV data within a broader monitoring framework, where satellite observations can guide the identification of zones of interest, and UAV surveys can provide the detailed structural information needed for targeted agronomic decisions (Guebsi et al., 2024; Pitton, 2025; Voss et al., 2025).

## CONCLUSIONS

Recent advances in geospatial technology have led to a significant transformation in how agricultural land is monitored, analysed and managed. This paper puts forward a contemporary approach to using drone-based aerial photogrammetric technologies to monitor crops and agricultural land. This method is recognised for providing accurate, georeferenced data quickly, and it is also transforming the traditional approach to managing agricultural land (Enemark, 2007). The results show that photogrammetric products, including 3D models and orthophotos, allow detailed assessment of crop conditions, supporting the identification of stress factors such as diseases, pests, and water deficits. In addition, the approach proves effective for precise parcel delineation, contributing to land use updates.

The study also confirms the practical value of UAV-based photogrammetric data in agricultural management, including reliable are estimation, productivity assessment, and documentation support for subsidy applications. Furthermore, 3D terrain and surface models enhance the understanding of land characteristics, supporting better land management.

Overall, the purposed approach contributes to improving efficiency, resource optimization, and non-invasive monitoring in agriculture. However, its application remains constrained by factors such as limited flight duration, weather dependence, and the need for technical expertise.

In conclusion, UAV-based photogrammetry represents a reliable and versatile tool for modern agriculture, offering significant benefits for crop monitoring, land management, and decision support.

## REFERENCES

Amarasingam, N., Salgadoe, A. S. A., Powell, K., Gonzalez, L. F., & Natarajan, S. (2022). A review of UAV platforms, sensors, and applications for monitoring of sugarcane crops. *Remote Sensing Applications: Society and Environment, 26*, 100712. https://doi.org/10.1016/j.rsase.2022.100712

Bendig, J., Bolten, A., Bennertz, S., Broscheit, J., Eichfuss, S. & Bareth, G. (2014). Estimating biomass of barley using crop surface models derived from UAV imagery. *Remote Sensing, 6*, 10395-10412. DOI: 10.3390/rs61110395

Delgado Vera, C., Aguirre Munizaga, M., Jiménez, M., Manobanda, N., & Rodríguez-Méndez, A. (2017). A photogrammetry software as a tool for precision agriculture: A case study. pp. 282–295. Springer. https://doi.org/10.1007/978-3-319-67283-0_21

Dreghici, S. A., Tulbure, I., & Coposesc, C. (2024). Applying computer supported media in land-use management for getting sustainability on local level. *RevCAD, 36*, 127–135

Enemark, S. (2007). Integrated land-use management for sustainable development. FIG. https://www.fig.net/resources/monthly_articles/2007/april_2007/april_2007_enemark.pdf

Food and Agriculture Organization of the United Nations. (2017). The future of food and agriculture: Trends and challenges. FAO. https://openknowledge.fao.org/handle/20.500.14283/i7011e

Guebsi, R., Mami, S., & Chokmani, K. (2024). Drones in precision agriculture: A comprehensive review of applications, technologies, and challenges. *Drones, 8*(11), 686. https://doi.org/10.3390/drones8110686

Gulaiya, S., Sharma, A., Singh, S., Kumar, R., Chaudhary, D., Yadav, K., Kumar, M., & Kumar, R. (2024). Precision agriculture: Transforming farming efficiency with cutting-edge smart technologies: A comprehensive review. *Journal of Experimental Agriculture International, 46*, 1126–1138. https://doi.org/10.9734/jeai/2024/v46i92909

International Food Federation. (2025). Geopolitical crises and their impact on global food supply chains. https://iff-uo.org/2025/08/09/geopolitical-crises-and-their-impact-on-global-food-supply-chains/

Kalischuk, M., Paret, M., Freeman, J., Raj, D., Silva, S., Eubanks, S., Wiggins, Z., Lollar, M., Marois, J., Mellinger, C., & Das, J. (2019). An improved crop scouting technique incorporating UAV-assisted multi-spectral crop imaging into conventional scouting practice for gummy stem blight in watermelon. *Plant Disease, 103*. https://doi.org/10.1094/PDIS-08-18-1373-RE

Pitton, G. (2025). *The use of modern technology in monitoring agricultural crops* (Bachelor's thesis). "1 Decembrie 1918" University of Alba Iulia

Sakthivel, N., Adhisankaran, K., Kabilan, M., Balachandar, D., Ragunath, K. P., Raja, R., Manivannan, V., & Vasumathi, V. (2025). A review on advancing agricultural practices using photogrammetric images. *Plant Science Today, 12*(sp1). https://doi.org/10.14719/pst.8813

Sreenatha, A., Nagaraja, K. S., Anil Kumar, S., Manjunatha Reddy, T. B., Mushrif, S. K., Narabenchi, G., Krishna, H. C., & Dhananjaya, P. (2025). Applications of unmanned aerial vehicles (UAVs) in agriculture: A review. *International Journal of Research in Agronomy, 8*(9, SP), 292–298, https://doi.org/10.33545/2618060X.2025.v8.i9Sd.3843

Tang, Z., Parajuli, A., Chen, C. J.,Hu, Y., Revolinski, S.,Medina, A. C.,Lin & S.,Zhang, Z. (2021). Validation of UAV-based alfalfa biomass predictability using photogrammetry with fully automatic plot segmentation. *Scientific Reports, 11*, 3336. https://doi.org/10.1038/s41598-021-82797-x

Todmal, A. (2023). Precision agriculture: Technology-driven approaches for efficient farming. https://doi.org/10.25215/9358791152.07

Tomaštík, J., Mokroš, M., Saloň, Š., Chudý, F., & Tunák, D. (2017). Accuracy of photogrammetric UAV-based point clouds under conditions of partially-open forest canopy. *Forests, 8*(5), 151. https://doi.org/10.3390/f8050151

Turlea, I. A., Dancea, E. M., Dragomir, L. O., & Popescu, G. (2023). Photogrammetric methods used to create orthophoto plans in the context of territory organization. *Research Journal of Agricultural Science, 55*(4), 260–272

Voss, G., May, M., Shackelford, N., Kelley, J., Stephen, R., & Bone, C. (2025). Evaluating the potential of UAVs for monitoring fine-scale restoration efforts in hydroelectric reservoirs. *Drones, 9*(7), 488. https://doi.org/10.3390/drones9070488

Zhu, J., Zhai, R., Ren, H.,Xie, K.,Du, A.,He, X.,Cui, C.,Wang, Y., Ye, J.,Wang, J.,Jiang, X., Wand, Y.,Huang, C., & Yang, W. (2024). Crops3D: A diverse 3D crop dataset for realistic perception and segmentation toward agricultural applications. *Scientific Data, 11*, 1438. https://doi.org/10.1038/s41597-024-04290-0

Scientific Papers. Series E. Land Reclamation, Earth Observation & Surveying, Environmental Engineering. Vol. XV, 2026
Print ISSN 2285-6064, CD-ROM ISSN 2285-6072, Online ISSN 2393-5138, ISSN-L 2285-6064

# ASSESSING WINTER MICROCLIMATES AND URBAN-RURAL THERMAL DIFFERENCES: A MOBILE MONITORING PILOT STUDY IN SOUTH-EASTERN ROMANIA

**Sorin FRĂSINA[1, 2], Adrian ROȘU[1, 3], Bogdan ROȘU[1, 3], Maxim ARSENI[1, 3], Daniel-Eduard CONSTANTIN[1, 3], Mădălin CRISTEA[1], Lucian SFÎCĂ[4], Cătălina ITICESCU[1, 2], Silvia DRAGAN[5]**

[1]"Dunarea de Jos" University of Galati, Faculty of Sciences and Environment, Department of Chemistry, Physics and Environment, 111 Domneasca Street, Galati, Romania
[2]"Dunarea de Jos" University of Galati, Faculty of Engineering, 111 Domneasca Street, Galati, Romania
[3]"Dunarea de Jos" University of Galati, REXDAN Research Infrastructure, 98 George Cosbuc Street, Galati, Romania
[4]"Alexandru Ioan Cuza" University, Faculty of Geography and Geology, Department of Geography, 20A Carol I Street, 700506, Iași, Romania
[5]EnviroEcoSmart S.R.L., Tecuci Street no. 189, Galati, Romania

Corresponding author email: adrian.rosu@ugal.ro

***Abstract***

*Rapid urbanization alters the thermal environment of cities, leading to the urban heat island effect. Because fixed meteorological stations cannot adequately capture high-resolution intra-urban microclimate variability, mobile monitoring has emerged as an essential complementary approach. This exploratory pilot study evaluated the utility of high-resolution mobile measurements for capturing winter microclimatic signatures along a regional transect in South-Eastern Romania, encompassing small and medium-sized urban hubs. Data were collected on February 10, 2026, under stable atmospheric conditions, using a vehicle-mounted weather station equipped with a radiation error correction system. To ensure scientific integrity, a three-stage quality control and normalization workflow was implemented. This included excluding data points recorded at speeds below 10 km/h to prevent thermal contamination, applying an altitude correction to a common reference level, and performing a time-drift correction based on official meteorological stations to isolate the spatial microclimatic signal. The spatially dense mobile data effectively identified critical thermal gradients and specific urban footprints. In conclusion, the study highlighted the value of mobile monitoring as a viable tool for assessing microclimatic spatial variations, providing detailed insights into urban-rural thermal contrasts during the cold season.*

***Key words:*** *altitude correction, Meteotracker, mobile measurements, temperature gradient, urban microclimate, urban-rural contrast.*

## INTRODUCTION

Rapid urbanization and significant land-use modifications have profoundly altered the thermal environment of cities, leading to the well-documented Urban Heat Island (UHI) effect (Oke, 1982). The canopy layer (CUHI), characterized by higher air temperatures in urbanized areas compared to their rural surroundings, poses severe challenges to urban variability of urban microclimates is critical for developing effective mitigation and adaptation strategies.

Traditionally, the assessment of urban thermal environments has relied on fixed meteorological sustainability, energy consumption, and human thermal comfort (Santamouris, 2015; Li et al., 2024). Urban overheating may significantly reduce climate resilience and increase thermal exposure risks for urban populations under future climate scenarios (Emmanuel & Krüger, 2012). As extreme weather events and heatwaves become more frequent, understanding the fine-scale spatial and temporal

stations. While these stations provide reliable, long-term synoptic data, their sparse spatial distribution makes them inadequate for capturing high-resolution intra-urban microclimate variability and the sharp

temperature gradients at urban-rural boundaries (Stewart & Oke, 2012; Martinez-Soto et al., 2025). Furthermore, previous studies demonstrated that urban-rural thermal contrasts are strongly influenced by land use and surface characteristics (Hart & Sailor, 2009). To address this spatial data gap, mobile monitoring has emerged as a robust complementary approach (Romero Rodríguez et al., 2020; Kousis et al., 2021; 2022; Martinez-Soto et al., 2025). Vehicle-based mobile measurements act as itinerant sensors, enabling the continuous recording of meteorological parameters across diverse land-cover types and topographical profiles within a short timeframe. Such approaches have been successfully applied to investigate fine-scale canopy layer thermal variability and spatial urban heat patterns (Brandsma & Wolters, 2012). Urban morphology, vegetation cover, and street geometry may substantially modify local thermal conditions and microclimatic variability at neighborhood scale (Middel et al., 2014).

Despite its advantages, mobile monitoring introduces challenges, primarily the "radiative error" caused by solar radiation heating the sensors at varying speeds. Recent technological advancements have led to the development of compact mobile sensors, such as the MeteoTracker (Barbano et al., 2024), which deploys a patented dual-sensor Radiation Error Correction System (RECS) (Jurato, 2020; MeteoTracker, 2025). This system ensures high-accuracy thermal measurements even under strong solar exposure, making it highly suitable for high-resolution investigations.

In Romania, recent studies have begun to map the UHI in major cities like Iași (Sfîcă et al., 2018; 2023), yet multi-city comparative transects investigating the thermal gradients between smaller urban hubs and rural plains remain scarce (Ichim et al., 2024). This is particularly true for winter conditions, which are often overlooked in favor of summer stress studies (Crétat et al., 2024), despite the important role of nighttime urban thermal retention under stable atmospheric conditions (Eliasson, 1996).

Therefore, this study is designed as an exploratory pilot study aiming to evaluate the interpretative value of high-resolution mobile surveys during a single winter day in South-Eastern Romania. The measurement date, 10 February 2026, was selected because it was characterized by stable winter atmospheric conditions, weak wind, absence of precipitation, and limited synoptic variability, which are favorable for identifying spatial thermal contrasts between different land-use environments. By utilizing the MeteoTracker sensor on a complex transect intersecting Focșani, Râmnicu Sărat, Buzău, Ianca, Brăila, and Galați, this paper explores the potential of spatially dense mobile data to capture fine-scale microclimatic signatures (Chàfer et al., 2022). The aim of the study was not to provide a climatological assessment of the winter urban heat island, but to test whether mobile monitoring can identify localized thermal gradients and urban footprints during suitable atmospheric conditions. While recognizing the temporal limitations of a single-day measurement, the study emphasizes the spatial richness of the data as a tool for identifying critical thermal gradients in Urban, Rural, and Road environments. In addition, high-resolution spatial observations provide valuable support for understanding local thermal variability and improving urban climate assessment methodologies (Voogt & Oke, 2003).

Satellite-derived Land Surface Temperature (LST) may complement mobile air temperature measurements by describing surface thermal patterns. However, LST refers to the land surface, while this study analyzes near-surface air temperature measured at road level. For this reason, Landsat-derived LST was not included in the present quantitative analysis, but it should be considered in future studies.

## MATERIALS AND METHODS

### Study Area and Meteorological Context

The study area spans a complex regional transect in South-Eastern Romania, covering a diverse topographical and land-use profile. The mobile survey originated in the rural area of Slobozia Conachi (Galați County) and intersected several urban hubs of varying sizes: Focșani, Râmnicu Sărat, Buzău, Ianca, Brăila, and Galați (see Figure 2). Mobile measurements are recognized for their ability to capture high-resolution spatial variability that fixed station networks often miss

(Kousis et al., 2022; Martinez-Soto et al., 2025). To establish a synoptic baseline, air temperature data from the official National Meteorological Administration (ANM) stations WMO-15310 (Galați) and WMO-15350 (Buzău) were used to compensate for the temporal drift of the mobile measurements during the transect survey (*Meteo Buzău, 10.02.2026*, 2026; *Meteo Galaţi, 10.02.2026*, 2026). The reference meteorological data consisted of hourly air temperature observations recorded at the two WMO stations during the mobile survey interval. These hourly values were linearly interpolated to the timestamp of each mobile measurement and then averaged in order to obtain a regional temperature trend used for temporal normalization. The Galați and Buzău stations were selected because they were the most relevant official meteorological stations located near the main monitored sectors of the transects and provided representative information for the regional air mass evolution during the survey. Additional stations were not included because they were either farther from the monitored routes or less representative for the spatial domain covered by the mobile measurements. Therefore, the two-station approach was used only for correcting the temporal drift of the mobile observations, not for replacing the high-resolution spatial information provided by the mobile survey.

Figure 1 illustrates the air temperature evolution recorded at the Galați and Buzău WMO stations on 10 February 2026, highlighting stable winter atmospheric conditions and a gradual daytime warming trend during the survey period.

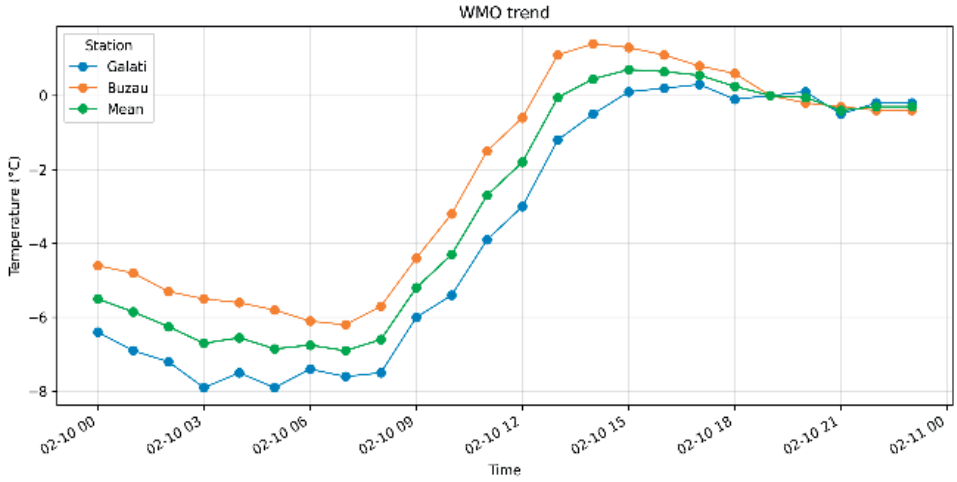



Figure 1.Temporal evolution of air temperature recorded at the WMO reference stations during the mobile survey. The blue line represents the Galați station (WMO-15310), the orange line represents the Buzău station (WMO-15350), and the green line indicates the mean regional temperature trend used for temporal normalization of the mobile measurements (Meteo Buzău, 10.02.2026, 2026; Meteo Galaţi, 10.02.2026, 2026)

These hourly reference data provided the regional synoptic background and were used for the temporal normalization of the mobile measurements. The hourly observations were interpolated to the exact time of each mobile record, and the mean trend of the two WMO stations was used to correct the mobile temperature values for the natural daytime thermal evolution.

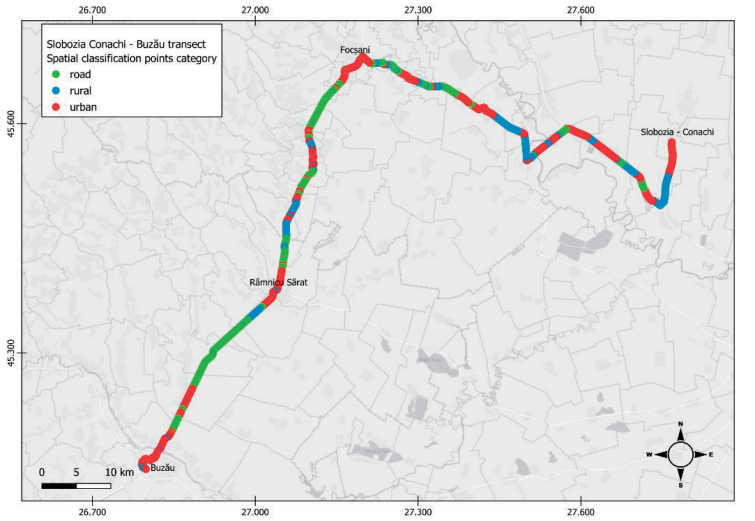
The measurements were conducted on 10 February 2026 in eastern Romania along two regional mobile transects between Slobozia Conachi-Buzău and Buzău-Galați (Figure 2), under stable winter atmospheric conditions favorable for the identification of microclimatic gradients and urban heat island (UHI) signatures (Crétat et al., 2024; Li et al., 2024). Data extracted from the official WMO stations in Galați and Buzău confirmed the persistence of these stable atmospheric conditions throughout the survey period (10:00-18:00 LT), characterized by weak wind speeds (generally 1-

3 m/s), absence of precipitation, and limited synoptic variability. These conditions reduced advective mixing processes that typically attenuate urban thermal contrasts, while the average measured thermal at WMO stations ranged between −3.4°C to +1.4°C, during the survey interval, favoring the preservation of local land-use-related temperature gradients (*Meteo Buzău, 10.02.2026*, 2026; *Meteo Galați, 10.02.2026*, 2026).

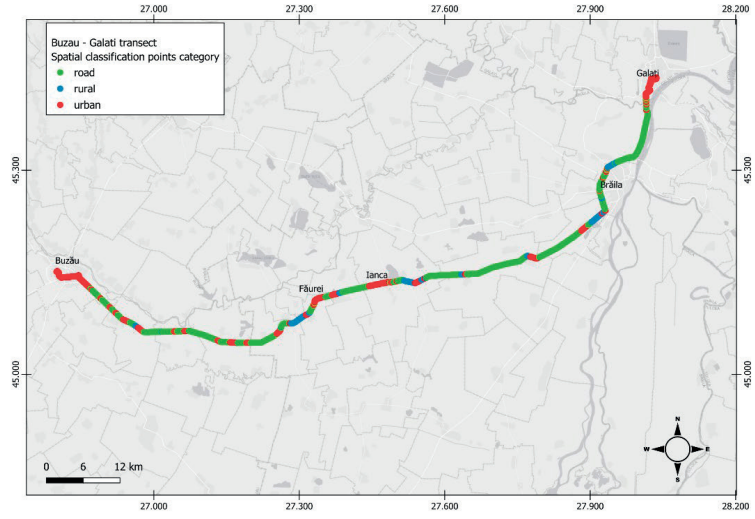
Following the quality-control and correction procedures, the mobile observations were spatially classified into three principal environmental categories: Urban, Rural, and Road environments. The classification was performed using OpenStreetMap-derived land-use and road-network information, combined with reverse geocoding and spatial proximity analysis (Boeing, 2017; *OpenStreetMap*, 2026). Urban sectors were identified based on the presence of continuous built-up areas characterized by increased building density and dominant residential, commercial, or industrial land-use classes. Rural sectors corresponded mainly to agricultural land, grasslands, open fields, and sparsely developed surfaces located outside compact settlements. Measurements situated directly along major transportation corridors or road infrastructure outside continuous urbanized areas were classified as Road environments. The spatial classification procedure enabled the differentiation and comparison of localized thermal signatures associated with urban morphology, land-use characteristics, and transportation-related environments along both regional transects.

Figure 2 presents the spatial configuration and automated environmental classification of the two mobile monitoring transects performed on 10 February 2026 between Slobozia Conachi-Buzău (Figure 2a) and Buzău-Galați (Figure 2b). The figure represents the output of a custom Python-based spatial classification workflow developed to process the corrected mobile temperature measurements. The classification algorithm automatically analysed the spatial distribution of each measurement point using land-use information, building-density characteristics, and road-network data extracted from the OpenStreetMap database (Boeing, 2017; *OpenStreetMap*, 2026). Unlike a simple administrative classification, the method was designed to identify the actual local microclimatic environment surrounding each measurement point. Thus, points located administratively inside city boundaries but lacking built-up characteristics were not automatically classified as Urban.

Urban environments were assigned only where clear built-up evidence was identified, including residential, commercial, industrial, or construction land-use polygons, the presence of at least six buildings within a 150 m radius, or a building-area ratio $\geq 0.015$ within the same search distance. Rural environments corresponded mainly to agricultural and open natural surfaces, while the Road category included measurements located within 60 m of transportation corridors outside continuous built-up areas. The resulting classification highlights the strong spatial heterogeneity encountered along both regional transects, with extended Rural sectors identified between Slobozia Conachi, Focșani, and Râmnicu Sărat, as well as between Buzău, Ianca, and Brăila, whereas the largest Urban environments were associated with the metropolitan sectors of Buzău, Brăila, and Galați.




(a)



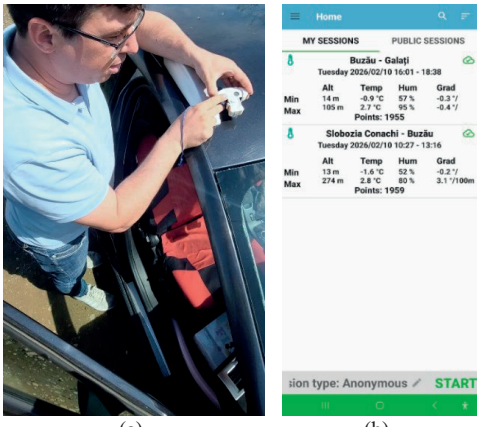

(b)

Figure 2 .Measurement track and results of spatial classification of the mobile monitoring transects from 10 February 2026 between Slobozia Conachi-Buzău (a) and Buzău-Galați (b). Red segments represent Urban environments associated with compact built-up areas and higher building density, dark blue segments indicate Rural environments dominated by agricultural and open land surfaces, while light green segments correspond to Road environments located mainly along transportation corridors outside continuous urbanized areas

**Instrumentation and mobile monitoring protocol**

Meteorological data were collected using the MeteoTracker (MTX-SA) standalone weather station, a device specifically engineered for high-resolution measurements on the move (MeteoTracker, 2025). The device features the patented dual-sensor Radiation Error Correction System (RECS), which dynamically corrects the "radiative error" caused by solar exposure (Jurato, J., 2020). The system ensures an air temperature accuracy of ±0.1°C (typical) and ±0.4°C under direct solar radiation at speeds exceeding 10 km/h (MeteoTracker, 2025). The performance of this sensor has been validated against reference meteorological equipment, confirming its suitability for urban microclimate investigations (Barbano et al., 2024; Loglisci et

al., 2024). During the mobile measurements performed on 10 February 2026, the device was mounted on the roof of a vehicle (see Figure 3) to minimize heat interference from the engine and asphalt, operating with a high temporal sampling resolution during the mobile survey , according to the manufacturer's specifications (Barbano et al., 2024b; Loglisci et al., 2024; MeteoTracker, 2025; Silva et al., 2025). The meteorological measurements recorded by the MeteoTracker (MTX-SA) weather station were transmitted in real time via Bluetooth to the MeteoTracker mobile application, where the data were continuously visualized and stored during the survey. Subsequently, the recorded datasets were automatically synchronized and uploaded to the MeteoTracker cloud platform, allowing remote access, download, and post-processing analysis from any location. The MeteoTracker application provides multiple visualization and statistical analysis functionalities, including real-time mapping of the measurement route with associated air temperature values, graphical representations of the recorded meteorological parameters, and the possibility to publicly share the monitoring project together with all corresponding spatial and temporal information (MeteoTracker / IoTopon Srl, 2026).




(a) (b)

Figure 3 . MeteoTracker mobile weather station mounting on the vehicle roof top during the mobile measurement campaign performed on 10 of February 2026 (a). Print screen from Meteo-Tracker app statistics data of the parameters recorded during measurements performed: Slobozia-Conachi – Buzău city and Buzău city – Galati city (b). Data Processing and Correction Procedures

Meteorological and positioning data acquired during the mobile transects conducted on 10 February 2026 were exported from the MeteoTracker+ application and subsequently processed using custom Python scripts.

The preprocessing workflow included data synchronization, quality-control procedures, filtering operations, and correction algorithms designed to remove anomalous records and improve the spatial and temporal consistency of the dataset. A three-stage quality control and normalization workflow was implemented.

The first stage aimed to prevent thermal contamination from the vehicle and surrounding traffic during stops. To this end, a speed-based filtering threshold was applied. Following the manufacturer's technical specifications and validated performance assessments, all data points recorded at speeds below 10 km/h were excluded from the final spatial analysis. This filtering ensures that the Radiation Error Correction System (RECS) operates within its optimal ventilation parameters, maintaining an accuracy of ±0.4°C even under solar exposure (MeteoTracker, 2025).

In the second stage, an altitude correction was applied to normalize the recorded air temperature ($T_{obs}$) to a common regional reference level ($H_{ref}$=50 m a.s.l.), accounting for the topographical variability of the Romanian Plain and Subcarpathian transitions areas. The corrected temperature ($T_{alt_corr}$) was calculated using the standard environmental lapse rate presented in the next equation:

$$T_{alt_corr} = T_{obs} + \Gamma\left(H_{obs} - H_{ref}\right) \quad (1)$$

where:

$\Gamma$ is the altitudinal temperature gradient of 0.0065°C/m (or 0.65°C/100 m);

$T_{obs}$ is the measured temperature;

$H_{obs}$- is the altitude of the observation point and $H_{ref}$ – is the altitudinal average reference calculated from all measurements altitudinal level.

In the third stage, a time-drift correction was performed to isolate the spatial microclimatic signal from the natural diurnal temperature variation. Given the segmented nature of the transect and the 3-hour stationary period in Buzău, a linear interpolation was applied between the hourly observations of the ANM

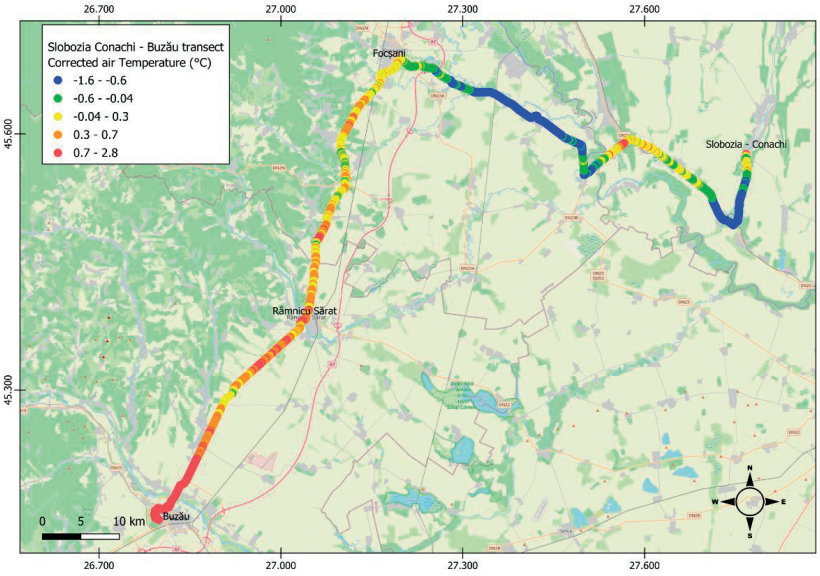
baseline stations (Galați and Buzău). This procedure adjusted each mobile observation relative to the regional heating/cooling rate of the air mass at the exact moment of sampling (data from Figure 2), ensuring that the observed gradients reflect land-use differences rather than the passage of time as stated by other studies (Chàfer et al., 2022; Kousis et al., 2022; Ichim et al., 2024). The corrected and normalized dataset obtained after the preprocessing workflow was subsequently used for the spatial classification and statistical analysis of the mobile measurements.

## RESULTS AND DISCUSSIONS

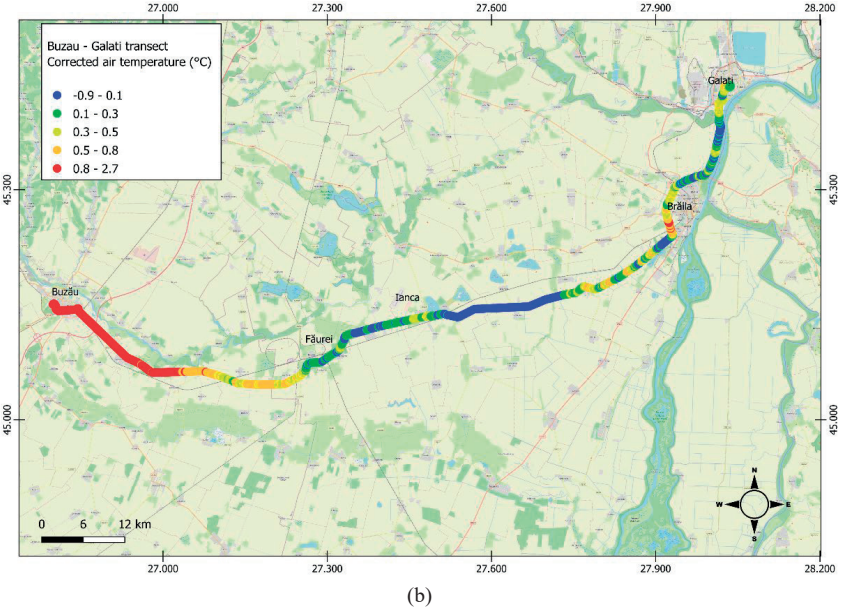
### Spatial distribution of corrected air temperature

The corrected mobile measurements presented in Figure 4 represent the spatial distribution of point-based air temperature observations after the application of the filtering and correction workflow described in the methodology section. The corrected temperatures are displayed directly along the monitored routes and highlight distinct thermal contrasts associated with differences in land use, urban density, road infrastructure, and surrounding rural landscapes. Figure 4a shows the point-based spatial distribution of corrected air temperature along the Slobozia Conachi-Buzău transect after filtering and correction procedures. The coldest sectors are observed mainly in the rural area west and south-west of Slobozia Conachi and on the eastern approach toward Focșani, where several segments fall within the blue class, corresponding to corrected temperatures between −1.6 and −0.6°C. These low values are associated with open rural surfaces, agricultural land, and low building density. Around Focșani, temperatures increase mostly into the −0.04 to +0.3°C and +0.3 to +0.7°C classes, indicating a transition toward more built-up and road-influenced environments. Between Focșani and Râmnicu Sărat, the route is dominated mainly by yellow and orange classes, with corrected temperatures generally ranging from −0.04 to +0.7°C, rather than by the coldest blue values. This suggests more moderate thermal conditions along the main road corridor and nearby settlements. The warmest sector appears toward Râmnicu Sărat and especially near Buzău, where orange and red classes dominate, with corrected temperatures exceeding +0.7°C and locally reaching the highest class of the transect, up to +2.8°C. This pattern indicates stronger heat retention in compact urbanized sectors compared with the surrounding rural landscape, as it was studied in other similar studies (Barbano et al., 2024; Loglisci et al., 2024).

Figure 4b shows the point-based spatial distribution of corrected air temperature along the Buzău–Galați transect after the filtering and correction procedures. The warmest sector is clearly observed near Buzău, where the route is dominated by red points corresponding to corrected temperatures between +0.8 and +2.7°C. This indicates a strong local thermal signal associated with the compact urban area of Buzău and nearby built-up surfaces. Immediately after leaving Buzău, the route gradually shifts toward orange and yellow classes, with temperatures decreasing to +0.5–+0.8°C and +0.3–+0.5°C, reflecting the transition from urbanized land toward more open road and rural environments. The central part of the transect, especially around Făurei and Ianca, is dominated by blue and green classes, with corrected temperatures generally between −0.9 and +0.3°C. The lowest values are observed mainly along the long road corridor east of Ianca, where blue points indicate temperatures between −0.9 and +0.1°C, corresponding to open agricultural landscapes, low building density, and reduced anthropogenic heat influence. Toward Brăila, temperatures increase again, with several yellow, orange, and red segments ranging from +0.3°C to +2.7°C, consistent with the transition into a more urbanized sector. North of Brăila and toward Galați, the route alternates between colder blue-green sections and warmer yellow-orange points, indicating a mixed thermal pattern influenced by the Danube corridor, road infrastructure, and urbanized surfaces near Galați.




(a)

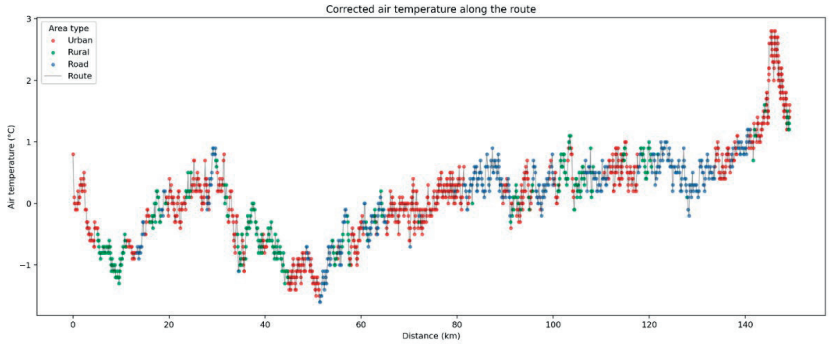



(b)

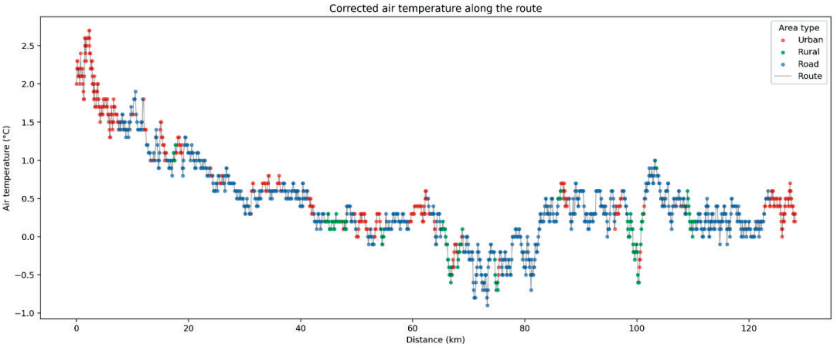
Figure 4. Spatial distribution of corrected air temperature along the Slobozia Conachi-Buzău transect (a) and the Buzău-Galați transect (b), based on mobile measurements performed on 10 February 2026. Warmer colors indicate higher corrected air temperatures, while colder colors indicate lower values

**Longitudinal thermal variability along the transects**

The longitudinal temperature profiles provided a detailed representation of the thermal variability recorded along the two mobile transects (Figure 5). The classification into Urban, Rural, and Road environments allowed the identification of localized thermal anomalies associated with urban morphology and transportation corridors.




(a)




(b)

Figure 5 Corrected air temperature variability along the Slobozia Conachi-Buzău transect (a) and the Buzău-Galați transect (b) classified by land-use category, based on mobile measurements performed on 10 February 2026. Red points indicate temperatures recorded within Urban sectors, green points represent Rural environments, and blue points correspond to Road-dominated areas

The longitudinal temperature profiles presented in Figure 5 reveal substantial small-scale thermal variability along both investigated transects, reflecting the strong influence of land-use characteristics and urban morphology on near-surface air temperature distribution.

Figure 5a highlights the longitudinal evolution of corrected air temperature along the Slobozia Conachi–Buzău transect, revealing a gradual transition from colder rural environments toward warmer urbanized sectors. In the first part of the route (0-15 km), corresponding mainly to rural landscapes near Slobozia Conachi, Rural measurements generally ranged between approximately −1.3°C and −0.5°C, while Road environments varied between approximately −0.9°C and −0.3°C. Between approximately 15 and 35 km, temperatures progressively increased toward positive values between approximately 0°C and +0.9°C across mixed Urban and Road sectors. The middle section of the transect (approximately 40-80 km) exhibits the coldest conditions, with several measurements below −1°C and minimum values approaching approximately −1.6°C around km 50-55. After approximately km 80, temperatures gradually increase again, while the strongest warm anomaly occurs near Buzău (approximately 140-150 km), where Urban measurements frequently exceed +2°C and locally approach +2.8°C, indicating a pronounced winter urban heat island effect.

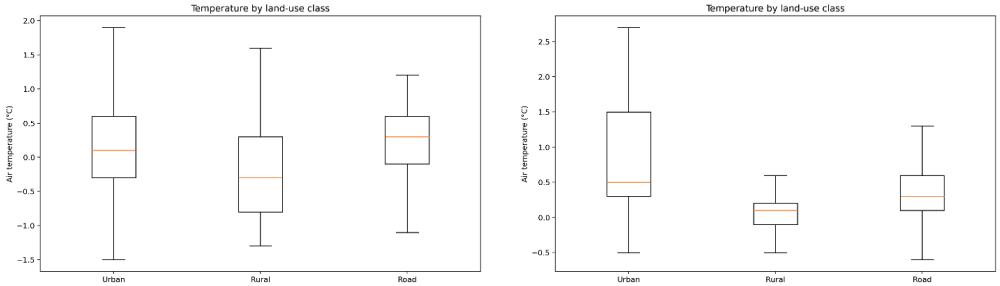
Along the Buzău-Galați transect (Figure 5b), the corrected temperature profile also reveals clear thermal contrasts between Urban, Rural, and Road environments. At the beginning of the transect (0-8 km), corresponding to the urban area of Buzău, Urban measurements remained consistently elevated, generally between +1.8°C and +2.7°C. Between approximately 10 and 40 km, temperatures progressively decreased toward less densely built and Road-dominated sectors, commonly ranging between approximately +0.3 °C and +1.2°C. The lowest

corrected temperatures were recorded in the central rural sector of the transect (approximately 55-80 km), where several measurements fall below 0°C and minimum values approach approximately −0.9°C around km 70-75. After approximately km 85, the thermal signal gradually increases again toward the Brăila-Galați metropolitan corridor, where Urban measurements remain predominantly positive, most frequently between approximately +0.5°C and +0.7°C.

**Statistical analysis of data**

To further evaluate the influence of land-use characteristics on local thermal conditions, the corrected air temperature values were statistically compared between Urban, Rural, and Road classes using boxplot analysis presented in Figure 6.

Figure 6 presents the boxplot distributions of corrected air temperature values for the Urban, Rural, and Road land-use categories along the two transects, providing a statistical overview of the median values, thermal dispersion, and variability ranges within each environmental class. For the Slobozia Conachi-Buzău transect (Figure 6a), the Urban category exhibits a broad thermal distribution, with values extending from approximately −1.5°C to nearly +1.9°C and a median close to +0.1°C. The central variability range (interquartile range) extends approximately between −0.3°C and +0.6°C, indicating substantial spatial heterogeneity within built-up environments. Rural sectors display lower median temperatures near −0.3°C and the coldest thermal conditions overall, with most values concentrated between approximately −0.8°C and +0.3°C. Road environments present intermediate thermal characteristics, with a median close to +0.3°C and a comparatively narrower central variability range extending approximately between −0.1°C and +0.6°C.




(a) (b)

Figure 6. Statistical distribution of corrected air temperature values for Urban, Rural, and Road environments along the Slobozia Conachi-Buzău transect (a) and the Buzău-Galați transect (b)

In the Buzău-Galați transect (Figure 6b), the Urban category again exhibits the highest positive temperatures and the widest thermal amplitude, ranging from approximately −0.5°C to +2.7°C, with a median close to +0.5°C. The central 50% of Urban temperature values are distributed approximately between +0.3°C and +1.5°C, reflecting enhanced thermal variability associated with compact built-up structures and anthropogenic heat influence. Rural environments show the narrowest thermal distribution, with a median close to +0.1°C and most values concentrated between approximately −0.1°C and +0.2°C, indicating relatively stable thermal conditions over open agricultural landscapes. Road sectors again display intermediate thermal behavior, with temperatures generally varying between approximately −0.9°C and +1.3°C and the central variability range extending approximately from +0.1°C to +0.6°C. Overall, the boxplots emphasize the stronger thermal variability and higher positive temperature anomalies associated with Urban environments, while Rural sectors remain characterized by lower and more homogeneous corrected temperature distributions along both transects.

## CONCLUSIONS

This exploratory pilot study demonstrated the capability of high-resolution mobile monitoring to identify winter urban-rural thermal gradients and localized urban heat island signatures in South-Eastern Romania. The preprocessing workflow, including speed filtering, altitude normalization, temporal correction using ANM reference stations, and automated land-use classification, improved the spatial consistency and interpretability of the mobile dataset.

The results revealed clear thermal differences between Urban, Rural, and Road environments along both transects. Urban sectors, especially near Buzău and within the Brăila-Galați corridor, showed higher corrected air temperatures and greater thermal variability, while Rural areas generally maintained lower and more stable thermal conditions. Road-dominated sectors displayed intermediate thermal behavior.

Urban-rural thermal differences are not specific only to winter conditions. They can be identified throughout the year, but their intensity, spatial expression, and controlling mechanisms vary depending on season, radiation balance, wind speed, cloud cover, land cover, vegetation activity, soil moisture, and anthropogenic heat release. During winter, stable atmospheric conditions, weak wind, and reduced turbulent mixing may favor the detection of heat retention within built-up areas. In contrast, during summer, urban–rural thermal contrasts may be amplified by stronger solar radiation, reduced evapotranspiration over impervious surfaces, and the thermal behavior of construction materials compared with vegetated rural areas. Therefore, the present winter case should be interpreted as one seasonal example of urban-rural thermal differentiation, not as the only period in which such contrasts can be detected.

The combined use of point-based temperature mapping, longitudinal profiles, and boxplot statistics showed that MeteoTracker mobile measurements can capture fine-scale thermal variability that is difficult to observe using fixed meteorological stations alone. The main strength of this study lies in the high spatial resolution of the mobile observations and in the integrated workflow combining speed filtering, altitude normalization, time-drift correction, and land-use-based classification into Urban, Rural, and Road environments. This approach allowed the identification of localized winter thermal gradients and urban-rural contrasts along regional transects in South-Eastern Romania.

Although limited to a single winter day, which does not allow seasonal or climatological generalization of the observed thermal contrasts. In addition, the present analysis focused on near-surface mobile air temperature measurements and did not include satellite-derived Land Surface Temperature. Future studies should include repeated mobile surveys during different seasons and meteorological conditions and may integrate Landsat-derived LST products to compare surface thermal patterns with near-surface air temperature variability. The study confirms the usefulness of this approach for future urban climate and UHI assessments in Romania.

## ACKNOWLEDGEMENTS

The authors acknowledge the support of the project An Integrated System for the Complex Environmental Research and Monitoring in the Danube River Area, REXDAN, SMIS code 127065, co-financed by the European Regional Development Fund through the Competitiveness Operational Program 2014-2020, contract no. 309/10.07.2020.

Lucian Sfîcă and Bogan Roșu contributions to this work was supported by a grant of the Ministry of Research, Innovation and Digitization, CNCS - UEFISCDI, project number PN-IV-P1-PCE-2023-0897, within PNCDI IV.

## REFERENCES

Barbano, F., Brattich, E., Cintolesi, C., Ghafoor Nizamani, A., Di Sabatino, S., Milelli, M., Peerlings, E. E. M., Polder, S., Steeneveld, G.-J., & Parodi, A. (2024). Performance evaluation of MeteoTracker mobile sensor for outdoor applications. *Atmospheric Measurement Techniques*, *17*(10), 3255–3278. https://doi.org/10.5194/amt-17-3255-2024

Boeing, G. (2017). OSMnx: New methods for acquiring, constructing, analyzing, and visualizing complex street networks. *Computers, Environment and Urban Systems*, *65*, 126–139. https://doi.org/10.1016/j.compenvurbsys.2017.05.004

Brandsma, T., & Wolters, D. (2012). Measurement and Statistical Modeling of the Urban Heat Island of the City of Utrecht (the Netherlands). *Journal of Applied*

*Meteorology and Climatology*, *51*(6), 1046–1060. https://doi.org/10.1175/JAMC-D-11-0206.1

Chàfer, M., Tan, C. L., Cureau, R. J., Hien, W. N., Pisello, A. L., & Cabeza, L. F. (2022). Mobile measurements of microclimatic variables through the central area of Singapore: An analysis from the pedestrian perspective. *Sustainable Cities and Society*, *83*, 103986. https://doi.org/10.1016/j.scs.2022.103986

Crétat, J., Richard, Y., Pohl, B., Emery, J., Dudek, J., Roy, D., Pergaud, J., Rega, M., Poupelin, M., Joly, D., Thévenin, T., Marquès, E., & Masson, V. (2024). Impact of topography and land cover on air temperature space-time variability in an urban environment with contrasted topography (Dijon, France, 2014–2021). *Theoretical and Applied Climatology*, *155*(3), 1941–1958. https://doi.org/10.1007/s00704-023-04742-4

Eliasson, I. (1996). Urban nocturnal temperatures, street geometry and land use. *Atmospheric Environment, Conference on the Urban Thermal Environment Studies in Tohwa*, *30*(3), 379–392. https://doi.org/10.1016/1352-2310(95)00033-X

Emmanuel, R., & Krüger, E. (2012). Urban heat island and its impact on climate change resilience in a shrinking city: The case of Glasgow, UK. *Building and Environment*, *53*, 137–149. https://doi.org/10.1016/j.buildenv.2012.01.020

Hart, M. A., & Sailor, D. J. (2009). Quantifying the influence of land-use and surface characteristics on spatial variability in the urban heat island. *Theoretical and Applied Climatology*, *95*(3), 397–406. https://doi.org/10.1007/s00704-008-0017-5

Ichim, P., Miron, R., Corocăescu, A.-C., Crețu, C.-Ștefănel, & Sfîcă, L. (2024). Land use as key element for urban heat island inception in small cities. Case study: Bârlad City, Romania. *Present Environment and Sustainable Development*, *18*(1). https://doi.org/https://doi.org/10.47743/pesd2024181006

Jurato, J. G. T. (2020). *System and method for calculating the temperature of an outdoor ambient air corrected from radiation error, and sensor device usable in such system* (European Patent Office Patent No. EP3645989).

Kousis, I., Manni, M., & Pisello, A. L. (2022). Environmental mobile monitoring of urban microclimates: A review. *Renewable and Sustainable Energy Reviews*, *169*, 112847. https://doi.org/10.1016/j.rser.2022.112847

Kousis, I., Pigliautile, I., & Pisello, A. L. (2021). Intra-urban microclimate investigation in urban heat island through a novel mobile monitoring system. *Scientific Reports*, *11*(1), 9732. https://doi.org/10.1038/s41598-021-88344-y

Li, Y., Yang, T., Zhao, G., Ma, C., Yan, Y., Xu, Y., Wang, L., & Wang, L. (2024). A systematic review of studies involving canopy layer urban heat island: Monitoring and associated factors. *Ecological Indicators*, *158*, 111424. https://doi.org/10.1016/j.ecolind.2023.111424

Loglisci, N., Milelli, M., Iurato, J., Galia, T., Galizia, A., & Parodi, A. (2024). Validation of Citizen Science Meteorological Data: Can They Be Considered a Valid Help in Weather Understanding and Community Engagement? *Sensors*, *24*(14), 4598. https://doi.org/10.3390/s24144598

Martinez-Soto, A., Vera-Fonseca, M., Valenzuela-Toledo, P., Melillan-Raguileo, A., & Shupler, M. (2025). Heat on the Move: Contrasting Mobile and Fixed Insights into Temuco's Urban Heat Islands. *Sensors*, *25*(4), 1251. https://doi.org/10.3390/s25041251

*Meteo Buzău, 10.02.2025*. (2026, February 10). [Database]. Https://Rp5.Ru/. https://rp5.ru/Arhiva_meteo_%C3%AEn_Buz%C4%83u

*Meteo Galați, 10.02.2026*. (2026, February 10). [Database]. Https://Rp5.Ru/. https://rp5.ru/Arhiva_meteo_%C3%AEn_Gala%C5%A3i

MeteoTracker / IoTopon Srl. (2026). *MeteoTracker Official Platform* [App database]. MeteoTracker+. https://play.google.com/store/apps/details?id=com.iotopon.meteotracker&hl=en

MeteoTracker, I. srl. (2025). *MeteoTracker X Standalone Datasheet* [Technical datasheet]. IoTopon Srl. https://meteotracker.com/wp-content/uploads/2025/06/METEOTRACKER-X-STANDALONE-DATASHEET_rev.3.pdf

Middel, A., Häb, K., Brazel, A. J., Martin, C. A., & Guhathakurta, S. (2014). Impact of urban form and design on mid-afternoon microclimate in Phoenix Local Climate Zones. *Landscape and Urban Planning*, *122*, 16–28. https://doi.org/10.1016/j.landurbplan.2013.11.004

Oke, T. R. (1982). The energetic basis of the urban heat island. *Quarterly Journal of the Royal Meteorological Society*, *108*(455), 1–24. https://doi.org/10.1002/qj.49710845502

*OpenStreetMap*. (2026). [OpenStreetMap geographic database.]. OpenStreetMap Contributors. https://www.openstreetmap.org/

Romero Rodríguez, L., Sánchez Ramos, J., Sánchez de la Flor, F. J., & Álvarez Domínguez, S. (2020). Analyzing the urban heat Island: Comprehensive methodology for data gathering and optimal design of mobile transects. *Sustainable Cities and Society*, *55*, 102027. https://doi.org/10.1016/j.scs.2020.102027

Santamouris, M. (2015). Regulating the damaged thermostat of the cities—Status, impacts and mitigation challenges. *Energy and Buildings*, *91*, 43–56. https://doi.org/10.1016/j.enbuild.2015.01.027

Sfîcă, L., Crețu, C.-Ștefănel, Ichim, P., Hrițac, R., & Breabăn, I.-G. (2023). Surface urban heat island of Iași city (Romania) and its differences from *in situ* screen-level air temperature measurements. *Sustainable Cities and Society*, *94*, 104568. https://doi.org/10.1016/j.scs.2023.104568

Sfîcă, L., Ichim, P., Apostol, L., & Ursu, A. (2018). The extent and intensity of the urban heat island in Iași city, Romania. *Theoretical and Applied Climatology*, *134*(3), 777–791. https://doi.org/10.1007/s00704-017-2305-4

Silva, T., Ramusga, R., Matias, M., Amaro, J., Bonifácio, A., Reis, C., Chokhachian, A., Lopes, G., Almeida, A., Frazão, J., Vasconcelos, J., Lopes, A., & Morgado, P.

(2025). Climate walking: A comparison study of mobile weather stations and their relevance for urban planning, design, human health and well-being. *City and Environment Interactions*, *27*, 100212. https://doi.org/10.1016/j.cacint.2025.100212

Stewart, I. D., & Oke, T. R. (2012). Local Climate Zones for Urban Temperature Studies. *Bulletin of the American Meteorological Society*, *93*(12), 1879–1900. https://doi.org/10.1175/BAMS-D-11-00019.1

Voogt, J. A., & Oke, T. R. (2003). Thermal remote sensing of urban climates. *Remote Sensing of Environment, Urban Remote Sensing*, *86*(3), 370–384. https://doi.org/10.1016/S0034-4257(03)00079-8.

Scientific Papers. Series E. Land Reclamation, Earth Observation & Surveying, Environmental Engineering. Vol. XV, 2026
Print ISSN 2285-6064, CD-ROM ISSN 2285-6072, Online ISSN 2393-5138, ISSN-L 2285-6064

# SATELLITE-DERIVED TURBIDITY AS AN INDICATOR OF SMALL-SCALE GOLD MINING ACTIVITY AROUND THE BROKOPONDO RESERVOIR, SURINAME

**Tamara MYSLYVA[1], Christiaan Max HUISDEN[1], Marek MROZ[2], Gerald TJON A SAN[1], Fauzia Gatoen ABDOELRAHMAN[3]**

[1]Anton de Kom University of Suriname, 86 Leysweg, Paramaribo, Republic of Suriname
[2]University of Warmia and Mazury in Olsztyn, 1 Michała Oczapowskiego Str., 10-719, Olsztyn, Poland
[3]Ministry of Foreign Affairs, International Business and Cooperation, 8 Henck Arronstraat, Paramaribo, Republic of Suriname

Corresponding author email: byrty41@yahoo.com

***Abstract***

*The rapid expansion of illegal gold mining over the past decade has emerged as one of the most critical environmental challenges in Suriname, driven by its severe impacts on both terrestrial and aquatic ecosystems. Monitoring these activities is difficult due to the remoteness of affected areas, limited accessibility, and safety constraints. This study explores the potential of Sentinel-2 Level-2A imagery for detecting and monitoring artisanal and small-scale gold mining (ASGM) activity around the Brokopondo Reservoir without relying on in-situ measurements. A Python-based workflow developed in Google Colab was used to pre-process the imagery and calculate the Normalized Difference Turbidity Index (NDTI) for the period 2021–2025. Spatial relationships between high and low NDTI clusters and their proximity to ASGM sites were examined using Moran's I, the Mann–Whitney U test, and Cliff's delta. The results suggest that NDTI has potential as a remote-sensing proxy for ASGM-related water turbidity, offering valuable support for environmental monitoring in remote tropical forest regions of the Guiana Shield.*

***Key words:*** *gold mining activity, indication, monitoring, proximity, water turbidity.*

## INTRODUCTION

Artisanal and small-scale gold mining (ASGM) is a critical livelihood activity in Suriname, supporting an estimated 20,000 people, particularly in interior regions such as Brokopondo and Sipaliwini (Seccatore & Theije, 2017; First National Action Plan, 2023). Although the sector contributes significantly to local economies, it also generates substantial environmental and public health risks due to the use of hazardous substances, especially mercury, during gold extraction (Marshall et al., 2020; Quispe Aquino et al., 2022; Malone et al., 2023). The environmental footprint of mercury use in artisanal and small-scale gold mining is especially pronounced in riverine and reservoir systems adjacent to mining areas, where disturbed soils and associated contaminants are mobilized into waterways, resulting in water quality degradation (Huisden et al., 2021). ASGM in Suriname primarily relies on hydraulic mining techniques that remove vegetation and mobilize large volumes of soil and sediment. These materials are commonly discharged directly into nearby rivers and creeks without sediment-control structures such as tailings ponds (Heemskerk & Kooye, 2003; Ouboter, 2015). The influx of fine sediments increases turbidity and facilitates the downstream transport of mercury-contaminated particles, as mercury readily binds to clay and fine sediment (Vreedzaam et al., 2023).

The Brokopondo Reservoir is located within one of Suriname's most active artisanal and small-scale gold mining regions, the Brokopondo district. Mining is a major driver of deforestation and ecological degradation in this area, with much of the activity occurring illegally (Global Forest Watch, 2025). Elevated sediment loads and turbidity within the reservoir and its tributaries have been directly linked to mining operations, posing risks to aquatic ecosystems and communities that rely on the water for

drinking, fishing, and other livelihood activities (Heemskerk et al., 2022). Despite the severity of ASGM-related environmental impacts, Suriname lacks a national system for systematic monitoring of water quality or mining activities (Rodríguez & Chavez, 2024). Reliable data on the extent and distribution of ASGM, particularly in the Brokopondo district, are limited (EMSAGS, 2023). Many mining sites are located in remote forested areas that are difficult to access and may pose safety risks for field researchers (United Nations Office on Drugs and Crime, 2025). These logistical and security constraints severely limit the feasibility of routine field sampling and make traditional monitoring approaches impractical in many ASGM-affected regions. Given these constraints, remote sensing provides a practical and effective alternative to ground-based monitoring.

Satellite imagery offers consistent, high-resolution, and high-frequency observations that enable the assessment of spatial and temporal variations in water quality where field measurements are not feasible (Espinoza et al., 2025). Sentinel-2, with its suitable spectral configuration and frequent revisit time, has become a widely used platform for monitoring optically complex inland waters (Elhag et al., 2019; Das et al., 2024). A substantial body of literature demonstrates that multispectral indices serve as reliable proxies for water-quality parameters such as turbidity (Steinbach et al., 2025), suspended sediment concentration (SSC), total suspended matter (TSM), chlorophyll-a (Chl-a), and coloured dissolved organic matter (CDOM) (Khan et al., 2021; Li et al., 2023; Chen et al., 2024; Tesfaye, 2024). Red–green reflectance contrasts are particularly effective in detecting sediment-laden waters associated with mining disturbances.

The Normalized Difference Turbidity Index (NDTI), derived from red and green spectral bands, has emerged as a robust indicator of relative turbidity and suspended sediments in both inland and coastal waters (Zhang et al., 2022; Amran & Daming, 2023). In river systems affected by ASGM, persistent turbidity hotspots downstream of mining areas provide strong qualitative evidence of sediment release even when in situ turbidity measurements are unavailable (Sousa & Veiga, 2009; Pereira & Lobo, 2024). Because many ASGM sites in Suriname are located in remote forested landscapes, including protected and Indigenous territories, satellite-based turbidity assessment is often the only feasible large-scale monitoring option. Remote sensing of water turbidity therefore offers a crucial means of detecting and understanding ASGM-induced sediment dynamics across the Brokopondo Reservoir and the broader Guiana Shield.

The purpose of this study is to evaluate the feasibility of using the Normalized Difference Turbidity Index, derived from Sentinel-2 imagery, as an indirect indicator of artisanal and small-scale gold mining activity around the Brokopondo Reservoir in Suriname in the absence of field-based water quality measurements. By generating multi-year, dry-season NDTI composites and analysing their spatial and temporal patterns, the study aims to determine whether elevated turbidity signals (NDTI hotspots) correspond spatially with known ASGM locations and can therefore be evaluated as a potential tool for environmental monitoring in remote, data-poor regions.

This study pursues five interconnected objectives: (1) to generate a spatial-temporal dataset of NDTI values for the Brokopondo Reservoir and its tributaries using Sentinel-2 imagery from 2021 to 2025, focusing on the dry-season months (July-November) when turbidity signals are most stable and comparable; (2) to characterize spatial turbidity using spatial autocorrelation methods, including Global Moran's I and Local Moran's I, in order to identify statistically significant clusters of high (HH) and low (LL) NDTI values across the study area; (3) to quantify the spatial relationship between ASGM sites and NDTI clusters by calculating distances from known ASGM locations to HH and LL clusters and evaluating whether mining sites are preferentially located near turbidity hotspots; (4) to statistically assess differences in proximity between ASGM sites and NDTI cluster types using the Mann-Whitney U test and Cliff's delta effect size, thereby testing the hypothesis that ASGM sites are significantly closer to HH clusters than to LL clusters; (5) to evaluate the potential of NDTI as a field-independent proxy for monitoring ASGM impacts, providing a scalable, replicable method for environmental surveillance in regions where ground-based

water quality monitoring is logistically constrained or unavailable.

## MATERIALS AND METHODS

*Study area*. The study was conducted in Suriname, a country situated north of the equator on the north-eastern coast of South America. Suriname's geographical coordinates extend from 1°50.45' N to 6°0.35' N and from 53°59.08' W to 54°33.49' W. Geologically, more than 80% of Suriname consists of the deeply weathered, rainforest-covered Precambrian Guiana Shield (Myslyva et al., 2024).

The area of interest is the Brokopondo Reservoir, officially known as the Professor Doctor Ingenieur W. J. van Blommestein Meer, also referred to as Brokopondostuwmeer (Leentvaar, 1975). It was formed in the 1960s following the construction of the Afobaka Dam on the Suriname River. The reservoir was primarily created to supply hydroelectric power to support the country's bauxite industry and general electricity needs. With a surface area that fluctuates around 1,560 km² depending on seasonal water levels, and catchment area approximately 12,200 km², it ranks among the largest human-made reservoirs in South America. The reservoir alone covers nearly one percent of Suriname's total land area. It lies in the Brokopondo district and extends between latitudes 4°20' N and 5°00' N and longitudes 54°50' W and 55°20' W (Figure 1).

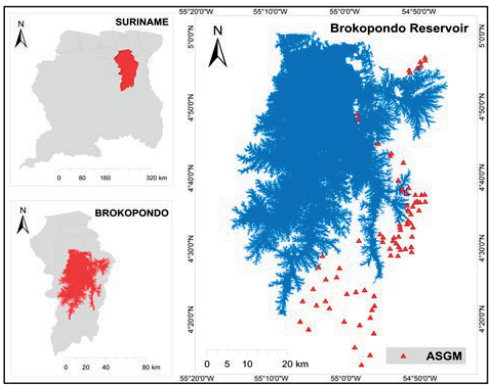



Figure 1. Location of the study area

The reservoir and its catchment are subject to various human activities, including artisanal and small-scale gold mining, agriculture, and logging, all of which affect water quality and sediment dynamics. Its size, hydrological characteristics, and environmental pressures make the Brokopondo Reservoir an important focus for remote sensing studies aimed at monitoring water turbidity, sediment transport, and land-use changes in tropical reservoirs.

The region of interest included the Brokopondo Reservoir and a 25-km buffer zone surrounding its shoreline. This extent was sufficiently large to capture the major tributaries and first-order streams flowing into the reservoir, as well as the majority of direct-impact ASGM sites and their associated drainage pathways. To estimate proximity to high-high (HH) and low-low (LL) water turbidity clusters, 80 ASGM activity points were selected.

Figure 2 presents a step-by-step methodological framework used to validate the application of the Normalized Difference Turbidity Index as an indicator of artisanal and small-scale gold mining activity by analyzing the spatial proximity of ASGM sites to major NDTI clusters within the Brokopondo Reservoir. The workflow integrates remote sensing, spatial autocorrelation analysis, proximity assessment, and statistical validation using the Mann-Whitney U test and Cliff's delta to quantify the association between ASGM activity and water turbidity patterns.

*Datasets used*. This study employed Sentinel-2 Level-2A surface reflectance imagery obtained from the harmonized collection available on the Google Earth Engine (GEE) platform. This dataset provides atmospherically corrected reflectance at 10-20 m spatial resolution and includes consistent radiometric calibration across the mission. Details of the other datasets used in this study are provided in Table 1.

Table 1. Characteristics of data collected

| Data | Source | Acquisition year | Scale/ Resolution |
|---|---|---|---|
| Digital Elevation Model (DEM) | 30-Meter SRTM Tile Downloader: https://dwtkns.com/srtm30m/ | 2018 | 1-arcsecond (3601x 3601 pixels) |
| Shape-file with locations of gold mining activity | National Environmental Authority: https://nimos.org/en/about-us/ | 2018 | – |
| Shapefile of the Brokopondo Reservoir boundary | National Land Monitoring System of Suriname (GONINI) https://www.gonini.sbb.sr/ | 2023 | – |

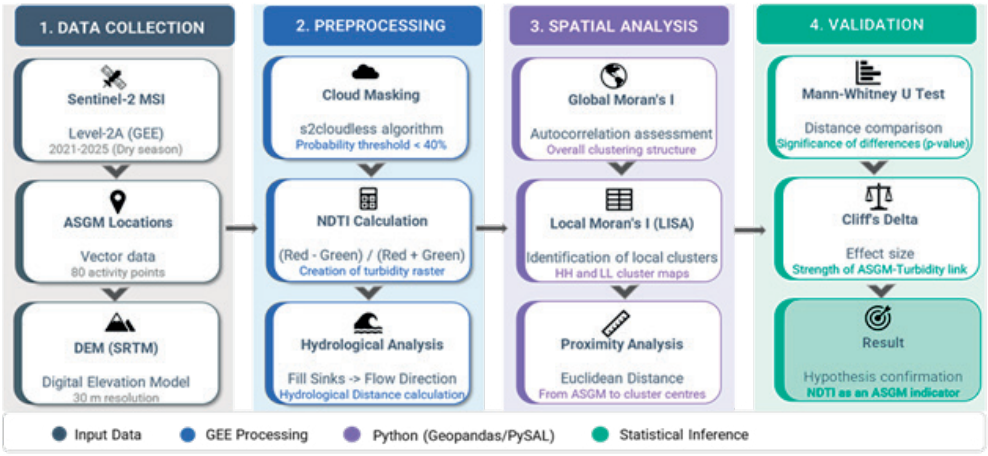



Figure 2. Overall scheme of the methodological approach for the research

The imagery was spatially filtered to the region of interest (ROI) covering the Brokopondo Reservoir and temporally constrained to the period from January 2021 to October 2025. A vector mask derived from a shapefile delineating the official boundaries of the Brokopondo Reservoir, obtained from the National Land Monitoring System of Suriname (GONINI), was used to define the reservoir extent. To exclude the influence of precipitation on water turbidity in the reservoir, only images acquired during July – November were retained.

*Cloud masking approach*. To minimize atmospheric contamination, all Sentinel-2 Level-2A surface reflectance data were corrected for cloud interference using the *s2cloudless* cloud-probability algorithm. The *s2cloudless* model is a machine-learning system based on gradient-boosted decision trees developed by ESA and Sinergise specifically for Sentinel-2 optical imagery. It generates a pixel-level cloud probability map (0-100%) provided in the COPERNICUS/S2_CLOUD_PROBABILITY dataset, which is temporally aligned with the Sentinel-2 SR image collection.

In this workflow, the cloud-probability band was added to each Sentinel-2 image by matching acquisition times. Cloud masking was performed using a probability-threshold approach commonly applied in Sentinel-2 pre-processing. Specifically, pixels with a cloud probability ≥ 40% were flagged as cloud-contaminated and removed from further analysis, while pixels with a probability < 40% were retained (GEE tutorial, 2025).

*Water turbidity index computation*. To quantify water turbidity, the Normalized Difference Turbidity Index (NDTI) was calculated for each cloud-free Sentinel-2 scene. NDTI is defined as:

$$NDTI = \frac{(R_{red} - R_{green})}{(R_{red} + R_{green})} \quad (1)$$

where $R_{Red}$ corresponds to Sentinel-2 Band 4 (665 nm) and $R_{Green}$ corresponds to Band 3 (560 nm) (Dewantoro et al., 2024).

This index is based on the relationship between turbidity and the spectral response of surface waters, where higher turbidity generally corresponds to higher NDTI values and vice versa. The index uses green and red band reflectance to estimate variations in suspended sediment concentration within the water column. This band combination effectively discriminates sediment-laden water; therefore, NDTI serves as a key indicator for turbidity mapping (Foteh et al., 2018).

NDTI was calculated for each selected scene and exported as raster layers for subsequent analysis.

Based on Sentinel-2 spectral characteristics and the typical optical behaviour of tropical inland waters, NDTI values were interpreted as follows: (i) NDTI < −0.1 – indicates clear water conditions, where green reflectance dominates (these values are typical of low suspended sediment concentrations and may occur in calm

reservoir areas, isolated ponds, or waters influenced by biological activity rather than mineral turbidity); (ii) −0.1 ≤ NDTI ≤ 0.1 – indicates low to moderate turbidity or transitional conditions, where red and green reflectance are comparable (this range is commonly observed in relatively stable reservoir waters with limited sediment input); (iii) < NDTI ≤ 0.3 – indicates moderate turbidity, often associated with increased suspended inorganic particles (such values may reflect seasonal runoff, shoreline disturbance, or early-stage mining impacts); (iv) NDTI > 0.3 – indicates high turbidity, dominated by mineral suspended matter (in the Brokopondo Reservoir, such values are consistent with sediment-laden inflows from upstream rivers and creeks affected by artisanal and small-scale gold mining activity).

*Hydrological distance calculation*. Hydrological distance was computed using ArcGIS 10.8 Hydrology toolbox to quantify flow-path connectivity within the Brokopondo Reservoir system. First, the digital elevation model was hydrologically corrected by filling sinks to ensure a continuous flow surface. Flow direction was then derived using the D8 algorithm, followed by flow accumulation to represent potential drainage pathways. Based on these layers, the stream identification step was used to delineate flow channels. The Flow Length tool was then applied in downstream mode to calculate the cumulative distance that water would travel along the flow network from each cell to the reservoir outlet.

The resulting hydrological distance raster represents a process-based metric of spatial connectivity constrained by the drainage network and was subsequently used in spatial statistical analyses to interpret the distribution, clustering, and downstream propagation of NDTI-derived turbidity signals.

*Global and Local Moran's Index calculations*. Spatial autocorrelation of the water turbidity values was assessed using Global Moran's I and Local Moran's I (LISA) statistics. These indices evaluate whether high or low values are spatially clustered or randomly distributed.

The *Global Moran's I* index provides a single summary statistic describing the overall spatial structure of the dataset. It was calculated following Mitchell (2005) using:

$$I = \frac{n}{\sum_{i=1}^{n}\sum_{j=1}^{n} w_{ij}} \cdot \frac{n\sum_{i=1}^{n}\sum_{j=i}^{n} w_{ij}(y_i-\bar{y})(y_j-\bar{y})}{\sum_{i=1}^{n}(y_i-\bar{y})^2]} \quad (2)$$

where $n$ represents the number of spatial units; $y_i$ is the attribute value at location $i$; $\bar{y}$ is the mean of the attribute and $w_{ij}$ is the spatial weight between locations $i$ and $j$.

Values of Moran's I greater than zero indicate positive spatial autocorrelation (clustering of similar values), values below zero indicate negative spatial autocorrelation (dispersion), and values near zero indicate spatial randomness.

*Local Moran's I* was applied to detect local clusters and spatial outliers, providing insight into the spatial heterogeneity of turbidity patterns. The Local Moran's I statistic for each location $i$ was computed as follows:

$$I_i = \frac{(y_i-\bar{y})}{m_2}\sum_{k=1}^{n} w_{ij}(y_j - \bar{y}) \quad (3)$$

where the normalization term $m_2$ is:

$$m_2 = \frac{1}{n}\sum_{k=1}^{n}(y_k - \bar{y})^2 \quad (4)$$

Positive and statistically significant $I_i$ values indicate HH or LL clusters, while negative values represent HL or LH outliers. This enables the identification of areas with anomalous turbidity behaviour within the reservoir.

*Statistical evaluation of ASGM-turbidity relationships*. The non-parametric Mann-Whitney U test was used to determine whether high-high turbidity clusters are significantly closer to ASGM sites than low-low clusters representing relatively clean-water areas. This test was selected because the distance data showed non-normal distributions and unequal variances, making non-parametric inference more appropriate than parametric alternatives. To complement the significance testing, Cliff's delta (δ) was calculated as a measure of effect size. Cliff's delta quantifies the probability that a randomly selected value from one group will exceed a randomly selected value from another group, minus the reverse probability. As a distribution-free statistic, it is well suited for skewed data, unequal sample sizes, and non-parametric comparison frameworks such as the Mann–Whitney test (Vargha & Delaney, 2000). Interpretation followed established thresholds,

where $\delta < 0.147$ indicates a negligible effect, $0.147 \leq \delta < 0.33$ a small effect, $0.33 \leq \delta < 0.474$ a medium effect, and $\delta \geq 0.474$ a large effect (Romano et al., 2006). Together, these metrics provide a robust assessment of both the statistical significance and the magnitude of differences between cluster types in relation to ASGM proximity.

*Software and computational workflow*. All image pre-processing, index computation, and spatial-statistical analyses were conducted in Google Colab (Python environment). Sentinel-2 imagery was accessed and processed using the Google Earth Engine Python API in combination with *geemap* and *xee*, enabling cloud-based filtering, cloud masking, and surface reflectance compositing.

Spatial data handling and vector operations were performed using *GeoPandas*, *Shapely*, and *STRtree*, while raster manipulation and masking were conducted with *rasterio* and *xarray*. Distance metrics, including hydrological distance and Euclidean distance between ASGM point locations and cluster pixels, were generated using *NumPy* and raster/vector spatial indexing routines. Non-parametric statistical testing was performed using *SciPy*.

## RESULTS AND DISCUSSIONS

A time series of NDTI maps spanning July 2021 to October 2025 reveals distinct cyclical patterns in the spatial distribution of water turbidity across the Brokopondo Reservoir (Figure 3).

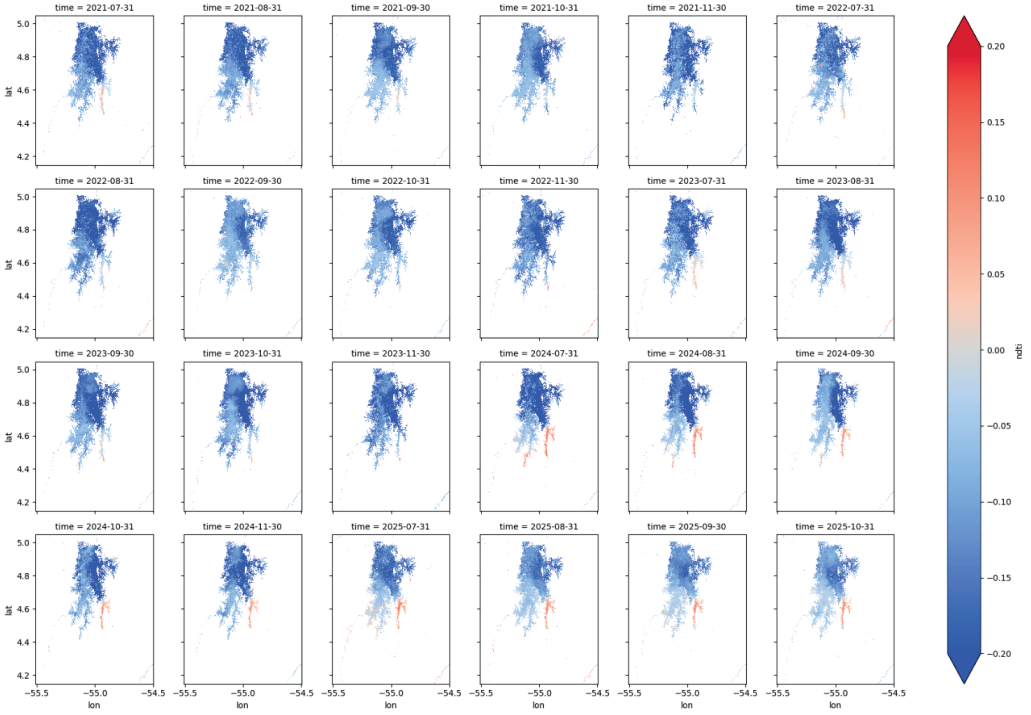



Figure 3. NDTI values and distribution for the Brokopondo Reservoir

The southern portion of the reservoir consistently exhibits the highest turbidity levels throughout the five-year period, corresponding to areas of intensive artisanal and small-scale gold mining activity. Temporal analysis indicates significantly lower turbidity during July 2021-November 2022 compared to July 2024-October 2025.

The suppressed turbidity observed in 2021 is likely a direct consequence of COVID-19 lockdown measures in Suriname, which restricted ASGM operations by limiting access to essential inputs such as fuel, equipment, and mercury used for amalgamation. Similarly, the reduced turbidity observed from July to November 2022 is associated with extreme

hydrological events. Unseasonably heavy rainfall in January and February 2022 – months typically classified as part of the short dry season – necessitated the controlled release of water from the Afobaka Dam on 28 February to mitigate rising reservoir levels. By 15 March, the resulting floods had propagated into the Upper Suriname, Tapanahoni, Lawa, and Marowijne river catchments, disrupting both mining operations and material transport. These hydrological disturbances temporarily curtailed gold mining activity and sediment mobilization from mining sites, as reflected in the NDTI-derived turbidity patterns. In contrast, the elevated turbidity observed in 2024-2025 corresponds to resumed and intensified ASGM activity under normal hydrological conditions, highlighting the strong coupling between anthropogenic sediment inputs and reservoir turbidity.

Considering these contextual factors, the period from July 2024 to October 2025 was selected for subsequent analysis, as it represents a more stable phase in which turbidity variations are more likely to reflect mining-related impacts rather than exceptional climatic or operational disruptions.

Global Moran's I was calculated to quantify the overall spatial structure of the NDTI dataset (Table 2).

Table 2. Spatial autocorrelation of NDTI-derived turbidity in the Brokopondo Reservoir based on Global Moran's I (July 2024-October 2025)

| Date | Global Moran's I | z-score | p-value |
|---|---|---|---|
| July 2024 | 0.834004 | 422.5635 | < 0.0001 |
| August 2024 | 0.854091 | 429.6744 | < 0.0001 |
| September 2024 | 0.812478 | 410.3696 | < 0.0001 |
| October 2024 | 0.821867 | 412.3634 | < 0.0001 |
| November 2024 | 0.82093 | 415.7692 | < 0.0001 |
| July 2025 | 0.869067 | 442.2297 | < 0.0001 |
| August 2025 | 0.810761 | 415.0792 | < 0.0001 |
| September 2025 | 0.838833 | 424.9217 | < 0.0001 |
| October 2025 | 0.799329 | 405.948 | < 0.0001 |

This indicator demonstrates consistently very strong and statistically significant positive spatial autocorrelation of NDTI-derived turbidity patterns across the Brokopondo Reservoir for all analyzed months between July 2024 and October 2025. Moran's I values range from 0.799 to 0.869, close to the theoretical upper limit of +1, indicating that high and low turbidity values are strongly clustered in space rather than randomly distributed.

The extremely high z-scores (405.9 to 442.2) and p-values < 0.0001 confirm that these clustering patterns are highly unlikely to have occurred by chance. The strongest spatial clustering was observed in July 2025 (I = 0.869), while slightly lower – but still very strong – clustering occurred in October 2025 (I = 0.799). These results suggest that sediment-rich and sediment-poor zones remain spatially stable over time. The strength and persistence of these spatial patterns support the suitability of NDTI as a robust indicator for identifying and monitoring persistent turbidity hotspots potentially linked to ASGM activity.

After confirming significant spatial clustering in the dataset, Local Moran's I was calculated to identify the spatial distribution of high and low NDTI values and to delineate HH and LL clusters, as well as spatial outliers (HL and LH) (Table 3).

Table 3. Non-parametric test statistics for spatial NDTI HH and LL cluster differentiation (July 2024-October 2025)

| Date | U statistic | p-value | Cliff's delta (effect size) |
|---|---|---|---|
| July 2024 | 284080.0 | < 0.000001 | 1.0 |
| August 2024 | 5606522.0 | < 0.000001 | 1.0 |
| September 2024 | 4997040.0 | < 0.000001 | 1.0 |
| October 2024 | 4105832.0 | < 0.000001 | 1.0 |
| November 2024 | 3652980.0 | < 0.000001 | 1.0 |
| July 2025 | 6580161.0 | < 0.000001 | 1.0 |
| August 2025 | 6075216.0 | < 0.000001 | 1.0 |
| September 2025 | 6224660.0 | < 0.000001 | 1.0 |
| October 2025 | 6107759.0 | < 0.000001 | 1.0 |

The Mann-Whitney U test results comparing HH and LL clusters reveal extremely strong and highly consistent differences between the two groups across all analyzed months. U statistics range from 284,080 (July 2024) to 6,580,161 (July 2025), with all pairwise comparisons yielding p-values < 0.000001, indicating robust statistical separation between the distributions.

Notably, Cliff's delta equals 1.0 for every month, representing the maximum possible effect size and demonstrating complete non-overlap between HH and LL cluster values. This uniform pattern indicates highly stable and persistent spatial differentiation of NDTI across both dry-season periods (2024 and 2025).

HH clusters consistently represent markedly higher turbidity-related index values, while LL

clusters represent persistently low values, with no intermediate overlap. Such effect sizes confirm that the spatial clustering of NDTI is both statistically significant and structurally robust.

Using the NDTI as an indicator of ASGM activity is a promising approach, but it has important limitations. In the Brokopondo Reservoir, increased water turbidity is not caused solely by gold mining; it can also be influenced by natural factors such as rainfall intensity, surface runoff, and local topography. To minimize precipitation-related effects, the analysis was restricted to the regional dry season (July-November), with particular emphasis on the driest months (September-November), consistently observed during 2021-2025. This temporal filtering allowed the analysis to focus on periods when anthropogenic sediment inputs from ASGM were less masked by rainfall-driven turbidity. A statistical assessment of the relationship between NDTI and precipitation for July 2021 – October 2025 showed a very weak correlation (Pearson's r = 0.08), indicating negligible linear dependence between rainfall and turbidity during the selected dry-season periods (Figure 4).

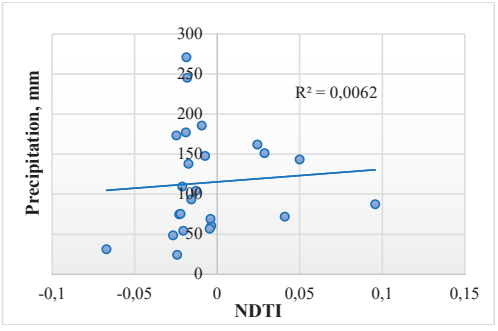



Figure 4. Relationship between NDTI and precipitation (2021-2025)

This weak correlation suggests that precipitation was not a dominant driver of turbidity variability within the area of interest during the analyzed periods, supporting the interpretation that the observed turbidity patterns are largely associated with anthropogenic disturbance.

To evaluate the influence of topography on turbidity patterns, hydrological distance was calculated and its relationship with the spatial distribution of high-high (HH) and low-low (LL) clusters were analysed (Table 4).

Table 4. Non-parametric test statistics for spatial relationships between NDTI clusters and hydrological distance (July 2024-October 2025)

| Date | U statistic | p-value | Cliff's delta (effect size) |
|---|---|---|---|
| July 2024 | 116882.0 | < 0.000001 | -0.1771 |
| August 2024 | 2617028.5 | 0.000053 | -0.0664 |
| September 2024 | 2341722.0 | 0.000171 | -0.0628 |
| October 2024 | 1872022.5 | < 0.000001 | -0.0881 |
| November 2024 | 1533951.0 | < 0.000001 | -0.1602 |
| July 2025 | 2858760.0 | < 0.000001 | -0.1311 |
| August 2025 | 2613307.0 | < 0.000001 | -0.1397 |
| September 2025 | 2955452.0 | 0.001388 | -0.0504 |
| October 2025 | 2884479.0 | 0.000454 | -0.0555 |

The non-parametric test results revealed no meaningful relationship between the spatial distribution of HH and LL clusters and hydrological distance. Although several months show statistically significant p-values, all Cliff's delta values are small and negative (–0.05 to – 0.18), indicating negligible effect sizes and confirming the absence of a systematic spatial trend. This means that neither HH nor LL clusters align with the longitudinal hydrological gradient of the reservoir. High-turbidity areas do not consistently occur upstream or downstream, and low-turbidity areas are not preferentially located farther from inflows. Instead, turbidity clusters appear spatially patchy and locally constrained, suggesting that hydrological distance is not a meaningful predictor of turbidity distribution. These results indicate that turbidity dynamics in the Brokopondo Reservoir are driven primarily by localized factors – such as ASGM activity, shoreline erosion, and small tributaries – rather than by overall hydrological connectivity.

To achieve the research objective, a proximity analysis was conducted to examine the relationship between high-intensity pollution sources (ASGM) and high-intensity effects (NDTI clusters). Euclidean distances were calculated from each ASGM location to all HH and LL cluster points within a 25 km zone around the Brokopondo Reservoir (Table 5).

Because field turbidity measurements were unavailable, nonparametric methods were used instead of regression modelling. The Mann–Whitney U test and Cliff's delta were applied to assess whether HH clusters are significantly closer to ASGM sites than LL clusters.

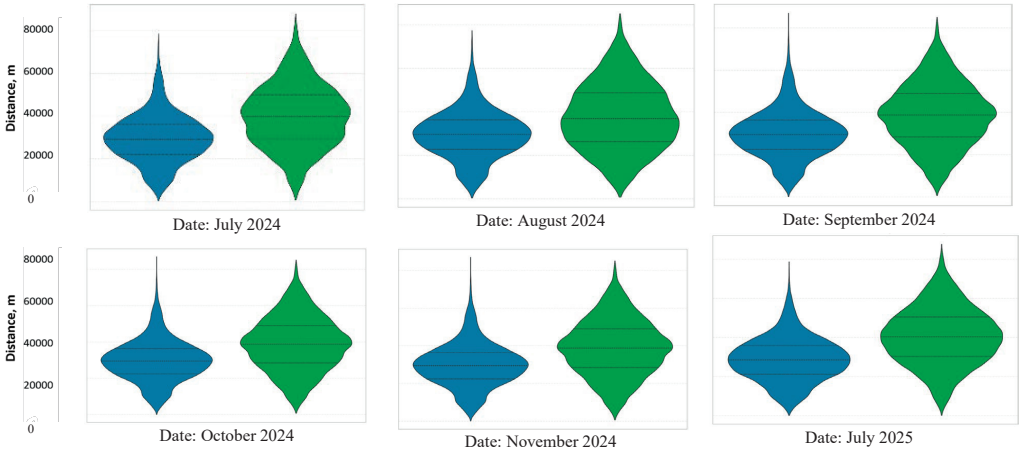
Across all months, HH clusters were consistently closer to ASGM sites than LL clusters. Mean distances ranged from 28,855 m to 30,798 m for HH clusters and from 37,791 m to 40,770 m for LL clusters.

U statistic and corresponding p-values (all p = 0.01) indicate statistically significant differences each month. Cliff's delta values were consistently negative (−0.3046 to −0.4715), confirming that ASGM locations are spatially associated with HH clusters rather than LL clusters. This pattern suggests a robust spatial correlation between areas of increased turbidity and proximal ASGM activity, supporting the use of NDTI clustering as an indicator for mining-related water quality impacts.

The violin plots (Figure 5) show a clear spatial separation between water turbidity cluster types and their proximity to artisanal and small-scale gold mining sites. Areas classified as high-high turbidity clusters are located, on average, at considerably smaller distances from ASGM operations compared to low-low turbidity clusters. This spatial relationship confirms the assumption that gold mining proximity is the primary driver of elevated sediment loads in the Brokopondo Reservoir.

Table 5. Distances between all ASGM locations and all HH and LL clusters points (July 2024-October 2025)

| Date | Cluster | Distance, m | | | U statistic | p-value | Cliff's delta (effect size) |
|---|---|---|---|---|---|---|---|
| | | min | max | mean | | | |
| July 2024 | HH | 452 | 78560 | 29558 | 32565897 | 0.01 | -0.4268 |
| | LL | 778 | 87877 | 40039 | | | |
| August 2024 | HH | 452 | 77395 | 29666 | 32754352 | 0.01 | -0.3046 |
| | LL | 778 | 85146 | 37791 | | | |
| September 2024 | HH | 244 | 78560 | 30209 | 663979890 | 0.01 | -0.3356 |
| | LL | 497 | 87886 | 39076 | | | |
| October 2024 | HH | 155 | 86971 | 29808 | 513405855 | 0.01 | -0.3748 |
| | LL | 779 | 85066 | 38905 | | | |
| November 2024 | HH | 155 | 88329 | 28916 | 435462823 | 0.01 | -0.4040 |
| | LL | 497 | 84353 | 38370 | | | |
| July 2025 | HH | 155 | 78853 | 28855 | 695519690 | 0.01 | -0.4715 |
| | LL | 130 | 87886 | 40609 | | | |
| August 2025 | HH | 155 | 78854 | 29644 | 682212917 | 0.01 | -0.4385 |
| | LL | 518 | 88102 | 40696 | | | |
| September 2025 | HH | 155 | 75740 | 29164 | 668830223 | 0.01 | -0.4628 |
| | LL | 131 | 88102 | 40770 | | | |
| October 2025 | HH | 155 | 78854 | 29598 | 721540967 | 0.01 | -0.4093 |
| | LL | 131 | 88102 | 39606 | | | |



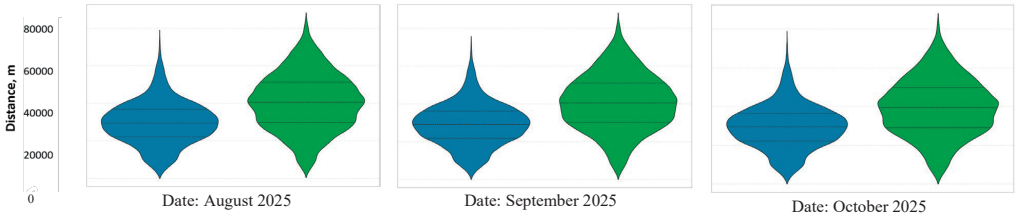



Figure 5. Violin plots showing the distribution of distances between ASGM sites and high–high (HH; blue) and low-low (LL; green) turbidity clusters

The results suggest that NDTI may provide an effective tool for identifying mining-related water turbidity. It relies solely on standard optical satellite imagery that is globally available, freely accessible, and frequently updated. Its calculation requires only red and green spectral bands, and is computationally simple and scalable. This makes it particularly valuable where field-based water quality data are limited or absent, enabling reproducible and cost-effective environmental monitoring of ASGM impacts in remote regions.

Future research could extend the proposed framework by integrating Land Surface Temperature (LST), the Normalized Difference Vegetation Index (NDVI), and the Bare Soil Index (BSI) with Normalized Difference Turbidity Index (NDTI)-based turbidity assessment. LST could provide complementary information on surface thermal changes associated with ASGM-related vegetation removal and soil exposure, while NDVI and BSI could help characterize vegetation loss and the expansion of disturbed or bare-soil areas around mining sites. Combining these indicators with NDTI could provide a more comprehensive assessment of the terrestrial–aquatic environmental footprint of ASGM and improve the monitoring of mining-induced landscape and water-quality changes.

## CONCLUSIONS

This study provides a comprehensive spatiotemporal assessment of turbidity dynamics in the Brokopondo Reservoir and evaluates the suitability of the NDTI as a proxy for monitoring the impacts of artisanal and small-scale gold mining.

By integrating five years of dry-season Sentinel-2 observations with spatial statistics and proximity analyses, the research demonstrates that turbidity in the reservoir is strongly structured spatially, highly persistent over time, and closely associated with the distribution of mining activities. Global Moran's I values consistently close to +1 confirm pronounced and stable clustering of high and low turbidity zones across all analyzed months, while Local Moran's I results show clear spatial segregation between HH and LL clusters with complete non-overlap in their distributions. These findings indicate that turbidity hotspots are not randomly distributed but represent persistent spatial features.

The analysis further reveals that neither precipitation nor hydrological distance meaningfully explains turbidity variability during the dry-season months. The very weak correlation between NDTI and rainfall ($r = 0.08$) indicates that seasonal filtering effectively removed climate-driven noise from the dataset, while negligible effect sizes derived from the hydrological distance analysis demonstrate that turbidity patterns do not follow the longitudinal structure of the reservoir. Instead, turbidity clusters are spatially localized and strongly influenced by nearby anthropogenic disturbances.

The proximity analysis confirms a significant and consistent spatial association between ASGM sites and HH turbidity clusters. Across all months from 2024-2025, HH clusters were systematically located closer to mining areas than LL clusters, with statistically significant results and moderate to strong effect sizes. These outcomes provide robust empirical support for the hypothesis that ASGM is a primary driver of elevated turbidity in the Brokopondo Reservoir.

Overall, the study suggests that NDTI has potential as a scalable, field-independent proxy

for mining-related turbidity. Its reliance on freely available optical satellite data, minimal spectral inputs, and straightforward computation makes it a potentially valuable tool for environmental monitoring in remote regions where conventional water-quality measurements are limited or unavailable. By combining spatial clustering metrics, non-parametric statistics, and proximity analysis, this research establishes a reproducible framework for detecting and tracking ASGM impacts on freshwater systems. The methodology and results highlight the potential for NDTI-based monitoring to support decision-making in environmental governance, early warning systems, and long-term assessments of mining-driven landscape change in tropical watersheds.

## REFERENCES

Amran, M., & Daming, W. (2023). Estimation of coastal waters turbidity using Sentinel-2 imagery. *Geodesy and Cartography*, 49(4), 180–185.

Chen, J., Wang, K., Li, X., Zhao, X., Cheng, X., Liu, Z., Zhang, J., & Zhang, S. (2024). Remote sensing inversion of water quality parameters (TSM, Chl-a, and CDOM) in subtidal seaweed beds and surrounding waters. *Ecological Indicators*, 167, 112716.

Das, S., Nandi, D., Thakur, R. R., Bera, D. K., Behera, D., Đurin, B., & Cetl, V. (2024). A novel approach for ex situ water quality monitoring using the Google Earth Engine and spectral indices in Chilika Lake, Odisha, India. *ISPRS International Journal of Geo-Information*, 13(11), 381.

Dewantoro, M. D. R., Ulfa, M., & Supatmanto, B. D. (2024). Water turbidity mapping using Sentinel-2A imagery and cloud-based Google Earth Engine in Saguling Reservoir. *IOP Conference Series: Earth and Environmental Science*, 1343(1), 012027.

Elhag, M., Gitas, I., Othman, A., Bahrawi, J., Gikas, P. (2019). Assessment of water quality parameters using temporal remote sensing spectral reflectance in arid environments. *Saudi Arabia. Water*, 11, 556.

EMSAGS Project. (2023). Final technical situational analysis: Artisanal and small-scale gold mining (ASGM) in Suriname (Final TSA report). EMSAGS / UNDP. Retrieved November 30, 2025, from https://emsags.org.

Espinoza, E., Baltodano, A., & Requena, N. (2025). Spatiotemporal analysis of water quality and optical changes induced by contaminants in lake Chinchaycocha Using Sentinel-2 and in situ data. *Water*, 17(15), 2195.

Foteh, R., Garg, V., Nikam, B. R., Khadatare, M. Y., Aggarwal, S. P., & Kumar, A. S. (2018). Reservoir sedimentation assessment through remote sensing and hydrological modelling. *Journal of the Indian Society of Remote Sensing*, 46, 1893–1905.

Global Forest Watch. (n.d.). Suriname. Retrieved November 30, 2025, from https://www.globalforestwatch.org.

Google Earth Engine tutorial. (n. d) Sentinel-2: Cloud masking with s2cloudless (community tutorial). Retrieved December 3, 2025, from https://developers.google.com.

Heemskerk, M. & Kooye, R. (2003). Challenges to Sustainable Small-Scale Mine Development in Suriname. 10.1201/9780203971284.ch36.

Heemskerk, M., Le Tourneau, F.-M., Hiwat, H., Cairo, H., & Pratley, P. (2022). In a life full of risks, COVID-19 makes little difference: Responses to COVID-19 among mobile migrants in gold mining areas in Suriname and French Guiana. *Social Science & Medicine*, 296, 114747.

Huisden, C. M., Landburg, G., Niram, A., Algoe, S., Dakriet, N. (2021) Mercury toxicity through fish consumption in Paramaribo, Suriname. *Academic Journal of Suriname*, (11)1, 25–32.

Khan, R. M., Salehi, B., Mahdianpari, M., & Mohammadimanesh, F. (2021). Water quality monitoring over Finger Lakes region using Sentinel-2 imagery on Google Earth Engine cloud computing platform. In ISPRS *Annals of the Photogrammetry, Remote Sensing and Spatial Information Sciences*, V-3-2021, 279–283.

Leentvaar, P. (1975). Hydrobiological observations in Surinam, with special reference to the manmade Brokopondo Lake. *Studies on the Fauna of Suriname and other Guyanas*, 15(56), 1–173.

Li, S., Kutser, T., Song, K., Liu, G., & Li, Y. (2023). Lake turbidity mapping using an OWTs-bp based framework and Sentinel-2 imagery. *Remote Sensing*, 15(10), 2489.

Malone, A., Figueroa, L., Wang, W., Smith, N. M., Ranville, J. F., Vuono, D. C., Alejo Zapata, F. D., Morales Paredes, L., Sharp, J. O., & Bellona, C. (2023). Transitional dynamics from mercury to cyanide-based processing in artisanal and small-scale gold mining: Social, economic, geochemical, and environmental considerations. *Science of the Total Environment*, 898, 165492.

Marshall, B. G., Veiga, M. M., da Silva, H. A. M., & Guimarães, J. R. D. (2020). Cyanide contamination of the Puyango-Tumbes River caused by artisanal gold mining in Portovelo-Zaruma, Ecuador. *Current Environmental Health Reports*, 7(3), 303–310.

Ministry of Natural Resources; National Institute for Environment and Development in Suriname (NIMOS); United Nations Development Programme (UNDP) (2023). First National Action Plan on Artisanal and Small-Scale Gold Mining (ASGM) in Suriname. EMSAGS Project. Retrieved December 5, 2025, from https://minamataconvention.org.

Mitchell, A. (2005). The ESRI Guide to GIS Analysis. *Esri Press*, 2.

Myslyva, T., Dasai, M., Huisden, C. M., Nadtochiy, P., Bilyavskyi, Y. (2024). Application of machine learning approaches for land use change modelling in Suriname. *Scientific Papers. Series E. Land Reclamation, Earth Observation and Surveying, Environmental Engineering*, 13, 830–840.

Ouboter, P. E. (2015). Review of mercury pollution in Suriname. *Academic Journal of Suriname*, 6, 531–543.

Pereira, B. M.& Lobo, F. d. L. (2024). Spatiotemporal analysis of total suspended solids in water bodies and mapping mining areas in Suriname and French Guiana. *Mining*, 4, 510–529.

Quispe Aquino, R., Malone, A., Smith, N. M., & García Zúñiga, F. F. (2022). Perceptions and realities of mercury contamination in a Peruvian artisanal and small-scale gold mining (ASGM) community. *Environmental Research*, 214, 114092.

Rodríguez, F., & Chavez, K. (2024). Small-scale gold mining study: Data to monitor environmental impacts in Suriname. Islamic Development Bank; Inter-American Development Bank; Global Partnership for Sustainable Development Data; Government of Suriname. Retrieved November 30, 2025, from https://www.data4sdgs.org.

Romano, J., Kromrey, J. D., Coraggio, J., Skowronek, J., & Devine, L. (2006). Exploring methods for evaluating group differences on the NSSE and other surveys: Are the t-test and Cohen's d indices the most appropriate choices? *Annual Meeting of the Southern Association for Institutional Research*.

Seccatore, J. & Theije, M. (2017). Socio-technical study of small-scale gold mining in Suriname. *Journal of Cleaner Production*, 144, 107–119.

Sousa, R. N., & Veiga, M. M. (2009). Using performance indicators to evaluate an environmental education program in artisanal gold mining communities in the Brazilian amazon. *Ambio*, 38, 40–46.

Steinbach, S., Bartels, A., Rienow, A., Thiongo, K., Zwart, S., & Nelson, A. (2025). Predicting turbidity dynamics in small reservoirs in central Kenya using remote sensing and machine learning. *International Journal of Applied Earth Observation and Geoinformation*, 136, 104390.

Tesfaye, A. (2024). Remote sensing-based water quality parameters retrieval methods: a review. *East African Journal of Environment and Natural Resources*, 7(1), 80-97.

United Nations Office on Drugs and Crime. (2025). Global analysis on crimes that affect the environment – Part 2b: Mineral's crime: Illegal gold mining. United Nations. Retrieved November 30, 2025, from https://www.unodc.org.

Vargha, A. & Delaney, H. D. (2000). A critique and improvement of the CL common language effect size statistics. *Journal of Educational and Behavioral Statistics*, 25(2), 101–132.

Vreedzaam, A., Ouboter, P. E., Hindori-Mohangoo, A. D., Lepak, R., Rumschlag, S., Janssen, S., Landburg, G., Shankar, A., Zijlmans, W., Lichtveld, M. Y., & Wickliffe, J. K. (2023). Contrasting mercury contamination scenarios and site susceptibilities confound fish mercury burdens in Suriname, *South America. Environmental Pollution*, 336, 122447.

Zhang, C., Liu, Y., Chen, X., & Gao, Y. (2022). Estimation of Suspended Sediment Concentration in the Yangtze Main Stream Based on Sentinel-2 MSI Data. *Remote Sensing*, 14(18), 4446.

Scientific Papers. Series E. Land Reclamation, Earth Observation & Surveying, Environmental Engineering. Vol. XV, 2026
Print ISSN 2285-6064, CD-ROM ISSN 2285-6072, Online ISSN 2393-5138, ISSN-L 2285-6064

# HIGH-RESOLUTION MAPPING OF VEGETATION TYPES, STRUCTURE, HEIGHT, AND DENSITY IN THE USAMV CLUJ-NAPOCA CAMPUS USING LiDAR, PHOTOGRAMMETRY AND MULTISPECTRAL SENSING

**Mircea Emil NAP, Tudor SĂLĂGEAN, Silvia CHIOREAN, Ioana POP, Florica MATEI, Cătălin VÂRBAN, Simion BRUMĂ, Elemer Emanuel ȘUBA**

University of Agricultural Sciences and Veterinary Medicine Cluj-Napoca,
3-5 Calea Mănăștur Street, 400372, Cluj-Napoca, Romania

Corresponding author emails: elemer-emanuel.suba@usamvcluj.ro, tudor.salagean@usamvcluj.ro

***Abstract***

*Metropolitan areas are most often affected by the weak presence of „green" infrastructure so that the climate can be affected. This work aims to evaluate the vegetation within the UASVM Cluj-Napoca campus, in terms of its spatial distribution, the types of vegetation and their characteristics. In an attempt to overcome the disadvantages of classical vegetation assessment methods, an approach that integrates several types of geospatial data was proposed. More specifically, LiDAR technology was used to determine, among other things, the height of forest vegetation and its density, aerial photogrammetric technology was used for contextual and texture information, and multispectral sensors helped to differentiate vegetation types. Data acquisition was carried out using the DJI MAVIC 3M, respectively the South SF 1200 with SG130 scanner. Data processing was carried out using various software. This research highlights the advantages brought by the use of the most modern geodetic and topographic technologies in the evaluation of green areas within large urban areas and their contribution to the most correct management of green areas.*

***Key words****: LiDAR, multispectral, photogrammetry, vegetation.*

## INTRODUCTION

The contemporary landscape is undergoing continuous transformation under the influence of natural processes and increasing anthropogenic pressures (Ali et al., 2026).

Romania has some of the largest remaining areas of old-growth forests in the European Union. This represents a very important part of the country's natural heritage. These forests continue to face increasing pressure due to inadequate management practices, despite their ecological significance, resulting in a gradual decline of their extent over recent decades. In this context modern surveying and monitoring technologies have become valuable tools for integrating spatial and descriptive data (Moatăr et al., 2026).

Rapid urbanization, land-use changes, and climate variability are altering the composition, structure, and spatial distribution of vegetation, highlighting the need for accurate and up-to-date monitoring approaches (Liang et al., 2020; Rai & Singh, 2026).

Traditional field-based vegetation surveys provide valuable information but are often time-consuming, labor-intensive, and difficult to implement over large or heterogeneous areas (Goebel & Iwaszczuk, 2026; Mohamad & Tahar, 2026).

Vegetation mapping with high accuracy is essential for monitoring plant distribution and for assessing ecosystem dynamics. Remote sensing has become one of the most effective methodologies in ths regard, being rapid and also cost efficient (Guan et al., 2019; Mohamad & Tahar, 2026).

Sattelite imagery has moderate spatial resolution being suitable for broad land cover classification, but high-resolution multispectral imagery which is also often combined with LiDAR data enables vegetation mapping with greater accuracy (Fernández-Guisuraga et al., 2018; Goebel & Iwaszczuk, 2023).

Equipped with a multitude of sensors, such as photogrammetric sensors, multispectral sensors and LiDAR, Unmanned Aerial Vehicles have become one of the most important technologies when it comes to remote sensing. Due to their ability to aquire high resolution spatial data, in a relatively short period of time, at relatively low cost, UAVs become essential tools in modern

vegetation assessment and monitoring (Hyyppä et al., 2020; Liu et al., 2026).

The objective of this study is to develop a high-resolution vegetation mapping framework for the UASVM Cluj-Napoca campus through 1the integration of UAV-based LiDAR, photogrammetric, and multispectral data. Specifically, the study aims to assess vegetation structure, estimate vegetation height and density, and generate a detailed vegetation inventory that can support future environmental monitoring and landscape management activities.

## MATERIALS AND METHODS

The investigated area covers approximately 26 hectares, with an elevation range of about 100 m, varying between 330 m and 440 m above sea level.

The study area consists of the USAMV Cluj-Napoca campus, Cluj County, Romania and a section of the adjacent Iuliu Prodan Park located in its immediate proximity.

The study site is characterized by an urban environment that includes numerous buildings, primarily dedicated to educational activities, while also containing extensive forest and horticultural vegetation. These characteristics, together with the easy and rapid access to the area, were the main reasons for selecting it as the case study site for this research.

LiDAR data were acquired using the South SF 1200 Unmanned Aerial System with SG130, which is 2kg aerial LiDAR system that combines a 45/61MP RGB camera with precise IMU/GNSS tracking. It has a ± 3 cm absolute accuracy. It features a 360° FOV, captures up to 800,000 pts/sec with 12 returns.

Photogrammetric and multispectral data was acquired using a DJI Mavic 3 Multispectral UAS equipped with an RTK-GNSS module providing positioning accuracies of approximately ± 0.10 m in both the horizontal and vertical components. The system integrates a 20 MP RGB camera for high-resolution photogrammetry and a 4-band 5 MP multispectral sensor (Green, Red, Red Edge, and NIR).

To complement the structural assessment, a series of spectral vegetation indices (Șuba et al., 2025) from the multispectral imagery were calculated, namely:

-NDVI (Normalized Difference Vegetation Index): It evaluates vegetation vigour, greenness, and photosynthetic activity based on red and near-infrared reflectance ((NIR - Red)/(NIR + Red));

-GNDVI (Green Normalized Difference Vegetation Index): It is sensitive to chlorophyll content and plant physiological condition through the use of the green spectral band. ((NIR - Green)/(NIR + Green));

-NDRE (Normalized Difference Red Edge Index): It assesses chlorophyll concentration and nitrogen status using the red-edge spectral region ((NIR - RedEdge)/(NIR + RedEdge));

-LCI (Leaf Chlorophyll Index): It estimates leaf chlorophyll content and vegetation productivity. ((NIR - RedEdge)/(NIR + Red));

-MCARI (Modified Chlorophyll Absorption Ratio Index): It enhances sensitivity to chlorophyll absorption and vegetation stress while reducing background effects ([(RedEdge - Red) - 0.2 (RedEdge - Green)]/times (RedEdge/Red));

-SIPI (Structure Insensitive Pigment Index): It evaluates pigment balance and vegetation stress while minimizing canopy structure influence ((NIR - Blue)/(NIR - Red)) (Șuba et al., 2025).

The workflow (Figure 1) which starts with UAV-based LiDAR, RGB, and multispectral data acquisition, followed by direct GNSS georeferencing.

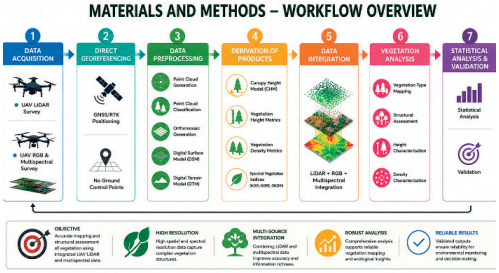



Figure 1. Workflow overview

After preprocessing, both structural and spectral vegetation metrics were derived, such as canopy height, density, and vegetation indices. These datasets were integrated and analysed together to provide a detailed assessment of vegetation.

## RESULTS AND DISCUSSIONS

In the first stage, a colorized LiDAR point cloud was generated from the acquired UAV data. This point cloud can be seen in Figure 2.



Figure 2. Colorized point cloud

Subsequently, the point cloud was analyzed based on elevation values, allowing the visualization and assessment of height variations across the study area and providing valuable information on vegetation structure and terrain morphology.

The LiDAR point cloud was subsequently classified into several categories, including ground points (brown), buildings (orange), and vegetation (green).

The classification was performed automatically using the Maximum Likelihood Estimation (MLE) algorithm (Figure 3).

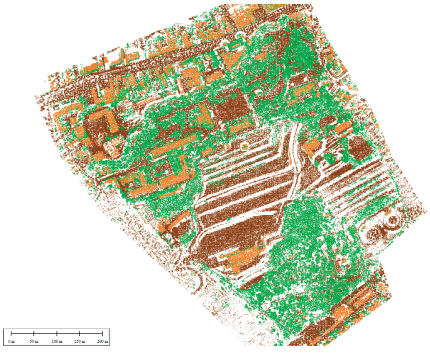


Figure 3. Ground points (brown), Buildings (orange), Vegetation (green)

Other valuable outputs derived from the LiDAR survey are the vertical cross-sections through the point cloud. These cross-sections provide detailed information on the vertical structure of vegetation and can support species identification (Figure 4).

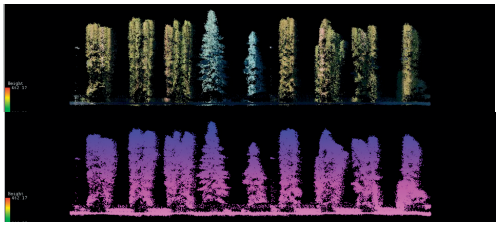


Figure 4. Thuja and spruce trees identified in the vertical cross-section

Tree and canopy extraction was also performed automatically using the Maximum Likelihood Estimation (MLE) algorithm combined with MultiScale Classification. This approach enabled the identification and delineation of individual trees and their crowns based on the structural characteristics of the LiDAR point cloud. The extracted tree attributes included elevation, tree height, mean crown diameter, and maximum crown diameter, providing detailed quantitative information for each identified tree (Figure 5).

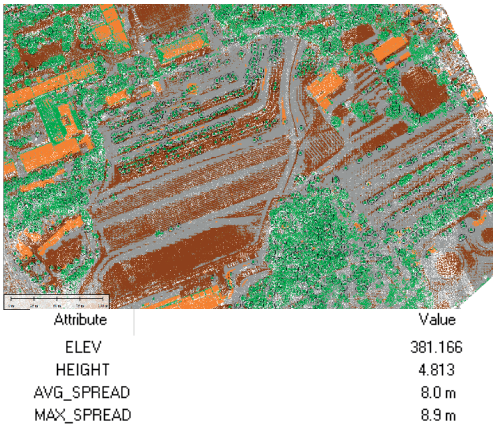



Figure 5. Tree and canopy extraction

The automated extraction of trees and canopy boundaries also presents several limitations, particularly regarding canopy delineation accuracy and trunk positioning. For example, large tree crowns may be divided into two or more individual trees, as major branches can be interpreted as separate crowns.

In Figure 6 it can be seen the Elevation-based representation A total of 1,645 trees exceeding 2.5 m in height were identified within the study area. The detected trees were distributed across different height classes, providing an overview of the vertical structure and composition of the vegetation.

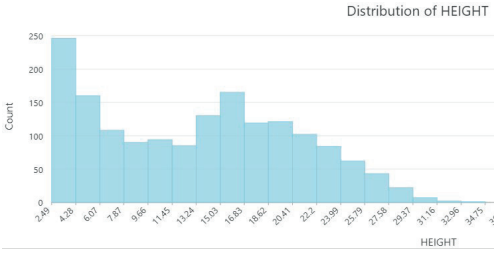



Figure 6. Elevation-based representation

Tree density map showing the distribution of trees per square meter across the study area is presented in Figure 7.

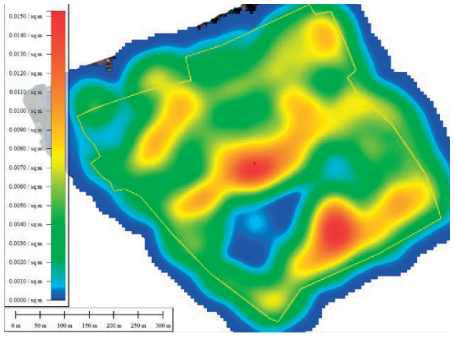


Figure 7. Tree density map

Multispectral images were acquired according to a predefined flight plan. A total of 2,796 images (RGB, Green band, Red band, Red Edge band) were collected during the survey. The study area covered approximately 262,330 m² (26.23 ha). Following image processing, a high-resolution orthomosaic was generated (Figure 8).

GNDVI quantifies vegetation health and vigour by comparing the reflectance recorded in selected spectral bands. Higher GNDVI values (approaching +1) indicate vegetation with elevated chlorophyll concentrations and intense photosynthetic activity, characteristics commonly associated with dense and healthy plant cover.



Figure 8. High-resolution orthomosaic

Intermediate GNDVI values correspond to areas with partial vegetation cover, such as grasslands or sparsely cultivated fields, where vegetation condition and density may vary. Lower GNDVI values (around 0) generally represent bare soil, built-up areas, or locations with limited vegetation cover. Negative GNDVI values are typically associated with water bodies, barren surfaces, or other non-vegetated land covers (Figure 9).

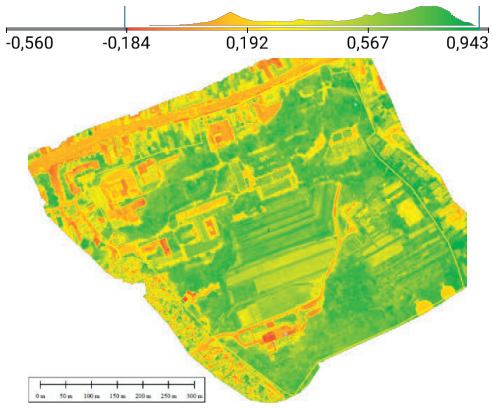



Figure 9. GNDVI

The Leaf Chlorophyll Index (LCI) is derived from the Near Infrared (NIR) and Red Edge spectral bands (Figure 10). The NIR band is particularly responsive to leaf internal structure and water content, whereas the Red Edge band is closely related to chlorophyll concentration, enabling an accurate assessment of vegetation condition. Low LCI values (grey to dark orange) generally indicate low chlorophyll concentrations and are commonly associated with bare soil, non-vegetated areas, or

vegetation affected by severe physiological stress. Moderate LCI values (yellow to light green) correspond to areas with partial vegetation cover, where reduced chlorophyll content may reflect nutrient limitations or environmental stress conditions. High LCI values (bright green) represent vigorous and healthy vegetation characterized by high chlorophyll concentrations, active photosynthesis, and strong plant development.

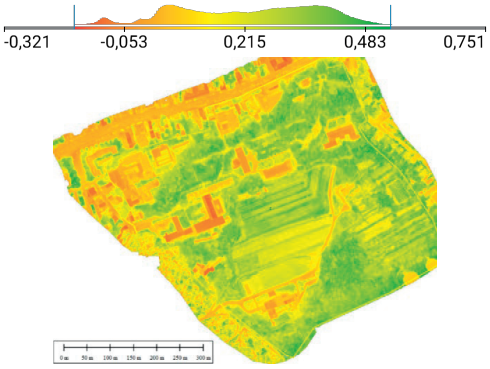



Figure 10. LCI

MCARI is highly responsive to changes in chlorophyll concentration and the Leaf Area Index (LAI), making it an effective indicator for evaluating vegetation health and detecting plant stress. High index values (dark to light green) are associated with elevated chlorophyll concentrations, reflecting healthy, vigorous vegetation with high photosynthetic activity. Moderate values (yellow to orange) indicate intermediate chlorophyll levels and may suggest the presence of mild plant stress or the onset of nutrient deficiencies. Low values (dark orange to red) are characteristic of vegetation with reduced chlorophyll content and are often linked to physiological stress, chlorosis, or diminished photosynthetic performance (Figure 11).

Because the NDRE index incorporates the Red Edge spectral band, it is particularly effective at identifying subtle changes in vegetation health before visible symptoms become apparent.

This capability makes it especially useful for precision agriculture applications, including crop health assessment, stress detection, and continuous crop monitoring. Negative values or values approaching zero (grey to dark orange) generally correspond to bare soil, non-vegetated surfaces, or vegetation in poor health.

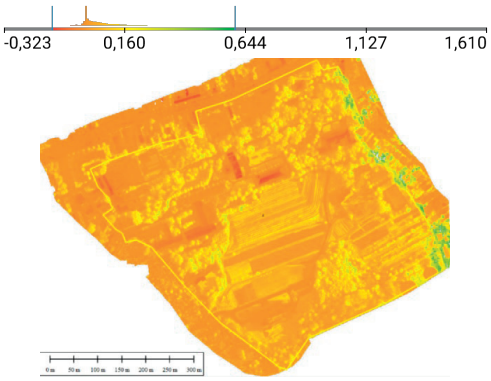



Figure 11. MCARI

Moderate values (yellow to light green) indicate the presence of vegetation with intermediate chlorophyll levels, which may reflect physiological stress or reduced plant vigour. High values (bright green) are characteristic of dense and healthy vegetation with high chlorophyll activity, indicating vigorous plant growth and optimal physiological condition (Figure 12).

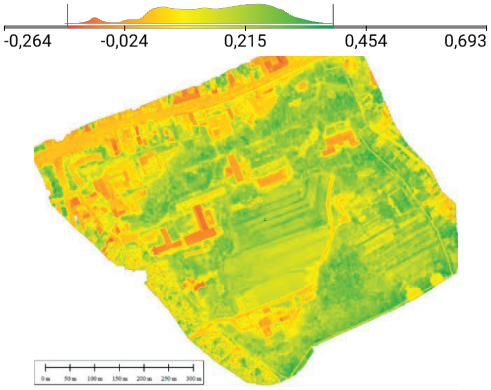



Figure 12. NDRE

In Figure 13 the NDVI applied on the studied area can be seen. High NDVI values (approaching +1) indicate dense, healthy vegetation with abundant chlorophyll content and active photosynthesis. On NDVI maps, these areas are typically displayed in bright green. Moderate NDVI values (around 0) are generally associated with sparse vegetation, grasslands, or areas with relatively low chlorophyll concentrations. These regions are commonly represented by yellow or light green shades. Low NDVI values (approaching −1)

correspond to bare soil, exposed rock, or other non-vegetated surfaces where vegetation is absent. On NDVI maps, these areas usually appear in brown or reddish colours.

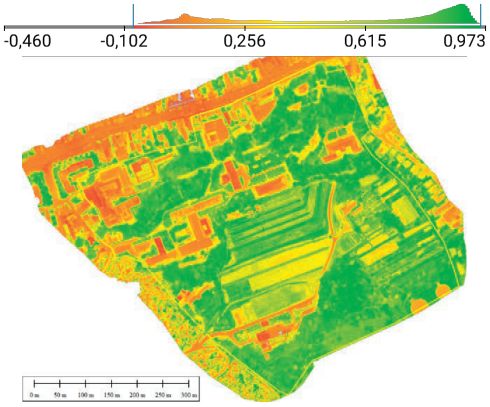



Figure 13. NDVI

The Structure Insensitive Pigment Index 2 (SIPI_2) (Figure 14) evaluates plant stress and pigment composition, particularly the carotenoid-to-chlorophyll ratio. Because it is less influenced by leaf structure, it provides a reliable assessment of vegetation health and photosynthetic performance.

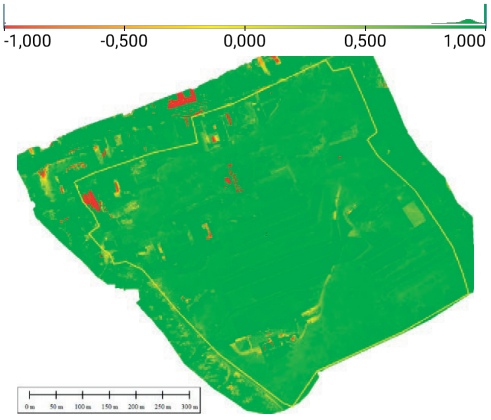



Figure 14. SIPI_2

The predominance of green areas indicates that most of the analysed vegetation is healthy and in good physiological condition.
Mean GNDVI values were calculated for each identified tree crown.
It can be observed that most trees fall within the higher GNDVI value range, indicating a generally good vegetation condition and relatively high chlorophyll content (Figure 15).

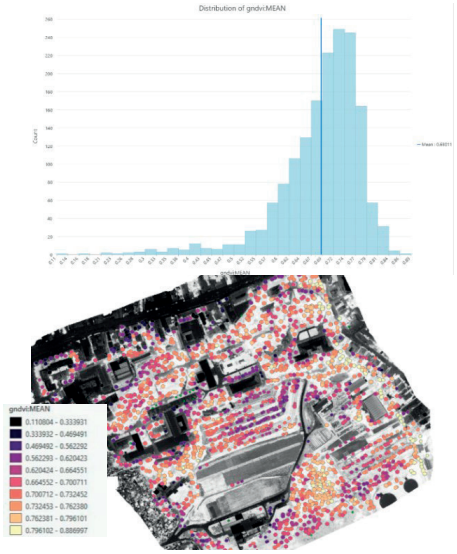



Figure 15. (Up) Mean GNDVI Values per Tree and (Down) Symbology of Mean GNDVI Values per Tree

The distribution of mean LCI values (Figure 16) appears relatively uniform across the study area, with a similar number of trees exhibiting values below and above the overall mean. This pattern suggests a relatively homogeneous distribution of chlorophyll content and vegetation condition among the identified trees.

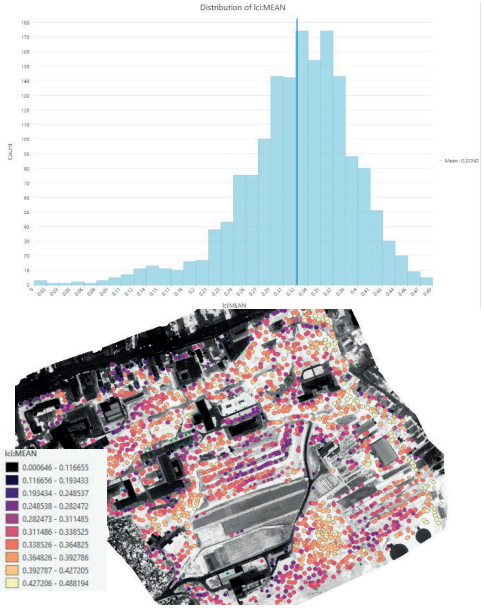



Figure 16. (Up) Mean LCI Values per Tree and (Down) Symbology of Mean LCI Values per Tree

The distribution of MCARI values (Figure 17) indicates that most trees are characterized by values below the overall mean. In addition, the range of values is relatively narrow, resulting in limited differentiation between distinct value classes across the study area.

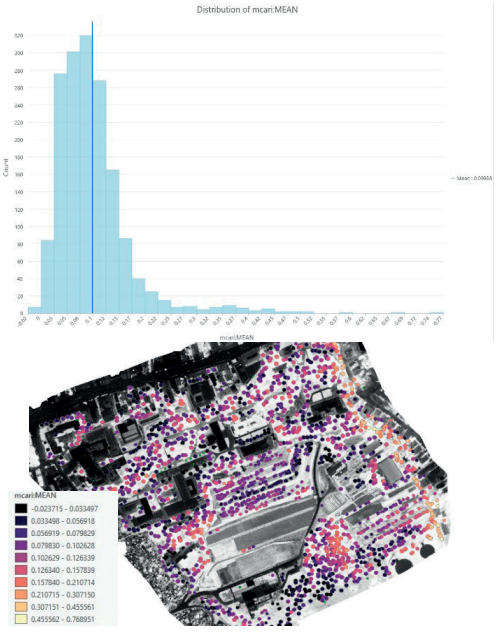
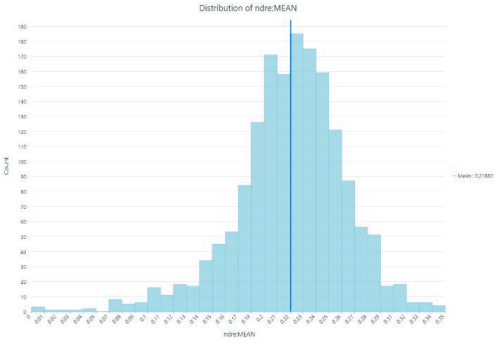



Figure 17. (Up) Mean MCARI Values per Tree and (Down) Symbology of Mean MCARI Values per Tree

The distribution of mean NDRE values (Figure 18) appears relatively uniform across the study area, with a similar number of trees exhibiting values below and above the overall mean.



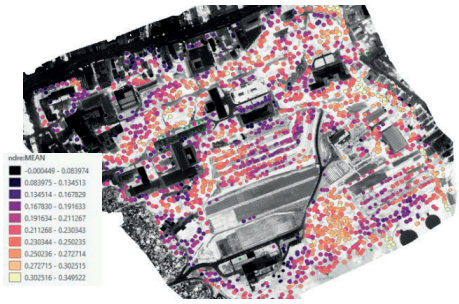
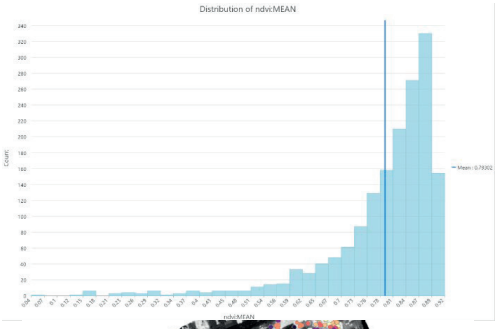




Figure 18. (Up) Mean NDRE Values per Tree and (Down) Symbology of Mean NDRE Values per Tree

The distribution of NDVI values (Figure 19) indicates that the majority of trees exhibit values above the overall mean. This suggests generally healthy vegetation conditions and a high level of photosynthetic activity throughout the study area.



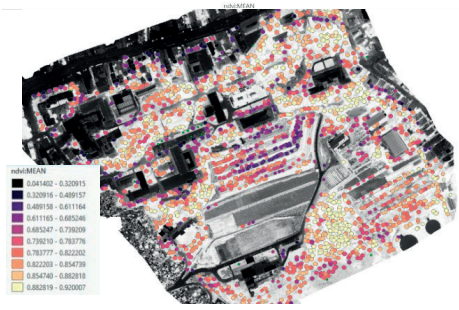




Figure 19. (Up) Mean NDVI Values per Tree and (Down) Symbology of Mean NDVI Values per Tree

The distribution of mean SIPI values (Figure 20) appears relatively uniform across the study area, with a similar number of trees exhibiting values below and above the overall mean.

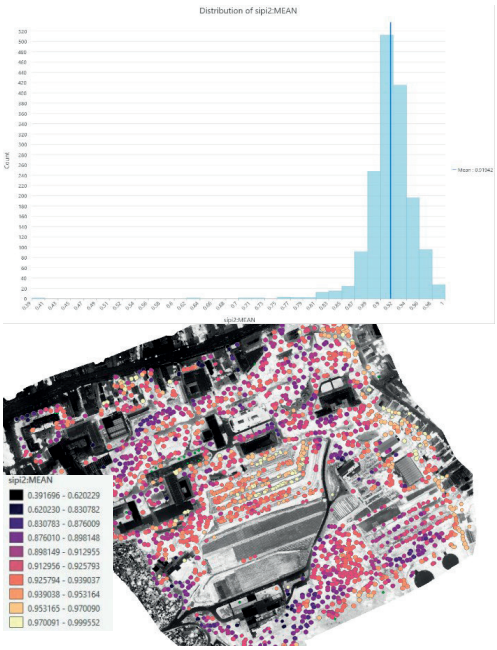



Figure 20. (Up) Mean SIPI_2 Values per Tree and (Down) Symbology of Mean SIPI_2 Values per Tree

All indices have median values close to 0 (distributed between -1 and +1, which also confirms their compliance with the theoretical thresholds), which is expected after standardization (Figure 21).

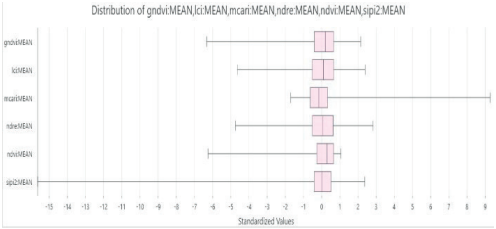



Figure 21. Boxplot Representation of Standardized Vegetation Indices

The boxplots are relatively narrow and similar in size, suggesting that most trees exhibit relatively homogeneous vegetation responses.
The main differences are observed in the length of the whiskers, which indicate the presence of trees with values that differ considerably from the rest of the population. This is most likely due to different species and unique specimens, especially those located within the agro-botanical garden area, although it may also result from canopy delineation errors.

## CONCLUSIONS

The LiDAR survey showed detailed information on both terrain and vegetation structure, thus being able to generate multiple high-value products from a single dataset. The automatic classification successfully separated ground, buildings, and vegetation, while tree and canopy extraction allowed the estimation of key dendrometric parameters, including tree height and crown dimensions.
Although the automated workflow proved efficient for processing large datasets, certain limitations were observed in the matter of canopy delineation, where large crowns were occasionally segmented into multiple individual trees. Nevertheless, the identification of 1,645 trees higher than 2.5 m and the generation of elevation and tree density maps demonstrate the potential of UAV-based LiDAR data for rapid and detailed forest inventory, vegetation analysis, and environmental monitoring.
Based on the images (in the following order: GNDVI → LCI → MCARI → NDRE → NDVI → SIPI2), a visual analysis of the consistency of tree classification can be performed.
There is no perfect correspondence between trees assigned to different classes across all images. The same tree that appears in a high-value class for one index may appear in a medium or even low-value class in another index. This is expected, as each index measures a different aspect of vegetation condition.
A partial correlation can be observed among the indices. Many trees maintain their general trend (high or low values) across several maps; however, they are not classified identically in all cases.
LCI and NDRE – The two maps exhibit a very similar distribution of values, indicating a strong correlation in identifying trees with different chlorophyll levels.
NDVI and GNDVI – Values are distributed similarly across most areas, highlighting a good correlation between vegetation vigor and chlorophyll content.
MCARI – This index reveals more pronounced differences among trees, and its results are only

partially similar to those obtained from NDVI and NDRE.

SIPI2 – The distribution of values differs the most from the other indices, suggesting that it captures distinct physiological characteristics, particularly those associated with vegetation stress.

A potential direction for future research is the correlation of vegetation indices with ground-collected data for tree species identification and condition assessment. By comparing GNDVI, LCI, MCARI, NDRE, NDVI, and SIPI2 values with direct field observations regarding species, health condition, stress level, defoliation, or the presence of degradation symptoms, it may be possible to determine whether certain species exhibit specific spectral signatures and whether they respond differently to stress factors. Such an approach would contribute both to improving species identification and to developing remote sensing–based models for monitoring tree health.

## ACKNOWLEDGEMENTS

This research work was carried out with the support of Ministry of Education and was financed through the CNFIS-FDI-2025-F-0030 project, funded by the National Council for Financing Higher Education (CNFIS).

## USE OF GENERATIVE ARTIFICIAL INTELLIGENCE (GenAI)

The authors declare the use of Generative Artificial Intelligence (GenAI) tools in the preparation of this manuscript. GenAI was used exclusively for language editing and text refinement and for the visual refinement of the sketch in Figure 1, which was previously drafted by the authors. All scientific content, data analysis, and interpretations were developed and verified by the authors.

## REFERENCES

Ali, M., Biswas, A., Iglseder, A., Kumar, V., Kumar, S., Gupta, S., Hollaus, M., Pfeiffer, N., & Lohani, B. (2026). Terrestrial and Airborne Laser Scanning Dataset of Trees in the Shivalik Range, India with Field Measurements and Leaf–Wood Classifications. *Scientific Data*, 13, 420.

Fernández-Guisuruga, J. M., Sanz-Ablanedo, E., Suárez-Seoane, S., & Calvo, L. (2018). Using Unmanned Aerial Vehicles in Postfire Vegetation Survey Campaigns through Large and Heterogeneous Areas: Opportunities and Challenges. *Sensors*, 18, 586.

Goebel, M., & Iwaszczuk, D. (2023). Spectral Analysis of Images of Plants Under Stress Using a Close-Range Camera. *The International Archives of the Photogrammetry, Remote Sensing and Spatial Information Sciences*, XLVIII-1, 63-69.

Goebel, M., & Iwaszczuk, D. (2026). Integrating Multispectral Imagery with Lidar Enhances 3D Mobile Mapping of Vegetation Condition. *Journal of Photogrammetry, Remote Sensing and Geoinformation Science.* https://doi.org/10.1007/s41064-026-00418-6

Hyyppä, E., Hyyppä, J., Hakala, T., Kukko, A., Wulder, M. A., White, J. C., Pyorala, J., Yu, X., Wang, Y., Virtanen, J. P., Pohjavirta, O., Liang, X., Holopainen, M., & Kaartinen. H. (2020). Under-canopy UAV Laser Scanning for Accurate Forest Field Measurements. *ISPRS Journal of Photogrammetry and Remote Sensing*, 164, 41-60.

Guan, S., Fukami, K., Matsunaka, H., Okami, M., Tanaka, R., Nakano, H., Sakai, T., Nakano, K., Ohdan, H., & Takahashi, K. (2019). Assessing Correlation of High-Resolution NDVI with Fertilizer Application Level and Yield of Rice and Wheat Crops using Small UAVs. *Remote Sensing*, 11, 112.

Liang, W., Abidi, M., Carrasco, L., McNelis, J., Tran, L., Li, Y., & Grant, J. (2020). Mapping Vegetation at Species Level with High-Resolution Multispectral and Lidar Data Over a Large Spatial Area: A Case Study with Kudzu. *Remote Sensing*, 12, 609.

Liu, S., Liu, Y., Zhang, X., Tian, B., Zhang, W., Huang, Y., Xie, W., Ke, T., Liu, K., Tao, P., Yao, Q., & Tan, K. (2026). Integrating drone multispectral and LiDAR data with machine learning: toward species-level biomass estimation in heterogeneous salt marsh vegetation. *Geo-Spatial Information Science,* 29(3), 1857-1875. https://doi.org/10.1080/10095020.2025.2574921

Moatăr, M. M., Dragomir, P. I., Salasan, C., Firu-Negoescu, G. A., Stefan, C. M., Panici, P. A., Bora, M., & Scedei, D. N. (2026). Forest Certification and Sustainable Forest Management in Romania—Benefits, Barriers, and a European Comparison. *Sustainability*. 18(18), 9556.

Mohamad, M. A. I., & Tahar, K. N. (2026). Tree Health Assessment Using UAV-Based Multispectral Imagery and NDVI Analysis. *International Journal of Geoinformatics*, 22(1), 38-46.

Rai, K., & Singh, G. (2026). Spatiotemporal Analysis of Forest Disturbance Dynamics in Maharashtra Using Remote Sensing Techniques. *The International Archives of the Photogrammetry, Remote Sensing and Spatial Information Sciences.* XLVIII-4, 73-81.

Șuba, E. E., Sălăgean, T., Pop, I. D., Matei, F., Chiorean, S., Nap, M. E., Sestraș, P., Brumă, S., Sabou, C. S., Păunescu, V., Dan, V.S., & Vakar, F. (2025). Monitoring different grass varieties using multispectral imagery based on different irrigation regimes. *Scientific Papers. Series E. Land Reclamation, Earth Observation & Surveying, Environmental Engineering*, XIV, 1006-1019.

Scientific Papers. Series E. Land Reclamation, Earth Observation & Surveying, Environmental Engineering. Vol. XV, 2026
Print ISSN 2285-6064, CD-ROM ISSN 2285-6072, Online ISSN 2393-5138, ISSN-L 2285-6064

# DEFORESTATION PREDICTIONS IN NORTHERN ROMANIA USING LONG SHORT-TERM MEMORY NEURAL NETWORKS

**Adina NITULESCU**

Polytechnic University of Timisoara, 300006, Timisoara, Romania

Corresponding author email: adina.nitulescu@upt.ro

***Abstract***

*Forests are among Earth's most important ecosystems, but unfortunately are vanishing at alarming rates. Thus, deforestation is a global challenge with serious impacts. This paper utilizes Google Earth Engine Landsat data, together with climatic and land-cover data in order to predict the annual deforestation rate in Suceava County. This is being accomplished by using deep learning techniques, more precisely by using Long Short-Term Memory Neural Networks in order to forecast the land changes. These offer distinct advantages in handling time-series data with long-term dependencies, thus making them particularly suitable for tracking changes in vegetation over time. The results have shown an average prediction of 0.45% tree cover loss every year for the next 10 years timeframe. Deforestation studies in Romania have largely focused on spatial analysis but predictive temporal modelling using LSTM remained underexplored. By leveraging the collected data, the paper demonstrates how deep learning techniques can enhance the monitoring and forecasting of forest loss, supporting more sustainable forest management and policy-making. Integrating such approaches could pave the way to anticipating risk and protecting high risk zones before deforestation occurs.*

***Key words****: climate protection, deep learning, deforestation, predictions.*

## INTRODUCTION

An important portion of the EU's biodiversity value forests lies in Romania, but unfortunately this wealth is not being protected enough. Romanian forests occupy around 6.5 million hectares, which translates to approximately 29% of the national territory (Romanian Ministry of Environment, Waters and Forests, 2023). Nowadays, thousands of hectares of forests have been logged and thus, it has emerged as a major environmental concern over the past three decades. Their symbolic value is as important as their ecological and economical one. It is being believed that up until today, illegal logging has cost Romania more than 5.7 billion dollars since the fall of the communism (Lawrence, 2015). One prime example is Suceava County in North-Eastern Romania, which has experienced significant tree-cover loss in the last few decades and which exhibits one of the highest levels of forest loss in Romania (Global Forest Watch, 2025). Yet there are no widely published, formal predictive models specifically for this county deforestation rates in the next 5-20 years available in popular sources. Using deep learning models, Suceava County can be modeled as a high-risk deforestation region, with predictions strongly influenced by past logging intensity, accessibility and climate stress.

Traditional deforestation monitoring methods rely heavily on satellite observation and manual interpretation, which can be time-consuming and less effective for early detection. Recent advances in machine learning, particularly Long Short-Term Memory (LSTM) neural networks, have made it possible to model and predict temporal patterns in environmental data. This study explores how LSTM-based models can be applied to Romanian forest data to predict future deforestation trends. As the drivers of deforestation are usually non-linear and heterogenous, neural networks might help overcome these challenges as they are very good at capturing non-linear functional forms and heterogeneity.

Romania's forests are among the most extensive and biologically diverse in Europe (European Environment Agency, 2024). Figure 1 presents an overview of the current deforestation status in all the EU countries. However, deforestation is not a problem for these countries as overall, Europe is experiencing a net reforestation.

Land-use change in Romania, particularly deforestation accelerated in the past few

decades. In Eastern Europe, land cover and use changes are a consequence of the combined conflict of economy and nature (Gurung et al., 2009). In order to analyze this and look at potential trends, spatially explicit land-use changes must be scale sensitive (Veldkamp et al., 2001; Lausch et al., 2015). Even though these forests are recognized for their exceptional diversity and vital roles in carbon storage, biodiversity conservation and sustainable resource management, the predictions for deforestation are alarming, with a significant amount of natural forest loss and a requirement for reforms to combat the underlying issue (Bohateret, 2012). This is being combined with a degradation of the land, as a result of irrational use of land resources, the abandon or even destruction of improvement systems as well as low fertization of agricultural land (Bălteanu & Popovici, 2010).

Thus, deforestation represents a critical environmental issue in Romania which needs rapid intervention and closer monitoring practices.

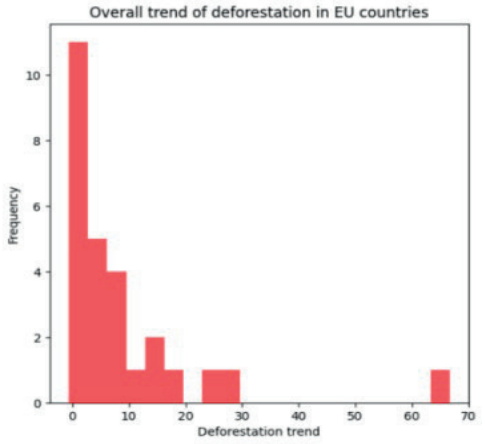



Figure 1. Overall trend of deforestation in EU

The use of AI's predictive power in deforestation forecasting represents a hot topic worldwide. This artificial intelligence enabled tools enable authorities to intervene before forest cover loss happens, providing a useful and reliable tool of real time monitoring and analysis. Similar tools have already been used by authorities in 6 countries but plans are already being developed in order to extend the usage of the AI tools to 12 countries by 2027. The Forest Foresight Model, developed by dutch scientists together with partners from Amazon Web Services aims to predict illegal deforestation up to six months before it occurs (WWF, n.d.). Also, artificial intelligence methods are embedded in platforms such as Google Earth Engine, where the satellite images are being analyzed using machine learning approaches, as well on the Global Forest Watch platform which provides real-time alerts of deforestation activities. These examples reinforce the need and importance of incorporating AI-powered systems in order to diminuate world forest loss (Chatrabhuj & Meshram, 2024).

This paper presents a methodological framework for predicting deforestation trends in Romania using Long Short-Term Memory (LSTM) neural networks. By leveraging satellite imagery, climatic variables, and land-cover data, the study demonstrates how deep learning techniques can enhance the monitoring and forecasting of forest loss, supporting more sustainable forest management and policy-making.

## MATERIALS AND METHODS

The shift from simply monitoring what's already gone to forecasting what is at risk in the future represented a breakthrough moment. Nowadays, predicting deforestation using machine learning has become a growing field. Previous studies have employed algorithms such as Random Forests, Support Vector Machines, and Convolutional Neural Networks (CNNs) on remote-sensing data. In this paper, a linear regression model has also been employed in order to forecast forest cover tree loss (Figure 2).

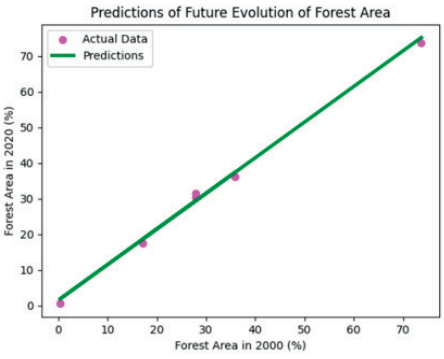



Figure 2. Forest cover loss forecast

Artificial intelligence driven deforestation prediction offers a numerous advantage over traditional monitoring techniques. By allowing less human participation for large-scale prognostic and research, it enables better and more accurate results.

The dataset used in this study includes: Landsat satellite images, collected between 2001 and 2024, vegetation indices, climatic variables, such as temperature, precipitation and soil moisture data as well as land cover data. Images are pre-processed through cloud masking, normalization, and temporal alignment. NDVI time-series are generated for each 1 km² grid cell. The dataset is then divided into training (70%), validation (15%), and test (15%) sets.

Neural networks are computational models of the brain. Artificial neurons are interconnected by edges, forming a neural network. Similar to the brain, the network receives input, internal processes such as activations of the neurons take place and the network yields output. Although these neural networks have a long history of research which dates back to 1943, the number of researchers involved was very small for the first 40 years. It was in 1983 that the funding of neural networks research began being funded in the US.

LSTM networks, a type of Recurrent Neural Network (RNN), offer distinct advantages in handling time-series data with long-term dependencies and are particularly suitable for tracking changes in vegetation over time. Deep learning is a sub-type of machine learning that uses deep neural networks to learn patterns from large amounts of data automatically. For deforestation detection, deep learning models can understand complex image features related to deforestation. Thus, more accurate detection results can be produced as a result (Yu et al., 2020). The collected and analyzed data for Suceava Country, Romania is between 2001 and 2024. Figure 3 presents the percentage of cover tree loss for the above-mentioned period of time.

Romanian forests display considerable variability, covering a broad spectrum of forest types, management approaches, and ecological characteristics, making them representative of wider European forest conditions. Deforestation is fundamentally a human process fuelled by a complex mixture of economic, political, and environmental factors (Malek et al., 2018; Rădulescu et al., 2022).

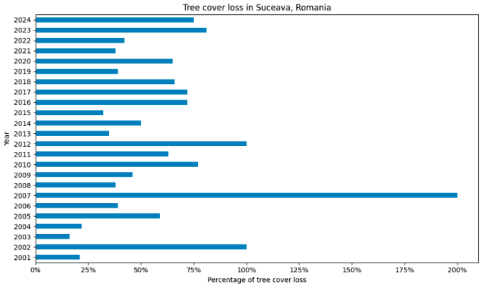



Figure 3. Tree cover loss 2001-2024 in NE Romania

Predicting deforestation is important for targeting interventions and for impact evaluation. Deforestation in general can have serious effects on the quality of life, such as: it worsens air pollution, affects biodiversity, disrupts water cycle and can even increase the risk of a pandemic. Deforestation has been proven to increase the risk of emergence of new diseases, as exemplified for the recent COVID-19 pandemic (Singhal et al., 2024). Predicting the location and timing of future loss is thus incredibly difficult (Cheval et al., 2022). In our paper, we solve this by utilizing Google Earth Engine data, together with climatic and land-cover data in order to provide accurate predictions for the analyzed region. Google Earth Engine is a cloud-based geospatial analysis platform that enables users to visualize, analyze and download satellite images. On top of providing raw imagery, Earth Engine contains several collections of associated data: SR, BAI, EVI, NBR, NDVI, and NDWI at 8-day, 32-day, and annual cadences, allowing for more in-depth analysis (Table 1). Google Earth's capabilities are further enhanced by GEE, which provides on-demand access to a large collection of remote sensing data, allowing for an in-depth and reliable analysis.

The data has been statistically processed and interpreted by building the trend line and setting up the forecast based on simulation models for the period 2025-2035. In Suceava, Romania, the annual deforestation rate has been significant in the past, with a loss of 1.1 kha of natural forest in 2024 only and thus represents a county of major interest.

Table 1. Vegetation indices, formula and description

| Index | Formula | Description |
|---|---|---|
| Normalized Difference Vegetation Index (NDVI) | $NDVI = \frac{(NIR - Red)}{(NIR + Red)}$ | Measures vegetation health by comparing NIR reflectance (healthy vegetation) with Red reflectance (chlorophyll absorption). Chosen for its widespread use in assessing vegetation cover and health |
| Shadow Index (SI) | $SI = (1 - Blue) \times (1 - Green) \times (1 - Red)$ | Custom index to detect shadowed areas in forests using visible bands. Selected to differentiate shadows from water and dark surfaces. |
| Enhanced Vegetation Index (EVI) | $EVI = \frac{(NIR - Red) \times 2.5}{(NIR - 6Red - 7.5Blue + 1)}$ | Enhances sensitivity to dense vegetation, reducing soil and atmospheric effects. Effective in monitoring forest canopy health. |
| Burn Area Index (BAI) | $BAI = \frac{1}{((0.1 - Red)^2 + (0.06 - NIR)^2)}$ | Highlights post-fire areas by assessing the spectral difference from charcoal reflectance. |
| Normalized Burn Ratio (NBR) | $NBR = \frac{NIR - SWIR}{NIR + SWIR}$ | A climatic index used to highlight burnt areas in large fire zones. |

## RESULTS AND DISCUSSIONS

As a summary, from 2001 to 2024, Romania lost around 6.0% of the 2000 tree cover area. Particularly for Suceava County, it meant a total loss of 15% from the 2000 tree cover area. Thus, Suceava County stands out as being one of the most extensively deforested areas in Romania.
The yearly forecast from 2025 to 2035 is approximately 0.45% forest cover loss for each subsequent year. The model predicts a prolongation of the incremental trend in deforestation. It represents a starting point and invites us all to take preventive actions in order to reduce the potential adverse effects deforestation has for the general population.
In this paper, a neural network, specifically the Long Short-Term Memory Neural one has been employed, together with 2001-2024 data in order to predict the deforestation trend in 2025-2035. Long Short-Term Memory Neural Networks have been specifically used for modelling the temporal data of deforestation (Hochreiter & Schmidhuber, 1997).
The LSTM model architecture is presented below in Figure 4.

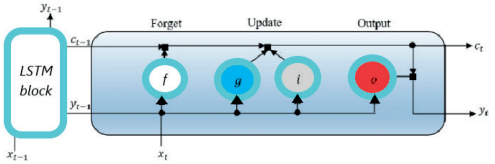



Figure 4. LSTM model architecture

The Long Short-Term Memory (LSTM) architecture is composed of linear units that include a self-recurrent connection with a constant weight of 1.0. This design enables values during the forward pass, as well as gradients during the backward pass, to be retained within the self-recurrent unit and accessed at the appropriate time step. Through this unit multiplier, the output or error from the previous time step is directly propagated to the subsequent time step. As a result, this self-recurrent unit, referred to as the memory cell, is able to store information over long temporal intervals, spanning dozens of time steps.
In our case, we have: one input layer represented by sequential NDVI and climatic data for each pixel, two hidden layers with 64 and 32 units, followed by dropout for regularization, a dense output layer represented by a sigmoid activation predicting the probability of deforestation occurrence in the next year, a binary-entropy loss function and as optimizer, Adam with a learning rate of 0.0001. The model's performance is assessed by using evaluation metrics described in Table 2.

Table 2. Evaluation metrics

| Model name | Accuracy | Precision | Recall | AUC |
|---|---|---|---|---|
| LSTM | 0.848169 | 0.848169 | 0.848169 | 0.950000 |

A variety of metrics can be employed to assess a model's performance, typically based on the counts of true positives (TP), true negatives (TN), false positives (FP) and false negatives (FN). One widely used evaluation tool is the Receiver Operating Characteristic (ROC) curve that has been plotted in order to evaluate classification performance (Figure 5). The ROC curve is a visual representation of model performance across all thresholds. It is drawn by calculating the true positive rate (TPR) and false positive rate (FPR) at every possible threshold (in practice, at selected intervals), then graphing TPR over FPR.

The trained LSTM model demonstrates high predictive accuracy, particularly in identifying high-risk zones in the Northern Eastern region of Romania and predicting the forest cover loss for the next 10 years timespan.

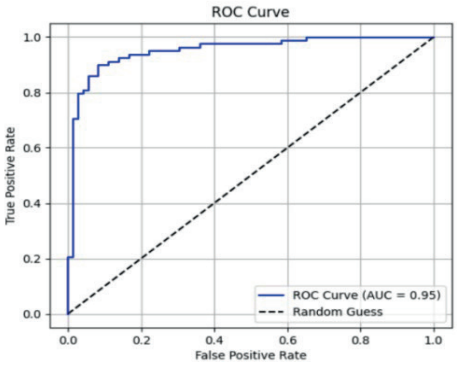



Figure 5. ROC-AUC curve

Areas in Suceava county especially show elevated predicted probabilities of deforestation due to intensive logging and road development. The model's time-series capability allows it to detect early NDVI declines indicative of forest degradation, even before clear-cutting occurs. Compared to the linear regression static model, the LSTM achieved a 10% improvement in F1-score. However, limitations include uneven data quality across regions and the difficulty of distinguishing legal from illegal logging activities. The area under the ROC curve (AUC) represents the capability of the model. The obtained value (0.95) highlights the great power and capability of the model and offers promises. In order to balance the deforestation, several countries bet on reforestation.

Figure 6 presents the differences in forest-cover distribution across European countries in 2000 and 2020, respectively.

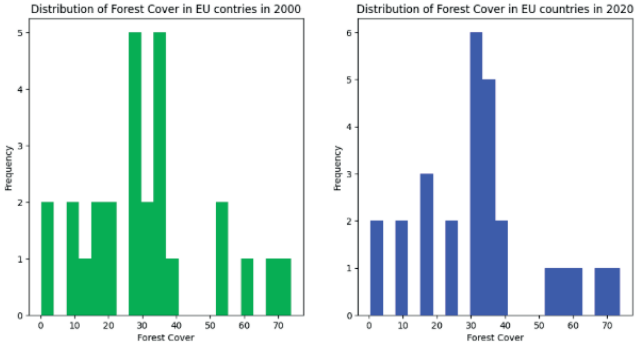



Figure 6. Distribution of Forest Cover in EU countries

Unfortunately, the reforestation trend has been going downwards lately in Romania, as last year (2024) it saw a decrease in forest regeneration efforts, with a total of 25,579 hectares reforested.

## CONCLUSIONS

Urgent attention must be paid to the problem of deforestation. However, Romanian forests face big challenges in being efficiently monitored at national scale. Thus, forecasts of deforestation risk could be a vital tool for prevention and protecting nature. Combining data collection, mapping and artificial intelligence approaches, the paper seeked to provide a 10-year overview of forest changes, a case study on the Suceava County in Northern Romania. The findings, exemplified by the percentage and impact of tree cover loss, can guide broader efforts to identify and address dangerous changes in forest cover.

This study demonstrates the feasibility and effectiveness of using LSTM networks for deforestation prediction in Romania. By analyzing temporal trends in vegetation indices and environmental factors, the model provides valuable foresight into forest loss dynamics. Future work should focus on integrating real-time data streams, expanding spatial resolution, and combining deep learning with socio-economic modelling for a more comprehensive understanding of deforestation drivers. These results provide useful insights for a better monitoring system and possible measures to be taken in advance by authorities in order to

prevent cover tree loss. This work lays the foundations of a deforestation prediction model for municipalities of Romania that combines dense neural and LSTM networks. Ultimately, this paper represents a major step forward in harnessing the power of artificial intelligence in forest monitoring and offers a pathway for better global efforts in preserving natural resources in the long-term.

## REFERENCES

Bălteanu, D., & Popovici, E. A. (2010). Land use changes and land degradation in post–socialist Romania. *Romanian Journal of Geography, 54*(2), 95–105.

Bohateret, V. M. (2012). Readjusting Romania's forestry policy with a view to the year 2050. *Journal of Settlements and Spatial Planning, 1,* 27–42.

Chatrabhuj, K., & Meshram, K. (2024). Design of an efficient satellite image analysis model for identification of sustainable construction area via ground subsidence monitoring and infrastructure moonitoring operations. *Indian Geotech. J. 54*(3), 1136-1151.

Cheval, S., Bulai, A., & Croitoru, A-E., Dorondel, S., Micu, D., Mihăilă, D., Sfîcă, L., & Tișcovschi, A. (2022). Climate Change Perception in Romania. *Theor. Appl. Clim., 149, 253-272.*

European Environment Agency (EEA). (2024). *Romania: Forest and Biodiversity Report.*

Global Forest Watch. (2025). *Suceava, Romania Deforestation Rates & Statistics,* https://www.globalforestwatch.org/dashboards/country/ROU/36

Gurung, A.B., Bokwa, A., Chelmicki, W., Elbakidze, M., Hirschmugl, M., Hostert, P., Ibisch, P., Kozak, J., Kuemmerle, T., Matei, E., Ostapowicz, K., Pociask-Karteczka, J., Schmidt, L., van der Linden, S., & Zebisch, M. (2009). Global change research in the Carpathian Mountain region. *Mt. Res. Dev.* 29, 282-288.

Hochreiter, S., & Schmidhuber, J. (1997). Long Short-Term Memory. *Neural Computation*. *9*(8), 1735–1780.

Lausch, A., Blaschke, T., Haase, D., Herzog, F., Syrbe, R.-U., Tischendorf, L., & Walz, U. (2015). Understanding and Quantifying Landscape Structure—A Review on Relevant Process Characteristics, Data Models and Landscape Metrics. *Ecol. Model.* 295, 31–41.

Lawrence, P. (2015) Romania acts to save forests from logging spree, *BBC* News, https://www.bbc.com/news/world-europe-33517854,

Malek, Ž., Zumpano, V., & Hussin, H. (2018). Forest management and future changes to ecosystem services in the Romanian Carpathians. *Environment Development and Sustainability*, *20*(3), 1275–1291.

Rădulescu, C. V., Bran, F., Ciuvăț, A. L., Bodislav, D. A., Buzoianu, O. C., Ștefănescu, M., & Burlacu, S. (2022). Decoupling the Economic Development from Resource Consumption: Implications and Challenges in Assessing the Evolution of Forest Area in Romania. *Land. 11(7)*, 1097.

Romanian Ministry of Environment, Waters and Forests. (2023). *National Forest Inventory Report*.

Singhal, V., Jinger, D., Rathore, A.C., Pal, R., Samal, I., Bhoi, T.K., Paramesh, V., Fahad, S., Jaremko, L., Abdelsalam, N.R., & Jaremko, M. (2024) COVID-19, Deforestation, and Green Economy. *Front. For. Glob. Chang.*, 6, 1305779.

Veldkamp, A., Verburg, P. H., Kok, K., de Koning, G. H. J., Priess, J., & Bergsma, A. R. (2001). The need for scale sensitive approaches in spatially explicit land use change modelling. *Environmental Modeling and Assessment, 6*, 111–121.

World Wide Fund for Nature (WWF). (n.d.). *Forest Foresight: technology for early action against deforestation.* https://www.wwf.org.ec/?392413/Forest-Foresight-technology-for-early-action-against-deforestation

Yu, H., Ni, W., Zhang, Z., Sun, G., & Zhang, Z. (2020). Regional forest mapping over mountainous areas in northeast China using newly identified critical temporal features of Sentinel-1 backscattering. *Remote Sens.* 12(9), 1485.

Scientific Papers. Series E. Land Reclamation, Earth Observation & Surveying, Environmental Engineering. Vol. XV, 2026
Print ISSN 2285-6064, CD-ROM ISSN 2285-6072, Online ISSN 2393-5138, ISSN-L 2285-6064

# THE ALTGORITHMIC LANDSCAPE OF AI BASED LAND USE INTERPRETATION

**Ioana Delia POP[1], Tudor SĂLĂGEAN[1], Mircea-Emil NAP[1], Elemer-Emanuel ȘUBA[1], Cristian MALINAS[1], Lucia-Adina TRUTA[1], Silvia CHIOREAN[1], Ferenc KAITAR[1], Adela-Maria NEAG[2], Florica MATEI[1]**

[1]University of Agricultural Sciences and Veterinary Medicine Cluj-Napoca, 3-5 Calea Mănăștur, 400372, Cluj-Napoca, Romania
[2]Technical University of Civil Engineering of Bucharest, 122-124 Lacul Tei Blvd, District 2, Bucharest, Romania

Corresponding author emails: faldea@usamvcluj.ro, adela-maria.neag@phd.utcb.ro

***Abstract***

*This study investigates the application of Artificial Intelligence (AI) techniques in land cover classification based on satellite imagery, with the objective of improving the accuracy and efficiency of traditional geospatial workflows. The research evaluates how conventional Geographic Information System (GIS) procedures can be enhanced through the integration of machine learning algorithms, particularly those designed for raster segmentation and automated image classification. A comparative analysis between classical supervised methods and AI-based approaches was conducted to detect land use and land cover (LULC) changes in the city of Satu Mare using multitemporal satellite data. Results show that AI-driven models offer improved classification consistency and reduced manual processing efforts. The results underline the relevance of AI-assisted image interpretation for land monitoring and its potential contribution to sustainable spatial planning. The proposed approach can be transferred to similar LULC studies.*

***Key words****: Artificial Intelligence, automated classification, land use and land cover (LULC), satellite imagery, urban expansion.*

## INTRODUCTION

Land use and land cover (LULC) dynamics are the indicator of human pressure on land resources and a major driver of environmental change with direct implications for agriculture, soil functions, and ecosystem services. Sustainable land management requires accurate and timely monitoring of land cover (LC), especially in rapidly evolving urban areas (Vitale & Lamonaca, 2026).

Urban expansion and peri-urban development often compete with agricultural land through land take, fragmentation, and the conversion of open or cultivated areas into sealed surfaces. These processes can alter infiltration and runoff regimes, reduce soil water storage capacity, and constrain the long-term productivity and resilience of agroecosystems. Recent European assessments underline soil sealing and land occupation as persistent and relevant pressures linked to spatial development, reinforcing the need for robust monitoring tools that can support sustainable land management and evidence-based planning (Arias-Navarro et al., 2024).

Earth observation (EO) provides an operational framework for consistent and repeatable LULC monitoring across large areas and multi-annual time spans. Among currently available EO missions, Sentinel-2 multispectral imagery offers a well-balanced combination of spatial resolution (10-20 m), revisit frequency, and spectral capability, enabling the detection and mapping of heterogeneous land-cover patterns.

Multitemporal analyses derived from such imagery can capture trajectories of change (e.g., densification, conversion of open land into built-up areas, or shifts between vegetated and non-vegetated surfaces) when acquisition dates are chosen to minimize seasonal bias. In the underlying study that informs this paper, Sentinel-2 imagery acquired in July 2017, July 2019, and July 2024 was selected to improve cross-year comparability and reduce confounding seasonal effects.

Conventional GIS LULC mapping typically relies on supervised classification algorithms (e.g., Random Forest/Random Trees, Support Vector Machines), supported training samples

and post-classification refinement. While these approaches remain widely used and can provide reliable outputs under appropriate conditions, their performance is often sensitive to training-sample representativeness and to class separability. This limitation becomes particularly pronounced in urban and peri-urban settings where spectral mixing, shadowing, and material heterogeneity increase confusion between classes (e.g., bare soil vs. construction surfaces; bright roofs vs. exposed ground).

In the Satu Mare case study, the baseline workflow required iterative training-sample refinement to mitigate overlaps between "bare soil" and "construction zones" and to address localized reflectance anomalies (e.g., highly reflective surfaces) that can propagate classification noise.

In recent years, Artificial Intelligence (AI), and especially deep learning (DL), has advanced LULC mapping by enabling models to learn complex spectral and spatial reform imagery. Unlike pixel-wise classifiers that often treat observations independently, DL methods can exploit contextual information (texture, morphology, neighbourhood structure), which tends to improve thematic consistency and reduce the characteristic "salt-and-pepper" effect in heterogeneous landscapes (Hurskainen et al., 2019).

A comprehensive review in Remote Sensing of Environment highlights how DL has accelerated urban land use mapping in scale, automation, and accuracy, particularly when integrated with modern geospatial data ecosystems (Li et al., 2024). Within DL, semantic segmentation has become a particularly relevant paradigm for EO-based LULC mapping because it produces dense, pixel-level predictions while implicitly capturing spatial structure. Recent empirical comparisons of segmentation architectures (e.g., U-Net, DeepLabV3+) demonstrate strong performance for multi-class land-cover tasks and suggest meaningful gains in both accuracy and robustness across diverse geographic contexts (Deressu et al., 2025). Furthermore, methodological work emphasizes that careful use of spectral information (including band-selection strategies) can strengthen segmentation outputs in applications relevant to urban planning and land-use management (Jia et al., 2024). Despite these advances, the practical adoption of AI in applied LULC monitoring still raises questions regarding labelling requirements, generalization across years and acquisition conditions, and integration into established GIS workflows.

This paper investigates how traditional Geographic Information System (GIS) LULC workflows can be enhanced through Artificial Intelligence approaches for raster segmentation and automated image classification. A comparative analysis is conducted between a classical supervised method implemented in a GIS environment and AI based approaches using multitemporal Sentinel-2 imagery for the municipality of Satu Mare, Romania. To ensure cross-temporal comparability, we employed a consistent four-class LULC classification scheme represented in Figure 1, for all acquisition years.

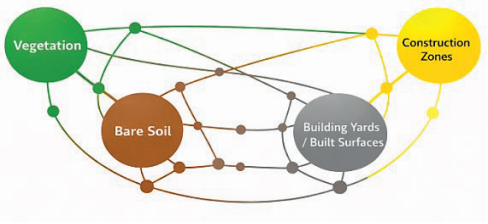



Figure 1. Land Cover classes

The study aims to evaluate improvements in classification consistency, quantify the reduction of manual effort linked to iterative training and correction, and to propose a transferable workflow for comparable LULC monitoring tasks at the urban and agricultural interface.

## MATERIALS AND METHODS

### *Study Area*

The selected case study is the municipality of Satu Mare, located in north-western Romania, in Satu Mare County, near the national borders with Hungary and Ukraine. The city is situated along the Someș River, mainly on its right bank, at approximately 47°47′24″ N latitude and 22°53′24″ E longitude. Positioned at an average altitude of about 126 m, Satu Mare lies within the lower floodplain of the Someș River, in a predominantly lowland area characterized by flat terrain.

Covering an area of approximately 120 km², Satu Mare represents an important administrative, economic, and cultural centre in the

north-western part of the country. Its geographical location, about 13 km from the border with Hungary and around 27 km from the border with Ukraine, provides the city with a strategic role as a connection point between different regions and cultural influences.
Therefore, understanding the spatial and urban evolution of Satu Mare is important for supporting future development strategies and planning, as illustrated in Figure 2.

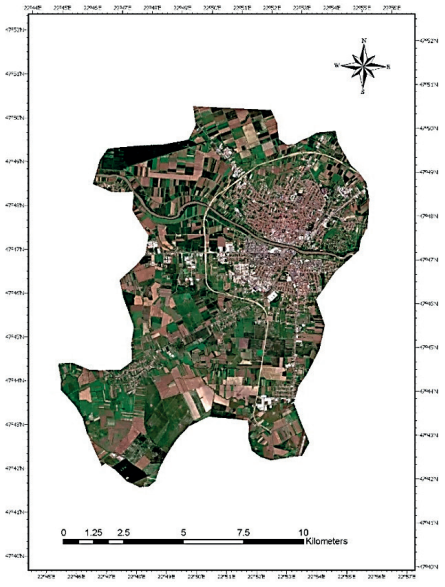



Figure 2. Localization of study area

***Evolution of AI in land cover mapping***

The methodological evolution of land use and land cover classification reflects a broader transformation in remote sensing, from conventional GIS image interpretation toward automated and data driven geospatial workflows. This transition is particularly relevant for multitemporal urban studies, where the objective is not limited to producing thematic maps, but also involves the consistent detection of spatial changes across different time periods. In the present study, focused on the city of Satu Mare, A.I is therefore approached as a complementary component of the GIS workflow, supporting the improvement of classification consistency, processing efficiency, and methodological transferability.
Classical supervised classification methods continue to provide an important basis for satellite image interpretation because they are relatively transparent, operational, and widely implemented in GIS environments. However, their performance may decrease in heterogeneous areas, where built-up surfaces, vegetation, agricultural land, bare soil, and water bodies can present overlapping spectral responses.
Recent comparative research confirms that urban LULC classification remains challenging because landscape heterogeneity directly influences feature extraction and model reliability. For this reason, comparative evaluations between traditional classifiers, machine learning algorithms, and deep-learning approaches are increasingly used to identify robust classification strategies for urban environments (Chowdhury, 2024).
The first major stage in the transition toward AI and LULC is represented by machine learning methods such as Random Forest, Support Vector Machine, and Artificial Neural Networks. These approaches are able to model nonlinear relationships between satellite-derived predictors and land cover categories more effectively than many conventional statistical methods. Their relevance is especially important in multitemporal studies, where the classification model must maintain stable performance across images acquired in different years. In this sense, machine learning contributes not only to classification accuracy, but also to the reproducibility of the change-detection workflow.
A further methodological development is represented by segmentation and object classification. Unlike the pixel methods, which classify each pixel independently, segmentation approaches group neighbouring pixels into spatially meaningful units before classification (Ma et al., 2020). This is particularly useful in urban and mixed landscapes, where land cover categories are often better represented as objects or patches rather than isolated pixels. More recently, deep learning has introduced a significant shift in classifications, by enabling automated feature extraction directly from remote sensing data. Instead of relying mainly on manually selected bands, indices, or predefined rules, deep-learning models can learn hierarchical spatial and spectral patterns from the imagery itself. This capacity is particularly

relevant for heterogeneous urban and peri-urban environments such as Satu Mare, where land-cover classes may vary in shape, texture, density, and spectral behaviour.

Recent reviews emphasize the growing role of deep learning in LULC classification using multispectral and hyperspectral Earth-observation data, while also noting persistent challenges related to training data availability, ground-truth quality, spatial resolution, and sensor-specific characteristics (Vali et al., 2020). Within this context, semantic segmentation is particularly important because it links classification with the spatial delineation of land-cover units. For raster LULC mapping, the objective is not only to assign thematic labels, but also to represent the spatial extent and configuration of land cover classes in a form suitable for change detection (Deressu et al., 2025). At a broader operational scale, AI has also evolved toward large area and frequently updated monitoring systems. Dynamic World is a relevant example of this development, providing near-real-time global LULC predictions at 10 m spatial resolution from Sentinel-2 imagery through a deep-learning workflow. Such products illustrate the movement from isolated map production toward continuous land-monitoring systems capable of supporting flexible temporal analysis and rapid interpretation of landscape change (Brown et al., 2022).

For the present research, this evolution provides the methodological foundation for comparing classical supervised GIS classification with AI assisted approaches in the multitemporal analysis of LULC change in Satu Mare. The purpose is not to replace GIS, but to enhance the geospatial workflow through greater automation, reproducibility, and classification stability. This is particularly important in urban and peri-urban change detection, where errors in individual classified maps may propagate into the final change analysis if the outputs are not produced and validated through a consistent methodological framework.

Therefore, AI classification must be supported by rigorous accuracy assessment. In LULC studies, the reliability of the final interpretation depends on the classification model, but also on the quality of reference data, sampling strategy, validation design, and the interpretation of accuracy indicators derived from the error matrix (Stehman & Foody, 2019). Consequently, the transition from classical GIS classification to AI can be understood as a progression toward more automated and reliable land monitoring workflows. In the case of Satu Mare, this approach supports the evaluation of how AI raster segmentation and automated image classification can improve the detection of land cover transformations.

***Data acquisition***

Nowadays, remote sensing applications rely on a wide range of satellite systems and observation platforms, each providing specific spatial, spectral and temporal perspectives of the Earth's surface. These multisource satellite observations, characterized by different levels of spectral and spatial detail, play an essential role in understanding landscape dynamics and monitoring land use and land cover transformations over time (Dong et al., 2020).

The methodological workflow presented in this study supports the analysis of AI land use interpretation by using Sentinel-2 satellite imagery acquired for three reference years: 2017, 2019 and 2024. The proposed approach highlights how artificial intelligence models can improve classification consistency and reduce the limitations of conventional manual geospatial procedures. By integrating multitemporal Sentinel-2 data with GIS preprocessing and AI assisted classification, the methodology provides a structured framework presented in the following Figure 3, for detecting and comparing land use and land cover changes across the selected study area.

***Sentinel-2***

The Sentinel-2 satellite constellation provides multispectral imagery composed of 13 spectral bands covering the visible, near-infrared and shortwave-infrared regions of the electromagnetic spectrum. With spatial resolutions of 10 m, 20 m and 60 m, depending on the spectral band, and a high temporal revisit frequency, Sentinel-2 data represent a valuable compromise between spatial detail, spectral information and temporal availability.

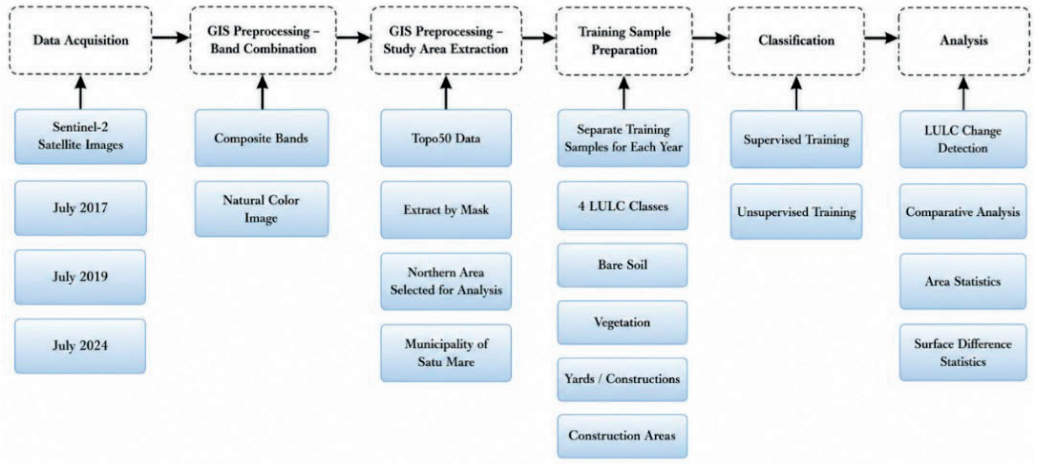



Figure 3. Worflow for AI land use interpretetion using multitemporal Sentinel-2 data in GIS

These characteristics make Sentinel-2 particularly suitable for land use and land cover mapping, especially in studies based on multitemporal image classification and comparative analysis (Vrieling et al., 2018; Rapinel et al., 2019; Le Dez et al., 2021).

In this context, remote sensing provides an efficient and reliable tool for identifying, mapping and monitoring landscape features, as well as areas affected by spatial transformation.

The analysis focuses on three reference years: 2017, 2019 and 2024 and evaluates different classification approaches in order to compare the resulting spatial patterns and highlight the main changes identified within the study area.

The satellite images used in this study were downloaded from the Copernicus platform. For the multitemporal comparative analysis, Sentinel-2 datasets were selected from dates as close as possible within the same month, but from different years, in order to minimize seasonal variations and ensure a more reliable comparison between the analysed periods. The selected images correspond to July and were chosen with 0% cloud cover so that the land surface features would not be obstructed. This selection criterion was important for improving the visual and spectral distinction between the land use and land cover classes used in the supervised classification process.

The Sentinel-2 products were downloaded in *. *safe* format, as this structure preserves the original satellite data and provides access to the complete set of spectral bands available at different spatial resolutions. Therefore, the extension format offered the necessary data quality and completeness for the subsequent preprocessing stages.

***GIS Preprocessing***

As presented in the Data Acquisition subsection in Figure 3, the GIS preprocessing stage was structured into two main components:

1. ***Band combination***;
2. ***Study area extraction*** - which involves the extraction of the study area based on official administrative boundary data.

These preprocessing steps were necessary to prepare the Sentinel-2 imagery for visual interpretation, supervised classification and subsequent comparative land use analysis.

For the first component, the Sentinel-2 datasets were imported into ArcGIS Pro, where the satellite information was available as separate multispectral bands. In order to obtain a visual representation that approximates the natural appearance of the Earth's surface, the Sentinel-2 spectral bands were combined using remote sensing processing techniques. The Natural Color composite was generated by assigning the red, green and blue spectral channels to Band 4, Band 3 and Band 2, respectively. Maintaining this band order is essential, as it ensures a correct RGB representation of the terrain. The band combination was performed in ArcGIS Pro using the Composite Bands function, which allowed the individual Sentinel-2 bands to be merged into a single multiband raster dataset.

The resulting natural color images provided a suitable basis for visual interpretation, further GIS preprocessing and subsequent land use and land cover classification.

Following the generation of the natural color composites, the study area was defined and extracted for the analysis. For this purpose, official administrative boundary data were obtained from the Geoportal ANCPI platform. The TopRo50 dataset was selected because it contains vector data representing administrative limits, including municipality boundaries. This dataset was imported into ArcGIS Pro and processed as a separate vector layer in order to identify and isolate the administrative boundary of Satu Mare Municipality, which represents the area of interest for this study.

Once the area of interest was defined, the boundary layer was used to extract the relevant portion from each Sentinel-2 natural color composite. This step ensured that the analysis was spatially limited to the selected study area and that all multitemporal datasets were processed using the same geographic extent, as illustrated in Figure 4.

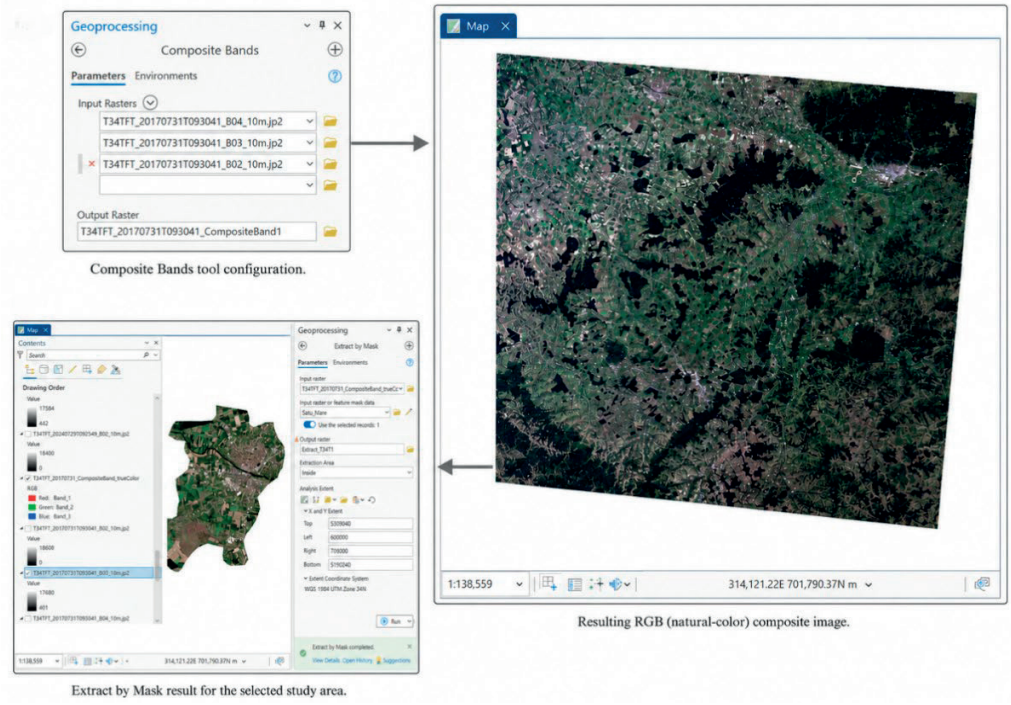



Figure 4. Band composition and study area extraction

***Training data preparation***

Training data preparation represents an essential stage in supervised land use and land cover classification, as this approach relies on labelled samples from the land cover classes of interest to train the classification algorithm (Moraes et al., 2024).

In remote sensing workflows, these samples consist of representative pixels or areas selected for each thematic category, enabling the classifier to associate the spectral characteristics of the satellite image with predefined land use and land cover classes. Their quality, spatial distribution and thematic consistency are important factors, as training sample selection and sample size can influence classification accuracy (Zhang et al., 2023).

In this study, separate training samples were created for each analysed year, namely 2017, 2019 and 2024. This approach was adopted to account for the specific spectral and spatial characteristics of each Sentinel-2 image, while maintaining a consistent classification scheme across the multitemporal analysis. Sentinel-2

imagery is widely used in land cover/use mapping due to its spectral characteristics, spatial resolution and temporal availability, which make it suitable for monitoring different types of land surface features (Phiri et al., 2020). For the differentiation of land use and land cover categories, four thematic classes were defined: *Bare Soil, Vegetation, Yards and Constructions, and Construction Areas.* These classes were selected according to the objective of the study, which focuses on identifying and comparing spatial changes. The prepared training samples were then used as reference data for the supervised classification process.

This step was carried out in ArcGIS Pro, using the Classify function available in the Imagery tab. The selected supervised classification method was Random Trees, which was applied to assign the Sentinel-2 pixels to one of the four predefined land use and land cover classes. This procedure allowed the generation of comparable thematic maps for 2017, 2019 and 2024, supporting the subsequent spatial and statistical analysis of land cover changes. The methodological approach is consistent with machine learning LULC classification, where satellite derived spectral information and predefined land cover classes are used to produce thematic maps for spatial interpretation (Talukdar et al., 2020).

***Supervised Pixel Based Classification***

Following the preparation of the training samples, the supervised classification stage was applied to transform the pre-processed Sentinel-2 imagery into thematic land use and land cover maps. This step represents the operational continuation of the training data stage, since the classifier uses the previously defined reference samples to associate the spectral characteristics of the raster pixels with the selected thematic classes. Supervised pixel-based classification is based on user defined classes within the raster dataset. The training samples are used to create spectral information that guides the classification process and supports the assignment of image pixels to the appropriate land use and land cover categories. Therefore, the reliability of this method depends on the quality of the training samples and on their capacity to represent the spectral variability of the surfaces present in the study area. According to the methodological guidelines, supervised classification relies on user-defined training samples, which are incorporated into a spectral signature file used for raster classification. The same perspective also highlights that training samples should represent the surfaces present in the study area through spectrally pure pixel samples.

In this study, the supervised classification was carried out in ArcGIS Pro using the classification tools available in the Imagery tab. The Random Trees algorithm was selected as the supervised classification method and was applied separately to the Sentinel-2 datasets corresponding to 2017, 2019 and 2024.

The classification was based on the four predefined land use and land cover categories, and a classified thematic raster was generated for each analysed year, providing the basis for the subsequent spatial comparison and statistical evaluation of land cover differences.

***Unsupervised Pixel Based Classification***

In parallel with the supervised approach, an unsupervised pixel-based classification was applied as a complementary method for interpreting the datasets. Unlike supervised classification, this method does not depend on predefined training samples. Instead, it automatically groups pixels into spectral clusters according to the similarity of their values. This makes the method useful for exploratory analysis, especially when the objective is to observe how the raster data are naturally organized based on their spectral characteristics.

The unsupervised classification process is automated, but the resulting clusters require interpretation after the classification has been completed. The methodology explains that the algorithm groups pixels according to similar spectral values, while the user must subsequently label the resulting clusters using additional raster information or visual interpretation. It also notes that the number of initial classes is often higher than the final number of visible land cover categories, because several spectral clusters may correspond to the same thematic class and may need to be merged during interpretation.

The purpose of this step was to provide an additional perspective on the spectral structure

of the images and to support the comparison between classification approaches. After processing, the spectral clusters were interpreted in relation to the main land use and land cover categories considered in the study.

***The role of AI in land use interpretation***

Artificial Intelligence techniques have become increasingly relevant in land use and land cover classification, particularly in studies based on satellite imagery and multitemporal geospatial datasets. The continuous development of remote sensing platforms, including satellite, UAV and airborne systems, has led to the generation of large volumes of spatial, spectral and temporal data. These datasets provide relevant information for understanding land surface dynamics, but their complexity requires analytical methods capable of supporting consistent and reproducible interpretation.

In this context, Geospatial Artificial Intelligence, or GeoAI, represents a methodological framework that integrates artificial intelligence, remote sensing and spatial data science. By combining machine learning and deep learning models with geospatial analysis principles, GeoAI can support the identification of spectral patterns, spatial structures and contextual relationships within heterogeneous landscapes (Dritsas & Trigka, 2026). This is particularly important in land use interpretation, as land cover classes are not defined only by individual pixel values, but also by their spatial distribution, neighbourhood relationships and variability across the landscape.

In the present study, AI is considered an algorithm implemented in the process of image. GIS methods provided the operational framework for Sentinel-2 data preparation and spatial analysis, including band composition, study area extraction, visualization, training sample preparation, map production and surface statistics. These procedures ensured that the classified rasters corresponding to 2017, 2019 and 2024 were spatially comparable and suitable for multitemporal analysis. The AI component is represented by a machine-learning classification algorithm that automatically assigns pixels to predefined LULC classes based on the characteristics learned from the training data.

Based on the training samples, the classifier learns the spectral characteristics associated with each class and applies this information to the entire raster image. In this way, AI assisted classification contributes to a more systematic interpretation of the Sentinel-2 imagery and reduces part of the repetitive manual effort involved in conventional image classification.

The use of Sentinel-2 imagery is appropriate for this type of analysis due to its multispectral characteristics and its balance between spatial, spectral and temporal resolution. Multispectral datasets such as Sentinel-2 and Landsat 8 are widely used for vegetation monitoring, land use classification and environmental assessment (Dritsas & Trigka, 2026). Within this research, Sentinel-2 data supported the supervised and unsupervised classification of the selected land cover classes and enabled the comparison of their spatial evolution over time.

Nevertheless, AI classification remains dependent on the quality of the input data, the representativeness of the training samples and the spectral separability of the selected classes. Therefore, the methodological approach adopted in this study can be understood as a GIS based land cover analysis enhanced by AI assisted classification.

## RESULTS AND DISCUSSIONS

*Multitemporal distribution of training samples*

The first stage of the results focuses on the spatial distribution of the training samples created for each analysed year as presented in the Material and Methods chapter. These samples were used to support the supervised classification process and to define the main land use categories considered in this study. Presenting the training samples separately it will allow to understand the importance of each classification and how the spectral characteristics of the study area varied across the analyses.

For the year 2017, the training samples were created according to the predefined classes. During this stage, an important classification issue was observed in relation to the Someș River, which crosses the selected study area as presented in Figure 5.

In the processed image, the river displayed a visual and spectral response similar to that of

vegetation, which generated ambiguity during the interpretation process.

As a result, parts of the river were associated with the vegetation class, highlighting one of the limitations of the pixel-based classification, when different land cover elements present similar spectral characteristics. A similar issue was also observed in other parts of the classified image, where the initial result was affected by the spectral resemblance between several classes. In particular, confusion occurred between the Bare Soil and Construction Areas classes, as exposed soil, construction surfaces and some building rooftops presented comparable pixel values. This led to partial class overlap and reduced the separability of these categories within the classification output.




Figure 5. River classification result for 2017 in ArcGIS Pro

For this reason, the workflow was returned to the previous stage, where the training samples were revised in the areas affected by classification errors. The first category that required correction was the Bare Soil class, for which additional training samples were created in order to better represent its spectral variability. These samples were adjusted and extended in the problematic areas, rather than being limited only to small and isolated polygons, because the Bare Soil class included surfaces with different tones, textures and pixel values. By incorporating a wider range of representative pixels, the revised training samples aimed to improve the separability of this class from spectrally similar categories, especially Construction Areas and certain built-up surfaces, and to obtain a more accurate supervised classification result, represented in Figure 6.

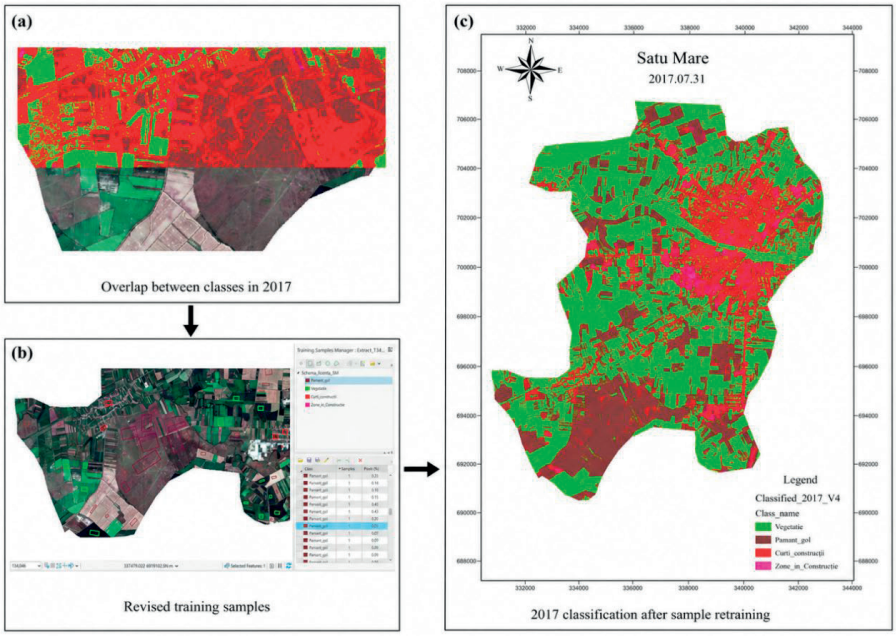



Figure 6. Overlap identification (a), training sample revision (b) and reclassified 2017 result (c)

***2019 training results***

Following the methodological approach applied to the 2017 dataset, a separate set of training samples was also created for the subsequent analysed image, using the same classification scheme and the same predefined land use and land cover classes. After the initial classification, a detailed visual assessment of the output revealed several limitations similar to those observed in the 2017 classification. The main issue was represented by the partial overlap between certain classes, which reduced the clarity and reliability of the thematic result. These inaccuracies indicated the need to refine the training samples in the areas where spectral confusion occurred, in order to improve class separability and obtain a more accurate classification output. Consequently, the workflow was returned to the training sample preparation stage. Additional samples were introduced in the problematic areas, with the purpose of better representing the local spectral variability and reducing the confusion between classes. This iterative correction process was necessary because some surface elements presented similar spectral responses, leading to misclassification in the initial result.

A particular anomaly was again observed in relation to the Yards and Constructions class as shown in Figure 7, similar to the situation identified in the 2017 dataset. In this case, the distortion may be associated with highly reflective surfaces, possibly solar panels, whose spectral response can influence the classification result and generate local errors.




Figure 7. a) Singularities identified for 2019; b) Training sample details

After revising the training samples and repeating the classification, the final output showed a visible improvement, with most of the previous class overlaps and impurities being reduced. Therefore, the corrected result provides a more reliable representation for 2019, demonstrated in Figure 8.

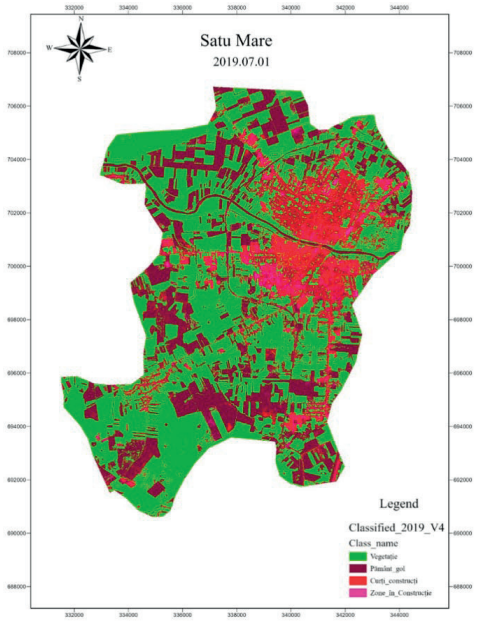



Figure 8. Final classified map for 2019

***2024 training results***

Consistent with the approach used for the previous two analysed years, the same methodological procedure was applied. The training sample preparation followed the same classification scheme used to maintain consistency across the multitemporal analysis.

However, although the images correspond to different years, the classification process revealed similar challenges related to the spectral overlap between certain land use and land cover classes. A recurrent issue identified in all three analysed datasets was the confusion between Construction Areas and Bare Soil. This overlap can be explained by the similar spectral response of exposed soil, construction surfaces and unfinished built-up areas, which makes their separation difficult in pixel-based classification. To reduce this problem, the Bare Soil class required larger and more representative training samples, capable of capturing a wider range of tones and pixel values associated with exposed soil surfaces. In contrast, for the Yards and Constructions class, smaller and more precise samples were necessary, especially in areas corresponding to rooftops and compact built-up elements. This adjustment allowed the classifier to better distinguish between surfaces that initially presented similar spectral characteristics. Therefore, as in the previous years, the 2024 classification required an iterative refinement of the training samples. The correction process was essential for reducing class overlap and improving the thematic clarity of the final classification result.

The final classified map for 2024, presented in Figure 9, illustrates the result obtained after the refinement of the training samples and the correction of the main classification inconsistencies.

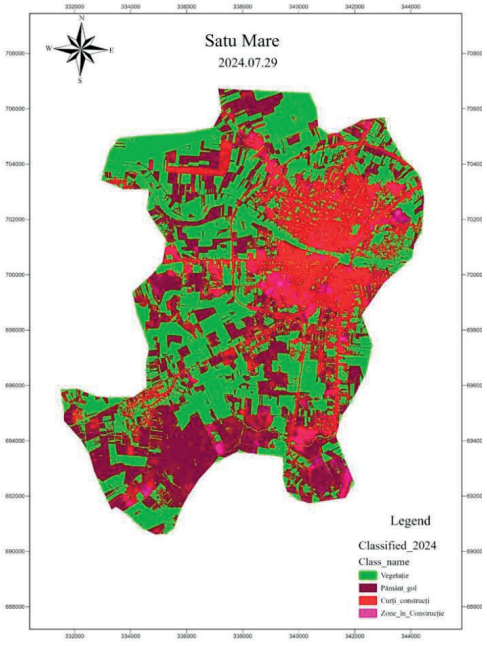



Figure 9. Classified map for 2024

***Comparative analysis based on land use classification results***

The analysis was conducted to evaluate the spatial dynamics of the selected land cover classes and to highlight the main changes

identified within the study area. The surface area of each land cover class was calculated using the raster attribute table generated after the classification process. In the classified raster, the count field represents the number of pixels assigned to each class. Since the Sentinel-2 raster used in this study has a spatial resolution of 10 m × 10 m, each pixel corresponds to an area of 100 m². Therefore, the surface area of each class was obtained by multiplying the number of pixels by 100 m² and then converting the result into hectares and square kilometres. This calculation was applied consistently to the classified rasters from 2017, 2019 and 2024, as presented in the following tables Table 1 for 2017, Table 2 for 2019 and Table 3 for 2024.

Table 1. Surfaces calculated for 2017

| Surface area of land cover classes in 2017 | | |
|---|---|---|
| Land cover class | Pixel count | Area (km²) |
| Vegetation | 598536 | 59.85 |
| Bare Soil | 414969 | 41.50 |
| Yards and Constructions | 174523 | 17.45 |
| Construction Areas | 52743 | 5.27 |
| Total | 1240771 | 124.08 |

Table 2. Surfaces calculated for 2019

| Surface area of land cover classes in 2019 | | |
|---|---|---|
| Land cover class | Pixel count | Area (km²) |
| Vegetation | 639505 | 63.95 |
| Bare Soil | 408773 | 40.88 |
| Yards and Constructions | 125082 | 12.51 |
| Construction Areas | 67411 | 6.74 |
| Total | 1240771 | 124.08 |

Table 3. Surfaces calculated for 2024

| Surface area of land cover classes in 2024 | | |
|---|---|---|
| Land cover class | Pixel count | Area (km²) |
| Vegetation | 496421 | 49.64 |
| Bare Soil | 483470 | 48.35 |
| Yards and Constructions | 209900 | 20.99 |
| Construction Areas | 50980 | 5.10 |
| Total | 1240771 | 124.08 |

The calculated surfaces show that vegetation represented the dominant class in 2017 and 2019, reaching its highest value in 2019 with 63.95 km². In 2024, vegetation decreased to 49.64 km², while bare soil increased to 48.35 km². The Yards and Constructions class also increased in 2024, reaching 20.99 km², compared with 12.51 km² in 2019 and 17.45 km² in 2017. Construction Areas remained the smallest class throughout the analysed period, with values ranging between 5.10 km² and 6.74 km².

The accuracy assessment was generated in ArcGIS Pro using the accuracy assessment points and the confusion matrix tool, resulting Figure 10.

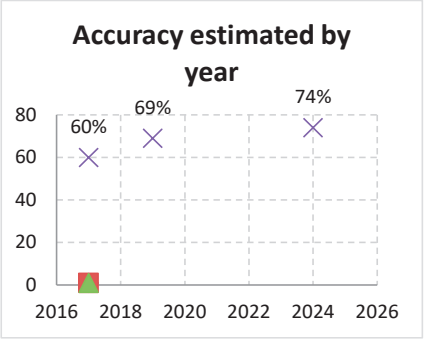



Figure 10. Accuracy estimation for each year classification

The overall accuracy increased from approximately 60% in 2017 to 74% in 2024, indicating a moderate improvement in classification performance. Given that all Sentinel-2 images were acquired using the same sensor and processed with the same classification methodology and algorithm, this improvement is associated with enhanced spectral separability among the land cover classes and the representativeness of the training samples used for each image. The accuracy assessment was performed using an independent set of validation samples, distinct from the training samples employed for model development, ensuring an unbiased evaluation of the classification performance.

In addition to these methodological aspects, the differences in accuracy may also be influenced by the climatic and phenological conditions recorded during the acquisition period. Although all Sentinel-2 images were selected from July, the spectral response of vegetation can vary from one year to another depending on precipitation, soil moisture, temperature and drought intensity. In drier years, vegetation may

show lower vigor and reduced spectral contrast, which can increase confusion with bare soil or transitional construction surfaces.

The lower accuracy obtained may therefore be partly related to the older temporal reference of the image and to possible vegetation stress during the summer period, which can reduce the spectral separability. For 2017, drought monitoring reports indicate a significant precipitation deficit in northern Romania, which may explain the lower spectral separability of vegetation. Under drought conditions, vegetation shows reduced vigor and can be more easily confused with bare soil or surfaces undergoing transformation. The year 2019 appears to have had more stable hydrological conditions for south-eastern Europe, which may support a clearer interpretation of the classes. In contrast, 2024 was characterized by very high temperatures and regional drought, factors that may introduce errors in the vegetation class, even though the image is the most recent and has better temporal relevance.

The results obtained from the classified maps were further analysed through class surface statistics, allowing the differences between the three years to be examined more clearly. The comparative Figure 11 illustrates the evolution of the identified classes.

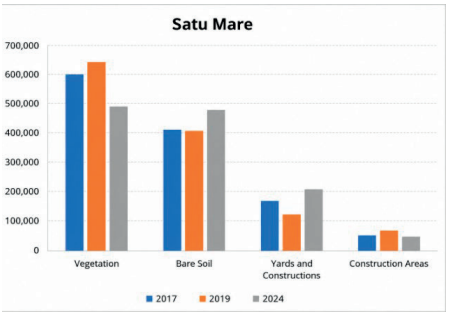



Figure 11. Surface area differences between the identified land cover classes across the analysed years

Vegetation represents the dominant class in all three analysed years, with the highest value recorded in 2019. However, a noticeable decrease can be observed in 2024, suggesting a reduction of vegetated surfaces compared to the previous two reference years. The bare soil class shows a relatively stable evolution between 2017 and 2019, followed by a clear increase in 2024. This may indicate the expansion of exposed or temporarily unused land surfaces, possibly related to land clearing, agricultural activity or areas prepared for future development.

As for the yards and constructions class, they fluctuated, decreasing in 2019 and increasing again in 2024, presented a more fluctuating evolution. A decrease was observed in 2019 compared to 2017, followed by an increase in 2024. This pattern may reflect changes in the built-up structure of the municipality, including residential, industrial or mixed-use developments.

In contrast, the areas classified as construction areas remained relatively limited in extent. The highest value was identified in 2019, while a decrease was observed in 2024. This may suggest that some of the construction sites detected in 2019 were completed by 2024 and were subsequently integrated into other classes, particularly yards and constructions. This evolution highlights the transitional character of construction areas, which often represent temporary land cover conditions rather than stable long-term classes.

## CONCLUSIONS

This study assessed the evolution of land use and land cover in Satu Mare Municipality between 2017, 2019 and 2024 through the integration of Sentinel-2 satellite imagery, GIS preprocessing and AI assisted classification methods.

The results indicate measurable variations in the spatial distribution of the analysed land cover classes. Changes were observed in the extent of Vegetation, Bare Soil, Yards and Constructions, and Construction Areas across the three reference years. These variations describe changes in the classified land cover structure of the study area, but they should not be interpreted as direct evidence of specific urban development processes, land reorganization or socio-economic transformations without additional field observations, cadastral data or planning documents.

A relevant example was identified in the southern part of the study area, where an area classified mainly as Bare Soil in 2017 was predominantly associated with Vegetation in 2019. By 2024, the same sector presented a more heterogeneous classification pattern, including Construction Areas, Bare Soil and smaller

vegetated surfaces. This research illustrates the capacity of multitemporal classification to detect changes in land cover patterns, while the causes of these changes require further validation through complementary data sources. The main contribution of the study is represented by the capacity of the proposed methodology to support a consistent multitemporal comparison. By applying the same classification scheme to the 2017, 2019 and 2024 datasets, the analysis provided both visual and quantitative information regarding land cover distribution and surface changes. This confirms the usefulness of integrating GIS preprocessing and AI assisted classification for territorial monitoring and comparative land cover analysis.

At the same time, several limitations were identified. The most important limitation is related to the spectral similarity between certain land cover classes. Confusion occurred especially between Bare Soil, Construction Areas and some built-up surfaces, while parts of the Someș River were associated with Vegetation due to similar spectral responses. These situations show that pixel classification can generate class overlap when different surface types present comparable pixel values. Another limitation is connected to the 10 m spatial resolution of Sentinel-2 imagery, which may not fully capture small or mixed urban features such as rooftops, courtyards, roads and construction materials.

Despite these limitations, the proposed workflow proved suitable for supporting multitemporal land cover analysis through the consistent processing and comparison of classified satellite imagery.

## REFERENCES

Arias-Navarro, C., Baritz, R., & Jones, A. (Eds.). (2024). *The state of soils in Europe: Fully evidenced, spatially organised assessment of the pressures driving soil degradation.* Publications Office of the European Union.

Brown, C. F., Brumby, S. P., Guzder-Williams, B., Birch, T., Brooks Hyde, S., Mazzariello, J., Czerwinski, W., Pasquarella, V. J., Haertel, R., Ilyushchenko, S., Schwehr, K., Weisse, M., Stolle, F., Hanson, C., Guinan, O., Moore, R., & Tait, A. M. (2022). Dynamic World, near real-time global 10 m land use land cover mapping. *Scientific Data, 9.*

Chowdhury, M. S. (2024). Comparison of accuracy and reliability of random forest, support vector machine, artificial neural network and maximum likelihood method in land use/cover classification of urban setting. *Environmental Challenges, 14.*

Deressu, T. F., Bojer, A. K., Debelee, T. G., Negera, W. G., Nadarajah, S., & Gebissa, K. W. (2025). Enhancing land use and land cover classification with deep learning-based satellite imagery segmentation. *International Journal of Applied Earth Observation and Geoinformation, 144*.

Dong, S., Zhuang, Y., Yang, Z., Pang, L., Chen, H., & Long, T. (2020). Land cover classification from VHR optical remote sensing images by feature ensemble deep learning network. *IEEE Geoscience and Remote Sensing Letters, 17*. 1396-1400.

Dritsas, E., & Trigka, M. (2026). Advances in geospatial artificial intelligence for remote sensing applications. *Computer Science Review, 60.* 100913.

Hurskainen, P., Adhikari, H., Siljander, M., Pellikka, P. K. E., & Hemp, A. (2019). *Auxiliary datasets improve accuracy of object-based land use/land cover classification in heterogeneous savanna landscapes.* Remote Sensing of Environment, 233.

Jia, P., Chen, C., Zhang, D., Sang, Y., & Zhang, L. (2024). Semantic segmentation of deep learning remote sensing images based on band combination principle: Application in urban planning and land use. *Computer Communications, 217.* 97-106.

Le Dez, M., Robin, M., & Launeau, P. (2021). Contribution of Sentinel-2 satellite images for habitat mapping of the Natura 2000 site 'Estuaire de la Loire' (France). *Remote Sensing Applications: Society and Environment, 24.* 100637.

Li, Z., Chen, B., Wu, S., Su, M., Chen, J. M., & Xu, B. (2024). Deep learning for urban land use category classification: A review and experimental assessment. *Remote Sensing of Environment, 311.* 114290.

Ma, L., Schmitt, M., & Zhu, X. X. (2020). Uncertainty analysis of object-based land-cover classification using Sentinel-2 time-series data. *Remote Sensing, 12*(22). 3798.

Moraes, D., Campagnolo, M. L., & Caetano, M. (2024). Training data in satellite image classification for land cover mapping: A review. *European Journal of Remote Sensing, 57*(1).

Phiri, D., Simwanda, M., Salekin, S., Nyirenda, V. R., Murayama, Y., & Ranagalage, M. (2020). Sentinel-2 data for land cover/use mapping: A review. *Remote Sensing, 12*(14). 2291.

Rapinel, S., Mony, C., Lecoq, L., Clément, B., Thomas, A., & Hubert-Moy, L. (2019). Evaluation of Sentinel-2 time-series for mapping floodplain grassland plant communities. *Remote Sensing of Environment, 223.* 115-129.

Stehman, S. V., & Foody, G. M. (2019). Key issues in rigorous accuracy assessment of land cover products. *Remote Sensing of Environment, 231*. 111199.

Talukdar, S., Singha, P., Mahato, S., Shahfahad, Pal, S., Liou, Y.-A., & Rahman, A. (2020*).* Land-use land-cover classification by machine learning classifiers for satellite observations: A review. *Remote Sensing, 12*(7). 1135.

Vali, A., Comai, S., & Matteucci, M. (2020). Deep learning for land use and land cover classification

based on hyperspectral and multispectral Earth observation data: A review. *Remote Sensing, 12*(15). 2495.

Vitale, A., & Lamonaca, F. (2026). Enhancing GeoAI land cover classification via hyperparameter tuning and cross-validation: A case study in Ravenna, Italy. *Measurement, 257*.

Vrieling, A., Meroni, M., Darvishzadeh, R., Skidmore, A. K., Wang, T., Zurita-Milla, R., Oosterbeek, K., O'Connor, B., & Paganini, M. (2018). Vegetation phenology from Sentinel-2 and field cameras for a Dutch barrier island. *Remote Sensing of Environment, 215*. 517-529.

Zhang, H., He, J., Chen, S., Zhan, Y., Bai, Y., & Qin, Y. (2023). Comparing three methods of selecting training samples in supervised classification of multispectral remote sensing images. *Sensors, 23*(20). 8530.

Scientific Papers. Series E. Land Reclamation, Earth Observation & Surveying, Environmental Engineering. Vol. XV, 2026
Print ISSN 2285-6064, CD-ROM ISSN 2285-6072, Online ISSN 2393-5138, ISSN-L 2285-6064

# LAND USE CHANGES INDUCED BY CONSTRUCTION MATERIAL EXTRACTION IN SURFACE QUARRIES WITHIN THE INEU ADMINISTRATIVE TERRITORY (BIHOR COUNTY, ROMANIA)

**Karoly Alexandru RACZ[1], Claudia Simona TIMOFTE[2], Nicu Cornel SABĂU[3]**

[1]Doctoral School of Engineering Sciences, Field of Agriculture, University of Oradea, Faculty of Environmental Protection, 24 Gen. Magheru Street, Oradea, Romania
[2]University of Oradea, Faculty of Law, 26 Gen. Magheru Street, Oradea, Romania
[3]University of Oradea, Faculty of Environmental Protection, 24 Gen. Magheru Street, Oradea, Romania

Corresponding author email: alex.racz@yahoo.com

***Abstract***

*This study analyses land use and land cover changes within the administrative territory of Ineu Commune, Bihor County, Romania, over the period 1990-2025, using GIS techniques and multi-temporal Earth observation data. The methodology integrates CORINE Land Cover datasets for the years 1990, 2000, 2006, 2012, and 2018 with high-resolution Sentinel-2 imagery for 2025, processed in QGIS. To ensure temporal comparability, the 2025 classification was harmonized according to CORINE Land Cover (CLC) schemes. Quantitative indicators, including absolute change, percentage change, and average annual rate of change, were calculated. The analysis reveals a significant expansion of construction material extraction areas and associated artificial lakes, accompanied by a reduction in heterogeneous agricultural surfaces. Mineral extraction sites increased from 0 ha to 243.14 ha, while the formation of 52 anthropogenic lakes was identified. The results indicate a simplification of the agricultural landscape and a transition towards a more specialized and partially industrialized territorial structure. The study also highlights major discrepancies between official local statistics and satellite-derived data, emphasizing the importance of geospatial monitoring for sustainable spatial planning. The research provides a robust methodological framework that can be replicated in other rural areas affected by extractive activities.*

***Key words****: anthropogenic lakes, CORINE Land Cover, GIS, gravel extraction, Sentinel-2, spatial planning.*

## INTRODUCTION

Land use change represents one of the most pressing environmental and socio-economic challenges in Europe, with a particularly strong impact on rural areas affected by resource extraction activities. In Romania, the rapid expansion of sand and gravel quarries has significantly altered local landscapes, leading to the loss of agricultural land and the formation of a considerable number of anthropogenic lakes (Ghirardi et al., 2023).

Although land use dynamics have been extensively studied at national and regional scales, detailed analyses at the level of administrative-territorial units remain limited, despite the fact that transformations are often more intense and spatially heterogeneous at local scale.

Geographic Information Systems (GIS) (https://qgis.org/, 2024), Graser (2013), Mouloudi et al. (2025) and Copernicus programs, particularly CORINE Land Cover and the Sentinel missions, provide essential tools for the long-term monitoring and quantification of these changes.

This study analyses and quantifies land use changes within the Ineu administrative-territorial unit, Bihor County, Romania, over the period 1990-2025. Ineu Commune (Ineu, n.d.), located approximately 20 km east of Oradea Municipality and included within the Oradea Metropolitan Area, is subject to specific anthropogenic pressures generated by gravel extraction activities carried out in the floodplain and former riverbed of the Crișul Repede River. The research highlights the reduction of agricultural land and the emergence of 52 artificial lakes, together with other major landscape transformations.

By integrating multi-temporal CORINE Land Cover (Copernicus, 2025; ESA 2025), datasets

with high-resolution Sentinel-2 (Simonetti et al., 2021) imagery and quantitative indicators, the study proposes a robust methodological framework for assessing the impact of extractive activities and supports sustainable land management in rural areas undergoing transition.

## MATERIALS AND METHODS

The study area corresponds to the Ineu Administrative-Territorial Unit, located in the central-eastern part of Bihor County, Romania, approximately 20 km east of Oradea Municipality. The commune is part of the Oradea Metropolitan Area and includes the villages of Ineu (administrative centre), Husasău de Criș, and Botean. The total surface area is 49.51 km² (4,951 ha) (Figure 1).

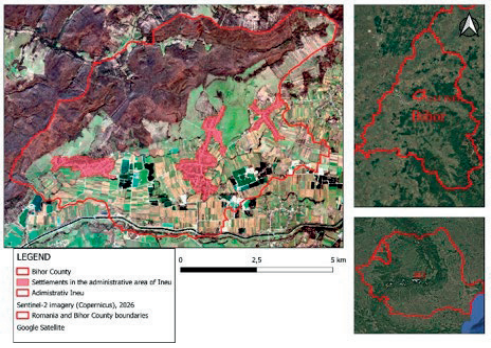



Figure 1. Geographic location of the Ineu Administrative-Territorial Unit within Bihor County, Romania (source: Sentinel-2 imagery, 2025, and administrative boundaries)

The territory is situated within the Oradea–Vad Borod Depression, on the floodplain and former riverbed of the Crișul Repede River, and is characterized by predominantly low plain relief with Quaternary deposits consisting of sands, gravels, and clays. The comparative analysis between the georeferenced historical map from 1782 and the current territorial configuration indicates a significant spatial overlap between the former riverbed of the Crișul Repede River and the main present-day mineral aggregate extraction areas (Figure 2).

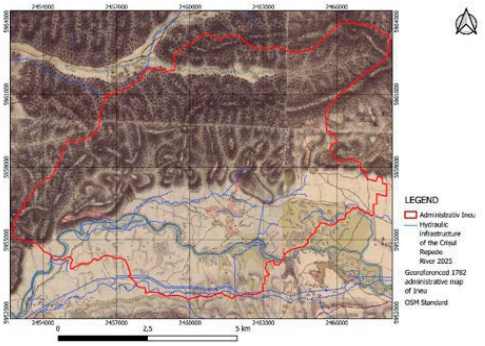



Figure 2. Comparative overlay between the 1782 historical map and the current landscape (2025), highlighting extraction areas on the former Crișul Repede riverbed

The multi-temporal analysis was based on two main categories of geospatial data and GIS processing techniques. The methodological workflow applied in the present study, including data acquisition, georeferencing, spatial processing, land use classification, vectorization, quantitative indicator calculation, and change detection analysis, is summarized in Figure 3.

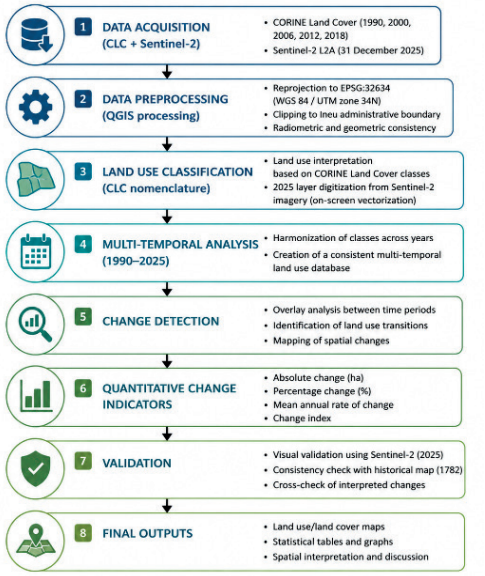



Figure 3. General methodological workflow applied for land use change analysis

CORINE Land Cover (CLC) (Copernicus, 2025; EEA, n.d.) datasets for the years 1990, 2000, 2006, 2012 and 2018 were downloaded from the Copernicus Land Monitoring Service (LandMonitoring, 2021; Şener & Arslanoğlu, 2023; Gómez-Fernández et al., 2024) (100 m spatial resolution, minimum mapping unit of 25 ha). A Sentinel-2 Level-2A multispectral image acquired on 31 December 2025 was downloaded from the Copernicus Data Space Ecosystem (10 m resolution for visible bands and 20 m resolution for vegetation bands). Applications of this type, made available to users, are employed in a wide range of fields, including urban spatial planning, forest management, water management, agriculture, food security, nature conservation and restoration, rural development, ecosystem accounting, and climate change mitigation and adaptation (Skilodimou et al., 2021; Alzurqani et al., 2024). All spatial datasets were clipped to the administrative boundary of Ineu commune. Polygon vector layers were generated through manual digitization and spatial overlay procedures in QGIS. Surface calculations were extracted from the polygon attribute tables and converted into hectares and percentages.

Land use classification was performed consistently for all six temporal reference periods using the CORINE Land Cover nomenclature (Skilodimou et al., 2021). The 2025 layer, derived from Sentinel-2 imagery, was harmonized with this nomenclature to ensure temporal comparability. The evolution of the surface areas and proportions of the main land use classes is presented in Table 1.

Table 1. Evolution of land use/land cover classes in the Ineu Administrative Territory, Bihor, Romania (1990-2025)

| CLC | CORINE LAND COVER LEGEND | 1990 | | 2000 | | 2006 | | 2012 | | 2018 | | 2025 | |
|---|---|---|---|---|---|---|---|---|---|---|---|---|---|
| | | Ha | % | Ha | % | Ha | % | Ha | % | Ha | % | Ha | % |
| 324 | Transitional woodland-shrub | 0,00 | 0,00 | 0,00 | 0,00 | 0,00 | 0,00 | 30,99 | 0,60 | 30,99 | 0,60 | 90,82 | 1,83 |
| 211 | Non-irrigated arable land | 1307,33 | 26,40 | 1307,71 | 26,30 | 1804,28 | 36,40 | 1766,59 | 35,60 | 1735,00 | 35,00 | 1598,11 | 32,27 |
| 222 | Fruit trees and berry plantations | 0,00 | 0,00 | 0,00 | 0,00 | 107,53 | 2,20 | 107,53 | 2,20 | 107,53 | 2,20 | 83,10 | 1,68 |
| 231 | Pastures | 745,97 | 15,10 | 745,97 | 15,10 | 783,98 | 15,80 | 775,64 | 15,70 | 775,64 | 15,60 | 748,24 | 15,12 |
| 221 | Vineyards | 192,21 | 3,80 | 192,21 | 3,90 | 82,32 | 1,70 | 82,32 | 1,70 | 82,32 | 1,70 | 82,55 | 1,67 |
| 131 | Mineral extraction sites | 0,00 | 0,00 | 0,00 | 0,00 | 33,26 | 0,70 | 155,20 | 3,10 | 186,78 | 3,80 | 243,14 | 4,91 |
| 242 | Complex cultivation patterns | 161,74 | 3,30 | 161,78 | 3,30 | 45,37 | 0,90 | 45,37 | 0,90 | 45,37 | 0,90 | 40,98 | 0,83 |
| 243 | Land principally occupied by agriculture, with significant areas of natural vegetation | 521,52 | 10,50 | 521,41 | 10,50 | 156,15 | 3,20 | 64,58 | 1,30 | 64,58 | 1,30 | 77,30 | 1,56 |
| 112 | Discontinuous urban fabric | 304,56 | 6,20 | 304,56 | 6,20 | 259,50 | 5,20 | 275,17 | 5,60 | 275,17 | 5,60 | 313,70 | 6,34 |
| 311 | Broad-leaved forest | 1657,78 | 33,50 | 1657,60 | 33,50 | 1618,86 | 32,70 | 1587,87 | 32,10 | 1587,87 | 32,10 | 1613,57 | 32,59 |
| 511 | Water courses | 60,34 | 1,20 | 60,34 | 1,20 | 60,34 | 1,20 | 60,34 | 1,20 | 60,34 | 1,20 | 60,34 | 1,20 |
| | **TOTAL** | | 100,00 | 4951,58 | 100,00 | 4951,59 | 100,00 | 4951,60 | 100,00 | 4951,59 | 100,00 | 4951,85 | 100,00 |

Considering the limitations of the CORINE Land Cover nomenclature at local scale, the newly formed lakes resulting from mineral aggregate extraction activities were mapped as water surfaces associated with extractive activities (Ghirardi et al., 2023).

To ensure a quantitative and comparable assessment of land use and land cover dynamics within the Ineu administrative-territorial unit over the period 1990-2025, a set of mathematical indicators was applied. These indicators allow the evaluation of both the magnitude and the intensity of changes across different land use categories.

In order to capture the specific temporal dynamics and the inflection points of landscape transformations, the quantitative indicators were calculated separately for two distinct periods: 1990-2006 (the post-communist agricultural intensification period) and 2006-2025 (the period of accelerated expansion of extractive activities and transition towards a partially industrialized landscape).

Quantitative indicators of land use change

Relative percentage change (%) of land use categories

$$\Delta P(\%) = \frac{A_{t2} - A_{t1}}{A_{t1}} \times 100$$

where:

$\Delta P(\%)$= relative percentage change of the land use category;

$A_{t1}$= area of the land use category at the initial time period (ha);

$A_{t2}$= area of the land use category at the final time period (ha).

Absolute change: $\Delta A = A_{t2} - A_{t1}$

where:

$\Delta A$= absolute change (ha);

$A_{t1}$= area at the initial time period;

$A_{t2}$= area at the final time period.

Average annual rate of change

$$R = \frac{A_{t2} - A_{t1}}{t_2 - t_1}$$

where:

$R$= average annual rate of change (ha/year);

$A_{t1}$= area at the initial time period (ha);

$A_{t2}$= area at the final time period (ha);

$t_2 - t_1$= time interval between the two reference periods (years).

Change index

$$I_c = \frac{A_{t2}}{A_{t1}}$$

where:

$I_c$= change index (dimensionless);

- $I_c > 1$= increase;
- $I_c < 1$= decrease;
- $I_c = 1$= stability.

All calculations were performed in Microsoft Excel and validated in QGIS.

Change detection was performed through post-classification analysis based on the spatial overlay of vector layers. For the year 2025, an additional validation procedure was carried out through overlay analysis with the georeferenced historical map from 1782, confirming that the majority of anthropogenic lakes were formed on the former riverbed of the Crișul Repede River.

Note: Since no official CORINE Land Cover product is available for 2025, the Sentinel-2-derived layer was manually created and harmonized with the CLC nomenclature in order to ensure temporal comparability.

## RESULTS AND DISCUSSIONS

Comparison between official statistics and satellite-derived data:

According to the Sustainable Development Strategy of Ineu Commune (2021-2027) (Lillemets et al., 2025; ZMO), agricultural land represents the dominant land use category, covering 60.41% of the total surface area (2,991 ha), followed by forest areas (32.94%), built-up surfaces (3.43%), water surfaces (1.01%), and communication routes (2.20%).

The comparison with CORINE Land Cover 2018 data reveals significant differences (Bodog et al., 2024) (Table 2).

Table 2. Comparative Analysis of Land Use Categories According to the Sustainable Development Strategy of Ineu Commune (2021-2027) and CORINE Land Cover 2018

| Category | Strategy (ha) | Strategy (%) | CLC 2018 (ha) | CLC 2018 (%) | Difference (ha) | Difference (%) |
|---|---|---|---|---|---|---|
| Agricultural land | 2991 | 60,41 | 2807,99 | 56,71 | -183,01 | -3,70 |
| Forest land | 1631 | 32,94 | 1617,85 | 32,67 | -13,15 | -0,27 |
| Built-up areas | 170 | 3,43 | 320,86 | 6,48 | +150,86 | +3,05 |
| Water bodies / Lakes | 0 | 0 | 144,57 | 2,92 | +144,57 | +2,92 |
| Total | 4951,59 | 100 | 4951,59 | 100 | | |

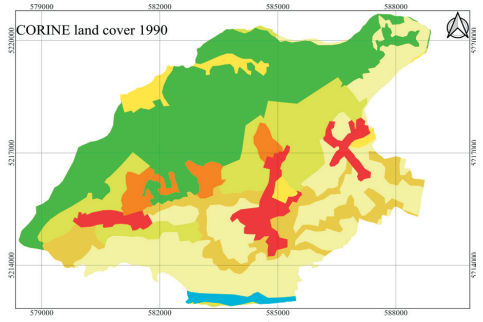
The share of agricultural land decreases to 56.71%, while built-up surfaces increase to 6.48%, and water bodies reach 2.92%. The most significant discrepancy concerns water surfaces: the local Strategy reports 0 ha of lakes, whereas satellite-derived data identify 144.57 ha, most of them representing anthropogenic lakes generated by extraction activities.

These discrepancies highlight the limitations of administrative statistics and the superiority of satellite-based monitoring in capturing recent anthropogenic transformations.

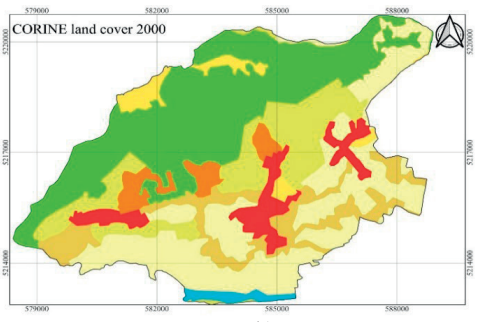
The analysis of the six temporal reference periods (1990, 2000, 2006, 2012, 2018, and 2025) highlights profound structural transformations of the landscape within the Ineu Administrative-Territorial Unit (Table 1, Figure 4). Table 3 presents the detailed evolution of the surface area and proportion of the main land use classes throughout the entire analysed period.

The general dynamics reveal two major processes:

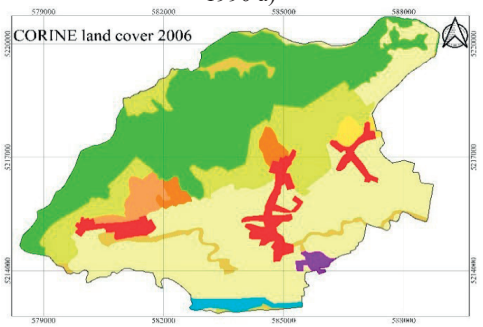
1. Intensification and simplification of agricultural land use during the first part of the analysed period (1990-2006) (Table 3).
2. Strong expansion of extractive activities after 2006, accompanied by the formation of anthropogenic lakes and the fragmentation of agricultural land (Table 4).



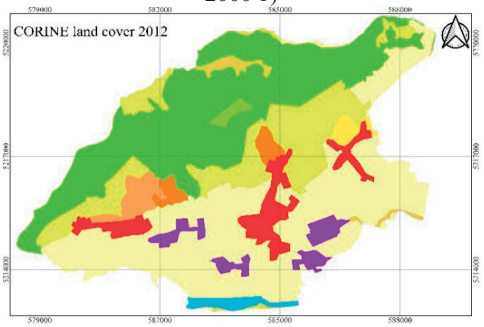

1990 a)



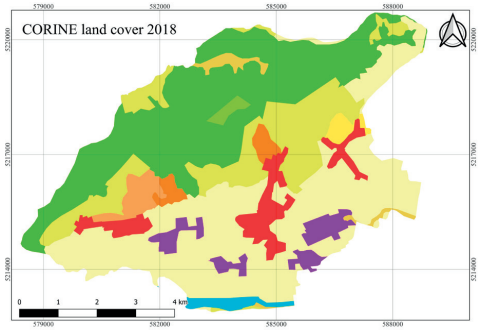

2000 b)



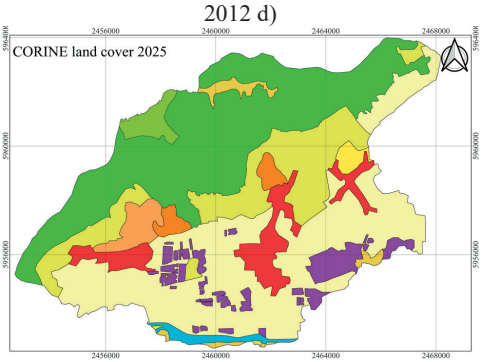

2006 c)




2012 d)




2018 e)




2025 f)

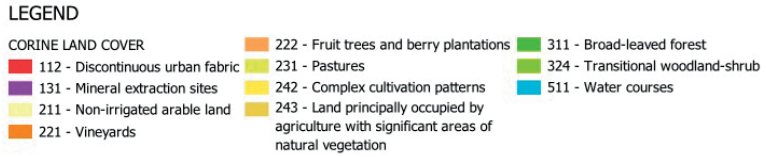



Figure 4. Temporal evolution of land use changes within the administrative-territorial unit of Ineu: 1990 a), 2000 b), 2006 c), 2012 d), 2018 e), and 2025 f). (CORINE Land Cover and Sentinel-2 data).

Table 3. Land use changes during the period 1990-2006 (16 years)

| CLC class (code) | 1990 (ha) | 2006 (ha) | Absolute change (ha) | Percentage change (%) | Average annual rate of change (%) |
|---|---|---|---|---|---|
| Non-irrigated arable land (211) | 1307,33 | 1804,28 | +496,95 | +38,01 | +2,03 |
| Pastures (231) | 745,97 | 783,98 | +38,01 | +5,10 | +0,31 |
| Vineyards + Fruit trees and berry plantations (221+222) | 192,21 | 189,85 | -2,36 | -1,23 | -0,08 |
| Complex cultivation patterns + Land principally occupied by agriculture, with significant areas of natural vegetation (242+243) | 683,26 | 201,52 | -481,74 | -70,50 | -7,45 |
| Total agricultural land (211+221+222+231+242+243) | 2928,77 | 2979,63 | +50,86 | +1,74 | +0,11 |
| Mineral extraction sites (131) | 0,00 | 33,26 | +33,26 | – | – |
| Discontinuous urban fabric (112) | 304,56 | 259,50 | -45,06 | -14,80 | -1,00 |
| Broad-leaved forest (311) | 1657,78 | 1618,86 | -38,92 | -2,35 | -0,15 |
| Water courses (511) | 60,34 | 60,34 | 0,00 | 0,00 | 0,00 |

Table 4. Land use changes in the Ineu Administrative-Territorial Unit during the period 2006-2025

| CLC class (code) | 2006 (ha) | 2025 (ha) | Absolute change (ha) | Percentage change (%) | Average annual rate of change (%) |
|---|---|---|---|---|---|
| Non-irrigated arable land (211) | 1804,28 | 1598,11 | -206,17 | -11,43 | -0,64 |
| Pastures (231) | 783,98 | 710,37 | -73,61 | -9,39 | -0,52 |
| Vineyards + Fruit trees and berry plantations (221+222) | 189,85 | 165,65 | -24,20 | -12,75 | -0,72 |
| Complex cultivation patterns + Land principally occupied by agriculture, with significant areas of natural vegetation (242+243) | 201,52 | 118,28 | -83,24 | -41,30 | -2,79 |
| Total agricultural land (211+221+222+231+242+243) | 2979,63 | 2592,41 | -387,22 | -12,99 | -0,73 |
| Mineral extraction sites (131) | 33,26 | 243,14 | +209,88 | +631,03 | +11,04 |
| Discontinuous urban fabric (112) | 259,50 | 313,70 | +54,20 | +20,89 | +1,00 |
| Broad-leaved forest (311) | 1618,86 | 1613,57 | -5,29 | -0,33 | -0,02 |
| Water courses (511) | 60,34 | 98,21 | +37,87 | +62,76 | +2,60 |

The period 1990-2006 is characterized by an intensification of agriculture on arable land (+496.95 ha, +38%), accompanied by a drastic reduction in heterogeneous and complex agricultural surfaces (-481.74 ha, -70.5%). This period reflects the transition from an extensive and fragmented agricultural system towards a more specialized form of agriculture after 1990. Mineral extraction activities emerged on a limited scale (33.26 ha), while the total agricultural surface recorded a slight increase (+1.74%).

The period 2006-2025 marks a major structural transformation of the landscape. Agricultural land experienced a continuous and significant decrease (-387.22 ha, -12.99%), particularly affecting arable land (-206 ha) and pastures (-73.61 ha). At the same time, mineral extraction sites expanded dramatically (+209.88 ha, +631%), while the surface occupied by discontinuous urban fabric increased steadily (+54.20 ha, +20.89%). The increase in water surfaces (+37.87 ha) corresponds to the formation of 52 anthropogenic lakes generated by gravel extraction activities in the former riverbed of the Crișul Repede River (Petrovszki & Timár, 2010; Pınar & Karahasan, 2024).

At the same time, important hydrotechnical interventions were carried out, especially on the

Crișul Repede River, which underwent major modifications, as well as within the secondary network of streams, ponds, canals, and drainage systems (Osei et al., 2025). The embankment and canalization of secondary watercourses were primarily intended to protect the locality of Ineu from floods (Osawa, 2024), contributing to significant alterations of the natural landscape.

These trends confirm the transition from a predominantly rural agricultural landscape towards a more specialized and partially industrialized landscape dominated by extractive activities. Similar land use transitions associated with agricultural restructuring and extractive activities have also been reported in other European rural regions (Alawode et al., 2025; Lillemets et al., 2025).

The identified transformations also highlight the increasing importance of efficient and transparent territorial governance. The guiding principles of public administration in many democratic countries include flexibility, transparency, autonomy, and efficiency, considered essential for the proper functioning of administrative systems. In the contemporary context, citizens increasingly expect public administration to become more efficient, flexible, and transparent in managing territorial resources and environmental transformations (Timofte, 2023; Timofte & Racz, 2025).

Spatial analysis indicates that the most significant transformations are concentrated within the floodplain and former riverbed of the Crișul Repede River.

The expansion of gravel quarries and the formation of 52 anthropogenic lakes have led to a pronounced fragmentation of agricultural land and to the reconfiguration of the local hydrographic network (Figures 5 and 6).

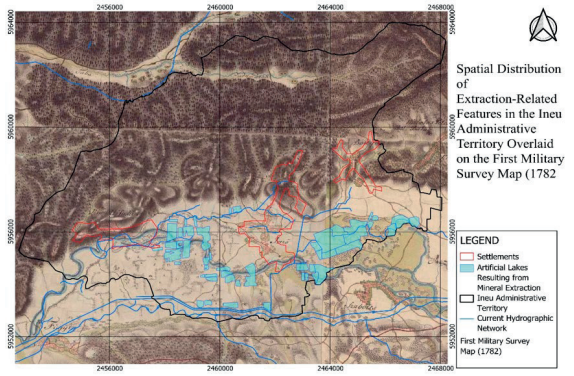



Figure 5. Comparative overlay between the 1782 historical map and the current situation (2025), highlighting the location of quarries on the former Crișul Repede riverbed.

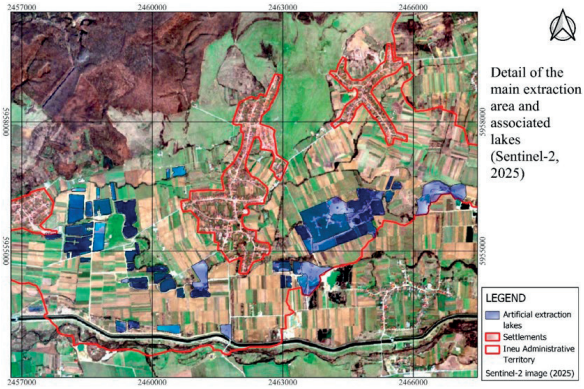



Figure 6. Detail of the main extraction area and the associated anthropogenic lakes. (Sentinel-2, 2025).

The results indicate a clear transition from a heterogeneous agricultural landscape (1990) towards a more specialized and partially industrialized system (2025), dominated by extractive activities.

The identified transformations present a dual character:

- *Negative aspects*: reduction of high-quality agricultural land, landscape fragmentation, and potential impacts on food security.
- *Opportunities:* economic benefits generated by extractive activities, recreational and fishery potential of anthropogenic lakes, and the possibility of using water resources for irrigation purposes.

The integration of high-resolution satellite monitoring (Sentinel-2) with CORINE Land Cover data and quantitative indicators provides a robust methodological framework for local spatial planning and for supporting public policies in rural areas affected by extractive activities.

## CONCLUSIONS

This study provides a comprehensive assessment of land use and land cover changes within the Ineu Administrative-Territorial Unit, Bihor County, during the period 1990-2025, through the integration of CORINE Land Cover data, Sentinel-2 satellite imagery, and quantitative indicators.

The results highlight a significant structural transformation of the landscape, marked by the transition from a heterogeneous agricultural system towards a more simplified and partially industrialized landscape. The most important change is represented by the expansion of mineral extraction sites, which led to the formation of 52 anthropogenic lakes and to a major reconfiguration of the territorial structure. At the same time, heterogeneous agricultural land recorded a pronounced decline, indicating a process of agricultural simplification and the gradual disappearance of traditional mixed farming systems. Arable land experienced a moderate increase, while broad-leaved forest areas remained relatively stable, demonstrating the structural resilience of natural landscape components. Quantitative analysis confirms that extractive activities represent the main pressure factor affecting land use, influencing both the spatial configuration and the functionality of the landscape.

The study also reveals significant discrepancies between official local statistics (Sustainable Development Strategy 2021-2027) and satellite-derived data, emphasizing the need to integrate geospatial technologies into territorial monitoring and spatial planning processes. The systematic use of satellite imagery and GIS analyses can contribute to a more objective evaluation, closer to the actual situation in the field, facilitating the development of public policies and administrative decisions based on updated and verifiable data.

From a socio-economic perspective, the identified transformations generate both challenges and opportunities. The reduction of high-quality agricultural land may affect the long-term productive capacity of the area, while the emergence of anthropogenic lakes creates new opportunities for economic diversification through tourism, recreation, and aquaculture.

The methodological approach applied in this study - combining standardized CORINE datasets, high-resolution Sentinel-2 imagery, and quantitative indicators - provides a robust and replicable framework for analysing land use dynamics at local scale, applicable to other rural areas affected by extractive activities. Future research should focus on the integration of higher-resolution datasets, field validation, and environmental impact assessment, particularly regarding soil degradation, water quality, and microclimatic changes.

In the context of the identified transformations, the study results underline the necessity of a rational and balanced use of land resources, especially in rural areas affected by extractive activities. The conversion of agricultural land towards industrial or extractive uses should be carried out on the basis of clear, objective, and sustainable criteria, ensuring the balance between economic development, environmental protection, and the conservation of agricultural resources. At the same time, the regulatory framework governing extractive activities could consider the introduction of territorial indicators and limits adapted to local carrying capacity, including by relating exploited surfaces to the total available agricultural land.

In conclusion, the study highlights the need for sustainable land management strategies capable

of reconciling economic development with environmental protection and the preservation of agricultural productive capacity. Satellite monitoring and quantitative analysis should become essential components of local and regional spatial planning, ensuring informed decision-making in the context of increasingly intense anthropogenic pressures.

## REFERENCES

Alawode, G. L., Oluwajuwon, T. V., Hammed, R. A., Olasuyi, K. E., Krasovskiy, A., Ogundipe, O. C., & Kraxner, F. (2025). Spatiotemporal assessment of land use land cover dynamics in Mödling district, Austria, using remote sensing techniques. *Heliyon, 11*(11), e43454. https://doi.org/10.1016/j.heliyon.2025.e43454

Alzurqani, S. A., Zurqani, H. A., White, D., Jr., Bridges, K., & Jackson, S. (2024). Google Earth Engine application for mapping and monitoring drought patterns and trends: A case study in Arkansas, USA. *Ecological Indicators, 168*, 112759. https://doi.org/10.1016/j.ecolind.2024.112759

Bodog, M., Racz, K. A., & Sabau, N. C. (2024). Past and future – a 10 – year perspective and the evolution of Ineu's forest. *Agriculture for Life, Life for Agriculture, Vol. XIII*. Retrieved from https://landreclamationjournal.usamv.ro/pdf/2024/Art93.pdf

Copernicus, E. E. (2025). *https://www.copernicus.eu/en/about-copernicus*. Retrieved from https://www.copernicus.eu/en.

ESA (European Spatial Agency). (2025). *esa.int*. Retrieved from https://www.esa.int/Applications/Observing_the_Earth/Copernicus/The_Sentinel_missions

EEA (European Enironment Agency). (n.d.). *land.copernicus.eu/en/products/corine-land-cover*. Retrieved from https://land.copernicus.eu/en/products/corine-land-cover

Ghirardi, N., Bresciani, M., Pinardi, M., Nizzoli, D., & Viaroli, P. (2023). Pit lakes from gravel and sand quarrying in the Po River basin: An opportunity for riverscape rehabilitation and ecosystem services improvement. *Ecological Engineering, 196*, 107103. https://doi.org/10.1016/j.ecoleng.2023.107103

*GIS*. https://qgis.org/. (2024).

Gómez-Fernández, D., Salas-López, R., Zabaleta-Santisteban, J. A., Medina-Medina, A. J., Goñas, M., Silva-López, J. O., Oliva-Cruz, M., & Rojas-Briceño, N. B. (2024). Landsat images and GIS techniques as key tools for historical analysis of landscape change and fragmentation. *Ecological Informatics, 82*, 102738. https://doi.org/10.1016/j.ecoinf.2024.102738

Graser, A. (2013). *Learning QGIS.* Packt Publishing Ltd.

Ineu, S. (n.d.). *ineu-bh.ro*. Retrieved from ineu-bh.ro: https://ineu-bh.ro/

LandMonitoring, C. S. (2021). *Land Cover/Land Use Change 2012-2018 (vector), Europe, 6-yearly*. Retrieved from https://land.copernicus.eu/en/products/n2k/n2k-change-2012-2018

Lillemets, J., Viira, A.-H., & Fertő, I. (2025). The intertwined geographies of agricultural land and human settlement in Europe. *Land Use Policy, 153*, 107527. https://doi.org/10.1016/j.landusepol.2025.107527

Mouloudi, A., Mili, E. M., El Faleh, E. M., Ait Said, B., & Mehdaoui, R. (2025). Mapping the impact of quarrying on karst groundwater resources in a semi-arid region using GIS and remote sensing: A case study of the Agourai aquifer, Middle Atlas, Morocco. *Journal of African Earth Sciences, 227*, 105635. https://doi.org/10.1016/j.jafrearsci.2025.105635

Osawa, T. (2024). Agricultural land around river confluences could strongly suppress floods occurrences. *Environmental and Sustainability Indicators*, 24, 100533. https://doi.org/10.1016/j.indic.2024.100533

Osei, J. D., Reed-Jones, Q., Twumasi, Y. A., & Ning, Z. H. (2025). A GIS-based flood hazard mapping in the Alsen St./Irma Lee Community Village in the Louisiana state of USA. *Natural Hazards Research, 5*(4), 778–799. https://doi.org/10.1016/j.nhres.2025.03.006

Petrovszki, J., & Timár, G. (2010). Channel sinuosity of the Körös River system, Hungary/Romania, as possible indicator of the neotectonic activity. *Geomorphology*, 122(3–4), 223–230. https://doi.org/10.1016/j.geomorph.2010.06.002

Pınar, M., & Karahasan, B. C. (2024). Asymmetric effects of EU cohesion policy on EU regional growth: The role of macroeconomic uncertainty. *The Journal of Economic Asymmetries, 30*, e00382. https://doi.org/10.1016/j.jeca.2024.e00382

Simonetti, D., Pimple, U., Langner, A., & Marelli, A. (2021). Pan-tropical Sentinel-2 cloud-free annual composite datasets. *Data in Brief, 39*, 107488. https://doi.org/10.1016/j.dib.2021.107488

Skilodimou, H. D., Bathrellos, G. D., & Alexakis, D. E. (2021). Flood Hazard Assessment Mapping in Burned and Urban Areas. *Sustainability*, *13*(8), 4455. https://doi.org/10.3390/su13084455

Şener, M., & Arslanoğlu, M. C. (2023). Morphometric analysis in Google Earth Engine: An online interactive web-based application for global-scale analysis. *Environmental Modelling & Software, 162*, 105640. https://doi.org/10.1016/j.envsoft.2023.105640

Timofte, C. S. (2023). E-administration and Public Administration Transparency in Bihor County, Romania. *LAW AND SOCIAL VALUES*. Retrieved from http://www.prafak.ni.ac.rs/en/pf-law-publishing/collection-of-papers-law-nis

Timofte, C., & Racz, K. (2025). Conversion of pasturelands into community forests: technical and administrative implications - the case of Ineu (Bihor county, Romania). *AgroLife Scientific Journal, 14*. https://doi.org/10.17930/AGL2025219

ZMO. (n.d.). *chrome-extension://efaidnbmnnnibpcajpcglclefindmkaj/https://zmo.ro/download/SDD%20INEU_2021_2027_FINAL.pdf*. Retrieved from chrome-extension://efaidnbmnnnibpcajpcglclefindmkaj/https://zmo.ro/download/SDD%20INEU_2021_2027_FINAL.pdf

Scientific Papers. Series E. Land Reclamation, Earth Observation & Surveying, Environmental Engineering. Vol. XV, 2026
Print ISSN 2285-6064, CD-ROM ISSN 2285-6072, Online ISSN 2393-5138, ISSN-L 2285-6064

# HIGH-DENSITY AIRBORNE LiDAR POINT CLOUD FOR DIGITAL TERRAIN MODELS IN SMALL STREAM ASSESSMENT AND REHABILITATION

**Tudor SĂLĂGEAN[1, 2, 3], Ioana POP[1], Florica MATEI[1], Silvia CHIOREAN[1], Mircea-Emil NAP[1], Catalin-Stefanel SABOU[1, 2], Andreea-Catalina MOSNEAG[2]**

[1]University of Agricultural Sciences and Veterinary Medicine Cluj-Napoca,
3-5 Calea Manastur Street, Cluj-Napoca, Romania
[2]Technical University of Civil Engineering of Bucharest, Doctoral School,
122-124 Lacul Tei Blvd, District 2, Bucharest, Romania
[3]Technical Sciences Academy of Romania, 26 Dacia Blvd, District 2, 030167, Bucharest, Romania

Corresponding author emails: catalin.sabou@usamvcluj.ro, catalinamosneag@gmail.com

***Abstract***

*Accurate topographic data are essential for the assessment and planning of interventions along small streams and narrow valleys, where traditional survey methods are often constrained by limited access, dense vegetation, and complex terrain. Airborne LiDAR represents a reliable solution, producing high-density point clouds that capture topographic variations, channel geometry, old hydraulic works, and subtle landscape features often missed by conventional techniques. This study aims to demonstrate the workflow for UAV-LiDAR data acquisition and processing, including flight planning, PPK data processing, point cloud classification and filtering, and the generation of high-resolution Digital Terrain Models (DTMs). These results provide a basis for hydrological analysis, planning, and regulatory approvals, supporting engineers and hydrologists in intervention design planning.*

***Key words****: design planning, Digital Terrain Models, LiDAR, small streams, UAV.*

## INTRODUCTION

Small streams represent essential components of fluvial systems, providing important ecological, hydrological, and socio-economic functions in fluvial landscapes. Despite their relatively small size, these watercourses contribute significantly to watershed connectivity, sediment transport, nutrient cycling, and ecosystem services, supporting both natural habitats and human activities (Ferreira et al., 2023). In many regions, small tributaries are particularly vulnerable to morphological alterations and channel instability, driven by both natural processes and anthropogenic pressures. These factors can increase flood susceptibility, accelerate bank erosion, and affect the performance of existing hydraulic infrastructure (Lin et al., 2020; Wang et al., 2021).

These processes are closely linked to the dynamic nature of fluvial environments, where erosion, sediment transport, and deposition continuously reshape channel and floodplain configuration. The interaction between natural processes and anthropogenic influences controls river corridor evolution and flow behaviour. Understanding these mechanisms allows a more accurate evaluation of channel stability and contributes to effective river management strategies (Sabou et al., 2025).

Accurate terrain representation is therefore required for the assessment, planning, and design of river engineering interventions, since topography governs flow direction, velocity, and water distribution. Digital Terrain Models (DTMs) are commonly used as input for hydraulic simulations, including flood modelling, channel morphology assessment, and hazard mapping (Muhadi et al., 2020). In small stream environments, where micro-topographic variations can significantly alter flow patterns, the quality and resolution of topographic data strongly influence modelling reliability (Li et al., 2021).

Conventional surveying methods, such as Global Navigation Satellite System (GNSS) receivers and total station measurements, face significant limitations in small stream environments, where restricted accessibility, dense vegetation, and steep terrain reduce data

coverage and increase acquisition time, often resulting in incomplete terrain representation (Sestras et al., 2025a). Traditional cross-sectional surveying approaches, although accurate, are time-consuming, costly, and may involve operational risks, while also failing to provide spatially continuous and sufficiently dense topographic representation of river environments (Gou et al., 2026). These constraints highlight the need for alternative approaches capable of capturing detailed topographic information in complex conditions.

LiDAR (Light Detection and Ranging) technology has proven to be an effective solution for acquiring high-resolution topographic data, as it generates dense three-dimensional point clouds that capture terrain morphology, channel geometry, and surrounding features (Marotta et al., 2021). Unlike photogrammetric methods, LiDAR data can be acquired under a wide range of conditions, including low-light or cloudy environments, while its capacity to penetrate vegetation enables the extraction of ground points in densely vegetated and urban areas, supporting the generation of reliable DTMs (Muhadi et al., 2020). At the same time, the integration of UAV photogrammetry and LiDAR enhances terrain modelling by leveraging the strengths of each method, enabling more accurate representation under varying surface and environmental conditions (Sestras et al., 2025b).

The development of unmanned aerial systems has further extended the use of LiDAR in environmental and engineering applications. UAV (Unmanned Aerial Vehicle) platforms enable flexible data acquisition at high spatial resolution, particularly in areas where existing elevation data are limited or insufficient in detail for accurate analysis (Trepekli et al., 2022). These systems are increasingly applied in flood modelling and terrain representation, especially in small basins where detailed topography is required for reliable simulations (Annis et al., 2020; Li et al., 2021). UAV-based LiDAR surveys can achieve centimetric accuracy, enabling the detection of topographic features such as small channels, roads, or surface irregularities that influence flow behaviour and flood propagation (Li et al., 2021).

High-density LiDAR datasets enable a detailed representation of terrain morphology, including channel features and floodplain topography, improving the accuracy of flood simulations. These datasets also support the identification of stream channels and tributary networks, as well as the extraction of morphological characteristics of river corridors (Grau et al., 2021). LiDAR-derived data have proven effective in generating Digital Elevation Models (DEMs) for hydraulic modelling and flood hazard assessment, particularly when integrated with simulation tools such as HEC-RAS (Mihu-Pintilie et al., 2019; Stoleriu et al., 2020).

The application of hydraulic models is often constrained by the need for large volumes of input data, including detailed stream geometry and flow characteristics, which are not always available in small or urban stream environments (Bolick et al., 2023). Most modelling studies also focus on larger river systems, while small streams are less frequently analysed, mainly due to the limited availability of consistent high-resolution topographic data, which increases uncertainty in hydrological and hydraulic analyses (Annis et al., 2020).

Beyond terrain modelling, LiDAR data support the analysis of geomorphological processes and terrain dynamics. Repeated acquisitions enable the detection of surface changes and the quantification of erosion and deposition through Digital Elevation Model of Difference (DoD) approaches (Li et al., 2024). The reliability of such analyses depends on factors such as point density and local terrain variability, which influence the accuracy of detected changes.

LiDAR-derived products also support advanced terrain analysis and feature extraction workflows. High-resolution Digital Elevation Models enable the identification of drainage patterns, small channels, and geomorphological structures through terrain analysis and machine learning techniques (Regmi et al., 2024; Busarello et al., 2025). These approaches support the analysis of channel morphology and geomorphological processes. LiDAR data also facilitate the monitoring of channel adjustments and bank erosion, providing insight into river dynamics over time (El-Khoury et al., 2025; Andualem et al., 2024).

The integration of Digital Surface Models (DSMs) and DEMs allows the selective incorporation of structural features such as embankments, bridges, and other built

structures, improving the representation of their hydraulic influence on flow behaviour and flood extent (Lee et al., 2025).

Despite these advantages, the use of high-resolution LiDAR point clouds also introduces practical limitations. Sub-meter resolution leads to large data volumes, often requiring simplification, such as subsampling, or scale adaptation for efficient use in hydrological applications, particularly over extended areas (Almeida et al., 2024). LiDAR systems are also limited in water-covered areas, as laser pulses are reflected by the water surface, preventing the acquisition of reliable information on channel bed morphology (Gou et al., 2026).

This study presents a complete UAV-LiDAR workflow for small stream assessment and rehabilitation, from data acquisition and point cloud processing to the generation of topographic products and hydraulic modelling inputs. The proposed methodology was applied to an urban stream sector requiring rehabilitation works and resulted in the generation of a classified point cloud, vectorized topographic features, a Digital Terrain Model and cross-sections used for hydraulic modelling. The generated datasets supported both the preparation of the topographic documentation submitted for technical acceptance by the Office of Cadastre and Real Estate Publicity (OCPI) and the evaluation of existing and proposed hydraulic conditions in HEC-RAS.

## MATERIALS AND METHODS

### *Study area*

The study area is located in north-western Romania, within Bihor County, in the built-up area of Peștiș village, administratively belonging to Aleșd town (Figure 1). The investigated watercourse is Valea Secătura, also known locally as Valea Șinteu, cadastral code III.1.44.19.2.0.0, situated within the Crișul Repede River basin. Figure 1 illustrates the geographical location of the study area at multiple spatial scales, including the position of Bihor County within Romania (Figure 1A), the location of Aleșd administrative territory within the county (Figure 1B), and the hydrographic context of Valea Secătura within the local drainage network (Figure 1C).

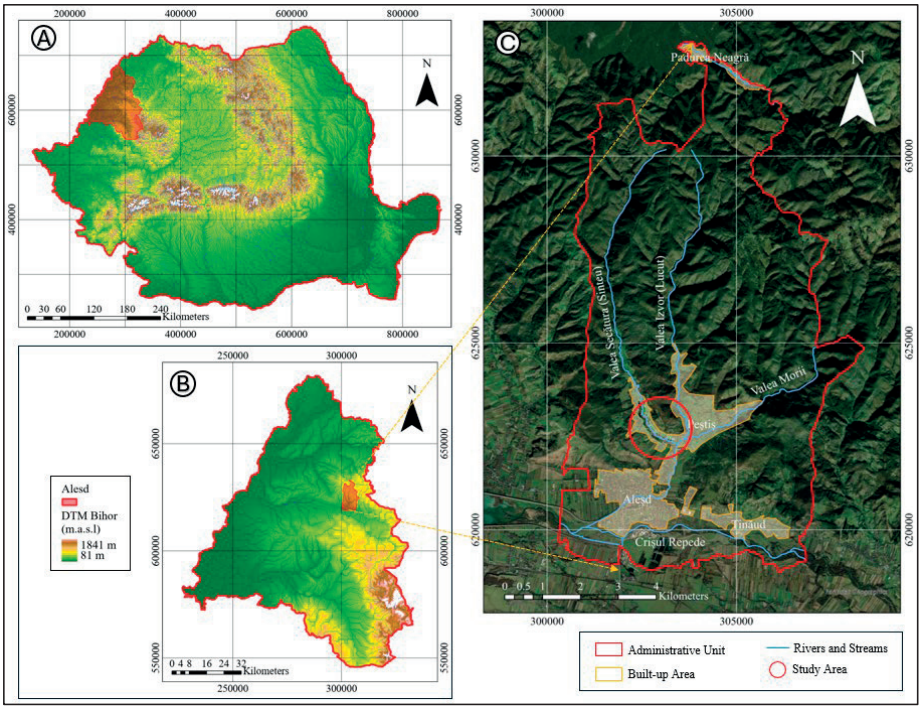



Figure 1. Geographic location of the study area and hydrographic context of Valea Secătura

According to the national hydrographic data and the technical documentation prepared for the rehabilitation project, Valea Secătura is a right-bank tributary of Valea Izvor (locally known as Valea Lucut), while Valea Izvor also collects the waters of Valea Morii (Valea Peștiș) in its upstream sector. Through this drainage network, the waters of Valea Secătura and Valea Morii are collected by Valea Izvor and ultimately discharge into the Crișul Repede River.

Based on cadastral records, Valea Secătura has a total length of approximately 9.6 km and drains a catchment area of about 14 km². The present study focuses on a 1.7 km sector of Valea Secătura situated within the built-up area of Peștiș village. The UAV-LiDAR survey covered the entire investigated sector, including the area targeted by the rehabilitation project entitled *"Amenajarea Valea Secătura (Șinteu)"*, for which engineering design and topographic documentation were required. The proposed rehabilitation works are concentrated on a channel sector of approximately 1 km located within the LiDAR survey corridor. In the built-up area of Peștiș village, the stream corridor is strongly influenced by anthropogenic activities and existing infrastructure, including local roads, residential properties, access crossings, bridges, retaining walls, and other hydraulic protection structures, as illustrated in Figure 2.



Figure 2. Aerial view of the investigated sector of Valea Secătura within the built-up area of Peștiș village

As a result, the channel is highly constrained and its morphology is largely controlled by previous engineering interventions. The technical documentation describes the watercourse as being bordered by roads and adjacent properties throughout the regulated sector. Existing hydraulic structures and the current channel configuration are presented in Figure 3.



Figure 3. Existing hydraulic infrastructure and anthropogenic constraints

Many of the existing hydraulic structures were originally constructed as part of the *"Regularizare Valea Izvor și afluenți"* project in 1987. Subsequent technical inspections revealed substantial deterioration of the hydraulic infrastructure, including damage to retaining walls, erosion of the channel bed and banks, discontinuities within existing protection works, sediment accumulation within the channel, and local reductions in flow capacity caused by bridges, footbridges, and access crossings. Combined with recurrent flood events, these processes progressively reduced the functionality of the existing works and highlighted the need for rehabilitation measures.

The rehabilitation project developed for the investigated sector proposes the demolition of approximately 1,819 m of existing retaining walls, reprofiling of 1,028 m of channel, and the construction of 2,056 m of new bank protection structures. Additional measures include the rehabilitation of existing crossings and the reconstruction of channel stabilization works designed to improve flow capacity and enhance the long-term stability of the channel.

Given the complexity of the site, the presence of ageing hydraulic infrastructure, and the need for detailed geometric information to support engineering design, the study area provides an appropriate framework for demonstrating the applicability of high-density UAV-LiDAR surveys in stream rehabilitation projects. The generated topographic datasets support the creation of high-resolution Digital Terrain Models, the extraction of engineering features, and the preparation of hydraulic modelling inputs required for stream assessment and rehabilitation works.

***UAV-LiDAR data acquisition and processing workflow***

The methodological framework adopted in this study integrates UAV-LiDAR data acquisition, GNSS-supported trajectory correction, LiDAR data processing, and the generation of topographic products required for hydraulic modelling and rehabilitation design. The complete workflow adopted in this study is presented in Figure 4.

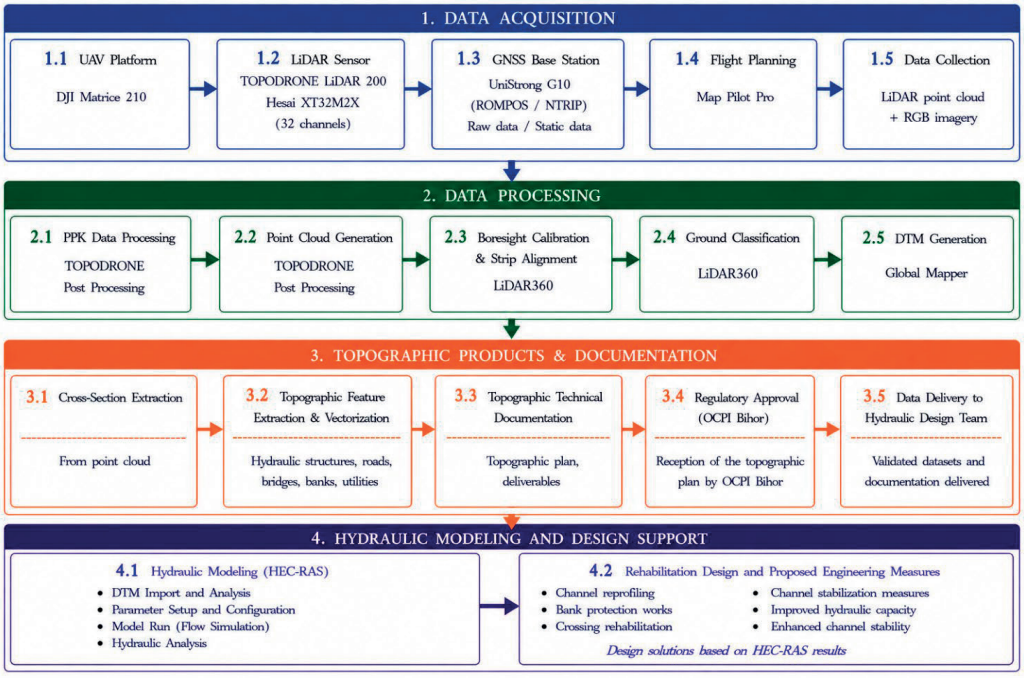



Figure 4. UAV-LiDAR data acquisition and processing workflow

The UAV-LiDAR survey was designed to acquire high-density airborne LiDAR data suitable for the generation of detailed topographic products required for stream assessment, hydraulic analysis, and rehabilitation planning along Valea Secătura. Attention was given to ensuring complete coverage of the stream corridor and adjacent infrastructure, including retaining structures, bridges, access crossings, roads, and neighbouring properties, while maintaining a consistent point density throughout the surveyed area.

Data acquisition was carried out using a DJI Matrice 210 unmanned aerial platform equipped with a TOPODRONE LiDAR 200 system integrating a Hesai XT32M2X laser scanner. The sensor incorporates 32 laser channels and a maximum acquisition rate of up to 640,000 points per second, enabling the collection of high-density point clouds suitable for detailed terrain modelling and the representation of both natural and engineered features within the investigated stream corridor. Simultaneously, RGB imagery was acquired using the onboard Zenmuse X4S camera. Although the primary objective of the survey was the acquisition of LiDAR data, the imagery was subsequently used for orthophoto generation and RGB colorization of the LiDAR point cloud.

Flight planning was performed in Map Pilot Pro using terrain-following functionality based on the Copernicus DEM. The mission was conducted at an average altitude of 100 m above ground level, allowing the UAV to maintain a nearly constant distance from the terrain surface throughout the survey. This approach reduced variations in point density associated with terrain elevation changes and improved the geometric consistency of the acquired dataset. The survey covered the entire 1.7 km study corridor along Valea Secătura, extending

beyond the proposed rehabilitation sector in order to capture the surrounding terrain and infrastructure necessary for the preparation of topographic documentation and hydraulic analyses. The main UAV-LiDAR mission parameters are presented in Table 1.

Table 1. UAV-LiDAR mission parameters

| Parameter | Value |
|---|---|
| Flight mission | Linear mission |
| Survey area | 30.22 ha |
| Survey corridor length | 3.45 km |
| Flight altitude (AGL) | 100 m |
| Flight speed | 6.0 m/s |
| Flight duration | 11 min 15 s |
| Number of flight lines (passes) | 2 |
| Forward/Side overlap | 75% / 75% |

The flight configuration consisted of two parallel flight lines following the longitudinal axis of the watercourse, ensuring complete coverage of the investigated corridor and sufficient overlap between the LiDAR strips.
The flight plan and survey coverage area are presented in Figure 5.

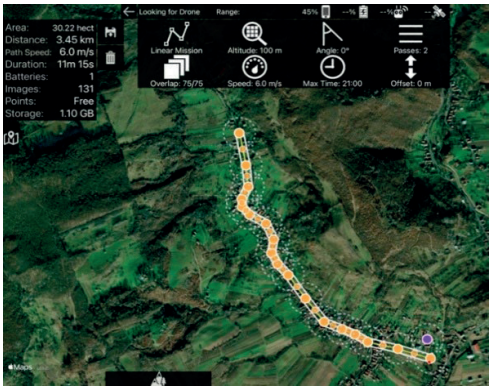



Figure 5. UAV-LiDAR mission planning

A dual-frequency UniStrong G10 GNSS receiver was installed at a location providing favourable satellite visibility and connected to the Romanian Positioning System (ROMPOS) through the Networked Transport of RTCM via Internet Protocol (NTRIP) service. The coordinates of the receiver position were initially determined using Real-Time Kinematic (RTK) positioning, after which the receiver was switched to static mode and continuously recorded raw GNSS observations during the survey. Following the initialization of the GNSS base station, the UAV-LiDAR survey was conducted while both the ground receiver and the onboard GNSS receiver (Helix antenna) simultaneously recorded raw satellite observations.
Data acquisition was conducted under favourable meteorological conditions, characterized by low wind speeds and the absence of precipitation. These conditions reduced vegetation movement during scanning and improved the quality of the acquired LiDAR data, supporting subsequent point cloud processing and ground classification.
Raw GNSS observations recorded by both the reference station and the onboard UAV receiver were processed using Post-Processed Kinematic (PPK) techniques to refine the flight trajectory and improve the positional accuracy of the LiDAR dataset. The TOPODRONE LiDAR Post Processing interface and the main processing parameters are presented in Figure 6.

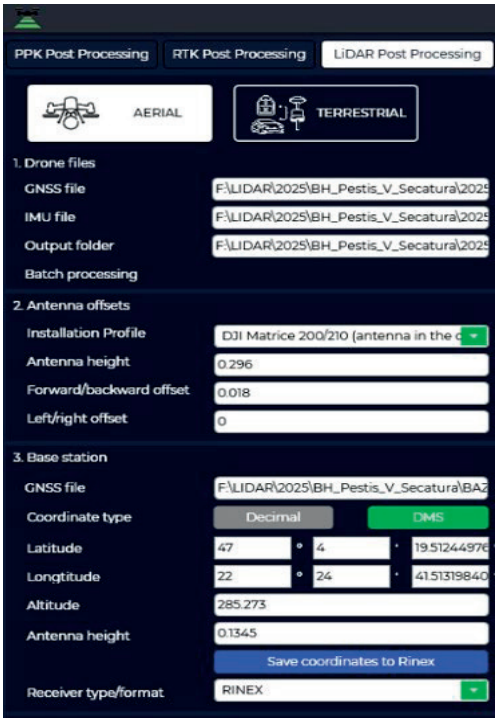



Figure 6. TOPODRONE LiDAR Post Processing interface and configuration parameters

The observations collected by the UniStrong G10 reference station were exported and converted to Receiver Independent Exchange Format (RINEX) files before being imported

into TOPODRONE Post Processing software together with the GNSS and Inertial Measurement Unit (IMU) data recorded by the UAV platform. The processing procedure incorporated UAV data files, antenna offsets, reference station coordinates, and the corresponding RINEX file to compute a corrected trajectory. The resulting solution enabled accurate reconstruction of the UAV trajectory and precise positioning of the LiDAR observations throughout the survey.

Following trajectory refinement, the LiDAR observations stored in PCAP format and the corresponding POS trajectory file were imported into TOPODRONE software for point cloud generation. This procedure integrated the corrected trajectory with the LiDAR measurements, enabling the calculation of the spatial coordinates of individual laser returns and the generation of the point cloud, as illustrated in Figure 7.

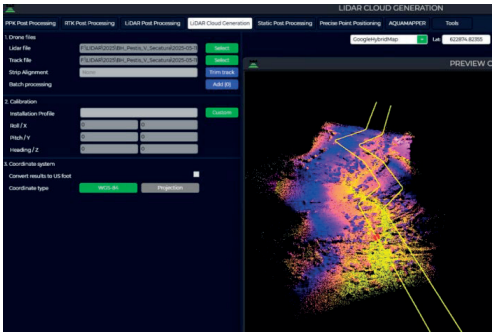



Figure 7. Point cloud generation in TOPODRONE software

The generated point cloud was processed in LiDAR360. Point cloud segments affected by increased positional uncertainty during UAV manoeuvres at flight-line transitions were excluded from further processing. These areas are typically associated with larger roll and pitch variations, which may introduce geometric distortions and reduce local accuracy. Boresight calibration was then performed to compensate for residual angular offsets between the GNSS receiver, IMU, and LiDAR sensor. Strip alignment procedures were subsequently applied to minimize positional discrepancies between overlapping flight strips. The aligned point cloud and a cross-sectional view of the dataset are presented in Figure 8.

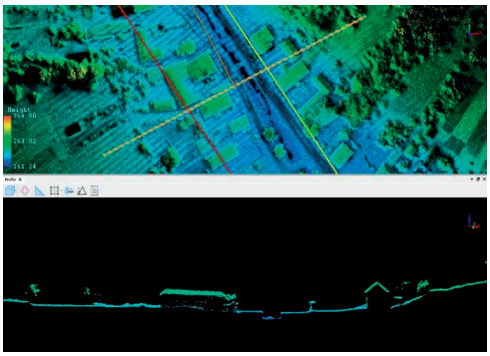


Figure 8. Strip alignment results and cross-sectional view of the LiDAR point cloud

The effectiveness of the calibration and strip alignment procedures was evaluated using the alignment statistics generated in LiDAR360. Boresight corrections involving roll, pitch, and heading adjustments were applied during the calibration process. The adjustment process reduced the maximum alignment error from 2.073 m to 0.079 m and the RMSE from 0.820 m to 0.029 m. The calibration report and alignment statistics are shown in Figure 9.

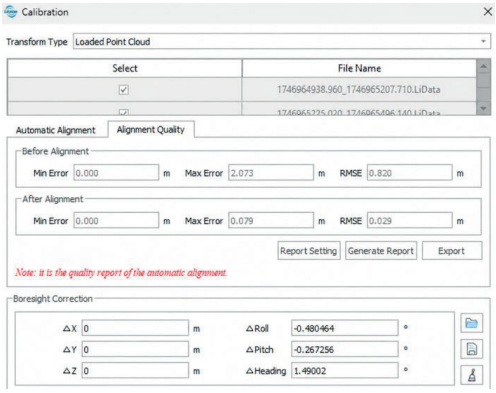



Figure 9. Calibration report and alignment statistics obtained in LiDAR360

The calibrated point cloud was further classified in LiDAR360 using the ground filtering algorithm to separate ground points from vegetation and other non-terrain features. Accurate ground classification is particularly important in stream environments, where riparian vegetation may significantly influence terrain representation and obscure the underlying terrain surface. Non-ground points were subsequently removed and the ground

class was extracted to generate a filtered dataset representing the bare-earth surface.

The extraction of the ground class represents a necessary stage in the LiDAR processing workflow, as the accuracy of the Digital Terrain Model depends on the correct identification of terrain points. Inaccurate classification may result in the inclusion of vegetation or other non-terrain features within the terrain model, potentially introducing local distortions in channel geometry and bank morphology. Particular attention was therefore given to the inspection of the classified dataset to ensure a continuous representation of the terrain throughout the surveyed corridor, including areas characterized by dense riparian vegetation. The resulting ground-filtered point cloud is presented in Figure 10.

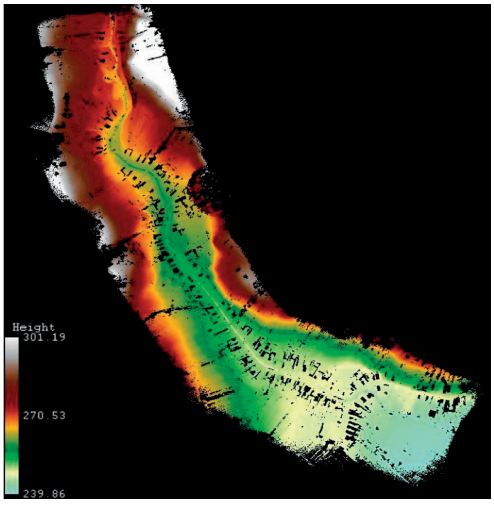



Figure 10. Ground-classified LiDAR point cloud

The ground-classified point cloud was processed in Global Mapper to generate the DTM. The terrain model captured the geometry of the stream channel, bank morphology, adjacent infrastructure, and surrounding terrain, providing spatial information for topographic and hydraulic applications. The density of the UAV-LiDAR dataset allowed the preservation of fine-scale terrain characteristics that are often difficult to identify using conventional surveying methods. The DTM generated for the investigated sector together with an example cross-section extracted from the terrain model are shown in Figure 11.

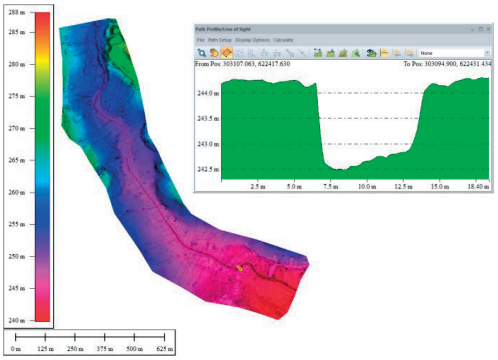


Figure 11. Digital Terrain Model and sample cross-section derived from the terrain model

Classified ground point cloud was used to derive the topographic information required to satisfy the beneficiary's requirements. Using the longitudinal axis of the watercourse as a reference, a total of 52 cross-sections were automatically generated in 3Dsurvey software and manually reviewed to identify and remove potential geometric irregularities resulting from the extraction process. Vector features required for topographic mapping, including points, breaklines, and other terrain elements, were extracted from the classified point cloud. The extracted datasets were used for the preparation of the topographic documentation submitted for technical acceptance by the Office of Cadastre and Real Estate Publicity (OCPI). Following acceptance, the approved topographic plan, together with the DTM and extracted cross-sections, was delivered to the beneficiary and subsequently used by the design team as input data for hydraulic analyses and the development of rehabilitation solutions for the investigated sector. The resulting products and their applications are presented in the following section.

## RESULTS AND DISCUSSIONS

### *Topographic products*

The generated topographic products provided the geometric information required for both engineering documentation and hydraulic modelling. These products included the classified point cloud, DTM, cross-sections, and the topographic plan submitted for technical acceptance by OCPI. A portion of the generated topographic plan is shown in Figure 12.

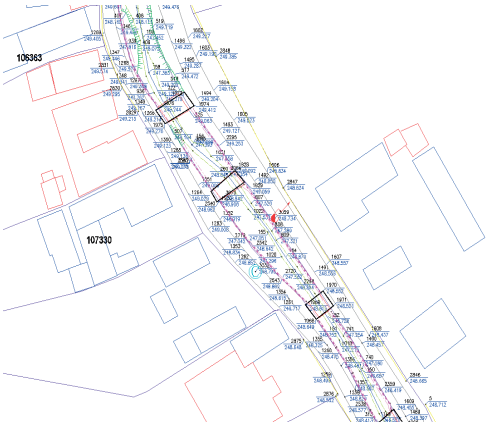



Figure 12. Topographic plan derived from the UAV-LiDAR survey.

The level of detail provided by the generated products enabled the identification of channel banks, hydraulic structures, road crossings, and other natural and anthropogenic features required for hydraulic modelling. The resulting DTM preserved subtle terrain variations along the stream corridor, allowing local morphological features to be represented with a level of detail that is difficult to achieve using conventional surveying methods. Similar findings have highlighted the importance of accurate ground point classification for generating reliable DTM suitable for engineering applications (Oniga et al., 2024).
The adopted workflow and the obtained results demonstrate that UAV-LiDAR surveys provide the topographic information required for engineering projects developed along narrow stream corridors. Comparable findings have been reported for the use of high-density LiDAR datasets in detailed terrain characterization supporting hydraulic analyses and river management applications (Stoleriu et al., 2020; Li et al., 2021).

***Hydraulic assessment of existing conditions***

The topographic products derived from the UAV-LiDAR survey constituted the basis for hydraulic modelling of the investigated sector.
The DTM, extracted cross-sections, and vectorized infrastructure elements were integrated into the HEC-RAS modelling environment to simulate hydraulic conditions corresponding to the climate change-adjusted design discharge with a 1% exceedance probability (Q1% = 47.70 m³/s). Two hydraulic modelling scenarios were analysed: the existing channel conditions at the time of the UAV-LiDAR survey and the proposed engineering solution developed for the investigated sector.
The hydraulic modelling results for the existing channel conditions and the proposed engineering solution are presented in Figures 13 and 14, respectively.

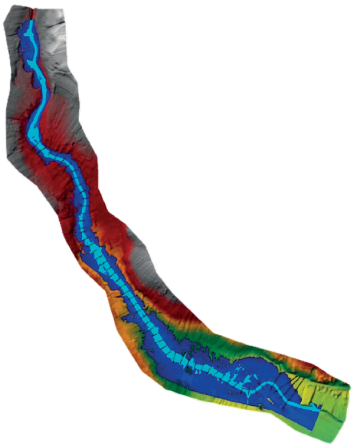


Figure 13. HEC-RAS hydraulic model of the investigated sector under existing conditions

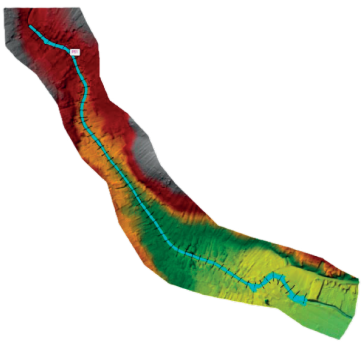


Figure 14. HEC-RAS hydraulic model of the proposed engineering solution

The comparison of these scenarios enabled the evaluation of the expected hydraulic performance of the proposed rehabilitation measures under identical hydrological conditions.
Simulation of the existing channel conditions revealed the influence of local geometric constraints associated with ageing hydraulic structures, channel degradation, sediment accumulation, and the consequent reduction in

flow conveyance capacity within several sections of the investigated corridor.

The reliability of hydraulic simulations is strongly dependent on the quality of the DTM and the geometric datasets used to construct the hydraulic model, including extracted cross-sections and vectorized infrastructure elements. Previous studies have demonstrated that high-resolution UAV-derived topographic datasets improve terrain representation and provide a reliable geometric basis for hydraulic modelling, flood hazard assessment, and the evaluation of engineering solutions (Mihu-Pintilie et al., 2019; Bilașco et al., 2021). The results obtained in the present study are consistent with these findings, demonstrating that the generated DTM and extracted cross-sections provided the geometric detail required for a realistic representation of hydraulic conditions within the investigated stream corridor.

### *Rehabilitation design and hydraulic performance*

Based on the hydraulic assessment, a rehabilitation solution was proposed for the investigated sector of Valea Secătura. The proposed design comprised channel reprofiling over approximately 1 km, reconstruction of bank protection structures with a total length of approximately 2 km, replacement of deteriorated retaining walls, and additional stabilization measures intended to improve hydraulic performance and channel stability.

The main hydraulic parameters for the representative cross-section (P20) under existing and proposed conditions are compared in Table 2. Both simulations were performed using the same climate change-adjusted design discharge (Q1% = 47.70 m³/s), allowing the differences in the hydraulic response to be attributed exclusively to the proposed channel geometry.

Table 2. Comparative hydraulic indicators for representative cross-section P20

| Hydraulic parameter | Existing | Proposed |
|---|---|---|
| Design discharge (m³/s) | 47.7 | 47.7 |
| Channel bed elevation (m) | 244.45 | 243.37 |
| Wetted area (m²) | 22.44 | 14.42 |
| Wetted perimeter (m) | 26.33 | 10.49 |
| Hydraulic radius (m) | 0.85 | 1.37 |
| Roughness coefficient (left bank) | 0.04 | 0.02 |
| Roughness coefficient (channel) | 0.04 | 0.03 |
| Roughness coefficient (right bank) | 0.04 | 0.02 |
| Mean flow velocity (m/s) | 2.13 | 3.31 |
| Maximum water level (m) | 246.65 | 245.69 |

Figure 15 presents the representative cross-section (P20), showing the existing ground profile together with the proposed engineering solution. The trapezoidal channel geometry was designed to provide adequate flow capacity while accommodating the local topographic and infrastructural constraints. The proposed design also accounted for existing crossings, adjacent properties, and the demolition and reconstruction of deteriorated hydraulic structures as part of the planned rehabilitation works.

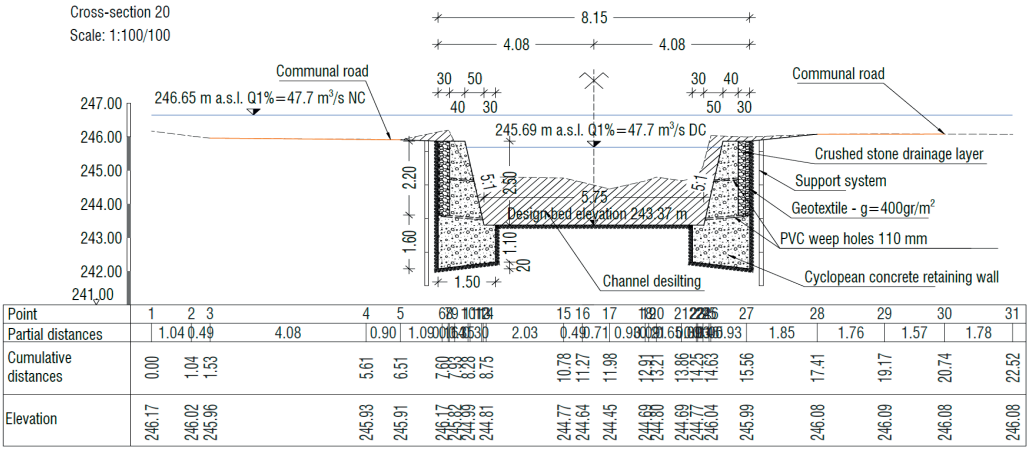



Figure 15. Designed cross-section (P20)

The comparison between the existing and proposed channel conditions demonstrated the importance of detailed topographic information for evaluating the hydraulic response of the investigated sector prior to implementation. High-resolution UAV-LiDAR datasets enabled the realistic representation of channel geometry and surrounding infrastructure, providing the basis required for hydraulic modelling and engineering design. Similar integrated approaches combining detailed terrain models, GIS analyses, and hydraulic simulations have been shown to support the evaluation and optimization of river rehabilitation solutions (Bilașco et al., 2021).

## CONCLUSIONS

This study demonstrated the applicability of UAV-LiDAR technology for acquiring high-resolution topographic data to support small stream assessment and rehabilitation planning. The proposed workflow, integrating PPK trajectory correction, LiDAR point cloud generation and calibration, ground classification, and terrain modelling, produced high-resolution topographic datasets suitable for cadastral documentation and hydraulic modelling.

The adopted methodology generated a DTM, a classified ground point cloud, vectorized topographic features required for the preparation of the topographic plan, and 52 cross-sections along the investigated sector of Valea Secătura. The resulting topographic plan was submitted for technical acceptance by the OCPI. Following technical approval, the approved topographic plan, together with the DTM, classified point cloud, and extracted cross-sections, was delivered to the design team.

Integration of these topographic datasets into the HEC-RAS modelling environment enabled the evaluation of existing hydraulic conditions and the assessment of the proposed engineering solution under the climate change-adjusted design discharge. The resulting analyses supported the identification of channel deficiencies and the design of channel reprofiling, bank protection structures, retaining walls, and additional stabilization measures adapted to the characteristics of the investigated sector.

The obtained results confirm that UAV-LiDAR surveys provide an efficient alternative to conventional topographic surveying methods for engineering projects involving small watercourses. The high density of the acquired point cloud enabled detailed representation of channel geometry, surrounding infrastructure, and terrain morphology.

At the time of manuscript preparation, the rehabilitation solution developed using the generated topographic and hydraulic datasets is under implementation within the investigated sector. This demonstrates the practical applicability of the proposed workflow and highlights the value of integrating UAV-LiDAR technology with hydraulic modelling to support real-world small stream rehabilitation projects.

## REFERENCES

Almeida, A. A. R. D., Mendonça, R. L., Silva, N. M. M., & da Paz, A. R. (2024). Evaluation of LiDAR-derived river networks coarsening with spatial patterns preservation. *Computers & Geosciences*, *189*, 105639.

Andualem, T. G., Peters, S., Hewa, G. A., Myers, B. R., Boland, J., & Pezzaniti, D. (2024). Channel morphological change monitoring using high-resolution LiDAR-derived DEM and multi-temporal imageries. *Science of the Total Environment*, *921*, 171104.

Annis, A., Nardi, F., Petroselli, A., Apollonio, C., Arcangeletti, E., Tauro, F., Belli, C., Bianconi, R., & Grimaldi, S. (2020). UAV-DEMs for small-scale flood hazard mapping. *Water*, *12*(6), 1717.

Bilașco, Ș., Roșca, S., Vescan, I., Fodorean, I., Dohotar, V., & Sestras, P. (2021). A GIS-based spatial analysis model approach for identification of optimal hydrotechnical solutions for gully erosion stabilization. Case Study. *Applied Sciences*, *11*(11), 4847.

Bolick, M. M., Post, C. J., Naser, M. Z., Forghanparast, F., & Mikhailova, E. A. (2023). Evaluating urban stream flooding with machine learning, LiDAR, and 3D modeling. *Water*, *15*(14), 2581.

Busarello, M. D. S. T., Ågren, A. M., Westphal, F., & Lidberg, W. (2025). Automatic detection of ditches and natural streams from digital elevation models using deep learning. *Computers & Geosciences*, *196*, 105875.

El-Khoury, L., Kurki-Fox, J., & Doll, B. (2025). Quantifying streambank erosion: A comparison of physical surveys, aerial imagery and UAS LiDAR surveys. *Earth Surface Processes and Landforms*, *50*(6), e70039.

Ferreira, V., Albariño, R., Larrañaga, A., LeRoy, C. J., Masese, F. O., & Moretti, M. S. (2023). Ecosystem services provided by small streams: an overview. *Hydrobiologia*, *850*(12), 2501-2535.

Gou, J., Lee, H., Park, J., Jang, S., Lee, N., & Song, I. (2026). Development of a stream DTM generation methodology using UAV-based SfM and LiDAR point cloud. *Scientific Reports*, *16.* 5178.

Grau, J., Liang, K., Ogilvie, J., Arp, P., Li, S., Robertson, B., & Meng, F. R. (2021). Using unmanned aerial vehicle and lidar-derived DEMs to estimate channels of small tributary streams. *Remote Sensing*, *13*(17), 3380.

Lee, S. J., Han, Y. S., Kim, J. S., & Yun, H. S. (2025). High-Resolution Flood Risk Assessment in Small Streams Using DSM–DEM Integration and Airborne LiDAR Data. *Sustainability*, *17*(21), 9616.

Li, B., Hou, J., Li, D., Yang, D., Han, H., Bi, X., Wang, CX., Hinkelmann, R., & Xia, J. (2021). Application of LiDAR UAV for high-resolution flood modelling. *Water Resources Management*, *35*(5), 1433-1447.

Li, P., Li, D., Hu, J., Fassnacht, F. E., Latifi, H., Yao, W., Gao, J., Chan, F.K., Dang, T., & Tang, F. (2024). Improving the application of UAV-LiDAR for erosion monitoring through accounting for uncertainty in DEM of difference. *Catena*, *234*, 107534.

Lin, L., Li, M., Chen, H., Lai, X., Zhu, H., & Wang, H. (2020). Integrating landscape planning and stream quality management in mountainous watersheds: A targeted ecological planning approach for the characteristic landscapes. *Ecological Indicators*, *117*, 106557.

Marotta, F., Teruggi, S., Achille, C., Vassena, G. P. M., & Fassi, F. (2021). Integrated laser scanner techniques to produce high-resolution DTM of vegetated territory. *Remote Sensing*, *13*(13), 2504.

Mihu-Pintilie, A., Cîmpianu, C. I., Stoleriu, C. C., Pérez, M. N., & Paveluc, L. E. (2019). Using high-density LiDAR data and 2D streamflow hydraulic modeling to improve urban flood hazard maps: A HEC-RAS multi-scenario approach. *Water*, *11*(9), 1832.

Muhadi, N. A., Abdullah, A. F., Bejo, S. K., Mahadi, M. R., & Mijic, A. (2020). The use of LiDAR-derived DEM in flood applications: A review. *Remote Sensing*, *12*(14), 2308.

Oniga, V. E., Loghin, A. M., Macovei, M., Lazar, A. A., Boroianu, B., & Sestras, P. (2024). Enhancing LiDAR-UAS derived digital terrain models with hierarchic robust and volume-based filtering approaches for precision topographic mapping. *Remote Sensing*, *16*(1), 78.

Regmi, N. R., Webb, N. D., Walter, J. I., Heo, J., & Hayman, N. W. (2024). Mapping landforms of a hilly landscape using machine learning and high-resolution LiDAR topographic data. *Applied Computing and Geosciences*, *24*, 100203.

Sabou, C. S., Bruma, S., Ioana, P. O. P., Matei, F., Sestras, P., Deak, J., ... & Salagean, T. River corridor change detection using satellite imagery and LiDAR data: a case study of the Siret river near Corbu Vechi village. *Scientific Papers. Series E. Land Reclamation, Earth Observation & Surveying, Environmental Engineering. XIV*, 985-993

Sestras, P., Badea, G., Badea, A. C., Salagean, T., Roșca, S., Kader, S., & Remondino, F. (2025a). Land surveying with UAV photogrammetry and LiDAR for optimal building planning. *Automation in Construction*, *173*, 106092.

Sestras, P., Badea, G., Badea, A. C., Salagean, T., Oniga, V. E., Roșca, S., ... & Nedevschi, S. (2025b). A novel method for landslide deformation monitoring by fusing UAV photogrammetry and LiDAR data based on each sensor's mapping advantage in regards to terrain feature. *Engineering Geology*, *346*, 107890.

Stoleriu, C. C., Urzica, A., & Mihu-Pintilie, A. (2020). Improving flood risk map accuracy using high-density LiDAR data and the HEC-RAS river analysis system: A case study from north-eastern Romania. *Journal of flood risk management*, *13*, e12572.

Trepekli, K., Balstrøm, T., Friborg, T., Fog, B., Allotey, A. N., Kofie, R. Y., & Møller-Jensen, L. (2022). UAV-borne, LiDAR-based elevation modelling: A method for improving local-scale urban flood risk assessment. *Natural Hazards*, *113*(1), 423-451.

Wang, R., Kim, J. H., & Li, M. H. (2021). Predicting stream water quality under different urban development pattern scenarios with an interpretable machine learning approach. *Science of the Total Environment*, *761*, 144057.

Scientific Papers. Series E. Land Reclamation, Earth Observation & Surveying, Environmental Engineering. Vol. XV, 2026
Print ISSN 2285-6064, CD-ROM ISSN 2285-6072, Online ISSN 2393-5138, ISSN-L 2285-6064

# UAV-DERIVED VEGETATION INDICES FOR SPATIAL ASSESSMENT OF WEED INFESTATION IN ARABLE CROPS

**Claudiu-Daniel UTOIU[1], Bogdan DRAGANCEA[2], Elena UTOIU[2], Catalin LAZAR[3], Mihai GIDEA[1]**

[1]University of Agronomic Sciences and Veterinary Medicine of Bucharest,
59 Marasti Blvd, District 1, Bucharest, Romania
[2]National Institute of Research & Development for Food Bioresources,
6 Dinu Vintila Street, District 2, Bucharest, Romania
[3]National Agricultural Research and Development Institute Fundulea, 915200,
Fundulea, Călăraşi County, Romania

Corresponding author email: claudiu.utoiu@gmail.com

***Abstract***

*Early identification of weed infestation is essential for improving the efficiency and sustainability of crop protection practices. This paper presents a spatial assessment of weed infestation in arable crops based on vegetation indices derived from unmanned aerial vehicle (UAV) multispectral imagery. UAV flights were conducted during early crop development stages, and the acquired data were processed to generate NDVI-based spatial maps. Spatial variability analysis was applied to differentiate crop-dominated areas from zones affected by weeds and to identify infestation hotspots within the field. The results indicate that UAV-derived vegetation indices provide valuable information for early weed detection and support site-specific management decisions. The proposed approach contributes to reducing unnecessary agrochemical inputs and promotes more environmentally responsible weed control strategies. This work highlights the potential of UAV-based monitoring as a practical tool for supporting precision agriculture and integrated weed management in arable farming systems.*

***Key words****: NDVI, precision farming, spatial analysis, UAV, weed infestation.*

## INTRODUCTION

Weed infestation remains a major constraint on crop productivity, input-use efficiency, and the sustainability of arable farming systems. Because weeds are rarely distributed uniformly within a field and instead tend to occur in patches, uniform herbicide application often leads to unnecessary chemical use, higher production costs, and greater environmental pressure. Site-specific weed management addresses this limitation by targeting interventions only where weed pressure justifies treatment, provided that reliable spatial information is available at the appropriate stage of crop development (López-Granados, 2011; Peña et al., 2013).

In this context, unmanned aerial vehicles (UAVs) provide an effective remote-sensing platform for early weed assessment in arable crops. Their flexibility in acquisition timing, low flight altitude, and centimetre-level spatial resolution make them especially useful during early growth stages, when crop and weed plants are still small and spatially distinguishable. When equipped with multispectral sensors, UAVs can capture reflectance in the visible, red-edge, and near-infrared regions, enabling the calculation of vegetation indices such as NDVI, NDRE, GNDVI, and chlorophyll-related metrics that support vegetation discrimination, crop vigor assessment, and the detection of anomalous zones associated with weed infestation (Clevers & Gitelson, 2013; Schlemmer et al., 2013; Stroppiana et al., 2018). Even so, spectral information alone is rarely sufficient for reliable weed discrimination, because crops and weeds may show similar reflectance patterns at early developmental stages. For this reason, vegetation indices are most useful when interpreted together with spatial variability analysis, crop-row structure, field observations, and management-zone delineation. This integrated approach strengthens weed mapping, hotspot identification, and the practical implementation of targeted herbicide application or other

integrated weed management strategies. Weed mapping is therefore one of the most promising UAV applications in precision agriculture, although its wider use still depends on robust classification under variable field conditions (López-Granados, 2011).

Despite the increasing number of studies addressing UAV-based weed mapping, several methodological limitations remain insufficiently resolved. First, many approaches rely on vegetation indices as direct indicators of weed presence, although crop and weed plants may exhibit similar spectral responses during early growth stages. Second, the transition from spectral variability maps to agronomically meaningful weed-management zones is not always clearly described, particularly in relation to crop-row structure, vegetation masking, and hotspot delineation. Third, the operational feasibility of these workflows remains uneven, as some studies emphasize classification accuracy while providing limited discussion on radiometric calibration, field-side processing, and practical decision-support outputs. These gaps indicate the need for an integrated methodological framework that links UAV-derived vegetation indices with spatial analysis, crop geometry, validation requirements, and site-specific weed management decisions.

The practical relevance of UAV multispectral imagery in arable systems lies in its narrow spectral bands, typically including blue, green, red, red-edge, and near-infrared wavelengths, as used by platforms such as the MicaSense RedEdge family and DJI agricultural multispectral systems (MicaSense, 2024a). These bands support both conventional vigor indices and chlorophyll-sensitive or soil-adjusted metrics that become increasingly informative as canopy conditions vary. Therefore, the aim of this study was to evaluate how UAV-derived vegetation indices can be integrated with spatial analysis for the early assessment of weed infestation in arable crops. The specific objectives were: (i) to develop a structured image-processing workflow for generating radiometrically corrected vegetation-index maps; (ii) to assess the complementary role of NDVI, red-edge, chlorophyll-sensitive, and soil-adjusted indices in identifying vegetation variability; (iii) to translate index-based outputs into probable weed hotspots and management-oriented spatial layers; and (iv) to discuss the operational relevance, limitations, and scientific contribution of UAV-based weed assessment for site-specific weed management. The working hypothesis was that vegetation indices alone are insufficient for reliable weed discrimination, but their integration with crop-row structure, spatial aggregation, and field validation can improve the interpretation of weed infestation patterns and support more targeted crop-protection decisions.

Among lightweight multispectral solutions used in agricultural UAV applications, the Parrot Sequoia and Sequoia+ sensors are notable for integrating four narrow spectral bands - green, red, red-edge, and near-infrared - with an RGB camera and a sunshine sensor for radiometric correction. This configuration supports the generation of vegetation indices under changing illumination conditions and makes the system suitable for crop monitoring, vigor assessment, and weed-mapping workflows in precision agriculture (Parrot, 2025).

## MATERIALS AND METHODS

### *Study design and data acquisition*

Multispectral data acquisition was designed for photogrammetric reconstruction rather than routine RGB inspection. Flight plans followed grid missions with about 75% frontlap and 75% sidelap, extended beyond the field boundary, and, where crop rows were clearly visible, were oriented perpendicular to the rows to improve both row detection and image alignment. Illumination conditions were controlled by scheduling flights close to local solar noon and avoiding rapidly changing cloud cover. Reflectance-panel images were collected immediately before and after each mission, and these observations were complemented, when available, by downwelling light sensor measurements. Ground observations recorded during the flights were used to label crops, weed, mixed-vegetation, and bare-soil samples and to provide independent validation for the final maps (MicaSense, 2024b).

### *Orthomosaic generation and analytical workflow*

After image acquisition, the dataset was processed into a radiometrically corrected orthomosaic and, where useful, a digital surface

model, since UAV-derived 3-D information can support the structural interpretation of vegetation patterns and crop canopy variability (Torres-Sánchez et al., 2015). The workflow comprised reflectance calibration, image alignment, camera optimization, dense reconstruction, orthomosaic generation, and the derivation of vegetation-index layers for subsequent analysis. This sequence is consistent across the main software environments used for multispectral UAV processing, including Pix4D, Agisoft Metashape, OpenDroneMap/WebODM, and ArcGIS Drone2Map, even though implementation details differ among platforms (Agisoft, 2026).

For weed assessment, the analytical workflow moved from calibrated imagery to management-oriented outputs. Vegetation masks were created first, followed by crop-row or crop-object detection, and vegetation occurring outside expected crop positions was classified as probable weed cover. Where crop and weed signatures overlapped, additional multispectral, textural, or structural features were used to improve discrimination. The final weed layers were then aggregated into management cells to identify hotspots and support prescription mapping, in line with established UAV weed-mapping approaches in row and narrow-row crops (Torres-Sánchez et al., 2014).

***Image processing and vegetation index formulas***

*Radiometric and geometric preprocessing*

Radiometric and geometric preprocessing was treated as a prerequisite for any meaningful vegetation-index analysis. Raw multispectral values were first normalized and then corrected for sensor-specific effects such as black level, exposure, gain, and vignette distortion before conversion to radiance and reflectance. Panel-based calibration was used to scale imagery to certified reflectance values, while incident-light measurements provided an additional correction pathway for platforms equipped with light sensors. Band co-registration was then applied to ensure spatial correspondence among spectral channels before index calculation (DJI, 2020; DJI, 2023; MicaSense, 2026; MicaSense, n.d.).

$$p_n = \frac{DN}{2^N}$$

where DN is the raw pixel value and N is the sensor bit depth. This normalization step follows standard radiometric calibration workflows for multispectral sensors (MicaSense, 2026).

A practical panel-based reflectance conversion can then be expressed as:

$$k_\lambda = \frac{\rho_{\text{panel},\lambda}}{\bar{L}_{\text{panel},\lambda}}$$

$$R_\lambda(x,y) = k_\lambda\, L_\lambda(x,y)$$

where: ρpanel,λ is the certified reflectance of the calibration panel at wavelength λ, L̄panel,λ is the mean radiance measured over the panel region, and Rλ(x,y) is the reflectance image for that band. This panel-scaling approach is consistent with published multispectral image-processing workflows (MicaSense, n.d.).

If the sensor platform uses an incident light sensor, the reflectance formulation can be written in ratio form:

$$R_\lambda \propto \frac{X_{\text{camera},\lambda}}{X_{\text{incident},\lambda}}$$

Incident-light formulations estimate band reflectance as the ratio between reflected and incoming radiation, with band-specific calibration parameters used for sensor harmonization in DJI multispectral systems (DJI, 2023).

A generic vignette correction can be modeled with a radial polynomial:

$$I_c(x,y) = I(x,y)(k_6 r^6 + k_5 r^5 + \cdots + k_1 r + 1)$$

where is the distance from the optical center and is the corrected image. Radial-polynomial vignette correction and band co-registration through homography-based alignment are standard steps in DJI multispectral image processing (DJI, 2020).

$$\begin{bmatrix} x' \\ y' \\ w' \end{bmatrix} = H \begin{bmatrix} x \\ y \\ 1 \end{bmatrix}, \qquad (x_r, y_r) = \left(\frac{x'}{w'}, \frac{y'}{w'}\right),$$

where is the alignment matrix estimated between bands, consistent with DJI multispectral preprocessing workflows (DJI, 2020).

*Vegetation indices appropriate for weeds and crop vigor*

NDVI was retained as the principal indicator because it is well suited to early crop development and sparse to moderate canopy cover, which matches the objective of early weed detection. To reduce the known limitations of NDVI under dense canopies or strong soil background, the analysis also included red-edge, chlorophyll-sensitive, and soil-adjusted indices.

Together, these indices provide a more stable description of vegetation status, chlorophyll-related variability, and partial soil exposure than NDVI alone (MicaSense, 2024c).

$$NDVI = \frac{NIR - Red}{NIR + Red}$$

$$NDRE = \frac{NIR - RedEdge}{NIR + RedEdge}$$

$$GNDVI = \frac{NIR - Green}{NIR + Green}$$

$$SAVI = \left(\frac{NIR - Red}{NIR + Red + L}\right)(1 + L)$$

$$MSAVI2 = \frac{1}{2}\left[2(NIR + 1) - \sqrt{(2NIR + 1)^2 - 8(NIR - Red)}\right]$$

$$VARI = \frac{Green - Red}{Green + Red - Blue}$$

$$CI_{green} = \frac{NIR}{Green} - 1$$

$$CI_{red-edge} = \frac{NIR}{RedEdge} - 1$$

$$MTCI = \frac{B6 - B5}{B5 - B4}$$

These formulas correspond to index definitions described in sensor documentation, GIS platforms, and remote-sensing literature. NDVI and NDRE are detailed by MicaSense and Esri, while GNDVI, SAVI, MSAVI2, VARI, $CI_{green}$, $CI_{red\text{-}edge}$, and related indices are available in common geospatial processing environments used for vegetation analysis (MicaSense, 2024a; Esri, 2026).

In interpretive terms, NDVI was used to characterize vegetation presence and overall crop vigor, whereas NDRE, GNDVI, and chlorophyll indices were used to capture chlorophyll-related variation when foliage became denser and NDVI sensitivity declined. SAVI and MSAVI2 improved performance in areas with partial soil exposure, and VARI remained a useful visible-band alternative when only RGB data were available. The combined use of these layers provided a more robust basis for weed discrimination under varying crop and soil conditions (Clevers & Gitelson, 2013; Schlemmer et al., 2013; MicaSense, 2024a; 2024c; Esri, 2026).

***Software ecosystems and real-time workflows***

*Photogrammetry and geospatial processing software*

The software ecosystem was organized by analytical function rather than by brand name. Photogrammetric reconstruction and orthomosaic generation were supported by platforms such as PIX4Dfields, Agisoft Metashape, DJI Terra, ArcGIS Drone2Map, and OpenDroneMap/WebODM, all of which provide multispectral processing, radiometric correction, and export of index layers. GIS and raster analysis were then used for thresholding, map algebra, and spatial aggregation, while Python- and AI-based tools supported more advanced feature extraction and weed classification when row geometry alone was insufficient. This functional workflow reflects current practice in multispectral crop analysis and allows both standard mapping and more advanced computer-vision pipelines to be integrated within the same methodological framework (DJI, 2024; Agisoft, 2026; QGIS Project, 2026; Pix4D, n.d.).

***Real-time and near-real-time processing options***

Real-time implementation was considered as a spectrum of processing speeds rather than a single technical mode. The most operationally mature approach remains near-real-time fieldside processing, in which imagery is transferred to a laptop immediately after landing and processed into orthomosaics and index maps using software such as PIX4Dfields, DJI Terra, or ArcGIS Drone2Map. Fully onboard edge inference is increasingly feasible with embedded GPU platforms such as NVIDIA Jetson devices, particularly for lightweight detection or segmentation models, while cluster or server reconstruction remains useful when multispectral datasets are too large for rapid single-machine processing. In practical terms, near-real-time fieldside mapping currently offers the best balance between speed, robustness, and field usability for multispectral weed monitoring (DJI, 2024; Pix4D, 2024; NVIDIA, n.d.).

***Chlorophyll and weed quantification***

*Chlorophyll calculations*

Chlorophyll estimation from UAV multispectral imagery was approached as a calibrated remote-sensing problem rather than as a fixed biochemical conversion. The most defensible indicators for arable crops were chlorophyll-sensitive and red-edge indices such as $CI_{green}$,

$CI_{red\text{-}edge}$, MTCI, and NDRE, which have been shown to respond well to canopy chlorophyll and nitrogen variation. Because the relationship between index values and chlorophyll content depends on crop type, growth stage, canopy architecture, illumination, and soil background, empirical calibration against field or laboratory measurements remained necessary for quantitative interpretation (Clevers & Gitelson, 2013; Schlemmer et al., 2013; Tian et al., 2025).

$$CI_{green} = \frac{NIR}{Green} - 1$$

$$CI_{red-edge} = \frac{NIR}{RedEdge} - 1$$

$$MTCI = \frac{B6 - B5}{B5 - B4}$$

$$NDRE = \frac{NIR - RedEdge}{NIR + RedEdge}$$

$$\widehat{Chl} = \beta_0 + \beta_1 CI_{red-edge} + \varepsilon$$

$$\widehat{Chl} = f(NDRE,\ CI_{green},\ MTCI,\ texture,\ height)$$

$$C_a = 12.25A_{663.2} - 2.79A_{646.8}$$

$$C_b = 21.50A_{646.8} - 5.10A_{663.2}$$

$$C_{x+c} = \frac{1000A_{470} - 1.82C_a - 85.02C_b}{198}$$

These spectrophotometric equations provide a laboratory reference for chlorophyll a, chlorophyll b, and total carotenoid determination and may be used to validate UAV-derived chlorophyll-sensitive indices when destructive pigment analysis is available (Lichtenthaler & Buschmann, 2001).

*Weed calculations*

Weed quantification translated spectral outputs into agronomically meaningful metrics. A binary vegetation mask was first generated from an index threshold, after which crop-row geometry was used to separate probable weeds from crop vegetation. Weed cover, weed pressure, and weed density were then calculated within grid cells or management zones to support hotspot detection and variable-rate treatment decisions. Where needed, a combined stress layer integrating weed presence with crop physiological status was used as a decision-support indicator. Validation focused on weed-specific accuracy measures such as overall accuracy, omission error, and commission error, which provide a more useful assessment of management performance than visual interpretation alone (Torres-Sánchez et al., 2014; Stroppiana et al., 2018; Esri, 2026).

$$M_v(i) = \begin{cases} 1, & VI(i) \geq T_v \\ 0, & VI(i) < T_v \end{cases}$$

$$M_w = M_v \wedge \neg M_c$$

$$WC_j = \frac{A_{\text{weed},j}}{A_{\text{cell},j}} \times 100$$

$$WP_j = \frac{A_{\text{weed},j}}{A_{\text{weed},j} + A_{\text{crop},j}} \times 100$$

$$WD_j = \frac{n_{\text{weed},j}}{A_{\text{cell},j}}$$

$$H_j = z(WC_j) - z(CI_{red-edge,j})$$

$$OA = \frac{TP + TN}{TP + TN + FP + FN}$$

$$OE = \frac{FN}{TP + FN}$$

$$CE = \frac{FP}{TP + FP}$$

## RESULTS AND DISCUSSIONS

The proposed workflow illustrates how UAV-derived vegetation indices can provide a consistent basis for the early spatial assessment of weed infestation in arable crops. As shown in Figure 1, NDVI provided a useful first screening of vegetated areas and highlighted within-field variability that would not be captured by uniform field inspection. When interpreted alone, however, NDVI could not fully separate crop and weed signals, particularly where crop cover was already developing or where soil background remained visible.

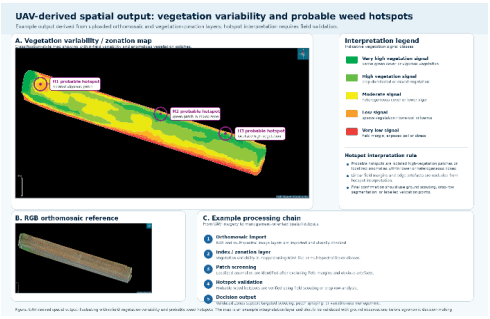



Figure 1. Example of a UAV-derived spatial output highlighting vegetation variability and probable weed hotspots within an arable field

The most informative interpretation was obtained when index maps were combined with crop-row structure and field observations, allowing anomalous vegetation outside expected crop positions to be interpreted more confidently as probable weed patches.

A second important result concerns the complementarity of the vegetation indices. As summarized in Table 1, NDVI remained useful for broad vegetation detection, but red-edge and chlorophyll-sensitive indices such as NDRE, GNDVI, $CI_{green}$, and $CI_{red-edge}$ added interpretive value where canopy density reduced NDVI sensitivity.

Table 1. Comparative relevance of selected vegetation indices for weed assessment in arable crops

| Ind | Veg. | Soi. | Den. | Ch | Wee | Prac |
|---|---|---|---|---|---|---|
| NDVI | High | Modera te | Moderate | Low | High | Initial screening |
| NDRE / red-edge | High | Modera te | High | High | High | Dense-canopy use |
| SAVI / MSAVI2 | Moderate | High | Moderate | Low–mod. | Modera te | Soil correction |

Soil-adjusted indices, including SAVI and MSAVI2, were particularly relevant during early growth stages or in sparsely covered areas, where bare soil influenced reflectance patterns. Taken together, these layers produced a more stable representation of crop vigor and weed-related spatial anomalies than any single index alone, improving the agronomic relevance of the resulting weed maps.

From an operational perspective, the main value of the approach lies in its ability to transform multispectral imagery into management-oriented outputs. Once vegetation masks and crop-row information were integrated, the analysis could delineate localized weed hotspots and aggregate them into treatment zones suitable for targeted intervention. This is directly aligned with site-specific weed management, where the objective is not only to detect weeds but also to support variable-rate herbicide application and reduce unnecessary chemical use. In this sense, the results reinforce the practical role of UAV monitoring as a decision-support tool for precision agriculture rather than as a purely descriptive remote-sensing exercise.

The hotspot labels indicate probable areas requiring field verification rather than confirmed weed infestation classes.

The results demonstrate that UAV-derived vegetation indices should be interpreted not only as descriptive indicators of vegetation vigor, but also as spatial decision-support layers for weed assessment. In scientific terms, the main significance of the workflow lies in its capacity to convert multispectral reflectance variability into agronomically interpretable patterns. NDVI provided an initial map of vegetation presence and within-field heterogeneity, while red-edge, chlorophyll-sensitive, and soil-adjusted indices helped refine the interpretation under variable canopy density and soil-background conditions. This supports the view that weed assessment cannot rely on a single spectral index, but requires a multi-layer interpretation that combines spectral, spatial, and agronomic information.

The internal validation of the proposed approach can be assessed against the study objectives and working hypothesis. The methodological workflow generated the expected sequence of outputs: calibrated imagery, vegetation-index layers, vegetation masks, probable weed hotspots, and management-oriented spatial units. At the same time, the analysis supported the working hypothesis that vegetation indices alone are not sufficient for robust weed discrimination. Their value increases when they are combined with crop-row geometry, spatial aggregation, and field observations. This confirms that the scientific contribution of the study is not the isolated use of NDVI, but the integration of vegetation-index mapping into a structured weed-assessment workflow.

The findings are consistent with previous UAV weed-mapping studies carried out in different crop systems. Peña et al. (2013) demonstrated the importance of object-based UAV image analysis for early-season weed mapping in maize, while Torres-Sánchez et al. (2014) showed that multitemporal UAV imagery can support early site-specific weed control in narrow-row crops such as wheat. Similarly, Stroppiana et al. (2018) highlighted the relevance of multispectral UAV data for early-season weed mapping in rice crops. Compared with these studies, the present approach emphasizes the methodological link between vegetation-index selection, crop-row interpretation, chlorophyll-sensitive indicators, and management-zone delineation. This comparison suggests that UAV-based weed assessment is transferable across crop systems, but its reliability depends on adapting the workflow to crop architecture, canopy closure, weed distribution, and the timing of image acquisition.

From a conceptual perspective, the study contributes to the advancement of site-specific weed management by framing UAV-derived vegetation indices as components of an integrated diagnostic system rather than as standalone classification tools. The proposed workflow connects remote-sensing outputs with practical weed-management decisions by moving from pixel-level vegetation variability to hotspot delineation and treatment-zone prioritization. This is important because the scientific and practical value of UAV monitoring depends not only on detecting spectral differences, but also on translating those differences into actionable agronomic decisions. In this sense, the study contributes a methodological bridge between UAV multispectral imaging, spatial weed ecology, and precision crop-protection planning.

Several limitations should nevertheless be acknowledged. First, the interpretation of probable weed hotspots remains dependent on field validation, because spectral similarity between crop and weed vegetation may lead to classification uncertainty. Second, the workflow is sensitive to illumination conditions, sensor calibration, flight altitude, crop growth stage, and the presence of exposed soil. Third, within-row weeds remain more difficult to detect than between-row weeds, especially in dense cereal crops or in fields with irregular crop emergence. Future research should therefore include larger multi-date datasets, ground-truth weed-density measurements, quantitative accuracy assessment, and comparison between index-based, object-based, and machine-learning classification approaches. Additional work is also needed to evaluate the feasibility of near-real-time processing under operational farm conditions and to connect UAV-derived weed maps with variable-rate herbicide application systems.

## CONCLUSIONS

This study addressed the need for a more integrated interpretation of UAV-derived vegetation indices in weed assessment by linking multispectral image processing, vegetation-index analysis, crop-row structure, and management-zone delineation. The results support the working hypothesis that NDVI and related indices are valuable for early vegetation screening but are insufficient as standalone weed-detection tools. Their scientific and practical relevance increases when they are combined with red-edge and chlorophyll-sensitive indicators, soil-adjusted indices, spatial aggregation, and field validation. NDVI remains an effective primary screening layer because it captures general vegetation presence and within-field variability, but it should not be used in isolation. Red-edge and chlorophyll-sensitive indices, including NDRE, $CI_{red\text{-}edge}$, and MTCI, become more informative when canopy density increases or when the objective extends beyond simple vegetation detection to physiological differentiation. Soil-adjusted indices further strengthen early-season analysis under partial soil exposure (Clevers & Gitelson, 2013; Schlemmer et al., 2013; MicaSense, 2024c).

Methodologically, the analysis supports the interpretation that multispectral data alone are rarely sufficient for reliable weed discrimination in complex arable scenes. Classification becomes more robust when spectral information is combined with crop-row geometry, spatial aggregation, and field-based validation, especially where weeds and crops share similar reflectance during early growth. This also helps explain why UAV weed mapping is often more straightforward in wide-row crops than in dense cereal systems, where plant separation is inherently more difficult (López-Granados, 2011; Torres-Sánchez et al., 2014; Stroppiana et al., 2018).

From an operational perspective, near-real-time fieldside processing currently offers the most practical balance between speed, robustness, and agronomic usefulness, whereas fully onboard inference remains promising but more constrained by model complexity and hardware limitations. Overall, the most effective framework combines calibrated multispectral acquisition, NDVI-based screening, complementary red-edge and chlorophyll-sensitive indices, row-aware weed calculations, and management-zone aggregation. In this form, UAV-based monitoring can support more precise herbicide application, reduce unnecessary chemical inputs, and strengthen the implementation of site-specific weed management in arable farming systems (López-

Granados, 2011; DJI, 2024; Pix4D, 2024; Bohra et al., 2025; NVIDIA, n.d.).

## ACKNOWLEDGEMENTS

This work was carried out with the institutional support of the National Institute of Research and Development for Food Bioresources – IBA Bucharest and the University of Agronomic Sciences and Veterinary Medicine of Bucharest. The study was developed in connection with research activities on integrated weed management and precision agriculture carried out within the ADER 2.1.4 project.

## USE OF GENERATIVE ARTIFICIAL INTELLIGENCE (GENAI)

The authors declare the use of Generative Artificial Intelligence (GenAI) tools in the preparation of this manuscript. GenAI was used for language editing, text refinement, formatting support, and drafting assistance. All scientific content, data interpretation, methodological assumptions, references, and final conclusions were reviewed and verified by the authors.

## REFERENCES

Agisoft. (2026, April 6). MicaSense RedEdge MX processing workflow (including Reflectance Calibration) in Agisoft Metashape Professional. Helpdesk Portal. https://agisoft.freshdesk.com/support/solutions/articles/31000148780-micasense-rededge-mx-processing-workflow-including-reflectance-calibration-in-agisoft-metashape-pro

Bohra, L. S., Radhamani, S., Fanish, S. A., Ravichandran, V., & Maragatham, S. (2025). Advances in site-specific weed management techniques for sustainable crop production. *Plant Science Today*, 12(sp3), 01–09. https://doi.org/10.14719/pst.8262

Clevers, J. G. P. W., & Gitelson, A. A. (2013). Remote estimation of crop and grass chlorophyll and nitrogen content using red-edge bands on Sentinel-2 and -3. *International Journal of Applied Earth Observation and Geoinformation,* 23, 344–351. https://doi.org/10.1016/j.jag.2012.10.008

DJI. (2020). P4 Multispectral Image Processing Guide. https://dl.djicdn.com/downloads/p4-multispectral/20200717/P4_Multispectral_Image_Processing_Guide_EN.pdf

DJI. (2023). Mavic 3M Image Processing Guide. https://dl.djicdn.com/downloads/DJI_Mavic_3_Enterprise/20230829/Mavic_3M_Image_Processing_Guide_EN.pdf

DJI. (2024). DJI Terra User Manual v4.0. https://dl.djicdn.com/downloads/dji-terra/20240118/DJI_Terra_User_Manual_v4.0__EN.pdf

Esri. (2026). Band Arithmetic function. ArcGIS Pro documentation. https://doc.esri.com/en/arcgis-pro/latest/help/analysis/raster-functions/band-arithmetic-function.html

Lichtenthaler, H. K., & Buschmann, C. (2001). Chlorophylls and carotenoids: Measurement and characterization by UV-VIS spectroscopy. Current Protocols in Food Analytical Chemistry, 1: F4.3.1-F4.3.8. https://doi.org/10.1002/0471142913.faf0403s01

López-Granados, F. (2011). Weed detection for site-specific weed management: Mapping and real-time approaches. *Weed Research*, 51(1), 1–11. https://doi.org/10.1111/j.1365-3180.2010.00829.x

MicaSense. (2024a, January 31). Creating agricultural indices (NDVI, NDRE) in QGIS. MicaSense Knowledge Base. https://support.micasense.com/hc/en-us/articles/226531127-Creating-agricultural-indices-NDVI-NDRE-in-QGIS

MicaSense. (2024b, March 26). Best practices: Collecting data with MicaSense sensors. MicaSense Knowledge Base. https://support.micasense.com/hc/en-us/articles/224893167-Best-practices-Collecting-Data-with-MicaSense-Sensors

MicaSense. (2024c, April 15). Overview of agricultural indices. MicaSense Knowledge Base. https://support.micasense.com/hc/en-us/articles/227837307-Overview-of-Agricultural-Indices

MicaSense. (2026, May 25). Radiometric Calibration Model for MicaSense sensors. MicaSense Knowledge Base. https://support.micasense.com/hc/en-us/articles/115000351194-Radiometric-Calibration-Model-for-MicaSense-Sensors

MicaSense. (n.d.). MicaSense RedEdge Image Processing Tutorial 1. MicaSense Image Processing. https://micasense.github.io/imageprocessing/MicaSense%20Image%20Processing%20Tutorial%201.html

NVIDIA. (n.d.). NVIDIA Jetson Orin Nano Super Developer Kit. https://www.nvidia.com/en-us/autonomous-machines/embedded-systems/jetson-orin/nano-super-developer-kit/

Parrot. (2025). Sequoia documentation. Parrot Support Center. https://www.parrot.com/en/support/documentation/sequoia

Peña, J. M., Torres-Sánchez, J., De Castro, A. I., Kelly, M., & López-Granados, F. (2013). Weed mapping in early-season maize fields using object-based analysis of unmanned aerial vehicle (UAV) images. *PLOS ONE,* 8(10), e77151. https://doi.org/10.1371/journal.pone.0077151

Pix4D. (2024). From drone to application: A full PIX4Dfields workflow training video. PIX4D Community. https://community.pix4d.com/t/from-drone-to-application-a-full-pix4dfields-workflow-training-video/33751

Pix4D. (n.d.). Processing options - PIX4Dfields. PIX4D Documentation. https://support.pix4d.com/hc/en-us/articles/360028421272

QGIS Project. (2026). Raster Analysis. In QGIS Desktop User Guide/Manual (QGIS 3.44). https://docs.qgis.org/3.44/en/docs/user_manual/working_with_raster/raster_analysis.html

Schlemmer, M., Gitelson, A., Schepers, J., Ferguson, R., Peng, Y., Shanahan, J., & Rundquist, D. (2013). Remote estimation of nitrogen and chlorophyll contents in maize at leaf and canopy levels. *International Journal of Applied Earth Observation and Geoinformation*, 25, 47–54. https://doi.org/10.1016/j.jag.2013.04.003

Stroppiana, D., Villa, P., Sona, G., Ronchetti, G., Candiani, G., Pepe, M., Busetto, L., Migliazzi, M., & Boschetti, M. (2018). Early season weed mapping in rice crops using multi-spectral UAV data. *International Journal of Remote Sensing*, 39(15–16), 5432–5452. https://doi.org/10.1080/01431161.2018.1441569

Tian, F., Zhou, J., Ransom, C. J., Aloysius, N., & Sudduth, K. A. (2025). Estimating corn leaf chlorophyll content using airborne multispectral imagery and machine learning. *Smart Agricultural Technology*, 10, 100719. https://doi.org/10.1016/j.atech.2024.100719

Torres-Sánchez, J., López-Granados, F., de Castro, A. I., & Peña, J. M. (2014). Multitemporal weed mapping using UAV imagery for early site-specific control: The case of wheat as a narrow row crop. *In Proceedings of the Second International Conference on Robotics and Associated High-Technologies and Equipment for Agriculture and Forestry (RHEA Conference),* Madrid, Spain. https://www.researchgate.net/publication/263673460_Multitemporal_weed_mapping_using_UAV_imagery_for_early_site-specific_control_the_case_of_wheat_as_a_narrow_row_crop

Torres-Sánchez, J., López-Granados, F., Serrano, N., Arquero, O., & Peña-Barragán, J. M. (2015). High-throughput 3-D monitoring of agricultural-tree plantations with unmanned aerial vehicle (UAV) technology. *PLOS ONE*, 10(6), e0130479. https://doi.org/10.1371/journal.pone.0130479

Scientific Papers. Series E. Land Reclamation, Earth Observation & Surveying, Environmental Engineering. Vol. XV, 2026
Print ISSN 2285-6064, CD-ROM ISSN 2285-6072, Online ISSN 2393-5138, ISSN-L 2285-6064

# GIS-BASED SCREENING OF ROAD-INDUCED SPATIAL FRAGMENTATION IN NATURA 2000 SITES IN ROMANIA

**Răzvan Lucian VOICU, Cristina CĂLIN, Sorin Mihai CÎMPEANU**

University of Agronomic Sciences and Veterinary Medicine of Bucharest,
Faculty of Land Reclamation and Environmental Engineering, 59 Mărăști Blvd,
District 1, 011464 Bucharest, Romania

Corresponding author email: cristina.calinn@gmail.com

***Abstract***

*Road infrastructure can alter the spatial continuity of protected areas by subdividing habitat blocks and increasing edge-related pressures. This study aims to assess road-induced structural (spatial) fragmentation - derived from GIS analysis rather than from measures of functional ecological connectivity - in Natura 2000 sites in Romania using a GIS-based screening approach focussed on motorways, express roads and national roads. Natura 2000 site boundaries were overlaid with the major road network to identify crossed sites, quantify the number of road segments located within each site, and analyse the spatial distribution and area of the resulting fragments in selected highly affected sites. The analysis showed that 119 out of 232 Natura 2000 sites were crossed by at least one major road segment, while several were traversed by multiple segments. Four sites were selected for detailed interpretation: ROSCI0290 Ialomița Corridor, ROSAC0162/ROSPA0071 Lower Siret Floodplain, ROSCI0206 Porțile de Fier/ROSPA0080 Almăjului-Locvei Mountains and ROSPA0091 Babadag Forest. Although the study does not quantify direct ecological effects, it provides a spatial screening framework that can support field surveys, roadkill monitoring, connectivity assessment and mitigation planning.*

***Key words:*** *ecological connectivity, GIS, Natura 2000, road infrastructure, spatial fragmentation.*

## INTRODUCTION

Road infrastructure is one of the most widespread forms of linear infrastructure and can produce important changes in habitat continuity. Roads generate direct habitat loss, edge effects, noise, light pollution, wildlife mortality, barriers to movement and increased human access. These effects may extend beyond the physical footprint of the road and can influence the functional integrity of protected areas.

In landscape ecology, fragmentation is not limited to the geometric division of a polygon. It has a structural component, related to the size, number and distribution of fragments, and a functional component, related to species movement, permeability and ecological connectivity. Road networks are therefore frequently treated as drivers of both landscape subdivision and ecological isolation.

Classical road ecology studies have shown that roads may have ecological effects disproportionate to the area that they occupy (Forman & Alexander, 1998; Trombulak & Frissell, 2000). Later reviews emphasised that roads affect species abundance, behaviour and population persistence through multiple pathways, including mortality, avoidance and reduced connectivity (Coffin, 2007; Fahrig & Rytwinski, 2009; Benítez-López et al., 2010).

In protected areas, the issue is particularly important because legal designation does not automatically guarantee ecological coherence. Natura 2000 sites are designated for the conservation of habitats and species of Community interest, but their spatial continuity may be affected where major roads cross or dissect protected landscapes. European studies have used GIS-based approaches to assess the role of roads and roadless areas in protected networks, including Natura 2000 sites (Selva et al., 2011; Votsi et al., 2012; Zomeni & Vogiatzakis, 2014; Kati et al., 2020).

However, these studies have largely addressed roadlessness and road density at continental scale or within individual Mediterranean countries, and have generally treated protected areas as units characterised by an aggregate

pressure index rather than as geometries physically subdivided by infrastructure.
Furthermore, no comparable screening exists for Romania, which hosts one of the largest and most biodiverse Natura 2000 networks in the EU. The present study addresses this gap by quantifying road-induced structural fragmentation across all Romanian Natura 2000 sites and by identifying the most affected sites as priorities for subsequent field-based and functional connectivity assessment.
The present study does not aim to demonstrate direct ecological impacts on species or habitats, because it does not include field surveys, roadkill monitoring, telemetry, species movement data or habitat-quality measurements. Instead, it provides a GIS-based spatial screening of potential road-fragmentation pressure in Natura 2000 sites in Romania. The purpose is to identify where the major road network crosses protected areas and where more detailed ecological assessment may be justified.

## MATERIALS AND METHODS

### Study scope

The study was designed as a GIS-based screening of road-induced spatial fragmentation in Natura 2000 sites. The analysis focused on the geometric relationship between protected-area boundaries and the major road network. Results were interpreted as spatial indicators of potential pressure and not as confirmed biological impacts.

### Spatial data and coordinate reference system

Two spatial datasets were used. The boundaries of the Romanian Natura 2000 sites (Sites of Community Importance/Special Areas of Conservation and Special Protection Areas) were obtained from Ministry of Environment, Waters and Forests - Romania, https://mmediu.ro/portal-gis/date-spatiale/arii-naturale-protejate-de-interes-national-si-international/, downloaded on 15.01.2025. The major road network of Romania was obtained from geo-spatial.org, https://geo-spatial.org/vechi/download/re-eaua-rutiera-na-ionala-a-romaniei-set-de-date-vectorial, downloaded on 16.01.2025. From the road dataset, only the categories relevant to the present screening were retained, namely motorways, express roads and national roads; county roads, communal roads and forest roads were excluded. The source geometries were not edited, generalised or topologically corrected, in order to preserve the reproducibility of the results against the original datasets. All spatial layers used for area calculations were processed in the Romanian national projected coordinate reference system Stereo 70 (EPSG:3844). This metric coordinate system is suitable for calculating areas and distances on Romanian territory.

### Operational definition of fragmentation

For this study, road-induced fragmentation was defined operationally as the intersection of a Natura 2000 site by one or more motorway, express-road or national-road segments, resulting in the spatial subdivision of the protected-area polygon into two or more fragments. This definition captures spatial fragmentation and should not be interpreted as a direct measure of ecological isolation or species-level impact.

### GIS workflow

• all spatial analyses were performed in QGIS Desktop 3.12.1.
• harmonisation of spatial datasets in Stereo 70 / EPSG:3844;
• selection of the major road categories: motorways, express roads and national roads;
• overlay of the major road network with Natura 2000 site boundaries;
• identification of sites crossed by at least one major road segment;
• counting of major road segments crossing each Natura 2000 site (i.e. the road sections resulting from the intersection of the road network layer with the site polygon, located within the site boundary);
• spatial subdivision of selected sites into fragments obtained by splitting the site polygon with the major road segments located inside it;
• calculation of fragment areas in hectares;
• selection of highly subdivided sites for detailed cartographic interpretation;
For the selected case-study sites, the conservation-management context was also cross-checked with official Romanian conservation documents, including ANANP Decision No. 125/2022 for the Lower Siret

Floodplain and ANANP Decision No. 144/2021 for the Porțile de Fier site, together with the official ministerial notes on minimum conservation measures for Ialomița Corridor and Babadag Forest (ANANP, 2021, 2022; Ministry of Environment, Waters and Forests, 2021, 2023).

**Screening indicators**

The analysis was based on four indicators, all derived exclusively from the GIS overlay: (i) the number of Natura 2000 sites crossed by the major road network; (ii) the number of major road segments located within each site; (iii) the number of fragments resulting from the subdivision of the selected case-study sites; and (iv) the area of the largest and smallest fragment in each selected site.

**Supporting contextual information**

Conservation-status information was not used as a screening indicator. It was consulted only as qualitative background for the interpretation of the four case-study sites and did not contribute to any calculation, to the ranking of sites or to the selection of the case studies. Conservation status was not used to infer causality between roads and species condition.

## RESULTS AND DISCUSSIONS

**National GIS screening of sites crossed by major roads**

The GIS overlay indicated that the major road network intersects a substantial number of Natura 2000 sites in Romania. According to the source dataset, 119 out of 232 analysed sites were intersected at least once by a major road. This result indicates that the spatial overlap between the major road network and the Natura 2000 network is widespread at the national level. The ecological significance of this overlap cannot be inferred from the geometric analysis alone, and the presence of a major road segment within a site should therefore be interpreted as a spatial warning signal rather than as evidence of high ecological impact (Figure 1).

A second GIS layer isolated the road segments located inside Natura 2000 site boundaries, providing a clearer spatial view of the road sections located within protected-area boundaries (Figure 2).

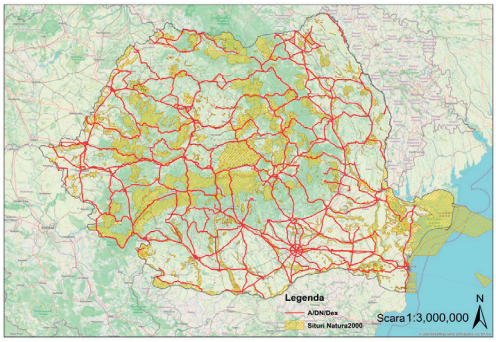



Figure 1. Natura 2000 sites crossed by the major road network in Romania

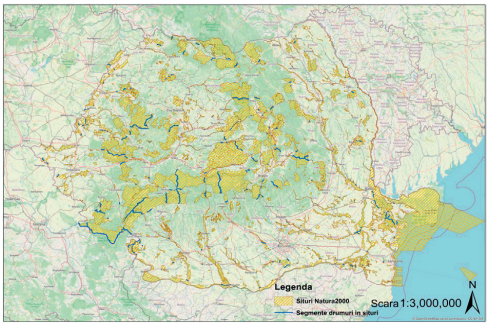



Figure 2. Major road segments located within Natura 2000 sites in Romania

**Number of major road segments per site**

The frequency distribution shows an uneven pattern of road-induced spatial subdivision. Most crossed sites contain one or two major road segments, whereas a smaller group of sites contains a larger number. Sites containing several road segments should be prioritised for detailed connectivity analysis because multiple crossings may reduce internal continuity and increase edge-related pressures (Figure 3).

**Selected case-study sites**

Four sites were selected for detailed spatial interpretation on the basis of two combined criteria. First, all four belong to the group of sites showing the highest number of major road segments identified in the national screening. Second, within this group the sites were selected so as to represent contrasting spatial configurations: a corridor-like protected area (ROSCI0290 Ialomița Corridor), a riparian system (ROSAC0162/ ROSPA0071 Lower Siret Floodplain), a large protected-area complex

(ROSCI0206 Porțile de Fier/ROSPA0080 Almăjului - Locvei Mountains) and a forested landscape (ROSPA0091 Babadag Forest). The selection is therefore illustrative of the most subdivided group of sites and of the diversity of geometric situations encountered, and it does not constitute an exhaustive ranking of the most fragmented sites in the national network.

Two distinct quantities are reported for each case-study site. The number of major road segments located within the site boundary was obtained by intersecting the road network layer with the site polygon, whereas the number of fragments was obtained separately by splitting the site polygon with those road lines. The two are not equivalent: a segment that fully traverses a site produces two fragments, a segment terminating inside the site produces none, and two segments intersecting within the same site may produce more than two. On this basis, the GIS screening identified 7 major road segments crossing the Ialomița Corridor, dividing the site into 9 fragments ranging from 59.59 to 11,078.09 ha; 7 segments within the Lower Siret Floodplain, giving 9 fragments of 58.16-17,413.10 ha; 7 segments within Porțile de Fier/Almăjului-Locvei Mountains, giving 7 fragments of 441.52-94,966.59 ha; and 5 segments within Babadag Forest, giving 6 fragments of 29.74-21,258.49 ha. The values reported for each case-study site refer to the number of major road segments located within the site boundary, obtained by intersecting the road network layer with the site polygon.

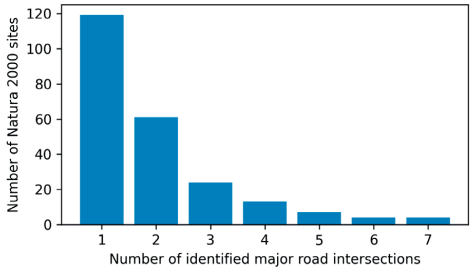



Figure 3. Distribution of Natura 2000 sites according to the number of major road segments located within the site boundary

The cartographic outputs for the selected sites show that multiple road segments may occur both in corridor-like sites and in large protected-area complexes. The maps also indicate strong differences in the spatial distribution of fragments, from narrow riparian sections to large habitat blocks (Figures 4-7).

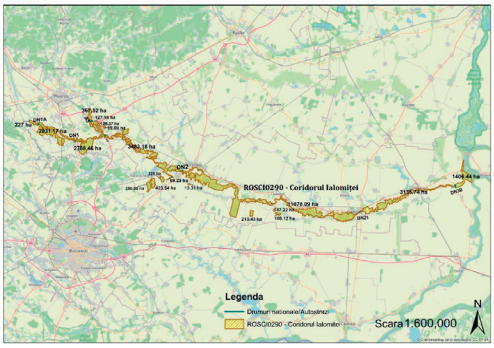



Figure 4. Road-induced spatial subdivision of ROSCI0290 Ialomița Corridor

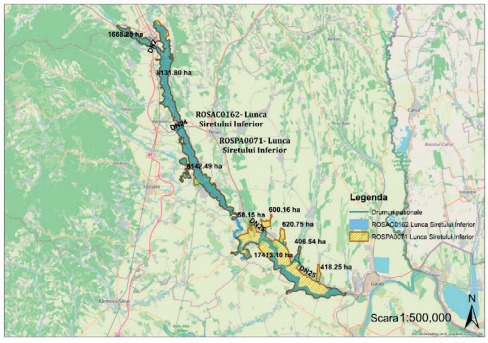



Figure 5. Road-induced spatial subdivision of ROSAC0162/ROSPA0071 Lower Siret Floodplain




Figure 6. Road-induced spatial subdivision of ROSCI0206 Porțile de Fier/ROSPA0080 Almăjului-Locvei Mountains




Figure 7. Road-induced spatial subdivision of ROSPA0091 Babadag Forest

## Interpretation of fragment size and site geometry

The results indicate that the number of road crossings alone is not sufficient to characterise the degree of spatial subdivision of a site. Fragment-size distribution and site geometry are equally important. Corridor-like and riparian sites, such as Ialomița Corridor and Lower Siret Floodplain, may be particularly sensitive to transversal road crossings because such crossings can interrupt longitudinal continuity. Conversely, large protected-area complexes may retain extensive fragments but still require analysis of permeability, wildlife crossing opportunities and roadkill risk (Figure 8).

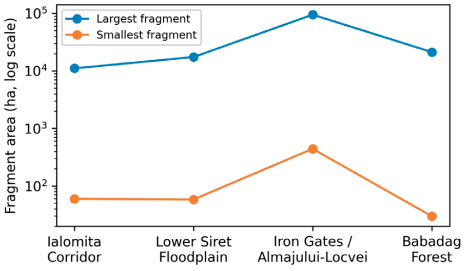



Figure 8. Contrast between the largest and smallest fragments in selected Natura 2000 sites

The contrast between the largest and smallest fragments is relevant for management. Very small fragments may be more exposed to edge effects, human access and functional isolation, even when their contribution to total site area is limited. Therefore, screening outputs should be interpreted together with local habitat maps, species data and field observations.

## Conservation-status context

The conservation-status graphs and official conservation context were treated as supporting background, based on the available site-specific documents, including ANANP decisions for the Lower Siret Floodplain and Porțile de Fier sites and official ministerial notes for Ialomița Corridor and Babadag Forest (ANANP, 2021, 2022; Ministry of Environment, Waters and Forests, 2021, 2023). The available conservation-status information was not interpreted as proof of a causal relationship between road fragmentation and species condition. In some sites, the presence of unfavourable or unknown conservation status indicates that spatial fragmentation overlaps with areas already requiring conservation attention, but additional ecological data are necessary to assess biological effects (Figure 9).

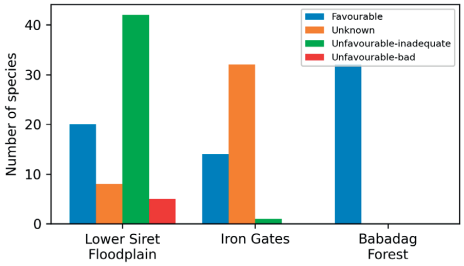



Figure 9. Conservation-status context for selected Natura 2000 sites, based on the values extracted from the existing graphs

## Management relevance

The GIS screening can support Natura 2000 management by identifying sites where detailed ecological assessment is justified. Priority actions may include field verification of road-crossing zones, roadkill monitoring, permeability assessment, mapping of existing culverts and bridges, habitat-connectivity modelling and evaluation of the need for wildlife passages or ecological bridges.

The approach is particularly useful as a preliminary planning tool because it is transparent, reproducible and based on spatial layers that can be updated as road networks or protected-area boundaries change. However, it should be complemented by ecological surveys before site-specific mitigation measures are designed.

## CONCLUSIONS

This study provides a GIS-based screening of road-induced spatial fragmentation in Romanian Natura 2000 sites. The analysis shows that a substantial number of sites are crossed by the major road network and that several sites are divided into multiple fragments. These findings do not demonstrate direct ecological impact, but identify the sites in which the geometry of the protected area is subdivided by the major road network, and in which a subsequent assessment of habitat continuity and of functional ecological connectivity would therefore be justified. Whether this structural subdivision translates into a reduction of functional connectivity can only be established through species-specific data on movement, permeability and mortality, which fall outside the scope of the present screening.

The selected case studies show that the degree of spatial subdivision depends not only on the number of road crossings, but also on-site geometry and on the size distribution of resulting fragments. The results can support the prioritization of detailed ecological surveys, roadkill monitoring, connectivity modelling and mitigation planning in Natura 2000 management.

## ACKNOWLEDGEMENTS

This study was developed as part of the doctoral research of Răzvan Lucian Voicu, carried out within the Doctoral School of Engineering and Management of Plant and Animal Resources - University of Agronomic Sciences and Veterinary Medicine of Bucharest.

## REFERENCES

Benítez-López, A., Alkemade, R., & Verweij, P. A. (2010). The impacts of roads and other infrastructure on mammal and bird populations: A meta-analysis. *Biological Conservation*, *143*(6), 1307-1316. https://doi.org/10.1016/j.biocon.2010.02.009

Coffin, A. W. (2007). From roadkill to road ecology: A review of the ecological effects of roads. *Journal of Transport Geography*, *15*(5), 396-406. https://doi.org/10.1016/j.jtrangeo.2006.11.006

Fahrig, L., & Rytwinski, T. (2009). Effects of roads on animal abundance: An empirical review and synthesis. *Ecology and Society*, *14*(1), 21. https://doi.org/10.5751/ES-02815-140121

Forman, R. T. T., & Alexander, L. E. (1998). Roads and their major ecological effects. Annual Review of *Ecology and Systematics*, *29*, 207-231. https://doi.org/10.1146/annurev.ecolsys.29.1.207

Kati, V., Kassara, C., Psaralexi, M., Tzortzakaki, O., Petridou, M., Galani, A., & Hoffmann, M. T. (2020). Conservation policy under a roadless perspective: Minimizing fragmentation in Greece. *Biological Conservation, 252*, 108828. https://doi.org/10.1016/j.biocon.2020.108828

Ministry of Environment, Waters and Forests. (2021). Note No. 262390/BT/03.12.2021 approving the minimum set of special protection and conservation measures for ROSPA0091 Babadag Forest. Bucharest, Romania.

Ministry of Environment, Waters and Forests. (2023). Note No. 20519/CA/26.06.2023 supplementing the minimum set of special protection and conservation measures for ROSCI0290 Ialomița Corridor. Bucharest, Romania.

National Agency for Protected Natural Areas (ANANP). (2021). Decision No. 144 of 08.04.2021 approving the methodological norms for implementing the conservation objectives of the Natura 2000 site ROSCI0206 Porțile de Fier. Bucharest, Romania.

National Agency for Protected Natural Areas (ANANP). (2022). Decision No. 125 of 28.03.2022 approving the methodological norms for implementing the conservation objectives of ROSPA0071 Lower Siret Floodplain and overlapping protected areas. Bucharest, Romania.

Selva, N., Kreft, S., Kati, V., Schluck, M., Jonsson, B. G., Mihok, B., Okarma, H., & Ibisch, P. L. (2011). Roadless and low-traffic areas as conservation targets in Europe. *Environmental Management*, *48*(5). 865-877. https://doi.org/10.1007/s00267-011-9751-z

Trombulak, S. C., & Frissell, C. A. (2000). Review of ecological effects of roads on terrestrial and aquatic communities. *Conservation Biology*, 14(1). 18-30. https://doi.org/10.1046/j.1523-1739.2000.99084.x

Votsi, N. E. P., Mazaris, A. D., Kallimanis, A. S., Zomeni, M., Vogiatzakis, I. N., Sgardelis, S. P., & Pantis, J. D. (2012). Road effects on habitat richness of the Greek Natura 2000 network. *Nature Conservation, 1*. 53-71. https://doi.org/10.3897/natureconservation.1.2086

Zomeni, M., & Vogiatzakis, I. N. (2014). Roads and roadless areas in Cyprus: Implications for the Natura 2000 network. *Journal of Landscape Ecology*, *7*(1). 75-90. https://doi.org/10.2478/jlecol-2014-0010

Scientific Papers. Series E. Land Reclamation, Earth Observation & Surveying, Environmental Engineering. Vol. XV, 2026
Print ISSN 2285-6064, CD-ROM ISSN 2285-6072, Online ISSN 2393-5138, ISSN-L 2285-6064

# RESEARCH ON FREE SURFACE ENERGY DISSIPATION

**Nicolae ALBOIU, Daniel CORNEA, Georgiana Daniela VULPE**

Technical University of Civil Engineering Bucharest,
122-124 Lacul Tei Blvd, District 2, Bucharest, Romania

Corresponding author email: nalboiu@gmail.com

***Abstract***

*The paper is a general presentation of the studies undertaken as part of a research project focused on a solution used for energy dissipation applied to free surface currents. The research has involved a series of studies on special shaped artificial roughness elements proposed by the authors of the preset paper. Several placement patterns of these elements were tested. Based on the result, conclusions could be drawn regarding the effects that these elements and their placement have on the flow. Based on the results obtained experimentally, new research directions are possible to be developed, which are aiming at new building materials and maybe a more versatile implementation technology compared to the classical one.*

***Key words****: artificial roughness, energy dissipation, free surface current, water current.*

## INTRODUCTION

Dissipation of free surface kinetic energy is a necessity when certain flow conditions, specific to hydropower structures, gutters and channels adjacent to highways, roads and water transport systems used in agriculture are met. Uncontrolled discharge of water is a major threat for both the integrity of hydrotechnical and water transport infrastructure, and for the environment such as riverbeds, lake basins, and coastal areas. From the hydro engineering point of view, the general purpose of dissipating the kinetic energy of water streams is the reduction of riverbed erosion, structural protection and flood control by reducing the water velocity. Another category of problems for which energy dissipation is necessary is related to the ecology field. For example, the protection of aquatic habitats.

Several energy dissipation solutions were developed over time. Each situation has its own particularities. Broadly speaking, establishing the energy dissipation solution is related to the particularities of the flow and the generating cause that produces a high kinetic energy flow. Common, widely applied technical solutions for dissipating the kinetic energy of water streams are: *stilling basins* - reinforced pools placed at the base of structures like spillways, that use the hydraulic jump as main mechanism of dissipation; *stepped spillways* - a series of steps placed on the downstream face of the hydro-structure that divide the main high energy stream in small waterfalls will have a dissipative effect due to aeration and friction (Kiselev, 1988; Chanson, 2021; Mei et al., 2025); *baffle/chute blocks* (Figure 1) - obstacles placed in the channel to break the water stream reducing thus the water velocity; *bucket dissipators* - deflectors with a curved shape that lunch a water jet which energy is dissipated due to the resistance, water-air friction and finally as a result of the impact with the downstream water surface; c*heck dams* - small structures designed to break the riverbed slope reducing thus the stream velocity; *tumbling flow systems* - a sequence of concrete elements/obstacles or small steps which create falls and pools along steep channels (10 - 35% channel slope). Out of the above-mentioned solutions, as they increase the flow resistance, baffle blocks and chute blocks represent *artificial roughness* (Figure 1) methods of energy dissipation. Beside those two types of blocks, the artificial roughness category includes also *sills and ribs* - horizontal ridges built into the bed of the channel that act as a brake for the lower layer of water, and *rip-rap or boulders* - anchored rocks used in channels to enhance friction zones.

Although they have been studied and successfully applied for many years, these techniques continue to be of interest to researchers in the field of hydraulics. The

problems that remain open are related to the problem of cavitation, but also to the optimization of dissipative elements, a fact confirmed by recent research carried out in the last decade.

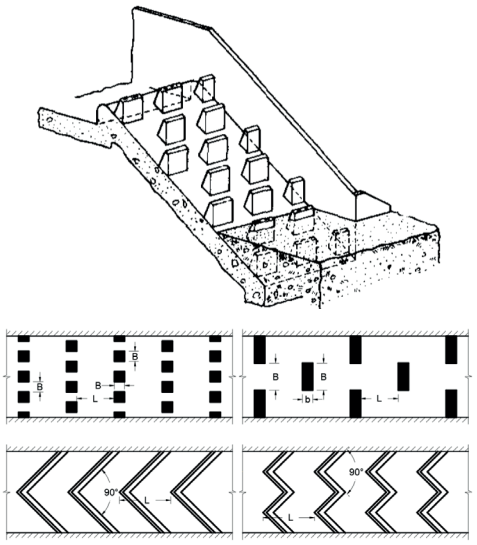



Figure 1. Example of baffle blocks (Peterka, 1984) and some increased artificial roughness types (Cioc, 1975) used for energy dissipation

Besides the presented solutions, a different but interesting dissipation method addressed to spillways, called *pre-aerated stilling basin spillway* (PSBS) is studied and presented in (Zhou et al., 2025).

Considering the technological evolution in the field of hydraulic phenomena research, both experimental and numerical (CFD), but also the evolution of building materials and execution technologies, the authors of this paper proposed a new shape of artificial roughness elements used for energy dissipation.

The research is focused on induced tumbling flow by using these elements. The development of the studies involved a succession of activities based on which the most efficient methods and approaches were used to draw valid conclusions regarding the behavior of the proposed roughness elements under operation conditions.

The research is a part of the *National Research Grants of the Technical University of Civil Engineering Bucharest GnaC ARUST 2024, DERA project, number TUCEB- No.1411/2025*.

## MATERIALS AND METHODS

To carry out the proposed research, both theoretical and experimental methods were considered.

*The theoretical studies* involved preliminary evaluations on which the future experimental research was developed. The subjects of interest were related on one hand to the main physical quantities used to describe and quantify free surface water streams and on the order hand to the potential effect of the roughness elements on a theoretical stream. Both evaluations were used to establish the future experimental framework and to provide a qualitative picture of the fluid flow kinetics in the presence of the artificial roughness elements.

For the numerical evaluation of the flow the well-known analytical relationships and the HEC-RAS software were used (Cioc, 1975; French, 1986). The qualitative relative effect of the roughness elements was evaluated prior to any test via the COMSOL Multiphysics CFD software. The analysis was based on a hypothetical scenario. Under this scenario four types of roughness elements were compared. The shape of the compared elements is shown in Figure 2.

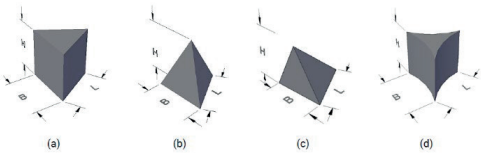



Figure 2. Shapes of the evaluated artificial roughness elements

All the four elements shown in figure 2 are considered 10 cm high (H) and 10 cm wide (B). The characteristics of the modeled domain are 1.5 m length and 1.2 m width. The artificial roughness elements were placed alternately as a single row, facing the water stream at 0.3 m downstream from the inlet of the domain. Considering the characteristics of the studied problem, a RANS k-ε turbulence model was used.

Based on the results of the qualitative, relative, evaluation, the shape depicted by image (d) was chosen for the future experimental tests (Figure 3).

The elements were made from plastic sheets cut on CNC machines and subsequently glued together. To obtain a uniform average roughness between the elements, the resulting pieces were wrapped in adhesive aluminum foil. Twenty-two central elements were placed in the flow field, and 4 lateral elements were placed near the channel walls.

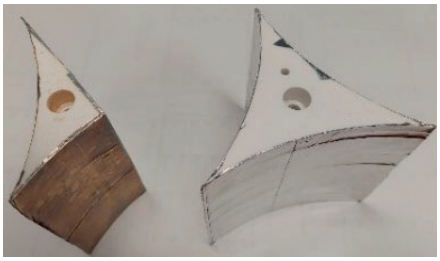


Figure 3. Lateral and central artificial roughness elements selected for the experimental study

*The experimental studies* were carried out in the „Dumitru Cioc" Hydraulics Laboratory (HL) part of the Technical University of Civil Engineering Bucharest (TUCEB).
To perform these experimental studies, some of the main infrastructure of the HL was used, namely the variable slope channel, the pumping station and the related hydraulic network.
The characteristics of the variable slope open channel are: a rectangular cross section, 1.20 m wide and 0.75 m depth (of which 0.65 m is the usable depth), the total length of the channel is 33.20 m, the maximum elevation difference at the downstream end, compared to the horizontal position, is 0.35 m that corresponds roughly to a channel slope of 1% (Figure 4).



Figure 4. The variable slope channel - „Dumitru Cioc" Hydraulics Laboratory; TUCEB

The pumping station is equipped with four centrifugal pumps, ensuring a maximum flow rate of 0.6 $m^3/s$.
The flow rate is measured using electromagnetic flowmeters placed on the laboratory water supply network pipes. The supply of the variable slope channel is ensured by two pipes connected to the tank placed at the upstream end. Each of these is equipped with a flow meter and a control valve. The diameters of these pipes are 200 mm and 250 mm, respectively.
To carry out the experimental study, a series of adjustments were necessary which mainly consisted of doubling the bottom of the channel and creating a well-defined experimental area. The solution to doubling the bottom was considered the only acceptable option for fixing the artificial roughness elements in a safe manner that would not affect the integrity of the channel. Three plastic plates were placed in the upstream area of the channel and fixed with metal strips to its walls. The total length occupied by these plates is 6.5 m. The first and last plates do not present any particularities. However, the central plate was provided with recessed nuts, their role is to ensure fixing of the roughness elements. The arrangement of the fixing nuts makes it possible to achieve a placement of the artificial roughness elements at a minimum distance of 10 cm on both main directions of the horizontal plane.
The theoretically obtained results regarding the flow characteristics were used as a starting point for the planning of future experiments. Thus, the precise experimental framework was established.
The measurements monitored the main physical quantities that are used for the description, characterization and classification of free surface currents, namely flow rates, depths and local velocities.
For flow rate measurements, the flow meters placed on the water supply pipes were used. The water depth was monitored using an ultrasonic probe, and the local velocity using an acoustic Doppler velocimeter (ADV) and, subsidiary, a Pitot tube connected to a pressure transducer (Figure 5).



Figure 5. Measuring equipment used

Due to the low water depth, a 2D side looking ADV probe was used. the acquisition frequency

of the measured values was set at 20Hz. To avoid measuring errors related to noise and sampling faults and post processing, several bibliographic works were consulted, including (Kazemi et al., 2021; Park & Hwang, 2021; Chen et al., 2024).

The first action aimed to establish the framework for the tests to be carried out. In this regard, the theoretical estimates initially made were experimentally verified. Based on these tests, the flow-depth-slope relationship which ensures the desired experimental framework was established.

First, to obtain high velocity values for the water stream the maximum possible slope ($i_{max}$) of the channel was set ($i_{max}$ = 1%). The experimental medium flowrate was Q = 0.096 $m^3/s$. The measured mean depth along the channel was $h_{med}$ = 0.10 m. For this setup, an unfavorable aspect that was observed was the deformation of the third bottom plate because of the lifting force generated by the water current.

The solution chosen to avoid this issue was to set a smaller slope for the channel and to increase the velocity of the water strictly in the first part of the experimental zone, by placing a sluice gate at the inlet section of the channel (Figure 6).

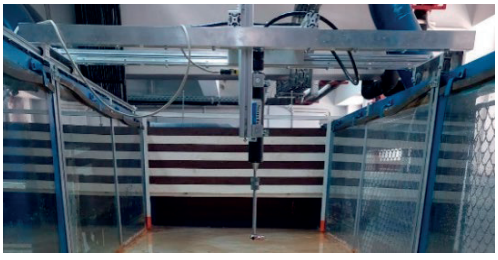


Figure 6. The sluice gate placed
at the upstream of the testing zone

After computation and experimental tests, the convenient experimental setup was established (Dumitrescu & Răzvan, 1972; French, 1986): the channel slope *i = 0.1%;* the experimental medium flow rate Q = 0.096 m3/s; the gate opening *a = 7 cm.* For the experiments a single arrangement and three different orientations (patterns) were considered (Figure 7).

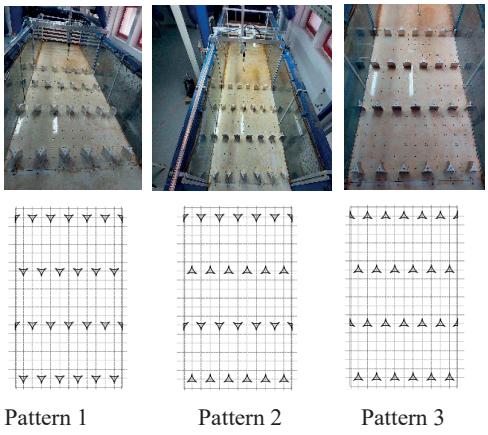



Figure 7. Patterns used for experimental test

The single arrangement for the three patterns is justified by the dissipation mechanism that is studied, namely tumbling flow.

For further reference of the studied arrangement, we will use the following names Pattern 1, Pattern 2 and Pattern, as shown in Figure 7, and for the "free" channel, i.e. without roughness elements, we will use the name Pattern 0.

Experiments carried out in the past by various researchers on alternatingly placed concrete cubes and the experience gained by applying this solution show, according to (Certousov, 1966; Dumitrescu & Răzvan, 1972; Morris & Wiggert, 1972; Peterka, 1984; Kiselev, 1988; Novak et al., 2005) referenced literature, recommended ratios between the height of the element and the depth of the current at the design flow rate and distances for placing the roughness elements in the direction of the current and transverse to it.

Although we proposed a new shape for the roughness elements, we considered these recommendations a rational starting point. However, a determined criterion was also the size of the area designated for mounting the roughness elements, this being used to the maximum extent. Considering the height of the elements, the longitudinal, the transversal spacing and the water depth, the studies were driven on a prototype (geometric scale coefficient $\alpha_l$ = 1).

## RESULTS AND DISCUSSIONS

*The CFD results* obtained on the modeling that assumes a hypothetical scenario, allowed a general qualitative analysis of the influence of the four roughness elements geometry. The conclusions are strictly valid within the assumptions and numerical conditions adopted. In the absence of experimental validation, the results cannot be considered from a quantitative point of view. Thus, they were used only as a starting point for choosing the geometry of roughness element used for future experimental tests.

The experimental tests were performed along the flow axis, tracking velocities at various depths for two relevant monitoring sections. The placement of those monitoring sections, $S_{ust}$ and $S_{dst}$, are upstream and respectively downstream the bottom plate where the roughness elements are fixed (Figure 8).



Figure 8. Measuring equipment placed at $S_{ust}$ and at $S_{dst}$

A first image of the effect generated by the three patterns compared to the "free" channel is plotted in Figure 9.

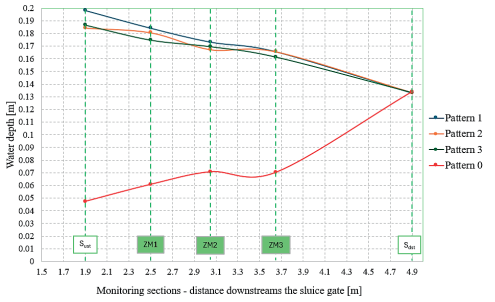



Figure 9. Comparative plot of the free surface shape

As shown in Figure 9, each of the Patterns P1, P2 and P3 are modifying the water depth along the experimental area. The water depth increases significantly in all the first three monitoring sections. In the last one, $S_{dst}$, the water reaches the same depth for all four patterns (Table 1).

Table 1. Water depth values along the experimental area

| Monitoring section | $S_{ust}$ | ZM1 | ZM2 | ZM3 | $S_{dst}$ |
|---|---|---|---|---|---|
| Water depth [m] | | | | | |
| Pattern 0 | 0.047 | 0.061 | 0.071 | 0.070 | 0134 |
| Pattern 1 | 0.198 | 0.184 | 0.173 | 0.166 | 0.133 |
| Pattern 2 | 0.184 | 0.181 | 0.167 | 0.166 | 0.133 |
| Pattern 3 | 0.187 | 0.175 | 0.170 | 0.161 | 0.133 |
| Water depth difference – Reference "Pattern 0" [m] | | | | | |
| Δ h1 | 0.151 | 0.123 | 0.102 | 0.096 | ≈0 |
| Δ h2 | 0.137 | 0.120 | 0.096 | 0.096 | ≈0 |
| Δ h3 | 0.140 | 0.114 | 0.099 | 0.091 | ≈0 |

After the $S_{dst}$ section the flow becomes uniform with a normal depth of roughly 0.16 m.

The presence of the artificial roughness generates a local resistance which influences the channel's flow rate. As the water depth rises upstream the artificial roughness elements, the orifice created by the sluice gate become submerged. Thus, the orifice head ($H_{orif}$) changes with respect to the degree of submergence. This fact is reflected in the flow rate (Table 2).

Table 2. Values influenced by orifice submergence

| Pattern | $h_{ust}$ | $H_{orif}$ | $Q$ |
|---|---|---|---|
| | [m] | [m] | [m$^3$/s] |
| 0 | 0.047 | 0.22 | 0.0955 |
| 1 | 0.198231 | 0.3 | 0.0950 |
| 2 | 0.184333 | 0.285 | 0.0947 |
| 3 | 0.186583 | 0.255 | 0.0945 |

The flow rate values shown in Table 2 are plotted in Figure 10 against orifice head ($H_{orif}$) by which the flow rate changes due to the head upstream the orifice are obtained.

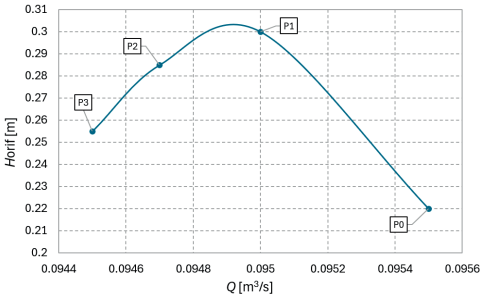



Figure 10. Flow rate curve Q($H_{orif}$)

Also, the flow rate plotted against the water depth in the $h_{uts}$ monitoring section, which is placed downstream the sluice gate, is useful to observe this influence (Figure 11).

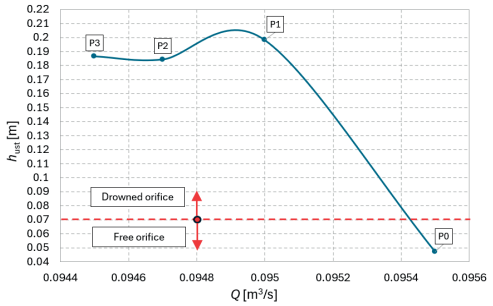



Figure 11. Flow rate curve Q($h_{ust}$)

Starting from the observation on the drowning effect of the gate orifice, the experiments on the dissipative effect generated by the three patterns were carried out at a same flowrate value, namely Q = 0.095 m3/s.

As the present paper focuses only on the whole ensemble of artificial roughness elements, the data obtained for the monitoring sections $S_{ust}$ and $S_{dst}$ are analyzed and discussed.

For Pattern 0 (Figure 9), the water depth is increasing significantly between $S_{ust}$ and $S_{dst}$. The shape of the water surface and the Froude number upstream ($Fr_1$ = 6.33) and downstream ($Fr$ = 0.36) are highlining a hydraulic jump. The flow upstream the testing area is supercritical and downstream the testing area is subcritical.

Thus, the goal of the artificial roughness is to reduce the kinetic energy of the water stream at $S_{ust}$ and to ensure a similar specific energy to the normal flow conditions one at $S_{dst}$. The graph in Figure 9 suggests the achievement of this goal.

A comparison between the values obtained for monitoring section $S_{ust}$ is shown in Table 3.

Table 3. Monitoring section $S_{ust}$ - values obtained for the main quantities

| Pattern | $h_{ust}$ [m] | $\Delta h_{ust}$ [m] | $V_{ust}$ [m/s] | $\Delta V_{ust}$ [m/s] | $KT_{ust}$ [m] | $\Delta KT_{ust}$ [m] |
|---|---|---|---|---|---|---|
| P0 | 0.047 | - | 1.815 | - | 0.168 | - |
| P1 | 0.198 | 0.151 | 0.338 | -1.477 | 0.006 | -0.162 |
| P2 | 0.184 | 0.137 | 0.510 | -1.304 | 0.014 | -0.154 |
| P3 | 0.187 | 0.140 | 0.368 | -1.446 | 0.007 | -0.161 |

The values shown in Table 3 for the four analyzed patterns are the water depth $h_{ust}$, the mean velocity $V_{ust}$ resulted from averaging the values obtained through local measurements and $KT_{ust}$ the specific kinetic energy value of the generalized Bernoulli equation. Also, the difference between a considered reference value, which corresponds to pattern P0, and the corresponding value obtained for the other three patterns are presented. The notations used are $\Delta h_{ust}$ for the obtained water depth difference, $\Delta V_{ust}$ for the mean velocity difference and $\Delta KT_{ust}$ the specific kinetic energy difference.

As shown in Table 1 and Table 3 the water depth increases due to the presence of any of the three patterns of the artificial roughness (P1, P2 and P3). Obliviously, this increase of the water depth generates a decreasing of the water velocity and consequently of the specific kinetic energy. The minus sign of those two differences is showing this decrease. The velocity decreases 81.37% for P1, 71.88 % for P2 of and 79.71% for P3. Also, a significant decrement is noticed for specific kinetic energy: for P1, 96.36%, for P2, 91.94% and for P3, 95.84%.

As a general conclusion, all the data obtained confirms the expected changes in the water surface profile for patterns P1 to P3. Namely, the presence of a high roughness area leads to rise in upstream water level and decrease in the downstream water level.

The analysis of the general effect produced by the presence of artificial roughness is driven by comparing the main quantities derived from the water depth and the water velocity measurements (Bekheet et al., 2025; Ghomri et al., 2023; Yang et al., 2025).

The first driven physical quantity was the difference of the total head corresponding to $S_{ust}$ and respectively to $S_{dst}$, for each of the three patterns of artificial roughness. This friction loss was obtained by applying the energy equation (the generalized Bernoulli equation) between the two monitoring sections. The results obtained are shown in Figure 12.

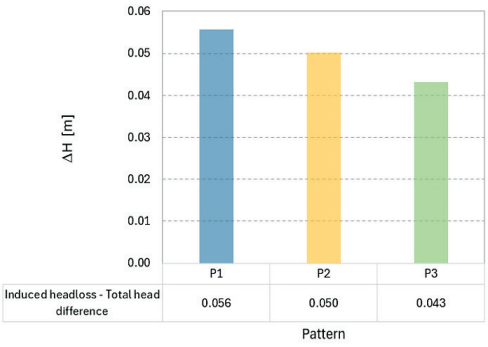



Figure 12. Fiction loss $\Delta H$ induced by the three patterns

As shown in Figure 12, pattern P1 induces a drop of the hydraulic head of 5.6 cm. Compared to this value, the drop generated by P2 is 10.71% less, and the third one, P3, 23.22% lower than P1.

Another way to quantify the dissipative effect between Sust and Sdst is by using the dissipated power (Figure 13).

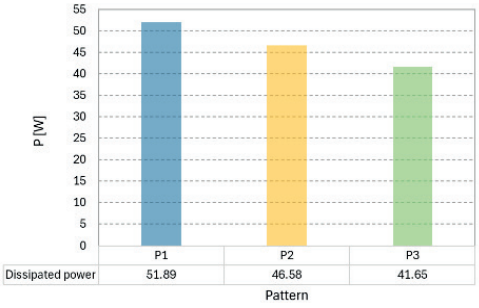



Figure 13. Dissipated power by the three patterns

The results obtained on the efficiency of each of the three patterns are plotted in Figure 14.

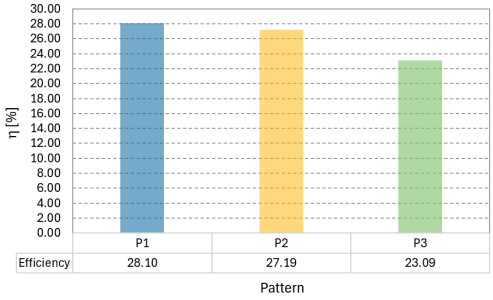



Figure 14. Efficiency of each of the three patterns

As shown in Figure 14, the most effective pattern is P1. Compared to P1, the dissipation efficiency decreases 3% for P2 and 17.83 % for P3.

## CONCLUSIONS

The experimental tests carried out in the „Dumitru Cioc" Hydraulics Laboratory, part of the Technical University of Civil Engineering Bucharest, are seen as a starting point for future tests.

The results obtained are considered encouraging for developing future research on the shapes proposed for the roughness elements.

The future possible research may follow two paths. The first one continues the hydraulic experimental tests with different flow rate values, diverse channel slopes and various distances between the artificial roughness elements. To obtain a complete image of the flow in the wake of the experimental area, transvers measurements at different depths are necessary. Also, the evaluation of turbulence like studies on turbulent kinetic energy and Reynolds stress provides important information about energy dissipation and is considered for future research.

A shortcoming of the experiments was the reduced number of available artificial roughness elements and consequently the low extent of the test area. Also, the lifting phenomenon of the bottom plates has dictated the maximum velocity value that can be used for the experiments (1.82 m/s). After correcting the previously mentioned aspects a comparative study, carried out in the same flow condition, on the behavior of the proposed artificial roughness elements and a classical shape like cubic elements is considered useful.

The second path that can be followed is related to the use of new materials for building the artificial roughness elements. New materials and new technologies are now available. A series of interdisciplinary studies involving the hydraulics laboratory personnel and the chemistry and building materials department of the TUCEB are considered of interest.

## REFERENCES

Bekheet, A. A., AboulAtta, N. M., Saad, N. Y., & Molla, D. A. (2025). Energy dissipation in stepped spillways: a comprehensive review of the recent research. *Innovative Infrastructure Solutions*, 10. 10.1007/s41062-025-02042-6.

Certousov, M. D. (1966). *Hidraulica. Curs special* [Hydraulics. Special course]. Bucharest, RO: Technical Publishing House.

Cioc, D. (1975). *Hidraulică* [Hydraulics]. Bucharest, RO: Didactic and Padagogic Publishing House.

Chanson, H. (2021). Hydraulics and Energy Dissipation on Stepped Spillways – Prototype and Laboratory Experiences. *Proceedings of the 2nd International Symposium of Water Disaster Mitigation and Water Environment Regulation*. Chengdu, China.

Chen, Y., Yang, W., & Lin, H. (2024). Reproducing the temporal averaging process of the acoustic Doppler velocimeter and assessing its impact on turbulence measurements. *Measurement*, 226. 114093. 10.1016/j.measurement.2023.114093.

Dumitrescu, D., & Răzvan, E. (1972*). Disiparea energiei și disipatori de energie* [Energy dissipation and energy dissipators]. Bucharest, RO: Technical Publishing House.

French, R. H. (1986). *Open-channel Hydraulics.* New York, USA: McGraw-Hill Book Company.

Ghomri, A., Lacheheb, S., & Djamaa, W. (2023). Effect of roughness on the characteristics of the hydraulic jump evolving into a rectangular channel of compound section. *Journal of Fundamental and Applied Sciences*, 13. 50. 10.4314/jfas.1300.

Kazemi, M., Khorsandi, B., & Mydlarski, L. (2021). Effect of Acoustic Doppler Velocimeter Sampling Volume Size on Measurements of Turbulence. *Journal of Atmospheric and Oceanic Technology*, 38. 10.1175/JTECH-D-20-0174.1.

Kiselev, P.G. (1988). *Îndreptar pentru calcule hidraulice* [Hydraulic Calculation Guide]. Bucharest, RO: Technical Publishing House.

Mei, J., Zhou, Y., Xu, K., Shu, Z., Gan, Q., Yu, Q., & Qian, J. (2025). Energy Dissipation on Inclined Stepped Spillways. *Water*, 17. 251. 10.3390/w17020251.

Morris, M.H., & Wiggert, J.M. (1972). *Applied Hydraulics in Engineering.* New York, USA: Ronald Press Company.

Novak, P., Moffat, A.I.B., Nalluri, C., & Narayanan, R. (2005). *Hydraulic Structures.* London, UK: Taylor & Francis.

Park, H., & Hwang, J.H. (2021). A Standard Criterion for Measuring Turbulence Quantities Using the Four-Receiver Acoustic Doppler Velocimetry. *Frontiers in Marine Science*, 8. 681265. 10.3389/fmars.2021.681265.

Peterka, A. J. (1984). *Hydraulic Design of Stilling Basins and Energy Dissipators. Engineering Monograph No. 25.* Denver Colorado, U.S: Department of the Interior Bureau of Reclamation.

Yang, J., Li, S., Farooq, U., & Helgesson, A. (2025). Energy Dissipation in Chute Spillway with Labyrinth Roughness Appurtenances. *Water*, 17. 3417. 10.3390/w17233417.

Zhou, Y., Huang, T., Xu, K., Mei, J., Jia, S., Yu, Q., & Qian, J. (2025). Hydraulic performance of a pre-aerated stilling basin: Experimental study. *PLOS ONE,* 20. 10.1371/journal.pone.0318191.

Scientific Papers. Series E. Land Reclamation, Earth Observation & Surveying, Environmental Engineering. Vol. XV, 2026
Print ISSN 2285-6064, CD-ROM ISSN 2285-6072, Online ISSN 2393-5138, ISSN-L 2285-6064

# EFFICIENT USE OF AGRICULTURAL LAND BY ORGANIZING AND DIMENSIONING CROP ROTATION

**Marius Nicolae CIOBOATĂ, Dragomir BRUMAR, Marilena Alina PRIOTEASA**

University of Craiova, Faculty of Agriculture, 19 Libertăţii Street, Craiova, Dolj, Romania

Corresponding author email: alinapri76@gmail.com

***Abstract***

*There are many discussions globally related to the efficient use of agricultural land. An important role in the valorization of these agricultural lands is represented by the size of the exploited plot of land. Through this work, the concentration of agricultural areas in units of optimal size was achieved to allow the application of modern agricultural methods and technologies. This paper presents a way of agricultural land consolidation of the plots of land in the category of arable use belonging to the cadastral plots T225-T226-T227, Izbiceni locality, Olt county, South-West Oltenia region of Romania. From the documents studied, the initial situation presented for the three cadastral plots a total area of 419.33 ha and a number of 517 individual lots, and for an individual lot there was an average area of 8110.83m$^2$, less than 1 ha, which determines the difficulty in the efficient exploitation of agricultural land. Through agricultural land consolidation, the individual plots were grouped into 9 fields of similar size, and the resulting average area for these fields being 46.48 ha, a corresponding area for optimal exploitation. At the same time as the analysis and sizing of the exploitation areas, the natural conditions (soil type, climate, vegetation) specific to the area were also analysed, in order to identify the crops suitable for the area and establish the crop rotation. Two field crop rotations were carried out: crop rotation C1 (185.61 ha), consisting of 4 fields and 4 crops (corn, barley, rapeseed, wheat) for a 4-year period, and crop rotation C2 (233.72 ha), consisting of 5 fields and 5 crop groups (sunflower, barley, soybeans, peas and wheat) for a 5-year period. The aim was for these crops to also meet the requirements of the agricultural products market.*

***Key words****: agricultural land, crop rotation, territory organization.*

## INTRODUCTION

Territorial organization is clearly defined as the set of measures, actions and works that intervene in a given territory in order to efficiently use the existing potential and ensure a coordinated development of economic and social activities (Bold, 1994). Territorial organization and agricultural planning plans represent the only way in which the coordination of spatial elements and the adopted solutions are aimed at improving the technical and economic organization of space, in order to adapt it to the various purposes foreseen by society (Brumar, 2006).

According to Eurostat (2026) and according to the latest baseline data from 2023, the EU had 8.8 million farms, of which 2.9 million, or 32.6%, were located in Romania alone – more than twice as many as in the next Member State, Italy, which had 1.3 million farms, or 14.3% of the EU total, followed by Poland with 1.2 million (14.5%) and Spain with 0.8 million (9.1%). The size of farms across the EU is small: almost two-thirds of farms had less than 5 hectares (ha) in 2023, respectively 62.8%, while at the opposite pole only 7.6% of farms reached 50 ha or more, and these accounted for 68.3% of the EU's utilised agricultural area (UAA). The average size of agricultural holdings at EU level was 17.8 ha, a threshold reached or exceeded by about 17% of farms (Eurostat, 2026).

Political, economic and social changes have a direct influence on the use of agricultural land over time (Ovreiu et al., 2021).

In Romania, the way of using and exploiting agricultural land was influenced by the following events:

1) Between 1949 and 1990 the land passed into the administration of the state. The socialist agricultural system appeared, characterized by the exploitation of large and homogeneous agricultural areas by categories of use. This period had a significant influence on the measures of organization and exploitation of the territory that are still felt today. Each agricultural unit in that period was obliged to

carry out a Territorial Organization Project and to review it periodically. Through this project, the following were carried out: the sizing of the plots, the realization of the circulation network, the characterization of the soils, the establishment of soil improvement measures, the establishment of the categories of use according to the creditworthiness notes, the arrangement of the irrigation surfaces, the drainage and elimination of flooded areas, the sizing of the production units, the regularization of water courses, etc.

2) After 1990, the political evolution led to the elimination of the centralized exploitation of agricultural land, the elimination of those agricultural cooperatives. During this period, private property was reconstituted through massive expropriations, which led to transformations in the exploitation of agricultural land, determining a high degree of fragmentation of agricultural areas (Ovreiu et al., 2021). This aspect generated economic disadvantages, caused the degradation of agricultural land and influenced the way agricultural land was exploited. The fragmentation of agricultural land, after 1990, also had a negative effect on the surface arranged with a drainage system. The cultivation of the land without taking into account the position of the network of drainage canals and sometimes even impossible to take into account due to the small size of the plot, caused the reappearance of excess moisture, which led to low crop yields (Oprea, 2022).

3) Romania's accession to the European Union (2007) was characterized by the existence of funds and subsidies for agriculture. New farms were developed that gradually increased the areas. New high-performance machinery was purchased that offers high yields on large areas. Farmers are starting to apply long-term sustainable technologies.

Fragmented use of agricultural land leads to high operating expenses but also low productivity, resulting in inefficient use and poor agricultural performance, but property fragmentation increases the trading value (Isenhardt et al., 2025). Land fragmentation plays an important role in determining the productivity of a farm, and the higher the weighted average of the plots worked, the higher the productivity of the farm (Looga et al., 2018).

The analysis of agricultural land fragmentation is multidimensional, encompassing several aspects: the number of plots that a farm operates, the size of these plots, how regular their shape is, the distance from the farm premises, and how dispersed the plots are from each other. Greater fragmentation tends to increase production costs while reducing yields, income, profitability and overall efficiency (Latruffe & Piet 2014).

A study by Valtiala et al. (2023) in Finland reviewed previous results on the relationship between plot size and exploitation efficiency. They found that there is an increase in labour efficiency in larger plots, and once a plot exceeds around 20 ha, any further increase in size brings few additional technical benefits.

Spatial planning is a way of exploiting agricultural land according to specific rules, determining the necessary measures for the conservation and improvement of land quality, a way of managing property rights and a solution for the development of agricultural businesses (Moteva & Marinova, 2020).

When there are good quality soils, characterized by high fertility, which have a favourable structure, texture and porosity, they can only provide high crop yields by applying appropriate technologies to normal environmental conditions (Balan et al., 2024).

Agricultural Land Use Planning involves the spatial organization of agricultural land for the purpose of rational exploitation, it involves the rational use of agricultural machinery, it involves the preservation of the natural properties of soils, it determines the economic efficiency of farms and the prosperity of rural areas (Moteva & Spalevic, 2016).

From the research carried out by Dorosh et al., 2020, on spatial planning and organization of agricultural land use in Ukraine, it follows that the rational use of land to ensure ecological and economic sustainability must be achieved by analysing the following indicators: territory – landscape – plot of land – soil (Dorosh et al., 2020).

The diversity of the relief, the intensity of anthropogenic productive activities and climate change favour the extension of soil degradation processes, with significant effects on agricultural productivity, and agricultural performance is directly influenced by the way

the territory is organized (Balan & Nitu, 2025).
The spatial organization of the territory aims at the most efficient use of agricultural land, by maintaining their balance, achieving a stable environment within the agroecosystems and at the same time the main goal being to obtain a maximum yield (Shkuratov et al., 2020).
Agricultural land is efficiently exploited by achieving high yields, these are influenced by the biological material used and the technology applied, as well as by environmental factors, climate, soil type, relief, etc. Soil fertility can be limited to varying degrees of limitations caused by human or industrial actions, which can sometimes act negatively (Oprea & Curea, 2022).
Within this work, the aim was to organize and arrange arable land for an arable area in Izbicéni, Olt County, Romania. This work offers a partial solution for the exploitation of agricultural land. It should be noted that the work refers to the identification of an optimal solution in terms of the size of a plot of land as a production unit, not in terms of the general size of the agricultural farm.
Through the works of organizing the arable territory, the amalgamation of agricultural land is also carried out. Romania is the country with the most fragmented agricultural territory in Europe (Eurostat, 2026), there has been an attenuation of this phenomenon in recent years, but progress is still needed to this end. The amalgamation of agricultural land can be influenced by legislative actions (mandatory) and by the free will of the land owner (optional actions). Currently, in Romania, private initiative is the only option that determines the amalgamation or grouping of arable areas, through sale-purchase contracts, association, lease, rental, but not according to a specific law, but according to the legislation regulating civil law. All these laws do not impose mandatory rules for the organization and location of parcels, which is why these actions result in random areas in size and with minimal effects on agricultural performance. Another problem that has arisen is the reduction of crop diversity at farm level, or the practice of a short rotation, farms have emerged that cultivate one, two or maximum three species of wheat, rapeseed, corn or sunflower. To this end, the European Parliament has tried to condition those direct payments to farmers (subsidies) on compliance with crop rotation and the minimum area.
This study aims to reduce the level of fragmentation of agricultural land in the analysed area, to create plots of optimal size and to draw up a crop rotation over a period of four years, in accordance with economic requirements and agrotechnical criteria. Such an approach ensures an economic development of the farm as well as the possibility of using irrigation in the future (Cioboată et al., 2023). In that area there is an irrigation system that requires small repairs.

## MATERIALS AND METHODS

The documentation for the organization and arrangement of agricultural land for agricultural farms aims to highlight the main factors that ensure the optimal framework for development in agricultural production. From a technical point of view, this is achieved through two stages: 1. Identification/ knowledge of the land fund (owner, category of use, conditions and natural resources) and grouping the neighbouring plots or lots in compact areas of larger size, establishing the boundaries and maintaining the obligatory limits; 2. Grouping the land by quality classes, establishing the crops and their rotation within fields adapted to the natural conditions and the economic criteria specific to the competitive market. All these should be achieved by observing the scientific criteria of territorial organization (Order no. 212, 2002)
In order to achieve the objectives of the work, the stages were followed according to the technical norms for the preparation of projects for the organization of the territory of agricultural holdings, as well as the indications in the specialized literature.
The present documentation is expressed by the cadastral plans scale 1:10000, 1:5000, the material base in digital and analogue format existing at the Olt Cadastre and Real Estate Advertising Office and at the Izbiceni Local Council.
Based on these, the cartographic documents (analogue and digital) that were made available by the Olt OCPI and the Izbiceni Local Council for the plots T225, T226, T227 were examined,

in question: orthophoto plan; cadastral plans 1:5000-1:10000; property titles; cadastral documentation resulting from the registration process; database resulting from the PAD conversion; other graphic and textual data possessed by OCPI and the Izbiceni Local Council, for the plots T225, T226, T227.

The identification of the site was achieved by locating it in the field.

Then the limits of the plots were established through direct measurements on the ground. The target of this action was to precisely determine the limits of the plots from T225 to T227, through measurements on the ground in order to be able to determine the location, respectively the surface. Topographic measurements were carried out in the coordinate system of the state geodetic network.

The accuracy of determining the points was determined according to ODG no. 634 and Decision no. 1 regarding the performance of kinematic GNSS measurements, issued by the director of the Directorate of Geodesy and Cartography within the ANCPI.

The measurements were performed with a GPS receiver, type Leica GS08 CS 10, of the dual-frequency geodetic accuracy class, the method used was RTK.

The processing of GPS measurements was carried out using the specialized Leica GeoOffice program, for the calculation of the coordinates at the determined points, observations from the permanent stations CORA (CORABIA) and SLA (SLATINA) were used.

The conversion of coordinates from the WGS 84 system to the STEREO 1970 projection system was carried out using the TransDat RO program.

Following the measurements with the GPS device, stereographic coordinates were obtained on the WGS 84 ellipsoid, these coordinates being transformed in the official reference system of Romania, using the coordinates of the existing geodetic points.

The plans were drawn up at a scale of 1:5000, 1:10000, using the BricsCAD V13 program.

The determination of the areas for each individual owner and on each plot was carried out through multiple detachments according to the parcel tables, using the TopoLt automatic program. Also in this program, simulations were made to identify the optimal option for organizing the agricultural territory, respectively for sizing the plots (soles/fields) for crop rotation. Several variants of dividing the total area into approximately equal plots were analyzed, but only 2 variants are presented in the paper that are exposed in the chapter results and discussions.

In order to establish the crop rotation, it is necessary to carry out the evaluation of agricultural land and its grouping in Homogeneous Ecological Territory (TEO), this is done on the basis of the creditworthiness grades calculated with the help of data from soil studies (Order no. 212, 2002). The following indicators are used: temperature, precipitation, texture at 20 cm depth, gleying, pseudogleying, salinization/alkalinization, pollution, slope, landslides, groundwater depth, flood susceptibility, subsidence, carbonate content, soil reaction, degree of saturation, edaphic volume, humus content, and excess moisture. The homogeneous ecological territory (TEO) for T225-T226-T227 in Izbiceni, Olt County, have been determined.

## RESULTS AND DISCUSSIONS

### Presentation of the studied area

The analysed territory belongs to the south-western Oltenia region of Romania, the category of use – arable. Official statistics show that, at the level of the entire region, the categories of land use have undergone significant changes after 1990 (Miluț et al., 2020). The increase in non-productive areas is interesting, another observation that must be taken into account is related to the accentuation of land degradation phenomena, so in this context it is necessary to identify sustainable land monitoring measures that balance agricultural productivity with environmental protection (Călina et al., 2025). In order to implement measures to mitigate land degradation, it is necessary to identify the spatial spread and intensity of these processes at a landscape level (Filipciuc et al., 2019).

The reconstitution of the right of ownership, after the application of Law 18/1991, determined the appearance of plots with small widths of 8-10-12 m, in the form of strips, in the N-S or E-W directions, and on different

lengths, this aspect determined the decrease of the yield per hectare (Popescu & Bălan, 2024).
The commune of Izbiceni consists of a single locality, bearing the same name, being placed on the right bank of the Olt River, in the Romanați Plain, a sub-branch of the Oltenia Plain, in the southern part of Olt County (Figure 1).
The commune is positioned on the northern latitude 43°49'; eastern longitude 24°39' and the maximum altitude 48.2 m on the mound in the northwest of the estate and the minimum 39.9 m at the water level of the Olt River, the north of the Danube river.

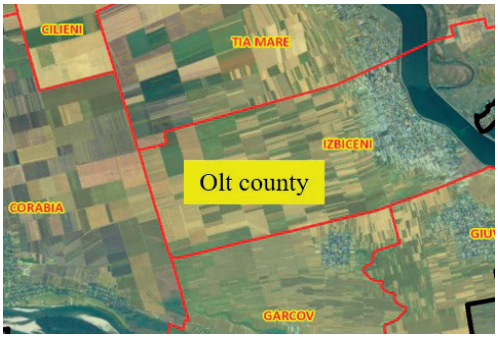



Figure 1. Location of Izbiceni (https://geoportal.ancpi.ro)

The area of Izbiceni commune is 5115 ha, of which 4130 ha are agricultural land and 985 ha are non-agricultural lands. The number of existing households in Izbiceni is 1320.
The climatic factors found in the commune of Izbiceni are:
- the average annual temperature oscillates between 10-12 degrees;
- precipitation is different from one year to the next and also from one season to another (the annual average being 450-570 mm/m$^2$);
- wind: the north wind blows intensely in winter, blowing snow, forming squalls (it reaches speeds of 60-70 km/h, in the northeast to southwest direction); the south wind, the second most important wind, blows more in spring, being humid and warm in the cold season and dry in the warm season (it reaches speeds of 20-30 km/hour, in the west-east); Bălțărețul, blows in the warm season from the southeast to the northwest; Zephyr blows from the south and brings heat. Austrul, Baltărețul and Zephyr are the winds with the main role in pollinating flowering plants.

The most common groups of soils in the locality are: chernozem; sandy soils; marshy soils, resulting from the rotting of plants, buried with the passage of time (Popescu, 2016).
The local flora is diversified, here we find the steppe combined with the flora of the lowlands (acacia, mulberry, apricot, chervil, sycamore, quince) which are combined with willow, poplar, mulberry, etc. and on the other hand, the places cultivated with cereals are often interspersed with places where meadow plants grow freely. Here we find numerous trees, vines, plants of all kind.
Characterization of soil types**.** According to the observations and determinations in the field and the results of the analyses obtained from the samples taken, we can state that the soils of the Izbiceni communal territory are part of soil unit 9 (US 9).
Soil unit 9 (US9), which is found on the territory of the plots T225-T226-T227, is the chernozem, cambic chernozem, very deep profile, with a loamy, loamy-sandy or loamy-clayey texture, the parent material is represented by loess, loess-like material, clays, marls, alluvial-proluvial deposits, etc., extremely rich in basic elements. The relief is a plain, which is characterized by flat or slightly undulating surfaces.
Chernozem properties (Popescu, 2017):
Am horizon: 40-60 cm; blackish colour (chromes and values less than or equal to 2); loamy, sandy loam or clayey loam texture; medium and large, well-formed glomerular structure; porous medium; compact medium; intense biological activity; gradual transition.
ACk horizon: 80-100 cm; brown-gray colour, with chromes and values <3.5 at least in the upper half; loamy texture, sometimes sandy loam or clayey loam depending on the nature of the parent material; less well-formed glomerular structure; porous medium; compact medium; frequent whitish stains and streaks of calcium carbonate; obvious effervescence; gradual transition.
Horizon Cca: 80-100 cm; lighter colour, different texture; unstructured; frequent spots and calcium carbonate concretions; strong effervescence.
For the evaluation of the agricultural land in plots T225-T226-T227 in Izbiceni, Olt county, only one TEO unit resulted, and the results obtained are presented in Tables 1-3.

From the studied documents, the owners of the lands in the T225-T226-T227 plots were identified as follows: T225 = 171 owners and a measured area of 1377559 $m^2$; T226 = 183 owners and a measured area of 1438009 $m^2$; T227 = 163 owners and a measured area of 1380317 $m^2$ (Figure 2). In order not to upload the document, the data referring to the parcel tables were not included.

Table 1. Eco pedological indicators of soil quality

| No. TEO | US 9 |
|---|---|
| Temperature | 10-12 |
| Precipitation | 400-500 |
| Gleying | Umed |
| Pseudogleying | 0 |
| Salinization/alkalinization | 0/0 |
| Texture at 20 cm depth | Loamy |
| Pollution | 0 |
| Slope | 1 |
| Landslides | 0 |
| Groundwater depth | Small |
| Flood susceptibility | 0 |
| Subsidence | unsettled |
| Carbonate Content | Medium |
| Soil Reaction | Weakly Alkaline |
| Degree of Saturation | High |
| Edaphic Volume | Very high |
| Humus Content | Very high |
| Excess Moisture | Permeable |

Table 2. Ratings and quality classes of TEO

| No. TEO US9 arable land (surface = 419.33 ha) | Ratings | Quality classes |
|---|---|---|
| Wheat | 70 | II |
| Barley | 71 | II |
| Corn | 81 | I |
| Beans | 75 | II |
| Potato | 59 | III |
| Sugar beet | 76 | II |
| Soybean | 80 | II |
| Peas | 70 | II |
| Flax | 77 | II |
| Rape | 90 | I |
| Hemp | 70 | II |
| Alfalfa | 77 | II |
| Clover | 56 | III |
| Vegetables | 62 | III |
| Arable | 81 | I |

Table 3. Classification of TEO into suitability classes

| No. TEO | | US9 |
|---|---|---|
| Surface | | 419.33 ha |
| Area by suitability classes | I | 0 |
| | II | 419.33 |
| | III | 0 |
| | IV | 0 |
| | V | 0 |
| | VI | 0 |
| Indicative requirements for improvement work | | Irrigation |

The initial situation of the land areas within the three plots before the organization of the territory was presented: in T225 the average area of a plot was 8,055.90 $m^2$; in T226 the resulting average area was 7,857.90 $m^2$, and in T227 the average area was 8,468.20 $m^2$.

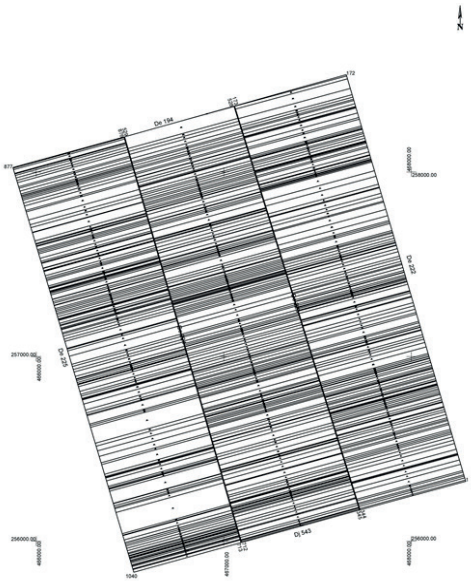


Figure 2. Summary presentation of the land fund

Using the automatic TopoLt program, the detachment of each area was carried out, simulations were carried out in order to achieve areas that correspond to the criteria for crop rotation, respectively for their sizing according to the arable land organization plans.

**Organization and arrangement of arable land**

The territory proposed for the organization is identified as part of the arable use category, belonging to the Izbiceni commune, Olt County and is recognized by the parcels from T225 to T227, and the demarcation in the field was carried out by the measurement sheet and by the exploitation roads.

Legally, these areas are privately owned. Currently, the studied area is entirely leased by an agricultural company. For the most efficient exploitation of the land, according to the principles of arable land organization (Brumar, 2006), two variants of dividing the

topographically raised land into approximately equal plots have been proposed.

The first variant of the territorial arrangement (Figure 3) includes 3 soles/fields/plots that have the areas of: Sola 227 = 1380317 m$^2$; Sola 226 = 1438009 m$^2$; Sola 225 = 1377559 m$^2$.

The roads cover the area of: De 223 – 9072 m$^2$; De 224 – 9500 m$^2$.




Figure 3. First variant of organizing and arranging agricultural land through crop rotations

The existing exploitation roads were preserved: De 223 and De 224 and the existing plots of land were divided into 3, resulting in 3 plots with an area almost to 140.00 ha, (137.75 ha; 138.03 ha; 143.80 ha). This variant is difficult to exploit, because it leads to the opening of very large plots, but also a crop rotation of only 3 years, and the shape of the resulting plots offers a very large gap between length and width.

The second variant proposed and recommendation for the exploitation of the territory (Figure 4) is characterized by the construction of a road De 194/1 with an area of 2484 m$^2$ and the maintenance of the existing ones (De 223 and De 224), as well as the division into nine soles, represented as follows:

- Sola I C1 (T 227) = 46.26 ha;
- Sola II C1 (T 227) = 46.22 ha;
- Sola III C1 (T 226) = 46.40 ha;
- Sola IV C1 (T 225) = 46.73 ha;
- Sola I C2 (T 226) = 48.04 ha;
- Sola II C2 (T 225) = 46.05 ha;
- Sola III C2 (T 225) = 44.97 ha;
- Sola IV C2 (T 226) = 49.11 ha;
- Sola V C2 (T 227) = 45.55 ha.

It is worth mentioning that the entire area subject to development is surrounded by existing exploitation roads that were not taken into analysis, but which can serve the surface.

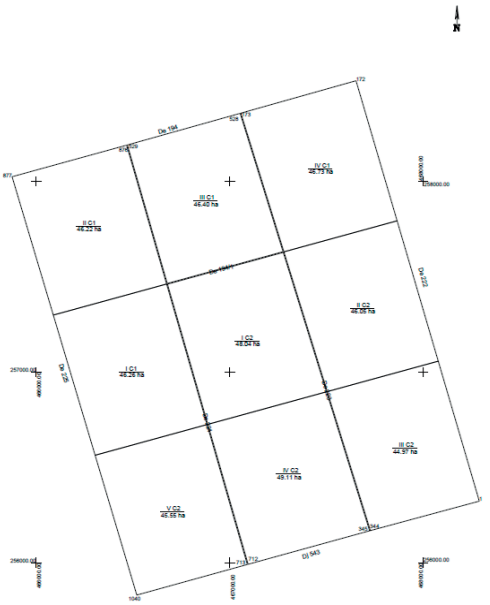



Figure 4. Second variant of organizing and arranging agricultural land through crop rotations

The roads cover the following areas: plot 223 – 9,072 m²; plot 224 – 9,500 m²; and plot 194/1 – 2,484 m².

In order to obtain the best possible results and to comply with the rules of arable land organization, the most suitable option is the second option (Figure 4), which helps to rotate the crops as well as possible, grouping the entire area in a crop rotation with 9 fields distributed in approximately equal areas, between 44.97 ha and 49.11 ha (Tables 4 and 5). These areas are very close to the size of 50 ha, a size recommended by the specialized literature and by many studies. The shape of the 9 fields resulting from the second variant is a shape close to the square, but due to the obligatory limits existing in the area (irrigation

canals, exploitation roads) parallelograms with 4 sides resulted, and the ratio between length and width (L:W) being a maximum of 1:0.8.

In order to ensure the most efficient circulation and flow throughout the exploitation of arable land, it was considered to keep the already existing exploitation roads, as well as the establishment of a new De 194/1 road, so that access on at least 3 sides for monitoring and exploitation is possible for each field. The result was a set of fields with at least two parallel sides.

Due to market trends, the organization of crops for the next period is influenced by the large share held by cereals (corn, wheat, barley) and oilseeds (rapeseed, sunflowers), but the introduction of plants that play a role in nitrogen fixation (peas and soybeans) was also taken into account. In selecting the crops to be introduced into rotation, their suitability for the analyzed area was also taken into account according to the data in Table 2.

From the analysis of the natural conditions specific to the area, it was found that for the entire area there is the same soil category. This aspect does not impose restrictions in terms of crop rotation. A very important aspect that was taken into account in designing the crop rotation, as presented below, was the compliance with agrotechnical principles. Thus, the alternation of cereals with row crops, the alternation of plants with different resistance to diseases and pests, the observance of the restrictive conditions of rotation (rapeseed-sunflower, barley-wheat, the recovery time of a crop), the time between harvest and sowing of the next plant, the required interval before returning the same crop to a field, the alternation of the root system, etc.

In terms of field size-of the surfaces, nine fields were delineated, meeting the technical requirements for agricultural land organization, thus it is proposed to divide the studied area into two crop rotations: C1 (crop rotation 1) with 4 fields and C2 (crop rotation 2) with 5 fields. The C1 crop rotation includes the fields (plots): I C1(T 227), II C1(T 227), III C1(T 226), IV C1(T 225), and the C2 crop rotation is made up of the fields (plots): I C2(T 226), II C2(T 225), III C2(T 225), IV C2(T 226), V C2(T 227).

The C1 and C2 crop rotations have in their configuration crops of wheat, corn, rapeseed, sunflower, barley, peas and soybeans, they are developed for a period of 4 years for the C1 rotation and for 5 years for the C2 rotation, or even 9 years.

The rotation for both rotations, C1 and C2, as well as the location and composition of the crops is described in Table 4 and Table 5.

Table 4. C1 organization and crop rotation

| Crop organization and rotation C1 (185.61 ha) | | | | | |
|---|---|---|---|---|---|
| Sola | | 1 | 2 | 3 | 4 |
| Field | | 227 | 227 | 226 | 225 |
| Surface (ha) | | 46.26 | 46.22 | 46.40 | 46.73 |
| Year | 1 | Corn | Barley | Rape | Wheat |
| | 2 | Barley | Rape | Wheat | Corn |
| | 3 | Rape | Wheat | Corn | Barley |
| | 4 | Wheat | Corn | Barley | Rape |

Table 5. C2 organization and crop rotation

| Crop organization and rotation C2 (233.72 ha) | | | | | | |
|---|---|---|---|---|---|---|
| Sola | | 1 | 2 | 3 | 4 | 5 |
| Field | | 226 | 225 | 225 | 226 | 227 |
| Surface (ha) | | 48,04 | 46,05 | 44,97 | 49,11 | 45,55 |
| Year | 1 | Sunflower | Barley | Soybeans and peas | Wheat | Wheat |
| | 2 | Barley | Soybeans and peas | Wheat | Wheat | Sunflower |
| | 3 | Soybeans and peas | Wheat | Wheat | Sunflower | Barley |
| | 4 | Wheat | Wheat | Sunflower | Barley | Soybeans and peas |
| | 5 | Wheat | Sunflower | Barley | Soybeans and peas | Wheat |

Territorial organization plans comprise a set of measures aimed at managing agricultural land efficiently, making effective use of its existing potential, and further improving it (Cioboată & Brumar, 2022).

## CONCLUSIONS

Through this work, the land area of approximately 419.33 ha, in the Izbiceni locality, Olt County, located in the southwestern part of the locality, was arranged and organized, being identified as part of the arable use category.

The researched area is located in a excessively continental climate zone, characterized by a temperate climate, with frosty winters and slushy snows and warm and generally dry

summers with sufficient precipitation but not being distributed everywhere throughout the year, being deficient in moisture in the months of March, April, August, September and October.

Following the identification on the ground and subject to the organization of the territory, the soils are part of the class of chernisols, more precisely chernozem and cambic chernozem.

Due to the high fertility and favourable climate, cereals and legumes can be grown in the studied area. Thus, wheat, rapeseed, sunflower, barley, soybeans and peas and, last but not least, corn were included in the rotation.

In the first proposed variant, a three-year field rotation was established with three approximately equal soils close to 140 ha (Figure 3), being inadequate.

In the second proposed variant, two land rotations were established, one for four years and one for five years, with approximately equal plot areas, close to 50 ha (Figure 4).

Through crop rotation, a combination of territorial conditions and the production potential of the land has been determined, the efficient use of agricultural machinery and equipment has been ensured, and hydro-ameliorative systems (irrigation) can be put into practice.

Carrying out such work at the level of an agricultural holding provides numerous advantages from an administrative and economic point of view:

- clear record of the areas and owners in each plot;
- the possibility of ordering and monitoring lease or sale-purchase transactions with agricultural land;
- identification of the type of soil present within the studied plot;
- the possible use of agricultural machinery equipped with satellite guidance infrastructure, resulting from the identification of coordinates;
- the advantage of easily creating a business plan in the following periods;
- the ratio of crops and also the cost over a period convenient for the rotation.

## ACKNOWLEDGEMENTS

This research work was conducted without external support or funding.

## REFERENCES

Balan M., Popescu C., & Nitu O. A., (2024). Agroproductive differences between two luvosol units at the Preajba Gorj Experimental Center, Romania. *Scientific Papers Series Management, Economic Engineering in Agriculture and Rural Development Vol. 24, Issue 2, 145-156*, https://managementjournal.usamv.ro/pdf/vol.24_2/Art13.pdf.

Balan, M., & Nițu, O. A. (2025). Study on land affected by erosion in Gorj county. *Scientific Papers. Series A. Agronomy, 68(1).* https://chrome-extension://efaidnbmnnnibpcajpcglclefindmkaj/https://agronomyjournal.usamv.ro/pdf/2025/issue_1/Art1.pdf.

Bold, I., 1994, *Farm – Organization, development, exploitation* [Exploatația agricolă – Organizare, dezvoltare, exploatare] , Mirton Publishing House.

Brumar, D., 2006, *Organization and spatial planning* [Organizarea şi amenajarea teritoriului], Sitech Publishing House, Craiova.

Călina, A., Călina, J., & Vangu, G. M. (2025). Study on the management of land use change by land use categories in the south-west Oltenia development region, during the period 1990-2023. *AgroLife Scientific Journal*, *14*(2), 45-53. https://doi.org/10.17930/AGL202524.

Cioboată, M., & Brumar, D. (2022). Study regarding choosing the optimal territorial planning of an arable land. *Annals of the University of Craiova-Agriculture Montanology Cadastre Series", 52(2), 215-222*. https://doi:10.52846/aamc.v52i2.1407, wosuid: rc:149105393_s24.

Cioboată, M., Brumar, D., & Călina, J. (2023). Study on the analysis of pedoclimatic and hydrographic conditions in order to introduce irrigation in an agricultural farm in the hilly area*. Annals of the University of Craiova-Agriculture Montanology Cadastre Series", 53(2), 161-170.* https://doi: 10.52846/aamc.v53i2.1494.

Dorosh, O., Dorosh, I., Butenko, Y., Svyrydova, L., & Dorosh, A. (2020). Methodology of spatial planning of agricultural land use*. Scientific Papers Series Management, Economic Engineering in Agriculture and Rural Development. 20, PRINT ISSN 2284-7995, E-ISSN 2285-3952.* https://chrome-extension://efaidnbmnnnibpcajpcglclefindmkaj/https://managementjournal.usamv.ro/pdf/vol.20_1/Art23.pdf.

Eurostat, (2026). Farms and farmland in the European Union – statistics, https://ec.europa.eu/eurostat/statistics-explained/index.php?title=Farms_and_farmland_in_the_European_Union_-_statistics#Farms

Filipciuc, V., Rozloga, I., Cojocaru, O., & Boaghe, L. (2019), Study of pedogenetic processes in soils long irrigated - monitoring and projecting their evolution. *Scientific Papers. Series A. Agronomy, Vol. LXII, Issue 1, ISSN 2285-5785, 48-55 https://agronomyjournal.usamv.ro/index.php/18-articles/articles-2019-issue-1/933.*

Isenhardt, L., Seifert, S., Wiltfang, T., & Hüttel, S. (2025). Costs of Farmland Fragmentation: Evidence

from Farmland Transactions in Eastern Germany. *German Journal of Agricultural Economics, 74*. https://doi.org/10.52825/gjae.v74i.2537.

Latruffe, L., & Piet, L. (2014): Does land fragmentation affect farm performance? A case study from Brittany, France. *Agricultural Systems 129: 68-80.* https://doi.org/10.1016/j.agsy.2014.05.005.

Looga, J., Jürgenson, E., Sikk, K., Matveev, E. & Maasikamäe, S. (2018). Land fragmentation and other determinants of agricultural farm productivity: The case of Estonia. *Land use policy, 79, 285-292*. https://doi.org/10.1016/j.landusepol.2018.08.021.

Miluț, M., Stan, I., Călina, J., Călina, A., Croitoru, A., Medelete, D., Bădescu, G. & Ionică, C. (2020). Observations regarding the evolution of the agricultural land fund in Romania on categories of use after 1990. *Scientific Papers. Series A. Agronomy*, *63*(1). http://agronomyjournal.usamv.ro/pdf/2020/issue_1/Art12.pdf.

Moteva, M., & Spalevic, V. (2016). Towards a new concept for the agricultural land-use planning in the new socio-economic conditions in Bulgaria. *Agrofor. International Journal, 1(1),* https://doi: 10.7251/agreng1601076m.

Moteva, M., & Marinova, B. (2020). Agricultural land protection by spatial planning in Bulgaria. *Geomatics and Environmental Engineering*, *14*(3), 89-105. https://doi.org/10.7494/geom.2020.14.3.89.

Oprea, R. (2022). Consequences of fragmentation of agricultural land arrangement with drying-drainage works. *Scientific Papers. Series E. Land Reclamation, Earth Observation & Surveying, Environmental Engineering*, XI.

Oprea, R., & Curea, D. (2022). Limitation of the production capacity of agricultural land in Raducaneni commune, Iași county. *Scientific Papers. Series A. Agronomy, LXV, 1, ISSN 2285-5785, 141-146*. https://WOS:000861074500019, https://agronomyjournal.usamv.ro/index.php/scientific-papers/past-issues?id=1379.

Order no.212 of 15 May 2002. (2002) for the approval of the Technical Norms for the preparation of projects for the organization of the territory of agricultural holdings, *Ministry of Agriculture, Food and Forestry*, *OFFICIAL GAZETTE no. 705 of 27 September 2002*. https://legislatie.just.ro/Public/DetaliiDocument/38610

Ovreiu, A. B., Bărsoianu, I. A., Nistor, C., Nedelea, A., & Comănescu, L. (2021). Long-Term Dynamics of Land Use in the Romanian Plain—The Central Bărăgan, Romania. Agriculture, 11(5), 423. https://www.mdpi.com/2077-0472/11/5/423, https://doi.org/10.3390/agriculture11050423.

Popescu, C. (2016). *Pedologie Cadrul natural de geneză, clasificarea, răspândirea şi caracterizarea solurilor din România* [Pedology: The Natural Framework of Genesis, Classification, Distribution and Characterization of Soils in Romania], Editura Sitech, Craiova, ISBN 978-606-11-7934-3.

Popescu, C. (2017). *Pedologie Formarea, evoluția, alcătuirea şi proprietățile solurilor din România* [Pedology: Formation, Evolution, Composition and Properties of Soils in Romania], Editura Sitech, Craiova, ISBN 978-606-11-7933-6.

Popescu, C., & Balan, M., (2024). Evaluation through natural bonitation work of the soils in the zone of confluence of Dolj and Mehedinti Counties and the estimation of crop plant productions specific to the area*. Scientific Papers Series Management, Economic Engineering in Agriculture and Rural Development, 24, 2,* 809-816, PRINT ISSN 2284-7995 E-ISSN 2285-3952.

Shkuratov, O., Dorosh, O., Gorodyska, O., & Patiyuk, O. (2020). Assessment of influence of spatial organization of the territory on economic efficiency of agrarian enterprises. *Scientific Papers Series Management, Economic Engineering in Agriculture and Rural Development. 20, 2, PRINT ISSN 2284-7995, E-ISSN 2285-3952*, chrome-extension://efaidnbmnnnibpcajpcglclefindmkaj/https://managementjournal.usamv.ro/pdf/vol.20_2/Art57.pdf

Valtiala, J., Niskanen, O., Torvinen, M., Riekkinen, K., & Suokannas, A. (2023). The relationship between agricultural land parcel size and cultivation costs. *Land Use Policy, 131*, 106728. https://doi.org/10.1016/j.landusepol.2023.106728.

Scientific Papers. Series E. Land Reclamation, Earth Observation & Surveying, Environmental Engineering. Vol. XV, 2026
Print ISSN 2285-6064, CD-ROM ISSN 2285-6072, Online ISSN 2393-5138, ISSN-L 2285-6064

# THREE-DIMENSIONAL BUILDING MODELING AS A DIGITAL STRATEGY FOR ENHANCING RURAL TOURISM PROMOTION

**Levente DIMEN, Silvia Alexandra DREGHICI, Tudor BORȘAN, George COZA**

"1 Decembrie 1918" University of Alba Iulia, 5 Gabriel Bethlen, Alba Iulia, Romania

Corresponding author email: ldimen@uab.ro

***Abstract***

*This article investigates the role of three-dimensional building modelling as a digital tool for promoting rural tourism and enhancing the visibility of underrepresented destinations. Rural areas often face challenges related to limited accessibility, low digital presence, and insufficient promotional resources, which constrain their tourism potential. To address these issues, the proposed approach integrates high-resolution spatial data, photogrammetry, and geographic information systems to generate accurate and interactive 3D building models of rural settlements. The methodology emphasizes cost-effective data acquisition and scalable modelling workflows suitable for small municipalities. The resulting 3D models are deployed within web-based visualization platforms and virtual tour environments to support destination marketing and visitor engagement. Results indicate that the use of 3D building models significantly improves the perceived attractiveness and spatial understanding of rural areas, facilitating remote exploration and informed travel planning. The study demonstrates that 3D modelling constitutes an effective and sustainable digital strategy for strengthening rural tourism promotion.*

***Key words****: 3D building modelling, rural tourism, digital heritage, spatial visualization, destination promotion.*

## INTRODUCTION

Nowadays, we face an increasing tourism, weather it is urban or rural. The challenges in rural tourism promotion refer mainly to limited visibility, low digital presence, fragmented information, and lack of immersive visitor experiences, and therefore a division between urban and rural tourism destinations.

Digital technologies of three-dimensional modelling play an important role in promoting tourism destinations. In this context, it is important to mention the evolution from two-dimensional maps and static images to immersive three-dimensional environments (eg. VR, AR, or web-based platforms) that allow users to visualize, explore, manipulate, and experience virtual worlds in real-time and lead to a growing relevance of 3D building models in smart tourism, virtual tourism, and tourism destination marketing (Rosmani, 2014; Caciora et al., 2021).

3D building modelling generates detailed, three-dimensional digital representations of structures integrating both geometric form and semantic information (meaning/attributes), used to simulate, visualize, and analyse buildings as tourism offer. Digital models are characterized by their Level of Detail (LoD) – which determines the precision of their geometry – and their semantic richness, which defines the level of information embedded within the model, such as material, function, or interior layout (Brenner, 2005; Biljecki et al., 2016). Three-dimensional building models come with many advantages over conventional models, especially where tourism is considered. 3D models offer immersive, interactive experiences, such as virtual tours, 360° videos, and holographic projections, that improve marketing and destination, cultural heritage, and touristic attraction exploration. These digital techniques allow for detailed, realistic, and accessible, or "pre-visit" exploration, finally increasing visitor engagement, satisfaction, and intent to travel (Rosmani, 2014; Caciora et al., 2021).

However, comparing to urban digital tourism promotion, there are limited empirical studies on the application of three-dimensional building modelling specifically for rural tourism promotion. There is also a lack of evaluation frameworks linking three-dimensional models to tourism attractiveness and visitor engagement.

Considering all the aspects mentioned above, the present paperwork aims to investigate how 3D building modelling can function as a digital strategy to enhance rural tourism promotion. The main objective is to assess its role in improving touristic rural destination visibility, visitor understanding, and promote rural and natural values (Rosmani, 2014; Caciora et al., 2021).

## MATERIALS AND METHODS

Due to the times we live in and the innovative opportunities offered by modern equipment currently available, the chosen topic for the present paperwork is the 3D modelling of an agritourist guesthouse located in a mountain hamlet, Apuseni Mountains, Romania, specifically for the purpose of promoting rural tourism. The preservation of this place through modern digital methods is the main priority, in order to promote it to all those who wish to understand and preserve the rural culture of our country, which is gradually disappearing due to the limited resources allocated to it.

The guesthouse in question is called "La Mărișcuța Citeră". It is a traditional house built in 1849, referred to by locals as the "Monument" House, located in the hamlet of Citeră, which belongs to the town of Zlatna, Alba County. The building represents a valuable source of traditions and historical heritage of the rural landscape. The "Monument" House holds particular importance as it is the oldest building on the site. It consists of two rooms and a basement and was constructed using adobe (a mixture of clay soil, straw, and equine/bovine manure), wood, and a manually crafted shingle roof. The foundation of the building is made of stone, while the interior structure is made of wooden posts and beams (Lacitera, n.d.).

Since 2021, many rehabilitation activities have been carried out, aiming to restore the site and transform it into a tourist area, which now comprises a total of ten buildings. The three-dimensional representation of the "Monument" House will be used to document, preserve, and facilitate the complete restoration of this building, both in the present and for future studies, through the creation of a virtual tour that will stimulate the public's imagination regarding such a place and encourage visitation (Lacitera, n.d.).

**Data collection**

The creation of high-quality three-dimensional models of buildings is contingent on the data collection method employed. Whether the images are meant for use in the field of architecture, cultural heritage, construction, or real estate, the manner in which they are captured has a direct impact on the accuracy, level of detail, and practical utility of the obtained model.

Terrestrial imaging is the process where images are captured from ground level. This method offers high detail for vertical surfaces, ornaments, entrances, and interiors. In order to achieve optimal results, it is essential to ensure consistent lighting, to avoid motion blur, and to maintain overlap of 60-80%. Terrestrial photogrammetry is a process that offers numerous advantages, including the capability to produce high-resolution textures for facades, comprehensive interior coverage, enhanced control over exposure and focus, but also a range of limitations, such as restricted access to roofs or elevated areas and a more protracted time commitment in the field (Brenner, 2005; Rosmani, 2014).

Conversely, the most prevalent technique for building reconstruction is aerial photogrammetry, which is ordinarily executed through the utilisation of drones. This method is highly effective in the image capture of roofs, facades, and the surrounding environment, with a particular emphasis on oblique photos. In order to achieve best results, it is imperative to adhere to the established flight parameters, with particular emphasis on the side overlap. The range of forward overlap was found to be between 75-85%, whilst the altitude was between 80-90%. It varies between 30 and 60 metres, contingent upon the height of the structure. Aerial photogrammetry has been proven to offer significant advantages, including efficient coverage of large areas, access to rooftops, and RTK/GNSS accuracy. However, it is important to note that there are also limitations, such as the capture of less detailed façade data and the restriction to narrow urban canyons (Brenner, 2005; Rosmani, 2014).

In the context of the present paperwork, the most reliable method for building reconstruction is hybrid, combining aerial and terrestrial imagery. This approach is suites best for restoration of

historical buildings, ensuring optimal coverage and detail across all elements of the structure. The integration of terrestrial and aerial imagery produces a high-fidelity 3D model, incorporating comprehensive details both of the roof, walls, and ground. The quality of the reconstruction is contingent not solely on the quantity of images available, but also on the consistency, overlap, lighting, and perspective variation of these images. The selection of capture methods and parameters should be made with consideration for factors such as the accessibility of the site, the level of detail required, and the availability of tools (Dreghici et al., 2016; Coza, 2025).

**3D Modelling Workflow**

The initial phase in the three-dimensional modelling workflow is the pre-processing one. During this first step, captured images and correlated data are analysed all together, and growth errors are eliminated. The photo histogram is uniformised, and images are calibrated if deemed necessary. Subsequently, the proper conversion of photographs into three-dimensional models is undertaken, adhering to the established workflow (Dreghici et al., 2016; Coza, 2025):

- The software's 'align photos' function involves the calculation of camera positions, resulting in the generation of a sparse point cloud. Following processing, a sparse point cloud representing the 3D space captured by the photographs will be displayed – Figure 1 a.
- The densifying of the point cloud enhances the intricacy of the model. In this step, the quality settings are configured, and depth filtering is established – Figure 1 b.
- The mesh is a 3D surface generated from the dense point cloud, which is used as the source data. Given that the model is a 3D object, not a terrain, the selected surface type is arbitrary. Upon completion, the model will possess a complete 3D geometry – Figure 1 c.
- Textures are a crucial element in achieving a realistic colour and appearance in the model. The texture will be mapped directly onto the 3D mesh, thereby enhancing visual realism – Figure 1 d.

While the software can generate high detail 3D models from captured images, it should be noted that the results are often presented in an arbitrary unit scale, unless the scale is set accordingly. It is important to recognise that, without scaling, measurements of distances, areas, and volumes will invariably differ from their real-world dimensions. The scale calibration is of high importance and is widely regarded as the best approach to ensure precision. The 3D model has emerged as a versatile solution that finds application in diverse domains, including surveying, archaeology, construction, mining, and numerous other fields (Coza, 2025).

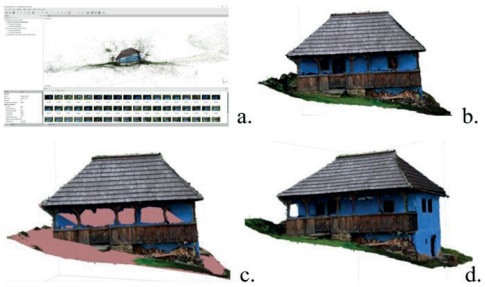



Figure 1. 3D modeling workflow: a. Photos alignment; b. Point cloud densifying; c. Mesh generation; d. Texture application (Coza, 2025)

By default, the software builds models based on image geometry, meaning measurements are relative rather than absolute. The process of converting the scale to real-world units is of high importance in achieving the needed transformation. This step is of crucial importance, as measurements become meaningful, allowing the calculation of distances, areas, and volumes in metric units, not inarbitrary values as opposed. The model is shown to be consistent with other datasets, thus allowing for integration with GIS data, CAD files and engineering designs. When executed with appropriate scaling, the model is capable of achieving both visual accuracy and reliability for quantitative analysis (Borsan et al., 2025; Coza, 2025).

**Web-Based Visualization**

The final step in the process will be the creation of a brief video comprising a 360-degree tour of the building (Figure 2). This will be used in future to promote both the area and the building on the guesthouse's official website. The software incorporates fundamental animation tools. The camera track feature allows the

generation of animations flythrough that is akin to those produced by professional studios. These animations are suite well to a variety of purposes, including presentations, reports, and online visualizations. Animated flythroughs have been demonstrated to enhance the visual appeal of three-dimensional models (Coza, 2025).

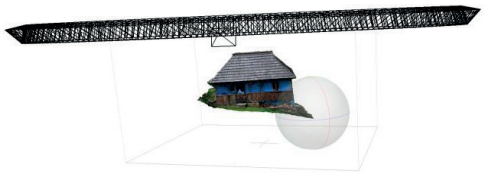


Figure 2. Video tour creation for web-based visualization (Coza, 2025)

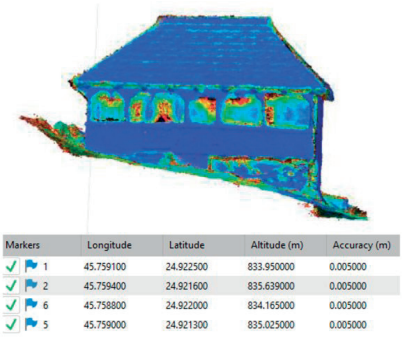
The usage of animated videos in professional contexts, including architecture, archaeology, land surveying, construction monitoring, and tourism promotion, represent a valuable tool. These videos present the capability to visualize the terrain and 3D building models from different angles, guide utilizers through a designated visualization route, virtually articulate model characteristics within online portfolios or client meetings and generate promotional information or instructional visuals.

In order to promote rural virtual tourism, it is essential to integrate the 3D model into digital platforms. Firstly, the 3D model must be rendered in a web-based visualisation format. Finally, the utilisation of mobile or VR-based tourism applications is necessary. The focus of mobile applications for rural tourism is on enhancing the physical experience through augmented reality (AR) and smart, location-based data, while virtual reality (VR) allows users to experience rural environments remotely, offering a "sense of presence" and emotional connection, which can inspire future travel or provide a substitute for those with limited mobility (Parra-Sanchez & Viviescas-Jaimes, 2024; Ilie et al., 2025).

**Evaluation Methods**

The evaluation of a 3D model is a process which is multi-layered in constitution, necessitating a balance between mathematical precision and visual and functional integrity. Regardless of whether one's profession lies within the fields of gaming, engineering, or 3D printing, the evaluation process is typically divided into three primary categories. The following aspects must be given due consideration (Grande et al., 2024; Coza, 2025):

- Geometric and structural accuracy (Figure 3). Geometric and structural accuracy metrics are utilised to ascertain the degree to which the three-dimensional data corresponds with its intended real-world dimensions or a reference "ground truth" model.
- Topology and performance (Figure 4). The evaluation of the model's construction is pivotal in determining its efficacy in software environments, such as game engines, or in the realm of animations.
- Visual and aesthetic quality. From the perspective of visual and aesthetic quality, the model's appearance under illumination is as significant as its structural design.



| Markers | Longitude | Latitude | Altitude (m) | Accuracy (m) |
|---|---|---|---|---|
| 1 | 45.759100 | 24.922500 | 833.950000 | 0.005000 |
| 2 | 45.759400 | 24.921600 | 835.639000 | 0.005000 |
| 6 | 45.758800 | 24.922000 | 834.165000 | 0.005000 |
| 5 | 45.759000 | 24.921300 | 835.025000 | 0.005000 |

Figure 3. Geometric and structural accuracy assessment (Coza, 2025): the confidence level of points in the dense point cloud and accuracy of control markers

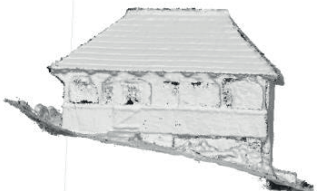


Figure 4. The class of points in the dense point cloud (Coza, 2025)

The evaluation of the 3D model from the perspective of tourism promotion entails the measurement of perceived attractiveness, usability, and engagement. Furthermore, a comparative analysis is to be conducted between

2D promotional materials and 3D models. Finally, qualitative feedback from tourists and local stakeholders is to be considered (Ahtik et al., 2025).

## RESULTS AND DISCUSSIONS

The following results are derived from the 3D model of the "monument" house. The model's output is characterised by its accuracy, realism and level of detail (LOD) (Shashi & Jain, 2007; Rahman & Cahyono, 2023):

- The 3D model of the building that has been generated offers a high level of accuracy, with a margin of error of between 1 and 3 centimetres. Whilst it is generally acknowledged that this method provides slightly less precision than alternative techniques, such as LiDAR, it is nevertheless highly cost-effective and sufficient for applications in the field of rural tourism promotion. The accuracy of the generated 3D model depends primarily on three key elements: the resolution of the input images, the level of overlap between consecutive photographs, and the operator's level of experience.
- The 3D model of the building, obtained through photogrammetric methods, provides a high degree of realism, as it preserves authentic textures, colours, and geometric details derived directly from real-world data.

Comparing to manual modelling, this process generates a digital twin characterised by high-fidelity detail, thus it has been set as a standard in the area of web visualisation.

- The level of detail (LOD) is the degree to which real-world objects are abstracted, ranging from raw footprints to sophisticated three-dimensional models. The present case study of the paperwork demonstrates that the 3D model generation, with high levels of detail (LoD), is optimised by the integration of aerial photogrammetry for roofs and site context with terrestrial (ground-based) imagery for facade, vertical, and complex details. This hybrid approach provides a complete coverage, bridging the gap between low-accuracy offered by aerial views and high-resolution offered by ground images, in order to achieve accurate LoD3 models.

In recent practice, 3D modelling together with interactive GIS maps and virtual visualisation tools has been increasingly applied to the presentation of major tourism sites, particularly historic houses. The use of these technologies improves the quality of documentation and at the same time makes the visitor experience more engaging. At the same time, they make it possible to develop digital twin models that support virtual visits, easier navigation within historical spaces, and spatial analyses useful for both heritage conservation and tourism promotion. The following visualisation techniques are to be employed for the purpose of promoting tourism at historic houses: the utilisation of three-dimensional modelling techniques in the preservation and marketing of historic structures enables users to observe these structures from diverse angles and levels of detail, web-based maps facilitate the spatial visualisation of historic houses across the designated territory, thereby enhancing identification and accessibility, and digital platforms have the capacity to curate the narrative surrounding historic houses, integrating visual data with historical, architectural and personal narratives to enhance user engagement (Ugwitz et al., 2021; Kourtit et al., 2025).

In the context of user perception and engagement, survey results have been demonstrated to reveal changes in destination understanding, interest in visiting, and perceived authenticity. These changes can be confirmed through statistical or thematic analysis of feedback (Ugwitz et al., 2021; Kourtit et al., 2025).

A comparison of three-dimensional models and traditional promotional tools, including brochures, photographs and maps, has been undertaken previously. The results of this comparison demonstrate that three-dimensional models significantly outperform traditional promotional tools in modern marketing, by the engender higher customer engagement, faster conversion rates and superior adaptability. Whilst conventional tools boast lower initial expenses and authenticity, three-dimensional visualisations have been demonstrated to enhance conversion rates. A preponderance of users has been observed to demonstrate a predilection for interacting with three-dimensional views as opposed to static images. The utilisation of three-dimensional models enables users to manipulate their environment through rotations and zooms in real-time, thereby sustaining attention for extended periods when compared with two-dimensional

media that is static and passive. Virtual tours represent a significant development in the realm of tourism promotion, offering visitors the opportunity to view the internal and external design of a destination prior to their physical arrival. In the domain of tourism, three-dimensional site models facilitate the provision of interactive, 360-degree views of the surrounding area, terrain, and amenities, thereby offering enhanced contextual information in comparison to two-dimensional maps. Whilst the initial financial outlay required for the creation of a 3D model may be significant, such an investment is frequently justified by the long-term benefits that such a model can deliver. Substantial research has demonstrated that, on average, three-dimensional imaging is six times more cost-effective than traditional photography when used in complex campaigns (Forbes Technology Council, 2021; Ugwitz et al., 2021; Kourtit et al., 2025).

The use of three-dimensional building modelling has been shown to improve spatial awareness and emotional connection by transforming abstract, two-dimensional building plans into tangible, virtual immersive environments that simulate reality. The technology in question is designed to facilitate an intuitive understanding of proportions and flow, in addition to promoting the development of a personal bond through the use of realistic lighting, textures, and interactive, personalised experiences. Three-dimensional modelling has been demonstrated to offer a superior, more intuitive grasp of space than its 2D counterpart, as well as impacting experiences, and thus provides several key benefits (Esri, n.d.; Gómez-Tone et al., 2021):

- It is possible for users to comprehend the true scale, volume, and proportions of a space.
- Interactive walkthroughs and 360° virtual tours have been shown to empower users by allowing them to "walk through" buildings and understand the flow and organisation of the layout.
- The capacity to manipulate, zoom and rotate models has been proven to facilitate superior spatial reasoning, as it enables viewers to observe the structure from different angles, thereby overcoming the limitations imposed by a single static viewpoint.
- Three-dimensional modelling also enables the consideration of environmental aspects, including daylight conditions and nearby contextual features. In this way, a clearer understanding of the relationship between the studied building and its surrounding environment can be obtained.
- The use of virtual 3D models generates a strong sense of presence for the user, who may perceive the simulated space in a manner similar to physical experience. As a consequence, emotional and perceptual reactions tend to be more pronounced.
- Furthermore, three-dimensional animation can be applied in the development of guided tours with narrative support, contributing to a better perception of spatial rhythm and continuity within the analysed space. The integration of these components within the framework of 3D modelling transforms the architectural design process from a technical undertaking to an emotional and experiential journey (Esri, n.d.; Gómez-Tone et al., 2021).

## CONCLUSIONS

Three-dimensional building modelling can transform rural tourism promotion by shifting from passive representation to immersive, spatially informed digital experiences. The case study of the "monument" house concluded that the combination of aerial and terrestrial photogrammetry is an effective method for creating an accurate, high-quality 3D model. This model can be utilised for the promotion of the area and the tracking of the construction's progress over time. The application of the present study may also be utilised in the future for the purpose of a past and present comparison, as well as in designing the future appearance of the construction (Coza, 2025).

The present study brings a relevant contribution to both the scientific and applied domains, with a particular focus on digital rural tourism and geospatial visualisation. The paper proposes a practical framework addressed to specialists involved in rural tourism activities and may be considered a useful reference for both academic research and professional practice (Coza, 2025).

The use of modern three-dimensional visualisation technologies in rural tourism promotion is gradually transforming the traditional approach to nature-based tourism by integrating digital, interactive and immersive

components. These tools enable tourists to virtually explore rural landscapes, agricultural areas and cultural heritage objectives from a distance, while also enhancing on-site visits through access to real-time information. In this context, such technologies contribute to the development of rural tourism in a more sustainable, educational and accessible manner. The main advantages of 3D modelling are presented below (Parra-Sanchez & Viviescas-Jaimes, 2024; Coza, 2025; Ilie et al., 2025).

- The utilisation of realistic visualisation techniques facilitates prospective visitors' ability to visualise the appearance of the destination prior to their arrival.
- The utilisation of three-dimensional modelling in the design and architectural professions has been demonstrated to have numerous advantages, including the potential for cost and time reduction in instances where renovation is necessary. This is due to the ability of designers and architects to modify an object without the need for physical reconstruction, thus ensuring a more efficient process.
- The process of monitoring the progression of construction projects over time is undertaken for the purposes of conducting studies or implementing rehabilitation work.
- 3Dmodelling sets out the argument for the importance of digital documentation and preservation for monuments and heritage sites.
- The calculation of volume is imperative for the planning and execution of excavation in case of intervention works.
- The creation of three-dimensional reconstructions of buildings is a key component of cadastral plan development, facilitating the creation of interactive maps.
- The promotion of tourism is achieved through the creation of virtual tours of areas intended for promotion.
- 3D models allow virtual tours of the touristic attractions, such as historic wooden churches or cultural sites, providing a way to virtually visit and appreciate them remotely.
- Modern technologies are used for interactive marketing, generate captivating experiences that increase interest in destinations.
- 3D models help in mapping and preserving architectural heritage, making it accessible for education and research.
- 3D models provide realistic, detailed views, helping tourists better understand the layout of destinations and, consequently, improving their overall experience.
- 3D models, such as 3D mesh models, are being used for interactive, web-based, or VR-driven, 360° virtual, and 3D web-based experiences, that are often more engaging than 2D and can also be used in city-wide planning.

The following key benefits and impact of the project are identified (Parra-Sanchez & Viviescas-Jaimes, 2024; Coza, 2025; Ilie et al., 2025):

- The provision of digital alternatives by modern technologies has been demonstrated to reduce the environmental impact of physical over-tourism in fragile rural areas.
- The removal of barriers for individuals with physical or financial constraints by modern technologies has been shown to provide access to remote or rugged rural locations.
- Digital technologies assist in the preservation of rural cultural identities and the promotion of local products, thereby fostering economic growth and the development of new business models within rural communities.
- The integration of physical and digital experiences, often termed 'hybrid' or 'phygital', has been demonstrated to enhance visitor satisfaction and emotional engagement with rural cultural heritage.

Three-dimensional modelling has also its limitations, which must be considered when undertaking such projects (Coza, 2025):

- The expense of high-quality projects involving large-scale work can be considerable, including the cost of drones, 3D scanners and software licenses for each device.
- The processing time for complex work requiring high precision can be lengthy, necessitating the purchase of high-performance computers capable of supporting and processing data at a high level.
- The use of such equipment and software requires advanced technical skills.
- The outcome is dependent on weather and lighting conditions for photogrammetry.
- The process is susceptible to loss of accuracy if the correct steps are not followed in data processing.
- The limitations imposed by a single case study.

- The existence of dependencies in the technological and infrastructural domains.

The following prospective research directions are hereby put forward (Coza, 2025):

- In order to facilitate the access to equipment such as photogrammetric equipment and high-precision devices, collaboration with local institutions, including universities and heritage NGOs, is imperative.
- The promotion of tourism is achieved through the creation of interactive virtual tours of various tourist attractions within a specific geographical area, such as a city or county.
- The creation of training courses and workshops is a collaborative endeavour undertaken in conjunction with construction, planning, and design companies for the benefit of educational institutions.
- The creation of a database or thematic map for the purpose of promoting tourism is hereby proposed. The objectives of this initiative would include the incorporation of this case study.
- The integration of AR/VR and metaverse tourism platforms is a subject that has been the focus of much recent discussion.
- The long-term ramifications on tourist arrivals and local economies must be given due consideration.
- The scalability of 3D modelling approaches for wider rural regions is a subject that merits further investigation.

## REFERENCES

Ahtik, J., Reberšek-Gavrič, Ž. & Gabrijelčič Tomc, H. (2025). Evaluating the impact of 3D visualizations on website usability and user experience. *Acta graphica, 33* (3), 96-106. https://doi.org/10.25027/ag.33.3.2

Biljecki, F., Ledoux, H., & Stoter, J. (2016). An improved LOD specification for 3D building models. *Computers, Environment and Urban Systems, 59*, 25–37. https://doi.org/10.1016/j.compenvurbsys.2016.04.005

Borsan, T., Dimen, L., Begov, A., & Dreghici, S. A. (2025). Considerations on the acquisition, processing, and mathematical interpretation of the georeferencing process. *Pangeea, 25*. https://doi.org/10.29302/Pangeea.25.09

Brenner, C. (2005). Building reconstruction from images and laser scanning. *International Journal of Applied Earth Observation and Geoinformation, 6*(3–4), 187–198. https://doi.org/10.1016/j.jag.2004.10.006

Caciora, T., Herman, G. V., Ilieș, A., Baias, Ș., Ilieș, D. C., Josan, I., & Hodor, N. (2021). The use of virtual reality to promote sustainable tourism: A case study of wooden churches historical monuments from Romania. *Remote Sensing, 13*(9), 1758. https://doi.org/10.3390/rs13091758

Coza, Ș.-G. (2025). *Reprezentarea 3D a unei construcții în vederea promovării turismului* [*3D representation of a building for tourism promotion*] [Bachelor's thesis]. "1 Decembrie 1918" University of Alba Iulia

Dreghici, S. A., Dimen, L., Koncsag, E., & Gazdac, A. (2016). 3D photogrammetric modeling of the historical monuments. In *SGEM2016 conference proceedings* (pp. 733–738). https://doi.org/10.5593/SGEM2016/B22/S10.094

Esri. (n.d.). 3D analysis. Retrieved from https://www.esri.com/en-us/capabilities/3d-gis/features/3d-analysis

Forbes Technology Council. (2021, December 30). Why product visuals in 3D are more cost-effective than photography. Retrieved from Forbes. https://www.forbes.com/councils/forbestechcouncil/2021/12/30/why-product-visuals-in-3d-are-more-cost-effective-than-photography/

Gómez-Tone, H. C., Martin-Gutierrez, J., Bustamante-Escapa, J., & Bustamante-Escapa, P. (2021). Spatial skills and perceptions of space: Representing 2D drawings as 3D drawings inside immersive virtual reality. *Applied Sciences, 11*(4), 1475. https://doi.org/10.3390/app11041475

Grande, R., Albusac, J., Vallejo, D., Glez-Morcillo, C., & Castro-Schez, J. J. (2024). Performance evaluation and optimization of 3D models from low-cost 3D scanning technologies for virtual reality and metaverse e-commerce. *Applied Sciences, 14*(14), 6037. https://doi.org/10.3390/app14146037

Ilie, M. R., Arghiroiu, G. A., & Beciu, S. (2025). A decade of rural tourism in Romania (2013–2023) and the potential of emerging technologies for sustainable development. *Scientific Papers Series Management, Economic Engineering in Agriculture and Rural Development, 25*(1)

Kourtit, K., Nijkamp, P., Scholten, H., & van Iersel, Y. (2025). Methodology and application of 3D visualization in sustainable cultural tourism planning. In B. Neuts, J. Martins, & M. Ioannides (Eds.), *Advances in cultural tourism research. Springer*. https://doi.org/10.1007/978-3-031-65537-1_11

Lacitera. (n.d.). Blog. Retrieved from https://lacitera.ro/#blog

Parra-Sanchez, D. T., & Viviescas-Jaimes, P. A. (2024). Application of digital technologies in nature-based tourism: A scientometric analysis. *Journal of Digital Economy, 3*, 249–259. https://doi.org/10.1016/j.jdec.2025.05.003

Rahman, A. D. M., & Cahyono, A. B. (2023). Analysis of 3-D building modeling using photogrammetric software: AgisoftMetashape and MicMac. *IOP Conference Series: Earth and Environmental Science*, 1276, 012044. https://doi.org/10.1088/1755-1315/1276/1/012044

Rosmani, A. F., Mazlan, U. H., Ahmad, S. Z., & Mohd Kharul Apendi, A. A., (2014). Developing an architectural visualization using 3D for photo tourism. *In Proceedings of the 2014 International Conference on Computer, Communications, and Control*

*Technology (I4CT)*. Langkawi, Malaysia, 429-433, 10.1109/I4CT.2014.6914220.

Shashi, M., & Jain, K. (2007). Use of photogrammetry in 3D modeling and visualization of buildings. *ARPN Journal of Engineering and Applied Sciences,* 2(2).

Ugwitz, P., Herman, L., & Stachoň, Z. (2021). *3D visualization of historical buildings: Methods, their utility in the tourism industry and beyond.*

Scientific Papers. Series E. Land Reclamation, Earth Observation & Surveying, Environmental Engineering. Vol. XV, 2026
Print ISSN 2285-6064, CD-ROM ISSN 2285-6072, Online ISSN 2393-5138, ISSN-L 2285-6064

# A DECISION-SUPPORT FRAMEWORK FOR SUSTAINABLE MANAGEMENT OF NATURAL SPORTS TURF UNDER TEMPERATE-CONTINENTAL CONDITIONS - A REVIEW AND CASE STUDY

**Alexandru DUMITRU, Mihai Sorin CÎMPEANU**

University of Agronomic Sciences and Veterinary Medicine of Bucharest,
59 Mărăști Blvd, District 1, Bucharest, Romania

Corresponding author email: dumitrualexandrumail@gmail.com

***Abstract***

*Managing natural sports turf under a temperate-continental climate requires maintenance operations to be sequenced within short climatic windows and triggered by measured site conditions rather than by a fixed calendar. This review synthesizes the scientific and technical literature on aeration, scarification, topdressing, fertilization, evapotranspiration-based irrigation, integrated pest and disease management and monitoring technologies, and organizes it into a circular decision-support framework with five components: diagnosis, planning, intervention, monitoring and adjustment. The framework is made operational through a seasonal calendar and a set of alert thresholds, and is applied in a case study of a 9,600 m² natural-turf rugby field with loamy sand soil, no subsurface drainage and a history of low-input maintenance. For this field, the case study derives the annual maintenance programme and the expected 12-month changes in five turf-quality indicators. The operating parameters of the framework fall within the ranges recommended in the literature, and the expected changes agree in direction with published empirical results. Because these changes are estimates rather than measured outcomes, monitoring of the field over several seasons is needed to validate the framework.*

***Key words****: decision-support framework, sports turf management, turf maintenance operations, alert thresholds, temperate-continental climate, case study.*

## INTRODUCTION

Natural turf sports fields remain, for football and rugby, the technical and functional benchmark against which every alternative surface is judged: they offer a combination of impact absorption, controlled traction, evaporative cooling and ecological reversibility that synthetic surfaces reproduce only partially (Cumberbatch et al., 2025). Unlike a construction material, sports turf is a living system, permanently subject to the combined action of climatic factors, the mechanical stress generated by matches and training, and the maintenance resources available.

The temperate-continental climate of much of Central and Eastern Europe, including Romania, adds a further layer of complexity. Large annual temperature ranges, winters with freeze–thaw episodes and summers with drought and heatwaves, together with increasingly variable precipitation driven by climate change (Hatfield, 2017), require intervention windows that differ from those recommended in manuals developed for oceanic or Mediterranean climates. The updated Köppen-Geiger classification of Beck et al. (2018) places most of Romania within the humid continental climate classes, with warm summers in the hilly and plateau regions and hot summers in the southern lowlands. For the cool-season species used on sports fields, this pattern restricts active growth mainly to spring and autumn, with summer heat and drought stress and winter dormancy in between (Fan et al., 2020; Braun et al., 2022). Observations on a football pitch in south-western Romania illustrate this seasonal pressure: frequent spring rainfall disrupted mowing, weed control and fungicide applications, and the disease resistance of the sward declined during spring (Corlan et al., 2019).

There is a recognized gap, both in the scientific literature and in the practice of sports field management, between technical knowledge of effective maintenance operations and their

systematic application on the ground: correct operations, applied at the wrong time or without justification based on measurements, produce poorer results than a coherent programme based on diagnosis and explicit decision thresholds. International standards for natural turf, such as the FIFA Quality Programme for Natural Playing Surfaces (FIFA, 2021), the FIFA Natural Turf Guidelines (FIFA, 2023) and the Sport England guidance on natural turf (Sport England, 2011), set targets for surface hardness, stability, evenness and agronomic condition, but only partially prescribe the temporal and decisional logic through which these targets can be achieved and maintained under specific climatic conditions.

This study pursues two complementary objectives. The first is to synthesize critically the scientific and technical literature on the maintenance methods applied to sports turf, organized around the five components of a decision cycle: diagnosis, planning, intervention, monitoring and adjustment. The second is to apply the resulting framework in a case study of a natural-turf rugby field, deriving its maintenance programme and expected effects, and to compare these with the ranges reported in the literature.

## MATERIALS AND METHODS

This article combines a narrative review of the scientific and technical literature with a case study. Sources were identified through searches in academic databases and publisher platforms (Wiley Online Library, ScienceDirect, SpringerLink, MDPI, Taylor & Francis Online, Emerald, PubMed and Google Scholar) and through direct consultation of technical documents issued by FIFA, World Rugby, Sport England, FAO and the European Commission. Search terms included: turfgrass management, sports turf, soil compaction sports field, turfgrass wear tolerance, turfgrass irrigation evapotranspiration, turfgrass integrated pest management, decision support system turfgrass, remote sensing turfgrass monitoring and turfgrass biodiversity pollinators, alone and in combination. The search covered publications from 2000 to 2026, together with a small number of standard reference texts on turf science. Sources were included if they were peer-reviewed articles, scientific monographs or technical documents of sports governing bodies and public authorities; dealt with cool-season turfgrass or with soil, water and pest processes transferable to sports turf; and reported quantitative results or operational recommendations. Studies on warm-season species were excluded.

The case study applies the framework to a natural-turf rugby field of 9,600 m² (120 × 80 m, including in-goal areas and run-off zones), with loamy sand soil, no subsurface drainage and a history of low-input maintenance. For this field, the authors established the starting condition, the annual maintenance programme, and the expected changes in five turf-quality indicators after 12 months. The expected changes are estimates made by the authors, not field measurements, and are reported as such in the **Results and discussions** section. The case study concerns a natural-turf rugby field located in Oltenia Plain. The starting values were obtained from field measurements carried out in March - April, penetration resistance with a cone penetrometer (0-10 cm), infiltration rate with a ring infiltrometer, and thatch thickness on soil cores, at 15 points distributed over the playing area. The expected changes after 12 months were estimated by applying to these starting values the effect ranges reported in the literature for the same operations (Table 3).

The literature was synthesized thematically, around the main groups of maintenance operations and the five components of the decision-support framework. For each theme, the relevant contributions were identified and, where possible, compared with the corresponding operating parameters of the framework, in order to show both where they agree and the limits of the comparison.

Within the framework, each intervention (aeration, scarification, topdressing, fertilization, irrigation, deep decompaction and drainage, overseeding, integrated pest and disease management) uses operating parameters taken from the specialized literature (Table 1). The authors' contribution lies in integrating these parameters into a seasonal calendar adapted to the temperate-continental climate and into a set of decision rules based on

alert thresholds that are measured periodically and recorded in a field register (Table 2). An operation is scheduled only when the diagnosis or a threshold exceedance calls for it, which avoids both under- and over-maintenance and makes management decisions transparent, justifiable and adjustable from one season to the next.

## RESULTS AND DISCUSSIONS

### 1. Soil physical properties: compaction, aeration, topdressing and drainage

Soil compaction, generated by repeated traffic from players and maintenance equipment, is consistently identified as one of the main causes of sports turf degradation, through reduced porosity, gas exchange and water infiltration (Adams & Gibbs, 1994; Christians et al., 2016). The review by Hamza and Anderson (2005) on soil compaction in cropping systems confirms, at a more general scale, the same physical mechanisms: reduced macroporosity, restricted root growth and decreased infiltration.

Mechanical aeration is the reference operation for counteracting compaction. Recent research refines the effectiveness of different aeration technologies: Dalsgaard et al. (2020) compared Shockwave-type aeration with conventional core aeration on athletic fields and found relevant differences in surface disruption and infiltration recovery, while Isom and Thompson (2026) analysed, on putting greens, the effect of aerator-pass frequency on sand incorporation and organic-matter accumulation. Sand topdressing complements aeration: Chen et al. (2025) showed, on creeping bentgrass, that the fineness of the topdressing sand significantly influences turf quality and surface characteristics, while the monograph edited by Stier et al. (2013) synthesizes the mechanisms of thatch formation and the options for its control. Surface and subsurface drainage are treated as structural components of performance sports fields, since the capacity for rapid water removal directly determines the number of available playing hours (Adams & Gibbs, 1994; Puhalla et al., 2020).

The framework translates these principles into explicit operating parameters (Table 1): two to four aeration passes per year within the April-May and September-October windows, scarification at a depth matched to the thatch layer, and topdressing with fine quartz sand at 1-3 mm per application. Within each window, the actual date is set by field conditions rather than by the calendar: operations are carried out while the turf is actively growing and the soil is neither frozen nor saturated. This level of operational detail, rarely made explicit in review articles, shows how general recommendations from the literature can be turned into an applicable annual programme.

Table 1. Operating parameters used in the framework for the main maintenance operations applied to sports turf (values set by the authors on the basis of the cited literature)

| *Operation* | Operating parameters | Optimal window (temperate-continental climate) | References |
|---|---|---|---|
| *Mechanical aeration* | Solid tines 5-10 cm, core aeration 8-12 cm, or pneumatic 10-20 cm; 2-4 passes/year | April-May; September-October | Beard, 2002; Christians et al., 2016; Dalsgaard et al., 2020 |
| *Scarification / verticutting* | Working depth 5-15 mm, matched to the depth of the thatch layer; 1-2 passes/year | April; September | Christians et al., 2016; Stier et al., 2013 |
| *Topdressing* | Quartz sand 0.2-0.8 mm (70-90%) + organic matter (10-30%); 1-3 mm/application, 2–3 applications/year | After aeration, spring and autumn | Chen et al., 2025; Stier et al., 2013 |
| *Fertilization* | N 15-25 g/m²/year, $P_2O_5$ 5-8 g/m²/year, $K_2O$ 15*20 g/m²/year, in 4-6 applications; rates adjusted to annual soil analysis | Seasonal programme (spring-summer-autumn) | Carrow et al., 2001; Carey et al., 2012 |
| *Irrigation* | ETc = Kc × ETo, with Kc 0.90–0.95 for cool-season turf; irrigation when depletion reaches 40% of available soil water (p = 0.40) | April-September, during active growth | Allen et al., 1998; Braun et al., 2022; Leinauer et al., 2025 |
| *Deep decompaction and drainage* | Deep decompaction 40-60 cm (every 5-10 years); drains 80-110 mm at 30-60 cm depth | Outside the competition period, on soil neither frozen nor saturated (late summer-early autumn) | Adams & Gibbs, 1994; Puhalla et al., 2020 |
| *Overseeding* | 10-20 g/m² (general), 20-40 g/m² (worn areas), mainly *Lolium perenne* | April-May; September | Christians et al., 2016; Corlan et al., 2019 |
| *Integrated pest management (IPM)* | Intervention thresholds: 2-5% affected area (diseases); about 30-120 larvae/m², depending on species (soil-dwelling larvae) | Continuous monitoring; targeted treatment | Potter, 1998; Sapkota et al., 2022; Batistič & Trdan, 2025 |

## 2. Species selection, nutrient management and water management

Turfgrass species and cultivar selection is a structural decision with long-term effects on a field's capacity to withstand intense traffic. Wear tolerance is determined by anatomical and morphological factors, analysed in detail by Głąb et al. (2015). Under actual tennis match play, Ebdon et al. (2021) found that Kentucky bluegrass and perennial ryegrass had the highest wear tolerance and carrying capacity among the cool-season species tested, well above fine fescues. Fan et al. (2020) synthesize, at a more general level, the physiological mechanisms of environmental-stress tolerance in turfgrass.

Balanced fertilization supports turf density, colour and recovery capacity, but excess nitrogen is associated with losses through leaching and runoff, with implications for water quality (Carey et al., 2012). Fertilizer rates are best adjusted to the nutrient status measured by soil analysis rather than applied as a fixed routine (Carrow et al., 2001). Scheduling irrigation from reference evapotranspiration is a documented alternative to fixed-calendar irrigation. FAO-56 gives crop coefficients of 0.90-0.95 and an allowable depletion fraction of 0.40 for cool-season turf (Allen et al., 1998); Leinauer et al. (2025) developed and tested variable crop coefficients, and Meza et al. (2025) showed, using high-resolution imagery, the spatial relationship between turf quality and actual evapotranspiration. The review by Braun et al. (2022) on water requirements and drought-stress responses provides a directly applicable reference for the cool-season species used in the temperate-continental climate.

The fertilization programme of the framework follows the same seasonal logic: balanced NPK in spring, reduced nitrogen and increased potassium in summer (for tolerance to heat and drought stress), and potassium and phosphorus in autumn, with annual nitrogen rates of 15-25 g/m² split into four to six applications. Splitting moderate rates into several applications is one of the practices that Carey et al. (2012) associate with a lower risk of nitrogen losses.

## 3. Integrated pest and disease management

Integrated Pest Management (IPM) is established as the best-practice standard for sports turf protection: cultural and preventive measures come first, the field is monitored regularly, and chemical treatments are used only when intervention thresholds are exceeded. The recent review by Batistič and Trdan (2025) highlights both the effectiveness of combining cultural and biological methods and the growing influence of climatic variability on disease dynamics. Microdochium patch and pink snow mould (*Microdochium nivale*), favoured by cool, wet weather and prolonged snow cover, whose virulence was recently investigated at genome scale by Tsers et al. (2023), and dollar spot (*Clarireedia jacksonii*), favoured by warm, humid weather, long periods of leaf wetness and low nitrogen fertility (Sapkota et al., 2022), illustrate the phytosanitary challenges of the temperate-continental climate. The framework uses intervention thresholds of 2-5% of the affected area for diseases and about 30-120 larvae/m² for soil-dwelling larvae, the latter corresponding to the species-dependent thresholds of roughly 3-12 larvae per square foot used in turfgrass entomology (Potter, 1998). The exact thresholds remain dependent on species, cultivar, irrigation and regional context.

## 4. Quality standards, safety and monitoring technologies

International sports organizations have developed technical standards for the quality and safety of playing surfaces. For natural turf, the FIFA Quality Programme for Natural Playing Surfaces (FIFA, 2021) assesses surface hardness, stability and evenness, ball–surface interaction and agronomic condition, while the FIFA Natural Turf Guidelines (FIFA, 2023) describe construction and maintenance practices adapted to local climate and soil. In rugby, impact-attenuation requirements are defined mainly for artificial surfaces through World Rugby Test Method 01, whose head injury criteria were recently re-examined by Colino et al. (2026); these values are a useful benchmark for natural turf, although they were not developed for it. The link between surface quality and injury risk is supported by a worldwide survey in which elite football players associated specific surface characteristics with injury (Mears et al., 2018),

although perception data cannot by themselves establish causality.

For monitoring technologies, the framework proposed by Helps et al. (2024) for evaluating pest management decision support systems offers criteria that can be transferred to sports turf management, while the review by Benos et al. (2021) on machine learning in agriculture shows a rapid expansion of predictive models. Alahmad et al. (2023) document how Internet of Things (IoT) sensors and big-data analysis support precision crop production, a direction with potential for large sports facilities. The review by Parra et al. (2024) on drones for turfgrass monitoring highlights the usefulness of multispectral imaging for early detection of drought stress, while Huang et al. (2021) draw attention to the interpretive limits of the NDVI index. The framework, in turn, uses a field register (date, indicator, value, operation applied), which applies the principles of a decision support system on a smaller scale.

## 5. Sustainability, circular economy and biodiversity

The EU Soil Strategy for 2030 (European Commission, 2021) sets explicit objectives on soil health and the reduction of compaction, which also apply to sports infrastructure. Strandberg et al. (2012) identify environmental regulation, pressure on water, energy and land, ecosystem services and biodiversity, integrated pest management and adaptation to climate change as priorities for sustainable turfgrass management, and argue that managers who minimize labour, energy and agronomic inputs are best placed to respond. Lower inputs are consistent with circular-economy principles, as illustrated by the recovery of organic matter through composting (Manea et al., 2024). The comparison between natural and synthetic turf by Cumberbatch et al. (2025) shows that natural turf offers relevant ecological advantages, provided that it is actively and continuously managed. For biodiversity, Lerman et al. (2018) showed that mowing less often increased bee abundance and diversity in suburban lawns, a result that may be transferable to the non-playing margins of sports facilities, while Lindsey et al. (2025) synthesize the broader ecological benefits of turfgrass in urban landscapes.

## 6. An integrated decision-support framework

The literature reviewed in sections 1-5 converges on a common principle: effective sports turf management is not mainly a matter of access to individual technologies, but of sequencing and triggering operations on the basis of up-to-date diagnostic information. This is consistent with the criteria for effective decision support systems identified by Helps et al. (2024). The framework proposed here puts this principle into practice in five stages (Figure 1).

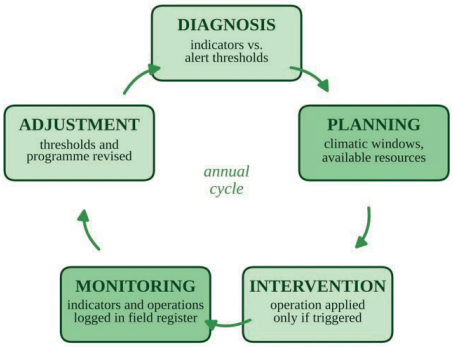



Figure 1. The five-stage decision-support cycle for natural sports turf management

Diagnosis establishes the condition of the field through indicators measured at set intervals (Table 2). Planning places the required operations within the climatic windows of the temperate-continental climate (Table 1) and within the resources available. Intervention applies an operation only when an alert threshold is exceeded. Monitoring records indicator values and the operations applied in the field register, and adjustment uses these records to revise the thresholds and the programme for the next cycle.

The five stages form a loop rather than a sequence: monitoring results feed into adjustment, and adjustment redefines the diagnosis and planning of the following cycle. This adaptive design is needed under a climate with marked year-to-year variability (Hatfield, 2017), where the same calendar cannot be applied unchanged from one season to the next. The thresholds in Table 2 are operational values set by the authors on the basis of the literature cited in sections 1-3; they are starting points to be recalibrated with the data accumulated in the field register.

Table 2. Indicators, alert thresholds and triggered operations in the decision-support framework (operational thresholds set by the authors)

| *Indicator (method)* | Monitoring frequency | Alert threshold | Triggered operation |
|---|---|---|---|
| *Penetration resistance, 0–10 cm (cone penetrometer)* | Spring and autumn, before the aeration windows | > 2.0 MPa | Core or solid-tine aeration; if compaction persists after two aeration cycles, deep decompaction is recommended |
| *Infiltration rate (ring infiltrometer)* | Spring and autumn | < 10 mm/h | Aeration + sand topdressing; drainage works if < 5 mm/h after two cycles |
| *Thatch thickness (soil cores)* | Spring and autumn | > 10 mm | Scarification; > 15 mm: scarification + topdressing in both windows |
| *Soil water balance (ETo, rainfall)* | Weekly, April–September | Depletion ≥ 40% of available water | Irrigation replacing ETc |
| *Turf cover (visual or image-based, % of area)* | Monthly and after matches | < 90% cover, or bare patches in high-wear areas | Overseeding and spot repair |
| *Disease incidence (% of area affected)* | Weekly in high-risk periods | 2-5% | Targeted fungicide treatment |
| *Soil-dwelling larvae (soil sampling)* | Late summer | About 30-120 larvae/m², depending on species | Targeted insecticide or biological control |
| *Soil nutrient status and pH (soil analysis)* | Annually, late winter | Below sufficiency range | Adjustment of the fertilization programme |

## 7. Application of the framework: case study of a natural-turf rugby field

The case study applies the framework to a 9,600 m² natural-turf rugby field in Oltenia Plain (120 × 80 m, including in-goal areas and run-off zones) with loamy sand soil, no subsurface drainage and a history of low-input maintenance (see Materials and methods). The starting conditions for the field were: penetration resistance of 3.2 MPa, infiltration rate of 7.8 mm/h and a thatch layer of 18 mm. All three values exceed the alert thresholds in Table 2, so the diagnosis called for aeration, scarification and topdressing in both growing-season windows.

The programme can be scaled to three levels of intensity (minimum, standard and premium) according to the resources available, in line with the emphasis placed by Strandberg et al. (2012) on minimizing labour, energy and agronomic inputs; heavy works (drainage, deep decompaction) are planned separately. The case study presents the standard level.

At the standard level, the annual programme combines core and solid-tine aeration, scarification, topdressing, fertilization in five applications, general overseeding and spot repairs, and two phytosanitary treatments planned for the case in which thresholds are exceeded. After 12 months, the authors expect the infiltration rate to increase from 7.8 to 17.2 mm/h (+121%), penetration resistance to fall from 3.2 to 1.8 MPa (−44%), thatch thickness to fall from 18 to 8 mm (−56%), turf density to increase by 39% and weed cover to fall by 76% (Figure 2), while the recovery time after heavy rain is expected to drop from about 48 hours to under 24 hours. These values are estimates, not field measurements, and serve as the targets against which the monitoring stage will assess the programme. The expected reductions in penetration resistance and recovery time are at the upper end of what can be achieved without subsurface drainage and depend on the deep decompaction work carried out separately.

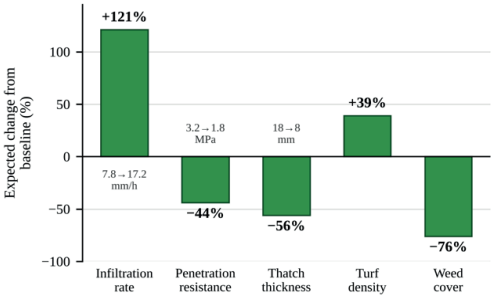



Figure 2. Expected changes in turf-quality indicators after 12 months of the standard programme on the case-study field (authors' estimates)

The direction of these changes is consistent with the effects reported in the empirical literature reviewed above: the improvement in infiltration through combined aeration and topdressing agrees with the comparative results of Dalsgaard et al. (2020) and Craft et al. (2017), and the reduction in weed cover through a denser sward agrees with the general principle that a dense, wear-tolerant sward is the most effective barrier to weed

establishment (Christians et al., 2016; Ebdon et al., 2021). The magnitude of the expected changes cannot, however, be generalized: it refers to a single combination of soil, climate and intensity of use, and for most of these indicators the literature does not offer reference ranges narrow enough for a strict quantitative comparison (Table 3). The agreement is therefore one of direction and plausible order of magnitude; it does not amount to an empirical validation of the framework, which requires repeated measurements on the field.

Table 3. Trends reported in the international literature compared with the parameters and expected results of the case study

| Parameter | Trend / range reported in the literature | Value in the case study | References |
|---|---|---|---|
| Aeration frequency | Recommended within active-growth windows, typically a few times per year | 2–4 passes/year (April–May, September–October) | Beard, 2002; Christians et al., 2016 |
| Nitrogen application (annual) | Moderate rates, split applications; controlled-release sources as best practice | 15–25 g N/m²/year, in 4–6 applications | Carey et al., 2012 |
| Infiltration rate (response to aeration + topdressing) | Consistent improvement, magnitude study-dependent | +121% expected (7.8 → 17.2 mm/h) | Craft et al., 2017; Dalsgaard et al., 2020 |
| Penetration resistance (response to aeration) | Reduced compaction, magnitude variable with soil and technique | −44% expected (3.2 → 1.8 MPa) | Hamza & Anderson, 2005; Craft et al., 2017 |
| Thatch thickness (target) | Below 10 mm considered non-limiting; above 10–15 mm requires intervention | 18 → 8 mm expected, through scarification + topdressing | Stier et al., 2013 |

## CONCLUSIONS

This review shows that the management of natural sports turf under a temperate-continental climate depends on sequencing maintenance operations within short climatic windows and on triggering them by measured field conditions. The literature supports the following conclusions:

(i) aeration, scarification and topdressing are the main operations for controlling compaction and thatch accumulation, and are best carried out in the April–May and September–October windows, while the turf is actively growing;

(ii) fertilization and irrigation should be treated as decision variables conditioned by soil analyses and reference evapotranspiration, not as calendar routine;

(iii) integrated pest and disease management, with explicit intervention thresholds, is the recommended approach for reducing reliance on chemical treatments;

(iv) international quality standards and remote-sensing tools provide reference values and data for the monitoring stage, although standards developed for artificial turf can serve only as benchmarks for natural turf;

(v) the case study shows how the five-stage framework (diagnosis, planning, intervention, monitoring and adjustment) translates into an annual programme and measurable targets for a specific field, and the expected effects agree in direction with published empirical results.

The main limitations of this study are that the case-study effects are estimates rather than measured outcomes, and that the reviewed literature comes largely from other climatic and institutional contexts, with few studies from Central and Eastern Europe. Monitoring the case-study field over several seasons and testing the framework on other soil types in the temperate-continental zone are the next steps, together with the integration of remote-sensing data into the diagnostic stage and an assessment of the cost–benefit ratio of precision monitoring on small and medium-sized fields.

## REFERENCES

Adams, W. A., & Gibbs, R. J. (1994). *Natural turf for sport and amenity: Science and practice*. CAB International.

Alahmad, T., Neményi, M., & Nyéki, A. (2023). Applying IoT sensors and big data to improve precision crop production: A review. *Agronomy*, 13(10), 2603. https://doi.org/10.3390/agronomy13102603

Allen, R. G., Pereira, L. S., Raes, D., & Smith, M. (1998). *Crop evapotranspiration: Guidelines for computing crop water requirements* (FAO Irrigation and Drainage Paper 56). Food and Agriculture Organization of the United Nations.

Batistič, L., & Trdan, S. (2025). Synergistic pest management strategies for turfgrass: Sustainable control of insect pests and fungal pathogens. *Agronomy*, 15(9), 2036. https://doi.org/10.3390/agronomy15092036

Beard, J. B. (2002). *Turf management for golf courses* (2nd ed.). Ann Arbor Press.

Beck, H. E., Zimmermann, N. E., McVicar, T. R., Vergopolan, N., Berg, A., & Wood, E. F. (2018). Present and future Köppen-Geiger climate classification maps at 1-km resolution. *Scientific Data*, 5, 180214. https://doi.org/10.1038/sdata.2018.214

Benos, L., Tagarakis, A. C., Dolias, G., Berruto, R., Kateris, D., & Bochtis, D. (2021). Machine learning in agriculture: A comprehensive updated review. *Sensors*, 21(11), 3758. https://doi.org/10.3390/s21113758

Braun, R. C., Bremer, D. J., Ebdon, J. S., Fry, J. D., & Patton, A. J. (2022). Review of cool-season turfgrass water use and requirements: II. Responses to drought stress. *Crop Science*, 62(5), 1685–1701. https://doi.org/10.1002/csc2.20790

Carey, R. O., Hochmuth, G. J., Martinez, C. J., Boyer, T. H., Nair, V. D., Dukes, M. D., Toor, G. S., Shober, A. L., Cisar, J. L., Trenholm, L. E., & Sartain, J. B. (2012). A review of turfgrass fertilizer management practices: Implications for urban water quality. *HortTechnology*, 22(3), 280–291. https://doi.org/10.21273/HORTTECH.22.3.280

Carrow, R. N., Waddington, D. V., & Rieke, P. E. (2001). *Turfgrass soil fertility and chemical problems: Assessment and management*. Ann Arbor Press.

Chen, H., Hempfling, J. W., Schmid, C. J., Xu, Z., Samaranayake, H., & Murphy, J. A. (2025). Finer topdressing sand affects creeping bentgrass quality and surface characteristics. *Agronomy Journal*, 117(2), e70039. https://doi.org/10.1002/agj2.70039

Christians, N. E., Patton, A. J., & Law, Q. D. (2016). *Fundamentals of turfgrass management* (5th ed.). Wiley.

Colino, E., Felipe, J. L., Douglas, M., Harrison, E., Webb, C., del Corral, J., Gallardo, L., & Garcia-Unanue, J. (2026). Review of World Rugby's Test Method 01 head injury criteria: Procedure analysis and optimisation. *Proceedings of the Institution of Mechanical Engineers, Part P: Journal of Sports Engineering and Technology*, 240(1), 29–36. https://doi.org/10.1177/17543371231219738

Corlan, C. E., Sărăţeanu, V., Cotuna, O., & Durău, C. C. (2019). Analysis of the seasonal evolution of a sport turf surface from Motru (Gorj County) – case study. *Research Journal of Agricultural Science*, 51(3), 206–212.

Craft, J., Baldwin, C. M., McCurdy, J. D., Stewart, B. R., Philley, H. W., Blythe, E. K., & Tomaso-Peterson, M. (2017). Maintaining soil physical properties in athletic fields using alternative technology. *International Turfgrass Society Research Journal*, 13(1), 636–641. https://doi.org/10.2134/itsrj2016.05.0360

Cumberbatch, I. S., Richardson, L., Grant-Bier, E., Kayali, M., Mbithi, M., Riviere, R. F., Xia, E., Spinks, H., Mills, G., & Tuininga, A. R. (2025). Artificial turf versus natural grass: A case study of environmental effects, health risks, safety, and cost. *Sustainability*, 17(14), 6292. https://doi.org/10.3390/su17146292

Dalsgaard, T. O., Thoms, A. W., Christians, N. E., Mertz, I., & Horton, R. (2020). Comparison of Shockwave aerification and conventional aerification methods on athletic fields. *Agronomy Journal*, 112(5), 3470–3477. https://doi.org/10.1002/agj2.20255

Ebdon, J. S., James, I., DaCosta, M., & Lu, J. (2021). Interspecific comparisons of C3 turfgrass for tennis use: I. Wear tolerance and carrying capacity under actual match play. *Crop Science*, 61(1), 750–762. https://doi.org/10.1002/csc2.20270

European Commission. (2021). *EU soil strategy for 2030 – Reaping the benefits of healthy soils for people, food, nature and climate* (COM(2021) 699 final). Publications Office of the European Union.

Fan, J., Zhang, W., Amombo, E., Hu, L., Kjorven, J. O., & Chen, L. (2020). Mechanisms of environmental stress tolerance in turfgrass. *Agronomy*, 10(4), 522. https://doi.org/10.3390/agronomy10040522

FIFA. (2021). *FIFA Quality Programme for Natural Playing Surfaces*. Fédération Internationale de Football Association.

FIFA. (2023). *FIFA Natural Turf Guidelines*. Fédération Internationale de Football Association.

Głąb, T., Szewczyk, W., Dubas, E., Kowalik, K., & Jezierski, T. (2015). Anatomical and morphological factors affecting wear tolerance of turfgrass. *Scientia Horticulturae*, 185, 1–13. https://doi.org/10.1016/j.scienta.2015.01.013

Hamza, M. A., & Anderson, W. K. (2005). Soil compaction in cropping systems: A review of the nature, causes and possible solutions. *Soil and Tillage Research*, 82(2), 121–145. https://doi.org/10.1016/j.still.2004.08.009

Hatfield, J. L. (2017). Turfgrass and climate change. *Agronomy Journal*, 109(4), 1708–1718. https://doi.org/10.2134/agronj2016.10.0626

Helps, J. C., van den Bosch, F., Paveley, N., Nistrup Jørgensen, L., Holst, N., & Milne, A. E. (2024). A framework for evaluating the value of agricultural pest management decision support systems. *European Journal of Plant Pathology*, 169(4), 887–902. https://doi.org/10.1007/s10658-024-02878-1

Huang, S., Tang, L., Hupy, J. P., Wang, Y., & Shao, G. (2021). A commentary review on the use of normalized difference vegetation index (NDVI) in the era of popular remote sensing. *Journal of Forestry Research*, 32(1), 1–6. https://doi.org/10.1007/s11676-020-01155-1

Isom, C., & Thompson, C. (2026). Effects of within-event aerator-pass frequency and tine size on sand incorporation and organic matter accumulation in cool-season putting greens of the Pacific Northwest. *Crop, Forage & Turfgrass Management*, 12(1), e70104. https://doi.org/10.1002/cft2.70104

Leinauer, B., VanLeeuwen, D. M., Sallenave, R., Kardashina, T., & Smeal, D. (2025). Actual evapotranspiration and variable crop coefficients for scheduling turfgrass irrigation. *Agronomy Journal*, 117(3), e70080. https://doi.org/10.1002/agj2.70080

Lerman, S. B., Contosta, A. R., Milam, J., & Bang, C. (2018). To mow or to mow less: Lawn mowing frequency affects bee abundance and diversity in

suburban yards. *Biological Conservation*, 221, 160–174. https://doi.org/10.1016/j.biocon.2018.01.025

Lindsey, A. J., Schiavon, M., Unruh, J. B., & Kenworthy, K. (2025). Urban landscapes: Turfgrass benefits. *Grasses*, 4(1), 3. https://doi.org/10.3390/grasses4010003

Manea, E. E., Bumbac, C., Dinu, L. R., Bumbac, M., & Nicolescu, C. M. (2024). Composting as a sustainable solution for organic solid waste management: Current practices and potential improvements. *Sustainability*, 16(15), 6329. https://doi.org/10.3390/su16156329

Mears, A. C., Osei-Owusu, P., Harland, A. R., Owen, A., & Roberts, J. R. (2018). Perceived links between playing surfaces and injury: A worldwide study of elite association football players. *Sports Medicine – Open*, 4(1), 40. https://doi.org/10.1186/s40798-018-0155-y

Meza, K., Torres-Rua, A. F., Hipps, L., Kopp, K., Straw, C. M., Kustas, W. P., Christiansen, L., Coopmans, C., & Gowing, I. (2025). Relating spatial turfgrass quality to actual evapotranspiration for precision golf course irrigation. *Crop Science*, 65(1), e21446. https://doi.org/10.1002/csc2.21446

Parra, L., Ahmad, A., Zaragoza-Esquerdo, M., Ivars-Palomares, A., Sendra, S., & Lloret, J. (2024). A comprehensive survey of drones for turfgrass monitoring. *Drones*, 8(10), 563. https://doi.org/10.3390/drones8100563

Potter, D. A. (1998). *Destructive turfgrass insects: Biology, diagnosis, and control*. Ann Arbor Press.

Puhalla, J. C., Krans, J. V., & Goatley, J. M. (2020). *Sports fields: Design, construction, and maintenance* (3rd ed.). Wiley.

Sapkota, S., Catching, K. E., Raymer, P. L., Martinez-Espinoza, A. D., & Bahri, B. A. (2022). New approaches to an old problem: Dollar spot of turfgrass. *Phytopathology*, 112(3), 469–480. https://doi.org/10.1094/PHYTO-11-20-0505-RVW

Sport England. (2011). *Natural turf for sport*. Sport England Technical Guidance Note.

Stier, J. C., Horgan, B. P., & Bonos, S. A. (Eds.). (2013). *Turfgrass: Biology, use, and management* (Agronomy Monograph 56). American Society of Agronomy, Crop Science Society of America, Soil Science Society of America.

Strandberg, M., Blombäck, K., Dahl Jensen, A. M., & Knox, J. W. (2012). Priorities for sustainable turfgrass management: A research and industry perspective. *Acta Agriculturae Scandinavica, Section B: Soil & Plant Science*, 62(sup1), 3–9. https://doi.org/10.1080/09064710.2012.682163

Tsers, I., Marenina, E., Meshcherov, A., Petrova, O., Gogoleva, O., Tkachenko, A., Gogoleva, N., Gogolev, Y., Potapenko, E., Muraeva, O., Ponomareva, M., Korzun, V., & Gorshkov, V. (2023). First genome-scale insights into the virulence of the snow mold causal fungus *Microdochium nivale*. *IMA Fungus*, 14(1), Article 2. https://doi.org/10.1186/s43008-022-00107-0

Scientific Papers. Series E. Land Reclamation, Earth Observation & Surveying, Environmental Engineering. Vol. XV, 2026
Print ISSN 2285-6064, CD-ROM ISSN 2285-6072, Online ISSN 2393-5138, ISSN-L 2285-6064

# SPECIFIC REHABILITATION WORKS OF DEGRADED AGROSILVOPASTORAL SYSTEMS, IN NONCOLLECTIVIZED AREAS

**Călin Ioan IOVAN[1], Sorin Lucian DOROG[1], Călin Gheorghe PĂŞCUŢ[1], Flavia-Mălina CIOFLAN[2], Eugenia ŞERBAN[3]**

[1]University of Oradea, Faculty of Environmental Protection, Department of Forestry and Forestry Engineering, Oradea, 26 Gen. Magheru Street, 410048, Romania
[2]Doctoral School of Engineering Sciences, Agronomy Field, University of Oradea, Faculty of Managerial and Technological Engineering, 1 University Street, 410087, Oradea, Romania
[3]University of Oradea, Faculty of Environmental Protection, Department of Environmental Engineering, 26 Gen. Magheru Street, 410048, Oradea, Romania

Corresponding author email: calin_iovann@yahoo.com

***Abstract***

*Agrosilvopastoral systems represented alternative and differentiated systems of exploitation of lands with reduced fertility, especially in the non-collectivized areas of medium and high hills. As a result, in these land exploitation systems, the productive potential of the land is exploited through agricultural, horticultural, forestry and zootechnical production. The objectives of the work are represented by the study and analysis of the works necessary for the rehabilitation of the exploitation process of agrosilvopastoral systems in the area of medium and high hills, abandoned after 1989, in the locality of Vîrfurile, Arad county, an area that was not collectivized. Consequently, field observations, inventories, analyses of information from the agricultural register and from the plot plan of the buildings in the study area were carried out. Also, a series of works necessary for the rehabilitation of the exploitation of agro-forestry and pastoral systems were experimented on experimental areas, making a series of comparisons with their situation prior to 1989. In conclusion, the rehabilitation of these land exploitation systems can be efficiently achieved by establishing owners' associations and respectively by accessing financing projects.*

***Key words****: agricultural production, agrosilvopastoral systems, forestry production, horticultural production, land exploitation systems, livestock production, non-collectivized area.*

## INTRODUCTION

Optimizing the exploitation of arable land has an important influence in ensuring the production of quality, healthy food in optimal quantities, the adequate and secure provision of ecosystem services (e.g. biodiversity, clean air and water) as well as in effectively mitigating and removing the negative effects of climate change (Smith et al., 2022).

The worrying evolution of climate change and the modest standard of living in rural areas, especially in developing countries, require a change towards new, high-performance strategies, relating to agricultural practices and collaboration between farmers and, respectively, to the relationships between them and nature (Cialdella et al., 2023).

Adaptive management of agricultural activities related to arable land needs to be achieved without expanding existing cultivated land areas, in parallel with the protection and conservation of natural resources, but by promoting efficient, systemically integrated production technologies. Consequently, paradoxically, these multiple problems are very clear and relatively easy to solve, at least at the algorithmic level, they represent one of the greatest obstacles facing humanity today (Smith et al., 2022).

Agrosilvopastoral systems are cropping systems that integrate agricultural crops, fodder, woody perennials with livestock, on the same plot of land, promoting a more efficient and sustainable use of resources, compared to monocultures, as a consequence of the structural and functional diversification of the components (Fahad et al., 2022; Chappa et al. 2024).

Integration of forest trees and, respectively, fruit trees in the arable land exploitation system, optimizes soil fertility and its physical, biological and chemical properties, and ensures

the production of fruits, seeds, wood, fodder and animal protection (Fahad et al., 2022).

Relatively recent research shows that agroforestry systems have the capacity to store 3-4 times more carbon in the soil than in biomass, and agro-silvopastoral systems achieve a more efficient, respectively higher, storage of carbon in both soil and biomass, compared to the former. These results show that climatic zones and soil type directly influence carbon stocks and sequestration rates within agro-silvopastoral systems (Ribeiro et al., 2023; Mazumder et al., 2025).

By creating a specific habitat, characterized mainly by the particularities of each type of activity (crop), the microclimate associated with these complex land use systems can optimize biodiversity more than monocultures. Consequently, the internal restoration potential of activities in agro-silvopastoral systems is high, being able to offer effective solutions for inefficiently exploited lands (Fahad et al., 2022). Also, agrosilvopastoral and agrosilvopastoral systems substantially increase functional diversity and overall biodiversity within agricultural landscapes, consequently being necessary and appropriate priority programs and strategies in European agri-environmental financing schemes (Santos et al., 2022).

From the analysis of the component elements of agrosilvopastoral systems, they can be integrated into all agricultural systems, from various areas of Europe. Currently, the way to obtain them can be achieved relatively simply and efficiently, by planting trees, shrubs and fruit trees on agricultural land, by introducing agriculture (agricultural systems) in existing forests, wooded pastures (e.g. silvopastures) and in existing orchards (https://euraf.isa.utl.pt/about/ agroforestry-europe).

On the European continent there is currently a unique heritage of traditional agroforestry and agrosilvopastoral systems, which are characterized by a high ecological and cultural value. Similarly, in Europe, in the last two decades, the activities of research centers related to agroforestry activities have facilitated the promotion of modern and innovative agroforestry systems, capable of optimally exploiting the productive potential of agricultural and forestry land (https://euraf.isa.utl.pt/about/agroforestry-europe).

Agrosilvopastoral systems can be classified according to several criteria, established according to their location, structural and functional characteristics. As a result, depending on their age and tradition, they can be classified into traditional and innovative (Smith et al., 2022).

Traditional exploitations are made up of agricultural, horticultural and forestry crops as well as animal husbandry activities, long-term production activities, which are ultimately managed for the production of quality, diversified food, generally of an ecological nature.

The most representative agrosilvopastoral system known on the world map is the Spanish dehesa (Figure 1) (or montado in Portuguese) existing since the Neolithic period, first mentioned in 924 AD.



Figure 1. Dehesa agrosilvopastoral system (https://www.madr.ro/attachments/article/495/ADER-1521-FAZA-I.pdf).

Although traditional, it is constantly updated, and is perceived as one of the most efficient systems, because it harmoniously combines biodiversity conservation and sustainable rural development. The area related to this type of exploitation is approximately 3.5-5.5 million ha in Spain and Portugal and 1-1.5 million ha in Italy, Greece, western North America, and the specific habitat is characterized by the Mediterranean climate and low soil fertility (https://www.madr.ro/attachments/article/495/ADER-1521-FAZA-I.pdf).

The type of dehesa system in Spain and montado in Portugal, used for the extensive raising of animals, especially cattle, on meadows with rare trees, can also be called a pastoral-silvo-agricultural system, and is carried out on very poorly productive (with very low fertility) or non-agricultural lands. Also, in these farms, firewood, branches, acorns, cork can be

obtained, and various cereals such as oats, barley, rye, wheat are often cultivated, to supplement animal feed and to combat a series of shrubs that invade permanent pastures (https://www.madr.ro/attachments/article/495/ADER-1521-FAZA-I.pdf).

Innovative agrosilvopastoralism refers to multifunctional systems, designed to obtain biomass, ecosystem services and integrated wood (Smith et al., 2022). Some current representative variants of farms are represented by alley groves, alley crops and raising forest hens (Budău et al., 2023).

Although agroforestry and agrosilvopastoral exploitations have been known and have been operating for thousands of years, the agroforestry research field is relatively young and presents a number of opportunities, due to the importance of the context in which agroforestry practices develop, and their future trend (Cialdella et al., 2023).

In Romania, with the exception of forest curtains protecting arable land with various crops, which expanded considerably in the mid-20th century, some authors consider that agroforestry and agrosilvopastoral systems represent a new concept, which is not perceived, for example, as an independent science (Popovici et al., 2018; Budău et al., 2023), although the activities related to agroforestry and agrosilvopastoral exploitations in many historical provinces of our country are known at least two centuries ago (Crainic et al., 2023a).

On hilly lands with relatively low fertility, the promotion of agrosilvopastoral systems can mitigate huge soil losses, and can promote carbon sequestration with high efficiency, ultimately contributing decisively to increasing farmers' income (Sirimalle et al., 2025).

In western Romania, especially in hilly and mountainous areas that were not collectivized, a number of lands were efficiently exploited within agrosilvopastoral systems until 1989, after which the management method gradually changed. As a result, a number of lands were exploited inappropriately, and others were abandoned, for various reasons. The reasons are represented by the depopulation of the areas, economic instability, the drastic reduction of the number of animals, the lack of subsidies, the lack of adequate facilities, the high degree of fragmentation of the plots that prevented the creation of associations, the low fertility of the soils, the trend of climatic conditions in the last three decades, and last but not least the socio-political context.

The paper aims to analyze the climatic conditions, the works and measures necessary for the rehabilitation and reintroduction into the productive circuit of degraded agro-silvopastoral systems and respectively ensuring the premises for their sustainable exploitation.

## MATERIALS AND METHODS

Vârfurile village is located in the east of Arad County, in the commune of the same name. The commune also includes the villages of Avram Iancu, Vidra, Măgulicea, Lazuri, Groși, Mermești and Poiana. Geographically, Vârfurile village is located in the northwest of the Hălmagiu Depression in the Apuseni Mountains, being situated at the foot of the Zarandului, Codru-Moma and Bihor Mountains, in the valley of the Crișul Alb River. Vârfurile Commune has an area of 136 $km^2$ and a population of over 2,200 inhabitants (https://primariavirfurile.ro/despre-noi/prezentare/; https://ro.wikipedia.org/wiki/Comuna_Vârfurile_Arad).

The Hălmagiu Depression is connected to the northwest with the Zarandului Depression. The latter, having a wide opening to the west, towards the Western Plain, favors the easy penetration of humid, oceanic air masses coming from western Europe, but also of Mediterranean air masses, which cause abundant precipitation. As a result, Vârfurile Commune has a temperate-continental, moderate climate, with slight Mediterranean influences, the winters being milder, and the summers being cooler. The commune's location in the shelter of the mountains, in the depression sector, means that it is protected from storms, but during the winter this causes frequent thermal inversions, associated with dense fogs. During the hot summer months, when continental-tropical air masses penetrate southwestern Romania, droughts can also occur in this territory. Overall, the thermally moderate climate with abundant rainfall makes the region well forested (Pop, 2005; https://primariahalmagiu.ro/download/urvqbaO3Rf0Eh7w9f690f8ugJ6lAzB8W4JBO4a7g.pdf).

In the present paper, meteorological data on the monthly and annual average air temperature and the monthly and annual amount of precipitation were used, from the closest weather station to Vârfurile village, respectively Gurahonț. The station has the geographical coordinates 46°27' N latitude, 22°33' E longitude, the code 15182 and the altitude 177 m (www.meteomanz.com). The analyzed period was 1990-2025 (36 years). The deviations of the annual average values of air temperature and precipitation from the multiannual average of the period 1966-2025 (60 years) were calculated (expressed in °C and in mm, respectively). Reporting to the multiannual average of a longer period than the one analyzed better highlights the climatic fluctuations of recent years. The temporal variability of the positive and negative annual deviations of temperature and precipitation, the linear trend of the annual deviations of air temperature and the polynomial trend of the annual deviations of precipitation were analyzed. Subsequently, the maximum and minimum values of monthly average temperatures and monthly precipitation amount from the period 1990-2025 were analyzed.

All meteorological data used in the paper came from the database of the National Meteorological Administration (N.M.A.) of Romania and from the rp5.ru (https://rp5.ru/) and Meteomanz.com (www.meteomanz.com) websites.

The observations were made on the route and respectively at the representative points of the agrosilvopastoral systems studied and analyzed in the Vârfurile commune, using cartographic materials and cadastral records in analog and digital format.

For a complex analysis of the agrosilvopastoral systems, their components were analyzed separately, and in order to establish and propose the necessary rehabilitation works, a similarity was made with the related activities in the agricultural, forestry and zootechnical sectors.

To simulate the spatial structure related to the tree biogroups within the agrosilvopastoral systems, inventories were carried out in experimental areas, and the data recorded in the field were processed with the PROARB 2.0 program (Popa, 1999), obtaining the related spatial profiles.

The recording on digital support of edifying images for the objectives of the case study was used for an objective presentation of the reality in the field.

Finally, the comparative analysis of the current components of the abandoned agrosilvopastoral systems with the functional ones was used to rigorously justify and substantiate the works necessary for their efficient rehabilitation.

The logistical base used is represented by treaties, publications and specialized papers, statistical data from the agricultural register, data from cadastral records, time and production norms for activities in the agroforestry sector, the EXCEL program, the PROARB 2.0 program for generating the structure of forest stands, digital cameras.

## RESULTS AND DISCUSSIONS

The multiannual average air temperature for the period 1990-2025 (10.9°C) was higher than the multiannual average temperature of the period 1966-2025 (10.5°C), at the Gurahonț weather station.

Figure 2 shows the positive and negative deviations of the annual average air temperature from the multiannual average of the period 1966-2025 (10.5°C), considered "normal". Warm years (with positive deviations > 0.5°C), cold years (with negative deviations < -0.5°C) and normal years (with deviations between -0.5 and 0.5°C) are highlighted. It is observed that most years of the period 1990-2025 have positive deviations from normal (23 years out of 36). In the 1990-2006 interval, negative deviations prevailed. But only 5 years are cool, 3 years are warm (1994, 2000 and 2002), and 9 are normal.

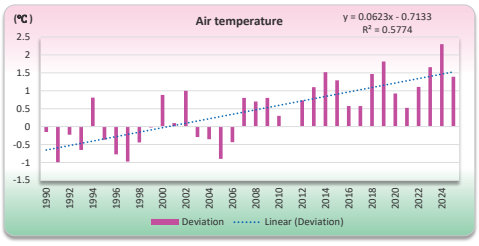



Figure 2. Deviations of the annual average air temperature (1990-2025) from the multiannual average (1966-2025), at the Gurahonț weather station; the linear trend of deviations

Starting with 2007, only positive annual deviations are present. Only 2 years are normal (2010 and 2011), the others being warm or hot. There are 9 hot years, with a deviation of more than 1°C. Of these, 4 years have a deviation of more than 1.5°C: 2024 (+2.3°C), 2019 (+1.8°C), 2023 (+1.7°C) and 2014 (+1.5°C). These are the hottest years of the period 1990-2025.

The linear trend of annual deviations of air temperature is strongly upward (Figure 2). The period 1990-2025 was a very warm one, the 2007-2025 interval being the warmest.

The multiannual average amount of precipitation for the period 1990-2025 (747.5 mm) was slightly lower than the multiannual average amount of the period 1966-2025 (752.0 mm), at the Gurahonț weather station.

Figure 3 shows the positive and negative deviations of the annual precipitation amounts from the multiannual average of the period 1966-2025 (752.0 mm), considered "normal". There are 17 years with positive deviations of precipitation and 19 years with negative deviations. The highest positive deviations exceed 100 mm. There are 9 years with a rainfall surplus of over 100 mm, of which 3 years with over 200 mm: 2005 (+244.2 mm), 2001 (+224.4 mm) and 2004 (+215.5 mm). These are the rainiest years of the period 1990-2025. The highest negative deviations exceed 100 mm, also. There are 8 years with a rainfall deficit of over 100 mm, of which 3 years with over 200 mm and 1 year with over 300 mm: 2025 (-313.6 mm), 2024 (-268.7 mm), 2000 (-257.4 mm) and 2011 (-218.4 mm). They are the driest years of the period 1990-2025.

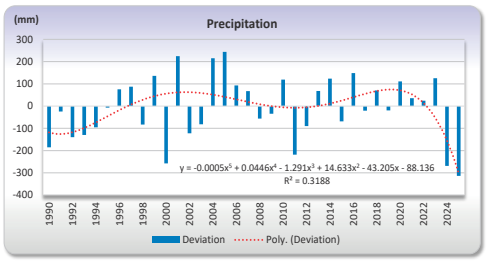



Figure 3. Deviations of the annual precipitation amounts (1990-2025) from the multiannual average (1966-2025), at the Gurahonț weather station; the polynomial trend of deviations

It is noted that the negative deviations are greater than the positive ones – as is usually recorded at the weather stations in Romania. The polynomial trend, represented using the 5th order polynomial, highlights the existence of two long rainy periods (1995-2007 and 2013-2023), interspersed with short dry periods (1990-1994, 2008-2012 and 2024-2025) (Figure 3).

Figure 4 shows the multiannual monthly average air temperature, as well as the highest and lowest monthly average temperatures recorded at the Gurahonț station, during the period 1990-2025. The highest monthly average temperatures were recorded in summer, in July 2024 (24.0°C), July 2012, July 2021, August 1992, August 2024 (all with 23.8°C). They especially occurred towards the end of the analyzed period, in hot weather conditions generated by the advection of the very hot and dry continental-tropical air masses, coming from northern Africa. The lowest monthly average temperatures were reported in winter, in Feb. 2012 (-5.3°C), Jan. 2017 (-5.0°C), Jan. 2000 (-4.0°C), Feb. 2003 (-3.9°C), Dec.1991 (-3.4°C). They occurred due to the advections of continental-arctic or polar air masses, which generate cold waves.

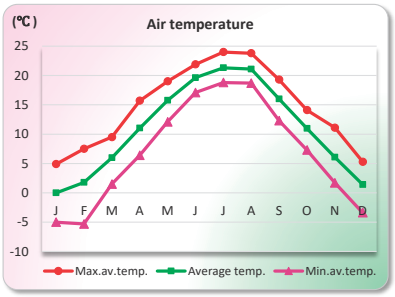



Figure 4. Multiannual monthly average air temperature and the highest/lowest monthly average temperatures, at the Gurahonț weather station (1990-2025)

The highest monthly precipitation amounts exceeded 100 mm, even 200 mm (218.2 mm in June 2020 - the month of the rainfall maximum) (Figure 5). The highest values were reported in the June-September interval (over 150 mm): July 2001 (184.6 mm), July 2011 (181.0 mm), July 2014 (180.4 mm), etc. Such large amounts are linked to the presence of very active cold fronts, which occur after a very hot period. The lowest monthly precipitation amounts ranged between 0 and 26.4 mm. Such small amounts occur when the anticyclonic baric formations persist, generating droughts.

During the period covered by the study, the components of agrosilvopastoral systems were affected by a series of disturbances, which were caused by abiotic and biotic factors, as well as by significant changes in the political and social context.

Consequently, their exploitation changed considerably, with implications for the efficient and sustainable use of the land.

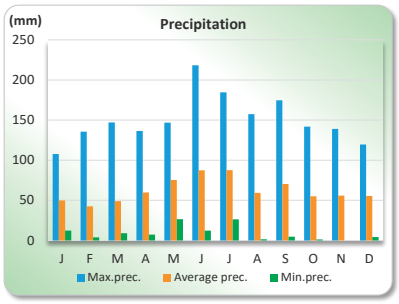



Figure 5. Average, maximum and minimum multiannual monthly amounts of precipitation, at the Gurahonț weather station (1990-2025)

Thus, a series of areas, which were used for grazing animals, in the period after 1989, were partially abandoned, with shrubs and trees of pioneer and invasive species settling on them (Crainic, 2017), which affected the production capacity of the respective lands (Figure 6).



Figure 6. Species of trees and shrubs that have settled on pasture areas within agrosilvopastoral systems

Replacing degraded pastures with agrosilvopastoral systems, especially on lands with clay soils, contributes to increasing soil organic carbon stocks and optimizing microelement circuits, ensuring the premises for sustainable management of these complex systems, against the backdrop of climate change, which is becoming increasingly evident (Ribeiro et al., 2023).

The specific work of rehabilitating agrosilvopastoral systems and reintroducing them into the productive circuit presents a particular specificity, since it is necessary to know the dynamics of how the different components interact during their complex production cycles (Lehmann et al., 2020).

As a result, the works related to the agricultural component, the forestry component, the livestock breeding component (zootechnics) will be analyzed, and last but not least, the aspects related to the sustainable use of the products obtained.

The works necessary for the rehabilitation of the agricultural component of the respective areas are represented by: cutting bushes, shrubs and thin trees, removing stumps by uprooting, works to fill holes and level the land following the uprooting of stumps, plowing the land, cultivating crops for green rotation and for animal feed, respectively. These will be carried out on those areas intended for agricultural crops, meadows and pastures for animal feed (Maruşca, 2018), and classic fruit tree orchards.

Cutting of bushes, shrubs and thin trees, can currently be done mechanized (Table 1), with high efficiency, and the resulting material will be transported and stored at a maximum distance of 20 m from the harvesting site, for recovery, depending on the owner's options.

To remove the stumps, by manual uprooting, excavations will be carried out with hand tools around them, the lateral roots and the central pivot will be cut, the stump will be dislocated and raised on the edge of the pit, later being transported and stored on a specially arranged surface (Table 2), for recovery. Finally, works will be carried out to plug the pits and level the land following the uprooting of the stumps (Table 3).

Table 1. Elements related to the work of cutting bushes, shrubs and thin trees with a Stihl chainsaw, on areas being afforested (processing after Unified time and production standards for forestry work (1997))

| Norm symbol | Operation name | Coverage level | Unit of measurement | Framing grid | T.O.[1] (lei/hour)/(€/hour) | N.P.[2] (ari/8hours) | N.T.[3] (hours-man/ar) | T.U.[4] (lei/ar)/(€/ar) |
|---|---|---|---|---|---|---|---|---|
| D.25.a. | Cutting and gathering wood | < 33 | ha | a 8-a | 30.496/5.92 | 0.227 | 70.46 | 2148.75/417.23 |
| D.25.b. | | 34 - 66 | ha | a 8-a | 30.496/5.92 | 0.156 | 102.81 | 3135.29/608.79 |
| D.25.b. | | > 66 | ha | a 8-a | 30.496/5.92 | 0,120 | 133.33 | 4066,03/789.31 |

T.O.[1] - hourly rate, N.P.[2] - production rate, N.T.[3] - time rate, T.U.[4] - unit rate. Conversion level used 1€ = 5.15 lei

Table 2. Elements related to manual uprooting of softwood and resinous hardwood stumps (processing after Unified time and production standards for forestry work (1997))

| Norm symbol | Diameter of the stump (cm) | Unit of measurement | Framing grid | T.O. (lei/hour)/(€/oră) | N.P. (pcs./8hours) | N.T. (hours-man/pcs.) | T.U. (lei/buc.)/(€/pcs.) |
|---|---|---|---|---|---|---|---|
| C.5.a | 11-20 | piece | a 2-a | 25.685/4.99 | 20.18 | 0.40 | 10.27/2.00 |
| C.5.b | 21-30 | piece | a 2-a | 25.685/4.99 | 8.48 | 0.94 | 24.14/4.69 |
| C.5.c | 31-40 | piece | a 2-a | 25.685/4.99 | 6.35 | 1.26 | 32.36/6.29 |
| C.5.d | 41-50 | piece | a 2-a | 25.685/4.99 | 4.02 | 1.99 | 51.11/9.93 |
| C.5.e | 51-60 | piece | a 2-a | 25.685/4.99 | 3.31 | 2.42 | 62.16/12.08 |
| C.5.f | 61-70 | piece | a 2-a | 25.685/4.99 | 1.92 | 4.17 | 107.11/20.81 |
| C.5.g | > 70 | piece | a 2-a | 25.685/4.99 | 1.56 | 5.13 | 131.76/25.60 |

Table 3. Elements related to the works of filling holes and leveling the land following the uprooting of stumps (processing after Unified time and production standards for forestry work (1997))

| Norm symbol | Average pit volume ($m^3$) | Unit of measurement | Framing grid | T.O. (lei/hour)/(€/hour) | N.P. (buc./8hours) | N.T. (hours-man/ pcs.) | T.U. (lei/pcs.)/(€/pcs.) |
|---|---|---|---|---|---|---|---|
| C.7.a | până la 0.25 | piece | heavy work | 25.126/4.88 | 109 | 0.07 | 1.76/0.34 |
| C.7.b | 0.26-0.40 | piece | heavy work | 25.126/4.88 | 79 | 0.10 | 2.51/0.49 |
| C.7.c | 0.41-0.60 | piece | heavy work | 25.126/4.88 | 36 | 0.22 | 5.53/1.07 |
| C.7.d | Peste 0.60 | piece | heavy work | 25.126/4.88 | 26 | 0.30 | 7.54/1.46 |

To achieve the necessary crops, the soil will be plowed with a three-furrow plow at a plowing depth of 29-31 cm (Table 4), since it has been experimentally proven that the largest carbon reserves in the soils of agrosilvopastoral systems are found at a depth of 0-15 cm (Salazar et al., 2024). The plowing work will also be carried out with a harrow pulled by a tractor (Table 5).

A particularly important work is represented by the fertilization of the areas intended for crops and grazing, respectively (Maruşca, 2022). Recent research has shown that on the land areas exploited in the agrosilvopastoral system, the application of chemical fertilizers has been limited to the point of total elimination (Tsufac, et al., 2022). Consequently, organic fertilizer represented by manure will be used, or where possible, mulching will be carried out.

Manure fertilization can be carried out with specialized trailers of the MIG type (Figure 7a), of different capacities, depending on the topography of the land and the surface being worked. In areas relatively difficult to access for mechanized means, animal-drawn means can also be used successfully, especially those with hypotraction.



Figure 7a. Fertilization with manure, using the MIG trailer

Table 4. Elements related to soil plowing works with a plow, with three furrows, in medium-textured soils, at a plowing depth of 29-31 cm (processing after Unified time and production standards for forestry work, 1997)

| Norm symbol | Furrow length (m) | Unit of measurement | Framing grid | T.O. (lei/hour)/(€/hour) | N.P. (ha./8hours) | N.T. (hours-man/ha) | T.U. (lei/ha)/(€/ha) |
|---|---|---|---|---|---|---|---|
| D.7.III.b.17 | 100-200 | ha | a 7-a | 29.184/5.67 | 0.85 | 9.41 | 274.62/53.35 |
| D.7.III.b.18 | 201-400 | ha | a 7-a | 29.184/5.67 | 0.92 | 8.70 | 253.90/49.33 |
| D.7.III.b.19 | 401-600 | ha | a 7-a | 29.184/5.67 | 0.96 | 8.33 | 243.10/47.23 |
| D.7.III.b.20 | Peste 600 | ha | a 7-a | 29.184/5.67 | 0.98 | 8.16 | 238.14/46.27 |

Table 5. Elements related to the work of disc ploughing with a tractor-drawn harrow (processing after Unified time and production standards for forestry work, 1997)

| Norm symbol | Disc harrow type | Working depth | Unit of measurement | Framing grid | T.O. (lei/hour)/(€/hour) | N.P. (ha/8hours) | N.T.(hours-man/ha) | T.U. (lei/ha)/(€/ha) |
|---|---|---|---|---|---|---|---|---|
| D.9.a | G.D -2.5 | 10-15 | ha | a 7-a | 29.184/5.67 | 4.37 | 1.83 | 53.41/10.38 |
| D.9.b | G.D -3.2 | 10-15 | ha | a 7-a | 29.184/5.67 | 5.69 | 1.41 | 41.15/7.99 |
| D.9.c | G.D -4.0 | 10-15 | ha | a 7-a | 29.184/5.67 | 6.79 | 1.18 | 34.44/6.69 |

The use of manure spreading at present, in the studied location, is currently reported on relatively small areas, due to the low number of cattle and sheep, but it can be expanded in the context of establishing associations between livestock breeders, and submitting financing projects for the development of these activities.
The increasing complexity of agrosilvopastoral systems, as a result of the way the soil is worked, with direct implications on enzymatic activities, nutrient availability, texture, fertility and implicitly on production diversification, actively contributes to optimizing synergies between the nutrient cycle and soil organic carbon storage (Steinfeld et al., 2023; Ngaba et al., 2024).
Fertilization works are also assimilated to those in the forestry sector, carried out in nurseries and plantations, and respectively on areas intended for obtaining complementary food for fauna of hunting interest. The incorporation of seeds into the previously processed soil, for the crops to be installed, can be done manually or mechanically, depending on their specifics. To ensure peace and protection of the crops grown, temporary or permanent fences can be made, depending on the way the land is exploited and the available material possibilities. Currently, a modern variant of making fences is represented by the electric fence (Maruşca, 2022).
The provision of complex ecosystem services, such as diversified fruit production, resistant to diseases and pests, will be of particular importance in the future, given climate change and the growing interest in food security (Špulerová et al., 2025). The specific works for fruit tree cultivation refer to the maintenance of traditional orchards, which are partially or totally abandoned, and to the restoration of some that have been destroyed, or which are at the upper limit of longevity, being dry or in the process of drying (Figure 7b).



Figure 7b. Orchard of local plum varieties in the process of drying, in which specimens of common juniper *Juniperus comunis* L. have been installed, and which needs to be restored

As a result, these works explicitly refer to maintaining optimal tree vegetation conditions and, respectively, to the appropriate management of their crowns, in order to obtain optimal fruit production. In this context, it is necessary to clear the biogroups of woody, shrubby and subshrubby species (Figure 8; Table 1), remove and utilize them, if possible, as well as administer natural fertilizers, namely manure, over the entire surface, with a periodicity of 3-5 years, depending on the soil type.



Figure 8. Apple orchard where black locust specimens *Robinia pseudacacia* L. are being installed, and where crown pruning is required

For the proper management of the crowns, regeneration, management and formation works are necessary, depending on the age, growth and development vigor and respectively the phytosanitary condition of the trees (Figure 9). These works will be assimilated to those related to the formation, maintenance and correction cuts of the crowns in the plantations and seed orchards related to deciduous species (Table 6).



Figure 9. Example of a local apple variety that was grown in a traditional orchard, requiring specific pruning of the crown and removal of surrounding tree vegetation

Also, if the orchards are totally or partially destroyed, they will be restored by planting some fruit tree specimens, if possible, from the original species, or from other local species, which are successfully acclimatized and naturalized in the area. It is preferable to promote in culture trees grafted on freely generative rootstocks, from the apple and pear species. These rootstocks are obtained from seeds, and are optimal for vigorous, long-lived and frost and drought-resistant trees, developing a deep taproot, presenting high adaptability to less fertile soils, representing the perfect solution for the creation of traditional orchards (https://pomfruct.ro/blog/informatii-privind-caractéristiques-portaltoiului/), and present an increased resistance to diseases and pests.

In this situation, the work of obtaining planting material by grafting (Table 7) and respectively its planting (Table 8) can be assimilated to those in the forestry sector, carried out in nurseries, plantations and forest seed orchards.

Consequently, the rehabilitation and preservation of classic (traditional) orchards is very important, because in addition to producing high-quality, organic fruits, it contributes to the preservation of regional traditions and identity, attractive places for recreation, aesthetic appreciation, inspiration for artists, for locals as well as for potential tourists, from the country and abroad (Špulerová et al., 2025).

The works related to the forestry component of agrosilvopastoral systems (Figure 10) refer to:

- ensuring an appropriate phytosanitary condition of the biogroups formed by trees belonging to the fundamental natural forest type;
- appropriate regulation of intraspecific and interspecific competition,
- artificial pruning and trimming works for trees that present an excessive crowning process;
- controlling the succession process of pioneer and invasive species;
- regeneration of tree biogroups that have reached their physiological limit.

Table 6. Elements related to crown formation, maintenance and correction pruning in deciduous tree seed plantations and orchards (processing after Unified time and production standards for forestry work, 1997)

| Norm symbol | Species group | Time since planting (years) | Unit of measurement | Framing grid | T.O. (lei/hour) (€/hour) | N.P. (pcs./8hours) | N.T. (hours-man/pcs.) | T.U. (lei/pcs.) (€/pcc.) |
|---|---|---|---|---|---|---|---|---|
| C.48.a | hardwood | 2-3 | pieces | a 7-a | 29.184/5.67 | 42.33 | 0.19 | 5.54/1.08 |
| C.48.b | hardwood | 4-6 | pieces | a 7-a | 29.184/5.67 | 29.74 | 0.27 | 7.88/1.53 |
| C.48.c | hardwood | 7-10 | pieces | a 7-a | 29.184/5.67 | 21.51 | 0.37 | 10.80/2.10 |
| C.48.d | hardwood | >10 | pieces | a 7-a | 29.184/5.67 | 16.03 | 0.50 | 1459/2.84 |

Table 7. Elements related to grafting works for deciduous forest saplings
(processing after Unified time and production standards for forestry work, 1997)

| Norm symbol | Specifications | Unit of measurement | Framing grid | T.O. (lei/hour)/(€/oră) | N.P. (1000 pcs./8hours) | N.T. (hours-man/buc) | T.U. (lei/1000 pcs.) (€/1000 pcs.) |
|---|---|---|---|---|---|---|---|
| B.83.I.b.1 | Prepared rootstock and scion, grafted and tied with raffia | (1000 pieces) | a 7-a | 29.184/5.67 | 0.12 | 65.57 | 1913.59/371,78 |
| B.83.I.b.1 | Glue graft with mastic | (1000 pieces) | a 7-a | 29.184/5.67 | 0.53 | 15.24 | 444.76/86,41 |

Table 8. Elements related to the planting works of seedlings grown or transplanted in polyethylene bags (processing after Unified time and production standards for forestry work, 1997)

| Norm symbol | Pit dimensions (cm) | Working conditions[1] | Unit of measurement | Framing grid | T.O. (lei/hour)/ (€/hour) | N.P. (buc./ 8hours) | N.T. (hours-man/ 100seedlings) | T.U. (lei/100 seedlings)/ (€/100 seedlings) |
|---|---|---|---|---|---|---|---|---|
| C.40.I.a | 30x30x30 | light[2] | 100 seedlings | a 6-a | 28.407/5,51 | 2.06 | 3.88 | 99,89/21.38 |
| C.40.I.b | 30x30x30 | medium[3] | 100 seedlings | a 6-a | 28.407/5,51 | 1.28 | 6.24 | 160,66/34.38 |
| C.40.I.c | 30x30x30 | heavy[4] | 100 seedlings | a 6-a | 28.407/5,51 | 0.91 | 8.75 | 225,28/48.21 |
| C.40.II.a | 40x40x40 | Light | 100 seedlings | a 6-a | 28.407/5,51 | 1.09 | 7.35 | 189,23/40.50 |
| C.40.II.b | 40x40x40 | Medium | 100 seedlings | a 6-a | 28.407/5,51 | 0.66 | 12.06 | 310,50/66.45 |
| C.40.II.c | 40x40x40 | Heavy | 100 seedlings | a 6-a | 28.407/5,51 | 0.48 | 16.84 | 433,56/92.79 |

[1]Working conditions are determined by soil texture and moisture, skeletal content, degree of weed and woody species coverage, and terrain slope. [2]Light conditions 5-7 points. [3]Medium conditions 8-11 points. [4]Heavy conditions 12-15 points.

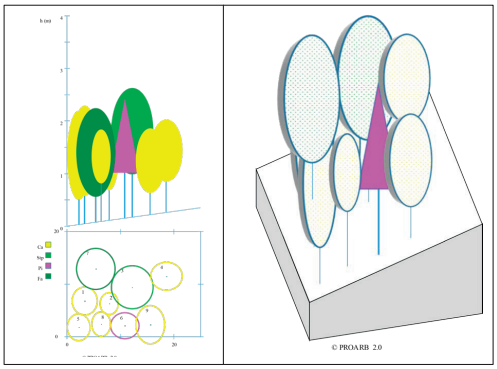



Figure 10. Tree biogroups within an agrosilvopastoral system in Vârfurile locality, Arad county.
The identified species are: Ca - *Carpinus betulus* L., Stp - *Quercus robur* L., Pi - *Pinus sylvestris* L., and Fa - *Fagus sylvatica* L.

The regeneration of tree biogroups, which build the fundamental natural type of forest bordering agrosilvopastoral systems, can be achieved naturally, from certified seed, coming from seed reserves (Crainic et al., 2023b), or mixed, also using bare-root forest seedlings (Dorog & Crainic, 2015). As a result, the tree species of *Quercus robur*, *Quercus ceris*, *Quercus petraea*, *Acer campestre*, *Fagus sylvatica*, *Carpinus betulus*, *Prunus avium*, and *Alnus glutinosa* will be regenerated, which are native species and have a very important role in improving and maintaining soil fertility and in the efficient functioning of the land exploitation system (Cheruto et al., 2025). Also, the wood that will be obtained from these tree species can be valued differently, depending on the needs of the owners. The aforementioned interventions will comply with the recommendations of the technical norms related to activities in the forestry sector, as well as some technical solutions offered by local experience, which have been shaped over decades of exploitation (activity).

It is also aimed at removing biogroups of shrubs and subshrubs that cannot be exploited, and which frequently colonize considerable areas.

The wood resulting from the application of the interventions mentioned above can be exploited

in compliance with the regulations in force regarding forest vegetation outside the national forest fund (Forestry Code - Law 331/2024), and the cultivation of some fruit tree species, such as walnut and cherry. Agrosilvopastoral systems have a high potential to store more carbon and improve the physical and chemical characteristics of the soil, compared to conventional pastoral systems (Salazar et al., 2024). Consequently, at present, the zootechnical component, namely animal husbandry, must be maintained and rehabilitated in these complex land use systems in the studied area, and for this reason.

The works related to the zootechnical component mainly refer to the partial redevelopment of animal shelters, watering places and, last but not least, the design of modern enclosures and electric fences, activities that can be carried out relatively easily by the owners, given the current logistical possibilities. To make the process of monitoring the exploitation and health of agro-forestry systems, and carbon sequestration more efficient on a large scale, remote sensing applications can be used with high efficiency (Sirimalle et al., 2025).

Although the elements related to the specifics and cost of the mentioned works have been assimilated to those in the corresponding activity sectors, however, currently the economic evaluation of the activities presented is carried out through direct negotiation between the owner and the provider, or they can be carried out by the owner himself, including a series of expenses determined by various materials, fuels, taxes, etc.

For the plains and low hills, the value of the works related to the installation of oat crops is approximately 2100 lei (407.76 euros) per hectare of land, and in the high hills area, where the case study was conducted, the value of these works is currently estimated at 2600 lei (504.85 euros) per hectare.

These aspects, regarding the method used to evaluate the works, are relevant for the correct quantification of all expenses and obviously for establishing an efficient financing approach.

It is known that at the European level, for example in Switzerland, the valorization of the productions of meadows and orchards related to agroforestry systems is declining, although these are managed within the framework of extensive agri-environmental schemes (SAE) (Nishizawa et al., 2022).

At the national level, although part of the areas exploited in the agrosilvopastoral system are declared for APIA subsidies (www.agroinfo.ro, www.agrointel.ro, Table 9), their amount can only finance (financially support) a relatively small percentage of the works necessary for their rehabilitation and introduction into the productive circuit.

Table 9. General summary of APIA support (€/ha), for hill and mountain areas (www.apia.org.ro)

| Use category | Estimated payment range (€/ha) |
|---|---|
| Permanent grassland (simple) | 120 - 180 |
| Mountain/alpine grassland | 200 - 300 |
| Agri-environmental grassland | 250 - 350 |
| Traditional orchards | 150 - 300 |

The revival of activities in this type of exploitation requires an efficient strategy for the valorization of the products obtained.

Although the production of animal and plant-based foods related to agro-silvopastoral systems is of superior quality, with some products being organic, in some situations production costs are higher, which may influence market competitiveness.

But the quality of the products, namely the taste, healthy character, naturalness, flavor, seriously attract the attention of consumers, who are interested in these essential characteristics. Consequently, consumers, through the actions of purchasing products, can support the activity in these systems (Philipp & Zander, 2023).

In this context, the creation of a modern, efficient system for the valorization of animal products, especially a series of dairy products from cattle, (represented by milk, cream, fresh cheese) which are sold locally, through a vending machine and a retail store, respectively, was initiated. As a result, the companies Lazurana Lact SRL and Lazurana Ferm Lact Agricultural Cooperative represent a local producer located in Lazuri Village, Vârfurile ATU, Arad County, which processes milk from local farms within the Vârfurile ATU, Arad County, and which exploits the lands in an agrosilvopastoral system, producing a wide range of organic dairy products.

Also, to capitalize on the fruits obtained from traditional orchards that are exploited in agro-

forestry systems, a complete line with industrial capacity was purchased for processing fruits and obtaining various types of pasteurized and unpasteurized, organic juices in the locality of Măgulicea, UAT Vârfurile, Arad County.

Agrosilvopastoral systems are characterized by a high level of biodiversity and superior production capacity, but their related activities require considerable time and financial effort, in order to optimally and sustainably capitalize on the productive potential of the land (Philipp & Zander, 2023).

The climatological analysis presented above shows that the period 1990-2025 was very warm, with 2/3 of the years analyzed having positive thermal deviations from normal. The 2007-2025 interval was the warmest, recording only positive annual temperature deviations. That caused the linear trend of annual thermal deviations to be strongly upward. The precipitation analysis highlighted that the negative annual deviations were greater than the positive ones, but the rainy periods were longer than the dry ones. However, the rainfall extremes were very well highlighted in the analyzed period 1990-2025: there were very rainy and excessively rainy years interspersed with very dry or excessively dry years. As a result, the very high temperatures and long droughts in the dry years negatively influenced the plant and animal yield in the studied area, and the excessive rains in the rainy years favored obtaining rich yields.

The necessary works for the rehabilitation and introduction into the productive circuit of the abandoned agrosilvopastoral systems have to be carried out in an integrated manner, for each of their components, depending on the objective reality on the ground. The specifics of the works and the way they are carried out have to be correlated with the technical and financial possibilities of the owners. Also, the way of valorizing the products of plant and animal origin obtained have to be optimal, in order to efficiently support the expenses related to the production process, with a view to sustainable management of these complex systems. The financing options that can be accessed through various projects or non-refundable payments and interventions, constitute an important support for the owners of agrosilvopastoral systems. According to the aspects presented above, it follows that the objectives of the study have been achieved.

The results obtained in this study contributed to the advancement of scientific knowledge in the addressed field, by the fact that for the rehabilitation and introduction into the productive circuit of the abandoned agrosilvopastoral systems, an integrated approach to the necessary works is required, depending on the specifics of the system component, in direct correlation with the vegetation conditions and the yield obtained, making it possible to predict the expenses and income obtained, with high accuracy.

The extension of research to other locations in Vârfurile Commune, Arad County, is mainly limited by the way in which agrosilvopastoral systems are exploited, which differs from one owner to another, with several differences regarding the exploitation of the productive potential of each component of the systems. Research may also be limited by the refusal of owners to facilitate the access to information from the agricultural register and to information relating to the plant and animal yields obtained.

Research and studies on agrosilvopastoral systems can be continued in the future for each village in the Vârfurile commune, in order to analyze their condition and the real possibilities for their rehabilitation and introduction into the productive circuit.

## CONCLUSIONS

The period 1990-2025 was a very warm one, the 2007-2025 interval being the warmest. Most years of the period 1990-2025 had positive deviations of the annual average air temperature from normal. Compared to the precipitation recorded in the period 1966-2025, the period 1990-2025 was relatively rich in precipitation, but in which the rainfall extremes were highlighted (there were very rainy and excessively rainy years interspersed with very dry or excessively dry years). Thermal and rainfall extremes are very damaging to forests, representing a major stress for them, weakening the resistance of trees and favoring the emergence of diseases and pests.

Agro-silvopastoral systems in uncultivated areas of medium and high hills were exploited differently over time, and after 1989, interest in

productive activities gradually decreased, some of them being abandoned, even today.

The work required to rehabilitate these complex land valorization systems has specific features for their functional components, requiring considerable financial support.

Although the measures that need to be adopted are relatively easy for owners, in order to make them more efficient, it is necessary to achieve an ownership, at least at the village level.

The initiation of the valorization of animal and plant products resulting from productive activities, mostly locally, in an organized manner, given the facilities that are currently available, represents for the studied area a definite possibility of rehabilitation and reintegration into the productive circuit of agro-silvopastoral systems.

## ACKNOWLEDGEMENTS

For the support given to the optimal development of the case study, we would like to thank the management of the Local Council of the Vârfurile City Hall, Arad County, the managers of the commercial companies Lazurana Lact SRL and Lazurana Ferm Lact Agricultural Cooperative. We would also like to thank the owners of the agrosilvopastoral systems that are currently carrying out productive activities, for facilitating access on the ground and to a series of information regarding the local experience accumulated over decades of activity.

## REFERENCES

Budău, R., Apăfăian, A., Caradaică, M., Bratu, I., Timofte, C., & Enescu, C. (2023). Expert-Based Assessment of the Potential of Agroforestry Systems in Plain Regions across Bihor County, Western Romania. *Sustainab*, 15:15724. https://doi.org/10.3390/su152215724.

Cialdella, N., Jacobson, M., & Penot, E. (2023). Economics of agroforestry: links between nature and society. *Agroforestry Systems*, 97.3, 273-277. https://doi.org/10.1007/s10457-023-00829-z.

Chappa, L. R., Nungula, E. Z., Makwinja, Y. H., Ranjan, S., Sow., S, Alnemari, A. M., Maitra, S., Seleiman, M. F., Mwadalu, R., Harun, I., & Raj, A. G. (2024). Outlooks on Major Agroforestry Systems In Jhariya, M.K., Banerjee, A., Jha R.K., Singh K.P. (Eds.), *Agroforestry*. 21–48, Scrivener Publishing LLC. https://doi.org/10.1002/9781394231164.ch2.

Cheruto, G., Nungula E. Z., Nyawira L., Chappa, L. R., Kahuthia-Gathu, R., Mwadalu, R., Dlamini, J., C., Ranjan, S., Sow S., Maitra, S., Nasar, J., & Gitari, H. (2025). Agroforestry tree species: *Acacia tortilis*, biology, importance, agroforestry production, and biotechnology application. *Tree Biology and Biotechnology*. https://doi.org/10.1007/978-981-96-0002-1_10.

Crainic, G. C., Covaci, F., Sabău, N. C., Sicoe, S. I., Irimie (Cioflan), F., Bodog, M. F., & Iovan, C. I. (2023a). Works specific to the introduction of silvopastoral systems in the forest fund. *Scientific Papers. Series E. Land Reclamation, Earth Observation & Surveying, Environmental Engineering*. XII, Print ISSN 2285-6064, CD-ROM ISSN 2285-6072, Online ISSN 2393-5138, ISSN-L 2285-6064. https://landreclamationjournal.usamv.ro/pdf/2023/Art10.pdf.

Crainic, G. C., Sicoe, S. I., Irimie, F., Irimie (Cioflan), Flavia., Iovan, C. I. & Bodog, M. F. (2023b). The particularities of the ecological rehabilitation works of the sessile oak stands (*Quercus petraea* (Matt.) Liebl), from the seed reserve. *Scientific Papers. Series E. Land Reclamation, Earth Observation & Surveying, Environmental Engineering*. XII, Print ISSN 2285-6064, CD-ROM ISSN 2285-6072, Online ISSN 2393-5138, ISSN-L 2285-6064. https://landreclamationjournal.usamv.ro/pdf/2023/Art29.pdf.

Crainic, G. C., (2017). Specific Works For The Maintenance Of Agroforestry Systems, *Analele Universităţii din Oradea, Fascicula Protecţia Mediului*. XXIX, 2017, 153-164, ISSN 1224-6255.

Dorog, L.S., & Crainic, G.C. (2015). Shrubs and trees regeneration in silvopastorale systems in the counties of Bihor and Arad, *Research Journal of agriculture science, 47.4.* University of Agriculture sciences and veterinar medicine of the Banat, Timişoara, 2015, pp. 64-69, https://www.cabdirect.org/cabdirect/abstract/20163022043.

Fahad, S., Chavan, S. B., Chichaghare, A. R., Uthappa, A.R., Kumar, M., Kakade, V., Pradhan, A., Jinger, D., Rawale, G., Yadav, D. K., Kumar, V., Farooq, T. H., Ali, B., Sawant, A. V., Saud. S., Chen, S., & Poczai, P. (2022). Agroforestry Systems for Soil Health Improvement and Maintenance. *Sustainability*, 14(22):4877. https://doi.org/10.3390/su142214877.

Hălmagiu Commune City Hall, Draft Decision No. 4548/20.09.2022 regarding the update of the Risk Analysis and Coverage Plan in Hălmagiu Commune for 2022, Chapter II – Climatic Characteristics, https://primariahalmagiu.ro/download/urvqbaO3Rf0Eh7w9f690f8ugJ6lAzB8W4JBO4a7g.pdf.

Lazurana Lact SRL. https://listafirme.ro/lazurana-lact-srl-52243169/ (22.05.2026, 9:30 a.m.);

Lazurana Ferm Lact Agricultural Cooperative. https://www.risco.ro/verifica-firma/lazurana-ferm-lact-cooperativa-agricola-cui-44666788?srsltid=AfmBOoo3Wr_SuSSKuwVrxynt4VFGu_voZSGsGqqoCojte1amm6ePUuBE (22 05 2026, 9.35 am). https://targetare.ro/44666788/lazurana-ferm-lact-cooperativa-agricola (22.05.2026, 9.45).

Law 331/2024 Forestry Code, *Official Gazette of Romania*, Part I no. 7 of January 9, 2025.

Lehmann, L. M., Smith, J., Westaway, S., Pisanelli, A., Russo, G., Borek, R., Sandor, M., Gliga, A., Smith, L., & Ghaley, B. B. (2020). Productivity and economic evaluation of agroforestry systems for sustainable production of food and non-food products. *Sustainability*, 12(13), 5429. https://doi.org/10.3390/su12135429.

Maruşca, T. (2022). *Praticulture and pastoralism in scientific research: own achievements and perspectives*. Transylvania University Publishing House of Braşov, Romania.

Maruşca T. (2018). *Agrosilvopastoral confessions*. Transylvania University Publishing House of Braşov, Romania.

Mazumder, S. Y., Bania, J. K., Sileshi, G. W., Paul, M. K., Das, A. K., & Nath, A. J. (2025), Variation in biomass and soil carbon storage and sequestration rates in different agroforestry systems with climatic zones and soil types. *Environ. Sustain. Indic*. 26:100642. https://doi.org/10.1016/j.indic.2025.100642.

Meteomanz.com, www.meteomanz.com (accessed on 2-5 Feb. 2026).

Ngaba, M. J.Y., Mgelwa, A. S., Gurmesa, G. A., Uwiragiye, Y., Zhu, F., Qiu, Q., Fang, Y., Hu, B., & Rennenberg, H. (2024). Meta-analysis unveils differential effects of agroforestry on soil properties in different zonobiomes. *Plant Soil* 496:589-607. https://doi.org/10.1007/s11104-023-06385-w.

Nishizawa, T., Kay, S., Schuler, J., Klein, N., Herzog, F., Aurbacher, J., & Zander, P. (2022). Ecological–Economic Modelling of Traditional Agroforestry to Promote Farmland Biodiversity with Cost-Effective Payments. *Sustainab* 14:5615. https://doi.org/10.3390/su14095615.

Philipp, S. M., & Zander, K. (2023). Orchard meadows: consumer perception and communication of a traditional agroforestry system in Germany. *Agroforest Syst.* 97:939–951. https://doi.org/10.1007/s10457-023-00840-4.

Popa, I. (1999). Useful computer applications in forestry research. The Carota Program and the Proarb Program. *Forestry Journal*, 2:41-42.

Pop, G. (2005). *Romania. The Western Hills and the Western Plain*, University of Oradea Publishing House, pp. 84-89 (In Romanian).

Popovici, L., Mihăilă, E., Costăchescu, C., & Constandache, C. (2018). Can Agroforestry Systems Be Ordinary Practices in Romania? *Can Agrofor. Syst. Be Ordinary Pract. Rom.* 61, 263-268. Lucrări ştiinţifice seria horticultură, 61 (1) / 2018, USAMV Iaşi. https://www.uaiasi.ro/revista_horti/files/Nr1_2018/43.%20Popovici%20L..pdf.

Ribeiro, J.M., Costa de Freitas, I., Souza e Brito, B. G., Fernandes, L. A., Carvalho Leite, L.F., de Almeida Barbosa, D.L., Santos, M. V., Pellegrino Cerri, C. E., & Frazão, L. A. (2023). Agrosilvopastoral system as a potential model for increasing soil carbon stocks: a century model approach. soil processes and properties, soil chemistry. *Rev. Bras. Ciênc. Solo*. 47(spe):e0220136. http://dx.doi.org/10.36783/18069657rbcs20220136.

rp5.ru, https://rp5.ru/ (accessed on 9-12 Feb. 2026).

Salazar, R., Alegre, J., Pizarro, D., Duff, A. J., Garcia, C., & Gomez, C. (2024). Soil carbon stock potential in pastoral and silvopastoral systems in the Peruvian Amazon. *Agroforest Syst* 98:2157-2167. https://doi.org/10.1007/s10457-024-00969-w.

Santos, M., Cajaiba, R. L., Bastos, R., Gonzalez, D., Petrescu Bakis, A. L., Ferreira, D., Leote, P., Barreto da Silva, W., Cabral, J. A., Gonçalves, B., & Mosquero-Losada, M. R. (2022). Why Do Agroforestry Systems Enhance Biodiversity? Evidence From Habitat Amount Hypothesis Predictions. *Front. Ecol. Evol*. 9:630151. https://doi.org/10.3389/fevo.2021.630151.

Sirimalle, M., Kumawat, C., Jiménez-Ballesta, R., Meena, R., Sharma, K. K., Patra, A., Mohapatra, K. K., & Kumawat, A. (2025). Impact of Long-Term Agroforestry Systems on Carbon Pools and Sequestration in Top and Deep Soil Layers of Semi-Arid Region of Western India. *Forests* 16(6):946. https://doi.org/10.3390/f16060946.

Smith, L. G., Westaway, S., Mullender, S., Ghaley, B. B., Xu, Y., Lehmann, L. M., Pisanelli, A., Russo, G., Borek, R., & Wawer, R. (2022). Assessing the Multidimensional Elements of Sustainability in European Agroforestry Systems. *Agric. Syst* 197:103357. https://doi.org/10.1016/j.agsy.2021.103357.

Špulerová, J., Bartlett, D., Kruse, A., Bürckmann, H., Eiter, S., Šmid Hribar, M., Kladnik, D., Kučera, Z., Melicher, J., Philipp, S., Potthoff, K., Renes, H., Roth, M., & Sigura, M. (2025). A review of the cultural significance of traditional orchards using examples from selected European countries. *Landsc Ecol.* 40:159. https://doi.org/10.1007/s10980-025-02169-y.

Steinfeld, J. P., Bianchi, J. J. A. F., Locatelli, L. J., Rodnei, R., Bispo de Resende, M. E., Ballester, R. M. V., Cerri, C. E. P., Bernardi, A. C. C., & Creamer, R. E. (2023). Increasing complexity of agroforestry systems benefits nutrient cycling and mineral-associated organic carbon storage, in south-eastern Brazil. *Geoderma* 440:116726. https://doi.org/10.1016/j.geoderma.2023.116726

Tsufac, A. R., Awazi, N. P., & Tchamba, M. N. (2022). Agroforestry as an Agro-Ecological Pathway to Phase Out Chemical Fertilizer Application in Smallholder Farms in Cameroon: State-of-the-Art and Policy Implications. Effects. *Curr World Environment* 17(1). http://dx.doi.org/10.12944/CWE.17.1.9.

Unified time and production standards for forestry work (1997). Ministry of Waters, Forests and Environmental Protection, National Forestry Administration. S.C. ROF Publishing House. S.A., Suceava, Romania.

Vârfurile Commune, Arad, https://ro.wikipedia.org/wiki/Comuna_Vârfurile_Arad (accessed on 23 Feb. 2026).

Vârfurile Commune City Hall – Presentation, https://primariavirfurile.ro/despre-noi/prezentare/ (accessed on 23 Feb. 2026).

Scientific Papers. Series E. Land Reclamation, Earth Observation & Surveying, Environmental Engineering. Vol. XV, 2026
Print ISSN 2285-6064, CD-ROM ISSN 2285-6072, Online ISSN 2393-5138, ISSN-L 2285-6064

# THE *SPHAGNUM* PEATBOGS OF MOLHAȘUL DE LA RÂȘCA - DEALUL NEGRU, CLUJ COUNTY

**Ana-Maria MOROȘANU, Miruna-Maria ȘTEFĂNUȚ, Sorin ȘTEFĂNUȚ**

Institute of Biology Bucharest of Romanian Academy, 296 Splaiul Independenţei, District 6, Bucharest, Romania

Corresponding author email: miruna.stefanut@ibiol.ro

***Abstract***

*Molhaşul de la Râşca - Dealul Negru is a montane oligotrophic peatbog complex in Cluj County (1042-1070 m a.s.l.), within the alpine biogeographical region of north-western Romania. Covering 35 ha, it comprises a mosaic of Sphagnum-dominated peat-forming communities, and for S. affine is the only site in Romania. The structure and hydrology of the site have been slightly altered by past drainage, grazing pressure, surrounding land-use changes and the expansion of woody vegetation, leading to anthropogenic habitat fragmentation and partial isolation from the neighbouring Râşca Răchitiş mire. Based on new field surveys, the present study documents the diversity, distribution patterns and habitat preferences of Sphagnum species across the active raised bog and evaluates the conservation value of Molhaşul de la Râşca - Dealul Negru as one of the regional reference sites for Sphagnum-dominated ecosystems in the Gilău Massif.*

***Key words****: Molhaşul de la Râşca, Natura 2000, peatbog, Romania, Sphagnum.*

## INTRODUCTION

Peatlands represent critical reservoirs of carbon worldwide, covering about 3.0% of the total land area but storing much more carbon than any terrestrial ecosystem (Scharlemann et al., 2014; Keane et al., 2025). One of the key ecosystem services that peatlands provide is biodiversity support, or even refugia for some rare species. Alongside climate regulation, water management and cultural heritage, this makes peatlands essential for sustainable environmental stewardship and long-term conservation. These ecosystems host a unique variety of species, many rare, endangered, or even adapted to wet, acidic, and nutrient-poor environments (Joosten et al., 2017). Therefore, protecting increasingly threatened peatlands thus directly supports biodiversity conservation.

Molhaşul de la Râşca - Dealul Negru Peatbog (CJ-016) represents one of the largest peatbogs in the Apuseni Mountains (21.59 ha).

From a historical perspective, E. Pop first described Molhaşul de la Râşca Peatbog (also known as *Mohuş-ul de la Dealul Negru* or *"Lágyas"*) in 1947 as being the only Apuseni site with natural *Pinus sylvestris*, though it was already invaded by trees (*Picea*, *Pinus*, *Betula pendula*, *B. pubescens,* and *Populus tremula*) and generally drier (with *Calluna vulgaris*, *Empetrum nigrum*, and *Vaccinium myrtillus*) (Pop, 1947). He noted early signs of degradation due to the nearby village (Pop, 1947; Pop, 1960). Later, he reported a 2.2 m-thick peat layer (ca. 120,000 $m^3$ formed mainly of sub-Atlantic origin, pH 3.90-5.00), along with some crises: underground peat burning (1910-1912) and exploitation from 1952 onwards (Pop, 1960).

Concerning the bryophyte flora of the study site, Györffy and Péterfi (1919) recorded two *Sphagnum* taxa from "*Lágyas*": *Sphagnum compactum* var. *squarrosa* and *Sphagnum imbricatum* var. *cristata* fo. *fuscescens*. Between 1936 and 1946, E. Pop collected additional *Sphagnum* species from Molhaşul de la Râşca and nearby sites, later determined and published by T. Ștefureac (1958) as *S. acutifolium* Ehrhardt (*S. nemoreum* Scop.), *S. capillaceum* (Weis.) Schrank (1936) and var. *versicolor* Warnst. (1936), and *S. magelanicum* Brid. (currently referred to as *S. medium* Limpr; 1936).

*Sphagnum* represents one of the most dominant plants in many peatlands. It engineers favourable conditions for its proliferation through moisture retention via capillary action,

nutrient efficiency, acidification, slow decomposition (due to the polyphenol content), and microbial suppression by specialized metabolites (Keane et al., 2025). As a *Sphagnum*-dominated peatbog, Molhașul de la Râșca - Dealul Negru`s accumulated organic matter - peat - is composed of a high percentage of this specific decomposed species due to its known resistance to decomposition (Kuhry & Vitt, 1996).

Some *Sphagnum* species from this site have a conservative importance, being the keystone of the ecosystem. *Sphagnum affine* Renauld & Cardot holds NE (not evaluated) conservation status in Romania due to data deficiency (Ștefănuț & Goia, 2012; Hodgetts et al., 2020). Recently confirmed in one site in Romania (Molhașul de la Râșca - Dealul Negru), therefore the conservation status changed from NE to CR (critically endangered) B1ab (ii, iii) + B2ab (ii, iii) (Sabovljević et al., 2025; Sass-Gyarmati et al., 2025; Ștefănuț et al., 2026). *S. affine*`s occurrence could be underestimated due to morphological similarities with *S. palustre*, particularly as they co-occur (Figure 1). Until now, we could consider *S. affine* a threatened species nationally, and it should have a protected conservation status.



Figure 1. *Sphagnum affine* mixed with *S. palustre,* Molhașul de la Râșca - Dealul Negru, 6.10.2025 (photo by Ștefănuț S.)

Similarly, *Hamatocaulis vernicosus* (Mitt.) - varnished hook-moss - is listed in Annex II of the EU Habitats Directive (European Union. Council Directive 92/43/EEC), with a 'Vulnerable' status in the Red Data Book of European Bryophytes (European Committee for the Conservation of Bryophytes) and the Red List of Romanian Bryophytes (Ștefănuț & Goia, 2012).

It faces a projected pessimistic future scenario of major range losses due to climate change (Ștefănuț et al., 2025), underscoring the need to protect it alongside peatland habitats.

Even though many Romanian peatlands face severe degradation, Molhașul de la Râșca Peatbog represents a rare functional oligotrophic system with Atlantic affinities (Sass-Gyarmati et al., 2025).

Despite historical documentation, no comprehensive bryophyte inventories have existed for over several decades. This data deficiency for conservation assessments of Molhașul de la Râșca Peatbog shaped this study`s objectives: (1) inventory bryophyte biodiversity, (2) assess PeatRO-identified pressures and conservation priorities, and (3) propose management measures for long-term protection. These efforts provide the scientific basis for the integration of Molhașul de la Râșca Peatbog within Apuseni Natural Park (RONPA0004) or its designation as a Natura 2000 Site of Community Importance (SCI).

## MATERIALS AND METHODS

### Study Area and Site Importance

Molhașul de la Râșca - Dealul Negru (CJ-016; 46.710460° N, 23.050730° E) lies within Râșca commune, Cluj County, Romania. Biogeographically, it belongs to the alpine region, situated in the northwest of Romania on the Dealul Negru plateau between Călata and Râșca valleys 1042-1070 m a.s.l., Gilău Massif, covering 35 ha (Figure 2). The site is located at 0.6 km to Apuseni Natural Park (RONPA0004) and Apuseni Natura 2000 site (ROSCI0002).



Figure 2. Geographical limits of Molhașul de la Râșca - Dealul Negru (grey). In blue is the Apuseni Natural Park

Pop (1947) positioned Molhașul de la Râșca – Dealul Mare and Molhașul de la Călățele (the largest peat bogs in the area) opposite each other across adjacent watersheds drained by Valea Călățele (Figure 3, a and b). Geologically, he describes the parent rock in the area as consisting primarily of nutrient-poor Eocene sandy clay, with exceptional outcrops of crystalline schists in contact with sandstone substratum (Pop, 1960).

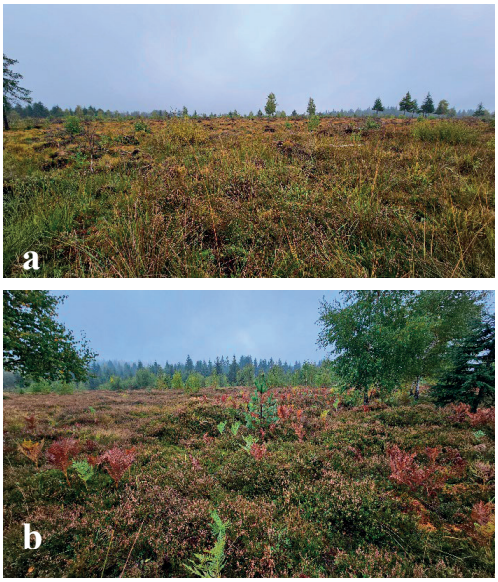



Figure 3. Molhașul de la Râșca Peatbog, ground view (a and b), 6.10.2025 (photo by Ștefănuț S.)

Currently, the general aspect of the site is an oligotrophic bog, with a deficient water regime. Dominant vegetation includes mosses (mainly *Sphagnum*) and the presence of some nano-phanerophytes such as *Calluna vulgaris*, *Empetrum nigrum*, *Vaccinium myrtillus*, *V. vitis-idaea,* and *Juncus squarrosus* - the latter representing its only national occurrence as an Atlantic species (Frink et al., 2017; Sass-Gyarmati et al., 2025; PeatRO Project).

**Field survey and sample collection**

Molhașul de la Râșca Peatbog was selected due to underreported bryophyte diversity, highlighting the need for additional conservation assessments. To inventory bryophytes, a field survey was made in order to collect samples on 6 October 2025.

For each species population, we recorded GPS coordinates (Garmin 64s, <50 cm accuracy), captured aerial imagery (DJI Mini 2 drone), and integrated the ground-based data to map habitat distribution.

The collected samples of bryophytes were morphologically identified under the light microscope, and the nomenclature of *Sphagnum* species was made after Hodgetts et al. (2020) and Hassel et al. (2025).

**Pressures and threats**

As a part of the PeatRO Project (2015-2017), Molhașul de la Râșca - Dealul Negru (CJ-016) and 215 other Romanian peatlands were evaluated for their conservation status in order to inform national strategies limiting biodiversity loss. Anthropogenic and environmental pressures noted during this project included drainage, cattle grazing, land-use changes and woody vegetation encroachment. Main threats comprise climate change and habitat fragmentation linked to the adjacent Râșca Răchitiș mire. Subsequent to the identification of these existing pressures, the project proposed restoration measures aimed to mitigate these pressures and to preserve the habitats.

## RESULTS AND DISCUSSIONS

During our field surveys, we identified a number of ten *Sphagnum* species, of which many are specific to the peat bogs of the Apuseni Mountains, and others are bryophyte species with great conservation potential, such as *Hamatocaulis vernicosus*.

***Sphagnum affine*** Renauld & Cardot

The species was first reported from Molhașul de la Râșca Peatbog as *Sphagnum imbricatum* Hornsch. var. *cristata* fo. *fuscescens* Warnst Comit. Kolozs: in turfosis Lágyas supra Magyarvalkó, alt. cca 920 m.s.m., 1915.25.X., leg. & det. Györffy I. and Péterfi M., BP (Budapest Herbarium) 7450/S, 7451/S, rev. Ștefănuț M-M. (Györffy & Péterfi, 1919; Sabovljević et al., 2025).

The species was rediscovered at the same site on 26 July 2013 (46.70849° N, 23.05224° E, 1070 m a.s.l.), *leg*. Sass-Gyarmati A., Jakab G., *det*. Sass-Gyarmati A., 2014, EGR (Eger

Herbarium), CL (Cluj-Napoca Herbarium), reported on 30 June 2025 (Sass-Gyarmati et al., 2025), BUCA (Institute of Biology Bucharest Herbarium), *B12946* (*conf.* Ștefănuț M.-M., 23 June 2025).

Both records were a compelling reason for us to look further for *S. affine* (Figure 4) in Molhașul de la Râșca peatbog, being the only location in Romania where it has been reported. Therefore, we confirmed its presence on 6 October 2025 at Molhasul de la Râsca - Dealul Negru, 46.709174° N, 23.049022° E, 1053 m a.s.l., *leg*. Ștefănuț M.-M., Moroșanu A.-M., Ștefănuț S., *det*. Ștefănuț M.-M., confirmed by Ștefănuț S., BUCA *B12617* (Ștefănuț et al., 2026).



Figure 4. *Sphagnum affine*, close-up (photo by Ștefănuț S.)

***Sphagnum compactum*** Lam. & DC.

An Atlantic species which was previously reported as *Sphagnum compactum* DC. var. *squarrosa* Russ., *Comit Kolozs: in turfosis Lágyas prope pagum Magyarvalkó, alt. 1000 m.s.m.* (25.10.1915), by Györffy and Péterfi (1919), confirmed by Sass-Gyarmati et al. (2025).

We also found *S. compactum* at Molhașul de la Râșca Peatbog, 46.708450° N, 23.051975° E, 1063 m a.s.l., 6.10.2025, *leg*. Ștefănuț M.-M., Moroșanu A.-M., Ștefănuț S., *det*. Ștefănuț M.-M., confirmed by Ștefănuț S., BUCA *B12671-B12672* (Figure 5).

We did not find two *Sphagnum* species previously recorded: *Sphagnum platyphyllum* (Lindb. ex Braithw.) Warnst. (Meleshko et al., 2025; Sass-Gyarmati et al., 2025), and *S. subsecundum* Nees (Meleshko et al., 2025).



Figure 5. *Sphagnum compactum*, close-up (photo by Ștefănuț M.-M.)

***Hamatocaulis vernicosus*** (Mitt.) Hedenäs

Even though drier, but an oligotrophic peatbog, Molhașul de la Râșca proved to be a suitable host for *H. vernisosus*, as it prefers such habitat conditions. We recorded for the first time this species in this site, 46.707762° N, 23.051411° E, 1065 m a.s.l., 6.10.2025, *det*. Ștefănuț S., Moroșanu A.-M., Ștefănuț M.-M. Also, we confirm the presence of *H. vernisosus* in Dâmbu Negru – La Pod site, 46.691190° N, 23.037044°E, 1079 m a.s.l., 7.10.2025, *det*. Ștefănuț S., Moroșanu A.-M., and Ștefănuț M.-M. (Figure 6).



Figure 6. *Hamatocaulis vernicosus,* close-up (photo by Moroșanu A.-M.)

Also, we found *Sphagnum angustifolium* (C.E.O. Jensen ex Russow) C.E.O. Jensen, *S. capillifolium* (Ehrh.) Hedw. (Figure 7), *S. divinum* Flatberg & Hassel (Figure 8), *S. girgenshonii* Russow, *S. inundatum* Russow (Figure 9), *S. medium* Limpr. (Figure 10), and *S. palustre* L. (Figure 11).



Figure 7. *Sphagnum capillifolium*, close-up (photo by Ștefănuț M.-M.)



Figure 8. *Sphagnum divinum*, close-up (photo by Ștefănuț S.)



Figure 9. *Sphagnum inundatum*, close-up (photo by Ștefănuț M.-M.)

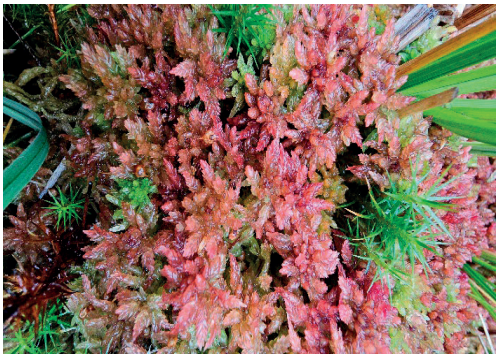


Figure 10. *Sphagnum medium*, close-up (photo by Ștefănuț S.)



Figure 11. *Sphagnum palustre*, close-up (photo by Ștefănuț M.-M.)

**Management recommendations**

The relatively dry conditions mentioned several decades ago by Pop (1947), also currently observed, alongside the decreasing abundance of peat-forming bryophytes, will materialise into a reduction of the peat accumulation and therefore a significant atmospheric carbon release. Bryophytes thus serve as key indicators for the structure and function of the peatland ecosystems (Vitt & House, 2021).

Furthermore, the vascular plant encroachment proved to be an early indicator of peatland degradation, a warning signal of warming- and drought-driven *Sphagnum* decline which accelerates ecosystem transition (Yu et al., 2026).

Considering all the anthropogenic and environmental pressures identified during the PeatRO Project (2015-2017), we consider that some priority conservation measures are

essential across short-, medium- and long-term periods, supported by a national legal framework, in order to protect the site and its biodiversity.

Short-term measures include grazing prohibition (fencing) and control of woody encroachment (manual removal), while medium-term measures include rehydration (dam construction and restoring the hydrological connectivity with Râșca Răchitiș mire CJ-017) and periodic monitoring efforts. In the long-term, the legal designation of Molhasul de la Râsca-Dealul Negru (CJ-016) as a Site of Community Importance (SCI) under the Natura 2000 umbrella or integration within Apuseni Natural Park (RONPA0004).

## CONCLUSIONS

Molhașul de la Râșca - Dealul Negru is remarkable as a key reference site for oligotrophic peat bogs in Apuseni Mountains, housing Romania`s unique *Sphagnum affine* (CR) population, alongside other rare bryophytes (*S. compactum*, *Hamatocaulis vernicosus* - VU).

This study inventories eleven *Sphagnum* species, bridging historical records while highlighting populations` resilience despite the PeatRO-identified pressures.

Current reports underscore the importance of continuous monitoring, given the anthropic pressures and habitat fragmentation.

Priority management measures recommended are short-term (grazing prohibition and control of woody encroachment), and medium-term (rehydration efforts and monitoring), which, alongside long-term legal measures (integration within Apuseni Natural Park RONPA0004 or designation as a SCI Natura 2000), will contribute to site conservation in a declining climate change context.

## ACKNOWLEDGEMENTS

This research work was carried out with the support of the Institute of Biology Bucharest, Romanian Academy, through the Projects RO1567-IBB03/2025 and RO1567-IBB06/2025, and was also financed from the "Restoration strategies of the deteriorated peatland ecosystems from Romania PeatRO)" Project through the EEA Grants and PDD project, SMIS 336936, "Enhancing knowledge of biodiversity through the implementation of the monitoring system for the conservation status of species and habitats of community interest in Romania and reporting under Article 17 of the Habitats Directive 92/43/EEC".

## REFERENCES

European Committee for the Conservation of Bryophytes. Red Databook of European Bryophytes; European Committee for the Conservation of Bryophytes: Trondheim, Norway, 1995; p. 291.

European Union. Council Directive 92/43/EEC of 21 May 1992 on the Conservation of Natural Habitats and of Wild Fauna and Flora (Habitats Directive), Anex IIb. Available at: https://eur-lex.europa.eu/eli/dir/1992/43/oj/eng (Accessed on 13 February 2026).

Frink, J. P., Coldea, G., Sass-Gyarmati, A., Pócs, T., & Jakab, G. (2017). *Juncus squarrosus* (Juncaceae) in Romania: its first certain occurrence and a new plant association for the Romanian vegetation. *Polish Botanical Journal, 62*(2), 233-240.

Györffy, I. & Péterfi M. (1919). Schedae et animadversions diversae ad "Bryophyta regni Hungariae exsicata, edita a sectione botanica Musei Nationalis Transsilvanici". Tom. II-III. No. 51-150 (Sphagna). *Botanikai Múzeum Füzetei,* 3, 43-74.

Hassel, K., Kyrkjeeide, M. O., Bengtson, F., Meleshko, O., & Flatberg, K. I. (2025). Nomenclatural inconsistencies in European species of *Sphagnum* subgen. *Subsecunda* with typification of *Sphagnum denticulatum* Brid. and *S. inundatum* Russow. *Lindbergia, 2025*, 1–12. https://doi.org/10.25227/linbg.027383.

Hodgetts, N. G. & Lockhart, N. (2020). *Checklist and country status of European bryophytes – update 2020*. Irish Wildlife Manuals, No. 123. National Parks and Wildlife Service, Department of Culture, Heritage and the Gaeltacht, Ireland.

Hodgetts, N. G., Söderström, L., Blockeel, T. L., Caspari, S., Ignatov, M. S., Konstantinova, N. A., Lockhart, N., Papp, B., Schröck, C., Sim-Sim, M., Bell, D., Bell, N. E., Blom, H. H., Bruggeman-Nannenga, M. A., Brugués, M., Enroth, J., Flatberg, K. I., Garilleti, R., Hedenäs, L., Holyoak, D. T., Hugonnot, V., Kariyawasam, I., Köckinger, H., Kučera, J., Lara, F. & Porley, R. D. (2020). An annotated checklist of bryophytes of Europe, Macaronesia and Cyprus. *Journal of Bryology, 42*(1), 1–116. https://doi.org/10.1080/03736687.2019.1694329.

Joosten, H., Tanneberger, F., & Moen, A. (2017). *Mires and peatlands of Europe: Status, distribution and conservation.* Schweizerbart Science Publishers.

Keane, B., Alderson, D. M., Clay, G. D., Evans, M. G., Field, C. D., Johnston, A., Limpens, J., McCarter, C. P. R., Overtoom, N., Ritson, J. P., Robroek, B. J. M., Rochefort, L., Shuttleworth, E. L., Telgenkamp, Y.,

Turetsky, M. R., & Waddington, J. M. (2025). The effects of drought on *Sphagnum* moss species and the implications for hydrology in peatlands. *New Phytologist*, *247*(5), 2003–2021. https://doi.org/10.1111/nph.70361.

Kuhry, P. & Vitt, D.H. (1996). Fossil carbon/nitrogen ratios as a measure of peat decomposition. *Ecology* 77: 271–275. https://doi.org/10.2307/2265676

Meleshko O., Kyrkjeeide M.O., Petlund H.T., Flatberg K.I., Eriksen L.B., Martin S.L.F., & Hassel K. (2025). Molecular species delimitation of *Sphagnum* subgenus *Subsecunda* in Europe. *Botanical Journal of the Linnean Society*, 1–13. https://doi.org/10.1093/botlinnean/boaf077.

PeatRO Project – "*Restoration strategies of the deteriorated peatland ecosystems from Romania (PeatRO)*" financed through the EEA Grants financial mechanism run by Iceland, Liechtenstein and Norway under the Programme RO02 – "Biodiversity and ecosystem services", Available at: https://www.ibiol.ro/peatro/en/index.html, (Accessed on 13 February 2026).

Pop, E. (1947). Semnalări de tinoave și de plante de mlaștini din România. III Mlaștinile din regiunea Călățele. *Buletinul grădinii botanice și al muzeului botanic dela Universitatea din Cluj* [Records of Peat Bogs and Marsh Plants in Romania. III. The Peat Bogs of the Călățele Region. Bulletin of the Botanical Garden and Botanical Museum of the University of Cluj], RO: Cartea Românească, 27: 65-79.

Pop, E. (1960). *Mlaştinile de turbă din Republica Populară Română.* [Peat Bogs in the Romanian People's Republic] Bucureşti, RO: Editura Academiei Republicii Populare Române.

Sabovljević, M. S., Tomović, G., Sabovljević, A. D., Kunev, G., Palpurina, S., Kutnar, L., Ilchev, I., Assyov, B., Djordjević, V., Papp, B., Dragićević, S., Szűcs, P., Stanković, S., Mežaka A., Shivarov, V. V., & Ștefănuț, M.-M. (2025). New records and noteworthy data of plants, algae and fungi in SE Europe and adjacent regions, 21. *Comprehensive Plant Biology,* *49*(1), 131–137. https://doi.org/10.2298/CPB2501131S.

Sass-Gyarmati, A., Jakab, G., Magyari-Sáska, Z., & Frink, J. P. (2025). Bryofloristic researches with new records in selected peatlands of the Apuseni Mountains (Western Romanian Carpathians). *AgroLife Scientific Journal, 14*(1): 172-190.

Scharlemann, J. P. W., Tanner, E. V. J., Hiederer, R., & Kapos, V. (2014). Global soil carbon: Understanding and managing the largest terrestrial carbon pool. *Carbon Management*, *5*(1), 81–91. https://doi.org/10.4155/cmt.13.77.

Ștefănuț, M.-M., Ștefănuț, S., & Moroșanu, A.-M. (2026). The conservation status of the Sphagnum species in Romania.*Plants, 15*(1), Article 140. https://doi.org/10.3390/plants15010140

Ștefănuț, S. & Goia, I. (2012). Checklist and Red List of Bryophytes of Romania. *Nova Hedwigia, 95*(1-2), 59–104. https://doi.org/10.1127/0029-5035/2012/0044

Ștefănut, S., Ștefănut, M.-M., Bită-Nicolae, C., Sahlean, T., Bîrsan, C.-C., Paica, I. C., Nicoară, G.-R., Helepciuc, F.-E., & Moroșanu, A.-M. (2025). Climate change projected effects on *Hamatocaulis vernicosus* occurrence in Romania. *Plants, 14*(21), Article 3354. https://doi.org/10.3390/plants14213354.

Ștefureac, T. I. (1958). Contribuțiuni la cunoașterea și răspândirea speciilor genului *Sphagnum* L. în bryoflora țării. *Contribuții Botanice*, 90-114. [Contributions to the Knowledge and Distribution of Species of the Genus *Sphagnum* L. in the Country's Bryoflora. Botanical Contributions, 90-114].

Vitt, D. H. & House, M. (2021). Bryophytes as key indicators of ecosystem function and structure of northern peatlands. *Bryophyte Diversity and Evolution, 43*(1), 253–264. https://doi.org/10.11646/bde.43.1.18.

Yu, M. J., Wang, T., & Wang, J. P. (2026). Vascular plant encroachment drives soil carbon loss and microbial assembly shifts across a successional gradient in a subtropical *Sphagnum*-dominated peatland. *Soil Ecology Letters, 8*, Article 260388. https://doi.org/10.1007/s42832-026-0388-5.

Scientific Papers. Series E. Land Reclamation, Earth Observation & Surveying, Environmental Engineering. Vol. XV, 2026
Print ISSN 2285-6064, CD-ROM ISSN 2285-6072, Online ISSN 2393-5138, ISSN-L 2285-6064

# GEOMETRY AND PHYSICS

**Cosmin-Constantin NIȚU**

University of Agronomic Sciences and Veterinary Medicine of Bucharest,
59 Marasti Blvd, District 1, Bucharest, Romania

Corresponding author email: cosmin.nitu@fifim.ro

***Abstract***

*All science is connected and the main connection is through the language of mathematics. Some of the most spectacular scientific results are obtained transdisciplinary. The relationship between geometry and physics is one of the most profound in science, evolving from a tool for measurement into the very language used to describe the fundamental laws of the universe. Geometry and physics are deeply intertwined disciplines, where geometry provides the formal language and structural framework for physical laws, while physics often drives the development of new mathematical theories. Differential geometry, for example, is essential for understanding gauge theories in particle physics and Riemannian geometry is fundamental in cosmology. Other branches of mathematics, such topology and Lie groups contribute to both classical and modern physics. In this article we investigate some geometric results obtained via physical methods and we emphasize some other links between geometry and physics.*

***Key words****: geometry, physics, string theory, theory of relativity, vectors.*

**"As far as the laws of mathematics refer to reality, they are not certain; and as far as they are certain, they do not refer to reality"- Albert Einstein, 1921**

## INTRODUCTION

The deep and enduring relationship between geometry and physics has played a central role in the development of modern scientific thought. From the early formulation of classical mechanics to the emergence of contemporary theories of spacetime, geometric concepts have provided a powerful language for describing the fundamental structure of physical reality. In particular, the use of mathematical frameworks such as Euclidean and non-Euclidean geometry has enabled physicists to model space, motion, and interactions with increasing precision and abstraction.

In classical physics, geometry was primarily viewed as a static and absolute stage upon which physical processes unfold. However, this perspective underwent a profound transformation with the advent of modern physics. The development of theories such as general relativity demonstrated that geometry is not merely a passive background, but an active and dynamic component of the physical universe. In this context, the curvature of spacetime becomes directly related to the distribution of mass and energy, illustrating a deep interplay between geometric structures and physical phenomena.

Geometry lies at the very heart of relativity, transforming it from a theory about forces into one about the structure of spacetime itself. In special relativity, the geometry is that of Minkowski space, where time and space are unified into a four-dimensional continuum with a non-Euclidean metric that determines invariant intervals between events. General relativity deepens this connection by describing gravity not as a force, but as the curvature of spacetime induced by mass and energy. The mathematical language of differential geometry-manifolds, metrics, geodesics, and curvature tensors-provides the framework for this description. Objects move along geodesics, which generalize the notion of straight lines to curved spacetime, and the Einstein field equations relate the geometric properties of spacetime directly to the physical distribution of matter and energy.

Geometry plays a central and indispensable role in string theory, where the fundamental objects are not point particles but one-dimensional strings whose vibrational modes depend sensitively on the geometry of the space in

which they propagate. In this framework, spacetime is typically extended beyond four dimensions, and the extra dimensions are assumed to form compact geometric spaces, often modelled by Calabi-Yau manifolds. The specific shape and topology of these compact spaces determine crucial physical properties, such as particle spectra and interaction strengths. Moreover, concepts from modern geometry-such as complex geometry, topology, and mirror symmetry-are deeply intertwined with the structure of string theory, revealing surprising dualities between seemingly distinct physical models. In this way, geometry is not merely a background setting, but an active ingredient that shapes the physical content of the theory itself (Steiner, 1992; Bailly et al., 2011; Rédei, 2020). This paper aims to explore fundamental connections between classical geometry and physics, highlighting how geometric methods contribute to our understanding of physical laws. By examining key theoretical frameworks and their applications, we seek to demonstrate that geometry is not only a mathematical tool, but also an essential foundation for the formulation and interpretation of physical theories.

## MATERIALS AND METHODS

### I. Vectors in geometry

In mathematics and physics, vectors are the same, as numerical support, but in physics they have an interpretation in some phenomena.

From the algebraic point of view, a *vector* is an element $x = (x_1, x_2, \dots, x_n) \in \mathbb{R}^n$. Vectors can naturally be added, substracted and multiplied by a scalar, in the same way as matrices, so $\mathbb{R}^n$ has a natural structure of vectorial space.

From the geometric point of view, a vector (Figure 1) is an "arrow" between two points (Berger, 1987).

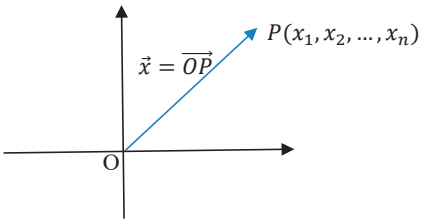



Figure 1. Vector

The Euclidian *scalar product* of two vectors $x, y \in \mathbb{R}^n$ is defined by the equality

$$x \cdot y = x_1 y_1 + x_2 y_2 + \cdots x_n y_n.$$

The Euclidian *norm* of a vector is

$$\|x\| = \sqrt{x_1^2 + x_2^2 + \cdots + x_n^2}.$$

*Remark 1.* $x^2 = x \cdot x = \|x\|^2$.

From *Cauchy-Buniakovski-Schwarz* inequality we have

$$|x \cdot y| \leq \|x\| \cdot \|y\|.$$

Thus, the angle between the two vectors is defined by

$$\cos\theta = \frac{x \cdot y}{\|x\| \cdot \|y\|} \in [-1, 1].$$

*Remark 2.* $x \perp y \Leftrightarrow x \cdot y = 0$.

### II. Mass centers

It is well known that the mass center G of system of material points in plane, of coordinates $P_i(x_i, y_i)$ in which there are concentrated the weights $m_i \geq 0,\ i = \overline{1,n}$ is given by (Solomentsev, 2001),

$$x_G = \frac{m_1 x_1 + m_2 x_2 + \cdots m_n x_n}{m_1 + m_2 + \cdots m_n}$$

and

$$y_G = \frac{m_1 y_1 + m_2 y_2 + \cdots m_n y_n}{m_1 + m_2 + \cdots m_n}$$

Therefore, considering the masses $m_i = m\ (constant)$ in the vertices of a triangle ABC, the mass center of the system

$$S = \{A(m), B(m), C(m)\}$$

has the same coordinates of the geometric mass center of the triangle ABC, which is the intersection of its medians:

$$x_G = \frac{x_A + x_B + x_C}{3}$$

and

$$y_G = \frac{y_A + y_B + y_C}{3}$$

The mass center of the plate ABC is $G(x_G, y_G)$, where.

$$x_G = \frac{\iint_{ABC} x\, \rho(x,y)\, dxdy}{\mu}$$

and

$$y_G = \frac{\iint_{ABC} y\,\rho(x,y)dxdy}{\mu}$$

where the mass of the plate ABC is

$$\mu = \iint_{ABC} \rho(x,y)\,dxdy.$$

***Definition 1.*** We consider the points $P_i(x_i, y_i) \in \mathbb{R}^2$, forming a polygon $P_1P_2 \dots P_n$. If

$$x_m = \min_{i=\overline{1,n}} x_i\ ,\ x_M = \max_{i=\overline{1,n}} x_i,$$

$$y_m = \min_{i=\overline{1,n}} y_i \text{ and } y_M = \max_{i=\overline{1,n}} y_i$$

then we call the rectangle

$$D_{P_1P_2\dots P_n} = [x_m, x_M] \times [y_m, y_M]$$

the ***rectangle cover*** of the polygon $P_1P_2 \dots P_n$.

## APPLICATIONS

### I. Applications of physics in geometry

***Theorem of Pythagoras*** (Figure 2)

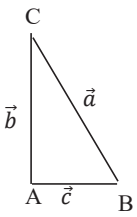



Figure 2. Rectangle triangle

By denoting $\overrightarrow{AB} = \vec{c},\ \overrightarrow{CB} = \vec{a}$ and $\overrightarrow{CA} = \vec{b}$, and $AB = c,\ BC = a\ and\ AC = b$ we have

$$\vec{b} + \vec{c} = \vec{a}\Big|^2$$

$$\vec{b}^2 + 2\underbrace{\vec{b}\cdot\vec{c}}_{0} + \vec{c}^2 = \vec{a}^2$$

$$\left\|\vec{b}\right\|^2 + \|\vec{c}\|^2 = \|\vec{a}\|^2$$

Thus, we obtain the theorem of Pythagoras.

$$b^2 + c^2 = a^2$$

***Stewart's relation*** (Figure 3)

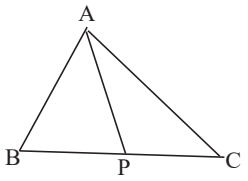



Figure 3. A scalene triangle with a cevian

By denoting $\overrightarrow{AB} = \vec{c},\ \overrightarrow{CB} = \vec{a}$ and $\overrightarrow{CA} = \vec{b}$, $\overrightarrow{AP} = \vec{p}$, and $AB = c, BC = a\ and\ AC = b$.

If $\frac{BP}{BC} = k \in (0,1)$, then $\frac{PC}{BC} = 1 - k$

$$\vec{c} = \vec{p} + k\vec{a}$$

$$\vec{b} = \vec{p} + (k-1)\vec{a}.$$

By raising the above equalities to square, we obtain

$$\vec{c}^2 = \vec{p}^2 + k^2\vec{a}^2 + 2k\vec{a}\vec{p}\ |\cdot(1-k)$$

$$\vec{b}^2 = \vec{p}^2 + (1-k)^2\vec{a}^2 + 2(k-1)\vec{a}\vec{p}\ |\cdot k$$

After the multiplication, we add the relation and it results an equivalent to Stewart's theorem:

$$AB^2 \cdot PC + AC^2 \cdot PB - BC^2 \cdot PA = PA \cdot PB \cdot PC$$

**Theorem 1**. Let ABC be a triangle with all the angles smaller than 120°. Then the point P in the plane of the triangle, for which the sum

$$PA + PB + PC = minimum$$

is the one which has the property that

$\widehat{APB} = \widehat{APC} = \widehat{BPC} = 120^o$, denoted by T
(the *Torricelli point* of the triangle - Figure 4)

*Proof*. We consider in the plane of the triangle ABC, assumed parallel to the ground, 3 threads tied at a point P, equal in length, passing through the points A, B and C and having the same weight $m$ at the other end. The forces $\overrightarrow{F_1}, \overrightarrow{F_2}$ and $\overrightarrow{F_3}$ that act on the point P are equal in module to the gravitational forces $\overrightarrow{G_1}, \overrightarrow{G_2}$ and $\overrightarrow{G_3}$.

This system of forces reaches the equilibrium state when its potential gravitational energy is minimum. If we denote by $h_1, h_2$ and $h_3$ the distances from the weights to the ground then the potential gravitational energy is

$$E_p = mgh_1 + mgh_2 + mgh_3$$
$$= mg(h_1 + h_2 + h_3)$$

Therefore, the sum

$h_1 + h_2 + h_3$ is minimum,

which implies that

$PA + PB + PC$ is minimum.

Also, at equilibrium

$$\overrightarrow{F_1} + \overrightarrow{F_2} + \overrightarrow{F_3} = \vec{0}$$

which proves that the angles between these forces are all equal with $120^o$ and ends the proof (Nicolescu & Boskoff, 1990).

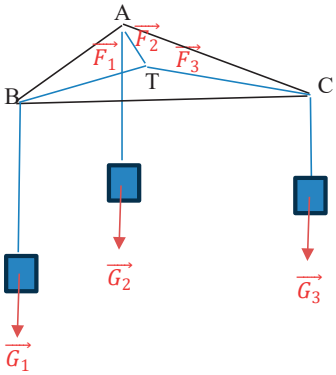



Figure 4. Torricelli's point

## II. Aplications of geometry in physics

**Theorem 2**. Considering a fixed triangle ABC in a plane, and the variable masses $m_1, m_2, m_3 \geq 0$, not all nulls, the mass center of the system $S = \{A(m_1), B(m_2), C(m_3)\}$ can be any point of the rectangle $D_{ABC}$ (Figure 5).

*Proof.*

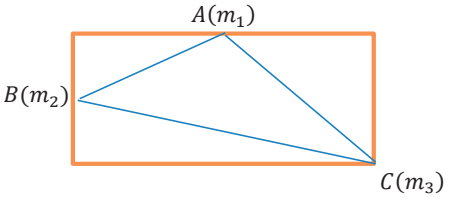



Figure 5. The rectangle cover of a triangle

We consider the points

$$A(x_1, y_1), B(x_2, y_2), C(x_3, y_3) .$$

Without loss of generality, we can assume that

$$m_1 + m_2 + m_3 = 1.$$

Otherwise, we can replace them with

$$m_i' = \frac{m_i}{m_1+m_2+m_3},$$

which have the property

$$m_1' + m_2' + m_3' = 1.$$

We observe that the mass center of the system $S = \{A(m_1), B(m_2), C(m_3)\}$ verifies the inequalities:

$$x_G = \frac{m_1x_1 + m_2x_2 + m_3x_3}{m_1 + m_2 + m_3} = m_1x_1 + m_2x_2 + m_3x_3 \geq (m_1 + m_2 + m_3)x_m = x_m$$

and also

$$x_G = \frac{m_1x_1 + m_2x_2 + m_3x_3}{m_1 + m_2 + m_3} = m_1x_1 + m_2x_2 + m_3x_3 \leq (m_1 + m_2 + m_3)x_M = x_M$$

Thus $x_G \in [x_m, x_M]$ and in the same way it can be shown that $y_G \in [y_m, x_M]$ .

So

$$G(x_G, y_G) \in [x_m, x_M] \times [y_m, y_M] = D_{ABC}.$$

Now we show that any point $(a, b) \in D_{ABC}$ is the mass center of a unique system $S = \{A(m_1), B(m_2), C(m_3)\}$, with $m_1 + m_2 + m_3 = 1$.

In this scope, we have to prove that the system of linear equations:

$$\begin{cases} m_1x_1 + m_2x_2 + m_3x_3 = a \\ m_1y_1 + m_2y_2 + m_3y_3 = b \\ m_1 + m_2 + m_3 = 1 \end{cases}$$

has a unique solution

$$(m_1, m_2, m_3).$$

This is true, by Cramer's rule, because the determinant of the system's matrix is

$$\Delta = \begin{vmatrix} x_1 & x_2 & x_3 \\ y_1 & y_2 & y_3 \\ 1 & 1 & 1 \end{vmatrix}$$

and $\Delta \neq 0$, as $Area\,(ABC) = \frac{1}{2}|\Delta| \neq 0$, which ends the proof.

**Theorem 3**. Considering a fixed triangle ABC in a plane, with the sides [AB], [AC] and [BC] made of homogenous materials of masses $\mu_1, \mu_2, \mu_3 \geq 0$, the mass center of the the triangle ABC can be any point of $D_{MNP}$, where M, N and P are the middle points of the sides [AB], [AC] and [BC].

*Proof.* From the physical point of view, the triangle ABC can be viewed as mass equivalent to the the system $S = \{M(\mu_1), N(\mu_2), P(\mu_3)\}$ and, by applying Theorem 1, we obtain the desired result.

**Theorem 4**. Let be a triangular plate ABC, where A, B and C are fixed points in a plane and we assume that the density function $\rho: ABC \to \mathbb{R}_+$ is integrable. Then, any point of $D_{ABC}$ can be the mass center of such a triangle plate.

*Proof.* The mass center of the plate ABC is $G(x_G, y_G)$, where

$$x_G = \frac{\iint_{ABC} x\,\rho(x,y)dxdy}{\mu}$$

$$y_G = \frac{\iint_{ABC} y\,\rho(x,y)dxdy}{\mu}$$

and the mass of the plate ABC is

$$\mu = \iint_{ABC} \rho(x,y)\,dxdy.$$

The triangle ABC, along with its interior, is a compact set in $\mathbb{R}^2$, as it is closed and bounded and we consider the projections

$x_m = \min pr_{Ox}ABC$ , $x_M = \max pr_{Ox}ABC$, and

$y_m = \min pr_{Oy}ABC$ , $y_M = \max pr_{Oy}ABC$

We have the inequalities:

$$x_m \le x \le x_M, \forall\, x \in \text{ABC}$$

Therefore, by integrating, we obtain

$$x_m = \frac{x_m \iint_{ABC} \rho(x,y)\,dxdy}{\mu} \le x_G$$

$$\le \frac{x_M \iint_{ABC} \rho(x,y)\,dxdy}{\mu} = x_m$$

Analogue,

$$y_m \le y_G \le x_M.$$

Now, for a fixed point $(a,b) \in D_{ABC}$, we consider the case from the Theorem 1, which ends the proof.

## CONCLUSIONS

The interplay between geometry and physics reveals a profound unity between mathematical abstraction and the description of the natural world. The results presented in this paper reinforce the idea that geometric frameworks are not merely auxiliary tools, but essential components in the formulation of physical theories. Through the analysis conducted, it becomes evident that physical phenomena can often be more deeply understood when interpreted through a geometric lens.

Moreover, the continued development of modern physics suggests that geometry will remain a fundamental pillar in future theoretical advancements. As new models and approaches emerge, the refinement of geometric methods will likely play a crucial role in addressing unresolved questions and extending the boundaries of current knowledge (Jost, 2009; Landi et al., 2017).

Ultimately, this article highlights the enduring significance of geometry in physics, emphasizing its capacity to unify concepts, clarify complex relationships, and provide insight into the understanding the structure of reality, because physics and geometry are inseparable.

## REFERENCES

Bailly, F., & Longo, G. (2011). *Mathematics and the natural sciences: the physical singularity of life.* World Scientific.

Berger, M. (1987). *Geometry I*, Springer Berlin, Heidelberg.

Einstein, A. (1921). *Geometry and Experience* (lecture).

Jost, J. (2009), *Geometry and Physics*, Springer Berlin, Heidelberg.

Nicolescu, L., & Boskoff, V. (1990). *Probleme practice de geometrie (Practical problems of geometry)*, Ed. Tehnică.

Rédei, M. (2020). On the tension between physics and mathematics, *J Gen Philos Sci 51*, pp. 411–425.

Solomentsev, E.D. (2001). Euclidean space. In *Encyclopedia of Mathematics,* EMS Press. encyclopediaofmath.org.

Landi, G., Rubtsov, V., & Sala, F. (2017). Interactions between Geometry and Physics: A Special Issue in Honor of Ugo Bruzzo's 60th Birthday. *Journal of Geometry and Physics*, 118, 1–3.

Steiner, M. (1992). Mathematical Rigor in Physics. In M. Detlefsen (Ed.), *Proof and Knowledge in Mathematics* (pp. 158–170). Routledge.

Scientific Papers. Series E. Land Reclamation, Earth Observation & Surveying, Environmental Engineering. Vol. XV, 2026
Print ISSN 2285-6064, CD-ROM ISSN 2285-6072, Online ISSN 2393-5138, ISSN-L 2285-6064

# THE USE OF FUNCTIONAL APPROACHES TO ANALYZE THE DIFFERENCES IN LAKE WATER MICROBIOME ASSEMBLAGES

**Paula POP, Vlad STOIAN, Bianca POP, Alexandra GHEORGHIȚĂ, Roxana VIDICAN**

Department of Microbiology, Faculty of Agriculture, University of Agricultural Sciences and Veterinary Medicine Cluj-Napoca, 3-5 Calea Mănăștur, Cluj-Napoca, Romania

Corresponding author email: vlad.stoian@usamvcluj.ro

***Abstract***

*Clean water and sanitation are one of the Sustainable development goals of the United Nations, and this resource needs constant monitoring due to its importance for human health. The aim of this paper was to assess the potential use of functional microbiome method to identify the geographical differences in functional microbiome in Lake Vârșolț, from Sălaj county. Basal community showed small-daily changes due to incubation, which represents a constant activity for the general microbial population. Guild activities presented a 50-100% increase each 24 hours, which sustain both the phenomenon of adaptation to substrate and proliferation due to favorable conditions. In terms of separate activities for functional groups, a different pattern of activity increases was observed for the entire 96 period of incubation. In terms of total microbial activity, the growth curves were 4-5 times in 96 hours, which represents an efficient indicator for short-term monitoring potential microbial development. The analysis of the entire database showed that functional profile is a suitable tool that enables the detection of difference in the microbiome assemblage and the forecasting of functional shifts in the community.*

***Key words****: activity patterns, functional microbiome, geographical distribution, guild and group assemblage, water monitoring.*

## INTRODUCTION

Microbial communities are essential components of aquatic ecosystems, playing a major role in global energy fluxes and biogeochemical cycles (Falkowski et al., 2008). They exhibit high species and genetic diversity, which makes them sensitive to environmental disturbances (Amann & Rossello-Mora, 2016; Levi et al., 2017; Ren et al., 2017). In lakes, the balance of external nutrient loading influences microbial functional genes and associated metabolic processes (Liu et al., 2020).

Microorganisms populate nearly all aquatic ecosystems and are usually among the first to respond to physical and chemical disturbances. As a result, changes in the microbial community structure frequently led to broader changes in the overall health and stability of the environment.

One of the most important services performed by microbial communities in aquatic ecosystems, is the regulation of energy flows and biogeochemical cycles, with bacteria playing a central role. The microorganisms in these ecosystems exhibit high diversity and considerable biomass (Whitman et al., 1998; Battin et al., 2003; Lennon & Locey, 2016).

In lake ecosystems, most microorganisms are found in benthic biofilms, where they play a key role in organic matter mineralization, nutrient, and contaminant transformation (Schiller et al., 2007; Findlay, 2010; Buchkowski et al., 2015). Microbial communities exhibit high genetic diversity, and their taxonomic and functional changes are visible in the flow of ecosystem processes (Newton et al., 2011; Ylla et al., 2014; Hayden & Beman, 2016; Peter & Sommaruga, 2016).

Community-level physiological profiling (CLPP) is a proven approach for identifying spatial and temporal variations in aquatic microbial communities (Nowak et al., 2025; Torrús-Castillo et al., 2026). In the studies of applied ecology, EcoPlates™ are commonly used to assess the stability of microbial communities and detect functional changes triggered by environmental disturbances.

The aim of this paper is to analyze the structure of the functional microbiome within a lake ecosystem based on the community-level physiological profiling approach. The

hypotheses tested were proposed to answer a series of research questions:
i) Is there a difference between functional microbiomes due to geographical distance within the same ecosystem?
ii) Can continuous monitoring of functional activity reveal changes in the community stability?
iii) Do the dominant functional groups show shifts within the community during the incubation time?

## MATERIALS AND METHODS

EcoPlate™ contains 31 organic carbon substrates and a control well, each in three replicates, with redox-sensitive tetrazolium dye, used for community-level physiological profiling (CLPP) of metabolically active heterotrophic bacteria (Stefanowicz et al., 2006). Key CLPP indicators include average well color development (AWCD), which reflects total metabolic activity, and the Sum of activities, which shows both the physiological diversity of microbial communities and the ability of a microbiome to metabolize different substrates (Kenarova et al., 2014; Muniz et al., 2014). Three sampling points were chosen in the lake and analyzed with the EcoPlate tool to score the difference between functional microbiomes recorded on a 96 hour incubation period.
The guilds used in the description of microbial metabolic activity follow the proposal of Stoian et al. (2022). The list of them is separated in 5 large guilds; CX - Carboxylic & acetic acids; AA - Amino acids; CH - Carbohydrates; PX - Polymers; AM - Amines/amides to which is added the SUM, as total metabolic activity; Water - bazal respiration; AWCD-average well color development.
All data were analysed with RStudio (R Core Team, 2024), with a flow of tests created to explore the trends of activity and community assemblage from a general view to an in-depth one. Data from 24, 48, 72 and 96 hours were supposed to a Principal Component Analysis (PCA), in "vegan" package, for the assessment of community stability and differences between sampling points (Oksanen et al., 2022). The ordinations of microbiome and environmental fitting of guild vectors were projected to determine the links between guilds and community stability. A second step for data analysis was performed with "agricolae" package, from which ANOVA and LSD tests were used to record the significant differences between sampling points in terms of guild activity and the total activity (de Mendiburu, 2023). The plate was read continuously every 24 hours up to 120 hours using a BioTek Epoch plate reader at an optical density of 590 nm.
The third step in data analysis was to extract the group with the highest activity within each guild, separately for each sampling point and incubation period. This procedure was performed to create a pattern analysis that can be developed further into a screening for indicator groups at different incubation time.
Biolog EcoPlates were selected for their power to characterize the entire microbial community in environmental matrices and providing insights on spatio-temporal changes and the kinetics of microbiome response to a set of standardized substrates (Zhao et al., 2021; Angelova et al., 2025).

## RESULTS AND DISCUSSIONS

Principal Component Analysis (PCA) highlighted a clear functional differentiation between the three sampling points (W1, W2, and W3), demonstrating the ability of functional microbiome profiling to differentiate geographical variations within the lake (Figure 1, Table 1). The first principal component (PC1) explained most of the variability and distinctly separated the samples from W3 from those from W1 and W2, suggesting the existence of a functional ensemble specific to this area and a different pattern of substrate use. W1 and W2 showed relatively similar profiles, being positioned in the negative region of PC1, but a moderate separation on PC2 indicates subtle differences in the dynamics of microbial activities. The more pronounced dispersion of samples from W1 suggests higher functional variability, while the compact grouping of samples from W2 indicates a more stable structure. The vectors associated with the model highlight the differentiated contribution of certain metabolic activities to the total explained variance (95%). Both Sum and CH vectors were oriented parallel with Axis 1, showing a high degree of importance of CH guild within the

entire community activities. At the opposite, AA vector associated with W3 show an angle toward PC1, which indicate the potential of this guild to reshape the entire microbiome and gain a higher importance within community.

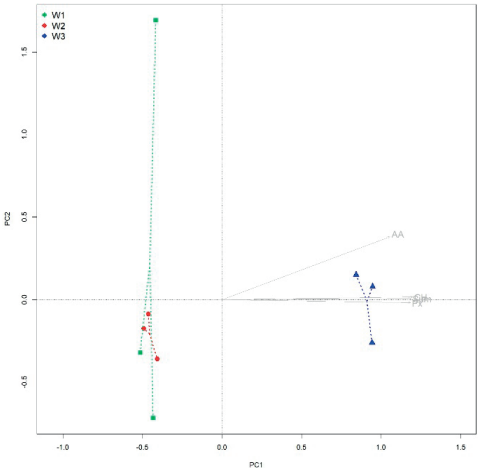



Figure 1. PCA projection of microbial communities and guild vectors at 24 h of incubation

Table 1. Vector fitting and importance on PCA projection (24 h)

| | PC1 | PC2 | r2 | p.val | |
|---|---|---|---|---|---|
| Sum | 0.99999 | 0.00518 | 0.9795 | 0.002 | ** |
| PX | 0.99987 | -0.01593 | 0.974 | 0.005 | ** |
| CH | 0.99992 | 0.01284 | 0.9973 | 0.001 | *** |
| CX | 0.64094 | -0.76759 | 0.05 | 0.887 | |
| AA | 0.94095 | 0.33854 | 0.875 | 0.002 | ** |
| AM | -0.58727 | -0.80939 | 0.6007 | 0.066 | . |

Note: * - significant; ** - distinct significant; *** - very significant. Variance explained by Axis 1=92.64% and Axis 2=2.76%.

PCA analysis highlights a clear separation of the three sampling points along the PC1 axis (Figure 2, Table 2). W3 is positioned in the positive region of PC1 and is associated with variables oriented in the same direction (particularly AM, AA, PX, and Sum), suggesting increased intensity of metabolic activities corresponding to these functional groups. In contrast, W1 and W2 are located in the negative region of PC1, indicating functional profiles distinct from W3. The separation on PC2 further differentiates W1 (negative values) from W2 (positive values), suggesting differences in the dynamics of microbial activities between these two locations. Longer vectors indicate a significant contribution of certain metabolic activities to the total variation explained by the model, confirmed by the existence of pronounced functional heterogeneity between the analyzed points.

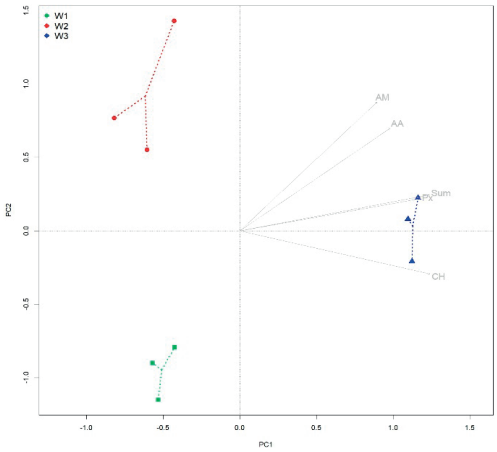



Figure 2. PCA projection of microbial communities and guild vectors at 48 h of incubation

Table 2. Vector fitting and importance on PCA projection (48 h)

| | PC1 | PC2 | r2 | p.val | |
|---|---|---|---|---|---|
| Sum | 0.98097 | 0.19416 | 0.9571 | 0.001 | *** |
| PX | 0.983 | 0.18362 | 0.8653 | 0.011 | * |
| CH | 0.97276 | -0.23183 | 0.9766 | 0.001 | *** |
| CX | 0.63794 | 0.77009 | 0.5259 | 0.103 | |
| AA | 0.81389 | 0.58102 | 0.8735 | 0.001 | *** |
| AM | 0.7142 | 0.69994 | 0.9454 | 0.001 | *** |

Note: * - significant; ** - distinct significant; *** - very significant. Variance explained by Axis 1=77.68% and Axis 2=11.62%.

The variance explained by the two axis is 89%, indicating both the dispersion of data in the ordination plan and the amplification of differences between communities. The Sum of activities and PX guild have coupled vectors, indicating the potential perturbation role of this guild within community. AM and AA vectors are oriented toward the higher part of the ordination and their opposite direction against W2 and W1 indicate the reduced activity within community. CH vector makes an angle with these two guilds, with a lower trend of direction. This guild is associated with one of the W3 points, indicating the potential arise of a different assembled community. Both W1 and

W3 show community similarity and stability, due to the low dispersion of points, and only small differences due to the group-activity pattern.

In this analysis, the separation on PC1 is even more pronounced, with W3 showing a clear separation in the positive area of the axis and correlated with the variables AA, AM, and PX, indicating a specific functional profile characterized by metabolic activity oriented to these substrates. W1 and W2 are grouped in the negative area of PCA but show a clear separation through PC1 and a corner position (Figure 3, Table 3).

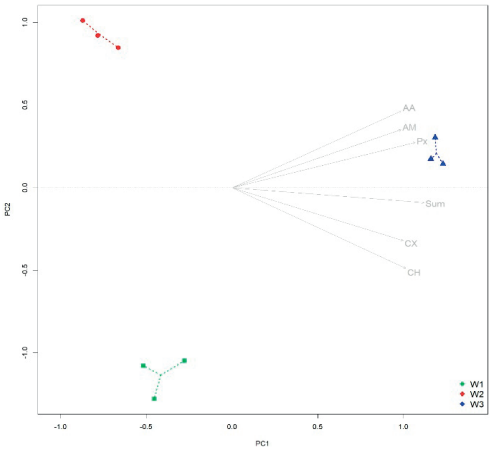



Figure 3. PCA projection of microbial communities and guild vectors at 72 h of incubation

Table 3. Vector fitting and importance on PCA projection (72 h)

| | PC1 | PC2 | r2 | p.val | |
|---|---|---|---|---|---|
| Sum | 0.9968 | -0.07997 | 0.9949 | 0.001 | *** |
| PX | 0.96861 | 0.24857 | 0.9584 | 0.012 | * |
| CH | 0.90068 | -0.43448 | 0.9954 | 0.001 | *** |
| CX | 0.95199 | -0.30614 | 0.8663 | 0.001 | *** |
| AA | 0.90497 | 0.42548 | 0.9366 | 0.001 | *** |
| AM | 0.94205 | 0.33549 | 0.8627 | 0.018 | * |

Note: * - significant; ** - distinct significant; *** - very significant. Variance explained by Axis 1=66.78% and Axis 2=18.58%.

The 85% of variance explained by the entire PCA is associated with the increased general activity (Sum vector), while all three communities became stable. The differences between communities are more visible due to their position in different quadrants. In the upper part of the ordination, AA, AM and PX guilds are associated within the same community, and their position makes them the candidates for W3 shift. All the guild vectors have an orientation against W1 and W2, indicating that a mix of group activities are responsible for the community specific assemblage.

PC1 represents the central axis of geographical differentiation, clearly separating W3 from W1 and W2 (Figure 4, Table 4). The samples from W3 are strongly positively correlated with the AA and AM, suggesting a functional profile characterized by increased metabolic activity. W1 and W2 are in the negative section of PC1, but they're different on PC2, showing extra variation in functional dynamics. W1 shows more negative values on PC2, while W2 is in the positive area, indicating a different structure of microbial activities. The direction of the vectors in the positive area of PC1 confirms the important role of certain functional groups in the spatial separation of microbial communities.

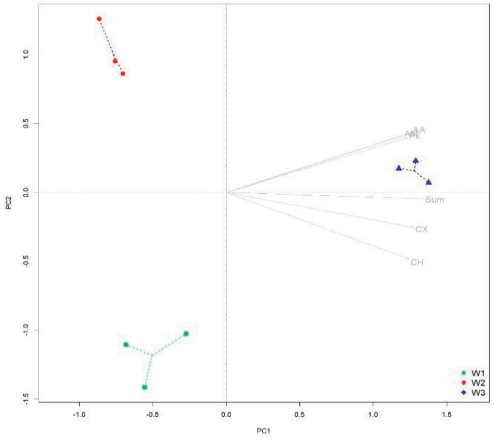



Figure 4. PCA projection of microbial communities and guild vectors at 96 h of incubation

At plateau phase, the variance explained reach 82%, with the Sum vector being the only very significant one. This vector is closed to PC1, in the middle of the angel formed by AA+AM and CH+CX vectors. This indicate that each of the two community types can be observed during the continuous evolution of the microbiome. While AA and AM are closed to each other, indicating a correlated evolution of this community type, in the case of CX and CH, a small angle can be observed, which indicates a direction to one of these guilds.

Table 4. Vector fitting and importance on PCA projection (96 h)

| | PC1 | PC2 | r2 | *p* - value | |
|---|---|---|---|---|---|
| Sum | 0.9994 | -0.03458 | 0.9962 | 0.001 | *** |
| PX | 0.95188 | 0.30647 | 0.9248 | 0.005 | ** |
| CH | 0.93178 | -0.36302 | 0.9817 | 0.001 | *** |
| CX | 0.98066 | -0.19573 | 0.9333 | 0.011 | * |
| AA | 0.94472 | 0.32789 | 0.98 | 0.002 | ** |
| AM | 0.94688 | 0.3216 | 0.8845 | 0.007 | ** |

Note: * - significant; ** - distinct significant; *** - very significant. Variance explained by Axis 1=65.54% and Axis 2=16.51%

In the initial phase (Table 5), all groups (CH, CX, PX, AA, AM) show low values, which are characteristic of the period of substrate adaptation. CH and AA have more significant contributions in W1 and W2, indicating initial activity focused on the use of more easily metabolizable compounds. CX shows moderate variability between samples, with no significant differences, while PX and AM record the lowest values, suggesting limited activity of these guilds in the initial phase. W2 has the highest total value (SUM), which suggests a community with more active initial metabolic potential, but the overall.

Table 5. General and guild activity at 24 h of incubation

| Sample | CH | CX | PX | AA | AM | SUM |
|---|---|---|---|---|---|---|
| W1 | 0.27±0.16 b | 0.06±0.03 a | 0.14±0.08 b | 0.21±0.12 b | 0.13±0.07 a | 0.51±0.29 b |
| W2 | 0.33±0.19 b | 0.34±0.19 a | 0.17±0.10 b | 0.20±0.11 b | 0.01±0.00 a | 0.86±0.49 b |
| W3 | 0.23±0.13 a | 0.13±0.07 a | 0.12±0.07 a | 0.14±0.08 a | 0.03±0.02 a | 0.53±0.30 a |

After 48 hours, all guilds show significant increases, indicating the start of the proliferation phase (Table 6). CH and CX are dominant, especially in W3, where they show the highest values and contribute significantly to the increase in total activity. PX and AA also show a clear intensification of activity, suggesting an expansion of the range of substrates used. The AM guild, although still lower in number than the others, begins to grow more visible, suggesting the activation of additional metabolic pathways. The differences between samples become clearer, with W3 highlighted by a higher functional response.

Table 6. General and guild activity at 48 h of incubation

| Sample | CH | CX | PX | AA | AM | SUM |
|---|---|---|---|---|---|---|
| W1 | 6.52±0.36b | 4.56±0.26a | 1.96±0.27b | 2.74±0.11b | 0.49±0.10b | 16.2±0.84b |
| W2 | 4.43±0.59c | 5.47±0.43a | 2.38±0.31b | 4.07±0.95ab | 1.27±0.23a | 17.6±2.19b |
| W3 | 11.0±0.16a | 5.68±0.36a | 4.04±0.15a | 5.62±0.20a | 1.71±0.17a | 28.0±0.27a |

Note: Different letters after means ± SE indicate significant differences at $p<0.05$ based on LSD test.

CH and CX remain dominant in the functional profile, especially in W3, where values are significantly higher compared to W1 and W2 (Table 7). PX and AA show constant increases, suggests a diversification of metabolism and a more complex use of available substrates. AM becomes better represented, which may indicate microbial succession processes and trophic interactions. W2 shows the lowest values for most groups, suggesting a limited metabolic capacity.

Table 7. General and guild activity at 72 h of incubation

| Sample | CH | CX | PX | AA | AM | SUM |
|---|---|---|---|---|---|---|
| W1 | 8.94±0.34b | 7.25±0.13b | 2.39±0.28b | 3.54±0.09b | 0.71±0.20b | 22.8±0.84b |
| W2 | 4.01±0.55c | 6.02±0.29b | 2.66±0.25b | 4.48±0.21b | 1.03±0.19b | 18.2±0.85c |
| W3 | 12.4±0.13a | 8.71±0.52a | 5.63±0.15a | 6.95±0.46a | 2.52±0.25a | 36.2±0.76a |

At 96 hours, the highest values for all groups are observed, and the differences between samples are most evident at this stage (Table 8). W3 has the highest values for CH, CX, PX, AA, and AM, which indicates a higher capacity to utilize different types of substrates. CH and CX remain the dominant groups, but PX, AA, and especially AM also increase significantly, indicating a more advanced microbial community structure and a more diversified use of resources. W1 has an intermediate level of activity, and W2 has the lowest values for most groups. The evolution of groups over time shows consistent functional differences between sampling locations and confirms the value of group analysis in the determination of variations in the microbial community (Table 9).

Table 8. General and guild activity at 96 h of incubation

| Sample | CH | CX | PX | AA | AM | SUM |
|---|---|---|---|---|---|---|
| W1 | 10.1±0.57b | 8.82±0.12b | 2.78±0.39b | 4.61±0.28c | 0.81±0.28b | 27.1±1.31b |
| W2 | 5.70±0.79c | 7.38±0.27c | 3.56±0.46b | 5.51±0.14b | 1.28±0.37b | 23.4±0.85c |
| W3 | 15.1±0.49a | 11.9±0.36a | 6.61±0.15a | 8.85±0.24a | 3.16±0.25a | 45.6±0.22a |

Table 9. Group-activity pattern analysis in the 24-96 time range

| | W1 | | | | | W2 | | | | | W3 | | | | |
|---|---|---|---|---|---|---|---|---|---|---|---|---|---|---|---|
| **Guild** | **CH** | **CX** | **P** | **AA** | **AM** | **CH** | **CX** | **P** | **AA** | **AM** | **CH** | **CX** | **P** | **AA** | **AM** |
| 24 h | CH3 | CX9 | P1 | AA2 | AM2 | CH3 | CX9 | P2 | AA2 | AM2 | CH4 | CX6 | P4 | AA4 | AM2 |
| 48 h | CH8 | CX2 | P1 | AA1 | AM2 | CH7 | CX2 | P2 | AA2 | AM2 | CH7 | CX3 | P4 | AA2 | AM2 |
| 72 h | CH8 | CX2 | P1 | AA1 | AM2 | CH8 | CX3 | P2 | AA2 | AM2 | CH7 | CX3 | P4 | AA2 | AM1 |
| 96 h | CH8 | CX2 | P2 | AA2 | AM2 | CH8 | CX3 | P2 | AA1 | AM2 | CH7 | CX3 | P4 | AA2 | AM1 |

Seasonal stratification is a major factor influencing the dynamics of microbial communities, especially in deep lakes, where temperature, oxygen, and nutrient gradients form distinct ecological niches (Winder & Sommer, 2012; Liu & Santamarina, 2024). Microbial communities are influenced by both deterministic, niche-based processes and stochastic mechanisms, including environmental selection and ecological drift (Chase & Myers, 2011; Stegen et al., 2013; Zhang et al., 2021).

Flowing water systems (rivers – lotic ecosystems) and standing water systems (lakes – lentic ecosystems) are essential components of terrestrial aquatic ecosystems, playing a major role in global biogeochemical processes (Maavara et al., 2020; Battin et al., 2023).

Hydrological factors, such as flow rates, water levels, retention times, and precipitation, influence the nutrient cycle and, shaping the structure of bacterial communities, can lead to biodiversity decline (Shabarova et al., 2021; Zhang et al., 2021; Chen et al., 2023).

## CONCLUSIONS

The study highlights that functional analysis of the aquatic microbiome is an effective tool for identification of spatial differences between microbial communities in lake ecosystems. Results from CLPP analysis with EcoPlate™ showed distinct metabolic profiles between the sample points (W1, W2, and W3). PCA analysis revealed a distinct separation of samples, especially from W3, which indicates the existence of a functional profile specific to this location and a different pattern of organic substrate utilization. While points W1 and W2 showed relatively similar functional profiles, W3 was characterized by higher metabolic intensity and a greater capacity to utilize different types of substrates.

The functional dynamics of microbial communities showed a progressive increase in metabolic activity during incubation. In the initial stage, the values of all functional groups (CH, CX, PX, AA, and AM) were low, which reflects the period of adaptation of microorganisms to the substrate. After 24 hours, a significant increase in metabolic activity was observed, mainly for the CH and CX groups, which were dominant in the functional profile. As incubation progressed, all groups showed a gradual increase in metabolic activity, suggesting a diversification of metabolism and a more complex use of available resources.

At 96 hours, the highest values were recorded for all functional groups, with differences between sampling points being more evident. W3 showed the highest metabolic activity and substrate utilization capacity, which indicates a more active and diverse microbial community. In contrast, W2 recorded the lowest values for most functional groups, suggesting a lower metabolic capacity or a faster stabilization of microbial activity.

The results show that the analysis of functional groups and substrate utilization can highlight important differences between microbial communities in different areas of the lake. These methods are useful for understanding the metabolic dynamics and adaptation of the microbiome to environmental conditions, confirming the value of functional analyses for monitoring spatial variations and ecological changes in aquatic ecosystems.

The results support the fact that functional analysis is an effective tool for identifying spatial heterogeneity and monitoring potential functional changes in microbial communities in lake ecosystems.

## ACKNOWLEDGEMENTS

This paper is part of a PhD study in the thematic area of *"Microbiological quality of water and its role in ensuring the safety of agri-food products"*, conducted by the first author P.P., under the coordination of Prof. dr. Roxana Vidican (R.V.).

## REFERENCES

Amann, R., & Rossello-Mora, R. (2016). Reply to "The underestimation of global microbial diversity". *mBio*, *7*(5), e01623-16.

Angelova, B., Traykov, I., Boteva, S., Tsvetkov, M., & Kenarova, A. (2025). Bacterial Metabolic Activity of High-Mountain Lakes in a Context of Increasing Regional Temperature. *Microorganisms*, *13*(6), 1375.

Battin, T. J., Kaplan, L. A., Denis Newbold, J., & Hansen, C. M. (2003). Contributions of microbial biofilms to ecosystem processes in stream mesocosms. *Nature*, *426*, 439–442.

Battin, T. J., Lauerwald, R., Bernhardt, E. S., Bertuzzo, E., Gener, L. G., Hall Jr, R. O., Hotchkiss, E.R., Maavara, T., Pavelsky, T.M., Ran, L., Raymond, P., Rosentreter, J.A., & Regnier, P. (2023). River ecosystem metabolism and carbon biogeochemistry in a changing world. *Nature*, *613*, 449–459.

Buchkowski, R. W., Schmitz, O. J., & Bradford, M. A. (2015). Microbial stoichiometry overrides biomass as a regulator of soil carbon and nitrogen cycling. *Ecology*, *96*(4), 1139–1149.

Chase, J. M., & Myers, J. A. (2011). Disentangling the importance of ecological niches from stochastic processes across scales. *Philosophical transactions of the Royal Society of London. Series B, Biological sciences, 366*(1576), 2351–2363.

Chen, Y., Xia, R., Jia, R., Hu, Q., Yang, Z., Wang, L., Zang, K., Wang, Y., & Zhang, X. (2023). Flow backward alleviated the river algal blooms. *Water Research, 245*, 120593.

de Mendiburu F. (2023). *Agricolae: Statistical Procedures for Agricultural Research* (Version1.3-7) [R package]. https://CRAN.R-project.org/package=agricolae

Falkowski, P. G., Fenchel, T., & Delong, E. F. (2008). The microbial engines that drive Earth's biogeochemical cycles. *Science, 320*, 1034–1039.

Findlay, S. (2010). Stream microbial ecology. *Journal of the North American Benthological Society*, *29*(1), 170–181.

Hayden, C. J., & Beman, J. M. (2016). Microbial diversity and community structure along a lake elevation gradient in Y osemite N ational P ark, C alifornia, USA. *Environmental Microbiology*, *18*(6), 1782–1791.

Kenarova, A., Radeva, G., Traykov, I., & Boteva, S. (2014). Community level physiological profiles of bacterial communities inhabiting uranium mining impacted sites. *Ecotoxicology and Environmental Safety, 100*, 226–232.

Lennon, J. T., & Locey, K. J. (2016). The underestimation of global microbial diversity. *mBio 7*, e01623-16.

Levi, P. S., Starnawski, P., Poulsen, B., Baattrup-Pedersen, A., Schramm, A., & Riis, T. (2017). Microbial community diversity and composition varies with habitat characteristics and biofilm function in macrophyte-rich streams. *Oikos*, *126*(3), 398–409.

Liu, M., Park, J., & Santamarina, J. C. (2024). Stratified water columns: homogenization and interface evolution. *Scientific Reports*, *14*(1), 11453.

Liu, Y., Ren, Z., Qu, X., Zhang, M., Yu, Y., Zhang, Y., & Peng, W. (2020). Microbial community structure and functional properties in permanently and seasonally flooded areas in Poyang Lake. *Scientific Reports*, *10*(1), 4819.

Maavara, T., Chen, Q., Van Meter, K., Brown, L. E., Zhang, J., Ni, J., & Zarfl, C. (2020). River dam impacts on biogeochemical cycling. *Nature Reviews Earth & Environment*, *1*(2), 103–116.

Muniz, S., Lacarta, J., Pata, M. P., Jimenez, J. J., & Navarro, E. (2014). Analysis of the diversity of substrate utilisation of soil bacteria exposed to Cd and earthworm activity using generalised additive models. *PLoS One*, 9(1), e85057.

Newton, R. J., Jones, S. E., Eiler, A., McMahon, K. D., & Bertilsson, S. (2011). A guide to the natural history of freshwater lake bacteria. *Microbiology and Molecular Biology Reviews*, *75*(1), 14–49.

Nowak, A., Pacwa-Płociniczak, M., & Marchlewicz, A. (2025). The effect of long-term exposure to diatrizoate on microbial communities in activated sludge. *Scientific Reports*, *15*(1), 17441

Oksanen, J., Simpson, G., Blanchet, F., Kindt, R., Legendre, P., Minchin, P., O'Hara. R., Solymos, P., Stevens, M., Szoecs. E., Wagner, H., Barbour, M., Bedward, M., Bolker, B., Borcard, D., Carvalho, G., Chirico, M., De Caceres, M., Durand, S., Evangelista, H., FitzJohn, R., Friendly, M., Furneaux, B., Hannigan, G., Hill, M., Lahti, L., McGlinn, D., Ouellette, M., Ribeiro Cunha, E., Smith, T., Stier, A., Ter Braak, C., Weedon, J. (2022). Vegan: Community Ecology Package. R package version 2.6-4, https://CRAN.R-project.org/package=vegan.

Peter, H., & Sommaruga, R. (2016). Shifts in diversity and function of lake bacterial communities upon glacier retreat. *The ISME Journal*, *10*(7), 1545–1554.

R Core Team (2024). *R: A Language and Environment for Statistical Computing*. R Foundation for Statistical Computing, Vienna, Austria. https://www.R-project.org/

Ren, Z., Wang, F., Qu, X., Elser, J. J., Liu, Y., & Chu, L. (2017). Taxonomic and functional differences between microbial communities in Qinghai Lake and its input streams. *Frontiers in Microbiology, 8*, 2319.

Schiller, D. V., Martí, E., Riera, J. L., & Sabater, F. (2007). Effects of nutrients and light on periphyton biomass and nitrogen uptake in Mediterranean streams with contrasting land uses. *Freshwater Biology*, *52*(5), 891–906.

Shabarova, T., Salcher, M. M., Porcal, P., Znachor, P., Nedoma, J., Grossart, H. P., Sed'a, J., Hejzlar, J., & Šimek, K. (2021). Recovery of freshwater microbial communities after extreme rain events is mediated by

cyclic succession. *Nature Microbiology*, 6(4), 479–488.

Stefanowicz, A. (2006). The Biolog plates technique as a tool in ecological studies of microbial communities. *Polish Journal of Environmental Studies*, *15*(5).

Stegen, J. C., Lin, X., Fredrickson, J. K., Chen, X., Kennedy, D. W., Murray, C. J., Rockhold, M.L., & Konopka, A. (2013). Quantifying community assembly processes and identifying features that impose them. *The ISME Journal*, *7*(11), 2069–2079.

Stoian, V., Vidican, R., Florin, P., Corcoz, L., Pop-Moldovan, V., Vaida, I., Vâtcă, S.D., Stoian, V.A., & Pleșa, A. (2022). Exploration of soil functional microbiomes A concept proposal for long-term fertilized grasslands. *Plants, 11*(9), 1253.

Torrús-Castillo, M., Macan, G. P., Landa, B. B., & Gómez, J. A. (2026). Effect of Regenerative Agriculture on Soil Health, Ecosystem Services and Economic Performance in a Commercial Olive Orchard in Southern Spain. *Soil Use and Management*, *42*(1), e70181.

Whitman, W. B., Coleman, D. C., & Wiebe, W. J. (1998). Prokaryotes: the unseen majority. *Proceedings of the National Academy of Sciences*, *95*(12), 6578-6583.

Winder, M., & Sommer, U. (2012). Phytoplankton response to a changing climate. *Hydrobiologi*a, *698*, 5–16.

Ylla, I., Canhoto, C., & Romaní, A. M. (2014). Effects of warming on stream biofilm organic matter use capabilities. *Microbial Ecology*, *68*(1), 132–145.

Zhang, L., Yin, W., Wang, C., Zhang, A., Zhang, H., Zhang, T., & Ju, F. (2021). Untangling microbiota diversity and assembly patterns in the world's largest water diversion canal. *Water Research, 204*, 117617.

Zhao, Q., Zhou, K., Zhang, F., Zhao, Y., Sun, H., & Xie, F. (2021). Effect of aquaculture water eutrophication on color development in Biolog EcoPlates. *Aquaculture International*, *29*(1), 373–386.

Scientific Papers. Series E. Land Reclamation, Earth Observation & Surveying, Environmental Engineering. Vol. XV, 2026
Print ISSN 2285-6064, CD-ROM ISSN 2285-6072, Online ISSN 2393-5138, ISSN-L 2285-6064

# ASSESSING STUDENTS' COMPETENCIES IN ADVANCED TECHNOLOGIES FOR A SUSTAINABLE GREEN FUTURE IN ENERGY, AGRICULTURE, AND INDUSTRY

**Nicoleta RADU[1, 2], Mihai Dan CARAMIHAI[3], Francisca BLANQUEZ CANO[4], Adrian SILVA[5], Narcisa BABEANU[1], Laura IOSUB[1], Razvan Ionut TEODORESCU[1]**

[1]University of Agronomic Sciences and Veterinary Medicine of Bucharest,
59 Marasti Blvd., District 1, Bucharest, Romania
[2]Institute of Research and Development for Plant Protection Bucharest, Romania,
8 Ion Ionescu de la Brad Blvd, Bucharest, Romania
[3]National University of Sciences and Technologies Politehnica Bucharest,
313 Splaiul Independentei Street, District 6, Bucharest, Romania
[4]University Autonoma de Barcelona, 08193, Bellaterra, Barcelona, Spain
[5]University of Porto, Praça de Gomes Teixeira, 4099-002, Porto, Portugal

Corresponding author email: nicoleta.radu@biotehnologii.usamv.ro

***Abstract***

*A sustainable green future depends on developing competencies in advanced technologies across energy, agriculture, and industry for graduate students of Master`s and Doctoral programs. This study aimed to assess graduate students' perceptions from three European universities regarding the key sustainability strategies through a structured survey focusing on digitalisation, agriculture, biodiversity conservation, and the circular economy. The majority of graduate students agreed that renewable energy reduces carbon footprint, air and water pollution, and enhances public health. Students demonstrated a clear understanding of the EU Green Agriculture objectives, emphasizing food security and environmental footprint reduction. Positive perceptions extended to biodiversity conservation, with support for effective management, monitoring, and clear conservation goals. Respondents endorsed circular economy principles, including resource efficiency, material redesign, and waste recapture, and aligned with the EU's industrial strategy for a progressive and sustainable economic transition. These findings indicate that the graduate students possess both awareness and favourable attitudes toward advanced technological solutions for sustainability. The results underscore the successful implementation of digital resources developed in academic curricula for students from Master`s and Doctoral programs from three European universities.*

***Key words****: graduate student competencies, green agriculture, sustainable.*

## INTRODUCTION

In the context of the profound structural transformations driven by the European Green Deal, European higher education plays a major role in shaping a new professional elite capable of operationalising the transition towards a climate-neutral economy (Borel-Saladin et al., 2013). The success of complex macro-structural initiatives such as the Common Agricultural Policy (CAP) or the "Farm to Fork" strategy is directly contingent upon the translation of theoretical directives into applied technical competencies and digital literacy (Matthews, 2013). These policy frameworks increasingly rely on data-driven decision-making, sustainability metrics, and cross-sectoral knowledge integration (Pe'er et al., 2020). Agricultural digitalisation (smart agriculture), precision farming systems, and the integration of Geographic Information Systems (GIS) are widely recognised as fundamental pillars of modern agro-ecosystem management (Wolfert et al., 2017; Mathenge et al., 2022). In parallel, advanced biotechnologies such as genomics, bioinformatics, and molecular breeding, alongside Big Data analytics and artificial intelligence infrastructures, are reshaping the resilience and productivity of primary production systems (Kamilaris et al., 2017; Liakos et al., 2018). These technological paradigms collectively underpin the ongoing transition towards Agriculture 4.0 and data-intensive sustainability governance (Klerkx et

al., 2019). To mitigate these asymmetries and ensure integrated training, an advanced educational programme was designed and implemented in the form of an intensive course, type blending learning with digital tools. This course adopted an interdisciplinary approach, addressing the pillars of sustainable development, the application of digital technologies in optimising primary production systems, and policy mechanisms for biodiversity conservation and ecosystem resilience The studies performed aimed to assess the competencies of doctoral and master's students in advanced technologies related to a sustainable green future in energy, agriculture, and industry, within the context of completion of a short intensive training program type blending learning, regarding the European Green Deal, using an anonymous cross-sectional survey

## MATERIALS AND METHODS

The studies performed were based on cross-sectional survey questionnaires involving 51 doctoral and master's students from five universities that participated at a short intensive learning training teaching program in the field of the European Green Deal. At the end of this session, participants in the intensive courses were invited to answer a specific survey questionnaire anonymously in order to assess their competencies in advanced technologies for a sustainable green future in energy, agriculture, and industry.

The participants (students) belong to the following universities:

- University of Agronomic Sciences and Veterinary Medicine of Bucharest (USAMVB), Romania;
- National University of Sciences and Technology Politehnica of Bucharest (UNSTPB), Romania;
- University Autonoma de Barcelona Spain (UAB Spain);
- University of Porto Portugal (UPorto Portugal);
- Uzhhorod National University Ukraine (Uzhhorod Univ_Ukraine).

Each group consisted of at least 10 participants per university.

The Survey Questionnaires were completed anonymously. Data were structured in a survey questionnaire based on a 5-point Likert scale, as follows:

1 = No, not at all;
2 = Only to a certain extent;
3 = More or less;
4 = Mostly yes;
5 = Yes, always.

The questionnaire assessed the students' perceptions regarding the following sentences:

B1: Do you think that the utilization of renewable energy reduces carbon footprint, air pollution and water environmental impact, but also improves public health?

B2: Do you think that remote sensing and GIS-based technologies for sustainable management of agriculture are important?

B3: Do you consider that the main objective of the EU Green Agriculture politics is to ensure food security by reducing environmental footprint and assuring competitive sustainability from farm to fork?

B4: Do you agree that the EU's Common Agricultural Policy is central to the EU Green Deal & its Farm to Fork and Biodiversity strategies?

B5: Do you think that genomics, bioinformatics, and big data in sustainable food production are useful for agriculture and food production systems

B6: Do you think that the EU target for Biodiversity conservation is effectively managing all protected areas, defining clear conservation objectives and measures, and monitoring them appropriately?

B7: Do you think that digitalization can be useful in the Global Biodiversity Assessment

**Statistical analysis**: All data are presented as means ± standard errors.

## RESULTS AND DISCUSSIONS

The results highlight a high level of student awareness regarding the role of digital technologies and European policies in promoting agricultural sustainability, biodiversity conservation, and the transition towards a green economy. With respect to the environmental impact of renewable energy sources (Figure 1), most respondents assigned

high scores (4 and 5), with 80% of responses falling within these categories. This finding indicates a solid understanding of the benefits of renewable energy in reducing carbon emissions, pollution, and natural resource degradation. Similar results have been reported in studies examining environmental literacy among European students, which indicate growing awareness of renewable energy as a key component of sustainable development and climate change mitigation strategies (Probst, 2022; Sanchez et al., 2025). The increasing visibility of renewable energy within European sustainability policies may further contribute to students' positive perceptions of its environmental benefits. Regarding the importance of GIS in agriculture (Figure 2), responses were largely positive, with 80% of students assigned scores of 4 or 5. This fact indicates strong awareness of the role of geospatial technologies in agricultural monitoring and management optimisation. This result is consistent with recent research demonstrating that GIS, remote sensing, precision agriculture, and artificial intelligence technologies contribute significantly to improving resource-use efficiency, crop monitoring, and sustainable land management practices (Finger, 2023; Wójcik-Gront et al., 2024).

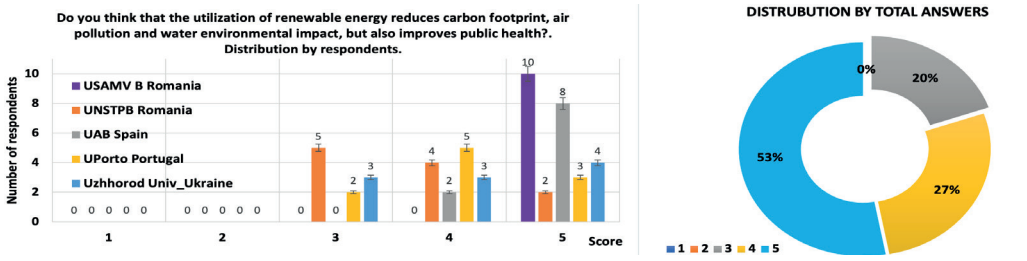



Figure 1. Assessment of the students' perceptions regarding the environmental impact of renewable energy sources

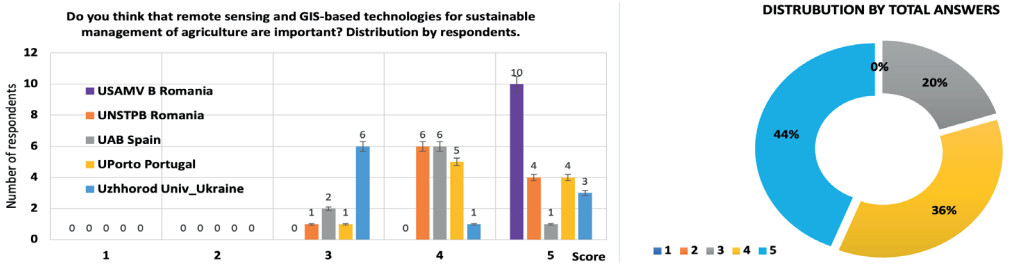



Figure 2. Assessment of the students' perceptions regarding the importance of GIS in agriculture

The high level of agreement observed among respondents suggests that students increasingly understand and recognise the importance of Agriculture 4.0 technologies in supporting sustainable and resilient agricultural systems. Assessment of students' perceptions regarding the objectives of EU green agricultural policies in relation to food security, the reduction of environmental impacts, and the promotion of sustainable competitiveness throughout the food supply chain is presented in the Figure 3.

The predominance of answers with scores 4 and 5 (71%) suggests that respondents understand and recognise the strategic importance of these policies in balancing food security with environmental sustainability This perception aligns with the objectives of the European Green Deal and the Farm to Fork Strategy, which aim to transform food systems by reducing environmental pressures while ensuring food security, economic viability, and social sustainability (Guyomard et al., 2023; Hamam et al., 2021; Radu et al., 2007; Radu et al., 2020). The relatively high proportion of moderate-agreement responses may reflect uncertainties about the practical implementation, economic feasibility, or long-term effectiveness of these measures.

Regarding the connection between the Common Agricultural Policy (CAP) and European Green Deal (Figure 4), the results reveal a predominantly positive perception of the CAP as a key policy instrument supporting the EU Green Deal, the Farm to Fork Strategy, and the Biodiversity Strategy too.

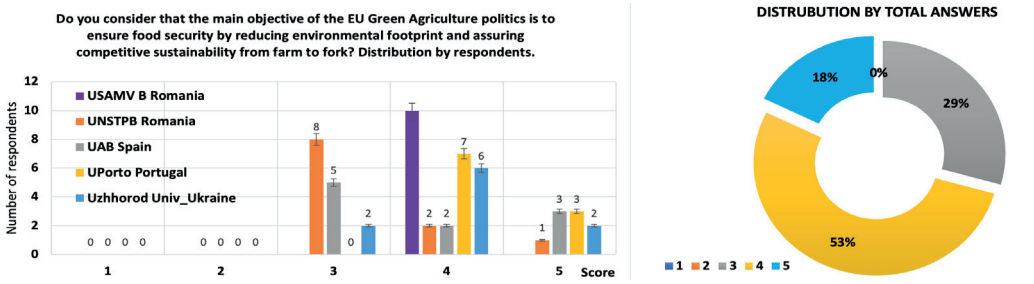



Figure 3. Assessment of students' perceptions regarding the objectives of EU green agricultural policies in relation to food security, the reduction of environmental impacts, and the promotion of sustainable competitiveness throughout the food supply chain

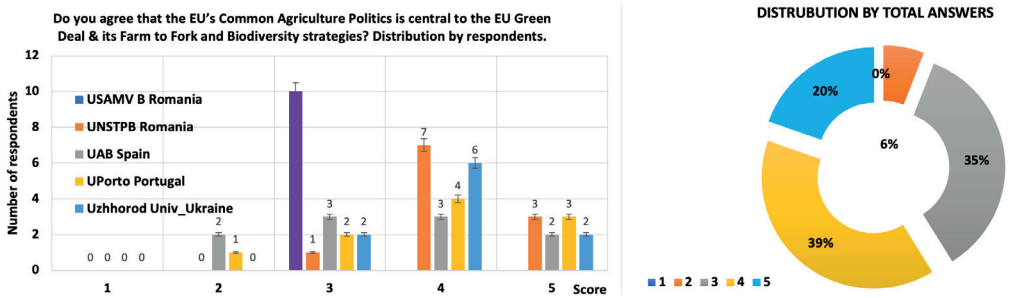



Figure 4. Assessment of the students' perceptions regarding the connection between the Common Agricultural Policy (CAP) and European Green Deal

The combined proportion of agreement and strong agreement responses (59%) demonstrates substantial support for the CAP's role in advancing sustainable agricultural development and environmental objectives across Europe. Similar findings have been reported by (Probst, 2022; Sanchez et al., 2025), who observed that university students increasingly recognise the importance of policy instruments in achieving sustainability transitions within agri-food systems. However, 35% of respondents selected score 3, indicating a moderate level of agreement. The overall findings suggest moderate-to-high awareness of the relationship between agricultural policy and sustainability goals. Responses concerning the contribution of genomics, bioinformatics, and big data to sustainable food systems (Figure 5) were predominantly positive, with 66% of respondents assigning scores of 4 or 5. This finding suggests that students acknowledge the potential of advanced biotechnologies to improve sustainability, productivity, and resource-use efficiency. Recent studies have highlighted the growing role of genomics, artificial intelligence, and data-driven approaches in supporting climate-smart agriculture, precision farming, and sustainable food production systems (Finger, 2023; Getahun et al., 2024; Ronzhin et al., 2025). These technologies are increasingly regarded as essential tools for addressing global challenges related to food security, environmental degradation, and climate change. Biodiversity conservation policies (Figure 6) were strongly acknowledged, with nearly 67% of responses receiving scores of 4-5, suggesting a high level of awareness of ecosystem protection priorities and conservation strategies. This result is in agreement with the increasing of biodiversity conservation within international policy agendas, particularly following the adoption of

the Kunming-Montreal Global Biodiversity Framework, which established ambitious targets for halting biodiversity loss by 2030 (Hughes & Grumbine, 2023).

The findings indicate that students are aware of the importance of biodiversity conservation as a prerequisite for ecosystem resilience and sustainable development. The usefulness of digitalisation in global biodiversity assessment (Figure 7) was positively evaluated, with 75% of respondents assigning high scores. This result demonstrates strong confidence in the contribution of digital technologies to biodiversity monitoring and management. The finding is supported by recent literature highlighting the transformative role of artificial intelligence, remote sensing, geographic information systems (GIS), and big data analytics in biodiversity assessment and conservation planning (Jetz et al., 2019; Hughes & Grumbine, 2023).

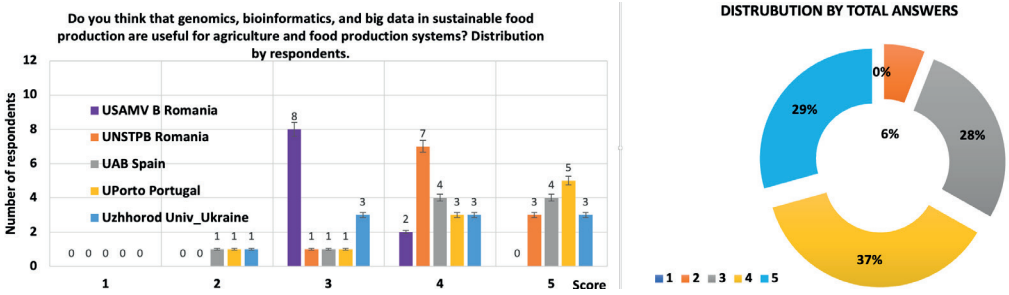



Figure 5. Assessment of the students' perceptions regarding the contribution of genomics, bioinformatics, and big data to sustainable food systems

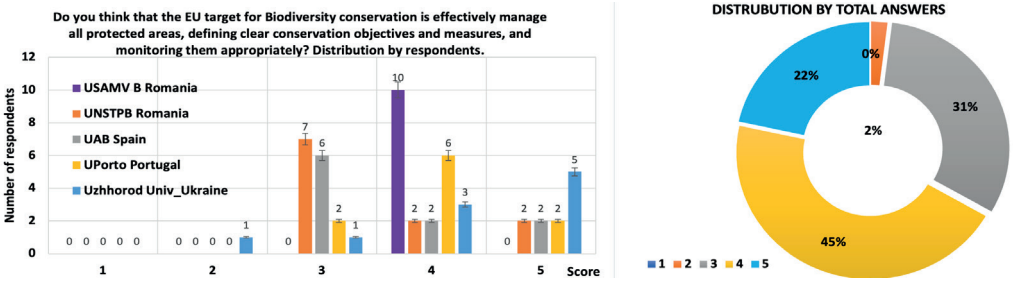



Figure 6. Assessment of the students' perceptions regarding EU Biodiversity conservation policies

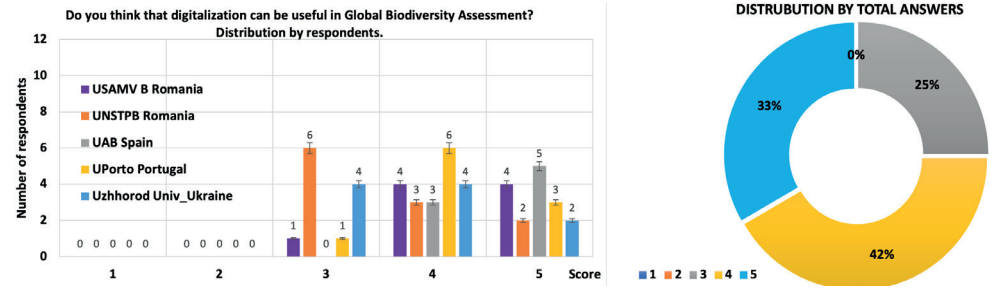



Figure 7. Assessment of the students' perceptions regarding the usefulness of digitalisation in global biodiversity assessment

Digital technologies enable large-scale ecological monitoring, improve data integration, and support evidence-based decision-making processes. Furthermore, advances in digital monitoring systems are considered essential for achieving the targets

established by the Kunming-Montreal Global Biodiversity Framework and for strengthening biodiversity governance at regional and global levels (Hughes & Grumbine, 2023).

Overall, the results indicate high levels of sustainability awareness and understanding among students from Romania, Spain, Portugal, and Ukraine, with limited inter-university variation and broadly consistent response patterns across cohorts.

A high level of environmental literacy among university students across Romania, Spain, Portugal, and Ukraine was obtained, particularly in relation to biodiversity conservation and the perceived role of digital technologies in ecological monitoring. This aligns with a broader shift in environmental education, which increasingly emphasizes systems thinking and the integration of technological competencies into sustainability-related curricula (Pauw et al., 2015; Reid, 2019).

A key finding is the strong endorsement (75%) of digitalisation in global biodiversity assessment. This reflects growing recognition of the role of emerging technologies such as artificial intelligence, remote sensing, geographic information systems (GIS), and big data analytics in transforming conservation science. These technologies enable continuous collection and integration of ecological data across spatial and temporal scales, improving biodiversity modelling, forecasting, and risk assessment (Radu et al., 2006; Dima et al., 2007; Pettorelli et al., 2014; Kissling et al., 2018; Jetz et al., 2019). Recent developments in digital Earth observation systems and AI-driven ecological monitoring further reinforce this transition toward data-intensive conservation paradigms (van der Plas et al., 2025; Miao et al., 2026). The expansion of global biodiversity platforms and digital infrastructure has also been identified as central to strengthening biodiversity governance and decision-making under rapid environmental change (Güntsch et al., 2025). The results are consistent with global scientific consensus that digital innovation is becoming indispensable for biodiversity governance. Similarly, the Kunming–Montreal Global Biodiversity Framework explicitly calls for strengthened monitoring systems, improved data accessibility, and the use of digital tools to support the implementation and evaluation of biodiversity targets. In this context, the positive student evaluations suggest an awareness of not only ecological challenges but also of the governance mechanisms required to address them. Furthermore, the limited variation across universities indicates a relatively homogeneous perception of sustainability and digitalisation in biodiversity contexts. This may reflect the increasing harmonisation of environmental science curricula across Europe, driven by the Bologna Process and the integration of sustainability competencies into higher education frameworks (Malmio & Liwång, 2023). Such consistency is important, as it suggests that future professionals across these countries may share a common conceptual foundation for addressing transboundary environmental challenges.

Overall, the data indicate a strong alignment between student perceptions and current scientific and policy directions in biodiversity conservation.

However, while optimism toward digital tools is justified, the literature also highlights persistent challenges, including unequal access to technology, data governance issues, and the need for interdisciplinary capacity building to ensure effective implementation (Pettorelli et al., 2014; Hughes & Grumbine, 2023).

## CONCLUSIONS

The survey revealed a generally high level of awareness among students regarding digitalization, biodiversity conservation, sustainable agriculture, and circular economy principles.

Digital technologies were widely recognized as valuable tools for biodiversity assessment and environmental monitoring, reflecting current trends in digital transformation and ecological management. Students demonstrated a good understanding of the relationship between the Common Agricultural Policy, the European Green Deal, and the Farm to Fork and Biodiversity strategies, although some neutral responses suggest opportunities for further educational interventions.

Genomics, bioinformatics, and big data were perceived as important contributors to future

sustainable food production systems, indicating growing acceptance of advanced agricultural technologies.

Biodiversity conservation and protected area management received strong support, highlighting the perceived importance of effective environmental governance.

The circular economy obtained the highest level of agreement among respondents, emphasizing the increasing relevance of resource efficiency and waste valorization concepts within sustainability education.

Collectively, these findings indicate that students from the participating European universities possess substantial sustainability literacy and recognize the importance of technological innovation and policy integration in addressing global environmental challenges.

## ACKNOWLEDGEMENTS

This research work was carried out with the support of the University of Agronomic Science and Veterinary Medicine of Bucharest, Romania, and was financed by the Project number: 2023-1-RO01-KA220-HED-000154433 entitled: Gender, Digitalization, Green: Ensuring a Sustainable Future for all in Europe.

## REFERENCES

Borel-Saladin, J.M., & Turok, I.N. (2013). The Green Economy: Incremental Change or Transformation? *Env. Pol. Gov.,* 23(4): 209-220.

Dima, G., Radu, N., Chirvase, A., & Pena, E. L. (2007). Studies regarding using biomass in bioremediation of wastewater with heavy metal. *Revista de Chimie, 58*(6), 561–565.

Finger, R. (2023). Digital innovations for sustainable and resilient agricultural systems. *European Review of Agricultural Economics*, Volume 50, Issue 4, September 2023, 1277–1309

Getahun, S., Kefale, H., & Gelaye, Y. (2024). Application of Precision Agriculture Technologies for Sustainable Crop Production and Environmental Sustainability: A Systematic Review. *The Scientific World Journal*, *2024*, 2126734.

Güntsch, A., Overmann, J., Ebert, B., Bonn, A., Le Bras, Y., Engel, T., Hovstad, K. A., Lange Canhos, D. A., Newman, P., van Ommen Kloeke, E., Ratcliffe, S., le Roux, M., Smith, V. S., Triebel, D., Fichtmueller, D., & Luther, K. (2025). National biodiversity data infrastructures: ten essential functions for science, policy, and practice. *Bioscience*, *75*(2), 139–151.

Guyomard, H., Soler, L.-G., Détang-Dessendre, C., & Réquillart, V. (2023). The European Green Deal improves the sustainability of food systems but has uneven economic impacts on consumers and farmers. *Communications Earth & Environment,* 4, 358.

Hamam, M., Chinnici, G., Di Vita, G., Pappalardo, G., Pecorino, B., Maesano, G., & D'Amico, M. (2021). Circular Economy Models in Agro-Food Systems: A Review. *Sustainability*, *13*(6), 3453.

Hughes, A. C., & Grumbine, R. E. (2023). The Kunming-Montreal Global Biodiversity Framework: what it does and does not do, and how to improve it. *Frontiers in Environmental Science***,** 11, 1281536.

Jetz, W., McGeoch, M. A., Guralnick, R., Ferrier, S., Beck, J., Costello, M. J., Fernandez, M., Geller, G. N., Keil, P., Merow, C., Meyer, C., Muller-Karger, F. E., Pereira, H. M., Regan, E. C., Schmeller, D. S., & Turak, E. (2019). Essential biodiversity variables for mapping and monitoring species populations. *Nature ecology & evolution*, *3*(4), 539–551.

Kamilaris, A., Kartakoullis, A., & Prenafeta-Boldú, F. X. (2017). A review on the practice of big data analysis in agriculture. *Computers and Electronics in Agriculture, 143*, 23–37.

Kissling, W.D., Walls, R., Bowser, A., Jones, M. O., Kattge, J., Agosti, D., Amengual, J., Basset, A., van Bodegom, P. M., Cornelissen, J. H. C., Denny, E. G., Deudero, S., Egloff, W., Elmendorf, S. C., Alonso García, E., Jones, K. D., Jones, O. R., Lavorel, S., Lear, D., Navarro, L. M., Pawar, S., Pirzl, R., Rüger, N., Sal, S., Salguero-Gómez, R., Schigel, D., Schulz, K. S., Skidmore, A., & Guralnick, R. P. (2018). Towards global data products of Essential Biodiversity Variables on species traits. *Nat Ecol Evol* 2, 1531–1540.

Klerkx, L., Jakku, E., & Labarthe, P. (2019). A review of social science on digital agriculture, smart farming and agriculture 4.0: New contributions and a future research agenda. *NJAS: Wageningen Journal of Life Sciences, 90–91*, 100315.

Liakos, K. G., Busato, P., Moshou, D., Pearson, S., & Bochtis, D. (2018). Machine Learning in Agriculture: A Review. *Sensors*, *18*(8), 2674.

Malmio, I., & Liwång, H. (2023). Education for sustainable development. In Filho, W. L., Azul, A. M., Doni, F., & A. L. Salvia (Eds.), *Handbook of sustainability science in the future*. Springer, Cham.

Mathenge, M., Sonneveld, B. G. J. S., & Broerse, J. E. W. (2022). Application of GIS in Agriculture in Promoting Evidence-Informed Decision Making for Improving Agriculture Sustainability: A Systematic Review. *Sustainability*, *14*(16), 9974.

Matthews, A. (2013). Greening agricultural payments in the EU's Common Agricultural Policy. *Bio-Based and Applied Economics*, *2*(1), 1–27.

Miao, Z., Zhang, Y., Fabian, Z., Hernandez Celis, A., Beery, S., Li, C., Liu, Z., Gupta, A., Nasir, M., Li, W., Holmberg, J., Palmer, M., Gaynor, K., Arbelaez, P., Wang, P., Dodhia, R., & Ferres, J. L. (2026). New frontiers in artificial intelligence for biodiversity research and conservation with multimodal language models. *Methods in Ecology and Evolution*, 17, 238–256.

Pauw, J. B.-D., Gericke, N., Olsson, D., & Berglund, T. (2015). The Effectiveness of Education for Sustainable Development. *Sustainability*, *7*(11), 15693-15717.

Pe'er, G., Bonn, A., Bruelheide, H., Dieker, P., Eisenhauer, N., Feindt, P. H., Hagedorn, G., Hansjürgens, B., Herzon, I., Lomba, Â., Marquard, E., Moreira, F., Nitsch, H., Oppermann, R., Perino, A., Röder, N., Schleyer, C., Schindler, S., Wolf, C., Zinngrebe, Y., & Lakner, S. (2020). Action needed for the EU Common Agricultural Policy to address sustainability challenges. *People and Nature*, 2(2), 305–316.

Pettorelli, N., Laurance, W. F., O'Brien, T. G., Wegmann, M., Nagendra, H., & Turner, W. (2014) Satellite remote sensing for applied ecologists: opportunities and challenges. *Journal of Applied Ecology*, 51(4), 839–848.

Probst, L. (2022). Higher Education for Sustainability: A Critical Review of the Empirical Evidence 2013–2020. *Sustainability*, *14*(6), 3402.

Radu, N., Bondar, E., Meghea, A., & Rau, I. (2006). Removal of copper and cobalt from diluted aqueous system by biosorption process. *Revista de Chimie* 7, 711-717.

Radu, N., & Meghea, A. (2007). Studies concerning the use of microbial biomass in fertilizer manufacture. *Journal of Environmental Protection and Ecology*, 875–890.

Radu, N., Chirvase, A. A., Babeanu, N., Popa, O., Cornea, P., Pîrvu, L., Bostan, M., Ciric, A., Mațe, E., Radu, E., Doni, M., Constantin, M., Răuț, I., Gurban, A. M., & Begea, M. (2020). Study regarding the potential use of a spent microbial biomass in fertilizer manufacturing. *Agronomy, 10*, 299.

Reid, A. (2019). Environmental education research - milestones and celebrations. *Environmental Education Research*, *25*(1), 1–5.

Ronzhin, A., Figurek, A., Surovtsev, V., & Dibirova, K. (2025). Digital Transformation and Precision Farming as Catalysts of Rural Development. *Land*, *14*(7), 1464.

Sanchez, S. J., Piedrahita Guzman, Y., Sosa-Molano, J., Robertson, D., Ahern, S., & Garza, T. (2025). Systematic literature review: A typology of sustainability literacy and environmental literacy. *Frontiers in Education*, 10, 1490791. https://doi.org/10.3389/feduc.2025.1490791

van der Plas, T. L., Alexander, D. G., & Pocock, M. J. O. (2025). Monitoring protected areas by integrating machine learning, remote sensing and citizen science. *Ecological Solutions and Evidence*, 6, e70040.

Wójcik-Gront, E., Zieniuk, B., & Pawełkowicz, M. (2024). Harnessing AI-Powered Genomic Research for Sustainable Crop Improvement. *Agriculture*, 14(12), 2299.

Wolfert, S., Ge, L., Verdouw, C., & Bogaardt, M.-J. (2017). Big Data in Smart Farming - A review, *Agricultural Systems*, 153, 69-80.

Scientific Papers. Series E. Land Reclamation, Earth Observation & Surveying, Environmental Engineering. Vol. XV, 2026
Print ISSN 2285-6064, CD-ROM ISSN 2285-6072, Online ISSN 2393-5138, ISSN-L 2285-6064

# GAMIFICATION AS A TOOL FOR ENHANCING PARTICIPATION AND LEARNING IN GREEN DIGITISATION EDUCATION

**Nicoleta RADU[1, 2], Mihai Dan CARAMIHAI[3], Francisca BLANQUEZ CANO[4], Adrian SILVA[5], Narcisa BABEANU[1], Laura IOSUB[1], Razvan Ionut TEODORESCU[1]**

[1]University of Agronomic Sciences and Veterinary Medicine of Bucharest,
59 Marasti Blvd, District 1, Bucharest, Romania
[2]National Institute for Research and Development in Chemistry and Petrochemistry - ICECHIM
Bucharest, Romania
[3]National University of Sciences and Technologies Politehnica Bucharest,
313 Splaiul Independentei Street, District 6, Bucharest, Romania
[4]University Autonoma de Barcelona, 08193, Bellaterra, Barcelona, Spain
[5]University of Porto, Praça de Gomes Teixeira, 4099-002, Porto, Portugal

Corresponding author email: nicoleta.radu@biotehnologii.usamv.ro

***Abstract***

*This study evaluates the students' satisfaction with gamification tools in learning sessions on green digitization across Spain, Romania, and Portugal. Graduate participants were surveyed to assess how the gaming-based system influenced engagement, learning, and motivation. Questions focused on the effectiveness of gamification in encouraging participation, the perceived value of participation awards, the correlation between game points and progress, and the impact on learning outcomes. Results indicate that students responded positively, reporting increased participation due to gamified elements, satisfaction with awards, and a clear alignment between points and game levels. Moreover, participants highlighted improved learning outcomes and a deeper understanding of course content as a direct result of the gaming system. These findings suggest that gamification can be a powerful tool in higher education for Master`s and Doctoral programs, particularly for courses addressing digital and green transformation, fostering both motivation and effective learning among graduate students from three European universities.*

***Key words****: gamification, green, learning tools.*

## INTRODUCTION

The integration of gamification into digital education has become a prominent strategy for enhancing student engagement, motivation, and learning effectiveness in higher education environments. Gamification, defined as the use of game design elements in non-game contexts, has been increasingly applied to support active learning and improve learner participation in digitally mediated instructional settings (Christopoulos & Mystakidis, 2023). Recent studies emphasize that gamified learning environments can enhance intrinsic motivation through mechanisms such as feedback loops, points systems, and progress visualization, which align with self-determination theory and flow-based learning models (Ratinho & Martins, 2023; Oliveira & Hamari, 2024). In parallel, the concept of green digitisation education has emerged as a critical interdisciplinary domain, combining sustainability literacy with the development of digital competence. This educational paradigm aims to equip learners with the skills necessary to navigate and contribute to environmentally sustainable digital transformation processes (Spilotro et al., 2026). Within this context, gamification has been proposed as a pedagogical tool capable of bridging abstract sustainability concepts with interactive and experiential learning models (Seaborn & Fels, 2015; Oliveira et al., 2023). Despite growing theoretical support, empirical evidence regarding the effectiveness of gamification in enhancing participation and learning outcomes in green digitisation education remains limited, particularly across multi-institutional European cohorts. This study aimed to evaluate the students' perceptions regarding the use of gamified educational tools, implemented across five European universities, focusing on

engagement, perceived learning, motivation, and overall satisfaction. The digital tool with gamification elements was developed to improve students' knowledge and understanding of the European Green Deal principles across European universities in the Cycle I and II programs.

## MATERIALS AND METHODS

### Study design and participants

The studies performed were based on cross-sectional survey questionnaires involving 51 doctoral and master's students from five universities:

- University of Agronomic Sciences and Veterinary Medicine of Bucharest (USAMV), Romania (PhD Biotechnologies program);
- National University of Sciences and Technology Politehnica of Bucharest (UNSTPB), Romania (Master Computer Science program);
- University Autonoma de Barcelona (UAB), Spain (PhD Biochemistry and Environment program);
- University of Porto (UPorto), Portugal (PhD Chemical Engineering and Environment program);
- Uzhhorod National University (Uzhhorod), Ukraine (Master of Computer Science program).

Each group consisted of at least 10 participants. The Survey Questionnaires were completed anonymously

### Instrument and measurement scale

Data were structured in a survey questionnaire based on a 5-point Likert scale, as follows:

1 = No, not at all;
2 = Only to a certain extent;
3 = More or less;
4 = Mostly yes;
5 = Yes, always.

The questionnaire assessed five dimensions:

A. Gamification-induced participation;
B. Perceived correlation between points and games;
C. Perceived learning improvement;
D. Course satisfaction;
E. Motivation toward digital and green competences.

### Statistical analysis

Responses were analyzed using the mean Likert scores. Statistical analysis was made applying one-way ANOVA (to assess differences across universities), with Tukey post hoc analysis to identify the differences between pairs. The value $p < 0.05$ was considered significant.

Notation:

* $p < 0.05$;
** $p < 0.01$;
*** $p < 0.001$.

## RESULTS AND DISCUSSIONS

### Gamification-driven participation across disciplinary profiles

The results from Question A indicate a pronounced heterogeneity in perceived participation enhancement induced by gamification (Figure 1). The PhD students from the biotechnology program (USAMV of Bucharest, Romania) and biochemistry/environmental sciences (UAB Spain) reported uniformly negative perceptions of participation increase, whereas computer science students (Uzhhorod University and UNSTPB Romania) demonstrated substantially higher engagement levels, feedback loops, which may enhance perceived coherence of gamified systems.

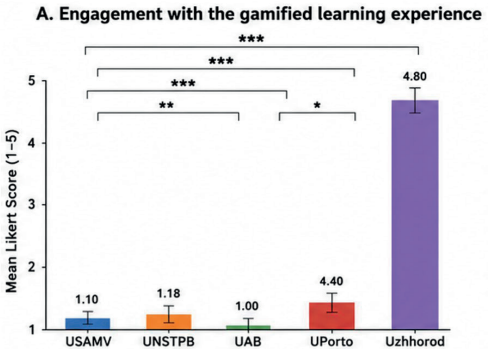



Figure 1. Engagement with the gamified learning experience of the students from USAMV, UNSTPB, UAB, UPorto and Uzhhorod

This disciplinary divergence aligns with recent findings suggesting that learners with stronger computational or systems-oriented backgrounds exhibit higher receptivity to

structured gamified environments, particularly those involving point systems and progression logic (Oliveira et al., 2025; Klock et al., 2026). Computer science students are typically more familiar with algorithmic reward structures and iterative. Conversely, students in biotechnology and biochemical engineering domains often engage in problem-based and experimental learning environments where intrinsic cognitive engagement is less dependent on external reward mechanisms. This may explain their lower responsiveness to gamified participation triggers, consistent with evidence that gamification effects are mediated by prior exposure to digital learning ecosystems (Dicheva et al., 2015). These results indicate statistically significant inter-university differences in perceived engagement (ANOVA $p < 0.05$), suggesting that gamification effectiveness is context-dependent and may be influenced by disciplinary or pedagogical culture.

**Perceived coherence of gamification mechanics (points–game alignment)**

Across all institutions, Question B (Figure 2) revealed generally positive evaluations regarding the alignment between points and game mechanics.

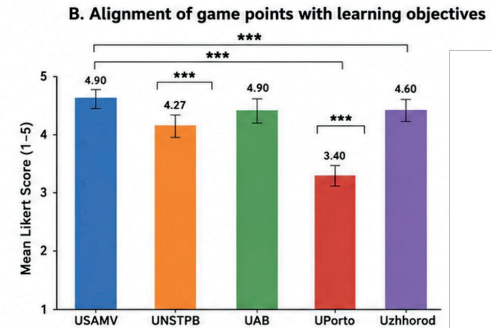



Figure 2. Alignment of the gamification tools with the learning objectives. Answers of the students from USAMV, UNSTPB, UAB, UPorto, and Uzhhorod

However, variation was observed in environmental and chemical engineering students (University of Porto), who reported lower coherence perception compared to computer science cohorts. This finding supports the argument that perceived transparency and structural clarity of gamified reward systems are critical determinants of engagement (Seaborn & Fels, 2015). In particular, students trained in computational disciplines may more easily interpret rule-based scoring systems as logically consistent, while students from life sciences or environmental engineering backgrounds may require more explicit contextual framing of gamification logic. The strong positive responses from USAMV, Uzhhorod University and UAB Spain suggest that when gamification is clearly mapped onto learning tasks, even interdisciplinary cohorts can achieve high perceived system coherence, reinforcing the importance of instructional design consistency (Seaborn & Fels, 2015; Toda et al., 2019; Rodriguez-Calzada et al., 2024).

**Perceived learning outcomes and cognitive integration**

The results for Question C (Figure 3) indicate moderate but consistent perceived learning improvements across all disciplines, with the highest scores observed in computer science students and the lowest in environmental chemical engineering students (University of Porto). This pattern may reflect differences in how gamified systems interact with domain-specific cognitive processing. In computer science education, learning tasks are often procedural and modular, which aligns naturally with gamified structures such as levels, scoring, and incremental progression. This structural compatibility enhances perceived learning gains, as supported by prior studies on gamification in STEM education (Rodrigues et al., 2022; Buenadicha-Mateos et al., 2025). In contrast, biotechnology and biochemical engineering education relies heavily on conceptual integration and experimental reasoning, which may not be directly enhanced by point-based gamification alone. As Ryan and Deci (2020) emphasize, perceived competence and autonomy are key mediators of learning motivation, suggesting that gamification must be carefully calibrated to avoid reducing complex scientific reasoning to superficial reward accumulation (Sailer & Homner, 2020; Ryan & Deci, 2020). Overall, ANOVA results indicate moderate but significant differences between institutions ($p < 0.05$), suggesting that gamification contributes to perceived learning

improvement, but with varying effectiveness across educational contexts.

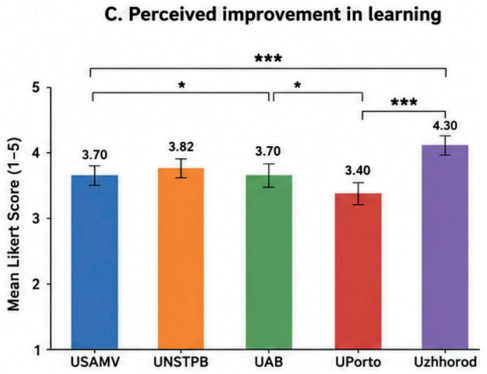



Figure 3. Perceived improvement in the learning process. Opinion of students from USAMV, UNSTPB, UAB, UPorto and Uzhhorod

## Course satisfaction as a function of disciplinary alignment

Overall satisfaction (Question D, Figure 4) was highest among computer science students and lowest among environmental chemical engineering students. This suggests that satisfaction is not only influenced by gamification design but also by disciplinary alignment between pedagogy and cognitive expectations.

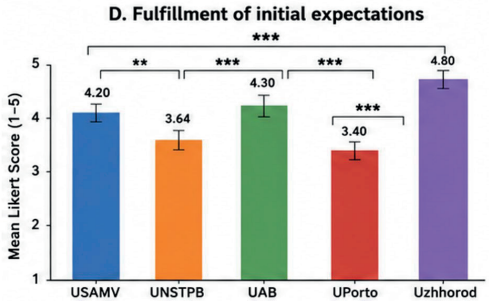



Figure 4. Students' initial expectations fulfilment at USAMV, UNSTPB, UAB, UPorto, and Uzhhorod

Gamified systems appear particularly effective when they reinforce structured problem-solving workflows, as is typical in computer science curricula. This is consistent with findings that gamification increases satisfaction when it supports goal clarity and immediate feedback mechanisms (Ratinho & Martins, 2023; David & Weinstein, 2024). However, in disciplines such as biotechnology and biochemical engineering, where learning is often exploratory and experimental, overly structured gamification may reduce perceived authenticity of learning experiences, leading to lower satisfaction despite similar instructional quality.

## Synthesis: disciplinary mediation of gamification effectiveness

Overall, the data suggest that gamification effectiveness in green digitization education is strongly mediated by disciplinary background. Computer science students consistently exhibit higher engagement, satisfaction, and perceived learning gains, likely due to cognitive alignment with structured digital systems (Question E, Figure 5).

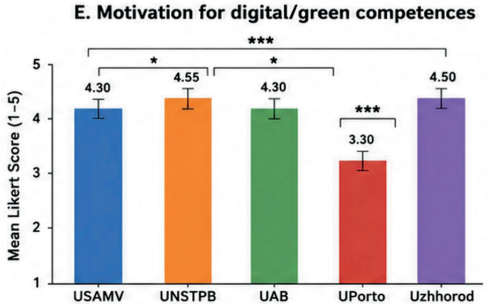



Figure 5. Motivation for digital/green competencies of students from USAMV, UNSTPB, UAB, UPorto and Uzhhorod

In contrast, biotechnology and biochemical engineering students demonstrate more selective responsiveness, indicating that gamification alone may not be sufficient to enhance engagement in domains requiring deeper conceptual reasoning or experimental interpretation. Environmental chemical engineering students occupy an intermediate position, benefiting from gamification when sustainability contexts are explicitly emphasized (Question E, Figure 5). This supports the notion that gamification is not universally effective but rather context-sensitive, requiring alignment with disciplinary epistemologies (van Roy & Zaman, 2018; Santiago et al., 2025; Klock et al., 2026). These findings reinforce the importance of adaptive

gamification design in higher education, particularly in interdisciplinary sustainability-oriented curricula. Across all five questions, a consistent pattern emerges: gamification tends to be more effective in institutions where participants report higher alignment between game mechanics and learning structure. The strongest overall effects were observed in Uzhhorod University, while the University of Porto consistently reported lower engagement and motivation scores. This heterogeneity highlights the importance of contextual factors such as disciplinary background, prior exposure to digital learning tools, and instructional design quality.

The integration of European Green Deal principles into educational processes through gamification-based tools facilitates the understanding of systemic relationships among the environment, production systems, and human well-being. In agriculture, such tools contribute to strengthening the transition toward sustainable and circular production models by simulating the impacts of resource-use decisions on soil degradation, greenhouse gas emissions, and biodiversity loss, as well as by promoting regenerative practices and the valorisation of biological residues in alignment with circular bioeconomy principles.

In the field of healthcare, gamification supports the development of an integrated One Health perspective, highlighting the interdependencies between environmental quality, food safety, and the incidence of diseases associated with ecological factors (Dima et al., 2007; Ciric et al., 2023). By incorporating game mechanics such as simulation, feedback loops, and structured progression, gamified learning environments enhance systems thinking across human, animal, and environmental health domains (Deterding et al., 2011; Ying & Wan Yahaya, 2026). Scenario-based serious games and outbreak simulations, in particular, improve engagement and facilitate applied learning in interdisciplinary contexts. Furthermore, gamified approaches contribute to the development of collaborative competencies essential for One Health practice, including cross-sector communication, coordinated decision-making, and data-driven reasoning. Such methods have been associated with improved knowledge retention and behavioral alignment in areas such as antimicrobial resistance stewardship and outbreak preparedness (Gan & Duan, 2026; van den Broek et al., 2026). However, limitations remain, including the risk of oversimplifying complex ecological systems and the potential disconnect between simulated environments and real-world operational performance. Therefore, gamification should be considered a complementary educational tool rather than a standalone methodology.

## CONCLUSIONS

This multi-university European study demonstrates that gamification can significantly enhance participation, motivation, and perceived learning outcomes in green digitization education. However, its effectiveness is not uniform across institutions and is strongly influenced by contextual and pedagogical factors. The results suggest that successful implementation of gamified learning systems requires careful alignment between game mechanics and educational objectives, as well as adaptation to disciplinary and cultural differences.

## ACKNOWLEDGEMENTS

This research work was carried out with the support of the University of Agronomic Science and Veterinary Medicine of Bucharest, Romania, and was financed by the Project number: 2023-1-RO01-KA220-HED-000154433 entitled: Gender, Digitalization, Green: Ensuring a Sustainable Future for all in Europe.

## REFERENCES

Buenadicha-Mateos, M., Sánchez-Hernández, M. I., González-López, O. R., & Tato-Jiménez, J. L. (2025). From Engagement to Achievement: How Gamification Impacts Academic Success in Higher Education. *Education Sciences*, *15*(8), 1054.

Christopoulos, A., & Mystakidis, S. (2023). Gamification in Education. *Encyclopedia*, 3(4), 1223-1243.

Ciric, A., Radu, N., Zaharie, M. G. O., Neagu, G., Pîrvu, L. C., Begea, M., & Stefaniu, A. (2023). Potential antitumor effect of functional yogurts formulated with prebiotics from cereals and a consortium of probiotic bacteria. *Foods, 12*, 1250.

David, L., & Weinstein, N. (2024). The how and how much of technology use in the classroom: A

motivational approach to teachers' technology use. *European Journal of Education, 59*(4)*,* e12674.

Deterding, S., Dixon, D., Khaled, R., & Nacke, L. (2011). From game design elements to gamefulness: Defining "gamification". *Proceedings of the 15th International Academic MindTrek Conference: Envisioning Future Media Environments.* 9–15.

Dicheva, D., Dichev, C., Agre, G., & Angelova, G. (2015). Gamification in education: A systematic mapping study. *Educational Technology & Society, 18*(3), 75–88.

Dima, G., Radu, N., Chirvase, A., & Pena, E. L. (2007). Studies regarding using biomass in bioremediation of wastewater with heavy metals. *Revista de Chimie, 58*(6), 561–565.

Gan, C., & Duan, L. (2026). The relationship between challenge and feedback mechanisms in gamified learning experiences and learning engagement: The mediating role of flow. *Acta Psychologica, 267*, 107054.

Klock, A. C. T., Palomino, P. T., Rodrigues, L. A. L., Toda, A. M., Simanke, S., Spors, V., Santana, B. S., & Hamari, J. (2026). Gamification towards and alongside equity, diversity and inclusion: Looking back to move forward. *New Media & Society, 28*(2), 899–924.

Oliveira, W., Dantas Scaico, P., Hamari, J., Li, Z., & Shi, L. (2025). The effects of gamification on students' flow experience. *Journal of Computer Assisted Learning, 41*(5), e70120.

Oliveira, W. & Hamari, J. (2024). Flow experience analysis in gameful educational environments: A systematic literature review. 2024 *IEEE International Conference on Advanced Learning Technologies (ICALT)*, 44–46.

Oliveira, W., Hamari, J., Shi, L., Toda, A. M., Rodrigues, L., Palomino, P. T., & Isotani, S. (2023). Tailored gamification in education: A literature review and future agenda. *Education and Information Technologies, 28*(1), 373–406.

Ratinho, E., & Martins, C. (2023). The role of gamified learning strategies in student's motivation in high school and higher education: A systematic review. *Heliyon*, *9*(8), e19033.

Rodrigues, L., Pereira, F. D., Toda, A. M., Palomino, P. T., Pessoa, M., Carvalho, L. S. G., Fernandes, D., Oliveira, E. H. T., Cristea, A. I., & Isotani, S. (2022). Gamification suffers from the novelty effect but benefits from the familiarization effect: Findings from a longitudinal study. *International Journal of Educational Technology in Higher Education, 19*, 13.

Rodriguez-Calzada, L., Paredes-Velasco, M., & Urquiza-Fuentes, J. (2024) The educational impact of a comprehensive serious game within the university setting: Improving learning and fostering motivation. *Heliyon*, *10*(16), e35608.

Ryan, R. M., & Deci, E. L. (2020). Intrinsic and extrinsic motivation from a self-determination theory perspective: Definitions, theory, practices, and future directions. *Contemporary Educational Psychology, 61*, 101860.

Sailer, M., & Homner, L. (2020). The gamification of learning: A meta-analysis. *Educational Psychology Review, 32*, 77–112.

Santiago, C. P., Silva, A. R. dos S., Menezes, J. W. M., & Aquino, F. J. A. de. (2025). Gamification and Self-Determination Theory in teaching computational thinking: An experience with Quizizz software. *Informatics in Education, 24*(3), 587–615.

Seaborn, K., & Fels, D. I. (2015). Gamification in theory and action: A survey. *International Journal of Human-Computer Studies, 74*, 14–31.

Spilotro, C., Posa, M., Secundo, G., & De Turi, I. (2026). Disclosing the twin transition: Digital and green transformation in Italian universities from an institutional perspective. *Journal of Innovation & Knowledge, 14*, Article 100964.

Toda, A. M., Oliveira, W., Shi, L., Bittencourt, I. I., Isotani, S., & Cristea, A. I. (2019). *Planning gamification strategies based on user characteristics and DM: A gender-based case study.* In Desmarais, M. C., Lynch, C. F., Merceron, A., & Nkambou, R. (Eds.). Proceedings of the 12th International Conference on Educational Data Mining (EDM 2019) *4*38–443.

van den Broek, G.S.E., Scholten, S, van Thuil, B.,van Rijn H., van Gog, T., & van der Velde, M. (2026). Gamified feedback in adaptive retrieval practice: Points and progress-bars enhance motivation but not learning. *Computers in Human Behavior, 177*, 108862.

van Roy, R., & Zaman, B. (2018). Need-supporting gamification in education: An assessment of motivational effects over time. *Computers & Education, 127*, 283–297.

Ying, H., & Wan Yahaya, W. A. J. (2026). AI-mediated feedback in gamified programming education: Effects on vocational students' achievement and motivation. *Frontiers in Education, 11*, 1846699.

Scientific Papers. Series E. Land Reclamation, Earth Observation & Surveying, Environmental Engineering. Vol. XV, 2026
Print ISSN 2285-6064, CD-ROM ISSN 2285-6072, Online ISSN 2393-5138, ISSN-L 2285-6064

# NUTRITIONALLY RELEVANT MINERALS IN PARSLEY ROOT: AN X-RAY FLUORESCENCE STUDY

**Laura RADULESCU[1], Calin JIANU[1], Ersilia ALEXA[1], Ariana-Bianca VELCIOV[1], Virgil-Dacian LALESCU[1], Antoanela COZMA[2], Corina Iuliana MEGYESI[1], Daniela STOIN[1], Diana MOIGRADEAN[1], Simion ALDA[3], Mariana-Atena POIANA[1], Carmen-Daniela PETCU[4], Viorica BOACA[2], Despina-Maria BORDEAN[1]**

[1]University of Life Sciences "King Mihai I" from Timisoara, Faculty of Food Engineering, 119 Aradului Street, 300645, Timisoara, Romania
[2]University of Life Sciences "King Mihai I" from Timisoara, Faculty of Agriculture, 119 Aradului Street, 300645, Timisoara, Romania
[3]University of Life Sciences "King Mihai I" from Timisoara, Faculty of Engineering and Applied Technologies, 119 Aradului Street, 300645, Timisoara, Romania
[4]University of Agronomic Sciences and Veterinary Medicine of Bucharest, Faculty of Veterinary Medicine, 105 Splaiul Independentei, 050097, District 5, Bucharest, Romania

Corresponding author emails: carmen.petcu@fmvb.usamvb.ro, despinabordean@usvt.ro

***Abstract***

*Parsley (Petroselinum crispum* Mill*.) is a plant valued for its high nutritional content and functional properties, being an important source of vitamins and essential minerals for human health. This study aims to evaluate the mineral composition of parsley root and assess its potential health benefits. The concentrations of macroelements (calcium, magnesium, potassium, and phosphorus) and microelements (iron, zinc, manganese, and copper) were determined using X-ray fluorescence spectrometry (XRF). Parsley root samples were collected from various supermarkets in Romania and the results were compared with data reported in the literature. The mineral analysis revealed a high and relatively consistent content of essential macro- and microelements across all samples. The measured levels of potassium, calcium, iron, manganese, and zinc were comparable to or slightly higher than those previously reported, highlighting the nutritional potential of parsley root as a natural mineral source. Variations among samples can be attributed to differences in soil composition and cultivation conditions, without significantly impacting the overall nutritional quality. These findings support the inclusion of parsley root as a valuable ingredient in balanced diets and functional food formulations.*

***Key words:*** *health benefits, mathematical model, Petroselinum crispum, X-ray fluorescence spectrometry.*

## INTRODUCTION

The vegetables with leaf and roots are valued due to their rich content in essential nutrients. They are also recognized for their significant contribution to human health. Among these, parsley (*Petroselinum crispum* Mill.), both the leaf and the root, represent a promising plant with relevant minerals content and considerable potential to facilitate various favorable health effects (Ahmed et al., 2025).

This work investigates the mineral composition of parsley roots using the X-ray fluorescence (XRF) technique.

Parsley *(Petroselinum crispum* Mill.*)* is an herbaceous leguminous plant that belongs to the Apiaceae family. According to the classification of A. L. de Jussieu, parsley (*Petroselinum crispum* Mill.) belongs to the Rosidae class and is known under the name of Umbelliferae. For this reason, it is often called the umbrella plant (Chauhan & Aishwarya, 2018). Native to Europe and western Asia it is currently widespread in many regions of the world (Mahmood et al., 2014). Parsley (*Petroselinum crispum* Mill.) is cultivated for its white taproot and intensely aromatic leaves. It is used for food, cosmetic, and pharmaceutical industries for their aromatic and culinary properties as well as for their medicinal benefits (Zaaboul & Liu, 2022). Also, it is wealthy in nutrients, vitamins, minerals (Zaaboul & Liu, 2022) and apiol, which is an organic compound found in parsley

seeds with therapeutic properties (Gogoaşă et al., 2014; Ajmera et al., 2019).

Parsley (*Petroselinum crispum* Mill.) is well known as an aromatic plant and it is widely used in both traditional and international cuisine. Generally, parsley is considered an auxiliary and decorative ingredient rather than a valuable source of nutrients (Ajmera et al., 2019; Bahramsoltani et al., 2024). The chemical composition of parsley root includes: 85% water, 3% protein, 6% carbohydrates, volatile oils and a significant amounts of minerals (especially potassium), phosphorus, magnesium, calcium, iron, as well as a number of vitamins (A, B, C). It is low in calories, one hundred grams of parsley root contains 36 kcal (Cozma et al., 2022; Wszelaczyńska et al., 2024). Among all root vegetables, parsley is characterized by a significant content of K (399 mg/100 g) and calcium (Ca) (43 mg/100 g). Moreover, parsley is also rich in folate (180 µg/100 g). Consumption of 100 g of parsley covers the daily requirement of folic acid by 30-40% (Knez et al., 2022).

Due to the diversity of bioactive compounds, parsley stands out as a vegetable with therapeutic potential and has been described in the scientific literature as exhibiting tonic, antianemia, antirachitic, antiasthmatic, anti-xerophthalmic, antiscorbutic, antifebrile, anti-inflammatory, mineralizing, depurative, diuretic, secretolytic, vasodilatory, expectorant, vermifuge, and uterotonic effects (Gogoaşă et al., 2014; Ajmera et al., 2019; Bahramsoltani et al., 2024).

Researcher's analyses have demonstrated the significance of dietary minerals, vital for disease prevention and maintaining overall good health. Although they constitute a relatively small proportion of approximately 4-6% of body weight, minerals are key components of the human diet (Özcan, 2004; Knez et al., 2022).

The minerals present in parsley have major importance, as each of them contributes significantly to the proper functioning of the body. Iron is a mineral vital for haemoglobin formation and oxygen transport in the blood. Magnesium plays an important role in the proper functioning of the nervous system, in regulating blood pressure, and has a relaxing effect on muscles. Calcium contributes to bone and dental health. Potassium has a key role in well function of hearth and blood pressure regulation, while zinc has beneficial effects to the immune system and protein synthesis, and phosphorus is essential for cellular energy production (Alobaidi, 2024).

The minerals present in parsley play an important role in maintaining optimal physiological functions, and their consumption contributes to overall health and helps prevent mineral deficiencies (Ajmera et al., 2019). Therefore, a healthy diet is based on a balanced and varied eating plan, which includes appropriate portions of vegetables, fruits and cereals rich in fiber and protein, along with a moderate consumption of fats, sugar and salt (Rădulescu et al., 2025).

To assess the mineral content of parsley roots and to identify variations determined by cultivation conditions and also by soil composition, it is necessary to apply an efficient and non-invasive analytical technique. Thus, X-ray fluorescence (XRF) is a rapid and precise method, which allows the simultaneous quantification of major minerals as well as trace elements without complex chemical preparation of the samples (Jenkins et al., 1995; Wszelaczyńska et al., 2024). The application of XRF in this study of parsley roots allows the determination of the complete mineral profile, thus providing valuable data for both nutrition and health as well as agricultural research.

## MATERIALS AND METHODS

Parsley roots were purchased from five different supermarkets in Romania, then cleaned to remove impurities, scraped, and initially air-dried at room temperature. Subsequently, the roots were dried in an oven until the moisture content decreased below 5%, a level recommended for accurate mineral determination. The dried samples were then finely ground, packed in sterile airtight bags, properly labelled, and stored for further analyses and determinations.

For X-ray fluorescence (XRF) analyses, the powdered samples were examined using a Hitachi X-MET8000 portable spectrometer, which can measure a wide range of atomic elements, from sodium (Z11) to uranium (Z92), providing detection limits from a few parts per

million (ppm) up to high percentages (% by weight). This method was selected because XRF is an essential technique for the evaluation of soil and plant samples at medium air pressure, and it is frequently used for both qualitative and quantitative analyses. The method is based on the fact that each mineral present in the analysed material (parsley root) emits a characteristic set of fluorescent X-rays, a "fingerprint" specific to each element (Rădulescu et al., 2024). XRF spectrometry is advantageous because it provides rapid determination of elemental concentrations and presence, with high accuracy (Panebianco et al., 2023). Measurements were performed in triplicate to ensure precision and consistency, and the results were expressed in parts per million (ppm).

Statistical evaluation of the data was performed using PAST software, version 2.17c (Hammer et al., 2001). Data obtained from the mineral determinations were processed using descriptive statistics and expressed as mean values ± standard deviation.

## RESULTS AND DISCUSSIONS

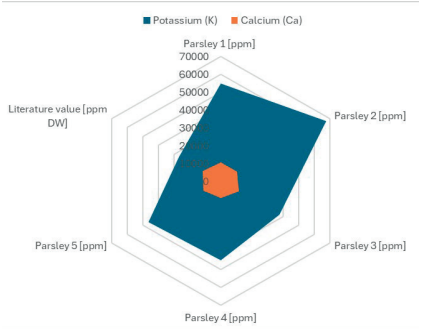
The analyzed parsley roots revealed high concentrations of several essential minerals, predominantly K and Fe, above literature reference values, demonstrating high nutritional potential. However, the increased levels of Cu, Ni, and Pb suggest possible environmental or soil-related contamination impacts. The variability between samples shows distinct geochemical or anthropogenic signatures connected with their provenience. Further soil–plant transfer factor assessment and comparison with regulatory maximum allowable limits are recommended to evaluate food safety implications (Table 1).

Table 1. Mineral composition of parsley root samples

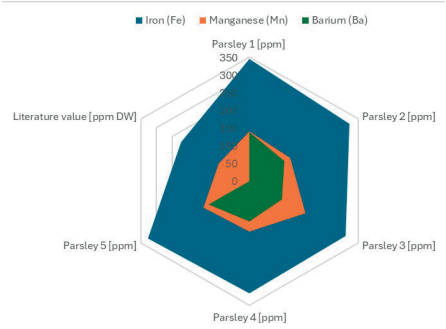
| Mineral | Parsley 1 [mg/kg] | Parsley 2 [mg/kg] | Parsley 3 [mg/kg] | Parsley 4 [mg/kg] | Parsley 5 [mg/kg] | Literature value (mg/kg DW) |
|---|---|---|---|---|---|---|
| Potassium (K) | 54707.00 ± 700.00 | 67462.00 ± 3,142.00 | 37,793.00 ± 930.00 | 44758.00 ± 315.00 | 46185.00 ± 1,690.00 | 63000.00 (Nutrition Data Hub, 2026) |
| Calcium (Ca) | 10525.00 ± 19.00 | 10585.00 ± 779.00 | 11732.00 ± 396.00 | 9811.00 ± 285.00 | 10906.00 ± 197.00 | 1760.00 (Nutrition Data Hub, 2026) |
| Iron (Fe) | 345.00 ± 8.00 | 323.00 ± 9.00 | 309.00 ± 7.00 | 317.00 ± 14.00 | 326.00 ± 18.00 | 539 (Nutrition Data Hub, 2026) |
| Copper (Cu) | 34.00 ± 1.00 | 47.00 ± 0.00 | 39.00 ± 0.00 | 40.00 ± 0.01 | 31.00 ± 3.00 | 4.6 (Nutrition Data Hub, 2026) |
| Manganese (Mn) | 140.00 ± 18.00 | 130.00 ± 23.00 | 181.00 ± 7.00 | 142.00 ± 21.00 | 149.00 ± 11.00 | 134 (Nutrition Data Hub, 2026) |
| Molybdenum (Mo) | 13.00 ± 3.00 | 7.00 ± 2.00 | 7.00 ± 0.00 | 10.00 ± 3.00 | 7.00 ± 3.00 | - |
| Zinc (Zn) | 52.00 ± 4.00 | 56.00 ± 1.00 | 47.00 ± 0.00 | 54.00 ± 1.00 | 53.00 ± 0.00 | 61.1 (Nutrition Data Hub, 2026) |
| Nickel (Ni) | 19.00 ± 1.00 | ND | 20.00 ± 4.00 | 22.00±0.00 | ND | 1.30 (Arsenov et al., 2021) |
| Barium (Ba) | 138.00 ± 16.00 | 113.00 ± 0.00 | 104.00 ± 0.02 | 114.00 ± 0.03 | 131.00 ± 0.00 | - |
| Strontium (Sr) | 48.00 ± 0.00 | 60.00 ± 2.00 | 79.00 ± 5.00 | 44.00 ± 2.00 | 57.00 ± 2.00 | - |
| Rubidium (Rb) | 10.00 ± 0.00 | 44.00 ± 3.00 | 25.00 ± 0.00 | 16.00 ± 0.00 | 21.00 ± 0.00 | - |
| Mercury (Hg) | 5.00 ± 0.00 | 20.00 ± 0.00 | 22.00 ± 2.00 | 17.00 ± 0.00 | 24.00 ± 5.00 | - |
| Lead (Pb) | 4.00 ± 0.00 | 10.00 ± 0.00 | 6.00 ± 0.00 | 7.00 ± 2.00 | 6.00 ± 0.00 | 0.55 (Winiarska-Mieczan et al., 2023) |

Data are presented as mean ± standard deviation
Legend: ND = Not Detected (below the detection limit of the XRF spectrometer).

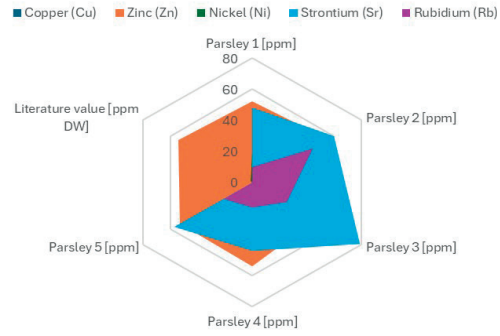
The five parsley root samples displayed diverse mineral fingerprints reflecting variances in their provenience (Figure 1). Parsley 2 was characterized by high K, Cu, Pb, and Rb, whereas Parsley 3 showed enrichment in Mn and Sr. The occurrence of Ni in only three samples supplementary supports site-specific soil influence. These results indicate that mineral composition in parsley roots is strongly designed by environmental and geochemical factors rather than solely by plant physiological control.



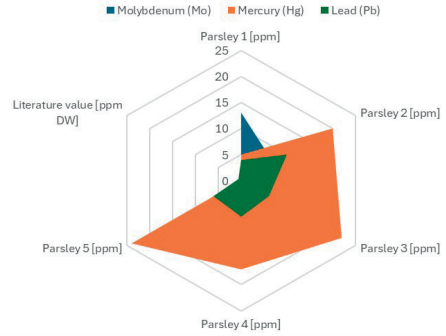

Comparative Mineral Profile of K and Ca in the investigated Parsley Root Samples




Comparative Mineral Profile of Fe, Mn and Ba in the investigated Parsley Root Samples




Comparative Mineral Profile of Cu, Zn, Ni, Sr and Rb in in the investigated Parsley Root Samples




Comparative Mineral Profile of Mo, Hg and Pb in in the investigated Parsley Root Samples

Figure 1. Mineral Fingerprint of Parsley Roots Based on Mineral Content

Each sample presents a distinct mineral fingerprint**,** indicating different soil characteristics and possibly different anthropogenic pressures. As we can observe, the mineral composition of the parsley roots is shaped by different particularities like: Physiological regulation (Ca, Zn stability); Soil fertility differences (K variability), Geochemical background (Ba, Sr, Rb) and local environmental influence (Ni, Pb, Hg).

Radar plot analysis revealed distinct mineral fingerprints among the five parsley root samples. While calcium and zinc displayed limited variability, indicating physiological regulation, potassium showed pronounced variation, with Parsley 2 exhibiting the highest concentration. Trace elements such as Ni, Pb, Hg, Rb, and Sr demonstrated strong inter-sample differences, suggesting provenance-dependent geochemical and environmental influences. Parsley 3 was characterized by elevated Mn and Sr, whereas Parsley 2 exhibited increased Cu, Pb, and Rb levels. These findings confirm that mineral accumulation patterns in parsley roots are primarily shaped by soil composition and local environmental conditions rather than intrinsic plant physiology alone.

The PCA biplot illustrates the mineral composition of the investigated parsley root samples after standardization (Figure 2). PC1 (the first principal component) represents the major source of variance in the dataset and primarily reflects differences in mineral enrichment, predominantly determined by K, Zn, Fe, Ba, and Mo. Along PC1, Parsley 1 indicates a relatively enriched mineral profile, while Parsley 3 is positioned on the opposite side, showing lower concentrations of several macro- and microelements. This separation suggests that PC1 presents the differences primarily related to soil fertility and mineral availability.

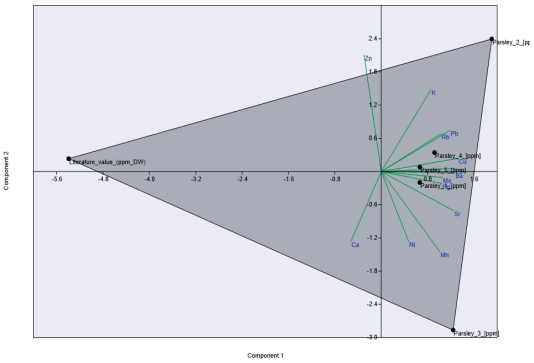



Figure 2. PCA Biplot of Mineral Composition in Parsley Roots Samples

PC2 (the second principal component) differentiates the samples based on the metals Pb, Rb, Cu, and Hg, which display stronger inter-sample variability and environmental sensitivity. Parsley 2 is clearly shifted upward along PC2, reflecting elevated Pb and Rb levels and thus a distinct geochemical signature. Parsley 3 appears in the lower quadrant, influenced more by Mn and Ca.

Parsley 2 is distinctly positioned in the positive PC2 quadrant, associated with high Pb and Rb levels, indicating a specific geochemical or environmental signature. In contrast, Parsley 3 appears in the lower quadrant, influenced more by Mn and Ca. The orientation and length of the vectors confirm that Rb, Pb, and Ni are among the strongest discriminant elements, contributing substantially to sample separation.

Overall, the PCA confirms that the mineral composition of parsley roots is governed by provenance-dependent factors. While some elements (e.g., Ca and Zn) appear relatively stable and physiologically regulated, others (notably Rb, Pb, Ni, and Mn) are responsible for the distinct mineral fingerprints observed among samples, highlighting the influence of soil geochemistry and localized environmental conditions.

## CONCLUSIONS

The analysis of parsley roots indicated high levels of essential minerals, potassium (K) and iron (Fe), exceeding the reference values reported in the scientific literature, thus reflecting a high nutritional potential. Trace elements such as copper (Cu), nickel (Ni), and lead (Pb) were present only in some of the samples, their occurrence highlighting possible influences of the environment or soil on contamination. The differences between the five studied samples reflect distinct geochemical or anthropogenic fingerprints, particularly related to their provenance and soil conditions. XRF analysis proved to be a very efficient, rapid, and non-destructive method, allowing both qualitative and quantitative assessment of the mineral composition of the parsley samples. The results obtained from principal component analysis (PCA) demonstrate that this composition is largely influenced by the provenance of the samples: elements such as Ca and Zn appear relatively stable and physiologically regulated, while other elements, such as Rb, Pb, Ni, and Mn, generate distinct mineral fingerprints, reflecting the influence of soil geochemistry and localized environmental conditions. Considering the above, further studies are recommended to evaluate the soil–plant transfer factor and to compare the values with the maximum allowable limits established by regulations, in order to assess implications for food safety. The high concentrations of potassium (K) and iron (Fe) emphasize the nutritional value of parsley root, while the analysis of trace elements and mineral fingerprints through XRF and PCA provides relevant data on provenance and environmental influences, thereby confirming the potential of parsley root as a source of essential minerals and the need for monitoring food safety.

## ACKNOWLEDGEMENTS

This work was carried out using the own research funds of the University of Life Sciences “King Mihai I” from Timișoara. The research was conducted with the support of the Interdisciplinary Research Platform of the University of Life Sciences “King Mihai I” from Timișoara. The acquisition of the XRF Hitachi X-MET8000 spectrometer was financed through the Interreg-IPA Cross-border Cooperation Romania-Serbia Programme, under the project “Modern technologies for monitoring land covered with waste in order to restore their initial use”, 2019-2021, e-MS code: RORS 365.

## REFERENCES

Ahmed, W. E., Almutairi, A. A., Almujaydil, M. S., Algonaiman, R., Mirghani Mousa, H., & Alhomaid, R. M. (2025). Nutraceutical potential of parsley (*Petroselinum crispum* Mill.): Comprehensive overview. *Italian Journal of Food Science, 37*(1). 194–209. https://doi.org/10.15586/ijfs.v37i1.2806

Ajmera, P., Kalani, S., & Sharma, L. (2019). Parsley - benefits & side effects on health. *International Journal of Physiology, Nutrition and Physical Education, 4*(1), 1236–1242.

Alobaidi, S. (2024). Renal health benefits and therapeutic effects of parsley (*Petroselinum crispum*): A review. *Frontiers in Medicine, 11*. 1494740.

Arsenov. D., Župunski, M., Pajević, S., Nemeš, I., Simin, N., Alnuqaydan, A.M., Watson, M., Aloliqi, A.A., & Mimica-Dukić, N. (2021). Roots of Apium graveolens and *Petroselinum crispum* - Insight into Phenolic Status against Toxicity Level of Trace Elements. *Plants (Basel),* 10(9). 1785. doi: 10.3390/plants10091785. PMID: 34579318; PMCID: PMC8472699.

Bahramsoltani, R., Ahmadian, R., Daglia, M., & Rahimi, R. (2024). *Petroselinum crispum* (Mill.) Fuss (Parsley): An updated review of the traditional uses, phytochemistry, and pharmacology. *Journal of Agricultural and Food Chemistry, 72*(2). 956–972.

Chauhan, E. S., & Aishwarya, J. (2018). Nutraceuticals potential of Petroselinum Crispum: A review. *J. Complement. Med. Altern. Healthc*, *7*(2).

Cozma, A., Velciov, A., Popescu, S., Alexa, E., Popescu, S., Mărăzan, V., Cozma B., & Rada, M. (2022). Fresh root vegetables as mineralizing foods. *Research Journal of Agricultural Science, 54*(2).

Gogoașă, I., Maria, A. L., Velciov, A., Bordean, D.M., Rada, M., Moigradean, D., Alda S., & Gergen, I. (2014). Preliminary research regarding the use of some vegetables (carrot, parsley, celery, and tomato) as supplementary sources of bio minerals. *Journal of Horticulture, Forestry and Biotechnology, 18*(4). 102–107.

Hammer, O., Harper, D. A. T., & Paul, D. R. (2001). PAST: Paleontological statistics software package for education and data analysis. *Palaeontologia Electronica, 4*(1). 9. https://palaeo-electronica.org/2001_1/past/issue1_01.htm

Jenkins, R., Gould, R. W., & Gedcke, D. (1995). *Quantitative X-ray spectrometry* (2nd ed.). CRC Press.

Knez, E., Kadac-Czapska, K., Dmochowska-Ślęzak, K., & Grembecka, M. (2022). Root vegetables - Composition, health effects, and contaminants. *International Journal of Environmental Research and Public Health, 19*(23). 15531.

Mahmood, S., Hussain, S., & Malik, F. (2014). Critique of medicinal conspicuousness of parsley (*Petroselinum crispum*): A culinary herb of Mediterranean region. *Pakistan Journal of Pharmaceutical Sciences, 27*(1). 193–202.

Nutrition Data Hub. (2026). Parsley, freeze-dried. Vegetables and Vegetable Products. Retrieved June 16, 2026, from https://nutritiondatahub.com/food/parsley-freeze-dried-170486

Özcan, M. (2004) Mineral Contents of Some Plants Used as Condiments in Turkey. *Food Chemistry*, 84. 437-440. http://dx.doi.org/10.1016/S0308-8146(03)00263-2

Panebianco, S., Pellegriti, M. G., Finocchiaro, C., Musumarra, A., Barone, G., Caggiani, M. C., Cirvilleri, G., Lanzafame, G., Pulvirenti, A., Scordino, A., & Mazzoleni, P. (2023). XRF analysis searching for fingerprint elemental profile in south-eastern Sicily tomatoes. *Scientific Reports, 13*(1). 13739.

Rădulescu, L., Velciov, A. B., Megyesi, C. T., Alda, S., & Bordean, D. M. (2025). Impact of cooking on the nutritional profile of parsnip (*Pastinaca sativa*). *International Multidisciplinary Scientific GeoConference: SGEM, 5*(1). 171–178.

Rădulescu, L., Tarkanyi, P., Velciov, A. B., Alda, L. M., Alda, S., & Bordean, D. M. (2024). Nettle bread, a potential functional product. *Scientific Papers. Series A. Agronomy, 67*(2).

Winiarska-Mieczan, A., Jachimowicz, K., Kwiecień, M., Krusiński, R., Kislova, S., Sowińska, L., Zasadna, Z., Yanovych, D. (2023). The Content of Cd and Pb in Herbs and Single-Component Spices Used in Polish Cuisine. *Biol Trace Elem Res*., *201*(7).3567-3581. doi: 10.1007/s12011-022-03437-7. Epub 2022 Oct 7. PMID: 36205876; PMCID: PMC10160165.

Wszelaczyńska, E., Poberežny, J., Gościnna, K., Retmańska, K., & Kozera, W. J. (2024). Nutritional value of parsley roots depending on nitrogen and magnesium fertilization. *Agriculture, 14*(1). 143.

Zaaboul, F., & Liu, Y. (2022). Vitamin E in foodstuff: Nutritional, analytical, and food technology aspects. *Comprehensive Reviews in Food Science and Food Safety, 21*(2). 964–998.

Scientific Papers. Series E. Land Reclamation, Earth Observation & Surveying, Environmental Engineering. Vol. XV, 2026
Print ISSN 2285-6064, CD-ROM ISSN 2285-6072, Online ISSN 2393-5138, ISSN-L 2285-6064

# ANALYSIS OF SPATIAL GEODETIC METHODS FOR MONITORING MINING GEOSYSTEMS

**Gabriel TĂNASIE[1], Nicolae DIMA[1], Larisa-Ofelia FILIP[1], Gabriel BĂDESCU[2]**

[1]University of Petroșani, 20 Universității Street, Petroșani, Romania
[2]University of Craiova, 13 A. I. Cuza Street, Craiova, Romania

Corresponding author email: LarisaFilip@upet.ro

***Abstract***

*The increasing availability of satellite and airborne technologies has changed the way mining-affected areas are monitored and analyzed. Spatial geodetic methods such as GNSS, satellite radar interferometry (InSAR), multispectral remote sensing, and UAV-based photogrammetry and LiDAR now allow continuous and accurate observation of ground behavior over large areas. This paper presents an overview of the main spatial geodetic techniques used for monitoring mining geosystems, focusing on their practical application in detecting ground subsidence, slow surface deformations, structural instabilities, and volumetric changes of waste dumps and tailings dams. The strengths and limitations of each method are discussed from a practical perspective, taking into account accuracy, spatial coverage, operational constraints, and cost efficiency. Examples from Romania and other European mining regions highlight the benefits of combining GNSS, InSAR, UAV data, and GIS platforms into integrated monitoring systems. Such approaches support early detection of hazardous processes and contribute to safer and more sustainable management of mining and post-mining environments.*

***Key words:*** *geotechnical monitoring, GIS, GNSS, InSAR, LiDAR, mining waste dumps, remote sensing, spatial geodesy, tailings dams, UAV.*

## INTRODUCTION

Mining geosystems (open pits, underground operations, waste rock dumps, ash deposits, and tailings storage facilities) are dynamic engineered–natural systems that can evolve rapidly under changes in loading, groundwater, drainage, and material properties. Their deformation may remain subtle for long periods, then accelerate into hazardous states such as progressive slope failure, dam crest settlement, or wide-area subsidence. Internationally, the consequences of tailings failures have strengthened the demand for demonstrable monitoring capacity and transparent risk governance, including the Global Industry Standard on Tailings Management (UNEP, 2020). In the European Union, the management of waste from extractive industries is framed by Directive 2006/21/EC, which requires appropriate control and risk prevention measures throughout the lifecycle of tailings facilities and waste dumps (European Parliament & Council, 2006). These drivers, together with the availability of Copernicus Sentinel missions, have accelerated the uptake of spatial geodetic and Earth observation techniques for operational monitoring.

Spatial geodetic methods complement classical geotechnical instrumentation by providing geometrically consistent, often remotely acquired observations that link local deformation at critical structures to regional patterns. GNSS networks offer absolute 3D positioning with high temporal sampling, supporting early detection of deviations from expected behavior and serving as validation for remote sensing products (Scaioni et al., 2018). Multi-temporal InSAR provides dense, wide-area displacement measurements along the radar line of sight (LOS) and can reveal slow subsidence or creep processes that are difficult to capture with sparse ground points (Ferretti et al., 2001; Berardino et al., 2002; Crosetto et al., 2016; Aswathi et al., 2022). UAV-based photogrammetry (Structure-from-Motion, SfM) and UAV LiDAR deliver centimeter- to decimeter-scale 3D surface models and enable volumetric change analysis over waste dumps, tailings beaches, and open-pit benches (Westoby et al., 2012; Nex et al., 2022; Liu et al., 2023). Multispectral and hyperspectral

remote sensing add information on surface cover and mineralogical indicators that relate to erosion, dust emission, or acid mine drainage (Seifi et al., 2019; Dkhala et al., 2020).

The aim of this paper is to synthesize, from a practical perspective, the main spatial geodetic techniques used for monitoring mining-affected areas and to compare their accuracy, spatial and temporal coverage, operational constraints, and cost efficiency. We also emphasize integrated monitoring architectures that combine GNSS, InSAR, UAV-derived 3D products and GIS-based decision layers to support early warning and sustainable mine closure and post-mining management (Del Soldato et al., 2019; Poncoș et al., 2022).

## MATERIALS AND METHODS

This study is a structured review and comparative analysis of spatial geodetic approaches for deformation and change monitoring in mining geosystems. The comparison follows four practical criteria: (i) geometric performance (precision, accuracy, and sensitivity to deformation components), (ii) scale (point, object, and regional coverage), (iii) temporal sampling and operational availability, and (iv) implementation effort and costs (hardware, field time, data processing, and expertise). As the literature spans multiple domains (geodesy, remote sensing, mining engineering and risk management), we focus on methods with established workflows and demonstrated applications to subsidence, slope instability, and volumetric change.

For satellite radar interferometry, we adopt the standard distinction between single-pair DInSAR and multi-temporal techniques. PSI relies on stable radar targets to estimate long time-series displacement with reduced atmospheric noise (Ferretti et al., 2001; Hanssen, 2001). SBAS and related small-baseline methods exploit short temporal and spatial baselines to increase coherence over distributed targets (Berardino et al., 2002). In operational contexts, Sentinel-1 provides systematic C-band acquisitions with a 12-day repeat cycle for a single satellite and 6 days for a two-satellite constellation, with robust day-and-night and all-weather capability (Copernicus Data Space, 2025; SentiWiki, 2025). For optical remote sensing, Sentinel-2 MSI provides 13 spectral bands supporting land cover, moisture and mineral mapping at 10-60 m resolution (Copernicus Data Space, 2025; ESA, 2025).

For UAV surveys, we consider two principal data products: (a) dense point clouds and digital surface models (DSMs) from SfM photogrammetry, and (b) LiDAR point clouds acquired from airborne laser scanners mounted on UAVs. Change detection between epochs can be performed using DEM-of-difference or point-cloud-to-point-cloud approaches such as M3C2, which is well suited to rough, three-dimensional surfaces common in dumps and benches (Williams et al., 2021; Liu et al., 2023).

For GNSS monitoring, we consider both permanent stations (continuous) and campaign networks, with processing options ranging from relative positioning to PPP solutions depending on infrastructure and required accuracy (Scaioni et al., 2018).

The integrated monitoring concept is represented as a data pipeline where each observation type is quality controlled and co-registered into a consistent reference frame, then fused within a GIS platform for interpretation, thresholding, and alerting. This aligns with modern risk-based monitoring guidance for tailings facilities emphasizing defensible data, traceability, and timely escalation (UNEP, 2020).

An integrated workflow for multi-sensor spatial monitoring is summarized in Figure 1.

An effective monitoring system for mining geosystems requires the integration of several complementary data sources, because each observation technique provides different information about surface deformation and environmental change. Satellite SAR data processed through PSI/SBAS techniques allow regional detection of slow ground movements, while GNSS networks provide precise reference measurements and local validation of displacement trends. UAV photogrammetry and UAV LiDAR add high-resolution three-dimensional information, useful for analysing local changes in waste dumps, tailings dams, open-pit slopes and other unstable mining structures. The combined interpretation of these datasets within a GIS/database environment makes it possible to perform quality control, compare independent measurements, detect

abnormal deformation patterns and transform geodetic observations into practical risk indicators. Figure 1 presents the proposed integrated workflow, from data acquisition and processing to GIS-based quality assessment and early warning support.

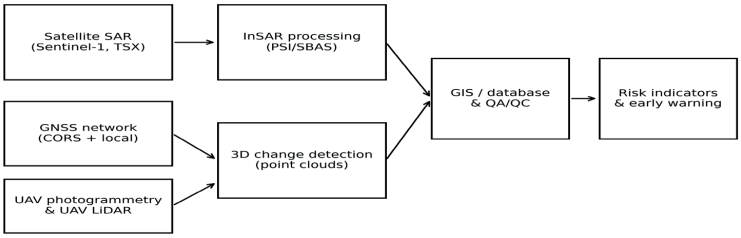



Figure 1. Integrated workflow combining satellite SAR, GNSS, UAV products and GIS decision layers

## RESULTS AND DISCUSSIONS

Table 1 highlights that no single method optimally satisfies precision, coverage and update frequency simultaneously. For operational risk management, method selection should be hazard-driven and multi-scale. Regional screening (e.g., subsidence bowls and creep zones) is effectively addressed by multi-temporal InSAR (Ferretti et al., 2001; Berardino et al., 2002; Crosetto et al., 2016), while structural performance at crest monuments or critical facilities requires high-fidelity ground measurements such as GNSS or classical geodetic control (Scaioni et al., 2018). For rapidly evolving geometry (bench retreat, dump reshaping, tailings beach migration), UAV point clouds enable frequent volumetric updates and local instability mapping (Westoby et al., 2012; Liu et al., 2023).

Table 1. Comparative overview of spatial geodetic methods for mining geosystem monitoring

| **Method** | **Main outputs** | **Typical deformation sensitivity** | **Spatial/temporal coverage** | **Strengths** | **Key limitations** |
|---|---|---|---|---|---|
| GNSS (campaign/continuous) | 3D point displacement; velocity; reference frame control | mm–cm at monitored points (daily–subdaily for permanent stations) | Points to networks; high rate possible | Absolute 3D; real-time options; strong for validation and critical structures | Sparse spatial sampling; requires installation and maintenance |
| InSAR (PSI/SBAS, Sentinel-1 or high-res SAR) | LOS displacement maps and time series; regional deformation patterns | mm–cm along LOS for coherent targets | $10^2$-$10^5$ km²; revisit 6-12 days (Sentinel-1) | Wide-area, dense measurements; retrospective analysis; cost-efficient at scale | LOS-only; decorrelation on vegetation/water; atmospheric artefacts; phase unwrapping issues |
| UAV photogrammetry (SfM) | Dense point clouds, orthomosaics, DSM/DTM; volumetric change | cm-dm (site dependent) | 0.1-10 km² per flight; on-demand | Very high spatial resolution; flexible survey geometry; low equipment cost | Requires safe access/flight permissions; lighting/wind constraints; GCP/direct georeferencing needed |
| UAV LiDAR | LiDAR point clouds; vegetation-penetrating surface; change vectors | dm to few cm (platform dependent) | 0.1-10 km²; on-demand (lower speed than photogrammetry) | Performs in low texture; less sensitive to illumination; better in vegetation | Higher sensor cost; calibration/boresight; point density depends on flight plan |
| Multispectral / hyperspectral EO (Sentinel-2, airborne) | Land cover, moisture proxies, mineral/contamination indicators | Indirect (not deformation); complements geometric monitoring | 10-60 m (Sentinel-2); revisit days | Supports environmental context: erosion, seepage, AMD indicators | Cloud sensitivity; mixed pixels; requires field validation for mineralogical interpretation |

The relationship between spatial coverage and vertical precision is an important criterion when selecting monitoring techniques for mining geosystems. Methods such as levelling, GNSS and terrestrial laser scanning provide high vertical accuracy, but their spatial coverage is

usually limited to points, profiles or local areas (Calina et al., 2021). In contrast, satellite-based InSAR offers regional coverage over very large surfaces, although the vertical precision is influenced by radar geometry, coherence, atmospheric effects and the need to convert line-of-sight displacement into vertical deformation. UAV photogrammetry and UAV LiDAR occupy an intermediate position, providing high-resolution spatial products over site-scale areas, which makes them particularly useful for monitoring waste dumps, tailings dams and open-pit slopes. Therefore, the choice of method should not be based only on precision, but also on the required monitoring scale, update frequency, accessibility of the site and the type of deformation process being investigated. Figure 2 illustrates this practical trade-off between typical spatial coverage and vertical precision for the main geodetic and remote-sensing techniques used in mining-area monitoring.

The practical value of spatial methods depends on uncertainty communication. InSAR products, for instance, are susceptible to atmospheric artefacts and may exhibit spatially correlated errors (Table 2); multi-temporal processing and the use of stable reference areas are therefore essential (Hanssen, 2001; Crosetto et al., 2016).

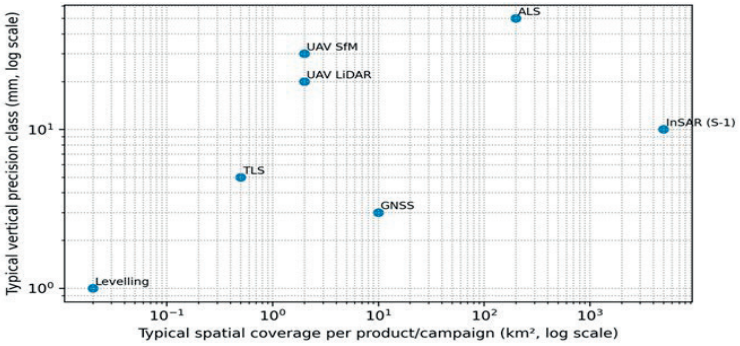



Figure 2. Trade-off between typical spatial coverage and precision class for common monitoring approaches (illustrative)

Table 2. Major error sources and mitigation strategies for spatial geodetic monitoring in mining areas

| Technique | Dominant error sources | Mitigation / QA-QC | Practical notes |
|---|---|---|---|
| InSAR (PSI/SBAS) | Atmospheric delay; temporal/spatial decorrelation; unwrapping errors; geometry (LOS) | Use multi-temporal methods; atmospheric filtering; ascending/descending decomposition; GNSS tie points | Best for slow deformation; interpret LOS; validate locally where possible |
| GNSS | Multipath; antenna stability; reference frame drift; troposphere modelling | Stable monuments; choke-ring antennas; network adjustment; PPP/relative processing; redundancy | High temporal sampling; critical points on crests and abutments |
| UAV SfM | Camera calibration; GCP quality; poor texture; wind; rolling shutter; time-varying shadows | Robust GCP network or RTK/PPK; calibration checks; overlap planning; independent checkpoints | Excellent for geometry and volumes; repeatable flight plans improve consistency |
| UAV LiDAR | Boresight misalignment; IMU drift; scan geometry; strip adjustment | Calibration flights; strip adjustment; ground truth targets; stable control points | Better than SfM on low-texture surfaces and in vegetation; higher sensor cost. |

Where deformation vectors are needed, combining ascending and descending tracks allows decomposition into vertical and east–west components, although the north–south component typically remains weakly observed (Crosetto et al., 2016). For UAV change detection, point-cloud-to-point-cloud techniques (e.g., M3C2) reduce bias introduced by gridding and are well suited for rough quarry and dump surfaces (Williams et al., 2021; Liu et al., 2023).

A typical integration pattern is to use GNSS time series to validate InSAR trends and to strengthen interpretation of low-rate deformation (Figure 3).

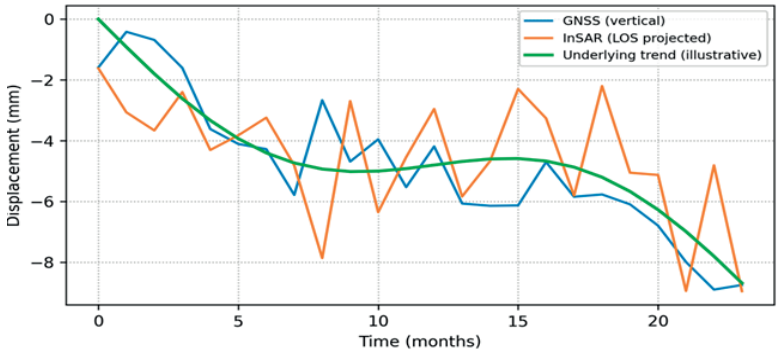



Figure 3. Example of GNSS-InSAR time series consistency for slow deformation

Integration is most effective when each method is assigned a clear role. In mining subsidence, for example, InSAR can provide long-term regional context and reveal residual subsidence beyond the footprint of active panels, while GNSS and classical control networks constrain absolute displacement at infrastructure points. This complementarity has been demonstrated in multiple European mining regions. In Poland's Upper Silesian Coal Basin, multi-decadal InSAR analysis revealed both active subsidence troughs and residual deformation zones over thousands of square kilometers (Przyłucka et al., 2022). In southeast Spain (La Unión), advanced DInSAR was used to map small-scale subsidence affecting built-up areas within historic mining districts (Herrera et al., 2007).

Romania provides diverse mining settings where integrated approaches are increasingly relevant (Stefan et al., 2009). A Sentinel-1 based study in the Călimani area demonstrated the use of interferometric processing for terrain reconstruction and monitoring in a former sulphur quarry, motivated by high costs and accessibility constraints of terrestrial surveys (Gheorghe & Vodă Marc, 2020). National-scale services have also been developed: a ground motion monitoring product for Romania highlighted the potential of InSAR to detect subtle deformation patterns and to support infrastructure and environmental assessment (Terrasigna, 2020). More recently, integrated EO monitoring of the Roșia Poieni copper mine has been discussed as a pathway to link geomorphic evolution and environmental indicators to operational decision-making (Herban et al., 2024; Kirsch et al., 2025).

From an operational point of view, decision makers often need a simplified comparison of method attributes; a qualitative scoring example is shown in Figure 4.

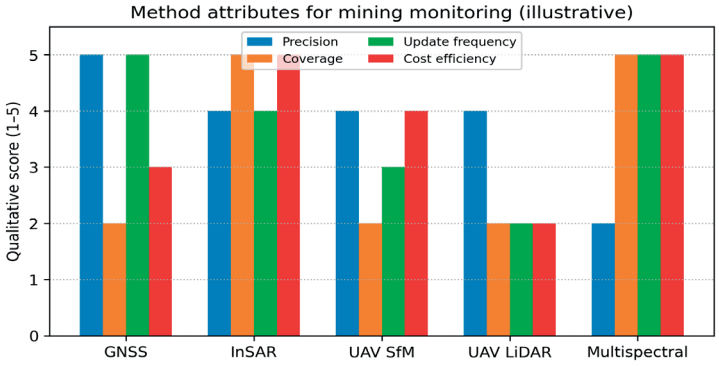



Figure 4. Qualitative comparison of method attributes relevant for mining monitoring

Table 3 summarizes practical configurations that align method capability with hazards. For tailings facilities, integrated schemes are increasingly coupled with numerical modelling and risk assessment. For instance, combining InSAR with modelling has been shown to improve interpretation and to support early detection of slope instability patterns in tailings ponds (Lu et al., 2025). InSAR-based ground motion services can also support prioritization, directing limited field resources to zones showing acceleration or anomalous trends (Del Soldato et al., 2019; Poncoș et al., 2022).

Table 3. Recommended integrated monitoring configurations by mining object and dominant hazard

| Object / hazard | Regional screening | Local high-resolution monitoring | Decision layer |
|---|---|---|---|
| Tailings dam: crest settlement, slope instability | InSAR (PSI/SBAS) + optical change detection for seepage indicators | GNSS on crest/abutments + UAV LiDAR/SfM for beach and slope geometry | Thresholds on velocities/accelerations; integration with geotechnical readings and GISTM controls |
| Waste rock dump: creep, erosion, runout susceptibility | InSAR + multispectral (moisture/vegetation) for surface condition | UAV SfM for frequent 3D updates; TLS for critical scarps; GNSS targets where needed | Change maps and volume budgets; trigger surveys after intense rainfall or operational regrading |
| Open pit slopes: bench instability, rockfall precursors | InSAR where coherent; regional context for surrounding infrastructure | UAV SfM/LiDAR + TLS for detailed discontinuity mapping and change detection | Spatial zoning of deformation; hazard maps; coupling with operational plans |
| Underground mining: subsidence bowls and infrastructure impact | InSAR time series (long-term) | GNSS/levelling lines along critical assets; UAV mapping for local cracks | Subsidence prediction vs observations; maintenance prioritization; public safety communication |

Beyond deformation, multispectral and hyperspectral remote sensing provides environmental context relevant for post-mining management, such as the spatial pattern of mineralogical anomalies in tailings and surrounding soils (Dkhala et al., 2020; Milut et al., 2020), or the mapping of acid mine drainage potential using spectral information (Seifi et al., 2019). Early Romanian work using Landsat data demonstrated the feasibility of mapping mining waste deposits across large areas in Romania and Slovakia (Vîjdea et al., 2004), while more recent local studies have applied Landsat and Sentinel imagery to monitor land-cover change around Roșia Poieni (Herban et al., 2024).

The main limitation of integrated monitoring is not data availability but operationalization: stable reference frames, repeatable acquisition plans, and transparent uncertainty reporting are required to avoid false alarms or missed detections. The monitoring chain should therefore include (i) a well-defined geodetic reference network anchored in stable ground, (ii) standardized processing and metadata, (iii) cross-validation between independent methods, and (iv) governance rules for escalation and documentation consistent with risk-based standards (Scaioni et al., 2018; UNEP, 2020).

## CONCLUSIONS

Spatial geodetic monitoring has become central to mining geosystem risk management because it links point-scale structural observations to regional deformation patterns.

Multi-temporal InSAR is the most cost-efficient option for wide-area screening of slow deformation, but it requires careful treatment of LOS geometry, coherence and atmospheric artefacts, and benefits from local GNSS validation.

GNSS remains indispensable for absolute 3D control at critical structures (e.g., dam crests) and for near-real-time trend detection at selected points.

UAV SfM photogrammetry and UAV LiDAR provide high-resolution 3D geometry and volumetric change estimates, enabling detailed assessment of dumps, benches and tailings beaches when flights can be conducted safely and repeatably.

Integrated monitoring architectures combining InSAR, GNSS, UAV products and GIS decision layers support early warning, efficient field prioritization and defensible reporting aligned with modern tailings governance standards.

## ACKNOWLEDGEMENTS

The authors acknowledge the open-access Copernicus Sentinel data and the scientific community that provides processing tools and methodological developments supporting operational deformation monitoring in mining and post-mining environments.

## REFERENCES

Aswathi, J., Binoj Kumar, R. B., Oommen, T., Bouali, E. H., & Sajinkumar, K. S. (2022). InSAR as a tool for monitoring hydropower projects: A review. *Energy Geoscience*, 3(2), 160–171. https://doi.org/10.1016/j.engeos.2021.12.007

Berardino, P., Fornaro, G., Lanari, R., & Sansosti, E. (2002). A new algorithm for surface deformation monitoring based on small baseline differential SAR interferograms. *IEEE Transactions on Geoscience and Remote Sensing*, 40(11), 2375–2383. https://doi.org/10.1109/TGRS.2002.803792.

Calina, J., Calina, A., Milut, M., Badescu, G., & Cioboata, M. (2021). Study on the use of land scanning in soil erosion inventory works for sustainable agriculture in agritouristic farms. *Scientific Papers. Series A. Agronomy*, 64(1), 659–668.

Copernicus Data Space. (2025). Sentinel-1 documentation. Copernicus Data Space Ecosystem.

Copernicus Data Space. (2025). Sentinel-2 documentation. Copernicus Data Space Ecosystem.

Crosetto, M., Monserrat, O., Cuevas-González, M., Devanthéry, N., & Crippa, B. (2016). Persistent scatterer interferometry: A review. ISPRS *Journal of Photogrammetry and Remote Sensing*, 115, 78–89.

Del Soldato, M., Solari, L., Raspini, F., Bianchini, S., Ciampalini, A., Montalti, R., Ferretti, A., Pellegrineschi, V., & Casagli, N. (2019). Monitoring ground instabilities using SAR satellite data: A practical approach. *ISPRS International Journal of Geo-Information,* 8(7), 307. https://doi.org/10.3390/ijgi8070307

Dkhala, B., Mezned, N., Gomez, C., & Abdeljaouad, S. (2020). Hyperspectral field spectroscopy and Sentinel-2 Multispectral data for minerals with high pollution potential content estimation and mapping. *Science of the Total Environment*, 740, 140160.

ESA. (2025). Sentinel-2: The mission. European Space Agency.

European Parliament & Council. (2006). Directive 2006/21/EC on the management of waste from extractive industries. Official Journal of the European Union.

Ferretti, A., Prati, C., & Rocca, F. (2001). Permanent scatterers in SAR interferometry. *IEEE Transactions on Geoscience and Remote Sensing*, 39(1), 8–20. https://doi.org/10.1109/36.898661

Gheorghe, M., & Vodă Marc, A.-I. (2020). InSAR digital terrain models for mining areas based on Sentinel-1 imagery: A case study in Căliman area. *GeoPatterns*, 5, 21–26. https://doi.org/10.5719/GeoP.5/3

Hanssen, R. F. (2001). *Radar interferometry: Data interpretation and error analysis*. Springer.

Herban, S., Vilceanu, C.-B., Crisan, A., & Nistor-Lopatenco, L. (2024). Analysis of Landsat and Sentinel satellite images for Roșia Poieni quarry and Valea Șesii decantation pond. *Scientific Papers. Series E. Land Reclamation, Earth Observation & Surveying, Environmental Engineering, XIII*, 805–812.

Herrera, G., Tomás, R., López-Sánchez, J. M., Delgado, J., Mallorquí, J. J., Duque, S., & Mulas, J. (2007). Advanced DInSAR analysis on mining areas: La Unión case study (Murcia, SE Spain). *Engineering Geology*, 90(3–4), 148–159. https://doi.org/10.1016/j.enggeo.2007.01.001

Kirsch, M., Lorenz, S., Gloaguen, R., Baciu, C., Kerekes, A.-H., Deaconu, L.-T., Djaddaoui, F., Monserrat, O., & Pavel, N. (2025). Satellite-based, integrated environmental monitoring of mine sites: An example from the Roșia Poieni copper mine, Romania. *EGU General Assembly (EGU25)*, EGU25-13273. https://doi.org/10.5194/egusphere-egu25-13273

Lu, L., Li, M., & Chao, L. (2025). Integration of InSAR and numerical modelling to assess tailings pond slope deformation affected by reservoir water. Scientific Reports, 15, 43304. https://doi.org/10.1038/s41598-025-27314-0

Liu, X., Zhu, W., Lian, X., & Xu, X. (2023). Monitoring mining surface subsidence with multi-temporal three-dimensional unmanned aerial vehicle point cloud. *Remote Sensing*, 15(2), 374. https://doi.org/10.3390/rs15020374

Milut, M., Stan, I., Calina, J., Calina, A., Croitoru, A., Medelete, D., Badescu, G., & Ionica, C. (2020). Observations regarding the evolution of the agricultural land fund in Romania on categories of use after 1990. *Scientific papers. Series A. Agronomy*, 63(1), 92-97.

Nex, F., Armenakis, C., Cramer, M., Cucci, D. A., Gerke, M., Honkavaara, E., Kukko, A., Persello, C., & Skaloud, J. (2022). UAV in the advent of the twenties: Where we stand and what is next. *ISPRS Journal of Photogrammetry and Remote Sensing*, 184, 215–242. https://doi.org/10.1016/j.isprsjprs.2021.12.006

Poncoș, V., Stanciu, I., Teleagă, D., Maţenco, L., Bozsó, I., Szakács, A., Birtas, D., Toma, Ş.-A., Stănică, A., & Rădulescu, V. (2022). An integrated platform for ground-motion mapping, local validation and interpretation using InSAR and GNSS. *Remote Sensing*, 14(4), 1046. https://doi.org/10.3390/rs14041046

Przyłucka, M., Kowalski, Z., & Perski, Z. (2022). Twenty years of coal mining-induced subsidence in the Upper Silesia in Poland identified using InSAR. *International Journal of Coal Science & Technology*, 9, 86, 1–17. https://doi.org/10.1007/s40789-022-00541-w

Scaioni, M., Marsella, M., Crosetto, M., Tornatore, V., & Wang, J. (2018). Geodetic and remote-sensing sensors for dam deformation monitoring: A review. *Sensors*, 18(11), 3682. https://doi.org/10.3390/s18113682

Seifi, A., Hosseinjanizadeh, M., Ranjbar, H., & Honarmand, M. (2019). Identification of acid mine drainage potential using Sentinel 2a imagery and field

data. *Mine Water and the Environment*, 38, 707–717. https://doi.org/10.1007/s10230-019-00632-2

SentiWiki. (2025). Sentinel-1 mission. Copernicus SentiWiki.

Stefan, O., Badescu, G., Badescu, R., Badea, G., Badea, A. C., & Didulescu, C. (2009). GIS applications in the field of the Maramures subterranean mining exploitations. In *Proceedings of the 5th WSEAS International Conference on Remote Sensing (REMOTE '09)*, pp. 27–32.

TERRASIGNA. (2020). National ground motion monitoring: Romania between 2015–2019 (Ground motion report). TERRASIGNA.

UNEP - United Nations Environment Programme, International Council on Mining and Metals, & Principles for Responsible Investmen. (2020). Global Industry Standard on Tailings Management. United Nations Environment Programme.

Vîjdea, A. M., Sommer, S. R., & Mehl, W. (2004). Use of remote sensing for mapping and evaluation of mining waste anomalies at national to multi-country scale (EUR 21185 EN). European Commission, Joint Research Centre. ISBN 92-894-7792-X.

Westoby, M. J., Brasington, J., Glasser, N. F., Hambrey, M. J., & Reynolds, J. M. (2012). 'Structure-from-Motion' photogrammetry: A low-cost, effective tool for geoscience applications. *Geomorphology*, 179, 300–314. https://doi.org/10.1016/j.geomorph.2012.08.021

Williams, J. G., Anders, K., Winiwarter, L., Zahs, V., & Höfle, B. (2021). Multi-directional change detection between point clouds. *ISPRS Journal of Photogrammetry and Remote Sensing*, 172, 95–113. https://doi.org/10.1016/j.isprsjprs.2020.12.002

Scientific Papers. Series E. Land Reclamation, Earth Observation & Surveying, Environmental Engineering. Vol. XV, 2026
Print ISSN 2285-6064, CD-ROM ISSN 2285-6072, Online ISSN 2393-5138, ISSN-L 2285-6064

# COST EFFECTIVE SYSTEM FOR HUMAN PRESENCE DETECTION IN RURAL ENVIRONMENT

**Peter UDVARDY[1], Levente DIMEN[2], Gergely VAKULYA[1]**

[1]Obuda University, Alba Regia Faculty, 45 Budai, Szekesfehervar, Hungary
[2]University of Alba Iulia, 5 Gabriel Bethlen, Alba Iulia, Romania

Corresponding author email: udvardy.peter@uni-obuda.hu

***Abstract***

*The present study investigates methods for detecting human presence in remote natural environments, including nature reserves and protected areas. Such regions play a critical role in environmental sustainability, and excessive human activity may adversely affect these sensitive ecosystems. Conversely, accurate estimation of visitor numbers is essential for effective management and long-term preservation of these areas. Several approaches exist for human detection, including optical systems based on visible-spectrum or infrared imaging. However, these techniques may raise concerns regarding privacy and personal data protection. To address these limitations, this research explores the application of Wi-Fi-based detection methods. Given that a significant proportion of mobile device users keep Wi-Fi functionality enabled, passive monitoring systems can identify and record Wi-Fi signal activity without direct personal identification. A dedicated hardware and software framework was developed to quantify mobile Wi-Fi activity within a designated remote study area. Validation was conducted by simultaneous visual counting, and the results indicate that Wi-Fi-based detection provides a reliable method for estimating the absolute number of visitors, as well as their temporal distribution.*

***Key words****: environment monitoring, data collection, sensor network, Wi-Fi.*

## INTRODUCTION

Detecting human presence in nature has become increasingly vital for balancing conservation, education, and sustainable recreation. As more people seek connection with the outdoors, understanding where and when humans interact with wild spaces allows us to protect fragile ecosystems while highlighting nature's educational value. Nature trails, scenic overlooks, and biodiversity hotspots serve as living classrooms, demonstrating the importance of preserving habitats, biodiversity, and ecological processes. By monitoring visitation patterns - such as peak days of the week, time-of-day surges, seasonal trends, and rough visitor counts - land managers and educators can optimize trail maintenance, crowd-flow strategies, and interpretive programs that foster deeper public appreciation for the natural world (Leverington et al., 2010; Wu et al., 2015).

At the same time, certain sensitive areas must remain largely undisturbed to safeguard endangered species, prevent soil erosion, or maintain pristine habitats. Over-visitation in these zones can cause irreversible damage, from compacted trails and habitat fragmentation to the spread of invasive species carried on hikers' boots. Real-time or near-real-time detection of human presence enables authorities to identify emerging pressure points, issue timely alerts, or temporarily close sections before degradation accelerates. This dual approach - encouraging responsible access to "welcome" areas while quietly guarding "avoid" zones - helps ensure that nature's educational and recreational benefits endure for future generations (Lindgren et al., 2016).

The ubiquity of smartphones makes passive, cost-effective monitoring possible without invasive cameras or expensive sensor networks. Even when a phone's Wi-Fi is turned off, modern devices periodically broadcast 802.11 probe request frames in search of known networks. These tiny, anonymous radio signals can be captured by simple, low-power receivers placed discreetly along trails or at trailheads. By analysing the volume, timing, and movement patterns of these packets, researchers and park managers can estimate human presence and movement with surprising accuracy. This technique offers a privacy-

friendly, scalable solution that requires minimal infrastructure and can be deployed in remote locations where traditional counting methods (cameras, trail counters, or manual surveys) are impractical or cost-prohibitive (Wang et al., 2013; Farshad et al., 2014).

Ultimately, the goal is to present a practical, affordable methodology that transforms everyday smartphone emissions into actionable ecological intelligence. By turning the invisible digital chatter of visitors into meaningful insights about human-nature interactions, we can better protect wild places, enhance educational experiences, and promote truly sustainable outdoor recreation - all while keeping deployment costs low enough for widespread adoption by conservation organizations, national parks, and local communities.

## MATERIALS AND METHODS

### The test area

The Sóstó Natural Reserve is situated on the periphery of the city, in close proximity to the urban center. The area has a long-standing history of land use, having functioned as a recreational zone for approximately two centuries. Following the World War II, the site was repurposed as a municipal waste disposal area for nearly 40 years, during which both solid waste and sewage sludge were deposited.

Subsequent to the political transitions of the 1990s, extensive remediation and ecological restoration efforts were undertaken. As a result, the area was rehabilitated and officially designated as a protected natural reserve, ultimately becoming a prominent recreational destination for local residents. The hydrological conditions of the reserve are artificially supported: the wetland ecosystem is maintained through the daily input of approximately 550 $m^3$ of treated water supplied from a wastewater treatment facility (Udvardy et al., 2023).

The core of the reserve is located adjacent to the main sports arena of Székesfehérvár, reflecting a notable integration of urban infrastructure and environmental sustainability. The site attracts several hundred thousand visitors annually, and it also serves an important educational function, hosting structured environmental and sustainability programs in collaboration with local schools and the reserve's managing authority. Figure 1 shows the Sóstó natural reserve area with the city's contours as it locates very close to the city centre.



Figure 1. The Sóstó natural reserve test area

### Human presence detection

Cameras, paired with computer vision algorithms (using edge AI or cloud-based processing), can identify humans based on shape, motion, or facial features. This approach provides the most accurate approximation of the number of people and can support additional attributes, such as age estimation. Cameras perform best in daylight conditions, although infrared (IR) cameras are available for low-light environments. However, machine-vision–based systems typically have high power consumption and significant cost. Their operation requires a clear line of sight, making them sensitive to occlusions and adverse weather conditions. Privacy concerns represent an additional and often critical limitation (Berger & Lu, 2022).

PIR (Passive Infrared) detectors sense differential infrared radiation emitted by warm, moving bodies as they pass through segmented Fresnel lenses. These sensors are highly attractive due to their ultra-low power consumption, cost-effectiveness, simple installation, and completely passive operation with no active emissions. However, PIR detectors have several inherent limitations (Andrews et al., 2020).

Their effective detection range is relatively short, typically between 5 and 12 meters, and they exhibit a high false-trigger rate caused by animals, direct sunlight, wind-blown vegetation, or environmental thermal gradients. In addition, PIR sensors are unable to count people, determine movement direction, or detect stationary humans. It is important to

emphasize that PIR sensors respond only to motion and provide a strictly binary output, offering no estimate of the number of people present (Gami, 2018).

Microwave Doppler sensors are compact radar modules, operating mostly at 5.8 GHz or 10.525 GHz, emit continuous-wave microwave signals and measure Doppler frequency shifts produced by moving objects. Their advantages include the ability to penetrate light foliage, clothing, or thin barriers, reliable operation in total darkness and adverse weather conditions such as fog, rain, or snow, a moderate detection range, and relatively low power consumption (Arab et al., 2022).

The main disadvantages are the inability to reliably distinguish humans from animals, swaying vegetation, or even moving water surfaces. These sensors are also sensitive to environmental vibrations and can detect only motion rather than static presence. In addition, regulatory restrictions on transmitted power apply in some countries, and the limited spatial resolution makes precise trail-segment counting or accurate crowd-size estimation challenging (Tada et al., 2022).

Ultrasonic transducers emit short acoustic pulses at approximately 40 kHz and measure the time of flight of echoes reflected from nearby objects. Their advantages include excellent short-range accuracy, very low cost, immunity to lighting conditions, and the ability to perform precise distance-based presence detection without relying on visual or thermal signatures. However, ultrasonic sensing has significant limitations in outdoor environments. The effective range is extremely limited in open natural settings, as sound waves attenuate rapidly and scatter due to wind and vegetation such as leaves. Performance is also highly sensitive to temperature, humidity, wind, rain, and ambient acoustic noise. Ultrasonic waves cannot penetrate vegetation or physical obstacles, and frequently produce false readings due to insects or small animals (Biryukova & Koretskaya, 2020).

**Architecture**

Wi-Fi communication is defined by the IEEE 802.11 standard. It is built entirely around the exchange of structured packets called frames.

Every transmission – whether announcing a network, requesting information, establishing a connection, or carrying actual data – takes one of three broad categories:

- Management frames are responsible for discovering access points, joining them, roaming between them, and maintaining the connection.
- Control frames manage medium access and acknowledge successful receptions.
- Data frames carry the actual user payload, mostly IP traffic.

The management frames are identified by the Type field in the Frame Control field being set to 00 (binary). The 4-bit Subtype field then specifies the exact kind of management frame. These frames handle network discovery, joining/leaving a Basic Service Set (BSS), authentication, association, and other administrative functions. Figure 2 shows the 802.11 packet structure which is the base for the system architecture (Du et al., 2025).

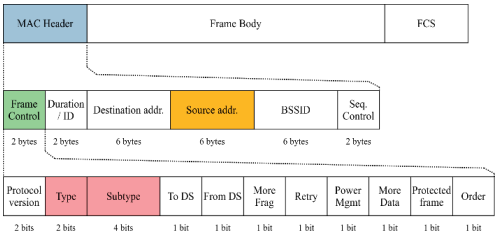



Figure 2. The 802.11 packet structure with the MAC header detailed

The defined management frame subtypes (as per the core 802.11 standard and its amendments up through recent revisions) are as follows, listed with their binary subtype values and common names:

- 0000 - Association Request;
- 0001 - Association Response;
- 0010 - Reassociation Request;
- 0011 - Reassociation Response;
- 0100 - Probe Request;
- 0101 - Probe Response;
- 0110 - Timing Advertisement (introduced in later amendments for synchronization);
- 1000 - Beacon;
- 1001 - Announcement Traffic Indication Message (ATIM) - used in Independent BSS (ad-hoc) networks for power-save coordination

- 1010 - Disassociation
- 1011 - Authentication
- 1100 - Deauthentication
- 1101 - Action (used for various management actions, spectrum management, radio measurement, etc.)
- 1110 - Action No ACK (a variant of Action frames that does not require acknowledgment, added in later amendments for efficiency in certain scenarios)

Subtypes 0111 and 1111 are typically reserved (unused or for future extensions), depending on the specific 802.11 amendment.

To connect to a Wi-Fi network, client devices such as smartphones and laptops must first discover which networks are available in their vicinity. One key method for this discovery is passive scanning, in which the device quietly listens across available channels without transmitting any frames. Access points (APs) in IEEE 802.11 wireless networks actively broadcast their Service Set Identifier (SSID) – the human-readable name of the Wi-Fi network – primarily through periodic beacon frames, which serve as the network's ongoing advertisement and synchronization signal.

These beacon frames are management frames transmitted at regular intervals, typically every 100-time units (approximately 102.4 milliseconds), on the AP's operating channel and at the lowest supported basic data rate to ensure maximum reachability by all potential clients in range. The SSID is included as a mandatory information element within the beacon frame body, allowing nearby devices performing passive scanning to discover available networks. This broadcast enables client devices to collect and list visible Wi-Fi networks (Gollier & Vanhoef, 2024).

Passive scanning requires a client device to listen on each Wi-Fi channel long enough to reliably capture at least one beacon frame from any nearby access point, since beacons are transmitted periodically – typically every 100-time units (approximately 102.4 ms), though the exact timing is asynchronous and unknown in advance. In the 2.4 GHz band, where most consumer devices operate in regions supporting channels 1 through 11 (or up to 13/14 depending on regulatory domain), this means the radio must remain powered on in receive mode for roughly 110-120 ms per channel to account for the beacon interval plus a small safety margin for channel switching overhead and potential beacon jitter. With 11 channels, a full passive scan can thus consume around 1.2-1.7 seconds of continuous operation of the radio, drawing significant power, often hundreds of milliwatts, during active listening. This energy cost is particularly burdensome for battery-powered smartphones. Figure 3 shows the in situ prototype of the detecting equipment.



Figure 3. Prototype of the Wi-Fi detection system deployed in situ

Another approach for network discovery is active scanning, in which client devices (such as smartphones and laptops) actively transmit probe request frames - management frames broadcast to the destination address ff:ff:ff:ff:ff:ff - targeting either specific known SSIDs (directed probes) or any available network (wildcard or null probes). This method is significantly faster than passive scanning because the device does not need to wait for the asynchronous arrival of beacon frames; instead, nearby access points that receive the probe request promptly reply with probe response frames containing the same essential BSS information (SSID, capabilities, security parameters, etc.) as beacons (Choi et al., 2017).

**Hardware architecture**

The hardware architecture of the human presence detection system is depicted in Figure 4. It is based on the ESP32-CAM module, originally designed to extend the ESP32 microcontroller with camera capabilities.

The board integrates a camera interface, an SD card slot, a Wi-Fi antenna, multiple IO ports, and a programming interface. In this implementation, the camera interface was not utilized. The ESP32-CAM was selected primarily because it offered the simplest design among available options that included a built-in SD card slot, while also being one of the most cost-effective solutions.

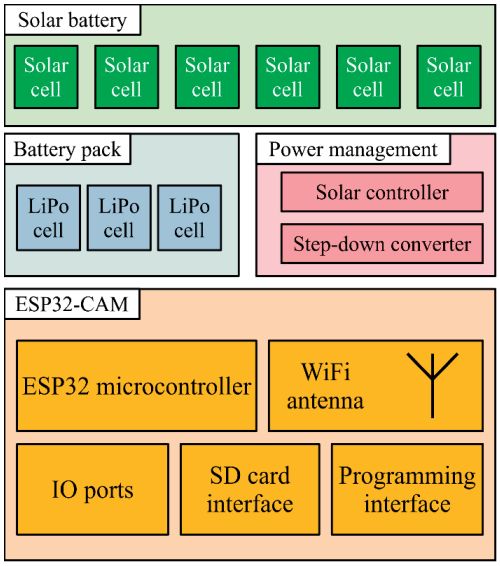



Figure 4. The hardware architecture of the system

The main component of the ESP32-CAM board is the ESP32 microcontroller. This device has two 32-bit xTensa CPU cores running at 240 MHz. The cores have IO port connections, high-speed serial buses (I2C and SPI) with DMA capability, timers and other common peripherals. The ESP32 stands out from the 32-bit ARM or RiscV families with its versatile Wi-Fi capabilities. It can act as a Wi-Fi client (station), access point (AP), or can even capture raw Wi-Fi packets.

The microcontroller is equipped with a 4 MB flash memory and 320 kB RAM to store the firmware and store the runtime data.

The ESP32 has several compatible sensor and other peripheral options from temperature, light, acceleration sensors to servos, SD card interfaces or even cameras.

The power source of the system is a 3-cell 2500 mAh lithium-polymer battery pack that provides a nominal voltage of 11.1 V. Power regulation and distribution are handled by a dedicated power management module, which incorporates both a solar charge controller and a step-down voltage regulator. Optionally, the battery pack can be recharged using a solar panel consisting of 6 photovoltaic cells connected in series.

**Software architecture**

The software of the human presence detection system is built on the FreeRTOS real-time operating system. FreeRTOS provides essential multitasking capabilities, including task management, scheduling, synchronization primitives, and message queues, along with direct access to the Wi-Fi subsystem and other hardware peripherals. Additional drivers handle SD card access and file system operations.

Upon boot, the Wi-Fi interface is configured in client (station) mode and attempts to connect to a predefined access point. Once connected, the system synchronizes its clock using the Network Time Protocol (NTP). Both the Wi-Fi connection and NTP synchronization are retried until successful. After time synchronization is completed, the Wi-Fi module is switched to a passive packet capture mode in which it listens continuously for all decodable packets, with probe request frames specifically filtered for processing.

Each captured probe request is placed into a message queue. Data from this queue is periodically flushed to the SD card as a CSV file at regular intervals (default: 30 minutes) or when the queue is nearing capacity. The CSV file is opened only during actual write operations and closed immediately afterward.

This approach, as opposed to writing after every packet or keeping the file continuously open, significantly extends the lifespan of the SD card and reduces the risk of file system corruption.

Each record in the CSV file contains the capture timestamp (year, month, day, hour, minute, and second), the source MAC address, the received signal strength (RSSI), and the

probed SSID. It should be noted that modern Android and iOS devices employ MAC address randomization and frequently transmit broadcast probe requests with an empty SSID field.
Consequently, a unique captured MAC address does not necessarily correspond to a unique physical device, and unique devices cannot be reliably distinguished based on the SSID field alone. Nevertheless, this method provides a practical and reasonably accurate approximation of the number of nearby Wi-Fi-enabled devices.

## RESULTS AND DISCUSSIONS

To evaluate the performance and usefulness of the human presence detection system, the device was deployed at the Sóstó Natural Reserve in a remote area far from residential buildings and other human infrastructure. This placement ensured that the system would detect primarily visitors genuinely present in the protected natural area rather than nearby residents or passers-by.
Figure 5 presents the recorded data for a single day. The logged probe requests were aggregated into one-hour intervals, and for each hour the number of unique MAC addresses from which at least one probe request was received was counted.

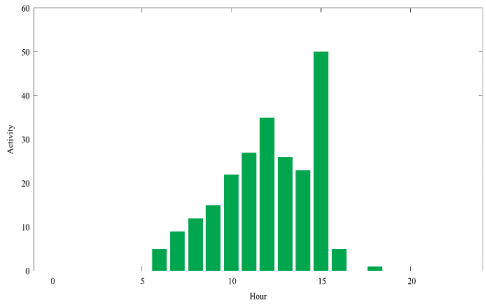


Figure 5. The collected and visualized activity data during a spring workday

As it was early spring, no visitors were detected before 6:00 a.m. or after 7:00 p.m. During the day, visitor activity showed a clear increase, reaching a first peak around noon. After a temporary decline, a second and larger peak occurred at 3:00 p.m., which corresponds to the most pleasant time of day for outdoor walks in early spring. A small additional peak was observed at 5:00 p.m., shortly after the typical end of a workday.
The absence of any detections during night time hours confirms that the system produced no false positives. The remote placement of the device, far from any residential areas, significantly contributed to this result by minimizing external interference.
This represents a notable advantage over many conventional human-presence monitoring systems, which often struggle with false triggers in populated environments. It is important to note that these detection-free periods were not caused by power loss, as any interruption in power supply is clearly visible in the system's log files.
The system's power consumption was also evaluated. After the initial setup phase, the average current draw stabilized at 39 mA. This low power requirement can be easily met by a moderately sized solar panel, even under modest lighting conditions. Furthermore, the system can operate autonomously for several days without solar input, with runtime depending primarily on battery capacity. For example, a compact 6 Ah battery can reliably power the system for approximately four days.
The robustness of the system was also evaluated through multiple power cycle tests. The log files remained fully consistent after each cycle, with no data loss or corruption observed.

## CONCLUSIONS

The Wi-Fi-based sensing systems represent a robust, scalable, and privacy-aware solution for monitoring human presence in remote natural environments, such as protected areas and nature reserves. Unlike conventional optical or infrared-based detection systems, which may raise significant concerns regarding personal data protection and require favourable environmental conditions, the proposed approach leverages passive monitoring of Wi-Fi probe signals. This enables an indirect yet effective detection of human presence without capturing personally identifiable information, thus aligning well with increasing legal expectations related to privacy.
The newly constructed hardware and software framework demonstrated reliable performance

in a real-world scenario. The system was capable of continuously capturing Wi-Fi signal activity and transforming it into meaningful indicators of visitor presence and movement patterns.

Comparative validation using simultaneous visual counting showed a strong correspondence between measured Wi-Fi activity and the actual number of individuals present in the monitored area. In addition to estimating absolute visitor counts, the system also provided valuable insights into temporal dynamics, such as peak visitation periods and fluctuations in human activity over time.

These capabilities are particularly relevant for environmental management and conservation practices. Accurate, continuous, and non-intrusive monitoring can support decision-makers in assessing anthropogenic pressure on sensitive ecosystems, optimizing the number of visitors and implementing adaptive management strategies. Furthermore, the relatively low cost, ease of deployment, and minimal maintenance requirements of Wi-Fi-based systems make the system especially suitable for large-scale or hard-to-access regions where traditional monitoring infrastructure may be impractical. Solar powered solutions contribute to solve sustainability challenges.

Despite the many advantages there are certain limitations that must be considered. The method inherently depends on the proportion of visitors carrying Wi-Fi-enabled devices with active signal broadcasting, which may introduce bias in absolute estimations under specific demographic or behavioural conditions. Additionally, environmental factors such as terrain, vegetation density, and signal interference can influence detection range and accuracy. Addressing these challenges may require calibration procedures, site-specific parameter tuning, or the integration of complementary sensing modalities.

Future research directions include the fusion of Wi-Fi sensing with other non-invasive technologies such as another environmental sensor, the application of advanced data analytics and machine learning techniques for improved signal interpretation, and the development of adaptive algorithms capable of compensating for environmental variability. Expanding long-term deployments across diverse ecological contexts would further validate the generalizability and reliability of the approach.

In summary, the presented Wi-Fi-based detection methodology offers a promising pathway toward sustainable, privacy-conscious and data-driven monitoring of human activity in ecologically sensitive areas, contributing to more effective conservation and management practices.

## REFERENCES

Andrews, J., Kowsika, M., Vakil, A., & Li, J. (2020). A motion induced passive infrared (PIR) sensor for stationary human occupancy detection. In *Proceedings of the 2020 IEEE/ION Position, Location and Navigation Symposium (PLANS)*. 1295–1304. https://doi.org/10.1109/PLANS 46316.2020.9109909

Arab, H., Ghaffari, I., Chioukh, L., Tatu, S. O., & Dufour, S. (2022). A convolutional neural network for human motion recognition and classification using a millimeter-wave Doppler radar. *IEEE Sensors Journal*, 22(5). 4494–4502. https://doi.org/10.1109/JSEN.2022.3140787

Berger, J., & Lu, S. (2022). A multi-camera system for human detection and activity recognition. *Procedia CIRP, 112*. 191–196. https://doi.org/10.1016/j.procir.2022.09.071

Biryukova, O. V., & Koretskaya, I. V. (2020). Selection of ultrasonic sensors for distance monitoring. In *Proceedings of the 2020 Systems of Signal Synchronization, Generating and Processing in Telecommunications (SYNCHROINFO).* 1–4. https://doi.org/10.1109/SYNCHROINFO49631.2020.9166089

Choi, T., Chon, Y., & Cha, H. (2017). Energy-efficient WiFi scanning for localization. *Pervasive and Mobile Computing, 37*. 124–138. https://doi.org/10.1016/j.pmcj.2016.07.005

Du, R., Hua, H., Xie, H., Song, X., Lyu, Z., & Hu, M. (2025). An overview on IEEE 802.11bf: WLAN sensing. *IEEE Communications Surveys & Tutorials, 27(1)*.

Farshad, A., Marina, M. K., & Garcia, F. (2014). Urban WiFi characterization via mobile crowdsensing. *IEEE Network Operations and Management Symposium (NOMS)*. 1–9. https://doi.org/10.1109/NOMS.2014.6838233

Gami, H. (2018). Movement direction and distance classification using a single PIR sensor. *IEEE Sensors Letters, 2(1)*. https://doi.org/10.1109/LSENS.2018.2792419

Gollier, H., & Vanhoef, M. (2024). SSID confusion: Making Wi-Fi clients connect to the wrong network. *Proceedings of the 17th ACM Conference on Security and Privacy in Wireless and Mobile Networks (WiSec*

*'24)*. 156–161. https://doi.org/10.1145/3643833.3656126

Leverington, F., Costa, K. L., Pavese, H., Lisle, A., & Hockings, M. (2010). A global analysis of protected area management effectiveness. *Environmental Management, 46*. 685–698. https://doi.org/10.1007/s00267-010-9564-5

Lindgren, J. F., Andersson, K., Brynolf, S., & Wilewska-Bien, M. (2016). The natural environment and human impacts. In K. Andersson, S. Brynolf, J. Lindgren, & M. Wilewska-Bien (Eds.), *Shipping and the environment* (pp. 23–52). Springer. https://doi.org/10.1007/978-3-662-49045-7_2

Tada, M., Yoshida, T., Hamada, Y., Kurihara, Y., Kobayashi, K., & Watanabe, K. (2022). Application of microwave Doppler sensor for remote vibration measurement. *IEEE Sensors Journal, 22(20).* 19975–19982. https://doi.org/10.1109/JSEN.2022. 3203080

Udvardy, P., Dimen, L., & Vakulya, G. (2023). Data collection in the wild: Challenges and solutions. *Scientific Papers. Series E. Land Reclamation, Earth Observation & Surveying, Environmental Engineering, 12*. ISSN 2285-6064

Wang, W., Joshi, R., Kulkarni, A., Leong, W. K., & Leong, B. (2013). Feasibility study of mobile phone WiFi detection in aerial search and rescue operations. *Proceedings of the 4th Asia-Pacific Workshop on Systems (APSys '13), Article 7*. 1–6. https://doi.org/10.1145/2500727.2500729

Wu, W., Zhang, X., Yang, Z., Qin, W., Wang, F., & Wang, C. (2015). Ecotourism suitability and zoning from the tourist perspective: A nature reserve case study. *Polish Journal of Environmental Studies, 24(6)*, 2683–2697. https://doi.org/10.15244/pjoes/5942202




ISSN 2285 – 6064
ISSN-L 2285 – 6064